FINAL REPORT

Defense Coastal/Estuarine Research Program (DCERP)

SERDP Project RC-2245

JANUARY 2018

Dr. Patricia Cunningham
Research Triangle Institute

Distribution Statement A
This document has been cleared for public release

SERDP
DOD ▪ EPA ▪ DOE

Page Intentionally Left Blank

This report was prepared under contract to the Department of Defense Strategic Environmental Research and Development Program (SERDP). The publication of this report does not indicate endorsement by the Department of Defense, nor should the contents be construed as reflecting the official policy or position of the Department of Defense. Reference herein to any specific commercial product, process, or service by trade name, trademark, manufacturer, or otherwise, does not necessarily constitute or imply its endorsement, recommendation, or favoring by the Department of Defense.

Page Intentionally Left Blank

REPORT DOCUMENTATION PAGE

Form Approved
OMB No. 0704-0188

Public reporting burden for this collection of information is estimated to average 1 hour per response, including the time for reviewing instructions, searching existing data sources, gathering and maintaining the data needed, and completing and reviewing this collection of information. Send comments regarding this burden estimate or any other aspect of this collection of information, including suggestions for reducing this burden to Department of Defense, Washington Headquarters Services, Directorate for Information Operations and Reports (0704-0188), 1215 Jefferson Davis Highway, Suite 1204, Arlington, VA 22202-4302. Respondents should be aware that notwithstanding any other provision of law, no person shall be subject to any penalty for failing to comply with a collection of information if it does not display a currently valid OMB control number. **PLEASE DO NOT RETURN YOUR FORM TO THE ABOVE ADDRESS.**

1. REPORT DATE *(DD-MM-YYYY)*
31-01-2018

2. REPORT TYPE
Final Technical Report

3. DATES COVERED *(From - To)*
April,2013 - December,2017

4. TITLE AND SUBTITLE

Defense Coastal/Estuarine Research Program 2 (DCERP2) Final Report

5a. CONTRACT NUMBER
W912HQ-13-C-0004

5b. GRANT NUMBER

5c. PROGRAM ELEMENT NUMBER

6. AUTHOR(S)
Cunningham, Patricia; Anderson, Iris; Brush, Mark; Christensen, Norman; Currin, Carolyn; Boezio, Danette; Ensign, Scott; Fegley, Stephen; Halpin, Patrick; Harrell, Peter; Kirwan, Matt; Matthews, Kimberly; Mckee, Brent; McNinch, Jesse; Mitchell, Steve; Paerl Hans; Piehler, Michael; Rodriguez, Antonio; Simms, Aaron; Tobias, Craig; and Walters, Jeffery

5d. PROJECT NUMBER
SERDP RC-2245

5e. TASK NUMBER

5f. WORK UNIT NUMBER

7. PERFORMING ORGANIZATION NAME(S) AND ADDRESS(ES)

RTI International
3040 Cornwallis Road
PO Box 12194
Research Triangle Park, NC
27709-2194

8. PERFORMING ORGANIZATION REPORT NUMBER
RC-2245

9. SPONSORING / MONITORING AGENCY NAME(S) AND ADDRESS(ES)

SERDP/ESTCP
4800 Mark Center Drive
Alexandria, VA 22350-3605

10. SPONSOR/MONITOR'S ACRONYM(S)
SERDP

11. SPONSOR/MONITOR'S REPORT NUMBER(S)
RC-2245

12. DISTRIBUTION / AVAILABILITY STATEMENT

Approved for public distribution; distribution is unlimited.

13. SUPPLEMENTARY NOTES

14. ABSTRACT

The Defense Coastal/Estuarine Research Program 2 (DCERP2) is a research-based program that was sited at Marine Corps Base Camp Lejeune (MCBCL), NC. The overall objective of DCERP2 was to recommend adaptive management strategies to sustain ecosystem natural resources within the context of an active military installation and predict plausible changes to these resources from future climate conditions including rising sea level. To address these challenges, the DCERP Team developed and implemented a research and monitoring program with the following objectives: 1. To understand MCBCL's diverse ecosystems and the effects man-made and natural drivers have on critical ecosystem processes (i.e., nutrient utilization and sediment transport); 2. To develop a carbon budget for the estuarine/coastal ecosystem that includes exchanges among these coastal ecosystems; and 3. To convey program results to DoD and other users through easy-to-use, Web-based tools and products. Another objective was to provide research support to other DoD installations in addition to MCBCL and research was also conducted at Marine Corps Air Station Cherry Point NC, Fort Bragg NC, and Eglin Air Force Base FL. This report includes the results and conclusions from 13 research projects and associated monitoring and modeling activities conducted as part of DCERP2.

15. SUBJECT TERMS
Ecosystem-based management, coastal wetlands, coastal barrier, aquatic-estuarine, terrestrial, climate change, sea level rise, carbon cycle, adaptation, resiliency, New River Estuary, Camp Lejeune, and translating science into practice

16. SECURITY CLASSIFICATION OF:			**17. LIMITATION OF ABSTRACT**	**18. NUMBER OF PAGES**	**19a. NAME OF RESPONSIBLE PERSON**
					Kimberly Matthews
a. REPORT	**b. ABSTRACT**	**c. THIS PAGE**			**19b. TELEPHONE NUMBER** *(include area code)*
Unclassified	Unclassified	Unclassified		1,306	919-316-3366

Standard Form 298 (Rev. 8-98)
Prescribed by ANSI Std. Z39.18

Page Intentionally Left Blank

Table of Contents

Abstract v

Chapter 1. Introduction 1-1

Chapter 2. Significant Findings and Management Implications 2-1

Chapter 3. Development of Uniform Historical and Projected Climate to Support Integrated Coastal Ecosystem Research (Research Project CC-1) 3-1

Chapter 4. Aquatic/Estuarine Module Monitoring Activity AEM-4: New River 4-1

Chapter 5. Aquatic/Estuarine Module Monitoring Activity AEM-2: Tributary Creeks 5-1

Chapter 6. Aquatic/Estuarine Module Monitoring Activity AEM-1: Main Channel of the New River Estuary 6-1

Chapter 7. Aquatic/Estuarine Module Monitoring Activity AEM-3: Shallow Zone of the New River Estuary 7-1

Chapter 8. Climate and Land-Use Impacts on Exports of Carbon, Suspended Solids, and Nutrients from Coastal Subwatersheds (Research Project AE-5) 8-1

Chapter 9. Nutrient-Driven Eutrophication and Carbon Flux Modulated by Climate Change in the New River Estuary (Research Project AE-4) and Climatic Drivers Regulating Benthic-Pelagic Carbon and Associated Nutrient Exchanges in the New River Estuary (Research Project AE-6) 9-1

Chapter 10. Coupled Ecosystem Modeling of the NRE for Research, Synthesis, and Management (Research Project TSP-2) 10-1

Chapter 11. Coastal Wetlands Module Monitoring Activity CWM-1 11-1

Chapter 12. Carbon Burial in Estuarine, Wetland, and Coastal Barrier Environments (Research Project AE-6, CW-4, CB-5) 12-1

Chapter 13. Improving Model Predictions for Marsh Response to Sea Level Rise and Implications for Natural Resource Management (Research Project CW-4) 13-1

Chapter 14. Marsh–Atmosphere and Marsh–Creek Exchanges of Carbon (Research Project CW-5) 14-1

Chapter 15. Predicting Sustainability of Coastal Military Training Environments: Developing and Evaluating a Simplified, Numerical Morphology Model (Research Project CB-4) 15-1

Chapter 16. Linking Barrier Island Transgression Induced by Storms and Sea Level Rise to the Carbon Cycle (Research Project CB-5). 16-1

Chapter 17. Effects of Different Understory/Midstory Restoration Management Options on Terrestrial Ecosystem Plant and Bird Communities (Research Project T-1) 17-1

Chapter 18. Forest Management, Species Habitat, and Implications for Carbon Flux and Storage (Research Project T-3) 18-1

Chapter 19. Impacts of Climate Change on Management of Red-Cockaded Woodpeckers at MCBCL (Research Project T-4). 19-1

Chapter 20. Using LiDAR to Measure Forests at Marine Corps Base Camp Lejeune (Research Project TSP-1) 20-1

Chapter 21. Development of a Spatial Decision-Support Framework: Translating Science into Practice Module (Research Project TSP-1) 21-1

Abstract (DCERP2 Final Report)

Objectives

Critical military training and testing on lands along the nation's coastal and estuarine shorelines are increasingly placed at risk because of encroachment pressures in surrounding areas, impairments due to other anthropogenic disturbances, and changes in climate and sea level. The U.S. Department of Defense (DoD) intends to enhance and sustain its training and testing assets and also optimize its stewardship of natural resources through the development and application of an ecosystem-based management approach on DoD installations. To accomplish this goal, particularly for installations in estuarine/coastal environments, the Strategic Environmental Research and Development Program (SERDP) launched the Defense Coastal/Estuarine Research Program (DCERP) as a 10-year effort at Marine Corps Base Camp Lejeune (MCBCL) in North Carolina. The results of the second 5 years of the program (DCERP2) are presented in the *DCERP2 Final Report.*

There were four overarching objectives of DCERP2. The first objective was to understand the effects of climate change impacts, including warming temperatures, variability in the hydrological cycle, storm events, and sea level rise on the coastal ecosystems at MCBCL from observations and measurements made over the 10-year program. The second objective was to understand the carbon cycle of the coastal and terrestrial ecosystems at MCBCL through a highly integrated sampling program. The third objective was to develop models, tools, and indicators to evaluate current and projected future ecosystem state changes and translate scientific findings into actionable information for installation managers. The last objective was to recommend adaptive management strategies to sustain ecosystem natural resources within the context of an active military installation.

Technical Approach

DCERP2 was implemented in two phases. The first phase was a 3-month planning period for identifying ecosystem processes and stressors, developing conceptual models to identify knowledge gaps, and working iteratively with DoD end-users to refine approaches to support MCBCL natural resource management. This effort resulted in the development of the *DCERP2 Monitoring Plan* and the *DCERP2 Research Plan*, which collectively served as the foundation for all DCERP2 activities. The DCERP Team approached and implemented the research and monitoring work by dividing the landscape into four distinct ecosystem modules: Aquatic/Estuarine, Coastal Wetlands, Coastal Barrier, and Terrestrial Modules. Because the effects of climate change have an overarching influence on all four ecosystem modules, climate change was treated as a fifth module (i.e., the Climate Change Module).

Implementation of the DCERP2 plans began in April 2013 and resulted in 13 research projects and five monitoring activities, as well as the enhancement of the DCERP Data and Information Management System (DIMS), which contains monitoring and research data from DCERP1 and DCERP2. DIMS provides optimized data storage and retrieval for integrated analysis, fostering information exchange among the various DCERP partners, other interested researchers, and stakeholders.

Results

Climate Change Impacts on Ecosystem Processes

MCBCL encompasses 153,000 acres and occupies 80% of the shoreline of the New River Estuary (NRE), thus making the NRE a core consideration to the management of the installation. The remainder of MCBCL consists of terrestrial habitat (i.e., 90,000 acres), which is managed for training and is also a wildlife habitat. To understand the potential impacts of climate change, the DCERP2 Team selected the climate drivers that would have the most influence on the MCBCL ecosystems and the region of study. The climate drivers selected included temperature, precipitation, storminess, and sea level rise. The DCERP2 Team used empirical data to understand the present state of the ecosystems and their natural variability under current climate conditions and developed ecological process models to understand the potential climate impacts on the ecosystems in the future.

To study these future impacts, we developed an ensemble of 24 climate model projections that represent the worst-case scenario of increasing concentrations of greenhouse gases in the future. This ensemble showed agreement regarding the magnitude of future temperature changes (e.g., increases) as compared with the magnitude of changes in precipitation, which will increase, decrease, or remain the same. Understanding the future temperatures is important because temperatures affect the function of natural systems in fundamental ways, including determining the rates of chemical reactions, an organism's metabolism, and the timing of critical life cycle events (phenology). In the terrestrial ecosystem, warming temperatures measured over the past 33 years were shown to have advanced egg-laying dates (5 days earlier) of red-cockaded woodpeckers (RCWs; *Picoides borealis*) at MCBCL and nearby at Fort Bragg, NC, and increased productivity at Fort Bragg. However, warmer temperatures are also associated with a lower coincidental survival rate of juvenile RCWs. Other considerations related to higher future temperatures may further complicate RCW management, such as the ability to maintain a regular prescribed fire regime, without which the RCW's longleaf pine (*Pinus palustris*) habitat cannot be sustained.

These complicated temperature interactions can also be observed in estuarine water quality. Under the Estuarine Simulation Model (ESM) scenarios that increased temperatures from +1°C (+1.8°F) to +5°C (+9°F) above current temperatures, hypoxia (i.e., low dissolved oxygen concentrations caused by decomposition of organic matter) in the NRE would increase, subsequently stressing the fish and shellfish living in these waters. In contrast, the ESM predicted water quality improvements such as decreases in chlorophyll *a* concentrations and days with chlorophyll *a* concentrations exceeding the state standard of greater than 40 µg/L. These temperature responses are also subject to modulation by changes in freshwater inflow and loadings due to inter-annual precipitation variability. However, the future impacts of precipitation at MCBCL are difficult to determine for all ecosystems because down-scaled climate projections indicated either a slight decrease or increase in the amount and intensity of rainfall.

Although there will be interactions with temperature and precipitation in the future, the effects of sea level rise on MCBCL's coastal marshes and the coastal barrier, Onslow Island, are more significant. Marsh resilience will depend upon the rate of sea level rise in combination with marsh plant productivity, suspended sediment inputs that regulate vertical accretion, and the

slope of the adjacent uplands for marsh migration. The DCERP2 Team developed the Geospatial Marsh Model, which predicted that marshes throughout the estuarine gradient gain area under the lowest sea level rise scenario (0.3 m by 2100) through a combination of expansion via marsh migration upslope and enhanced vertical accretion. Above the medium sea level rise scenario (1.3 m by 2100), the model predicted that both middle and lower NRE marshes drown because of limited sediment supply and reduced ability to continue to migrate landward. The marsh that demonstrated the highest resilience is located along the Intracoastal Waterway. This marsh that has the highest sediment supply and the lowest surrounding slope was only predicted to drown at the highest sea level rise rate (greater than 1.8 m by 2100).

Over the past 70 years, measured changes to the coastal barrier indicated that storms (defined here by decadal hurricane frequency) and sea level rise, not military training use, had the largest influence on beach position and overwash. The DCERP2 Beach Morphology Model, which used the lowest (0.3 m) and highest (2.5 m) sea level rise by 2100, projected a substantial loss of infrastructure on the southern portion of the barrier island regardless of sea level rise rate by 2035 and a complete loss of usable beach by 2065. Conversely, the same model scenarios indicated that the northern portion of Onslow Island will remain stable and likely grow seaward, thereby allowing MCBCL managers to consider moving the amphibious assault training areas to the more stable northern end of Onslow Beach.

Carbon Cycles in Coastal Ecosystems

Quantifying carbon cycling in the estuarine/coastal landscape within MCBCL's boundaries hinged upon measuring intra-ecosystem carbon inventories and inter-ecosystem fluxes at appropriate spatial and temporal scales. Coastal carbon fluxes are highly variable in space and time and are challenging to measure; thus, few coastal carbon budgets are currently available, and most of these have relied on limited observational scales. The DCERP2 Team conducted novel research that captured daily, seasonal, annual, and inter-annual variabilities in carbon fluxes and exchanges across the shallow and pelagic areas of the estuary from the head of the estuary to its discharge into the coastal ocean to determine the main drivers of the carbon cycle for the NRE. The team also measured carbon fluxes before and after a major storm event and determined that significant fluxes resulted from the storm's passage that were not considered in most other carbon studies.

The NRE carbon budget quantified flows and tracked the complex processes that control whether carbon supplied from the watershed or formed in the estuary is stored internally, exported into the ocean, or emitted into the atmosphere. The NRE was in near metabolic balance annually, with only minor exchanges of carbon dioxide between the atmosphere and estuary. Depending upon river discharge, the NRE was either slightly net heterotrophic (more respiration than photosynthesis) or slightly autotrophic (more photosynthesis than respiration). This small variation around net neutral metabolism was maintained by counter-balancing multiple reactions and exchanges between the deeper estuarine channel and shallow shoals and between the upper and lower portions of the estuary. Daily variations in carbon fluxes were as large as those on seasonal time scales, which have been ignored in many other estuarine carbon studies, thus demonstrating the need to perform high-resolution temporal and spatial measurements to understand the mechanisms driving the observed carbon fluxes.

The DCERP2 Team determined that the flux of carbon across the estuary to the coastal salt marshes and the barrier island boundaries was relatively minor. Overall, the annual net carbon balance in the marshes was driven by carbon exchanges with the atmosphere and short-term sediment deposition. Lateral fluxes of carbon between the estuary and marsh, both through drainage of the marsh platform during ebbing tides and via porewater advection, were small when compared with the atmospheric exchanges. Most marshes at MCBCL fixed more carbon than they respired; however, the small aerial extent of coastal wetlands relative to the total area of MCBCL limits their contribution to the larger landscape carbon budget. The other ecosystem services, such as fisheries habitat and attenuating wave energy, provided by these marshes at MCBCL may be a more important role than carbon storage. The carbon flux measurement of the coastal barrier showed that storms drove the transition of the island from being a carbon sink to a carbon source. This transition occurs because storms increased carbon loss through shoreface erosion of peat deposits buried beneath the island and reduced carbon storage through washover sand deposition that buries backbarrier marshes. Future changes in the magnitude and frequency of storms could accelerate carbon loss through increased erosion.

In contrast to the estuarine ecosystems, the terrestrial portion of the MCBCL landscape represents the largest carbon management potential in both size and quantities of carbon that could be stored. Results of forest carbon modeling showed that above-ground live carbon storage for three prevalent pine species on MCBCL was highest in longleaf pine, moderate in loblolly pine (*Pinus taeda*), and lowest in pond pine (*Pinus serotina*) forests. Longleaf pine is the forest species of greatest focus and management aboard MCBCL and at several other DoD installations in the Southeastern United States. Longleaf pine represents the greatest opportunity for carbon storage into the future under management scenarios designed to maintain or restore longleaf habitat, primarily through using prescribed fire.

Models, Tools, and Indicators to Assess Ecosystem State Change and Recommend Adaptive Management Strategies

The DCERP2 Team developed ecosystem models, tools, and environmental indicators to assist installation managers in making more informed management decisions. The DCERP2 Team identified several indicators of changes in ecosystem state that can serve as useful targets for managers and inform decisions about land-use changes, point source discharges, forest management practices, and marsh mitigation activities. The communication of information to DoD managers and other end-users was an ongoing process and involved maps, user guides, easy-to-interpret model outputs, annual reports, workshops, and one-on-one meetings. These outreach efforts and products were designed to share DoD–relevant information and provide MCBCL with adaptive management strategies. All DCERP products were collected throughout the program in DIMS, which is currently available to all registered users at https://dcerp.rti.org. The DIMS data portal fulfills the SERDP's data management goal for DCERP by providing an accessible Web-based platform for distributing all DCERP data, tools, models, and other products to all three target audiences: researchers, DoD installation managers, and local stakeholders, including the public.

Benefits

The research, monitoring, and modeling efforts conducted as part of DCERP2 resulted in a greater understanding of MCBCL's diverse ecosystems and their interactions with respect to the carbon cycle, management of carbon, and plausible future climate conditions. In addition, the research results provided an understanding of which on- and off-installation activities are currently affecting these ecosystems and what management actions could be implemented to best sustain the military's training mission and natural resource assets of MCBCL. The DCERP2 Team recommended that MCBCL continue long-term monitoring in a scaled-back manner in several of the ecosystems of study. Long-term monitoring data provide information about the status of critical indicators such as chlorophyll *a* concentration, thus allowing shifts in baseline conditions or increases in historic variation to be detected. These shifts in baseline conditions or historic variability may suggest changes to the way in which an ecosystem functions. The knowledge gained from DCERP2 will provide benefits to other DoD installations in similar coastal settings and to the scientific community, other coastal managers, and the public at large.

Chapter 1

Introduction

SERDP Project Number: RC-2245

Principal Investigator:

Dr. Patricia Cunningham
RTI International
E-mail: patc@rti.org

Supporting Researchers:

Kim Matthews, kmatthews@rti.org

November 2017

Final

This report was prepared under contract to the U.S. Department of Defense (DoD) Strategic Environmental Research and Development Program (SERDP). The publication of this report does not indicate endorsement by DoD, nor should the contents be construed as reflecting the official policy or position of DoD. References herein to any specific commercial product, process, or service by trade name, trademark, manufacturer, or otherwise, do not necessarily constitute or imply its endorsement, recommendation, or favoring by DoD.

Table of Contents

List of Acronyms 1-v
Introduction 1-1
DCERP Goals and Objectives 1-1
Background 1-2
Site Selection 1-2
Integration of DCERP with MCBCL's Natural Resources Management 1-3
Program Organization 1-4
DCERP2 Management Team 1-4
DCERP2 Research Team 1-5
DCERP2 Executive Committee 1-6
DCERP2 Modules 1-6
Thematic Areas 1-6
Description of Themes 1-6
Climate Change 1-7
Carbon Cycle and Carbon Management 1-7
Translating Science into Practice 1-8
DCERP Strategy—Planning Phase 1-9
DCERP Strategy—Implementation Phase 1-11
Design and Implement DCERP2 Research Projects 1-11
Design and Implementation of Monitoring Activities 1-13
Identify Indicators, Develop Tools, and Design Models 1-14
Translate Relevant Findings into Actionable Information for DoD Installation Managers 1-14
Data Management 1-15
Report Organization 1-15
Literature Cited 1-16
Appendix 1-A: DCERP2 Technical Advisory Committee 1-A-1
Appendix 1-B: DCERP2 Regional Coordinating Committee 1-B-1
Appendix 1-C: DCERP2 Logic Model 1-C-1

List of Figures

Figure 1-1. Site map of MCBCL 1-3
Figure 1-2. The organization of DCERP2, with the DCERP2 Research Team shown within the blue border 1-5
Figure 1-3. The carbon budget for the New River and its surrounding coastal area. 1-8
Figure 1-4. The overall process used for meeting DCERP's objectives. 1-10
Figure 1-5. The overarching conceptual model for DCERP2 at MCBCL. 1-11

List of Tables

Table 1-1. Programmatic Themes for DCERP 1-7
Table 1-2. Examples of Military, Non-Military, Legacy, and Natural Stressors to an Ecosystem 1-10
Table 1-3. Research Projects from DCERP1 and DCERP2 1-12
Table 1-4. Summary of DCERP2 Module-Specific Monitoring Activities 1-14
Table 1-5. Models Developed and/or Applied During DCERP2 1-14

List of Acronyms

AE	Aquatic/Estuarine (Module)
Air	Atmospheric (Module)
BMA	benthic microalgae
C	carbon
CB	Coastal Barrier (Module)
CC	Climate Change (Module)
CDOM	chromophoric dissolved organic matter
CO_2	carbon dioxide
CW	Coastal Wetlands (Module)
DCERP	Defense Coastal/Estuarine Research Program
DCERP1	first cycle of the Defense Coastal/Estuarine Research Program
DCERP2	second cycle of the Defense Coastal/Estuarine Research Program
DIMS	Data and Information Management System
DoD	U.S. Department of Defense
EMD	Environmental Management Division
EPA	U.S. Environmental Protection Agency
iMAP	interactive mapping application
ICW	Intracoastal Waterway
INRMP	Integrated Natural Resources Management Plan
IPR	In-Progress Review
km	kilometer
MARDIS	Monitoring and Research Data and Information System
MCBCL	Marine Corps Base Camp Lejeune
mm/yr	millimeters per year
N	nitrogen
NAVFAC EXWC	Naval Facilities Engineering and Expeditionary Warfare Center
NOAA	National Oceanic and Atmospheric Administration
NRE	New River Estuary
OSC	On-site Coordinator
PI	Principal Investigator
RC	Resource Conservation and Climate Change (a SERDP program area)

RCC	Regional Coordinating Committee
RCCC	Resource Conservation and Climate Change (Program)
SERDP	Strategic Environmental Research and Development Program
RCW	red-cockaded woodpecker
T	Terrestrial (Module)
TAC	Technical Advisory Committee
TSP	Translating Science into Practice (Module)
USACE	U.S. Army Corps of Engineers

Introduction

The overall intent of the Defense Coastal/Estuarine Research Program (DCERP) was "to develop the knowledge required to assess the interaction between military [training] activities and ecological resources in a coastal/estuarine setting, monitor those interactions, and identify adaptive, ecosystem management approaches for sustainment of military lands and adjacent waters" (SERDP, 2005). DCERP1, conducted from 2007 to 2012, focused on the overall intent of the Strategic Environmental Research and Development Program (SERDP) goals for DCERP. During DCERP2, conducted from 2013 to 2017, SERDP expanded these goals to understanding the potential impacts of future climate change on the sustainability of the U.S. Department of Defense's (DoD's) military training mission, understanding the carbon cycle and the potential for managing natural resources to maximize natural carbon storage, and developing easy-to-use tools and models to help DoD installation managers make more informed management decisions. The purpose of this *DCERP2 Final Report* is to summarize the research, monitoring, and modeling activities and results from work conducted during DCERP2, which builds on work accomplished previously during DCERP1.

This chapter of the *DCERP2 Final Report* provides a programmatic background to DCERP activities conducted at Marine Corps Base Camp Lejeune (MCBCL) in North Carolina (the primary study site) and secondary DoD installations. This chapter also highlights the overall program organization and objectives and describes the activities conducted during DCERP2. This chapter describes how the DCERP Team engaged with other team members and MCBCL natural resources management staff during DCERP2's initial planning and throughout the conduct of the program. The planning period was used to prepare the *DCERP2 Monitoring Plan* (RTI, 2013a) and *DCERP2 Research Plan* (RTI, 2013b), which both follow and complement the overarching research strategy developed at the start of the 10-year program (RTI, 2007a). This chapter discusses the development of the Data and Information Management System (DIMS) for the program to facilitate translation of findings to scientists, managers, and stakeholders.

DCERP Goals and Objectives

Critical military training and testing on lands along our nation's coastal and estuarine shorelines are increasingly placed at risk because of civilian development pressures in surrounding areas encroaching on installation boundaries, impairments due to other man-made disturbances, climate change (e.g., extreme weather events, rising sea level), and increasing requirements for compliance with federal and state environmental standards and regulations (RTI, 2013b). DoD intends to enhance and sustain its military training and testing assets and to optimize its stewardship of natural resources through the development and application of an ecosystem-based management approach on DoD facilities (SERDP, 2005). DoD's policy has established ecosystem-based management as the preferred approach for military lands (Goodman, 1996). This approach focuses on sustaining and enhancing military training and testing activities by monitoring and managing the interdependent natural resource assets on which the future of these activities depends (RTI, 2007a). To expand its commitment to improving military readiness while demonstrating the science behind this approach, SERDP made a 10-year commitment to implementing an integrated research and monitoring effort to support the sustainability of military training and testing in ecologically and economically important coastal ecosystems.

Background

The four objectives of DCERP2 are to

- Build on previous DCERP1 findings to identify additional indicators that can serve to assess the state of the ecosystem that could affect sustainability of the military training mission
- Determine how ecosystem processes (within active military training environments) respond to climatically-driven change to understand the sensitivity and adaptive capacity of these ecosystems
- Assess opportunities for adaptive management of estuarine, coastal, and terrestrial ecosystems to enhance carbon storage at MCBCL and other DoD installations in similar coastal settings
- Convey significant scientific findings to installation managers and decision makers by developing easy-to-use decision-support tools and models hosted on a readily accessible Web-based platform.

Site Selection

SERDP launched DCERP at MCBCL in 2006 (**Figure 1-1**). As a U.S. Marine Corps installation, MCBCL has a primary mission: military training and preparedness. MCBCL provides an ideal environmental setting for DCERP because it encompasses four distinct ecosystems (aquatic/estuarine, coastal wetlands, coastal barrier, and terrestrial ecosystems), within the installation boundaries.

MCBCL was selected as the primary DCERP study site for many reasons, including the following:

- The New River watershed, which is entirely contained within Onslow County and encompasses the majority of MCBCL training and cantonment areas, is a relatively small watershed; therefore, it is a manageable study site.
- MCBCL occupies and controls management of a substantial portion (approximately 80%) of the New River Estuary (NRE) shoreline.
- The barrier island and coastal dune system of Onslow Beach provide the premier amphibious assault training environment in the contiguous United States.
- The wide spectrum of ongoing military training and testing operations at MCBCL enables researchers to examine these training impacts on a broad range of ecosystems, from upland pine forests to aquatic and estuarine waters to coastal marshes and barrier islands.

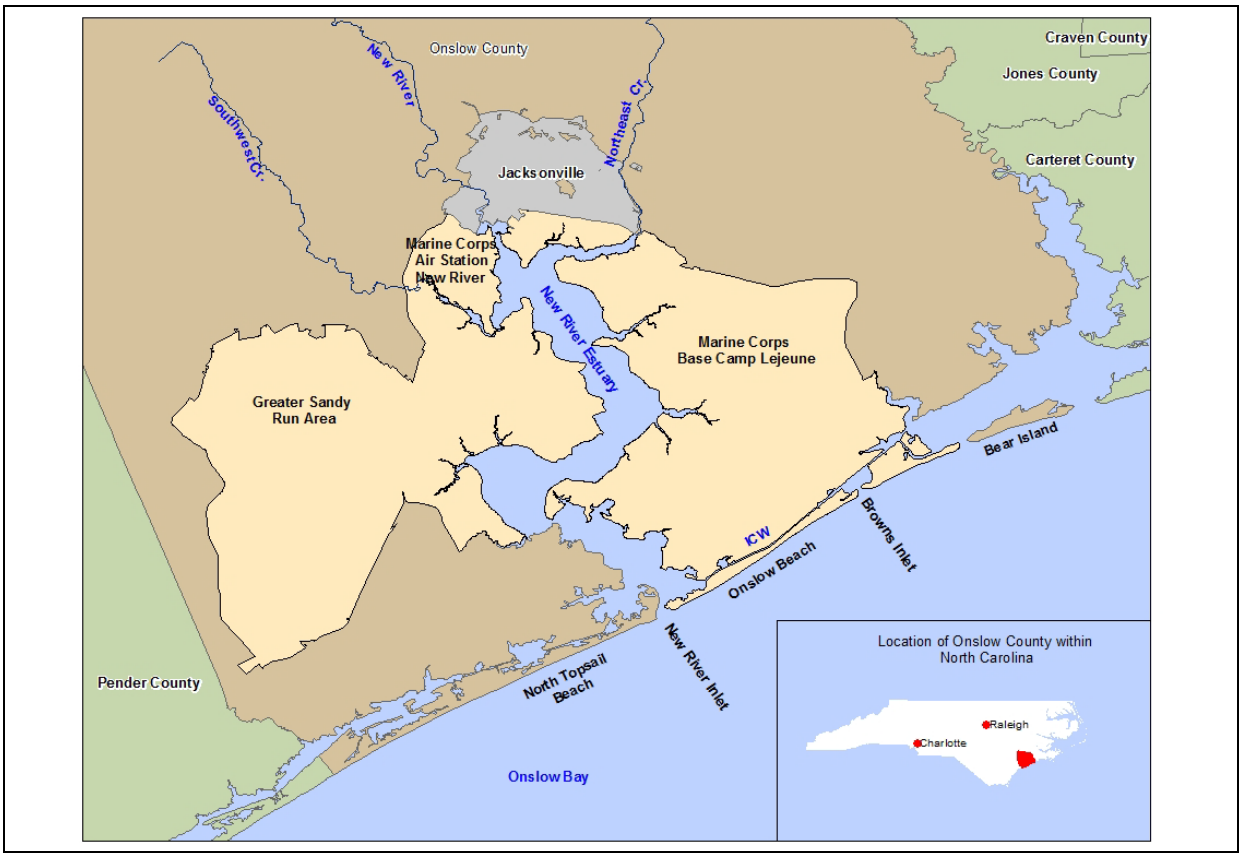

Figure 1-1. Site map of MCBCL.

As part of DCERP2, SERDP wanted to expand the program beyond MCBCL to other DoD installations in similar environmental settings. To address this program goal, the DCERP2 Team conducted a variety of research activities at three other coastal DoD installations in southeastern United States. These installations are Marine Corps Air Station Cherry Point (50 miles northwest of MCBCL on the Neuse River Estuary in North Carolina), Fort Bragg (120 miles west of MCBCL in the Sandhills ecoregion of North Carolina), and at Eglin Air Force Base (on the Panhandle of Florida on the Choctawhatchee Estuary along the Gulf of Mexico).

Integration of DCERP with MCBCL's Natural Resources Management

MCBCL's primary mission is to provide military training that promotes the combat readiness of expeditionary forces, and all MCBCL natural resource management activities on the installation support this mission (MCBCL, 2006). As an active DoD installation, MCBCL must ensure its mission readiness can continue without significant disruption. As with all federal facilities, MCBCL must comply with appropriate environmental laws and regulations, such as the federal Endangered Species Act, Clean Air Act, and Clean Water Act. To ensure such compliance, MCBCL uses a long-term planning document, the Integrated Natural Resources Management Plan (INRMP; MCBCL, 2006 and 2015). The MCBCL INRMP guides implementation of the natural resources program with the objective of ensuring consistency with MCBCL's military mission and to support the ability to train Marines, while providing for the conservation, rehabilitation, and the sustainable multiple-faceted uses of natural resources on the installation.

DCERP's objectives were designed to assist MCBCL in achieving its mission goals (RTI, 2007a). To achieve this goal, MCBCL's natural resource and environmental management staff participated throughout the program in all planning workshops, annual review meetings, and ecosystem-specific meetings. In addition, DCERP team researchers and installation staff met one-on-one to exchange information about research and monitoring findings. These meetings were important because they provided opportunities for the DCERP researchers to obtain additional information about any changes to military training procedures and practices planned for the installation. Throughout the 10-years of DCERP, the research team made every effort to include the MCBCL natural resources management issues of concern in the DCERP research activities, where appropriate, and to communicate DCERP activities, research findings, and management recommendations to Base staff.

Program Organization

DCERP is a multi-disciplinary and multi-organizational collaborative research effort among SERDP, the Naval Facilities Engineering and Expeditionary Warfare Center (NAVFAC EXWC), MCBCL, and RTI International. RTI assembled a diverse team of experts from federal agencies, academic institutions, and the private sector to design and implement the DCERP2 monitoring and research programs. The DCERP Management Team and the DCERP Research Team are further discussed in the following subsections of this chapter.

DCERP2 Management Team

SERDP is an environmental research and development program that is planned and implemented by DoD in full partnership with the U.S. Department of Energy and the U.S. Environmental Protection Agency (EPA; SERDP, 2017). The SERDP Resource Conservation and Climate Change (RCCC) Program Office ensured that DCERP activities would enhance the knowledge of ecosystem and military interactions within approved scopes of work and budgets. The overarching federal management for DCERP and the On-Site Coordinator (OSC) was assigned to the NAVFAC EXWC. SERDP ensured that the tasks identified in the Statement of Work were properly performed by the DCERP2 Research Team. The DCERP2 Research Team was led by Dr. Patricia Cunningham of RTI (the DCERP Principal Investigator [PI]). The DCERP PI was responsible for the overall scientific quality, cohesiveness, and relevance of DCERP monitoring and research activities. DCERP activities conducted at MCBCL were coordinated through the OSC, with assistance from the MCBCL Director of the Environmental Management Division (EMD; Mr. John Townson), and the Head of the Environmental Conservation Branch (Mr. Marty Korenek).

Two external committees (i.e., Technical Advisory Committee [TAC] and the Regional Coordinating Committee [RCC]) also provided guidance and input to DCERP during annual meetings held throughout the 10-year program. The TAC was a group of discipline experts from academia, industry, government, and the military that was assembled by the NAFVAC EXWC to provide scientific and technical review and guidance to ensure the quality and relevance of DCERP. Members of the DCERP2 TAC are listed in **Appendix 1-A** of this chapter. The RCC was a group of local, regional, and state stakeholders that served as one of the recipients of outreach from MCBCL, the DCERP PI, the DCERP OSC, and the SERDP RCCC Program Manager, thereby fostering relationships among the representative organizations and the DCERP

research team. Members of the DCERP2 RCC are listed in **Appendix 1-B** of this chapter. During the annual meetings held at MCBCL, the DCERP Team provided a summary of research and monitoring findings to MCBCL staff, the TAC, and the RCC. **Figure 1-2** illustrates the DCERP organization and lines of communication during DCERP2; the lines of communication were similar to those used during DCERP1.

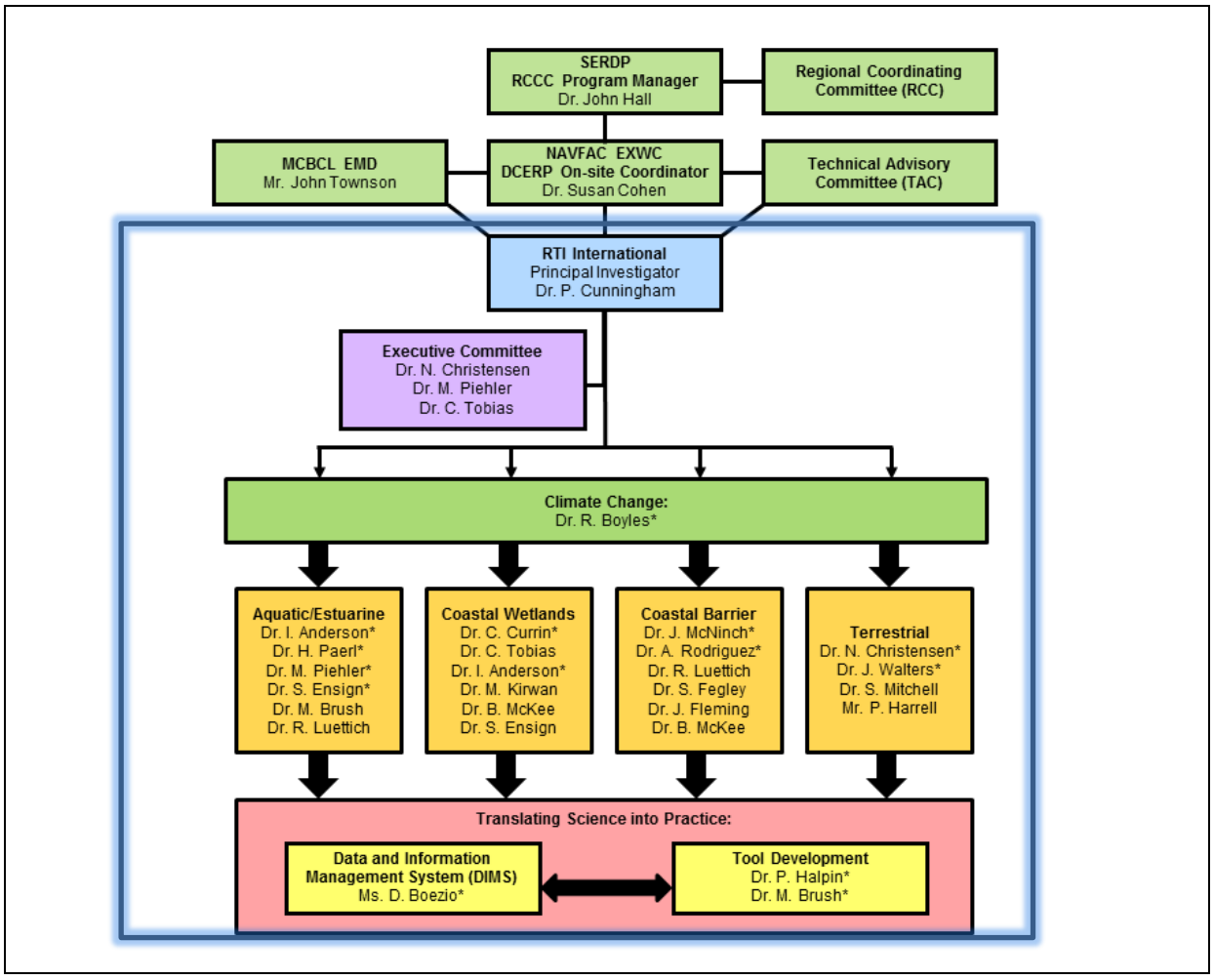

Figure 1-2. The organization of DCERP2, with the DCERP2 Research Team shown within the blue border.

Note: Asterisks denote Lead Researchers.

DCERP2 Research Team

RTI, the prime contractor for DCERP2, selected members of the DCERP Team because of their expertise in relevant environmental and ecosystem research disciplines and substantial previous experience in working collaboratively on interdisciplinary aquatic/estuarine, coastal, and terrestrial ecosystem projects. The team included the DCERP PI, environmental and data scientists from RTI, researchers from six academic institutions, two federal agencies, and three small businesses.

DCERP2 Executive Committee

The DCERP2 Executive Committee, which consisted of three senior researchers (i.e., Drs. Norman Christensen, Craig Tobias, and Michael Piehler), provided guidance to the DCERP PI to inform programmatic decisions, prioritize research proposals, and help present significant DCERP findings to the SERDP In-Progress Review (IPR) Committee and Scientific Advisory Board (SAB). These three researchers on the DCERP2 Executive Committee represented distinct disciplines that cut across several of the ecosystems of the program and augmented the expertise of the DCERP PI.

DCERP2 Research Team

The researchers, collectively referred to as the DCERP2 Team, are from the following organizations:

- AquaCo, LLC
- Duke University
- Geodynamics, LLC
- National Oceanic and Atmospheric Administration (NOAA)
- North Carolina State University
- RTI International
- Seahorse Consulting
- University of Connecticut
- University of North Carolina at Chapel Hill's Institute of Marine Sciences
- U.S. Army Corps of Engineers (USACE)
- Virginia Institute of Marine Science
- Virginia Tech.

DCERP2 Modules

As occurred during DCERP1, the DCERP2 Research Team was organized into four separate, but integrated, ecosystem modules (i.e., Aquatic/Estuarine, Coastal Wetlands, Coastal Barrier, and Terrestrial) based on the ecosystem-based management objectives for the program (RTI, 2007a). Two major changes were made to the cross-cutting modules created during DCERP1 to address the new DCERP2 thematic areas of climate change, and translating complex scientific data into actionable information. The Atmospheric Module from DCERP1 was eliminated, and a Climate Change Module was assembled for developing downscaled climate model data for eastern North Carolina, including MCBCL lands. The Data Management Module from DCERP1 was expanded to encompass the needs of translating science into practice.

The Data Management Module included the following two components: (1) a data archive and (2) a model and tool development component (RTI, 2007a). These two components were combined to create the Translating Science into Practice Module that directly addressed the thematic area of translating relevant scientific findings into actionable information for MCBCL managers and other users. The Translating Science into Practice Module implemented a one-stop Web-based system for all DCERP data, findings, tools, models, and products.

Thematic Areas

Description of Themes

The specific thematic areas represented overarching themes that had broad application within and among the ecosystem modules and provided additional pathways for integrating research and monitoring activities (**Table 1-1**). During DCERP1, the team addressed the initial DCERP objectives of developing monitoring approaches and identifying key ecological processes (i.e., hydrodynamics, nutrient cycling, and sediment transport), with the goal of supporting ecosystem-

based management for coastal DoD installations in similar ecological settings (RTI, 2007a). During DCERP2, the team addressed the expanded objectives that included the new thematic areas. These areas are (1) determining the effects of climate change on estuarine/coastal systems, (2) understanding the carbon cycle and management of carbon storage in estuarine/coastal ecosystems, and (3) translating science into practice by providing findings in clear, easy-to-understand language and by developing Web-accessible models and tools for DoD installation managers and other users (RTI, 2013b).

Table 1-1. Programmatic Themes for DCERP

DCERP1	DCERP2
Hydrodynamics of the NRE and coastal ecosystems	Climate change impacts on the coastal ecosystems of MCBCL
Sediment transport in the estuary, marshes, and coastal barrier	Understanding the estuarine/coastal carbon cycle and carbon management
Nutrient cycling and primary productivity	Translating science into practice
Military training and land management	

Climate Change

The first DCERP theme included determining the effects of climate change on estuarine/coastal ecosystems. DoD recognized that projected climate changes will impact installations, operations, and missions in the United States and globally (DoD, 2010 and 2012; SERDP, 2013). To address DoD's concerns about the impacts of climate change, the DCERP2 Team identified four major climate drivers to study at MCBCL. The four climate drivers that were assessed by the DCERP2 Team were temperature, precipitation, storminess, and sea level rise. Detailed summaries of the potential ecosystem and military mission impacts were provided in the *DCERP2 Research Plan* (RTI, 2013b). It is important to note that the impacts may be more severe because of a combination of two or more of these climatic drivers acting synergistically.

The DCERP2 Team developed uniform historical climate data and future downscaled climate projections for consistent use in the ecosystem models at appropriate scales. Based on the needs of the ecosystem modeling efforts, precipitation and temperature data were calculated at daily timescales at a maximum spatial scale of 10 km. Wind data were provided at the appropriate temporal and spatial scales for predicting the future wind conditions on Onslow Beach. Sea level rise scenarios were based on five global sea level rise models with local adjustments for MCBCL based on guidance developed by SERDP (Hall et al., 2016). Each of the DCERP ecosystem modules have research projects that contain a climate change component that addressed one or more of the four climate drivers. Most of the climate change research involved the development of models by using historical data, and then forecasting ecosystem changes into future decades. (Note: A list of these models is provided in **Table 1-5**.)

Carbon Cycle and Carbon Management

The second DCERP theme was understanding the carbon cycle and managing carbon storage in estuarine/coastal systems. DoD is one of the largest institutional consumers of fossil fuels in the world, representing 93% of all federal fuel consumption annually (Lengyel, 2007). Fossil fuel

consumption by DoD peaked in 2007 at 125 million barrels per year, and then declined by 30% to 87.4 million barrels per year in 2014 (DoD, 2016). This rate of fossil fuel consumption results in the release of large quantities of carbon dioxide (CO_2) into the atmosphere. Increased atmospheric CO_2 has been the leading cause of global warming over the past century (IPCC, 2013). To mitigate these impacts, the U.S. Congress set targets for reducing energy use by all federal agencies, including DoD, through the Energy Policy Act of 2005, the National Defense Authorization Act of 2006, and the Energy Independence and Security Act of 2007 (Schwartz et al., 2012). As a result, DoD is interested in the possibility of offsetting its carbon footprint through natural resource management activities such as management of wetlands and forested lands as carbon stores. DCERP's study of the carbon cycle was undertaken to add to knowledge of carbon cycling in estuarine/coastal systems and how best to manage these natural assets for the future when the use of carbon credits and trading may become more widespread.

The DCERP2 Team developed an integrated approach to quantifying carbon cycling throughout the coastal landscape bounded by MCBCL (**Figure 1-3**). The DCERP2 Team applied a common methodology that quantified atmospheric carbon fluxes, burial, carbon exchanges, and attribution of carbon sources across ecosystems. The symmetry of experimental approaches built into each module (i.e., common spatial and temporal scales or measurements, as well as common units of flux) led to a more seamless integration. This approach yielded contemporaneous mass balances that served as snapshots of carbon inventory and transformation rates and contributed to the mechanistic understanding of how probable changes in climatic and localized anthropogenic drivers will impact carbon cycling.

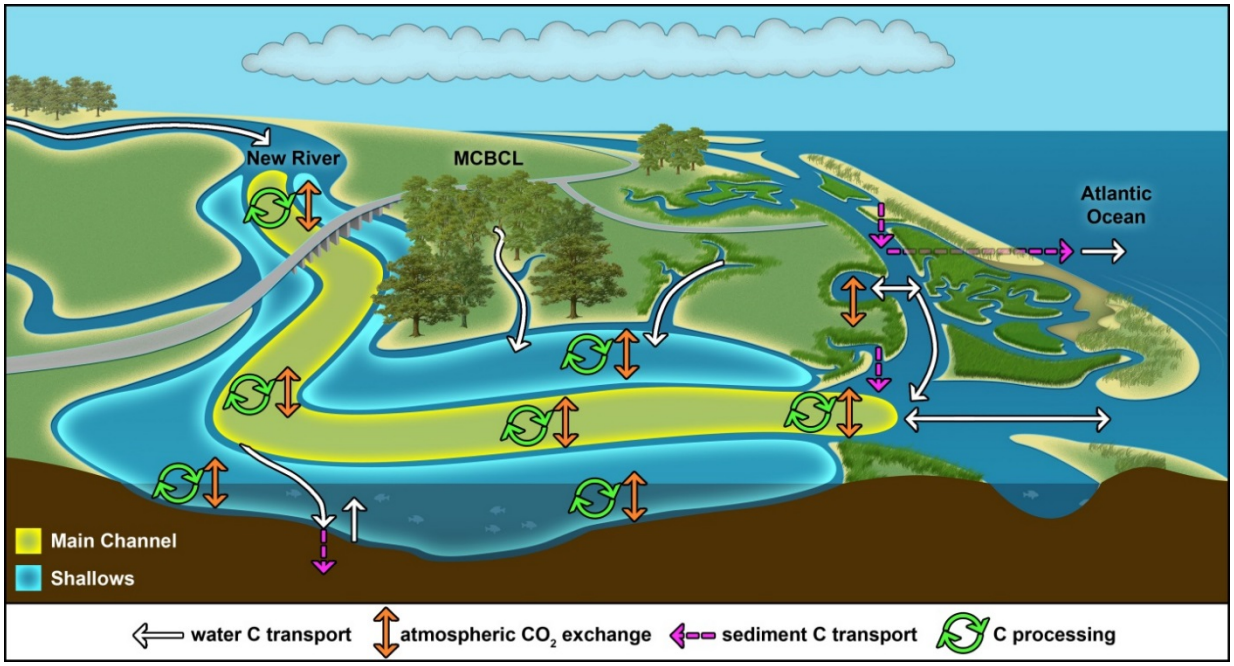

Figure 1-3. The carbon budget for the New River and its surrounding coastal area.

Translating Science into Practice

The third DCERP2 theme, translating science into practice, required communicating often complex scientific findings to three target audiences: the scientific community, DoD managers,

and local stakeholders including the public. DCERP researchers excel at communicating their findings through peer-reviewed journal articles and presentations to academic audiences at many symposia and conferences. However, it is challenging to make findings both understandable and actionable for DoD managers, and even more difficult—but of major importance—to explain the science to the public. With input from MCBCL environmental staff, the researchers used a variety of methods to showcase the scientific findings in ways that were useful in making management decisions, while promoting an understanding of the science behind the tools and models. A logic model (**Appendix 1-C**) was developed to determine which activities would apply for each audience and the short-, medium-, and long-term desired outcomes for these activities. The DCERP2 Translating Science into Practice Module directly addressed the thematic area through the development of a one-stop, Web-based system for all three audiences to access all DCERP data, findings, tools, models, and products.

DCERP Strategy—Planning Phase

During the planning periods for DCERP1 and DCERP2, the team followed guidance on ecosystem-based management from the Ecological Society of America (Christensen et al., 1996) and recommendations of the U.S. Commission on Ocean Policy (2004), including adaptive management principles (Walters, 2001). Based on interconnectivity, this strategy helped separate underlying natural (e.g., climatic) and man-made regional processes from locally driven processes. This strategy also helped identify stressor-specific indicators of ecosystem state change that provide managers with assessment points that identify shifts in conditions that could threaten ecosystem sustainability (RTI, 2007a).

Integration of the research and monitoring effort across ecosystems is a hallmark of DCERP and occurred at the thematic, module, and project levels. Integration started with identifying ecosystem processes and stressors, incorporating these into an overarching conceptual model of the ecosystems across MCBCL, and then creating individual conceptual models for each of the four major ecosystem types with the same emphasis on processes and stressors (**Figure 1-4**). (RTI, 2007a). The team then developed the integrated monitoring and research activities and used the results from these activities to identify indicators, design models, and develop decision-support tools. These significant findings were translated into actionable information for installation managers. Throughout this process, feedback from MCBCL staff was used to provide critical evaluation of the DCERP2 Team's understanding of the ecosystems and address MCBCL's management needs.

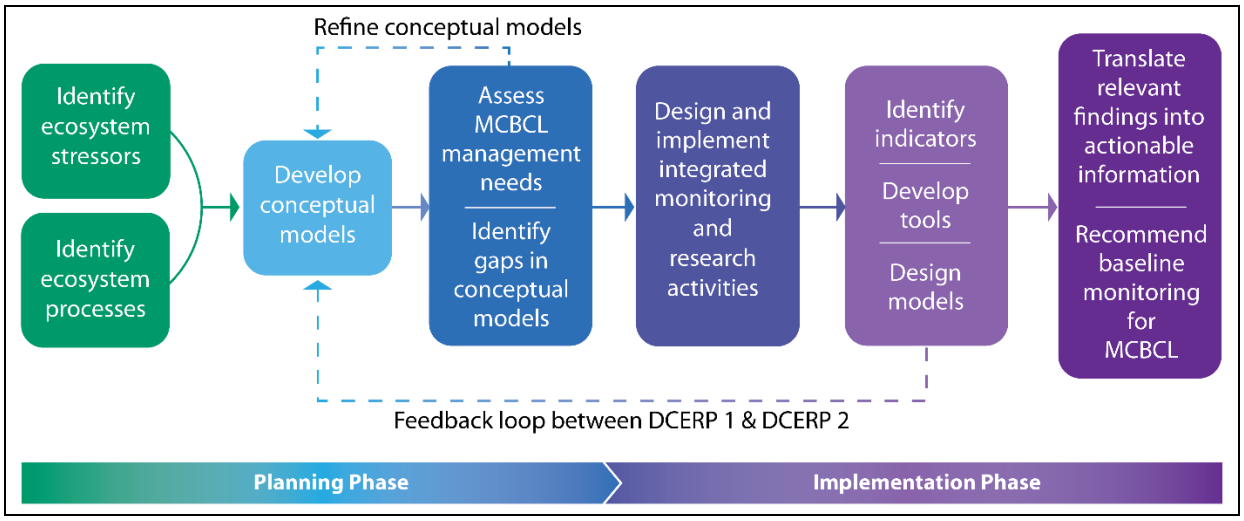

Figure 1-4. The overall process used for meeting DCERP's objectives.

The DCERP Team defined "stressors" as activities or events that alter ecological processes. Natural ecosystem stressors include natural forces (e.g., hurricanes, sea level rise) whose effects are enhanced by anthropogenic activity (e.g., global warming). The increased intensity and frequency of natural events, in combination with enhanced anthropogenic contributions, could cause ecosystem perturbations outside the range of natural variation in the future (RTI, 2007a). During DCERP1, the team grouped the stressors into four major categories: military, non-military, legacy, and natural. **Table 1-2** provides a definition for each category of stressor and lists specific examples relevant to DCERP.

Table 1-2. Examples of Military, Non-Military, Legacy, and Natural Stressors to an Ecosystem

Stressors	Examples
Military	Activities or events that are uniquely associated with military training and testing at MCBCL. Some examples of military activities include the use of military tracked vehicles and amphibious watercraft, troop movements on the Base, and the use of firing ranges, drop zones, and impact areas for training.
Non-military	Any anthropogenic (non-military) activities that can occur on or off Base. Some examples of non-military activities include industrial and municipal discharges, local residential or commercial development, and nutrient runoff from confined animal feeding operations. agricultural practices, and forest or urban lands. Additional stressors in this category include atmospheric deposition of nutrients and other contaminants, groundwater withdrawals, and prescribed burning activities.
Legacy	Anthropogenic activities that have occurred in the past, but whose effects are continuing today. Some examples of legacy stressors that are relevant to MCBCL include the original construction and continued maintenance of the Intracoastal Waterway (ICW), early ditching activities to drain land, historic use of fire, and timber harvesting.
Natural	Natural stressors can include sea level rise whose effects are enhanced by anthropogenic activity (e.g., global warming), as well as changes in temperatures, precipitation, and storminess (e.g., hurricanes).

Once the DCERP Team defined and grouped the stressors into the four major categories, the team developed the overarching conceptual model of DCERP for the MCBCL region (RTI, 2007a). The conceptual model for DCERP2 was built on the findings from DCERP1 and included an expansion of the study areas to understand the carbon cycle and climate impacts to the estuarine/coastal area of MCBCL both now and into the future (**Figure 1-5**; RTI, 2013b). The conceptual model also included four climate drivers: temperature, precipitation, storminess, and rising sea level. All the modules developed module-level conceptual models for their respective ecosystems that can be found in Chapter 2 of this *DCERP2 Final Report*.

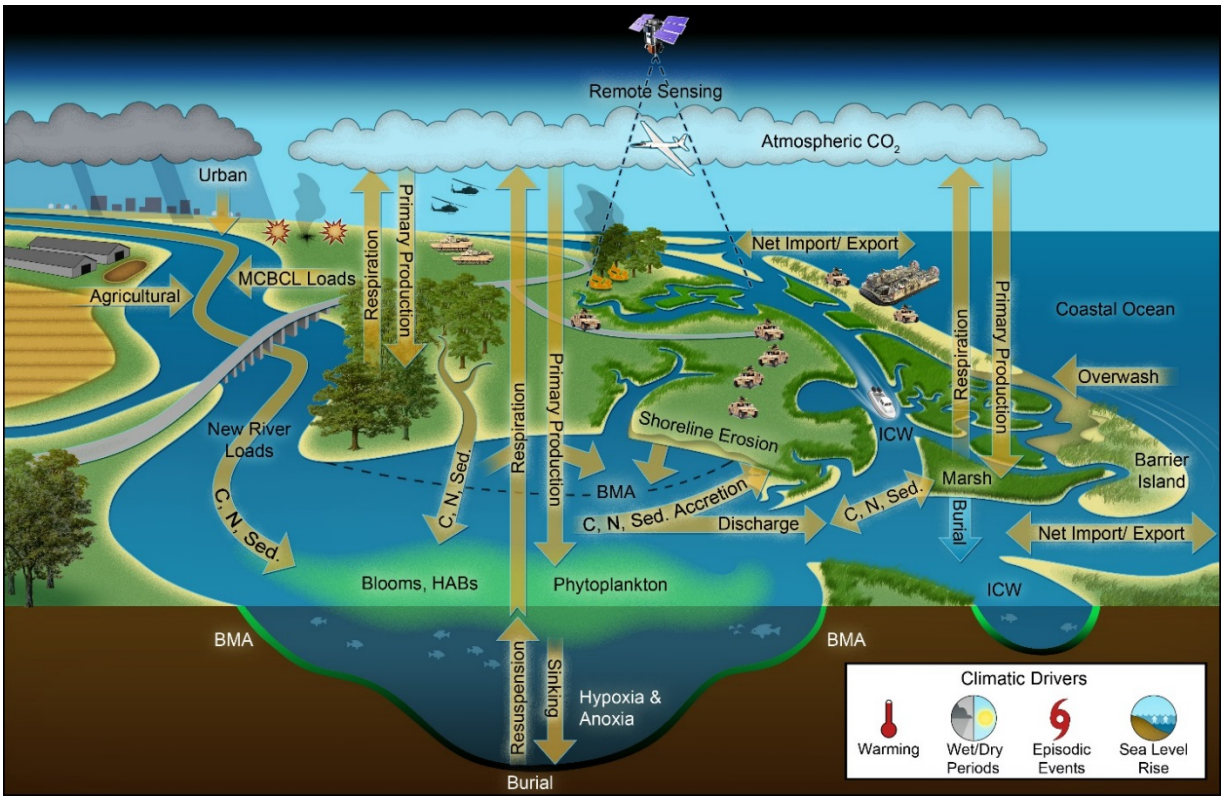

Figure 1-5. The overarching conceptual model for DCERP2 at MCBCL.

DCERP Strategy—Implementation Phase

Design and Implement DCERP2 Research Projects

To meet DCERPs overarching objectives, the DCERP Team conducted 13 research projects during DCERP1 and another 13 research projects during DCERP2 (**Table 1-3**). Some DCERP2 projects continued to build on information obtained during DCERP1, but with the introduction of the three new programmatic themes, most research projects had to develop new or expanded areas of research. Additionally, DCERP1 research findings provided feedback regarding the adaptive DCERP monitoring program so that changes in sampling frequency, spatial extent of sampling locations, and/or parameters to be sampled during DCERP2 could be made as necessary to fill remaining data gaps (RTI, 2007a).

Table 1-3. Research Projects from DCERP1 and DCERP2

DCERP1 Research Project Title	DCERP2 Research Project Title	Researcher
Aquatic/Estuarine Module		
AE-1: Develop and Deploy Microalgal Indicators as Measures of Water Quality, Harmful Algal Bloom Dynamics, and Ecosystem Condition	**AE-4:** Nutrient–Driven Eutrophication and Carbon Flux Modulated by Climate Change in the NRE	Hans Paerl
AE-2: Quantifying and Predicting Watershed Inputs of Nutrients, Sediments, and Pathogens to Tributary Creeks on MCBCL	**AE-5:** Climate and Land-Use Impacts on Exports of Carbon, Sediments, and Nutrients from Coastal Subwatersheds	Michael Piehler
AE-3: Developing Indicators of Ecosystem Function for Shallow Estuaries: Benthic Functional Responses in the NRE	**AE-6:** Climatic Drivers Regulating Benthic-Pelagic Carbon and Associated Nutrient Exchanges in the NRE	Iris Anderson
Coastal Wetlands Module		
CW-1: Drivers and Forecasts of the Responses of Tidal Salt Marshes to Sea Level Rise	**CW-4:** Improving Model Predictions for Marsh Response to Sea Level Rise and Implications for Natural Resource Management	Jim Morris, CW-1; Carolyn Currin, CW-4
CW-2: Forecasting Influence of Natural and Anthropogenic Factors on Estuarine Shoreline Erosion Rates	None	Mark Fonseca
CW-3: Hydraulic Exchange and Nutrient Reactivity in the NRE Wetlands	**CW-5:** Marsh–Atmosphere and Marsh–Creek Exchanges of Carbon	Craig Tobias, CW-3; Iris Anderson, CW-5
Coastal Barrier Module		
CB-1: Short-Term Barrier Evolution: Overwash at Onslow Beach Through Assessment of Training Activities and Model Predictions	**CB-4:** Predicting Sustainability of Coastal Military Training Environments: Developing and Evaluating a Simplified, Numerical Morphology Model	Jesse McNinch
CB-2: Long-Term Barrier Evolution Related to Variations in Underlying Geology and Land Use	**CB-5:** Linking Barrier Island Transgression Induced by Storms and Sea Level Rise to the Carbon Cycle	Tony Rodriguez
CB-3: Understanding the Top-Down and Bottom-Up Drivers of Shorebird Nest Success and Habitat Use in Relation to Beach Management Practices on MCBCL	None	Sarah Karpanty and Jim Fraser
Terrestrial Module		
T-1: Effects of Different Understory Restoration Management Options on Terrestrial Ecosystem Structure and Function	**T-1:** Effects of Different Understory/Midstory Restoration Management Options on Terrestrial Ecosystem Plant and Arthropod Communities **(This project continued from DCERP1)**	Norman Christensen
None	**T-3:** Forest Management, Species Habitat, and Implications for Carbon Flux and Storage	Stephen Mitchell

(continued)

Table 1-3. Research Projects from DCERP1 and DCERP2 (continued)

DCERP1 Research Project Title	DCERP2 Research Project Title	Researcher
T-2: Effects of Habitat Management for Red-Cockaded Woodpeckers (RCWs) on Bird Communities	**T-4:** Impacts of Climate Change on Management of RCWs at MCBCL	Jeffrey Walters
Climate Change Module		
None	**CC-1:** Development of Uniform Historical and Projected Climate to Support Integrated Coastal Ecosystem Research	Aaron Sims
Translating Science into Practice Module		
(This project was part of Data Management and Tool Development during DCERP1)	**TSP-1:** Development of a Common Spatial Decision Support System (SDSS) Framework	Pat Halpin and Danette Boezio
(This project was part of Research Project AE-3 during DCERP1)	**TSP-2:** Coupled Ecosystem Modeling of the NRE for Research, Synthesis, and Management	Mark Brush
Atmospheric Module		
Air-1: Optimization of Prescribed Burning by Considering Mechanical Thinning as a Viable Land Management Option	None	Karsten Baumann
Air-2: Nitrogen Deposition to Terrestrial and Aquatic Ecosystems	None	Wayne Robarge

Design and Implementation of Monitoring Activities

DCERP2 baseline monitoring included sampling of basic parameters that supported the broader research agenda, provided data that were useful to more than one ecosystem module, must be monitored for 5–10 years, and would be transitioned in a scaled-down form to MCBCL to monitor Base lands at the end of the DCERP efforts (RTI, 2013b). The DCERP1 baseline monitoring program is summarized in the *DCERP Baseline Monitoring Plan* (RTI, 2007b).

The *DCERP2 Monitoring Plan* (RTI, 2013a) was narrowed from DCERP1 to focus on the New River watershed and coastal marshes with an emphasis on the relationships between nutrients, sediment, and carbon fluxes as mediated by natural (hydrologic and thermal) and anthropogenic drivers. The *DCERP2 Monitoring Plan* was designed to gather systematic, time-series observations regarding responses to ecosystem stressors and indicators over a sufficient period to determine the existing status, trends, and natural variation of measured parameters. The plan was also designed to record, assess, and archive extreme events and ecosystem trends and to be responsive to changing research, modeling, adaptive management and decision-support tool development to meet MCBCL management needs. The DCERP2 monitoring program included the activities in **Table 1-4**. The ultimate goal of both the DCERP1 and DCERP2 monitoring programs was to provide recommendations to MCBCL regarding a scaled-down monitoring program that could provide data to assess long-term trends in key parameters of importance for each of the MCBCL ecosystems.

Table 1-4. Summary of DCERP2 Module-Specific Monitoring Activities

Module	Activities
Aquatic/ Estuarine	Hydrodynamics: Stream flow and discharge (New River, tributary creeks) Chemistry: Chromophoric dissolved organic matter (CDOM), nutrients (nitrogen, phosphorus, carbon), salinity, pH, oxygen concentration, and temperature Sedimentology: Total suspended solids (NRE), turbidity (NRE), and suspended sediment concentration (New River) Biology: Primary productivity, phytoplankton biomass, and benthic microalgal biomass
Coastal Wetlands	Shoreline delineation: Surface elevation change, topography, morphology, and marsh edge erosion Hydrodynamics: Tide gauges (hydroperiod, water level, temperature, and salinity) Marsh vegetation: Distribution, composition, stem height, and grazer density (snails) Sedimentology: Accretion rates.

Identify Indicators, Develop Tools, and Design Models

The DCERP2 Team used results from the integrated research and monitoring efforts to identify indicators of ecosystem state change, develop decision-support tools, and design models that addressed MCBCL's management needs. The DCERP2 Team also designed and developed a variety of models and tools to help Base managers understand the impacts of specific management practices or climate change impacts on installation natural resources sustainability, both now and into the future. A list of the models developed for MCBCL and other DoD installations appears as **Table 1-5**.

Table 1-5. Models Developed and/or Applied During DCERP2

Model Name and Research Project	Purpose of the Model for Installation Managers
Estuarine Simulation Model (Research Project TSP-2)	Identify water quality impairment from nutrients and sediment, and carbon dynamics in the NRE under current and future land-use and climate scenarios
Geospatial Marsh Model (Research Project CW-4)	Estimate the sustainability of marshes under different sea level rise scenarios specified by SERDP (Hall et al., 2016) through 2100
Beach Morphology Model (Research Project CB-4)	Predict shoreline location and elevation of Onslow Beach under different sea level rise scenarios specified by SERDP and storminess scenarios (i.e., future wind speed) through 2100
Forest Carbon Management Tool (Research Project T-3)	Estimate carbon storage capacity of forested areas based on different forestry management practices and climate scenarios through 2100 by using the LANDIS-II model
Red-Cockaded Woodpecker (RCW) Decision Support System (Research Project T-4)	Predict the demographics of RCW populations in MCBCL based on habitat changes from future climate and forest management practices derived from the Forest Carbon Management Tool

Translate Relevant Findings into Actionable Information for DoD Installation Managers

Based on research and monitoring results, the DCERP2 Team translated relevant findings into actionable information and communicated these findings to MCBCL personnel to assist them in making more informed management decisions. The findings were translated in peer-reviewed publications, written reports, during formal and information presentations and training

workshops, and through maps and other visualization online tools available through the DCERP DIMS Web site. In addition, the DCERP Team has provided baseline monitoring recommendations and produced factsheets and ecosystem guidebooks specifically for MCBCL to help direct future monitoring and management needs for each of the four ecosystems.

Data Management

The voluminous amounts of research and monitoring data collected over the 10 years of DCERP required the development of an efficient data management system early in the program. The DCERP1 Data Management Module Team were responsible for designing and implementing the DIMS. During DCERP2, the DIMS was expanded to focus on translating the results into actionable information. The DCERP DIMS was designed to facilitate collection, integration, and exchange of environmental data, tools, and models. The model and tool development component provides the ultimate cross-cutting function of incorporating the simple models, which were developed by the individual research projects, into integrated management tools and decision-support models for MCBCL managers (RTI, 2013c).

The DCERP DIMS is composed of the following components:

- A Monitoring and Research Data and Information System (MARDIS), which is used to access research and monitoring data
- A Document Database, which is used to access unstructured data such as reports, maps, photographs, and graphics
- An interactive mapping application (iMAP)
- A public Web site.

All data, tool, models, and products produced during DCERP are archived in the DCERP DIMS that is currently available at https://dcerp.rti.org. DIMS fulfills SERDP's data management goal for the program by providing an accessible Web-based platform for distributing all DCERP data, tools, models, and other products to all three of the DCERP target audiences: researchers, installation managers, and local stakeholders, including the public. Detailed summaries of this system and its functionalities are provided in Chapter 21 of this report.

Report Organization

This *DCERP2 Final Report* summarizes the DCERP activities conducted from November 2012 through November 2017. Chapter 2 summarizes the major findings, results, and conclusions of the 13 research projects and the major findings and trends in the Aquatic/Estuarine and Coastal Wetlands monitoring data. Chapters 3 through 22 provide detailed research project reports for each of the DCERP2 research activities listed in **Table 1-3** and the monitoring activities listed in **Table 1-4**.

Literature Cited

Christensen, N.L., A. Bartuska, J.H. Brown, S. Carpenter, C. D'Antonio, R. Francis, J.F. Franklin, J.A. MacMahon, R.F. Noss, D.J. Parsons, C.H. Peterson, M.G. Turner, and R.G. Woodmansee. 1996. The scientific basis for ecosystem management. *Ecological Applications 6*:665–691.

DoD (U.S. Department of Defense). 2016. *Department of Defense 2016 Operational Energy Strategy*. Washington, DC. Available at http://www.acq.osd.mil/eie/Downloads/OE/2016%20OE%20Strategy_WEBd.pdf

DoD (U.S. Department of Defense). 2012. *Department of Defense FY 2012 Climate Change Adaptation Roadmap*. U.S. Department of Defense. September 18. Available at http://www.dodworkshops.org/Appendix_A_-_DoD_Climate_Change_Adaption_Roadmap_20120918.pdf

DoD (U.S. Department of Defense). 2010. *Quadrennial Defense Review Report*. February. http://www.defense.gov/qdr/images/QDR_as_of_12Feb10_1000.pdf

Goodman, S.W. 1996. Ecosystem management at the Department of Defense. *Ecological Applications 6*:706–707.

Hall, J.A., S. Gill, J. Obeysekera, J., W. Sweet, K. Knuuti, and J. Marburger. 2016. *Regional Sea Level Scenarios for Coastal Risk Management: Managing the Uncertainty of Future Sea Level Change and Extreme Water Levels for the Department of Defense Coastal Sites Worldwide*. U.S. Department of Defense, SERDP. 224 pages. Available at https://www.serdp-estcp.org/Program-Areas/Resource-Conservation-and-Resiliency/Infrastructure-Resiliency/Regional-Sea-Level-Scenarios-for-Coastal-Risk-Management

IPCC (Intergovernmental Panel on Climate Change). 2013. *Climate Change 2013: The Physical Science Basis*. Contribution of Working Group I to the Fifth Assessment Report of the Intergovernmental Panel on Climate Change. Available at http://www.ipcc.ch/report/ar5/wg1/

Lengyel, G.J. 2007. *Department of Defense Energy Strategy: Teaching an Old Dog New Tricks*. 21st Century Defense Initiative. Foreign Policy Studies. The Brookings Institution, Washington, DC. August. Available at https://web.archive.org/web/20140529175335/http://www.brookings.edu/~/media/research/files/papers/2007/8/defense%20lengyel/lengyel20070815.pdf

MCBCL (Marine Corps Base Camp Lejeune). 2015. *2015–2020 Integrated Natural Resource Management Plan*. Marine Corps Base Camp Lejeune, North Carolina. Available at http://www.lejeune.marines.mil/Portals/27/Documents/EMD/2015-2020_MCBCL_INRMP_(MASTER).pdf

MCBCL (Marine Corps Base Camp Lejeune). 2006. *Integrated Natural Resource Management Plan (INRMP)*. U.S. Marine Corps, Camp Lejeune, NC.

RTI (RTI International). 2013a. *DCERP2 Monitoring Plan*. Prepared for Strategic Environmental Research and Development Program (SERDP), Arlington, VA.

RTI (RTI International). 2013b. *DCERP2 Research Plan*. Prepared for Strategic Environmental Research and Development Program (SERDP), Arlington, VA.

RTI (RTI International). 2013c. *DCERP1 Final Research Report*. Prepared for Strategic Environmental Research and Development Program (SERDP), Arlington, VA.

RTI (RTI International). 2007a. *Defense Coastal/Estuarine Research Program (DCERP) Strategic Plan*. Prepared for Strategic Environmental Research and Development Program (SERDP), Arlington, VA.

RTI (RTI International). 2007b. *DCERP Baseline Monitoring Plan*. Prepared for Strategic Environmental Research and Development Program (SERDP), Arlington, VA.

Schwartz, M., K. Blakeley, and R. O'Rourke. 2012. *Department of Defense Energy Initiatives: Background and Issues for Congress*. CRS Report for Congress. Available at http://www.fas.org/sgp/crs/natsec/R42558.pdf

SERDP (Strategic Environmental Research and Development Program). 2017. About SERDP. Available at https://www.serdp-estcp.org/About-SERDP-and-ESTCP/About-SERDP

SERDP (Strategic Environmental Research and Development Program). 2013. *Assessing Impacts of Climate Change on Coastal Military Installations: Policy Implications*. U.S. Department of Defense. January. Available at https://www.serdp-estcp.org/content/download/17219/192680/file/SERDP%20Coastal%20Assessment%20White%20Paper_January%202013.pdf

SERDP (Strategic Environmental Research and Development Program). 2005. *Workshop Proceedings for the Defense Coastal/Estuarine Research Program*. Atlantic Beach, NC. February 10–12, 2004. Available at https://www.serdp-estcp.org/content/download/7258/93109/file/SI-1413-WR.pdf

U.S. Commission on Ocean Policy. 2004. *An Ocean Blueprint for the 21st Century*. Final report. Washington, DC. Available at http://govinfo.library.unt.edu/oceancommission/documents/full_color_rpt/000_ocean_full_report.pdf

Walters, C. 2001. *Adaptive Management of Renewable Resources*. The Blackburn Press: Caldwell, NJ.

Appendix 1-A
DCERP2 Technical Advisory Committee

Name	Affiliation
Mr. Alan Anderson	Construction Engineering Research Laboratory, Engineer Research and Development Center, U.S. Army Corps of Engineers (USACE)
Dr. William Boicourt	Horn Point Environmental Laboratory, University of Maryland
Dr. Bob Christian	Department of Biology, East Carolina University
Dr. Leda Kobziar	School of Forest Resources and Conservation, University of Florida
Mr. Kevin Knuuti	Cold Regions Research and Engineering Laboratory, USACE
Mr. Lee Mulkey	Private consultant
Dr. Robert R. Twilley	Louisiana Sea Grant College Program, Louisiana State University

Appendix 1-B
DCERP2 Regional Coordinating Committee

Members of the DCERP2 Regional Coordinating Committee

Name	Affiliation	Location
Dr. Dean Carpenter	Albemarle–Pamlico National Estuary Program	Raleigh, NC
Ms. Anne Deaton	North Carolina Division of Marine Fisheries	Wilmington, NC
Ms. Pat Donovan-Potts	City of Jacksonville and New River Roundtable	Jacksonville, NC
Dr. John Fear	North Carolina Sea Grant	Raleigh, NC
Mr. Jim Gumm	U.S. Forest Service, Croatan Forest	New Bern, NC
Mr. John Hammond	U.S. Fish and Wildlife Service	Raleigh, NC
Mr. Tommy Hughes	North Carolina Wildlife Resource Commission	New Bern, NC
Mr. Carmen Lombardo	Environmental Affairs, Marine Corps Air Station Cherry Point	Havelock, NC
Mr. Hervey McIver	The Nature Conservancy	Durham, NC
Dr. Diana Rashash	North Carolina Cooperative Extension	Jacksonville, NC
Dr. Linda Rimer	U.S. Environmental Protection Agency	Research Triangle Park, NC
Mr. John Townsend	Marine Corps Base Camp Lejeune	Jacksonville, NC
Dr. Lexia Weaver	North Carolina Coastal Federation	Newport, NC

Appendix 1-C
DCERP2 Logic Model

Logic Model: DCERP Strategic Vision for Translating Science into Practice

Needs	Inputs	Outputs: Activities	Outputs: Target Audience	Outcomes	
To communicate science-based findings to multiple audiences with a variety of goals	• MCBCL as primary study site; Eglin Air Force Base, Marine Corps Air Station Cherry Point, and Fort Bragg as secondary sites • MCBCL management questions • SERDP funding • DCERP Team (researchers, graduate students, post-doctoral students, and research technicians) • Monitoring and research data • Climate histories and climate futures data • Equipment and materials • Technology	Develop and maintain DIMS, including the interactive mapping application [iMAP] visualization and query tools, MARDIS data archive, Document Database, and other outreach products for different target audiences Determine ecosystem responses to future management and climate scenarios and provide recommendations to MCBCL	MCBCL and other DoD installation staff	Short term	Increased MCBCL understanding of ecosystem processes, stressors, and potential changes in the ecosystems driven by management actions and future climate conditions
				Mid term	Evaluation of DCERP management recommendations and implementation of ecosystem–based management changes to MCBCL lands
				Long term	Enhanced sustainability of MCBCL (and other DoD) training lands, the integration of research and monitoring as a part of adaptive management decisions, and provision of a basis for setting carbon goals under future management and climate conditions
		Organize workshops with DoD end users to refine suitability of products and establish relationships between DCERP data and DoD management goals. Create reference guides to communicate findings and recommendations for MCBCL managers	Stakeholders (local, state, and regional)	Short term	Better understanding of estuarine/coastal ecosystem processes and potential changes to these systems under future management and climate conditions
				Mid term	Application of this understanding to the stakeholders' estuarine /coastal settings and transition lessons learned regionally, where applicable
				Long term	Improved management and condition of estuarine/coastal ecosystems in the southeastern United States and Gulf Coast
		Host annual briefings for Regional Coordinating Committee, MCBCL, and TAC to share information and gain feedback about scientific methods Publish manuscripts in peer-reviewed journals and make presentations at relevant scientific conferences	Scientific community	Short term	Improved understanding of nutrient cycles (nitrogen and phosphorus), carbon cycle, and processes in estuarine and coastal ecosystems now and under future climate conditions
				Mid term	Contributions to basic science and advancements in our understanding of coastal plain processes and function in a changing environment
				Long term	Possible changes in natural resource management policies because of an expanded body of literature on coastal ecosystem science

Assumptions

- End users (i.e., DoD installations, scientific community, other managers, and stakeholders) have questions and/or decisions that DCERP data can help answer

Challenges

- Time scale of models versus time scale of the planning process
- Matching the appropriate DCERP products to specific, but ever-evolving short-, medium-, and long-term regulatory and/or planning needs

Chapter 2

Significant Findings and Management Implications

SERDP Project Number: RC-2245

Principal Investigator:

Dr. Patricia Cunningham
RTI International
E-mail: patc@rti.org

Note: Input for this chapter was provided by the entire DCERP2 Team.

November 2017

Final

This report was prepared under contract to the U.S. Department of Defense (DoD) Strategic Environmental Research and Development Program (SERDP). The publication of this report does not indicate endorsement by DoD, nor should the contents be construed as reflecting the official policy or position of DoD. References herein to any specific commercial product, process, or service by trade name, trademark, manufacturer, or otherwise, do not necessarily constitute or imply its endorsement, recommendation, or favoring by DoD.

Table of Contents

List of Acronyms 2-vi
Introduction 2-1
DCERP Themes 2-2
Theme 1: Climate Change 2-2
Theme 2: Carbon Cycle and Carbon Management 2-6
Theme 3: Translating Science into Practice 2-11
Aquatic/Estuarine Module 2-13
Aquatic/Estuarine Module Research and Monitoring 2-13
Scientific Findings of the Aquatic/Estuarine Module 2-14
Findings with Implications for DoD and Other Coastal Managers 2-16
Coastal Wetlands Module 2-17
Coastal Wetlands Module Research and Monitoring 2-17
Scientific Findings of the Coastal Wetlands Module 2-18
Findings with Implications for DoD and Other Coastal Managers 2-19
Coastal Barrier Module 2-21
Coastal Barrier Module Research 2-21
Scientific Findings for the Coastal Barrier Module 2-22
Findings with Implications for DoD and Other Coastal Managers 2-24
Terrestrial Module 2-25
Terrestrial Module Research 2-25
Scientific Findings of the Terrestrial Module 2-26
Findings with Implications for DoD and Other Coastal Managers 2-27
Identification of Ecosystem Indicators 2-28
Data and Information Management System 2-30
DCERP Public Web Site 2-30
DCERP Data Portal 2-30
Legacy of DCERP 2-31
Literature Cited 2-33

List of Figures

Figure 2-1. DCERP2 themes. 2-1

Figure 2-2. Neuse River Estuary temperature scenarios. 2-3

Figure 2-4. A comparison of water levels of the New River at Gum Branch from May 7–12, 1972, when no tidal signal was evident and for the same period in 2013 when a tidal signal was evident. 2-4

Figure 2-3. The wave action from storms will be enhanced by sea level rise and cause changes in shoreline position and dune structure. 2-4

Figure 2-5. The domain for marsh modeling at Freeman Creek, Traps Bay, and French Creek. 2-5

Figure 2-6. Residual flow carbon budget showing annual carbon exchanges as dissolved inorganic carbon (DIC) and total organic carbon (TOC) flows (in gigagrams of carbon [Gg-C; 10^9 g-C]). 2-7

Figure 2-7. Transects of the difference of estuarine versus atmospheric pCO_2 (ΔpCO_2) before and after passage of Hurricane Joaquin in fall 2015. 2-8

Figure 2-8. Carbon from peat deposits eroding from the shoreface of Onslow Beach. 2-10

Figure 2-9. Translating Science into Practice. 2-11

Figure 2-10. Conceptual model for the Aquatic/Estuarine Module. 2-14

Figure 2-11. A comparison of diel (day versus night) variation of partial pressure of CO_2 (pCO_2) to average seasonal variation within each box. 2-15

Figure 2-12. Hypoxia in bottom waters can cause fish kills. 2-16

Figure 2-13. Stormwater detention ponds are used to treat stormwater runoff from developed areas of MCBCL. 2-17

Figure 2-14. Conceptual model for the Coastal Wetlands Module. 2-18

Figure 2-15. Landward migration of salt marsh is determined by topography and the absence of development. 2-20

Figure 2-16. Living Shoreline suitability index for MCBCL available at http://maps.coastalresilience.org/northcarolina/. 2-21

Figure 2-17. Conceptual model for the Coastal Barrier Module. 2-22

Figure 2-18. Area of the washover at Onslow Beach through time. 2-24

Figure 2-19. CSHORE-C15 predictions of shoreline and beach position in 2065 across the Onslow Beach northern portion of the training area under highest and lowest sea level rise scenarios. 2-25

Figure 2-20. Conceptual model for the Terrestrial Module. 2-26

Figure 2-21. Red-cockaded woodpecker. 2-27

Figure 2-22. Components of the DCERP Data and Information Management System (DIMS). 2-30

List of Tables

Table 2-1. Sea Level Rise Scenarios Used by DCERP Based on SERDP Guidance (Hall et al., 2016) 2-5

Table 2-2. Indicators and Associated Benchmark of Ecosystem State Change Identified During DCERP 2-29

List of Acronyms

ΔpCO_2	difference in partial pressure of carbon dioxide
°C	degree Celsius
°F	degree Fahrenheit
$\mu g\ L^{-1}$	micrograms per liter
AVP	autonomous vertical profiler
C	carbon
CAR	carbon accumulation rate
CDOM	chromophoric dissolved organic matter
chl *a*	chlorophyll *a*
cm	centimeter
CO_2	carbon dioxide
DCERP	Defense Coastal/Estuarine Research Program
DCERP1	first cycle of DCERP
DCERP2	second cycle of DCERP
DIC	dissolved inorganic carbon
DIMS	Data and Information Management System
DOC	dissolved organic carbon
DoD	U.S. Department of Defense
ESM	Estuarine Simulation Model
ft	feet, foot
$g\ C\ m^{-2}\ yr^{-1}$	grams of carbon per square meter per year
Gg-C	gigagrams of carbon
GIS	geographic information systems
ha	hectare
ICW	Intracoastal Waterway
iMAP	interactive mapping application
$J\ m^{-1}$	joules per meter
km	kilometer
km^2	square kilometer
LCAC	Landing Craft Air Cushion (vehicle)
m	meter
m^2	square meter
m^3	cubic meter
$m^3\ s^{-1}$	cubic meters per second
MARDIS	Monitoring and Research Data Information System
MCBCL	Marine Corps Base Camp Lejeune
$mg\ m^{-2}$	milligrams per square meter

mg/L	milligrams per liter
Mg/yr	megagrams per year
mi	mile
mi^2	square mile
mph	miles per hour
NH_4^+	ammonium
NPP	net primary production
NRE	New River Estuary
pCO_2	partial pressure of CO_2
POC	particulate organic carbon
RC	Resource Conservation and Climate Change (a SERDP program area)
RCW	red-cockaded woodpecker
RWE	representative wave energy
SCM	stormwater control measure
SERDP	Strategic Environmental Research and Development Program
SSC	suspended sediment concentration
TOC	total organic carbon
TSP	Translating Science into Practice (Module)
USGS	U.S. Geological Survey
YR1	Year 1
YR2	Year 2

Introduction

DCERP2 focused on understanding the factors that regulate carbon, nutrient, and sediment processes and the responses of these processes in various coastal ecosystems to potential climate conditions. This knowledge has important implications for operations, military training, and ecosystem management at the U.S. Department of Defense's (DoD's) numerous installations across the Southeastern United States. DCERP2 has also made major efforts to translate this scientific knowledge into formats that are understandable not only to the DoD installation managers, but also to the scientific community, other coastal managers, and the public.

This chapter of the *DCERP2 Final Report* highlights the significant findings and management implications of the Defense Coastal/Estuarine Research Program (DCERP) conducted at Marine Corps Base Camp Lejeune (MCBCL) from February 2013 through November 2017. The findings are presented first at the thematic level (i.e., climate change, carbon, and translating science into practice [TSP]; **Figure 2-1**) and then at the ecosystem module level (i.e., Aquatic/Estuarine, Coastal Wetlands, Coastal Barrier, and Terrestrial Modules). The three themes served as major cross-module integrating objectives, and the modules were developed to organize the program around common management units.

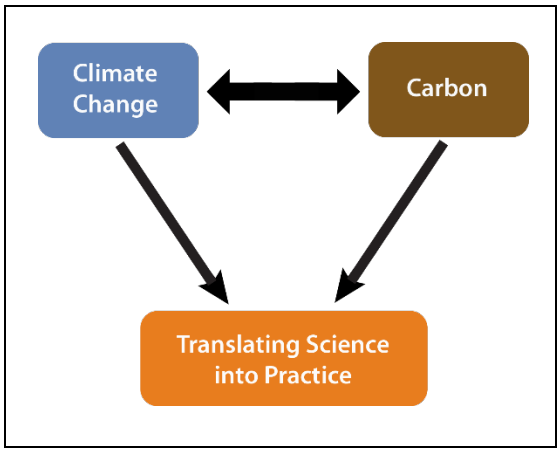

Figure 2-1. DCERP2 themes.

A summary of the DCERP Data and Information Management System (DIMS) is also included in this chapter. DIMS is the database-driven, Internet system that provides a means to access and manage the DCERP data collections, and it provides a framework that supports DCERP's dynamic outreach products and ecosystem-based management tools. DCERP DIMS serves as the permanent repository for DCERP data, information, and modeling results collected during DCERP's implementation. Detailed information and additional findings to those summarized in this chapter are provided in the individual chapters for each monitoring activity and research project in Chapters 3 through 22 of this *DCERP2 Final Report*.

This chapter also discusses the legacy of this 10-year research and monitoring program that includes a summary of scientific publications, presentations, and outreach activities conducted by the DCERP2 Team. DCERP should serve as a model for other long-term ecosystem monitoring and research programs that can be conducted to address natural resources management needs at other DoD installations and provide findings that are useful to the broader community of scientists, natural resource managers, and other stakeholders, including the public.

DCERP Themes

Theme 1: Climate Change

Nearly all DCERP2 research projects incorporated one or more components of climate change to drive the ecological process models and to project plausible impacts on natural ecosystem processes through the end of this century. The climate drivers that were considered included temperature, precipitation, storminess (wind speed), and sea level rise. An ensemble of downscaled climate projections, based on worst case scenario of increasing concentrations of greenhouse gases, was developed to study future climate conditions in Eastern North Carolina. This ensemble allowed the uncertainty associated with the climate projections to be represented and translated into climate change impact assessments. The ensemble included both dynamic and statistical downscaling techniques and contained climate variables of temperature, precipitation, and wind at the daily time scale needed by the DCERP2 Team.

Ecosystem Reponses to Climate Change

Increasing Temperature

Temperature affects the function of natural ecosystems in fundamental ways such as impacting the rates of chemical reactions, organisms' metabolism, and the timing of critical life cycle events (phenology). Based on the ensemble of climate projections, by 2100 the number of days with maximum temperature greater than 90°F (32°C) was projected to increase at MCBCL. For example, in July, the ensemble predicted an increase from 15 days with temperatures greater than 90°F (32°C) to between 23 and 32 days by 2100. Higher air temperatures influence water temperatures, which can affect the solubility of gaseous constituents such as oxygen (O_2) and carbon dioxide (CO_2) and also the trophic status of estuaries. The Estuarine Simulation Model (ESM) developed for the New River Estuary (NRE) predicted a long-term trend towards increased heterotrophy (i.e., respiration exceeds photosynthesis) with the predicted increase in temperature. Increased heterotrophy will be accompanied by water column and sediment hypoxia (low dissolved oxygen concentration harmful to aquatic life) and increased fluxes of CO_2 into the atmosphere due both to the decreased solubility of O_2 and CO_2 in the warmer water and increased uptake of O_2 and release of CO_2 by microbial respiration in the sediment. The ESM developed for the Neuse River at Marine Corps Air Station Cherry Point (in North Carolina), predicted that higher temperatures will cause earlier spring phytoplankton blooms and an increase in phytoplankton net primary production compared with current conditions (**Figure 2-2**). These two examples show the challenges that DoD managers may experience in the future regarding water quality management and the importance of maintaining a routine monitoring program to detect critical estuarine responses.

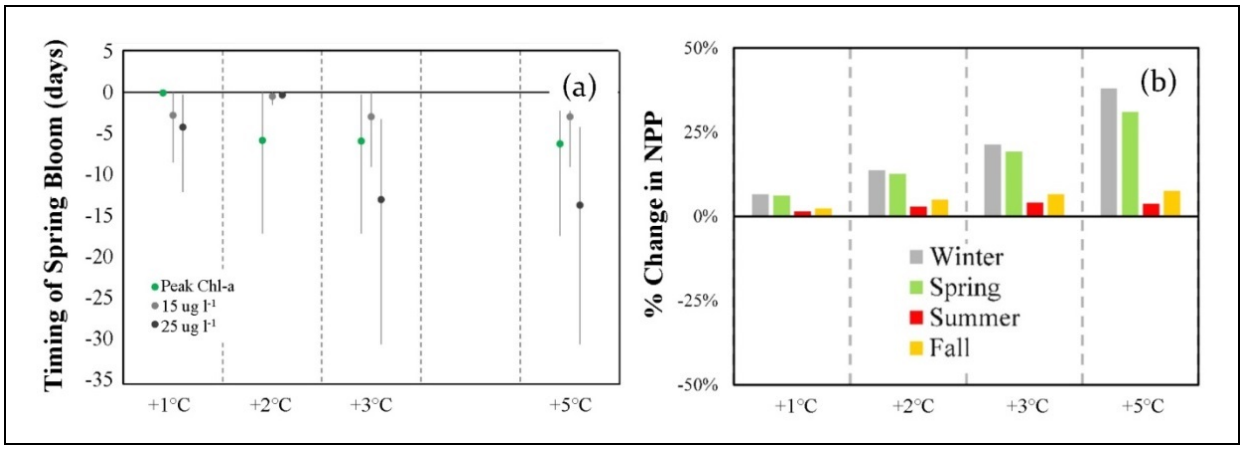

Figure 2-2. Neuse River Estuary temperature scenarios.

Neuse River ESM output under a series of temperature-warming scenarios relative to current conditions. (a) Timing of the spring bloom as defined by various chlorophyll *a* (chl *a*) thresholds, with negative values indicating an earlier bloom; (b) the percent change in seasonal phytoplankton net primary production (NPP).

In terrestrial landscapes, modeling results indicated that increasing temperatures will inhibit the growth and regeneration of loblolly pine (*Pinus taeda)*, a dominant tree in forest communities in Eastern North Carolina. Thus, towards the end of the century, conditions may become less suitable to loblolly pine and more suitable to slash pine (*Pinus elliottii*), a more southerly occurring species. Landscape model results also suggest that longleaf pine (*Pinus palustris*)—a key habitat for the federally endangered red-cockaded woodpecker (RCW; *Picoides borealis*)—may also be more resilient to warmer temperatures than loblolly pine, benefiting RCWs.

Variability in Precipitation

Precipitation drives the hydrologic cycle to both the aquatic and terrestrial ecosystems. The current annual precipitation for MCBCL is 54 inches (137 cm), which some models indicate will increase in the future while others indicate will decrease or remain the same in the future. When examining the range of future projections (encompassing 95% of the distribution of the climate ensemble data), a slight decrease or an increase in the number of days with heavy rain (greater than 1 inch [2.54 cm]) is projected to occur for all months of the year. New River flow was found to be the major source of nutrients, sediments, and carbon to the NRE. Thus, changes in the magnitude or the distribution of precipitation events during a year will impact both the amounts and timing of loading of these materials to the estuary. River flow was also a strong predictor of algal bloom dynamics in the estuary, due not only to its role in delivering nutrients, but also to its role in modulating estuarine residence time. In years with lower than average river flows, algal blooms occurred in the upper reaches of the estuary near Jacksonville, NC. During moderate flow periods, blooms occurred in the middle to lower estuary. At the highest flows, blooms did not develop because the algae did not have enough time to assimilate nutrients that had been transported into the estuary.

Changes in precipitation patterns also impact terrestrial systems. MCBCL forest managers rely on prescribed burning to meet RCW habitat restoration goals; however, precipitation extremes will cause significant complications in conducting prescribed burns. Foresters typically have a window for conducting prescribed burning that lasts from November through April each year. Conditions that are either too wet or too dry can limit the ability to conduct prescribed burns,

thus increasing risks for wildfires, especially high-intensity crown fires that can kill mature pine trees. Complicating management further, changes in precipitation delivery in concert with temperature changes will also increase challenges to the prescribed fire regime. Both of these climate conditions that prevent regular application of prescribed fire would not be beneficial to attaining RCW recovery goals.

Changes in Storminess

Wind magnitude, used as a measure of storminess, is an important driver of ecological processes in coastal ecosystems, affecting sediment transport and resuspension, shoreline erosion, and mixing of estuarine waters. The DCERP2 Team used 40 mph (tropical storm winds) as a threshold for storminess. However, the climate models consist of daily average wind speed information, and thus, none of the climate models simulated daily average wind speed that met that threshold criterion.

Figure 2-4. The wave action from storms will be enhanced by sea level rise and cause changes in shoreline position and dune structure.

However, storm events are currently the major cause of changes to the coastal barrier island (**Figure 2-3**), especially in the southwestern portion of Onslow Beach where storms are the initial driver of overwash events. Washover fans that develop during such storm-driven events can be further modified by frequent, overwash events associated with spring tides, wave runup, and small storms, that continue to transport sand across the barrier before the washover area finally stabilizes. Even without an increase in storminess above current levels, accelerated rates of sea level rise will cause erosion of carbonaceous sediment at the ocean shoreline which will shift Onslow Beach from a carbon reservoir towards a net source of carbon to adjacent environments such as the coastal ocean and the atmosphere.

Rising Sea Level

Sea level changes are a central forcing feature in estuaries and coastal areas because they control the exchanges of materials at the upstream and downstream endpoints of the estuary. Sea level impacts the physiology of important organisms, such as marsh plants, and influences estuarine and coastal barrier hydrodynamics and the processes of accretion and erosion. An analysis of long-term data from the upper New River revealed striking changes in the historic water level (i.e., gage height) recorded at the long-term U.S. Geological Survey (USGS) Gum Branch stream gaging station (**Figure 2-4**). A trend of increasing daily minimum and maximum water levels was observed during periods of low discharge from 1987 through 2013, presumably due to changes in both freshwater discharge and sea level. Similar to the New River mainstem, tributary creeks are currently conduits for loading of nutrients, sediment, and carbon into

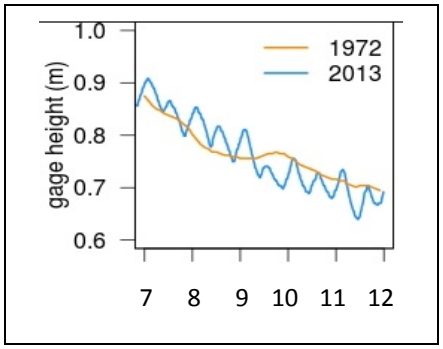

Figure 2-3. A comparison of water levels of the New River at Gum Branch from May 7–12, 1972, when no tidal signal was evident and for the same period in 2013 when a tidal signal was evident.

the estuary. Although no significant changes in loading occurred at the tributary creek monitoring sites, which are located above the area of tidal influence, future sea level rise will likely mean that higher salinity waters will move farther upstream of their current point of influence in these tributary creeks. This shift in salinity could have impacts on aquatic organisms in areas of the NRE designated as primary and secondary nursery areas.

Coastal marshes are located at the land–water interface and must increase their surface elevation by the accumulation of sediment and biomass, or risk being inundated by rising sea level. The Geospatial Marsh Model was used to predict the fate of three different coastal marshes at MCBCL in response to five scenarios of sea level rise (**Table 2-1**). The response of MCBCL marshes to sea level rise can be characterized by differing combinations of four main responses. These responses are as follows: (1) horizontal expansion or movement via upland migration, (2) transition to flood tolerant vegetation (i.e., black needle rush [*Juncus roemerianus*] replaced by smooth cordgrass [*Spartina alterniflora*]), (3) enhanced vertical accretion of the marsh, and (4) drowning of the marsh vegetation.

Table 2-1. Sea Level Rise Scenarios Used by DCERP Based on SERDP Guidance (Hall et al., 2016)

Scenario	Increase in Sea Level by 2100
Lowest	1.0 ft (0.3 m)
Low	2.6 ft (0.8 m)
Medium	4.3 ft (1.3 m)
High	5.9 ft (1.8 m)
Highest	8.2 ft (2.5 m)

All three of the modeled MCBCL marshes gained area under the lowest sea level rise scenario (1.0 ft [0.3 m] by 2100) through a combination of expansion via marsh migration toward the uplands and marsh maintenance through enhanced vertical accretion (**Figure 2-5**). The response of Freeman Creek, which is on the Intracoastal Waterway (ICW), was dominated by marsh expansion without any substantial change in the proportion of *Spartina alterniflora* (flood tolerant) and *Juncus roemerianus* (irregularly flooded) vegetation types. The modeled response of Traps Bay, which is in the lower estuary, showed a transition from *Juncus roemerianus* to the more flood tolerant *Spartina alterniflora*, with limited area for upland expansion. The response of the French Creek marsh, which is in the middle estuary, was dominated by drowning, with an extensive loss of marsh and swamp coverage at all scenarios beyond the lowest sea level rise scenario (1.0 ft [0.3 m] by 2100). Above the medium sea level rise scenario (1.3 m by 2100), marshes at French Creek and Traps Bay drown because of limited sediment supply and reduced ability to continue to migrate landward. The marsh that demonstrated the highest resilience was Freeman Creek. This marsh had the highest sediment supply and the lowest surrounding slope; therefore, it was only predicted to drown at the highest sea level rise rate (greater than 1.8 m by 2100).

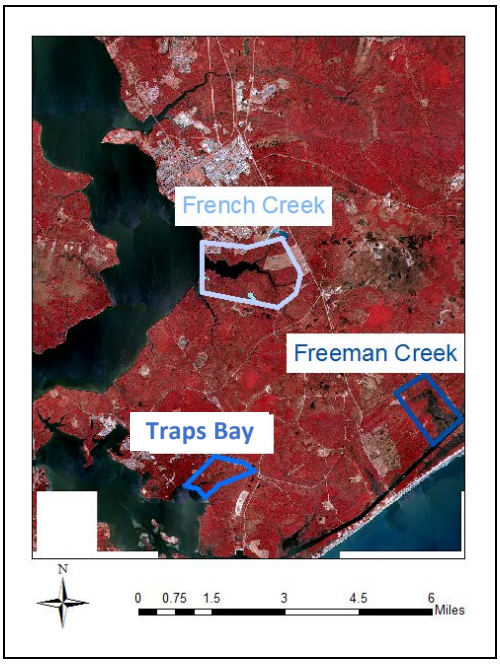

Figure 2-5. The domain for marsh modeling at Freeman Creek, Traps Bay, and French Creek.

As with the marshes, sea level rise is the predominant force that shapes the coastal barrier island of Onslow Beach. Using the CSHORE-C15 Beach Morphology Model, projected sea level rise was found to exert a greater influence on shoreline position than wind magnitude (storminess). Using the lowest (0.3 m) and highest sea level rise (2.5 m) rates through 2100 as the range of possible solutions, the CSHORE-C15 model forecasted shoreline position for all sea level rise scenarios indicated a substantial loss of infrastructure south of the Onslow Beach Bridge by 2035 and a loss of usable beach by 2065. Conversely, the model indicated that the island north of the bridge will remain stable and likely grow seaward. This information has implications for the sustainability of the critical Marine Corps amphibious training area in its current location on Onslow Beach.

Theme 2: Carbon Cycle and Carbon Management

The second theme of DCERP2 was to develop an understanding of carbon cycling and exchanges between the estuary, marshes, coastal barrier, and the atmosphere and to explore terrestrial carbon dynamics resulting from different forest management practices. Quantifying carbon cycling in the estuarine/coastal landscape within MCBCL's boundaries hinges upon measuring intra-ecosystem carbon inventories and inter-ecosystem fluxes at the appropriate spatial and temporal scales. Carbon budgets provide a tool to quantify carbon flows and track the complex processes that control whether carbon is stored internally or exported into the ocean and atmosphere (Crosswell et al., 2017).

New River Estuary Carbon Budget

The NRE is representative of lagoonal estuaries that are common along temperate coastlines of the Southeast and Gulf Coasts of the United States. Carbon processing within, delivery to, and export from the NRE was assessed at unprecedented spatial and temporal resolution by the DCERP2 Team. On an annual basis and across the entire estuary, the NRE was in near metabolic balance with gross primary production approximating community respiration. Depending on river discharge, the NRE was either slightly net heterotrophic (more respiration than photosynthesis) or slightly autotrophic (more photosynthesis than respiration). This small variation around net neutral metabolism was maintained by counterbalancing metabolic rates and exchanges spatially between the channel and the shoals, between the upper and lower estuary, and temporally between seasons.

The NRE varied from a small sink for CO_2 during a relatively dry year to a small source for atmospheric CO_2 during a year when river discharge was higher (**Figure 2-6**). Net CO_2 exchanges between the atmosphere and the estuary were small components of the estuary-wide carbon budget, and up to one order of magnitude less than exchanges reported from some European (Frankignoulle et al., 1998) and Asian (Chen et al., 2013) estuaries, but similar to other microtidal estuaries such as the Neuse River in North Carolina (Crosswell et al., 2012), York River in Virginia (Anderson et al., 2014), and several tropical estuaries in Australia (Maher and Eyre, 2012). At times, the flux of CO_2 to and from the atmosphere was divergent in magnitude and direction from net metabolism. This finding indicates that physical–chemical factors such as water temperature, pulsed delivery of inorganic and organic carbon and nutrients from the watershed, and temporal patterns in destratification were as or more important than gross primary productivity and community respiration for setting the air–water CO_2 exchange.

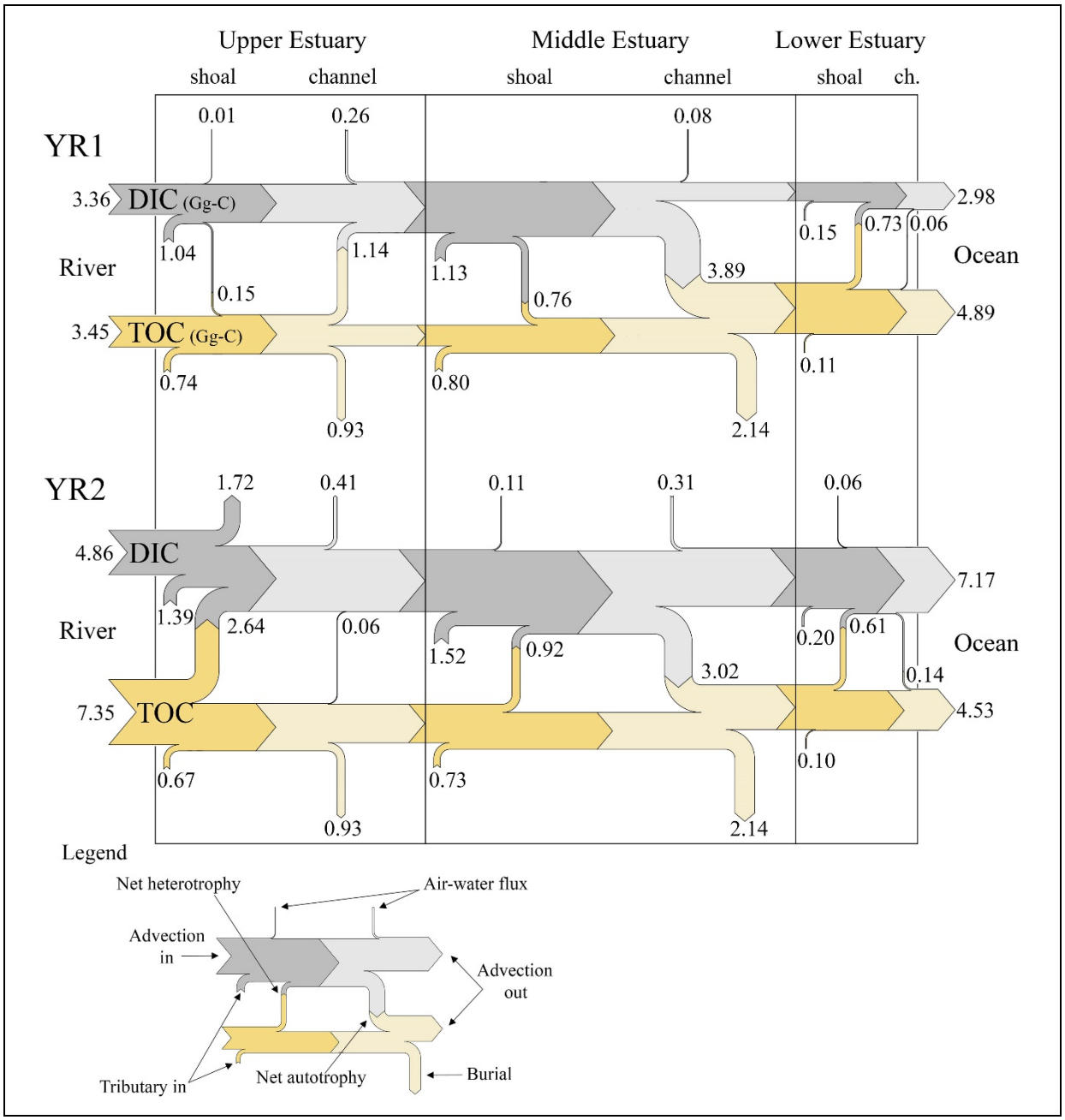

Figure 2-6. Residual flow carbon budget showing annual carbon exchanges as dissolved inorganic carbon (DIC) and total organic carbon (TOC) flows (in gigagrams of carbon [Gg-C; 10^9 g-C]).

Flow width is proportional to magnitude, and the length of each region from left to right is proportional to the area of that region in the NRE. Year 1 (YR1) was a dry year, and Year 2 (YR2) was a wet year with rainfall almost double the dry year.

The NRE was a source of both inorganic and organic carbon into the coastal ocean, in part reflecting inputs from the New River. Passage through the NRE changed the total carbon flux to the coastal ocean minimally (approximately 10%), but was important for changing the allocation between inorganic and organic carbon before export. Wet years delivered more organic carbon

than inorganic carbon from the NRE watershed. Within the estuary, organic carbon was attenuated by 20% to 30%, resulting in greater export of inorganic carbon than organic to the coastal ocean. During dry years, inorganic and organic carbon loads from the watershed were lower and approximately equivalent. The estuary tips towards metabolic balance or slight autotrophy under these conditions, resulting in net production of organic carbon and uptake of inorganic carbon, augmenting the estuarine organic carbon export to the coastal ocean by up to 40%. Lability experiments suggested that organic carbon produced by primary production in the estuary is more labile than the humic-rich organic carbon delivered from the watershed. Therefore, this estuarine-mediated alteration of organic carbon load and composition has implications for carbon dynamics in the coastal ocean.

Small, tributary creeks from MCBCL deliver relatively consistent amounts of both organic and inorganic carbon into the NRE regardless of wet or dry years. Inputs of dissolved inorganic carbon (DIC) from adjacent marshes were not a factor in the estuarine carbon budget, in contrast to some other estuarine systems (Cai, 2011). This lack of marsh influence is likely due to the low tidal amplitude and limited extent of fringing marshes bordering the NRE. However, enhanced mixing and delivery of organic and inorganic carbon caused by large storm events were important to the estuarine carbon budget. Effluxes of CO_2 during a 5-week period following Hurricane Joaquin were 10 times higher than pre- and post-fluxes and approximately equivalent to several months of net CO_2 exchange during non-storm periods, illustrating the importance of quantifying the contribution of storm events to annual budgets (**Figure 2-7**). We suggest that river discharge, at least in a coarse sense, is a reasonable proxy for the NRE carbon impact on the coastal ocean and atmosphere, given the incumbent uncertainty in estuarine carbon budgets.

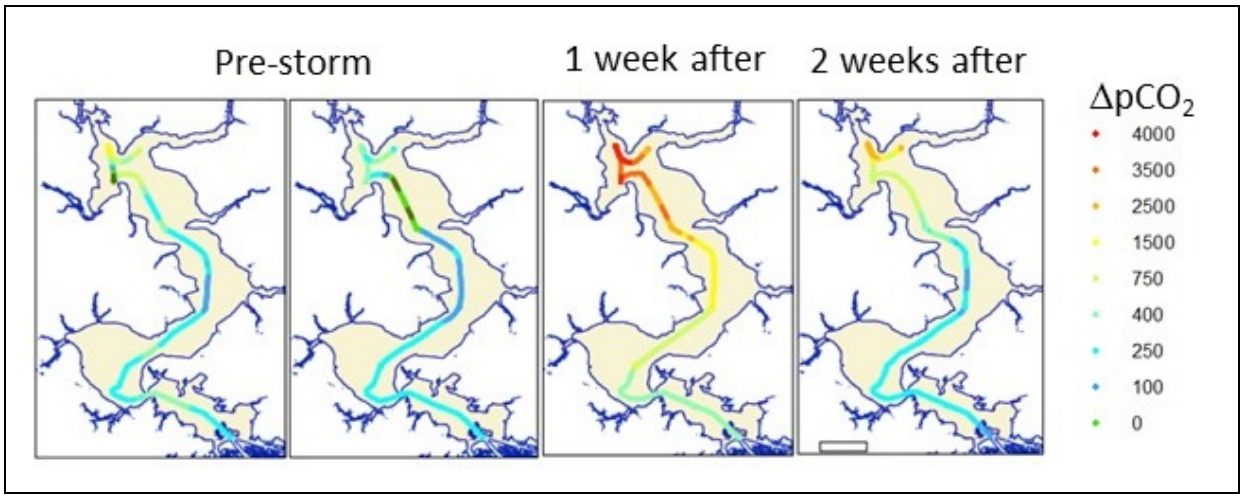

Figure 2-7. Transects of the difference of estuarine versus atmospheric pCO_2 (ΔpCO_2) before and after passage of Hurricane Joaquin in fall 2015.

Carbon accumulates in estuarine sediments on annual to decadal scales and is important for assessing whether the NRE transports carbon offshore or traps carbon locally. Carbon accumulation rates (CARs) in the upper portion of the NRE were correlated to sediment accumulation rates and were among the highest rates reported in the literature from other estuaries (Gordon and Goñi, 2004; Herrmann et al., 2015; Kemp et al., 1997; Maher and Eyre, 2012; Roden et al., 1995; Warnken et al., 2008). Based on age-dating of the sediments, carbon

accumulation increased over the past century and exceeded the local rate of sea level rise by two- to four-fold. The high deposition rates mirror the increased rates of sea level rise, watershed development, and hydrologic forcings. Although storm-driven pulses of terrestrial-derived soils coincide with peak CARs, these event-driven influxes are less carbon rich than sediments that accumulate during storm-free periods.

Purely based on a mass balance, carbon accumulation in sediments of the NRE could not be supported by watershed delivery of terrestrial soil carbon alone. Substantial amounts of particulate organic carbon (POC) derived from estuarine productivity must accumulate in sediments to help offset some of the respiration of carbon delivered from the watershed. Although influxes of terrestrial soil are required to maintain the high rates of sediment accretion, that soil carbon is modified or likely supplemented by non-terrestrial carbon to achieve the current carbon composition in the NRE sediments.

The secondary effect of adding new carbon to the estuarine sediment is that the new carbon helps fuel sediment respiration, which drives anoxia and optimizes carbon burial. Over the past few decades, the magnitude and composition of the new carbon has changed in response to point nutrient sources, reflecting changes in watershed delivery from changing land use upstream of the NRE. Regardless of evolving sources of carbon, the current CAR is well above local sea level rise and likely unsustainable. As accommodation space for more sediment in the upper NRE decreases, a future redistribution of sediment carbon throughout the estuary would be expected. The geomorphology of the NRE poses significant impediments to export of sediment carbon to the coastal ocean. Further research is needed to determine whether this process of carbon redistribution within the NRE affects the total mass of carbon stored in sediments or facilitates the release of sediment carbon (either previously stored or recently delivered to the NRE) from the watershed to the coastal ocean. However, the NRE appears to be a transient, short-term sink for carbon that can easily divest itself of stored carbon via emissions of CO_2 into the atmosphere with the passage of severe storms as has occurred in other East Coast estuaries (Crosswell et al., 2014).

Carbon Flux in Coastal Marshes

Salt marshes occupy more than 10 km^2 on MCBCL and range from large *Spartina*–dominated marshes along the ICW to smaller areas of *Juncus*–dominated fringing marshes on embayments and tributaries of the NRE. Although all MCBCL marshes are accumulating carbon as they increase surface elevation, short-term flux measurements show that while some MCBCL marshes take up more CO_2 from the atmosphere than is released (autrotrophic), others exhibit a net release of CO_2 (heterotrophic). The net carbon efflux in the heterotrophic marshes is likely due to microbial respiration of imported external carbon or marsh carbon released via local erosion. The supply of carbon from the watershed is trivial compared with carbon delivered in tidal waters and produced by plant primary production. Overall, the annual net carbon balance in the marshes is driven by CO_2 exchanges with the atmosphere and sediment deposition. Lateral fluxes of carbon, both through drainage of the marsh platform during ebbing tides, and via porewater advection were small in comparison.

Sediment CARs are the sum of sediment accretion, biogenic growth, microbial decay, and physical compaction. The mean sediment accumulation rates over the past 150 years in MCBCL

marshes are similar to the local rate of sea level rise. All marshes showed increased CARs over the past century compared with rates greater than 500 years ago, coincident with an acceleration of sea level rise. However, if the rate of sea level rise exceeds net elevation change in the future, then the marshes will cease to be sites for carbon accumulation and the carbon that has accumulated and been buried over the past hundreds to thousands of years will be subject to erosion and subsequent decomposition. These processes would release CO_2 back into the atmosphere and make the marshes an increasing source of CO_2.

The fate of potentially drowned and eroded marsh carbon remains poorly constrained. Controlled in vitro decomposition experiments of *Spartina*–derived material revealed that decomposition to CO_2 was influenced by age of the material and temperature. Methane production was negligible. Annual carbon decomposition rates of 17% to 23% per year were obtained from marsh sediment collected from depths of 10 cm to 35 cm and incubated under oxic conditions at constant temperatures. At face value, these results suggest that the conversion to CO_2 could occur on a decadal timescale. However, this is highly dependent on erosion rate, the age distribution of the carbon eroded, how quickly it is redeposited, and the environmental conditions of the "redepositional" environment, which might greatly reduce the decomposition rate. Given the high loads of sediment that are reworked and redistributed within the marsh, it is likely that much of the eroded carbon is redeposited onto the marsh surface on timescales that are faster than the decomposition rate. Once redeposited on the marsh away from erosional edges, carbon can be preserved and stored on longer timescales. Some MCBCL marshes have served as a long-term sink for carbon for more than 1,000 years and will continue to increase their carbon content as sea level rises, unless they drown and carbon is no longer accumulated.

Carbon Dynamics of Onslow Beach

Backbarrier island salt marshes provide important ecosystem functions, which include the sequestration of atmospheric CO_2 and below-ground carbon storage in the form of peat and organic-rich sediment. As the barrier island moves landward and sand overwashes the backbarrier marshes in the southwestern portion of Onslow Beach, this carbon is buried beneath the island for centuries (less than 500 years) before it becomes exposed by the ocean's hydrodynamic processes and is eroded and released on the beach front (**Figure 2-8**). Transgressive barrier islands with a wide backbarrier marsh primarily function as carbon sinks, but will transition to sources temporarily during storms when ocean shoreline erosion rates increase and overwash deposition onto backbarrier marshes occurs. As a barrier island continues to migrate landward, the backbarrier marsh narrows beyond a critical width, where the island primarily functions as a carbon source, and the carbon reservoir continually decreases. During this phase of barrier island transgression, carbon export rates will likely continuously exceed storage rates across the narrow backbarrier

Figure 2-8. Carbon from peat deposits eroding from the shoreface of Onslow Beach.

marsh. This decreasing (negative) trajectory of the carbon reservoir endures until the reservoir is depleted or when the coastal barrier merges with the mainland (the previous highstand shoreline). Our modeling results and field observations on Onslow Beach advocate for the consideration of barrier island transgressive processes in regional and global coastal carbon budgets. Proper assessment of present and future transgressive barrier island carbon budgets must consider erosion and overwash, as well as the island's backbarrier setting.

Carbon Stores on Forested Lands

MCBCL terrestrial forests provide the greatest opportunity for carbon storage. The terrestrial carbon research conducted during DCERP2 assessed the effects of different forest management practices on long-term carbon stores across MCBCL's landscape. Results of terrestrial carbon modeling scenarios (using LANDIS-II) suggested that above-ground live carbon storage is highest in longleaf pine compared with loblolly pine and is lowest in pond pine (*Pinus serotina*) forests. The amount of above-ground live carbon stores depends upon site conditions, stand development age, and variations and frequency of management practices (e.g., cutting interval and prescribed fire rotations). Model simulations of different forest management practices across MCBCL's landscape reinforced the findings that carbon storage was highest with management strategies designed to promote the restoration and maintenance of longleaf pine ecosystems. This finding was true for two prescribed fire regimes (3- and 6-year fire return intervals). Carbon storage at MCBCL and through much of the Southeastern United States, therefore, can be increased through active management strategies for restoring longleaf pine stands.

Theme 3: Translating Science into Practice

The third cross-cutting theme involved translating the scientific findings of DCERP's integrated monitoring, research, modeling, and adaptive management activities into practice for several different target audiences (**Figure 2-9**). The audiences that received information included the scientific community, DoD installation and regional managers, and local stakeholders. Practical application of DCERP information involves bridging the gap between scientific findings, in which researchers have comprehensive knowledge of a domain and in which installation managers and planners may interface with summary information or use the data only infrequently.

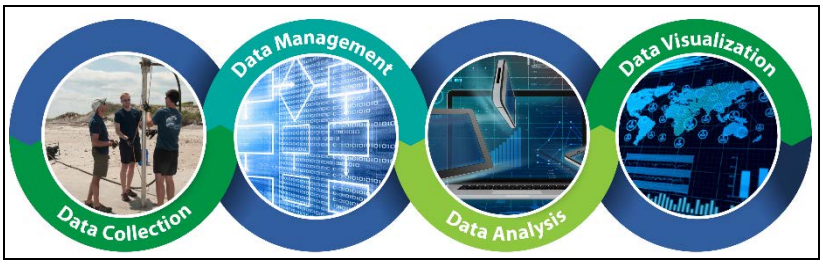

Figure 2-9. Translating Science into Practice.

The primary means used by the DCERP2 Team to translate results to the scientific community were through publishing findings in peer-reviewed journal articles or books and presenting research findings at international, national, or regional scientific meetings. For example, the DCERP2 Team presented during special sessions of the 2014 Joint Aquatic Sciences Meeting and the 2017 Coastal Estuarine Research Foundation Conference. Members of the DCERP2 Team collaborated on a paper about the estuarine carbon budget that was published in *Limnology*

and Oceanography, and our findings about the importance of sea level rise anomalies on coast barrier morphology were featured in *Nature*.

Although publishing results in scientific journals and presenting research at scientific conferences are both vitally important outreach activities to the scientific community, these activities often do not provide the scientific results in a format that is directly usable or actionable by DoD installation managers. Specifically, DCERP2 researchers expanded the functionality of DIMS to provide common mapping and data access functionality so that DIMS and the comprehensive suite of tools could help turn the extensive amount of DCERP data into accessible and usable information. The expanded DIMS provides a one-stop-shop data portal for accessing the various DCERP data, tools, models, and other information and products so that DoD managers can use them to make informed ecosystem-based management decisions. This effort of DCERP2 provided scientific research results in easy-to-understand documents and via models and decision-support tools developed to directly address installation management needs. These models and tools include mechanistic models, geographic information systems (GIS) data layers and associated analyses, and maps and reports that provide information needed by installation managers to make ecosystem-based management decisions. The DCERP2 Team has disseminated these products through various meetings, including annual Technical Advisory Committee meetings with MCBCL's Environmental Management Division staff, lunch and learn presentations to various installation personnel, and topic-specific technical briefings and Webinars with appropriate installation technical committees or staff from other DoD installations. These types of formal and informal meetings continued throughout the 10-year program.

The DCERP2 Team's efforts to bring findings and information to the broadest audience were reflected in the large number of engagements with stakeholders at the national, state, and local levels. For example, in 2014, the estuarine/coastal carbon research was presented to representatives of the U.S. Global Change Research Program, which provides a coordinated and focused scientific strategy for conducting carbon cycle research at the national level. Throughout DCERP, various researchers were interviewed by National Public Radio for *The State of Things* and *Science Friday* programs and provided interviews to several coastal and regional newspapers. Presentations of results were also given to local and regional stakeholder groups such as the New River Roundtable and the Albemarle-Pamlico Sound National Estuary Partnership. Additionally, the team developed other outreach products such as fact sheets about specific topics and published a quarterly newsletter to clearly and concisely explain the results of DCERP2 research to outside audiences. These products were posted and easily accessed via the DCERP public Web site (available at http://dcerp.rti.org).

During the final year of DCERP2, the team led a 1-day meeting for stakeholders in Jacksonville, NC, to inform local Onslow County, the City of Jacksonville, and MCBCL staff about DCERP's findings that are relevant to water quality and natural resource management. The team also conducted a 2-day scientific symposium in Raleigh, NC, for the scientific community, including regulators from the State of North Carolina, environmental consultants, university faculty and students, and non-governmental organization scientists.

Although all DCERP researchers were individually responsible for translating their significant scientific findings into actionable information for MCBCL managers, other coastal managers,

and the public, Research Project TSP-1 focused on helping DCERP researchers with bringing data, information, tools, and model results into various visual formats that made the results clear and easy to understand for various end users. Specifically, DIMS was developed to provide a one-stop-shop data portal for accessing the various DCERP data, tools, models, and other information and products developed by the DCERP Team so managers can use them to make informed ecosystem-based management decisions.

More Information About Ecosystem Module Monitoring and Research

The next four sections of this chapter emphasize the key scientific accomplishments and findings relevant to natural resource managers from the aquatic/estuarine, coastal wetlands, coastal barrier, and terrestrial ecosystems. Detailed information that describes each ecosystem, including their drivers, stressors, and knowledge gaps in the conceptual model, are provided in the *DCERP2 Research Plan* (RTI International, 2013).

Aquatic/Estuarine Module

Aquatic/Estuarine Module Research and Monitoring

DCERP Aquatic/Estuarine Module researchers studied the tidal reach of the NRE from the head of the estuary near Jacksonville, NC, to the tidal inlet at Onslow Bay, including inputs from the New River and several tributary creeks within MCBCL lands that flow into the NRE. The NRE is a relatively small (88 km^2 [34 mi^2]), shallow, microtidal Coastal Plain estuary. More than 50% of the NRE area is less than 2 m deep relative to mean sea level. Most of the estuary's shoreline (80%) is contained within the boundaries of MCBCL's land. The NRE consists of a series of lagoons and is confined by barrier islands that restrict water exchange with the Atlantic Ocean.

The Aquatic/Estuarine Module investigated how anthropogenic loadings (carbon, nutrient, and sediment inputs) from the New River watershed and MCBCL tributaries affected benthic microalgae and pelagic phytoplankton of the estuary. Furthermore, the effects of climatic variability, including acute or episodic events (e.g., tropical systems, floods, droughts) and longer term trends (e.g., warming, precipitation changes), on estuarine structure and function were characterized and quantified to better understand the interactive and potentially confounding impacts of climate (change) on water quality and habitat condition (**Figure 2-10**).

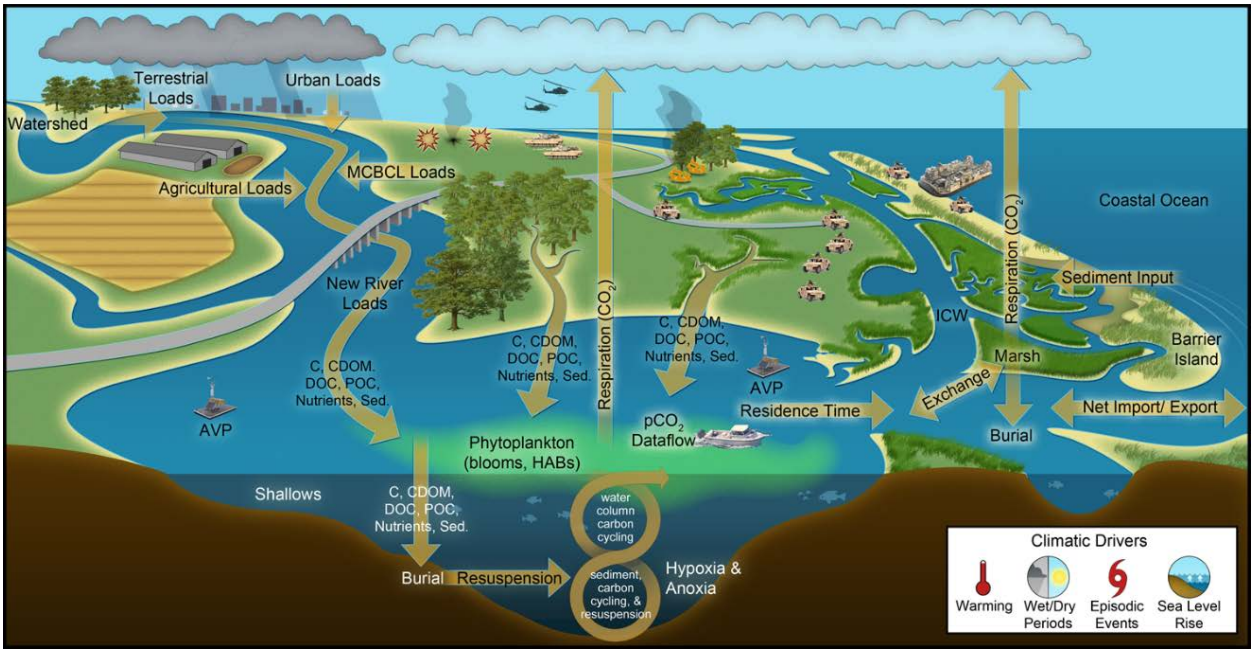

Figure 2-10. Conceptual model for the Aquatic/Estuarine Module.

Scientific Findings of the Aquatic/Estuarine Module

The NRE is a dynamic ecosystem in which primary production and the cycling of carbon and nutrients are strongly controlled by physical (i.e., hydrologic, tidal, wind, light) and chemical (i.e., nutrients, organic matter) interactions operating over highly variable temporal and spatial scales (Crosswell et al., 2017; Ensign et al., 2004; Hall et al., 2013; Mallin et al., 2005; Paerl et al., 2014; Peierls et al., 2012). Phytoplankton production and community structure are controlled by nutrient inputs, residence time, and the degree of stratification in the estuary. In contrast, benthic microalgae production is controlled by water clarity. Water clarity is reduced by the presence of suspended sediments, chromophoric dissolved organic matter, and pelagic phytoplankton biomass—all parameters regulated by climate-driven hydrologic flows from the New River and from sediment erosion from tidal activity and wave energy (Anderson et al., 2014). During the 10-year DCERP study period, the New River discharge at the USGS Gum Branch stream gaging station varied widely, spanning greater than three orders of magnitude. This stream flow variability represents nearly the full range of flow conditions captured in the historic discharge record for this station dating back to 1949.

Estuarine carbon fluxes varied up to four-fold between day and night.

Measurements of partial pressure of CO_2 (pCO_2) in the surface waters of the NRE showed up to a four-fold difference over the diel or day–night cycle, indicating the importance of high resolution spatial surveys to detect daily variations of CO_2 flux when developing estimates of system-wide fluxes (**Figure 2-11**).

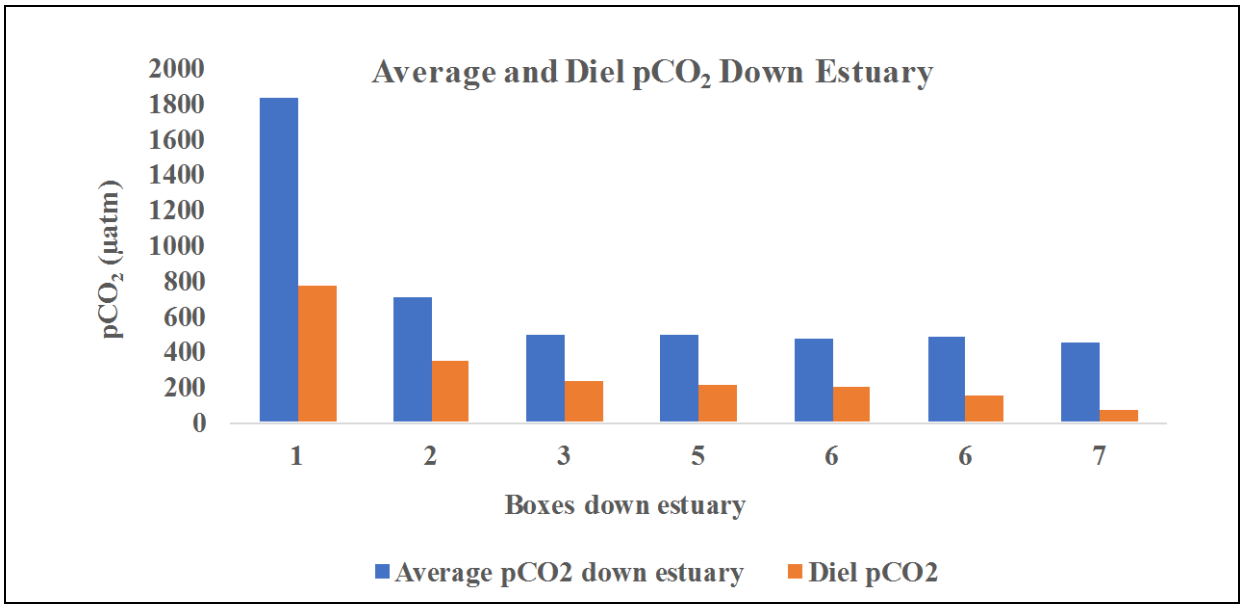

Figure 2-11. A comparison of diel (day versus night) variation of partial pressure of CO_2 (pCO_2) to average seasonal variation within each box.

The upper estuary is a sink for carbon when algal blooms are present.

The pattern of CO_2 exchanges varied both spatially and temporally across the estuary. During a wet year, the highest effluxes of CO_2 were at the head of the estuary, due primarily to decomposition of total organic carbon (TOC) transported from the New River into the estuary. CO_2 exchanges were the highest during periods of high temperature and were the lowest when algal blooms were occurring. However, overall CO_2 exchanges were negligible compared with fluxes of other forms of carbon, mainly DIC and TOC. TOC was the dominant form of carbon exported from the estuary during a dry year, whereas DIC was the dominant carbon species exported in a wet year. The TOC exported was mainly produced by photosynthesis within the estuary and was likely quite labile and, therefore, more likely to impact carbon dynamics in the coastal ocean.

The nutrient load from small coastal streams is lower than expected.

Overall, nutrient loading from tributary streams originating on MCBCL land was low compared with other coastal plain streams, and their total nutrient load to the NRE was small relative to other watershed sources, including the New River. However, increased watershed development on the installation (measured by percent imperviousness) increased in-stream concentrations and loading of most constituents (i.e., nutrients, sediment, and carbon). Dissolved organic carbon (DOC) was an exception because its source is wetlands and flood plains that are lost during development. This finding could alter future stormwater management requirements.

Hypoxia is linked to increased temperature and stratification, not to algal blooms.

Bottom water hypoxia (low oxygen conditions) was closely linked to increasing water temperature (because of oxygen solubility characteristics) and stratification of the water column, but had no clear-cut relationship to contemporaneous algal blooms in the estuary. Spatially, hypoxia was most common in the middle and upper estuary and was never observed at the two lowest estuarine stations. Most hypoxia events were detected when bottom water temperatures ranged between 77°F and 90°F (25°C and 32°C). As future temperatures increase toward the year 2100, hypoxic events may become more frequent and of longer duration, which could result in an increasing number of fish kills and loss of benthic shellfish populations in the estuary (**Figure 2-12**).

Figure 2-12. Hypoxia in bottom waters can cause fish kills.

Findings with Implications for DoD and Other Coastal Managers

The findings from DCERP2 inform management needs in various ways. The remainder of this section discusses some of the more significant findings that are meant to directly inform current or future management actions at MCBCL.

Future management efforts need to control nitrogen inputs to the NRE.

The New River watershed is the major source of nitrogen to the NRE, with approximately 64% of the external nitrogen originating in the watershed. Additional sources include Onslow Bay (15%), MCBCL lands (8%), the MCBCL wastewater treatment facility (7%), and atmospheric deposition (6%). Scenarios developed by using the ESM can be employed to set nutrient reduction targets for the NRE both now and under future climate conditions and to compute carbon storage in the estuary resulting from these scenarios. The ESM is a widely applicable tool that provides help to installation managers with adjacent estuarine systems.

Long-term increasing trends in chlorophyll *a*, ammonium, and light attenuation and decreasing dissolved oxygen concentrations in bottom water may be related to increasing anthropogenic eutrophication of the NRE associated with changes in land use and increasing population growth over the past two decades. Future water quality management efforts must minimize nitrogen inputs to sustain water quality in the NRE. A comprehensive management effort among MCBCL, Onslow County, and the City of Jacksonville will be required to reduce nitrogen loadings into the estuary from all point and nonpoint sources in the watershed.

Stream temperature is elevated in more developed watersheds.

Summer mean stream temperatures were up to 9°F (5°C) higher in more developed than less developed watersheds, and there was an apparent upward trend in stream temperature throughout

the 8-year study period (2008 to 2015). Warmer temperatures are likely to result in increased nutrient fluxes from the sediments and decaying organic matter, but they are also likely to cause increased rates of denitrification.

Stormwater wet detention ponds may not be the most appropriate best management practices for coastal plain conditions.

Aging stormwater wet pond sediments may contribute nitrogen to receiving waters (**Figure 2-13**). Net nitrogen fixation measured in stormwater wet pond sediments showed that the typical design of large, deep ponds may not be the most effective solution for improving the quality of urban stormwater in southeastern coastal areas, especially during summer months. Because of the negative effects on water quality from wet ponds in coastal areas, use of an alternative stormwater control measure (SCM) design may be more appropriate for MCBCL. Using SCMs with shallower water or no standing water at all could facilitate net denitrification during the summer by reducing stratification and anoxic conditions in the sediments and bottom water of SCMs. Alternative SCMs such as stormwater wetlands and bioretention cells could control similar volumes of stormwater and might produce higher quality water than existing wet ponds. In existing ponds, aeration to improve the circulation of pond water to reduce stratification, as well as frequent excavation of pond sediments could also reduce anoxic conditions, thereby reducing nitrogen fixation.

Figure 2-13. Stormwater detention ponds are used to treat stormwater runoff from developed areas of MCBCL.

Coastal Wetlands Module

Coastal Wetlands Module Research and Monitoring

Coastal wetlands are a vital component of the coastal landscape that links terrestrial and freshwater habitats with the sea or estuary. Marshes provide a variety of ecosystem services, including improving water quality by transforming nutrients and trapping sediment, attenuating wind wave and boat wake energy on shorelines, stabilizing the coastal barrier island, accreting sediments and building land, and providing recreational opportunities for people (**Figure 2-14**).

Salt marshes within the MCBCL region occur in the lower and middle NRE and along both shores (mainside and backbarrier) of the ICW and are typically dominated by *Spartina alterniflora* and *Juncus roemerianus*, the dominant plant species in salt marshes of the Atlantic Ocean and Gulf Coast; thus, DCERP research results are readily transferrable to other locations. DCERP2 Coastal Wetlands Module research and monitoring activities investigated the sources and fates of carbon to the marshes and the factors that affect the ability of marshes to keep pace with current and projected rates of sea level rise, thus addressing issues of resilience and vulnerability. The monitoring and research activities are summarized in **Appendices A and B**, respectively.

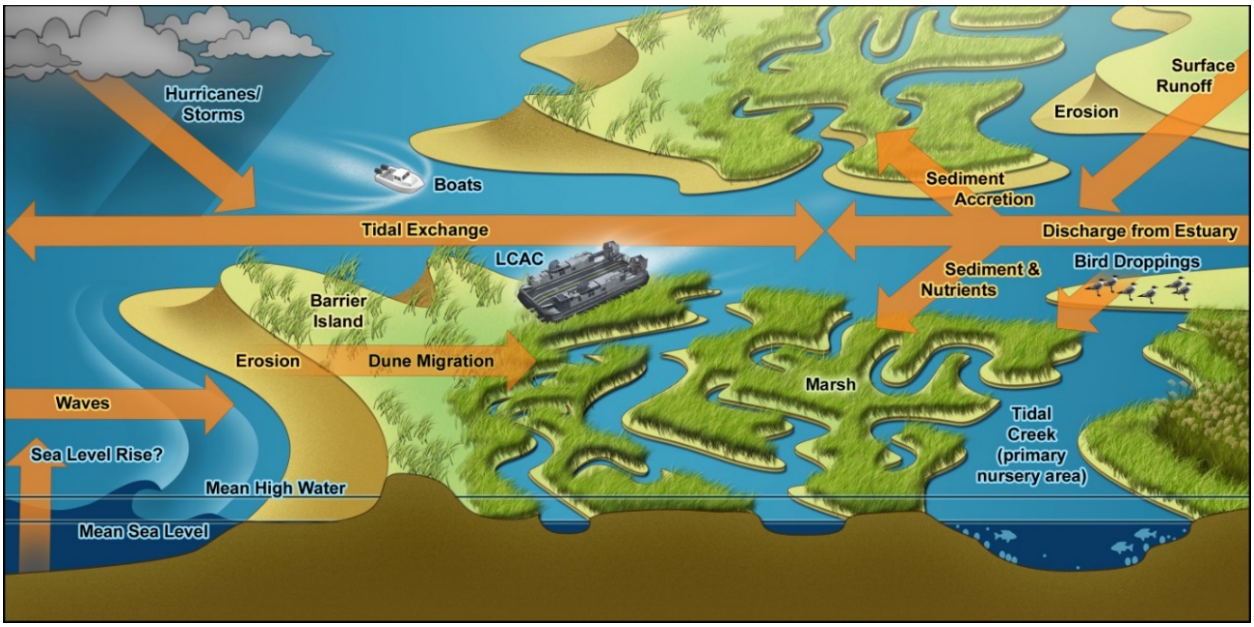

Figure 2-14. Conceptual model for the Coastal Wetlands Module.

Scientific Findings of the Coastal Wetlands Module

Carbon fluxes from salt marshes were determined over multiple spatial and temporal scales. Significant variability between sites, and the fact that many MCBCL marsh systems are in relative isolation from each other and the NRE, precluded the development of a single MCBCL marsh carbon budget. Instead, the DCERP2 Team focused on understanding the drivers of net carbon turnover and storage within the marshes and transport across the marsh boundaries to help inform the estuarine carbon budget and predict carbon accumulation potential of marshes along the ICW and NRE. Understanding the relationship between physical characteristics of the marsh location, pore water chemistry, responses to fertilization, and the rates of carbon cycling processes may improve carbon budget assessments within a marsh ecosystem and help identify which marsh locations may be most sensitive to carbon loss because of human impacts. The factors that affect marsh resilience to sea level rise include marsh elevation, sediment availability, the rate of sea level rise, the density of marsh vegetation, and variables such as nutrient enrichment and salinity that affect the density and species distribution of marsh vegetation.

Sea level rise is an important variable in forecasting marsh CARs.

Past CARs were studied at the middle estuary (French Creek), lower estuary (Traps Bay), and along the ICW (Freeman Creek; **Figure 2-5**). These rates varied from 19.7 to 147 g C m^{-2} yr^{-1} over marsh ages ranging from 200 to 3,200 years before the present. Some of the highest CARs were associated with younger, more surficial marsh sections, which we attribute to a response to recent accelerated sea level rise and incomplete decomposition of recently deposited material. In contrast, some of the lowest CARs integrate carbon accumulated over the past 2,000 years, during which North Carolina experienced little sea level rise. Therefore, sea level rise is an important component in forecasting future CARs for marshes, and contemporary observations are needed to accurately predict carbon dynamics.

The surface microlayer is a novel mechanism for redistributing sediment in marshes.

Models of marsh response to sea level rise rely on the spatial patterns of sediment transport in water moving from the tidal creek across the marsh where sediment deposition occurs on a daily tidal cycle. The DCERP2 Team identified a novel mechanism by which suspended sediments were redistributed across the marsh surface via the surface microlayer, which can float sand-sized particles (Ensign and Currin, 2017). This microlayer of suspended material carried approximately three times more sediment in the marsh over every tidal cycle than the amount that entered the creek from the watershed during one of the largest flood events.

Tidal creek structure is a surrogate for suspended sediment concentrations needed for marshes to keep pace with sea level rise.

Suspended sediment concentration (SSC), a critical variable for evaluating the sensitivity of salt marshes to sea level rise, is used in parameterizing marsh models; therefore, considerable effort was expended during DCERP to measure sediment dynamics in the MCBCL coastal wetland sites. A correlation between SSC and tidal creek structure was discovered that provides a practical alternative to conducting extremely labor-intensive field surveys of SSC (Ensign et al., 2017). Tidal creeks with wide, bay-like mouths had only half the SSC of narrow, winding tidal creeks. This correlation is useful because it allows researchers and managers to make general predictions of SSC in tidal creeks from remote imagery instead of having to collect in situ water samples, and will help increase the accuracy of broad-scale, high-resolution marsh modeling efforts.

Changes in predominant marsh plant species may signal an early response to sea level rise.

Marshes in the lower estuary appear to be transitioning from *Juncus*–dominated to *Spartina*–dominated. When *Juncus roemerianus* declined in 2012, *Spartina alterniflora* biomass began a 4-year increase. This trend is consistent with other monitoring parameters, including the percentage of plots containing each species, species percent cover, and stem density. Increases in salinity and/or more frequent inundation in response to sea level rise would be expected to favor *S. alterniflora* over *J. roemerianus*, and the data suggest that changes in response to these climate-related drivers may already be underway.

Findings with Implications for DoD and Other Coastal Managers

At MCBCL, salt marshes occupy approximately 1,100 ha (2,718 acres), ranging from *Spartina*–dominated marshes along the ICW to *Juncus*–dominated fringing marshes on embayments and tributaries of the middle and lower NRE. These marshes provide important ecosystem services, including support for amphibious assault training, and protection of the shorelines and MCBCL infrastructure from erosion and flooding. Projected rates of sea level rise along the North Carolina coast in conjunction with storms and changing land use threaten sustainability of these coastal wetlands. Our research findings on coastal wetlands can inform the ecosystem-based, adaptive management on MCBCL and for other coastal communities.

The most cost-effective adaptive management approach for maintaining MCBCL marshes is land management.

The most proactive and cost-effective adaptive management approach for sustaining MCBCL marshes into the future is to locate installation infrastructure away from the estuarine shoreline to minimize the need for shoreline hardening and maximize the potential for marsh migration into upland areas as sea level rises (**Figure 2-15**).

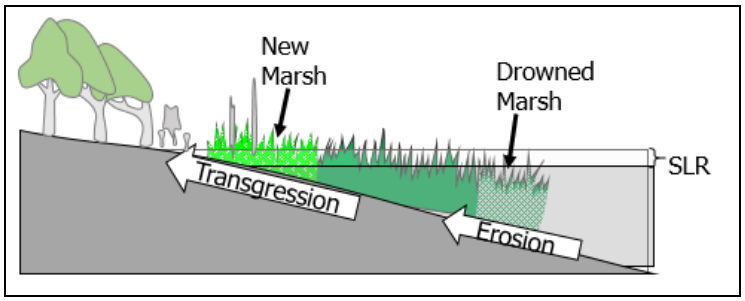

Figure 2-15. Landward migration of salt marsh is determined by topography and the absence of development.

Fertilization improves stem growth of Spartina alterniflor*a, but not* Juncus roemerianus *marshes.*

Coastal salt marshes must increase in elevation at a rate equal to or greater than the rate of sea level rise to maintain their intertidal position. Studies were conducted to determine whether fertilization of marshes is a viable management strategy because surface elevation increase is positively correlated with total standing biomass (above-ground stem growth plus below-ground root growth). After 1 year of fertilization, stem growth in marshes dominated by *Spartina alterniflora* increased by factors ranging from 2 to 4, but stem growth in marshes dominated by *Juncus roemerianus* did not increase. This finding has important implications for the potential use of fertilization as an adaptive management tool to enhance biomass and surface elevation increase for transplanted or restored *Spartina*–dominated marshes. Initial fertilization of transplanted or restored *Spartina alterniflora* plants will increase their success and enhance recovery of their ecosystem function. However, fertilization also decreases the ratio of aboveground to belowground biomass; thus, for established marshes, especially those close to the creek bank, fertilization may increase the likelihood of marsh collapse and erosion. Large-scale fertilization of marsh habitat does not appear to have a substantial impact on long-term (century-time scale) marsh survival because model simulations suggest that positive impacts of fertilization decrease with flooding duration and sea level rise.

Living Shoreline approaches to shoreline stabilization are suitable for the entire NRE area.

If shoreline stabilization is required, then the representative wave energy (RWE) conditions on the NRE and ICW shorelines are low enough that Living Shoreline approaches to shoreline stabilization are suitable for the entire area. At lower wave energy sites (RWE less than 300 J m^{-1}), a Living Shoreline with marsh and/or oyster reefs is appropriate, but at higher energy sites (RWE between 300 J m^{-1} and 700 J m^{-1}), a Living Shoreline protected with rock sills would be more appropriate (**Figure 2-16**; Currin et al., 2017).

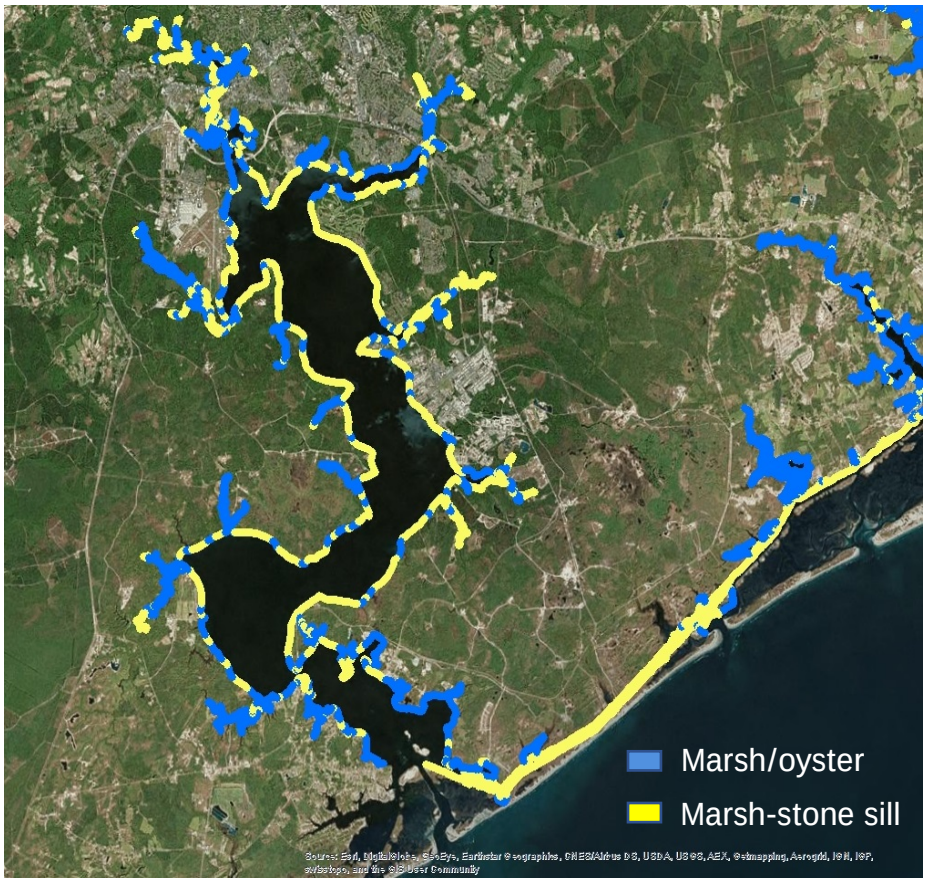

Figure 2-16. Living Shoreline suitability index for MCBCL available at http://maps.coastalresilience.org/northcarolina/.

Coastal Barrier Module

Coastal Barrier Module Research

Onslow Beach is a northeast–southwest trending, wave-dominated barrier island located 20 km south of where the Outer Banks barrier-island chain ends. This 12-km (8 mi)–long barrier fronts salt marsh and is bounded by the New River Inlet to the southwest and Browns Inlet to the northeast. The Onslow Beach shoreline is sinusoidal with a central headland separating two shallow, cuspate embayments. The northern embayment has an 80-m wide beach with multiple well-developed dune ridges that are 7-m to 9-m high. The headland area has a narrow beach (20-m wide) with a single discontinuous dune ridge less than 4-m high.

The Coastal Barrier Module examined the coastal barrier island ecosystem that lies at the interface between the continental shelf and the protected NRE. This barrier island ecosystem encompasses the shallow subtidal and intertidal shoreface, tidal inlet, backshore beach, aeolian dune, shrub zone, maritime forest, and washover sand-flat habitats. These habitats are defined by intrinsic ecological processes, but are linked by sediment transport, nutrient exchange, and biological uses, each of which undergoes substantial changes over multiple time scales (**Figure 2-17**).

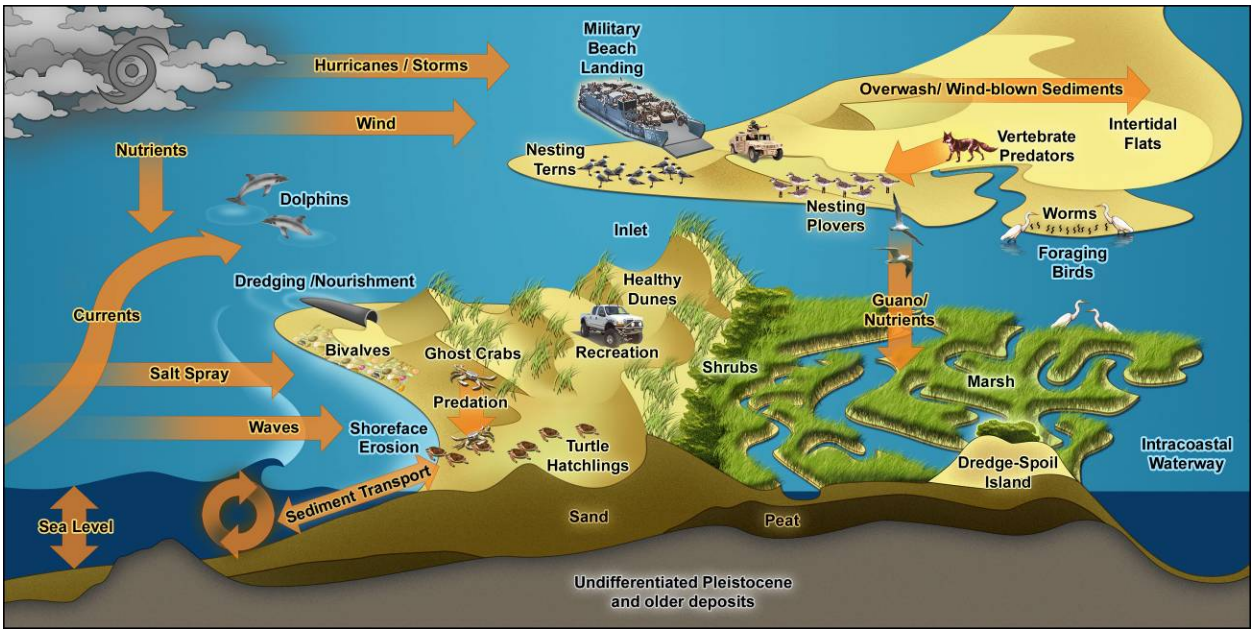

Figure 2-17. Conceptual model for the Coastal Barrier Module.

Scientific Findings for the Coastal Barrier Module

The conceptual framework for barrier island rollover and associated implications for the carbon budget of a transgressive barrier island were examined by developing a numerical along-shore averaged carbon-budget model and parameterizing that model with data collected at two sites along survey transects on Onslow Beach. Our methods were chosen to elucidate those main processes responsible for transitioning transgressive barrier islands from being carbon sinks to sources and to evaluate the timescale over which that transition can occur. To estimate the net carbon budget at both sites, carbon storage and export were both calculated.

Although storm events can result in major changes to shoreline position and erosion over decadal time scales, sea level anomalies can cause as much or more beach erosion than a hurricane on an annual time scale. Sea level anomalies are small vertical increases in water level that are sustained for 2 weeks or longer. These small wave events on top of these prolonged increases in water level need to be considered and included in predictive coastal barrier erosion models. Onslow Beach will continue to be impacted by tropical and extra-tropical events and by high erosion rates because of the island's position, near-shore geomorphology and limited sand supply.

Transgressive barrier carbon storage is related to the width of the backbarrier salt marsh.

Carbon storage in transgressive barrier islands such as Onslow Beach is directly related to the width of the backbarrier salt marsh, whereas carbon export occurs in response to erosion associated with the landward movement of the island. Sea level rise principally forces barrier islands to migrate landward across continental shelves and during migration the width of backbarrier marsh changes because of erosion and storm overwash. This width change can be positive if overwash creates new marsh width through washover or flood-tidal delta deposition at intertidal elevations, or it can be negative if erosion and overwash (burial of marsh) reduces

marsh width. With the progressive narrowing of the backbarrier marsh, Onslow Beach will begin to function more persistently as a carbon source until the stored carbon reservoir is depleted at the point when the barrier island welds with the mainland. With accelerated sea level rise and the potential for increased intensity of storms, erosion of carbonaceous sediment at the ocean shoreline will more frequently shift the carbon budget of Onslow Beach towards being a net source of carbon.

The carbon flux for the coastal barrier shows large fluctuations.

Carbon budgets were examined at two sites on Onslow Beach. Both sites showed large fluctuations in net carbon storage associated with storm overwash, erosion, and subsequent recovery. For example, before Hurricane Fran (1996), one site stored carbon at a rate of 2.5 Mg/yr because of the expansive backbarrier salt marsh and moderate rates of beach erosion, which released old, buried carbon (carbon stored as peat and eroded from the shoreface) into the ocean. Immediately after Hurricane Fran, that portion of the island transitioned to being a source of carbon (releasing carbon at a rate of 0.7 Mg/yr) because the area available for marsh carbon sequestration was reduced because of marsh burial by deposition of a washover terrace. Over the past 7 years, no beach erosion has occurred at this site. Currently, carbon is being sequestered in the backbarrier marshes at a rate of 13.9 Mg/yr.

Onslow Beach is a very young barrier island, younger than 500 years old.

Radiocarbon dating of peat cores from below Onslow Beach suggests that the island is very young, younger than 500 years old and approximately 2,000 years younger than the Outer Banks barrier island chain to the north. Because of rapid rates of transgression of the southwestern portion of Onslow Island toward the mainland, the duration of carbon storage as peat deposited in this portion of the barrier island is no older than 500 years.

Washover fans are not necessarily created by one overwash event.

We discovered that the conceptual model for washover fan development is not applicable to narrow portions of a barrier island where backbarrier elevation is low. Washover fans are not necessarily created by one overwash event, but an integration of different processes occurring during both fair and stormy weather over time. We measured the formation of a washover fan that formed as the results of 81 overwash events over 3 years. After a washover deposit initially formed in 2011 by Hurricane Irene, we measured the evolution of that washover fan as the result of 81 overwash events over 3 years (**Figure 2-18**). Between November 2012 and May 2013, the washover fan increased in areal extent from 3,300 m^2 to 29,000 m^2 and in volume from 2,200 m^3 to 16,700 m^3. After that 10-fold increase in washover fan size, the morphology of the area eventually stabilized and vegetation began to recolonize. These data highlight that overwash during fair-weather conditions is an important process in transporting sand across a barrier island. In addition, researchers must be cautious when interpreting storm power from the landward extent of ancient washover fans.

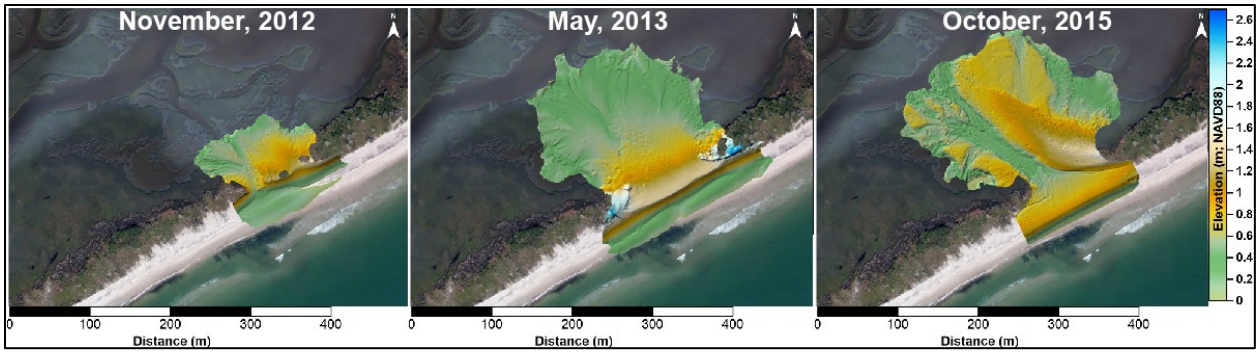

Figure 2-18. Area of the washover at Onslow Beach through time.

Findings with Implications for DoD and Other Coastal Managers

Onslow Beach is a critical asset to MCBCL as the primary Atlantic Coast location where amphibious military training maneuvers occur. Onslow Beach also serves as a habitat for several species of concern, which MCBCL must also protect. Research efforts were designed to support the long-term sustainability of Onslow Beach as an important coastal resource necessary for amphibious military training and for maintaining important habitats for protected species of shorebirds and sea turtles.

The model predicted substantial loss of training area on Onslow Beach within 20 years and complete loss in 50 years.

The lowest (0.3 m) and highest (2.5 m by 2100) sea level rise rates were used in the CSHORE-C15 Beach Morphology Model to forecast shoreline position under future sea level rise scenarios (**Table 2-1**). According to the model, both scenarios indicated substantial loss of the use of training areas south of the Onslow Beach Bridge within 20 years and a complete loss (defined by the primary dune within 100 m of ICW) within 50 years (**Figure 2-19**). Island width will be less than 100 m south of the bridge in the northern portion of the training area within 50 years. Conversely, the model forecast, using the same range of sea level rise rates and climate forces, indicated shoreline position, and its associated beach and dunes will remain stable and likely grow seaward along the entire beach north of the Onslow Beach Bridge.

Sea turtles will false crawl more on flat beaches with scarped dunes.

Beach landscape data revealed that sea turtle false crawls (i.e., unsuccessful attempts in finding beach nest sites) are more frequent on flat beaches with steeply eroded, scarped dunes. With increased rates of sea level rise, scarped dunes and low-slope beaches will become more extensive, which could result in a higher occurrence of false crawls that could have detrimental effects on sea turtle reproduction. Increased numbers of false crawls could delay a sea turtle's search for a suitable nesting location and lead to eggs being laid later in the season, when they may not have enough time to develop because of cooler temperatures.

Figure 2-19. CSHORE-C15 predictions of shoreline and beach position in 2065 across the Onslow Beach northern portion of the training area under highest and lowest sea level rise scenarios.

Terrestrial Module

Terrestrial Module Research

The Terrestrial Module's ecosystem-based research was conducted along the gradient of vegetation from the salt marsh at the estuary margin, through brackish and freshwater marsh, to the longleaf pine savannas and pocosins (i.e., shrub bogs) that dominate the upland terrestrial environments on MCBCL. Variation in the biota and ecosystem processes along this gradient are driven by variations in hydrology, soils, and fire behavior. **Figure 2-20** presents the conceptual model for the Terrestrial Module and illustrates the complementary nature of these critical physical, chemical, and biotic processes; disturbances; and interactions.

The research projects of the Terrestrial Module constitute an integrated effort designed to provide a greater understanding of how forest restoration treatments affect the interrelationships among the vegetation and avifaunal communities across sites representing a wide range of soil conditions and a wide spectrum of RCW foraging habitat quality. Research focused on the critical knowledge gaps related to efforts to restore longleaf pine ecosystems and used models to predict the impacts of future landscape condition and climate on terrestrial carbon stores and RCW demographics.

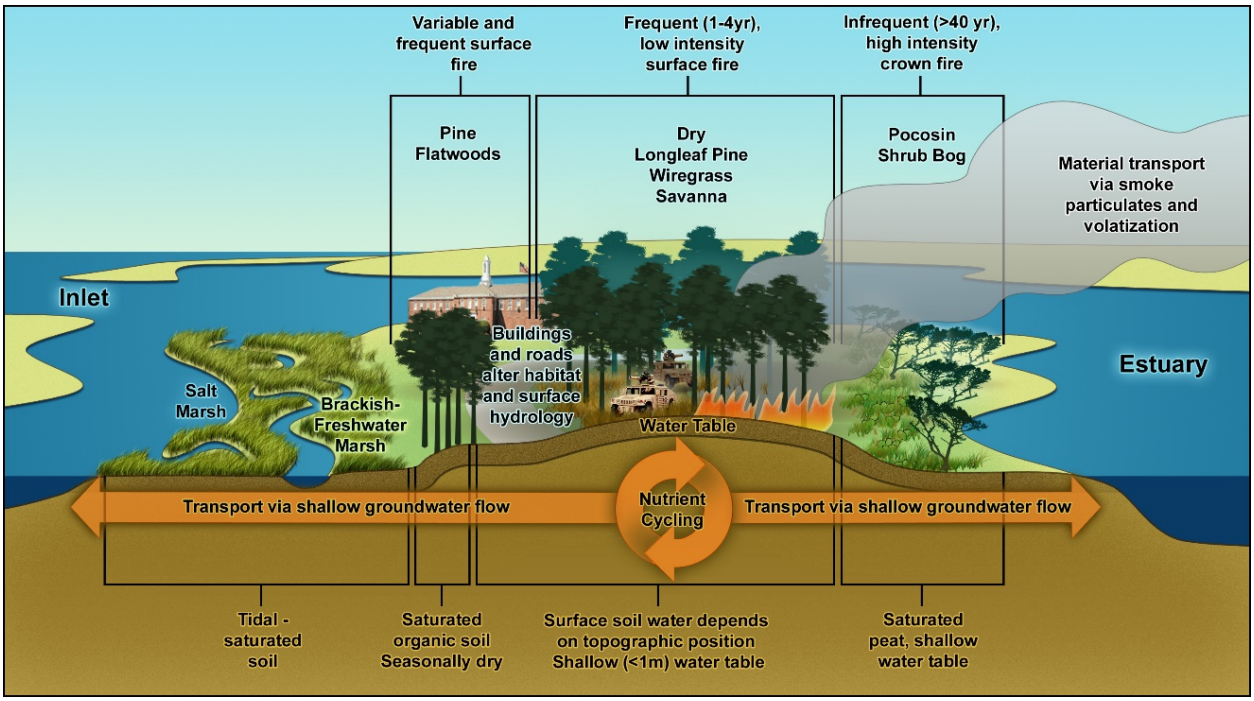

Figure 2-20. Conceptual model for the Terrestrial Module.

Scientific Findings of the Terrestrial Module

The terrestrial landscape across MCBCL represents the greatest potential for managing carbon to off-set greenhouse gas emissions. As previously mentioned in this chapter, the type of forest that represents the greatest carbon storage capacity is that of longleaf pine, which is also the species of greatest focus and management aboard MCBCL. Although carbon storage is not currently a forest management objective at MCBCL, the current management regimes and goals coincide with the greatest potential for carbon storage and position the installation well for future carbon management considerations.

Carbon storage was the highest with management efforts to promote longleaf pine restoration.

LANDIS-II model simulations of different forest management practices across the MCBCL landscape reinforced the finding that carbon storage was highest with management efforts designed to promote restoration of longleaf pine. This finding reinforces the longleaf pine restoration efforts of forest managers at MCBCL as well as at other DoD installations across the Southeastern United States. The no management scenario (i.e., stands without prescribed fires) stored less carbon than actively managed stands (with prescribed fires). Thus, carbon storage at MCBCL and throughout the Southeastern United States can be increased most effectively through active management practices that also support longleaf pine restoration goals.

RCW life history traits have changed in response to climate conditions.

An analysis of historic climate data (1980 through 2011) shows that several RCW life history traits have changed during this 31-year period. Egg-laying dates are earlier and juvenile survival rates are higher at both sites, and many other traits have changed at Fort Bragg (e.g., larger clutches, more partial brood loss, higher fledgling production). Life history traits are linked to climate, which has changed more over time at the inland Sandhills site than at coastal MCBCL. Changes in traits in the Sandhills region are linked to a non-linear warming trend, characterized by increasing temperatures through the 1980s and into the early 1990s, followed by a period of stability, and then renewed warming beginning in the mid-2000s. Many of the changes in demography in the Sandhills region follow this same, non-linear pattern. At MCBCL, traits were linked to precipitation and to temperatures. We hypothesize that the effects of climate change on RCWs in the Sandhills region of North Carolina (Fort Bragg) will be positive (with rising temperatures), at least in the immediate future. This hypothesis is not surprising, given that North Carolina represents the northern most range of this species. Rising temperatures may also have positive effects on RCWs at MCBCL, but another possible scenario is that greater variability in precipitation will have adverse effects on productivity in this coastal RCW population.

Findings with Implications for DoD and Other Coastal Managers

Across southeastern United States, vast areas that were once dominated by open longleaf pine savanna now support closed canopy stands of loblolly pine with a dense understory and midstory of broadleaved shrubs and trees. The absence of fire on these landscapes has exacerbated this trend, and this situation still exists on a significant portion of forested land at MCBCL, although much of the habitat has been restored to open savanna conditions. A primary motivator for longleaf pine restoration is to meet Endangered Species Act goals in management for the RCW (**Figure 2-21**). In addition to understanding the impacts of forestry management actions, we evaluated the possible impacts of climate change on RCW demography and population dynamics at MCBCL and Fort Bragg, NC.

RCWs in North Carolina are benefiting from higher temperatures, but Florida populations of RCWs are not.

To date, the impacts of climate change (e.g., increasing temperature) on RCWs on MCBCL and Fort Bragg at the northern end of the species' range have been positive to neutral, resulting in increased productivity. These effects, coupled with effective habitat restoration and aggressive management, have resulted in population increases and larger group sizes, and thus more viable populations. However, there is additional evidence of negative effects of climate change on the productivity of RCWs at Eglin Air Force Base in Florida at the southern end of the RCW's range (Walters, unpublished data).

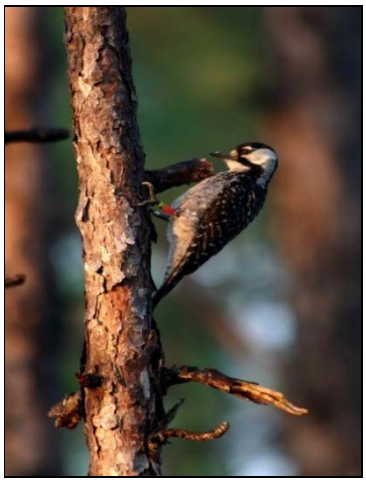

Figure 2-21. Red-cockaded woodpecker.

If higher temperatures result in less productivity and/or survivorship of RCWs at installations in the southern portion of its range, then MCBCL and Fort Bragg may be under additional pressure to attain or surpass their RCW recovery goals.

The benefits of midstory thinning restoration treatments in longleaf pine habitats are lost if they are not followed by regular prescribed fire.

Short-term results indicated significant benefits from mechanical thinning in reducing density of understory woody stems and restoring plant diversity and composition of 50- to 60-year old loblolly dominated forests to conditions such as those of longleaf pine savannas. However, after 5 or 6 years without regular prescribed burning applications, no differences were observed among controls and thinning treatments. These results indicate that if thinning treatments are not followed by regular prescribed fire, then the benefits of thinning are quickly lost. Furthermore, ingrowth of woody stems results in an increase in understory fuels and may cause more severe wildfires at MCBCL in the future if prescribed burning is not conducted.

In the year after thinning treatment followed by prescribed fire, there was a detectable shift in understory plant species composition toward the characteristic composition of longleaf pine savannas (the MCBCL restoration goal). Understory plant species richness was significantly higher in treatment plots compared with the control in 2010 and 2011; however, in the absence of additional prescribed fire, species richness was lower in all plots by 2016, and the differences among treatments disappeared. Bird species richness also was consistently lower in 2016 when compared with 2010 and 2011, and no differences were observed among treatments at either sample time. To achieve longleaf pine restoration goals, mechanical restoration treatments such as understory thinning must be accompanied by a regular prescribed fire program. However, as we approach the 21st century, the requirement for prescribed burning will become more challenging with the potential for changing precipitation regimes and with increasing temperatures.

Identification of Ecosystem Indicators

One of the four objectives of DCERP2 was to build on DCERP1 research and monitoring findings to identify environmental conditions that could serve as indicators of ecosystem state change that may affect the sustainability of MCBCL's training mission or impact ecosystem function. The overarching strategy developed during DCERP1 helped to separate underlying natural (e.g., climatic, biogenic) and man-made regional processes from locally driven processes and to identify stressor-specific indicators of ecosystem state change. These indicators provide benchmark values for MCBCL managers to use as early signs of changing conditions that could threaten ecosystem sustainability (**Table 2-2**). Some of these indicators are specific to MCBCL; however, other indicators may have broader applications at other DoD installations or coastal areas in similar ecological settings.

Table 2-2. Indicators and Associated Benchmark of Ecosystem State Change Identified During DCERP

Indicator	Benchmark Value	Ecological Consequence of This Change
Flow rate of the NRE	27 m^3 s^{-1}	River flow of >27 m^3 s^{-1} shortens water residence time in the estuary, and this is too short to allow for phytoplankton bloom development. Above this flow rate, nutrients and phytoplankton blooms are essentially flushed out of the estuary, removing concentrations of nutrients from runoff events that could result in algal blooms or harmful algal blooms under lower flow situations.
Benthic chlorophyll *a*	77 mg m^{-2}	Benchmark predicts the sediment-water ammonium (NH_4^+) flux. For values below this benchmark, the benthic microalgal filter released NH_4^+ into the water column (net respiration), which stimulates further pelagic phytoplankton blooms. Above this threshold range, the benthos absorbed NH_4^+ from the water column (net photosynthesis), effectively reducing further eutrophication by the phytoplankton.
Land imperviousness	>20% impervious surface	Runoff of sediment and nutrients into the tributary creeks and ultimately into the estuary increase from land-use areas with >20% imperviousness.
Prescribed fire interval	Prescribed fire every 3 years	Application of prescribed fire at >3-year fire intervals results in increasing understory and midstory vegetation regrowth similar to no burning at all; this impedes the recovery of longleaf pine restoration efforts, reduces value of the habitat for RCW recovery, and impacts utility of the land for military training uses.
Suspended Sediment Concentration (SSC)	>25 mg/L	SSCs >25 mg/L are required to provide NRE marshes with adequate sediment to keep pace with moderate to high sea level rise. SSCs <25 mg/L do not provide adequate sediment for marsh accretion and may result in the drowning of MCBCL marshes.
Representative Wave Energy (RWE)	RWE ≤300 J m^{-1}	(Note: Nearly all MCBCL shoreline segments are candidates for one of these Living Shoreline approaches, which are cost effective and preserve the fishery habitat, water quality, and other ecosystem functions of salt marshes.) **Natural Living Shoreline** designs are those that incorporate marsh vegetation and/or oyster reefs and can persist on shorelines where RWE values are ≤300 J m^{-1}.
	RWE >300 to ≤700 J m^{-1}	**Hybrid Living Shoreline** designs are those that incorporate marsh vegetation with low rock sills and can provide effective erosion protection at RWE values up to 700 J m^{-1}.

Data and Information Management System

The management of DCERP data and information evolved during the 10 years of DCERP1 and DCERP2 to serve not only as a secure archive for the voluminous amounts of collected data, but also as a dynamic data and information management system that allows interested users to access, analyze, and visualize the DCERP data and other synthesis products. DIMS consists of several distinct component systems as shown in **Figure 2-22** and supports data archiving, searching, and retrieval functionalities.

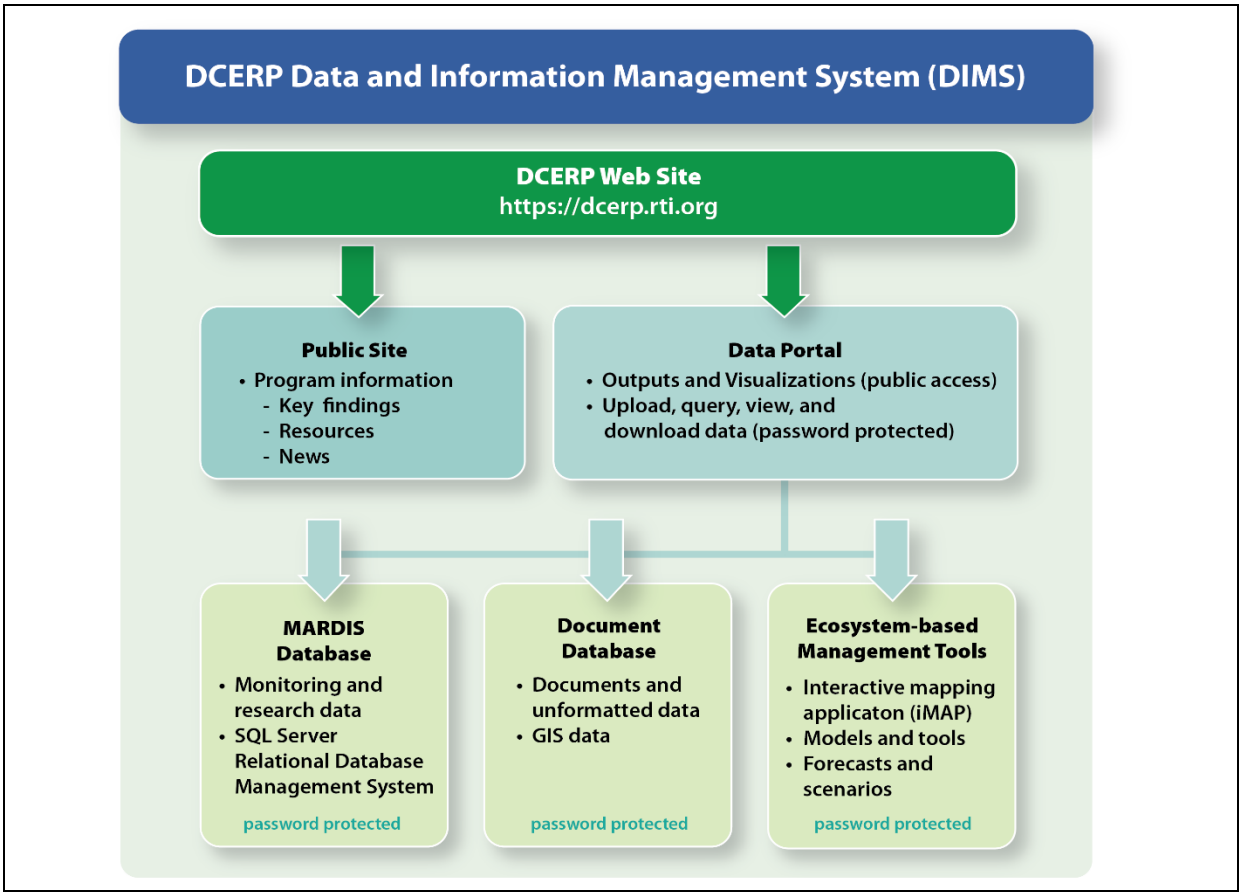

Figure 2-22. Components of the DCERP Data and Information Management System (DIMS).

DCERP Public Web Site

The DCERP public Web site (available at http://dcerp.rti.org) provides comprehensive information about the entire program, including the background, objectives, and research activities; the benefits to military installations; and descriptions of the research and monitoring efforts. Technical reports, presentations, and other outreach materials are also posted to this site.

DCERP Data Portal

The DCERP data portal, which is part of the DCERP Web site, is the front-end interface to the data and tool components of DIMS and includes the Monitoring and Research Data Information

System (MARDIS) database, the Document Database, and ecosystem-based management tools, including the interactive mapping application (iMAP). In addition, the DCERP data portal provides access to various output products and tools such as story maps, model pages containing information and outputs, the Water Quality Dashboard, and topic-driven queries.

DIMS was expanded under Research Project TSP-1 with various ecosystem-based management tools that assist users in accessing, sharing, and viewing the data and enable users to view the vast amounts of DCERP data in more meaningful and manageable ways. The three primary components of the enhanced DIMS include the following:

- The iMAP component is used to visualize DCERP geospatial data and provide spatial and topic-driven search capabilities for data from MARDIS and other sources. The primary objective of iMAP was to allow end users to assess relationships and discover data to support natural resources management decisions.
- The models and tools component contains integrated decision-support models developed by the DCERP2 researchers including the ESM, Geospatial Marsh Model, and the CSHORE-C15 Beach Morphology Model.
- A forecasts and scenarios component allows users to review previously generated management and climate change scenario outputs prepared by the model and tool developers. The outputs are maintained in a library for easy access by users who do not need customized scenarios.

Full integration of these tools with MARDIS and within DIMS resulted in the implementation of a common framework in DIMS. In addition, this framework provides a centralized location for accessing DCERP data, models, and tools; a common Internet mapping framework; and tools for viewing data synthesized over space and time. This framework also offers improved access to DCERP and MCBCL data collections and improved usability and understanding of the data. The framework allows the integration of specific models directly with DIMS and the DCERP data and provides model outcomes in formats directly accessible by MCBCL and other DoD installation staff. Having access to the DCERP data, tools, models, and other information and products enables MCBCL managers to make informed decisions that support their long-term mission for military training and preparedness and for the sustainability of MCBCL ecosystems.

Legacy of DCERP

The legacy of DCERP is the well designed and implemented methodology used to collect, archive, synthesize, and produce significant scientific findings that have actionable applications for multiple end-users, including DoD installations, the scientific community, and other stakeholders. DCERP is an exemplar of a well-integrated research and monitoring program that provided long-term data of four major component ecosystems across MCBCL—the aquatic/estuarine, coastal wetlands, coastal barrier and terrestrial environments. DCERP also provides insights about ecosystem processes and management solutions for enhancing the sustainability of these systems.

During the process of conducting research and monitoring efforts for over a decade, the team has produced innovative monitoring devices and new methodologies for tracking and evaluating various environmental processes. For example, the team applied an innovative Dataflow system to monitor CO_2 fluxes in the estuary over a diel cycle. Coastal wetland researchers developed a new method for collecting sediment associated with the marsh surface microlayer that showed that this mechanism transported more sediment over a tidal cycle than was introduced into the marshes from the uplands during a storm event. In addition, the researchers discovered a correlation between tidal creek morphology and the amount of SSC available to the marsh. This relationship was tested and validated for seven different tidal creeks in various geographical regions of the North Carolina coast. The Coastal Barrier Module researchers changed conventional thinking that overwash was a one-time event. This change resulted after a discovery was made in which one washover site was overwashed more than 80 different times in both fair and stormy weather conditions over several years before the washover fan was stabilized. Finally, Terrestrial Module researchers showed that prescribed burning at 3-year intervals improves herbaceous understory vegetation and bird population diversity and is the best burning interval for restoring RCW habitat. It is important to note that model results also showed that using this burning interval improves potential carbon storage at MCBCL in the future.

These innovative methods and novel findings have been communicated throughout DCERP by the team through a strong publication record. Collectively, the DCERP Team has published more than 75 papers in peer-reviewed journals and book chapters. The team is preparing additional papers for publication at the time of this final report. The DCERP Team members and their students have given more than 125 presentations about DCERP findings at different scientific conferences, symposia, and meetings. The program also provided training to undergraduate and graduate students and to postdoctoral candidates at seven different academic institutions. This scientific research opportunity resulted in master's and doctoral degrees for 20 students and research opportunities for 12 postdoctoral candidates.

Another legacy of DCERP, which will allow for the widest continuing distribution of data, models, tools, and other products, is the continuance of the DCERP DIMS. Open access to all registered users will make DCERP information available for comparison with other coastal research and monitoring data, allow the use of tools and models to analyze data, and provide examples of translating complex information into easy-to-understand and actionable information for a wide variety of audiences.

The short-term goal is that DCERP findings have increased MCBCL staff's understanding of ecosystem processes, stressors, and potential changes in the ecosystems driven by management actions and future climate conditions. The medium-term goal is that MCBCL should conduct an evaluation of DCERP management recommendations and implementation strategies. The long-term goal is that the recommendations made through DCERP will enhance the sustainability of MCBCL and other installation training lands in similar ecological settings, integrate research and monitoring as part of adaptive management decisions, and provide a basis for setting carbon goals under future management and climate conditions.

Literature Cited

Anderson, I.C., M.J. Brush, M.F. Piehler, C.A. Currin, J.W. Stanhope, A.R. Smyth, J.D. Maxey, and M.L. Whitehead. 2014. Impacts of climate related drivers on the benthic nutrient filter in a shallow photic estuary. *Estuaries and Coasts 37*(Supp 1):46–62. doi: 10.1007/s12237-013-9665-5

Cai, W. 2011. Estuarine and coastal ocean carbon paradox: CO_2 sinks or sites of terrestrial carbon incineration? *Annual Review of Marine Science 3*:123–145. doi: 10.1146/annurevmarine-120709-142723

Chen, C.T.A., T.H. Huang, Y.C. Chen, Y. Bai, X. He, and Y. Kang. 2013. Air–sea exchanges of CO_2 in the world's coastal seas. *Biogeosciences 10*:6509–6544.

Crosswell, J.R., I.C. Anderson, J.W. Stanhope, B. Van Dam, M.J. Brush, S. Ensign, M.F. Piehler, B. McKee, M. Bost, and H.W. Paerl. 2017. Carbon budget of a shallow, lagoonal estuary: Transformations and source-sink dynamics along the river–estuary–ocean continuum. *Limnology and Oceanography.* doi: 10.1002/lno.10631

Crosswell, J.R., M.S. Wetz, B. Hales, and H.W. Paerl. 2014. Extensive CO_2 emissions from shallow coastal waters during passage of Hurricane Irene (August 2011) over the Mid-Atlantic Coast of the USA. *Limnology and Oceanography 59*:1651–1665.

Crosswell, J.R., M.S. Wetz, B. Hales, and H.W. Paerl. 2012. Air–water CO_2 fluxes in the microtidal Neuse River Estuary, North Carolina. *Journal of Geophysical Research: Oceans 117*(C8):C08017. doi:10.1029/2012JC007925

Currin, C.A., J. Davis, and A. Malhotra. 2017. Response of salt marshes to wave energy provides guidance for successful living shoreline implementation. *Living Shorelines: The Science and Management of Nature-based Coastal Protection.* Edited by Bilkovic, D.M., J. Toft, M. Mitchell, and M. La Peyre. CRC Press, Taylor & Francis Group.

Ensign, S.H., and C.A. Currin. 2017. Geomorphic implications of particle movement by water surface tension in a salt marsh. *Wetlands 37*:245–256. doi: 10.1007/s13157-016-0862-4

Ensign, S.H., J.N. Halls, and M.A. Mallin. 2004. Application of digital bathymetry data in an analysis of flushing times of two North Carolina estuaries. *Computers and Geosciences 30*:501–511.

Ensign, S., C. Currin, M. Piehler, and C. Tobias. 2017. A method for using shoreline morphology to predict suspended sediment concentration in tidal creeks. *Geomorphology 276*:280–288.

Frankignoulle, M., G. Abril, A. Borges, I. Bourge, C. Canon, B. Delille, E. Libert, and J-M. Théate. 1998. Carbon dioxide emission from European estuaries. *Science 282*:434–436.

Gordon, E.S., and M.A. Goñi. 2004. Controls on the distribution and accumulation of terrigenous organic matter in sediments from the Mississippi and Atchafalaya river margin. *Marine Chemistry 92*:331–352.

Hall, J.A., S. Gill, J. Obeysekera, J., W. Sweet, K. Knuuti, and J. Marburger. 2016. *Regional Sea Level Scenarios for Coastal Risk Management: Managing the Uncertainty of Future Sea Level Change and Extreme Water Levels for the Department of Defense Coastal Sites Worldwide*. U.S. Department of Defense, Strategic Environmental Research and Development Program (SERDP). 224 pages. Available at https://www.serdp-estcp.org/Program-Areas/Resource-Conservation-and-Resiliency/Infrastructure-Resiliency/Regional-Sea-Level-Scenarios-for-Coastal-Risk-Management

Hall, N.S., H.W. Paerl, B.L. Peierls, A.C. Whipple, and K.L. Rossignol. 2013. Effects of climatic variability on phytoplankton biomass and community structure in the eutrophic, microtidal, New River Estuary, North Carolina, USA. *Estuarine and Coastal Shelf Science 117*:70–82. doi: http://dx.doi.org/10.1016/j.ecss.2012.10.004

Herrmann, M., R.G. Najjar, W.M. Kemp, R.B. Alexander, E.W. Boyer, W. Cai, and R.A. Smith. 2015. Net ecosystem production and organic carbon balance of U.S. East Coast estuaries: A synthesis approach. *Global Biogeochemical Cycles 29*(1):96–111.

Kemp, W.M., E.M. Smith, M. Marvin-DiPasquale, and W.R. Boynton. 1997. Organic carbon balance and net ecosystem metabolism in Chesapeake Bay. *Marine Ecology Progress Series 150*:229–248.

Maher, D.T., and B.D. Eyre. 2012. Carbon budgets for three autotrophic Australian estuaries: Implications for global estimates of the coastal air–water CO_2 flux. *Global Biogeochemical Cycles 26*:GB1032. doi: 10.1029/2011GB004075

Mallin, M.A., M.R. McIver, H.A. Wells, D.C. Parsons, and V.L. Johnson. 2005. Reversal of eutrophication following sewage treatment upgrades in the New River Estuary, North Carolina. *Estuaries 28*:750–760.

Paerl, H.W., N.S. Hall, B.L. Peierls, and KL. Rossignol. 2014. Evolving paradigms and challenges in estuarine and coastal eutrophication dynamics in a culturally and climatically stressed world. *Estuaries and Coasts 37*(2):243–258.

Peierls, B.L., N.S. Hall, and H.W. Paerl. 2012. Non-monotonic responses of phytoplankton biomass accumulation to hydrologic variability: A comparison of two coastal plain North Carolina estuaries. *Estuaries and Coasts 35*(6):1376–1392.

Roden, E.E., J.H. Tuttle, W.R. Boynton, and W.M. Kemp. 1995. Carbon cycling in mesohaline Chesapeake Bay sediments 1: POC deposition rates and mineralization pathways. *Journal of Marine Research 53*:779–819.

RTI International. 2013. *DCERP2 Research Plan*. Prepared for Strategic Environmental Research and Development Program (SERDP), Arlington, VA.

Warnken, K.W., P.H. Santschi, K.A. Roberts, and G.A. Gill. 2008. The cycling and oxidation pathways of organic carbon in a shallow estuary along the Texas Gulf Coast. *Estuarine, Coastal and Shelf Science 76*:69–84.

Chapter 3

Development of Uniform Historical and Projected Climate to Support Integrated Coastal Ecosystem Research

SERDP Project Number: RC-2245

Climate Change Module

Research Project Number: CC-1

Lead Researchers:

Adrienne Wootten, Aaron Sims
State Climate Office of North Carolina, North Carolina State University
amwootte@ncsu.edu, apsims@ncsu.edu

Supporting Researchers:

Heather Aldridge, heather_aldridge@ncsu.edu
Geneva Gray, Geneva_Gray@ncsu.edu

November 2017

Final

This report was prepared under contract to the U.S. Department of Defense (DoD) Strategic Environmental Research and Development Program (SERDP). The publication of this report does not indicate endorsement by DoD, nor should the contents be construed as reflecting the official policy or position of DoD. References herein to any specific commercial product, process, or service by trade name, trademark, manufacturer, or otherwise, do not necessarily constitute or imply its endorsement, recommendation, or favoring by DoD.

Table of Contents

Acronyms 3-vii
Abstract 3-1
Objectives of the Research Project 3-3
Background 3-3
Introduction 3-3
Historical Observations 3-4
Downscaling 3-4
Ensembles 3-5
Uncertainty 3-5
Dependence 3-6
Climate Data Scale 3-6
Materials and Methods 3-6
Task 1—Compilation of Historical Climate Observations 3-7
Task 2—Compilation of Future Climate Projections 3-10
Task 3—Historical Evaluation of Downscaled Climate Projections 3-13
Task 4—Influence of Climate Data Scale 3-18
Results and Discussion 3-18
Task 1—Compilation of Historical Climate Observations 3-18
Task 2—Compilation of Future Climate Projections 3-25
Task 3—Historical Evaluation of Downscaled Climate Projections 3-36
Task 4—Influence of Climate Data Scale 3-49
Conclusions and Implications for Future Research and Implementation 3-53
Response to Research Questions 3-55
Findings with Implications for Future Batse Management 3-56
Literature Cited 3-57
Appendix 3-A: Supporting Data 3-A-1
Appendix 3-B: List of Scientific/Technical Publications 3-B-1
Appendix 3-C: List of Students 3-C-1

List of Figures

Figure 3-1. Historical evaluation domain, with two military bases (Fort Bragg and MCBCL) in red and 25 ECONet stations in blue. 3-9

Figure 3-2. Domain over MCBCL (black box). 3-14

Figure 3-3. (Left panel) A time series of the annual number of days with precipitation greater than 0 inches (0 mm) and (right panel) maximum temperature greater than 90°F (32.22°C) at Kinston, NC (KINS shown in Figure 3-1) for the ECONet data (black), PRISM (green), METDATA (blue), and NLDAS-2 (red). 3-19

Figure 3-4. RMSE and correlation for each location in the study domain for METDATA as compared with ECONet observations for daily maximum temperature (a and b, respectively) and daily precipitation (c and d, respectively). 3-23

Figure 3-5. Composite probability distribution functions of daily error for between gridded climate products and all ECONet stations. 3-24

Figure 3-6. Monthly historical average and future projected ranges over MCBCL for the critical threshold of average number of days with maximum temperatures >90°F. 3-26

Figure 3-7. Monthly historical average and future projected ranges over MCBCL for the critical threshold of average number of days with maximum temperatures >100°F. 3-27

Figure 3-8. Monthly historical average and future projected ranges over MCBCL for the critical threshold of average number of days with minimum temperatures <28°F. 3-28

Figure 3-9. Monthly historical average and future projected ranges over MCBCL for the critical threshold of average number of days with minimum temperatures <32°F. 3-28

Figure 3-10. Monthly historical average and future projected ranges over MCBCL for the critical threshold of average number of days with precipitation >0 inches. 3-29

Figure 3-11. Monthly historical average and future projected ranges over MCBCL for the critical threshold of average number of days with precipitation >1 inch..... 3-30

Figure 3-12. Spread of future uncertainty for annual average maximum temperature, with the full ensemble (76 members) in gray and the reduced ensemble (24 members) in blue..... 3-35

Figure 3-13. Spread of future uncertainty for annual average minimum temperature, with the full ensemble (76 members) in gray and the reduced ensemble (24 members) in blue..... 3-36

Figure 3-14. Spread of future uncertainty for annual total precipitation, with the full ensemble (76 members) in gray and the reduced ensemble (24 members) in blue. 3-36

Figure 3-15. RMSE for climate model baseline (1979–1999): Average number of days with maximum temperature greater than 100°F. 3-37

Figure 3-16. RMSE for climate model baseline (1979–1999): Average number of days with maximum temperature greater than 90°F. 3-38

Figure 3-17. RMSE for climate model baseline (1979–1999): Average number of days with minimum temperature less than 28°F. 3-40

Figure 3-18. RMSE for climate model baseline (1979–1999): Average number of days with minimum temperature less than 32°F. 3-40

Figure 3-19. RMSE for climate model baseline (1979–1999): Average number of days with precipitation greater than 0 inches. 3-42

Figure 3-20. RMSE for climate model baseline (1979–1999): Average number of days with precipitation greater than 1 inch. 3-43

Figure 3-21. RMSE for climate model baseline (1979–1999): Average number of days with daily average wind speed less than 3 miles per hour. 3-45

Figure 3-22. Percent contribution to the total uncertainty from each source of uncertainty across time for Fort Bragg (left) and MCBCL (right) for projections of the decadal mean of the annual average daily high temperature. 3-46

Figure 3-23. Percent contribution to the total uncertainty from each source of uncertainty across time for Fort Bragg (left) and MCBCL (right) for projections of the decadal mean of the annual number of days with high temperature greater than 95°F. 3-47

Figure 3-24. Percent contribution to the total uncertainty from each source of uncertainty across time for Fort Bragg (left) and MCBCL (right) for projections of the decadal mean of the annual number of days with low temperature less than 32°F. 3-47

Figure 3-25. Percent contribution to the total uncertainty from each source of uncertainty across time for Fort Bragg (left) and MCBCL (right) for projections of the decadal mean of the annual total precipitation. 3-48

Figure 3-26. Percent contribution to the total uncertainty from each source of uncertainty across time for Fort Bragg (left) and MCBCL (right) for projections of the decadal mean of the annual number of days with precipitation greater than 1 inch. 3-49

Figure 3-27. Delta AICc by spatial resolution for each location. 3-51

Figure 3-28. Delta AICc by spatial resolution for each location. Values at zero have the strongest relationship with the climate variables for RCW nest survival. 3-51

Figure 3-29. Delta AICc by spatial resolution for each location. Values at zero have the strongest relationship with the climate variables for local RCW recruitment. 3-52

Figure 3-30. Delta AICc by spatial resolution for each location. Values at zero have the strongest relationship with the climate variables for the number of RCWs fledged..... 3-53

List of Tables

Table 3-1. Advantages and Disadvantages of Dynamic and Statistical Downscaling Techniques 3-5

Table 3-2. Climate Sensitivities of Each DCERP2 Ecosystem Model 3-7

Table 3-3. Historical Climate Data Sets Evaluated in DCERP2 3-8

Table 3-4. Variables and Critical Levels Evaluated by Research Project CC-1 3-10

Table 3-5. Downscaled Projections Used in the Development of the Reduced Ensemble 3-11

Table 3-6. Average RMSE for Daily ECONet Compared with Historical Climate Data Sets 3-19

Table 3-7. Average RMSE (Days) for Each Critical Level 3-20

Table 3-8. Average Correlation for Daily ECONet Compared with Historical Climate Data Sets 3-20

Table 3-9. Average Correlation for Days with Each Critical Level..... 3-21

Table 3-10. Final Reduced Ensemble of Downscaled Climate Projections..... 3-25

Table 3-11. Monthly Historical Average and Future Projected Ranges over MCBCL for Critical Thresholds of Interest..... 3-31

Table 3-12. Annual Sum of Monthly RMSE for Maximum Temperature Critical Levels..... 3-38

Table 3-13. Annual Sum of Monthly RMSE for Minimum Temperature Critical Levels.... 3-41

Table 3-14. Annual Sum of Monthly RMSE for Precipitation Critical Thresholds 3-43

Table 3-15. Related Climate Variables and Highest Ranked Spatial Resolution for Each Location and Trait..... 3-50

Acronyms

°C	degree Celsius
°F	degree Fahrenheit
AC	agglomerative coefficient
AICc	Akaike Information Criterion
CB	Coastal Barrier (Module)
CC	Climate Change (Module)
CCR	Center for Climatic Research
DCERP	Defense Coastal/Estuarine Research Project
DCERP1	first cycle of DCERP
DCERP2	second cycle of DCERP
DoD	U.S. Department of Defense
ECONet	North Carolina Environment and Climate Observing Network
ESM	Estuarine Simulation Model
GCM	global climate model
KINS	location of the ECONet station in Kinston, NC
km	kilometer
km^2	square kilometers
LAM	limited area model
m	meter
m/s	meters per second
MCBCL	Marine Corps Base Camp Lejeune
METDATA	University of Idaho's Gridded Surface Meteorological Data
mm	millimeter
mph	miles per hour
NASA	National Aeronautics and Space Administration
NLDAS-2	North American Land Data Assimilation System version 2
NOAA	National Oceanic and Atmospheric Administration
PRISM	Parameter-elevation Regressions on Independent Slopes Model
RC	Resource Conservation and Climate Change (a SERDP program area)
RCM	regional climate model
RCW	red-cockaded woodpecker
RCW DSS	Red-Cockaded Woodpecker Decision-Support System
RMSE	root mean square error
SERAP	Southeast Regional Assessment Project
SERDP	Strategic Environmental Research and Development Program
W/m^2	watts per meter squared

Abstract

The objective of Research Project CC-1 was to identify relevant historical weather observations and future climate projections that influence installation operations and environmental research at Marine Corps Base Camp Lejeune (MCBCL) in North Carolina. The project involved validating historical gridded climate estimates, studying influences of climate data scale on ecological processes, evaluating historical climate model projections, developing an ensemble of future climate projections for use by the DCERP2 Team, and examining the contribution of downscaling to the total uncertainty of climate projections. As part of this effort, these data were evaluated for the following pre-defined critical thresholds of interest: the average number of days with temperature >90°F, >100°F, <32°F, and <28°F; precipitation >0 inches and >1 inch; and daily average wind speed <3 mph and >40 mph.

Because weather station observations were limited near MCBCL, the feasibility of using historical gridded estimates as surrogate observations was evaluated. Three high-resolution historical gridded estimates, Parameter-elevation Regressions on Independent Slopes Model (PRISM; Daly et al., 2008), North American Land Data Assimilation System version 2 (NLDAS-2; Xia et al., 2012a and 2012b), and the University of Idaho's Gridded Surface Meteorological Data (METDATA; Abatzoglou, 2011), were evaluated using observations from the North Carolina Environment and Climate Observing Network (ECONet). Based on the results from these analyses, the Research Project CC-1 Team recommended using the METDATA gridded estimates as the historical data set for DCERP2.

The application of climate data scale on ecological processes was studied by varying the spatial resolution of METDATA. These climate data were used as inputs to an environmental model that simulates the life history traits of the red-cockaded woodpecker (RCW; *Picoides borealis*). No single climate data scale was ideal for simulating all RCW traits. Some traits were better represented with higher resolutions of climate data (e.g., <30 km for lay date and nest survival), whereas other traits were better captured by coarser resolutions (e.g., >40 km for local recruitment and number fledged).

METDATA was also used to evaluate the climate projection data sets for the historical climate model baseline period. The evaluation was performed over the MCBCL area for the eight critical thresholds of interest. Results indicated that the error in the average number of days per month for any individual model was less than 5 days for most climate thresholds. However, it is important to examine these errors in conjunction with the historical occurrences of these variables. Based on this error analysis, no single downscaling method consistently performed better than any other method. The accuracy of the equally weighted ensemble average of the climate model baselines varied monthly. In addition, the ensemble average performed better than at least 50% of the individual model members annually for any given threshold. No single model consistently outperformed the ensemble average for all metrics.

Given the large volume of future climate data, efforts were made to reduce the number of data sets used in the DCERP2 ecological process models, while preserving the expected spread and uncertainty in the future projections. A hierarchal clustering technique was used to reduce the ensemble from 76 to 24 future climate models and the number of downscaling techniques from

seven to three. This reduced ensemble of climate models was provided to the other DCERP2 ecosystem modules.

Based on the results of the downscaling uncertainty analysis, there were two recommendations for impact assessments to adequately represent all sources of uncertainty. These recommendations were as follows: (1) studies should use multiple downscaled climate projections, and (2) independent downscaled global climate models with common time periods should be utilized.

Keywords: Climate, clustering, downscaling, ensemble, environment, extremes, observations, precipitation, projection, temperature, uncertainty, weather

Objectives of the Research Project

Climate change is a long-term challenge that could impact the U.S. Department of Defense's (DoD's) management of terrestrial, coastal, and aquatic/estuarine resources. There are also fundamental challenges in identifying the specific climate factors that drive ecosystem processes and in projecting changes to these climate factors into the future at ecosystem process scales. Research Project CC-1 attempted to address both challenges.

The main goal of Research Project CC-1 was to develop uniform and consistent historical and projected climate inputs to support the DCERP2 Team's research and ecosystem modeling efforts. Specific objectives of this research project included the following:

1. Integration of climate change data and science into the DCERP2 Team's research process through extensive engagement with team researchers and installation managers.
2. Identification and documentation of critical climate variables and levels at the appropriate temporal and spatial scales for the ecosystems being studied and modeled.
3. Development of uniform historical climate data and future climate scenarios for consistent use across the entire DCERP2 Team at scales sufficient to adequately test and evaluate ecosystem process models. These climate data were based on input from DCERP2 Team researchers and were derived from the results of ongoing research efforts by other SERDP–funded climate change studies (i.e., Research Projects RC-1702 and RC-2206). It is important to note that Research Project CC-1 did not provide input about sea level rise because SERDP provided guidance (Hall et al., 2016) to the DCERP2 Team about appropriate sea level rise scenarios.

Background

Introduction

Ecosystems can be susceptible to extreme weather and climate events. It was necessary to identify critical levels at which ecological impacts in the New River Estuary and the associated ecosystems of Marine Corps Base Camp Lejeune (MCBCL) become significant or irreversible, especially because extreme weather and climate events across the Southeastern United States have the potential to change over the next century. Recent research has indicated an increase in the frequency of extreme heat events, with a decrease in the frequency and severity of extreme cold events (Christensen et al., 2007; DeGaetano and Allen, 2002; Diffenbaugh et al., 2005). In addition, extreme precipitation events are projected to decrease in frequency and increase in magnitude (Diffenbaugh et al., 2005; Kunkel et al., 2003), which may lead to an increase in drought frequency and possibly more flooding when rainfall events do occur. To better understand the impacts of extreme events on localized ecosystem processes, climate data sets (historical and future) with high spatial and temporal resolution were needed.

Historical climate observations and the future projections of climate were utilized in DCERP2 as inputs to ecological process models. It was important to assess climate conditions in the recent past before exploring how those conditions might change in the future by using downscaled climate projections. Downscaling methods relate future changes in broader climate patterns produced by global climate models (GCMs) to local or regional spatial scales. However, no

standard method for downscaling currently exists, and to the best of our knowledge, no methods have been evaluated for application to ecosystem process models and decisions.

Historical Observations

Gridded estimates of historical climate data were used for the evaluation of climate projections and the calibration of ecosystem models. These gridded estimates covered a period in the past and were based upon station observations, remotely sensed observations, and statistical interpolation techniques. In addition, these estimates provided a complete record in time (e.g., no missing data records) and an improvement in spatial coverage (e.g., no data gaps exist between weather stations).

To meet the needs of the DCERP2 ecosystem modeling teams, we evaluated the representativeness of multiple historical gridded data sets in eastern North Carolina. The most accurate of these gridded estimates was then used to evaluate downscaled climate projections.

Downscaling

To assess how climate change could affect multiple sectors (e.g., ecosystems), climatologists have created climate projections by using techniques that translate coarse GCM outputs to regional or local scales. The process of creating these more localized projections is called downscaling, which can be generated by using a broad range of statistical or numerical modeling techniques. A common definition of downscaling is described by Benestad and Chen (2008) as "the process of making the link between the state of some variable representing the large space and the state of some variable representing a much smaller space." Downscaling is crucial for studies on regional or local scales (e.g., research on ecosystems) because GCMs are too coarse to simulate local-scale climate processes that impact these systems. Although many techniques fall under this definition, downscaling can generally be categorized into two groups: dynamic downscaling and empirical statistical downscaling, which are further described as follows:

- Dynamic downscaling employs physical relationships like those of GCMs. This process usually refers to the use of limited area models (LAMs) as in studies by Giorgi (1990), Frogner et al. (2006), and Tudor and Termonia (2010). LAMs are high-resolution numerical models deployed over a constrained domain and use the GCMs as an input data set. LAMs used for climate-scale time periods (i.e., a season or longer) are commonly called regional climate models (RCMs).
- Empirical statistical downscaling (also known as statistical downscaling) uses statistical methods and observed climate data to determine a relationship between regional and global scales.

Table 3-1 highlights the advantages and disadvantages associated with each type of downscaling approach (Goodess et al., 2003; Varis et al., 2004; von Storch et al., 2000; Wootten et al., 2014). Using numerical modeling to simulate environmental conditions, dynamic downscaling techniques estimate projected future changes for more than 30 climate variables. However, the number of GCMs that can be translated to regional and local scales by using dynamic downscaling is limited by the computational expense of these techniques. Typically, input from fewer GCMs (e.g., three to five) are used for this type of downscaling as compared to

statistically downscaled data sets (e.g., 15 to 20) and thus, less uncertainty associated with the GCMs can be characterized.

Table 3-1. Advantages and Disadvantages of Dynamic and Statistical Downscaling Techniques

Technique	Advantages	Disadvantages
Dynamic	• Remains physically consistent • Provides a full suite of physical variables • Contains no constraints by in situ observations	• Is computationally expensive • Inherits biases of the native GCM • Contains multiple parameterization schemes
Statistical	• Is computationally inexpensive • Can be easily tailored to specific applications • Incorporates historical climate information	• Assumes statistical stationarity • Requires long records of in situ observations • Inherits biases of the native GCM

Statistical downscaling is more computationally efficient; thus, a higher number of GCMs can be translated to local scales, which allows for a more thorough characterization of uncertainty of future climates. However, the long observational record (greater than 20 years) required by statistical downscaling techniques restricts the number of available variables. In most cases, these variables are limited to temperature and precipitation.

Both downscaling techniques inherit the biases of the native GCMs. Statistical downscaling tends to correct this bias, but dynamically downscaled projections are often not bias corrected. Thus, bias correction should be considered prior to evaluating this type of downscaled data set.

Ensembles

Studies by Chaturvedi et al. (2012) and Wootten et al. (2014) suggested that a set of multiple GCMs (referred to as an ensemble) provided higher accuracy during the historical period than any single GCM. An ensemble allows for the uncertainty associated with climate projections to be represented and translated into climate change impact assessments (Mote et al., 2011). Recent literature suggested that building an ensemble of climate projections with only one downscaling technique represented does not provide a robust assessment of future climate change (Chen et al., 2011; Eum et al., 2014; Khan et al., 2006). Using an ensemble with multiple downscaling techniques allows for the uncertainty of the projections to be more adequately captured. Thus, for DCERP2, we created an ensemble of downscaled climate projections that incorporated the uncertainty associated with multiple downscaling techniques as well as multiple GCMs.

Uncertainty

Uncertainty in the GCM projections comes from the following three main sources (Gettelman and Rood, 2016; Hawkins and Sutton, 2009): natural variability, GCM uncertainty, and scenario uncertainty.

Uncertainty associated with the climate system is called natural variability; it is the variation associated with natural cycles, such as the El Niño Southern Oscillation or the North Atlantic

Oscillation. GCM uncertainty arises from the differences in the solutions from each GCM. Scenario uncertainty arises from all the different possibilities for human emission concentrations and societal action in the future. The contribution of different sources of uncertainty in GCM projections was thoroughly explored during previous research (e.g., Hawkins and Sutton, 2009 and 2011). However, downscaling uncertainty—associated with the differences between downscaling techniques—is an active area of research. The contribution from the different sources of uncertainty (i.e., natural variability, GCM, scenario, and downscaling) is important to understanding and improving projections of climate change.

Dependence

Some evaluations of climate model ensembles assume that the structure is a random sample from a distribution of plausible models centered on the true climate (Sanderson and Knutti, 2012). Under this assumption, the mean of the ensemble is more accurate than any individual model. In addition, this assumption implies that each member of an ensemble is independent of the other members.

However, several studies have noted issues with independence in a multi-model ensemble of GCMs (e.g., Sanderson and Knutti, 2012; Sanderson et al., 2015). Sanderson and Knutti (2012) found that the assumption of independence is not usually met because many GCMs used the same components or parameterizations. Given that GCMs are used to drive the creation of downscaled projections, independence is also an issue in downscaled projections. To address this dependence issue, a clustering methodology was used in the creation of an ensemble of downscaled projections for DCERP2.

Climate Data Scale

Downscaled projections are produced at multiple spatial resolutions, with some projections as fine as 800 meters. Previous literature has suggested that for a robust impact assessment, the resolution of the climate data should be 4 km or less (Franklin et al., 2013; Trivedi et al., 2008). However, it is important to note that such assessments have primarily focused on mountainous regions. There is speculation that for coastal regions, climate data at a resolution of 10 km or less are sufficient for robust climate change impact assessments (Tom Smith, Southeast Ecological Science Center, personal communication).

Formal research regarding the influence of scale on impact assessment in eastern North Carolina has not been previously performed. This analysis in eastern North Carolina allowed guidance to be created that is applicable to future assessments for determining appropriate climate data resolution. In addition, the results provide guidance for future decision making at the ecosystem level.

Materials and Methods

For the first 2 years of DCERP2, Research Project CC-1 focused on identifying the known climate sensitivities for the ecosystem models being used in other modules of DCERP2. This process included identifying the relevant temporal scale (e.g., hourly, daily, monthly) and spatial scale associated with those sensitivities needed for each DCERP2 ecosystem module (e.g.,

Aquatic/Estuarine, Coastal Wetlands, Coastal Barrier, and Terrestrial). The specific factors of interest to each ecosystem module were obtained through discussions held during the 2014 Technical Advisory Committee Meeting and in the weeks following. **Table 3-2** summarizes the sensitivities of interest for each process model based on this interaction with the DCERP2 Team.

Table 3-2. Climate Sensitivities of Each DCERP2 Ecosystem Model

Process Model (Module)	Climate Sensitivities	Temporal Resolution	Spatial Resolution
Estuarine Simulation Model (ESM) (Aquatic/Estuarine)	Temperature, precipitation, sea-level rise,[a] winds, relative humidity,[a] total solar radiation, and photosynthetically active radiation	Daily	Approximately 40 km^2
Marsh Model (Coastal Wetlands)	Sea level rise [a]	Annual	Approximately 10 km^2
CSHORE-C15 (Coastal Barrier)	Wave height, wave period, water level (surge, tides, sea level rise)[a]	Hourly	300 m
LANDIS-II (Terrestrial)	Temperature (average minimum, average, average maximum, standard deviation), precipitation (average and standard deviation), and average photosynthetically active radiation	Monthly	Approximately 10 km^2
Red-Cockaded Woodpecker Decision-Support System (RCW DSS) (Terrestrial)	Precipitation (total and variance), and temperature (average maximum, average minimum)	Monthly	Base level approximately 20 km^2

[a] Note: The focus of Research Project CC-1 was on winds, temperature, precipitation, and solar radiation projections. This project did not provide historical observations or future projections of sea level rise, wave height, wave period, water level, tides, or storm surge. Guidance for sea level rise came directly from SERDP (Hall et al., 2016); however, data for these other variables (wave height, wave period, water level, tides, storm surge) came from SERDP Research Project RC-1702 and data collected by Research Project CB-1 as part of DCERP1. In addition, Research Project CC-1 did not provide relative humidity data.

Based upon the information provided by the ecosystem modules, several climate variables were chosen to form the basis of evaluation and research for Research Project CC-1. Existing research gaps influenced the breakdown of Research Project CC-1 module efforts into four tasks, which are listed as follows and further described in the remainder of this section:

- Task 1—Compilation of Historical Climate Observations
- Task 2—Compilation of Future Climate Projections
- Task 3—Historical Evaluation of Downscaled Climate Projections
- Task 4—Influence of Climate Data Scale

Task 1—Compilation of Historical Climate Observations

To determine the gridded historical climate data set used in DCERP2, three known and widely used data sets were evaluated. These data sets are as follows: (1) Parameter-elevation Regressions on Independent Slopes Model (PRISM; Daly et al., 2008), (2) North American Land

Data Assimilation System version 2 (NLDAS-2; Xia et al., 2012a and 2012b), and (3) the University of Idaho's Gridded Surface Meteorological Data (METDATA; Abatzoglou, 2011). NLDAS-2 and METDATA contain information about temperature, precipitation, wind speed, solar radiation, and specific humidity, whereas PRISM only provides information about temperature and precipitation. Additional characteristics of these three sets of historical climate data are provided in **Table 3-3**.

Table 3-3. Historical Climate Data Sets Evaluated in DCERP2

Name (Reference)	Provider	Spatial Resolution	Variables Available
PRISM (Daly et al., 2008)	Oregon State University	Approximately 4 km	Daily high temperature, low temperature, and precipitation
NLDAS-2 (Xia et al., 2012a and 2012b)	National Aeronautics and Space Administration (NASA) and National Oceanic and Atmospheric Administration (NOAA)	Approximately 12 km	Hourly temperature, solar radiation, precipitation, winds, and specific humidity
METDATA (Abatzoglou, 2011)	University of Idaho's Northwest Knowledge Network	Approximately 4 km	Daily low temperature, high temperature, solar radiation, precipitation, winds, and specific humidity

The three historical climate data sets had differing spatial resolutions (**Table 3-3**). Thus, before performing the evaluation, historical observations were re-gridded to a consistent spatial resolution (15-km grid lengths). For the evaluation, the three historical climate data sets were compared with an independent weather station observational data set called the North Carolina Environment and Climate Observing Network (ECONet), which consists of research-grade quality measurements of common variables (e.g., temperature, precipitation, winds, relative humidity). ECONet is comprised of about 40 stations across North Carolina – 25 of which were located within the eastern North Carolina study region as shown in **Figure 3-1** (blue dots). For the three historical observed data sets, time series were extracted for the grid cell closest to the latitude and longitude of each ECONet weather station.

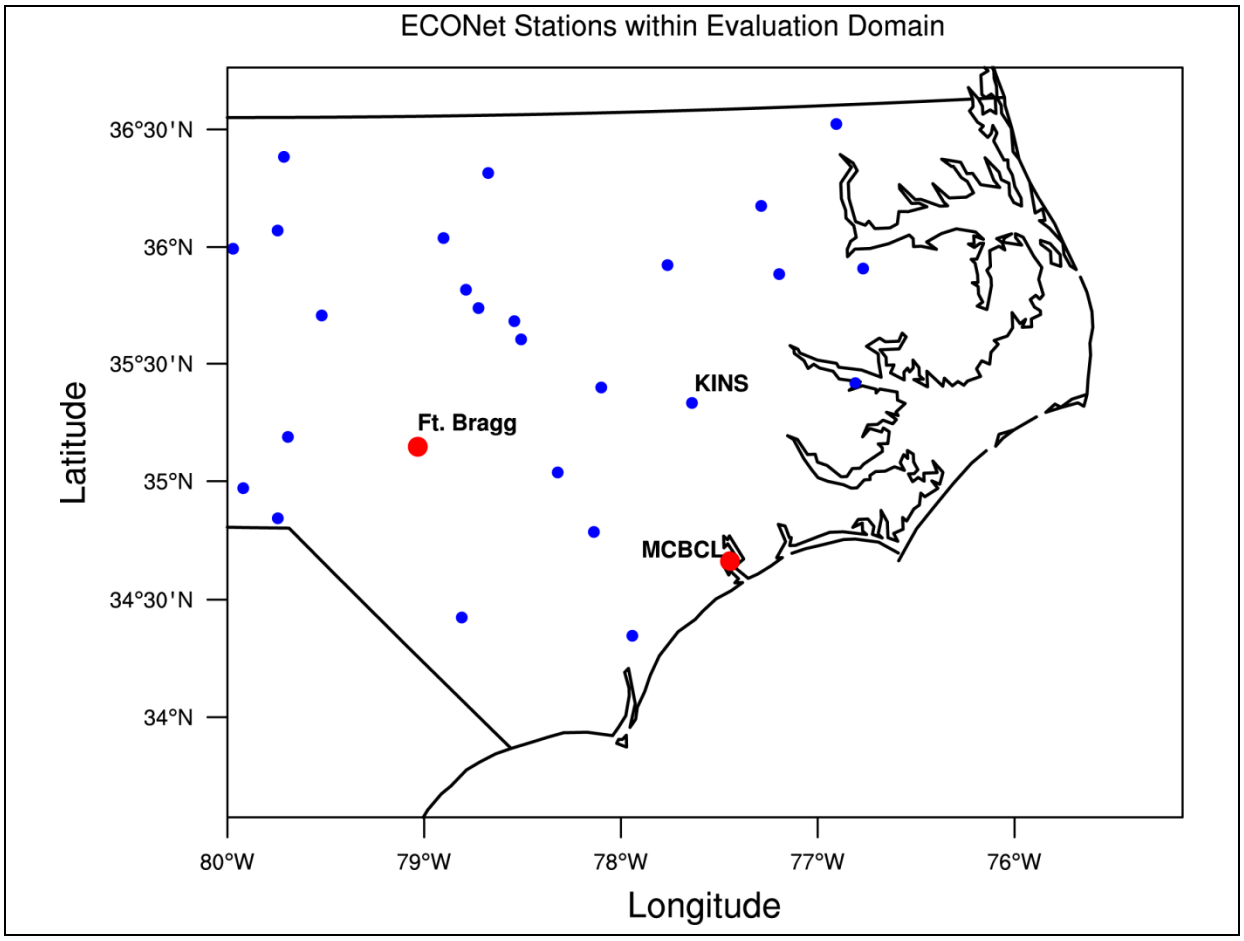

Figure 3-1. Historical evaluation domain, with two military bases (Fort Bragg and MCBCL) in red and 25 ECONet stations in blue.

The blue dot labeled KINS represents the location of the ECONet station in Kinston, NC.

The daily variables and monthly critical thresholds of interest (monthly totals per year) shown in **Table 3-4** were evaluated for the period 2003–2012. For each variable, several error metrics (root mean square error [RMSE], correlation, and mean bias) were computed to examine the accuracy of the three historical data sets as compared with the ECONet observations. In addition, the probability distribution functions were analyzed to further explore the differences between ECONet observations and each set of historical gridded observations.

Table 3-4. Variables and Critical Levels Evaluated by Research Project CC-1

Variable (Daily)	Critical Levels (Monthly)
Maximum temperature	Average number of days >90°F (32.22°C) Average number of days >100°F (37.78°C)
Minimum temperature	Average number of days <32°F (0°C) Average number of days <28°F (−2.22°C)
Total precipitation	Average number of days >0 inches (0 mm) Average number of days >1 inch (25.4 mm)
Average wind speed	Average number of days <3 mph (1.34 m/s) Average number of days >40 mph (17.88 m/s)
Average solar radiation	Not applicable

Task 2—Compilation of Future Climate Projections

Development of the Reduced Ensemble

Previous guidance suggested using all available GCM data when building an ensemble of climate projections that have not yet been downscaled. However, recent literature has found limitations with that approach (Pennell and Reichler, 2011; Sanderson et al., 2015) and thus, a reduced ensemble methodology is recommended. The approach of decreasing the number of downscaled datasets, while also preserving the physical independence of each downscaled GCM, was used in DCERP2. This type of study had not been previously performed on a regional level.

Task 2 aimed to develop a reduced ensemble using the downscaled climate projections shown in **Table 3-5**. These downscaled climate projections cover the continental United States and represent a wide range of downscaling techniques (types and approaches), time periods, emissions scenarios, and GCMs. In addition, two generations of GCMs were used—CMIP3 and CMIP5—from the Fourth and Fifth Assessment Reports, respectively, from the Intergovernmental Panel on Climate Change.

The two dynamically downscaled data sets were bias corrected using the QQ-mapping technique (Dobler et al., 2012). This technique was used because it effectively captures the extremes of temperature, precipitation, and wind speed (e.g., the critical thresholds of interest to the DCERP2 Team). In addition, each downscaled data set has different grid lengths ranging from 4 km to 15 km. For consistency among the data sets, all data were re-gridded to the same 15-km grid for this analysis.

Table 3-5. Downscaled Projections Used in the Development of the Reduced Ensemble

Downscaling Data Set	Time Periods	GCM Generation	Downscaling Type	Downscaling Approach	Number of GCMs	Number of Emissions Scenarios
Hostetler (Hostetler et al., 2011)	1968–1999; 2010–2099	CMIP3	Dynamic	RegCM3	3	1
MACA (Abatzoglou and Brown, 2012)	1950–2005; 2006–2099	CMIP5	Statistical	Analog or weather typing	20	2
BCCA CMIP3 (Brekke et al., 2013)	1961–2000; 2046–2065; 2081–2100	CMIP3	Statistical	Analog or weather typing	9	3
BCCA CMIP5 (Brekke et al., 2013)	1950–2099	CMIP5	Statistical	Analog or weather typing	21	4
Southeast Regional Assessment Project (SERAP; Hayhoe et al., 2013)	1960–2099	CMIP3	Statistical	Transfer functions	16	4
Center for Climatic Research (CCR; Lorenz, n.d.)	1961–2000; 2046–2065; 2081–2100	CMIP3	Statistical	Transfer functions	13	3
CLAREnCE10 (Lydia Stefanova, Florida State University, personal communication)	1968–2000; 2038–2070	CMIP3	Dynamic	Regional Spectral Model	3	1

Clustering Technique

The clustering analysis was performed over eastern North Carolina. The methodology is similar to Kaufman and Rousseeuw (2005) and Pennell and Reichler (2011). To find dependencies in downscaled climate model data, Ward's agglomerative hierarchical clustering (Ward, 1963) was used in this analysis. This method uses relationships of similarity, dissimilarity, or distance to sort the most similar data in a stepwise manner until all the data sets merge to a single, agglomerative point.

To identify groups in these data, model similarity was calculated. To do so, bias from the METDATA observations for each variable was computed for each of the climate model baseline periods, as shown in Equation 1:

$$bias(i,j,t)_n = METDATA(i,j,t) - model_n(i,j,t) \qquad \text{(Eq. 3-1)}$$

where *i,j* is the spatial dimension, *t* is the number of days in the historical evaluation period, and *n* is the number of models.

The bias for each model was then correlated with the bias of every other model at each grid point and time step to find a measure of independence (e.g., higher correlations increase the likelihood that the models are not fully independent), as shown in Equation 2a:

$$\rho(i,j)_{k,l} = corr(bias(i,j,\mathrm{t})_k, bias(i,j,\mathrm{t})_l) \qquad \text{(Eq. 3-2a)}$$

where *k*l* is the number of model to model combinations.

A single correlation value for each variable was obtained by calculating a domain average using Equation 2b:

$$\rho(v)_{k,l} = \frac{\sum_1^G \rho(g)_{k,l}}{G} \quad \text{(Eq. 3-2b)}$$

where *g=(i,j)*, *G* is the number of grid cells, and *v* is the number of meteorological variables.

Correlations were also averaged over the meteorological variables, as shown Equation 3:

$$\rho_{k,l} = \frac{\sum_1^v \rho(v)_{k,l}}{v} \quad \text{(Eq. 3-3)}$$

Ward's agglomerative hierarchical method was then used to identify groups of the most similar downscaled climate models by calculating distances between models and grouping the closest values through an iterative process (Kaufman and Rousseeuw, 2005). The robustness of this clustering analysis was quantified using the agglomerative coefficient (AC). According to Kaufman and Rousseeuw (2005), the AC is a measure of how well the data structure is represented. The AC can range from zero to one, with zero indicating the internal structure of the data cannot be captured with this agglomerative method and one being a perfect model of the internal structure of the data. This coefficient is defined as shown in Equation 4:

$$AC = \frac{1}{n}\sum_{i=1}^{n} l(i) \quad \text{(Eq. 3-4)}$$

where *n* is the number of data points and *l(i)* is the normalized length of the modeled structure.

This dataset had an AC value of 0.76, which captured the internal structure of the data represented by the clustering solution. Nodes that have AC values close to zero were more similar, whereas nodes further from zero were less similar.

Choosing Ensemble Members

After the models were grouped, the number of models in the reduced ensemble was selected by iteratively varying the number of clusters based on the level of similarity. Ultimately, 24 different clusters of models were chosen based on the size of the clusters, e.g., the number of models per group. A skill score and RMSE were used to determine which model from each cluster group was selected for the reduced ensemble. The skill score measures the distribution fit between the modeled and observed values. Values of zero did not overlap at all, and values of one overlapped perfectly. Selection of a member out of each branch was performed by using the model that had either the lowest RMSE or the highest skill score. Each iteration and metric was ranked based on how well the reduced ensemble captured the distribution of the full ensemble. Once a branch pattern was selected, the full ensemble of yearly average maximum temperature, yearly average minimum temperature, and yearly total precipitation was compared with the reduced ensemble for that same parameter.

Comparison of the Reduced Ensemble

Historical average (1979–1999) and a range of future projected averages (2026–2045, 2045–2065, 2081–2099) were calculated on a monthly time step for the eight DCERP2 critical thresholds of interest listed in **Table 3-4**. The three downscaling techniques in the reduced ensemble covered different time periods; thus, the number of models included in each future time period varied as follows:

- 2026–2045 (21 out of 24 ensemble members)
- 2046–2065 (24 out of 24 ensemble members)
- 2081–2099 (23 out of 24 ensemble members).

To compute the future values, projected changes of the critical thresholds were averaged across all available models in the reduced ensemble. In addition, two standard deviations above and below the average of these projected changes were calculated, which represents the range in future climate and encompasses 95% of the distribution of the data among reduced ensemble models. The projected future changes (average and two standard deviations above and below the average) were also added back to the historical averages (1979–1999) to obtain a range of future projected averages. Any negative values resulting from adding these two quantities (e.g., if a large negative projected future change was added to a small historical average) were set to zero since number of days cannot be less than zero. These negative values were most likely the result of high model error. All values were averaged across a domain over MCBCL (**Figure 3-2**).

Uncertainty of the Reduced Ensemble

The reduced ensemble uncertainty was investigated for three variables of interest: annual average minimum temperature, annual average maximum temperature, and annual total precipitation. For each variable, the uncertainty and spread of the reduced ensemble of 24 downscaled models was qualitatively compared with the full distribution of the 76 downscaled climate projections.

Task 3—Historical Evaluation of Downscaled Climate Projections

Evaluation of Downscaled Projections

The three downscaled data sets in the reduced ensemble (i.e., Southeast Regional Assessment Project [SERAP], MACA, and CLAREnCE10) were evaluated using the recommended gridded historical data set, METDATA, from Task 1. The climate model baseline data and gridded historical observations spanned across different time periods so a common 21-year period of 1979–1999 was used in this analysis. Each historical baseline period was evaluated on a monthly time scale for the critical thresholds of interest listed in **Table 3-4**. MACA was the only downscaled data set in the reduced ensemble that contained wind speed data and thus, only 13 out of the 24 members were analyzed for the wind speed critical thresholds. RMSE was used to evaluate the historical projections as compared to the historical gridded data set, METDATA, within a domain over MCBCL (**Figure 3-2**).

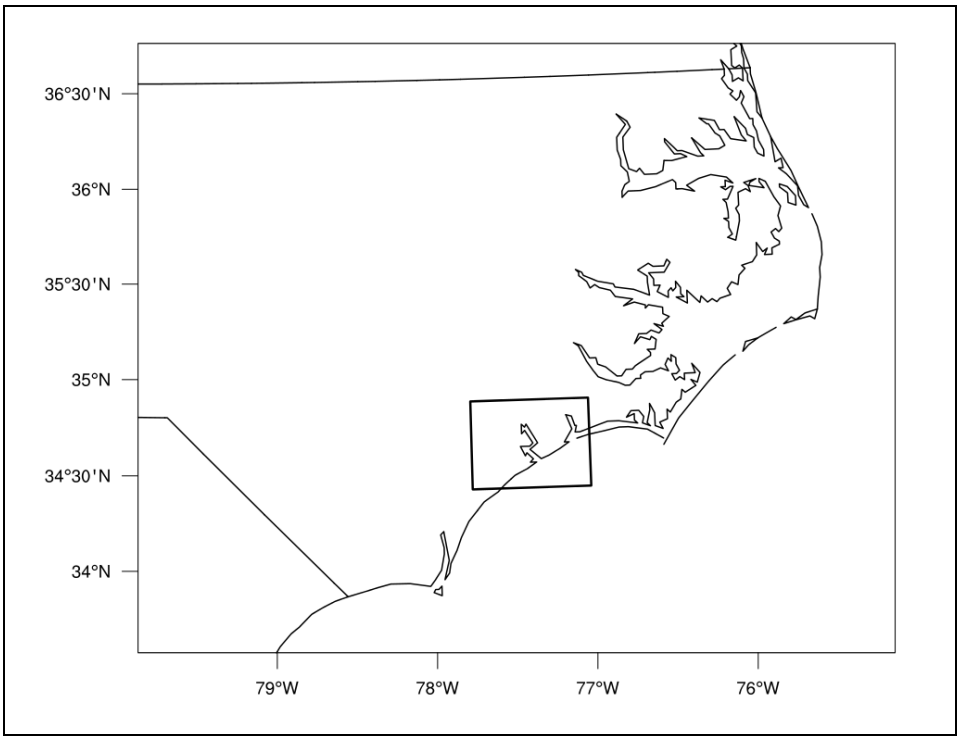

Figure 3-2. Domain over MCBCL (black box).

Ensemble Accuracy versus Individual Accuracy

The historical accuracy of the reduced ensemble and each individual model member was evaluated for the monthly critical levels of interest (average number of days with temperature >90°F, >100°F, <28°F, and <32°F; precipitation >0 inches and >1 inch; and daily average wind speed <3 mph and >40 mph) over the MCBCL domain (**Figure 3-2**). The equally weighted ensemble average for the climate model baseline was calculated on a monthly time step. That monthly ensemble average and each individual ensemble member were evaluated using RMSE.

Downscaling Uncertainty

Recent studies have explored the contribution of various sources of uncertainty with regards to ensembles of global climate projections, most notably Hawkins and Sutton (2009) and (2011). Based on those studies, the following three sources of uncertainty are defined for ensembles of GCMs: natural variability, GCM uncertainty, and scenario uncertainty. Impact assessments that guide management and decision making have recently started using downscaled climate projections (e.g., Argüeso et al., 2015; Basso et al., 2015; Koutroulis et al., 2015; Parmesan et al., 2015; Werth and Chen, 2014) that contribute an additional source of uncertainty. This uncertainty results from differences between downscaling techniques. This analysis assessed the contribution from the three commonly used sources of uncertainty as well as the uncertainty due to downscaling.

Previous literature that characterized the contribution from downscaling uncertainty have been limited to a combination of small domains (areas less than 46,000 km^2), mountainous regions, and/or one type of downscaling technique (Chen et al., 2011; Dobler et al., 2012; Kay et al.,

2012; Mandal et al., 2016; Minville et al., 2008; Pourmokhtarian et al., 2016). Results of these studies are not necessarily applicable in the Piedmont (e.g., Fort Bragg) or Coastal Plain (e.g., MCBCL) regions of North Carolina. These regions contain less complex topographical features and different land-surface processes, such as the sea breeze. For DCERP2, an uncertainty analysis was performed using multiple downscaling techniques in these non-mountainous areas.

Five of the seven downscaled data sets used in the development of the reduced ensemble (**Table 3-5**) were also utilized for the uncertainty analyses in eastern North Carolina (i.e., Fort Bragg and MCBCL): Hostetler, MACA, BCCA CMIP5, SERAP, and the Center for Climatic Research [CCR]. Note: CLAReNCE10 was not included because the data set did not cover the entire domain for Dr. Adrienne Wootten's dissertation work. In addition, BCCA CMIP3 was not included because that data set had not yet been downloaded when Dr. Wootten was working on that portion of her analysis. To address how the contribution of each source of uncertainty was represented by the different time periods used by different downscaled climate projections, the following two evaluations were performed:

1. ALLDATA—This evaluation includes all five downscaled projection data sets, including all emissions scenarios and GCMs in addition to time periods that are not continuous.
2. IDEAL—This subset has 16 GCMs and two emissions scenarios in common from MACA and BCCA CMIP5. These two sets of downscaled projections are also continuous in time.

For the ALLDATA and IDEAL evaluations, the original methodology for GCMs by Hawkins and Sutton (2009) was extended to incorporate downscaling uncertainty (Wootten et al., 2017). To incorporate the influence of downscaling uncertainty (Wootten, 2016), the differences between downscaling techniques were directly incorporated into the fourth order polynomial base equation, as shown in Equation 5:

$$X_{m,d,s,t} - i_{m,d,s} = x_{m,d,s,t} - \varepsilon_{m,d,s,t} \qquad \text{(Eq. 3-5)}$$

where $X_{m,d,s,t}$ is the value of the variable in time (t) for each combination of GCM (m), downscaling technique (d), and emissions scenario (s), and $i_{m,d,s}$ is the average of the variable over the time period from 1981–2000. In addition, $x_{m,d,s,t}$ and $\varepsilon_{m,d,s,t}$ are the fitted values and residuals, respectively, from a fourth order polynomial fit in time (t) for each combination of m, d, and s. The fourth order polynomial fit represents the slowly varying signal of anthropogenic climate change (Benestad, 2003), and the residuals of that fit represent the remaining fluctuations. Thus, downscaling was incorporated at the outset, which enabled the variance decomposition method to include this source of uncertainty. The entire time period available for each data set was used for each fit. Variance decomposition was applied to the fitted values and residuals.

We also included a weighting scheme to account for the accuracy of the GCMs and downscaling techniques for the historical anomaly by using Equations 6 and 7, respectively:

$$w_m = \frac{1}{x_{obs} + \left|\frac{1}{N_d}\sum x_{m,d,1999} - x_{obs}\right|} \qquad \text{(Eq. 3-6)}$$

$$w_d = \frac{1}{x_{obs} + \left|\frac{1}{N_m}\sum x_{m,d,1999} - x_{obs}\right|} \quad \text{(Eq. 3-7)}$$

where w_m is the weight for the GCM and w_d is the weight for the downscaling technique. In these weighting schemes, $x_{m,d,1999}$ is the anomaly from the fourth order polynomial fit of the variable in 1999 from the PRISM data set, which is designated as x_{obs} (Daly et al., 2008); and N is the number of observations for each combination of downscaling technique (d) and GCM (m). The year 1999 was used as the reference year because it is common among all the downscaled projections. The anomaly from the fourth order polynomial in 1999 was used to assess the ability of the models to simulate the recent change of a variable of interest, allowing the best performing GCMs and downscaling techniques in recent history to retain the highest weights in the variance decomposition equations. To assess the historical accuracy of each individual GCM or downscaling technique, the mean weights across GCMs or downscaling techniques were used as shown in Equations 8 and 9, respectively:

$$W_m = \frac{w_m}{\sum_{i=1}^{N_m} w_m} \quad \text{(Eq. 3-8)}$$

$$W_d = \frac{w_d}{\sum_{i=1}^{N_d} w_d} \quad \text{(Eq. 3-9)}$$

where W_m is the rescaled weights for the GCMs; W_d is the rescaled weights for the downscaling techniques; and N_m and N_d are the number of GCMs and downscaling techniques, respectively. This weighting is similar to that of Hawkins and Sutton (2009), in which the weighting is used to reduce the weights of GCMs and downscaling techniques for which the recent anomaly is too large or too small. However, there are limitations associated with model weighting. The available sample of models and downscaling techniques cannot be considered an unbiased sample (Sanderson and Knutti, 2012). To account for situations in which the entire complement of GCM and downscaling combinations is not available for variance decomposition, additional rescaling was also applied using Equations 10 and 11, respectively:

$$\omega_{m(exists)} = \frac{W_{m(exists)}}{\sum W_{m(exists)}} \quad \text{(Eq. 3-10)}$$

$$\omega_{d(exists)} = \frac{W_{d(exists)}}{\sum W_{d(exists)}} \quad \text{(Eq. 3-11)}$$

Values of $\omega_{m(exists)}$ and $\omega_{d(exists)}$ depended on the availability of the GCMs or downscaling techniques in the sample. Therefore, the values of $\omega_{m(exists)}$ and $\omega_{d(exists)}$ did not remain constant, but the values of $W_{m(exists)}$ and $W_{d(exists)}$ remained constant. More importantly, as more combinations become available, the values of $\omega_{m(exists)}$ and $\omega_{d(exists)}$ approach $W_{m(exists)}$ and $W_{d(exists)}$. In addition, the calculation of $\omega_{m(exists)}$ and $\omega_{d(exists)}$ forced the weights used in future combinations to sum to one, thereby ensuring that the estimates of mean and variance in Equations 12 through 15 were unbiased.

The calculation for each source of uncertainty used the fitted values, residuals, and weights as described in the following four steps (Equations 12 through 15):

1. Natural variability:

$$V = \sum_m \omega_m \sum_d \omega_d Var(\varepsilon) \quad \text{(Eq. 3-12)}$$

where V is the natural variability source of uncertainty. The values of ω_m and ω_d are the rescaled weights previously described. In addition, $Var(\varepsilon)$ is the variance of the residuals of the polynomial fit (ε). The value of V is assumed to be constant in time.

2. GCM uncertainty:

$$M(t) = \frac{1}{N_s}\frac{1}{N_d}\sum_s \sum_d Var_m^{\omega}(x_{m,.,.,t}) \quad \text{(Eq. 3-13)}$$

where $M(t)$ is the GCM uncertainty for each time t. N_s and N_d represent the total number of emissions scenarios and downscaling techniques, respectively. In addition, $\sum_s \sum_d Var_m^{\omega}(x_{m,.,.,t})$ is the weighted variance across the GCMs of the fitted polynomial values (x), with ω_m as the weights.

3. Downscaling uncertainty:

$$D(t) = \frac{1}{N_s}\frac{1}{N_m}\sum_s \sum_m Var_d^{\omega}(x_{.,d,.,t}) \quad \text{(Eq. 3-14)}$$

where $D(t)$ is the downscaling uncertainty for each time t. Similar to the calculation of $M(t)$ in Equation 13, the weighted variance is taken using ω_d as the weights. N_m represents the total number of GCMs available.

4. Scenario uncertainty:

$$S(t) = Var_s\left(\sum_m \omega_m \sum_d \omega_d x_{m,d,.,t}\right) \quad \text{(Eq. 3-15)}$$

where $S(t)$ is the scenario uncertainty each time t. The values of ω_m and ω_d are the rescaled weights previously described and the fitted polynomial values (x) are used in this equation. The variance is taken across the emissions scenarios.

Assuming that each source of uncertainty is independent, the total variance from the climate model projections was then defined as shown in Equation 16:

$$T(t) = V + M(t) + D(t) + S(t) \quad \text{(Eq. 3-16)}$$

These four sources of uncertainty were analyzed for the decadal mean of the following variables: (1) annual average daily high temperature, (2) annual number of days with high temperature greater than 95°F, (3) annual number of days with low temperature below 32°F, (4) annual total precipitation, and (5) annual number of days with precipitation greater than 1 inch. The 95°F temperature threshold was selected for the uncertainty analysis (part of Dr. Adrienne Wootten's dissertation work) since this threshold was used in the Southeast Chapter of the National Climate Assessment (Carter et al., 2014) and the North Carolina State Climate Summary (Frankson et al., 2017). The uncertainty contribution analysis was performed at Fort Bragg and MCBCL although additional analyses for a broader Southeastern United States domain were included in Wootten et al. (2017) and the dissertation published by Wootten (2016).

Task 4—Influence of Climate Data Scale

The Research Project CC-1 Team worked with Vicki Garcia (Terrestrial Module) on Task 4, which included an assessment of the effect of the spatial resolution of climate data on the life history traits of the red-cockaded woodpecker (RCW; *Picoides borealis*). Local spring weather variables measured at 4 km were found to be associated with RCW life history trait annual means at two study sites in North Carolina: MCBCL near Jacksonville, NC in the Coastal Plain and Fort Bragg near Southern Pines, NC in the Sandhills (Garcia, 2014). To examine how the spatial resolution of these weather variables affected our ability to predict RCW life history traits, the highest ranked weather variable—which varied by trait (i.e., date the egg was laid, nest survival, local recruitment, and number of fledglings) and by location (i.e., Fort Bragg or MCBCL)—was used for the traits examined in Garcia (2014). That same weather variable was calculated by using METDATA gridded estimates at different resolutions: its native resolution (4 km) as well as 10, 15, 20, 30, 40, and 50 km. The spatial resolution of most publicly available downscaled projections falls within this range. For each spatial resolution, METDATA values for the grid cells closest to Fort Bragg and MCBCL were used.

The corrected Akaike Information Criterion (AICc; Anderson, 2008; Burnham and Anderson, 2002) was used to compare models with weather variables measured at different spatial resolutions, as well as a model with no weather variables (intercept only), and to determine which spatial resolution best represented the selected RCW life history trait. Additionally, egg lay dates and the other traits were examined by using generalized linear models with either Poisson or binomial distributions, depending on the trait.

Results and Discussion

Task 1—Compilation of Historical Climate Observations

Evaluation of the historical climate observations were performed by comparing these data to the ECONet stations for the period 2003–2012. A sample time series at Kinston, NC is shown in **Figure 3-3**, with ECONet data compared to each historical data set for the annual number of days with precipitation greater than 0 inches and the maximum temperature greater than 90°F.

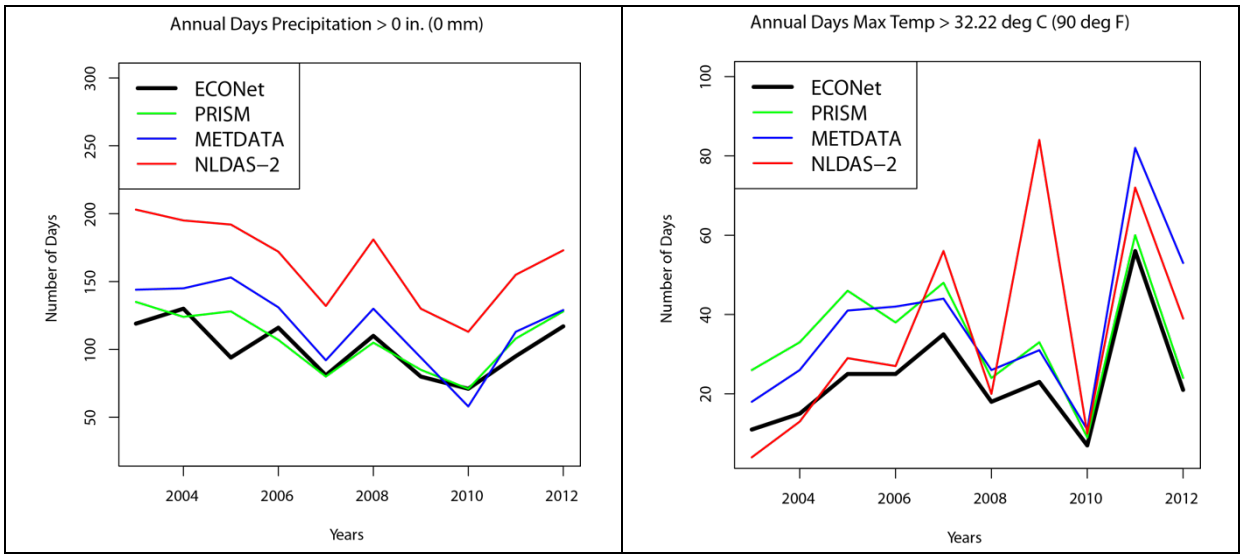

Figure 3-3. (Left panel) A time series of the annual number of days with precipitation greater than 0 inches and (right panel) maximum temperature greater than 90°F at Kinston, NC (KINS shown in Figure 3-1) for the ECONet data (black), PRISM (green), METDATA (blue), and NLDAS-2 (red).

The average RMSE for all ECONet stations as compared with each historical climate data set is provided in **Table 3-6** for five daily variables of interest: maximum temperature, minimum temperature, precipitation, average wind speed, and average solar radiation. PRISM had the lowest error for minimum and maximum temperature and precipitation. METDATA and NLDAS-2 had similar errors for these variables, but NLDAS-2 had overall slightly lower RMSE for three out of the five variables.

Table 3-6. Average RMSE for Daily ECONet Compared with Historical Climate Data Sets

Variables	PRISM	METDATA	NLDAS-2
Maximum temperature (°C)	1.06	2.32	2.02
Minimum temperature (°C)	1.28	2.13	2.29
Precipitation (inches)	0.18	0.26	0.22
Average wind speed (m/s)	Not applicable	1.86	1.62
Average solar radiation (W/m^2)	Not applicable	48.13	48.14

A summary of the RMSE for critical levels for temperature, precipitation, and wind (previously described in **Table 3-4**) is provided in **Table 3-7**. PRISM had the lowest errors for both maximum temperature critical levels (>90°F and >100°F) and one of the precipitation critical levels (>0 inches). However, NLDAS-2 had lower errors for the number of days with very cold temperatures (<28°F and <32°F) and for days with heavy rainfall (>1 inch). Comparing only the results for NLDAS-2 with METDATA, the latter performed better for one of the warm day thresholds (>90°F) and for days with measurable rain (>0 inches).

Table 3-7. Average RMSE (Days) for Each Critical Level

Variables	PRISM	METDATA	NLDAS-2
Maximum temperature >90°F	1.91	2.61	2.85
Maximum temperature >100°F	0.23	0.86	0.77
Minimum temperature <32°F	1.74	1.91	1.59
Minimum temperature <28°F	1.54	1.55	1.35
Precipitation >0 inches	2.48	3.13	5.87
Precipitation >1 inch	0.76	0.75	0.73
Average wind speed <3 mph	Not applicable	5.87	4.87

The average correlations between ECONet and each gridded climate product for the five daily variables (maximum temperature, minimum temperature, precipitation, average wind speed, and average solar radiation) are provided in **Table 3-8**. PRISM had the highest correlation with ECONet observations for minimum and maximum temperature and precipitation. METDATA and NLDAS-2 performed similarly in terms of correlation. For average wind speed and average solar radiation, which were not available in the PRISM data set, METDATA had a higher correlation for wind speed as compared to that of NLDAS-2 yet an identical correlation for solar radiation. Comparing only the results for NLDAS-2 with METDATA for the other three variables, the latter had slightly lower correlations compared with the former for maximum temperature and precipitation yet an identical correlation for minimum temperature.

Table 3-8. Average Correlation for Daily ECONet Compared with Historical Climate Data Sets

Variables	PRISM	METDATA	NLDAS-2
Maximum temperature	0.996	0.971	0.976
Minimum temperature	0.992	0.975	0.975
Precipitation	0.870	0.725	0.790
Average wind speed	Not applicable	0.841	0.765
Average solar radiation	Not applicable	0.877	0.877

A summary of the average correlation between ECONet and each gridded climate product for each critical level (previously described in **Table 3-4**) is provided in **Table 3-9**. All historical data sets had similar correlations with ECONet observations. For the six variables in common, PRISM had the highest correlation except for the heavy precipitation critical level (>1 inch). However, for this critical level, correlations for the other two data sets were basically identical to that of PRISM, with correlations only ~0.001 higher or lower. Comparing only the results for NLDAS-2 with METDATA for all critical levels, the latter had slightly higher correlations than the former for days with warm temperatures (>90°F), both minimum temperature levels, and days with precipitation >0 inches.

Table 3-9. Average Correlation for Days with Each Critical Level

Variables	PRISM	METDATA	NLDAS-2
Maximum temperature >90°F	0.958	0.925	0.886
Maximum temperature >100°F	0.808	0.650	0.703
Minimum temperature <32°F	0.970	0.962	0.959
Minimum temperature <28°F	0.953	0.950	0.943
Precipitation >0 inches	0.807	0.788	0.770
Precipitation >1 inch	0.659	0.658	0.660
Average wind speed <3 mph	Not applicable	0.303	0.481

RMSE, correlation, and mean bias were analyzed spatially to determine whether geographical influences, such as elevation or proximity to the ocean, had any effect on the comparative statistics. Examples for two error metrics, two variables, and one historical climate data set are provided in **Figure 3-4**. However, no consistent spatial pattern was observed in any error statistics (RMSE, correlation, and mean bias) for any variable or gridded climate data set. Therefore, the performance of any of these three gridded climate products performed equally well across the entire domain.

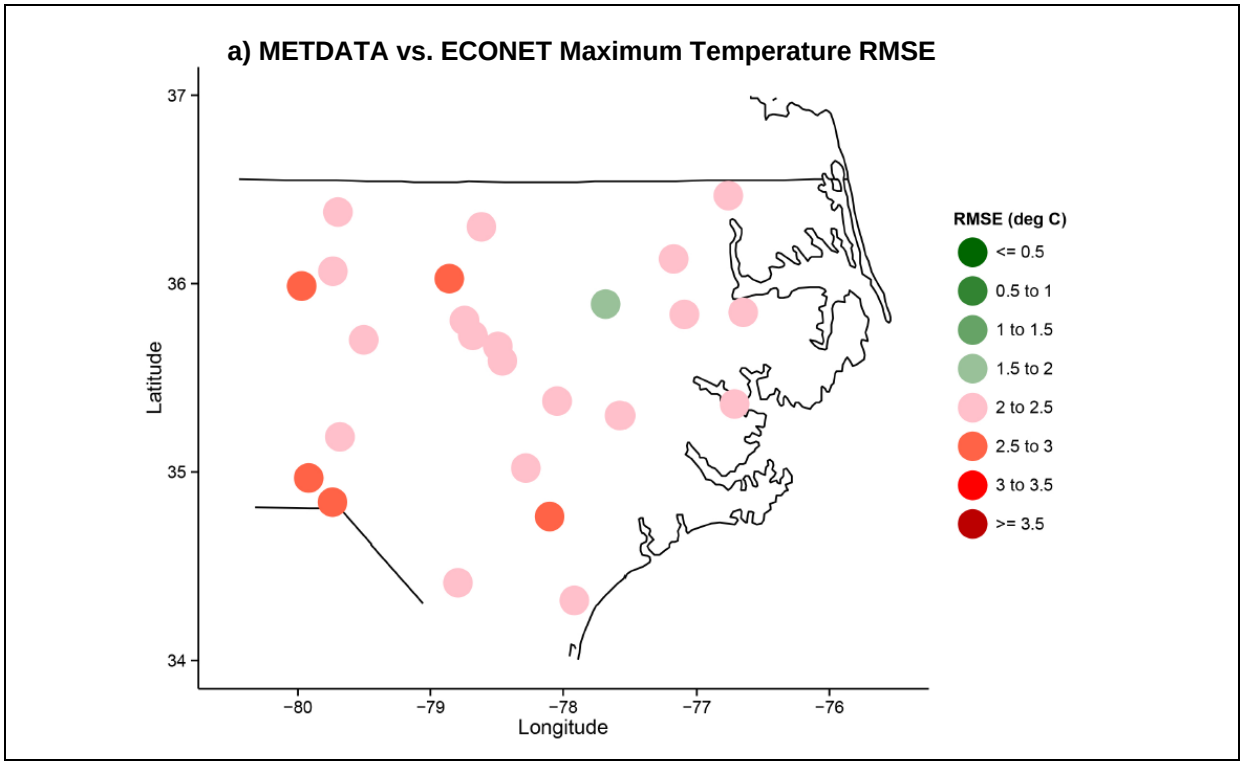

Figure 3-4. RMSE and correlation for each location in the study domain for METDATA as compared with ECONet observations for daily maximum temperature (a and b, respectively) and daily precipitation (c and d, respectively) (continued below)

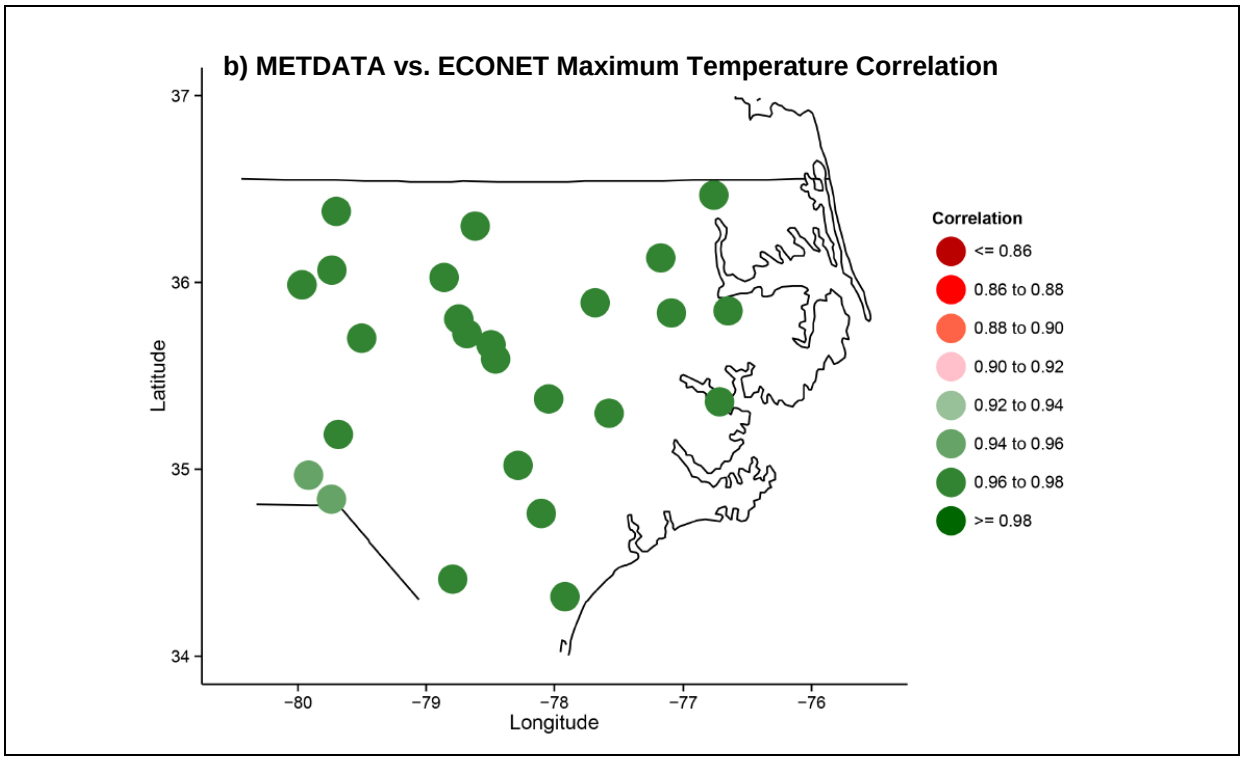

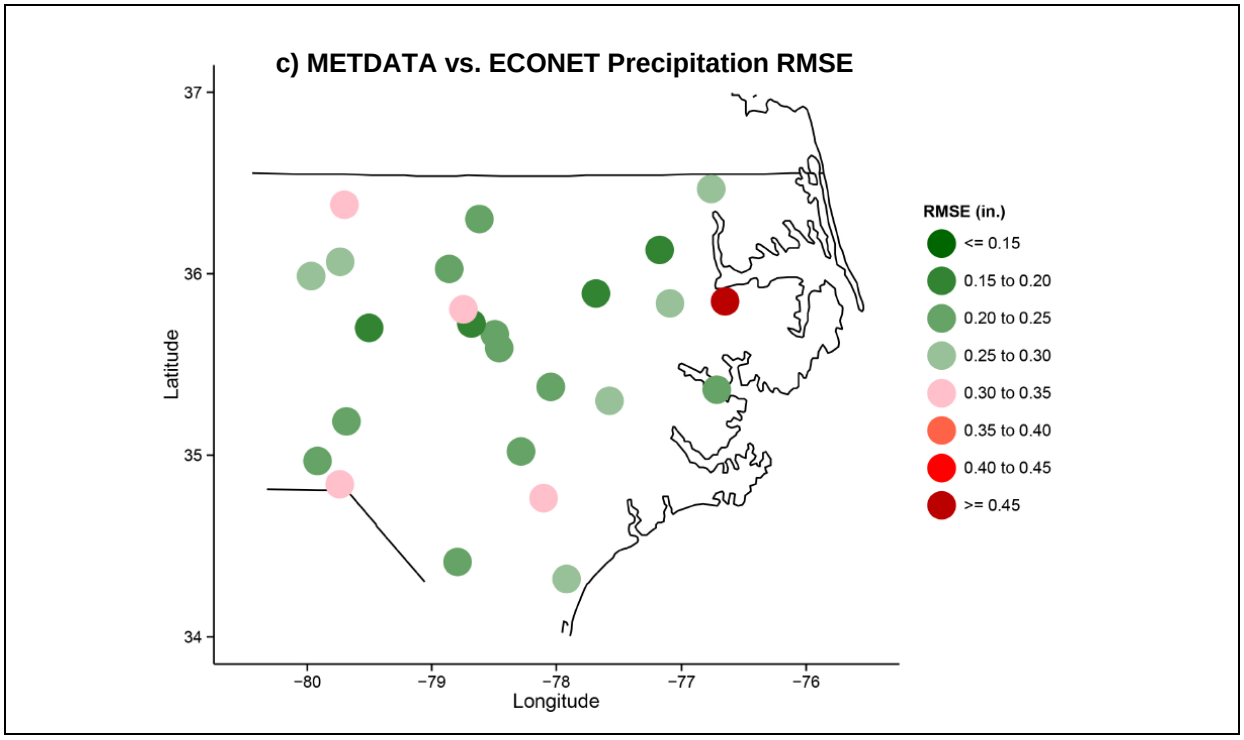

Figure 3-4. RMSE and correlation for each location in the study domain for METDATA as compared with ECONet observations for daily maximum temperature (a and b, respectively) and daily precipitation (c and d, respectively) (continued below)

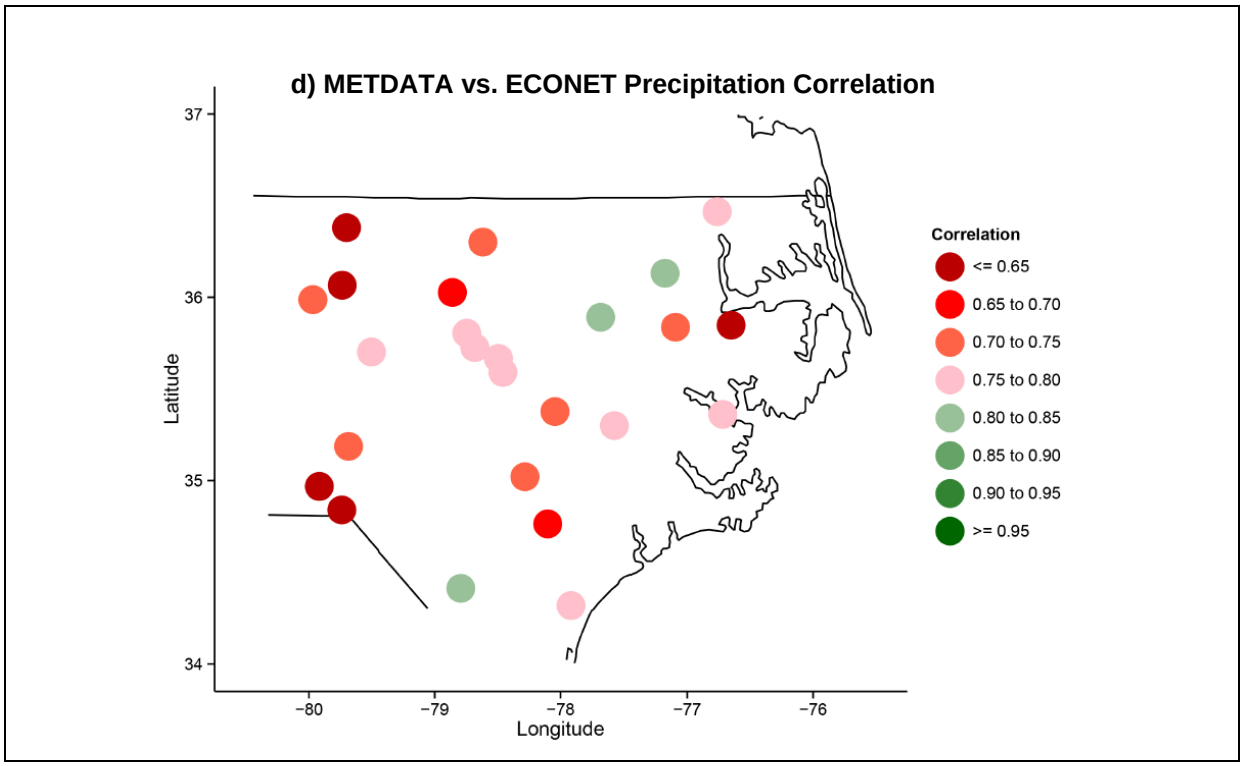

Figure 3-4. RMSE and correlation for each location in the study domain for METDATA as compared with ECONet observations for daily maximum temperature (a and b, respectively) and daily precipitation (c and d, respectively).

Figure 3-5 shows the composite probability distribution function of error for five variables of interest: maximum temperature, minimum temperature, non-zero precipitation, wind speed, and solar radiation. The error for PRISM was concentrated close to zero for minimum and maximum temperature, whereas the errors for METDATA and NLDAS-2 had higher spread. The non-zero precipitation error distribution of NLDAS-2 was similar to that of PRISM. The error in METDATA for wind speed was more narrowly concentrated, but was generally more positive when compared to that of NLDAS-2. The error for METDATA and NLDAS-2 solar radiation was effectively identical.

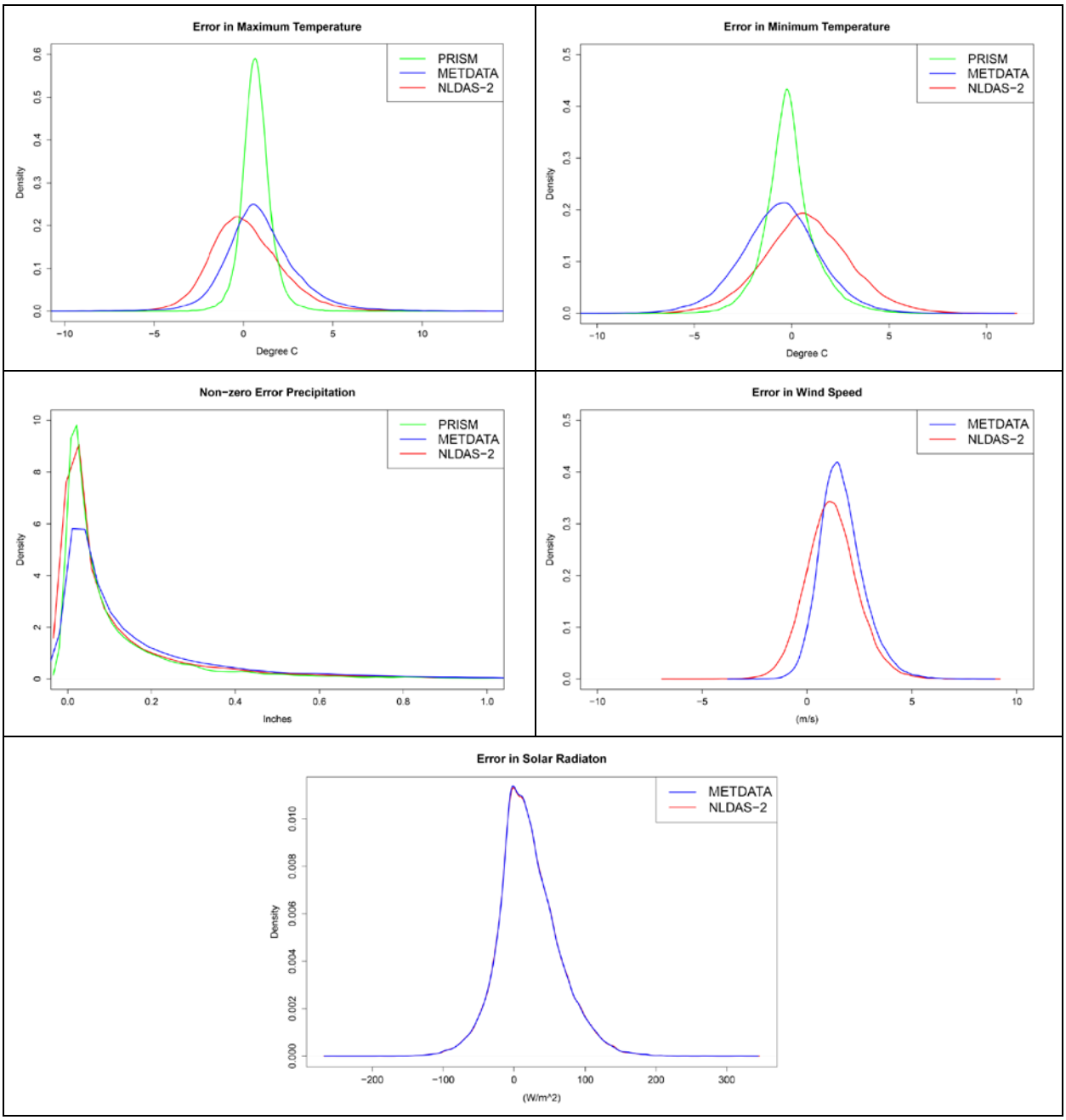

Figure 3-5. Composite probability distribution functions of daily error for between gridded climate products and all ECONet stations.

Three different historical climate data sets were compared with daily ECONet observations for the period from 2003 to 2012. Overall, PRISM performed best for minimum and maximum temperature and precipitation yet did not contain wind speed and solar radiation variables. Both METDATA and NLDAS-2 provide estimates of wind and incoming solar radiation, but had generally higher errors and lower correlations with ECONet as compared with PRISM. METDATA and NLDAS-2 had similar errors overall. METDATA has a native spatial resolution of 4 km, whereas NLDAS-2 has a native spatial resolution of 12 km. Given the need for wind observations, the comparable performance against NLDAS-2, and the advantages of higher

native spatial resolution, METDATA was recommended as the gridded historical climate observations for DCERP2.

Task 2—Compilation of Future Climate Projections

Development of the Reduced Ensemble

Many of the full ensemble members were based on permutations of the same GCMs, and thus, each ensemble member was not fully independent from the other members. Clustering reduced the dependency between the final ensemble members, providing a more robust reduced ensemble data set. Based on the agglomerative hierarchal clustering results, ensemble members were more likely to be clustered together if they shared the same parent GCM or were downscaled using the same methodology. GCM influences appeared to be stronger than influences from the downscaling type.

For the reduced ensemble, the selection of a member out of each branch was performed by using the model that had either the lowest RMSE or the highest skill score. The selection criteria that maximized the full ensemble distribution (76 downscaled climate projections) were chosen as the final reduced ensemble (24 downscaled climate projections) for DCERP2 (**Table 3-10**).

Table 3-10. Final Reduced Ensemble of Downscaled Climate Projections

MACA: bcc-csm1-1	MACA: MIROC5	SERAP: echam5
MACA: BNU-ESM	MACA: MIROC-ESM-CHEM	SERAP: echo
MACA: CanESM2	MACA: MIROC-ESM	SERAP: gfdl-2-0
MACA: CNRM-CM5	MACA: MRI-CGCM3	SERAP: gfdl-2-1
MACA: CSIRO-Mk3-6-0	MACA: NorESM1-M	SERAP: hadgem
MACA: GFDL-ESM2G	SERAP: ccsm	SERAP: miroc-med
MACA: GFDL-ESM2M	SERAP: cgcm3-t47	SERAP: mri-cgcm2
MACA: inmcm4	SERAP: cnrm	CL10: HadCM3

Comparison of the Reduced Ensemble

This analysis focused on monthly time scales; however, projections of temperature and precipitation on annual time scales were discussed in Frankson et al. (2017). According to that study, average annual temperatures in North Carolina are projected to increase in the future. However, the range of this increase varies widely by end-of-century for the lower and higher future emissions pathways, with increases of ~2°F to ~8°F and ~7°F to ~13°F, respectively. In addition, annual precipitation is projected to increase in North Carolina although not all portions of the state lie within the area where the majority of global climate models indicate that this change is statistically significant.

Table 3-11 contains historical average (1979-1999) and a range of future projected averages (2026–2045, 2045–2065, and 2081–2099) for the DCERP2 critical thresholds of interest listed in **Table 3-4** on a monthly time scale. The average number of days with daily average wind speed greater than 40 mph was not included in **Table 3-11** since none of the days in the historical or future periods of interest met that daily average wind speed threshold criteria. For the future time

periods in **Table 3-11**, the range (minimum to maximum) in critical threshold values is shown and encompasses 95% of the distribution of the data among reduced ensemble models. Temperature and precipitation critical threshold data from **Table 3-11** are also displayed graphically in **Figures 3-6 through 3-11**. All values represent a domain average over MCBCL (**Figure 3-2**).

Maximum Temperature Critical Thresholds

The average number of days with temperature greater than 90°F is historically approximately 10 days in the summer months (June, July, and August). This critical threshold is projected to increase by 3 to 17 days per month in 2026–2045 as shown in **Table 3-11** and **Figure 3-6**. For the same period, the critical threshold of greater than 100°F, which is historically on average close to 0 days per month, is expected to remain the same or increase by up to 2 days **(Table 3-11** and **Figure 3-7**) during summer months. For 2046–2065, the critical maximum temperature level of greater than 90°F is projected to increase by 6 to 19 days per month during the peak of the warm season (June, July, and August). Up to 5 additional days per month above 100°F during summer are expected for this mid-century time period. A similar trend is possible for the average number of days with temperature greater than 90°F in 2081–2099, with up to almost 1 month of additional days per month (8 to 26 more days) above this threshold during summer and early fall (i.e., June, July, August, and September). For the same time period, the critical level greater than 100°F is projected to increase up to 19 days per month during the warm season (June, July, and August).

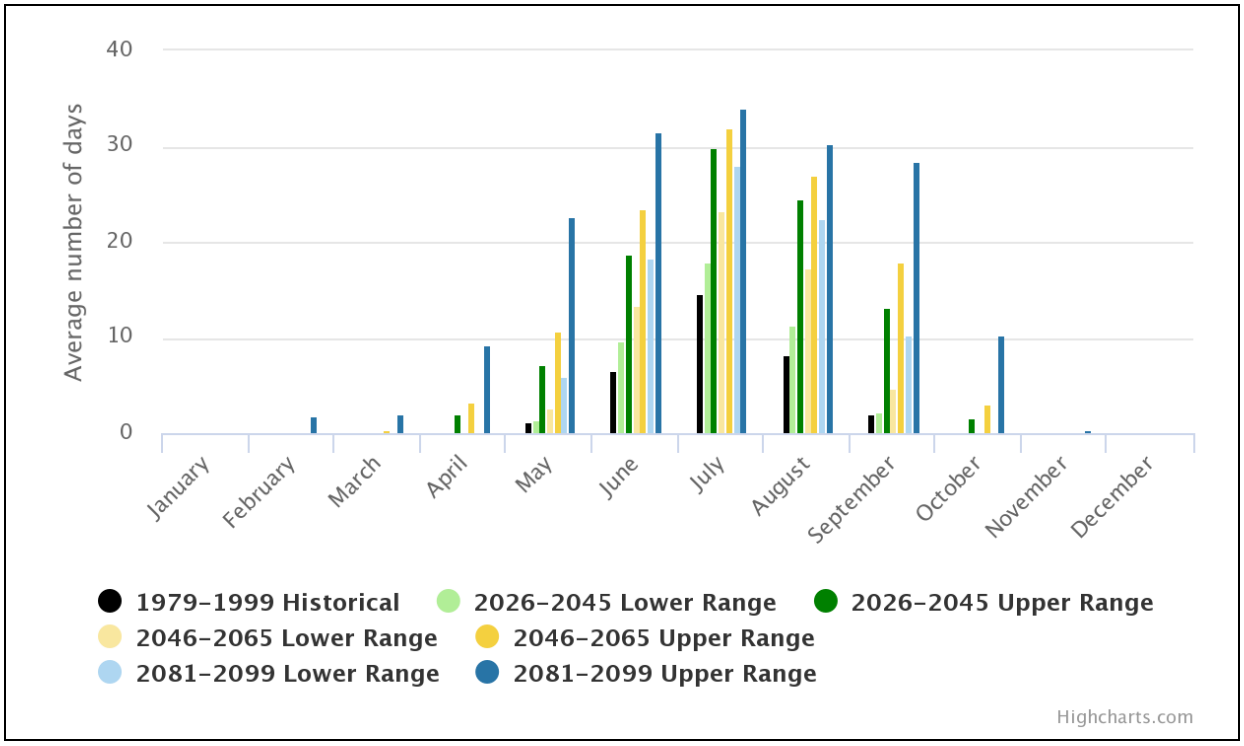

Figure 3-6. Monthly historical average and future projected ranges over MCBCL for the critical threshold of average number of days with maximum temperatures >90°F.

Note that the slight decrease that is sometimes seen in the projected number of days above 90°F and 100°F is likely due to the high error of some of the downscaled climate models in the reduced ensemble. The magnitude of this error can exceed the future projected change, resulting in more uncertainty in those values.

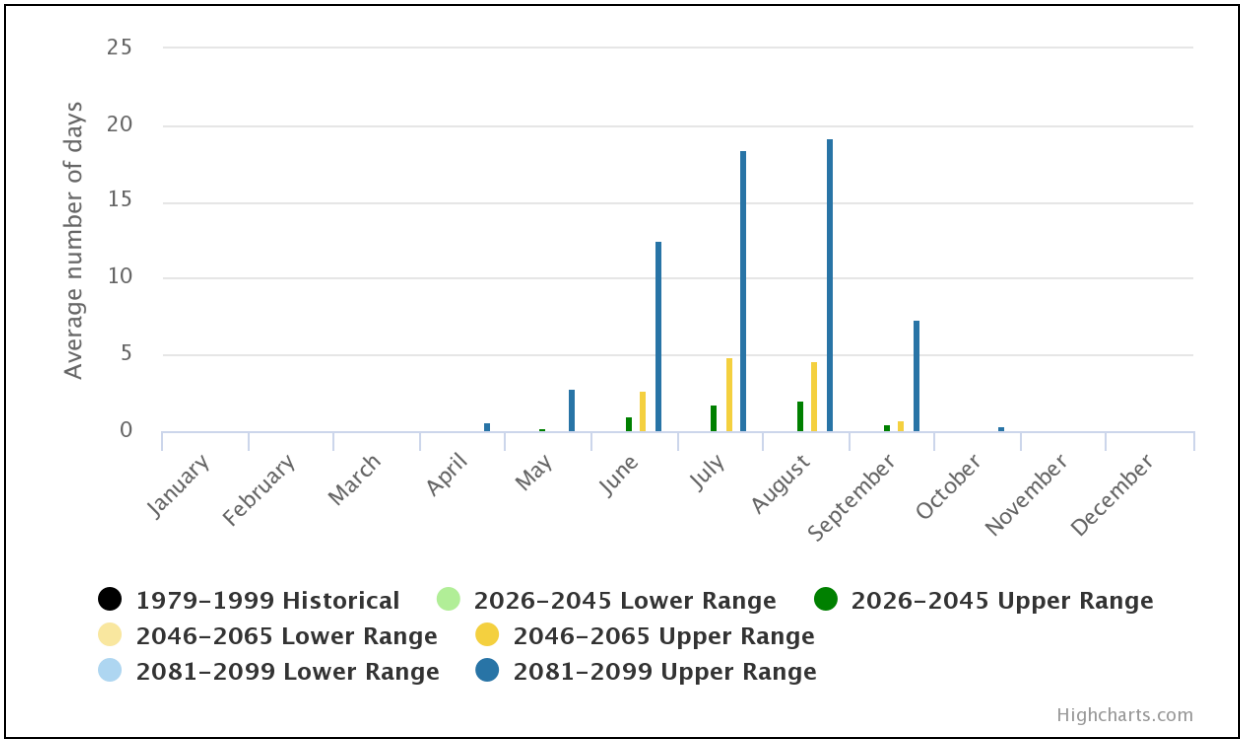

Figure 3-7. Monthly historical average and future projected ranges over MCBCL for the critical threshold of average number of days with maximum temperatures >100°F.

Minimum Temperature Critical Thresholds

Historically, the average number of days with temperature less than 28°F ranges from a few days to approximately 8 days per month during the cool season (e.g., November through March). This variable is projected to remain about the same or decrease by 5 days or less during these months in 2026–2045 as shown in **Table 3-11** and **Figure 3-8**. Similar results are expected for the below 32°F threshold in 2026–2045, which historically averages about 5 to 13 days per month during the cool season (**Table 3-11** and **Figure 3-9**). For the 2046–2065 time period, approximately the same number or a decrease of as many as 7 days per month could occur for the critical level of less than 28°F during the cold season (i.e., November through March), but 1 to 9 fewer days below freezing per month are projected. For days with temperature below 28°F, the projected range in values on any given month during the coldest months (i.e., December through February) in 2081–2099 is 0 to 5 days, which is up to 8 fewer days per month as compared with the historical average. A similar decreasing trend is expected for the average number of freezing days in 2081–2099, with up to 12 fewer days per month.

Note that the slight increase that is sometimes seen in the projected number of days below 28°F and 32°F is likely due to the high error of some of the downscaled climate models in the reduced ensemble. Similar to the analysis for the number of days above 90°F and 100°F, the magnitude

of this error can exceed the future projected changes, resulting in more uncertainty in those values.

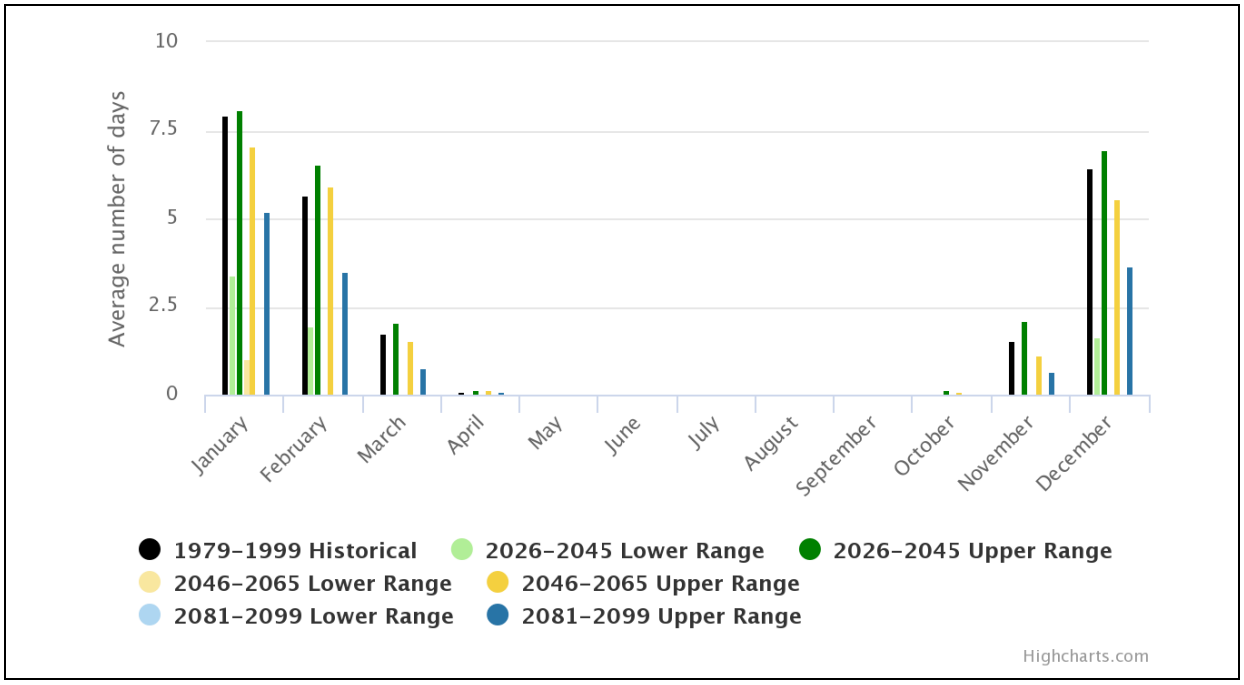

Figure 3-8. Monthly historical average and future projected ranges over MCBCL for the critical threshold of average number of days with minimum temperatures <28°F.

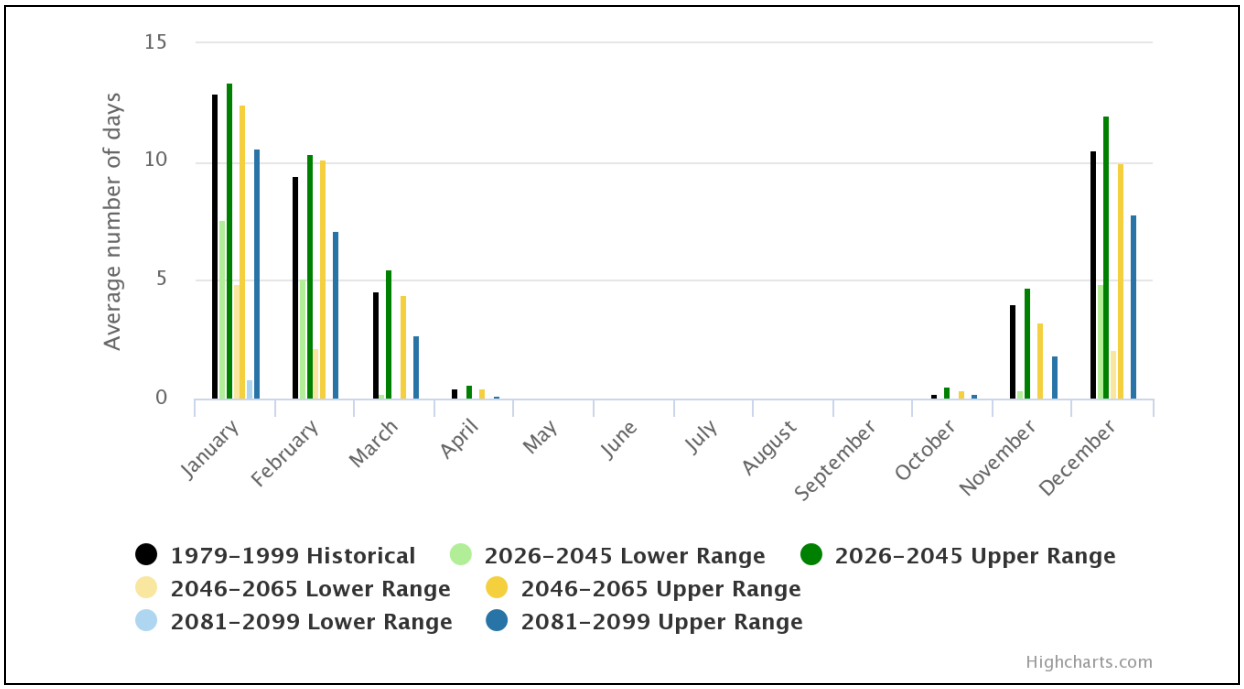

Figure 3-9. Monthly historical average and future projected ranges over MCBCL for the critical threshold of average number of days with minimum temperatures <32°F.

Precipitation Critical Thresholds

The historical average number of days per month with precipitation greater than 0 inches and greater than 1 inch ranges from approximately 10 to 20 days and approximately 0 to 2 days, respectively. For the three future time periods (i.e., 2026–2045, 2046–2065, and 2081–2099), the change in the monthly average number of days with precipitation greater than 0 inches ranges from 3 fewer days to 5 more days, 4 fewer days to 5 more days, and 5 fewer days to 7 more days, respectively (**Table 3-11** and **Figure 3-10**). A similar trend (possible decrease or increase) is observed for greater than 1 inch of precipitation during all future time periods (i.e., 2026–2045, 2046–2065, 2081–2099), with either 1 fewer day or up to 2 additional days per month **(Table 3-11** and **Figure 3-11)**. Overall, this trend indicated that the downscaled models in the reduced ensemble did not agree about whether these precipitation critical thresholds will increase or decrease in the future. Similarly, Kunkel et al. 2013 also found a large spread in future changes of annual mean precipitation and seasonal mean precipitation for a domain in the Southeast US. This large range of future changes is likely because climate models have limited skill in simulating precipitation (Walsh et al., 2014) and thus, precipitation projections are generally more uncertain than temperature projections (Carter et al., 2014).

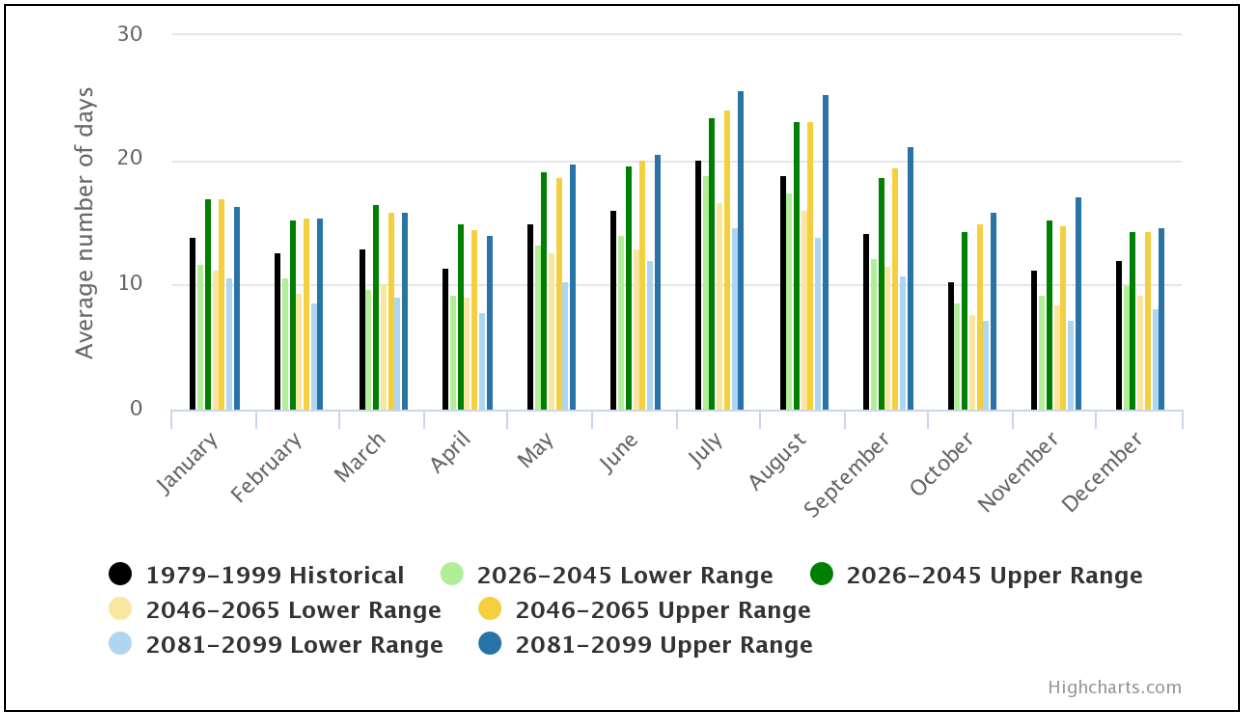

Figure 3-10. Monthly historical average and future projected ranges over MCBCL for the critical threshold of average number of days with precipitation >0 inches.

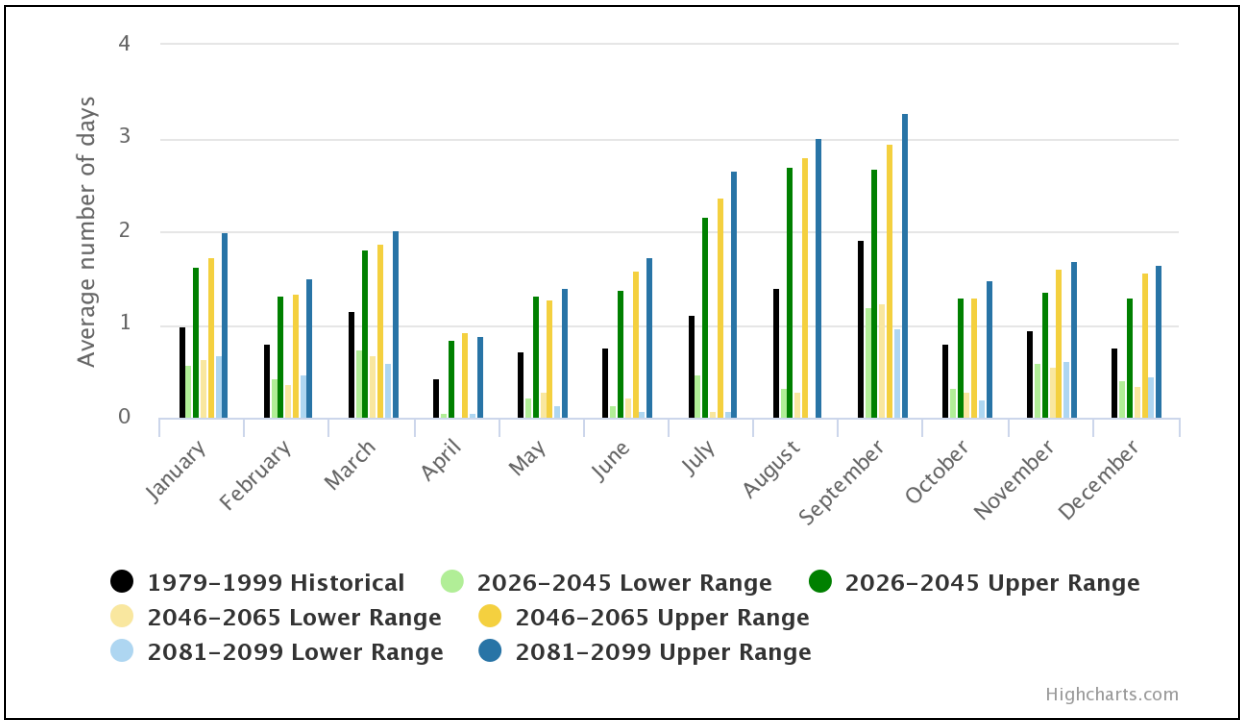

Figure 3-11. Monthly historical average and future projected ranges over MCBCL for the critical threshold of average number of days with precipitation >1 inch.

Wind Speed Critical Threshold

Historically, the average number of days per month with daily average wind speed below 3 mph is about 0 to 1 day. This critical threshold is projected to stay approximately the same or increase by 1 or 2 days per month for the future time periods of 2026–2045 and 2046–2065, as shown in **Table 3-11**. A similar increasing trend is observed for the average number of days per month below 3 mph in 2081–2099, with up to 3 additional days in October. Results for the critical threshold of the average number of days with daily average wind speed greater than 40 mph were not included because none of the days in the historical or future periods of interest met that daily average wind speed threshold criteria.

Table 3-11. Monthly Historical Average and Future Projected Ranges over MCBCL for Critical Thresholds of Interest

Average Number of Days >90°F	Jan	Feb	Mar	Apr	May	June	Jul	Aug	Sept	Oct	Nov	Dec
Historical METDATA (1979–1999)	0.00	0.00	0.01	0.26	1.23	6.70	14.65	8.26	1.98	0.13	0.00	0.00
Future projected range (2026–2045)	0.00–0.01	0.00–0.18	0.00–0.21	0.00–2.16	1.54–7.20	9.75–18.81	17.92–29.80	11.42–24.58	2.23–13.16	0.00–1.69	0.00–0.02	0.00–0.01
Future projected range (2046–2065)	0.00–0.00	0.00–0.20	0.00–0.48	0.00–3.21	2.64–10.62	13.38–23.51	23.23–31.90	17.23–27.00	4.65–17.90	0.00–3.16	0.00–0.09	0.00–0.02
Future projected range (2081–2099)	0.00–0.01	0.00–1.78	0.00–2.07	0.00–9.24	5.94–22.71	18.38–31.52	27.94–33.98	22.56–30.40	10.21–28.48	0.00–10.24	0.00–0.50	0.00–0.13
Average Number of Days >100°F	**Jan**	**Feb**	**Mar**	**Apr**	**May**	**June**	**Jul**	**Aug**	**Sept**	**Oct**	**Nov**	**Dec**
Historical METDATA (1979–1999)	0.00	0.00	0.00	0.00	0.00	0.02	0.08	0.05	0.00	0.00	0.00	0.00
Future projected range (2026–2045)	0.00–0.00	0.00–0.00	0.00–0.00	0.00–0.02	0.00–0.20	0.00–1.05	0.00–1.79	0.00–2.00	0.00–0.50	0.00–0.00	0.00–0.00	0.00–0.00
Future projected range (2046–2065)	0.00–0.00	0.00–0.00	0.00–0.00	0.00–0.06	0.00–0.17	0.00–2.71	0.00–4.85	0.00–4.66	0.00–0.78	0.00–0.06	0.00–0.00	0.00–0.00
Future projected range (2081–2099)	0.00–0.00	0.00–0.17	0.00–0.16	0.00–0.59	0.00–2.79	0.00–12.44	0.00–18.45	0.00–19.17	0.00–7.32	0.00–0.43	0.00–0.00	0.00–0.00

(continued)

Table 3-11. Monthly Historical Average and Future Projected Ranges over MCBCL for Critical Thresholds of Interest (continued)

Average Number of Days <28°F	Jan	Feb	Mar	Apr	May	June	Jul	Aug	Sept	Oct	Nov	Dec
Historical METDATA (1979–1999)	7.95	5.68	1.75	0.08	0.00	0.00	0.00	0.00	0.00	0.01	1.56	6.45
Future projected range (2026–2045)	3.39–8.08	1.96–6.56	0.00–2.04	0.00–0.14	0.00–0.01	0.00–0.00	0.00–0.00	0.00–0.00	0.00–0.00	0.00–0.15	0.00–2.09	1.66–6.97
Future projected range (2046–2065)	1.04–7.08	0.00–5.93	0.00–1.56	0.00–0.18	0.00–0.00	0.00–0.00	0.00–0.00	0.00–0.00	0.00–0.00	0.00–0.09	0.00–1.14	0.00–5.57
Future projected range (2081–2099)	0.00–5.21	0.00–3.52	0.00–0.76	0.00–0.11	0.00–0.00	0.00–0.00	0.00–0.00	0.00–0.00	0.00–0.00	0.00–0.06	0.00–0.66	0.00–3.68
Average Number of Days <32°F	**Jan**	**Feb**	**Mar**	**Apr**	**May**	**June**	**Jul**	**Aug**	**Sept**	**Oct**	**Nov**	**Dec**
Historical METDATA (1979–1999)	12.90	9.40	4.55	0.44	0.00	0.00	0.00	0.00	0.00	0.23	4.02	10.51
Future projected range (2026–2045)	7.60–13.37	5.11–10.34	0.20–5.48	0.00–0.60	0.00–0.06	0.00–0.00	0.00–0.00	0.00–0.00	0.00–0.00	0.00–0.53	0.35–4.69	4.88–11.99
Future projected range (2046–2065)	4.89–12.46	2.19–10.14	0.00–4.38	0.00–0.45	0.00–0.04	0.00–0.00	0.00–0.00	0.00–0.00	0.00–0.00	0.00–0.36	0.00–3.21	2.12–9.95
Future projected range (2081–2099)	0.84–10.57	0.00–7.08	0.00–2.73	0.00–0.18	0.00–0.03	0.00–0.00	0.00–0.00	0.00–0.00	0.00–0.00	0.00–0.24	0.00–1.86	0.00–7.79

(continued)

Table 3-11. Monthly Historical Average and Future Projected Ranges over MCBCL for Critical Thresholds of Interest (continued)

Average Number of Days >0 Inches	Jan	Feb	Mar	Apr	May	June	Jul	Aug	Sept	Oct	Nov	Dec
Historical METDATA (1979–1999)	13.98	12.64	13.00	11.46	15.04	16.10	20.14	18.88	14.16	10.38	11.29	12.01
Future projected range (2026–2045)	11.77–16.99	10.71–15.33	9.72–16.55	9.21–15.04	13.30–19.15	14.03–19.67	18.83–23.54	17.43–23.15	12.14–18.71	8.64–14.36	9.22–15.31	10.02–14.31
Future projected range (2046–2065)	11.35–16.94	9.42–15.53	10.18–15.92	9.09–14.56	12.61–18.71	12.92–20.11	16.65–24.19	16.04–23.25	11.54–19.43	7.71–15.04	8.58–14.82	9.28–14.41
Future projected range (2081–2099)	10.62–16.41	8.66–15.47	9.06–15.93	7.87–14.12	10.31–19.72	12.09–20.51	14.70–25.63	13.96–25.29	10.80–21.12	7.23–16.00	7.25–17.12	8.23–14.72
Average Number of Days >1 Inch	**Jan**	**Feb**	**Mar**	**Apr**	**May**	**June**	**Jul**	**Aug**	**Sept**	**Oct**	**Nov**	**Dec**
Historical METDATA (1979–1999)	0.99	0.80	1.16	0.44	0.72	0.77	1.11	1.40	1.91	0.80	0.94	0.76
Future projected range (2026–2045)	0.58–1.63	0.43–1.32	0.74–1.81	0.07–0.84	0.22–1.31	0.15–1.39	0.48–2.16	0.32–2.71	1.19–2.68	0.32–1.30	0.60–1.37	0.41–1.29
Future projected range (2046–2065)	0.64–1.73	0.38–1.34	0.68–1.87	0.03–0.93	0.29–1.27	0.22–1.59	0.09–2.38	0.29–2.80	1.23–2.95	0.29–1.29	0.55–1.61	0.35–1.56
Future projected range (2081–2099)	0.68–2.01	0.48–1.50	0.60–2.03	0.07–0.89	0.15–1.41	0.09–1.74	0.09–2.67	0.00–3.02	0.97–3.27	0.21–1.48	0.62–1.70	0.46–1.65

(continued)

Table 3-11. Monthly Historical Average and Future Projected Ranges over MCBCL for Critical Thresholds of Interest (continued)

Average Number of Days <3 mph	Jan	Feb	Mar	Apr	May	June	Jul	Aug	Sept	Oct	Nov	Dec
Historical METDATA (1979–1999)	0.05	0.04	0.00	0.08	0.11	0.08	0.35	0.43	0.46	0.34	0.12	0.13
Future projected range (2026–2045)	0.00–0.72	0.00–0.88	0.00–0.77	0.00–0.74	0.00–1.29	0.00–1.40	0.00–1.20	0.00–1.01	0.00–1.36	0.00–1.62	0.00–1.33	0.00–1.39
Future projected range (2046–2065)	0.00–0.56	0.00–0.84	0.00–1.12	0.00–0.90	0.00–1.04	0.00–1.24	0.00–1.02	0.00–1.66	0.00–1.89	0.00–2.04	0.00–1.02	0.00–1.15
Future projected range (2081–2099)	0.00–0.70	0.00–0.91	0.00–0.95	0.00–0.96	0.00–1.41	0.00–1.16	0.00–1.41	0.00–1.70	0.00–2.12	0.00–2.86	0.00–1.81	0.00–1.07

Uncertainty of the Reduced Ensemble

A reduced ensemble of 24 downscaled models best represents the uncertainty and spread of the full distribution of the 76 downscaled climate projections. Based on the iterative process of selecting the reduced ensemble, the spread of the future uncertainty was best captured by using these 24 selected models. The annual average maximum temperature for the full distribution and the reduced ensemble are shown in **Figure 3-12**. The annual average minimum temperature for the full distribution and the reduced ensemble are shown in **Figure 3-13**. The annual total precipitation for the full distribution and the reduced ensemble is shown in **Figure 3-14**. It is important to note that the process of reducing the ensemble included all three variables at the same time to generate the ensemble. Thus, the spread of individual variables may not necessarily be reflected in the reduced ensemble at all time steps.

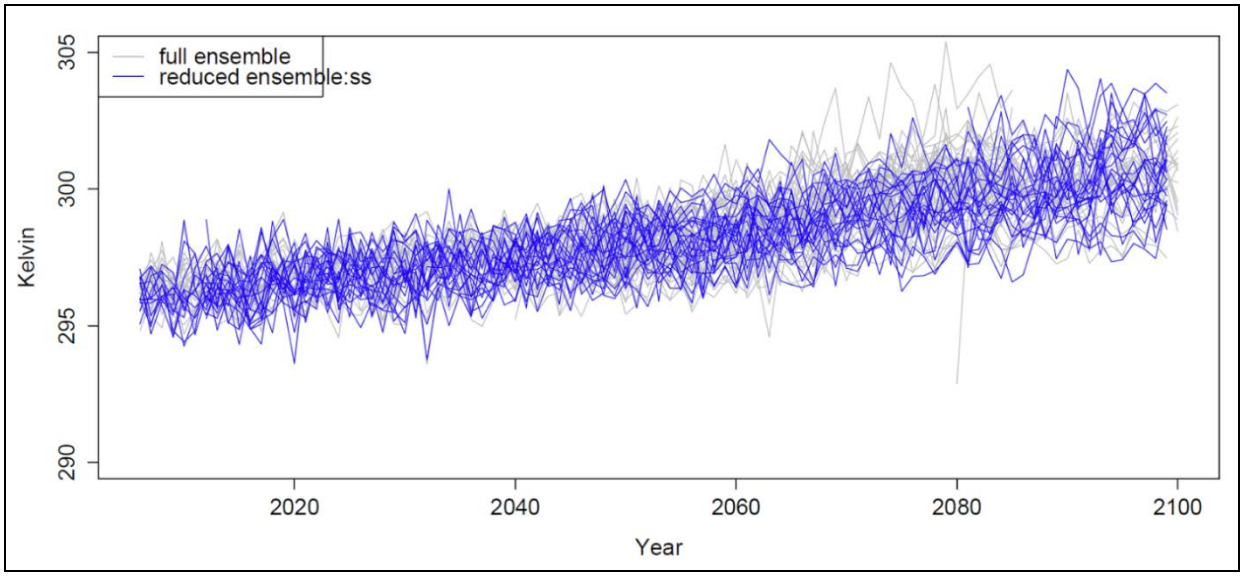

Figure 3-12. Spread of future uncertainty for annual average maximum temperature, with the full ensemble (76 members) in gray and the reduced ensemble (24 members) in blue.

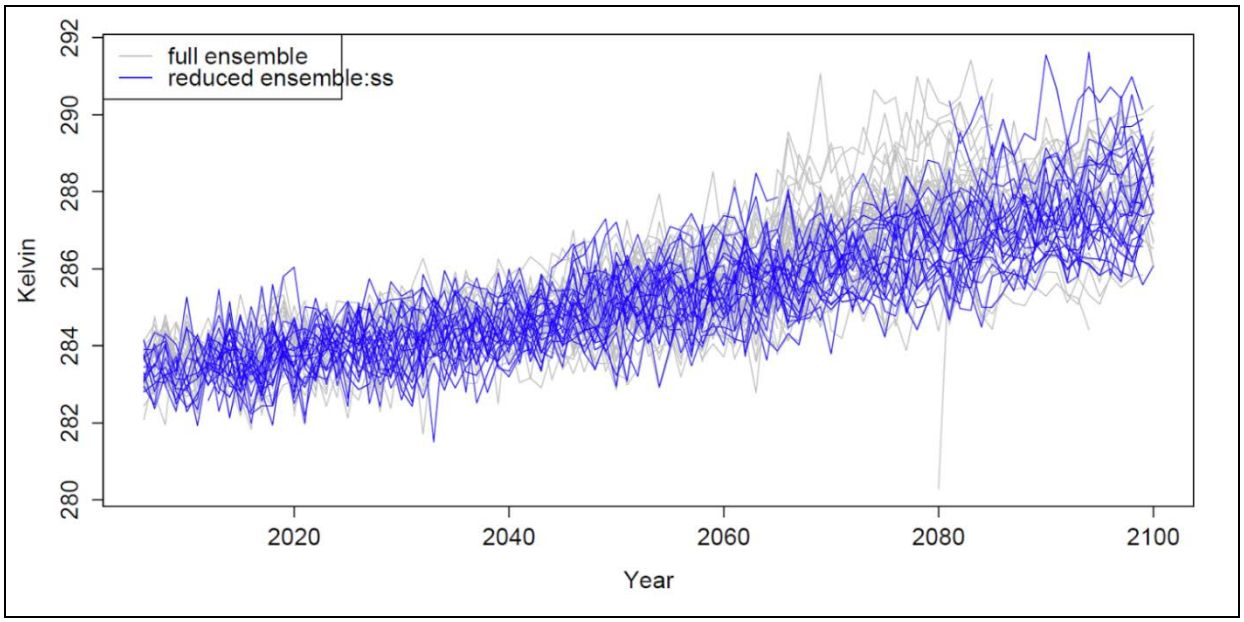

Figure 3-13. Spread of future uncertainty for annual average minimum temperature, with the full ensemble (76 members) in gray and the reduced ensemble (24 members) in blue.

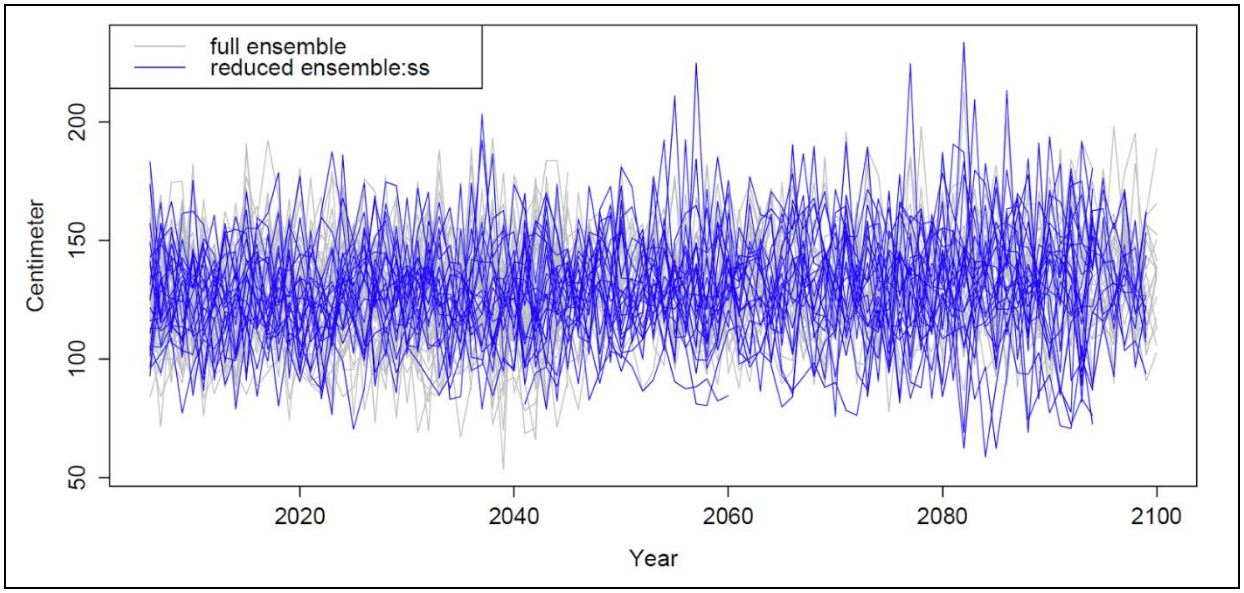

Figure 3-14. Spread of future uncertainty for annual total precipitation, with the full ensemble (76 members) in gray and the reduced ensemble (24 members) in blue.

Task 3—Historical Evaluation of Downscaled Climate Projections

Evaluation of Downscaled Projections

The DCERP2 critical thresholds of interest listed in **Table 3-4** were evaluated in this study. However, the average number of days with daily average wind speed greater than 40 mph was not included in this analysis because none of the days in the historical or future periods of

interest met that daily average wind speed threshold criteria. In addition, MACA was the only downscaled data set in the reduced ensemble that contains wind speed data and thus, only 13 out of the 24 members were analyzed for the wind speed critical thresholds.

It is important to examine these errors in conjunction with the historical occurrences of the number of days associated with each threshold as shown in **Figures 3-6 through 3-11** and **Table 3-11**. As an example, the average number of days with precipitation >1 inch occurred less frequently (**Figures 3-11**) and had lower RMSE (**Figure 3-20**) than the average number of days with precipitation >0 inches (**Figures 3-10 and 3-19**).

Maximum Temperature Critical Thresholds

Both maximum temperature critical thresholds exhibited similar trends over time, with higher RMSE values and larger differences among the models during summer months (**Figures 3-15 and 3-16**) when the most occurrences have historically occurred (**Figures 3-6 and 3-7**). For the average number of days with maximum temperature greater than 100°F, the ensemble average of the climate model baselines had the lowest RMSE for all months except for July, which had one model (inmcm4) with RMSE that was 0.01 days lower than the ensemble average of the baselines. A similar temporal pattern was observed with the critical threshold of greater than 90°F, with higher values and larger differences among models during the warm season. For this greater than 90°F threshold, the ensemble average of the climate model baselines had lower RMSE than most models during all months except July, August, and September. This threshold exhibited larger errors during summer as compared to the average number of days greater than 100°F, which is most likely due to the higher frequency of occurrence of days above 90°F, as shown in **Figures 3-6 and 3-7**.

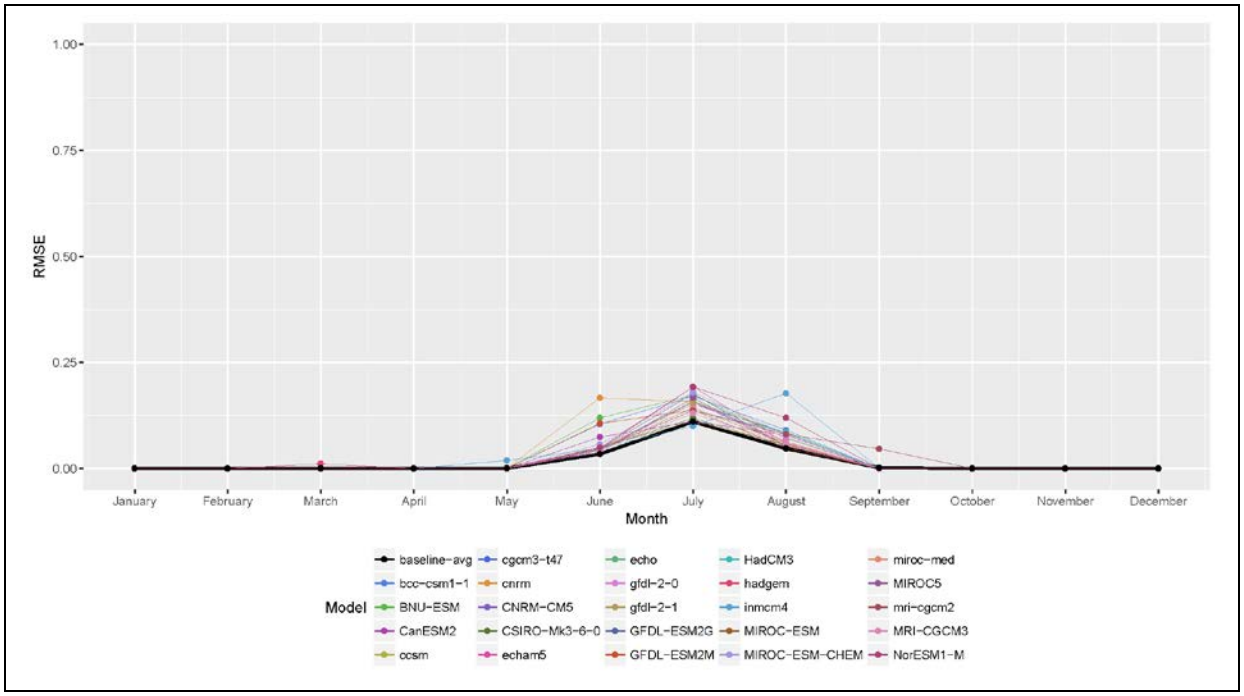

Figure 3-15. RMSE for climate model baseline (1979–1999): Average number of days with maximum temperature greater than 100°F.

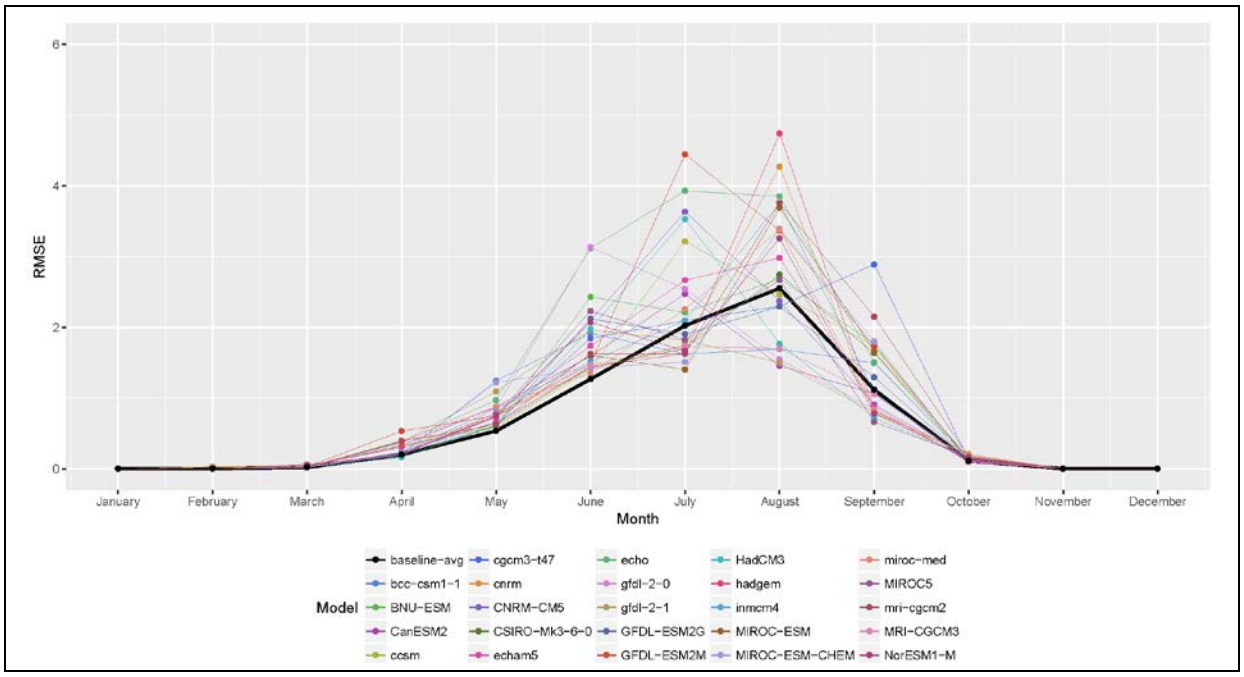

Figure 3-16. RMSE for climate model baseline (1979–1999): Average number of days with maximum temperature greater than 90°F.

For both maximum temperature critical thresholds, the annual sums of monthly RMSE were ranked from lowest (1) to highest (25) in **Table 3-12**. In the rank column of this table, green colors represent models in the lower tercile (e.g., ranked in the top eight), yellow colors indicate models in the middle tercile (e.g., ranks 9 through 16), and red colors represent models in the upper tercile (e.g., ranked between 17 and 25). The 25 models include the 24 reduced ensemble members plus one "model" that is the ensemble average of the baselines. For the two maximum temperature thresholds, the ensemble average of the baselines ranked in the top three out of 25 total models. In addition, a higher number of MACA models were ranked in the top 10 as compared with SERAP models.

Table 3-11. Annual Sum of Monthly RMSE for Maximum Temperature Critical Levels

Model	Downscaling Data Set	Number of Days >90°F	Rank
baseline-avg	ALL	7.84	3
HadCM3	CLAREnCE10	8.93	10
MRI-CGCM3	MACA	7.02	1
CanESM2	MACA	7.94	4
bcc-csm1-1	MACA	8.34	5
CSIRO-Mk3-6-0	MACA	8.48	6
GFDL-ESM2G	MACA	8.55	7
MIROC5	MACA	8.57	8
NorESM1-M	MACA	8.91	9
MIROC-ESM	MACA	9.53	14

Model	Downscaling Data Set	Number of Days >100°F	Rank
baseline-avg	ALL	0.20	1
HadCM3	CLAREnCE10	0.27	11
MIROC-ESM	MACA	0.22	2
CSIRO-Mk3-6-0	MACA	0.22	3
MRI-CGCM3	MACA	0.23	4
MIROC5	MACA	0.26	7
CNRM-CM5	MACA	0.26	8
CanESM2	MACA	0.26	10
GFDL-ESM2G	MACA	0.28	13
GFDL-ESM2M	MACA	0.29	17

(continued)

Table 3-12. Annual Sum of Monthly RMSE for Maximum Temperature Critical Levels (continued)

Model	Downscaling Data Set	Number of Days >90°F	Rank
inmcm4	MACA	9.66	16
MIROC-ESM-CHEM	MACA	9.72	17
CNRM-CM5	MACA	10.11	20
BNU-ESM	MACA	10.17	22
GFDL-ESM2M	MACA	12.47	24
gfdl-2-1	SERAP	7.79	2
miroc-med	SERAP	9.30	11
echam5	SERAP	9.39	12
gfdl-2-0	SERAP	9.41	13
cnrm	SERAP	9.55	15
hadgem	SERAP	9.76	18
ccsm	SERAP	9.93	19
cgcm3-t47	SERAP	10.16	21
mri-cgcm2	SERAP	10.36	23
echo	SERAP	13.92	25

Model	Downscaling Data Set	Number of Days >100°F	Rank
MIROC-ESM-CHEM	MACA	0.32	20
inmcm4	MACA	0.34	21
NorESM1-M	MACA	0.36	22
BNU-ESM	MACA	0.36	23
bcc-csm1-1	MACA	0.37	24
ccsm	SERAP	0.25	5
miroc-med	SERAP	0.25	6
echam5	SERAP	0.26	9
gfdl-2-0	SERAP	0.27	12
cgcm3-t47	SERAP	0.28	14
gfdl-2-1	SERAP	0.28	15
echo	SERAP	0.29	16
hadgem	SERAP	0.31	18
mri-cgcm2	SERAP	0.31	19
cnrm	SERAP	0.38	25

Minimum Temperature Critical Thresholds

For both minimum temperature critical level variables, the ensemble average of the baselines outperformed approximately 50% of the individual models in terms of RMSE during cool season months as shown in **Figures 3-17 and 3-18**. Both minimum temperature critical thresholds also exhibited similar trends over time, with the highest overall error during January and December, which is when most occurrences are likely to occur. The spread of RMSE for average number of days below 32°F was higher than that of the error for the number of days below 28°F.

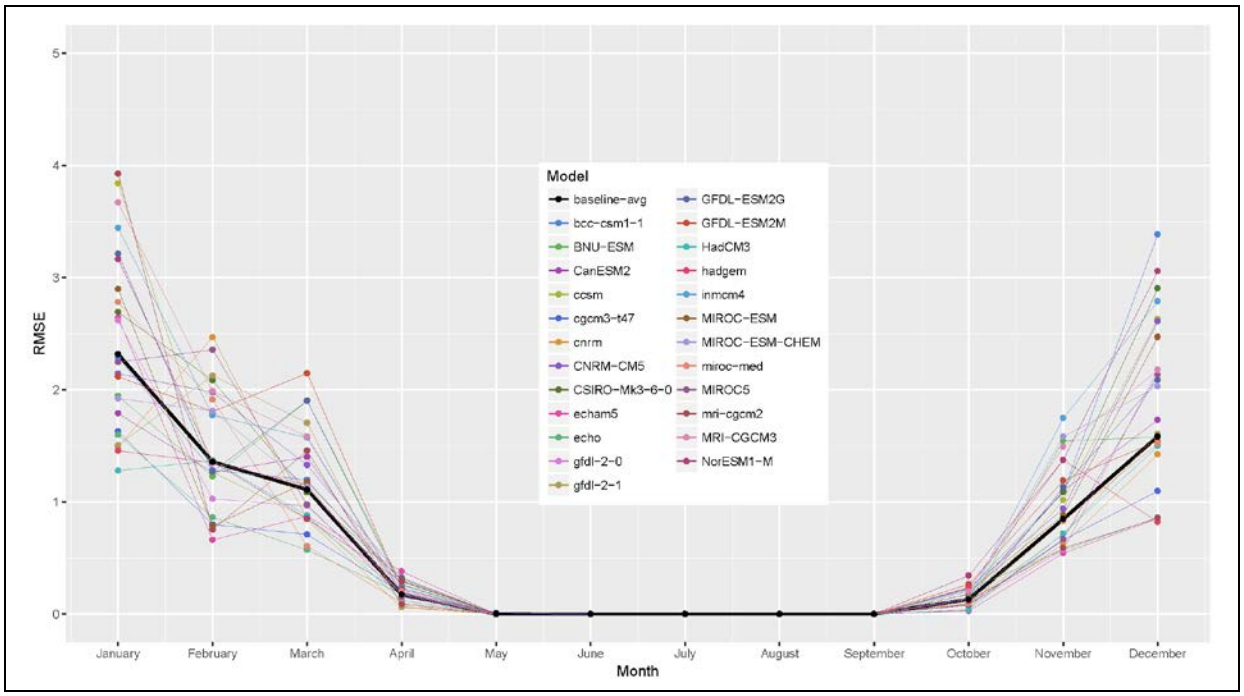

Figure 3-17. RMSE for climate model baseline (1979–1999): Average number of days with minimum temperature less than 28°F.

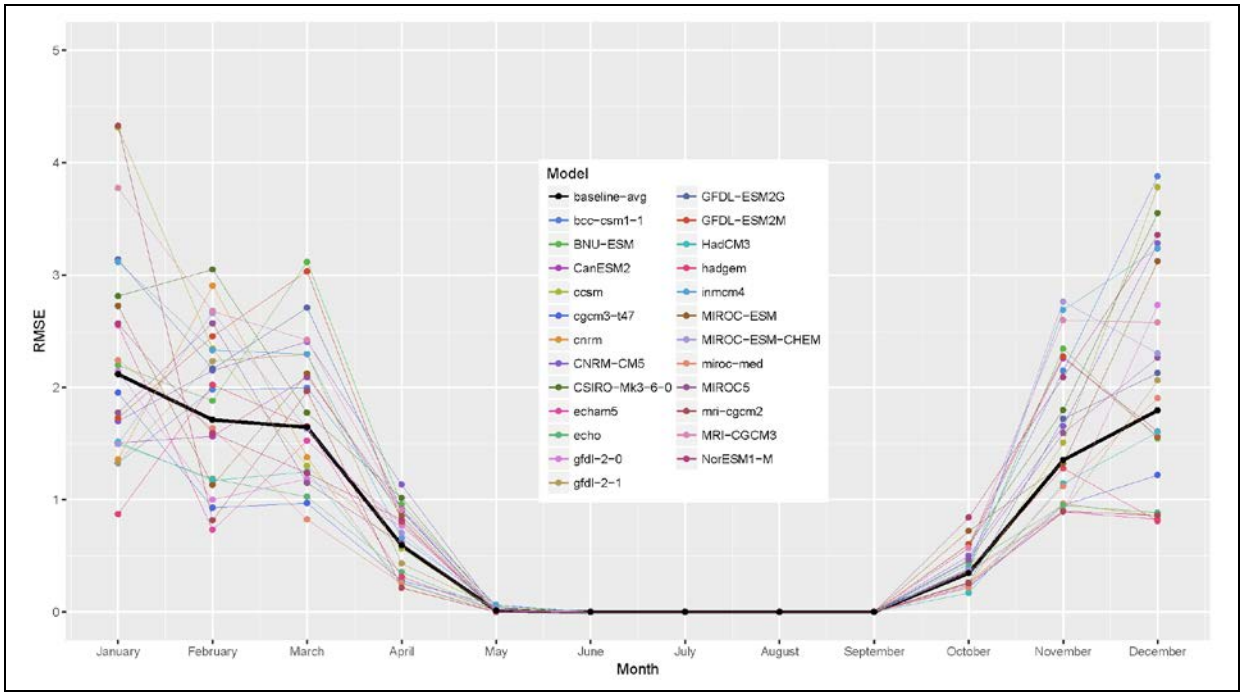

Figure 3-18. RMSE for climate model baseline (1979–1999): Average number of days with minimum temperature less than 32°F.

For both minimum temperature critical thresholds, the annual sums of monthly RMSE were ranked from lowest (1) to highest (25) in **Table 3-13**. In the rank column of this table, green colors represent models in the lower tercile (e.g., ranked in the top eight), yellow colors indicate

models in the middle tercile (e.g., ranks 9 through 16), and red colors represent models in the upper tercile (e.g., ranked between 17 and 25). The 25 models include the 24 reduced ensemble members plus one "model" that is the ensemble average of the baselines.

The only model in the reduced ensemble from the CLAREnCE10 downscaled data set (HadCM3) ranked in the top three out of 25 models for these two minimum temperature thresholds. In addition, most of the SERAP models had lower error than the majority of the MACA models. For both minimum temperature thresholds, the ensemble average of the baselines ranked in the top 10 out of 25 models.

Table 3-12. Annual Sum of Monthly RMSE for Minimum Temperature Critical Levels

Model	Downscaling Data Set	Number of Days <32°F	Rank
baseline-avg	ALL	9.57	10
HadCM3	CLAREnCE10	7.11	3
MIROC5	MACA	10.44	12
CanESM2	MACA	10.57	13
MIROC-ESM-CHEM	MACA	11.95	14
MIROC-ESM	MACA	11.99	15
BNU-ESM	MACA	12.45	16
GFDL-ESM2M	MACA	12.45	17
NorESM1-M	MACA	12.50	18
bcc-csm1-1	MACA	12.67	19
CNRM-CM5	MACA	12.83	20
GFDL-ESM2G	MACA	13.02	21
CSIRO-Mk3-6-0	MACA	14.60	23
inmcm4	MACA	14.77	24
MRI-CGCM3	MACA	15.54	25
echo	SERAP	6.33	1
cgcm3-t47	SERAP	6.57	2
hadgem	SERAP	7.33	4
echam5	SERAP	7.55	5
cnrm	SERAP	7.93	6
miroc-med	SERAP	8.19	7
gfdl-2-0	SERAP	9.09	8
mri-cgcm2	SERAP	9.34	9
gfdl-2-1	SERAP	9.65	11
ccsm	SERAP	14.06	22

Model	Downscaling Data Set	Number of Days <28°F	Rank
baseline-avg	ALL	7.52	7
HadCM3	CLAREnCE10	5.91	3
CanESM2	MACA	7.62	8
BNU-ESM	MACA	8.55	13
MIROC5	MACA	8.62	14
MIROC-ESM	MACA	8.72	15
MIROC-ESM-CHEM	MACA	8.80	16
GFDL-ESM2M	MACA	9.29	17
CNRM-CM5	MACA	9.56	18
bcc-csm1-1	MACA	9.72	19
GFDL-ESM2G	MACA	9.92	21
CSIRO-Mk3-6-0	MACA	10.34	22
NorESM1-M	MACA	10.44	23
MRI-CGCM3	MACA	11.31	24
inmcm4	MACA	11.65	25
echo	SERAP	4.87	1
cgcm3-t47	SERAP	5.18	2
echam5	SERAP	5.98	4
hadgem	SERAP	6.55	5
cnrm	SERAP	7.00	6
gfdl-2-0	SERAP	7.63	9
mri-cgcm2	SERAP	7.79	10
gfdl-2-1	SERAP	7.82	11
miroc-med	SERAP	7.85	12
ccsm	SERAP	9.84	20

Precipitation Critical Thresholds

The model spread and magnitude of the monthly RMSE values had no discernable trend over time for each precipitation critical threshold (**Figures 3-19 and 3-20**). The ensemble average of the baselines consistently had less error than approximately 50% of the individual models for the critical threshold of precipitation greater than 0 inches. In addition, larger spread among the models was observed for the average number of days greater than 0 inches of precipitation as compared with the critical threshold of greater than 1 inch of precipitation, especially during cooler months (October through March).

The only dynamically downscaled model in the reduced ensemble (HadCM3) had anomalously high error for critical threshold greater than 1 inch during April, May, June, and July as compared to most of the other models, with the RMSE during June and July being approximately two times larger than most of the other models. For this greater than 1 inch threshold, the ensemble average of the baselines had lower error than approximately 50% of the individual models for each month except during the warm months, which was primarily because of the high error values of the HadCM3 model during late spring into summer.

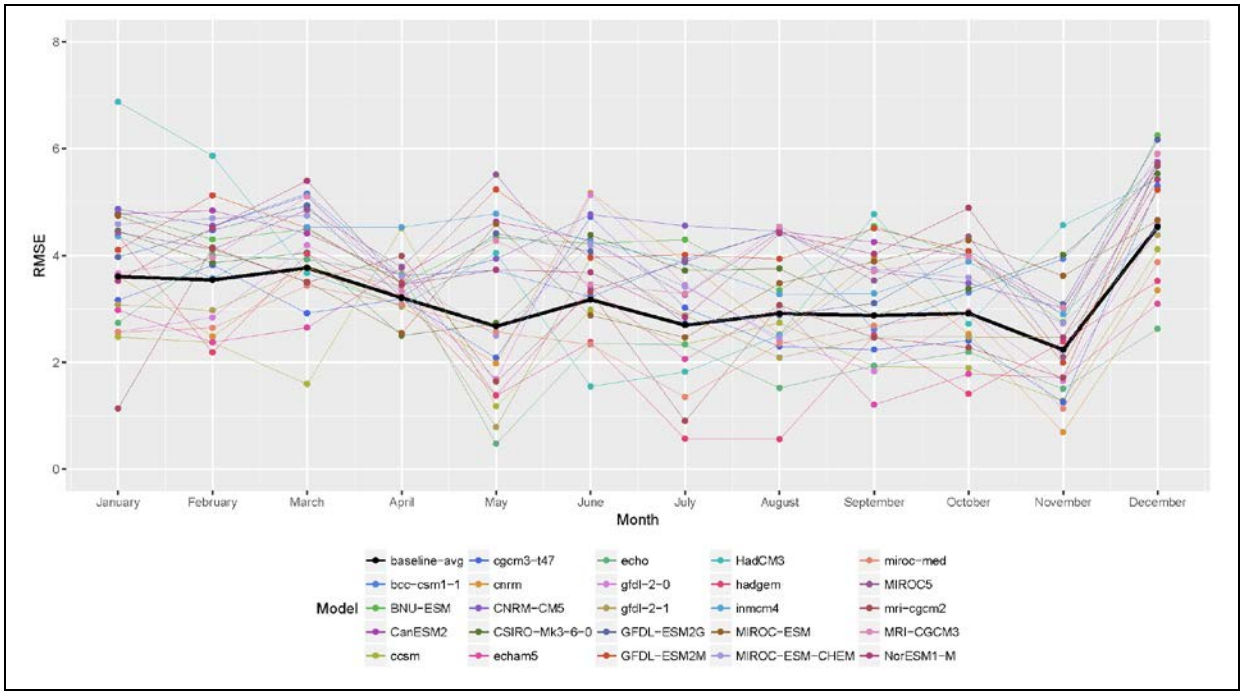

Figure 3-19. RMSE for climate model baseline (1979–1999): Average number of days with precipitation greater than 0 inches.

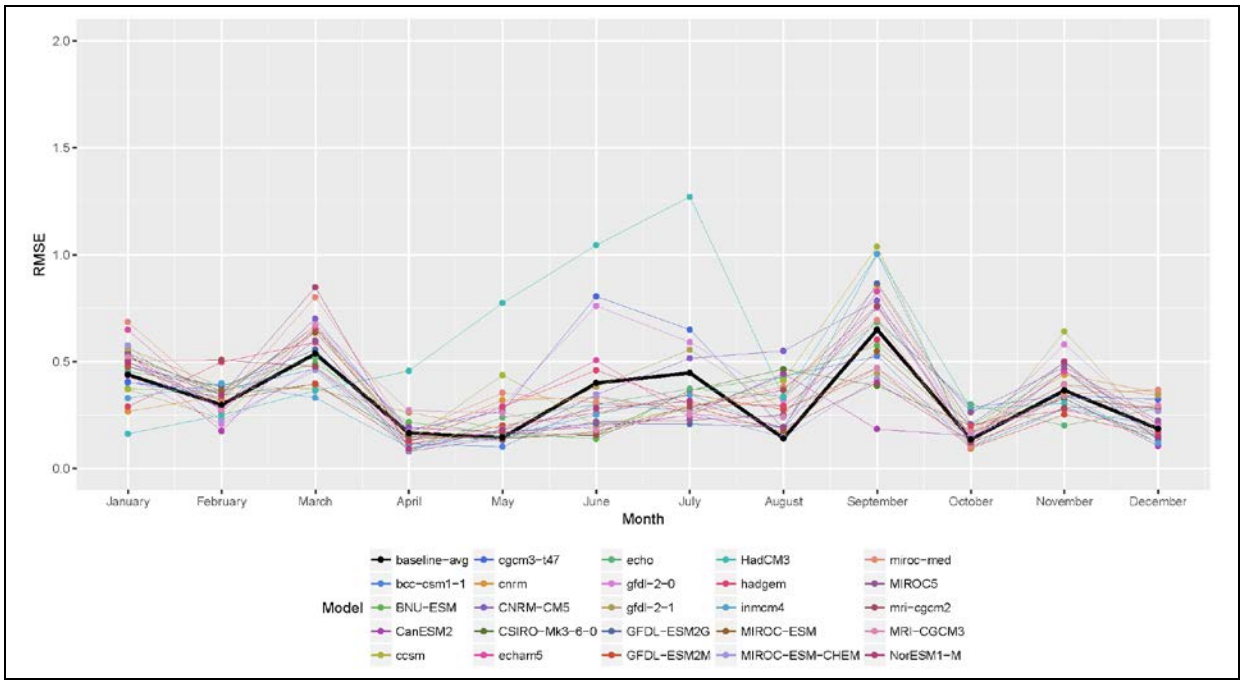

Figure 3-20. RMSE for climate model baseline (1979–1999): Average number of days with precipitation greater than 1 inch.

For both precipitation critical thresholds, the annual sums of monthly RMSE were ranked from lowest (1) to highest (25) in **Table 3-14**. In the rank column of this table, green colors represent models in the lower tercile (e.g., ranked in the top eight), yellow colors indicate models in the middle tercile (e.g., ranks 9 through 16), and red colors represent models in the upper tercile (e.g., ranked between 17 and 25). The 25 models include the 24 reduced ensemble members plus one "model" that is the ensemble average of the baselines.

In general, SERAP had less error for simulating non-zero precipitation, and MACA performed better with higher amounts of precipitation (>1 inch). The dynamically downscaled model (HadCM3) did not perform well for either of the precipitation thresholds, especially precipitation greater than one inch when it ranked 25th out of 25 models. In addition, the ensemble average of the baselines ranked in the top 11 out of 25 models.

Table 3-13. Annual Sum of Monthly RMSE for Precipitation Critical Thresholds

Model	Downscaling Data Set	Number of Days >0 inches	Rank
baseline-avg	ALL	38.17	11
HadCM3	CLAREnCE10	46.89	15
MIROC-ESM	MACA	44.80	12
MIROC-ESM-CHEM	MACA	44.83	13
CSIRO-Mk3-6-0	MACA	45.27	14

Model	Downscaling Data Set	Number of Days >1 inch	Rank
baseline-avg	ALL	3.91	9
HadCM3	CLAREnCE10	6.39	25
GFDL-ESM2M	MACA	3.37	1
CanESM2	MACA	3.39	2
MIROC-ESM-CHEM	MACA	3.46	3

(continued)

Table 3-14. Annual Sum of Monthly RMSE for Precipitation Critical Thresholds (continued)

Model	Downscaling Data Set	Number of Days >0 inches	Rank
GFDL-ESM2G	MACA	47.14	16
inmcm4	MACA	47.77	17
MRI-CGCM3	MACA	48.23	18
NorESM1-M	MACA	48.37	19
bcc-csm1-1	MACA	49.13	20
MIROC5	MACA	50.07	21
GFDL-ESM2M	MACA	50.20	22
BNU-ESM	MACA	50.83	23
CanESM2	MACA	51.17	24
CNRM-CM5	MACA	51.62	25
hadgem	SERAP	28.55	1
echo	SERAP	29.27	2
ccsm	SERAP	29.43	3
echam5	SERAP	29.50	4
miroc-med	SERAP	30.95	5
mri-cgcm2	SERAP	33.85	6
gfdl-2-1	SERAP	34.76	7
cgcm3-t47	SERAP	36.43	8
gfdl-2-0	SERAP	36.63	9
cnrm	SERAP	37.01	10

Model	Downscaling Data Set	Number of Days >1 inch	Rank
bcc-csm1-1	MACA	3.56	4
CSIRO-Mk3-6-0	MACA	3.59	5
inmcm4	MACA	3.66	6
MIROC-ESM	MACA	3.79	7
BNU-ESM	MACA	3.91	8
NorESM1-M	MACA	3.93	10
MRI-CGCM3	MACA	4.00	11
GFDL-ESM2G	MACA	4.02	12
MIROC5	MACA	4.06	13
CNRM-CM5	MACA	4.67	21
mri-cgcm2	SERAP	4.06	14
hadgem	SERAP	4.10	15
echo	SERAP	4.16	16
gfdl-2-1	SERAP	4.32	17
cnrm	SERAP	4.50	18
echam5	SERAP	4.56	19
ccsm	SERAP	4.66	20
miroc-med	SERAP	4.81	22
gfdl-2-0	SERAP	4.93	23
cgcm3-t47	SERAP	5.14	24

Wind Speed Critical Thresholds

As shown in **Figure 3-21**, the highest monthly RMSE values occurred during August for the critical threshold of daily average wind speed less than 3 mph. The ensemble average of the baselines consistently outperformed approximately 50% of the individual models in terms of RMSE. For most months, the variance among models for this wind speed threshold was approximately the same (1 day). August and September were exceptions, the latter of which was due to the RMSE of a MACA model (GFDL-ESM2M) being anomalously lower by almost 1 day as compared with the remainder of the models. Results for the critical threshold of average number of days with daily average wind speed greater than 40 mph were not included because none of the days in the period of interest (1979–1999) met that daily average wind speed threshold criterion.

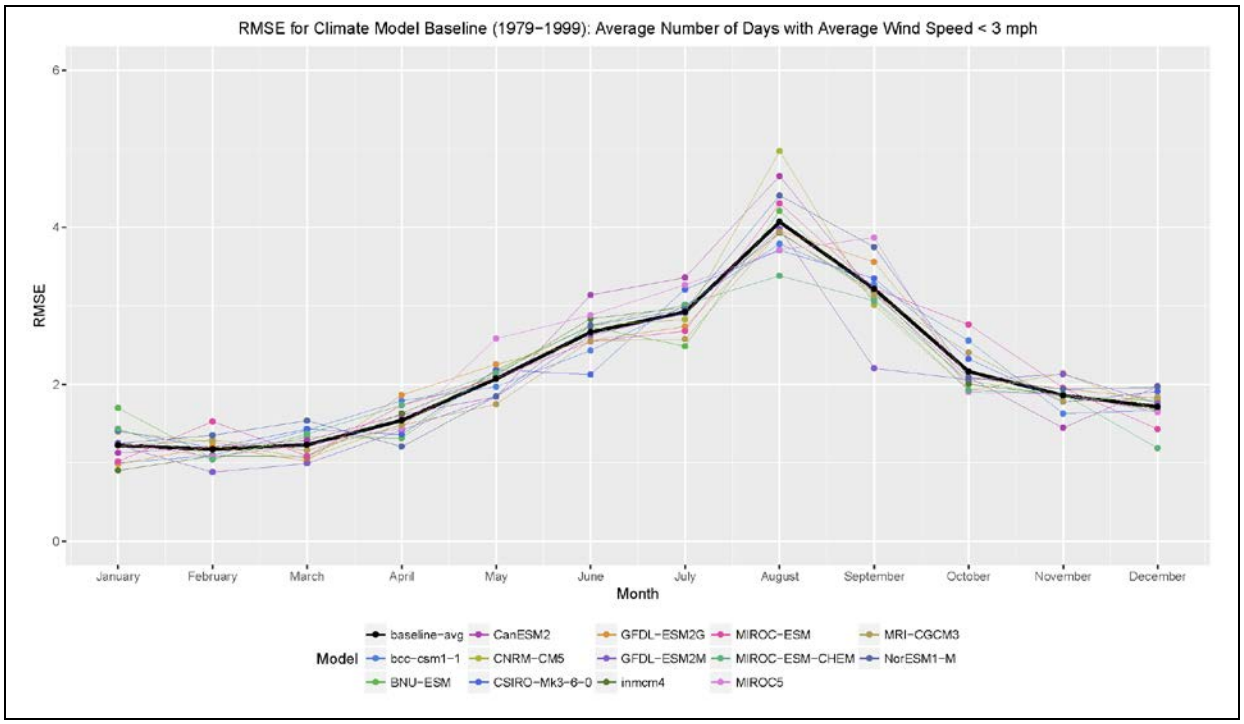

Figure 3-21. RMSE for climate model baseline (1979–1999): Average number of days with daily average wind speed less than 3 mph.

Ensemble Accuracy versus Individual Accuracy

The historical accuracy of the reduced ensemble and each individual model member was evaluated for the critical levels of interest (average number of days with temperature >90°F, >100°F, <28°F, and <32°F; precipitation >0 inches and >1 inch; and daily average wind speed <3 mph and >40 mph) over the MCBCL domain (**Figure 3-2**). For the climate model baseline equally weighted ensemble average, accuracy varied monthly and had lower RMSE than at least 50% of the individual model members annually for any given threshold (**Figures 3-15 through 3-21**). No single model consistently outperformed the ensemble average for all metrics, which is consistent with previous work by Chaturvedi et al. (2012) and Wootten et al. (2014). However, it is important to note that non-linear interactions in climate models and downstream process-based ecological models cannot be properly represented by an ensemble average. Therefore, when running this type of process-based ecological model, it is recommended to use all individual downscaled GCM members of the entire reduced ensemble to fully capture the range of possibilities of a future climate (e.g., **Table 3-11**). After the simulation of this ecological model is performed, similar metrics (e.g., average, standard deviations) can be applied to that model's output to capture the range of future outcomes.

Downscaling Uncertainty

The downscaling uncertainty results were based on two experiments: (1) a continuous time series with common GCMs and emissions scenarios (IDEAL), and (2) a discrete time series with GCMs and emissions scenarios that are not necessarily shared in common among all of the

downscaled data sets (ALLDATA)—the latter of which investigated the influence of different time periods on the representation of uncertainty in the downscaled climate projection data sets.

Downscaling uncertainty was not the dominant source (defined as greater than 50% of the total contribution) in the IDEAL experiment at Fort Bragg or MCBCL for projections of the decadal mean of the annual average daily high temperature (**Figure 3-22**). For this variable, the dominant sources of uncertainty changed throughout the century in the IDEAL experiment. Natural variability was the dominant source of uncertainty in earlier years; GCM uncertainty became dominant around 2020–2040, followed by scenario uncertainty toward the end of the century. These results agree with the findings from Hawkins and Sutton (2009).

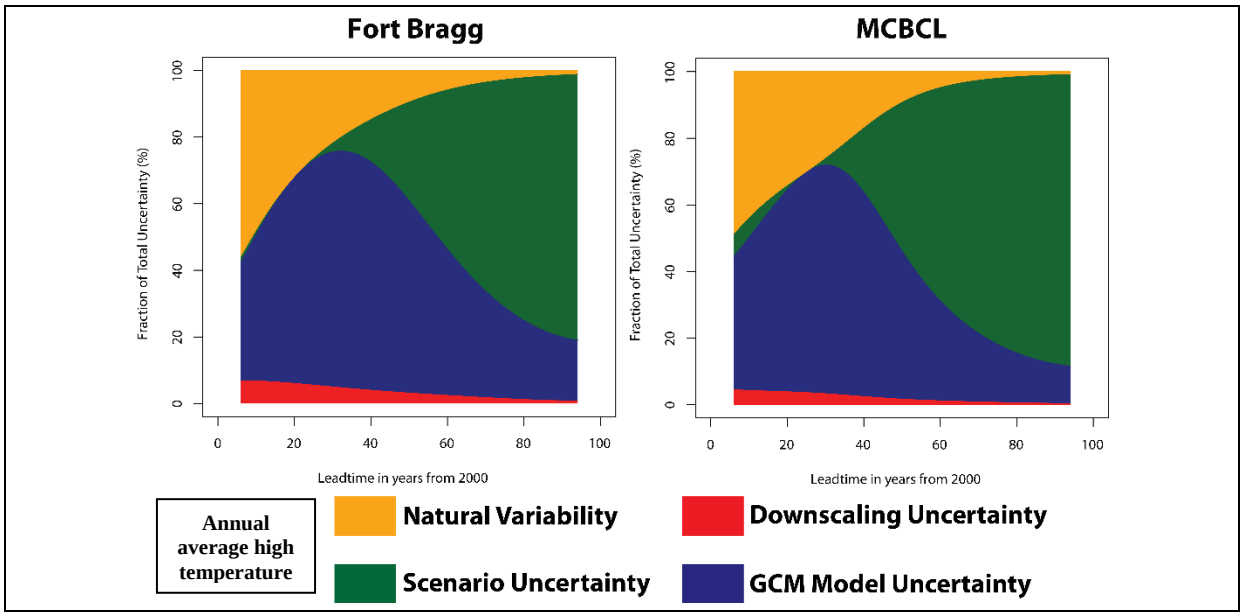

Figure 3-22. Percent contribution to the total uncertainty from each source of uncertainty across time for Fort Bragg (left) and MCBCL (right) for projections of the decadal mean of the annual average daily high temperature.

For the decadal mean of the annual number of days with high temperature greater than 95°F in the IDEAL experiment, downscaling was a dominant source of uncertainty at MCBCL from 2020 to 2030 and was at least 10% of the contribution at Fort Bragg for most time periods (**Figure 3-23**). In addition, for this variable and experiment, scenario uncertainty was the dominant source at both locations by the end of the century.

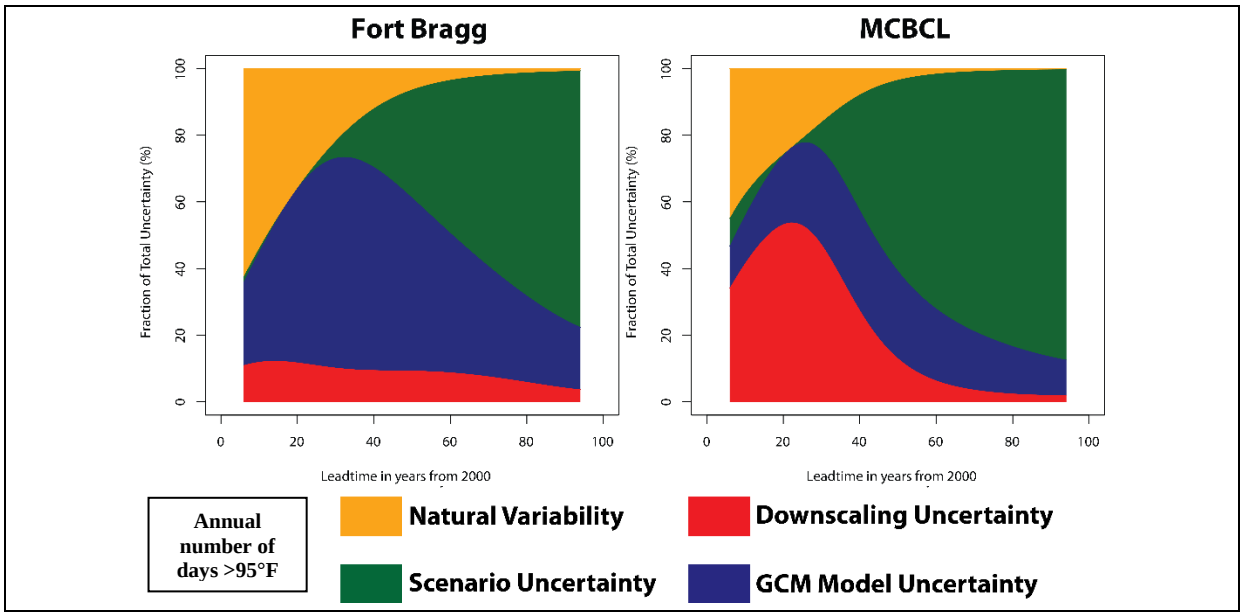

Figure 3-23. Percent contribution to the total uncertainty from each source of uncertainty across time for Fort Bragg (left) and MCBCL (right) for projections of the decadal mean of the annual number of days with high temperature greater than 95°F.

The IDEAL experiment results for projections of the decadal mean of the annual number of days with low temperature below 32°F are shown in **Figure 3-24**. For this variable and experiment, the pattern of dominant sources throughout time was similar to that of annual average daily high temperature (**Figure 3-22**) except the downscaling uncertainty for number of days below freezing reached approximately 10% of the total uncertainty at MCBCL around 2030.

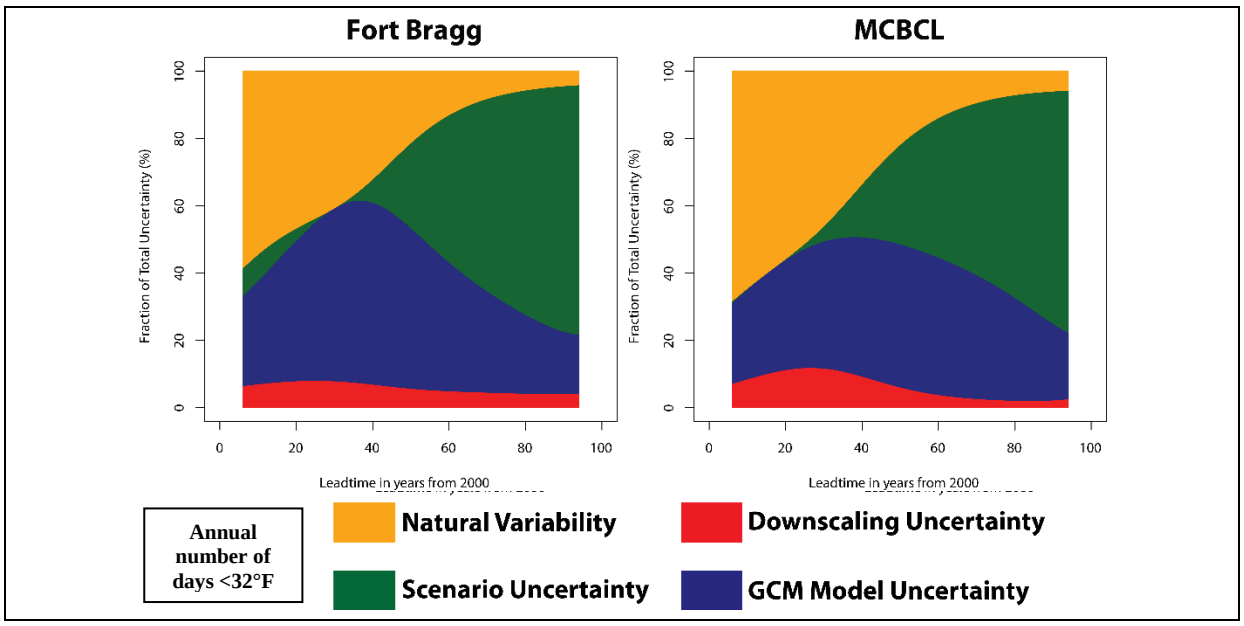

Figure 3-24. Percent contribution to the total uncertainty from each source of uncertainty across time for Fort Bragg (left) and MCBCL (right) for projections of the decadal mean of the annual number of days with low temperature less than 32°F.

Although scenario uncertainty was the dominant source of uncertainty by the end of the century for all three temperature variables (**Figures 3-22 through 3-24**), it was not the dominant source of uncertainty for either of the precipitation variables during any time period (**Figures 3-25 and 3-26**). By the end of the century, GCM uncertainty was the dominant source for projections of the decadal mean of the annual total precipitation at Fort Bragg and MCBCL during the IDEAL experiment (**Figure 3-25**). For this same experiment, similar results occurred for projections of the decadal mean of the annual number of days with precipitation greater than 1 inch, with GCM uncertainty as the dominant (largest) source at MCBCL (Fort Bragg) by end of century (**Figure 3-26**).

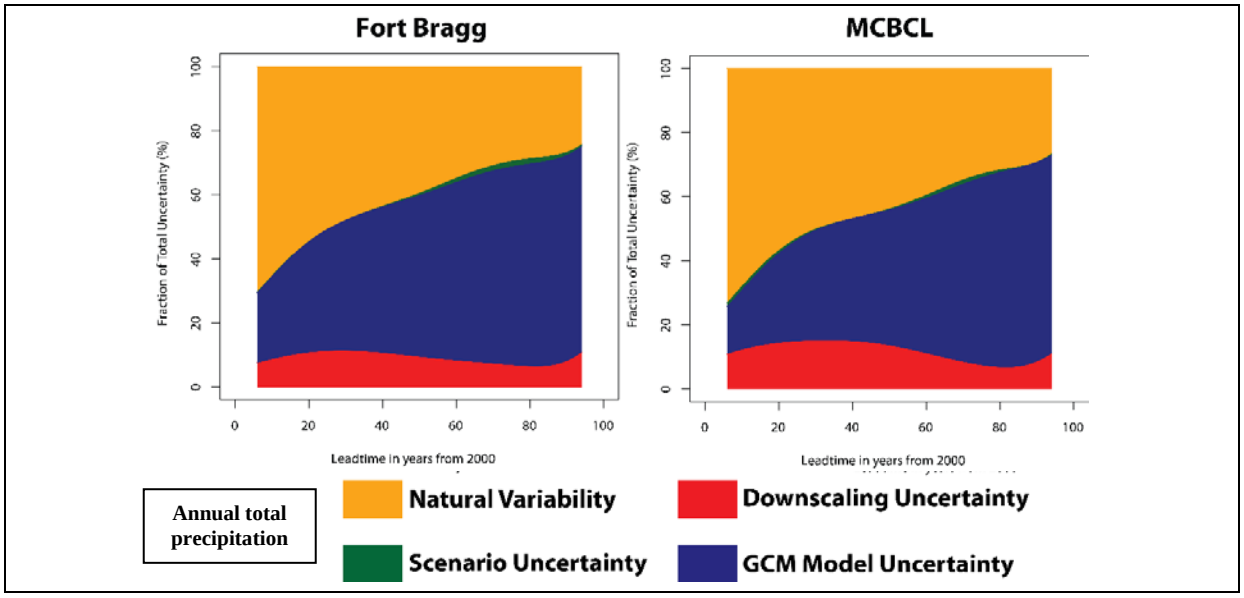

Figure 3-25. Percent contribution to the total uncertainty from each source of uncertainty across time for Fort Bragg (left) and MCBCL (right) for projections of the decadal mean of the annual total precipitation.

For both precipitation variables, downscaling uncertainty was not the dominant source of uncertainty during any of the time periods in the IDEAL experiment at Fort Bragg or MCBCL. However, for both of these variables, uncertainty due to downscaling contributed to about 10% to 20% of the total uncertainty at both locations throughout the entire time period (**Figures 3-25 and 3-26**).

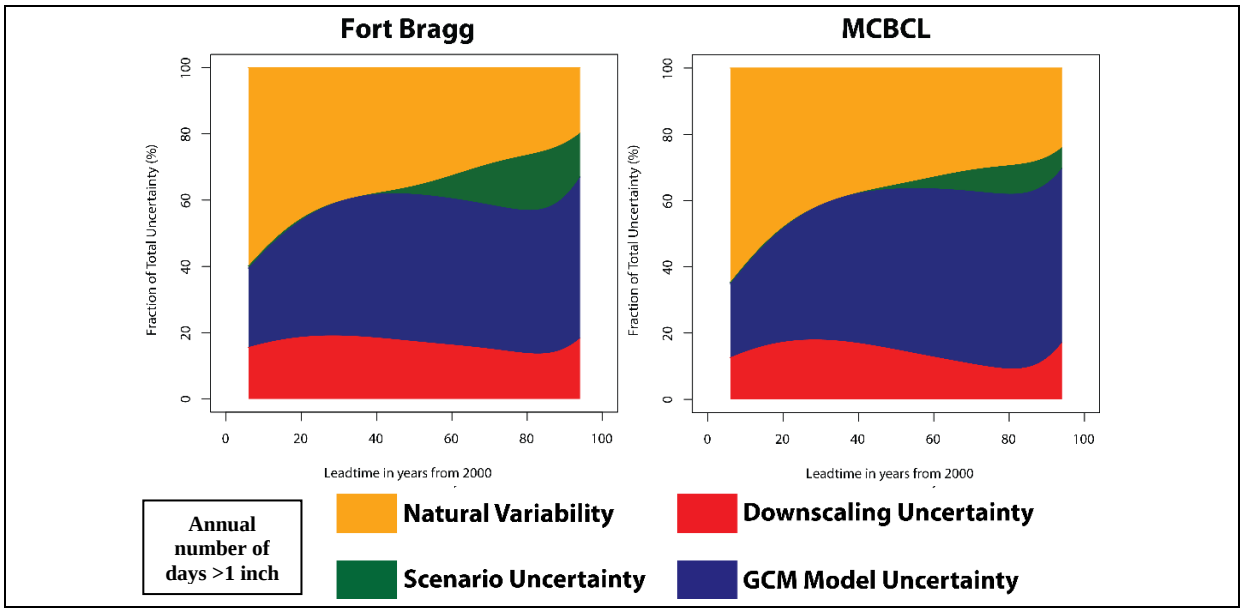

Figure 3-26. Percent contribution to the total uncertainty from each source of uncertainty across time for Fort Bragg (left) and MCBCL (right) for projections of the decadal mean of the annual number of days with precipitation greater than 1 inch.

Overall, the IDEAL experiment findings suggest that, although downscaling was not the dominant source of uncertainty for most of the temperature and precipitation variables, it was often a significant source (approximately between 10% and 20% of the total uncertainty) in the study region of DCERP2 Research Project CC-1. Therefore, particularly for projections of extreme temperature and precipitation, multiple downscaling techniques should be considered.

The results of the ALLDATA experiment (not shown) indicated that the contribution of different sources of uncertainty changed during time periods that were not common between the different downscaled climate projection data sets. The resulting impact assessments that use these downscaled projections with uncommon time periods may have higher uncertainty due to the lack of downscaling techniques represented. Therefore, there were two recommendations for impact assessments to adequately represent all sources of uncertainty: (1) studies should utilize multiple downscaled climate projections, and (2) independent downscaled GCMs with common time periods should be used.

Task 4—Influence of Climate Data Scale

The four traits considered critical for RCWs were evaluated at MCBCL and Fort Bragg. The trait that had the strongest relationship with a climate variable at each location is shown in **Table 3-15**. In addition, the highest ranked spatial resolution for each trait and location is shown in this table. The native 4-km resolution of the climate data did not provide the strongest relationship to any of the traits at either location.

Table 3-14. Related Climate Variables and Highest Ranked Spatial Resolution for Each Location and Trait

Trait	MCBCL		Fort Bragg	
	Highest Ranked Climate Variable	**Highest Ranked Resolution (km)**	**Highest Ranked Climate Variable**	**Highest Ranked Resolution (km)**
Lay date	Number of days with minimum temperature <5°C in March	10	Mean maximum temperature in April	15
Nest survival	Variance in precipitation in January	10	Number of days with maximum temperature >35°C in June	30
Local recruitment	Mean temperature during the previous May	50	Mean maximum temperature during the previous April	40
Number fledged	Sum of the total precipitation in May	50	Number of days with minimum temperature <5°C in April	50

Climate data at 10-km resolution had the strongest relationship with RCW lay date and nest survival at MCBCL. In contrast, the 15- and 30-km resolution had the strongest relationship with lay date and nest survival, respectively, at Fort Bragg. At MCBCL, the highest ranked climate variables for lay date and nest survival may be influenced by the proximity to the Atlantic Ocean (e.g., sea breeze effect). Thus, finer resolution climate data at 10 km were required at MCBCL since these local climate influences can be better represented at this resolution as compared to coarser resolutions (e.g., 30 or 50 km). Fort Bragg is further inland with fewer coastal influences and thus, the climate variable with the strongest relationships to RCW nest survival did not change as quickly over short distances. This could explain why the coarser climate data resolution (30 km) had a stronger relationship with nest survival at Fort Bragg as compared with the 10-km resolution at MCBCL.

Overall, for lay date, the strength of the relationship with the climate variables increased with decreasing resolution (<20 km) at both locations (**Figure 3-27**). The two locations did not share the same pattern for nest survival (**Figure 3-28**), with the strongest relationship at higher resolutions at MCBCL (<40km), decreasing rapidly from 50 km to 30 km. Conversely, at Fort Bragg, the relationship was the strongest at coarser resolutions between 30 km and 50 km.

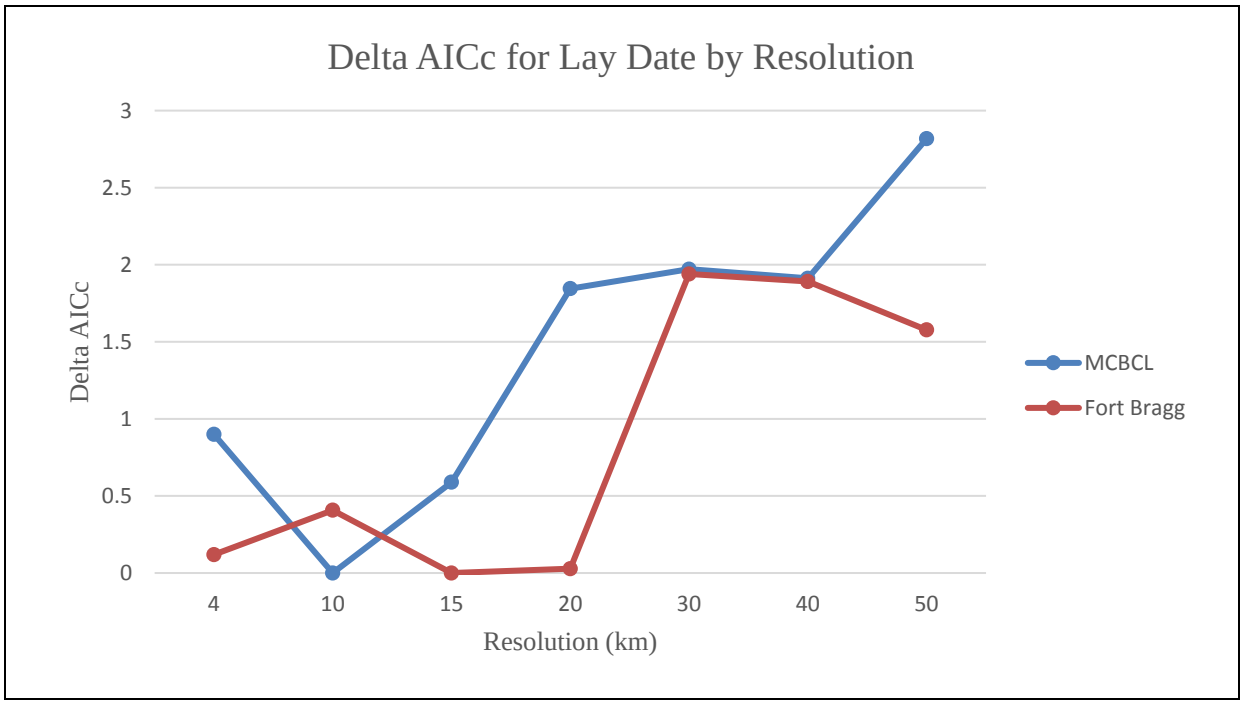

Figure 3-27. Delta AICc by spatial resolution for each location.

Values at zero have the strongest relationship with the climate variables for lay date.

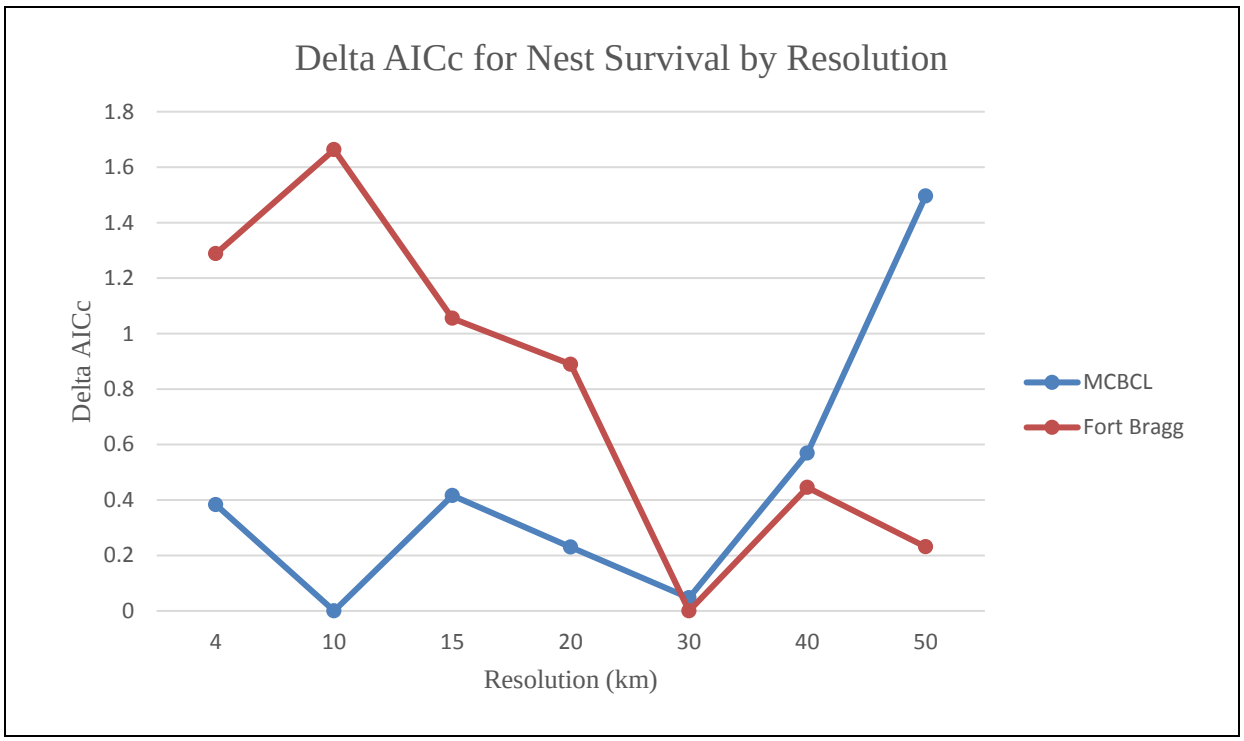

Figure 3-28. Delta AICc by spatial resolution for each location. Values at zero have the strongest relationship with the climate variables for RCW nest survival.

As shown in **Table 3-15**, climate data at coarser spatial resolutions (e.g., 40 and 50 km) had the strongest relationship with local recruitment and number fledged at MCBCL and Fort Bragg. In general, the relationship between climate data and recruitment strengthened with decreasing spatial resolution (>15 km) at Fort Bragg (**Figure 3-29**). In contrast, there was little change in the strength of this relationship at MCBCL for resolutions between 4 km and 40 km. However, the strongest relationship between climate data and recruitment at this location existed at a spatial resolution of 50 km. For number fledged, there was a stronger overall relationship at MCBCL than at Fort Bragg when considering the delta AICc pattern across all spatial resolutions (**Figure 3-30**). However, both locations showed the strongest relationships between climate data and number of fledglings at the 50-km resolution.

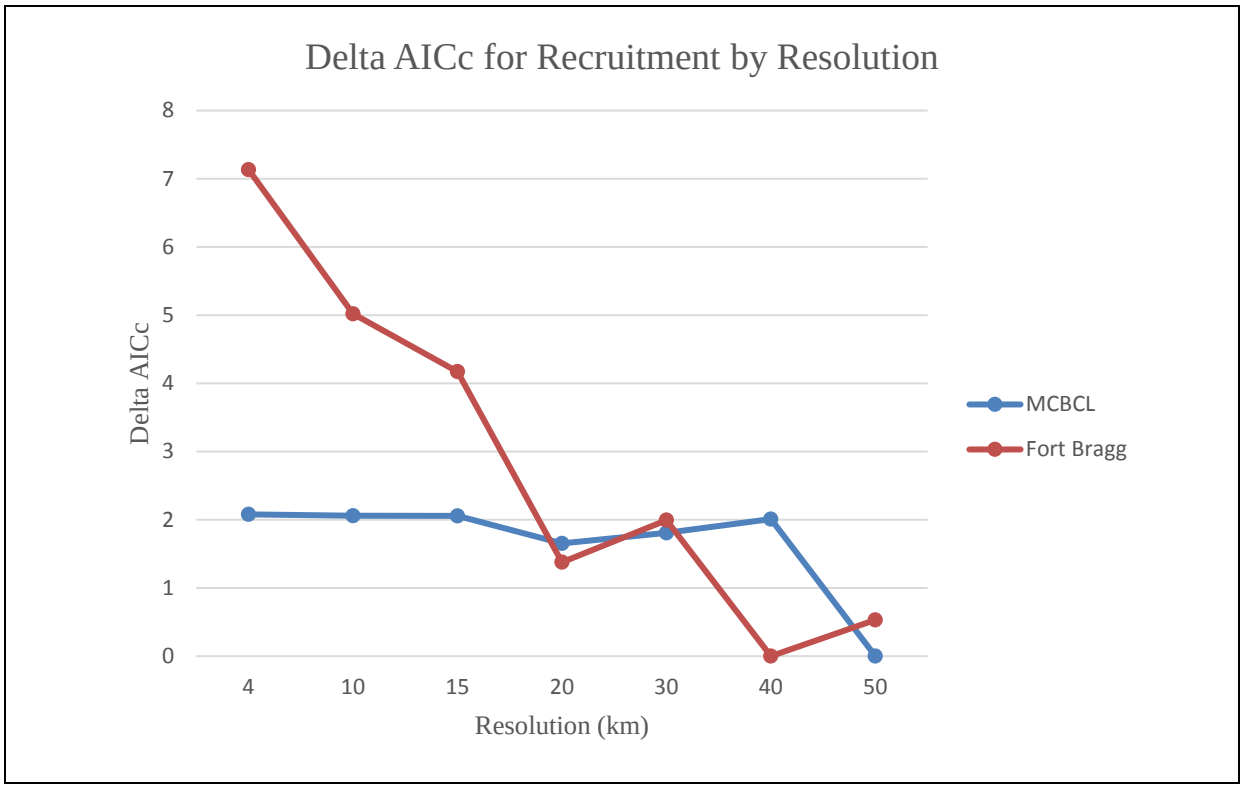

Figure 3-29. Delta AICc by spatial resolution for each location. Values at zero have the strongest relationship with the climate variables for local RCW recruitment.

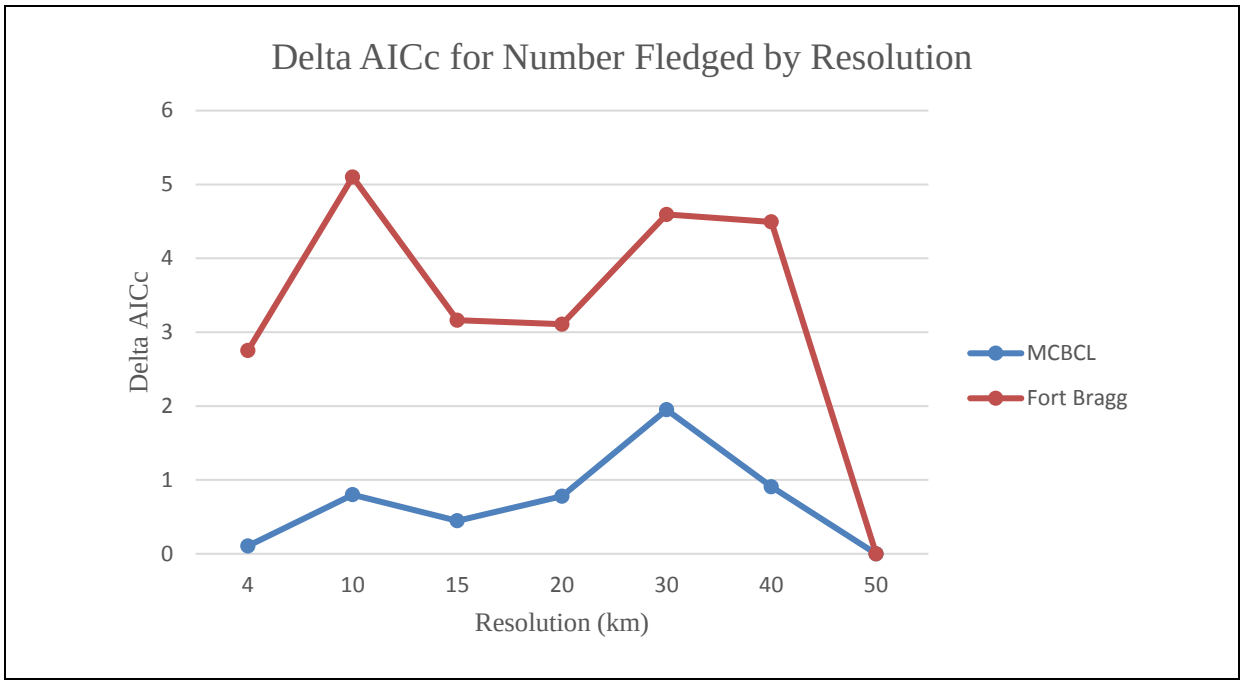

Figure 3-30. Delta AICc by spatial resolution for each location. Values at zero have the strongest relationship with the climate variables for the number of RCWs fledged.

Overall, the finest resolution (4 km) climate data did not have the strongest relationship with any of the RCW demographic variables. These results disagreed with previous studies, such as Franklin et al. (2013) and Trivedi et al. (2008), that suggest a spatial resolution of 4 km or finer is required for climate impact assessments of certain species. However, those previous studies focused on mountainous regions where climate variables can change rapidly over short distances. In Eastern North Carolina, the topography changes less rapidly than mountainous regions. In addition, the climate variables that influence RCWs do not typically change rapidly over short distances. However, there is more variation closer to the coast, and the land–sea boundary can cause changes in temperature and precipitation.

It is important to note the differences in spatial resolution of the strongest climate data relationships with the RCW demographics. The lay date and nest survival had the strongest relationship with finer resolutions (10 km, 15 km, and 30 km) while local recruitment and the number RCWs fledged had the strongest relationship with coarser resolutions (40 km and 50 km). One possible explanation is that RCW lay date and nest survival are more strongly affected by climate conditions in the tree cavity, such as temperature and the resulting incubation duration required to keep the birds' eggs viable. In comparison, the number fledged and recruitment are more likely to be influenced by conditions in the wider landscape (e.g., available food supply or predator activity) than within the local area.

Conclusions and Implications for Future Research and Implementation

Research Project CC-1 provided a historical gridded data set and an ensemble of downscaled future climate projections to guide the assessment of climate impacts and development of visualizations by the other DCERP2 modules. Those assessments will inform installation

managers who are interested in how ecosystems are impacted by climate (e.g., changes in flow regime or forested area). In addition, the Research Project CC-1 Team developed new methodologies to answer research questions posed for DCERP2, addressed additional research questions in climate science, and fulfilled the needs of stakeholder groups seeking to use future climate projections.

The critical threshold analysis revealed that the average number of days with temperature greater than 90°F and 100°F are both projected to increase by end of the century. In contrast, the average number of days with temperature below 28°F and 32°F are projected to decrease by 2100. The future values for both precipitation critical thresholds (>0 inches and >1 inch) ranged from fewer days to more days per month as compared to the historical average. Thus, the downscaled climate models in the reduced ensemble did not agree about whether the number of days for these precipitation thresholds will increase or decrease in the future. The average number of days per month with daily average wind speed below 3 mph is projected to stay approximately the same or slightly increase by the end of the century.

A historical evaluation of the climate model baselines was performed over MCBCL for the critical levels of interest (e.g., average number of days with temperature >90°F, >100°F, <28°F, and <32°F; precipitation >0 inches and >1 inch; and daily average wind speed <3 mph and >40 mph). None of the days in the historical (or future periods) of interest met the daily average wind speed threshold criteria of greater than 40 mph and thus, that wind speed threshold was not included in this analysis. For most of these thresholds, the error in the average number of days per month for any individual model was less than 5 days. However, it is important to examine these errors in conjunction with the historical occurrences of the number of days associated with each threshold. As an example, the average number of days with precipitation >1 inch occurred less frequently and had lower RMSE than the average number of days with precipitation >0 inches. In addition, using multiple downscaling methods is recommended since no single downscaling method consistently performed better than any other method. Also, no single model consistently outperformed the ensemble average of the climate model baselines for these critical levels of interest. This finding is consistent with studies by Chaturvedi et al. (2012) and Wootten et al. (2014). It is important to note that non-linear interactions in climate models and downstream process-based ecological models cannot be properly represented by an ensemble average. Therefore, when running this type of process-based ecological model, it is recommended to use all individual downscaled GCM members of the entire reduced ensemble to fully capture the range of possibilities of a future climate. After the simulation of this ecological model is performed, similar metrics (e.g., average, standard deviations) can be applied to that model's output to capture the range of future outcomes.

The practice of downscaling GCMs is important for studying local or regional changes in climate. The contribution of downscaling to the total uncertainty in climate projections had not been previously evaluated in the Southeastern United States. Therefore, the Research Project CC-1 Team created a methodology to examine the contribution from downscaling uncertainty. The contribution of different sources of uncertainty changed through time when using multiple downscaled climate projection data sets that did not contain common time periods. Downscaling techniques can be a significant source of uncertainty (approximately 10% to 20% of the total uncertainty) for future projections of precipitation at MCBCL and Fort Bragg throughout time and the dominant source of uncertainty (greater than 50% of the total uncertainty) for projections

of maximum temperature greater than 95°F at MCBCL around 2020–2030. Therefore, impact assessments and planning efforts that require information from climate projections should include more than one downscaling technique and have independent downscaled GCMs with common time periods to adequately represent all sources of uncertainty. It is important to note that impact variables, such as streamflow or species distribution, tend to have a non-linear relationship with climate variables (e.g., Jin et al., 2005). Thus, the 10% to 20% contribution of downscaling to the total uncertainty of the climate projections might translate to a higher or lower percentage of contribution for future projections of impact variables.

Since downscaled climate projection data sets often use the same GCMs and downscaling can be a significant source of uncertainty, it was necessary to consider GCM independence when developing the DCERP2 ensemble of future climate projections. It is important to note that similar analyses should be performed in other regions of the United States because the dependence relationships in other regions of the country could be different. In addition, DCERP2 ecosystem modules identified that using all available downscaled climate projections (76 members) was not feasible because of the large size of the ensemble. Thus, a methodology was developed to create an ensemble of projections with fewer members. This reduced ensemble (24 members) reflected the range of uncertainty in the future projections.

The Research Project CC-1 Team partnered with the Terrestrial Module researchers to study the effects of climate data scale on life traits of RCWs at MCBCL and Fort Bragg. No single climate data scale was ideal for all RCW traits (e.g., egg lay date, recruitment) at both locations. The modeling of some traits was improved with higher resolutions of climate data (e.g., <30 km for lay date and nest survival) while other traits were better represented by coarser resolutions (e.g., >40 km for local recruitment and number fledged). These results were contrary to previous studies in mountainous regions (e.g., Franklin et al. [2013]; Trivedi et al. [2008]), which recommended the use of finer spatial resolutions (<4 km) for climate impact assessments. Therefore, further research is warranted to assess the ideal spatial resolution for other ecological impact assessments in coastal regions.

Response to Research Questions

1. Which downscaling techniques are appropriate to address changes in variables and critical levels of interest to the DCERP research modules?

According to the clustering results in Task 2, the downscaling techniques used to create the MACA, SERAP, and CLAREnCE10 data sets were appropriate to address changes in variables of interest to DCERP2 research modules: annual average minimum temperature, annual average maximum temperature, and annual total precipitation. The reduced ensemble—containing three downscaling techniques—was selected to maximize independence of the downscaled GCMs in the ensemble and capture the uncertainty in future projections.

A historical evaluation of the climate model baselines of MACA, SERAP, and CLAREnCE10 models over MCBCL was performed for the critical levels of interest (average number of days with temperature >90°F, >100°F, <28°F, and <32°F; precipitation >0 inches and >1 inch; and daily average wind speed <3 mph and >40 mph). Based on this error analysis, no single downscaling method consistently performed better than other methods. For most thresholds, the

error in the average number of days per month for any individual model was less than 5 days. However, it is important to examine these errors in conjunction with the historical occurrences of the number of days associated with each threshold. As an example, the average number of days with precipitation >1 inch occurred less frequently and had lower RMSE than the average number of days with precipitation >0 inches.

2. How does the historical accuracy of an ensemble of downscaled climate projections compare to the accuracy of the individual downscaled projections in eastern North Carolina?

The historical accuracy of the reduced ensemble and each individual model member was evaluated for the critical levels of interest (average number of days with temperature >90°F, >100°F, <28°F, and <32°F; precipitation >0 inches and >1 inch; and daily average wind speed <3 mph and >40 mph) over the MCBCL domain. For the climate model baseline equally weighted ensemble average, accuracy varied monthly, and it performed better than at least 50% of the individual model members annually for any given threshold. In addition, no single model consistently outperformed the ensemble average of the climate model baselines for all the critical thresholds identified by DCERP2. However, non-linear interactions in climate models and downstream process-based ecological models cannot be properly represented by an ensemble average. Therefore, when running this type of process-based ecological model, it is recommended to use all individual downscaled GCM members of the entire reduced ensemble to fully capture the range of possibilities of a future climate. After the simulation of this ecological model is performed, similar metrics (e.g., average, standard deviations) can be applied to that model's output to capture the range of future outcomes.

3. At what point does adding more downscaled projections to an ensemble no longer influence the uncertainty of the projections?

Using the clustering method developed in Task 2, the climate projections for 76 models were analyzed for variables of interest (annual average minimum temperature, annual average maximum temperature, and annual total precipitation) and grouped by similarity. Spread and uncertainty were captured by the 24 individual models shown in the analysis. Including more model members in the ensemble (beyond those 24) did not appear to substantially change the ensemble spread and uncertainty.

Findings with Implications for Future Base Management

Due to the large volume of data, using all available downscaled climate projections is challenging for users, such as those within DoD installations. The ensemble in this study contained 24 model members (reduced from 76 members), which is a set of projections that captured the range of future uncertainty for MCBCL. This reduction in the amount of data is more feasible for DoD to use for adaptation planning, impact assessments, and decision making. The methodology for reducing an ensemble of climate projections can be implemented at other installations and in similar contexts for other species, local hydrology, and habitat evolution.

The influence of climate data on ecological processes was evaluated, including simulation of the life history traits of the RCW. Although future climate projections seemed to affect RCW

demographic variables, installation managers should also consider other influential factors (e.g., food supply, landscape change, predators) that may have stronger impacts on RCW management.

It is important for long-term installation management to consider future climate projections based upon multiple downscaling techniques and downscaled GCMs that are independent. Overall, installation managers should consider a range of future climate scenarios in their decision-making processes. In addition, applications of the research conducted during Research Project CC-1 should be reassessed periodically (e.g., 5 to 10 years) to incorporate new downscaled climate projection data sets.

Literature Cited

Abatzoglou, J.T. 2011. Development of gridded surface meteorological data for ecological applications and modeling. *International Journal of Climatology 33*(1):121–131.

Abatzoglou, J.T., and T.J. Brown. 2012. A comparison of statistical downscaling method suited for wildfire applications. *International Journal of Climatology 32*:720–780.

Anderson, D.R. 2008. *Model-Based Inference in the Life Sciences: A Primer on Evidence*. Springer: New York, NY.

Argüeso D., J.P. Evans, A.J. Pitman, and A. Di Luca. 2015. Effect of city expansion on heat stress under climate change conditions. *PLoS ONE 10*:1–19. doi: 10.1371/journal.pone.0117066

Basso, B., D.W. Hyndman, A.D. Kendall, P.R. Grace, and G.P. Robertson. 2015. Can impacts of climate change and agricultural adaptation strategies be accurately quantified if crop models are annually re-initialized? *PLoS ONE 10*:1–12. doi: 10.1371/journal.pone.0127333

Benestad, R.E., I. Hanssen-Bauer, and D. Chen. 2008. *Empirical-Statistical Downscaling*. World Scientific Publishing. 228 pages.

Benestad, R.E. 2003. What can present climate models tell us about climate change? *Climatic Change 59*:311–331. doi:10.1023/A:1024876611259

Brekke, L. B.L. Thrasher, E.P. Maurer, and T. Pruitt. 2013. *Downscaled CMIP3 and CMIP5 Climate Projections: Release of Downscaled CMIP5 Climate Projections, Comparison with Preceding Information, and Summary of User Needs*. U.S. Department of the Interior, Bureau of Reclamation, Technical Service Center, Denver, CO. 116 pages. Available at http://gdo-dcp.ucllnl.org/downscaled_cmip_projections/techmemo/downscaled_climate.pdf

Burnham, K.P., and D.R. Anderson. 2002. *Model Selection and Multimodel Inference: A Practical Information–Theoretic Approach*. Springer: New York, NY.

Carter, L.M., J.W. Jones, L. Berry, V. Burkett, J.F. Murley, J. Obeysekera, P.J. Schramm, and D. Wear. 2014. Southeast and the Caribbean. Pp. 396–417, Chapter 17 in *Climate Change Impacts in the United States: The Third National Climate Assessment*. Edited by Melillo, J.M., T.C. Richmond, and G.W. Yohe. U.S. Global Change Research Program. doi:10.7930/J0NP22CB

Chaturvedi, R.K., J. Joshi, M. Jayaraman, G. Bala, and N.H. Ravindranath. 2012. Multi-model climate change projections for India under representative concentration pathways. *Current Science 103*(7):791–802.

Chen, J., F.P. Brissette, and R. Leconte. 2011. Uncertainty of downscaling method in quantifying the impact of climate change on hydrology. *Journal of Hydrology 401*:190–202. doi: 10.1016/j.jhydrol.2011.02.020

Christensen, J.H., B. Hewitson, A. Busuioc, A. Chen, X. Gao, I. Held, R. Jones, R.K. Kolli, W.-T. Kwon, R. Laprise, V. Magaña Rueda, L. Mearns, C.G. Menéndez, J. Räisänen, A. Rinke, A. Sarr, and P. Whetton. 2007. Regional climate projections. In *Climate Change 2007: The Physical Science Basis. Contribution of Working Group I to the Fourth Assessment Report of the Intergovernmental Panel on Climate Change*. Edited by Solomon, S., D. Qin, M. Manning, Z. Chen, M. Marquis, K.B. Averyt, M. Tignor, and H.L. Miller. Cambridge University Press: Cambridge, United Kingdom, and New York, NY.

Daly, C., M. Halbleib, J.I. Smith, W.P. Gibson, M.K. Doggett, G.H. Taylor, J. Curtis, and P.P. Pasteris. 2008. Physiographically sensitive mapping of climatological temperature and precipitation across the conterminous United States. *International Journal of Climatology 28*:2031–2064. doi: 10.1002/joc.1688

DeGaetano, A.T., and R.J. Allen. 2002. Trends in twentieth-century temperature extremes across the United States. *Journal of Climate 15*:3188–3205.

Diffenbaugh, N.S., J.S. Pal, R.J. Trapp, and F. Giorgi. 2005. Fine-scale processes regulate the response of extreme events to global climate change. In *Proceedings of the National Academy of Sciences USA 102*:15774–15778.

Dobler, C., S. Hagemann, R.L. Wilby, and J. Stötter. 2012. Quantifying different sources of uncertainty in hydrological projections in an Alpine watershed. *Hydrology and Earth System Sciences 16*(11):4343–4360.

Eum, H., D. Yonas, and T. Prowse. 2014. Uncertainty in modeling the hydrologic responses of a large watershed: A case study of the Athabasca River basin, Canada. *Hydrological Processes 28*:4272–4293. doi: 10.1002/hyp.10230

Franklin, J., F.W. Davis, M. Ikegami, A.D. Syphard, L.E. Flint, A.L. Flint, and L. Hannah. 2013. Modeling plant species distributions under future climates—How fine scale do climate projections need to be? *Global Change Biology 19*:473–483. doi: 10.1111/gcb.12051

Frankson, R., K. Kunkel, L. Stevens, D. Easterling, W. Sweet, A. Wootten, and R. Boyles. 2017. North Carolina State Summary. NOAA Technical Report NESDIS 149-NC. 3 pages. Available at: https://statesummaries.ncics.org/nc

Frogner, I., H. Haakenstad, and T. Iversen. 2006. Limited-area ensemble predictions at the Norwegian Meteorological Institute. *Quarterly Journal of the Royal Meteorological Society 132*:2785–2808. doi:10.1256/qj.04.178

Gettelman, A., and R.B. Rood. 2016. *Demystifying Climate Models—A Users Guide to Earth System Models*. Springer-Verlag Berlin: Heidelberg, Germany. 274 pages.

Garcia, V. 2014. *Lifetime Fitness and Changing Life History Traits in Red-Cockaded Woodpeckers*. Ph.D. dissertation, Virginia Tech, Blacksburg, VA. Available at https://vtechworks.lib.vt.edu/handle/10919/71347?show=full

Giorgi, F. 1990. Simulation of regional climate using a limited area model nested in a general circulation model. *Journal of Climate 3*:941–964.

Goodess, C., T. Osborn, and M. Hulme. 2003. *The Identification and Evaluation of Suitable Scenario Development Methods for the Estimation of Future Probabilities of Extreme Weather Events*. Tyndall Centre for Climate Change Research. Available at http://library.umac.mo/ebooks/b13623382.pdf

Hall, J.A., S. Gill, J. Obeysekera, W. Sweet, K. Knuuti, and J. Marburger. 2016. Regional Sea Level Scenarios for Coastal Risk Management: Managing the Uncertainty of Future Sea Level Change and Extreme Water Levels for Department of Defense Coastal Sites Worldwide. U.S. Department of Defense, Strategic Environmental Research and Development Program. 228 pp.

Hawkins, E., and R. Sutton. 2011. The potential to narrow uncertainty in projections of regional precipitation change. *Climate Dynamics 37*:407–418. doi: 10.1007/s00382-010-0810-6

Hawkins E., and R. Sutton. 2009. The potential to narrow uncertainty in regional climate predictions. *Bulletin of the American Meteorological Society 90*:1095–1107. doi: 10.1175/2009BAMS2607.1

Hayhoe, K., A. Stoner, X. Yang, C. Crow, R. Swaminathan, I. Scott-Fleming, J-H. Ryu, R. Gelca, and S. Swain. 2013. Development and Dissemination of a High-Resolution National Climate Change Dataset. Available at https://cida.usgs.gov/thredds/fileServer/dcp/files/Hayhoe_USGS_downscaled_database_final_report.pdf

Hostetler, S.W., J.R. Alder, and A.M. Allan. 2011. *Dynamically Downscaled Climate Simulations over North America: Methods, Evaluation, and Supporting Documentation for Users*. U.S. Geological Survey Open-File Report 2011–1238. 64 pages. Available at http://pubs.usgs.gov/of/2011/1238

Jin, Y., A. Kawamura, K. Jinno, and R. Berndtsson. 2005. Nonlinear multivariable analysis of SOI and local precipitation and temperature. *Nonlinear Processes in Geophysics 12*:67–74.

Kaufman, L., and P.J. Rousseeuw. 2005. *Finding Groups in Data: An Introduction to Cluster Analysis.* John Wiley, Hoboken. doi:10.1002/9780470316801.ch1

Kay, A.L., H.N. Davies, V.A. Bell, and R.G. Jones. 2012. Comparison of uncertainty sources for climate change impacts: Flood frequency in England. *Climate Change 92*:41–63. doi: 10.1007/s10584-008-9471-4

Khan, M.S., P. Coulibaly, and Y. Dibike. 2006. Uncertainty analysis of statistical downscaling methods using Canadian global climate model predictors. *Hydrological Processes 20*:3085–3104. doi: 10.1002/hyp.6084

Koutroulis, A.G., M.G. Grillakis, I.K. Tsanis, and D. Jacob. 2015. Exploring the ability of current climate information to facilitate local climate services for the water sector. *Earth Perspectives.* doi: 10.1186/s40322-015-0032-5

Kunkel, K. E., L. E. Stevens, S. E. Stevens, L. Sun, E. Janssen, D. Wuebbles, C. E. Konrad, II, C. M. Fuhrman, B. D. Keim, M. C. Kruk, A. Billet, H. Needham, M. Schafer, and J. G. Dobson. 2013. Regional Climate Trends and Scenarios for the U.S. National Climate Assessment: Part 2. Climate of the Southeast U.S. NOAA Technical Report 142-2. 103 pp., National Oceanic and Atmospheric Administration, National Environmental Satellite, Data, and Information Service, Washington D.C.

Kunkel, K.E., D.R. Easterling, K. Redmond, and K. Hubbard. 2003. Temporal variations of extreme precipitation events in the United States: 1895–2000. *Geophysical Research Letters 30*:1900.

Lorenz, D. n.d. Downscaled climate projections. Available at https://djlorenz.github.io/downscaling2/main.html

Mandal, S., P.A. Breach, and S.P. Simonovic. 2016. Uncertainty in precipitation projection under changing climate conditions: A regional case study. *American Journal of Climate Change 5*:116–132. doi: 10.4236/ajcc.2016.51012

Minville, M., F. Brissette, and R. Leconte. 2008. Uncertainty of the impact on climate change on the hydrology of a Nordic watershed. *Journal of Hydrology 358*:70–83. doi: 10.1016/j.jhydrol.2008.05.033

Mote, P., L. Brekke, P.B. Duffy, and E. Maurer. 2011. Guidelines for constructing climate scenarios. *Eos Transactions, American Geophysical Union 92*:257–258.

Parmesan, C., A. Williams-Anderson, M. Moskwik, A.S. Mikheyev, and M.C. Singer. 2015. Endangered Quino checkerspot butterfly and climate change: Short-term success but long-term vulnerability? *Journal of Insect Conservation 19*:185–204. doi: 10.1007/s10841-014-9743-4

Pennell, C., and T. Reichler. 2011. On the effective number of climate models. *Journal of Climate 24*:2358–2367. doi:10.1175/2010JCLI3814.1

Pourmokhtarian, A., C.T. Driscoll, J.L. Campbell, K. Hayhoe, and A.N.M. Stoner. 2016. The effects of climate downscaling technique and observation dataset on modeled ecological responses. *Ecological Applications 26*:1321–1337. doi: 10.1890/15-0745

Sanderson B.J., and R. Knutti. 2012. On the interpretation of constrained climate model ensembles. *Geophysical Research Letters 39*:L16708. doi: 10.1029/2012GL052665

Sanderson, B.J., R. Knutti, and P. Caldwell. 2015. Addressing interdependency in a multimodel ensemble by interpolation of model properties. *Journal of Climate 28*:5150–5170. doi: 10.1175/JCLI-D-14-00361.1

Trivedi, M.R., P.M. Berry, M.D. Morecroft, and T.P. Dawson. 2008. Spatial scale affects bioclimate model projections of climate change impacts on mountain plants. *Global Change Biology 14*:1089–1103. doi:10.1111/j.1365-2486.2008.01553.x

Tudor, M., and P. Termonia. 2010. Alternative formulations for incorporating lateral boundary data into limited-area models. *Monthly Weather Review 138*:2867–2882. doi:10.1175/2010MWR3179.1

Varis, O., T. Kajander, and R. Lemmela, R. 2004. Climate and water—From climate models to water resources management and vice versa. *Climatic Change 66*:321–344.

von Storch, H., B.C. Hewitson, and L.O. Mearns. 2000. Review of empirical downscaling techniques. *Regional Climate Development Under Global Warming, Conference Proceedings of the RegClim Spring Meeting*, Jevnaker, Norway. May 8–9. Kjeller, Norway, Norwegian Institute for Air Research, General Technical Report No. 4:29–46. Edited by Iversen, T., and B.A.K. Høiskar.

Walsh, J., D. Wuebbles, K. Hayhoe, J. Kossin, K. Kunkel, G. Stephens, P. Thorne, R. Vose, M. Wehner, J. Willis, D. Anderson, S. Doney, R. Feely, P. Hennon, V. Kharin, T. Knutson, F. Landerer, T. Lenton, J. Kennedy, and R. Somerville. 2014. Our Changing Climate. Pp. 19–67, Chapter 2 in *Climate Change Impacts in the United States: The Third National Climate Assessment*. Edited by Melillo, J.M., T.C. Richmond, and G.W. Yohe. U.S. Global Change Research Program. doi:10.7930/J0KW5CXT

Ward, J.H. 1963. Hierarchical grouping to optimize an objective function. *Journal of the American Statistical Association 58*(301):236–244.

Werth, D., and K.-F. Chen. 2014. The application of statistical downscaling process to derive 21st century river flow predications using a global climate simulation. *Water Resources Management 29*:849–861. doi: 10.1007/s11269-014-0847-0

Wootten, A. 2016. *Uncertainty in Climate Projections: An Investigation of the Contribution from Downscaling*. *Atmospheric Science*. Ph.D. dissertation, North Carolina State University, Raleigh, NC.

Wootten, A., A. Terando, B.J. Reich, R.P. Boyles, and F. Semazzi. 2017. Characterizing sources of uncertainty from global climate models and downscaling techniques. *Journal of Applied Meteorology and Climatology.* doi: 10.1175/JAMC-D-17-0087.1

Wootten, A., K. Smith, R. Boyles, A. Terando, L. Stefanova, V. Misra, T. Smith, D. Blodgett, and F. Semazzi. 2014. *Downscaled Climate Projections for the Southeast U.S.—Evaluation and Use for Ecological Applications*. U.S. Geological Survey Open-File Report 2014-1190. Available at https://pubs.er.usgs.gov/publication/ofr20141190

Xia, Y., K. Mitchell, M. Ek, J. Sheffield, B. Cosgrove, E. Wood, L. Luo, C. Alonge, H. Wei, J. Meng, B. Livneh, D. Lettenmaier, V. Koren, Q. Duan, K. Mo, Y. Fan, and D. Mocko. 2012a. Continental-scale water and energy flux analysis and validation for the North American Land Data Assimilation System project phase 2 (NLDAS-2): 1. Intercomparison and application of model products. *Journal of Geophysical Research, Atmospheres* 117(D3).

Xia, Y., K. Mitchell, M. Ek, B. Cosgrove, J. Sheffield, L. Luo, C. Alonge, H. Wei, J. Meng, B. Livneh, Q. Duan, and D. Lohmann. 2012b. Continental-scale water and energy flux analysis and validation for the North American Land Data Assimilation System project phase 2 (NLDAS-2): 2. Validation of model-simulated streamflow. *Journal of Geophysical Research, Atmospheres* 117(D3).

Appendix 3-A
Supporting Data

Climate data were provided to the following DCERP2 ecosystem modules:

Aquatic/Estuarine

- Estuarine Simulation Model (ESM; provided to Dr. Mark Brush)—The final 24 reduced ensemble members were provided.

Coastal Barrier

- CSHORE-C15 beach morphology model (provided to Dr. Jesse McNinch)—Of the 24 downscaled climate models that were chosen as the reduced ensemble members, only 13 of the models in the DCERP2 ensemble contained wind speed so those 13 were included in the beach morphology model. The 13 downscaled climate models were as follows: inmcm4, bcc-csm1-1, NorESM1-M, MRI-CGCM3, MIROC5, MIROC-ESM, MIROC-ESM-CHEM, GFDL-ESM2M, GFDL-ESM2G, CanESM2, CSIRO-Mk3-6-0, CNRM-CM5, and BNU-ESM. These models contained daily data for the entire climate model baseline period (1950–2005) and for the entire future Representative Concentration Pathway 8.5 scenario/pathway (2006–2099).

Terrestrial

- LANDIS-II (provided to Dr. Steve Mitchell)—An average of the final 24 reduced ensemble members was provided as the climate projection dataset for LANDIS-II. The reduced ensemble included models from three downscaled data sets: (1) MACA (bcc-csm1-1, BNU_ESM, CanESM2, CNRM-CM5, CSIRO-Mk3-6-0, GFDL-ESM2G, GFDL-ESM2M, inmcm4, MIROC5, MIROC-ESM, MIROC-ESM-CHEM, MRI-CGCM3, and NorESM1-M), (2) SERAP (ccsm, cgcm3-t47, cnrm, echam5, echo, gfdl-2-0, gfdl-2-1, hadgem, miroc-med, and mri-cgcm2), and (3) CL10 (HadCM3). However, these three downscaled data sets were run for different historical and future time periods and thus, not all 24 members were always included in the average. The final 24 reduced ensemble members were also provided and Dr. Mitchell was encouraged to input as many models as possible into LANDIS-II.

Recommended Best Practices for Use with Climate Projections

The following best practices were recommended for use with climate projections:

- An ensemble of climate model projections can provide insight regarding the future climate. A member of an ensemble—an individual model simulation—represents one possible future scenario. Non-linear interactions in climate models and downstream process-based ecological models cannot be properly represented by an ensemble average. Therefore, when running this type of process-based ecological model, it is recommended to use all individual downscaled GCM members of the entire reduced ensemble to fully

capture the range of possibilities of a future climate. After the simulation of this ecological model is performed, similar metrics (e.g., average, standard deviations) can be applied to that model's output to capture the range of future outcomes.

- Calculating the future climate change over time from any model consists of several important steps. Since all models have inherent biases, it is important to calculate the future climate change by comparing the climate model projection to the respective climate model baseline period. The climate model baseline period is the results from a climate model that has been simulated over a historical period. To calculate the future change over time (e.g., deltas), the climate model baseline must be subtracted from the future climate projection. These deltas can then be added back to the historical observations, not to the climate model baseline, to obtain values for a future climate. This process helps to eliminate any inherent model biases by using the rate of change as compared to the climate model baseline simulation.
- When evaluating future climate data, it is important to use the appropriate time scale. Although climate model data are output on daily or monthly time steps, using these data at this temporal resolution is not recommended. Longer temporal time periods of future climate projections (approximately 20-year averages in DCERP2) are needed to provide meaningful guidance on climate time scales.
- When using climate projections as inputs into ecological models, such as estuarine or land system models, it is important to use the climate variables (e.g., temperature, precipitation) from the same climate model projection data set.

Appendix 3-B
List of Scientific/Technical Publications

Papers

Wootten, A., A. Terando, B.J. Reich, R.P. Boyles, and F. Semazzi. 2017. Characterizing sources of uncertainty from global climate models and downscaling techniques. *Journal of Applied Meteorology and Climatology.* doi: 10.1175/JAMC-D-17-0087.1

Thesis and Dissertation

Wootten, A. 2016. *Uncertainty in Climate Projections: An Investigation of the Contribution from Downscaling*. *Atmospheric Science*. Ph.D. dissertation, North Carolina State University, Raleigh, NC.

Presentations

Bedsworth, L., R. De La Rosa, G. Franco, M. McCormick, J. Parfrey, R. McPherson, D. Rosendahl, and A. Wootten. 2015. *Speaking Truth to Power and Power to Truth: Building a Two-Way Street in Climate Change Assessments*. Presented to a Working Group at the 2015 National Adaptation Forum, St. Louis, MO.

Boyles, R., and A. Wootten. 2015. *Testing Process Models with Climate Model Outputs in the Southeast*. Presented at the Strategic Environmental Research and Development Program (SERDP) Climate Change Program Review and National Oceanic and Atmospheric Administration's Partnership Meeting, Boulder, CO.

Brackett, M., A. Wootten, G. Ely, and R. Boyles. 2016. *Finding the Best Historical Climate Dataset for Ecological Modeling*. Presented at the 22nd Conference on Applied Climatology, New Orleans, LA. Available at https://ams.confex.com/ams/96Annual/webprogram/Paper289418.html

Brackett, M. 2015. *Finding the Best Historical Climate Dataset for Ecological Modeling*. Presented at North Carolina State University's Summer 2015 Undergraduate Research Symposium, Raleigh, NC.

Gray, G.M.E., and R. Boyles. 2017. *Model Independence in Downscaled Climate Projections: A Case Study in the Southeast United States*, 458. Presented at the 2017 Annual Meeting of the American Meteorological Society, Seattle, WA.

Gray, G.M.E., and R. Boyles. 2016. *Ensemble Creation with Downscaled Climate Projections for Ecological Use*. Presented at the 22nd Conference on Applied Climatology, New Orleans, LA. Available at https://ams.confex.com/ams/96Annual/webprogram/Paper285053.html

Gray, G.M.E. and R. Boyles. 2016. *Model Independence in Downscaled Climate Projections: A Case Study in the Southeast United States*. Presented at the 2016 Fall Meeting of the American Geophysical Union, San Francisco, CA.

Wootten, A., B. Reich, A. Terando, and R. Boyles. 2016. *How Much Does Downscaling Contribute to Uncertainty in Downscaled Climate Projections? A Case Study in Eastern North Carolina*. Presented at the 28th Conference on Climate Variability and Change, New Orleans, LA. Available at https://ams.confex.com/ams/96Annual/webprogram/Paper289112.html

Wootten, A. 2015. *Climate Change and Southeast Ecosystems.* Presented at the Wildlife Conservation Society's Climate Adaptation for Conservation Training and Coaching Session, Memphis, TN. Available at https://globalchange.ncsu.edu/secsc/wp-content/uploads/CC-and-SE-Ecosystems_Wootten.pdf

Wootten, A., B. Reich, A. Terando, and R. Boyles. 2015. *How Much Does Downscaling Contribute to the Uncertainty in Downscaled Climate Projections? A Case Study in Eastern North Carolina*. Presented at the American Geophysical Union's Annual Fall Meeting, San Francisco, CA. Available at https://agu.confex.com/agu/fm15/meetingapp.cgi/Paper/81680

Appendix 3-C
List of Students

- Michael Brackett, B.S., Meteorology, North Carolina State University, Raleigh, NC, 2016.
- Adrienne Wootten, Ph.D., Atmospheric Science, North Carolina State University, Raleigh, NC, 2016.
- Geneva Gray, M.S., Atmospheric Science, North Carolina State University, Raleigh, NC, in progress.

Chapter 4

AEM-4: New River

SERDP Project Number: RC-2245

Aquatic Estuarine Module

AEM-4

Lead Researcher:

Dr. Scott Ensign
Aquatic Analysis and Consulting, LLC
Morehead City, NC
E-mail: scott@aquaco.us

August 2017

Final

This report was prepared under contract to the U.S. Department of Defense (DoD) Strategic Environmental Research and Development Program (SERDP). The publication of this report does not indicate endorsement by DoD, nor should the contents be construed as reflecting the official policy or position of DoD. References herein to any specific commercial product, process, or service by trade name, trademark, manufacturer, or otherwise, do not necessarily constitute or imply its endorsement, recommendation, or favoring by DoD.

Table of Contents

Acronyms 4-v
Abstract 4-1
Objectives of the Monitoring Activity 4-3
Background 4-3
Materials and Methods 4-3
Sample Collection and Analysis 4-3
Temporal Trend Analysis 4-4
Prediction of Carbon and Sediment Fluxes to the NRE 4-6
Sensitivity of River Flux to Changes in Discharge Due to Climate Change 4-7
Results and Discussion 4-7
Temporal Trend in Discharge and Tidal Flow 4-7
Statistical Summary and Temporal Trends 4-10
Prediction of Carbon Flux to the NRE 4-12
Prediction of Sediment Flux to the NRE 4-13
Storm Flows on the New River: The Example of Hurricane Matthew 4-15
Sensitivity of River Flux to Changes in Discharge Due to Climate Change 4-17
Assessment of Directionality/Trends 4-18
Conclusions and Implications for Future Research and Implementation 4-18
Key Findings 4-18
Findings with Implications for Future Base Management 4-20
Literature Cited 4-21
Appendix 4-A: Supporting Data 4-A-1
Appendix 4-B: List of Scientific/Technical Publications 4-B-1
Appendix 4-C: List of Students 4-C-1
Appendix 4-D: Supplemental Study 4-D-1

List of Figures

Figure 4-1. A trend analysis of high and low flows at the New River at Gum Branch from 1988 through 2016 by using daily discharge measurements from the USGS. 4-8

Figure 4-2. (Top panel) The water levels on the New River at Gum Branch from 28 April through 10 May (typical low discharge period) over individual years spanning three decades. (Middle panel) The statistical distributions of daily range in water levels at the site from 1969 through 2015 when river stage

was less than 1.5 m and the daily change in water level was less than 0.03 m, representing periods of consistently low watershed discharge. (Bottom panel) The relationship between monthly stream water level range and monthly mean sea level at the NOAA tide gage at Beaufort, NC (Stream Gaging Station 8656483) from 1988 through 2013. 4-9

Figure 4-3. The relationships between DIC, DOC, POC, and the discharge used for estimating carbon fluxes to the NRE at Jacksonville 4-12

Figure 4-4. The relationship between (top panel) SSC and discharge with model fits and uncertainty and (bottom panel) cumulative sediment flux and uncertainty from 1988 through 2015. 4-14

Figure 4-5. (Top panel) The effects of Hurricane Matthew on water level and turbidity), (middle panel) the relationship between SSC and turbidity at Gum Branch, and (bottom panel) the predicted SSC during Hurricane Matthew 4-16

List of Tables

Table 4-1. Statistical Summary of Parameters Measured in situ in the New River at Gum Branch During DCERP1 and DCERP2, 2008 Through 2016 4-10

Table 4-2. Statistical Summary of Nitrogen and Phosphorus Concentrations Measured in the New River at Gum Branch During DCERP1 and DCERP2 (2008 Through 2016) 4-11

Table 4-3. Changes in Flow-Normalized Concentration and Flow-Normalized Flux in Constituents from 2008 through 2016 at the New River at Gum Branch; Analyses Were Performed by Using EGRET 4-11

Table 4-4. Statistical Summary of Carbon, chl a, and SSC in the New River at Gum Branch During DCERP1 and DCERP2 (2008 Through 2016) 4-11

Table 4-5. Annual Flux and Yield Estimates of Carbon Constituents in the New River at Gum Branch by Using Relationships Shown in Figure 4-3 4-13

Table 4-6. Sediment Budget for the NRE 4-15

Table 4-7. Summary Results from Frequency-Magnitude Analysis of Constituent Fluxes Past the New River at Gum Branch 4-17

Acronyms

µatm	microatmosphere
µg L^{-1}	micrograms per liter
µm	micrometer
µS cm^{-1}	microsiemens per centimeter
A	flux of CO_2 from water into the atmosphere
AE	Aquatic/Estuarine (Module)
AEM	Aquatic/Estuarine Monitoring
°C	degree Celsius
C	carbon
CB	Coastal Barrier (Module)
chl *a*	chlorophyll *a*
CO_2	carbon dioxide
DCERP	Defense Coastal/Estuarine Research Program
DCERP1	first cycle of DCERP
DCERP2	second cycle of DCERP
DIC	dissolved inorganic carbon
DOC	dissolved organic carbon
DoD	U.S. Department of Defense
EGRET	Exploration and Graphics for RivEr Trends, (a USGS modeling program)
g	gram
G	flux at Gum Branch
g C g^{-1}	grams of carbon per gram
g cm^{-3}	grams per cubic centimeter
g km^{-2} yr^{-1}	grams per square kilometer per year
g yr^{-1}	grams per year
J	flux at Jacksonville
k	light attenuation
kg yr^{-1}	kilograms per year
km	kilometer
km^2	square kilometers
m, m^{-1}	meter
m^{-2} yr^{-1}	square meters per year
m^3 s^{-1}	cubic meters per second
m^3 yr^{-1} FOIA	cubic meters per yearFreedom of Information Act
MARDIS	Monitoring and Research Data Information System
MCBCL	Marine Corps Base Camp Lejeune
mg/L, mg L^{-1}	milligrams per liter
mmol C m^{-2} hr^{-1}	millimoles of carbon per square meter per hour
µM	micromolar
N	nitrogen
NH_4	ammonium
NO_3	nitrate
NOAA	National Oceanic and Atmospheric Administration
NRE	New River Estuary

NTU	Nephelometric Turbidity Unit
O^2	oxygen
P	phosphorus
P	DIC production via photomineralization
PAR	photosynthetically active radiation
pCO_2	partial pressure of carbon dioxide
PN	particulate nitrogen
PO_4	orthophosphate
POC	particulate organic carbon
PP	particulate phosphorus
ppt	parts per thousand
PVC	polyvinyl chloride
RC	Resource Conservation and Climate Change (a SERDP program area)
RT	residence time
s^{-1}	second
SERDP	Strategic Environmental Research and Development Program
SSC	suspended sediment concentration
TDN	total dissolved nitrogen
TDP	total dissolved phosphorus
TSP	Translating Science into Practice (Module)
USGS	United States Geological Survey
WRTDS	Weighted Regression on Time, Discharge, and Season
YSI	Yellow Springs Instruments, Inc.

Abstract

Objectives and Technical Approach: The objectives of Aquatic/Estuarine Monitoring Activity AEM-4 were to: (1) analyze trends in river hydrology from 1988 to 2016, (2) analyze trends in water chemistry constituents and flux to the New River Estuary (NRE) over the DCERP1 and DCERP2 periods (i.e., 2008 through 2016), and (3) estimate the loss of nitrate (NO_3), dissolved inorganic carbon (DIC), and dissolved organic carbon (DOC) between Gum Branch and Jacksonville. During DCERP2, sampling was conducted 12 times throughout the year at the U.S. Geological Survey's (USGS's) New River gaging station near Gum Branch (USGS Stream Gaging Station 02093000). Constituent concentrations, fluxes, and river discharge were analyzed for long-term trends by using various statistical models relating constituent concentrations with discharge. Lagrangian and synoptic measurements were made along the tidal freshwater portion of the New River to calculate reductions in NO_3, DIC, and DOC flux.

Results: There are four results. First, between 1988 and 2016, the 7-day and 30-day minimum flows at Gum Branch increased by 0.22 $m^3 s^{-1}$ (100% increase) and 0.33 $m^3 s^{-1}$ (116% increase), respectively. The daily range in water level showed an increase in the median daily water level range from 0.02 m in 1969 and 1988 to 0.06 m 2015. These data indicate that tidal extension has occurred and that this site is now experiencing sea level rise.

Second, for flow-normalized concentrations and fluxes at Gum Branch between 2009 and 2016, ammonium (NH_4) concentrations likely decreased, but NH_4 flux did not change. In addition, NO_3 concentration did not change, but it was highly likely that NO_3 flux decreased; total dissolved nitrogen (TDN) concentration and flux likely decreased; and particulate nitrogen (PN) concentration likely decreased, but PN flux did not change. Also, orthophosphate (PO_4) concentration decreased significantly, but PO_4 flux did not change; particulate organic carbon (POC) concentration did not change, but POC flux likely increased; and chlorophyll *a* (chl *a*) concentration likely decreased, but chl *a* flux did not change.

Third, carbon flux at Gum Branch was dominated by DIC (46%), followed by DOC (44%) and POC (10%). Estuarine shoreline erosion was predicted to account for 63% of sediment and 25% of the POC inputs into the NRE because watershed sediment fluxes are low in the New River watershed.

Lastly, during the summer when discharge at Gum Branch is low, 11% of the NO_3 flux at Gum Branch may be denitrified before reaching Jacksonville, NC. DIC flux at Jacksonville is 1.4–fold greater than at Gum Branch, and DOC flux at Jacksonville is 31% lower than at Gum Branch.

Benefits: The tidal freshwater portion of the NRE is extending farther inland as sea level rises. This tidal extension is also likely happening throughout Marine Corps Base Camp Lejeune (MCBCL) in low elevation stream channels. If these riparian areas are not disturbed by development or engineering practices (e.g., culverts, weirs), then MCBCL will receive additional ecosystem service (e.g., enhanced denitrification flux) from these low elevation, tidal streams. TDN flux into the tidal freshwater NRE decreased over the DCERP monitoring period, and PO_4 concentration declined. If these trends continue, they may decrease the propensity for intensive algal growth to occur in the NRE in the future. The extent to which algal growth may be reduced

will require continued monitoring at both Gum Branch and the NRE. The accuracy of the DCERP2 estuarine carbon budget and Estuarine Simulation Model will be improved by adjusting the watershed flux assumptions used for scaling-up watershed yields at Gum Branch to fluxes at Jacksonville.

Keywords: Sea level rise, river flux, river fluxes, river discharge, trend analysis, hurricane, carbon, nitrogen, phosphorus, suspended sediment

Objectives of the Monitoring Activity

The objective of Aquatic/Estuarine Monitoring Activity AEM-4 was to characterize the watershed inputs of carbon, nitrogen, and phosphorus into the New River Estuary (NRE) from the New River watershed upstream of Jacksonville, NC. The concentrations of these constituents were combined with river discharge reported by the U.S. Geological Survey (USGS) to calculate constitute fluxes to the NRE. These data inform Research Projects AE-4, AE-5, AE-6, CB-5, and TSP-2 and Monitoring Activities AEM-1, AEM-2, and AEM-3 to develop the DCERP2 estuarine carbon budget. Additional objectives of Monitoring Activity AEM-4 were to analyze long-term trends in constituent concentrations and fluxes over the DCERP1 and DCERP2 periods, analyze long-term trends in hydrology, and explore the sensitivity of nutrient fluxes from the upper New River watershed to potential future changes in river discharge.

Background

During DCERP1, monitoring on the New River occurred at the following two stations: the main stem of the New River at Jacksonville (USGS Stream Gaging Station 0209303205) and the mainstem of the New River at Gum Branch (USGS Stream Gaging Station 02093000). The Jacksonville station was only operational during DCERP1. The USGS operated the Gum Branch station from 1949 through 1973, but moved the gage to its present position in 1969. The station was discontinued from 1974 through 1987, and operation resumed in 1987 and has operated continuously to the present. Results from DCERP1 showed that nitrate (NO_3) and, to a lesser extent orthophosphate (PO_4), declined between the two sites. Most sampling for water chemistry was conducted during low flow periods, leaving uncertainty about constituent fluxes during higher flow periods. Mean annual flows during DCERP1 (2007–2012) except 2010 were below the long-term (1988–2012) mean of 3.286 $m^3 s^{-1}$ (see **Table 4-A1** in **Appendix 4A**); therefore, the DCERP1 New River monitoring was limited in describing event-scale fluxes. The Marine Corps Base Camp Lejeune (MCBCL) watershed is downstream of the Gum Branch station, and, therefore, the water and chemical fluxes at the Gum Branch station are independent of any MCBCL activities or management actions. However, water quality at Gum Branch does encompass activities within the management area of both Onslow County and the City of Jacksonville.

Materials and Methods

Sample Collection and Analysis

Sampling was conducted at the New River near Gum Branch (34.84924° N, 77.51914° W), from the downstream side of Northwest Bridge Road. Discharge data from the USGS stream gauging station on the New River near Gum Branch was downloaded from the USGS's National Water Information System Web interface (USGS Stream Gaging Station 02093000). The instantaneous discharge reported closest to the time of sampling was used to calculate the instantaneous flux of carbon, nitrogen, phosphorus, and particulate constituents.

Sampling was conducted six times per year during low flow and six times per year at high flow after storm events. Sampling began on 21 March 2013 and concluded on 20 September 2016. A pair of low and high flow samples was collected every 2 months (i.e., January and February,

March and April, May and June, July and August, September and October, and November and December).

Salinity, conductivity, temperature, dissolved oxygen, and turbidity were measured onsite by using a Yellow Springs Instruments, Inc. (YSI) 6820 multiprobe datasonde. All probes were calibrated before collecting measurements and checked for drift after sampling was performed; violations from acceptable calibration were noted and logged in the Monitoring and Research Data Information System (MARDIS) data set. Water samples for analysis of ammonium (NH_4), NO_3, dissolved organic nitrogen (DON), orthophosphate (PO_4), dissolved inorganic carbon (DIC), dissolved organic carbon (DOC), particulate organic carbon (POC), and suspended sediment concentration (SSC) were collected mid-stream by using a DH-81 isokinetic sampler. Sampling was performed by profiling and compositing water from the surface to 0.25 m above the bottom. With the exception of DIC and SSC, samples were stored on ice until filtration through pre-combusted Whatman glass fiber filters (0.7 µm) and frozen until sample analysis at the University of North Carolina at Chapel Hill's Institute of Marine Sciences. DIC samples were refrigerated until analyzed, usually within 2 days of sample collection. Samples were analyzed for SSC by using ASTM International's Method D 3977-97 (ASTM International, 2013) and for chlorophyll *a* (chl *a*) by using the approach used by Arar and Collins (1997).

Temporal Trend Analysis

A trend analysis was performed on river discharge and physio-chemical parameters. The period of analysis for river discharge trends was 1 January 1988 (earliest date of continuous measurement at the current USGS stream gaging station at Gum Branch) through 31 December 2016. The period of analysis for physio-chemical parameters was for the DCERP1 and DCERP2 periods. Only those parameters collected through both periods of DCERP were analyzed. The parameters are as follows: NH_4, NO_3, total dissolved nitrogen (TDN), particulate nitrogen (PN), PO_4, POC, and chl *a*. The calendar year, not water year, is the basis for all analyses.

In rivers, constituent concentrations are often a function of river discharge. For this reason, analysis of long-term trends in constituent concentrations requires attention to the discharge when sampling was performed. Many statistical tools have been developed for this purpose; the one selected for use here is the Exploration and Graphics for RivEr Trends (EGRET) analysis package (Hirsch and De Cicco, 2015) developed by the USGS because it is specifically designed for analyzing and detecting long-term trends. EGRET uses a Weighted Regression on Time, Discharge, and Season (WRTDS) to interpolate across the monthly sample intervals. Weighting of predictions across the time series is performed by using a moving window that gives samples close to the center of the moving window more weight than values farther from the center. This process produces a smoothed time series that enables visual examination of trends in constituent concentrations. Given the relatively short period of analysis (8 full years in DCERP, 2008 through 2016, while EGRET performs best with 50 year records), a 4-year averaging window (2-year half window) was set without edge correction. A discharge window was set to 4 orders of magnitude in the natural log of discharge due to the relatively small sample set (less than 100 samples from DCERP, while EGRET is designed for data sets of at least 200 samples).

Long-term trends in constituent concentration in a river may indicate changes in watershed sources or biogeochemical processing upstream. In the context of DCERP, these changes in the

New River watershed sources and biogeochemical processes upstream of the Gum Branch gage are of less interest than long-term trends in flux (concentration × discharge, expressed as mass per year) to the NRE. Changes in flux to the NRE could occur because of one, or a combination of two factors: constituent concentration change or discharge change. By normalizing the predicted flux by expected concentration at a given discharge, the EGRET model enhances interpretation of long-term trends. For example, if sampling was conducted at low flows for one period of time and subsequently sampled at high flows during a second period of time, measured flux would increase because of its dependence on discharge. It would be incorrect to interpret the increase in flux as indicative of a change in loading to the river upstream or biogeochemical processes in-stream because sampling during the two periods was systematically biased by the increase in river discharge over the two periods of sampling. Instead, the dependence of concentration on discharge must be accounted for to interpret changes in flux. That is the challenge that the EGRET model helped to address.

An additional challenge is concluding whether a change in flow-normalized concentration or flux over time is meaningful, given inter- and intra-annual variability in concentration and its relationship with discharge. The EGRET model includes a bootstrap method for estimating uncertainty in trends generated by the WRTDS model (Hirsch et al., 2015). The method applies a standard null hypothesis testing approach (α=0.10), but also provides a description of the likelihood of a change between two time periods. A Bayesian posterior mean estimate of the probability of a trend uses “very likely” to describe a probability of 0.90 to 0.95, “likely” to describe a probability of 0.66 to 0.90, “about as likely as not” to describe a probability of 0.33 to 0.66, and “unlikely” to describe a probability of 0.10 to 0.33. Because of the relatively short period of DCERP monitoring at Gum Branch (from 2009 through 2016), the probability-based interpretation of trends is most appropriate for analysis of the DCERP Gum Branch data.

One shortcoming of the EGRET model is that it assumes a linear relationship between ln(concentration), which is the natural logarithms of concentration, and ln(discharge), which is the natural logarithms of discharge. Although the slope of this relationship varies in the model over time and over a range of discharge, the assumption of linearity in the relationship may not be accurate. One reason a linear relationship between concentration and discharge may not be accurate is because of hysteresis over the base flow, storm flow, and base flow cycle. However, the influence of a poorly characterized concentration–discharge relationship on aggregate flux over annual periods is diminished in small rivers, such as the New River, because relative changes in discharge are often larger than the relative changes in constituents over that range in discharge.

The EGRET package also enables analysis of trends in river discharge through summary metrics (annual 7-day low flow, annual 30-day low flow, annual mean, annual median, annual 30-day high flow, and annual 7-day high flow). Given the influence of sea level rise on water level at the Gum Branch gage, a filtering algorithm was developed to investigate the tidal influence at Gum Branch during low discharge. Here, tidal influence was interpreted as the daily range in water level during low flow periods. “Low flow” was defined as days having a mean water level that is less than 1.5 m. Days when water level was affected by storm events (>0.03 m change in water level between 1 day and the next) were excluded from analysis.

An additional analysis was performed on all the carbon, nitrogen, phosphorus, and SSC constituents to determine the effects of sampling frequency (e.g., monthly, biweekly, weekly) on uncertainty in calculated annual fluxes. Uncertainty in the calculated annual flux arises from errors in concentrations predicted by using the regression between the constituent concentration and discharge. Errors in concentration predictions during high discharge impart the most uncertainty in calculated annual fluxes if the regression slope between concentration and discharge is positive during high discharge. Thus, the uncertainty in annual flux calculated for each constituent varies based on whether the constituent concentration increases or decreases at high discharge. Generally, higher sampling frequency measures a greater range in river discharge, thereby reducing uncertainty in the regression between concentration and discharge at high discharge. Monitoring at Gum Branch targeted high-discharge events to reduce this source of error, and non-linear regression was performed (discussed below) that gave special treatment to the prediction of concentrations at high discharge. Higher frequency sampling may have further reduced the imprecision and bias in annual flux calculations. Moatar et al. (2012) provide a method to estimate how imprecision and bias of annual fluxes change with sampling frequency. This method required calculations of the proportion of the historic total water volume discharged in the 98th percentile of mean daily discharge (22.3%) and the slope of the regression relationship at higher flows. This method was applied to the Gum Branch data to determine the extent to which calculated annual flux accuracy would increase had monitoring been performed biweekly or weekly rather than monthly.

Prediction of Carbon and Sediment Fluxes to the NRE

Constituent fluxes in the New River measured at Gum Branch originate from a 243 km^2 watershed. Downstream from this point, an additional 394 km^2 of watershed contributes to the constituent fluxes in the river at the Highway 17 Bridge in Jacksonville, NC. Therefore, the constituent fluxes measured at Gum Branch must be scaled-up to account for this additional watershed contribution. This additional flux was estimated by assuming the yield of a constituent (mass area time^{-1}) from this 394 km^2 area was the same as that measured from the 243 km^2 contributing area at Gum Branch, and then the constituent yield at Gum Branch was multiplied by 2.6 to account for this ungauged area.

The flux of carbon at the Gum Branch station was analyzed to develop the DCERP2 carbon budget (see *DCERP2 Final Report*, Chapter 9). Three constituents were analyzed: DIC, DOC, and POC. To generate annual fluxes of these constituents over the 2013–2014 and 2014–2015 periods, regression relationships were developed between concentration and discharge. This regression was then applied to the daily discharge data to interpolate between sampling events, and then was scaled-up for the predicted discharge at Jacksonville by using the ratio of discharge between Jacksonville and Gum Branch. Non-linear regression models were selected for fitting relationships between concentration and discharge. Uncertainty was estimated based on the 95% confidence limits of the regression coefficients.

Knowledge of the suspended sediment flux at Gum Branch is critical for interpreting the patterns in estuary sediment accumulation produced by Dr. Brent McKee of the University of North Carolina at Chapel Hill (see *DCERP2 Final Report*, Chapter 12). Dr. McKee concluded from sediment core geochronologies that sediment accumulation has increased in recent decades, potentially because of more frequent or larger magnitude floods. To help examine that

hypothesis, long-term trends in sediment flux to the NRE were explored. Using methods identical to those used for DIC, DOC, and POC, the non-linear regression between SSC and discharge was performed to interpolate between measurements and extrapolate backward through the discharge record to 1988.

The most uncertainty in estimating the long-term river fluxes is the response of constituent concentration during extreme discharge events. On 8 October 2016, Hurricane Matthew provided an opportunity to investigate the effects of the seventh largest storm since 1949 on the New River, as measured by the mean daily discharge at Gum Branch. On 6 October 2016, a YSI turbidity probe and HOBO water level logger were deployed in the New River 5 km upstream from Jacksonville (34.77025^{o} N, 77.46452^{o} W). Data were collected while Hurricane Matthew was occurring until 14 October 2016. Additionally, an SSC sample was collected from Gum Branch during the day of peak discharge (i.e., 9 October 2016). Using a regression between turbidity and SSC from previous measurements at Gum Branch, the effects of the flood on sediment delivery to the NRE were estimated.

Sensitivity of River Flux to Changes in Discharge Due to Climate Change

River discharge largely controls the flux of nitrogen, phosphorus, and carbon from watersheds, and future changes in the precipitation regime over annual timescales may change river discharge and subsequently elemental flux. It should be noted that in addition to river discharge, land-use changes in the watershed can also impact these fluxes. The extent to which future precipitation patterns may change is highly uncertain, and do not permit predictions of how watershed nitrogen, phosphorus, and carbon flux may change. However, it is possible to analyze the current distribution of elemental flux across the range in discharge. This analysis was performed for the New River at Gum Branch to address the following question: Under what threshold of discharge does 75% and 90% of constituent fluxes occur? A frequency–magnitude approach was used to address this question, synthesizing river discharge and constituent fluxes over the DCERP monitoring period.

Results and Discussion

Temporal Trend in Discharge and Tidal Flow

At Gum Branch between 1988 and 2016, the annual 7-day minimum flow increased by 0.22 m^3 s^{-1} (100% increase) and the 30-day minimum flow increased by 0.28 m^3 s^{-1} (98% increase) (**Figure 4-1**). No consistent trends were observed in maximum flows, although a slight increase in mean discharge did occur (**Figure 4-1**). The daily range in water level, filtered to exclude high flow periods and transitions from low flow to high flow, showed an increase in the median daily water level range from 0.02 m in 1969 to 0.06 m in 2016 (**Figure 4-2**).

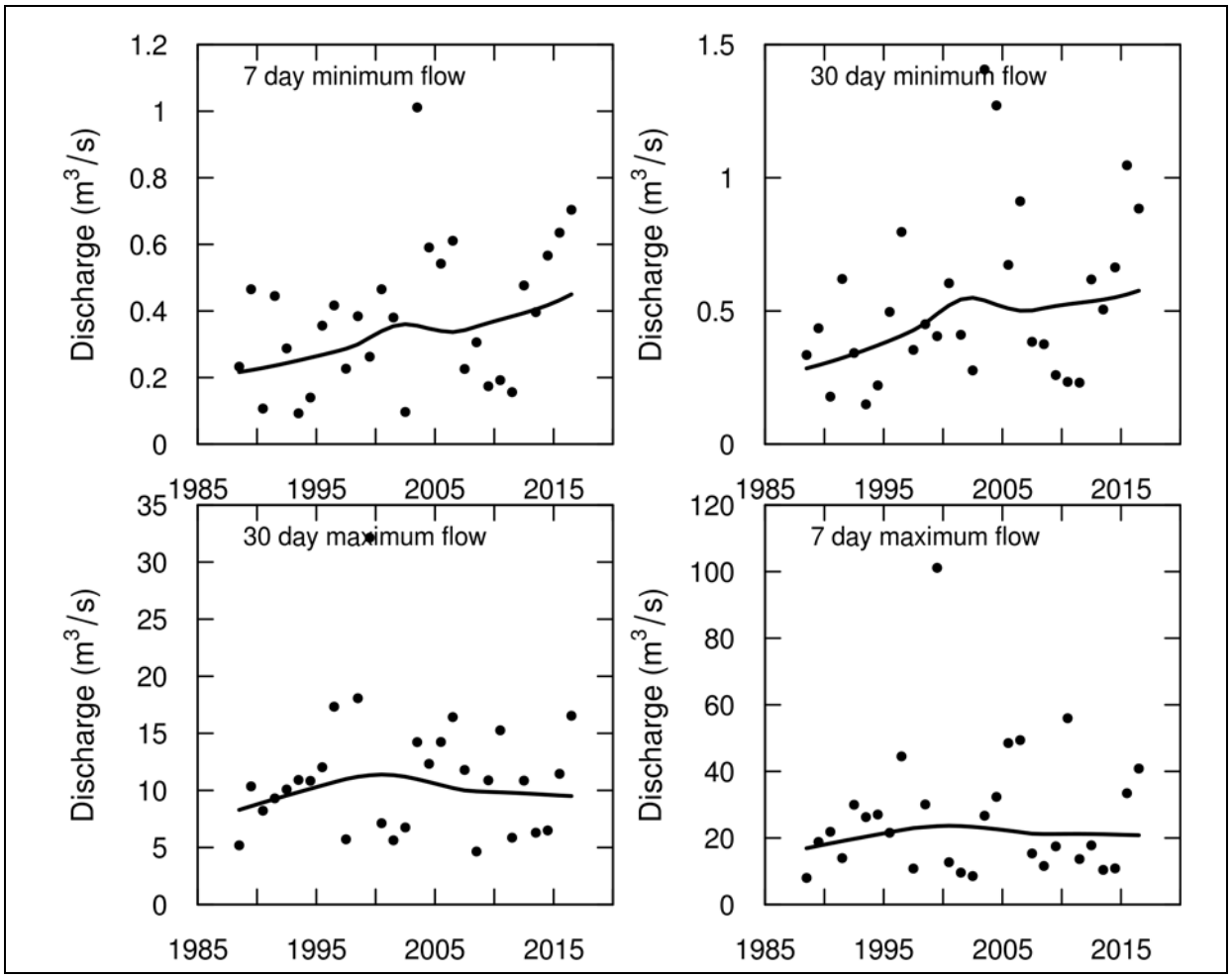

Figure 4-1. A trend analysis of high and low flows at the New River at Gum Branch from 1988 through 2016 by using daily discharge measurements from the USGS.

The combination of these trends indicates that sea level rise has affected the hydrology of the New River at Gum Branch. The increase in 7-day and 30-day minimum discharges may be because of a back-water effect of tide on river flow. The strongest evidence for the onset of tidal flow is shown by the semi-diurnal tide at Gum Branch that has only become evident after 1972 (**Figure 4-2**, top panel).

There are two potential factors contributing to this trend. First, channel dredging may have enhanced tidal exchange at the estuary mouth or decreased channel friction farther into the estuary and allowed more tidal energy to propagate upstream. A 3.2-km section of the New River tidal freshwater zone was straightened and dredged in the 1950s and 1960s, but this activity preceded the observed change in hydrology. The New River Inlet has been dredged repeatedly, although historic National Oceanic and Atmospheric Administration (NOAA) charts do not provide sufficient detail to quantify an increase in channel volume and subsequent tidal attenuation. On 23 July 2015, a Freedom of Information Act request was made to the Wilmington District U.S. Army Corps of Engineers to obtain dredge material records for the New River Inlet, but no action has been made to address this request.

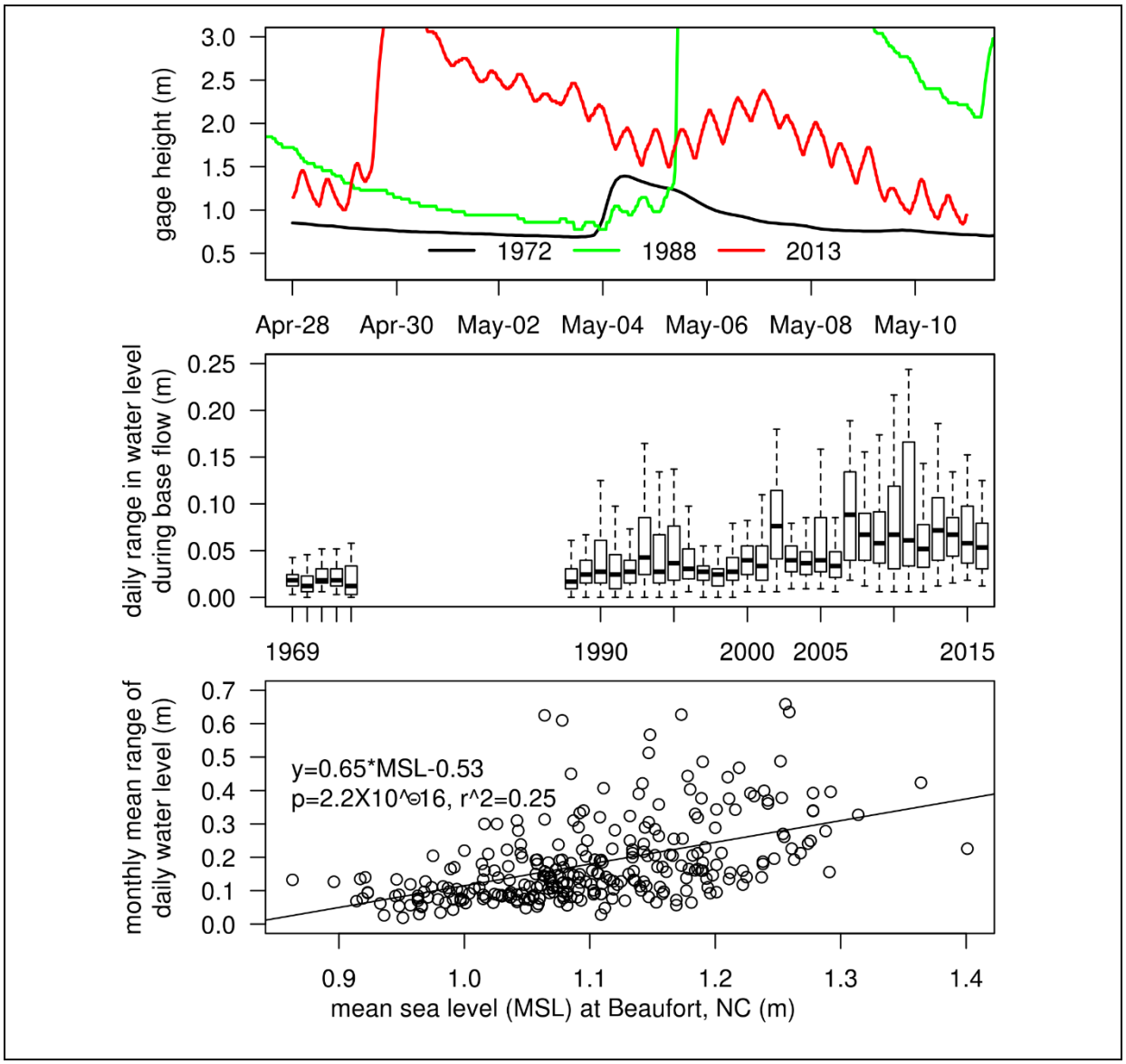

Figure 4-2. (Top panel) The water levels on the New River at Gum Branch from 28 April through 10 May (typical low discharge period) over individual years spanning three decades. (Middle panel) The statistical distributions of daily range in water levels at the site from 1969 through 2015 when river stage was less than 1.5 m and the daily change in water level was less than 0.03 m, representing periods of consistently low watershed discharge. (Bottom panel) The relationship between monthly stream water level range and monthly mean sea level at the NOAA tide gage at Beaufort, NC (Stream Gaging Station 8656483) from 1988 through 2013.

The second explanation for the increase in tidal hydrology is that sea level rise has raised the surface elevation of the New River such that tide can travel farther upriver with less attenuation. A correlation was found between the daily range in water level (a proxy for tidal influence at Gum Branch) and the water level at the NOAA tide gage in Beaufort, NC (**Figure 4-2**, bottom panel). This correlation supports the conclusion that sea level rise has gradually affected the

hydrology at Gum Branch. The onset of tidal conditions at Gum Branch is referred to as "tidal extension" (Ensign and Noe, in revision).

Statistical Summary and Temporal Trends

Sampling was conducted at Gum Branch 43 times between 21 March 2013 and 9 October 2016 for DCERP2. The statistical distribution of the results, including those data collected during DCERP1, are summarized in **Tables 4-1, 4-2, and 4-3**, and in **Figures 4-A1 through 4-A5**.

Table 4-1. Statistical Summary of Parameters Measured in situ in the New River at Gum Branch During DCERP1 and DCERP2, 2008 Through 2016

Parameters	n	Minimum	25th Percentile	Median	Mean	75th Percentile	Maximum
Temperature (°C)	42	3.75	13.70	18.10	17.09	22.27	24.59
Specific conductivity (µS cm^{-1})	42	77	158	219	241	329	432
Salinity	42	0.04	0.07	0.1	0.11	0.16	0.21
Dissolved oxygen (mg L^{-1})	39	4.3	6.6	7.6	7.9	9.1	11.6
Dissolved oxygen (% saturation)	39	50	74.1	80.3	79.9	87.6	111.7
Turbidity (NTU)	42	0	1.33	5.8	21.6	27	136

The WRTDS model results predicted the mean annual concentration, mean annual flow–normalized concentration, mean annual flux, and mean annual flow–normalized flux for a subset of constituents measured for the duration of DCERP1 and DCERP2 (2008 through 2016) in **Table 4-2** (nitrogen and phosphorus) and **Table 4-3** (carbon, chl *a*, and SSC). The mean annual flow–normalized concentrations and flux are reported in **Table 4-4**, and **Figures 4-A7 through Figure 4-A13** in **Appendix 4-A** of this chapter provide graphical representations of all metrics. The green flow-normalized trend line in these appendix figures provides evidence of trends over time that are useful for interpreting data in **Table 4-4**. Discussion here will focus on the flow-normalized values presented in **Table 4-4** because they remove the influence of discharge from the modeled concentration and subsequent trend analysis. Between 2009 and 2016, NH_4 concentrations likely decreased, but NH_4 fluxes did not change, indicating that NH_4 concentrations during high flow events may be increasing. NO_3 concentrations were unlikely to have changed, but it was highly likely that NO_3 fluxes decreased. Both TDN concentrations and fluxes likely decreased. PN concentrations likely decreased, but PN fluxes were unlikely to have changed. It was highly likely that PO_4 concentrations decreased, but unlikely that PO_4 fluxes changed. It was unlikely that POC concentrations changed, but POC fluxes likely increased. Finally, chl *a* concentrations likely decreased, but chl *a* fluxes were unlikely to have changed.

Table 4-2. Statistical Summary of Nitrogen and Phosphorus Concentrations Measured in the New River at Gum Branch During DCERP1 and DCERP2 (2008 Through 2016)

Constituent	N	Minimum	25th Percentile	Median	Mean	75th Percentile	Maximum
NH_4 (µg L^{-1})	97	17	41	58	100	103	807
NO_3 (µg L^{-1})	97	130	1,120	1,470	1,537	1,900	3,420
TDN (µg L^{-1})	94	881	1,802	2,140	2,168	2,500	3,710
PN (µg L^{-1})	94	2.85	41.7	71.4	183.9	202.4	1,791
PO_4 (µg L^{-1})	87	20	56	84	125	166	494

Table 4-3. Changes in Flow-Normalized Concentration and Flow-Normalized Flux in Constituents from 2008 through 2016 at the New River at Gum Branch; Analyses Were Performed by Using EGRET

Constituent	Concentration Change (mg L^{-1})	Change (%)	Flux Change (10^3 kg yr^{-1})	Change (%)
NH_4	−0.0082	−12 Decrease likely	1.2	13 Increase as likely as not
NO_3	−0.27	−15 Decrease as likely as not	−54	−32 Decrease highly likely
TDN	−0.31	−13 Decrease likely	−46	−19 Decrease likely
PN	−0.023	−18 Decrease likely	−0.0099	−0.038 Decrease as likely as not
PO_4	−0.052	−46 Decrease highly likely	−1.7	−11 Decrease as likely as not
POC	0.064	6.7 Increase as likely as not	59	31 Increase likely
Chl *a*	−0.00019	−18 Decrease likely	0.02	16 Increase as likely as not

Table 4-4. Statistical Summary of Carbon, chl a, and SSC in the New River at Gum Branch During DCERP1 and DCERP2 (2008 Through 2016)

Constituent	N	Minimum	25th Percentile	Median	Mean	75th Percentile	Maximum
DIC (mg L^{-1})	42	2.9	8.415	15.88	16.34	23.8	30.62
DOC (mg L^{-1})	41	4.15	6.51	11.14	11.41	14.73	26.08
POC (µg L^{-1})	87	203.1	510.3	927.3	1,934	2,274	12,790
Chl *a* (µg L^{-1})	97	0	0.56	0.9	1.48	1.65	8.08
SSC (mg L^{-1})	52	0.10	2.0	8.0	37.3	56.5	217

Prediction of Carbon Flux to the NRE

Prediction of New River discharge at Highway 17 in Jacksonville during DCERP2 was made by scaling water yield (volume per watershed area per time) at Gum Branch by watershed area at the New River at Jacksonville. This equates to multiplying Gum Branch discharge by 2.6 to yield the discharge at Jacksonville. The root mean square error of these predictions was 6.6 $m^3 s^{-1}$.

Prediction of carbon and sediment fluxes to the NRE over the DCERP lifespan required interpolation daily between the monthly measurements. With discharge as the only continuously measured variable, this interpolation required that relationships be established between constituent concentrations and discharge. Instead of assuming a linear relationship between ln(concentration) and ln(discharge), as in the EGRET model (Hirsch and De Cicco, 2015), non-linear models were fit to each constituent that maximized the utility of the data collected. Three unique regression models were generated between DIC, DOC, and POC, and discharge (**Figure 4-3**). DIC decreased as discharge increased, whereas DOC increased. POC peaked at a low discharge and decreased thereafter.

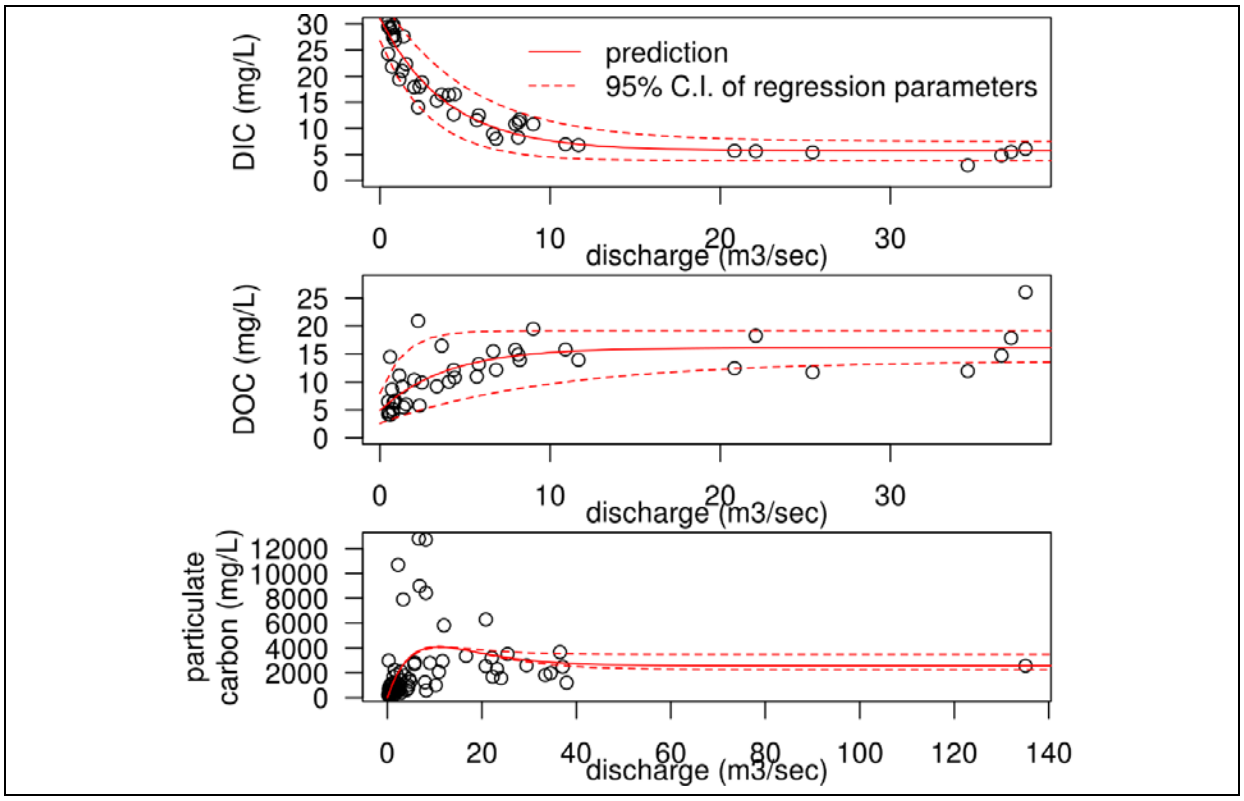

Figure 4-3. The relationships between DIC, DOC, POC, and the discharge used for estimating carbon fluxes to the NRE at Jacksonville.

These relationships were applied to the 2013–2014 and 2014–2015 daily discharge observations to calculate fluxes as carbon input data to the DCERP2 carbon budget (**Table 4-5**). Uncertainty in each flux was calculated from the 95% confidence interval of parameter estimates. As an additional check on the potential imprecision and bias of these flux estimates, the method of Moatar et al. (2012) was applied to the linear regression between concentration and discharge for

each constituent given the frequency of sample collection. In general, imprecision in calculated annual flux was predicted to decrease by approximately half if sampling was conducted weekly versus monthly (with the exception of SSC; **Table 4-A3**). These predictions are instructive for assessment of the estuarine carbon budget. Of the three carbon constituents measured (i.e., DIC, DOC, and POC), POC showed the largest decrease in imprecision, from 45% to 24%, when sampling frequency increased from monthly to weekly. However, POC was a small fraction of the overall carbon budget at Gum Branch, and thus an additional sampling effort would not have yielded a worthwhile increase in accuracy of the carbon budget. It is important to note that the method of annual flux analysis was not based on linear regression between constituent concentration and discharge, so the calculated annual fluxes of carbon are less susceptible to the imprecision and bias predicted by Moatar et al. (2012).

Table 4-5. Annual Flux and Yield Estimates of Carbon Constituents in the New River at Gum Branch by Using Relationships Shown in Figure 4-3

Year (July–June)	POC Flux 10^6 g yr^{-1}	DOC Flux 10^6 g yr^{-1}	DIC Flux 10^6 g yr^{-1}	Total Organic Carbon Yield 10^6 g km^{-2} yr^{-1}	DIC Yield 10^6 g km^{-2} yr^{-1}
2013–2014	224 (222–225)	962 (542–1,398)	1,179 (818–1,556)	4.88 (3.14–6.68)	4.85 (3.37–6.40)
2014–2015	433 (431–447)	1,881 (1,185–2,552)	1,610 (1,071–2,181)	9.52 (6.65–12.3)	6.63 (2.41–8.98)

Prediction of Sediment Flux to the NRE

Sediment flux at Gum Branch was calculated by using a similar approach as POC, in which a model was fitted to the data that captured the apparent plateau in concentration at higher discharge rates (**Figure 4-4**, top panel). The sediment flux over decadal time spans is of particular relevance to the geomorphology of the New River, so extrapolation was performed beginning in 1988, when the present Gum Branch gage position was established. The cumulative suspended sediment flux at Gum Branch from 1988 through 2016 was 1.6×10^{11} g, which averages to 5.6×10^{9} g yr^{-1}.

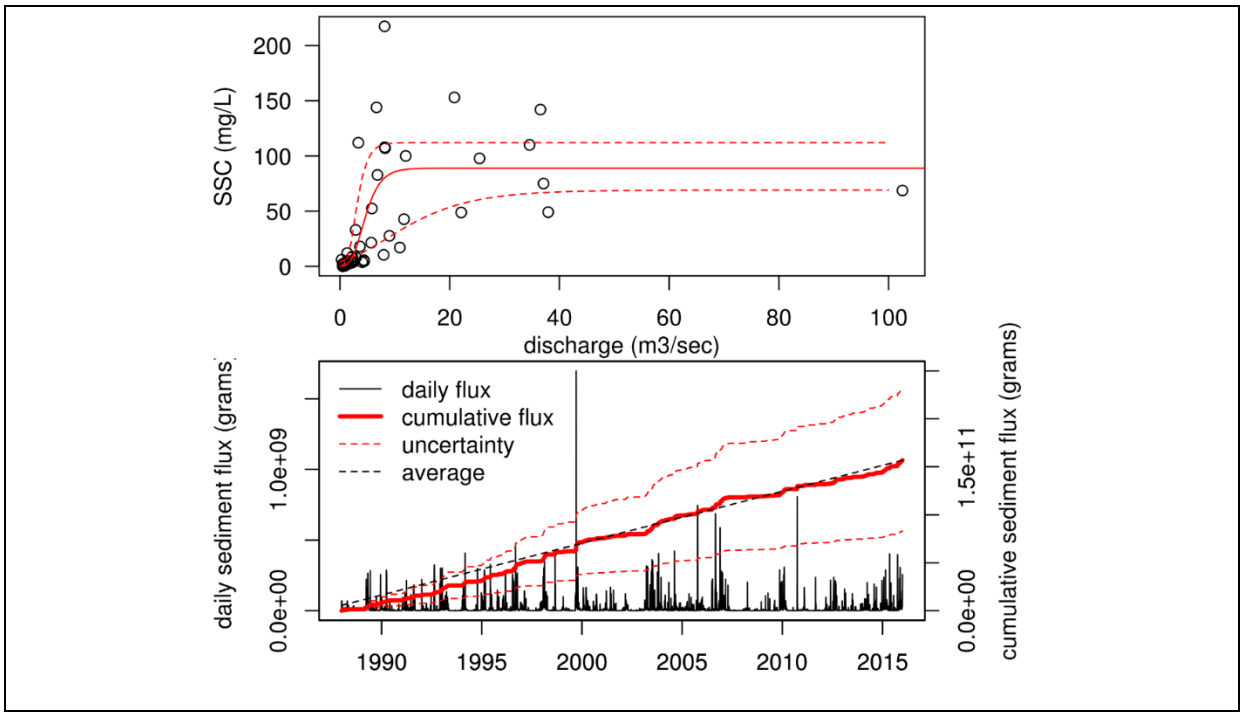

Figure 4-4. The relationship between (top panel) SSC and discharge with model fits and uncertainty and (bottom panel) cumulative sediment flux and uncertainty from 1988 through 2015.

Note: The dashed black line shows the cumulative sediment flux of the annual average.

When normalized by the 243 km^2 watershed upstream from Gum Branch, the resultant 23×10^6 g km^{-2} yr^{-1} is higher than most long-term sediment yields for coastal plain rivers from New Jersey through Florida (Ensign and Noe, in revision). Consideration of how this sediment flux is transported to the NRE is a critical component of the DCERP estuarine sediment and carbon budgets. Without further information about floodplain dynamics within the tidal freshwater zone of the New River, the DCERP Team assumed that 100% of this sediment is passed through the tidal freshwater zone into the saline estuary below Jacksonville. It is more likely that a high proportion of this sediment is trapped by tidal riparian wetlands before reaching Jacksonville.

Tidal freshwater forested wetlands in the Eastern United States accrete an average of 4,629 grams of sediment m^{-2} yr^{-1} (Noe et al., in review). Applying this accretion rate to a 50-m wide riparian floodplain on either side of the 19-km long tidal freshwater New River (Ensign et al., 2012), as much as 8.8×10^9 grams of sediment per year are removed from fluvial transport before reaching the oligohaline estuary at Jacksonville (**Table 4-6**). Fluvial suspended sediment that does reaches the oligohaline portion of the estuary may be further attenuated by capture in salt marshes, such as fringing wetlands at Freeman Creek, which can easily trap the total annual watershed sediment flux from their watersheds (Piehler, 2013).

Table 4-6. Sediment Budget for the NRE

	Source: Watershed Above Gum Branch	Source: Watershed Below Gum Branch off Base	Source: Watershed on Base	Source: NRE Shoreline Erosion	Sink: Tidal River Floodplain Deposition	Total Delivery to NRE
Watershed area (km^2)	243	473 [a]	308	—	—	1,024
Annual average yield (10^6 g km^{-2} yr^{-1})	23.0	23.0	9.6 [b]	—	—	—
Annual average flux (10^9 g yr^{-1})	5.60	10.9	3.0	18.6 [c]	8.80 [d]	29.3

[a] Includes the 394 km^2 watershed between Gum Branch and Jacksonville, and the off-Base portion of the tributaries entering the New River downstream from Jacksonville.

[b] Yield measured from 10 watersheds during Monitoring Activity AEM-2 is averaged annually from 2008 through 2011.

[c] Assuming a shoreline erosion of 18,618 m^3 yr^{-1} to the NRE and a bulk density of 1,000,000 g m^{-3}.

[d] Assuming a deposition of 4,629 g m^{-2} yr^{-1}, a river length of 19 km, and an active floodplain width of 50 m on either side of the channel.

In addition to sediment erosion and transport from the watershed, shoreline erosion is a source of sediment to the NRE. Using the measurement of 18,618 m^3 yr^{-1} of shoreline erosion in the NRE (Currin et al., 2015) and assuming a bulk density of 1 g cm^{-3}, it is estimated that 18.6×10^9 grams of sediment per year enters the NRE from shoreline erosion. In contrast, the average annual sediment yield at Gum Branch (23×10^6 g km^{-2} yr^{-1}) scaled to the entire NRE watershed drainage area (1,024 km^2) would produce a flux of 37×10^9 g yr^{-1}. Thus, shoreline erosion supplies 63% of the sediment flux to the NRE (after accounting for sediment loss from tidal river floodplain deposition).

Deposition of POC in riparian wetlands must also be considered in an analysis of estuarine carbon budgets and sediment carbon stocks. Assuming an average allochthonous carbon trapping in riparian zones of 150 g m^{-2} yr^{-1} (Noe et al., in review), this equates to a loss of 285×10^6 g of carbon along the 19-km reach from Gum Branch to Jacksonville with a 50-m wide riparian zone on either side of the channel. This estimated annual loss is similar to the POC flux at Gum Branch (**Tables 4-5** and **4-A2**), indicating that the entire flux of POC past Gum Branch may be trapped on the riparian floodplain before reaching the estuary at Jacksonville. The effect of this POC trapping on POC flux to the estuary at Jacksonville is offset by tributaries entering the river within the tidal freshwater zone. An additional source of carbon to the NRE is from shoreline erosion. Using an estimated 18,618 m^3 yr^{-1} of shoreline erosion in the NRE (Currin et al., 2015), and soil carbon density of 0.02 g C g^{-1} of sediment, carbon flux to the NRE is estimated at 372×10^6 g C yr^{-1}. This shoreline source flux of POC to the NRE is estimated to be 25% of total delivery.

Storm Flows on the New River: The Example of Hurricane Matthew

In the week preceding Hurricane Matthew, a YSI 600OMS with a turbidity probe was deployed 5-km upstream of Jacksonville. Turbidity measured during the event was used to estimate SSC

based on a regression relationship between turbidity and SSC at the Gum Branch station. The water level on the New River at Gum Branch increased by 5 m during the storm, but the water level upstream of Jacksonville increased by less than 1 m. This attenuation of the storm flow, the second highest in the past 53 years, was likely because of widespread inundation of the riparian floodplain. A similar decrease in the water level between a river gage and tidal freshwater zone was reported on the Choptank River, MD (a similar-sized watershed), following its largest flood in more than 50 years (Ensign et al., 2014). The wide floodplain of these coastal plain river systems attenuates flood height.

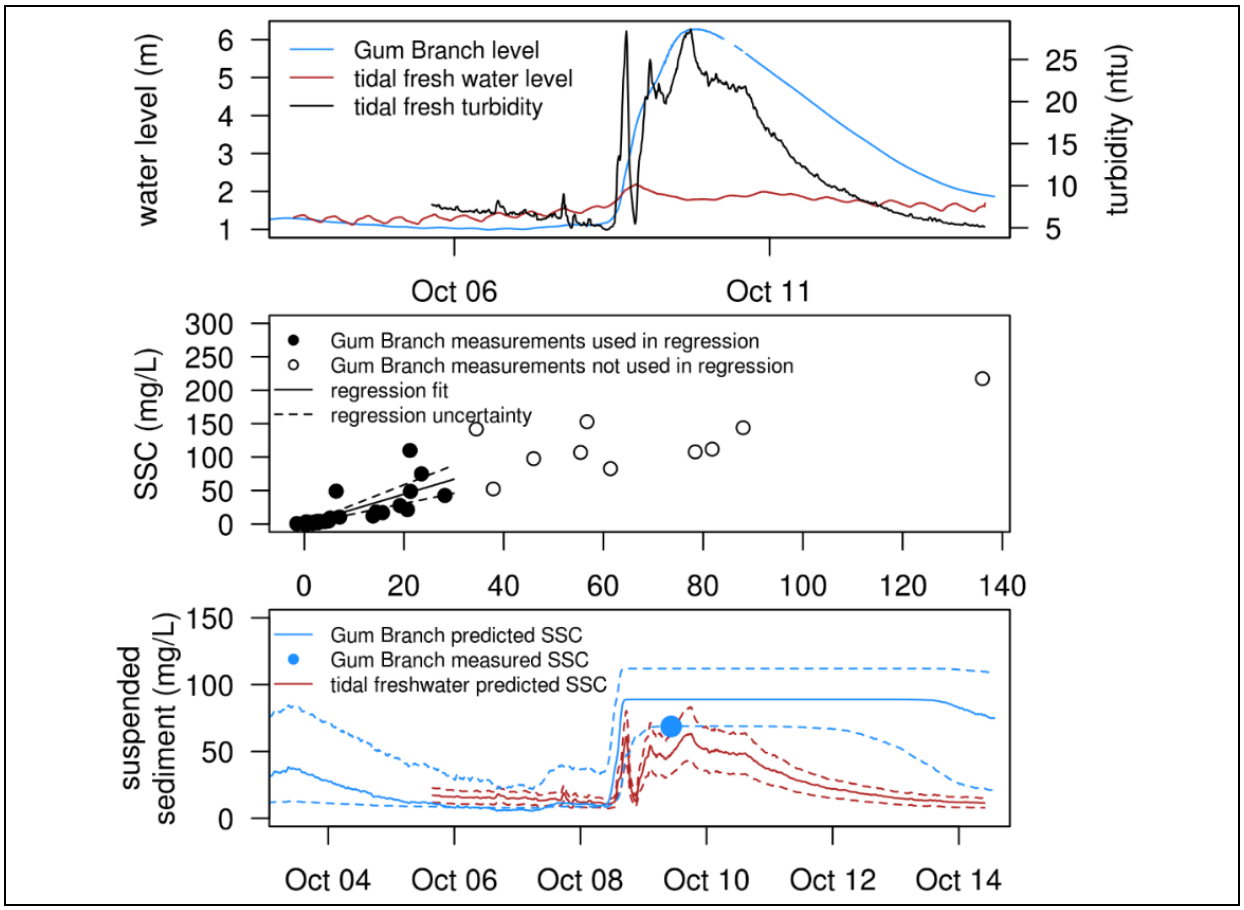

Figure 4-5. (Top panel) The effects of Hurricane Matthew on water level and turbidity), (middle panel) the relationship between SSC and turbidity at Gum Branch, and (bottom panel) the predicted SSC during Hurricane Matthew.

Note: Dashed blue and red lines represent the 95% confidence interval of the predictions. The regression in the middle panel was based only on the turbidity values within the range shown in the top panel.

This broad inundation of the floodplain also allows sediment deposition to occur. Using a regression relationship between SSC and turbidity at Gum Branch (**Figure 4-5**, middle panel) and measured turbidity from the deployed probe. We estimated SSC in the tidal freshwater New River upstream from Jacksonville. The predicted SSC during Hurricane Matthew at Gum Branch was higher than the tidal freshwater site throughout the event. Although uncertainty in these predictions is relatively large, it appears likely that SSC decreased downstream of Gum Branch as the suspended flux was deposited on the inundated riparian floodplain. However, without

discharge measurements at the head of this reach, it is impossible to determine the mass of sediment deposited in the floodplain.

Sensitivity of River Flux to Changes in Discharge Due to Climate Change

River discharge, rather than constituent concentration, largely controls the flux of constituents downstream. Therefore, changes in discharge regime because of climate change in the future may alter constituent fluxes to the NRE. An analysis of discharge (as a cumulative frequency distribution) and the magnitude of constituent flux across that range of discharge provides insight regarding how future changes in discharge regime may affect long-term constituent flux. The relationships between discharge and concentration previously discussed in this chapter were combined with the discharge record at Gum Branch from 1949 to 2016. **Table 4-7** provides a summary of results for two percentiles of the total constituent fluxes from 1949 to 2016. For example, 75% of the DIC flux has occurred at discharges less than 7.08 $m^3 s^{-1}$ (the 90.4th percentile of mean daily discharge from 1949 to 2016), and 90% of DIC flux has occurred at discharges less than 17.8 $m^3 s^{-1}$ (97.6th percentile of mean daily discharge). Graphical representations of each constituent's frequency-magnitude flux are provided in **Figures 4-A15 through 4-A19** in **Appendix 4-A** of this chapter.

Table 4-7. Summary Results from Frequency-Magnitude Analysis of Constituent Fluxes Past the New River at Gum Branch

Constituent	Discharge ($m^3 s^{-1}$) at the 75th Percentile of Constituent Flux	Percentage of Discharge Record	Discharge ($m^3 s^{-1}$) at the 90th Percentile of Constituent Flux	Percentage of Discharge Record
DIC	7.08	90.4%	17.8	97.6%
DOC	22.4	98.3%	44.7	99.6%
POC	17.8	97.6%	35.5	99.3%
SSC	22.4	98.3%	44.7	99.6%
NO_3	11.2	95.1%	28.2	98.9%
PO_4	28.2	98.9%	56.2	99.8%

With the exception of DIC, 25% of the total constituent fluxes occurred during relatively high discharge events (>95th percentile). This finding means that 25% of the annual constituent flux occurs during just 18 days of the year. Constituent fluxes to the NRE are sensitive to future changes in climate that could focus precipitation into more clustered storm events. Even if the total river discharge remains constant in the future, the distribution of that flow over the year may affect constituent fluxes to the NRE. DCERP2 Research Project CC-1 (*DCERP2 Final Report*, Chapter 3) does not predict any significant change in precipitation for the New River watershed through 2030, but the 2060–2090 period may have an increase in the number of days with more than 1 inch of rainfall. Therefore, significant changes in constituent fluxes to the NRE due to precipitation patterns affected by climate change are not expected for another 30 years.

Assessment of Directionality/Trends

- Sampling at Gum Branch during DCERP2 consisted of a pair of low and high discharge samples collected every 2 months. This effort to collect samples during high-discharge events improved the accuracy of subsequent calculations of annual constituent fluxes. A statistical analysis of the relationship between constituent concentration and discharge during high-discharge events further improved the annual constituent flux estimates. In addition, estimates of annual flux would have been further improved by sampling weekly or biweekly (every 2 weeks) rather than monthly: precision of DIC and NO_3 flux would improve 7%; precision of DOC, NH_4, and TDN flux would improve 10%; and precision of POC, PN, PO_4, and SSC flux would improve 21%.
- The 7-day and 30-day minimum flows at Gum Branch and tidal influence have increased over the past 28 years, likely because of sea level rise. The onset of tides in the 1970s or 1980s changed the New River at Gum Branch into an estuary, and this change in hydrology will have a profound influence on biogeochemical and sedimentary processes between Gum Branch and Jacksonville.
- The flux of dissolved nitrogen (including organic and inorganic forms) at Gum Branch likely decreased during the DCERP monitoring period. Some of this decrease in flux was because of a decrease in NO_3 flux and NH_4 concentration. While Gum Branch represents the head of the NRE, its watershed only represents 24% of the overall New River Basin. Therefore, although a decrease in dissolved nitrogen to the head of the NRE can be concluded with some confidence, it is unclear whether this trend has occurred throughout the broader watershed downstream.
- PO_4 concentration has likely decreased at Gum Branch during the DCERP monitoring period. However, a change in PO_4 flux was not likely to have occurred. This may indicate that sources of PO_4 to the New River upstream of Gum Branch have decreased, but that there is sufficient PO_4 mobilized during storms to offset the decrease in concentration.
- A decrease in the delivery of dissolved nitrogen to the NRE may reduce phytoplankton growth and biomass accumulation during some periods of the year. Knowledge of these changes in river flux and subsequent algal response are essential to any future data interpretation in the NRE. Therefore, continued monitoring of nitrogen and phosphorus at the New River at Gum Branch should be a core component of any future monitoring effort in the NRE.

Conclusions and Implications for Future Research and Implementation

Key Findings

A key finding of this monitoring effort was that the NRE extends upstream to the mainstem New River at Gum Branch, where sea level rise is increasing the daily range in water level and increasing the minimum annual flows. This is the first instance where the onset of tidal condition has been detected at a river gaging station in the United States. The tidal freshwater portion of the NRE is currently extending upstream because of sea level rise, and this hydrologic change between Jacksonville and Gum Branch may have affected in-stream biogeochemical processes, floodplain dynamics and vegetation, and the flux and processing of materials as they traverse the

New River's tidal freshwater zone. The shifting boundaries of estuarine condition offer exciting opportunities for future research. For example, how are rates of ecosystem processes (e.g., denitrification, sulfate reduction, tree mortality, fin fish habitat use) changing across the estuarine gradient, and what is the net result on each process? How do changes in those processes interact over time? How should management action anticipate these changes to maximize preservation and function of these processes? Answering these questions is not directly relevant to MCBCL management activities because the New River tidal freshwater estuary is off-Base. However, this same process of tidal extension is likely occurring in the tributaries to the NRE that are on MCBCL, such as Southwest Creek and Northeast Creek. Efforts by MCBCL to monitor and manage riparian wetland habit should be aware that tidal extension may be occurring in these habitats and may explain shifts in flora and fauna as the hydrology changes.

A second key finding of this monitoring effort was that dissolved nitrogen flux to the NRE has likely decreased during the past 9 years. Furthermore, it is likely that the PN concentrations decreased, and it is highly likely that PO_4 concentrations decreased during this period. No data were collected upstream of Gum Branch regarding river or watershed processes; therefore, it is unclear why nitrogen and phosphorus levels have declined. However, from a land and estuary management perspective, these are positive changes. Phytoplankton in the NRE are growth-limited by nitrogen and phosphorus during some periods of the year, so decreased riverine delivery may help limit growth rates for some species that potentially pose a direct or indirect problem to the estuarine ecosystem. This trend analysis accomplishes a major objective of the DCERP monitoring effort. Stakeholders with interests in water quality of the NRE should be encouraged by the decreasing trend in nitrogen and phosphorus as potentially indicating the effectiveness at nutrient reduction strategies implemented in the watershed, but should keep in mind that past trends do not guarantee a continued change in the future. Monitoring of nitrogen and phosphorus should continue at Gum Branch and tributaries on MCBCL so that more robust trend detection can be performed over time. Interpretation of future changes in phytoplankton in the NRE requires co-occurring measurements of nitrogen and phosphorus flux to the estuary.

A third key finding of this monitoring effort was that sediment flux to the NRE is mainly a local process, not a watershed-scale process. The sediment yield of the New River watershed, while relatively high compared with other Coastal Plain rivers, is low enough that all of the sediment passing Gum Branch is expected to be trapped and stored on the floodplain before reaching Jacksonville. This finding means that most of the sediment entering the NRE is from shoreline erosion along the estuary, itself. Similarly, the very low yield of POC and extensive trapping on storage of river floodplains leave shoreline erosion as a significant source of POC to the NRE. Although river floods (such as those that occurred after Hurricane Matthew) increase sediment and POC flux at Gum Branch, the water level and sediment concentrations are greatly attenuated prior to reaching Jacksonville. These data and conclusions resolve the knowledge gap that exists in DCERP regarding sediment and carbon budget input to the NRE. From a management perspective, the conclusion is that preserving riparian wetland buffers is an extremely effective strategy for keeping sediment from developed land from reaching the NRE.

A final key finding resulted from the supplemental research on tidal transport, nitrogen, and carbon transformation in the tidal freshwater zone of the NRE (**Appendix 4D**). A critical gap in DCERP was knowledge of the time-scale of constituent transport from the head of the estuary at

Gum Branch to Jacksonville. Deployment of Lagrangian drifters showed that travel time through this reach took between 2.8 and 6.1 days, depending on river discharge. This travel time served as the basis for estimating the transformation of NO_3 and DOC entering the estuary at Gum Branch and before arriving at Jacksonville. During this travel time, approximately 10% of the NO_3 load at Gum Branch was predicted to be removed by denitrification, and 31% of the DOC flux was predicted to be converted to DIC by photomineralization. In addition, the flux of DIC at Jacksonville was 1.4 times the flux at Gum Branch. These predictions inform the DCERP effort to parameterize a carbon budget by providing estimates of how fluxes at Gum Branch should be modified to represent the budget boundary at Jacksonville. For stakeholders and MCBCL, the value of this research is the estimated travel time of potential pollutants (such as what occurred during a swine lagoon spill on the New River in 1995) from Gum Branch to Jacksonville. Although travel time was not measured during a high-discharge event, the data provide an indication of how long managers may have to alert the public of a water quality hazard in Jacksonville if a pollutant is detected at Gum Branch.

Findings with Implications for Future Base Management

The tidal freshwater portion of the NRE is extending farther inland as sea level rises. This tidal extension is also likely occurring throughout MCBCL in low elevation stream channels: this is a net benefit to operations at MCBCL. Tidal extension into low elevation streams at MCBCL provides additional capacity for trapping and storage of watershed sediment that may otherwise impair estuarine waters. If these riparian areas are not disturbed by development or engineering practices (e.g., culverts, weirs), then MCBCL will receive additional ecosystem services from these low elevation, tidal streams that trap sediment. The ecosystem services provided by this altered hydrology may be disproportionately large relative to the small footprint of wetland change. Furthermore, tidal extension and changes in hydrology may help explain observed changes in flora and fauna in riparian habitats.

Monitoring in the off-Base portion of the New River watershed revealed decreases in nitrogen and phosphorus. These changes may affect phytoplankton growth and its direct and indirect effects on the NRE. To detect future changes in nitrogen and phosphorus flux to the New River, MCBCL should continue monitoring at Gum Branch and select locations on-Base that have been monitored continuously during DCERP. Without continuous data about nitrogen and phosphorus flux at Gum Branch and other locations, explaining the cause of future changes in phytoplankton in the NRE will be impossible. Continuous data about nitrogen and phosphorus flux to the NRE would dramatically simplify the research required to evaluate the need for point and non-point nutrient regulations in the future, while reducing uncertainty about causes of water quality impairment.

The extensive tidal riparian zones of the NRE tributaries on MCBCL provide an extremely important function of trapping watershed sediment. This function is particularly valuable on MCBCL in areas of recent land clearing or development where sediment loads to streams may be temporarily elevated. Preservation of existing riparian zones and restoration of degraded riparian zones on MCBCL will greatly reduce sediment flux to the NRE.

Finally, the location of MCBCL surrounding the NRE makes it vulnerable to pollutant spills upstream on the New River and its watershed. Major spills have occurred upstream in the past

and ultimately affected water quality at MCBCL access points on the NRE. One aspect of emergency preparedness on MCBCL is knowledge of how long it takes spills to travel from upstream sources to the NRE. Under low discharge conditions, the travel time is between 3 and 6 days. Research needs to be conducted to determine what this spill travel time would be during high-discharge events, so more precise measurements can be made for individual locations on MCBCL.

Literature Cited

Arar, E.J., and G.B. Collins. 1997. Method 445.0: In vitro determination of chlorophyll *a* and pheophytin in marine and freshwater algae by fluorescence. U.S. Environmental Protection Agency (EPA), Washington, DC.

ASTM International. 2013. ASTM D3977-97: Standard test methods for determining sediment concentration in water samples. ASTM International, West Conshohocken, PA.

Currin, C., J. Davis, L. Cowart Baron, A. Malhotra, and M. Fonseca. 2015. Shoreline change in the New River Estuary, North Carolina: Rates and consequences. *Journal of Coastal Research 31*(5):1069–1077.

Ensign, S.H., and G.B. Noe. In revision. Tidal extension and sea level rise: Recommendations for a research agenda. *Frontiers in Ecology and the Environment.*

Ensign, S.H., G.B. Noe, and C.R. Hupp. 2014. Linking channel hydrology with riparian wetland accretion in tidal rivers. *Journal of Geophysical Research: Earth Surface*

Ensign, S.H., M.W. Doyle, and M.F. Piehler. 2012. Tidal geomorphology affects phytoplankton at the transition from forested streams to tidal rivers. *Freshwater Biology 57*:2141–2155.

Hirsch, R.M., and L.A. De Cicco. 2015. *User Guide to Exploration and Graphics for RivEr Trends (EGRET) and Data Retrieval—R Packages for Hydrologic Data.* Version 2.0, February 2015. U.S. Geological Survey Techniques and Methods, Book 4, Chapter A10. 93 pages.

Hirsh, R.M., S.A. Archfield, and L.A. De Cicco. 2015. A bootstrap method for estimating uncertainty of water quality trends. *Environmental Modelling and Software 73*:148–166. doi:

Moatar F., M. Meybeck, S. Raymond, F. Birgand, and F. Curie. 2012. River flux uncertainties predicted by hydrological variability and riverine material behaviour. *Hydrological Processes 27*(25):3535–3546. doi:10.1002/hyp

Noe, G.B., C. Hupp, E. Schenk, K. Krauss, S. McMillan, D. Kroes, S. Ensign, J. Gillespie, K. Wolf, and C. Ahn. In review. Nutrient and sediment inputs change soil structure and biogeochemistry in floodplain ecosystems: A cross-study analysis of consequences of hydrologic connectivity.

Piehler, M.F. 2013. *Defense Coastal/Estuarine Research Program (DCERP1) Final Monitoring Report*. Chapter 4: Tributary Creeks. RTI International, Research Triangle Park, NC.

Appendix 4-A
Supporting Data

Table 4A-1. Annual Mean of Daily Mean Streamflow for the New River near Gum Branch (U.S. Geological Survey Stream Gaging Station 02093000)

Calendar Year	Annual Mean Streamflow
2007	2.056
2008	1.500
2009	2.724
2010	3.320
2011	1.571
2012	3.066
2013	2.226
2014	3.157
2015	5.834
2016	4.963
Period of record[a]	3.268

[a] Calendar years 1950–1973 and 1988–2016.

Table 4A-2. Particulate Organic Carbon (POC) Budget for the NRE

	Source: Watershed Above Gum Branch	Source: Watershed Below Gum Branch off-Base	Source: Watershed on-Base	Source: NRE Shoreline Erosion	Sink: Tidal River Floodplain Deposition	Total Delivery to NRE
Watershed area (km^2)	243	473[a]	308	—	—	1,024
Annual average yield (10^6 g C km^{-2} yr^{-1})	1.35	1.35	1.35	—	—	—
Annual average flux (10^6 g C yr^{-1})	328[a]	639	416	372	285	1,470

[a] Average of both annual periods reported in **Table 4-5**.

Table 4A-3. Predicted Median Imprecision and Bias of Annual River Fluxes at Gum Branch Predicted by Using the Methods of Moatar et al. (2012)

Parameter	7-Day Imprecision	7-DayBias	15-Day Imprecision	15-DayBias	30-Day Imprecision	30-DayBias
DIC	±8	1	±10	1	±15	2
DOC	±10	0	±13	0	±20	0
POC	±24	−3	±32	−7	±45	−14
NH_4	±10	0	±13	0	±20	0
NO_3	±8	1	±10	1	±15	2
TDN	±10	0	±13	0	±20	0
PN	±24	−3	±32	−7	±45	−14
PO_4	±24	−3	±32	−7	±45	−14
SSC	±50	−8	±60	−22	±70	−36

Note: DIC = dissolved inorganic carbon; DOC =dissolved organic carbon; NH_4 = ammonium; NO_3 = nitrate; PN = particulate nitrogen; POC = particulate organic carbon; PO_4 = orthophosphate; TDN = total dissolved nitrogen; SSC = suspended sediment concentration.

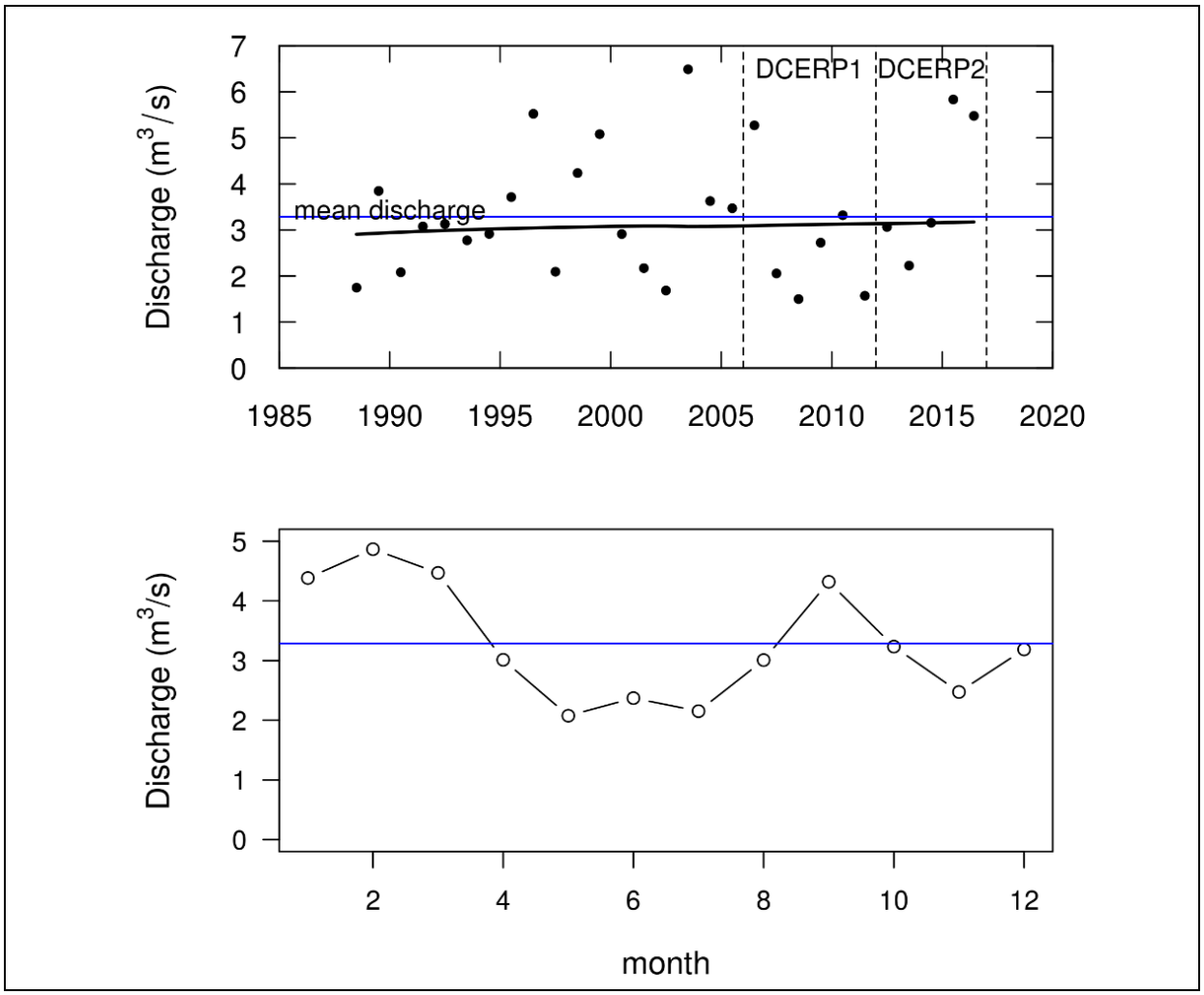

Figure 4A-1. Annual mean discharge at Gum Branch from 1988 through 2016, showing overall mean (blue line) and (top panel) Exploration and Graphics for RivEr Trends (EGRET)–predicted trend (black line), and (bottom panel) monthly mean discharge at Gum Branch over the same period.

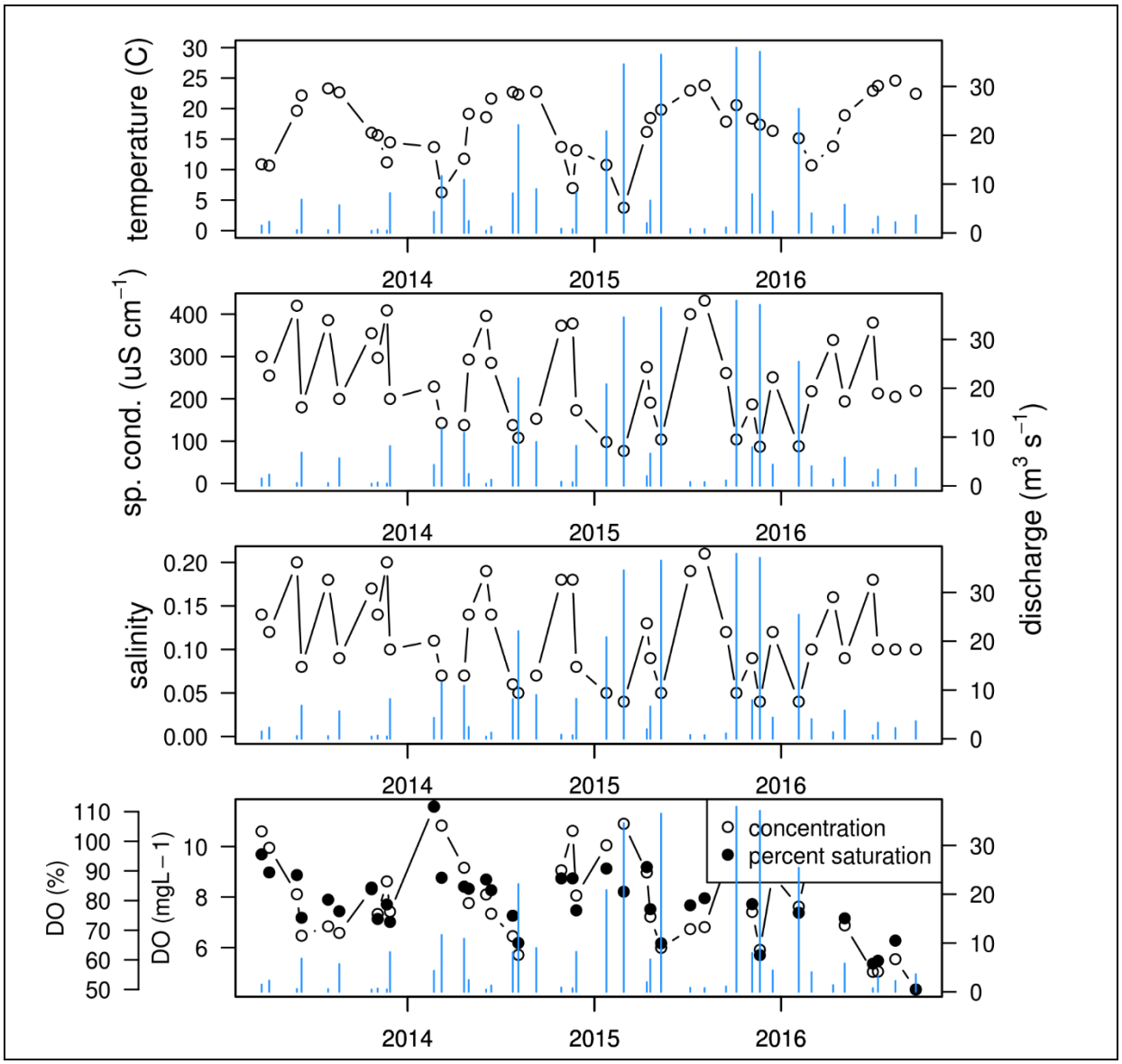

Figure 4A-2. Temperature, specific conductivity, salinity, dissolved oxygen, and discharge at the New River at Gum Branch during the DCERP2 monitoring period.

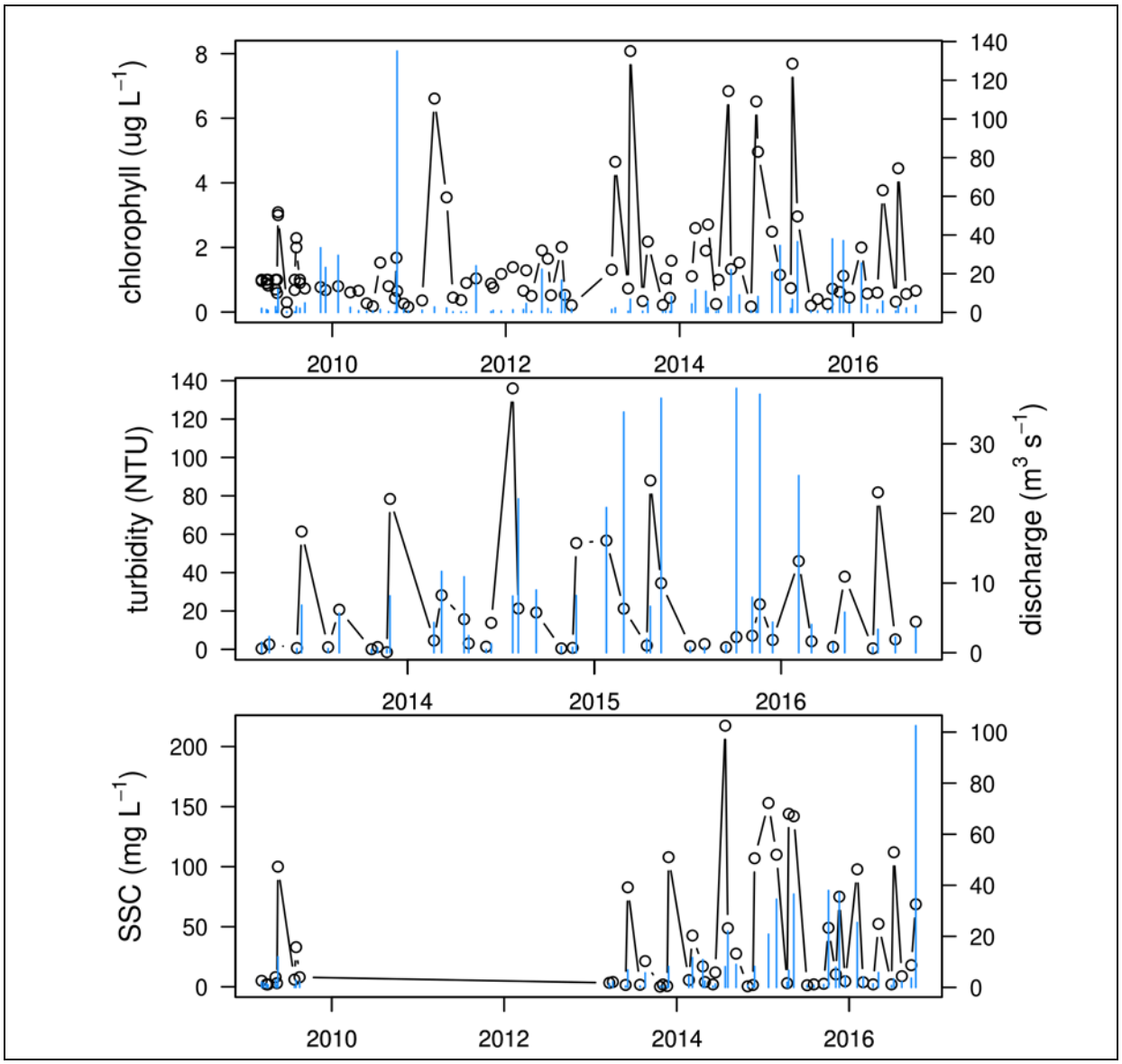

Figure 4A-3. Chlorophyll *a*, turbidity, and suspended sediment concentrations (SSC) at the New River at Gum Branch during the DCERP1 and DCERP2 monitoring period.

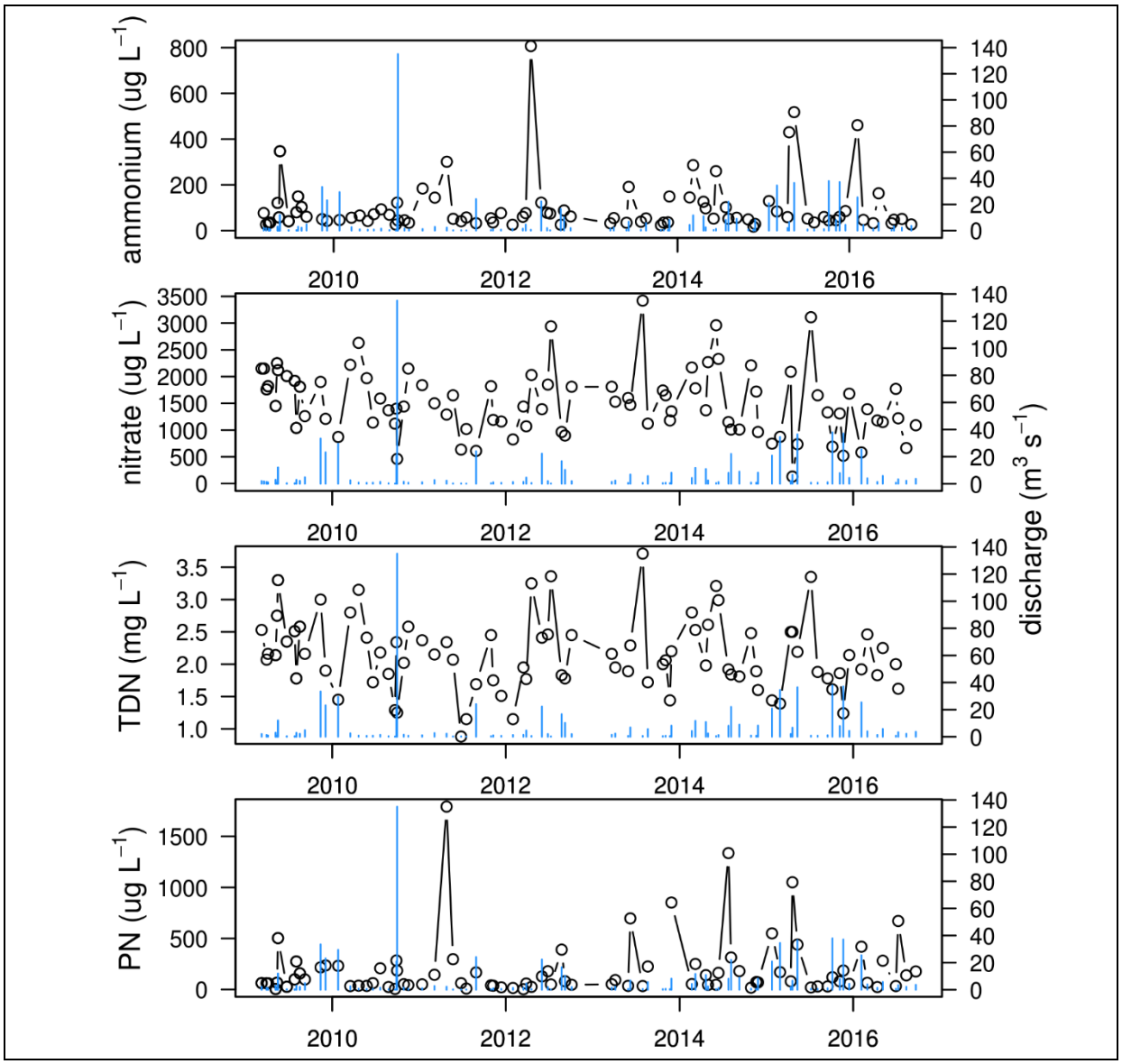

Figure 4A-4. Ammonium (NH_4), nitrate (NO_3), total dissolved nitrogen (TDN), and particulate nitrogen (PN) at the New River at Gum Branch during the DCERP1 and DCERP2 monitoring period.

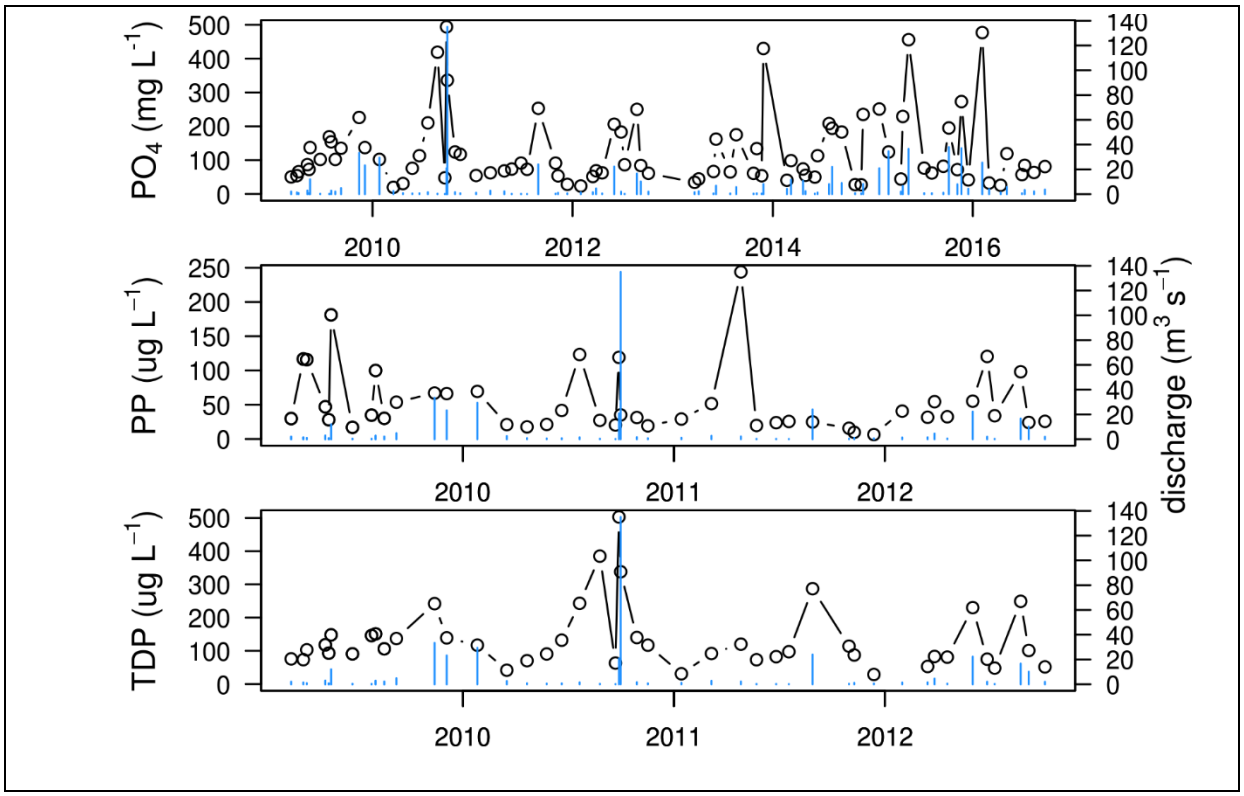

Figure 4A-5. Orthophosphate (PO_4), particulate phosphorus (PP), and total dissolved phosphorus (TDP) at the New River at Gum Branch during the DCERP1 and DCERP2 monitoring period.

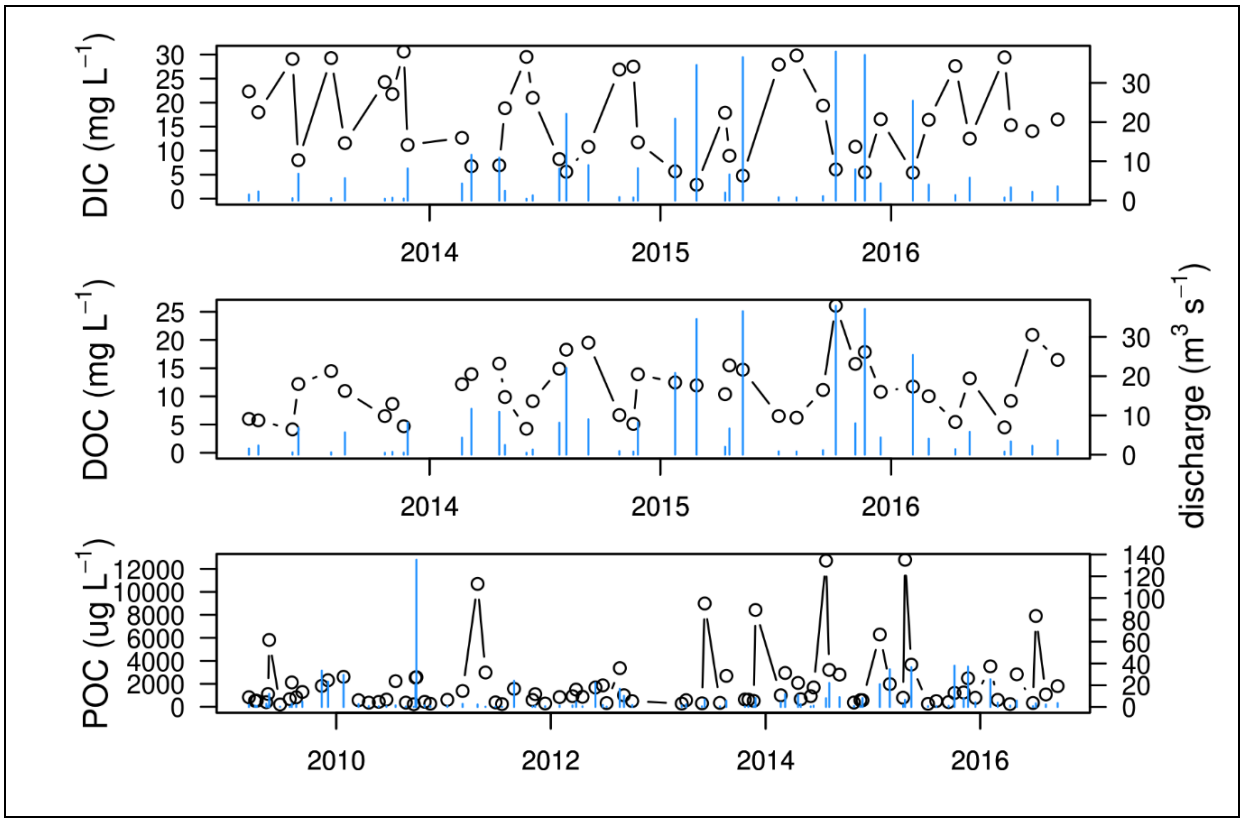

Figure 4A-6. Dissolved inorganic carbon (DIC), dissolved organic carbon (DOC), and particulate organic carbon (POC) at the New River at Gum Branch during the DCERP1 and DCERP2 monitoring period.

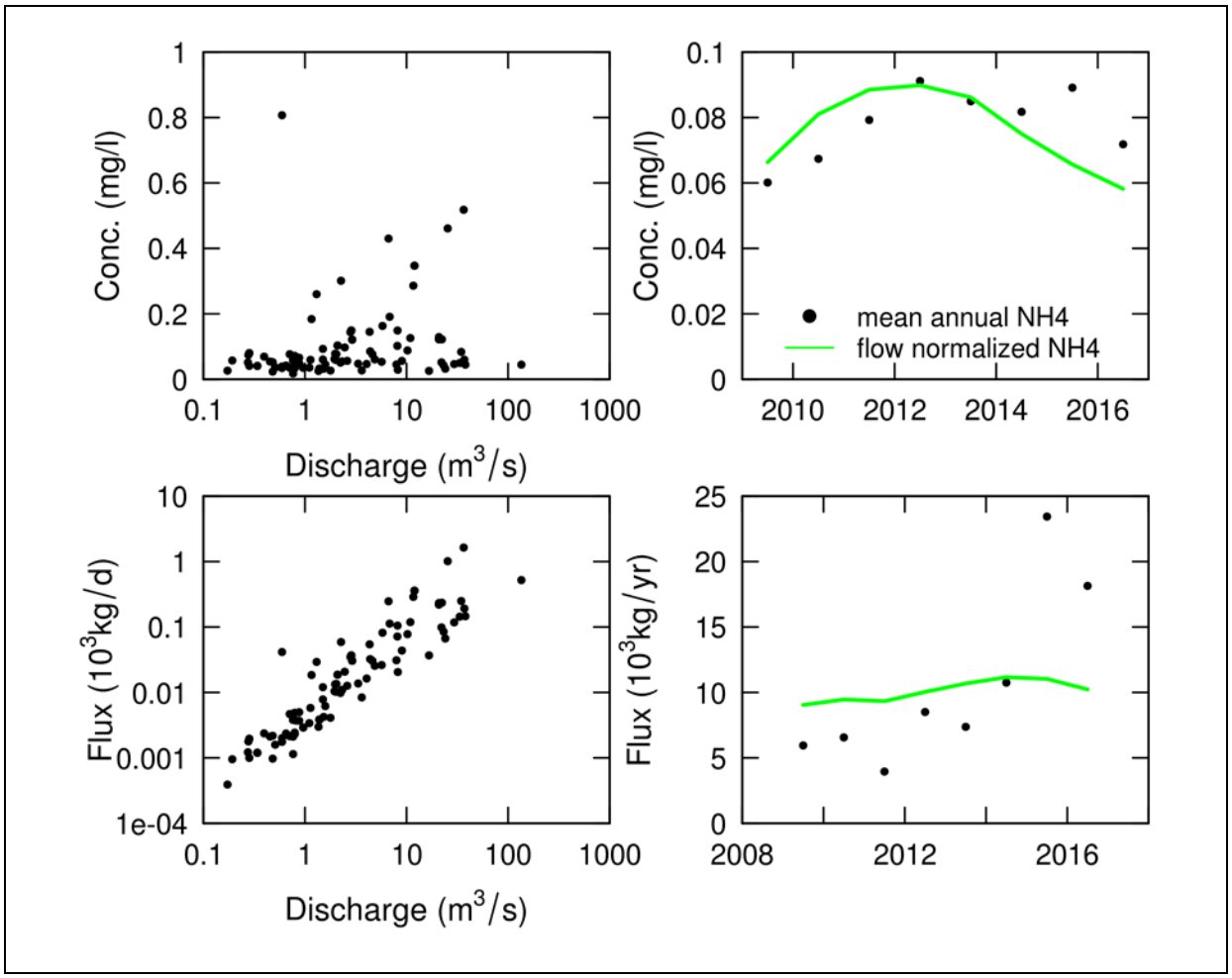

Figure 4A-7. The EGRET Weighted Regression on Time, Discharge, and Season (WRTDS) model trend analysis of ammonium (NH_4) at the New River at Gum Branch.

The EGRET confidence interval analysis showed that the change in flow-normalized concentration between 2010 and 2016 was not statistically significant, but it is likely that NH_4 concentration decreased. The change in flow-normalized flux between 2010 and 2016 was not statistically significant, and it is unlikely that NH_4 flux changed.

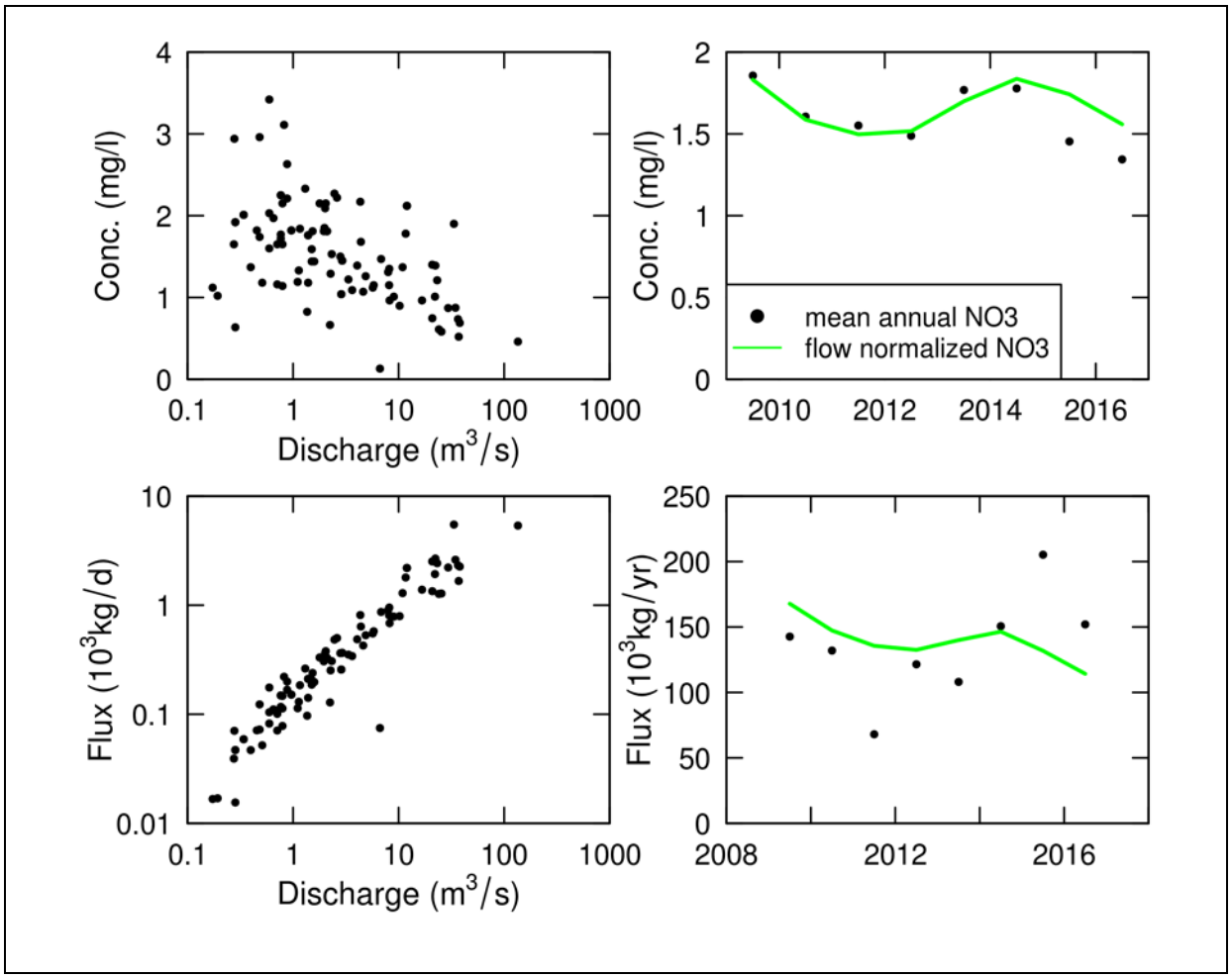

Figure 4A-8. The EGRET WRTDS model trend analysis of nitrate (NO_3) at the New River at Gum Branch.

The EGRET confidence interval analysis showed that the change in flow-normalized concentration between 2010 and 2016 was not statistically significant, and it is unlikely that NO_3 concentration changed. The change in flow-normalized flux between 2010 and 2016 was not statistically significant, but it is likely that NO_3 flux decreased.

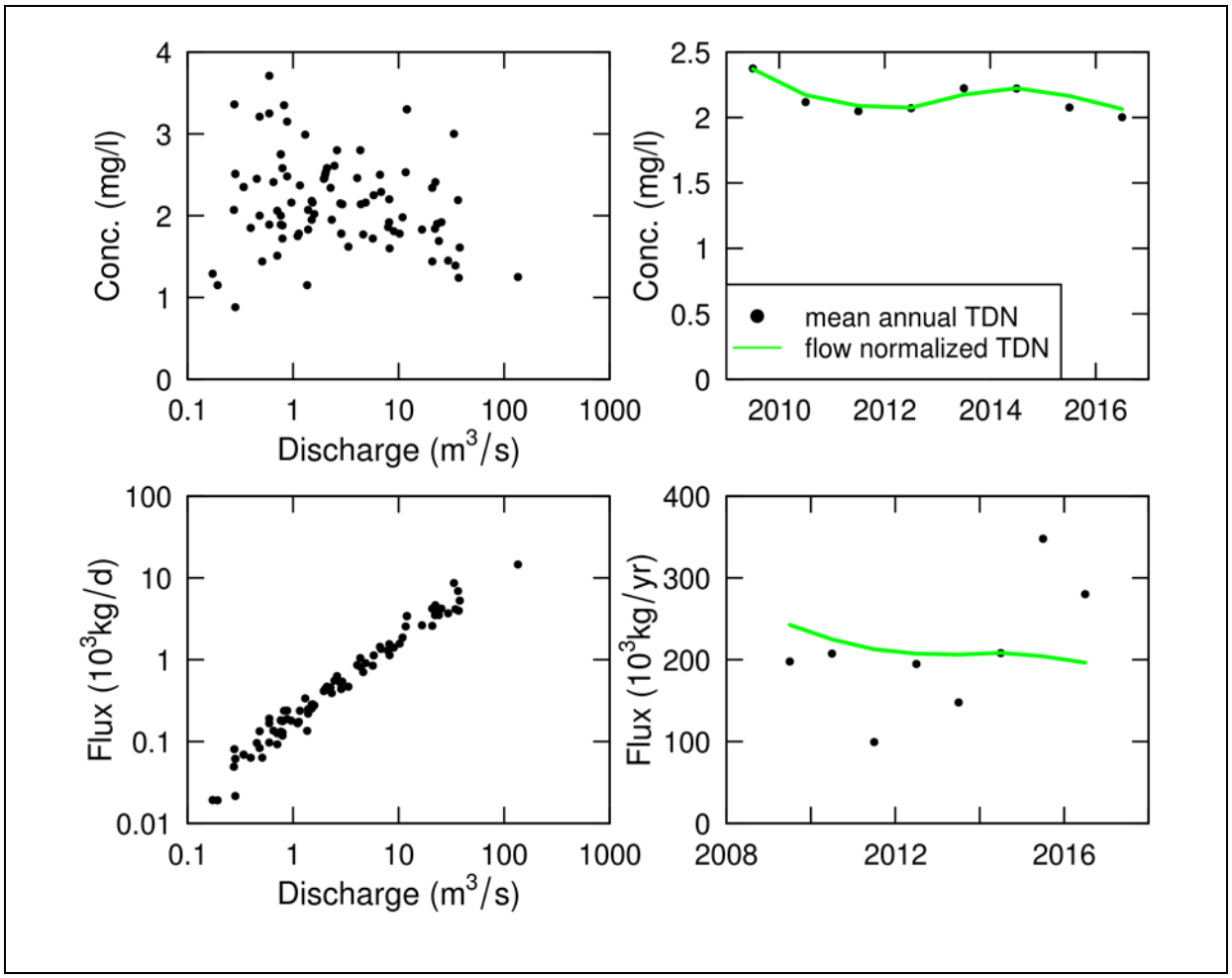

Figure 4A-9. The EGRET WRTDS model trend analysis of total dissolved nitrogen (TDN) at the New River at Gum Branch.

The EGRET confidence interval analysis showed that the change in flow-normalized concentration between 2010 and 2016 was not statistically significant, but it is likely that TDN concentration decreased. The change in flow-normalized flux between 2010 and 2016 was not statistically significant, but it is very likely that TDN flux decreased.

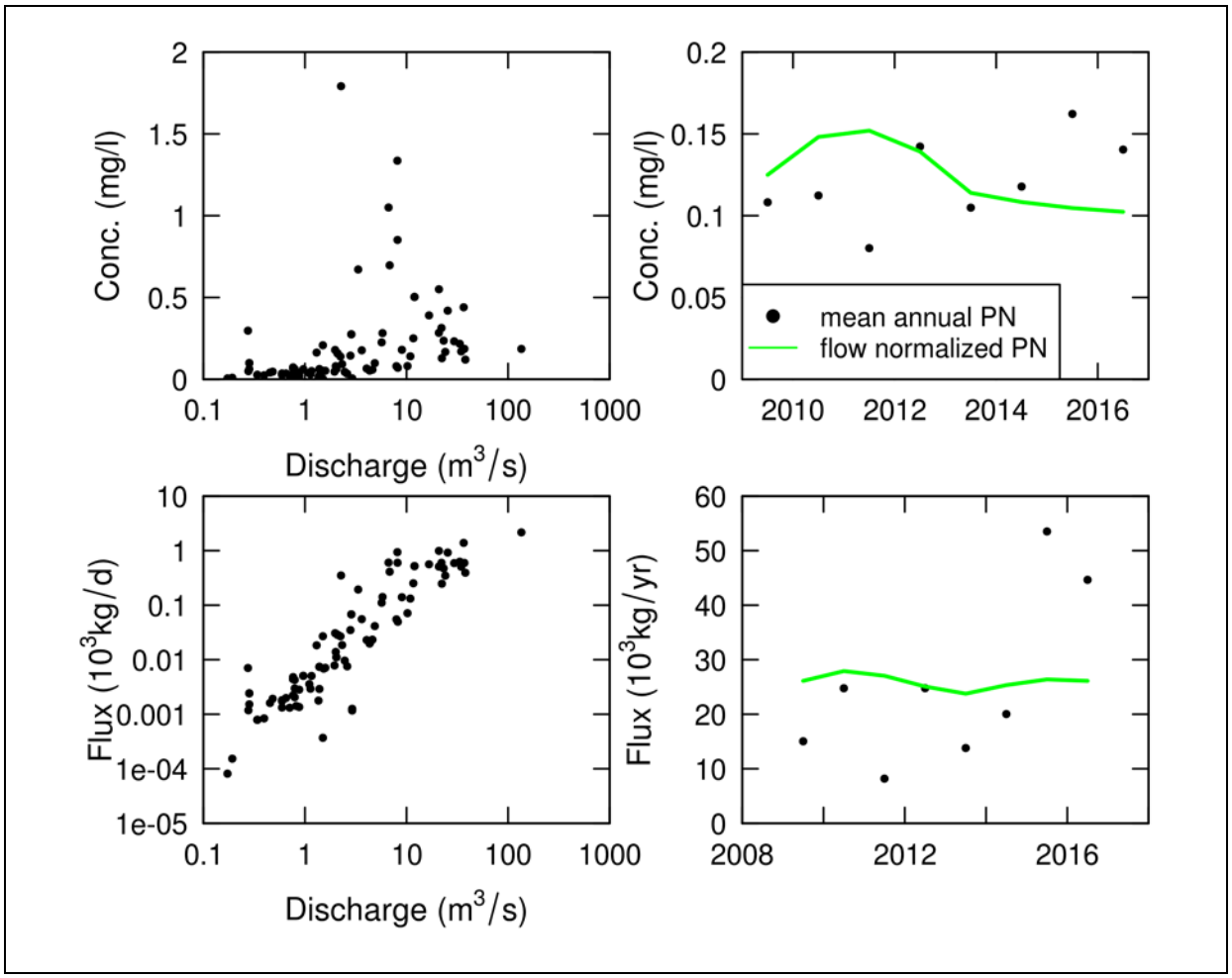

Figure 4A-10. The EGRET WRTDS model trend analysis of particulate nitrogen (PN) at the New River at Gum Branch.

The EGRET confidence interval analysis showed that the change in flow-normalized concentration between 2010 and 2016 was not statistically significant, and it is unlikely that PN concentration changed. The change in flow-normalized flux between 2010 and 2016 was not statistically significant, and it is unlikely that PN flux changed.

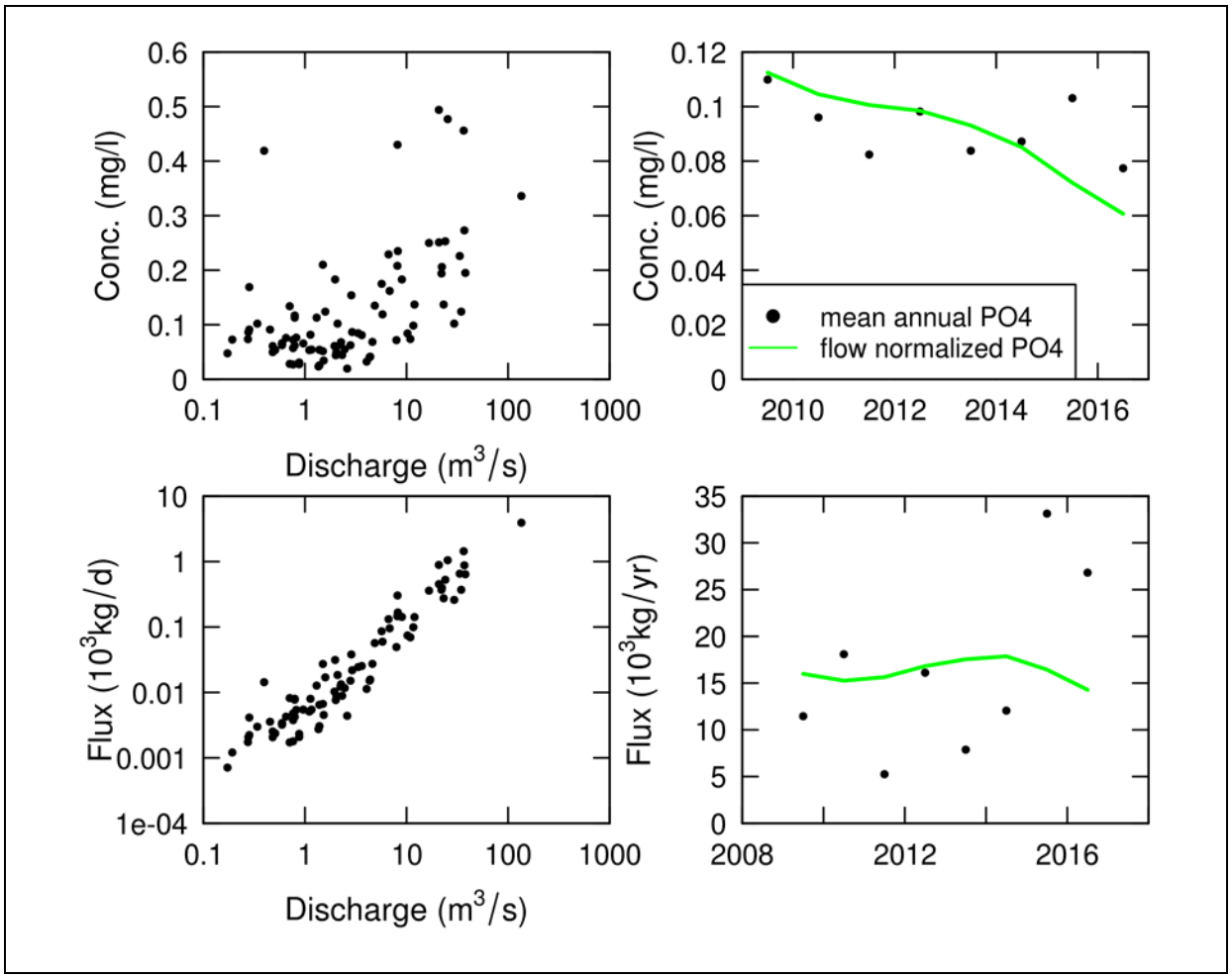

Figure 4A-11. The EGRET WRTDS model trend analysis of orthophosphate (PO_4) at the New River at Gum Branch.

The EGRET confidence interval analysis showed that the decrease in flow-normalized concentration between 2010 and 2016 was statistically significant, and it is highly likely that PO_4 concentration decreased. The change in flow-normalized flux between 2010 and 2016 was not statistically significant, and it is unlikely that PO_4 flux changed.

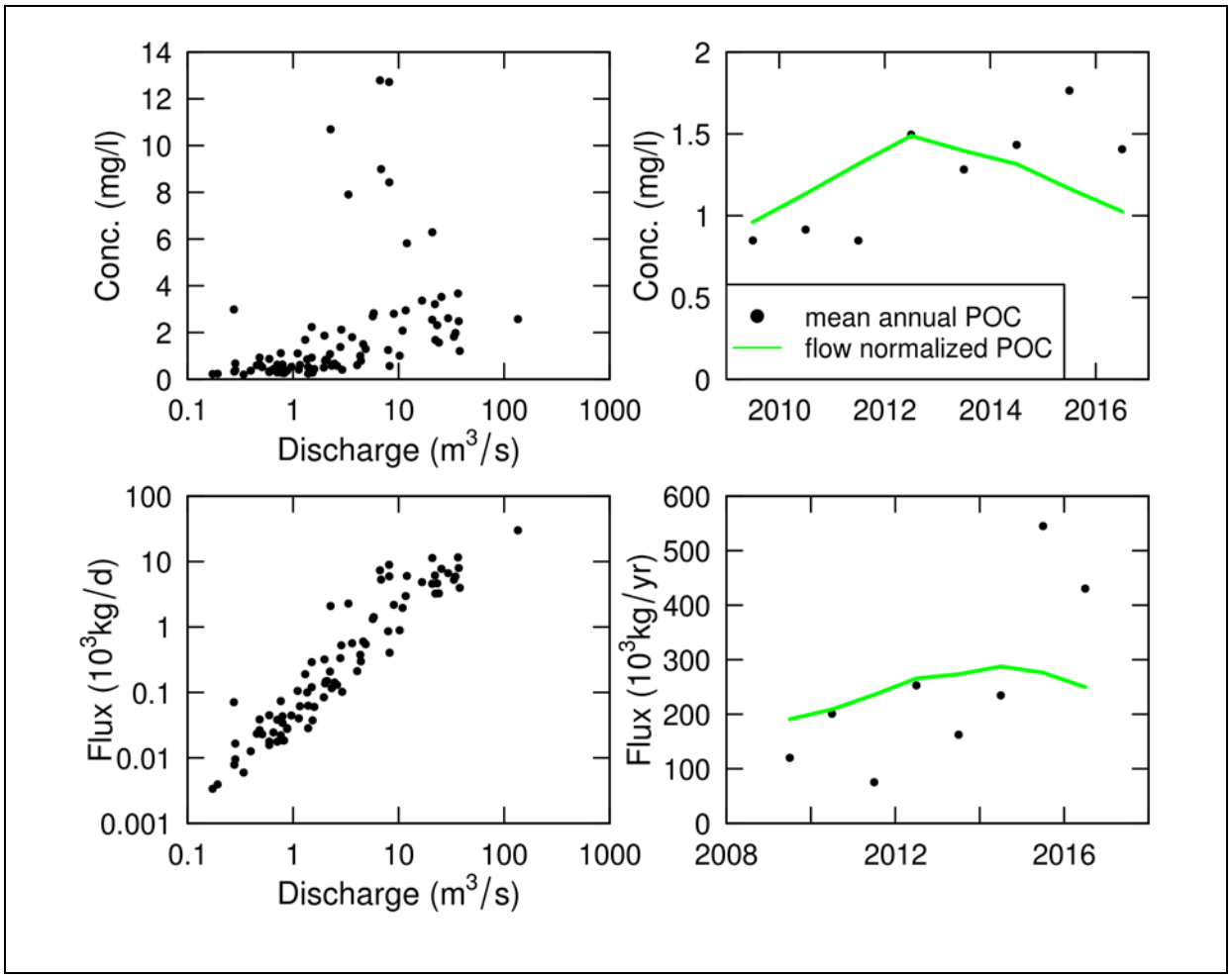

Figure 4A-12. The EGRET WRTDS model trend analysis of particulate organic carbon (POC) at the New River at Gum Branch.

The EGRET confidence interval analysis showed that the change in flow-normalized concentration between 2010 and 2016 was not statistically significant, and it is unlikely that POC concentration changed. The change in flow-normalized flux between 2010 and 2016 was not statistically significant; however, it is likely that POC flux increased.

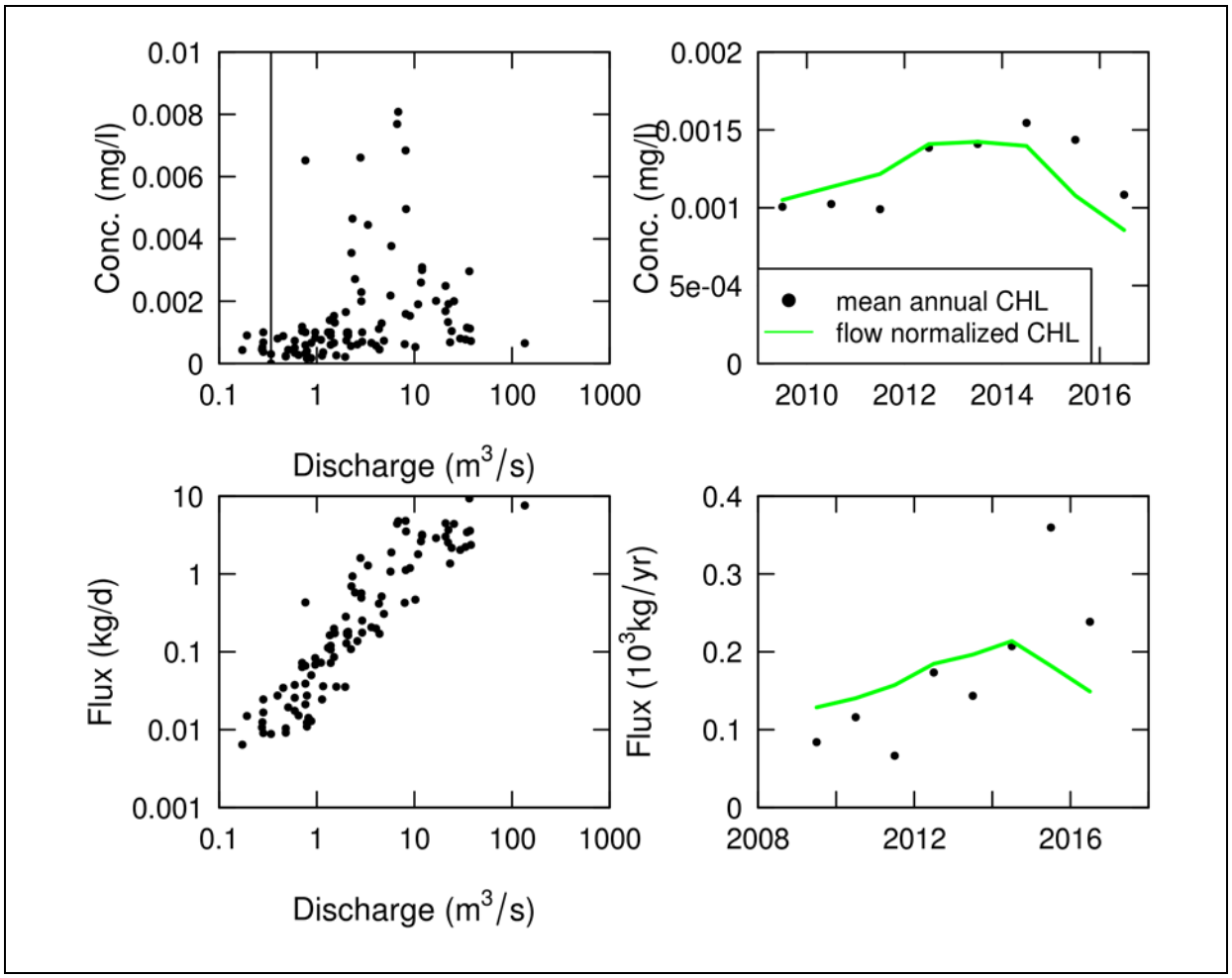

Figure 4A-13. The EGRET WRTDS model trend analysis of chlorophyll *a* (chl *a*) at the New River at Gum Branch.

The EGRET confidence interval analysis showed that the change in flow-normalized concentration between 2010 and 2016 was not statistically significant, but it is likely that chl *a* concentration decreased. The change in flow-normalized flux between 2010 and 2016 was not statistically significant, and it is unlikely that chl *a* flux changed.

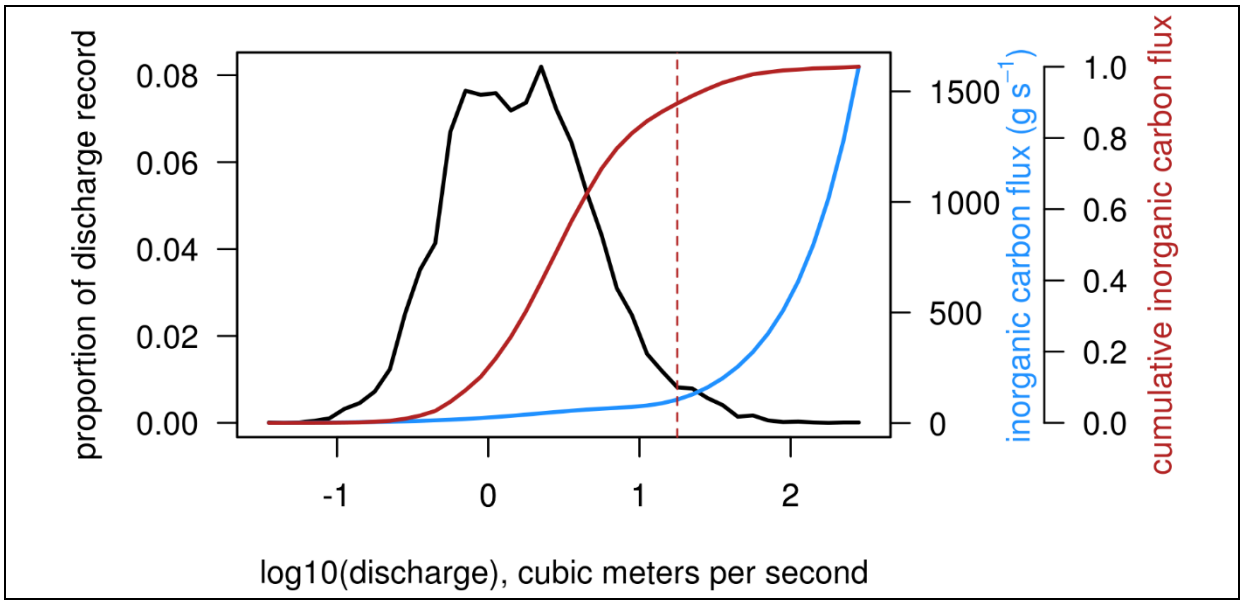

Figure 4A-14. The frequency-magnitude analysis of dissolved inorganic carbon (DIC) at the New River at Gum Branch.

The dashed vertical line denotes the 90th percentile of cumulative dissolved inorganic carbon (DIC) flux.

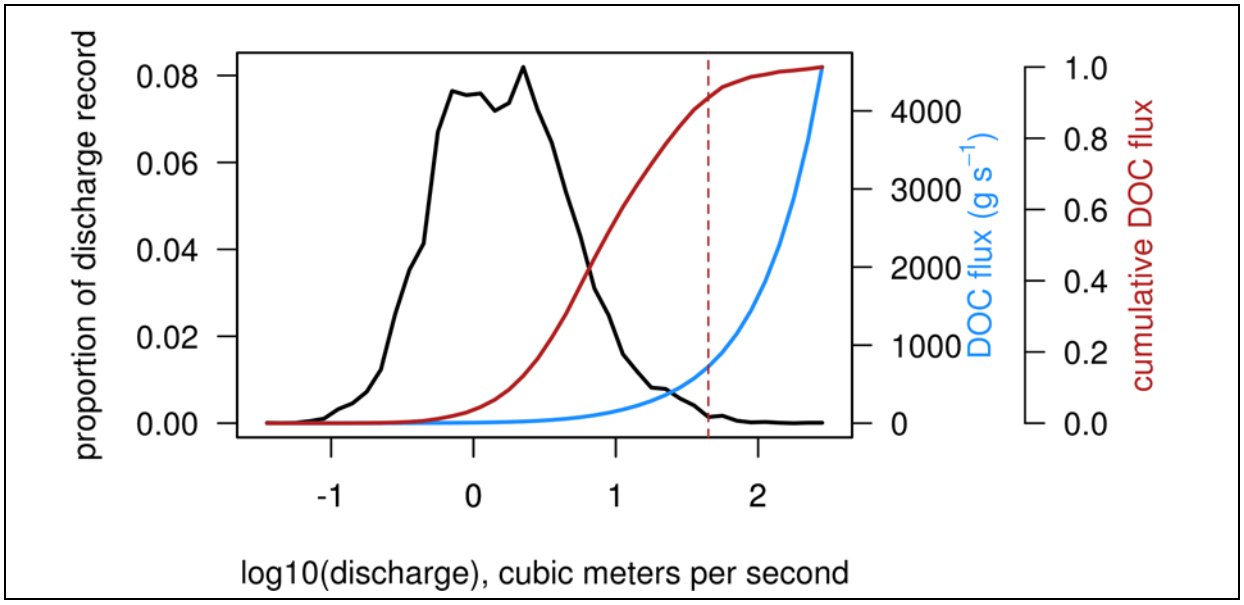

Figure 4A-15. The frequency-magnitude analysis of dissolved organic carbon (DOC) at the New River at Gum Branch.

The dashed vertical line denotes the 90th percentile of cumulative DOC flux.

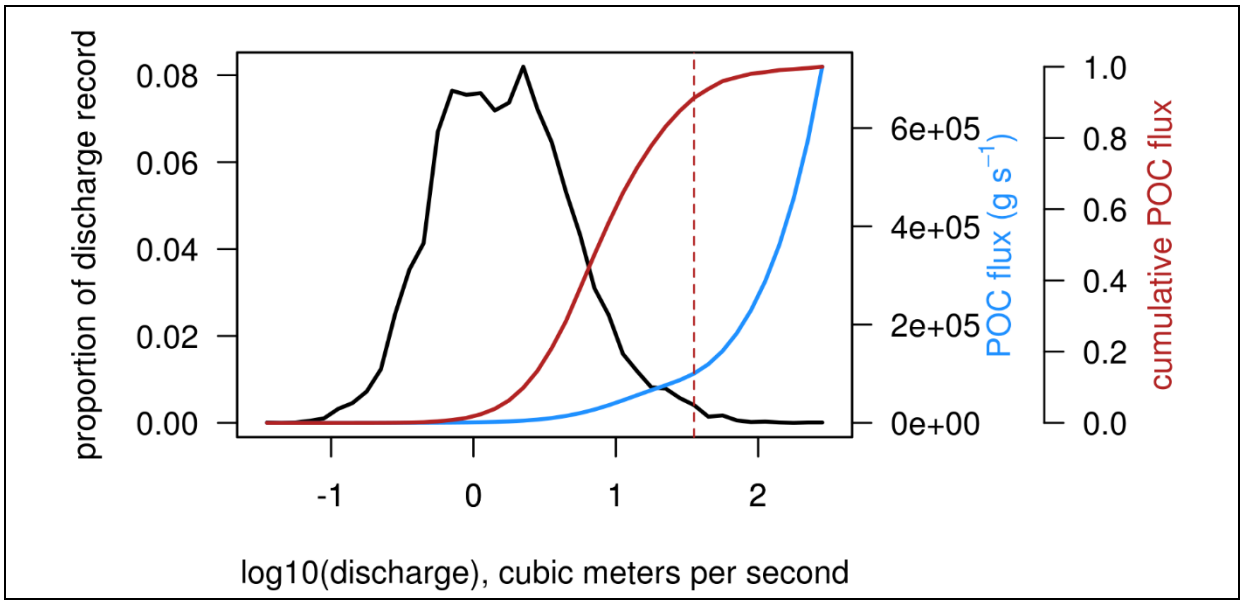

Figure 4A-16. The frequency-magnitude analysis of particulate organic carbon (POC) at Gum Branch.

The dashed vertical line denotes the 90th percentile of cumulative POC flux.

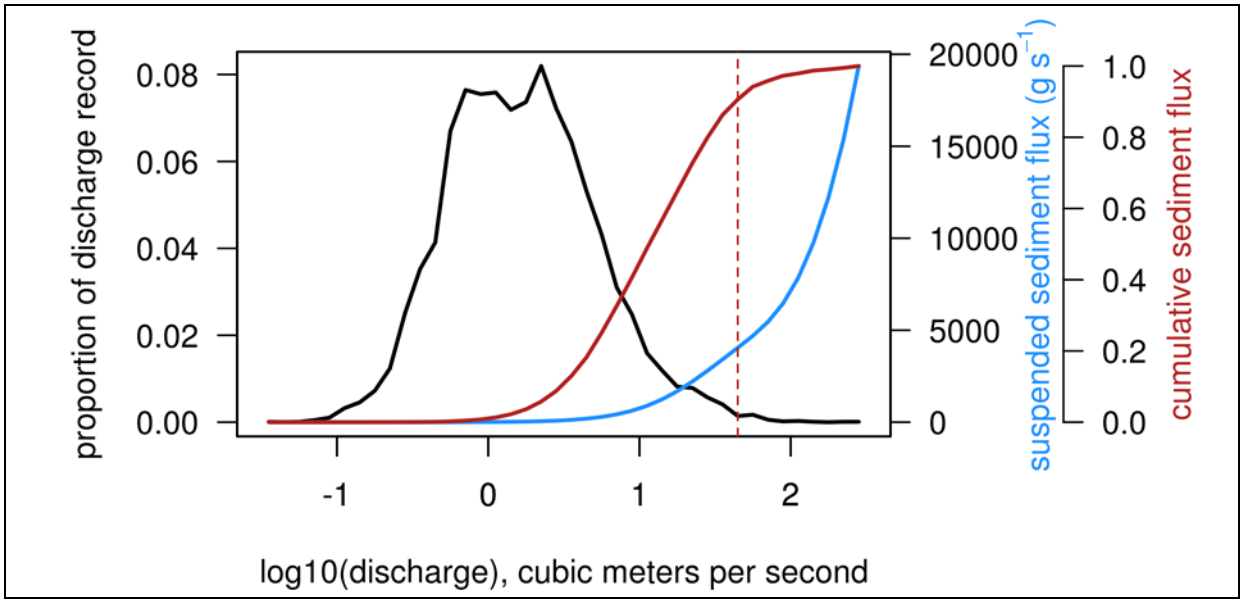

Figure 4A-17. The frequency-magnitude analysis of sediment at the New River at Gum Branch.

The dashed vertical line denotes the 90th percentiles of cumulative sediment flux.

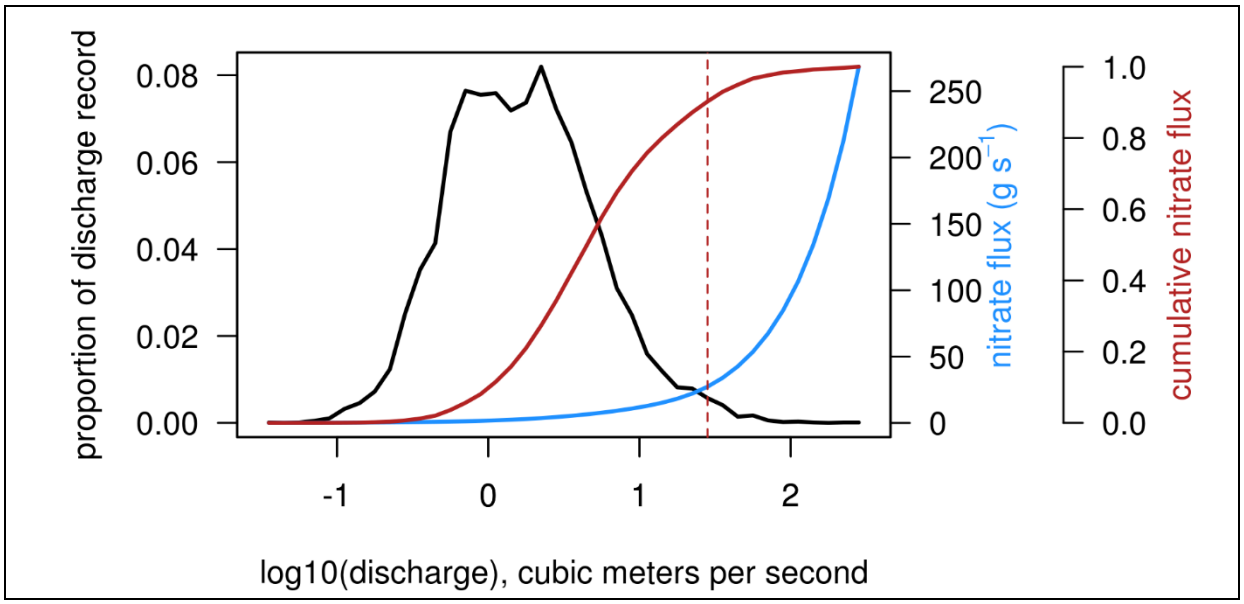

Figure 4A-18. The frequency-magnitude analysis of nitrate (NO_3) at the New River at Gum Branch.

The dashed vertical line denotes the 90th percentile of cumulative NO_3 flux.

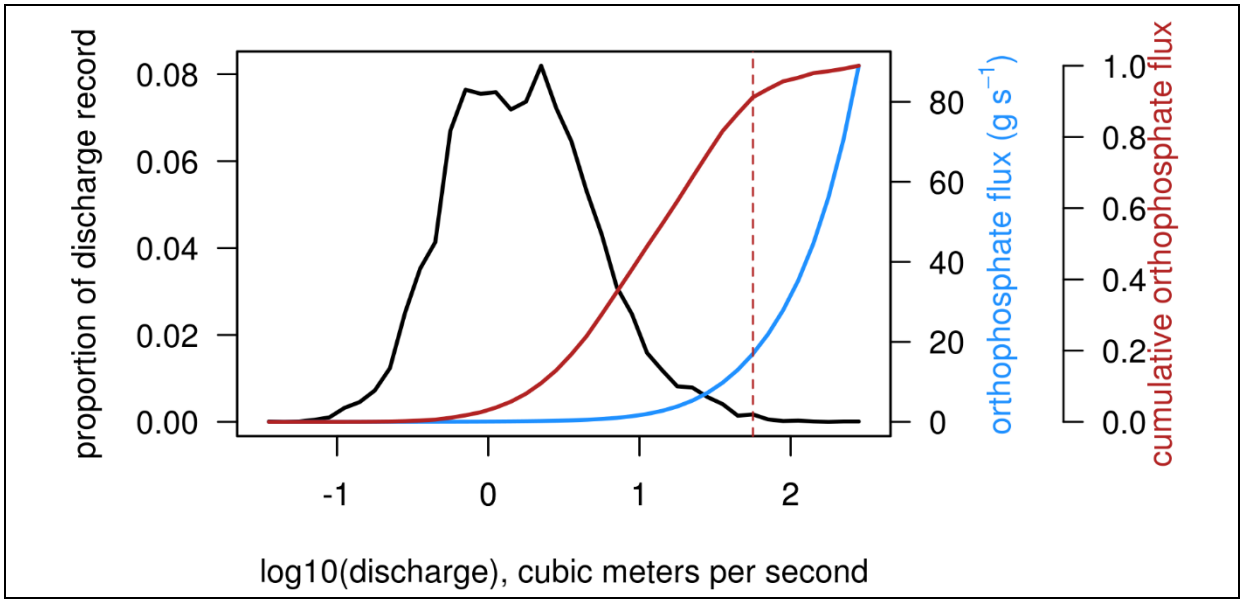

Figure 4A-19. Frequency-magnitude analysis of orthophosphate (PO_4) at the New River at Gum Branch.

The dashed vertical line denotes the 90th percentile of cumulative PO_4 flux.

Appendix 4-B
List of Scientific/Technical Publications

Papers

Ensign, S.H., and G.B. Noe. In revision. Tidal extension and sea level rise: Recommendations for a Research Agenda. Frontiers in Ecology and the Environment. *Frontiers in Ecology and the Environment*.

Thesis

Not applicable

Presentations

Ensign, S.H., G.B. Noe, and C.R. Hupp. 2016. *Tidal Freshwater Landscapes and Salinity Intrusion*. Presented at the Summer Meeting of the Association for the Sciences of Limnology and Oceanography, Santa Fe, NM.

Ensign, S.H. 2016. *Tidal Freshwater Ecosystem: The Ecologic, Economic, and Policy Landscape at the Front Lines of Sea Level Rise*. Presented at the Departmental Seminar, University of Texas, Austin, Marine Science Institute. December 4.

Ensign, S.H. 2015. *Tidal Freshwater Ecosystem*. Presented at the Departmental Seminar, Virginia Institute of Marine Sciences, Gloucester Point, VA. September 17.

Ensign, S.H. 2015. *Tidal Freshwater Ecosystem: Ecological Processes at the Front Lines of Sea Level Rise*. Presented at the Departmental Seminar, Biology, East Carolina University, Greenville, NC. April 2.

Ensign, S.H. 2014. *Environmental and Ecological Process at the Front Lines of Sea Level Rise*. Presented at the Departmental Seminar, Curriculum in Ecology, University of North Carolina at Chapel Hill, Chapel Hill, NC. November 13.

Appendix 4-C
List of Students

None

Appendix 4-D
Supplemental Study

Improving Estimates of Nutrient and Carbon Loading to the Upper New River Estuary Using Floating Drifters

Dr. Scott H. Ensign and Bryce R. Van Dam

Objectives

The first objective of this study was to characterize the travel time of water and solutes through the tidal freshwater portion of the New River. The travel time of particles and solutes is fundamental for estimating their exposure to reaction sites where biogeochemical processes occur. The exposure time provides the time scale for calculating biogeochemical process rates that alter constituent fluxes between the head-of-tide and the upstream boundary of the DCERP Estuarine Simulation Model (Dr. Mark Brush) at Jacksonville, NC.

The second objective of the study was to estimate nitrogen uptake as a function of denitrification and ecosystem metabolism within the tidal freshwater zone. Nitrate (NO_3) uptake was calculated by using measured metabolic rates and literature values of denitrification. Uptake was expressed as the percent reduction between the NO_3 flux entering the tidal freshwater zone at Gum Branch and the flux entering the NRE at Jacksonville. This percent reduction provides a scalar for making more accurate predictions of NO_3 flux at the upstream boundary (Highway 17 at Jacksonville) of the Estuarine Simulation Model (see the *DCERP2 Final Report*, Chapter 10).

The third objective of the study was to estimate photolytic transformation of dissolved organic carbon (DOC) to dissolved inorganic carbon (DIC) during transit through the tidal freshwater zone and DIC exchange with the atmosphere. These transformations and exchanges will improve the accuracy of carbon budget estimates to the New River Estuary (NRE), and ultimately improve the accuracy of ecosystem processes estimated by the Estuarine Simulation Model.

Background

The NRE contains an extensive oligohaline and tidal freshwater zone extending from Jacksonville to the U.S. Geological Survey (USGS) gage on the New River near Gum Branch. This 19-km zone of the estuary tapers in width going upstream, becoming a meandering channel bordered by extensive tidal freshwater forested wetlands. Over-bank flooding from the channel into the wetlands occurs during high tide, and this hydrologic coupling between river and riparian zone affects solute and particle transport downstream. The morphologic changes in channel width, tree canopy shading, and irradiance along this zone may also influence biological production and photochemical processes.

These geomorphic, hydrologic, and biogeochemical gradients may alter the New River's solute, particle, and elemental fluxes between the DCERP monitoring station on the New River near Gum Branch and the upper extent of DCERP estuarine monitoring and modeling at Highway 17 in Jacksonville. Despite these anticipated changes in flux, the DCERP Estuarine Simulation

Model and empirical carbon budget apply the measured yield at Gum Branch as the upstream boundary flux. The absence of monitoring data between Jacksonville and Gum Branch has repeatedly been cited in DCERP as a limitation to both the Estuarine Simulation Model and the empirical carbon budget. If attenuation (net uptake) of elemental fluxes occurred within this zone, then the models would over-estimate inputs across the upstream model boundary. If augmentation (net input) of elemental flux occurred, then the upstream model boundary would under-estimate this input. In either event, the resultant interpretation of environmental process rates in the upper portion of the Estuarine Simulation Model and empirical carbon budget would be in error.

During DCERP1, supplemental data on river discharge was collected by the USGS along this zone of the New River. The study found reverse (upstream) tidal flow occurred as much as 10 km upstream from Highway 17. The bi-directional, unsteady flow within the tidal freshwater zone is a difficult challenge to estimating elemental transformations during transport through the tidal freshwater zone. Estimation of these transformations requires knowledge of transport time and channel volume through the tidal freshwater zone. The supplemental monitoring activity described here fills that gap.

Methods and Materials

Study Sites

The tidal freshwater zone of the New River begins at the Northwest Bridge Road crossing at the USGS New River Gum Branch stream gaging station (34.84918º N 77.51932º W; **Figure 4D-1**). The next 10 km downstream exhibit a semi-diurnal tide year-round with an approximate 0.2-m range and never contains saltwater, even under severe droughts. The channel in this zone is approximately 2-m deep and between 10- and 15-m wide. Except during severe droughts, the tidal freshwater zone extends another 5 km downstream to 34.77025º N 77.46452º W (15 km on **Figure 4D-1**). This zone is approximately 3-m deep and between 15- and 20-m wide, and the tidal amplitude is approximately 0.2 m. Except for a 2-km dredged zone (34.79623º N 77.47028º W to 34.80992º N 77.42339º W), the riparian zone of the tidal freshwater New River consists of bottomland hardwood forest (cypress, black gum, red maple) that floods during the semi-diurnal tide. The dredged section is the only portion of this zone of the New River where channel levees are apparent.

Downstream of 34.77025º N 77.46452º W (15 km on **Figure 4D-1**), the New River morphology and riparian zone change distinctly, and the oligohaline conditions and water column salinity stratification occur in this stretch during normal flow conditions. The channel widens to approximately 100 m and deepens to 8 m. Riparian vegetation is scrub-shrub with no bald cypress. One kilometer upstream from Jacksonville, the river widens to greater than 500 m, and the depth decreases to 2 m.

Sampling

Data were collected during three measurement periods: 10–12 May 2016, 22–24 August 2016, and 2–5 October 2016. During each period, two YSI 600OMS datasondes (Yellow Springs Instruments, OH) were deployed to measure temperature, salinity, specific conductivity, and dissolved oxygen. One datasonde was located at the upstream end of the study zone (5 km on

Figure 4D-1), and the other datasonde was located at the downstream end (15 km on **Figure 4D-1**). The datasondes were secured to polyvinyl chloride (PVC) poles that were driven into the river bed along the edge of the channel. Onset HOBO pressure transducers were also secured to the PVC poles to measure water depth. Datasondes and pressure transducers were deployed for 48 hours. Light attenuation (k [in m^{-1}]) was measured during each measurement period by using a LiCor photosynthetically active radiation (PAR) sensor deployed from a research vessel in the mid-channel. Additional measurements of dissolved oxygen and salinity were made by using a YSI 6920 datasonde.

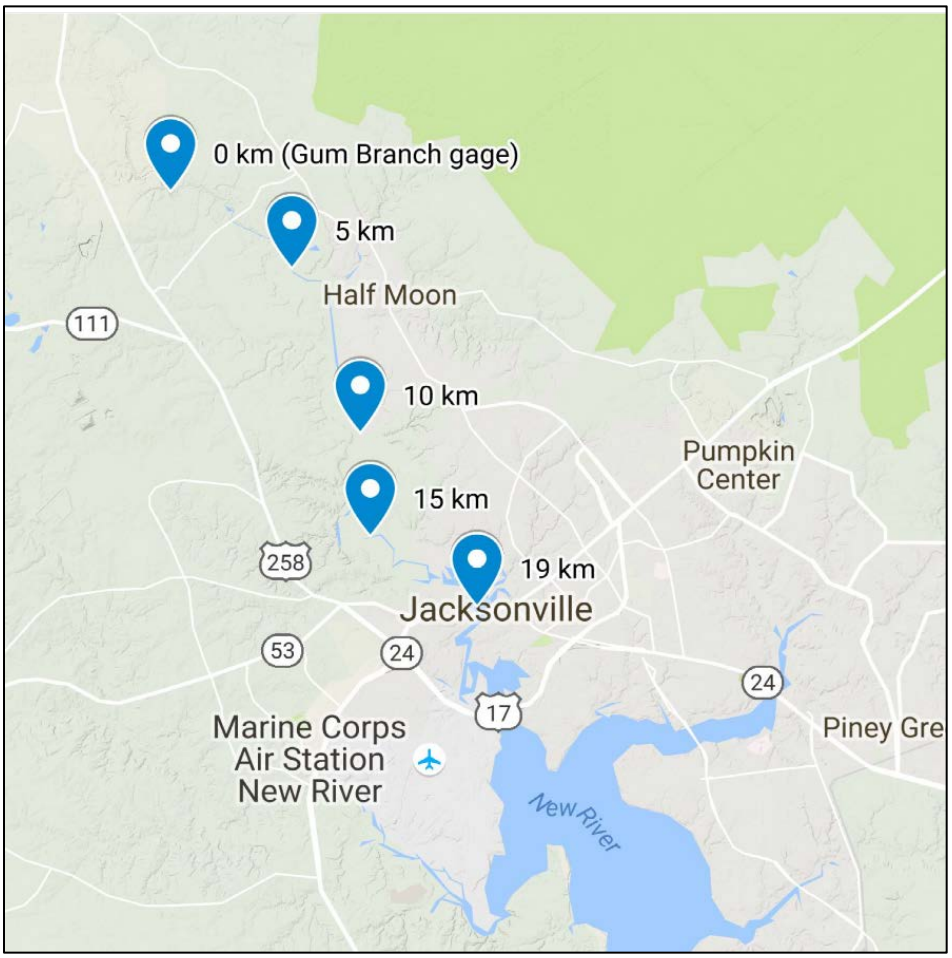

Figure 4D-1. A map of the tidal freshwater zone of the New River, starting at 0 km at Gum Branch and ending at 19 km at Jacksonville.

During each measurement period, a pair of HydroSphere drifters (Planktos Instruments, LLC, Morehead City, NC) were deployed along the zone. During the deployment in May and August 2016, one drifter was deployed at the surface (floating) and the other was deployed subsurface (neutrally buoyant). The neutrally buoyant drifters were not effective at traveling unimpeded because of the very low flow velocities that prevented lateral and vertical mixing. In response, both drifters were deployed floating in the October deployments. Very low flow velocities and subsequent low cross-channel mixing frequently resulted in even the floating drifters getting snagged by shoreline debris. During daylight, the drifters were monitored carefully; the drifters were freed when they reached the shore to maximize their free-drift path length. This was

important for estimating travel time along the reach. On several occasions, the drifters were deployed at strategic areas to capture additional flow information or for point source detection.

Water travel times from Gum Branch to Highway 17 in Jacksonville were estimated from the drifter velocities. Drifter velocities during periods of free-flowing travel were measured on the ebb and flood tide, and then were extrapolated across the study reach. The estimated travel time of a particle (the HydroSphere) through the study reach was assumed to represent the average replacement time of freshwater within the reach by inflowing water at the head-of-tide. The estimated travel time includes the effects of oscillating flow direction. For the calculations described in the remainder of this section, we assumed that once the travel path reached the downstream boundary (Highway 17 at Jacksonville) the water (or solute) was lost from the study reach.

The air–water carbon dioxide (CO_2) flux and DIC inventories were measured during each survey. Fluxes were determined by using the floating dome technique (Marino and Howarth, 1993), and the partial pressure of carbon dioxide (pCO_2) was measured by using the same flow-through analyzer that was built for the DCERP Research Project AE-4. DIC was measured at 12 stations in the tidal freshwater zone during each cruise. Measured air–water fluxes were scaled up over the study reach per residence time (*RT*; see **Table 4D-1**) by using Equation 1, as follows:

$$CO_2 \text{ atmospheric flux (g)} = \text{measured flux} \times \text{study reach area} \times RT \qquad \text{(Eq. 1)}$$

The study reach surface area was assumed to be equal to the river channel widths reported by Siporin (2010), multiplied by reach length, totaling 836,629 m^2. Synoptic surveys of temperature, pH, salinity, oxygen (O_2), CO_2, and DIC were conducted along the study reach while the drifters were deployed. The flow-through analyzer previously described was fitted with a YSI 6000 series datasonde, which measured temperature, pH, salinity, and O_2. Measurements were made at 30-second intervals and summarized by 3-km reaches.

We predicted the mass of NO_3, DOC, and DIC that entered the tidal freshwater zone at the head-of-tide during a period equal to the water replacement time. Non-linear regression of NO_3 concentration versus discharge, DOC concentration versus discharge, and DIC concentration versus discharge are presented in Chapter 4 of the *DCERP2 Final Report*. These masses of constituents were assumed to react across the benthic and air–water surfaces during the water replacement time. For NO_3, it was assumed that the mass was exposed to the entire benthic surface area of the channel and mixed completely. A flat river–bottom morphology was assumed, acknowledging that this may under-estimate the surface area for denitrification. Denitrification rates from that benthic surface were taken from Von Korff et al. (2014), who measured denitrification during four seasons in the tidal freshwater zone of the New River. Uncertainty for each calculation of denitrification included uncertainty in travel time (flushing time), NO_3 concentration entering the reach, and denitrification rate.

Photomineralization from DOC to DIC was predicted by using the formula from Granéli et al. (1998), as shown in Equation 2:

$$\text{DIC production (g m}^{-3}\text{ 6 hr}^{-1}) = 0.04 \times \text{DOC} - 0.117 \qquad \text{(Eq. 2)}$$

Next, the DIC production was applied to the photic depth (10% of surface irradiance: $-\ln(0.1)/k$ of the study reach. Attenuation of ultraviolet A and ultraviolet B was not measured; therefore, the approximation of the total radiation spectrum had to be assumed from the measured PAR values. DIC production across the study reach during *RT* of water was calculated as shown in Equation 3, where DIC is in grams of carbon per cubic meter:

$$\text{DIC production (g)} = \text{DIC production (g m}^{-3}\text{ 6 hr}^{-1}) \times 836{,}629 \times (-\ln(0.1)/k) \times (RT/6) \qquad \text{(Eq. 3)}$$

Application of these rates implies that the active depth of irradiance is 1-m deep. Uncertainty for each calculation of photomineralization included uncertainty in travel time (water replacement time), DOC concentration entering the reach, and DIC concentration entering the reach.

A mass balance of DIC was constructed by using the measured and estimated fluxes. Measured fluxes include the DIC flux at Gum Branch and the CO_2 loss to the atmosphere across the air–water interface. DIC production via photomineralization was estimated by using Equation 3. The net DIC flux at Jacksonville was calculated as the average DIC concentration closest to Jacksonville during synoptic sampling multiplied by discharge at Gum Branch scaled to Jacksonville discharge (for an explanation, see Chapter 4 of the *DCERP2 Final Report*). Unmeasured fluxes include lateral inputs, groundwater inputs, and DIC produced by respiration. These combined unmeasured DIC fluxes into the study reach (*L*) were calculated as shown in Equation 4:

$$L = J - G - P + A \qquad \text{(Eq. 4)}$$

where, *J* is the flux at Jacksonville, *G* is the flux at Gum Branch, *P* is DIC production via photomineralization (Eq. 3), and *A* is flux of CO_2 from water into the atmosphere (Eq. 1).

Results and Discussion

Field Measurements in May 2016

In May 2016, the tidal amplitude was 0.19 m at the upstream site and 0.28 m at the downstream station (**Figure 4D-2**). The surface HydroSphere drifter traveled 3.4 km unimpeded, but the subsurface drifter was snagged on the bottom for most of the measurement period. The surface drifter velocities during flood and ebb tide were interpolated from Gum Branch through the end of the study reach: by the conclusion of the 48-hr monitoring period a particle released at Gum Branch would have traveled between 11.0 and 13.4 km. It would have taken between 83 and 146 hours for the drifter to reach Highway 17 in Jacksonville (**Table 4D-1**).

Table 4D-1. Estimated Drifter Travel Time from the New River at Gum Branch to Highway 17, Jacksonville; the Numbers in Parentheses Are Lower and Upper Bounds of Travel Time Estimates

Travel time	10–12 May 2016	22–24 August 2016	3–4 October 2016
Hours	115 (83, 146)	83 (68, 98)	76 (63, 89)
Days	4.8 (3.4, 6.1)	3.5 (2.8, 4.1)	3.2 (2.6, 3.7)

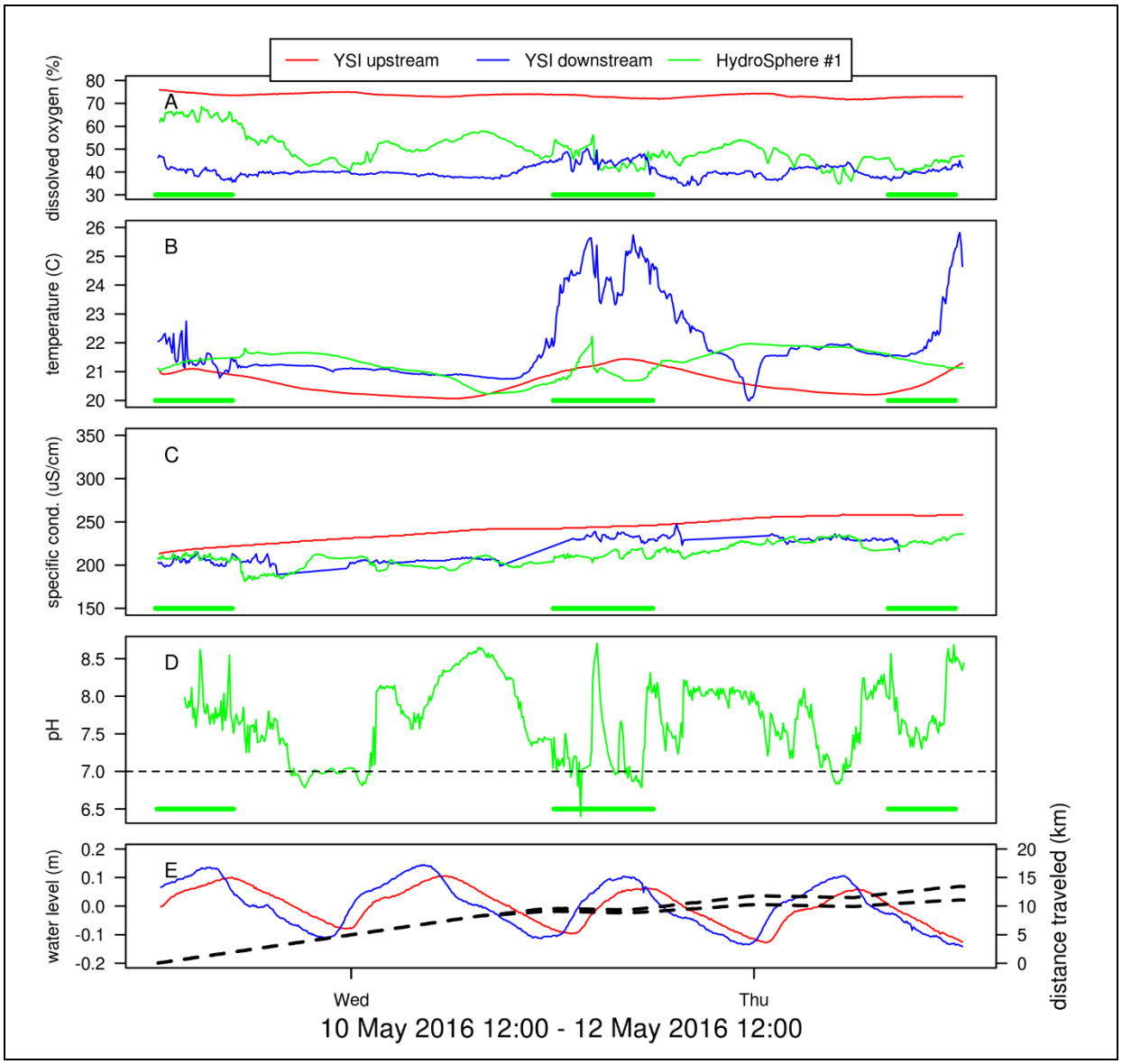

Figure 4D-2. Stationary and drifter measurements made in the tidal freshwater zone of the New River over 48 hours in May 2016.

Green bars denote periods when HydroSphere #1 was traveling freely at the surface. Black dashed lines in bottom panel show estimated distance traveled for water parcel introduced at the head of the study reach (YSI upstream).

The surface drifter measured a 25% drop in dissolved oxygen concentration in the upper 1.9 km of the study reach, indicating either a point source or rapid consumption of oxygen in the channel. Dissolved oxygen decreased from an average 6.6 mg L^{-1} (73% saturation) to 3.5 mg L^{-1} (40% saturation) between the upstream and downstream stations, which is consistent with the synoptic measurements. No consistent diurnal pattern in oxygen was observed at either measurement location. A diurnal temperature change of 1°C occurred in the afternoon at the upstream station, while a 5°C increase occurred downstream. The downstream increase corresponded with rising stage of the tide, so warmer water could have been advected past the sensor. The drifter measured large fluctuations in pH, from 7 to 8.5, and the synoptic measurements showed a decrease from 7.3 upstream to 7.0 downstream. The vertical attenuation

coefficient of PAR averaged −4.0 m^{-1} (**Table 4D-2**). In addition, pCO_2 increased from 2,155 µatm upstream to 3,613 µatm at 12 km (**Figure 4D-3**). DIC decreased from 1.51 µM upstream to 1.16 µM downstream. The downstream end of the study reach had estuarine-influenced salinity of 0.4 ppt.

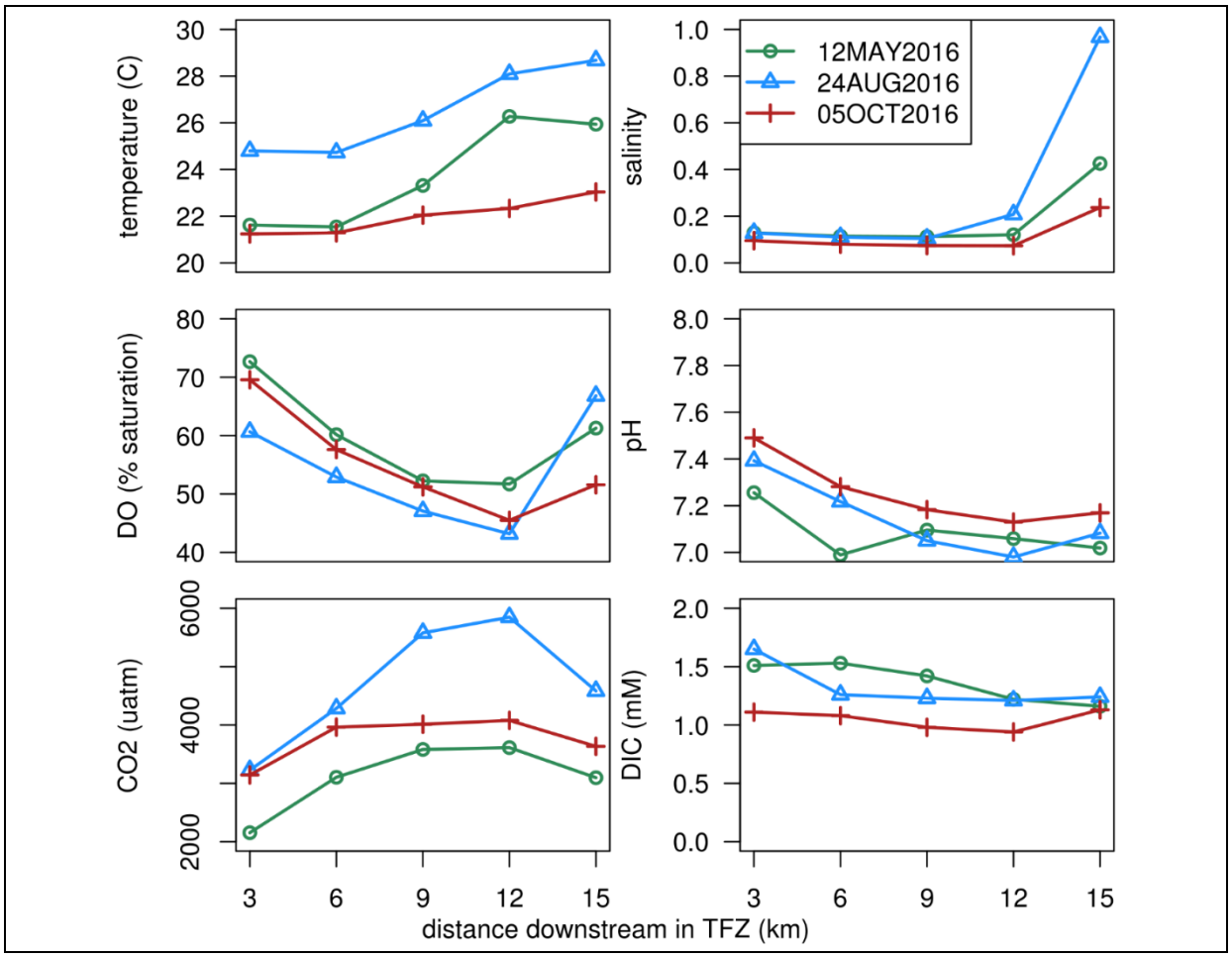

Figure 4D-3. Synoptic measurements in the tidal freshwater zone of the New River.

Field Measurements in August 2016

In August 2016, the tidal amplitude was 0.24 m at the upstream site and 0.28 m at the downstream station (**Figure 4D-4**). The surface drifter (HydroSphere #3) traveled 2.8 km unimpeded, but the subsurface drifter (HydroSphere #2) became snagged. Extrapolation of drifter velocities during ebb and flood tide indicated that the drifter would have traveled 12.8 km from Gum Branch during the study period if it had not been snagged. It would have taken between 68 and 98 hours for the particle to travel from Gum Branch to Highway 17 in Jacksonville (**Table 4D-1**).

Dissolved oxygen decreased from an average of 4.9 mg L^{-1} (60% saturation) at the upstream station to 2.0 mg L^{-1} (25% saturation) at the downstream station. Synoptic measurements showed a similar pattern (**Figure 4D-3**). Temperature showed mid-afternoon warming at both stations. A pulse in specific conductivity occurred at the downstream station during the two high-tide

periods at the end of the study. The drifters measured pH between 7 and 8 during the first day, and then below 7 during the second day. Synoptic measurements of pH were between 7.4 and 7.0. Estuarine salinity was detectable at 12 km and increased to 1 ppt at the downstream end of the study reach. The vertical attenuation coefficient of PAR averaged −3.7 m^{-1} (**Table 4D-2**). The pCO_2 increased from 3,225 µM at the upstream end of the study reach to 5,846 µatm at 12 km (**Figure 4D-3**). DIC decreased from 1.65 µM to 1.21 µM at 12 km.

Table 4D-2. Attenuation of PAR in the New River Tidal Freshwater Zone

Date	Time (hh:mm)	Location (dd.d N, dd.d W)	PAR attenuation coefficient (m^{-1})
10 May 2016	12:40	34.82939, 77.48001	−3.4
12 May 2016	09:16	34.79099, 77.46340	−4.5
22 August 2016	12:05	34.82939, 77.48001	−3.8
22 August 2016	16:45	34.79835, 77.47068	−3.9
23 August 2016	11:35	34.76771, 77.46793	−3.7
23 August 2016	12:40	34.79076, 77.46319	−3.8
24 August 2016	10:25	34.79067, 77.46314	−3.5
3 October 2016	12:25	34.82939, 77.48001	−5.2
3 October 2016	16:05	34.78366, 77.46560	−7.2
5 October 2016	14:45	34.77045, 77.46526	−5.6

Field Measurements in October 2016

In October 2016, tidal amplitude was 0.24 m upstream and 0.26 m downstream (**Figure 4D-5**). The two surface drifters traveled a total of 5.3 km unattended. Extrapolation of the drifter velocities during ebb and flood tides yielded a prediction that a particle passing Gum Branch would travel between 13.8 km and 16.4 km during the 48-hour period. It would have taken between 63 and 89 hours for the particle to travel from Gum Branch to Highway 17 in Jacksonville.

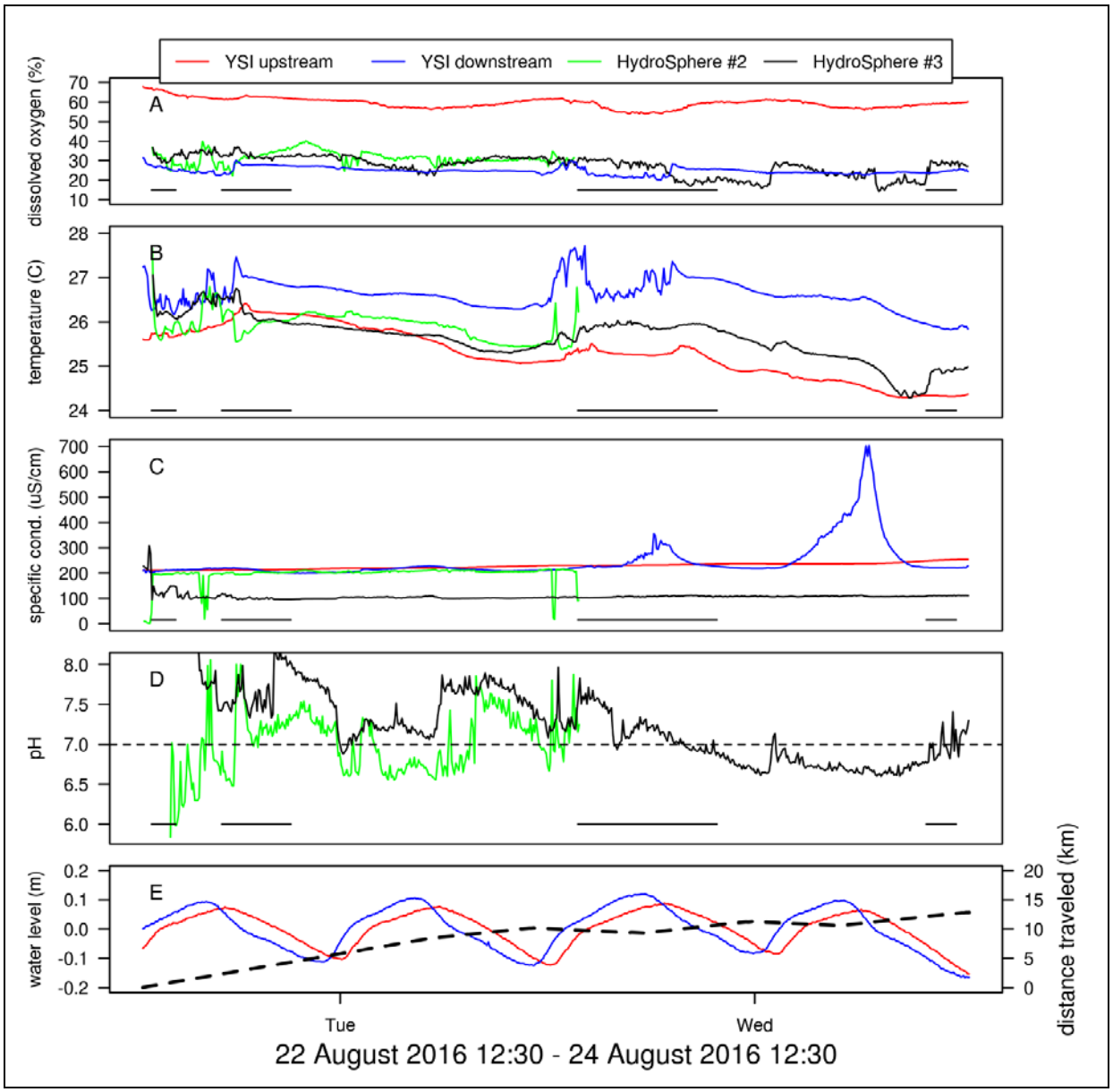

Figure 4D-4. Stationary and drifter measurements of the New River tidal freshwater zone in August 2016. Black bars denote periods when HydroSphere #3 was traveling freely. The black dashed line in the bottom panel shows the estimated distance traveled for a water parcel introduced at the head of the study reach (YSI upstream).

Dissolved oxygen decreased from 6.2 mg L^{-1} (71% saturation) upstream to 3.2 mg L^{-1} (37% saturation) downstream (**Figure 4D-5**), and synoptic measurements showed a decrease from 70% saturation to 45% saturation at 12 km (**Figure 4D-3**). Temperature fluctuated in a diurnal pattern at all study sites. Specific conductivity declined from the upstream site and the downstream site, but no temporal pattern was apparent. The HydroSpheres measured pH ranging from 6.5 to 7.5. The vertical attenuation coefficient of PAR averaged −6.0 m^{-1} (**Table 4D-2**). In addition, pCO_2 increased from 0 km to 12 km, but DIC concentration remained relatively constant (**Figure 4D-3**).

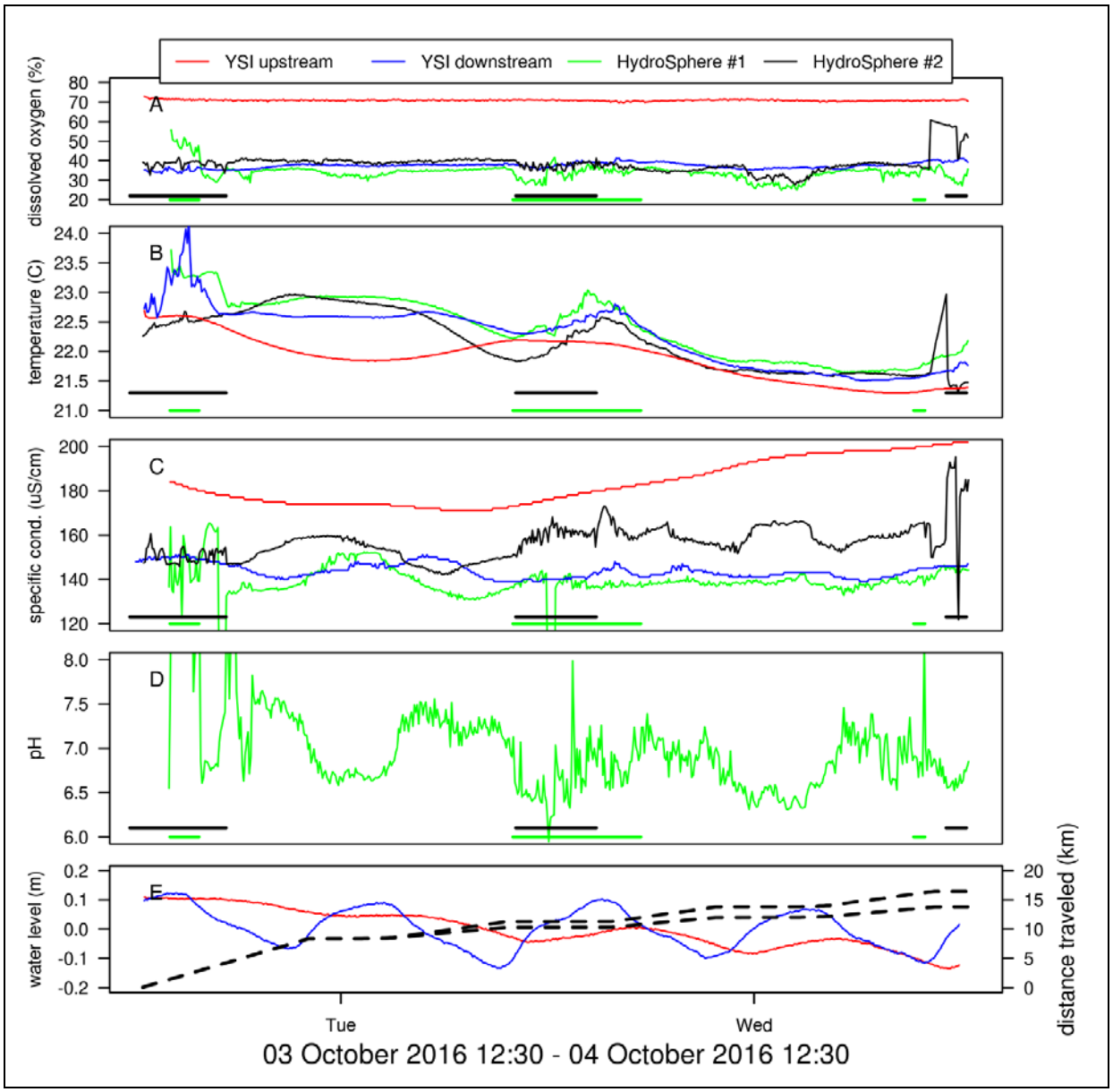

Figure 4D-5. Stationary and drifting measurements of the New River tidal freshwater zone in October 2016.

Green and black bars denote periods when HydroSpheres were traveling freely. The black dashed lines in the bottom panel show the estimated distance traveled for water parcel introduced at the head of the study reach (YSI upstream).

Higher river discharge during the October sampling allowed detection of tributary inputs to the New River that were previously undetected. In particular, Half Moon Creek enters the New River at 34.81137º N 77.47367º W through a subsurface pipe buried beneath the channel levee. Although the pipe was not visible below the water surface, a plume of highly colored, turbidity-free water was visible in the main channel. A HydroSphere was released upstream from this point to test the responsiveness of the drifter to detecting this source. **Figure 4D-6** shows a clear drop in dissolved oxygen from 5.1 mg L^{-1} (58% saturation) above the confluence to 4.5 mg L^{-1} (50% saturation) below. Specific conductivity decreased from 191 µS cm^{-1} above the confluence

to 184 µS cm^{-1} below the confluence after mixing was complete. All parameters rebounded within 15 minutes (0.12 km), as complete mixing occurred. Temperature continued to increase presumably due to diurnal warming.

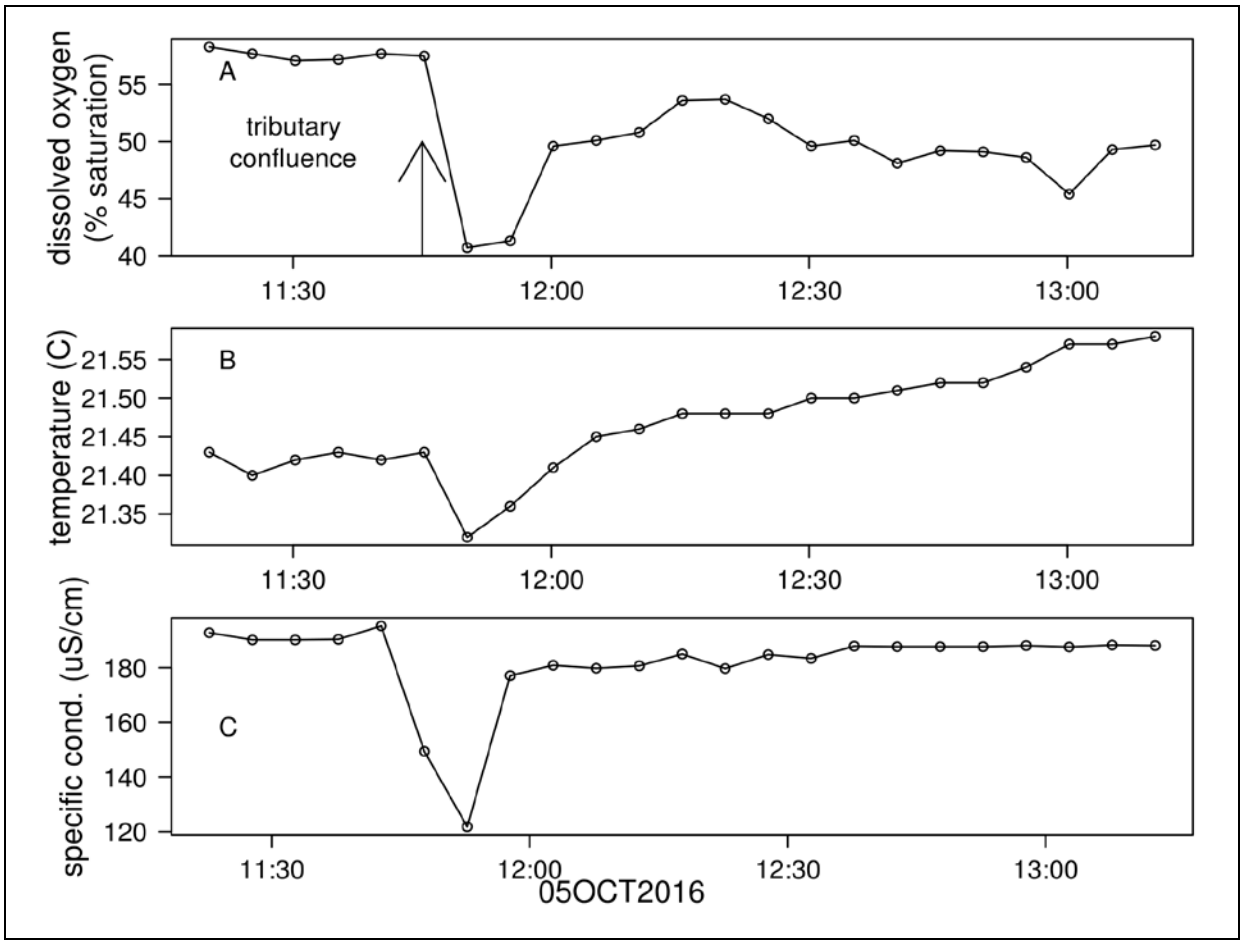

Figure 4D-6. Drifter measurements passing Half Moon Creek in October.

Mass Balances

Nitrate

Nitrogen removal via denitrification within the Gum Branch to Jacksonville (Highway 17) reach of the New River was estimated based on flux of nitrogen into the reach and literature values of denitrification rate in the New River tidal freshwater zone. The predicted nitrogen removal was 5%, 18%, and 10% of the incoming NO_3 flux at Gum Branch in the May, August, and October sample periods, respectively (**Table 4D-3**). For the purposes of estimating NO_3 flux to the NRE, the accuracy of the predicted NO_3 flux at Jacksonville could be improved by subtracting a proportion of the estimated flux at Gum Branch. The intermediate value of the three estimates made here (10%) could be used to approximate this NO_3 loss.

Table 4D-3. Estimated Nitrate (NO_3) Flux and Uptake Through the Tidal Freshwater Zone of the NRE. Numbers in Parentheses Are the Lower and Upper Bounds of Estimates

Parameter	Units	10–12 May 2016	22–24 August 2016	3–5 October 2016
Gum Branch discharge	$m^3 s^{-1}$	2.677	1.123	3.228
Predicted NO_3 concentration	$g\ m^{-3}$	1.597 (0.873, 2.669)	1.756 (0.976, 3.019)	1.548 (0.841, 2.562)
NO_3 flux at Gum Branch	10^6 g per *RT* [a]	1.761 (0.698, 3.755)	0.589 (0.268, 1.196)	1.367 (0.616, 2.649)
Denitrification rate [b]	$mg\ m^{-2}\ hr^{-1}$	1.610 (1.428, 1.792)	2.772 (2.254, 3.290)	3.808 (2.912, 4.704)
NO_3 removal	10^3 g per *RT*	154 (99, 219)	192 (128, 270)	242 (153, 350)
Gum Branch NO_3 flux denitrified	%	4.9 (1.5, 17.7)	18.4 (6.0, 56.6)	10.0 (3.3, 32.0)

[a] *RT* = Water replacement time (see **Table 4-D1**).

[b] Rates from Von Korff et al. (2014).

Carbon

Study reach segment-averaged pCO_2 was always highly supersaturated, ranging from 2,155 to 5,847 μatm (atmospheric pCO_2 is approximately 380 μatm; **Figure 4D-3**). Average CO_2 fluxes from river water to the atmosphere averaged 7.4, 10.9, and 22.4 mmol C $m^{-2}\ hr^{-1}$ during May, August, and October, respectively (**Figure 4D-7**). The tidal freshwater New River is a large source of CO_2 into the atmosphere, but it is also apparent that pCO_2 does not vary substantially along the study reach. This is in contrast to the main body of the NRE, where pCO_2 generally decreases with distance downstream. To maintain this constant pCO_2 despite the large air–water exchange, a significant internal or external source must bring CO_2 into the system. **Figure 4D-7** shows the relationship between modeled CO_2 flux and O_2 flux (calculated based on measured O_2 and measured gas transfer velocity). The apparent linear relationship suggests that net ecosystem heterotrophy is the source of this large degassing CO_2 flux; however, more research is needed to rule out the importance of tributary inputs.

Photomineralization was estimated based on the area of the study reach, the predicted travel time of water through the study reach, and the literature values of photomineralization. Predicted photomineralization consumed 24%, 54%, and 14% of the DOC entering the study reach past Gum Branch in May, August, and October 2016 (**Table 4D-4**).

Table 4D-4. Estimates of DIC and DOC Fluxes Within the Tidal Freshwater Zone of the NRE

Parameter	Units	10–12 May 2016	22–24 August 2016	3–5 October 2016
Gum Branch discharge	$m^3\ s^{-1}$	2.677	1.123	3.228
Predicted DOC	g C m^{-3}	10.6 (5.2, 17.6)	7.8 (3.8, 14.2)	11.3 (5.7, 18.1)
Predicted DIC	g C m^{-3}	18 (13, 24)	25 (19, 30)	17 (11, 22)
Predicted DOC	10^6 g C per *RT* [a]	11.7 (4.2, 24.7)	2.6 (1.0, 5.6)	10.0 (4.2, 18.7)
Predicted DIC	g C per *RT*	20.2 (10.2, 33.6)	8.3 (5.3, 11.8)	14.7 (8.2, 23.0)
DIC production via photomineralization [b]	g C m^{-3} 6 hr^{-1}	0.307 (0.092, 0.586)	0.196 (0.035, 0.451)	0.337 (0.11, 0.607)
DIC production via photomineralization [c]	10^6 g C per *RT*	2.82 (0.612, 6.86)	1.41 (0.206, 3.84)	1.37 (0.371, 2.89)
DOC loss from photomineralization	Percent reduction in Gum Branch flux	24 (15, 28)	54 (2, 68)	14 (9, 15)
DIC loss to atmosphere [d]	10^6 g C per *RT*	8.5 (6.2, 11)	9.1 (7.4, 11)	19.1 (14, 20)

[a] *RT* = Water replacement time (see **Table 4D-1**).
[b] See Equation 2.
[c] See Equation 3.
[d] See Equation 1.

The air–water exchange of CO_2 was fast enough in August and October to remove all of the DIC entering the tidal freshwater zone at Gum Branch (**Tables 4D-4 and 4D-5**). However, the DIC concentration decreased only 19%, 27%, and 15% along the tidal freshwater zone in May, August, and October, respectively (**Figure 4D-3**). Replacement of the initial pool of DIC delivered at Gum Branch must have been countered by an internal source of DIC. Photomineralization along the tidal freshwater zone was predicted to contribute 2.82×10^6, 1.41×10^6, and 1.37×10^6 g of carbon to the study reach during the May, August, and October study periods (**Table 4D-5**). These were generally a minor contribution to the additional DIC entering the study reach, and we calculated that there must have been respiratory DIC production and lateral inputs of 25.5×10^6, 12.4×10^6, and 11.8×10^6 g of carbon during the May, August, and October study periods, respectively.

The large decrease in dissolved oxygen along the tidal freshwater zone may indicate a high rate of microbial respiration, although a lateral input was found to contribute low-oxygen water. The consistent rate of decrease in dissolved oxygen in synoptic surveys provides evidence for a consistent process rate, not sporadic lateral inputs. Moreover, the oxygen and CO_2 air–water fluxes were nearly 1:1, suggesting the rapid re-oxygenation with atmospheric oxygen was driven by respiratory losses.

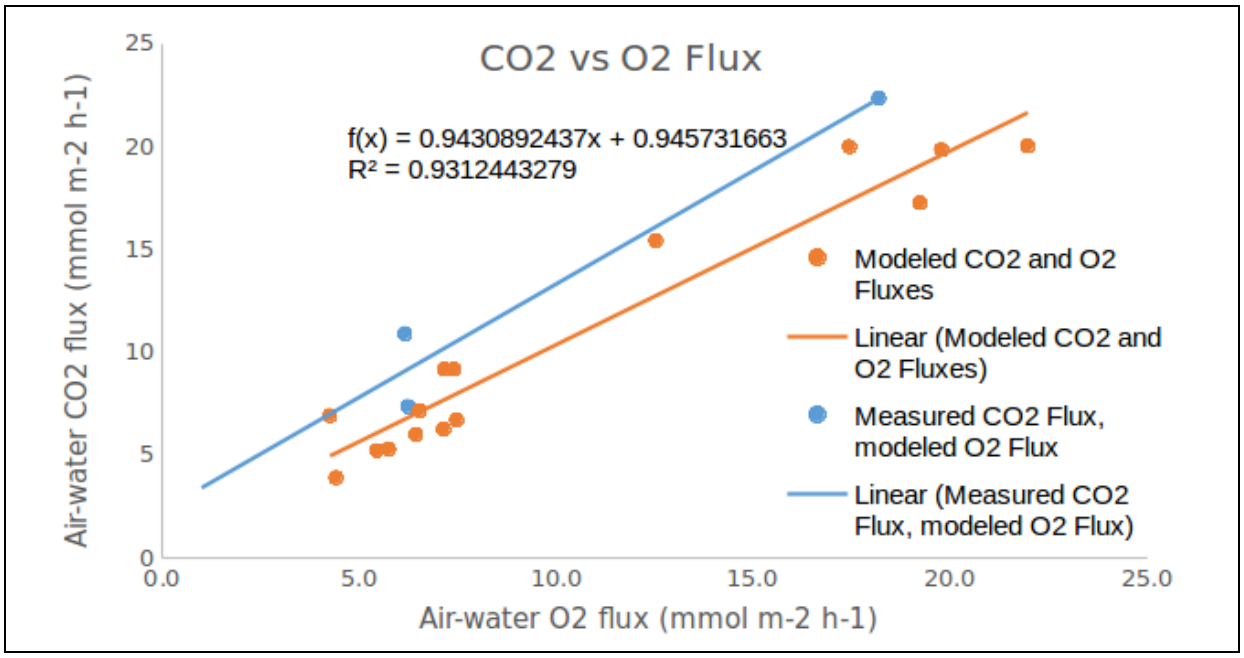

Figure 4D-7. The relationship between CO_2 and O_2 air–water flux.

Table 4D-5. Mass Balance of DIC for the Tidal Freshwater Zone of the NRE; Letters Following Each Flux Refer to Equation 4

Flux (10^6 g C per Water Replacement Time)	10–12 May 2016	22–24 August 2016	3–5 October 2016
Upstream input from Gum Branch (*G*)	20.2	8.26	14.7
CO_2 loss to atmosphere (*A*)	8.51	9.08	17.1
CO_2 gain from photomineralization (*P*)	2.82	1.41	1.37
Lateral input + respiration (*L*)	25.5	12.4	11.8
Export past Highway 17 in Jacksonville (*J*)	40.1	13.0	10.8
Jacksonville export and Gum Branch import	2.0	1.6	0.7

Conclusions

Physicochemical characteristics and river morphology changed dramatically 8 km upstream from Jacksonville's Highway 17 Bridge. The synoptic data showed consistent longitudinal changes in patterns in temperature, salinity, dissolved oxygen, pH, pCO_2, and DIC at this location. The tidal freshwater zone above this point shows a consistent increase in temperature, a decrease in dissolved oxygen saturation, and an increase in pCO_2. These patterns highlight a shift in the hydrologic and biogeochemical processes along the New River that distinguish the oligohaline estuary from tidal freshwater zone.

The data allowed prediction that a drifting particle or parcel of water took between 2.8 and 6.1 days to travel from Gum Branch to Jacksonville. Although the very slow flow velocity of the tidal freshwater New River made it difficult to deploy Lagrangian drifters, they did provide

crucial information about the travel time of water and solutes through this zone that helped us quantify internal cycling of NO_3, DIC, and DOC. There did not appear to be a relationship between discharge at Gum Branch and predicted travel time through the tidal freshwater zone during low discharge conditions. This lack of relationship is partly due to the uncertainty in measured travel time, but it may also be a hydrologic feature of the tidal freshwater zone. Higher discharge at Gum Branch may not have a strong influence on travel time to Jacksonville because of the influence of tides and because higher water levels are quickly spread over-bank. Over-bank, tidal flooding dramatically decreases the average flow velocity of water conveyed downstream.

Denitrification was predicted to approximately 10% of the flux at Gum Branch. Although it is unclear how this fraction changes with discharge, particularly above 4 $m^3 s^{-1}$ at Gum Branch, this 10% fraction can be used to better approximate NO_3 flux into the NRE from upstream.

The relatively long, tidally influenced travel time and large river surface area allowed all of the DIC input at Gum Branch to escape from the river before reaching Jacksonville. This loss was compensated mostly by a combination of lateral inputs, groundwater inputs, and microbial respiration. A significant mass of DOC (31% of the flux at Gum Branch) was predicted to be converted to DIC within the tidal freshwater zone by photolysis. From a mass balance of DIC, we predict that DIC flux at Jacksonville is 1.4 times the flux at Gum Branch. This estimate can be applied during low-flow conditions (less than 4 $m^3 s^{-1}$) at Gum Branch to improve the estimated fluxes to the NRE at Jacksonville.

No consistent diurnal oxygen production was observed in the tidal freshwater zone from which to estimate ecosystem metabolism. Pulses of phytoplankton primary production have been measured in neighboring black water rivers (Ensign et al., 2012), but monitoring in the New River did not capture any of these seasonal events. The tidal freshwater New River was highly heterotrophic—a strong and spatially consistent decrease in dissolved oxygen saturation was measured during all sampling trips.

Literature Cited

Ensign, S.H., M.W. Doyle, and M.F. Piehler. 2012. Tidal geomorphology affects phytoplankton at the transition from forested streams to tidal rivers. *Freshwater Biology 57*:2141–2155.

Granéli, W., M. Lindell, B.M. De Faria, and F.D.A. Esteves. 1998. Photoproduction of dissolved inorganic carbon in temperate and tropical lakes: Dependence on wavelength band and dissolved organic carbon concentration. *Biogeochemistry 43*:175–195.

Marino, R., and R.W. Howarth. 1993. Atmospheric oxygen exchange in the Hudson River: Dome measurements and comparison with other natural waters. *Estuaries 16*:433.

Siporin, K. 2010. Geomorphology, hydrology, and vegetation of North Carolina tidal rivers and their floodplains. Honors Thesis, Institute for the Environment, University of North Carolina at Chapel Hill, Chapel Hill, NC.

Von Korff, B.H., M.F. Piehler, and S.H. Ensign. 2014. Comparison of denitrification between river channels and their adjoining tidal freshwater wetlands. *Wetlands 34*:1047–1060.

Chapter 5

MCBCL Tributary Creeks

SERDP Project Number: RC-2245

Aquatic and Estuarine Module

Monitoring Activity AEM-2

Lead Researchers:

Dr. Michael F Piehler
University of North Carolina at Chapel Hill, Institute of Marine Sciences
Morehead City, NC
piehler@unc.edu

Supporting Researchers:

Adam Gold, acgold@live.unc.edu
Suzanne Thompson, sthompso@email.unc.edu

November 2017

Final

This report was prepared under contract to the U.S. Department of Defense (DoD) Strategic Environmental Research and Development Program (SERDP). The publication of this report does not indicate endorsement by DoD, nor should the contents be construed as reflecting the official policy or position of DoD. References herein to any specific commercial product, process, or service by trade name, trademark, manufacturer, or otherwise, do not necessarily constitute or imply its endorsement, recommendation, or favoring by DoD.

Table of Contents

Acronyms 5-v
Abstract 5-1
Objectives of the Monitoring Activity 5-2
Background 5-2
Materials and Methods 5-3
    Eight Watershed Streamflow Analyses 5-3
    Five Watershed Stream Analyses 5-5
Results and Discussion 5-5
    Eight Watershed Stream-Flow Analyses 5-5
    Changes in Hydrology Because of Urbanization 5-7
    Possible Solutions to Mitigate Changes in Hydrology 5-8
    Five Watershed Stream Analyses 5-8
Conclusions and Implications for Future Research and Implementation 5-13
    Monitoring Goals and Response 5-14
Literature Cited 5-14
Appendix 5-A: List of Scientific/Technical Publications 5-A-1
Appendix 5-B: List of Students 5-B-1
Appendix 5-C: Other Supporting Information 5-C-1

List of Figures

Figure 5-1. Overview map of the eight study watersheds wih stream sample points and manually delineated impervious area..... 5-3

Figure 5-2. The relationship between watershed imperviousness and mean flow per unit area (cubic meters per second) for low flows (lowest 20% of flows), total flow, and high flows (highest 20% of flows)..... 5-6

Figure 5-3. The relationship between watershed imperviousness and the R-B flashiness index..... 5-7

Figure 5-4. Stream temperature in the five study streams..... 5-9

Figure 5-5. Comparison of air and stream temperature through DCERP1 and DCERP2..... 5-10

Figure 5-6. Mean stream conductivity through the study period plotted versus watershed imperviousness. 5-11

Figure 5-7. The relationship between annual precipitation and mean annual conductivity in 2011–2014. 5-11

Figure 5-8. Time series of stream discharge from five study watersheds (gray), moving average of stream discharge (red), and measured precipitation (bars). 5-12

Figure 5-9. The relationship between watershed area and R-B flashiness index with more developed watersheds (orange) and more natural watersheds (blue). 5-13

List of Tables

Table 5-1. Attributes of the Eight Study Watersheds..... 5-4

Acronyms

°C	degree Celsius
AE	Aquatic/Estuarine (Module)
AEM	Aquatic/Estuarine Monitoring
CC	Climate Change (Module)
CHB	Courthouse Bay
COG	Cogdels
DCERP	Defense Coastal/Estuarine Research Program
DCERP1	first cycle of DCERP
DCERP2	second cycle of DCERP
DoD	U.S. Department of Defense
FR	French
ha	hectare
m	meter
MCBCL	Marine Corps Base Camp Lejeune
NRE	New River Estuary
ppt	part per thousand
q	streamflow every 6 hours
r^2	r squared
R-B	Richards-Baker
RC	Resource Conservation and Climate Change (a SERDP program area)
SCM	stormwater control measure
SERDP	Strategic Environmental Research and Development Program
TAR	Tarawa Terrace
TRAP	Traps

Abstract

The relationship between watershed imperviousness and hydrology in the coastal plain of the Southeastern United States has not been extensively studied for all prevalent soil types in the area, but changes in hydrology because of development affect important and sensitive coastal waters. To determine how hydrology changes with development for well-drained coastal watersheds, this study used a long-term data set of stream discharge measurements from coastal watersheds on Marine Corps Base Camp Lejeune, NC, that span a range of watershed imperviousness. Results from this study provide information about changes in streamflow along the Southeastern Coast of the United States that may negatively affect human infrastructure development and water quality.

The goals of this study were to

1. Determine the impact of impervious surface coverage on stream hydrology
2. Determine the possible causes for differences in urban and non-urban hydrology
3. Compare well-drained and poorly drained coastal plain watersheds and how they are affected by impervious surface coverage and human development
4. Characterize the relationship between watershed imperviousness and stream conductivity
5. Assess the relationship between air and creek temperatures along a gradient of watershed imperviousness.

Keywords: Coastal plain, conductivity, hydrology, imperviousness, streamflow, temperature, watershed development

Objectives of the Monitoring Activity

We measured streamflow in eight coastal creeks for 2 years (February 2009–February 2011) and conductivity, temperature, and streamflow in five coastal creeks for a period of 5 years (July 2010–July 2015) on Marine Corps Base Camp Lejeune (MCBCL) to assess the impacts of land use on those factors and to use in conjunction with data from Research Project AE-5 to estimate loading to the New River Estuary (NRE). Creek sampling stations were spatially stratified to assess variability within the estuarine salinity zones and to determine the effects of land activities on streamflow and on sediment and nutrient delivery to the estuary. Elements of streamflow are related to land use to link land activities and aquatic and estuarine ecosystem function.

Background

Changes in the watersheds due to human infrastructure development affect water quality through impacts on hydrology and the sources and composition of materials (e.g., sediment, nutrients, fecal material; Paul and Meyer, 2001). The transition from a natural to a developed landscape increases the amount of impervious cover and decreases in forested area, among other changes. These changes typically decrease infiltration of precipitation, creating periods of increased peak storm flows (Leopold, 1968) of diminished duration (Seaburn, 1969) with the potential for changes, either increases or decreases, in base flows (Bhaskar et al., 2016; Price, 2011). The net effect is an overall increase in runoff volume, particularly in the storm flow component.

Few studies have examined the effects of increased watershed imperviousness on hydrology within the southeastern coastal plain and even fewer studies have focused on coastal areas. There are important distinctions in soil types even between areas within the coastal plain. These distinctions likely affect how development and increased imperviousness might change a watershed's hydrology. In the southeastern coastal plain, forest management studies have found that watersheds in the coastal plain have higher rates of evapotranspiration than other physiographic regions such as mountains (Sun et al., 2002). Also, forest thinning or removal (clear cutting) increases the volume of water exported from a watershed as streamflow (Kim et al., 2013; Mclaughlin et al., 2013). One study in the inner coastal plain on poorly drained soils found a decline in water table elevation, an increase in channel incision, and a decrease in the relative amount of baseflow with increased watershed imperviousness (Hardison et al., 2009). These studies inform predictions of the effects of urbanization on hydrology in urban and forested coastal plain watersheds, but direct measurements are also necessary for well-drained urban watersheds.

Coastal streams are important conduits for nutrients and contaminants in stormwater runoff to receiving waters (DiDonato et al., 2009; Mallin and Lewitus, 2004). Managing nutrient and sediment loading poses a challenge because sufficient quantities of each are necessary for proper aquatic/estuarine ecosystem functioning, but excessive amounts can be detrimental. Nutrients are necessary to support primary production to support higher trophic levels. Ecologically valuable salt marshes that are downstream in many coastal creeks require sediment to maintain their elevation in the face of rising sea levels and wave-driven erosion. Sediment delivered in rivers and streams is thought to make an important contribution to salt marsh accretion (Morris, 2002). However, sediments and nutrients in excess overwhelm ecosystem requirements and can degrade coastal habitats.

Materials and Methods

Eight Watershed Streamflow Analyses

Watershed Imperviousness

Watersheds on MCBCLwere delineated by using 1-m resolution elevation data provided by MCBCL and the Hydrology toolbox from ArcMap 10.2 (ESRI) (**Figure 5-1**). Drainage networks, including where streams flowed underground or under roads, were "burned" into the elevation data, and high-resolution orthoimagery was used to confirm the location of the drainage network in these places. National Agriculture Imagery Program imagery (USDA, 2009) were used to manually delineate impervious areas in each of the study watersheds for the initial year of data collection (**Table 5-1**). The impervious area was divided by the total watershed area to calculate percent watershed imperviousness. This watershed imperviousness metric was used for the entire study period (February 2009–February 2011), so this assumes that there was no significant change in impervious area during the study period.

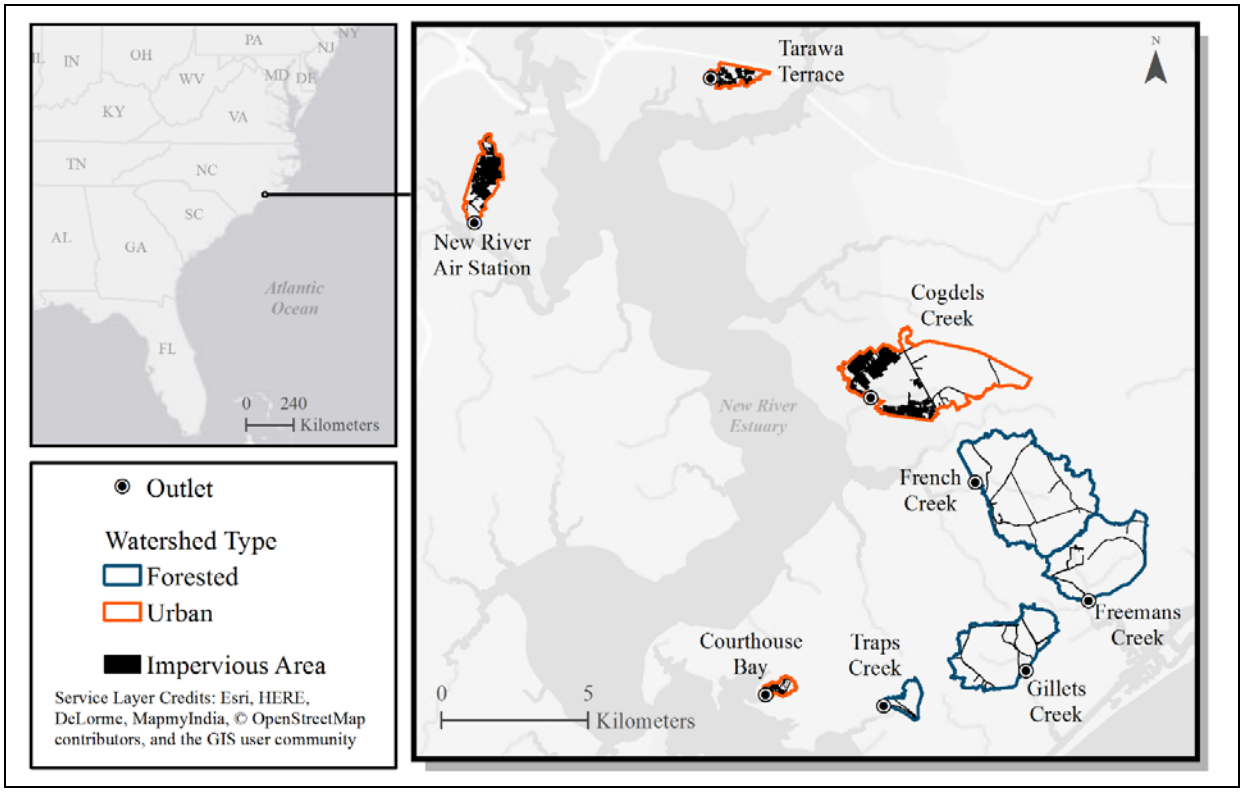

Figure 5-1. Overview map of the eight study watersheds wih stream sample points and manually delineated impervious area.

Table 5-1. Attributes of the Eight Study Watersheds

Name	Total Area (ha)	Impervious Area (ha)	Impervious-ness (%)	Type	% Well-drained soils	Mean watershed slope (%)
Cogdels Creek	725.41	130.45	17.98	Urban	75.94	6.41
Courthouse Bay	31.77	7.67	24.15	Urban	100	4.92
Freeman Creek	468.50	6.80	1.45	Forested	45.48	5.70
French Creek	835.05	7.99	0.96	Forested	35.65	4.96
Gillets Creek	433.20	12.59	2.91	Forested	37.98	6.28
New River Air Station	142.10	75.11	52.86	Urban	100	5.12
Tarawa Terrace	70.16	18.55	26.44	Urban	83.48	4.87
Traps Bay Creek	61.48	2.41	3.93	Forested	41.36	8.33

Streamflow Measurement

Stream discharge was measured every 30 minutes for 2 years in eight streams, consisting of four forested and four urban sites, by using Teledyne Isco flow and depth sensors combined with measurements of stream cross-sectional area. These data sets were aggregated into 6-hour means for each of the eight study watersheds and were used for all calculations within this study. To account for varying watershed areas, streamflow data were divided by watershed area. Study streams were chosen to encompass a wide range of watershed percent imperviousness.

Flow Duration Curves

The R package HydroTSM was used to calculate flow duration curves for each watershed's stream discharge data (Zambrano-Bigiarini, 2017), and stream-flow data were partitioned into different flow classes. The lowest 20% of stream-flow measurements (low flows) were grouped together, and the highest 20% of stream-flow measurements (high flows) were grouped together. The means of the complete record of stream-flow measurements or total flow, low flows, and high flows were calculated.

Flashiness of Flow

The flashiness of streamflow, a dimensionless metric that indicates how quickly streamflow changes, was calculated for each watershed over the 2-year study period by using the Richards-Baker (R-B) flashiness index (Baker et al., 2004), as shown in Equation 5-1:

$$R - B\ Index = \frac{\sum_{i=1}^{n} |q_i - q_{i-1}|}{\sum_{i}^{n} q_i} \qquad \text{(Eq. 5-1)}$$

Where

q = Streamflow every 6 hours. Larger watersheds typically have lower values of flashiness, but the addition of impervious area can also increase flashiness.

Five Watershed Stream Analyses

Watershed Imperviousness

Watersheds on MCBCLwere delineated by using 1-m resolution elevation data provided by MCBCL and the Hydrology toolbox from ArcMap 10.2 (ESRI) (**Figure 5-1**). Drainage networks, including where streams flowed underground or under roads, were "burned" into the elevation data, and high-resolution orthoimagery was used to confirm the location of the drainage network in these places. National Agriculture Imagery Program imagery (USDA, 2009) were used to manually delineate impervious areas in each of the study watersheds for the initial year of data collection (**Table 5-1**). The impervious area was divided by the total watershed area to calculate percent watershed imperviousness. This watershed imperviousness metric was used for the entire study period (February 2009–February 2011), so this assumes that there was no significant change in impervious area during the study period.

Stream Temperature and Conductivity

We analyzed stream temperature patterns for stream data and compared seasonal temperature patterns to watershed imperviousness, forested area, and other measures of development to determine the likely causes of differences in temperature from the five streams. Our study streams flow directly into the NRE, potentially leading to increased estuarine temperatures in streams with increased temperatures. We provided temperature data to Research Project AE-6 to inform the design of their temperature manipulation experiments. Additionally, stream water conductivity measurements were collected, and the relationship between conductivity and watershed imperviousness was analyzed.

Streamflow Measurements

Stream discharge was measured every 30 minutes for 5 years in five watersheds spanning a range of watershed percent imperviousness by using Teledyne Isco flow and depth sensors combined with measurements of stream cross-sectional area. These data set were aggregated into 6-hour means. To account for varying watershed areas, streamflow data were divided by watershed area whenever the magnitude of streamflow or water load was compared between watersheds.

Results and Discussion

Eight Watershed Stream-Flow Analyses

Flow Duration Curves

By utilizing area-normalized streamflow and values from flow duration curves, the effects of watershed imperviousness on various types of streamflow can be determined. Mean low flow, or the mean of the lowest 20% of flows, and watershed imperviousness were significantly (α=0.05) correlated (**Figure 5-2**, r^2=0.97, $p<0.01$). Similar relationships were found between mean total flow from the complete stream-flow record and watershed imperviousness (**Figure 5-2**, r^2=0.94, $p<0.01$), as well as mean high flow, or the mean of the highest 20% of flows, and watershed

imperviousness (**Figure 5-2**, r^2=0.93, p<0.01). These results indicate that watershed imperviousness increases the amount of streamflow during all three of these types of flow.

Flashiness of Flow

Streamflow flashiness was significantly (α=0.05) and positively correlated with watershed imperviousness (**Figure 5-3**, r^2=0.77, p<0.01). Although **Figure 5-3** shows a linear function to model the relationship between stream-flow flashiness and watershed imperviousness, flashiness did not increase above levels observed in the watersheds of the forested study until watershed imperviousness exceeded approximately 20%. Increased flashiness can have negative impacts on the stability of stream ecosystems and downstream waters and can possibly indicate larger amounts of stream incision and nutrient loading.

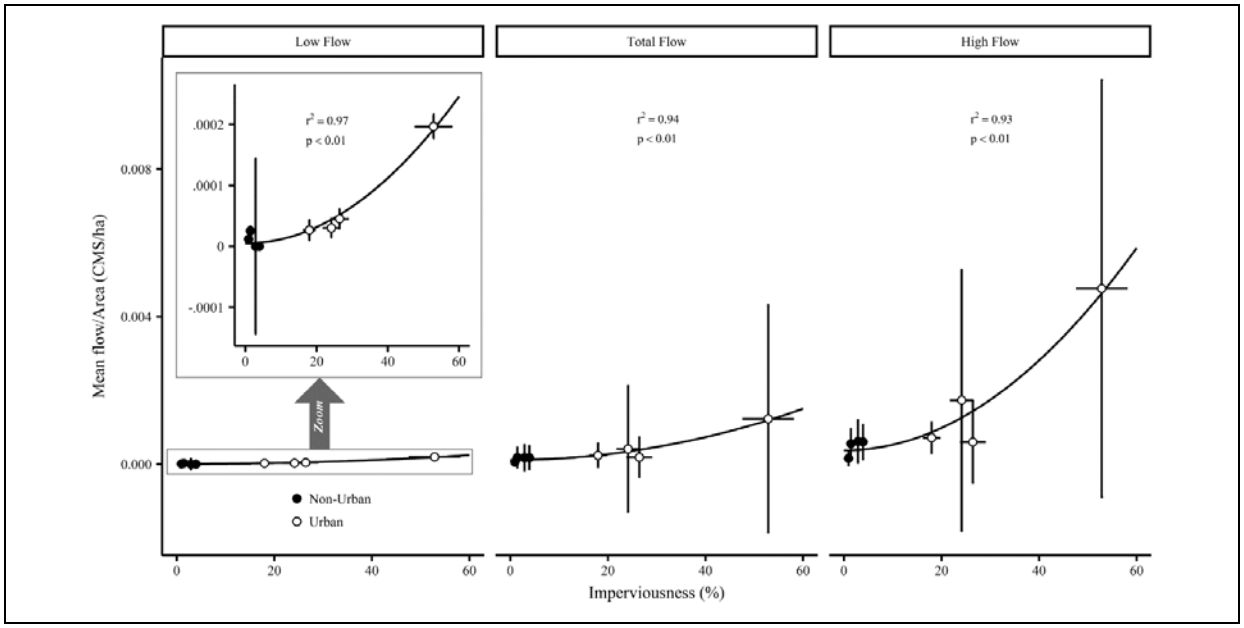

Figure 5-2. The relationship between watershed imperviousness and mean flow per unit area (cubic meters per second) for low flows (lowest 20% of flows), total flow, and high flows (highest 20% of flows)

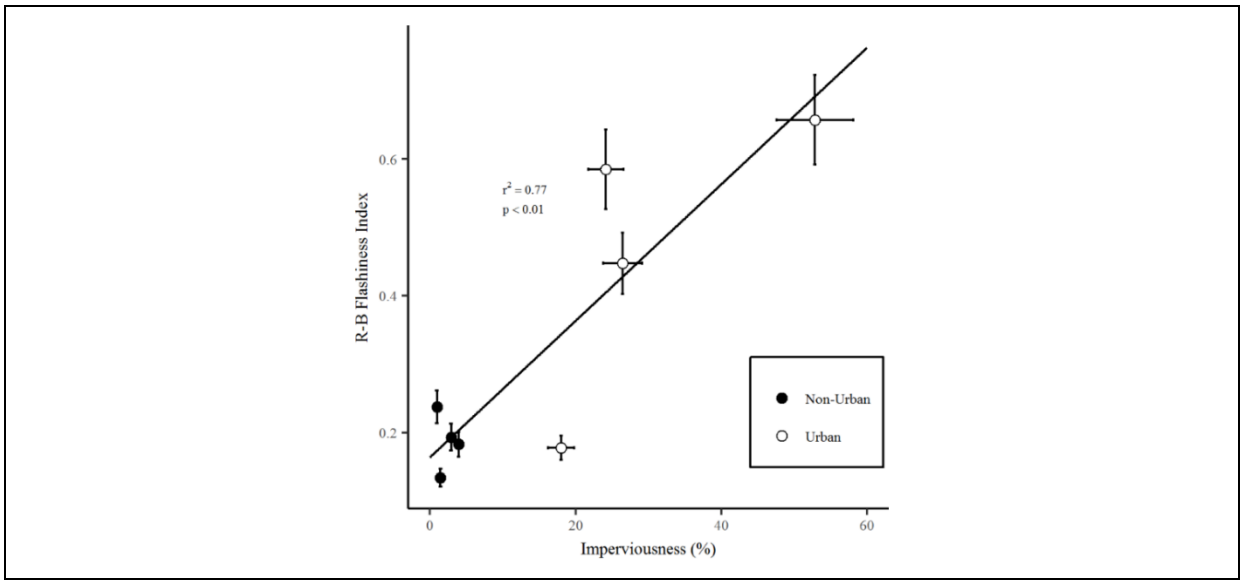

Figure 5-3. The relationship between watershed imperviousness and the R-B flashiness index.

Changes in Hydrology Because of Urbanization

Our monitoring activities revealed that the mean low flow (normalized by area) elevated as watershed imperviousness increased. Many past studies have documented decreases in baseflow after increased imperviousness because of decreased infiltration (Price, 2011), but the opposite is shown in this study. Possible reasons for this increase in low flow could be decreased evapotranspiration and stream incision (Bhaskar et al., 2016; Price, 2011). Although a survey of human water consumption, water infrastructure, and stream morphology was beyond the scope of this study, we did evaluate the soil type of the watersheds to obtain some insight regarding impervious area, evapotranspiration, and infiltration.

The coastal Southeastern United States, including this study area, naturally has longleaf pine (*Pinus palustris*) forests (Outcalt and Sheffield, 1996), but human development clears away these established and deep-rooted trees in favor of lawn turf and pavement, thus decreasing evapotranspiration because of differences in water use (Bosch et al., 2014). Additionally, the soil type and soil drainage in this study area are heterogeneous (NRCS, 2015), and the desire to protect property and infrastructure by building on well-drained land leads to larger amounts of development and forest clearing on well-drained soils (**Table 5-1**). These well-drained patches then likely become even more important recharge areas because of both decreased evapotranspiration and increased infiltration, possibly contributing to the increased low flow with imperviousness observed during this study. Previous studies of watersheds that underwent vegetation clearing with development observed large decreases in evapotranspiration (Barron et al., 2013; Roy et al., 2009), possibly increasing baseflow (Bhaskar et al., 2016). Increases in low flows can have negative consequences on stream ecology and human infrastructure. For example, increased low flow can increase nutrient loading (Stanford and Ward, 1993), alter stream food webs (Reich et al., 2010), elevate flooding risk for areas near streams (Barron et al., 2013), and lead to infiltration of groundwater to wastewater systems (Bhaskar et al., 2016).

In addition to increased area-normalized low flow with increased imperviousness, the area-normalized total flow and high flows also increased. These increases are more straightforward and easier to predict, mainly because stormwater management over the past few decades favored an efficient drainage network that quickly routes runoff from impervious surfaces to streams (Burns et al., 2012). The hydrologic effects of impervious area and the efficient drainage of these areas are illustrated by the significant (α=0.05) positive relationship between the R-B flashiness index and imperviousness of each watershed (**Figure 5-3**). Increased high flows can lead to stream incision (Hardison et al., 2009), increased nutrient loading (Wahl et al., 1997; Walsh et al., 2005), and other negative ecological effects (Paul and Meyer, 2001; Walsh et al., 2005).

Possible Solutions to Mitigate Changes in Hydrology

To account for the reduced evapotranspiration and increased infiltration, appropriate stormwater control measures (SCMs) could be used. Instead of using conventional SCMs, such as stormwater ponds, other measures could be employed. For instance, SCMs designed to reduce water volume through evapotranspiration and stormwater harvesting could be used to reduce overall water volume.

An emerging stormwater management strategy dubbed as the “ecohydrologic approach” (Fletcher et al., 2014) or “flow regime approach” (Burns et al., 2012), inspired by Poff et al. (1997), could be used. The strategy focuses on restoring a “natural flow regime with similar flow magnitude, duration, timing, frequency, and variability of flows” (Fletcher et al., 2014). Studies detailing these similar approaches concluded that mimicking natural flow regimes would be unlikely without reducing runoff volume (Fletcher et al., 2014; Walsh et al., 2012), or, in this case, reducing infiltration, increasing evapotranspiration, and reducing runoff volume caused by urbanization. Examples of such SCMs are lined bioretention cells, reforestation, and stormwater harvesting. Lined bioretention cells reduce runoff and infiltration by encouraging evapotranspiration. For example, one study showed that a bioretention cell evapotranspired 19% if its inflow water volume (Li et al., 2009). Restoring swaths of forested area (Trimble et al., 1987) or tree planting throughout an urban watershed (Bell et al., 2016) can decrease overall water volume, and reclaimed stormwater can reduce runoff volumes and be used for non-potable purposes (Fletcher et al., 2007). This stormwater management strategy has been successful elsewhere in the United States (Dietz and Clausen, 2008; Jarden et al., 2016) and has been suggested in the coastal plain to improve water quality (Gold et al., 2017).

Five Watershed Stream Analyses

Stream Temperature

Temperature is an important controlling factor for biological and chemical processes in streams. Research suggests that urbanization affects stream temperature (Nelson and Palmer, 2007). Data from DCERP1 and DCERP2 were used to test the hypothesis that increased imperviousness in sub-watersheds would increase coastal stream temperature. Coastal stream temperature responses to urbanization may be distinctive from their upland analogues due to generally lower relief in coastal watersheds. **Figure 5-4** depicts seasonal mean temperatures for the five streams that have been monitored in both DCERP1 and DCERP2. Elevated temperatures in streams with more developed watersheds were observed throughout the record. Summer mean temperatures were as

much as 5°C higher in more developed streams as compared with less developed streams. There is an apparent upward trend in stream temperature through the period of record (2008–2015).

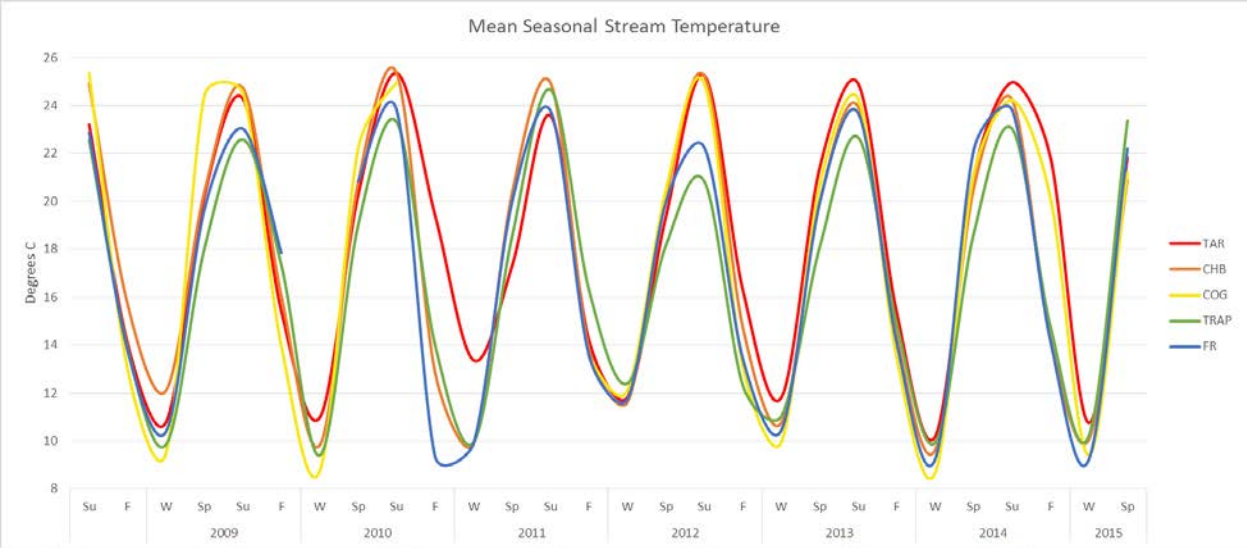

Figure 5-4. Stream temperature in the five study streams.

Temperature (in °C) and is presented for each season from 2008–2013. Sites are presented from least developed (cool colors) to most developed (warm colors).

In collaboration with the Research Project CC-1, we assessed the relationship between air and stream temperatures during DCERP1 and DCERP2. Our past results revealed impacts of land development on stream temperature. Increased imperviousness correlated with increasing storm flow stream temperature, and decreased forest cover correlated with increased base flow stream temperature. The strong correlations between air and stream temperature shown in **Figure 5-5** support the potential to forecast future changes in stream temperatures based on air temperature. There were no significant differences in the slopes of the regressions for each of the streams, although their respective watersheds exhibited varied levels of development. This finding suggests that a single forecast of future temperature changes could be made for all streams on MCBCL.

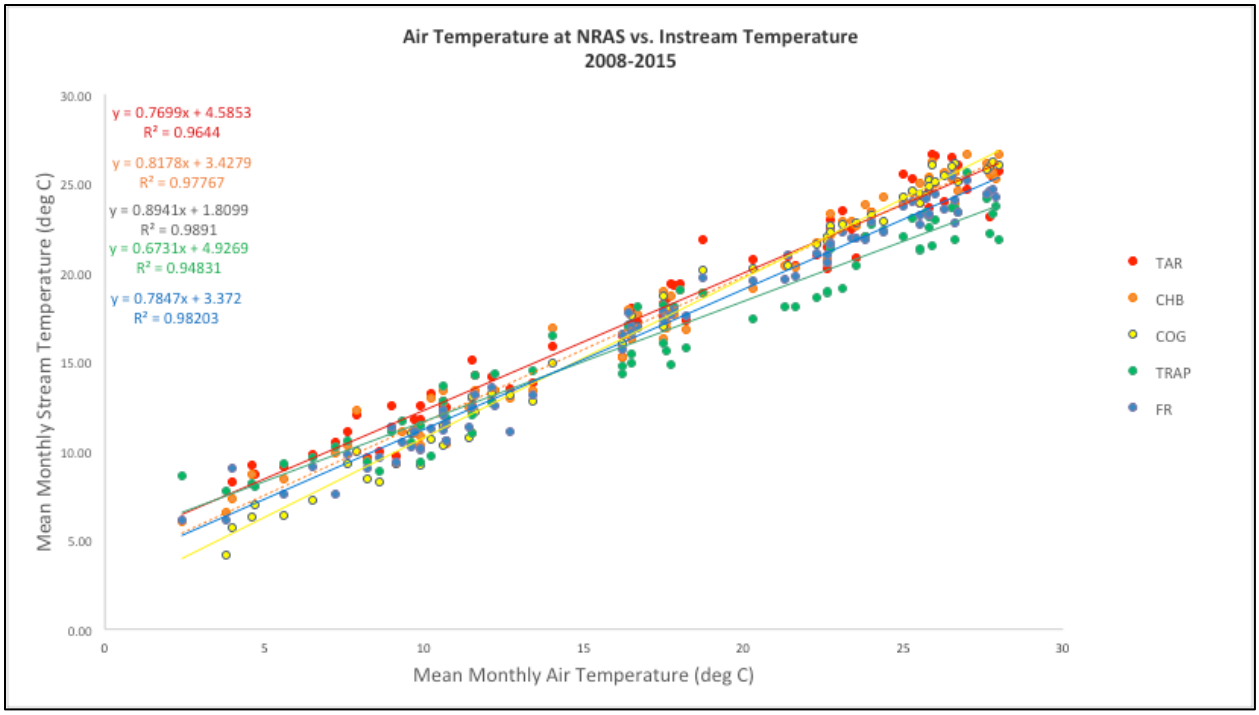

Figure 5-5. Comparison of air and stream temperature through DCERP1 and DCERP2.

Warmer colors represent more developed streams and cooler colors represent streams with less watershed development. Results of linear regressions are color coded for each stream. Streams were Tarawa Terrace (TAR), Courthouse Bay (CHB), Cogdels Creek (COG), Traps Bay Creek (TRAP) and French Creek (FR).

Stream Conductivity

Conductivity measures water's capacity to pass electrical flow (conduct an electric current), which is directly related to the concentration of ions in the water. In coastal streams, the most likely source of ions is from seawater. We tested the hypothesis that development in coastal stream watersheds affects stream conductivity. The relationship between mean stream conductivity from 2011 to 2014 was contrasted with imperviousness (**Figure 5-6**). There was no clear relationship between stream conductivity and imperviousness and all conductivity levels were very low (the maximum conductivity was a small fraction of a part per thousand [ppt] in salinity). The highest conductivity was at Courthouse Bay and was likely attributable to that site's proximity to the inlet and ocean. To further examine our hypothesis, we examined conductivity in all streams and stratified the data by annual precipitation (**Figure 5-7**). Again, all stream conductivity levels were very low. There was a pattern of higher stream conductivity during years with less precipitation, but these increases were mostly quite small. The exception again was Courthouse Bay, which we believe was driven by its proximity to the New River Inlet. Using DCERP data (2008–2015), we found that watershed development did not have a predictable effect on stream conductivity, but that lower precipitation did result in higher stream conductivity (though no conductivity values were greater than the equivalent of 1 ppt salinity). Therefore, we found no effect of imperviousness on in-stream conductivity.

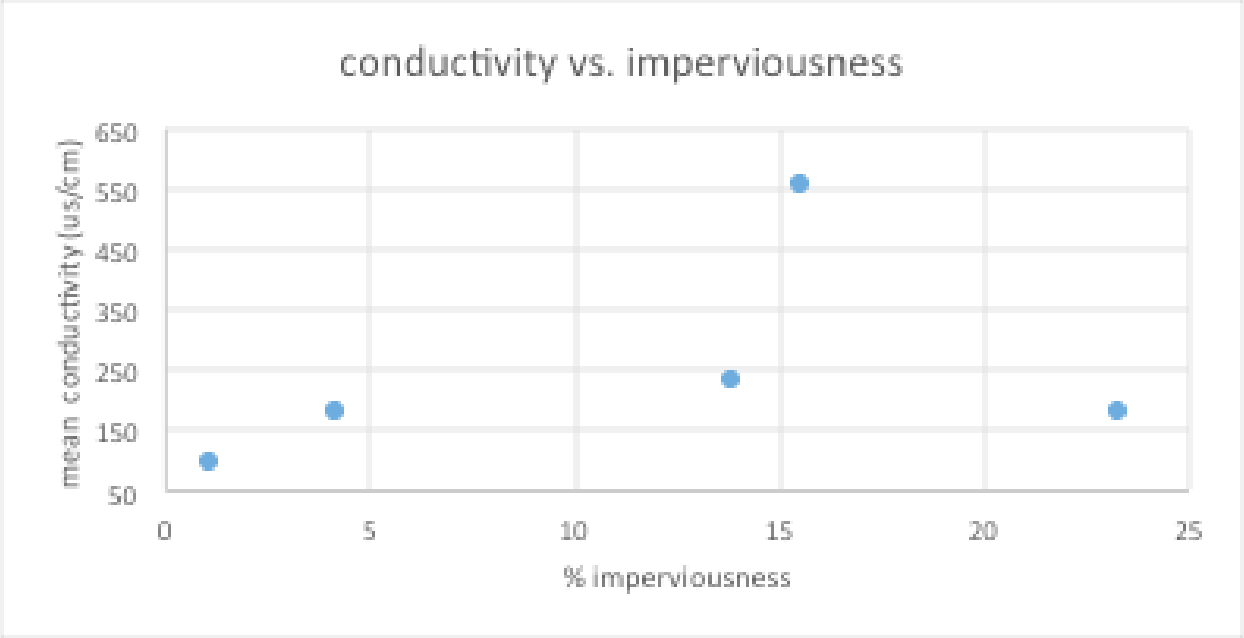

Figure 5-6. Mean stream conductivity through the study period plotted versus watershed imperviousness.

The slightly higher conductivity level was observed at Courthouse Bay.

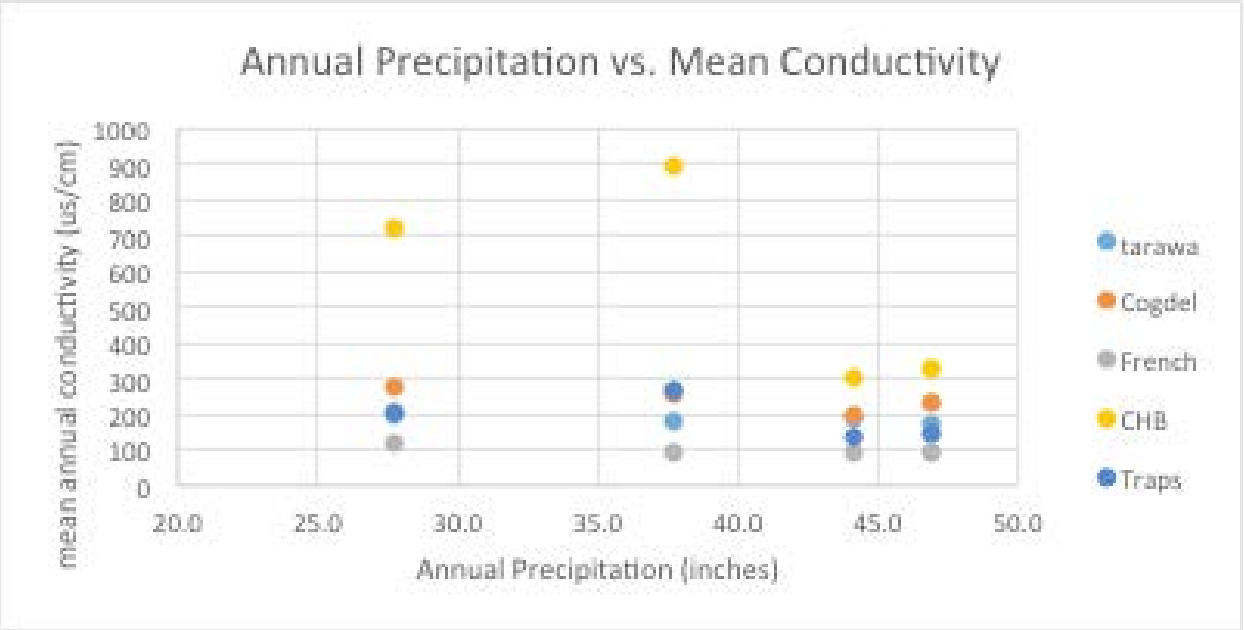

Figure 5-7. The relationship between annual precipitation and mean annual conductivity in 2011–2014.

Streamflow

The record of streamflow between July 2010 and July 2015 for the five study watersheds shows inter-annual and seasonal variations in streamflow (**Figure 5-8**), but unlike the eight watershed

streamflow analysis, only weak correlations (R^2 <0.25) were found between watershed imperviousness and mean streamflow, streamflow flashiness, and low/high flow metrics. These weak relationships were likely due to inter-annual variability in precipitation and streamflow that obscured differences among streams. The eight watershed streamflow analyses more clearly show differences between watershed imperviousness and streamflow. There was a strong relationship between watershed area and flashiness (**Figure 5-9**, R^2=0.86). This finding indicates that flashiness was generally controlled by watershed area rather than watershed imperviousness, but more developed watersheds had flashiness metrics that fell above the logarithmic regression line and more natural watersheds had flashiness metrics that fell below the logarithmic regression line (**Figure 5-9**). This pattern suggests that while watershed area is the main control for streamflow flashiness, watershed imperviousness may increase streamflow flashiness as previously discussed in the section titled Eight Watershed Streamflow Analyses.

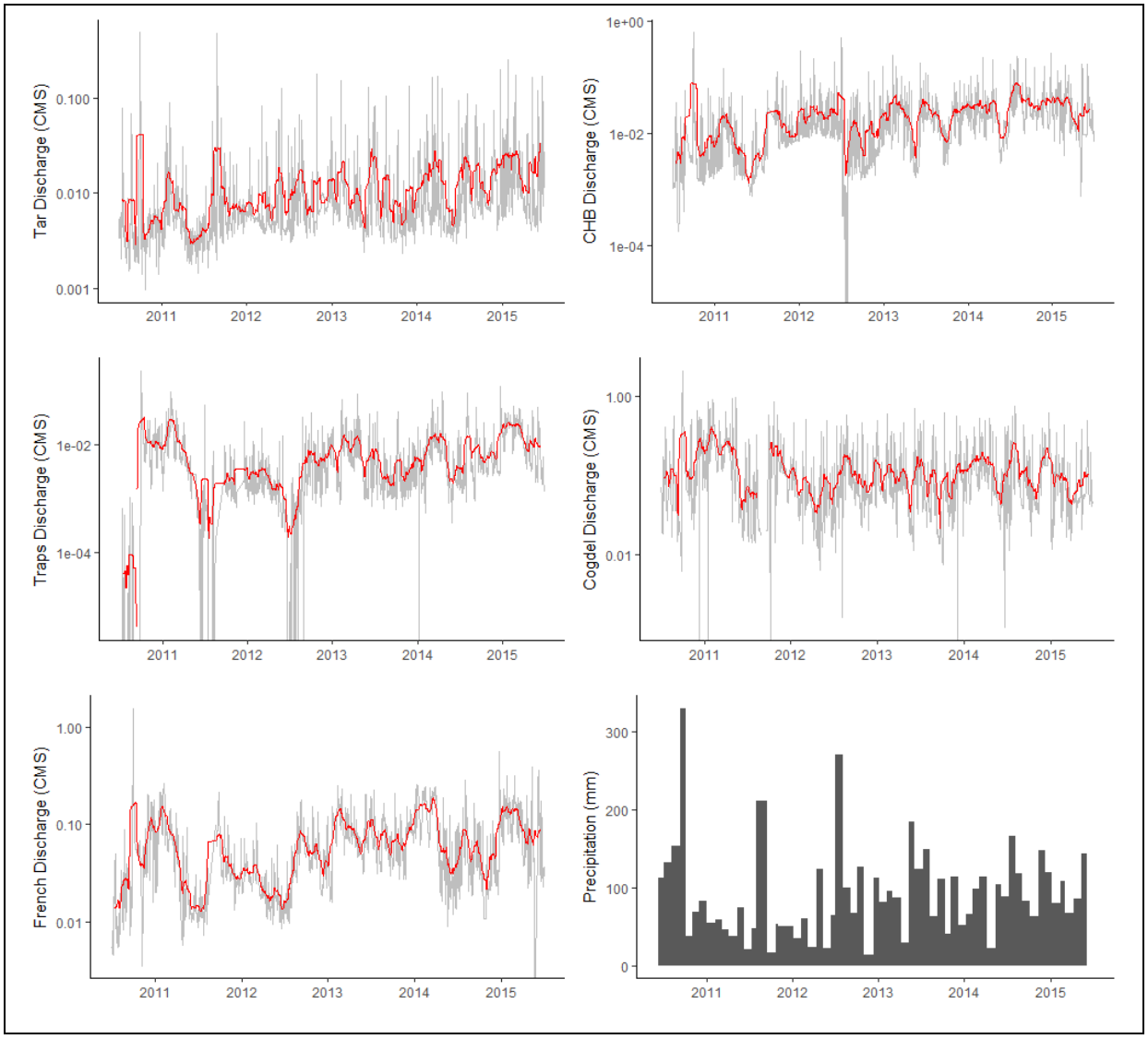

Figure 5-8. Time series of stream discharge from five study watersheds (gray), moving average of stream discharge (red), and measured precipitation (bars).

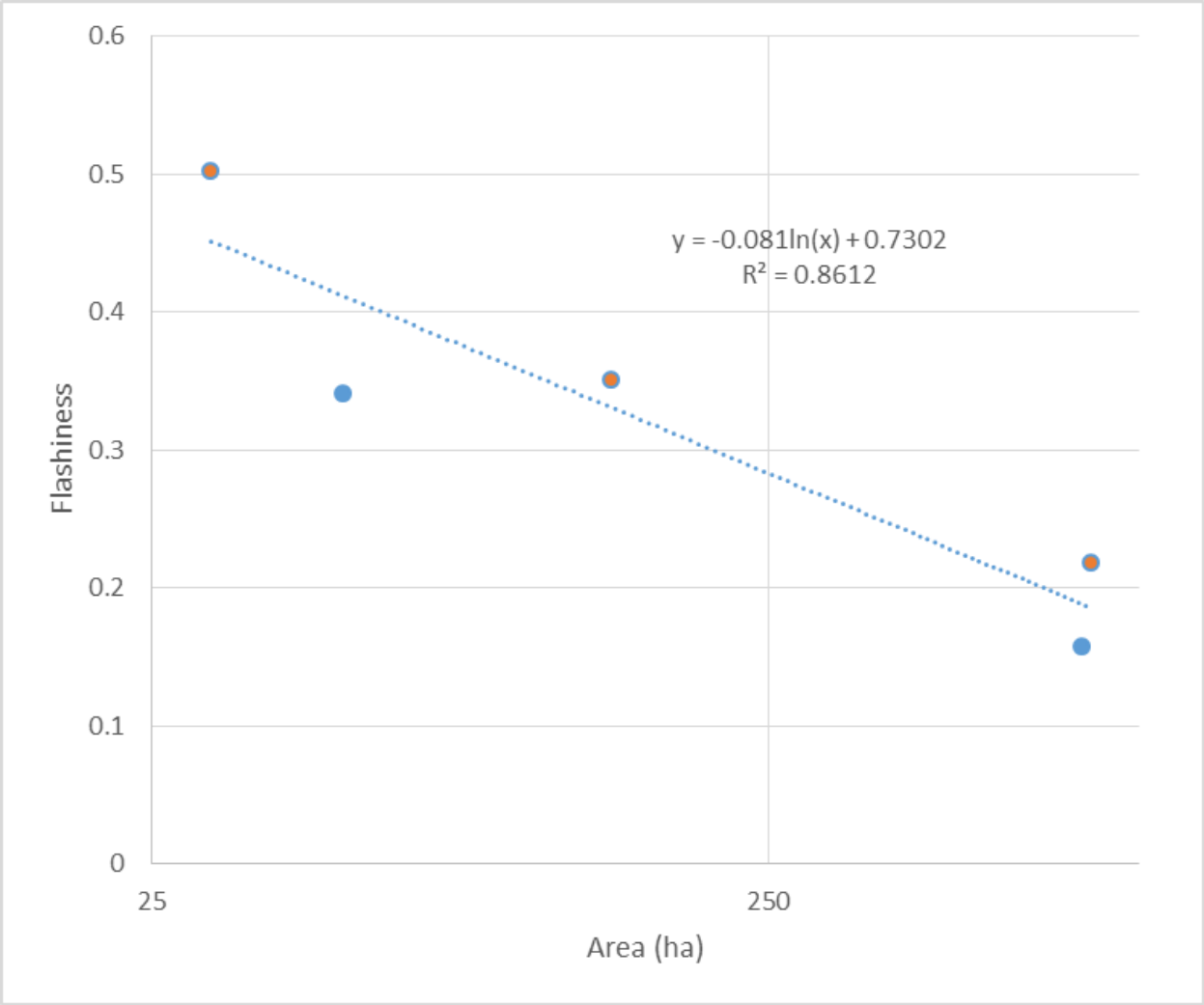

Figure 5-9. The relationship between watershed area and R-B flashiness index with more developed watersheds (orange) and more natural watersheds (blue).

Conclusions and Implications for Future Research and Implementation

Results from MCBCL tributary stream monitoring showed that watershed imperviousness was significantly and positively correlated with mean stream, low flow, high flow, total flow, and stream flashiness. Preferential development and deforestation on well-drained soils likely led to increased infiltration and decreased evapotranspiration in watersheds with greater imperviousness. The positive relationship between all presented metrics of flow with watershed imperviousness suggests that an ecohydrological stormwater management approach that focuses on increasing evapotranspiration and stormwater harvesting (i.e., rain barrels and cisterns) could successfully mitigate the negative hydrologic effects of development in well-drained areas of the coastal plain such as the area on which MCBCL is located.

Monitoring Goals and Response

1. **Determine the impact of impervious surface coverage on stream hydrology.**

   Results from MCBCL tributary stream monitoring showed that watershed imperviousness was significantly and positively correlated with mean stream low flow, high flow, total flow, and stream flashiness. The observed difference was detected at 20% imperviousness within the watershed.

2. **Determine possible causes for differences in urban and non-urban hydrology.**

   The increases in total flow and high flows in urban watersheds were expected and are because of decades of stormwater management that favored an efficient drainage network that quickly routes runoff from impervious surfaces to streams (Burns et al., 2012). The increase in low-flow hydrology for urban watersheds was unexpected, but could be attributed to decreased evapotranspiration from the conversion of forested lands to turf grass and the subsequent recharge of base flow through infiltration on well-drained soils.

3. **Characterize the relationship between watershed imperviousness and stream conductivity.**

   We hypothesized that salinity intrusion may have been more prevalent in undeveloped watersheds due to less flashy hydrology. However, imperviousness was not a good predictor of conductivity in our study watersheds. Additional research below the head of tide could provide more information regarding the influence of development on stream conductivity.

4. **Assess the relationship between air and creek temperatures along a gradient of watershed imperviousness.**

   Air and stream temperatures were highly correlated at all sites through the duration of the study. This finding is useful because it supports using future forecasts for air temperature for stream temperature forecasting.

Literature Cited

Baker, D.B., R.P. Richards, T.T. Loftus, and J.W. Kramer. 2004. A new flashiness index: Characteristics and applications to midwestern rivers and streams. *Journal of the American Water Resources Association 40*:503–522. doi:10.1111/j.1752-1688.2004.tb01046.x

Barron, O.V., A.D. Barr, and M.J. Donn. 2013. Effect of urbanisation on the water balance of a catchment with shallow groundwater. *Journal of Hydrology 485*:162–176. doi:10.1016/j.jhydrol.2012.04.027

Bell, C.D., S.K. McMillan, S.M. Clinton, and A.J. Jefferson. 2016. Hydrologic response to stormwater control measures in urban watersheds. *Journal of Hydrology 541*:1488–1500. doi:10.1016/j.jhydrol.2016.08.049

Bhaskar, A.S., L. Beesley, M.J. Burns, T.D. Fletcher, P. Hamel, C.E. Oldham, and A.H. Roy. 2016. Will it rise or will it fall? Managing the complex effects of urbanization on base flow. *Freshwater Science 35*:293–310. doi:10.1086/685084

Bosch, D.D., L.K. Marshall, and R. Teskey. 2014. Forest transpiration from sap flux density measurements in a southeastern coastal plain riparian buffer system. *Agricultural and Forest Meteorology 187*:72–82. doi:10.1016/j.agrformet.2013.12.002

Burns, M.J., T.D. Fletcher, C.J. Walsh, A.R. Ladson, and B.E. Hatt. 2012. Hydrologic shortcomings of conventional urban stormwater management and opportunities for reform. *Landscape and Urban Planning 105*:230–240. doi:10.1016/j.landurbplan.2011.12.012

DiDonato, G.T., J.R. Stewart, D.M. Sanger, B.J. Robinson, B.C. Thompson, A.F. Holland, and R.F. Van Dolah. 2009. Effects of changing land use on the microbial water quality of tidal creeks. *Marine Pollution Bulletin 58*(1):97–106.

Dietz, M.E., and J.C. Clausen. 2008. Stormwater runoff and export changes with development in a traditional and low impact subdivision. *Journal of Environmental Management 87*:560–566. doi:10.1016/j.jenvman.2007.03.026

Fletcher, T.D., G. Vietz, and C.J. Walsh. 2014. Protection of stream ecosystems from urban stormwater runoff: The multiple benefits of an ecohydrological approach. *Progress in Physical Geography 38*:543–555. doi:10.1177/0309133314537671

Fletcher, T.D., V.G. Mitchell, A. Deletic, T.R. Ladson, and A. Séven. 2007. Is stormwater harvesting beneficial to urban waterway environmental flows? *Water Science and Technology 55*:265–272.

Gold, A.C., S.P. Thompson, and M.F. Piehler. 2017. Water quality before and after watershed-scale implementation of stormwater wet ponds in the coastal plain. *Ecological Engineering 105*:240–251. doi:10.1016/j.ecoleng.2017.05.003

Hardison, E.C., M.A. O'Driscoll, J.P. Deloatch, R.J. Howard, and M.M. Brinson. 2009. Urban land use, channel incision, and water table decline along coastal plain streams, North Carolina. *Journal of the American Water Resources Association 45*:1032–1046. doi:10.1111/j.1752-1688.2009.00345.x

Jarden, K.M., A.J. Jefferson, and J.M. Grieser. 2016. Assessing the effects of catchment-scale urban green infrastructure retrofits on hydrograph characteristics. *Hydrological Processes 30*:1536–1550.

Kim, H.W., D.M. Amatya, G.M. Chescheir, W.R. Skaggs, and J.E. Nettles. 2013. Hydrologic effects of size and location of fields converted from drained pine forest to agricultural cropland. *Journal of Hydrologic Engineering 18*:552–566. doi:10.1061/(ASCE)HE.1943-5584.0000566

Leopold, L.B. 1968. *Hydrology for Urban Land Planning—A Guidebook on the Hydrologic Effects of Urban Land Use*. U.S. Geological Survey Circular 554. U.S. Department of the Interior, U.S. Geological Survey, Reston, VA.

Li, H., L.J. Sharkey, W.F. Hunt, and A.P. Davis. 2009. Mitigation of impervious surface hydrology using bioretention in North Carolina and Maryland. *Journal of Hydrologic Engineering 14*:407–415. doi:10.1061/(ASCE)1084-0699(2009)14:4(407)

Mallin, M.A., and A.J. Lewitus. 2004. The importance of tidal creek ecosystems. *Journal of Experimental Marine Biology and Ecology 298*(2):145–149.

Mclaughlin, D.L., D.A. Kaplan, and M.J. Cohen. 2013. Managing forests for increased regional water yield in the southeastern U.S. coastal plain. *Journal of the American Water Resources Association 49*:953–965. doi:10.1111/jawr.12073

Morris, J.T., P.V. Sundareshwar, C.T. Nietch, B.R. Kjerfve, and D.R. Cahoon. 2002. Responses of coastal wetlands to rising sea level. *Ecology 83*:2869–2877.

Nelson, K.C., and M.A. Palmer. 2007. Stream temperature surges under urbanization and climate change: data, models, and responses. *Journal of the American Water Resources Association 43*(2):440–452.

NRCS (Natural Resources Conservation Service). 2015. Web Soil Survey. Available at https://websoilsurvey.sc.egov.usda.gov

Outcalt, K.W., and R.M. Sheffield. 1996. *The Longleaf Pine Forest: Trends and Current Conditions*. Resource Bulletin SRS-9, U.S. Department of Agriculture, Forest Service, Southern Research Station, Asheville, NC.

Paul, M.J., and J.L. Meyer. 2001. Streams in the urban landscape. *Annual Review of Ecology and Systematics 32*:333–365. doi:10.1146/annurev.ecolsys.32.081501.114040

Poff, N.L., J.D. Allan, M.B. Bain, J.R. Karr, K.L. Prestegaard, B.D. Richter, R.E. Sparks, and J.C. Stromberg. 1997. The natural flow regime. *Bioscience 47*:769–784. doi:10.2307/1313099

Price, K. 2011. Effects of watershed topography, soils, land use, and climate on baseflow hydrology in humid regions: A review. *Progess in Physical Geography 35*:465–492. doi:10.1177/0309133311402714

Reich, P., D. McMaster, N. Bond, L. Metzeling, and P.S. Lake. 2010. Examining the ecological consequences of restoring flow intermittency to artificially perennial lowland streams:patterns and predictions from the Broken—Boosey Creek system in northern Victoria, Australia. *River Research and Applications 26*:529–545.

Roy, A.H., A.L. Dybas, K.M. Fritz, and H.R. Lubbers. 2009. Urbanization affects the extent and hydrologic permanence of headwater streams in a midwestern U.S. metropolitan area. *Journal of the North American Benthological Society 28*:911–928. doi:10.1899/08-178.1

Seaburn, G.E. 1969. *Effects of Urban Development on Direct Runoff to East Meadow Brook, Nassau County, Long Island, New York*. U.S. Geological Survey Professional Paper 627-B. (14 pages).

Stanford, J.A., and J.V. Ward. 1993. An ecosystem perspective on alluvial rivers: Connectivity and the hyporheic corridor. *Journal of the North American Benthological Society 12*:48–60.

Sun, G., S.G. McNulty, D.M. Amatya, R.W. Skaggs, L.W. Swift, J.P. Shepard, and H. Riekerk, 2002. A comparison of the watershed hydrology of coastal forested wetlands and the mountainous uplands in the Southern U.S. *Journal of Hydrology 263*:92–104. doi:10.1016/S0022-1694(02)00064-1

Trimble, S.W., F.H. Weirich, and B.L. Hoa. 1987. Reforestation and the reduction of water yield on the Southern Piedmont since circa 1940. *Water Resources Research 23*:425–437. doi:10.1029/WR023i003p00425

USDA (U.S. Department of Agriculture). 2009. *National Agriculture Imagery Program (NAIP) (WWW Document).* Available at https://lta.cr.usgs.gov/NAIP

Wahl, M.H., H.N. McKellar, and T.M. Williams. 1997. Patterns of nutrient loading in forested and urbanized coastal streams. *Journal of Experimental Marine Biology and Ecology 213*(1):111–131. doi:10.1016/S0022-0981(97)00012-9

Walsh, C.J., T.D. Fletcher, and M.J. Burns. 2012. Urban stormwater runoff: a new class of environmental flow problem. *PLoS One 7*:e45814. doi:10.1371/journal.pone.0045814

Walsh, C.J., A.H. Roy, J.W. Feminella, P.D. Cottingham, P.M. Groffman, and R.P. Morgan. 2005. The urban stream syndrome: Current knowledge and the search for a cure. *Journal of the North American Benthological Society 24*(3):706–723.

Zambrano-Bigiarini, M. 2017. Package “hydroTSM.” August 7. Available at https://cran.r-project.org/web/packages/hydroTSM/hydroTSM.pdf

Appendix 5-A
List of Scientific/Technical Publications

Papers

Ensign, S.H., C.A. Currin, M.F. Piehler, and C. Tobias. 2017. A method for using shoreline morphology to predict suspended sediment concentration in tidal creeks. *Geomorphology 276*:280–288.

Gold, A.C., S.P. Thompson, and M.F. Piehler. 2017. Water quality before and after watershed-scale implementation of stormwater wet ponds in the coastal plain. *Ecological Engineering 105*:240–251. doi:10.1016/j.ecoleng.2017.05.003

Gold, A.C., S.P. Thompson, and M.F. Piehler. 2017. Coastal stormwater wet pond sediment nitrogen dynamics. *Science of the Total Environment 609*:672–681. doi:10.1016/j.scitotenv.2017.07.213

Von Korff, B.H., M.F. Piehler, and S.H. Ensign. 2014. Comparison of denitrification between river channels and their adjoining tidal freshwater wetlands. *Wetlands 34*:1047–1060.

Thesis

Gold, A.C. 2017. *Impacts of Coastal Stormwater Pond Nitrogen Cycling on Downstream Water Quality*. M.S. thesis, University of North Carolina at Chapel Hill, Chapel Hill.

White, C.A. 2014. *Quantifying Coastal Stream Metabolism Across a Gradient of Human Watershed Development*. M.S. thesis, University of North Carolina at Chapel Hill, Chapel Hill.

Presentations

White, C.L., M.F. Piehler, L.I. Couper, and S.P. Thompson. 2013. *Impacts of Land Use on Coastal Stream Metabolism*. Presented at the Southeast Tidal Creeks Summit, Wilmington, NC. December 16–17.

Piehler, M.F. 2013. *Science to Support Ecosystem Management and Restoration: Synergy Through Cooperation at APNEP*. Invited lunchtime keynote presentation at the 2013 Albemarle–Pamlico Ecosystem Symposium: Embarking on a New Voyage, New Bern, NC. November.

Piehler, M.F. 2013. *Integrating an Estuarine Research and Monitoring Program (DCERP) into North Carolina Coastal Decision-Making*. Presented at the 2013 Albemarle–Pamlico Ecosystem Symposium: Embarking on a New Voyage, New Bern, NC. November.

White, C.L., M.F. Piehler, L.I. Couper, and S.P. Thompson. 2013. *Assessing Impacts of Land Use on Coastal Stream Metabolism*. Presented at the Conference of the Coastal and Estuarine Research Federation, San Diego, CA. November 3–7.

Appendix 5-B
List of Students

- Caitlin White, M.S., Marine Sciences, University of North Carolina at Chapel Hill, Chapel Hill, NC, 2014.
- Adam Gold, M.S., Ecology, University of North Carolina at Chapel Hill, Chapel Hill, NC, 2017
- Adam Gold, Ph.D., Ecology, University of North Carolina at Chapel Hill Chapel Hill, NC, currently pursuing.

Appendix 5-C
Other Supporting Information

- Adam Gold, University of North Carolina at Chapel Hill's Graduate Education Advancement Board Impact Award, 2017. For more information, see http://gradschool.unc.edu/news/2017/impact/awards.html#Gold

Chapter 6

Aquatic/Estuarine Module

Aquatic/Estuarine Main Channel Monitoring Program

SERDP Project Number: RC-2245

Aquatic/ Estuarine Module

AEM-1

Lead Researchers:

Dr. Hans Paerl, University of North Carolina at Chapel Hill Institute of Marine Sciences
Dr. Mike Piehler, University of North Carolina at Chapel Hill Institute of Marine Sciences
Dr. Iris Anderson, Virginia Institute of Marine Science
Dr. Scott Ensign, Aquatic Analysis and Consulting, LLC

Supporting Researchers:

Dr. Rick Luettich, UNC-IMS
Ms. Jennifer Stanhope, VIMS
Matthew McIver, Aquatic Analysis and Consulting, LLC
Dr. Nathan S. Hall, UNC-IMS
Dr. Benjamin L. Peierls, UNC-IMS
Bryce Van Dam, UNC-IMS

November 2017

Final

This report was prepared under contract to the U.S. Department of Defense (DoD) Strategic Environmental Research and Development Program (SERDP). The publication of this report does not indicate endorsement by DoD, nor should the contents be construed as reflecting the official policy or position of DoD. References herein to any specific commercial product, process, or service by trade name, trademark, manufacturer, or otherwise, do not necessarily constitute or imply its endorsement, recommendation, or favoring by DoD.

Table of Contents

Acronyms 6-vii
Abstract 6-1
Objectives of the Monitoring Activity 6-3
Background 6-4
Materials and Methods 6-5
Monthly Discrete Sampling 6-6
Monthly Vertical Profiles 6-7
Dataflow Transects 6-8
Autonomous Vertical Profilers 6-8
Freshwater Inputs and Flushing Time 6-9
Nutrients, Carbon, and Total Suspended Solids Concentrations 6-10
Phytoplankton Biomass and Primary Productivity 6-11
Data Analyses and Statistical Approaches 6-11
Results and Discussion 6-11
Freshwater Inputs to the NRE 6-11
Spatial and Temporal Variabilities of Water Quality and Estuarine Function 6-14
Seasonality of Water Quality 6-15
Covariations Between Water Quality Parameters 6-16
Relationship Between Phytoplankton Biomass and Flushing Time 6-17
Phytoplankton Blooms 6-19
Dynamics of Dissolved Carbon Dioxide 6-22
Frequency of Bottom Water Hypoxia 6-24
Spatial Gradients of Salinity, Nutrients, Phytoplankton Biomass, and Carbon 6-26
Compliance with the Chlorophyll Water Quality Standard 6-29
Assessment of Directionality and Trends in Estuarine Water Quality 6-31
Long-Term Temporal Trends 6-31
Assessment of Monitoring Design 6-36
Spatial Resolution 6-36
Temporal Resolution 6-39
Comparison of the Effectiveness of Temporal and Spatial Sampling Resolution During DCERP 6-43
Redundancy Analysis of Monthly Monitoring Stations 6-44

Recommendations for Continued Monitoring of the New River Estuary 6-46
Parameters 6-46
Temporal and Spatial Resolution 6-47
Continuity 6-48
Conclusions and Implications for Future Research and Implementation 6-48
Key Findings 6-48
Findings with Implications for Base Management 6-49
Literature Cited 6-50
Appendix 6-A: List of Scientific/Technical Publications 6-A-1
Appendix 6-B: List of Students 6-B-1
Appendix 6-C: Other Supporting Information 6-C-1
Appendix 6-D: Response to Research Questions 6-D-1

List of Figures

Figure 6-1. Conceptual diagram of the linkages between external and internal processes that affect NRE water quality. 6-5
Figure 6-2. Map of the NRE and location of sampling stations. 6-7
Figure 6-3. The Dataflow system is used to gather high-resolution downstream transects of water quality. 6-8
Figure 6-4. A schematic diagram of an AVP and a photograph of the instrument deployed in Morgan Bay. 6-9
Figure 6-5. Time series of the New River discharge over the DCERP study period. 6-12
Figure 6-6. Time series of the annual mean New River discharge from 1949 to 2016. 6-13
Figure 6-7. Physical–chemical and phytoplankton biomass response to changes in discharge and temperature in the New River Estuary from October 2007 to December 2016. 6-14
Figure 6-8. Long- and short-term variabilities in key water quality parameters measured by the AVPs at Stones Bay and Morgan Bay. 6-15
Figure 6-9. A scatter plot of phytoplankton biomass as chlorophyll a versus flushing time. 6-17
Figure 6-10. Box and whisker plots of flushing time at each of the eight monthly DCERP monitoring stations in the NRE. 6-18
Figure 6-11. Summary of the number of phytoplankton blooms dominated (highest percentage of total biovolume) by algal classes in the NRE from October 2007 to December 2016. 6-20

Figure 6-12. The relationship between freshwater age and estuarine pCO_2. Data were collected from July 2013 to July 2015. 6-23

Figure 6-13. Dataflow transects of the difference of estuarine versus atmospheric pCO_2 (ΔpCO_2) before and after passage of Tropical Storm Joaquin in fall 2015. 6-24

Figure 6-14. A histogram of bottom water temperatures from all data from Stations 1 through 8 and during moderate (less than 4 mg L^{-1} DO) and severe (less than 2 mg L^{-1}) bottom water hypoxia; x-axis labels are the centroids of 2°C bins. 6-26

Figure 6-15. Box and whisker plots of the along stream distribution of salinity, nutrients, phytoplankton biomass, and carbon. 6-27

Figure 6-16. A map of the NRE that shows delineation of NCDEQ's assessment units and station locations where chl a was sampled by AEM-1 (UNC-IMS), AEM-3 (VIMS), and NCDEQ. 6-28

Figure 6-17. Time series of chlorophyll a values within each assessment unit over the DCERP project period from 2007 through 2016. 6-30

Figure 6-18. Compliance determinations for chlorophyll a for each NRE assessment unit during overlapping 5-year windows. 6-31

Figure 6-19. Example of method used to remove hydrological impacts on water quality before long-term trend analyses. 6-33

Figure 6-20. Example results of seasonal Kendall tests for long-term trend in chlorophyll a (chl a) data and salinity-corrected chl a data from Station 5. 6-34

Figure 6-21. A map showing the track lines of 81 Dataflow sampling transects in relation to the eight monitoring stations sampled monthly in the NRE. 6-36

Figure 6-22. Dataflow transect data from 4 November 2015 that have been formatted for analyzing the effects of sampling at different spatial resolutions. 6-37

Figure 6-23. The influence of spatial sampling interval on the precision of estimates of the transect means for 81 Dataflow transects of temperature, salinity, dissolved oxygen, turbidity, chlorophyll a, and 16 transects of pCO_2. 6-39

Figure 6-24. The influence of temporal sampling interval on the precision of estimates of the record means for six complete annual records from the AVPs at Stones and Morgan Bays. 6-40

Figure 6-25. Box and whisker plots of the standard error of Dataflow transect means of key water quality parameters across a range of potential spatial sampling intervals. 6-41

Figure 6-26. Box and whisker plots of the standard error of annual means across a range of potential temporal sampling intervals for water quality data produced by the AVPs at Stones Bay and Morgan Bay. 6-42

Figure 6-27. Box and whisker plots of the slopes of the exponential decay of the variance of the mean transect evaluated at 4-km spatial resolution for the

Dataflow (DF) transects and at 30-day temporal resolution for the Morgan Bay (MB-AVP) and Stones Bay (SB-AVP) AVP annual records..... 6-44

Figure 6-28. Quantile–quantile regression of chlorophyll a data from two pairs of stations within the eight station, monthly monitoring program. 6-44

Figure 6-29. Quantile–quantile regression of chlorophyll a data from all possible pairs of stations with SSEs and dissimilarity rankings. 6-45

Figure 6-30. Average dissimilarity rankings for nine water quality parameters for each station pair within the eight stations monitored monthly..... 6-46

List of Tables

Table 6-1. Description of Monitoring Activities for the NRE Water Column..... 6-6

Table 6-2. Results of Pearson's Correlations for Key Water Quality Parameters from the AVPs at Stones Bay and Morgan Bay 6-16

Table 6-3. Summary of phytoplankton bloom composition in the New River Estuary from October 2007 through December 2016 6-20

Table 6-4. Frequency of Bottom Water Hypoxia by Water-Year and by Station with Water-Depth and Stratification Intensity. (The measurement depth was 0.5 m above the bottom.) 6-25

Table 6-5. Results from Seasonal Kendall Tests for Long-Term Trends in Important Indicators of Water Quality, Habitat Conditions, and Carbon Cycling Along the Main Channel of the NRE..... 6-32

Table 6-6. Results from Seasonal Kendall Tests for Long-Term Trends in Important Indicators of Water Quality and Habitat Conditions Along the Main Channel of the NRE from 1998 to 2016 Using the Combination of UNC Wilmington and DCERP Data Sets 6-35

Table 6-7. Recommended Eutrophication and Habitat Condition Related Parameters for Continued Monitoring in the NRE 6-47

Acronyms

°C	degrees Celsius
µg L^{-1}	micrograms per liter
µm	micrometer
µmol	micromole
ΔpCO_2	difference in partial pressure of CO_2 between air and estuary
α	coefficient that describes the rate of decay
ADCP	acoustic Doppler current profiler
AE	Aquatic/Estuarine (Module)
AEM	Aquatic/Estuarine Monitoring Activity
AEMP	Aquatic/Estuarine Monitoring Program
AMS	NCDEQ's Ambient Monitoring System
AU	assessment unit
AVP	autonomous vertical profiler
AWAC	acoustic wave and current
β	proportionality constant
B	bottom water
CB	Coastal Barrier (Module)
CDOM	chromophoric dissolved organic matter
chl *a*	chlorophyll *a*
cm	centimeter
CO_2	carbon dioxide
CW	Coastal Wetlands (Module)
d	day
DCERP	Defense Coastal/Estuarine Research Program
DCERP1	first cycle of DCERP
DCERP2	second cycle of DCERP
DF	Dataflow
DIC	dissolved inorganic carbon
DIN	dissolved inorganic nitrogen
DO	dissolved oxygen
DO_{bott}	bottom water dissolved oxygen
DOC	dissolved organic carbon
DoD	U.S. Department of Defense
ESM	Estuarine Simulation Model
GF/F	glass fiber filter
Hz	hertz
ICW	Intracoastal Waterway
JACK	Jacksonville (Site)
K_d	PAR attenuation coefficient
km	kilometer
km hr^{-1}	kilometer per hour
kPa	kilopascal
K_{PAR}	attenuation coefficient for photosynthetically active radiation
L, L^{-1}	liter

LOESS	local regression
m	meter
m s^{-1}	meters per second
m^2 s^{-1}	square meters per second
m^3 s^{-1}	cubic meters per second
MB-AVP	Morgan Bay AVP annual record
MCBCL	Marine Corps Base Camp Lejeune
mg L, mg L^{-1}	milligrams per liter
N	number of samples
NA	salinity correction is not applicable to salinity data
NCDEQ	North Carolina Department of Environmental Quality
NH_4^+	ammonium
NO_2^-	nitrite
NO_3^- + NO_2^-	nitrate + nitrite
NPDES	National Pollution Discharge Elimination System
NRE	New River Estuary
NS	not significant
NTU	Nephelometric Turbidity Unit
PAR	photosynthetically active radiation
pCO_2	partial pressure of carbon dioxide
PO_4^{3-}	orthophosphate
POC	particulate organic carbon
PPR	primary productivity
R	daily respiration
RC	Resource Conservation and Climate Change (a SERDP program area)
S	surface water
SB-AVP	Stones Bay AVP annual record
SD	standard deviation
SERDP	Strategic Environmental Research and Development Program
SiO_3^{-2}	silicate
SSE	sum squared error
TDN	total dissolved nitrogen
TSP	Translating Science into Practice (Module)
TSS	total suspended solids
UNC-CH	University of North Carolina at Chapel Hill
UNC-IMS	University of North Carolina at Chapel Hill's Institute of Marine Sciences
UNCW	University of North Carolina at Wilmington
USGS	U.S. Geological Survey
VIMS	Virginia Institute of Marine Science
WWTP	wastewater treatment plant
y^{-1}	year
y_k	means of the resampled data sets
$\bar{Y}$	"true" transect mean
$\bar{y}_{sys}$	variance of the estimated transect mean
YSI	Yellow Springs Instruments, Inc.

Abstract

Goals and Objectives: The goal of this monitoring effort was to provide data to evaluate the roles of natural and anthropogenic stressors on water quality and habitat condition within the New River Estuary (NRE) to assess the compatibility of Marine Corps Base Camp Lejeune activities with desirable water quality and habitat conditions. To accomplish this goal, the monitoring objectives were to quantify the input, distribution, use, cycling, and fate of nutrients, inorganic and organic carbon, sediments and other physico-chemical parameters (e.g., dissolved oxygen, pH, salinity) affecting productivity, trophic state, water quality, and habitat condition. Data from this monitoring activity also provided information about carbon stocks, as well as the environmental conditions that modulate rates of carbon processing. These data were critical for the development of the estuarine carbon budget by Research Projects AE-4 and AE-6 and for construction and evaluation of the Estuarine Simulation Model (ESM) developed by Research Project TSP-2.

Technical Approach: Water quality and trophic status, as well as the natural and anthropogenic drivers of these indicators of ecological condition were monitored in the water column of the NRE from October 2007 through December 2016. Conditions within the estuary were assessed by monthly transect surveys consisting of discrete water sample collection and Dataflow measurements and continuous autonomous vertical profiling systems to measure critical physical and chemical drivers (e.g. circulation, salinity, dissolved oxygen, temperature, pH, nutrients, inorganic and organic carbon, light availability) and ecological response variables (e.g., phytoplankton biomass, productivity, community composition) associated with trophic status and water quality. Physical drivers of water quality were assessed by analyzing the effects of New River discharge.

Results: Analyses of the monitoring data indicate that physical processes such as riverine freshwater discharge, stratification, wind stress, and sediment resuspension are dominant drivers of variability in water quality and habitat condition. Bottom water hypoxia was closely linked to temperature and stratification with no apparent relationship to algal blooms, which may have resulted from anthropogenic nutrient loading. Periods of high algal biomass were linked to optimal levels of river flow, which provided enough nutrients for phytoplankton biomass development, but also sufficient residence time within the estuary for growth to occur. Dynamics of partial pressure of carbon dioxide (pCO_2) were found to be highly dependent on phytoplankton production with significant net uptake occurring only during periods of high algal biomass. Although short-term variability in phytoplankton biomass, dissolved oxygen, water clarity, and nutrients were strongly linked to physical factors that are not under human control, trend analyses detected long-term increases in chlorophyll *a*, ammonium, and light attenuation and decreases in bottom water dissolved oxygen may be due to long-term anthropogenically-driven eutrophication of the NRE.

Benefits: Data collected from this monitoring program served as a comprehensive baseline against which the longer term anthropogenic trends in water quality, ecological condition, regulatory compliances (e.g., chlorophyll *a*, dissolved oxygen, pH) may be assessed. Characterization of the temporal and spatial scales of variability has provided guidance for the design of future research and monitoring efforts for the NRE and similar estuarine systems.

Monitoring data were additionally used to support DCERP2 research projects to examine the environmental controls of nutrient and carbon cycling (Research Projects AE-4, AE-5, AE-6, CW-4, CW-5, and CB-5), develop an estuary-wide carbon budget (Research Projects AE-4 and AE-6), parameterize a mechanistic ESM (Research Project TSP-2), and provide supporting data to contextualize the research projects of the Aquatic/Estuarine and Coastal Wetlands Modules.

Keywords: Carbon, dissolved oxygen, estuary, nitrogen, phosphorus, residence time, riverine discharge, salinity, tides, turbidity

Objectives of the Monitoring Activity

The objectives of the Aquatic/Estuarine Monitoring Activity AEM-1 activity are to provide information to

1. Understand the context in which complex interacting physical, chemical, and biotic processes drive estuarine water and habitat quality, including carbon, nutrient, dissolved oxygen (DO), and sediment fluxes under current conditions and for different climate change scenarios (i.e., warming, hydrologic changes, extreme events, and sea level rise)
2. Differentiate climatic, including extreme events, from anthropogenic stressors and their impacts on nutrient and carbon cycling
3. Ensure compatibility and compliance of Marine Corps Base Camp Lejeune (MCBCL) activities with water and habitat quality management goals, currently and into the future
4. Identify the ecosystem services provided by these natural resources for ecosystem, recreational, and economic benefits
5. Provide data for decision-support tools and model calibration and verification. The Aquatic/Estuarine Monitoring Program (AEMP) will support the data needs of Research Projects AE-4, AE-5, AE-6, TSP-2, CW-4, CW-5, and CB-5.

The main objective of this monitoring activity was to monitor the input, distribution, use, cycling, and fate of nutrients, inorganic and organic carbon and sediments and other physico-chemical parameters (e.g., DO, pH, salinity) affecting the productivity, trophic state, water quality, and habitat condition of the New River Estuary (NRE). Sampling locations were distributed along the downstream axis of the estuary to assess the variability within the estuarine salinity zones, tidal, and mixing regimes. The sampling design allowed us to examine the impacts of terrestrial, atmospheric, coastal wetlands, and oceanic exchanges of materials (e.g., sediment, nutrients) on the estuary and to evaluate the effects of processes and activities on MCBCL (i.e., erosion/sedimentation, nutrient releases, and discharge events) versus off-Base human and natural (climatic) drivers of ecological condition. This monitoring activity was designed to evaluate the short- and long-term effects of these drivers on the structure, function, and sustainability of the NRE in a regime of climatic variability. The monitoring activity also served as a critical source of data for supporting the Aquatic/Estuarine Module research projects and modeling activities.

Aquatic/Estuarine Monitoring Activity AEM-1 was designed to achieve multiple goals (**Table 6-1**). These goals include improving the understanding of the physical, chemical, and biological processes and interactions that drive water, sediment, and habitat quality; supporting AE and CW research components; and helping to differentiate the magnitudes and effects of natural and anthropogenic ecosystem stressors. Differentiating the stressors includes the consideration of extreme weather-related events, such as hurricanes, nor'easters, floods, and droughts, which have thus far been shown to be very important drivers whose impacts vary greatly among years. Additional goals include providing information for designing and implementing a long-term monitoring program that ensures compatibility of MCBCL's activities with desirable estuarine water, sediment, and habitat quality and potential regulatory issues such as chlorophyll *a* (chl *a*) exceedances, DO and pH conditions and facilitating the conservation of regional natural resources for ecosystem, recreational, and economic benefits.

Background

Estuaries integrate inputs from terrestrial, freshwater, oceanic, and atmospheric systems (Day and Kemp, 1989; Hobbie, 2000; Valiela et al., 1997), and the accurate assessment and management of estuaries necessitate consideration of their connections to, and interactions with, these other systems. Many estuaries also exist in regions of rapidly expanding and diversifying human activity (Boesch et al., 2001; Cloern, 2001; Nixon, 1995; Paerl et al., 2014). In the context of the MCBCL region, the Aquatic/Estuarine Module examined the tidal reach of the NRE from near Jacksonville, NC, to the tidal inlet at Onslow Bay. Development of strategies and tactics to maintain and/or improve estuarine water quality and habitat conditions in the NRE cannot occur without quantifying and distinguishing natural processes from human-influenced watershed- and airshed-based impacts, as well as human activities that occur in the estuary (Boesch et al., 2001; Malone et al., 1999; Nixon, 1995; Paerl, 1997; Paerl et al., 2014, see **Figure 6-1**). Furthermore, the effects of climatic variability, including acute or episodic events (e.g., tropical cyclones, floods, droughts) and longer term trends (e.g., precipitation patterns, warming), on estuarine structure and function must be characterized and quantified to understand and take into consideration the interactive and potentially confounding impacts of climate (change) on water quality and habitat condition (Cloern and Jassby, 2010; Kennish and Paerl, 2010; Paerl et al., 2010 and 2014).

When combined with AEM-4 New River monitoring activities, previous monitoring activities during DCERP1 (DCERP1 AEM-3) and historical monitoring data collected by the University of North Carolina at Wilmington (UNCW), provide a substantial long-term record of key water quality data to evaluate long-term change, and the roles of climatic and human drivers. Pre-DCERP data (1998–2007) collected by UNCW demonstrated historically poor water quality conditions in the upper estuary, but strong improvements in estuarine water quality were achieved following upgrades to wastewater treatment by Jacksonville and MCBCL (Mallin et al., 2005). During the following decade of DCERP monitoring, no acute, large-scale human influences such as wastewater spills were observed. However, DCERP water quality monitoring on the NRE demonstrated significant, and at times, dominant effects that climatic events and change can have on the nutrient inputs, water quality, trophic state, overall ecological condition, resourcefulness, utility (for military training, commercial, and recreational purposes), and sustainability of the NRE.

The Aquatic/Estuarine Module monitoring network was designed to capture the level of complexity and variability in biogeochemical and trophic responses needed to assess ecological conditions and changes of the NRE. Only long-term monitoring and modeling will reveal the full extent of anthropogenic and climatically induced perturbations and changes impacting this system. The Aquatic/Estuarine Module's monitoring activities were closely coupled to and provided critical baseline data for the research activities within this module (see **Figure 6-1** and **Table 6-1**). Additionally, coordination and information exchange occurred in conjunction with the monitoring and research activities for the Coastal Wetlands, Atmospheric, Terrestrial, and Coastal Barrier Modules.

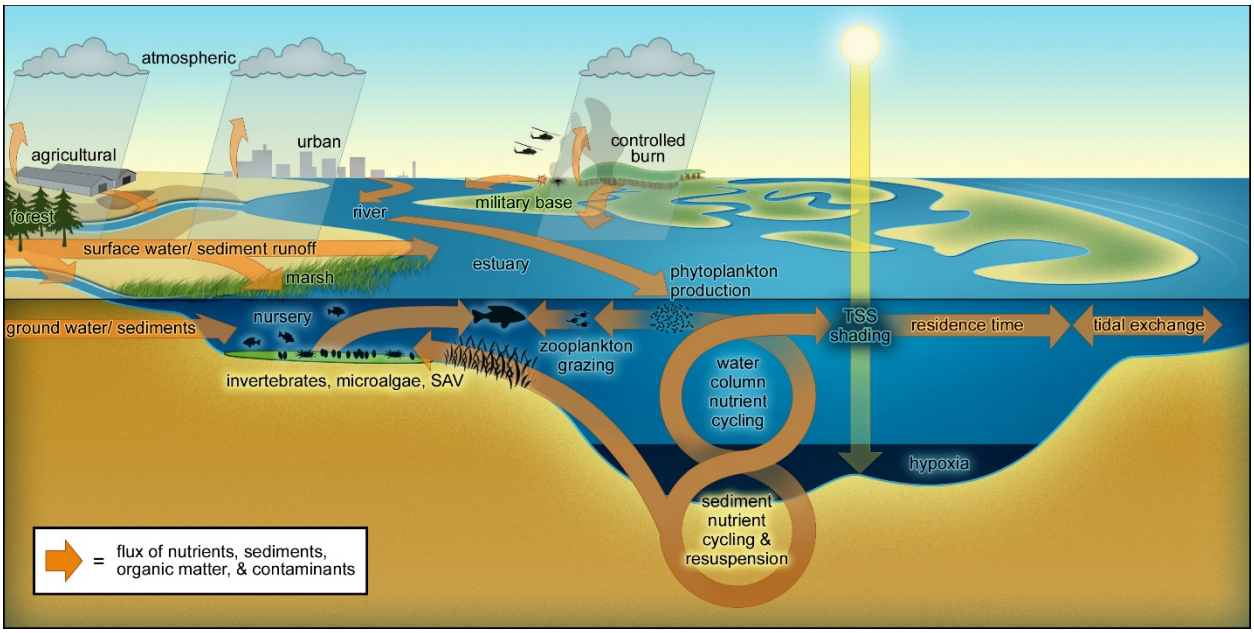

Figure 6-1. Conceptual diagram of the linkages between external and internal processes that affect NRE water quality.

Materials and Methods

A multi-faceted monitoring program provided key information about biogeochemistry, water quality, and ecosystem function within the main water column of the NRE (**Table 6-1**). The four components of the Aquatic/Estuarine Monitoring Activity (AEM-1) were designed to capture the full range of temporal and spatial variability inherent to dynamic estuarine systems. This monitoring activity complements the other DCERP1 efforts conducted by Aquatic/Estuarine Monitoring Activities AEM-1 in the New River, AEM-2 in tributary creeks of MCBCL, and AEM-3 in the shallow portions of the NRE. These activities are summarized in Chapters 4, 5, and 7 of the *DCERP2 Final Report*.

Table 6-1. Description of Monitoring Activities for the NRE Water Column

Monitoring Component	Variables	Spatial Scale	Temporal Scale
Discrete sampling	Nutrients, dissolved inorganic and organic carbon, phytoplankton biomass and primary production, phytoplankton community composition, suspended sediments, particulate carbon, and chromophoric dissolved organic matter	Surface (0.2 m) and bottom water (0.5 m above the bottom) from 8 stations from Highway 17 to the Intracoastal Waterway	Monthly spring through fall; every other month during winter
Vertical profiles	Depth profiles of temperature, salinity, DO, pH, turbidity, chlorophyll (via in vivo fluorescence), photosynthetically active radiation	Profiles conducted with 0.5-m vertical resolution at the 8 discrete sampling stations	Coincident with discrete sampling
Dataflow transects	Surface water transects of temperature, salinity, DO, pH, turbidity, chlorophyll (via in vivo fluorescence)	Near Highway 17 to the Intracoastal Waterway, 10-m spatial resolution	Coincident with discrete sampling
Autonomous vertical profilers	Depth profiles of temperature, salinity, DO, pH, turbidity, chlorophyll (via in vivo fluorescence) and measurements of wind speed and direction	Two stations, Stones Bay and Morgan Bay, with 10-cm depth resolution	Year round, 2 profiles per hour

Monthly Discrete Sampling

A monitoring transect of eight stations (Stations 1–8 in **Figure 6-2**) was conducted by using a 25-foot Parker research vessel for collecting water samples from the surface (0.2 m) and bottom (0.5 m above the bottom) by using a non-destructive diaphragm pump. These stations spanned the NRE from the upstream Station 7 just south of Jacksonville to Station 1 just inside the New River inlet. During DCERP1, transects were conducted monthly. During DCERP2, transects were conducted monthly from March through November and every other month from December through February. Sample collection occurred during the hours of 0800 through 1300. Water samples were dispensed into pre-cleaned 4-polyethylene bottles and maintained under dark, in situ temperature conditions by placing them in coolers until samples were delivered to the laboratory at the University of North Carolina at Chapel Hill's Institute of Marine Sciences (UNC-IMS) by mid-afternoon, approximately 15:00. Upon delivery to the laboratory, the samples were processed immediately to obtain measurements of nutrients, phytoplankton biomass, inorganic and organic carbon, suspended sediments, and particulate organic matter (see the Materials and Methods section of this chapter).

In addition to the eight monthly sampling stations, additional sampling efforts were conducted upstream of Highway 17 by Dr. Scott Ensign (Aquatic/Estuarine Monitoring Activity AEM-4, Chapter 4 of the *DCERP2 Final Report*). Surface water grab samples were collected with biweekly to monthly frequency into pre-cleaned polyethylene bottles at two USGS stream gaging stations that continuously monitored water level, temperature, salinity, and flow velocity. USGS Stream Gaging Station 0209303205 (**Figure 6-2**) is at the head of the NRE near Jacksonville, NC. USGS Stream Gaging Station 02093000 near Gum Branch is the only station along the freshwater reaches of the New River. Discrete sampling at Gum Branch occurred throughout the DCERP study period (2007 to 2016, but sampling at USGS Stream Gaging Station 020903205

began April 2008 and ended in 2012. Starting in November 2010 and ending in December 2011, additional samples were collected near Wilson Bay and upstream of the old Highway 17 Bridge. Collectively, these upstream samples collected by staff at USGS and the North Carolina Cooperative Extension provided data regarding the loading of nutrients, sediments, and phytoplankton biomass to the estuary and aided in elucidating processes that occurred within the freshwater to brackish water transition zone, a region of intense chemical and biological activities within many estuaries (Boynton and Kemp, 1985; Cloern, 1999; Fisher et al., 1988; Paerl et al., 1995 and 2010).

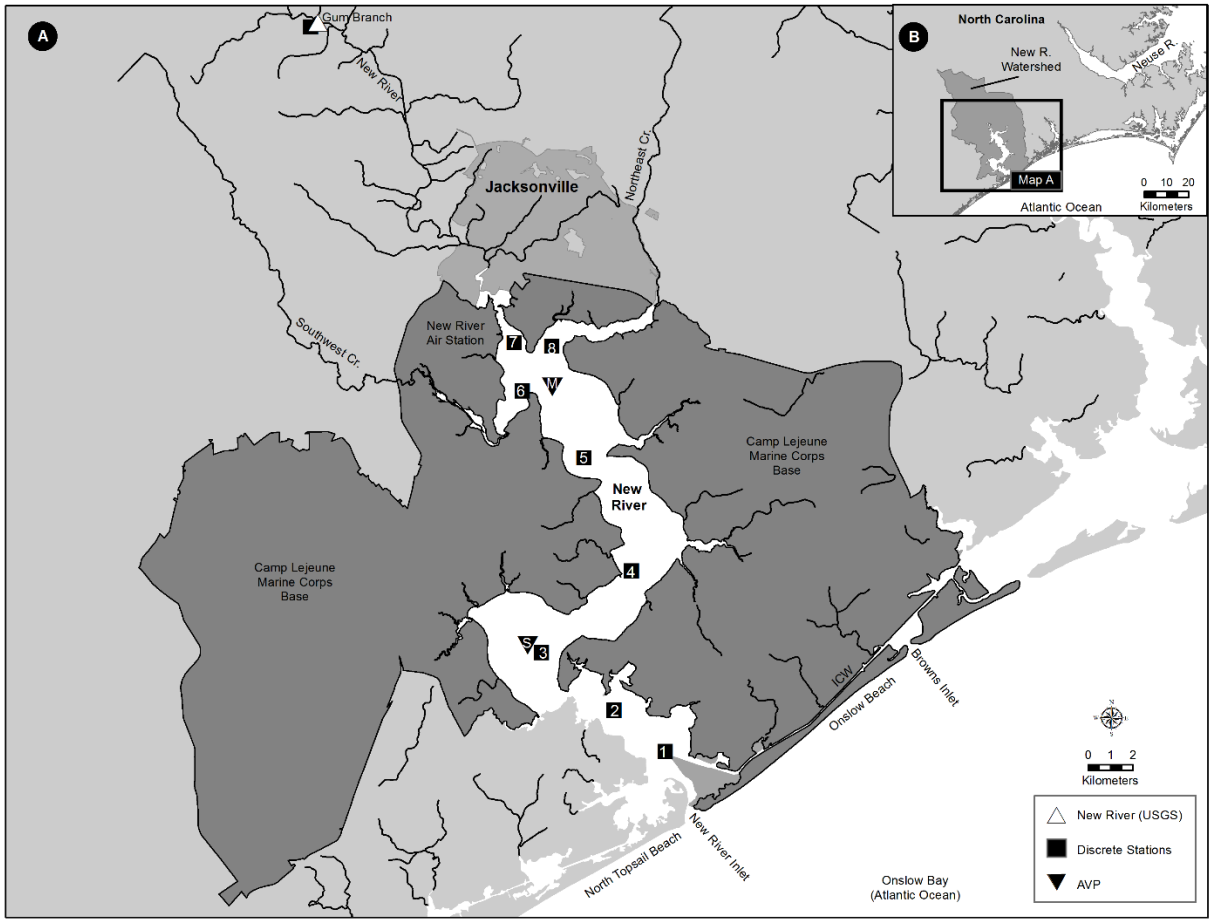

Figure 6-2. Map of the NRE and location of sampling stations.

Monthly Vertical Profiles

Coincident with monthly discrete sample collection, vertical profiles of key water quality parameters were collected from each of the eight stations by using a Yellow Springs Instrument Inc. (YSI) 6600 multiparameter water quality datasonde coupled to a Li-Cor 2 π photosynthetically active radiation (PAR) sensor. Temperature, salinity, pH, DO, turbidity, chl *a* (by in vivo fluorescence), and PAR were measured at 0.5 m–depth intervals throughout the water column. The *in vivo* fluorometer measures the sum of chlorophyll types *a*, *b*, *c1*, *c2*, and *c3*. However, chl *a* dominates this sum (Hall et al., 2012). Therefore, henceforth, in vivo fluorescence measurements are described in terms of chl *a*. YSI instruments were calibrated

before each monthly monitoring cruise. PAR attenuation coefficients (K_d) were calculated as the slope of the natural log of PAR versus depth according to Beer's law.

Dataflow Transects

Transects of water quality parameters were produced for surface waters of the NRE by using a Dataflow system (see Madden and Day, 1992) shown in **Figure 6-3**. Use of the Dataflow system commenced in DCERP1 (February 2009) and went through DCERP2 (December 2016) and was used coincidentally with monthly sampling efforts to expand the spatial resolution of the downstream transect produced by the eight discrete sampling stations. While the vessel is underway, surface waters enter the Dataflow system in a through-hull fitting in the bottom of a research vessel (Parker 25). Water is then pumped through a debubbler into a flow chamber attached to a YSI 6600 multiparameter water quality datasonde, which measures salinity, temperature, DO, turbidity, pH, and chl *a* (via in vivo fluorescence). With a 0.5-Hz sampling frequency, the spatial resolution is approximately 10 m at a normal forward speed of approximately 20 km hr^{-1}. Dataflow datasondes were calibrated before each sampling event.

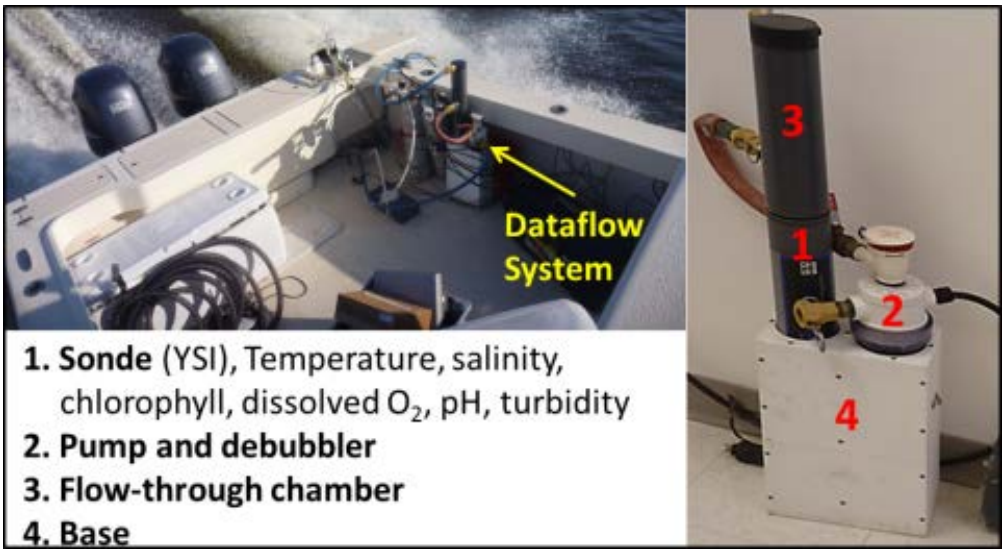

Figure 6-3. The Dataflow system is used to gather high-resolution downstream transects of water quality.

Autonomous Vertical Profilers

Autonomous vertical profilers (AVPs) were deployed and used to continuously monitor key water quality parameters (**Table 6-1**) from June 2008 through June 2016 in central Stones Bay at Station 3 (see **Figure 6-2**) and from June 2008 through October 2016 in Morgan Bay upstream of Station 5 (**Figure 6-2**). The AVPs consist of a moored floating platform housing a computer-controlled winch mechanism that lowers and raises a YSI Model 6600 multiparameter water quality datasonde at programmable time intervals (**Figure 6-4**; Reynolds-Fleming et al., 2002). Winch speed and sampling frequency of the AVP system and datasonde were configured to produce full water column profiles of temperature, salinity, DO concentration, chl *a* concentration (by in vivo fluorescence), and turbidity every 30 minutes and achieve vertical depth resolution of approximately 10 cm. An anemometer (RM Young) affixed to the mast of the

AVP measured 6-minute averages of wind speed and direction every 30 minutes (**Figure 6-4**). Data were stored locally on the AVP computers and telemetered back to the laboratory each night. Datasondes were exchanged with freshly cleaned and calibrated datasondes as necessary, but at least monthly.

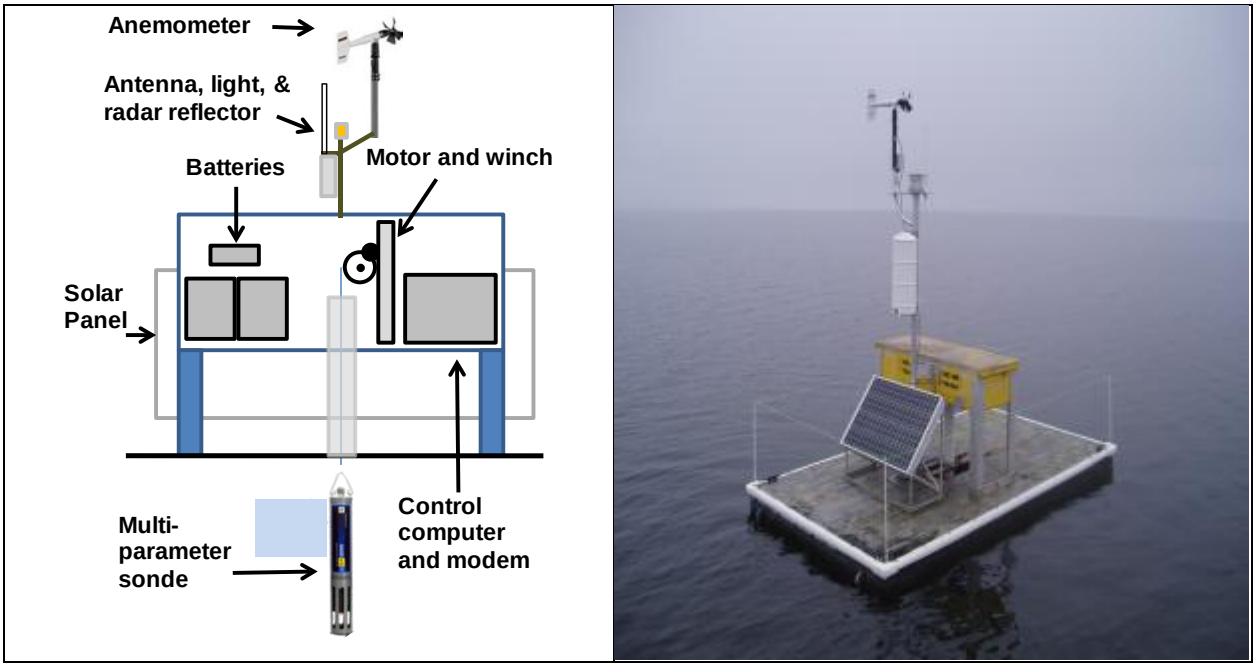

Figure 6-4. A schematic diagram of an AVP and a photograph of the instrument deployed in Morgan Bay.

Freshwater Inputs and Flushing Time

Throughout DCERP1 and DCERP2, freshwater discharge into the NRE was continuously quantified by the USGS Stream Gaging Station 02093000 near Gum Branch (**Figure 6-2**). The historical record extending back to 1949 provided context for the recent decade of river flow conditions. The Gum Branch gage accounts for only approximately 22% of the New River watershed and an assumed equivalent fraction of discharge to the NRE (Ensign et al., 2004). Ungaged freshwater inputs were estimated by multiplying the gauged freshwater discharge by the ratio of ungaged to gaged watershed area, exclusive of the estuary water surface (Ensign et al., 2004).

The flushing time was calculated by using the date-specific freshwater replacement method (Alber and Sheldon, 1999). Flushing time is the amount of time necessary for the combination of riverine discharge and seawater inflows to replace the volume of an estuary or estuarine segment (Sheldon and Alber, 2006). The date-specific version of this traditional measure of transport time scale was chosen because it accounts for changing river flow conditions and the time lags between river gage and downstream locations (Alber and Sheldon, 1999). Flushing time, as calculated here, is also correctly interpreted as the average age of freshwater within an estuary (Sheldon and Alber, 2006). This interpretation is used to provide time scales for the biological transformation of riverine nutrient loads into phytoplankton biomass as freshwater is advected and mixed downstream within the NRE.

To calculate flushing time, the estuary was divided into nine segments encompassing sampling Stations 1–8 and USGS Stream Gaging Station 0209303205 near Jacksonville (**Figure 6-2**). Volumes for each segment were estimated by using raster bathymetry data from the National Geophysical Data Center's Coastal Relief Model according to methods detailed by Ensign et al. (2004). Salinity of each segment was taken as the vertically averaged salinity of the monthly profiles at each of the eight monthly sampling stations. For the most upstream segment, encompassing the USGS Stream Gaging Station 0209303205, salinity at the approximately 1-m instrument depth was assumed to be representative of the entire water column. The flushing time for each segment was calculated by using the cumulative freshwater volume upstream of the downstream boundary of each segment and represents the average time freshwater spent upstream of each segment (i.e., average freshwater age within the estuary). Calculating the cumulative flushing times from the head to the exit of the estuary in this manner allows the use of the discretely sampled snapshots of phytoplankton biomass and nutrient concentrations to reconstruct the time course of phytoplankton biomass development and nutrient draw down during downstream transport within the estuary (Hall et al., 2013; Paerl et al., 2014; Peierls et al., 2012).

Nutrients, Carbon, and Total Suspended Solids Concentrations

Nutrient analyses were conducted on water collected monthly from the eight estuarine stations and from the Gum Branch USGS gaging station. All water samples were gently filtered (less than 25 kPa) through 25 mm in diameter Whatman GF/F glass fiber filters (0.7 µm nominal pore size). Total dissolved nitrogen (TDN), nitrate (NO_3^- + nitrite [NO_2^-], labeled as NO_3^-), ammonium (NH_4^+), orthophosphate (PO_4^{-3}), and silicate (SiO_3^{-2}) concentrations were determined by using colorimetric flow injection analyses (Lachat QuikChem 8000, Lachat Instruments, Milwaukee, WI) and standard protocols (Lachat QuikChem Methods 31-107-04-3-B, 31-107-04-1-C, 31-107-06-1-A, and 31-115-01-3-C, respectively). Mean detection limits were 2.33 (TDN), 0.03 (NO_3^-), 0.22 (NH_4^+), 0.03 (PO_4^{-3}), and 0.53 (SiO_3^{-2}) µmol L^{-1}.

Total suspended solids (TSS) were measured according to Standard Methods 2540 D (APHA, 1998): water samples were filtered on pre-rinsed, pre-dried, tared Whatman GF/F filters, filters were dried at 105°C, and then weighed by using a calibrated Mettler Toledo AB-S analytical balance. Solids concentration is the difference in filter weights before and after filtration divided by volume of water filtered.

Concentrations of chromophoric dissolved organic matter (CDOM), a key determinant of light attenuation, were measured monthly at the eight estuarine stations by using fluorometry according to methods detailed in Lunetta et al. (2009) and are expressed as quinine sulfate equivalents (in µg L^{-1}). Water samples were vacuum filtered (less than 25 kPa) by using pre-combusted Whatman GF/F filters, and the filtrate was stored in scintillation vials in the dark at 4°C until fluorometric analysis by using a Turner Designs TD-700 fluorometer. Particulate organic carbon (POC) and particulate organic nitrogen were measured on seston collected on pre-combusted GF/F filters, which were then analyzed by high temperature combustion, by using a Costech ECS 4010 analyzer (Peierls and Paerl, 2011). Dissolved inorganic carbon (DIC) and dissolved organic carbon (DOC) concentrations were measured on a Shimadzu total organic carbon analyzer (TOC-5000A; Crosswell et al., 2012; Paerl et al., 2001).

Phytoplankton Biomass and Primary Productivity

Chlorophyll *a* (chl *a*), a common measure of phytoplankton biomass, was determined from all water samples collected monthly from the routine transect stations and from the two USGS stream gaging stations. (**Figure 6-2**). Fifty-milliliter aliquots were filtered onto 25-mm diameter Whatman GF/F filters. Storage, extraction, and fluorometric analyses were in accordance with Wetz et al. (2011).

Primary productivity was measured monthly via the in situ ^{14}C method (Paerl, 2002) for surface waters from the eight transect stations from the hours of approximately 0900 to 1300 on the day after sample collection. Water samples were maintained overnight, and incubations were performed under ambient light and temperature conditions in the UNC-IMS's outdoor pond with circulating seawater (Mallin and Paerl, 1992). Light conditions associated with vertical mixing were simulated by using a field light simulator (Mallin and Paerl, 1992). Light availability was measured throughout each incubation period with a Li-Cor 2π PAR meter. The average PAR flux during the incubations was 234 µmol photons m^{-2} s^{-1} (standard deviation [SD]=94). Light-dark ^{14}C assay methods followed those described in Paerl (2002), with the exception that activity of samples was measured on a Beckman Coulter LS 6500 liquid scintillation counter. Also, DIC concentration was measured on a Shimadzu total organic carbon analyzer (TOC-5000A).

Data Analyses and Statistical Approaches

A wide variety of data analyses and statistical procedures was used to explore spatial and temporal variabilities and interrelationships between water quality parameters and their drivers. Analysis and statistical methods are described in detail within each section, followed by the results of the analyses.

Results and Discussion

Freshwater Inputs to the NRE

Freshwater input is associated with loading of nutrients, sediment, and terrestrial carbon including light attenuating CDOM. Additionally, freshwater input flushes the estuary and promotes estuarine circulation, which can create strong vertical density gradients. Consequently, freshwater input is a dominant driver of water quality and ecological condition within the estuary. The New River dominates freshwater inputs into the NRE, and freshwater contributions from smaller tributaries generally follow similar temporal patterns (Ensign et al., 2004; Peierls et al., 2012). The New River discharge at the USGS Gum Branch stream gaging station varied widely over the study period (2007-2016), spanning greater than three orders of magnitude from approximately 0.1 to 135 m^3 s^{-1} (**Figure 6-5**). The extreme level of stream flow variability represents nearly the full range of conditions captured in the long-term discharge record that dates back to 1949 (Hall et al., 2012). Despite the occurrence of very high flows associated with tropical storms (notably Tropical Storm Nicole in 2010, Hurricane Irene in 2011, and Tropical Storm Joaquin in 2015) and nor'easters, most of the 9-year study period was characterized by drought conditions with annual mean discharge at or below the long-term average (**Figure 6-6**).

On an annual average basis, 2008, 2009, 2011, and 2013 were dryer than average (**Figure 6-6**); 2010 had slightly above-average discharge (**Figure 6-6**), but this was largely due to a single, large flood pulse that followed the passage of the remnants of Tropical Storm Nicole. Discharge was slightly below the long-term average during 2012 and 2014; the flow conditions were only significantly above average during 2015 and 2016.

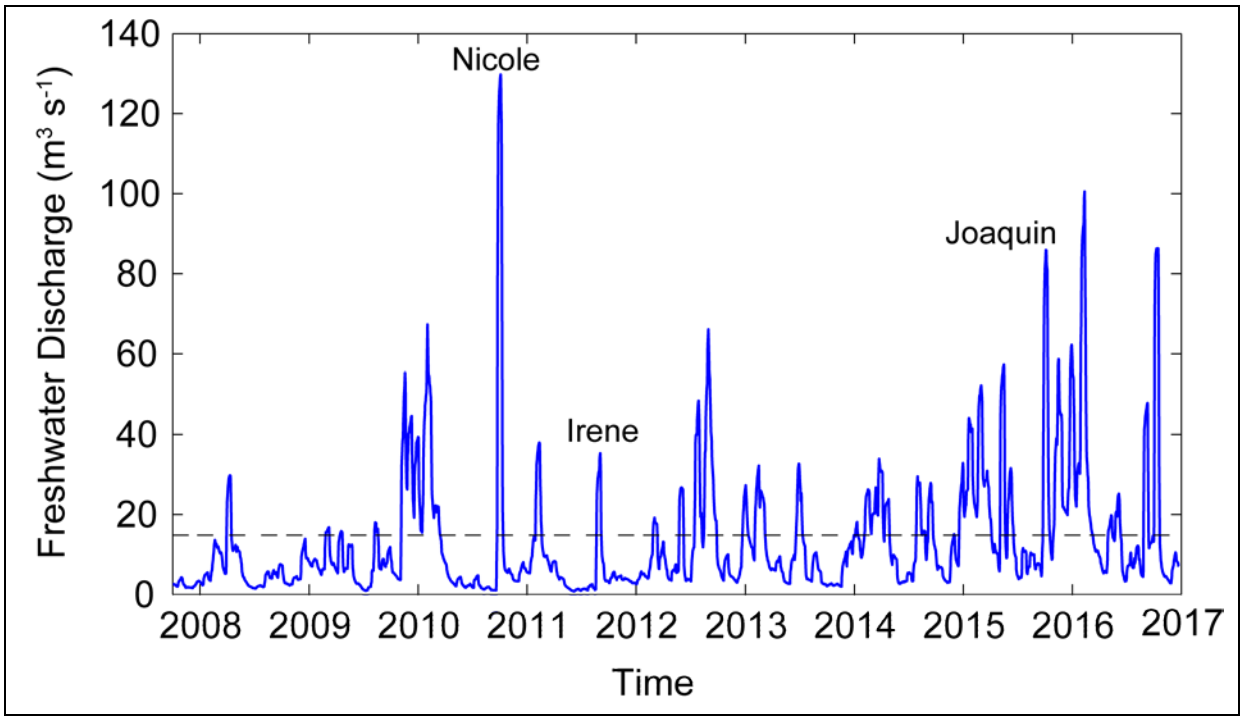

Figure 6-5. Time series of the New River discharge over the DCERP study period.

Discharge values have been smoothed with a 2-week running average. The dashed line is the long-term (1949–present) average.

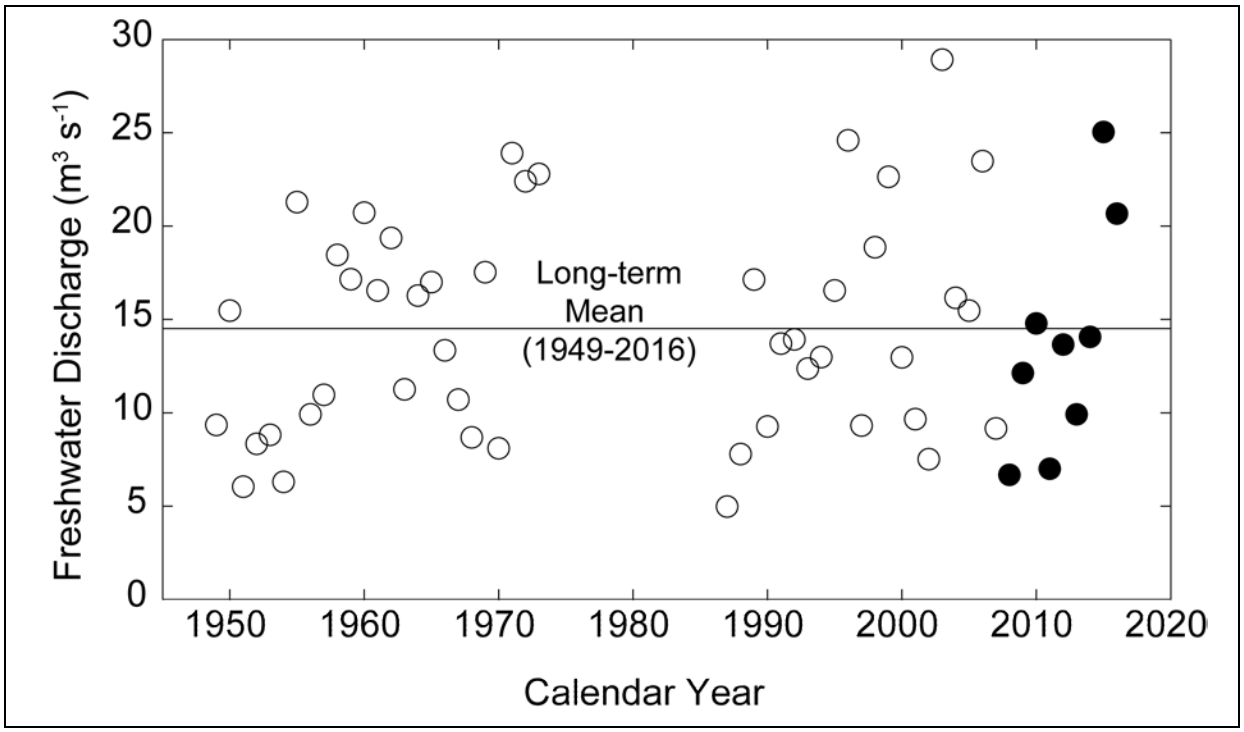

Figure 6-6. Time series of the annual mean New River discharge from 1949 to 2016.

Discharge values during DCERP are represented as filled symbols.

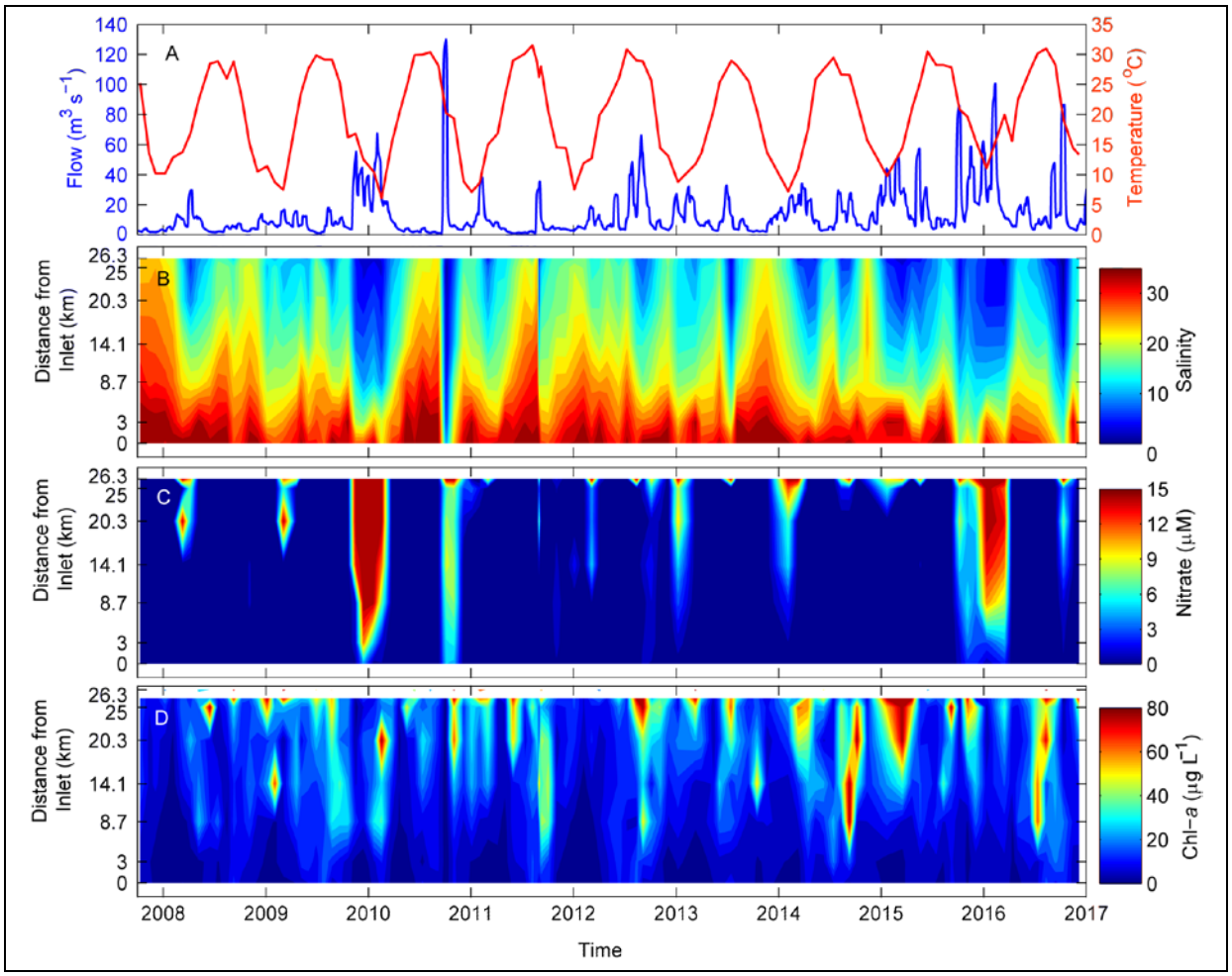

Figure 6-7. Physical–chemical and phytoplankton biomass response to changes in discharge and temperature in the New River Estuary from October 2007 to December 2016.

Contour plot *y*-axes are the distance upstream from the inlet. The labels of the *y*-axes correspond to the locations of eight main channel monitoring stations. Data from Stations 6 and 8 (distance 25 km) were averaged for each sampling date.

Spatial and Temporal Variabilities of Water Quality and Estuarine Function

Hydrology was a dominant driver of water quality throughout DCERP (**Figure 6-7**). Because of the relatively small watershed, large precipitation events were routed quickly through the watershed and resulted in a very flashy hydrologic regime (Peierls et al., 2012). Despite smoothing of the discharge record, these spikes in New River discharge are still evident and had immediate impacts on salinity (**Figure 6-7B**) and on bioavailable nitrogen (**Figure 6-7C**), the primary limiting nutrient for phytoplankton in the estuary as indicated by NO_3^- (Altman and Paerl, 2012; Mallin et al., 2005). During periods of base flow, the riverine NO_3^- load was assimilated upstream of the study area and therefore, most of the time, NO_3^- was undetectable even at Station 7, which is the most upstream station (**Figure 6-7C**). During high discharge, particularly during the winter, NO_3^- was detectable at upstream stations; during very high discharge, NO_3^- was detectable throughout the estuary. The phytoplankton biomass response to changes in river nutrient loading was complicated by the dual impacts of riverine pulses (i.e.,

while the pulses increase the load of growth-stimulating nutrients, they also create a rapid flushing of the estuary). Consequently, large pulses of NO_3^- were not immediately translated to phytoplankton biomass, and there was often a lagged response of chl *a* to strong nutrient pulses (**Figure 6-7D**).

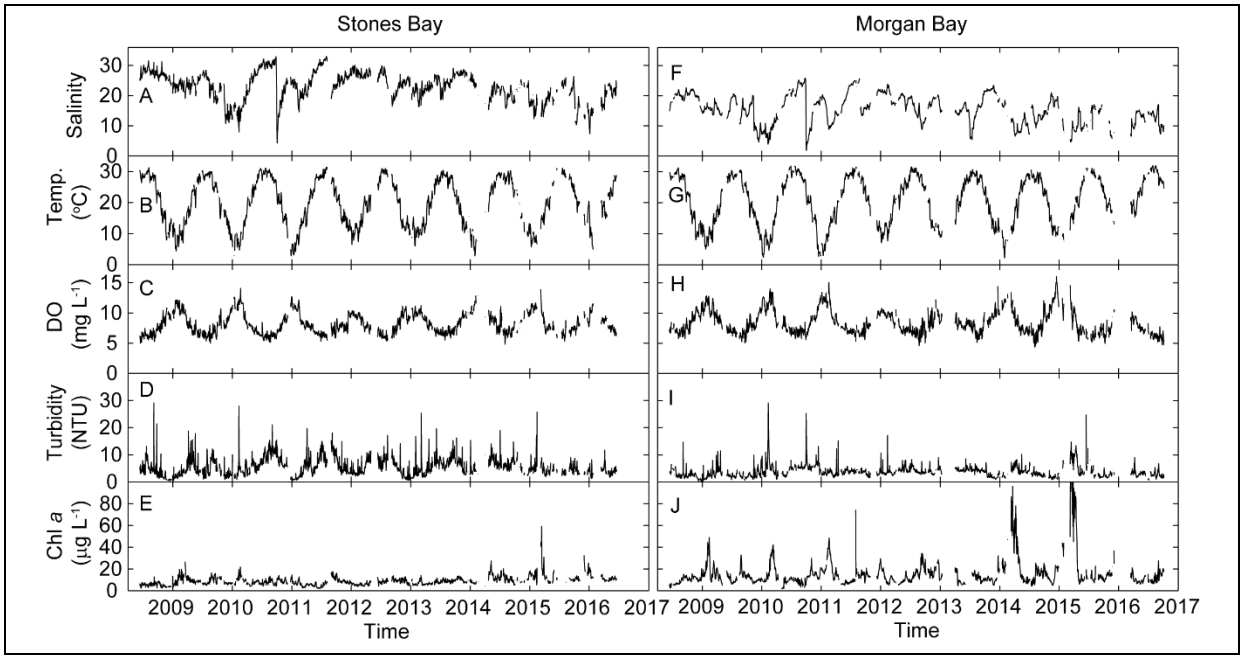

Figure 6-8. Long- and short-term variabilities in key water quality parameters measured by the AVPs at Stones Bay and Morgan Bay.

Data shown are daily averages of vertically averaged values.

Seasonality of Water Quality

The multi-annual, semi-hourly time series of key water quality parameters produced by the AVPs at Stones Bay and Morgan Bay demonstrate a large degree of seasonality of key water quality parameters (**Figures 6-8**). Maximum annual salinities generally occurred during the summer, but decreases in salinity were highly variable during the winter (**Figures 6-8A and F**). The most notable depressions in salinity occurred during the wet fall and winter in 2009 through early 2010. In addition, dramatic salinity drops occurred after Tropical Storm Nicole in late September 2010, after Hurricane Irene in late August 2011, and after Tropical Storm Joaquin in September and October 2015. The temperature oscillated between summer highs of approximately 30°C in late July and early August to winter lows of approximately 2°C in late January (**Figures 6-8B and G**).

DO was strongly impacted by temperature because of solubility characteristics. Winter maxima ranged between approximately 12–14 mg L^{-1} and summer minima ranged between approximately 5–6 mg L^{-1} (**Figures 6-8C and H**). Turbidity (**Figures 6-8D and I**) and chl *a* (**Figures 6-8E and J**) also showed oscillations at seasonal time scales, with both generally showing maxima during the spring and late summer periods. This trend is more evident in the Morgan Bay record (**Figure 6-8J**) for chl *a* and for turbidity in the Stones Bay record

(**Figure 6-8E**). These differences between sites suggest potential differences in drivers of turbidity and chl *a* between the two sites.

Covariations Between Water Quality Parameters

The interrelationships between daily average water quality parameters at the two AVP sites were assessed by using Pearson's correlations. Results are shown in **Table 6-2**. Because of autocorrelation within each parameter, the number of samples (*N*) in each data record is much greater than the true degrees of freedom. The use of *N* as an estimate of the degrees of freedom would result in unacceptable Type 1 error in testing the null hypothesis that no correlation exists. Estimates of equivalent degrees of freedom, which take into account autocorrelation, were calculated according to Emery and Thomson (1997) and are used to calculate the *p* values for each parameter pair.

Table 6-2. Results of Pearson's Correlations for Key Water Quality Parameters from the AVPs at Stones Bay and Morgan Bay

Parameters				
Temperature	**Salinity**	**DO**	**Turbidity**	**Chl *a***
Stones Bay				
{55}	**0.34**	**−0.85**	**0.38**	−0.04
0.0062	{50}	**−0.37**	0.15	**−0.42**
2.1×10^{-27}	0.0037	{71}	**−0.35**	0.22
0.0018	0.14	0.0014	{159}	0.13
0.39	8.3×10^{-4}	0.057	0.17	{53}
Morgan Bay				
{53}	0.087	**−0.81**	−0.03	**−0.23**
0.26	{64}	−0.06	**−0.22**	**−0.36**
2.1×10^{-14}	0.31	{67}	0.01	**0.31**
0.41	0.036	0.47	{184}	**0.34**
0.045	0.0016	0.0042	3.2×10^{-5}	{127}

Pearson's *R* lies above and the *p* values lie below the diagonal. Equivalent degrees of freedom for each parameter lie along the diagonal in brackets. Bold *R* values are significant at α=0.05.

Most of the interrelationships between water quality variables were of similar sign (i.e., positive or negative) between AVP sites. Positive relationships between temperature and salinity at both sites reflect the tendency toward higher freshwater inputs during the winter and spring, when evapotranspiration within the watershed is at an annual minimum (Litaker et al., 1987). Because of the strong influence of temperature on gas solubility, DO showed a significant negative correlation with temperature (**Table 6-2**). The negative relationship between salinity and DO at both stations is most likely a product of the covariation of these two variables with temperature. The strong negative relationships between chl *a* and salinity underscore the influence of the riverine nutrient load delivered by freshwater riverine inputs that fuels higher phytoplankton biomass.

Significant differences in interrelationships between water quality parameters did exist between the two AVP stations. At Stones Bay, turbidity was highly correlated with temperature (by covariation with DO as well), but at Morgan Bay, no relationship between turbidity and temperature was observed (**Table 6-2**). It is unclear what drives this seasonal pattern in turbidity at Stones Bay. Sediment resuspension due to wind and wave energy is a dominant source of turbidity within the NRE. However, it seems unlikely that physical processes drive this seasonal pattern because tidal energy is fairly constant throughout the year, and wind energy to the NRE reaches an annual minimum during the summer months. It seems likely that the seasonal turbidity signal is of biological or anthropogenic origin, perhaps because of foraging of demersal finfish or perhaps because of the shrimp trawling industry. At Morgan Bay, turbidity showed a strong positive relationship with chl *a* and with salinity. The high correlation between turbidity and chl *a* is likely because of the turbidity created by high cell densities during phytoplankton blooms, which are common in Morgan Bay. The negative correlation between turbidity and salinity may be because of covariation between chl *a* and salinity (i.e., turbidity due to phytoplankton decreases at higher salinity) or may be due to the effect of riverine sediment loading that enhances turbidity while depressing salinity.

Relationship Between Phytoplankton Biomass and Flushing Time

The strongest relationship between hydrology and phytoplankton biomass was observed by calculating the flushing time from river discharge and salinity in the estuary. The flushing time is the amount of time necessary to replace the amount of freshwater in the estuary, and therefore also measures how much time freshwater has spent in the estuary after being discharged by the river (i.e., flushing time is a measure of freshwater age; Lucas et al., 2009; Monsen et al., 2002). Higher discharge results in shorter flushing times, and upstream segments of the estuary always have shorter flushing times than downstream segments.

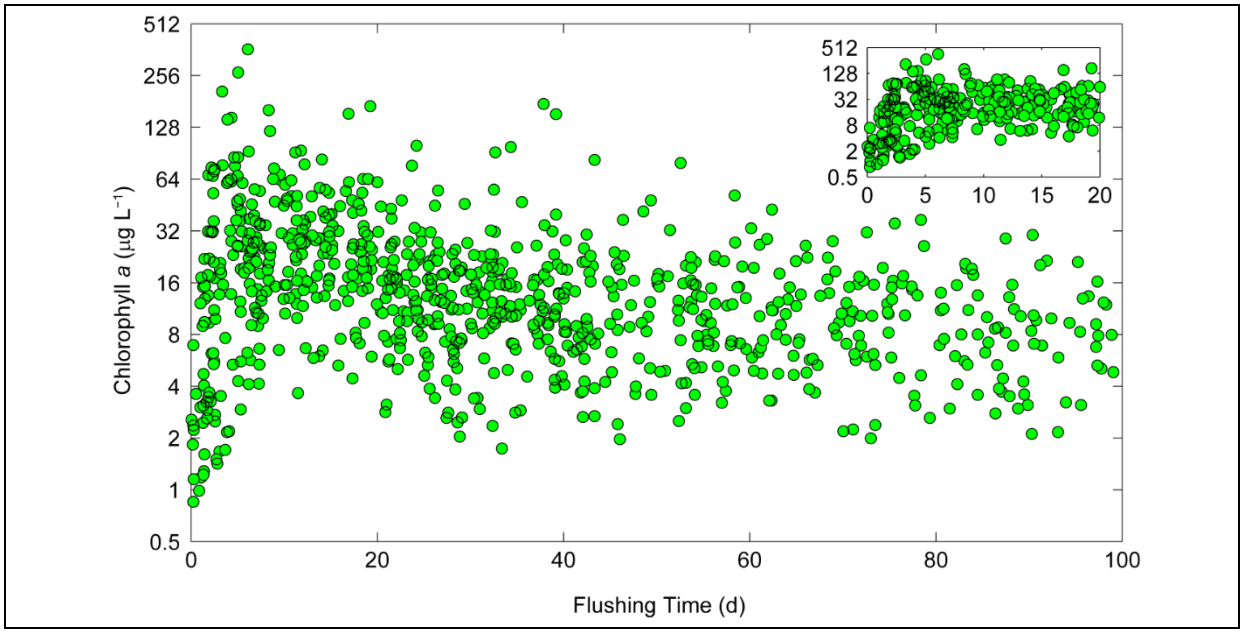

Figure 6-9. A scatter plot of phytoplankton biomass as chlorophyll *a* versus flushing time.

Data are from the eight DCERP sampling stations monitored monthly for all sampling dates from October 2007 through December 2016. The inset shows an expansion of the relationship up to a flushing time of 20 days (d).

Chl *a* in the NRE exhibited a strong non-monotonic relationship with flushing time (**Figure 6-9**), and this relationship explains much of the observed spatial and temporal variation of phytoplankton biomass in the NRE (Hall et al., 2013; Paerl et al., 2014; Peierls et al., 2012). Under short flushing time conditions (less than approximately 10 days) associated with high flows or moderate flow conditions in the upper estuary, despite the delivery of high concentrations of riverine nutrients, there is insufficient time for phytoplankton to grow. After freshwater has spent 1 to 2 weeks in the estuary, enough time has lapsed for phytoplankton to grow and completely assimilate the riverine nitrogen load. Consequently, biomass peaks at a freshwater age of 1 to 2 weeks while nutrient concentrations reach growth limiting levels (Peierls et al., 2012). Following the peak, phytoplankton production is reliant on regenerated nutrients from the water column and sediments. Nutrient regeneration is never completely efficient due to losses of nutrients from burial, denitrification, and transfer to higher trophic levels. All three nutrient-removal processes result in a slow decline of phytoplankton biomass as the freshwater is slowly transported downstream away from its riverine nutrient source. This pattern appears to be common to shallow, microtidal estuaries where rivers are the main source of nutrients and phytoplankton growth in the river is strongly light limited (Hall et al., 2013; Peierls et al., 2012).

Within the set of DCERP monthly monitoring stations, Stations 6, 7, and 8 in the upper estuary most often had flushing times of 1 to 2 weeks (**Figure 6-10**). Therefore, it should not be surprising that these stations were most likely to experience significant phytoplankton blooms and exceedances of the North Carolina chl *a* water quality standard (see **Figure 6-10**).

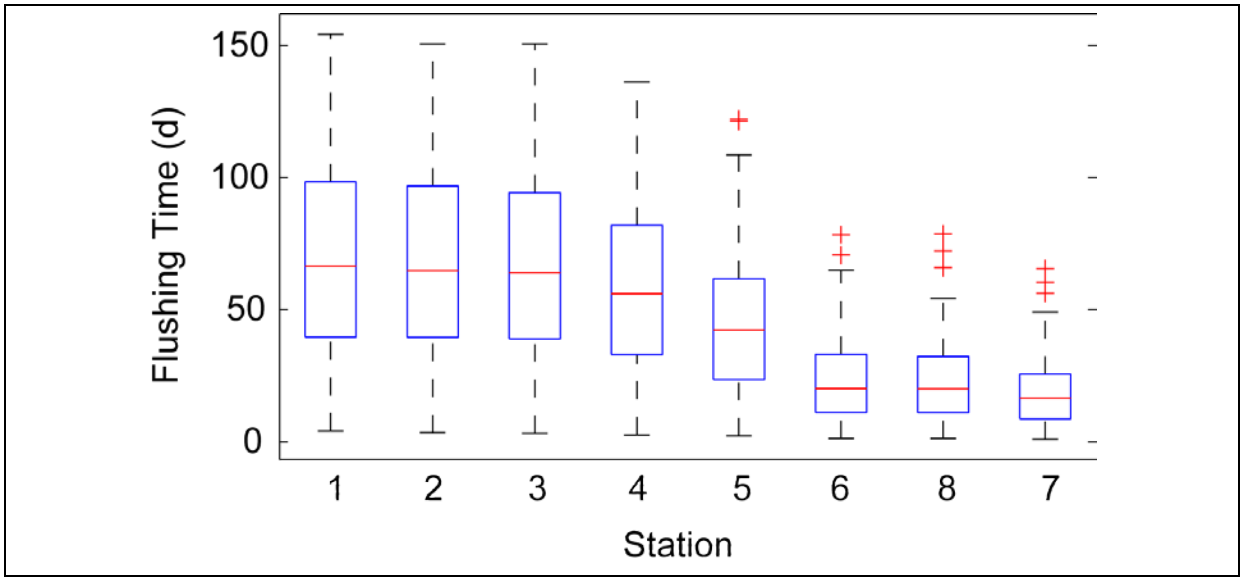

Figure 6-10. Box and whisker plots of flushing time at each of the eight monthly DCERP monitoring stations in the NRE.

Stations are arranged by increasing distance from the inlet. Boxes represent the interquartile range. Red horizontal lines are the median values. Whiskers represent 1.5 times the interquartile range. Values outside the whiskers are represented with red "+" symbols.

These measures of freshwater age can also be used to determine the residence time within a particular section of the estuary. The difference in freshwater age between an upstream and adjacent downstream station represents the amount of time that water spent in the section of the

estuary between those two stations. This measure of residence time is more appropriate (than flushing time) for determining what the likely impacts of siting a point source of nutrients would be within a particular section of the estuary (Monsen et al., 2002). As shown in **Figure 6-10**, freshwater age changes by only a couple of days between Station 3 and Station 1 at the New River inlet. This finding indicates rapid movement of water through this narrow, highly tidal region of the estuary. Results from the Estuarine Simulation Model corroborate this finding, indicating a residence time of less than 2 days downstream of the Highway 172 Bridge (for more information about this model, see Research Project TSP-2, Chapter 10 of the DCERP2 Final Report).

Based on these results, siting any new nutrient point sources downstream of the Highway 172 Bridge would be less problematic for water quality because the residence time is likely too short for phytoplankton bloom development, and there are no downstream segments of the estuary to impair. Currently, MCBCL's wastewater treatment plant (WWTP) effluent is discharged into Farnell Bay, where residence time is more than long enough for nutrients to be assimilated by phytoplankton. Although the associated nutrient loads are currently too small to cause major water quality problems, changing the effluent discharge position to downstream of Highway 172 should be considered during any future expansion in loading from the WWTP.

Phytoplankton Blooms

Phytoplankton species that dominated blooms were identified and quantified by using inverted microscopy following methods detailed by Hall et al. (2013). A bloom sample was defined as a sample exceeding the 40 $\mu g\ L^{-1}$ chl *a* water quality standard adopted by the North Carolina Department of Environment and Natural Resources (NCDEQ; recently renamed the Department of Environmental Quality). When multiple bloom samples were collected at spatially contiguous stations on the same sampling date, only the sample with the highest chl *a* concentration was examined. On 41 separate dates, phytoplankton biomass reached bloom levels at locations (mostly middle and upper) in the NRE (**Table 6-3**). Dinoflagellates dominated the majority of the blooms (27 out of 41) (**Figure 6-11**). Although eight species of dinoflagellates were observed to dominate biomass across all the blooms, three species dominated 22 out of the 27 dinoflagellate–dominated blooms (**Table 6-3**). *Gyrodinium instriatum* and *Polykrikos hartmanii* were common bloom dominants during the summer and fall, and *Prorocentrum minimum* was the most common bloom dominating dinoflagellate during the cooler months from early winter through early spring. None of these species are known to be particularly harmful (i.e., produce toxins). Raphidophytes composed the next most common class of dominant bloom-forming phytoplankton, and blooms occurred during the warmer months from late spring through early fall. Because of poor preservation in Lugol's solution, raphidophytes could not be identified to the species level. However, previous characterization of raphidophyte blooms in the NRE from live samples has shown that the dominant species in the NRE are *Heterosigma akashiwo*, *Chattonella subsalsa*, *Chattonella c.f. verruculosa*, and *Fibrocapsa japonica* (Tomas et al., 2007). All of these raphidophyte species have been associated with fish kill events in other estuaries. However, no fish kills were observed during these blooms in the NRE (see NCDEQ's fish kill database of the North Carolina Department of Environmental Quality [NCDEQ, 2017]). Euglenophytes and diatoms were the only two other phytoplankton classes that dominated blooms in the NRE during the DCERP. The diatom blooms were dominated by small, solitary,

centric diatoms, whereas the euglenophyte blooms were dominated by *Euglena sp.* and *Eutreptia sp.*

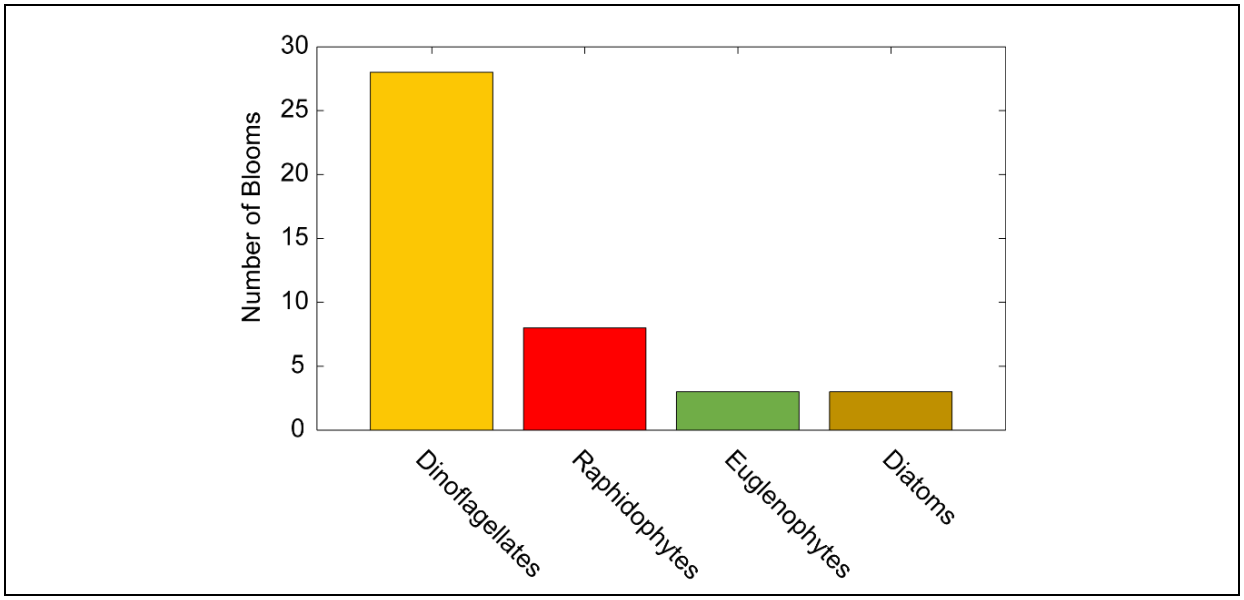

Figure 6-11. Summary of the number of phytoplankton blooms dominated (highest percentage of total biovolume) by algal classes in the NRE from October 2007 to December 2016.

It is notable that out of the total of 41 blooms, there were only three cases (the three diatom blooms) in which the dominant bloom-forming species was not a highly motile flagellate species. Using the AVPs to track the vertical distribution of phytoplankton biomass over time, it is clear that the flagellates in the NRE conduct a regular pattern of diel vertical migration whereby the cells swim upwards near to the surface during the day and deeper into the water column at night. The ability to vertically migrate in this shallow, CDOM–stained estuary provides access to near surface light during the day and may provide access to higher levels of nutrients in deeper waters at night (Hall et al., 2015). Motility can also lead to a greater level of cell retention in estuaries, which enhances the ability of their populations to reach bloom levels (Anderson and Stolzenbach, 1985; Seliger et al., 1970).

Table 6-3. Summary of phytoplankton bloom composition in the New River Estuary from October 2007 through December 2016

Date	Stations Impacted	Highest Chl *a* (µg L^{-1})	Division or Class	Species	% Biovolume
16 June 2008	**6S**,8	170	Raphidophyte	Undeterminable	92
8 September 2008	**7S**	74	Raphidophyte Dinoflagellate	Undeterminable Gymnodinoid	53 27
5 January 2009	6,**7S**,8	88	Dinoflagellate Euglenophyte	*Akashiwo sanguinum* *Eutreptia* sp.	51 25
2 February 2009	**4S**	67	Dinoflagellate Dinoflagellate	*Akashiwo sanguinum* *Heterocapsa triquetra*	74 18

(continued)

Table 6-3. Summary of phytoplankton bloom composition in the New River Estuary from October 2007 through December 2016 (continued)

Date	Stations Impacted	Highest Chl *a* (µg L^{-1})	Division or Class	Species	% Biovolume
4 March 2009	**7S**	224	Euglenophyte Cryptophyte	*Euglena* sp. *Cryptomonas* sp.	47 29
29 June 2009	6,**7S**	54	Raphidophyte Euglenophyte	Undeterminable *Euglena* sp.	70 6
24 August 2009	5,6,7,**8S**	70	Dinoflagellate Dinoflagellate	*Gyrodinium instriatum* *Karlodinium veneficum*	68 11
17 February 2010	**5S**	106	Dinoflagellate	*Heterocapsa triquetra*	96
17 May 2010	**6S**,8	56	Raphidophyte	Undeterminable	94
14 June 2010	**7S**	46	Raphidophyte	Undeterminable	82
1 November 2010	5,**7S**,8	149	Dinoflagellate Ciliophora Euglenophyte	*Gyrodinium instriatum* *Myrionecta rubra* *Eutreptia* sp.	50 22 10
1 February 2011	6,**7S**,8	68	Diatom Dinoflagellate Dinoflagellate	*Cyclotella sp.* cf. *Gymnodinium aureolum* *Heterocapsa triquetra*	39 30 28
2 March 2011	6,**7S**	58	Diatom	*Cyclotella sp.*	83
31 May 2011	5,**6S**,7	87	Raphidophyte	Undeterminable	99
8 August 2011	**6S**	56	Raphidophyte	Undeterminable	87
31 August 2011	**4S**	55	Dinoflagellate	*Polykrikos hartmanii*	97
7 September 2011	**3S**	45	Dinoflagellate	*Polykrikos hartmanii*	99
7 September 2011	5,**7S**	62	Euglenophyte Dinoflagellate Raphidophyte Dinoflagellate	*Eutreptia sp.* *Gyrodinium instriatum* Undeterminable *Polykrikos hartmanii*	32 21 18 8
3 October 2011	3,**4S**	46	Dinoflagellate	*Polykrikos hartmanii*	98
13 August 2012	6,7,**8S**	158	Dinoflagellate	*Polykrikos hartmanii* *Scrippsiella trochoidea*	73 15
4 September 2012	5,6,**7S**,8	120	Dinoflagellate Raphidophyte	*Scrippsiella trochoidea* Undeterminable	74 23
5 November 2012	7,**8S**	60	Dinoflagellate	*Polykrikos hartmanii*	95
11 March 2013	**7S**,8	146	Dinoflagellate	*Prorocentrum minimum*	98
16 July 2013	5,**6S**,7,8	90	Diatom	*Cyclotella sp.*	91
4 February 2014	**7B**	46	Dinoflagellate Unidentified flagellate	*Prorocentrum minimum* Undeterminable	60 36

(continued)

Table 6-3. Summary of phytoplankton bloom composition in the New River Estuary from October 2007 through December 2016 (continued)

Date	Stations Impacted	Highest Chl *a* (µg L^{-1})	Division or Class	Species	% Biovolume
11 March 2014	5, 6, 7, **8S**	79	Dinoflagellate	*Prorocentrum minimum*	84
16 April 2014	5, **6S**, 7	84	Dinoflagellate	*Prorocentrum minimum*	99
10 June 2014	**7S**	51	Raphidophyte	Undeterminable	99
11 August 2014	5, **8S**	58	Dinoflagellate	c.f. *Peridinium aciculaferum*	76
10 September 2014	**3S**, 4	192	Dinoflagellate	*Polykrikos hartmanii*	99
7 October 2014	**5S**, 6, 7, 8	88	Dinoflagellate	*Polykrikos hartmanii*	99
22 January 2015	5, 6, **7S**, 8	95	Dinoflagellate Diatom	*Prorocentrum minimum* *Cyclotella sp.*	72 12
18 March 2015	4, 5, 6, 7, **8S**	350	Dinoflagellate	*Prorocentrum minimum*	99
21 April 2015	7, **8S**	94	Dinoflagellate	*Prorocentrum minimum*	92
8 September 2015	**6S**, 7	324	Dinoflagellate Raphidophyte	*Polykrikos hartmanii* Undeterminable	55 40
4 November 2015	7, **8S**	95	Dinoflagellate Dinoflagellate	*Gyrodinium instriatum* *Polykrikos hartmanii*	50 45
3 December 2015	**6S**	72	Euglenophyte	Undetermined	99
11 July 2016	**3S**, 4, 5, 8	66	Dinoflagellate	*Polykrikos hartmanii*	99
10 August 2016	5, **7S**, 8	99	Dinoflagellate Raphidophyte	*Gyrodinium instriatum* undeterminable	62 20
12 September 2016	**7S**	57	Dinoflagellate	*Gyrodinium instriatum*	75
5 December 2016	6, **7S**, 8	204	Dinoflagellate	*Prorocentrum minimum*	99

Note: A bloom event was defined as a sampling date with surface water concentrations greater than 40. Spatially contiguous stations with bloom level chlorophyll *a* were considered to be impacted by the same bloom, and the surface (S) water or bottom (B) water sample from the impacted station with the highest chlorophyll *a* (in bold) was microscopically enumerated to determine the dominant phytoplankton. Taxa listed comprised greater than 75% of total phytoplankton biovolumes within each bloom sample.

Dynamics of Dissolved Carbon Dioxide

By modulating phytoplankton biomass, changes in flushing time also strongly modulated the net air–sea exchange of carbon dioxide (CO_2) in the estuary (**Figure 6-12**). Riverine freshwater was always supersaturated (up to 10 times higher than the atmosphere) with CO_2, and the estuary was a strong net source of CO_2 to the atmosphere when freshwater ages were only a few days. As freshwater age increased beyond approximately 2 weeks, high rates of phytoplankton primary

production, mixing with well buffered ocean water, and prior outgassing, led to much lower partial pressure of carbon dioxide (pCO_2). During peak phytoplankton production, the estuary was on average still a small source of CO_2 into the atmosphere. In many cases, however, the estuary actually became a sink for atmospheric CO_2 (pCO_2 less than atmospheric equilibrium in **Figure 6-12**). These net CO_2 uptake events only occurred when freshwater age was greater than approximately 2 weeks. At even greater freshwater ages, respiration of the declining and increasingly nutrient limited phytoplankton carbon resulted in the estuary resuming its function as a source of CO_2 with positive fluxes that declined to near zero at the oldest freshwater ages.

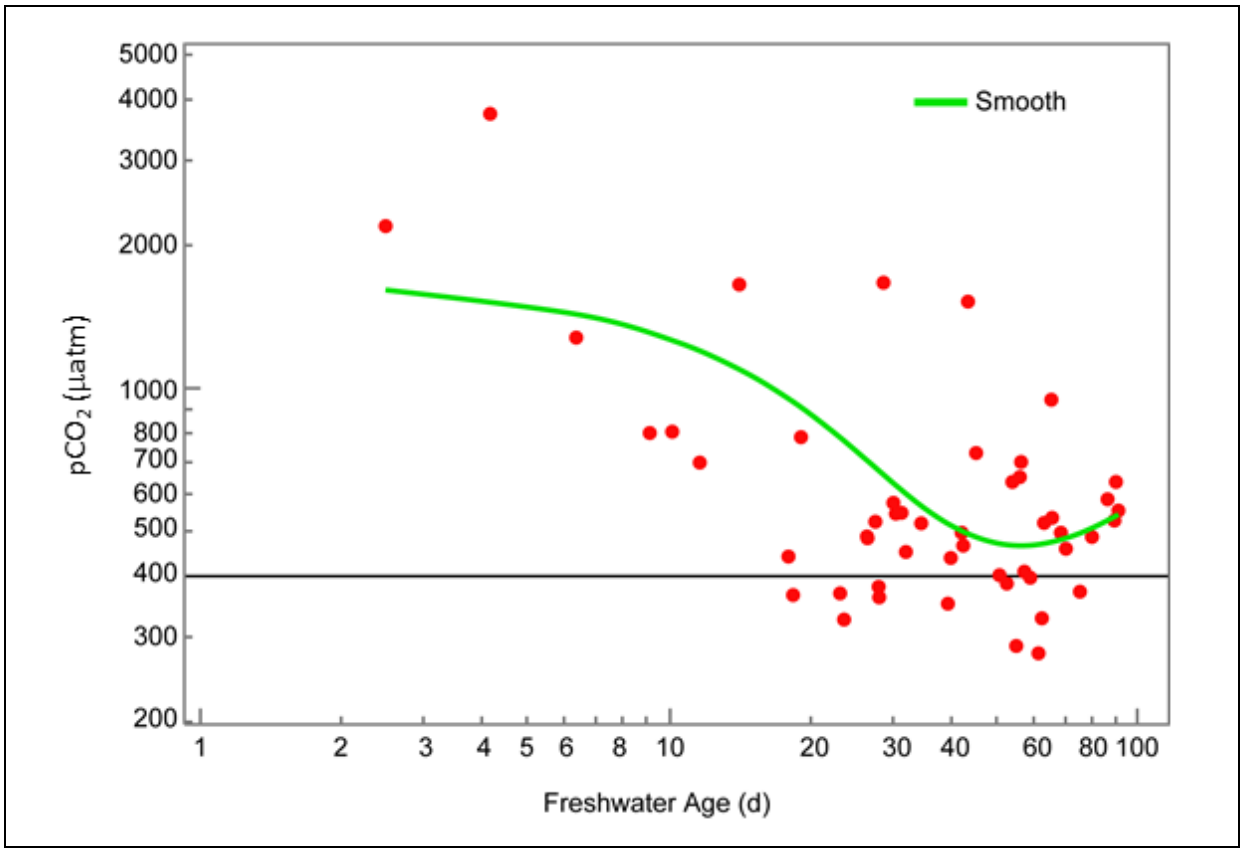

Figure 6-12. The relationship between freshwater age and estuarine pCO_2.
Data were collected from July 2013 to July 2015.

The AEMP was designed to provide data to Research Projects AE-4 and AE-6. Findings from these research projects suggested that parameters relevant to the carbon cycle (e.g., pCO_2, DOC) are highly variable on time scales shorter than the measurement frequency used for these research projects (2 months). Some of this variability was attributed to the impact of episodic events, which may deliver water and nutrients or enhance vertical mixing. When Hurricane Joaquin impacted the NRE in late September and early October 2015, Research Project AE-4 researchers were afforded the opportunity to directly measure the impacts of such an event on carbon cycling in the estuary. Research Projects AE-4 and AE-6 of this DCERP2 Final Report provide more detail. The estuary was a source of CO_2 to the atmosphere at all locations during the 2 weeks before the storm. Greatly enhanced fluxes of CO_2 into the atmosphere during the approximately 2-week period during which Hurricane Joaquin impacted the study area demonstrated the significance of storm events on estuarine carbon processing (**Figure 6-13**).

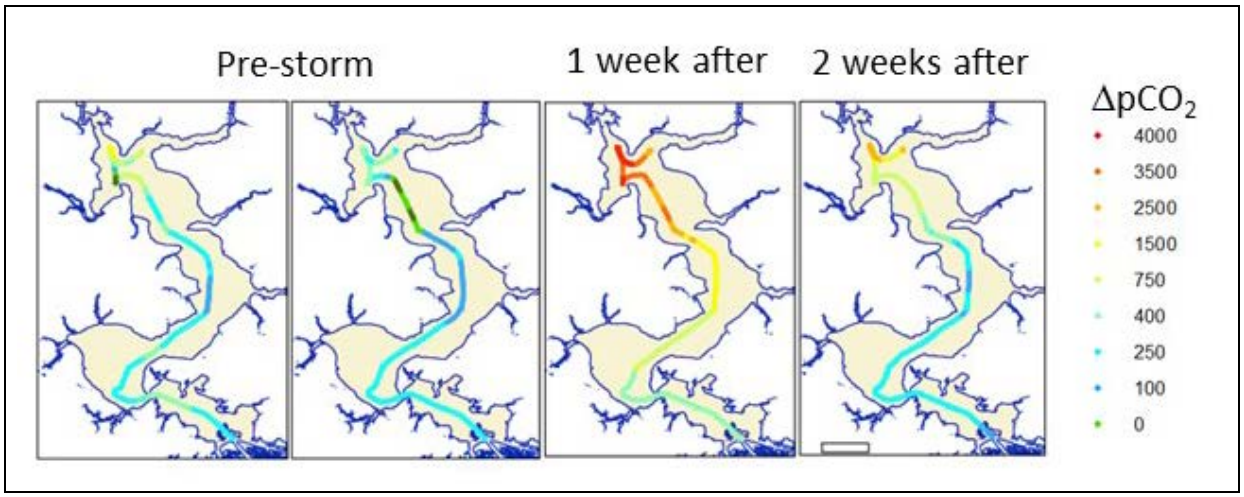

Figure 6-13. Dataflow transects of the difference of estuarine versus atmospheric pCO_2 (ΔpCO_2) before and after passage of Tropical Storm Joaquin in fall 2015.

Frequency of Bottom Water Hypoxia

The frequency of hypoxic conditions was determined by year and by station by using near-bottom readings from the vertical profile data AVP (**Table 6-4**). Hypoxia can be defined by a range of DO concentrations. We followed the moderate (less than 4 mg L^{-1}) and severe hypoxia (less than 2 mg L^{-1}) definitions from Buzzelli et al. (2002). Note that we did not examine the vertical or across-channel spatial extent of these hypoxic conditions. **Figure 6-14** shows a histogram of the frequency of moderate and severe bottom water hypoxia in relation to the temperature of the bottom water. The frequencies of all measured bottom water temperatures are shown for comparative purposes. It is clear that both moderate and severe hypoxia were restricted to times of the year when water temperatures were relatively high. Very few bottom water hypoxia events were detected when the bottom water temperatures were below 25°C.

Between years, the greatest frequency of hypoxia was observed in 2015, followed by 2009 and 2011 (**Table 6-4**). Years 2007, 2008, 2010, and 2013 were notable for their low frequencies of occurrence of hypoxic events. Spatially, hypoxia was most common at Stations 4, 5, 6, and 8 in the middle and upper estuary. Hypoxia was never observed at the downstream Stations 1 and 2.

Table 6-4. Frequency of Bottom Water Hypoxia by Water-Year and by Station with Water-Depth and Stratification Intensity. (The measurement depth was 0.5 m above the bottom.)

		Total Sample Number (N)	Hypoxic Sample Number		Mean (SD) Water Depth (m)	Stratification Intensity Bottom–Surface Salinity
			Moderate (<4 mg L^{-1})	Severe (<2 mg L^{-1})		
By Year	2007	24	0	0	2.4 (0.6)	0.8 (0.9)
	2008	96	6	0	2.8 (0.7)	2.1 (2.3)
	2009	104	13	7	2.8 (0.6)	3.3 (3.1)
	2010	96	0	0	2.8 (0.8)	2.7 (3.7)
	2011	112	11	3	2.8 (0.7)	2.5 (3.4)
	2012	96	9	3	2.7 (0.6)	2.0 (1.7)
	2013	80	4	1	2.4 (0.8)	2.3 (2.7)
	2014	80	7	2	2.3 (0.9)	2.0 (3.1)
	2015	88	17	6	2.5 (0.9)	3.7 (2.9)
	2016	88	9	2	2.4 (0.8)	2.8 (2.6)
By Station[a]	CL-1	108	0	0	3.5 (0.8)	1.0 (1.7)
	CL-2	108	0	0	2.4 (0.4)	2.4 (2.7)
	CL-3	108	2	0	1.8 (0.3)	2.4 (2.3)
	CL-4	108	17	3	3.0 (0.4)	4.5 (3.3)
	CL-5	108	17	5	2.5 (0.3)	3.3 (3.1)
	CL-6	108	14	7	1.9 (0.3)	2.1 (3.4)
	CL-7	108	10	1	1.6 (0.2)	2.4 (2.7)
	CL-8	108	19	8	2.0 (0.3)	2.3 (2.7)

Bottom water hypoxia is a complicated phenomenon that results from a combination of biological and physical drivers (Malone et al., 1988; Sanger et al., 2011). As previously mentioned, temperature is both a physical driver through its impact on oxygen solubility and is a strong biological driver by controlling rates of microbial respiration. Climate-related warming can be expected to exacerbate bottom water hypoxia in the NRE. The availability of organic carbon as a substrate for respiration is another important biological driver of bottom water hypoxia; consequentially, bottom water hypoxia is often intimately related to the production and deposition of organic matter by phytoplankton in the overlying surface waters (Malone et al., 1988). Riverine discharge delivers nutrients that fuel phytoplankton production, but also decreases surface water salinity and enhances stratification. Riverine discharge, therefore, also has important impacts on both the biological and physical drivers of hypoxia. Shelf waters of Onslow Bay are generally near saturation with respect to oxygen (Dafner et al., 2007). As high oxygen water in Onslow Bay is advected upstream in the bottom layer, oxygen depletion proceeds at a rate that is dependent on the balance between oxygen loss via respiration and oxygen inputs that occur when oxygen is mixed or diffuses into the bottom water from above. Turbulent mixing, driven by winds and tides, is generally much more important than diffusion in re-aerating the bottom waters; therefore, this is likely the reason why hypoxia was not observed

at the downstream stations. Bottom waters at these stations were likely too "new" and the vertical mixing due to the tides was too vigorous for hypoxia to occur.

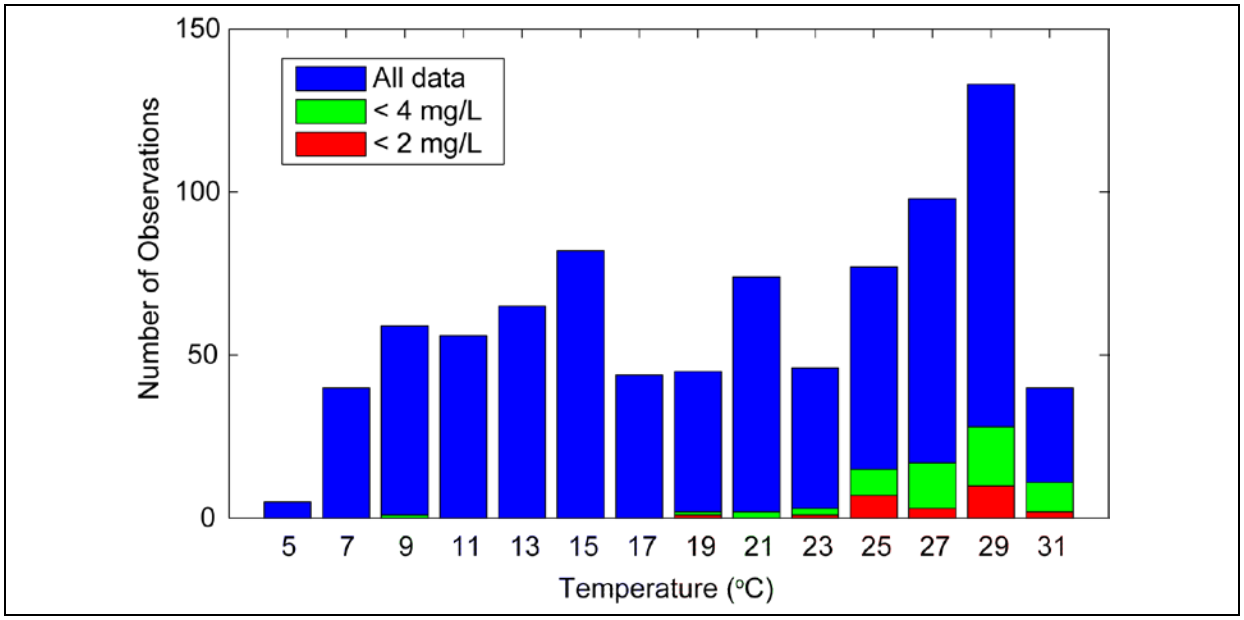

Figure 6-14. A histogram of bottom water temperatures from all data from Stations 1 through 8 and during moderate (less than 4 mg L^{-1} DO) and severe (less than 2 mg L^{-1}) bottom water hypoxia; *x*-axis labels are the centroids of 2°C bins.

To gain a greater understanding of the roles that physical drivers play in the temporal and spatial occurrence of hypoxic events, we compared the frequency of hypoxia to water column depth and stratification intensity. Depth is an important determinant of oxygen penetration because stronger vertical mixing is required to mix oxygen downward into deeper layers and because bottom waters of deeper stations are more like to lie below the pycnocline, which acts as a barrier to vertical mixing. Additionally, deeper areas are often low-energy, depositional centers for fine-grained, organic-rich sediments, which contribute to high biological oxygen demand. The difference between bottom and surface water salinity is used as a surrogate for density differences between the two layers (Hall et al., 2012), an indicator of the intensity of vertical mixing which ventilates the bottom waters.

The analyses reveal that some of the prominent temporal and spatial patterns can be explained by water depth and stratification intensity. The high frequency of hypoxic events during 2015 and 2009 coincided with the highest observed average stratification intensities. Spatially, the high frequencies of hypoxia at Stations 4 and 5 are also explained by high degrees of stratification and by the greatest water depths. The comparatively high frequency of hypoxia at Station 8 cannot be explained either by depth or particularly strong stratification, but this might be due to a higher degree of oxygen demand in this bloom-prone region of the estuary.

Spatial Gradients of Salinity, Nutrients, Phytoplankton Biomass, and Carbon

Station J16 (37.6 km upstream from the inlet) was generally the upper limit of salt water intrusion in the NRE (**Figure 6-15**). However, during the lowest observed flows, salinity reached

approximately 6 at Station L1 (41.9 km upstream). Dissolved inorganic nitrogen (DIN) decreased in a near monotonic manner from Gum Branch toward the inlet. The exception was a tendency for DIN to increase between Stations L2 and L1. The approximately 0.4 mg L^{-1} increase between these stations located only 400 m apart was statistically significant (p=0.015, N=13, paired *t*-test for samples collected on the same days) and is likely because of effluent from the Lauradale WWTP outflow (National Pollution Discharge Elimination System [NPDES] permit NC0036226) near Station L1 (NCDENR, 2007).

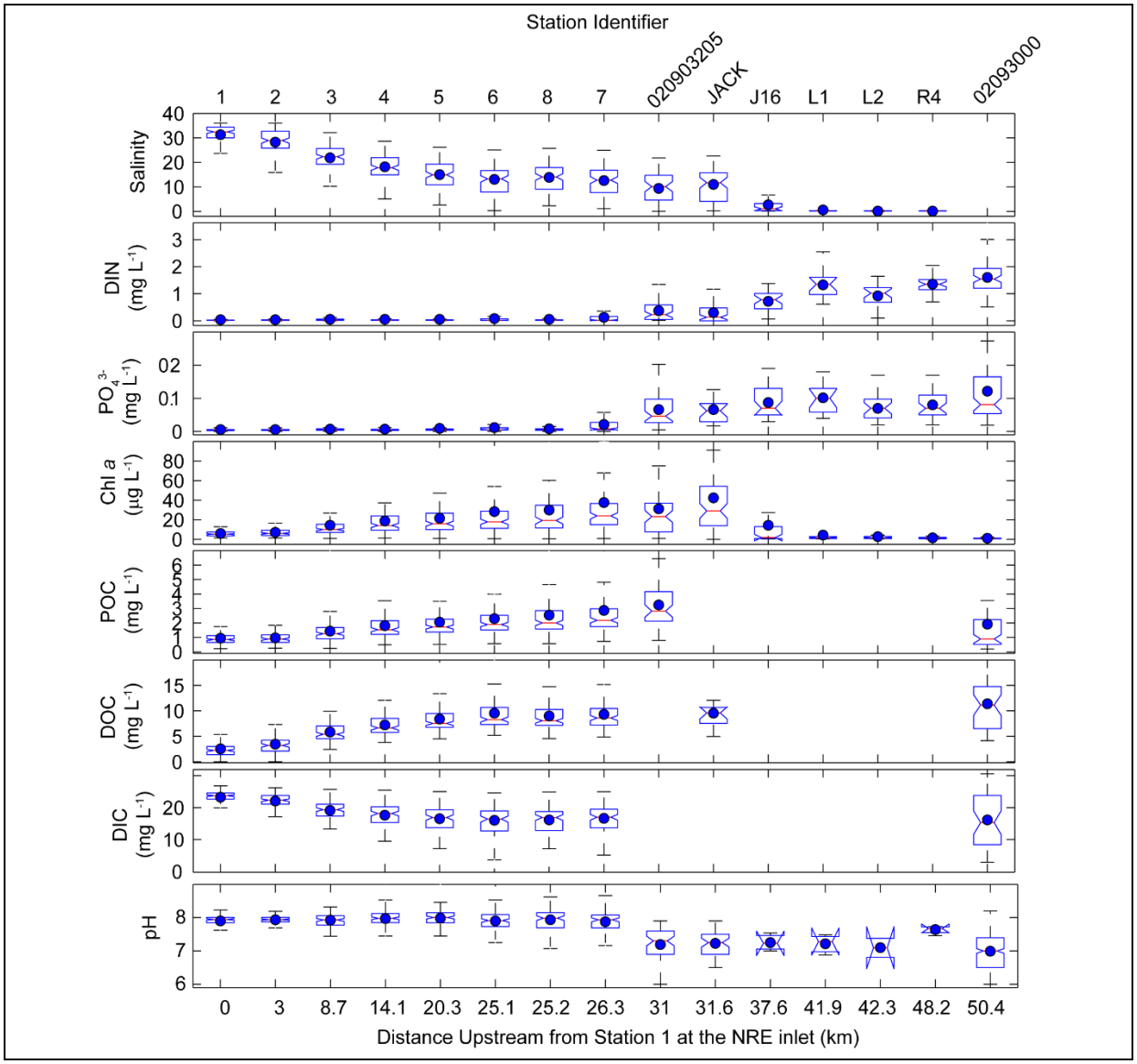

Figure 6-15. Box and whisker plots of the along stream distribution of salinity, nutrients, phytoplankton biomass, and carbon.

Boxes represent the interquartile range. Red horizontal lines are the median values. Blue dots are mean values. Whiskers represent 1.5 times the interquartile range. Note: Stations 1 through 8 were sampled from October 2007 through December 2016; Stations upstream of Station 7 were only sampled from November 2010 through December 2011.

The steep decline in DIN in the upper 10 km of the river was not accompanied by increases in chl *a* (**Figure 6-15**). Also, PO_4^{-3} did not decline in a similar manner to NO_3^- as would be expected if phytoplankton uptake were the dominant driver of the observed downstream decline in DIN within the freshwater reaches. DIN in the freshwater reaches is dominated by NO_3^- (Hall et al., 2012), and denitrification rates within the tidal fresh region of the New River can be significant during the warmer months (Von Korf et al., 2014). Together, the evidence suggests that DIN attenuation in the freshwater reaches of the New River is most likely because of denitrification rather than phytoplankton uptake.

The downstream gradient of POC matches the downstream gradient of chl *a* (**Figure 6-15**), which suggests that algal carbon is a dominant source of POC in the NRE. POC fluxes to the sediment are the major mechanism for long-term carbon storage within estuaries (Day and Kemp, 1989; Hobbie, 2000). Therefore, denitrification within the freshwater reaches may also impact the net carbon budget of the estuary by reducing algal primary production because of the decreased downstream flux of bioavailable nitrogen.

Unlike POC, DOC concentrations were higher at upstream stations, which suggests that the major source is terrestrially derived material from within the watershed. Spectral absorbance analyses of New River DOC completed by DCERP2 Research Projects AE-4 and AE-6 corroborate the dominant terrestrial origin of the DOC pool. On average, DOC concentrations were approximately two times higher than POC concentrations. Research Projects AE-4 and AE-6 have demonstrated that the majority of this large flux of organic matter to the NRE is largely refractive. Even with exposure to sunlight, which can break down refractive, high molecular weight DOC into smaller, more bioavailable forms (Osburn et al., 2012), only between 10–40% of the DOC pool was oxidized to CO_2.

DIC was highly variable within the freshwaters near Gum Branch (USGS Stream Gaging Station 02093000) and generally increased down-estuary. Increases in DIC along the salinity gradient are expected because of the high bicarbonate content of seawater. Median pH was generally near 7 in the upstream, tidal fresh section of the NRE, but ranged from almost 6 to greater than 8. Below Jacksonville, pH was higher with a median value near 8 and a significant reduction in variability going downstream toward the inlet. Near neutral pH in blackwater, coastal streams such as the New River is uncommon, but is likely due to the buffering effect of the underlying limestone bedrock. The downstream, increasing trend in pH and reduction in its variability are likely due to the chemical effects of higher pH and increased buffering capacity of bicarbonate rich seawater combined with the biological effect of reduced magnitudes of biological production and respiration.

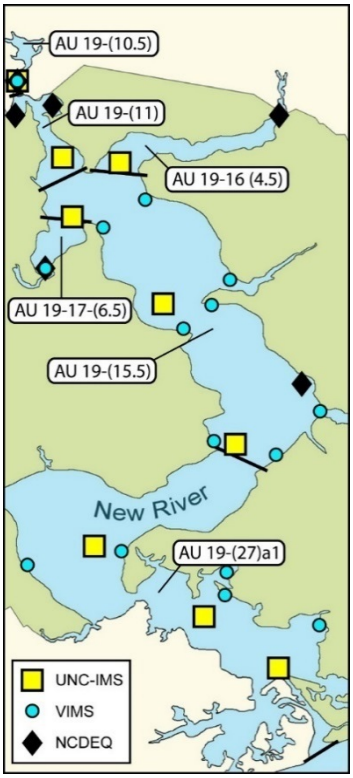

Figure 6-16. A map of the NRE that shows delineation of NCDEQ's assessment units and station locations where chl *a* was sampled by AEM-1 (UNC-IMS), AEM-3 (VIMS), and NCDEQ.

Compliance with the Chlorophyll Water Quality Standard

Through DCERP1 and DCERP2, the AEM-1 has amassed a substantial database of chl *a* concentrations that are highly valuable for assessing compliance of the NRE with the North Carolina's water quality standard of 40 $\mu g\ L^{-1}$. To account for the high natural variation in chl *a*, the North Carolina compliance determination procedure allows for 10% of water samples collected to exceed the 40 $\mu g\ L^{-1}$ standard. The State's standard compliance determination procedure specifies the use of a binomial statistical test to determine whether the exceedance percentage (percentage of samples that exceed 40 $\mu g\ L^{-1}$) is significantly greater than 10% at the 90% statistical confidence level (i.e., α=0.10). This test is used for all chl *a* data collected within each assessment unit of the estuary every 5 years.

Chl *a* data were assembled from Aquatic/Estuarine Monitoring Activities AEM-1 and AEM-3 and from NCDEQ's DWR's Ambient Monitoring System database for each of the six assessment units for the period from 2007 through 2016. Station locations and the delineation of the assessment units are shown in **Figure 6-16**. For each assessment unit, the frequency of chl *a* exceedance percentages was then calculated for running 5-year windows.

Figure 6-17 shows the distribution of chl *a* values for each assessment unit for the period from October 2007 through 2016. The two assessment units upstream near Jacksonville, AU 19 (10.5) and AU 19 (11), and the assessment units comprised by Northeast Creek (AU 19-16 [4.5]) and Southwest Creek (AU 19-17 [6.5]) had exceedance percentages greater than 10%.

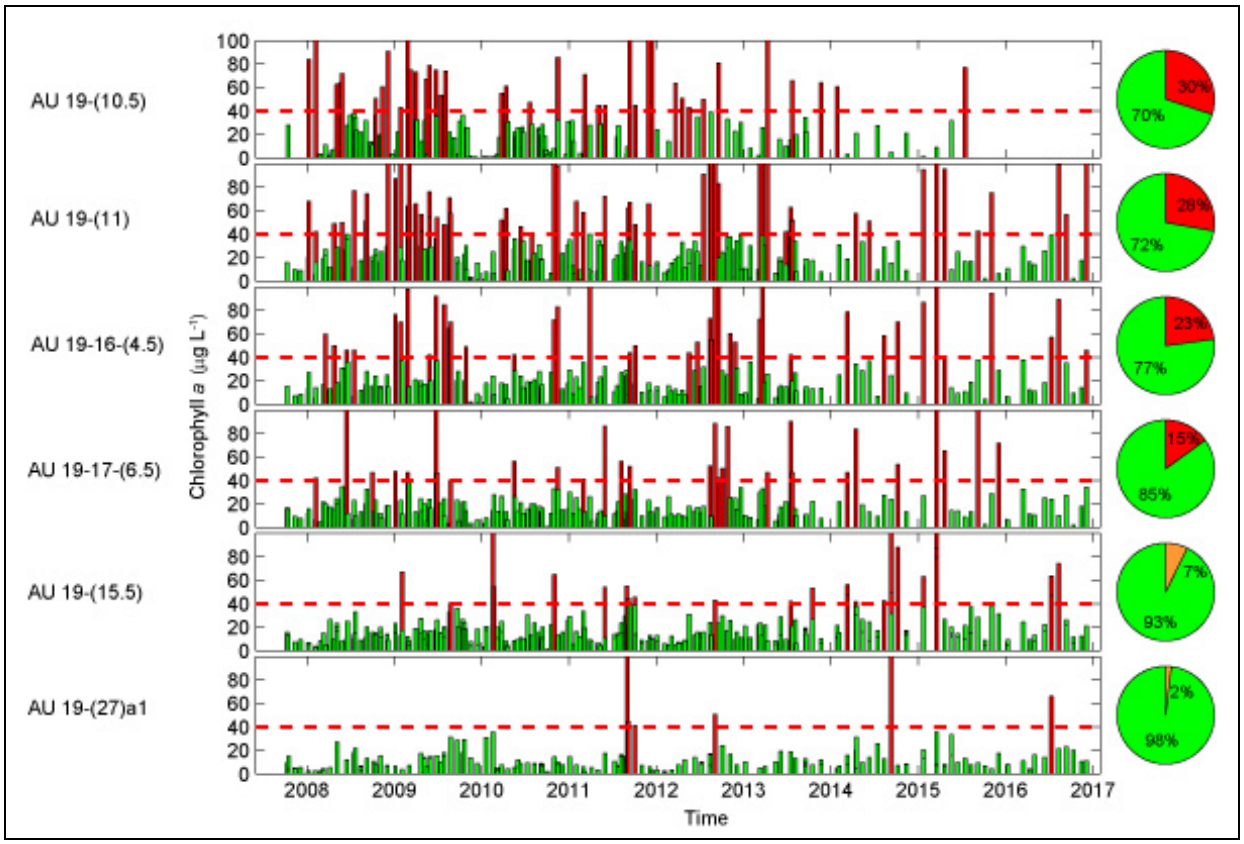

Figure 6-17. Time series of chlorophyll *a* values within each assessment unit over the DCERP project period from 2007 through 2016.

Samples greater or less than the 40 µg L^{-1} standard (red dashed line) are shown as red or green bars, respectively. Pie charts to the right show the percentages of samples less than (green) or greater than (red or orange) the NCDEQ standard. Red indicates that the percentage of samples greater 40 µg L^{-1} was greater than 10% with a 90% confidence level.

Binomial tests were run for each assessment unit for each 5-year window from 2007 through 2016. **Figure 6-18** shows the final compliance determination derived from the statistical tests. With the exception of one assessment period, the upper two assessment units and Northeast and Southwest Creeks were significantly non-compliant with the State chl *a* standard. The exception to this trend was for Northeast Creek during the 2007 through 2011 assessment period. During this period, the exceedance percentage at Northeast Creek was 12% and was not statistically greater than the 10% allowance specified in the compliance determination procedure. Exceedance percentages of the upper two segments, AU 19 (10.5) and AU 19 (11), were consistently approximately 30%, a value much higher than the allowable 10%. These assessment units do not directly receive nutrient inputs from MCBCL. Much of the data from Northeast and Southwest Creeks were gathered near the creek mouths (Monitoring Activity AEM-1 Stations 8 and 6). Water at these sampling stations reflects a mix of creek waters, main channel water (AU 19-16 [4.5]), and eutrophic waters from the upstream assessment unit AU 19 (11). It seems highly likely that inputs from upstream are a primary cause of the high exceedance

percentages at the two creek assessment units. Therefore, the areas of the NRE that are of greatest concern with respect to compliance with State and federal water quality standards are likely being impacted by upstream nutrient inputs that are not controllable by MCBCL. Over the course of 9 years of DCERP, there was a general trend of increasing exceedance frequency. For example, for AU 19 (5.5), which encompasses the middle of the estuary, the exceedance frequency steadily increased from 5% in the first 5-year period to 11% in the final 5-year period. Similar increases were observed for AU 19-16 (4.5) and AU 19-17 (6.5). The following section discusses whether this trend was because of hydrology or increased anthropogenic nutrient loading.

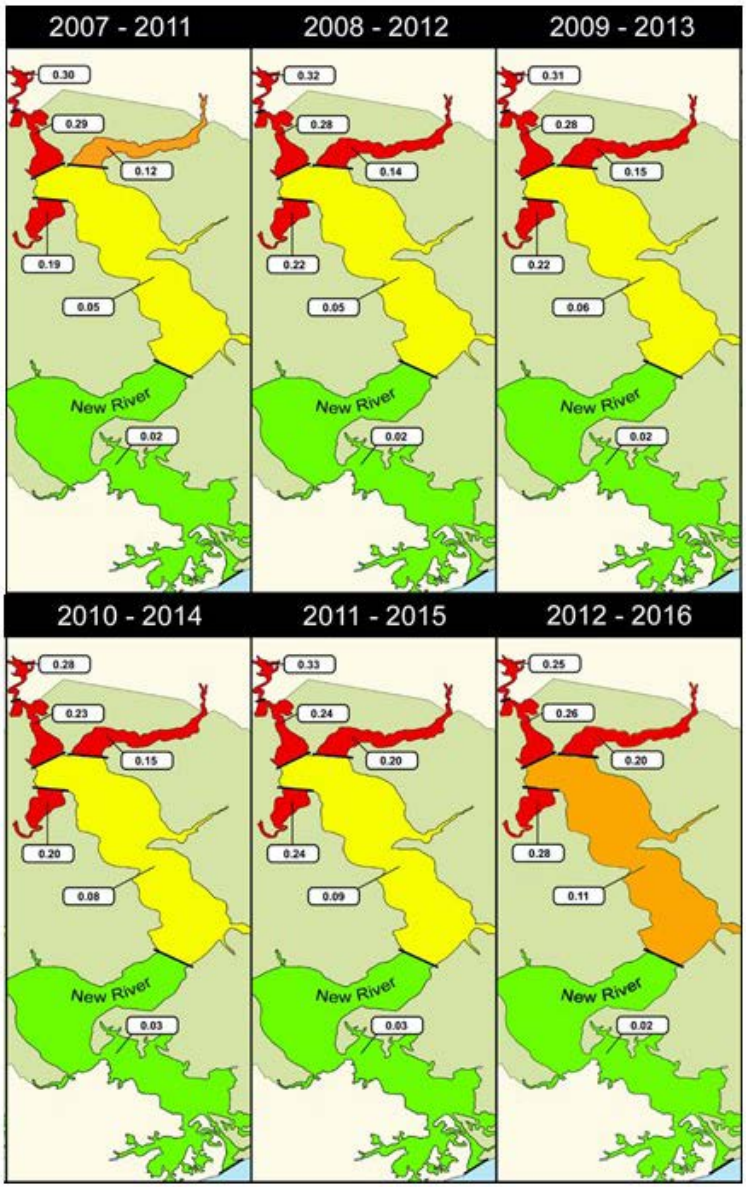

Figure 6-18. Compliance determinations for chlorophyll *a* for each NRE assessment unit during overlapping 5-year windows.

Assessment units in red were determined to be non-compliant; those in green were determined to be compliant. Assessment units in yellow were compliant, but had exceedance percentages greater than 5%. Assessment units in orange had exceedance percentages (labeled values) greater than 10%, but the percentage was not statistically greater than 10% at a 90% confidence level.

Assessment of Directionality and Trends in Estuarine Water Quality

Long-Term Temporal Trends

Seasonal Kendall tests (Hirsch et al., 1982) were performed to detect and quantify significant, monotonic long-term trends for 11 important indicators of water quality, habitat conditions, and carbon cycling for the 9-year (October 2007 through December 2016) data set produced by DCERP's. *P* values were adjusted to account for autocorrelation according to Hirsch and Slack (1984). When significant positive or negative long-term trends were determined, Sen slopes were calculated to quantify the average magnitude of change over each data record (Hirsch et al., 1982). Prior to analyses, each record was natural log transformed. Because the seasonal Kendall test is non-parametric, this transformation does not affect the detection of

statistically significant trends. However, because of the log transformation, all Sen slopes share the common unit (y^{-1}), which can facilitate a comparison of trend magnitudes between water quality parameters. A slope of approximately 0.7 y^{-1} is equivalent to a factor of 2 increase per year. For some parameters, a variable number of sample values fell below the method detection limit, and the detection limits for many of the parameters changed over the course of the study period. All left-censored values (i.e., below detection limit) were assigned the value of the maximum detection limit reported over the study period. Additionally, all non-censored values less than the maximum reported detection limit were assigned the value of the maximum detection limit (Hirsch et al., 1982).

Over the 9-year study period, salinity declined significantly at all stations, with the steepest declines occurring near the head of the estuary (**Table 6-5**). Chl *a* increased significantly at Stations 5 and 8. NO_3^- and total nitrogen displayed no significant trends, and NH_4^+ increased significantly only at Station 7. PO_4^{-3} increased significantly at all stations except for Stations 3 and 7 and generally showed stronger increases at upstream stations. Light availability decreased at most stations as indicated by increases in the attenuation coefficient for PAR. The strongest declines in light availability occurred at upstream stations, and only Stations 3 and 4 showed no trends in light availability. Despite increases in light attenuation, turbidity decreased at the upstream stations (6 through 8). No trends were detected for surface water DO, but bottom water oxygen decreased at Stations 7 and 8. No trends were observed for POC, but DOC increased significantly at mid-estuarine stations (3 through 5) and in the tributary mouth stations (6 and 8).

Table 6-5. Results from Seasonal Kendall Tests for Long-Term Trends in Important Indicators of Water Quality, Habitat Conditions, and Carbon Cycling Along the Main Channel of the NRE

Values shown are Sen slopes of natural log transformed, salinity corrected water quality parameters for cases when seasonal Kendal tests detected a significant (adjusted *p* value <0.05) monotonic trend over time. NS indicates the trend was "not significant." NA indicates that salinity correction is "not applicable" to salinity data. Data analyzed were from surface samples only, with the exception of bottom water dissolved oxygen (DO_{bott}). Because of log transformation, all slopes are in years (y^{-1}). K_{PAR}=vertical attenuation of photosynthetically active radiation; TN=total nitrogen. Data were collected during the DCERP project from October 2007 to December 2016 at eight main channel stations. Data analyzed were from surface samples only with the exception of bottom water dissolved oxygen (DO_{bott}). The lower set of "corrected" results have taken hydrological impacts into account by subtracting off a local regression (LOESS) of salinity from the parameter data.

Station	Salinity	Chl *a*	NO_3^-	NH_4^+	PO_4^{3-}	TN	K_{PAR}	Turbidity	DO_{surf}	DO_{bott}	POC	DOC
1	−0.011	NS	NS	NS	+0.107	NS	+0.040	NS	NS	NS	NS	NS
2	−0.020	NS	NS	NS	+0.056	NS	+0.039	NS	NS	NS	NS	NS
3	−0.041	NS	NS	NS	NS	NS	NS	NS	NS	NS	NS	+0.046
4	−0.052	NS	NS	NS	+0.066	NS	NS	NS	NS	NS	NS	+0.045
5	−0.058	+0.069	NS	NS	+0.086	NS	+0.056	NS	NS	NS	NS	+0.037
6	−0.071	NS	NS	NS	+0.080	NS	+0.050	−0.032	NS	NS	NS	+0.035
7	−0.076	NS	NS	+0.070	NS	NS	+0.051	−0.040	NS	−0.019	NS	NS
8	−0.078	+0.061	NS	NS	+0.075	NS	+0.066	−0.035	NS	−0.034	NS	+0.038
1 corrected	NA	NS	NS	NS	NS	NS	NS	NS	NS	NS	NS	NS
2 corrected	NA	NS	NS	NS	NS	NS	NS	NS	NS	NS	NS	NS
3 corrected	NA	NS	NS	NS	NS	NS	NS	NS	NS	NS	NS	NS
4 corrected	NA	NS	NS	NS	NS	NS	NS	NS	NS	NS	NS	NS
5 corrected	NA	NS	NS	NS	NS	NS	NS	NS	NS	NS	NS	NS
6 corrected	NA	NS	NS	NS	NS	NS	NS	−0.042	NS	NS	NS	NS
7 corrected	NA	NS	NS	NS	NS	NS	NS	−0.065	NS	NS	NS	NS
8 corrected	NA	NS	NS	NS	NS	NS	NS	−0.051	NS	NS	NS	NS

In an estuary that has long experienced symptoms of cultural eutrophication (Bricker et al., 1999; Mallin et al., 2005; Tomas et al., 2007), the observed increases in nutrients, phytoplankton, and organic carbon and declines in water clarity and DO are potentially emblematic of continued, anthropogenic degradation of water quality. However, water quality conditions in the NRE are tightly linked to freshwater inputs (Hall et al., 2013; Paerl et al., 2014; Peierls et al., 2012). Elevated freshwater discharge is accompanied by higher loads of nutrients that fuel phytoplankton biomass, sediments, DOC, CDOM that attenuate light and a greater degree of salinity-based vertical stratification that can lead to hypoxic bottom water conditions. As previously discussed and as evidenced by the strong decreasing trends in salinity, the DCERP project occurred during a period of naturally increasing precipitation and freshwater delivery to the estuary. Consequently, it is unclear from the previous analyses whether the results indicate human or climatically or hydrologically driven change.

The ability to correct for changes in freshwater delivery is critical for removing climatic variation to reveal human induced change (Beck and Hagy, 2015; Hirsch et al., 1982). Statistical removal of the impact of changing freshwater inputs was achieved by calculating the residuals of each water quality parameter (excluding salinity) from a local regression (LOESS) of concentration on salinity according to Aroner (2000) and Beck and Hagy (2015). **Figure 6-19** shows an example of how this process eliminated hydrologic influences on chl *a* concentrations at Station 5, where a significant increase in chl *a* occurred (**Table 6-5**, **Figure 6-20** top panel). After the relationship between salinity and chl *a* is removed, any remaining temporal trends are more likely because of anthropogenic influences rather than changing climatic or hydrologic conditions.

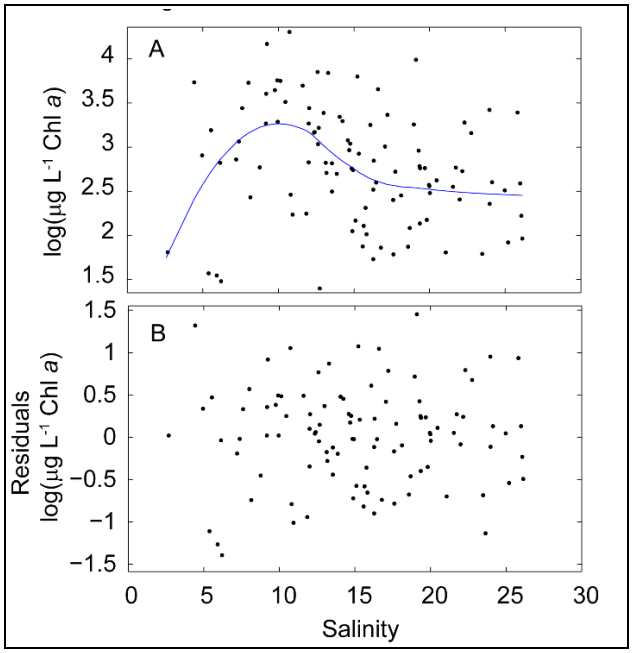

Figure 6-19. Example of method used to remove hydrological impacts on water quality before long-term trend analyses.

(A) The relationship between salinity and chlorophyll *a* (chl *a*) from Station 5 that shows the local regression (LOESS) curve (blue line) used to remove hydrological effects before the long-term trend analyses. (B) Residual chl *a* after subtraction of the LOESS against salinity.

As shown in the bottom panel of **Figure 6-20**, elimination of the hydrological impact of increased freshwater delivery resulted in the elimination of the observed, statistically significant trend in chl *a* at Station 5 (p=0.21). Similarly, most of the other previously detected significant trends were also eliminated after the removal of the hydrological influence of freshwater delivery. Only the decreasing trend in turbidity near the head of the estuary remained statistically significant, and these trends grew stronger. It appears most likely that the observed declining trends in water quality were primarily driven by the climatic impact of sampling through consecutive time periods of drought, moderate rainfall, and above average rainfall conditions during the 9-year DCERP study period. **These results underscore the dominant role of hydrology in determining water quality of the NRE**

and the necessity of taking hydrology into account when assessing human influences on trends in water quality, habitat conditions, and carbon cycling. Although the trends in these indicators of ecological condition were strongly linked to physical factors that are not under human control, this does not indicate a lack of anthropogenic effects on water quality. Anthropogenic effects such as the accumulated impact of changes in land use within the basin are likely to form a slower moving trend that may not be captured even within a robust 9-year study period.

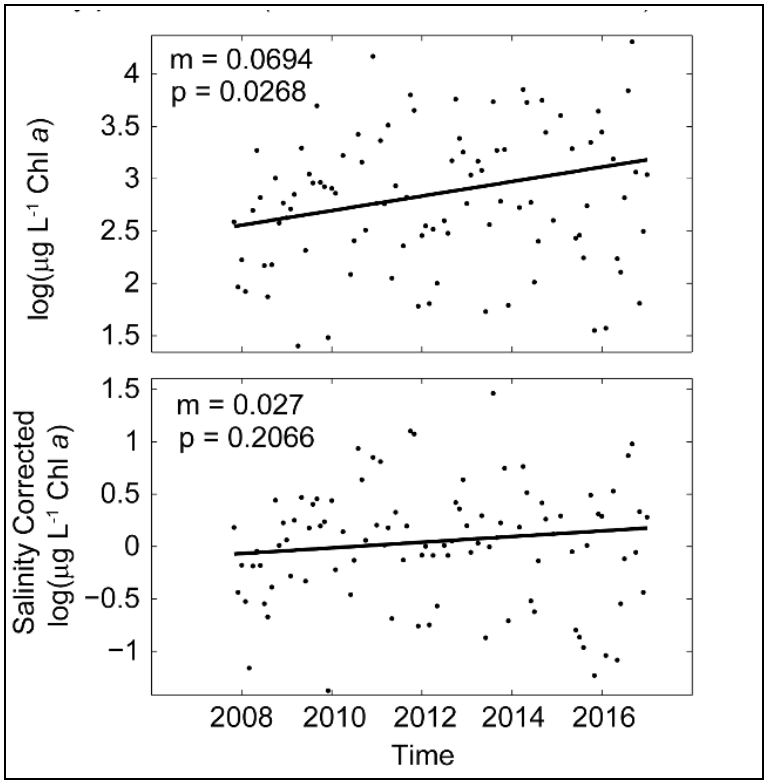

Figure 6-20. Example results of seasonal Kendall tests for long-term trend in chlorophyll *a* (chl *a*) data and salinity-corrected chl *a* data from Station 5.

The m-values are Sen slopes, and *p* values represent the probability of achieving as high a value of the Kendall test statistic when no true trend exists.

Before DCERP, approximately 10 years of NRE water quality data were collected by UNCW. DCERP's AEM main channel monitoring stations are co-located with six of the UNCW sampling stations. By combining DCERP's AEMP data with data collected from 1998 to 2007 by the UNCW, approximately 19, uninterrupted years of monthly water quality data have been collected at DCERP Stations 1, 2, 3, 4, 5, and 7. Extending the water quality record deeper into the past provides a greater possibility of detecting anthropogenic impacts on water quality. As with the DCERP data records, seasonal Kendal tests on log transformed, salinity-corrected values were used to detect and quantify the magnitude of long-term trends for a set of parameters that were measured by both monitoring programs. These parameters included surface and bottom water salinity and DO; surface water NO_3^-, NH_4^+, PO_4^{-3}, chl *a*, and turbidity; and the attenuation coefficient for PAR.

Unlike the shorter 9-year record under DCERP, there was no long-term trend in salinity within the longer term 19-year record. The most consistent trends throughout the 19-year period were marked increases in chl *a* and NH_4^+ at all stations and declines in turbidity (**Table 6-6**). These trends were statistically significant regardless of whether hydrological variability was removed from the records. PO_4^{-3} increased at Station 3 in the salinity corrected record, but NO_3^- showed no discernible trends. DO also decreased in the surface and bottom waters at middle and lower estuary stations, but removal of the influence of changing freshwater inputs eliminated significant declining trends in surface water DO. Decreasing light availability (increasing attenuation coefficient for photosynthetically active radiation [K_{PAR}]) was detected at Stations 2 and 7 in the salinity corrected records and at Station 2 in the uncorrected record.

Table 6-6. Results from Seasonal Kendall Tests for Long-Term Trends in Important Indicators of Water Quality and Habitat Conditions Along the Main Channel of the NRE from 1998 to 2016 Using the Combination of UNC Wilmington and DCERP Data Sets

Table configuration follows **Table 6-5**.

Station	Salinity	Chl *a*	NO_3^-	NH_4^+	PO_4^{3-}	K_{PAR}	DO_{surf}	DO_{bott}	Turbidity
1	NS	+0.066	NS	+0.058	NS	NS	NS	NS	–0.036
2	NS	+0.060	NS	+0.069	NS	+0.0107	NS	NS	–0.041
3	NS	+0.063	NS	+0.089	NS	NS	–0.0040	–0.0047	–0.046
4	NS	+0.056	NS	+0.075	NS	NS	–0.0047	–0.0089	–0.054
5	NS	+0.069	NS	+0.052	NS	NS	–0.0025	NS	–0.051
7	NS	+0.071	NS	+0.050	NS	NS	NS	NS	–0.050
$1_{corrected}$	NA	+0.061	NS	+0.056	NS	NS	NS	–0.0026	–0.032
$2_{corrected}$	NA	+0.058	NS	+0.063	NS	+0.0094	NS	NS	–0.038
$3_{corrected}$	NA	+0.057	NS	+0.093	+0.031	NS	NS	–0.0037	–0.042
$4_{corrected}$	NA	+0.059	NS	+0.082	NS	NS	NS	–0.0069	–0.046
$5_{corrected}$	NA	+0.061	NS	+0.055	NS	NS	NS	NS	–0.046
$7_{corrected}$	NA	+0.066	NS	+0.047	NS	+0.0072	NS	NS	–0.052

With the exception of decreasing turbidity, increases in chl *a*, NH_4^+, and light attenuation and decreases in bottom water oxygen levels are indicative of declining water quality and habitat conditions within the estuary over the past two decades. However, potential biases because of changes in sampling and analytical methodology between the two monitoring programs could also produce an apparent trend where none exists. For example, during the UNCW monitoring period, sampling was conducted on ebb tide (Mallin et al., 2005). Therefore, it might be expected that turbidity would be higher on average in the UNCW monitoring data because of sediment resuspension by tidal currents. Elevated turbidity during the first half of the combined record may produce a long-term declining trend in the 19-year data set. However, the decrease in turbidity at the upstream stations during the 9-year DCERP record suggests that the trend is probably a true reflection of a general decline of turbidity within the estuary.

It is also possible that the increase in chl *a* is because of a small change in methodology. During DCERP, GF/F filters containing retained phytoplankton cells were mechanically disrupted during the extraction process by using a tissue grinder in a pestle prior to steeping in 90% acetone solvent. During the UNCW monitoring period, filters were steeped in 90% acetone, but no mechanical disruption was used, which likely would result in a reduced extraction efficiency and lower values (Wasmund et al., 2006). To test the potential for this methodological bias to have produced the observed increasing trends in chl *a*, all of the chl *a* values were increased by the maximum loss of extraction efficiency (22%) because of the omission of mechanical disruption (Wasmund et al., 2006). Using this worst case approach, the magnitudes of the increasing slopes for chl *a* decreased from a station-wide average of 0.06 y^{-1} to 0.046 y^{-1}, but the trends were still statistically significant. Thus, it seems unlikely that the differences in extraction methodology could have produced an artifactual increasing trend in chl *a*. Although we could use additional information to gauge the validity of trends within this combined data record, it is impossible to determine with certainty how the changes in methodology may have impacted the

ability to detect and quantify long-term trends. Strict consistency of methods, including sampling, handling, laboratory analyses, equipment, and reporting, are optimal for producing long-term data sets. In such data sets, any observed trends can only be explained by conditions in the environment without the need to worry about possible effects of methodological artifacts.

Assessment of Monitoring Design

Spatial Resolution

Data collected from the Dataflow instrumentation provided high spatial resolution (approximately 10 m) data necessary to determine the dominant spatial distribution patterns of six key parameters related to water quality, habitat condition, and carbon cycling (temperature, salinity, DO, turbidity, chl *a*, and pCO_2). These data were used to determine the spatial distribution of variability of these parameters along the main axis of the estuary. This information was used to quantitatively assess the degree with which the down-stream spacing of the eight monitoring stations sampled monthly was capable of capturing the spatial variability of key water quality components.

Figure 6-21. A map showing the track lines of 81 Dataflow sampling transects in relation to the eight monitoring stations sampled monthly in the NRE.

From February 2009 through December 2016, 84 Dataflow transects were conducted on an approximate monthly basis. For one profile, data were lost because of instrument malfunction and some of the water quality parameters for two transects were impacted by an instrument malfunction and were eliminated from the subsequent analyses. The spatial coverage of the 81 transect lines are shown in **Figure 6-21**. During 16 of the 81 transects, the pCO_2 was measured in addition to the five key water quality parameters previously mentioned. Before analyses of the remaining 81 Dataflow transects, cross-river excursions and loops were removed to produce a single transect line along the main axis of the estuary. Latitude and longitude data were converted to distance (km) from the beginning of each transect. Linear interpolation was used to produce an evenly spaced data series with a 0.02 km (20 m) sampling interval. This interpolation resulted in only minor adjustments to data values because of the close proximity of the raw sample spacing (mean=15.3 m; SD=6.2 m) to the extrapolated interval. This transect was considered to represent the “true” variability of water quality within the NRE.

Figure 6-22 shows an example Dataflow transect data set collected on 4 November 2015 that has been formatted and interpolated as previously described. It is clear that the magnitude and

spatial scales of variability differ considerably among the six parameters. Temperature was near 20°C and showed almost no variability across the estuary. Salinity decreased smoothly from approximately 25 near the inlet to near 10 upstream. DO was fairly constant throughout the estuary, but showed some peaks and troughs with spatial scales on the order of a few kilometers. In contrast to these three rather smoothly varying parameters, turbidity and chl *a* displayed higher degrees of variability at smaller spatial scales with several peaks that were 1- to 2-km wide. The high chl *a* and high degree of spatial correlation between chl *a* and turbidity upstream of 15 km was caused by the bloom-level densities of two large dinoflagellates in the upper estuary (**Table 6-3**). In addition, pCO_2 varied little in the lower estuary, but exhibited both larger scale (2- to 4-km) peaks and smaller (less than 1-km) peaks in concentration in the upper area that was impacted by the dinoflagellate bloom.

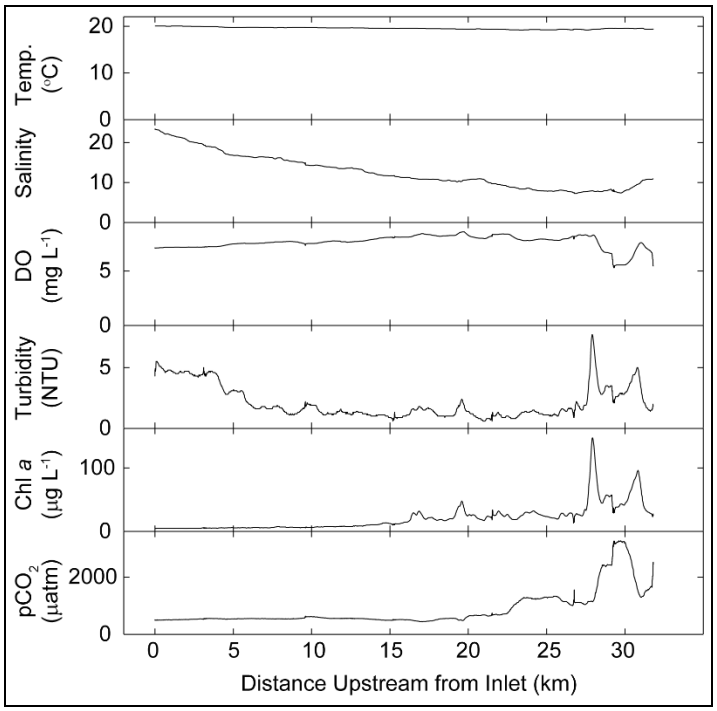

Figure 6-22. Dataflow transect data from 4 November 2015 that have been formatted for analyzing the effects of sampling at different spatial resolutions.

Assuming that the Dataflow sampler captures the vast majority of the variability in water quality along the axis of the estuary, we statistically determined the effects of increasing or decreasing the spatial sampling resolution on the percentage of water quality variability that is captured. The methodology employed is described in detail by Jassby et al. (1997). Data from the "true" transect were then resampled across a range of potential equidistant spatial sampling intervals from very coarse (tens of km) to very fine intervals (tens of m).

If the original "true" transect contained *N* data points, and the resampled transect contained *n* data points, then there are *m=N/n* possible resampled transects for each sampling interval. Cases in which *m* was not an integer value were handled by using circular systematic sampling whereby sampling was wrapped back to the beginning of the record (Jassby et al., 1997). For each transect, the means of the resampled data sets (y_k) were then compared with the "true" transect mean ($\bar{Y}$) to determine the influence of spatial sampling interval on precisely representing the "true" transect mean. This comparison was accomplished by calculating the variance of the estimated transect mean ($\bar{y}_{\text{sys}}$) as shown in Equation 6-1, where *k* represents individual resampled transects from 1 to *m*.

$$\text{var}(\bar{y}_{\text{sys}}) = \frac{1}{m}\sum_{k=1}^{m}(y_k - \bar{Y})^2 \qquad \text{(Eq. 6-1)}$$

In **Figure 6-23**, var($\bar{y}_{\mathrm{sys}}$) has been normalized by var($\bar{y}_{\mathrm{sys}}$) for the case when k=1, and the data points represent the mean values and SDs for the normalized var($\bar{y}_{\mathrm{sys}}$) from the complete set of Dataflow transects. As sample spacing decreases (equivalently, the sample number is increased), the resampled transects approach the "true" full transect (n=N) and the error in reproducing the "true" transect mean (variance of the transect mean) approaches zero. This methodology produces a set of exponential decay curves that provide an objective tool for: (1) estimating the number of equally spaced sampling stations necessary to provide a given level of precision in estimation of estuary-wide mean water quality conditions, and (2) comparing the spatial autocorrelation structure of water quality parameters, between transects, and between estuarine systems (Jassby et al., 1997). The slope of the decay functions describes the sensitivity of accurately depicting mean water quality conditions within the estuary to changes in sampling interval. As will be discussed in the section of this chapter that is titled Comparison of the Effectiveness of Temporal and Spatial Sampling Resolution During DCERP), this information is useful for evaluating how changes in either temporal or spatial sampling resolution will impact the ability of monitoring efforts to accurately and precisely represent mean estuarine water quality conditions.

These analyses of the spatial and temporal variabilities of water quality conditions involve only those values that can be measured rapidly and in situ to produce a very high resolution data set. These basic water quality parameters represent a small subset of the water quality parameters measured during the project period. However, given the strong relationships between these variables and other water quality parameters, it is likely that the underlying spatial and temporal structures of unassessed parameters are similar. For example, the structure of the variability of CDOM is likely to be similar to that of salinity because freshwater inputs are the dominant source of CDOM to the estuary. Similarly, the variance structure of nutrient concentrations is likely similar to those of salinity and chl *a* because freshwater inputs and phytoplankton uptake represent primary sources and sinks, respectively, of nutrients within the NRE.

For each water quality parameter, the number of equidistant samples required to precisely capture the "true" transect mean decreased rapidly from 32 km (one sample per transect) through approximately 8-km spacings (**Figure 6-23**). Below spacings of approximately 8 km, the rate of decline in the error started to asymptote toward zero. Differences in dominant modes of variability between water quality parameters determined the rate of decay of error in the mean estimate as sample number increased. Variations in salinity were generally smooth through space and, as a result, estimates of mean transect salinity with a relative variance of less than 10% could be made with a sampling interval of 8-km or approximately 4-km equidistant sampling stations within the estuary. At a 4-km interstation sampling interval, which is the approximate sampling interval for the monthly discrete sampling stations, the relative variance for salinity was consistently less than 5% for all 81 transects. Temperature, DO, turbidity, and chl *a* contained a higher degree of small-scale variability and a greater degree of variability in spatial structure between transects. For these parameters, an 8-km interstation interval resulted in approximately a 5% to 30% relative variance of the transect mean. At a 4-km spacing, the relative variance ranged from less than 5% to greater than 10%.

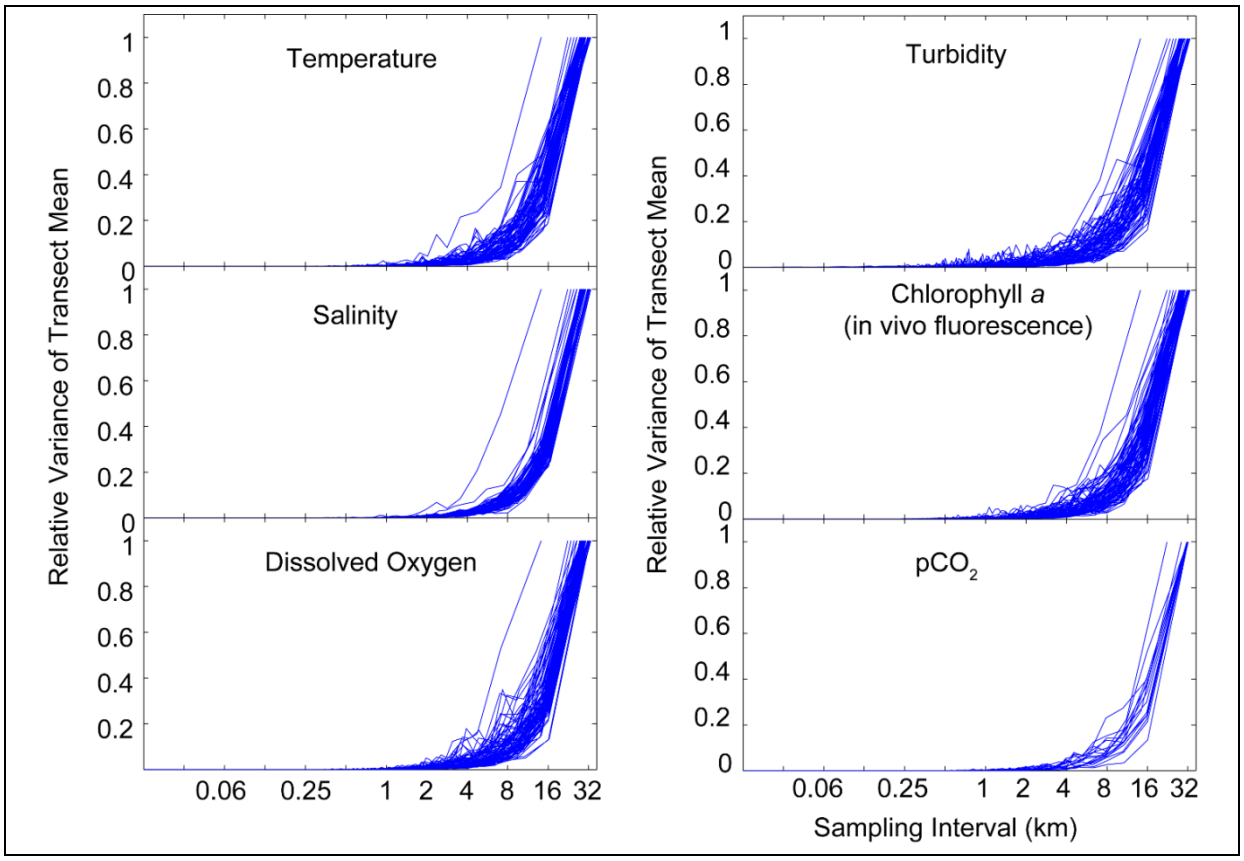

Figure 6-23. The influence of spatial sampling interval on the precision of estimates of the transect means for 81 Dataflow transects of temperature, salinity, dissolved oxygen, turbidity, chlorophyll *a*, and 16 transects of pCO_2.

Curves represent the variance of the transect means normalized by the variance with only one sample per transect (n=1).

Temporal Resolution

To assess the effectiveness of the temporal resolution of the monthly water quality monitoring program, data from the AVPs were similarly used to produce high temporal resolution time series of these key water quality parameters. For each parameter, data for each bihourly profile were averaged to produce a mean water column concentration. Missing data values were linearly interpolated from nearest stations. Each data set from the two AVPs was broken down into four, year-long records that ran from June to June from 2008 through 2012. As with the Dataflow records, annual means of these records were considered to represent "true" mean conditions within the NRE against which the means produced with increasingly large sampling intervals were compared. An analysis of these four separate annual records, rather than a combined analysis of the entire 4-year records, was performed to increase the confidence of estimates of how the variance of the record means changes with decreased temporal sampling resolution. Splitting the data into annual periods precludes an assessment of the impact of sampling intervals greater than 1 year. However, such a crude level of temporal resolution for estuarine monitoring is rarely considered.

The vast majority of variability in temperature lies in the annual cycle. As a result, the decay of temperature variance with increased sampling resolution is consistently very steep when sampling resolution increases from one sample per year to four samples per year (**Figure 6-24**). Bimonthly sampling (approximately 64-day sampling period) results in a relative variance for temperature of approximately 1%. Because DO is so closely tied to temperature through its solubility characteristics, it exhibited a similar consistent decay and bimonthly sampling resulted in a relative variance of less than 5%. Short-term variability was more important for salinity, turbidity, and chl *a*. However, even for these variables that are highly impacted by short-term effects, such as precipitation and nutrient loading events, tidal oscillations, and wind events, the relative variance of the annual mean decreased to approximately 5% at a monthly sampling period.

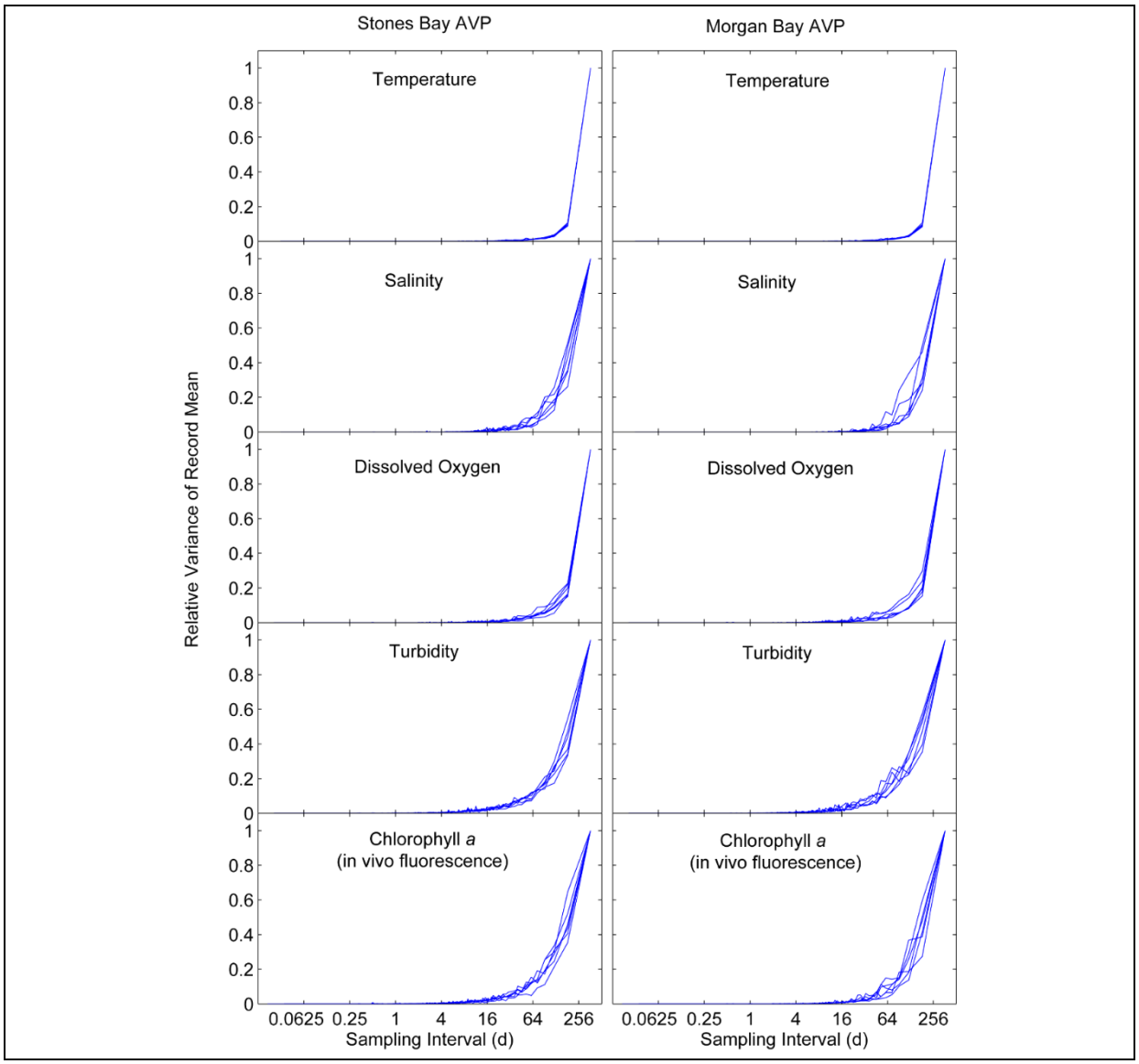

Figure 6-24. The influence of temporal sampling interval on the precision of estimates of the record means for six complete annual records from the AVPs at Stones and Morgan Bays.

Curves represent the variance of the transect means normalized by the variance with only one sample per annual record (*n*=1).

Figure 6-25 shows the standard error of estimated means for spatial (Dataflow) records across a range of potential spatial sampling intervals. Within a transect, variabilities in temperature and DO were relatively minor, and these resulted in a estimations with low standard errors less than 10% in transect means with the approximately 4-km sampling resolution employed by the routine monthly monitoring program. The spatial patchiness of turbidity and chl *a* and the strong downstream salinity gradient resulted in much higher (10–30%) standard errors for these variables at a 4-km sampling resolution. Chl *a*, in particular, demonstrated a high degree of small-scale patchiness. As a result, to consistently produce a standard error less than 10% would require a spatial sampling resolution of less than 0.25 km.

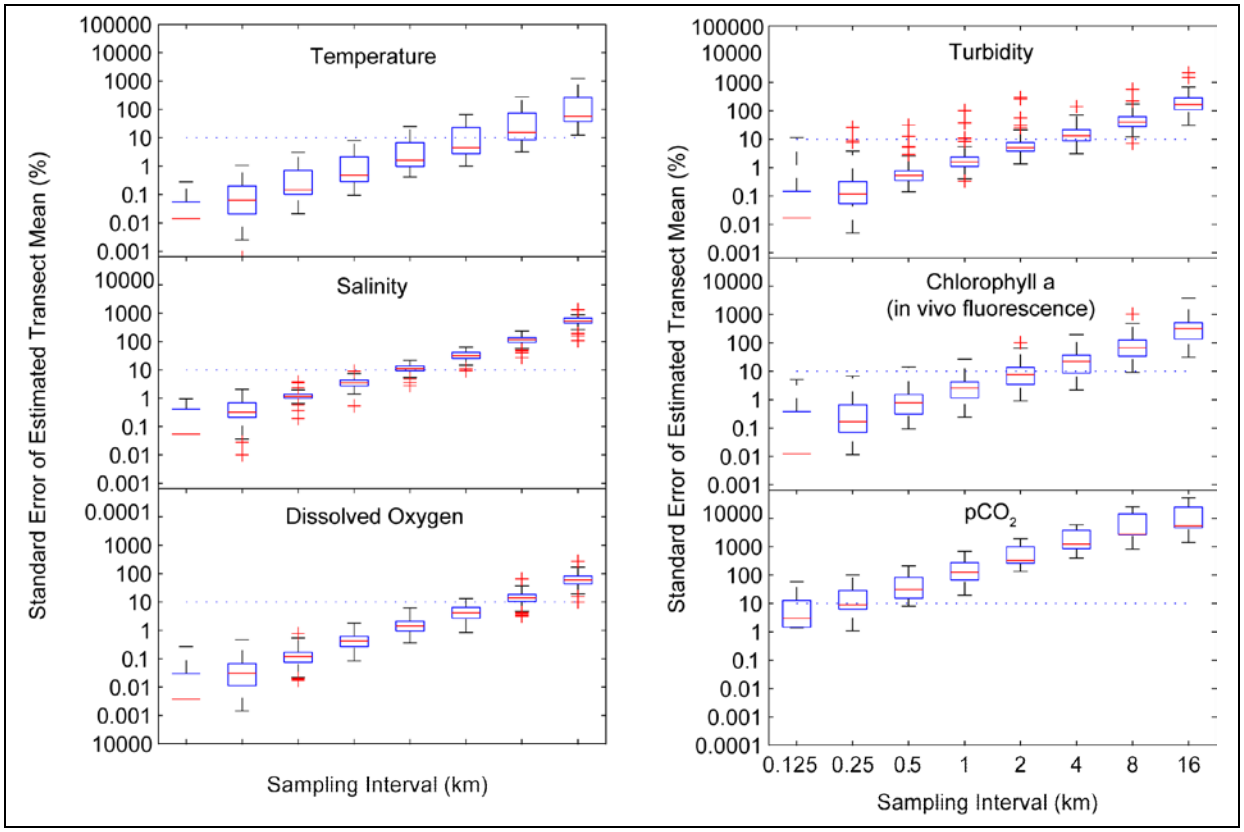

Figure 6-25. Box and whisker plots of the standard error of Dataflow transect means of key water quality parameters across a range of potential spatial sampling intervals.

Boxes represent the interquartile range for the standard errors of the 81 Dataflow transects for temperature, salinity, dissolved oxygen, turbidity, chlorophyll *a*, and 16 transects for pCO_2. Red horizontal lines are the median values. Whiskers represent 1.5 times the interquartile range. Values outside the whiskers are represented with red "+" symbols. Dashed lines indicate a standard error of 10%.

Figure 6-26 shows the standard error of estimated means for temporal records captured by the AVPs across a range of potential temporal sampling intervals. Compared with variability in standard errors among transects, variability in standard errors among years was much smaller as indicated by the tight interquartile ranges and lack of outliers within the box plots for the AVP records. The two AVP records also displayed very similar patterns of decline in standard errors

as temporal sampling interval increased. For both AVP records, standard errors for temperature and DO fell to approximately 10% with only quarterly sampling (90 day) as a result of strong seasonal components to their variability. Standard errors for salinity also decreased rapidly, with the Morgan Bay record having a standard error below 10% at a 90-day sampling. Standard error for the Stones Bay record did not fall to 10% at a 90-day sampling interval. This difference is likely because of the higher degree of short-term, tidal variability at Stones Bay as indicated by the greater drop in standard error from 1-day to 0.5-day sampling intervals. For both AVP records, chl *a* and turbidity had standard errors of between 10–30% at a quarterly sampling interval, but fell below 10% with monthly sampling.

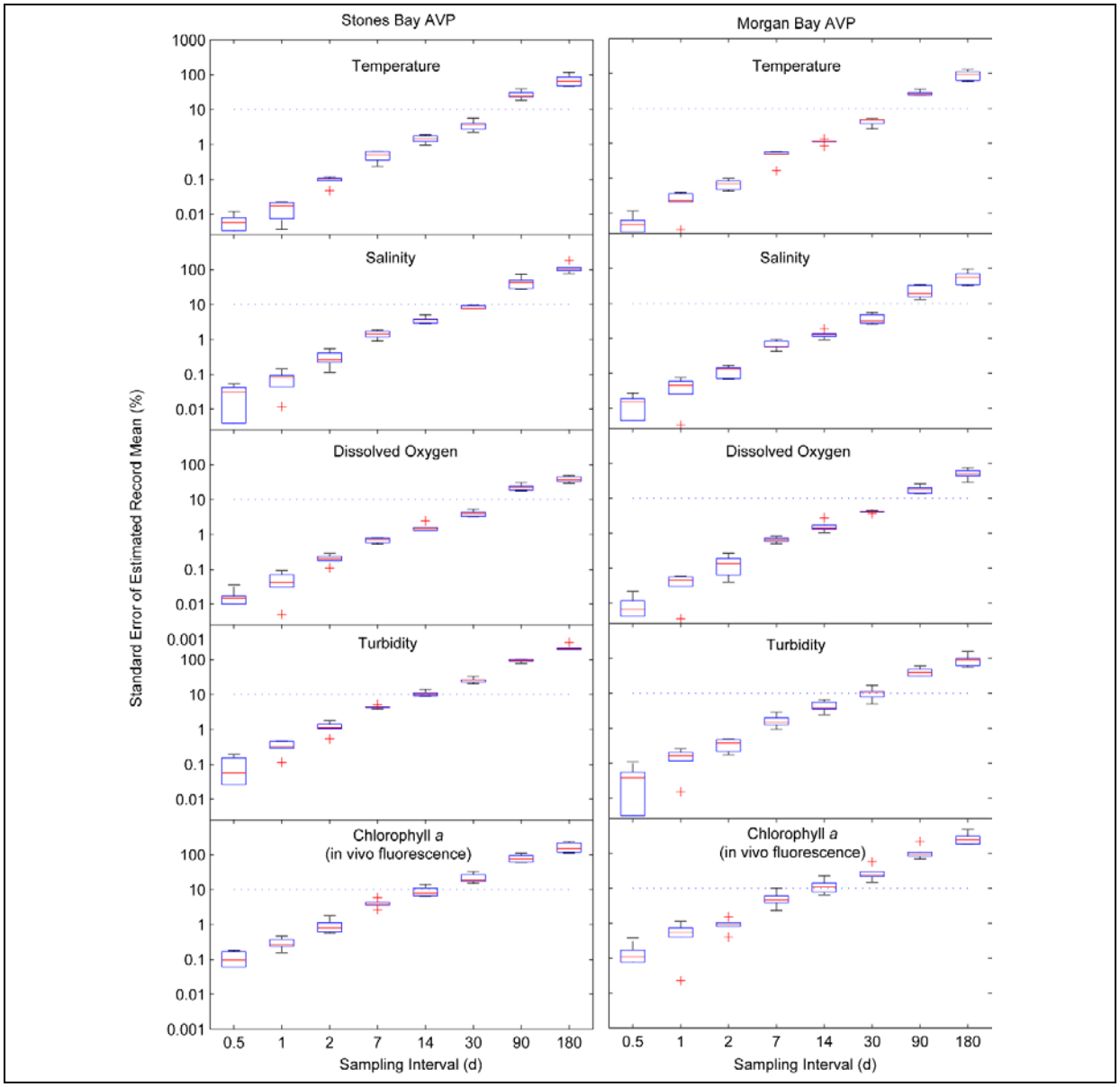

Figure 6-26. Box and whisker plots of the standard error of annual means across a range of potential temporal sampling intervals for water quality data produced by the AVPs at Stones Bay and Morgan Bay.

Figure configuration follows Figure 6-22.

Comparison of the Effectiveness of Temporal and Spatial Sampling Resolution During DCERP

To compare how changes in spatial or temporal sampling resolution would affect the monitoring program's ability to reproduce record means, slopes of the exponential decay of the variance of the record means were compared within the region of the decay curves (**Figures 6-23 and 6-24**) that approximated the sampling resolution of the monitoring program.

The exponential decay of variance of the record means as sampling interval decreases can be expressed as shown in Equation 6-2.

$$\mathrm{var}\left(\bar{y}_{\mathrm{sys}}\right) = \beta \frac{1}{n^{\propto}} \qquad \text{(Eq. 6-2)}$$

Where α is a coefficient that describes the rate of decay as sample number (*n*) increases and β is a proportionality constant (Jassby et al., 1997). Decay of the variance of the record means as shown in **Figures 6-23 and 6-24** were fit to this function by using a least-squares minimization procedure ("lsqcurvefit," MATLAB version R2010b, Natick, MA) to obtain estimates for α and β. The derivative of Equation 2 with respect to *n* is shown in Equation 6-3:

$$\frac{d\mathrm{var}\left(\bar{y}_{\mathrm{sys}}\right)}{dn} = \propto \beta n^{\propto - 1} \qquad \text{(Eq. 6-3)}$$

Using the best-fit parameters for α and β, we evaluated Equation 5-3 with *n* values that corresponded to the sampling intervals (approximately 4-km spatial, and approximately 30-day temporal) of the monthly monitoring program, the slope of the exponential decay provides a quantitative measure of the sensitivity of the variance of the mean to changes in spatial and temporal sampling interval from the current monitoring program design. These slope calculations allow for an objective means for determining how enhancing or reducing spatial or temporal monitoring efforts will affect the monitoring program's ability to accurately and precisely quantify the average condition of the estuary.

Figure 6-27 shows box plots of the slopes of the exponential decay of the variance of the mean evaluated at the sample number corresponding to the temporal and spatial resolution of the monthly monitoring program. Higher values indicate a greater sensitivity to change in the number of equidistant samples or equivalently sampling interval. Median values of the slopes of the exponential decay of variance were of the same order of magnitude at the spatial and temporal sampling resolution of the eight station, monthly monitoring program. Additionally, there was no consistent trend across variables in sensitivity to changes in spatial or temporal sampling interval. The similarity in slopes indicates that, in general, the spatial and temporal resolutions of the monitoring program were well balanced with respect to its ability to reproduce spatial and temporal averages of estuarine conditions. However, for a unit increase in sampling effort, better approximations for salinity could be gained by increasing spatial resolution, but the opposite is true for temperature. For turbidity and chl *a*, the impacts of changes in temporal resolution versus spatial resolution varied depending on which AVP record was examined. For Stones Bay, which is more prone to turbidity events driven by wind-induced resuspension and tidal advection of suspended sediments, increased temporal resolution would more effectively reduce error of mean estimates than increased spatial resolution. Similarly, at Morgan Bay,

which is prone to short-lived, but high biomass algal blooms, the estimation of mean chl *a* was more sensitive to changes in temporal sampling resolution.

Redundancy Analysis of Monthly Monitoring Stations

The previously mentioned analyses demonstrate that the current station spacing and monthly sampling frequency are nearly optimal for balancing temporal and spatial sampling efforts against the ability to reproduce a "true" transect mean. However, that does not mean that each of the eight stations that monitor monthly would contribute equally to capturing variability in key water quality parameters. It is possible that water quality conditions at some stations are so similar to another that monitoring those stations is essentially a duplicated and, therefore, a wasted effort.

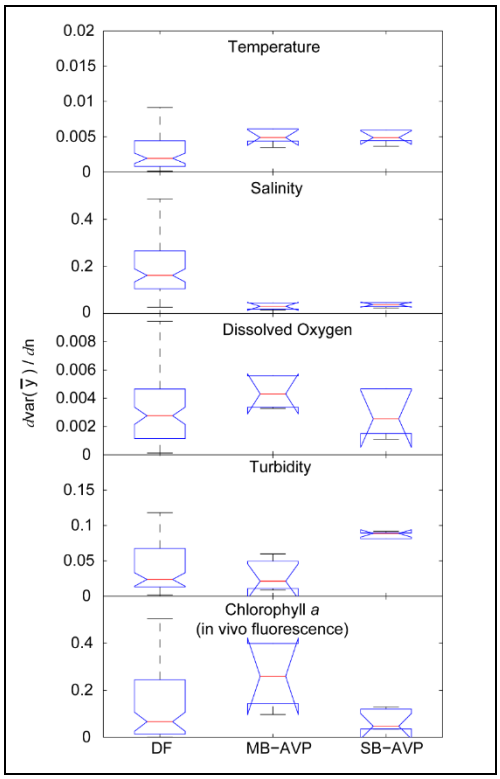

Figure 6-27. Box and whisker plots of the slopes of the exponential decay of the variance of the mean transect evaluated at 4-km spatial resolution for the Dataflow (DF) transects and at 30-day temporal resolution for the Morgan Bay (MB-AVP) and Stones Bay (SB-AVP) AVP annual records.

A comparison of data distributions among all possible pairs of the eight monitoring stations was used to examine potential redundancy of information provided by each station. A set of key eutrophication-related water quality parameters and indicators of general habitat condition was chosen for the analyses. These parameters were chl *a*, turbidity, TSS, DIN, PAR attenuation coefficient, total nitrogen, total phosphorus, dissolved inorganic phosphorus (PO_4^{-3}), bottom water DO, and salinity. For each parameter at each station, data were sorted and correlated with the sorted data from all other stations (i.e., a quantile–quantile regression). **Figure 6-28** shows quantile–quantile regressions for cases in which the two station pairs exhibit very similar and very different data distributions for chl *a*. In this case, it is clear that chl *a* at Stations 1 and 2 are much more similar than between Stations 3 and 6.

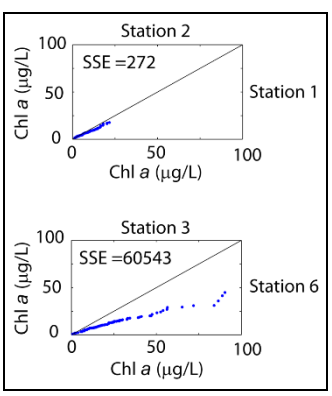

Figure 6-28. Quantile–quantile regression of chlorophyll *a* data from two pairs of stations within the eight station, monthly monitoring program.

Sum squared errors (SSEs) from these regressions provide an objective measure of the dissimilarity between the data distributions of each station pair. These quantile–quantile regressions were performed for all 28 possible station pairs and for each of the nine selected water quality parameters. For each parameter, dissimilarity was ranked based on the magnitude of the SSE of the quantile–quantile regression. **Figure 6-29** shows all of the quantile–quantile

regressions, SSEs, and dissimilarity rankings for chl *a*. Averages of these rankings across all nine selected water quality parameters were then used as objective criteria for determining the overall similarity of water quality conditions among stations (**Figure 6-30**). Station pairs with very low average rankings indicate a high degree of consistency in their water quality data distributions and suggest that one of the two stations may be removed from the monitoring program without significant loss of information.

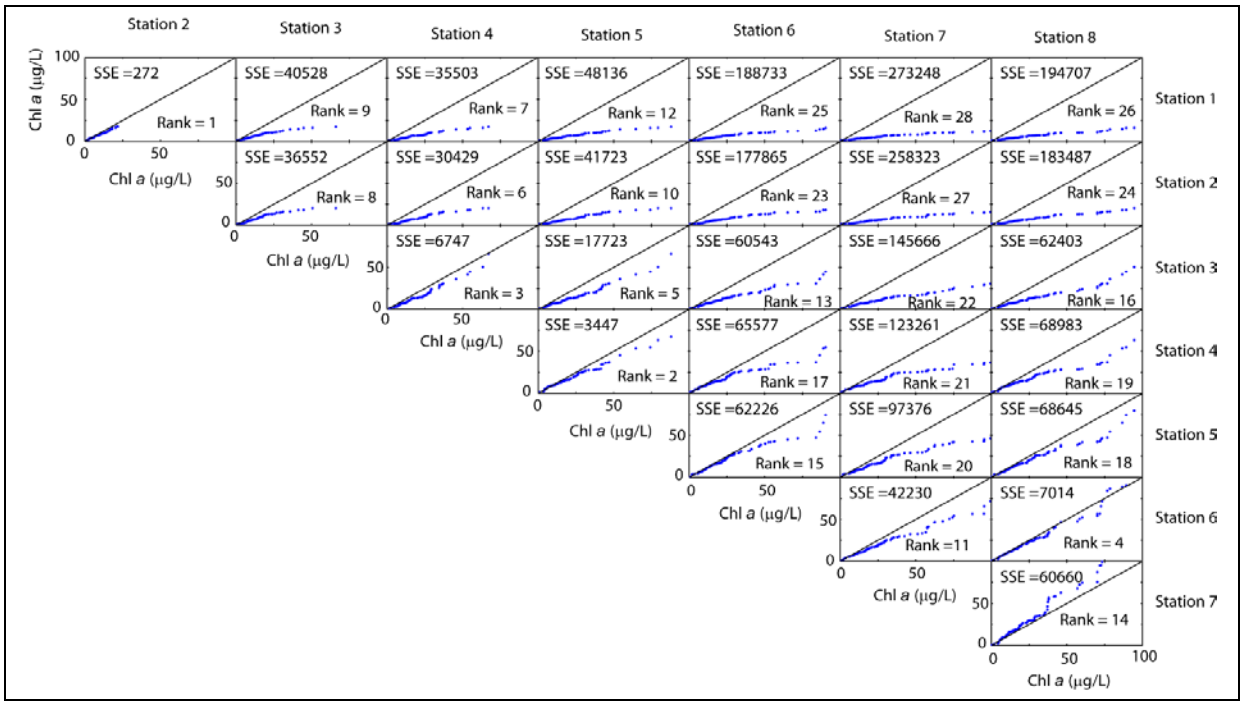

Figure 6-29. Quantile–quantile regression of chlorophyll *a* data from all possible pairs of stations with SSEs and dissimilarity rankings.

As expected, adjacent stations showed a greater degree of similarity in water quality conditions than those spaced farther apart along the estuary (**Figure 6-30**). Two station pairs showed the highest degree of similarity: Stations 1 and 2 nearest the inlet and Stations 4 and 5 within Farnell and Morgan Bays. Station 7 showed the greatest degree of dissimilarity with all stations. Based on these results, either Station 1 or 2 and either Station 4 or 5 could be removed from the monitoring program without significant loss of information about the condition of the estuary. More discussion about these options is provided in the section of this chapter that is titled Recommendations for Continued Monitoring.

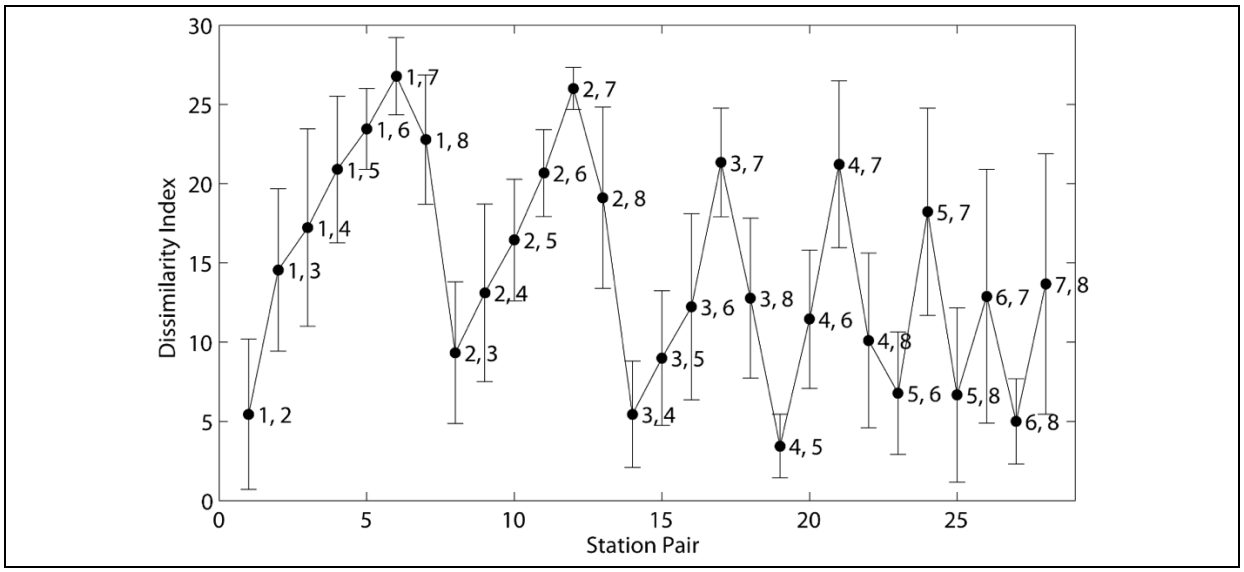

Figure 6-30. Average dissimilarity rankings for nine water quality parameters for each station pair within the eight stations monitored monthly.

Error bars are standard deviations from the mean ranking.

Recommendations for Continued Monitoring of the New River Estuary

Continued monitoring of the NRE will serve multiple purposes that will guide effective management of water quality and habitat conditions to ensure sustainable use of its natural resources. These purposes include the following:

- Assessing status and trends
- Detecting environmental and human health threats (e.g., toxic algal blooms)
- Determining cause–effect relationships
- Determining compliance with water quality standards
- Providing data for water quality and habitat model inputs (e.g., total maximum daily load [TMDL]).

The design of a cost-effective monitoring program that serves these purposes should consider four design features: the parameters or indicators to measure, appropriate temporal resolutions, appropriate spatial resolutions, and continuity with prior monitoring efforts. The following discussions in the remainder of this subsection address each of these design elements.

Parameters

Because eutrophication is the primary threat to the health and sustainability of the NRE, water quality parameters and indicators that track the causal factors (nutrient concentrations and loads), response factors (e.g., phytoplankton, DO, pH, turbidity), important physical drivers (river flow), and habitat conditions (temperature, salinity) should form the basis for continued monitoring. Within the set of parameters, it is critical to include parameters for which current State of North Carolina standards exist or are likely to exist in the future. Additionally, it is important to include

both particulate and dissolved forms of nutrients so that it is possible to determine the fraction of nutrient available for phytoplankton growth and the fraction already contained within biota. A list of recommended parameters for continued monitoring is provided in **Table 6-7**.

Table 6-7. Recommended Eutrophication and Habitat Condition Related Parameters for Continued Monitoring in the NRE

Parameter Categories	Recommended Parameters	Recommended Frequency
Causal	NO_3^-, NH_4^+, PO_4^{-3}, total nitrogen, total phosphorus, particulate nitrogen, dissolved organic nitrogen, and dissolved silicon	Monthly
Response	Chl *a*, accessory photopigments, DO, pH, turbidity, light attenuation, and Secchi disk	Monthly
Habitat	Temperature, salinity, TSS, and CDOM	Monthly
Physical	New River discharge	Continuous

The suite of nutrients listed in **Table 6-7** includes those forms that determine algal growth and biomass levels within the NRE. All forms of nitrogen are measured because the estuary is primarily nitrogen limited. Phytoplankton biomass is quantified via chl *a* and community composition is quantified via class level–specific accessory pigment. It is important to maintain monitoring of phytoplankton community composition because potentially harmful taxa are prevalent in the NRE, and because shifts in taxa can aid in understanding ecosystem responses to climatic and human induced ecosystem change. Multiple indicators pertaining to water clarity are recommended including turbidity, CDOM, TSS, light attenuation, and Secchi disk depth are recommended because it is important to understand what optically active constituents are responsible for any observed changes in light availability within the estuary. A full set of parameters quantifying the nutrient, light, and phytoplankton fields will greatly enhance any future modeling efforts (e.g., in the event of TMDL development). As response variables for eutrophication, DO, pH, and chl *a* are parameters with North Carolina water quality standards and are therefore important to measure for assessing compliance. These recommended parameters also include all of the parameters that were collected before DCERP by UNCW and therefore will maintain a long-term continuous record for many of these critical water quality parameters. New River discharge data are invaluable for understanding water quality in the NRE, and continued operation by the USGS of the stream gaging station at Gum Branch should be a high priority for MCBCL, the City of Jacksonville, and Onslow County.

Temporal and Spatial Resolution

Analyses of the AEM-1 data have shown that the current station spacing and monthly sampling frequency are nearly optimal for balancing sampling effort against the ability to reproduce a “true” transect mean. Additionally, the current sampling regime has the advantage of data continuity with previous monitoring data because UNCW sampled most of the same stations and also at monthly resolution. Based on the redundancy analysis, Station 2 is highly redundant of Station 1, and Station 4 is highly redundant of Station 5. Both Stations 2 and 4 could be eliminated without significant loss of information regarding the distribution of water quality data throughout the estuary. However, MCBCL staff pointed out that Station 4 is located near the outfall from MCBCL’s sewage treatment plant and that retaining Station 4 would help meet

NPDES monitoring requirements. Given this information, it is recommended to remove Station 2 from the current monitoring program. Maintaining Station 1 is important for providing a downstream boundary condition for any future modeling efforts, and Station 5 is representative of Morgan Bay, which represents a large fraction of the surface area of the NRE.

Continuity

Ideally, the station locations, sampling intervals, and field and laboratory methodologies for sample measurements would remain consistent through time. This greatly facilitates the determination of long-term trends in estuarine conditions by eliminating potential sampling and analytical biases. However, the goals of the monitoring program will change after DCERP, likely creating different priorities for sampling. A major goal of DCERP was to support the Aquatic/Estuarine Module research projects that required a clear understanding of the vertical gradients of water quality conditions within the estuary. Consequently, discrete samples were collected from the surface and bottom of the water column. After DCERP, the monitoring program will shift its focus to supporting compliance assessment and long-term trend detection. As such, it would be prudent to adopt sampling methodologies that are consistent with the ongoing routine monitoring conducted by NCDEQ's Ambient Monitoring System (AMS). Adopting consistent sampling methodologies involves a depth-integrated sample of the euphotic zone and would obviate the need to collect two discrete samples at each station. Integrated photic zone sampling would result in substantial cost reduction to the monitoring program, but may result in some biases when comparing previously collected data. If this change in methods is made, it is highly recommended to conduct a comparison of the two sampling methods to determine whether a bias is created and if so, to determine an appropriate correction factor to eliminate the bias for any long-term trend analyses.

Conclusions and Implications for Future Research and Implementation

Key Findings

A primary goal of this monitoring project was to determine how natural and anthropogenic stressors impact water quality and habitat condition of the NRE and, when possible, to identify stressors that are readily manageable from those that are not. Nutrient concentrations, chl *a*, turbidity, and DO are common indicators of estuarine water quality that are used to establish ratings of overall estuarine health and habitat condition (U.S. EPA, 2012). Regarding these indicators, a common theme emerged from the analysis of this comprehensive 9-year data set: natural processes such as riverine discharge, temperature, wind stress, stratification, and tidal currents exhibited the strongest and most direct linkages with water quality and habitat condition.

Bottom water hypoxia was closely linked with temperature and stratification, with no clear relationships to algal blooms, which might have resulted from anthropogenic nutrient loading. Periods of high algal biomass were linked with optimal levels of river flow which provided enough nutrients for phytoplankton biomass development, but also sufficient residence time within the estuary for growth to occur. During periods when flows were too high for phytoplankton biomass development, nutrient concentrations within the estuary were high. Thus, nutrient concentrations within the estuary were also largely determined by riverine discharge.

Additionally, long-term trends in nutrient loads and phytoplankton biomass were determined primarily by long-term patterns in river flow.

Although the short-term variability in these indicators of ecological condition were strongly linked to physical factors that are not under human control, this does not indicate a lack of anthropogenic effects on water quality. The significant increase in nitrogen concentrations below the Lauradale WWTP provides a clear example of how human activities are enhancing nutrient loading to the estuary. Additionally, acute anthropogenic events such as sewage spills or upgrades to sewage treatment facilities have had readily observable impacts on water quality within the NRE (Mallin et al., 2005). However, these types of acute anthropogenic events did not occur during the 9-year study period. Rather than not having an impact, the human impacts on the NRE simply did not change appreciably over the 9-year study period and thus were not strongly reflected in the observed variability of water quality within the estuary during DCERP.

Anthropogenic effects such as the accumulated impact of changes in land use within the basin are likely to form a slower moving trend that are difficult to detect over short study periods, but are more likely to be detected with long-term multi-decade records. When DCERP data were combined with previous data collected by UNCW researchers, long-term trends in water quality became evident. Increasing trends in chl *a* and NH_4^+, as well as decreases in bottom water DO concentrations and water clarity, indicated a general pattern of declining water quality associated with cultural eutrophication of the NRE. It is unclear what might have caused the observed decreases in turbidity and whether this trend is related to the general pattern of increasing trophic status. It is also impossible to determine with certainty that these trends are not because of slight differences in methodology between the two monitoring programs. However, it seems unlikely that any potential sampling biases would systematically and artificially produce eutrophication-like trends in four key water quality parameters. The ability to determine long-term trends with a high degree of certainty is greatly facilitated by maintaining uninterrupted long-term monitoring with consistent sampling and laboratory analytical methodologies.

Findings with Implications for Base Management

High levels of nutrient loading to the estuary is a primary concern for water quality and habitat condition. Downstream gradients of nutrient concentrations along the river to upper estuary indicate that most of the nutrient load to the estuary is from riverine sources that lie upstream of MCBCL. Consequently, managing water quality within the estuary will require a watershed-level approach to reduce nutrient loads with significant cooperation between MCBCL, Onslow County, the City of Jacksonville, and smaller municipalities.

Under all but the highest river flow conditions, residence times of the NRE are long enough that phytoplankton have time to fully assimilate nutrient loads. The result is that within much of the estuary, including most of the region surrounded by MCBCL, phytoplankton growth is strongly nutrient limited and any increases in nutrient load would result in higher levels of phytoplankton biomass. The region downstream of the Highway 172 Bridge appears less susceptible to eutrophication due to strong tidal flushing. The poorly flushed regions from Stones Bay upstream to Jacksonville are particularly susceptible to eutrophication. As MCBCL plans future land development and infrastructure projects in areas that drain to this region of the estuary, mitigation of nutrient loading to this region of the estuary should be emphasized. Any

enhancement of point source loads (i.e., WWTP effluent) should consider siting the discharge point downstream of the Highway 172 Bridge.

Compared with loading from upstream sources, the comparatively low load of nutrients, sediments, and other pollutants from the land area comprising MCBCL likely stems from the large areas of undeveloped forest and wetlands within the Base. Future development of these areas would likely enhance non-point source pollution because of land-use change and increases in impervious surface area. Effective strategies for mitigating non-point source impacts on water quality from future Base development could include minimizing sediment losses by maintaining natural vegetation and ground cover particularly within riparian areas, (2) minimizing impervious surfaces (e.g., parking lots, pave lots), (3) minimizing the use of chemical fertilizers in residential areas (e.g., lawns, gardens, golf courses), and (4) promoting retention of water within tributary watersheds by preserving and reclaiming wetlands, using retention ponds, minimizing ditching, and controlling stormwater runoff in developed areas.

Literature Cited

Alber, M., and J.E. Sheldon. 1999. Use of a date-specific method to examine variability in the flushing times of Georgia estuaries. *Estuarine, Coastal and Shelf Science 49*:469–482.

Altman, J.C., and H.W. Paerl. 2012. Composition of inorganic and organic nutrient sources influences phytoplankton community structure in the New River Estuary, North Carolina. *Aquatic Ecology 42*:269–282.

Anderson, D.M., and K.D. Stolzenbach. 1985. Selective retention of two dinoflagellates in a well-mixed estuarine embayment: The importance of diel vertical migration and surface avoidance. *Marine Ecology Progress Series 25*:39–50.

APHA (American Public Health Association). 1998. *Standard Methods for the Examination of Water and Wastewater*. American Public Health Association, Washington, DC.

Aroner, E.R. 2000. *Water Quality/Hydrology Graphics/Analysis System. User's Manual.* WQHYDRO Consulting, Portland, OR.

Beck, M.W., and J.D. Hagy III. 2015. Adaptation of a weighted regression approach to evaluate water quality trends in an estuary. *Environmental Modeling & Assessment 20*(6):637–655. doi: 10.1007/s10666-015-9452-8

Boesch, D.F., E. Burreson, W. Dennison, E. Houde, M. Kemp, V. Kennedy, R. Newell, K. Paynter, R. Orth, and W. Ulanowicz. 2001. Factors in the decline of coastal ecosystems. *Science 293*:629–638.

Boynton, W.R., and W.M. Kemp. 1985. Nutrient regeneration and oxygen-consumption by sediments along an estuarine salinity gradient. *Marine Ecology Progress Series 23*:45–55.

Bricker, S.B., C.G. Clement, D.E. Pirhalla, S.P. Orlando, and D.R.G. Farrow. 1999. *National Estuarine Eutrophication Assessment: Effects of Nutrient Enrichment in the Nation's*

Estuaries. National Oceanic and Atmospheric Administration, National Ocean Service, Special Projects Office and the National Centers for Coastal Ocean Science, Silver Spring, MD. 71 pages.

Buzzelli, C.P., R.A. Luettich, S.P. Powers, C.H. Peterson, J.E. McNinch, J.L. Pinckney, and H.W. Paerl. 2002. Estimating the spatial extent of bottom-water hypoxia and habitat degradation in a shallow estuary. *Marine Ecology Progress Series 230*:103–112.

Cloern, J.E. 2001. Our evolving conceptual model of the coastal eutrophication problem. *Marine Ecology Progress Series 210*:223–253.

Cloern, J.E. 1999. The relative importance of light and nutrient limitation of phytoplankton growth: A simple index of coastal ecosystem sensitivity to nutrient enrichment. *Aquatic Ecology 33*:3–16.

Cloern, J.E., and A.D. Jassby. 2010. Patterns and scales of phytoplankton variability in estuarine-coastal ecosystems. *Estuaries and Coasts 33*:230–241.

Crosswell, J.R., M.S. Wetz, B. Hales, and H.W. Paerl. 2012. Air–water CO_2 fluxes in the microtidal Neuse River Estuary, North Carolina. *Journal of Geophysical Research 117*:C08017. doi:10.1029/2012JC007925

Dafner, E.V., M.A. Mallin, J.J. Souza, H.A. Wells, and D.C. Parsons. 2007. Nitrogen and phosphorus species in the coastal and shelf waters of Southeastern North Carolina, Mid-Atlantic U.S. coast. *Marine Chemistry 103*:289–303.

Day, J.W., and W.M. Kemp (Eds.). 1989. *Estuarine Ecology*. Wiley Interscience: New York, NY.

Emery, W.J., and R.E. Thomson. 1997. *Data Analysis Methods in Physical Oceanography*. Elsevier Science Inc.: New York, NY.

Ensign, S.H., J.N. Halls, and M.A. Mallin. 2004. Application of digital bathymetry data in an analysis of flushing times of two North Carolina estuaries. *Computers and Geosciences 30*:501–511.

Fisher, T.R., L.W. Harding, D.W. Stanley, and L.G. Ward. 1988. Phytoplankton, nutrients, and turbidity in the Chesapeake, Delaware, and Hudson estuaries. *Estuarine Coastal and Shelf Science 27*:61–93.

Hall, N.S, A.C. Whipple, and H.W. Paerl. 2015. Vertical spatio-temporal patterns of phytoplankton due to migration behaviors in two shallow, microtidal estuaries: Influence on phytoplankton function and structure. *Estuarine, Coastal and Shelf Science 162*:7–21.

Hall, N.S., H.W. Paerl, B.L. Peierls, A.C. Whipple, and K.L. Rossignol. 2013. Effects of climatic variability on phytoplankton biomass and community structure in the eutrophic, microtidal, New River Estuary, North Carolina, USA. *Estuarine and Coastal Shelf Science 117*:70–82. doi: http://dx.doi.org/10.1016/j.ecss.2012.10.004

Hirsch, R.M., and J.R. Slack. 1984. A non-parametric test for seasonal data with serial dependence. *Water Resources Research 20*:727–732.

Hirsch, R.M., J.R. Slack, and R.A. Smith. 1982. Techniques of trend analysis for monthly water quality data. *Water Resources Research 18*:107–121.

Hobbie, J.E. (Ed.). 2000. *Estuarine Sciences—A Synthetic Approach to Research and Practice*. Island Press: Washington, DC.

Jassby, A.D., B.E. Cole, and J.E. Cloern. 1997. The design of sampling transects for characterizing water quality in estuaries. *Estuarine Coastal and Shelf Science 45*:285–302.

Kennish M., and H.W. Paerl. 2010. *Coastal Lagoons: Critical Habitats of Environmental Change*. CRC Marine Science Series. CRC Press: Boca Raton, FL.

Litaker, R.W., C.S. Duke, B.E. Kenney, and J. Ramus. 1987. Short-term variability and phytoplankton abundances in a shallow tidal estuary. I. Winter and summer. *Marine Biology 96*:115–121.

Lucas, L.V., J.K. Thompson, and L.R. Brown. 2009. Why are diverse relationships observed between phytoplankton biomass and transport time? *Limnology and Oceanography 54*: 381–390.

Lunetta, R.S., J.F. Knight, H.W. Paerl, J.J. Streicher, B.L. Peierls, T. Gallo, J.G. Lyon, T.H. Mace, and C.P. Buzzelli. 2009. Measurements of water colour using AVIRIS imagery to assess the potential for an operational monitoring capability in the Pamlico Sound Estuary, USA. *International Journal of Remote Sensing 30*:3291–3314.

Madden, C.J., and J.W. Day. 1992. An instrument system for high-speed mapping of chlorophyll *a* and physiochemical variables in surface waters. *Estuaries 15*:421–427.

Mallin, M.A., and H.W. Paerl. 1992. Effects of variable irradiance on phytoplankton productivity in shallow estuaries. *Limnology and Oceanography 37*:54–62.

Mallin, M.A., M.R. McIver, H.A. Wells, D.C. Parsons, and V.L. Johnson. 2005. Reversal of eutrophication following sewage treatment upgrades in the New River Estuary, North Carolina. *Estuaries 28*:750–760.

Malone, T.C., A. Malej, L.W. Harding Jr., N. Smodlaka, and R.E. Turner (Eds.). 1999. Coastal and estuarine studies. *Ecosystems at the Land-Sea Margin: Drainage Basin to Coastal Sea (Volume 55*). American Geophysical Union: Washington, DC.

Malone, T.C., L.H. Crocker, S.E. Pike, and B.W. Wendler. 1988. Influences of river flow on the dynamics of phytoplankton production in a partially stratified estuary. *Marine Ecology Progress Series 48*:235–249.

Monsen, N.E., J.E. Cloern, L.V. Lucas, S.G. Monismith. 2002. A comment on the use of flushing time, residence time, and age as transport time scales. *Limnology and Oceanography 47*:1545–1553.

Nixon, S.W. 1995. Coastal marine eutrophication: A definition, social causes, and future concerns. *Ophelia 41*:199–219.

NCDENR (North Carolina Department of Environment and Natural Resources). 2007. *White Oak River Basin Wide Water Quality Plan*. North Carolina Department of Environment and Natural Resources, Division of Water Quality, Planning Section, Raleigh, NC. May.

NCDEQ (North Carolina Department of Environmental Quality). *Online Fish Kill Events Database*. Available at https://deq.nc.gov/about/divisions/water-resources/water-resources-data/water-sciences-home-page/nc-fish-kill-activity

Osburn, C.L., L.T. Handsel, M.P. Mikan, H.W. Paerl, and M.T. Montgomery. 2012. Fluorescence tracking of dissolved and particular organic matter in a river-dominated estuary. *Environmental Science & Technology 46*:8628–8636.

Paerl, H.W. 2002. Primary productivity and producers. Pp. 329–341 in *Manual of Environmental Microbiology (2nd edition)*. Edited by C.J. Hurst. ASM Press: Washington, DC.

Paerl, H.W. 1997. Coastal eutrophication and harmful algal blooms: Importance of atmospheric deposition and groundwaters as “new” nitrogen and other nutrient sources. *Limnology and Oceanography 42*:1154–1165.

Peierls, B.L., and H.W. Paerl. 2011. Longitudinal and depth variation of bacterioplankton productivity and related factors in a temperate estuary. *Estuarine and Coastal Shelf Science 95*:207–215.

Paerl, H.W., N.S. Hall, B.L. Peierls, and KL. Rossignol. 2014. Evolving paradigms and challenges in estuarine and coastal eutrophication dynamics in a culturally and climatically stressed world. *Estuaries and Coasts 37(2)*:243–258.

Paerl, H.W., K.L. Rossignol, N S. Hall, B.L. Peierls, and M.S. Wetz. 2010. Phytoplankton community indicators of short- and long-term ecological change in the anthropogenically and climatically impacted Neuse River Estuary, North Carolina, USA. *Estuaries and Coasts 33*:485–497.

Paerl, H.W., J.D. Bales, L.W. Ausley, C.P. Buzzilli, L.B. Crowder, L.A. Eby, J.M. Fear, M. Go, B.J. Peierls, T.L. Richardson, and J.S. Ramus. 2001. Ecosystem impacts of three sequential hurricanes (Dennis, Floyd, and Irene) on the United States’ largest lagoonal estuary, Pamlico Sound, NC. *Proceedings of the National Academy of Sciences 98*(10):5655–5660.

Paerl, H.W., M.A. Mallin, C.A. Donahue, M. Go, and B.L. Peierls. 1995. *Nitrogen Loading Sources and Eutrophication of the Neuse River Estuary, NC: Direct and Indirect Roles of*

Atmospheric Deposition. University of North Carolina Water Resources Research Institute Report No. 291. 119 pages.

Peierls, B.L., N.S. Hall, and H.W. Paerl. 2012. Non-monotonic responses of phytoplankton biomass accumulation to hydrologic variability: A comparison of two coastal plain North Carolina estuaries. *Estuaries and Coasts 35*(6):1376–1392.

Reynolds-Fleming, J.V., F.G. Fleming, and R.A. Luettich. 2002. Portable autonomous vertical profiler for estuarine applications. *Estuaries 25*(1):142–147.

Sanger, D.M., E.M. Smith, G. Voulgaris, E.T. Koepfler, S.M. Libes, G.H.M. Riekerk, D.C. Bergquist, D.I. Greenfield, P.A. Wren, C.A. McCoy, R.F. Viso, R.N. Peterson, and J.D. Whitaker. 2011. Constrained enrichment contributes to hypoxia formation in Long Bay, South Carolina (USA), an open water urbanized coastline. *Marine Ecology Progress Series 461*:15–30.

Seliger, H.H., J.H. Carpenter, M. Loftus, and W.D. McElroy. 1970. Mechanisms for accumulation of high concentrations of dinoflagellates in a bioluminescent bay. *Limnology and Oceanography 15*:234–245.

Sheldon, J.E., and M. Alber. 2006. The calculation of estuarine turnover times using freshwater fraction and tidal prism models: A critical evaluation. *Estuaries and Coasts 29*:133–146.

Tomas, C.R., J. Peterson, and A.O. Tatters. 2007. *Harmful Algal Species from Wilson Bay, New River, North Carolina: Composition, Nutrient Bioassay and HPLC Pigment Analyses*. North Carolina Water Resources Research Institute Report No. 369. 31 pages.

Vervollkommnung der Quantitativen Phytoplankton-Methodik. *Internationale Verhandlung für Theoretische und Angewandte Limnologie 9*:1–38.

U.S. EPA (U.S. Environmental Protection Agency). 2012. *National Estuary Program Coastal Condition Report IV*. Report number EPA-842-R-10-003. U.S. Environmental Protection Agency, Washington, DC. April.

Valiela, I., G. Collins, J. Kremer, K. Lajtha, M. Geist, B. Seely, J. Brawley, and C.H. Sham. 1997. Nitrogen loading from coastal watersheds to receiving estuaries: New method and application. *Ecological Applications 7*:358–380.

Von Korff, B.H., M.F. Piehler, and S.H. Ensign. 2014. Comparison of denitrification between river channels and their adjoining tidal freshwater wetlands. *Wetlands 34*:1047–1060.

Wasmund, N., I. Topp, and D. Schories. 2006. Optimising the storage and extraction of chlorophyll samples. *Oceanologia 48*:125–144.

Wetz, M.S., E.A. Hutchinson, R.S. Lunetta, H.W. Paerl, and J.C. Taylor. 2011. Severe droughts reduce estuarine primary productivity with cascading effects on higher trophic levels. *Limnology and Oceanography 56*:627–638.

Appendix 6-A
List of Scientific/Technical Publications

Peer Reviewed Papers

Paerl, H.W., N.S. Hall, B.L. Peierls, K.L. Rossignol, and A.R. Joyner 2013. Hydrologic variability and its control of phytoplankton community structure and function in two shallow, coastal, lagoonal ecosystems: The Neuse and New River Estuaries, North Carolina, USA. *Estuaries and Coasts 37*(Supp 1):31–45. doi: 10.1007/s12237-013-9686-0

Paerl, H.W., N.S. Hall, B.L. Peierls, and KL. Rossignol. 2014. Evolving paradigms and challenges in estuarine and coastal eutrophication dynamics in a culturally and climatically stressed world. *Estuaries and Coasts 37(2)*:243–258.

Crosswell, J.R., M.S. Wetz, B. Hales, and H.W. Paerl. 2014. Extensive CO_2 emissions from shallow coastal waters during passage of Hurricane Irene (August 2011) over the Mid-Atlantic Coast of the USA. *Limnology and Oceanography 59*:1651–1665.

Paerl, H. W., J.T. Scott, M.J. McCarthy, S.E. Newell, W.S. Gardner, K.E. Havens, D.K. Hoffman, S.W. Wilhelm, and W.A. Wurtsbaugh. 2016. It takes two to tango: When and where dual nutrient (N & P) reductions are needed to protect lakes and downstream ecosystems. *Environmental Science & Technology 50*:10805–10813.

Crosswell, J.R., I.C. Anderson, J.W. Stanhope, B. Van Dam, M.J. Brush, S. Ensign, M.F. Piehler, B. McKee, M. Bost, and H.W. Paerl. 2017. Carbon budget of a shallow, lagoonal estuary: Transformations and source-sink dynamics along the river-estuary-ocean continuum. *Limnology and Oceanography.* doi: 10.1002/lno.10631

Hall, N.S., A.C. Whipple, and H.W. Paerl. 2015. Vertical spatio-temporal patterns of phytoplankton due to migration behaviors in two shallow, microtidal estuaries: Influence on phytoplankton function and structure. *Estuarine Coastal and Shelf Science* 162:7–21.

Hall, N.S., R.W. Litaker, W.J. Kenworthy, M.W. Vandersea, W.G. Sunda, J.P. Reid, D.H. Slone, and S. Butler. 2017. Environmental conditions promoting a consortial brown tide—picocyanobacteria bloom in Guantánamo Bay, Cuba. *Harmful Algae*. In review.

Presentations

Anderson, I., J. Stanhope, B. Van Dam, N. Hall, J. Croswell, H. Paerl, and M. Brush. 2015. *Bio-Physical Controls of CO_2 Fluxes Along a River–Estuary Continuum*. Presented at the Coastal and Estuarine Research Federation Conference, Portland, OR. November.

Paerl, H.W. 2017. *The Ultimate Challenge: Mitigating Harmful Algal Blooms in a World Experiencing Human Nutrient Enrichment and Climatic Change.* Invited Presentation at the EPA Region 9 Conference on Harmful Algal Blooms, Costa Mesa, CA. April.

Paerl, H.W. 2016. *Fighting the "Mean Green": Controlling Proliferation of Harmful Cyanobacterial Blooms in a World Experiencing Human- and Climatic-Induced Change.* Invited Seminar presented at Old Dominion University, Norfolk, VA. September.

Paerl, H.W. 2015. *The Grand Challenge of Nutrient Pollution in World's Water Resources: Global Eutrophication and Harmful Algal Bloom Dynamics.* Invited talk presented at the United Nations Educational, Scientific and Cultural Organization's Water Quality Symposium, Kyoto, Japan. June.

Paerl, H.W. 2014. *Managing Eutrophication Along the Freshwater–Marine Continuum in Coastal Watersheds: Why the Need for Dual Nutrient (N & P) Controls?* Invited seminar presented to the Biology Department, East Carolina University, Greenville, NC, September.

Paerl, H.W., I.C. Anderson, W.S. Gardner, M.J. McCarthy, N.S. Hall, B.L. Peierls, and K.L. Rossignol. 2015. *Controlling Eutrophication Along the Freshwater–Marine Continuum: Why the Need for Dual Nutrient Input Constraints?* Presented at the Coastal and Estuarine Research Federation Conference, Portland, OR. November.

Paerl, H.W., J.R. Crosswell, B.R. Van Dam, J.W. Stanhope, I.C. Anderson, B. Abare, K.L. Rossignol, B.L. Peierls, and N.S. Hall. 2015. *Impacts of Human and Climatic Perturbations on Blue, Green, and Black Carbon in Our Estuaries*. Keynote address presented at the Atlantic Estuarine Research Society Conference, Wanchese, NC. March.

Peierls, B.L, A.G. Hounshell, C.L. Osburn, and H.W. Paerl. 2016. *Bioavailability of Riverine Dissolved Organic Matter in an Estuarine System: Evidence of the Priming Effect?* Presented at the Association for the Sciences of Limnology and Oceanography (ASLO) Ocean Sciences 2016, New Orleans, LA. February 25.

Stanhope, J.W., I.C. Anderson, J.R. Crosswell, B.R. Van Dam, H.W. Paerl, and H.S. Walker. 2015. *The New River Estuary, North Carolina: A Source or Sink of CO_2?* Presented at the Atlantic Estuarine Research Society Conference, Wanchese, NC. March.

Van Dam, B.R., J.W. Stanhope, I.C. Anderson, J.R. Crosswell, and H.W. Paerl. 2015. *Diel and Seasonal pCO_2 Variability in the New River Estuary, North Carolina.* Presented at the Atlantic Estuarine Research Society Conference, Wanchese, NC. March.

Van Dam, B., J. Stanhope, I. Anderson, and H. Paerl. 2015. *Estuarine CO_2 Flux: A Comparison of Two North Carolina Estuaries.* 2015. Presented at the Coastal and Estuarine Research Federation Conference, Portland, OR. November.

Appendix 6-B
List of Students

- Julia Altman, M.Sc., Marine Science, University of North Carolina at Chapel Hill (UNC-CH), spring 2012.
- Joey Croswell, Ph.D., Marine Science, UNC-CH, fall 2015.
- Tim Otten, Ph.D., Environmental Sciences and Engineering, UNC-CH, spring 2014.
- Bryce Van Dam, Ph.D., Marine Science, UNC-CH, anticipated in spring 2018.

Appendix 6-C
Other Supporting Information

Honors

Dr. Hans W. Paerl received the 2011 Odum Award from the Coastal and Estuarine Research Federation for addressing the causes, consequences, and controls of eutrophication in aquatic ecosystems. In 2015, Dr. Paerl was named a Fellow of the American Geophysical Union for his work on human and climatic alterations of freshwater and marine nutrient cycling and their impacts on harmful algal blooms.

Appendix 6-D
Response to Research Questions

1. How do meteorological events such as high precipitation storms, tropical cyclones, and droughts modify phytoplankton community structure and function (rates of primary production and planktonic respiration) and will the changes significantly impact carbon flux and budgets for the NRE?

Meteorological events strongly regulated phytoplankton biomass and production due to the linkage between precipitation and river flow. Very high flows dampened phytoplankton production due to high flushing rates and light limitation. In combination with high rates of allocthonous carbon loading (rapidly respired in the upper estuary, contributing to large carbon dioxide [CO_2] fluxes), minimal autotrophic production led to net heterotrophy under high flow conditions. During drought, low nutrient inputs dampened autotrophic production. Consequently, these long residence time periods were associated with low biomass and CO_2 fluxes that fluctuated around zero. Highest production and biomass occurred during moderate flow regimes which provided enough nutrients for phytoplankton biomass development, but also sufficient residence time within the estuary for growth to occur. When nutrient inputs and flushing rates were appropriate for high biomass accumulation, the estuary was a sink for atmospheric CO_2.

2. What is the relationship between allochthonous organic carbon loading from freshwater discharge events and respiration and heterotrophic conditions?

Allocthonous loads of organic carbon dominated near the head of the estuary. The majority (80%) of the riverine organic load was refractory, but degradation of the labile fraction supported net heterotrophy under most river flow conditions. The proportion of allocthonous versus autochthonous production was strongly governed by river flow with higher flows leading to a higher proportion of allochthonous carbon due to delivery from the watershed and lower flows leading to higher autochthonous production due to longer residence times and higher light availability. During higher discharge years, heterotrophic conditions drove the NRE to export more carbon to Onslow Bay than during low-flow years.

3. **Do warmer conditions favor potentially harmful cyanobacterial, dinoflagellate, and raphidophyte HAB species over more desirable diatoms? If so, how will these changes impact NRE fertility, nutrient cycling, and carbon utilization and flux?**

While the raphidophytes are considered harmful, the cyanobacteria observed in the NRE are primarily picoplanktonic cyanobacteria, and generally are not harmful. Estuarine Simulation Model results showed little impact on the abundance of cyanobacteria or raphidophytes with elevated temperature scenarios due to higher temperatures also leading to higher rates of grazing losses.

Chapter 7

Aquatic/Estuarine Monitoring

SERDP Project Number: RC-2245

Aquatic/Estuarine Module

Monitoring Activity AEM-3

Lead Researchers:

Dr. Iris Anderson
Virginia Institute of Marine Science
Gloucester Point, VA
E-mail: iris@vims.edu

Supporting Researchers:

Dr. Scott Ensign, scott@aquaco.us
Jennifer Stanhope, jwu@vims.edu

November 2017

Final

This report was prepared under contract to the U.S. Department of Defense (DoD) Strategic Environmental Research and Development Program (SERDP). The publication of this report does not indicate endorsement by DoD, nor should the contents be construed as reflecting the official policy or position of DoD. References herein to any specific commercial product, process, or service by trade name, trademark, manufacturer, or otherwise, do not necessarily constitute or imply its endorsement, recommendation, or favoring by DoD.

Table of Contents

Acronyms 7-v
Abstract 7-1
Objectives of AEM-3 7-3
Background 7-3
Materials and Methods 7-5
Study Site 7-5
Results and Discussion 7-8
Spatial Patterns of Water Quality Across the NRE 7-8
Temporal Variation of Water Quality Parameters Across the NRE 7-9
Responses of Water Quality Parameters to Storm Activity 7-9
Effects of Climate and Storm Events on DO–Based Metabolism 7-18
Assessment of Directionality and Trends 7-20
Conclusions and Implications for Future Research and Implementation 7-21
Findings with Implications for Future Base Management 7-21
Literature Cited 7-21
Appendix 7-A: List of Scientific/Technical Publications 7-A-1
Appendix 7-B: List of Students 7-B-1

List of Figures

Figure 7-1. NRE shallow water monitoring stations (SW-1 through SW-10) and path of the Dataflow cruises. 7-5
Figure 7-2. For the purpose of developing a carbon budget for Research Projects AE-4 and AE-6, the NRE was subdivided into Boxes 1 through 7. 7-6
Figure 7-3. NRE shallow water (SW-1 through SW-10) shown in black and channel (C-1 through C-8) monitoring stations shown in red. 7-6
Figure 7-4. Samples taken during Dataflow cruises in the NRE. 7-7
Figure 7-5. Box plots of water quality variables for Stations SW-1 through SW-10 from July 2013 through July 2014. 7-10
Figure 7-6. Box plots of water quality variables for Stations SW-1 through SW-10 from July 2014 through July 2015. 7-11
Figure 7-7. Box plots of water quality variables for Stations SW-1 through SW-10 from July 2015 through July 2016. 7-12

Figure 7-8. Spatial variations of salinity, chlorophyll a (chl a), chromophoric dissolved organic matter (CDOM), and dissolved organic carbon (DOC) averaged across all dates from July 2013 through July 2016. 7-13

Figure 7-9. The difference in pCO_2 variation from Boxes 1 through 7 (down estuary) from July 2013 through July 2015. 7-13

Figure 7-10. Variation in dissolved inorganic nitrogen (DIN) concentrations between dates and sites located down estuary and sampled from July 2013 through July 2015. 7-14

Figure 7-11. Freshwater discharge at Jacksonville from July 2013 through July 2016; sum of discharge shown per year. 7-14

Figure 7-12. Contour plots of nitrate plus nitrite (NO_x), ammonium (NH_4^+), chlorophyll a (chl a, in vitro), and salinity by shallow water stations from July 2013 through July 2016. 7-15

Figure 7-13. Temporal variability in chlorophyll a (chl a), ammonium (NH_4^+), and dissolved organic carbon (DOC), with freshwater discharge from July 2013 through July 2015. 7-16

Figure 7-14. Temporal variability in the partial pressure of carbon dioxide (pCO_2) with water temperature from July 2013 through July 2015. 7-16

Figure 7-15. Temporal variability in the partial pressure of carbon dioxide (pCO_2), chlorophyll a (chl a), and freshwater (FW) discharge from July 2013 through July 2015. 7-17

Figure 7-16. A comparison of water quality variables in the presence and absence of Hurricane Joaquin. 7-18

Figure 7-17. Daily respiration (R), gross primary production (GPP), and net ecosystem metabolism (NEM) rates at shallow water Stations (SW-1, SW-3, and SW-9) versus daily air temperature (Marine Corps Air Station New River [KNCA]) from July 2013 through December 2015. 7-19

Figure 7-18. Daily net ecosystem metabolism (NEM) rates at shallow water Stations (SW-1, SW-3, and SW-9), daily precipitation (Marine Corps Air Station New River [KNCA]), and daily mean discharge at Gum Branch (USGS Stream Gaging Station 02093000) from July 2013 through December 2015. 7-20

List of Tables

Table 7-1. Summary of Analytical Methods Used for AEM-3 7-7

Acronyms

°C	degree Celsius
ΔpCO_2	difference in partial pressure of carbon dioxide between water and the atmosphere
µatm	microatmosphere of pressure
µg L^{-1}	micrograms per liter
µM	micromole
µmol L^{-1}	micromoles per liter
AE	Aquatic/Estuarine (Module)
AEM	Aquatic/Estuarine Monitoring Activity
AVP	autonomous vertical profiler
BMA	benthic microalgae
C	channel
CB	Coastal Barrier (Module)
CDOM	chromophoric dissolved organic matter
CDOM abs	chromophoric dissolved organic matter absorption at 440-nm wavelength
CFS	cubic feet per second
chl *a*	chlorophyll *a*
cm	centimeter
CO_2	carbon dioxide
CW	Coastal Wetlands (Module)
DCERP	Defense Coastal/Estuarine Research Program
DCERP1	first cycle of DCERP
DCERP2	second cycle of DCERP
DIC	dissolved inorganic carbon
DIN	dissolved inorganic nitrogen
DIP	dissolved inorganic phosphorus
DMSO	dimethyl sulfoxide
DO	dissolved oxygen
DOC	dissolved organic carbon
DoD	U.S. Department of Defense
DON	dissolved organic nitrogen
FW	freshwater
g C m^{-2} y^{-1}	grams of carbon per meter squared per year
GPP	gross primary production
Io	irradiance at the surface
km^2	square kilometer
KNCA	station name of Marine Corps Air Station New River
m, m^{-1}	meter
m^{-2} d^{-1}	square meters per day
MCBCL	Marine Corps Base Camp Lejeune
mg L^{-1}	milligrams per liter
mg mL^{-2}	milligrams per square meter
mM	millimolar
mmol	millimole

MSL	mean sea level
N_2O	nitrous oxide
NEM	net ecosystem metabolism
NH_4^+	ammonium
nm	nanometer
NO_x	nitrate plus nitrite
NRE	New River Estuary
PAR	photosynthetically active radiation
pCO_2	partial pressure of carbon dioxide
PO_4^{3-}	orthophosphate
POC	particulate organic carbon
ppb	parts per billion
R	daily respiration
RC	Resource Conservation and Climate Change (a SERDP program area)
SERDP	Strategic Environmental Research and Development Program
SW	shallow water
TDN	total dissolved nitrogen
TOC	total organic carbon
TSP	Translating Science into Practice (Module)
USGS	U.S. Geological Survey
YSI	Yellow Springs Instruments, Inc.

Abstract

The New River Estuary (NRE) in North Carolina, surrounded by Marine Corps Base Camp Lejeune (MCBCL) and by the City of Jacksonville at its head, is a shallow system with more than half of the estuary at depths less than 2 m at MSL. Results of DCERP1 demonstrated that the benthic zone in the shoal areas of the NRE plays an important role in regulating water quality within the estuary by mitigating nutrient enrichment delivered in freshwater discharge from the New River; thus, it is essential to make measurements both in the channel (Aquatic/Estuarine Monitoring Activity AEM-1) and the shoal zone (Monitoring Activity AEM-3) to identify the patterns and drivers of carbon variability in the estuary. The primary goal of AEM-3 was to provide water quality data from the shoal area to support the research effort of Research Projects AE-4 and AE-6 to develop a carbon budget for the NRE. The NRE is highly dynamic, with water quality varying in response to site location down estuary, to fresh water discharge and storm activity, and to physical variables such as wind, temperature, light availability and attenuation. Rates of metabolism are important drivers of water quality variables (e.g., dissolved inorganic carbon [DIC], partial pressure of carbon dioxide [pCO_2], dissolved organic carbon [DOC]), but these rates are themselves regulated by nutrient availability, freshwater discharge, light availability, and temperature. The measurements made by AEM-3 were essential for the calculations of metabolism made by Research Projects AE-4 and AE-6 and for determinations of transformations and exchanges of carbon species as they move down the estuary and between the estuary, atmosphere, sediments, and coastal ocean.

Bimonthly from July 2013 through July 2016, water quality parameters were measured in the shallow zone along the periphery of the NRE. These parameters include pCO_2, dissolved oxygen (DO), DIC, DOC, dissolved organic nitrogen, dissolved inorganic nitrogen, dissolved inorganic phosphorus, total suspended solids, chlorophyll *a* (chl *a)*, and benthic chl *a* (a measure of benthic microalgal biomass). In addition, multi-sensor datasondes were deployed in shallow water to capture diel variations of DO and water quality in the upper, middle, and lower estuary. Additional deployments of datasondes were made to capture changes in shallow DO and water quality during and after episodic events that were necessary for calibrating and validating models of estuarine productivity and trophic state. Shallow water sampling stations were spatially stratified to assess variability within the estuarine salinity zones. The uppermost estuary site, closest to the City of Jacksonville, was a hot spot of biogeochemical activity, demonstrating high concentrations of nutrients, chromophoric dissolved organic matter, pCO_2, and chl *a*, which is a proxy for phytoplankton. Major drivers of both spatial and temporal variability in water quality, as shown in both DCERP1 and DCERP2, were temperature and freshwater discharge from the New River. Passage of Hurricane Joaquin (October 2 and 3, 2015) caused major water quality responses in the estuary. Overall, the NRE was poised in near metabolic balance during the years of our study; however, extreme storm events such as Joaquin, which are likely to increase in response to climate change, will impact the cycling of carbon in the estuary, with increased fluxes of carbon dioxide (CO_2) to the atmosphere. The greatest net heterotrophy and the largest exchanges of CO_2 between the estuary and the atmosphere were observed at the uppermost station monitored in the estuary where the New River flow first enters the estuary above the City of Jacksonville.

Keywords: Ammonium, chlorophyll *a*, chromophoric dissolved organic matter, dissolved inorganic carbon, dissolved inorganic nitrogen, dissolved inorganic phosphorus, dissolved organic carbon, dissolved oxygen, freshwater discharge, hurricane response, metabolism, nitrate, partial pressure of carbon dioxide, salinity

Objectives of AEM-3

1. Provide water quality data from the shoal zone to support the research efforts of Research Projects AE-4 and AE-6 to develop a carbon budget for the New River Estuary (NRE)

2. Identify the patterns and drivers of water quality variability in the shoal zone of the NRE

3. Provide the environmental context, explaining the biogeochemical processes that drive the carbon budget in the NRE

4. Determine the impacts of storm activity on metabolic processes in the NRE

5. Provide data for decision-support tools and model calibration and verification. AEM-3 supported the data needs of Research Projects AE-4, AE-5, AE-6, TSP-2, CW-4, CW-5, and CB-5.

During DCERP1, the Aquatic/Estuarine Module Team noted strong biotic responses to natural and anthropogenic disturbances. The benthos was shown to account for more than 40% of primary production in the entire estuary. Thus, it is essential to monitor water quality in the shallow water zone where benthic and pelagic production and respiration are strongly linked to determine sources, sinks, and transformations of carbon in the NRE. The primary objective of AEM-3 was to provide background data on water quality within the shallow zone of the NRE. These data provide the context for understanding the metabolic responses (photosynthesis, respiration, net ecosystem metabolism), measured by Research Projects AE-4 and AE-6, that occur in the estuary and that regulate transformations and speciation of carbon and the resulting net exchanges of carbon species with the atmosphere, sediment, and coastal ocean. As such, AEM-3 responds to the thematic focus areas of carbon cycling and climate change. As demonstrated in DCERP1, physical factors also play an important role in determining variability in water quality parameters across locations and over time. To determine physical–biological interactions, AEM-3 assessed temporal and spatial variabilities in response to freshwater discharge, salinity, storm activity, and temperature. These data are essential as input for model calibration and verification, for model predictions of water quality in response to disturbances caused by land use and climate change, and for development of the decision-support tools by Research Project TSP-2.

Background

Estuaries are key sites of organic carbon production, respiration, and transformation. The extent of these processes and their impacts on the coastal ocean and atmosphere are influenced by a variety of natural and anthropogenic factors, including nutrient and organic carbon enrichment, land use, freshwater input, and episodic perturbation by storms (Bauer et al., 2013; Canuel et al., 2012; Crosswell et al., 2014 and 2017). For example, estuaries that receive elevated rates of inorganic nutrient loading may produce more organic carbon than they consume, which they may export as total organic carbon (TOC), the sum of dissolved organic carbon (DOC) and particulate organic carbon (POC) into the coastal ocean (Kemp et al., 1997; Nixon, 1995). Estuaries that receive carbon derived from adjacent highly productive coastal wetlands or from watersheds dominated by agriculture may be important sources of carbon dioxide (CO_2) emissions to the

atmosphere (Borges and Abril, 2011; Cai, 2011). In deep estuarine systems, primary production and water column concentration of chlorophyll *a* (chl *a*), which is a proxy for phytoplankton biomass, exhibit predictable responses to inputs of nutrients. However, in shallow systems (e.g., like the NRE), in which the benthos are exposed to light, the relationship no longer appears to hold, and production is far less than predicted (McGlathery et al., 2007; Nixon et al., 2001). One explanation for the behavior of shallow photic systems is that benthic microbial processes play an important role in regulating the fate of both carbon and nitrogen. Benthic microalgae (BMA) are important primary producers in shallow estuaries, releasing DOC, which can then be respired by bacteria. Depending on light availability, nitrogen is taken up by BMA to produce biomass, and, in addition, the microbial processes denitrification and ammonium oxidation (i.e., anammox) can convert nitrogen to nitrous oxide (N_2O) and nitrogen gas (Anderson et al., 2003, 2010; Eyre et al., 2011; Joye and Anderson, 2008; McGlathery et al., 2007; Sundbäck et al., 2004). Benthic microbial processes also play an important role in remineralizing DOC delivered from the New River and smaller tributaries (allochthonous inputs) or produced by photosynthesis (autochthonous inputs). Benthic microbial processes are impacted by changes in available light, nutrients, the delivery of TOC from watersheds and resuspension events because of winds, tides and currents, temperature, and salinity (Joye and Anderson, 2008). The NRE (**Figure 7-1**) can serve as a model system for study of the interacting biological and physical variables that regulate carbon and nitrogen cycling in estuarine systems.

DCERP1 Research Project AE-3 demonstrated that the NRE is a moderately eutrophic estuary with rates of benthic primary production (g C m^{-2} y^{-1}) that accounted for 41% of total average annual primary production across the estuary. Although phytoplankton dominated total gross primary production (GPP) in the NRE, an active benthic microbial community in the shallow photic zone was highly productive and effective in mitigating watershed nutrient loads, and thereby serving as a benthic filter. The benthos served as both a source of recycled nutrients supporting pelagic primary production, as well as a benthic filter, sequestering and removing nutrients by BMA uptake, denitrification, and anammox and thereby mitigating eutrophication. The effectiveness of the benthic filter was dependent on light availability and photic area of the estuary (≥1% Io), which varied as a function of freshwater discharge. Chromophoric dissolved organic matter (CDOM) delivered in freshwater discharge increases light attenuation in the water column, thereby reducing light availability to the benthos. From 2008 through 2011, photic area in the NRE varied from 46% to 97% of total estuarine bottom area. When light availability was low, the benthos switched from net autotrophic (photosynthesizing their food) to heterotrophic (using organic compounds for food) and from a net sink to a source of nitrogen to the water column. Estuary-wide benthic processes sequestered from 41% to 67% of the inorganic nitrogen remineralized from organic matter in sediments in spring and from 27% to 63% in summer. Whereas the uptake of regenerated nitrogen by photosynthesizing BMA sequestered more nitrogen when sufficient light was available, denitrification proved to be more important for removal of nitrogen when light was limiting. Benthic chl *a* was an excellent indicator of the effectiveness of the BMA nitrogen "filter." During summer 2010 and spring 2011, a threshold for benthic chl *a* was observed that ranged from 70–83 mg m^{-2}, below which the benthos was a source of nutrients supporting primary production and above which was a sink, sequestering nutrients. In high discharge years with high nutrient inputs, high pelagic primary production, and low photic area, the BMA "filter" is likely to be less effective because of light limitation and low biomass. Wind also affected benthic processes by resuspending particulates in shallow waters and by reducing light availability throughout the water column. Particle-size of suspended

particulate matter increased down estuary. CDOM and sediment loads were dominant factors controlling light attenuation, benthic metabolism, and nutrient exchange up estuary; resuspension and phytoplankton abundance were likely more important drivers down estuary. These data from DCERP1 Research Project AE-3 not only revealed important information about the state of the NRE, but the information also provided an important context for understanding carbon cycling in the shoal zone of the NRE. AEM-3 of DCERP2 builds on the work of DCERP1 by further consideration of the biological–physical interactions that regulate inputs of nutrients, TOC, CDOM, and light availability, which then drive carbon transformations, speciation, and exchanges in both the pelagic and benthic zones throughout the estuary.

Materials and Methods

Study Site

The NRE is a shallow, microtidal system of 79 km^2 that is located in North Carolina, USA and is surrounded by Marine Corps Base Camp Lejeune (MCBCL; 631 km^2), with the City of Jacksonville at the head of the estuary (**Figure 7-1**). More than 50% of the NRE area is less than 2-m deep relative to MSL; thus, light reaches the benthic surface throughout much of the estuary, and both phytoplankton and benthic microalgae are important contributors to total primary production (Anderson et al., 2014; Hall et al., 2013). The system is semi-lagoonal, consisting of a number of shallow embayments and connected to the ocean via a restricted inlet. Most freshwater input comes from the New River, which drains a 716-km^2 watershed and enters at the head of the estuary above Jacksonville. Additional freshwater input comes from small tributary creeks that span the length of the system and drain the 308-km^2 lateral watershed. The NRE channel zone is seasonally stratified in the upper and middle reaches of the estuary and is generally well mixed in the lower estuary. Tides are semi-diurnal with a mean daily range of 0.43 m in the lower estuary and 0.17 m in the upper estuary (Currin, 2013). The system is highly sensitive to variations in freshwater discharge; freshwater flushing times range from 1 to 150 days, with a mean of 34 days (Ensign et al., 2004; Hall et al., 2013; Peierls et al., 2012).

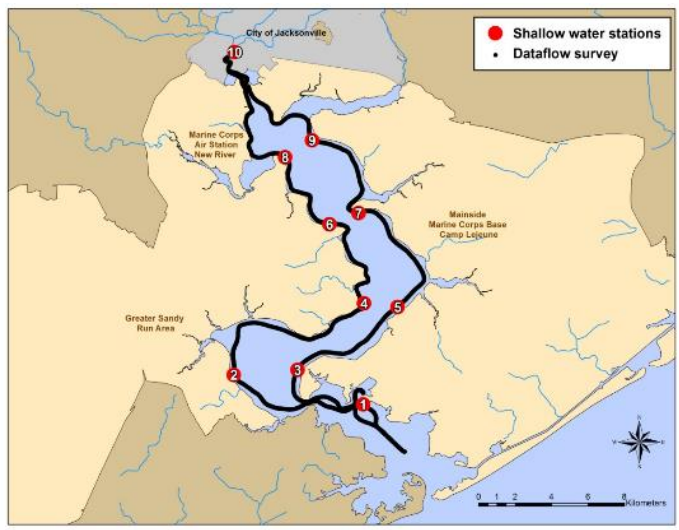

Figure 7-1. NRE shallow water monitoring stations (SW-1 through SW-10) and path of the Dataflow cruises.

For the purpose of developing a carbon budget, the NRE was divided into seven boxes (1 through 7, see **Figure 7-2**) and three regions, the upper, middle, and lower estuary, based on major geographic constrictions and hydrography (**Figures 7-1, 7-2, and 7-3**). Grab samples for determinations of all analytes were collected at fixed stations during AEM-3 in the shoal zone (SW-1 to SW-10) and by AEM-1 in the channel zone (C-1 through C-8) (**Figure 7-3**). Sampling by AEM-1 and AEM-3 was highly coordinated and performed at the same time periods to

provide needed data for Research Projects AE-4 and AE-6. Shoal and channel components were delineated in each section using the 2-m contour (MSL) as the boundary. The channel and shoal areas are relatively balanced in the upper and middle estuary, whereas the lower estuary is almost entirely comprised of shoal (94%). Although maximum depths in the estuary reach 5 m, the depths in the channel sections range between 2.4 m to 3 m, and the mean depth on the shoals is approximately 1 m. The tributary watershed areas for the upper, middle, and lower estuary are 138, 150, and 20 km^2, respectively.

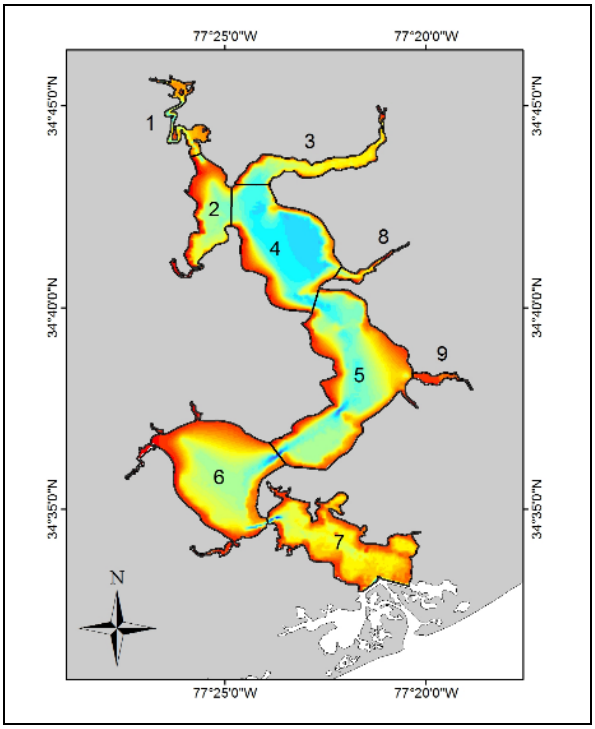

Figure 7-2. For the purpose of developing a carbon budget for Research Projects AE-4 and AE-6, the NRE was subdivided into Boxes 1 through 7.

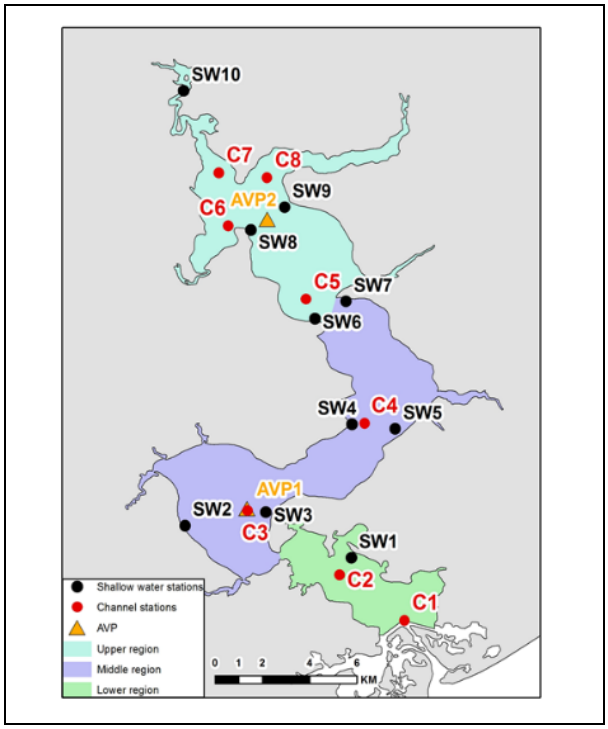

Figure 7-3. NRE shallow water (SW-1 through SW-10) shown in black and channel (C-1 through C-8) monitoring stations shown in red.

Autonomous vertical profilers (AVPs) located mid-channel are represented by AVP-1 and AVP-2 shown in yellow.

Bimonthly, a Dataflow system (modified from Madden and Day [1992]) was used to sample the periphery of the NRE in the shallow water zone (**Figure 7-4**) (approximately every 30 m or 2 seconds). The Dataflow system was fitted with sensors for salinity, pH, temperature, dissolved oxygen (DO), turbidity, chlorophyll a, and CDOM, and coupled to a showerhead-equilibration chamber with a non-dispersive infrared absorbance analyzer (Li-Cor LI-840, modified from Hales et al., 2004). Additional grab samples of water and sediment were collected at Stations SW-1 to SW-10 to determine dissolved inorganic carbon (DIC) and dissolved organic carbon (DOC), dissolved inorganic nitrogen (DIN), and dissolved inorganic phosphorus (DIP), total suspended solids, chl *a*, and benthic chl *a* (a measure of benthic microalgal biomass) (**Figure 7-4**). In addition, YSI multi-sensor datasondes (Yellow Springs Instruments, Inc. [YSI]) were deployed for approximately 1-week periods to measure diel variations in DO and water

quality in the shallows of three regions (SW-1, SW-3, and SW-9) of the estuary and to estimate metabolic rates by using the Open Water method (Caffrey, 2003). Additional deployments of datasondes were made to capture changes in shallow DO and water quality during and after episodic storm events that are necessary for calibrating and validating models of estuarine productivity and trophic state. Shallow water sampling stations were spatially stratified to assess the variability within the estuarine salinity zones. All analytes, sampled in triplicate, were analyzed as described in **Table 7-1**.

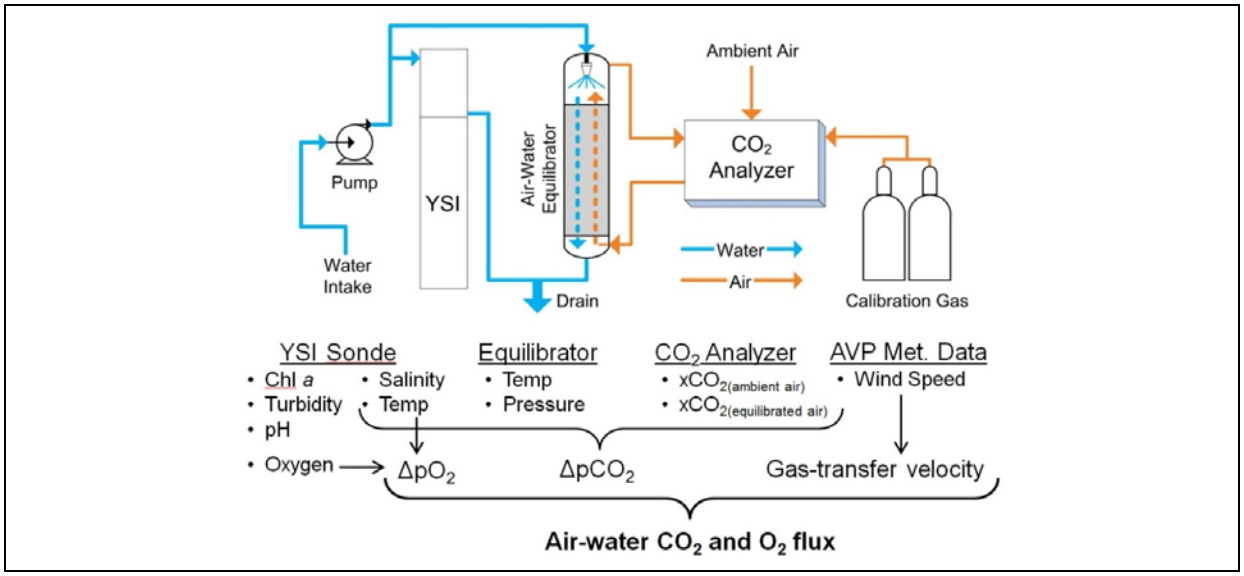

Figure 7-4. Samples taken during Dataflow cruises in the NRE.

Table 7-1. Summary of Analytical Methods Used for AEM-3

Analyses	Methods or Instrument	References
Sediment characterization		
Sediment organic content	Loss on ignition (500°C)	Not applicable
Benthic chl *a* and phaeophytin (microalgae biomass)	Chl *a*—acetone extract and spectrophotometry (Beckman Coulter DU800 spectrophotometer)	Lorenzen, 1967; Neubauer et al., 2000
Sediment nutrients	Potassium chloride extraction	Keeney and Nelson, 1982
Water quality		
Temperature, salinity, DO, turbidity, chl *a* (in vivo) (field measurements)	YSI 6600 multi-parameter datasonde	Not applicable
DO (metabolism experiments)	Hach luminescence DO sensor	Hach Method 10360
Chl *a* (extracted; phytoplankton biomass)	Chl *a*—Acetone; dimethyl sulfoxide (DMSO) extract and fluorometry (Turner Designs Fluorometer, Model 10-AU)	Arar and Collins, 1997; Shoaf and Lium, 1976
CDOM	WetLabs CDOM sensor (Beckman Coulter DU800 spectrophotometer; absorption read at wavelength 440 nm)	Gallegos and Neale, 2002; Green and Blough, 1994; Kirk, 1994
Photosynthetically active radiation (PAR)	Li-Cor LI-192SA underwater and LI-190SA quantum sensors	Not applicable

(continued)

Table 7-1. Summary of Analytical Methods Used for AEM-3 (continued)

Analyses	Methods or Instrument	References
Nutrient		
Nitrate, nitrite	Cadmium reduction and diazotization (Lachat)	Smith and Bogren, 2001
Ammonium	Phenol hypochlorite method (Lachat)	Liao, 2001
DIP (phosphate)	Molybdate method (Lachat)	Knepel and Bogren, 2001
Total dissolved nitrogen (TDN) and dissolved organic nitrogen (DON)	Alkaline persulfate digestion (Lachat)	Koroleff, 1983
DIC	Acidification to CO_2; LI-6252 CO_2 analyzer	Not applicable
POC and particulate nitrogen	Fison Model EA 1108 elemental analyzer	Not applicable
DOC	680°C catalytically aided combustion oxidation and non-dispersive infrared detection (Shimadzu TOC-V analyzer)	Neubauer and Anderson, 2003

Results and Discussion

Spatial Patterns of Water Quality Across the NRE

Data are shown for stations ordered from down to up estuary (SW-1 to SW-10) or from up to down estuary (Boxes 1 through 7). Box plots of water quality variables up estuary across Stations SW-1 to SW-10 are shown for July 2013 through July 2014 (**Figure 7-5**), July 2014 through July 2015 (**Figure 7-6**), and July 2015 through July 2016 (**Figure 7-7**). Spatial patterns were similar across all 3 years. As salinity decreased up estuary, DOC, chl *a*, the difference in partial pressure of carbon dioxide between water and the atmosphere (ΔpCO), and CDOM increased (**Figures 7-8 and 7-9**). Although DIN (**Figure 7-10**) was highest at the head of the estuary, concentrations decreased rapidly down estuary as nutrients were assimilated by phytoplankton and benthic microalgal primary production. In addition, pH was similar across the estuary except at Station SW-10 in **Figures 7-5, 7-6, and 7-7**, where pH was lowest and partial pressure of carbon dioxide (pCO_2), DOC, and CDOM (**Figures 7-8 and 7-9**) were highest, suggesting export from the New River at sites closest to the City of Jacksonville. The location of peak pelagic and benthic chl *a* shifted between Years 1, 2, and 3 of the study, during which time annual freshwater discharge increased (**Figures 7-11**). The increasingly low benthic chl *a* observed at the head of the estuary during Years 2 and 3 of the study suggests light limitation of primary production because of the high export of CDOM to the head of the estuary as freshwater discharge increased during Years 2 and 3 (**Figures 7-5, 7-6, and 7-7**).

Box 1 (SW-10) at the head of the estuary was a hot spot of biological activity, given the high concentrations of DOC, which may be derived from allochthonous sources in the New River or from autochthonous primary production at the head of the estuary. The high concentrations of pCO_2 often observed at the head of the estuary (**Figure 7-9**) suggest that a portion of the DOC introduced from the New River was labile (approximately 15% to 20%, as shown in lability experiments run by Research Projects AE-4 and AE-6) and rapidly respired, whereas the rapid loss of DIN down estuary suggests high rates of primary production.

Temporal Variation of Water Quality Parameters Across the NRE

Water quality varied between seasons and years, mainly because of changes in physical drivers such as freshwater discharge and temperature. Freshwater discharge increased from 33,984 CFS from July 2013 through July 2014; to 58,394 CFS from July 2014 through July 2015; and increased again to 71,163 CFS from July 2015 through July 2016 (**Figure 7-11**). As shown in **Figure 7-12**, during periods of high freshwater discharge and resulting low salinity, chl *a* and nutrients tended to be higher throughout the estuary. The impacts of Hurricane Joaquin, which crossed the North Carolina coast on October 2 and 3, 2015, accompanied by heavy rainfall can be observed by the low salinities throughout the estuary. Periods of high freshwater discharge often correlate with high concentrations of DOC, ammonium (NH_4^+), and chl *a* (**Figure 7-13**), as one might expect with increased transport of allochthonous DOC and nutrients from the watershed to the estuary. Variations in pCO_2 concentrations track well with water temperature (**Figure 7-14**) and somewhat with chl *a* and freshwater discharge (**Figure 7-15**).

Responses of Water Quality Parameters to Storm Activity

To compare water quality variables in the presence versus absence of an extreme storm event (i.e., Hurricane Joaquin), we plotted average and median values measured during October 2015 and March 30, 2016, a period impacted by the hurricane, as well as average and median values for all periods from July 2013 through July 2016 that were not impacted by the event. Results shown in the box and whiskers plots in **Figure 7-16** demonstrate decreased average salinity and DIC concentrations and increased average DOC, NH_4^+, CDOM, and nitrate plus nitrite (NO_x) across the entire NRE. One might expect increased chl *a* because of the added nutrients; however, high freshwater discharge decreases freshwater residence time such that phytoplankton are washed out of the estuary so quickly they are unable to multiply and assimilate the added nutrients. In addition, the increased CDOM may reduce light availability, further constraining primary production.

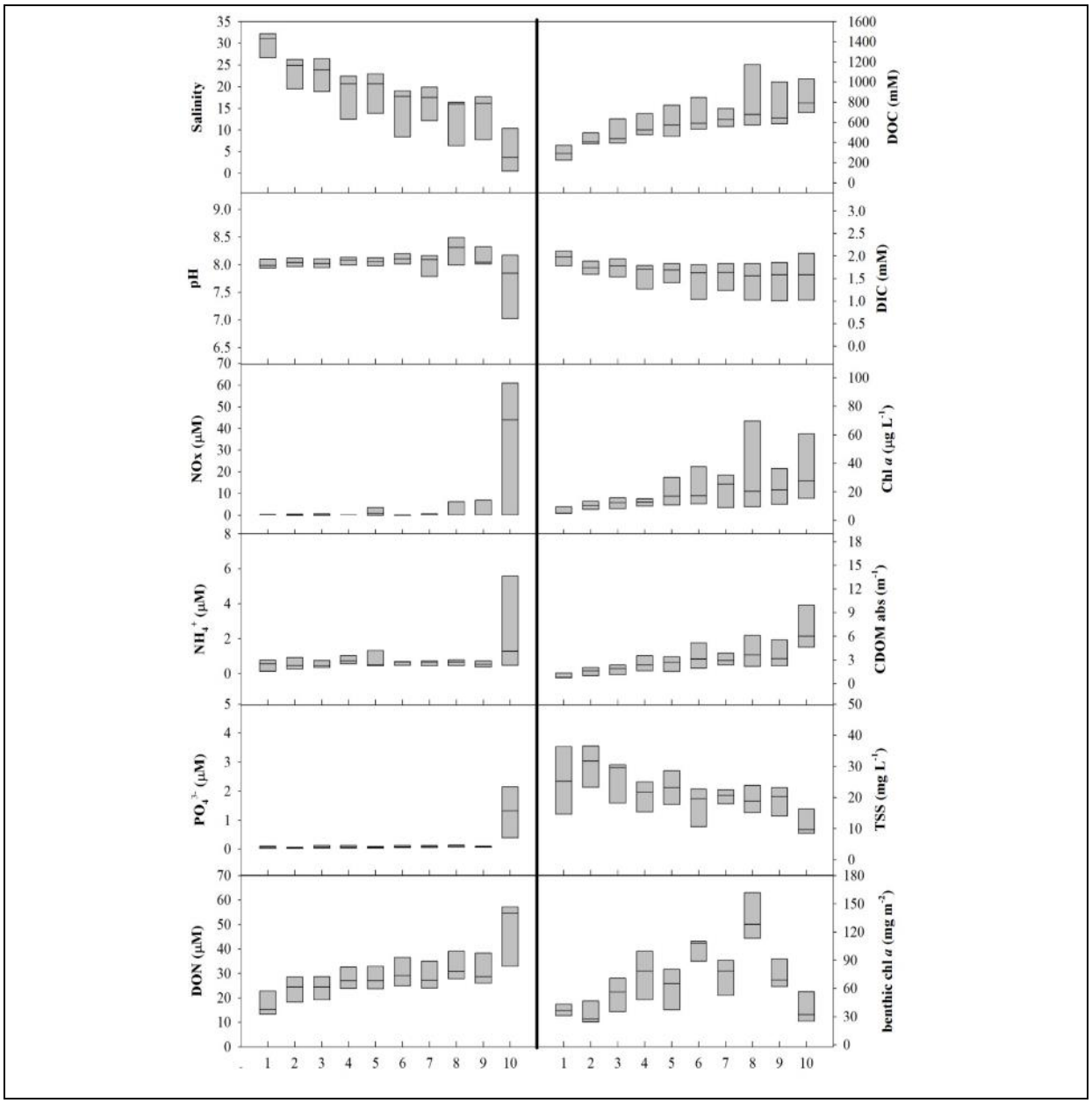

Figure 7-5. Box plots of water quality variables for Stations SW-1 through SW-10 from July 2013 through July 2014.

The box is 25th and 75th percentile and line within the box is the median. CDOM abs=chromophoric dissolved organic matter absorption at 440 nm wavelength; chl *a*=chlorophyll *a* in vitro; DIC=dissolved inorganic carbon; DOC=dissolved organic carbon; DON=dissolved organic nitrogen; TSS=total suspended solids.

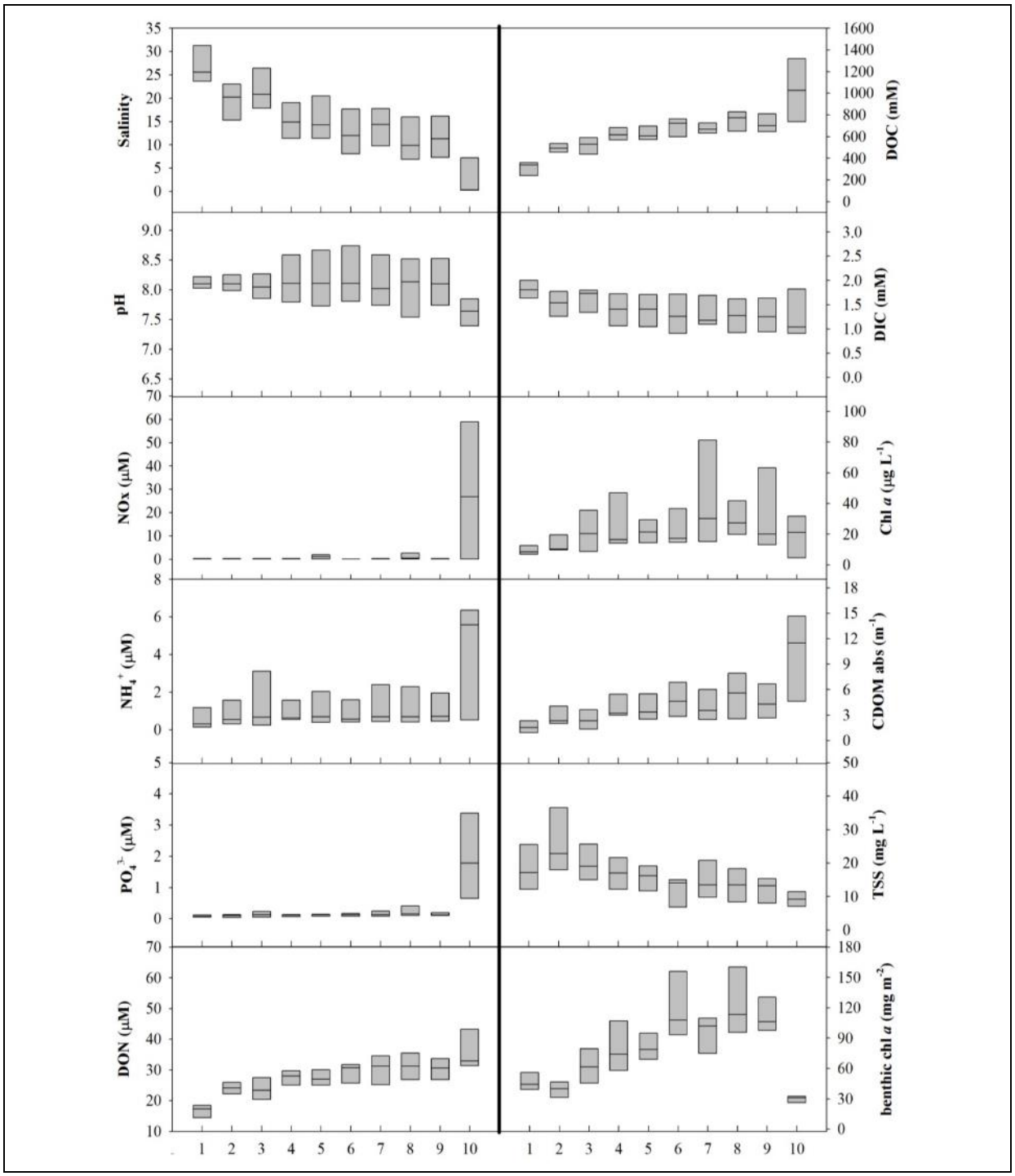

Figure 7-6. Box plots of water quality variables for Stations SW-1 through SW-10 from July 2014 through July 2015.

The box is 25th and 75th percentile and line within the box is the median. CDOM abs=chromophoric dissolved organic matter absorption at 440 nm wavelength; chl *a*=chlorophyll *a* in vitro; DIC=dissolved inorganic carbon; DOC=dissolved organic carbon; DON=dissolved organic nitrogen; TSS=total suspended solids.

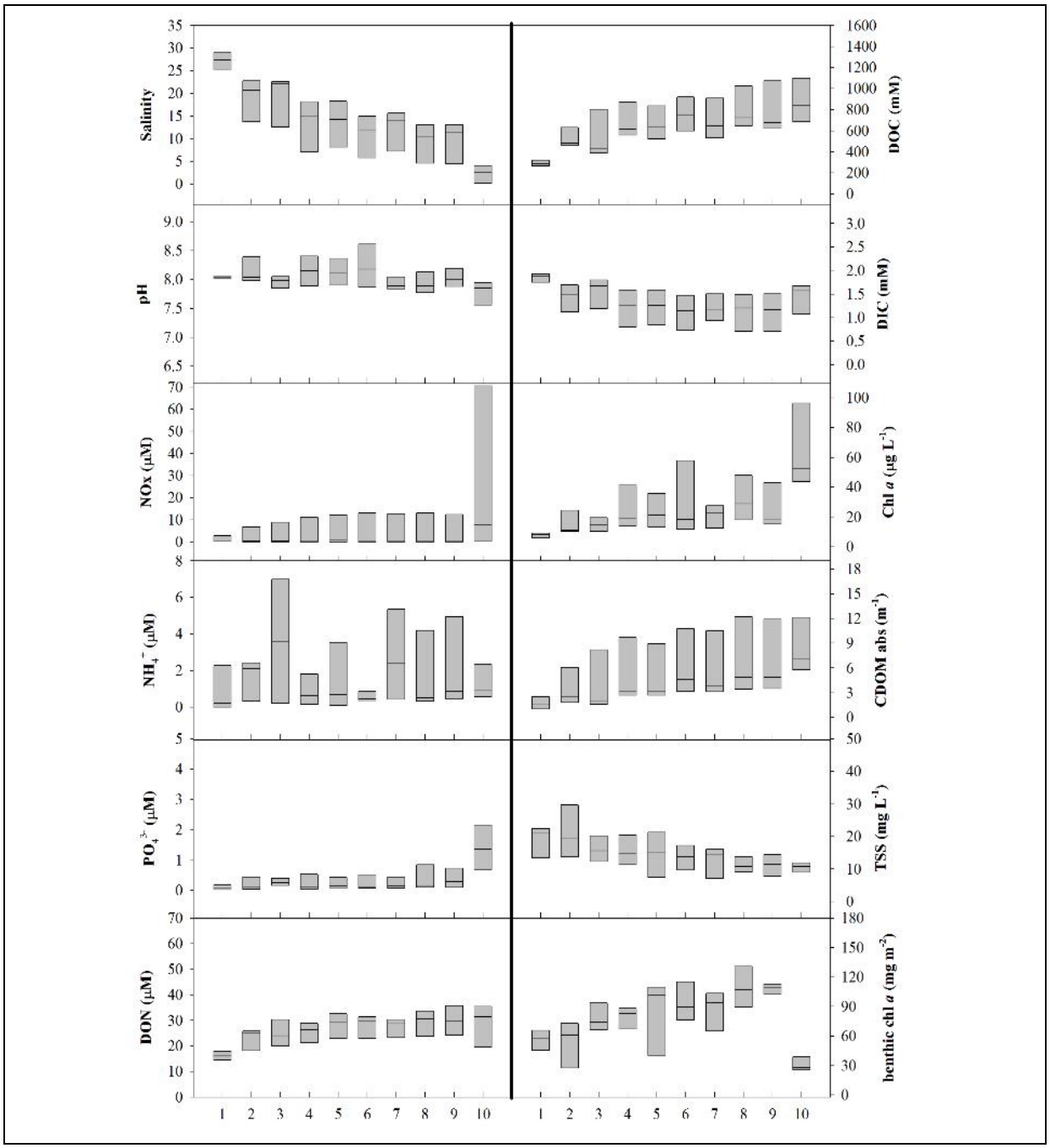

Figure 7-7. Box plots of water quality variables for Stations SW-1 through SW-10 from July 2015 through July 2016.

The box is 25th and 75th percentile and line within the box is the median. CDOM abs=chromophoric dissolved organic matter absorption at 440 nm wavelength; chl *a*=chlorophyll *a* in vitro; DIC=dissolved inorganic carbon; DOC=dissolved organic carbon; DON=dissolved organic nitrogen; TSS=total suspended solids.

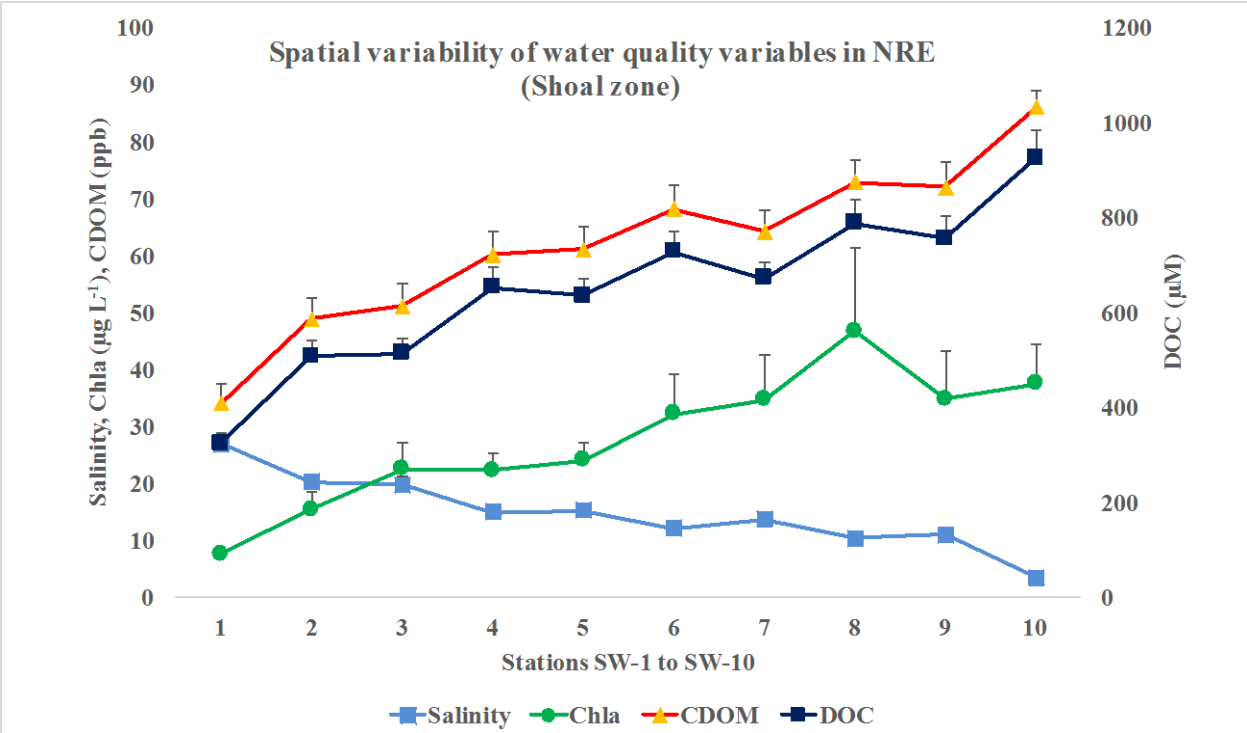

Figure 7-8. Spatial variations of salinity, chlorophyll *a* (chl *a*), chromophoric dissolved organic matter (CDOM), and dissolved organic carbon (DOC) averaged across all dates from July 2013 through July 2016.

Sampling locations ranged from SW-1, Box 7, (down estuary) to SW-10, Box 1 (up estuary).
Error bars represent standard errors.

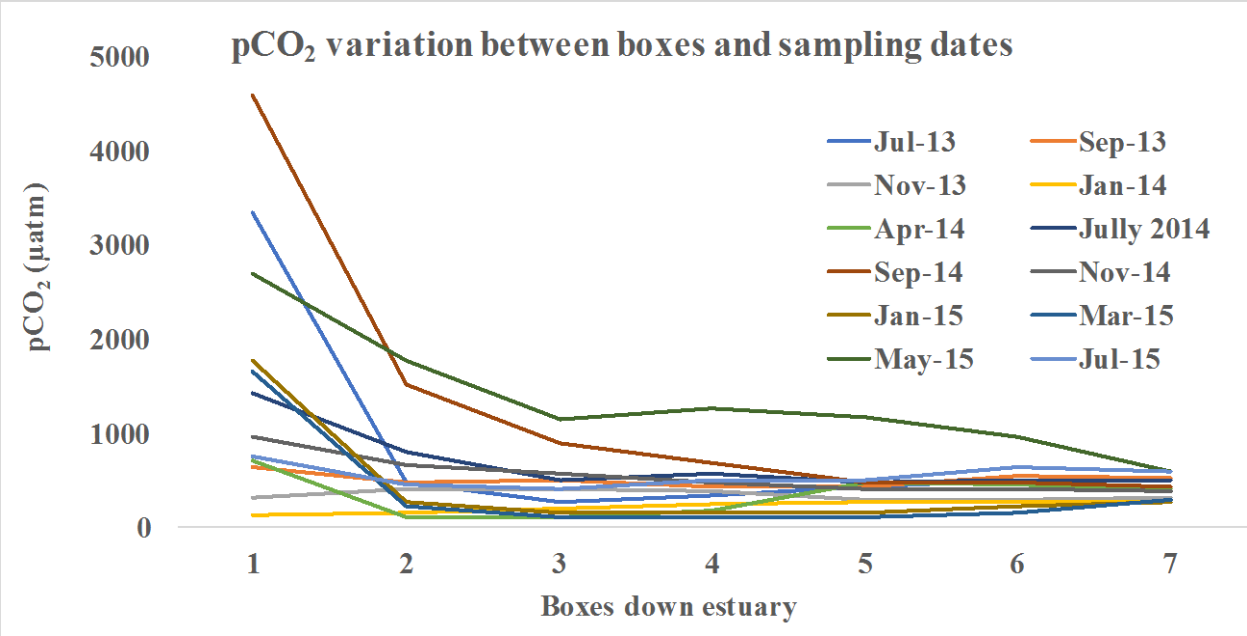

Figure 7-9. The difference in pCO_2 variation from Boxes 1 through 7 (down estuary) from July 2013 through July 2015.

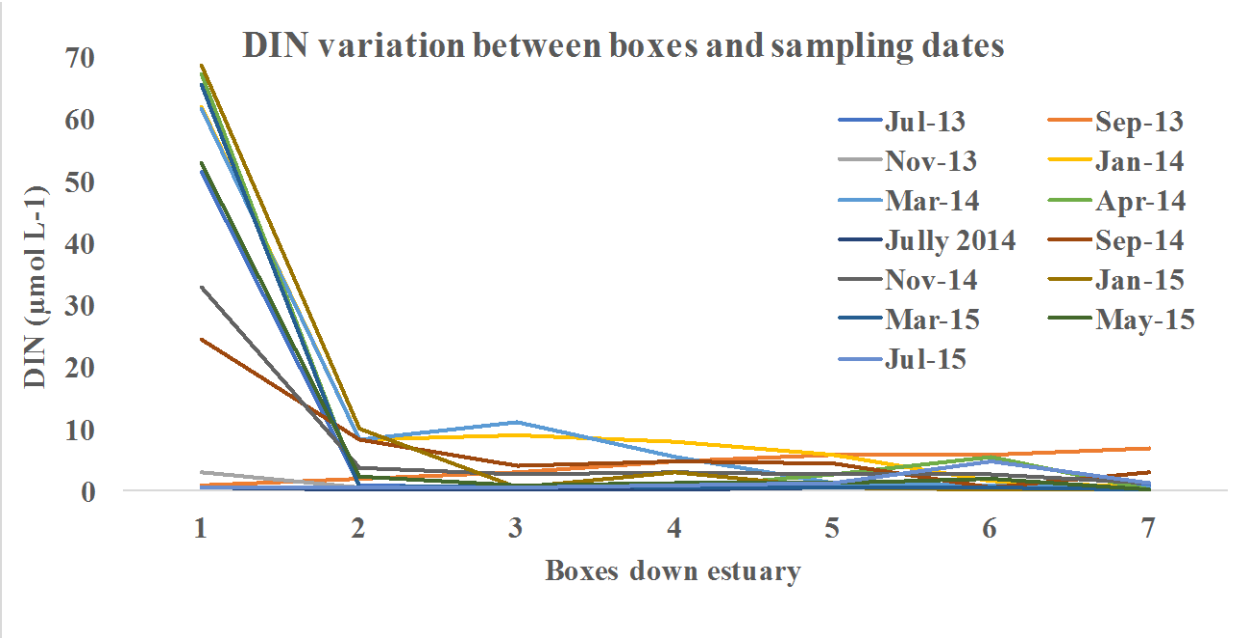

Figure 7-10. Variation in dissolved inorganic nitrogen (DIN) concentrations between dates and sites located down estuary and sampled from July 2013 through July 2015.

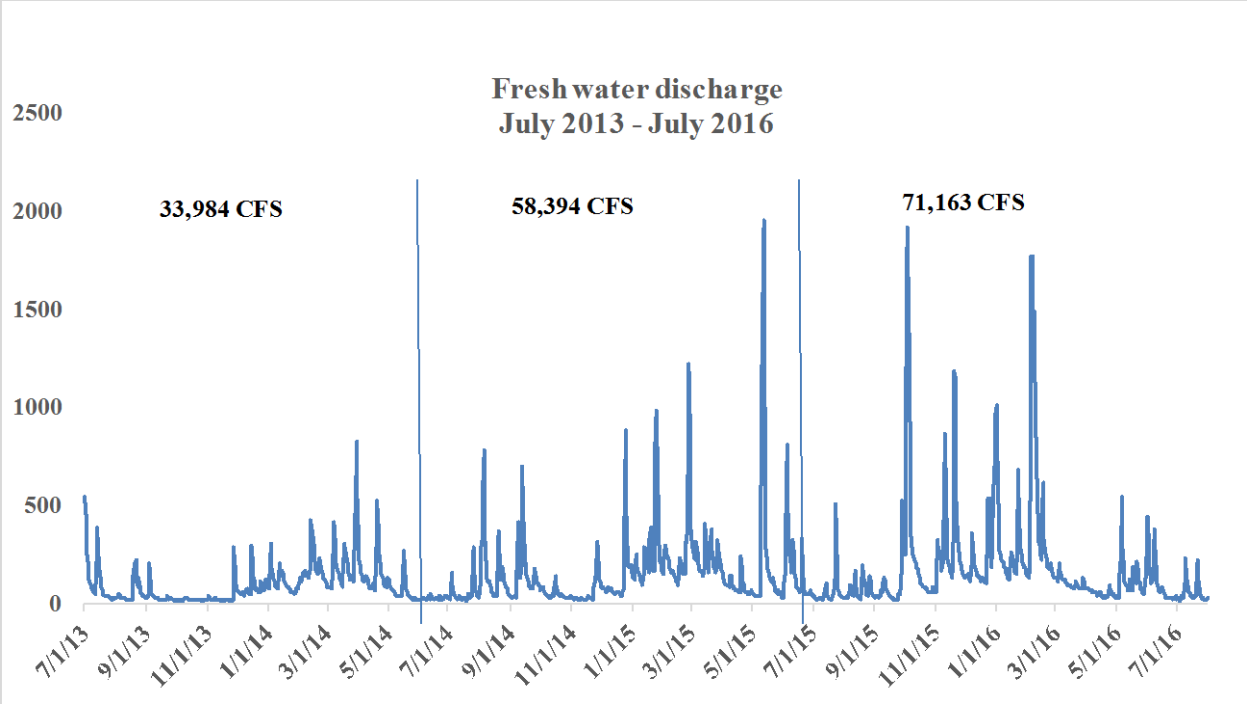

Figure 7-11. Freshwater discharge at Jacksonville from July 2013 through July 2016; sum of discharge shown per year.

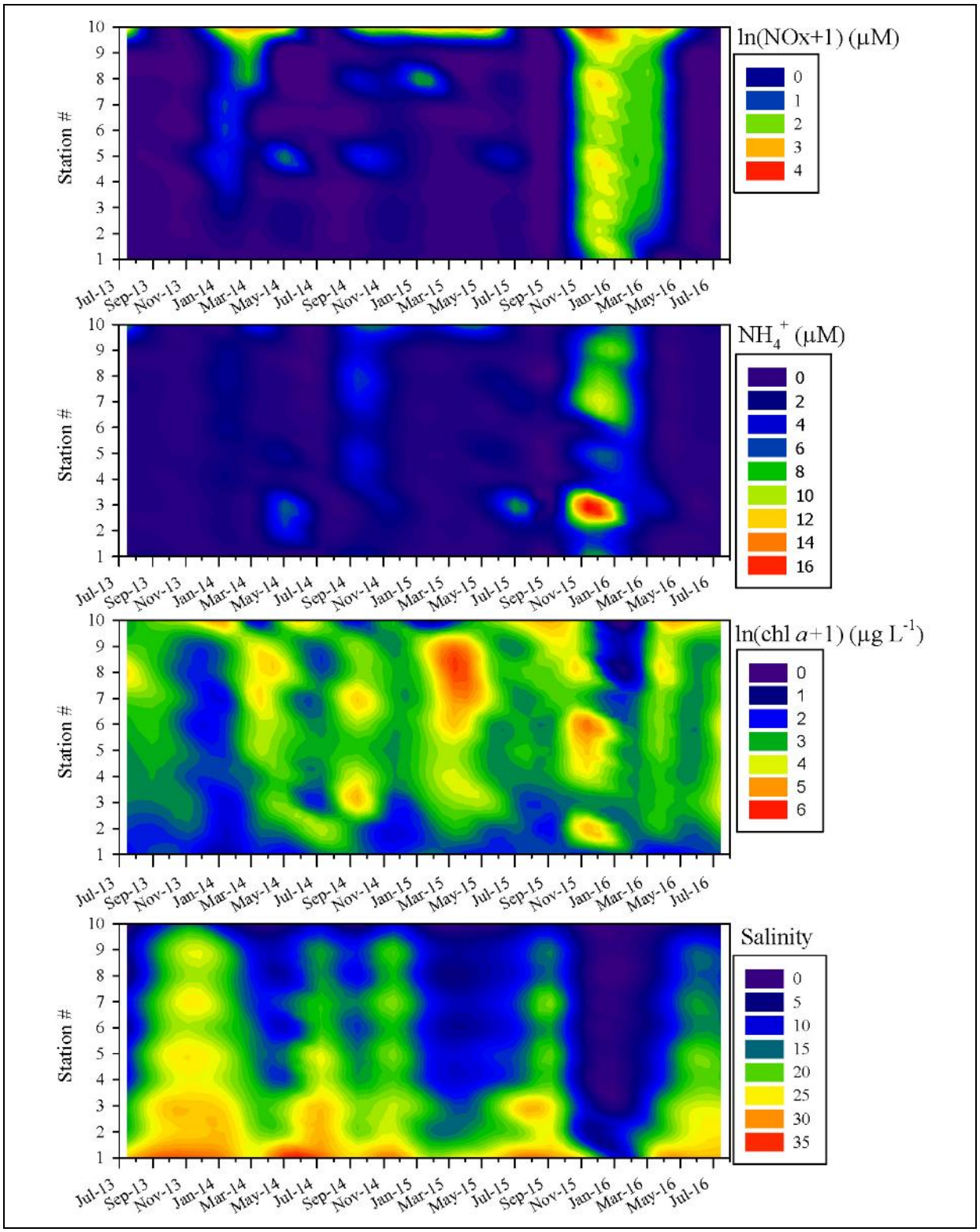

Figure 7-12. Contour plots of nitrate plus nitrite (NO_x), ammonium (NH_4^+), chlorophyll *a* (chl *a*, in vitro), and salinity by shallow water stations from July 2013 through July 2016.

NO_x and chlorophyll *a* are natural log transformed.

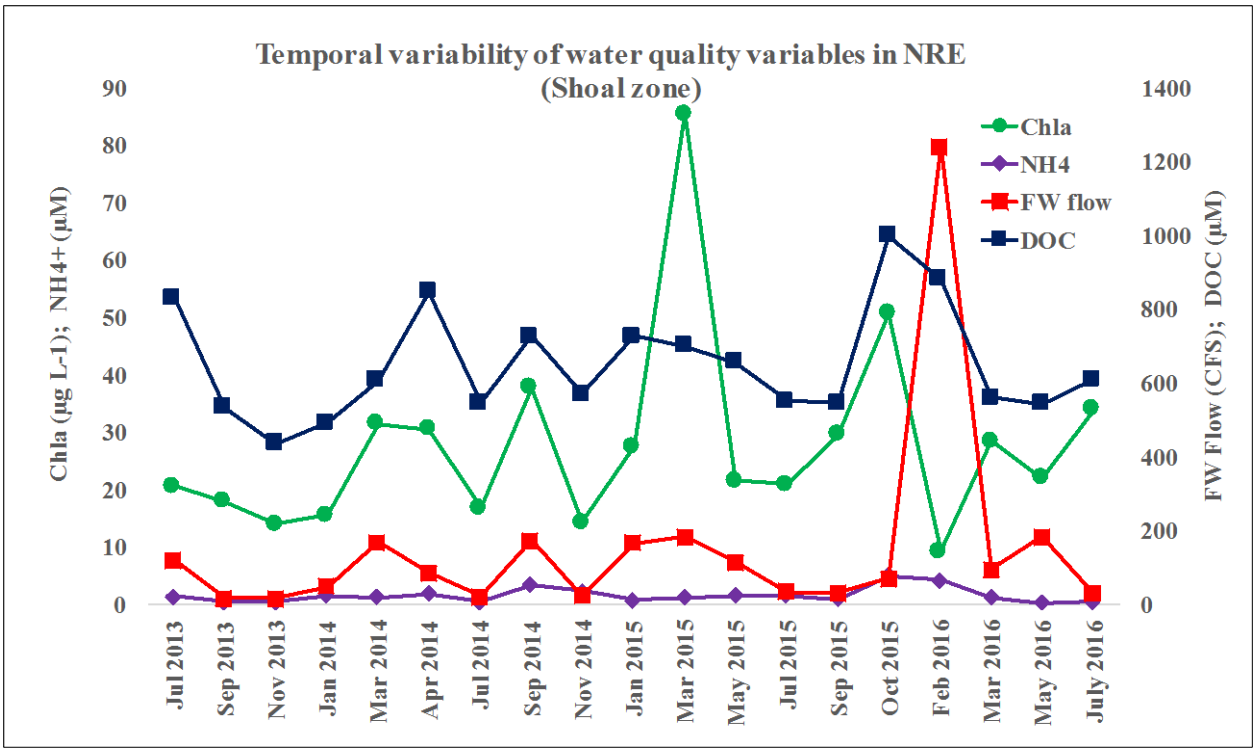

Figure 7-13. Temporal variability in chlorophyll *a* (chl *a*), ammonium (NH_4^+), and dissolved organic carbon (DOC), with freshwater discharge from July 2013 through July 2015.

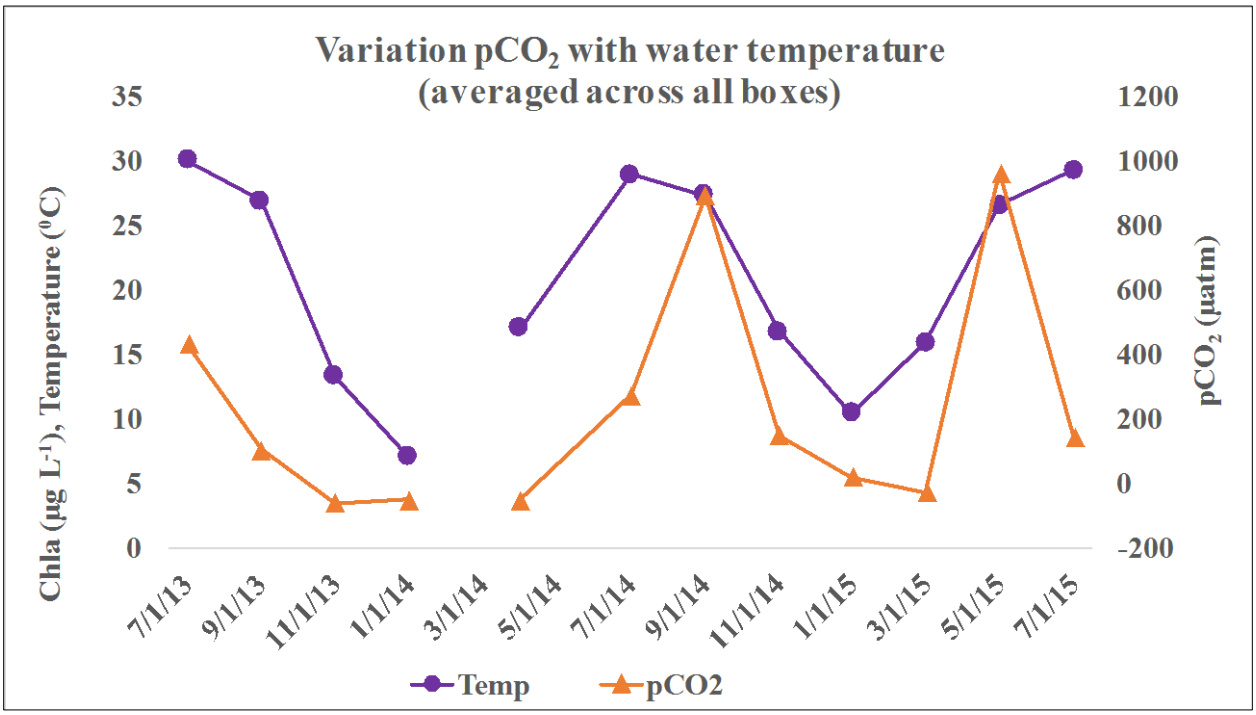

Figure 7-14. Temporal variability in the partial pressure of carbon dioxide (pCO_2) with water temperature from July 2013 through July 2015.

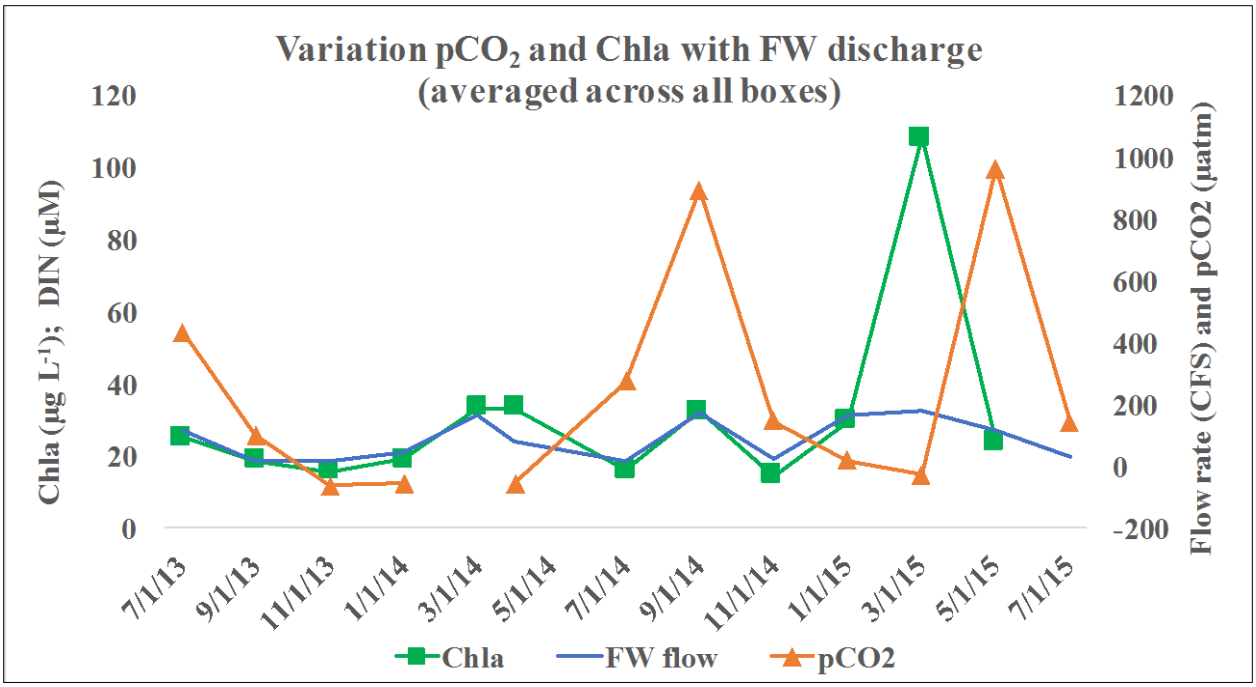

Figure 7-15. Temporal variability in the partial pressure of carbon dioxide (pCO_2), chlorophyll *a* (chl *a*), and freshwater (FW) discharge from July 2013 through July 2015.

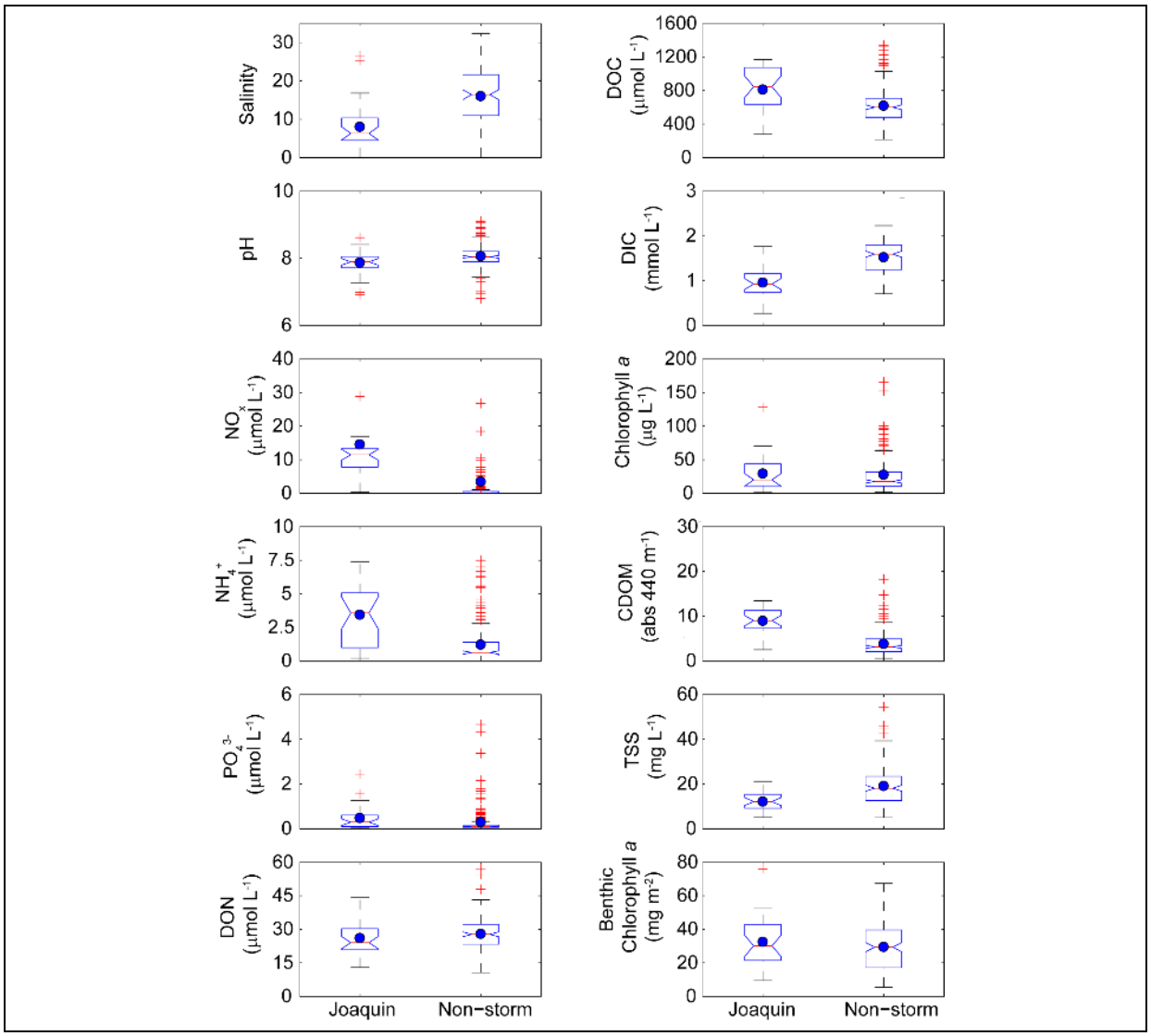

Figure 7-16. A comparison of water quality variables in the presence and absence of Hurricane Joaquin.

Note: The data marked Joaquin were collected from October 1, 2015 through March 30, 2016. Non-storm data were collected from July 2013 through July 2016. The boxes are interquartile range. Red lines are medians, blue dots are means, whiskers are 1.5 times interquartile range. Values outside of whiskers are red "+" symbols.

Effects of Climate and Storm Events on DO–Based Metabolism

DO–based metabolism rates were calculated for Stations SW-1, SW-3, and SW-9 by using the Open Water method (Caffrey, 2003); continuous DO was measured by YSI datasondes to assess potential effects due to climate and storm events. As observed in Year 1 of the study (from July 2013 through June 2014), daily respiration (R) and GPP generally varied with daily mean air temperature (Marine Corps Air Station New River [station name: KNCA]), with greater and more variable R and GPP rates in the warmer months (**Figure 7-17**). Temperature had only a small effect on net ecosystem metabolism, which is based on the difference between GPP and R and was less variable in the colder months. **Figure 7-18** shows net ecosystem metabolism versus daily precipitation. There were no obvious metabolic responses to small storm events (greater

than 2.5 cm of precipitation, but not including nor'easters and hurricanes). We did observe strongly heterotrophic conditions (less than −200 mmol of oxygen m^{-2} d^{-1}) at the upper estuarine station in Morgan Bay (Station SW-9) during and after Hurricane Joaquin and its associated nor'easters. During these events, there was daily precipitation from September 24 through October 5, 2015 (greater than 15 cm over the last 4 days) and very high river discharge at Gum Branch (U.S. Geological Survey [USGS] Stream Gaging Station 02093000). However, similarly high heterotrophy was observed at Station SW-9 from September 20 through 24, 2014, when there was lower river discharge and no major storm occurring before these dates other than two small storms on September 8 and 13 (6.7 cm and 5.3 cm, respectively). Storm events of similar magnitude and frequency during other time periods did not produce this metabolic response, suggesting that other potential drivers of increased heterotrophy or that metabolism may have been masked by the normally high day-to-day variability in oxygen flux.

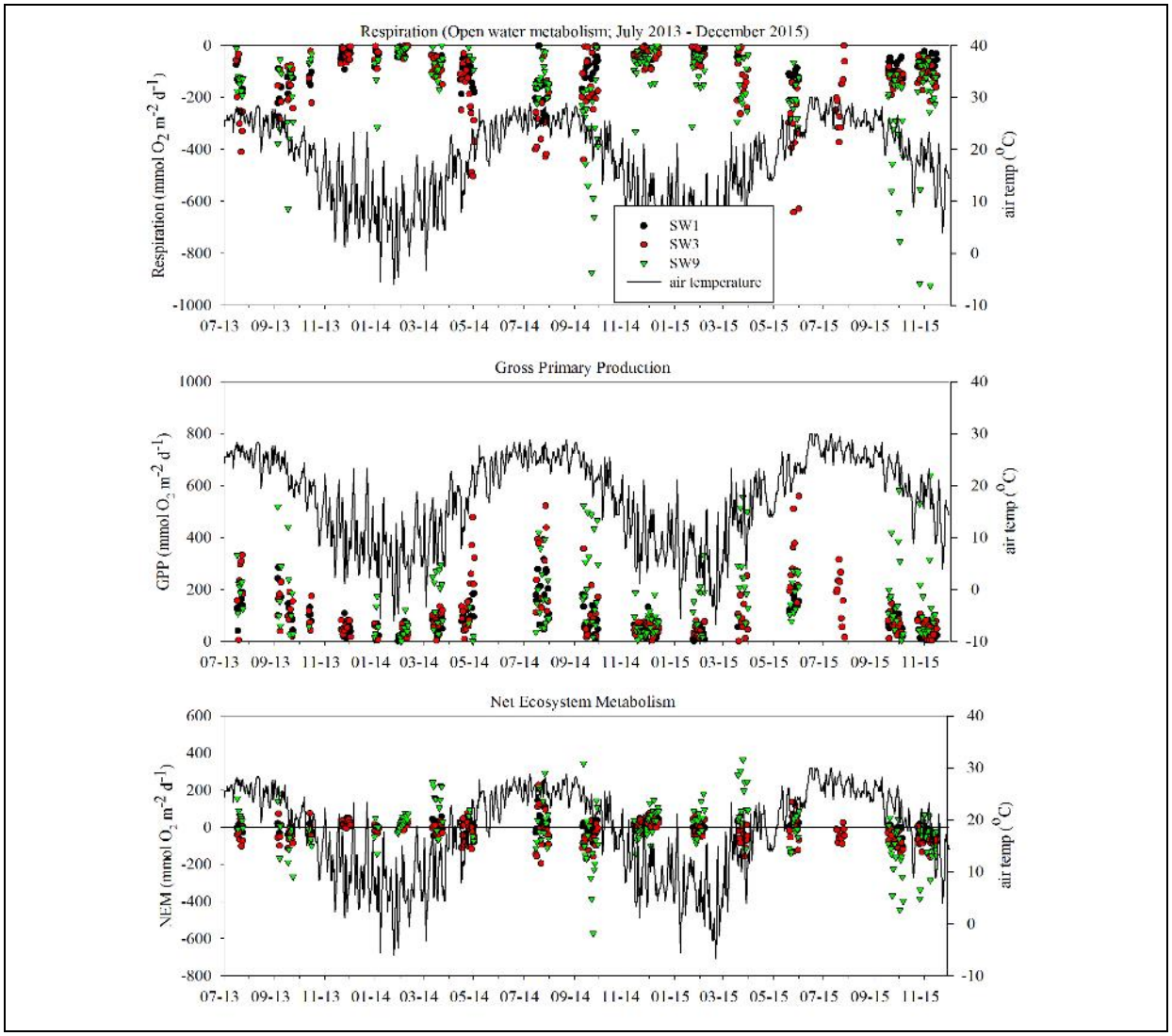

Figure 7-17. Daily respiration (R), gross primary production (GPP), and net ecosystem metabolism (NEM) rates at shallow water Stations (SW-1, SW-3, and SW-9) versus daily air temperature (Marine Corps Air Station New River [KNCA]) from July 2013 through December 2015.

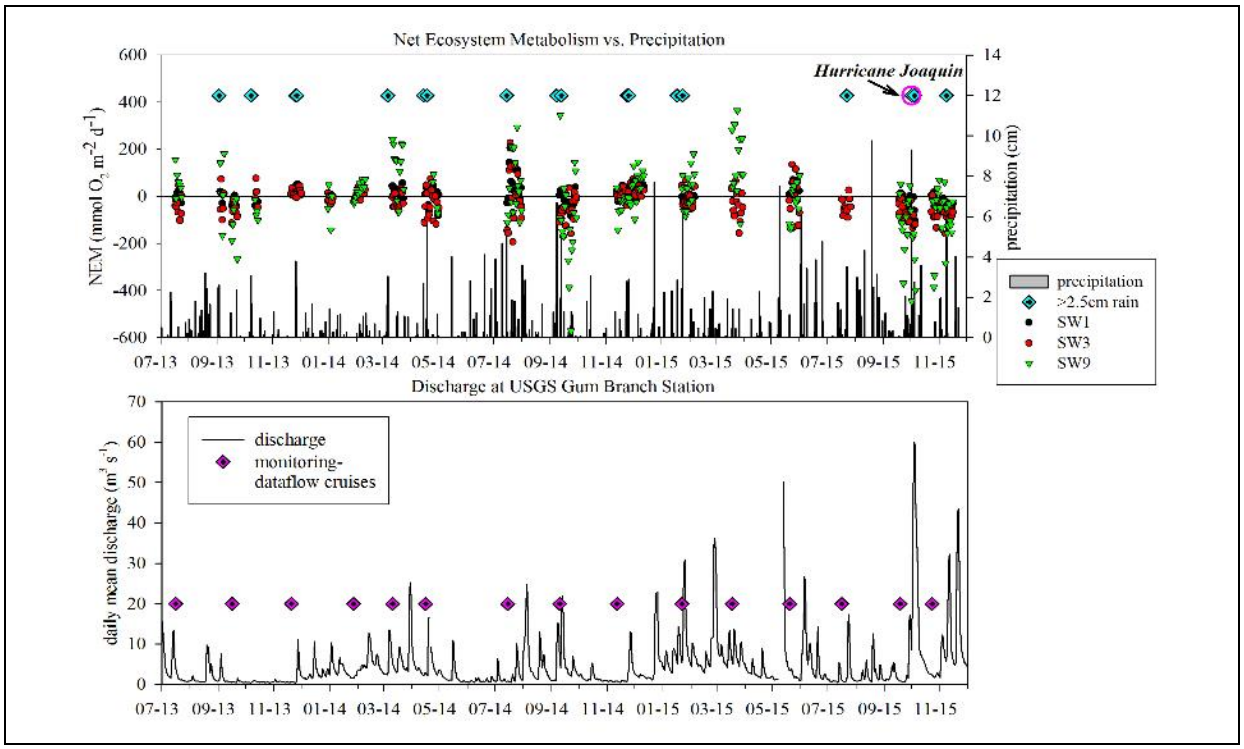

Figure 7-18. Daily net ecosystem metabolism (NEM) rates at shallow water Stations (SW-1, SW-3, and SW-9), daily precipitation (Marine Corps Air Station New River [KNCA]), and daily mean discharge at Gum Branch (USGS Stream Gaging Station 02093000) from July 2013 through December 2015.

Blue diamonds (upper panel) denote dates with greater than 2.5 cm of daily precipitation and are within 3 days prior to a YSI deployment. Pink diamonds (lower panel) denote dates when monitoring grab samples were collected and Dataflow cruises were conducted.

Assessment of Directionality and Trends

The AEM-3 was only in effect during DCERP2. The only monitoring in the shoal zone that occurred during DCERP1 was performed as part of Research Project AE-3. The focus of Research Project AE-3 was to determine the role of the benthos in mitigating nutrient pollution in the NRE. To fulfill its objectives, the sites chosen for study in Research Project AE-3 were located mainly in the mouths of the New River and other tributaries directly delivering nutrients to the estuary, Thus, the Research Project AE-3 sites were not the same as those used during DCERP2. For the AEM-3 sites, the focus was to assess the cycling of carbon in the estuary and to help develop a carbon budget for the entire ecosystem. As a result, we are unable to assess long-term trends over the 10-year program of DCERP1 and DCERP2; however, we did discuss the drivers of short-term variability (diel, seasonal, annual, and inter-annual) observed in the estuary during DCERP2 both in the previous paragraphs of this chapter and in the final report for Research Projects AE-4 and AE-6. Variability in carbon cycling in the NRE is also discussed in detail in a newly published paper by Crosswell et al. (2017).

Conclusions and Implications for Future Research and Implementation

Variability in both carbon and nutrient cycling is mainly because of natural drivers, in particular freshwater discharge, exacerbated by storm activity in the dynamic NRE. Nutrients and TOC from the watersheds both off-Base and within MCBCL are transported to the estuary in freshwater discharge. In the estuary, the nutrients support phytoplankton production and TOC is respired. The net ecosystem metabolism, either net autotrophy or heterotrophy, which results from these processes, controls the exchanges of carbon that occur between the estuary and the atmosphere, sediments, and coastal ocean. A net autotrophic estuary will act as a sink for atmospheric CO_2, may accumulate more sediment carbon, and will export more TOC than DIC to the ocean, whereas a net heterotrophic estuary will act as a source of atmospheric CO_2 and export more DIC than TOC to the coastal ocean. Overall, the NRE was poised in near metabolic balance during the years of our study; however, extreme storm events, which are likely to increase in response to climate change, will impact the cycling of carbon in the estuary, with increased fluxes of CO_2 into the atmosphere. Greatest net heterotrophy and the largest exchanges of CO_2 between the estuary and the atmosphere were at Station SW-10 near the City of Jacksonville. Water quality managers at MCBCL and in the region can help to reduce negative water quality impacts by promoting the use of best management practices on farmlands and confined animal feeding operations (CAFOs) in the region and by reducing erosion and nutrient release on MCBCL.

The studies conducted by AEM-3 and Research Projects AE-4 and AE-6 resulted in the development of one of the most highly resolved and complete carbon budgets for an estuary in the United States. The studies have also demonstrated that most of the estuarine carbon budgets currently available are limited because of insufficient sampling on temporal and spatial scales.

Findings with Implications for Future Base Management

The results and methodology to achieve results of AEM-3 and Research Projects AE-4 and AE-6 are currently being transferred to the York River Estuary in Virginia where the National Science Foundation has funded a new project to determine the effects of intense phytoplankton blooms on the carbon cycle and other biogeochemical and microbial community metrics. The National Science Foundation grant will provide Drs. Iris Anderson and Mark Brush with the opportunity to apply methods developed for DCERP to track the fate of carbon and nutrients derived from the harmful algal blooms, which are increasing in intensity and frequency in the York River Estuary.

Literature Cited

Anderson, I.C., M.J. Brush, M.F. Piehler, C.A. Currin, J.W. Stanhope, A.R. Smyth, J.D. Maxey, and M.L. Whitehead. 2014. Impacts of climate related drivers on the benthic nutrient filter in a shallow photic estuary. *Estuaries and Coasts 37*:S46–S62. doi: 10.1007/s12237-013-9665-5

Anderson, I.C., J.W. Stanhope, A.K. Hardison, and K.J. McGlathery. 2010. Sources and fates of nitrogen in Virginia coastal bays. Chapter 3, pp. 43–72 in *Coastal Lagoons: Critical*

Habitats of Environmental Change. Edited by Kennish, M.J., and H.W. Paerl. CRC Press.

Anderson, I.C., K.J. McGlathery, and A.C. Tyler. 2003. Microbial mediation of reactive nitrogen in a temperate lagoon. *Marine Ecology Progress Series 246*:73–84.

Arar, E.J., and G.B. Collins. 1997. *In vitro Determination of Chlorophyll a and Phaeophytin a in Marine and Freshwater Algae by Fluorescence*. Method 445.0, Revision 1.2. National Exposure Research Laboratory, Office of Research and Development, U.S. Environmental Protection Agency, Cincinnati, OH.

Bauer, J.E., W. Cai, P.A. Raymond, T.S. Bianchi, C.S. Hopkinson, and P.A. Regnier. 2013. The changing carbon cycle of the coastal ocean. *Nature 504*:61–70. doi: 10.1038/nature12857

Borges, A.V., and G. Abril. 2011. Carbon dioxide and methane dynamics in estuaries. Pp. 119–161 in *Treatise on Estuarine and Coastal Science. Volume 5: Biogeochemistry*. Edited by Wolanski, E., and D. McLusky. Academic Press.

Caffrey, J.M. 2003. Production, respiration, and net ecosystem metabolism in U.S. estuaries. *Environmental Monitoring and Assessment 81*:207–219.

Cai, W.J. 2011. Estuarine and coastal ocean carbon paradox: CO_2 sinks or sites of terrestrial carbon incineration? *Annual Review of Marine Science 3*:123–145.

Canuel, E.A., S.S. Cammer, H.A. McIntosh, and C.R. Pondell. 2012. Climate change impacts on the organic carbon cycle at the land-ocean interface. *Annual Reviews Earth Planetary Science 40*:685–711. doi:10.1146/annurev-earth-042711-105511

Crosswell, J.R., I.C. Anderson, J.W. Stanhope, B. Van Dam, M.J. Brush, S. Ensign, M.F. Piehler, B. McKee, M. Bost, and H.W. Paerl. 2017. Carbon budget of a shallow, lagoonal estuary: Transformations and source-sink dynamics along the river–estuary–ocean continuum. *Limnology and Oceanography 62*: S29–S45. doi: 10.1002/lno.10631

Crosswell, J.R., M.S. Wetz, B. Hales, and H.W. Paerl. 2014. Extensive CO_2 emissions from shallow coastal waters during passage of Hurricane Irene (August 2011) over the Mid-Atlantic Coast of the USA. *Limnology and Oceanography 59*:1651–1665. doi:10.4319/lo.2014.59.5.165

Currin, C.A. 2013. Marsh surface elevation. Chapter 7 in *Defense Coastal/Estuarine Research Program (DCERP1) Final Monitoring Report*. Project SERDP RC-1413. Edited by Cunningham, P. RTI International, Research Triangle Park, NC.

Ensign, S.H., J.N. Halls, and M.A. Mallin. 2004. Application of digital bathymetry data in an analysis of flushing times of two large estuaries. *Computers and Geosciences 30*(5):501–511.

Eyre, B.D., A.J.P. Ferguson, A. Webb, D. Maher, and J.M. Oakes. 2011. Metabolism of different benthic habitats and their contribution to the carbon budget of a shallow oligotrophic sub-

tropical coastal system (southern Moreton Bay, Australia). *Biogeochemistry 102*(1–3):87–110.

Gallegos, C.L., and P.J. Neale. 2002. Partitioning spectral absorption in case 2 waters: Discrimination of dissolved and particulate components. *Applied Optics 41*(21):4220–4233.

Green, S.A., and N.V. Blough. 1994. Optical absorption and fluorescence properties of chromophoric dissolved organic matter in natural waters. *Limnology and Oceanography 39*:1903–1916.

Hales, B., D. Chipman, and T. Takahashi. 2004. High-frequency measurement of partial pressure and total concentration of carbon dioxide in seawater using microporous hydrophobic membrane contactors. *Limnology and Oceanography Methods 2*:356–364. doi:10.4319/lom.2004

Hall, N.S., H.W. Paerl, B.L. Peierls, A.C. Whipple, and K.L. Rossignol. 2013. Effects of climatic variability on phytoplankton community structure and bloom development in the eutrophic, microtidal, New River Estuary, North Carolina, USA. *Estuarine, Coastal and Shelf Science 117*:70–82.

Joye, S.B., and I. Anderson. 2008. Nitrogen cycling in estuarine and nearshore sediments. Chapter 19, pp. 868–915 in *Nitrogen in the Marine Environment.* Edited by Capone, D., D. Bronk, E. Carpenter, and M. Mulholland. Springer Verlag.

Keeney, D.R., and D.W. Nelson. 1982. Nitrogen—Inorganic forms. Pp. 643–693 in *Methods of Soil Analysis*. (2nd Edition). Edited by Page, A.L., et al. ASA, CSSA, and SSSA: Madison, WI.

Kemp, W.M., E.M. Smith, M. Marvin-DiPasquale, and W.R. Boynton. 1997. Organic carbon balance and net ecosystem metabolism in Chesapeake Bay. *Marine Ecology Progress Series 150*:229–248. doi:10.3354/meps150229

Kirk, J.T.O. 1994. *Light and Photosynthesis in Aquatic Ecosystems*. (2nd edition). Cambridge University Press: Cambridge, United Kingdom. 509 pages.

Knepel, K., and K. Bogren. 2001. Determination of orthophosphate by flow injection analysis. QuikChem Method 31-115-01-1-H, Lachat Instruments, Milwaukee, WI.

Koroleff, F. 1983. Total and organic nitrogen. Pp. 162–169 in *Methods of Seawater Analysis*. Edited by Grasshoff, K., M. Ehrhardt, and K. Kremling. Verlag-Chemie, Weinheim.

Liao, N. 2001. Determination of ammonia in brackish or seawater by flow injection analysis. QuikChem Method 31-107-06-1-B, Lachat Instruments, Milwaukee, WI.

Lorenzen, C. 1967. Determination of chlorophyll and phaeopigments: Spectrophotometric equations. *Limnology and Oceanography 12*:343–346.

Madden, C., and J. Day. 1992. An instrument system for high-speed mapping of chlorophyll *a* and physicochemical variables in surface waters. *Estuaries 15*:421–427. doi:10.2307/1352789

McGlathery, K.J., K. Sundbäck, and I.C. Anderson. 2007. Eutrophication in shallow coastal bays and lagoons: The role of plants in the coastal filter. *Marine Ecology Progress Series 348*:1–18.

Neubauer, S.C., and I.C. Anderson. 2003. Transport of dissolved inorganic carbon from a tidal freshwater marsh to the York River estuary. *Limnology and Oceanography 48*(1):299–307.

Neubauer, S.C., W.D. Miller, and I.C. Anderson. 2000. Carbon cycling in a tidal freshwater marsh ecosystem: A gas flux study. *Marine Ecology Progress Series 199*:13–30.

Nixon, S. W. 1995. Coastal marine eutrophication: A definition, social causes, and future concerns. *Ophelia* 41: 199–219. doi: 10.1080/00785236.1995.10422044

Nixon, S.W., B. Buckley, S. Granger, and J. Bintz. 2001. Response of very shallow marine ecosystems to nutrient enrichment. *Human and Ecological Risk Assessment 7*(5):1457−1481.

Peierls, B.L., N.S. Hall, and H.W. Paerl. 2012. Non-monotonic responses of phytoplankton biomass accumulation to hydrologic variability: A comparison of two coastal plain North Carolina estuaries. *Estuaries and Coasts 35*:1376–1392. doi:10.1007/s12237-012-9547-2

Shoaf, W.T., and B.W. Lium. 1976. Improved extraction of chlorophyll *a* and *b* from algae using dimethylsulfoxide. *Limnology and Oceanography 21*:926–928.

Smith, P., and K. Bogren. 2001. Determination of nitrate and/or nitrite in brackish or seawater by flow injection analysis colorimetry. QuikChem Method 31-107-04-1-E, Lachat Instruments, Milwaukee, WI.

Sundbäck, K., F. Linares, F. Larson, A. Wulff, and A. Engelsen. 2004. Benthic nitrogen fluxes along a depth gradient in a microtidal fjord: The role of denitrification and microphytobenthos. *Limnology and Oceanography 49*:1095–1107.

Appendix 7-A
List of Scientific/Technical Publications

Papers

Anderson, I.C., M.J. Brush, M.F. Piehler, C.A. Currin, J.W. Stanhope, A.R. Smyth, J.D. Maxey, and M.L. Whitehead. 2014. Impacts of climate-related drivers on the benthic nutrient filter in a shallow photic estuary. *Estuaries and Coasts 37*(Suppl 1):S46–S62. doi: 10.1007/s12237-013-9665-5

Crosswell, J.R., I.C. Anderson, J.W. Stanhope, B. Van Dam, M.J. Brush, S. Ensign, M.F. Piehler, B. McKee, M. Bost, and H.W. Paerl. 2017. Carbon budget of a shallow, lagoonal estuary: transformations and source-sink dynamics along the river–estuary–ocean continuum. *Limnology and Oceanography*. doi: 10.1002/lno.10631

Van Dam, B., J.R. Crosswell, I.C. Anderson, and H.W. Paerl. In review. Watershed-scale drivers of air-water CO_2 exchanges in two lagoonal, North Carolina (USA) estuaries. *Limnology and Oceanography*.

Presentations

Anderson, I., J. Crosswell, K. Czapla, and B. Van Dam. 2017. *Carbon Transformations and Source-Sink Dynamics Along a River, Marsh, Estuary, Ocean Continuum*. (Invited speaker). Presented at the American Geophysical Union, New Orleans, LA. December.

Anderson, I., C. Currin, C. Tobias, K. Czapla, N. McTigue, and S. Ensign. 2017. *Lateral Export of Carbon from Salt Marshes to Adjacent Aquatic Systems*. Presented to the Coastal Estuarine Research Federation, Providence, RI. November.

Czapla, K., I. Anderson, J. Stanhope, M. Fogarty, C. Currin, N. McTigue, and E. Herbert. 2017. *Spatial Patterns of Net Community Production in Response to Fertilization in a Polyhaline Marsh*. Presented to the Coastal Estuarine Research Federation, Providence, RI. November.

Anderson, I., K. Czapla, and E. Herbert. 2017. *Salt Marsh Metabolism and Carbon Accumulation*. Invited presentation at the Ocean Carbon and Biogeochemistry Workshop, Woods Hole, MA. June.

Czapla, K., I. Anderson, E. Herbert, and M. Fogarty. 2017. *Salt Marsh Metabolism and Carbon Accumulation: Effects of Location and Fertilization*. Poster presented at the Ocean Carbon and Biogeochemistry Workshop, Woods Hole, MA. June.

Anderson, I., M. Brush, J. Stanhope, J. Crosswell, H. Paerl, M. Piehler, B. McKee, and B. Van Dam. 2017. *Carbon Budget of a Shallow, Lagoon Estuary: Transformations and Source-Sink Dynamics*. Invited plenary talk at the University of South Alabama, Dauphin Island Sea Laboratory, Dauphin Island, AL. April.

Anderson, I., J. Crosswell, and B. Van Dam. 2017. *Carbon Transformations and Source–Sink Dynamics Along a River, Estuary, Ocean Continuum*. Invited presentation at the Annual Meeting of the North America Carbon Program, Bethesda, MD. February.

Czapla, K., I. Anderson, and J. Stanhope. 2016. *Effective Edges: Salt Marsh Creek Banks as Hotspots for N Removal*. Presented to the Atlantic Estuarine Research Society, Virginia Beach, VA. March.

Anderson, I., J. Stanhope, B. Van Dam, N. Hall, J. Croswell, H. Paerl, and M. Brush. 2015. *Bio-physical Controls of CO_2 Fluxes Along a River–Estuary Continuum*. Presented at the Coastal and Estuarine Research Federation Conference, Portland, OR. November.

Stanhope, J., I. Anderson, J. Croswell, B. Van Dam, H. Paerl, and H. Walker. 2015. *A Shallow Photic Estuary in North Carolina: A Source or Sink of Carbon Dioxide?* Presented at the Coastal and Estuarine Research Federation Conference, Portland, OR. November.

Van Dam, B., J. Stanhope, I. Anderson, and H. Paerl. 2015. *Estuarine CO_2 Flux: A Comparison of Two North Carolina Estuaries*. Presented at the Coastal and Estuarine Research Federation Conference, Portland, OR. November.

Paerl, H.W., I.C. Anderson, W.S. Gardner, M.J. McCarthy, N.S. Hall, B.L. Peierls, and K.L. Rossignol. 2015. *Controlling Eutrophication Along the Freshwater–Marine Continuum: Why the Need for Dual Nutrient Input Constraints?* Presented at the Coastal and Estuarine Research Federation Conference, Portland, OR. November.

Stanhope, J.W., I.C. Anderson, M.J. Brush, C.A. Currin, and M.F. Piehler. 2013. *Benthic Microbial Responses to Interacting Physical–Biological Drivers in a Shallow Estuary*. Presented at Biennial Conference of the Coastal and Estuarine Research Federation, CERF 2013, San Diego, CA. November.

Anderson, I.C. 2015. *Estuaries as Sources or Sinks of Carbon: Climatic Drivers.* Invited presentation at the Laura Randall Schweppe Endowed Lecture Series in Marine Science, University of Texas, Austin, TX. March.

Anderson, I.C. 2014. *Interacting Drivers Regulating the Fate of Nitrogen in Shallow Photic Marine Systems*. Presented at the Joint Aquatic Sciences Meeting, Portland, OR. May.

Anderson, I.C. 2012. *Responses of the Benthic Filter to Physical Drivers.* Presented at the University of Parma, Parma, Italy. October.

Anderson, I.C. 2012. *The Role of the Benthic Filter in Shallow Estuaries.* Invited presentation at the East China Normal University, Shanghai, China. June.

Anderson, I.C. 2012. *Tracking the Fate of Carbon and Nitrogen in a Shallow Photic Coastal Lagoon.* Invited presentation at the East China Normal University, Shanghai, China. June.

Appendix 7-B
List of Students

- Czapla, K., Ph.D. expected in August 2018, Virginia Institute of Marine Science, College of William and Mary, Williamsburg, VA.

Chapter 8

Climate and Land-Use Impacts on Exports of Carbon, Suspended Solids, and Nutrients from Coastal Subwatersheds

SERDP Project Number: RC-2245

Aquatic and Estuarine Module

Research Project AE-5

Lead Researchers:

Dr. Michael F Piehler
University of North Carolina at Chapel Hill's Institute of Marine Sciences
piehler@unc.edu

Supporting Researchers:

Suzanne Thompson, sthompso@email.unc.edu
Adam Gold, acgold@live.unc.edu

November 2017

Final

This report was prepared under contract to the U.S. Department of Defense (DoD) Strategic Environmental Research and Development Program (SERDP). The publication of this report does not indicate endorsement by DoD, nor should the contents be construed as reflecting the official policy or position of DoD. References herein to any specific commercial product, process, or service by trade name, trademark, manufacturer, or otherwise, do not necessarily constitute or imply its endorsement, recommendation, or favoring by DoD.

Table of Contents

Acronyms 8-v
Abstract 8-1
Objectives of the Research Project 8-2
Background 8-2
Materials and Methods 8-4
Tributary Stream Carbon and Nutrient Loading 8-4
Stream Temperature and Conductivity 8-7
Forestry Impacts on Carbon and Nutrient Loading 8-7
Stormwater Best Management Practices 8-8
Results and Discussion 8-10
Tributary Stream Nutrient and Carbon Loading 8-10
Forestry Impacts on Carbon and Nutrient Loading 8-13
Stream Temperature and Conductivity 8-15
Stormwater Best Management Practices 8-17
Conclusions and Implications for Future Research and Implementation 8-21
Research Questions 8-21
Findings with Implications for Future Base Management 8-22
Literature Cited 8-23
Appendix 8-A: Supporting Data 8-A-1
Appendix 8-B: List of Scientific/Technical Publications 8-B-1
Appendix 8-C: List of Students 8-C-1
Appendix 8-D: Other Supporting Information 8-D-1

List of Figures

Figure 8-1. Overview map of the study watersheds and impervious area. 8-5
Figure 8-2. Location of forested stream sample points and the watersheds. 8-8
Figure 8-3. Locations of the five retention ponds sampled for net N_2 fluxes and nutrient fluxes at the sediment–water interface. 8-9
Figure 8-4. Mid-aged stormwater wet pond at Tarawa Terrace. Cattails (Typha spp.) fringe the pond and alligator weed (Alternanthera philoxeroides) floats along the surface around the pond edge. 8-10
Figure 8-5. Nitrate (NO_x) loading from watersheds on MCBCL. 8-12

Figure 8-6. (Left panel) Annual loads of POC, DOC, and DIC from streams organized from low to high imperviousness, French Creek (French), Traps Bay Creek (Traps), Cogdels Creek (Cogdels), Courthouse Bay (CHB), and Tarawa Terrace (Tarawa). (Right panel) The relationship between the ratio of DOC:DIC loading and watershed imperviousness. 8-13

Figure 8-7. Annual loads of water from watersheds being managed to restore longleaf pine (MIXED), longleaf pine–dominated (LLYP), and unmanaged, loblolly pine–dominated (LOBLOLL). 8-14

Figure 8-8. Annual load of DOC (top) and DIC (bottom) in storm (s) and baseflow(b) from watersheds being managed to restore longleaf pine (MIXED), longleaf pine–dominated (LLYP), and unmanaged, loblolly pine–dominated (LOBLOLL). 8-14

Figure 8-9. Stream temperatures of the five study streams. 8-15

Figure 8-10. Comparison of stream and air temperatures through DCERP1 and DCERP2. 8-16

Figure 8-11. Mean stream conductivity through the study period plotted versus watershed imperviousness. 8-17

Figure 8-12. The relationship between annual precipitation and mean annual conductivity from 2010 through 2015 8-17

Figure 8-13. Nutrient (µM), total suspended solids (TSS; mg/L), and chlorophyll a (Chl-a; µg/L) concentrations for the pre-construction (Pre) and post-construction (Post) periods of development during both baseflow and stormflow. 8-18

Figure 8-14. Net sediment N_2 fluxes as a function of pond age for both ambient and nitrate–enriched conditions. 8-19

Figure 8-15. Boxplots of net sediment N_2 fluxes in different portions of a single wet pond. Measurements were taken during late summer. 8-20

List of Tables

Table 8-1. Land Cover and Watershed Area of Study Sites 8-6

Table 8-2. Forested Watershed Attributes 8-7

Table 8-3. Descriptions of Data and Equations Used to Create Maps of Estimated Monthly Loads for Various Water Quality Variables 8-11

Table 8-4. Mean Change and Mean Percent Change for Each Water Quality Constituent During the Monitoring Period of the Single, Mid-aged Pond (from July 2016 through January 2017) 8-20

Acronyms

°C	degree Celsius
µg/L	micrograms per liter
µm	micrometer
µM	micromoles
µs/cm	microseconds per centimeter
AE	Aquatic/Estuarine (Module)
AEM	Aquatic/Estuarine monitoring activity
b	baseflow
BMP	best management practice
CC	Climate Change (Module)
CHB	Courthouse Bay
Chl-*a*	chlorophyll *a*
CHN	carbon, hydrogen, and nitrogen
cm	centimeter
COG	Cogdels Creek
DCERP	Defense Coastal/Estuarine Research Project
DCERP1	first cycle of DCERP
DCERP2	second cycle of DCERP
DIC	dissolved inorganic carbon
DOC	dissolved organic carbon
DoD	U.S. Department of Defense
FR	French Creek
g/ha	grams per hectare
ha	hectare
HCl	hydrochloric acid
kg/ha	kilograms per hectare
LLYP	longleaf pine
LOBLOLL	loblolly pine
m	meter
m^3/ha	cubic meters per hectare
MCBCL	Marine Corps Base Camp Lejeune
mg/L	milligrams per liter
mL	milliliter
mm	millimeter
$NaNO_3$	sodium nitrate
NH_4^+–N	ammonium-nitrogen (referred to as NH_4)
NLCD	National Land Cover Dataset
NO_3^-+NO_2^-	nitrate plus nitrite-nitrogen (referred to as NO_x)
NRE	New River Estuary
ON	organic nitrogen
PO_4^{3+}–P	orthophosphate (referred to as PO_4)
POC	particulate organic carbon
Post	post-construction
ppt	part per thousands

Pre	pre-construction
RC	Resource Conservation and Climate Change (a SERDP program area)
s	storm
SERDP	Strategic Environmental Research and Development Program
TAR	Tarawa Terrace
TDN	total dissolved nitrogen
TOC	total organic carbon
TRAP	Traps Bay Creek
TSS	total suspended solids
YSI	Yellow Springs Instruments, Inc.

Abstract

Streams originating on the coastal plain are understudied, despite being both a critical component of coastal ecosystem function and a priority for land managers due to their importance in significant regulations related to clean water. Marine Corps Base Camp Lejeune (in North Carolina) was the location of a study to assess the connection of land activities to changes in water quality. We measured streamflow, temperature, conductivity, and concentrations of nutrients, carbon, and sediments at sites above the influence of tide in watersheds with distinctive land use. Development, as represented by increases in imperviousness, was found to increase concentrations and loading of most constituents. Dissolved organic carbon was an exception because its sources are wetlands and flood plains that are often lost during development. Maximum summer temperature was found to increase in streams with more developed watersheds, likely due to loss of shading from vegetation and increased warming potential on impervious surfaces. Conductivity was not found to be affected by development at our stream stations. Different forestry management practices for longleaf pine (*Pinus palustris*), unmanaged loblolly pine (*Pinus taeda*), and forests being managed to transition to longleaf pine were found to have impacts on nutrient and carbon loading, but not on water budgets. The longleaf pine watershed had higher exports of all carbon and nutrient forms. Finally, stormwater pond efficacy was assessed by using both a time series approach and targeted pond measurements. All data indicated that stormwater ponds were not comprehensively maintaining water quality. Particular challenges were identified with nitrogen, including measuring consistent and significant rates of microbially mediated nitrogen fixation in pond sediments. Overall, nutrient loading from Marine Corps Base Camp Lejeune streams was found to be on the low end, relative to similar streams. Additionally, the total load of nutrients from streams on Base to the New River Estuary was found to be small relative to other sources. Models developed from our data permit prediction of the impacts of future watershed development on nutrient loading. Assessments of stormwater ponds also offered a potential rationale for maintenance that could lead to enhanced stormwater pond function. Information summarized here provides a robust tool that the Base can use for future decision making, including the negotiation of a regional water quality plan for the New River Estuary.

Keywords: Best management practices, carbon, land use, nitrogen, phosphorus, stormflow, stream, watershed

Objectives of the Research Project

Research Project AE-5 builds on our understanding of the linkages between land-use activities and the tributary streams, with a focus on the impacts of climate change and climate variability on the processing and export of materials (particularly carbon) by coastal tributary creeks. Specific objectives of Research Project AE-5 are to

1. Assess Marine Corps Base Camp Lejeune's (MCBCL's) land-use effects on tributary creek loading of carbon (both dissolved and particulate) and its delivery mechanism to the estuary (e.g., in baseflow or stormflow). Measure carbon, nutrient, and sediment concentrations through baseflow and stormflow in five MCBCL tributaries to the New River Estuary (NRE) with representative land uses over a 2-year period (2013–2015). Employ flow and water level from monitoring activity AEM-2 (tributary creek monitoring) to calculate loading, and then use these loads during Research Project AE-6 to assess in-stream attenuation of loading. Conduct analyses to determine the quantity of carbon loaded, and the type of carbon (e.g., labile versus refractory). Use these data to determine the load of carbon from MCBCL lands through streams to the NRE with specific details on the effects of MCBCL land use.

2. Measure the impacts of forestry management on exports of carbon, suspended solids, and nutrients. Make targeted deployments in forestry management areas adjacent to streams in land areas subjected to midstory and understory thinning and prescribed burning. Collect similar measurements at a reference stream draining from a similar forest type that is not subject to active management.

3. Quantify the linkage between tributary creek temperature and MCBCL land use and determine the potential effects on the ecology of both the tributary creeks and the estuary. Compare temperatures in tributaries to the NRE and determine the impacts of stream delivery of varied temperature water to the NRE.

4. Determine the extent to which stormwater best management practices (BMPs) restore ecosystem function by decreasing sub-watershed scale export of carbon, nutrients, and sediments through tributary streams. During recent construction activities at MCBCL, a significant number of stormwater management structures were built on the installation. Through targeted deployments (portions of 2016), determine the mass balance of materials (nutrients, sediments, and carbon) entering and leaving several of these BMP structures. Assess the extent to which the BMP engineering solution reduces excessive levels of nutrients, suspended solids, and carbon to the levels observed in less developed watersheds.

Background

Changes in watersheds associated with human development affect ecosystem function through impacts on both the hydrology and the sources and composition of materials (e.g., carbon, nitrogen, sediments; Paul and Meyer, 2001). The transition from an undeveloped to a developed landscape results in increases in the amount of impervious cover and decreases in forested area, among other changes. These changes decrease infiltration of rainfall, creating periods of

increased peak stormflows of shorter duration and a corresponding potential for decreased baseflows. Some changes in land use, associated with development, likely increase sources of materials or decrease the effectiveness of sinks of materials.

In coastal regions, managing stream loading of nutrients and suspended matter can pose a challenge to managers because sufficient quantities of each are necessary for coastal wetlands ecosystem to function, but in excess, they are pollutants. Some proportional amounts of nitrogen and phosphorus are necessary to support primary production to meet the consumptive needs of higher trophic levels in coastal ecosystems. Additionally, sea level rise is currently counteracted by accretion of mineral and organic materials in marshes, necessitating the delivery of ample amounts of sediment to coastal areas, in part, via riverine networks (Morris et al., 2002). Balancing the need for some nutrients and suspended materials within coastal management programs generally designed to minimize loading requires reliable information about the magnitudes and timing of material loading from coastal streams.

A variety of modeling approaches have been used to estimate material loading by streams over a range of systems (Alexander et al., 2002; Seitzinger et al., 2005). The models reviewed by Alexander et al. (2002) predicted nitrogen export within 50% of measured export for large watersheds; however, this potential discrepancy may be too large if the information is being compared with relatively small-scale changes in the landscape. One central challenge for modeling coastal stream loading is the tendency for a shallow water table, which significantly affects stream function by delivering water and nutrients to streams through groundwater flow that is difficult to measure.

Directly measuring coastal stream material load is important for understanding the effects of development on coastal receiving waters, as is the need for standardized methods that enable cross-watershed comparisons. Several studies have used direct measurements of material concentration and discharge to calculate load (Birgand et al., 2006; Kaushal et al., 2008; Sobota et al., 2009). Measuring discharge and multiple parameters of water chemistry is the most robust method and rigorously connects changes in the watershed to stream carbon, nutrient, and sediment loading. Natural coastal subwatersheds deliver high dissolved organic carbon (DOC) loads due to the prevalence of wetlands (Mulholland and Kuenzler, 1979). Urbanization in coastal watersheds has been linked to changes in DOC loading (Hatt et al., 2004). Quantitative connections between the degree of development and the patterns and magnitudes of loading of dissolved carbon and other constituents (i.e., suspended materials, nutrients) require direct measurements at several representative sites.

Recent increases in stream and river temperatures have been reported throughout the United States (Kaushal et al., 2010). Water temperatures affect the metabolic rates of organisms and the speed of chemical reactions (Harris et al., 2006; O'Connor et al., 2009) and water characteristics, including vapor pressure, surface tension, density, and viscosity (Stevens et al., 1975), that affect ecosystem function (Vogel, 1994). Metabolic rates are known to increase exponentially with temperature (Brown, 2004); however, the change in these rates is not uniform across all organisms. Harris et al. (2006) found that consumer (heterotrophic) respiration increases twice as rapidly as net primary production rates with temperature increases due to larger consumer biomass and a lower autotrophic activation energy. This difference could shift the ecosystem balance and impose limits on heterotrophic biomass or deplete autotrophic standing stock

(O'Connor et al., 2009). Changes in temperature can also influence the organisms' presence in an area because these organisms have specific temperature preferences and tolerances.

Stormwater runoff can have negative ecological effects on coastal waters (Sanger et al., 2013), and one of these negative effects is eutrophication caused by nitrogen enrichment (Howarth and Marino, 2006). One way to mitigate increased nitrogen loads from urbanized watersheds is to use structural BMPs to treat stormwater. The most common type of BMP is to employ the use a stormwater pond (Collins et al., 2010). Stormwater ponds collect runoff from a landscape and either fully drain to a stream over time ("dry pond") or drain partially and maintain a permanent pool of water ("wet pond"). The main purpose of these ponds is to slow down the delivery of water from impervious surfaces to the stream and settle out particulate pollutants (Hancock et al., 2010; NCDENR, 2009), but these ponds are also thought to be important sites for nitrogen removal via denitrification (Bettez and Groffman, 2012; Collins et al., 2010; Groffman et al., 2004 and 2009; Zhu et al., 2004). Previous studies on stormwater ponds or other BMPs have used methods that do not directly measure nitrogen removal processes or have used acetylene assays that significantly alter the microbial community (Fulweiler et al., 2015). Additionally, no studies have directly measured nitrogen removal processes in stormwater ponds or BMPs in coastal areas. We applied state-of-the-art field and analytical methodologies to better understand the impacts of stormwater wet ponds on coastal water quality.

Materials and Methods

Tributary Stream Carbon and Nutrient Loading

Using five creeks (**Figure 8-1** and **Table 8-1**) with watersheds on a development gradient from 3% to 63% developed area (impervious area and open developed area) and a wide range of imperviousness (1%–23%), we measured sample concentration of carbon, nutrients, and suspended sediments for 2 years (June 2013–July 2015). We deployed automated water samplers (Teledyne Isco, Inc.) equipped with datasondes (Yellow Springs Instruments, Inc. [YSI]) to continuously collect stream discharge data. We calculated loading of nutrients, sediments, and dissolved inorganic carbon (DIC) and DOC (including quantity of reactive carbon) from the sum of daily water volume based on 0.5-hour records of water velocity and level, which were measured in monitoring activity AEM-2 and paired with nutrient, sediment, and carbon concentrations from monthly baseflow conditions and stormflow periods.

Water sampling consisted of manual sampling (i.e., water grab sample, water depth measurement, and water velocity confirmation by using a Sontek Flowtracker Acoustic Doppler Velocimeter) of all five creeks every other week and after a rain event (defined as greater than 2.5 cm of rain in 24 hours). In addition, we conducted more frequent automated sampling to enhance resolution during storm events with automated samplers. We programed the samplers to collect storm water samples above a threshold stream velocity set for storms and at flow-paced intervals once enabled. We collected automated grab samples as soon as possible after a rain event and transported them on ice to the laboratory for processing. We selected water samples from the automated samplers to encompass a period that included before, rising, peak, and falling limbs of hydrographs, for each storm at each site.

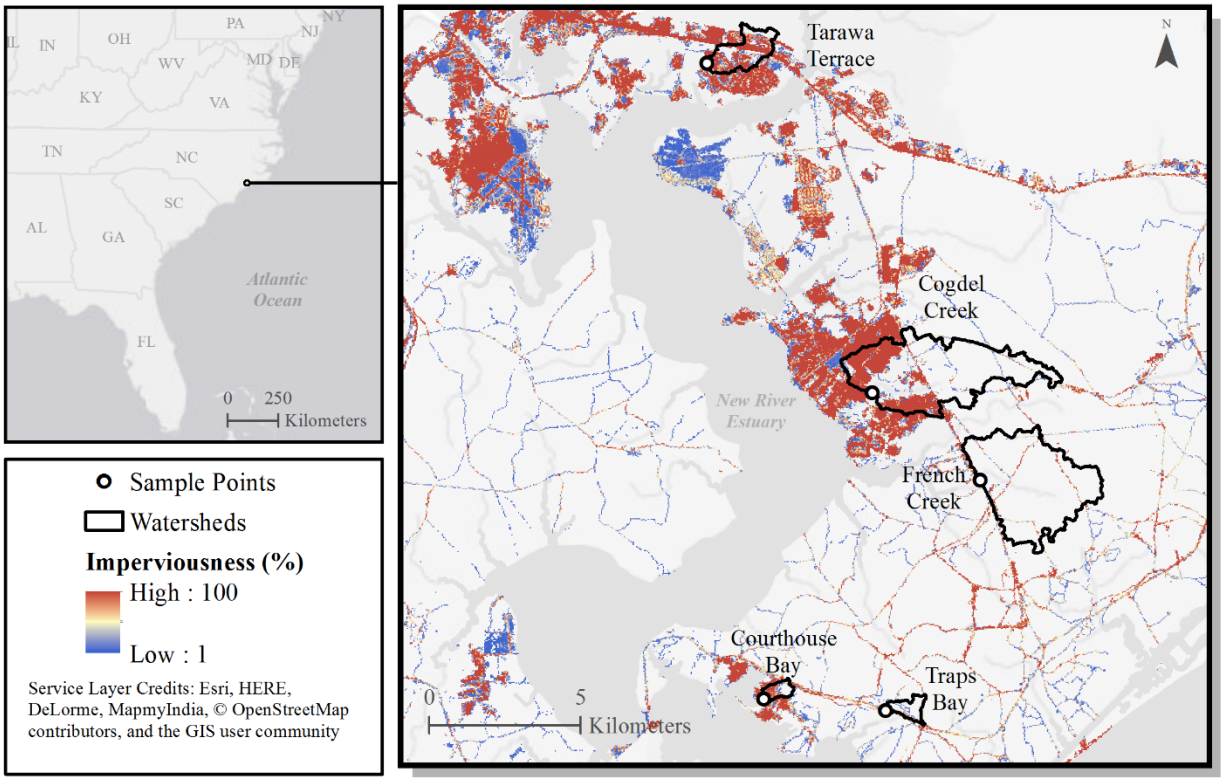

Figure 8-1. Overview map of the study watersheds and impervious area.

We analyzed all water samples collected for total suspended solids (TSS) and nutrients, including nitrate plus nitrite-nitrogen (NO_3^-+NO_2^-, referred to as NO_x), ammonium-nitrogen (NH_4^+−N, referred to as NH_4), orthophosphate (PO_4^{3+}−P, referred to as PO_4), and total dissolved nitrogen (TDN). We filtered water samples through Whatman glass fiber filters (25 mm in diameter, 0.7-µm nominal pore size) and will analyze the filtrate with a Lachat QuickChem 8000 automated ion analyzer by using standard protocols (NO_x Method 31-107-04-1-A; NH_4 Method 31-107-06-1-A; and PO_4 Method 31-115-01-3-G, Lachat Instruments, Milwaukee, WI). We filtered additional water through pre-cleaned and dried Whatman glass fiber pre-filters (47 mm in diameter, 0.7-µm nominal pore size) and dried and weighed residue for measurement of total suspended solids (TSS) by using standard protocols (Method 2540 D, 2-57 [Clesceri et al., 1998]). We used a carbon, hydrogen, and nitrogen (CHN) analyzer to measure particulate organic carbon (POC) and employed a total organic carbon (TOC) analyzer to measure DOC. For POC analysis, we filtered stormflow and baseflow water samples on 25-mm pre-combusted glass fiber filters and stored the samples frozen in small, plastic Petri dishes. We fumed the filters with concentrated hydrochloric acid (HCl) for 6 hours and allowed them to dry before analyzing the filters on a CHN analyzer. For DOC analysis, we filtered water samples on 25-mm pre-combusted glass fiber filters. We collected 5 mL of filtrate in a combusted glass scintillation vial and capped it with an acid rinsed, Teflon-lined cap. Samples were stored frozen on their side until analysis on a TOC analyzer. Samples were run once on the TOC analyzer, and then were acidified and re-run to allow for the calculation of DIC by difference.

Table 8-1. Land Cover and Watershed Area of Study Sites

Site	Forested Land (in ha)	Impervious Surface (in ha)	Developed Land (in ha)	Total Area (in ha)
Cogdels Creek	280.53 (33.6%)	115.25 (13.8%)	209.16 (25.0%)	835.83
French Creek	80.28 (9.9%)	8.56 (1.1%)	27.72 (3.4%)	807.30
Tarawa Terrace	24.48 (17.6%)	32.28 (23.2%)	63.90 (45.9%)	139.14
Courthouse Bay	3.06 (9.8%)	4.85 (15.5 %)	19.62 (62.6%)	31.32
Traps Bay Creek	5.76 (11.3%)	2.11 (4.1%)	6.39 (12.5%)	51.03

We separated stream loading into storm load, which occurs during rain events, and base load, which represents the groundwater contribution to the load. We used a hydrograph separation method to divide the flow into stormflow and baseflow. Using this method, we manually inspected continuous flow data to determine storm events based on peaks in flow (Ward and Robinson, 2000). We interpolated the baseflow during storm events between a point prior to the peak and after the peak to yield a reasonable estimate for baseflow during storm conditions. Storm events increase shallow groundwater flow, thus increasing baseflow. Because our sites are generally above the range of tidal influence, assessing the impacts of tidal elevation on the hydrograph is not routinely required. Analyzing baseflow load and stormflow load separately provided insight regarding the differences in loading that occurred due to changes in land coverage that may influence flow patterns and runoff characteristics.

To estimate the mean monthly nutrient and sediment loading from MCBCL watersheds into the NRE, mean watershed imperviousness of watersheds draining into the NRE from the MCBCL were calculated, and regression equations were used to calculate predicted nutrient and sediment loading. Specifically, concentration measurements for each variable were combined with discharge measurements to calculate monthly loads. Mean monthly nutrient loads for each water quality variable for each watershed were derived by calculating the mean of monthly nutrient loads between July 2008 and July 2015. Mean watershed imperviousness was calculated by taking the mean of 2011 National Land Cover Dataset (NLCD) percent imperviousness data (Xian et al., 2011) within each watershed. A linear model was created for each water quality variable by using the mean monthly nutrient load as the dependent variable and percent watershed imperviousness (imperviousness) as the independent variable. When necessary, outlier watersheds were removed from the linear model due to exceptionally high nutrient loads. ESRI's ArcMap and aerial imagery were used to place 225 points around the NRE at the mouth of streams that flow into the NRE. The watershed for each of these points was delineated by using 1-m resolution elevation data. The regression equations were then used to calculate an estimated mean monthly load of each water quality variable for all 225 watersheds. Maps of estimated mean monthly nutrient and sediment loads were created from stream water quality data collected between 2008 and 2015 on five watersheds across MCBCL. NLCD data detailing the amount of impervious area was from 2011; therefore, the previously mentioned maps may not reflect current conditions. For future projections of mean monthly nutrient loading, the regression equations calculated and presented in this report may be used with updated impervious area data.

The contribution of MCBCL watersheds to overall nitrogen loading was calculated by scaling loading terms from stream and river measurements, measurements from wastewater treatment facilities, and estimates of atmospheric deposition and loading from Onslow Bay.

We conducted analyses to determine the quantity of carbon loaded and the reactivity of the carbon. We can use these data to determine any differences in biological availability of the load of carbon from MCBCL watersheds to the NRE.

Stream Temperature and Conductivity

We analyzed stream temperature patterns for stream data and compared seasonal temperature patterns to watershed imperviousness, forested area, and other measures of development to determine the likely causes of differences in temperature from the five streams. Our study streams flow directly into the NRE, potentially leading to increased estuarine temperatures in streams with increased temperatures. We provided temperature data to Research Project AE-6 to inform the design of its temperature manipulation experiments. Additionally, stream water conductivity measurements were collected, and the relationship between conductivity and watershed imperviousness was analyzed.

Forestry Impacts on Carbon and Nutrient Loading

We made targeted stream monitoring deployments at three forested streams in land areas subjected to mechanical midstory and understory thinning and prescribed burning for habitat enhancement for red cockaded woodpeckers (*Picoides borealis*; **Table 8-2** and **Figure 8-2**). These watersheds included loblolly pine–dominated (LOBLOLL), mixed forest in the process of being restored to longleaf pine (MIXED), and longleaf pine–dominated forest (LLYP). For managed and reference watersheds, we gauged streams as previously described and recorded base loading and storm loading of carbon, nutrients, and sediments as previously detailed. Stream loading data provided an export term for carbon, nutrients, and sediments under varied forest management regimes.

Table 8-2. Forested Watershed Attributes

Watershed Forest Cover	Size (in ha)	Managed (Yes or No)
Mixed forest undergoing restoration to longleaf pine (MIXED)	96.65	Yes
Longleaf pine-dominated (LLYP)	47.87	No
Loblolly pine-dominated (LOBLOLL)	143.4	No

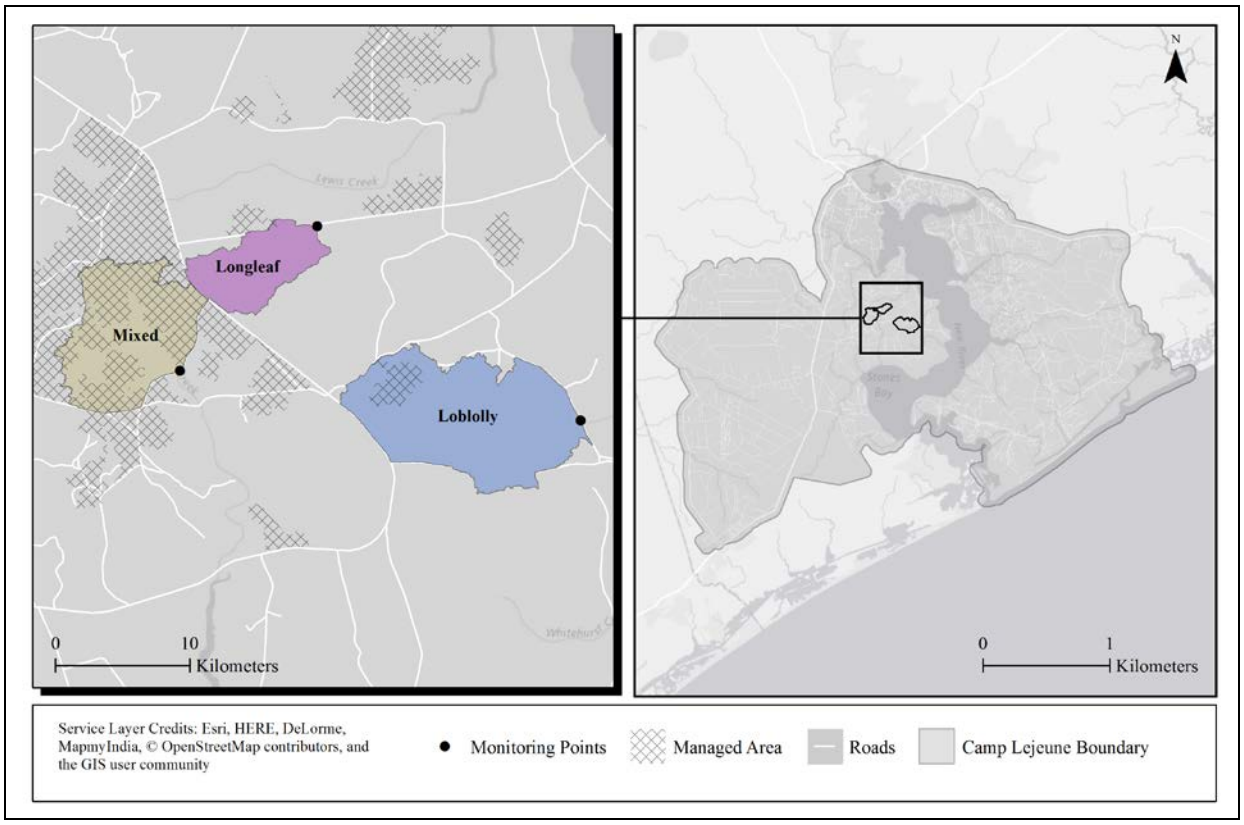

Figure 8-2. Location of forested stream sample points and the watersheds.

Stormwater Best Management Practices

Best Management Practice Function

We evaluated stormwater BMP function through targeted a deployment of a flow and water sampling array identical to that previously described to measure nutrient loading. We determined the mass balance of materials (i.e., nutrients, sediments, and carbon) entering and leaving study structures. We determined the range of stormwater BMPs present on MCBCL and focused on stormwater wet retention ponds, which are the most common type of BMP on the installation (**Figure 8-3**). We ran an extended deployment at a stormwater retention structure at Tarawa Terrace. The analysis of water quality was identical to those previously described for nutrient loading, except concentrations of water quality variables were measured instead of loads. We also used stream water quality data from a subwatershed with the monitored BMP and other BMPs (Tarawa Terrace) to a less developed reference subwatershed (French Creek). We also collected grab samples at a range of BMPs in several watersheds during baseflow and stormflow conditions to provide a broader examination of the extent to which the engineering solution has reduced excessive loading of nutrients and suspended solids to the concentrations observed in less developed watersheds. Understanding not only the function of coastal stormwater BMPs as engineering solutions, but also their role in the broader context of coastal landscape biogeochemistry were important focuses of the research.

Internal Nitrogen Dynamics and Pollutant Removal

Five wet retention ponds of similar size and soil type, but varying ages (between 3.25 and 10 years) were selected for measurement of net N_2 fluxes and nutrient fluxes from the sediment–water interface during the summer, specifically in late June and early August (**Figure 8-3**). All retention ponds were fringed with cattails (*Typha* spp.*)* and had alligator weed (*Alternanthera philoxeroides)* floating along the surface around the pond edge and extending into the open water (**Figure 8-4**). Ponds had not been excavated or had vegetation removed. Both types of fluxes were measured during ambient conditions, and nitrate-enriched conditions that matched nitrate concentrations were observed during storms by using triplicate sediment cores taken from the bottom of ponds, a flow-through sediment core experimental setup, and a membrane inlet mass spectrometer. Nitrate concentrations during storms were simulated by creating a solution of sodium nitrate ($NaNO_3$) and adding the solution to the feed water of the flow-through sediment core experiment to raise the concentration of nitrate to approximately 30 µM. A single pond (6.16 years, "mid-aged") was selected for further measurement of sediment–water interface fluxes and extended water quality monitoring from July 2016 to January 2017. For single pond sediment–water interface fluxes, various sites within the pond (i.e., forebay, main pond) and different vegetation covers (i.e., marsh edge, shallow water with floating vegetation, and deep water without vegetation) were compared. The removal and percent removal of water quality constituents were calculated for each sampling event during monitoring of the single pond by subtracting the concentration of each water quality constituent at the outflow from the concentration at the inflow. These values were aggregated to determine the mean removal and mean percent removal of each water quality constituent.

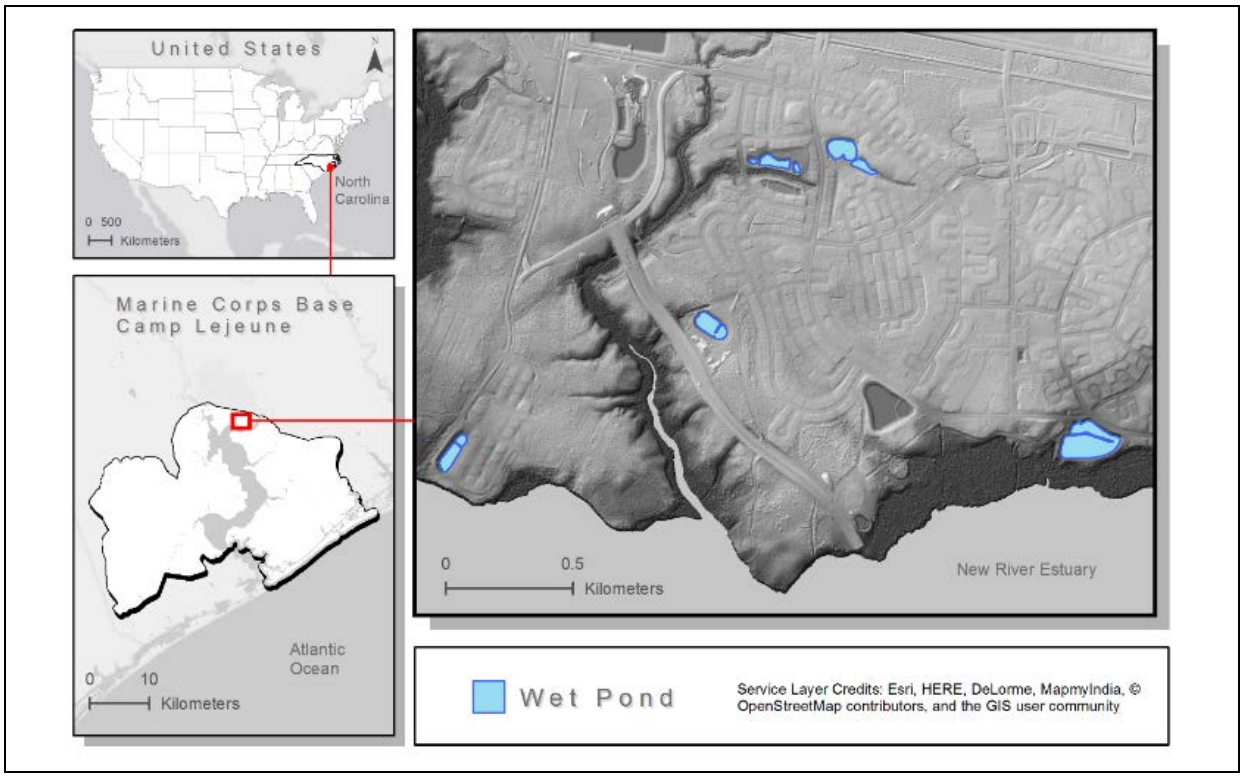

Figure 8-3. Locations of the five retention ponds sampled for net N_2 fluxes and nutrient fluxes at the sediment–water interface.

Figure 8-4. Mid-aged stormwater wet pond at Tarawa Terrace. Cattails (*Typha* spp.) fringe the pond and alligator weed (*Alternanthera philoxeroides)* floats along the surface around the pond edge.

Results and Discussion

Tributary Stream Nutrient and Carbon Loading

Nutrient Loading

Our research sites encompassed a range of watershed development. The value of these data is enhanced through the development of regression equations relating development (as represented by imperviousness) to the loading of nitrogen, phosphorus, and TSS as detailed in **Table 8-3**. These equations can be used to predict changes in watershed loads that may result from future changes in imperviousness.

Coastal streams are both the receiving waters and the transport conduits for land-derived materials (e.g., nutrients, sediment, carbon). This high level of connectivity to the surrounding watershed makes headwater streams sentinels of impacts that may occur due to changing land uses. Determining the impacts of land use and rainfall patterns on material delivery by streams is necessary for quantifying and reducing degradation resulting from watershed development. Results indicated that in more developed watersheds with a higher percentage of impervious surfaces (e.g., roofs, paved roads, parking lots), loading of most constituents increased when compared with less developed watersheds with lower percentages of impervious surfaces. Notably, organic nitrogen loads did not exhibit a strong relationship with watershed imperviousness, so increased development likely does not have a large impact on organic nitrogen loads. Organic nitrogen loads make up the vast majority of total nitrogen loads, so the weak relationship between organic nitrogen loads and watershed imperviousness explains that weak relationship between total nitrogen loads and watershed imperviousness. Overall, the strong relationships between dissolved inorganic forms of nitrogen, dissolved phosphorus, and TSS with watershed imperviousness indicate that increased development on MCBCL has

negative effects on water quality, and these effects align with the previous scientific consensus of development and stream water quality degradation.

Regression modeling determined the relationship between development and loading and was used to map loads from NRE watersheds by using methods previously described. The spatially distributed data for nitrate are shown in **Figure 8-5**. Additional maps of loading of dissolved organic nitrogen, phosphate, TDN, and TSS are available in **Appendix 8-A**.

Table 8-3. Descriptions of Data and Equations Used to Create Maps of Estimated Monthly Loads for Various Water Quality Variables

Variable	Regression Equation	R^2	Number of Watersheds
NO_x	NO_x (g/ha)=0.7934×mean imperviousness	0.7811	4
ON	ON (g/ha)=−1.2462×mean imperviousness+103.99	0.2094	4
PO_4	PO_4 (g/ha)=0.0608×mean imperviousness+1.6268	0.8648	4
TDN	TDN (g/ha)=−0.2949×mean imperviousness+108.74	0.0139	4
TSS	TSS (kg/ha)=1.2461×mean imperviousness	0.7492	5

Note: The date range for all variables was July 2008 through July 2015.

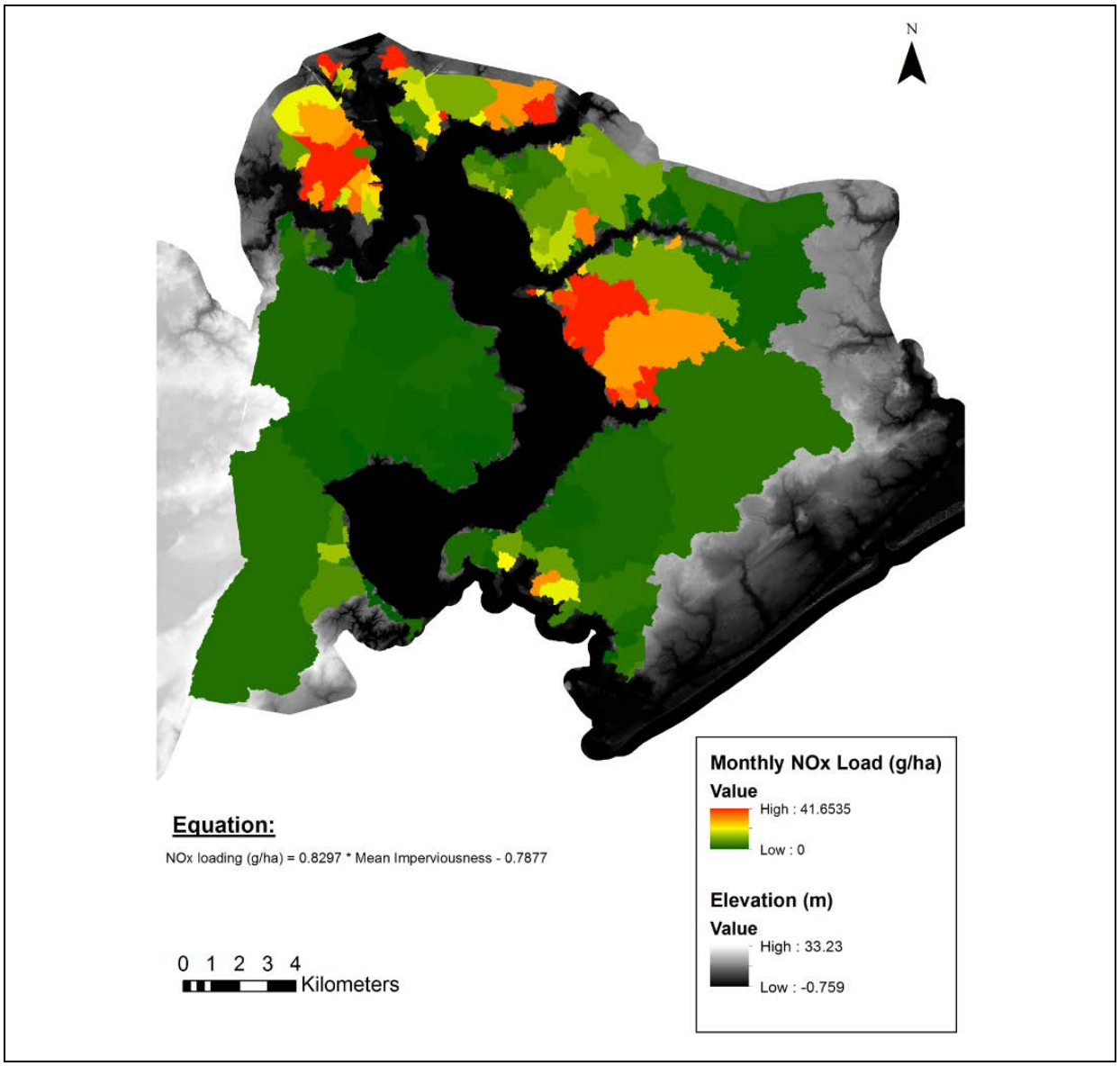

Figure 8-5. Nitrate (NO_x) loading from watersheds on MCBCL.

Warmer colored values (orange and red) represent higher loads and are extrapolated based on the observed relationship between imperviousness and nitrate loading.

Stream Carbon Loading

Loadings of POC, DOC, and DIC were quantified for all five study streams. **Figure 8-6** (left panel) shows the measured annual load of several carbon types. Patterns and magnitudes of loading of POC and DOC were very similar relative to development, as was observed from 2013 and 2014. DIC loading in several streams was much higher than either DOC or POC. There was a general pattern of increased DIC loading with increased development. We compared the ratio of DOC:DIC across the range of watershed development (**Figure 8-6**, right panel) and found a distinctive pattern of decrease in DOC:DIC with increased watershed development. This is the first comparison of DOC and DIC loading that we are aware of in the literature. Shifts from organic to inorganic carbon loading as development occurs in coastal streams have significant

implications for the estuarine carbon budget and the ecology of the receiving waters. These data were extrapolated by using ratios of ungauged to gauged stream watershed area and included in the development of a estuarine carbon budget (see Chapter 6, Research Projects AE-4 and AE-6). Streams in undeveloped coastal watersheds are renowned for their high DOC loads (i.e., blackwater) that are derived from floodplains and contiguous riparian wetlands. Altering this balance could create conditions that are more favorable to fast growing, bloom-forming algal species.

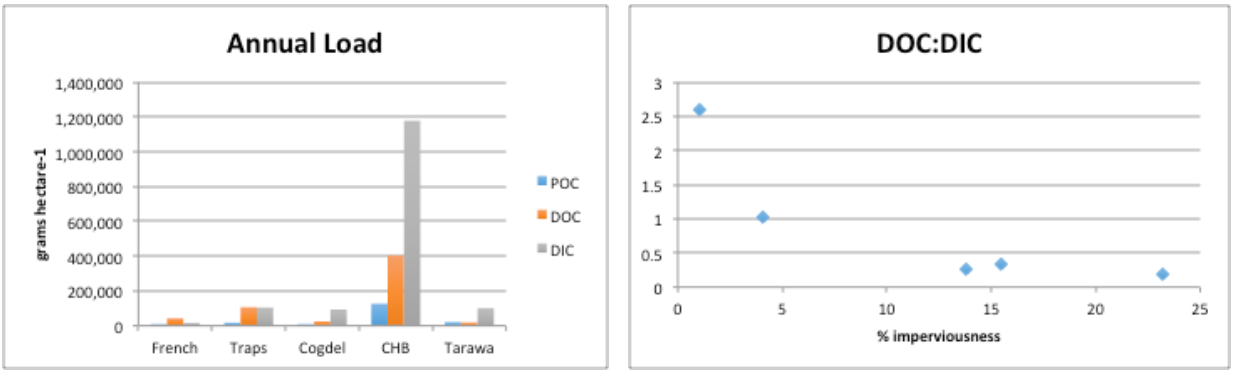

Figure 8-6. (Left panel) Annual loads of POC, DOC, and DIC from streams organized from low to high imperviousness, French Creek (French), Traps Bay Creek (Traps), Cogdels Creek (Cogdels), Courthouse Bay (CHB), and Tarawa Terrace (Tarawa). (Right panel) The relationship between the ratio of DOC:DIC loading and watershed imperviousness.

Forestry Impacts on Carbon and Nutrient Loading

Stream delivery of nutrients and carbon was assessed from forested watersheds with varied forest management. The goal of this research was to compare the export of carbon and nutrients from watersheds that were loblolly pine–dominated, mixed forest in the process of being restored to longleaf pine, and longleaf pine–dominated forest. Streams with homogenous land use of these forest management types were sampled to test the hypothesis that forest management does not affect export of carbon and nutrients.

We found that water delivery from all three study watersheds was very similar in both stormflow and baseflow (**Figure 8-7**). Carbon loading had similar patterns for both DOC and DIC (**Figure 8-8**). Longleaf pine (LLYP) had the highest load for both forms of carbon. Carbon loading patterns were very similar to the loading patterns for all nutrients measured (**Appendix 8-A**). These results are relevant because they increase the breadth of MCBCL's information regarding the export of materials from land managed by the Base and because it provides general information for land in the Southeastern United States with similar land use. If this pattern holds true across similar watersheds on Base, forestry management may contribute to determining Base-wide exports of stream carbon. Because pristine coastal plain watersheds are the largest exporters of DOC, this finding is not likely to have any detrimental environmental implications.

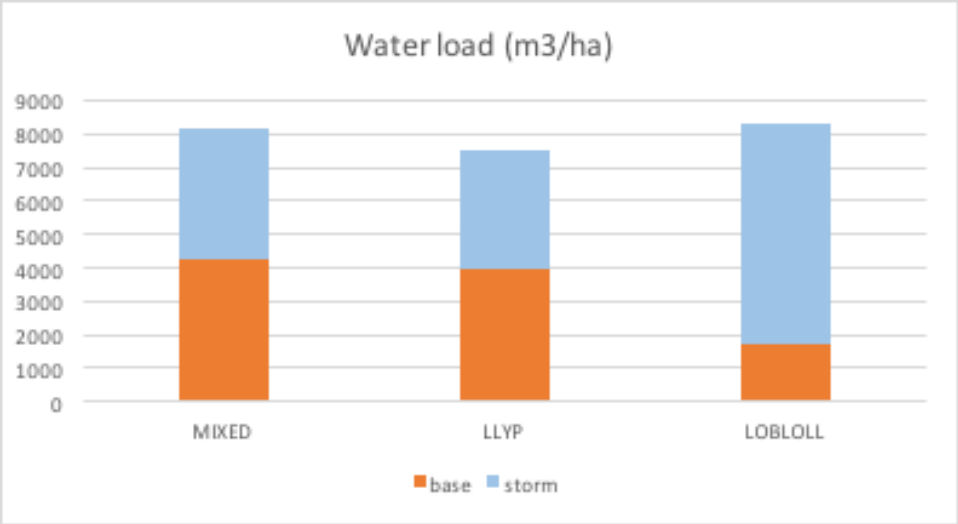

Figure 8-7. Annual loads of water from watersheds being managed to restore longleaf pine (MIXED), longleaf pine–dominated (LLYP), and unmanaged, loblolly pine–dominated (LOBLOLL).

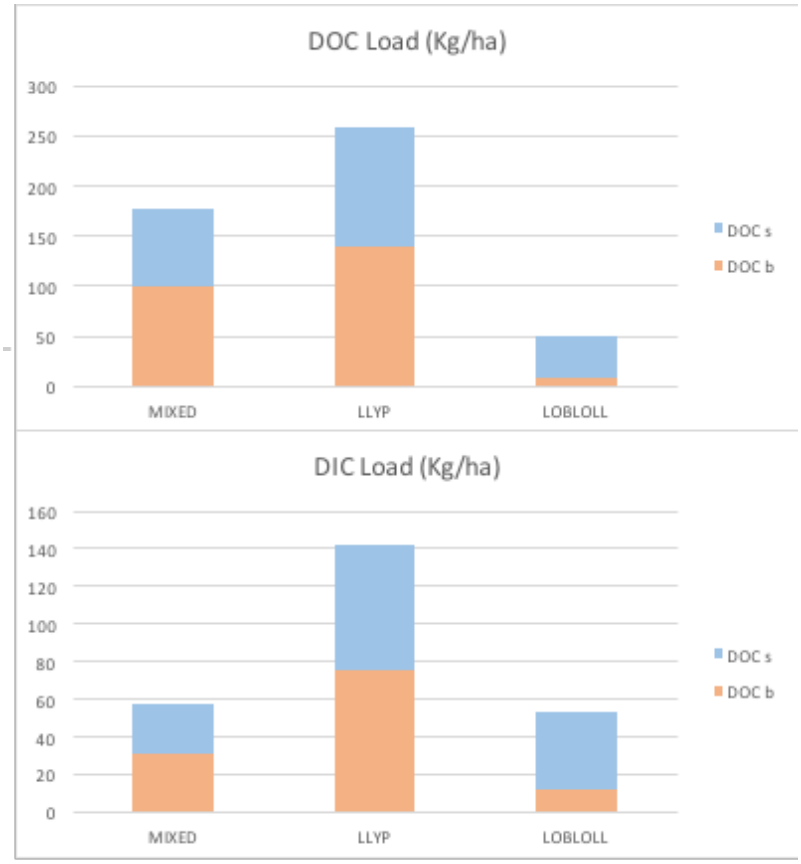

Figure 8-8. Annual load of DOC (top) and DIC (bottom) in storm (s) and baseflow(b) from watersheds being managed to restore longleaf pine (MIXED), longleaf pine–dominated (LLYP), and unmanaged, loblolly pine–dominated (LOBLOLL).

Stream Temperature and Conductivity

Stream Temperature

Temperature is an important controlling factor for biological and chemical processes in streams. Research suggests that urbanization affects stream temperature (Nelson and Palmer, 2007). Data from DCERP1 and DCERP2 were used to test the hypothesis that increased imperviousness in sub-watersheds would increase coastal stream temperature. Coastal stream temperature responses to urbanization may be distinctive from their upland analogues due to generally lower relief in coastal watersheds. **Figure 8-9** depicts seasonal mean temperatures during all flow conditions for the five streams that have been monitored during both DCERP1 and DCERP2. Elevated temperatures in streams with more developed watersheds were observed throughout the record. Summer mean temperatures were as much as 5°C higher in more developed streams compared with less developed streams. There is an apparent upward trend in stream temperature through the period of record (2008–2015).

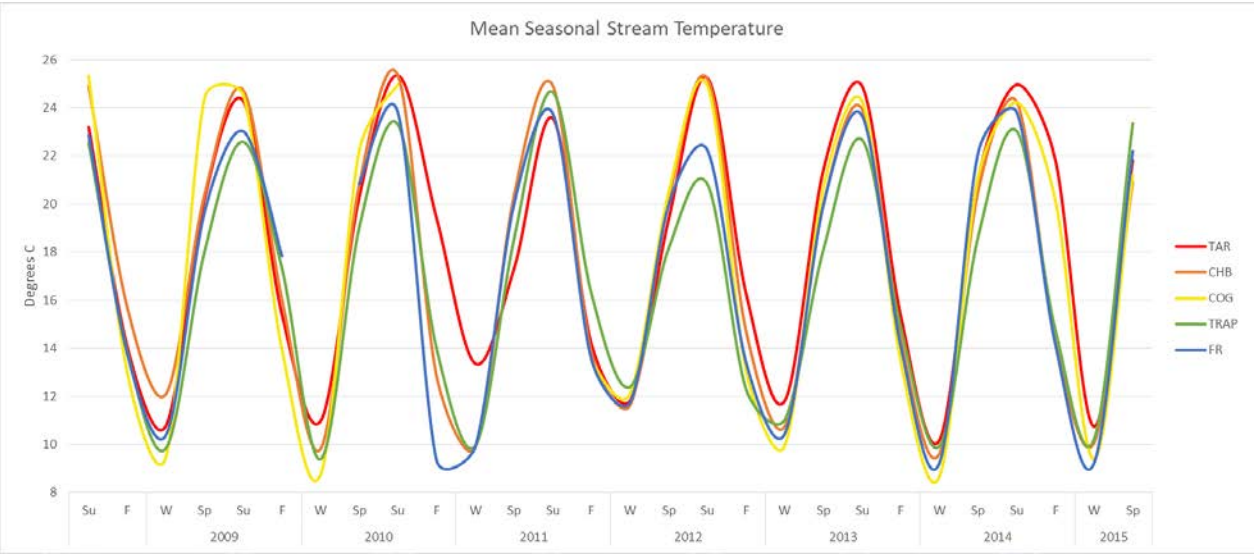

Figure 8-9. Stream temperatures of the five study streams.

Temperature (in °C) is presented for each season from 2008–2015. Sites are presented from least developed (cool colors) to most developed (warm colors).

In collaboration with Research Project CC-1, we conducted an assessment of the relationship between air temperature and stream temperature during both DCERP1 and DCERP2. Our past results revealed impacts of land development on stream temperature. Increased imperviousness correlated with increasing stormflow stream temperature and decreased forest cover correlated with increased baseflow stream temperature (RTI, 2013). The strong correlations between air and stream temperature shown in **Figure 8-10** support the potential to forecast future changes in stream temperatures based on air temperatures. There were no significant differences in the slopes of the regressions for each of the streams, although their respective watersheds exhibited varied levels of development. This finding suggests that a single forecast of future temperature changes could be made for all streams on MCBCL due to the similar slopes of regressions between mean monthly stream temperature and mean monthly air temperature.

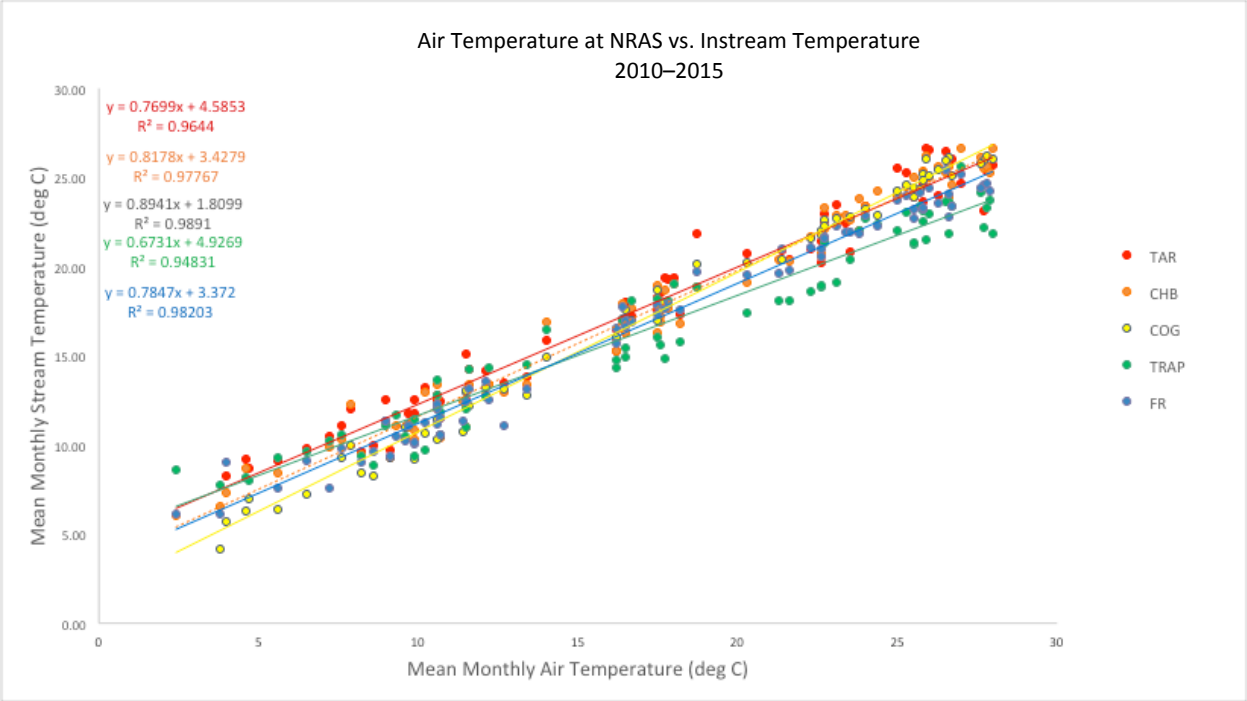

Figure 8-10. Comparison of stream and air temperatures through DCERP1 and DCERP2.

Warmer colors (red and orange) represent more developed streams and cooler colors (blue and green) represent streams with less watershed development. Results of linear regressions are color coded for each stream. Streams were Tarawa Terrace (TAR), Courthouse Bay (CHB), Cogdels Creek (COG), Traps Bay Creek (TRAP), and French Creek (FR).

Stream Conductivity

Conductivity measures water's capacity to pass electrical flow (conduct an electric current), which is directly related to the concentration of ions in the water. In coastal streams, the most likely source of ions is from seawater. We tested the hypothesis that development in coastal stream watersheds affects stream conductivity. The relationship between mean stream conductivity from 2010 to 2015 was contrasted with imperviousness (**Figure 8-11**). There was no clear relationship between stream conductivity and imperviousness, and all conductivity levels were very low (the maximum conductivity was a small fraction of a part per thousand [ppt] in salinity). The highest conductivity was at Courthouse Bay and was likely attributable to that sites proximity to the inlet and ocean. To further examine our hypothesis, we evaluated the conductivity in all streams and stratified the data by annual precipitation (**Figure 8-12**). Again, all stream conductivity levels were very low. There was a pattern of higher stream conductivity in years with less precipitation, but these increases were mostly quite small. The exception again was at Courthouse Bay, which we believe was driven by its proximity to the New River Inlet. Using DCERP data from 2010 through 2015, we found that watershed development did not have a predictable effect on stream conductivity, but that lower precipitation did result in higher stream conductivity (though no conductivity values were greater than the equivalent of 1 ppt salinity). Therefore, we found no effect of imperviousness on instream conductivity.

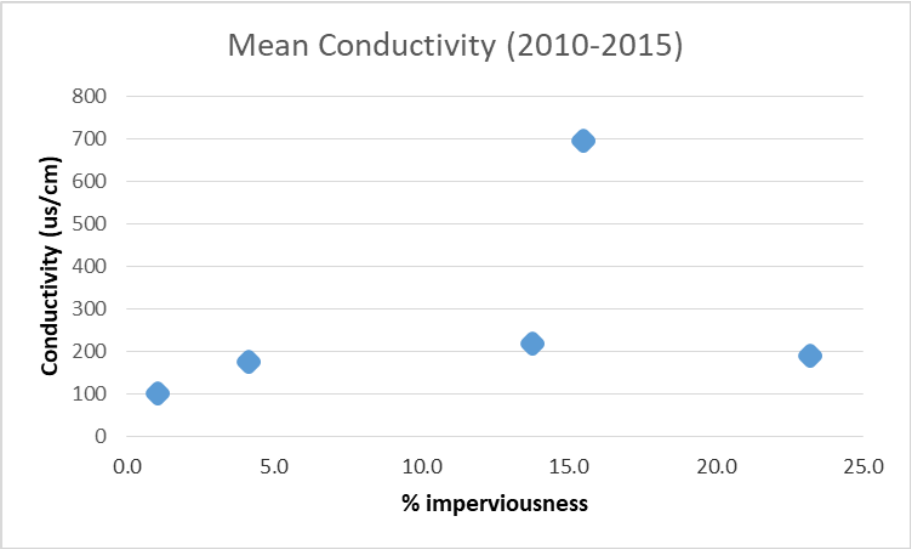

Figure 8-11. Mean stream conductivity through the study period plotted versus watershed imperviousness.

The slightly higher conductivity level was observed at Courthouse Bay.

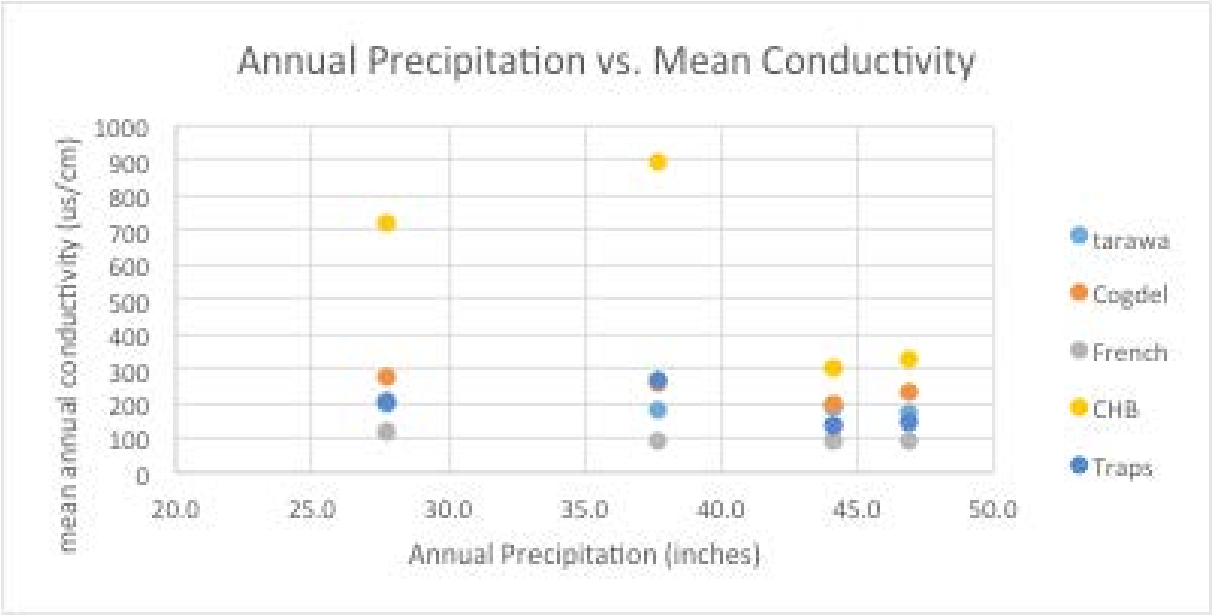

Figure 8-12. The relationship between annual precipitation and mean annual conductivity from 2010 through 2015.

Stormwater Best Management Practices

Best Management Practice Function

Tarawa Terrace Creek and French Creek were monitored for 7 years from mid-2008 through mid-2015. During this time period, the watershed of Tarawa Creek was further developed from

22.8% mean imperviousness to 28.0% watershed imperviousness and outfitted with retention ponds that collected water from 97% of the watershed area. There were previously no BMPs used within the watershed. During the same time, there was no increase in watershed imperviousness and no BMPs were installed in French watershed. To determine the effectiveness of stormwater BMPs (retention ponds) in mitigating the negative effects of development on water quality, the tributary creek time series data were divided into three sections: pre-construction (January 2008 through January 2009), mid-construction (January 2009 through March 2011), and post-construction (March 2011 through June 2015). The concentrations of various water quality constituents were compared for the pre-construction and post-construction periods. The mid-construction period data were not included in the analysis because of difficulty in distinguishing between the effects of construction within the Tarawa Creek watershed and the effects of BMPs **(Figure 8-13).**

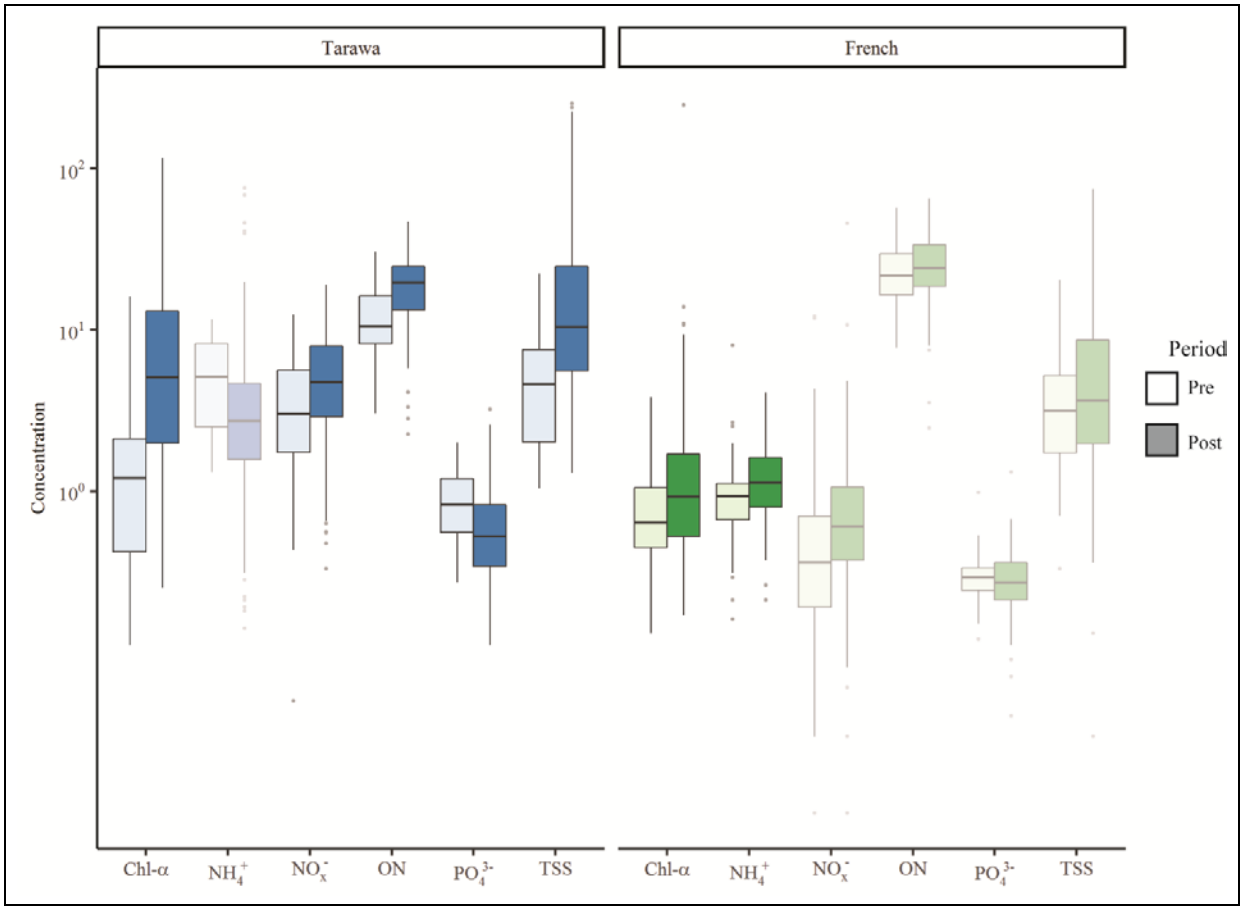

Figure 8-13. Nutrient (µM), total suspended solids (TSS; mg/L), and chlorophyll *a* (Chl-*a*; µg/L) concentrations for the pre-construction (Pre) and post-construction (Post) periods of development during both baseflow and stormflow.

Full color boxplots indicate water quality variables that changed significantly between pre- and post-construction periods based on Student's *t*-tests (α=0.05).

In the Tarawa Terrace stream, the mean chlorophyll *a*, NO_x, ON, and TSS concentrations significantly increased; the mean orthophosphate (PO_4) concentration significantly decreased, and the mean NH_4 concentration did not change. In the French Creek, chlorophyll *a* and NH_4

significantly increased between pre-construction and post-construction periods, although the increases were much smaller than changes in the Tarawa Terrace stream and only significant because the concentrations were extremely low. The changes in concentration in the French stream were likely due to natural variability in precipitation or temperature. These data suggest that the installation of retention ponds did not mitigate all of the negative effects of increased development in the Tarawa Terrace watershed, and centralized stormwater management may not be the most effective method for maintaining water quality in this area. Other stormwater management strategies for reducing the volume of stormwater runoff and treating all stormwater generated from impervious surfaces, such as low impact development, could possibly better protect stream water quality from watershed development. Examples of low impact development include street curb cuts draining to bioretention cells, rain gardens, gutter downspout diversion to pervious surfaces, permeable pavement, green roofs, and stormwater harvesting and reuse (i.e., using rain barrels for irrigation or toilet flushing).

Internal Nitrogen Dynamics and Pollutant Removal

Five stormwater ponds of varying ages were sampled during the summer (i.e., June and August 2016) to analyze internal nitrogen dynamics **(Figure 8-14**). Additionally, a single pond was monitored for 6 months to determine the amount of pollutant removal occurring in the pond (**Table 8-4)** and the net sediment N_2 fluxes in various portions of the pond **(Figure 8-15).**

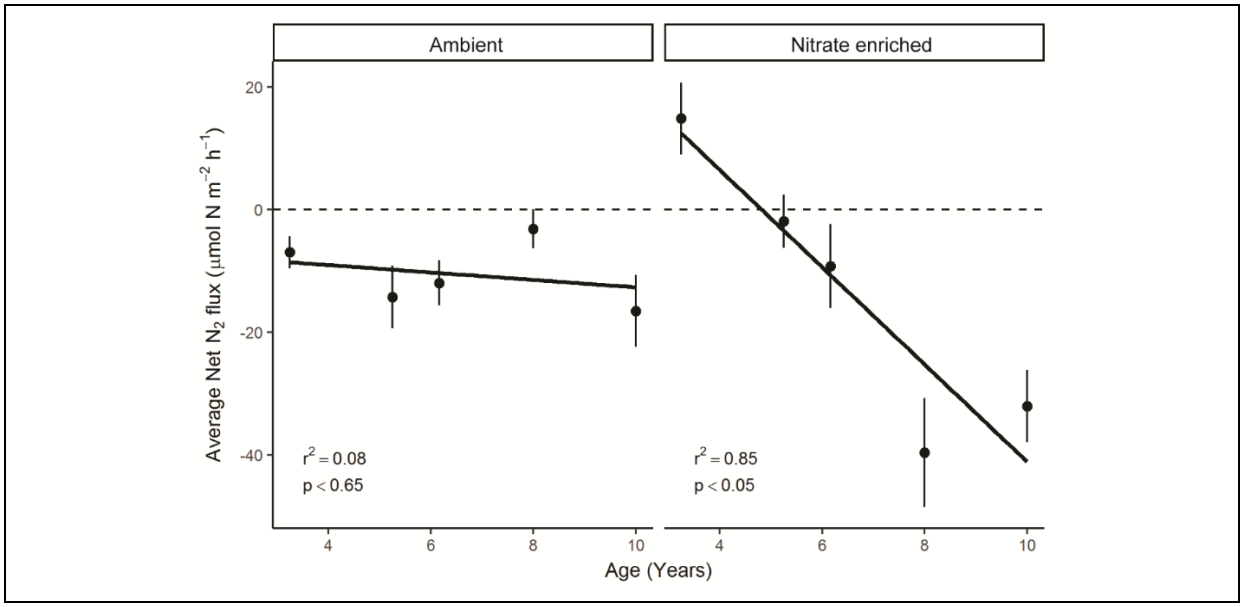

Figure 8-14. Net sediment N_2 fluxes as a function of pond age for both ambient and nitrate–enriched conditions.

Measurements were taken during early summer. Error bars indicate standard error.

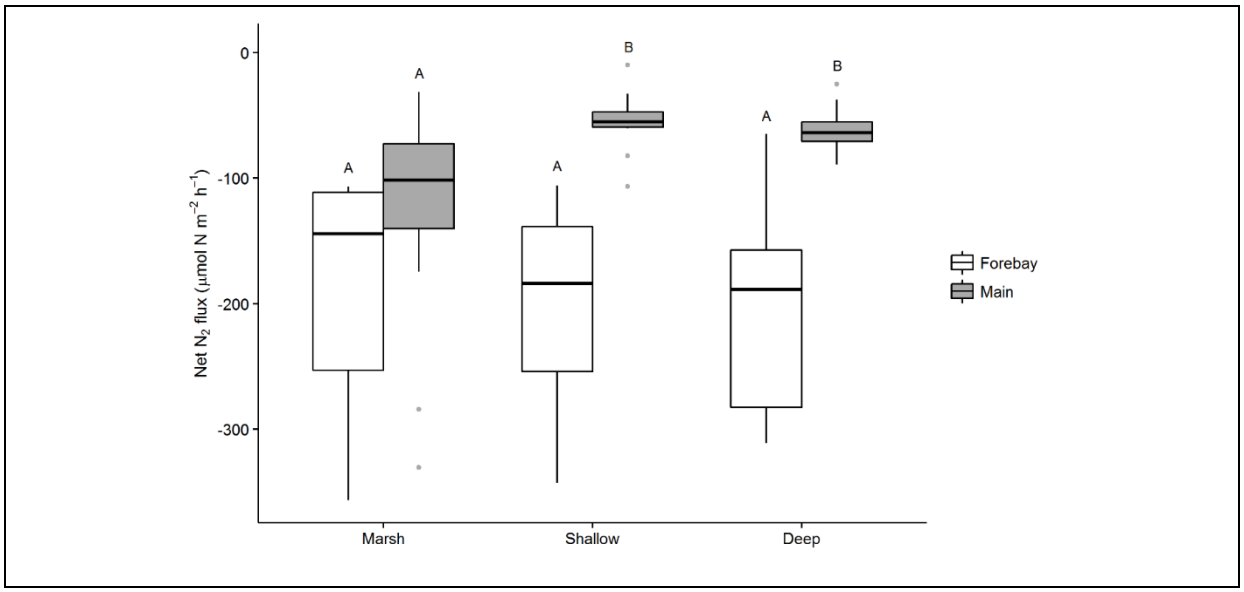

Figure 8-15. Boxplots of net sediment N_2 fluxes in different portions of a single wet pond.
Measurements were taken during late summer.

All pond sediments exhibited negative net N_2 fluxes during ambient (i.e., baseflow) conditions, indicating net nitrogen fixation (**Figure 8-14**). After a nitrate enrichment, raising the nitrate concentration to 30 µM NO_x^-, younger pond sediment net N_2 fluxes shifted towards net denitrification, and older pond sediments had even more extreme rates of net nitrogen fixation (**Figure 8-14**). Net nitrogen fixation was likely caused by extreme nitrogen limitation, resulting from low nitrogen concentrations, thermal stratification, and large PO_4 fluxes from the sediments. These PO_4 fluxes were due to low oxygen conditions resulting from organic matter decomposition within the ponds. There was a significant negative relationship between TDN concentrations in the pond water and pond age, and the percent sediment organic matter increased with pond age, but was not significant (Gold et al., 2017). Rates of net N_2 fluxes became much more negative between early summer and late summer (**Figure 8-15**), indicating that temperature or pond stratification were important drivers of increased net sediment nitrogen fixation. Higher rates of net nitrogen fixation within the shallow and deep sections of the pond's forebay compared with the main basin could be caused by increased sediment and organic matter deposition due to the forebay's proximity to the pond inlet.

Table 8-4. Mean Change and Mean Percent Change for Each Water Quality Constituent During the Monitoring Period of the Single, Mid-aged Pond (from July 2016 through January 2017)

	TSS (mg/L)	NO_x (µM)	NH_4 (µM)	PO_4 (µM)	TDN (µM)	ON (µM)	Chl-a (µg/L)
Baseflow							
Mean change	6.96	−20.99	−55.40	−2.52	−81.08	−4.69	2.34
Standard deviation	16.95	14.38	103.56	3.80	112.36	9.13	31.38
Mean % change	108.01	−92.75	−47.68	−58.49	−50.97	−12.82	256.25
Standard deviation	156.61	12.70	48.16	30.14	35.89	29.53	275.50

(continued)

Table 8-4. Mean Change and Mean Percent Change for Each Water Quality Constituent During the Monitoring Period of the Single, Mid-aged Pond (from July 2016 through January 2017) (continued)

	TSS (mg/L)	NO_x (µM)	NH_4 (µM)	PO_4 (µM)	TDN (µM)	ON (µM)	Chl-a (µg/L)
Stormflow							
Mean change	−17.07	−9.52	−2.37	−1.47	−11.51	0.38	4.85
Standard deviation	16.15	9.98	2.60	0.70	12.87	4.22	7.03
Mean % change	−76.67	−95.74	−53.45	−67.59	−27.93	4.72	362.86
Standard deviation	13.67	9.19	19.65	12.54	19.24	25.59	279.57
Total							
Mean change	−1.05	−17.41	−38.83	−2.19	−59.34	−3.11	3.13
Standard deviation	19.92	13.95	88.30	3.16	97.82	8.14	25.90
Mean % change	34.91	−93.74	−49.48	−61.34	−43.77	−7.34	289.56
Standard deviation	149.97	11.40	40.70	25.82	32.85	28.75	272.12

Overall, a large percentage of all inorganic nitrogen species was removed in the pond, TSS concentrations increased slightly in the pond, and there was a large percent increase in phytoplankton biomass, as determined by measuring chlorophyll *a* concentrations, in the pond. These results indicate that the pond was a large producer of phytoplankton during summer and fall, possibly accounting for, and offsetting most of the nitrogen removal observed in the pond.

Pond excavation and/or pond mixing could discourage net sediment nitrogen fixation during the summer and possibly reduce the amount of phytoplankton biomass exported from retention ponds. Net sediment nitrogen fixation appears to have been driven by extreme nitrogen limitation and low-oxygen conditions at the sediment–water interface. These conditions could be reduced by removing sediment organic matter that causes oxygen depletion during summer via respiration and mixing pond water to provide oxygenated water to the sediment−water interface.

Conclusions and Implications for Future Research and Implementation

Research Questions

1. **Will the intensity and type of watershed development alter stream loading of carbon, nutrients, and suspended solids? Will there be shifts in carbon forms (DOC versus POC) related to watershed land cover?**

Development altered loading of nutrients, suspended solids, and carbon into MCBCL tributary creeks. Increased development was associated with increases in loading of nitrogen, phosphorus, and sediments. Dissolved organic carbon loading decreased with increased development, but particulate organic carbon loading increased. Increases in nutrient loading that contribute to excessive nutrient supplied to the estuary could have detrimental impacts. Carbon loading, in the form of DOC, is very high in pristine streams. The shift in carbon loading because of development is unlikely to have environmental impacts.

2. **Will forest management to enhance habitat for red-cockaded woodpeckers affect stream export of carbon relative to forested streams not being managed for this species?**

Water export from watersheds dominated by unmanaged loblolly, mixed forests being managed for restoration to longleaf pine, and longleaf pine–dominated forests had very similar water budgets. Loads of DOC and DIC were both highest in the longleaf pine watershed. Because pristine coastal watersheds export large amounts of carbon (primarily as DOC), the fact that restored longleaf pine watersheds export more carbon is unlikely to have detrimental environmental effects.

3. **Stormwater BMPs are generally designed to reduce nutrient, pathogen, and suspended material loading. How effective are the BMPs selected for this study?**

Long-term monitoring showed that some BMPs (stormwater wet ponds) were not comprehensively effective in returning water quality to pre-construction levels. In particular, stormwater ponds were not effective in removing nitrogen. Flux incubations revealed that wet pond sediments were rarely denitrifying (removing nitrogen) and were often fixing nitrogen, which may have led to the growth and export of large amounts of phytoplankton biomass. These results indicate that wet ponds may be sources of new nitrogen rather than removing nitrogen as has been the presumption.

4. **What are the impacts of variations in watershed land cover on coastal stream temperatures? Are there variable impacts on baseflow and stormflow temperatures? If observed, are distinctions in temperature ecologically significant for the streams and/or estuary?**

Increased development was associated with higher maximum temperatures during the summer. Distinctions in temperature within creeks varied by as much as 5°C. This is an ecologically meaningful difference in the context of trophic interactions and nutrient cycling. Additionally, this warmer water has the potential to affect the ecology of the NRE in the bays that receive the stream discharge.

5. **How will predicted changes in air temperature and freshwater pulses affect the magnitude and patterns of stream loadings of carbon, nutrients, and sediments in these coastal creeks?**

Increases in freshwater pulses will increase loading of carbon, nutrients, and sediments in coastal creeks. Water volume was the major driver of loading, indicating that heavy rainfall events cause more freshwater pulses that will result in larger loads to the tributary creeks. Temperature is likely to have a more complex impact. Warmer temperatures are likely to result in increased nutrient fluxes from sediments and decaying organic matter, but higher temperatures are also likely to cause increased rates of denitrification.

Findings with Implications for Future Base Management

Water export from watersheds dominated by unmanaged loblolly, mixed forests being managed for restoration to longleaf pine, and longleaf pine–dominated forests had very similar water

budgets. Loads of DOC and DIC were both highest in the longleaf pine watershed. Because pristine coastal watersheds export large amounts of carbon (primarily as DOC), the fact that restored longleaf pine watersheds export more carbon is unlikely to have detrimental environmental effects.

Stormwater retention ponds did not mitigate the negative effects of development in a residential watershed. Sediment flux experiments showed that stormwater retention ponds rarely removed nitrogen via denitrification, but rather added nitrogen via nitrogen fixation. Through the summer and fall, a single stormwater pond produced large amounts of phytoplankton biomass and removed large amounts of nitrogen. More frequent excavation and/or pond mixing could improve nitrogen removal via denitrification in stormwater retention ponds and possibly decrease the export of phytoplankton biomass.

Literature Cited

Alexander, R.B., A.H. Elliott, U. Shankar, G.B. McBride. 2002. Estimating the sources and transport of nutrients in the Waikato River Basin, New Zealand. *Water Resources Research 38*(12):4-1–4-23. doi:10.1029/2001WR000878

Bettez, N.D., and P.M. Groffman. 2012. Denitrification potential in stormwater control structures and natural riparian zones in an urban landscape. *Environmental Science Technology 46*(20):10909–10917. doi:10.1021/es301409z

Birgand, F., T.W. Appelboom, G.M. Chescheir, R.W. Skaggs, and J.W. Gilliam. 2006. Evaluation of time proportional sampling strategies for estimating annual nutrient fluxes at the outlets of coastal plain watersheds. Pp. 208–217 in *Proceedings of the American Society of Agricultural and Biological Engineers*, New Bern, NC.

Brown, J.H., J.F. Gillooly, A.P. Allen, V.M. Savage, and G.B. West. 2004. Toward a metabolic theory of ecology. *Ecology 85*:1771–1789.

Clesceri, L.S., A.E. Greenberg, and A.D. Eaton. 1998. *Standard Methods for the Examination of Water and Wastewater*. 20th Edition. Washington, DC: American Public Health Association, American Water Works Association, Water Environment Federation.

Collins, K.A., T.J. Lawrence, E.K. Stander, R.J. Jontos, S.S. Kaushal, T.A. Newcomer, N.B. Grimm, and M.L. Cole Ekberg. 2010. Opportunities and challenges for managing nitrogen in urban stormwater: A review and synthesis. *Ecological Engineering 36*(11):1507–1519. doi:10.1016/j.ecoleng.2010.03.015

Fulweiler, R.W., E.M. Heiss, M.K. Rogener, S.E. Newell, G.R. LeCleir, S.M. Kortebein, and S.W. Wilhelm. 2015. Examining the impact of acetylene on N-fixation and the active sediment microbial community. *Frontiers in Microbiology 6*:418. doi:10.3389/fmicb.2015.00418

Gold, A.C., S.P. Thompson, and Piehler. 2017. Coastal stormwater wet pond sediment nitrogen dynamics. *Science of the Total Environment 609*:672–681. doi:10.1016/j.scitotenv.2017.07.213

Groffman, P.M., K. Butterbach-Bahl, R.W. Fulweiler, A.J. Gold, J.L. Morse, E.K. Stander, C. Tague, C. Tonitto, and P. Vidon. 2009. Challenges to incorporating spatially and temporally explicit phenomena (hotspots and hot moments) in denitrification models. *Biogeochemistry 93*:49–77. doi:10.1007/s10533-008-9277-5

Groffman, P.M., N.L. Law, K.T. Belt, L.E. Band, and G.T. Fisher. 2004. Nitrogen fluxes and retention in urban watershed ecosystems. *Ecosystems 7*:393–403. doi:10.1007/s10021-003-0039-x

Hancock, G.S., J.W. Holley, and R.M. Chambers. 2010. A field-based evaluation of wet retention ponds: How effective are ponds at water quantity control? *JAWRA: Journal of the American Water Resources Association* 46(6):1145–1158. doi:10.1111/j.1752-1688.2010.00481.x

Harris, L.A., C.M. Duarte, and S.W. Nixon. 2006. Allometric laws and prediction in estuarine and coastal ecology. *Estuaries and Coasts 29*:340–344. doi:10.1007/BF02782002

Hatt, B.E., T.D. Fletcher, C.J. Walsh, and S.L. Taylor. 2004. The influence of urban density and drainage infrastructure on the concentrations and loads of pollutants in small streams. *Environmental Management 34*(1):112–124. doi:10.1007/s00267-004-0221-8

Howarth, R.W., and R. Marino. 2006. Nitrogen as the limiting nutrient for eutrophication in coastal marine ecosystems: Evolving views of three decades. *Limnology and Oceanography 51*:364–376.

Kaushal, S.S., G.E. Likens, N.A. Jaworski, M.L. Pace, A.M. Sides, D. Seekell, K.T. Belt, D.H. Secor, and R.L. Wingate. 2010. Rising stream and river temperatures in the United States. *Frontiers in Ecology and the Environment 8*(9):461–466. doi:10.1890/090037

Kaushal, S.S., P.M. Groffman, L.E. Band, C.A. Shields, R.P. Morgan, M.A. Palmer, K.T. Belt, C.M. Swan, S.E.G. Findlay, and G.T. Fisher. 2008. Interaction between urbanization and climate variability amplifies watershed nitrate export in Maryland. *Environmental Science and Technology* 42(16):5872–5878. doi:10.1021/es800264f

Morris, J.T., P.V. Sundareshwar, C.T. Nietch, B.R. Kjerfve, and D.R. Cahoon. 2002. Responses of coastal wetlands to rising sea level. *Ecology 83*:2869–2877.

Mulholland, P.J., and E.J. Kuenzler. 1979. Organic carbon export from upland and forested wetland watersheds. *Limnology and Oceanography 24*:960–966. doi:10.4319/lo.1979.24.5.0960

NCDENR (North Carolina Department of Environment and Natural Resources). 2009. Stormwater BMP manual. Chapter 10 in *Wet Detention Basin*. Available at https://ncdenr.s3.amazonaws.com/s3fs-public/Water Quality/Surface Water Protection/SPU/SPU - BMP Manual Documents/BMPMan-Ch10-WetPonds-20090616-DWQ-SPU.pdf

Nelson, K.C., and M.A. Palmer. 2007. Stream temperature surges under urbanization and climate change: Data, models, and responses. *Journal of the American Water Resources Association 43*(2):440–452.

O'Connor, M.I., M.F. Piehler, D.M. Leech, A. Anton, and J.F. Bruno. 2009. Warming and resource availability shift food web structure and metabolism. *PLoS Biology 7*(8):e1000178. doi:10.1371/journal.pbio.1000178

Paul, M.J., and J.L. Meyer. 2001. Streams in the urban landscape. *Annual Review of Ecology and Systematics 32:333–365*. doi:10.1146/annurev.ecolsys.32.081501.114040

RTI International. 2013. *DCERP1 Final Research Report*. RTI International. Research Triangle Park, NC

Sanger, D., A. Blair, G. DiDonato, T. Washburn, S. Jones, G. Riekerk, E. Wirth, J. Stewart, D. White, L. Vandiver, and A.F. Holland. 2013. Impacts of coastal development on the ecology of tidal creek ecosystems of the U.S. southeast including consequences to humans. *Estuaries and Coasts 38*:49–66. doi:10.1007/s12237-013-9635-y

Seitzinger, S.P., J.A. Harrison, E. Dumont, A.H.W., Beusen, and A.F. Bouwman. 2005. Sources and delivery of carbon, nitrogen, and phosphorus to the coastal zone: An overview of Global Nutrient Export from Watersheds (NEWS) models and their application. *Global Biogeochemical Cycles 19*(4) doi:10.1029/2005GB002606

Sobota, D.J., J.A. Harrison, and R.A. Dahlgren. 2009. Influences of climate, hydrology, and land use on input and export of nitrogen in California watersheds. *Biogeochemistry 94*:1–20. doi:10.1007/s10533-009-9295-y

Stevens, H.H., J.F. Ficke, and G.F. Smoot. 1975. Water temperature, influential factors, field measurement, and data presentation. Book 1, Chapter D1 in *U.S. Geological Survey Techniques of Water Resources Investigations*.

Vogel, S. 1994. *Life in Moving Fluids: The Physical Biology of Flow*. Princeton University Press.

Ward, R.C., and M. Robinson. 2000. *Principles of Hydrology*. 4th Edition. McGraw-Hill: London, UK.

Xian, G., C. Homer, J. Dewitz, J. Fry, N. Hossain, and J. Wickham. 2011. The change of impervious surface area between 2001 and 2006 in the conterminous United States. *Photogrammetric Engineering and Remote Sensing 77*(8):758–762.

Zhu, W-X., N.D. Dillard, and N.B. Grimm, 2004. Urban nitrogen biogeochemistry: Status and processes in green retention basins. *Biogeochemistry 71*:177–196. doi:10.1007/s10533-004-9683-2

Appendix 8-A
Supporting Data

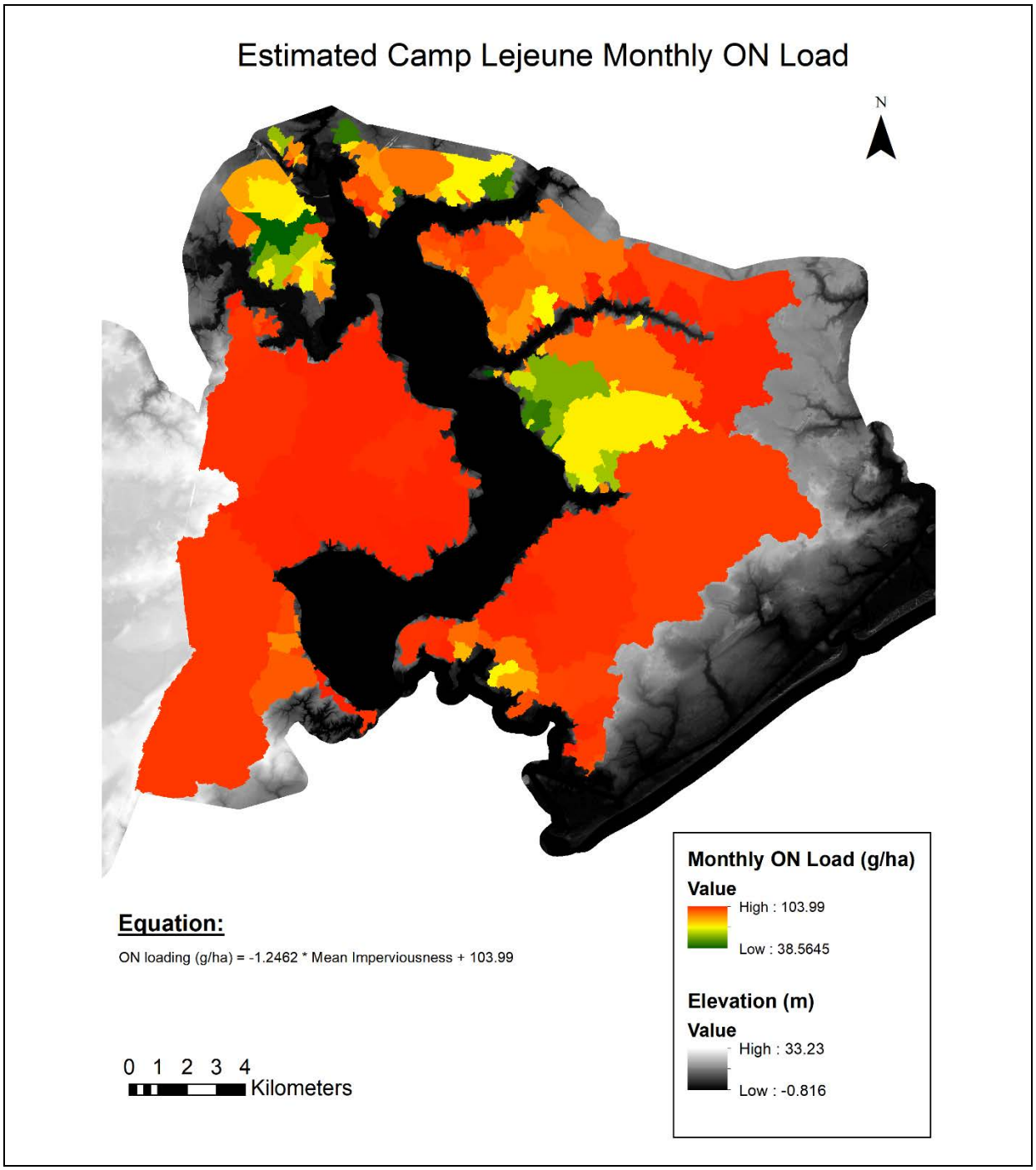

Figure 8A-1. Estimated monthly organic nitrogen (ON) load at Marine Corps Base Camp Lejeune.

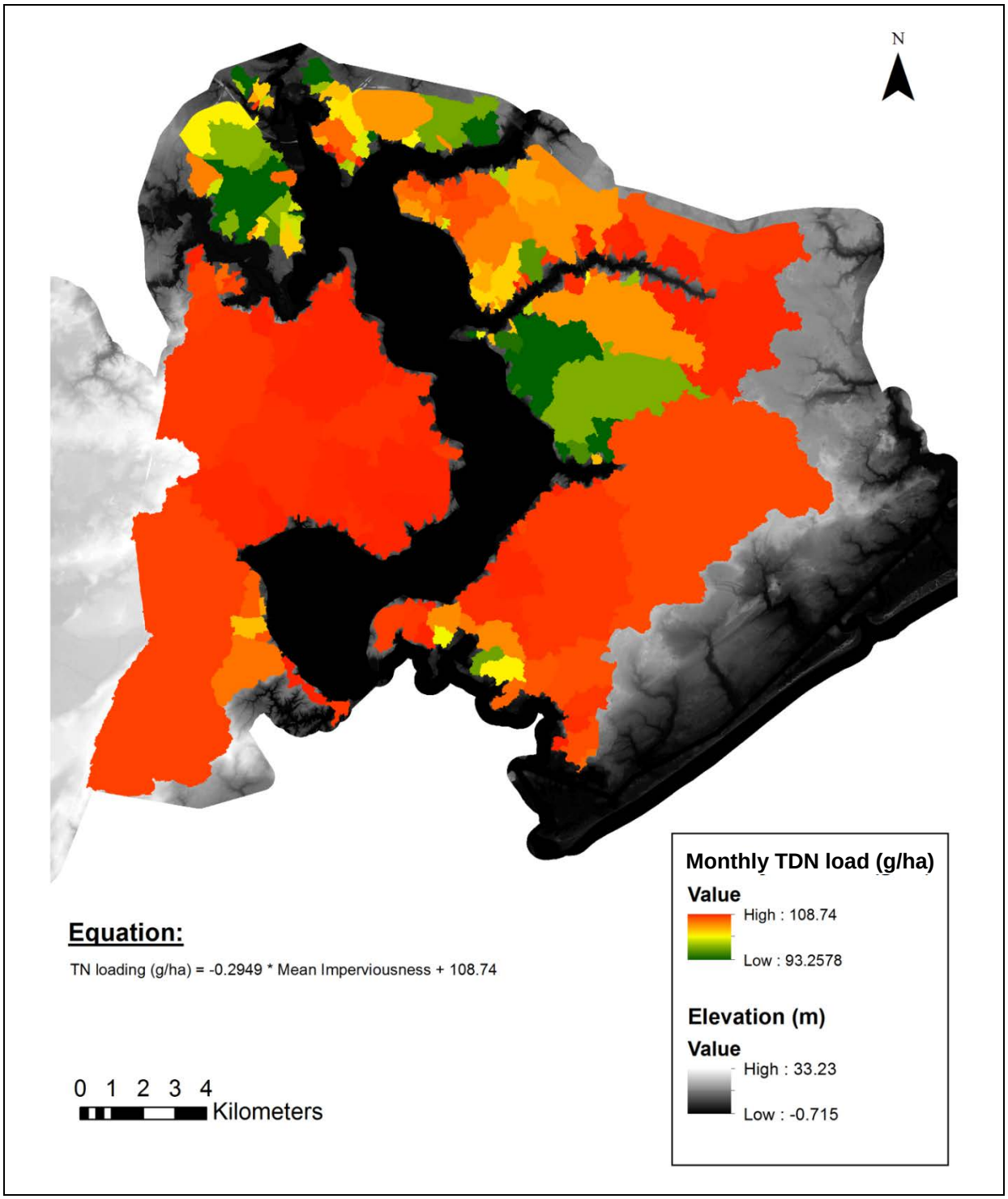

Figure 8A-2. Estimated monthly total nitrogen (TDN) load at Marine Corps Base Camp Lejeune.

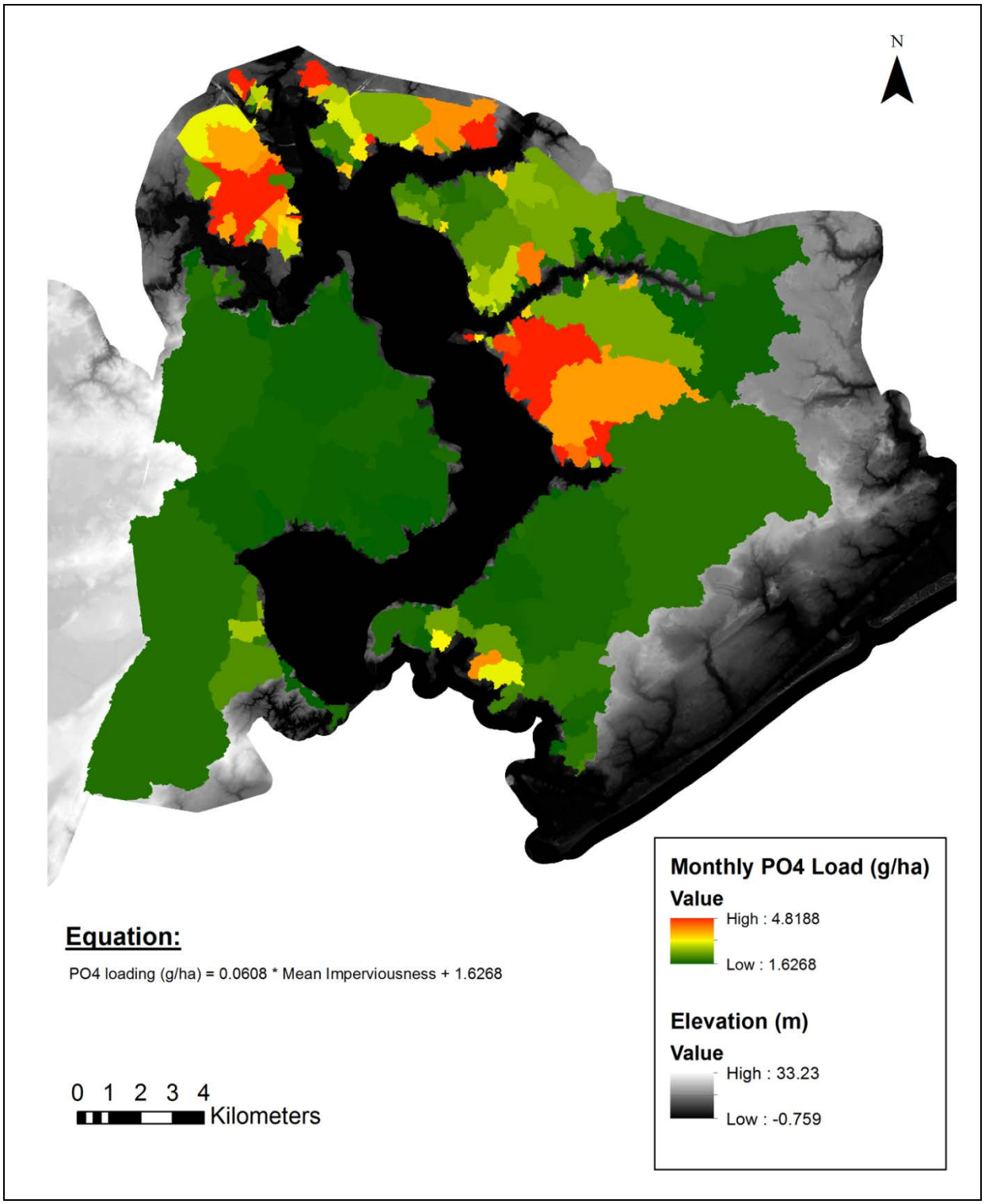

Figure 8A-3. Estimated monthly orthophosphate (PO_4) load at Marine Corps Base Camp Lejeune.

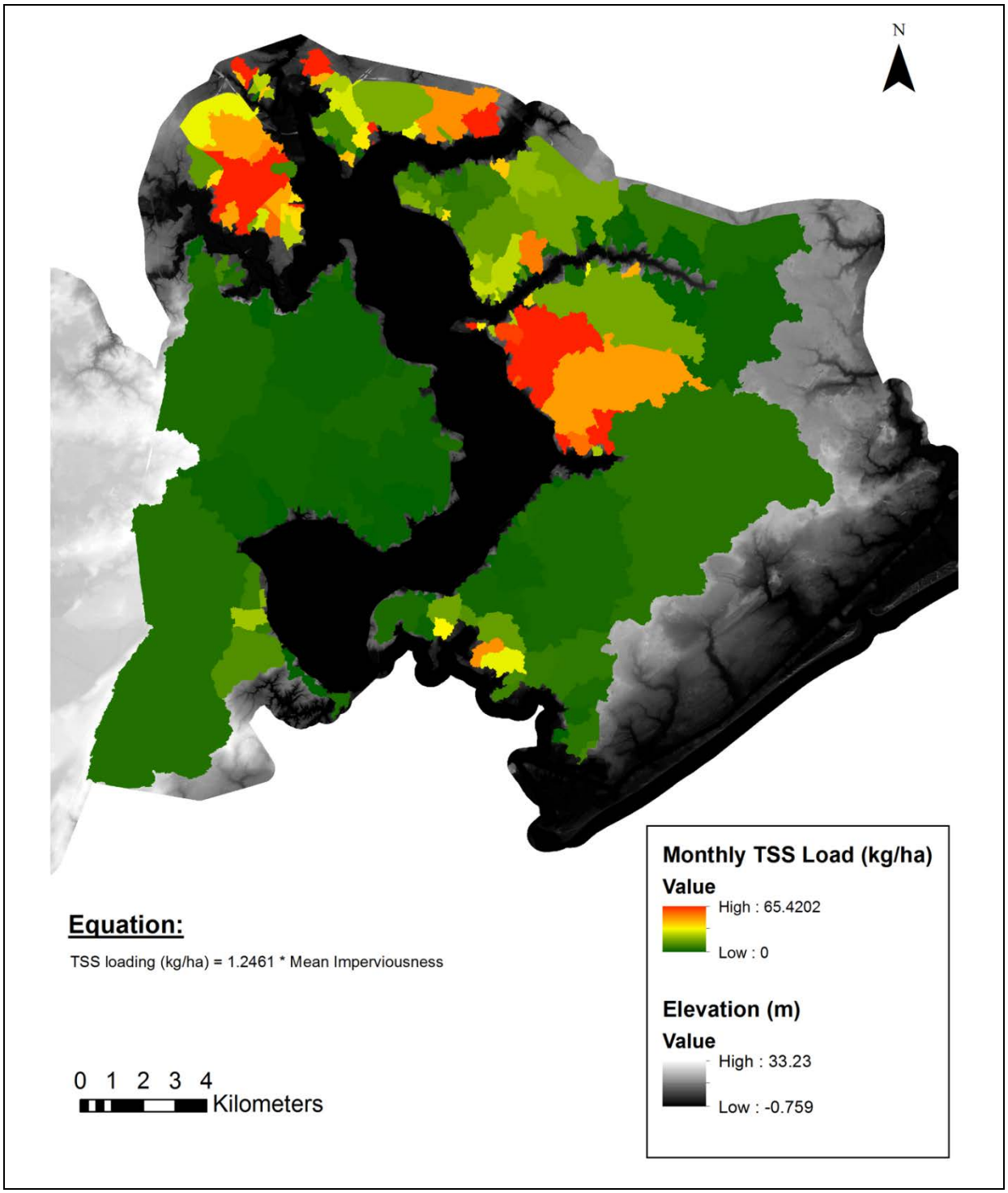

Figure 8A-4. Estimated monthly total suspended solids (TSS) load at Marine Corps Base Camp Lejeune.

Appendix 8-B
List of Scientific/Technical Publications

Papers

Ensign, S.H., C.A. Currin, M.F. Piehler, and C. Tobias. 2017. A method for using shoreline morphology to predict suspended sediment concentration in tidal creeks. *Geomorphology 276*:280–288.

Gold, A.C., S.P. Thompson, and M.F. Piehler. 2017. Water quality before and after watershed-scale implementation of stormwater wet ponds in the coastal plain. *Ecological Engineering 105*:240–251. doi:10.1016/j.ecoleng.2017.05.003

Gold, A.C., S.P. Thompson, and M.F. Piehler. 2017. Coastal stormwater wet pond sediment nitrogen dynamics. *Science of the Total Environment 609*:672–681. doi:10.1016/j.scitotenv.2017.07.213

Von Korff, B.H., M.F. Piehler, and S.H. Ensign. 2014. Comparison of denitrification between river channels and their adjoining tidal freshwater wetlands. *Wetlands 34*:1047–1060.

Thesis

Gold, A.C. 2017. *Impacts of Coastal Stormwater Pond Nitrogen Cycling on Downstream Water Quality*. M.S. thesis, University of North Carolina at Chapel Hill, Chapel Hill.

White, C.A. 2014. *Quantifying Coastal Stream Metabolism Across a Gradient of Human Watershed Development*. M.S. thesis, University of North Carolina at Chapel Hill, Chapel Hill.

Presentations

White, C.L., M.F. Piehler, L.I. Couper, and S.P. Thompson. 2013. *Impacts of Land Use on Coastal Stream Metabolism*. Presented at the Southeast Tidal Creeks Summit, Wilmington, NC. December 16–17.

Piehler, M.F. 2013. *Science to Support Ecosystem Management and Restoration: Synergy Through Cooperation at APNEP*. Invited lunchtime keynote presentation at the 2013 Albemarle–Pamlico Ecosystem Symposium: Embarking on a New Voyage, New Bern, NC. November.

Piehler, M.F. 2013. *Integrating an Estuarine Research and Monitoring Program (DCERP) into North Carolina Coastal Decision-Making*. Presented at the 2013 Albemarle–Pamlico Ecosystem Symposium: Embarking on a New Voyage, New Bern, NC. November.

White, C.L., M.F. Piehler, L.I. Couper, and S.P. Thompson. 2013. *Assessing Impacts of Land Use on Coastal Stream Metabolism*. Presented at the Conference of the Coastal and Estuarine Research Federation, San Diego, CA. November 3–7.

Appendix 8-C
List of Students

- Caitlin White, M.S., Marine Sciences, University of North Carolina at Chapel Hill, Chapel Hill, NC, 2014.
- Adam Gold, M.S., Ecology, University of North Carolina at Chapel Hill, 2017; currently pursuing Ph.D., Ecology, University of North Carolina at Chapel Hill, Chapel Hill, NC.

Appendix 8-D
Other Supporting Information

- Adam Gold, University of North Carolina at Chapel Hill's Graduate Education Advancement Board Impact Award, 2017. For more information, see http://gradschool.unc.edu/news/2017/impact/awards.html#Gold

Chapter 9

Nutrient-Driven Eutrophication and Carbon Flux Modulated by Climate Change in the New River Estuary

and

Climatic Drivers Regulating Benthic-Pelagic Carbon and Associated Nutrient Exchanges in the New River Estuary

SERDP Project Number: RC-2245

Aquatic/Estuarine Module

Research Projects AE-4 and AE-6

Lead Researchers:

Dr. Iris Anderson, Virginia Institute of Marine Science
E-mail: iris@vims.edu

Dr. Hans Paerl, University of North Carolina at Chapel Hill's Institute of Marine Sciences
E-mail: hpaerl@email.unc.edu

Supporting Researchers:

Dr. Mark Brush, VIMS
Dr. Joseph Crosswell, UNC-IMS; VIMS
Dr. Carolyn Currin, NOAA
Dr. Scott Ensign, Aquatic Analysis and Consulting, LLC
Dr. Brent McKee, UNC-CH
Dr. Michael Piehler, UNC-IMS
Jennifer Stanhope, VIMS
Dr. Craig Tobias, UCONN

November 2017

Final

This report was prepared under contract to the U.S. Department of Defense (DoD) Strategic Environmental Research and Development Program (SERDP). The publication of this report does not indicate endorsement by DoD, nor should the contents be construed as reflecting the official policy or position of DoD. References herein to any specific commercial product, process, or service by trade name, trademark, manufacturer, or otherwise, do not necessarily constitute or imply its endorsement, recommendation, or favoring by DoD.

Table of Contents

Abstract 9-1
Objectives of the Research Projects 9-2
Background 9-2
Materials and Methods 9-4
Integration of Research Projects AE-4 and AE-6 9-4
Carbon Data Collection 9-6
Air–Water CO_2 Flux 9-7
Metabolism 9-7
River and Tributary Loading (Data from Monitoring Activity AEM-4, Dr. Scott Ensign, Chapter 4, and Research Project AE-5, Dr. Michael Piehler, Chapter 8) 9-8
Addressing Uncertainty in Long-Term pCO_2 Variability Due to Bimonthly Sampling Frequency 9-9
Burial (Data from Dr. Brent McKee, Chapter 12) 9-10
Carbon Budget 9-10
Lability of DOC 9-10
Results and Discussion 9-11
River and Tributary Loading 9-11
Air–Water CO_2 Flux 9-12
CO_2 Efflux in Response to Hurricane Joaquin 9-15
Variations in pCO_2 During 7-Week Gaps Between Monthly Dataflow Cruises 9-16
Metabolism 9-17
Lability of DOC 9-18
Burial 9-19
Export to Ocean 9-19
Carbon Budget 9-21
Conclusions and Implications for Future Research and Implementation 9-22
Spatial Scales of Metabolic Balance 9-22
Temporal Scales of Air–Water CO_2 Exchange 9-23
Uncertainty 9-24
Scaling and Prediction of Coastal Carbon Fluxes 9-25
Findings with Implications for Future Base Management 9-26
Literature Cited 9-26
Appendix 9-A: Additional Information: Research Project AE-6 ..... 9-A-1
Appendix 9-B: Research Project AE-6: Research Questions and Answers 9-B-1
Appendix 9-C: Research Project AE-4: Research Questions and Answers 9-C-1
Appendix 9-D: List of Scientific/Technical Publications 9-D-1
Appendix 9-E: List of Students 9-E-1
Appendix 9-F: Other Supporting Information 9-F-1

List of Figures

Figure 9-1. Sampling sites and spatial data used in the NRE carbon budget: (A) NRE regions, river (Gum Branch station) and tributary sampling stations; (B) shoal and channel sampling stations used in metabolism estimates; (C) meteorological AVP stations and survey tracks for air–water CO_2 flux measurements in channel and shoal; and (D) sites used in burial estimates, and the shoal-channel boundary (2-m depth contour) applied within sections and regions. 9-5

Figure 9-2. Comparison of diel (day versus night) variation of pCO_2 to average seasonal variation within each box. 9-13

Figure 9-3. (A) Areal daily CO_2 flux in shoal and channel; (B) Areal daily chlorophyll a (Chl a) concentration in shoal and the channel. 9-14

Figure 9-4. Influence of water temperature on daily CO_2 fluxes in shoal and channel. 9-14

Figure 9-5. CO_2 flux response to the passage of Hurricane Joaquin. 9-16

Figure 9-6. Gross Primary Production (GPP), ecosystem respiration (R), and net ecosystem metabolism (NEM) in the upper, middle, and lower NRE and integrated across the entire estuary. 9-18

Figure 9-7. Lability of DOC in water samples collected offshore of Jacksonville, NC. 9-19

Figure 9-8. Residual flow carbon budget showing annual carbon exchanges as DIC and TOC flows in Gg-C (10^9 g-C). 9-20

List of Tables

Table 9-1. Components of Research Projects AE-4 and AE-6[a] 9-4

Table 9-2. Annual Carbon Budget Terms (10^6 g-C) 9-12

Table 9-3. Annual Regional Air – Water CO_2 Fluxes 9-15

Table 9-4. Comparison of CO_2 Fluxes Calculated by Linear Interpolation and Based on Continuous in situ Measurements (mmol C m^{-2} hr^{-1}) 9-16

Table 9-5. Carbon Export from the NRE to Onslow Bay (10^9 g-C)[a] 9-21

Acronyms

°C	degree Celsius
µatm	microatmosphere
µg L^{-1}	micrograms per liter
µL	microliter
µm	micro meter
ΔDIC_g	portion of the total DIC change that is due to air–water CO2 flux
ΔDIC_q	portion of the total DIC change associated with a change in salinity
ΔDIC_t	total change in DIC between water samples
ΔpCO_2	difference between the gas concentrations in the surface water and atmosphere
AE	Aquatic/Estuarine (Module)
AEM	Aquatic/Estuarine Monitoring Activity
AVP	autonomous vertical profiler
BMA	benthic microalgae
BMA-N	benthic microalgal-nitrogen
C	carbon
C/N	total organic carbon to total nitrogen ratio
CDOM	chromophoric dissolved organic matter
Chl *a*, chl *a*	chlorophyll *a*
cm	centimeter
cm h^{-1}, cm/hr	centimeters per hour
cm y^{-1}, cm yr^{-1}	centimeters per year
cm^3	cubic centimeter
CO_2	carbon dioxide
CO-OPS	Center for Operational Oceanographic Products and Services
CW	Coastal Wetlands (Module)
DCERP	Defense Coastal/Estuarine Research Program
DCERP1	first cycle of DCERP
DCERP2	second cycle of DCERP
DIC	dissolved inorganic carbon
DIN	dissolved inorganic nitrogen
DIP	dissolved inorganic phosphorus
DNF	denitrification
DO	dissolved oxygen
DOC	dissolved organic carbon
DoD	U.S. Department of Defense
DON	dissolved organic nitrogen
EA-IRMS	elemental analyzer–continuous flow isotope ratio mass spectrometry
ESM	Estuarine Simulation Model
F	metabolic DIC flux
F_1	dawn1–dusk
F_2	dusk–dawn2
F_b	metabolic DIC flux in the bottom water
F_s	metabolic DIC flux in the surface water
g	gram

g C	grams of carbon
g C m^{-2} d^{-1}	grams of carbon per square meter per day
g-C m^{-3}	grams of carbon per cubic meter
g C y^{-1}, g C yr^{-1}	grams of carbon per year
Gg-C yr^{-1}	gigagram of carbon per year (10^9 grams of carbon per year)
GPP	gross primary production
h, hr	hour
ha	hectare
HCl	hydrochloric acid
$HgCl_2$	mercury chloride
IRGA	infrared gas analyzer
K_0	solubility coefficient
k_{660}	gas exchange coefficient
kg	kilogram
kg TN y^{-1}, kg TN yr^{-1}	kilograms of total nitrogen per year
km	kilometer
km^2	square kilometer
kg km^{-1} yr^{-1}	kilograms per kilometer per year
KNCA	Marine Corps Air Station New River weather station
L min^{-1}	liters per minute
m	meter
m s^{-1}	meters per second
m^2	square meter
m^3	cubic meter
m^3 s^{-1}	cubic meters per second
MCBCL	Marine Corps Base Camp Lejeune
MIN	gross nitrogen mineralization
mL	milliliter
mmol C m^{-2} hr^{-1}	millimoles of carbon per square meter per hour
msl	mean sea level
N	nitrogen
NACD 88	North American Vertical Datum of 1988
NDIR	nondispersive infrared
NEM	net ecosystem metabolism
NFix	nitrogen fixation
nm	nanometer
NOAA	National Oceanic and Atmospheric Administration
NRE	New River Estuary
O^2	oxygen
OC	organic carbon
PAR	photosynthetically active radiation
pCO_2	partial pressure of carbon dioxide
POC	particulate organic carbon
PPr	primary production
ppt	parts per thousand
Q	river discharge

R	respiration
RC	Resource Conservation and Climate Change (a SERDP program area)
Sc	Schmidt number for ambient surface temperature and salinity
SERDP	Strategic Environmental Research and Development Program
TOC	total organic carbon
SW	shallow water
TN	total nitrogen
TSP	Translating Science into Practice (Module)
u_{10}	function of wind speed normalized to 10 m above the water surface
UCONN	University of Connecticut
UNC-CH	University of North Carolina at Chapel Hill
UNC-IMS	University of North Carolina at Chapel Hill's Institute of Marine Sciences
USGS	U.S. Geological Survey
VIMS	Virginia Institute of Marine Science
yr	year
YR1	Year 1
YR2	Year 2
z_b	average depth of the respective section minus z_s
z_s	depth of the pycnocline at the respective station

Abstract

Coastal ecosystems, such as the New River Estuary (NRE), are composed of many connected environments, and carbon can undergo significant transformation as it moves through this aquatic network. Carbon budgets provide a tool to quantify carbon flows and track the complex processes that control whether carbon is stored internally or exported into the ocean and atmosphere. However, coastal carbon fluxes are highly variable in space and time and are challenging to measure. Currently, there are few available coastal carbon budgets, and most have relied on limited observational scales. The **overarching objective** of Research Projects AE-4 and AE-6 was to develop a comprehensive carbon budget for the NRE via coordinated measurements of dissolved inorganic carbon (DIC) and total organic carbon (TOC) fluxes across the entire estuary. The **technical approach** involved measurements of carbon exchanges via river and tributary input, air–water flux, burial and metabolism over the 2-year period: July 2014 through July 2015 (a dry year) and July 2015 through July 2016 (a wet year). Air–water carbon dioxide (CO_2) fluxes and metabolic variables were simultaneously measured in the channel and shoal by conducting a series of novel high-resolution surveys at dawn, dusk, and the following dawn. Carbon flows between estuary regions and export into the coastal ocean were calculated by quantifying residual transport of DIC and TOC down the estuary as the flows were modified by sources, sinks, and internal transformations. Variability in flows within regions and across the entire estuary were determined at time scales ranging from diel to seasonal to annual and inter-annual. **Results** of the study demonstrated that net ecosystem metabolism (NEM), which can vary from net autotrophic, in which case production (photosynthesis) in the system exceeds decomposition (respiration), to net heterotrophic, in which case decomposition exceeds production, was the primary driver of carbon flow and speciation in the NRE. Annually, the entire NRE was in near metabolic balance, maintained by counteracting carbon fluxes spatially across lateral gradients from channel to shoal, longitudinally down the estuarine gradient, and temporally between day and night and various seasons. The NRE varied from a small sink for CO_2 during Year 1 to a small source for atmospheric CO_2 during Year 2. Variation in CO_2 fluxes was as large over diel as for seasonal time scales and has been ignored in most other published studies. The NRE was a source of both DIC and TOC to the coastal ocean; however, the dominant carbon species exported varied, depending on whether the system was net autotrophic (mainly a source of TOC) or net heterotrophic (mainly a source of DIC). A major **benefit** of this study is that it demonstrates the importance of and need to perform high temporal and spatial resolution measurements of carbon fluxes at appropriate scales to understand the mechanisms responsible for the observed exchanges and to predict how they might change in response to future increased storm activity, temperature, and land-use change.

Keywords: Burial, carbon, carbon budget, carbon dioxide, dissolved inorganic carbon, dissolved organic carbon, flux, gross primary production, microtidal estuary, net ecosystem metabolism, photosynthesis, phytoplankton, respiration, total organic carbon

Objectives of the Research Projects

The primary objective of this research was to develop a carbon budget for the New River Estuary (NRE) by tracking the fate of total inorganic and organic carbon, loaded into the estuary from the New River, smaller tributaries, and the atmosphere, as they are transformed by metabolic processes. The species and magnitude of carbon exchanged with the atmosphere, coastal ocean, and sediment, which depend upon the transformations within the estuary, were quantified on diel, seasonal, and annual time scales through the integration of high-resolution sampling programs in the main channel (Research Project AE-4) and shallow waters (Research Project AE-6) of the NRE. The open water method used to measure metabolism integrated the influences of both phytoplankton in the water column and benthos, building on nutrient and hydrologic input and water quality data collected during DCERP1 and by DCERP2 Monitoring Activities AEM-1 (NRE channel), AEM-2 (NRE tributaries), AEM-3 (NRE shallows), and AEM-4 (New River). System-scale carbon exchange data were combined with results from Research Projects AE-5, CW-4, and CW-5 to develop a net carbon budget based on residual carbon flows for the estuarine region of Marine Corps Base Camp Lejeune (MCBCL). The Residual Carbon Flow model tracked dissolved inorganic carbon (DIC) and total organic carbon (TOC) as they moved from the watersheds of the New River and those of smaller tributaries on MCBCL into the NRE, where they were transformed by metabolic processes and then exported into the atmosphere as carbon dioxide (CO_2), buried in sediment or released into the coastal ocean as DIC or TOC. Data collected by Research Projects AE-4 and AE-6 were used to validate the Estuarine Simulation Model (ESM) as part of Research Project TSP-2. The ESM predicts estuarine responses to human perturbations and future climatic change for developing management decision-support tools (see Chapter 10 of this DCERP2 Final Report).

Background

The NRE is a shallow, microtidal, lagoonal system with a long average flushing time (64 days), and more than half of the estuary has water depths less than 2 m (msl). In such systems, light, nutrients (nitrogen and phosphorus), temperature, and salinity regulate net ecosystem metabolism (NEM), which determines to a large extent the speciation of carbon (DIC, pCO_2, particulate organic carbon [POC], or dissolved organic carbon [DOC]), and exchanges with the atmosphere, sediments, and coastal ocean (Caffrey, 2003; Gazeau et al., 2005; Kennish and Paerl, 2010; Paerl et al., 2010; Raymond et al., 2000). Data collected during DCERP1 demonstrated that the delivery of carbon, nitrogen, and phosphorus in dissolved and particulate forms from watersheds to the estuary were strongly affected by freshwater discharge during episodic (e.g., storms) and chronic (e.g., drought) events and, in turn, regulated both benthic and pelagic gross primary production (GPP; Peierls et al., 2012). The fate of carbon, nitrogen, and phosphorus derived from external sources depends upon the sources and lability of the organic components and uptake of inorganic components by benthic and pelagic primary producers, provided that sufficient light is available (Kemp et al., 1997 and 2005). As planktonic biomass moves down-estuary and settles to the sediment surface, it is recycled by benthic microorganisms, micro- and macro-fauna to organic and inorganic forms of carbon, nitrogen, and phosphorus, some of which may be sequestered in the benthos by benthic microorganisms and eventually buried, some released to support planktonic production, and some exchanged with the atmosphere and ocean (Anderson et al., 2010; Crosswell et al., 2012; Hardison et al., 2011; Nixon, 1986; Zimmerman and Canuel, 2000). Regional and global carbon budgets have generally ignored the transformations and

exchanges that occur as carbon moves from the terrestrial zone down river and across an estuary to the coastal ocean (Regnier et al., 2013). Attempts to synthesize carbon budgets for coastal regions of North America have identified major data gaps for many budget terms (Benway et al., 2015; Najjar et al., 2012), including NEM, respiration (R), air–water CO_2 fluxes, and burial. Biological and physical drivers that regulate the fate of carbon moving through the estuarine continuum include nutrient loading, the loading ratio of dissolved inorganic nitrogen (DIN) to TOC, benthic community composition, freshwater discharge, flushing time, water-column stratification, erosion, burial and light availability (diel variation) (Blair and Aller, 2012; Najjar et al., 2012). An improved understanding of the relative importance of these various drivers requires greater temporal and spatial resolution of data than are currently available (Crosswell et al., 2014; Maher et al., 2015).

NEM, the balance between production and consumption of organic carbon within an aquatic system, regulates carbon transformation and influences the pathways by which carbon is exported to adjacent systems (Kemp and Testa, 2011). A net autotrophic system imports inorganic nutrients and DIC and exports or buries TOC, which includes DOC plus POC, whereas a net heterotrophic system imports TOC and exports DIC and nutrients (Boynton and Kemp, 2000; Nixon et al., 1996). In a review of 79 estuaries around the world, Borges and Abril (2011) noted that 66 of them were net heterotrophic, and in most, the partial pressure of CO_2 (pCO_2) was supersaturated relative to atmospheric levels. Raymond et al. (2000) suggest that pCO_2 supersaturation is an indicator of a net heterotrophic system; however, Maher et al. (2013) and Neubauer and Anderson (2003) note that the source of the DIC may be from adjacent wetlands and, thus, may not necessarily indicate net heterotrophy in the estuary.

Primary production within an estuary depends upon both external nutrient loading and internal recycling of organic matter (Kemp et al., 1997; Testa and Kemp, 2008). Nixon et al. (1995) demonstrated that in Narragansett Bay, RI, most of the carbon fixed is respired within the estuary. Kemp et al. (1997) suggested that the loading ratio of DIN to TOC can, to a large extent, determine whether an estuary will be net autotrophic or heterotrophic. A recent study by Herrmann et al. (2015) estimated NEM and carbon burial and export for 52 estuaries located along the East Coast of the United States based on the ratio of DIN:TOC loading. Overall, most of these systems were estimated to be net heterotrophic, although estuaries along the mid-Atlantic Bight tended to be almost in balance. From these data, Herrmann et al. (2015) calculated that East Coast estuaries export approximately 60% of the inputs of TOC to the continental shelf. In making these estimates, Herrmann et al. (2015) recognized that data, especially those related to burial, marsh inputs, and NEM, are very limited, and the scientists emphasized that additional research was needed to assess their modeling method.

Shallow estuaries such as the NRE comprise nearly half of estuarine surface area in the United States (NOAA Coastal Assessment Framework, 2017), and metabolic processing in these estuaries is different than in deeper estuaries. In shallow systems where the benthos is exposed to sufficient light, primary production by benthic microalgae (BMA), seagrasses, or macroalgae plays an important role in sequestering (at least temporarily) nutrients and DIC (Anderson et al., 2014; Eyre et al., 2011; McGlathery et al., 2007; Nixon et al., 2001). NEM in the shallow zone is strongly regulated by light, which varies on diel and seasonal cycles, but also with factors such as freshwater discharge carrying chromophoric dissolved organic matter (CDOM) and nutrients.

The biotic and abiotic conditions that drive metabolism interact in a complex manner, varying spatially and temporally and thereby require intensive data collection (Anderson et al., 2014).

The overarching objective of the research reported herein was to develop an empirical carbon budget for the NRE by using high-resolution temporal and spatial data, which allow more accurate measurements of metabolic variables and air–water CO_2 exchanges. Simultaneous water-quality mapping surveys were conducted in the channel and shoal to capture diel and seasonal variability during both wet and dry years. Carbon inputs from the inland and lateral watersheds were directly monitored in the river and tributaries, and burial was estimated from an analysis of sediment cores taken throughout the estuary. The NRE carbon budget was constructed from empirical data by using a residual carbon flow approach that focused on ecosystem connectivity.

Materials and Methods

Integration of Research Projects AE-4 and AE-6

Development of an estuary-wide carbon budget for the NRE required measurement of carbon exchanges at pertinent time–space scales. Accordingly, we integrated the sampling programs of Research Projects AE-4 and AE-6 to: (1) conduct simultaneous spatial surveys of the main channel and peripheral shallow waters of the NRE and (2) deploy autonomous monitoring systems to collect parallel diel measurements of surface pCO_2 and auxiliary parameters on autonomous vertical profilers (AVPs) and nearby shallow-water stations (**Table 9-1 and Figure 9-1**). By synchronizing research activities, we were able to directly compare the physical and biological controls on primary production and carbon fluxes in the deep and shallow waters of the NRE. This collective data set allowed us to determine the net metabolic status of the NRE system and the source or sink term of estuarine waters for atmospheric CO_2.

Table 9-1. Components of Research Projects AE-4 and AE-6[a]

Research Project	Variable	Temporal Scale	Spatial Scale	Method
AE-4: Main channel of NRE	Water temperature, salinity, DO, pCO_2, pH, turbidity, chlorophyll fluorescence (in vivo)	Continuous (AVPs) Bimonthly (Dawn–dusk–dawn surveys)	2 stations (AVPs); pCO_2, Dataflow cruises	YSI multiparameter datasonde; Li-Cor pCO_2 shower-head analyzer
	DIC, water temperature, chlorophyll in vivo, DO, pH, turbidity, PAR; PPr	Bimonthly (Dawn–dusk–dawn surveys)	8 stations (surface and near bottom)	YSI multiparameter datasonde, IRGA (DIC), and Li-Cor quantum sensor; ^{14}C method for PPr
AE-6: Shallow NRE	Water temperature, salinity, DO, pCO_2, pH, turbidity, DIC, CDOM, PAR, and chlorophyll in vivo	Bimonthly (Dawn–dusk–dawn surveys)	6 stations (DIC); pCO_2 on Dataflow cruises	YSI multiparameter datasonde, Li-Cor shower-head pCO_2 analyzer, IRGA (DIC), and WetLabs CDOM sensor

Note: DO = dissolved oxygen; IRGA = infrared gas analyzer; PAR = photosynthetically active radiation; PPr = primary production.

[a] Data used by Research Projects AE-4 and AE-6 were also generated by Monitoring Activities AEM-1 and AEM-3.

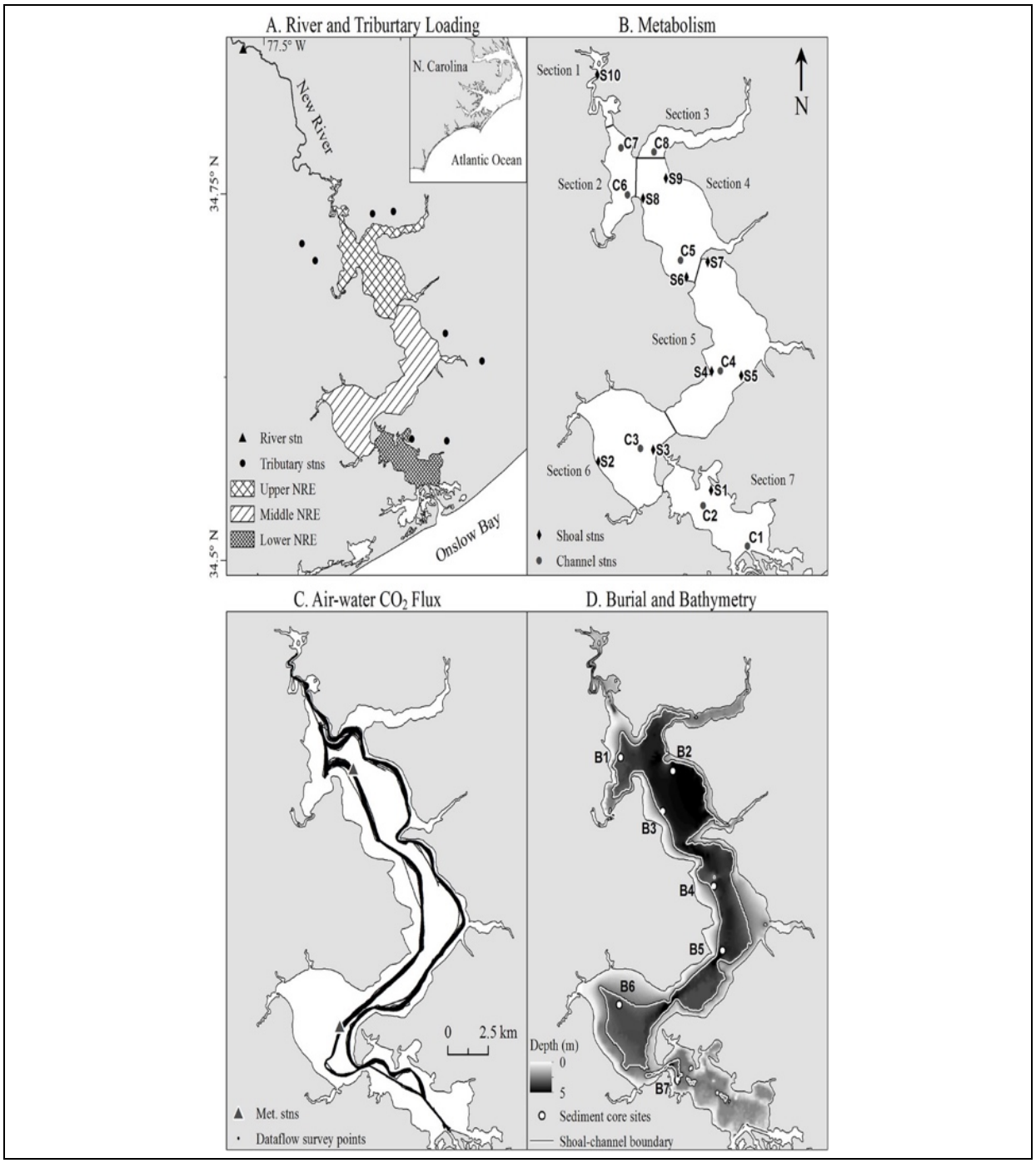

Figure 9-1. Sampling sites and spatial data used in the NRE carbon budget: (A) NRE regions, river (Gum Branch station) and tributary sampling stations; (B) shoal and channel sampling stations used in metabolism estimates; (C) meteorological AVP stations and survey tracks for air–water CO_2 flux measurements in channel and shoal; and (D) sites used in burial estimates, and the shoal-channel boundary (2-m depth contour) applied within sections and regions.

For the purposes of developing a carbon budget, the NRE was divided into three regions, the upper, middle, and lower estuary, based on major geographic constrictions and hydrography (Figure 9-1A). Estuary regions were further divided into seven sections to improve scaling of carbon fluxes to representative areas (Figure 9-1B). Shoal and channel components were delineated in each section using the 2-m contour (msl) as the boundary (Figure 9-1D). Based on area, the upper estuary contains more channel (55%) than shoal (45%), the middle estuary is relatively balanced (51% shoal, 49% channel), and the lower estuary is almost entirely comprised of shoal (94%). Although maximum depths in the estuary reach 5 m, depths in the channel sections range from 2.4 to 3 m, and mean depth on the shoals is approximately 1 m. Surface (<2 m) salinities typically range from 11 to 19 (mean 14.7) in the upper estuary, from 18 to 25 (mean 21.2) in the middle estuary, and from 29 to 34 (mean 30.7) in the lower estuary. The MCBCL tributary creek watershed areas for the upper, middle, and lower estuary were 138, 150, and 20 km^2, respectively. Most of the tidal marshes around the NRE are located outside the system along the nearby Intracoastal Waterway, although 15%, 9%, and 48% of the shoreline is fringed by marshes in the upper, middle, and lower regions of the estuary, respectively (Currin et al., 2015).

Carbon Data Collection

Spatial surveys were conducted at bimonthly intervals from July 2013 to July 2015, where Year 1 (YR1) refers to the first 12 months and Year 2 (YR2) refers to the past 12 months. Each bimonthly (i.e., every 2 months) survey interval consisted of a series of three high-resolution surveys that were conducted at dawn, dusk, and the following dawn. Surveys began approximately 45 minutes prior to sunrise or sunset and required approximately 1.5 hours to cover the entire NRE from the New River Inlet (Station C1, Figure 9-1B) to the mouth of the New River at Jacksonville, NC (Station S10, Figure 9-1B). Each survey involved two research vessels that conducted simultaneous transects of the estuary channel and shoal by using identical high-resolution water quality mapping systems. Water was continuously pumped to a multi-parameter datasonde (Yellow Springs Instruments, Model 6600) in a flow-thru cell (Dataflow, modified from Madden and Day, 1992) and a showerhead-equilibration chamber. Equilibrated air was directed to a nondispersive infrared (NDIR) absorbance detection analyzer (Li-Cor LI-840, modified from Hales et al., 2004). Surface water pCO_2, temperature, and salinity were measured at a rate of 0.5 Hz. Spatial data were corrected for the total system response time (average of 46 s), which was measured on each individual survey. Atmospheric pCO_2 was measured at the beginning and end of each survey after a series of CO_2 standard gases (120, 2,000, and 5,000 µatm) were run for NDIR calibration.

To calculate metabolism, surface water DIC samples were collected at shoal stations along the eastern shore (i.e., S1, S3, S5, S7, S9, and S10), and surface and bottom water DIC samples and salinity measurements were collected at all channel stations (i.e., C1 through C8; Figure 9-1B). An additional survey was conducted after the first dawn survey of each series to collect water-column profiles and discrete samples for DOC and POC at all stations. Shoal POC samples were only collected during YR2. Shoal POC concentrations in YR1 were estimated based on discrete chlorophyll samples and using a chlorophyll *a* (chl *a*): POC regression determined on each survey from channel samples.

DIC samples, collected in 10-mL vials (n=2) were pre-spiked with 10 µL of mercuric chloride ($HgCl_2$) saturated solution. Vials were sealed without a headspace by using butyl stoppers, were stored inverted in water until analysis, and were analyzed within 1 week as described by Neubauer and Anderson (2003). Data were calibrated based on a periodic analysis of certified reference materials from the A. Dickson laboratory at the Scripps Institution of Oceanography. Bulk water samples for DOC and POC analysis were stored on ice, filtered within 24 hr of collection, and the filtrate analyzed on a Shimadzu TOC-V for DOC. The POC was determined by combusting the GF/F filter in a CNH elemental analyzer (Costech Analytical Technologies Model ECS 4010 or Perkin-Elmer 2400 Series II).

Air–Water CO_2 Flux

For each spatial survey, Dataflow and pCO_2 data were aggregated by NRE section into distance-weighted averages for the channel and shoal (Figure 9-1B and 9-1C). Daily means were estimated for each survey series and interpolated between bimonthly survey intervals. Distance-weighted averages were also interpolated within the 24-hour survey interval so that DIC–based metabolism estimates could be corrected for gas exchange, as described in the Metabolism subsection. Air–water flux was calculated for each section according to Equation 9-1.

$$\text{Flux}=K_0(k_{660})(\Delta pCO_2)(Sc/660)^{-0.5} \qquad \text{Eq. 9-1}$$

where K_0 is the solubility coefficient (Weiss, 1974), k_{660} is the gas exchange coefficient, ΔpCO_2 is the air–water pCO_2 gradient (µatm) and Sc is the Schmidt number at ambient surface temperature and salinity (Wanninkhof, 1992). The gas transfer parameterization of Jiang et al. (2008) was selected to estimate k_{660} because it represents a wide range of estuarine gas exchange studies. Hourly air–water CO_2 fluxes between the dawn and dusk survey intervals were calculated by using the average hourly wind speed from two meteorological AVP stations in the NRE (Figure 9-1). Daily CO_2 fluxes between bimonthly intervals were calculated by using daily wind speeds and daily interpolation of surface water data. To approximate uncertainty, air–water fluxes were also calculated by using the gas transfer parameterizations of Ho et al. (2006) and Prytherch et al. (2010). These parameterizations represent the minimum and maximum gas transfer rates that have been applied in estuaries (Crosswell et al., 2014).

Metabolism

GPP, R, and NEM were estimated based on the change in DIC of discrete water samples between surveys. At each station, the hourly metabolic DIC flux (F) was calculated based on the difference between the dawn1–dusk (F_1) surveys and the dusk–dawn2 (F_2) surveys (Equation 9-2). Daily R, GPP, and NEM were then determined by following Equations 3 through 5.

$$F=\Delta DIC_t-\Delta DIC_q-\Delta DIC_g \qquad \text{Eq. 9-2}$$

$$R=(F_2)\times 24 \qquad \text{Eq. 9-3}$$

$$GPP=(F_1-F_2)\times h_1 \qquad \text{Eq. 9-4}$$

$$NEM=GPP-R \qquad \text{Eq. 9-5}$$

where ΔDIC_t is the total change in DIC between water samples, ΔDIC_q is the portion of the total DIC change associated with a change in salinity, and ΔDIC_g is the portion of the total DIC change that is due to air–water CO_2 flux. ΔDIC_q was estimated as the change in salinity between consecutive water samples multiplied by the slope of the DIC:salinity regression, which was calculated separately for channel and shoal stations by using data from the two surveys of the respective interval. At channel stations, F in the surface water (F_s) and bottom water (F_b) were integrated into a single term according to Equation 9-6.

$$F=z_s(F_s)-z_b(F_b) \qquad \text{Eq. 9-6}$$

where z_s is the depth of the pycnocline at the respective station, and z_b is the average depth of the respective section minus z_s. The ΔDIC_g term was excluded from F_b. The pycnocline depth was represented as the depth at which the salinity profile equaled the average surface and bottom salinity. If the total vertical salinity gradient at any station was less than 1.5, the station was considered well mixed, and Equation 2 was applied by using the average of the DIC values. For each survey series, R, GPP, and NEM at stations within or near each NRE section were combined into separate sectional averages for the channel and shoal. These averages were scaled to the three estuary regions based on area. Finally, regional values were interpolated daily between survey dates to yield annual estimates.

Daily metabolism rates based on direct measurement of DIC represent six 24-hour intervals per year. A recent study of uncertainty propagation in ecosystem budgets showed that spatial and temporal variability were the dominant sources of error in scaling discrete observations to annual budget terms (Lehrter and Cebrian, 2010). Following Lehrter and Cebrian (2010), we represent uncertainty as the 95% confidence interval around the scaled annual budget term, ignoring measurement, systematic, and model errors. However, we take a more conservative approach than applied in most prior methods to account for unknown uncertainty in our open-water metabolism estimates. The annual standard error for each section was determined by including all respective sectional metabolism data (g-C m^{-2} d^{-1}) within that year. The metabolism data were assumed to be a randomly sampled regardless of the time of the year or the location within the section. This approach makes no distinction between the channel and shoal and accounts for uncertainty in our representation of shoals as all areas less than a 2-m depth. The 95% confidence interval for each section were then scaled to the annual carbon budget terms based on the channel and shoal areas.

River and Tributary Loading (Data from Monitoring Activity AEM-4, Dr. Scott Ensign, Chapter 4, and Research Project AE-5, Dr. Michael Piehler, Chapter 8)

Riverine carbon flux to the upper section of the NRE was calculated from constituent concentrations and river discharge (Q, m^3 s^{-1}) at the U.S. Geological Survey (USGS) gaging station at Gum Branch (Station 02093000). Water samples for DIC, DOC, and POC were collected at Gum Branch from March 2013 through December 2015. During each of these years, six samples were collected during low discharge and six were collected during high discharge. Carbon loads were calculated by first developing a relationship between constituent concentration and discharge, based on exploratory plots and model fitting before applying a non-linear least squares regression. Three-parameter exponential models were developed for DIC (n=34) and DOC (n=33) (g-C m^{-3}), explaining 94% and 65% of the variance, respectively

(Equations 9-7 and 9-8). A more complex model form showed the best fit for POC (n=76), explaining 31% of the variance (Equation 9-9).

$$DIC=5.7+25e^{-0.26Q} \quad \text{Eq. 9-7}$$

$$DOC=17-12e^{-0.18Q} \quad \text{Eq. 9-8}$$

$$POC=1.1Q\, e^{-0.12Q}+1.5(1-e^{-0.10Q}) \quad \text{Eq. 9-9}$$

The models were applied to discharge data during the period from 01 July 2013 to 30 June 2015 to derive an integrated mass flux (Gg-C yr^{-1}) of each constituent. These fluxes were then scaled to the New River watershed below the Gum Branch gauging station based on drainage area to yield the upper watershed carbon input for YR1 and YR2. Uncertainty in the predicted loads was calculated by using the 95% confidence interval of the estimated concentration values.

Water discharge and DIC, DOC, and POC were measured at eight stations in five tributaries draining directly into the upper, middle, and lower NRE (Figure 9-1A) (Piehler et al., 2013). Water samples were collected manually every other week and after rainfall events yielded greater than 2.5 cm in 24 hours. Sampling resolution was increased during storm events by using automated water samplers (Teledyne Isco), and discharge was measured every 30 minutes. Carbon loads, fluxes, and yields were calculated for each sub-catchment for the period 01 July 2013 to 30 June 2015. Tributary DIC samples were only collected during YR2. For YR1, DIC loading was estimated by scaling YR2 loads by tributary discharge. The median of the five sub-catchment yields was applied across the entire tributary catchment area for the NRE. Uncertainty in the predicted constituent loads to the estuary was estimated by using the second lowest and second highest of the five sub-catchment constituent yields.

To estimate regional flushing times, freshwater discharge at Gum Branch and in the NRE tributaries was scaled to the total NRE watershed area as previously described. Flushing times were calculated for each sampling date by using the date-specific freshwater replacement method (Alber and Sheldon, 1999). Briefly, this method integrates salinity profiles, region-specific water volumes, and freshwater input corrected for lag due to watershed hydrology. Additional details about the calculation of NRE flushing time are provided by Ensign et al. (2004) and Peierls et al. (2012).

Addressing Uncertainty in Long-Term pCO_2 Variability Due to Bimonthly Sampling Frequency

To develop the carbon budget for the NRE, the estuary was sampled bimonthly, and fluxes of CO_2 were interpolated between the bimonthly samplings. It was assumed that pCO_2 increased or decreased linearly during the approximately 7 weeks between sampling efforts. To determine how much uncertainty was introduced by the interpolation method, we deployed a C-sense in situ CO_2 sensor (Turner Designs) in at the AVP stations in Stone and Morgan Bays seven times between September 2015 and September 2016, covering all seasons and a wide range of environmental conditions. We calculated daily average CO_2 fluxes (mmol C m^{-2} hr^{-1}) by using directly measured pCO_2, and then compared those values with the fluxes that were determined by assuming a linear change in pCO_2 between the beginning and end of the deployment (simulating our bimonthly trips).

Burial (Data from Dr. Brent McKee, Chapter 12)

Seven cores (50 cm total depth) were collected across the NRE in 2013 (Fig. 1D). Each core was extruded and sub-sampled at 1 cm intervals within 24 hours of collection. Samples were weighed wet, frozen and lyophilized then re-weighed for porosity and bulk density determinations. Samples were split into two aliquots for radiochemical analysis and organic geochemical analyses. Organic geochemical analyses were performed via elemental analyzer - continuous flow isotope ratio mass spectrometry, and the Constant Rate of Supply/Constant Flux model (Sanchez-Cabeza and Ruiz-Fernandez 2012) was applied for data interpretation. Short-term (< 5yr) carbon accumulation rates were determined based on the ^{210}Pb dating, dry bulk density, and percent organic carbon (Supporting information). Burial terms applied to the 2013–2015 carbon budgets represent the mean short-term accumulation rate for each estuarine section. Uncertainty bounds were estimated using the minimum and maximum rate for each group of cores.

Carbon Budget

An empirical carbon budget was developed that resolved fluxes within each region of the NRE. To conceptualize the carbon budget in terms of organic and inorganic carbon flows, DOC and POC were combined as TOC; thus, net heterotrophy converted TOC to DIC and net autotrophy converted DIC to TOC. It was assumed that all major carbon fluxes were defined except for advective exchanges between regions and at the ocean boundary. Beginning in the upper estuary, the advective carbon exchanges across subsequent regional boundaries were quantified based on the residual carbon flow. That is, the advective exchange at each regional boundary balanced the carbon sources and sinks in the upstream region and enabled the next residual to be estimated in the seaward region. Channel and shoal carbon fluxes were resolved as separate inputs and exports for each region, but were integrated to estimate the residual carbon flows.

The water column DIC and TOC pools were assumed to be at steady state on annual scales. This assumption was tested by scaling the DIC and TOC at each station to regional volumes following the same methods as described for metabolism. Additional carbon budget terms, including marsh deposition, shoreline erosion, and atmospheric deposition were estimated based on literature values and first-order scaling estimates. These terms were found to be relatively minor and were excluded from the carbon budget because they were not directly measured in this study. Estimates for each term are tabulated and discussed in the Conclusions and Implications for Future Research and Implementation section of this chapter. Atmospheric deposition was calculated based on aerosol and rainwater carbon concentrations from Willey et al. (2000) and Wozniak et al. (2011), and annual rainfall measured at Marine Corps Air Station New River (KNCA). Marsh deposition and shoreline erosion were based on recent NRE estimates from Currin et al. (2015).

Lability of DOC

The lability of DOC was determined in 2-week-long incubations of filtered water with added bacterial inoculum (McCallister et al., 2006; Wiegner et al., 2006). Water samples were collected in July and October 2015 from the New River at Jacksonville (Station S10 in **Figure 9-1B**) and in marsh groundwater wells, marsh creeks, and headwaters of Freeman and Traps Bay Creeks.

Water was filter-sterilized (0.2 μm) and dispensed in ultraviolet-transmissable Tedlar bags with the addition of bacterial inocula (filtrate of marsh creek water passed through combusted 0.7-μm GF/F) from the sample locations. In July 2015, water samples were incubated at in situ temperature in the dark and ambient light in flow-through, outdoor tanks at the Virginia Institute of Marine Science; sub-samples collected on Days 0, 2, 5, 7, and 14 were analyzed for DIC, dissolved organic nitrogen (DON), DOC, DIN, and dissolved inorganic phosphorus (DIP) concentrations (Anderson laboratory) and spectral analysis (Piehler laboratory). Spectral slopes between 275–295 nm (S275–295) and 350–400 nm (S350–400) were determined by applying a linear fit to natural log-transformed spectral absorbance data. These slopes are used as indicators of CDOM source and structure (Helms et al., 2008). In October 2015, water samples were incubated at an in situ temperature in the dark, and samples were collected at Days 0, 2, 7, and 14 for chemical and spectral analyses as previously mentioned. All nutrient analyses were performed as listed in Table 9-1 and Table 7-1 of Chapter 7 of the DCERP2 Final Report (RTI International, 2017).

Results and Discussion

River and Tributary Loading

Mean New River discharge at Gum Branch for YR1 (2.51 $m^3 s^{-1}$), YR2 (4.39 $m^3 s^{-1}$), and YR3 (5.10 $m^3 s^{-1}$) constrained approximately 60% of the annual river discharge conditions from 1950 to 2013 (mean=3.20; standard deviation=1.15 $m^3 s^{-1}$). YR1 represents a relatively dry year, where the freshwater input from the river and all tributaries equaled 346 × 10^6 m^3. The average flushing times for the upper, middle, and lower estuary during YR1 were 32, 12, and 2 days, respectively. YR2 represents a wet year, with a total freshwater input of 465 × 10^6 m^3 and average flushing times of 18, 8, and 2 days for the upper, middle, and lower estuary, respectively. Riverine discharge at Gum Branch in YR2 was almost twice the discharge in YR1, and YR2 flushing times in the upper estuary were approximately half as long as in YR1 (**Figure 9-2**). Rainwater input ranged from 89 to 125 × 10^6 m^3 yr^{-1} (114 to 159 cm yr^{-1}) in YR1 and YR2, respectively. The estimated groundwater input of 8.2 × 10^6 m^3 yr^{-1} (10.4 cm yr^{-1}) was comparable to rates observed in the neighboring White Oak Estuary (0.6 to 39.4 cm yr^{-1}; Kogan and Paull, 2005).

Riverine inputs of organic and inorganic carbon were approximately equal in YR1 (**Table 9-2**). As river discharge increased from YR1 to YR2, TOC accounted for a larger portion of the total riverine carbon load (Table 9-2). Tributary loading was also a major input of DIC and TOC in YR1, accounting for approximately one-third of the total freshwater carbon load (Table 9-2). Most of this input occurred in the upper and middle NRE, as the lower estuary drained only 4% of tributary catchments. During the higher discharge conditions in YR2, TOC loading was dominated by riverine discharge, representing more than 80% of the freshwater TOC input. Freshwater DIC loading was less variable between the wet and dry years because greater freshwater input was partially offset by lower DIC concentrations. Total carbon loading from other freshwater sources was minor due to the low volume of groundwater discharge and low carbon concentrations in rainwater.

Air–Water CO_2 Flux

A large range in surface water pCO_2 was observed during spatial surveys (11 to 6,503 µatm). Diel variability in ΔpCO_2 was comparable to spatial and seasonal variability (Figure 9-2), ranging from 16 to 49% of seasonally averaged pCO_2 per box to 9 to 61% of spatially averaged pCO_2 per season. Surface waters changed from an atmospheric CO_2 source at dawn to a CO_2 sink at dusk during 25% to 60% of the bimonthly survey series, depending on the region. The amplitudes of CO_2 efflux or influx were increasingly dampened with distance down-estuary and followed similar patterns in the channel and shoal (**Figure 9-3**). The largest influxes coincided with the highest chl *a* concentrations, a proxy for phytoplankton blooms (Figure 9-3). Peak seasonal CO_2 effluxes were correlated with water temperatures (**Figure 9-4**). Hourly wind speeds showed no apparent diel or seasonal trend, and the average daily winds speeds (YR1: 4.3 m s^{-1}; YR2: 4.2 m s^{-1}) were typical for coastal regions. Flux estimates showed low sensitivity to the gas transfer parameterization used, except in the upper estuary during YR2.

Table 9-2. Annual Carbon Budget Terms (10^6 g-C)

Component	Region	YR1 (Drier Year)				YR2 (Wetter Year)			
				Uncertainty Bounds				Uncertainty Bounds	
		DIC	TOC	DIC	TOC	DIC	TOC	DIC	TOC
New River		3,359	3,448	(2,100–4,685)	(2,762–4,987)	4,857	7,350	(3,085–6,717)	(5,306–10,824)
Tributaries	Upper	1,036	736	(1,291–1,447)	(430–791)	1,393	666	(1,291–1,447)	(562–1,712)
	Middle	1,129	802	(1,407–1,576)	(468–862)	1,518	726	(1,407–1,576)	(613–1,866)
	Lower	150	107	(187–210)	(62–115)	202	96	(187–210)	(81–248)
Air–water CO_2 flux[a]	Upper shoal	11	—	(−15, 7)	—	1,721	—	—	(1,050, 1,815)
	Upper channel	−261	—	(−186, −275)	—	414	—	—	(218, 435)
	Middle shoal	2	—	(7, −2)	—	110	—	—	(45, 104)
	Middle channel	85	—	(57, 88)	—	−311	—	—	(−220, −338)
	Lower shoal	−1	—	(−3, −3)	—	−56	—	—	(−44, −63)
	Lower channel	7	—	(5, 7)	—	−2	—	—	(−2, −2)
NEM[b]	Upper shoal	−146		(±1,247)		2,644		(±1,814)	
	Upper channel	1,140		(±1,161)		56		(±1,708)	
	Middle shoal	−761		(±2,018)		919		(±2,592)	
	Middle channel	−3,891		(±1,921)		−3,021		(±2,349)	
	Lower shoal	733		(±733)		613		(±739)	
	Lower channel	55		(±50)		−137		(±50)	

(continued)

Table 9-2. Annual Carbon Budget Terms (10^6 g-C) (continued)

Component	Region	YR1 (Drier Year)				YR2 (Wetter Year)			
				Uncertainty Bounds				Uncertainty Bounds	
		DIC	TOC	DIC	TOC	DIC	TOC	DIC	TOC
Burial[c]	Upper	—	928	—	(701–1,200)	—	928	—	(701–1,200)
	Middle	—	2,136	—	(2,136–10,537)	—	2,136	—	(2,136–10,537)
	Lower	—	0	—		—	0	—	

a Negative values indicate flux from air to water. Uncertainty represented according to Ho et al. (2006) and Prytherch et al. (2010).

b Negative values indicate net autotrophy (i.e., conversion of DIC to TOC).

c Based on short-term (<5-yr) burial rates.

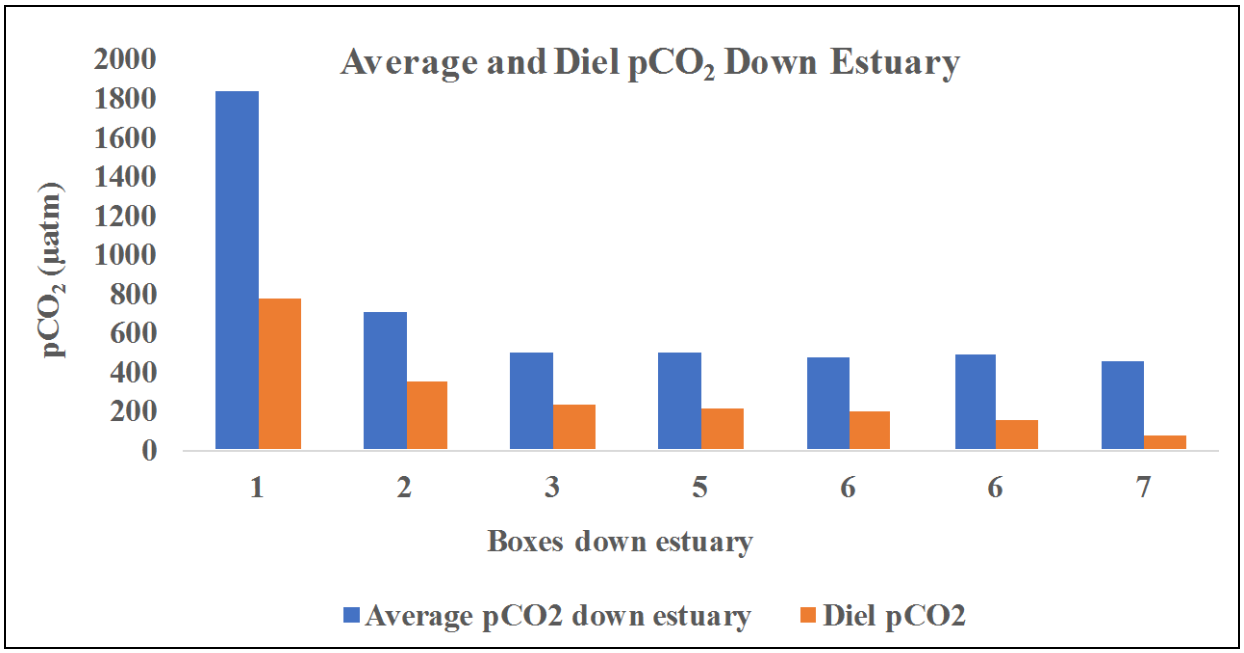

Figure 9-2. Comparison of diel (day versus night) variation of pCO_2 to average seasonal variation within each box.

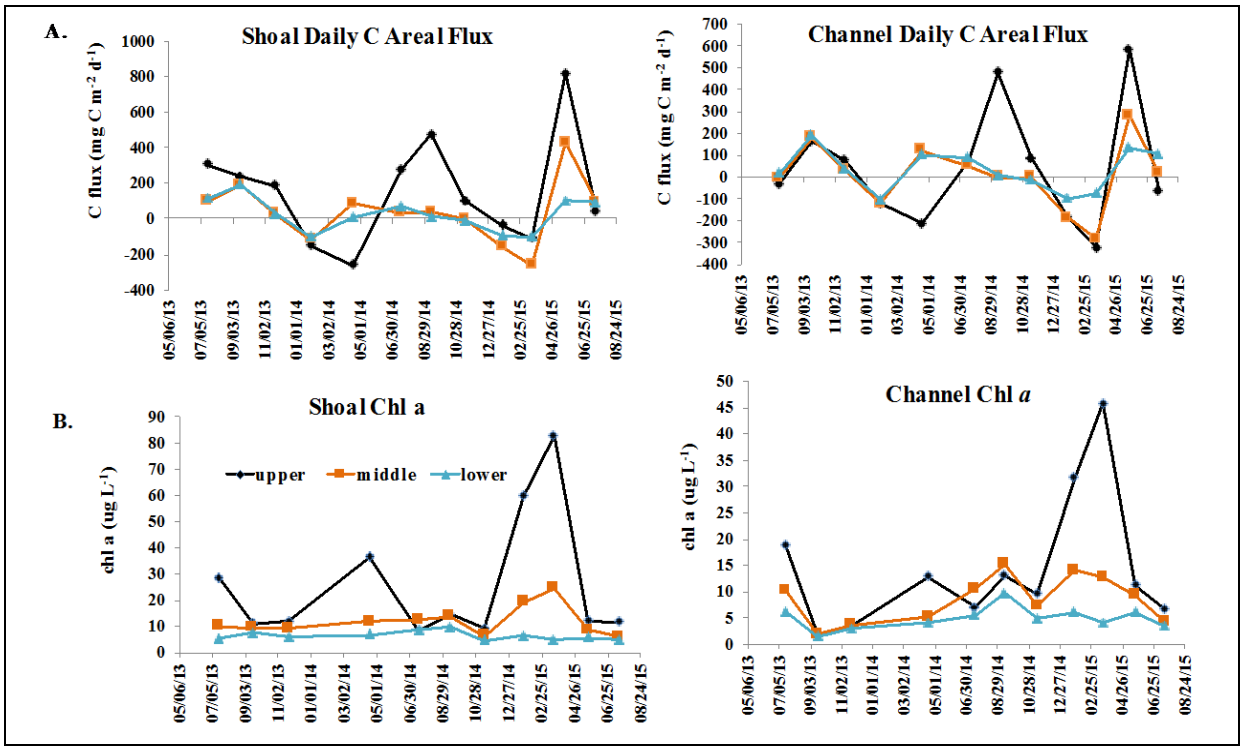

Figure 9-3. (A) Areal daily CO_2 flux in shoal and channel; (B) Areal daily chlorophyll *a* (Chl *a*) concentration in shoal and the channel.

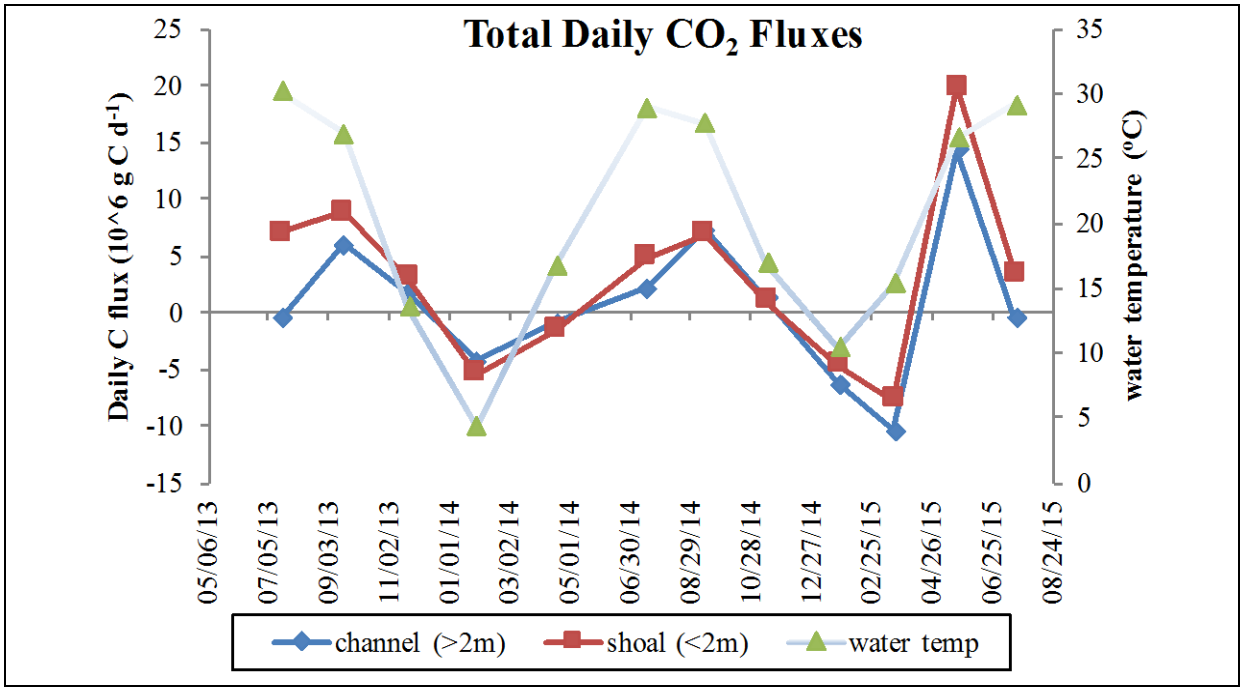

Figure 9-4. Influence of water temperature on daily CO_2 fluxes in shoal and channel.

The NRE was a minor sink for atmospheric CO_2 during YR1 (-157×10^6 g C yr^{-1}) and a small CO_2 source during YR2 ($1{,}876 \times 10^6$ g C yr^{-1}) (Table 9-2 and **Table 9-3**). The upper estuary

shoal in YR2 was the only region with a large air–water CO_2 flux (1,721 × 10^6 g C yr^{-1}), which was linked to high riverine input (Table 9-3). Annual air–water fluxes in all other regions were among the lowest yet observed in estuaries (Laruelle et al., 2013). Despite the relatively large range in ΔpCO_2, short-term variations at diel and seasonal scales were nearly balanced when aggregated to annual budget terms.

Table 9-3. Annual Regional Air – Water CO_2 Fluxes

Site	Year 1		Year 2	
	CO_2 Flux (10^6 g-C y^{-1})	**Uncertainty Bounds**	**CO_2 Flux (10^6 g-C y^{-1})**	**Uncertainty Bounds**
Upper shoal	11	−15, 7	1,721	1,050, 1,815
Upper channel	−261	−186, −275	414	218, 435
Middle shoal	2	7, −2	110	45, 104
Middle channel	85	57, 88	−311	−220, −338
Lower shoal	−1	−3, −3	−56	−44, −63
Lower channel	7	5, 7	−2	−2, −2
Total	**−157**	—	**1,876**	—

CO_2 Efflux in Response to Hurricane Joaquin

The NRE was indirectly impacted by the passage of Hurricane Joaquin and associated nor'easters during late September and early October 2015. We were able to sample just before and after the storm impacted the area. Two Dataflow and pCO_2 cruises were conducted during the 3 weeks before the storm, and two were conducted during the 2 subsequent weeks. With these four cruises bracketing the storm, we assumed a linear change between sampling dates, and then used daily average wind speed (from the AVPs) to estimate CO_2 fluxes during the storm. Before Hurricane Joaquin, pCO_2 in the NRE was approximately at equilibrium with atmosphere (as a system-wide average), but quickly shifted to a large source of CO_2 once floodwaters entered the estuary. As seen in **Figure 9-5**, there was a period of intense CO_2 degassing during the few weeks surrounding the storm, likely driven by both high wind speeds and elevated pCO_2. Fluxes during the storm period were the highest ever measured during DCERP2, only surpassed by the impact of Hurricane Irene measured on the nearby Neuse River Estuary in 2011 (Crosswell et al., 2014). As a first effort to approximate the drivers of these storm-induced CO_2 effluxes, a simple mass balance was constructed between carbon (DIC+DOC+POC) supplied from the river and loss to the atmosphere as CO_2. This approach suggested that the estuarine CO_2 degassing observed was largely supported by riverine loading of TOC and CO_2. <u>This analysis provides additional support for the broad finding of the Aquatic/Estuarine Module, that estuarine carbon processing is tightly linked with the quantity and quality of inorganic and organic carbon supplied by rivers</u>.

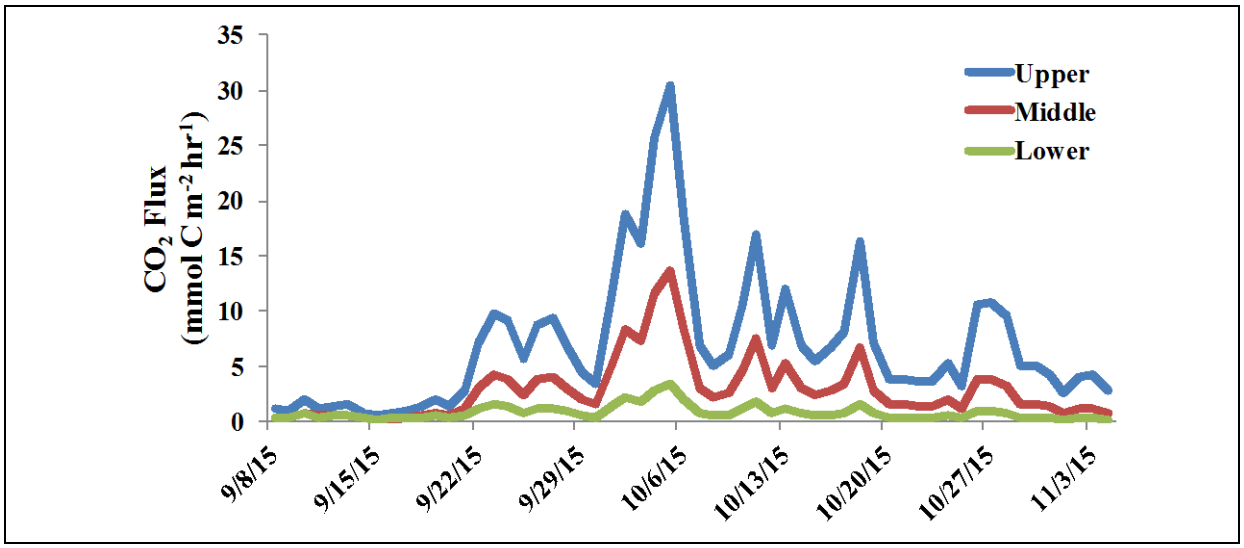

Figure 9-5. CO_2 flux response to the passage of Hurricane Joaquin.

Variations in pCO_2 During 7-Week Gaps Between Monthly Dataflow Cruises

Daily average CO_2 fluxes (mmol C m^{-2} hr^{-1}) based on pCO_2, continuously measured using a carbon-sense pCO_2 sensor, were compared to fluxes determined by assuming a linear change in pCO_2 between the beginning and end of a deployment (simulating bimonthly trips) (**Table 9-4**). Although there was variability between these methods, the differences were generally small and were not consistently positive or negative. On average, CO_2 fluxes determined by linearly interpolating pCO_2 underestimated measured values by approximately 0.2 mmol C m^{-2} hr^{-1}. This difference is far less than the typical spatial or temporal variation in CO_2 fluxes, suggesting that the use of linear interpolation of our high spatial resolution pCO2 data contributed little to any error on an annual basis.

Table 9-4. Comparison of CO_2 Fluxes Calculated by Linear Interpolation and Based on Continuous in situ Measurements (mmol C m^{-2} hr^{-1})

Date	Measured using Turner C- Sense)	Using Linear Interpolation	Difference
September 2016	1.965	1.776	−0.188
March 2016	0.103	0.580	0.477
January 2016	−0.147	−0.148	−0.001
November 2015	2.886	1.069	−1.817
October 2015	1.406	1.266	−0.140
September 2015	−0.347	−0.218	0.129
September 2015	2.226	2.401	0.175
Average	—	—	−0.195

Metabolism

The NRE was net autotrophic during YR1 (NEM of −3.0 ±3.3 mol C m^{-2} yr^{-1}) and in near metabolic balance during YR2 (NEM of 1.1 ±4.4 mol C m^{-2} yr^{-1}) (**Figure 9-6**). The channel showed a trend of high GPP in the upper estuary that was twice the GPP in the middle and lower estuary channel for both years (Figure 9-6). The upper estuary channel was slightly net heterotrophic, whereas the middle estuary channel was strongly net autotrophic. The upper and middle estuary shoal were both net autotrophic during YR1, but were net heterotrophic during YR2 (Figure 9-6). At a system-wide scale, annual metabolism was relatively consistent between years. However, there was an apparent shift in the spatial relationships that maintain overall metabolic balance. During YR1, NEM was balanced along the longitudinal axis of the estuary. Strong net autotrophy in the middle estuary channel and shoal offset net heterotrophy in the upper and lower estuary. Both the channel and shoal were net autotrophic at the system-wide scale. During YR2, NEM was balanced by across-axis coupling of net autotrophy in the channel and net heterotrophy in the shoal (**Figure 9-6**).

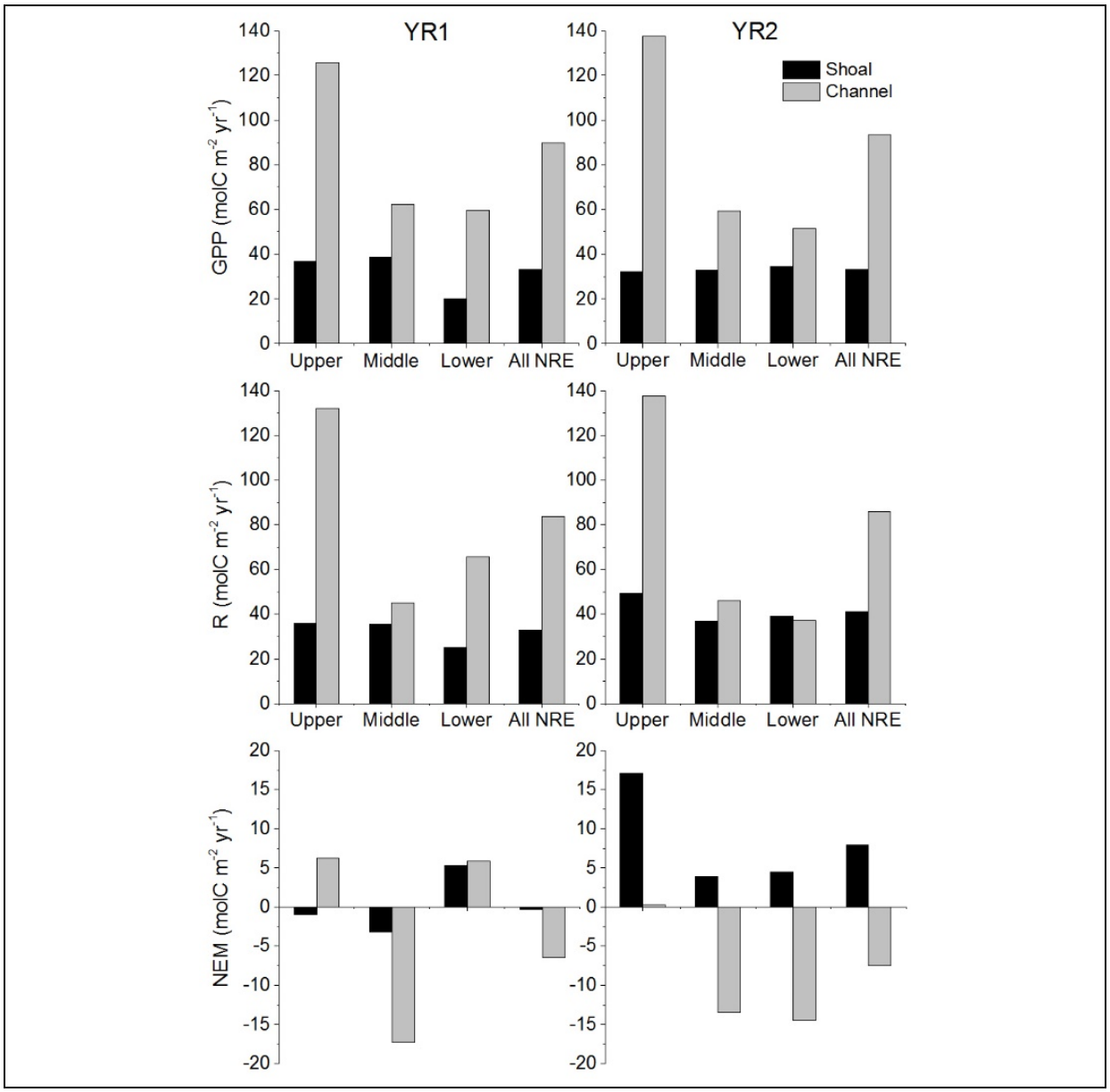

Figure 9-6. Gross Primary Production (GPP), ecosystem respiration (R), and net ecosystem metabolism (NEM) in the upper, middle, and lower NRE and integrated across the entire estuary.

Uncertainties in NEM estimates are listed in Table 9-2.

Lability of DOC

In July, in samples from the head of the estuary offshore of Jacksonville (Station SW10), 16% of DOC decomposed to DIC during both light and dark incubations (**Figure 9-7**). In October 2015, 13% of the DOC broke down during incubation in the dark (Figure 9-7). The photochemical lability of DOC was greater in the headwaters of tributary creeks, whose watersheds were located on MCBCL. In July 2015, between 17 and 33% of the DOC decomposed in the light, and only 1–10% broke down in the dark (data not shown). In October 2015, samples lability was

high in the dark, with 11 to 41% decomposing to DIC (data not shown). The spectral data supported the incubation results. The slope ratios (ratio of absorbances 275–295/350–400) of the DOC sampled in the headwaters of Traps Bay and Freeman Creek were the lowest of any of our water samples and increased in samples down stream, suggesting that the DOC in headwater creeks was allochthonous (terrestrial) in origin, had a higher molecular weight, and was less photodegraded than samples taken from stations further down creek.

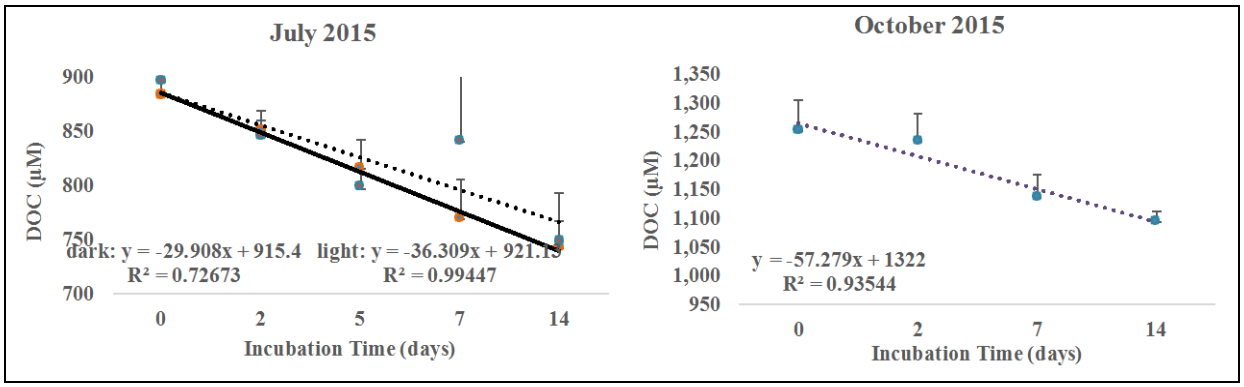

Figure 9-7. Lability of DOC in water samples collected offshore of Jacksonville, NC.

Error bars are standard errors.

Burial

The short term (<5-yr) burial rates in the upper and middle estuary were relatively high. Carbon burial appeared to be spatially homogenous in the upper estuary, with a mean rate of 4.85 mol C m^{-2} yr^{-1} and a range of 3.85 to 6.59 mol C m^{-2} yr^{-1}. Burial rates in the middle estuary were spatially variable, ranging from 46.99 mol C m^{-2} yr^{-1} at Core Site 4 to no net burial at Core Site 5 (Figure 9-1D). Carbon burial rates in the lower estuary were negligible because this area is non-depositional and dominated by a sandy bottom.

Export to Ocean

Residual carbon flows out of the estuary were generally similar in magnitude to net exports computed from freshwater discharge and observed concentrations. Residual flows of TOC (4.53–4.89 Gg-C yr^{-1}, **Figure 9-8**) showed good agreement with the computed exports (3.5–6.4 Gg-C yr^{-1}) and fell within the estimated uncertainty (**Table 9-5**). Similarly, the residual flow of DIC during YR2 (7.17 Gg-C yr^{-1}, Figure 9-8) was close to the computed export (9.4 Gg-C yr^{-1}) and fell just outside the estimated uncertainty (Table 9-5). There was a greater discrepancy between the computed DIC export (7.3 Gg-C yr^{-1}) during YR1 and the residual DIC flow (2.98 Gg-C yr^{-1}, Table 9-5), although both estimates show significant export of DIC that appears to be correlated with river discharge.

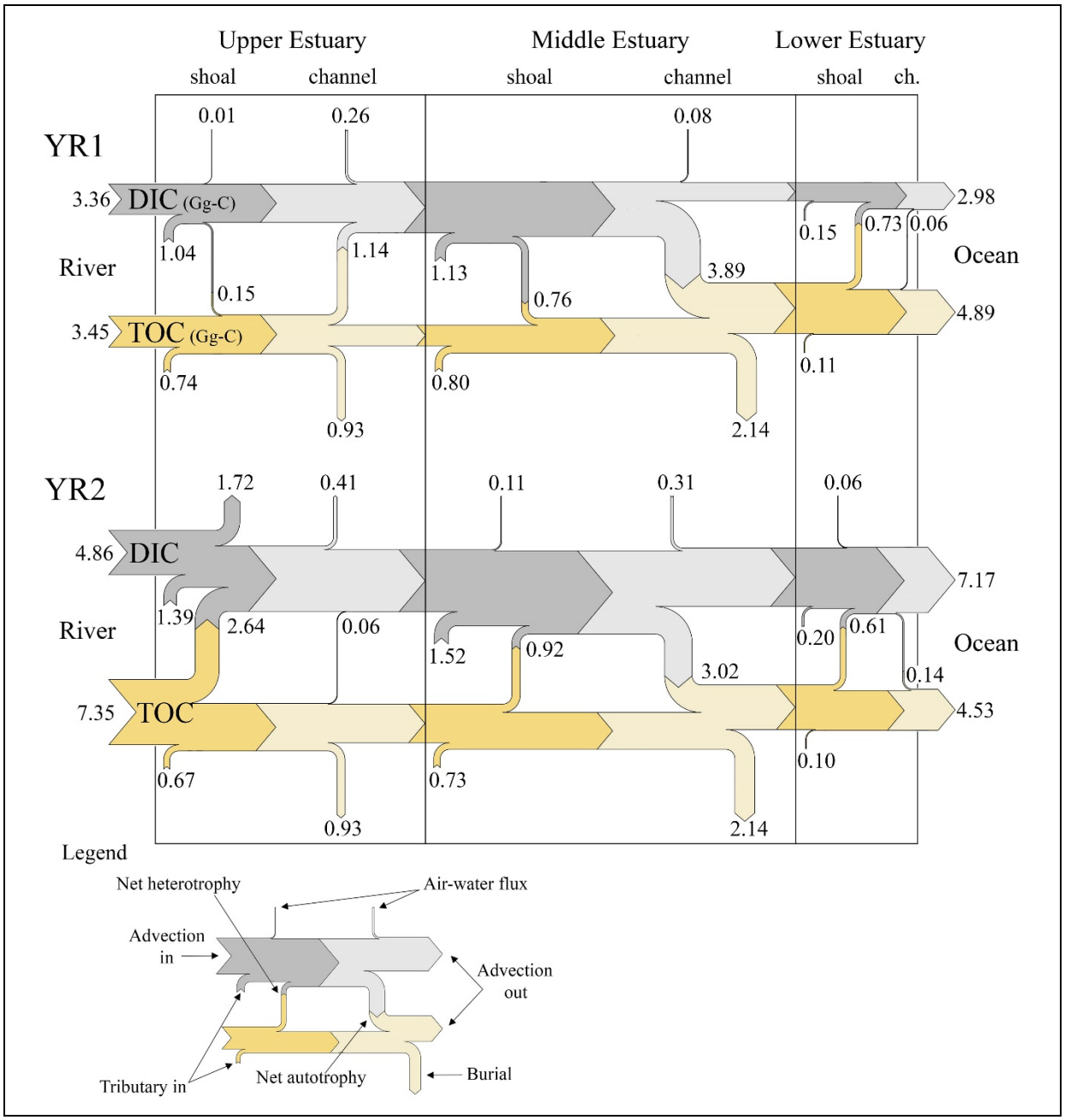

Figure 9-8. Residual flow carbon budget showing annual carbon exchanges as DIC and TOC flows in Gg-C (10^9 g-C).

Flow width is proportional to magnitude, and the length of each region from left to right is proportional to the area of that region in the NRE.

Table 9-5. Carbon Export from the NRE to Onslow Bay (10^9 g-C)[a]

Year	Method	DIC	TOC	Uncertainty Bounds	
				DIC	TOC
1	Computed	7.27	3.50	(6.08–9.66)	(0.85–6.20)
	Residual	2.98	4.89	(−0.60–6.56)	(0.80–8.98)
2	Computed	9.39	6.36	(7.24–13.9)	(1.45–11.3)
	Residual	7.17	4.53	(2.43–11.7)	(−0.43–9.49)

[a] Computed exports were based on freshwater inflow and observed DIC and TOC concentrations. Residual exports were based on the sum of other carbon budget terms as described in Materials and Methods section of this chapter.

Carbon Budget

Entire Estuary

Annual carbon budget terms are represented as mean DIC and TOC flows in Figure 9-8, with uncertainty bounds in Table 9-2. We first summarize the carbon budget at the system-wide scale, then discuss carbon flow by region and year in the remainder of this section. Residual carbon flow for each region was always positive, indicating net transport of DIC and TOC from the river, through the estuary, and into the coastal ocean (Figure 9-8). Riverine input of TOC and flushing times were the main differences in external forcing between years. Metabolism was the most significant internal control on net carbon flow. Air–water CO_2 fluxes were minor except during high discharge during YR2, when the surface waters transitioned from large atmospheric CO_2 efflux to small CO_2 uptake along the river–ocean gradient (Figure 9-8). The export of TOC into Onslow Bay appeared to be consistent between years, whereas the export of DIC to Onslow Bay during YR2 was approximately 2.5 times higher than during YR1 (Figure 9-8).

Upper Estuary

During YR1, the upper estuary shoal was slightly net autotrophic (Figure 9-6). Prior studies of the NRE have shown that during similar low-discharge conditions, nearly all of the terrestrial nutrient load was assimilated by phytoplankton near the head of the estuary (see the previous section titled Entire Estuary, Figure 9-1B; Hall et al., 2013; Paerl et al., 2013; Peierls et al., 2012). It follows that downstream transport of phytoplankton detritus to areas with nutrient depleted conditions could explain the strong net heterotrophy observed in the upper estuary channel (Figure 9-6). Regardless of the pathway, at least 20% of the riverine TOC input must have been degraded to support the net heterotrophy in the upper estuary. Lability tests run in July and October of YR1 showed DOC decomposition of between 13 and 16% in waters offshore of Jacksonville (Figure 9-7). The upper NRE channel was the most heterotrophic region of the estuary, but also the largest sink for atmospheric CO_2 (Table 9-2, Figure 9-8). During YR2, higher riverine input had a major impact on net carbon flow in the upper estuary (Figure 9-8). Strong net heterotrophy in the shoal converted approximately one-third of the TOC input into DIC. Net heterotrophy in the channel decreased during YR2, but there was still significant air–water CO_2 efflux. At least half of the DIC produced by net heterotrophy in the upper estuary was rapidly lost to the atmosphere, even if an assumption is made that all excess CO_2 in river water was also ventilated (Figure 9-8). Burial rates in the upper estuary were relatively consistent

between the three cores. The mean 5-year burial estimate of 0.93 Gg-C yr^{-1} would account for between 10 and 20% of the freshwater TOC input.

Middle Estuary

Metabolic controls dominated carbon flow in the middle estuary (Figure 9-8). During YR1, strong net autotrophy in both the channel and shoal converted approximately 70% of the net DIC input into TOC. During YR2, the middle estuary had a less significant impact on the overall NRE carbon flow due to higher DIC input and counteracting metabolic rates in the channel and shoal (Figure 9-8). Net autotrophy in the channel converted approximately 40% of the DIC input to TOC during YR2, and the channel was a sink for atmospheric CO_2. Approximately one-third of these carbon exchanges in the channel were offset by net heterotrophy and CO_2 efflux from the shoal (Table 9-2, Figure 9-8). The middle estuary appeared to be the depositional center of the NRE, but we could not determine the relative contribution of allochthonous and autochthonous sources to TOC burial based on the carbon budget alone. Only approximately 20% of the freshwater TOC input was in the form of POC, which suggests that burial of autochthonous POC would be required to support the middle estuary burial term.

Lower Estuary

Net heterotrophy in the shoal was the only significant carbon exchange in the lower estuary other than advection (Figure 9-8). Shoal heterotrophy may have been supported by degradation of organic matter input from the middle estuary or from surrounding marshes. Alternatively, the metabolic signal measured by the open water method may reflect processes that occurred within the marshes before the water is transported to the shoal (Neubauer and Anderson, 2003). In either case, it appeared that the primary role of the lower estuary in the carbon budget was as a conduit for the transport of material from the middle estuary to Onslow Bay (Figure 9-8).

Conclusions and Implications for Future Research and Implementation

Spatial Scales of Metabolic Balance

By delivering labile DOC and nutrients that support primary production, riverine discharge was the most significant control on the NRE carbon budget, especially in the upper estuary (Figure 9-8). However, differences in NEM between the channel and shoal were comparable to the variability observed along the river–ocean axis of the estuary (Figure 9-6). The influence of lateral variability on the carbon budget was most significant during YR2, when counteracting fluxes in the channel and shoal acted to preserve metabolic balance (Figure 9-6). Our results are consistent with prior studies that show significant lateral variability in shallow estuaries (Eyre et al., 2011; Gazeau et al., 2005; Maher and Eyre, 2012). Kemp et al. (1997) estimated that all littoral regions in Chesapeake Bay were net autotrophic and that all pelagic regions were net heterotrophic. In these previous studies, channel and shoal observations were separated by days or years, during which the controls on metabolism may have changed. By collecting contemporaneous observations, we show that metabolic balance in a shallow estuary can be maintained by counteracting fluxes along the river–ocean gradient (YR1) or across the channel–shoal gradient (YR2), depending on riverine influence.

Results from the NRE were also consistent with observations from microtidal estuaries in which vertical stratification was identified as an important control on carbon cycling. Crosswell et al. (2012), Gazeau et al. (2005), and Koné et al. (2009) found evidence that CO_2 generated by net heterotrophy at depth remained stored in the bottom water of microtidal systems under stratified conditions. This decoupling would explain how the upper NRE channel could be net heterotrophic and also a sink for atmospheric CO_2 during YR1 (Figures 9-6 and 9-8). The impact of destratification on carbon cycling is still not well understood in partially stratified estuaries such as the NRE. Previous studies found a positive correlation between water flushing time and net heterotrophy. Based on this correlation, Kemp and Testa (2011) and Smith et al. (2005) suggested that at longer flushing times, a larger portion of imported organic matter is degraded in estuaries, thereby increasing net heterotrophy; at shorter flushing times, imported and internally produced organic matter are exported out of the system, thereby increasing net autotrophy. An opposite relationship was observed in the NRE. As flushing times decreased from YR1 to YR2, net autotrophy did increase in the channel, but this impact was outweighed by a larger shift toward net heterotrophy in the shoal (Figure 9-8). Our results, which explicitly resolve channel and shoal fluxes, demonstrate how traditional estuary sampling designs that only consider longitudinal variability can lead to errors in ecosystem metabolism estimates. In systems such as the NRE, these errors could potentially lead to misinterpretation of key functional relationships. We found that changes in flushing time may shift how carbon processing is partitioned among habitats, but it had a relatively minor impact on annual, system-wide metabolism.

Temporal Scales of Air–Water CO_2 Exchange

Estuaries have been traditionally viewed as heterotrophic ecosystems with globally significant emissions of CO_2 to the atmosphere (Borges and Abril, 2011; Cai, 2011). Our results and those of other recent flux studies indicate that estuaries are more dynamic than previously thought and that accurate quantification of CO_2 exchange requires analysis at annual, seasonal, and diel timescales. Inter-annual variability in system-wide NRE CO_2 fluxes was small (−0.17 to 1.99 mol C m^{-2} yr^{-1}) and was comparable to results from a 3-year study in a macrotidal north Atlantic estuary (2.1 to 5.1 mol C m^{-2} yr^{-1}; Hunt et al., 2014). Greater inter-annual variability has been observed in the nearby Neuse River Estuary in response to droughts, floods, and storms (−16 to 4.7 mol C m^{-2} yr^{-1}; Crosswell et al., 2014), but there are few other multi-year, high-resolution CO_2 flux data sets. Seasonal trends in CO_2 fluxes have been documented in several other estuaries along the U.S. East Coast and worldwide. Estuaries have been shown to vary seasonally from large CO_2 sources to moderate CO_2 sinks due to changes in temperature, water chemistry, and biological activity (Evans et al., 2012; Hunt et al., 2014; Joesoef et al., 2015). Diel variation in CO_2 fluxes has thus far been poorly constrained, with observations limited to a single season or a single sampling station (Dai et al., 2009; Maher et al., 2015; Mørk et al., 2016). Our data from 72 spatial surveys show that diel variability was comparable to seasonal variability (Figure 9-2). Prior studies in marsh- and mangrove-dominated estuaries have suggested that diel trends may be influenced by tidal pumping of DIC from surrounding wetlands (Maher et al., 2015; Neubauer and Anderson, 2003). Marsh input to most of the NRE is minor on short timescales due to low tidal amplitudes and limited extent of fringing marshes (Currin et al., 2015). Thus, it is reasonable to assume that the difference between pCO_2 during dawn and dusk surveys was driven by internal metabolic activity.

Most prior spatial CO_2 surveys in estuaries have been conducted over hours or days, and diel variability has typically been ignored. Diel variability in ΔpCO_2 was comparable to spatial and seasonal variability (Figure 9-2), ranging from 16–49% of seasonally averaged pCO_2 per box to 9–61% of spatially averaged pCO_2 per season. In the NRE, time of sampling relative to diel variation can determine whether the system appears to be an atmospheric CO_2 source or CO_2 sink. Significant diel variation in pCO_2 has been reported in a few other estuary types (Dai et al., 2009; Maher et al., 2015; Mørk et al., 2016); however, more high-resolution flux observations are needed to characterize temporal trends in coastal air–water CO_2 fluxes. Currently, the available data suggest that inter-annual variability is small in the absence of extreme events and that the time of day may be as important as the time of year when scaling pCO_2 observations to annual carbon budgets.

Uncertainty

Carbon exchanges within the coastal aquatic continuum are highly variable and lead to large uncertainties that are difficult to quantify. A meaningful assessment of uncertainty is even more challenging when individual fluxes and their associated errors are integrated into system-scale budgets (Kemp and Testa, 2011). In the NRE carbon budget, we estimated advective exchanges based on the residual carbon flow between regions. This approach lends itself to a conceptual understanding of ecosystem connectivity whereby a change in carbon flux in one region may influence fluxes in other regions (Figure 9-8). Exports of DIC and TOC computed from discharge and observed concentrations provided an independent check on the residual carbon flows. Both methods showed large (approximately Gg yr^{-1}) transport of carbon from the NRE to Onslow Bay, and the mean residual flow estimates either fell within or just outside of the uncertainty bounds of the computed export, with the exception of DIC during YR1. Considering these uncertainty bounds together with those for all measured rates (Table 9-4), the computed exports confirm the estimated residual flows in Figure 9-8. We note that the two approaches measure different processes. Although the computed exports help validate the budget, only the residual method applied here can provide an estimate of estuarine trophic status and insights into the primary controls on carbon cycling, which in the NRE is internal metabolism.

Atmospheric gas exchange was previously identified as a major uncertainty in carbon budget estimates (Gazeau et al., 2005). Our sampling methods were designed to reduce this uncertainty via high-resolution surveys that captured both diel and spatial variability across the entire estuary. The role of air–water flux in the carbon budget was minor, regardless of the gas transfer parameterization used (Tables 9-1 and 9-2). Uncertainty in freshwater carbon loading was also relatively low (approximately 30%), as input was well constrained by regular monitoring and event-based sampling in the New River and NRE tributaries (Table 9-1).

Uncertainty in regional metabolic rates was generally approximately 100%; therefore, most estimates were not significantly different from zero (Table 9-1). This was an expected result from scaling net exchanges for cycles that are nearly balanced (Eyre et al., 2011; Kemp et al., 1997), and our estimated uncertainty was still comparable to or lower than the NEM uncertainty in other published carbon budgets (Herrmann et al., 2015; Hopkinson and Smith, 2005; Kemp and Testa, 2011; Maher and Eyre, 2012). The open water method for calculating metabolism requires that approximately the same mass of water is measured on dawn and dusk surveys and that non-metabolic controls on DIC are sufficiently quantified. To account for unknown errors in

these assumptions, we took a conservative approach in estimating uncertainty, which did not distinguish between channel and shoal. As a result, the uncertainties were higher for all metabolism estimates, particularly in the upper and middle estuary (Table 9-1). This uncertainty is outweighed by the advantages of the open water method in quantifying carbon budget terms, particularly compared to incubation methods (Gazeau et al., 2005). The open water method integrates the active metabolic components of the system, it can be applied over relatively large spatial scales, and it does not affect the environmental conditions.

Uncertainty in burial estimates was large, mostly due to the middle estuary (Table 9-1). Burial rates in the upper estuary only varied by approximately 25%, and the lower estuary showed no net burial. By contrast, burial in the middle estuary varied from zero to 46.99 mol C m^{-2} yr^{-1}, which was one of the largest fluxes by area in the NRE. The wide range of burial rates in the middle estuary may be partly due to site selection. We attempted to select coring sites that were representative of the large depositional areas in the middle estuary. Potential overestimation of burial rates due to this sampling approach was reduced by scaling only the median burial estimate (9.53 g-C m^{-2} yr^{-1}) in the middle estuary.

Scaling and Prediction of Coastal Carbon Fluxes

There have been relatively few ecosystem-scale carbon budgets in estuaries, and only a handful of studies have quantified both organic and inorganic carbon fluxes (Benway et al., 2015; Testa et al., 2017). The complete carbon budget constructed in the DCERP2 study provides a pertinent data set for comparison with modeled carbon fluxes along the U.S. East Coast. The USGS–developed Spatially Referenced Regression on Watershed Attributes SPARROW) model estimates riverine export of TOC to estuaries across the conterminous United States based on watershed land use and stream photosynthesis. If we apply the SPARROW model's estimates of TOC yield (kg km^{-1} yr^{-1}; USGS, 2017) to the respective NRE watershed areas used in the DCERP2 study, the model predicts riverine TOC input of 4.96 Gg-C yr^{-1} and tributary input of 0.96, 0.89, and 0.12 Gg-C yr^{-1} in the upper, middle, and lower estuary, respectively. These model estimates are in strong agreement with the average river and tributary TOC inputs for YR1 and YR2 (Table 9-1, Figure 9-8). The modeled riverine TOC input was also remarkably similar to our residual estimates of TOC export from the NRE (Figure 9-8). This finding might suggest that the average annual TOC load from rivers provides a reasonable approximation of TOC export from small estuaries to the coastal ocean, an assumption applied in a recent biogeochemical-circulation model of the U.S. eastern continental shelf by Cahill et al. (2016). However, our NRE budget also shows that as carbon moves along the river–ocean continuum, a significant portion of TOC can be mineralized to DIC and subsequently converted back to TOC through autotrophic production (Figure 9-8). This transformation of allochthonous TOC to autochthonous TOC in estuaries represents an important biogeochemical process, as it can influence the ultimate fate of carbon that is exported to the coastal ocean.

It is challenging to scale carbon budgets between systems, even where there appear to be similarities. This challenge is demonstrated by comparing our carbon budget to a recent modeling study by Herrmann et al. (2015) that estimated organic carbon budgets in estuaries along the entire eastern U.S. coastline. Applying the authors' rates for the NRE (Hermann et al. (2015) supplemental; New River best estimate) to the 79 km^2 NRE surface area yields a riverine TOC load of 29.6 Gg-C yr^{-1}, NEM of −6.3 Gg-C yr^{-1}, burial of 0.67 Gg-C yr^{-1}, and ocean TOC

export of 22.5 Gg-C yr^{-1}. These estimates differ from our budget terms by a factor of five, and we found that the NRE was net autotrophic on average rather than heterotrophic, as predicted by Herrmann et al. (2015). The two studies cover different timescales, and our budget terms mostly fall within the 95% confidence intervals from Hermann et al. (2015), which is comparable to other site-specific studies cited by Hermann et al. Nevertheless, the large discrepancies underscore current model limitations in representing ecosystem diversity. It is impossible to measure all relevant coastal carbon fluxes at regional and global scales. Therefore, recent efforts to assess the current state and future direction of carbon cycle research have established more practical recommendations: choose a small number of representative coastal systems, coordinate research efforts to quantify the relevant fluxes, and constrain a range of environmental conditions that influence carbon cycling (Benway et al., 2015; Najjar et al., 2012). The shallow aquatic continuum of the NRE is representative of lagoonal estuaries that are broadly distributed along temperate coastlines (Laruelle et al., 2013). The observational methods applied in the DCERP2 study can also help identify processes that regulate carbon cycling in other estuary types. A better understanding of these controls is needed to improve models for scaling carbon fluxes and predicting how coastal ecosystems will respond to climatic and anthropogenic change.

Findings with Implications for Future Base Management

Overall the NRE was poised in near metabolic balance during the years of our study; however, extreme storm events, likely to increase in response to climate change, will impact the cycling of carbon in the estuary with increased fluxes of CO_2 to the atmosphere. Greatest net heterotrophy and the largest exchanges of CO_2 between the estuary and the atmosphere were at station SW-10 near the city of Jacksonville. Water quality managers both on MCBCL and in the region can help to reduce negative water quality impacts by promoting use of best management practices on farmlands and CAFOs in the region and by reducing erosion and nutrient release on MCBCL.

Literature Cited

Alber, M., and J.E. Sheldon. 1999. Use of a date-specific method to examine variability in the flushing times of Georgia estuaries. *Estuarine, Coastal and Shelf Science 49*(4):469–482.

Anderson, I.C., M.J. Brush, M.F. Piehler, C.A. Currin, J.W. Stanhope, A.R. Smyth, J.D. Maxey, and M.L. Whitehead. 2014. Impacts of climate related drivers on the benthic nutrient filter in a shallow photic estuary. *Estuaries and Coasts 37*(Supp 1):46–62. doi: 10.1007/s12237-013-9665-5

Anderson, I.C., J.W. Stanhope, A.K. Hardison, and K.J. McGlathery. 2010. Sources and fates of nitrogen in Virginia coastal bays. Chapter 3, pp. 43–72 in *Coastal Lagoons: Critical Habitats of Environmental Change*. Edited by Kennish, M.J., and H.W. Paerl. CRC Press.

Benway, H., S. Alin, E. Boyer, W.-J. Cai, P. Coble, J. Cross, M. Friedrichs, M. Goñi, P. Griffith, M. Herrmann, S. Lohrenz, J. Mathis, G. McKinley, R. Najjar, C. Pilskaln, S.A. Siedlecki, and R. Smith. 2015. *A Science Plan for Carbon Cycle Research in North American Coastal Waters*. Report of the Coastal CARbon Synthesis (CCARS) Community

Workshop, Woods Hole, MA. August 19–21, 2014, Ocean Carbon and Biogeochemistry Program and North American Carbon Program, 84 pages.

Blair, N.E., and R.C. Aller. 2012. The fate of terrestrial organic carbon in the marine environment. *Annual Review of Marine Science 4*:401–423. doi: 10.1146/annurev-marine-120709-142717

Borges, A.V., and G. Abril. 2011. Carbon dioxide and methane dynamics in estuaries. Pp. 119–161 in *Treatise on Estuarine and Coastal Science. Volume 5: Biogeochemistry*. Edited by Wolanski, E., and D. McLusky. Academic Press.

Boynton, W.R., and W.M. Kemp. 2000. Influence of river flow and nutrient loads on selected ecosystem processes: A synthesis of Chesapeake Bay data. Pp. 269–298 in Estuarine Science: A Synthetic Approach to Research and Practice. Edited by Hobbie, J.E. Island Press.

Caffrey, J.M. 2003. Factors controlling net ecosystem metabolism in U.S. estuaries. *Estuaries 27*(1):90–101.

Cahill, B., J. Wilkin, K. Fennel, D. Vandemark, and M.A.M. Friedrichs. 2016. Interannual and seasonal variabilities in air–sea CO_2 fluxes along the U.S. eastern continental shelf and their sensitivity to increasing air temperatures and variable winds. *Journal of Geophysical Research: Biogeosciences 121*(2):295–311. doi: 10.1002/2015JG002939

Cai, W.J. 2011. Estuarine and coastal ocean carbon paradox: CO_2 sinks or sites of terrestrial carbon incineration? *Annual Review of Marine Science 3*:123–145.

Crosswell, J.R., M.S. Wetz, B. Hales, and H.W. Paerl. 2014. Extensive CO_2 emissions from shallow coastal waters during passage of Hurricane Irene (August 2011) over the mid-Atlantic Coast of the USA. *Limnology and Oceanography 59*(5):1651–1665. doi: 10.4319/lo.2014.59.5.1651

Crosswell, J.R., M.S. Wetz, B. Hales, and H.W. Paerl. 2012. Air–water CO_2 fluxes in the microtidal Neuse River Estuary, North Carolina. *Journal of Geophysical Research: Oceans 117*(C8). 12 pages.

Currin, C., J. Davis, L. Cowart Baron, A. Malhotra, and M. Fonseca. 2015. Shoreline change in the New River Estuary, North Carolina: Rates and consequences. *Journal of Coastal Research 31*:1069–1077.

Dai, M., Z. Lu, W. Zhai, B. Chen, Z. Cao, K. Zhou, W.-J. Cai, and C.-T.A. Chen. 2009. Diurnal variations of surface seawater pCO_2 in contrasting coastal environments. *Limnology and Oceanography 54*(3):735–745. doi:10.4319/lo.2009.54.3.0735

Ensign, S.H., J.N. Halls, and M.A. Mallin. 2004. Application of digital bathymetry data in an analysis of flushing times of two large estuaries. *Computers and Geosciences 30*(5):501–511.

Evans, W., B. Hales, P.G. Strutton, and D. Ianson. 2012. Sea–air CO_2 fluxes in the western Canadian coastal ocean. *Progress in Oceanography 101*(1):78–91. doi: 10.1016/j.pocean.2012.01.003

Eyre, B.D., A.J.P. Ferguson, A. Webb, D. Maher, and J.M. Oakes. 2011. Metabolism of different benthic habitats and their contribution to the carbon budget of a shallow oligotrophic sub-tropical coastal system (southern Moreton Bay, Australia). *Biogeochemistry 102*(1–3):87–110.

Gazeau, F., A.V. Borges, C. Barrón, C.M. Duarte, N. Iversen, J.J. Middelburg, B. Delille, M-D. Pizay, M. Frankignoulle, J-P. Gattuso. 2005. Net ecosystem metabolism in a micro-tidal estuary (Randers Fjord, Denmark): Evaluation of methods. *Marine Ecology Progress Series 301*:23–41.

Hales, B., D. Chipman, and T. Takahashi. 2004. High-frequency measurement of partial pressure and total concentration of carbon dioxide in seawater using microporous hydrophobic membrane contactors. *Limnology and Oceanography: Methods, 2*(11):356–364. doi: 10.4319/lom.2004.2.356

Hall, N.S., H.W. Paerl, B.L. Peierls, A.C. Whipple, and K.L. Rossignol. 2013. Effects of climatic variability on phytoplankton community structure and bloom development in the eutrophic, microtidal, New River Estuary, North Carolina, USA. *Estuarine, Coastal and Shelf Science 117*:70–82.

Hardison, A.K., I.C. Anderson, E.A. Canuel, C.R. Tobias, and B. Veuger. 2011. Carbon and nitrogen dynamics in shallow photic systems: Interactions between macroalgae, microalgae, and bacteria. *Limnology and Oceanography 56*(4):1489–1503.

Hedges, J.I., and J.H. Stern. 1984. Carbon and nitrogen determinations of carbonate-containing solids. *Limnology and Oceanography 29*(3):657–663.

Helms, J.R., A. Stubbins, J.D. Ritchie, E.C. Minor, D.J. Kieber, and K. Mopper. 2008. Absorption spectral slopes and slope ratios as indicators of molecular weight, source, and photobleaching of chromophoric dissolved organic matter. *Limnology and Oceanography 53*(3):955–969.

Herrmann, M., R.G. Najjar, W.M. Kemp, R.B. Alexander, E.W. Boyer, W-J. Cai, P.C. Griffith, K.D. Kroeger, S.L. McCallister, and R.A. Smith. 2015. Net ecosystem production and organic carbon balance of U.S. East Coast estuaries: A synthesis approach. *Global Biogeochemical Cycles 29*:96–111. doi: 10.1002/2013GB004736

Ho, D.T., C.S. Law, M.J. Smith, P. Schlosser, M. Harvey, and P. Hill. 2006. Measurements of air–sea gas exchange at high wind speeds in the Southern Ocean: Implications for global parameterizations. *Geophysical Research Letters 33*(16):L16611.

Hopkinson, C.S., and E.M. Smith. 2005. Estuarine respiration: An overview of benthic, pelagic, and whole system respiration. Pp. 122–146 in *Respiration in Aquatic Ecosystems*. Edited by del Giorgio, P., and P. Williams. Oxford University Press.

Hunt, C.W., J.E. Salisbury, and D. Vandemark. 2014. CO_2 input dynamics and air–sea exchange in a large New England estuary. *Estuaries and Coasts 37*(5):1078–1091.

Jiang, L.Q., W.J. Cai, and Y. Wang. 2008. A comparative study of carbon dioxide degassing in river- and marine-dominated estuaries. *Limnology and Oceanography 53*(6):2603–2615. doi: 10.4319/lo.2008.53.6.2603

Joesoef, A., W.J. Huang, Y. Gao, and W.J. Cai. 2015. Air–water fluxes and sources of carbon dioxide in the Delaware estuary: Spatial and seasonal variability. *Biogeosciences 12*(20):6085–6101.

Kemp, W.M., and J.M. Testa. 2011. Metabolic balance between ecosystem production and consumption. Pp. 83–118 in *Treatise on Estuarine and Coastal Science. Volume 5: Biogeochemistry*. Edited by Wolansky, E., and D. McLusky. Academic Press.

Kemp, W.M., W.R. Boynton, J.E. Adolf, D.F. Boesch, W.C. Boicourt, G. Brush, J.C. Cornwell, T.R. Fisher, P.M. Gilbert, J.D. Hagy, L.W. Harding, E.D. Houde, D.G. Kimmel, W.D. Miller, R.I.E. Newell, M.R. Roman, E.M. Smith, and J.C. Stevenson. 2005. Eutrophication of Chesapeake Bay: Historical trends and ecological interactions. *Marine Ecology Progress Series 303*:1–29. doi: 10.3354/meps303001

Kemp, W.M., E.M. Smith, M. Marvin-Dipasquale, and W.R. Boynton. 1997. Organic carbon balance and net ecosystem metabolism in Chesapeake Bay. *Marine Ecology Progress Series 150*(1–3):229–248. doi: 10.3354/meps150229

Kennish, M., and H.W. Paerl. 2010. *Coastal Lagoons: Critical Habitats of Environmental Change*. CRC Marine Science Series. CRC Press.

Kogan, I., and C.K. Paull. 2005. Coastal seismic wipe-outs: Distribution controlled by pore water salinity. *Marine Geology 217(1–2)*:161–175.

Koné, Y.J.M., G. Abril, K.N. Kouadio, B. Delille, and A.V. Borges. 2009. Seasonal variability of carbon dioxide in the rivers and lagoons of Ivory Coast (West Africa). *Estuaries and Coasts 32*(2):246–260. doi: 10.1007/s12237-008-9121-0

Laruelle, G.G., H.H. Dürr, R. Lauerwald, J. Hartmann, C.P. Slomp, N. Goossens, and P.A.G. Regnier. 2013. Global multi-scale segmentation of continental and coastal waters from

the watersheds to the continental margins. *Hydrology and Earth System Science 17*(5):2029–2051. doi: 10.5194/hess-17-2029-2013

Lehrter, J.C., and J. Cebrian. 2010. Uncertainty propagation in an ecosystem nutrient budget. *Ecological Applications 20*(2):508–524.

Madden, C., and J. Day. 1992. An instrument system for high-speed mapping of chlorophyll a and physico-chemical variables in surface waters. *Estuaries 15*(3):421–427.

Maher, D.T., and B.D. Eyre. 2012. Carbon budgets for three autotrophic Australian estuaries: Implications for global estimates of the coastal air–water CO_2 flux. *Global Biogeochemical Cycles 26*(1):GB1032. doi: 10.1029/2011GB004075

Maher, D.T., K. Cowley, I.R. Santos, P. Macklin, and B.D. Eyre. 2015. Methane and carbon dioxide dynamics in a subtropical estuary over a diel cycle: Insights from automated in situ radioactive and stable isotope measurements. *Marine Chemistry 168*:69–79. doi: 10.1016/j.marchem.2014.10.017

Maher, D.T., I.R. Santos, L. Golsby-Smith, J. Gleeson, and B.D. Eyre. 2013. Groundwater-derived dissolved inorganic and organic carbon exports from a mangrove tidal creek: The missing mangrove carbon sink? *Limnology and Oceanography 58*(2):475–488.

McCallister, S.L., J.E. Bauer, and E.A. Canuel. 2006. Bioreactivity of estuarine dissolved organic matter: A combined geochemical and microbiological approach. *Limnology and Oceanography 51*(1):94–100.

McGlathery, K.J., K. Sundbäck, and I.C. Anderson. 2007. Eutrophication in shallow coastal bays and lagoons: The role of plants in the coastal filter. *Marine Ecology Progress Series 348*:1–18.

Mørk, E.T., M. Sejr, P.A. Stæhr, and L.L. Sørensen. 2016. Temporal variability of air–sea CO_2 exchange in a low-emission estuary. *Estuarine, Coastal and Shelf Science 176*: 1–11. doi: 10.1016/j.ecss.2016.03.022

Najjar, R.G., M.A.M. Friedrichs, and W.-J. Cai (Eds). 2012. *Report of the U.S. East Coast Carbon Cycle Synthesis Workshop, January 19–20, 2012*. Ocean Carbon and Biogeochemistry Program and North American Carbon Program.

Neubauer, S.C., and I.C. Anderson. 2003. Transport of dissolved inorganic carbon from a tidal freshwater marsh to the York River estuary. *Limnology and Oceanography 48*(1):299–307.

Nixon, S.W., S.L. Granger, and B.L. Nowicki. 1995. An assessment of the annual mass balance of carbon, nitrogen, and phosphorus in Narragansett Bay. *Biogeochemistry* 31:15–61.

Nixon, S.W. 1986. Nutrient dynamics and the productivty of marine coastal waters. Pp. 97–115 in *Marine Environment and Pollution*. Edited by Halwagy, R., D. Clayton, and M. Behbehani. The Alden Press.

Nixon, S.W., B. Buckley, S. Granger, and J. Bintz. 2001. Response of very shallow marine ecosystems to nutrient enrichment. *Human and Ecological Risk Assessment 7*(5):1457–1481.

Nixon, S.W., J.W. Ammerman, L.P. Atkinson, V.M. Berounsky, G. Billen, W.C. Boicourt, W.R. Boynton, T.M. Church, D.M. Ditoro, R. Elmgren, J.H. Garber, A.E. Giblin, R.A. Jahnke, N.J.P. Owens, M.E.Q. Pilson, and S.P. Seitzinger. 1996. The fate of nitrogen and phosphorus at the land–sea margin of the north Atlantic Ocean. *Biogeochemistry 35*(1):141–180.

NOAA (National Oceanic and Atmospheric Administration) Office for Coastal Management. 2017. Coastal Assessment Framework. Available at https://data.noaa.gov/dataset/coastal-assessment-framework-national-assessment-of-estuary-and-coastal-habitats

Paerl, H. W., N. S. Hall, B. L. Peierls, K. L. Rossignol, and A.R. Joyner. 2013. Hydrologic variability and its control of phytoplankton community structure and function in two shallow, coastal, lagoonal ecosystems: The Neuse and New River Estuaries, North Carolina, USA. *Estuaries and Coasts* 37: 31–45. doi:10.1007/s12237-013-9686-0

Paerl, H.W., K.L. Rossignol, N.S. Hall, B.L. Peierls, and M.S. Wetz. 2010. Phytoplankton community indicators of short- and long-term ecological change in the anthropogenically and climatically impacted Neuse River Estuary, North Carolina, USA. *Estuaries and Coasts 33*(2):485–497.

Peierls, B.L., N.S. Hall, and H.W. Paerl. 2012. Non-monotonic responses of phytoplankton biomass accumulation to hydrologic variability: A comparison of two coastal plain North Carolina estuaries. *Estuaries and Coasts 35*:1376–1392.

Piehler, M., M. Brush, C. Tobias, and R. Noble. 2013. Quantifying and predicting watershed inputs of nutrients, sediments, and pathogens to tributary creeks on Marine Corps Base Camp Lejeune. Chapter 6 in *Defense Coastal/Estuarine Research Program (DCERP1) Final Research Report*. SERDP Project No. RC-1413. Edited by Cunningham, P. RTI International, Research Triangle Park, NC.

Prytherch, J., M.J. Yelland, R.W. Pascal, B.I. Moat, I. Skjelvan, and M.A. Srokosz. 2010. Open ocean gas transfer velocity derived from long-term direct measurements of the CO_2 flux. *Geophysical Research Letters 37*:L23607. doi: 10.1029/2010GL045597

Raymond, P.A., J.E. Bauer, and J.J. Cole. 2000. Atmospheric CO_2 evasion, dissolved inorganic carbon production, and net heterotrophy in the York River estuary. *Limnology and Oceanography 45*(8):1707–1717.

Regnier, P., P. Friedlingstein, P. Ciais, F.T. Mackenzie, N. Gruber, I.A. Janssens, G.G. Laruelle, R. Lauerwald, S. Luyssaert, A.J. Andersson, S. Arndt, C. Arnosti, A.V. Borges, A.W. Dale, A. Gallego-Sala, Y. Goddéris, N. Goossens, J. Hartmann, C. Heinze, T. Ilyina, F, Joos, D.E. LaRowe, J. Leifeld, F.J.R. Meysman, G. Munhoven, P.A. Raymond, R. Spahni, P. Suntharalingam, and M. Thullner. 2013. Anthropogenic perturbation of the carbon fluxes from land to ocean. *Nature Geoscience 6*:597–607. doi: 10.1038/NGEO1830

Sanchez-Cabeza, J.A., and A.C. Ruiz-Fernandez. 2012. ^{210}Pb sediment radiochronology: An integrated formulation and classification of dating models. *Geochimica et Cosmochimica Acta 82*:183–200. doi:10.1016/j.gca.2010.12.024

Smith, S., R. Buddemeier, F. Wulff, D. Swaney, V. Camacho-Ibar, L. David, V. Dupra, J. Kleypas, M. San Diego-McGlone, C. McLaughlin, and P. Sandhei. 2005. C, N, P fluxes in the coastal zone. Pp. 95–143 in *Coastal Fluxes in the Anthropocene*. Edited by Crossland, C.J., H.H. Kremer, H.J. Lindeboom, J.I. Marshall Crossland, and M.D.A. Le Tissier. Global Change—The IGBP Series. Springer.

Testa, J.M., and W.M. Kemp. 2008. Variability of biogeochemical processes and physical transport in a partially stratified estuary: A box-modeling analysis. *Marine Ecology Progress Series 356*:63−79.

Testa, J.M., W.M. Kemp, L.A. Harris, R.J. Woodland, and W.R. Boynton. 2017. Challenges and directions for the advancement of estuarine ecosystem science. *Ecosystems 20*(1) 14−22.

USGS (U.S. Geological Survey). 2017. *SPARROW Decision Support System*. Available at https://cida.usgs.gov/sparrow

Wanninkhof, R. 1992. Relationship between wind speed and gas exchange. *Journal of Geophysical Research: Oceans 97*(C5):7373–7382. doi: 10.1029/92JC00188

Weiss, R. 1974. Carbon dioxide in water and seawater: The solubility of a non-ideal gas. *Marine Chemistry 2*(3):203–215. doi: 10.1016/0304-4203(74) 90015-2

Wiegner, T.N., S.P. Seitzinger, P.M. Glibert, and D.A. Bronk. 2006. Bioavailability of dissolved organic nitrogen and carbon from nine rivers in the eastern United States. *Aquatic Microbial Ecology 43*:277–287.

Willey, J.D., R.J. Kieber, M.S. Eyman, and G.B. Avery, Jr. 2000. Rainwater dissolved organic carbon: Concentrations and global flux. *Global Biogeochemical Cycles 14*(1):139–148.

Wozniak, A.S., J.E. Bauer, and R.M. Dickhut. 2011. Fossil and contemporary aerosol particulate organic carbon in the eastern United States: Implications for deposition and inputs to watersheds. *Global Biogeochemical Cycles 25*(2):GB2013.

Zimmerman, A.R., and E.A. Canuel. 2000. A geochemical record of eutrophication and anoxia in Chesapeake Bay sediments: Anthropogenic influence on organic matter composition. *Marine Chemistry 69*(1–2):117–137.

Appendix 9-A
Additional Information: Research Project AE-6

Estimates of the Estuarine-Wide Effectiveness of the Benthic Filter

Background

In the shallow New River Estuary (NRE), the benthos plays an important role in mitigating the effects of nutrient enrichment. Data collected during DCERP1 demonstrated that the NRE is moderately eutrophic, with the benthos contributing more than 40% of the total production for the entire estuary. The effectiveness of the benthic filter for nutrient and carbon sequestration is determined primarily by light availability and a variety of physical variables such as wind, residence time, and temperature (Anderson et al., 2010; McGlathery et al., 2007; Sundbäck et al., 2004). A net autotrophic system will either sequester organic carbon as particulate organic carbon (POC) in sediments or export it as POC and dissolved organic carbon (DOC) into the ocean, whereas a net heterotrophic system will be a source of carbon dioxide (CO_2) into the atmosphere and dissolved inorganic carbon (DIC) into the coastal ocean (Cai, 2011; Hopkinson and Smith, 2005). Macrotidal and large estuaries have generally been thought to be net heterotrophic because of the processing of external dissolved organic matter (Caffrey, 2003; Gazeau et al., 2005; Smith and Hollibaugh, 1997; Staehr et al., 2012). However, much less is known about net ecosystem metabolism (NEM) in microtidal, shallow, lagoonal systems such as the NRE, which may be representative of up to half of the estuarine surface area in the United States (NOAA, 2011). Shifts toward net heterotrophy due to natural or anthropogenic disturbances are likely to result in reductions in water and sediment quality with increased occurrences of hypoxia or anoxia and potential impacts on higher trophic levels.

Objectives

- Determine estuarine-wide effectiveness of the benthic filter by measuring:
  - benthic metabolic and nutrient cycling process rates, including nutrient fluxes, autotrophic nitrogen demand, gross nitrogen mineralization (MIN), nitrogen fixation (NFix), and denitrification (DNF) on sediment cores sampled at representative water depths in the upper, middle, and lower estuary in the fall, as conducted in the summer and spring (July 2010 and April 2011 during DCERP1.
  - Calculate annual areal rates by scaling measurements to area in estuary at each water depth.
  - On an annual basis for the New River Estuary determine the percentage of nitrogen mineralized in the benthos by microbial processes that is removed by benthic microalgal uptake and by microbial denitrification, which together represent the benthic filter.

Methods and Materials

To scale benthic processes to system-wide estimates for the entire estuary, we measured benthic metabolic and nutrient cycling rates (e.g., nutrient fluxes, autotrophic nitrogen demand, gross nitrogen mineralization [MIN], nitrogen fixation [NFix], and denitrification [DNF]) in sediment cores sampled in October 2013 at representative water depths across the entire estuary. As conducted in summer (July 2010) and spring (April 2011) during DCERP1, sediment cores were collected at sites in the upper, middle, and lower regions of the NRE at three different water depths (approximately 0.5 m, 1.5 m, and 3 m msl) (**Figure 9A-1**). Benthic microalgal nitrogen demand was calculated as described by Anderson et al. (2014). Additional analytical methods were described in the *DCERP2 Research Plan* (RTI, 2013a).

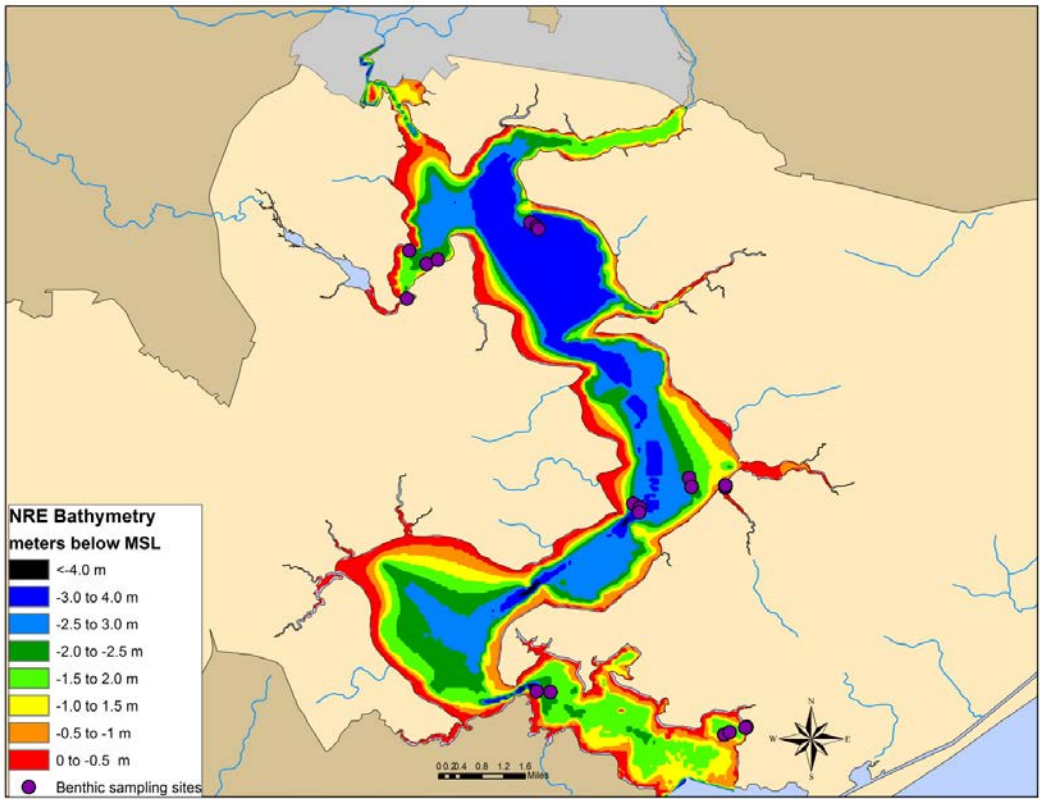

Figure 9A-1. NRE bathymetry (North American Vertical Datum of 1988 [NAVD 88]) and depth experiment benthic sampling stations in the upper, middle, and lower regions of the estuary.

The NAVD 88 to msl offset is +0.01 m for the Wilmington, NC, Center for Operational Oceanographic Products and Services (CO-OPS) Station 8658120 (National Tidal Datum Epoch of 1983–2001; NOAA, 2004).

Using the bathymetry data for the upper, middle, and lower regions of the NRE, areas encompassing water depths ranging from 0.0–1.0 m were combined to represent the 0.5-m treatment. The area with 1.0- to 2.0-m depth range represented the 1.5-m treatment, and the area greater than the 2.0-m depth represented the 3.0-m treatment (**Table 9A-1**). Benthic microalgal nitrogen demand, MIN, and gross DNF (net DNF+NFix) measured at the square meter scale (see Anderson et al., 2014) at the various depths and locations within the NRE were multiplied by the area within a depth range at each location and summed to provide an estuarine-wide estimate for

each of the various benthic nitrogen sources and sinks. To estimate winter rates, benthic gross primary production (GPP), MIN, and NFix rates measured in March 2010 at 0.5-m water depth were used to predict 1.5-m and 3-m rates based on linear and non-linear regressions of mean GPP, MIN, and NFix versus water depth by estuarine region measured in the spring, summer, and fall depth experiments. DNF rates were predicted based on seasonal relationships between winter and the other three seasons measured by Von Korff et al. (2014) in the tidal freshwater zone.

Table 9A-1. NRE Area by NRE Region and Depth Treatment

(1 ha=10,000 m^2)

Region	Water Depth (m)	Total Area (m^2)	Percentage (%) of Total
Upper	0.5	6,242,438	7.9
	1.5	6,337,720	8.1
	3.0	15,456,384	19.6
Middle	0.5	10,280,682	13.1
	1.5	9,352,179	11.9
	3.0	18,671,774	23.7
Lower	0.5	4,259,293	5.4
	1.5	7,293,870	9.3
	3.0	785,581	1.0

Results and Discussion

To determine the overall impact of the benthic filter on allochthonous and autochthonous loads of nitrogen supplied to the NRE, we scaled rates of benthic MIN, benthic microalgal nitrogen demand, and gross DNF and measured seasonally at various depths in the upper, middle, and lower NRE, to the entire estuary. Seasonally and for individual estuarine regions, benthic processes were estimated to remove between 12% to greater than 100% of the total nitrogen produced by autochthonous processes, measured as benthic MIN. A greater percentage of autochthonous nitrogen was removed in the lower estuary than in the middle and upper estuary, likely because of greater light availability in that region (**Figure 9A-2**). When scaled up to the estuarine level, winter had the lowest percentage of MIN removed (30%), whereas summer had the highest (50%). Annually and averaged over all regions, benthic microalgal nitrogen demand and DNF together removed 41% of total benthic autochthonous nitrogen, with DNF representing a slightly large proportion of the total sinks than benthic microalgae (BMA; 55% versus 45%). In the absence of the benthic filter, organic matter remineralized in sediments would have been released into the water column to support eutrophication. Benthic processes also potentially accounted for much of the removal of allochthonous nitrogen that entered the NRE and was taken up by phytoplankton and subsequently deposited in the benthos. As shown in **Figure 9A-3**, across the entire estuary, benthic sinks were capable of removing 100% of the estimated annual average load of allochthonous nitrogen that entered the NRE between 1998–2011 (794,000 kg of total nitrogen [TN] y^{-1}; for more information, see Chapter 5 of *DCERP1 Final Research Report* [RTI, 2013b]). It is clear that in a shallow system such as the NRE, the benthic filter plays a

critical role in reducing fluxes of nitrogen from the benthos to the water column and thereby provides a buffer against accelerating pelagic eutrophication.

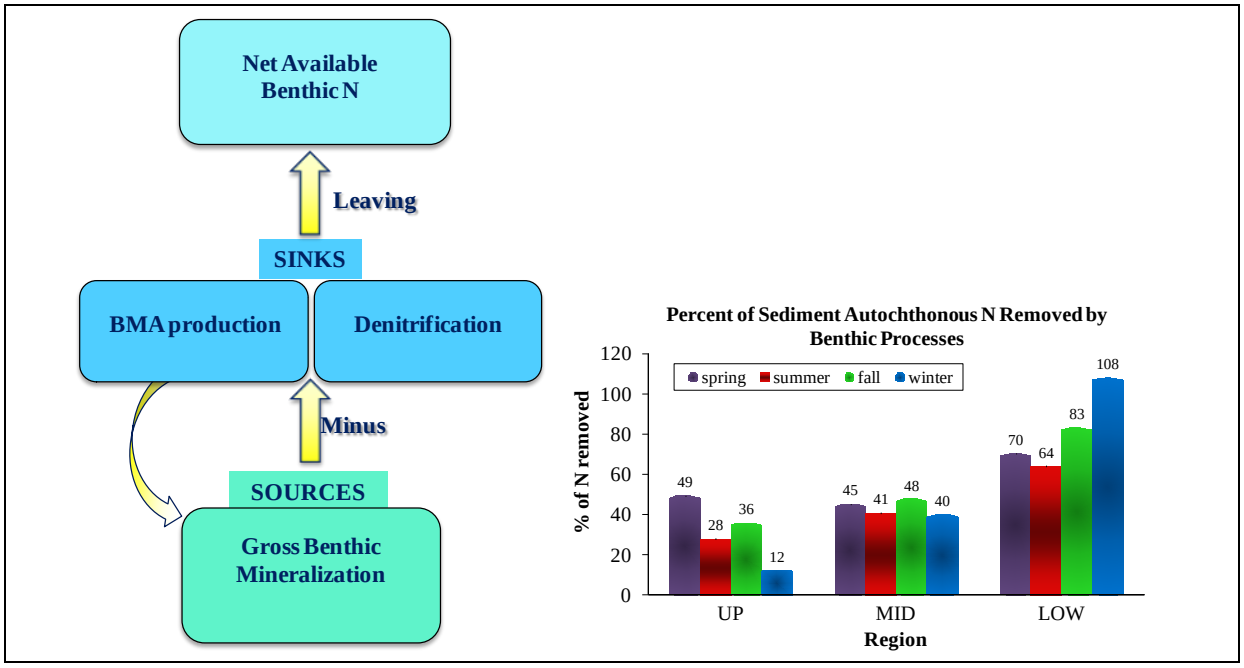

Figure 9A-2. The percentage of sediment autochthonous nitrogen (N) removed by benthic processes scaled up to the NRE by region and season.

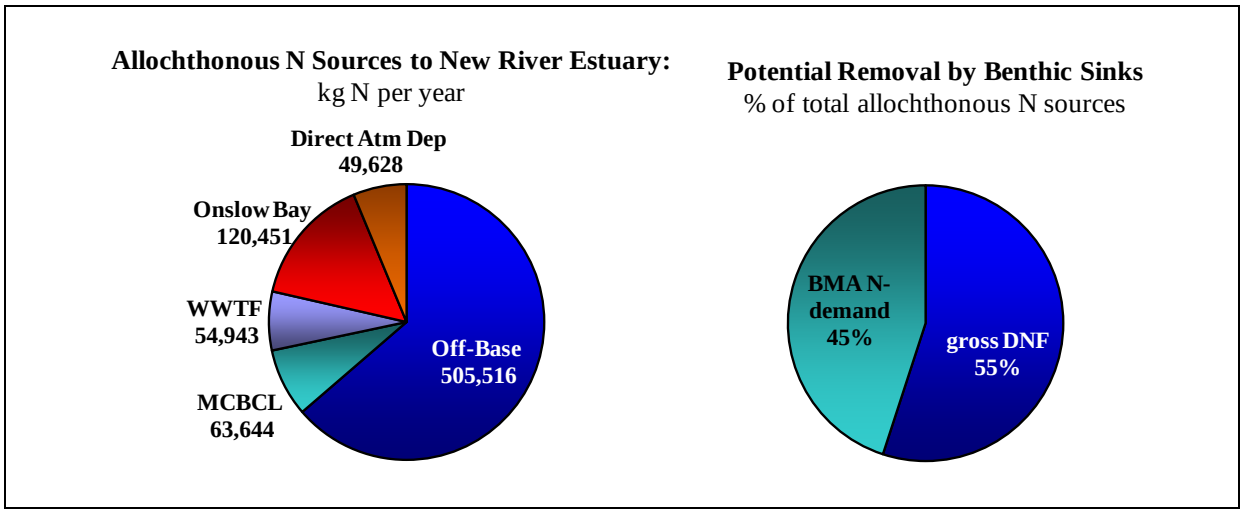

Figure 9A-3. Allochthonous nitrogen (N) sources to the NRE (modified from RTI, 2013b) (left) and the percent removal of total allochthonous N by benthic sinks of BMA N demand and denitrification (DNF; right).

Conclusions

The AE-3 research module of DCERP1 demonstrated that the NRE is a moderately eutrophic estuary with rates of benthic primary production (gC m^{-2} y^{-1}) that accounted for 41% of total average annual primary production across the estuary. Although phytoplankton dominated total GPP in the NRE, an active benthic microbial community in the shallow photic zone was highly

productive and effective in mitigating watershed nutrient loads, and thereby serving as a benthic filter. The benthos served as both a source of recycled nutrients supporting pelagic primary production as well as a benthic filter, sequestering and removing nutrients by BMA uptake, denitrification, and anaerobic ammonium oxidation (i.e., anammox) and thereby mitigating eutrophication. The effectiveness of the benthic filter was dependent on light availability and photic area of the estuary (≥1% Io), which varied as a function of FW discharge. Between 2008–2011, photic area in the NRE varied between 46–97% of total estuarine bottom area. When light availability was low, the benthos switched from net autotrophic (photosynthesizing their food) to heterotrophic (using organic compounds for food) and from a net sink to a source of N to the water column. Estuary-wide benthic processes sequestered from 41–67% of the inorganic nitrogen remineralized from organic matter in sediments in spring and from 27–63% in summer.

Literature Cited

Anderson, I.C., M.J. Brush, M.F. Piehler, C.A. Currin, J.W. Stanhope, A.R. Smyth, J.D. Maxey, and M.L. Whitehead. 2014. Impacts of climate related drivers on the benthic nutrient filter in a shallow photic estuary. *Estuaries and Coasts 37*(Supp 1):46–62. doi: 10.1007/s12237-013-9665-5

Anderson, I.C., J.W. Stanhope, A.K. Hardison, and K.J. McGlathery. 2010. Sources and fates of nitrogen in Virginia coastal bays. Chapter 3, pp. 43–72 in *Coastal Lagoons: Critical Habitats of Environmental Change*. Edited by Kennish, M.J., and H.W. Paerl. CRC Press.

Caffrey, J.M. 2003. Production, respiration, and net ecosystem metabolism in U.S. estuaries. *Environmental Monitoring and Assessment 81*:207–219.

Cai, W.J. 2011. Estuarine and coastal ocean carbon paradox: CO_2 sinks or sites of terrestrial carbon incineration? *Annual Review of Marine Science 3*:123–145.

Gazeau, F., A.V. Borges, C. Barrón, C.M. Duarte, N. Iversen, J.J. Middelburg, B. Delille, M-D. Pizay, M. Frankignoulle, J-P. Gattuso. 2005. Net ecosystem metabolism in a micro-tidal estuary (Randers Fjord, Denmark): Evaluation of methods. *Marine Ecology Progress Series 301*:23–41.

Hopkinson, C.S., and E.M. Smith. 2005. Estuarine respiration: An overview of benthic, pelagic, and whole system respiration. Pp. 122–146 in *Respiration in Aquatic Ecosystems*. Edited by del Giorgio, P., and P. Williams. Oxford University Press.

McGlathery, K.J., K. Sundbäck, and I.C. Anderson. 2007. Eutrophication in shallow coastal bays and lagoons: The role of plants in the coastal filter. *Marine Ecology Progress Series 348*:1–18.

NOAA (National Oceanic and Atmospheric Administration). 2011. *NOAA Coastal Geospatial 653 Data Project*. Available at http://coastalgeospatial.noaa.gov/data_gis.html

NOAA (National Oceanic and Atmospheric Administration). 2004. *North Carolina Bathymetry/Topography Sea Level Rise Project: Determination of Sea Level Trends*. NOAA Technical Report NOS CO-OPS 041. Silver Spring, MD. May.

RTI. 2013a. *DCERP2 Research Plan*. Strategic Environmental Research and Development Program (SERDP) Research Project RC-2245. RTI International, Research Triangle Park, NC.

RTI. 2013b. *DCERP1 Final Research Report*. Strategic Environmental Research and Development Program (SERDP) Research Project RC-1413. RTI International, Research Triangle Park, NC.

Smith, S.V., and J.T. Hollibaugh. 1997. Annual cycle and inter-annual variability of ecosystem metabolism in a temperate climate embayment. *Ecological Monographs 67*(4):509–533.

Staehr, P.A., J.M. Testa, W.M. Kemp, J.J. Cole, K. Sand-Jensen, and S.V. Smith. 2012. The metabolism of aquatic ecosystems: History, applications, and future challenges. *Aquatic Science 74*(1):15–29.

Sundbäck, K., F. Linares, F. Larson, A. Wulff, and A. Engelsen. 2004. Benthic nitrogen fluxes along a depth gradient in a microtidal fjord: The role of denitrification and microphytobenthos. *Limnology and Oceanography 49*(4):1095–1107.

Von Korff, B.H., M.F. Piehler, and S.H. Ensign. 2014. Comparison of denitrification between river channels and their adjoining tidal freshwater wetlands. *Wetlands 34*(6):1047–1060.

Appendix 9-B
Research Project AE-6: Research Questions and Answers

1. At the estuarine-wide scale, what are the annual net benthic–pelagic exchanges of carbon, nitrogen, and phosphorus (this will build on data collected during DCERP1)?

To determine the overall impact of the benthic filter on external and internal loads of nitrogen supplied to the New River Estuary (NRE), we scaled rates of benthic gross nitrogen mineralization (MIN), benthic microalgal nitrogen demand, and denitrification (DNF) and measured seasonally at various depths in the upper, middle, and lower NRE, to the entire estuary. Because nitrogen is the limiting nutrient, the majority of nitrogen as dissolved inorganic nitrogen (DIN) is utilized by the phytoplankton as it enters the estuary from the New River, but ultimately the phytoplankton sinks to the bottom of the estuary, where further transformation of the nutrient occurs. Seasonally and for individual estuarine regions, benthic processes were estimated to remove from 12% to greater than 100% of the DIN produced by internal processes, measured as benthic MIN. Annually and averaged over all regions of the NRE, benthic microalgal-nitrogen (BMA-N) demand and DNF together removed 41% of the total benthic internal DIN, with DNF representing a slightly large proportion of the total nitrogen sinks than benthic microalgae (BMA; 55% versus 45%). In the absence of the BMA benthic filter, organic matter remineralized in sediments would have released DIN back into the water column to support additional pelagic phytoplankton growth. Across the entire estuary, benthic nitrogen sinks were capable of removing 100% of the estimated annual average load of external sources of DIN that entered the NRE between 1998 and 2011 (794,000 kg TN yr^{-1}). We did not show exchanges for carbon and phosphorus from this study because nitrogen is the limiting nutrient in the NRE and carbon data are shown in the carbon budget developed for the period from July 2013 through July 2015.

2. Based on diel variations in dissolved inorganic carbon, dissolved oxygen, and ^{18}O signatures, what is the net metabolic status (autotrophy versus heterotrophy) of the shallow estuarine zone of the NRE?

Net ecosystem metabolism (NEM) in the shallow shoal and deeper channel zones of the NRE followed similar patterns, varying with time of day, season, and year. Net heterotrophy increased seasonally with increasing water temperature. Counteracting dissolved inorganic carbon (DIC) fluxes, measured across and along the estuary and seasonally, maintained NEM in near metabolic balance over annual time scales. However, NEM was sensitive to river discharge, demonstrating slight net autotrophy during Year 1 (YR1, from July 2013 through July 2014) of our study, a dry year, and shifting to slight net heterotrophy during Year 2 (YR2, from July 2014 through July 2015), a year with twice the rainfall as YR1. Metabolic patterns were similar when calculated based on diel variation of DIC or dissolved oxygen (DO); however, for most of our calculations, we relied on DIC measurements, which are not as sensitive as DO to anaerobic conditions in the estuary. We did not use ^{18}O signatures when developing the carbon budget for the NRE.

3. How do air–water partial pressure of carbon dioxide (CO_2) exchanges in the shallow estuarine zone vary spatially (along the estuary) and temporally at diel, seasonal, and inter-annual scales?

The air–water CO_2 exchanges in the shallow estuarine zones of the estuary varied in a similar way both spatially in the upper, middle, and lower estuary and temporally over the seasons. However, when aggregated annually over the entire estuary, CO_2 exchanges were small, showing slight CO_2 uptake in YR1 (from July 2013 through July 2014), a drier year when the NRE was slightly net autotrophic, and showing slight CO_2 releases in YR2 (from July 2014 through July 2015), a wetter year when the NRE was slightly net heterotrophic. CO_2 effluxes were highest during seasons with high temperatures, but often shifted to CO_2 influxes during periods of maximum photosynthesis during phytoplankton blooms, especially at the head of the estuary near Jacksonville, NC.

4. How do the sources and fates of particulate organic carbon and dissolved organic carbon derived from the NRE watersheds vary temporally and spatially?

Sources of particulate organic carbon (POC) and dissolved organic carbon (DOC) may come from both external sources from the upper watershed and internal sources from processes occurring in the estuarine sediments. Sources of external total organic carbon (TOC=POC+DOC) include the New River and the smaller tributary creeks located on Marine Corps Base Camp Lejeune lands. During periods of high freshwater discharge, riverine sources of TOC dominate. Lability of the DOC in the upper NRE ranges from 15 to 20% and in the headwaters of the smaller tributaries, this may be as high as 40%. TOC declines rapidly during transport down estuary due to sedimentation of the POC, decomposition of the DOC, and dilution with tidal seawater. Based on our metabolic measurements, internal sources of TOC are recycled rapidly during transport supporting production of phytoplankton down-estuary.

5. What are the metabolic and nutrient flux responses of the shallow zone to climatic drivers (e.g., fresh water delivery [salinity]) and temperature (based on controlled experimental manipulations)?

A 10-day reciprocal transfer experiment was performed in July 2015 and March 2016. The experiment involved taking sediment from the upper estuary and incubating it at higher salinity and two elevated temperatures and taking sediment from the lower estuary and incubating it at lower salinity and two elevated temperatures for a period of 10 days. However, the results of the experiment were not conclusive. To adequately examine the effects of different salinities and elevated temperature on metabolic and nutrient flux responses, experiments should be conducted for a longer period of time than was allowed in our study.

Appendix 9-C
Research Project AE-4: Research Questions and Answers

1. How do meteorological events such as high precipitation storms, tropical cyclones, and droughts modify phytoplankton community structure and function (rates of primary production and planktonic respiration) and will the changes significantly impact carbon flux and budgets for the New River Estuary (NRE)?

Major storm events can alter phytoplankton community biomass and composition in multiple ways. If the storm delivers a lot of rain, accompanied by high freshwater runoff containing elevated nutrient loads, primary production (as well as respiration) and phytoplankton biomass can increase rapidly (within a matter of days; **Figure 9C-1**). However, if freshwater discharge rates are very high, increased flushing rates (decreased water residence times) can rapidly "wash" plankton out of the estuary. There is a "tradeoff" between nutrient-stimulated growth and flushing, with an "optimum" for the New River and nearby Neuse River Estuary described by Peierls et al. (2012).

As far as impacts on phytoplankton composition go, typically fast-growing diatoms, cryptophytes and chlorphytes (green algae) are favored by high flushing rates, while dinoflagellates and cyanobacteria prefer more quiescent. Longer residence time periods. These categorizations can vary, depending on the nutrient loads accompanying the storm-based runoff.

Reference

Peierls, B.L., N.S. Hall, and H.W. Paerl. 2012. Non-monotonic responses of phytoplankton biomass accumulation to hydrologic variability: a comparison of two coastal plain North Carolina estuaries. *Estuaries and Coasts 35*:*1*376–1392.

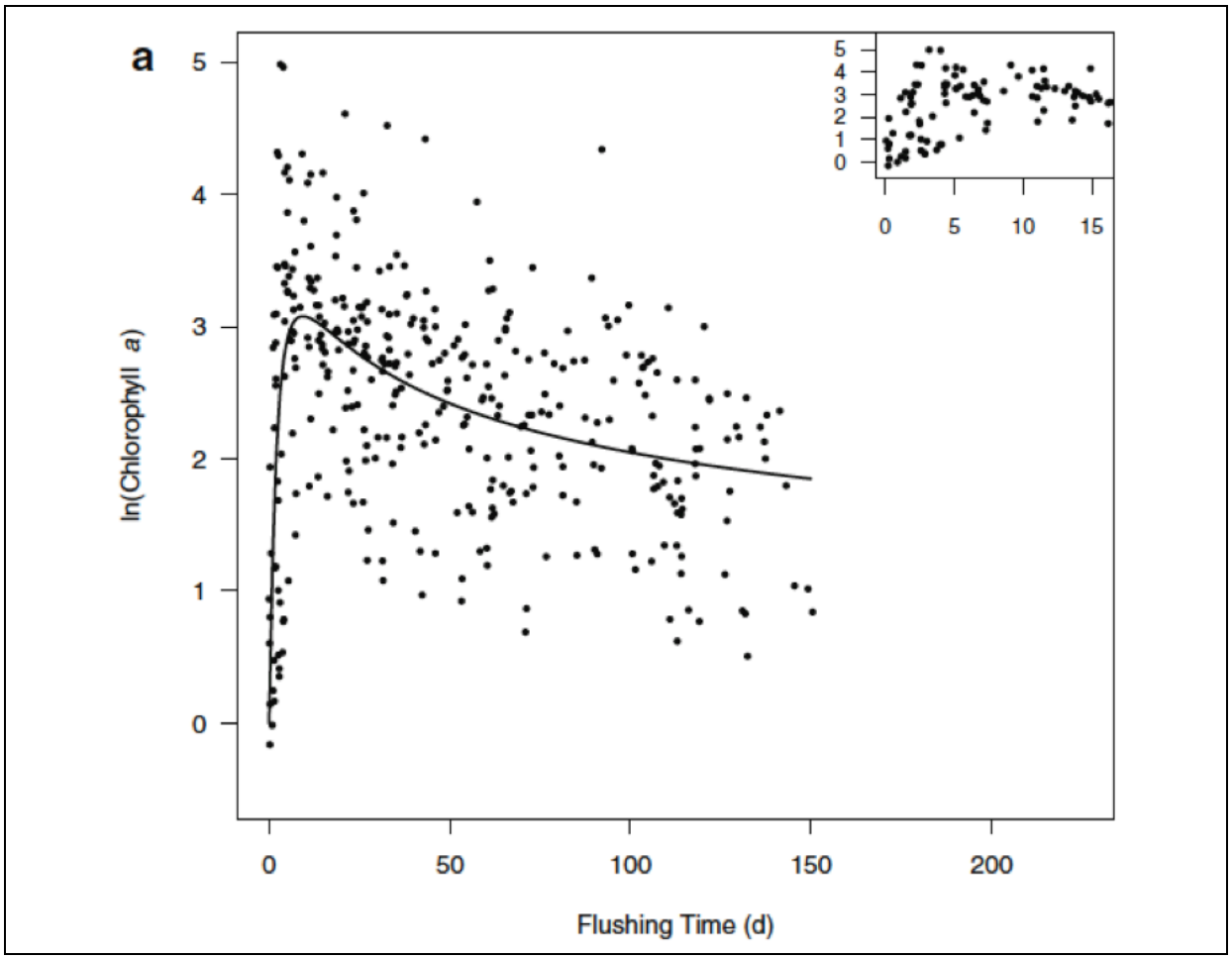

Figure 9C-1. A scatter plot of phytoplankton biomass as chlorophyll *a* versus flushing time.

Data are from the eight DCERP sampling stations monitored monthly for all sampling dates from October 2007 through December 2016. Inset shows an expansion of the relationship up to a flushing time of 15 days (d).

2. What is the relationship between allochthonous organic carbon loading from freshwater discharge events and respiration and heterotrophic conditions?

Obviously, allochthonous organic carbon (OC) loading will stimulate respiration, but autochthonous OC loading (i.e., algal blooms) will also increase respiration rates. If the rate of respiration (i.e., O_2 consumption) from these inputs is less than the rates of O_2 production from photosynthesis (on a 24-h basis), the system will tend to remain "net autotrophic," but if the converse occurs, it will tend to be "net heterotrophic." Of course, a lot depends on how the benthic communities respond as well; therefore, both planktonic and benthic respiration and photosynthesis need to be assessed contemporaneously.

3. Do warmer conditions favor potentially harmful cyanobacterial, dinoflagellate, and raphidophyte harmful algal bloom species over more desirable diatoms? If so, how will these changes impact NRE fertility, nutrient cycling, and carbon utilization and flux?

The short answer is yes. The second part of this question would require at least another 5-year study. One would have to examine the food web and nutrient cycling ramifications of these changes, which were not assessed in the current study. It has been assumed that a shift towards cyanobacteria, which "like it hot" would have negative effects on food web transfer, because larger cyanobacterial bloom species are not readily consumed and are poor food sources even if they are consumed. They would end up playing a larger role in internal nutrient cycling n=because a larger fraction of their biomass would end up in the sediments, rather than being exported out of the system as zooplankton and fish (see **Figure 9C-2**). We have no idea what happens to the picoplanktonic cyanobacteria, but there is some evidence that they could be consumed by microzooplankton and make their way up the food chain in that manner. Dinoflagellates and Raphidophytes can sometime be consumed by macrozooplankton and benthic grazers, and thus could be good food sources. However, so toxin-producing species may be detrimental to grazers and hence cause food web problems. Also, large blooms can die suddenly and sink to the bottom, aggravating hypoxia and impeding food web transfer and altering biogeochemical cycling. **Figure 9C-2** is from Paerl (2017).

Reference

Paerl, H.W. 2017. Controlling harmful cyanobacterial blooms in a climatically more extreme world: Management options and research needs. *Journal of Plankton Research 39*(5):763–771. doi: 10.1093/plankt/fbx042

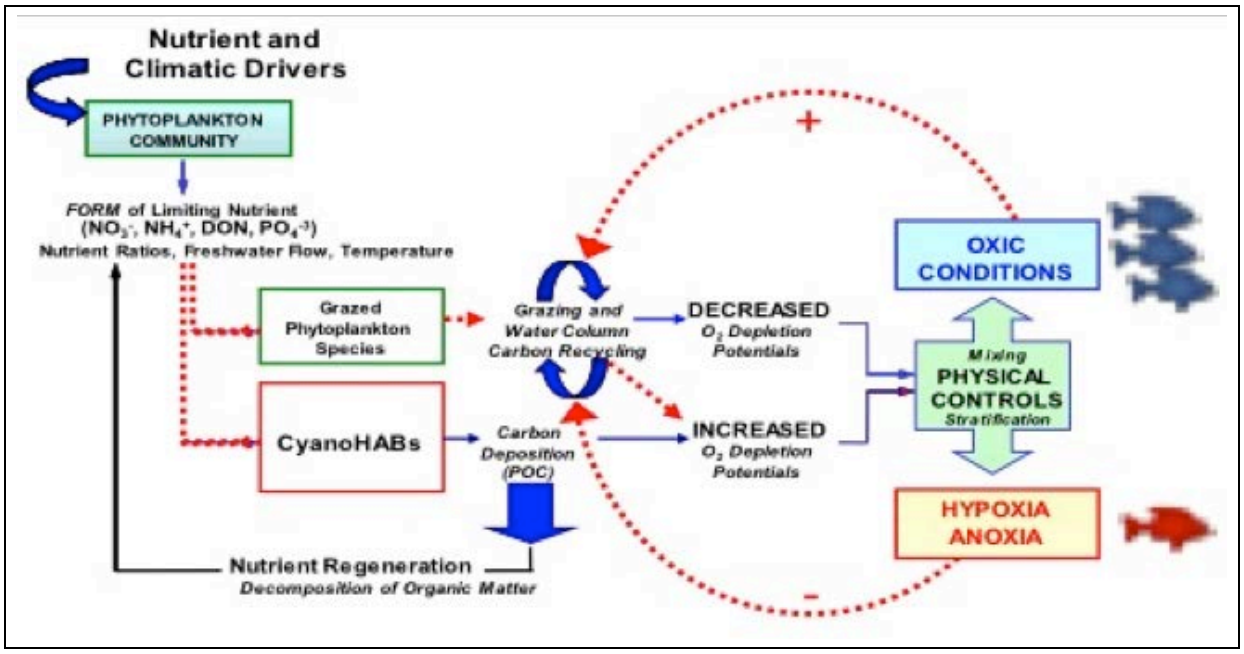

Figure 9C-2. Conceptual diagram, showing the interactions and feedback loops between nutrient supply, freshwater flow (flushing/residence time), temperature and vertical stratification and cyanobacteria bloom growth potential in a eutrophic system experiencing anthropogenic nutrient loading and climatically driven (altered freshwater flow, warming) environmental change

Appendix 9-D
List of Scientific/Technical Publications

Papers

Anderson, I.C., M.J. Brush, M.F. Piehler, C.A. Currin, J.W. Stanhope, A.R. Smyth, J.D. Maxey, and M.L. Whitehead. 2014. Impacts of climate related drivers on the benthic nutrient filter in a shallow photic estuary. *Estuaries and Coasts 37*(Supp 1):46–62. doi: 10.1007/s12237-013-9665-5

Brym, A., H.W. Paerl, M.T. Montgomery, L.T. Handsel, K. Ziervogel, and C.L. Osburn. 2014. Optical and chemical characterization of base-extracted particulate organic matter in coastal marine environments. *Marine Chemistry 162*:96–113.

Crosswell, J.R., I.C. Anderson, J.W. Stanhope, B. Van Dam, M.J. Brush, S. Ensign, M.F. Piehler, B. McKee, M. Bost, and H.W. Paerl. 2017. Carbon budget of a shallow, lagoonal estuary: Transformations and source-sink dynamics along the river–estuary–ocean continuum. *Limnology and Oceanography*. In press.

Crosswell, J.R., M.S. Wetz, B. Hales, and H.W. Paerl. 2014. Extensive CO_2 emissions from shallow coastal waters during passage of Hurricane Irene (August 2011) over the mid-Atlantic Coast of the USA. *Limnology and Oceanography 59*(5):1651–1665.

Murphy, A.E., K.A. Emery, I.C. Anderson, and M.L. Pace. 2016. Quantifying the effects of commercial clam aquaculture on carbon and nitrogen cycling: An integrated ecosystem approach. Submitted to *Estuaries and Coasts*.

Murphy, A.E., I.C. Anderson, A.R. Smyth, B. Song, and M.W. Luckenbach. 2016. Microbial nitrogen processing in hard clam (*Mercenaria mercenaria*) aquaculture sediments: The relative importance of denitrification and dissimilatory nitrate reduction to ammonium (DNRA). *Limnology and Oceanography 61*(5):1589–1604.

Murphy, A.E., I.C. Anderson, and M.W. Luckenbach. 2015. Enhanced nutrient regeneration at commercial hard clam (*Mercenaria mercenaria*) beds and the role of macroalgae. *Marine Ecology Progress Series 530*:135–151.

Nojavan A.F., S.S. Qian, H.W. Paerl, K.H. Reckhow, and E.A. Albright. 2014. A study of anthropogenic and climatic disturbance of the New River Estuary using a Bayesian belief network. *Marine Pollution Bulletin 83*:107–115.

Paerl, H.W. 2016. Impacts of climate change on cyanobacteria in aquatic environments. Pp. 3–31 in *Climate Change and Microbial Ecology: Current Research and Future Trends*. Edited by Marxsen. J. Caister Academic Press.

Paerl, H.W. 2014. Mitigating harmful cyanobacterial blooms in a human- and climatically impacted world. *Life 4*(4):988–1012.

Paerl, H.W., W.S. Gardner, K.E. Havens, A.R. Joyner, M.J. McCarthy, S.E. Newell, B. Qin, and J.T. Scott. 2016. Mitigating cyanobacterial harmful algal blooms in aquatic ecosystems impacted by climate change and anthropogenic nutrients. *Harmful Algae 54*:213–222.

Paerl, H.W., N.S. Hall, B.L. Peierls, and K.L. Rossignol. 2014. Evolving paradigms and challenges in estuarine and coastal eutrophication dynamics in a culturally and climatically stressed world. *Estuaries and Coasts 37*(2):243–258.

Paerl, H.W., W.S. Gardner, M.J. McCarthy, B.L. Peierls, and S.W. Wilhelm. 2014. New insights on old paradigms—Shifting thoughts on freshwater eutrophication. *Science 346*:175.

Paerl, H.W., N.S. Hall, B.L. Peierls, K.L. Rossignol, and A.R. Joyner. 2014. Hydrologic variability and its control of phytoplankton community structure and function in two shallow, coastal, lagoonal ecosystems: The Neuse and New River Estuaries, North Carolina, USA. *Estuaries and Coasts 37*(Supp 1):31. doi: 10.1007/s12237-013-9686-0

Van Dam, B., J.R. Crosswell, I.C. Anderson, and H.W. Paerl. In review. Watershed-scale drivers of air–water CO_2 exchanges in two lagoonal, North Carolina (USA) estuaries. *Limnology and Oceanography*.

Thesis or Dissertation

Maxey, J.D. 2012. Shedding Light on the Estuarine Coastal Filter: The Relative Importance of Benthic Microalgae in Shallow Photic Systems. M.S. thesis, Virginia Institute of Marine Science, William and Mary, Williamsburg, VA.

Whitehead, M. 2012. The Role of Benthic Nitrogen Fixation as a Source of new Nitrogen to the New River Estuary, NC. M.S. thesis, Virginia Institute of Marine Science, William and Mary, Williamsburg, VA.

Presentations

Anderson, I., J. Crosswell, K. Czapla, and B. Van Dam. 2017. *Carbon Transformations and Source-Sink Dynamics Along a River, Marsh, Estuary, Ocean Continuum*. Invited presentation to the American Geophysical Union, New Orleans, LA. December.

Anderson, I., C. Currin, C. Tobias, K. Czapla, N. McTigue, and S. Ensign. 2017. *Lateral Export of Carbon from Salt Marshes to Adjacent Aquatic Systems*. Presented to the Coastal Estuarine Research Federation, Providence, RI. November.

Anderson, I., K. Czapla, and E. Herbert. 2017. *Salt Marsh Metabolism and Carbon Accumulation.* Invited presentation at Ocean Carbon and Biogeochemistry, Woods Hole MA. June.

Anderson, I., M. Brush, J. Stanhope, J. Crosswell, H. Paerl, M. Piehler, B. McKee, and B. Van Dam. 2017. *Carbon Budget of a Shallow, Lagoon Estuary: Transformations and Source-Sink Dynamics*. Invited plenary talk at the University of South Alabama, Dauphin Island Sea Laboratory. April.

Anderson, I., J. Crosswell, and B. Van Dam. 2017. *Carbon Transformations and Source–Sink Dynamics Along a River, Estuary, Ocean Continuum*. Presented at the North America Carbon Program Annual Meeting, Bethesda MD. February.

Czapla, K., I. Anderson, E. Herbert, and M. Fogarty. 2017. *Salt Marsh Metabolism and Carbon Accumulation: Effects of Location and Fertilization*. Poster presented at Ocean Carbon and Biogeochemistry, Woods Hole, MA. June.

Czapla, K., I. Anderson, J. Stanhope, M. Fogarty, C. Currin, N. McTigue, and E. Herbert. 2017. *Spatial Patterns of Net Community Production in Response to Fertilization in a Polyhaline Marsh*. Presented to the Coastal Estuarine Research Federation. Providence, RI. November.

Czapla, K., I. Anderson, and J. Stanhope. 2016. *Effective Edges: Salt Marsh Creek Banks as Hotspots for N Removal*. Presented to the Atlantic Estuarine Research Society. March.

Anderson, I., J. Stanhope, B. Van Dam, N. Hall, J. Croswell, H. Paerl, and M. Brush. 2015. *Bio-Physical Controls of CO_2 Fluxes Along a River–Estuary Continuum*. Presented at the Coastal and Estuarine Research Federation Conference, Portland, OR. November.

Anderson, I. 2015. *Impacts of Clam Aquaculture on Eutrophication: A Matter of Scale*. Presented at Virginia Commonwealth University, Richmond, VA. February. Also presented at Colby College, Waterville, ME. April.

Anderson, I. 2015. *Estuaries as Sources or Sinks of Carbon: Climatic Drivers*. Presented at the Laura Randall Schweppe Endowed Lecture Series in Marine Science, University of Texas, Austin, TX. March.

Anderson, I. 2015. *Clam Aquaculture: Impacts on Marine Ecosystems*. Presented at the Laura Randall Schweppe Endowed Lecture Series in Marine Science, University of Texas, Austin, TX. March.

Anderson, I.C., J.W. Stanhope, M. Brush, A. Smyth, C. Currin, and M. Piehler. 2014. *Interacting Drivers Regulating the Fate of Nitrogen in Shallow Photic Marine Systems.* Invited presentation at the Joint Aquatic Sciences Meeting, Portland, OR. May.

Crosswell, J.R. 2015. *A Stormy Future for Coastal Carbon: Assessing Impacts of Climatic Perturbation on Carbon Transport, Processing, and Storage in Coastal Regions.* Invited talk presented at the North American Carbon Project Principal Investigators' Meeting, Washington, DC. January.

Crosswell, J.R., and H.W. Paerl. 2015. *Bubble Clouds in Coastal Waters and Their Role in Air–Water Gas Exchange*. Poster presented at the Ameriflux Principal Investigators' Meeting, Washington, DC. January.

Paerl, H.W., I.C. Anderson, W.S. Gardner, M.J. McCarthy, N.S. Hall, B.L. Peierls, and K.L. Rossignol. 2015. *Controlling Eutrophication Along the Freshwater-Marine Continuum: Why the Need for Dual Nutrient Input Constraints?* Presented at the Coastal and Estuarine Research Federation Conference, Portland, OR. November.

Paerl, H.W., J.R. Crosswell, B.R. Van Dam, J.W. Stanhope, I.C. Anderson, B. Abare, K.L. Rossignol, B.L. Peierls, and N.S. Hall. 2015. *Impacts of Human and Climatic Perturbations on Blue, Green and Black Carbon in Our Estuaries*. Keynote address presented at the Atlantic Estuarine Research Society Conference, Wanchese, NC. March.

Paerl, H.W., N.S. Hall, B.L. Peierls, K.L. Rossignol, and A.R. Joyner. 2014. *Managing Eutrophication Along the Freshwater–Marine Continuum in Coastal Watersheds: Why the Need for Dual Nutrient (N&P) Controls?* Invited seminar presented at East Carolina University, Greenville, NC. October.

Paerl, H.W., N.S. Hall, B.L. Peierls, K.L. Rossignol, and A.R. Joyner. 2014. *Coastal Eutrophication Dynamics and Controls in a Culturally and Climatically Stressed World.* Keynote talk presented at the Deltas in Times of Climate Change Conference, Rotterdam, The Netherlands. September.

Paerl, H.W. 2014. *Field-Based Assessments of Human and Climatically Driven Environmental Change in Estuarine System, North Carolina, USA*. Invited talk presented at American Chemical Society Meetings, San Francisco, CA. August.

Paerl, H.W. 2014. *What Controls Harmful Algal Blooms in North Carolina Estuaries and What Can We Do About It?* Invited lecture presented at the N.C. Teachers' Workshop, sponsored by the Duke Energy Foundation, Pine Knoll Shores, NC. July.

Paerl, H.W. 2014. *Environmental Controls of Harmful Algal Bloom Formation Along the Freshwater–Marine Continuum*. Invited lecture presented at the Nanjing Institute of Geography and Limnology, Nanjing, China. June.

Paerl, H.W. 2014. *Environmental Controls of Harmful Cyanobacterial Blooms*. Invited talk and U.S. Environmental Protection Agency Prevention, Control and Mitigation of Cyanobacteria and Cyanotoxins Webinar. May. Available at http://www2.epa.gov/sites/production/files/2014-07/documents/cyanohab-webinar-5142014.pdf

Paerl, H.W. 2014. *Impact of Human and Climatic Forcing on Estuarine Phytoplankton Production and CO_2 Flux.* Keynote talk presented at the Scientific Committee of Ocean Research (SCOR) Working Group 137 Meeting, Busan, South Korea. April.

Paerl, H.W. 2014. *Human and Climatic Drivers of Phytoplankton Community Structure and Function: What's Manageable and What's Not?* Invited seminar presented to the Departments of Microbiology and Biology, Oregon State University, Corvallis, OR. April.

Paerl, H.W. 2014. *Teasing Apart Water Quality and Habitat Impacts of Human and Climatic Perturbations in Our Estuaries.* Keynote talk presented at the Annual Symposium of the Everglades Wetlands Research Park, Kapnick Center, Florida Gulf Coast University, Naples, FL. January.

Peierls, B.L, A.G. Hounshell, C.L. Osburn, and H.W. Paerl. 2016. *Bioavailability of Riverine Dissolved Organic Matter in an Estuarine System: Evidence of the Priming Effect?* Presented at the Association for the Sciences of Limnology and Oceanography (ASLO) Ocean Sciences 2016, New Orleans, LA. February.

Stanhope, J., I. Anderson, J. Croswell, B. Van Dam, H. Paerl, and H. Walker. 2015. *A Shallow Photic Estuary in North Carolina: A Source or Sink of Carbon Dioxide?* Presented at the 23rd Biennial Conference of the Coastal and Estuarine Research Federation, Portland, OR. November.

Stanhope, J.W., I.C. Anderson, J.R. Crosswell, B.R. Van Dam, H.W. Paerl, and H.S. Walker. 2015. *The New River Estuary, North Carolina: A source or Sink of CO_2?* Presented at the Atlantic Estuarine Research Society Conference, Wanchese, NC. March.

Van Dam, B., J. Stanhope, I. Anderson, and H. Paerl. 2015. Estuarine CO_2 Flux: A Comparison of Two North Carolina Estuaries. Presented at the Coastal and Estuarine Research Federation Conference, Portland, OR. November.

Van Dam, B.R., J.W. Stanhope, I.C. Anderson, J.R. Crosswell, and H.W. Paerl. 2015. *Diel and Seasonal pCO_2 Variability in the New River Estuary, North Carolina*. Presented at the Atlantic Estuarine Research Society Conference, Wanchese, NC. March.

Appendix 9-E
List of Students

- Bryce Van Dam, Ph.D., Marine Science, University of North Carolina at Chapel Hill, Chapel Hill, NC. Anticipated in spring 2018.
- Kenneth Czapla, Ph.D., Virginia Institute of Marine Science, William and Mary, Williamsburg, VA. Anticipated in spring 2012.

Appendix 9-F
Other Supporting Information

Dr. Hans Paerl received the Odum Lifetime Achievement Award in 2011 from the Estuarine and Coastal Research Federation for his work on the cause and consequences of eutrophication and harmful algal blooms in estuarine and coastal waters. In December 2015, Dr. Paerl was recognized as a Fellow of the American Geophysical Union.

Dr. Iris Anderson received the Virginia Institute of Marine Science (VIMS) Lifetime Achievement Award in 2015 and the William and Mary Plumeri Award for Faculty Excellence in 2012. In addition, Dr. Anderson was selected as a visiting scholar for the Laura Randall Schweppe Endowed Lecture Series in Marine Science at the University of Texas, Austin, in March 2015. At the university, Dr. Anderson gave a series of lectures based on studies of the climactic drivers of carbon cycling in estuaries performed for DCERP2.

Chapter 10

Coupled Ecosystem Modeling of the NRE for Research, Synthesis, and Management

SERDP Project Number: RC-2245

Translating Science into Practice

Research Project TSP-2

Lead Researchers:

Dr. Mark J. Brush
Virginia Institute of Marine Science
College of William and Mary
Gloucester Point, VA 23062
brush@vims.edu

Supporting Researchers:

Dr. Samuel J. Lake, sjlake@vims.edu
Ms. Sara Blachman, sablachman@vims.edu
Ms. Shanna Williamson, swilliamson@vims.edu

January 2018

Final

This report was prepared under contract to the U.S. Department of Defense (DoD) Strategic Environmental Research and Development Program (SERDP). The publication of this report does not indicate endorsement by DoD, nor should the contents be construed as reflecting the official policy or position of DoD. References herein to any specific commercial product, process, or service by trade name, trademark, manufacturer, or otherwise, do not necessarily constitute or imply its endorsement, recommendation, or favoring by DoD.

Table of Contents

Acronyms 10-vii
Abstract 10-1
Objectives of the Research Project 10-3
Background 10-3
Materials and Methods 10-4
Estuarine Simulation Model 10-4
ESM Expansion and Calibration/Validation 10-8
ESM Scenarios 10-9
Phytoplankton Functional Group Model 10-10
ReNuMa Model 10-13
Application in Other Estuarine Systems 10-15
Online Decision-Support Tool 10-19
Results and Discussion 10-20
New River ESM Calibration and Validation 10-20
Phytoplankton Functional Group Model 10-28
ReNuMa Model 10-37
ESM Scenarios 10-41
Phytoplankton Functional Group Scenarios 10-47
ReNuMa Model Scenarios 10-49
Application in Other Estuarine Systems—Neuse River ESM 10-51
Application in Other Estuarine Systems—Choctawhatchee Bay ESM 10-60
Cross-System Comparisons 10-69
Online Decision-Support Tool 10-71
Conclusions and Implications for Future Research and Implementation 10-79
Findings with Implications for Future Base Management 10-80
Literature Cited 10-82
Appendix 10-A: List of Scientific/Technical Publications 10-A-1
Appendix 10-B: List of Students 10-B-1

List of Figures

Figure 10-1. A schematic of the DCERP Estuarine Simulation Model (ESM) 10-5
Figure 10-2. Domain of the New River Estuary (NRE) Estuarine Simulation Model (ESM) 10-7
Figure 10-3. Vertical structure and simulated exchanges in the New River Estuary (NRE) Estuarine Simulation Model (ESM). 10-7
Figure 10-4. New River discharge at Gum Branch during the Estuarine Simulation Model (ESM) simulation period. 10-9

Figure 10-5. Schematic of the multi-group phytoplankton model. 10-10
Figure 10-6. Associations between accessory photopigments and New River Estuary (NRE) phytoplankton. 10-13
Figure 10-7. Sub-watersheds and stream gaging stations used in the ReNuMa model calibration and validation. 10-14
Figure 10-8. New estuaries selected for Estuarine Simulation Model (ESM) application in DCERP2 10-15
Figure 10-9. Domain of the Neuse River Estuary Estuarine Simulation Model (ESM). 10-16
Figure 10-10. Addition of Slocum and Hancock Creeks to the Neuse River Estuarine Simulation Model (ESM). 10-17
Figure 10-11. Neuse River and Trent River discharge during the Estuarine Simulation Model (ESM) simulation period. 10-17
Figure 10-12. Domain of the Choctawhatchee Bay Estuarine Simulation Model (ESM)..... 10-18
Figure 10-13. Choctawhatchee River discharge during the Estuarine Simulation Model (ESM) simulation period. 10-19
Figure 10-14. Flushing times of the New River Estuary (NRE). 10-20
Figure 10-15. Simulated New River Estuary parameters, 2007–2015. 10-22
Figure 10-16. Simulated New River Estuary parameters, 2007–2015. 10-23
Figure 10-17. Simulated New River Estuary parameters, 1998–2007. 10-24
Figure 10-18. Simulated New River Estuary parameters, 1998–2007. 10-25
Figure 10-19. Modeled above- and below-ground biomass of Ruppia maritima in three spatial elements of the middle and lower New River Estuary. 10-26
Figure 10-20. Modeled above- and below-ground biomass of Halodule wrightii in three spatial elements of the middle and lower New River Estuary. 10-26
Figure 10-21. Simulated carbon parameters in the New River Estuary. 10-27
Figure 10-22. Simulated air–sea carbon dioxide (CO_2) flux in the New River Estuary. 10-28
Figure 10-23. Average annual cycles of chlorophyll a (chl a) and gross primary production (GPP), functional group model. 10-30
Figure 10-24. Simulated group dynamics from the functional group model, 2007–2012. 10-33
Figure 10-25. Modeled diatom and raphidophyte biomass. 10-34
Figure 10-26. Modeled dinoflagellate biomass. 10-35
Figure 10-27. Modeled cyanobacteria biomass. 10-36
Figure 10-28. Modeled watershed loads at Gum Branch using the ReNuMa model. 10-38
Figure 10-29. Modeled watershed loads from Cogdels Creek using the ReNuMa model. 10-39
Figure 10-30. Nutrient loading scenarios. 10-42

Figure 10-31. Wastewater treatment facility (WWTF) expansion scenarios. 10-43
Figure 10-32. Summary of Climate Projections for the New River Estuary. 10-44
Figure 10-33. Simulated New River Estuary (NRE) response to climate warming. 10-45
Figure 10-34. Interactive effects of nutrient loading and climate warming on water quality. 10-46
Figure 10-35. Effects of nutrient loading and climate warming on carbon cycling. 10-47
Figure 10-36. Simulated response of phytoplankton functional groups to changes in temperature, nutrient loading, and discharge. 10-48
Figure 10-37. Simulated response of watershed inputs to climate change. 10-50
Figure 10-38. Simulated response of watershed inputs to land-use change. 10-51
Figure 10-39. Flushing times of the Neuse River Estuary. 10-52
Figure 10-40. Final calibration of the Neuse River Estuarine Simulation Model. 10-53
Figure 10-41. Final calibration of the Neuse River Estuarine Simulation Model. 10-54
Figure 10-42. Modeled total suspended solids (TSS) in Slocum Creek, Neuse River, NC. .. 10-56
Figure 10-43. Impact of watershed loading on dissolved inorganic nitrogen (DIN) in Slocum Creek. 10-57
Figure 10-44. Impact of watershed loading on chlorophyll-a (Chl-a) in Slocum Creek. 10-58
Figure 10-45. Impact of the Marine Corps Air Station (MCAS) Cherry Point wastewater treatment facility (WWTF) on Neuse River water quality. 10-59
Figure 10-46. Combined loading and climate warming scenarios in the Neuse River Estuary. 10-60
Figure 10-47. Example interpolations of Choctawhatchee Basin Alliance (CBA) vertical profiling surveys. 10-61
Figure 10-48. Flushing times of Choctawhatchee Bay. 10-62
Figure 10-49. Final calibration of the Choctawhatchee Bay Estuarine Simulation Model. ... 10-63
Figure 10-50. Final calibration of the Choctawhatchee Bay Estuarine Simulation Model. ... 10-64
Figure 10-51. Effects of atmospheric and Gulf of Mexico loads in Choctawhatchee Bay. ... 10-66
Figure 10-52. Effects of total organic carbon (TOC) loads to Choctawhatchee Bay. 10-66
Figure 10-53. Choctawhatchee Bay nutrient-reduction scenarios. 10-67
Figure 10-54. Coupled nutrient-climate scenarios in Choctawhatchee Bay. 10-68
Figure 10-55. A screen capture of the currently available versions of the online New River Estuarine Simulation Model. 10-71
Figure 10-56. A screen capture of the currently available versions of the online Neuse River Estuarine Simulation Model. 10-72

Figure 10-57. A screen capture of the currently available versions of the online Choctawhatchee Bay Estuarine Simulation Model..... 10-72

Figure 10-58. The Home page of the online New River Estuarine Simulation Model (ESM)..... 10-74

Figure 10-59. The Scenario Analysis page of the online New River Estuary Estuarine Simulation Model (ESM)..... 10-75

Figure 10-60. An example Model Output page of the online New River Estuary Estuarine Simulation Model (ESM)..... 10-76

Figure 10-61. The custom page for total suspended solids (TSS) stormwater loading in the online Neuse River Estuarine Simulation Model (ESM)..... 10-77

Figure 10-62. The downloadable user's guide for the New River Estuary Estuarine Simulation Model (ESM)..... 10-78

Figure 10-63. Coastal systems in which the Estuarine Simulation Model is currently applied..... 10-80

List of Tables

Table 10-1. Forcing Functions and State Variables of the DCERP Estuarine Simulation Model (ESM)..... 10-6

Table 10-2. Range of Parameter Values Found in the Literature for Each Phytoplankton Functional Group..... 10-11

Table 10-3. Initial and Final (Calibrated) Parameter Values for the Phytoplankton Functional Group Model..... 10-12

Table 10-4. Functional Group Model Skill Assessment 10-31

Table 10-5. Additional Assessment of Functional Group Model Output 10-32

Table 10-6. Skill Assessment for Modeled Streamflow Using the ReNuMa model 10-40

Table 10-7. Skill Assessment for Modeled TDN Loading Using the ReNuMa Model 10-40

Table 10-9. Skill Assessment of the Neuse River Estuarine Simulation Model..... 10-55

Table 10-10. Skill Assessment of the Choctawhatchee Bay Estuarine Simulation Model... 10-64

Table 10-11. Characteristics of the Three Research Project TSP-2 Study Systems 10-70

Acronyms

% error	percent mean and median error
°C	degree Celsius
µatm	microatmosphere
µg l^{-1}	micrograms per liter
µmol N l^{-1}	micromoles of nitrogen per liter
µmol P l^{-1}	micromoles of phosphorus per liter
ABS Error	absolute error
ADCIRC	Advanced Circulation (hydrodynamic) model
AE	Aquatic/Estuarine (Module)
AFB	Air Force Base
AG (subscript)	above-ground biomass (shoots)
AT (subscript)	atmospheric-derived
B	bottom layer
BG (subscript)	below-ground biomass (roots/rhizomes)
BMA	benthic microalgae
C	carbon
CBA	Choctawhatchee Basin Alliance
CC	Climate Change (Module)
CDOM	chromophoric dissolved organic matter
chl *a*, Chl-*a*	chlorophyll *a*
cm mo^{-1}	centimeters per month
CO_2	carbon dioxide
C_{SED}	sediment carbon pool
CV	coefficient of variation
C_{WC}	water column carbon pool
Cyano	cyanobacteria
d^{-1}	per day
DCERP	Defense Coastal/Estuarine Research Program
DCERP1	first cycle of DCERP
DCERP2	second cycle of DCERP
DEM	Digital Elevation Model
DIC	dissolved inorganic carbon
DIN	dissolved inorganic nitrogen
Dino	dinoflagellates
DIP	dissolved inorganic phosphorus
DNF	denitrification
DO	dissolved oxygen
DoD	U.S. Department of Defense
ESM	Estuarine Simulation Model
g C m^{-2}, gC m^{-2}	grams of carbon per square meter
g C m^{-2} d^{-1}	grams of carbon per square meter per day
g C m^{-2} yr^{-1}	grams of carbon per square meter per year
g dw m^{-2}	grams dry weight per square meter
gC g^{-1} chl-*a* d^{-1}	grams of carbon per gram of chlorophyll *a* per day

GIS	geographic information systems
GPP	gross primary production
k_D	vertical attenuation coefficient for light
kg mo^{-1}	kilograms per month
m d^{-1}	meters per day
m, m^{-1}	meter, per meter
M.S.	Master of Science (degree)
m^3 d^{-1}	cubic meters per day
MCAS	Marine Corps Air Station
MCBCL	Marine Corps Base Camp Lejeune
mg/L, mg l^{-1}, mg L^{-1}	milligrams per liter
mg m^{-3}	milligrams per cubic meter
mm	millimeter
mmol m^{-2} d^{-1}	millimoles per square meter per day
mmol m^{-3}	millimoles per cubic meter
mmol m^{-3} d^{-1}	millimoles per cubic meter per day
ModMon	Neuse River Estuary Modeling and Monitoring Program
mol mol^{-1}	mole per mole
N	nitrogen
N/A	not applicable
NC DENR	North Carolina Department of Environment and Natural Resources
NEM	net ecosystem metabolism
NLCD	National Land Cover Database
NOAA	National Oceanic and Atmospheric Administration
NPP	net primary production
NTU	Nephelometric Turbidity Unit
NRE	New River Estuary
O_2	dissolved oxygen (in water)
OMF	overall model fit
P	phosphorus
PAR	photosynthetically active radiation
pCO_2	partial pressure of carbon dioxide in water
PHYTO	phytoplankton
PPT	precipitation
Raphido	raphidophytes
R	respiration
RC	Resource Conservation and Climate Change (a SERDP program area)
ReNuMa	Regional Nutrient Management (model)
RMS Error	root mean squared error
S	salinity
SAV	submerged aquatic vegetation
SED (subscript)	sediment
SERDP	Strategic Environmental Research and Development Program
SSURGO	National Resources Conservation Service Soil Survey Geographic (Database)
T_a	air temperature

T, TEMP	temperature (water)
TDN	total dissolved nitrogen
TDP	total dissolved phosphorus
TOC	total organic carbon
TP	total phosphorus
TSP	Translating Science into Practice (Module)
TSS	total suspended solids
T_w	water temperature
USGS	U.S. Geological Survey
USLE	Universal Soil Loss Equation
VIMS	Virginia Institute of Marine Science
WC (subscript)	water column
WIND	daily mean wind speed
WS (subscript)	watershed-derived
WWTF	wastewater treatment facility

Abstract

Objectives: Research Project TSP-2 synthesized DCERP data into an Estuarine Simulation Model (ESM) for analysis of New River Estuary (NRE) water quality and the ecosystem carbon budget and for predicting NRE response to changes in nutrient loading and climate. The project demonstrated the wider applicability of the ESM through application in two new estuaries and provided online, decision-support versions of each ESM for translating scientific information into practice.

Technical Approach: The DCERP1 ESM was extended through 2015 and sub-models were added for the inorganic carbon system and two new seagrass species. The model was re-calibrated to pre-DCERP (1998–2007) and DCERP1 data (2008–2012), and independently validated by using DCERP2 data (2013–2015). A phytoplankton functional group model was developed to simulate the dynamics of diatoms, dinoflagellates, cyanobacteria, and raphidophytes and was validated against DCERP1 data. The DCERP1 Regional Nutrient Management (ReNuMa) model was extended through 2015, re-calibrated against DCERP1 data (2008–2012), and validated against DCERP2 data (2013–2015). Climate scenarios from Research Project CC-1 were run through the ReNuMa model and the ESM together with nutrient loading scenarios to predict changes in water quality and the system carbon budget. The ESM was also applied to the Neuse River, NC, and Choctawhatchee Bay, FL, to demonstrate its wider applicability.

Results: The ESM reproduced observed NRE water quality, the inorganic carbon system, and major features of the carbon budget. The phytoplankton functional group model reproduced chlorophyll *a*, productivity, and group dynamics. The ReNuMa model reproduced discharge and nutrient loading from the upper watershed and most smaller watersheds monitored during DCERP. Simulated warming tended to reduce watershed inputs, while changes in precipitation were positively correlated to inputs; however, changes in land use have the potential to overwhelm the effects of climate on watershed loading. ESM scenarios highlighted the interactive effects of nutrient loading and climate. Although warming was predicted to reduce chlorophyll concentrations, this effect could be offset by increases in freshwater discharge in the absence of nutrient load reductions. Although hypoxia responded to load reductions, greater reductions will be required in a warmer climate to achieve the same improvement achievable under current conditions. Climate warming shifted the phytoplankton community towards cyanobacteria, and increased freshwater discharge and nutrient loading favored diatoms, dinoflagellates, and raphidophytes. Both nutrient reductions and climatic warming drove the NRE to greater heterotrophy, reducing carbon storage and increasing carbon dioxide fluxes into the atmosphere. Scenarios highlight a trade-off in managing for nutrient loading versus carbon storage; reductions in nutrient loading to mitigate eutrophication will also reduce the potential for carbon storage. The ESM successfully reproduced observed water quality in the Neuse River and Choctawhatchee Bay.

Benefits: Model scenarios can be used to set nutrient reduction targets for the NRE both now and under future climatic conditions and to compute carbon dynamics resulting from these scenarios. The ESM is a widely applicable tool for supporting management on installations with

adjacent estuarine systems. The online models developed for DCERP provide user-friendly decision-support tools directly usable by DoD installations and local coastal managers.

Keywords: Benthic microalgae, carbon, carbon dioxide, climate change, decision-support tool, dissolved inorganic carbon, estuary, land use, net ecosystem metabolism, nitrogen, nutrients, oxygen, phytoplankton, phytoplankton, simulation model, water quality, watershed

Objectives of the Research Project

Research Project TSP-2 synthesized DCERP data into an ecosystem modeling platform for analysis of New River Estuary (NRE) water quality and the ecosystem carbon budget and for predicting NRE response to changes in nutrient loading and climate. The project also demonstrated the wider applicability of the Estuarine Simulation Model (ESM) through application in two new estuaries and provided an online, decision-support tool in each system for translating scientific information into actionable information for water quality managers. Specific objectives of Research Project TSP-2 were to

1. Expand the utility of the DCERP1 ESM by extending the model through 2015, adding new ecosystem state variables, and refining the DCERP1 Regional Nutrient Management (ReNuMa) model

2. Simulate the NRE carbon budget for comparison to the empirical carbon budget

3. Simulate NRE response to changes in nutrient loading and climate, particularly with respect to water quality, carbon cycling, the role of the estuary as a carbon source or sink, and ecosystem services

4. Quantify potential tradeoffs between management to increase carbon storage and reduce nutrient-fueled eutrophication

5. Demonstrate the broad applicability of the ESM by applying the model to the Neuse River, NC (Marine Corps Air Station [MCAS] Cherry Point) and Choctawhatchee Bay, FL (Eglin Air Force Base [AFB])

6. Develop and deliver readily transferable, online decision-support versions of the New River, Neuse River, and Choctawhatchee Bay ESMs to facilitate water quality management.

Background

Dynamic simulation models have a long history as heuristic and synthetic research tools in the study of coastal marine ecosystems (Brush and Harris, 2016; Canham et al., 2003; Kremer and Nixon, 1978; Riley et al., 1949; Steele, 1974). These models have been increasingly applied to guide management, particularly related to the effects of nutrient loading on cultural eutrophication (Giblin and Vallino, 2003; Harris et al., 2003; NRC, 2000; U.S. EPA, 1999). In the United States, large investments over many years have been made in the development of high-resolution, biogeochemically complex ecosystem models of major estuarine and coastal systems, including the Chesapeake Bay (Cerco and Noel, 2004), the Long Island Sound (HydroQual, 1991), and the Massachusetts Bay/Boston Harbor (Chen et al., 2010; Jiang and Zhou, 2008).

Although these models typically focus on biogeochemical cycling of carbon and nutrients and the effects of changing nutrient loads on estuarine water quality, using models to predict coastal ecosystem response to climate change is just beginning (Brito et al., 2012; Carr et al., 2012;

Justić et al., 2005; Lake and Brush, 2015a; Neumann, 2010). Many estuaries are currently undergoing a "natural experiment" in which nutrient loads are being reduced concurrent with climate change (Nixon, 2009). In other cases, estuarine dynamics are changing primarily due to climatic influences without concurrent changes in nutrient loads (Nixon et al., 2009). As climate continues to change, with increases or decreases in nutrient loading, predictive tools are required for determining the synergistic effects of these changes on estuarine water quality, ecosystem function, and the ability of estuaries to process, sequester, and remove carbon and nutrients.

With the increasing demand for models to inform management decisions across a wide range of estuarine and coastal systems (e.g., total maximum daily loads for all impaired waterbodies in the United States; U.S. EPA, 1999), managers need readily applied, generally transferable modeling tools that can be applied quickly to a variety of systems with limited resources. During the past two decades, a growing body of research has been conducted that examined the role of complexity and spatial resolution in models (Baird et al., 2003; Denman et al., 2003; Friedrichs et al., 2006; Fulton et al., 2003 and 2004; Ménesguen et al., 2007; Raick et al., 2006). In addition, multiple calls have been made for the development of simpler, "reduced complexity" models for use in management (Duarte et al., 2003; NRC, 2000; Pace, 2001; Rigler and Peters, 1995). Such reduced complexity modeling tools have the potential for rapid application in the myriad of smaller coastal systems around the nation, including those adjacent to U.S. Department of Defense (DoD) installations, which do not often have the resources to support long-term development of more complex models. Simpler models can also be characterized by fast run times, enabling the efficient use of the models directly by stakeholders, either on desktop computers or over the Internet.

During DCERP1, we developed a reduced complexity ESM to understand New River Estuary (NRE) structure and function, and predict NRE response to natural and anthropogenic stressors, primarily nutrient loading (Brush, 2013). The ESM was calibrated to Marine Corps Base Camp Lejeune (MCBCL) monitoring data (1998–2007) and DCERP1 monitoring and research data (2007–2010). The model was primarily used to determine (1) the characteristics of the NRE ecosystem that control its response to anthropogenic nutrient loading and (2) NRE response to these loads under inter-annual hydrologic variability in terms of water quality and ecosystem function (Brush, 2013). The modeling work in Research Project TSP-2 as part of DCERP2 expanded the ESM to include additional components and management endpoints (e.g., two new seagrass species, phytoplankton functional groups, the dissolved inorganic carbon [DIC]-carbon dioxide [CO_2] system), and expanded the focus of model simulations to carbon cycling and response to climate change. Additionally, the wider applicability of the model was demonstrated through application of the ESM in two new coastal systems adjacent to DoD installations (MCAS Cherry Point and Eglin AFB), and all three models were delivered online as decision-support tools.

Materials and Methods

Estuarine Simulation Model

The ESM (**Figure 10-1**) is a mechanistic, process-based model that was initially applied to the period 1998–2010. The DCERP1 ESM simulated daily concentrations of phytoplankton (PHYTO) and benthic microalgal (BMA) biomass (in units of chlorophyll *a* [chl *a*], carbon [C],

nitrogen [N], and phosphorus [P]); biomass of eelgrass (*Zostera marina*; as C, N, and P); and concentrations of dissolved inorganic nitrogen (DIN), dissolved inorganic phosphorus (DIP), dissolved oxygen (DO), and the water column and sediment pools of labile organic carbon (C_{WC} and C_{SED}, respectively) and their associated N and P. The ESM aggregates key state variables and formulates selected rate processes using robust, cross-system empirical linkages to avoid use of multiple loosely constrained parameters and enable direct comparison of model predictions to observations (Brush and Nixon, 2017). The ESM is in line with recent calls for models of reduced complexity for use in management (Duarte et al., 2003; NRC, 2000).

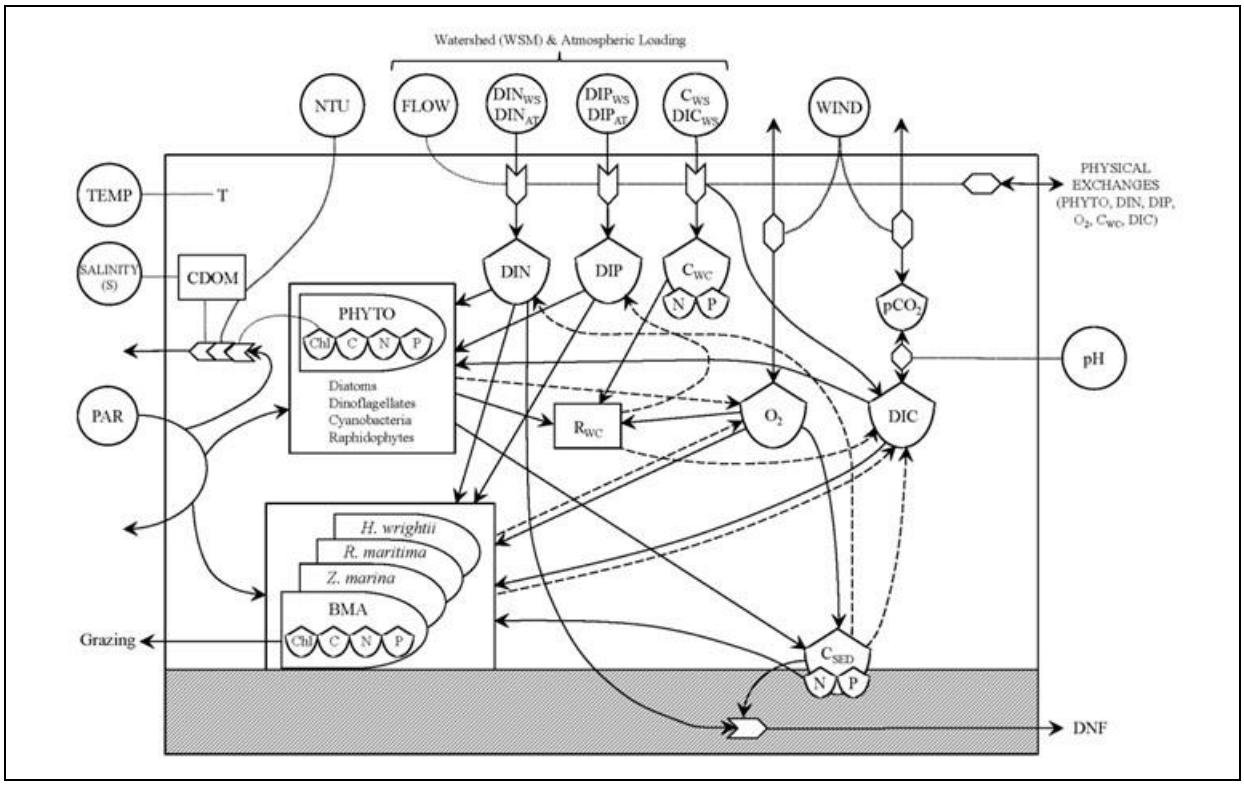

Figure 10-1. A schematic of the DCERP Estuarine Simulation Model (ESM).

Terms are defined in the list of acronyms, the text, and in **Table 10-1**. Symbols are those of Odum (1994). Flows that consume material are shown with solid arrows; flows that produce material are shown with broken arrows. **Figure 10-1** shows the final version of the model from DCERP2; note that the phytoplankton functional groups are not included in the primary ESM, but were implemented in a separate, stand-alone version of the model.

The ESM is forced with measured water temperature, salinity, and turbidity, meteorological time series, atmospheric nitrogen deposition, and watershed loads of freshwater and nutrients (**Table 10-1**). The model runs in a series of coarse spatial elements, each with surface and bottom layers (**Figures 10-2 and 10-3**). Exchanges among spatial elements are computed from forced freshwater inputs and salinity distributions using an Officer (1980) box model approach with partitioning between advective and non-advective exchanges based on Officer and Kester (1991). Although boxed schemes lose spatial resolution, they capture the major down-estuary and surface-to-bottom gradients in water quality, facilitate rapid implementation in new study systems, and make multiple fast runs (seconds to minutes) possible during model testing and

subsequent use as decision-support tools. Recent work has confirmed the utility of boxed approaches (Brush and Nixon, 2017; Kremer et al., 2010; Lake and Brush, 2015b; Ménesguen et al., 2007; Testa and Kemp, 2008).

Table 10-1. Forcing Functions and State Variables of the DCERP Estuarine Simulation Model (ESM)

Components in red font were added for DCERP2.

Forcing Functions		
Temperature (air, water)	Photosynthetically active radiation (PAR)	
Salinity[a]	Watershed loading (water, DIN, DIP, DIC, total organic carbon [TOC])	
Turbidity	Wastewater treatment facility [WWTF] loading (water, TN, total phosphorus [TP], TOC)	
Precipitation	Atmospheric N deposition (wet and dry)	
Relative humidity	Onslow Bay chl *a*, DIN, DIP, dissolved oxygen in water [O_2], DIC, TOC	
Wind speed	pH	
State Variables		
Phytoplankton (PHYTO)[b]	Benthic microalgae (BMA)[b]	DIC
Eelgrass growth index	DIN	pCO_2
Widgeon grass growth index	DIP	Water column TOC (C_{WC})[c]
Shoal grass growth index	O_2	Sediment TOC (C_{SED})[c]

[a] Forced salinity is used to compute chromophoric dissolved organic matter through a linear regression.

[b] Computed in carbon (C) units; nitrogen (N), phosphorus (P), and chlorophyll *a* (chl *a*) are computed stoichiometrically. An independent, multi-group phytoplankton sub-model was also implemented which divided this state variable into four functional groups: diatoms, dinoflagellates, cyanobacteria, and raphidophytes.

[c] These pools include associated N and P computed stoichiometrically.

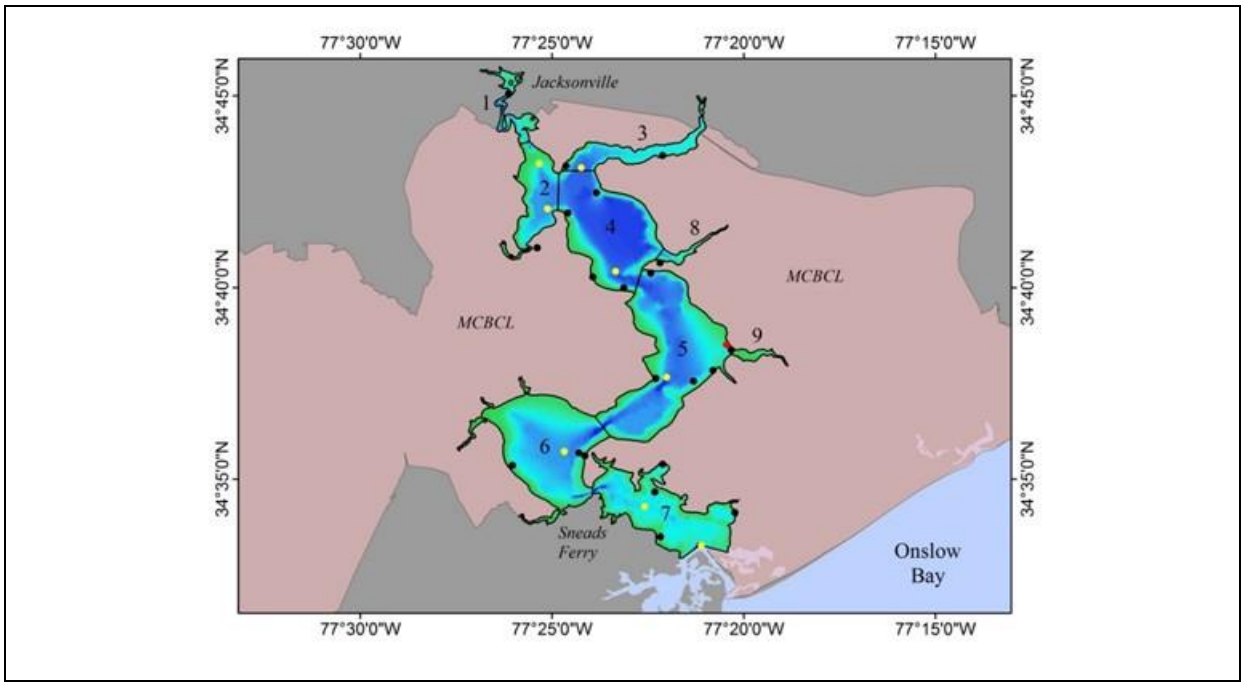

Figure 10-2. Domain of the New River Estuary (NRE) Estuarine Simulation Model (ESM).

Spatial elements of the NRE ESM, along with the primary DCERP stations (yellow circles = water column; black circles = benthic) used for model forcing and calibration. Boxes 1–7 have a surface layer and a bottom layer. Shading indicates bathymetry with darker blue indicating deeper water. The red circle shows the location of the Marine Corps Base Camp Lejeune (MCBCL) wastewater treatment facility outfall.

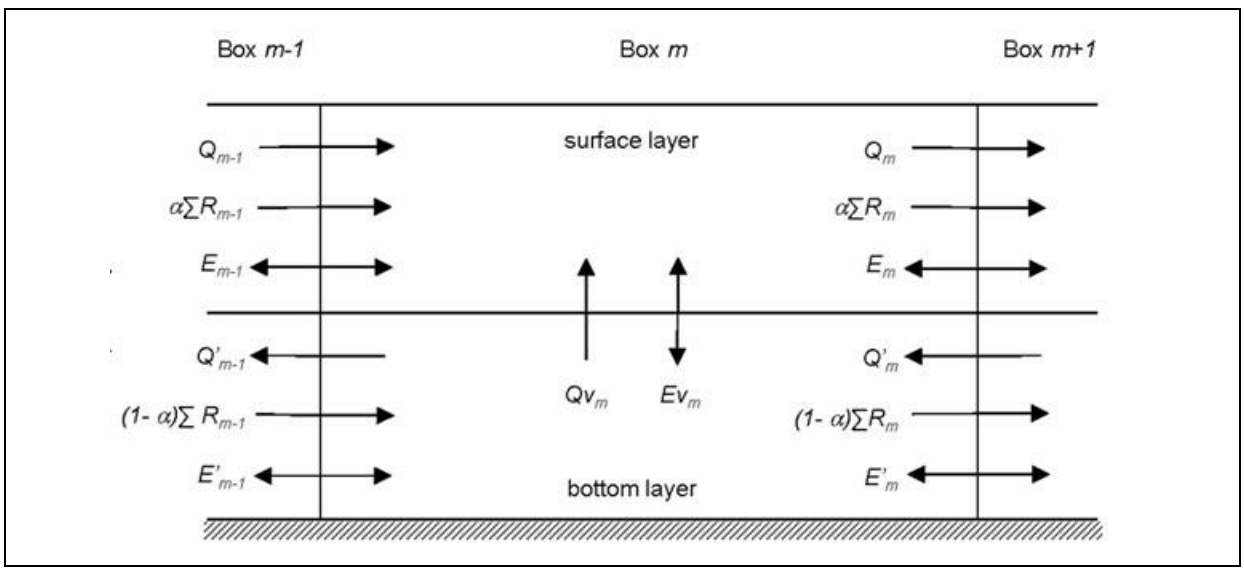

Figure 10-3. Vertical structure and simulated exchanges in the New River Estuary (NRE) Estuarine Simulation Model (ESM).

The model computes exchanges across all box faces including advective (i.e., gravitational circulation) flows *Q* and *Qv*, and non-advective (i.e., tidal) flows *E* and *Ev*, as well as down-estuary flows of cumulative freshwater inputs (ΣR), divided among the surface and bottom layers using the parameter α. Subscript (*m*) denotes box number; superscript (’) denotes the bottom layer.

ESM Expansion and Calibration/Validation

The ESM was first expanded with additional components to increase its utility for addressing the foci of DCERP2 research on carbon and climate change, and its ultimate use as a decision-support tool for MCBCL (**Figure 10-1 and Table 10-1**). To simulate the inorganic carbon system, a state variable was added for DIC with inputs from the watershed and Onslow Bay, and consumption and production due to modeled photosynthesis and respiration, respectively. pH was added as a forcing function based on DCERP monitoring data, and the equations of Pilson (1998) were used to compute the partial pressure of carbon dioxide in water (pCO_2) from modeled DIC and forced pH. Air–sea exchange of CO_2 was added using the equations of Crosswell et al. (2017). The DCERP1 model already had a state variable for water column total organic carbon (TOC), and inputs from the watershed and Onslow Bay were added based on DCERP2 measurements; watershed inputs were modified by observed lability from Research Project AE-6.

The lower NRE supports growth of three seagrass species, eelgrass (*Zostera marina*), widgeon grass (*Ruppia maritima*), and shoal grass (*Halodule wrightii*). Eelgrass was included in the DCERP1 model; the other two species were added during DCERP2 to simulate the entire community, using the models of Burd and Dunton (2001) and Cerco and Moore (2001). Because biomass and areal coverage data are lacking for the NRE, formulations were used not to predict annual biomass cycles, but rather to compute the net growth rate (photosynthetic growth less respiration, mortality, and translocation) as an index of potential survival.

The ESM was updated with DCERP2 monitoring data to run through 2015, and meteorological forcing was replaced with historical reconstructions for the entire simulation period (1998–2015) provided by Research Project CC-1. The full model simulation period encompasses an approximately 5.5-fold range in discharge conditions (**Figure 10-4**), with a mean and range nearly identical to those for the entire record of the gauge since it was installed in 1949 (mean = 281; min = 117; max = 561 x 10^3 m^3 d^{-1}; no data 1973–1987). The ESM is thus applicable across the full range of discharge conditions experienced in the NRE. To translate DCERP2 climate projections from Research Project CC-1 into ESM scenarios, regressions were developed between air and water temperatures, and New River discharge and NRE salinity using DCERP monitoring data and discharge from the U.S. Geological Survey (USGS) stream gaging station at Gum Branch, NC. The model was re-calibrated to both the pre-DCERP (1998–October 2007) and DCERP1 (November 2007–2012) periods and was independently validated with DCERP2 data (2013–2015). Model skill was assessed by computing absolute, percent, and root mean squared error for several state variables in each spatial element. A simulated carbon budget was developed from the model output for each year of the simulation, as well as for the periods of July 16, 2013–July 15, 2014 and July 16, 2014–July 15, 2015, which correspond with Years 1 and 2, respectively, of the empirical carbon budget developed in Research Projects AE-4 and AE-6.

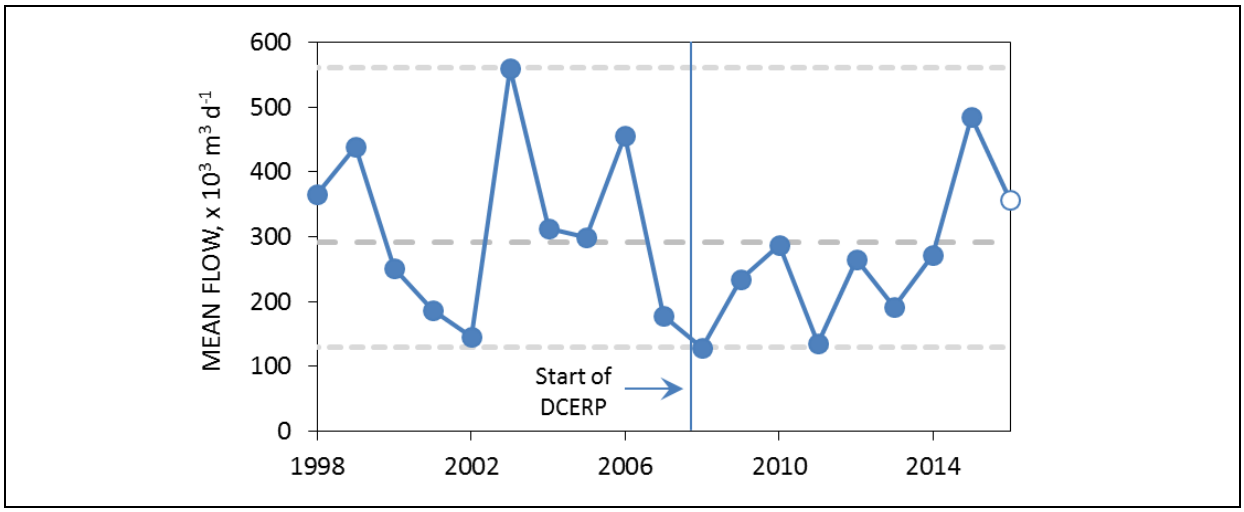

Figure 10-4. New River discharge at Gum Branch during the Estuarine Simulation Model (ESM) simulation period.

Mean daily discharge of the New River at Gum Branch (U.S. Geological Survey stream gaging station 02093000) for each year during the ESM simulation period. Middle dashed line is the mean during this period; lower and upper lines denote the minimum and maximum, respectively. Although DCERP2 monitoring data were collected during 2016 (open circle), the ESM does not currently run for that year.

ESM Scenarios

Following calibration and validation, the ESM was used to conduct a series of scenarios to predict NRE response to changes in nutrient loading and climate. First, the DCERP1 scenario in which nutrient loads were removed separately from the (1) MCBCL watershed, (2) MCBCL wastewater treatment facility (WWTF), and (3) off-Base watershed, was updated to span the entire period of the ESM. This scenario enables identification of the nutrient sources most important in driving water quality in the NRE, the potential for improvements with load reductions, and the influence of inter-annual hydrologic variability. Second, a series of runs were made in which discharge and associated loads from the MCBCL WWTF were increased to simulate potential future expansion of the facility to accommodate additional troops or tie-in a portion of the off-Base population.

Next, scenarios were run to quantify the potential impacts of projected changes in climate on NRE water quality, net ecosystem metabolism (NEM), and the system carbon budget. Output from Research Project CC-1 was synthesized to compute average, minimum, and maximum predicted changes in temperature and annual precipitation across all climate models for the periods 2030–2040, 2055–2065, and 2089–2099. Scenarios were first run with increasing temperature alone, followed by combined scenarios with increasing temperature and projected changes in precipitation. Climate scenarios were then run in combination with changes in nutrient loads to examine their interactive effects on NRE response. Finally, load reduction scenarios were used to quantify potential trade-offs in managing to reduce nutrient-fueled eutrophication versus managing to enhance carbon storage.

Phytoplankton Functional Group Model

The DCERP ESM computes phytoplankton biomass as a single, aggregated state variable, but changes in nutrient loading and climate have the potential to differentially affect various phytoplankton functional groups. An independent, stand-alone version of the ESM was therefore developed that replaced the aggregated phytoplankton state variable with sub-models of the major functional groups present in the NRE. The NRE assemblage is comprised of a variety of species, but blooms are dominated by four primary groups: diatoms, cyanobacteria, dinoflagellates, and raphidophytes (Hall et al., 2013); these groups were therefore included in the functional group model. Well-established formulations of phytoplankton growth and loss were combined to create a mathematical process-based simulation model of the NRE phytoplankton community, represented by four separate state variables for each of the primary groups (**Figure 10-5**). The model captures daily fluctuations in diatom, dinoflagellate, cyanobacteria, and raphidophyte biomass in g C m^{-2} and was formulated after the mechanistic primary production model used in the Chesapeake Bay Program water quality model (Cerco and Noel, 2004 and 2013; Cerco et al., 2010). Formulations are described in full by Blachman (2016).

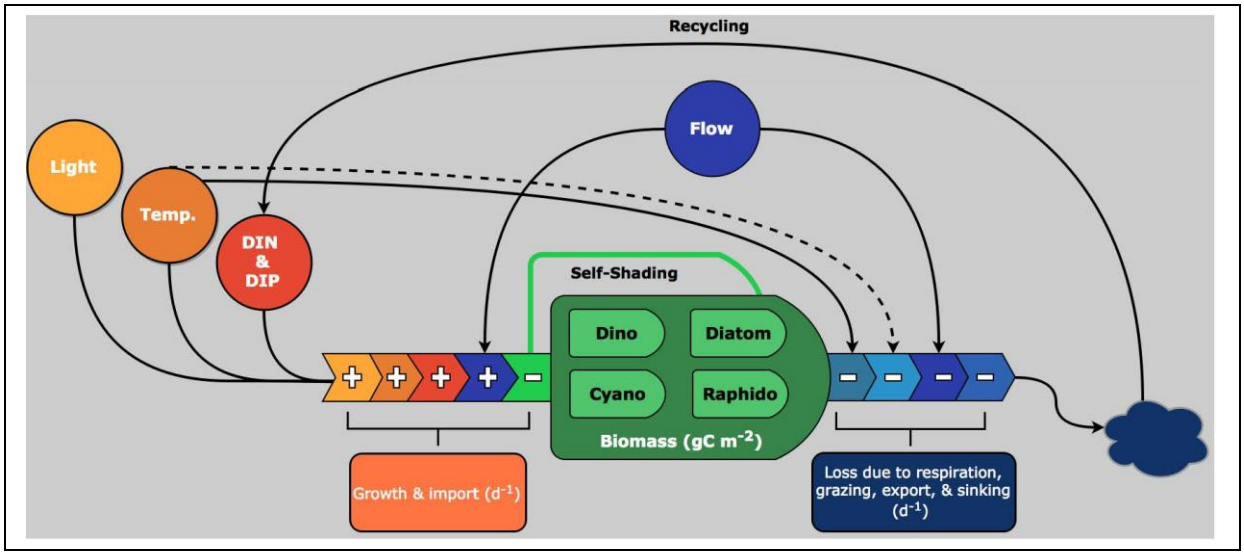

Figure 10-5. Schematic of the multi-group phytoplankton model.

Growth is a function of light, temperature (temp.), and nutrients. Self-shading occurs through absorption of light by chlorophyll *a*. Losses include respiration and grazing (temperature-dependent), sinking, and mixing. Note: Cyano = cyanobacteria; Dino = dinoflagellates; Raphido = raphidophytes.

Model parameters were initially determined based on a literature synthesis of growth and loss rates of estuarine phytoplankton species, focusing on species that are endemic to the NRE and the surrounding region (**Table 10-2**). An initial review of the literature was conducted to find well-established taxonomic group differences in growth and loss rates that could be used to constrain the parameters. Then species and genus specific parameters for algae known to bloom in the NRE were collected. The review included data from other multi-group phytoplankton models and multiple meta-analyses. In both cases, the parameter values collected were group specific, rather than species specific. Data on the species composition of the diatoms and dinoflagellates that are abundant in the system were collected during DCERP1 by Paerl et al. (2013a). However, the species composition of cyanobacteria and raphidophytes in the NRE are

unreported. The cyanobacteria in the nearby shallow Neuse River Estuary are not typical freshwater species, but instead are predominantly marine picoplankton similar to *Synechococcus* species (Paerl et al., 2010). The parameters for the cyanobacteria group are focused on rates and values reported for that genus. Parameter values for the raphidophyte sub-model primarily come from literature about the species *Heterosigma akashiwo*, a species identified as contributing to raphidophyte blooms in the NRE (N. Hall, personal communication). The parameter values from meta-analyses of other flagellate groups were also included in the raphidophyte review to associate the less abundant NRE phytoplankton groups, such as chlorophytes, cryptophytes, chrysophytes, and euglenophytes, with one of the modeled groups.

Table 10-2. Range of Parameter Values Found in the Literature for Each Phytoplankton Functional Group

Model Parameters		Diatom	Dinoflagellate	Cyanobacteria	Raphidophyte
P_{MAX}	(gC g^{-1}chl-a d^{-1})	40 - 300	25 - 450	41 - 200	23 - 114
C:CHL	(gC g^{-1}chl-a)	17 - 107	27 - 80	30 - 176	19 - 67
α	(gC g^{-1}chl-a (E m^{-2})$^{-1}$)	3 - 16	3 - 10	3 - 12	3 - 6
T_{opt}	(°C)	16 - 25	20 - 30	28 - 34	20 - 30
K_N	(µmol N l^{-1})	0.6 - 2.3	1.4 - 8.8	0.1 - 1.0	0.3 - 2.6
K_P	(µmol P l^{-1})	0.1 - 1.1	0.1 - 3.1	0.1 - 1.0	1.0 - 2.0
BM	(d^{-1})	0.01 - 0.2	0.01 - 0.05	0.01 - 0.06	0.05 - 0.1
W	(m d^{-1})	0.2 - 1.0	0.2 - 0.5	0 - 0.1	0.2
V_{MAX}	(µmol g^{-1} dry weight hr^{-1})	700 - 1200	100 - 400	400	400 - 550

See Blachman (2016) for full details of the literature synthesis and parameter definitions.

The four phytoplankton sub-models were integrated into an independent version of the ESM, replacing the aggregated phytoplankton state variable (PHYTO) and its associated formulations, and were connected to the other components of the ESM as appropriate (i.e., calculation of light attenuation, nutrient uptake and recycling, dissolved oxygen production and consumption, and sinking to the sediment carbon pool). Model output for total chl *a* and biomass of each functional group were calibrated to DCERP1 monitoring data collected by Paerl et al. (2013a). Final parameter values (**Table 10-3**) were determined during model calibration by adjusting parameters within the reported ranges to obtain the best possible fit to the observations, while retaining appropriate differences among phytoplankton groups.

Table 10-3. Initial and Final (Calibrated) Parameter Values for the Phytoplankton Functional Group Model

		Diatom		Dinoflagellate		Cyanobacteria		Raphidophyte	
		Initial	Final	Initial	Final	Initial	Final	Initial	Final
P_{MAX}	(gC g^{-1}chl-a d^{-1})	96	192	83	195	120	154	38	99
C:CHL	(gC g^{-1}chl-a)	40	40	55	50	75	70	38	38
α	(gC g^{-1}chl-a (E m^{-2})$^{-1}$)	10	11	7	9	9	10	4	5
K_{T1}	(°C^{-2})	0.005	0.005	0.006	0.006	0.003	0.003	0.01	0.01
K_{T2}	(°C^{-2})	0.02	0.02	0.012	0.012	0.005	0.005	0.004	0.004
T_{opt}	(°C)	22	22	24	25	30	30	27	27
K_N	(µmol N l^{-1})	1.6	1.6	5.3	2.8	1	1	1.8	1.8
K_P	(µmol P l^{-1})	0.7	0.8	1.6	1.4	0.6	0.6	1.5	1.2
BM	(d^{-1})	0.06	0.1	0.05	0.05	0.05	0.05	0.05	0.1
PR	(m^2 g^{-1}C d^{-1})		0.4		0.2		0.3		0.1
W	(m d^{-1})	0.5	0.25	0.2	0.1	0.1	0.1	0.2	0.15
V_{MAX}	(µmol g^{-1} dry weight hr^{-1})	700	700	300	400	400	400	400	400

Statistical metrics including mean and median absolute error, mean and median percent error, and root mean squared error were computed to compare observed and modeled chl *a*. To determine whether the model was accurately capturing seasonality, the volume-weighted, estuary-wide average annual cycles of modeled chl *a* and phytoplankton production were visually compared to the volume-weighted, estuary-wide annual cycles of chl *a* and ^{14}C productivity calculated from DCERP1 data (Paerl et al., 2013a) using linear interpolation. Daily ^{14}C production rates were obtained from 4-hour, mid-day incubations; this method provides an estimate somewhere between gross primary production (GPP) and net primary production (NPP), depending on incubation length. Values were scaled to daily rates assuming that 32% of primary production occurred during the incubation period, based on photosynthesis–irradiance curves developed during DCERP1 (Brush, unpublished data).

Qualitative comparisons were made between contour plots of model output of individual group chl *a* biomass and observed diagnostic accessory photopigment concentrations corresponding with specific phytoplankton groups, collected during DCERP1 by Paerl et al. (2013a) (**Figure 10-6**). Phytoplankton classes were categorized by accessory photopigments as outlined in Paerl et al. (2013a) and in additional examinations of the NRE phytoplankton assemblage (Altman and Paerl, 2012; Hall et al., 2013). The pigment peridinin was used for comparison to modeled dinoflagellate biomass, the pigment zeaxanthin was used for comparison to modeled cyanobacteria biomass, and the pigment fucoxanthin was used for comparisons to modeled diatom and raphidophyte biomass (Hall et al., 2013; Paerl et al., 2003 and 2013a). There is ambiguity in these comparisons, preventing the use of quantitative metrics, because accessory photopigments are not specific to certain species within phytoplankton functional groups, but are shared across multiple taxonomic classifications. Additionally, there is no evidence that the pigment-to-chlorophyll or pigment-to-carbon ratios are constant. However, there is precedence for their use as diagnostic tools to monitor phytoplankton communities in shallow coastal plain systems and as biomarkers to interpret seasonal and environmental patterns in assemblages (Paerl et al., 2007 and 2010; Pinckney et al., 2001).

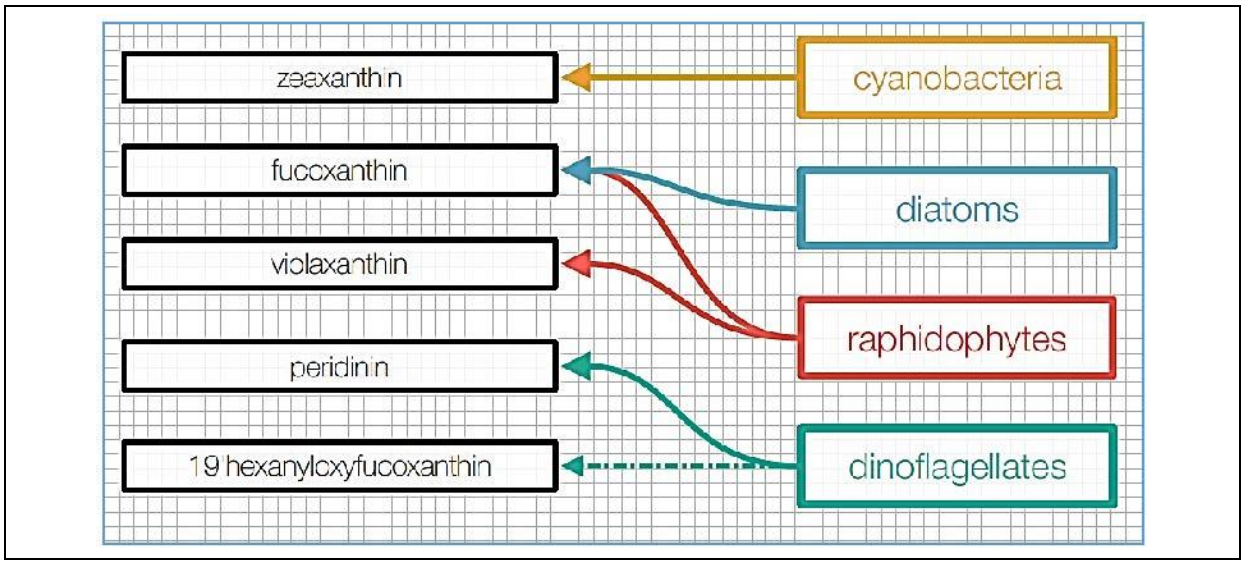

Figure 10-6. Associations between accessory photopigments and New River Estuary (NRE) phytoplankton.

Linkages between primary accessory photopigments and the phytoplankton groups most commonly found in the NRE as reported in Paerl et al. (2013a).

The final component of model validation used the limited cell count data collected when bloom events (chl *a* greater than 40 mg m^{-3}) were identified during DCERP1 (N. Hall, unpublished data). There are 20 dates and locations for which these data were available. These data were supplemented with cell counts collected periodically at two stations in the upper and mid-estuary by the North Carolina Division of Water Resources. The cell counts had been converted to biovolume by the phycologists who collected the data. Biovolume estimates were then converted to biomass using the density of seawater, a dry-to-wet weight ratio of 0.25:1, and a carbon-to-dry weight ratio of 0.45:1 (Duarte, 1992; Reynolds, 2006). The observed biomass estimates for each group were linearly regressed against the closest model output during a 2-week period either before or after the corresponding sample collection date.

The completed model was used to run scenarios with changes in climate, including temperature, freshwater delivery, and nutrient loading, to predict potential effects on the NRE phytoplankton community.

ReNuMa Model

To translate projected changes in temperature and precipitation into changes in watershed discharge and nutrient loading to the NRE, the ReNuMa model developed during DCERP1 (Brush, 2013) was re-parameterized and extended through 2015. The model was calibrated against observations at Gum Branch and the 10 small watersheds on MCBCL monitored during DCERP (Research Projects AE-2 and AE-5) for the period 2008–2012, and independently validated against data from the period 2013–2015 (**Figure 10-7**). Climate input data (i.e., air temperature and precipitation) over this period were obtained from the historical reconstruction provided by Research Project CC-1 for Onslow County. Land cover was determined in ArcMap using shapefiles obtained from the National Land Cover Database (NLCD) for the years 2006 and 2011 (Fry et al., 2011; Homer et al., 2015). Areas in the off-Base watershed classified as

"Cultivated Crops" by the NLCD were split into soybean (39%), corn (33%), cotton (17%), and wheat (11%) based on the percentage contribution of each crop at the county level (U.S. Department of Agriculture's National Agriculture Statistics Service 2000–2008). Population density was computed using U.S. Census Bureau data (TIGER 2010), and the fraction of the population on septic tanks in the off-Base watershed was estimated using a geographic information systems (GIS) shapefile of sewer service areas in the watershed in 2004 (NCCGIA, 2007). Point-source discharges were obtained from the U.S. Environmental Protection Agency's Water Discharge Permits Web site (EPA-PCS 2009).

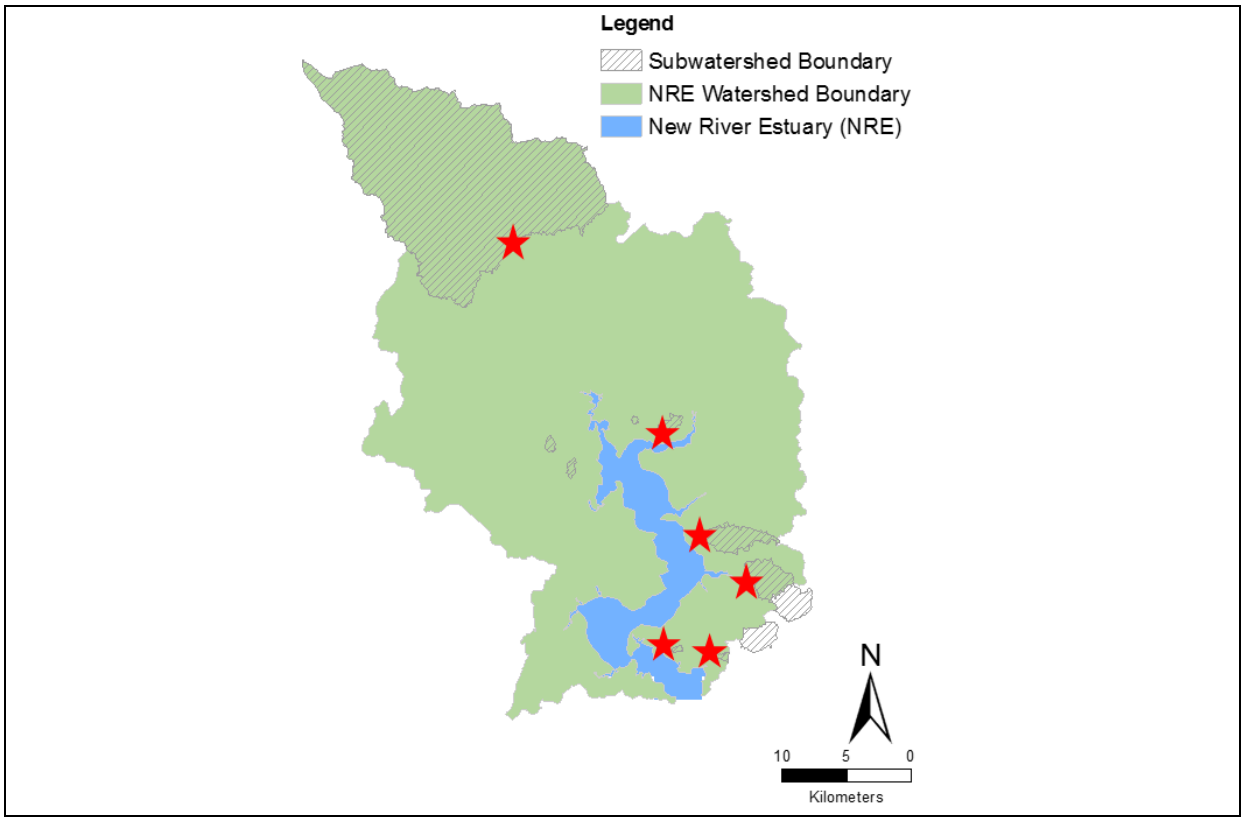

Figure 10-7. Sub-watersheds and stream gaging stations used in the ReNuMa model calibration and validation.

Watershed measured by the U.S. Geological Survey stream gaging station at Gum Branch and the 10 sub-watersheds on Marine Corps Base Camp Lejeune monitored by Research Projects AE-2 and AE-5. Red stars denote those watersheds with data for the full simulation period (through 2015).

Stream recession coefficients were calculated using daily discharge data over nine separate precipitation events in each of the 11 calibration sub-watersheds between the years 2008–2011. Runoff curve numbers and Universal Soil Loss Equation (USLE) parameter values were computed from soil characteristics data obtained from the National Resources Conservation Service Soil Survey Geographic (SSURGO) Database for Onslow County. A 20-foot Digital Elevation Model (DEM) GIS coverage obtained from the USGS National Elevation Dataset was used to calculate the slope length for each land use type using the "Flow Length" tool in ArcMap, while application of the "Slope" tool in ArcMap allowed for calculation of the percent slope for each land use type (Hickey, 2000). Remaining model parameters were estimated using look-up tables and default values in the ReNuMa model user's manual (Hong and Swaney, 2007)

and the Generalized Watershed Loading Functions manual upon which the ReNuMa model is based (Haith et al., 1996).

The model was calibrated to observed streamflow and loading of total dissolved nitrogen (TDN) and total dissolved phosphorus (TDP) from the 11 calibration sub-watersheds (**Figure 10-7**) for the period from 2008 through 2012. Once calibrated, the model was run through 2015 to provide an independent validation of model output for the period from 2013 through 2015. Model skill was computed through regression of observed and modeled monthly flow and loads, with a focus on the slope, r^2, and *p*-value of the regressions. A ranking scheme was developed to assess the quality of model fit in each watershed:

- Good: Slope not significantly different from 1, intercept not significantly different from 0, and an overall significant linear relationship (α=0.05)
- Intermediate: Slope significantly different from 1 and/or intercept significantly different from 0, but an overall significant linear relationship (α=0.05)
- Poor: Slope significantly different from 1 and/or intercept significantly different from 0, and no significant linear relationship (α=0.05).

Once calibration and validation were complete, the ReNuMa model was applied over the entire NRE watershed, distinguishing between the off- and on-Base portions of the watershed, and used to compute discharge and nutrient loading over the full simulation period (2008–2015) and under a range of land-use and climate change scenarios.

Application in Other Estuarine Systems

The wider utility of the ESM was demonstrated by applying the original DCERP1 version to estuaries adjacent to two other coastal DoD installations from which monitoring data were available for calibration: the Neuse River Estuary, NC (MCAS Cherry Point), and Choctawhatchee Bay, FL (Eglin AFB) (**Figure 10-8**).

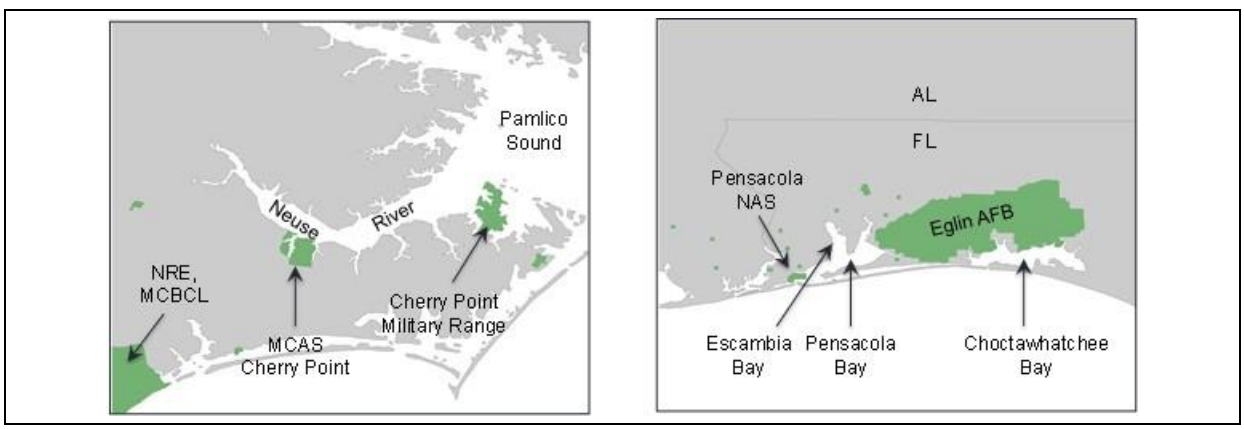

Figure 10-8. New estuaries selected for Estuarine Simulation Model (ESM) application in DCERP2.

The ESM was applied to the Neuse River Estuary, NC (left) and Choctawhatchee Bay, FL (right). Green polygons show the adjacent U.S. Department of Defense facilities (Marine Corps Air Station Cherry Point and Eglin Air Force Base).

The Neuse River Estuary was subdivided into eight spatial elements along the mainstem of the estuary based on geomorphic constrictions and the location of long-term water quality monitoring data from the Neuse River Estuary Modeling and Monitoring (ModMon) Program (**Figure 10-9**). Each element contains a surface layer and a bottom layer separated by the mean position of the pycnocline, determined from ModMon temperature and salinity profiles. Watershed boundaries for each element were delineated using the USGS National Hydrography Dataset and the National Oceanic and Atmospheric Administration (NOAA) Coastal Relief Model. Vertically homogenous boxes were added for Slocum and Hancock Creeks, which are adjacent to MCAS Cherry Point (**Figure 10-10**), and the portion of the watersheds of these creeks draining from the Base was delineated. A state variable for total suspended solids (TSS) was added at the request of MCAS Cherry Point to simulate the impact of stormwater runoff on creek sediment concentrations. Bathymetric soundings were obtained from the NOAA National Geophysical Data Center and used to compute mean depths and volumes of each element. Model forcing data were obtained for photosynthetically active radiation (PAR; NOAA National Climatic Data Center station at Kinston, NC); meteorology (NOAA National Climatic Data Center station at MCAS Cherry Point); Neuse and Trent River discharge (USGS); WWTFs (New Bern, Havelock, Fairfield Harbor, Bridgeton, and MCAS Cherry Point); water temperature, salinity, and turbidity in each element (ModMon); and the tidal fresh and marine boundary conditions (ModMon). The model was set up for the period 2007–2010 to match the original focus of the New River ESM during DCERP1, and the model was calibrated to ModMon data over the same period, focusing on simulated vertical light attention coefficient (k_D), surface chl *a*, TSS, DIN, and DIP, and surface and bottom concentrations of O_2. The 2007–2010 calibration period reflects relatively dry conditions in the estuary (**Figure 10-11**). After calibration, model skill metrics were computed as previously described and a series of nutrient reduction and climate warming scenarios were run to understand the response of the Neuse River Estuary to these impacts.

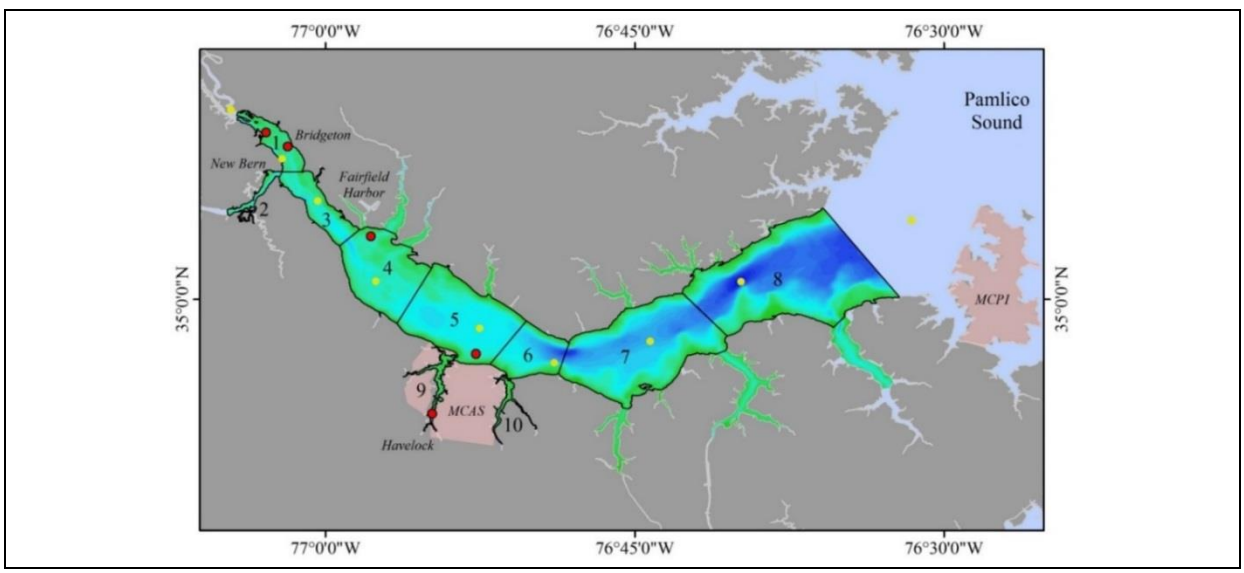

Figure 10-9. Domain of the Neuse River Estuary Estuarine Simulation Model (ESM).

Spatial elements of the Neuse River ESM, along with ModMon monitoring stations used for model forcing and calibration (yellow circles). Shading indicates bathymetry, with the darker blue indicating deeper waters. Boxes 9 and 10 have a single vertical layer; all other boxes have a surface and bottom layer. The red circles show the locations of wastewater treatment facility outfalls included in the model.

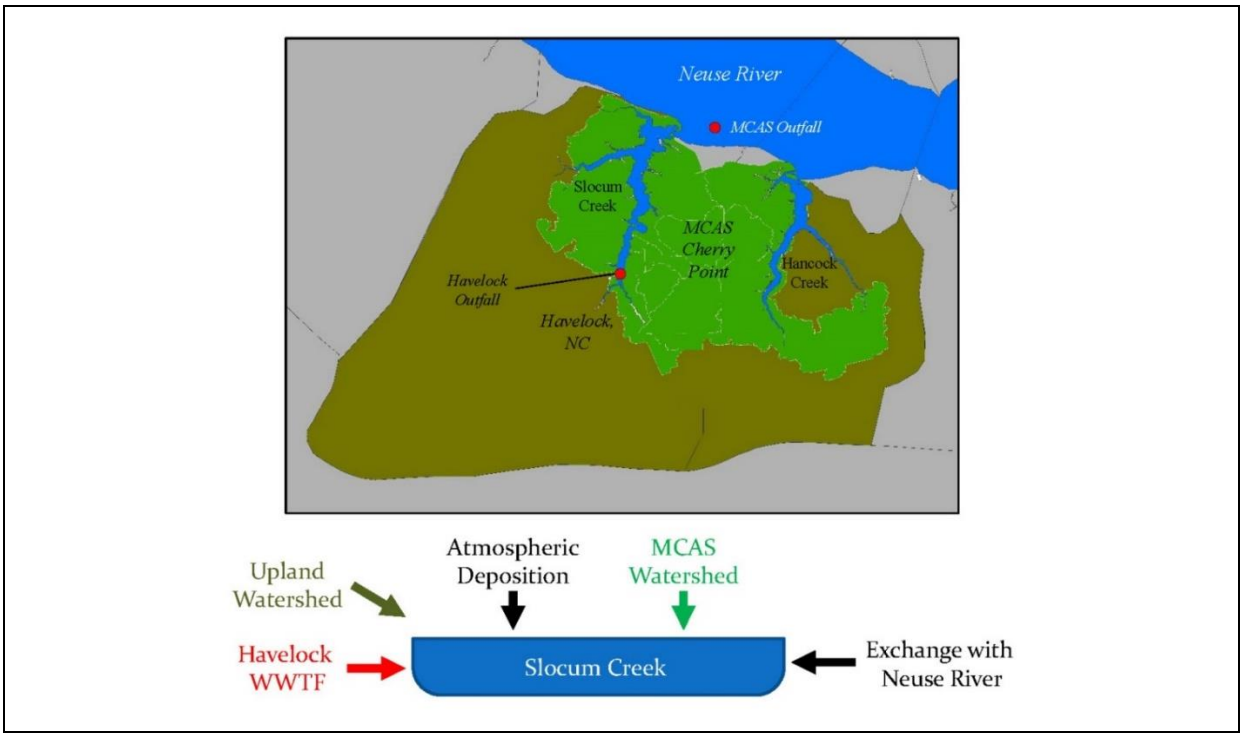

Figure 10-10. Addition of Slocum and Hancock Creeks to the Neuse River Estuarine Simulation Model (ESM).

Map shows Marine Corps Air Station (MCAS) Cherry Point boundaries (green), watershed area draining to Slocum and Hancock Creeks (brown), and locations of Havelock and MCAS Cherry Point wastewater treatment facility outfalls (red circles). The lower diagram illustrates the watershed inputs by using Slocum Creek as an example.

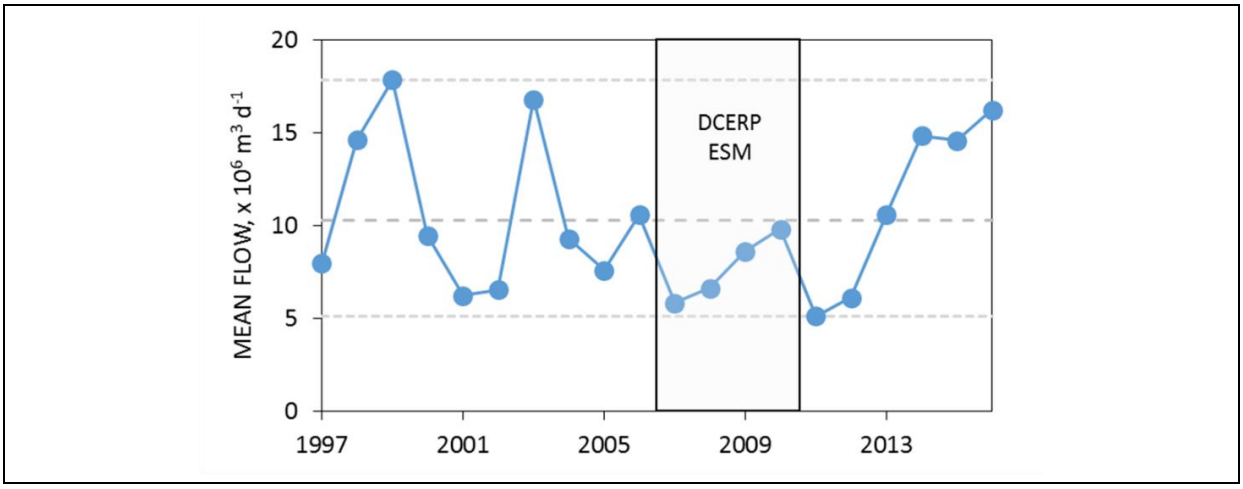

Figure 10-11. Neuse River and Trent River discharge during the Estuarine Simulation Model (ESM) simulation period.

The combined mean daily discharge rate of the Neuse River near Fort Barnwell (U.S. Geological Survey [USGS] stream gaging station 02091814) and Trent River near Trenton (USGS stream gaging station 02092500) for each year during the ESM simulation period. The dashed line in the middle is the mean during this period; lower and upper lines denote the minimum and maximum, respectively. Graph encompasses the entire period of record at Fort Barnwell.

Choctawhatchee Bay was subdivided into six spatial elements along the mainstem of the estuary based on geomorphic constrictions and the location of water quality monitoring data from the Choctawhatchee Basin Alliance (CBA) and Florida Department of Environmental Protection (**Figure 10-12**). Spatial elements were also included for three bayous adjacent to Eglin AFB. Each element contains a surface layer and a bottom layer separated by the mean position of the pycnocline, determined from CBA temperature and salinity profiles. Watershed boundaries for each element were delineated using the USGS National Hydrography Dataset and NOAA Coastal Relief Model. Bathymetric soundings were obtained from the NOAA National Geophysical Data Center and used to calculate mean depths and volumes of each element. Model forcing data were obtained for PAR and meteorology (NOAA National Climatic Data Center station at Fairhope, AL); Choctawhatchee River and Alaqua Creek discharge (USGS); water temperature, salinity, and turbidity in each element (CBA); and riverine and marine boundary conditions (CBA, USGS). The model was set up for the period 2010–2014 to match the availability of monitoring data and was calibrated to CBA and Florida Department of Environmental Protection data over the same period, focusing on simulated Secchi depth, surface chl *a*, DIN, and DIP, and surface and bottom concentrations of O_2. The 2010–2014 calibration period reflects a wide range of discharge (**Figure 10-13**). After calibration, model skill metrics were calculated as previously described, and a series of nutrient reduction and climate warming scenarios were run to understand the response of Choctawhatchee Bay to these impacts.

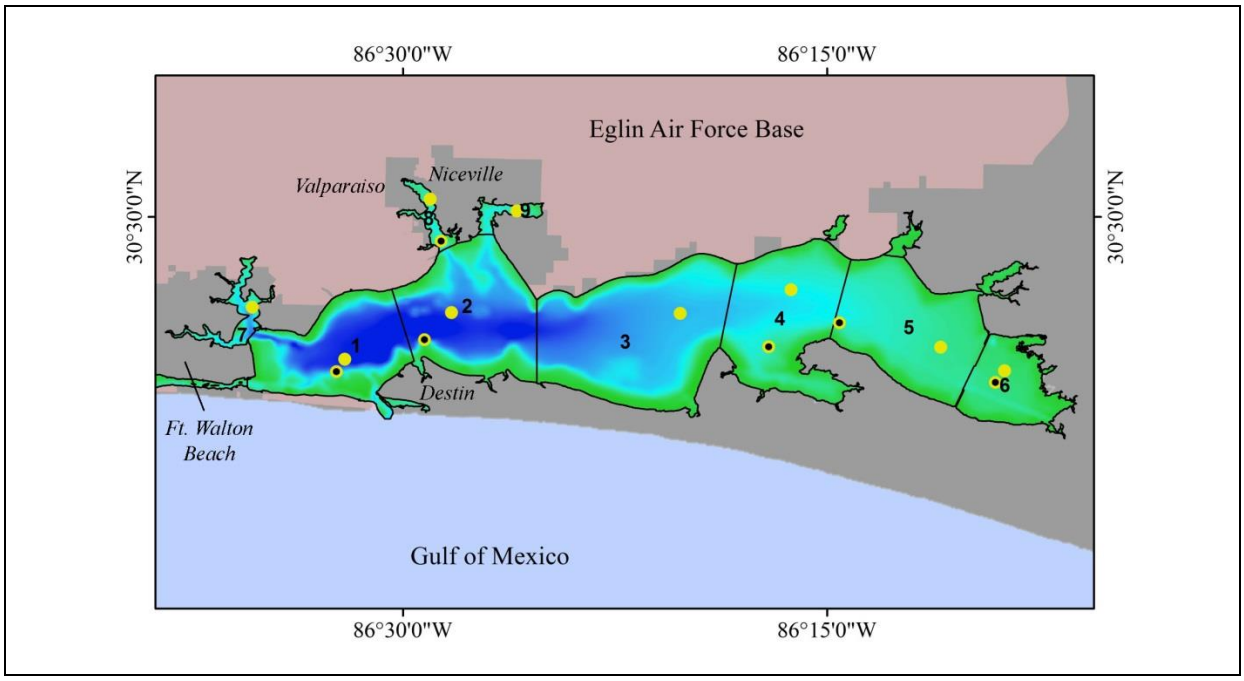

Figure 10-12. Domain of the Choctawhatchee Bay Estuarine Simulation Model (ESM).

Spatial elements of the Choctawhatchee ESM, along with Choctawhatchee Basin Alliance (yellow circles) and Florida Department of Environmental Protection (black circles) monitoring stations used for model forcing and calibration. All boxes have a surface layer and a bottom layer. Shading indicates bathymetry, with darker blue indicating deeper water.

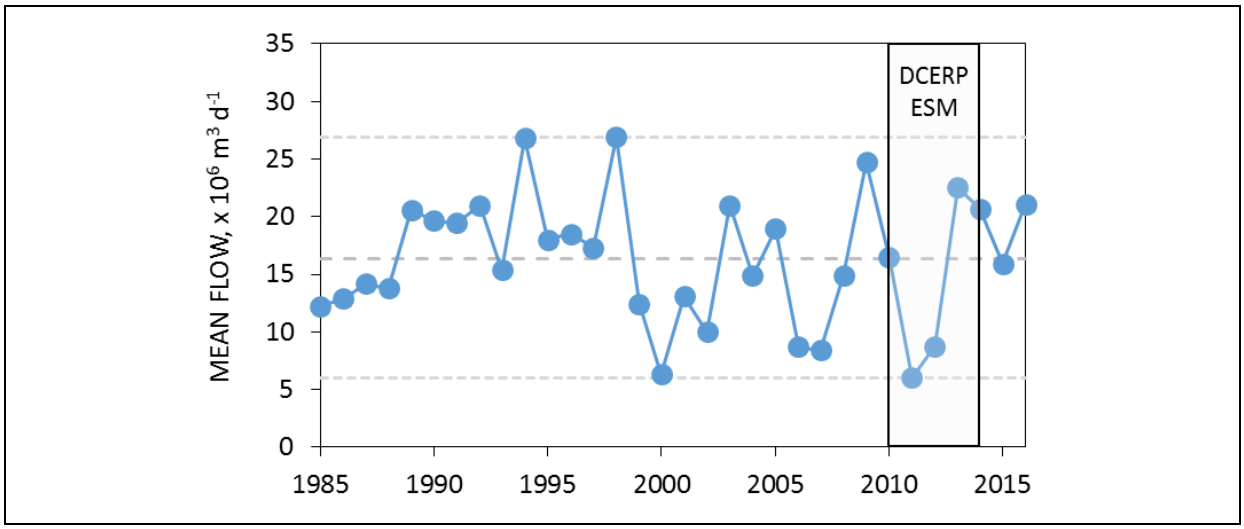

Figure 10-13. Choctawhatchee River discharge during the Estuarine Simulation Model (ESM) simulation period.

Mean daily discharge rate of the Choctawhatchee River near Bruce, FL (U.S. Geological Survey [USGS] stream gaging station 02366500) for each year during the ESM simulation period. The dashed line in the middle is the mean during this period; lower and upper lines denote the minimum and maximum, respectively. The gauge record begins in 1930.

Online Decision-Support Tool

To transfer each ESM to staff at each Base and to local stakeholders, and to facilitate its use as a management tool, online decision-support versions of each model were created and made available online through the Virginia Institute of Marine Science (VIMS) Coastal Systems Ecology and Modeling Program Web site.

Each ESM is available on the Virginia Institute of Marine Science (VIMS) Coastal Systems Ecology and Modeling Program Web site.

http://www.vims.edu/research/departments/bio/programs/semp/models/index.php

The approach enables use of the models by Base personnel and local stakeholders without the need for extensive modeling expertise, equipment, or software, through a Web browser on a personal computer. User-friendly, graphical user interfaces and short user guides were constructed for each model with documentation, instructions for running simulations, and user-defined inputs for key parameters, primarily nitrogen and phosphorus loading rates from various sources and water temperature. The interfaces include the ability to visualize results, including time modeled parameters were out of compliance with state criteria, compare results across multiple scenarios, and download results to the users' personal computer for further analysis. The interfaces were developed with feedback from Base personnel and local stakeholders at workshops conducted in 2014 (MCBCL and MCAS Cherry Point), 2015 (Eglin AFB), and 2017 (at all three Bases).

Results and Discussion

New River ESM Calibration and Validation

Freshwater flushing times computed with the Officer box model within the New River ESM displayed a great deal of variability, both within months, over the annual cycle, and inter-annually (**Figure 10-14a**). The overall median and mean flushing times were 68 and 78 days, respectively, with a standard deviation of 46 days. Flushing times were generally lower in the winter and early spring, corresponding with higher river discharge, and increased during summer when discharge was lower. Flushing times within a given month were highly variable, reflecting strong inter-annual variability in discharge among years; overall, flushing times were strongly controlled by freshwater inputs to the estuary, as represented by discharge at Gum Branch (**Figure 10-14b**).

The median and mean flushing times from the ESM closely match the values of 64 and 70 days, respectively, calculated for the period 1996–2000 by using similar methods by Ensign et al. (2004). These authors similarly reported a strong negative relationship between flushing time and discharge. Median flushing times also compare well to residence times computed during DCERP1 with the highly resolved, physically based Advanced Circulation (ADCIRC) hydrodynamic model. Residence times in the ADCIRC model were estimated under conditions of mean discharge at Gum Branch and at two times and 10 times the mean discharge, and resulted in values of 74, 37, and 18 days, respectively (Paerl et al., 2013b). The value under mean discharge falls between the median and mean values estimated with the ESM, and the relationship with discharge similarly matches that from the ESM. Paerl et al. (2013b) also report a flushing time of 80 days for the estuary based on a date-specific freshwater age method, which similarly corresponds closely to values from the ESM.

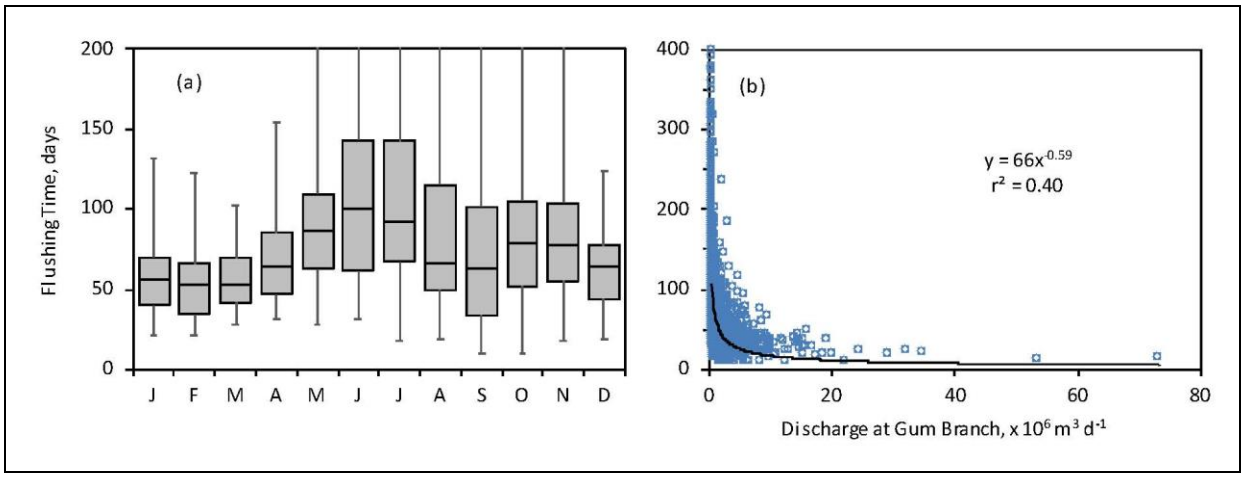

Figure 10-14. Flushing times of the New River Estuary (NRE).

(a) Box plots depicting monthly median flushing times in the NRE (central lines) along with first and third quartiles (boxes) and minima and maxima (error bars), for the period 1998–2015. The *y*-axis was intentionally truncated to resolve the seasonal cycle. (b) The relationship between flushing time and discharge at Gum Branch.

The ESM was successfully re-calibrated to DCERP1 (2007–2012) data and was extended through 2015 to provide an independent validation from 2013 to 2015 (**Figures 10-15 and**

10-16). The model reproduces the approximate magnitudes, down-estuary gradients, and dynamics of water quality variables and rate processes for which monitoring data are available. Light attenuation (k_D) is computed using the multiple linear regression with chlorophyll *a*, turbidity, and chromophoric dissolved organic matter (CDOM) developed during DCERP1 (Anderson et al., 2014). Although this regression appears to overestimate k_D to a limited degree in the upper estuary, calculated values are nevertheless reasonable and follow the temporal patterns in the observations (**Figure 10-15**). Dissolved inorganic nutrient concentrations (both nitrogen and phosphorus) are closely reproduced by the model, with values generally at low concentrations except during events which are primarily driven by peaks in discharge. Phytoplankton biomass (as chlorophyll *a*) is similarly reproduced by the model, including a number of the observed bloom events and clear water phases. The model does particularly well at reproducing the marked down-estuary declines in nutrients and chlorophyll *a*, which are key features of the NRE.

The model captures the seasonal cycle of dissolved oxygen in both surface and bottom waters, as well as several hypoxic events in the upper estuary (**Figure 10-16**). The regular seasonal cycling of oxygen apparent in the data and model is driven by the seasonal saturation cycle, which is in turn driven by seasonal changes in temperature and salinity, whereas event-scale dynamics are driven primarily by the metabolic production and consumption of oxygen. The model also appears to be capturing the correct range of phytoplankton NPP, although these comparisons are subject to uncertainty. Modeled NPP represents net daytime production, whereas observations were based on ^{14}C incubations (Paerl et al., 2013a), which represent rates between GPP and NPP. The latter were conducted for 4 hours at approximately mid-day in a rotating wheel that moves bottles through a light gradient designed to represent in situ conditions. Extrapolating these rates to daily values for comparison to the model assumes that incubation light conditions match in situ conditions, and requires one to assume the fraction of daily production that occurred during the 4-hour incubation. Finally, the model captures the approximate biomass of BMA (**Figure 10-16, bottom**). BMA are simulated in 0.5-m depth increments in the model. Because field measurements were made at 0.5 m, these values should be bracketed by model predictions in the 0- to 0.5-m and 0.5- to 1-m depth increments.

The completed model was also used to simulate the pre-DCERP years during which monitoring was conducted by the University of North Carolina at Wilmington (1998–2007; Mallin et al., 2005); this data set was originally used during DCERP1 to conduct the first application of the ESM to the NRE. Although not all parameters are available in this data set, the updated model again captured the magnitudes, down-estuary gradients, and major dynamics of k_D, nutrients, chlorophyll *a*, and DO (**Figures 10-17 and 10-18**).

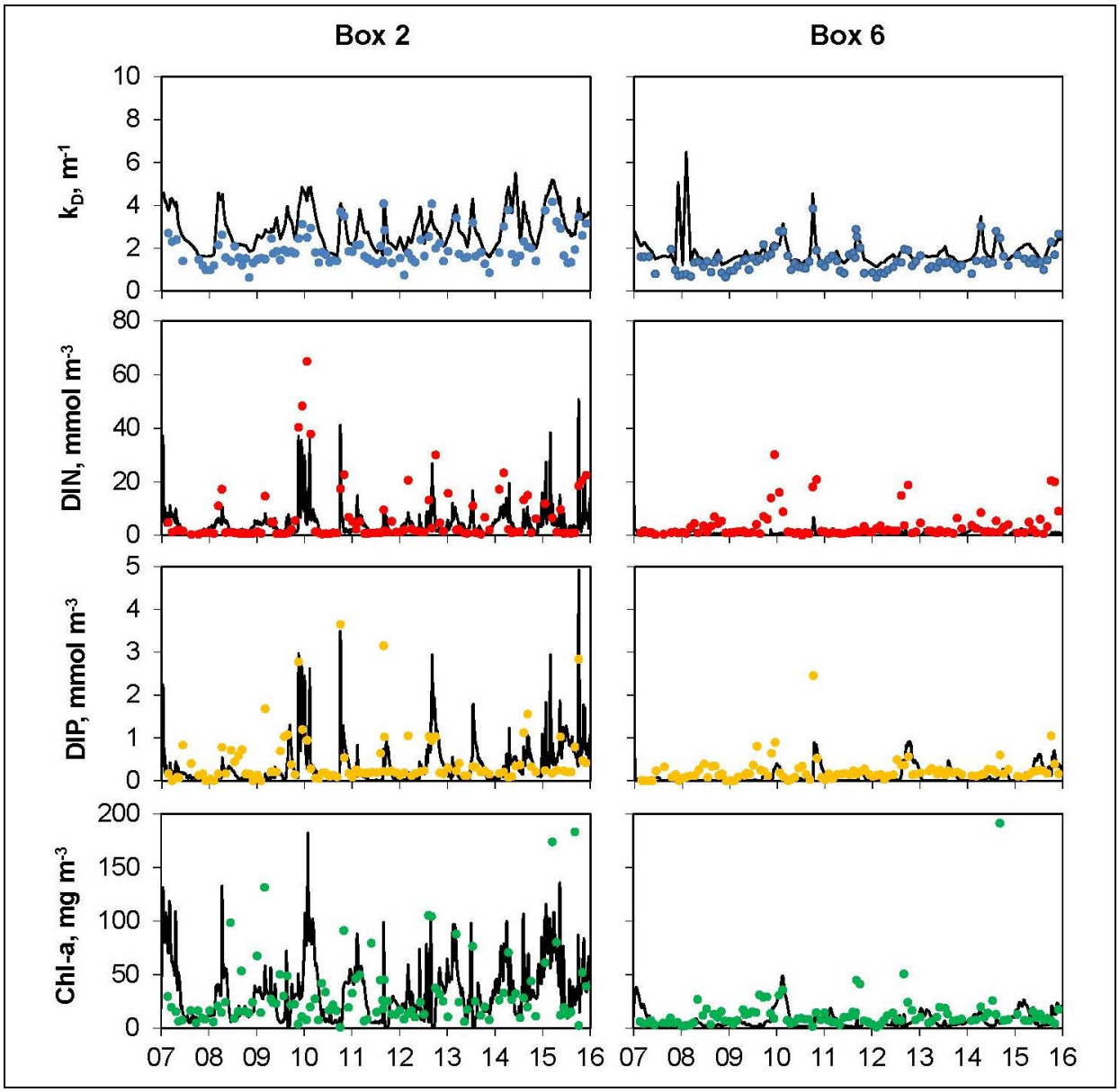

Figure 10-15. Simulated New River Estuary parameters, 2007–2015.

A comparison of Estuarine Simulation Model–predicted (black lines) and observed (colored points) water quality parameters in the surface layers of two representative spatial elements (Box 2 = up-estuary; Box 6 = down-estuary) through DCERP1 and DCERP2. Data were collected as part of the DCERP Monitoring Program.

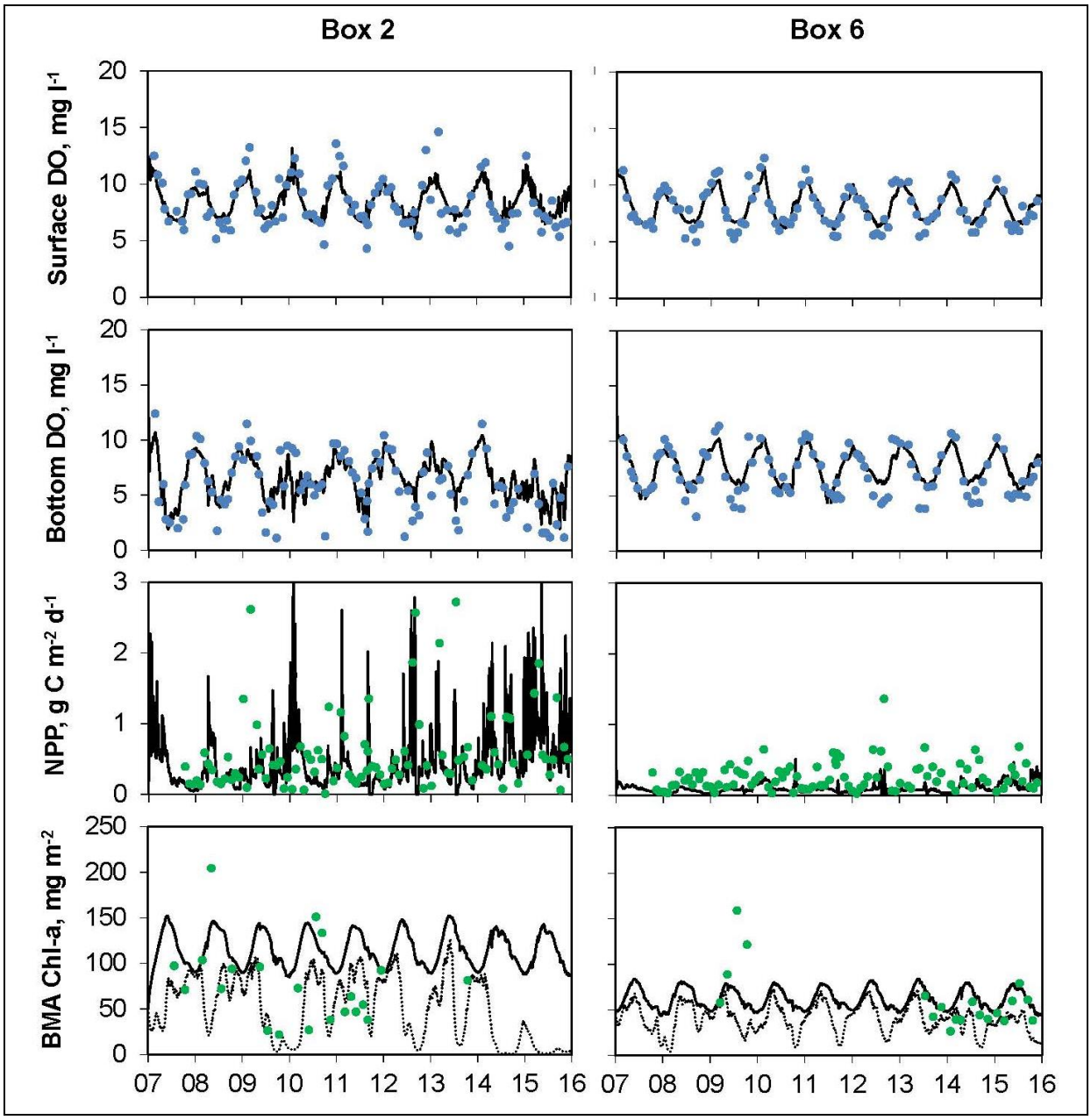

Figure 10-16. Simulated New River Estuary parameters, 2007–2015.

A comparison of Estuarine Simulation Model–predicted (black lines) and observed (colored points) dissolved oxygen (DO), phytoplankton net primary production (NPP), and benthic microalgal biomass (in the top 3 mm of sediment) in two representative spatial elements (Box 2 = up-estuary; Box 6 = down-estuary) through DCERP1 and DCERP2. Data regarding benthic microalgae (BMA) were collected at 0.5-m depth and should be bracketed by model predictions for the 0- to 0.5-m (solid lines) and 0.5- to 1-m (broken lines) depth segments. Data were collected as part of the DCERP Monitoring Program.

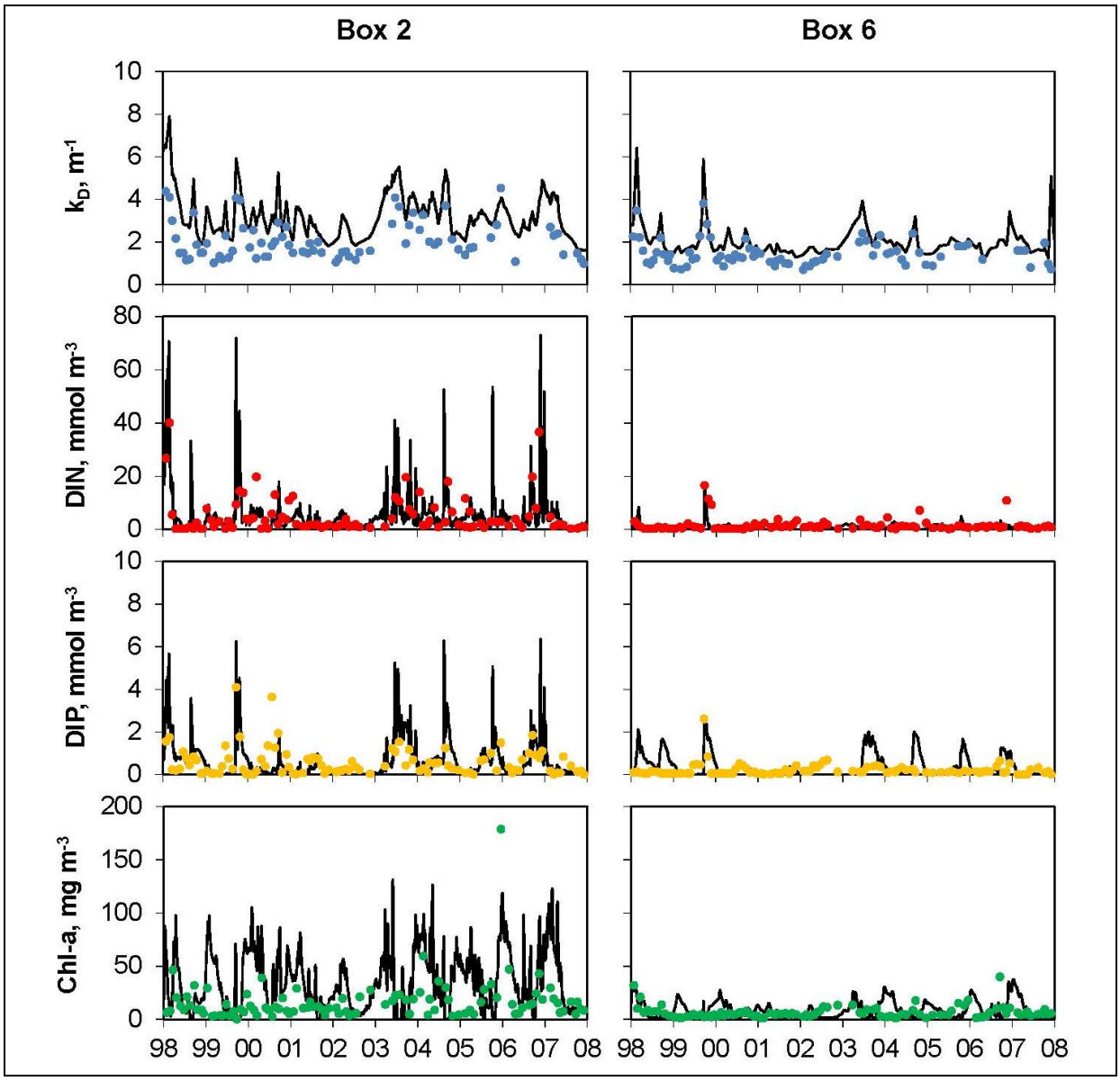

Figure 10-17. Simulated New River Estuary parameters, 1998–2007.

A comparison of Estuarine Simulation Model–predicted (black lines) and observed (colored points) water quality parameters in the surface layers of two representative spatial elements (Box 2 = up-estuary; Box 6 = down-estuary) before DCERP. Data were collected for Marine Corps Base Camp Lejeune by the University of North Carolina at Wilmington.

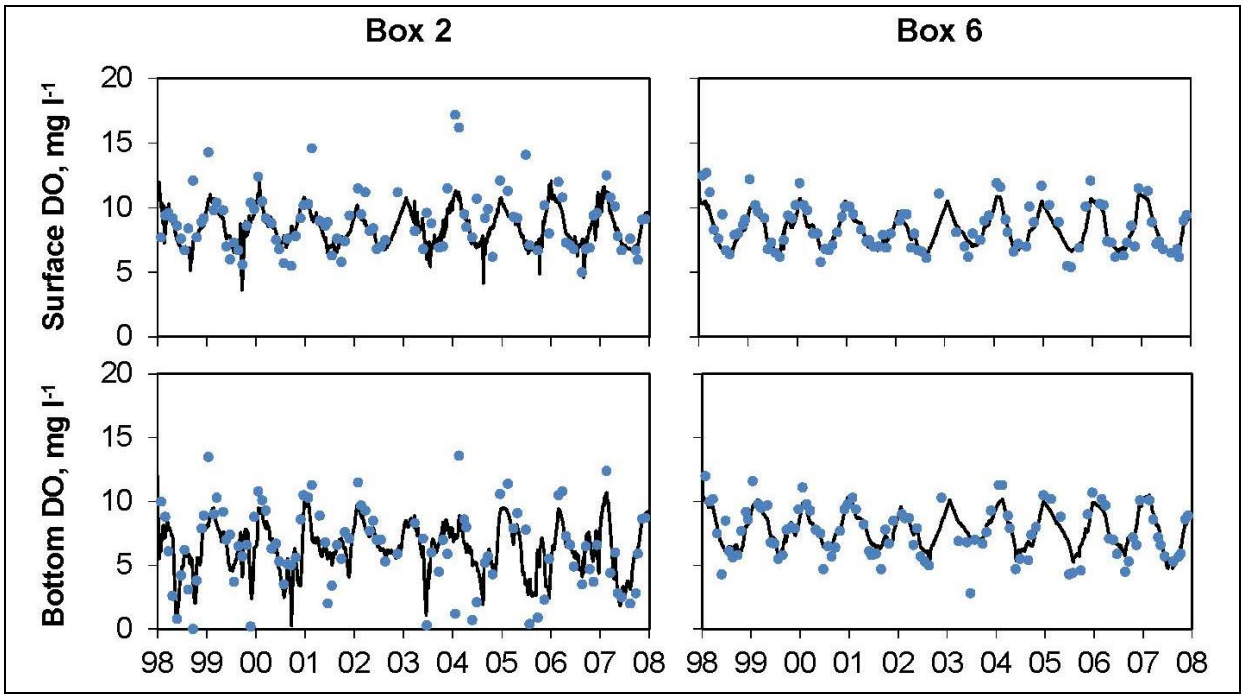

Figure 10-18. Simulated New River Estuary parameters, 1998–2007.

A comparison of Estuarine Simulation Model–predicted (black lines) and observed (colored points) dissolved oxygen (DO) in the surface and bottom layers of two representative spatial elements (Box 2 = up-estuary; Box 6 = down-estuary) before DCERP. Data were collected for the Marine Corps Base Camp Lejeune by the University of North Carolina at Wilmington.

Model expansion during DCERP2 included the addition of two new seagrass species (i.e., *Ruppia maritima* and *Halodule wrightii*) that are found in the lower NRE along with *Zostera marina*, which was included in the DCERP1 ESM. The *R. maritima* model reproduces repeatable seasonal cycles of above-ground and below-ground biomass in the New River (**Figure 10-19**). Although biomass data are not available from the NRE, Cerco and Moore (2001) presented data from the Chesapeake Bay in which *R. maritima* reaches a summertime peak above-ground biomass of approximately 40 g C m^{-2}, which is in the range of model predictions for the New River.

The *H. wrightii* model also reproduces repeatable seasonal cycles of above-ground and below-ground biomass in the New River (**Figure 10-20**). Although biomass data are again unavailable from the NRE, two publications provide data from nearby Core and Bogue Sounds, NC. Fonseca and Bell (1998) reported biomass ranging from near zero to more than 3,300 g dw m^{-2}, with a seasonal mean between 215 and 454 g dw m^{-2}, and Hovel et al. (2002) reported peak biomass between 30 and 80 g dw m^{-2}. These wide ranges make it difficult to choose an appropriate calibration target in the model; however, the model is reproducing values within the range of these published estimates.

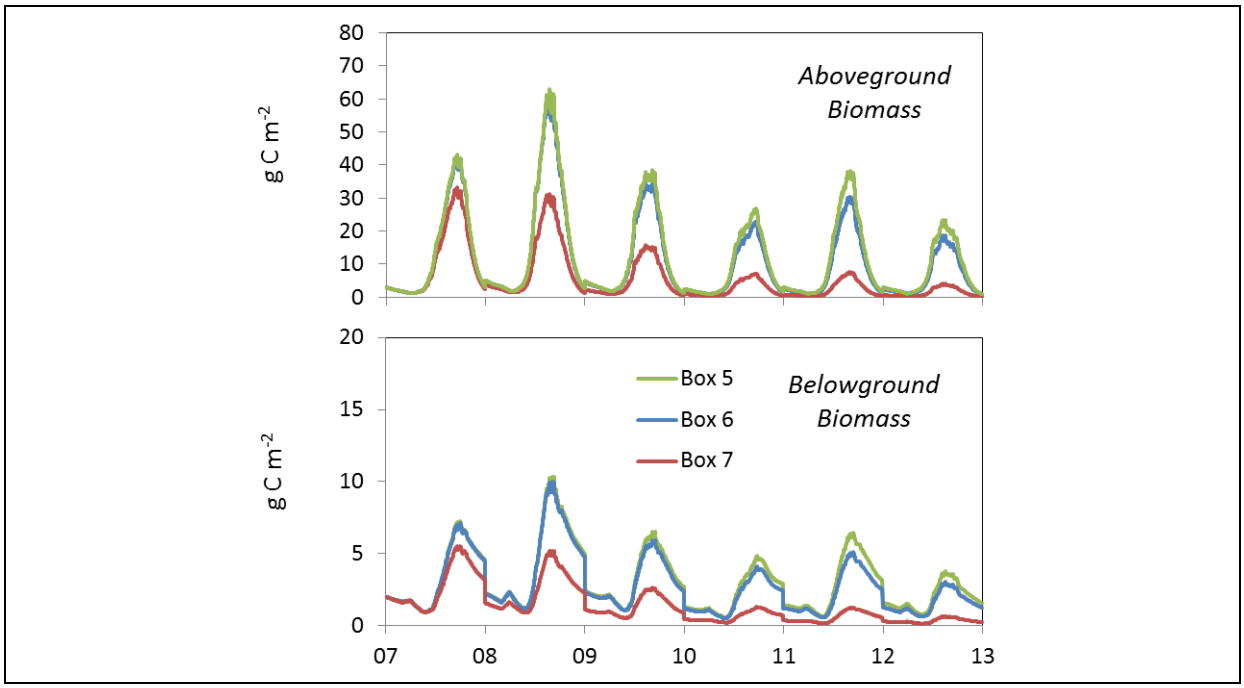

Figure 10-19. Modeled above- and below-ground biomass of *Ruppia maritima* in three spatial elements of the middle and lower New River Estuary.

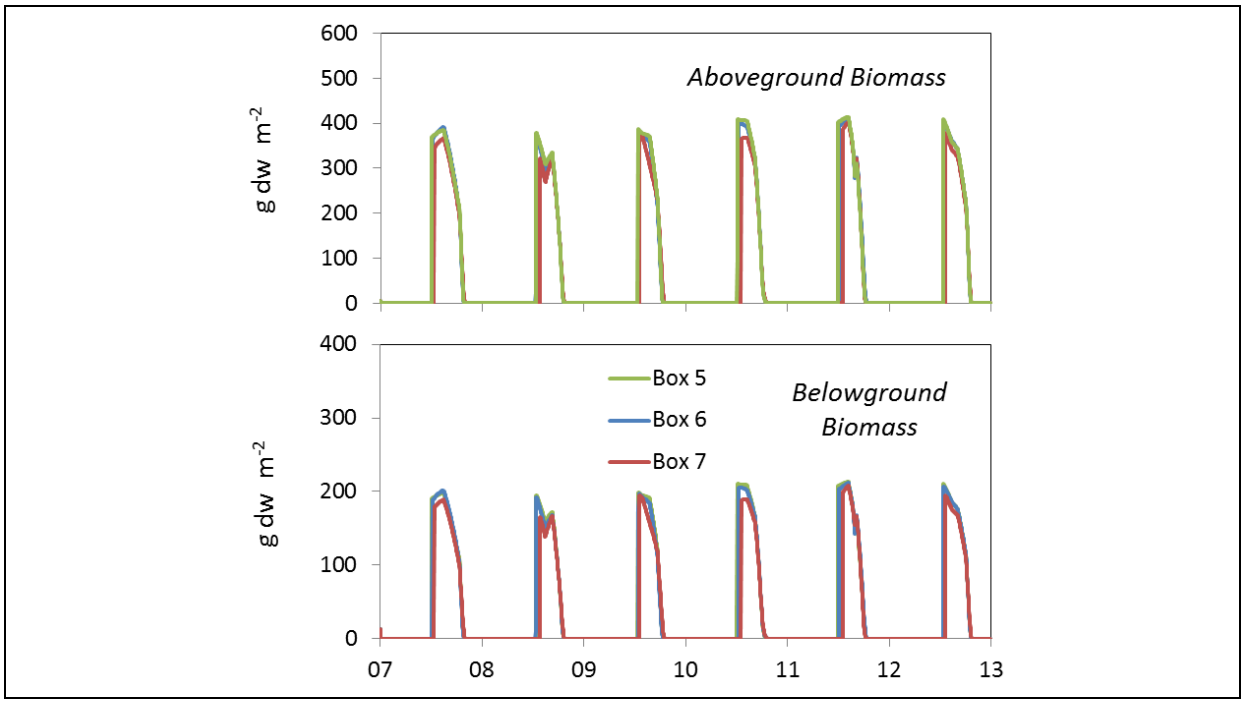

Figure 10-20. Modeled above- and below-ground biomass of *Halodule wrightii* in three spatial elements of the middle and lower New River Estuary.

ESM expansion during DCERP2 also included the addition of a state variable for DIC and calculation of pCO_2 and air–sea diffusion of CO_2 to enable a greater focus on carbon cycling. DIC data are available for the entire DCERP period, and the model captures the magnitudes and

dynamics of DIC throughout the estuary (**Figure 10-21, top**). With regard to pCO_2, data are only available for 2 years during DCERP2 (July 2013 through July 2015), and the model again captured the magnitudes and dynamics throughout the system (**Figure 10-21, bottom**). Similarly, the model is capturing the approximate values and dynamics of air–sea CO_2 exchange as measured by Research Projects AE-4 and AE-6 (**Figure 10-22**). The correspondence between model and data is especially good in the upper estuary (Boxes 1–4 and 8) and middle estuary (Boxes 5, 6, and 9), but not as good for the lower estuary (Box 7). The former regions comprise the majority of both estuarine area and volume, so when analyzed for the entire system, the model again closely follows the observations.

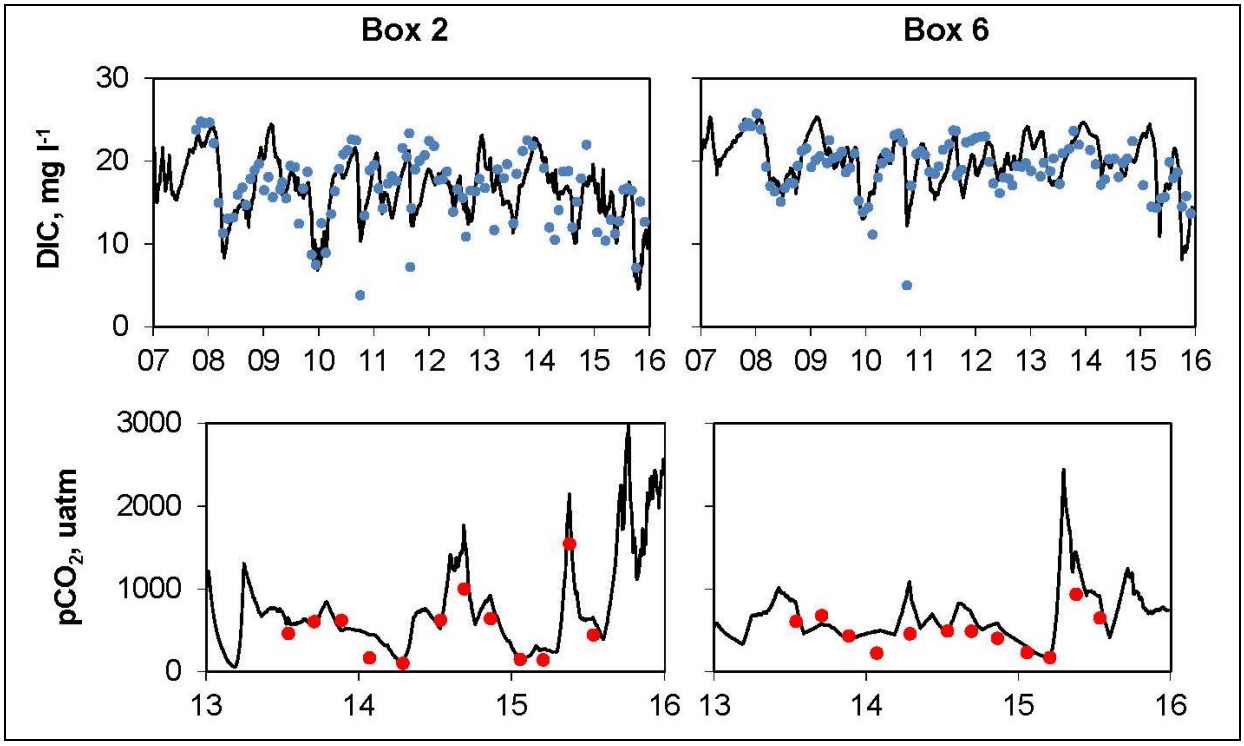

Figure 10-21. Simulated carbon parameters in the New River Estuary.

A comparison of Estuarine Simulation Model–predicted (black lines) and observed (colored points) dissolved inorganic carbon (DIC) concentrations (upper panels) and partial pressure of carbon dioxide in water (pCO_2) (lower panels) in the surface layers of the upper (Box 2) and lower (Box 6) estuary. Data were collected as part of the DCERP Monitoring Program.

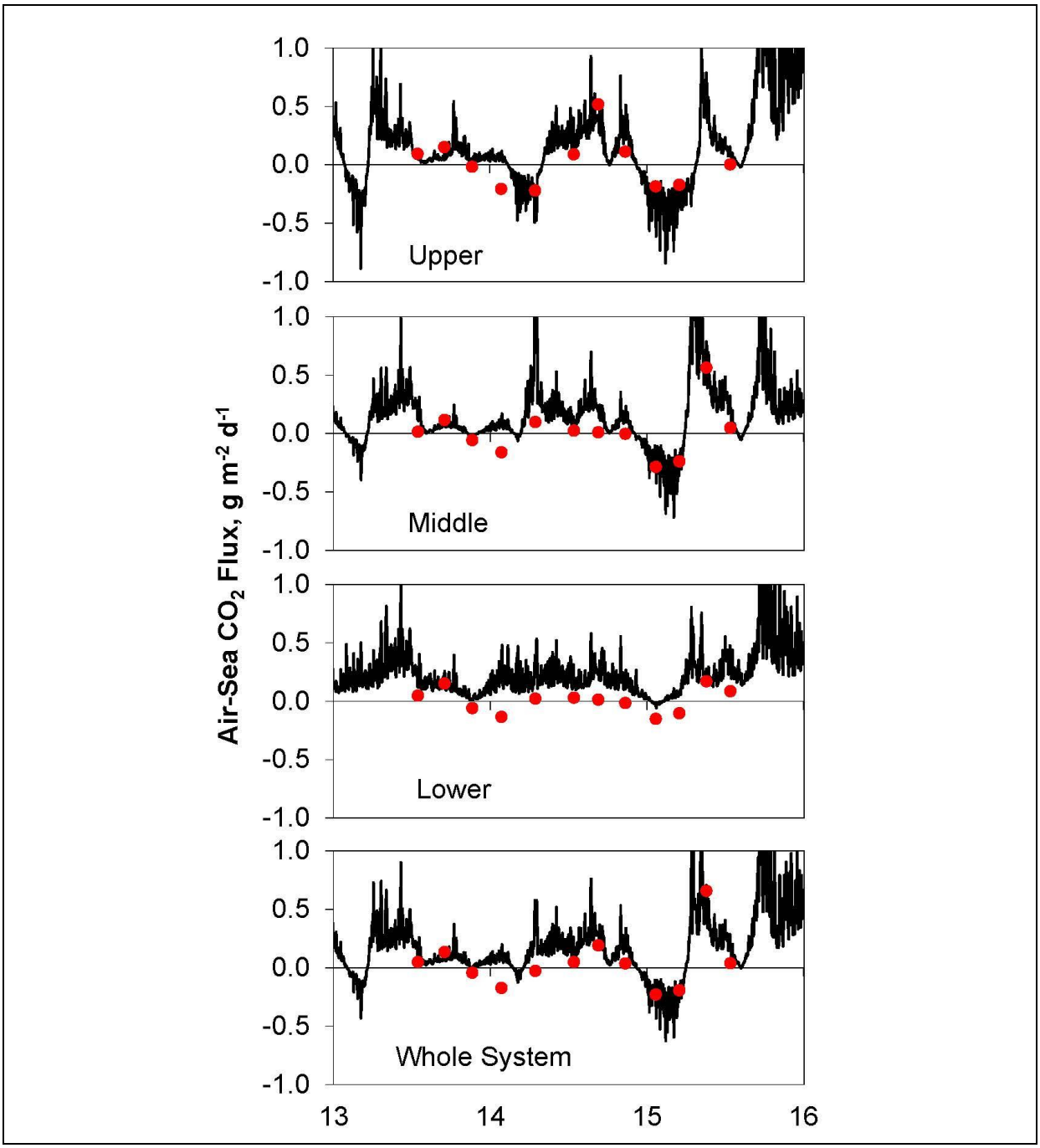

Figure 10-22. Simulated air–sea carbon dioxide (CO_2) flux in the New River Estuary.

A comparison of Estuarine Simulation Model–predicted (black lines) and observed (colored points) CO_2 flux across the air–water interface in the upper, middle, and lower regions of the estuary and area-weighted for the entire system. Rates were measured as part of the DCERP Monitoring Program. Positive rates represent exchanges from the water to the atmosphere; negative rates represent uptake by the water.

Phytoplankton Functional Group Model

Full details of the phytoplankton functional group model calibration, output, and simulations are discussed by Blachman (2016). The model successfully reproduced observed chl *a*

concentrations throughout the estuary, as well as the typical seasonal cycle of chl *a* and primary production (**Figure 10-23**). Volume-weighted average daily surface concentration of chl *a* in the NRE was 15.9 mg m^{-3} according to the model output compared with 15.6 mg m^{-3} based on interpolated DCERP1 observations.

The average annual cycles of modeled and observed chl *a* overlap within two standard deviations of one another for most of the year. The quality of the fit varies by season; it appears to be particularly good during winter and early spring as well as during late summer and most of the fall. However, the model overestimated average chl *a* from the end of April through the beginning of May. The mean interpolated cycle was within two standard deviations of the mean model output for 90% of the year or 327 days. Conversely, the average model output was within two standard deviations of the interpolated mean 95% of the year or 347 days.

The average annual cycles of modeled and observed primary production followed a similar pattern, with modeled values falling within the range of the observations for most of the year, although the model appears to overestimate production during some parts of the year. Some overestimation is to be expected since model predictions represent GPP while observed values lie between GPP and NPP. The comparison is also dependent on the assumptions used to convert observed hourly productivity into daily values (see above). Production incubations were conducted for approximately 4 hours at approximately noon, with samples rotating through multiple irradiance levels (Paerl et al., 2013a). Scaling up to daily values required assumptions about the in situ light environment and fraction of daily production occurring during the incubation period. Given that, it is as important to match the correct seasonal pattern as the absolute magnitude of production; the model appears to correctly reproduce the seasonal pattern except for elevated rates during the spring.

Model predictions of total chl *a* were within the range of DCERP observations across all mainstem boxes. When comparing observed chl *a* across the 64 sampling dates (2007–2012) to the model output on the same days, mean absolute error was 11.0 mg m^{-3}, mean percent error was 96.5%, and root mean squared error was 17.3 mg m^{-3} for the entire system (n=364; **Table 10-4**). Skill metrics improved when the median values were used and when observations were compared with the closest model output within 1 week of each sampling date (mean absolute error = 7.8 mg m^{-3}; mean percent error 82.4%, and root mean squared error = 14.4 mg m^{-3}). Annual mean simulated surface chl *a* also compared favorably to observations from an independent set of shallow water sites sampled seasonally from 2007 to 2011 (Anderson et al., 2014; **Table 10-5a**). Average annual GPP predicted by the model also matched productivity estimates scaled up from DCERP1 monitoring data (154 versus 150 gC m^{-2} yr^{-1}, respectively; Paerl et al., 2013a; **Table 10-5b**). However, the model does not capture the full range of the inter-annual variability in observed production.

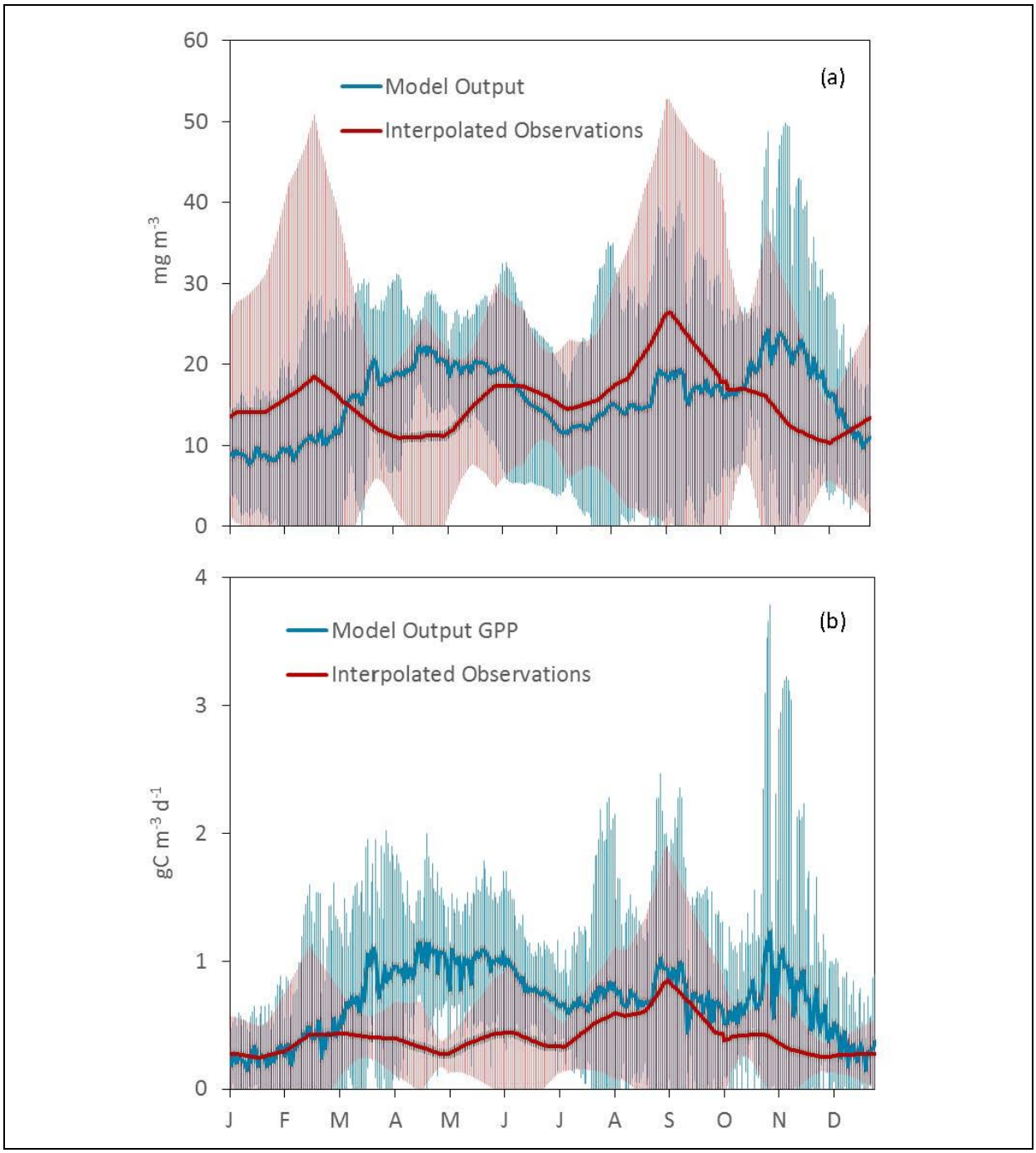

Figure 10-23. Average annual cycles of chlorophyll *a* (chl *a*) and gross primary production (GPP), functional group model.

Water column average annual cycles (±2 standard deviations) of NRE (a) chl *a* and (b) GPP from the functional group model and interpolated monitoring data, 2007–2012.

Table 10-4. Functional Group Model Skill Assessment

(a) exact date		Box 2	Box 3	Box 4	Box 5	Box 6	Box 7	**All Sites**
ABS Error	Mean	19.2	14.7	12.2	9.4	7.1	3.6	**11.0**
	Median	13.4	12.2	9.1	8.3	5.0	3.0	**7.3**
% Error	Mean	119.2	133.4	110.8	80.8	80.4	54.6	**96.5**
	Median	60.4	54.5	57.2	53.6	52.4	49.5	**54.0**
RMS Error		28.2	19.2	18.4	13.4	9.9	4.9	**17.3**
n =		*64*	*64*	*64*	*64*	*64*	*64*	*384*

(b) closest ±7 days		Box 2	Box 3	Box 4	Box 5	Box 6	Box 7	**All Sites**
ABS Error	Mean	13.6	9.8	8.6	6.8	5.4	2.8	**7.8**
	Median	7.5	7.8	5.5	5.0	3.7	1.9	**4.2**
% Error	Mean	78.6	95.6	82.6	60.4	57.2	35.7	**82.4**
	Median	31.9	29.2	35.2	31.8	43.5	31.0	**39.1**
RMS Error		23.5	14.9	16.3	10.8	8.3	4.1	**14.4**
n =		*64*	*64*	*64*	*64*	*64*	*64*	*384*

Absolute mean and median error (ABS error [mg m^{-3}]), percent mean and median error (% error), and root mean squared error (RMS error [mg m^{-3}]) were calculated for surface chlorophyll *a* (chl *a*) by using (a) the model output on the exact date each observation was collected and (b) the closest model output within a ±1-week period around the date when samples were collected.

Table 10-5. Additional Assessment of Functional Group Model Output

(a) Predicted mean surface chlorophyll *a* (chl *a*) values by box compared to mean values observed at six shallow water sites across the New River Estuary (NRE) seasonally from 2008 to 2011 (Anderson et al., 2014). (b) Predicted and observed (Paerl et al., 2013a) values of water column-integrated, surface area-weighted annual gross primary production (GPP) by year.

(a) Mean chl *a* (mg m^{-3})		
Box Number	**Model Predictions**	**DCERP Estimates**
1	41.3	50.4
2	27.7	16.5
4	20.5	14.4
5	15.1	13.8
7	4.2	11.6[a]

[a] The value is the mean of data from two sites.

(b) Annual phytoplankton GPP		**Year**	**Model Predictions**	**DCERP Estimates**
Surface-area weighted	(gC m^{-2} yr^{-1})	2008	144	102
Surface-area weighted	(gC m^{-2} yr^{-1})	2009	146	154
Surface-area weighted	(gC m^{-2} yr^{-1})	2010	147	156
Surface-area weighted	(gC m^{-2} yr^{-1})	2011	160	186
Surface-area weighted	(gC m^{-2} yr^{-1})	2008–2011	154	150[b]
Total NRE GPP	(×10^{6} gC yr^{-1})	10/2007–12/2011	12,848	11,954

[b] Adjusted from the original value of 146, which included 3 months of data from 2007. These data were excluded, and GPP from 2008 to 2011 was averaged.

Modeled diatom biomass contributed most (41%) to total chl *a*, followed by dinoflagellates (24%), cyanobacteria (21%), and raphidophytes (13%). The model reproduced the expected seasonal succession in group biomass, with diatoms peaking in late winter and early spring and reaching their minimum each summer, generally in August (**Figure 10-24**). Simulated dinoflagellate biomass was highest in mid-to-late spring, but there was also a late summer peak, more prominent in some years than in others. The dinoflagellate and cyanobacteria sub-models both predicted their lowest biomass in early-to-mid winter. Modeled cyanobacteria concentrations were the converse of dinoflagellates with a high most years in the late summer and a substantial peak in the late spring. Simulated raphidophyte concentrations were also highest in late summer, and lowest in the late winter and early spring.

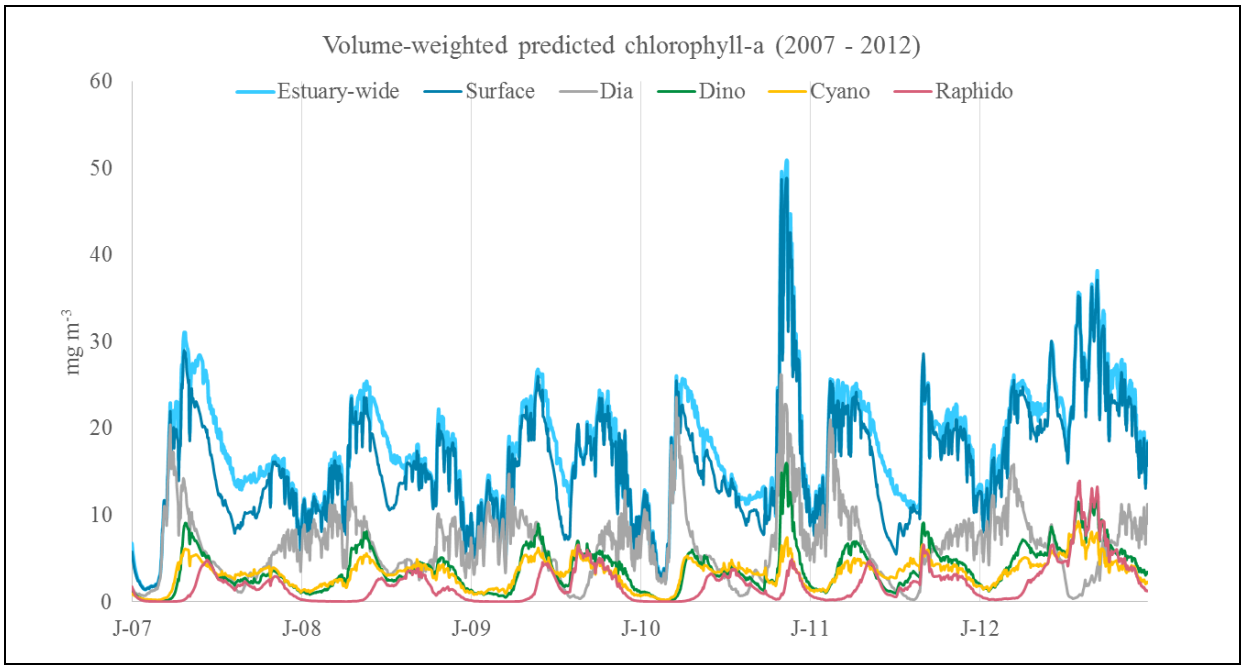

Figure 10-24. Simulated group dynamics from the functional group model, 2007–2012.

Volume-weighted mean surface chlorophyll-*a* concentrations (total and in each functional group), as well as estuary-wide (surface and bottom layers combined) concentrations, for Boxes 1 through 7. Note: Cyano = cyanobacteria; Dia = diatom; Dino = dinoflagellates; Raphido = raphidophytes.

The model captures some of the spatial and temporal distributions of the NRE phytoplankton community based on comparisons to photopigment observations, though the matches are imperfect. The correspondence of modeled diatom and raphidophyte biomass with observed fucoxanthin concentrations was the most ambiguous (**Figure 10-25**). The late summer peak in dinoflagellate chl *a* simulated by the model corresponded with elevated concentrations of peridinin that in some years spanned the length of the estuary (**Figure 10-26**). The most equivalent observable patterns were between the plots of modeled cyanobacteria biomass and observed zeaxanthin concentrations (**Figure 10-27**). Simulated peaks of cyanobacteria chl *a* corresponded to elevated zeaxanthin concentrations in fall 2007, spring and summer 2008, summer and fall 2010, and spring and summer 2012. The comparison was less strong in 2009, and in 2011, there was an elevated mid-year zeaxanthin concentration that was not captured by the model.

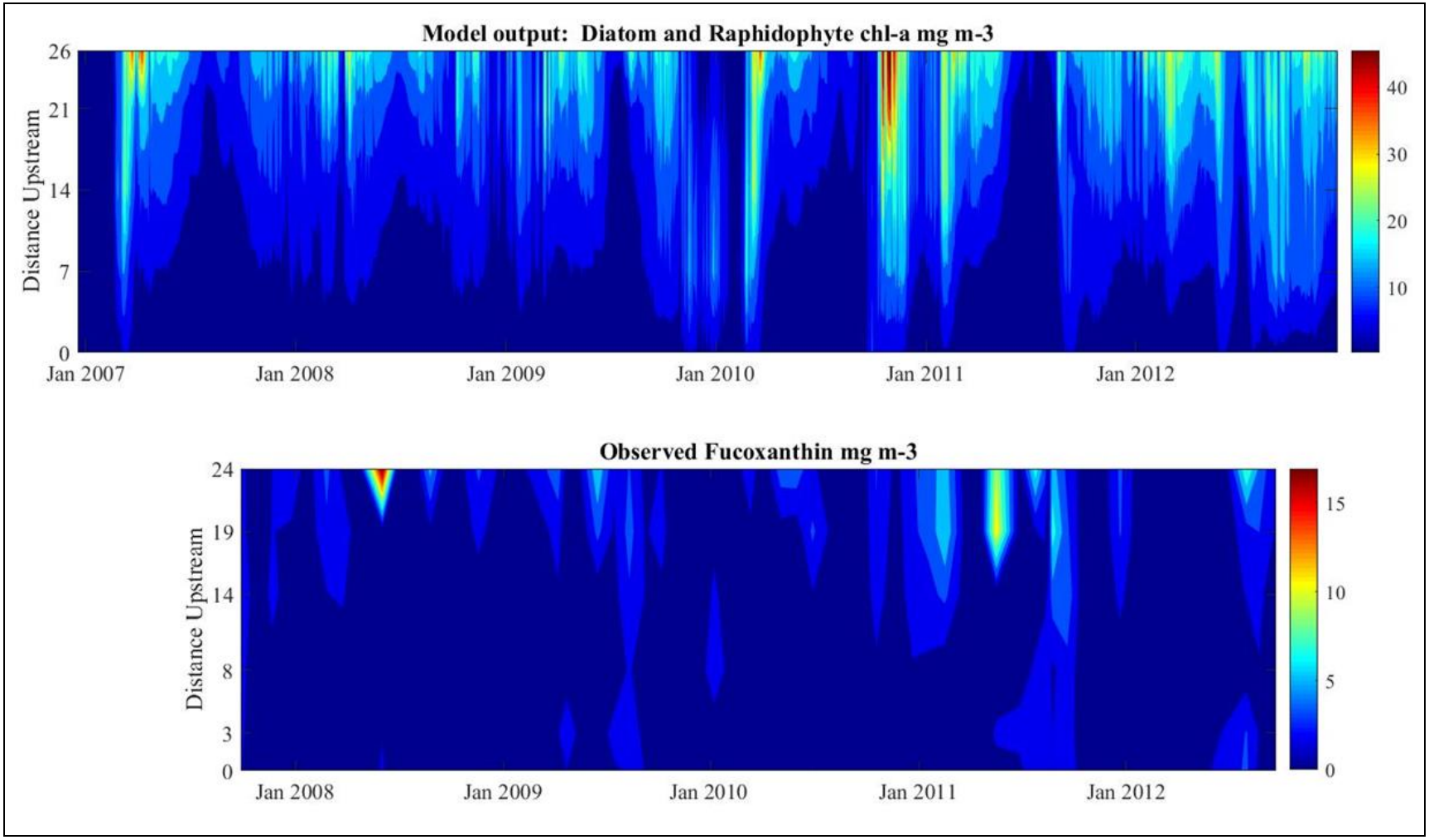

Figure 10-25. Modeled diatom and raphidophyte biomass.

Modeled diatom and raphidophyte chlorophyll-*a* (chl-*a*) concentrations and the corresponding observed fucoxanthin concentrations (Paerl et al., 2013a) in the surface layer of the New River Estuary.

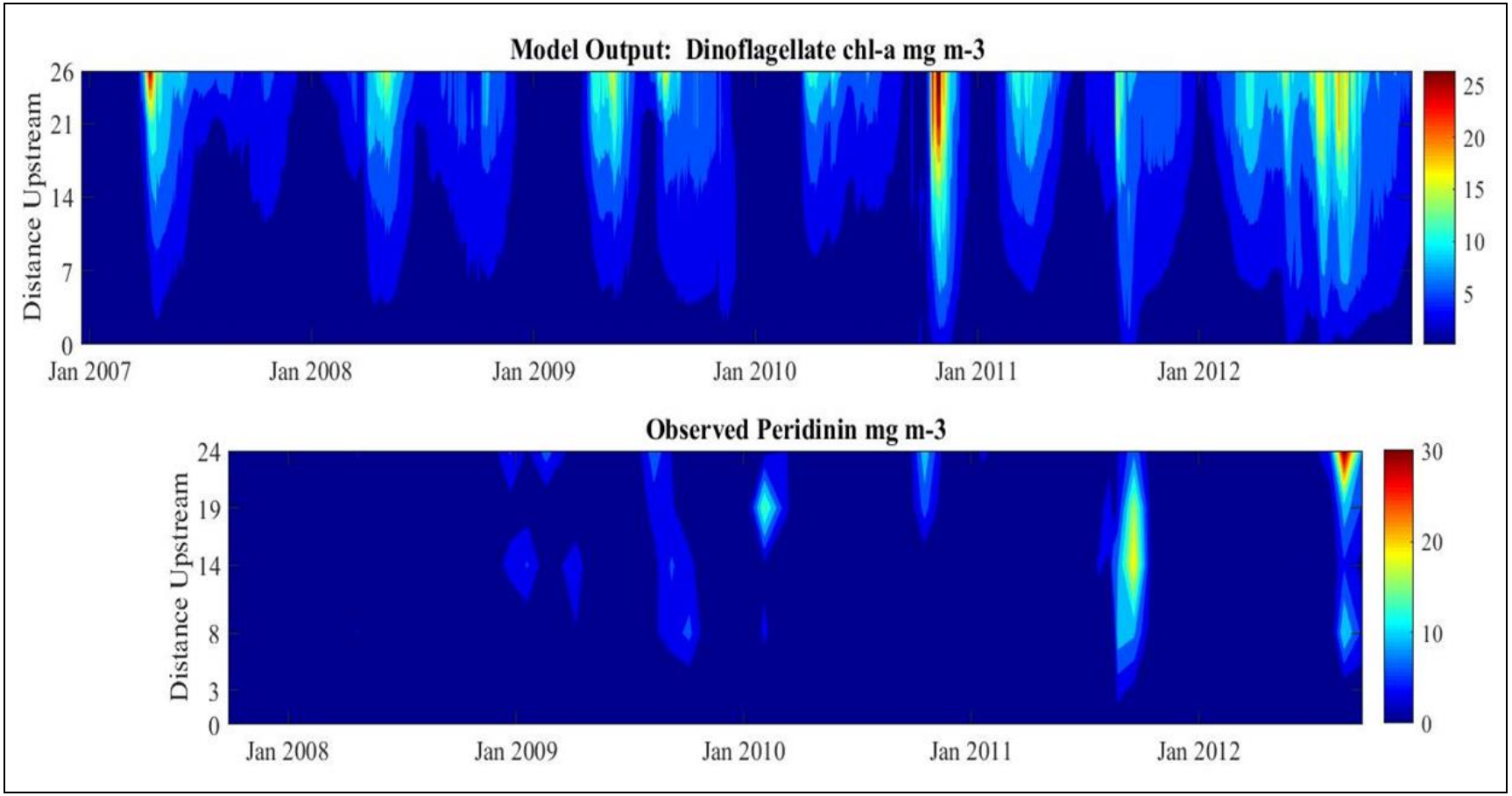

Figure 10-26. Modeled dinoflagellate biomass.

Modeled dinoflagellate chlorophyll-*a* (chl-*a*) concentrations and the corresponding observed peridinin concentrations (Paerl et al., 2013a) in the surface layer of the New River Estuary.

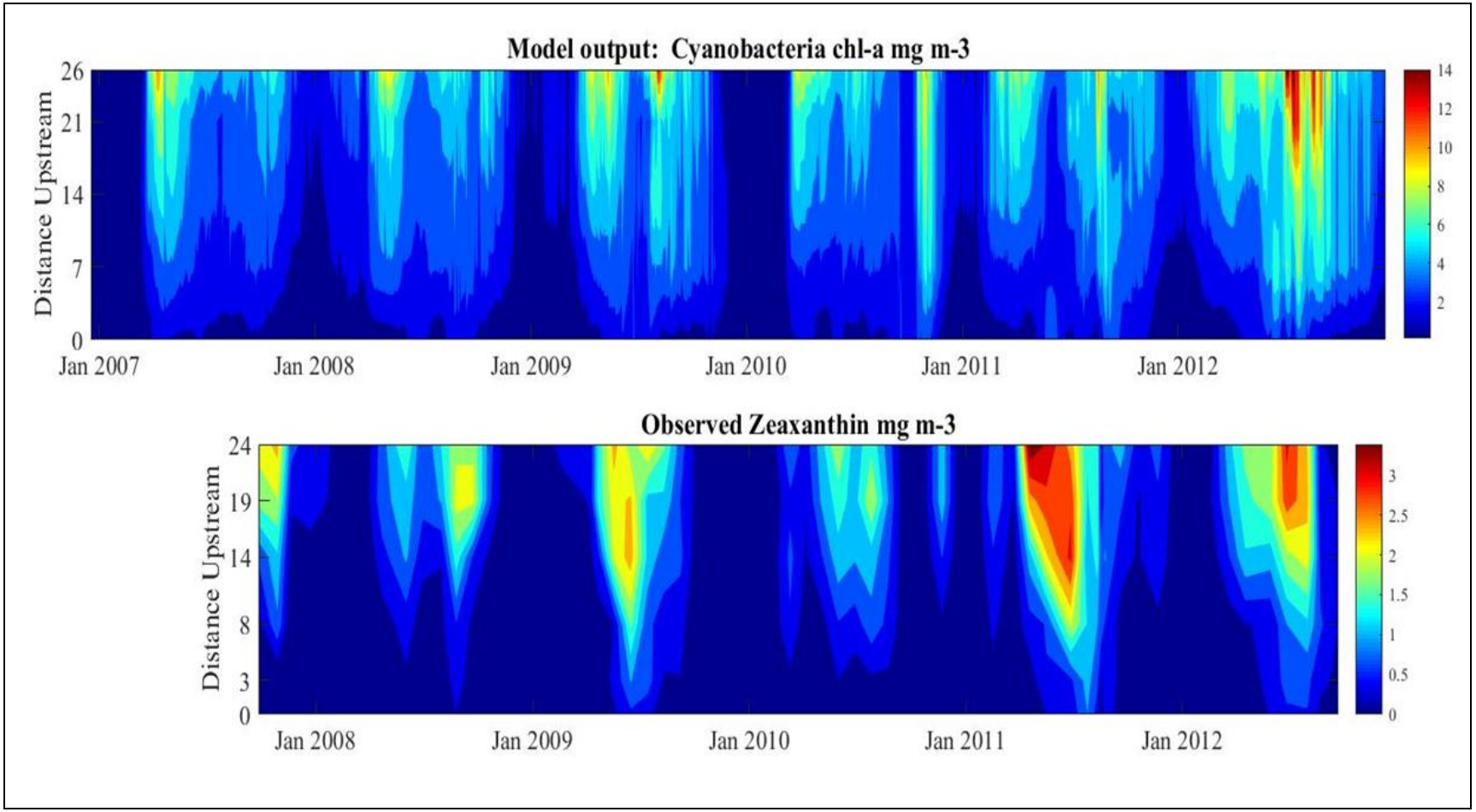

Figure 10-27. Modeled cyanobacteria biomass.

Modeled cyanobacteria chlorophyll-*a* (chl-*a*) concentrations and the corresponding observed zeaxanthin concentrations (Paerl et al., 2013a) in the surface layer of the New River Estuary.

ReNuMa Model

Complete ReNuMa model results will be documented in a forthcoming VIMS M.S. thesis by Ms. Shanna Williamson. The model reproduced discharge and nutrient loading from the Gum Branch watershed and a majority of on-Base sub-watersheds monitored during DCERP (**Figures 10-28 and 10-29; Tables 10-6, 10-7, and 10-8**). Six out of the 11 sub-watersheds used in calibration and validation had good model fits for streamflow. These included two sub-watersheds with data only through the calibration period (i.e., Freeman Creek and Gillets Creek), and four with data through the entire research period (i.e., Cogdels Creek, French Creek, Gum Branch, and Tarawa Terrace). The ReNuMa model captured between 8% and 53% of the variability in the measured data. Three sub-watersheds had intermediate model fits, two with data that spanned the entire research period (i.e., Courthouse Bay and Traps Bay Creek) and one with data only for the calibration period (Camp Johnson). The ReNuMa model captured between 17% and 58% of the variability in these watersheds. The two watersheds with poor fits (i.e., Airport and Southwest Creeks) only had data that extended to the end of the calibration period.

Four out of the 11 sub-watersheds used in calibration and validation had good model fits for TDN loading. Three sub-watersheds (i.e., Cogdels and French Creeks, Gum Branch) had data extending over the entire research period, while one (i.e., Freeman Creek) only had data through the calibration period. The ReNuMa model captured between 10% and 53% of the variability in the measured data. Five sub-watersheds had intermediate model fits, three with data extending for the entire research period (i.e., Courthouse Bay, Tarawa Terrace, and Traps Bay Creek) and two with data only through the calibration period (Camp Johnson and Gillets Creek). The ReNuMa model captured between 9% and 51% of the variability in these sub-watersheds. Airport and Southwest Creeks had poor fits.

Only one out of the 11 sub-watersheds had a good model fit for TDP loading. This sub-watershed (i.e., Freeman Creek) had data only through the calibration period, and the ReNuMa model captured 63% of the variability in the measured data. Seven sub-watersheds had intermediate model fits, six with data through the entire research period (i.e., Cogdels Creek, Courthouse Bay, French Creek, Gum Branch, Tarawa Terrace, and Traps Bay Creek) and one with data only extending through the calibration period (Camp Johnson). The ReNuMa model captured between 11% and 54% of the variability in these watersheds. Three sub-watersheds had poor fits (i.e., Airport, Gillets, and Southwest Creeks) with all having data only extending through the calibration period.

Overall, the ReNuMa model reproduced discharge and loads in most sub-watersheds, providing confidence in its ability to provide estimates of inputs across the entire NRE watershed. Most importantly, fits for discharge and TDN load were particularly good for Gum Branch, which delivers most of the fresh water and nutrients into the NRE (Brush, 2013) and is thus the most critical watershed to simulate with accuracy. The ReNuMa model also reproduced watershed inputs in several of the smaller, on-Base sub-watersheds, and only two watersheds (i.e., Airport and Southwest Creeks) had poor fits for streamflow and TDN. Both are very small, and the former is characterized by a great deal of impervious surface and ditching, which are difficult conditions to reproduce in a watershed model. The ReNuMa model was less successful at reproducing TDP loads, although it still produced good or intermediate fits in most sub-watersheds. Because the NRE is primarily nitrogen limited (Paerl et al., 2013a), it is more important to accurately reproduce TDN loading.

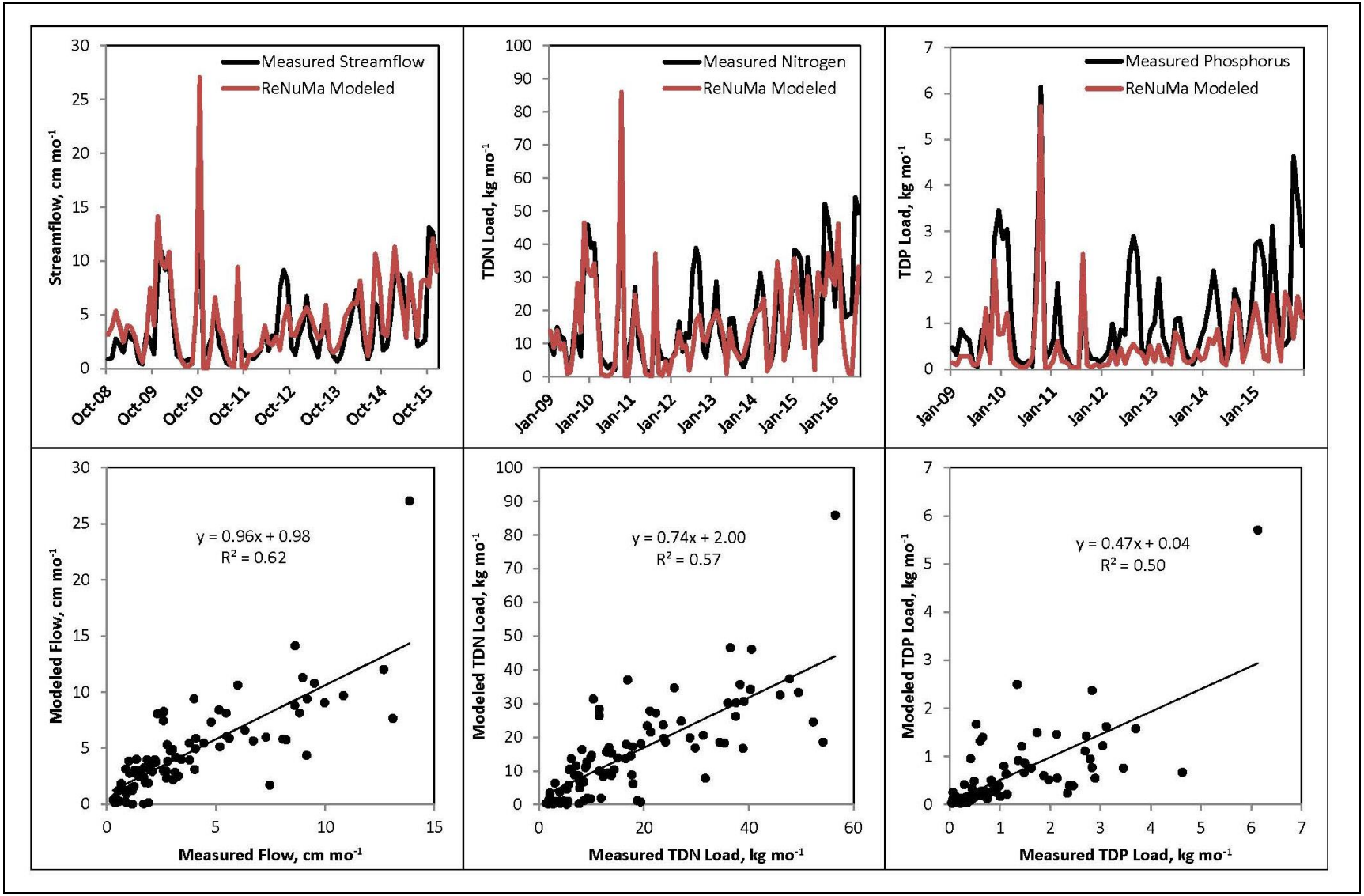

Figure 10-28. Modeled watershed loads at Gum Branch using the ReNuMa model.

Modeled discharge is expressed as a watershed yield (cm mo^{-1}), which is equivalent to cubic meters of discharge per square meter of watershed per month (× 100). Total dissolved nitrogen (TDN) and total dissolved phosphorus (TDP) loads are in kilograms per month (kg mo^{-1}).

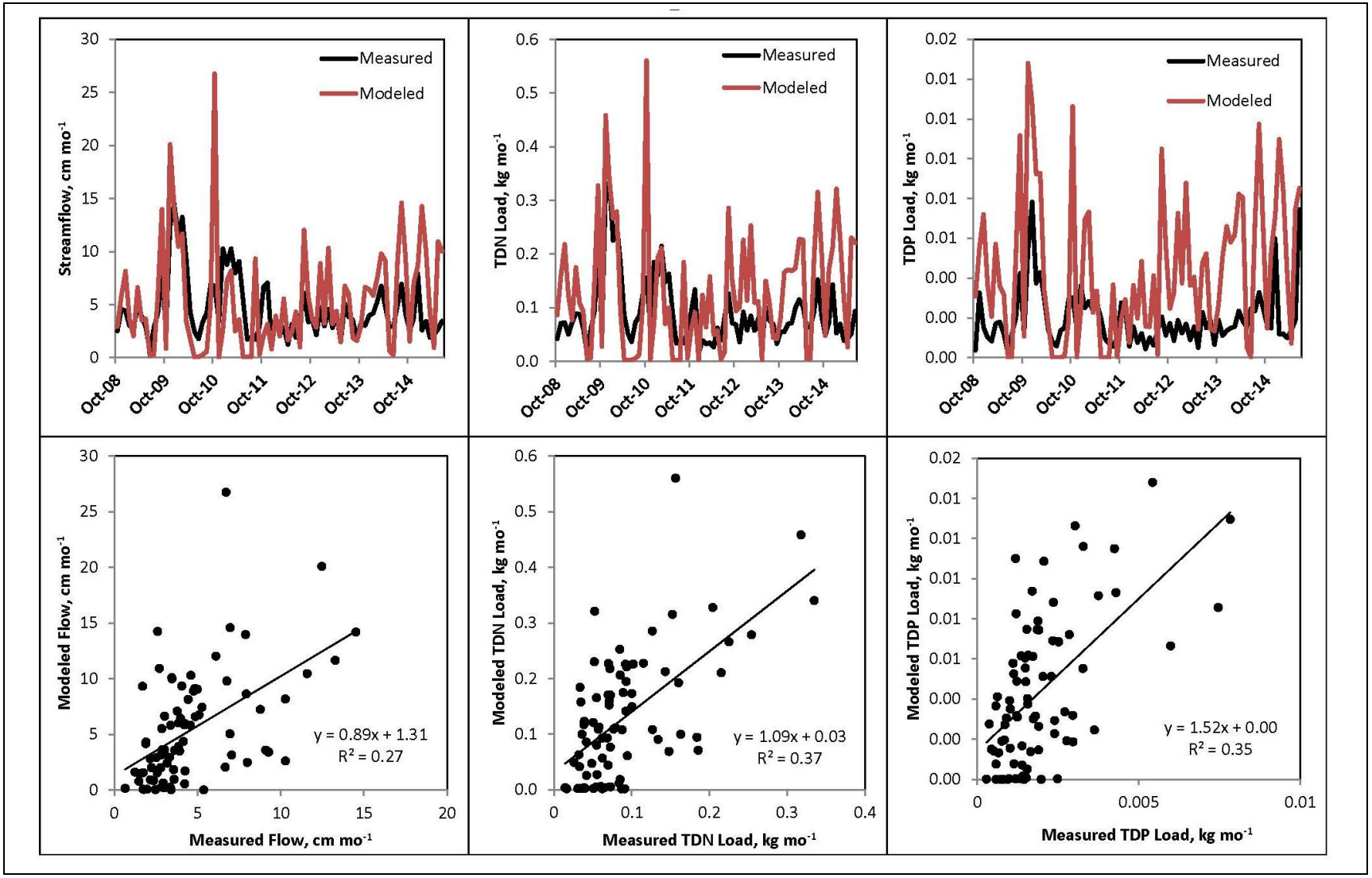

Figure 10-29. Modeled watershed loads from Cogdels Creek using the ReNuMa model.

Cogdels Creek on Marine Corps Base Camp Lejeune is presented as an example of a good fitting sub-watershed. Modeled discharge is expressed as a watershed yield (cm mo^{-1}), which is equivalent to cubic meters of discharge per square meter of watershed per month (× 100). Total dissolved nitrogen (TDN) and total dissolved phosphorus (TDP) loads are in kilograms per month (kg mo^{-1}).

Table 10-6. Skill Assessment for Modeled Streamflow Using the ReNuMa model

Watershed	Slope (Streamflow)	Intercept (Streamflow)	r^2 (Streamflow)	p (Streamflow)		
				Slope	Intercept	OMF
1. Airport	0.19	23.32	0.07	<<0.001	0.015	0.13
2. Camp Johnson	0.52	-0.08	0.17	0.024	0.97	0.016
3. Cogdels	0.94	1.27	0.26	0.73	0.19	<<0.001
4. Courthouse	0.27	4.19	0.24	<<0.001	<<0.001	<<0.001
5. Freeman	1.23	-1.45	0.45	0.38	0.23	<<0.001
6. French	0.88	0.95	0.13	0.87	0.22	<<0.001
7. Gillets	1.14	-1.7	0.49	0.51	0.12	<<0.001
8. Gum Branch	0.9	-0.12	0.53	0.27	0.79	<<0.001
9. Southwest	0.16	3.55	0.08	<<0.001	0.016	0.09
10. Tarawa	0.73	0.41	0.08	0.35	0.61	0.013
11. Traps	0.63	1.72	0.58	<<0.001	<<0.001	<<0.001

Note: Regression statistics between measured and modeled values; *p* indicates significance level; OMF = overall model fit. Watersheds with good (green), intermediate (yellow), and poor (red) fits as defined in the methods.

Table 10-7. Skill Assessment for Modeled TDN Loading Using the ReNuMa Model

Watershed	Slope (TDN)	Intercept (TDN)	r^2 (TDN)	p (TDN)		
				Slope	Intercept	OMF
1. Airport	0.15	0.04	0.06	<<0.001	0.01	0.18
2. Camp Johnson	0.40	-6.8e-04	0.19	<<0.001	0.55	0.013
3. Cogdels	1.12	0.02	0.28	0.56	0.34	<<0.001
4. Courthouse	0	0.09	0.21	<<0.001	0.0013	<<0.001
5. Freeman	0.79	-0.02	0.45	0.22	0.33	<<0.001
6. French	0.73	0.03	0.1	0.29	0.17	0.0043
7. Gillets	0.59	-0.02	0.46	0.001	0.21	<<0.001
8. Gum Branch	1.1	-1.65	0.53	0.38	0.50	<<0.001
9. Southwest	0.1	0.01	0.08	<<0.001	0.026	0.085
10. Tarawa	0.54	0.002	0.09	0.022	0.57	0.008
11. Traps	0.36	0.001	0.51	<<0.001	0.017	<<0.001

Note: Regression statistics between measured and modeled values; *p* indicates significance level; OMF = overall model fit. Watersheds with good (green), intermediate (yellow), and poor (red) fits as defined in the methods.

Table 10-8. Skill Assessment for Modeled TDP Loading Using the ReNuMa Model

Watershed	Slope (TDP)	Intercept (TDP)	r^2 (TDP)	p (TDP)		
				Slope	Intercept	OMF
1. Airport	0.05	0.002	0.004	<<0.001	<<0.001	0.71
2. Camp Johnson	0.65	-1.6e-05	0.44	0.01	0.63	<<0.001
3. Cogdels	1.23	0.0019	0.26	0.32	0.001	<<0.001
4. Courthouse	1.9e-04	0.24	0.21	<<0.001	<<0.001	<<0.001
5. Freeman	1.13	-4.1e-04	0.63	0.44	0.24	<<0.001
6. French	0.44	0.001	0.11	<<0.001	<<0.001	0.003
7. Gillets	-0.0003	0.001	1.7e-06	<<0.001	<<0.001	0.99
8. Gum Branch	0.48	-0.04	0.54	<<0.001	0.65	<<0.001
9. Southwest	0.07	2.9e-04	0.06	<<0.001	<<0.001	0.14
10. Tarawa	0.14	1.02e-04	0.16	<<0.001	<<0.001	0.00017
11. Traps	1.33	1.01e-04	0.48	0.037	<<0.001	<<0.001

Note: Regression statistics between measured and modeled values; *p* indicates significance level; OMF = overall model fit. Watersheds with good (green), intermediate (yellow), and poor (red) fits as defined in the methods.

ESM Scenarios

The re-calibrated, expanded ESM was used to update the DCERP1 scenario analysis in which nutrient loads were removed separately from the on-Base portion of the NRE watershed, MCBCL WWTF, and the off-Base portion of the watershed (**Figure 10-30**). As demonstrated during DCERP1 (Brush, 2013), water quality was almost unchanged when loading from the Base was removed, and only slightly altered when the WWTF was removed, with small improvements near the facility. Conversely, major improvements in water quality were predicted when loading from the off-Base portion of the watershed was removed. Results confirm findings from DCERP1 that the off-Base watershed provides the bulk of the nutrient loading to the NRE (51–68% of all external sources; between 70% and 82% of watershed loads; Brush, 2013). Findings indicate that MCBCL (in Jacksonville, NC) has minimal impacts on NRE water quality at the scale of the ESM boxes and that future improvements in water quality will be best achieved by reducing loading from the upland, off-Base watershed.

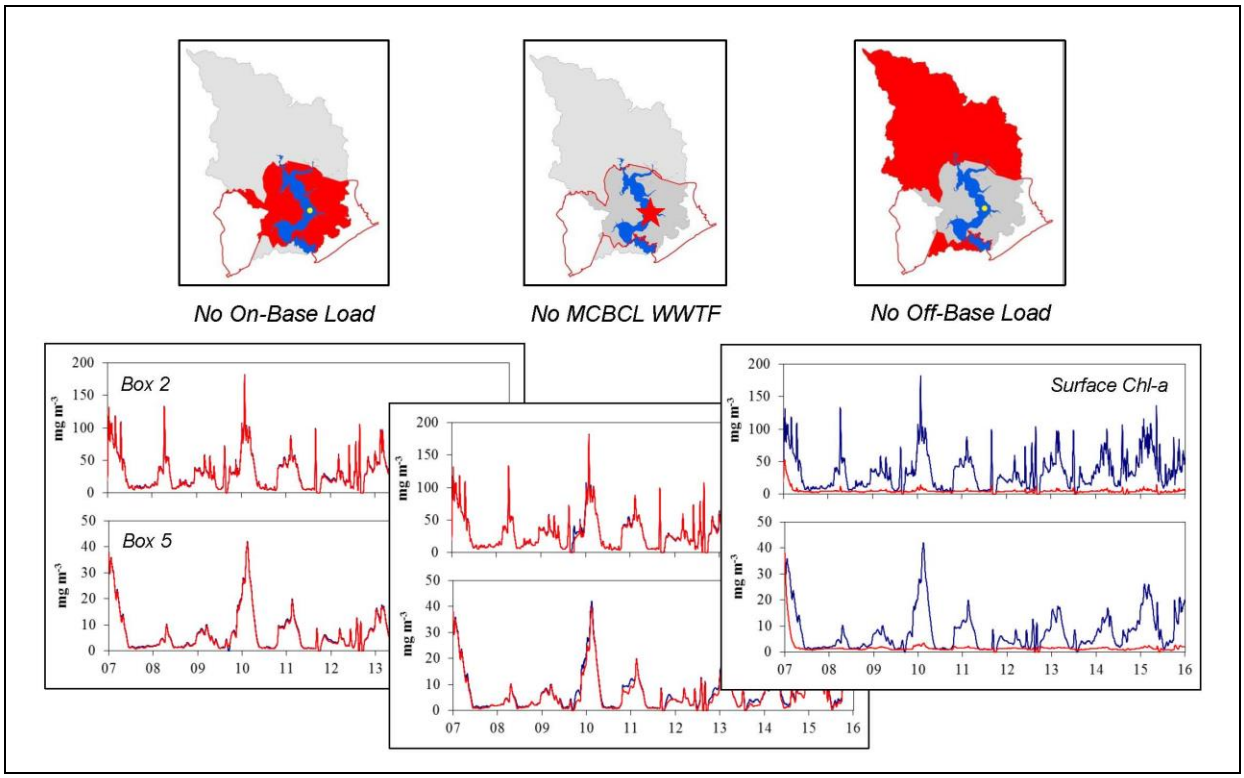

Figure 10-30. Nutrient loading scenarios.

Model predicted surface chlorophyll-*a* (Chl-*a*) concentrations in two representative spatial elements resulting from simulations in which the on-Base (left), Marine Corps Base Camp Lejeune (MCBCL) wastewater treatment facility (WWTF; middle), and off-Base (right) nutrient loads were removed (red lines), compared to predictions under current conditions (blue lines).

A second nutrient-management scenario was conducted with the ESM to simulate potential expansion of the MCBCL WWTF, as Base personnel have previously considered the possibility of tying in a portion of the MCBCL population to the facility. Facility discharge and associated loads of nutrients and organic carbon were increased from current conditions (1 time) up to a doubling of output (two times), also including increases of 10%, (1.1 times) 25% (1.25 times), 50% (1.5 times), and 75% (1.75 times) (**Figure 10-31**). Model results indicate that a doubling of treatment plant inputs to the NRE will have no discernable impact on estuarine water quality at the scale of the ESM boxes, with only minor increases in DIN and decreases in bottom O_2 in the boxes (4 and 9) just upstream of Farnell Bay (Box 5) where the facility discharges its effluent.

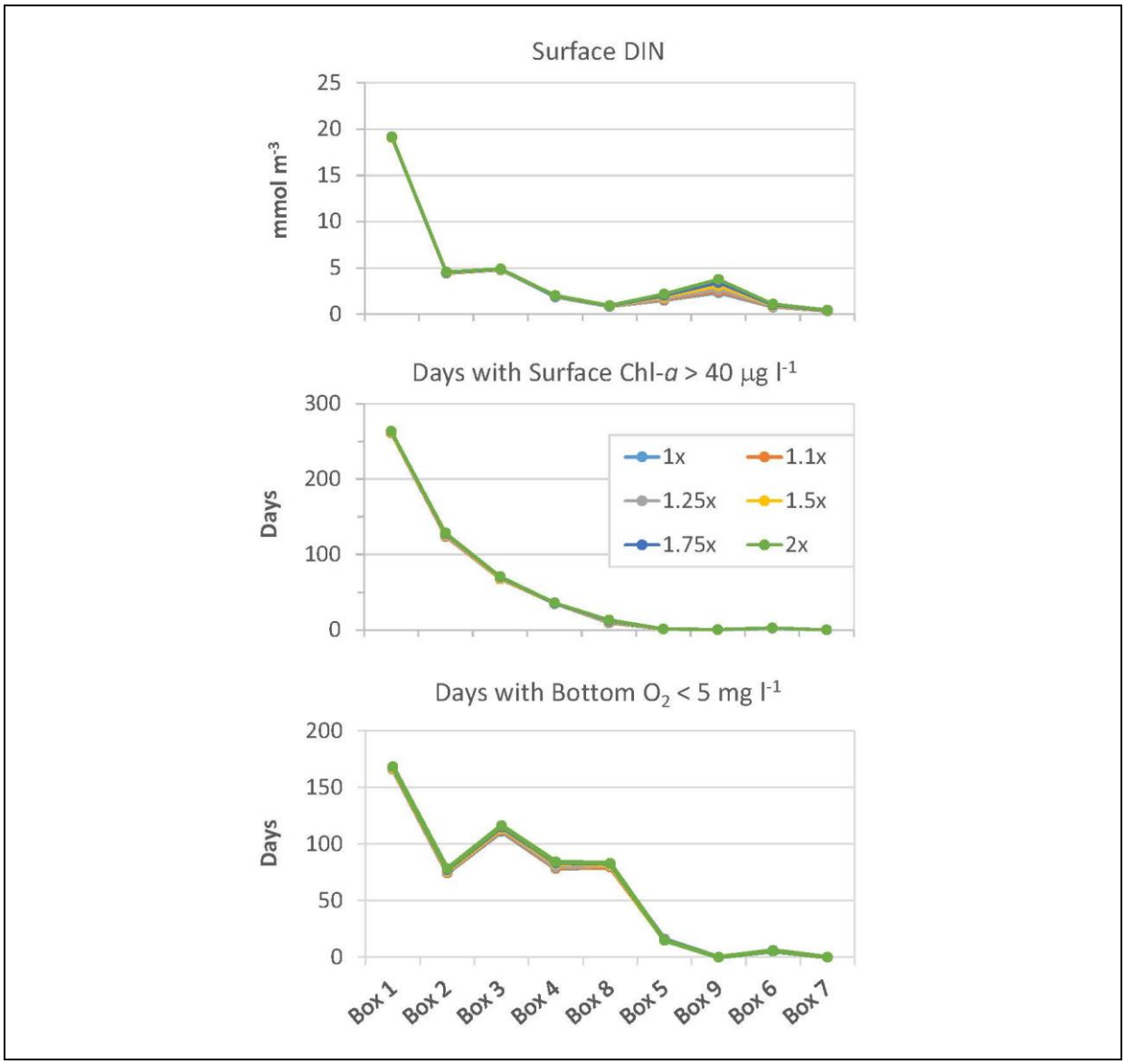

Figure 10-31. Wastewater treatment facility (WWTF) expansion scenarios.

Model predicted water quality in a series of runs in which Marine Corps Base Camp Lejeune (MCBCL) WWTF discharge and resultant loads were increased from current (1 time) to double current (two times) inputs. Values represent annual averages over the period from 2007 through 2015.

Climate projections of air temperature and annual precipitation through 2100 provided by Research Project CC-1 were used to determine the magnitude of likely changes by 2035, 2060, and 2099 relative to current conditions. To account for inter-annual variability, projections were averaged over 10-year periods (2030–2040, 2055–2065, and 2089–2099). The median projection for increases in air temperatures by 2099 was 4.3°C, with first quartile of 3.8°C and the third quartile of 5.0°C (**Figure 10-32**). Air temperatures (T_a) averaged over the NRE during the DCERP years provided by Research Project CC-1 were strongly correlated to surface and bottom water temperatures (T_w) in the NRE (surface: T_w=1.06T_a, r^2=0.80; bottom: T_w=1.05T_a, r^2=0.77), indicating that changes in air temperature directly correlate to changes in water temperature with a 1:1 conversion.

Precipitation projections were more varied, with some predicting increases in annual precipitation and others predicting decreases, and with variations in the magnitude of those changes (**Figure 10-32**). The median projection was for precipitation to increase by 9% by 2099, with first and third quartiles of −5% and +13%, respectively, and minimum and maximum values of ±28%. These changes fall within the typical range in annual precipitation because of current inter-annual variability, so ESM scenarios below focus on changes to temperature.

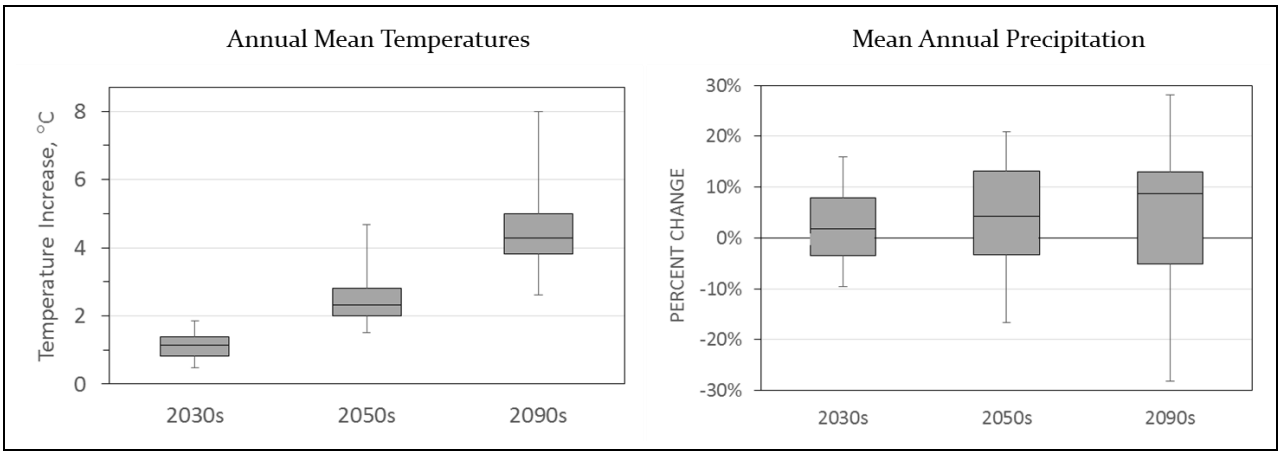

Figure 10-32. Summary of Climate Projections for the New River Estuary.

Box plots showing median (middle line), first and third quartiles (boxes), and minimum and maximum (error bars) projected changes in air temperature and annual precipitation relative to current conditions. Projections were summarized by using the 24 model runs provided by Research Project CC-1 for three decades (the label "2050s" refers to the period 2055–2065).

Simulated warming in increments of +1°C resulted in moderate decreases in average chlorophyll *a* concentrations, and in days with chlorophyll *a* exceeding the state criterion of 40 µg l^{-1}, although phytoplankton NPP changed only slightly (**Figure 10-33**). This result is due to increased respiration and grazing, and is in line with the Metabolic Theory of Ecology that predicts respiration to increase faster with increasing temperatures relative to photosynthesis. Hypoxia was predicted to worsen with warming, with large increases in the number of days with bottom oxygen concentrations below 5 mg l^{-1}. This is a combined result of increased respiration and decreased solubility at warmer temperatures.

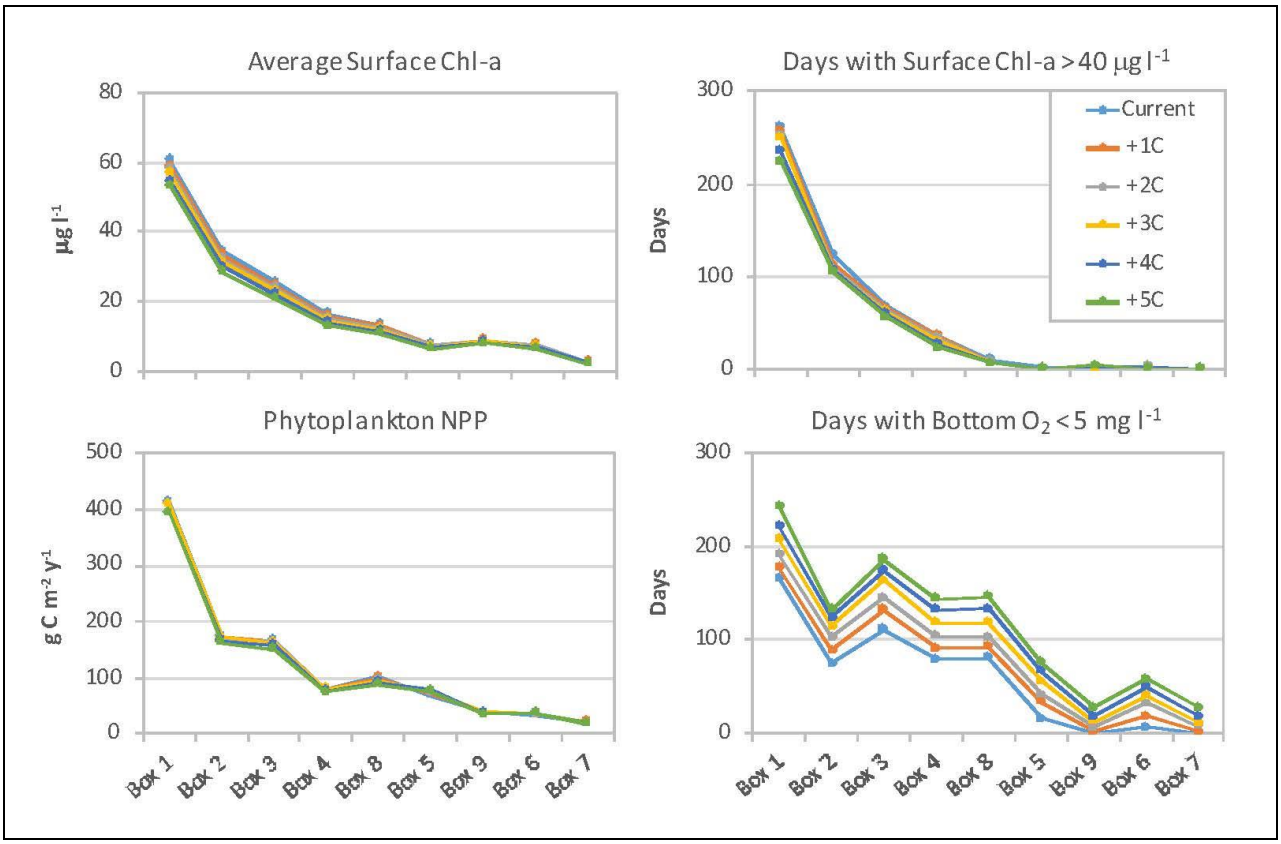

Figure 10-33. Simulated New River Estuary (NRE) response to climate warming.

Predicted phytoplankton chlorophyll-*a* (Chl-*a*), phytoplankton net primary production (NPP), and dissolved oxygen (O_2) throughout the NRE under current conditions and in simulations in which temperatures were increased in 1°C increments. Values represent means over the period 2007–2015.

The interactive effects of nutrient loading and climate warming were assessed by running the model with nutrient loading reduced by half (0.5 times), and with this same reduction concurrent with a +5°C warming (0.5 times, +5°C). Phytoplankton responses were primarily driven by the load reduction, with large decreases in chlorophyll *a* biomass, days above 40 µg l^{-1}, and NPP under the 0.5-times scenario, and only small additional effects when a 5°C warming was combined with the load reduction (**Figure 10-34**). Conversely, all improvements in hypoxia under the load reduction were lost in the combined scenario, with predicted hypoxia becoming worse compared to current conditions. This result implies that climate warming will require larger load reductions to achieve the same level of water quality improvement achievable under current conditions, and is in line with similar findings in the York River Estuary (Lake and Brush, 2015a) and Neuse River Estuary as part of this project (see below).

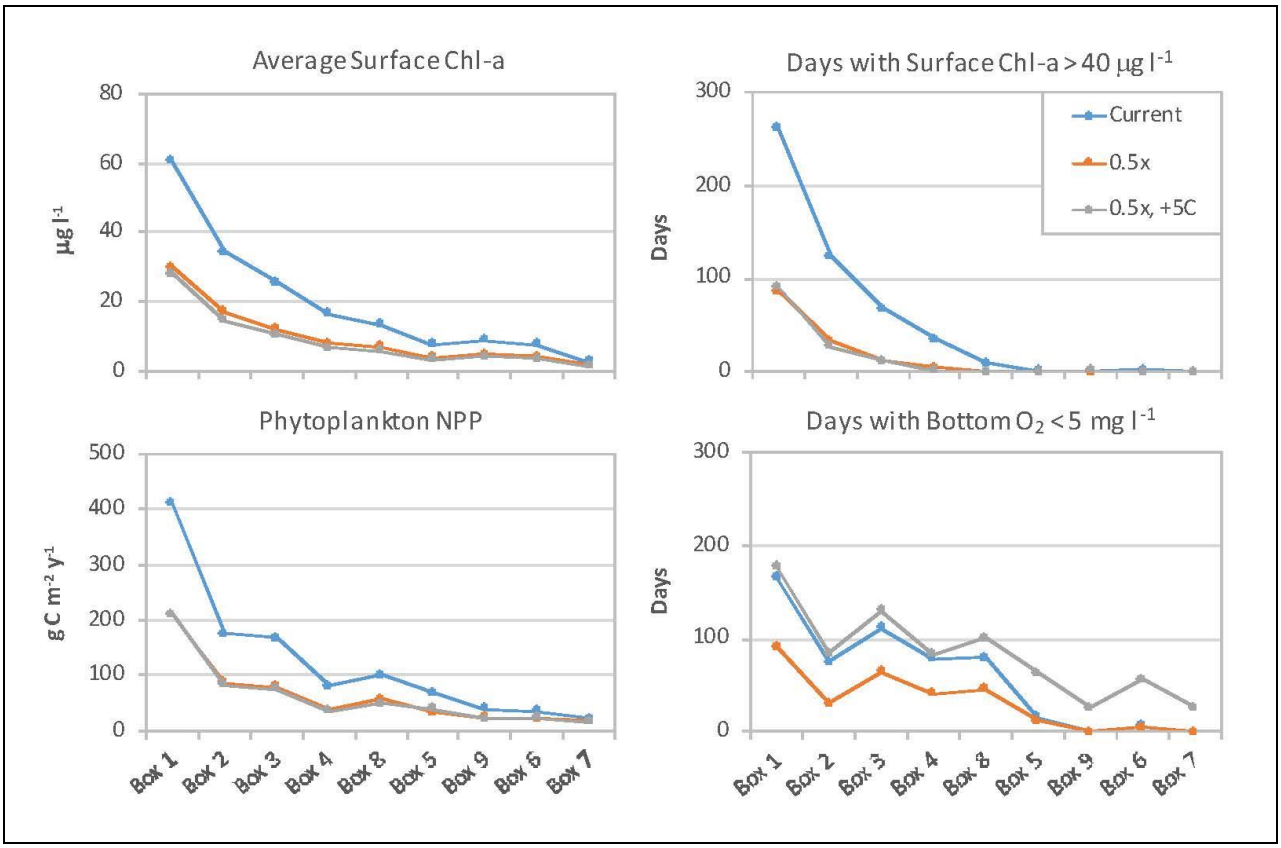

Figure 10-34. Interactive effects of nutrient loading and climate warming on water quality.

Predicted phytoplankton chlorophyll-*a* (Chl-*a*), phytoplankton net primary production (NPP), and dissolved oxygen (O_2) throughout the New River Estuary under current conditions and in simulations in which nutrient loads were reduced by half (0.5 times), with and without a concurrent increase in temperatures by 5°C. Values represent means over the period 2007–2015.

Climate warming was predicted to have a substantial impact on estuarine carbon cycling (**Figure 10-35**). The estuary was predicted to become increasingly net heterotrophic under a warmer climate, with increased efflux of CO_2 to the estuary. A 5°C increase in temperature resulted in a 142% increase in net heterotrophy and a 29% increase in CO_2 efflux. Thus, climate warming will increase the role of the NRE as a source of CO_2 and reduce its potential as a sink or exporter of fixed carbon.

Nutrient load reductions also caused the estuary to become more heterotrophic and a slightly greater source of CO_2 (**Figure 10-35**). Reducing the load by 50% (0.5 times) resulted in a 46% increase in net heterotrophy and a 3.5% increase in annual CO_2 efflux. These results highlight a trade-off in managing for nutrients versus carbon. The 0.5 times scenario resulted in large improvements in water quality, with system-wide reductions in chlorophyll *a* (48%), DIN (42%), and phytoplankton NPP (49%) and an 8.7% increase in bottom O_2 in the upper estuary (Boxes 1–4). However, these improvements come at the expense of reduced potential for carbon storage. Although water quality improvements under this scenario were much greater than the small increase in CO_2 efflux, changes in NEM were much larger, indicating reduced potential of the estuary to store or export fixed carbon.

Finally, nutrient reductions and climate warming interacted to result in even greater increases in net heterotrophy and CO_2 efflux. These rates increased by 181% and 32%, respectively, in the 0.5 times, +5°C scenario (**Figure 10-35**).

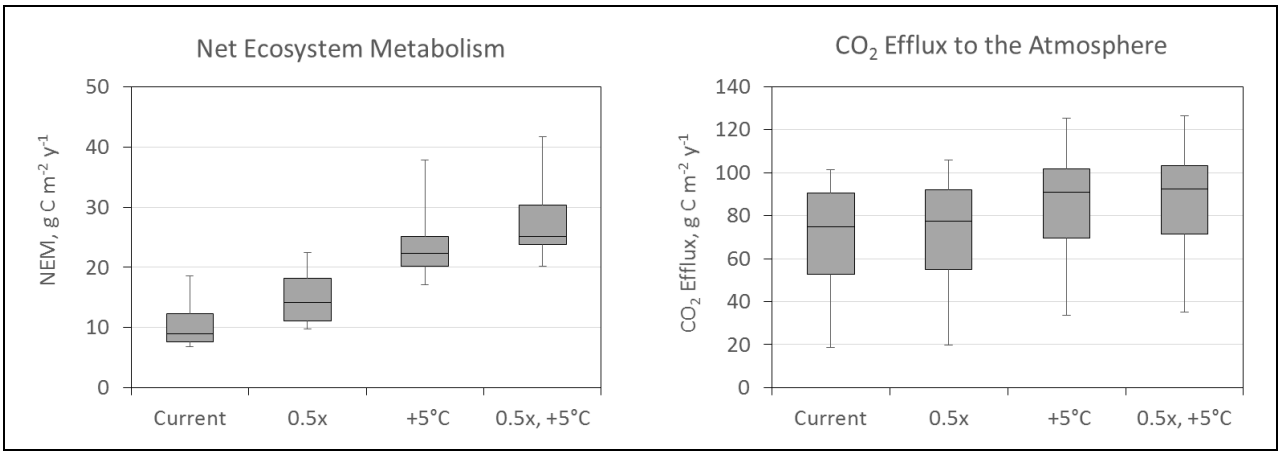

Figure 10-35. Effects of nutrient loading and climate warming on carbon cycling.

Predicted net ecosystem metabolism (NEM) and carbon dioxide (CO_2) efflux for the entire NRE under current conditions and in simulations in which nutrient loads were reduced by half (0.5 times), with and without a concurrent increase in temperatures by 5°C. Box plots summarize annual average values over the period 2007–2015. Positive NEM and CO_2 efflux represent net heterotrophy and release of CO_2 to the atmosphere, respectively.

Phytoplankton Functional Group Scenarios

Simulations with changes in temperature, nutrient loading, and freshwater discharge all resulted in changes to phytoplankton community composition (**Figure 10-36**). The contribution of diatoms to total chl *a* was predicted to decline steadily with increasing temperature, while the contributions of the other groups generally grew. Group biomass and community composition were more sensitive to changes in nutrient loading and discharge. Predicted chl *a* biomass of all groups increased with increasing nutrient loads, but the cyanobacteria sub-model was the least sensitive. Simulations with altered freshwater inflow had a similar, but moderated effect on group chl *a* compared with the nutrient simulations. Although biomass continued to increase with increases in nutrient loading, values leveled off at higher rates of discharge, suggesting diminishing returns due to concomitant increases in light attenuation due to CDOM and decreases in flushing time.

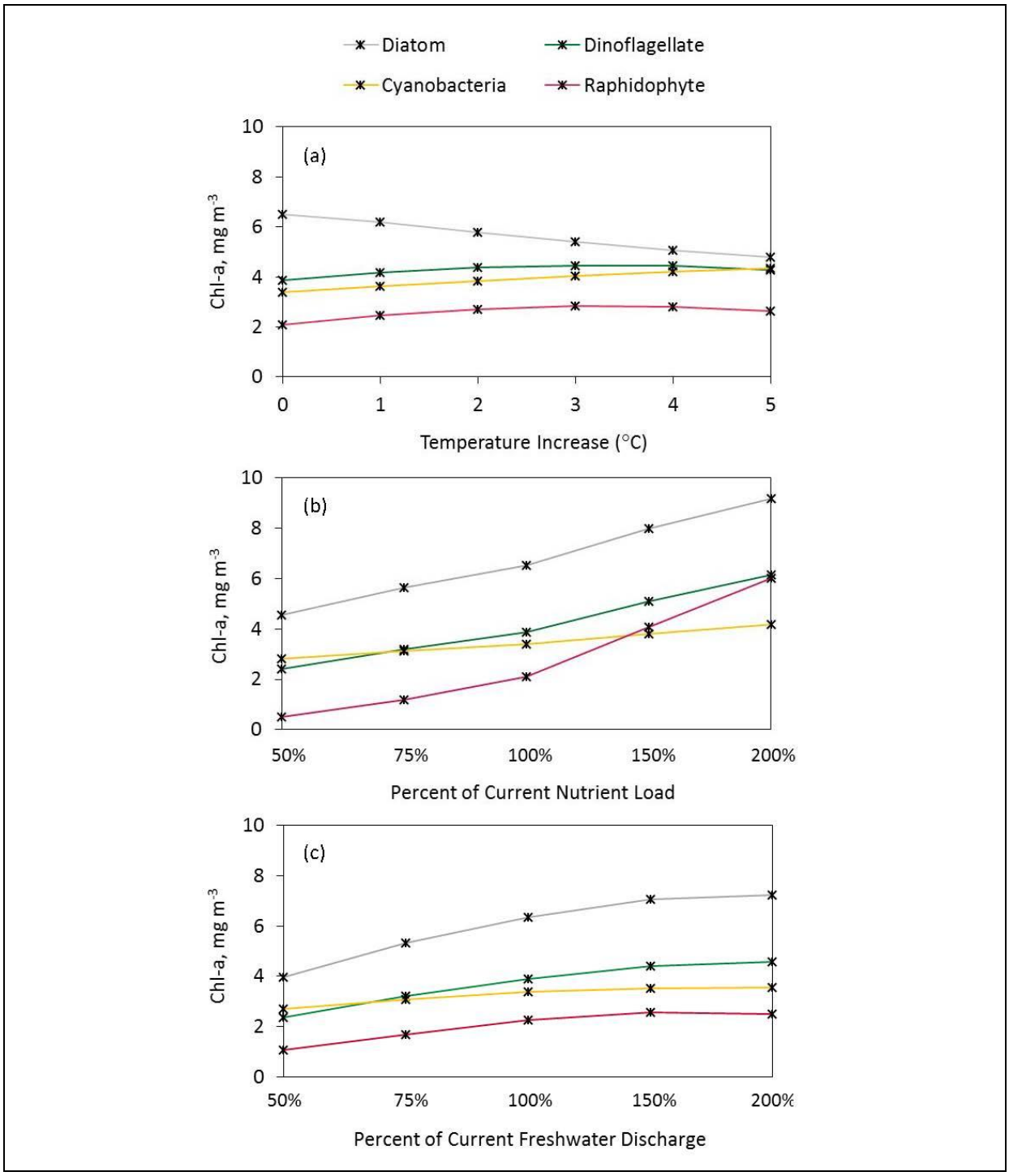

Figure 10-36. Simulated response of phytoplankton functional groups to changes in temperature, nutrient loading, and discharge.

Average daily surface chlorophyll-*a* (Chl-*a*) concentration in each phytoplankton functional group as a function of (a) temperature warming, (b) watershed nutrient loading, and (c) freshwater inflow (with concomitant changes in nutrient loading, salinity, flushing, and chromophoric dissolved organic matter).

ReNuMa Model Scenarios

Model scenarios with increasing air temperatures indicated monotonic decreases in discharge and nutrient loading (**Figure 10-37a**), resulting from increased rates of evapotranspiration in the watershed. Except for TDP from the on-Base watershed, inputs increased no more than 12% with a 5°C warming. Impacts from changes in annual precipitation up to ±20% caused comparatively greater changes in watershed inputs, with greater discharge and nutrient loading in wetter years (**Figure 10-37b**). In scenarios with combined warming and altered precipitation, warming and reduced precipitation resulted in greater decreases in watershed inputs than from either change alone, and warming partially reduced the increases in watershed inputs due to increased precipitation (**Figure 10-37c**).

Simulated increases in developed land cover resulted in differing responses among discharge, TDN, and TDP loading in the off- and on-Base watersheds, but generally, changes in these inputs were small (**Figure 10-38a**). In contrast, increases in agricultural land uses in the off-Base watershed resulted in larger increases in nutrient loading, although changes in discharge were small (**Figure 10-38b**). Taken together, results indicate that projected climatic warming and changes in precipitation (whether increases or decreases) have the potential to substantially alter watershed delivery of fresh water and nutrients to the NRE, with the direction of the change dependent primarily on precipitation. Changes in land use which are nutrient intensive (e.g., agriculture) will interact with these climate-mediated effects, and they have the potential to exacerbate increased loading in wetter years.

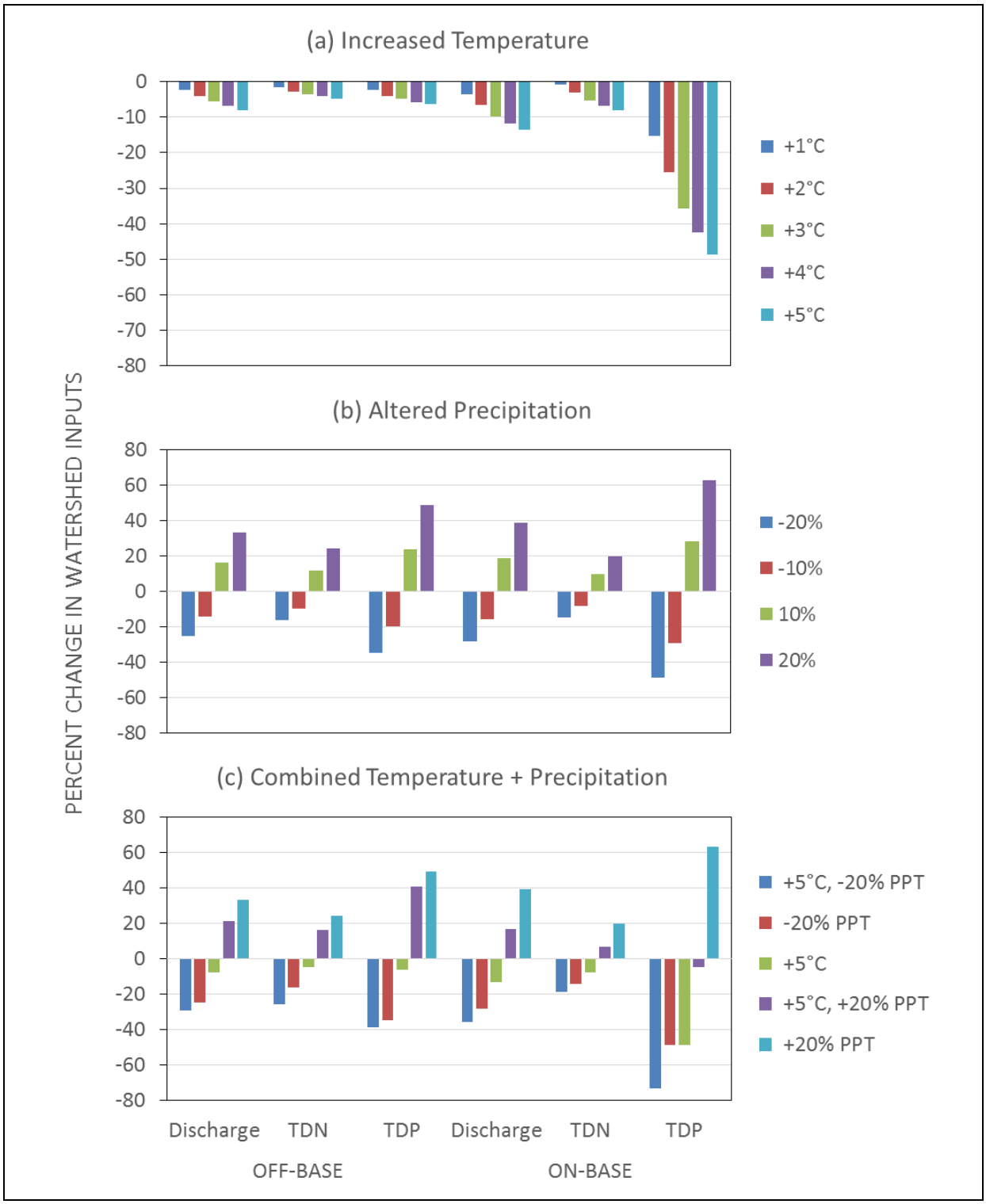

Figure 10-37. Simulated response of watershed inputs to climate change.

Percent change in average annual discharge and nutrient loading from the off- and on-Base watersheds of the New River Estuary as a function of climatic warming and altered precipitation (PPT).

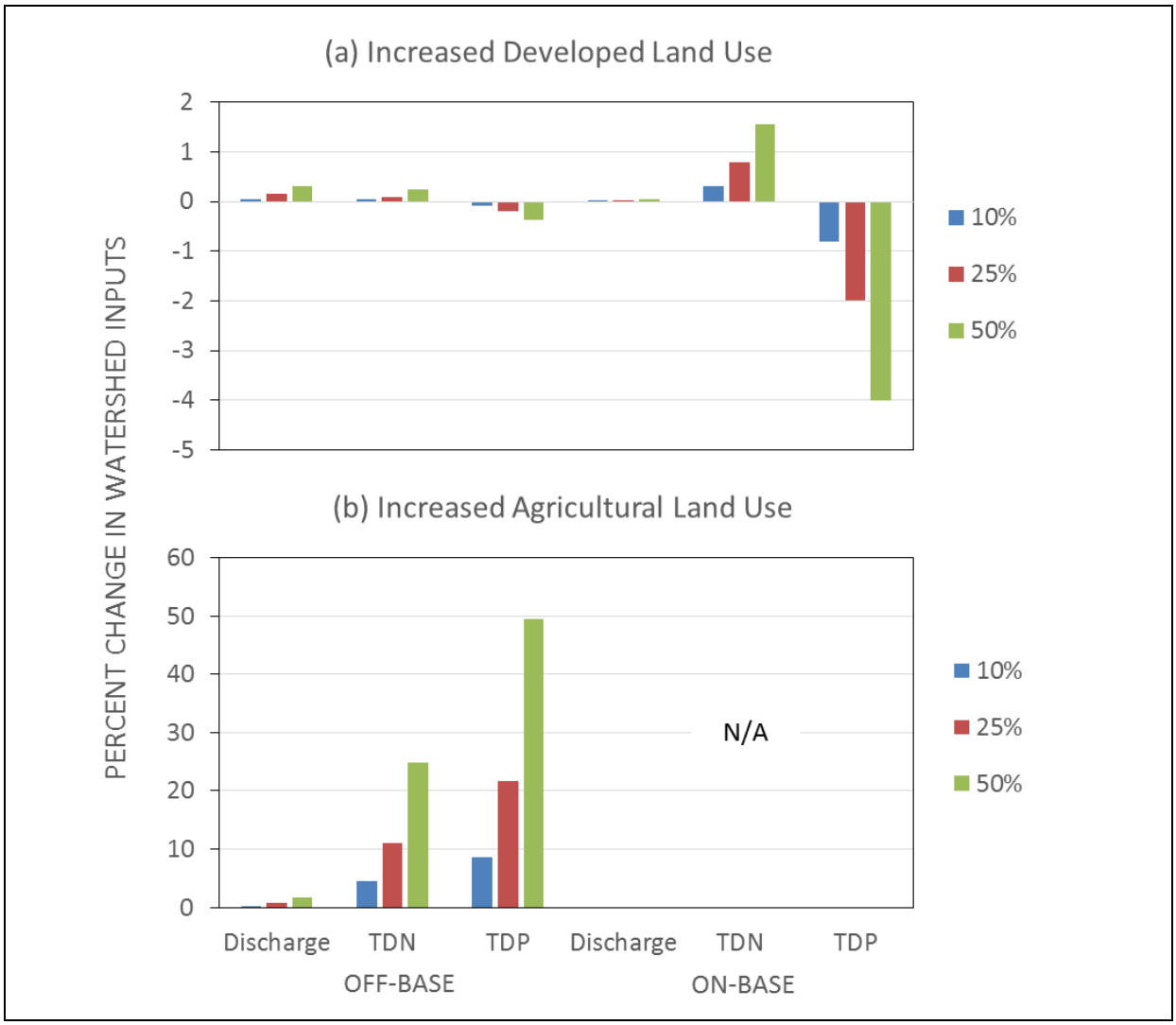

Figure 10-38. Simulated response of watershed inputs to land-use change.

Percent change in average annual discharge and nutrient loading from the off- and on-Base watersheds of the New River Estuary (NRE) as a function of increasing developed and agricultural land. The latter was simulated only for the off-Base watershed. N/A = Not applicable.

Application in Other Estuarine Systems—Neuse River ESM

Median modeled flushing time in the Neuse River was 33 days, with large seasonal and shorter term variations associated with changes in freshwater discharge (**Figure 10-39**). The ESM reproduced the magnitudes, down-estuary gradients, and approximate dynamics of multiple parameters from the ModMon monitoring database (**Figures 10-40 and 10-41**). The model was tested against observed light attenuation (K_D); concentrations of DIN, DIP, chl *a*, and DO in surface and bottom waters; and phytoplankton primary production, with low absolute, percent, and RMS errors (**Table 10-9**). At the request of MCAS Cherry Point, the model was also set up to simulate concentrations of TSS, which were reproduced with relatively low error once stormwater inputs were included (**Figure 10-42 and Table 10-9**). The model also reproduced the relatively limited data compiled from the literature for sediment chl *a*, water column and

sediment respiration, BMA primary production, sediment nutrient fluxes, and denitrification (not shown).

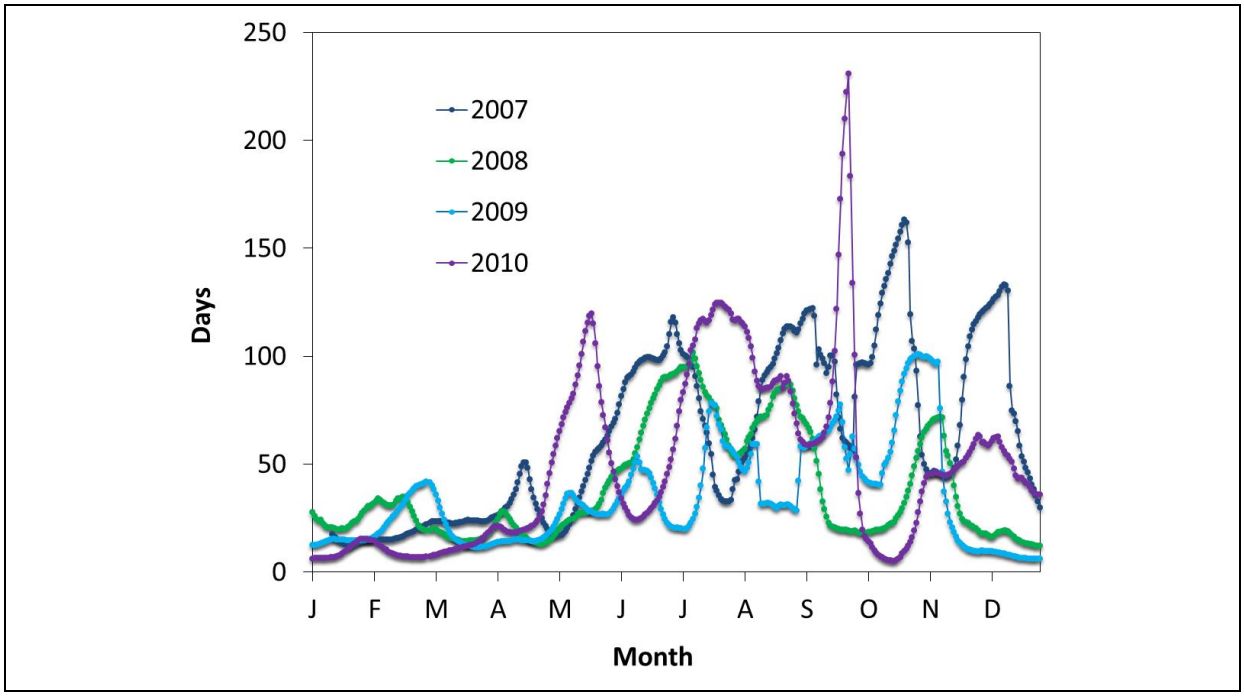

Figure 10-39. Flushing times of the Neuse River Estuary.

Fresh water flushing times computed with the Neuse River Estuarine Simulation Model for each year of the model simulation.

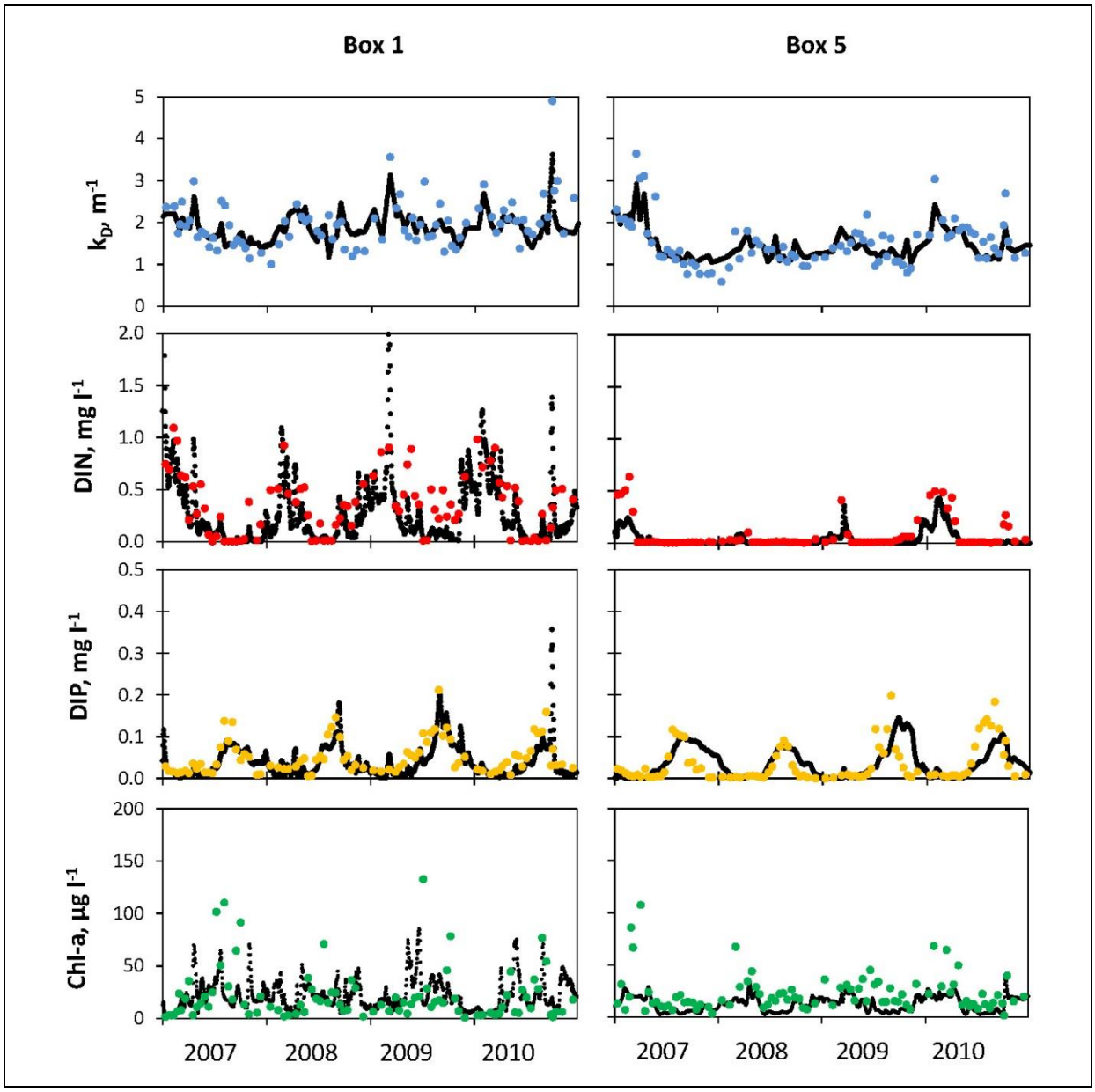

Figure 10-40. Final calibration of the Neuse River Estuarine Simulation Model.

Modeled (black points) and observed (colored points) light attenuation (k_D) and surface dissolved inorganic nitrogen (DIN), dissolved inorganic phosphorus (DIP), and chlorophyll-*a* (Chl-*a*) concentrations in two spatial elements of the Neuse River Estuary (see **Figure 10-9**).

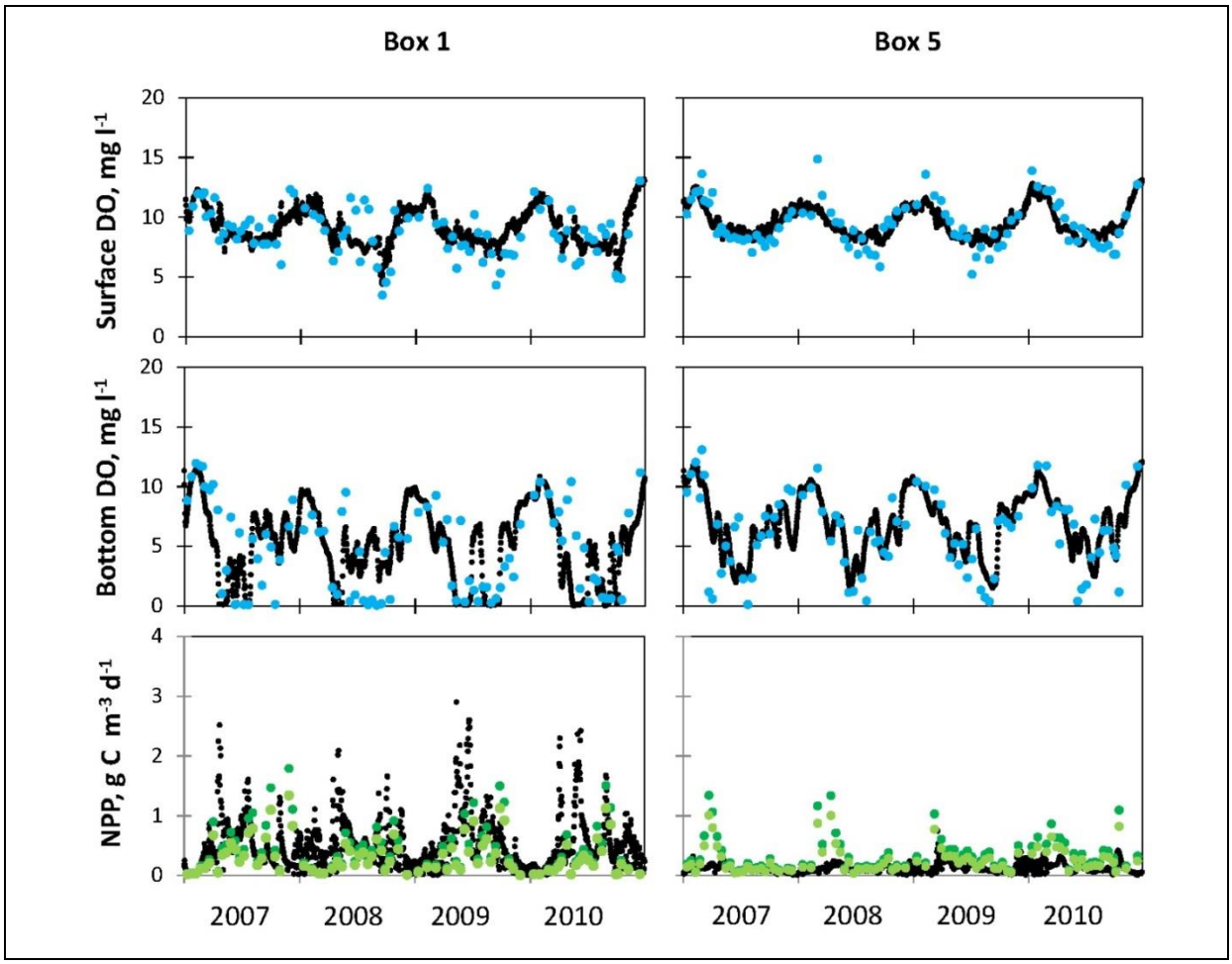

Figure 10-41. Final calibration of the Neuse River Estuarine Simulation Model.

Modeled (black points) and observed (colored points) surface and bottom dissolved oxygen (DO) concentrations and phytoplankton net primary production (NPP) in two spatial elements of the Neuse River Estuary (see **Figure 10-9**).

Table 10-9. Skill Assessment of the Neuse River Estuarine Simulation Model

		K_D	TSS_S	TSS_B	$PHYTO_S$ Chl-*a*	$PHYTO_B$ Chl-*a*	DO_S	DO_B	DIN_S	DIN_B	DIP_S	DIP_B	$PHYTO_S$ NPP
		m^{-1}	$g\ m^{-3}$	$g\ m^{-3}$	$\mu g\ L^{-1}$	$mg\ m^{-2}$	$mg\ O_2\ L^{-1}$	$mg\ O_2\ L^{-1}$	$g\ N\ m^{-3}$	$g\ N\ m^{-3}$	$g\ P\ m^{-3}$	$g\ P\ m^{-3}$	$g\ C\ m^{-2}\ d^{-1}$
	n =	*432*	*83*	*83*	*618*	*614*	*619*	*619*	*614*	*614*	*595*	*592*	*614*
Boxes 1 - 8	**ABS Error**	**0.13**	**1.97**	**2.40**	**6.05**	**2.46**	**0.47**	**0.73**	**0.01**	**0.04**	**0.01**	**0.02**	**0.04**
	% Error	**9.47**	**23.34**	**25.73**	**39.49**	**24.39**	**5.16**	**12.80**	**62.67**	**63.80**	**39.22**	**98.67**	**25.01**
	RMS Error	**0.30**	**3.41**	**4.32**	**26.88**	**17.31**	**1.08**	**2.02**	**0.12**	**0.10**	**0.03**	**0.06**	**0.22**
	Nash-Sutcliffe	**0.76**	**0.29**	**0.05**	**0.06**	**0.17**	**0.72**	**0.65**	**0.73**	**0.68**	**0.53**	**0.42**	**0.29**
	n =	*432*	*130*	*83*	*659*	*614*	*686*	*619*	*661*	*614*	*642*	*592*	*614*
All Sites	**ABS Error**	**0.13**	**2.18**	**2.40**	**6.31**	**2.46**	**0.55**	**0.73**	**0.01**	**0.04**	**0.01**	**0.02**	**0.04**
	% Error	**9.47**	**26.56**	**25.73**	**41.80**	**24.39**	**6.03**	**12.80**	**63.13**	**63.80**	**43.20**	**98.67**	**25.01**
	RMS Error	**0.30**	**4.77**	**4.32**	**27.30**	**17.31**	**1.27**	**2.02**	**0.11**	**0.10**	**0.05**	**0.06**	**0.22**
	Nash-Sutcliffe	**0.76**	**0.21**	**0.05**	**0.04**	**0.17**	**0.63**	**0.65**	**0.73**	**0.68**	**0.20**	**0.42**	**0.29**

Model skill was calculated for 2007 through 2010 using available monitoring data. Skill metrics were calculated by comparing the observations to the closest modeled value within 1 week (±7 days). Subscripts "S" and "B" refer to surface layers and bottom layers, respectively.

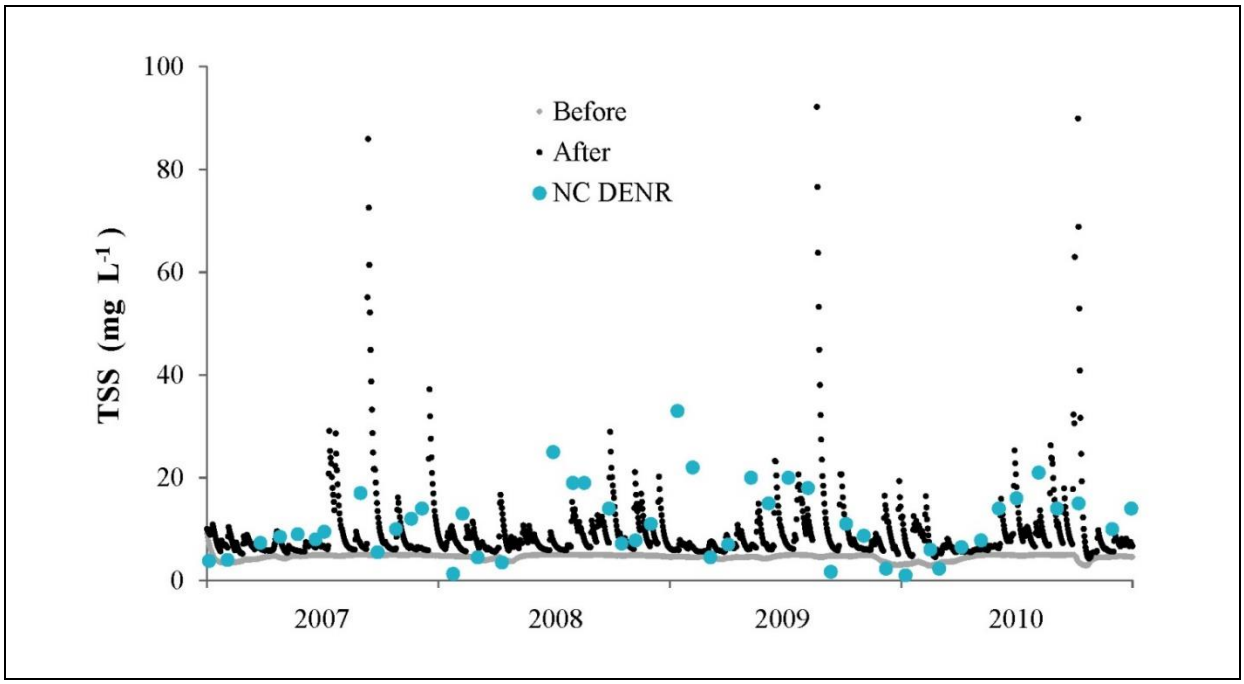

Figure 10-42. Modeled total suspended solids (TSS) in Slocum Creek, Neuse River, NC.

Observed (colored points) surface concentrations of TSS in Slocum Creek, adjacent to Marine Corps Air Station Cherry Point, and modeled values before (grey points) and after (black points) inclusion of stormwater loads from the watershed. Observations were collected by the North Carolina Department of Environment and Natural Resources (NC DENR).

The Neuse River ESM was used to conduct a series of simulations to determine the major drivers of water quality in the Neuse and the role of inputs from MCAS Cherry Point. First, simulations were conducted to assess the impact of land-based nutrient inputs into Slocum and Hancock Creeks which lie adjacent to MCAS Cherry Point. Simulations were run in which inputs from the watershed on the Base, the watershed off the Base, the Havelock WWTF, and all three were removed. Removal of watershed nutrient loads from MCAS Cherry Point had little impacts on water quality in Slocum Creek; however, removal of loads from the off-Base watershed had larger effects; removal of those loads together with the Havelock WWTF had the biggest effects (**Figures 10-43 and 10-44**). We note, however, that we have no direct measurements of nutrient loading from MCAS Cherry Point; rather loads were estimated by scaling measured watershed yields at the USGS monitoring station in Kinston, NC, to the area of each watershed draining to the Neuse River Estuary. This approach is the best available method for estimating these loads, but they are nevertheless uncertain. We also note that the Havelock WWTF outfall has recently been relocated (after the ESM simulation period) to Box 5 in the mainstem of the Neuse River Estuary, near the outfall for the MCAS Cherry Point WWTF.

Second, the model was run with and without discharges from the MCAS Cherry Point WWTF, which discharges directly into the Neuse River (Box 5), to assess the impacts of this discharge on water quality within the Neuse River Estuary. Model results indicate that the WWTF discharge has no detectable influence on water quality, at least at the scale of the coarse boxes used in the ESM (**Figure 10-45**).

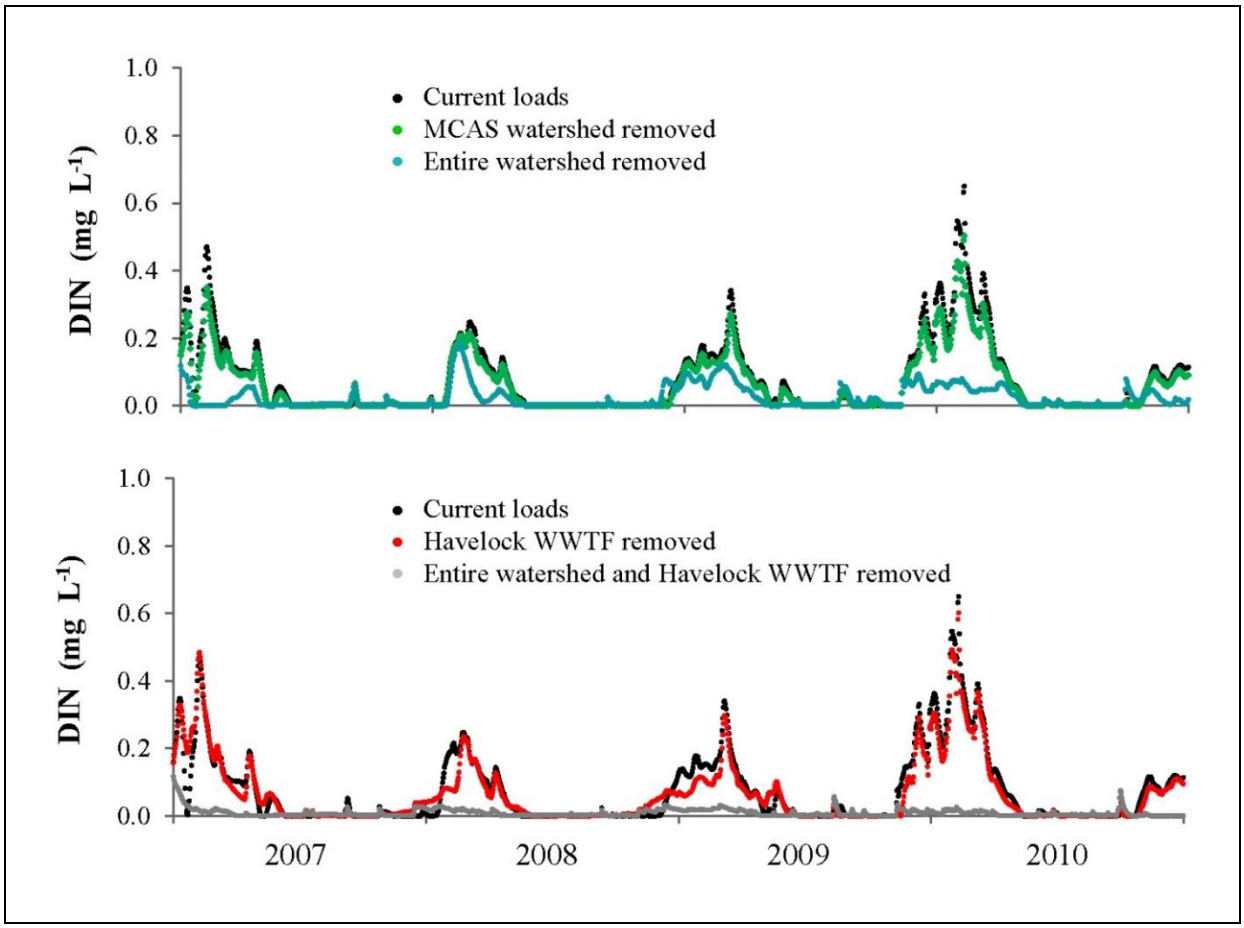

Figure 10-43. Impact of watershed loading on dissolved inorganic nitrogen (DIN) in Slocum Creek.

Output of surface DIN from the Neuse River Estuarine Simulation Model in Slocum Creek (Box 9) under current watershed loads and in several simulations in which various loading sources were removed.

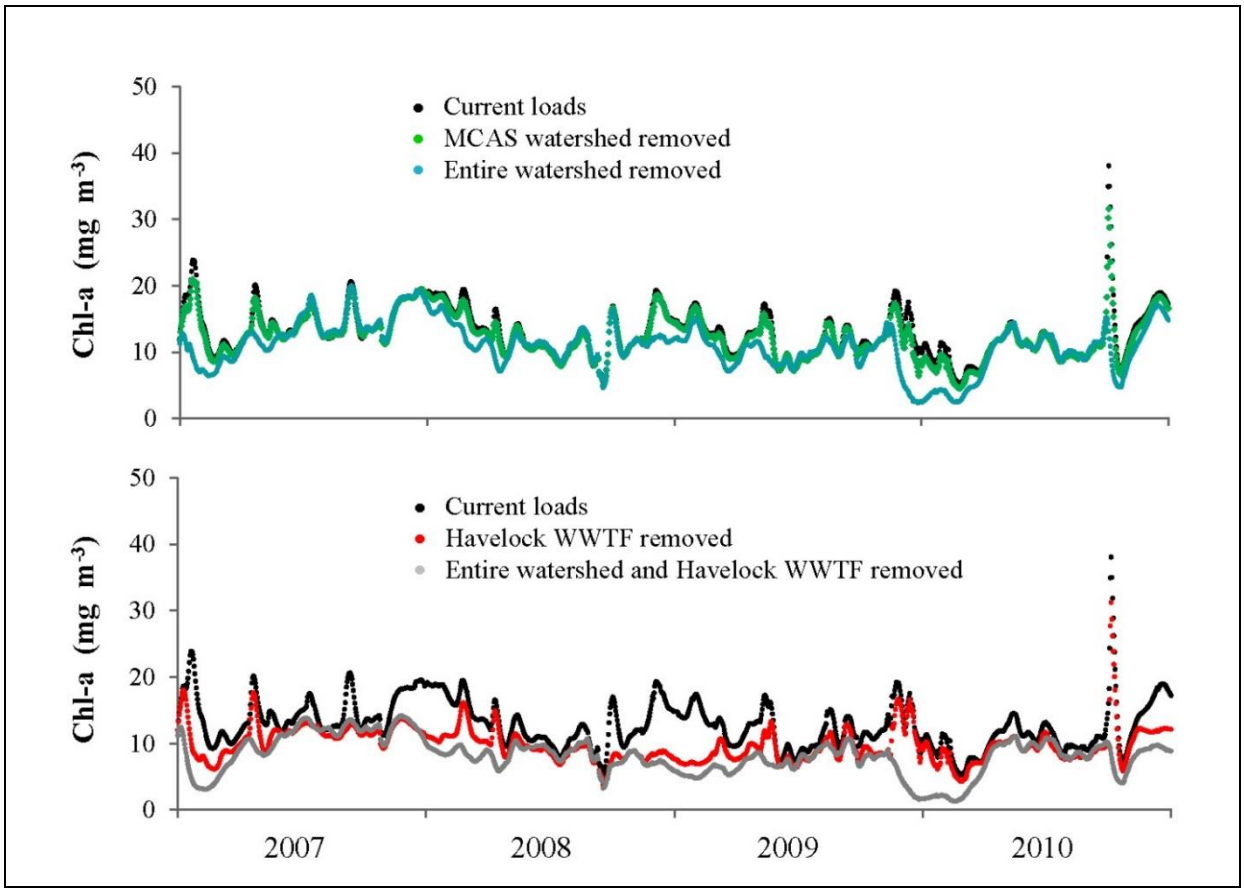

Figure 10-44. Impact of watershed loading on chlorophyll-*a* (Chl-*a*) in Slocum Creek.

Output of surface Chl-*a* from the Neuse River Estuarine Simulation Model in Slocum Creek (Box 9) under current watershed loads and in several simulations in which various loading sources were removed.

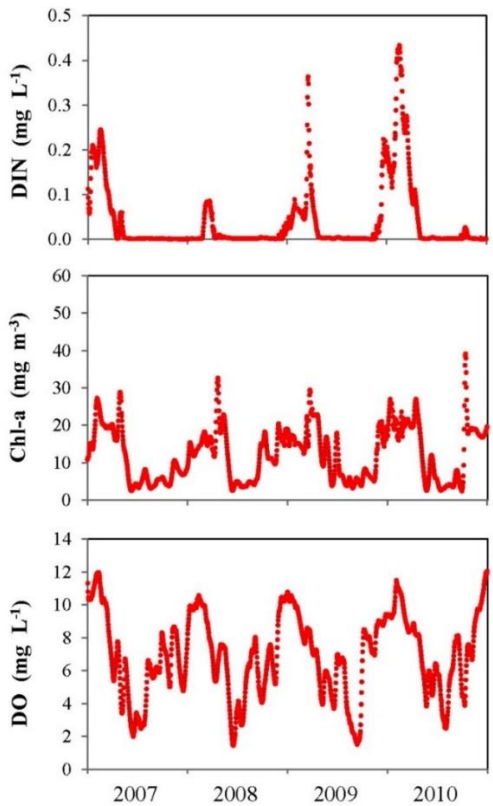

Figure 10-45. Impact of the Marine Corps Air Station (MCAS) Cherry Point wastewater treatment facility (WWTF) on Neuse River water quality.

Output of surface dissolved inorganic nitrogen (DIN), surface chlorophyll-*a* (Chl-*a*), and bottom water dissolved oxygen (DO) in Box 5 of the Neuse River Estuarine Simulation Model under calibration conditions (black) and a simulation in which the MCAS Cherry Point wastewater outfall was removed (red) (black symbols are underneath the red).

Finally, a series of nutrient load reductions combined with climate warming scenarios were run to assess their impact on phytoplankton dynamics and hypoxia in the Neuse River Estuary. The estuary was predicted to respond to simulated climate warming similarly to what we report above for the New River and previously reported for the York River Estuary, VA (Lake and Brush, 2015a and b). Simulated warming in increments of +1°C resulted in earlier spring phytoplankton blooms and an increase in phytoplankton NPP in the model (**Figure 10-46a, b**). An earlier spring bloom is in line with other studies in estuarine and coastal systems, which have demonstrated a change in the phenology of phytoplankton blooms in response to climate change (e.g., Nixon et al., 2009). Most of the increase in NPP was predicted to occur in winter–spring as in the York River Estuary, whereas rates were only marginally increased in summer–fall, in contrast to the York River Estuary where they were predicted to decrease.

The frequency of simulated hypoxia in the Neuse River Estuary responded strongly to external inputs of nutrients and organic matter from the watershed and Pamlico Sound (**Figure 10-46c, d**). The upper estuary responded strongly to watershed load reductions, but was unresponsive to inputs from Pamlico Sound (**Figure 10-46c**), matching the response in the upper York River Estuary. The lower estuary responded to reductions from both sources, but more so to reductions

from Pamlico Sound (**Figure 10-46d**), similar to the lower York River Estuary, which is also a tributary estuary. The implication for both estuaries is that to eliminate hypoxia, reductions in local watershed inputs may not be enough to improve water quality in the lower reaches of the system, which also responds to inputs from farther field sources that advect across the estuary mouth and may be more difficult to control.

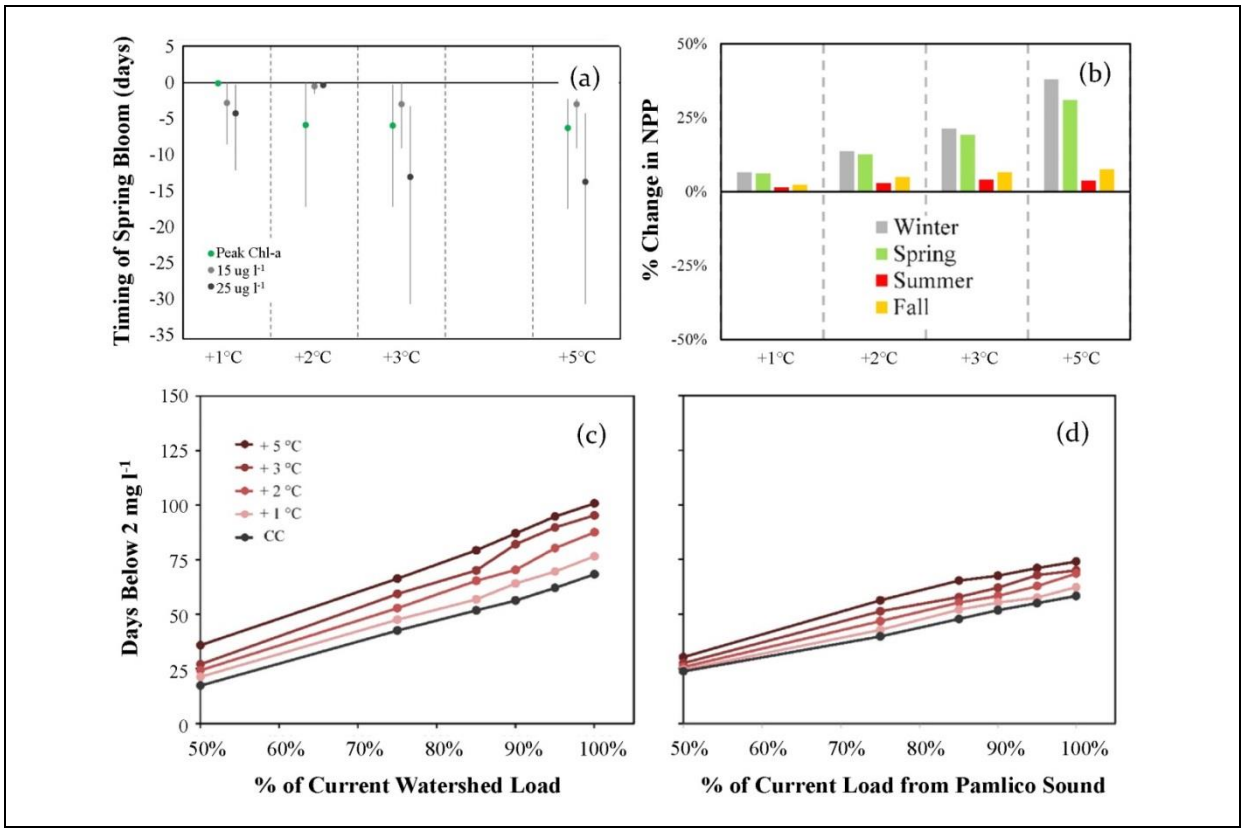

Figure 10-46. Combined loading and climate warming scenarios in the Neuse River Estuary.

Output of the Neuse River Estuarine Simulation Model under a series of temperature-warming scenarios relative to current conditions (CC). (a) Timing of the spring bloom as defined by various chlorophyll-*a* (Chl-*a*) thresholds, with negative values indicating an earlier bloom; (b) percent change in seasonal phytoplankton net primary production (NPP); (c, d) the number of hypoxic days in the upper (Boxes 1–4) and lower (Boxes 5–8) estuary, respectively, as a function of external loading (nutrients and total organic carbon) and temperature.

The response of Neuse River Estuary hypoxia to load reductions was also strongly sensitive to water temperature as in the York River Estuary (**Figures 10-46c, d**). For a given reduction in the load, the number of hypoxic days increased with simulated warming. The implication is that under climatic warming, load reductions will need to be increased to produce the same improvement in water quality predicted under current climatic conditions.

Application in Other Estuarine Systems—Choctawhatchee Bay ESM

Analysis of hypoxia in Choctawhatchee Bay using monthly CBA monitoring surveys revealed relatively persistent and severe hypoxia (DO concentrations down to 0–0.5 mg l^{-1}) from March through October 2014 (**Figure 10-47**). Colder months were characterized by less severe hypoxia,

although low DO conditions (often as low as 2–3 mg l^{-1}) were still present along large sections of the estuary bottom or in smaller patches. The head of the bay was frequently strongly stratified because of inflow from the Choctawhatchee River, whereas the remainder of the system was only partially stratified, particularly during summer.

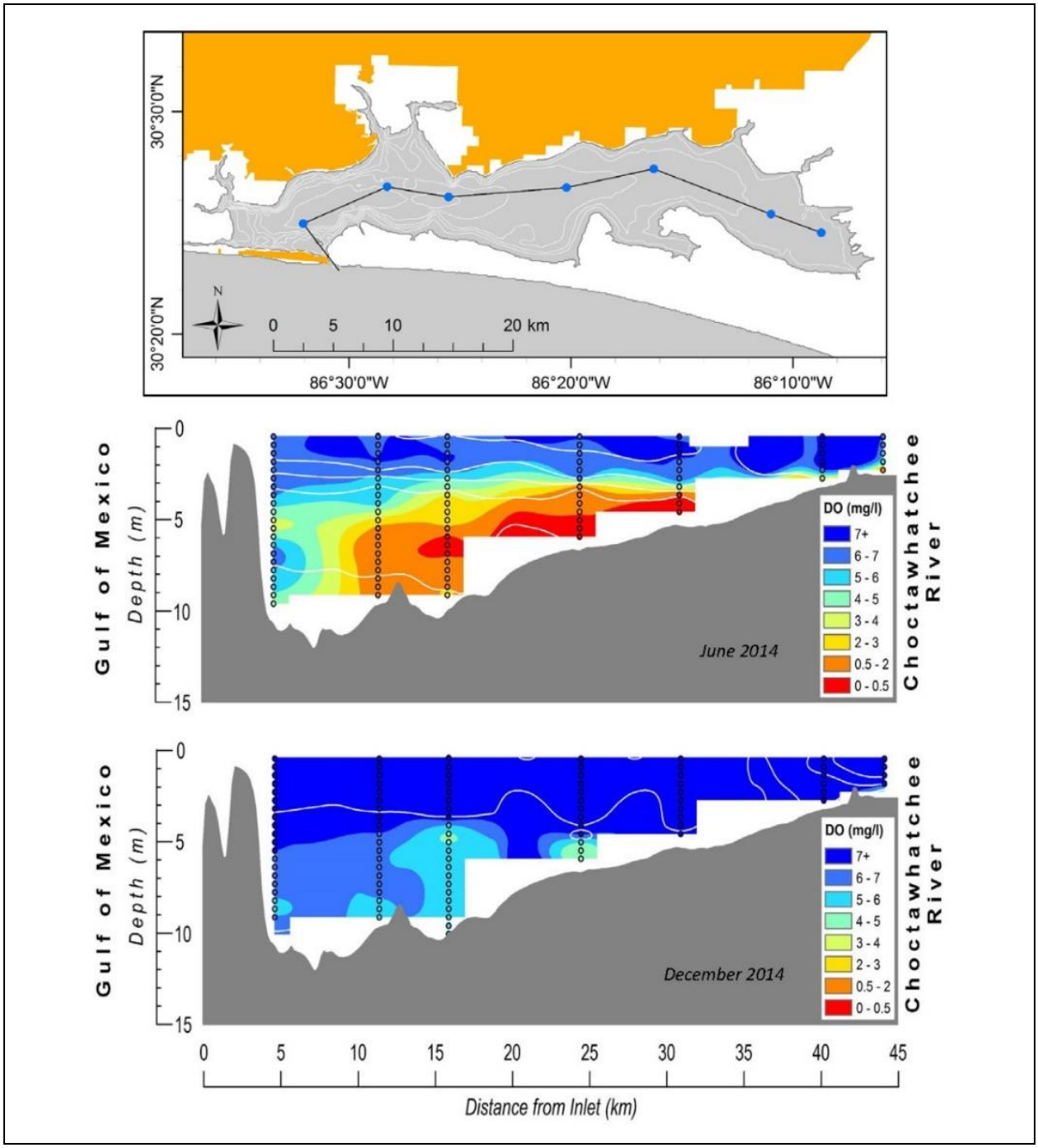

Figure 10-47. Example interpolations of Choctawhatchee Basin Alliance (CBA) vertical profiling surveys.

Data from CBA vertical profiles along the axis of Choctawhatchee Bay (upper) were interpolated to produce an animation of monthly dissolved oxygen and density. Examples are shown for hypoxic (middle, June 2014) and normoxic (lower, December 2014) conditions. White lines are contours of seawater density.

Median modeled flushing time in Choctawhatchee Bay was 42 days, with large seasonal and shorter-term variations associated with changes in freshwater discharge (**Figure 10-48**). The Choctawhatchee Bay ESM generally reproduced Secchi depth, DIN, DIP, chl *a*, and DO in most boxes, although fewer data are available for model calibration in this system, particularly for nutrients (**Figures 10-49 and 10-50**). The model tended to overestimate chl *a* in the uppermost boxes (i.e., 5 and 6), which are relatively shallow and close to the major watershed input from the Choctawhatchee River, and did not always capture the full extent of hypoxia, but nevertheless the ESM captured the main ecosystem dynamics and approximate magnitudes of state variables in most boxes. The model reproduced the observations with low absolute, percent, and root mean squared errors (**Table 10-10**).

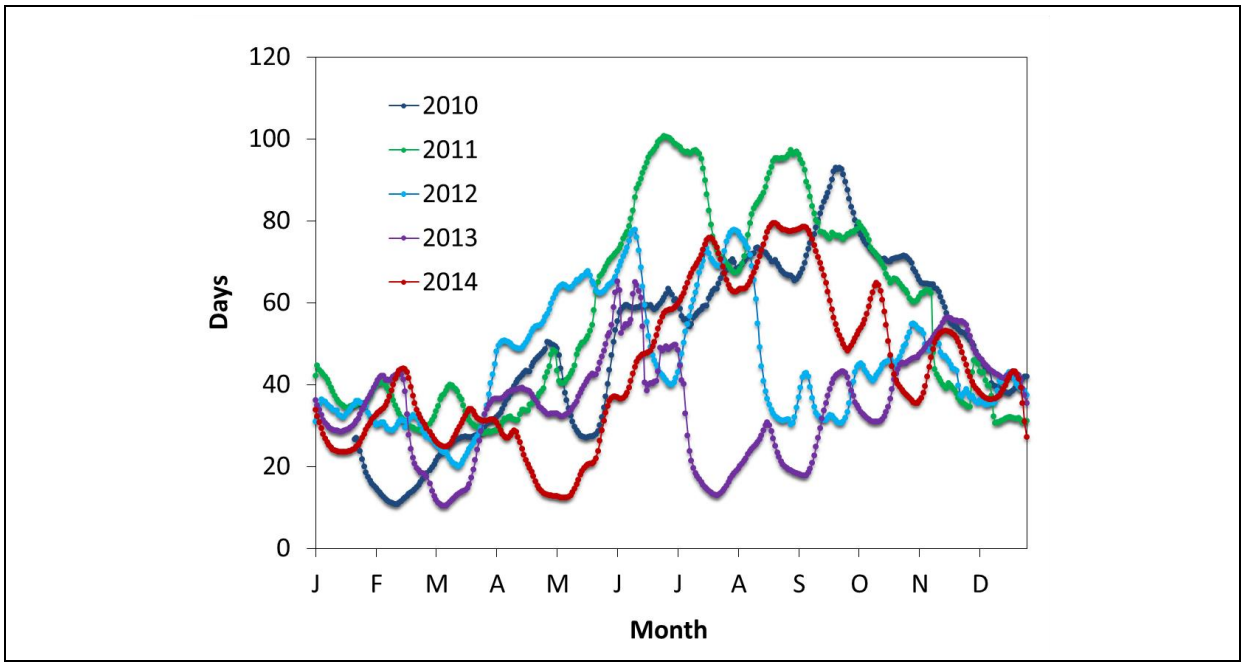

Figure 10-48. Flushing times of Choctawhatchee Bay.

Fresh water flushing times computed with the Choctawhatchee Bay Estuarine Simulation Model; for each year of the model simulation.

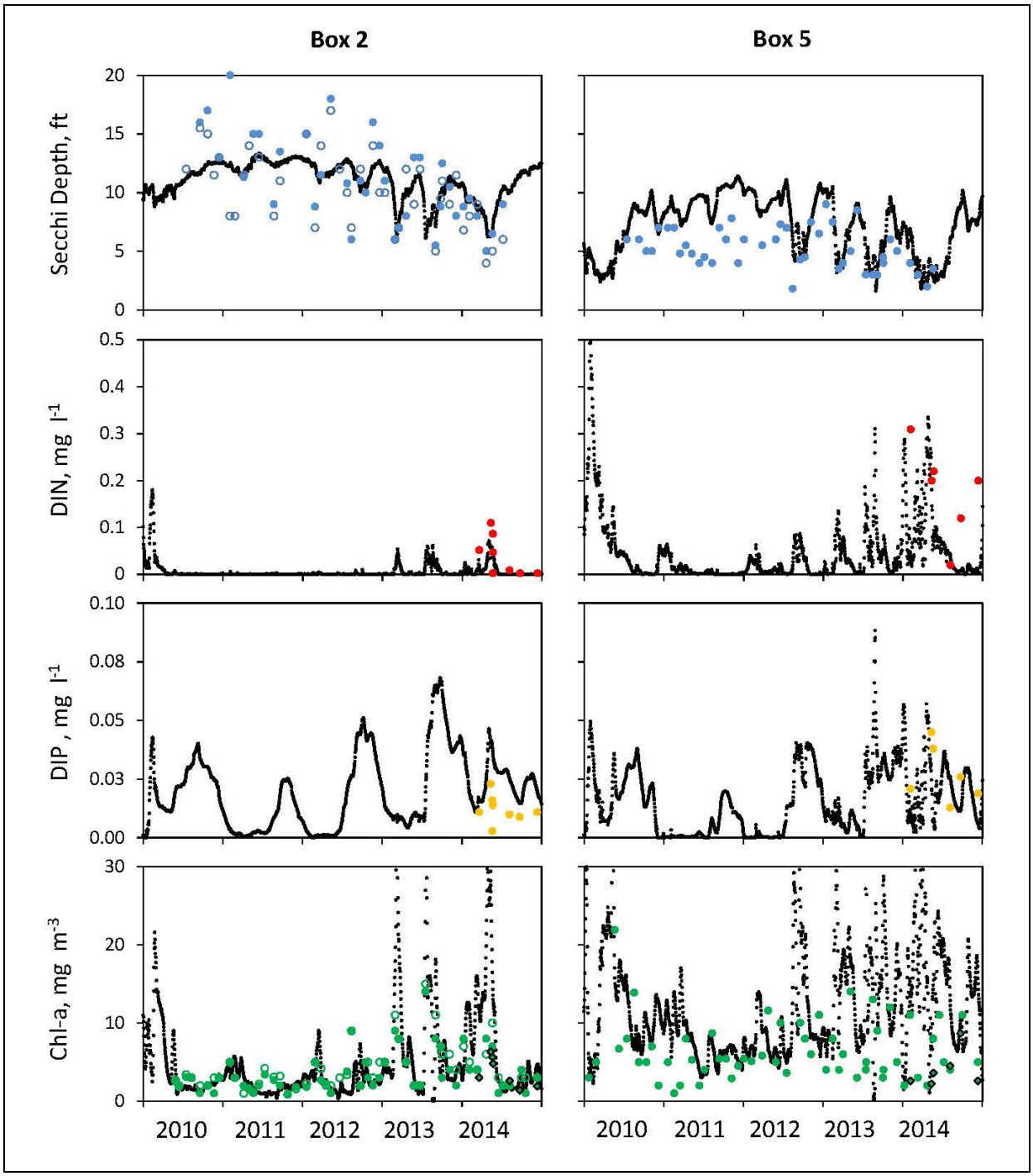

Figure 10-49. Final calibration of the Choctawhatchee Bay Estuarine Simulation Model.

Modeled (black points) and observed (colored points) Secchi depth and surface dissolved inorganic nitrogen (DIN), dissolved inorganic phosphorus (DIP), and chlorophyll-*a* (chl-*a*) concentrations in two spatial elements of Choctawhatchee Bay (see **Figure 10-12**). Different symbols denote different stations.

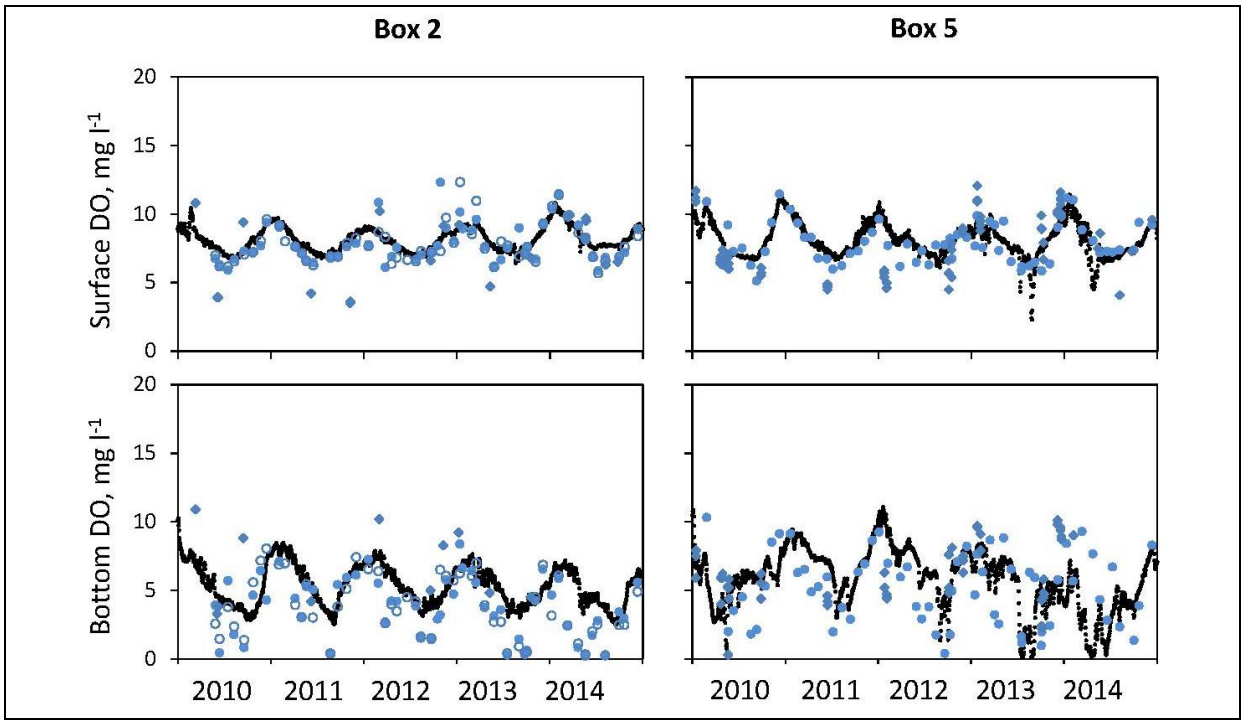

Figure 10-50. Final calibration of the Choctawhatchee Bay Estuarine Simulation Model.

Modeled (black points) and observed (colored points) surface and bottom dissolved oxygen (DO) concentrations in two spatial elements of Choctawhatchee Bay (see **Figure 10-12**). Different symbols denote different stations.

Table 10-10. Skill Assessment of the Choctawhatchee Bay Estuarine Simulation Model.

		Secchi Depth	PHYTO$_S$ Chl-*a*	DO$_S$	DO$_B$	DIN$_S$	DIP$_S$
		ft^{-1}	µg L^{-1}	mg O$_2$ L^{-1}	mg O$_2$ L^{-1}	g N m^{-3}	g P m^{-3}
	n =	*228*	*340*	*346*	*179*	*28*	*22*
Boxes 1 - 6	**ABS Error**	**0.27**	**0.87**	**0.19**	**0.33**	**0.00**	**0.00**
	% Error	**3.10**	**18.77**	**2.42**	**5.83**	**39.12**	**7.47**
	RMS Error	**0.66**	**4.92**	**0.36**	**0.63**	**0.01**	**0.00**
	Nash-Sutcliffe	**0.95**	**0.20**	**0.90**	**0.86**	**0.72**	**0.90**
	n =	*334*	*486*	*487*	*264*	*28*	*22*
All Sites	**ABS Error**	**0.23**	**0.57**	**0.18**	**0.31**	**0.00**	**0.00**
	% Error	**2.62**	**15.55**	**2.27**	**5.54**	**39.12**	**7.47**
	RMS Error	**0.60**	**4.13**	**0.33**	**0.57**	**0.01**	**0.00**
	Nash-Sutcliffe	**0.95**	**0.31**	**0.91**	**0.89**	**0.72**	**0.90**

Note: Model skill was computed for the years 2010 through 2014 by using available monitoring data. Skill metrics were computed by comparing the observations to the closest modeled value within 1 week (±7 days). Subscripts "S" and "B" refer to the surface and bottom layers, respectively.

A series of nutrient load-reduction and climate-warming scenarios were performed with the Choctawhatchee Bay ESM analogous to those performed with the New and Neuse River models. The model was first run without DIN and DIP inputs from the atmosphere or exchange with the Gulf of Mexico, and resulting water quality was nearly identical to the calibrated run with these inputs present (**Figure 10-51**). Results confirm that the major source of DIN and DIP loading is from the surrounding watershed.

Model runs were focused on reducing nutrient loads, but the bay also receives substantial TOC inputs from both the watershed and Gulf of Mexico, and these loads appear to have an important influence on bay water quality. When the model was run without these inputs, simulated chl *a* markedly decreased (**Figure 10-52a**), presumably because of a reduction in remineralization of nutrients (with subsequent uptake by phytoplankton) as the TOC is respired. Removal of TOC loading resulted in increased simulated oxygen concentrations (**Figure 10-52b**), resulting from a reduction in respiratory load.

To assess the role of DIN and DIP loading originating from on- versus off-Base (i.e., Eglin AFB versus the surrounding watershed), the model was run with each source removed and was run again with both sources removed (**Figure 10-53a, b**). Predicted concentrations of DIN and chl *a* in the mainstem of Choctawhatchee Bay (Boxes 1 through 6) responded strongly to reductions in off-Base loads, but not to removal of on-Base loads, indicating the strong control of bay water quality by inputs from the Choctawhatchee River at the head of the system. In contrast, DIN and chl *a* in the bayous adjacent to the Base (Boxes 7 through 9) responded to reductions from both sources.

Predicted duration of hypoxia responded to nutrient load reductions in varied ways. Removal of off-Base loads resulted in marked reductions in severe (<2 mg l^{-1}) hypoxia in Boxes 5 and 6 near the mouth of the Choctawhatchee River, whereas reductions in on-Base loads had little effect (**Figure 10-53c, d**). Removal of off-Base loads had the opposite effect elsewhere in the estuary, resulting in increases in severe hypoxia, and moderate (<4 mg l^{-1}) hypoxia increased throughout the system. Additional simulations suggested that these increases in hypoxia resulted from a reduction in phytoplankton production of oxygen below the pycnocline in the relatively clear waters of this system as opposed to the more turbid estuarine systems in North Carolina. Removal of on-Base loads had little effect on modeled hypoxia, again highlighting the dominant influence of the Choctawhatchee River.

Simulations with combined nutrient load reductions and climate warming confirmed the influence of nutrient loading described previously, with reductions in chl *a* biomass and severe hypoxia, but slight increases in moderate hypoxia (**Figure 10-54**). Warming was predicted to slightly reduce chl *a* biomass, but markedly increase both moderate and severe hypoxia, with a much larger effect than that caused by nutrients. As in the New River and Neuse River Estuary scenarios, results suggest that greater nutrient load reductions will be required in a warmer world to achieve the same level of water quality improvement as currently achievable with smaller load reductions.

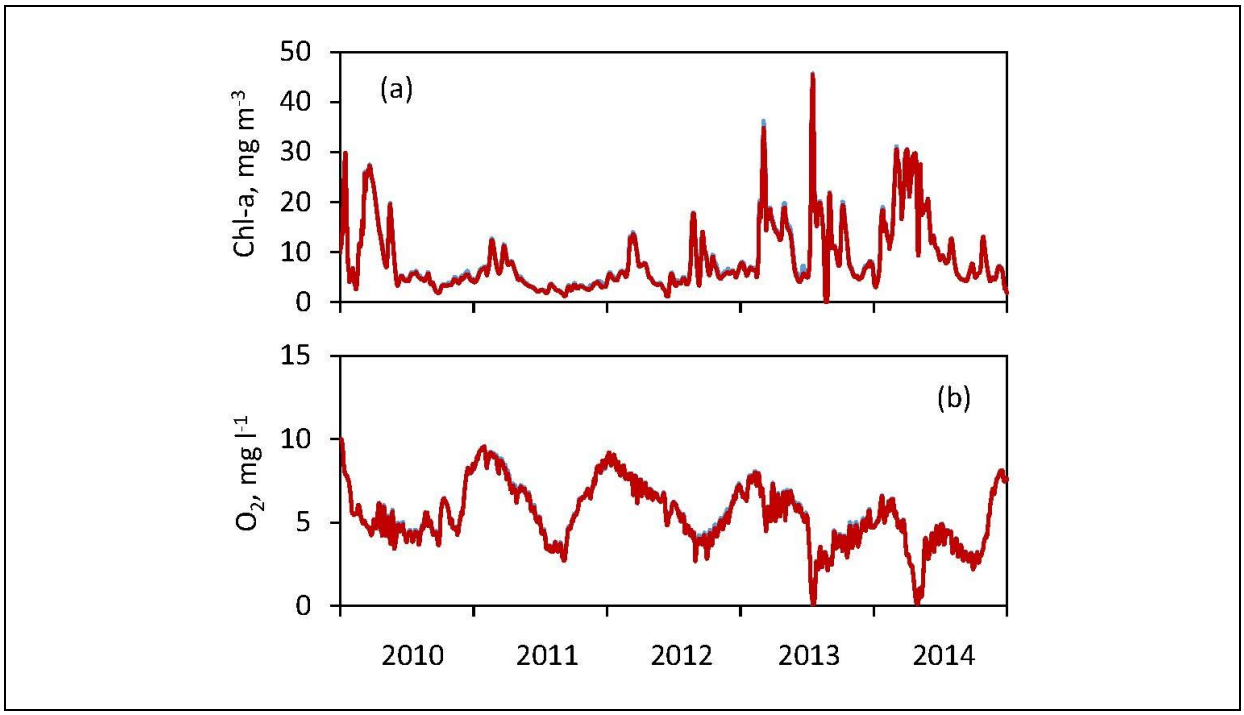

Figure 10-51. Effects of atmospheric and Gulf of Mexico loads in Choctawhatchee Bay.

Model predictions of (a) surface water chlorophyll-*a* (Chl-*a*) and (b) bottom water oxygen (O_2) in Box 4 under current conditions (blue) and with atmospheric nitrogen deposition and Gulf of Mexico dissolved inorganic nitrogen (DIN) and dissolved inorganic phosphorus (DIP) inputs removed (red).

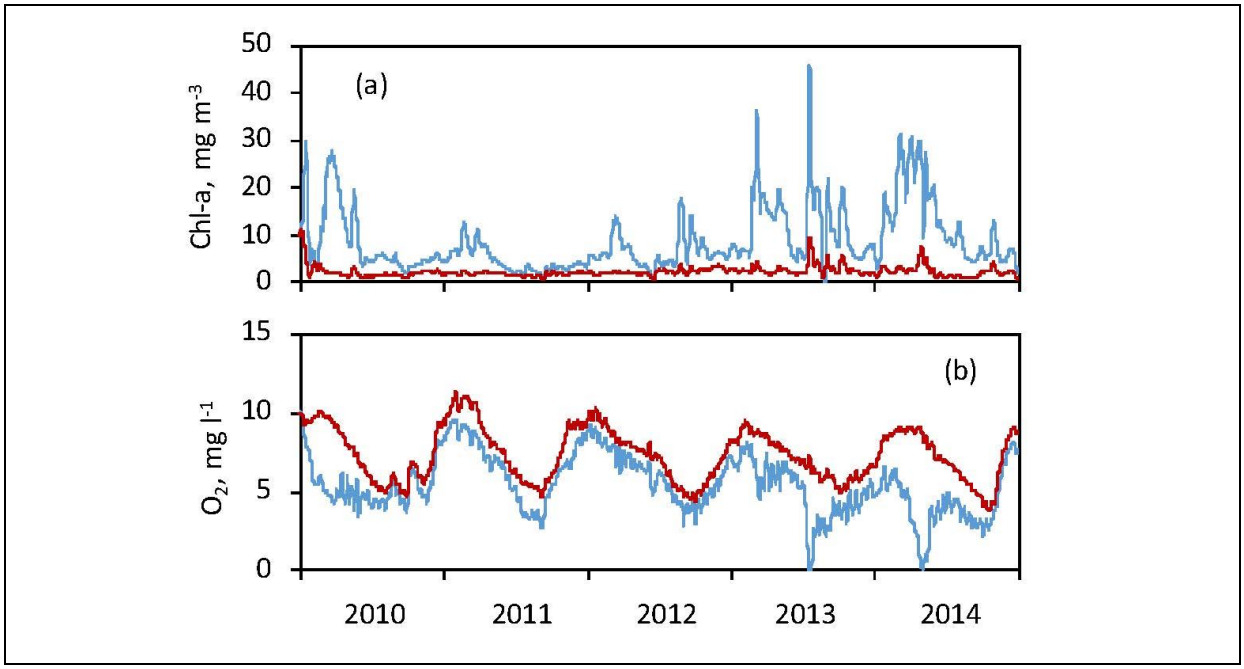

Figure 10-52. Effects of total organic carbon (TOC) loads to Choctawhatchee Bay.

Model predictions of (a) surface water chlorophyll-*a* (Chl-*a*) and (b) bottom water oxygen (O_2) in Box 4 under current conditions (blue) and with watershed and Gulf of Mexico total organic carbon (TOC) inputs removed (red).

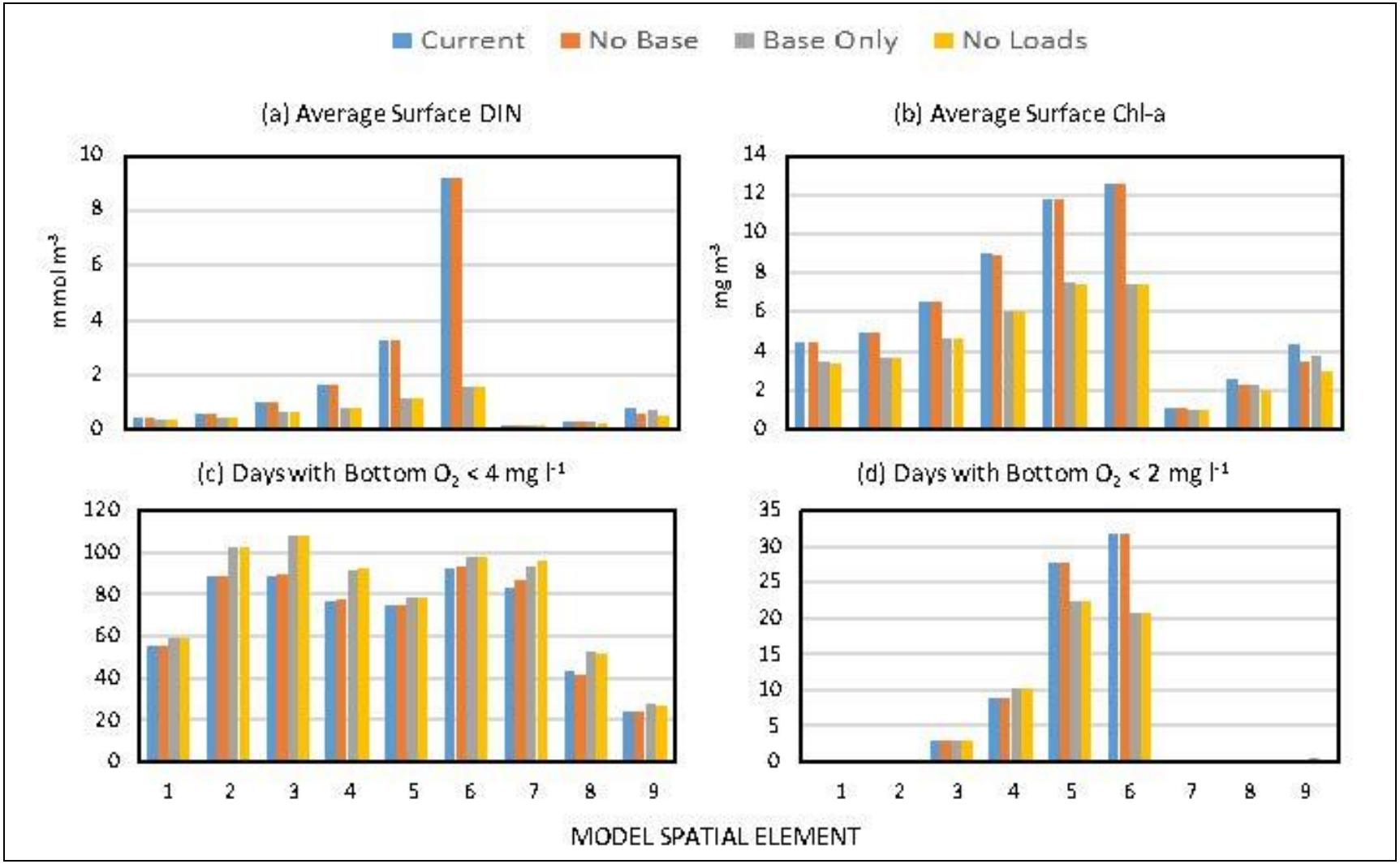

Figure 10-53. Choctawhatchee Bay nutrient-reduction scenarios.

Average modeled water quality for 2010–2014 under current dissolved inorganic nitrogen (DIN) and dissolved inorganic phosphorus (DIP) loading (blue), loading from Eglin Air Force Base removed (orange), loading from the off-Base watershed removed (grey), and loading from all watersheds removed (yellow).

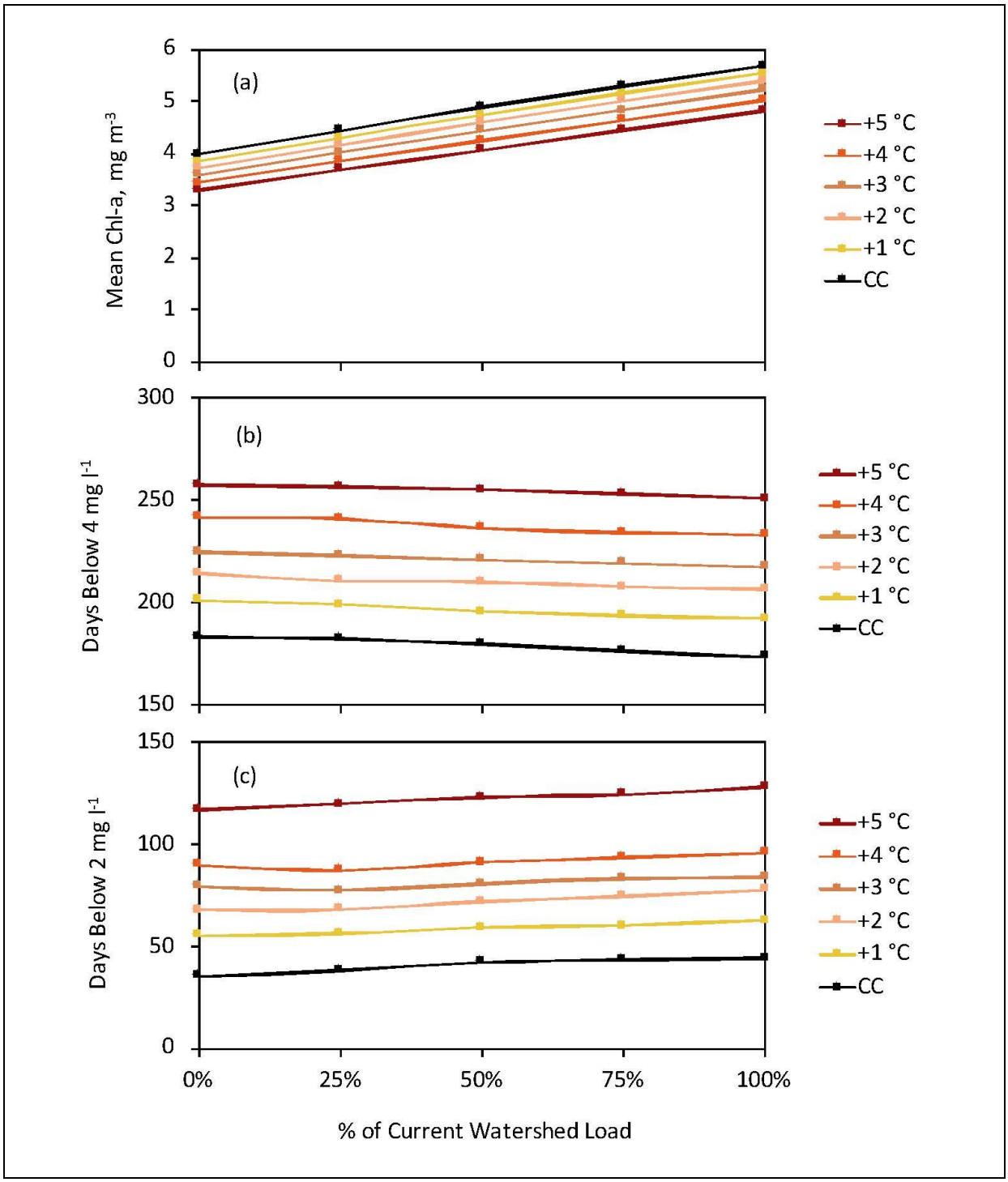

Figure 10-54. Coupled nutrient-climate scenarios in Choctawhatchee Bay.

Model runs were conducted across a range in watershed load reductions in increments of 25% and with climate warming in increments of 1°C. (a) Average chlorophyll-*a* (Chl-*a*), (b) days when bottom water oxygen (O_2) was <4 mg l^{-1}; and (c) days when bottom water O_2 was <2 mg l^{-1}.

Cross-System Comparisons

The three modeled estuaries provide some useful contrasts, from the small, shallow NRE with a relatively small watershed to the larger, relatively deeper Neuse River Estuary and Choctawhatchee Bay with much larger watersheds (**Table 10-11**). The three systems span an approximately 13-fold difference in mean freshwater inputs, with flows and variability in flow (expressed as standard deviation) increasing from the NRE to the Neuse River Estuary to Choctawhatchee Bay. Despite differences in overall flow variability, coefficients of variation are similar in each system.

The three systems also have contrasting flushing times as computed by each ESM (**Table 10-11**). Mean flushing times are longer in the NRE, on the order of 2 to 2.5 months, than in the other systems where they are approximately 1 to 1.5 months, suggesting a greater potential in the NRE for water quality problems associated with elevated nutrient loading and eutrophication. Flushing times in all three systems vary substantially between relatively wet and dry years, and within each year due to the annual cycle of freshwater inflow and storm events. The overall range in flushing times is greatest in the NRE, intermediate in the Neuse River Estuary, and smallest in Choctawhatchee Bay.

External loading of DIN, DIP, and TOC from the watershed, WWTFs, and atmospheric deposition calculated within each ESM also vary across the three systems to different degrees (Table 10-11). Rates of DIN loading are similar across the systems, and DIP loading is similar between the NRE and Neuse River Estuary, but is approximately 50% lower in Choctawhatchee Bay. Greater separation occurs among TOC loads, with the lowest values in the Neuse River Estuary and higher values in the NRE and Choctawhatchee Bay. Loading ratios of DIN to DIP also vary dramatically across the three systems, but all are above the Redfield ratio, suggesting overall nitrogen limitation, which is in line with bioassay results for the NRE and Neuse River Estuary (Mallin et al., 2005; Paerl, 2009; Paerl et al., 2013a). The ratio of DIN load to TOC load has been shown to be a predictor of NEM in estuarine systems and therefore their ability to serve as sources or sinks for CO_2 and TOC, with a value of approximately 0.2 mol mol^{-1} marking the transition between net heterotrophy (systems <0.2) and net autotrophy (systems >0.2) (Kemp et al., 1997; Testa et al., 2013). The NRE and Choctawhatchee Bay are below this threshold, but the Neuse River Estuary is above it.

Finally, normalizing loading to typical flushing rates (or in this case multiplying loads by flushing time) provides an estimate of the steady-state concentration that would occur because of simple dilution alone (i.e., in the absence of biological processing) (Nixon et al., 2001). These calculations indicate much higher steady-state concentrations in the NRE and lowest values in Choctawhatchee Bay for DIN and DIP, whereas steady-state TOC is highest in the NRE and lowest in the Neuse River Estuary (**Table 10-11**).

Table 10-11. Characteristics of the Three Research Project TSP-2 Study Systems

Characteristic	New	Neuse	Choctawhatchee
Surface area, × 10^6 m^2	78.7	294	336
Volume, × 10^6 m^3	143	1,062	1,596
Mean Depth, m	1.8	3.6	4.7
Watershed: Estuarine Area	13.0	48.0	40.0
Freshwater inflow, × 10^6 m^3 d^{-1}			
Mean	1.3	9.8	17.7
Median	0.8	5.1	11.2
SD	1.9	10.9	18.3
CV	1.5	1.1	1.0
Flushing time, days			
Mean	79.4	46.5	46.2
Median	69.3	33.4	41.7
SD	46.9	35.8	20.0
CV	0.59	0.77	0.43
Loading rate, mmol m^{-2} d^{-1}			
DIN	0.97	1.5	1.3
DIP	0.034	0.037	0.018
TOC	18.8	6.2	24.4
Loading rate, mmol m^{-3} d^{-1}			
DIN	0.54	0.42	0.28
DIP	0.019	0.010	0.004
TOC	10.5	1.7	5.1
Load ratios, mol mol^{-1}			
DIN:DIP	28.7	41.0	74.2
DIN:TOC	0.05	0.25	0.05
Steady-state concentration, mmol m^{-3}			
DIN	42.9	19.7	12.8
DIP	1.49	0.48	0.17
TOC	830	80.4	238

Note: Summary dimensions, freshwater inflow, flushing time, and loading computed from the Estuarine Simulation Models in each study system.

Online Decision-Support Tool

User-friendly, graphical user interfaces were developed for the New River, Neuse River, and Choctawhatchee Bay ESMs, and are available through the VIMS Coastal Systems Ecology and Modeling Program Web site (see http://www.vims.edu/research/departments/bio/programs/semp/models/index.php).

Models are served for each simulation year in each estuary, specifically for 2007–2015 in the New River (**Figure 10-55**), 2007–2010 in the Neuse River (**Figure 10-56**), and 2010–2014 in Choctawhatchee Bay (**Figure 10-57**). Simulation years 1998–2006 are also available in the NRE and can be provided if useful to MCBCL or other stakeholders. To guide users in selecting the most appropriate year for selection, the Web site lists annual precipitation and mean daily freshwater discharge from the major rivers entering each system, together with long-term mean values, and any tropical storms or hurricanes that occurred during the year.

- **DCERP New River Estuarine Simulation Model** (v.1a, December 2013; updated July 2014):

Year	Annual Precipitation[a], cm y^{-1}	Freshwater Inflow[b], x 10^3 m^3 d^{-1}	Major Storms[c]
2007	73	178	
2008	126	129	
2009	125	235	
2010	122	287	TS Nicole
2011	99	136	Hurricane Irene
2012	136	265	TS Beryl
2013	135	192	
2014	156	273	Hurricane Arthur
2015	189	486	

[a] Annual precipitation, NOAA station MCAF New River (1995-2015 mean is 136 cm y^{-1}).
[b] Mean daily discharge, USGS Gum Branch station (1995-2015 mean is 294 x 10^3 m^3 d^{-1}).
*[c] Tropical storms (TS) and hurricanes passing by the North Carolina coast (Source: National Hurricane Center; **http://www.nhc.noaa.gov/data/tcr/**).*

Figure 10-55. A screen capture of the currently available versions of the online New River Estuarine Simulation Model.

- **DCERP Neuse River Estuarine Simulation Model** (v.1, Aug 2014; updated Apr 2015):

Year	Annual Precipitation[a], cm y^{-1}	Freshwater Inflow[b], x 10^6 m^3 d^{-1}	Major Storms[c]
2007	103	5.8	
2008	133	6.6	
2009	173	8.6	
2010	150	9.8	TS Nicole

[a] Annual precipitation, NOAA station MCAS Cherry Point (1997-2016 mean is 134 cm y^{-1}).
[b] Mean daily discharge, USGS stations 02091814 (Neuse River near Fort Barnwell) and 02092500 (Trent River near Trenton) (1997-2016 mean is 10.3 x 10^6 m^3 d^{-1}).
*[c] Tropical storms (TS) and hurricanes passing by the North Carolina coast (Source: National Hurricane Center; **http://www.nhc.noaa.gov/data/tcr/**).*

Figure 10-56. A screen capture of the currently available versions of the online Neuse River Estuarine Simulation Model.

- **DCERP Choctawhatchee Bay Estuarine Simulation Model** (v.1, Oct 2017):

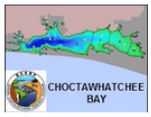

Netsim-logo-Choc.jpg

Year	Annual Precipitation[a], cm y^{-1}	Freshwater Inflow[b], x 10^6 m^3 d^{-1}	Major Storms[c]
2010	138	16.5	
2011	104	6.0	
2012	145	8.8	
2013	178	22.5	
2014	178	20.7	

[a] Annual precipitation, NOAA station at Fairhope, AL (2007-2016 mean is 156 cm y^{-1}).
[b] Mean daily discharge, USGS station 02366500 (Choctawhatchee River near Bruce) (1985-2016 mean is 16.3 x 10^6 m^3 d^{-1}).
*[c] Tropical storms (TS) and hurricanes passing by the Florida coast (Source: National Hurricane Center; **http://www.nhc.noaa.gov/data/tcr/**).*

Figure 10-57. A screen capture of the currently available versions of the online Choctawhatchee Bay Estuarine Simulation Model.

The online interfaces for each ESM include a description of the model, instructions for running scenarios, a dashboard page for conducting scenario analyses, and a series of pages that display model output for several parameters. Selected screen captures from the NRE ESM are shown in **Figures 10-58, 10-59, and 10-60** as examples. Upon selecting a model year to run, the model Home page appears. Navigation buttons guide users through a series of pages with background information about the model, what it simulates, and what data are used to drive it. For users who have already reviewed these pages, the Home page has a button that when clicked will take users directly to the Scenario Analysis page. The Scenario Analysis page allows users to run the model under current conditions, or modify nitrogen and phosphorus loading (together or separately) from each major source. For example, for the NRE ESM, users can change loading from the off-Base watershed, on-Base watershed, MCBCL WWTF, atmosphere, and Onslow Bay. Users can also increase water temperatures up to 5°C and modify annual precipitation by ±30% based on projections through 2100 from Research Project CC-1. Changes can be made individually or in combination. At the request of MCAS Cherry Point, a second scenario page was added to the online Neuse River ESM. This page allows users to enter stormwater TSS concentrations and discharge from the Base into Slocum and Hancock Creeks via sketch pads (**Figure 10-61**), allowing the Base to enter its stormwater monitoring data and predict impacts to the adjacent creeks.

Once the model is run, output is made available for viewing and downloading on the following pages (**Figure 10-60**). All models provide a standard set of output, including surface water chl *a*, bottom water O_2, and surface water DIN and DIP. The NRE ESM also provides output for submerged aquatic vegetation (SAV) survival and the Neuse River Estuary ESM provides output for TSS. Graphs on each page display model predictions for the entire year, and users can click through the graph to view output for each spatial element of the model. Graphs are comparative in that they will overlay results from successive scenarios until the user clears them. The output pages for chl *a* and O_2 also include tables that show the cumulative number of days during the simulation year that values exceeded (chl *a*) or were below (O_2) established state criteria or approximate threshold concentrations. For example, the NRE and Neuse River Estuary ESMs show the number of days chl *a* exceeded the North Carolina state criterion of 40 µg l^{-1}, and number of days O_2 was below 5 mg l^{-1}, an approximate threshold below which organisms show negative impacts from hypoxia. Each output page also includes a button that when clicked will allow a user to copy output (daily modeled values for the full year across all spatial elements) to his or her computer clipboard, for pasting into a spreadsheet program. A user can thus obtain model output for his or her own post-processing and analysis. A three-page user's guide has also been developed for each model to provide more details and guide users through scenario analyses. The user's guide (**Figure 10-62**) is available for download at the VIMS Coastal Systems Ecology and Modeling Web site.

Pilot versions of the online models were presented via workshops at each Base to provide an overview of model capabilities, present example scenario results, and solicit feedback from Base personnel and local stakeholders to enhance the utility of the models and fine-tune them to local needs. Initial workshops were conducted at MCBCL and MCAS Cherry Point in July 2014 and at Eglin AFB in June 2015. Final workshops were conducted at each Base in September and October 2017. Final modifications were made to the interfaces based on the feedback received.

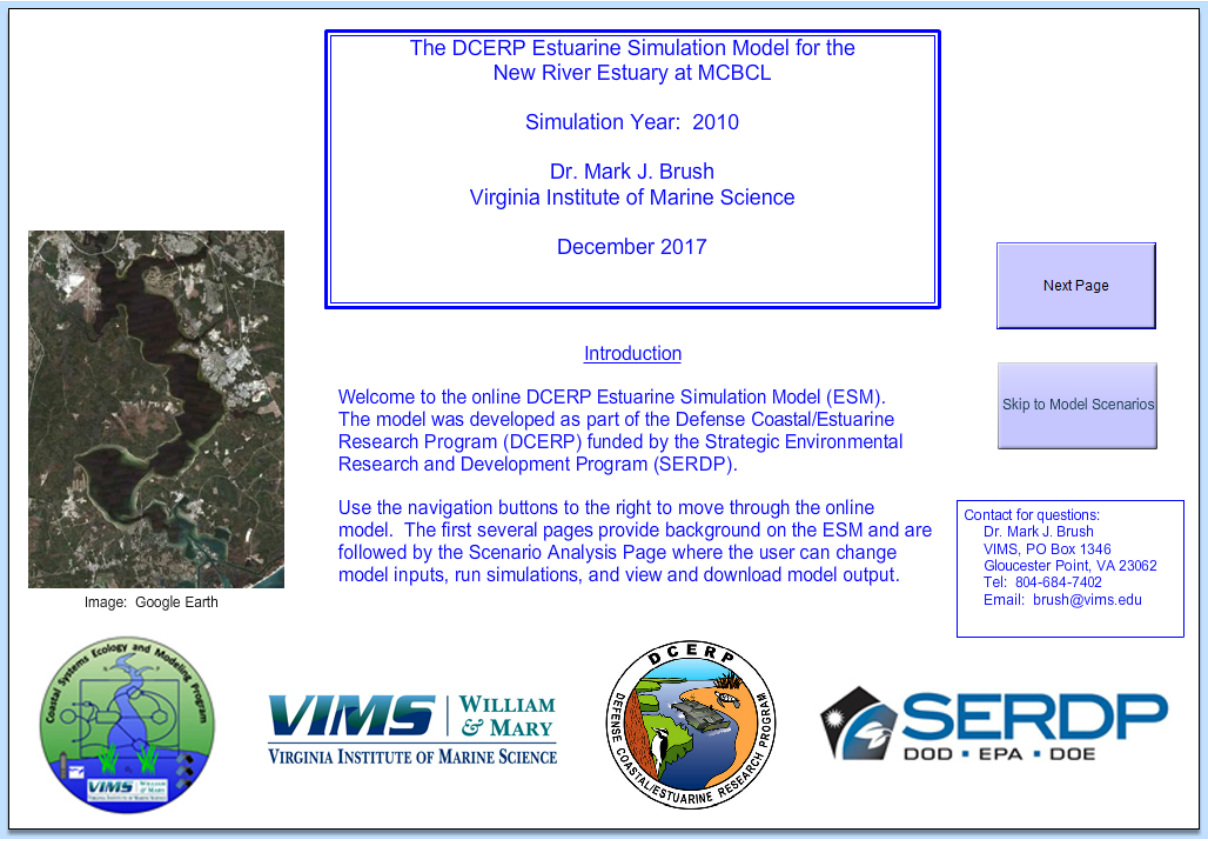

Figure 10-58. The Home page of the online New River Estuarine Simulation Model (ESM).
Users can navigate through pages that describe the model, or they can skip directly to running model scenarios.

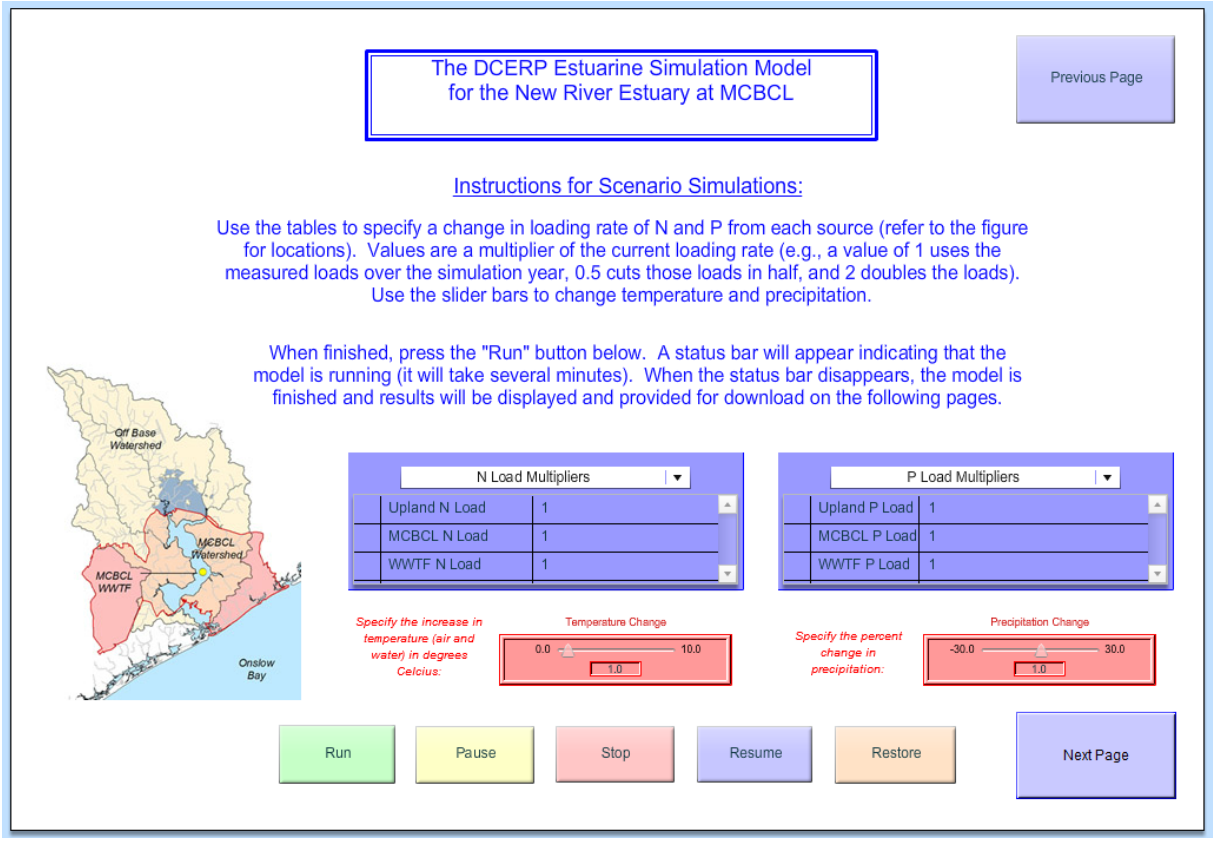

Figure 10-59. The Scenario Analysis page of the online New River Estuary Estuarine Simulation Model (ESM).

Users can change the nitrogen and phosphorus loading from various sources, water temperature, and precipitation, and can run the model. Output is provided on the following pages.

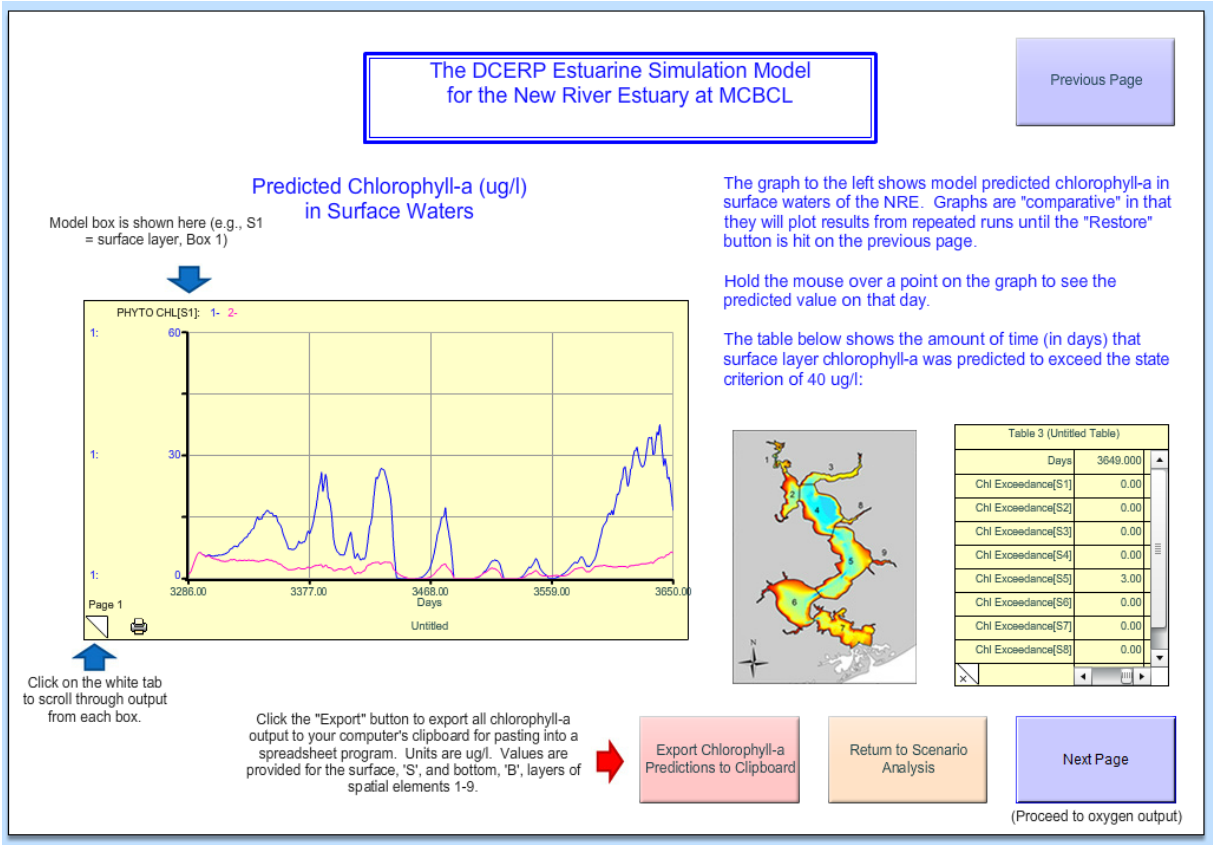

Figure 10-60. An example Model Output page of the online New River Estuary Estuarine Simulation Model (ESM).

Output pages are available for chlorophyll-*a* (chl-*a*), oxygen (O_2), dissolved inorganic nitrogen (DIN), dissolved inorganic phosphorus (DIP), and submerged aquatic vegetation (SAV) survival. **Figure 10-60** shows output for chl-*a* in a run under current conditions (blue line) and a scenario in which the upland watershed load was removed (pink line). The table shows the time in which predicted chl-*a* exceeded the state criterion of 40 µg l^{-1} in the latter scenario. Clicking on the "Export Chlorophyll-a Predictions to Clipboard" (red) button will export the model output to the user's computer clipboard for pasting into a spreadsheet program.

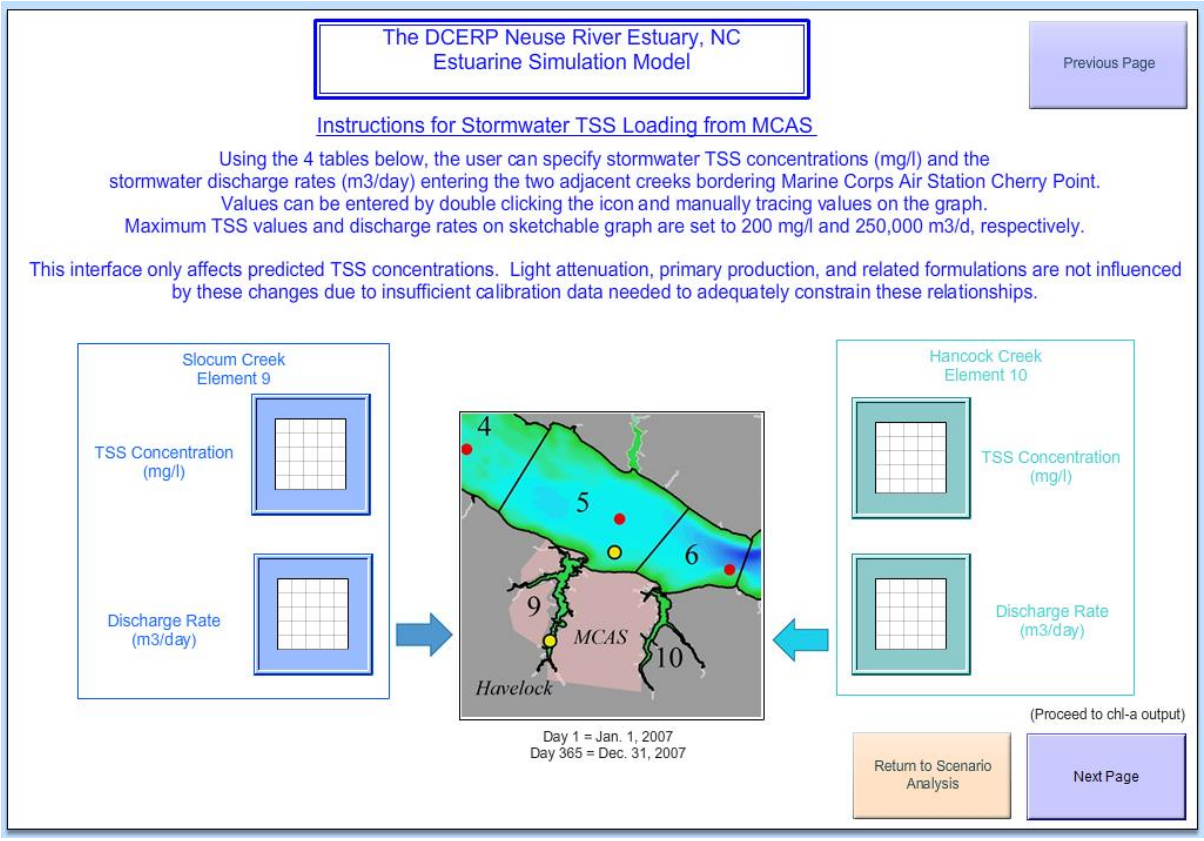

Figure 10-61. The custom page for total suspended solids (TSS) stormwater loading in the online Neuse River Estuarine Simulation Model (ESM).

This page allows users to enter data for stormwater TSS concentrations and discharge into Slocum and Hancock Creeks. This page was created at the request of Marine Corps Air Station (MCAS) Cherry Point staff.

DCERP Estuarine Simulation Model for the New River Estuary: User Guide (December 2017)

1. INTRODUCTION

Thank you for your interest in the DCERP Estuarine Simulation Model (ESM) for the New River Estuary (NRE), NC available at: http://www.vims.edu/research/departments/bio/programs/semp/models/index.php. This document provides instructions for navigating the online model interface, including step-by-step instructions with screen capture images to assist in conducting model simulations and obtaining model output for analysis.

2. NAVIGATION

Use the navigation buttons on the right of each page to move through the ESM. These are highlighted in red in the image to the right. On the ***Introduction*** page the user can proceed to site specific information by selecting the 'Next Page' button, or advance to the model ***Scenario Simulations*** page by selecting the 'Skip to Model Scenarios' button.

Once you have navigated beyond the ***Scenario Simulation*** page, an additional navigation button 'Return to Scenario Analysis' will be available on the bottom right of each page.

3. SITE SPECIFIC INFORMATION

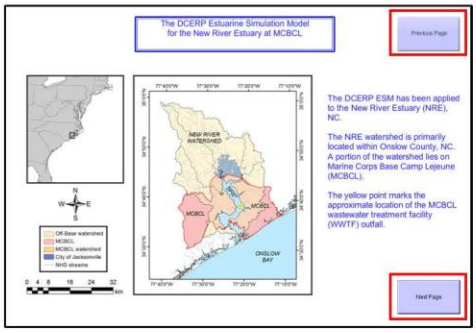

The next seven pages following the ***Introduction*** provide background information on the ESM and its application to the NRE. The pages include:

- Location of the NRE
- Model boxes and bathymetry
- Dimensions of the boxes and watersheds (2 pages)
- Components of the ESM
- Diagram of the ESM
- Source of loading data

Use the navigation buttons on the right to move between pages.

4. RUNNING THE MODEL

On the ***Scenario Simulations*** page the user can specify a change in current nutrient loading (both N and P) from each major source. Values in the table represent multipliers of the current loading rates (e.g., a value of 1 uses the measured loads, a value of 0.5 cuts those loads in half, and a value of 2 doubles the loads).

Figure 10-62. The downloadable user's guide for the New River Estuary Estuarine Simulation Model (ESM).

Conclusions and Implications for Future Research and Implementation

Major conclusions from Research Project TSP-2 are presented as follows:

1. Climate change will interact with nutrient loading to influence future NRE conditions.

NRE response to climate change will be strongly modulated by changes in nutrient loading, and vice versa. Although climate change will substantially alter watershed discharge and nutrient loading, changes in land use and thus loading from the upper watershed have the potential to overwhelm these effects. Although warming is predicted to reduce estuarine chlorophyll *a* concentrations and favor less desirable cyanobacteria, this effect could be offset by increases in discharge in the absence of nutrient load reductions. NRE hypoxia is sensitive to watershed loading, but greater load reductions will be necessary in a warmer climate to obtain the same improvement achievable under current conditions.

2. The NRE carbon budget responds to both nutrient loading and climate change.

Simulated nutrient load reductions and climatic warming drove the NRE to greater heterotrophy, reducing the potential for carbon storage and increasing CO_2 fluxes to the atmosphere. Scenarios highlight a trade-off in managing for nutrient loading versus carbon storage. Reductions in loading to mitigate nutrient-fueled eutrophication will also reduce the potential for carbon storage; conversely, increased loading will enhance the role of the NRE as a sink for carbon, but at the expense of degraded water quality.

3. The ESM is a widely applicable research and management tool.

Given the increasing demand for models to inform management decisions across a wide range of estuarine and coastal systems, managers need readily applied, generally transferable modeling tools that can be applied to a variety of systems with limited resources. Successful application of the ESM to the NRE in DCERP1 and DCERP2, to the Neuse River Estuary and Choctawhatchee Bay as part of DCERP2, and to several other systems from New England through the Mid-Atlantic region of the United States as part of other projects confirm the general applicability of the ESM across a wide range of estuarine systems (**Figure 10-63**). The online version of the ESM provides a readily accessible, user-friendly decision-support tool directly usable by resource managers.

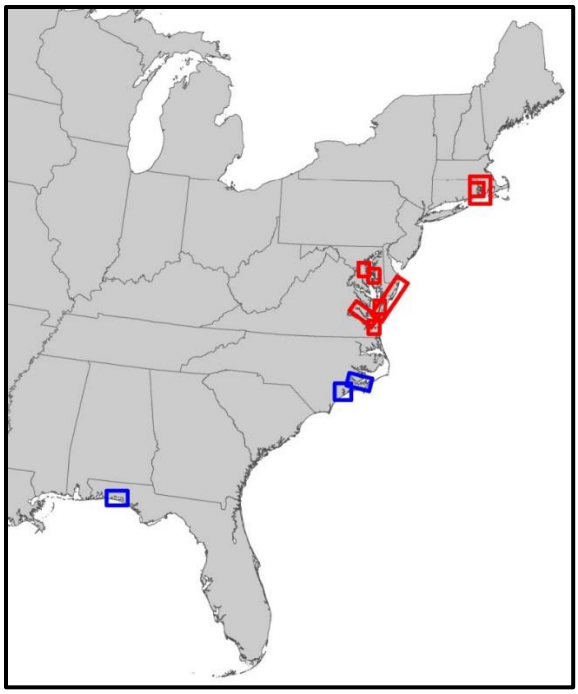

Figure 10-63. Coastal systems in which the Estuarine Simulation Model is currently applied.

Models developed through DCERP are highlighted in blue. Models developed through other projects are highlighted in red.

Findings with Implications for Future Base Management

Results confirm the DCERP1 conclusion that MCBCL has minimal impacts on NRE water quality at the scale of ESM spatial elements. Future improvements in estuarine water quality will be primarily achieved through reductions in loads from the upland, off-Base watershed. The MCBCL WWTF is a small point source to the estuary and could be expanded at least to double its current output, with minimal to no discernible impact on NRE water quality at the scale of the ESM. Although MCBCL has minimal impact on NRE water quality, it is worth noting that future management to control nutrients may result in a reduced potential for carbon storage and increase the role of the NRE as a CO_2 source.

MCAS Cherry Point also appears to have little impact on water quality in the Neuse River or its adjacent creeks as resolved by the ESM, with the potential exception of stormwater TSS inputs. Water quality in the Neuse River mainstem is primarily controlled by inputs from the Neuse and Trent Rivers, as well as from Pamlico Sound. Recent relocation of the Havelock WWTF by that community was a positive decision.

The major source of nutrients to Choctawhatchee Bay is from the Choctawhatchee River, so Eglin AFB has minimal impacts on water quality in the main bay. In contrast, water quality within the local bayous appears to be partly controlled by inputs from Eglin watersheds.

Although all three Bases have relatively limited impacts on nutrient-driven water quality, results in all three systems suggest that greater nutrient load reductions will be required in a warmer

world to achieve the same level of water quality improvement as currently achievable with smaller load reductions.

The models and online interfaces developed here provide directly-usable, management-relevant, decision-support tools to inform Base resource management. The ESM is widely applicable to estuaries and similar coastal marine ecosystems along the U.S. East and Gulf Coasts and should be applicable in other regions. Although the coarse, boxed approach and simplified physical mixing scheme of the ESM limit its ability to resolve fine-scale impacts on water quality and effects of fine-scale circulation patterns, the model nevertheless serves as a valuable tool for performing ecosystem-level scenario analyses. The online version of the ESM provides a readily accessible, user-friendly tool for resource managers and other local stakeholders to directly perform their own management-relevant scenario analyses through a Web browser without the need for costly software, modeling infrastructure, or extensive modeling expertise. The ESM and online capabilities are widely applicable and readily transferable to other coastal installations in similar ecological settings.

Literature Cited

Altman J.C., and H.W. Paerl. 2012. Composition of inorganic and organic nutrient sources influences phytoplankton community structure in the New River Estuary. *Aquatic Ecology 46*:269–282.

Anderson, I.C., M.J. Brush, M.F. Piehler, C.A. Currin, J.W. Stanhope, A.R. Smyth, J.D. Maxey, and M.L. Whitehead. 2014. Impacts of climate-related drivers on the benthic nutrient filter in a shallow photic estuary. *Estuaries and Coasts 37*:46–62.

Baird, M.E., S.J. Walker, B.B. Wallace, I.T. Webster, and J.S. Parslow. 2003. The use of mechanistic descriptions of algal growth and zooplankton grazing in an estuarine eutrophication model. *Estuarine, Coastal and Shelf Science 56*(3–4):685–695.

Blachman, S.A. 2016. *Modeling Phytoplankton Community Response to Nutrient Loading and Climate Change in a Shallow Temperate Estuary*. M.S. thesis, College of William and Mary, Gloucester Point, VA.

Brito, A.C., A. Newton, P. Tett, and T.F. Fernandese. 2012. How will shallow coastal lagoons respond to climate change? A modeling investigation. *Estuarine, Coastal and Shelf Science 112*:98–104.

Brush, M.J. 2013. *Development and application of watershed and estuarine simulation models for the New River Estuary*. Final report, Synthetic Modeling, Defense Coastal/Estuarine Research Program 1 (DCERP1), SERDP Project RC-1413. RTI International, Research Triangle Park, NC.

Brush, M.J., and L.A. Harris. 2016. Ecological modeling. Pp. 214–223 in *Encyclopedia of Estuaries*. Edited by Kennish, M.J. Encyclopedia of Earth Sciences Series, Springer Netherlands.

Brush, M.J., and S.W. Nixon. 2017. A reduced complexity, hybrid empirical-mechanistic eutrophication and hypoxia model for shallow marine ecosystems. Pp. 61–93 in *Modeling Coastal Hypoxia: Numerical Simulations of Patterns, Controls and Effects of Dissolved Oxygen Dynamics*. Edited by Justic, D., K.A. Rose, R.D. Hetland, and K. Fennel. Springer.

Burd, A.B., and K.H. Dunton. 2001. Field verification of a light-driven model of biomass changes in the seagrass *Halodule wrightii*. *Marine Ecology Progress Series 209*:85–98.

Canham, C.D., J.J. Cole, and W.K. Lauenroth (Eds.). 2003. *Models in Ecosystem Science*. Princeton University Press: Princeton, NJ.

Carr, J.A., P. D'Odorico, K.J. McGlathery, and P.L. Wiberg. 2012. Modeling the effects of climate change on eelgrass stability and resilience: Future scenarios and leading indicators of collapse. *Marine Ecology Progress Series 448*:289–301.

Cerco, C.F., and M.R. Noel. 2013. Twenty-one-year simulation of Chesapeake Bay water quality using the CE-QUAL-ICM Eutrophication Model. *Journal of the American Water Resources Association*, *49*(5):1119–1133.

Cerco, C.F., and M.R. Noel. 2004. *The 2002 Chesapeake Bay Eutrophication Model*. Report 903-R-04-004. Chesapeake Bay Program Office, U.S. Environmental Protection Agency, Annapolis, MD.

Cerco, C.F., and K. Moore. 2001. System-wide submerged aquatic vegetation model for Chesapeake Bay. *Estuaries 24*(4):522–534.

Cerco, C.F., S. Kim, and M.R. Noel. 2010. *The 2010 Chesapeake Bay Eutrophication Model*. U.S. EPA Chesapeake Bay Program, Annapolis, MD.

Chen, C., R. Tian, R.C. Beardsley, J. Qi, and Q. Xu. 2010. *Modeling 2008 in Massachusetts Bay Using an Upgraded Unstructured-Grid Bays Eutrophication Model*. Report 2010-15. Massachusetts Water Resources Authority, Boston, MA. 118 pages.

Crosswell, J.R., I.C. Anderson, J.W. Stanhope, B. Van Dam, M.J. Brush, S. Ensign, M.F. Piehler, B. McKee, and H.W. Paerl. 2017. Carbon budget of a shallow, lagoonal estuary: transformations and source-sink dynamics along the river–estuary–ocean continuum. *Limnology and Oceanography* doi: 10.1002/lno.10631.

Denman, K.L. 2003. Modelling planktonic ecosystems: Parameterizing complexity. *Progress in Oceanography 57*(3–4):429–452.

Duarte, C.M., J.S. Amthor, D.L. DeAngelis, L.A. Joyce, R.J. Maranger, M.L. Pace, J. Pastor, and S.W. Running. 2003. The limits to models in ecology. Pp. 437–451 in *Models in Ecosystem Science*. Edited by Canham, C.D., J.J. Cole, and W.K. Lauenroth. Princeton University Press: Princeton, NJ.

Duarte, C.M. 1992. Nutrient concentration of aquatic plants: patterns across species. *Limnology and Oceanography 37*:882–889.

Ensign, S.H., J.N. Halls, and M.A. Mallin. 2004. Application of digital bathymetry data in an analysis of flushing times of two North Carolina estuaries. *Computers and Geosciences 30*:501–511.

Fonseca, M.S., and S.S. Bell. 1998. Influence of physical setting on seagrass landscapes near Beaufort, North Carolina, USA. *Marine Ecology Progress Series*, *171*:109–121.

Friedrichs, M.A.M., R.R. Hood, and J.D. Wiggert. 2006. Ecosystem model complexity versus physical forcing: Quantification of their relative impact with assimilated Arabian Sea data. *Deep-Sea Research Part II 53*:576–600.

Fry, J., G.Z. Xian, S. Jin, J. Dewitz, C.G. Homer, L. Yang, C.A. Barnes, N.D. Herold, and J.D. Wickham. 2011. Completion of the 2006 National Land Cover Database for the

conterminous United States. *Photogrammetric Engineering and Remote Sensing 77(9)*:858–864.

Fulton, E.A., A.D.M. Smith, and C.R. Johnson. 2004. Effects of spatial resolution on the performance and interpretation of marine ecosystem models. *Ecological Modelling 176*(1–2):27–42.

Fulton, E.A., A.D.M. Smith, and C.R. Johnson. 2003. Effect of complexity on marine ecosystem models. *Marine Ecology Progress Series 253*:1–16.

Giblin, A.E., and J.J. Vallino. 2003. The role of models in addressing coastal eutrophication. Pp. 327–343 in *Models in Ecosystem Science*. Edited by Canham, C.D., J.J. Cole, and W.K. Lauenroth. Princeton University Press: Princeton, NJ.

Haith, D.A., R. Mandel, and R.S. Wu. 1996. *Generalized Watershed Loading Functions: Version 2.0 User's Manual*. Cornell University, Ithaca NY.

Hall, N.S., H.W. Paerl, B.L. Peierls, A.C. Whipple, and K.L. Rossignol. 2013. Effects of climatic variability on phytoplankton community structure and bloom development in the eutrophic, microtidal, New River Estuary, North Carolina, USA. *Estuarine, Coastal and Shelf Science 117*:70–82.

Hickey, R. 2000. Slope angle and slope length solutions for GIS. *Cartography 29(1)*:1–8.

Harris, G.P., S.W. Bigelow, J.J. Cole, H. Cyr, L.L. Janus, A.P. Kinzig, J.F. Kitchell, G.E. Likens, K.H. Reckhow, D. Scavia, D. Soto, L.M. Talbot, and P.H. Templer. 2003. The role of models in ecosystem management. Pp. 299–307 in *Models in Ecosystem Science*. Edited by Canham, C.D., J.J. Cole, and W.K. Lauenroth. Princeton University Press: Princeton, NJ.

Homer, C.G., J.A. Dewitz, L. Yang, S. Jin, P. Danielson, G. Xian, G., J. Coulston, N. Herold, J. Wickham, and K. Megown. 2015. Completion of the 2011 National Land Cover Database for the conterminous United States—Representing a decade of land cover change information. *Photogrammetry Engineering and Remote Sensing 81*:345–354. doi: 10.14358/PERS.81.5.345

Hong, B., and D.P. Swaney. 2007. *Regional Nutrient Management (ReNuMa) Model Version 1.0 User's Manual*. Cornell University, Ithaca, NY. Available at http://www.eeb.cornell.edu/biogeo/nanc/usda/renuma.htm

Hovel, K.A., M.S. Fonseca, D.L. Myer, W.J. Kenworthy, and P.E. Whitfield. 2002. Effects of seagrass landscape structure, structural complexity and hydrodynamic regime on macrofaunal densities in North Carolina seagrass beds. *Marine Ecology Progress Series, 243*:11–24.

HydroQual. 1991. *Water Quality Modeling Analysis of Hypoxia in Long Island Sound*. Report to the Management Committee of the Long Island Sound Estuary Study and the New

England Interstate Water Pollution Control Commission, HydroQual, Inc., Mahwah, NJ. 280 pages.

Jiang, M.S., and M. Zhou. 2008. *Massachusetts Bay Eutrophication Model: 2005 Simulation*. Report 2008-13. Massachusetts Water Resources Authority, Boston, MA. 85 pages.

Justić, D., N.N. Rabalais, and R.E. Turner. 2005. Coupling between climate variability and coastal eutrophication: Evidence and outlook for the northern Gulf of Mexico. *Journal of Sea Research 54*:25–35.

Kemp, W.M., E.M. Smith, M. Marvin-DiPasquale, and W.R. Boynton. 1997. Organic carbon balance and net ecosystem metabolism in Chesapeake Bay. *Marine Ecology Progress Series 150*:229–248.

Kremer, J.N., and S.W. Nixon. 1978. *A Coastal Marine Ecosystem: Simulation and Analysis*. Springer-Verlag: New York, NY.

Kremer, J.N., J. Vaudrey, D. Ullman, D. Bergondo, N. LaSota, C. Kincaid, D. Codiga, and M.J. Brush. 2010. Simulating property exchange in estuarine ecosystem models at ecologically appropriate scales. *Ecological Modelling 221*(7):1080–1088.

Lake, S.J., and M.J. Brush. 2015a. Modeling estuarine response to load reductions in a warmer climate: The York River Estuary, Virginia, USA. *Marine Ecology Progress Series 538*:81–98.

Lake, S.J., and M.J. Brush. 2015b. Contribution of nutrient and organic matter sources to the development of periodic hypoxia in a tributary estuary. *Estuaries and Coasts 38*:2149–2171.

Mallin, M.A., M.R. McIver, H.A. Wells, D.C. Parsons, and V.L. Johnson. 2005. Reversal of eutrophication following sewage treatment upgrades in the New River Estuary, North Carolina. *Estuaries 28*:750–760.

Ménesguen, A., P. Cugier, S. Loyer, A. Vanhoutte-Brunier, T. Hoch, J-F. Guillaud, and F. Gohin. 2007. Two- or three-layered box-models versus fine 3-D models for coastal ecological modelling? A comparative study in the English Channel (Western Europe). *Journal of Marine Systems 64*(1–4):47–65.

NCCGIA (North Carolina Center for Geographic Information and Analysis). 2007. *Type A Current Public Sewer Systems*. GIS shapefile available at www.nconemap.com. NCCGIA, Raleigh, NC.

Neumann, T. 2010. Climate-change effects on the Baltic Sea ecosystem: A model study. *Journal of Marine Systems 81*:213–224.

Nixon, S.W. 2009. Eutrophication and the macroscope. *Hydrobiologia 629*: 5–19.

Nixon, S., B. Buckley, S. Granger, and J. Bintz. 2001. Responses of very shallow marine ecosystems to nutrient enrichment. *Human and Ecological Risk Assessment 7*(5):1457–1481.

Nixon, S.W., R.W. Fulweiler, B.A. Buckley, S.L. Granger, B.L. Nowicki, and K.M. Henry. 2009. The impact of changing climate on phenology, productivity, and benthic-pelagic coupling in Narragansett Bay. *Estuarine, Coastal and Shelf Science 82*:1–18.

NRC (National Research Council). 2000. *Clean Coastal Waters: Understanding and Reducing the Effects of Nutrient Pollution*. National Academy Press: Washington, DC.

Odum, H.T. 1994. *Ecological and General Systems: An Introduction to Systems Ecology.* Second edition. University Press of Colorado: Niwot, CO.

Officer, C.B. 1980. Box models revisited. Pp. 65–114 in *Estuarine and Wetland Processes with Emphasis on Modeling*. Edited by Hamilton, P., and K.B. MacDonald. Plenum Press: New York, NY.

Officer, C.B., and D.R. Kester. 1991. On estimating the non-advective tidal exchanges and advective gravitational circulation exchanges in an estuary. *Estuarine, Coastal and Shelf Science 32*:99–103.

Pace, M.L. 2001. Prediction and the aquatic sciences. *Canadian Journal of Fisheries and Aquatic Sciences 58*(1):63–72.

Paerl, H.W. 2009. Controlling eutrophication along the freshwater–marine continuum: dual nutrient (N and P) reductions are essential. *Estuaries and Coasts 32*:593–601.

Paerl, H.W., N.S. Hall, B.L. Peierls, K.L. Rossignol, A.R. Joyner, T. Otten, K.H. Reckhow, and F. Nojavan. 2013a. Develop and deploy microalgal indicators as measures of water quality, harmful algal bloom dynamics, and ecosystem condition. Chapter 3 in *Defense Coastal/Estuarine Research Program (DCERP1) Final Research Report*. RTI International, Research Triangle Park, NC.

Paerl, H., R. Luettich, N. Hall, B. Peierls, A. Whipple, and J. Reynolds-Fleming. 2013b. New River Estuary—Water column. Chapter 5 in *Defense Coastal/Estuarine Research Program (DCERP1) Final Monitoring Report*. Edited by Cunningham, P. RTI International, Research Triangle Park, NC.

Paerl, H.W., K.L. Rossignol, S.N. Hall, B.L. Peierls, and M.S. Wetz. 2010. Phytoplankton community indicators of short- and long-term ecological change in the anthropogenically and climatically impacted Neuse River Estuary, North Carolina, USA. *Estuaries and Coasts 33*:485–497.

Paerl, H.W., L.M. Valdes-Weaver, A.R. Joyner, and V. Winkelmann. 2007. Phytoplankton indicators of ecological change in the eutrophying Pamlico Sound system, North Carolina. *Ecological Applications 17*(sp5):S88–S101.

Paerl, H.W., L.M. Valdes, J.L. Pinckney, M.F. Piehler, J. Dyble, and P.H. Moisander. 2003. Phytoplankton photopigments as indicators of estuarine and coastal eutrophication. *Bioscience 53*:953–964.

Pilson, M.E.Q. 1998. *An Introduction to the Chemistry of the Sea*. Prentice Hall: Upper Saddle River, NJ.

Pinckney, J.L., T.L. Richardson, D.F. Millie, and H.W. Paerl. 2001. Application of photopigment biomarkers for quantifying microalgal community composition and in situ growth rates. *Organic Geochemistry 32*:585–595.

Raick, C., K. Soetaert, and M. Gregoire. 2006. Model complexity and performance: How far can we simplify? *Progress in Oceanography 70*(1):27–57.

Reynolds, C.S. 2006. *Ecology of Phytoplankton.* First edition. Cambridge University Press, Cambridge.

Rigler, F.H., and R.H. Peters. 1995. Science and limnology. Book 6 in *Excellence in Ecology*. Edited by Kinne, O. International Ecology Institute, Oldendorf/Luhe. 239 pages.

Riley, G.A., H. Stommel, and D.F. Bumpus. 1949. Quantitative ecology of the plankton of the Western North Atlantic. *Bulletin of the Bingham Oceanographic Collection 12*:1–169.

Steele, J.H. 1974. *The Structure of Marine Ecosystems*. Harvard University Press: Cambridge, MA.

Testa, J.M., and W.M. Kemp. 2008. Regional, seasonal, and inter-annual variability of biogeochemical processes and physical transport in a partially stratified estuary: A box-modeling analysis. *Marine Ecology Progress Series 356*:63–79.

Testa, J.M., W.M. Kemp, C.S. Hopkinson, Jr., and S.V. Smith. 2013. Ecosystem metabolism. Chapter 15 in Estuarine Ecology (2nd edition). Edited by Day, Jr., J.W., B.C. Crump, W.M. Kemp, and A. Yáñez-Arancibia. Wiley-Blackwell, Hoboken, N.J.

U.S. EPA (Environmental Protection Agency). 1999. Protocol for developing nutrient TMDLs. U.S. EPA report 841-B-99-007. U.S. Environmental Protection Agency, Office of Water, Washington, DC.

Appendix 10-A
List of Scientific/Technical Publications

Papers

Anderson, I.C., M.J. Brush, M.F. Piehler, C.A. Currin, J.W. Stanhope, A.R. Smyth, J.D. Maxey, and M.L. Whitehead. 2014. Impacts of climate related drivers on the benthic nutrient filter in a shallow photic estuary. *Estuaries and Coasts 3* (Suppl 1):S46–S62.

Blachman, S.A., and M.J. Brush. In preparation. Modeling phytoplankton community response to nutrient loading and climate change in a shallow temperate estuary.

Brush, M.J. and L.A. Harris. 2016. Ecological modeling. Pp. 214–223 in *Encyclopedia of Estuaries*. Edited by Kennish, M.J. Encyclopedia of Earth Sciences Series, Springer Netherlands.

Crosswell, J.R., I.C. Anderson, J.W. Stanhope, B. Van Dam, M.J. Brush, S. Ensign, M.F. Piehler, B. McKee, M. Bost, and H.W. Paerl. 2017. Carbon budget of a shallow, lagoonal estuary: Transformations and source-sink dynamics along the river–estuary–ocean continuum. *Limnology and Oceanography 62*(S1):S29–S45.

Ganju, N.K., M.J. Brush, B. Rashleigh, A.L. Aretxabaleta, P. del Barrio, J.S. Grear, L.A. Harris, S.J. Lake, G. McCardell, J. O'Donnell, D.K. Ralston, R.P. Signell, J.M. Testa, and J.M.P. Vaudrey. 2016. Progress and challenges in coupled hydrodynamic-ecological estuarine modeling. *Estuaries and Coasts 39*:311–332.

Kennish, M.J., M.J. Brush, and K.A. Moore. 2014. Drivers of change in shallow coastal photic systems: An introduction to the special issue. *Estuaries and Coasts 37*(Suppl 1): S3–S19.

Kennish, M.J., M.J. Brush, and K.A. Moore (eds). 2014. Drivers of change in shallow coastal photic systems. Special issue, *Estuaries and Coasts 37*(Suppl 1):3–19.

Thesis

Blachman, S.A. 2016. Modeling phytoplankton community response to nutrient loading and climate change in a shallow temperate estuary. M.S. thesis, College of William and Mary, Gloucester Point, VA.

Williamson, S. In preparation. Assessing the impacts of land use and climate change on streamflow and nutrient delivery to the New River Estuary, NC. M.S. thesis, College of William and Mary, Gloucester Point, VA.

Presentations

Anderson, I.C., J. Stanhope, B. Van Dam, N. Hall, J. Crosswell, H. Paerl, and M. Brush. 2015. *Bio-physical Controls of CO_2 Fluxes Along a River–Estuary Continuum*. Presented at the Coastal and Estuarine Research Federation Biennial Meeting, Portland, OR.

Anderson, I., J. Stanhope, M. Brush, A. Smyth, C. Currin, and M. Piehler. 2014. *Interacting Drivers Regulating the Fate of Nitrogen in Shallow Photic Marine Systems*. Presented at the Joint Aquatic Sciences Meeting, Portland, OR.

Blachman, S. and M.J. Brush. 2015. *A Multi-group Phytoplankton Model to Predict Shifts in Community Composition in a Changing Environment*. Poster presented at the Coastal and Estuarine Research Federation Biennial Meeting, Portland, OR.

Blachman, S. and M.J. Brush. 2015. *Modeling Phytoplankton Community Composition of the New River Estuary, North Carolina*. Poster presented at the Atlantic Estuarine Research Society Spring Meeting, Wanchese, NC. (Received Outstanding Student Poster Presentation award)

Brush, M.J. 2017. *New River Estuarine Simulation Model (ESM)*. Final workshop with MCBCL personnel and local stakeholders (two separate meetings) to present the ESM, major findings, and the online interface. Presented at MCBCL, Jacksonville, NC.

Brush, M.J. 2016. *Introduction to Estuarine Ecosystem Modeling*. Invited keynote lecture as part of the workshop, Modelling Estuarine Ecosystems. Presented at the Atlantic Canada Coastal and Estuarine Science Society Annual Meeting, Charlottetown, Prince Edward Island.

Brush, M.J. 2016. *Modeling Through the Macroscope: Reduced Complexity Models for Coastal Ecosystem Science and Management*. Invited keynote research seminar as part of the workshop, Modelling Estuarine Ecosystems. Presented at the Atlantic Canada Coastal and Estuarine Science Society Annual Meeting, Charlottetown, Prince Edward Island.

Brush, M.J. 2014. *Further Adventures in Modeling Through the Macroscope*. Invited seminar presented at the Chesapeake Biological Laboratory, Solomons, MD.

Brush, M.J. 2014. *Nutrient-Fueled Eutrophication: Reflections and Ruminations from the "Right Coast."* Invited presentation, part of the Lower Food Web Dynamics in California's Bay-Delta Ecosystem, Delta Science Program, and University of California, Davis's Center for Aquatic Biology & Aquaculture seminar, Davis, CA.

Brush, M.J. 2013. *Modeling the Response of Coastal Ecosystems to Nutrient Loading and Climate Change*. Invited presentation featured at the Mini-symposium on Dynamics of Marine Ecosystems at the Conference on Application of Dynamical Systems, Society for Industrial and Applied Mathematics, Snowbird, UT.

Brush, M.J., and S.J. Lake. 2017. *Neuse River Estuarine Simulation Model (ESM)*. Final workshop with Marine Corps Air Station Cherry Point personnel to present the ESM, the major findings, and the online interface. Marine Corps Air Station Cherry Point, Havelock, NC.

Brush, M.J., and S.J. Lake. 2017. *Choctawhatchee Bay Estuarine Simulation Model (ESM)*. Final workshop with Eglin Air Force Base and Choctawhatchee Basin Alliance personnel to

present the ESM, the major findings, and the online interface. Eglin Air Force Base, Niceville, FL.

Brush, M.J., and S.J. Lake. 2013. *Predicting the Response of Coastal Ecosystems to Nutrient Loading and Climate Change Using Models with Simplified Physics and Biology*. Linking Hydrodynamic and Ecological Models in Estuaries: A Workshop to Discuss Recent Advances and Approaches, U.S. Geological Survey Woods Hole Science Center, Woods Hole, MA. September 10–11.

Brush, M.J. 2015. *Carbon budgeting in the New River Estuary, NC*. Session organized at the Spring 2015 Meeting of the Atlantic Estuarine Research Society, Wanchese, NC.

Brush, M.J., and S.J. Lake. 2015. Site visit and presentation to Eglin Air Force Base personnel and local environmental groups regarding implementation of the Choctawhatchee Bay ESM. Eglin Air Force Base, Niceville, FL.

Brush, M.J., and S.J. Lake. 2014. Presentation to MCBCL personnel and local stakeholders regarding implementation of the online New River ESM. MCBCL, Jacksonville, NC.

Brush, M.J., and S.J. Lake. 2014. Site visit and presentation to Marine Corps Air Station Cherry Point personnel regarding implementation of the Neuse River ESM. Marine Corps Air Station Cherry Point, Havelock, NC.

Lake, S.J., and M.J. Brush. 2015. *User-Friendly, Online Decision-Support Models for Nutrient and Carbon Management in the Neuse and New River Estuaries, NC*. Poster presented at the Atlantic Estuarine Research Society Spring Meeting, Wanchese, NC.

Lake, S.J., and M.J. Brush. 2015. *Response of the Neuse and York River Estuaries to Load Reductions in a Warmer Climate*. Presented at the Coastal and Estuarine Research Federation Biennial Meeting, Portland, OR.

Stanhope, J.W., I.C. Anderson, M.J. Brush, C.A. Currin, and M.F. Piehler. 2013. *Benthic Microbial Responses to Interacting Physical-Biological Drivers in a Shallow Estuary*. Poster presented at the 22nd Biennial Conference of the Coastal and Estuarine Research Federation, San Diego, CA.

Williamson, S.C., and M.J. Brush. 2017. *Assessing the Impact of Land Use and Climate Change on Streamflow and Nutrient Delivery to the New River Estuary, NC*. Presented at the Atlantic Estuarine Research Society Spring Meeting, St. Mary's City, MD.

Appendix 10-B
List of Students

- Sara A. Blachman, M.S., Virginia Institute of Marine Science, College of William and Mary, Williamsburg, VA, December 2016.
- Shanna Williamson, M.S. candidate, Virginia Institute of Marine Science, College of William and Mary, Williamsburg, VA, degree pending.

Chapter 11

Coastal Wetland Monitoring Program

SERDP Project Number: RC-2245

Coastal Wetlands

CWM-1

Lead Researchers:

Dr. Carolyn A. Currin
NOAA National Ocean Service
National Centers for Coastal Ocean Science
Carolyn.currin@noaa.gov

Supporting Researchers:

Anna Hilting, NOAA, anna.hilting@noaa.gov
Michael Greene, NOAA, Michael.greene@noaa.gov
Dr. Scott Ensign, Aquatic Analysis and Consulting, LLC

November 2017

Final

This report was prepared under contract to the U.S. Department of Defense (DoD) Strategic Environmental Research and Development Program (SERDP). The publication of this report does not indicate endorsement by DoD, nor should the contents be construed as reflecting the official policy or position of DoD. References herein to any specific commercial product, process, or service by trade name, trademark, manufacturer, or otherwise, do not necessarily constitute or imply its endorsement, recommendation, or favoring by DoD.

Table of Contents

Acronyms 11-vii
Abstract 11-1
Objectives of the Monitoring Activity 11-3
Background 11-3
Materials and Methods 11-6
Research Location and Design 11-6
Bench Mark and Surface Elevation 11-9
Temperature, Salinity, Water Level, and Inundation 11-11
Marsh Vegetation 11-12
Marsh Surface Elevation Change and Sediment Accretion 11-14
Shoreline Change 11-15
Net Volume Change 11-16
Results and Discussion 11-17
Elevation 11-17
Temperature and Salinity 11-17
Water Level and Tidal Datums 11-19
Inundation 11-22
Marsh Vegetation 11-30
Inundation, Rainfall, and Vegetation 11-38
Marsh Surface Elevation Change 11-41
Inundation and Elevation Change 11-47
Sediment Accretion 11-47
Shoreline Change 11-49
Assessment of Directionality and Trends 11-51
Conclusions and Implications for Future Research and Implementation 11-53
Key Findings 11-53
Findings with Implications for Future Base Management 11-55
Literature Cited 11-55
Appendix 11-A: Supporting Data 11-A-1
Appendix 11-B: List of Scientific/Technical Publications 11-B-1

List of Figures

Figure 11-1. Location of Marine Corps Base Camp Lejeune in Onslow County, NC. 11-4

Figure 11-2. Location of the six coastal wetland monitoring sites. 11-7

Figure 11-3. Example of the relationship between vegetation monitoring sites, SET stations, and vegetation sample plots at two sites. 11-13

Figure 11-4. Marker Horizon results from the DCERP marsh monitoring sites (2008–2016). 11-15

Figure 11-5. Example of the DSAS analysis process at Traps Bay Bridge (TBB). 11-17

Figure 11-6. Inter-annual monthly mean (±standard deviation) and maximum and minimum temperature at Gottschalk Marina Wallace Creek (GMWC) and Mile Hammock Bay (MHB). 11-18

Figure 11-7. Inter-annual monthly mean (±standard deviation) and maximum and minimum salinity values at Gottschalk Marina Wallace Creek (GMWC) and Mile Hammock Bay (MHB). 11-19

Figure 11-8. Six-minute water level data from Beaufort, NC (NWLON Station 8656483), Mile Hammock Bay (MHB) and Gottschalk Marina Wallace Creek (GMWC). 11-20

Figure 11-9. Inter-annual monthly mean (±standard deviation), maximum, and minimum water level at Gottschalk Marina Wallace Creek (GMWC) and Mile Hammock Bay (MHB). 11-21

Figure 11-10. Inundation of the marsh surface at each SET station for the period between quarterly SET measurements. 11-24

Figure 11-11. The mean elevation of the vegetation plots at each monitoring station. 11-31

Figure 11-12. The average annual percent cover of Juncus roemerianus and Spartina alterniflora for each vegetation monitoring station. 11-32

Figure 11-13. Percentage of vegetation plots by year and monitoring station where species other than Spartina alterniflora, Juncus roemerianus, and Littoraria irrorata (snails) were found. 11-33

Figure 11-14. The Spartina alterniflora die-off area at Mile Hammock Bay in 2015. 11-34

Figure 11-15. Annual Juncus roemerianus and Spartina alterniflora biomass and snail density at eight monitoring stations from 2009 to 2016. 11-34

Figure 11-16. Average annual S. alterniflora and J. roemerianus biomass at Traps Bay Bridge (TBB) and Traps Bay Creek (TBC). 11-35

Figure 11-17. Changes in average annual snail (Littoraria irrorata) density and S. alterniflora biomass at Mile Hammock Bay (MHB), Onslow Beach Backbarrier (OBB), Traps Bay Bridge (TBB), and Traps Bay Creek (TBC) from 2009 to 2016. 11-37

Figure 11-18. The Palmer Drought Severity Index (PDSI) for the Southern Coastal Plain of North Carolina, which includes MCBCL. 11-38

Figure 11-19. Annual growing season inundation for vegetation plots within the monitoring sites. 11-40

Figure 11-20. The relationship between starting elevation and the rate of net surface elevation change (Table 11-11) for all 16 SETs (slope=−28 mm y^{-1} m of starting elevation, r^2=0.42, p<0.01). 11-42

Figure 11-21. Marsh surface elevation recorded from the six SETs at Freeman Creek (FC). 11-44

Figure 11-22. Marsh surface elevation recorded from SETs at Onslow Beach Backbarrier (OBB) and Mile Hammock Bay (MHB). 11-45

Figure 11-23. Marsh surface elevation recorded from the SETs at Traps Bay Bridge (TBB), Trays Bay Creek (TBC), Pollock's Point Shoreline (PPS), Pollock's Point Woods (PPW), French Creek Shoreline (FNS) and French Creek Woods (FNW). 11-46

Figure 11-24. (A) Elevation change for each quarter at all SETs plotted by inundation between measurements with the regression slope. (B) The standard error of quarterly SET measurements plotted by inundation. 11-47

Figure 11-25. The relationship between net surface elevation change and sediment accretion as measured by SETs and Marker Horizons, respectively, across the study period. 11-49

Figure 11-26. Images of the cut-fill analysis results for (A) Traps Bay Bridge, (B) Traps Bay Creek, (C) Pollocks Point Shoreline, and (D) French Creek. 11-51

List of Tables

Table 11-1. Components of the Coastal Wetlands Monitoring Program 11-6

Table 11-2. List of Vegetation Monitoring Sites and Water Level Stations and Descriptions of Monitoring Parameters 11-7

Table 11-3. Baseline Length and Transect Distance of DSAS Stations Associated with SET Marks..... 11-16

Table 11-4. The Mean Annual Water Level Measured at the Beaufort NWLON Station, Mile Hammock Bay (MHB) and Gottschalk Marina Wallace Creek (GMWC)..... 11-21

Table 11-5. Tidal Datums Determined by Using the Modified Range Ratio Method with the Beaufort, NC NWLON Station 8656483 as a Control..... 11-22

Table 11-6. Average ± Standard Error (SE) Annual Marsh Elevation and Inundation (Hours and Percentage of Time) by Treatment for the SETs at Each Site..... 11-25

Table 11-7. Average (±Standard Error [SE]) SET Elevations and Inundation (Hours and Percentage of Time) by Season 11-28

Table 11-8. Inundation Duration Calculated from September 15, 2016 to October 30, 2016 by Using Water Level Data and the Average SET Sediment Surface Elevation at Each Site or Station..... 11-30

Table 11-9. Significant Relationships ($p<0.05$) Between Growing Season Rainfall (Total Inches of Precipitation Between April 1 of Each Year and the Date of the Annual Survey) and Annual Average Vegetation Parameters at MCBCL Vegetation Monitoring Stations 11-38

Table 11-10. Standard Least Squares Regression Results for the Relationship Between a Series of Dependent Variables with Growing Season Inundation (Total Hours of Growing Season with Sediment Surface Inundated)..... 11-40

Table 11-11. The mean (±Standard Error) Rate of Elevation Change at Each SET over the 9-Year Study Period (2008–2016) Determined by Two Applications of Linear Regression Analysis (see the Materials and Methods Section of This Chapter)..... 11-43

Table 11-12. Results of the Cut-Fill Analysis by Using the Digital Shoreline Analysis System (DSAS) for French Creek (FN), Pollocks Point Shoreline (PPS), Traps Bay Bridge (TBB), and Traps Bay Creek (TBC) and from 2008 (2011 for FN) to 2016 for the Digital Elevation Model (DEM) area indicated 11-50

Acronyms

°C	degree Celsius
AE	Aquatic/Estuarine (Module)
C	control
CB	Coastal Barrier (Module)
cm	centimeter
CO-OPS	Center for Operational Oceanographic Products and Services
CORS	Continuously Operating Reference Station
CP	control point
CVS	Carolina Vegetation Survey
CW	Coastal Wetlands (Module)
CWMP	Coastal Wetland Monitoring Program
DCERP	Defense Coastal/Estuarine Research Program
DCERP1	first cycle of DCERP
DCERP2	second cycle of DCERP
DD	decimal degree
DEM	Digital Elevation Model
DoD	U.S. Department of Defense
DSAS	Digital Shoreline Analysis System
EPR	end point rate
F	fertilized
FC	Freeman Creek
FC-C	Freeman Creek control
FC-F	Freeman Creek fertilized
FN	French Creek
FNS	French Creek Shoreline
FNW	French Creek Woods
GMWC	Gottschalk Marina Wallace Creek (water level station)
GNSS	Global Navigation Satellite System
GPS	global positioning system
GRS 80	Geodetic Reference System 1980
ICW	Intracoastal Waterway
IGS08	International GNSS Service 2008
KNCA	New River Air Station
m	meter

m^2, m^{-2}	square meter
m^3	cubic meter
MARDIS	Monitoring and Research Data Information System
MCBCL	Marine Corps Base Camp Lejeune
mg m^{-2}	milligrams per square meter
MHB	Mile Hammock Bay
MHB-C	Mile Hammock Bay control
MHB-F	Mile Hammock Bay fertilized
MHHW	Mean of all higher high water heights observed over a specific NTDE (or calculated equivalent); mean high high water
MHW	Mean of all high water heights observed over a specific NTDE (or calculated equivalent); mean high water
MLLW	Mean of all lower low water heights observed over a specific NTDE (or calculated equivalent); mean low low water
MLW	Mean of all low water heights observed over a specific NTDE (or calculated equivalent); mean low water
mm	millimeter
mm y^{-1}	millimeters per year
MN	Difference in elevation between MHW and the MLW
MSL	Mean of all hourly heights observed over a specific NTDE (or calculated equivalent); mean sea level
NAD 83	North American Datum of 1983
NAVD 88	North American Vertical Datum of 1988
NGS	National Geodetic Service
NOAA	National Oceanic and Atmospheric Administration
NRE	New River Estuary
NSRS	National Spatial Reference System
NTDE	National Tidal Datum Epoch
NWLON	National Water Level Observation Network
OBB	Onslow Beach Backbarrier
OBB-C	Onslow Beach Backbarrier control
OBB-F	Onslow Beach Backbarrier fertilized
OPUS	Online Positioning User Service (Projects)
PDSI	Palmer Drought Severity Index
PP	Pollocks Point (Shoreline and Woods)
PPS	Pollocks Point Shoreline
PPW	Pollocks Point Woods

r^2	r-squared (value) or coefficient of determination
RC	Resource Conservation and Climate Change (a SERDP program area)
RSLR	relative sea level rise
RTK-GPS	real-time kinematic global positioning system
SE	standard error
SERDP	Strategic Environmental Research and Development Program
SET	surface elevation table
SLP	Sensor Leveling Point
TB	Traps Bay (Bridge and Creek)
TBB	Traps Bay Bridge
TBC	Traps Bay Creek
TSP	Translating Science into Practice (Module)
USGS	U.S. Geological Survey
VRP	vertical reference point
VRS	Virtual Reference Station
YSI	Yellow Springs, Inc.

Abstract

The primary objectives of the Coastal Wetlands monitoring activity were to: (1) improve understanding of the climate drivers and ecological processes that determine the stability and community structure of the coastal wetland ecosystem; (2) quantify spatial and temporal variability in key parameters affecting marsh carbon, nutrient, and sediment fluxes; and (3) provide data to support development of forecasting tools, models, and adaptive management actions to improve the sustainability of coastal wetlands. Present-day salt marshes have developed during a prolonged (thousands of years) period of sea level rise, and positive feedbacks between plant production and biomass, sediment accretion, and tidal inundation, enable marshes to maintain the intertidal elevation required for their growth. Predictions of how marshes will fare under the projected accelerated sea level rise of the twenty-first century rely upon accurate knowledge of present-day marsh surface elevation, sediment accretion rates, contribution of subsurface processes to net elevation change, and tidal dynamics of the study area.

Two secondary tide gage stations provided data for the calculation of local tidal datums and documented seasonal and annual variabilities in water level. During the study period (2008–2016), mean water level in Wallace Creek in the upper New River Estuary (NRE), and in the Mile Hammock Bay harbor, adjacent to the Intracoastal Waterway (ICW), increased 10 and 14 mm y^{-1}, respectively, rates much higher than the local long-term rate of relative sea level rise (RSLR), which is 3.0 mm y^{-1}. Our study period included one of the recurring, short-lived, rapid sea level rise accelerations (Southeast United States, 2011–2015) associated with decadal oscillations in ocean–atmospheric processes. Intra-annual monthly variation in mean water level was 23 cm at both stations, nearly twice the 12-cm increase in mean annual water level over the study period. Shorter term deployment of pressure sensors at study sites demonstrated that marshes near Browns Inlet experience twice the tidal amplitude as marshes near the New River Inlet and up to six times the tidal amplitude of marshes in the upper NRE. Inundation, which is dependent upon marsh elevation and water level, also had strong spatial and seasonal components. The low-lying marshes at Freeman Creek near Browns Inlet were the most frequently and regularly inundated marshes, with lowest inundation (38%) occurring in the winter and spring and the highest inundation in the fall (52%). Marshes in the NRE had more seasonal variability in inundation. At French Creek, where tidal amplitude is reduced and mean sea level is higher than other sites, inundation ranged from 17% in spring to 56% in fall.

We used surface elevation tables (SETs) and Marker Horizons to measure net marsh surface elevation change and sediment accretion rates, respectively, at six salt marsh monitoring sites on Marine Corps Base Camp Lejeune (MCBCL) between early 2008 and November 2016. Three of the sites were dominated by *Spartina alterniflora* and were adjacent to the ICW. The remaining sites were in the NRE, where dominant vegetation ranged from mixed *S. alterniflora–Juncus roemerianus* to predominantly *J. roemerianus*. A total of 16 SETs were installed. Five out of the 10 SETs at ICW sites were installed in experimental fertilized plots. None of the six NRE SETs were in fertilized plots. The two SETs at each NRE site were placed in different geomorphic or hydrodynamic settings (i.e., shore versus upland boundary or creek versus bay front). Fifteen out of the 16 SETs showed a significant increase in marsh surface elevation during the study period, with slopes ranging from 10 mm y^{-1} at a low-elevation (zero m North American Vertical Datum

of 1988 [NAVD 88]), *S. alterniflora* site to 0.5 mm y^{-1} at locations higher in the intertidal area. Four SETs, all at Freeman Creek, exhibited surface elevation change rates greater than RSLR, and all but four SETs on MCBCL were at least keeping pace with RSLR. At two of the ICW sites, fertilized SETs exhibited greater elevation increase than non-fertilized SETs.

Across the study period, sediment accretion rates exceeded net elevation change rates in 76% of 194 paired measurements. MCBCL marsh surface elevation change is primarily driven by sediment accretion, but below-ground plant production, sediment compaction, and shallow subsidence also contribute to net marsh surface elevation change.

Marsh floral species composition and percent cover, and *Spartina alterniflora* and *Juncus roemerianus* above-ground biomass, were monitored annually in permanent 1-m^2 plots at each of the six monitoring sites. The density of the marsh periwinkle snail (*Littoraria irrorata*), the occurrence of oysters and mussels in vegetation plots, and the elevation of each permanent plot were recorded annually. Declines in marsh vegetation (both *S. alterniflora* and *J. roemerianus)* were observed in 2012–2013 at all sites after a period of moderate drought as indicated by the Palmer Drought Severity Index. A die-off of *S. alterniflora*, which resulted in large bare areas, was observed at several sites and was most widespread and persistent at Mile Hammock Bay, where the average % cover of *S. alterniflora* across the monitoring site declined from over 50% to less than 25 %, and *S. alterniflora* aboveground biomass declined from over 300 g m^{-2} to less than 125 g m^{-2}. One year after the initial marsh decline at Mile Hammock Bay, snail density increased from 100 snails per square meter (m^{-2}) to more than 250 m^{-2}. Neither measure of marsh vegetation recovered to pre-die-off values by 2016, although snail density declined to pre-die-off densities. Similar patterns were observed at Onslow Bay and Traps Bay sites, although at these sites, *S. alterniflora* percent cover and biomass recovered by 2014.

Annual marsh monitoring also revealed a change in marsh vegetation cover at Traps Bay Creek during the study period. Traps Bay Creek is in the lower NRE, and *J. roemerianus* was the dominant marsh vegetation in terms of percent cover and biomass until 2012. After 2012, *J. roemerianus* biomass declined and *S. alterniflora* biomass increased at Traps Bay Creek. A similar trend in percent cover of the marsh vegetation was noted at Traps Bay Creek and at a nearby site and is indicative of an expansion of *S. alterniflora*, a more salt and inundation tolerant plant, at marsh sites in the lower estuary.

The fate of sediment eroded from marsh shorelines was examined at four sites in the NRE by constructing detailed Digital Elevation Models to analyze both horizontal and vertical changes in the salt marsh shoreline. Three out of the four stations exhibited shoreline erosion between 2008 and 2016. The fourth station showed a slight seaward movement of the zero elevation contour line. Erosion of the marsh edge was correlated with an increase in marsh surface elevation landward of the shoreline, indicating a conservation of marsh sediment within the system. This mechanism both increases resiliency of the marshes to sea level rise and limits the loss of sediment carbon via erosion.

Keywords: Accretion, dieback, elevation, Intracoastal Waterway, *Juncus roemerianus*, Marker Horizon, New River Estuary, North Carolina, salt marsh, sea level rise, sediment, *Spartina alterniflora*, surface elevation table, tidal datum, water level

Objectives of the Monitoring Activity

The Coastal Wetlands Monitoring Program (CWMP) is designed to

1. Improve understanding of the physical, biological, and ecological processes that determine the stability and community structure of the coastal wetlands ecosystem
2. Quantify spatial and temporal (inter-annual) variability in key parameters affecting marsh carbon, nutrient, and sediment fluxes
3. Provide data to support development of forecasting tools and models
4. Use these tools to guide adaptive management actions to improve the sustainability of coastal wetlands to climate change and man-made impacts.

Specific variables include those that characterize the system at the plant-community structure level, landscape-scale measures of marsh geomorphology, and tide and water quality data to assess hydrodynamic features that shape the landscape. The CWMP data are used by Research Projects AE-4, AE-6, CW-4, CW-5, and CB-5 and provide inputs to the Estuarine Simulation Model being refined as part of Research Project TSP-2.

Specific objectives of Coastal Wetlands Module monitoring, and the research projects using the data, include the following:

- Determining the net change in surface elevation across the estuarine tidal and salinity gradient in Marine Corps Base Camp Lejeune (MCBCL) marshes (Research Project CW-4)
- Measuring sediment accretion rates across the estuarine tidal and salinity gradient in MCBCL marshes (Research Projects CW-4 and CW-5)
- Determining inter-annual variability in marsh above-ground biomass and species composition (Research Project CW-4)
- Measuring temporal and spatial variability in snail density of MCBCL marshes and determining the relationship to marsh above-ground biomass
- Estimating the volume of eroded marsh shoreline to support an estuarine carbon budget (Research Projects AE-4, AE-6, CW-4, and CW-5)
- Providing tide gage data in the lower and upper portions of the New River Estuary (NRE) to support hydrodynamic models and inundation calculations to assess the impact of storm events (Research Projects CW-4 and CW-5).

Background

Critical military training and testing on lands along the nation’s coastal and estuarine shorelines are increasingly placed at risk because of development pressures in surrounding areas, impairments due to other anthropogenic disturbances, and increasing requirements for compliance with environmental regulations. The U.S. Department of Defense (DoD) has established ecosystem-based management as the preferred approach for military lands (Goodman, 1996). To accomplish this goal in coastal environments, the Strategic Environmental

Research and Development Program (SERDP) launched the Defense Coastal/Estuarine Research Program (DCERP) at MCBCL in North Carolina (**Figure 11-1**) in 2006. As a U.S. Marine Corps installation, MCBCL has a single and exclusive mission: military preparedness. MCBCL provides an ideal platform for DCERP because it integrates coastal barrier, aquatic/estuarine, coastal wetlands, and terrestrial ecosystems, all within the boundaries of DoD properties.

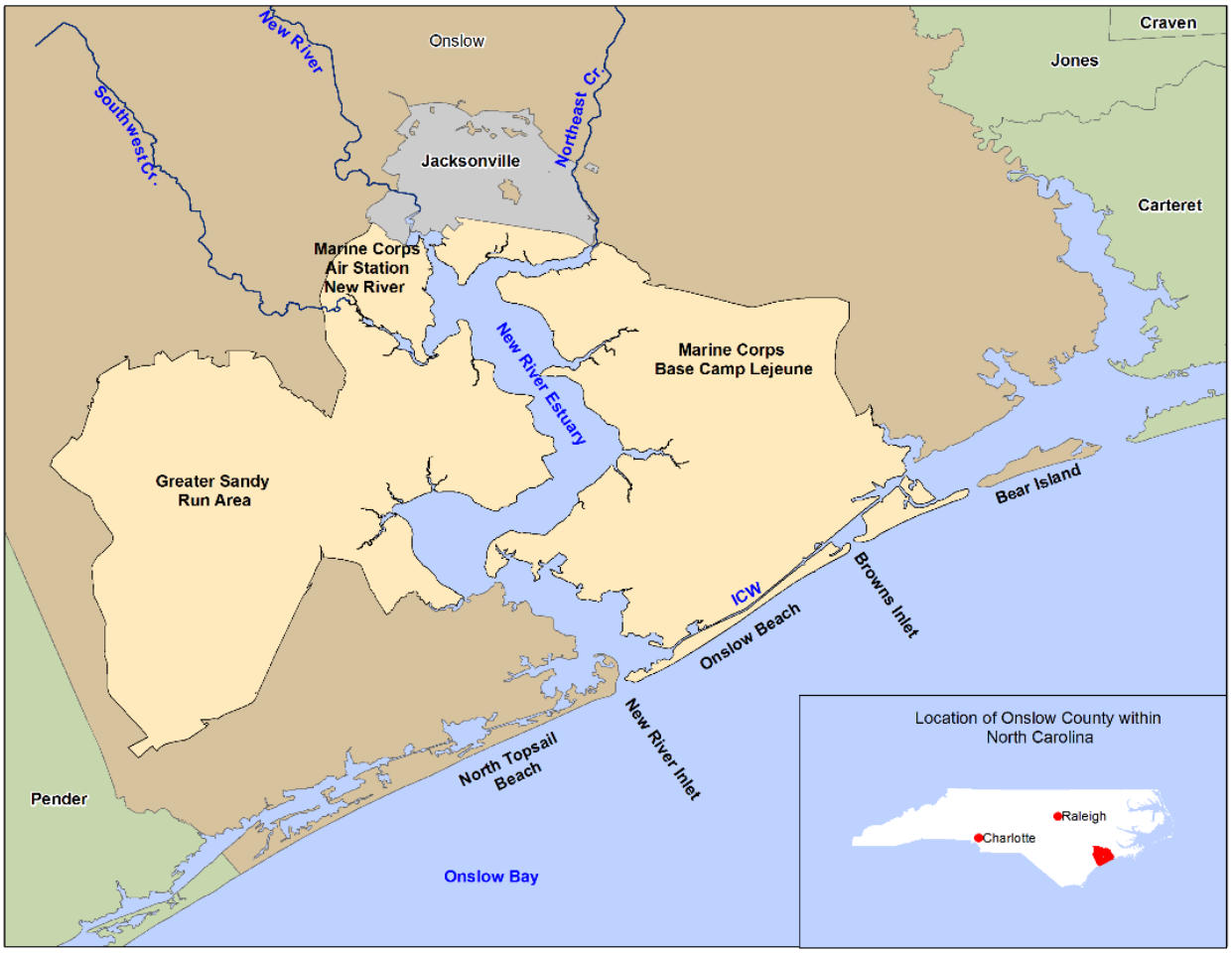

Figure 11-1. Location of Marine Corps Base Camp Lejeune in Onslow County, NC.

The potential impacts of climate change on military training have been identified as a growing challenge to our nation's military readiness. DoD facilities in coastal/estuarine areas are at additional risk from climate change, including changes in rising sea level and extreme weather (Hall et al., 2016). In addition, installation managers need to understand the trade-offs between carbon management and other adaptive management decisions to reach future installation carbon goals in a changed climate. To balance military training needs and sustainable natural resource management, installation managers need easy-to-use decision-support tools, models, and other products to assist them in making often complex management decisions.

Coastal marshes are a vital component of the estuarine landscape and link terrestrial and freshwater habitats with the sea (Levin et al., 2001). In the intertidal zone, marshes help to stabilize sediments and minimize erosion (Currin et al., 2015; Knutson et al., 1982; Möller et al.,

1999). Wetlands improve water quality by acting as nutrient transformers and by trapping sediment (Morris, 1991; Tobias et al., 2001; Valiela and Teal, 1979). In generally, marshes consume (denitrify) nitrate dissolved in flood water and, thus, have a beneficial effect on estuarine water quality. In addition, coastal wetlands provide critical habitat area for a diverse group of estuarine organisms, serve as nursery habitat for commercially important fishery species (Kneib, 1997), and provide recreational opportunities for people.

However, across the United States, coastal salt marshes have declined in area over the past 200 years, and they are currently being lost at a higher rate than any other wetland category (Dahl, 2011). Much of this loss results from the conversion of salt marsh to open water and is a result of sea level rise, storm events, erosion, and changes in land-use practices (Cahoon et al., 2006; Kirwan and Blum, 2011; Mattheus et al., 2010; Morris et al., 2002). Projected acceleration in sea level rise (Bindoff et al., 2007; Vermeer and Rhamstorf, 2009) will exacerbate these processes and will require both improved modeling efforts and adaptive management approaches to minimize the adverse impact of marsh loss on coastal ecosystems.

Coastal wetlands on MCBCL include backbarrier island marshes that are crucial to island dynamics, *Spartina alterniflora*–dominated marshes on the mainland adjacent to both Browns and the New River Inlets and along the Intracoastal Waterway (ICW), and fringing marshes in embayments and tributaries of the main stem NRE, which transition from *Spartina*–dominated in the lower estuary to *Juncus roemerianus*–dominated in the mid-estuary. However, the distribution and productivity of marsh vegetation vary along elevation, nutrient, and salinity gradients and are sensitive to annual variations in rainfall and sea level (Pennings and Bertness, 2001). Furthermore, tidal dynamics and wave energy exert significant controls on the shape of the marsh landscape, as well as its response to short- and long-term changes in sea level (Friedrichs and Perry, 2001; Kolker et al., 2009). The CWMP strategy is to measure forcing factors affecting marsh distribution, production, and erosion/accretion and to document annual variability in marsh production and sedimentation rates across landscape-scale gradients in elevation, tidal amplitude, and wave exposure. Monitoring variables and the temporal and spatial scale of measurement are listed in **Table 11-1**.

Monitoring stations (**Table 11-2**) were co-located with stations used by the Research Project CW-4 and CW-5 Teams. Suspended sediment concentration sampling conducted by Drs. Scott Ensign and Carolyn Currin occurred at Freeman Creek (FC), Traps Bay Creek (TBC), and French Creek (FN) stations as part of the Research Project CW-4 study. Marsh cores for geochronology (Research Projects CW-4 and CB-5) were collected at FC, Onslow Beach Backbarrier (OBB), Mile Hammock Bay (MHB), TBC and FN stations. The impacts of fertilization on above- and below-ground biomass were examined at FC, OBB, MHB, TBC and FN (CW-4). CWMP data from FC, TBC and FN were used to model the marsh response to sea level rise (Research Project CW-4).

Table 11-1. Components of the Coastal Wetlands Monitoring Program

Variable	Temporal Scale	Spatial Scale	Method
Shoreline erosion	Every 2–3 years	Sites	RTK-GPS and DEM
Water level, temperature, and salinity	Continuous (every 6 minutes, with a few gaps	2 stations	Tide gages
Marsh vegetation and snails	Annually	Permanent 1-m^2 plots, 15–30 plots per site	*Spartina* and *Juncus* stem density, height, biomass and marsh species percent cover; density of *Littoraria irrorata*
Marsh surface elevation change and accretion	Quarterly	16 SETs and associated Marker Horizon plots at 6 sites	SETs and Marker Horizons

DEM=Digital Elevation Model; RTK-GPS=real-time kinematic global positioning system; SET=surface elevation table.

Materials and Methods

Research Location and Design

The coastal wetlands that are the focus of this module are defined as the vegetated inter-tidal habitat in salt and brackish waters and include the salt marshes along the lower NRE shoreline and ICW to the brackish marshes along the upper NRE shoreline and tributaries of the NRE. The monitoring sites are stratified along the salinity and tidal gradient and include wetlands in both the NRE and ICW (**Figure 11-2 and Table 11-2**).

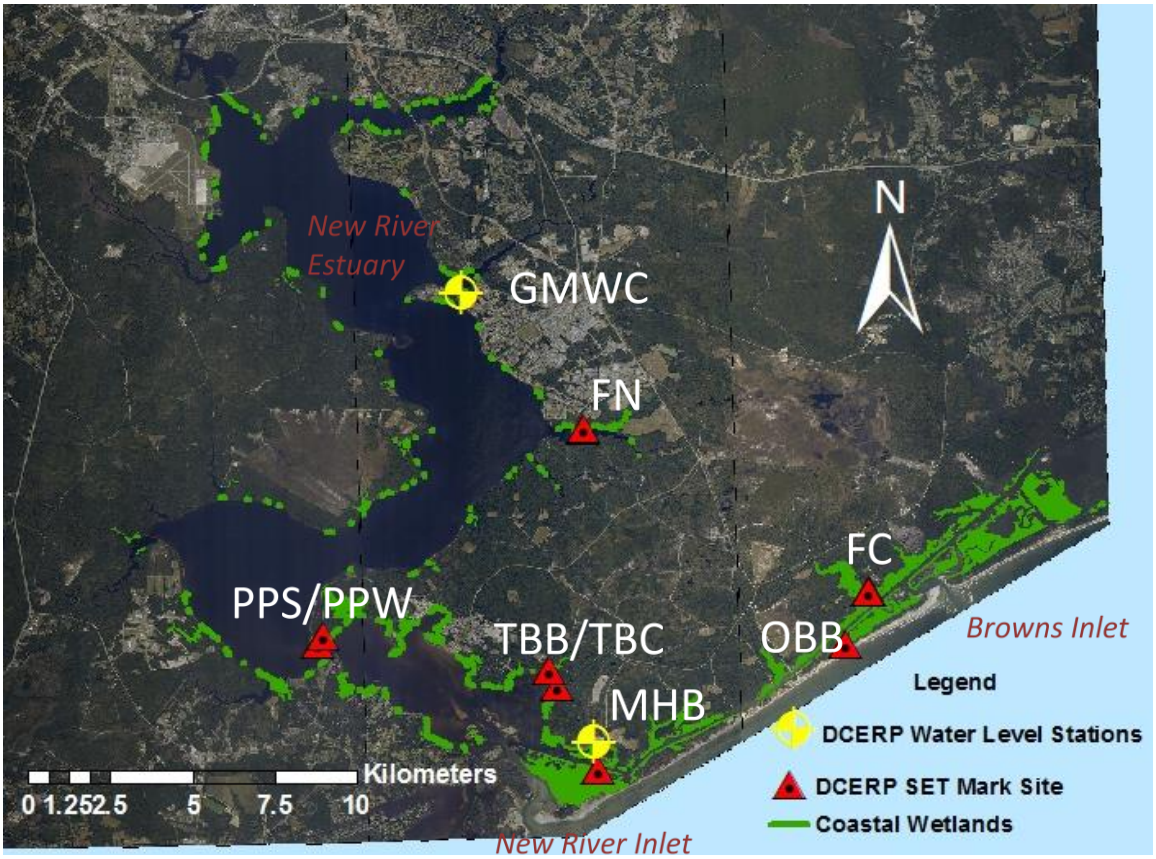

Figure 11-2. Location of the six coastal wetland monitoring sites.

Surface elevation tables (SETs; red triangles) and two secondary tide gage (water level) stations (yellow and black circles) are indicated by symbols and abbreviations. Freeman Creek (FC), Mile Hammock Bay (MHB), and Onslow Beach Backbarrier (OBB) are located along the Intracoastal Waterway. Traps Bay (TB; Traps Bay Bridge [TBB] and Traps Bay Creek [TBC]), Pollocks Point (PP; Pollocks Point Shoreline [PPS] and Pollocks Point Woods [PPW]), French Creek (FN; [French Creek Shoreline and French Creek Woods]), and Gottschalk Marina Wallace Creek (GMWC) are within the NRE. Green areas denote coastal wetlands.

Table 11-2. List of Vegetation Monitoring Sites and Water Level Stations and Descriptions of Monitoring Parameters

Site/Station	ID	Parameter	Sample Frequency	Sampling Duration	Sampling Notes
Freeman Creek	FC	Surface elevation	Quarterly	2008–2016	Surface elevation tables (SETs; 6)
Control	FC-C	Sediment accretion	Quarterly to annually	2008–2016	Marker Horizons (3–6)
Fertilized	FC-F	Vegetation and snail density; vegetation biomass	Annually	2008–2016	Permanent plots (25)
		Water level	Continuous	2014–2016	Water level loggers

(continued)

Table 11-2. List of Vegetation Monitoring Sites and Water Level Stations and Descriptions of Monitoring Parameters (continued)

Site/Station	ID	Parameter	Sample Frequency	Sampling Duration	Sampling Notes
Onslow Beach Backbarrier	OBB	Surface elevation	Quarterly	2008–2016	SETs (2)
Control	OBB-C	Sediment accretion	Quarterly to annually	2008–2016	Marker Horizons (3–6)
Fertilized	OBB-F	Vegetation and snail density; vegetation biomass	Annually	2008–2016	Permanent plots (25)
		Water level	Continuous	2015–2016	Water level loggers
Mile Hammock Bay	MHB	Water level, temperature, and salinity	Continuous	2008–2017	YSI 600 LS datasondes surveyed to bench marks
Control	MHB-C	Surface elevation	Quarterly	2008–2016	SETs (2)
Fertilized	MHB-F	Sediment accretion	Quarterly to annually	2008–2016	Marker Horizons (3–6)
		Vegetation and snail density; vegetation biomass	Annually	2008–2016	Permanent plots (25)
		Water level	Continuous	2015–2016	Water level loggers
Traps Bay	TB	Surface elevation	Quarterly	2008–2016	SETs (2)
Bridge	TBB	Sediment accretion	Quarterly	2008–2016	Marker Horizons (2–8)
Creek	TBC	Vegetation and snail density; vegetation biomass	Annually	2009–2016	Permanent plots (30)
		Water level	Continuous	2014–2016	Water level loggers
		Shore erosion	Biannual	2013–2016	Digital Elevation Model (DEM)
Pollocks Point	PP	Surface elevation	Quarterly	2008–2016	SETs (2)
Shoreline	PPS	Sediment accretion	Quarterly to annually	2008–2016	Marker Horizons (2–8)
Woods	PPW	Vegetation and snail density; vegetation biomass	Annually	2009–2016	Permanent plots (30)
		Shore erosion	Biannual	2013–2016	DEM
Gottschalk Marina Wallace Creek	GM WC	Water level, temperature, and salinity	Continuous	2008–2016	YSI 600 LS datasondes surveyed to bench marks
French Creek	FN	Surface elevation	Quarterly	2008–2016	SETs (2)
Shoreline	FNS	Sediment accretion	Quarterly to annually	2008–2016	Marker Horizons (1–4)
Woods	FNW	Vegetation and snail density; vegetation biomass	Annually	2009–2016	Permanent plots (15)
		Water level	Continuous	2014–2016	Water level loggers
		Shore erosion	Biannual	2013–2016	DEM

Bench Mark and Surface Elevation

A bench mark is a specific type of survey mark that has a known elevation relative to a datum. Bench marks may be permanent or temporary. A survey mark refers to any permanent mark or disk placed in the ground or attached to permanent structure with known latitude, longitude, or height information. Within the DCERP project, the bench mark coordinate position and elevation are available through the Monitoring and Research Data Information System (MARDIS), but are not published for public use or survey control. Bench marks associated with surface elevation tables (SETs) are referred to as SET marks (Cahoon, 2002a). Select SET marks are also designated as control points, which are used to reference nearby SET marks, surface elevations, and Global Navigation Satellite System (GNSS) accuracy during a particular survey (NOAA, 2007c). Bench marks and survey marks are classified by their stability. Class A is the most stable. DCERP SET marks are Class B, and all marks are Class C. No Class A marks exist in the survey area. More information on these different types of bench marks is provided by Floyd (1978).

Global positioning system (GPS) data were collected by using several techniques, and the procedures, processing, and accuracy of elevation measures vary with the collection technique used. Static and topographic surveys using high accuracy GNSS receivers (Trimble® 5800 and R6-3) were used to determine coordinate, ellipsoid and orthometric heights of specific points and structures (Zilkoski et al., 2008). The data receivers accessed the GPS and the National Spatial Reference System (NSRS) via Continuously Operating Reference Station (CORS) networks or through Virtual Reference Station (VRS) or real-time kinematic techniques. Receiver data were processed using Trimble software or transformed and submitted directly to National Geodetic Survey (NGS) Online Positioning User Service (OPUS; NOAA, 2014) or Trimble Business Center for post-processing, display, and reports.

The NGS OPUS Projects program was used to determine coordinate, ellipsoid and orthometric heights, and estimates of error of selected reference marks (**Appendix 11-A, Table 11-A-1**). OPUS Projects "offer Web-based access to simple visualization, management, and processing tools for multiple marks and multiple occupations" by using high accuracy GNSS receivers. This process technique ties all surveyed marks to the NSRS through the CORS hub station. A project that was specific for DCERP (DCERP_OP) was created within the program.

At each marsh monitoring site, one SET mark was designated as the control point for reference in all subsequent surveys or leveling operations (**Appendix 11-A, Table 11-A-2**). For GPS data collection, GNSS dual-phase receivers were set up on a brass disc located on the surface of each SET mark base. The brass disc is set in concrete and has mark numbers and name identifications stamped on its face. In 2008 and 2009, the OPUS static program was used to determine the SET mark coordinate position and heights (Davis et al., 2017). The mean of three static data collection sessions (greater than 2 hours) were used to determine a SET mark position and elevation, and the mean values were used for reference until 2016 when results were improved with the release of the new geoid model (G12B) and the NGS OPUS Projects program. All elevation data were updated and analyzed by using the G12B model for orthometric heights. In this report, orthometric height is reported as elevation in meters relative to North American Vertical Datum of 1988 (NAVD 88). In 2016, the previously mentioned OPUS Project DCERP_OP was used to determine all SET mark three-dimensional positions. In 2014 and 2015,

additional OPUS collections were made on SET marks and on new Class C bench marks and published NSRS bench marks. At a minimum, two static GPS data collection sessions (greater than 4 hours=mean of all DCERP_OP sessions) were collected simultaneously on multiple marks. These sessions were during different days and sessions times to include the changes in satellite ephemeris. Additional simultaneous collection sessions were made to improve the accuracy through redundant occupations. The best OPUS solution on non-published marks (control point marks) (based on overall Root Mean Square (RMS) and peak-to-peak error was designated the a priori position. Forty-five GPS static collections were used during project processing. The nearby Jacksonville, NC, CORS (identification=NCJV) was used as the hub mark for all session processing and final network adjustment. Ten additional CORS were used during the survey and in the final network adjustment; all CORS were fully constrained (X, Y, Z). Elevations of non-control point SETs and bench marks were determined by laser-leveling to the nearest control point SET or Class C bench mark by using techniques modified from the National Oceanic and Atmospheric Administration (NOAA; Hicks et al., 1987). In 2016, the reference point on SET marks (the brass disc) was transferred to the highest point on the SET receiver structure, designated as the vertical reference point (VRP) for sediment surface elevation calculations (Lynch et al., 2015).

NOAA's Beaufort Laboratory established two secondary water level stations, which are defined as being established for more than 1 year and less than 19 years (NOAA, 2003). The MHB station was installed on February 21, 2008 along the ICW. A second station, Gottschalk Marina Wallace Creek was installed on May 15, 2008 on a tributary of the NRE. The station at Gottschalk Marina Wallace Creek was removed on August 26, 2016. The station at Mile Hammock Bay is being maintained to support a joint project from NOAA and the U.S. Army Corps of Engineers to test the thin-layer application of dredged material on the marsh surface, which grew out of DCERP2 research and modeling results. At each station, new Class C bench marks and at least three reference marks were installed, surveyed, and leveled following NOAA's Center for Operational Oceanographic Products and Services (CO-OPS) protocols for secondary water level stations (NOAA, 2007a). Coordinates and heights of Class C bench marks were initially established by using the OPUS program in 2009. Coordinates and heights were updated in 2016 following processing in OPUS Projects (**Appendix 11-A, Table 11-A-1**).

At each station, a vented datasonde (Yellow Springs, Inc. [YSI] Model 600LS) was deployed at a stable elevation, which was measured precisely to a physical reference point, designated as the sensor leveling point on the supporting structure. The datasondes collected water level, temperature, and salinity data. Water levels, recorded as above the sensor zero point, were corrected to elevation in meters NAVD 88 by referencing the sensor leveling point elevation and correcting for the vertical offset to the datasonde sensor zero point (NOAA, 2015).

The sensor leveling point elevations were determined to be 1.61 m NAVD 88 at Gottschalk Marina Wallace Creek based on an OPUS Project and 2.12 m NAVD 88 at Mile Hammock Bay by laser leveling to bench mark MILE (with OPUS Projects–determined elevation; **Appendix 11-A, Table 11-A-1**).

The elevation of each permanent vegetation sample plot was obtained by laser leveling to the control point SET mark, except for 2009 at Mile Hammock Bay, where an average of measurements obtained by both RTK-GPS and laser leveling was used. Instrument and

measurement error due to uneven or soft ground, and operator error in maintaining a vertical pole position and reading the range finder, is estimated to be ±2 cm.

Temperature, Salinity, Water Level, and Inundation

YSI 600LS datasondes collected water level, temperature, and salinity data every 6 minutes, which is the sampling frequency required to calculate a National Tidal Datum Epoch (NTDE) equivalent tidal datum (NOAA, 2007b). Temperature, salinity, and water level data were downloaded at least every 2 months from the temporary tide gages, and datasondes were replaced every 3 to 9 months. The datasondes underwent calibration procedures before and after deployment to test for drift and data quality. Water level data were collected from May 15, 2008 to August 26, 2016 at Gottschalk Marina Wallace Creek (8.3 years) and from February 21, 2008 to December 24, 2016 at Mile Hammock Bay (8.8 years). The record was interrupted by four gaps at Mile Hammock Bay (13–48 days) and one gap at Gottschalk Marina Wallace Creek (6 days) because of instrument failure or boat strike damage. One year (2009) of Mile Hammock Bay and Gottschalk Marina Wallace Creek water level data were provided to NOAA's CO-OPS for quality assurance and quality control checks and tidal datum analysis. The data were referenced to the nearest National Water Level Observation Network (NWLON) Station (8656483 in Beaufort, NC) by using the modified range ratio method (NOAA, 2003) to determine Mile Hammock Bay and Gottschalk Marina Wallace Creek tidal datums referenced to the current (1983–2001). CO-OPS provided additional assistance by calculating datums for Freeman Creek, Traps Bay Creek, and French Creek by using short-term HOBO logger water level data. Because logger sensor stability is not rigorously controlled and deployment are short term, datums based on logger data are less accurate than Mile Hammock Bay and Gottschalk Marina Wallace Creek datums.

The entire records of water level at Gottschalk Marina Wallace Creek and Mile Hammock Bay were evaluated relative to water levels at the NWLON Station 8656483 in Beaufort, NC for quality control purposes (NOAA, 2007b) and to evaluate regional trends in water level.

One of the goals of collecting water level data at Mile Hammock Bay and Gottschalk Marina Wallace Creek throughout the study period was to determine the duration of inundation at each marsh monitoring site. Inundation at SET stations and vegetation plots was determined as the number of hours or percentage of time when a specified SET or vegetation plot elevation was lower than the local water level elevation for a specified period. Because Mile Hammock Bay was the only site near a water level station, HOBO and/or Troll water level loggers were deployed from periods ranging from several months to up to 2 years at several marsh monitoring sites. These observations were used to evaluate the tidal characteristics of the marshes relative to those of the longer term water level stations (Beaufort Station 8656483, Mile Hammock Bay, and Gottschalk Marina Wallace Creek). The analysis was limited to loggers deployed in creeks that captured the full tidal signal for at least several months (Freeman Creek, Onslow Beach Backbarrier, and French Creek). Because no loggers were deployed at Traps Bay Bridge, Pollocks Point Woods, and Pollocks Point Shoreline, and the full tidal signal at Traps Bay Creek was recorded for less than 2 months, we were unable to evaluate the relationship between the longer term stations and, therefore, the accuracy of site-specific inundation measurements over the entire study period. By comparing inundation calculated using short-term site-specific loggers with inundation calculated using data from Beaufort, Mile Hammock Bay, and

Gottschalk Marina Wallace Creek, we determined that Beaufort water level data could be used to calculate inundation at Freeman Creek and Onslow Beach Backbarrier and that Gottschalk Marina Wallace Creek water level data could be used to calculate inundation at French Creek.

Inundation was calculated for each SET marsh surface elevation for the period between quarterly SET measurements (winter, spring, summer, and fall) by using the elevation of the previous SET measurement. Growing season inundation was calculated as the total hours that each vegetation plot at Freeman Creek, Onslow Beach Backbarrier, Mile Hammock Bay, and French Creek was inundated between April 1 of each year until the date of the annual vegetation survey by using the elevation of each plot measured during the year's annual survey.

Monthly mean water levels were calculated as the mean of all hourly water level data. Monthly mean temperature and salinity values were determined from 6-minute data. Monthly means are not reported for months with less than 96% of the month recorded. Inter-annual monthly means are the average of the monthly means for a particular month over the entire study.

Growing season rainfall was calculated as the total number of inches of rainfall at the New River Air Station (KNCA) in Jacksonville, NC, between April 1 of each year until the date of the annual survey. Rainfall data were downloaded from MesoWest (http://mesowest.utah.edu).

Marsh Vegetation

Permanent 1-m^{-2} plots were established for vegetation surveys within the marsh area surrounding the SETs at each site during DCERP1, using a restricted random sampling plot layout (Elzinga et al., 1998). At NRE sites, 15 plots were established around each SET, which was separated within the site to sample different hydrodynamic regimes (shoreline versus upper marsh boundary at French Creek and Pollocks Point, bay front versus creek front at Traps Bay Bridge and Traps Bay Creek). French Creek is an exception to the plot number per site, where the proximity of the shoreline and upper marsh allowed for a smaller sampling area that was adequately covered with 15 plots. At each ICW site, 25 plots were established around the SETs, which were collocated within a site. The total area sub-sampled at each site ranged between 4,000 m^2 and 5,000 m^2 at the ICW sites and between 1, 000 m^2 and 2,000 m^2 at the NRE sites (**Figure 11-3**).

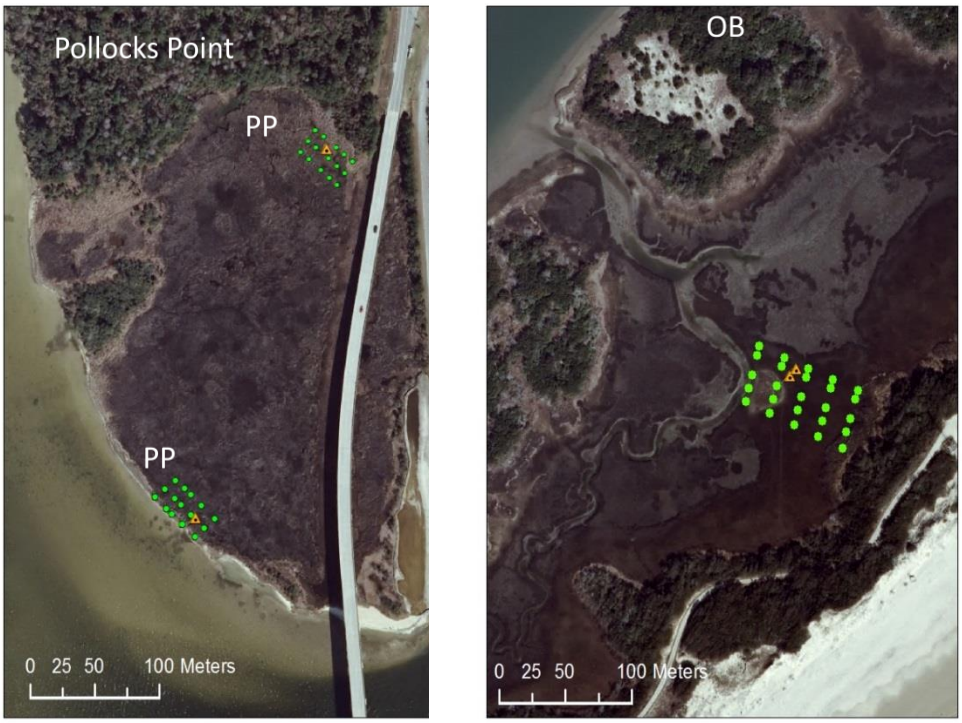

Figure 11-3. Example of the relationship between vegetation monitoring sites, SET stations, and vegetation sample plots at two sites.

(A) Pollocks Point site is in the lower portion of the NRE and consists of two vegetation monitoring areas, PPW and PPS. Each green dot represents a 1-m^2 sample plot. There are 15 sample plots around each NRE SET (orange triangles) except at French Creek, where two SETs are located within one vegetation monitoring area. (B) The Onslow Beach Backbarrier (OBB) vegetation monitoring site is near the Intracoastal Waterway (ICW), which can be seen in the upper left of the figure. The three monitoring sites located along the ICW include 25 1-m^2 sample plots, indicated by green dots, and two to six SETs, indicated by orange triangles. Half of the SETs at each ICW site were fertilized as part of the Research Project CW-4.

Measures of vegetation species composition and percent cover, *Juncus roemerianus* and *Spartina alterniflora* stem density and stem height, *Juncus roemerianus* biomass, marsh periwinkle snail density, and plot elevation were collected annually from 2009 to 2016 from each permanent plot (except for Pollocks Point Woods in 2012 and 2013). Sampling dates ranged from July 16–August 20, targeting the time of peak marsh biomass (Christian et al., 1990; Morris and Haskin, 1990). Pollocks Point Woods was not surveyed in 2011 and 2012.

The percent cover of each plant species, as well as mussels, live oysters, oyster cultch, and wrack (detritus) was visually estimated and assigned to a Carolina Vegetation Survey (CVS) category (Peet et al., 1998). The density (in m^{-2}) of the gastropod *Littoraria irrorata* (marsh periwinkle snail) was recorded from 1-m^2 plots, unless the number in a 0.25-m^2 subplot exceeded 25, in which case only snails from one subplot were counted (and multiplied by four). The density of live *S. alterniflora* stems was measured in 0.25-m^2 subplots and multiplied by four to estimate stem density per square meter. The heights of 10 live *S. alterniflora* stems were measured in each plot along a mid-plot transect and used to estimate biomass by using a height–weight regression model to estimate live above-ground biomass (Davis et al., 2017). The *S. alterniflora* biomass numbers reported here represent peak above-ground biomass, which is approximately 70% of

annual above-ground production (Currin unpublished data; Morris and Haskin, 1990). The high density of *Juncus roemerianus* stems precluded counting stems and heights to convert to above-ground biomass in the permanent plots; instead, destructive harvests from adjacent areas were used to determine *J. roemerianus* biomass. At the NRE sites, *J. roemerianus* stems were harvested from a 0.0625-m^2 plot located within 2 m of nine (every other transect) of the permanent sampling plots. At the ICW sites, *J. roemerianus* was found in only three plots at Onslow Beach Backbarrier and did not occur within the vegetation monitoring plots at Freeman Creek and Mile Hammock Bay. At Onslow Beach Backbarrier, *J. roemerianus* biomass was estimated as previously described for each plot where *J. roemerianus* occurred. At Freeman Creek, separate plots that were well outside the vegetation monitoring plot area were established to obtain additional measures of *J. roemerianus* biomass in marshes adjacent to the ICW. Upon return to the laboratory, *J. roemerianus* stems were washed, sorted into live and dead fractions, and weighed after drying. Live stems were used to determine above-ground biomass. The average sampling area *S. alterniflora* and *J. roemerianus* biomass was calculated by using data only from plots that contained the species.

Standard least squares regression analysis in JMP (SAS Institute Inc., 2015) was used to analyze the relationship between growing season rainfall and growing season inundation with snail density and *Spartina alterniflora* and *Juncus roemerianus* biomass, stem density, and stem height.

Marsh Surface Elevation Change and Sediment Accretion

Net marsh surface elevation change and sediment accretion rates were determined with SETs and feldspar Marker Horizon plots. These were established at six marsh sites in 2008 during DCERP1. The sediment elevation associated with each SET was obtained by measuring the distance (in millimeters) between the SET arm and sediment surface with 36 pins (Lynch et al., 2015). SET data were collected at least quarterly at all stations throughout DCERP1 and DCERP2. The mean and standard error (SE) of the rate of elevation change at each SET was used in a Student's *t*-test following methods in Lynch et al. (2015) to determine significant difference in the rate from zero and from the 3.0 mm y^{-1} RSLR at Beaufort, NC (NWLON Station 8656483; NOAA, 2017; Method 1). In Method 1, the rates of elevation change are determined by linear regression for each of the 36 pins per SET. Nine pin rates per SET arm are averaged to obtain rates of change for each arm, and then those rates are averaged to obtain mean rates and standard error. Average SET elevations measured during each quarter were used in the standard least squares regression model in JMP (Method 2) to determine slope, r^2, and p values of elevation change over time. Marker Horizon plots were established near the SETs by deploying a thin layer of feldspar clay on the marsh surface following the modified cryocore method based on the National Park Service protocol (Lynch et al., 2015). Marker Horizon data (sediment accretion) were collected in conjunction with SET measurements (except for 2013) and when site conditions allowed. The period between quarterly SET measurements ranged from 50 to 150 days, but the period of accretion represented by Marker Horizon measurements was often longer, for two reasons. First, at some sampling times, standing water prevented core collection on the same day, or even within the same quarter, as SET data collection. Second, from 2008 through 2011, we followed the approach of establishing a single 1-m^2 plot for repeated accretion measures over long time periods (years to decades; Lynch et al., 2015). We observed that measurements from Marker Horizons that had been installed for longer periods

resulted in lower rates of accretion (**Figure 11-4**), likely due to compaction over time. Marker Horizon methods were changed in 2011, so that new Marker Horizon plots were installed each quarter to minimize the effects of long-term compaction on accretion measures.

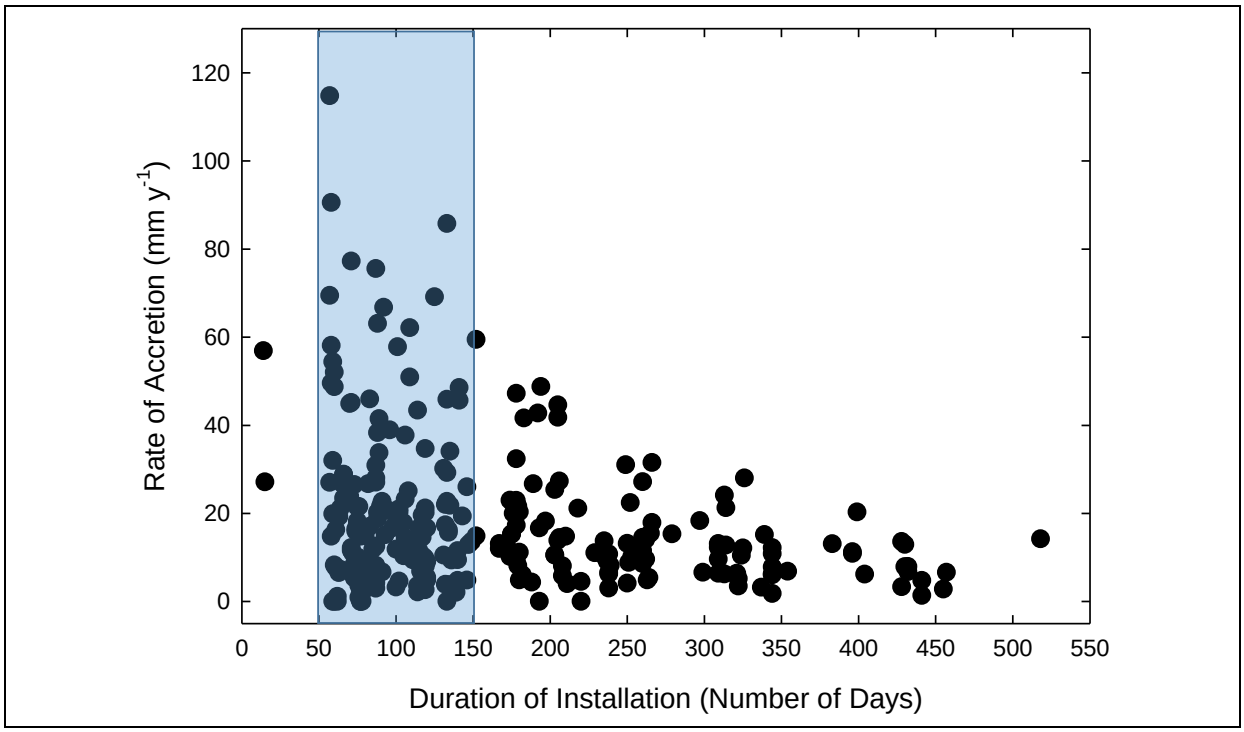

Figure 11-4. Marker Horizon results from the DCERP marsh monitoring sites (2008–2016).

Data from fertilized plots are not shown. The blue area corresponds to the range in time that occurred between quarterly SET readings and that represent the subset of data used for analysis.

At Freeman Creek, Mile Hammock Bay, and Onslow Beach Backbarrier, half of the SETs and Marker Horizon plots were fertilized three times during the growing season (February through August) from 2008 to 2010 as part of an experiment to detect the impacts of fertilization on elevation change. Results of this experiment were published by Davis et al. (2017). These SETs and accompanying Marker Horizon plots were re-fertilized between April 2015 and June 2016 in support of the Research Project CW-4 study (see Section 2).

We limited our analysis of the role of accretion in the marsh elevation change as measured with SETs to accretion data from unfertilized Marker Horizon plots that were installed for approximately the same duration (50 to 150 days) as the period between SET measurements. This subset of Marker Horizon data, shown in **Appendix 4-A-3** and in the shaded area of **Figure 11-4**, was used to calculate accretion rates for each site.

Shoreline Change

A shoreline position and marsh surface and volume change analysis was conducted at four NRE monitoring sites (i.e., Traps Bay Bridge, Traps Bay Creek, Pollocks Point Shoreline, and French Creek). Topographic surveys provided elevation data at each station. NOAA personnel

conducted surveys in 2008, 2009, and 2011, and Geodynamics Inc. conducted surveys in 2014 and 2016.

Field collections of VRSs and RTK-GPS data were conducted by using high-accuracy GPS receivers during early spring, when plants are dormant, and during low tide. Techniques were adapted from NGS and GNSS manufacturer processing guidelines. Both survey techniques referenced the designated SET control point for a station during the field collections. Raw field data were stored in a Trimble TSC2 or TSC3 hand-held units and imported to the vendor software program (Trimble Geomatics Office and Trimble Business Center), in which data were reviewed and edited for horizontal and vertical precisions.

Digital Elevation Models (DEMs) were created and analyzed by using ArcGIS v10+, Spatial Analyst Tools. Adjustments to topographic point elevations collected in the field were based on the mean static orthometric heights of the station SET control point and the difference in the mean SET control point elevation at the time of data collection.

Marsh DEMs were created from the adjusted point shapefiles by using the Natural Neighbor Interpolation rendering, cell size set at 1 m^2. To compare DEMs of equal area, polygons were created for each station and used as an extraction mask, which was determined by the largest area covered by the four collections. The contour line at zero (0) m NAVD88 was extracted from the DEM and used to calculate the horizontal change in shoreline position.

The Digital Shoreline Analysis System (DSAS) method, an ArcGIS extension (Thieler et al., 2017) was used to calculate the distances between the various zero-line contours through time. The *x* and *y* intercepts were extracted from the intersection of perpendicular transects and the shorelines (**Table 11-3 and Figure 11-5**). Shoreline change distances based on these intercepts include net shoreline measurement, the total distance from the earliest to the latest intercept and end point rate (EPR), and the annual rate of change in the shoreline.

Net Volume Change

Net volume change was calculated by using an ArcGIS Spatial Analyst Tool, the Cut Fill technique. DEMs were used to estimate local change in surface elevation based on change in sediment volume. The area used in subsequent comparisons was determined by the first DEM at each station. All DEM comparisons are conducted between the initial sample period (i.e., 2008, except for 2011 at French Creek) and 2014 and 2016.

Table 11-3. Baseline Length and Transect Distance of DSAS Stations Associated with SET Marks

Transect spacing was 5 m at all stations.

Station	Nearby SET Mark	Baseline Length (m)	Transects Used in Analysis (n)
Traps Bay Bridge	41	75	19
Traps Bay Creek	42	50	11
Pollocks Point	43	25	6
French Creek	45	40	9

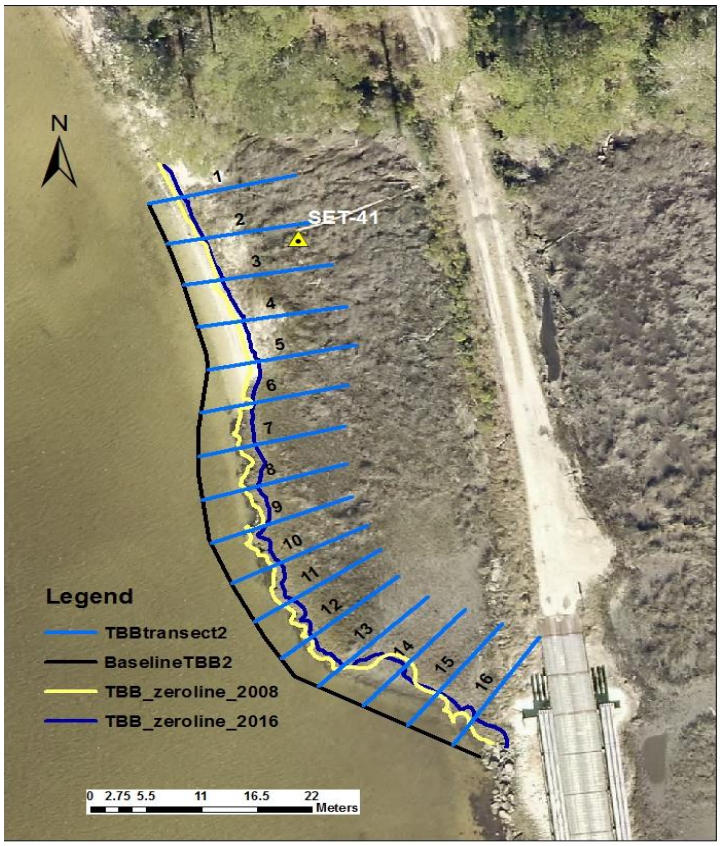

Figure 11-5. Example of the DSAS analysis process at Traps Bay Bridge (TBB).

Zero-m contour lines for 2008 and 2016 were established, and the distance between the two lines was calculated by using transects that are perpendicular to a baseline.

Results and Discussion

Elevation

The OPUS Projects processing results for the SET marks designated as control points (**Appendix 11-A, Table 11-A-2**) produced an accuracy of ±1.5 cm (68%) orthometric height (NAVD 88). Coordinate (±0.01 cm, North American Datum of 1983 [NAD 83, 2011]) and ellipsoid heights (Geodetic Reference System 1980 [GRS 80]) were (±0.01 cm) at the same confidence level. All sessions and the final adjustment applied the most current geoid model (G12B). Class C bench marks were also surveyed to an accuracy of ±1.5 cm.

Temperature and Salinity

Mile Hammock Bay and Gottschalk Marina Wallace Creek monthly water level, temperature, and salinity values (i.e., mean, maximum, and minimum) are shown in **Appendix 11-A (Figures 11-A-1 and 11-A-2)**. The average water temperature at both sites was 20°C, and the inter-annual monthly mean temperatures at the two stations differed by 1°C or less, with an annual range of between 8°C and 30°C (Gottschalk Marina Wallace Creek) and 9°C and 29°C (Mile Hammock Bay; **Figure 11-6**). The monthly water mean temperatures ranged between 6°C and 30°C at the Mile Hammock Bay station and between 6°C and 31°C at Gottschalk Marina Wallace Creek.

(**Figure 11-6 and Appendix 11-A, Figures 11-A-1 and 11-A-2**). Inter-annual variability was greatest in the winter months, especially in December and March (**Figure 11-6**). At Gottschalk Marina Wallace Creek, the highest observed temperatures (34°C) were observed from 2010 to 2013 and in 2016 in June or July. The lowest observed temperatures (0°C) were observed in December 2010, January 2014, and February 2015 (**Appendix 11-A, Figure 11-A-1**). At Mile Hammock Bay, maximum temperatures reached (33°C) in July 2011 and August 2016. Temperatures were as low as 2°C in December 2010 and February 2015 (**Appendix 11-A, Figure 11-A-2**).

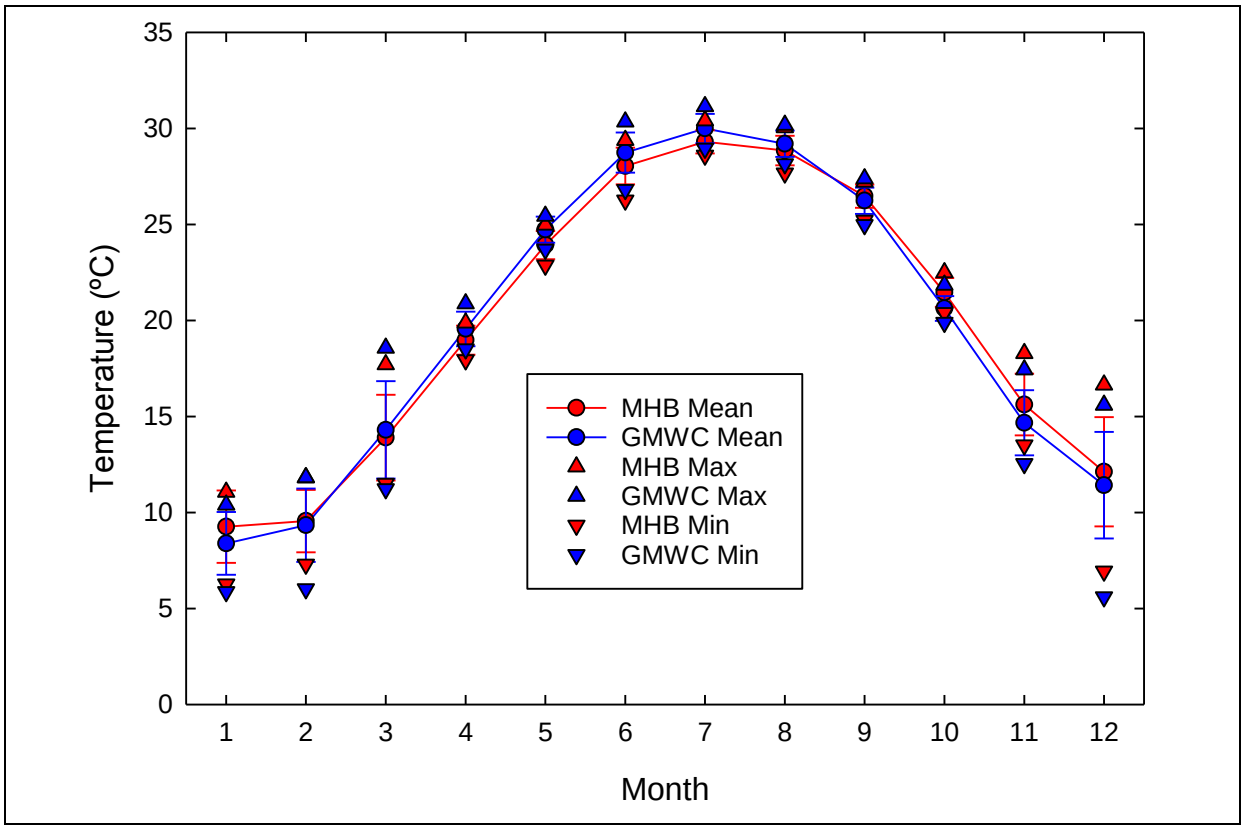

Figure 11-6. Inter-annual monthly mean (±standard deviation) and maximum and minimum temperature at Gottschalk Marina Wallace Creek (GMWC) and Mile Hammock Bay (MHB).

The number of years represented by each mean ranges from seven to nine. Inter-annual monthly means are the averages of the monthly means for a particular month over the entire study (**Appendix 11-A, Figures 11-A-1 and 11-A-2**).

Annual salinity trends were similar at Gottschalk Marina Wallace Creek and Mile Hammock Bay, although inter-annual monthly means were 14 to 18 lower and inter-annual variability was greater at Gottschalk Marina Wallace Creek (**Figure 11-7**). At Mile Hammock Bay, monthly mean salinity values during the study period ranged from 20 to 35 (**Appendix 11-A and Figure 11-A-2**) with inter-annual monthly means that ranged from 27 (February) to 32 (June, July, and August; **Figure 11-7**). A larger range in monthly mean salinity (2–25) was observed at Gottschalk Marina Wallace Creek (**Appendix 11-A, Figure 11-A-1**). Inter-annual monthly salinity means at Gottschalk Marina Wallace Creek were lowest (10) in February and March and highest (17) in June and July (**Figure 11-7**).

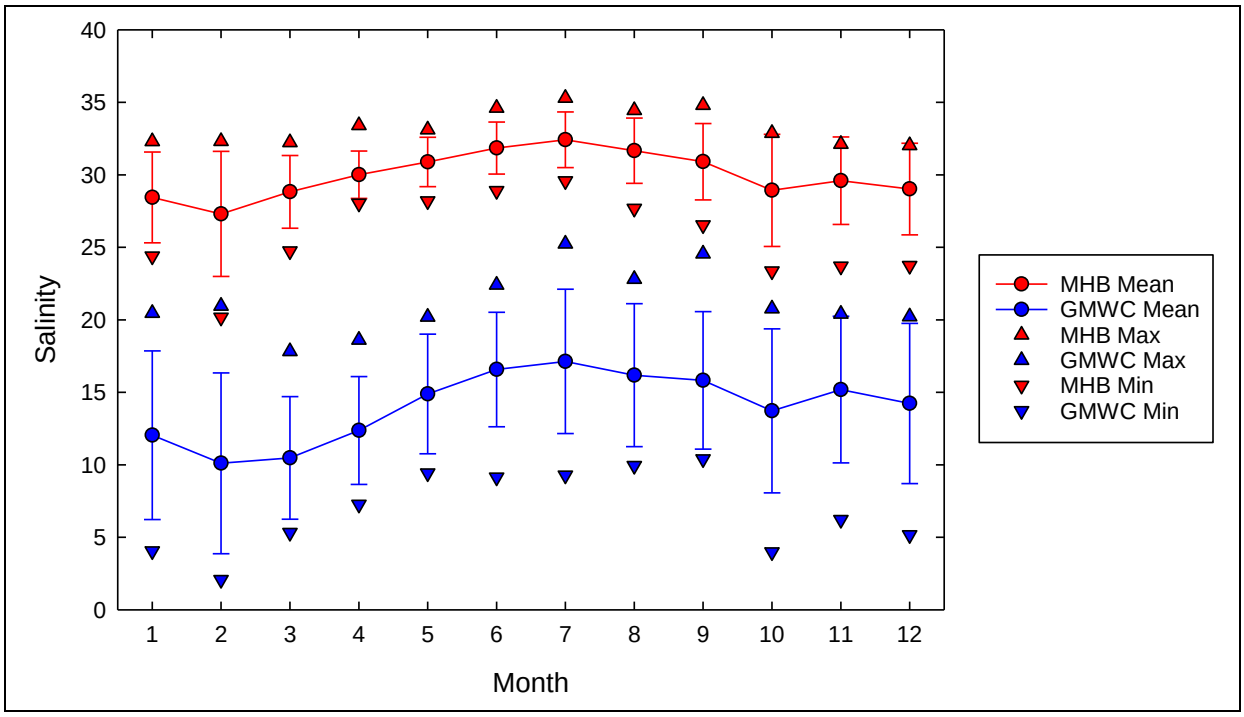

Figure 11-7. Inter-annual monthly mean (±standard deviation) and maximum and minimum salinity values at Gottschalk Marina Wallace Creek (GMWC) and Mile Hammock Bay (MHB).

The number of years represented by each mean ranges from seven to nine. Inter-annual monthly means are the averages of the monthly means for a particular month over the entire study (**Appendix 11-A, Figures 11-A-1 and 11-A-2**).

Water Level and Tidal Datums

Six-minute water level data at Mile Hammock Bay and Gottschalk Marina Wallace Creek exhibit similar water level trends to the NWLON control station in Beaufort, NC, but have reduced amplitudes (**Figure 11-8**).

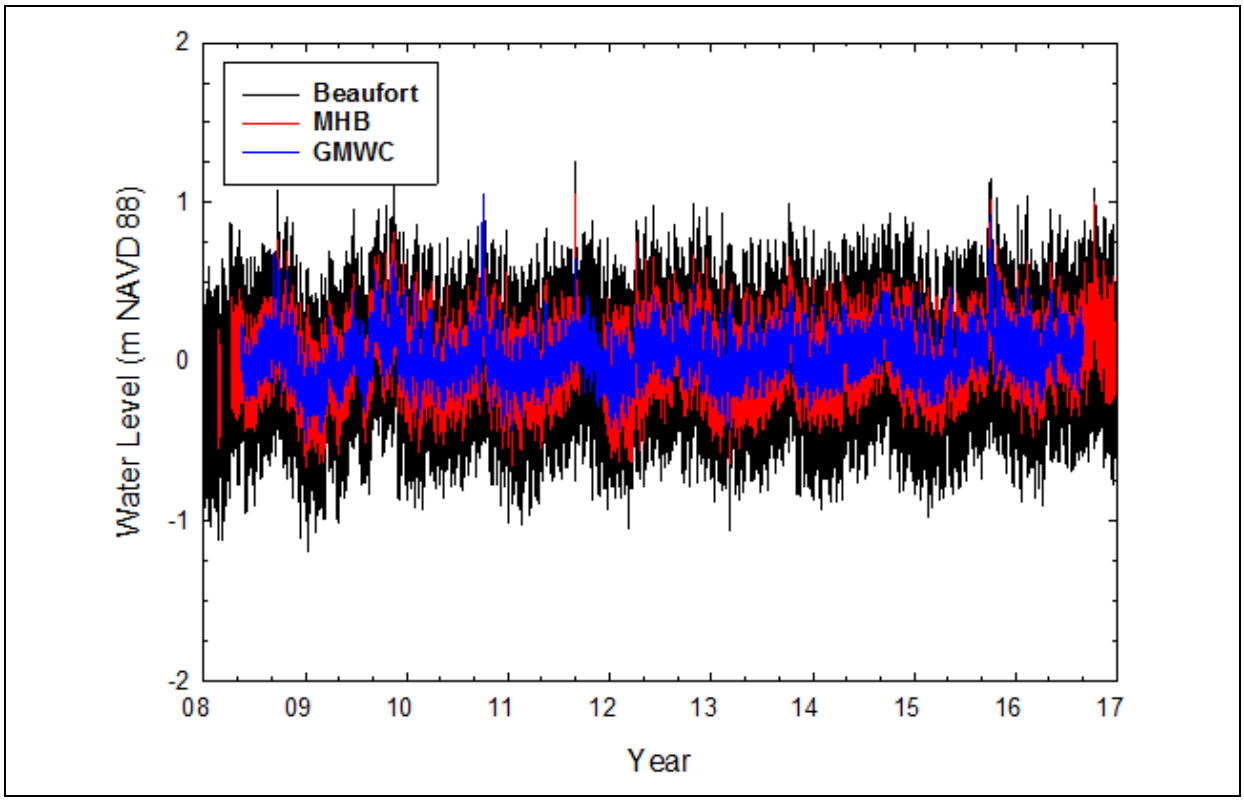

Figure 11-8. Six-minute water level data from Beaufort, NC (NWLON Station 8656483), Mile Hammock Bay (MHB) and Gottschalk Marina Wallace Creek (GMWC).

Mean water level at Mile Hammock Bay and Gottschalk Marina Wallace Creek varied on a seasonal and annual basis (**Figure 11-9 and Table 11-4**). There was a 23-cm difference in inter-annual monthly mean water level at each station, as well as a between-station difference in mean water level, which varied seasonally. From February to September, Gottschalk Marina Wallace Creek mean water level was 6 cm to 8 cm higher than at Mile Hammock Bay. From October to January, the difference was only 2 cm to 5 cm (**Figure 11-9**). Seasonal differences (fall minus spring) in water level at Gottschalk Marina Wallace Creek (16 cm) and Mile Hammock Bay (18 cm) were approximately twice the largest annual difference in water level at each station (for years with complete records in **Table 11-4**).

Between 2008 and 2016, the slope of monthly mean water level was 14 mm y^{-1} at Mile Hammock Bay and Beaufort and was 10 mm y^{-1} at Gottschalk Marina Wallace Creek. The 2008 to 2016 increase in monthly water levels at all three stations is much higher than the 3-mm y^{-1} long-term (1953–2016) RSLR rate at Beaufort, NC (NOAA, 2017). Within the period of our study (i.e., 2011–2015), sea level rise accelerated south of Cape Hatteras, including Beaufort, NC, to more than 20 mm y^{-1} (Valle-Levinson et al., 2017). Similar short-lived, rapid sea level rise accelerations associated with combined cumulative effects of El Niño Southern Oscillation and North Atlantic Oscillation have occurred at least six times on the U.S. East Coast since 1920 (Valle-Levinson et al., 2017). Relative sea level rise rates must be calculated over decades to obtain the variability in astronomic tidal constituents and oceanographic features that oscillate over decadal time scales (Douglas, 2001). Therefore, although the 10 mm y^{-1} to 14 mm y^{-1} increase in water level that we observed on MCBCL from 2008 to 2016 reflects the water level

changes experienced by installation coastal wetlands, the values should not be interpreted as the current local sea level rise rate (Douglas, 2001).

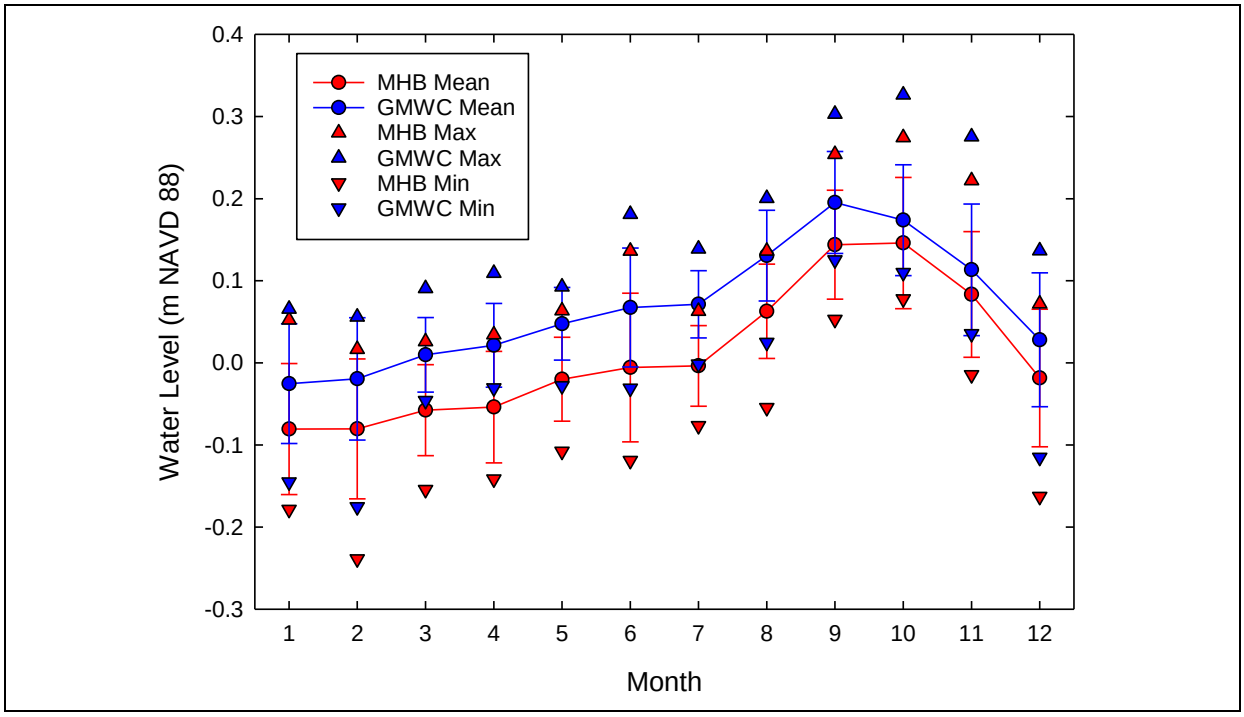

Figure 11-9. Inter-annual monthly mean (±standard deviation), maximum, and minimum water level at Gottschalk Marina Wallace Creek (GMWC) and Mile Hammock Bay (MHB).

The number of years represented by each mean ranges from seven to nine. Inter-annual monthly means are the averages of the monthly means for a particular month over the entire study (**Appendix 11-A, Figures 11-A-1 and 11-A-2**).

Table 11-4. The Mean Annual Water Level Measured at the Beaufort NWLON Station, Mile Hammock Bay (MHB) and Gottschalk Marina Wallace Creek (GMWC)

Years with incomplete data are italicized. Values are based on 63% of the year for 2008 and 2016 at GMWC. Values are based on 75% to 77% of the year for 2008 and 2011 and 89% to 98% of the year for 2009, 2013, and 2016 at MHB.

Mean Annual Water Level (m NAVD 88)			
Year	**Beaufort**	**MHB**	**GMWC**
2008	−0.09	*−0.01*	*0.02*
2009	−0.05	*0*	0.02
2010	−0.06	−0.02	0.01
2011	−0.06	*−0.04*	0.00
2012	−0.02	0	0.03
2013	−0.05	*−0.02*	0.01
2014	0.01	0.04	0.07
2015	−0.01	0.05	0.08
2016	0.03	*0.08*	*0.07*

A tidal datum refers to an elevation at which the height of a local predicted tide would occur, in reference to a fixed point or bench mark (NOAA, 2003). Calculated tidal datums for Mile Hammock Bay and Gottschalk Marina Wallace Creek, Freeman Creek, Traps Bay Creek, and French Creek referenced to the current NTDE are shown relative to the control station in Beaufort (NLWON Station 8656483) in **Table 11-5** (see the Materials and Methods section of this chapter for the methods applied and associated accuracy at each station). The datums illustrate the tidal gradient from Freeman Creek to Gottschalk Marina Wallace Creek. From stations nearest to Browns Inlet (Freeman Creek and Onslow Beach Backbarrier to Gottschalk Marina Wallace Creek in the upper NRE), mean sea level (MSL) increased by 5 cm, mean high water (MHW) decreased by 28 cm, mean low water (MLW) increased by 68 cm, and the tide range decreased by 66 cm.

The regional MSL values referenced to the NTDE (**Table 11-5**) are, on average, 8 cm lower than the annual MSL observations from 2008–2016 (**Table 11-4**). Tidal datums tied to the NTDE are necessary for comparing long-term and regional differences in water level, but short-term local observations are necessary for describing local conditions during the monitoring and research study periods.

Table 11-5. Tidal Datums Determined by Using the Modified Range Ratio Method with the Beaufort, NC NWLON Station 8656483 as a Control

Datums at Mile Hammock Bay and Gottschalk Marina Wallace Creek were calculated by using 1 year of data collected at the secondary water level stations in 2009. Freeman Creek and French Creek datums are based on short-term logger data. MHHW=mean high high water; MHW=mean high water; MLLW=mean low low water; MLW=mean low water; MN=mean range of tide; and MSL=mean sea level. French Creek datums were adjusted by 7 cm to correct for an error in sensor elevation.

Tidal Datums (m NAVD 88)					
Location	**Beaufort NLWON Station 8656483**	**Freeman Creek**	**Mile Hammock Bay**	**French Creek**	**Gottschalk Marina Wallace Creek**
Period of Data Used for Datum Calculation	**1983–2001 (19 Years)**	**2016–2017 (7 Months)**	**2009 (12 Months)**	**2014–2015 (11 Months)**	**2009 (12 Months)**
MHHW	0.445	0.398	0.193	0.053	0.062
MHW	0.358	0.319	0.15	0.029	0.039
MSL	−0.112	−0.099	−0.073	−0.046	−0.051
MLW	−0.59	−0.502	−0.278	−0.117	−0.127
MLLW	−0.633	−0.537	−0.309	−0.137	−0.15
MN	0.948	0.821	0.429	0.145	0.166

Inundation

Marsh inundation occurs when the tidal water level is above the marsh sediment surface, and it can be measured in the number of hours or the percentage of time that the marsh is below water. Inundation at a specific location and time depends on marsh elevation and water level, which, as previously described, varies with position along the tidal gradient, season, and year. Tidal amplitude decreases and MSL increases from Freeman Creek and Onslow Beach Backbarrier (as

represented by the Beaufort NWLON Station 8656483 amplitude) to Mile Hammock Bay to Gottschalk Marina Wallace Creek (**Table 11-5**), and this gradient in tidal characteristics, together with differences in marsh elevations, drives differences in inundation patterns at the four marshes (**Figure 11-10**). Seasonal and annual changes in water level (**Figure 11-9 and Table 11-4**) also influence inundation. Here, we introduce the results from inundation analysis. Later, these results will be used to evaluate their relationship to marsh biomass and marsh surface elevation change.

Average annual and seasonal inundation of the marsh surface surrounding each SET is shown in number of hours and percentage of time in **Tables 11-6 and 11-7**. Inundation was calculated quarterly to compare with SET measurements and during the growing season for comparison with vegetation measurements. The number of days in growing season inundation calculations ranges from 106 to 141, depending on the sampling area and year. The number of days between SET measurements ranged from 57 to 147, with fewer average days between SET measurements in the fall (80 days) than other seasons: winter (93 days), spring (98 days), and summer (95 days). Because of differences in the number of days in each calculation, inundation patterns may differ depending upon whether hours or the percentage of time were considered. Fall is a period of greater inundation (in units of percent time) at all four sites (**Figure 11-10 and Table 11-7**). Analysis of the relationship between inundation and vegetation parameters or elevation change was conducted by using the number of hours of inundation to match the measurement period. Seasonal and annual differences in inundation were analyzed in percentage of time to normalize for changes in sampling periods.

Annual inundation varies 4% to 6% at Freeman Creek, 7% at Onslow Beach Backbarrier, and 15% at Mile Hammock Bay and French Creek (**Table 11-6**). At each of these sites, marsh surface inundation (percentage of time) was significantly greater ($p<0.05$) during the fall (August SET measurement to November SET measurement) when seasonal water levels were higher (**Figure 11-9**). At Freeman Creek, inundation in the summer season was also significantly different from all other seasons. Inundation is typically lowest in the winter and spring (**Table 11-7**), but this can vary with site and year (**Figure 11-10**).

Seasonal variation in inundation at each site (**Table 11-7**) is two to three times greater than annual variations in inundation (**Table 11-6**). Seasonal variability in marsh inundation increases from Freeman Creek (15%) to Onslow Beach Backbarrier (25%) to French Creek (39%). This range in seasonal inundation is driven in part by seasonal changes in water level and elevation differences between sites. Onslow Beach Backbarrier and Freeman Creek experience similar tidal characteristics (and inundation for both was calculated by using the same source of water level data, Beaufort, NWLON Station 8656483), but Freeman Creek experiences lower seasonal variability because it is lower in the tidal frame and more frequently inundated (**Table 11-6**). Mile Hammock Bay is approximately 5 cm higher in elevation than French Creek, but water levels can be 2 cm to 8 cm higher at French Creek (as represented by Gottschalk Marina Wallace Creek water level) than at Mile Hammock Bay, depending on the season (**Figure 11-9**). In the winter, spring, and summer, Onslow Beach Backbarrier, Mile Hammock Bay, and French Creek experience similar periods of inundation even though Onslow Beach Backbarrier is at least 10 cm higher than Mile Hammock Bay and French Creek (**Table 11**-7).

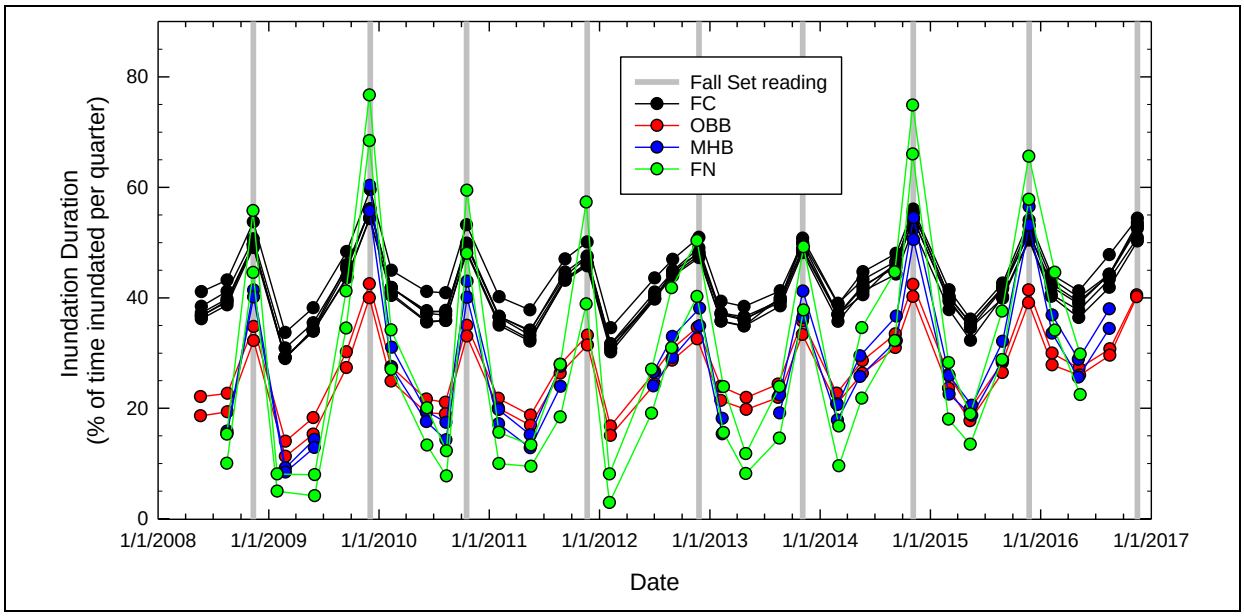

Figure 11-10. Inundation of the marsh surface at each SET station for the period between quarterly SET measurements.

Fall SET measurement dates are highlighted by gray vertical lines. FC=Freeman Creek; FN=French Creek; MHB=Mile Hammock Bay; and OBB=Onslow Beach Backbarrier.

Table 11-6. Average ± Standard Error (SE) Annual Marsh Elevation and Inundation (Hours and Percentage of Time) by Treatment for the SETs at Each Site

The number of SETs varies at each site (3 FC-C, 3 FC-F, 1 OBB-C, OBB-F, MHB-C, MHB-F, and 2 FN-C) as does the availability of water level data for inundation calculations. The average inundation for each year was calculated by using the elevation of the previous SET measurement. C=control; F=fertilized; FC=Freeman Creek; FN=French Creek; MHB=Mile Hammock Bay; and OBB=Onslow Beach Backbarrier.

Site Treatment	Year	SET Measures (n)	Inundation Values (n)	Average (±SE) Sediment Surface Elevation at the Start of the Inundation Period (m NAVD 88)	Average (±SE) Inundation (Hours)	Average (±SE) Inundation (% Time)
FC-C	2008	12	9	0.026±0.010	914±40	43±2
FC-C	2009	12	12	0.035±0.007	965±60	42±3
FC-C	2010	12	12	0.043±0.006	809±57	43±2
FC-C	2011	12	12	0.052±0.006	983±52	41±2
FC-C	2012	12	12	0.063±0.006	932±103	42±2
FC-C	2013	12	12	0.069±0.005	835±61	41±2
FC-C	2014	12	12	0.076±0.006	961±55	45±2
FC-C	2015	12	12	0.084±0.005	971±68	42±2
FC-C	2016	12	12	0.094±0.007	969±54	45±2
FC-F	2008	12	9	0.031±0.003	903±36	432
FC-F	2009	12	12	0.049±0.004	927±55	41±3
FC-F	2010	12	12	0.069±0.003	770 ± 51	41±2
FC-F	2011	12	12	0.076±0.002	939±50	40±2
FC-F	2012	12	12	0.079±0.002	908±99	41±2
FC-F	2013	12	12	0.074±0.002	831±61	40±2
FC-F	2014	12	12	0.072±0.004	964±54	45±2
FC-F	2015	12	12	0.085±0.003	967±66	42±2
FC-F	2016	12	12	0.104±0.005	948±51	44±2
OBB-C	2008	4	3	0.259±0.001	496±89	23±4
OBB-C	2009	4	4	0.258±0.001	518±120	23±6

(continued)

Table 11-6. Average ± Standard Error (SE) Annual Marsh Elevation and Inundation (Hours and Percentage of Time) by Treatment for the SETs at Each Site (continued)

Site Treatment	Year	SET Measures (n)	Inundation Values (n)	Average (±SE) Sediment Surface Elevation at the Start of the Inundation Period (m NAVD 88)	Average (±SE) Inundation (Hours)	Average (±SE) Inundation (% Time)
OBB-C	2010	4	4	0.260±0.001	455±63	24±3
OBB-C	2011	4	4	0.262±0.001	558±56	24±3
OBB-C	2012	4	4	0.266±0.000	546±130	25±4
OBB-C	2013	4	4	0.266±0.001	499±60	24±3
OBB-C	2014	4	4	0.267±0.000	619±64	30±4
OBB-C	2015	4	4	0.268±0.001	616±110	27±5
OBB-C	2016	4	4	0.271±0.000	664±76	31±3
OBB-F	2008	4	3	0.218±0.002	563±82	27±4
OBB-F	2009	4	4	0.224±0.001	582±119	26±6
OBB-F	2010	4	4	0.231±0.001	500±67	26±3
OBB-F	2011	4	4	0.241±0.001	600±54	25±3
OBB-F	2012	4	4	0.243±0.001	590±141	27±4
OBB-F	2013	4	4	0.240±0.000	549±62	27±3
OBB-F	2014	4	4	0.241±0.001	668±70	32±4
OBB-F	2015	4	4	0.244±0.002	666±114	29±5
OBB-F	2016	4	4	0.250±0.004	690±72	32±3
MHB-C	2008	4	2	0.131±0.001	606±268	29±13
MHB-C	2009	4	3	0.129±0.002	554±275	28±16
MHB-C	2010	4	4	0.130±0.001	519±93	28±6
MHB-C	2011	4	3	0.134±0.001	512±81	21±4
MHB-C	2012	4	3	0.142±0.001	744±125	33±3
MHB-C	2013	4	3	0.143±0.002	570±128	27±7

(continued)

Table 11-6. Average ± Standard Error (SE) Annual Marsh Elevation and Inundation (Hours and Percentage of Time) by Treatment for the SETs at Each Site (continued)

Site Treatment	Year	SET Measures (n)	Inundation Values (n)	Average (±SE) Sediment Surface Elevation at the Start of the Inundation Period (m NAVD 88)	Average (±SE) Inundation (Hours)	Average (±SE) Inundation (% Time)
MHB-C	2014	4	4	0.138±0.001	724±120	35±7
MHB-C	2015	4	4	0.136±0.001	771±169	34±8
MHB-C	2016	4	3	0.128±0.003	735±100	35±3
MHB-F	2008	4	2	0.135±0.000	588±259	28±12
MHB-F	2009	4	3	0.140±0.003	508±255	26±15
MHB-F	2010	4	4	0.149±0.002	465±93	25±6
MHB-F	2011	4	3	0.153±0.000	442±73	18±3
MHB-F	2012	4	3	0.161±0.001	673±118	29±3
MHB-F	2013	4	3	0.163±0.001	494±116	24±6
MHB-F	2014	4	4	0.161±0.001	643±108	32±7
MHB-F	2015	4	4	0.155±0.001	700±162	31±8
MHB-F	2016	4	3	0.148±0.002	663±93	31±3
FN-C	2008	6	4	0.100±0.008	656±232	31±11
FN-C	2009	8	8	0.097±0.007	648±196	31±10
FN-C	2010	8	8	0.102±0.006	509±101	28±7
FN-C	2011	8	8	0.105±0.007	537±115	24±6
FN-C	2012	8	8	0.103±0.009	591±122	28±6
FN-C	2013	8	8	0.112±0.007	485±96	23±5
FN-C	2014	8	8	0.113±0.008	722±116	38±8
FN-C	2015	8	8	0.115±0.007	774±146	34±7
FN-C	2016	8	4	0.120±0.005	670±98	33±5

Table 11-7. Average (±Standard Error [SE]) SET Elevations and Inundation (Hours and Percentage of Time) by Season

The number of SETs varies at each site (3 FC-C, 3 FC-F, 1 OBB-C, OBB-F, MHB-C, MHB-F, and 2 FN-C) as does the availability of water level data for inundation calculations. The season of greatest elevation (fall) is highlighted gray. C=control; F=fertilized; FC=Freeman Creek; FN=French Creek; MHB=Mile Hammock Bay; and OBB=Onslow Beach Backbarrier.

Site Treatment	Season	SET Measurements (n)	Inundation Values (n)	Average (±SE) Sediment Surface Elevation at the Start of the Inundation Period (m NAVD 88)	Average (±SE) Inundation Between SET Measurements (Hours)	Average (±SE) Inundation Between SET Measurements (% Time)
FC-C	Winter	27	24	0.068±0.006	833±39	38±1
FC-C	Spring	27	27	0.060±0.006	889±48	38±1
FC-C	Summer	27	27	0.059±0.006	1007±48	43±1
FC-C	Fall	27	27	0.062±0.006	969±28	52±1
FC-F	Winter	27	24	0.079±0.004	816±39	37±1
FC-F	Spring	27	27	0.070±0.004	865±44	37±1
FC-F	Summer	27	27	0.070±0.004	984±47	42±1
FC-F	Fall	27	27	0.075±0.004	951±27	51±1
OBB-C	Winter	9	8	0.264±0.002	456±48	21±2
OBB-C	Spring	9	9	0.264±0.002	486±56	20±1
OBB-C	Summer	9	9	0.265±0.001	578±59	26±1
OBB-C	Fall	9	9	0.264±0.002	686±34	36±1
OBB-F	Winter	9	8	0.240±0.004	506±50	23±2
OBB-F	Spring	9	9	0.237±0.003	539±58	23±1
OBB-F	Summer	9	9	0.236±0.004	629±62	28±1
OBB-F	Fall	9	9	0.239±0.004	724±33	38±1
MHB-C	Winter	9	7	0.135±0.002	509±68	23±3
MHB-C	Spring	9	7	0.135±0.002	523±75	22±2
MHB-C	Summer	9	8	0.135±0.002	646±97	28±3
MHB-C	Fall	9	7	0.133±0.002	889±70	48±3

(continued)

Table 11-7. Average (±Standard Error [SE]) SET Elevations and Inundation (Hours and Percentage of Time) by Season (continued)

Site Treatment	Season	SET Measurements (n)	Inundation Values (n)	Average (±SE) Sediment Surface Elevation at the Start of the Inundation Period (m NAVD 88)	Average (±SE) Inundation Between SET Measurements (Hours)	Average (±SE) Inundation Between SET Measurements (% Time)
MHB-F	Winter	9	7	0.154±0.003	448±60	20±3
MHB-F	Spring	9	7	0.151±0.003	466±69	20±2
MHB-F	Summer	9	8	0.151±0.003	571±86	25±3
MHB-F	Fall	9	7	0.152±0.003	826±68	44±3
FN-C	Winter	18	16	0.110±0.005	418±64	19±3
FN-C	Spring	16	16	0.105±0.006	402±54	17±2
FN-C	Summer	18	16	0.107±0.005	604±79	26±3
FN-C	Fall	18	16	0.110±0.004	1040±54	56±3

As previously mentioned, we were unable to calculate inundation at Traps Bay or Pollocks Point. The water level logger at Traps Bay Creek captured the full tidal signal in just a few short intervals, the longest of which was from September 15, 2016 to October 30, 2016. Traps Bay Creek had a similar timing of tides and high tide water levels as Mile Hammock Bay, but attenuated low tides due to distortion of the tidal wavelength by shallow water (NOAA, 2007b). Datums calculated based on 1 month of data indicate that Traps Bay Creek high tide elevations were similar to those at Mile Hammock Bay, that Traps Bay Creek low tides were in between Mile Hammock Bay and Gottschalk Marina Wallace Creek, and Traps Bay Creek that MSL was higher than MSL at both water level stations. We determined that using Mile Hammock Bay or Gottschalk Marina Wallace Creek water levels to calculate inundation duration would lead to an unacceptable error of up to 30%. However, we could use the short window of full signal tidal records to calculate inundation at Traps Bay Creek, Traps Bay Bridge, Pollocks Point Shoreline, and Pollocks Point Woods for a snapshot comparison of inundation with the other four marshes during the season and year (fall 2016) with the highest average water levels throughout the study period (**Table 11-4** and **Figure 11-9**). However, because this was a time of unusual high water, these results do not represent marsh inundation time during the entire study period. The station with the highest mean SET elevation, Onslow Beach Backbarrier, is least frequently inundated, followed by Freeman Creek, Mile Hammock Bay, and Traps Bay Creek (**Table 11-8**). Inundation at Traps Bay Bridge, Pollocks Point Shoreline, and Pollocks Point Woods was calculated by using the Traps Bay Creek short-term data, which were the closest source of water level data, but may not be representative of the tidal characteristics at those locations.

Table 11-8. Inundation Duration Calculated from September 15, 2016 to October 30, 2016 by Using Water Level Data and the Average SET Sediment Surface Elevation at Each Site or Station

Inundation results for stations in italics are estimates because water level data were not obtained from Traps Bay Bridge (TBB), Pollocks Point Shoreline (PPS), and Pollocks Point Woods (PPW). FC=Freeman Creek; FN=French Creek; MHB=Mile Hammock Bay; OBB=Onslow Beach Backbarrier; and TBC=Traps Bay Creek.

Site or Station	Mean SET Elevation (m NAVD 88)	Inundation Duration (% Time from September 15 Through October 30, 2016)	Water Level Data Source
FC	0.07	60	FC HOBO
OBB	0.25	62	FC HOBO
MHB	0.14	65	MHB water level station
TBB	0.10	92	*TBC HOBO*
TBC	0.10	92	TBC HOBO
PPS	0.14	85	*TBC HOBO*
PPW	0.13	88	*TBC HOBO*
FN	0.11	92	FN HOBO

Marsh Vegetation

Vegetation surveys were conducted at eight plot areas at the six monitoring sites from 2009 to 2016 in mid-July to mid-August, except for 2011 and 2012 at Pollocks Point Woods. The average surface elevation of permanent vegetation monitoring plots, by sampling area and year, ranged from −0.01 at Freeman Creek in 2010 to 0.30 m NAVD 88 at Onslow Bay Backbarrier in

2016 (**Figure 11-11**). The net change in average surface elevation from 2009 to 2016 was zero m at Mile Hammock Bay and Traps Bay Bridge; +0.01 m at Traps Bay Creek; +0.02 m at Onslow Beach Backbarrier, Pollocks Point Shoreline, French Creek, and Traps Bay Creek; and +0.03 m at Freeman Creek and Pollocks Point Woods.

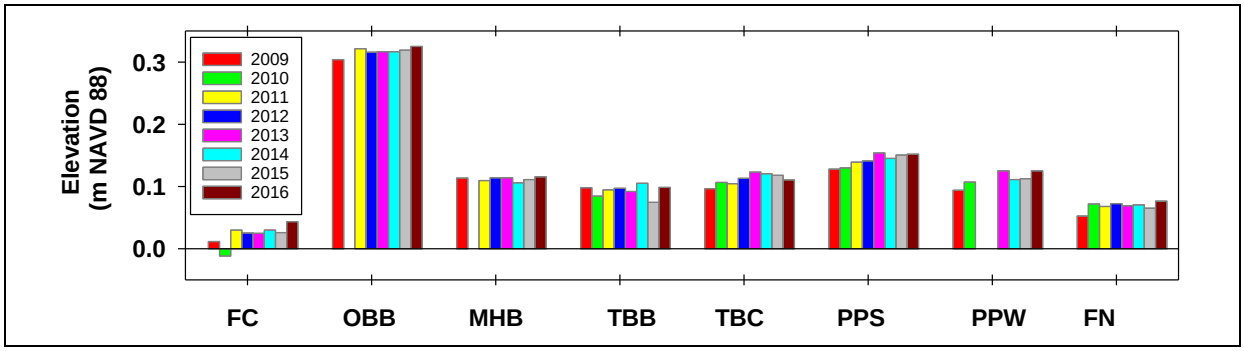

Figure 11-11. The mean elevation of the vegetation plots at each monitoring station.

Elevations were not measured in 2010 at Freeman Creek (FC) and Onslow Beach Backbarrier (OBB) or in 2011 and 2012 at Pollocks Point Woods (PPW). Sampling areas are ordered left to right from the most saline, highest tidal amplitude site (FC) to the least saline, least tidally influenced site (French Creek [FN]). FC, OBB, and Mile Hammock Bay (MHB) are adjacent to the Intracoastal Waterway; Traps Bay Bridge (TBB), Traps Bay Creek (TBC), Pollocks Point Shoreline (PPS), PPW, and FN are within the NRE.

Change in dominant marsh vegetation along the salinity and tidal gradient is demonstrated by the transition from *Spartina alterniflora*–dominated marshes in the ICW sites to *Juncus roemerianus*–dominated marshes at French Creek, approximately 20 km upstream of the NRE inlet (**Figure 11-12**). In the ICW sites, *J. roemerianus* was only found at Onslow Beach Backbarrier, within three sample plots 80 m from the shoreline. Note: *J. roemerianus* was measured outside of the sampling plot at Freeman Creek. Along the lower NRE, Traps Bay Creek, sheltered in the mouth of the creek, and Traps Bay Bridge, located along the shore of the estuary and exposed directly to waves, had similar percent cover of *S. alterniflora* (2% to greater than 50%) and *J. roemerianus* (0.1% to 25%).

At Pollocks Point Shoreline, located on the NRE shoreline, approximately 7 km upriver from Traps Bay Creek, cover was dominated by *J. roemerianus* (approximately 10% to 50%), and *S. alterniflora* (2% or less percent cover) was only observed along the shoreline. Pollocks Point Woods, located near the marsh-upland transition, and French Creek, which is in a brackish region of the NRE, were also dominated by *J. roemerianus*.

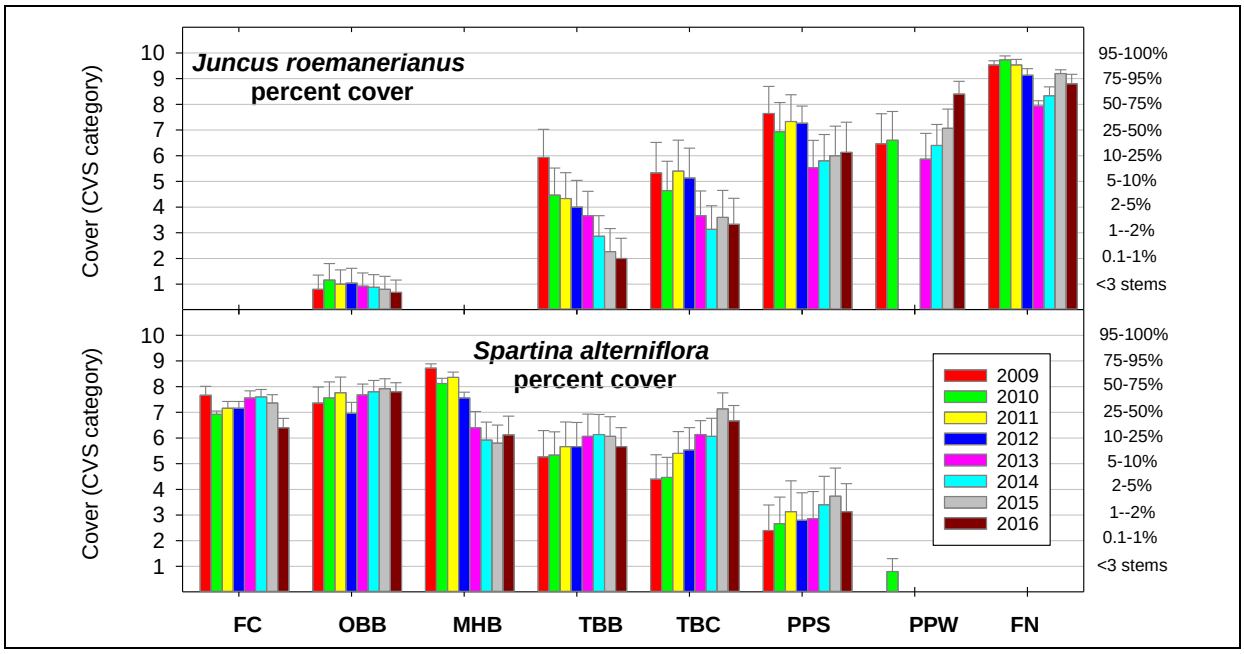

Figure 11-12. The average annual percent cover of *Juncus roemerianus* and *Spartina alterniflora* for each vegetation monitoring station.

The ranges of percent cover represented by the Carolina Vegetation Survey (CVS) category are shown on the *y* axes. FC=Freeman Creek; FN=French Creek; MHB=Mile Hammock Bay; OBB=Onslow Beach Backbarrier; PPS=Pollocks Point Shoreline; PPW=Pollocks Point Woods; TBB=Traps Bay Bridge; and TBC=Traps Bay Creek.

In addition to the *J. roemerianus* and *S. alterniflora*, seven other plant species, mussels, snails and oysters were recorded in marsh vegetation monitoring plots (**Figure 11-13**). The low diversity of marsh plants is consistent with that of coastal wetlands in the Southeast, and reflects the small change in elevation over the monitoring plots because marsh diversity increases closer to the upland border and at higher tidal elevations (Bertness and Pennings, 2000). We note that the absence of a plant species from the vegetation monitoring station does not necessarily mean that the species is absent from the overall marsh area. *J. roemerianus*, for example, can be found near the upper edges of the marsh at Freeman Creek, but not in areas within the vegetation plots. The use of permanent plots, however, does provide the opportunity to detect changes in plant species over time, particularly in marshes that are near transition zones. Traps Bay Bridge, Traps Bay Creek, and Pollocks Point Shoreline (located in the lower NRE) and Onslow Beach Backbarrier (the marsh at the highest elevation) exhibit the highest plant diversity in the vegetation monitoring plots (**Figure 11-13**).

Less common species found in our vegetation plots include *Guekensia demissa* (ribbed mussels), *Distichlis spicata* (salt grass), *Borrichia frutescens* (sea ox-eye), *Limonium carolinium* (sea lavender), *Phragmites, cf australis*, *Salicornia spp.*, *Spartina patens*, *Spartina cynosuroides*, *Typha sp.* (cattail), and oyster (*Crassostrea virginica*), both live and cultch (**Figure 11-13**). The occurrence of *Littoraria irrorata* (marsh periwinkle snails) varied by sampling area and is discussed below.

At Freeman Creek, the site with the lowest elevation and highest tidal amplitude, no plants were found other than *S. alterniflora*. Other species occasionally identified in Freeman Creek plots

include mussels, live oyster, and oyster cultch (**Figure 11-13**). The Onslow Beach Backbarrier is near Freeman Creek and experiences a similar tidal amplitude, but is much higher in the tidal frame than Freeman Creek, allowing for the occurrence of a wider range of marsh plant species.

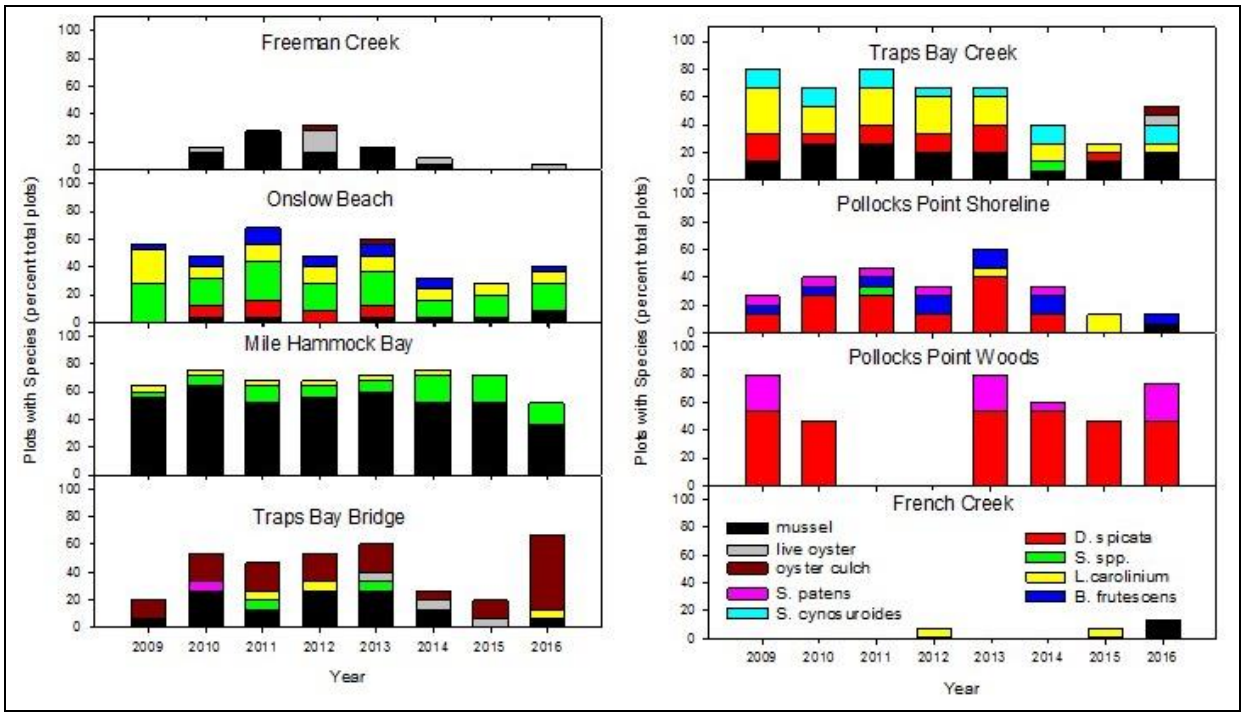

Figure 11-13. Percentage of vegetation plots by year and monitoring station where species other than *Spartina alterniflora*, *Juncus roemerianus*, and *Littoraria irrorata* (snails) were found.

Phragmites cf australis and *Typha Sp.* are not shown (see text).

In addition to *S. alterniflora*, *Salicornia spp*., mussels, and *L. carolinium* were observed at Mile Hammock Bay, which is approximately 20 cm lower in elevation than Onslow Beach Backbarrier with a lower tidal range. Diversity of plant species at Traps Bay Bridge, Traps Bay Creek, and Pollocks Point Shoreline were similar to that of Onslow Beach Backbarrier, but at Pollocks Point Woods and French Creek, only one or two species were found in addition to *J. roemerianus*.

In general, the occurrence and biomass of *J. roemerianus* increases and that of *S. alterniflora* decreases going up the estuarine gradient, as tidal amplitude and salinity decrease (**Figures 11-12 and 11-15**). An exception to this pattern is at Pollocks Point Shoreline, where the highest calculated biomass of *S. alterniflora* was recorded. At Pollocks Point Shoreline, *S. alterniflora* only occurs in the plots immediately adjacent to the shoreline and benefits from regular tidal exchange.

Over the study period, several sampling areas underwent changes in both percent cover and biomass of *S. alterniflora* and *J. roemerianus.* Mile Hammock Bay experienced an *S. alterniflora* die-off that started in 2012 and persisted through 2016 (**Figure 11-14**). *S. alterniflora* cover declined from more than 50% to less than 25% (**Figure 11-12**) and average biomass (for plots where the species was found) in 2012 was half the biomass observed in 2010 (**Figure 11-15**).

Figure 11-14. The *Spartina alterniflora* die-off area at Mile Hammock Bay in 2015.

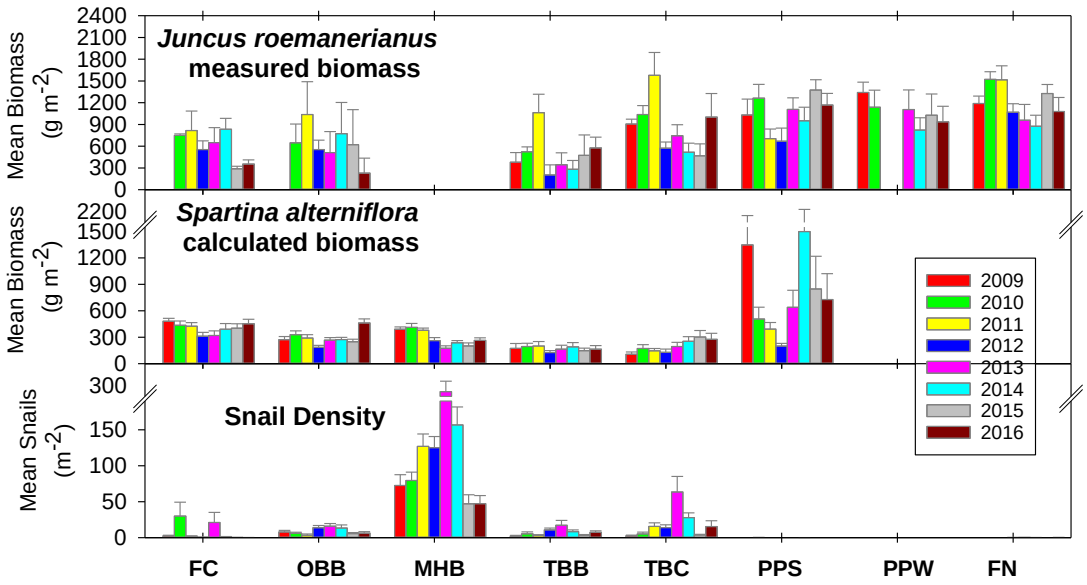

Figure 11-15. Annual *Juncus roemerianus* and *Spartina alterniflora* biomass and snail density at eight monitoring stations from 2009 to 2016.

At FC, *J. roemerianus* was measured outside of the vegetation station. At Onslow Beach Backbarrier (OBB), *J. roemerianus* was limited to three plots 80 m from the shoreline. FC=Freeman Creek; FN=French Creek; MHB=Mile Hammock Bay; OBB= Onslow Beach Backbarrier, PPS=Pollocks Point Shoreline; PPW=Pollocks Point Woods; TBB=Traps Bay Bridge; and TBC=Traps Bay Creek.

S. alterniflora biomass declined at all stations in 2012 (**Figure 11-15**), and biomass values reached the lowest point of the entire study period at Freeman Creek, Onslow Beach Backbarrier, Traps Bay Bridge and Pollocks Point Shoreline (**Figure 11-15**). At Mile Hammock Bay, biomass reached its lowest value the following year (2013), but all other monitoring stations showed an increase in *S. alterniflora* biomass from 2012 to 2013. At Onslow Beach Backbarrier and Traps Bay Creek, *Spartina* biomass continued to increase after 2012; the highest values of the study period were observed in 2016 at those sites (**Figure 11-15**).

J. roemerianus biomass was also lower in 2012 than from 2009 through 2011 at most monitoring areas (**Figure 11-15**) and was at its lowest recorded level over the entire study period at Traps Bay Bridge and Pollocks Point Shoreline. At two areas, Traps Bay Bridge and Traps Bay Creek, the 2012 decline in *J. roemerianus* percent cover and biomass co-occurred with an increase in *S. alterniflora* percent biomass through 2015, although the trend in biomass was reversed as was observed after the 2016 sampling (**Figures 11-12 and 11-16**).

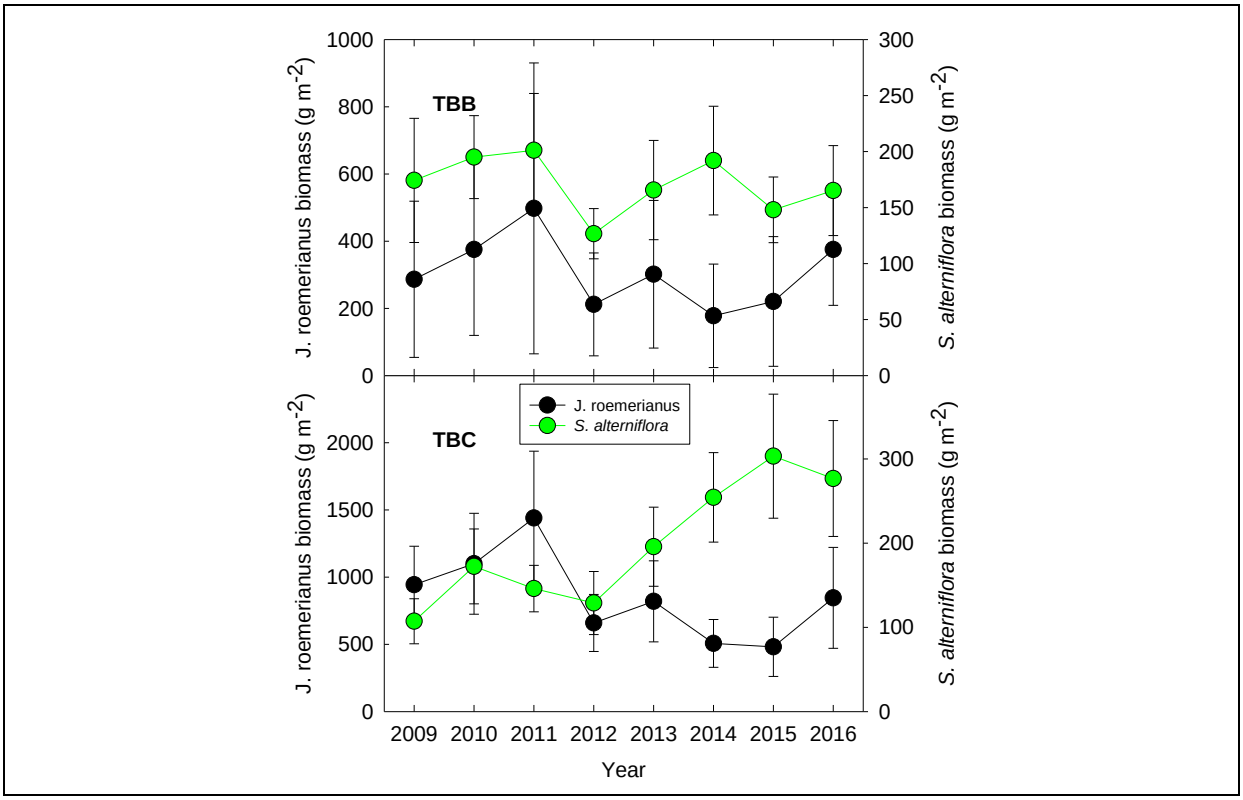

Figure 11-16. Average annual *S. alterniflora* and *J. roemerianus* biomass at Traps Bay Bridge (TBB) and Traps Bay Creek (TBC).

The biomass data are averages of plots in which each species was found (no plots with zero biomass values are included in the average). Note the change in scale with the sampling area.

Snail density (*Littoraria irrorata*) was greatest at the higher elevation ICW sites (Onslow Beach Backbarrier and Mile Hammock Bay; **Figure 11-15**). Location-specific average snail density peaked in 2013 at four sampling areas: Onslow Beach Backbarrier (16 m^{-2}), Mile Hammock Bay (271 m^{-2}), Traps Bay Bridge (17 m^{-2}), and Traps Bay Creek (63 m^{-2}), 1 year after the observed decline in marsh plant biomass (**Figure 11-17**). At Mile Hammock Bay and Traps Bay Creek,

snail density was significantly higher in 2013 than in other years except for 2014 at Traps Bay Creek. At each of these locations, snail density decreased after 2013. At Freeman Creek, snail density was less than 3 m^{-2} in all years except for in 2010 (30 m^{-2}) and 2013 (21 m^{-2}). Snails may contribute to the expansion of marsh dieback during periods of drought (Silliman et al., 2005). The reduction in snail density from 2014 through 2016 at Mile Hammock Bay is associated with a significant loss in plant biomass.

There were also temporal trends in the occurrence of some less common species. At both Traps Bay stations, there was a reduction in the number of plots where less common species were found in 2014 and 2015. In 2016, oyster cultch became more common at Traps Bay Bridge than in previous years and occurred for the first time at Traps Bay Creek. Other less common species were occasionally recorded. *Salicornia spp.* was found in 2011 and 2013 at Traps Bay Bridge, 2011 at Pollocks Point Shoreline and in 2014 at Traps Bay Creek. Sea oxeye (*Borrichia frutescens*) occurred only at Pollocks Point Shoreline, and *S. patens* was found just once (2010) at Traps Bay Bridge, 5 years at Pollocks Point Shoreline and never at Traps Bay Creek. Throughout the study, *S. cynosuroides* was limited to one station, Traps Bay Creek, where it was found every year except 2015. *Phragmites cf australis* was found only once, in a single plot at Traps Bay Creek in 2013. At Pollocks Point Woods, *D. spicata* was observed during each survey, and *S. patens* was observed in 4 out of the 6 years surveyed. During 2009 and 2010, *Typha sp*. was observed in 20% or less of the plots.

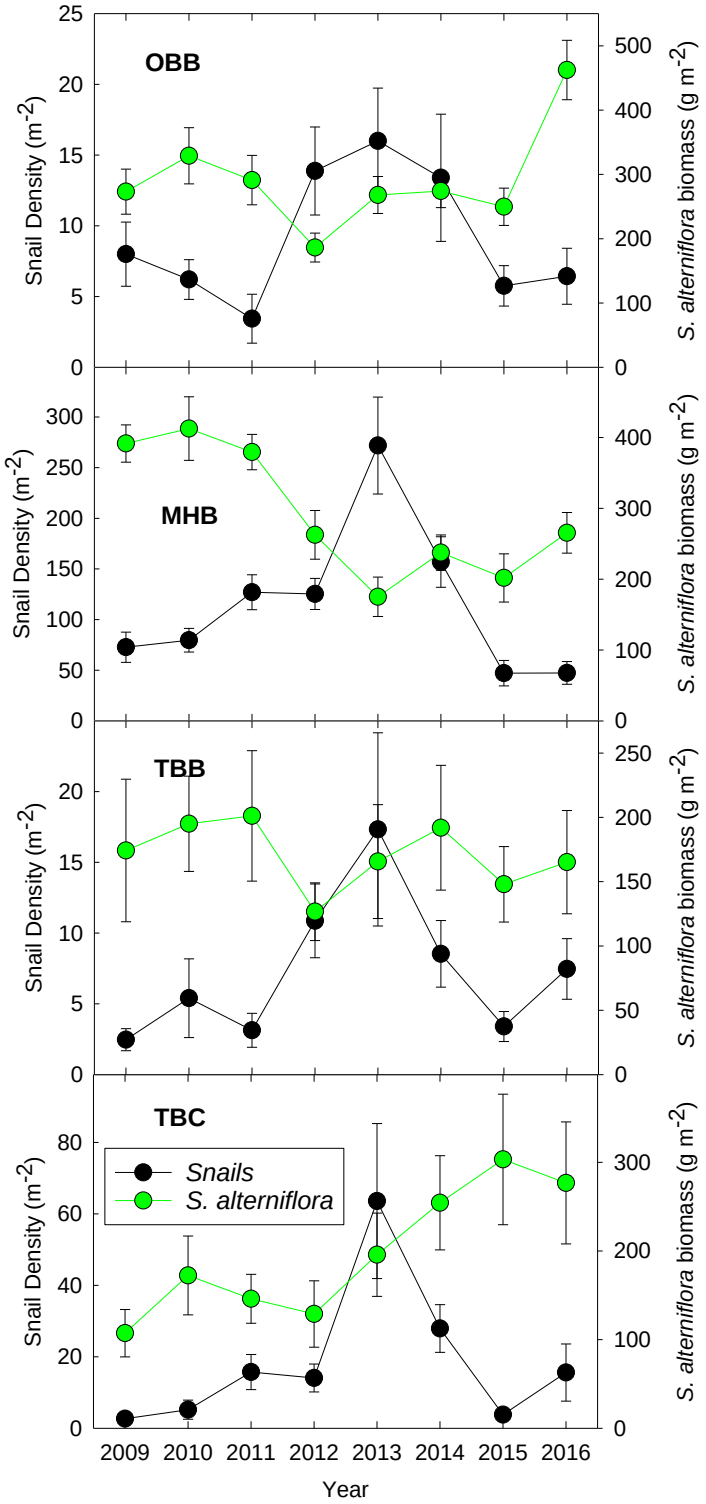

Figure 11-17. Changes in average annual snail (*Littoraria irrorata*) density and *S. alterniflora* biomass at Mile Hammock Bay (MHB), Onslow Beach Backbarrier (OBB), Traps Bay Bridge (TBB), and Traps Bay Creek (TBC) from 2009 to 2016.

Note the differences in scale between the locations.

Inundation, Rainfall, and Vegetation

The transition in the relative biomass of *Juncus roemerianus* and *Spartina alterniflora* at Traps Bay Bridge and Traps Bay Creek, and the changes in *S. alterniflora* biomass and snail density at Onslow Beach Backbarrier, Mile Hammock Bay, Traps Bay Bridge, and Traps Bay Creek, were associated with an extended period of drought (mid-2010 to mid-2012; **Figure 11-19**). The trends in the Palmer Drought Severity Index (PDSI; **Figure 11-18**). mirror those of growing season rainfall At Traps Bay Creek and Traps Bay Bridge there are significant ($p<0.05$) and moderate (r^2=0.29–0.65) negative relationships between *J. roemerianus* biomass and growing season rainfall totals, and positive relationships between *S. alterniflora* biomass and growing season rainfall at Traps Bay Creek and Traps Bay Bridge (**Table 11-9**). At other sites, including Mile Hammock Bay, where the changes in *S. alterniflora* biomass were most pronounced, there was no significant relationship between *S. alterniflora* biomass and growing season rainfall.

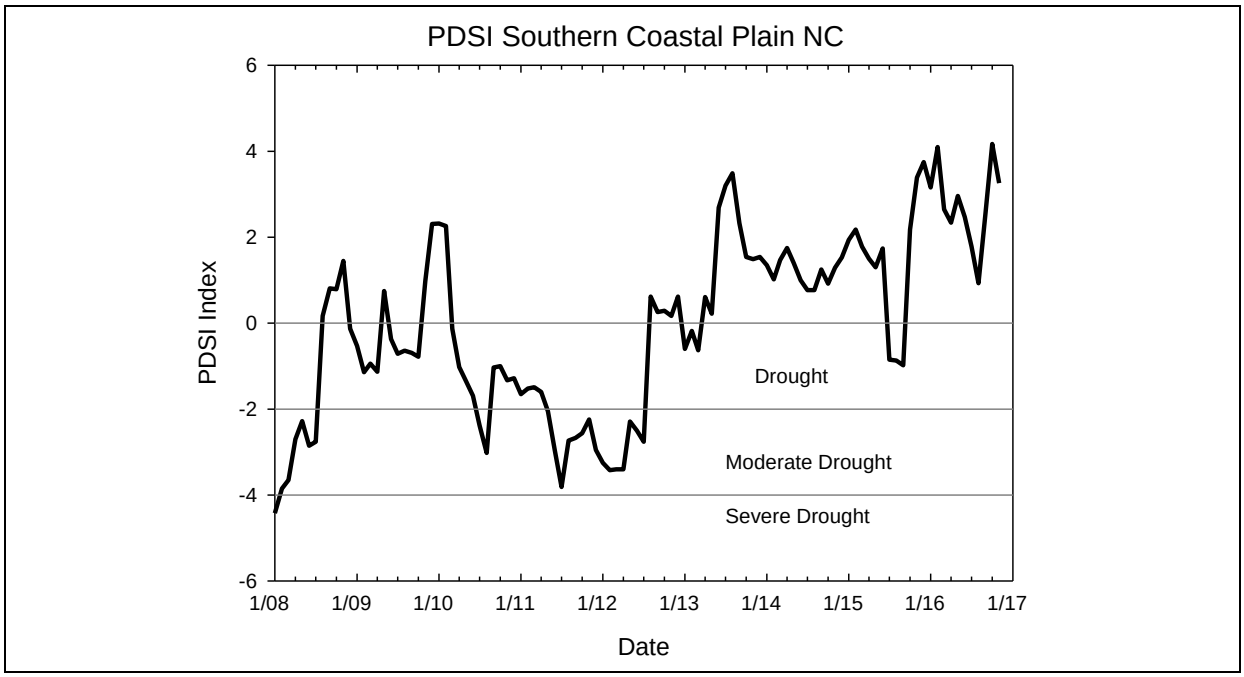

Figure 11-18. The Palmer Drought Severity Index (PDSI) for the Southern Coastal Plain of North Carolina, which includes MCBCL.

Data from the State Climate Office of North Carolina (http://climate.ncsu.edu/climate/climdiv.php).

Table 11-9. Significant Relationships ($p<0.05$) Between Growing Season Rainfall (Total Inches of Precipitation Between April 1 of Each Year and the Date of the Annual Survey) and Annual Average Vegetation Parameters at MCBCL Vegetation Monitoring Stations

Parameters tested include *Spartina alterniflora* and *Juncus roemerianus* biomass, stem density, stem height and percent cover, and snail density at all sites. Results are shown for sites and parameters with significant slopes. Freeman Creek (FC), Onslow Beach Backbarrier (OBB), Mile Hammock Bay (MHB), and French Creek (FN). The

biomass data are averages of plots in which each species was found (no plots with zero biomass values are included in the average). TBB = Traps Bay Bridge; TBC=Traps Bay Creek; and PPS = Pollocks Point Shoreline.

Station	Dependent Variable	Slope	r^2	P
TBC	*S. alterniflora* biomass (mg m^{-2})	3.53	0.65	0.01
TBC	*J. roemerianus* biomass (mg m^{-2})	−9.3	0.63	0.02
TBC	*J. roemerianus* density (m^{-2})	−7.4	0.29	0.03
TBB	*J. roemerianus* biomass (mg m^{-2})	−6.64	0.56	0.03
TBB	*J. roemerianus* density (m^{-2})	−8.38	0.53	0.04
PPS	*S. alterniflora* biomass (mg m^{-2})	7.51	0.45	0.07

Growing season inundation depends on water level and vegetation plot elevation. The duration (hours) of the growing season varies slightly depending upon the date of annual vegetation surveys. As illustrated in **Figure 11-19**, there are both between-site and intra-site (plot) differences in growing season inundation over the study period. Growing season inundation of French Creek and Mile Hammock Bay plots was more variable annually than at Onslow Beach Backbarrier and Freeman Creek (**Figure 11-19**), reflecting site-specific seasonal trends in water level (**Figure 11-10**). There were significant relationships between growing season inundation and *J. roemerianus* and *S. alterniflora* stem density, stem height, biomass, and between inundation and snail density at one or more sites. We limit our discussion to the significant results with an r^2>0.25 (shaded rows in **Table 11-11**), and note that no results had an r^2>0.44. At the three Onslow Beach Backbarrier plots with *J. roemerianus* observations, *J. roemerianus* stem density and biomass declined with growing season inundation. At Freeman Creek, *S. alterniflora* stem density declined with growing season inundation, in contrast to an observed increase in S. *alterniflora* stem height with increased growing season inundation that was observed at Freeman Creek, Mile Hammock Bay, and Onslow Beach Backbarrier combined.

The drivers of observed changes in vegetation cover, species composition, and biomass may vary across wetland ecosystems, which vary in elevation, tidal amplitude, and salinity. Between 2009 and 2016, we observed a drought and a short-term acceleration in RSLR. The drought is correlated with a decline in marsh biomass that occurred in 2012 at several stations and was most pronounced in higher elevation marshes and those with reduced tidal amplitude (Onslow Beach Backbarrier, Mile Hammock Bay, and Traps Bay). The recent increase (post-2012) in inundation and rainfall are coincident with shifts in dominant vegetation in the lower estuary. The drought may have been a tipping point at Mile Hammock Bay because there has been no recovery of *S. alterniflora* percent cover or biomass associated with the increase in rainfall or inundation after the die-off event. To a limited extent (e.g., significant relationships at only a few sites), we observed different responses of *S. alterniflora* and *J. roemerianus* to annual variability in growing season rainfall and inundation. Co-occurrence of increased growing season rainfall and inundation toward the end of the study period (2014–2016) make it difficult to distinguish the primary driver of marsh vegetation response and recovery from drought conditions.

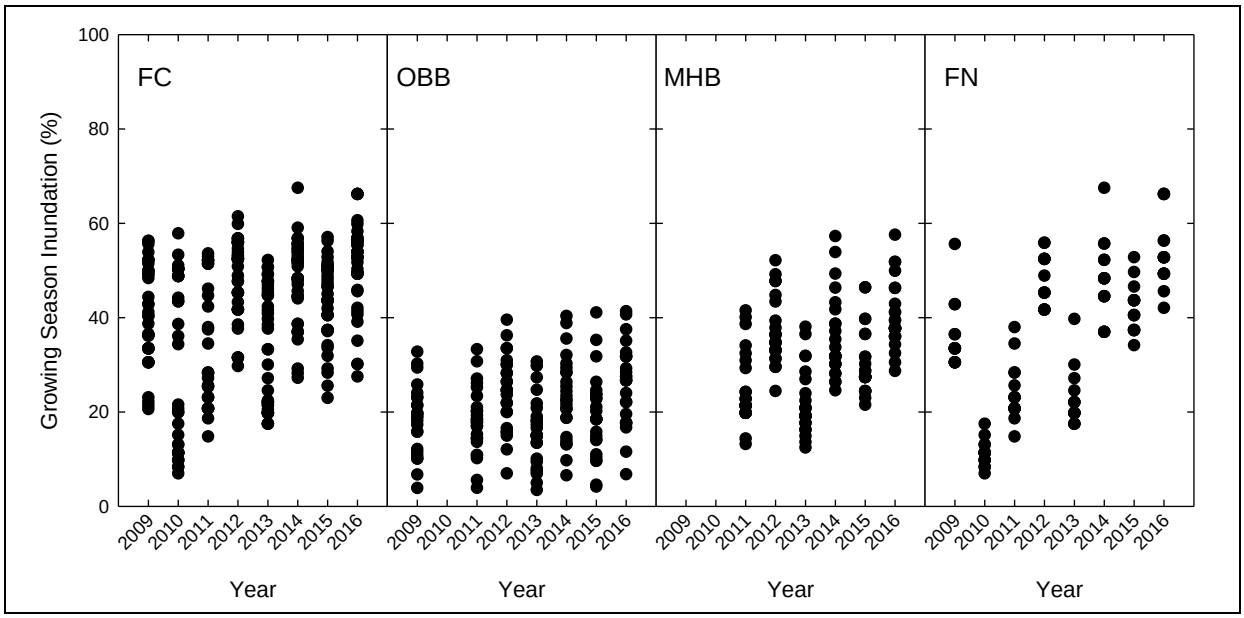

Figure 11-19. Annual growing season inundation for vegetation plots within the monitoring sites.

Missing data are due to incomplete water level records or lack of elevation measurements. Note that the number of days in the growing season ranges from 106 (2012) to 141 (2010), depending on the site and year. FC=Freeman Creek; OBB=Onslow Beach Backbarrier; MHB=Mile Hammock Bay; and FN=French Creek.

Table 11-10. Standard Least Squares Regression Results for the Relationship Between a Series of Dependent Variables with Growing Season Inundation (Total Hours of Growing Season with Sediment Surface Inundated)

Dependent Variable	Site	n	Slope	r^2
J. roemerianus stem density (m^{-2})	OBB	71	−1.27[a]	**0.35**
	FN	72	−0.16	0.02
	OBB and FN	143	0.23	0.02
J. roemerianus stem heigh+ (cm)	OBB	17	−0.07	0.19
	FN	72	0	0.01
	OBB and FN	89	0.00[a]	0.08
J. roemerianus biomass (g m^{-2})	OBB	17	−0.26[a]	**0.28**
	FN	72	−0.24	0.04
	OBB and FN	89	0.08	0.01
S. alterniflora stem density (m^{-2})	FC	187	−0.11[a]	**0.44**
	OBB	175	−0.18	0.02
	MHB	150	−0.12	0.01
	FC, MHB, and OBB	512	−0.30[a]	0.16

(continued)

Table 11-10. Standard Least Squares Regression Results for the Relationship Between a Series of Dependent Variables with Growing Season Inundation (Total Hours of Growing Season with Sediment Surface Inundated) (continued)

Dependent Variable	Site	n	Slope	r^2
S. alterniflora stem height (cm)	FC	187	0	0.0
	MHB	129	0.02[a]	**0.33**
	OBB	166	0.02[a]	0.15
	FC, MHB, and OBB	482	0.03[a]	**0.30**
S. alterniflora biomass (g m^{-2})	FC	187	−0.19[a]	0.07
	OBB	166	−0.05	0.00
	MHB	129	0.02	0.00
	FC, OBB, and MHB	482	0.03[a]	0.00
L. irrorata density (m^{-2})	FC	188	0.01	0.01
	OBB	175	0	0
	MHB	150	−0.14[a]	0.08
	FN	120	0	0.01
	FC, MHB, OBB, and FN	633	−0.02[a]	0.01

[a] Indicates a significance of 0.05. r^2 values greater than 0.25 are in bold. The biomass regressions excluded plots where the species was not found.

Marsh Surface Elevation Change

Initial marsh surface elevations at the 16 SET stations ranged from −0.01 to 0.26 m NAVD 88, and SET measurements of marsh surface elevation were obtained quarterly from early 2008 until November 2016 (**Appendix 11-A, Table 11-A-2**). Half of the SETs at Freeman Creek, Onslow Beach Backbarrier, and Mile Hammock Bay were fertilized in two experiments (2008–2011 and 2015–2016). These results are discussed by Davis et al. (2017) and are presented in Research Project CW-4 (Chapter 13, Section 3) of this report. Over the course of the study, the highest rates of elevation change occurred at Freeman Creek (3.9 to 10.2 mm y^{-1}) and the lowest (0.5 mm y^{-1}) occurred at Pollocks Point Woods and the Mile Hammock Bay control SET (**Table 11-11**). Surface elevation at four of the SETs at Freeman Creek (two fertilized and two control) is increasing at rates significantly greater than the long-term (1953–2016) RSLR rate of 3.0 mm y^{-1} (NOAA, 2017). Marsh surface elevations at SETs at Onslow Beach Backbarrier (38), Mile Hammock Bay (39 and 40), and Pollocks Point Woods (44) are increasing at rates significantly lower than local RSLR (**Table 11-11**). There was a negative relationship (r^2=0.49, $p<0.01$) between starting elevation and the 2008–2016 net rate of elevation change (**Figure 11-20**). We note that Onslow Beach Backbarrier SETs, which are at the highest elevation, are also located near Browns Inlet and experience more than twice the tidal amplitude than SETs at other sites with low elevation change (Mile Hammock Bay and French Creek).

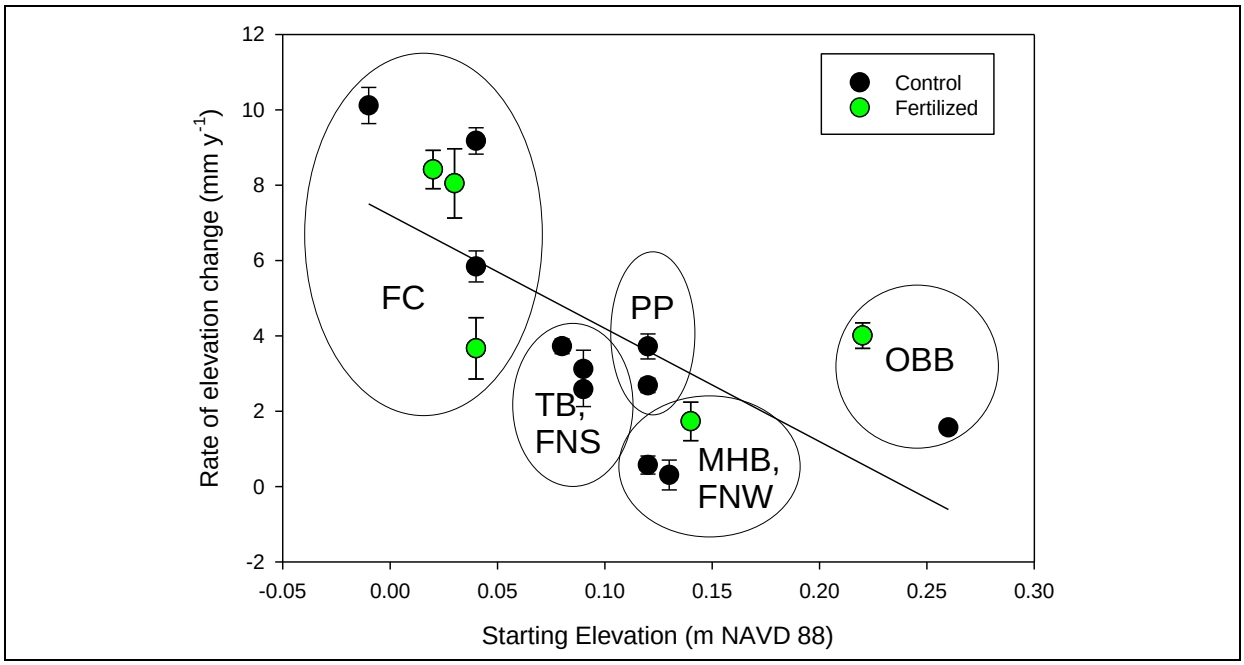

Figure 11-20. The relationship between starting elevation and the rate of net surface elevation change (Table 11-11) for all 16 SETs (slope=−28 mm y^{-1} m of starting elevation, r^2=0.42, p<0.01).

FC=Freeman Creek; FNS=French Creek Shoreline; FNW=French Creek Woods; MHB=Mile Hammock Bay; OBB=Onslow Beach Backbarrier; PP=Pollocks Point (Shoreline and Woods); and TB=Traps Bay (Bridge and Creek).

Table 11-11. The mean (±Standard Error) Rate of Elevation Change at Each SET over the 9-Year Study Period (2008–2016) Determined by Two Applications of Linear Regression Analysis (see the Materials and Methods Section of This Chapter)

All Method 1 rates were significantly different than zero except for PPW (marked by [a]). Bold rates are significantly greater than RSLR (3 mm y^{-1}) at an alpha of 0.05. Italicized rates are significantly less than RSLR. All Method 2 slopes are significant except for SET 39 ([a]). r^2 values are from Method 2. C= control; F=fertilized; FC=Freeman Creek; FNS=French Creek Shoreline; FNW=French Creek Woods; MHB=Mile Hammock Bay; OBB=Onslow Beach Backbarrier; PPS=Pollocks Point Shoreline; PPW=Pollocks Point Woods; TBB=Traps Bay Bridge; and TBC=Traps Bay Creek.

Site or Station	Treatment	SET	Starting Elevation (m NAVD 88)	Rate of Elevation Change (mm y^{-1}) Method 1	Rate of Elevation Change (mm y^{-1}) Method 2	Method 2 r^2
FC	C	31	−0.01	**10.2±1.3**	10.1±0.5	0.93
FC	C	33	0.04	5.9±1.6	5.8±0.4	0.84
FC	C	36	0.04	**9.2±0.6**	9.2±0.4	0.95
FC	F	32	0.02	**8.8±0.6**	8.4±0.5	0.89
FC	F	34	0.04	3.9±1.1	3.7±0.8	0.37
FC	F	35	0.03	**8.3±0.6**	8.1±0.9	0.69
OBB	C	38	0.26	*1.7±0.4*	1.6±0.1	0.86
OBB	F	37	0.22	3.7±0.4	4±0.3	0.76
MHB	C	39	0.13	*0.5±0.1*	0.3±0.4[a]	0.02
MHB	F	40	0.14	*2.0±0.2*	1.7±0.5	0.25
TBB	C	41	0.09	2.5±0.4	2.6±0.5	0.49
TBC	C	42	0.08	3.7±0.5	3.7±0.2	0.92
PPS	C	43	0.12	3.6±0.3	3.7±0.3	0.79
PPW	C	44	0.12	*0.5±0.2*[a]	0.6±0.2	0.15
FNS	C	45	0.09	3.1±0.6	3.1±0.5	0.54
FNW	C	46	0.12	2.7±0.3	2.7±0.2	0.86

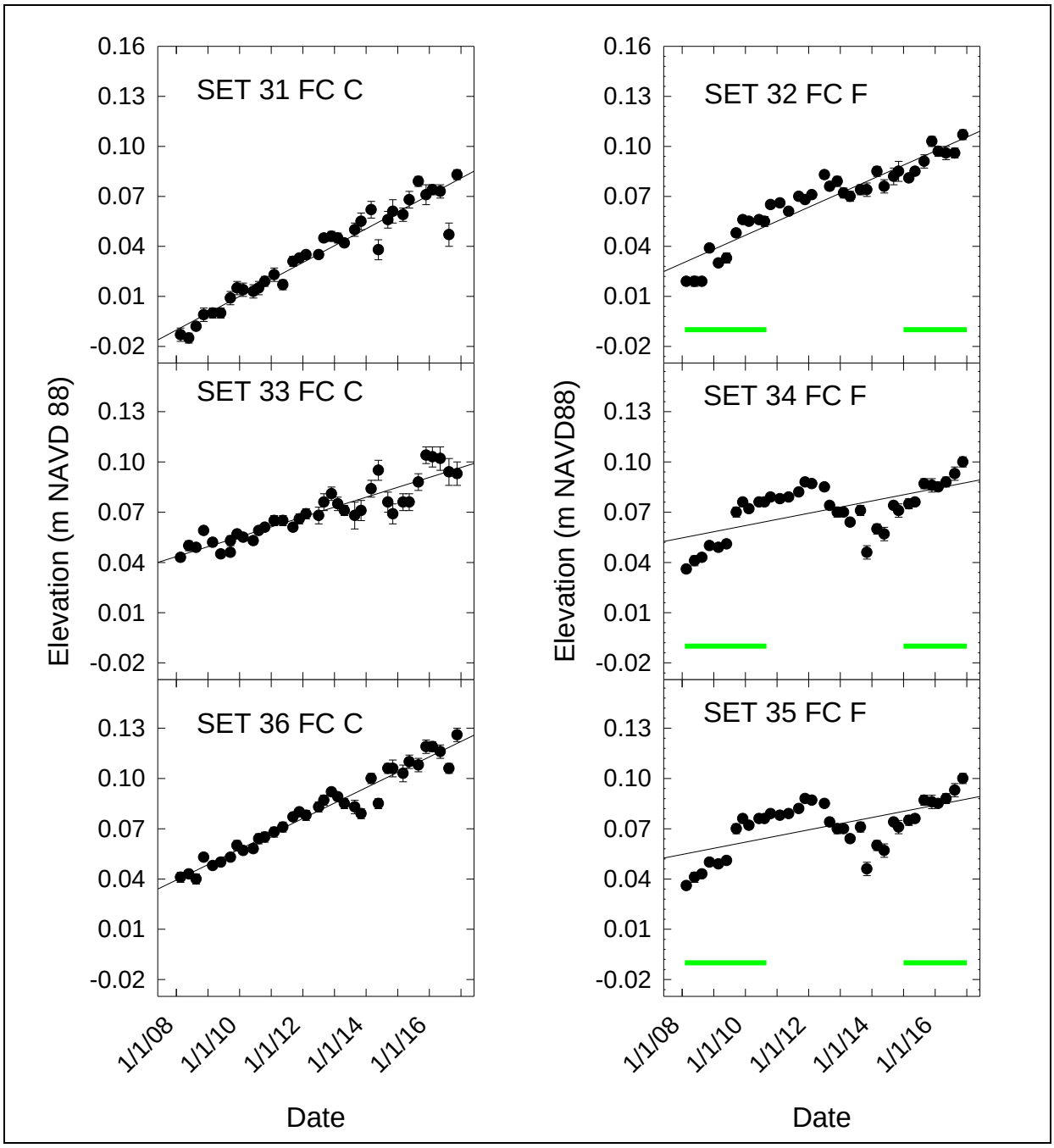

Figure 11-21. Marsh surface elevation recorded from the six SETs at Freeman Creek (FC).

Standard least squares regression line parameters are presented in **Table 11-10**. Green lines represent period of fertilizer application. C=control; and F=fertilized.

Freeman Creek SETs had the highest gain in elevation, with a net increase of between 5 cm and 10 cm from 2008 to 2016. The highest Freeman Creek rates occurred at two control (31 and 36) and two fertilized SETs (32 and 35; **Table 11-11**). SETs 33 (control) and 34 (fertilized) had the lowest rates of elevation change at Freeman Creek. The rate of change over time was variable, especially at two of the fertilized SETs (34 and 35; **Figure 11-21**). During the first fertilization period (from February 2008 through May 2010), the rate of increase at the fertilized SETs

exceeded that of the control stations. From 2012–2013, when the rate of increase slowed at the control stations, elevation decreased by 2 to 20 mm y^{-1} at the three fertilized Freeman Creek SETs, and then accelerated with the second fertilizer application (2015–2016). Losses in elevation were also observed during 2012–2013 at the control SETs.

At Onslow Beach Backbarrier and Mile Hammock Bay, the fertilized plots increased approximately two to four times faster than the control plots (**Figure 11-22 and Table 11-11**). Over the entire timeframe, the rate of elevation change at both the Mile Hammock Bay SET and the Onslow Beach Backbarrier control SET were significantly less than local RSLR (3.0 mm y^{-1}; **Table 11-11**). Despite its position relatively high in the tidal frame, the Onslow Beach Backbarrier fertilized plot elevation increased at a rate close to the RSLR (**Table 11-11**).

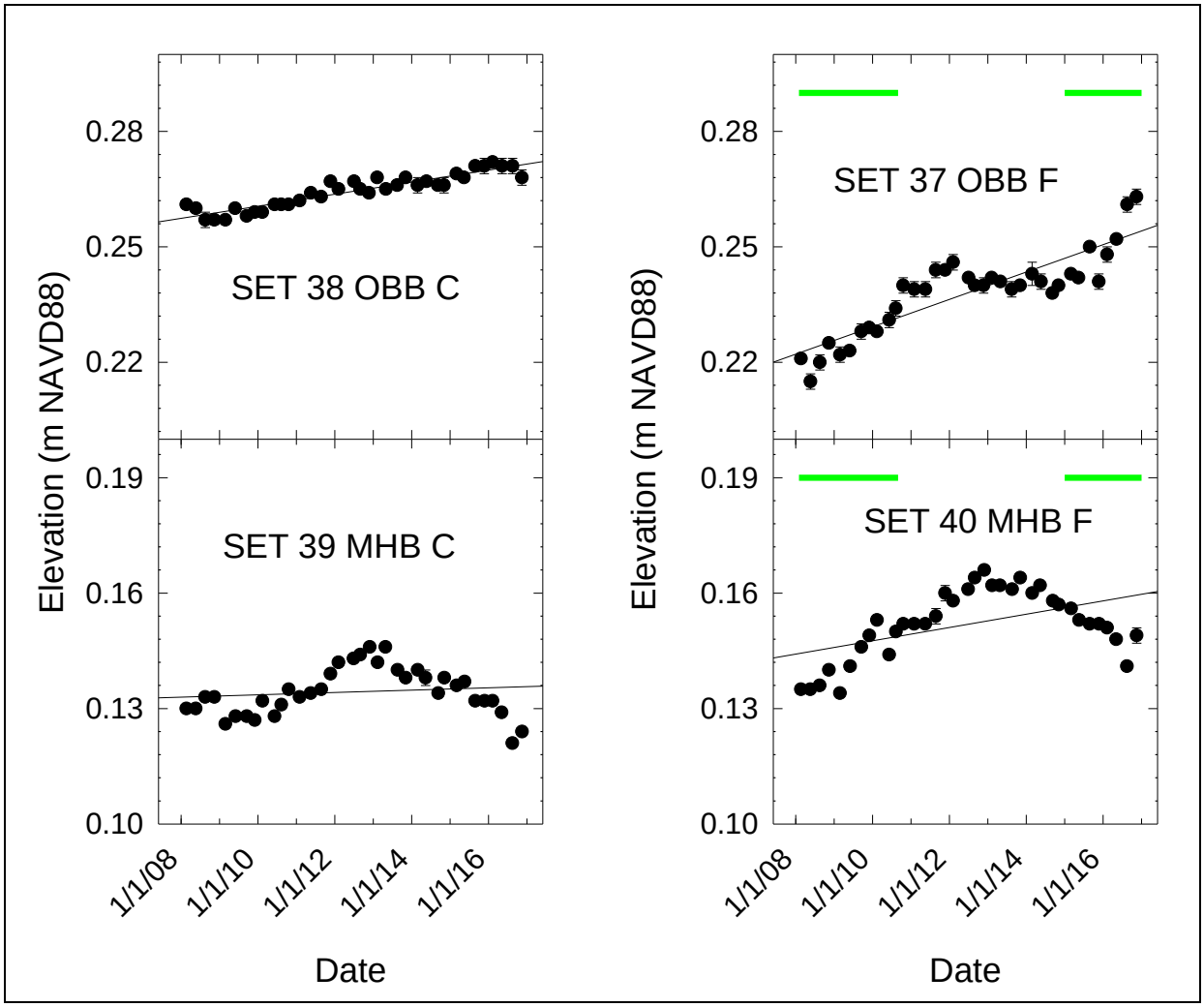

Figure 11-22. Marsh surface elevation recorded from SETs at Onslow Beach Backbarrier (OBB) and Mile Hammock Bay (MHB).

Standard least squares regression line parameters are presented in **Table 11-10**.
Green lines represent the period of fertilizer application. C=control; and F=fertilized.

At Traps Bay Bridge, Traps Bay Creek, Pollocks Point Shoreline, French Creek Shoreline, and French Creek Woods, marsh surface elevation increased by 2.5 to 3.7 mm y^{-1} (**Figure 11-22; Table 11-11**). Pollocks Point Woods was the only SET with a non-significant change rate (0.5 mm y^{-1}). Rates were more variable at the SETs adjacent to the shoreline (Traps Bay Bridge, Traps Bay Creek, Pollocks Point Shoreline, and French Creek Shoreline), where exposure to wind waves and shoreline erosion is greatest (**Table 11-11**).

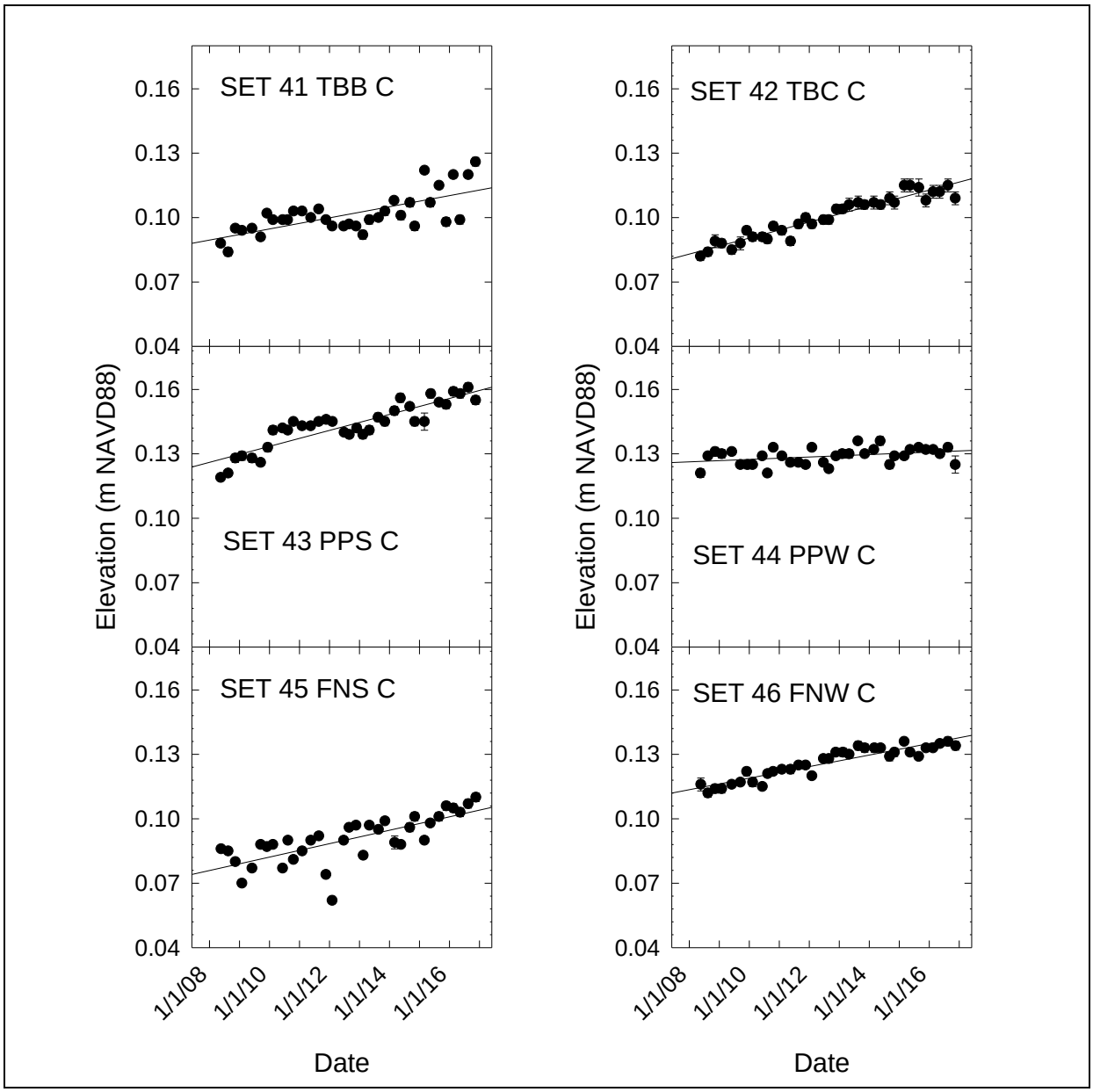

Figure 11-23. Marsh surface elevation recorded from the SETs at Traps Bay Bridge (TBB), Trays Bay Creek (TBC), Pollock's Point Shoreline (PPS), Pollock's Point Woods (PPW), French Creek Shoreline (FNS) and French Creek Woods (FNW).

Standard least squares regression line parameters are presented in **Table 10**. C=Control.

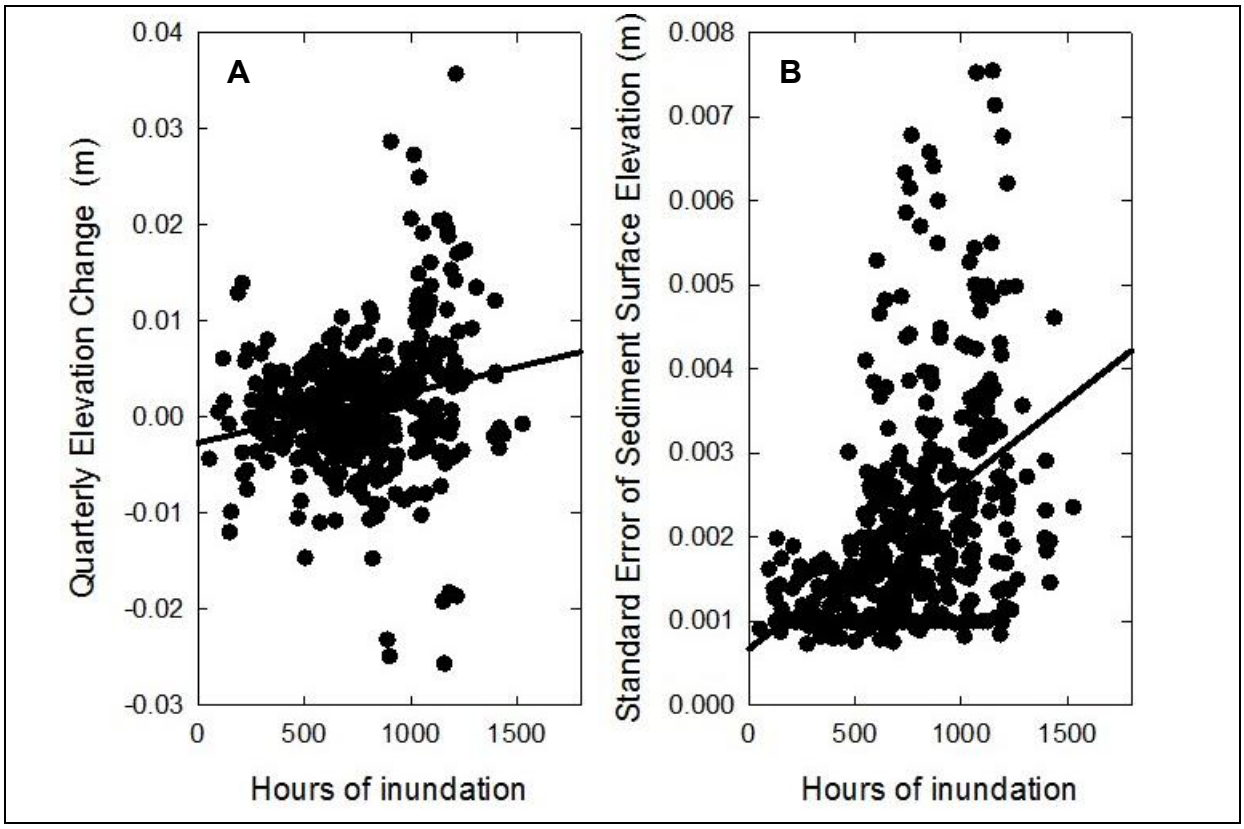

Figure 11-24. (A) Elevation change for each quarter at all SETs plotted by inundation between measurements with the regression slope. (B) The standard error of quarterly SET measurements plotted by inundation.

SETs with inundation values are limited to those at Freeman Creek, Onslow Beach Backbarrier, Mile Hammock Bay, and French Creek (a total of 402 quarterly measurements).

Inundation and Elevation Change

There was not a significant relationship between inundation and elevation change over the entire data set (Freeman Creek, Onslow Beach Backbarrier, Mile Hammock Bay, and French Creek; **Figure 11-23A**). At two fertilized SETs (32 and 34) and one control SET (36), there was a significant ($p<0.05$), but not a strong ($r^2=0.13$ to 0.37) positive relationship between inundation and elevation change. There was a significant, though small, positive relationship between the standard error of elevation and inundation (**Figure 11-23B**, $p<0.02$, $r^2=0.19$).

Sediment Accretion

The number of quarterly Marker Horizon measurements obtained with SET measures of elevation change ranged from 11 to 26 for each SET (**Appendix 11-A, Figures 11-A-4 and A-5**), resulting in a total of 194 paired elevation change rates and accretion rates over the course of the study (**Figure 11-24**). Net surface elevation change was negative for 41% of the paired rates. Because negative accretion is not recorded by Marker Horizon plots and accretion data collection was inconsistent relative to SET data collection (35 or 36 quarterly measurements per SET), our analysis of the role of sediment accretion in elevation change over the length of the study period is limited.

Freeman Creek had the highest average rate of accretion (43 mm y^{-1}). The stations adjacent to the NRE shoreline (Traps Bay Bridge and Pollocks Point Shoreline) had the next highest average accretion rates (27 mm y^{-1}), followed by Traps Bay Creek (24 mm y^{-1}), Mile Hammock Bay control and Onslow Beach Backbarrier (16 mm y^{-1}), and the more sheltered stations of French Creek and Pollocks Point Woods (12 mm y^{-1}). These average accretion rates are four to 32 times greater than the overall rate of elevation change observed from 2008–2016 (**Table 11-11**), but are within the range of positive quarterly elevation change rates (**Figure 11-24**).

The contribution of sediment accretion (*A*, measured by Marker Horizons) to surface elevation change (*E*, measured by SETs) provides an estimate of the role of subsurface processes to marsh surface elevation (Cahoon et al., 2002a and b). Subsurface processes include shallow subsidence, sediment compaction, and organic matter decomposition, which reduce marsh elevation and the accumulation of below-ground plant material and swelling, which would increase marsh elevation (Cahoon et al., 2002a and b). Where $E<A$ (above the 1:1 line in **Figure 11-24**), it is an indication that sediment compaction, organic matter decomposition, or soil shrinkage is occurring to reduce soil elevation. For 76% of paired elevation change and accretion measurements in this study, $E<A$, was often due to negative elevation change rates (**Figure 11-24**).

For 24% of the 194 paired quarterly measurements, $E>A$ (below the 1:1 line **in Figure 11-24**), suggesting that below-ground plant production can also make a significant contribution to marsh elevation (Nyman et al., 2006). This situation occurred more frequently (35% to 42% of the time) at Freeman Creek control (SET 33), Pollocks Point Shoreline (SET 43), Pollocks Point Woods (SET 44), and French Creek Shoreline (SET 45). It also was more likely to occur in the winter (approximately 41% of the time), which is the season with the lowest surface elevation increase and lowest water levels (**Figure 11-7**). Clearly, MCBCL marsh surface elevation change is driven by sediment accretion, although the processes of below-ground plant production, sediment compaction, and shallow subsidence are contributors to net marsh surface elevation change.

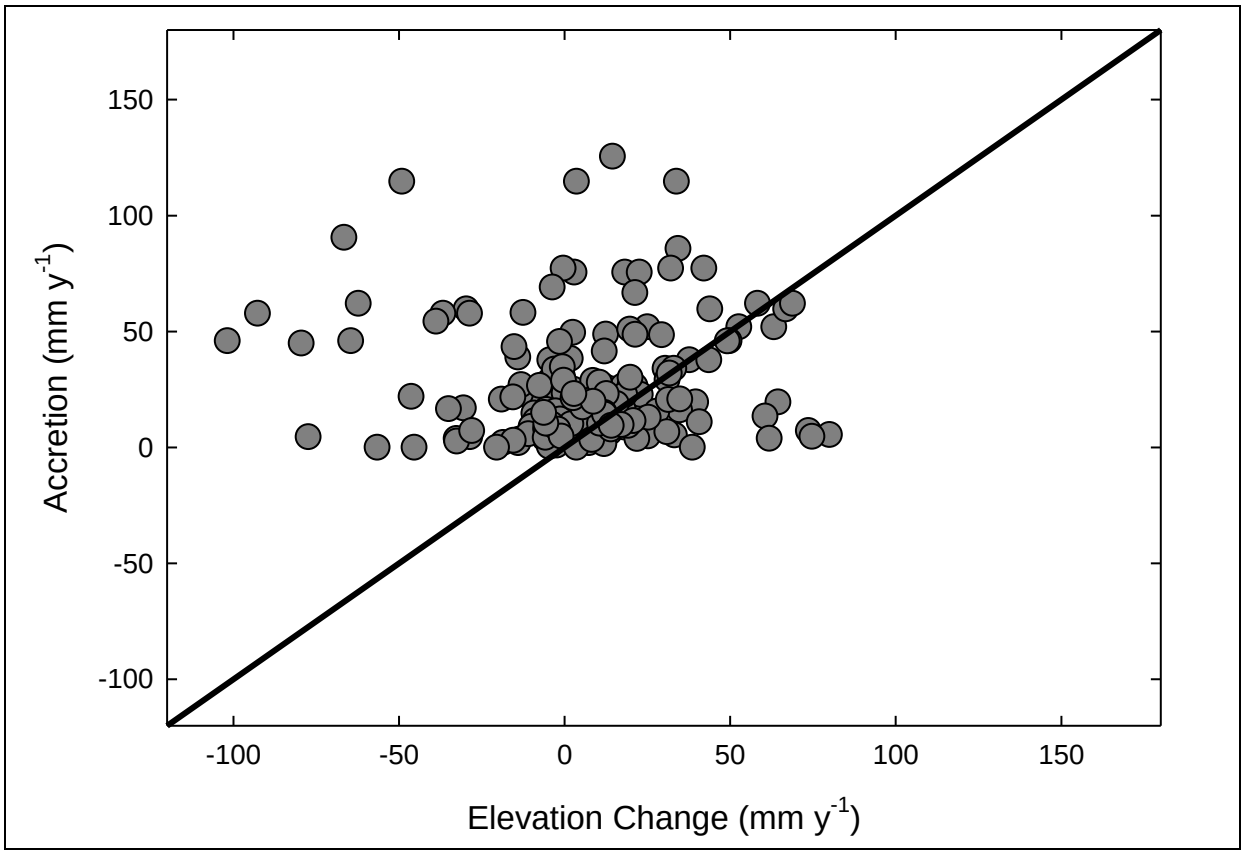

Figure 11-25. The relationship between net surface elevation change and sediment accretion as measured by SETs and Marker Horizons, respectively, across the study period.

The straight line represents a one-to-one relationship.

Shoreline Change

Three out of the four marsh stations in the NRE showed a net retreat in shoreline position, calculated by the zero m NAVD88 contour line (**Table 11-11**), during the DCERP study period. The greatest erosion occurred at the two stations that experience the highest wave energy: Traps Bay Bridge and Pollocks Point Shoreline (see *DCERP1 Final Monitoring Report* [RTI International, 2013]). The two NRE study stations located within a tidal creek system (Traps Bay Creek and French Creek Shoreline) experienced either very low shoreline erosion (Traps Bay Creek) or a seaward expansion of the zero m contour line (French Creek). The results of the DEM cut-fill analysis (**Figure 11-25**) demonstrate that at all sites, the loss of sediment elevation was most pronounced near the shoreline, and that landward areas of the marsh experienced an increase in sediment elevation. At three of the sites (Traps Bay Bridge, Traps Bay Creek, and French Creek), the total sediment volume in the cut-fill area increased over the study period. Traps Bay Bridge had the highest shoreline erosion rate, but also the highest increase in total sediment volume (**Table 11-12**). French Creek, which experienced a seaward expansion in the net zero contour line, had the highest mean surface elevation change. These results point to the importance of shoreline erosion in supplying sediment to maintain marsh surface elevation (Currin et al., 2015; Mariotti and Carr, 2014). In addition, the results suggest that eroded

sediment may not spend significant time in the estuarine water column, but may instead be quickly redeposited on the marsh surface.

Table 11-12. Results of the Cut-Fill Analysis by Using the Digital Shoreline Analysis System (DSAS) for French Creek (FN), Pollocks Point Shoreline (PPS), Traps Bay Bridge (TBB), and Traps Bay Creek (TBC) and from 2008 (2011 for FN) to 2016 for the Digital Elevation Model (DEM) area indicated

Shoreline movement analysis based on the extracted zero contour line from DEM of each site and sample year. EPR=end point rate or annual shoreline change rates.

Station	Start Date	End Date	Total Days	DEM Area (m^2)	EPR ($m\ y^{-1}$)	Total Volume Change (m^3)	Mean Surface Elevation Change (m)
TBB	12/3/2008	4/6/2016	2,681	1,579	−0.13	48.0	0.03
TBC	12/4/2008	4/15/2016	2,689	1,173	−0.01	15.0	0.01
PPS	12/3/2008	4/14/2016	2,689	129	−0.14	0.1	0.00
FN	12/3/2011	4/14/2016	1,594	238	0.13	16.3	0.07

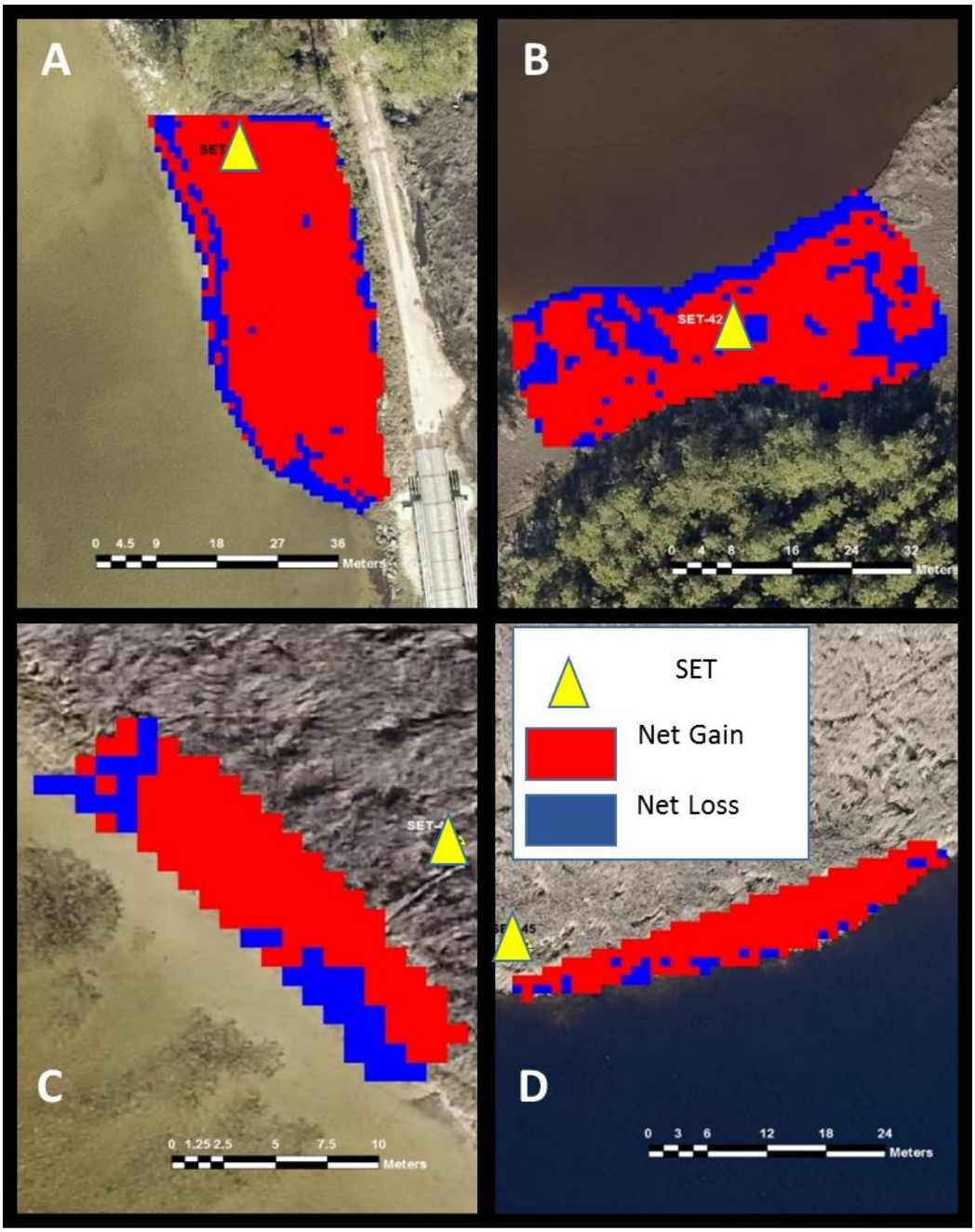

Figure 11-26. Images of the cut-fill analysis results for (A) Traps Bay Bridge, (B) Traps Bay Creek, (C) Pollocks Point Shoreline, and (D) French Creek.

Assessment of Directionality and Trends

During the CWMP, researchers deployed instruments to measure spatial and temporal changes in several parameters crucial to understanding the impact of climate drivers on salt marsh ecosystems on MCBCL, including water level and marsh elevation. Secondary tide gages were installed at the upper and lower ends of the NRE and collected temperature, salinity, and water level data at 6-minute intervals during the entire study period. The 6-minute data collection was

necessary to compute tidal datums and to detect seasonal changes in water level. The long-term record enabled the detection of inter-annual changes in water level linked to large-scale oceanic-atmospheric processes, which operate on decadal time scales. Additional water level sensors were deployed for shorter time periods at additional stations, which spanned the distribution of salt marsh habitat across salinity and tidal gradients. This effort successfully identified the 0.2-m to 0.9-m range in tidal amplitude that MCBCL salt marshes experience, which is a crucial parameter in modeling marsh response to RSLR.

Our analysis of water level data revealed that although a nearby CO-OPS station in Beaufort, NC can be used to estimate water levels experienced by marshes around Browns Inlet, it does not mirror observed water levels in the NRE, where local wind and rainfall events play a significant role in water level variation. The maintenance of a water level recorder or secondary tide gage near the New River Inlet should be considered to provide MCBCL with accurate information about trends in water level within the NRE. This may be of importance, given potential changes in New River Inlet hydrodynamics due to either dredging operations or storm events and their potential impacts on tidal water levels that may impact amphibious training operations within the NRE.

Coastal Wetlands Module's monitoring sites were chosen to encompass the wide range in salinity and geomorphological setting in which marshes occur on MCBCL. Along the ICW, marsh sites included a backbarrier island marsh (Onslow Beach Backbarrier), a marsh associated with a large tidal creek (Freeman Creek), and a marsh near the New River Inlet that was potentially impacted by military training exercises (Mile Hammock Bay). We selected sites from the lower to the upper NRE that included mixed *S. alterniflora* and *J. roemerianus* communities (Traps Bay) and a brackish site dominated by *J. roemerianus* (French Creek). We expected that patterns of marsh production might vary significantly by site. If so, this would inform our ability to use monitoring data to expand research results across the MCBCL landscape. Site variability was tested by performing univariate analysis of longitudinal data collected from permanent plots by using an analysis that was designed for repeated measures of experimental units. We found significant annual variability in marsh above-ground biomass at most sites. This variability was correlated with drought conditions, which occurred across the MCBCL landscape from 2011 through 2012. In addition, we found that growing season water level and precipitation also had significant, and different, impacts on the dominant marsh species, *S. alterniflora* and *J. roemerianus.*

Marsh surface elevation data from 16 SETs was collected over the entire DCERP1 and DCERP2 study period at quarterly intervals. A record of at least 5 years is recommended as sufficient time to assess the response of marsh surface elevation to RSLR (Lynch et al., 2015). Our data demonstrate that all but one of the marsh monitoring sites is significantly increasing surface elevation, although there are four sites that are not increasing at a rate equal to or greater than the current local RLSR rate of 3 mm $y^{-}1$. Monitoring data from three sites (Freeman Creek, Traps Bay, and French Creek), which differ in tidal amplitude, dominant marsh community, suspended sediment supply, and geomorphology, were used during Research Project CW-4 to generate predictive geospatial models on marsh response to several sea level rise scenarios. Model predictions for each site varied due to differences in site sediment accretion, plant community, and tidal amplitude, which were quantified during the CWMP.

Monitoring the NRE shoreline and determining the short- and long-term erosion rates supported the objectives of Research Project CW-4 and helped to identify vulnerable shorelines. Marsh erosion rates determined during DCERP1 at four research sites were extended by using EPR analysis and ArcGIS Spatial Analyst tools. This approach provided crucial information that was used to develop a hypothesis regarding the role of maintenance dredging in limiting sediment supply to marshes adjacent to the ICW. This approach also supported calculations regarding the amount and fate of marsh carbon released via shoreline erosion.

Conclusions and Implications for Future Research and Implementation

Key Findings

Temporal and Spatial Variability in Water Level

- During the study period, water levels in the NRE and ICW increased 10 and 14 mm y^{-1}, respectively, which are much higher rates than the long-term rate of RSLR (3.0 mm y^{-1}). Our study period included one of the recurring, short-lived, rapid sea level rise accelerations (Southeastern United States, 2011–2015) associated with decadal oscillations.
- Tidal amplitudes decrease from 0.95 m at Freeman Creek, to 0.43 m at Mile Hammock Bay, to 0.17 m at Gottschalk Marina Wallace Creek. Research Project CW-4 results indicate this is a key variable in marsh sustainability to sea level rise, and these data were crucial to model predictions on long-term marsh resiliency to sea level rise.
- MSLs increase from −0.11 m NAVD 88 at Freeman Creek, to −0.07 m NAVD 88 at Mile Hammock Bay, to −0.05 m NAVD 88 at Gottschalk Marina Wallace Creek.
- The inter-annual, seasonal range in water levels (0.23 m) is approximately twice the increase in mean annual water level over the 2008 to 2016 study period (0.12 m or less).
- Inundation of the marsh surface had strong spatial and seasonal components. The low Freeman Creek marsh near Browns Inlet (where tidal amplitude was greatest) was more frequently inundated (43% of the time), with lowest inundation (38%) occurring in the winter and spring and highest in the fall (52%). Other marshes were inundated 26% to 30% of the time on an annual basis, with a greater range in seasonal inundation. Inundation at all sites was highest in fall.

Monitoring of Above-Ground Plant Biomass and Species Composition Provided Evidence of Inter-annual Variability Associated with an Extended Drought (2010 through mid-2012)

- Average site *S. alterniflora* biomass began a decline at Onslow Beach Backbarrier, Mile Hammock Bay, and Traps Bay Creek in 2010 and at Traps Bay Bridge in 2011. These declines were coincident with the onset of drought conditions. *S. alterniflora* and *J. roemerianus* biomass declined at all monitoring sites in 2012 and reached the lowest levels recorded throughout the study at several sites.
- Snail (*Littoraria irrorata*) density increased after 2012 and peaked in 2013 at four sites (Onslow Beach Backbarrier, Mile Hammock Bay, Traps Bay Bridge, and Traps Bay

Creek). The decline in marsh biomass at Mile Hammock Bay continued and became a persistent marsh die-off event, which was also associated with a loss of surface elevation that began in 2013.

- A change in dominant marsh vegetation was observed at sites in the lower NRE. *J. roemerianus* biomass peaked in 2011 at Traps Bay Bridge and Traps Bay Creek and returned to half of the 2011 values from 2012–2016. In 2012, *S. alterniflora* began increasing its coverage and biomass, resulting in a shift in the relative proportions of *S. alterniflora* and *J. roemerianus* biomass at these two sites. A significant positive relationship between *S. alterniflora* biomass and rainfall and a negative relationship between *J. roemerianus* biomass and rainfall suggest the transition may be associated with the drought. However, higher tidal water levels occurred at the same time and may also have contributed to change in marsh vegetation.

Marsh Surface Elevation and Sediment Accretion Measures Reveal Patterns and Drivers of Marsh Response to Sea Level Rise

- During the accelerated sea level rise (10 to 14 mm y^{-1}) that was documented during the study period, SET results indicate that most of the MCBCL marshes are keeping pace with the long-term RSLR of 3 mm y^{-1}, but only three SETs at Freeman Creek kept pace with the short-term accelerated sea level rise. Marshes that did not keep pace with the long-term RLSR rate include an unfertilized SET at high elevation (Onslow Beach Backbarrier control), a marsh undergoing a die-off event (Mile Hammock Bay), and a mid-estuary, mixed species marsh near the upland marsh boundary (Pollocks Point Woods).
- The highest net elevation change and highest sediment accretion rates occurred at Freeman Creek. The SETs at this site are located near MSL, and the site also experiences the highest tidal amplitude and suspended sediment concentration observed in the study sites.
- Sediment accretion rates as measured with Marker Horizons were greater than net surface elevation time 75% of the time, demonstrating the importance of sediment to net elevation change, and demonstrating that subsurface compaction and decomposition are important processes controlling surface elevation.
- The sites experiencing the highest wave energy and shoreline erosion rates (Pollocks Point Shoreline and Traps Bay Bridge) had the next highest average accretion rate (27 mm y^{-1}) in the NRE, followed by another more sheltered, shoreline site (Traps Bay Creek with 24 mm y^{-1}). The marshes adjacent to the shoreline at Traps Bay Bridge and Pollocks Point Shoreline demonstrated an increase in sediment volume because the elevation increase in the marsh exceeded the loss of volume via erosion. These data illustrate the importance of eroded sediment as a source of sediment for marshes to maintain their surface elevation. These data also suggest that eroded marsh carbon may spend a limited time suspended in the water column.

Findings with Implications for Future Base Management

The variability in tidal amplitude and seasonal inundation that we documented across the MCBCL estuarine system has implications for coastal wetland ecosystems, natural resource management, and military training operations. The increase in tide range from Browns Inlet to New River Inlet means that salt marshes closer to the New River Inlet are more vulnerable to sea level rise. Future changes in dominant marsh vegetation and suspended sediment supply are also linked with tidal amplitude. Successful us of adaptive management options for salt marshes, including Living Shorelines and thin-layer applications of dredged material, will require an understanding of site-specific tide conditions and hydrodynamics.

The SETs and Class C bench marks that have been established at MCBCL provide long-term reference points for measuring changes in marsh surface elevation and water levels. These require little to no maintenance and can be used to address specific management needs in the future.

Literature Cited

Bertness, M.D., and S.C. Pennings. 2000. Spatial variation in process and pattern in salt marsh plant communities. Pp. 39–58 in *Concepts and Controversies in Tidal Marsh Ecology*. Edited by Weinstein, M. Kluwer Press: Boston, MA.

Bindoff, N.L., J. Willebrand, V. Artale, A, Cazenave, J. Gregory, S. Gulev, K. Hanawa, C. Le Quéré, S. Levitus, Y. Nojiri, C.K. Shum, L.D. Talley, and A. Unnikrishnan. 2007. Observations: Oceanic climate change and sea level. *Climate Change 2007: The Physical Science Basis. Contribution of Working Group I to the Fourth Assessment Report of the Intergovernmental Panel on Climate Change*. Edited by Solomon, S., D. Qin, M. Manning, Z. Chen, M. Marquis, K.B. Averyt, M. Tignor and H.L. Miller. Cambridge University Press: Cambridge, United Kingdom and New York, NY.

Cahoon, D.R., P.F. Hensel, T. Spencer, D.J. Reed, K.L. McKee, and N. Saintilan. 2006. Coastal wetland vulnerability to relative sea level rise: Wetland elevation trends and process controls. *Wetlands and Natural Resource Management: Ecological Studies 190*:271–292.

Cahoon, D.R., J.C. Lynch, P. Hensel, R. Boumans, B.C. Perez, B. Segura, and J.W. Day, Jr. 2002a. A device for high precision measurement of wetland sediment elevation: I. Recent improvements to the sedimentation-erosion table. *Journal of Sedimentary Research 72*(5):730–733.

Cahoon, D.R., J.C. Lynch, B.C. Perez, B. Segura, R.D. Holland, C. Stelly, G. Stephenson, and P. Hensel. 2002b. High-precision measurements of wetland sediment elevation: II. The rod surface elevation table. *Journal of Sedimentary Petrology 72*:734–739.

Christian, R.R., W.L. Bryant Jr., and M.M. Brinson. 1990. *Juncus roemerianus* production and decomposition along gradients of salinity and hydroperiod. *Marine Ecology Progress Series 68*:137–145.

Currin, C., J. Davis, L. Cowart Baron, A. Malhotra, and M. Fonseca. 2015. Shoreline change in the New River Estuary, North Carolina: Rates and consequences. *Journal of Coastal Research 31*(5):1069–1077.

Dahl, T.E. 2011. *Status and Trends of Wetlands in the Conterminous United States 2004–2009*. U.S. Department of the Interior; Fish and Wildlife Service, Washington, DC. 108 pages.

Davis, J., C. Currin, and J.T. Morris. 2017. Impacts of fertilization and tidal inundation on elevation change in microtidal, low relief salt marshes. *Estuaries and Coasts*:1–11. doi: 10.1007/s12237-017-0251-0

Douglas, B.C. 2001. Sea level change in the era of the recording tide gauge. Pp. 37–62 in Sea Level Rise History and Consequences. Edited by Douglas, B.C., M.S. Kearney, and S.P. Leatherman. Academic Press: San Diego, CA.

Elzinga, C.L., D.W. Salzer, and J.W. Willoughby. 1998. *Measuring and Monitoring Plant Populations*. Technical Reference 1730-1. U.S. Department of the Interior, Bureau of Land Management. Available at https://www.blm.gov/nstc/library/pdf/MeasAndMon.pdf

Friedrichs, C.T., and J.E. Perry. 2001. Tidal salt marsh morphodynamics: A synthesis. *Journal of Coastal Research 27*:7–37.

Floyd, R.P. 1978. Geodetic Bench Marks. NOAA Manual NOS NGS 1. Available at https://www.ngs.noaa.gov/PUBS_LIB/GeodeticBMs/

Goodman, S.W. 1996. Ecosystem management at the Department of Defense. *Ecological Applications 6*(3):706–707.

Hall, J.A., S. Gill, J. Obeysekera, W. Sweet, K. Knuuti, and J. Marburger. 2016. *Regional Sea Level Scenarios for Coastal Risk Management: Managing the Uncertainty of Future Sea Level Change and Extreme Water Levels for Department of Defense Coastal Sites Worldwide*. U.S. Department of Defense, Strategic Environmental Research and Development Program. 224 pp.

Hicks, S.D., P.C. Morris, H.A. Lippincott, and M.C. O'Hargan. 1987. *User's Guide for the Installation of Bench Marks and Leveling Requirements for Water Level Stations*. Final Report. U.S. Department of Commerce, National Oceanic and Atmospheric Administration, National Ocean Service, Rockville, MD. Available at https://tidesandcurrents.noaa.gov/publications/users_guide_for_installation_of_Bench_Mark.pdf

Kirwan, M.L., and L.K. Blum. 2011. Enhanced decomposition offsets enhanced productivity and soil carbon accumulation in coastal wetlands responding to climate change. *Biogeosciences 8*:987–993.

Kneib, R.T. 1997. The role of tidal marshes in the ecology of estuarine nekton. *Oceanography and Marine Biology 35*:163–220.

Knutson, P.L., R.A. Brochu, W.N. Seelig, and M. Inskeep, 1982. Wave damping in *Spartina alterniflora* marshes. *Wetlands 2*(1):87–104.

Kolker, A.S., S.L. Goodbred, S. Hameed, and J.K. Cochran. 2009. High-resolution records of the response of coastal wetland systems to long-term and short-term sea-level variability. *Estuarine, Coastal and Shelf Science 84*:493–508.

Levin, L.A., D.F. Boesch, A. Covich, C. Dahm, C. Erséus, K.C. Ewel, R.T. Kneib, A. Moldenke, M.A. Palmer, P. Snelgrove, D. Strayer, and J.M. Weslawski. 2001. The function of marine critical transition zones and the importance of sediment biodiversity. *Ecosystems 4*:430–451.

Lynch J.C., P. Hensel, and D.R. Cahoon. 2015. *The Surface Elevation Table and Marker Horizon Technique: A Protocol for Monitoring Wetland Elevation Dynamics*. Natural Resource Report NPS/NCBN/NRR–2015/1078. National Park Service, National Oceanic and Atmospheric Administration. Available at https://pubs.er.usgs.gov/publication/70160049

Mariotti, G., and J. Carr. 2014. Dual role of salt marsh retreat: Long-term loss and short-term resilience. *Water Resources Research 50*(4):2963–2974. doi: 10.1002/2013WR014676

Mattheus, C.R., A.B. Rodriguez, B.A. McKee, and C.A. Currin. 2010. Impact of land-use change and hard structures on the evolution of fringing marsh shorelines. *Estuarine, Coastal and Shelf Science 88*:365–376. doi: 10.1016/j.ecss.2010.04.016

Möller, I., T. Spencer, J. R. French, D. J. Leggett and M. Dixon. 1999. Wave transformation over salt marshes: A field and numerical modelling study from north Norfolk, England. *Estuarine Coastal and Shelf Science 49*:411–426.

Morris, J.T. 1991. Effects of nitrogen loading on wetland ecosystems with particular reference to atmospheric deposition. *Annual Review of Ecology and Systematics 22*:257–279.

Morris, J.T., and B. Haskin. 1990. A 5-yr record of aerial primary production and stand characteristics of *Spartina alterniflora*. *Ecology 71*:2209–2217.

Morris, J.T., P.V. Sundareshwar, C.T. Nietch, B. Kjerfve, and D.R. Cahoon. 2002. Responses of coastal wetlands to rising sea level. *Ecology 83*:2869–2877.

NOAA (National Oceanic and Atmospheric Administration). 2017. Mean Sea Level Trend: 8656483 Beaufort, North Carolina. Available at https://tidesandcurrents.noaa.gov/sltrends/sltrends_station.shtml?stnid=8656483

NOAA (National Oceanic and Atmospheric Administration). 2015. *Accurate Elevations for Sea Level Change Sentinel Sites*. Pending publication.

NOAA (National Oceanic and Atmospheric Administration). 2014. *Online Positioning User Service Baseline Processing and Adjustment Software, User Instructions and Technical*

Guide, version 2.3—January 31, 2014. Available at https://geodesy.noaa.gov/OPUS-Projects/OpusProjects.shtml

NOAA (National Oceanic and Atmospheric Administration). 2007a. *Guidelines for Determining Tidal Datums for Habitat Restoration and Monitoring Projects in North Carolina*. Draft Technical Report. U.S. Department of Commerce, NOAA, Center for Operational Oceanographic Products and Services. March.

NOAA (National Oceanic and Atmospheric Administration). 2007b. *Tidal Analysis and Prediction*. U.S. Department of Commerce NOAA Special Publication NOS CO-OPS 3. Library of Congress Control Number: 2007925298. Available at https://www.tidesandcurrents.noaa.gov/publications/Tidal_Analysis_and_Predictions.pdf

NOAA (National Oceanic and Atmospheric Administration). 2007c. *User's Guide for GPS Observations*. Technical Report. U.S. Department of Commerce, NOAA, National Ocean Service, Center for Operational Oceanographic Products and Services. March.

NOAA (National Oceanic and Atmospheric Administration). 2003. *Computational Techniques for Tidal Datums Handbook*. U.S. Department of Commerce National Oceanic and Atmospheric Administration Special Publication National Ocean Service CO-OPS 2. https://tidesandcurrents.noaa.gov/publications/Computational_Techniques_for_Tidal_Datums_handbook.pdf

Nyman, J.A., R.J. Walters, R.D. Delaune, and W.J. Patrick. 2006. Marsh vertical accretion via vegetative growth. *Estuarine Coastal Shelf Science 69*:370–380.

Peet, R.K., T.W. Wentworth, and P.S. White. 1998. A flexible, multipurpose method for recording vegetation composition and structure. *Castenea 63*:262–274.

Pennings, S.C., and M.D. Bertness. 2001. Salt marsh communities. Pp. 289–316 in *Marine Community Ecology*. Edited by Bertness, M.D., S.D. Gaines, and M.E. Hay. Sinauer Associates, Inc.: Sunderland, MA.

RTI International. 2013. *DCERP1 Final Monitoring Report.* Strategic Environmental Research and Development Program (SERDP) Research Project RC-1413. RTI, Research Triangle Park, NC.

Silliman, B.R., J. van de Koppel, M.D. Bertness, L.E. Stanton, and I.A. Mendelssohn. 2005. Drought, snails and large-scale die-off of southern U.S. salt marshes. *Science 310*:1803–1806.

Thieler, E.R., E.A. Himmelstoss, J.L. Zichichi, and A. Ergul. 2017. *Digital Shoreline Analysis System (DSAS) version 4.0-An ArcGIS extension for calculating shoreline change.* Version 4.4. July 2017: U.S. Geological Survey Open-File Report No. 2008-1278. Available at https://pubs.er.usgs.gov/publication/ofr20081278

Tobias, C.R., I.C. Anderson, E.A. Canuel, and S.A. Macko. 2001. Nitrogen cycling through a fringing marsh-aquifer ecotone. *Marine Ecology Progress Series 210*:25–39.

Valiela, I., and J.M. Teal. 1979. The nitrogen budget for a salt marsh ecosystem. *Nature 280*:652–656.

Valle-Levinson, A., A. Dutton, and J.B. Martin. 2017. Spatial and temporal variability of sea-level rise hotspots over the eastern United States. *Geophysical Research Letters 44*(15):7876–7882. doi: 10.1002/201/2017GL073926

Vermeer, M., and S. Rhamstorf. 2009. Global sea level linked to global temperature. *Proceedings of the National Academy of Sciences of the United States of America* 106(51):21527–21532. doi: 10.1073/pnas.0907765106

Zilkoski, D.B., E.E. Carlson, and C.L. Smith. 2008. Guidelines for establishing GPS–derived orthometric heights. *NOAA Technical Memorandum NOS NGS-59 Version, 1*, 1–19.

Appendix 11-A
Supporting Data

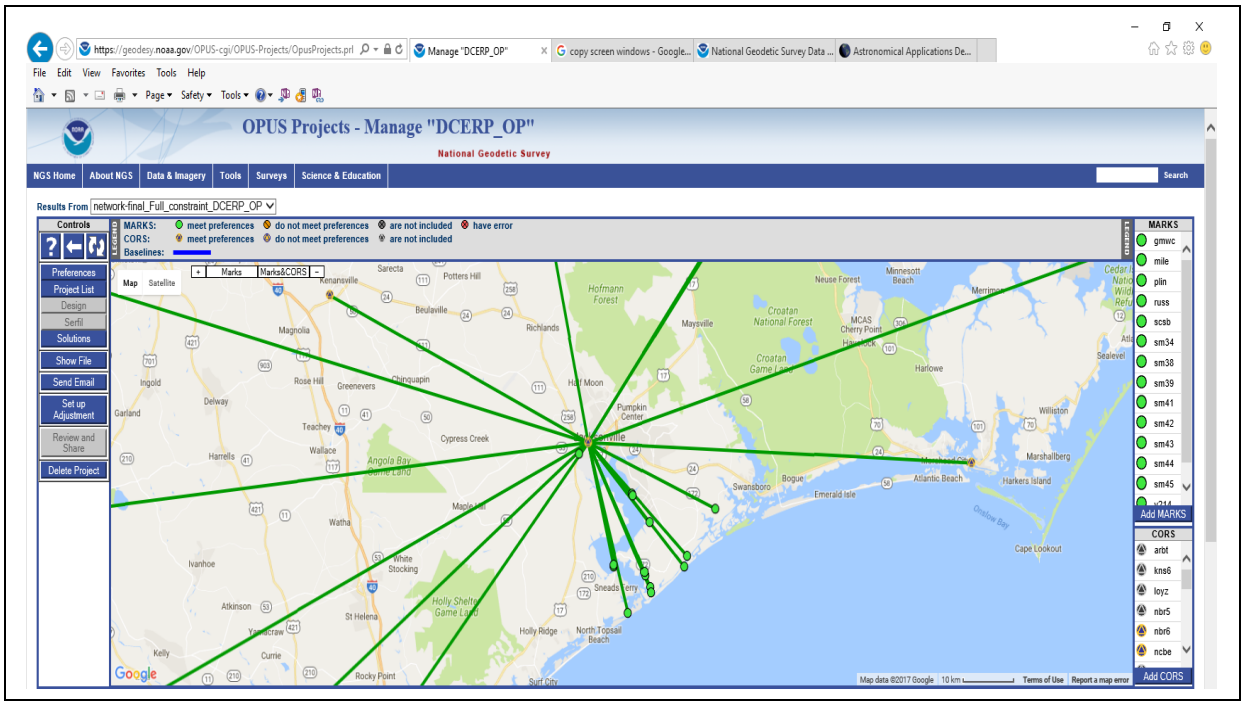

Figure 1111A-1. Screenshot of Online Positioning User Service (OPUS) Projects DCERP_OP showing the fully constrained processing with Continuously Operating Reference Station (CORS) and surface elevation table (SET) mark baselines.

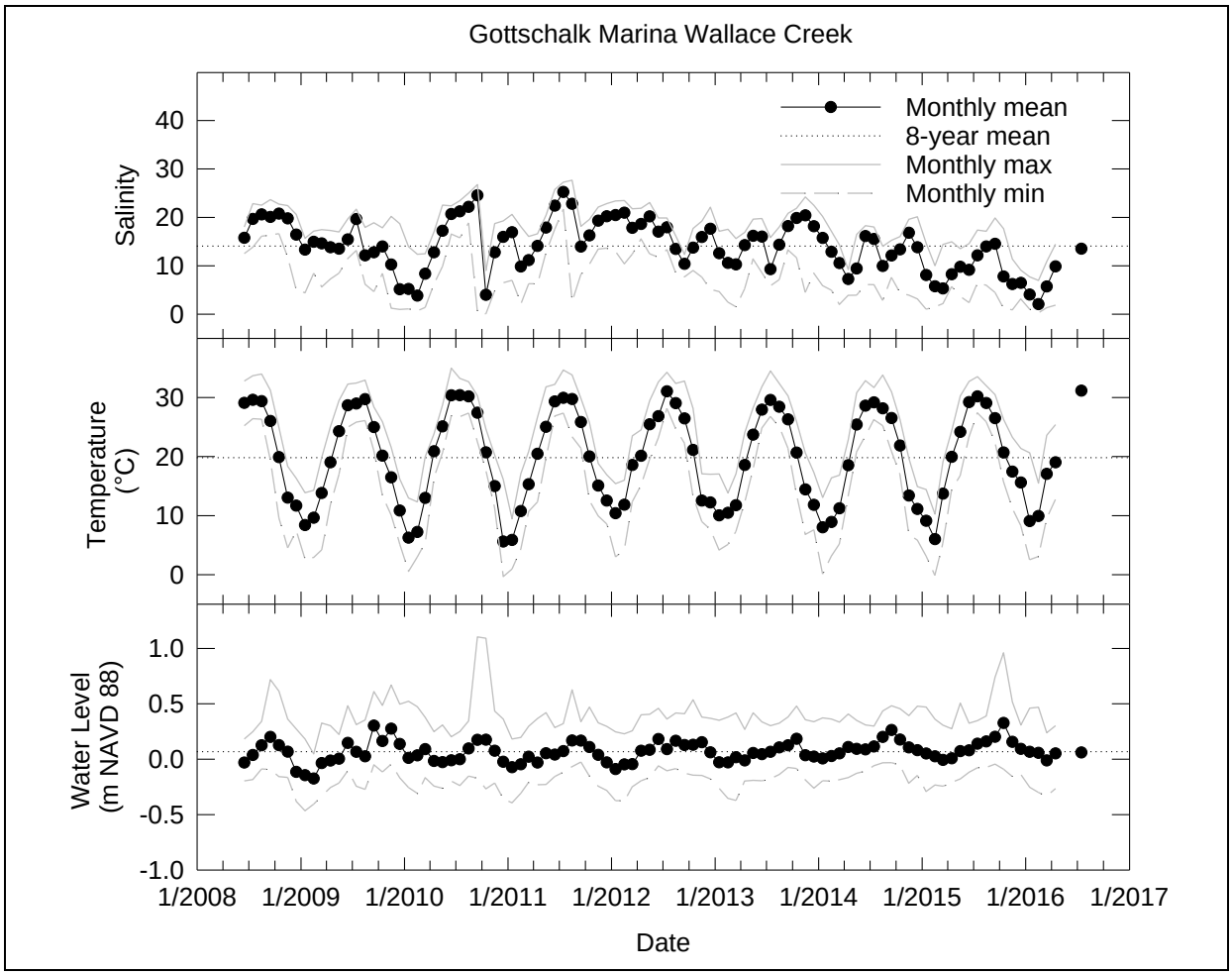

Figure 11A-2. Monthly salinity, temperature and water level at Gottschalk Marina Wallace Creek. May, June, and August 2016 are excluded because of incomplete records.

°C=degree Celsius; and NAVD 88=North American Vertical Datum of 1988.

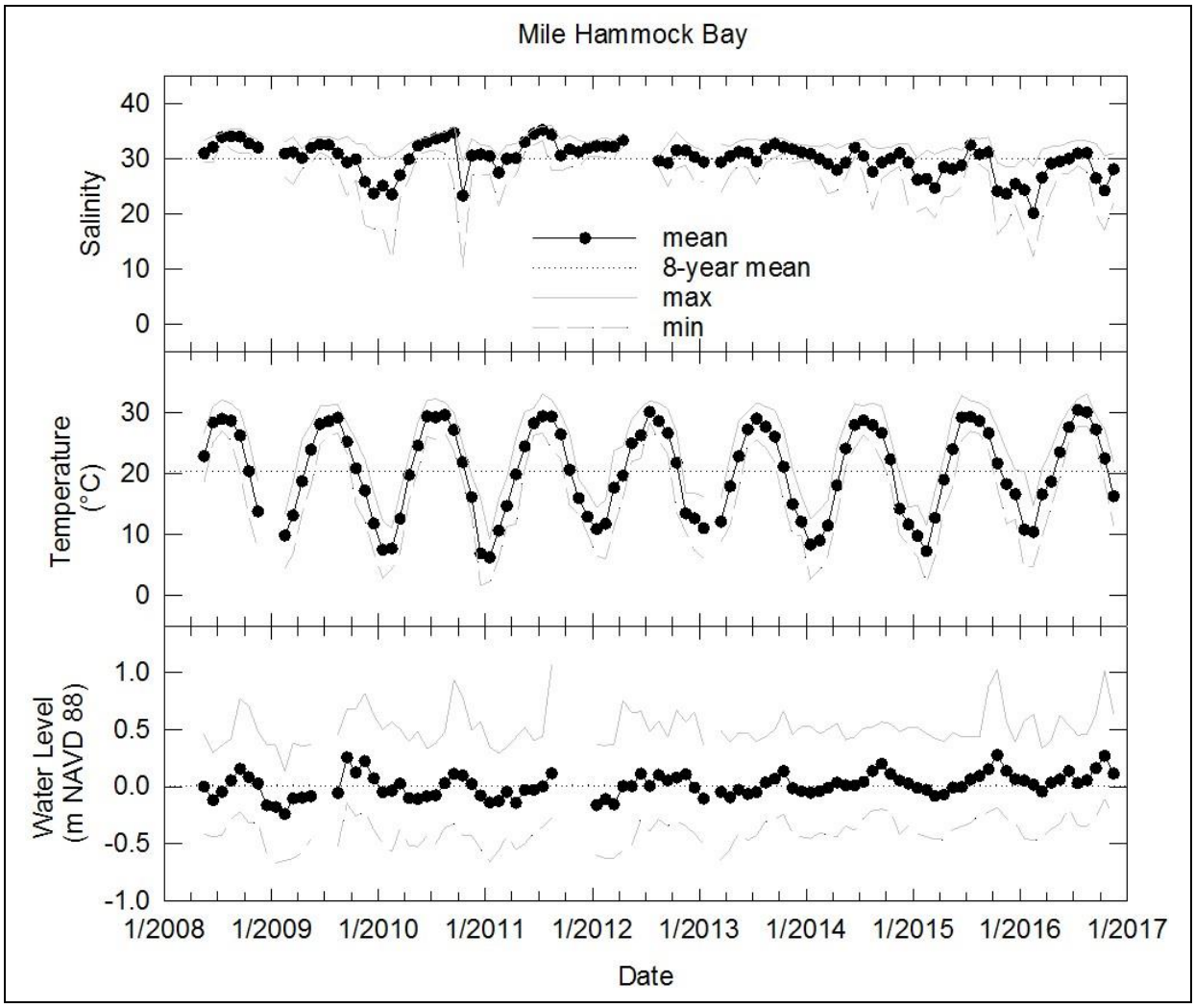

Figure 11A-3. Monthly salinity, temperature and water level at Mile Hammock Bay. Months with incomplete or missing records are excluded.

°C=degree Celsius; and NAVD 88=North American Vertical Datum of 1988.

Table 11A-1. Online Positioning User Service (OPUS) Projects Results for Control Point Surface Elevation Table (SET) and Class C Bench Marks.

Final adjusted latitude and longitudes are in North American Datum of 1983 (NAD 83) and International GNSS Service (IGS08) coordinates along with peak-to-peak errors. Orthometric heights (m NAVD 88) are determined using ellipsoid heights (m GRS 80). Latitude and longitude are given in degrees, minutes, and decimal seconds. Orthometric heights are determined by using the current GEOID (12B) and have an accuracy of ±1.5 cm. BM = bench mark; GMWC SLP = Gottschalk Marina Wallace Creek Sensor Leveling Point. MILE and PLINA are bench mark names.

Bench Mark (SET Number, or Class C Bench Mark Name)	Reference	NAD_83 (2011)	Peak-to-Peak Error	IGS08 (2012.8757)	Peak-to-Peak Error
SET 34	Latitude	34 35 40.57863	0.000 m	34 35 40.60582	0.000 m
	Longitude	77 15 04.18760	0.000 m	77 15 04.20436	0.000 m
	Ellipsoid height	-37.166 m	0.002 m	-38.579 m	0.002 m
	Orthometric height	0.04 m	0.015 m		
SET 38	Latitude	34 34 49.43649	0.000 m	34 34 49.46417	0.000 m
	Longitude	77 15 27.59996	0.000 m	77 15 27.61882	0.000 m
	Ellipsoid height	-36.914 m	0.002 m	-38.327 m	0.002 m
	Orthometric height	0.31 m	0.015 m		
SET 39	Latitude	34 32 45.01910	0.000 m	34 32 45.04670	0.000 m
	Longitude	77 19 30.25248	0.000 m	77 19 30.27140	0.000 m
	Ellipsoid height	-37.180 m	0.002 m	-38.594 m	0.002 m
	Orthometric height	0.15 m	0.015 m		
SET 41	Latitude	34 34 06.66797	0.000 m	34 34 06.69473	0.000 m
	Longitude	77 20 10.90241	0.000 m	77 20 10.91755	0.000 m
	Ellipsoid height	-37.186 m	0.002 m	-38.598 m	0.002 m
	Orthometric height	0.014 m	0.015 m		
SET 42	Latitude	34 34 23.64430	0.000 m	34 34 23.67136	0.000 m
	Longitude	77 20 18.68151	0.000 m	77 20 18.69798	0.000 m
	Ellipsoid height	-37.158 m	0.002 m	-38.571 m	0.002 m
	Orthometric height	0.016 m	0.015 m		
SET 43	Latitude	34 34 49.00160	0.000 m	34 34 49.02865	0.000 m
	Longitude	77 24 04.96046	0.000 m	77 24 04.97695	0.000 m
	Ellipsoid height	-37.056 m	0.002 m	-38.467 m	0.002 m
	Orthometric height	0.27 m	0.015 m		
SET 44	Latitude	34 34 57.42411	0.000 m	34 34 57.45117	0.000 m
	Longitude	77 24 01.21570	0.000 m	77 24 01.23228	0.000 m
	Ellipsoid height	-37.114 m	0.002 m	-38.525 m	0.002 m
	Orthometric height	0.21 m	0.015 m		
SET 45	Latitude	34 38 20.22280	0.000 m	34 38 20.25006	0.000 m
	Longitude	77 19 44.28365	0.000 m	77 19 44.30067	0.000 m
	Ellipsoid height	-37.057 m	0.002 m	-38.468 m	0.002 m
	Orthometric height	0.15 m	0.015 m		
BM MILE	Latitude	34 33 13.78302	0.000 m	34 33 13.81049	0.000 m
	Longitude	77 19 35.95232	0.000 m	77 19 35.97057	0.000 m
	Ellipsoid height	-35.235 m	0.001 m	-36.648 m	0.001 m
	Orthometric height	2.09 m	0.015 m		
BM PLINA	Latitude	34 40 31.34396	0.000 m	34 40 31.37138	0.000 m
	Longitude	77 21 43.21053	0.000 m	77 21 43.22829	0.000 m
	Ellipsoid height	-30.483 m	0.001 m	-31.892 m	0.001 m
	Orthometric height	6.66 m	0.015 m		
GMWC SLP	Latitude	34 40 38.03118	0.000 m	34 40 38.05888	0.000 m
	Longitude	77 21 45.79497	0.000 m	77 21 45.81398	0.000 m
	Ellipsoid height	-35.526 m	0.002 m	-36.936 m	0.002 m
	Orthometric height	1.61 m	0.015 m		

Table 11A-2. Attributes of Surface Elevation Table (SET) Stations at Marine Corps Base Camp Lejeune

The SETs are the Rod SET-Deep type designed by Cahoon et al., 2002. Orthometric heights (elevation in m NAVD 88) of eight SET reference marks (brass markers) designated as control points (CP) were determined through inclusion in an OPUS Project. Control point elevations are determined by using the current GEOID (12B) and have an accuracy of ±1.5 cm. All other reference mark elevations were obtained by laser leveling to a CP (see Methods). The vertical reference point (VRP) is located on the highest point of the rod receiver, and its elevation is used in calculations of sediment surface elevation. The VRP elevations were determined by close range optical leveling to each SETs reference mark. DD = decimal degrees.

SET Number	MARDIS Station Long Name	Site Abbre-viation	Latitude (DD)	Longitude (DD)	Installation Date	Rod Depth (m)	Elevation of Brass Disc Marker (m NAVD 88)	Elevation of Brass Disc Marker Measurement Technique	Elevation of VRP (m NAVD 88)	Elevation of Initial Mean Sediment Surface (m NAVD 88)
31	Coastal Wetlands—Freemans Creek–Marsh Control Plot—Rep 2	FC	34.59462	-77.25131	11/25/2007	10.9	0.01	Laser Leveling	0.16	-0.01
32	Coastal Wetlands—Freemans Creek—Marsh, Fertilized Plot—Rep 1	FC	34.59458	-77.25126	11/26/2007	8.5	0.02	Laser Leveling	0.18	0.02
33	Coastal Wetlands—Freemans Creek–Marsh, Control Plot—Rep 1	FC	34.59455	-77.25120	11/26/2007	8.5	0.08	Laser Leveling	0.23	0.04

SET Number	MARDIS Station Long Name	Site Abbre-viation	Latitude (DD)	Longitude (DD)	Installation Date	Rod Depth (m)	Elevation of Brass Disc Marker (m NAVD 88)	Elevation of Brass Disc Marker Measurement Technique	Elevation of VRP (m NAVD 88)	Elevation of Initial Mean Sediment Surface (m NAVD 88)
34	Coastal Wetlands—Freemans Creek—Marsh, Fertilized Plot—Rep 2	FC	34.59461	-77.25116	11/26/2007	8.5	0.04	OPUS Project (Control Point)	0.17	0.04
35	Coastal Wetlands—Freemans Creek—Marsh, Fertilized Plot—Rep 3	FC	34.59463	-77.25122	11/25/2007	9.7	0.08	Laser Leveling	0.23	0.03
36	Coastal Wetlands—Freemans Creek–Marsh, Control Plot—Rep 3	FC	34.59466	-77.25127	11/25/2007	9.7	0.13	Laser Leveling	0.24	0.04
37	Coastal Wetlands—Onslow Beach Backbarrier–Marsh, Fertilized Plot—Rep 1	OB	34.58040	-77.25767	12/6/2007	9.7	0.3	Laser Leveling	0.43	0.22
38	Coastal Wetlands—Onslow Beach Backbarrier–Marsh, Control Plot—Rep 1	OB	34.58044	-77.25762	12/6/2007	9.7	0.31	OPUS Project (Control Point)	0.44	0.26

SET Number	MARDIS Station Long Name	Site Abbre-viation	Latitude (DD)	Longitude (DD)	Installation Date	Rod Depth (m)	Elevation of Brass Disc Marker (m NAVD 88)	Elevation of Brass Disc Marker Measurement Technique	Elevation of VRP (m NAVD 88)	Elevation of Initial Mean Sediment Surface (m NAVD 88)
39	Coastal Wetlands—Mile Hammock Bay–Marsh, Control Plot—Rep 1	MHB	34.54584	-77.32507	11/27/2007	7.3	0.15	OPUS Project (Control Point)	0.32	0.13
40	Coastal Wetlands—Mile Hammock Bay–Marsh, Fertilized Plot—Rep 1	MHB	34.54578	-77.32509	11/27/2007	7.3	0.21	Laser Leveling	0.34	0.14
41	Coastal Wetlands—Traps Bay–Marsh, Juncus Plot—Bridge	TBB	34.56852	-77.33636	4/15/2008	9.7	0.14	OPUS Project (Control Point)	0.25	0.09
42	Coastal Wetlands—Traps Bay–Marsh, Juncus Plot—Creek	TBC	34.57323	-77.33852	4/15/2008	8.5	0.16	OPUS Project (Control Point)	0.27	0.08
43	Coastal Wetlands—Pollocks Point–Marsh, Juncus Plot—Lower	PP	34.58028	-77.40138	4/15/2008	8.5	0.27	OPUS Project (Control Point)	0.38	0.12

SET Number	MARDIS Station Long Name	Site Abbre-viation	Latitude (DD)	Longitude (DD)	Installation Date	Rod Depth (m)	Elevation of Brass Disc Marker (m NAVD 88)	Elevation of Brass Disc Marker Measurement Technique	Elevation of VRP (m NAVD 88)	Elevation of Initial Mean Sediment Surface (m NAVD 88)
44	Coastal Wetlands—Pollocks Point–Marsh, Juncus Plot—Upper	PP	34.58262	-77.40034	4/14/2008	8.5	0.21	OPUS Project (Control Point)	0.38	0.12
45	Coastal Wetlands—French Creek–Marsh, Juncus Plot—Lower	FN	34.63895	-77.32897	4/15/2008	8.5	0.15	OPUS Project (Control Point)	0.24	0.09
46	Coastal Wetlands—French Creek–Marsh, Juncus Plot—Upper	FN	34.63922	-77.32908	4/15/2008	8.5	0.17	Laser leveling	0.30	0.12

Table 11A-3. Results from Quarterly Set Measurements at Marine Corps Base Camp Lejeune (2008–2016)

NAVD 88 is the North American Vertical Datum in 1988. Elevations are reported at the mm level for change analysis. Orthometric Height accuracy is at the cm level (NOAA, 2014).

SET Number	Number of Pins per Reading	Year Read	Season Read	Date Read	Mean Sediment Surface Elevation (m NAVD 88)	SE Sediment Surface Elevation (m NAVD 88)	Maximum Sediment Surface Elevation (m NAVD 88)	Minimum Sediment Surface Elevation (m NAVD 88)
31	36	2008	Winter	2/19/2008	-0.013	0.004	0.030	-0.046
31	34	2008	Spring	5/23/2008	-0.015	0.003	0.023	-0.041
31	36	2008	Summer	8/16/2008	-0.008	0.002	0.023	-0.036
31	36	2008	Fall	11/11/2008	-0.001	0.004	0.028	-0.043
31	36	2009	Winter	2/24/2009	0.000	0.003	0.030	-0.037
31	35	2009	Spring	5/28/2009	0.000	0.003	0.029	-0.039
31	36	2009	Summer	9/16/2009	0.009	0.004	0.048	-0.020
31	36	2009	Fall	12/3/2009	0.015	0.004	0.048	-0.018
31	36	2010	Winter	2/11/2010	0.014	0.004	0.052	-0.015
31	36	2010	Spring	6/8/2010	0.013	0.004	0.051	-0.019
31	35	2010	Summer	8/10/2010	0.015	0.004	0.055	-0.018
31	36	2010	Fall	10/18/2010	0.019	0.003	0.048	-0.005
31	35	2011	Winter	2/3/2011	0.023	0.004	0.060	-0.006
31	36	2011	Spring	5/16/2011	0.017	0.003	0.053	-0.008
31	34	2011	Summer	9/9/2011	0.031	0.003	0.059	0.005
31	36	2011	Fall	11/21/2011	0.033	0.002	0.056	0.013
31	35	2012	Winter	2/7/2012	0.035	0.002	0.062	0.016
31	34	2012	Spring	7/2/2012	0.035	0.002	0.057	0.008
31	32	2012	Summer	8/31/2012	0.045	0.002	0.070	0.016
31	35	2012	Fall	11/26/2012	0.046	0.003	0.075	0.011
31	33	2013	Winter	2/7/2013	0.045	0.003	0.067	0.019
31	36	2013	Spring	4/24/2013	0.042	0.002	0.073	0.011
31	35	2013	Summer	8/22/2013	0.050	0.004	0.112	-0.010
31	36	2013	Fall	11/4/2013	0.055	0.005	0.098	-0.045
31	36	2014	Winter	3/1/2014	0.062	0.005	0.121	0.001
31	35	2014	Spring	5/23/2014	0.038	0.006	0.098	-0.038
31	36	2014	Summer	9/9/2014	0.056	0.005	0.092	-0.044

SET Number	Number of Pins per Reading	Year Read	Season Read	Date Read	Mean Sediment Surface Elevation (m NAVD 88)	SE Sediment Surface Elevation (m NAVD 88)	Maximum Sediment Surface Elevation (m NAVD 88)	Minimum Sediment Surface Elevation (m NAVD 88)
31	36	2014	Fall	11/5/2014	0.061	0.007	0.111	-0.063
31	36	2015	Winter	3/4/2015	0.059	0.004	0.096	-0.013
31	35	2015	Spring	5/14/2015	0.068	0.005	0.109	-0.014
31	36	2015	Summer	8/28/2015	0.079	0.003	0.104	0.031
31	36	2015	Fall	11/24/2015	0.071	0.006	0.104	-0.058
31	36	2016	Winter	2/5/2016	0.074	0.003	0.102	0.022
31	35	2016	Spring	5/6/2016	0.073	0.004	0.107	0.012
31	36	2016	Summer	8/15/2016	0.047	0.007	0.110	-0.054
31	36	2016	Fall	11/16/2016	0.083	0.003	0.116	0.033
32	35	2008	Winter	2/19/2008	0.019	0.002	0.045	-0.009
32	36	2008	Spring	5/23/2008	0.019	0.003	0.050	-0.022
32	36	2008	Summer	8/16/2008	0.019	0.002	0.046	-0.018
32	36	2008	Fall	11/11/2008	0.039	0.002	0.066	0.014
32	36	2009	Winter	2/24/2009	0.030	0.002	0.049	0.004
32	34	2009	Spring	5/28/2009	0.033	0.003	0.069	-0.021
32	35	2009	Summer	9/16/2009	0.048	0.002	0.064	0.026
32	36	2009	Fall	12/3/2009	0.056	0.002	0.079	0.037
32	35	2010	Winter	2/11/2010	0.055	0.001	0.077	0.039
32	36	2010	Spring	6/8/2010	0.056	0.001	0.072	0.042
32	36	2010	Summer	8/10/2010	0.055	0.003	0.092	0.000
32	35	2010	Fall	10/18/2010	0.065	0.001	0.084	0.047
32	35	2011	Winter	2/3/2011	0.066	0.002	0.084	0.042
32	36	2011	Spring	5/16/2011	0.061	0.002	0.079	0.035
32	34	2011	Summer	9/9/2011	0.070	0.001	0.085	0.057
32	36	2011	Fall	11/21/2011	0.068	0.001	0.082	0.051
32	36	2012	Winter	2/7/2012	0.071	0.002	0.088	0.042
32	36	2012	Spring	7/2/2012	0.083	0.002	0.112	0.045
32	36	2012	Summer	8/31/2012	0.076	0.002	0.099	0.056
32	34	2012	Fall	11/26/2012	0.079	0.003	0.113	0.050
32	36	2013	Winter	2/7/2013	0.072	0.003	0.101	0.033
32	36	2013	Spring	4/24/2013	0.070	0.003	0.093	0.018

SET Number	Number of Pins per Reading	Year Read	Season Read	Date Read	Mean Sediment Surface Elevation (m NAVD 88)	SE Sediment Surface Elevation (m NAVD 88)	Maximum Sediment Surface Elevation (m NAVD 88)	Minimum Sediment Surface Elevation (m NAVD 88)
32	35	2013	Summer	8/22/2013	0.074	0.003	0.108	0.027
32	36	2013	Fall	11/4/2013	0.074	0.004	0.126	0.004
32	36	2014	Winter	3/1/2014	0.085	0.003	0.116	0.058
32	36	2014	Spring	5/23/2014	0.076	0.004	0.109	0.013
32	36	2014	Summer	9/9/2014	0.082	0.005	0.112	-0.077
32	36	2014	Fall	11/5/2014	0.085	0.006	0.137	-0.079
32	36	2015	Winter	3/4/2015	0.081	0.002	0.112	0.054
32	36	2015	Spring	5/14/2015	0.085	0.002	0.127	0.066
32	36	2015	Summer	8/28/2015	0.091	0.004	0.126	0.025
32	34	2015	Fall	11/24/2015	0.103	0.003	0.131	0.039
32	34	2016	Winter	2/5/2016	0.097	0.003	0.128	0.065
32	36	2016	Spring	5/6/2016	0.096	0.004	0.144	0.036
32	36	2016	Summer	8/15/2016	0.096	0.003	0.128	0.035
32	36	2016	Fall	11/16/2016	0.107	0.003	0.142	0.067
33	36	2008	Winter	2/19/2008	0.043	0.002	0.064	0.014
33	35	2008	Spring	5/23/2008	0.050	0.003	0.078	0.012
33	33	2008	Summer	8/16/2008	0.049	0.002	0.066	0.012
33	36	2008	Fall	11/11/2008	0.059	0.002	0.091	0.031
33	36	2009	Winter	2/24/2009	0.052	0.002	0.079	0.025
33	34	2009	Spring	5/28/2009	0.045	0.002	0.069	0.026
33	35	2009	Summer	9/16/2009	0.050	0.002	0.073	0.027
33	36	2009	Fall	12/3/2009	0.057	0.002	0.076	0.033
33	35	2010	Winter	2/11/2010	0.055	0.002	0.075	0.043
33	36	2010	Spring	6/8/2010	0.053	0.002	0.069	0.031
33	35	2010	Summer	8/10/2010	0.059	0.002	0.082	0.038
33	36	2010	Fall	10/18/2010	0.061	0.002	0.085	0.026
33	35	2011	Winter	2/3/2011	0.065	0.003	0.097	0.030
33	36	2011	Spring	5/16/2011	0.065	0.003	0.092	0.033
33	35	2011	Summer	9/9/2011	0.061	0.002	0.081	0.035
33	35	2011	Fall	11/21/2011	0.066	0.003	0.093	0.031
33	31	2012	Winter	2/7/2012	0.069	0.003	0.094	0.035

SET Number	Number of Pins per Reading	Year Read	Season Read	Date Read	Mean Sediment Surface Elevation (m NAVD 88)	SE Sediment Surface Elevation (m NAVD 88)	Maximum Sediment Surface Elevation (m NAVD 88)	Minimum Sediment Surface Elevation (m NAVD 88)
33	28	2012	Spring	7/2/2012	0.068	0.005	0.098	0.023
33	31	2012	Summer	8/31/2012	0.076	0.005	0.122	-0.001
33	31	2012	Fall	11/26/2012	0.081	0.004	0.114	0.023
33	35	2013	Winter	2/7/2013	0.075	0.004	0.113	0.035
33	36	2013	Spring	4/24/2013	0.071	0.003	0.103	0.014
33	36	2013	Summer	8/22/2013	0.068	0.008	0.140	-0.040
33	36	2013	Fall	11/4/2013	0.071	0.006	0.154	0.010
33	36	2014	Winter	3/1/2014	0.084	0.005	0.143	0.005
33	36	2014	Spring	5/23/2014	0.095	0.006	0.138	-0.010
33	36	2014	Summer	9/9/2014	0.076	0.006	0.126	-0.039
33	35	2014	Fall	11/5/2014	0.069	0.006	0.125	0.011
33	35	2015	Winter	3/4/2015	0.076	0.005	0.133	0.006
33	36	2015	Spring	5/14/2015	0.076	0.005	0.126	-0.022
33	36	2015	Summer	8/28/2015	0.088	0.005	0.127	-0.013
33	36	2015	Fall	11/24/2015	0.104	0.005	0.138	0.015
33	36	2016	Winter	2/5/2016	0.103	0.006	0.154	-0.032
33	36	2016	Spring	5/6/2016	0.102	0.007	0.144	-0.022
33	34	2016	Summer	8/15/2016	0.094	0.008	0.158	-0.007
33	35	2016	Fall	11/16/2016	0.093	0.007	0.163	0.018
34	36	2008	Winter	2/19/2008	0.036	0.002	0.077	0.000
34	36	2008	Spring	5/23/2008	0.041	0.003	0.099	0.008
34	36	2008	Summer	8/16/2008	0.043	0.002	0.072	0.025
34	36	2008	Fall	11/11/2008	0.050	0.002	0.085	0.026
34	36	2009	Winter	2/24/2009	0.049	0.002	0.072	0.016
34	34	2009	Spring	5/28/2009	0.051	0.002	0.071	0.023
34	36	2009	Summer	9/17/2009	0.070	0.003	0.103	0.037
34	35	2009	Fall	12/1/2009	0.076	0.002	0.101	0.056
34	36	2010	Winter	2/11/2010	0.072	0.002	0.098	0.052
34	36	2010	Spring	6/8/2010	0.076	0.002	0.101	0.050
34	36	2010	Summer	8/10/2010	0.076	0.002	0.102	0.045
34	36	2010	Fall	10/18/2010	0.079	0.001	0.102	0.052

SET Number	Number of Pins per Reading	Year Read	Season Read	Date Read	Mean Sediment Surface Elevation (m NAVD 88)	SE Sediment Surface Elevation (m NAVD 88)	Maximum Sediment Surface Elevation (m NAVD 88)	Minimum Sediment Surface Elevation (m NAVD 88)
34	35	2011	Winter	2/3/2011	0.078	0.001	0.092	0.053
34	36	2011	Spring	5/16/2011	0.079	0.001	0.100	0.058
34	36	2011	Summer	9/9/2011	0.082	0.001	0.099	0.056
34	36	2011	Fall	11/21/2011	0.088	0.001	0.112	0.074
34	32	2012	Winter	2/7/2012	0.087	0.002	0.109	0.072
34	36	2012	Spring	7/2/2012	0.085	0.002	0.105	0.064
34	36	2012	Summer	8/31/2012	0.074	0.002	0.104	0.043
34	35	2012	Fall	11/26/2012	0.070	0.003	0.110	0.034
34	33	2013	Winter	2/7/2013	0.070	0.002	0.102	0.044
34	35	2013	Spring	4/24/2013	0.064	0.002	0.095	0.040
34	36	2013	Summer	8/22/2013	0.071	0.003	0.103	-0.006
34	36	2013	Fall	11/4/2013	0.046	0.004	0.100	-0.009
34	36	2014	Winter	3/1/2014	0.060	0.003	0.097	-0.002
34	36	2014	Spring	5/23/2014	0.057	0.004	0.093	0.009
34	36	2014	Summer	9/9/2014	0.074	0.002	0.105	0.039
34	36	2014	Fall	11/5/2014	0.071	0.004	0.104	-0.020
34	36	2015	Winter	3/4/2015	0.075	0.003	0.112	0.037
34	36	2015	Spring	5/14/2015	0.076	0.002	0.104	0.055
34	36	2015	Summer	8/28/2015	0.087	0.003	0.113	0.054
34	36	2015	Fall	11/24/2015	0.086	0.004	0.136	0.036
34	36	2016	Winter	2/5/2016	0.085	0.002	0.107	0.046
34	36	2016	Spring	5/6/2016	0.088	0.003	0.113	0.043
34	35	2016	Summer	8/15/2016	0.093	0.004	0.125	0.031
34	36	2016	Fall	11/16/2016	0.100	0.003	0.139	0.051
35	36	2008	Winter	2/19/2008	0.033	0.002	0.056	-0.003
35	36	2008	Spring	5/23/2008	0.036	0.001	0.063	0.019
35	35	2008	Summer	8/16/2008	0.036	0.002	0.062	0.009
35	36	2008	Fall	11/11/2008	0.051	0.002	0.066	0.031
35	36	2009	Winter	2/24/2009	0.048	0.001	0.060	0.030
35	36	2009	Spring	5/28/2009	0.051	0.002	0.070	0.026
35	36	2009	Summer	9/17/2009	0.071	0.001	0.089	0.060

SET Number	Number of Pins per Reading	Year Read	Season Read	Date Read	Mean Sediment Surface Elevation (m NAVD 88)	SE Sediment Surface Elevation (m NAVD 88)	Maximum Sediment Surface Elevation (m NAVD 88)	Minimum Sediment Surface Elevation (m NAVD 88)
35	36	2009	Fall	12/1/2009	0.078	0.002	0.104	0.043
35	35	2010	Winter	2/11/2010	0.075	0.001	0.092	0.063
35	36	2010	Spring	6/8/2010	0.077	0.002	0.094	0.058
35	35	2010	Summer	8/10/2010	0.076	0.002	0.090	0.048
35	35	2010	Fall	10/18/2010	0.082	0.001	0.105	0.067
35	35	2011	Winter	2/3/2011	0.084	0.002	0.103	0.065
35	36	2011	Spring	5/16/2011	0.083	0.001	0.098	0.069
35	34	2011	Summer	9/9/2011	0.079	0.001	0.097	0.069
35	36	2011	Fall	11/21/2011	0.084	0.002	0.108	0.070
35	36	2012	Winter	2/7/2012	0.079	0.002	0.115	0.067
35	36	2012	Spring	7/2/2012	0.075	0.002	0.102	0.046
35	36	2012	Summer	8/31/2012	0.082	0.002	0.106	0.060
35	35	2012	Fall	11/26/2012	0.087	0.002	0.111	0.061
35	36	2013	Winter	2/7/2013	0.087	0.002	0.113	0.063
35	34	2013	Spring	4/24/2013	0.084	0.003	0.122	0.047
35	36	2013	Summer	8/22/2013	0.064	0.004	0.098	-0.009
35	36	2013	Fall	11/4/2013	0.058	0.003	0.093	0.024
35	36	2014	Winter	3/1/2014	0.083	0.002	0.122	0.049
35	36	2014	Spring	5/23/2014	0.073	0.003	0.113	0.034
35	36	2014	Summer	9/9/2014	0.088	0.003	0.128	0.049
35	36	2014	Fall	11/5/2014	0.085	0.004	0.145	0.010
35	36	2015	Winter	3/4/2015	0.086	0.005	0.160	0.014
35	36	2015	Spring	5/14/2015	0.085	0.004	0.129	0.018
35	36	2015	Summer	8/28/2015	0.112	0.003	0.140	0.081
35	35	2015	Fall	11/24/2015	0.122	0.005	0.164	0.039
35	35	2016	Winter	2/5/2016	0.125	0.003	0.152	0.091
35	35	2016	Spring	5/6/2016	0.134	0.003	0.166	0.108
35	36	2016	Summer	8/15/2016	0.126	0.003	0.155	0.087
35	36	2016	Fall	11/16/2016	0.133	0.004	0.164	0.061
36	36	2008	Winter	2/19/2008	0.041	0.003	0.087	0.003
36	36	2008	Spring	5/23/2008	0.043	0.002	0.070	0.023

SET Number	Number of Pins per Reading	Year Read	Season Read	Date Read	Mean Sediment Surface Elevation (m NAVD 88)	SE Sediment Surface Elevation (m NAVD 88)	Maximum Sediment Surface Elevation (m NAVD 88)	Minimum Sediment Surface Elevation (m NAVD 88)
36	35	2008	Summer	8/16/2008	0.040	0.003	0.090	0.014
36	36	2008	Fall	11/11/2008	0.053	0.002	0.081	0.033
36	36	2009	Winter	2/24/2009	0.048	0.002	0.065	0.031
36	36	2009	Spring	5/28/2009	0.050	0.002	0.080	0.031
36	36	2009	Summer	9/17/2009	0.053	0.002	0.089	0.033
36	35	2009	Fall	12/1/2009	0.060	0.003	0.094	0.034
36	36	2010	Winter	2/11/2010	0.057	0.002	0.086	0.036
36	36	2010	Spring	6/8/2010	0.058	0.002	0.088	0.033
36	36	2010	Summer	8/10/2010	0.064	0.003	0.097	0.034
36	35	2010	Fall	10/18/2010	0.065	0.003	0.096	0.041
36	34	2011	Winter	2/3/2011	0.068	0.003	0.104	0.047
36	36	2011	Spring	5/16/2011	0.071	0.003	0.102	0.049
36	36	2011	Summer	9/9/2011	0.077	0.002	0.097	0.055
36	36	2011	Fall	11/21/2011	0.080	0.002	0.100	0.054
36	36	2012	Winter	2/7/2012	0.078	0.003	0.104	0.053
36	36	2012	Spring	7/2/2012	0.083	0.003	0.115	0.054
36	35	2012	Summer	8/31/2012	0.087	0.003	0.116	0.062
36	36	2012	Fall	11/26/2012	0.092	0.002	0.122	0.069
36	35	2013	Winter	2/7/2013	0.089	0.002	0.123	0.070
36	36	2013	Spring	4/24/2013	0.085	0.003	0.116	0.034
36	36	2013	Summer	8/22/2013	0.083	0.004	0.128	0.046
36	36	2013	Fall	11/4/2013	0.079	0.003	0.115	0.037
36	35	2014	Winter	3/1/2014	0.100	0.003	0.137	0.054
36	36	2014	Spring	5/23/2014	0.085	0.003	0.125	0.041
36	36	2014	Summer	9/9/2014	0.106	0.003	0.139	0.078
36	36	2014	Fall	11/5/2014	0.106	0.005	0.147	0.032
36	36	2015	Winter	3/4/2015	0.103	0.005	0.152	0.003
36	36	2015	Spring	5/14/2015	0.110	0.004	0.149	0.061
36	36	2015	Summer	8/28/2015	0.108	0.004	0.137	0.039
36	36	2015	Fall	11/24/2015	0.119	0.004	0.156	0.046
36	36	2016	Winter	2/5/2016	0.119	0.003	0.163	0.091

SET Number	Number of Pins per Reading	Year Read	Season Read	Date Read	Mean Sediment Surface Elevation (m NAVD 88)	SE Sediment Surface Elevation (m NAVD 88)	Maximum Sediment Surface Elevation (m NAVD 88)	Minimum Sediment Surface Elevation (m NAVD 88)
36	35	2016	Spring	5/6/2016	0.116	0.004	0.147	0.031
36	36	2016	Summer	8/15/2016	0.106	0.003	0.136	0.062
36	36	2016	Fall	11/16/2016	0.126	0.004	0.164	0.078
37	35	2008	Winter	2/20/2008	0.221	0.001	0.235	0.201
37	34	2008	Spring	5/20/2008	0.215	0.002	0.244	0.191
37	35	2008	Summer	8/17/2008	0.220	0.002	0.240	0.194
37	36	2008	Fall	11/12/2008	0.225	0.001	0.249	0.201
37	36	2009	Winter	2/25/2009	0.222	0.002	0.252	0.196
37	35	2009	Spring	5/28/2009	0.223	0.001	0.238	0.207
37	36	2009	Summer	9/15/2009	0.228	0.002	0.260	0.195
37	35	2009	Fall	11/30/2009	0.229	0.001	0.240	0.210
37	35	2010	Winter	2/10/2010	0.228	0.001	0.244	0.215
37	36	2010	Spring	6/7/2010	0.231	0.002	0.247	0.211
37	36	2010	Summer	8/9/2010	0.234	0.002	0.255	0.214
37	36	2010	Fall	10/19/2010	0.240	0.002	0.259	0.214
37	32	2011	Winter	1/31/2011	0.239	0.002	0.254	0.226
37	36	2011	Spring	5/18/2011	0.239	0.002	0.261	0.220
37	36	2011	Summer	8/24/2011	0.244	0.002	0.265	0.225
37	36	2011	Fall	11/22/2011	0.244	0.001	0.258	0.229
37	36	2012	Winter	2/6/2012	0.246	0.002	0.262	0.228
37	36	2012	Spring	7/2/2012	0.242	0.001	0.255	0.227
37	36	2012	Summer	8/29/2012	0.240	0.001	0.264	0.218
37	36	2012	Fall	11/20/2012	0.240	0.002	0.255	0.213
37	36	2013	Winter	2/6/2013	0.242	0.001	0.262	0.221
37	36	2013	Spring	5/1/2013	0.241	0.001	0.257	0.225
37	36	2013	Summer	8/15/2013	0.239	0.002	0.263	0.216
37	36	2013	Fall	11/3/2013	0.240	0.001	0.256	0.224
37	36	2014	Winter	2/25/2014	0.243	0.003	0.318	0.223
37	35	2014	Spring	5/21/2014	0.241	0.002	0.263	0.223
37	36	2014	Summer	9/7/2014	0.238	0.001	0.252	0.211
37	36	2014	Fall	11/4/2014	0.240	0.001	0.250	0.223

SET Number	Number of Pins per Reading	Year Read	Season Read	Date Read	Mean Sediment Surface Elevation (m NAVD 88)	SE Sediment Surface Elevation (m NAVD 88)	Maximum Sediment Surface Elevation (m NAVD 88)	Minimum Sediment Surface Elevation (m NAVD 88)
37	36	2015	Winter	3/2/2015	0.243	0.001	0.258	0.226
37	36	2015	Spring	5/12/2015	0.242	0.001	0.268	0.223
37	36	2015	Summer	8/27/2015	0.250	0.001	0.266	0.231
37	36	2015	Fall	11/22/2015	0.241	0.002	0.271	0.219
37	36	2016	Winter	2/8/2016	0.248	0.002	0.268	0.221
37	36	2016	Spring	5/7/2016	0.252	0.001	0.265	0.239
37	36	2016	Summer	8/17/2016	0.261	0.002	0.284	0.238
37	36	2016	Fall	11/14/2016	0.263	0.002	0.299	0.242
38	34	2008	Winter	2/20/2008	0.261	0.001	0.283	0.253
38	33	2008	Spring	5/20/2008	0.260	0.001	0.274	0.239
38	36	2008	Summer	8/17/2008	0.257	0.002	0.273	0.233
38	36	2008	Fall	11/12/2008	0.257	0.001	0.274	0.233
38	35	2009	Winter	2/25/2009	0.257	0.001	0.269	0.240
38	33	2009	Spring	5/28/2009	0.260	0.001	0.268	0.250
38	35	2009	Summer	9/15/2009	0.258	0.001	0.267	0.235
38	36	2009	Fall	11/30/2009	0.259	0.001	0.273	0.244
38	36	2010	Winter	2/10/2010	0.259	0.001	0.266	0.246
38	36	2010	Spring	6/7/2010	0.261	0.001	0.268	0.248
38	34	2010	Summer	8/9/2010	0.261	0.001	0.270	0.251
38	36	2010	Fall	10/19/2010	0.261	0.001	0.270	0.244
38	36	2011	Winter	1/31/2011	0.262	0.001	0.268	0.251
38	34	2011	Spring	5/18/2011	0.264	0.001	0.271	0.253
38	36	2011	Summer	8/24/2011	0.263	0.001	0.271	0.249
38	35	2011	Fall	11/22/2011	0.267	0.001	0.277	0.256
38	36	2012	Winter	2/6/2012	0.265	0.001	0.275	0.254
38	35	2012	Spring	7/2/2012	0.267	0.001	0.279	0.250
38	34	2012	Summer	8/29/2012	0.265	0.001	0.278	0.256
38	35	2012	Fall	11/20/2012	0.264	0.001	0.279	0.246
38	35	2013	Winter	2/6/2013	0.268	0.001	0.286	0.252
38	36	2013	Spring	5/1/2013	0.265	0.001	0.279	0.246
38	36	2013	Summer	8/15/2013	0.266	0.001	0.281	0.238

SET Number	Number of Pins per Reading	Year Read	Season Read	Date Read	Mean Sediment Surface Elevation (m NAVD 88)	SE Sediment Surface Elevation (m NAVD 88)	Maximum Sediment Surface Elevation (m NAVD 88)	Minimum Sediment Surface Elevation (m NAVD 88)
38	36	2013	Fall	11/3/2013	0.268	0.001	0.278	0.246
38	35	2014	Winter	2/25/2014	0.266	0.002	0.281	0.235
38	34	2014	Spring	5/21/2014	0.267	0.001	0.284	0.235
38	36	2014	Summer	9/7/2014	0.266	0.001	0.279	0.234
38	36	2014	Fall	11/4/2014	0.266	0.002	0.285	0.219
38	36	2015	Winter	3/2/2015	0.269	0.001	0.285	0.257
38	34	2015	Spring	5/12/2015	0.268	0.001	0.281	0.251
38	36	2015	Summer	8/27/2015	0.271	0.001	0.283	0.253
38	36	2015	Fall	11/22/2015	0.271	0.002	0.289	0.219
38	35	2016	Winter	2/8/2016	0.272	0.001	0.301	0.256
38	35	2016	Spring	5/9/2016	0.271	0.002	0.291	0.243
38	34	2016	Summer	8/17/2016	0.271	0.002	0.302	0.232
38	34	2016	Fall	11/14/2016	0.268	0.002	0.292	0.240
39	36	2008	Winter	2/20/2008	0.130	0.001	0.144	0.122
39	36	2008	Spring	5/19/2008	0.130	0.001	0.144	0.117
39	34	2008	Summer	8/16/2008	0.133	0.001	0.148	0.123
39	36	2008	Fall	11/12/2008	0.133	0.001	0.142	0.123
39	36	2009	Winter	2/25/2009	0.126	0.001	0.135	0.119
39	36	2009	Spring	6/1/2009	0.128	0.001	0.137	0.112
39	36	2009	Summer	9/16/2009	0.128	0.001	0.134	0.117
39	35	2009	Fall	12/1/2009	0.127	0.001	0.138	0.114
39	36	2010	Winter	2/12/2010	0.132	0.001	0.140	0.125
39	32	2010	Spring	6/7/2010	0.128	0.001	0.133	0.120
39	36	2010	Summer	8/11/2010	0.131	0.001	0.141	0.111
39	35	2010	Fall	10/20/2010	0.135	0.001	0.145	0.121
39	35	2011	Winter	2/1/2011	0.133	0.001	0.144	0.109
39	34	2011	Spring	5/17/2011	0.134	0.001	0.146	0.123
39	35	2011	Summer	8/25/2011	0.135	0.001	0.147	0.116
39	36	2011	Fall	11/21/2011	0.139	0.001	0.159	0.126
39	34	2012	Winter	2/6/2012	0.142	0.001	0.151	0.130
39	36	2012	Spring	6/28/2012	0.143	0.001	0.156	0.121

SET Number	Number of Pins per Reading	Year Read	Season Read	Date Read	Mean Sediment Surface Elevation (m NAVD 88)	SE Sediment Surface Elevation (m NAVD 88)	Maximum Sediment Surface Elevation (m NAVD 88)	Minimum Sediment Surface Elevation (m NAVD 88)
39	36	2012	Summer	8/30/2012	0.144	0.001	0.159	0.126
39	36	2012	Fall	11/28/2012	0.146	0.001	0.158	0.127
39	35	2013	Winter	2/11/2013	0.142	0.001	0.153	0.128
39	36	2013	Spring	4/26/2013	0.146	0.001	0.162	0.130
39	36	2013	Summer	8/20/2013	0.140	0.001	0.147	0.129
39	35	2013	Fall	11/5/2013	0.138	0.001	0.149	0.120
39	36	2014	Winter	2/27/2014	0.140	0.001	0.170	0.131
39	36	2014	Spring	5/13/2014	0.138	0.002	0.147	0.098
39	36	2014	Summer	9/10/2014	0.134	0.001	0.143	0.118
39	36	2014	Fall	11/6/2014	0.138	0.001	0.148	0.128
39	36	2015	Winter	3/4/2015	0.136	0.001	0.146	0.126
39	36	2015	Spring	5/18/2015	0.137	0.001	0.150	0.128
39	36	2015	Summer	8/28/2015	0.132	0.001	0.139	0.122
39	36	2015	Fall	11/24/2015	0.132	0.001	0.141	0.119
39	36	2016	Winter	2/8/2016	0.132	0.001	0.140	0.123
39	36	2016	Spring	5/5/2016	0.129	0.001	0.138	0.089
39	36	2016	Summer	8/15/2016	0.121	0.001	0.129	0.115
39	36	2016	Fall	11/15/2016	0.124	0.001	0.134	0.104
40	34	2008	Winter	2/20/2008	0.135	0.001	0.144	0.122
40	36	2008	Spring	5/19/2008	0.135	0.001	0.147	0.112
40	34	2008	Summer	8/16/2008	0.136	0.001	0.156	0.124
40	36	2008	Fall	11/12/2008	0.140	0.001	0.152	0.133
40	36	2009	Winter	2/25/2009	0.134	0.001	0.145	0.122
40	36	2009	Spring	6/1/2009	0.141	0.001	0.154	0.126
40	36	2009	Summer	9/16/2009	0.146	0.001	0.161	0.128
40	36	2009	Fall	12/1/2009	0.149	0.001	0.159	0.139
40	36	2010	Winter	2/12/2010	0.153	0.001	0.160	0.147
40	30	2010	Spring	6/7/2010	0.144	0.001	0.156	0.136
40	36	2010	Summer	8/11/2010	0.150	0.001	0.172	0.134
40	36	2010	Fall	10/20/2010	0.152	0.001	0.161	0.139
40	34	2011	Winter	2/1/2011	0.152	0.001	0.165	0.141

SET Number	Number of Pins per Reading	Year Read	Season Read	Date Read	Mean Sediment Surface Elevation (m NAVD 88)	SE Sediment Surface Elevation (m NAVD 88)	Maximum Sediment Surface Elevation (m NAVD 88)	Minimum Sediment Surface Elevation (m NAVD 88)
40	36	2011	Spring	5/17/2011	0.152	0.001	0.167	0.137
40	36	2011	Summer	8/25/2011	0.154	0.002	0.171	0.136
40	36	2011	Fall	11/21/2011	0.160	0.002	0.193	0.143
40	33	2012	Winter	2/6/2012	0.158	0.001	0.173	0.136
40	36	2012	Spring	6/28/2012	0.161	0.001	0.173	0.142
40	36	2012	Summer	8/30/2012	0.164	0.001	0.176	0.151
40	36	2012	Fall	11/28/2012	0.166	0.001	0.176	0.155
40	36	2013	Winter	2/11/2013	0.162	0.001	0.174	0.137
40	36	2013	Spring	4/26/2013	0.162	0.001	0.185	0.144
40	35	2013	Summer	8/20/2013	0.161	0.001	0.182	0.153
40	36	2013	Fall	11/5/2013	0.164	0.001	0.180	0.152
40	36	2014	Winter	2/27/2014	0.160	0.001	0.178	0.146
40	35	2014	Spring	5/13/2014	0.162	0.001	0.176	0.142
40	36	2014	Summer	9/10/2014	0.158	0.001	0.171	0.148
40	36	2014	Fall	11/6/2014	0.157	0.001	0.177	0.145
40	36	2015	Winter	3/4/2015	0.156	0.001	0.171	0.138
40	36	2015	Spring	5/18/2015	0.153	0.001	0.170	0.143
40	36	2015	Summer	8/28/2015	0.152	0.001	0.170	0.140
40	36	2015	Fall	11/24/2015	0.152	0.001	0.170	0.139
40	36	2016	Winter	2/8/2016	0.151	0.001	0.171	0.135
40	36	2016	Spring	5/5/2016	0.148	0.001	0.170	0.129
40	36	2016	Summer	8/15/2016	0.141	0.001	0.159	0.126
40	36	2016	Fall	11/15/2016	0.149	0.002	0.170	0.129
41	35	2008	Spring	5/16/2008	0.088	0.001	0.101	0.070
41	34	2008	Summer	8/14/2008	0.084	0.002	0.112	0.055
41	36	2008	Fall	11/10/2008	0.095	0.001	0.109	0.075
41	36	2009	Winter	1/29/2009	0.094	0.001	0.116	0.079
41	36	2009	Spring	6/2/2009	0.095	0.001	0.113	0.080
41	35	2009	Summer	9/15/2009	0.091	0.001	0.107	0.070
41	36	2009	Fall	11/30/2009	0.102	0.001	0.116	0.084
41	36	2010	Winter	2/11/2010	0.099	0.001	0.113	0.076

SET Number	Number of Pins per Reading	Year Read	Season Read	Date Read	Mean Sediment Surface Elevation (m NAVD 88)	SE Sediment Surface Elevation (m NAVD 88)	Maximum Sediment Surface Elevation (m NAVD 88)	Minimum Sediment Surface Elevation (m NAVD 88)
41	36	2010	Spring	6/9/2010	0.099	0.001	0.108	0.093
41	36	2010	Summer	8/9/2010	0.099	0.001	0.120	0.089
41	36	2010	Fall	10/20/2010	0.103	0.001	0.114	0.091
41	36	2011	Winter	1/31/2011	0.103	0.001	0.109	0.090
41	36	2011	Spring	5/19/2011	0.100	0.001	0.112	0.092
41	35	2011	Summer	8/23/2011	0.104	0.001	0.114	0.097
41	36	2011	Fall	11/18/2011	0.099	0.001	0.112	0.088
41	36	2012	Winter	2/3/2012	0.096	0.001	0.110	0.086
41	34	2012	Spring	6/22/2012	0.096	0.001	0.109	0.082
41	36	2012	Summer	8/27/2012	0.097	0.001	0.105	0.085
41	36	2012	Fall	11/19/2012	0.096	0.001	0.109	0.081
41	36	2013	Winter	2/11/2013	0.092	0.002	0.111	0.071
41	36	2013	Spring	4/30/2013	0.099	0.002	0.136	0.082
41	36	2013	Summer	8/19/2013	0.100	0.001	0.121	0.082
41	36	2013	Fall	11/7/2013	0.103	0.002	0.134	0.089
41	36	2014	Winter	2/26/2014	0.108	0.001	0.121	0.090
41	36	2014	Spring	5/19/2014	0.101	0.002	0.117	0.066
41	36	2014	Summer	9/6/2014	0.107	0.002	0.126	0.088
41	36	2014	Fall	11/3/2014	0.096	0.002	0.123	0.075
41	36	2015	Winter	3/3/2015	0.122	0.001	0.132	0.113
41	36	2015	Spring	5/12/2015	0.107	0.002	0.128	0.088
41	36	2015	Summer	8/27/2015	0.115	0.001	0.133	0.104
41	36	2015	Fall	11/22/2015	0.098	0.002	0.126	0.080
41	36	2016	Winter	2/17/2016	0.120	0.001	0.139	0.103
41	36	2016	Spring	5/7/2016	0.099	0.002	0.121	0.080
41	36	2016	Summer	8/17/2016	0.120	0.001	0.133	0.100
41	36	2016	Fall	11/14/2016	0.126	0.002	0.147	0.099
42	36	2008	Spring	5/16/2008	0.082	0.002	0.115	0.060
42	36	2008	Summer	8/14/2008	0.084	0.002	0.118	0.061
42	36	2008	Fall	11/10/2008	0.089	0.003	0.126	0.064
42	36	2009	Winter	1/29/2009	0.088	0.002	0.125	0.063

SET Number	Number of Pins per Reading	Year Read	Season Read	Date Read	Mean Sediment Surface Elevation (m NAVD 88)	SE Sediment Surface Elevation (m NAVD 88)	Maximum Sediment Surface Elevation (m NAVD 88)	Minimum Sediment Surface Elevation (m NAVD 88)
42	35	2009	Spring	6/2/2009	0.085	0.002	0.114	0.061
42	36	2009	Summer	9/15/2009	0.088	0.003	0.126	0.061
42	36	2009	Fall	11/30/2009	0.094	0.002	0.116	0.077
42	36	2010	Winter	2/11/2010	0.091	0.002	0.114	0.073
42	36	2010	Spring	6/9/2010	0.091	0.002	0.119	0.067
42	35	2010	Summer	8/9/2010	0.090	0.002	0.120	0.070
42	36	2010	Fall	10/21/2010	0.096	0.002	0.124	0.085
42	36	2011	Winter	1/31/2011	0.094	0.002	0.126	0.071
42	36	2011	Spring	5/19/2011	0.089	0.002	0.108	0.073
42	36	2011	Summer	8/23/2011	0.097	0.002	0.129	0.066
42	36	2011	Fall	11/18/2011	0.100	0.002	0.133	0.076
42	36	2012	Winter	2/3/2012	0.097	0.002	0.133	0.071
42	35	2012	Spring	6/22/2012	0.099	0.002	0.130	0.079
42	36	2012	Summer	8/27/2012	0.099	0.002	0.138	0.078
42	35	2012	Fall	11/27/2012	0.104	0.002	0.141	0.081
42	36	2013	Winter	2/11/2013	0.104	0.002	0.138	0.081
42	36	2013	Spring	4/30/2013	0.106	0.003	0.154	0.089
42	36	2013	Summer	8/19/2013	0.107	0.003	0.177	0.077
42	36	2013	Fall	11/3/2013	0.106	0.002	0.149	0.089
42	36	2014	Winter	2/26/2014	0.107	0.003	0.149	0.085
42	35	2014	Spring	5/19/2014	0.106	0.002	0.135	0.090
42	36	2014	Summer	9/6/2014	0.109	0.003	0.150	0.089
42	36	2014	Fall	11/3/2014	0.107	0.003	0.144	0.075
42	36	2015	Winter	3/3/2015	0.115	0.003	0.152	0.096
42	36	2015	Spring	5/13/2015	0.115	0.003	0.165	0.086
42	36	2015	Summer	8/27/2015	0.114	0.004	0.182	0.087
42	36	2015	Fall	11/22/2015	0.108	0.003	0.150	0.082
42	34	2016	Winter	2/17/2016	0.112	0.003	0.160	0.083
42	36	2016	Spring	5/7/2016	0.112	0.003	0.153	0.082
42	36	2016	Summer	8/17/2016	0.115	0.003	0.149	0.085
42	36	2016	Fall	11/14/2016	0.109	0.003	0.150	0.071

SET Number	Number of Pins per Reading	Year Read	Season Read	Date Read	Mean Sediment Surface Elevation (m NAVD 88)	SE Sediment Surface Elevation (m NAVD 88)	Maximum Sediment Surface Elevation (m NAVD 88)	Minimum Sediment Surface Elevation (m NAVD 88)
43	36	2008	Spring	5/16/2008	0.119	0.001	0.133	0.098
43	36	2008	Summer	8/14/2008	0.121	0.001	0.135	0.107
43	36	2008	Fall	11/10/2008	0.128	0.002	0.152	0.103
43	36	2009	Winter	1/29/2009	0.129	0.002	0.158	0.104
43	36	2009	Spring	6/1/2009	0.128	0.002	0.147	0.100
43	36	2009	Summer	9/15/2009	0.126	0.001	0.139	0.110
43	36	2009	Fall	12/10/2009	0.133	0.002	0.153	0.104
43	36	2010	Winter	2/12/2010	0.141	0.002	0.168	0.113
43	36	2010	Spring	6/7/2010	0.142	0.001	0.152	0.126
43	36	2010	Summer	8/11/2010	0.141	0.001	0.152	0.124
43	36	2010	Fall	10/18/2010	0.145	0.001	0.157	0.133
43	36	2011	Winter	2/1/2011	0.143	0.001	0.158	0.126
43	36	2011	Spring	5/17/2011	0.143	0.001	0.163	0.129
43	36	2011	Summer	8/23/2011	0.145	0.001	0.159	0.129
43	36	2011	Fall	11/21/2011	0.146	0.001	0.160	0.124
43	35	2012	Winter	2/6/2012	0.145	0.001	0.164	0.131
43	36	2012	Spring	6/28/2012	0.140	0.001	0.155	0.127
43	36	2012	Summer	8/30/2012	0.139	0.001	0.152	0.125
43	33	2012	Fall	11/28/2012	0.142	0.002	0.165	0.123
43	36	2013	Winter	2/11/2013	0.139	0.002	0.171	0.105
43	35	2013	Spring	4/30/2013	0.141	0.002	0.160	0.107
43	36	2013	Summer	8/15/2013	0.147	0.002	0.175	0.131
43	36	2013	Fall	11/5/2013	0.145	0.002	0.174	0.119
43	36	2014	Winter	3/2/2014	0.150	0.002	0.172	0.118
43	36	2014	Spring	5/14/2014	0.156	0.002	0.173	0.119
43	36	2014	Summer	9/5/2014	0.152	0.001	0.162	0.137
43	36	2014	Fall	11/3/2014	0.145	0.002	0.159	0.112
43	36	2015	Winter	3/2/2015	0.145	0.004	0.166	0.000
43	35	2015	Spring	5/18/2015	0.158	0.002	0.185	0.138
43	36	2015	Summer	8/28/2015	0.154	0.001	0.169	0.140
43	36	2015	Fall	11/22/2015	0.153	0.002	0.175	0.113

SET Number	Number of Pins per Reading	Year Read	Season Read	Date Read	Mean Sediment Surface Elevation (m NAVD 88)	SE Sediment Surface Elevation (m NAVD 88)	Maximum Sediment Surface Elevation (m NAVD 88)	Minimum Sediment Surface Elevation (m NAVD 88)
43	36	2016	Winter	2/19/2016	0.159	0.002	0.186	0.140
43	36	2016	Spring	5/11/2016	0.158	0.002	0.179	0.127
43	36	2016	Summer	8/17/2016	0.161	0.002	0.177	0.126
43	36	2016	Fall	11/15/2016	0.155	0.002	0.178	0.119
44	36	2008	Spring	5/16/2008	0.121	0.002	0.152	0.105
44	36	2008	Summer	8/15/2008	0.129	0.001	0.139	0.114
44	36	2008	Fall	11/10/2008	0.131	0.002	0.154	0.109
44	36	2009	Winter	1/29/2009	0.130	0.002	0.151	0.103
44	36	2009	Spring	6/1/2009	0.131	0.001	0.146	0.111
44	36	2009	Summer	9/15/2009	0.125	0.001	0.140	0.103
44	36	2009	Fall	12/10/2009	0.125	0.002	0.145	0.098
44	35	2010	Winter	2/10/2010	0.125	0.001	0.141	0.110
44	36	2010	Spring	6/8/2010	0.129	0.001	0.149	0.120
44	36	2010	Summer	8/9/2010	0.121	0.001	0.139	0.110
44	35	2010	Fall	10/20/2010	0.133	0.001	0.156	0.121
44	36	2011	Winter	2/2/2011	0.129	0.001	0.142	0.105
44	34	2011	Spring	5/17/2011	0.126	0.001	0.143	0.110
44	36	2011	Summer	8/23/2011	0.126	0.001	0.137	0.108
44	36	2011	Fall	11/18/2011	0.125	0.001	0.136	0.114
44	36	2012	Winter	2/3/2012	0.133	0.001	0.150	0.121
44	36	2012	Spring	6/22/2012	0.126	0.001	0.140	0.116
44	36	2012	Summer	8/27/2012	0.123	0.001	0.130	0.114
44	36	2012	Fall	11/20/2012	0.129	0.001	0.144	0.113
44	36	2013	Winter	2/6/2013	0.130	0.002	0.151	0.104
44	36	2013	Spring	4/30/2013	0.130	0.002	0.153	0.108
44	35	2013	Summer	8/15/2013	0.136	0.001	0.157	0.117
44	35	2013	Fall	11/7/2013	0.130	0.001	0.155	0.109
44	35	2014	Winter	2/25/2014	0.132	0.001	0.159	0.117
44	35	2014	Spring	5/14/2014	0.136	0.002	0.154	0.116
44	35	2014	Summer	9/6/2014	0.125	0.002	0.145	0.097
44	36	2014	Fall	11/4/2014	0.129	0.001	0.144	0.117

SET Number	Number of Pins per Reading	Year Read	Season Read	Date Read	Mean Sediment Surface Elevation (m NAVD 88)	SE Sediment Surface Elevation (m NAVD 88)	Maximum Sediment Surface Elevation (m NAVD 88)	Minimum Sediment Surface Elevation (m NAVD 88)
44	36	2015	Winter	3/3/2015	0.129	0.001	0.140	0.104
44	36	2015	Spring	5/12/2015	0.132	0.001	0.153	0.104
44	36	2015	Summer	8/26/2015	0.133	0.001	0.144	0.123
44	36	2015	Fall	11/22/2015	0.132	0.001	0.163	0.115
44	36	2016	Winter	2/19/2016	0.132	0.001	0.149	0.124
44	36	2016	Spring	5/11/2016	0.130	0.001	0.144	0.102
44	36	2016	Summer	8/17/2016	0.133	0.002	0.154	0.101
44	36	2016	Fall	11/14/2016	0.125	0.004	0.145	-0.008
45	36	2008	Spring	5/20/2008	0.086	0.001	0.097	0.075
45	36	2008	Summer	8/15/2008	0.085	0.001	0.102	0.071
45	36	2008	Fall	11/10/2008	0.080	0.001	0.096	0.067
45	36	2009	Winter	1/29/2009	0.070	0.001	0.089	0.059
45	35	2009	Spring	6/2/2009	0.077	0.001	0.089	0.061
45	36	2009	Summer	9/14/2009	0.088	0.001	0.103	0.065
45	36	2009	Fall	11/30/2009	0.087	0.001	0.108	0.064
45	36	2010	Winter	2/10/2010	0.088	0.001	0.103	0.068
45	36	2010	Spring	6/9/2010	0.077	0.001	0.094	0.066
45	36	2010	Summer	8/12/2010	0.090	0.001	0.102	0.077
45	36	2010	Fall	10/19/2010	0.081	0.001	0.092	0.069
45	36	2011	Winter	2/2/2011	0.085	0.001	0.096	0.075
45	36	2011	Spring	5/19/2011	0.090	0.001	0.104	0.073
45	36	2011	Summer	8/24/2011	0.092	0.001	0.108	0.078
45	36	2011	Fall	11/18/2011	0.074	0.001	0.084	0.061
45	36	2012	Winter	2/3/2012	0.062	0.001	0.075	0.050
45	36	2012	Spring	6/22/2012	0.090	0.001	0.105	0.080
45	36	2012	Summer	8/27/2012	0.096	0.001	0.107	0.086
45	36	2012	Fall	11/19/2012	0.097	0.001	0.107	0.088
45	36	2013	Winter	2/15/2013	0.083	0.001	0.091	0.072
45	36	2013	Spring	4/30/2013	0.097	0.001	0.124	0.073
45	35	2013	Summer	8/19/2013	0.095	0.001	0.108	0.084
45	36	2013	Fall	11/7/2013	0.099	0.001	0.116	0.073

SET Number	Number of Pins per Reading	Year Read	Season Read	Date Read	Mean Sediment Surface Elevation (m NAVD 88)	SE Sediment Surface Elevation (m NAVD 88)	Maximum Sediment Surface Elevation (m NAVD 88)	Minimum Sediment Surface Elevation (m NAVD 88)
45	36	2014	Winter	3/4/2014	0.089	0.003	0.120	0.015
45	36	2014	Spring	5/19/2014	0.088	0.001	0.101	0.058
45	36	2014	Summer	9/5/2014	0.096	0.002	0.111	0.055
45	36	2014	Fall	11/3/2014	0.101	0.002	0.117	0.051
45	36	2015	Winter	3/2/2015	0.090	0.001	0.106	0.072
45	36	2015	Spring	5/13/2015	0.098	0.001	0.119	0.081
45	36	2015	Summer	8/26/2015	0.101	0.002	0.122	0.084
45	36	2015	Fall	11/23/2015	0.106	0.002	0.124	0.070
45	36	2016	Winter	2/17/2016	0.105	0.002	0.128	0.087
45	35	2016	Spring	5/11/2016	0.103	0.002	0.128	0.090
45	36	2016	Summer	8/17/2016	0.107	0.002	0.127	0.071
45	36	2016	Fall	11/18/2016	0.110	0.002	0.132	0.091
46	36	2008	Spring	5/20/2008	0.116	0.003	0.156	0.078
46	36	2008	Summer	8/15/2008	0.112	0.002	0.137	0.089
46	36	2008	Fall	11/10/2008	0.114	0.002	0.136	0.092
46	36	2009	Winter	1/29/2009	0.114	0.002	0.140	0.089
46	36	2009	Spring	6/2/2009	0.116	0.001	0.134	0.104
46	36	2009	Summer	9/14/2009	0.117	0.001	0.137	0.107
46	36	2009	Fall	11/30/2009	0.122	0.002	0.144	0.099
46	36	2010	Winter	2/10/2010	0.117	0.002	0.140	0.097
46	36	2010	Spring	6/9/2010	0.115	0.001	0.126	0.096
46	36	2010	Summer	8/12/2010	0.121	0.001	0.144	0.108
46	36	2010	Fall	10/19/2010	0.122	0.001	0.132	0.110
46	36	2011	Winter	2/2/2011	0.123	0.001	0.138	0.109
46	36	2011	Spring	5/19/2011	0.123	0.002	0.154	0.110
46	36	2011	Summer	8/24/2011	0.125	0.001	0.139	0.109
46	36	2011	Fall	11/18/2011	0.125	0.001	0.139	0.117
46	36	2012	Winter	2/3/2012	0.120	0.001	0.132	0.108
46	35	2012	Spring	6/22/2012	0.128	0.001	0.155	0.113
46	35	2012	Summer	8/27/2012	0.128	0.002	0.152	0.116
46	36	2012	Fall	11/19/2012	0.131	0.001	0.145	0.118

SET Number	Number of Pins per Reading	Year Read	Season Read	Date Read	Mean Sediment Surface Elevation (m NAVD 88)	SE Sediment Surface Elevation (m NAVD 88)	Maximum Sediment Surface Elevation (m NAVD 88)	Minimum Sediment Surface Elevation (m NAVD 88)
46	36	2013	Winter	2/15/2013	0.131	0.002	0.158	0.119
46	36	2013	Spring	4/30/2013	0.130	0.001	0.152	0.117
46	36	2013	Summer	8/19/2013	0.134	0.002	0.165	0.117
46	36	2013	Fall	11/7/2013	0.133	0.002	0.150	0.114
46	36	2014	Winter	3/4/2014	0.133	0.002	0.151	0.107
46	36	2014	Spring	5/19/2014	0.133	0.001	0.154	0.118
46	36	2014	Summer	9/5/2014	0.129	0.002	0.155	0.115
46	36	2014	Fall	11/3/2014	0.131	0.002	0.156	0.117
46	36	2015	Winter	3/2/2015	0.136	0.001	0.153	0.124
46	36	2015	Spring	5/13/2015	0.131	0.001	0.151	0.115
46	36	2015	Summer	8/26/2015	0.129	0.001	0.151	0.115
46	36	2015	Fall	11/23/2015	0.133	0.001	0.151	0.122
46	36	2016	Winter	2/17/2016	0.133	0.001	0.153	0.120
46	36	2016	Spring	5/11/2016	0.135	0.001	0.150	0.121
46	36	2016	Summer	8/17/2016	0.136	0.002	0.161	0.120
46	36	2016	Fall	11/18/2016	0.134	0.002	0.167	0.115

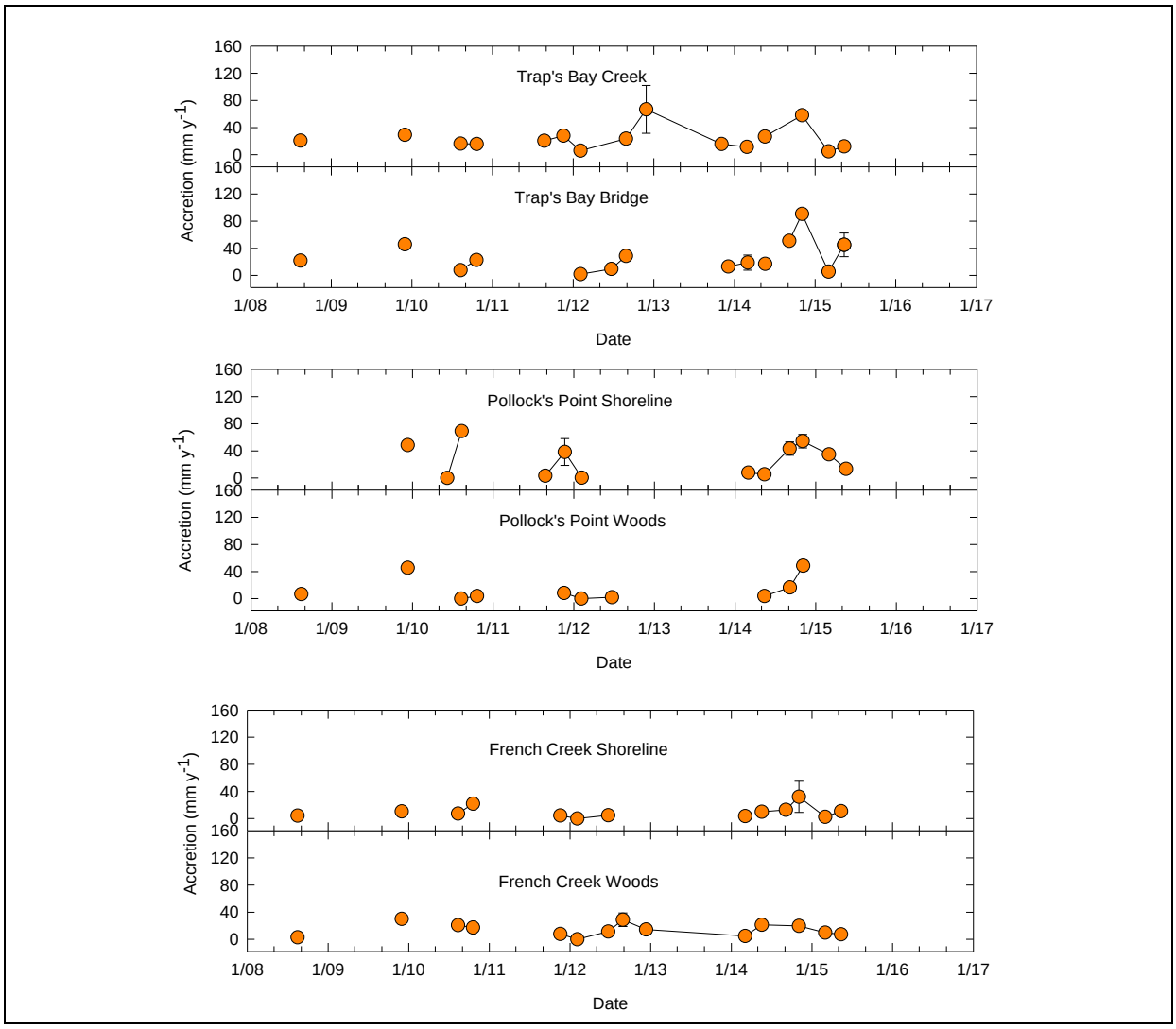

Figure 11A-4. Accretion rates measured from unfertilized Marker Horizon deployments of 50 to 150 days at the NRE sites.

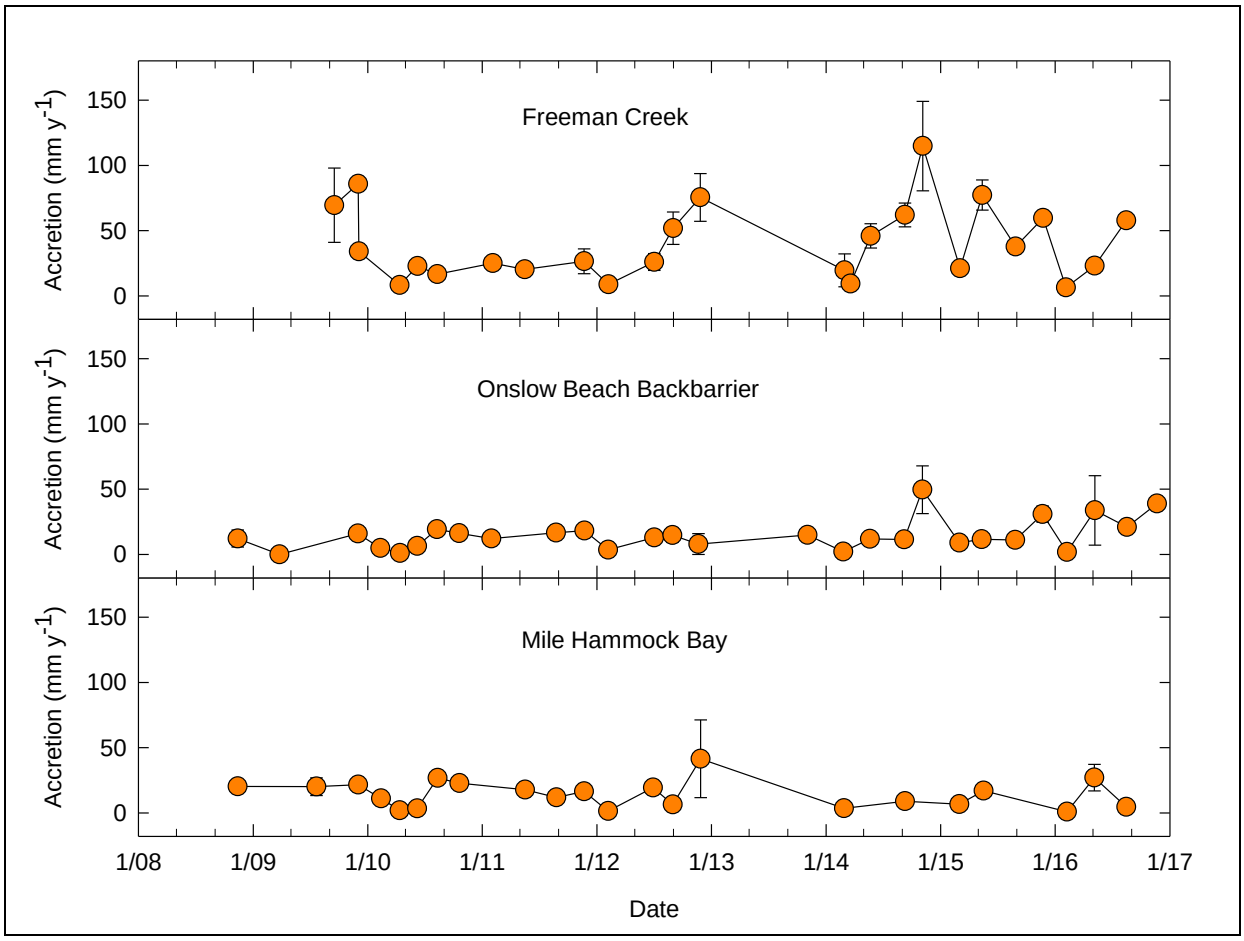

Figure 11A-5. Accretion rates measured from unfertilized Marker Horizon deployments of 50 to 150 days at the Intracoastal Waterway sites.

Appendix 11-B
List of Scientific/Technical Publications

See list of publications is Chapters 13 and 14 of the *DCERP2 Final Report* for Research Projects CW-4 and CW-5, respectively.

Chapter 12

Carbon Burial in Estuarine, Wetland, and Coastal Barrier Environments

SERDP Project Number: RC-2245

Carbon Burial

Research Projects AE-6, CW-4, and CB-5

Lead Researcher:

Dr. Brent McKee
University of North Carolina at Chapel Hill
Chapel Hill, NC
bmckee@unc.edu

Supporting Researchers:

Molly Bost (mbost@live.unc.edu)
Anna Atencio (aatencio@live.unc.edu)
Tony Rodriguez (abrodrig@email.unc.edu)
Carolyn Currin (carolyn.currin@noaa.gov)
Nathan McTigue (nathan.mctigue@noaa.gov)
Craig Tobias (craig.tobias@uconn.edu)
Rick Smith (globalaquaticresearch@gmail.com)

November 2017

Final

This report was prepared under contract to the U.S. Department of Defense (DoD) Strategic Environmental Research and Development Program (SERDP). The publication of this report does not indicate endorsement by DoD, nor should the contents be construed as reflecting the official policy or position of DoD. References herein to any specific commercial product, process, or service by trade name, trademark, manufacturer, or otherwise, do not necessarily constitute or imply its endorsement, recommendation, or favoring by DoD.

Table of Contents

Acronyms 12-v
Abstract 12-1
Objectives of the Research Project 12-2
Background 12-2
Materials and Methods 12-3
Results and Discussion 12-5
New River Estuary 12-5
Coastal Wetlands and Back Barrier Salt Marshes 12-16
Conclusions and Implications for Future Research and Implementation 12-24
Key Scientific Findings 12-24
Research Questions 12-25
Findings with Implications for Future Base Management 12-26
Literature Cited 12-27
Appendix 12-A: Supporting Data 12-A-1
Appendix 12-B: List of Scientific/Technical Publications 12-B-1
Appendix 12-C: List of Students 12-C-1

List of Figures

Figure 12-1. The locations of core sample collection sites used for studying sediment and organic carbon accumulation rates in the estuary, and salt marshes of MCBCL 12-4
Figure 12-2. Excess ^{210}Pb profile for New River estuarine sediment cores. 12-7
Figure 12-3. Sediment accumulation rates (SARs) of cores collected in the NRE. 12-8
Figure 12-4. Percent organic carbon profiles for NRE cores. 12-10
Figure 12-5. Carbon accumulation rates at NRE sites over the past 150 years. 12-11
Figure 12-6. Sediment organic matter was characterized with respect to %N, C:N, δ^{13}C, and δ^{15}N to constrain source contributions of organic carbon stored in sediments 12-14
Figure 12-7. Carbon accumulation rates from the upper, middle, and lower NRE. 12-16
Figure 12-8. Excess ^{210}Pb profile for marsh cores. 12-18
Figure 12-9. Sediment accumulation rates for MCBCL marsh sites. 12-20
Figure 12-10. Percent organic carbon (% OC) profiles from marsh cores. 12-22
Figure 12-11. Carbon accumulation rates in MCBCL marsh cores. 12-23

List of Tables

Table 12-1. Sediment and Organic Carbon Accumulation Rates for the NRE 12-9

Table 12-2. Carbon Accumulation Rates in the NRE and Other Sites Reported in the Literature 12-12

Table 12-3. Comparison of CF and CFCS Model Outputs (150 year time scale) 12-19

Table 12-4. SAR and CAR Values and Influencing Factors (Ranked) 12-21

Acronyms

%C	total organic carbon
%N	total nitrogen
$\delta^{13}C$	isotopic measurements of carbon
$\delta^{15}N$	isotopic measurements of nitrogen
AE	Aquatic/Estuarine (Module)
C	carbon
CA	constant activity
CAR	carbon accumulation rate
CB	Coastal Barrier (Module)
CF	constant flux
CFCS	constant flux constant sedimentation
CIC	constant initial concentration
cm	centimeter
C:N	ratio of carbon to nitrogen
CRS	constant rate of supply
CW	Coastal Wetlands (Module)
DCERP	Defense Coastal/Estuarine Research Project
DIC	dissolved inorganic carbon
DIN	dissolved inorganic nitrogen
DoD	U.S. Department of Defense
dpm g^{-1}	Disintegrations per minute per gram of sediment
EA-IRMS	elemental analyzer–isotope ratio mass spectrometer
g C m^{-2} y^{-1}	grams of carbon per square meter per year
g cm^{-2}	grams per square centimeter
g cm^{-3}	grams per cubic centimeter
g m^{-2} y^{-1}	grams per square meter per year
ICW	Intracoastal Waterway
km^2	square kilometer
MAR	mass accumulation rate
MCBCL	Marine Corps Base Camp Lejeune
mm	millimeter
mm y^{-1}	millimeters per year
mol C m^{-2} y^{-1}	moles of carbon per square meter per year
NAVD 88	North American Vertical Datum of 1988
NO_3^-	nitrate
NRE	New River Estuary
OC	organic carbon
RC	Resource Conservation and Climate Change (a SERDP program area)
SAR	sediment accumulation rate
SERDP	Strategic Environmental Research and Development Program
TBC	Traps Bay Creek
Tg C	terragrams of carbon
WWTP	wastewater treatment plant

Abstract

During the past century, the New River Estuary (NRE) and associated wetlands have been impacted by climate change and anthropogenic factors such as the construction of the Intracoastal Waterway and the establishment of Marine Corps Base Camp Lejeune (MCBCL). The overall focus of this study was to better understand how sediment and organic carbon (OC) accumulations within the system have been impacted by these changes. To examine these accumulations, seven cores were collected in the estuary, and six cores were collected from surrounding marshes. Each core was analyzed for ^{210}Pb (to establish sediment geochronologies), and rates of sediment and OC accumulation were determined.

Characteristic features of the upper estuary cores are a gradual increase in sedimentation rate from the bottom of the cores (early 1900s), followed by a more rapid increase in rates during the 1990s, peaking at 1999, the year of Hurricane Floyd's impact. In the upper estuary, the sediment accumulation rates (SAR) in the early 1900s range between 0.2 and 0.4 cm y^{-1} and peak at over 1 cm y^{-1} in 1999, returning present rates of 0.7 to 0.8 cm y^{-1}. The sediment accumulation rate (SAR) profiles in the middle estuary exhibit a steady increase during the past 150 years (from 0.1 to 0.4 cm y^{-1}) without well-defined peaks. The rate of sediment supply to the middle estuary is much lower than the supply to the upper bay and much higher than the lower estuary, which is non-depositional. Sedimentation rates in the upper NRE are high, relative to estuarine rates reported in the literature, and result from a medium rate of sediment supply, adequate accommodation space, and low wave energy to re-suspend or remobilize surface sediments. High surface water productivity and subsequent rapid remineralization within the water column lead to low oxygen conditions within bottom waters and surface sediments of the estuary. The low oxygen conditions optimize the preservation of terrestrial OC from the watershed. As a result, carbon accumulation rate (CAR) values in the upper NRE are among the highest reported in the literature and values for the middle estuary are within the middle range of values observed in other estuaries. The terrestrial OC source is generally restricted to the upper estuary because of the limited connectivity between the upper and middle estuary. Geomorphological controls on the estuary (limited fetch for wind waves, limited connectivity between individual lagoons and with the ocean) govern the CAR distributions within the NRE.

The mean SARs over the past 150 years in MCBCL marshes range from 1.1 to 3.4 mm y^{-1}. The current SARs (averaged over the past 5 years) range from 1.6 mm y^{-1} to 3.9 mm y^{-1}. The local rate of sea level rise, since 1860, is approximately 2.5 mm y^{-1} (Kemp et al., 2011). The world average SAR for marshes is 6.8 mm y^{-1}, and SARs for MCBCL marshes are among the lowest reported in the literature. The global mean for marsh CARs is 242.2 g C m^{-2} y^{-1}, with a range from 30 g C m^{-2} y^{-1} in the Arctic to 315 g C m^{-2} y^{-1} in the Mediterranean. CAR values for the coastal wetland and backbarrier sites examined in this study range from 15 g C m^{-2} y^{-1} to 150 g C m^{-2} y^{-1}. These CAR values are also amongst the lowest reported in the literature. One possibility for the low CAR values is that most the sites examined are either sediment starved (backbarrier environments) or have low OC supplies, or they have a combination of these two factors.

Keywords: Sediment, organic carbon, accumulation rate, estuary, marsh, geochronology, ^{210}Pb, terrestrial, geomorphology, lagoon, connectivity

Objectives of the Research Project

The overall objective of this research project was to determine the rates of sediment and carbon accumulation in estuarine, coastal wetland, and coastal barrier environments associated with Marine Corps Base Camp Lejeune (MCBCL). Specific objectives of this research project are discussed as follows.

For Aquatic/Estuarine Module (Research Project AE-6), the objectives were to

- Determine the sediment accumulation rates (SARs) within bottom sediment of the New River Estuary (NRE) during the past 150 years.
- Determine the long-term (150-year time scale) carbon sequestration rates by burial in estuarine sediments
- Relate long-term changes in land use (e.g., establishment of MCBCL) and climate to carbon burial.

For Coastal Wetlands Module (Research Project CW-4) and Coastal Barrier Module (Research Project CB-5), the objectives were to

- Determine the long-term (150-year) marsh SARs in marshes along the Intracoastal Waterway (ICW) and NRE
- Determine the carbon accumulation rates (CARs) in marshes along the ICW and NRE
- Evaluate how sea level rise will affect carbon storage in MCBCL marshes over the next century
- Assess the efficacy of carbon burial in the backbarrier marsh.

Background

The NRE consists of a series of broad, shallow lagoons linked together by narrow channels and confined by two barrier islands at the mouth in Onslow Bay. Seawater is exchanged from Onslow Bay through a single inlet at the mouth at the New River Inlet. Freshwater supply is dominated (>95%) by the New River upstream of Jacksonville, NC. The flushing time for the NRE varies seasonally, ranging from 8 to 187 days, with an average of 70 days (Altman and Paerl, 2012; Ensign et al. 2004). During the 1980s and 1990s, it was considered one of the most eutrophic estuaries in the southeastern United States, and in a 1996 National Oceanic and Atmospheric Administration survey, this estuary was considered to be one of the four most eutrophic estuaries in the southeastern United States (Bricker et al., 1999), with dense phytoplankton blooms and bottom water anoxia and hypoxia (Mallin et al., 2005). Beginning in 1998, the City of Jacksonville and MCBCL completed wastewater treatment plant (WWTP) upgrades that significantly reduced the total nitrogen input to the NRE and effectively ended a WWTP source of ammonium. However, low oxygen bottom water conditions continued to persist for at least another decade. Salinity stratification and slow flushing of the system exacerbated the low oxygen conditions (Ensign et al., 2004).

The NRE system has a distinct ("choked lagoon") geomorphology because of its series of poorly connected lagoons that are confined by barrier islands. This geomorphology of the NRE also limits the connectivity between the NRE and surrounding wetlands in the system. Since the 1930s, the NRE and associated wetlands have been impacted by climate change and anthropogenic factors such as the construction of the ICW and the establishment of the MCBCL.

Given these changes in the New River system (within the estuary and surrounding area marshes) during the past century, the overall focus of this study has been to better understand how these changes have impacted sediment and carbon accumulation within the system and what insights could be obtained regarding the future carbon dynamics of the system.

Materials and Methods

Seven 50-cm long cores were collected in the estuary by using 10-cm diameter core tubes (**Figure 12-1**). The cores were extracted by hand by using a push-coring device with a one-way valve to retain the sediments and an extension rod to access deeper water depths. Six marsh cores were collected by using 10-cm aluminum tubes driven into the marsh surface (**Figure 12-1**). It is important when doing geochronology work that the site selected be one that has been minimally disturbed so that the core record is not affected by either natural or human disturbances throughout its history. Estuarine and marsh cores were all subsampled at 1-cm intervals. Each interval was subsequently analyzed for ^{210}Pb (to establish sediment geochronologies) and for dry bulk density and carbon and nitrogen content. The methods for these analyses were the same for marsh and estuarine core samples.

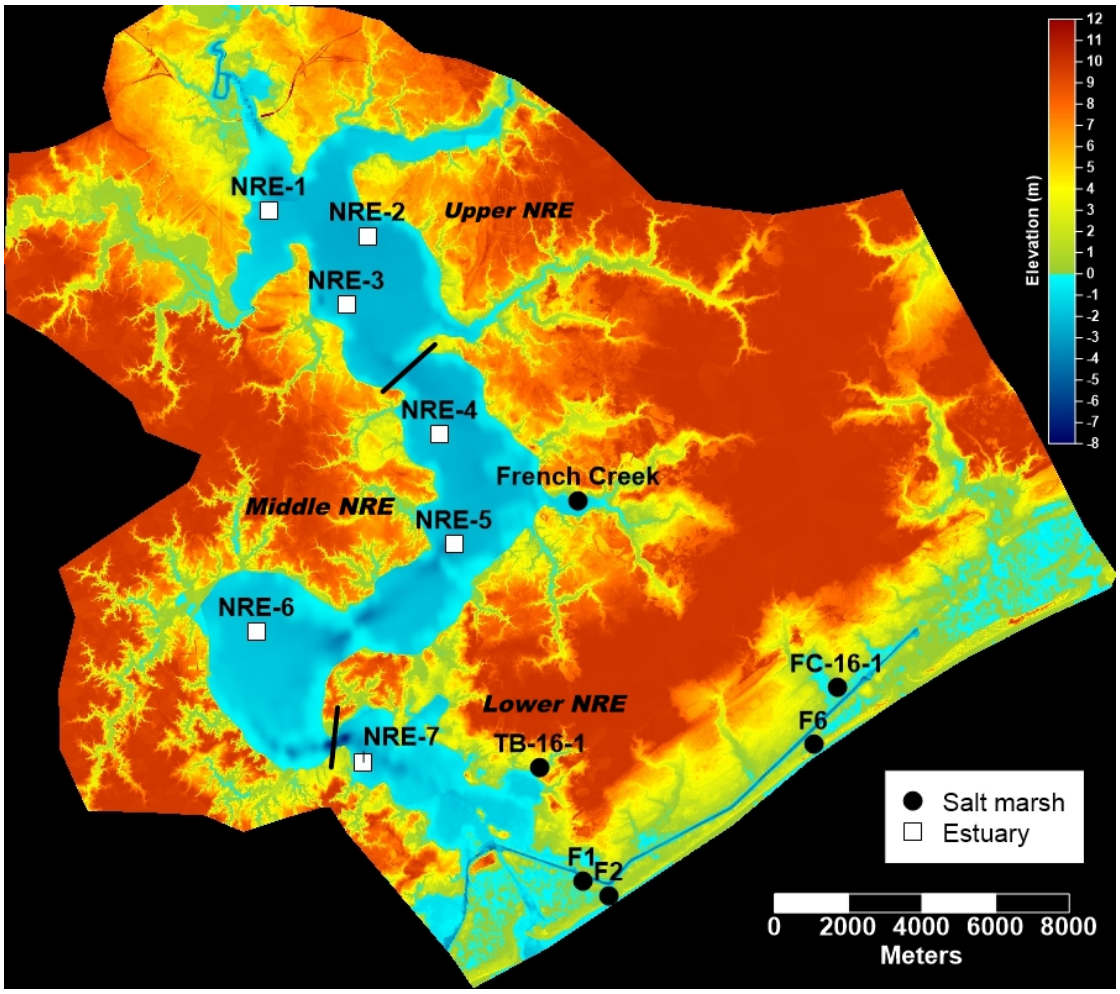

Figure 12-1. The locations of core sample collection sites used for studying sediment and organic carbon accumulation rates in the estuary, and salt marshes of MCBCL.

We determined ^{210}Pb activities by using an alpha spectrometry method in which the activities of ^{210}Po, the radiometric granddaughter of ^{210}Pb, were counted after methods described by DeMaster et al. (1985), McKee et al. (1983), and Nittrouer et al. (1979). Sediment samples from discrete intervals down-core were freeze-dried, spiked with a ^{209}Po tracer (to determine and correct for chemical yield), and leached with nitric and hydrochloric acids in a Teflon microwave digestion bomb. Polonium was spontaneously electroplated onto a stainless-steel planchet, and ^{210}Po /^{210}Pb ratio concentrations were measured by using silicon barrier detectors and an alpha spectrometer. Corrections were made for radioactive decay between times of collection and radiochemical counting. The time scale on which ^{210}Pb can be used as a chronometer is approximately 5 or 6 half-lives, or 120 to 150 years. When using the alpha spectrometry method, excess ^{210}Pb activity (above that supported by effective parent ^{226}Ra) is determined by analyses of “background” total ^{210}Pb activities deep in the core (>>100 years old).

^{210}Pb geochronologies have been used to document rates of sediment accumulation in a variety of coastal environments. ^{210}Pb (22.3-year half-life) is delivered to coastal environments from the atmosphere. For estuarine environments, an additional source of ^{210}Pb is supplied from surrounding waters from the in situ decay of ^{226}Ra; therefore, we can use sediment profiles of

excess ^{210}Pb to quantify the net SAR over the past 100+ years and to characterize changes in accumulation rates during that time period. SARs have units of length per time; in this study, the units cm y^{-1}or mm y^{-1} are used.

We modeled the excess ^{210}Pb data for each core by using a suite of geochronological dating models (Sanchez-Cabeza and Ruiz-Fernández, 2012) to derive SARs and MARs. The Constant Activity (CA) model, traditionally named the Constant Initial Concentration (CIC) model, assumes that the initial concentration of excess ^{210}Pb reaching the surface sediment at a site remains the same over the 150-year timescale of ^{210}Pb and also implies that the excess ^{210}Pb flux to the sediment surface is proportional to the MAR. The Constant Flux (CF) model, also known as the Constant Rate of Supply (CRS) model, assumes that the initial concentration of excess ^{210}Pb and the MARs may change, but they must be inversely proportional. Most importantly, for our purposes, the CF model does not assume constant sedimentation rates. The Constant Flux Constant Sedimentation (CFCS) model assumes simultaneously a constant flux of excess ^{210}Pb to the sediment surface and a constant rate of mass accumulation. Essentially, the CFCS model is a piecewise CA model in which sedimentation rates are constant over one section of the core, but can change to a different constant rate over another core section.

Dry bulk density is the mass of dry sediment contained in a known volume of wet sediment (in units of g cm^{-3}). Dry bulk density was measured by weighing, drying and re-weighing each 1-cm interval of the cores, and then dividing the dry mass by the know volume of each interval (81.1 cm^3 for each 1-cm interval). Carbon density is the product of dry bulk density and the fraction of organic carbon (OC) in the sample. For bulk sediment total organic carbon, total nitrogen, and isotopic measurements ($\delta^{13}C$ and $\delta^{15}N$), sediments were freeze-dried, ground, acidified to remove inorganic carbon, and then analyzed with an elemental analyzer coupled to a Thermo Delta V Plus isotope ratio mass spectrometer (EA-IRMS). CARs are derived by calculating the product of SAR and carbon density.

Results and Discussion

New River Estuary

Sediment Cores

In September 2013, cores were collected from the upper (Stations NRE-1 through NRE-3), middle (Stations NRE-4 through NRE-6), and lower (Station NRE-7) reaches of the NRE (**Figure 12-1**). Upon examination after preliminary analyses, the core collected from Station NRE-5 (middle estuary) appears to have been collected from a disturbed area of the estuarine bottom and was not used for further analyses. The core from Station NRE-7 (lower estuary) was difficult to collect because the site had a sandy bottom, which is representative of the entire lower estuary. Station NRE-7, and the entire lower estuary, is therefore considered to be non-depositional with respect to fine sediments and associated OC.

Sediment Accumulation Rates

Excess ^{210}Pb ($^{210}Pb_{xs}$) profiles for the upper estuary are presented in **Figure 12-2** as a function of sediment thickness, depth being expressed in cumulative mass depth in g cm^{-2} (to eliminate the

non-linear dependence between the accumulated dry mass and sediment depth due to different water content and sediment compaction). Mass depth incorporates the sediment bulk density and the sediment thickness of each depth interval and is used instead of depth to account for post-depositional compaction. Sediments in all five cores were fine grained (predominantly silt sized). At a hypothetical site where sedimentation rates have been constant over the past century, $^{210}Pb_{xs}$ concentrations will decrease exponentially when plotted in this mass depth format. The $^{210}Pb_{xs}$ concentrations (dpm g^{-1}) for each core and the exponential trendline for each profile is represented by the dotted curves in **Figure 12-2**. The upper estuary profiles follow the trendline closely (R^2=approximately 0.95) with some parts of the profile deviating from the trendline. These deviations indicate periods when the rate of sedimentation had either increased or decreased relative to the idealized constant rate over the past 150 years. Middle estuary profiles exhibit more frequent and larger deviations from the exponential trendline (R^2=0.54 to 0.81), indicating more variable rates of sedimentation at these sites. These changes in sedimentation rate result from changes in sediment supply from the watershed and/or re-suspension and remobilization of sediments within the estuary.

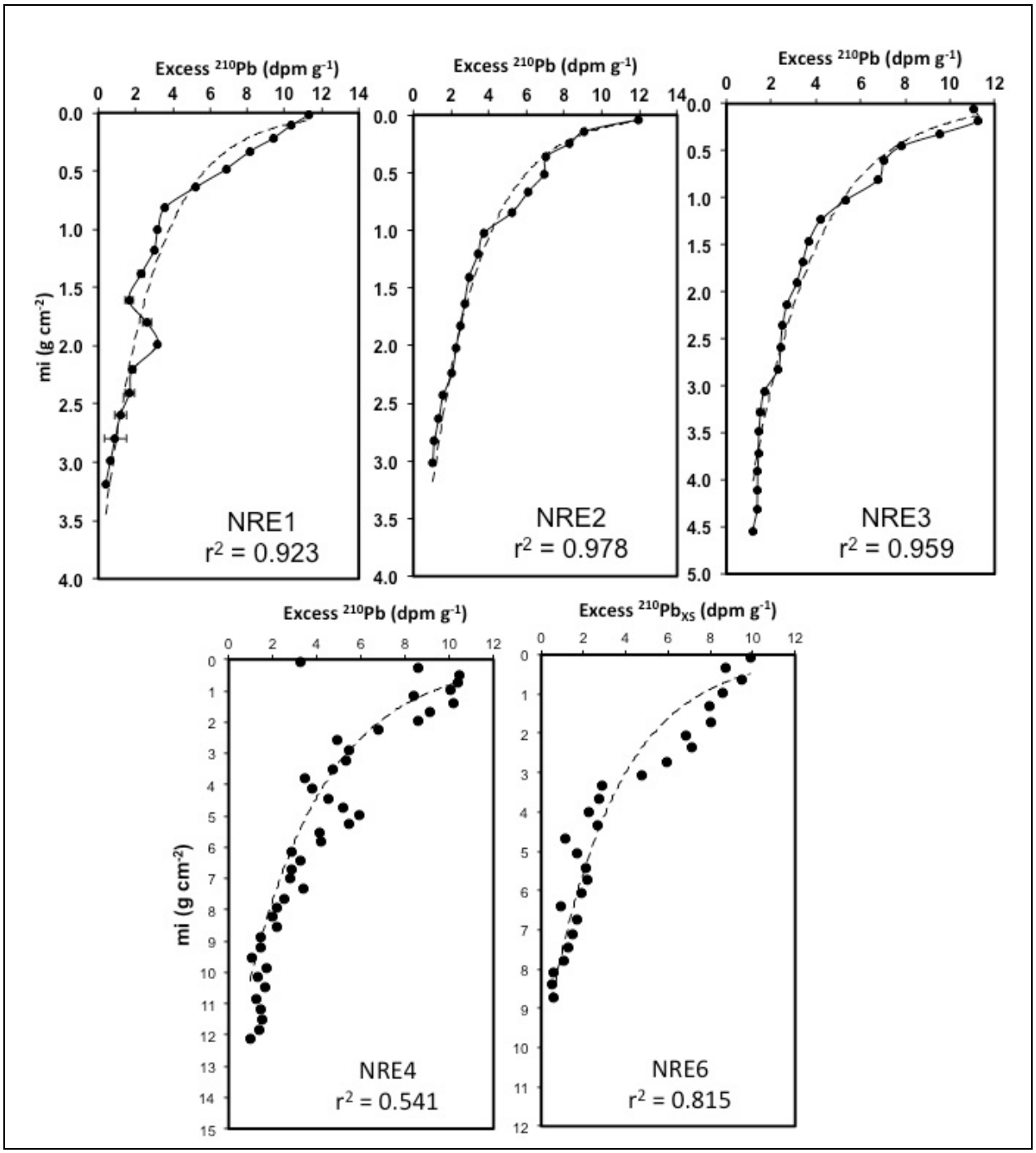

Figure 12-2. Excess ^{210}Pb profile for New River estuarine sediment cores.

The *y*-axis (m_i) is mass depth, which is the product of the interval thickness and the bulk density of the depth interval. The exponential trendline for each profile is represented by the dotted curves.

Geochronology models were applied to these profiles. Application of the CA model implies that deeper layers must be older and, for this reason, when using the CA model, the $^{210}Pb_{xs}$ concentration profile must decrease monotonically and closely follow the exponential trendline, but this is not the case for the NRE profiles, and the assumptions of the CA model are violated. Therefore, the CA model is not used in this study. The mean SARs derived from the CF and

CFCS models were very similar and because the CF model provides additional information about changes in sedimentation rates during the past 150 years, the SAR profiles using the CF model results are presented in **Figure 12-3**.

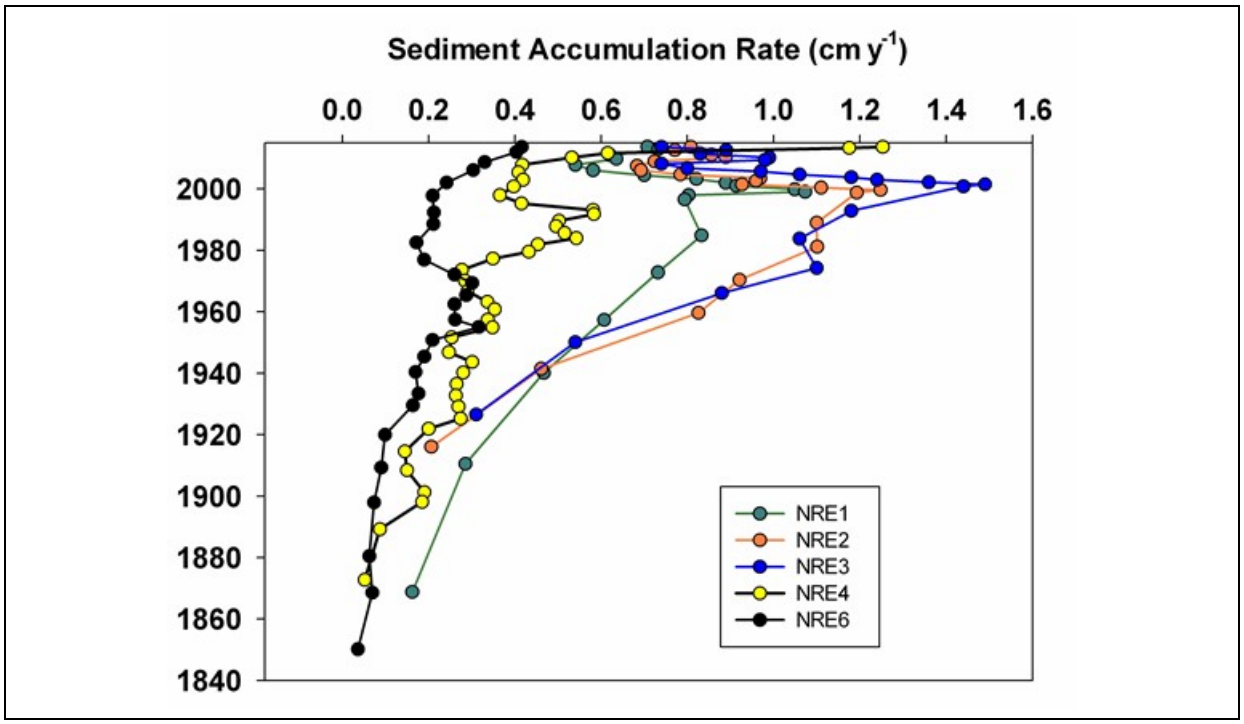

Figure 12-3. Sediment accumulation rates (SARs) of cores collected in the NRE.

Characteristic features of the upper estuary cores (Stations NRE-1 through NRE-3) are (1) a gradual increase in sedimentation rate from the bottom of the cores (late 1800s) to the 1980s; followed by (2) a more rapid increase in rates during the 1990s, peaking at 1999; (3) a decrease in sedimentation rates between 1999 and 2008; and (4) a final increase in SARs from 2008 to date with some indication of a minor peak around 2011. These trends are interpreted as follows:

1. An increase in population in the New River watershed during the twentieth century was accompanied by land-use changes that increased sediment yield in the basin and resulted in additional sediment sources to the estuary. The gradual increase in SAR is also facilitated by the increasing rate of sea level rise, which created additional accommodation space for sedimentation.

2. There was a dramatic increase in water discharge and associated erosion in the watershed resulting from a period of hurricane impacts in the New River system. During the middle to late 1990s, six major hurricanes (with winds exceeding 90 mph and associated heavy rain and flooding) impacted Onslow County, including the New River watershed. This stormy period was highlighted by four major hurricanes that made landfall during the 1998–1999 hurricane seasons. The most notable of these events was Hurricane Floyd, which made landfall September 16, 1999, and resulted in a 500-year flood in the basin. These events are likely to have greatly increased the sediment discharge into the upper estuary. Peak SAR values in the upper estuary range from 1.05 cm y^{-1} to 1.49 cm y^{-1} and

occur around 1999 (range: 1998.9 to 2000.9). These peak rates are 1.5 times the mean SARs for the past 150 years (**Table 12-1**).

3. The decrease in sedimentation during the decade following Hurricane Floyd was possibly the result of the extensive removal of alluvial and colluvial sediments in the watershed during the events of the late 1990s. This decrease would indicate that it takes approximately a decade for the watershed storage of sediments to be replenished in the New River system.

4. The increase in sedimentation in the upper estuary from approximately 2008 to date signals a return of sufficient sediment supply in the watershed to bring sediment discharge back to normal (pre-1990) rates.

Overall, it appears that sediment accumulation in the upper estuary is tied very closely to processes of deposition, erosion, and transport in the adjacent New River watershed; however, this does not seem to be the case for the middle estuary (Stations NRE-4 and 6). These SAR profiles exhibit a steady increase in the sedimentation rate during the past 150 years without well-defined peaks. The highest SAR values for NRE-4 and NRE-6 are at the sediment surface. The mean SARs in the middle estuary are much lower (by a factor of 2 to 4) than those in the upper estuary (**Table 12-1**). Therefore, the rate of sediment supply to the middle estuary is much lower than supply to the upper bay. This lower rate is probably because the connectivity between the sediment rich upper estuary and the middle estuary is limited by geomorphological restrictions and because the sandy lower estuary is not an immediate source of fine sediments.

Table 12-1. Sediment and Organic Carbon Accumulation Rates for the NRE

Rates	Upper Estuary			Middle Estuary	
	NRE-1	NRE-2	NRE-3	NRE-4	NRE-6
Mean SAR (past 150 years) (mm y^{-1})	7.0	8.6	9.9	4.2	2.1
Peak SAR (mm y^{-1})	10.7	12.5	14.9	6.1	4.2
Ratio of peak to mean SAR	1.5	1.5	1.5	1.5	2.0
SAR (past 5 years)[a] (mm y^{-1})	6.5	7.9	8.6	9.2	3.8
Mean CAR (past 150 years) (g C m^{-2} y^{-1})	103.3	107.6	125.3	53.4	20.8
Peak CAR (mm y^{-1})	205.5	163.8	210.3	134.2	33.5
Ratio of peak to mean CAR	1.9	1.5	1.7	2.5	1.6
CAR (past 5 years)[a] (g C m^{-2} y^{-1})	53.5	61.8	71.3	90.1	31.5

[a] Data from approximately 2008.7 to core collection 2013.7.

A balance between sediment supply, accommodation space, and available energy governs estuarine sedimentation rates (Zhu and Olsen, 2014). Storm events that impact the watershed increase the supply of sediments transported from the watershed to the estuary. Regarding the mean sedimentation rates observed in the NRE, accommodation space is very slowly decreasing there because SARs are greater than the rate of sea level rise; however, the NRE-6 area is a possible exception. Energy within the system is low because it is a micro-tidal environment and because the lagoonal geomorphology of the estuary limits connectivity with the ocean and limits

fetch-related wave energy sufficient to remobilize bottom sediments. Although no synthesis publication of sedimentation rates in estuaries exist, the SAR values are certainly among the highest published in the literature (Smith et al., 2015; Warnken et al., 2008).

The percent organic carbon (% OC) of NRE bottom sediments decreases in a seaward direction (**Figure 12-4**); surface values range from 8% at NRE-1 to 3% at NRE-6. The % OC values increase by between 10% and 15% with core depth from the surface at each site. The mean % OC (over all core depths) for the cores collected range from 8.4 at NRE-1 to 3.2 at NRE-6. At the upper estuary stations, a minimum in % OC is observed at a depth of approximately 10 cm, which corresponds to the 1999 horizon. This horizon is consistent with the SAR profiles interpretations previously mentioned that emphasize a large input of lower carbon content terrestrial sediment from the watershed driven by storm flooding. The decreasing influence of low % OC terrestrial sediments with distance from the New River also explains the orderly increase in % OC from NRE-1 to NRE-6 shown in **Figure 12-4**.

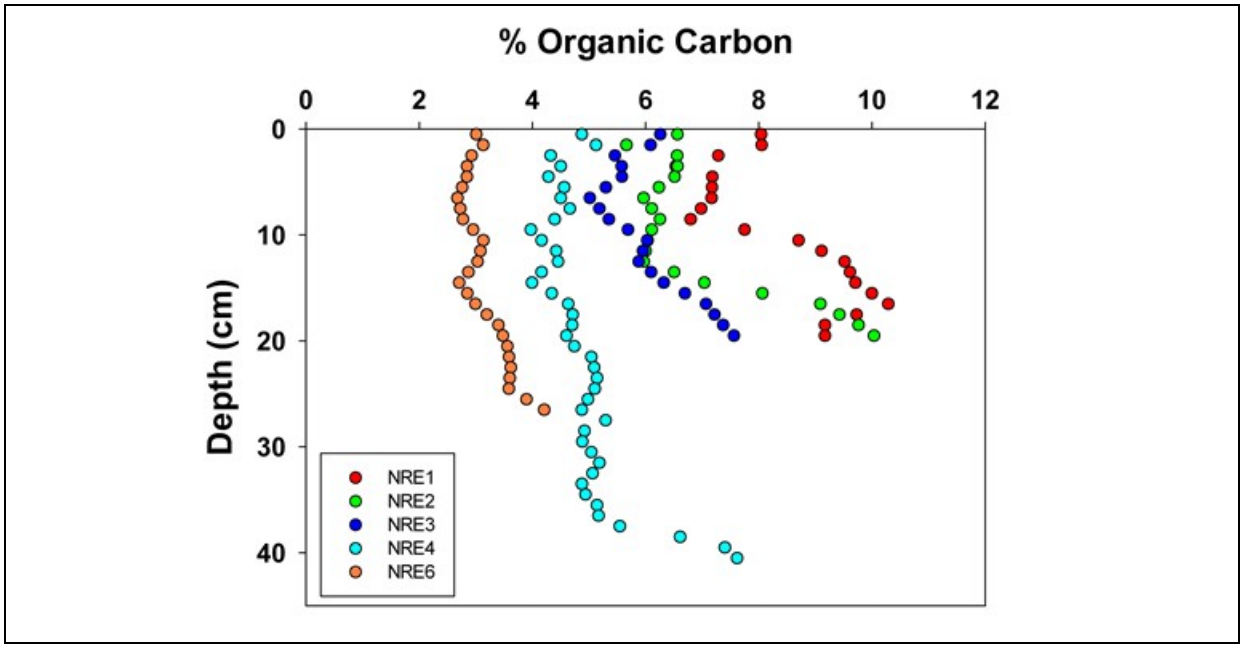

Figure 12-4. Percent organic carbon profiles for NRE cores.

Water content decreases and bulk density increases with depth in each core (Appendix 12-A); therefore, carbon density (the product of bulk density and fraction OC), increases by between 30% and 50% with depth in all cores. The CAR is the product of the SAR and carbon density for each core interval and is shown in **Figure 12-5**. CAR profiles exhibit down-core variations that are very similar to the SAR profiles previously discussed because SAR values are an order of magnitude greater than carbon density values for most intervals. Therefore, in the NRE, the CARs are controlled by the SARs, which, in turn, appear to be driven (spatially and temporally) by the input of the terrestrial material from the watershed because the energy to re-suspend and mobilize sediment is low and accommodation space (at present) is adequate.

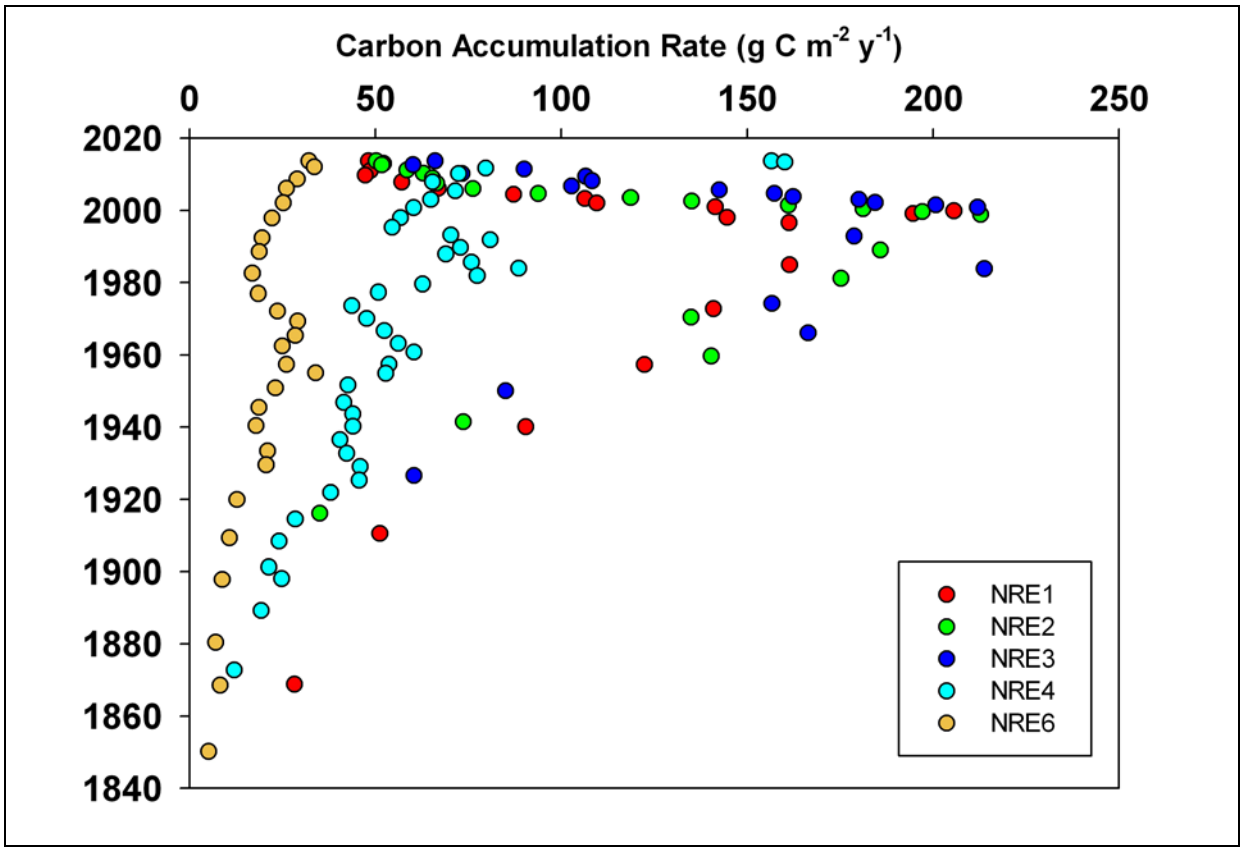

Figure 12-5. Carbon accumulation rates at NRE sites over the past 150 years.

Carbon Accumulation Rates in Estuaries

CAR values for the NRE range from 20.8 to 135.4 g C m^{-2} y^{-1} (1.7 to 11.3 mol C m^{-2} y^{-1}). An examination of estuarine OC accumulation in a large number of papers in the literature use molar units instead of mass; therefore, we are using both units here for easy comparisons (**Table 12-2**). The mean CAR for the upper estuary is 109.9 g C m^{-2} y^{-1} (9.9 mol C m^{-2} y^{-1}) with a range of 106.1 to 135.4 g C m^{-2} y^{-1} (8.8 to 11.3 mol C m^{-2} y^{-1}). The mean for the middle estuary is 39.3 g C m^{-2} y^{-1} (3.3 mol C m^{-2} y^{-1}) with a range of 20.8 to 57.8 g C m^{-2} y^{-1} (1.7 to 4.8 mol C m^{-2} y^{-1}). The upper estuary CAR values are the highest recorded in the literature (**Table 12-2**). The middle estuary (NRE-4 and NRE-6) range of CARs is within the middle to upper range of values reported in the literature (**Figure 12-5; Table 12-2**).

Table 12-2. Carbon Accumulation Rates in the NRE and Other Sites Reported in the Literature

Location	CAR ($g\ C\ m^{-2}\ y^{-1}$)	CAR ($mol\ C\ m^{-2}\ y^{-1}$)	Reference
New River Estuary, NC	***21–125***	***2–10***	***This Study***
Other estuaries	***3-79***	***0-7***	***Estuaries cited below***
Southeastern Australian estuaries	14–52	1–4	Maher and Eyre (2012)
52 East Coast U.S. estuaries (modeled)	9–20	1–2	Herrmann et al. (2015)
Atchafalaya Estuary, LA	42–72	4–5	Gordon and Goñi (2004)
Galveston Bay, TX	30–40	2-3	Warnken et al. (2008)
Chesapeake Bay	30–79	3–7	Kemp et al. (1997); Roden et al. (1995)
Worldwide Fjords	3–35	0–3	Smith et al. (2015)

Carbon accumulation in an estuary depends on the OC content, sedimentation rate, oxygen exposure time in the sediment, and the lability of incoming carbon sources (Hedges and Keil 1995). These factors are optimized in the NRE. The water column is shallow and upper sediments are seasonally hypoxic to anoxic (Mallin et al., 2005). The result is a limited oxygen exposure time. The OC content (3.2 to 8.4 % carbon) of sediments in the NRE is within the range of other estuarine environments reported in the literature (see the references cited in **Table 12-2**) and the lability of the sediments accumulating in the NRE are likely to be relatively low because of the substantial terrestrial carbon component, especially in the upper estuary. Finally, sedimentation rates in the NRE are high, especially peak values (greater than 1 cm y^{-1}), relative to most estuarine rates reported in the literature (Renfro et al., 2016; Ruiz-Fernández et al., 2002). As previously discussed, the relatively high rates of SAR result from conditions of a medium rate of sediment supply, adequate accommodation space, and low energy to re-suspend or remobilize surface sediments. High rates of sedimentation serve to limit the oxygen exposure time of OC in the estuary, and therefore optimize OC preservation in bottom sediments.

Sources of Organic Carbon Stored in NRE Sediments

Sediment organic matter was characterized with respect to total organic carbon (%C), total nitrogen (%N), the ratio of carbon to nitrogen (C:N), and the isotopic measurements of carbon ($\delta^{13}C$) and nitrogen ($\delta^{15}N$) in order to constrain source contributions of carbon stored in sediments, and how those sources may have changed over time (**Figure 12-6**). **Figure 12-6** illustrates the sediment profiles of carbon and nitrogen constituents for NRE-1. Profiles for the other stations (NRE-2, NRE-3, NRE-4, and NRE-6) are shown in **Appendix 12-A**. The % C profiles are shown in **Figure 12-4**. In the upper estuary, there is a higher accumulation of more carbon-rich sediment. Accumulation rates increased over the past century, and exceeded the local rate of sea level rise by two- to four-fold during some periods (**Figure 12-3**). The accelerated rate of deposition may mirror the increased rate of sea level rise, modification of the watershed, and/or changing hydrologic forcing. Using all of the data available, the C:N and $\delta^{13}C$ indicate that the NRE traps a mixture of allochthonous terrestrial (e.g., soil), and autochthonous (e.g., phytoplankton) material, and the relative contribution of the terrestrial source decreases with

distance downstream (**Figure 12-6, Appendix 12-A**). The 2 to 4 ‰ increase in $\delta^{15}N$ in the middle NRE cores relative to upper NRE cores further supports this conclusion. However, given the overlap in potential source end-members (Lamb et al., 2006), it is difficult to ascribe specific fractional contribution values from each source at this juncture.

Pulses and Transition of OC in the Upper NRE

Large changes in the character of sediment organic matter deposited were detected in the upper NRE in excess of what might be expected from post-depositional diagenetic effects. Five distinct periods were apparent: from the late-1800s through the mid 1950s; from the mid 1950s through the 1980s; during the 1990s; from the late-1990s through the late 2000s; and, from the late 2000s to date. These are the same salient periods previously identified for SAR values.

In the upper estuary, starting in the 1950s, accumulating sediment organic matter showed increasing %N and decreasing values of $\delta^{15}N$, and C:N (**Figure 12-6**). Because phytoplankton contributions are rich in nitrogen, these changes in the nitrogen organic matter metrics can reasonably be attributed to changes in this source. Local wastewater nutrient inputs over the period from the 1950s to the mid-1990s increased substantially and fueled the frequency and intensity of phytoplankton blooms, which peaked in the 1990s, declining thereafter with operation of the new MCBCL WWTP in 1998. It appears that a small, but higher, contribution (and preservation) of nitrogen-rich phytodetritus to sediments similarly increased during this period. The concurrent drop in $\delta^{15}N$ from 3 to 0.5 ‰ is wholly consistent with phytoplankton nitrogen assimilation under conditions of excess dissolved inorganic nitrogen in the water column (Mallin et al., 2005), where isotopic fractionation can be maximized. This wastewater effect appeared to be very localized to the upper NRE because similar patterns in these metrics were not found at NRE-4 or further downstream. Profiles for NRE-1 are displayed here. The profile sets for the other stations are presented in **Appendix 12-A**.

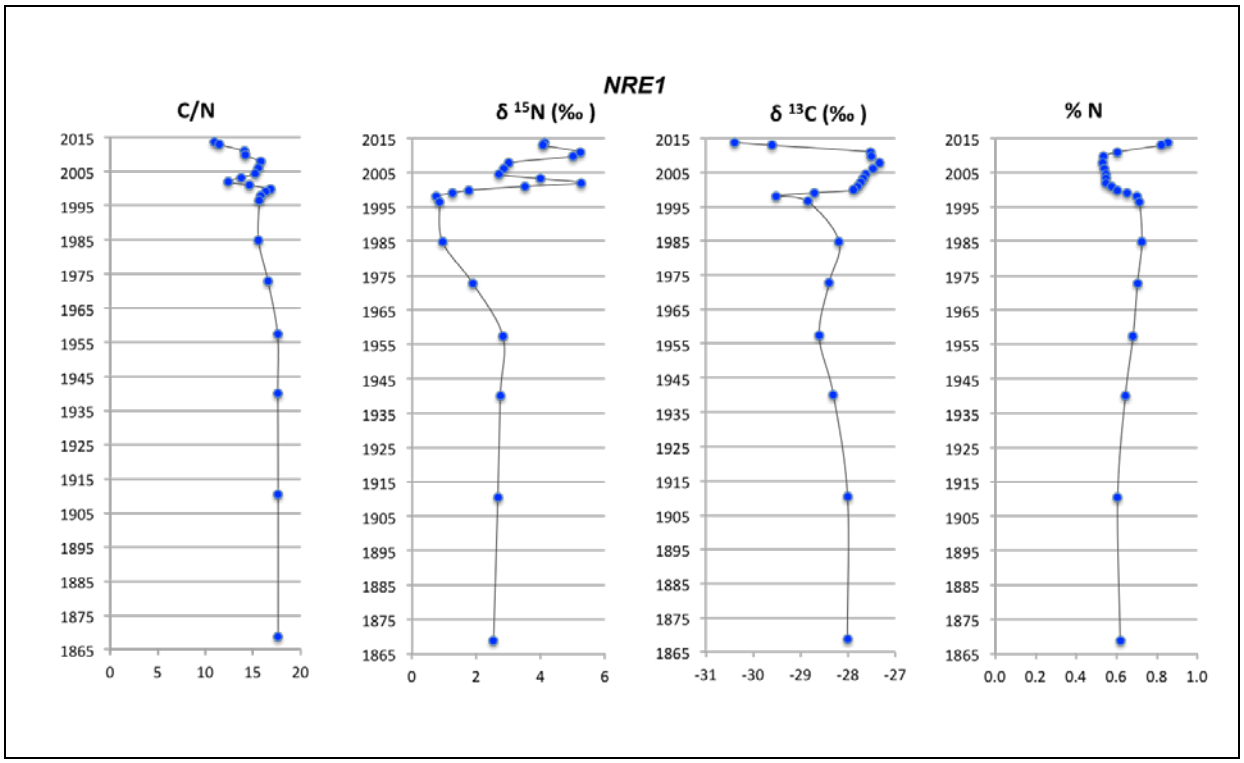

Figure 12-6. Sediment organic matter was characterized with respect to %N, C:N, $\delta^{13}C$, and $\delta^{15}N$ to constrain source contributions of organic carbon stored in sediments.

From the mid-1990s through the mid-2000s, the NRE was subject to two almost concurrent events that likely affected both autochthonous and allochthonous organic matter inputs to sediments. First, in 1998, the City of Jacksonville and MCBCL completed WWTP upgrades that significantly reduced the total nitrogen input to the NRE and effectively ended a WWTP source of ammonium. Primary production dropped by two-thirds relative to pre-1998 levels. After 1998, the major external source of nitrogen driving primary production switched from WWTP ammonium to nitrate (NO_3^-) loadings from the upper New River watershed. Second, in the late 1990s, Eastern North Carolina was hit with several storms, the largest of which was Hurricane Floyd in 1999, which caused a 500-year flood event. The spike in the SAR in NRE-1 over this period, in conjunction with a drop in %N and %C, is interpreted as the storm-induced delivery of mineral rich watershed soils. The drop in %N, combined with a large 5‰ enrichment in $\delta^{15}N$, could also be interpreted as the drop in the local phytoplankton contribution, where the isotopically heavier values reflect phytoplankton dissolved inorganic nitrogen (DIN) assimilation no longer in an excess DIN environment and/or a switch to a watershed NO_3^- source that was more ^{15}N enriched as a result of partial denitrification in transit to the NRE.

The localized WWTP effect on local organic matter sources observed from the 1950s through the mid-1990s in the upper estuary, propagates throughout estuary starting in the mid-1990s. This wider distribution could be partially attributable to a limited movement of sediment down-estuary. Similar patterns in %C, %N, ^{15}N, and ^{13}C are observed at all upper NRE stations, but there appears to be a time lag with distance downstream. There may also be a more widespread effect. Dropping the dominant WWTP influence enables us to better recognize the role of

watershed delivery of NO_3^-, soils, and other upstream organic matter sources of carbon on stored sediment carbon in the NRE. In all upper NRE cores, starting in the mid-1990s, there was an increase in the $\delta^{13}C$ of sediment carbon. The values are not outside the range of soils or phytoplankton, so source attribution is difficult. Furthermore, the $\delta^{13}C$–POC produced locally can be dependent on the local ^{13}C-dissolved inorganic carbon (DIC), which varies with salinity and system net metabolism. The simplest interpretation suggests that there has been relatively increasing source of ^{13}C rich carbon accumulating in the upper NRE since the mid-1990s. Such watershed sources have previously been attributed to either corn agriculture or grasslands (Goñi et al., 1997). There is a modest amount of acreage devoted to row crop agriculture in the NRE watershed; however, it is likely that there are significant amounts of corn imported into the watershed to support confined animal feeding operations locally (Mallin et al. 2005). The large range of $\delta^{13}C$ measured at the uppermost Station NRE-1, most notably very light $\delta^{13}C$ over the past 10 years combined with higher %N and lower C:N (**Figure 12-6**), indicates that the OC source contributions are either resetting to some new balance, or that variable contributions among soils, freshwater or estuarine phytoplankton, and other watershed sources is the new normal. It appears that the sediment organic matter response trajectory of the uppermost NRE started by the WWTP upgrade has given way to a new trajectory driven by factors or sources from the upper New River watershed.

Summary: Sediment and Organic Carbon Accumulation in the NRE

Figure 12-7 illustrates the down-estuary distribution of CARs in the NRE.). High surface water productivity and subsequent rapid remineralization within the water column leads to low oxygen conditions within bottom waters and surface sediments. The low oxygen conditions optimize the preservation of terrestrial OC inputs from the watershed. As a result, CAR values in the NRE are among the highest reported in the literature (Herrmann et al., 2015 The terrestrial OC source is generally restricted to the upper estuary because of the constricted lagoon geomorphology of the estuary limits connectivity between the upper and middle estuary.

Ultimately, it is the geomorphological controls on the estuary (limited fetch for wind waves, long residence times and limited connectivity between individual lagoons and with the ocean) that regulates CAR distributions within the NRE (**Figure 12-7**). Despite this lack of connection between the upper estuary and the ocean, the CAR values for the middle estuary are within the middle range of values observed in other estuaries (**Table 12-2**). CAR values (last 5 years; **Table 12-1**) for the upper estuary (NRE1, NRE2, NRE3) were averaged (g C m^2 y^{-1}) and multiplied by the surface area of the upper estuary (m^2) to calculate the carbon burial rates (g C y^{-1}) for the estuarine carbon budget. The same was performed for the CAR values (last 5 years; **Table 12-1**) for the middle estuary (NRE4, NRE6).

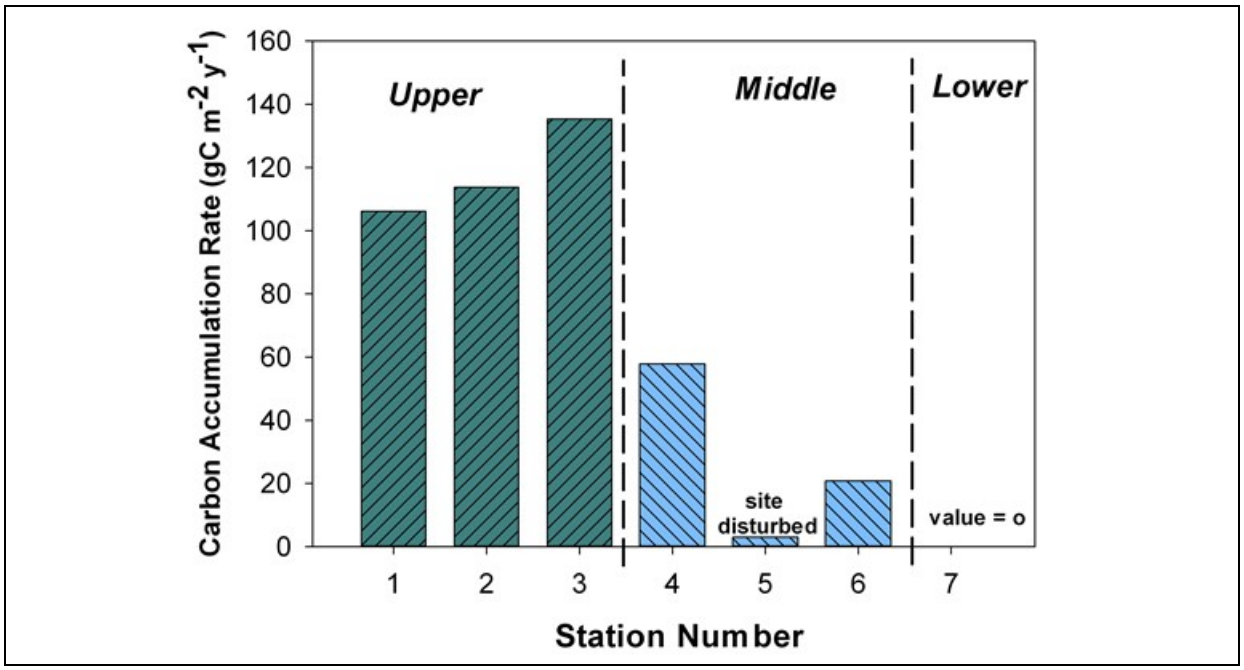

Figure 12-7. Carbon accumulation rates from the upper, middle, and lower NRE.

Coastal Wetlands and Back Barrier Salt Marshes

Background

Sediment accretion rate is among the most important parameters affecting marsh ecosystem health. The long-term stability of marsh ecosystems is governed by interactions between sea level, land elevation, primary production, and sediment accretion that regulate the elevation of the marsh sediment surface in equilibrium with mean sea level (Morris et al., 2002). The ability of marshes to keep up with current and projected rates of sea level rise depends upon sediment availability, the rate of sea level rise, the dominant macrophyte, and the density of marsh vegetation (Kirwan and Murray, 2007; Morris et al., 2002; Mudd et al., 2009). Other factors such as anthropogenic impacts (e.g., ICW creation in the 1930s, MCBCL establishment in 1940s) and the intensity and frequency of storm events on marsh sediment accretion rates (Kolker et al., 2009) are also important. The interactions between these factors are key. For example, rates of sea level rise and sediment accretion interact to control productivity. In turn, marsh productivity interacts with sediment availability and allocthonous sediment loading to influence sediment accretion by impacting the efficiency of the marsh as a sediment trap. The net rate of change in the elevation of the marsh surface and therefore the marsh's ability to survive in conditions of accelerated rates of sea level rise is intimately related to the net rate of sediment accretion (Morris et al., 2002). Finally, sediment accretion and sediment accumulation are not equivalent terms, although sedimentation is a very important part of accretion. This chapter discusses sediment accumulation, as a driving force for marsh accretion and as an important linkage to carbon accumulation in MCBCL marshes.

Sediment Cores

Salt marshes occupy more than 10 km^2 on MCBCL and range from *Spartina*-dominated marshes along the ICW to *Juncus*-dominated fringing marshes on embayments and tributaries of the NRE. *Spartina*-dominated sites include Freeman Creek (Station FC-16-1) and backbarrier sites (Stations F1, F2 and F6). French Creek is a *Juncus*-dominated site, and mixed species marsh sites include Traps Bay Creek (Station TB-16-1). Seven sediment cores were collected across the coastal barrier and coastal wetland ecosystems (**Figure 12-1**). Backbarrier marsh cores (Stations F1, F2, and F6) were collected on October 4, 2013. The coastal wetland cores were collected from Freeman Creek and Traps Bay Creek on January 8, 2016. An additional core was collected from French Creek on June 27, 2016. After initial analyses, it was determined that one of the cores at Freeman Creek was collected from a disturbed area and that the core from Station F2 contained no appreciable $^{210}Pb_{xs}$; therefore, no further analyses were performed on those two cores.

Excess ^{210}Pb ($^{210}Pb_{xs}$) profiles for all marsh cores are presented in **Figure 12-8** as a function of mass depth (m, g cm^{-2}). The exponential trendline for each profile is represented by the dotted curves in **Figure 12-8**. The coastal wetland profiles (Freeman, French, and Traps) follow the trendline closely (R^2=approximately 0.88) with some parts of the profile deviating from the trendline. These deviations indicate periods when the rate of sedimentation has either increased or decreased relative to the idealized constant rate over the past 150 years. The deeper sediments of the Traps Bay core, in particular, exhibit a large scatter from the trendline. The backbarrier marsh profiles exhibit more frequent and larger deviations from the exponential trendline, especially Station F1 (R^2=0.62), indicating more variable rates of sedimentation at these sites, possibly due to overwash processes. F1 is proximate to the washover fan created by Hurricane Fran.

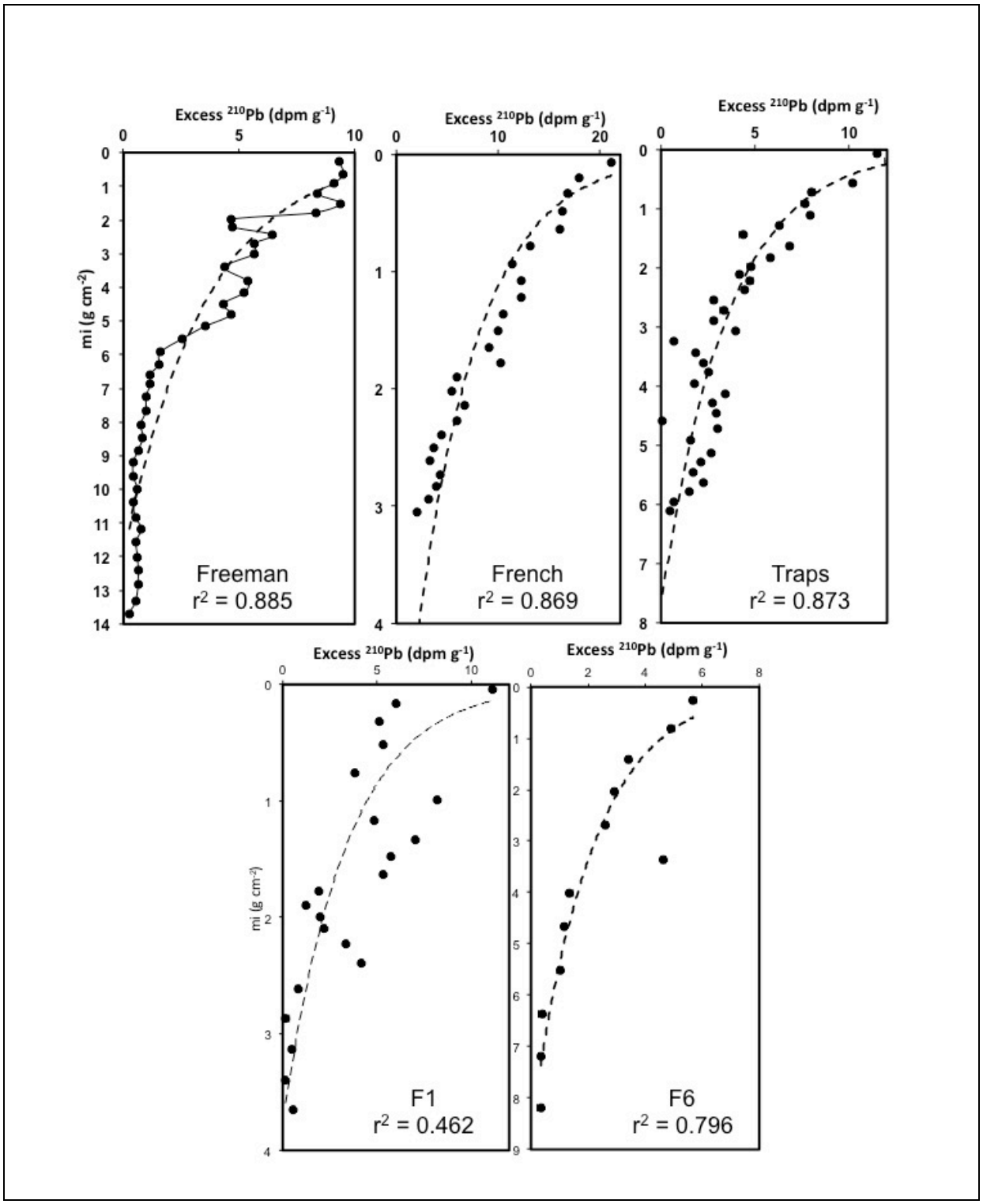

Figure 12-8. Excess ^{210}Pb profile for marsh cores.

The *y*-axis (m_i) is mass depth, which is the product of the interval thickness and the bulk density of the depth interval. The exponential trendline for each profile is represented by the dotted curves.

Geochronology models were applied to these profiles. Application of the CA model implies that deeper layers must be older and, for this reason, when using the CA model, the $^{210}Pb_{XS}$ concentration profile must decrease monotonically and closely follow the exponential trendline. Strictly speaking, this is not the case for the marsh profiles; therefore, the assumptions of the CA model are violated, and the CA model is not used in this study. In most cases, the mean SARs derived from the CF model are greater than 15% different from the SARs derived by using the CFCS model (**Table 12-3**). For all sites combined, the mean SAR values by using the CFCS model is 2.69 mm y^{-1} compared with 2.33 mm y^{-1} by using the CF model, or only a 15% difference.

Upon examination, it is clear that the higher rates derived when using the CFCS model result from the fact that CF–derived SARs generally increase from the bottom of the core (from the late 1800s to date; **Figure 12-9**). The CFCS model, which assumes a constant SAR throughout the core, can overestimate (and, in some cases, underestimate) the rates. It should be noted that a constant rate of accumulation is commonly assumed in sediment accretion and carbon accumulation studies cited in the literature (using impulse tracers such as ^{137}Cs or when CA or CFCS models are used for ^{210}Pb), so a re-examination of published rates may be in order, based on the differences observed in this study. Because the CF model provides additional information regarding changes in sedimentation rates during the past 150 years, the SAR profiles using the CF model are presented in **Figure 12-9**.

Table 12-3. Comparison of CF and CFCS Model Outputs *(150 year time scale)*

Model Outputs	Station F1	Station F6	Traps	French	Freeman
Mean SAR (CF)[a]	2.1	1.1	3.4	2.1	3.1
SAR (CFCS)[a]	1.5	1.1	4.5	3.5	2.7
Mean CAR (CF)[b]	44	15	151	98	67
CAR (CFCS)[b]	48	17	206	183	63
Mean Percent organic carbon (%)	14	2	26	44	6

[a] Units: mm y^{-1}

[b] Units: g C m^{-2} y^{-1}

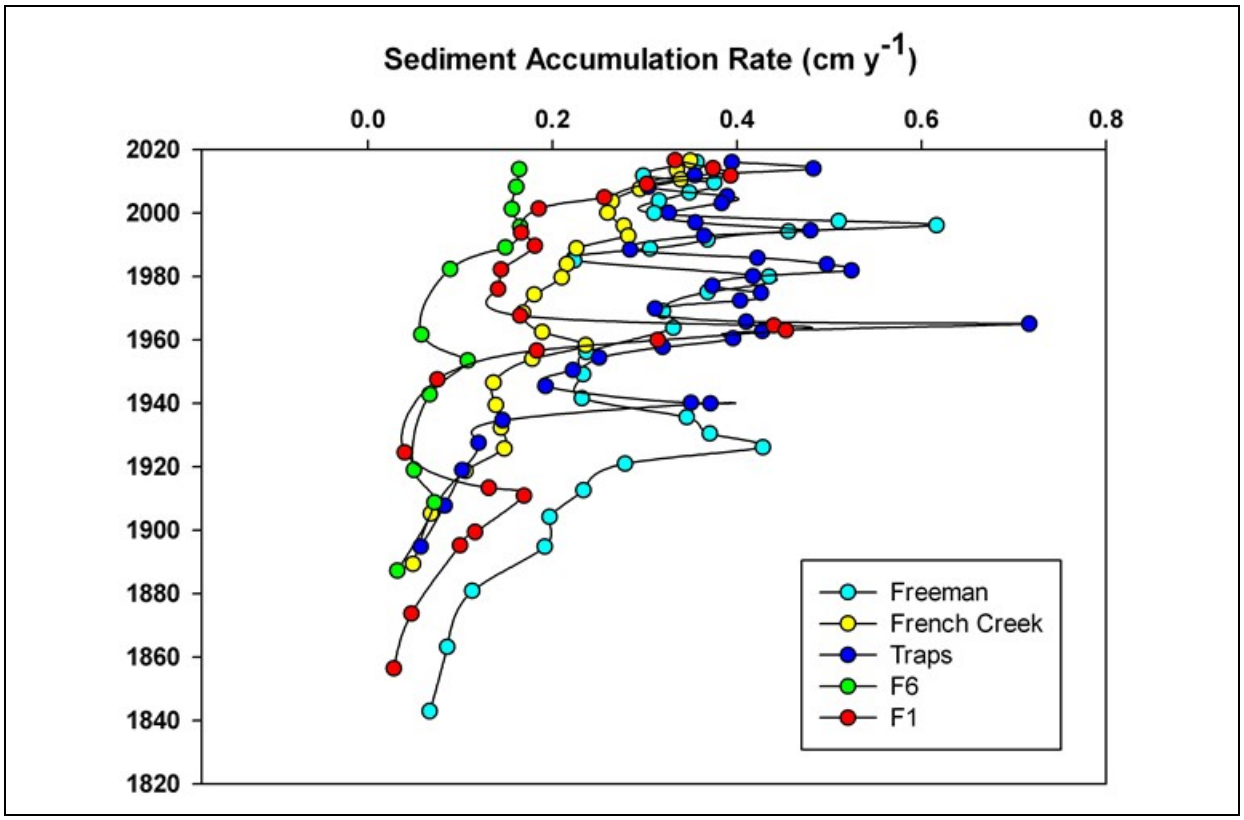

Figure 12-9. Sediment accumulation rates for MCBCL marsh sites.

Sediment Accumulation Rates in Marshes

A characteristic feature of all the marsh cores examined in MCBCL (**Figure 12-9**) is a gradual increase in sedimentation rate from the bottom of the cores (late 1800s). This gradual increase is likely a response to rising sea level. The mean SAR over the past 150 years is 2.06 mm y^{-1} for Station F1 and 1.06 mm $y^{-}1$ for Station F6; values that are below local rates of sea level rise (approximately 2.5 mm y^{-1} since 1860; Kemp et al., 2011). The mean sediment accumulation rates for the coastal wetland sites are 3.09 mm $y^{-}1$ for Freeman, 2.08 mm y^{-1} for French, and 3.40 mm y^{-1} for Traps. The current rates of sediment accumulation (averaged over the past 5 years) are 2.7 mm y^{-1} for Station F1, 1.6 mm y^{-1} for Station F6, 3.6 mm y^{-1} for Freeman, 3.5 mm y^{-1} for French, and 3.9 mm y^{-1} for Traps. These higher rates reflect the increasing rates observed over the past 150 years to date. At these current accretion rates, only Station F6 is not keeping up with the current rate of sea level rise. No distinguishable (multi-point) peaks are observed in the SAR profiles.

Factors Influencing SAR and CAR Values in Marshes

Some factors (elevation, dominant macrophyte, % OC) that potentially influence SAR and CAR values are shown in **Table 12-4**.

Table 12-4. SAR and CAR Values and Influencing Factors (Ranked)

Station	Elevation (m NAVD 88)	Dominant Macrophyte	SAR (mm y^{-1})	%C	CAR (g C m-2 y^{-1})
Freeman	−0.159 Lowest rank[a] (1)	*Spartina*	3.09 Rank (2)	6.1 Rank (4)	67 Rank (3)
Traps	0.068 Rank (2)	Mixed	3.40 Highest rank (1)	26.2 Rank (2)	151 Highest rank (1)
French	0.128 Highest rank (5)	*Juncus*	2.08 Rank (3)	44.2 Highest rank (1)	98 Rank (2)
Station F1	0.122 Rank (4)	*Spartina*	2.06 Rank (4)	13.9 Rank (3)	44 Rank (4)
Station F6	0.112 Rank (3)	*Spartina*	1.06 Lowest rank (5)	2.1 Lowest rank (5)	15 Lowest rank (5)

[a] Rank from highest to lowest except elevation (lowest to highest).

According to Chmura and Hung (2004), SAR decreases with distance from the nearest creek (i.e., low elevation marshes have higher SAR than high marsh). Since increasing distance from the nearest creek is usually proportional to increasing elevation, this decrease in SAR is probably due to shorter inundation time and thus reduced sediment input. Oenema and DeLaune (1988) developed a function describing the relationship between SAR and the distance of a marsh from the major creeks, showing that the SAR of low-elevation marsh is higher than that of high-elevation marsh. Low-elevation marshes have higher inundation frequency and are possibly linked to higher sediment availability (especially during storms). Freeman and Traps (the two lowest elevation marshes) have the two highest SARs. Traps, which has the second ranked % OC and the highest SAR, has the highest CAR value out of the marshes examined. In a related manner, Stations F1 and F6 (the two lowest SAR) are only connected to the ICW for sediment source (with occasional additions by overwash processes) and, therefore, may be limited by sediment availability. The nature of the sediments available can also be important. Station F6, which consists of mainly sandy sediments, has the lowest %C and the lowest SAR (no fine-grained source), and has the lowest CAR because of the inverse relationship between grain size and OC content.

Connor et al. (2001) reported that low-elevation marsh sediments were characterized by higher soil bulk densities and lower %C, whereas high-elevation marsh sediments are likely to have a higher carbon content (Connor et al., 2001; Zhou et al., 2007). In addition, it was observed that root productivity of salt marsh species is higher in low-inundation conditions than that in high-inundation conditions (Blum, 1993). The pattern of low marsh having higher CARs suggests that this increase in carbon content and root productivity is more than offset by the decrease in SAR and dry bulk density while going landward.

SAR and CAR values are also influenced by the dominant macrophyte at a site. French (the highest elevation) has only the third ranked SAR, but *Juncus* is the dominant macrophyte and as a consequence has by far the highest %C; therefore, French has the second highest CAR. Traps (a mixed macrophyte environment) has the second highest %C and the highest SAR and therefore is ranked first in CAR values.

SAR Comparisons to Other Marsh Environments

To put MCBCL marsh SAR values (range: 1.06 to 3.40 mm y^{-1}) in perspective, we can compare these rates to other global marsh data. In a recent compilation of marsh sedimentation rates (Ouyang and Lee, 2014) SAR values are provided from 141 sites worldwide; however, a geographic representation problem remains in this newest compilation. North American and European sites dominate the list; 70 sites (half of the total sites presented) are from the United States. However, this list is an improvement over previous accounting of marsh values. The world average SAR from Ouyang and Lee (2014) is 0.68 cm y^{-1} (6.8 mm y^{-1}) with a standard deviation of 0.77 cm y^{-1} (7.7 mm y^{-1}). MCBCL SAR values (mean: 2.34 mm y^{-1}) are below the published mean but comparable to the lower values cited in Ouyang and Lee (2014).

Pb-210 integrates over the past 150 years and therefore the SAR values derived in this study may not be directly comparable to overall values in Ouyang and Lee (2014). A large number of SAR values (62%) reported in that study were derived by using marker horizons, ^{137}Cs geochronologies or were back calculated from CAR and carbon density. Marker horizons and ^{137}Cs integrate over shorter times scales than ^{210}Pb and may not be directly comparable.

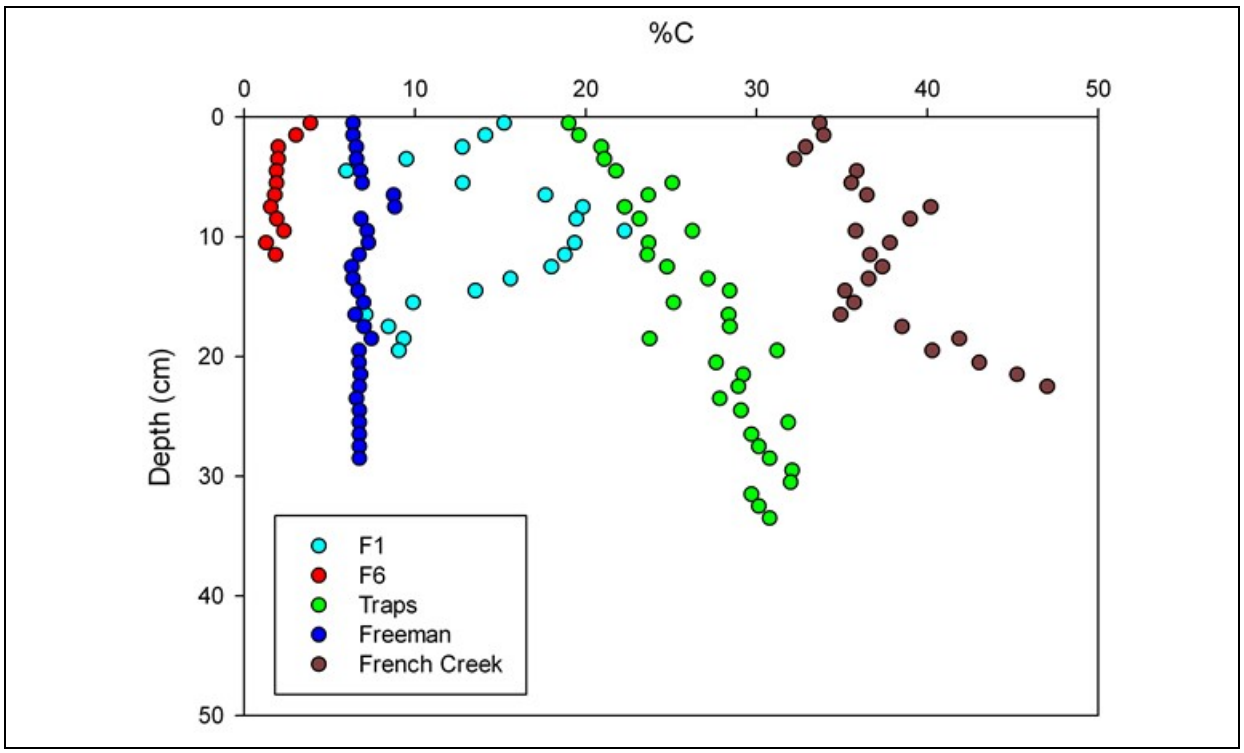

Figure 12-10. Percent organic carbon (% OC) profiles from marsh cores.

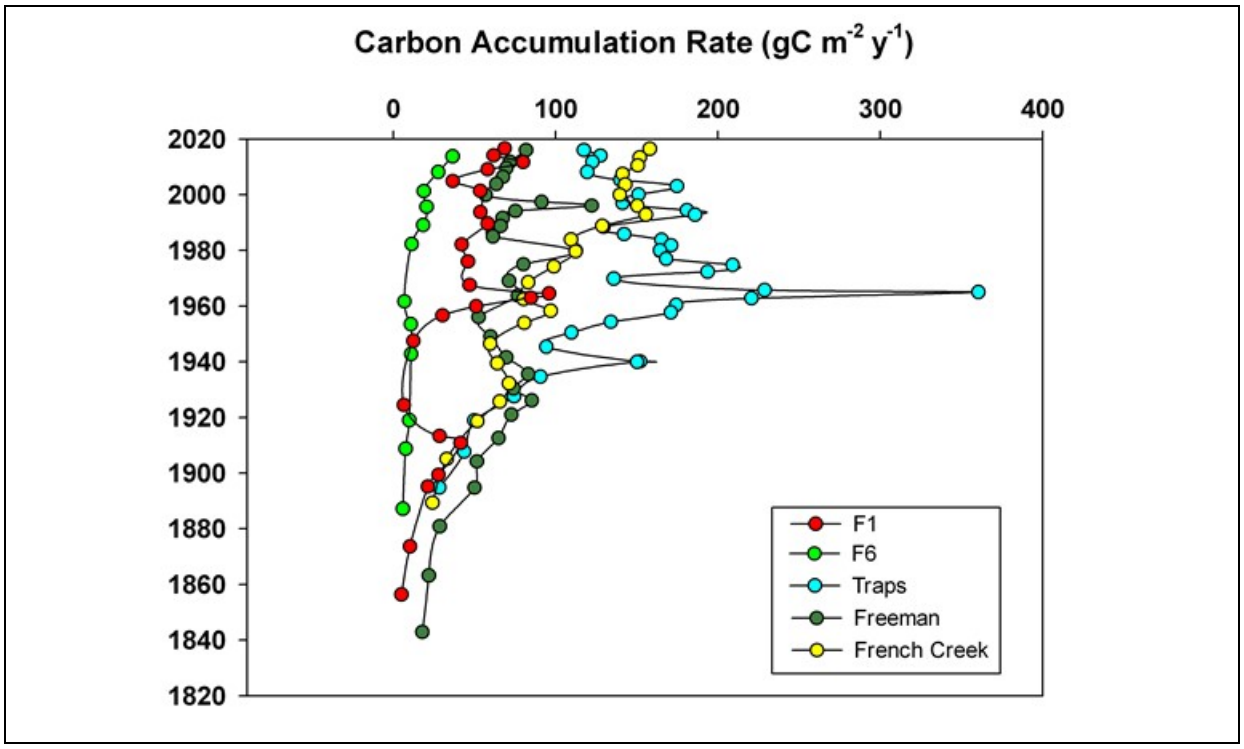

Figure 12-11. Carbon accumulation rates in MCBCL marsh cores.

CAR Comparisons to Other Marsh Environments

Vegetated coastal habitats (i.e., blue carbon habitats) cover less than 0.5% of seafloor bottom (Halpern et al., 2008), but they are disproportionately valuable carbon sinks. In particular, salt marshes (Cebrian, 2002; Duarte et al., 2005) are strongly autotrophic environments that fix carbon dioxide in excess of what is respired. This excess material accumulates in sediments at a rate accounting for approximately 46.9% of the approximately 250 Tg C buried throughout the entire ocean each year (Chmura et al., 2003; Duarte et al., 2005).

CAR values are the product of SAR and organic carbon fraction values. The % OC profiles for MCBCL marsh cores are presented in **Figure 12-10**. A wide range of values is observed in the cores examined (ranging from mean values of 2.12% at Station F6 to 44.2% at French). CAR profiles for MCBCL marsh cores are displayed in **Figure 12-11**.

In the latest compilation of global salt marsh CARs, Ouyang and Lee (2014) estimate the global mean to be 242.2 ±25.9 g C m^{-2} y^{-1}, with a range from 30 g C m^{-2} y^{-1} in the Arctic to 315 g C m^{-2} y^{-1} in the Mediterranean. CAR values for marshes examined in this study range from 15 to 150 g C m^{-2} y^{-1}. These CAR values are among the lowest reported in the literature. One possibility for this is that most of the sites examined are either sediment starved (back barrier environments at Stations F1 and F6) or have low OC supplies (Station F6 and Freeman), or they have a combination of these two factors. Only French and Traps have CAR values that are at or above 100 g C m^{-2} y^{-1}. Both these sites have high OC content (ranging from 26% to 44%).

The variation of CAR values in marshes at MCBCL and worldwide can be explained by its drivers. A CAR is driven by three parameters: SAR, dry bulk density of the soil, and its OC

content. Salt marshes have the highest rate of carbon accumulation of all vegetated coastal habitats because SARs generally approximate the rate of relative sea level rise (DeLaune et al., 1978; Ouyang and Lee, 2014); however, this is not the case (long term) for MCBCL marshes. Therefore, MCBCL CAR values are among the lowest documented in the literature.

Conclusions and Implications for Future Research and Implementation

Climatic and anthropogenic factors such as the construction of the Intracoastal Waterway and the establishment of Marine Corps Base Camp Lejeune (MCBCL) have impacted the New River Estuary (NRE) and associated wetlands, during the past century. The overall focus of this study was to better understand how sediment and organic carbon (OC) accumulations within the system have been impacted by these changes.

This is the first study to examine sediment and carbon accumulation rates in the NRE and marshes within MCBCL. This is the first quantification of sedimentation and carbon sequestration in the study area. Removal of organic carbon to estuarine and marsh sediments is an important parameter in the carbon budget for MCBCL. The results of this study are an important first step to filling this critical knowledge gap.

Key Scientific Findings

In the NRE, sediment accumulation rates have been increasing during the past century and, in the upper estuary, this general increase was punctuated by a dramatic increase in the 1990s (a period of high hurricane activity) peaking at 1999, the year of Hurricane Floyd's impact, which resulted in resulted in a 500-year flood in the basin. In the upper estuary sediment accumulation rates increase from 2 mm y^{-1} in the late 1800s to a present rate of 7.5 mm y^{-1} with a maxima in 1999 of over 10 mmy^{-1}. In the middle estuary, sediment accumulation rates increase from 1 mm y-1 in the late 1800s to a present rate of 4 mm y^{-1} without well-defined peaks in between. These findings indicate that the sediment input to the NRE has increased over the past century as a result of increased population and land use changes in the upper New river watershed. On top of this general increase, large storm events such as Hurricane Floyd have played an inordinate role in transferring sediments from the watershed to the NRE. The geomorphology of the NRE, which is a series of poorly connected lagoons, has been an important control on sediment retention within the estuary. As a result, sediment accumulation rates in the NRE are amongst the highest values recorded in the literature.

High surface water productivity and subsequent rapid remineralization within the water column lead to low oxygen conditions within bottom waters and surface sediments of the estuary. These low oxygen conditions optimize the preservation of terrestrial OC from the watershed. As a result, carbon accumulation rate (CAR) values in the upper NRE are also among the highest reported in the literature and values for the middle estuary are within the middle range of values observed in other estuaries. The terrestrial OC source is generally restricted to the upper estuary because of the limited connectivity between the upper and middle estuary. Geomorphological controls on the estuary (limited fetch for wind waves, limited connectivity between individual lagoons and with the ocean) govern the CAR distributions within the NRE.

The mean SARs over the past 150 years in MCBCL marshes range from 1 to 3 mm y^{-1}. The current SARs (averaged over the past 5 years) range from 2 mm y^{-1} to 4 mm y^{-1}. As a reference point, the local rate of sea level rise, since 1860, is approximately 2.5 mm y^{-1}. SARs for MCBCL marshes are generally below the present rate of sea level rise but sediment accumulation is only one factor that contributes to sediment accretion rates. This same story holds for CARs in MCBCL marshes. CAR values for the coastal wetland and back barrier sites examined in this study range from 15 g C m^{-2} y^{-1} to 150 g C m^{-2} y^{-1}. The global mean for marsh CARs is 242 g C m^{-2} y^{-1}, and the median value is 137 g C m^{-2} y^{-1}. CAR values in this study are comparable to the lower values cited in the literature and therefore, marshes in the MCBCL are vulnerable to SLR due to low sediment supply. Despite the lower values for SAR and CAR in MCBCL, these are very valuable environments in terms of ecosystem services as well as carbon sequestration.

Research Questions

1. **What are the rates of sediment accumulation within bottom sediment of the New River Estuary (NRE) and how are they distributed?**

Mean sediment accumulation rates (SARs) in the NRE range from 10 mm y^{-1} in the upper estuary to 2 mm y^{-1} in the middle estuary when integrated over the past 150 years. The lower estuary is non-depositional with sandy bottom sediments. The SAR values for the upper estuary are among the highest recorded in the literature. SAR values integrated over the past 5 years are similar (ranging from 4 to 9.mm y^{-1}). The high SAR values observed are primarily because the NRE consists of a series of lagoons that are poorly connected between lagoons and with the ocean. This geomorphology, coupled with low tidal and wave energy conditions, and long water residence times, results in most sediments remaining within the estuary. Upper estuary cores clearly show the importance of large storm floods such as Hurricane Floyd (which impacted the New River watershed in 1999) as major sources of sediment to the estuary.

2. **What are the rates of organic carbon (OC) accumulation within bottom sediment of the NRE and how are they distributed?**

Following the patterns of the SARs, CAR values range from 125 g C m^{-2} y^{-1} in the upper estuary to 21 g C m^{-2} y^{-1} in the middle estuary. The upper estuary CAR values are amongst the highest recorded in the literature (ranging from 3 to 79 g C m^{-2} y^{-1}). These high rates in the upper estuary result from the fact that it receives a large supply of terrestrial carbon, especially during storm floods. The low connectivity between the upper estuary and the ocean enable this terrestrial OC input to accumulate in the estuary. The low oxygen conditions of bottom waters and surface sediments in the upper estuary optimize terrestrial carbon preservation and OC accumulation.

3. **What impacts have land-use and climate change had on sediment and OC accumulations within bottom sediment of the NRE?**

The couplings between population increases and land-use changes during the past century have led to increases in the sediment yield in river basins worldwide. For rivers without substantial dams, this in turn has resulted in an increase in sediment loading to adjacent estuaries. Population increases and land-use changes have been prevalent within the New River watershed

during the past century. Therefore, as observed in other river-estuarine systems, the gradual increases in SAR and CAR in the NRE, since the late 1800, are likely due to increased sediment input from the basin. In addition, strong climate events, such as hurricanes, results in an episodic floods and pulses of particulate terrestrial carbon that is rapidly accumulated in estuarine bottom sediments.

4. What are the rates of sediment accumulation in marshes along the ICW and NRE?

SARs in the MCBCL marshes examined range from 1.06 to 3.40 mm y^{-1}. In contrast to sedimentation rates in the estuary, these marsh sedimentation rates are among the lowest reported in the literature. The world average SAR is 6.8 mm y^{-1} (two to six times higher than observed in MCBCL marshes). Globally, the lowest directly measured SAR value (1.33 mm y^{-1}) is from Greenland, and the highest measured value (14.5 mm y^{-1}) was from the sediment Mississippi delta in Louisiana. The lack of connectivity of the marshes (with the estuary and the ocean) is again the governing factor; the marshes are sediment starved.

5. What are the rates of OC accumulation in marshes along the ICW and NRE?

The CAR for marshes along the ICW and NRE range from 15 to 150 g C m^{-2} y^{-1}. The global mean for marsh CAR is 242.2 ±25.9 g C m^{-2} y^{-1}, with a range from 30 g C m^{-2} y^{-1} in the Arctic to 315 g C m^{-2} y^{-1} in the Mediterranean. The MCBCL marsh CAR values are amongst the lowest reported in the literature. One possibility for this low CAR value is that most the sites examined are either sediment starved (back barrier environments) or have low OC supplies, or they have a combination of these two factors.

6. How will sea level rise affect carbon storage in MCBCL marshes over the next century?

As a reference point, the current rate of sea level rise is approximately 2.5 mm y^{-1}, and the rate of rise is accelerating. The most important measurement for marsh environments is sediment accretion rate. Marshes with accretion rates that are less than the rate of sea level rise are eventually drowned. Sediment accretion rates are the sum of sediment accumulation, biogenic growth, microbial decay and physical compaction. During this study, we measured the SARs; for MCBCL marshes, the SAR range was from 1.06 to 3.40 mm y^{-1} (amongst the lowest rates reported for marshes). Sediment accretion and sediment accumulation are not equivalent terms, although SAR is a very important part of accretion. For SAR as a contribution to sediment accretion rates in MCBCL marshes, the prospect of the marshes remaining above sea level is low. Information about other factors regarding below-ground biomass and sediment compaction are needed to make a full assessment. If the rate of sea level rise exceeds accretion rates, then not only will the marshes cease to be sites for carbon accumulation, but also the OC that has been accumulation over the past century (or longer) will be subject to erosion and loss.

Findings with Implications for Future Base Management

Controls on sediment and carbon accumulation in the NRE are largely within the upper New River Watershed and therefore, there are no specific management changes that are needed to maintain sustainability with respect to sediment and carbon accumulation in the estuary. An

increase in intense storms resulting from climate change will serve to maintain or increase sediment and carbon accumulation in the NRE. The lack of conditions that connect the upper and middle NRE with the lower NRE and the ocean will help maintain sediment and carbon accumulation within the NRE. The low sediment supply to MCBCL marshes appears to be due to a combination of local geomorphology and past anthropogenic impacts such as the construction of the ICW. Therefore, no specific management changes are suggested to maintain the sustainability of MCBCL marshes. However, any future changes that lead to a greater connectivity between the marshes and potential sediment sources would certainly increase the viability of MCBCL marshes. The possibility of a future increase in intense storm activity will be a double-edged sword for MCBCL marshes. The potential for increased sediment supply from storm activity could be offset by increased shoreface erosion of existing marshes.

Literature Cited

Altman, J. C., and H. W. Paerl. 2012. Composition of inorganic and organic nutrient sources influences phytoplankton community structure in the New River Estuary, North Carolina. *Aquatic Ecology 46*(3):269–282.

Blum, L. 1993. *Spartina alterniflora* root dynamics in a Virginia marsh. *Marine Ecology Progress Series 102*:69–178.

Bricker, S.B., C.G. Clement, D.E. Pirtalla, S.P. Orlando, and D.R.G. Farrow. 1999. *National estuarine eutrophication assessment: Effects of nutrient enrichment in the nation's estuaries*. National Oceanic and Atmospheric Administration, National Ocean Service, Special Projects Office and the National Centers for Coastal Ocean Science, Silver Spring, MD. Report available at https://ian.umces.edu/neea/pdfs/eutro_report.pdf

Cebrian, J. 2002. Variability and control of carbon consumption, export, and accumulation in marine communities. *Limnology and Oceanography 47*(1):11–22.

Chmura, G.L., and G.A. Hung. 2004. Controls on salt marsh accretion: A test in salt marshes of Eastern Canada. *Estuaries 2*:70–81.

Chmura, G., S.C. Anisfeld, D.R. Cahoon, and J.C. Lynch. 2003. Global carbon sequestration in tidal, saline wetland soils. *Global Biogeochemical Cycles 17*:1111–1123.

Connor, R.F., G.L. Chmura, and C.B. Beecher. 2001. Carbon accumulation in Bay of Fundy salt marshes: Implications for restoration of reclaimed marshes. 2001. *Global Biogeochemical Cycles 15*(4):943–954.

DeLaune, R.D., W.H. Patrick, and R.J. Buresh. 1978. Sedimentation rates determined by ^{137}Cs dating in a rapidly accreting salt marsh. *Nature 275*(5680):532–533.

DeMaster, D.J., B.A. McKee, C. Nittrouer, Q. Jiangchu, and C. Guodong. 1985. Rates of sediment accumulation and particle reworking based on radiochemical measurement from continental shelf deposits in the East China Sea. *Continental Shelf Research 4*:143–158.

Duarte, C.M., J.J. Middelburg, and N. Caraco. 2005. Major role of marine vegetation on the oceanic carbon cycle. *Biogeosciences 2*:1–8.

Ensign, S.H., J.N. Halls, and M.A. Mallin. 2004. Application of digital bathymetry data in an analysis of flushing times of two large estuaries. *Computers and Geosciences 30*(5):501–511.

Goñi, M.A., K.C. Ruttenberg, and T.I. Eglinton. 1997. Sources and contribution of terrigenous organic carbon to surface sediments in the Gulf of Mexico. *Nature 389*:275–278.

Gordon, E.S., and M.A. Goñi. 2004. Controls on the distribution and accumulation of terrigenous organic matter in sediments from the Mississippi and Atchafalaya river margin. *Marine Chemistry 92*:331–352.

Halpern, B.S., S. Walbridge, K.A. Selkoe, C.V. Kappel, F. Micheli, C. D'Agrosa, J.F. Bruno, K.S. Casey, C. Ebert, H.E. Fox, R. Fujita, D. Heinemann, H.S. Lenihan, E.M.P. Madin, M.T. Perry, E.R. Selig, M. Spalding, R. Steneck, and R. Watson. 2008. A global map of human impact on marine ecosystems. *Science 319*:948–952.

Hedges, J.I., and R.G. Keil. 1995. Sedimentary organic matter preservation: an assessment and speculative synthesis. *Marine Chemistry 49*(2–3):137–139.

Herrmann, M., R.G. Najjar, W.M. Kemp, R.B. Alexander, E.W. Boyer, W. Cai, and R.A. Smith. 2015. Net ecosystem production and organic carbon balance of U.S. East Coast estuaries: A synthesis approach. *Global Biogeochemical Cycles 29*(1):96–111.

Kemp, A.C., B.P. Horton, and J.P. Donnelly. 2011. Climate related sea-level variations over the past two millennia. *Proceedings of the National Academy of Sciences 108*(27):11017–11022.

Kemp, W.M., E.M. Smith, M. Marvin-DiPasquale, and W.R. Boynton. 1997. Organic carbon balance and net ecosystem metabolism in Chesapeake Bay. *Marine Ecology Progress Series 150*:229–248.

Kirwan, M.L., and A.B. Murray. 2007. A coupled geomorphic and ecological model of tidal marsh evolution. *Proceedings of the National Academy of Sciences 104*:6118–6122.

Kolker, A.S., S.L. Goodbred, S. Hameed, and J.K. Cochran. 2009. High-resolution records of the response of coastal wetland systems to long-term and short-term sea level variability. *Estuarine, Coastal and Shelf Science 84*:493–508.

Lamb, A.L., G.P. Wilson, and M.J. Leng. 2006. A review of coastal palaeoclimate and relative sea-level reconstructions using delta C-13 and C/N ratios in organic material. *Earth-Science Reviews 75*(1–4):29–57.

Maher, D.T., and B.D. Eyre. 2012. Carbon budgets for three autotrophic Australian estuaries: Implications for global estimates of the coastal air–water CO_2 flux. *Global Biogeochemical Cycles 26*:GB1032.

Mallin, M.A., M.R McIver, H.A. Wells, D.C. Parsons, and V.L. Johnson. 2005. Reversal of eutrophication following sewage treatment upgrades in the New River Estuary, NC. *Estuaries 28*:750–760.

McKee, B.A., C.A. Nittrouer, and D.J. DeMaster. 1983. The concepts of sediment deposition and accumulation applied to the continental shelf near the mouth of the Yangtze River. *Geology 11*:631–633.

Morris, J.T., P.V. Sundareshwar, C.T. Nietch, B. Kjerfve, and D.R. Cahoon. 2002. Responses of coastal wetlands to rising sea level. *Ecology 83*:10:2869–2877.

Mudd, S.M., S.M. Howell, and J.T. Morris. 2009. Impact of dynamic feedbacks between sedimentation, sea level rise, and biomass production on near-surface marsh stratigraphy and carbon accumulation. *Estuarine, Coastal and Shelf Science 82*:377–389.

Nittrouer, C.A., R.W. Sternberg, R. Carpenter, and J.T. Bennett. 1979. The use of Pb-210 geochronology as a sedimentological tool: Application to the Washington coastal shelf. *Marine Geology 31*:297–316.

Oenema, O., and R.D. DeLaune.1988. Accretion rates in salt marshes in the Eastern Scheldt, Southwest Netherlands. *Estuarine, Coastal and Shelf Science 26*(4):379–394.

Ouyang, X., and S.Y. Lee. 2014. Updated estimates of carbon accumulation rates in coastal marsh sediments. *Biogeosciences 11*:5057–5071.

Renfro, A.A., J.K. Cochran, and D.J. Hirschberg. 2016. The sediment budget of an urban coastal lagoon (Jamaica Bay, NY) determined using Th-234 and Pb-210. *Estuarine, Coastal and Shelf Science 180*:136–149.

Roden, E.E., J.H. Tuttle, W.R. Boynton, and W.M. Kemp. 1995. Carbon cycling in mesohaline Chesapeake Bay sediments 1: POC deposition rates and mineralization pathways. *Journal of Marine Research 53*:779–819.

Ruiz-Fernández, A.C., Hillaire-Marcel, C., Ghaleb, B., Soto-Jimenez, M., and Paez-Osuna, F. 2002. Recent sedimentary history of anthropogenic impacts on the Culiacan River Estuary, northwestern Mexico: Geochemical evidence from organic matter and nutrients. *Environmental Pollution 118*(3):365–377.

Sanchez-Cabeza, J., and A. Ruiz-Fernández. 2012. ^{210}Pb sediment radiochronology: An integrated formulation and classification of dating models. *Geochimica et Cosmochimica Acta 82*:183–200.

Smith, R.W., T.S. Bianchi, and M. Allison. 2015. High rates of organic carbon burial in fjord sediments globally. *Nature Geoscience 8*(6):450–454.

Warnken, K.W., P.H. Santschi, K.A. Roberts, and G.A. Gill. 2008. The cycling and oxidation pathways of organic carbon in a shallow estuary along the Texas Gulf Coast. *Estuarine, Coastal and Shelf Science 76*:69–84.

Zhou J., Y. Wu, Q. Kang, and J. Zhang. 2007. Spatial variations of carbon, nitrogen, phosphorous and sulfur in the salt marsh sediments of the Yangtze Estuary in China. *Estuarine, Coastal and Shelf Science* 71(1–2):47-59.

Zhu, J., and C.R. Olsen. 2014. Sedimentation and organic carbon burial in the Yangtze River and Hudson River Estuaries: Implications for the global carbon budget. *Aquatic Geochemistry 20*(2–3):325–342.

Appendix 12-A
Supporting Data

Table 12A-1. Dry Bulk Density (g cm^3) versus Depth (cm) for NRE cores

Depth	NRE1	NRE2	NRE3	NRE4	NRE6
0.5	0.076	0.048	0.123	0.171	0.171
1.5	0.131	0.100	0.123	0.361	0.361
2.5	0.113	0.116	0.150	0.239	0.239
3.5	0.144	0.131	0.113	0.367	0.366
4.5	0.150	0.103	0.190	0.366	0.366
5.5	0.171	0.125	0.225	0.403	0.402
6.5	0.177	0.137	0.195	0.285	0.285
7.5	0.194	0.146	0.230	0.366	0.366
8.5	0.168	0.159	0.224	0.343	0.343
9.5	0.232	0.158	0.220	0.318	0.318
10.5	0.219	0.115	0.230	0.263	0.263
11.5	0.179	0.167	0.216	0.365	0.365
12.5	0.199	0.218	0.229	0.289	0.289
13.5	0.224	0.202	0.248	0.380	0.380
14.5	0.176	0.186	0.226	0.358	0.358
15.5	0.210	0.177	0.245	0.394	0.394
16.5	0.182	0.168	0.174	0.344	0.344
17.5	0.217	0.189	0.249	0.271	0.271
18.5	0.175	0.149	0.205	0.349	0.349
19.5	0.212	0.190	0.192	0.335	0.335
20.5	0.148	0.122	0.195	0.373	0.372
21.5	0.201	0.200	0.237	0.345	0.345
22.5	0.166	0.166	0.231	0.311	0.311
23.5	0.203	0.203	0.237	0.354	0.354
24.5	0.198	0.198	0.212	0.271	0.271
25.5	0.184	0.184	0.209	0.338	0.338
26.5	0.174	0.174	0.193	0.353	0.352
27.5	0.206	0.207	0.209	0.282	0.282
28.5	0.198	0.193	0.188	0.310	0.310
29.5	0.215	0.211	0.208	0.332	0.332
30.5	0.174	0.212	0.250	0.273	0.273
31.5	0.189	0.211	0.233	0.348	0.347
32.5	0.149	0.159	0.169	0.326	0.326
33.5	0.191	0.203	0.216	0.357	0.356

Depth	NRE1	NRE2	NRE3	NRE4	NRE6
34.5	0.226	0.210	0.194	0.412	0.412
35.5	0.210	0.222	0.233	0.352	0.352
36.5	0.159	0.166	0.173	0.270	0.270
37.5	0.213	0.215	0.217	0.135	0.135
38.5	0.218	0.189	0.161	0.270	0.270
39.5	0.239	0.223	0.207	0.329	0.329
40.5	0.208	0.186	0.164	0.282	0.282
41.5	0.199	0.220	0.241	0.354	0.354
42.5	0.189	0.185	0.181	0.313	0.312
43.5	0.218	0.217	0.215	0.304	0.304
44.5	0.223	0.229	0.235	0.275	0.275
45.5	0.257	0.236	0.215	0.297	0.297
46.5	0.185	0.208	0.231	0.244	0.244
47.5	0.199	0.223	0.248	0.295	0.295
48.5	0.184	0.203	0.223	0.244	0.244
49.5	0.193	0.227	0.261	0.296	0.295

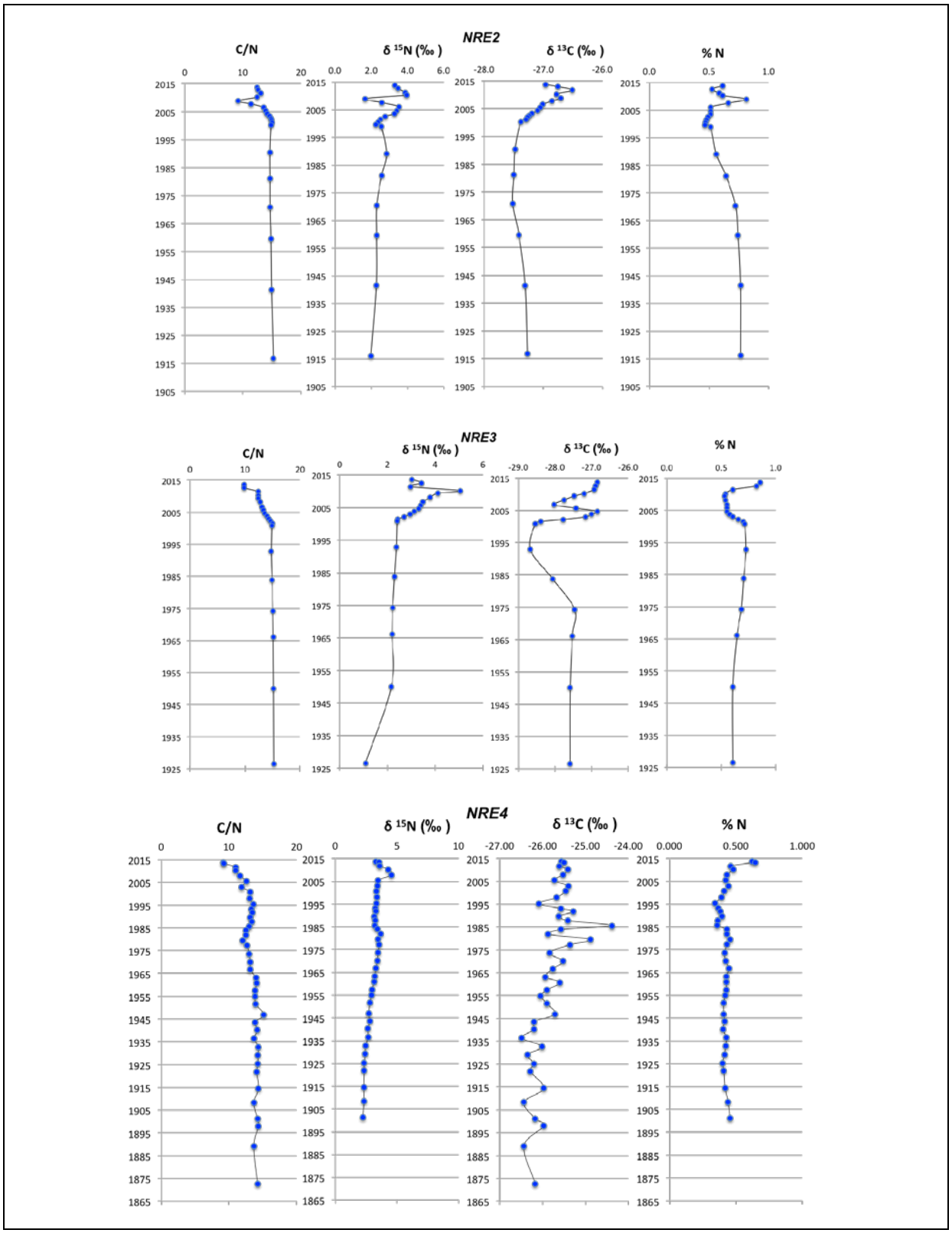

Figure 12A-1. Sediment organic matter was characterized with respect to %N, C:N, $\delta^{13}C$, and $\delta^{15}N$ to constrain source contributions of organic carbon stored in sediments (continued)

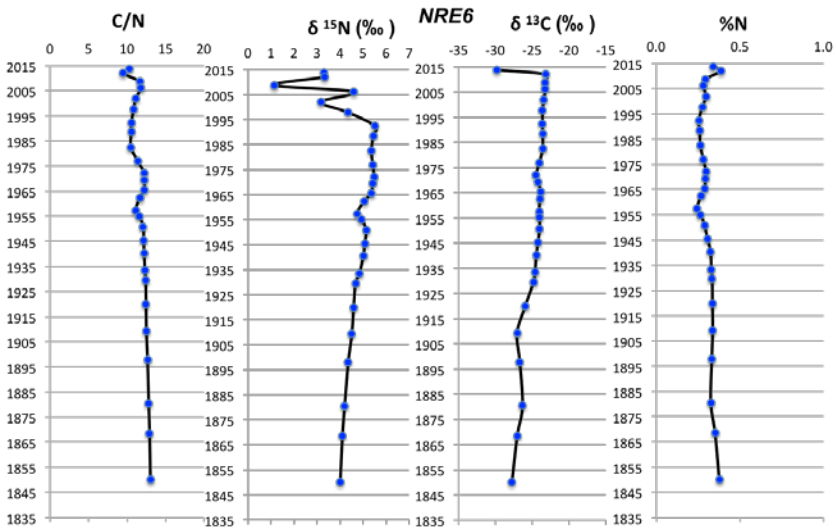

Figure 12A-1. Sediment organic matter was characterized with respect to %N, C:N, $\delta^{13}C$, and $\delta^{15}N$ to constrain source contributions of organic carbon stored in sediments.

Appendix 12-B
List of Scientific/Technical Publications

Papers

Crosswell. J., I. Anderson, J. Stanhope, B. Van Dam, M. Brush, S. Ensign, M. Piehler, B. McKee, M. Bost, H. Paerl. 2017. Carbon budget of a shallow, lagoonal estuary: Transformations and source-sink dynamics along the river-estuary-ocean continuum. *Limnology and Oceanography* 00:00.

Thesis

How storms affect carbon burial in the new river estuary, North Carolina. Molly Bost. University of North Carolina at Chapel Hill, Master of Science in the Department of Marine Sciences. 2016

Presentations

Temperature effects on the carbon content of marsh core subsamples through time. Atencio, A., B. McKee and T. Rodriguez. Oral Presentation. GSA Southeastern, March 31, 2017. Anadarko Annual Research Symposium, April 27, 2017

Oyster reef and marsh accretion rates in correspondence to sea-level rise. Poster Presentation, GSA, November 2, 2015. Atencio, A., T. Rodriguez, and B. McKee. Chancellor's Science Scholars Research Symposium, December 2015

Response of sediment accumulation rates in the new river estuary to storm events. Poster Presentation, CERF Meeting November 2015. Bost, M. and B. McKee

Appendix 12-C
List of Students

- Molly Bost, M.S., Marine Science, University of North Carolina at Chapel Hill, May 2016
- Anna Atencio, B.S., Geological Sciences, University of North Carolina at Chapel Hill, May 2017.

Chapter 13

Coastal Wetlands Module

SERDP Project Number: RC-2245

Coastal Wetlands

Research Project CW-4

Lead Researchers:

Dr. Carolyn A. Currin, National Oceanic and Atmospheric Administration's National Centers for Coastal Ocean Science, Beaufort Laboratory
E-mail: Carolyn.currin@noaa.gov

Supporting Researchers:

Dr. Iris Anderson, VIMS
Dr. Jenny Davis, NOAA
Dr. Scott Ensign, Aquatic Analysis and Consulting, LLC
Dr. Ellen Herbert, VIMS postdoctoral
Dr. Matt Kirwan, VIMS
Brent McKee, UNC-CH
Dr. Nathan McTigue, NOAA NRC postdoctoral
Dr. Craig Tobias, UCONN

November 2017

Final

This report was prepared under contract to the U.S. Department of Defense (DoD) Strategic Environmental Research and Development Program (SERDP). The publication of this report does not indicate endorsement by DoD, nor should the contents be construed as reflecting the official policy or position of DoD. References herein to any specific commercial product, process, or service by trade name, trademark, manufacturer, or otherwise, do not necessarily constitute or imply its endorsement, recommendation, or favoring by DoD.

Table of Contents

Acronyms 13-viii
Abstract 13-1
Objectives of the Research Project 13-4
Background 13-4
Section 1. Suspended Sediment Concentration and Transport Mechanisms 13-9
Introduction 13-9
Materials and Methods 13-9
Results and Discussion 13-11
Section 2. Variations in Below-Ground Biomass with Elevation and Nutrient Availability 13-19
Introduction 13-19
Materials and Methods 13-19
Results and Discussion 13-21
Section 3. Geospatial Marsh Model 13-37
Introduction 13-37
Methods and Materials 13-37
Results and Discussion 13-46
Section 4. Investigating Salt Marsh Sediment Carbon Decomposition After Erosion Events 13-61
Introduction 13-61
Materials and Methods 13-61
Results and Discussion 13-63
Section 5. Drivers of Organic Carbon Content and Accumulation Rates in Salt Marsh Sediments 13-70
Introduction 13-70
Materials and Methods 13-70
Results and Discussion 13-71
Conclusions and Implications for Future Research and Implementation 13-84
Research Questions 13-84
Other Key Scientific Findings 13-86
Literature Cited 13-88
Appendix 13-A: Supporting Data 13-A-1
Appendix 13-B: List of Scientific/Technical Publications 13-B-1
Appendix 13-C: Other Supporting Information 13-C-1

List of Figures

Figure 13-1. Conceptual model for the Coastal Wetlands Module. 13-5

Figure 13-2. Location of coastal wetland research and monitoring stations on Marine Corps Base Camp Lejeune. 13-7

Figure 13-3. Suspended sediment concentrations (SSCs) in Freeman, Traps, and French Creeks. 13-13

Figure 13-4. Suspended sediment concentrations (SSCs) in the marshes of Freeman, Traps, and French Creeks. 13-14

Figure 13-5. Channel width, wetland width, and sampling sites in Freeman, Traps, and French Creeks. 13-16

Figure 13-6. The relationship between the in-channel suspended sediment (upstream and downstream sites combined) and the position of the transition from embayed to wetland-dominated. 13-17

Figure 13-7. Distribution of below-ground biomass with respect to relative tidal elevation. 13-22

Figure 13-8. Annual below-ground biomass production measured as amount of root+rhizome material in ingrowth bags after 1 year at Mile Hammock Bay (MHB) and Onslow Beach Backbarrier (OBB). 13-23

Figure 13-9. Annual below-ground biomass production measured as amount of root+rhizome material in ingrowth bags after 1 year at Traps Bay Creek (TBC) and Freeman Creek (FC). 13-23

Figure 13-10. Estimated relative turnover rate of below-ground biomass. 13-24

Figure 13-11. Live+dead standing above- and below-ground J. romerianus biomass across the elevation gradient at French Creek (FN). 13-25

Figure 13-12. Average Spartina alterniflora above-ground biomass by site and year. 13-26

Figure 13-13. Standing belowground biomass (BGB; live+dead) in fertilized and control plots. 13-27

Figure 13-14. Measured porewater ammonium (NH_4^+) concentrations in fertilized and control plots sampled at 5 cm and 15 cm. 13-28

Figure 13-15. Measured porewater PO_4 concentrations in fertilized and control plots sampled at 5 cm and 15 cm. 13-29

Figure 13-16. Porewater hydrogen sulfide (H_2S) concentrations in fertilized (F) and control (C) plots. 13-30

Figure 13-17. Average measured sediment accretion by treatment. 13-34

Figure 13-18. Elevation change over time at Freeman Creek. Solid markers/solid lines represent fertilized plots, open markers/dashed lines represent control plots. 13-35

Figure 13-19. Elevation change over time at Onslow Bay (OB) and Mile Hammock (MH) Bay. 13-35

Figure 13-20. Domain for marsh modeling at Freeman Creek, Traps Bay, and French Creek at MCBCL. 13-37

Figure 13-21. Habitat classifications derived from MCBCL RGB and IR Ortho-Imagery for the three study domains. 13-39

Figure 13-22. Vegetation-corrected digital elevation maps of the three marsh domains at MCBCL. 13-41

Figure 13-23. Example plot of probability distribution function for vegetation types extracted from the DEM by using the habitat classification at Freeman Creek. 13-46

Figure 13-24. Modeled change in total marsh area (km^2) over five sea level scenarios for the three study domains: (top) Freeman Creek, (middle) Traps Bay, and (bottom) French Creek. 13-50

Figure 13-25. Modeled habitat coverage in 2100 under five sea level scenarios for the three study marsh domains at MCBCL: (left) Freeman Creek, (middle) Traps Bay, and (right) French Creek. 13-51

Figure 13-26. Modeled change in spatially averaged marsh accretion rate (mm/yr) over five sea level scenarios for the three study domains: (top) Freeman Creek, (middle) Traps Bay, and (bottom) French Creek. 13-52

Figure 13-27. Modeled habitat coverage in 2013, 2035, 2065, and 2100 under low (0.8 m) sea level rise scenario across the three model domains, illustrating three responses to rising sea level: transgression + accretion (Freeman Creek [left]), accretion + transition to flood tolerant vegetation (Traps Bay [middle]), and drowning (French Creek [right]). 13-53

Figure 13-28. Modeled change in average marsh carbon accumulation rate ($g\ m^2\ yr^{-1}$; left panel) and total carbon accumulation across each site (kg/yr; right panel) over five sea level scenarios for the three study domains: (top) Freeman Creek, (middle) Traps Bay, and (bottom) French Creek. 13-55

Figure 13-29. Modeled change in total marsh area (km^2), average accretion rate ($mm\ yr^{-1}$) and carbon burial rate (g carbon [C] $m^{-2}\ yr^{-1}$) at Traps Bay at the medium sea level rise (1.3 m by 2100) scenario under double ambient suspended sediment concentrations (SSCs; dark blue circles), current ambient SSC (medium blue triangles), and half ambient SSC (light blue squares). 13-57

Figure 13-30. Modeled change in total marsh area (km^2), average accretion rate ($mm\ yr^{-1}$) and carbon burial rate (g carbon [C] $m^{-2}\ yr^{-1}$) at Freeman Creek under double ambient suspended sediment concentrations (SSCs; dark blue circles), current ambient SSC (medium blue triangles), and half ambient SSC (light blue squares). 13-58

Figure 13-31. Accretion model validation comparing the measured marsh accretion rates and organic contents from SETs at three MCBCL marshes (i.e., Freeman Creek, Onslow Beach, and Mile Hammock Bay) with modeled accretion and organic content. 13-60

Figure 13-32. Maximum accretion rate modeled under unfertilized conditions (black), fertilized conditions by using the balanced growth model described in the text (green), and fertilized conditions with static root to shoot (R:S) allocation (blue) across suspended concentrations (0–60 mg/L). 13-60

Figure 13-33. Molar carbon to nitrogen (C:N) ratios of sediment from litter bottle experiment. 13-63

Figure 13-34. Litter bottle mass-loss change for each depth horizon over the course of the 77-day experiment. 13-64

Figure 13-35. Cumulative decomposition for shallow and deep sediment at 20°C and 30°C. 13-66

Figure 13-36. An example temperature profile from 1 year of monitoring data (left). 13-67

Figure 13-37. Conceptual schematic of the salt marsh carbon pump. 13-68

Figure 13-38. Regression plots for %OC and %OM for Freeman Creek (FC), French Creek (FN), and Traps Bay Creek (TB). 13-72

Figure 13-39. Profiles of organic matter content (%OM) in cores collected from MCBCL. 13-75

Figure 13-40. Profiles of organic carbon content (%OC) in cores collected from MCBCL. 13-75

Figure 13-41. Profiles of sediment carbon density (SCD) from cores collected at MCBCL. 13-77

Figure 13-42. Profiles of molar carbon to nitrogen ratios in cores collected at Freeman Creek (FC), French Creek (FN), and Traps Bay Creek (TB). 13-77

Figure 13-43. Profiles of stable carbon isotope values ($\delta^{13}C$) for Freeman Creek (FC) and Traps Bay Creek (TB) cores. Grey rectangles represent the $\delta^{13}C$ range of C_3 vegetation (e.g., Juncus roemarianus, maritime forest), and green rectangles represent C_4 vegetation (e.g., Spartina alterniflora, Distichilis sp). 13-78

Figure 13-44. Profiles of bulk density in cores collected from MCBCL. Profiles are color coded. 13-79

Figure 13-45. Box plots that represent the distribution of organic carbon content (left) and sediment carbon density (right) from MCBCL marsh sites. 13-79

Figure 13-46. Relationship between %OM and bulk density. 13-80

Figure 13-47. Source plot for marsh material collected at Freeman Creek (FC; black) and Traps Bay Creek (RB; red). 13-81

Figure 13-48. Scatterplot of carbon accumulation rate as a function of radiocarbon age. 13-82

List of Tables

Table 13-1. Suspended, Surface Microlayer, and Skimmed Matter at the Upstream Site: Mean (Minimum, Maximum) 13-12

Table 13-2. Suspended, Surface Microlayer, and Skimmed Matter at the Downstream Site: Mean (Minimum, Maximum) 13-12

Table 13-3. Tidal Constituents Modeled with T-Tide from 1 Year of Water Level Data .. 13-15

Table 13-4. Seasonal Mean NH_4^+ Concentrations 13-28

Table 13-5. Mean NH_4^+ Concentration by Site. Reported Values Are Averages Across All Depths (5 cm and 15 cm) and All Seasons by Site 13-29

Table 13-6. Mean Porewater Hydrogen Sulfide (H_2S) by Sample Date 13-30

Table 13-7. Mean Porewater H_2S by Site 13-30

Table 13-8. Sediment Particle Size and Bulk Density in Fertilized and Control Plots. 13-32

Table 13-9. Mean Daily Sediment Deposition by Site Across All Seasons 13-33

Table 13-10. Mean Daily Sediment Deposition by Season Across All Sites 13-33

Table 13-11. Starting Elevation, Elevation Change Rate, and Mean Biomass at Fertilized and Control Plots. 13-36

Table 13-12. Summary of Each Modeling Scenario, Corresponding with Global Scenarios to Which MCBCL–Specific Adjustments Were Added 13-38

Table 13-13. Site-Specific Model Parameters 13-44

Table 13-14. Global Model Parameters 13-45

Table 13-15. Initial Habitat Classification and Total Area (m^2) Based on RGB and IR Digital Ortho-Imagery from MCBCL 13-47

Table 13-16. Summary of Vegetation Errors, DEM Correction Factors, and Errors in DEMs Corrected for Vegetation Induced Errors in LiDAR–Derived Elevations 13-48

Table 13-17. Percent (%) Change in Marsh Area from Initial Condition (2013) for Each Sea Level Rise Scenario Under Ambient Sediment Conditions for Each Marsh 13-48

Table 13-18. Percent (%) Change in Annual Carbon Accumulation (kg/yr) Across the Entire Marsh from Initial Condition (2013) for Each Sea Level Rise Scenario Under Ambient Sediment Conditions for Each Marsh 13-54

Table 13-19. Characteristics of the Two Sediment Horizons Incubated During the 161-day Experiment 13-64

Table 13-20. Updated Calculations of Potential CO_2 Emissions After Salt Marsh Degradation 13-69

Table 13-21. Characteristics of March Cores Collected at MCBCL 13-74

Acronyms

% yr^{-1}	percentage per year
%OC	percent organic carbon content
%OM	percent organic matter content
°C	degree Celsius
µm	micrometer
µM	micromolar
AD	Anno Domini
ANCOVA	analysis of covariance
ANOVA	analysis of variance
BGB	below-ground biomass
C	carbon
C:N	carbon to nitrogen ratio
cal BP	calendar years before present
CAR	carbon accumulation rate
CH_4	methane
cm	centimeter
CO_2	carbon dioxide
CW	Coastal Wetlands (Module)
DCERP	Defense Coastal/Estuarine Research Program
DCERP1	first cycle of DCERP
DCERP2	second cycle of DCERP
DEM	Digital Elevation Model
EPA	U.S. Environmental Protection Agency
FC	Freeman Creek
FN	French Creek
g	gram
g/g	grams per gram
g C	grams of carbon
g C cm^{-3}	grams of carbon per cubic centimeter
g C m^{-2} y^{-1}	grams of carbon per square meter per year
g cm^{-3}	grams per cubic centimeter
g m^{-2}	grams per square meter
g m^2 yr^{-1}	grams per square meter per year
g ww	grams wet weight
GGA	greenhouse gas analyzer
GMWC	Gottschalk Marine/Wallace Creek
H_2S	hydrogen sulfide
HCl	hydrochloric acid
ICW	Intracoastal Waterway
IPCC	Intergovernmental Panel on Climate Change
IR	infrared
IRMS	isotope ratio mass spectrometer
kg	kilogram
kJ mol^{-1}	kilojoules per mole

km	kilometer
L	liter
LCAC	Landing Craft Air Cushion
LiDAR	light detection and ranging
LOI	loss on ignition
m	meter
M	mole
m/s	meter per second
m/yr	meter per year
m^2	square meter
m^2/s	square meter per second
MCBCL	Marine Corps Base Camp Lejeune
Mg C ha^{-1}	megagrams of carbon per hectare
Mg C yr^{-1}	megagrams of carbon per year
mg/L, mg L^{-1}	milligrams per liter
MH	Mile Hammock Bay
Mha	megahectare
MHB	Mile Hammock Bay
MHW	mean high water
MHW	mean high water
MHWL	mean high water level
mL	milliliter
mm	millimeter
mm y^{-1}, mm/yr	millimeter per year
mmol	micromole
mmol C mol C^{-1} yr^{-1}	micromoles of carbon per mole of carbon per year
mol N m^{-2} yr^{-1}	moles of nitrogen per square meter per year
mol P m^{-2} yr^{-1}	moles of phosphorus per square meter per year
MSL	mean sea level
NAVD 88	North American Vertical Datum of 1988
NDVI	Normalized Differential Vegetation Index
NH_4^+	ammonium
NH_4NO_3	ammonium nitrate
NO_3+NO_2	nitrate plus nitrite
NOAA	National Oceanic and Atmospheric Administration
NOSAMS	National Ocean Sciences Accelerator Mass Spectrometry
NRC	National Research Council
NRE	New River Estuary
NRE	New River Estuary
OBB	Onslow Beach Backbarrier
OC	organic carbon
OPUS	Online Positioning User Service
P_2O_5	phosphorus pentoxide
PDB	Pee Dee Belemnite
PES	polyethersulfone
PETG	polyethylene terephthalate copolyester, glycol modified

Pg C	petagrams of carbon
Pg C y^{-1}	petagrams of carbon per year
Pg CO_2	petagrams of carbon dioxide
Pg CO_2 yr^{-1}	petagrams of carbon dioxide per year
PO_4	orthophosphate
PPS	Pollocks Point Shore
ppt	parts per thousand
PPW	Pollocks Point Woods
PTFE	polytetrafluoroethylene
PVC	polyvinyl chloride
R:S	root to shoot ratio
RC	Resource Conservation and Climate Change (a SERDP program area)
RGB	red, green, and blue
RTK-GPS	real-time kinematic global positioning system
SCD	sediment carbon density
SD	standard deviation
SD	standard deviation
SERDP	Strategic Environmental Research and Development Program
SET	surface elevation table
SSC	suspended sediment concentration
STORET	STOrage and RETrieval
TBB	Traps Bay Bridge
TBC, TB	Traps Bay Creek
TSS	total suspended solids
UCONN	University of Connecticut
UNC-CH	University of North Carolina at Chapel Hill
VIMS	Virginia Institute of Marine Science
yr/cm^{-1}	year per centimeter

Abstract

The major objectives of the Research Project CW-4 were to improve our understanding of the factors controlling salt marsh response to sea level rise, provide predictive models of marsh response to sea level rise for managers, assess the carbon storage capacity of Marine Corps Base Camp Lejeune (MCBCL) salt marshes, and develop and assess adaptive management strategies for sustaining coastal wetlands on MCBCL. The response of salt marshes to sea level rise may be to drown or erode, to accrete vertically to maintain elevation, or to move landward. We examined the environmental and biological factors driving these responses across the MCBCL landscape and how erosion and vertical accretion may impact carbon burial rates in MCBCL salt marshes.

We used results from the Coastal Wetland Monitoring Program in addition to field and laboratory experiments to determine key aspects of the relationships between marsh vegetation, nutrients, sediment supply, and inundation, which are key to modeling the response of marshes to sea level rise. This work was performed at a series of sites across an estuarine gradient, ranging from brackish, low tidal amplitude (less than 20-cm tide) marshes dominated by *Juncus roemerianus* to polyhaline marshes with nearly a 1-m tidal amplitude dominated by *Spartina alterniflora*. Field experiments provided information about suspended sediment supply at sites spanning the estuarine gradient and about the transport of suspended sediment within a marsh. We found that wetland-dominated tidal creeks (Freeman Creek) have over twice the suspended sediment concentration (SSC) as embayed tidal creeks (French Creek) and that this relationship was consistent with other creek systems in Eastern North Carolina. We also found that sediment held in the surface microlayer was a significant source of sediment to the Freeman Creek marsh, such that during a tidal cycle, this sediment redistribution mechanism can move three times as much sediment as received from the watershed during the largest storm event measured during the study period. In situ examinations of the relationship between elevation and above- and below-ground marsh biomass revealed that in *Spartina alterniflora* marshes, there is a parabolic relationship between marsh above-ground production, although the elevation of optimal production varies with tidal amplitude. Below-ground biomass displayed a different, non-parabolic relationship across the elevation gradient, such that at all locations, marsh carbon burial is maximized at elevations near mean sea level. In contrast, there was not a strong relationship between elevation and *Juncus roemerianus* biomass. Experimental additions of nitrogen and phosphorus fertilizer consistently led to increased rates of belowground biomass and surface elevation gain in *Spartina alterniflora* marshes, and facilitated plant regrowth after a die-off event. There was no response to fertilizer by *Juncus roemerianus*.

A geospatial model to predict the response of marshes to five different sea level rise scenarios was applied to three MCBCL marshes, including French Creek, Traps Bay Creek, and Freeman Creek, by using field and remote sensing data. These sites represented a gradient in suspended sediment supply, dominant plant community and hydroperiod, thereby allowing us to assess the full suite of possibilities for MCBCL marshes. For each site, marsh habitat classification and digital elevation maps were generated and ground-truthed based on monitoring data. The response of MCBCL marshes to sea level rise can be characterized by a combination of four main responses: horizontal expansion via upland transgression, transition to flood-tolerant vegetation, enhanced vertical accretion, and drowning. The predominance of these responses is

governed by the rate of sea level rise, the combination of productivity and suspended sediment that regulate vertical accretion, and the slope of the upland. The model predicted that all three marshes gain area under the lowest sea level rise scenario (0.3 m by 2100) through a combination of expansion via marsh transgression upslope and marsh maintenance though enhanced vertical accretion. The response of Freeman Creek is dominated by marsh expansion without any substantial change in the proportion of vegetation types. The response of Traps Bay is via a transition from *Juncus roemerianus* to more flood tolerant *Spartina alterniflora*, with limited expansion due to topography. The primary marsh response to sea level rise at French Creek is drowning, as the creek system is predicted to lose extensive marsh and swamp coverage at all scenarios beyond the lowest sea level rise. At the two higher sea level rise scenarios (greater than 1.8 m by 2100), both Traps Bay and French Creek marshes drown due to limited sediment supply and reduced ability to move landward. Overall, Freemans Creek is predicted to be very resilient to sea level rise because it has the highest SSC and lowest surrounding slope, and is only predicted to drown at the highest sea level rise rate (greater than 2.5 m).

Carbon accumulation is a product of carbon concentration and sediment accumulation rate. Both field data and model results show that as MCBCL marshes experience sea level rise, the annual carbon accumulation will increase under low to moderate sea level rise scenarios. Past carbon accumulation rates (CARs) were investigated at French Creek, Traps Bay, and Freeman Creek, integrating contemporary sediment carbon stocks by age horizons determined by radiocarbon (^{14}C) dating. These rates varied from 19.7 to 147 g C m^{-2} y^{-1} over marsh ages from approximately 200 to 3,200 years before present. Although some of the highest CARs were associated with younger marsh sections, we attribute this to recent accelerated sea level rise and not incomplete decomposition. Moreover, some of the lowest rates were integrated over more than 2,000 years, a time when the North Carolina was experiencing little to no sea level rise. Therefore, we conclude that sea level rise is an important component in forecasting future CARs for marshes, and using millennial ages will underestimate CAR because they are heavily weighted by sea level rise rates much lower than contemporary observations.

The preserved sediment carbon in the salt marshes at MCBCL was composed of material produced from both C_3 (upland maritime forest or *Juncus roemarianus*) and C_4 (*Spartina alterniflora*) photosynthesis. One component of understanding a salt marsh's response to sea level rise is to predict the fate of the stored carbon in the sediments upon erosion or drowning. Decomposition experiments of C_4 material from Freeman Creek revealed a very slow decomposition of stored material once eroded to oxic horizons. Temperature was a major driver of salt marsh sediment decomposition, a process mediated by microbial extracellular enzymes, and sediment quality was a secondary factor. Therefore, we used annual temperature profiles of the tidal creeks at MCBCL to derive decomposition rates of 17% to 23% loss per year. Thus, our empirical findings greatly constrain and reduce previous reports of potential carbon dioxide emissions from marsh degradation ranged from 25% to 100% loss of eroded carbon within 1 year.

Results from research on coastal wetlands informs the ecosystem-based, adaptive management goals at MCBCL. We have identified where and why salt marsh habitat is vulnerable to sea level rise and erosion and have assessed adaptive management approaches for the conservation and restoration of marsh habitat. We provided guidance for the implementation of Living Shorelines for shoreline stabilization, initiated two pilot projects to test the use of thin-layer application of

dredged sediment to low-lying and fragmented marshes, and determined the situations in which fertilizer application to marshes would be valuable. Details of these approaches were provided to MCBCL in a separate document and can inform MCBCL management decisions.

Keywords: Adaptive management, carbon accumulation, carbon burial, decomposition, fertilization, geospatial model, inundation, *Juncus roemerianus,* marsh migration, salt marsh, sea level rise, sediment accretion, shoreline erosion, *Spartina alterniflora,* and suspended sediment.

Objectives of the Research Project

The major objectives for Research Project CW-4 were to improve our understanding of the factors controlling salt marsh responses to sea level rise, provide predictive models for managers incorporating climate forcing factors, assess the carbon storage capacity of Marine Corps Base Camp Lejeune (MCBCL) salt marshes, and develop and assess adaptive management strategies for sustaining coastal wetlands on MCBCL. In this chapter, we provide our research results in five sections, which address the first six specific objectives as described in the *DCERP2 Final Research Plan* (RTI International, 2013). The last specific objective of the module, which is an assessment of adaptive management strategies for MCBCL wetlands, including Living Shorelines, thin-layer sediment disposal, and fertilization, is addressed in a separate report (Currin, 2017), and a summary is provided in the Implications for Future Base Management section of this document. In this chapter, the first section provides detailed information about temporal and spatial variability of suspended sediment concentrations (SSCs) and discusses the development of a conceptual model of SSC delivery to the marsh surface to improve marsh elevation predictions. The second section provides information about factors controlling below-ground marsh biomass production and discusses experiments to evaluate marsh response to fertilization across a gradient of elevation and tidal amplitude. The third section describes results of a geospatial model, which improves and expands predictions of marsh sustainability under rising sea level on MCBCL and identifies the marsh locations that are particularly susceptible to loss. The fourth section investigates the factors that affect decomposition of marsh sediment carbon and long-term carbon burial rates. The third, fourth, and fifth sections provide predictions and hindcasts of carbon accumulation rates (CARs) and burial rates in MCBCL marshes.

Background

Coastal marshes are a vital component of the estuarine landscape (**Figure 13-1**) and link terrestrial and freshwater habitats with the sea (Levin et al., 2001). These interactions include the exchange of solutes, including carbon and nutrients (Cai, 2011; Jordan et al., 1983); fauna; and sediment between marsh, estuary, and adjacent landforms. In the intertidal zone, marshes help to stabilize sediments and minimize erosion (Gedan et al., 2011; Knutson et al., 1982; Möller et al., 1999). Wetlands improve water quality by acting as nutrient transformers and by trapping sediment (Harrison and Bloom, 1977; Morris, 1991; Valiela and Teal, 1979). Generally speaking, marshes consume (denitrify) nitrate dissolved in flood water and, thus, have a beneficial effect on estuarine water quality. In addition, coastal wetlands provide critical habitat area for a diverse group of estuarine organisms, serve as nursery habitat for commercially important fishery species (Kneib, 1997), and provide recreational opportunities for people.

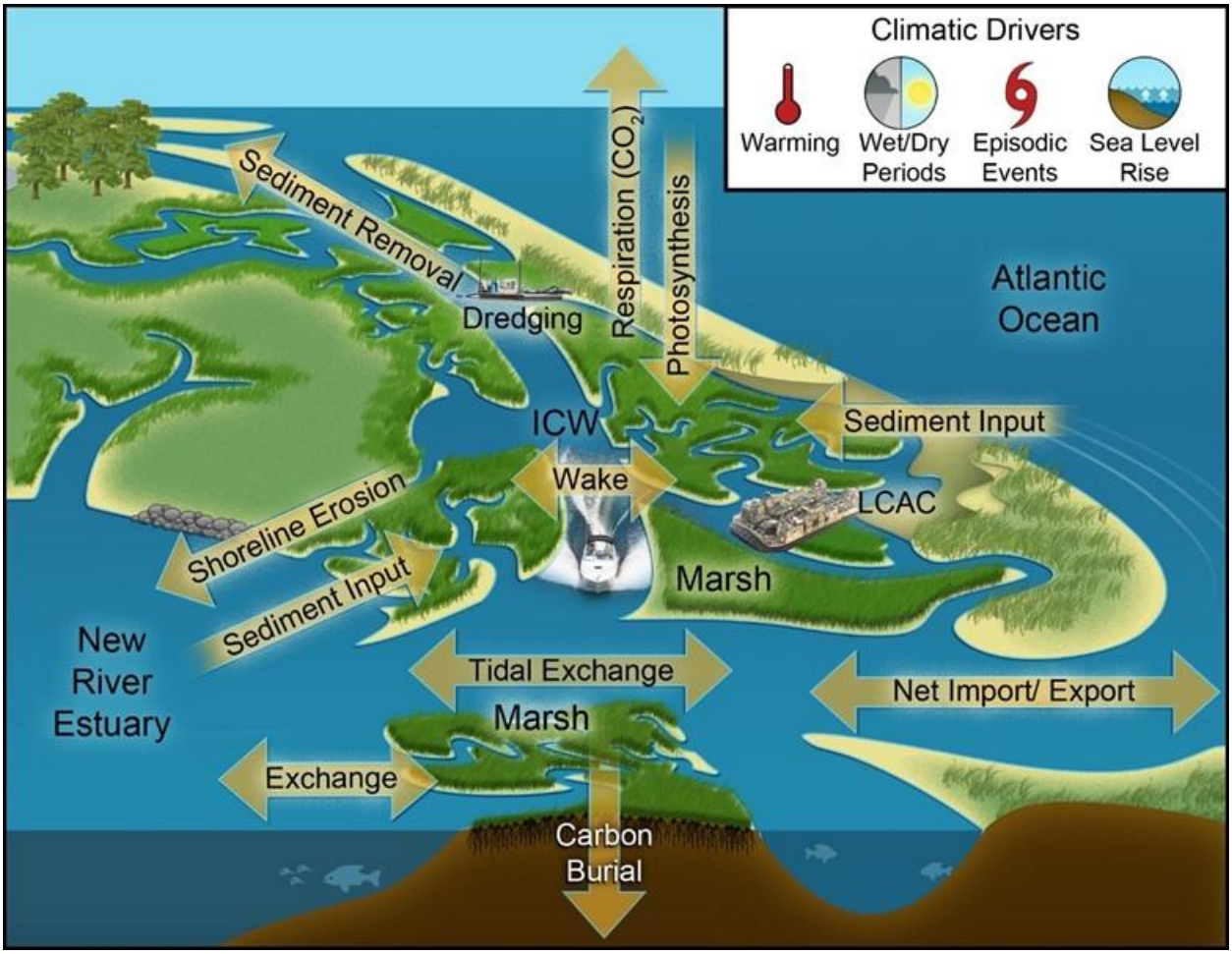

Figure 13-1. Conceptual model for the Coastal Wetlands Module.

Note: ICW = Intracoastal Waterway; and LCAC = Landing Craft Air Cushion.

Salt marshes also play an important role in the global carbon cycle. Recent estimates suggest that some coastal habitats store more carbon per area and take up more carbon annually than terrestrial habitats (Nellemann et al., 2009). As a result, it has been suggested that these coastal habitats, even though they account for a small percent of land cover, are approximately an equivalent carbon sink as other major terrestrial habitats, including temperate, tropical, and boreal forests (Mcleod et al., 2011; Nelleman et al., 2009). However, across the United States, coastal salt marshes have declined in area over the past 200 years, which, prior to the 1972 Clean Water Act, was primarily due to human activities. However, in the most recent assessment of U.S. coastal wetland status and trends, 99% of wetland loss was attributed to effects from "coastal storms, land subsidence, sea level rise and other ocean processes (Dahl, 2011), which resulted in the conversion of salt marsh to open water. This is consistent with recent literature, which has documented the loss of salt marsh as result of sea level rise, storm events, erosion, and changes in land-use practices (Cahoon et al., 2006; Kirwan and Blum, 2011; Mattheus et al., 2010; Morris et al., 2002). Projected acceleration in sea level rise (Bindoff et al., 2007; Vermeer and Rhamstorf, 2009) will exacerbate these processes and will require both improved modeling efforts and adaptive management approaches to minimize the adverse impact of marsh loss on coastal ecosystems.

Figure 13-1 presents the conceptual model for the Coastal Wetlands Module, illustrating the complementary nature of critical estuarine physical, chemical, and biotic processes and interactions. Integration of the marsh–barrier island is crucial because marshes provide a platform over which the barrier dune system can migrate, and the dunes protect the marshes from erosive wave energy that would otherwise degrade them. Along the estuarine shoreline, marshes protect uplands from flooding and storm surge. The marshes will also migrate over the terrestrial landscape in response to rising sea level where the topography allows. Exchanges of sediment and inorganic and organic carbon with estuarine waters occur (via diffusion and settling) when the marsh is submerged. Exchange of carbon with the atmosphere and estuarine waters (via diffusive flux to the atmosphere and advective exchange of marsh porewater) can occur during emergent periods. Marsh primary production that is not decomposed and lost to the atmosphere or estuary can be buried through sediment accretion and net surface elevation increase, and this represents a net carbon sink to the ecosystem.

The ability of marshes to keep up with current and projected rates of sea level rise depends upon sediment availability, the rate of sea level rise, the density of marsh vegetation, the intensity and frequency of storms, and variables such as nutrient enrichment and salinity that affect the density and species distribution of marsh vegetation (Kirwan and Murray, 2007; Morris et al., 2002; Mudd et al., 2009). The vulnerability of coastal wetlands to sea level rise is a function of the local tidal amplitude and marsh surface elevation relative to local mean and high water (Morris et al., 2002). As the rate of sea level rise increases, the equilibrium elevation of the marsh will decrease. As this elevation approaches the lower limit of a wetland's range of tolerance, the marsh will convert to open water upon any further increase in the rate of sea level rise.

Results from DCERP1 demonstrated that crucial uncertainties remain that limit our ability to translate current model predictions of marsh response to sea level rise to MCBCL coastal wetlands. These uncertainties include a lack of data on temporal and spatial variability in SSC; an incomplete understanding of how changes in tidal amplitude, which exist between Browns and New River Inlets alter the distribution of plant biomass within the tidal frame; and understanding the relative roles of mineral sediments versus below-ground primary production in contributing to marsh surface elevation change across salinity and elevation gradients (Cahoon et al., 2004; Nyman et al., 2006). Geochronology of marsh cores will provide a record of how past changes in sea level rise and plant community impact sediment and CARs at different locations within MCBCL. In conjunction with measures of below-ground biomass production and decomposition, these data will also provide estimates of the present and future carbon sequestration and burial of MCBCL marshes, which was a new research emphasis in DCERP2.

DCERP2 research was conducted at the research and monitoring stations established during DCERP1 (**Figure 13-2**). These stations span a gradient in tidal amplitude and salinity and provided data on marsh vegetation, surface elevation change, and water level to inform DCERP2 research and modeling efforts.

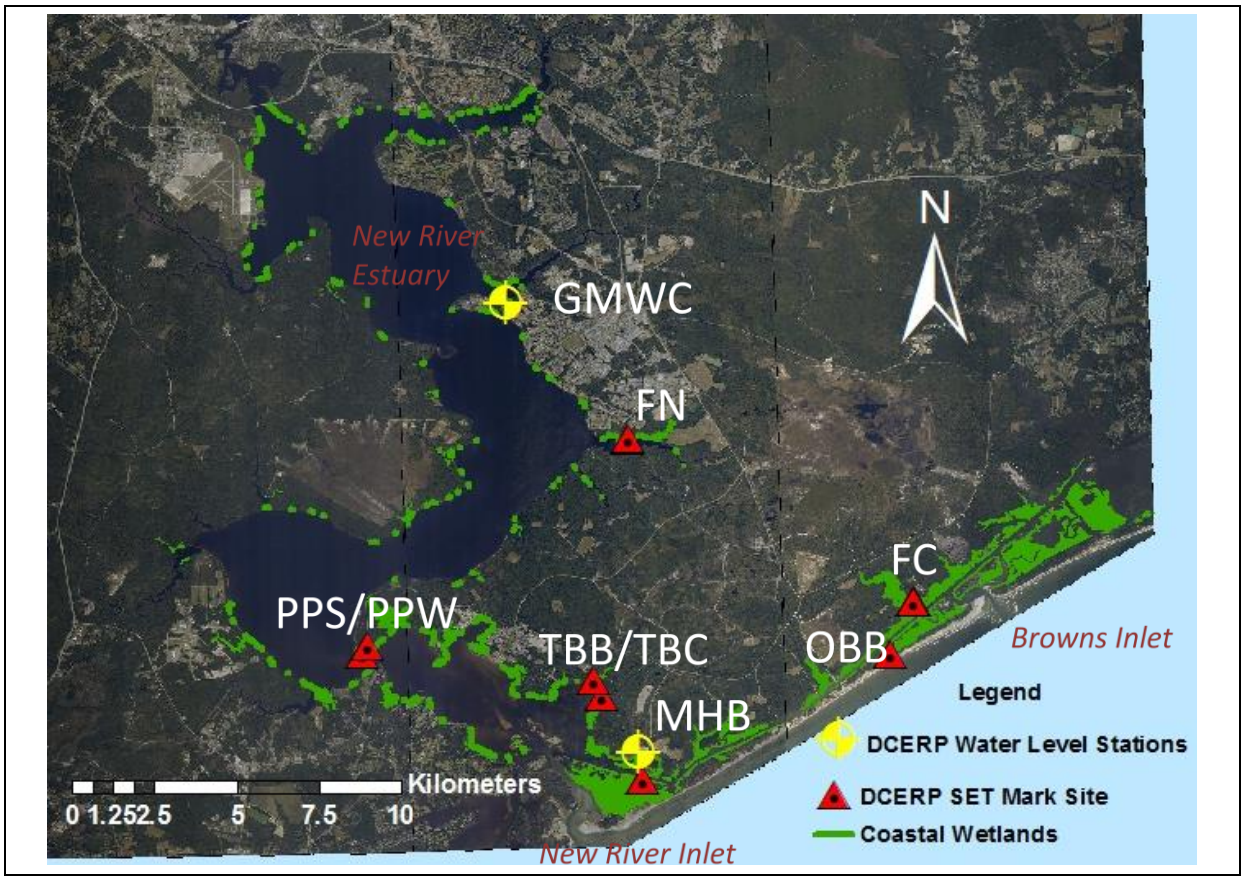

Figure 13-2. Location of coastal wetland research and monitoring stations on Marine Corps Base Camp Lejeune.

Water level stations were established at Gottschalk Marine/Wallace Creek (GMWC) and Mile Hammock Bay (MHB). Marsh monitoring stations include French Creek (FN), Pollocks Point Shore (PPS) and Pollocks Point Woods (PPW), Traps Bay Bridge (TBB) and Traps Bay Creek (TBC), MHB, Onslow Beach Backbarrier (OBB) and Freeman Creek (FC). Each monitoring station included two to five surface elevation tables ([SETs] mark sites). The extent of coastal wetlands is indicated by the green polygons.

Marsh Carbon Cycle

Several DCERP2 research projects address aspects of carbon sequestration and burial on the MCBCL landscape, including terrestrial habitats, the New River Estuary, barrier islands, and coastal wetlands. In this chapter, we discuss the results of experiments to determine factors affecting decomposition rates of marsh sediment organic carbon exposed to aerobic conditions, an inventory of carbon stored on MCBCL coastal wetlands and an estimate of the amount released via shoreline erosion, an examination of factors controlling carbon burial and accumulation rates over the past 2,000 years, and predictions of future carbon accumulation under a range of sea level rise scenarios. We provide the following definitions to support these findings, which are the result of a series of discussions among lead researchers in the Coastal Wetlands, Coastal Barrier, and Aquatic/Estuarine modules. These researchers addressed aspects of the estuarine and marine carbon cycle during DCERP2.

The Intergovernmental Panel on Climate Change (IPCC) defines ***carbon sequestration*** as the process of increasing the carbon content of a reservoir/pool other than the atmosphere (i.e., any process that removes carbon from the atmosphere regardless of the duration that carbon experiences out of the atmosphere). During DCERP2, we use three different terms to discuss carbon sequestration in the salt marsh: ***carbon deposition***, ***carbon accumulation***, and ***carbon burial***. Although the three terms possess different meanings, they share some similarities. They fall on a timescale continuum between when carbon is removed from the atmosphere via photosynthesis and retained within the marsh ecosystem over a period of years. The carbon to which these terms refer can be either autochthonous or allochthonous. The carbon fixation age (i.e., how many years prior to sequestration the carbon in the material/molecules was fixed from the atmosphere) is irrelevant in any of these definitions. They apply to salt marshes at MCBCL and are operational based on the geochronology tools available.

Carbon deposition—Recent carbon emplacement on the sediment surface. This refers to surface processes, mainly from allochthonous sediment settlement and can be measured with a feldspar marker horizon or ^{7}Be (i.e., beryllium isotope). With these techniques, it is difficult to resolve the degree that carbon deposition results in long-term, semi-permanent carbon storage in marsh sediments due to dynamic surface process that might ultimately transport or decompose the carbon. Thus, measurements of carbon deposition cannot be used to infer climate change mitigation potential for wetlands. The timescale for carbon deposition is months to years.

Carbon accumulation—Carbon incorporation within the sediment horizon. This can occur from previously deposited carbon becoming incorporated below the surface and/or from the production from plant below-ground biomass. It can be measured with ^{210}Pb (lead) and ^{14}C horizon markers that integrate at least 100 years of accumulation. We use this term differently than other previous syntheses that aggregate any sediment methods under this term without differentiating the timescale continuum in which they operate (e.g., Chmura et al., 2003; Mcleod et al., 2011; Ouyang and Lee, 2014). The 100-year timescale is in line with some IPCC climate scenarios and global warming potential calculations, but only 67% of a pulse of carbon dioxide (CO_2) emitted 100 years ago would be sequestered through these processes. Therefore, climate change mitigation potential can be carefully discussed with the previously mentioned caveat.

Carbon burial—Carbon integrated into salt marsh sediments to a depth at which surface processes no longer influence its gains or losses. The carbon that becomes buried is only a small fraction of the total initial carbon sequestered by the marsh ecosystem, but it will remain in the salt marsh sediments for timescales that are pertinent to climate change mitigation. We define this as greater than 300 years. In relation to CO_2 lifetime, 75% of a pulse of CO_2 emitted 300 years ago will be sequestered by Earth's ecosystems.

Note: Carbon accumulation/burial rates that integrate time periods when sea-level rise was much slower (greater than 1,000 years before present) will underestimate true contemporary and future rates. However, true burial rates under contemporary sea level rise cannot be made because the current accelerated sea level rise rates have not occurred for long enough timescales to measure carbon burial. Although these previously mentioned terms fall on a continuum, they do not necessarily overlap. For example, there is a gap between carbon deposition (less than several years) and carbon accumulation (approximately 100 years). Methods such as ^{137}Cs and sediment elevation tables integrate surficial processes and plant below-ground biomass production over time periods in this gap. Perhaps new terminology that diverges from traditional geology should be generated to describe the sediment carbon biogeochemistry measured in this timeframe of several years to decades (e.g., ***carbon accrual*** or ***carbon buildup***).

Section 1. Suspended Sediment Concentration and Transport Mechanisms

Lead Researcher: Scott Ensign

Introduction

A subset of the Research Project CW-4 objectives was to provide predictive models for managers to incorporate sea level rise into adaptive management strategies. One requirement of these predictive models is knowledge of the suspended sediment regime in a salt marsh and its adjoining estuary, and thus a specific objective of Research Project CW-4 was to measure the suspended sediment regime of Freeman, Traps, and French Creeks. In addition, tidal harmonics and wetland shoreline morphology were analyzed to identify predictive relationships between these metrics and the suspended sediment regime.

Materials and Methods

Suspended Sediment Concentration

Eleven field trips were conducted between June 2013 and December 2013 to sample suspended sediment within the tidal portion Freeman, Traps, and French Creeks. During each field trip, two sites were sampled: one in the embayed portion of the creek downstream and one in the wetland-dominated portion upstream. Sampling commenced approximately 3 hours before high tide and continued until 3 hours after high tide, with samples collected from the channel every 20 minutes at a depth of 0.25 m by using a DH-81 isokinetic sampler and 500-mL bottles. Samples were filtered through pre-weighed Whatman 934-AH filters and dried at 75°C until a constant weight was measured over sequential 1-hour periods (typically 12 to 24 hours) by using a Sartorious ED124S balance.

During 2014 and 2015, automated rising stage samples were used in Freeman Creek to collect suspended matter in the channel and the marsh. Stage samplers were constructed to hold five, 500-mL bottles horizontally stacked with bent copper tubing for sampler nozzles. Our design was based on the modified rising stage sampler described by Diehl (2008). In the marsh, the first stage sample was collected when water reached 9-cm depth above the marsh sediment and subsequent samples were collected at 9-cm depth intervals. In the channel, samplers were mounted on poles 3 m from the vegetated bank, and samples were collected at 9-cm intervals beginning at a water level approximately equal to the elevation of the marsh platform. The upward bend in the copper tube kept the sample bottles from filling until the nozzle was 2 cm below the water surface, thereby eliminating capture of material in the surface microlayer. Sample bottles were positioned to sample over a 0.45-cm range of water level above the sediment surface, which is the range of inundation at the study sites. Sampling continued through the entire period of rising tide, although the water level at high tide was sometimes not high enough to fill all sample bottles.

Surface Microlayer Sediment

The surface microlayer at each station was sampled by dipping a 48-mm × 152-mm glass plate into the water, and then using purified water to rinse material that adhered to the plate into a

bottle, and repeating this procedure for a total of three dips (total sampled area was 0.0438 m^2 of water surface). Material contained in the surface microlayer was calculated as dry mass (g) divided by 0.0438 m^2 to yield a mass per area which differs from the mass per volume approach use by previous researchers (Harvey and Burzell, 1972). This glass plate method was selected for surface microlayer sampling over alternatives such as screens due to the density of marsh grass, though the glass plate method has been found to under-represent chlorophyll *a* and some microorganisms (Agogué et al., 2004). In addition to measuring the concentration (mass per water surface area) of material in the surface microlayer using glass slides, we also measured material lifted by surface tension off a known area of marsh sediment. We developed a "skimmer" that enabled us to capture the surface microlayer that originated within a defined area of marsh sediment during flood tide (for details, see Ensign and Currin, 2017).

Particle Characterization

A Teflon decaport sample splitter (Rickly Hydrologic Company, Columbus, OH) was used to split field samples into subsamples for particle characterization. The mass of suspended and surface microlayer material was determined on pre-weighed Whatman 934-AH filters, rinsed with purified water, and dried at 75°C until a constant weight was measured over sequential 1-hour periods (usually between 12 and 24 hours) on a Sartorious ED124S balance with 0.0001-g precision. Each filter assessed for loss on ignition (LOI) was combusting for 4 hours at 500°C. All suspended and surface microlayer samples were analyzed for chlorophyll *a* by using the modified fluorometric technique (Arar and Collins, 1997).

The particle sizes of all samples were analyzed by using a Coulter Counter with a 200-micrometer (µm) aperture, which has an analytical range of 4 µm to 120 µm. Samples were pre-filtered through 125-µm NITEX mesh, and then added to 0.2 µm–filtered Gulfstream water. Data were summarized for statistical analysis by using the median particle size (D50) and the 84th percentile (D84).

Particulate organic carbon and nitrogen were analyzed by using a Costech elemental analyzer. Samples were filtered onto pre-combusted GF/F filters and fumed with concentrated hydrochloric acid (HCl) overnight. The presence of inorganic carbon after fuming was tested on every 10 to 20 samples by dropping concentrated acid on the fumed filter and looking for bubbles. No bubbling post-fuming was ever detected. The carbon to nitrogen ratio was used as an indicator of the biochemical composition of particulate material that could help distinguish between suspended and surface microlayer material.

Tidal Harmonic Analysis

One year of water level data were used to analyze tidal harmonics by using the MATLAB program T-tide (Pawlowicz et al., 2002) to examine potential flood or ebb tide asymmetry that would influence sediment transport. Water level data were measured at 15-minute intervals near the downstream site on the three creeks by using AquaTroll water level recorders (In-Situ Inc., Fort Collins, CO). The modeled amplitude and phase are reported here for constituents whose amplitude is greater than 1 cm for any of the creeks.

Morphometric Analysis

The embayed and wetland-dominated portions of each creek were delineated by using the methods discussed by Ensign et al. (2017). In summary, this method used existing shoreline delineations from the North Carolina Department of Coastal Management and Digital Elevation Model (DEM) data to measure the cross-channel width of open water versus intertidal vegetation extent at high tide. The quotient of these two values was calculated along the creek from near the head of tide to each creek's mouth. The point where this value exceeded unity marked the transition from wetland dominated (upstream) from embayed (downstream). The embayed index was calculated as the proportion of the overall tidal creek length, from upstream to downstream, where this value occurred.

To bolster our analysis of the relationship between estuary morphology and suspended sediment, we searched the U.S. Environmental Protection Agency's (EPA's) STOrage and RETrieval (STORET) database (for more information, see www.epa.gov/storet) for total suspended solids (TSS; SSC was not reported in the STORET database) in estuarine creeks in North Carolina. To remain comparable to Freeman, Traps, and French Creeks, we only selected stations that were within the boundaries of a tidal waterbody fringed by emergent marshes and having a total centerline length less than 15 km from the mouth to the upstream extent of the delineated channel. Morphological characteristics of these creeks were measured as described by Ensign et al. (2017).

Statistical Analysis

TSS data from DCERP2 Aquatic/Estuarine Module Monitoring Activity AEM-2 for Freeman, Traps, and French Creeks were included in the analysis of SSC. With three sampling locations on each of three creeks, comparisons between the locations are not likely to be independent of one another. Furthermore, repeated measurements at the same site are likely to have a lower variance than the broader population of sites. To accommodate this hierarchical data structure and inherent lack of independence between the SSC and TSS measurements, two mixed-effects linear regression models were used. To test whether sediment concentration differed among non-tidal, upstream tidal, and downstream tidal sites, site (n=3) was used as a fixed variable, and creek (n=3) was used as a random variable. To test whether sediment concentration differed between tidal creeks, creek was used as a fixed variable, and tidal site (upstream and downstream) was used as a random variable.

TSS from the additional creeks found in the STORET database were combined with SSC from Freeman, Traps, and French Creeks to examine the relationship between sediment concentration and creek morphology. A multiple contrast test was employed to test for differences between groups of creeks based on their embayment index. The data were tested for normality and equal variance before conducting the appropriate parametric or non-parametric test.

Results and Discussion

Suspended Sediment Concentration

A mixed effects model between sediment concentration and site (non-tidal [AEM-2], upper tidal [wetland dominated], and lower tidal [embayed]) with creek as a random effect showed that

concentration at the upper tidal and lower tidal sites did not differ (difference=0.15, t=0.08, p=0.94), but the non-tidal site was 9.1 mg L^{-1} lower than the lower tidal site (t=−6.02, p=0.0) (**Figure 13-3**). A separate mixed effects model between sediment concentration and creek, with site as a random effect showed French Creek was 5.9 mg L^{-1} lower than Freeman Creek (t=−4.2, p=0.0), but that Traps and Freeman Creeks were not different (t=1.3, p=0.20). SSC did not exhibit a consistent decline with increasing distance from the creek channel (**Figure 13-4**). The automated, rising stage samplers deployed at Freeman Creek during the 2014–2015 sampling campaign generally showed decreasing concentrations between the channel and marsh at the upstream site, whereas the downstream site generally showed an increase in concentration between the channel and marsh (**Appendix A, Figures 13-A1 and 13-A2**).

Surface Microlayer Sediment

Surface microlayer concentration in the channel ranged from a mean of 0.038 g m^{-2} on 17 December 2014 to 0.59 g m^{-2} on 10 August 2015 (**Tables 13-1 and 13-2**). Surface microlayer concentrations in the marsh were generally higher than the channel, with mean surface microlayer concentrations in the marsh ranging from 0.15 g m^{-2} on 17 December 2014 to 0.54 g m^{-2} on 22 April 2015.

Table 13-1. Suspended, Surface Microlayer, and Skimmed Matter at the Upstream Site: Mean (Minimum, Maximum)

Date	Site	Suspended (g m^{-2})	Surface Microlayer (g m^{-2})	Skimmed (g m^{-2} of Sediment Area)	Settled (g m^{-2})	Skimmed: Settled
20 August 2014	Channel	19 (4.3, 30.5)	0.13 (0.042, 0.24)	0.52	—	—
20 August 2014	Marsh	6.2 (2.2, 12.6)	0.25 (0.034, 0.75)	0.92 (0.78, 1.0)	4.5	0.2
17 December 2014	Channel	22 (2.3, 34)	0.038 (0.0, 0.18)	1.8 (0.55, 2.6)	—	—
17 December 2014	Marsh	1.1	0.15 (0.071, 0.27)	0.70	0.40	1.8
10 August 2014	Channel	34 (30, 39)	0.59 (0.11, 1.2)	1.3 (1.1, 1.6)	—	—
10 August 2014	Marsh	7.6 (2.3, 12)	0.48 (0.084, 1.5)	1.6 (1.1, 2.4)	4.3	0.37

Table 13-2. Suspended, Surface Microlayer, and Skimmed Matter at the Downstream Site: Mean (Minimum, Maximum)

Date	Site	Suspended (g m^{-2})	Surface Microlayer (g m^{-2})	Skimmed (g m^{-2} of Sediment Area)	Settled (g m^{-2})	Skimmed: Settled
24 June 2014	Channel	12 (2.3, 23)	0.054 (0.011, 0.061)	0.048	—	—
24 June 2014	Marsh	4.3 (1.9, 7.5)	0.47 (0.05, 1.1)	0.38 (0.027, 0.72)	2.0	0.19
29 October 2014	Channel	6.8 (4.3, 10.7)	0.076 (0.0, 0.17)	1.5	—	—
29 October 2014	Marsh	3.0 (0.99, 6.8)	0.47 (0.053, 2.1)	1.0 (0.024, 2.4)	2.4	0.42
22 April 2015	Channel	23 (2.0, 51)	0.13 (0.009, 0.54)	1.1 (0.65, 1.6)	—	—
22 April 2015	Marsh	3.5 (1.1, 7.8)	0.54 (0.0, 1.4)	1.3 (0.64, 1.9)	2.8	0.46

Particle entrainment within the surface microlayer is a redistribution mechanism of material, not an allochthonous source of new sediment to the marsh. Nonetheless, the magnitude of material moving via this mechanism dwarfs the mass of new, watershed-derived sediment in Freeman Creek. For example, over a 4-year period of continuous monitoring in Freeman Creek, the highest watershed material flux measured was 154 kg during a 12-hour period (Ensign et al., 2016). Based on the 450,000 m^2 of Freeman Creek marsh and a surface microlayer entrainment of 1.14 g m^{-2} per tidal cycle, we predict that 513 kg of material is redistributed throughout the marsh on every tidal cycle. Although the spatial scales of movement of the surface microlayer may be limited by the slow flow velocity within the marsh, the long-term influence of this transport mechanism on marsh morphology is significant.

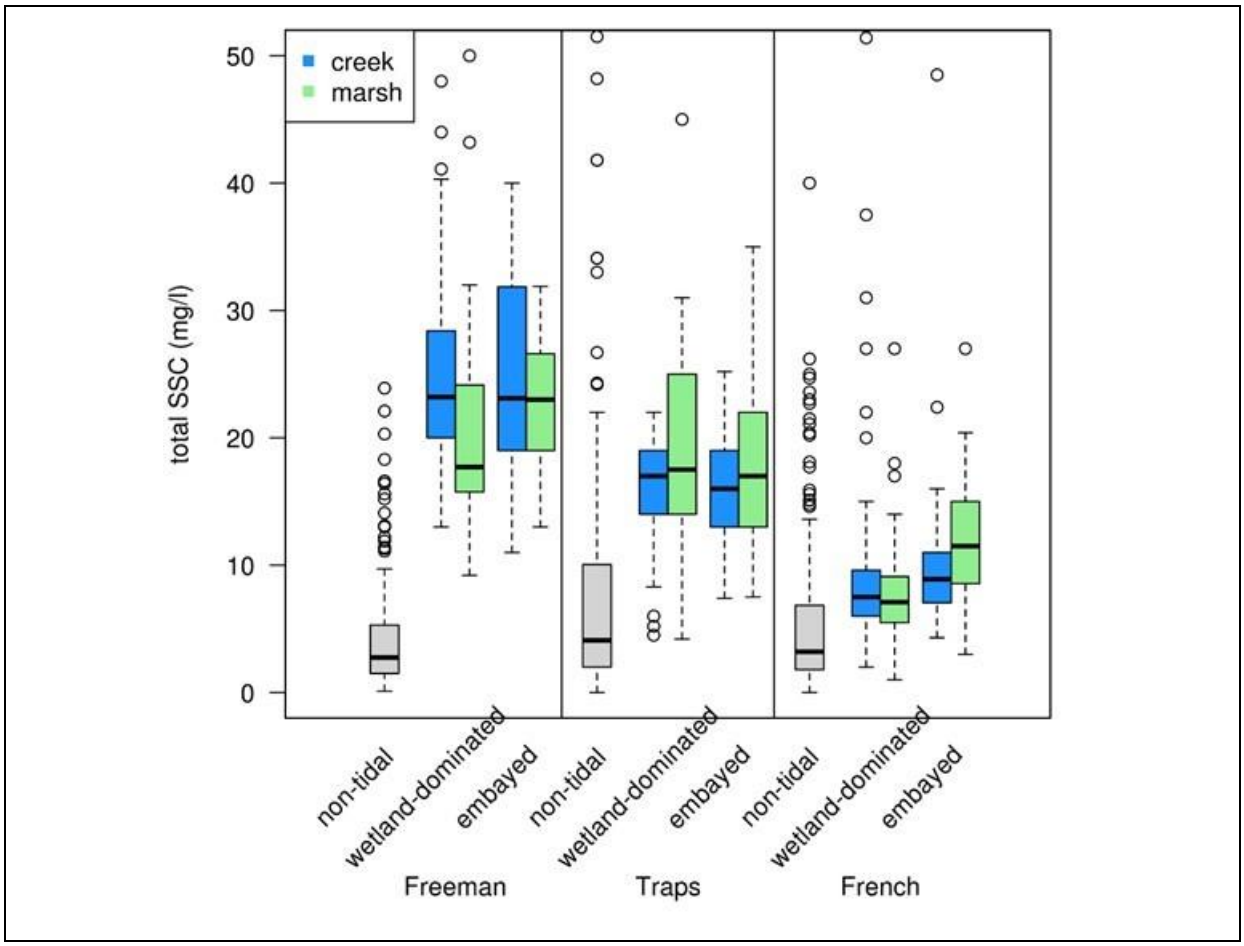

Figure 13-3. Suspended sediment concentrations (SSCs) in Freeman, Traps, and French Creeks.

Note: Boxes represent the interquartile range bisected by a solid line indicating the median, with whiskers representing limits of individual values less than 1.5 times the interquartile range. Circles show values beyond this limit.

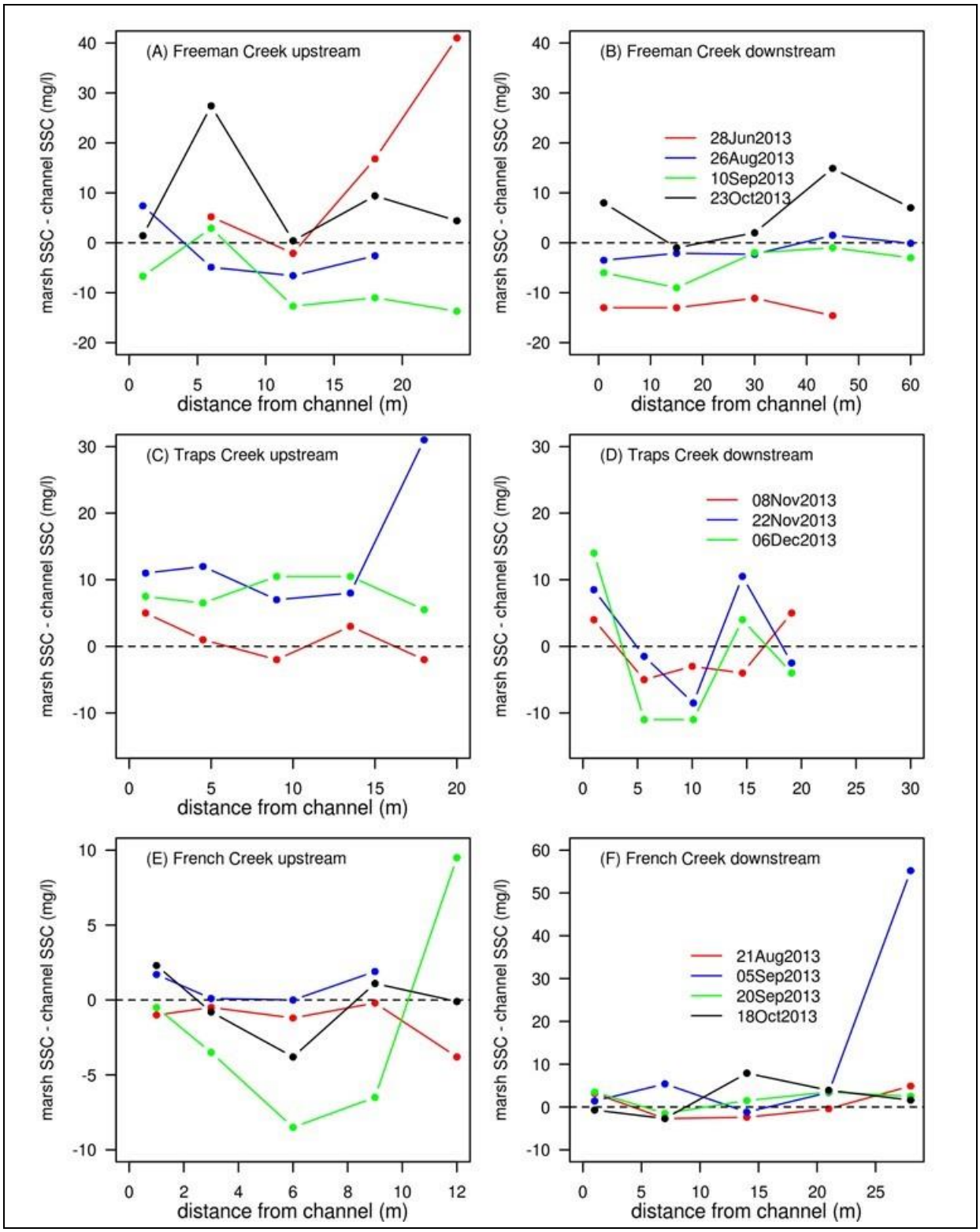

Figure 13-4. Suspended sediment concentrations (SSCs) in the marshes of Freeman, Traps, and French Creeks.

Note: Values are normalized to the SSC in the channel.

In addition to helping explain the higher deposition rates observed in the marsh interior, another consequence of surface microlayer transport is that it may help build natural levees from the back marsh toward the channel. At our downstream site, water first reached the back marsh through sloughs and sheet-flow, not from flow through or over the natural levee. We observed movement of the surface microlayer from the back marsh toward the levee, demonstrating an incremental movement of material and subsequent deposition that would supplement levee development from the reverse direction of conventional models (over-topping of levees and deposition from sediment-laden channel water). The back-filling of levees by surface microlayer transport would tend to strengthen the topographic patterns normally attributed to hydraulically driven suspended matter transport and deposition from the channel.

Particle Characterization

For samples collected in the marsh, mass LOI in surface microlayer material (mean=32%) was not different than suspended matter (mean=28%). The carbon to nitrogen ratio in the surface microlayer (mean=20) was not significantly different from suspended matter (mean=16). The median particle size (D50) in the surface microlayer (mean=5.6 μm) was significantly larger than suspended matter (mean=5.4 μm). Similarly, the 84th percentile of particle size (D84) in the surface microlayer (mean=8.7 μm) was larger than suspended matter (mean=7.6 μm).

Tidal Harmonics

Tidal amplitude was highest in Freeman Creek, intermediate in Traps Bay Creek, and lowest in French Creek (**Table 13-3**). Although not significant in Freeman or French Creeks, the solar annual and solar semiannual constituents were significant in Traps Creek, suggesting a more prominent seasonal variation in freshwater runoff and subsequent water levels in Traps Bay Creek. Weak harmonic distortion occurred in the M4 overtide of all creeks (M4:M2<0.17), indicating that flood-ebb asymmetry in current velocity and associated sediment transport was minimal (Friedrichs and Aubrey, 1988).

Table 13-3. Tidal Constituents Modeled with T-Tide from 1 Year of Water Level Data

Tidal Constituent	Freeman Creek		Traps Bay Creek		French Creek	
	Amplitude (mm)	Phase	Amplitude (mm)	Phase	Amplitude (mm)	Phase
M2	39	23	13	61	7	282
S2	6	124	2	33	1	305
N2	9	52	3	252	1	326
K1	8	304	3	4	2	275
M4	2	3	2	88	1	113
O1	6	123	3	120	2	104
L2	2	160	1	51	1	68
P1	2	183	1	60	1	55
SA	–	–	16	77	–	–
SSA	–	–	9	230	–	–
Total	74	–	53	–	16	–

Morphometric Analysis

Freeman Creek had an embayed section, but was mostly wetland-dominated (**Figure 13-5**). Classification of this middle portion as embayed was partly an analytical artifact of not accounting for dendritic channels interspersed with wetland in the shoreline digitization. Therefore, we consider Freeman to be a wetland-dominated creek (embayed index=0). Traps and French Creeks had embayed indices of 0.24 and 0.61, respectively. The increase in width along each creek corresponded with the increase in the channel to floodplain ratio, indicating that channel width was the predominant control on this ratio instead of a reduction in the valley width that would limit wetland extent.

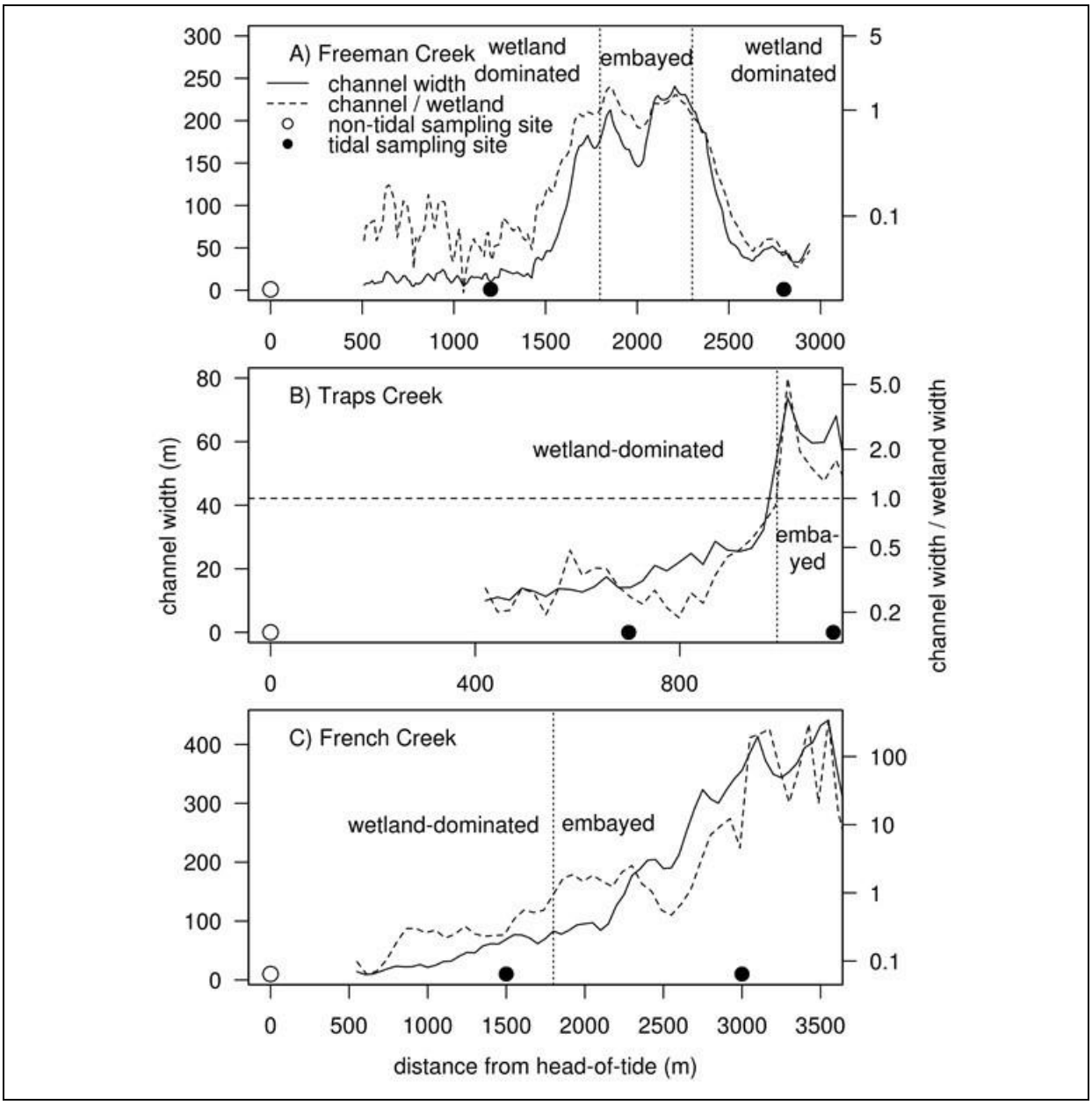

Figure 13-5. Channel width, wetland width, and sampling sites in Freeman, Traps, and French Creeks.

The search of EPA's STORET database found eight creeks that fit the morphologic criteria needed to allow comparison. Calabash Creek was not included in further analysis because it had extremely high TSS relative to all other creeks (the mean was 55 mg L^{-1} and maximum was greater than 500 mg L^{-1}), likely due to phytoplankton blooms that have led to its listing as an impaired creek under the Clean Water Act. The remaining seven creeks had embayed indices ranging from 0.0 (Oak Island Creek) to 0.74 (Slocum Creek; **Figure 13-6**). All creeks with embayed indices less than 0.5 had medians TSS between 20 and 30 mg L^{-1}, whereas the others had medians less than 10 mg L^{-1}.

Given the apparent grouping of high and low SSC in creeks on either side of the 0.5 embayed index (**Figure 13-6**), we tested for a statistical contrast between these two groups.

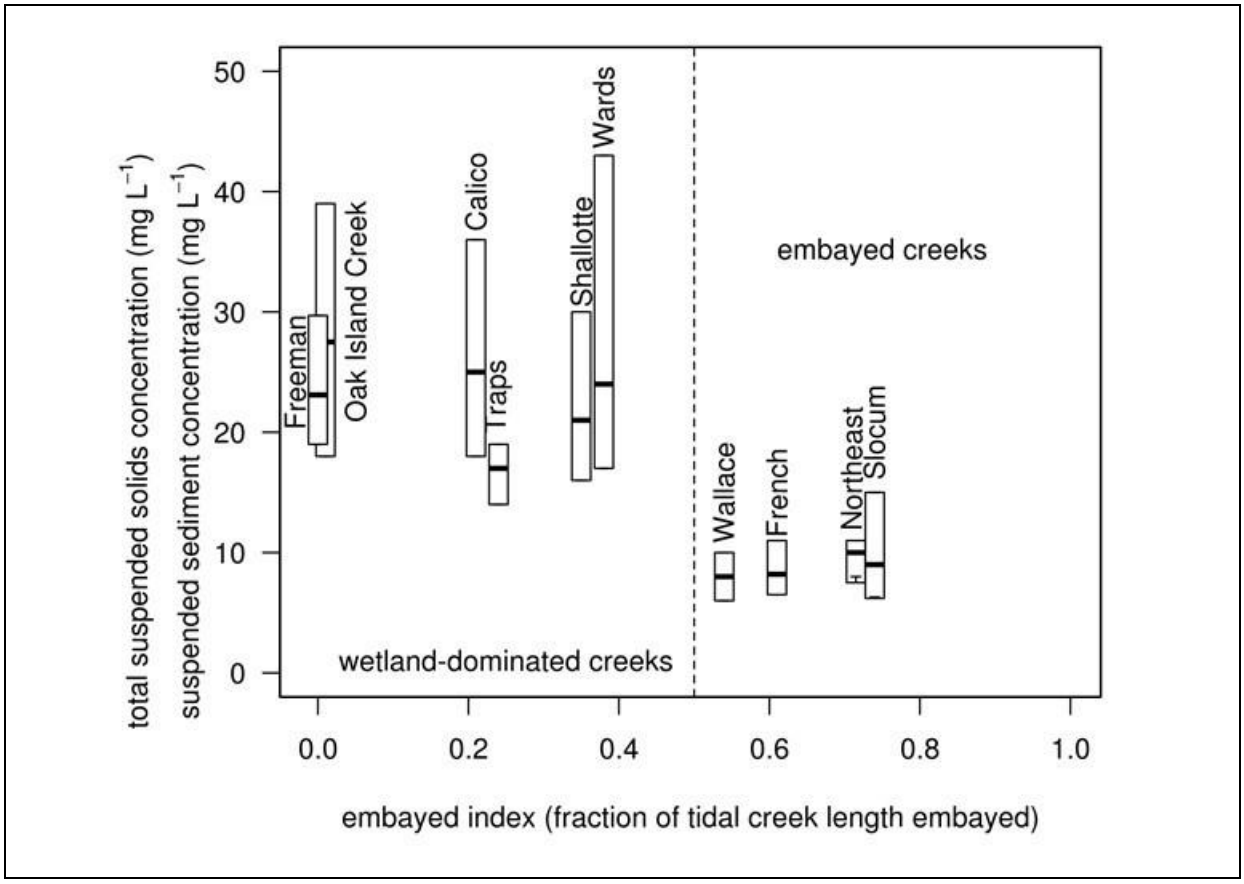

Figure 13-6. The relationship between the in-channel suspended sediment (upstream and downstream sites combined) and the position of the transition from embayed to wetland-dominated.

Note: Each box represents the interquartile range and the bar represents the median value.

The data could not be normalized by common transformation techniques, nor was there equal variance between groups. Therefore, a non-parametric contrast test was performed on the ranked values (Zar, 2010). The test statistic (14.7) did not exceed the chi-square critical value at a=0.05 (16.9), indicating that the sediment concentration in the more embayed creeks (median=8.9 mg L^{-1}, standard deviation [SD]=16.4) could not be considered different from the less embayed creeks (median=20 mg L^{-1}, SD=4.7). When the apparent outlier among the less

embayed creeks (Traps Creek) was removed, the test statistic (18.7) exceeded the critical value (15.5), indicating a difference ($p<0.05$) between groups.

A simple morphometric analysis of tidal creeks performed with freely available spatial data showed that creeks embayed for over half their length had approximately half the suspended sediment as less embayed creeks. In the North Carolina creeks we studied, this equated to a difference between median sediment concentration of 11 mg L^{-1}. A difference of this magnitude is predicted to affect the long-term stability of marshes exposed to sea level rise in the range that is occurring over much of the East Coast of the United States (Kirwan et al., 2010). Therefore, morphodynamic models of wetland shoreline change in the creeks studied here may predict opposing outcomes for marsh platforms (stability versus collapse) depending on which median SSC is considered. This model sensitivity indicates that the morphodynamic dichotomy proposed here and associated difference in SSC would improve the predictive power of wetland shoreline change models.

We assume that this correspondence between estuary shape and SSC in Freeman, Traps, and French Creeks was due to the influence of tidal currents and not watershed sediment loads because all creeks had similar watershed sediment concentrations (non-tidal sites) and discharge. Salt marsh accretion rates mirrored the patterns in SSC, with the highest accretion occurring in the least embayed (Freeman Creek) and the lowest accretion occurring in the most embayed (French Creek). Although marsh accretion does not necessarily equal marsh elevation change because of compaction, subsidence, root in-growth, and decomposition, accretion does indicate the availability and delivery of sediment from the channel to the marsh. The availability of sediment to the marsh is the key factor in morphodynamic models of wetland shoreline change, and our accretion data further support the link between morphology, suspended sediment, and wetland response.

Although the morphologic patterns and SSC observed here are representative of the North Carolina coast, further research will be needed to extend these methods to other regions with different tidal amplitude. Assuming the morphologic dichotomy-sediment concentration relationship applies in other regions, the absolute values of SSC for each morphology would need to be identified to enable effective application of this relationship to morphodynamic models elsewhere. In contemplating this future research, we emphasize that the landscape setting for this relationship appears to require small (less than 15-km long) tidal creeks with watershed influence, as well as alluvial stream valleys with relatively unconstrained tidal wetlands at the upper extent of tide. The small size of the tidal creeks examined here sets our research apart from previous investigations of morphology and sediment dynamics in large estuaries (Uncles et al., 2002), but further research is needed to identify the size range of creeks in which the dichotomy in morphology and relationship with SSC applies.

Section 2. Variations in Below-Ground Biomass with Elevation and Nutrient Availability

Lead Researchers: Jenny Davis and Carolyn Currin

Introduction

The goals of this work were to investigate the abundance of marsh below-ground biomass (roots and rhizomes) of *Spartina alterniflora* and *Juncus romerianus* across a marsh elevation gradient and to evaluate the response of below-ground biomass, porewater nutrient profiles, and sediment characteristics (i.e., deposition rate, particle size, and bulk density) to nutrient fertilization. During DCERP1, we established that above-ground biomass of *Spartina alterniflora* exhibits a parabolic distribution with elevation such that biomass is greatest at mid-marsh elevations and decreases at both lower and higher elevations. Plants are highly plastic with respect to root to shoot ratios, thus it is not clear whether below-ground biomass exhibits a similar parabolic distribution with elevation. Because below-ground marsh production is the primary source of carbon stored in marsh sediments, understanding its distribution is critical to our efforts to evaluate the carbon storage capacity of MCBCL marshes.

During DCERP1, we also confirmed that nutrient fertilization leads to significant increases in above-ground standing biomass of *Spartina alterniflora* and that fertilized plots gain elevation at higher rates than controls. Since that time, there has been an ongoing debate in the literature about the impact of fertilization on below-ground biomass. Some published results suggest that fertilization leads to enhanced decomposition of below-ground biomass and ultimately marsh deterioration and elevation loss, whereas others indicate either increased amounts of below-ground biomass, leading to elevation increases, or no net change. Thus, fertilization may be an effective adaptive management strategy for increasing the elevation of low-lying marshes, but not if it also results in a net loss of below-ground material. To investigate the response of below-ground biomass to fertilizer addition, we revisited the experimental plots occupied during DCERP1 and added additional sites, including one *Juncus roemerianus*–dominated marsh, in which we documented fertilizer response of both above- and below-ground biomass.

Materials and Methods

Below-Ground Biomass Elevation Gradients

We evaluated total root biomass and annual root production along shore-perpendicular transects at Freeman Creek, Onslow Beach, Mile Hammock Bay, Traps Bay Creek, and French Creek. Each marsh transect encompassed the full elevation gradient of the marsh, and five to six sampling points were spaced along each transect at equal elevation intervals. At each sampling point, we collected a large sediment core (15-cm diameter × 30-cm deep). The entire core was rinsed over a 2-mm sieve to remove sediment, until only clean root and rhizome tissue remained. The root material in these cores was considered to represent the standing stock of live and dead below-ground biomass. Ingrowth bags were used to estimate annual root production following the methods from Davis et al., (2015). Briefly, ingrowth bags (plastic mesh bags attached to metal wire frames (15 cm × 30 cm) were placed into the holes created by coring. Ingrowth bags were filled with sieved (2 mm) sediment collected from the creek bank at each site and were left

in place for 1 year. After 1 year, ingrowth bags were harvested and rinsed over a 2-mm sieve as previously described. Root material in the ingrowth bags was considered to represent annual growth. After rinsing, all root material was dried at 60°C for 48 hours and then weighed. We also collected above-ground biomass across the elevation gradient at French Creek, a site dominated by *Juncus romerianus* because the relationship between *Juncus romerianus* above-ground biomass and marsh elevation was not previously established for our study area. Biomass over the elevation gradient is presented in terms of relative tidal elevation (elevation of mean high water [MHW]–plot elevation) to facilitate comparison among sites.

Response to Fertilizer Addition Fertilization

Study plots (1.5 m on a side) were established at the Freeman Creek, Onslow Beach Backbarrier, Mile Hammock Bay, Traps Bay Creek, and French Creek study sites. The Freeman Creek site consisted of five treatment and five control plots; all remaining sites had three treatment and three control plots. At Freeman Creek, six of the plots (i.e., three treatment and three control) were established to encompass the area measured by a surface elevation table (SET); at both Mile Hammock Bay and Onslow Beach Backbarrier, two plots (i.e., one treatment and one control) encompassed the SET devices. The Freeman Creek, Mile Hammock Bay, and Onslow Beach Backbarrier SET–associated plots had been included in the DCERP1 study, and fertilizer treatments were made during the growing season from 2008 to 2010, and then were discontinued (Davis et al., 2017). None of the fertilizer study plots at French Creek or Traps Bay Creek were directly associated with SETs or had been previously fertilized.

Fertilizer was applied quarterly by broadcast application of granular ammonium nitrate (NH_4NO_3) and phosphorus pentoxide (P_2O_5) at a rate of 30 mol N m^{-2} yr^{-1} and 15 mol P m^{-2} yr^{-1}. Fertilization began in April 2015, and the final application occurred in June 2016. This dosage rate was that same as that used during DCERP1 fertilization experiments (Davis et al., 2017).

<u>Porewater</u>

To investigate fertilization-related changes in porewater nutrient composition, we sampled porewater from each treatment and control plot approximately 2 weeks after each fertilizer application. Samples for inorganic nitrogen and phosphorus were collected at depths of 5 cm and 15 cm by using porewater sippers that were installed in each plot for the duration of the study. Samples were filtered immediately upon collection (0.45 µm, polyethersulfone [PES] filters) and stored frozen until analysis. Porewater samples were analyzed for ammonium (NH_4^+), nitrate plus nitrite (NO_3+NO_2), and orthophosphate (PO_4) via an autoanalyzer by using standard wet chemistry methods (Knepel and Bogren, 2001; Liao, 2001; Smith and Bogren, 2001). Salinity of porewater samples was determined in the field via refractometer.

Each time samples were collected for nutrient analysis, we collected an additional sample from each experimental plot for analysis of porewater sulfide concentration. Sulfate reduction is the dominant form of heterotrophic respiration in salt marsh sediments, accounting for 50% or more of carbon mineralization (Howes et al., 1984). Sulfide samples were collected at a depth of 15 cm by using a portable push-point sampler and peristaltic pump with gas-tight tubing. Sulfide samples were stored refrigerated in zinc acetate until analysis by using the Clines method (Cline, 1969).

Biomass

Peak standing above-ground biomass was estimated for each plot annually by using a combination of previously established allometric relationships (Davis et al., 2017) and destructive harvest methods. Ingrowth bags were installed in two fertilized and two control plots at each site for the analysis of below-ground biomass (as previously described).

Sediment Characteristics

At each plot, two small sediment cores (6 cm × 20 cm) were collected in July 2016 after 1 full year of fertilization: one for analysis of bulk density and the other for particle size analysis (Davis et al., 2017). The core collected for bulk density was extruded in 5-cm increments, and each increment was dried at 60°C for 48 hours, weighed for bulk density characterization, and then ground coarsely and combusted at 450°C for 4 hours for analysis of percent organic matter (%OM). The second core was processed for particle size distribution by rinsing the entire core volume over successive 2-mm (to capture gravel and macroparticulate organic matter) and 63-µm (to capture sand) sieves and collecting all rinse water. The silt+clay fraction was quantified by collecting three 25-mL subsamples of the rinse water (with stirring), drying in a 60°C oven, and weighing. Total silt+clay weight was calculated from the average weight of the three 25-mL subsamples and the total volume of rinse water collected.

Sediment Deposition

Rates of sediment deposition were measured quarterly in two fertilized and two control plots (but not plots that were associated with SETs) from each site. Sediment deposition was measured by distributing a thin layer of feldspar clay on the marsh surface by hand. The edges of the deposition area were marked with flagging and polyvinyl chloride (PVC) poles. Deposition was estimated from the depth of new sediment overlying the feldspar after 3 months (Lynch et al., 2015).

Elevation Change

Rates of marsh surface elevation change were measured quarterly via SET in the SET–associated treatment and control plots at Freeman Creek, Mile Hammock Bay, and Onslow Beach Backbarrier. We did not have SETs directly associated with treatment plots at Traps Bay Creek and French Creek and consequently, did not make direct comparisons between treatment and elevation change rate for these sites. The SET data presented here are from the same SETs described in Chapter 4 of the *DCERP2 Final Report*.

Results and Discussion

Below-Ground Biomass Elevation Gradients

At Onslow Beach Backbarrier, Traps Bay Creek, and Freeman Creek, standing below-ground biomass of *Spartina alterniflora* (consisting of both live and dead roots and rhizomes) varied systematically over the elevation gradient, with peak biomass occurring at elevations near MHW. At Mile Hammock Bay, where experimental plots are higher in the tidal frame and the tidal range is narrower (Davis et al., 2017), peak below-ground biomass occurred at elevations slightly

higher than MHW (negative values on the *x*-axis of **Figure 13-7**). At all four sites, *S. alterniflora* below-ground biomass exhibited a parabolic distribution with elevation. Data from the *Juncus romerianus*–dominated French Creek marsh are discussed separately below. Results from DCERP1 showed that *S. alterniflora* above-ground biomass also exhibits a parabolic distribution with respect to elevation, but the peak values of above-ground biomass occur at lower relative tidal elevations (nearer mean sea level [MSL]), thus the peak above- and below-ground biomass elevations are spatially distinct. Standing below-ground biomass at Traps Bay Creek did not follow the same pattern. At this site, the lowest below-ground biomass occurred at mid-marsh elevations—though it should be noted that this fringing marsh has a very narrow elevation range (less than 20 cm), perhaps too narrow for a distinct pattern to develop.

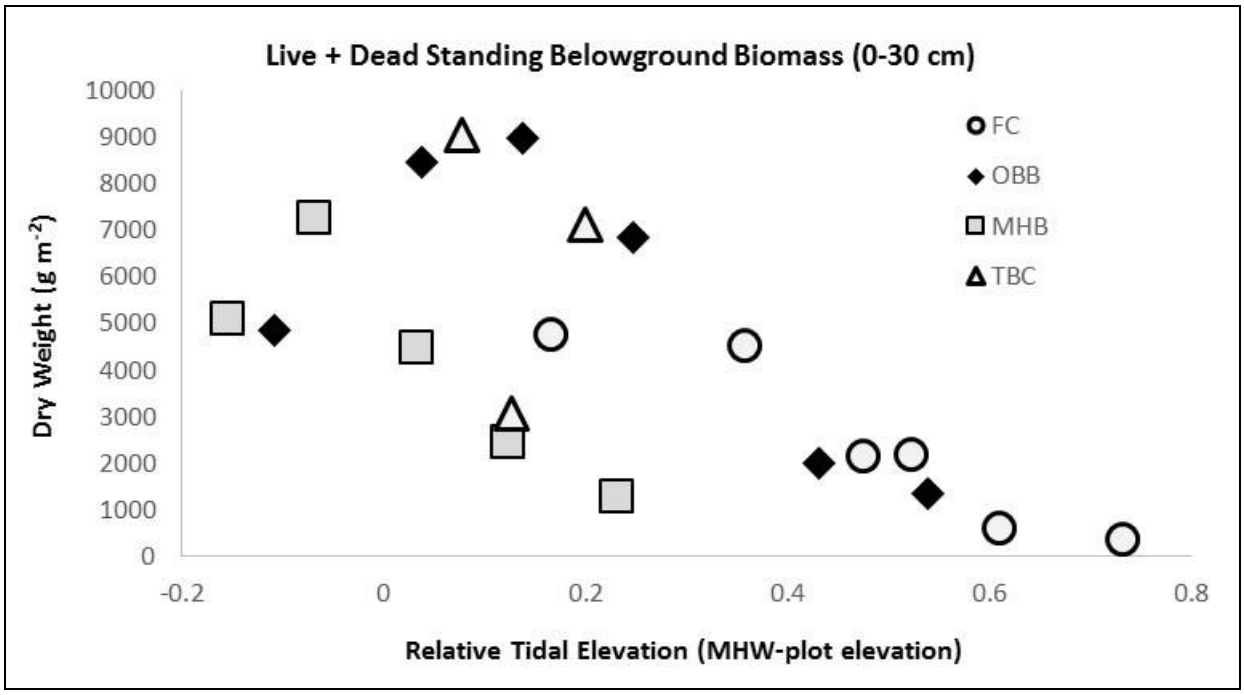

Figure 13-7. Distribution of below-ground biomass with respect to relative tidal elevation.

Note: FC=Freeman Creek; MHB=Mile Hammock Bay; MHW = mean high water; OBB=Onslow Beach Backbarrier; and TBC=Traps Bay Creek. Each point represents a single sample.

Net annual below-ground biomass production (estimated as the amount of root+rhizome material in ingrowth bags after 1 year) exhibited a clear pattern of higher production at higher elevations at both Mile Hammock Bay and Onslow Beach Backbarrier (**Figure 13-8**), but was less consistent with respect to elevation at Traps Bay Creek and Freeman Creek (**Figure 13-9**). At each of the latter sites, below-ground production at the shoreline was an order of magnitude above that of other samples from the same site. It is not clear why this occurs only at these two sites, but may have to do with differences in shoreline geomorphology/transect orientation. At both Freeman Creek and Traps Bay Creek, the lowest elevation point on the transect was directly adjacent to a tidal creek. At Onslow Beach Backbarrier and Mile Hammock Bay, the lowest point was adjacent to a mudflat forming a shallow marsh pond. Thus, the Onslow Beach Backbarrier and Mile Hammock Bay plots likely experienced less flushing than low elevation plots adjacent to tidal creeks.

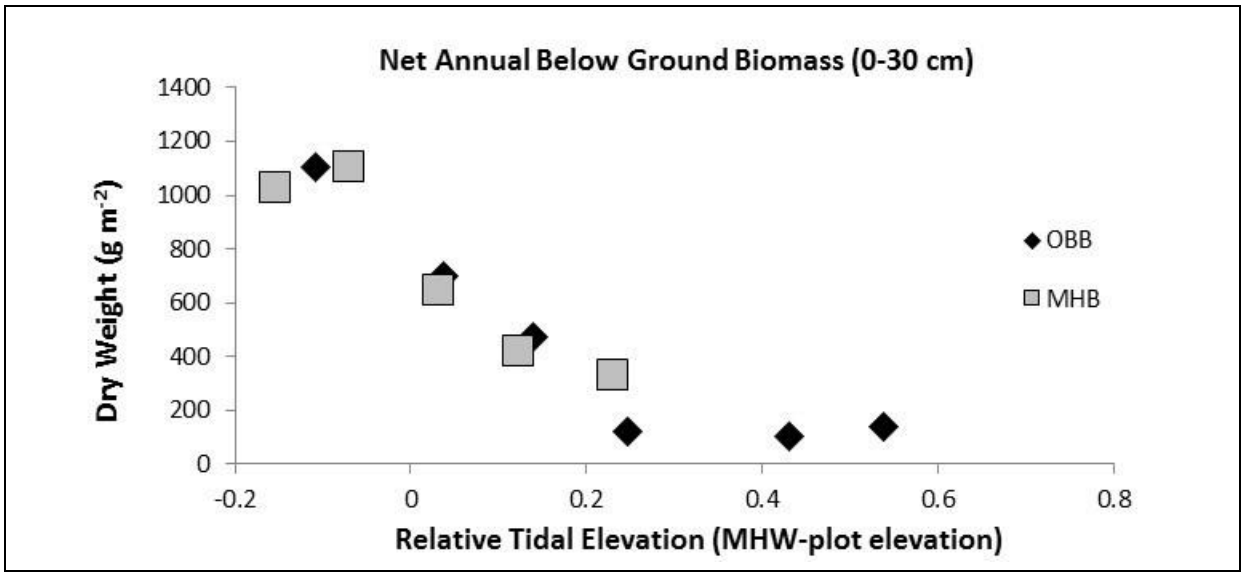

Figure 13-8. Annual below-ground biomass production measured as amount of root+rhizome material in ingrowth bags after 1 year at Mile Hammock Bay (MHB) and Onslow Beach Backbarrier (OBB).

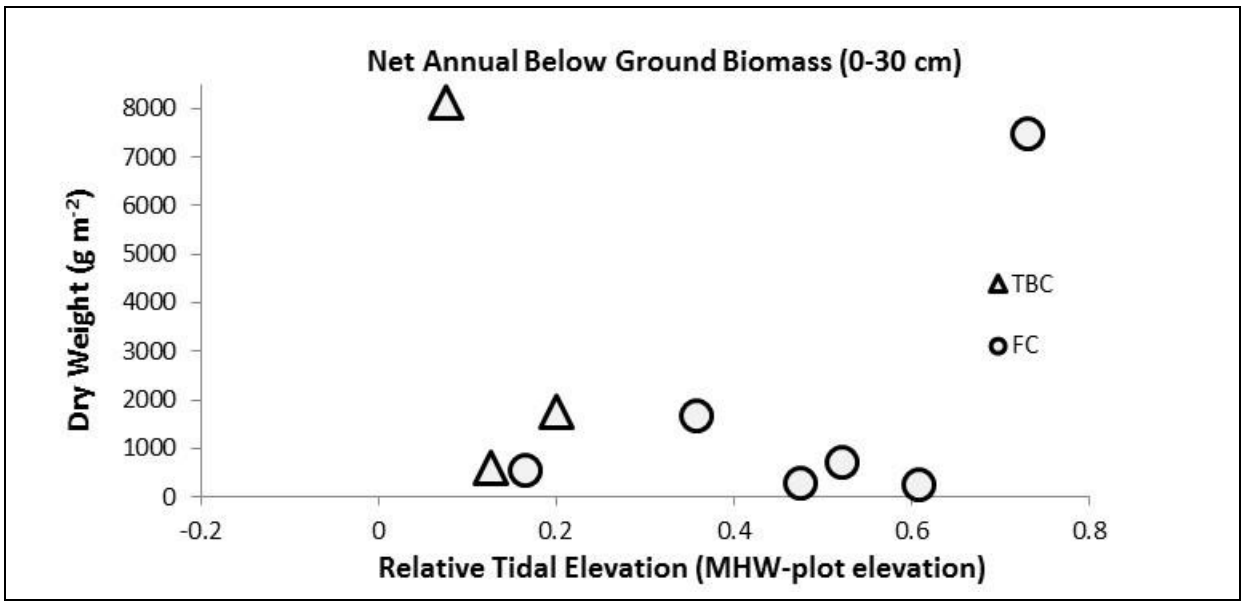

Figure 13-9. Annual below-ground biomass production measured as amount of root+rhizome material in ingrowth bags after 1 year at Traps Bay Creek (TBC) and Freeman Creek (FC).

To estimate the turnover of root+rhizome material in the soil, we compared annual production to standing stock (**Figure 13-10**). These data indicate that turnover is greater at both high and low ends of the marsh elevation gradient than at mid-marsh elevations. High rates of turnover can result from either decreased production or from increased decomposition. We expect both processes to vary with tidal elevation as more biomass is produced at higher elevations (**Figure 13-10**; Davis et al., 2015), and decomposition is likely to be slower at low elevations due to longer inundation times, which may result in less oxygen availability. The balance between these

two opposing factors leads to maximal preservation at mid-marsh elevations. If we assume that standing below-ground biomass is at steady state, this turnover rate suggests that on average, 10% of the root+rhizome material greater than 2 mm is lost annually, with values as high as 30% at Traps Bay Creek and low elevation plots at Freeman Creek.

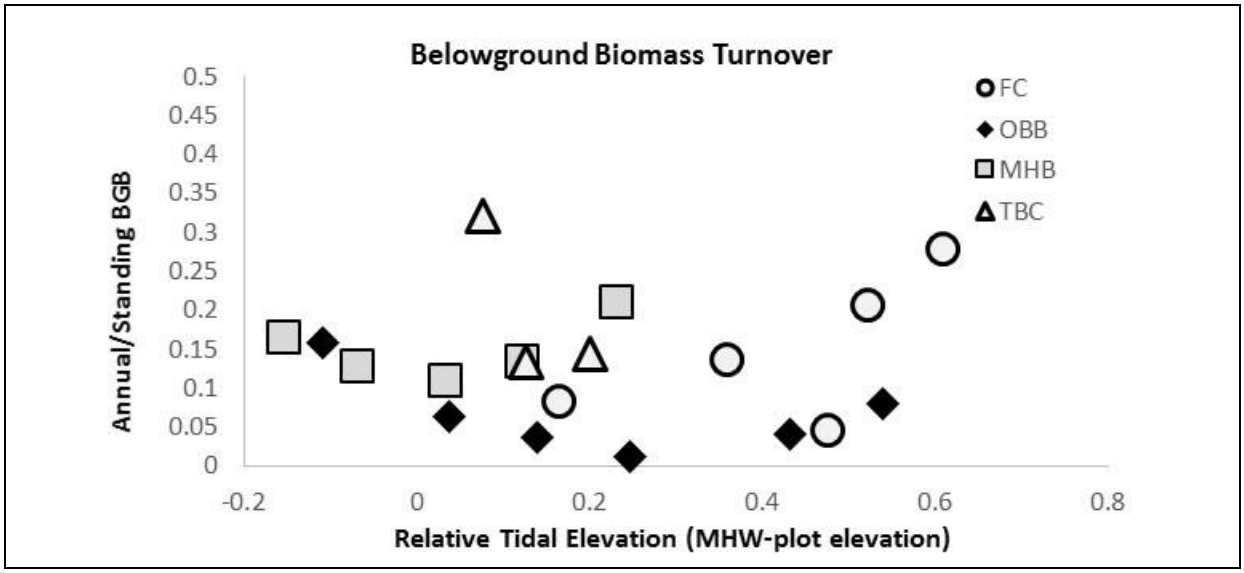

Figure 13-10. Estimated relative turnover rate of below-ground biomass.

Note: BGB = below-ground biomass; FC=Freeman Creek; OBB=Onslow Beach Backbarrier; MHB=Mile Hammock Bay; and TBC=Traps Bay Creek.

The *Juncus romerianus*–dominated French Creek marsh varied in elevation from creek edge to upland by a range of less than 20 cm, considerably less than most of the *Spartina alterniflora*–dominated marshes investigated here. At French Creek, there was not a significant trend in either above- or below-ground biomass with elevation (**Figure 13-11**). The lack of a trend may be a function of the narrow elevation range at this site, but is consistent with results from other *Juncus*–dominated marshes in North Carolina (R. Christian, personal communication). Standing stocks of above-ground *Juncus romerianus* biomass ranged between 1,171 g m^{-2} and 2,148 g m^{-2} and were within the range of previously reported values from the Mississippi coast and the Cape Lookout region of Central North Carolina (Eleuterius, 1984; Williams and Murdoch, 1972), but higher than other reported values from North Carolina (Woerner and Hackney, 1997). Although we did install root ingrowth bags at French Creek, the plots had not revegetated as of 1 year after installation. Thus, we are unable to estimate annual root production or turnover at this site.

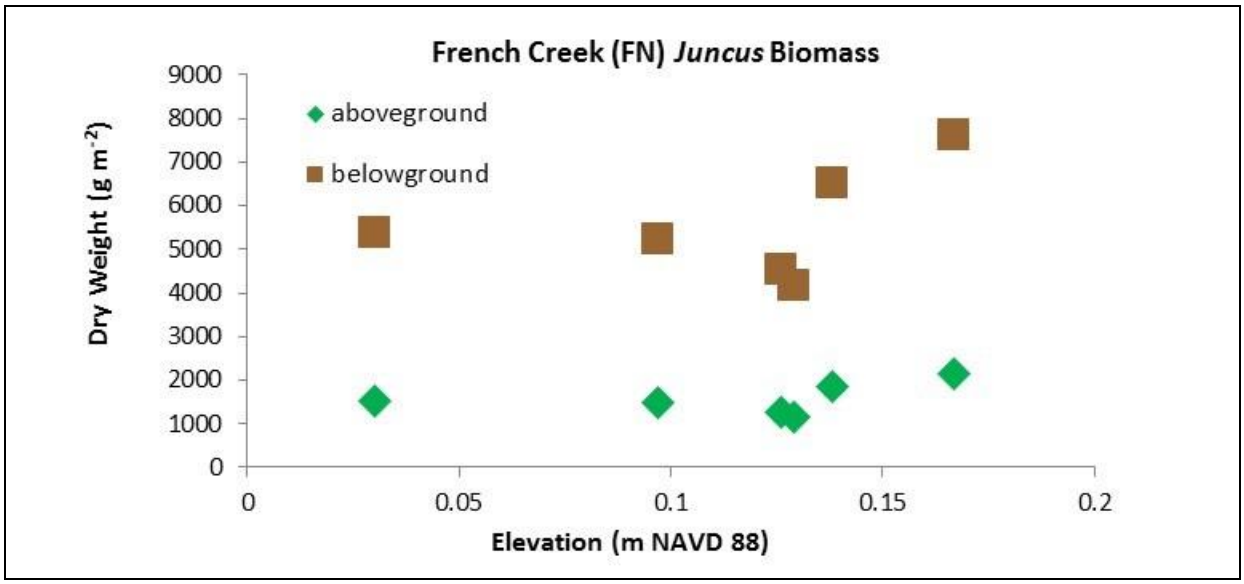

Figure 13-11. Live+dead standing above- and below-ground *J. romerianus* biomass across the elevation gradient at French Creek (FN).

Biomass Response to Fertilizer Addition

The Mile Hammock Bay marsh experienced a die-off event beginning in 2012 that left most of the study region devoid of vegetation during DCERP2 (Research Project CW-4, Coastal Wetland Monitoring). The only regions within the die off patch where *Spartina alterniflora* remained were the plots previously fertilized in DCERP1, and these contained only a few stems (between five and 10) each. As a result, we did not collect biomass data from this site during the 2015 sampling season. By the 2016 sampling (after 1 full year of fertilization), average above-ground biomass in fertilized plots at Mile Hammock Bay was 305 g m^{-2}, well below that of fertilized plots at the other *S. alterniflora* sites, but still a dramatic improvement over starting conditions. Among the other *S. alterniflora*–dominated sites (Freeman Creek, Onslow Beach Backbarrier, and Traps Bay Creek), average standing, live, above-ground *S. alterniflora* biomass ranged between 36 and 2,167 g dry weight per m^2 and was consistently greater in fertilized than control plots in both years ($F_{5,32}$=14.3, $p<0.001$; **Figure 13-12**). Morris et al (2013) showed that the growth response of *S. alterniflora* to fertilization is negatively correlated with in situ biomass. Biomass in *S. alternifora* marshes at MCBCL is on the lower end of previously reported values from the Southeastern United States (Davis et al., 2017), and so the observed increase may not be typical of all marshes. Fertilized plots also demonstrated greater resilience to, and regrowth from, the 2012 marsh dieback (RTI International, 2012). The 2012 marsh die-off event occurred during an extended period of drought, which has been identified as a probable cause of marsh die-off in other areas of the Southeast (Alber et al., 2008). The addition of ammonium nitrate to short form *Spartina alterniflora* has been shown to result in more plant growth and higher leaf concentrations of the osmoregulatory compounds proline and glycinebetaine, but had less effect on tall form plants (Cavalieri and Huang, 1981). Our results suggest that the nitrogen additions at Mile Hammock Bay provided *Spartina alterniflora* plants with a greater capacity for osmoregulation and increased capability to withstand drought conditions.

Juncus above-ground biomass did not exhibit a consistent trend with respect to fertilization. Average standing live biomass was greater in fertilized than control plots in 2015 (1,945 and 2,496 g dry weight m^{-2}, respectively). The pattern was reversed in 2016 with reduced biomass in fertilized relative to control plots (2,193 and 966 g dry weight m^{-2} respectively). Additionally, there were no significant between-treatment differences in stem height or in number of stems per square meter. The lack of consistent response may be a function of sampling bias. Because *J. romerianus* grows in clumps, rather than in the more even distribution characteristic of *Spartina alterniflora*, our sampling approach (counting stems within a $0.0625m^2$ quadrat and extrapolating to 1 m^2) may not have adequately captured fertilization-induced changes in *J. romerianus* biomass.

Previous studies of the *J. romerianus* response to nitrogen addition have found either no response (Hunter et al., 2015) or decreases in above-ground biomass with nitrogen addition (Pennings et al., 2005 and references therein). In the Pennings et al. (2005) review, most of the studies were conducted in marshes with mixed *S. alterniflora* and *J. romerianus* populations. In these cases, fertilization resulted in increases in *S. alterniflora* and concomitant decreases in *J. romerianus*. There is no *S. alterniflora* at French Creek, thus unlike the previous examples, our fertilizer addition did not lead to competitive displacement, but rather, measured the response of pure stands of *J. romerianus*. These data suggest that if *J. romerianus* responds to nutrient fertilization, then it may do so more slowly than *S. alterniflora*.

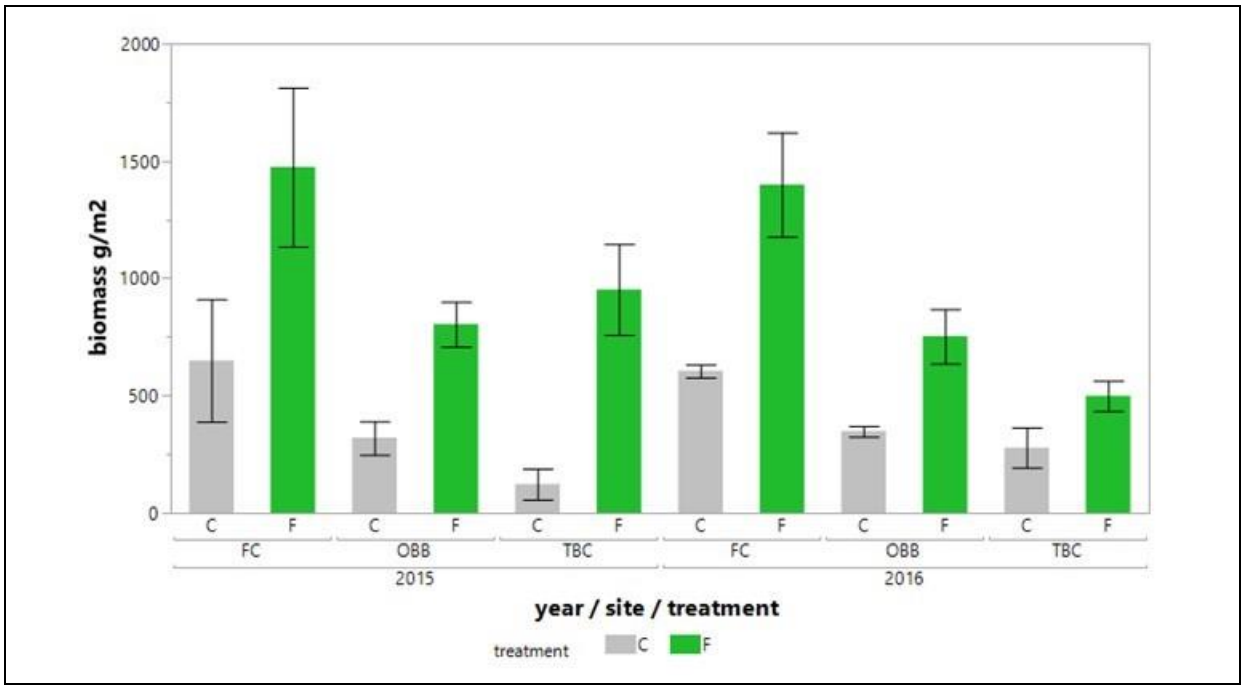

Figure 13-12. Average *Spartina alterniflora* above-ground biomass by site and year.

Note: C=control; F=fertilized. FC=Freeman Creek, OBB=Onslow Beach Backbarrier, MHB=Mile Hammock Bay, and TBC=Traps Bay Creek. Error bars represent standard error.

Fertilization led to greater amounts of standing below-ground biomass (organic material greater than 2 mm) across all sites (**Figure 13-13**; $t=4.59$, $p<0.0013$). The ratio of root to above-ground or shoot biomass in *S. alterniflora* has been shown to decrease as a result of fertilizer addition

because plants produce less root per unit of photosynthetic tissue when nutrients are abundant (Morris et al., 2013). We observed increases in root biomass of both *J. romerianus* and *S. alterniflora* in fertilized plots. Regarding *S. alterniflora*, the increase in root biomass in fertilized plots is correlated with significant increases in above-ground biomass; although each plant may produce less root per unit of shoot, there is so much more shoot material in fertilized plots that the overall abundance of root still increases (Morris et al., 2013). The increase in below-ground biomass with fertilization, similar to that of above-ground biomass, is a function of the low in situ biomass at these sites. Drs. Ellen Herbert and Matt Kirwan (see Section 4 of this chapter) show that as standing biomass increases, fertilization will no longer have a positive effect on below-ground *S alterniflora* biomass. The reason for increased below-ground biomass in *J. romerianus* where above-ground biomass did not respond consistently to fertilization is less clear, but suggests that fertilization differentially impacts above- and below-ground biomass in *Juncus*.

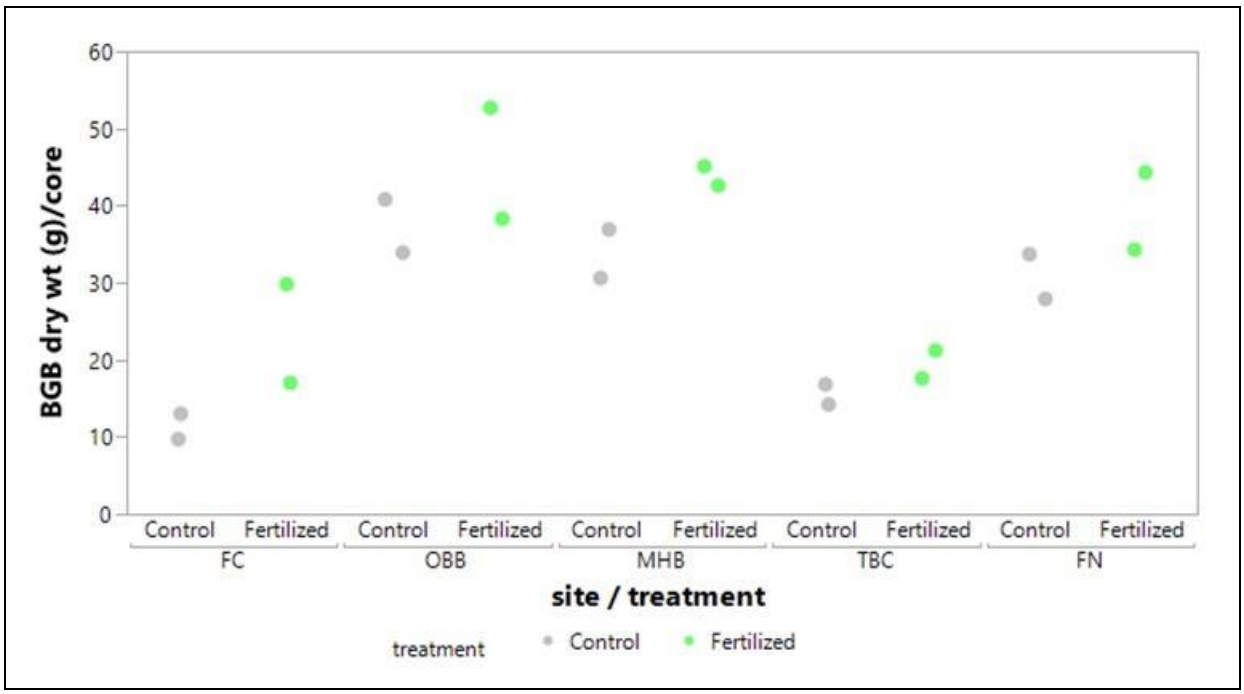

Figure 13-13. Standing belowground biomass (BGB; live+dead) in fertilized and control plots.

Symbols represent *Spartina alterniflora* in Freeman Creek (FC), Onslow Beach Backbarrier (OBB), and Mile Hammock Bay (MHB) plots, and *Juncus roemeranius* in the French Creek (FN) plots.

Porewater Nitrogen, Phosphorous, and Sulfide Concentrations

Porewater ammonium concentrations were log transformed before statistical analysis to meet normality and equal variance assumptions. Ammonium concentrations were consistently higher in fertilized than control plots (mean values across all sites, all time periods of 2,383 µM and 78 µM, respectively), but did not vary significantly by sample depth ($F_{2,337}$=200.38, p<0.0001). Significant variability was detected across sites and sample dates ($F_{7,270}$=4.94, p<0.0001), with lower concentrations in June than in all other sample times (**Figure 13-14 and Table 13-4**) and

lower concentrations detected in fertilized plots at Freeman Creek and Traps Bay Creek than at other sites (**Table 13-5**).

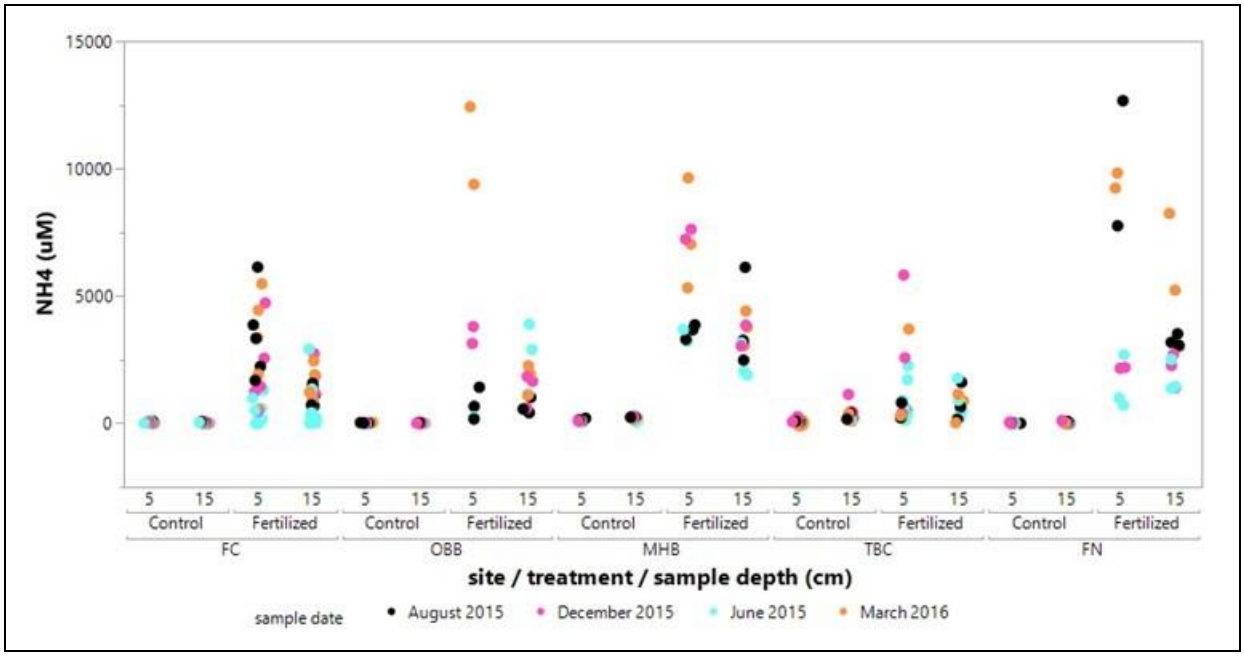

Figure 13-14. Measured porewater ammonium (NH_4^+) concentrations in fertilized and control plots sampled at 5 cm and 15 cm.

Note: FC=Freeman Creek, FN=French Creek; MHB=Mile Hammock Bay, OBB=Onslow Beach Backbarrier, and TBC=Traps Bay Creek.

Table 13-4. Seasonal Mean NH_4^+ Concentrations

Note: Reported values are averages across all depths (5 cm and 15 cm) and all sites by season. Samples were collected approximately 2 weeks after fertilizer application. Treatments with different superscripts were significantly different.

Sample Date	Mean NH_4^+ Control Plots (µM)	Mean NH_4^+ Fertilized Plots (µM)
March 2016	$62^{c, d}$	$3{,}934^{a}$
June 2015	46^{d}	$1{,}110^{b}$
August 2015	81^{c}	$2{,}543^{a}$
December 2015	135^{c}	$2{,}614^{a}$

Table 13-5. Mean NH_4^+ Concentration by Site. Reported Values Are Averages Across All Depths (5 cm and 15 cm) and All Seasons by Site

Note: Samples were collected approximately 2 weeks after fertilizer application. Treatments with different superscripts were significantly different.

Site	Mean NH_4^+ Control Plots (µM)	Mean NH_4^+ Fertilized Plots (µM)
Freeman Creek	30^{d}	1458^{b}
Onslow Beach Backbarrier	16^{d}	$2503^{a,b}$
Mile Hammock Bay	140^{c}	4364^{a}
Traps Bay Creek	203^{c}	1114^{b}
French Creek	19^{d}	4103^{a}

Porewater NO_3+NO_2 concentrations (data not shown) were frequently below detection. There were no significant differences in NO_3+NO_2 among fertilized and control plots or by site, sample depth, or season. Significant differences in PO_4 porewater concentrations ($F_{5, 335}$=6.0498, p<0.0001) occurred among treatments (mean PO_4 in fertilized plots=158 µM, in control plots=1.2 µM), and among sites with average concentrations at French Creek an order of magnitude greater than at all other sites (333 µM versus an average of 31 µM; **Figure 13-15**).

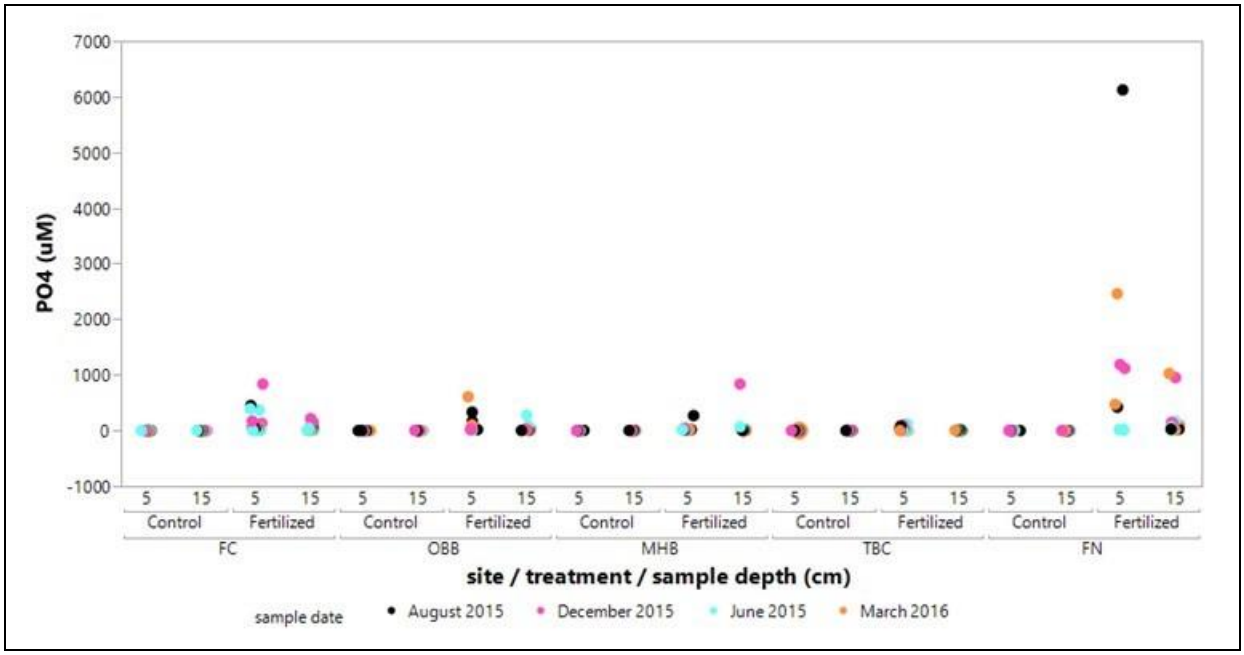

Figure 13-15. Measured porewater PO_4 concentrations in fertilized and control plots sampled at 5 cm and 15 cm.

Note: FC=Freeman Creek; FN=French Creek; MHB=Mile Hammock Bay; OBB=Onslow Beach Backbarrier; and TBC=Traps Bay Creek.

Porewater hydrogen sulfide (H_2S) concentrations were square-root transformed to meet normality criteria. Concentrations did not differ by treatment, but were significantly different by season and site ($F_{7, 124}$=21.17, P<0.0001) with consistently lower concentrations at Freeman Creek than at other sites, and the greatest concentrations across all sites occurring in December and lowest concentrations occurring in March (**Figure 13-16** and **Tables 13-6 and 13-7**).

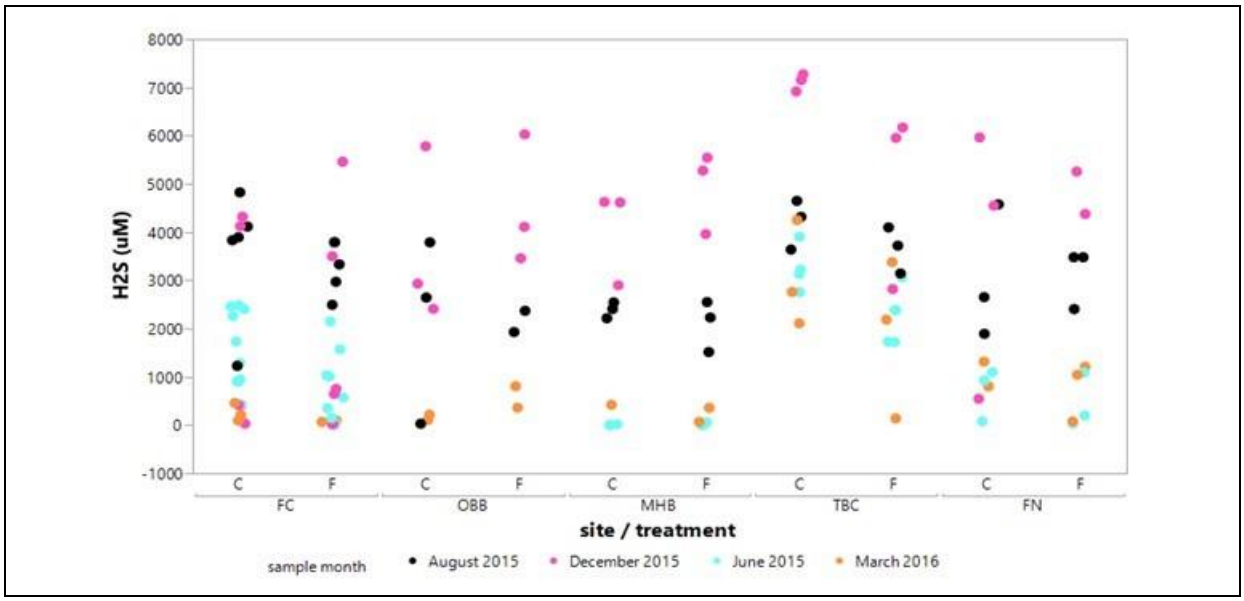

Figure 13-16. Porewater hydrogen sulfide (H_2S) concentrations in fertilized (F) and control (C) plots.

Note: All samples were collected at 15 cm; FC=Freeman Creek; FN=French Creek; MHB=Mile Hammock Bay; OBB=Onslow Beach Backbarrier; and TBC=Traps Bay Creek.

Table 13-6. Mean Porewater Hydrogen Sulfide (H_2S) by Sample Date

Note: Reported values are averages by sample date and treatment across all sites. Samples were collected approximately 2 weeks after fertilizer application. Treatments with different superscripts were significantly different.

Site	Mean H_2S Control Plots (µM)	Mean H_2S Fertilized Plots (µM)
Freeman Creek	1,904[b]	1,473[b]
Onslow Beach Backbarrier	2,239[a,b]	2,723[a,b]
Mile Hammock Bay	1,975[a,b]	1,960[b]
Traps Bay Creek	4,235[a]	3,063[a,b]
French Creek	2,219[a,b]	2,059[a,b]

Table 13-7. Mean Porewater H_2S by Site

Note: Reported values are averages by site and treatment across all seasons. Samples were collected approximately 2 weeks after fertilizer application. Treatments with different superscripts were significantly different.

Sample Date	Mean H_2S Control Plots (µM)	Mean H_2S Fertilized Plots (µM)
March 2016	1,159[c]	756[c]
June 2015	1,628[b,c]	932[c]
August 2015	3,132[a,b]	2,956[a,b]
December 2015	3,821[a]	3,958[a]

Differences in porewater nutrient concentrations among sites can occur for a variety of reasons, including differences in plant uptake, variable soil porosity or porewater flow rates, and variable nutrient cycling processes. Ammonium concentrations in fertilized plots at Mile Hammock Bay

and French Creek were consistently higher than those of control plots. This was not the case at Freeman Creek, Onslow Beach Backbarrier, or Traps Bay Creek, where, in many cases, fertilized plot ammonium concentrations approached those of controls plots (**Figure 13-14**). The difference is likely due to the influence of marsh vegetation. There was very little standing plant biomass at Mile Hammock Bay due to the ongoing die-off at this site, and the lack of above-ground biomass response to fertilization at French Creek suggests that the *Juncus* at this site was not nitrogen limited. Thus, porewater ammonium concentrations remained high at Mile Hammock Bay and French Creek relative to the other sites, all of which experienced significant increases in plant biomass fueled by uptake of porewater nutrients (**Figure 13-12**). Actively growing marsh vegetation influences porewater NH_4^+ concentrations via at least two pathways: (1) direct NH_4^+ uptake to support plant growth and (2) NH_4^+ oxidation (fueled by radial oxygen loss from live roots; Koop-Jakobsen and Wenzhöfer, 2015). Both pathways of NH_4^+ removal from pore waters should be maximized in the summer when plants are actively growing. Thus, the among-site differences in porewater NH_4^+ concentration detected here are at least partially driven by differences in the abundance and type of marsh vegetation present at each site.

Porewater sulfide was present in millimolar concentrations across all sites and did not vary with treatment. These values are similar to those reported for other salt marsh sediments and suggest that sulfate reduction is an important metabolic pathway in this system (Koretsky et al., 2005). Because sulfide is a product of sulfate reduction, its concentration in porewater may be indicative of the degree of carbon mineralization that is occurring. Porewater H_2S can undergo several transformations, including oxidation to sulfate in the presence of oxygen or pyrite formation in the presence of available iron. As a result, the amount of H_2S present does not translate directly to carbon mineralization rates. Still, the lack of variability between treatments suggests that fertilization did not directly lead to increased organic matter turnover. Similar to ammonium, porewater sulfide concentrations exhibited strong seasonal variability with lower concentrations during the growing season. The relatively low spring and summertime concentrations are most likely driven by plant-mediated oxygenation of the rhizosphere. Because H_2S is not stable under oxic conditions, oxygen loss from roots, which is likely to be greatest during the active growing season, leads to spontaneous sulfide oxidation (Lamers et al., 2013). This process also explains the elevated porewater sulfide concentrations during December, when plants are no longer actively growing.

Sediment Characteristics

Sediment properties varied widely among sites (**Table 13-8**). As a general rule, very organic soils tend to have low dry bulk densities (0.2–0.3 g cm^{-3}), and highly mineral soils tend to have high bulk density values (1.0–2.0 g cm^{-3}; Mitsch and Gosselink, 2007). All sites other than Onslow Beach Backbarrier exhibited bulk density values indicative of organic-rich soils (**Table 13-8**). Despite having as much or more below-ground biomass than the other sites (**Figure 13-13**), Onslow Beach Backbarrier exhibited much higher bulk density values due to a high sand content. The sand content at Mile Hammock Bay, although lower than that at Onslow Beach Backbarrier, was also elevated relative to that of the rest of the sites. These site-specific differences in soil characteristics provide important clues about the soil formation processes at each site. Both Onslow Beach Backbarrier and Mile Hammock Bay are located on barrier islands that are separated from the mainland by the Atlantic Intracoastal Waterway (AIWW). These sites receive sand inputs through aeolian transport of particles from the barrier island oceanfront

beach/dune system (Rodriguez et al., 2013), which results in greater sand content at these sites. The low sand content at Freeman Creek, which is directly across the AIWW from the barrier island suggests that sand does not travel across the AIWW in significant quantities. Soils at French Creek have approximately two times greater %OM than all other sites which suggests that plant root production is a strong driver of soil formation at this site. None of the sediment properties measured here varied by treatment, thus short-term fertilizer addition does not have measurable consequences in terms of sediment structure.

Table 13-8. Sediment Particle Size and Bulk Density in Fertilized and Control Plots.

One sample was collected from each non-SET associated plot at the end of the 2-year fertilization period.

Site	Treatment	Replicate	Percent Organic Matter	Bulk Density (g cm^3)	Percent Sand by Weight	Percent Silt by Weight
FC	Control	1	20.8	0.3087	0.37	0.63
		2	20	0.2669	0.21	0.79
	Fertilized	1	18.3	0.3229	0.34	0.66
		2	19.4	0.257	0.3	0.7
OBB	Control	1	12.2	0.8307	0.87	0.13
		2	14.1	0.7215	0.83	0.17
	Fertilized	1	21.5	0.547	0.85	0.15
		2	12.8	0.734	0.62	0.38
MHB	Control	1	33.3	0.1842	0.49	0.51
		2	33.4	0.219	0.38	0.62
	Fertilized	1	30.2	0.2162	0.48	0.52
		2	26.9	0.2322	0.47	0.53
TBC	Control	1	24.7	0.2245	0.22	0.78
		2	22.8	0.2341	0.31	0.69
	Fertilized	1	23.6	0.2377	0.17	0.83
		2	27.8	0.2139	0.21	0.79
FN	Control	1	54.2	0.1343	0.29	0.71
		2	53.8	0.1687	0.33	0.67
	Fertilized	1	58	0.1294	0.23	0.77
		2	49.8	0.1582	0.24	0.76

Note: %OM=percent organic matter; FC=Freeman Creek; FN=French Creek; MHB=Mile Hammock Bay; OBB=Onslow Beach Backbarrier; and TBC=Traps Bay Creek.

Sediment Deposition

Marker horizon-based estimates of sediment accretion were converted to daily rates by dividing the measured deposition at each site by the number of days between readings, and then were log transformed to satisfy equal variance criteria. A two-way analysis of variance (ANOVA) of log-transformed data indicated significant differences by season and site ($F_{7, 507}=70.11$, $p<0.001$). Average daily deposition rates were greatest at Freeman Creek and were lowest at French Creek (**Table 13-9**). Among-site differences in sediment deposition are driven by a combination of

inundation time and SSC, both of which effectively control the access that each marsh has to mineral sediments. Inundation times varied among sites such that French Creek > Traps Bay Creek > Mile Hammock Bay > Freeman Creek > Onslow Beach Backbarrier (see Chapter 4 of the *DCERP2 Final Report*). SSCs were similar at Freeman Creek and Traps Bay Creek and were on average approximately 5.9 mg L^{-1} greater at these sites than at French Creek (Ensign et al., 2016). Despite experiencing the longest inundation times, low SSCs appeared to limit deposition at French Creek. Although site-specific data on SSC were not available for Onslow Beach Backbarrier and Mile Hammock Bay, deposition at Onslow Beach Backbarrier was likely limited by the short inundation times experienced there. There was no marsh vegetation to trap and stabilize sediments at Mile Hammock Bay (in many cases, the feldspar marker horizon layers were washed away by tidal flow) resulting in low accumulation rates at this site. Across all sites, average daily deposition was highest in the fall and lowest in the winter (**Table 13-10**). This trend is also a function of inundation time because water levels are substantially higher in the fall across all sites (see Chapter 4 of the *DCERP2 Final Report*).

Table 13-9. Mean Daily Sediment Deposition by Site Across All Seasons

Sites that share the same superscript letter are not significantly different.

Site	Mean Daily Deposition Rate (mm)
FC[a]	0.15
TBC[b]	0.08
OBB[c]	0.05
MHB[c]	0.05
FN[d]	−0.01

Note: FC=Freeman Creek; FN=French Creek; MHB=Mile Hammock Bay; OBB=Onslow Beach Backbarrier; and TBC=Traps Bay Creek.

Table 13-10. Mean Daily Sediment Deposition by Season Across All Sites

Seasons that share the same superscript letter are not significantly different.

Season	Mean Daily Deposition Rate (mm)
Spring[a]	0.07
Summer[a]	0.07
Fall[b]	0.12
Winter[c]	0.01

One of the hypothesized mechanisms by which fertilization may lead to enhanced marsh elevation gain is through increased rates of sediment trapping (Morris et al., 2002). Under this scenario, increased plant biomass resulting from fertilization leads to greater particle trapping efficiency and thus higher elevation gain through mineral deposition. In the current study, fertilized plots experienced significantly greater rates of sediment deposition at only Freeman Creek and Traps Bay Creek (**Figure 13-17**) because these sites experienced higher SSCs, long inundation times, and significant increases in above-ground biomass. At each of the other sites, at least one of these criteria was not met.

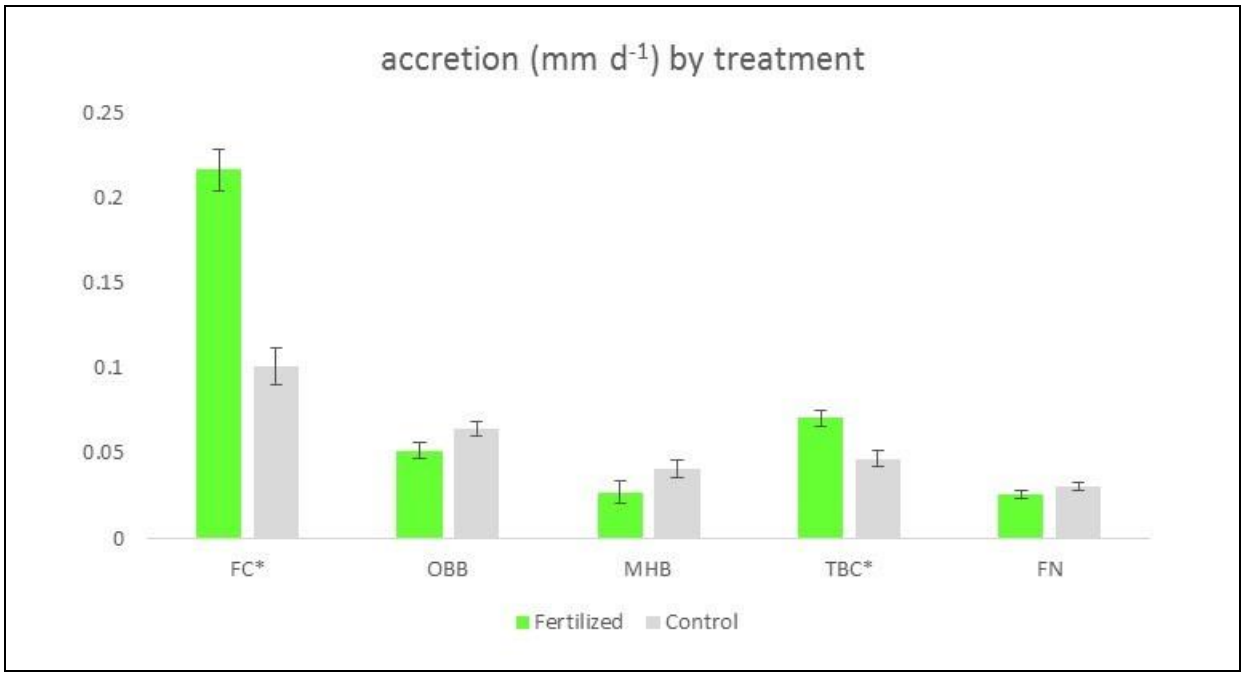

Figure 13-17. Average measured sediment accretion by treatment.

Note: * = significant difference between treatments; FC=Freeman Creek; FN=French Creek; MHB=Mile Hammock Bay; OBB=Onslow Beach Backbarrier; and TBC=Traps Bay Creek.

Elevation Change

The effect of fertilization on net marsh elevation change rates, as determined by SETs, was measured at Freeman Creek, Onslow Beach Backbarrier, and Mile Hammock Bay. Total cumulative elevation change was highest at Freeman Creek, and except for one control SET at Freeman Creek, was greater in fertilized than control SETs at all three sites (**Figures 13-18 and 13-19**). No significant relationships were detected between either starting elevation or standing live biomass of SET plots and elevation change (**Table 13-11**). Enhanced rates of elevation gain in fertilized plots at Mile Hammock Bay and Onslow Beach Backbarrier without enhanced deposition, implicates soil volume expansion via increased below-ground biomass production as the driver of elevation gain at these sites. Although it is likely that this also occurs at Freeman Creek and Traps Bay Creek, we do not have the data necessary to quantify the relative roles of below-ground production and sediment deposition to elevation gain.

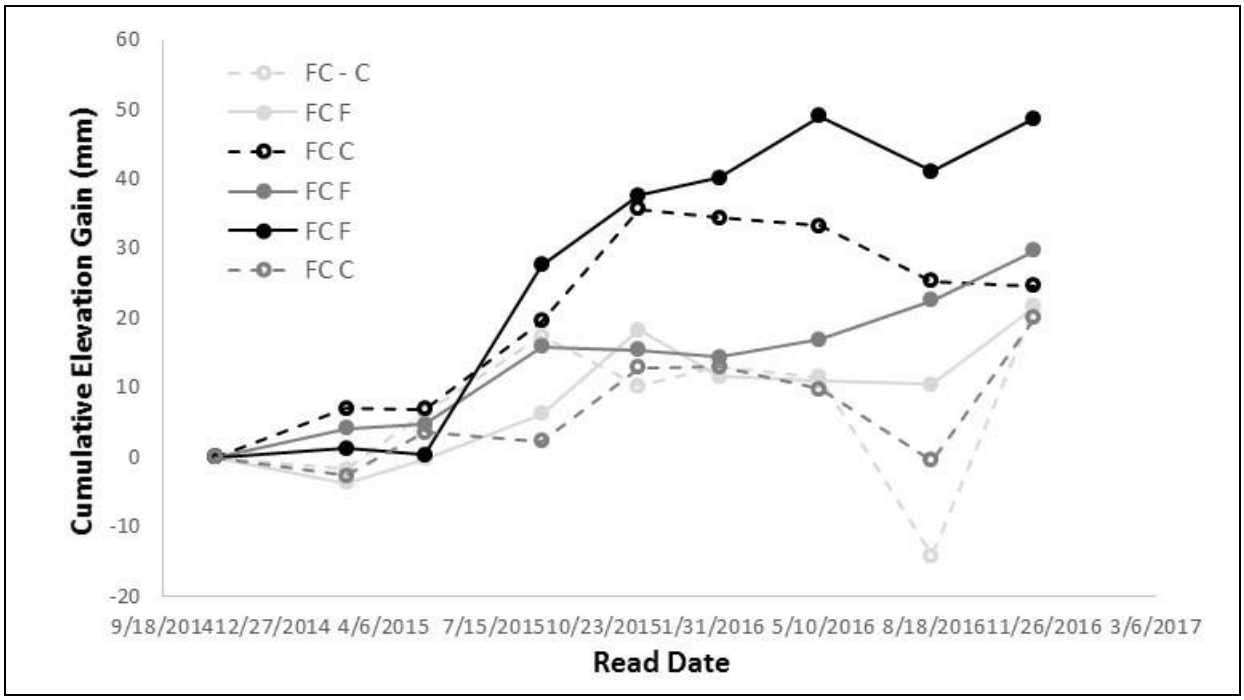

Figure 13-18. Elevation change over time at Freeman Creek. Solid markers/solid lines represent fertilized plots, open markers/dashed lines represent control plots.

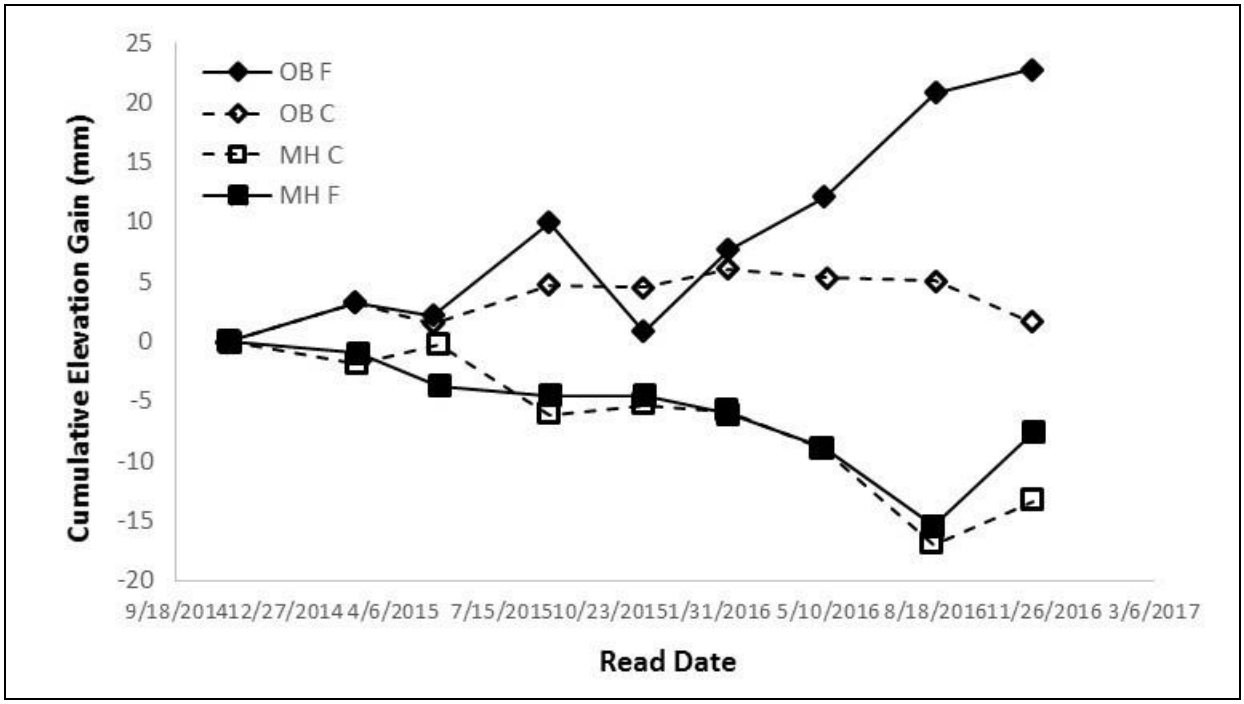

Figure 13-19. Elevation change over time at Onslow Bay (OB) and Mile Hammock (MH) Bay.

Solid markers/solid lines represent fertilized plots, open markers/dashed lines represent control plots.

Table 13-11. Starting Elevation, Elevation Change Rate, and Mean Biomass at Fertilized and Control Plots.

Site	Set Number	Treatment	Starting Elevation (m NAVD 88)	Mean Elevation Change Rate (mm yr^{-1})	Standing Live Biomass (g m^{-2})
FCFC	31	Control	0.061	3.68	437
	32	Fertilized	0.085	10.54	814
	33	Control	0.068	14.80	494
	34	Fertilized	0.07	13.32	1603
	35	Fertilized	0.084	28.44	1514
	36	Control	0.106	7.3	904
OBB	37	Fertilized	0.239	10.84	472
	38	Control	0.266	1.44	314
MHB	39	Control	0.137	−7.81	—
	40	Fertilized	0.156	−5.72	—

Note: FC=Freeman Creek; MHB=Mile Hammock Bay; NAVD 88= North American Vertical Datum of 1988; and OBB=Onslow Beach Backbarrier; and TBC=Traps Bay Creek.

Davis et al. (2017) compared SET data in fertilized and control plots of Freeman Creek, Onslow Beach Backbarrier, and Mile Hammock Bay from 2008 to 2012. This data record included the initial fertilization conducted during DCERP1 (2008–2010) and 2-year post fertilization. This analysis showed that fertilized plots at Onslow Beach Backbarrier and Mile Hammock Bay maintained an elevation advantage over control plots for up to 2 years after fertilizer application ceased. This was not the case at Freeman Creek, where control plots “caught up” to fertilized plots once fertilizer application ceased. The difference appears to be a function of naturally high deposition rates at Freeman Creek that result from its low position in the tidal frame and ample suspended sediment loads. Although the longevity of the fertilized plot elevation advantage over control plots varied among sites, elevation at all three sites responded positively to fertilization. We found no evidence of negative impacts to marsh sustainability from short-term fertilizer applications. Fertilized plots had an elevation advantage of between 0 cm and 20 cm over control plots at the same site by the end of the study (**Figures 13-18 and 13-19**). Model results (from Drs. Herbert and Kirwan presented in this chapter) indicate that the role of fertilization in increasing marsh surface elevation is a function of both in situ biomass and suspended sediment load. Both factors are likely to change with accelerated sea level rise, and thus, so is the effectiveness of fertilization as an adaptive management strategy. However, under current conditions, short-term fertilization appears to be an effective approach to building elevation capital.

Section 3. Geospatial Marsh Model

Lead Researchers: Drs. Ellen Herbert and Matt Kirwan

Introduction

As a subset of Research Project CW-4, we developed a geospatial model of the response of marshes to sea level rise by using field and remote sensing data from MCBCL marshes. The geospatial model predicts the horizontal migration of marsh habitats based on their elevation relative to MSL, thereby allowing marsh habitats to move upslope in response to increased flooding as sea level rises. The vertical evolution of the marsh surface is modeled for specific marsh vegetation types and simulates both above-ground sediment trapping and below-ground organic matter accumulation in response to variations in flooding time. The geospatial model includes a novel numerical simulation of plant resource allocation in response to nutrient supply that allows for the simulation of the influence of nutrients (fertilization) on above-ground productivity and sediment trapping and below-ground biomass accumulation.

Methods and Materials

Site Selection and Model Scenarios

We modeled three of the most well-studied MCBCL marshes, Freemans Creek, Traps Bay, and French Creek (**Figure 13-20**). These sites were selected based on the availability of biomass, elevation, water level, and suspended sediment data to parameterize the model. These sites were also selected because they represent a gradient in suspended sediment supply, dominant plant community and hydroperiod, thereby allowing us to assess the full suite of possibilities for MCBCL marshes. The modeling domain includes open water, mudflat, herbaceous marsh, swamp, and adjacent upland environments.

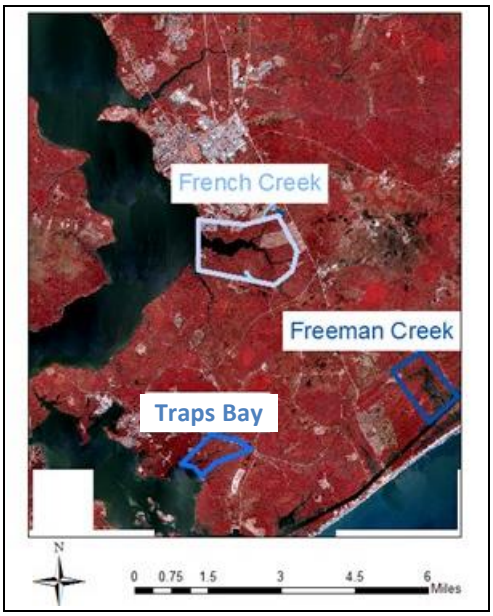

Figure 13-20. Domain for marsh modeling at Freeman Creek, Traps Bay, and French Creek at MCBCL.

For each site, we model elevation and habitat distributions under the five Global Sea Level Rise + Base Adjustment scenarios for MCBCL (**Table 13-12**) from 2013 (initial) to 2100. As it corresponded to the year of baseline Ortho-Imagery at MCBCL, 2013 was selected as the initial year. Sea level for each year was estimated by interpolating a curve though the total sea level rise (Global + Site-Specific Adjustments) specified for MCBCL by Hall et al. (2016). Because SSC is well known to be a dominant control on the ability of marshes to increase elevation with sea level rise (Fagherazzi et al., 2012; Kirwan et al., 2010), we simulated three sediment scenarios for each marsh under each sea level rise scenario (**Table 13-12**). The three scenarios are as follows: current average ambient SSC (Ambient), half of current average SSC (1/2 Ambient), and double

current average SSC (Double Ambient). Finally, because both field and modeling results from DCERP1 (RTI International, 2013) and DCERP2 (Davis et al., 2017) illustrate that the fertilization of marshes with nitrogen has a substantive impact on the ability of *Spartina alterniflora* marshes to gain elevation, we ran the medium sea level rise scenario (1.3 m) with three sediment scenarios under fertilized and unfertilized conditions.

Table 13-12. Summary of Each Modeling Scenario, Corresponding with Global Scenarios to Which MCBCL–Specific Adjustments Were Added

Ctrl=control; and N=nitrogen. Numerical values for sea level rise scenarios indicate sea level at 2100. For the Medium sea level rise scenario, each sediment scenario was run under fertilized and unfertilized conditions.

Sediment Scenario	Sea Level Rise Scenario	Lowest (0.3 m)	Low (0.8 m)	Medium (1.3 m)	High (1.8 m)	Highest (2.5 m)
½ Ambient				Ctrl / +N		
Ambient				Ctrl / +N		
Double Ambient				Ctrl / +N		

Geospatial Model—Input Data

Habitat Classification

We used the MCBCL 2010 Red, Green, and Blue (RGB) and Infrared (IR) Ortho-Imagery (0.3-m resolution) to generate a raster of habitat classifications by using the maximum likelihood classification method in ArcGIS 10.0. Initially, we computed the Normalized Differential Vegetation Index (NDVI) from the Ortho-Imagery by using the Image Analyst tool in ArcGIS 10.0. We then used field-confirmed polygons of habitat classes (**Figure 13-21**) to create a data set of training pixels or "Signature File" (10 to 20 polygons per habitat type). We then computed variances and covariance matrices based on RGB, IR, and NDVI values for each habitat in the "Signature File." These matrices were then used to compute the statistical probability that each pixel in the image belonged to a given habitat class, and the pixel was assigned to the habitat class with the greatest probability. Accuracy of the classification was tested by selecting 30 random points in each predicted habitat type by using Hawth's Tools in ArcGIS 10.0 and visually assessing areal imagery. Accuracy of the classification ranged from 78% for tidal swamp forest to 98% for *Spartina alterniflora* marsh. Maps of habitat class (**Figure 13-21**) were used to establish initial marsh accretion rates and elevation distribution in the geospatial model.

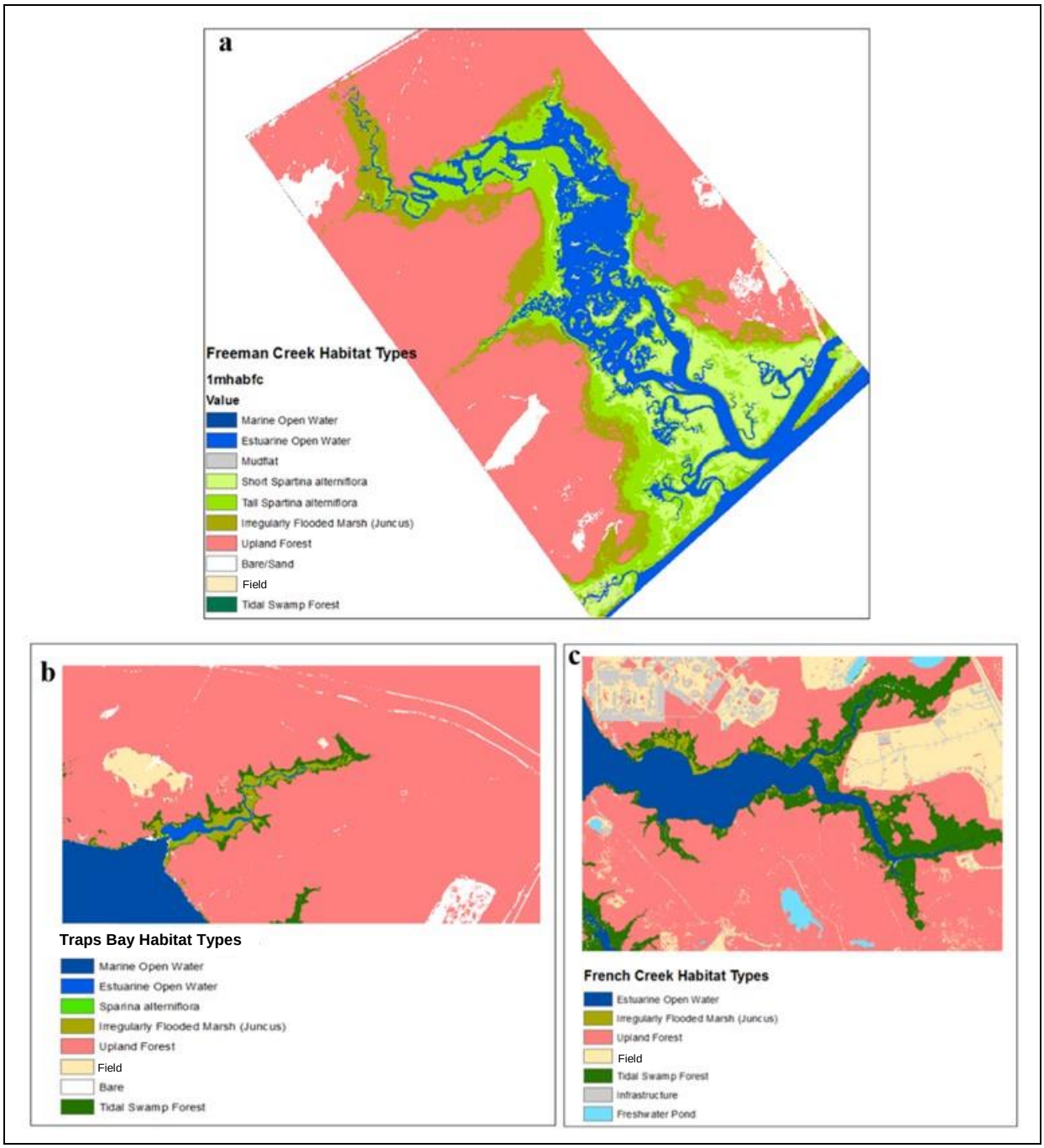

Figure 13-21. Habitat classifications derived from MCBCL RGB and IR Ortho-Imagery for the three study domains.

Digital Elevation Maps

Elevations were derived from MCBCL 2013 light detection and ranging (LiDAR) data. Given the observation that dense marsh vegetation can result in overestimates of marsh elevation by as much as 25 cm (Hladik and Alber, 2012), we used all available real-time kinematic global positioning system (RTK-GPS)–measured point elevations (ground control points) collected by Coastal Wetlands Monitoring (see Chapter 4 of the *DCERP2 Final Report*) from each site to

assess the accuracy of the DEM. The data were randomly divided into training and validation data sets by using ArcGIS 10.0. For each site, 50% of the RTK-GPS ground control points were used to calibrate tidal marsh elevation ranges and correction factors, and the remaining 50% were reserved as validation data for the modified DEM accuracy assessment. The training data were used to assess the accuracy of the LIDAR–derived DEM for marsh habitats following the method described by Hladik and Alber (2012). Habitat-specific "correction factors" were calculated as the mean error (i.e., the mean of the difference between the DEM and training RTK-GPS ground control point elevations for the marsh habitat classes at each site. Following the method described by Hladik and Alber (2012) and Hladik et al. (2013), the correction factor was subtracted from the original DEM in ArcGIS (Spatial Analyst toolbox) to produce a vegetation corrected DEM (**Figure 13-22**). After applying the correction factors, the accuracy of both the original and vegetation corrected DEMs were assessed by using the reserved RTK-GPS survey validation data, which were not used to derive the correction factors.

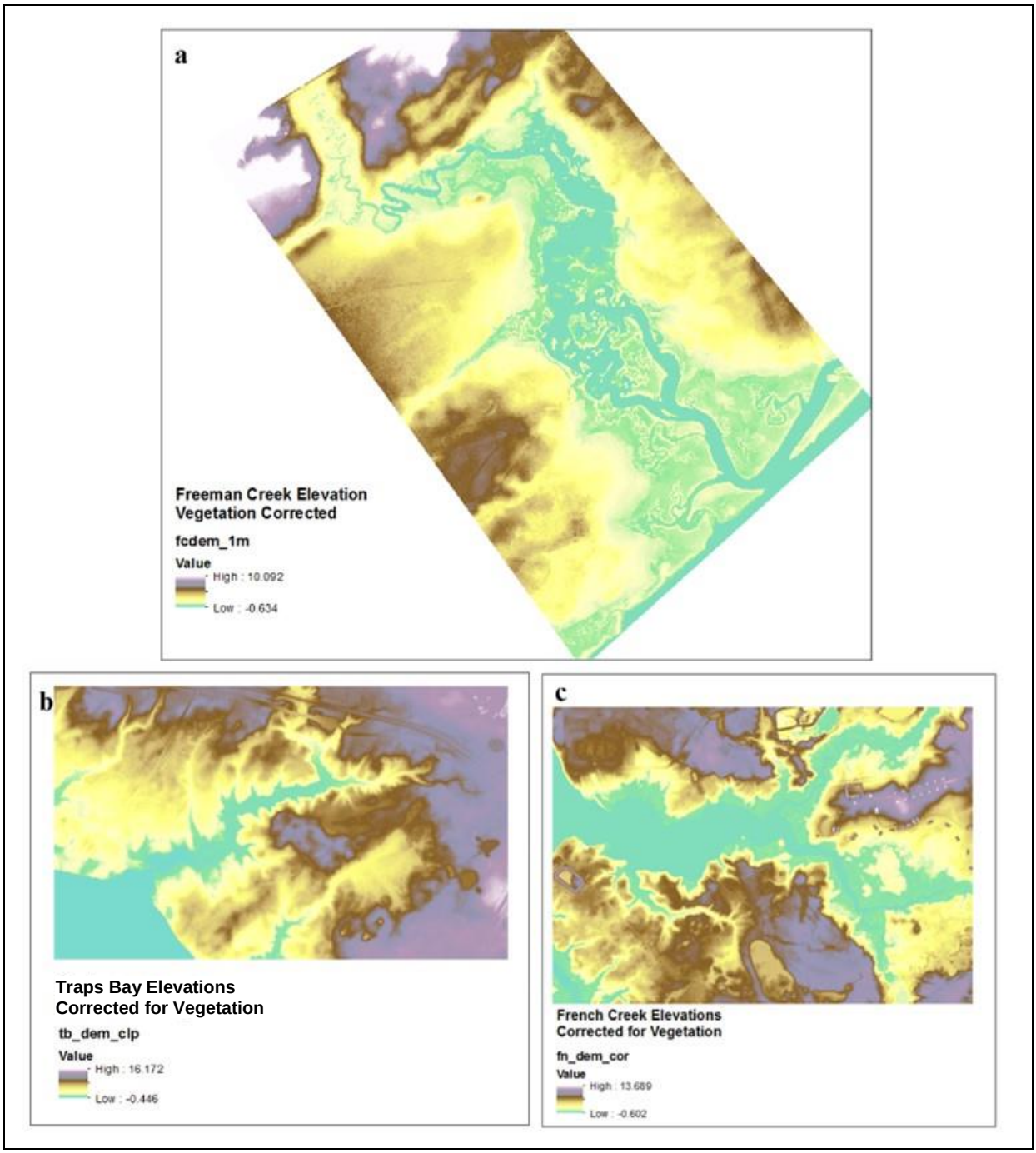

Figure 13-22. Vegetation-corrected digital elevation maps of the three marsh domains at MCBCL.

Model Development

We consider the following five distinct habitat groups in the model framework: (1) Subtidal, consisting of open water and unvegetated mudflat; (2) *Spartina alterniflora* low marsh; (3) *Juncus romerianus* high marsh; (4) tidal swamp forest; and (5) upland, including forest, field, bare, and infrastructure.

Vertical Marsh Evolution

Following previous models of salt marsh vertical accretion (Fagherazzi et al., 2012; Kirwan and Guntenspergen, 2010; Morris et al., 2002; Mudd et al., 2004), *Spartina* and *Juncus* marsh elevation $z(t)$ relative to mean sea level (R) is calculated annually as the sum of the mass of sediment trapping (q_t) and settling (q_s) and organic matter (a_o) deposited on the marsh divided by the density of the marsh soil formed (ρ_m). The calculation is shown in Equation 13-1.

$$dz/dt = -R + \frac{[q_s(z,L)+q_t(z,L)+ q_o(B)]}{\rho_m} \qquad \text{(Eq. 13-1)}$$

Where ρ_m is calculated from an empirical relationship between organic content and density in marsh soils (Neubauer, 2008), and L and B are the annually averaged above-ground and below-ground biomass, respectively. Settling (q_s) is the product of the sediment settling velocity (w_s) and the instantaneous SSC, $C(z, L, t)$, integrated over the tidal cycle. Throughout the tidal cycle, C is obtained by subtracting the mass deposited ($q_s + q_t$) at time (t) from the depth-integrated mass of sediment entering the marsh on the flood tide (e.g., from a tidal creek) with a fixed concentration of sediment (C_0). Based on the field measurements in Section 1 of the chapter, there is no significant spatial variation in suspended sediment load across the marsh surface (Ensign and Currin, 2017). We, therefore, hold C_0 constant across the marsh surface. Trapping (q_t) is proportional to C and the diameter ($\emptyset_s$), density (n_s), and height (h_s) of stems on the marsh surface (D'Alpaos et al., 2007). We use the formulation from Palmer et al. (2004) to calculate trapping as shown in Equation 13-2.

$$\boldsymbol{q_{dt} = C\ U\ \epsilon\ \emptyset_s\ d_s\ \min[h_s, \mathrm{D}]} \qquad \text{(Eq. 13-2)}$$

Where, D is instantaneous water depth below high tide and $\emptyset_s, n_s$, and $h_s$are related to L via empirically derived power-law functions, which vary with both habitat types (*Spartina* low marsh versus *Juncus* high marsh), fertilization status and elevation within the habitat (Davis et al., 2017; Mudd et al., 2010).

Following the methods from Mudd et al. (2009), L is a function of D. The maximum and minimum depth limits of plant growth are determined for each site by extracting initial (2013) range of elevation of each marsh habitat type from the DEM as described in detail below and by using the site-specific water level data to convert elevation (z) to depth relative to mean high water (D). For *Spartina*, we use the formulation Morris et al. (2002) approximate leaf biomass at any particular elevation, *L(z)*, by fitting a parabolic function through the minimum and maximum *D*, where biomass is 0 and the elevation of peak measured biomass, L_{max}, (Davis et al., 2017), as shown in Equation 13-3.

$$L = aD + bD^2 + c \qquad \text{(Eq. 13-3)}$$

Where, *a*, *b*, and *c* are the coefficients corresponding to the upper and lower depth limits and $L_{max.}$ Because site-specific data reveal no trend in *Juncus* biomass with elevation, we set L to the site-specific mean *Juncus* biomass across its entire elevation range. After $q_s$and q_t are calculated, the site-specific organic fraction of the suspended sediment (Ensign and Currin, 2017;) is subtracted to obtain the contribution of mineral sediment to accumulation.

Below-ground biomass is estimated by using a balanced growth model. Across biomes and plant species functional equilibrium exists in which the mass and uptake rate of carbon by leaf tissue (L) is balanced by the mass (Ro) and the uptake rate of nutrients (μ) by root tissue to optimize total growth (Agren and Ingestad, 1987; Reynolds and D'Antonio, 1996; Reynolds and Thornley, 1982). Because resource uptake is governed by Michaelis-Menton kinetics, as nitrogen concentrations in the environment (*N)* increase, the rate of nitrogen uptake per unit root area increases, and less root tissue is required to sustain growth. This mode of biomass allocation is particularly consistent in monospecific stands (Reynolds and D'Antonio, 1996). Root biomass in the model is determined from L to stoichiometrically balance carbon and nitrogen uptake based on an optimal tissue carbon to nitrogen ratio (α), which is calculated as shown in Equation 13-4.

$$Ro = L * \frac{\alpha\rho}{\mu} \qquad \text{(Eq. 13-4)}$$

Where, ρ is carbon uptake net of respiration estimated from Giurgevich and Dunn (1981). Nitrogen uptake is calculated as shown in Equation 13-5.

$$\mu = V_{max} \frac{[N]}{k_m + [N]} \qquad \text{(Eq. 13-5)}$$

Where V_{max} is the maximum nitrogen uptake velocity and $k_m$is the half-saturation constant (Bradley and Morris, 1990). The accumulation of sulfides at higher elevations inhibit nitrogen uptake, which is reflected in the model by approximating V_{max} and k_m as a linear function of elevation based on sulfide concentrations measured in marsh soils and measured experimentally (Bradley and Morris, 1990; Morris, 1984). Because the primary function of rhizome biomass is the storage of photo-assimilated carbon, we set R_h equal to L (Morris et al., 2013). Below-ground biomass (B) is the sum of root (R_o) and rhizome (R_h) biomass.

Organic accumulation, $q_o(B)$, is proportional to the refractory component (k_{rb}=0.19) of the annual below-ground root deposition, assuming 100% annual turnover, and below-ground rhizome deposition, assuming 30% annual turnover (Kirwan and Mudd, 2012; Morris et al., 2012), summed with the refractory component of the organic fraction of suspended sediment.

Subtidal and upland habitats are assumed to have negligible vertical growth in the model. Although tidal swamp forests display similar geomorphic feedbacks as *Spartina* and *Juncus* marshes, limited data are available to constrain a numerical approach; therefore, we assigned tidal swamp forests an accretion rate of 1.9 mm/yr based on long-term measurements of similar systems in the Southeastern United States (Craft, 2012).

<u>Simulation of Fertilization Conditions</u>

Fertilization has been shown to substantially impact both *Spartina* growth and marsh elevation gain in the marshes of MCBCL. To simulate fertilization, we altered key *Spartina* parameters that reflect field observations. The parameters are leaf biomass (L) increases with fertilization, canopy characteristics ($\emptyset_s$, n_s, h_s) that influence sediment trapping and setting change with fertilization, root to shoot ratio declines with fertilization (B), and decomposition increases with fertilization (k_{rb}). The effects of fertilization on leaf biomass are based on two global meta analyses of *Spartina* that show L decreases as in situ control biomass increases (Herbert et al., in

review; Morris, 1991; Morris et al., 2013). Fertilized above-ground biomass (L_f) is calculated by using an empirical formula relating unfertilized (control) leaf biomass (L) to a proportional increase in above-ground biomass as shown in

$$L_f = L + L * aL^{-b} \quad \text{(Eq. 13-6)}$$

Where, a is 9,377 and b is 0.7 according to Morris et al. (2013). Because the vegetation structure, the diameter ($\emptyset_s$), the density (n_s), and the height (h_s) of stems are altered by fertilization, we use empirical coefficients for fertilized *Spartina* (Mudd et al., 2010). R_h is calculated as proportional to L_f as in the unfertilized condition, and the effect of fertilization on R_o is simulated by doubling the environmental nitrogen concentration (N) in Equation 13-6, resulting in a higher uptake of nitrogen per unit root and a lower root to shoot ratio. Finally, fertilized tissue is higher in nitrogen and lower in lignin and has been observed to decomposed faster than unfertilized tissue, which is reflected in our model by lower concentration of refractory compounds (k_{rb}=0.12) in fertilized *Spartina alterniflora* based on field studies (Deegan et al., 2012; Hodson et al., 1984). *Juncus* above-ground biomass at MCBCL (see Section 2 of this chapter) and across other North American marshes (Pennings et al., 2005) does not respond to fertilization so parameterizations for *Juncus* marshes remained the same in fertilized and unfertilized simulations. A summary of site-specific model input values is provided in **Table 13-13**, and a summary of global model input values derived from the literature is provided in **Table 13-14**.

Table 13-13. Site-Specific Model Parameters

Site-Specific Parameter	Unit	Freeman Creek	Traps Bay	French Creek	Source
Peak biomass *Spartina*	g/m^2	648	648	648	Davis et al., 2017
Peak biomass *Juncus*	g/m^2	649	832	1,208	Section 2 of this chapter
Suspended sediment concentration (SSC)	mg/L	26.2	16.1	11.2	Ensign and Currin, 2017
Organic fraction of SSC	%	16.7	33	52	Ensign and Currin, 2017
Tide range	m	0.82	0.57	0.16	Ensign and Currin, 2017
Mean sea level	m North American Vertical Datum of 1988 (NAVD 88)	−0.099	−0.073	−0.046	Section 1 of this chapter
Mean high water level	m NAVD 88	0.398	0.191	0.053	Section 1 of this chapter

Table 13-14. Global Model Parameters

Global Parameter Description	Parameter	Unit	Value	Source
Initial rate of sea level rise	R	m/yr	0.0027	National Oceanic and Atmospheric Administration Tide Gauge
Effective settling velocity	w_s	—	—	—
Refractory fraction biomass	k_{rb}	%	19	Hodson et al., 1984
Reference flow velocity	U	m/s		Mudd et al., 2010
Average particle diameter	dp	µm	0.2	Mudd et al., 2010
Kinematic viscosity of water	v	m^2/s	1×10^{-6}	Mudd et al., 2010
Capture efficiency	α	unitless	0.223	Mudd et al., 2010
	β	unitless	0.718	Mudd et al., 2010
	λ	unitless	2.08	Mudd et al., 2010

Horizontal Marsh Migration

For each site, a map of habitats was overlain on a DEM of elevations relative to mean high water level (MHWL) to produce a set of probability distribution functions that describes the current distribution of habitats across the current distributions of depth (*D*) relative to MHW (**Figure 13-23**). For each time step of the model run, after elevations are updated annually following the methods previously described in the *Vertical Marsh Evolution* section, the probability distribution function was used to calculate habitat conversion for each *Spartina*, *Juncus*, tidal swamp forest, or upland cell such that if the rate of sea level rise exceeded elevation gain and the cell experienced a greater flooding depth, then its probability to convert to a more flood tolerant habitat type increased.

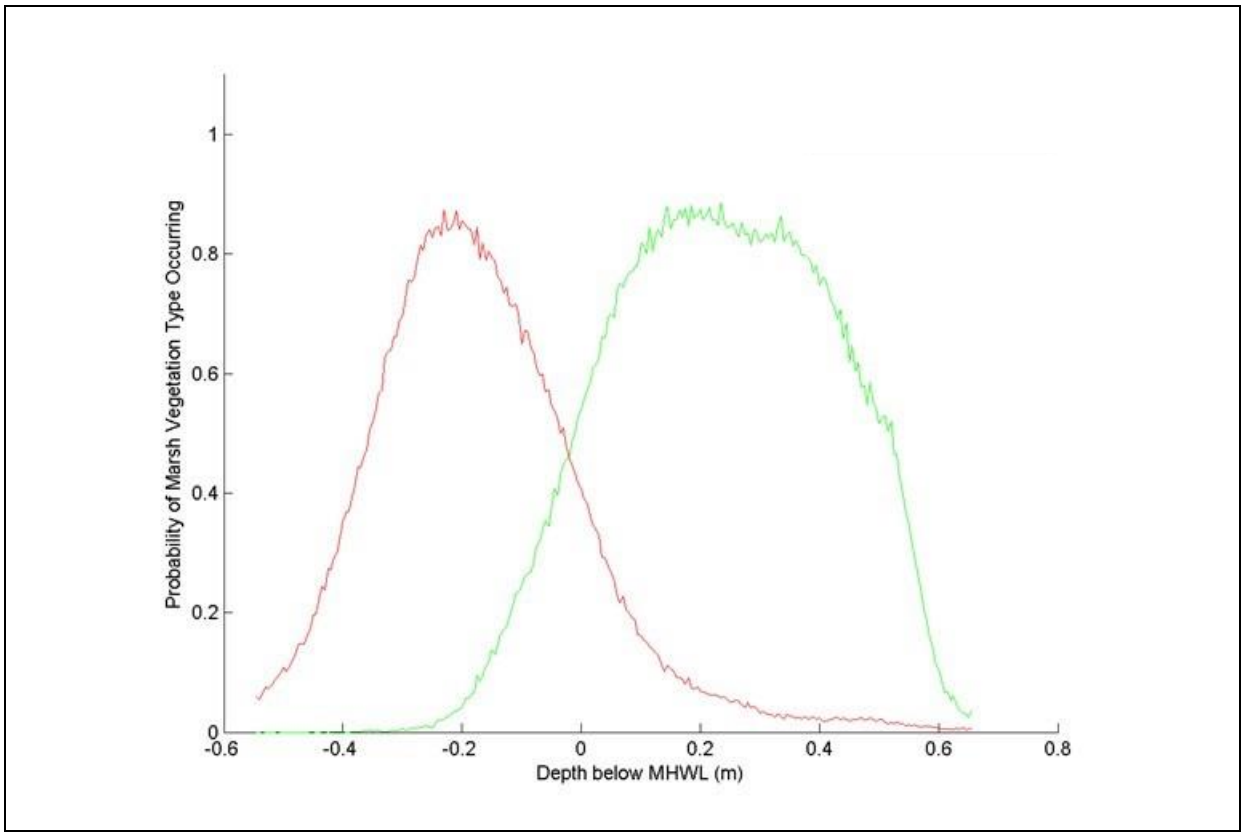

Figure 13-23. Example plot of probability distribution function for vegetation types extracted from the DEM by using the habitat classification at Freeman Creek.

Note: Green line indicates distribution of *Spartina alterniflora* and red line indicates distribution of *Juncus romerianus*. There is no tidal swamp forest in the Freeman Creek modeling domain. Other sites (French Creek and Traps bay) are included in Appendix 13A.

Sensitivity and Uncertainty Calculations

To quantify the uncertainty of model output, we conducted a global sensitivity analysis of the vertical accretion model to identify the model variables with the most influence on model outcomes. We computed the elementary effects of each input, including a mean and SD by using the UQLab 1.0 Uncertainty Quantification Package in MATLAB. Because we used a probability-based approach for the horizontal migration, we did not undertake sensitivity analysis for this portion of the model. Peak biomass (B) and SSC (C_0) were identified as the most important variables affecting the outcome of the model. We then ran the model using the 5th (low) and 95th (high) percentiles determined via bootstrapping for B and C_0 to generate an estimate of the variability of possible outcomes for each sea level rise scenario.

Results and Discussion

Habitat Classification and Vegetation-Induced Errors in LiDAR Elevation

The marshes across the estuarine gradient at MCBCL display a distinct gradient in vegetation cover **Table 13-15**), with Freeman Creek having the highest proportion of flood-tolerant *Spartina* (68%), followed by Traps Bay (4%), and finally French Creek (0%). There is also an

increasing proportion of tidal forest up-estuary, with tidal forest comprising most of French Creek. *Juncus* and *Spartina* distributions across flooding gradients (**Figures 13-23 and 13-A3**) are similar between Freeman Creek and Traps Bay. *Juncus* appears to colonize in deeper water depths at French Creek than at other sites.

Table 13-15. Initial Habitat Classification and Total Area (m^2) Based on RGB and IR Digital Ortho-Imagery from MCBCL

Class	Habitat	Freeman	Traps	French
0	Deepwater marine	303	240,037	0
1	Estuarine water	363,638	21,753	808,489
2	Mudflat	12,384	0	0
3	Short-form *Spartina alterniflora*	184,550	2,234	0
4	Tall-form *Spartina alterniflora*	287,863	0	0
5	Irregularly flooded marsh (dominated by *Juncus romerianus*)	230,943	53,210	89,273
6	Forest	1,283,320	261,326	407,408
7	Field	83,814	53,678	112,573
8	Bare/sand	55,080	79,786	
9	Tidal swamp forest	0	67,854	857,236
10	Infrastructure (buildings/roads)	0	0	374,322
11	Freshwater pond	0	0	91,798

Vegetation-induced errors in LiDAR–derived DEMs generally increase with the height and density of vegetation. We found the largest systematic errors associated with vegetation that exceeded 600 g/m^2, particularly the tall-form *Spartina* at Freeman Creek (vegetation induced error=0.1 m) and *Juncus* at French Creek (vegetation induced error=0.25 m). These errors are notable because they are the same order of magnitude as the lower rates of predicted sea level rise (**Table 13-16**), indicating that, absent corrections, the elevation of the marsh is overestimated by 0.1 to 0.25 m; therefore, the marsh survival will be overestimated, particularly under lower rates of sea level rise.

Table 13-16. Summary of Vegetation Errors, DEM Correction Factors, and Errors in DEMs Corrected for Vegetation Induced Errors in LiDAR–Derived Elevations

Note: These errors represent differences in ground control points measured by using RTK-GPS and the LiDAR DEM, not the fundamental vertical accuracy of the DEM.

Site	Habitat	Number of Training Points	Mean Error Unmodified DEM (m ± SD)	DEM Correction Factor (m)	Number of Validation Points	Mean Error of Vegetation Corrected DEM (m)
Freeman	Short *Spartina*	146	−0.0043 (±0.121)	0	137	−0.0043 (±0.120)
	Tall *Spartina*	44	0.1045 (±0.056)	0.1045	56	0.00625 (±0.116)
	Irregularly flooded	40	0.0509 (±0.075)	0.0509	33	0.014 (±0.132)
Traps	Short *Spartina*	108	0.100 (±0.1002)	0.100	109	−0.0388(±0.0895)
	Irregularly flooded	320	0.041 (±0.047)	0.0410	321	−0.0035(±0.0377)
French	Irregularly flooded (*Juncus*)	193	0.2545 (±0.08)	0.254	194	−0.022 (±0.18)

Marsh Response to Sea Level Rise Across the Estuarine Gradient

The response of MCBCL marshes can be characterized by a combination of the following four main responses: (1) horizontal expansion via upland transgression, (2) transition to flood-tolerant vegetation, (3) enhanced vertical accretion, and (4) drowning. The predominance of these responses at a given marsh complex is governed by the rate of sea level rise, the combination of productivity and suspended sediment that regulate vertical accretion (**Table 13-13**), and the slope of the upland. All three marshes gain area (**Table 13-17 and Figure 13-24**) under the lowest sea level rise scenario (0.3 m by 2100) through a combination of expansion via marsh transgression upslope (**Figure 13-25**) and marsh maintenance though enhanced vertical accretion (**Figure 13-26**). The low sea level rise scenario (0.8 m by 2100) best illustrates the difference in processes that dominate each of three marsh complexes (**Figure 13-27**). The response of Freeman Creek is dominated by marsh expansion without any substantial change in the proportion of *Spartina* (flood tolerant) and *Juncus* (irregularly flooded) vegetation types. The response of Traps Bay by a transition from *Juncus* to more flood-tolerant *Spartina*, with limited expansion of the marsh into the upland. French Creek is dominated by drowning, losing extensive marsh and swamp coverage at all scenarios beyond the lowest sea level rise.

Table 13-17. Percent (%) Change in Marsh Area from Initial Condition (2013) for Each Sea Level Rise Scenario Under Ambient Sediment Conditions for Each Marsh

% Change	2013	2035	2065	2100
Freeman Creek				
Lowest (0.3 m)	0.0	7.0	16.1	24.6
Low (0.8 m)	0.0	6.5	22.5	49.0
Medium (1.3 m)	0.0	14.6	40.6	76.7
High (1.8 m)	0.0	17.2	52.1	21.7
Highest (2.5 m)	0.0	22.7	35.6	−33.3

(continued)

Table 13-17. Percent (%) Change in Marsh Area from Initial Condition (2013) for Each Sea Level Rise Scenario Under Ambient Sediment Conditions for Each Marsh (continued)

% Change	2013	2035	2065	2100
Traps Bay				
Lowest (0.3 m)	0.0	10.2	21.1	31.2
Low (0.8 m)	0.0	9.4	28.7	64.8
Medium (1.3 m)	0.0	19.4	44.6	−9.0
High (1.8 m)	0.0	22.4	−3.2	12.7
Highest (2.5 m)	0.0	28.9	37.5	−21.8
French Creek				
Lowest (0.3 m)	0.0	2.0	4.4	14.1
Low (0.8 m)	0.0	1.9	11.3	−52.7
Medium (1.3 m)	0.0	3.8	−57.4	−40.5
High (1.8 m)	0.0	−82.3	−78.5	−86.5
Highest (2.5 m)	0.0	−6.6	−40.5	−41.5

Overall, Freeman Creek is predicted to be very resilient to sea level rise because it has the highest SSC and lowest surrounding slope. We predict the Freeman Creek marsh complex will maintain the current high rate of accretion (**Figure 13-26**) and expand via substantial horizontal migration (**Figure 13-25**), leading to marsh expansion under most scenarios. Only at the highest sea level rise scenario is wetland area lost at Freeman Creek, resulting in massive drowning of the marsh complex. The threshold rate of sea level rise for marsh loss at Traps Bay is between the medium and highest sea level rise scenarios. We define the "threshold rate of sea level rise for marsh loss" as the rate of sea level rise where marsh drowning outpaces marsh migration, leading to a net decrease in marsh area. Traps Bay maintains insufficient SSC to maintain the current marsh area through vertical accretion and is surrounded by higher slope topography, limiting migration. The French Creek marsh complex has the lowest suspended sediment, tide range, and measured accretion rate (see Chapter 11 of the *DCERP2 Final Report*), limiting vertical adaptation, while the steep slopes of the surrounding upland limit marsh transgression. Without major changes in ecosystem management (i.e., increased sediment supply, see below), the marsh is predicted to decline precipitously in area under most sea level rise scenarios, which is particularly concerning, given its proximity to MCBCL infrastructure (**Figure 13-25**). Although SSC is key to maintain current marshes, upland expansion will be a major factor in wetland survival. Complex topography at MCBCL results in complex, non-linear patterns of wetland change, particularly at Traps Bay and French Creek (**Figure 13-24 and 13-25**), where topography leads to alternating periods of wetland expansion and contraction through time due to distinct "terraces" in the antecedent topography. Freeman Creek is characterized by a low-gradient, smooth slope.

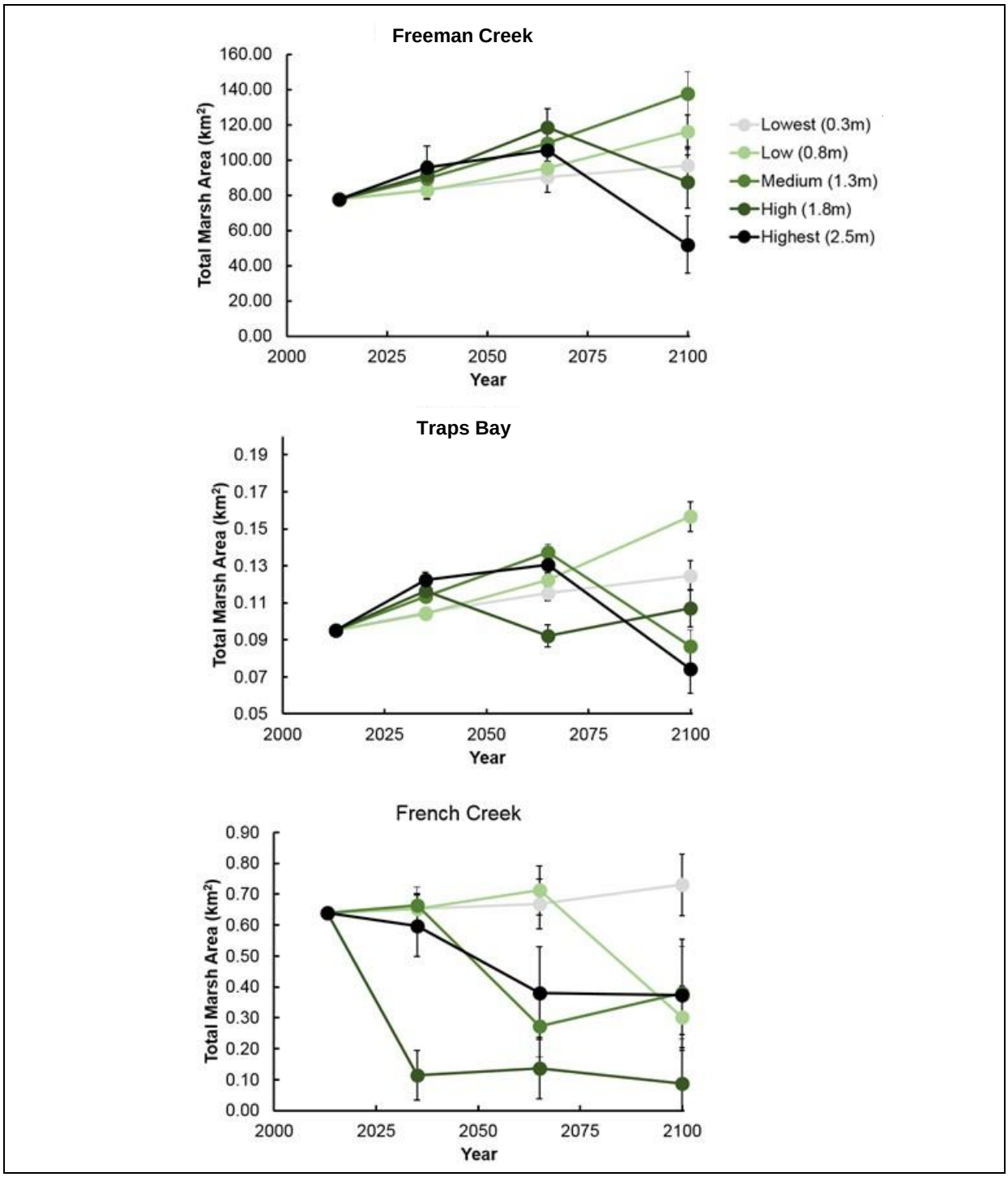

Figure 13-24. Modeled change in total marsh area (km^2) over five sea level scenarios for the three study domains: (top) Freeman Creek, (middle) Traps Bay, and (bottom) French Creek.

Error bars represent the variance in model output by using the highest (95%) and the lowest (5%) accretion parameters (biomass and SSC).

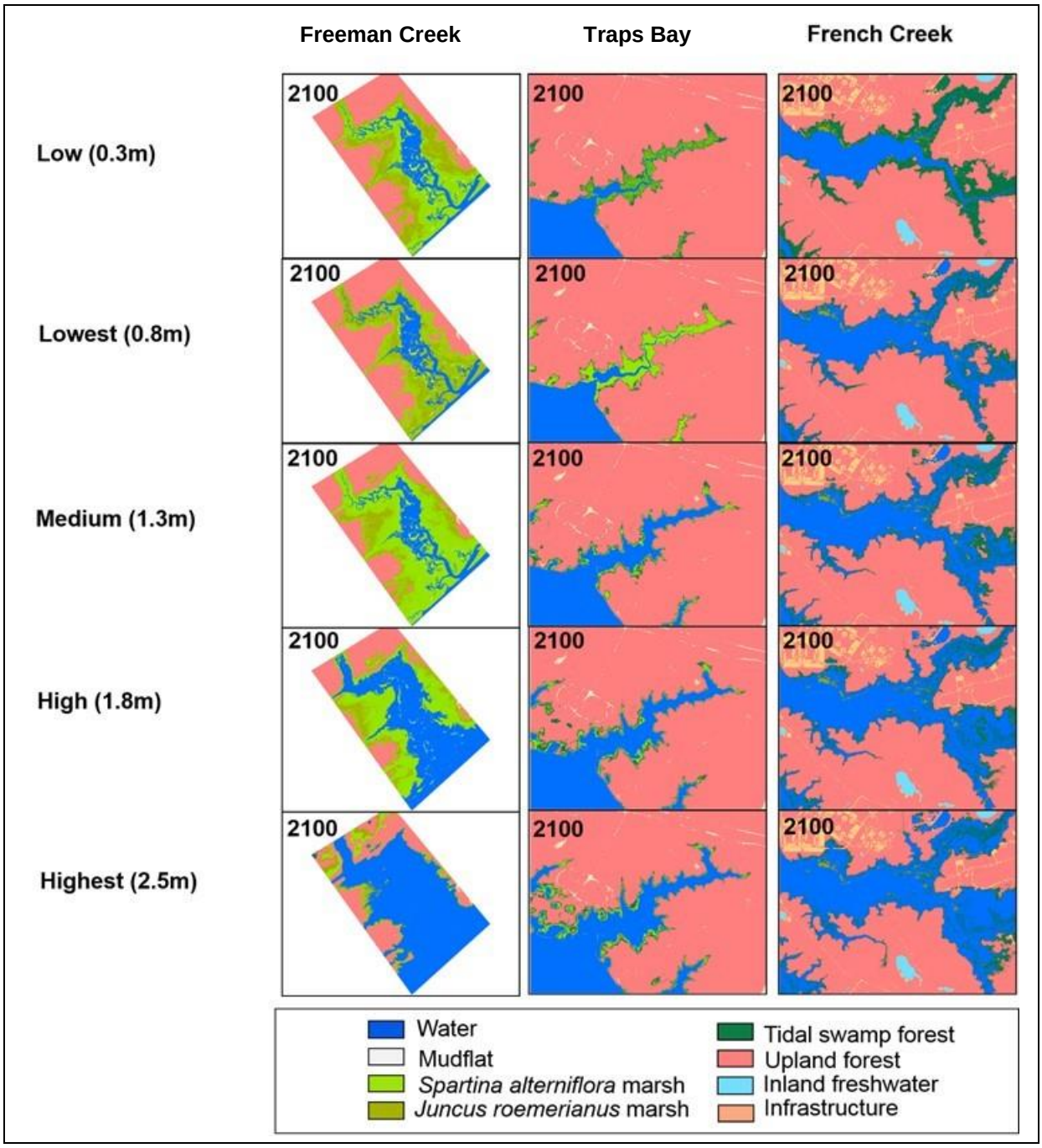

Figure 13-25. Modeled habitat coverage in 2100 under five sea level scenarios for the three study marsh domains at MCBCL: (left) Freeman Creek, (middle) Traps Bay, and (right) French Creek.

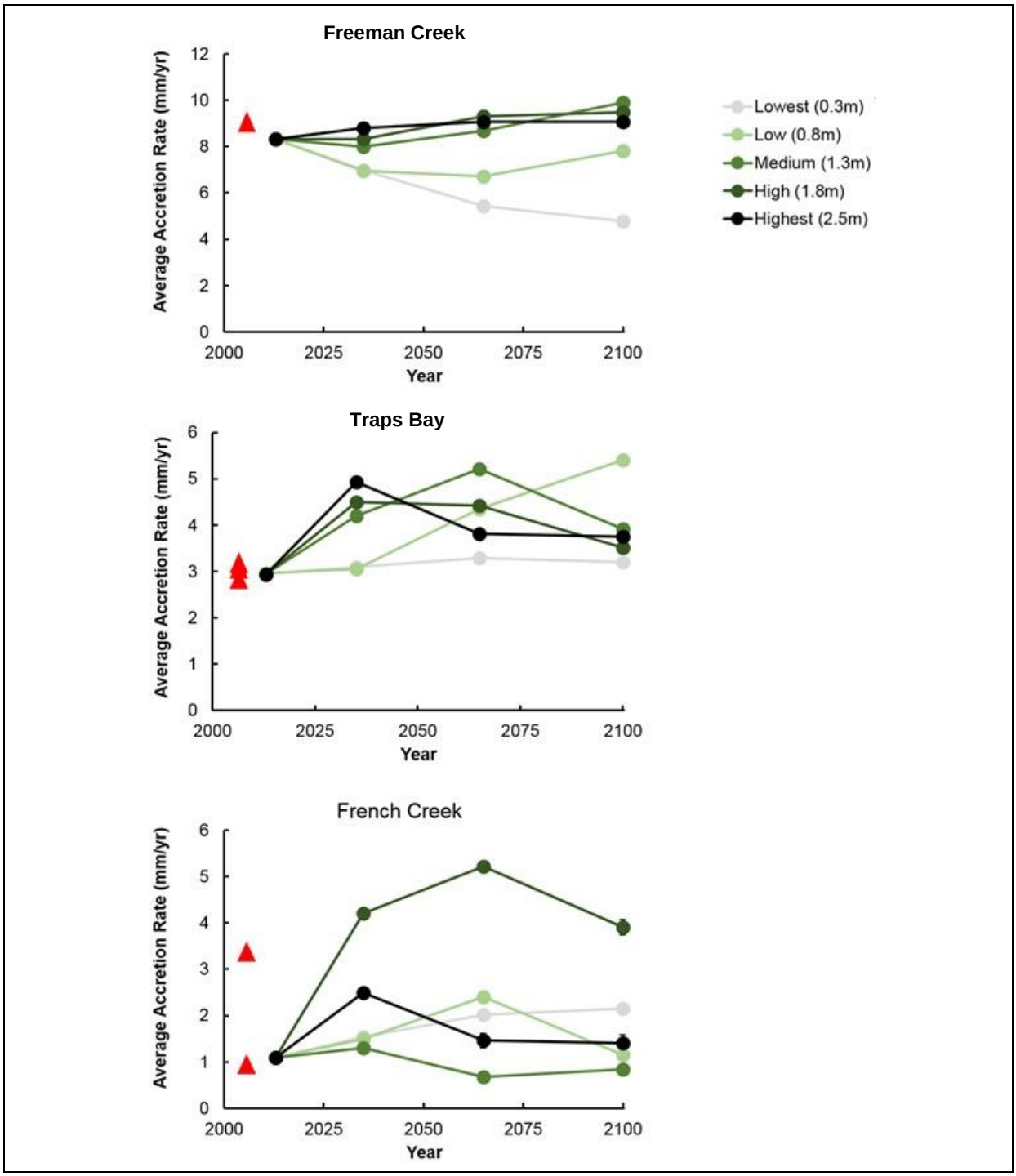

Figure 13-26. Modeled change in spatially averaged marsh accretion rate (mm/yr) over five sea level scenarios for the three study domains: (top) Freeman Creek, (middle) Traps Bay, and (bottom) French Creek.

Note: Measured accretion rates from SETs are plotted as red triangles.

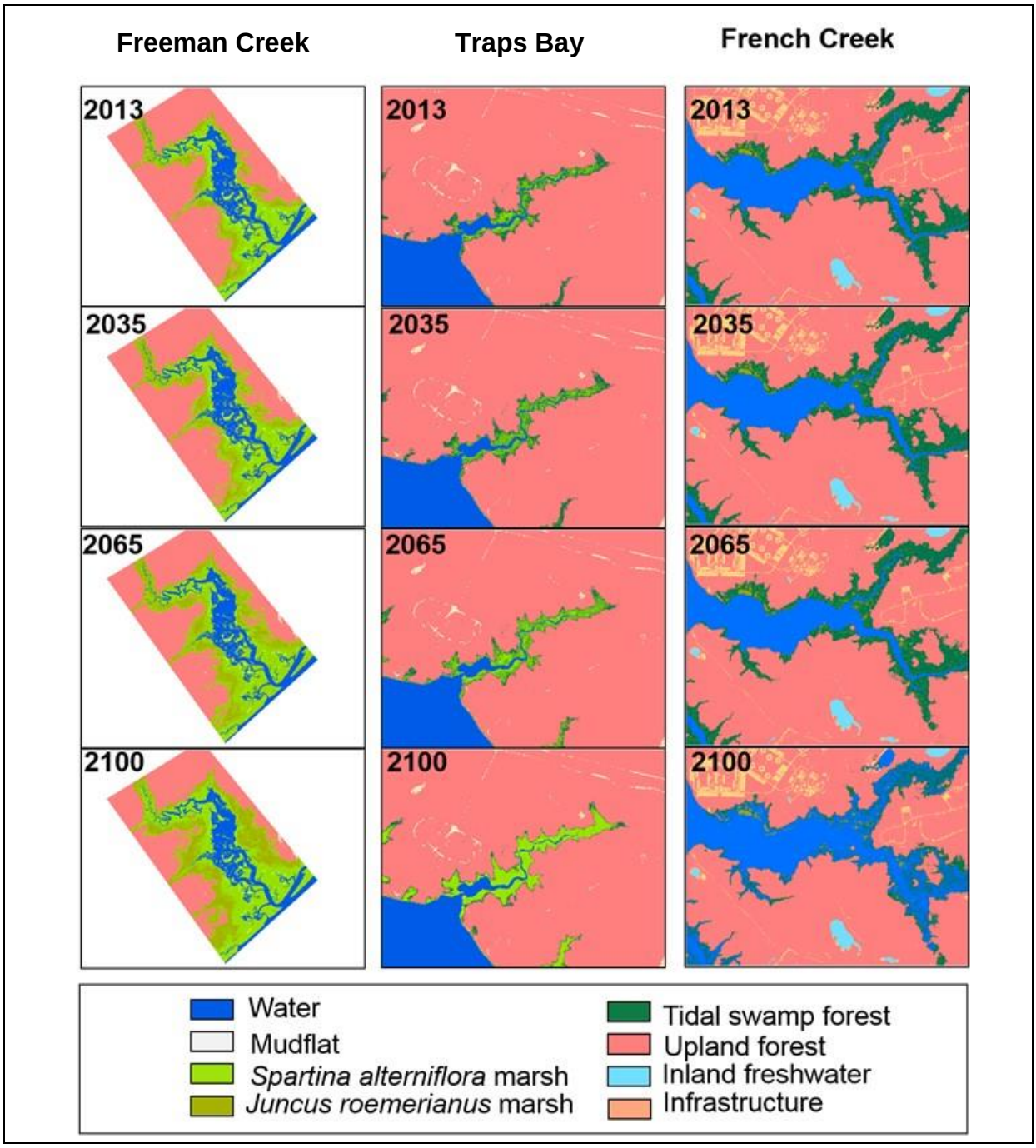

Figure 13-27. Modeled habitat coverage in 2013, 2035, 2065, and 2100 under low (0.8 m) sea level rise scenario across the three model domains, illustrating three responses to rising sea level: transgression + accretion (Freeman Creek [left]), accretion + transition to flood tolerant vegetation (Traps Bay [middle]), and drowning (French Creek [right]).

Marsh Carbon Accumulation Under Sea Level Rise

Carbon accumulation is a product of carbon concentration and accumulation rate. Generally, consistent with field data (Section 5 of this chapter), the model predicts that as MCBCL marshes

experience accelerated sea level rise, the annual carbon accumulation will increase (**Figure 13-28** and **Table 13-18**). This is primarily a function of increased vertical accumulation in response to water depth (**Figure 13-26**). Furthermore, the model predicts that site-wide areal carbon accumulation (kilograms per year over the entire wetland area) will increase (**Table 13-18 and Figure 13-28**), even as the size of the wetland declines (**Table 13-17 and Figure 13-24**), indicating that the increase in CAR (per square meter) is large enough to overcome the loss of wetland area to drowning. French Creek provides an excellent example of this phenomenon. Even though there is a 40% loss in wetland area at the highest sea level rise scenario, the rate of CAR increases from an average of approximately 30 to approximately 450 g m^2 yr^{-1} (150%). Despite annual carbon balances that indicate net carbon gain at the site scale, the long-term fate of this carbon is uncertain because wetlands will continue to drown and move up-slope over time. Model and field data are inadequate for understanding the fate of wetland carbon that is drowned, thus the fate of a large portion of the carbon buried over the lifetime of the wetland complex is unaccounted for.

Table 13-18. Percent (%) Change in Annual Carbon Accumulation (kg/yr) Across the Entire Marsh from Initial Condition (2013) for Each Sea Level Rise Scenario Under Ambient Sediment Conditions for Each Marsh

Actual rates (g m^{-2} yr^{-1}) are provided in Figure 13-28.

% Change	2013	2035	2065	2100
Freeman Creek				
Lowest (0.3m)	0.0	−0.7	2.6	5.7
Low (0.8m)	0.0	−0.5	0.0	3.4
Medium (1.3m)	0.0	−1.6	1.7	−3.9
High (1.8m)	0.0	−1.1	−2.1	35.2
Highest (2.5m)	0.0	−0.8	4.0	147.8
Traps Bay				
Lowest (0.3m)	0.0	8.2	18.6	18.2
Low (0.8 m)	0.0	6.6	47.0	66.0
Medium (1.3 m)	0.0	40.3	68.1	280.4
High (1.8 m)	0.0	48.4	157.0	372.2
Highest (2.5 m)	0.0	57.7	514.2	316.6
French Creek				
Lowest (0.3 m)	0.0	37.9	76.2	84.5
Low (0.8 m)	0.0	34.6	104.7	637.4
Medium (1.3 m)	0.0	28.1	300.5	466.8
High (1.8 m)	0.0	260.0	330.5	873.5
Highest (2.5 m)	0.0	158.6	841.2	2,161.7

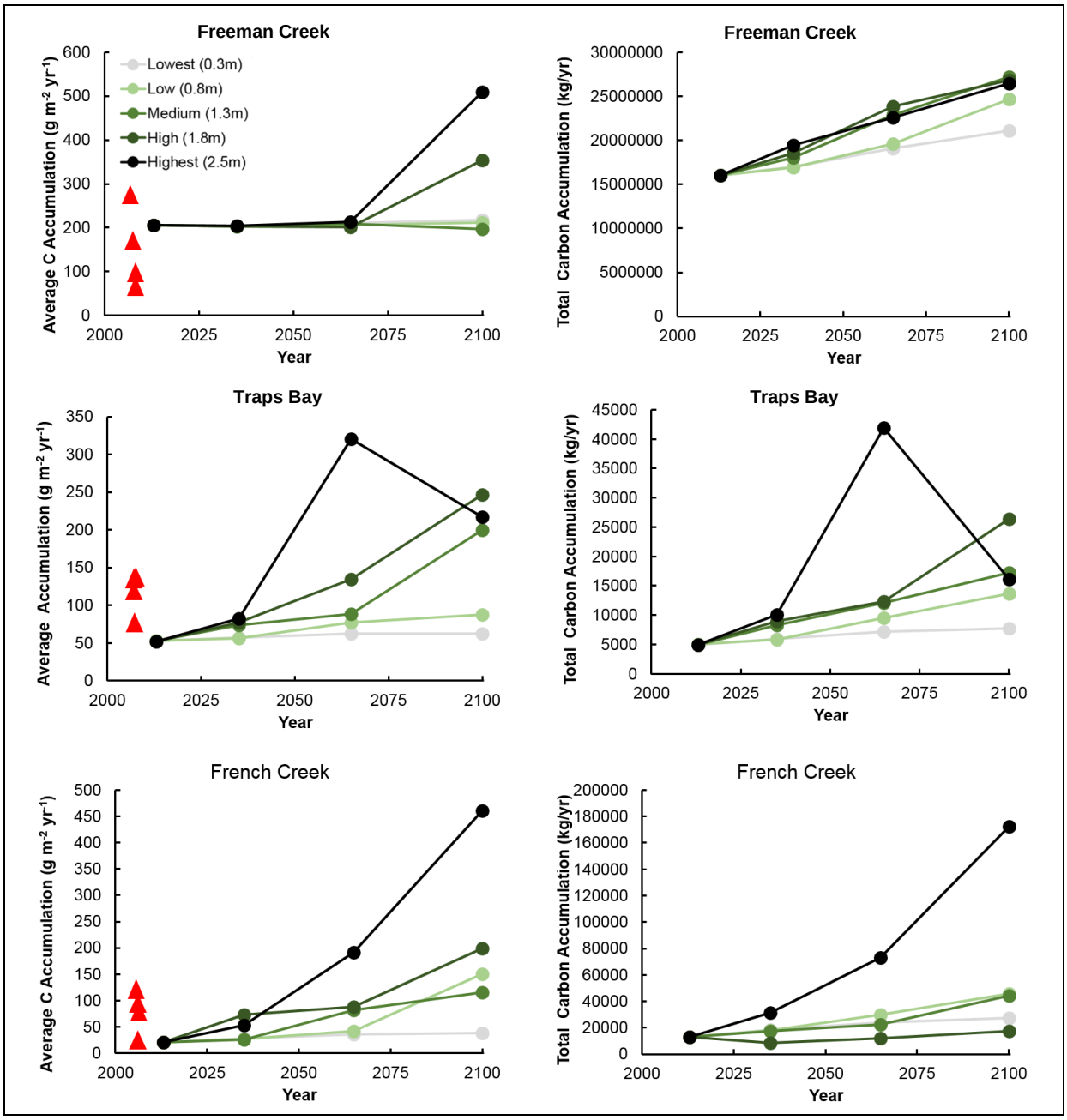

Figure 13-28. Modeled change in average marsh carbon accumulation rate (g m^2 yr^{-1}; left panel) and total carbon accumulation across each site (kg/yr; right panel) over five sea level scenarios for the three study domains: (top) Freeman Creek, (middle) Traps Bay, and (bottom) French Creek.

Measured accumulation rates from cores are plotted as triangles at initial year.

Model Sensitivity, Uncertainty, and Fit to Field Data

The model produces results consistent with measurements of accretion (**Figure 13-26**) and carbon burial (**Figure 13-28**) at each site, indicating that the model accurately represents physical processes (sedimentation) and biological processes (productivity and decomposition of

organic material). The model is most sensitive to the two parameters that influence vertical accretion: biomass production (B) and SSC (C_0). Varying these parameters within their measured range produces minimum and maximum estimates of marsh survival (range of uncertainty) under each scenario (error bars in **Figure 13-24**). This uncertainty estimate ranges from 7% to 50% of modeled area, and increases with time and sea level rise. However, even using the maximum value of the uncertainty range (i.e., parameter values leading to greatest marsh survival), the model predicts net marsh loss at French Creek and Traps Bay under the high sea level rise scenario (+1.8 m), and net marsh loss at all three sites under the highest sea level rise scenario (+2.5 m).

Marsh Response to Variation in Management: Suspended Sediment and Nutrients

The vertical accretion rate and therefore the ability of the marsh to keep pace with sea level rise is heavily influenced by SSC (see *Model Sensitivity, Uncertainty, and Fit to Field Data*). Management decisions such as erosion control, dam building, inlet dredging, and channel dredging can greatly influence the availability of sediment in the water column. At Traps Bay, marsh vertical accretion is dominated by organic matter accumulation under current, ambient SSC (16.5 mg/L). Simulations in which SSC is reduced in half (16.1 mg/L to 8.05 mg/L) does not substantially impact the marsh area at 2100, because mineral sediment deposition represents a small component of total vertical accretion (**Figure 13-29**). However, at Traps Bay doubling the ambient SSC (16.1 mg/L) to 32.2 mg/L nearly doubles the area of marsh remaining compared to the ambient SSC at 2100 under the medium sea level rise (1.3 m by 2100) scenario. This is a direct result of a doubling of the accretion rate, which becomes dominated by mineral sediment deposition under elevated SSC.

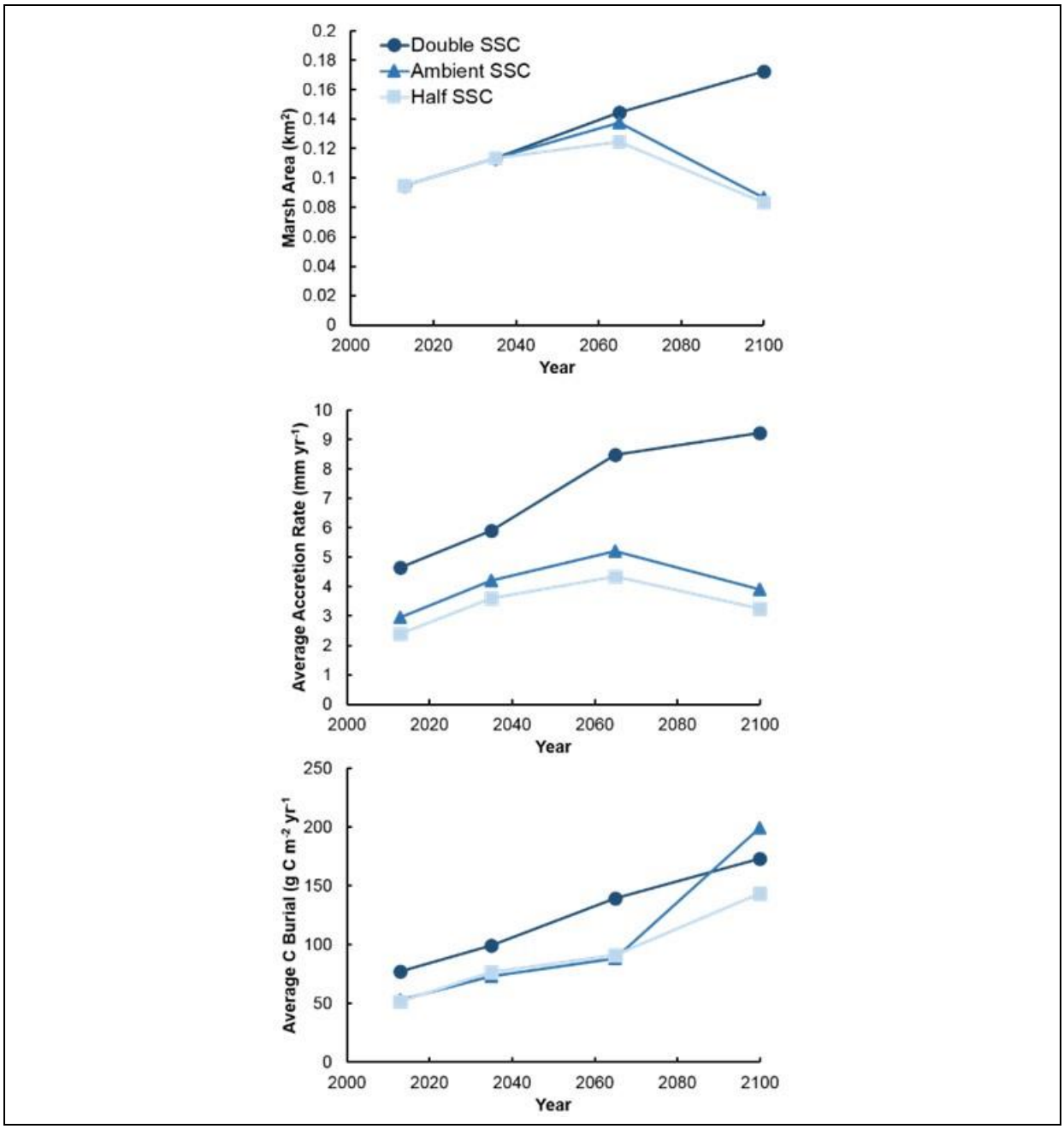

Figure 13-29. Modeled change in total marsh area (km^2), average accretion rate ($mm\ yr^{-1}$) and carbon burial rate (g carbon [C] $m^{-2}\ yr^{-1}$) at Traps Bay at the medium sea level rise (1.3 m by 2100) scenario under double ambient suspended sediment concentrations (SSCs; dark blue circles), current ambient SSC (medium blue triangles), and half ambient SSC (light blue squares).

Freeman Creek has a higher (26.2 mg/L) ambient SSC and displays a markedly different response to simulations of changes in sediment supply. Simulations suggest a doubling of the SSC at Freeman Creek will not increase marsh persistence, while a halving to 13.1 mg/L results in a substantial decline in marsh area by 2100 under the medium sea level rise (1.3 m by 2100) scenario (**Figure 13-30**). Together, these results suggest that across gradients in productivity and

hydrology at MCBCL, a SSC between 26.2 mg/L and 32.2 mg/L is needed to maintain marsh area under moderate (1.8 m by 2100) to high (2.5 m by 2100) rates of sea level rise. In both cases carbon accumulation is maximized at higher SSC in which deposition is maximized.

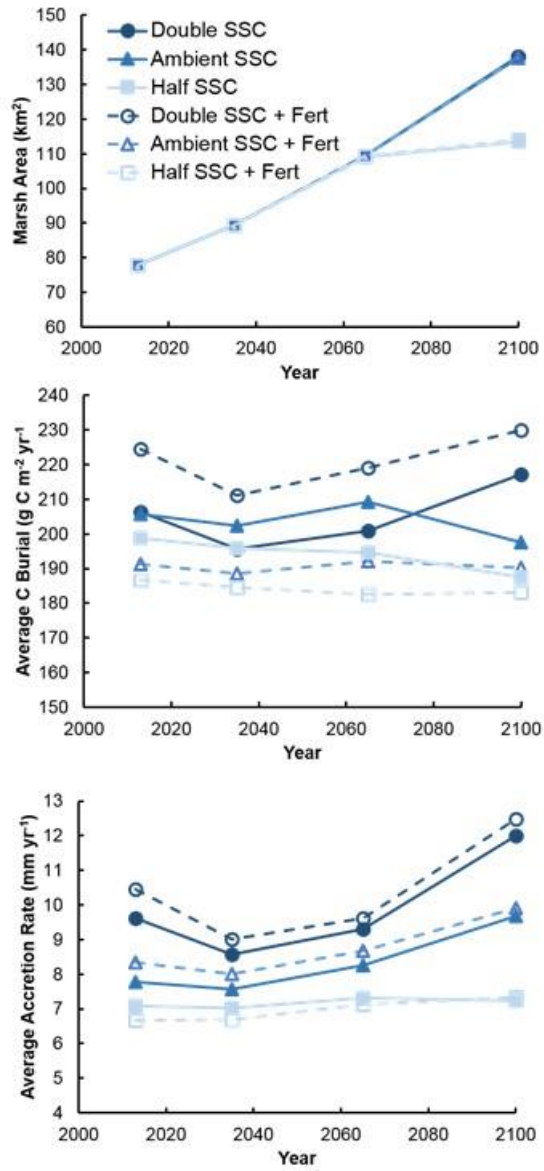

Figure 13-30. Modeled change in total marsh area (km^2), average accretion rate ($mm\ yr^{-1}$) and carbon burial rate (g carbon [C] $m^{-2}\ yr^{-1}$) at Freeman Creek under double ambient suspended sediment concentrations (SSCs; dark blue circles), current ambient SSC (medium blue triangles), and half ambient SSC (light blue squares).

Closed symbols connected by solid lines represent the unfertilized condition. Open symbols connected by dashed lines represent the fertilized condition.

Previous work at MCBCL illustrates how fertilization benefits marshes by stimulating above-ground productivity, sediment trapping, and below-ground production (Research Project CW-1 in the *DCERP1 Final Research Report* [RTI International, 2012]). Our model reproduces

patterns in accretion and organic deposition measured in field experiments at MCBCL (Davis et al., 2017) and captures the variability related to productivity and sediment gradients (**Figure 13-31**). Our model predicts that as suspended sediment increases, so do the positive effects of fertilization because increased biomass traps a greater proportion of sediment (see black and green lines in **Figure 13-32**). However, unlike the previous marsh elevation models developed during DCERP1 (see the blue line in **Figure 13-32**), our new geospatial marsh model predicts substantially less benefit from fertilization that is variable with space and elevation because the model considers the role of site condition in regulating the response of the marsh to fertilization. For instance, in the high marsh (Onslow Beach or Mile Hammock Bay fertilization plots, see Section 2 of this chapter) where growth is limited by nitrogen availability through physical and geochemical means, fertilization will produce a strong positive response, increasing growth of both above- and below-ground biomass and subsequently accretion, regardless of sediment. In areas of the marsh with naturally higher nitrogen, particularly creek banks and lower marsh areas, fertilization results in a net shift of biomass production from roots to shoots because roots are no longer needed to forage for nitrogen, leading to declines in root to shoot ratios and root biomass even if above-ground biomass is enhanced. This effect is important only when most MCBCL marshes become more frequently flooded, such as under scenarios of rapid sea level rise. Thus, as sea level rises and more nitrogen is naturally delivered into the marsh via increased flooding, marsh accretion will benefit less from artificial fertilization. With low SSCs (8–12 mg/L; see Figure **13-32**), the enhanced trapping of sediment above ground is not large enough to counter-balance the reduction in roots below ground under elevated rates of sea level rise (greater than 5 mm/yr). This effect is illustrated in **Figure 13-32**, where at low SSC, fertilization decreases the rates of accretion, but it enhances the rates at high SSC. As sea level rise accelerates towards the end of the century, marsh accretion no longer benefits from fertilization at the ambient and half ambient SSC. Currently, fertilization enhances marshes at all *Spartina* marshes (Section 2 of this chapter), but the model suggests that the benefits of fertilization for elevation gain will be attenuated with increased sea level rise if sediment concentrations are not elevated.

When applied spatially to Freeman Creek, the model suggests that fertilization will have a minimal impact on wetland survival under the medium sea level rise (1.3 m by 2100) scenario (**Figure 13-30**. Fertilization tends to negatively impact carbon accumulation even when accretion is maintained because it reduces root inputs to the soil and enhances the decomposition of soil carbon (consistent with findings of Research Project CW-5). Although fertilization enhances accretion and carbon accumulation when SSC is high (double ambient), leading to elevation gain and slightly longer times until drowning, this does not translate into enhanced marsh survival at the relevant management timescales.

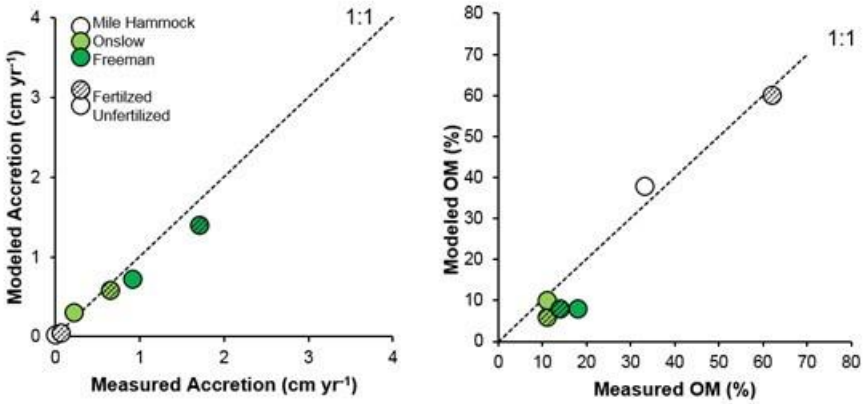

Figure 13-31. Accretion model validation comparing the measured marsh accretion rates and organic contents from SETs at three MCBCL marshes (i.e., Freeman Creek, Onslow Beach, and Mile Hammock Bay) with modeled accretion and organic content.

Crosshatched symbols are fertilized plots. Open symbols are control plots.

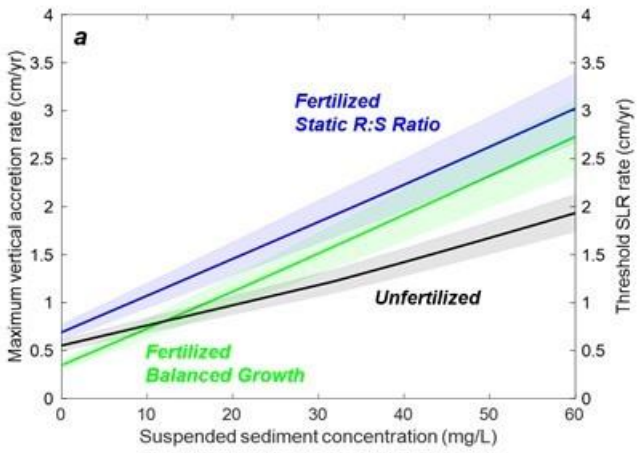

Figure 13-32. Maximum accretion rate modeled under unfertilized conditions (black), fertilized conditions by using the balanced growth model described in the text (green), and fertilized conditions with static root to shoot (R:S) allocation (blue) across suspended concentrations (0–60 mg/L).

Section 4. Investigating Salt Marsh Sediment Carbon Decomposition After Erosion Events

Senior Researcher: Nathan McTigue and Carolyn Currin

Introduction

Salt marshes have enormous potential to bury and store organic carbon in sediment for centuries to millennia. However, little is known about the fate of this carbon pool after disturbance events, particularly erosion that would unbury and expose it to aerobic and photo-oxidizing environments in tidal creeks. Current literature estimates of potential remineralization of wetland organic carbon after habitat destruction are vast; therefore, constraining the potential range is critical to fully understand the strength and permanence of the marsh carbon sink and its role in the global carbon cycle. Because few experimental data exist to substantiate this potential range, we devised an approach that measures carbon dioxide (CO_2) emissions from salt marsh sediment after simulated erosion to oxic horizons. Additionally, we apply a mass-loss strategy that mimics litterbag experiments to examine the same process. Within this section, we refer to decomposition and remineralization interchangeably and define these as the microbial enzymatic degradation of organic carbon in dark, oxic conditions.

Materials and Methods

Sediment and Water Sample Collection

Experiments were conducted on sediment collected from Freeman Creek at MCBCL. Twelve sediment cores were collected from the *Spartina alterniflora* zone by using a 5-cm diameter × 100-cm long Russian peat borer in September 2016. Cores were taken within the same 1 m^2 so that depth sections from each core could subsequently be combined, homogenized, and redistributed among sampling units. Two simultaneous, independent incubations were conducted to measure the decomposition of marsh material in oxic conditions: (1) a mass-loss experiment that mimics traditional litterbag designs and (2) a sediment respiration experiment that directly measures CO_2 and methane (CH_4) evolution.

Because litterbag experiments rely on an operational definition of decomposition based on the litterbag pore size, material that is small enough to fall through the litterbag is considered decomposed, including non-decomposed material in small particulate or dissolved phases. We avoided this assumption by incubating sediment in closed bottles with oxygenated seawater, henceforth referred to as a litter bottle. Decomposition was still considered mass-loss, but we ensured that non-decomposed material was not measured as lost. A parallel respiration experiment also used a closed-bottle approach, but instead of relying on a change of substrate mass, it directly measured the production of CO_2 and CH_4, inferring that the gases were products of microbial respiration of sediment carbon (i.e., decomposition). Henceforth, these results are referred to as greenhouse gas analyzer (GGA) experiments. Both experiments used homogenized sediment from the same sampling horizons at Freeman Creek: shallow (5–10 cm) and mid (20–25 cm) depths, and the litter bottle experiments used a third depth horizon denoted as deep (30–35 cm).

A 4-L seawater sample was collected every hour for 6 hours throughout the day to eliminate microbial community bias within the seawater. After collection, the seawater was filtered by using a 2-µm filter and combined in a 25-L carboy. The filtered creek water was aerated until its use in the experiment.

Litter Bottle Experimental Design

Sediment aliquots (approximately 10 g ww) from each of the three depth horizons (n=12) were placed in separate PETG (polyethylene terephthalate copolyester, glycol modified) 1-L bottles after wet weight was measured for each individual sample. Voucher subsamples from every sample aliquot (n=2) were placed in labeled aluminum dishes for analysis for bulk density, water content, and carbon and nitrogen content. Each 1-L bottle with sediment aliquot received 500 mL of filtered creek water as microbial community inoculum for decomposition. After sealing each bottle, they were placed outdoors in flowing seawater. Bottles were retrieved each evening to measure dissolved oxygen. Regularly, bottles were removed from tanks, uncapped, and left on shake tables for 48 hours to ensure oxygenation of water. Bottles were harvested (n=4 for each of the three depth treatments) at 25, 55, and 77 days for mass-loss measurements.

After harvest, the creek water from each bottle was vacuum filtered through an ashed, pre-weighed GF/F filters (pore size=0.45 µm). Filtered creek water was subsampled for dissolved organic carbon concentration. Dissolved organic carbon samples were frozen and shipped to the Virginia Institute of Marine Science (VIMS) for analysis. Filters were dried at 60°C and re-weighed to determine the mass of particulate matter retained on filters. The remaining sediment in each bottle was removed and dried at 60°C. Carbon and nitrogen content analyses were conducted on subsamples from each sediment fraction. Once converted to units of carbon, decomposition rate was determined as the difference in carbon content between the final litter bottle and its initial content.

GGA Experimental Design

Sediment from the shallow and mid horizons were weighed and placed in 500-mL PETG bottles. Each bottle was given 3 mL of filtered creek water as inoculum. Bottles were sealed with Nalgene 2–ported 38-430 polypropylene caps (Western Fluids Engineering, LLC, Wildomar, CA). Each threaded port was equipped with a PMC12 quick-connect valved in-line coupling insert (Colder Products Company, Saint Paul, MN) that mated with a PMC12 non-valved quick-connect coupling body. Coupling bodies were attached to the inlet and outlet of an ultra-portable GGA (Los Gatos, Inc., Santa Ana, CA) with quarter-inch polytetrafluoroethylene (PTFE) tubing. The GGA uses off-axis integrated cavity spectroscopy to measure simultaneously CO_2, CH_4, and water. Gas production rates were calculated as shown in Equation 13-7.

$$(C_{final} – C_{initial})/\Delta t \qquad \text{(Eq. 13-7)}$$

Where, *C* is the concentration of gas and Δt is the amount of time between each measurement.

Bottles with sediment from each depth horizon were incubated in either a 20°C or 30°C temperature baths (n=3 for each temperature) and measured regularly for gas production for 161 days, which was the time it took for all experimental units to reach at least 4% carbon loss.

The cumulative decomposition rates were used to calculate Q_{10} and activation energy (E_a), which are defined as shown in Equations 13-8 and 13-9, respectively.

$$Q_{10} = \frac{Rate\ at\ 30℃}{Rate\ at\ 20℃} \quad \text{(Eq. 13-8)}$$

$$\ln k_2 = -\frac{E_a}{R}\left(\frac{1}{T_2} - \frac{1}{T_1}\right) + \ln k_1 \quad \text{(Eq. 13-9)}$$

Q_{10} represents the rate of change for a reaction, given 10°C of increased temperature that generally describes the temperature sensitivity of a reaction. Most enzymatic reactions, such as those that we hypothesize govern microbial decomposition of marsh sediment organic matter, exhibit a Q_{10} of approximately 2. Activation energy (E_a) can be thought of as the energy required for a reaction to occur.

Sediment Analysis

Sediment analyses were conducted on all samples, including both initial voucher samples and final sediment samples from the litter bottle. Water content was measured as mass loss when dried at 60°C. Bulk density is defined as mass of dry sediment divided by volume. All sediment requiring elemental analysis was finely ground by using a mortar and pestle followed by further homogenization in a ball mill (Retsch MM301). Small subsamples were weighed and wrapped in tin capsules for analysis on a Costech ECS 4010 (Valencia, CA). Filters were wrapped in tin capsules and analyzed as previously mentioned.

Results and Discussion

Decomposition in Litter Bottles

Sediment carbon and nitrogen elemental ratios did not change over the course of the experiment (**Figure 13-33**). Sediment carbon content in litter bottles did not change within our detection limits over the course of the 77-day experiment (**Figure 13-34**). The detection limit of measured change in carbon mass was dependent upon the balance resolution we used for bulk sediment (10^{-5} g) and the variation on the elemental analyzer (±1.2%), which allowed us to measure changes larger than 3.9 mmol of carbon. The changes in the litter bottles were under this threshold; therefore, we conclude that less than 3.9 mmol of carbon decomposed during the 77-day experiment.

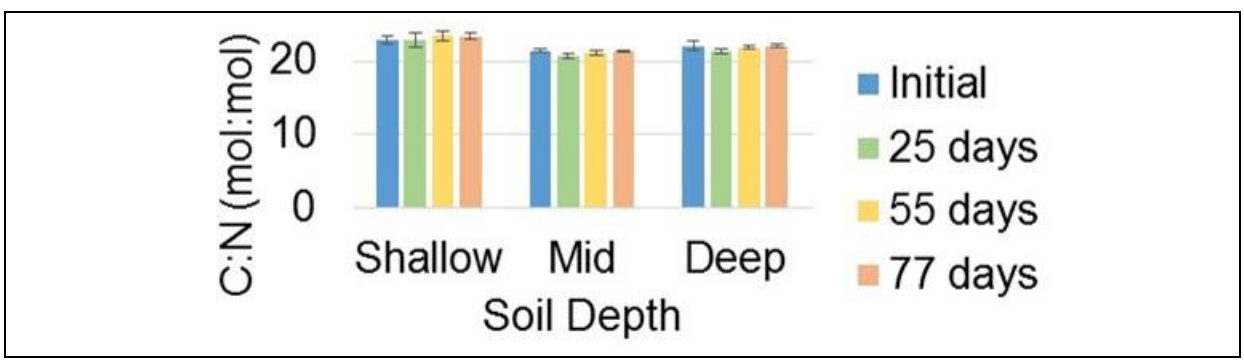

Figure 13-33. Molar carbon to nitrogen (C:N) ratios of sediment from litter bottle experiment.

Bars are grouped by depth horizon. Time of harvest is color coded.

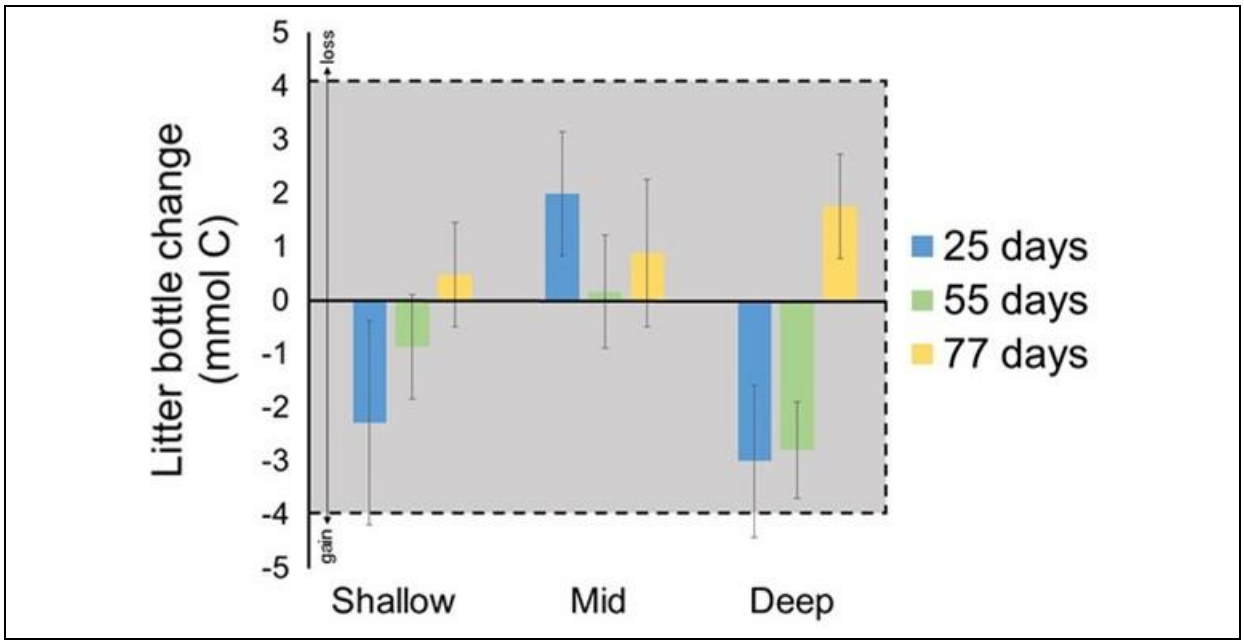

Figure 13-34. Litter bottle mass-loss change for each depth horizon over the course of the 77-day experiment.

The shaded box (dashed line) represents the detection limit for analysis.

GGA Experiments—Sediment Characteristics

Sediment from the shallow horizon contained slightly more organic carbon than its deeper counterpart (11.9±0.2 versus 9.5±0.1% organic carbon), but did not vary in molar carbon to nitrogen ratio (22.9±0.8 versus 21.4±0.4; see **Table 13-19**). Using a linear age-depth model, the age of the shallow sediment horizon is estimated at 110±35 cal BP, whereas the deeper sediment horizon is 320±35 cal BP (**Table 13-19**). However, fresh root material was likely collected in the shallow sediment horizon, whereas the deeper sediment horizon was below the active root zone.

Table 13-19. Characteristics of the Two Sediment Horizons Incubated During the 161-day Experiment

Sediment Horizon	Depth (cm)	^{14}C Age[a] (cal BP)	Organic Carbon Content (%)	Carbon to Nitrogen Ratio (mol:mol)	Q_{10}	Activation Energy (kJ mol^{-1})	Decomposition Rate (mmol C mol C^{-1} yr^{-1})
Shallow	5–10	110±35	11.9±0.2	22.9±0.8	2.0	49.7	230±3
Mid	20–25	320±35	9.5±0.1	21.4±0.4	2.2	58.8	168±2

[a] Estimated from a linear age-depth model: a sample of organic carbon from 92 cm was aged at 1,290 ±15 cal BP, or 14 yr/cm^{-1} However, younger organic carbon from the root zone was captured at the shallow depth.

GGA Experiments—Decomposition Rates

Over the 161-day experiment, the cumulative decomposition rate was linear, indicating relatively constant decomposition in all experimental units (**Figure 13-35**). CH_4 emissions were three to four orders of magnitude smaller than CO_2 flux; thus, methanogenesis pathways were not

important in our oxic experiment. Temperature was the most important factor regulating decomposition. Both shallow and deep sediment decomposed faster at 30°C than at 20°C, although the shallow sediment decomposed faster than the deeper sediment at both respective temperatures. Therefore, the relative lability or recalcitrance of the incubated sediment organic matter was a secondary controlling factor the decomposition process.

Q_{10} for decomposition in the shallow sediment over the course of the entire experiment was 2.0, and the deeper sediment exhibited slightly more temperature sensitivity with a Q_{10} of 2.2 (**Table 13-19**). However, decomposition processes in the deeper sediment required a higher activation energy (58.8 kJ mol^{-1}) than the reactions in the shallow sediment (49.7 kJ mol^{-1}; **Table 13-19**). The trend observed in this experiment follows the carbon-quality temperature hypothesis, which predicts that the decomposition reactions of refractory substrates (i.e., the deeper sediment with higher activation energy) are more sensitive to changes in temperature (Craine et al., 2010; Davidson and Janssens, 2006). This indicates that although the deeper sediment is more resistant to decomposition, given the same temperature (i.e., energy) increase, a larger proportion of the deeper sediment will decompose. Therefore, previously stable carbon in eroded sediments could remineralize to the atmosphere, given climate change-related temperature increases.

From the empirically defined activation energy for the shallow and deep decomposition reactions, theoretical decomposition rates at any temperature could be calculated by using Arrhenius kinetics (Eq. 13-9). Because temperature was the major controlling factor for the decomposition process for salt marsh sediment, it is somewhat arbitrary to report the decomposition rate at a single constant temperature, as was measured in this experiment. Instead, a decomposition rate that integrates the temperature regime that sediment organic matter might experience upon erosion is more ecologically relevant. We integrate temperature-dependent decomposition rates over 1 year of MCBCL creek temperature (recorded at Mile Hammock Bay) to determine annual decomposition rates. Annual decomposition rates for the shallow sediment horizon are estimated at 230±3.0 mmol C mol C^{-1} yr^{-1} (or 23.0%), which was slightly higher than the rate in deep sediment at 168±2.0 mmol C^{-1} yr^{-1} (or 16.8%) (**Table 13-19 and Figure 13-36**).

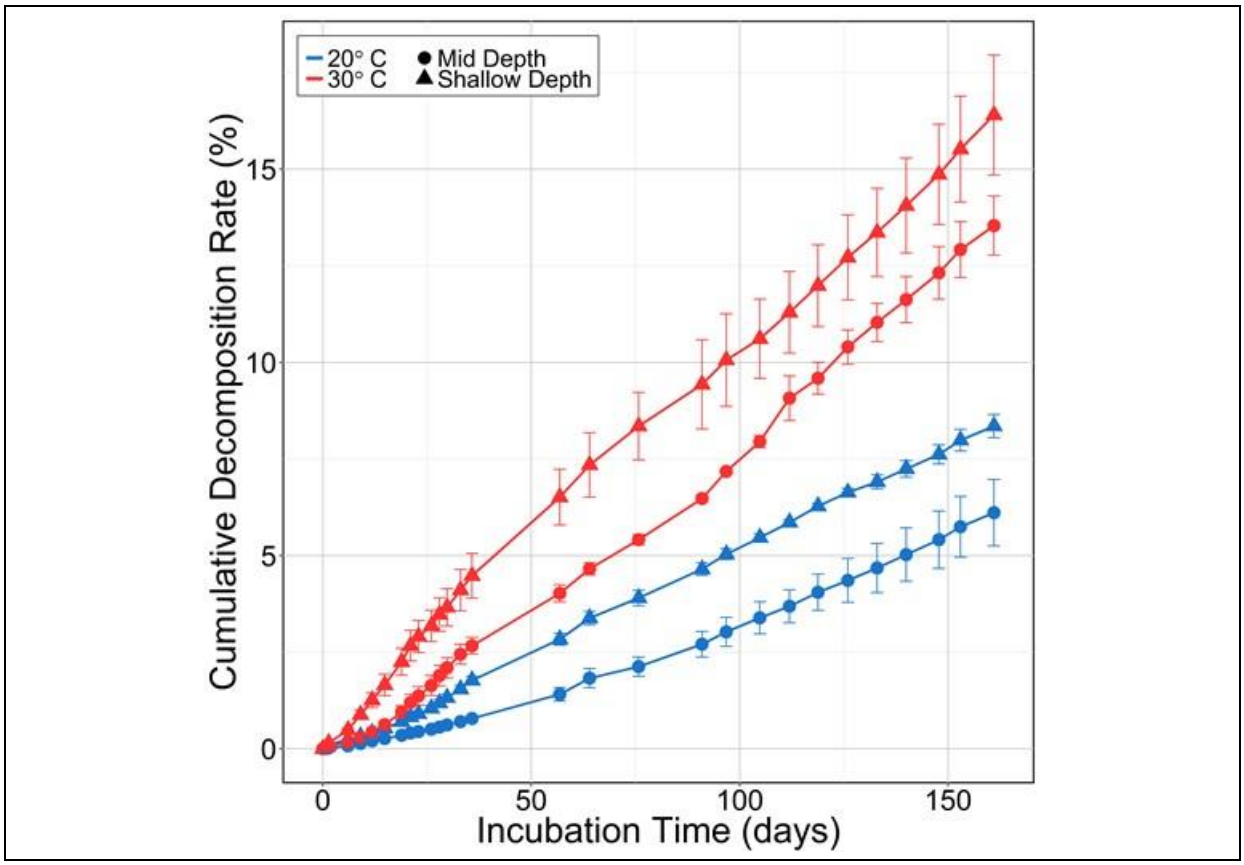

Figure 13-35. Cumulative decomposition for shallow and deep sediment at 20°C and 30°C.

There are several caveats that accompany these results. Notably, the rates are estimated for dark, oxic conditions. Most of the below-ground organic carbon stock of an intact marsh would also experience dark conditions, but the oxygen penetration depth in the marsh surface is very shallow, so these rates do not apply to un-eroded material still intact in a salt marsh. Because these in vitro rates are from a dark experiment, it is possible they could be higher if photo-oxidation accelerates remineralization. We estimate that the lifetime of eroded material is 1 year before it is either exported from the estuary or reburied in creek sediments or atop the marsh; thus, we acknowledge that the duration of "un-burial" for the material will affect its ultimate decomposition. To avoid the complications associated with carbonate chemistry equilibration, only a small volume of filtered creek water was used for inoculum in the experiment. Therefore, the microbial community that was captured in that sample was responsible for all the decomposition. The relatively linear decomposition rates suggest that the microbial community was quickly established and viable throughout the experiment (**Figure 13-35**). However, an experiment that measures decomposition with a varying microbial community that mimics actual conditions is a next step in clarifying the diagenetic processes of eroded marsh material, and it might yield higher rates.

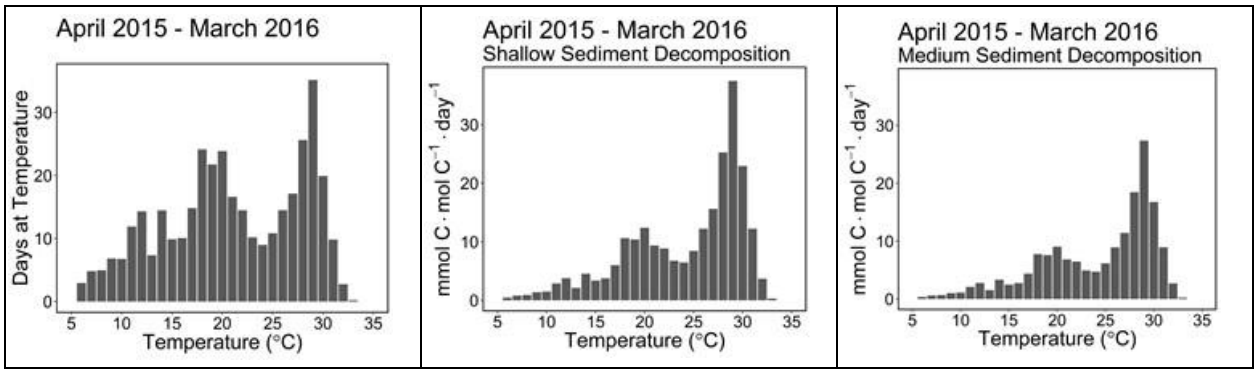

Figure 13-36. An example temperature profile from 1 year of monitoring data (left).

The temperature-dependent decomposition rates for both depth horizons were integrated over 1 year of temperature monitoring data to determine the total annual decomposition. This process was repeated for three different 1-year intervals to obtain average (±SD) decomposition rates (see Table 13-19).

Loss of Marsh Carbon from Eroded Sediment on MCBCL

The marshes along the New River Estuary (NRE) and Intracoastal Waterway (ICW) have experienced measurable shoreline erosion. The newly determined marsh decomposition of eroded material is useful to elucidate how much of the eroded material might result in CO_2 emissions. We estimate that approximately 177.2 Mg C yr^{-1} are eroded from the marsh shoreline on MCBCL. However, this loss translates to approximately 25.9–35.5 Mg C yr^{-1} released from decomposition (assuming the temperature profile from our estimate represents a typical annual cycle).

Therefore, much of the carbon lost from the marsh via erosion is not necessarily remineralized to the atmosphere. The fate of the remaining carbon is unknown, but we speculate that one of the following scenarios occur: (1) it is reburied in the creek bank, (2) it is transported atop the marsh (on flood tides) and becomes reincorporated into the marsh sediment, or (3) it is exported into the ocean. The retention of carbon within an eroding marsh ecosystem should be considered in future marsh carbon budgets.

It is well known that the dark, anoxic environment of the marsh sediment column preserves organic carbon. Contrary to previous conjectures that exposure to oxic environments would remineralize up to 100% of the material, eroded salt marsh sediment carbon slowly decomposes via temperature-driven processes. The semi-permanence of this material—even after erosion into environmental conditions that most other plant-derived material would decompose (e.g., algae, wrack, wood and other materials from terrestrial plants)—indicates the salt marsh ecosystem produces a quality of carbon that is preserved for long periods of time. This salt marsh carbon pump effectively stores CO_2 because the long-term net carbon accumulation of refractory OC resists rapid decomposition (**Figure 13-37**).

Decomposition of Eroded Material as a Source of Global CO_2 Emissions

There is a tremendous amount of carbon, on the order of 2,000 Pg C (1 Pg C=1 Gt C=10^{15} g C), stored in living plants and the soil carbon reservoirs of tropical-, temperate-, and boreal forests, peatlands, tundra, grasslands, and coastal ecosystems (Campbell et al., 2008). An important facet

of ecosystem management involves preserving these existing carbon stocks, which dwarf the average annual fossil fuel combustion and industrial emissions of 9.0±0.5 Pg C y^{-1}, measured from 2005–2014 (Le Quéré et al., 2015). These ecosystems, including salt marshes, have garnered increasing attention as a potential source of CO_2 into the atmosphere if the stored carbon stock is oxidized upon habitat degradation (Howard et al., 2017; Pendleton et al., 2012). Previous estimates for decomposition of wetland sediment upon oxidation after disturbance range from 25–100% (Howard et al., 2017; Pendleton et al., 2012; see **Table 13-20**). Our data constrain this wide range of possible values by providing empirical results from salt marsh sediment at MCBCL that reduce the decomposition rate from 25–100% to 17–23% per year (**Table 13-19**).

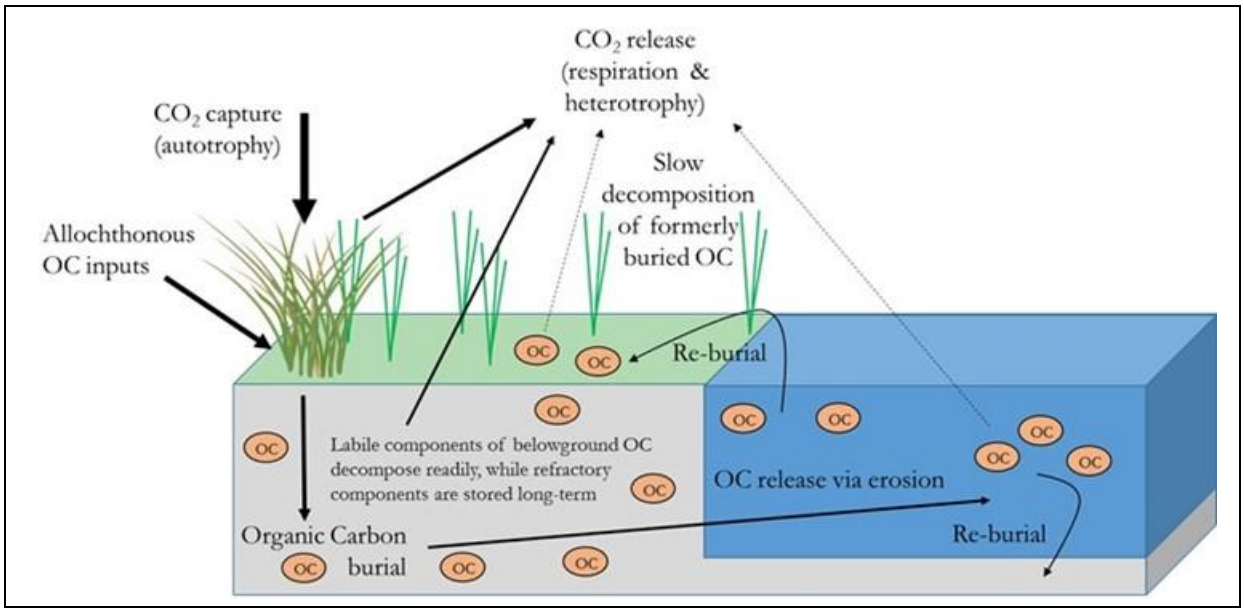

Figure 13-37. Conceptual schematic of the salt marsh carbon pump.

Upon marsh erosion, organic carbon (OC) that has passed through the pump resists rapid decomposition and is likely reburied before it completely remineralizes.

Pendleton et al. (2012) used the salt marsh geographic extent of 22,000 km^2–400,000 km^2, an annual global habitat loss of 1–2%, and potential decomposition rates of 25–100% to determine that salt marshes could emit 0.02–0.24 Pg CO_2 from habitat destruction (**Table 13-20**). Howard et al. (2017) uses the same geographic extent and habitat loss values, but instead assumed 100% conversion of stored carbon to CO_2 to estimate 0.02–0.76 Pg CO_2 potentially emitted from salt marsh destruction.

Table 13-20. Updated Calculations of Potential CO_2 Emissions After Salt Marsh Degradation

Study	Global Salt Marsh Extent (Mha)	Marsh Area Loss Rate (% yr^{-1})	Sediment Carbon Decomposition Rate (% yr^{-1})	Potential Salt Marsh Carbon Stock Remineralized in Top 1 m[a] (Mg C ha^{-1})	Potential CO_2 Emissions (Pg CO_2 yr^{-1})
Pendleton et al., 2012	2.2–40	1–2	25–100	65–259	0.02–0.24
This study	19–40	1–2	17–23	41–60	0.05–0.13

[a] Sediment carbon decomposition rate × 259 Mg C ha^{-1} (mean stock for above-ground biomass and top 1 m).

Although the immediate goal of this research was to constrain the wide range of potential decomposition rates of eroded marsh material, we note that the unacceptably large range of estimated salt marsh area, spanning 22,000 km^2–400,000 km^2, contributes to the uncertainty in estimating global carbon burial for wetlands (Howard et al., 2017; Mcleod et al., 2011; Morris et al., 2012). The low end of this range originated from Chmura et al., (2003), who tallied 22,000 km^2 of tidal salt marshes from Canada, Europe, the United States, and South Africa, but projected that the salt marshes along the coasts of Asia, South America, and Australia would substantially increase the estimate. The high end of the range is derived from Duarte et al. (2005), who used the estimate of 400,000 km^2 established by Woodwell et al. (1973). Recent remote sensing results have demonstrated an estimated global 1.66 million km^2 of marshes in tropical and temperate Asia, South America, and Australia, but could not differentiate tidal saline from freshwater wetlands (Gumbricht et al., 2017). Nahlik and Fennessy (2016) determined that the ratio of saline to freshwater marshes in the contiguous United States was approximately 1:10, and applying this ratio to estimates of tropical and temperate marshes adds 166,000 km^2 to the estimate of temperate tidal marshes made by Chmura et al. (2003).

Our recalculation of global salt marsh emissions from habitat loss differs from previous estimates of Pendleton et al. (2012) and Howard et al. (2017) because we use the following: (1) a different global extent of salt marsh (188,000–400,000 km^2) and (2) a more constrained decomposition rate for eroded salt marsh sediment (17–23%). We update the estimate of potential global emissions from eroded salt marsh ranges between 0.05 and 0.13 Pg CO_2 yr^{-1} (**Table 13-20**). This calculation also hinges on the assumption that 1% to 2% of salt marsh globally is lost and uses the previous assumption that average salt marsh sediment in the upper 1 m contains 259 Mg C ha^{-1} (see Pendleton et al., 2012), two assumptions that require further testing and updating. Our rates specifically pertain to eroded material that remains in the wetland ecosystem, whereas some of the global projected loss estimates include wetland drowning or conversion to upland pasture, which may be governed by different decomposition reactions.

Section 5. Drivers of Organic Carbon Content and Accumulation Rates in Salt Marsh Sediments

Lead Researchers: Nathan McTigue, Antonio Rodriguez, and Carolyn Currin

Introduction

One aspect of Research Project CW-4 was to elucidate how salt marshes respond to sea level rise in terms of carbon biogeochemistry (e.g., long-term carbon burial versus immediate decomposition of eroded material). Specifically, one technical objective of Research Project CW-4 was to determine long-term marsh sediment carbon burial rates. Related to this objective is how marsh elevation and accretion rates responds to sea level rise. Therefore, a specific research question was to address how marsh transgression into upland elevations will affect carbon sequestration rates (Question 6). In this section, we address these objectives by investigating how the salt marsh carbon biogeochemistry at MCBCL has responded in the past to changes in sea level rise. First, we present information on the carbon standing stock of six cores from five different sites at MCBCL. On select cores, we present stable isotope data that provide insight regarding the origin of the material (i.e., C_3 versus C_4 vegetation). Second, we use radiocarbon dating to determine the age of salt marsh cores and integrate the overlying carbon stocks into long-term sediment CAR and accretion rates. These rates are put into context by comparing them to historic sea level rise for the North Carolina coast and to CAR reported for salt marshes globally.

Materials and Methods

Sample Collection

In October 2014, seven cores were collected near Freeman Creek, Onslow Beach Backbarrier, and along the ICW with aluminum casing (diameter=7 cm) and driven into the marsh by hand. An additional set of cores were collected from Traps Bay Creek, Freeman Creek, and French Creek between January and March 2016 with a Russian peat corer. At each peat core location, elevation was measured with a laser level and stadia rod, relative to a Class B benchmark. The benchmark was a stainless-steel rod driven into the ground to the point of refusal, whose elevation (North American Vertical Datum of 1988 [NAVD 88]) was surveyed by using the National Geodetic Survey using the Online Positioning User Service (OPUS) Projects Program. Cores were collected with a stainless-steel Russian peat corer (diameter=5 cm). The peat corer was driven into the ground by hand until the point of resistance, which we define as the “marsh contact” because the corer cannot penetrate the basal paleoshoreline sand unit. We assume that no carbon from the current marsh lies below the marsh contact. Cores were collected in 1-m sections and transferred to PVC cradles. The distance from the creek bank was measured by meter tape to the nearest 0.1 m.

Sample Preparation and Analysis

Cores were cut into 2-cm depth intervals and dried at 60°C until a constant weight was reached. Once dried and re-weighed for bulk density determination, samples were homogenized by hand (mortar and pestle) or mechanically by a ball mill (Retsch MM301). A subsample from every 2-cm interval was weighed and ashed at 450°C for 6 hours to determine organic matter content

(i.e., %OM) by LOI (Nixon and Oviatt, 1973). A randomized subset of samples underwent elemental analysis (Costech ECS 4010) to determine the percent organic carbon content (%OC) at the National Oceanic and Atmospheric Administration (NOAA) Laboratory. For analysis of %OC, a homogenized subsample of sediment was subjected to an acidification treatment with 1 M HCl to remove carbonates that would bias the organic carbon content measurement. Using internal acetanilide standards, the elemental analysis coefficient of variance was less than 1.5%. Additional subsamples from every 5 cm to 10 cm were wrapped in silver capsules, subjected to the acidification procedure previously described, dried, and wrapped in an additional tin capsule for bulk stable carbon isotope analysis. This analysis measured via continuous flow isotope ratio mass spectrometer (IRMS) on a Thermo Delta V Advantage IRMS coupled to a Costech 4010 elemental analyzer at the University of Connecticut. Raw isotope values were corrected by two-point normalization by using U.S. Geographical Survey 40 and 41 glutamic acid reference materials. Analytical precision was 0.2 ppt or better for $\delta^{13}C$. Stable carbon isotope ratios are reported in standard δ notation relative to the Pee Dee Belemnite (PDB) standard, where $\delta^{13}C=([R_{sample}/R_{standard}]-1)\times1000$, and R is $^{13}C/^{12}C$.

Before drying core sections, a macro-particulate organic matter sample that was clearly identifiable as a single piece of vegetative material was removed from core sections 4, 14, and 24 cm above the basal marsh contact in Cores 1L, 2L, and 3L, respectively (**Table 13-21**). The sample was cleaned of extraneous sediment with deionized water under a dissecting scope. Samples were dried at 60°C in ashed glassware and shipped to the National Ocean Sciences Accelerator Mass Spectrometry (NOSAMS) laboratory in Woods Hole, MA, for radiocarbon (^{14}C) age analysis. Radiocarbon ages were calibrated by using CALIB 7.10 (Stuiver et al., 2017) and are reported as the mean probability age rounded to nearest decade ±2σ. By convention, radiocarbon ages use the year 1950 AD as the modern baseline (Stuiver and Polach, 1977). Thus, to determine the sample's actual age, we added the difference between sample collection date and 1950 (i.e., 66 years for our samples collected in 2016) to the calibrated age and henceforth report ages as calendar years before present (cal BP).

A set of samples (n=38) were run for %OC at both NOAA's Laboratory and the University of Connecticut for inter-laboratory calibration. These samples were highly correlated ($y=1.05x+0.05$, $r^2=0.97$) and justified our use of data from either laboratory as one combined data set. Because only some samples were measured for %OC, but all were measured for %OM, we derived a site-specific empirical relationship to predict %OC from %OM, based on the approach of Craft et al. (1991). The linear regression between %OC and %OM ($y=0.47x+1.1$, $r^2=0.92$) was used to convert %OM to %OC, which was subsequently used to calculate carbon inventories. Sediment %OC from each depth was integrated for each core section down to the marsh contact and extrapolated to 1 m^2. Sediment CAR was determined by the dividing carbon inventory (g C m^{-2}) by the age at the target depth (y).

Results and Discussion

Relationship Between Organic Matter (LOI) and Organic Carbon Content

Determining the relationship between %OM and %OC content is important for methodological reasons: %OM is determined via LOI and is simpler, less expensive, and quicker to analyze. However, when investigating questions that involve carbon biogeochemistry, %OM content,

which constitutes total organic matter mass (including carbon, nitrogen, sulfur, phosphorus, hydrogen, oxygen, and all other elements composed within the organic matter), is not as valuable as %OC content. For this reason, a subsample of the total samples run for %OM was also analyzed for %OC, and the relationship between the two measures were used to convert the remaining %OM values to %OC (Craft et al., 1991). Generally, all samples formed a linear trend, but significant differences existed between all three sites (analysis of covariance [ANCOVA], $F(2, 450)=753$, $p<0.01$; **Figure 13-38**). The samples from Freeman Creek and TB overlapped in %OC and %OM content, although the relationship between the two measurements were significantly different. French Creek possessed %OC and %OM values higher than either Freeman Creek or Traps Bay Creek, but the linear regression of the two variables formed the steepest slope between all sites (**Figure 13-38**).

It is important to note that significantly different conversion equations were derived from each site despite the proximity of each site to one another. The differences in tidal regime, emergent vegetation (e.g., *Spartina alterniflora* versus *Juncus roemarianus*), and porewater salinity are possible factors that contributed to the different quantity and quality of organic matter preserved in sediments. These data clearly demonstrate that organic matter contains different amounts of organic carbon, even among the salt marshes within proximity to each other on MCBCL. Therefore, we suggest using site-specific empirically derived relationships between %OM and %OC for each individual study site instead of using previously derived and published relationships as a "catch-all" for all study sites (e.g., Craft et al., 1991). The slope of our measured regressions is larger than that proposed by Craft et al. (1991); thus, if we relied on the previously published equation, we would underestimate %OC. In the following sections, %OC for each site (i.e., Freeman Creek, French Creek, and Traps Bay Creek) is represented by each respective conversion curve (**Figure 13-38**).

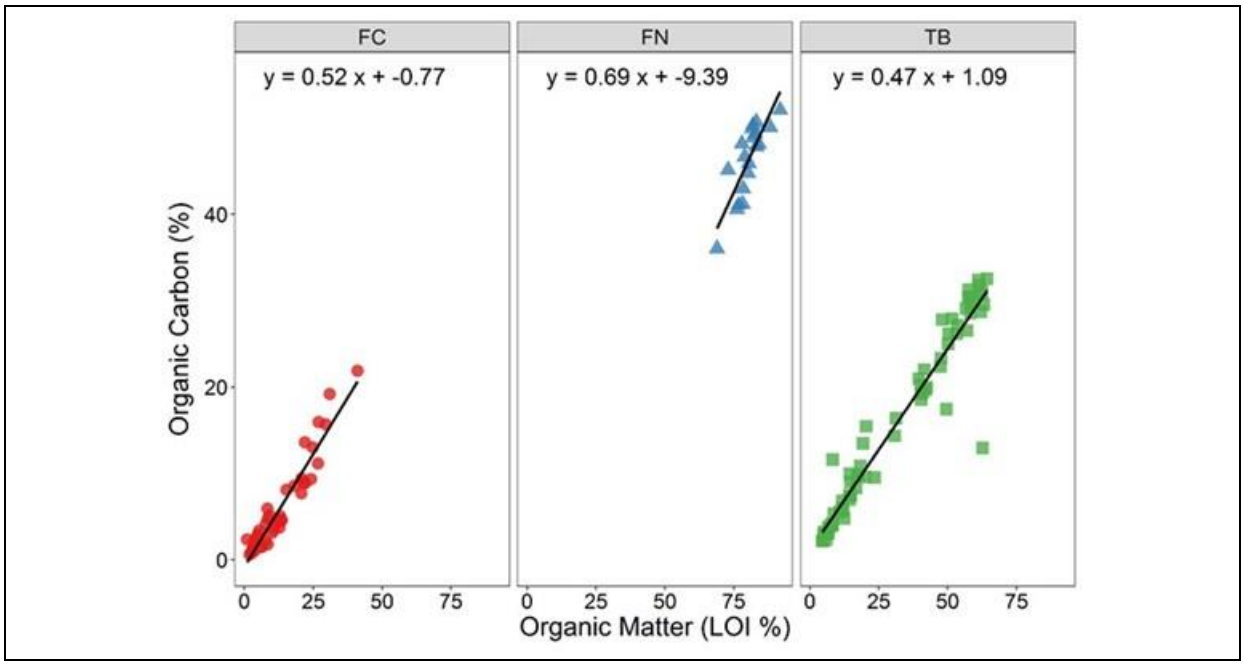

Figure 13-38. Regression plots for %OC and %OM for Freeman Creek (FC), French Creek (FN), and Traps Bay Creek (TB).

Regression equations are significantly different from one another ($p<0.05$).

Sediment Core Profiles: %OM, %OC, Sediment Carbon Density, and $\delta^{13}C$

Traps Bay Creek

The three cores collected with the peat corer from Traps Bay Creek (i.e., TB.16.1L, TB.16.2L, TB.16.3L) were 224-, 194-, and 90-cm long, respectively (**Table 13-21**). The marsh surface elevation of the three cores were within 2 cm relative to each other, ranging from 0.068 to 0.085 NAVD 88 (m). The %OM content in the cores ranged from 1.9% in the deepest portions of the core to 67.5% in the upper 30 cm of each core (**Figure 13-39**). The %OC content ranged from 2.0% to 32.6% for all cores at all depths (**Figure 13-40**). Much of core TB.16.1L contained between 20% and 30% organic carbon. Cores TB.16.2L and TB.16.3L exhibited higher carbon content in the upper parts of the core, whereas the carbon content was attenuated down-core and approached the lower threshold of measured values. Mean sediment carbon density (SCD) was 0.039±0.010 g C cm^{-3} for all three cores (**Figure 13-41**). The molar carbon to nitrogen ratios in core TB.16.1L ranged from 23.5 to 64.6 with a mean (±SD) of 32.5±10.7 (**Figure 13-42**). Sediment organic carbon $\delta^{13}C$ values from all three cores fell between −34.1% and −20.5‰, but only two of the 55 samples were heavier than −23‰ (**Figure 13-43**). Therefore, most of the carbon within the Traps Bay Creek cores is C_3–derived vegetation.

Freeman Creek

The four peat cores collected at Freeman Creek (FC.16.1L, FC.16.2L, FC.16.3L, FC.16.6L) and the one aluminum core (C-8) were between 26- and 94-cm long. The surface elevations of the peat cores spanned from the near-creek low lying marsh at −0.159 m NAVD 88 to the upland marsh at 0.536 m NAVD 88 (**Table 13-21**). The %OC content ranged from 0% to 24.8% (**Figure 13-40**), but most values were less than 10%. SCD for all four cores was 0.020±0.012 g C cm^{-3} (**Figure 13-41**). The molar carbon to nitrogen ratio for sediment at Freeman Creek cores ranged from 11.6 to 41.1 (mean±SD=21.6±7.1; **Figure 13-42**). The $\delta^{13}C$ values for sediment collected with the peat corer spanned from −29.4 to −15.9‰ (**Figure 13-43**), a range encapsulating both C_3 and C_4 vegetation (Lamb et al., 2006). In the surficial portions of cores FC.16.1L, FC.16.2L, and FC.16.3L, the stable carbon isotopes suggest a mixture of C_3– and C_4–derived material constitutes the organic carbon in the sediment. Deeper within these cores, there is a clear shift in $\delta^{13}C$ values that indicate C_3–derived material constitutes the preserved material under the marsh. There is a clear, notable shift in FC.16.3L at 45-cm deep (**Figure 13-43**). Core FC.16.6L, the most upland core collected, entirely consists of C_3–derived carbon despite having been collected where *Spartina patens* and *Distichilis* species. dominated the emergent vegetation.

French Creek

At French Creek, cores FN.16.1L and FN.16.2L were 247- and 86-cm long, respectively (**Table 13-21**). The French Creek cores exhibited the highest %OM (78.2±9.8%; **Figure 13-39**), which translated to the highest %OC (44.7±6.1%) observed among all study sites (**Figure 13-40**). Despite high carbon content throughout the cores, SCD was only slightly higher than the other sites at 0.042±0.010 g C cm^{-3} (**Figure 13-41**) due to low bulk density throughout both cores (**Figure 13-44**). The range of molar carbon to nitrogen ratios (21.6–56.3) overlapped with Freeman Creek and Traps Bay Creek (**Figure 13-42**).

Onslow Beach and the ICW

The cores collected from Onslow Beach and along the ICW were the lowest in carbon content at 1.5±1.7 %OC and 4.0±5.2 %OC, respectively (**Figure 13-40**). Their low carbon content yielded relatively low SCD at 0.009±0.008 g C cm^{-3} and 0.014±0.010 g C cm^{-3}, respectively (**Figure 13-41**). Several sections of these cores contained high sand volume from dredge spoils and, thus, contained much less carbon than those cores that consisted of marsh content throughout the entire core (e.g., cores C-17 and C-28 contain sections of core where SCD=0). However, salt marsh has colonized and vertically accreted on these dredge spoils based on the carbon content that exists in the upper-most sections of cores C-17 and C-28.

Table 13-21. Characteristics of March Cores Collected at MCBCL

CAR was calculated by dividing the carbon stock by calibrated ^{14}C age. A dash indicates parameters not measured.

Sample	Surface NAVD 88 (m)	Sample Depth (cm)	$\delta^{13}C$ (‰)	Calibrated ^{14}C Age (cal BP)	Carbon Stock (g C m^{-2})	CAR (g C m^{-2} y^{-1})
TB.16.1L	0.068	220	−28.7	2,416±20	95,575	38.9
TB.16.2L	0.082	180	−27.4	586±15	75,417	119
TB.16.3L	0.085	74	−24.7	186±25	33,356	147
FC.16.1L	0.057	94	−14.1	671±50	13,205	19.7
FC.16.2L	−0.159	26	−14.9	195±15	4,649	23.8
FC.16.3L	0.062	92	−26.1	1,351±15	34,053	25.2
FC.16.6L	0.536	60	−26.6	261±25	13,896	53.2
FN.16.1L	0.097	247	−28.6	3,226±50	104,012	32.2
C-1	−0.276	70	–	–	13,696	–
C-7	−0.138	104	–	–	13,104	–
C-8	−0.117	102	–	–	12,672	–
C-17	0.117	46	–	–	4,873	–
C-5	0.051	110	–	–	17,820	–
C-29	0.372	105	–	–	22,239	–
C-28	0.572	102	–	–	10,169	–

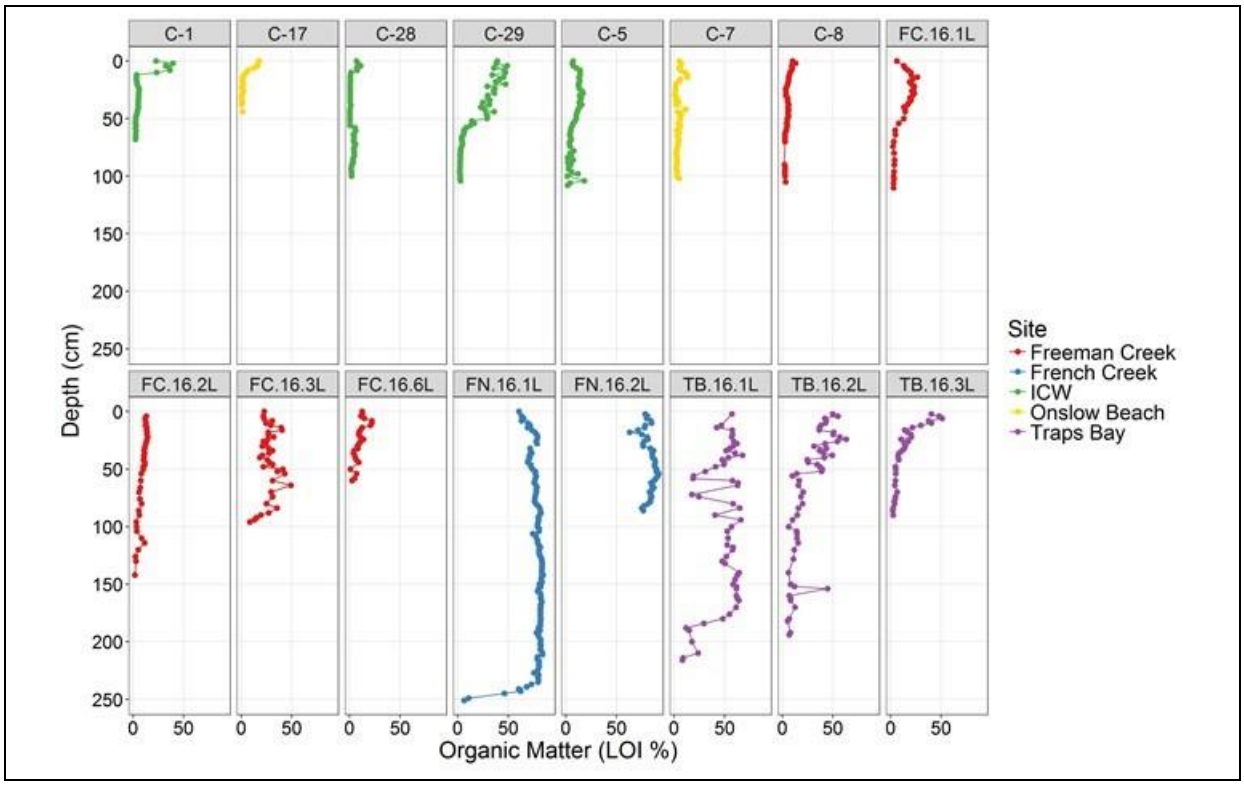

Figure 13-39. Profiles of organic matter content (%OM) in cores collected from MCBCL.

Profiles are color coded by site.

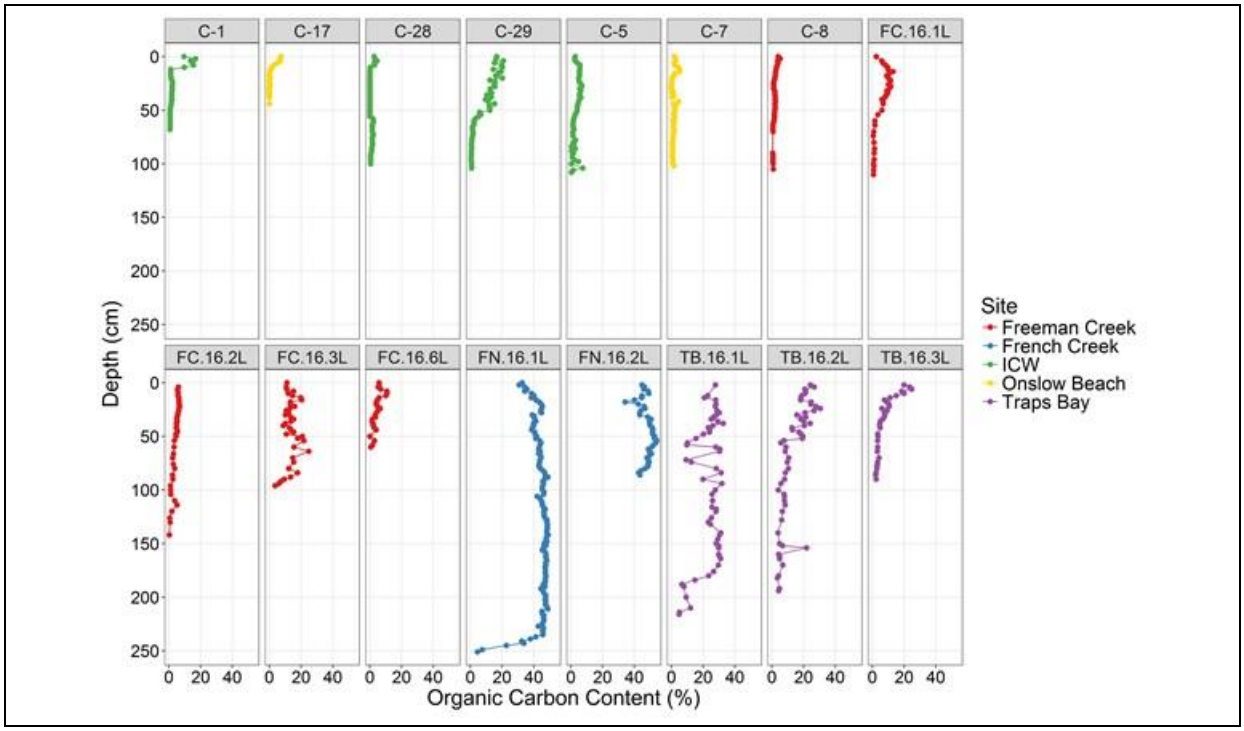

Figure 13-40. Profiles of organic carbon content (%OC) in cores collected from MCBCL.

Profiles are color-coded by site.

The organic carbon content in our sites on MCBCL exhibited a large range, and significant differences existed between sites (ANOVA, F [4, 760]=1,242, $p<0.01$; **Figure 13-45**). Pairwise post-hoc tests revealed that Onslow Beach possessed the lowest %OC of all sites, but was not significantly different than the ICW sites ($p>0.05$). Freeman Creek was not different from the ICW cores, but was significantly higher than the Onslow Beach cores ($p<0.05$). Traps Bay was significantly different than all other sites ($p<0.05$), as was French Creek with the highest %OC values of all sites ($p<0.05$).

SCD varied across MCBCL from 0–0.074 g C cm^{-3}, encompassing the range of values published for other salt marsh systems (Ouyang and Lee, 2014). SCD is the product of %OC and bulk density, so despite being related to %OC, it did not always mimic the same trend. Significant differences in SCD existed between sites (ANOVA, F [4, 760]=287, $p<0.01$; **Figure 13-45**). The SCD distributions from the ICW and Onslow Beach sites were not significantly different from each other ($p>0.05$). Likewise, regarding SCD distributions, there were no differences between French Creek and Traps Bay ($p>0.05$), but they were different from Onslow Beach, ICW, and Freeman Creek. The SCD distribution at Freeman Creek, although containing overlapping values with all other sites, was significantly different ($p<0.05$).

The sediment from the salt marshes on MCBCL is unique in that one study area spans almost the entire possible range of LOI, from approximately 0% to 92% (**Figures 13-39 and Figure 13-46**). These data allow us to investigate trends that would otherwise require a meta-analysis approach where data from multiple studies are compiled. LOI followed the predicted relationship with bulk density proposed by Morris et al. (2016), where the two variables form a power function described by the self-packing density of both pure organic matter and pure inorganic matter (**Figure 13-46**). This relationship ($y=0.11x^{-0.59}$, $r^2=0.79$) implies that measurement of dry bulk density in future samples can yield %OM content; moreover, with previously derived site-specific empirical relationships between %OM and %OC (**Figure 13-38**), carbon content can also be derived. This approach would be useful if rough estimates of carbon content are desired, but measuring carbon content directly would dramatically reduce the error associated within these relationships. However, the relationships previously mentioned are robust enough to be used for future sediment studies at MCBCL, which would then only require the measurement of bulk density to yield %OM and %OC.

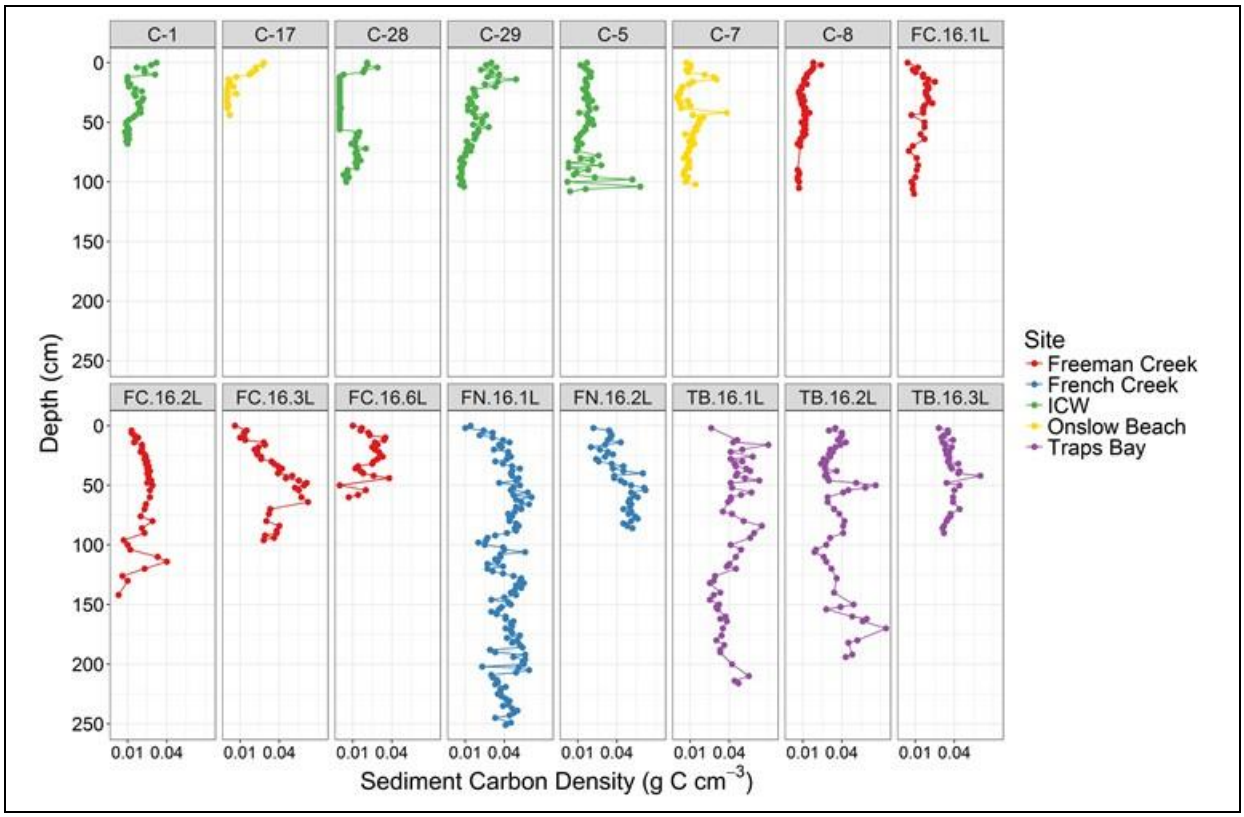

Figure 13-41. Profiles of sediment carbon density (SCD) from cores collected at MCBCL.

Profiles are color-coded. SCD is the product of %OC and bulk density.

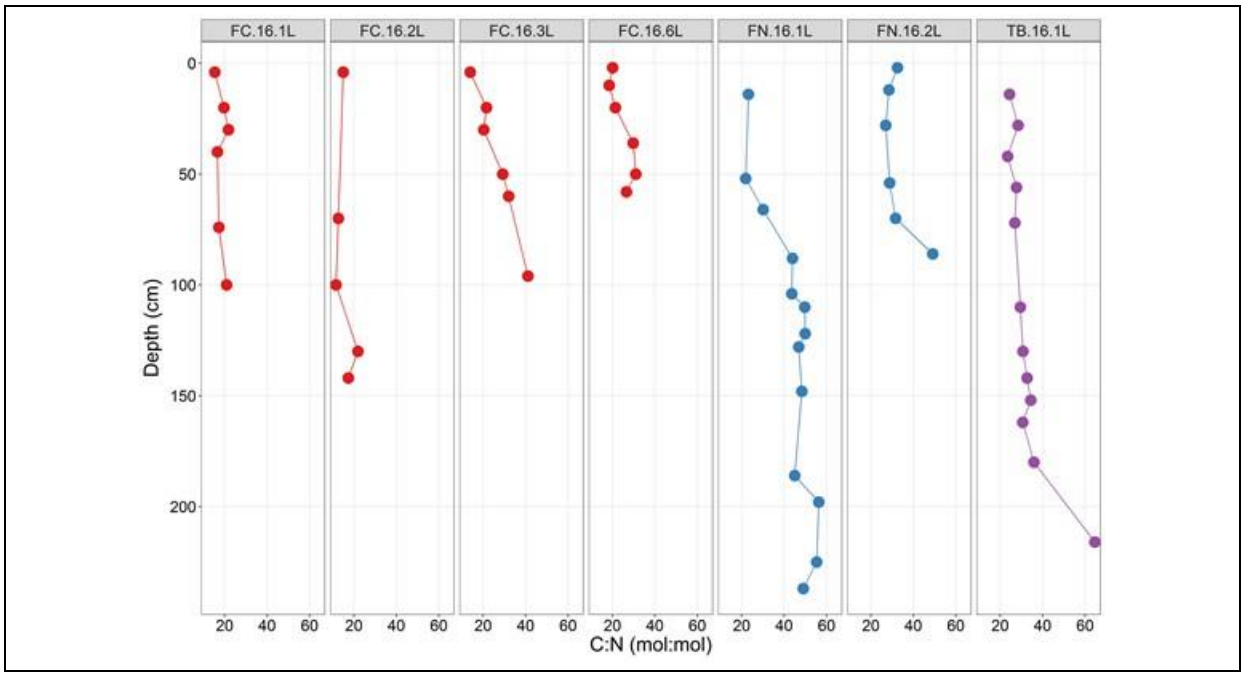

Figure 13-42. Profiles of molar carbon to nitrogen ratios in cores collected at Freeman Creek (FC), French Creek (FN), and Traps Bay Creek (TB).

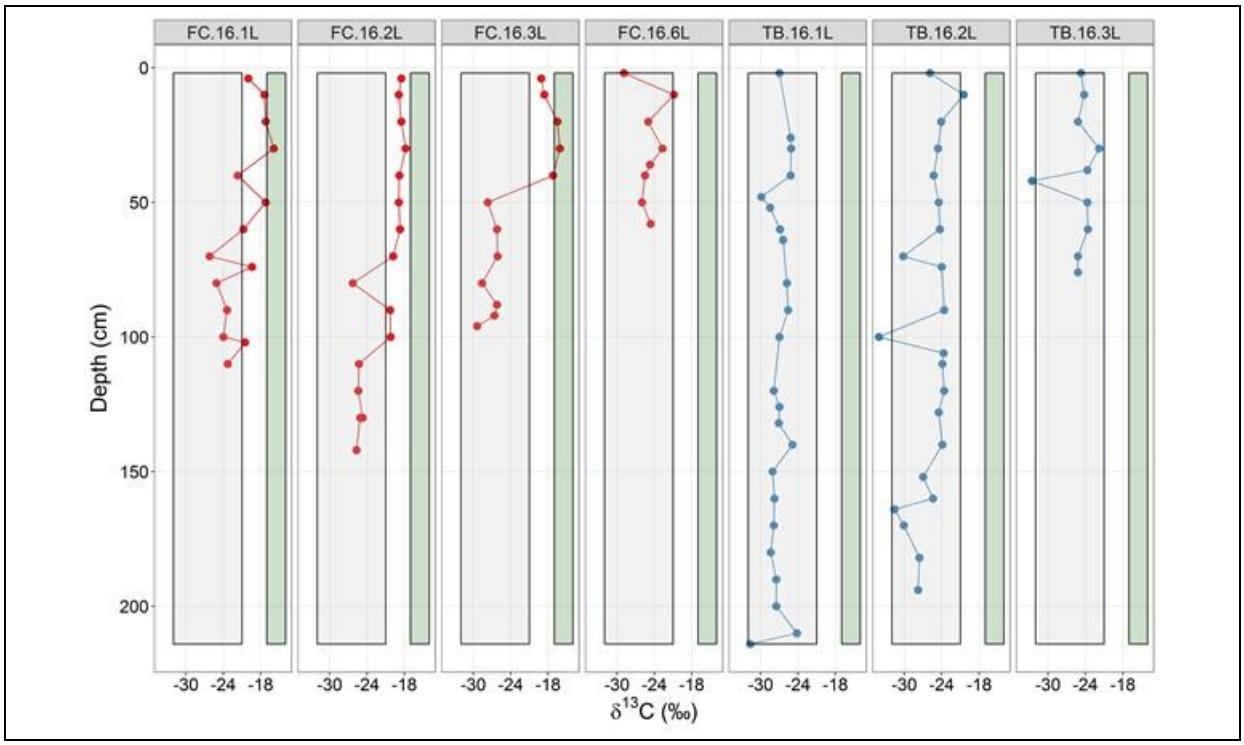

Figure 13-43. Profiles of stable carbon isotope values ($\delta^{13}C$) for Freeman Creek (FC) and Traps Bay Creek (TB) cores. Grey rectangles represent the $\delta^{13}C$ range of C_3 vegetation (e.g., *Juncus roemarianus,* maritime forest), and green rectangles represent C_4 vegetation (e.g., *Spartina alterniflora*, *Distichilis* sp).

Values from Lamb et al. (2006).

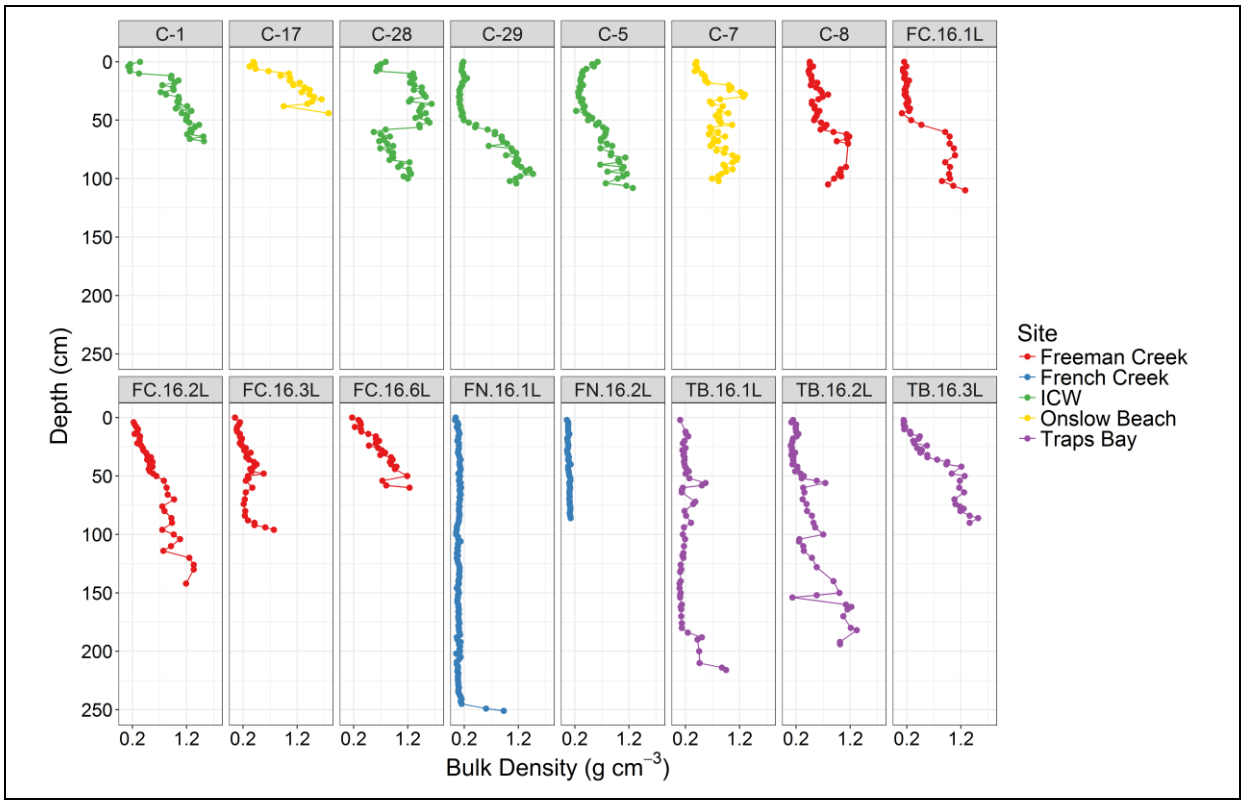

Figure 13-44. Profiles of bulk density in cores collected from MCBCL. Profiles are color coded.

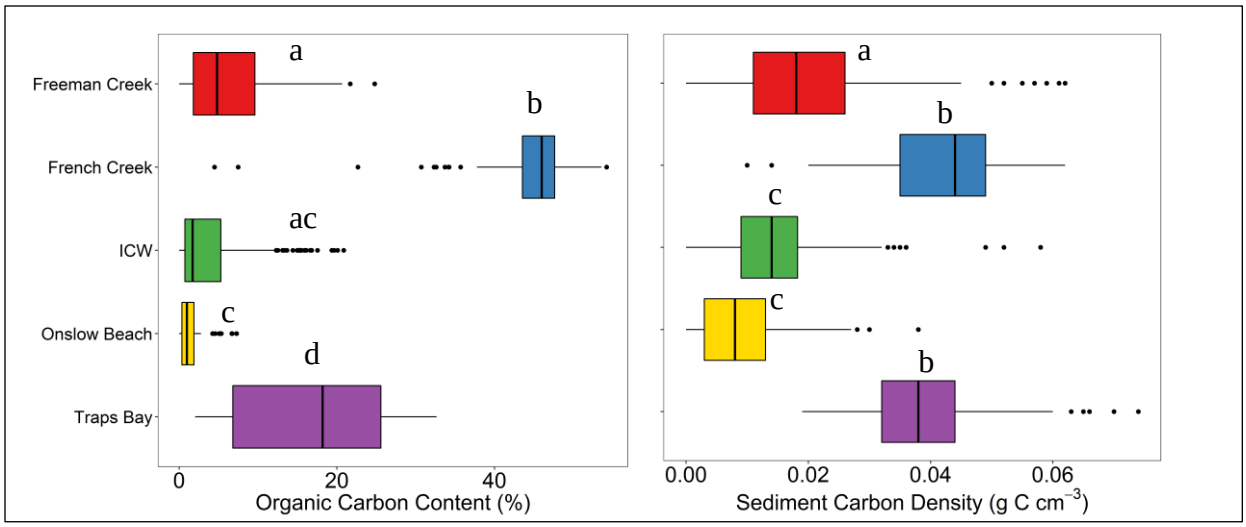

Figure 13-45. Box plots that represent the distribution of organic carbon content (left) and sediment carbon density (right) from MCBCL marsh sites.

Letters denote significant differences for each respective graph.

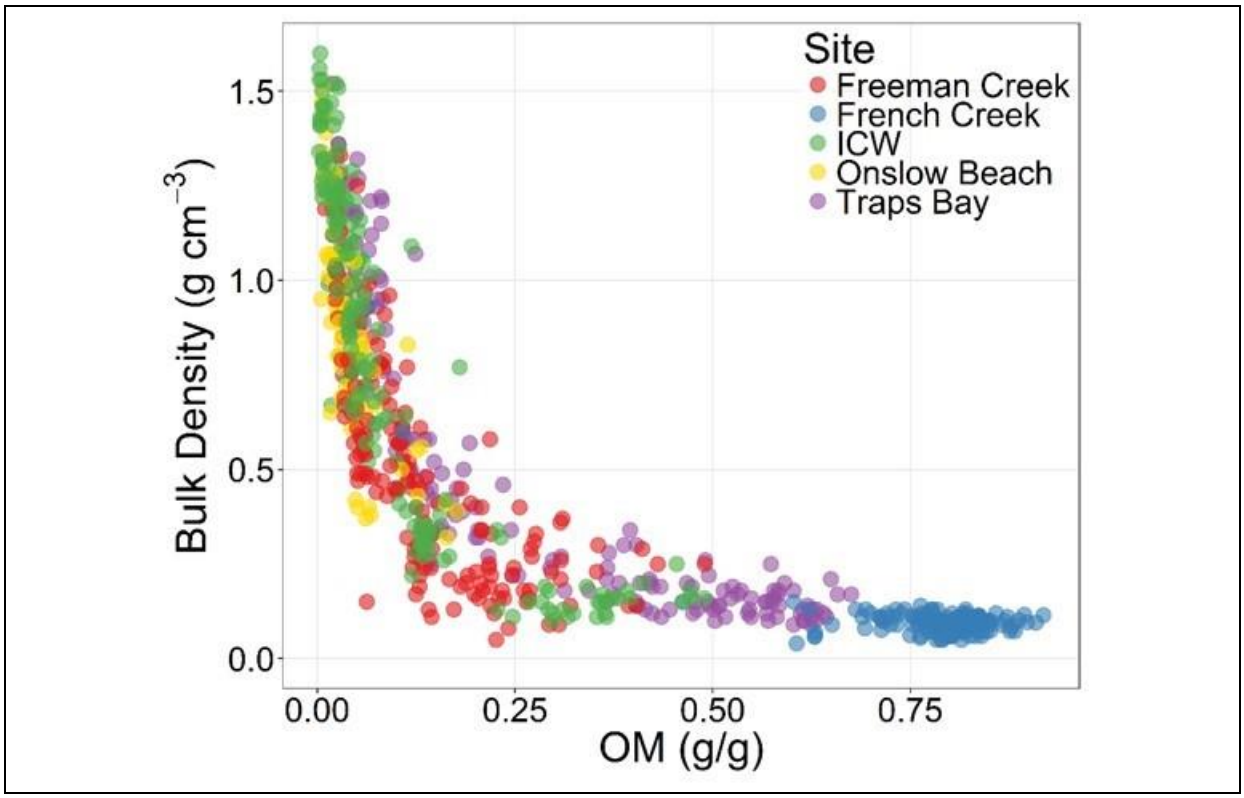

Figure 13-46. Relationship between %OM and bulk density.

The different salt marsh sites within MCBCL encapsulate almost the full range of possible %OM values, providing a robust predictive relationship between the two parameters.

Sources of Carbon to Salt Marshes

C_3 and C_4 vegetation differ in their stable carbon isotope values ($\delta^{13}C$) due to disparate photosynthetic strategies that discriminate $^{13}CO_2$ to different degrees during the carbon fixation process. Likewise, marine and freshwater algae and particulate organic matter differ in $\delta^{13}C$ as well, due to disparate sources of dissolved inorganic carbon that are ultimately fixed into biomass. These differences are useful in discerning the inputs of carbon to salt marshes. Although $\delta^{13}C$ values can overlap between marine algae and particulate organic matter and both C_3 and C_4 plants, molar carbon to nitrogen ratios do not, and thus, can be used to differentiate them. Using the approach by Lamb et al. (2006), we can examine the distribution of sediment samples plotted by molar carbon to nitrogen ratio and $\delta^{13}C$ value (**Figure 13-47**). Only one sample from Traps Bay Creek was analyzed for both parameters. This sample clearly fell within the bivariate space indicated as C_3 vegetation provenance. Freeman Creek samples were distributed between both C_3 and C_4 vegetation origin, and some samples that fell in between the distinct regions indicated a mixture of C_3 and C_4 content. This mixing model approach demonstrates that marine/freshwater algae or particulate organic matter is not stored in salt marsh sediments.

Samples were limited from other sites besides Freeman Creek, so these conclusions unfortunately only apply to one site. Without additional biomarkers (e.g., Λ8 for lignin), it is not possible to decipher upland C_3 plants (e.g., salt cedar, live oak, pine) from wetland C_3 vegetation

(e.g., *J. roemarianus*). This caveat not only applies to the source model (**Figure 13-47**), but also to the down-core profile where sediment $\delta^{13}C$ values fall within the range of C_3 vegetation (**Figure 13-43**).

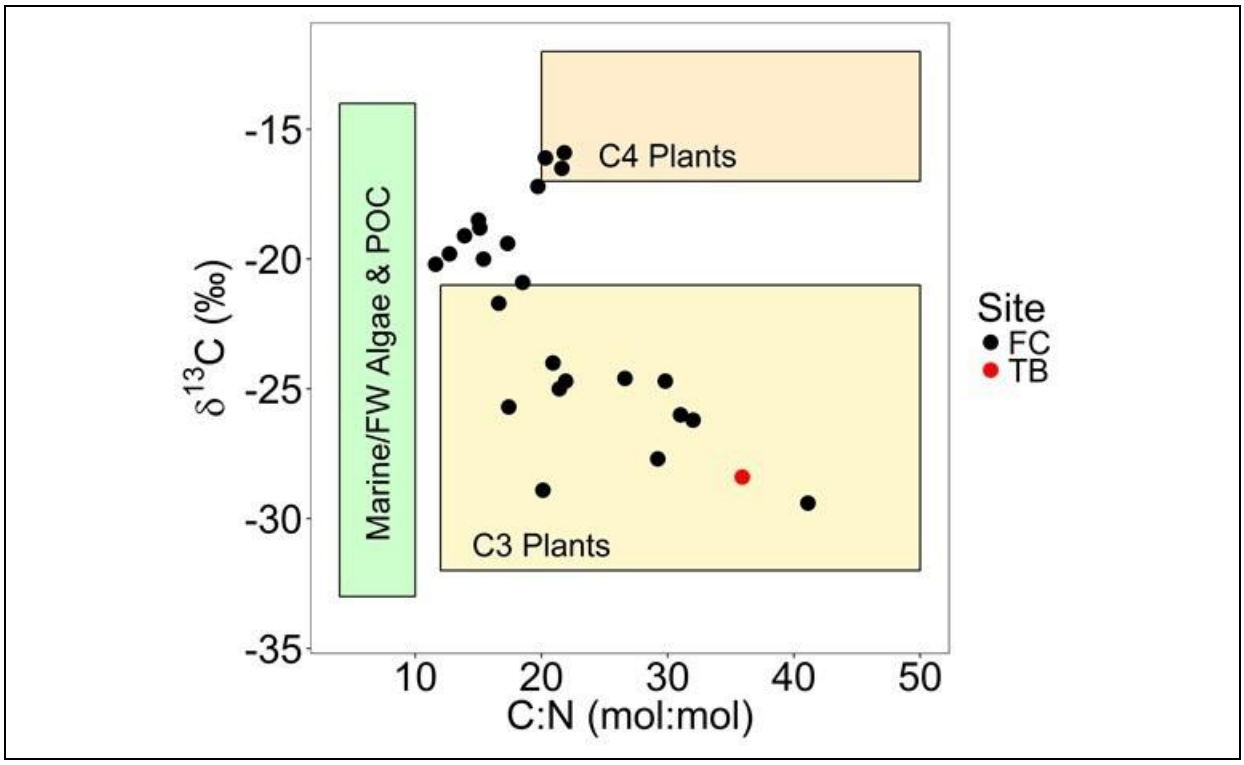

Figure 13-47. Source plot for marsh material collected at Freeman Creek (FC; black) and Traps Bay Creek (RB; red).

Values for source end-members are from Lamb et al. (2006).

Carbon Accumulation Rates at Freeman Creek, Traps Bay Creek, and French Creek

The calibrated age of the material sampled from the marsh cores ranged from 186±25 to 3,226±50 cal BP (**Table 13-21**). French Creek contained the oldest measured sample that was collected from 247-cm deep (3,226±50 cal BP). The age of organic carbon from Freeman Creek and Traps Bay Creek spanned an order of magnitude, from centuries to millennia (**Table 13-21**). Although the ages of the Freeman Creek material were not related to sample depth, Traps Bay Creek exhibited a clear relationship between age and depth.

Dividing the carbon stock (g C m^{-2}) that overlies each ^{14}C horizon marker by the age (year) of the material yields an assumed-linear average annual CAR represented in units of g C m^{-2} y^{-1}. At French Creek, where the oldest and deepest sample was collected, the CAR was 32.2±0.5 g C m^{-2} y^{-1}. At Freeman Creek, the CAR ranged from 19.7±1.5 to 53.2±5.1 g C m^{-2} y^{-1}, where the highest value was in the most-upland, youngest core. The CAR of 38.9±0.3 g C m^{-2} y^{-} from the deepest, oldest core at Traps Bay Creek (220 cm, 2,416±20 cal BP) was similar to that measured at Freeman Creek and French Creek. However, the other cores at Traps Bay Creek yielded much higher CARs at 119±3.0 and 147±20 g C m^{-2} y^{-1}.

Understanding the magnitude of the long-term carbon sink for salt marshes is important to assess their potential for climate change mitigation. Current surveys of salt marsh CAR range from 3–1,713 g C m^{-2} y^{-1}; these rates were determined with various tools, including marker horizons, ^{137}Cs, and ^{14}C (Ouyang and Lee, 2014). Based on this survey, the global mean CAR is estimated at 245 g C m^{-2} y^{-1}, but the median rate is much lower at 137 g C m^{-2} y^{-1} because the data distribution is skewed right (i.e., some very high CAR measurements skew the distribution).

One possible reason that the global rates span three orders of magnitude is that the methods employed to measure CAR vary in the timescales that they integrate the carbon stock so that the shorter integrations periods overestimate CAR by measuring labile carbon that will ultimately remineralize to the atmosphere. With these data, we can test the hypothesis that diagenesis controls CAR: the longer time (or older ^{14}C age) that CAR is integrated over, the smaller CAR will be because the carbon stock has had a longer time to decompose. Conversely, the shorter time (or youngest ^{14}C ages) that CAR is integrated over will yield the highest CAR because carbon that will ultimately decompose is being counted as "accumulated."

To test this hypothesis, we examined the relationship between CAR and radiocarbon age (**Figure 13-48**). Although the youngest radiocarbon ages yielded the highest CARs and the oldest radiocarbon ages yielded the lowest CARs, the trend was not universal among all samples, particularly those from Freeman Creek. These data demonstrate that diagenetic processes alone do not account for differences in CAR. Instead, site-specific differences (e.g., porewater salinity, tidal amplitude, sediment input) likely impart additional influences on the biogeochemical processes that accumulate, preserve, and bury carbon in wetland sediments.

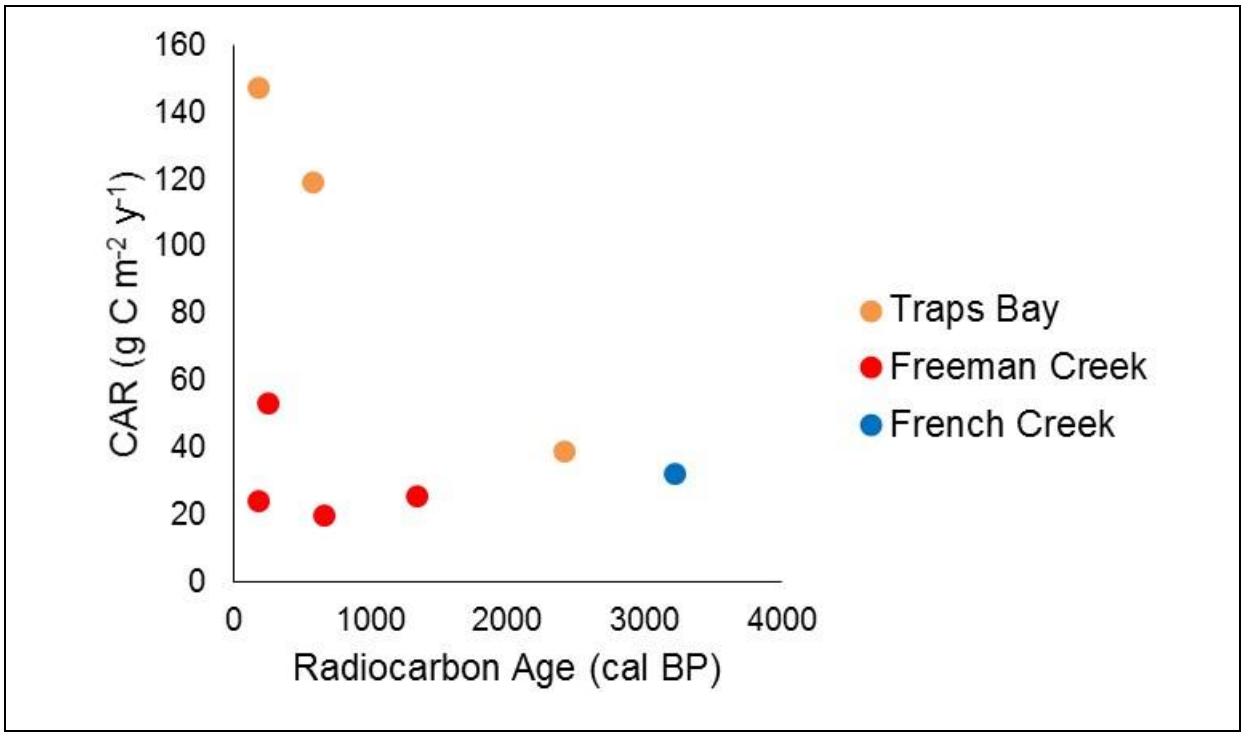

Figure 13-48. Scatterplot of carbon accumulation rate as a function of radiocarbon age.

Values are color-coded by site.

Our millennial CAR estimates align with other studies conducted elsewhere in the United States. Johnson et al. (2007) collected and dated a New England salt marsh core to 3,700 cal BP, and reported a CAR of 40 g C m^{-2} y^{-1}. Brevik and Homburg (2004) collected a core in Southern California whose provenance was 5,000 cal BP and measured a linear CAR of 30 g C m^{-2} y^{-1}. The trend exhibited by Traps Bay Creek and French Creek corroborates the findings of Choi and Wang (2004), who showed that centennial CAR measurements (130±9 g C m^{-2} y^{-1}) from a Florida *Juncus* marsh were approximately 10-fold higher than their CAR measurements integrated over the past 1,820 years (13±2 g C m^{-2} y^{-1}).

Several ecogeomorphic feedbacks exist in salt marshes that allow them to keep pace with sea level rise (Fagherazzi et al., 2012 and 2013; Kirwan and Guntenspergen, 2012). A positive relationship exists between tidal inundation and the deposition of allochthonous sediment to coastal wetlands, enhancing burial of organic matter (Reed, 1995). Therefore, sea level rise can increase the deposition of sediment and organic matter accumulation in salt marsh sediment given a sufficient sediment supply (Fagherazzi et al., 2013; Kirwan and Mudd, 2012; Mudd et al., 2009). Without sea level rise encouraging sediment accretion and subsequent elevation increase, a marsh can only bury carbon until reaching sediment-carbon saturation, then a marsh becomes carbon neutral and ceases its net greenhouse gas sink capacity, similar to terrestrial environments with carbon-saturated soils. Given these ecogeomorphic feedbacks, relative changes in marsh vertical accretion are proportional to changes in MSL. Relative sea level rise has changed for the North Carolina coast over past 3,000 years (Kemp et al., 2017) and is a possible driver of CAR. From 3000 to 2200 cal BP, relative sea level rise was unchanging or only slightly rising (less than 0.5 mm y^{-1}). Small increases occurred between 2200 and 2250 cal BP of 0.5–1.0 mm y^{-1}. In the most recent 300 years, relative sea level rise has accelerated dramatically, more than doubling its pre-industrial rate (Kemp et al. 2017). The historic marsh captured in the deep cores FN.16.1L and TB.16.1L, which were aged to 3226±50 and 2416±20 cal BP respectively, were exposed to low rates of relative sea level rise (0–0.5 mm y^{-1}) for approximately 1,000 years. During this time, because the marsh did not accrete vertically, CAR was limited by sediment carbon saturation, whereby a threshold of carbon content would be hypothetically reached when production and decomposition reached equilibrium. To determine CAR, the entire carbon stock for each core was integrated over millennial time horizons and presented here as a linear annual rate, essentially averaging the low (or non-existent) CARs from millennia ago with the recent most centuries that are clearly higher rates (e.g., CAR for TB.16.3L from the past 186±25 years was 147±20 g C m^{-2} y^{-1}). To demonstrate how CAR changes over time, even in the same marsh unit, we can recalculate CAR for core TB.16.1L for the upper 74 cm of marsh, where the horizon marker from core TB.16.3L (186±25 cal BP) was measured. In the top-most 74 cm of core TB.16.1L, the CAR was 152±20 g C m^{-2} y^{-1}, which is an order of magnitude higher than that of the entire core. The accelerated relative sea level rise in the recent 250 years causes higher CARs in salt marsh by inducing vertical sediment accretion. Decomposition undoubtedly also plays a role in regulating CAR, but it seems that it operates at timescales less than approximately 200 years, the approximate age of the youngest horizon marker measured in this study. For example, feldspar marker horizons are used to measure CAR and integrate time over months to years. Even ^{137}Cs horizon markers that integrate CAR over approximately 50 years are likely influenced more by carbon diagenesis than relative sea level rise.

The salt marsh at Freeman Creek exhibited relatively low CARs in all cores despite ranging in radiocarbon ages from 195–1,351 cal BP, a span of time that underwent an increase in relative sea level rise (Kemp et al., 2017). The contemporary processes we measure in the mineralogenic marsh may be different from historic processes due to its proximity to the ICW finished approximately 80 years ago, which may have altered its tidal regime, sediment supply, and its connection to the Atlantic Ocean through Browns Inlet. Another possibility to explain the divergence of this pattern is that radiocarbon aging was not the most advantageous method to use at this site for dating horizon markers. If the material analyzed for ^{14}C is older allochthonous material captured by the marsh, then CAR will be underestimated.

The amount of relative sea level rise captured in a CAR measurement (i.e., the age of the horizon marker) is critical because it is a driver of CAR. These data also suggest that if relative sea level rise continues to accelerate, then CAR will also continue to increase. However, salt marshes have thresholds at which their ecogeomorphic feedbacks can no longer keep pace with sea level rise (Fagherazzi et al., 2013; Mariotti and Fagherazzi, 2010). The complexities of these relationships forecasted into the future are discussed by Drs. Herbert and Kirwan (see Section 3 of this chapter). Overall, the CARs reported for marshes at MCBCL fall within the range of previously reported values (Mcleod et al., 2011; Ouyang and Lee, 2014). The assessment of global salt marsh CAR by Ouyang and Lee (2014) is overestimated due to the inclusion of measurements that include labile carbon that will ultimately remineralize to the atmosphere. Compared with the median value of CAR from Ouyang and Lee (2014) of 137 g C m^{-2} y^{-1}, the measurements from Traps Bay (from approximately 200–600 cal BP) align well with this range. The CARs from cores TB.16.1L and FN.16.1L that integrate the entire core over greater than 2,400 years were much lower than the reported global median rate, but by looking at the most recent 200 years of carbon accumulation in core TB.16.1L, it was much higher and aligned with the global median value.

Conclusions and Implications for Future Research and Implementation

Research Questions

1. **What is the relationship between *Spartina* and *Juncus* above-ground and below-ground biomass, and how does it change with marsh surface elevation and the MCBCL salinity gradient?**

Spartina above-ground biomass has a parabola-shaped relationship with surface elevation and inundation, which is attenuated in marshes with lower tidal ranges. Below-ground *Spartina* biomass decreases with inundation and lower elevation and is highest near MHW. We did not observe a significant relationship between *Juncus* above- and below-ground biomass. *Juncus is* found at higher tidal elevations in higher salinity marshes adjacent to the ICW than in lower salinity marshes adjacent to the NRE.

2. **How fast does marsh organic matter exposed via shoreline erosion decompose?**

Upon erosion to oxic horizons, marsh sediment organic carbon decomposition was primarily driven by temperature. Using average annual creek temperature from MCBCL to integrate annual decomposition rates for two sediment horizons, we estimate that sediment marsh carbon

will decompose by 7% to 23% in 1 year, given continual exposure to an oxic environment, which substantially constrains the range of previous estimates ranging between 25% and 100%.

3. How do tidal harmonics and amplitude influence SSC and sediment deposition in salt marsh creeks?

We found that tidal creek geomorphology (i.e., wetland dominated versus embayed creeks) was a stronger influence on SSC than tidal amplitude. We also documented an alternative mechanism for distributing SSC across the marsh because sediment was resuspended from the marsh surface into a surface microlayer and transported.

4. What is the fate of sediment eroded from fringing marshes, and does it vary with wave exposure?

In higher wave energy settings, eroded sediment is often returned to the marsh surface, where it increases surface elevation. In lower energy settings, it is deposited into the bottom of tidal creeks. Resuspended sediment can be transported long distances across the marsh when entrapped in the surface microlayer of tidal waters.

5. How does marsh vulnerability to sea level rise vary across the MCBCL landscape, and what factors are most important in vulnerable areas?

Because the contribution of plant productivity to elevation gain reaches a maximum of approximately 3 mm/yr, suspended sediment supply is the critical factor for maintaining marsh elevation at higher rates of sea level rise. Even when marshes drown at higher rates of sea level rise, new marshes are formed in adjacent uplands, a slope-dependent process; therefore, sediment supply and adjacent topography are the critical factors that regulate marsh vulnerability. Freeman Creek marshes along the ICW are the most resilient to sea level rise due to low topography that enables extensive marsh migration and adequate suspended sediment supply to maintain surface elevation. Freeman Creek marshes are predicted to expand significantly under a medium (1.3 m by 2100) scenario of sea level rise, whereas Traps Bay marshes in the lower estuary significantly declined under the medium scenario due to reduced sediment supply and steeper topography. French Creek marshes in the middle estuary are the most vulnerable due to reduced tidal amplitude, low suspended sediment supply, and steeper topography, and are predicted to decline significantly under all sea level rise scenarios. We found that SSCs between 26 and 32 mg/L are necessary to maintain the current extent of MCBCL marshes, yet most MCBCL marshes have SSC far lower than this threshold.

6. How will marsh migration into upland elevations affect carbon sequestration rates?

The migration of marshes into upland environments will increase the rate of soil carbon accumulation. Measurements of soil carbon accumulation under forests range from 4.1 g m^{-2} yr^{-1} to 55 g m^{-2} yr^{-1} (Richter et al., 1999), with the sandy, pine-dominated soils of MCBCL likely falling on the low end of this range. Measured rates of marsh soil carbon accumulation at the MCBCL sites are much higher (34 g m^{-2} yr^{-1} to 280 g m^{-2} yr^{-1}). Thus, the conversion of forest to marsh under accelerated sea level rise will lead to higher rates of carbon accumulation at the landscape level. In general, both the areal extent of wetland migration into uplands and the rate at which carbon accumulates in the wetland will increase proportionally to sea level rise.

7. How will sea level rise affect carbon storage in MCBCL marshes over the next century?

Model predictions are that as MCBCL marshes experience sea level rise in the future, the annual carbon accumulation will increase, which is primarily a function of increased vertical sediment accumulation in response to water depth. This prediction is matched by observations of sediment accumulation over the past two millennia, during which both sediment and carbon accumulation increased with an increasing rate of sea level rise. The increase in marsh migration into uplands, combined with increased CARs under accelerated sea level rise, result in enhanced carbon storage across the gradient of marshes in MCBCL and exceed the loss of wetland carbon via wetland drowning at the landscape scale, even at the highest rates of sea level rise.

Other Key Scientific Findings

- Suspended sediment concentration (SSC) is an important parameter determines the ability of marshes to keep up with sea level rise. We discovered a relationship between tidal creek morphology and SSC, thereby allowing the determination of sediment supply to a marsh system via analysis of aerial imagery instead of via labor-intensive water quality sampling and analysis. In addition, we identified a novel mechanism for the redistribution of suspended sediments across the marsh surface via the surface microlayer, which can float sand-sized particles. In Freeman Creek, this microlayer of suspended material carried three times as much sediment as the creek received from its watershed during the largest storm event measured during the DCERP2 study.
- The production and turnover of below-ground *Spartina alterniflora* biomass vary independently with tidal inundation, so that marsh carbon uptake and burial are maximized at elevations near MSL. Conservation and restoration efforts targeted at marshes near MSL will have the greatest benefit in terms of maximizing continued carbon burial in MCBCL marsh sediments.
- Short-term fertilizer addition to *Spartina alterniflora* marshes consistently led to increased rates of surface elevation gain. The elevation advantage in fertilized plots occurred because of increased above-ground biomass, which led to enhanced particle trapping efficiency; and below-ground biomass production, which led to soil volume expansion. The relative contributions of these two processes varies with tidal elevation and suspended sediment availability. We found no evidence of elevation loss or change in sediment properties because of fertilization.
- A marsh die-off event occurred in 2012 that was associated with drought conditions. Marsh periwinkles (*Littoraria irrorata*) increased in density after the die-off event began. Although *Spartina* biomass returned to pre-drought levels by 2015 at most sites, the Mile Hammock Bay marsh remained significantly impacted with many bare areas. Snail density returned to pre-die-off levels by 2015 at all sites. However, fertilized plots at Mile Hammock Bay exhibited greater regrowth after the die-off event than unfertilized plots, suggesting that fertilization may be an effective mechanism for stimulating recovery in marsh die-off areas.
- Model predictions suggest that MCBCL marshes will expand in area under very low sea level rise (0.3 m by 2100). Higher rates of sea level rise (0.8 m to 2.5 m by 2100) lead to changes in vegetation species composition and decreases in total marsh extent. The

greatest marsh losses (measured as a decrease in the percentage of existing marsh area) will occur in systems with low SSCs and steep marsh and upland boundaries, such as French Creek.

- SSCs on the order of 26 mg/L to 32 mg/L are necessary to maintain current marsh area under moderate to high sea level rise scenarios.
- As the rate of sea level rise increases, fertilization becomes less effective as an adaptive management strategy unless suspended sediment loads also increase. This is due to the changing nature of the impact of fertilization on plant biomass with increased inundation. Sea level rise leads to enhanced carbon accumulation, largely due to the increased rate of vertical accumulation of marsh surface. This response is so large that even as total marsh surface area begins to decrease, total marsh carbon accumulation continues to increase.
- Decomposition of organic carbon in eroded salt marsh sediments is primarily controlled by temperature, and secondarily by organic matter quality, which decreases with age. Shallower sediments have higher quality; therefore, they decompose faster than deeper sediments.
- We used 1 year of in situ temperature data to model decomposition rates for sediments within the active root zone and found that only between 17% and 23% of the organic carbon stored in sediments was respired over the course of 1 year. These data indicate that much of the marsh carbon lost to shoreline erosion remains in organic form for long enough to be re-deposited intact either on the marsh surface or in the bottom of the estuary.
- Our decomposition rates greatly constrain and reduce previous estimates of potential CO_2 emissions from eroded and decomposed salt marsh sediment. The semi-permanence of this material indicates that salt marshes are effective at storing carbon in their sediments for long-term, even with destructive forces such as drowning and erosion.
- We show the relationship between marsh sediment organic matter and organic carbon content is linear, but significant site-specific differences in the regression equations exist. Therefore, using literature conversion equations derived for different locations instead of independently determining a site-specific relationship may overestimate or underestimate the organic carbon content of marsh sediments.
- Organic carbon in the wetlands of MCBCL is up to 3,200 years old. The provenance of the aged marsh sediment carbon on MCBCL is mostly from plants with C_3 photosynthesis (upland maritime forest or *Juncus roemarianus*). Past shifts in dominant vegetation are apparent in Freeman Creek, where previous C_3 vegetation was outcompeted by C_4 vegetation (*Spartina alterniflora*, *Distichilis* sp.), possibly when tidal regimes shifted.
- There is an inverse relationship between sediment bulk density and organic matter content. This causes SCD to remain almost constant along a downcore profile. However, French Creek and Traps Bay marshes, consisting of C_3–derived material, possess significantly higher SCD than other sites.
- Generally, older integration ages for CAR yield smaller rates; the highest measured rates were from younger ages (approximately 200 years old). This trend suggests that sea level

rise plays an important role in both hindcasting and forecasting the capability of salt marshes to store carbon.

Implications for Future Base Management

- One of the most cost-effective adaptive management approaches for maintaining MCBCL salt marshes is land management; in particular, locating infrastructure away from the estuarine shoreline to minimize the need for shoreline hardening and maximize the potential for marsh migration into uplands with continued sea level rise.
- The wave energy conditions on the NRE and ICW shorelines are low enough that if shoreline stabilization is required, Living Shoreline approaches to shoreline stabilization are suitable for the entire area. A guidance tool that describes the type of Living Shoreline suitable for the wave energy of a specific site was developed for Central North Carolina, including MCBCL. The guidance tool is available at http://maps.coastalresilience.org/northcarolina. Additional resources that provide general guidance are also available under the Living Shoreline Explorer.
- Modeling and research results made a compelling case that fragmented and low-lying marshes near the New River Inlet and along the ICW are candidates for thin-layer application of dredged sediment to increase resiliency to sea level rise. NOAA leveraged DCERP2 research results to develop a collaborative project with the U.S. Army Corps of Engineers to design the regulatory framework for this approach and to obtain data about the effectiveness of the approach. Two thin-layer application pilot projects were funded by NOAA and commenced in March 2017. Preliminary results of these two pilot studies will be available in 2018.
- Transplanted and restored *Spartina alterniflora* marshes will benefit from initial fertilization, increasing their success and enhancing recovery of their ecosystem function. Large-scale fertilization of marsh habitat, however, does not appear to have a substantial impact on long-term (century-time scale) marsh survival.

Literature Cited

Agogué, H., E.O. Casamayor, F. Joux, I. Obernosterer, C. Dupuy, F. Lantoine, P. Catala, M.G. Weinbauer, T. Reinthaler, G.J. Herndl, and P. Lebaron. 2004. Comparison of samplers for the biological characterization of the sea surface microlayer. *Limnology and Oceanography Methods 2*(7):213–225.

Agren, G.I., and T. Ingestad. 1987. Root:shoot ratio as a balance between nitrogen productivity and photosynthesis. *Plant, Cell and Environment 10*:579–586. doi: 10.1111/j.1365-3040.1987.tb01838.x

Alber, M., E.M. Swenson, S.C. Adamowicz, and I.A. Mendelssohn. 2008. Salt marsh dieback: An overview of recent events in the U.S. *Estuarine, Coastal and Shelf Science 80*:1–11.

Arar, E.J., and G.B. Collins. 1997. *Method 445.0 In Vitro Determination of Chlorophyll a and Pheophytin a in Marine and Freshwater Algae by Fluorescence*. U.S. Environmental Protection Agency, Washington, DC.

Bindoff, N.L., J. Willebrand, V. Artale, A. Cazenave, J.M. Gregory, S. Gulev, K. Hanawa, C. Le Quéré, S. Levitus, Y. Nojiri, and C.K. Shum. 2007. Observations: Oceanic climate change and sea level.

Bradley, P.M., and J.T. Morris. 1990. Influence of oxygen and sulfide concentration on nitrogen uptake kinetics in *Spartina alterniflora*. *Ecology 71*:282–287.

Brevik, E.C., and J.A. Homburg. 2004. A 5,000 year record of carbon sequestration from a coastal lagoon and wetland complex, southern California, USA. *Catena 57(3)*:221–232.

Cahoon, D.R., P.F. Hensel, T. Spencer, D.J. Reed, K.L. McKee, and N. Saintilan. 2006. Coastal wetland vulnerability to relative sea-level rise: Wetland elevation trends and process controls. Pp. 271–292 in *Wetlands and Natural Resource Management*. Edited by Verheven, J.T.A., B. Beltman, R. Bobbink, and D.F. Whigham. Ecological Studies (Analysis and Synthesis) Series *190*. Springer: Berlin, Heidelberg, Germany.

Cahoon, D.R., M.A. Ford, and P.F. Hensel. 2004. Ecogeomorphology of *Spartina Patens*-dominated tidal marshes: Soil organic matter accumulation, marsh elevation dynamics, and disturbance. Pp. 247–266 in The Ecogeomorphology of Tidal Marshes. Edited by Fagherazzi, S., M. Marani, and L.K. Blum. American Geophysical Union: Washington DC.

Cai, W.J. 2011. Estuarine and coastal ocean carbon paradox: CO_2 sinks or sites of terrestrial carbon incineration? *Annual Review of Marine Science 3*:123–145.

Campbell, A., L. Lysenko, A. Hughes, and H. Gibbs. 2008. Carbon Storage in Protected Areas: Technical Report. United Nations Environment Programme World Conservation Monitoring Centre. Available at https://archive.org/details/carbonstorageinp08camp

Cavalieri, A.J., and A.H. Huang. 1981. Accumulation of proline and glycinebetaine in *Spartina alterniflora* Loisel. In response to NaCl and nitrogen in the marsh. *Oecologia 49*:224–228.

Chmura, G.L., S.C. Anisfeld, D.R. Cahoon, and J.C. Lynch. 2003. Global carbon sequestration in tidal, saline wetland soils. *Global Biogeochemical Cycles 17(4)*:1111.

Choi, Y., and Y. Wang. 2004. Dynamics of carbon sequestration in a coastal wetland using radiocarbon measurements. *Global Biogeochemical Cycles 18(4)*:311–319.

Cline, D. 1969. Spectrophotometric determination of hydrogen sulfide in natural waters. *Limnology and Oceanography 14*:454–458.

Craft, C.B. 2012. Tidal freshwater forest accretion does not keep pace with sea level rise. *Global Change Biology 18*:3615–3623. doi: 10.1111/gcb.12009

Craft, C.B., E.D. Seneca, and S.W. Broome. 1991. Loss on ignition and Kjeldahl digestion for estimating organic carbon and total nitrogen in estuarine marsh soils: Calibration with dry combustion. *Estuaries and Coasts 14(2)*:175–179.

Craine, J.M., N. Fierer, and K.K. McLauchlan. 2010. Widespread coupling between the rate and temperature sensitivity of organic matter decay. *Nature Geoscience 3*:854–857. doi: 10.1038/NGEO1009

Currin, C.A. 2017. *Adaptive Management Recommendations for Coastal Wetlands on Marine Corps Base Camp Lejeune*. July. Defense Coastal/Estuarine Research Program Report. 25 p.

D'Alpaos, A., S. Lanzoni, M. Marani, and A. Rinaldo. 2007. Landscape evolution in tidal embayments: Modeling the interplay of erosion, sedimentation, and vegetation dynamics. *Journal of Geophysical Research: Earth Surface 112*:1–17. doi: 10.1029/2006JF000537

Dahl, T.E. 2011. *Status and Trends of Wetlands in the Conterminous United States 2004 to 2009*. Report to Congress. U.S. Department of the Interior, U.S. Fish and Wildlife Service. *Fisheries and Habitat Conservation*. Available at https://www.fws.gov/wetlands/Documents/Status-and-Trends-of-Wetlands-in-the-Conterminous-United-States-2004-to-2009.pdf

Davidson, E.A., and I.A. Janssens. 2006. Temperature sensitivity of soil carbon decomposition and feedbacks to climate change. *Nature 440*:165–173.

Davis J., C. Currin, and J.T. Morris. 2017. Impacts of fertilization and tidal inundation on elevation change in microtidal, low relief salt marshes. *Estuaries and Coasts*. doi: 10.1007/s12237-017-0251-0Eleuterius, L. N. 1984

Davis, J., C. Currin, C. O'Brien, C. Raffenberg, and A. Davis. 2015. Living Shorelines: Coastal resilience with a blue carbon benefit. *PLoS ONE 10*(11):e0142595. doi: 10.1371/journal.pone.0142595

Deegan, L.A., D.S. Johnson, R.S. Warren, B.J. Peterson, J.W. Fleeger, S. Fagherazzi, and W.M. Wollheim. 2012. Coastal eutrophication as a driver of salt marsh loss. *Nature 490*:388–392. doi: 10.1038/nature11533

Diehl, T.H. 2008. *A Modified Siphon Sampler for Shallow Water*. U.S. Geological Survey Scientific Investigations Report 2007-5282. 11p. Available at https://pubs.usgs.gov/sir/2007/5282/pdf/sir20075282.pdf

Duarte, C.M., J.J. Middelburg, and N. Caraco. 2005. Major role of marine vegetation on the oceanic carbon cycle. *Biogeosciences 2*:1–8.

Eleuterius, L.N. 1984. Autecology of the black needlerush *Juncus roemerianus*. *Gulf Research Reports 7*(4):339–350.

Ensign, S.H., and C. Currin. 2017. Geomorphic implications of particle movement by water surface tension in a salt marsh. *Wetlands 37*(2):245–256. doi: 10.1007/s13157-016-0862-4.

Ensign, S.H., C. Currin, M. Piehler, and C. Tobias. 2017. A method for using shoreline morphology to predict suspended sediment concentration in tidal creeks. *Geomorphology 276*:280–288.

Fagherazzi, S., G. Mariotti, P.L. Wiberg, and K.J. McGlathery. 2013. Marsh collapse does not require sea level rise. *Oceanography 26*(3):70–77.

Fagherazzi, S., M.L. Kirwan, S.M. Mudd, G.R. Guntenspergen, S. Temmerman, A. D'Alpaos, J. van de Koppel, J.M. Rybczyk, E. Reyes, C. Craft, and J. Clough. 2012. Numerical models of salt marsh evolution: Ecological, geormorphic, and climatic factors. *Reviews of Geophysics 50*:RG1002. doi: 10.1029/2011RG000359.1.INTRODUCTION

Friedrichs, C.T., and D.G. Aubrey. 1998. Non-linear tidal distortion in shallow well-mixed estuaries: A synthesis. *Estuarine, Coastal and Shelf Science 27*:521–545.

Gedan, K.B., M.L. Kirwan, E. Wolanski, E.B. Barbier, and B.R. Silliman. 2011. The present and future role of coastal wetland vegetation in protecting shorelines: Answering recent challenges to the paradigm. *Climatic Change 106*:7–29.

Giurgevich, J.R., and E.L. Dunn. 1981. A comparative analysis of the CO_2 and water vapor responses of two *Spartina* species from Georgia coastal marshes. *Estuarine, Coastal and Shelf Science 12*:561–568. doi: 10.1016/S0302-3524(81)80082-5

Gumbricht, T., R.M. Roman-Cuesta, L. Verchot, M. Herold, F. Wittmann, E. Householder, N. Herold, and D. Murdiyarso. 2017. An expert system model for mapping tropical wetlands and peatlands reveals South America as the largest contributor. *Global Change Biology*:1–19.

Hall, J.A., S. Gill, J. Obeysekera, W. Sweet, K. Knuuti, and J. Marburger. 2016. *Regional Sea Level Scenarios for Coastal Risk Management: Managing the Uncertainty of Future Sea Level Change and Extreme Water Levels for Department of Defense Coastal Sites Worldwide*. U.S. Department of Defense, Strategic Environmental Research and Development Program. 224 pages.

Harrison, E.Z., and A.L. Bloom. 1977. Sedimentation rates on tidal salt marshes in Connecticut. *Journal of Sedimentary Petrology 47*(4):1484–1490.

Harvey, G.W., and L.A. Burzell. 1972. A simple microlayer method for small samples. *Limnology and Oceanography 17*(1):156–157.

Herbert, E.R., D.C. Walters, and M.L. Kirwan. Resolving contrasting salt marsh responses to eutrophication. In review.

Hladik, C., and M. Alber. 2012. Accuracy assessment and correction of a LIDAR-derived salt marsh Digital Elevation Model. *Remote Sensing of Environment 121*:224–235. doi: 10.1016/j.rse.2012.01.018

Hladik, C., J. Schalles, and M. Alber. 2013. Salt marsh elevation and habitat mapping using hyperspectral and LIDAR data. *Remote Sensing of the Environment 139*:318–330.

Hodson, R.E., R.R. Christian, and A.E. Maccubbin. 1984. Lignocellulose and lignin in the salt marsh grass Spartina alterniflora: Initial concentrations and short-term, post-depositional changes in detrital matter. *Marine Biology 81*:1–7. doi: 10.1007/BF00397619

Howard, J., A. Sutton-Grier, D. Herr, J. Kleypas, E. Landis, E. Mcleod, E. Pidgeon, and S. Simpson. 2017. Clarifying the role of coastal and marine systems in climate mitigation. *Frontiers in Ecology and the Environment 15*:42–50.

Howes, B.L., J.W.H. Dacey, and G.M. King. 1984. Carbon flow through oxygen and sulfate reduction pathways in salt marsh sediments. *Limnology and Oceanography 29*:1037–1051.

Hunter, A., J. Cebrian, J.P. Stutes, D. Patterson, B. Christiaen, C. Lafabrie, and J. Goff. 2015. Magnitude and trophic fate of black needlerush (*Juncus roemerianus*) productivity: Does nutrient addition matter? *Wetlands 35(2)*:401–417.

Johnson, B.J., K.A. Moore, C. Lehmann, C. Bohlen, and T.A. Brown. 2007. Middle to late Holocene fluctuations of C_3 and C_4 vegetation in a northern New England salt marsh, Sprague marsh, Phippsburg Maine. *Organic Geochemistry 38*:394–403.

Jordan, T.E., D.L. Correll, and D.F. Whigham. 1983. Nutrient flux in the Rhode River: Tidal exchange of nutrients by brackish marshes. *Estuarine, Coastal and Shelf Science 17(6)*:651–667.

Kemp, A.C., J.J. Kegel, S.J. Culver, D.C. Barber, D.J. Mallinson, E. Leorri, C.E. Bernhardt, N. Cahill, S.R. Riggs, A.L. Woodson, R.P. Mulligan, and B.P. Horton. 2017. Extended late Holocene relative sea-level histories for North Carolina, USA. *Quaternary Science Reviews 160*:13–30.

Kirwan, M.L., and L.K. Blum. 2011. Enhanced decomposition offsets enhanced productivity and soil carbon accumulation in coastal wetlands responding to climate change. *Biogeosciences 8*:987–993.

Kirwan, M.L., and G.R. Guntenspergen. 2012. Feedbacks between inundation, root production, and shoot growth in a rapidly submerging brackish marsh. *Journal of Ecology 100*(3):764–770.

Kirwan, M.L., and G.R. Guntenspergen. 2010. Influence of tidal range on the stability of coastal marshland. *Journal of Geophysical Research 115*:F02009. doi: 10.1029/2009JF001400

Kirwan, M.L., and S.M. Mudd. 2012. Response of salt-marsh carbon accumulation to climate change. *Nature 489*:550–553. doi: 10.1038/nature11440

Kirwan, M.L., and A.B. Murray. 2007. Ecological and morphological response of brackish tidal marshland to the next century of sea level rise: Westham Island, British Columbia. *Global and Planetary Change 60*(3):471–486.

Kirwan, M.L., G.R. Gunternspergen, A. D'Alpaos, J.T. Morris, S.M. Mudd, and S. Temmerman. 2010. Limits on the adaptability of coastal marshes to rising sea level. *Geophysical Research Letters* 37:L23401.

Kneib, R.T. 1997. The role of tidal marshes in the ecology of estuarine nekton. *Oceanography and Marine Biology: An Annual Review 35*:163–220.

Knepel, K., and K. Bogren. 2002. Determination of Orthophosphate by Flow Injection Analysis: QuikChem Method 31-115-01-1-H. Milwaukee, WI: Lachat Instruments:14.

Knutson, P.L, R.A. Brochu, W.N. Seelig, and M. Inskeep. 1982. Wave damping in *Spartina alterniflora* marshes. *Wetlands 2*:87–104.

Koop-Jakobsen, K., and F. Wenzhöfer. 2015. The dynamics of plant-mediated sediment oxygenation in *Spartina anglica* rhizospheres—A planar optode study. *Estuaries and Coasts 38*:951–963.

Koretsky, C.M., P. Van Cappekken, T.J. DiChristina, J.E. Kostka, K.L. Lowe, C.M. Moore, A.N. Roychoudhury, and E. Voillier. 2005. Salt marsh pore water geochemistry does not correlate with microbial community structure. *Estuarine, Coastal and Shelf Science 62*:233–251.

Lamb, A.L., G.P. Wilson, and M.J. Leng. 2006. A review of coastal palaeoclimate and relative sea-level reconstructions using $\delta^{13}C$ and C/N ratios in organic material. *Earth-Science Reviews 75*:29–57.

Lamers, L.P.M., L.L. Govers, I.C.J.M Janssen, J.J.M. Geurts, M.E.W. Van der Welle, M.M. Van Katwijk, T. Van der Heide, J.G.M. Roelofs, and A.J.P. Smolders. 2013. Sulfide as a soil-phytotoxin—A review. *Frontiers in Plant Science 4*:268.

Langley, J.A., K.L. McKee, D.R. Cahoon, J.A. Cherry, and J.P. Megonigal. 2009. Elevated CO_2 stimulates marsh elevation gain, counterbalancing sea-level rise. In *Proceedings of the National Academy of Sciences of the United States of America 106*:6182–6186. doi: 10.1073/pnas.0807695106

Le Quéré, C., R. Moriarty, R.M. Andrew, J.G. Canadell, S. Sitch, J.I. Korsbakken, P. Friedlingstein, G.P. Peters, R.J. Andres, T.A. Boden, R.A. Houghton, J.I. House, R.F. Keeling, P. Tans, A. Arneth, D.C.E. Bakker, L. Barbero, L. Bopp, J. Chang, F. Chevallier, L.P. Chini, P. Ciais, M. Fader, R.A. Feely, T. Gkritzalis, I. Harris, J. Hauck, T. Ilyina, A.K. Jain, E. Kato, V. Kitidis, K. Klein Goldewijk, C. Koven, P. Landschützer, S.K. Lauvset, N. Lefèvre, A. Lenton, I.D. Lima, N. Metzl, F. Millero, D.R. Munro, A. Murata, J.E.M.S. Nabel, S. Nakaoka, Y. Nojiri, K. O'Brien, A. Olsen, T. Ono, F.F. Pérez, B. Pfeil, D. Pierrot, B. Poulter, G. Rehder, C. Rödenbeck,

S. Saito, U. Schuster, J. Schwinger, R. Séférian, T. Steinhoff, B.D. Stocker, A.J. Sutton, T. Takahashi, B. Tilbrook, I.T. van der Laan-Luijkx, G.R. van der Werf, S. van Heuven, D. Vandemark, N. Viovy, A. Wiltshire, S. Zaehle, and N. Zeng. 2015. Global carbon budget 2015. *Earth System Science Data 7*:349–396.

Levin, L.A., D.F. Boesch, A. Covich, C. Dahm, C. Erséus, K.C. Ewel, R.T. Kneib, A. Moldenke, M.A. Palmer, P. Snelgrove, D. Strayer, and J.M. Weslawski. 2001. The function of marine critical transition zones and the importance of sediment biodiversity. *Ecosystems 4(5)*:430–451.

Liao, N. 2001. Determination of Ammonia in Brackish or Seawater by Flow Injection Analysis. QuikChem Method 31-107-06-1-B. Revised 2002. Lachat Instruments, Milwaukee, WI.

Lynch, J.C., P. Hensel, and D.R. Cahoon. 2015. The Surface Elevation Table and Marker Horizon Technique: A Protocol for Monitoring Wetland Elevation Dynamics. Natural Resource Report NPS/NCBN/NRR—2015/1078. National Park Service, Fort Collins, CO.

Mariotti, G., and S. Fagherazzi. 2010. A numerical model for the coupled long-term evolution of salt marshes and tidal flats. *Journal of Geophysical Research: Earth Surface 115(F1)*.

Mattheus, C.R., A. Rodriguez, B. McKee, and C.A. Currin. 2010. Impact of land-use change and hard structures on the evolution of fringing marsh shorelines. *Estuarine, Coastal and Shelf Science 88*:365–376.

Mcleod, E., G.L. Chmura, S. Bouillon, R. Salm, M. Björk, C.M. Duarte, C.E. Lovelock, W.H. Schlesinger, and B.R. Silliman. 2011. A blueprint for blue carbon: Toward an improved understanding of the role of vegetated coastal habitats in sequestering CO_2. *Frontiers in Ecology and the Environment 9(10)*:552–560.

Mitsch, W.J., and J.G. Gosselink. 2007. *Wetlands*. Fourth Edition. John Wiley & Sons: Hoboken, NJ. 600 pages.

Möller, I., T. Spencer, J.R. French, D.J. Leggett, and M. Dixon. 1999. Wave transformation over salt marshes: A field and numerical modelling study from north Norfolk, England. *Estuarine, Coastal and Shelf Science 49*:411–426.

Morris, J.T. 1991. Effects of nitrogen loading on wetland ecosystems with particular reference to atmospheric deposition. *Annual Review of Ecology and Systematics 22*:257–279. doi: 10.1146/annurev.es.22.110191.001353

Morris, J.T. 1984. Effects of oxygen and salinity on ammonium uptake by *Spartina alterniflora* Loisel. and *Spartina patens* (Aiton) Muhl. *Journal of Experimental Marine Biology and Ecology 78*:87–98. doi: 10.1016/0022-0981(84)90071-6

Morris, J.T., D.C. Barber, J.C. Callaway, R. Chambers, S.C. Hagen, C.S. Hopkinson, B.J. Johnson, P. Megonigal, S.C. Neubauer, T. Troxler, and C. Wigand. 2016. Contributions

of organic and inorganic matter to sediment volume and accretion in tidal wetlands at steady state. *Earth's future 4(4)*:110–121.

Morris, J.T., G.P. Shaffer, and J.A. Nyman. 2013. Brinson review: perspectives on the influence of nutrients on the sustainability of coastal wetlands. *Wetlands 33*:975–988.

Morris, J.T., J. Edwards, S. Crooks, and E. Reyes. 2012. Assessment of carbon sequestration potential in coastal wetlands. Pp. 517–531 in *Recarbonization of the Biosphere*. Springer: The Netherlands.

Morris, J.T., P.V. Sundareshwar, C.T. Nietch, B. Kjerfve, and D.R. Cahoon. 2002. responses of coastal wetlands to rising sea level. *Ecology 83*:2869–2877.

Mudd, S.M., A. D'Alpaos, and J.T. Morris. 2010. How does vegetation affect sedimentation on tidal marshes? Investigating particle capture and hydrodynamic controls on biologically mediated sedimentation. *Journal of Geophysical Research 115*:F03029. doi: 10.1029/2009JF001566

Mudd, S.M., S. Fagherazzi, J.T. Morris, and D.J. Furbish. 2004. Flow, sedimentation, and biomass production on a vegetated salt marsh in South Carolina: Toward a predictive model of marsh morphologic and ecologic evolution. *American Geophysical Union*:165–187. doi: 10.1029/CE059p0165

Mudd, S.M., S.M. Howell, and J.T. Morris. 2009. Impact of dynamic feedbacks between sedimentation, sea-level rise, and biomass production on near-surface marsh stratigraphy and carbon accumulation. *Estuarine, Coastal and Shelf Science 82*:377–389. doi: 10.1016/j.ecss.2009.01.028

Nahlik, A.M., and M.S. Fennessy. 2016. Carbon storage in U.S. wetlands. *Nature Communications 7(13835)*:1–9.

Nellemann, C., E. Corcoran, C.M. Duarte, L. Valdés, C. De Young, L. Fonseca, and G. Grimsditch. 2009. Blue Carbon: A Rapid Response Assessment. *United Nations Environment Programme, GRID-Arendal*, 80.

Neubauer, S.C. 2008. Contributions of mineral and organic components to tidal freshwater marsh accretion. *Estuarine, Coastal and Shelf Science 78*:78–88. doi: 10.1016/j.ecss.2007.11.011

Nixon, S.W., and C.A. Oviatt. 1973. Ecology of a New England salt marsh. *Ecological Monographs 43*:463–498.

Nyman, J.A., R.J. Walters, R.D. Delaune, and W.H. Patrick Jr. 2006. Marsh vertical accretion via vegetative growth. *Estuarine, Coastal and Shelf Science 69*:370–380.

Ouyang, X., and S.Y. Lee. 2014. Updated estimates of carbon accumulation rates in coastal marsh sediments. *Biogeosciences 11*:5057–5071.

Palmer, M.R., H.M. Nepf, and T.J.R. Pettersson. 2004. Observations of particle capture on a cylindrical collector. Implications for particle accumulation and removal in aquatic systems. *Limnology and Oceanography 49*:76–85.

Pawlowicz, R., B. Beardsley, and S. Lentz. 2002. Classical tidal harmonic analysis including error estimates in MATLAB using T_TIDE. *Computers and Geosciences 28*:929–937.

Pendleton, L., D.C. Donato, B.C. Murray, S. Crooks, W.A. Jenkins, S. Sifleet, C. Craft, J.W. Fourqurean, J.B. Kauffman, N. Marbà, P. Megonigal, E. Pidgeon, D. Herr, D. Gordon, and A. Baldera. 2012. Estimating global "blue carbon" emissions from conversion and degradation of vegetated coastal ecosystems. *PLoS ONE 7*(9):e43542. doi: 10.1371/journal.pone.0043542

Pennings, S.C., C.M. Clark, E.E. Cleland, S.L. Collins, L. Gough, K.L. Gross, D.G. Milchunas, and K.N. Suding. 2005. Do individual plant species show predictable responses to nitrogen addition across multiple experiments? *Oikos 110(3)*:547–555.

Reed, D.J. 1995. The response of coastal marshes to sea-level rise: survival or submergence? *Earth Surface Processes and Landforms 20*:39–48.

Reynolds, H.L., and C. D'Antonio. 1996. The ecological significance of plasticity in root weight ratio in response to nitrogen: Opinion. *Plant and Soil 185*:75–97. doi: 10.1007/BF02257566

Reynolds, J.F., and J.H.M. Thornley. 1982. A shoot:root partitioning model. *Annals of Botany 49*:585–597.

Richter, D.D., D. Markewitz, S.E. Trumbore and C.G. Wells. 1999. Rapid accumulation and turnover of soil carbon in a re-establishing forest. *Nature 400*:56–68.

Rodriguez, A.B., S.R. Fegley, J.T. Ridge, B.M. VanDusen, and N. Anderson. 2013. Contribution of aeolian sand to backbarrier marsh sedimentation. *Estuarine, Coastal and Shelf Science 117*:248–259.

RTI International. 2013. *DCERP2 Final Research Plan*. Strategic Environmental Research and Development Program (SERDP) Research Project RC-2245. RTI International, Research Triangle Park, NC.

RTI International. 2012. *DCERP1 Final Research Report*. Strategic Environmental Research and Development Program (SERDP) Research Project RC-1431. RTI International, Research Triangle Park, NC.

Smith, P., and K. Bogren. 2001. Determination of Nitrate and/or Nitrite in Brackish or Seawater by Flow Injection Analysis Colorimeter: QuikChem Method 31-107-04-1-E. Milwaukee, WI: Lachat Instruments:12.

Stuiver, M., and H.A. Polach. 1977. Discussion reporting of ^{14}C data. *Radiocarbon 19(3)*:355–363.

Stuiver, M., P.J. Reimer, and R.W. Reimer. 2017. CALIB 7.1. Available at http://calib.org on 2017-01-15.

Uncles, R.J., J.A. Stephens, and R.E. Smith. 2002. The dependence of estuarine turbidity on tidal intrusion length, tidal range, and residence time. *Continental Shelf Research 22*:1835–1856.

Valiela, I., and J.M. Teal. 1979. The nitrogen budget of a salt marsh ecosystem. *Nature 280(5724)*:652–656.

Vermeer, M., and S. Rahmstorf. 2009. Global sea level linked to global temperature. In *Proceedings of the National Academy of Sciences 106*(51):21527–21532.

Williams, R.B., and M.B. Murdoch. 1972. Compartmental analysis of the production of *Juncus romerianus* in a North Carolina salt marsh. *Chesapeake Science 13*:69–79.

Woerner, L.S., and C.T. Hackney. 1997. Distribution of *Juncus roemerianus* in North Carolina tidal marshes: The importance of physical and biotic variables. *Wetlands 17*(2):284–291.

Woodwell, G.M., P.H. Rich, and C.A.S. Hall. 1973. Carbon in estuaries. Pp. 221–240, volume 24 in *Carbon and the Biosphere*. Edited by Woodwell, G.M., and E.V. Pecan. U.S. Atomic Energy Commission: Springfield, VA.

Zar, J.H. 2010. *Biostatistical Analysis.* Fifth Edition. Upper Saddle River, NJ: Prentice Hall. 960 pages.

Appendix 13-A
Supporting Data

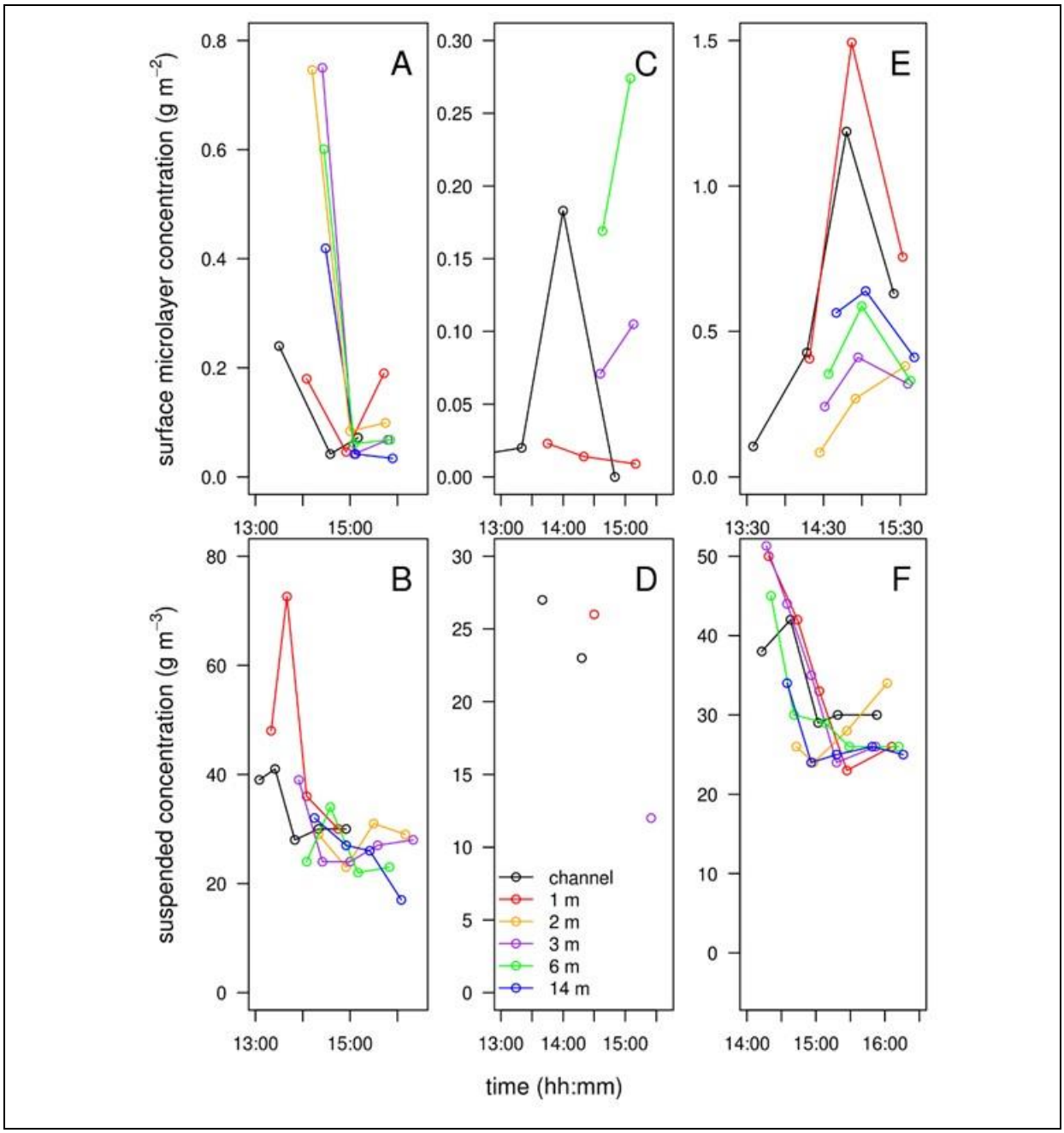

Figure 13A-1. Surface microlayer concentrations (panels A, C, and D) and suspended sediment concentrations (panels B, D, and F) at the Freeman Creek upstream site on 20 August 2014 (panels A and B), 17 December 2014 (panels C and D), and 10 August 2015 (panels E and F).

Distances shown in the legend (bottom of panel D) indicate the distance into the marsh from the channel edge.

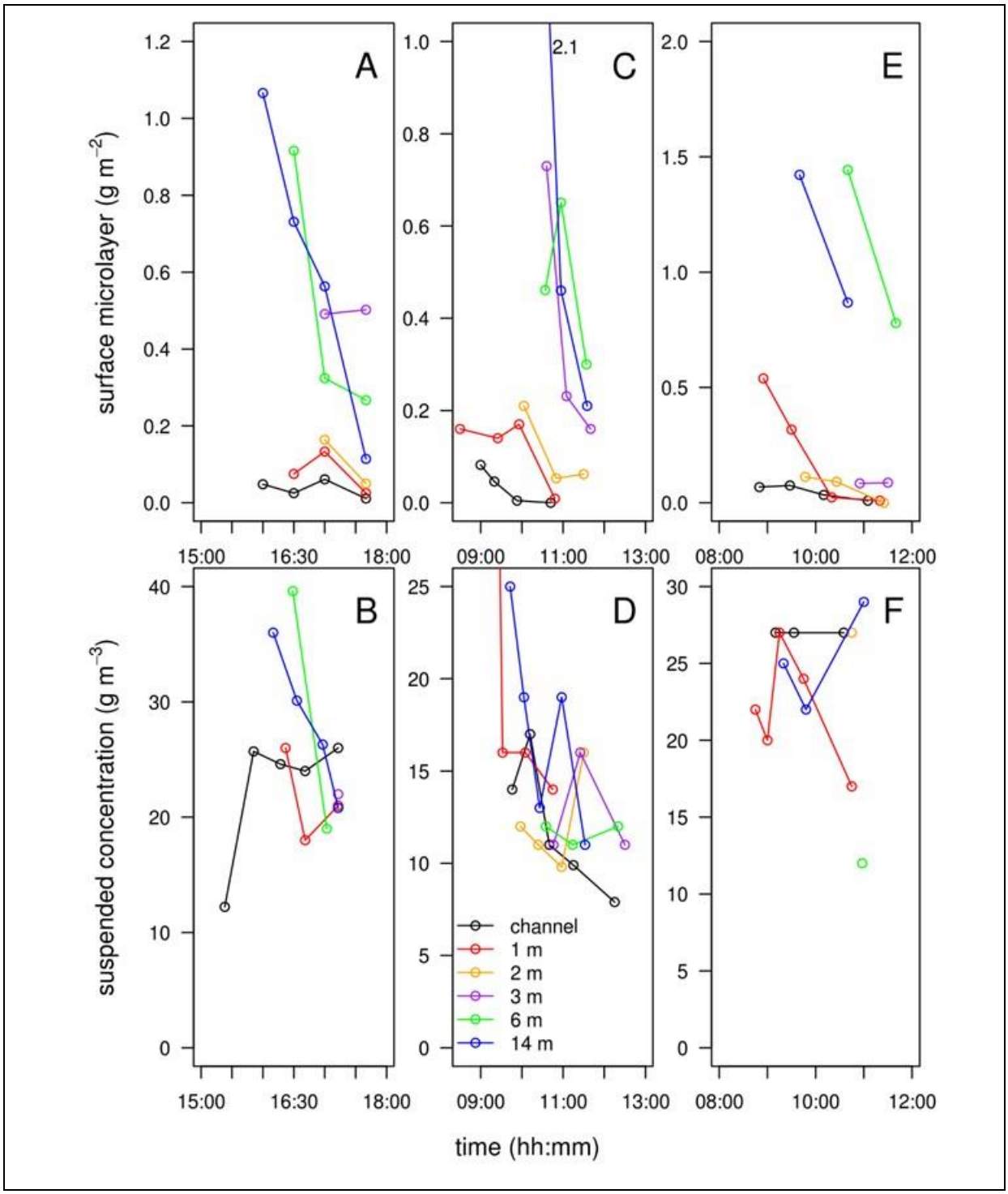

Figure 13A-2. Surface microlayer concentrations (panels A, C, and D) and suspended sediment concentrations (panels B, D, and F) at the Freeman Creek downstream site on 24 June 2014 (panels A and B), 29 October 2014 (panels C and D), and 22 April 2015 (panels E and F).

Distances shown in the legend indicate the distance into the marsh from the channel edge.

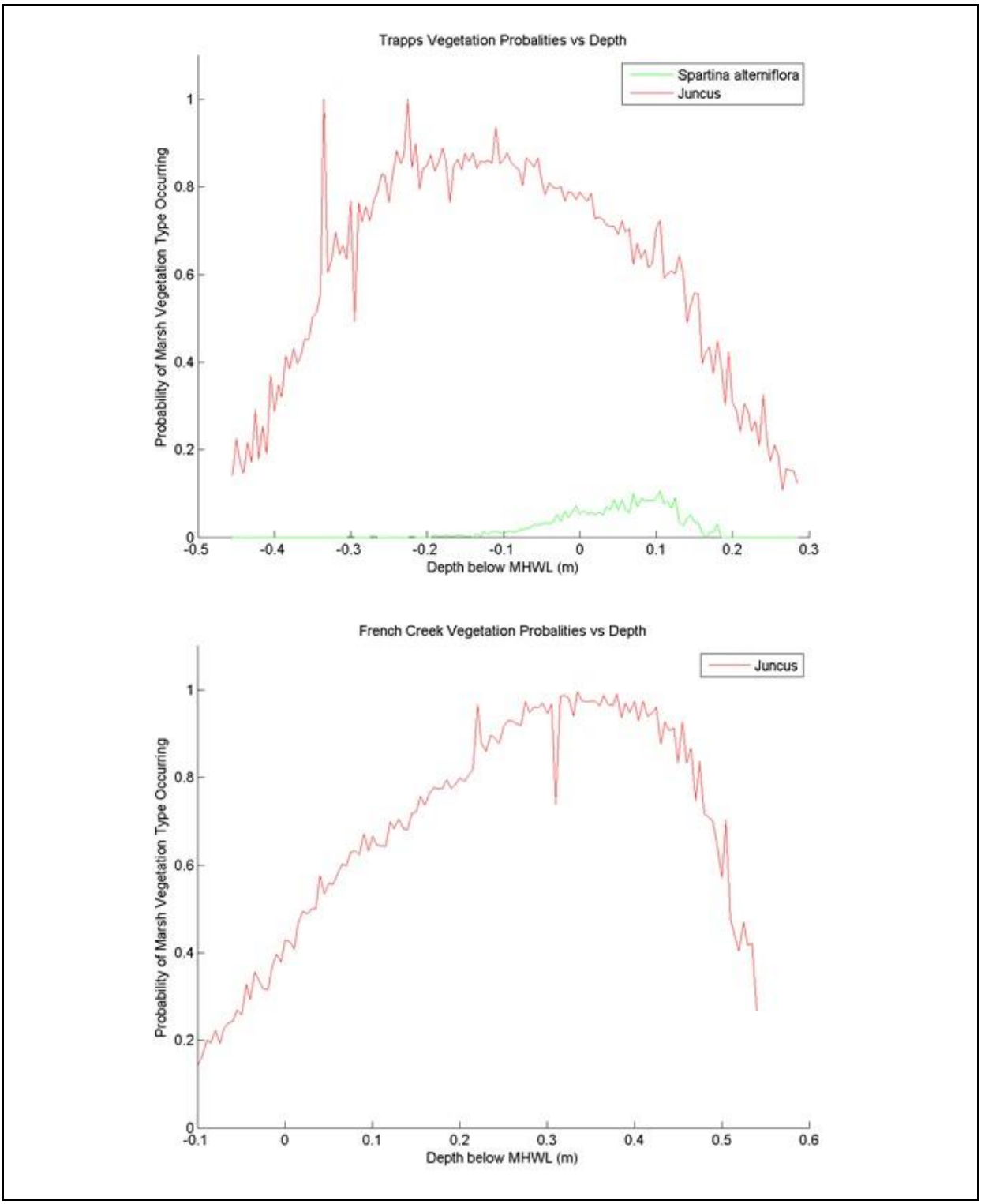

Figure 13A-3. Plots of the probability distribution function for vegetation types extracted from the Digital Elevation Model by using the habitat classification at Traps Bay Creek (top panel) and French Creek (bottom panel).

Appendix 13-B
List of Scientific/Technical Publications

Papers

Currin. C.A. 2017. *Adaptive Management Recommendations for Coastal Wetlands on Marine Corps Base Camp Lejeune*. July. Report prepared for Marine Corps Base Camp Lejeune. 25 pages.

Currin, C.A., J. Davis, and A. Malhotra. 2017. Response of salt marshes to wave energy provides guidance for successful living shoreline implementation. *Living Shorelines: The Science and Management of Nature-based Coastal Protection.* Edited by Bilkovic, D.M., J. Toft, M. Mitchell, and M. La Peyre. CRC Press, Taylor & Francis Group.

Davis, J., C. Currin, and J.T. Morris. 2017. Impacts of fertilization and tidal inundation on elevation change in microtidal, low relief salt marshes. *Estuaries and Coast 40*(6):16771687. doi: 10.1007/s12237-017-0251-0

Ensign, S.H., and C.A. Currin. 2017. Geomorphic implications of particle movement by water surface tension in a salt marsh. *Wetlands 37*:245–256. doi: 10.1007/s13157-016-0862-4

Ensign, S., C. Currin, M. Piehler, and C. Tobias. 2017. A method for using shoreline morphology to predict suspended sediment concentration in tidal creeks. *Geomorphology 276*:280–288.

Currin, C.A., J. David, L. Cowart, A. Malhotra, and M. Fonseca. 2015. Shoreline change in the New River Estuary, North Carolina: Rates and consequences. *Journal of Coastal Research 31*:1069–1077.

Davis, J.L., Currin, C.A., O'Brien, C. Raffenburg, and A. Davis. 2015. Living Shorelines: Coastal resilience with a blue carbon benefit. *PLoS One 10*(11):e0142595. doi: 10.1371/journal.pone.0142595

McTigue, N.D., J. Davis, A. Rodriguez, and C.A. Currin. In review. Measuring organic carbon accumulation in salt marsh sediments over the past two millennia: Insights to the climate change mitigation potential of blue carbon. *Global Biogeochemical Cycles*.

Thesis

None

Presentations

Cox, D., N.D. McTigue, and C. Currin. 2015. *Blue Carbon for How Long? Lability of Buried Salt Marsh Carbon Released via Erosion.* Presented at the American Geophysical Union's Fall Meeting, San Francisco, CA.

Currin, C. 2017. *Current Status of Coastal Marshes, Sediment Accumulation and Resilience to Sea Level Rise*. Presented at the DCERP Stakeholders' Meeting, Jacksonville, NC.

Currin, C.A. 2016. *A Longer View of Living Shorelines: Combining Habitat Conservation and Coastal Resiliency*. Presented at the University of North Carolina at Chapel Hill's Institute of Marine Sciences, Morehead City, NC.

Currin, C.A. 2016. *Climate Thresholds for Southeast Atlantic Marshes*. Presented at the National Oceanic and Atmospheric Administration's Climate Thresholds Webinar Series.

Currin, C.A. 2015. *Fringing Salt Marshes: Research to Assess Their Vulnerability, Resiliency and Adaptive Management Approaches*. Presented at the National Oceanic and Atmospheric Administration's Science Webinar Series.

Currin, C.A. 2014. *Estuarine Carbon Cycle Research on Marine Corps Base Camp Lejeune: From the River to the Barrier Island*. Presented at Restore America's Estuaries Blue Carbon Workshop, Beaufort, NC.

Currin, C.A. 2014. *Salt Marshes in an Era of Accelerated Sea Level Rise: Caught Between a Condo and the Rising Tide*. Presented at the Virginia Institute of Marine Sciences, Gloucester Point, VA.

Currin, C.A. and J. Davis. 2016. *Sustainability of Living Shorelines in a World of Rising Sea Level and Increasing Wave Energy*. Presented at Restore America's Estuaries, New Orleans, LA.

Davis, J., N. McTigue, and C. Currin 2017. *Blue Carbon Sequestration in Living Shorelines: (Lack of) Variability Across a Geographic Gradient*. Presented to the American Geophysical Union.

Davis, J.L. C. Currin, C. O'Brien, C. Raffenberg, and A. Davis. 2016. *The Blue Carbon Potential of Living Shorelines*. Presented as part of the National Oceanic and Atmospheric Administration's One Science Webinar Series.

Davis, J.L., N. McTigue, and C. Currin. 2015. *Production and Storage of Blue Carbon in Tidal Salt Marshes of Marine Corps Base Camp Lejeune*. Presented to the Atlantic Estuarine Research Society, Wanchese, NC.

Davis, J.L. C. Currin, C. O'Brien, C. Raffenberg, and A. Davis. 2015 *The Carbon Sequestration Potential of Living Shorelines*. Presented to the Society of Wetland Scientists, Providence, RI.

Ensign, S. 2017. *Improving Prediction of Salt Marsh Response to Sea Level Rise; New Methods and Novel Dynamics*. Presented as part of the National Oceanic and Atmospheric Administration's Science Webinar Series. January.

Ensign, S.H., and C.A. Currin. 2014. *Floating Material Is an Alternative Sediment Source for Salt Marshes*. Presented to the Southeast Estuarine Research Society, Carolina Beach, NC.

Herbert, E.R. 2017. *Marsh Maintenance: The Interactions Between Biology and Geology That Sustain Coastal Wetlands*. Presented at the Southeastern Virginia Postdoctoral Symposium, Gloucester Point, VA.

Herbert, E.R. 2016. *Eutrophication, Salinization and Sea-Level Rise: Measuring and Modeling the Effects of Multiple Stressors in Coastal Wetlands*. Presented at the Virginia Commonwealth University, Department of Biology, Richmond, VA.

Herbert, E.R. 2016. *Leveraging Monitoring Data to Improve Model Predictions for Marsh Response to Sea Level Rise*. Presented to the Governors South Atlantic Alliance (GSAA) Coastal Wetland Monitoring Workgroup, Ponte Vedra Beach, FL.

Herbert, E.R. 2016. *Modeling Tidal Marsh Resilience to Sea Level Rise: Integrating the Effects of Multiple Stressors to Inform Estuarine Management*. Presented at East Carolina University, Department of Biology, Greenville, NC.

Herbert, E.R. 2016. *Modeling Tidal Marsh Resilience to Sea-Level Rise and Human Impacts: Explicitly Representing Ecological Responses to Biogeochemical Regime Changes*. Presented at the Virginia Institute of Marine Science, Department of Physical Sciences, Gloucester Point, VA.

Herbert, E.R., D.C. Walter, and M.L. Kirwan. 2017. *Landscape Evolution of the Coastal Carbon Sink*. Presented at the Coastal and Estuarine Research Federation Annual Meeting, Providence, RI.

Herbert, E.R., C.B. Craft, and M.L. Kirwan. 2016. *Considering the Effects of Multiple Stressors When Predicting the Fate and Persistence of Blue Carbon*. Presented at the Ecological Society of America Annual Meeting, Ft. Lauderdale, FL.

Herbert, E.R., D.C. Walter, and M.L. Kirwan. 2016. *Robbing Peter to Pay Paul: Modeling the Dynamic Evolution of the Coastal Carbon Sink Across Multiple Landforms*. Presented at the American Geophysical Union Annual Meeting, San Francisco, CA.

Light, T., N.D. McTigue, and C. Currin. 2016. *Measuring the Decomposition of Organic Carbon Sequestered by Salt Marsh Sediment*. Presented at the American Geophysical Union's Fall Meeting, San Francisco, CA.

McTigue, N. 2017. *Measuring Organic Carbon Preservation in Salt Marsh Sediments over Two Millennia: Insights to the Climate Change Mitigation Potential of Blue Carbon*. Presented at the Southeastern Virginia Postdoctoral Symposium, Gloucester Point, VA.

McTigue, N.D., and C.A. Currin. 2016. *Decomposition of Semi-permanent Stored Sediment Organic Carbon from Eroding Salt Marshes*. Presented at the Association for the Sciences of Limnology and Oceanography's (ASLO's) Summer Meeting, Santa Fe, NM.

McTigue, N., Q. Walker, R. Giannelli, and C. Currin. 2017. *Revisiting the Blueprints for Blue Carbon*. Poster presented at the Ocean Carbon & Biogeochemistry Workshop, Woods Hole, MA.

McTigue, N.D., J. Davis, A.B. Rodriguez, and C.A. Currin. 2017. *Measuring Marsh Carbon Sequestration Across Time and Space: Does It Add up to Climate Mitigation?* Presented to the Coastal and Estuarine Research Federation, Providence, RI.

McTigue, N.D., J. Davis, and C. Currin. 2015. *Blue Carbon Blues: Identifying Carbon Storage and Loss Potential in Eroding Salt Marshes*. Presented to the Coastal and Estuarine Research Federation, Portland, OR.

McTigue, N.D., J. Davis, C.R. Tobias, B.A. McKee, A.B. Rodriguez, and C.A. Currin. 2016. *Measuring Organic Carbon Sequestration, Burial, and Preservation in Salt Marsh Sediments over the Past Two Millennia*. Presented at the American Geophysical Union's Fall Meeting, San Francisco, CA.

Rainville, K., J. Davis, and C. Currin. 2016. *Carbon Sequestration in Created and Natural Tidal Marshes of the Florida Panhandle*. Student poster presented at the American Geophysical Union's Fall Meeting, San Francisco, CA.

Appendix 13-C
Other Supporting Information

Currin, C. 2017. *Adaptive Management Recommendations for Coastal Wetlands on MCBCL*. Prepared for Marine Corps Base Camp Lejeune, NC. Available at dcerp.rti.org.

TNC (The Nature Conservancy). North Carolina's Living Shorelines Application. Available at http://coastalresilience.org/new-north-carolinas-living-shorelines-application

Chapter 14

Physical and Chemical Drivers of Salt Marsh Net Metabolism, Carbon Accumulation, and Responses to Fertilization

SERDP Project Number: RC-2245

Coastal Wetlands

CW-5

Lead Researchers:

Dr. Iris Anderson
Ken Czapla
Virginia Institute of Marine Science
Gloucester Point, VA
iris@vims.edu
kmczapla@vims.edu

Supporting Researchers:

Dr. Carolyn Currin, NOAA, ccurrin@noaa.gov
Dr. Craig Tobias, UCONN, craig.tobias@uconn.edu
Dr. Scott Ensign, Aquatic Analyses and Consulting, LLC, scott@aquaco.us
Jennifer Stanhope, VIMS, jwu@vims.edu

December 2017

Final

This report was prepared under contract to the U.S. Department of Defense (DoD) Strategic Environmental Research and Development Program (SERDP). The publication of this report does not indicate endorsement by DoD, nor should the contents be construed as reflecting the official policy or position of DoD. References herein to any specific commercial product, process, or service by trade name, trademark, manufacturer, or otherwise, do not necessarily constitute or imply its endorsement, recommendation, or favoring by DoD.

Table of Contents

Acronyms 14-vi
Abstract 14-1
Objectives of the Research Project 14-3
Background 14-3
Materials and Methods 14-5
Experimental Plan 14-5
Measurements 14-7
Results and Discussion 14-14
Pore Water Chemistry 14-14
Sediment Characterization 14-17
Biomass 14-20
Metabolism 14-22
NCM Measured with Static Chambers vs. an Eddy Covariance Tower 14-25
Net Ecosystem Metabolism 14-25
Greenhouse Gas Emissions 14-27
Total Carbon Accumulation at Freeman Creek Marsh 14-27
Carbon Mass Balance in Freeman Creek Marsh 14-30
Conclusions and Implications for Future Research and Implementation 14-32
Key Scientific Findings 14-32
Research Questions 14-33
Findings with Implications for Future Base Management 14-34
Literature Cited 14-35
Appendix 14-A: Influence of Salt Marshes on Nitrogen, Phosphorus, and Carbon in Tidal Creek Channels 14-A-1
Appendix 14-B: List of Scientific/Technical Publications 14-B-1
Appendix 14-C: List of Students 14-C-1

List of Figures

Figure 14-1. A map of the New River Estuary, showing the locations of two marsh sites. The darker orange area represents Marine Corps Base Camp Lejeune lands. 14-6

Figure 14-2. Plots were established by installing aluminum collars for chamber flux measurements and piezometers for pore water analysis at 5- and 15-cm depths. 14-7

Figure 14-3. A diagram of the experimental design. 14-7

Figure 14-4. Flux chamber setup, including (a) chambers, (b) Los Gatos greenhouse gas analyzer, (c) an ice water cooling system, and (d) a Campbell datalogger. 14-9

Figure 14-5. H_2S concentrations in pore water at 5 cm (top) and 15 cm (bottom) sediment depths and the three marsh sites at Marine Corps Base Camp Lejeune. 14-15

Figure 14-6. NH_4^+ concentrations in pore water at 5 cm (top) and 15 cm (bottom) sediment depths at the three marsh sites at Marine Corps Base Camp Lejeune. 14-16

Figure 14-7. Dissolved organic carbon (DOC) concentrations in pore water at 5 cm (top) and 15 cm (bottom) sediment depths at the three marsh sites at Marine Corps Base Camp Lejeune. 14-17

Figure 14-8. Dissolved inorganic carbon (DIC) concentrations in pore water at 5 cm (top) and 15 cm (bottom) sediment depths at the three marsh sites at Marine Corps Base Camp Lejeune. 14-18

Figure 14-9. Percent sediment organic matter at 0- to 2-cm (top) and 2- to 5-cm depths at the three marsh sites at Marine Corps Base Camp Lejeune. 14-19

Figure 14-10. Bulk density of sediment at 0- to 2-cm and 2- to 5-cm integrated depths at the three marsh sites at Marine Corps Base Camp Lejeune. 14-20

Figure 14-11. Above-ground biomass of S. alterniflora at the three marsh sites at Marine Corps Base Camp Lejeune. 14-21

Figure 14-12. Above-ground biomass (AGB) versus below-ground biomass (BGB; top) and root:shoot ratio (bottom) observed in fall 2016 at three marsh sites at Marine Corps Base Camp Lejeune. 14-22

Figure 14-13. Annual GPP and respiration (R) rates for the three marsh sites at Marine Corps Base Camp Lejeune. 14-23

Figure 14-14. Seasonal net community metabolism. Positive values represent net heterotrophy and CO_2 emissions. Negative values represent net autotrophy and CO_2 uptake for the three marsh sites at Marine Corps Base Camp Lejeune. 14-24

Figure 14-15. Net community metabolism extrapolated to annual scale. Positive values represent net heterotrophy and CO_2 emissions. Negative values represent

net autotrophy and CO_2 uptake **at three marsh sites** at Marine Corps Base Camp Lejeune. 14-24

Figure 14-16. Comparison of net CO_2 exchange at Freeman Creek measured with a static chamber system and with an eddy covariance tower from July 9 through 30, 2016. 14-25

Figure 14-17. Spatial analysis of Freeman Creek performed with ArcGIS showing tall-form S. alterniflora marsh (yellow), short-form S. alterniflora marsh (green), and S. alterniflora marsh within 5 m of creek bank (red). 14-26

Figure 14-18. Daily CH_4 fluxes at three marsh sites at Marine Corps Base Camp Lejeune. 14-27

Figure 14-19. Comparison of carbon (C) fluxes and total short-term C accumulation for each treatment. 14-29

Figure 14-20. Mass balance carbon (C) budget in Freeman Creek marsh to estimate net carbon accumulation. 14-31

Figure 14-21. Mass balance carbon (C) budget in Freeman Creek marsh with fertilization. 14-31

List of Tables

Table 14-1. Sampling Events and Measurements 14-13

Table 14-2. Methodology of Research Project CW-5. 14-13

Table 14-3. Freeman Creek NEM (10^5 kg C/year) Estimates Compared with and without Considering Edge Differences for Both Control and Fertilized Scenarios 14-26

Table 14-4. Annual Tidal, Groundwater, and Total Carbon Export for DIC, DOC, and Total Dissolved Carbon (mol m^{-2} $year^{-1}$) at Freeman Creek 14-28

Table 14-5. Sediment Carbon Input Rates (mol C m^{-2} yr^{-1}) 14-29

Acronyms

%OM	percent organic matter
°C	degree Celsius
°F	degree Fahrenheit
µE m^{-2} s^{-1}	microEinsteins per square meter per second
µL	microliter
µm	micrometer
µM	micromolar
µmol L^{-1} hr^{-1}	micromoles per liter per hour
µmol CH_4 m^{-2} day^{-1}	micromoles of methane per square meter per day
AGB	above-ground biomass
ANOVA	analysis of variance
BGB	below-ground biomass
C	carbon
CH_4	methane
cm	centimeter
cm/yr	centimeter per year
CO_2	carbon dioxide
CW	Coastal Wetlands (Module)
DIC	dissolved inorganic carbon
DOC	dissolved organic carbon
DoD	U.S. Department of Defense
FC	Freeman Creek
g cm^{-3}	grams per cubic centimeter
g m^{-2}	grams per square meter
GHG	greenhouse gas
GGA	greenhouse gas analyzer
GPP	gross primary production
H_2S	hydrogen sulfide
H_2SO_4	sulfuric acid
ha	hectare
$HgCl_2$	mercuric chloride
ICW	Intracoastal Waterway
kg C/year	kilograms of carbon per year
km^2	square kilometer
L	liter
m	meter
m^2	square meter
mL	milliliter
mm	millimeter
mM hr^{-1}	millimoles per hour
mm/year	millimeters per year
mmol L^{-1} hr^{-1}	millimoles per liter per hour
mmol m^{-2} hr^{-1}	millimoles per square meter per hour
mol	mole

mol C m^{-2} yr^{-1}	moles of carbon per square meter per year
mol CO2 m^{-2} hr^{-1}	moles of carbon dioxide per square meter per hour
mol m^{-2}	moles per square meter
mol m^{-2} $year^{-1}$	moles per square meter per year
N_2O	nitrous oxide
NaOH	sodium hydroxide
NAVD 88	North American Vertical Datum of 1988
NCM	net community metabolism
NEM	net ecosystem metabolism
NH_4^+	ammonium
NH_4NO_3	ammonium nitrate
NO_2^-	nitrite
NO_3^-	nitrate
NOAA	National Oceanic and Atmospheric Administration
NRE	New River Estuary
OM	organic matter
oz.	ounce
P_2O_5	phosphorus pentoxide
PAR	photosynthetic active radiation
P-I	photosynthesis–irradiance
PO_4^{3-}	phosphate
R	respiration
RC	Resource Conservation and Climate Change (a SERDP program area)
SE	standard error
SERDP	Strategic Environmental Research and Development Program
TBC	Traps Bay Creek
TOC	total organic carbon
UCONN	University of Connecticut
V	volt
VIMS	Virginia Institute of Marine Science

Abstract

Salt marshes are thought to have high carbon sequestration rates and store a globally significant pool of carbon. However, carbon sequestration rates vary in response to factors such as marsh elevation within the tidal framework, tidal amplitude, pore water residence time, sediment carbon inputs, dominant plant species and their above-ground biomass, distance from creek, and anthropogenic nitrogen loading. Tidal flushing and pore water residence time influence the delivery of sediment carbon and the accumulation of dissolved pore water compounds such as ammonium (NH_4^+) and hydrogen sulfide (H_2S), known to impact carbon cycling. Whereas anthropogenic nitrogen loading to marshes may increase above-ground biomass and rates of sediment carbon trapping, it may also increase net heterotrophy by stimulating plant and microbial respiration.

The primary objectives of Research Project CW-5 were to determine the following in fertilized and unfertilized *Spartina alterniflora* marshes: (1) atmosphere–marsh exchanges of carbon dioxide (CO_2) and methane (CH_4), (2) lateral exchanges of dissolved inorganic carbon (DIC) and dissolved organic carbon (DOC) between both the marsh surface and subsurface and adjacent creeks, (3) sediment carbon input to the marsh surface, and (4) total marsh carbon accumulation or loss. The technical approach included fertilization manipulations in *Spartina alterniflora* marsh sites differing in tidal amplitude, elevation, pore water residence time, and distance from the creek edge. Measurements were made seasonally for a year in triplicate unfertilized and fertilized plots across three different marsh locations: Freeman Creek marsh edge and interior, both with shorter pore water residence times and higher tidal amplitude, and Traps Bay Creek interior, with longer pore water residence time and lower tidal amplitude. Pore water H_2S, NH_4^+, DIC and DOC were measured at 5- and 15-cm depths within each site. Respiration, gross primary production, and net community metabolism were calculated based on net CO_2 exchanges measured in static chambers. Sediment carbon input was quantified based on Marker Horizon data and a predictive model. For determination of lateral carbon export, DIC and DOC were measured in overlying water and the creek at flood tide and in groundwater wells at the edge of the marshes. Results demonstrated that marsh location and pore water residence time influenced all pore water analytes with lower concentrations at the marsh edge than interior and higher concentrations at Traps Bay Creek than Freeman Creek. In addition, Freeman Creek was net heterotrophic in both edge and interior, but Traps Bay Creek was net autotrophic. Fertilization increased net heterotrophy in Freeman Creek, particularly on the edge, and decreased net autotrophy in Traps Bay Creek. Sediment deposition was an important source of organic carbon in Freeman Creek and Traps Bay interior marshes, but not in the Freeman Creek edge marsh, which had a high berm and a short inundation time. Lateral export of DIC and DOC to the creek was comparable to sediment carbon input plus net community metabolism in the interior, but not in the edge marshes at Freeman Creek. We concluded the following: (1) location is an important driver in determining pore water chemistry and resulting carbon accumulation potential of salt marshes; (2) fertilization increased net heterotrophy at Freeman Creek and decreased net autotrophy at Traps Bay Creek, thereby decreasing their potential to accumulate carbon through autochthonous processes; and (3) sediment input is vital to carbon accumulation and sustainability in net heterotrophic marshes such as Freeman Creek. This study provides benefits to the scientific and management communities by identifying the factors impacting salt marsh carbon accumulation or loss. The loss of carbon was greatest in marshes with short pore

water residence times, in locations at the creek edge, and in response to fertilization. Loss of carbon in net heterotrophic marshes may be mitigated by sediment organic carbon inputs. Thus, it is imperative to maintain sediment supply and low levels of nitrogen to sustain salt marshes.

Keywords: Carbon accumulation, carbon dioxide exchanges, fertilization, hydrogen sulfide, net community metabolism, net ecosystem metabolism, methane emission, nitrogen uptake, sediment accretion, *Spartina alterniflora*

Objectives of the Research Project

There are four primary objectives of Research Project CW-5. The first objective is to determine the seasonal and annual exchanges of carbon dioxide (CO_2) and methane (CH_4) between *Spartina alterniflora* marshes and the atmosphere in marshes of different elevations in the tidal framework, exposure to tides of different amplitudes, creek proximities, and nitrogen availability. The other three objectives are to determine lateral exchanges of dissolved inorganic carbon (DIC) and dissolved organic carbon (DOC), sediment carbon input, and total marsh carbon accumulation by using a mass balance approach. Because each of these processes may depend upon physical parameters, which vary with location, they will be examined in three different marsh locations: the edges and interiors of Freeman Creek marsh and Traps Bay Creek marsh. Traps Bay Creek, which is higher in the tidal framework than the edge and interior Freeman Creek sites, may behave more similar to a high marsh site (Currin, personal communication). Locational differences in fertilization effects are particularly important because increasing nitrogen loading is primarily anthropogenic on the East Coast of the United States and because understanding the effects it will have on different marshes within the same coastal system may lead to broader management applications for water quality management and salt marsh preservation.

Background

Salt marshes are an important component of the coastal North Carolina landscape, not only for the characteristic aesthetics on the coast, but also for their valuable ecosystem services. One crucial service that they provide is the accumulation of carbon into a globally significant carbon pool, potentially helping to buffer climate change (Duarte et al., 2005). Carbon accumulation rates may easily be overestimated (Wang et al., 2017) because the spatial heterogeneity that results from the physical characteristics of a location such as elevation, tidal amplitude, sediment flushing rate, and inundation time, is poorly understood. Human impacts at short time scales, such as nitrogen loading and change in sediment supply, may alter rates of carbon accumulation, potentially destabilizing salt marshes and accelerating the release of stored carbon into the atmosphere and adjacent tidal water. Increased storm activity and sea level rise resulting from climate change will further exacerbate responses to short time scale disturbances. Understanding the relationship between physical characteristics of the marsh location, pore water chemistry, and rates of carbon cycling processes may improve carbon budget assessments within a system and identify which marsh locations may be most sensitive to carbon loss because of human impacts.

Anoxic marsh sediments are prime locations for microbial carbon cycling, in part because of the high productivity of marsh grass species and abundance of organic matter (OM), which plays the role of electron donor in a variety of microbially mediated redox reactions, including aerobic, sulfate, and nitrate respiration. Sulfate reduction is primarily responsible for anaerobic respiration in salt marshes (Howarth and Giblin, 1983; Howes et al., 1984). CO_2, a highly soluble gas present in water as DIC, is a major product of both aerobic and anaerobic respiration, but may be taken up by the photosynthesis of *Spartina alterniflora*, benthic microalgae, and other autotrophs. The balance between gross primary production (GPP) and respiration (R) determines whether a marsh is net heterotrophic and a source of CO_2 into the atmosphere, or is net autotrophic and a sink for CO_2 from the atmosphere. CH_4 may also be produced through methanogenesis, but this process is thought to be largely suppressed by the presence of sulfate in

salt marsh sediments, typically causing relatively low CH_4 emissions in salt marshes (Poffenbarger et al., 2011). Stems of *Spartina alterniflora* may help transport CH_4 into the atmosphere by acting as a conduit through the zone of CH_4 oxidation in the sediments (Neubauer et al., 2005; Tong et al., 2012). Over 100 years, CH_4 has 45 times the sustained flux heat trapping capacity of CO_2 (Neubauer et al., 2015).

Pore water chemistry affects carbon cycling rates; the concentration of particular chemical components of pore water are likely to vary with physical characteristics of the salt marsh location. NH_4^+, the product of organic matter mineralization and dissimilatory nitrate reduction to NH_4^+, supports growth of *S. alterniflora* and may be oxidized by sediment microorganisms to nitrate (nitrification). The typically high concentrations of sulfide produced by sulfate reduction in salt marshes inhibits nitrification (Joye and Holibaugh, 1995), NO_3^- reduction by denitrification (Burgin and Hamilton, 2007), and uptake of NH_4^+ by *S. alterniflora* (Bradley and Morris, 1990). Thus, high concentrations of H_2S may impact carbon cycling by inhibiting plant growth and nitrate metabolism. DOC, a product of primary production or dissolution of particulate organic carbon, may vary in lability as a substrate for decomposition. *S. alterniflora* root exudates may be a source of particularly labile DOC (Zhang et al., 2013), which may rapidly decompose to DIC by sediment microbial respiration. Concentrations of these substrates in pore water may be affected by pore water flushing and residence time, redox conditions, transformation rates, oxygen exposure, and plant productivity. Marsh locations with proximity to tidal creeks may experience higher rates of pore water flushing and greater exposure to electron acceptors such as oxygen, nitrate, and sulfate in the tidal water, and thus are likely to be chemically distinct sub-habitats within salt marshes. *S. alterniflora* above-ground biomass and productivity are also dependent on elevation of the marsh within the tidal framework. As elevation decreases relative to mean sea level, productivity increases to a maximum threshold after which it begins to decrease with decreasing elevation (Morris et al., 2002). *S. alterniflora* may influence pore water chemistry by releasing oxygen, a product of photosynthesis, into the rhizosphere, potentially enhancing both aerobic metabolism and NO_3^- metabolism by fueling coupled nitrification–denitrification (Koop-Jakobsen and Giblin, 2010).

Salt marshes are vulnerable to high rates of sea level rise; however, eco-geomorphic feedbacks caused by the relationship between accretion rates, above-ground biomass, and rate of sea level rise allow many salt marshes to maintain elevation above sea level at sea level rise rates up to 50 mm/year, provided an ample supply of suspended sediment is available (Kirwan et al., 2016). Accretion may occur through below-ground expansion by autochthonous productivity or above ground by allochthonous sediment deposition, which depends upon physical and biological factors such as above-ground biomass, tidal amplitude, concentration of suspended sediments, and marsh platform elevation (Friedrichs and Perry, 2001). Because the above-ground stems of *S. alterniflora* inhibit tidal water velocity, causing suspended sediments to settle on the marsh surface, greater *Spartina* above-ground biomass has been observed to correlate with greater marsh sediment accretion (Morris et al., 2002). As sea level rises, longer inundation periods and increasing above-ground biomass cause greater deposition rates. The National Oceanic and Atmospheric Administration (Zervas, 2004) estimated that at Beaufort, NC, mean sea level rise over the 18-year period (i.e., 1983–2001) was 3.2 mm per year; however, mean sea level rise was 14 mm per year (Currin, unpublished data) during the most recent 8-year period. Because suspended sediments often have a high OM composition, they not only allow marshes to keep up with sea level rise, but may contribute a significant proportion of a salt marsh's total carbon

accumulation rate. However, accretion may be impacted by high rates of decomposition, thereby causing loss of carbon from both autochthonous production and deposited sediments.

The East Coast of the United States is a hot spot of increasing anthropogenic nitrogen loading (Scavia and Bricker, 2006). In North Carolina, hog farming and other agriculture, urbanization, and wastewater are major sources of nitrogen to estuaries, thereby causing increased nitrogen input to North Carolina's valuable coastal wetlands. The New River Estuary (NRE) and many other estuaries and smaller tidal creeks along North Carolina's coast are estimated to host approximately 60,000 ha of salt marsh, composing 11% of the total salt marsh area on the East Coast of the United States (Wiegert and Freeman, 1990). Although salt marsh sediments are known to improve water quality by removing nitrogen from adjacent waters (Nelson and Zavaleta, 2012), excess nitrogen removal may be accompanied by an increase in the emissions of carbon into the atmosphere. A 40-year history of salt marsh fertilization experiments aiming to determine the effects of increasing nitrogen availability (Valiela, 2015) has led to controversy and mixed conclusions. Some studies (Morris et al., 2013) conclude that fertilization leads to increased above-ground production and accretion rates; thus, it has recently been proposed as a sea-level rise management strategy (Davis et al., 2017). However, other studies (Darby and Turner, 2008; Deegan et al., 2012; Morris and Bradley, 1999) conclude that fertilization causes decreased below-ground biomass and increased microbial respiration, leading to marsh destabilization, carbon loss, and extreme erosion events. One explanation for these ostensibly conflicting results may be differences in the physical factors specific to the location where the experiments were conducted and which may drive different fertilization responses. If this hypothesis is true, then identifying locations where fertilization is likely to result in net positive effects while preventing marsh collapse would be valuable information for salt marsh conservation.

Materials and Methods

Experimental Plan

Sites: Experiments were conducted at two high salinity *Spartina alterniflora* sites: Freeman Creek and Traps Bay Creek (**Figure 14-1**). Freeman Creek is a marsh-dominated tidal creek that discharges into the Intracoastal Waterway (ICW). Traps Bay Creek contains a small fringing marsh and discharges directly into an embayment within the NRE. The Freeman Creek interior site, with an average elevation of −0.04 m, was lower in the tidal framework than the Traps Bay Creek site, with an average elevation of 0.08 m. However, the Freeman Creek edge site was higher in elevation (0.21 m) because there is a berm, a geomorphological characteristic resulting from faster rates of sediment accretion along the edge (elevations in North American Vertical Datum of 1988 [NAVD 88] datum, based on surface elevation table data). Tidal range averaged 0.83 m at Freeman Creek and 0.57 m at Traps Bay Creek (Ensign et al., 2017) and salinities ranged from 32–35 at Freeman Creek and from 25–32 at Traps Bay Creek.

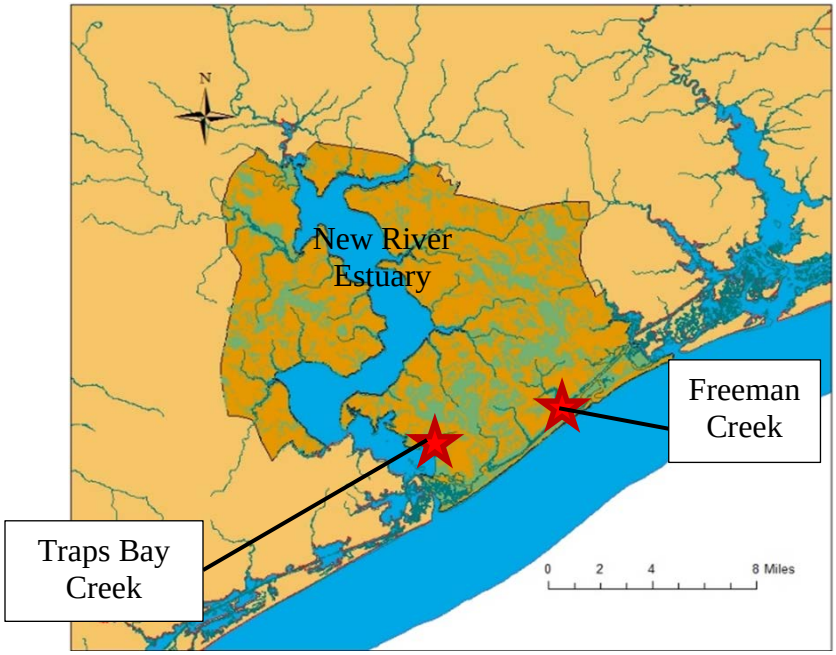

Figure 14-1. A map of the New River Estuary, showing the locations of two marsh sites. The darker orange area represents Marine Corps Base Camp Lejeune lands.

Experimental Design: Three pairs of plots (**Figure 14-2**), one control and one fertilized, were established within each of three locations: Freeman Creek edge, Freeman Creek interior, and Traps Bay Creek interior (**Figure 14-3**). Plot locations were selected based on representative plant communities, proximity to established boardwalks, and locations of previously established plots. Fertilized plots received 30 mol of nitrogen per year as ammonium nitrate (NH_4NO_3) and 15 mol of phosphorus per year as P_2O_5. Fertilizer was broadcast onto the marsh surface once per season, approximately one month before seasonal samplings described in **Table 14-1.** The control-fertilized plot pairs improved the detection of statistical differences despite significant random spatial heterogeneity within the marsh. Aluminum collars, 0.9 m × 0.9 m with drainage holes flush with the marsh surface, were positioned within each plot for measuring gas fluxes, with 0.9 m × 0.5 m side plots outside the collars for coring, making the total plot size 1.4 m × 0.9 m. A minimum distance of 1 m was maintained between plot pairs to avoid fertilizer effects within control plots. Sites were sampled once per season from summer 2015 to summer 2016, with a sampling in fall 2016 for end-of-experiment measurements (**Table 14-1**).

Figure 14-2. Plots were established by installing aluminum collars for chamber flux measurements and piezometers for pore water analysis at 5- and 15-cm depths.

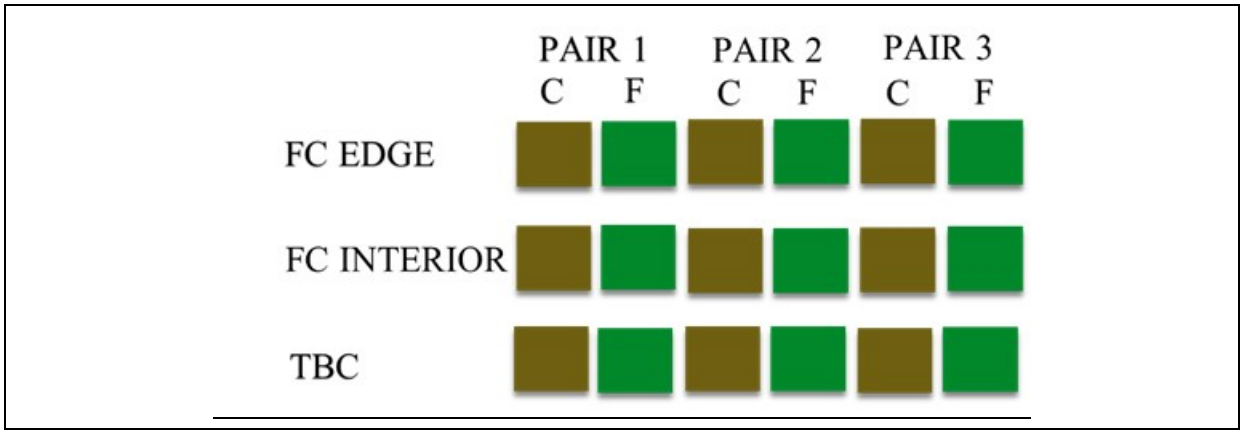

Figure 14-3. A diagram of the experimental design.

C=control plots (shaded brown); F=fertilized plots (shaded green); FC=Freeman Creek; TBC=Traps Bay Creek.

Measurements

Measurements are summarized in Table 14-2.

Pore Water Chemistry

Two piezometers, as described by Neubauer and Anderson (2003), were installed permanently in each plot to seasonally collect pore water at 5- and 15-cm sediment depths. Before sampling, the piezometers were pumped to remove water, flushed with nitrogen gas to prevent oxidation of reduced compounds, and allowed to refill with pore water. Samples collected by syringe were analyzed for concentrations of several analytes, which are discussed in the remainder of this section.

H_2S: To obtain this measurement, 3.0 mL of pore water were injected through a 0.45 µm polyethersulfone filter (Whatman) into 5.0 mL of 0.01 M zinc acetate solution, carefully

avoiding bubbles or exposure to the atmosphere. Samples were analyzed on a spectrophotometer by using Cline's reagent (Cline, 1969).

Dissolved Inorganic Carbon (DIC): To obtain this measurement, 8-mL Hungate tubes (Bellco Glass), pre-spiked with 8.0 µL of saturated mercuric chloride ($HgCl_2$), were filled and capped without headspace, and then stored refrigerated, upside-down in a container of deionized water. These samples were analyzed within 30 days by using an infrared gas analyzer (Li-Cor 6252) as described by Neubauer and Anderson (2003). Samples were injected into 0.05 M of sulfuric acid (H_2SO_4), continuously sparged with CO_2–free N_2 to convert all DIC to CO_2 gas.

Dissolved Nutrients (Ammonium [NH_4^+], Nitrite [NO_2^-], and Phosphate [PO_4^{3-}]): Pore water was immediately filtered through a 0.45-µm Whatman polyethersulfone filter into a 2-oz. Whirlpak bag, stored on ice in the field, and frozen within 12 hours of sampling. Samples were pre-processed before analysis to remove H_2S by acidifying to a pH less than 3 with sulfuric acid, sparging for 8 minutes with argon gas, and neutralizing to a pH between 6 and 7 with sodium hydroxide (NaOH). Samples were filtered or centrifuged after this process to remove precipitates, and then were analyzed on a Lachat QuikChem autoanalyzer.

DOC: Pore water was immediately filtered through a 0.45-µm Whatman filter into a pre-combusted 10-mL scintillation vial. Samples were analyzed by using a Shimadzu total organic carbon (TOC) analyzer.

Sediment Characterization

To characterize sediment, 5-cm deep sediment cores (2.2-cm in diameter) were taken from the area of the plot outside the gas flux collars. Cores were kept on ice, sectioned at 0- to 2-cm and 2- to 5-cm depths, and dried at 50°C for 2 to 3 weeks. Bulk density was assessed by weighing the dry mass of core sections and dividing by the core section volume. Percent organic content was measured by combusting the dried core sections in a muffle furnace at 500°C for 5 hours and determining the percent loss of mass after combustion.

Above-ground Biomass

During each season, stem density was estimated by counting the number of stems inside a 0.25 m^2 quadrat. The heights of the first 10 stems along a transect across the plot were measured, and the algorithm shown as Equation 1 was used to convert stem height to biomass (Davis et al., 2017):

$$\text{Average stem mass (g)} = (0.03467 \times H) - (0.000903 \times H^2) + (0.0000142 \times H^3) \qquad \text{(Eq. 1)}$$

Where

H = Stem height (in cm).

The average of the 10 stem masses was multiplied by the stem density to calculate biomass per square meter.

Below-ground Biomass

At the end of the experiment, 6.4-cm diameter cores were taken to a depth of 20 cm and passed through a 1-mm sieve to recover root biomass. Biomass was dried for 2 to 3 weeks at 50°C, weighed, and then divided by core surface area to determine grams of biomass per square meter.

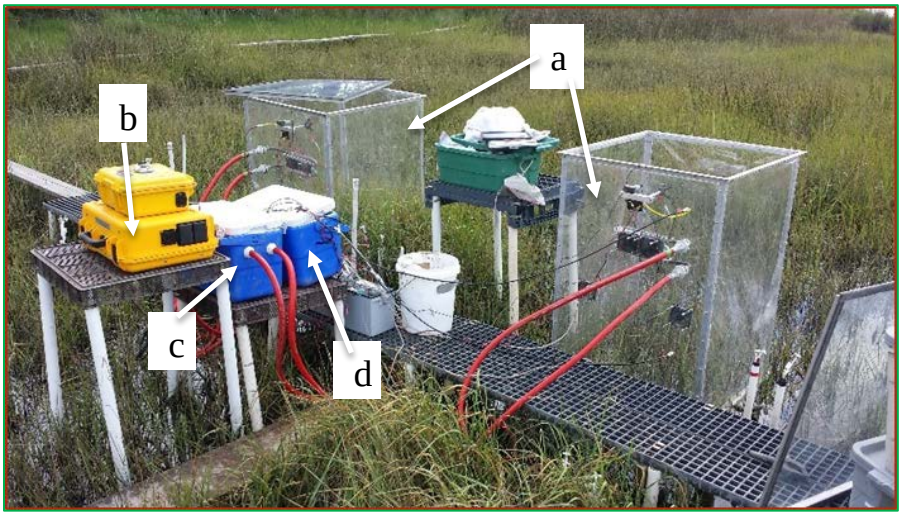

Figure 14-4. Flux chamber setup, including (a) chambers, (b) Los Gatos greenhouse gas analyzer, (c) an ice water cooling system, and (d) a Campbell datalogger.

CO_2 Flux

Fluxes of CO_2 were measured *in situ* by using static chambers (**Figure 14-4**, Miller et al., 2001; Neubauer et al., 2000) placed on a 0.9-m × 0.9-m aluminum collar installed permanently within each plot 3 months before the first sampling. The 1.5-m tall chambers were constructed of an aluminum frame covered with transparent 4-mil thick HydroBlock P-series TR film (Honeywell) on three vertical sides, and a hard transparent 1/8-inch thick Lexan composed one vertical side and lids. Each chamber container four 3.62-inch equipment-cooling fans powered by a 12-V battery for gas circulation. Foam rubber weather stripping was glued to the bottoms of the chambers and lids to create a seal when placed on the collars. Chambers were equipped with ice-water cooling systems as described by Neubauer et al. (2000) to keep chambers within 2°C of ambient temperatures. Air from the chambers were pumped through 1/4-inch Bev-A-Line XX tubing with AP Series Micro Air Pumps, Model 40 (Sensidyne Inc.) to a Los Gatos ultra-portable greenhouse gas analyzer (GGA), which recorded CO_2 and CH_4 concentrations every 2 seconds. Ambient photosynthetic active radiation (PAR), internal chamber PAR, ambient temperature, internal chamber temperature, and sediment temperature at 5-cm depth, were recorded every 15 seconds during flux measurements by using a Campbell CR1000 datalogger, thermocouple wire, and Li-Cor 190R Quantum sensors. Control and fertilized plot pairs were measured simultaneously by automating two, four-way Humphrey solenoid valves to switch the gas sample read by the GGA between two chambers every 45 seconds. The ice-water cooling system and solenoid valves were controlled by an A6REL-12 six-channel relay driver wired into the Campbell datalogger, powered by a 12-V battery. Drainage holes in collars were plugged with rubber stoppers before collecting flux measurements. Fluxes were measured between 10 a.m. and 3 p.m. during times when the marsh platform was not inundated with tidal water. Each

measurement consisted of four light treatments created by manipulating light exposure with chamber covers: 0% PAR (covered by a Mylar space blanket), 25% PAR (covered by two Phifer Pool and Patio charcoal fiberglass wire screens), 50% PAR (covered by one screen), and 100% PAR (no cover). Each light treatment was run for 7 to 10 minutes.

Respiration

Respiration was defined as the emission of CO_2 measured in the 0% PAR light treatment. Respiration rates were extrapolated to their respective seasons by using daily average sediment temperatures and an experimentally determined Q_{10} of 2.59. Q_{10} was determined by measuring CO_2 production in three interior marsh cores from Freeman Creek and three marsh cores from Traps Bay Creek held in the dark at 15°C and 25°C. Equation 2 was used to model hourly rates of respiration (R) throughout each respective season based on temperature:

$$R=R_i \times Q_{10}^{(\Delta T/10)} \qquad \text{(Eq. 2)}$$

Where

R_i = Respiration measured in the field (mmol m^{-2} hr^{-1})
ΔT = Hourly average change in temperature (°C) from ambient field temperature
R = Hourly respiration adjusted for hourly average temperature (mmol m^{-2} hr^{-1}).

Q_{10} results for all six cores were averaged because there was no significant difference between sites (Q_{10}=2.59, standard error [SE]=0.09). Seasonal and annual respiration were derived from totals of hourly respiration.

Gross Primary Production: Flux rates were calculated for each of the four light treatments. Respiration (0% PAR treatment) was subtracted from each flux, and photosynthesis–irradiance (P-I) curves were constructed with the formula (Jassby and Platt, 1976), as shown in Equation 3:

$$GPP=P_{max} \times \alpha \times \tanh(I/P_{max}) \qquad \text{(Eq. 3)}$$

Where

P_{max} = Maximum productivity (mmol m^{-2} hr^{-1})
α = Initial slope of photosynthesis versus irradiance
tanh = Hyperbolic tangent function
I = PAR (µE m^{-2} s^{-1}).

The phytotools package in the statistical software R (Silsbe and Malkin, 2015) was used to determine best fits for P-I curves. These curves were used to model hourly GPP throughout each respective season by using hourly averaged PAR data from a CRONOS weather station at the Pamlico Aquaculture Field Laboratory in Aurora, NC (for more information, see https://climate.ncsu.edu/cronos/?station=AURO) to model hourly GPP throughout each respective season. Seasonal and annual GPP were derived from totals of hourly GPP.

Net Community Metabolism

Net community metabolism (NCM) was defined as the difference between respiration and GPP and was calculated for every hour modeled throughout the year (positive NCM represents net CO_2 emission, and negative NCM represents net CO_2 uptake). Hourly NCM was totaled to calculate seasonal and annual NCMs. To examine the effects of inundation on net CO_2 exchanges, the timing of Freeman Creek inundation and exposure was mapped through the sampling seasons by using the water level indicated by the NOAA tidal gauge (Station ID 8656483) at Beaufort, NC (determined to be nearly identical in timing and amplitude compared to HOBO marsh water level loggers installed during Research Project CW-4 in Freeman Creek) and average elevations for each marsh location. All elevation calculations were determined based on the NAVD 88 datum. Inundated versus exposed marsh data from the eddy covariance tower at Freeman Creek marsh were compared with chamber flux extrapolations to determine the effects of inundation on CO_2 flux. A correction derived from this comparison was applied to times when the marsh was inundated.

Net Ecosystem Metabolism:

Net ecosystem metabolism (NEM), calculated for Freeman Creek only, is defined here as NCM (mol m^{-2} yr^{-1}) scaled to the entire Freeman Creek marsh area. ArcGIS was used to determine total Freeman Creek *S. alterniflora* marsh area and total edge marsh area, defined as marsh within 5 m of the tidal creek (corresponding approximately to the width of the high-elevation berm). The edge and interior NCMs were extrapolated to their respective total areas, and the interior and edge NEMs were totaled to determine the total annual NEM at Freeman Creek. Calculations were made for both control and fertilized conditions.

Greenhouse Gas Emissions

CH_4 and nitrous oxide (N_2O) exchanges were measured simultaneously with CO_2 exchanges in static chambers. CH_4 concentrations were analyzed using a Los Gatos GGA, and N_2O was manually sampled through septa in t-fittings connecting the tubing that pumps chamber air into the GGA. Thirty-mL gas samples, collected with a 60-mL syringe, were transferred into 12-mL Exetainers (LabCo) previously flushed with argon. After flushing the Exetainer with 25 mL of sample, the Exetainers were pressurized by adding 5 mL of gas and stored upside-down in deionized water before analyzing for N_2O within 30 days. The analysis was performed on a Shimadzu GC-8A with an electron capture detector set at 330°C, P-5 (5% CH_4, 95% argon mix) as the carrier gas, and a Porapak Q column set to 80°C.

Lateral Carbon Export

Lateral carbon export was calculated only for control sites in Freeman Creek marsh.

Tidal Water

Water overlying Freeman Creek interior at high tide was sampled at six randomly chosen sites each in April and August (see **Appendix 14-A**) for DIC and DOC concentrations and was analyzed by using the same methods previously described for pore water. The volume of water leaving the marsh was calculated based on water depth at high tide and the total area of the *S.*

alterniflora marsh and was multiplied by mean measured concentrations of DIC and DOC to determine lateral export of carbon by tidal exchange. Export was scaled up to annual values by multiplying the average of spring 2016 and summer 2016 export per tidal cycle by the number of tidal cycles per year.

Groundwater

Three 50-cm deep wells installed at the edge of Freeman Creek were sampled in July and October 2015 and in February and May 2016. Samples were analyzed for DIC and DOC as previously described. Seasonal estimates of lateral groundwater export of carbon were calculated by multiplying by the drainage flux of pore water (measured by Lettrich [2011]), which was based on hydraulic gradient and conductivity (Darcy method), by the measured concentrations of DIC and DOC.

Sediment Carbon Input

Marker Horizons were established in control and fertilized plots at Traps Bay Creek and Freeman Creek interior and were measured for sediment accretion every 3 months (see Chapter 13 [Research Project CW-4] of this report). Surface percent organic matter (%OM) and bulk density measured seasonally in the top 2 cm of Freeman Creek interior marsh sediment were used to calculate carbon content in accreted sediment. The Marsh model developed by DCERP researcher Dr. Ellen Herbert (described in Chapter 13 of the *DCERP2 Final Report*) was used to estimate carbon input along the Freeman Creek edge.

Statistics

Three-way analysis of variance (ANOVAs) with factors of season, location, and treatment (fertilized versus unfertilized) and Tukey post-hoc tests were used to assess the significant differences in pore water chemistry, sediment characteristics, biomass, and seasonal fluxes. H_2S, DIC, and DOC were square root–transformed, and NH_4^+ and above-ground biomass were log-transformed to meet the assumptions of data normality for ANOVAs (normality was assessed with quantile–quantile plot linearity in the software package R (R Core Team, 2014). In addition, $\alpha=0.05$ was used for all statistical testing. A linear mixed-effect model was performed with the lme4 package in R to compare respiration, GPP, and NCM with location and treatment as factors and plot pairs acting as a random effect nested within location to account for random spatial variability.

Table 14-1. Sampling Events and Measurements

Sampling Event	Dates	Temperature Range During Sampling (°C)	Measurements
Summer 2015	July 12–14, 2015	22–32	Pore water chemistry, sediment characteristics, above-ground biomass, and greenhouse gas (GHG) fluxes
Fall 2015	October 24–26, 2015	10–25	Pore water chemistry, sediment characteristics, above-ground biomass, and GHG fluxes
Winter 2015–2016	February 2–5, 2016	0–23	Pore water chemistry, sediment characteristics, and GHG fluxes
Spring 2016	May 5–7, 2016	7–24	Pore water chemistry, sediment characteristics, above-ground biomass, and GHG fluxes
Summer 2016	July 16–18, 2016	22–33	Pore water chemistry, sediment characteristics, above-ground biomass, and GHG fluxes
Fall 2016	November 10–14, 2016	3–22	Above-ground biomass and below-ground biomass

Table 14-2. Methodology of Research Project CW-5.

Analysis	Method	Reference(s)
Pore water DIC	Acidic sparge and Li-Cor 6252	Neubauer and Anderson, 2003
Pore water NH_4^+	Phenolhypochlorite; Lachat auto analyzer; sparge to remove H_2S	Modified from Liao, 2001
Pore water DOC	680°C catalytically aided combustion and non-dispersive infrared detection; Shimadzu TOC-V analyzer	Neubauer and Anderson, 2003
Pore water sulfide	Cline's reagent and methylene blue method; spectrophotometer	Cline, 1969
Above-ground biomass	Non-destructive assessment by using stem heights and density	Davis et al., 2017
Below-ground biomass	20-cm deep, 6.4-cm wide core	Modified from Davis et al., 2017
R	CO_2 flux in dark static chambers and Los Gatos GGA	Neubauer et al., 2000
GPP	CO_2 flux in static chambers at four light levels and Los Gatos GGA	Neubauer et al., 2000
NCM	Extrapolation by using Q_{10} and P-I curves	Silsbe and Malkin, 2015
Sediment organic content	Loss on ignition	[a]
Sediment bulk density	Dry mass in volume of core	[a]
CH_4	Static chambers and Los Gatos GGA	Neubauer et al., 2000

[a] Loss on ignition and bulk density do not have references because they are standard methods with no original publication.

Results and Discussion

Pore Water Chemistry

Freeman Creek interior, Freeman Creek edge, and Traps Bay Creek had distinct pore water characteristics. H_2S concentrations (**Figure 14-5**) were lowest at Freeman Creek edge and highest at Traps Bay Creek. This pattern is likely caused by high-energy creek water flushing edge pore water, whereas the interior with less flushing favors accumulation to higher concentrations. The three-way ANOVA and Tukey post-hoc test detected significantly greater H_2S on the Freeman Creek edge than interior ($p=7e^{-7}$ for 5 cm; $p=0.007$ for 15 cm) and significantly greater H_2S at Traps Bay Creek than at the Freeman Creek interior at 15-cm depth ($p=1e^{-7}$). NH_4^+ (**Figure 14-6**) was greater in the Freeman Creek interior than at the edge ($p<1e^{-7}$ for 5 cm and 15 cm), but greater at Traps Bay Creek than at Freeman Creek edge and interior at 15-cm depth ($p<1e^{-7}$). DOC (**Figure 14-7**) was greater in the Freeman Creek interior than at the edge
($p=2.8e^{-6}$ at 5 cm; $p=0.01$ at 15 cm) and greater at Traps Bay Creek than at the Freeman Creek interior ($p=1.7e^{-4}$ at 5 cm; $p<1e-^{7}$ at 15 cm). DIC (**Figure 14-8**) was greater in the Freeman Creek interior than at the edge ($p=0.005$), but greater at Traps Bay Creek than at Freeman Creek edge and interior at 15 cm ($p<1e^{-7}$). NH_4^+ was the only pore water analyte affected by fertilization, having greater concentrations in fertilized plots than control plots ($p=0.008$). A significant interaction was detected between fertilization and location at 15-cm depth ($p=0.007$), indicating that fertilization increased NH_4^+ concentrations more at Traps Bay Creek than at Freeman Creek.

Seasonal effects on pore water chemistry were generally less dramatic than differences among sites, showing significant differences only between specific seasons at all sites. H_2S was greater during fall than winter ($p=0.025$ at 5 cm; $p=0.002$ at 15 cm) and spring ($p=0.017$ at 5 cm; $p=1.5e^{-5}$ at 15 cm), and greater in summer 2016 than spring at 15 cm depth ($p=0.002$). No significant seasonal effect was detected for NH_4^+. DOC concentrations were greater in summer 2015 than winter ($p=0.006$ at 5 cm; $p=7.9e^{-6}$ at 15 cm), greater during fall than winter at 15 cm ($p=0.003$), and greater during summer 2015 than spring ($p=0.03$). DIC was greater during fall ($p=0.022$ at 5 cm; $p=0.014$ at 15 cm), summer 2015 (at 5 cm only, $p=0.011$), and summer 2016 ($p=0.019$) than winter.

These results suggest that the location of a salt marsh is a major driver for concentrations of pore water H_2S, NH_4^+, DIC, and DOC, likely caused by lower pore water residence time at Freeman Creek, creek water flushing at Freeman Creek edge, and the higher pore water residence time at Traps Bay Creek. The pattern observed in H_2S concentrations is particularly important because of previously described interactions between H_2S concentrations and nitrogen and carbon cycling, which may help drive spatial patterns in carbon accumulation, greenhouse gas (GHG) emissions, and marsh sustainability. In Freeman Creek interior and Traps Bay Creek, concentrations were found above 2,000 µM, the level experimentally determined to completely halt nitrogen uptake in *S. alterniflora* (Bradley and Morris, 1990). If nitrogen is the limiting nutrient, as has been found in many other salt marshes (Darby and Turner, 2008; Morris et al., 2013; Valiela, 2015), then one would expect that *S. alterniflora* would deplete pore water NH_4^+. However, NH_4^+ was found to accumulate more in locations with high H_2S concentrations, which indicates that the rate of nitrogen uptake rather than availability of NH_4^+ limits growth.

Fertilization may have increased pore water NH_4^+ more at Traps Bay Creek than at Freeman Creek edge and interior because rates of nitrogen uptake are likely inhibited by high H_2S concentrations at Traps Bay Creek. Because DOC, as a product of primary production, was greater at Traps Bay Creek than at Freeman Creek, the accumulation at Traps Bay Creek may be caused by greater pore water residence time, which is approximately 90 days at Traps Bay Creek and 12 days at Freeman Creek (Lettrich, 2011). Seasonal patterns of H_2S and DIC are most easily explained by variations in temperature, which influences the rates of plant metabolism and its production of oxygen and photosynthate, which is leached into the rhizosphere and respired along with DOC.

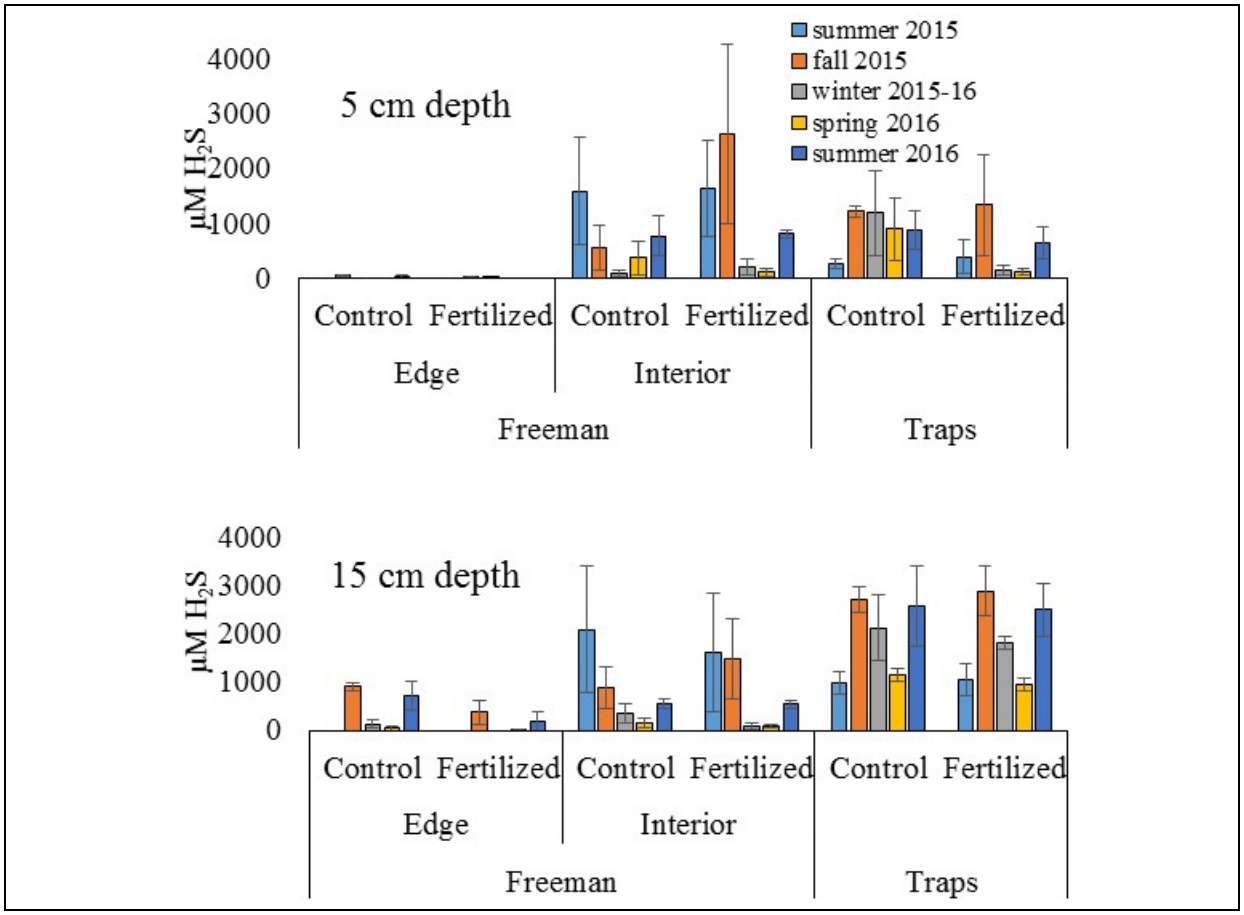

Figure 14-5. H_2S concentrations in pore water at 5 cm (top) and 15 cm (bottom) sediment depths and the three marsh sites at Marine Corps Base Camp Lejeune.

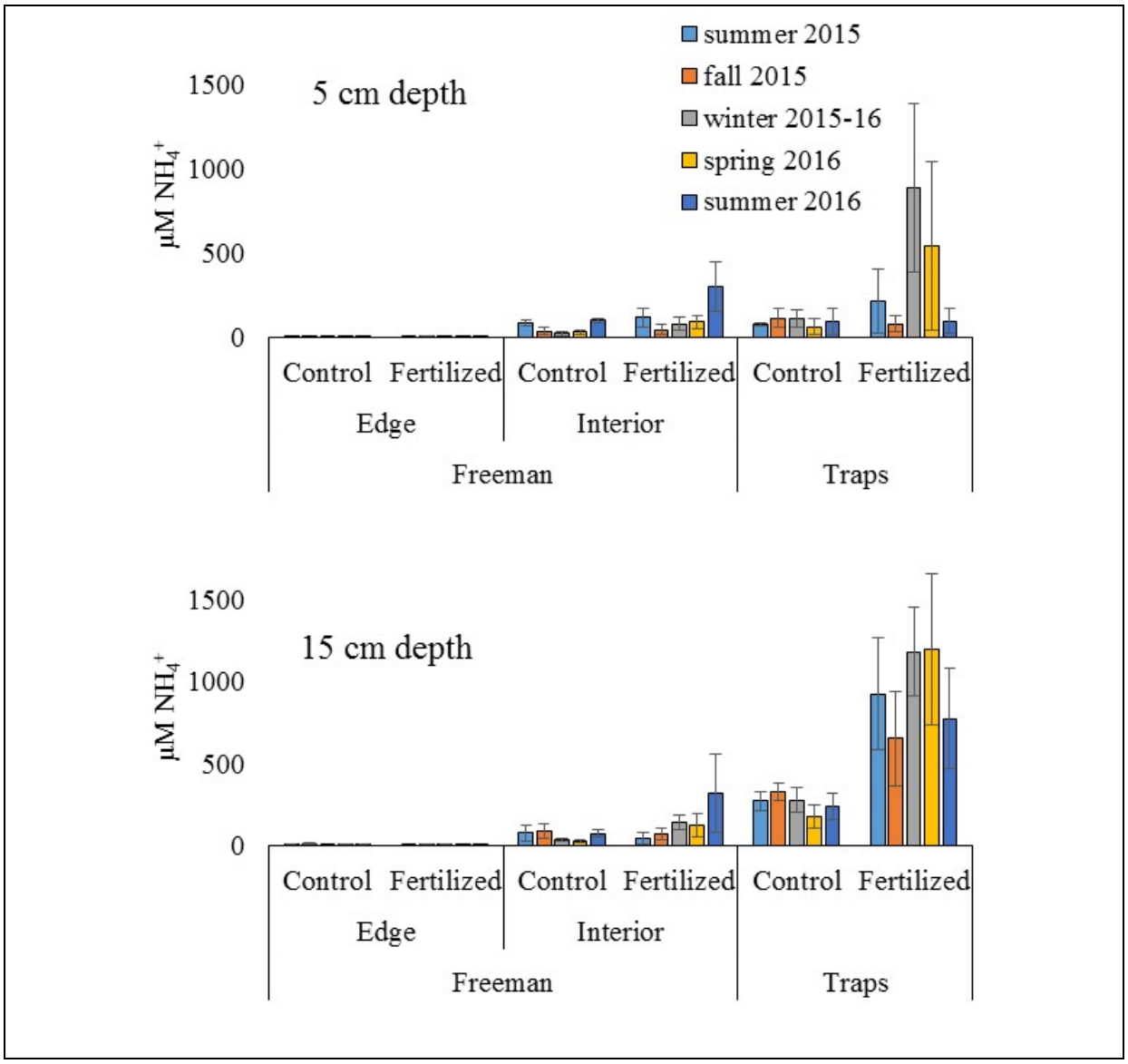

Figure 14-6. NH_4^+ concentrations in pore water at 5 cm (top) and 15 cm (bottom) sediment depths at the three marsh sites at Marine Corps Base Camp Lejeune.

Sediment Characterization

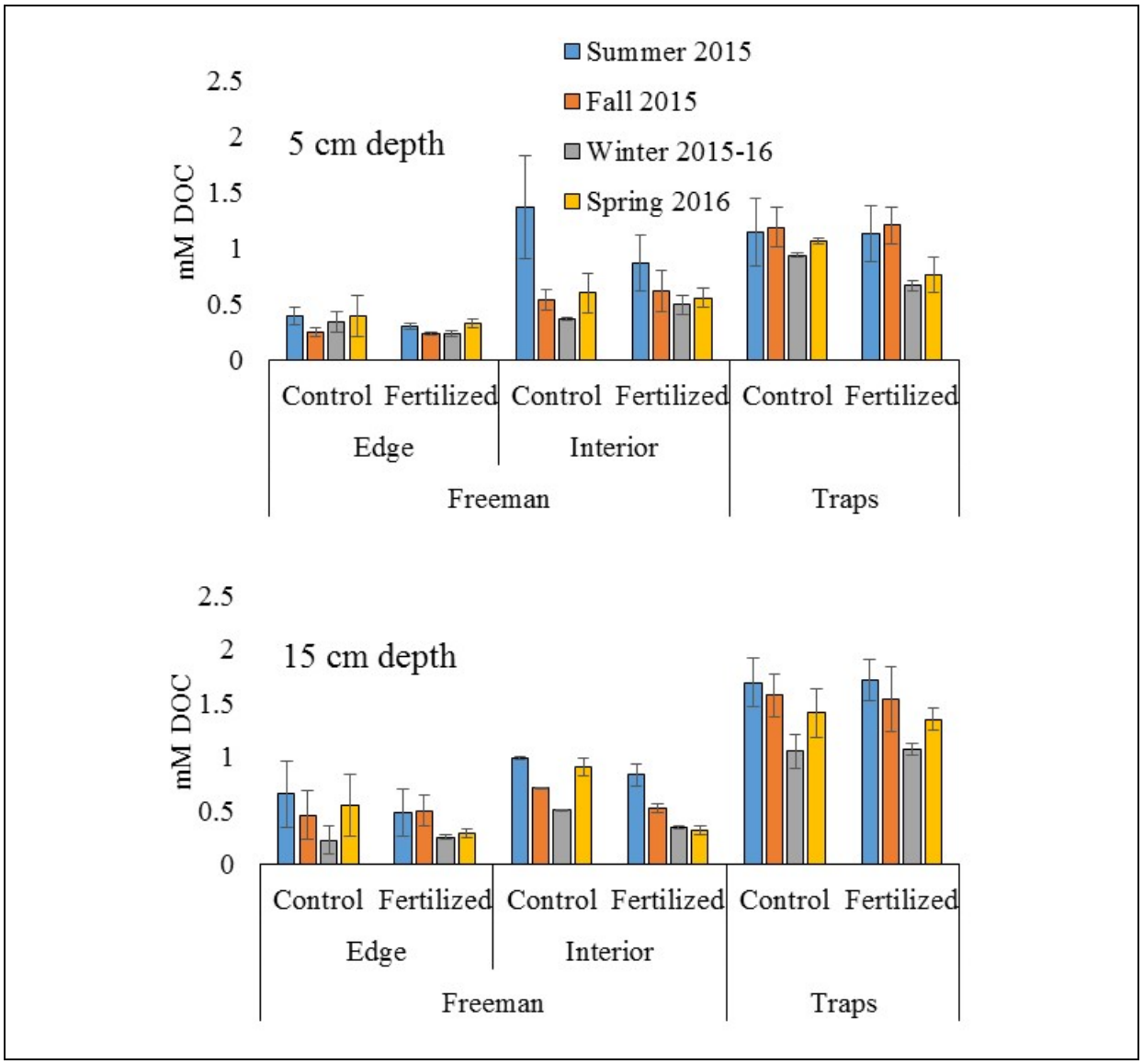

Figure 14-7. Dissolved organic carbon (DOC) concentrations in pore water at 5 cm (top) and 15 cm (bottom) sediment depths at the three marsh sites at Marine Corps Base Camp Lejeune.

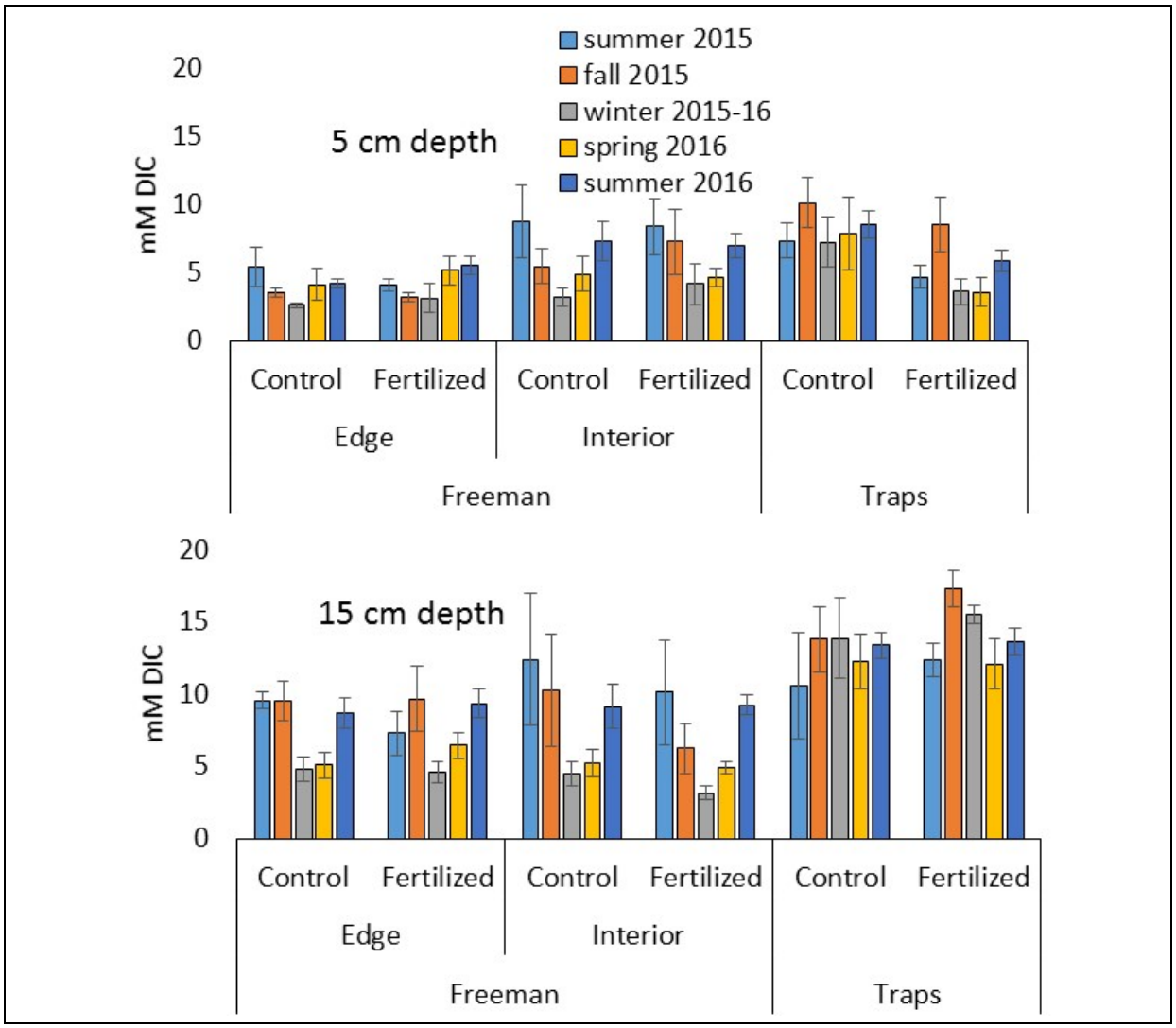

Figure 14-8. Dissolved inorganic carbon (DIC) concentrations in pore water at 5 cm (top) and 15 cm (bottom) sediment depths at the three marsh sites at Marine Corps Base Camp Lejeune.

In Freeman Creek interior, %OM (**Figure 14-9**) was approximately 15% in both the 0- to 2-cm and 2- to 5-cm depths, across all seasons in both fertilized and unfertilized plots. However, in Freeman Creek edge and Traps Bay Creek the %OM was more variable, exceeding 25% during some seasons at both 0- to 2-cm and 2- to 5-cm depths. No statistically significant seasonal or fertilization effects on %OM were detected. Traps Bay Creek had greater %OM than Freeman Creek interior and edge ($p<1e^{-7}$ for both 0- to 2-cm and 2- to 5-cm depths). Bulk density (**Figure 14-10**) was greater at the edge than in the interior at 0- to 2-cm depth ($p=0.043$), but greater at Freeman Creek edge and interior than at Traps Bay Creek ($p=7.3e^{-6}$ at 0- to 2-cm depth; $p<1e^{-7}$ at 2- to 5-cm depth); thus, differences in sediment %OM and bulk density are driven by location. In addition, bulk density was greater during winter than summer 2016 at 0- to 2-cm ($p=0.008$). Traps Bay Creek sediments contained greater %OM, which may be a result of decreased inorganic sediment input rate and increased pore water residence time (Lettrich, 2011). The edge may have been more variable in OM content than the interior because it is exposed to

the creek and may have received more organic sediment during events such as Hurricane Joaquin, which occurred 2 weeks before the October 2015 sampling.

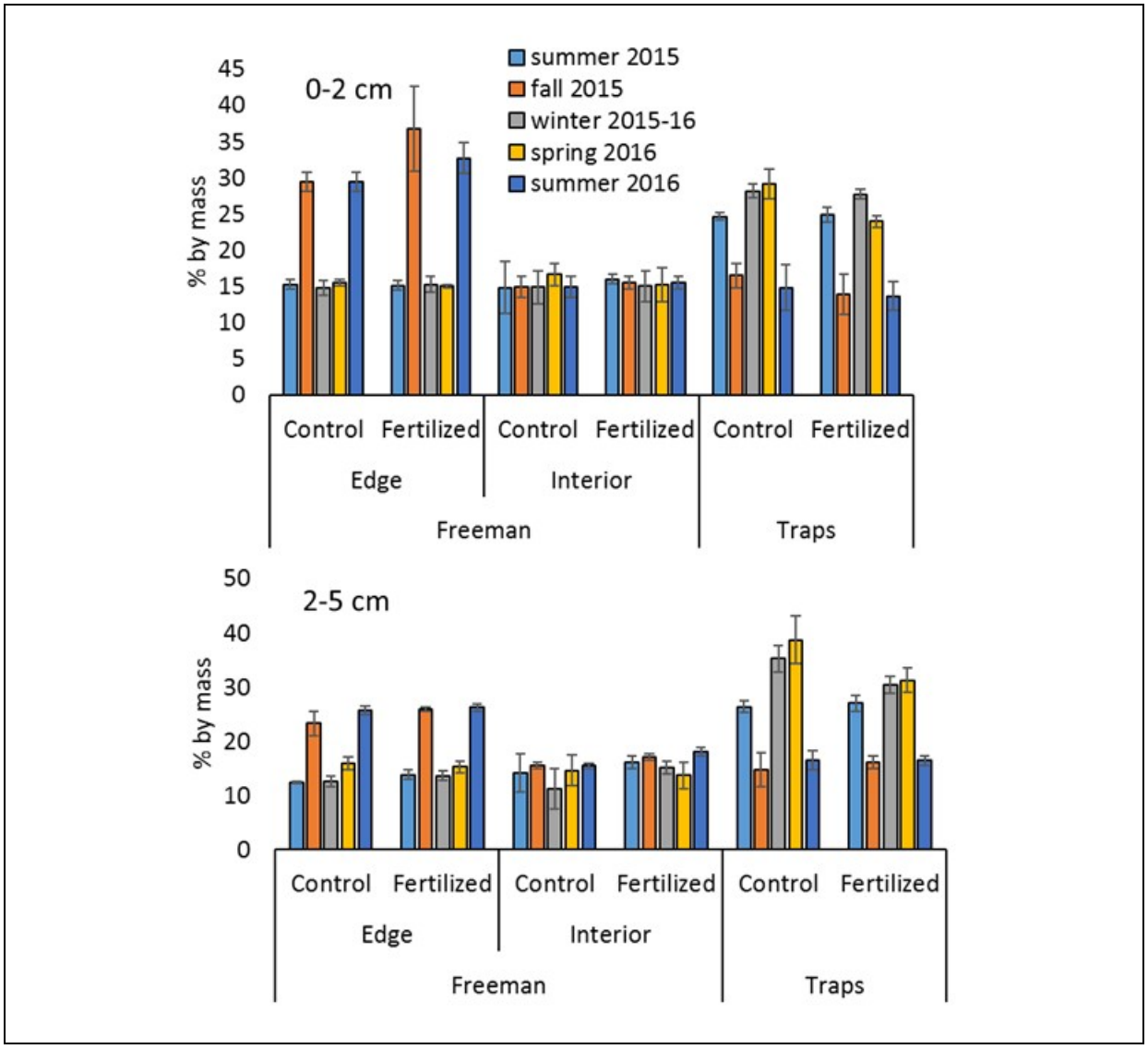

Figure 14-9. Percent sediment organic matter at 0- to 2-cm (top) and 2- to 5-cm depths at the three marsh sites at Marine Corps Base Camp Lejeune.

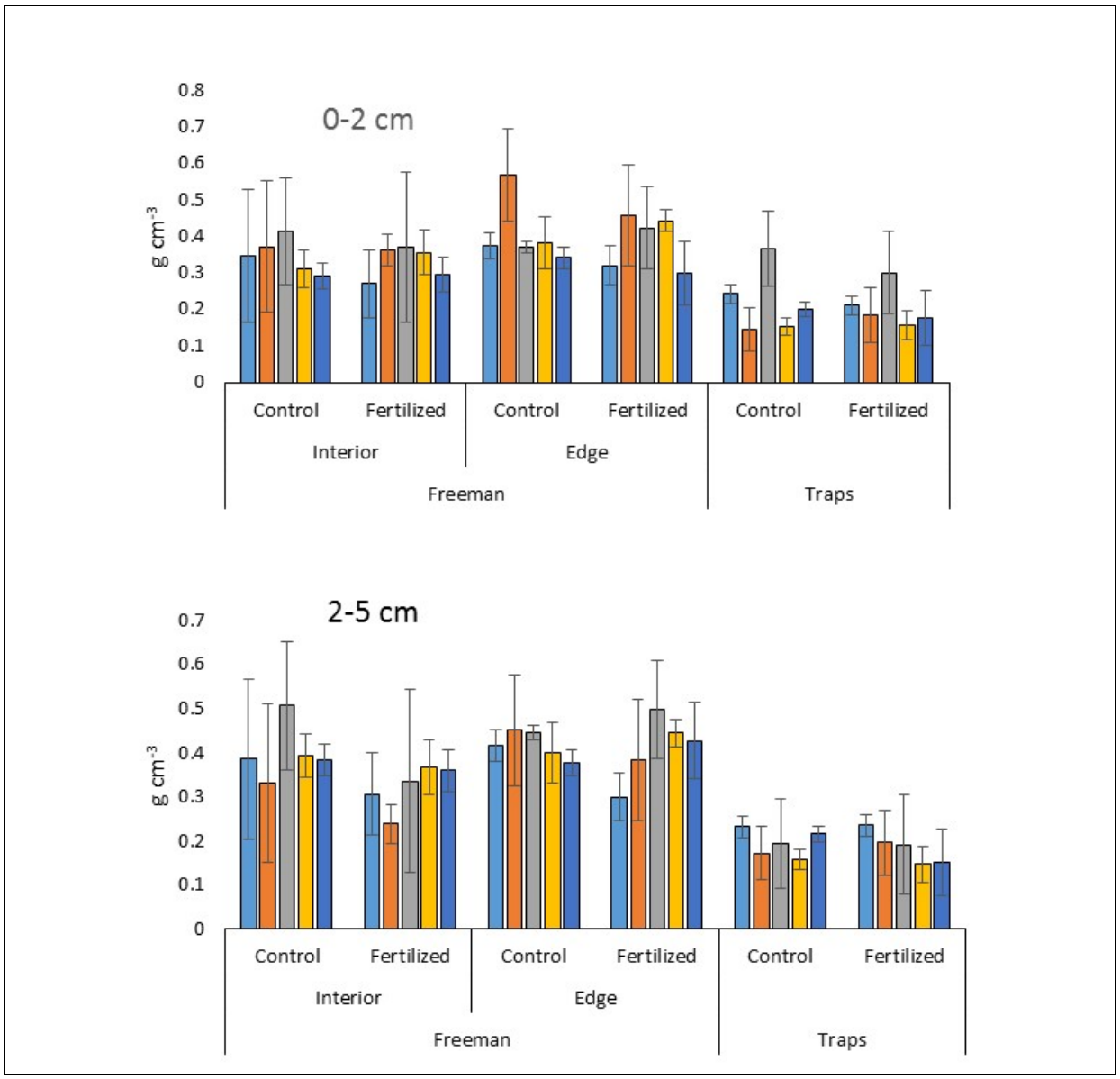

Figure 14-10. Bulk density of sediment at 0- to 2-cm and 2- to 5-cm integrated depths at the three marsh sites at Marine Corps Base Camp Lejeune.

Biomass

Above-ground biomass (**Figure 14-11**) was not different on the edge and interior at Freeman Creek, but Freeman Creek had greater above-ground biomass than Traps Bay Creek ($p=1.6e^{-4}$). Winter ($p=0.03$), spring ($p=0.002$), and summer 2016 ($p=0.03$) had greater above-ground biomass than summer 2015. Fertilization significantly increased above-ground biomass at all locations ($p=2e^{-16}$). There was a significant interaction between season and location ($p=0.005$). Above-ground biomass spiked dramatically with fertilization at the Freeman Creek edge during summer 2016, but this pattern was not observed in the interior of either Freeman Creek or Traps Bay Creek. Although above-ground biomass is important to consider because of its relationship with sediment trapping, it constituted only a small proportion of total biomass. Below-ground

biomass at Freeman Creek edge was lower than in Freeman Creek interior, with an average root:shoot ratio below 10 (**Figure 14-12**) and was not affected by fertilization. Fertilization in the interior of both Freeman Creek and Traps Bay Creek resulted in a decrease in both below-ground biomass and root:shoot ratio. A decrease in root:shoot ratio and below-ground biomass in response to fertilization has been observed in other studies (Morris et al., 2013; Tobias and Neubauer, 2009).

As previously described, pore water NH_4^+ was lower at Freeman Creek edge than at the interior. Increasing above-ground biomass with fertilization on the edge indicates that the fertilizer is not only flushed into the creek, but is also taken up by *S. alterniflora* to stimulate growth. In the interior, especially at Traps Bay Creek, pore water NH_4^+ accumulated, suggesting that uptake by *S. alterniflora* is inhibited by high H_2S concentrations. Long-term stability of the marsh platform is thought to increase with the root:shoot ratio (Darby and Turner, 2008); thus, fertilization may result in decreased marsh platform stability at Freeman Creek interior and at Traps Bay Creek; the response is less clear-cut for the Freeman Creek edge.

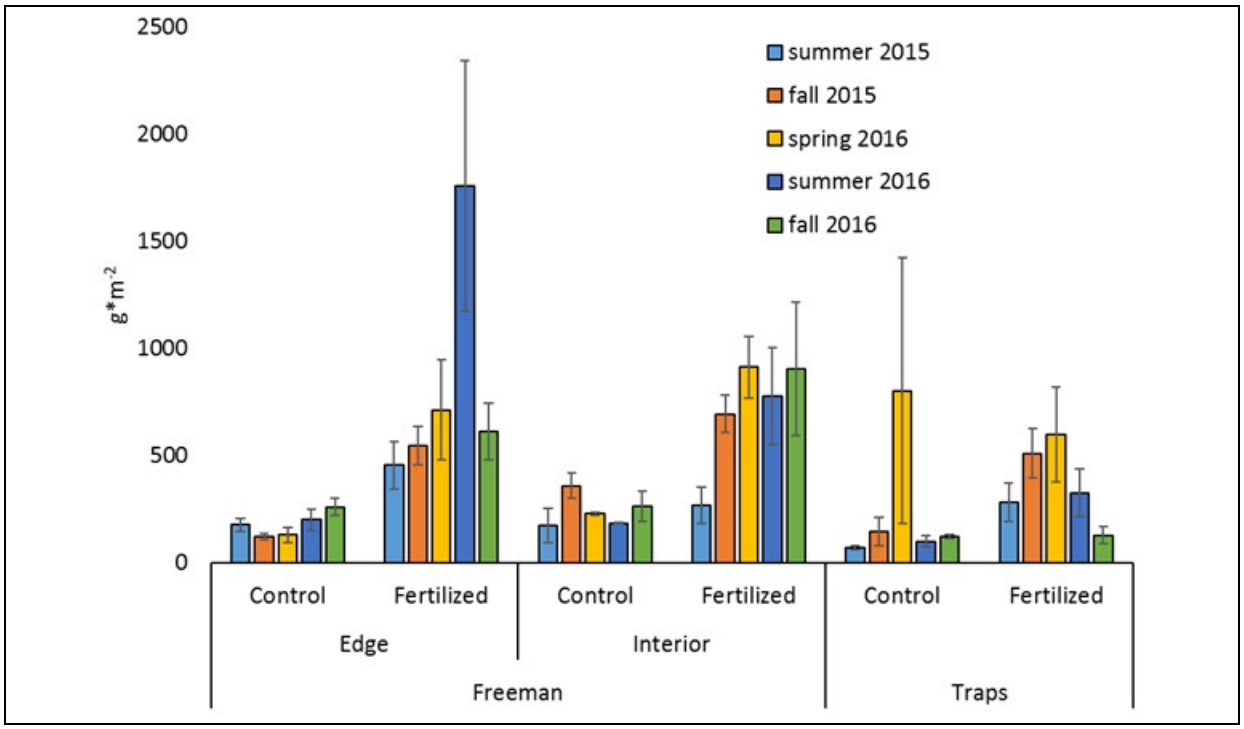

Figure 14-11. Above-ground biomass of *S. alterniflora* at the three marsh sites at Marine Corps Base Camp Lejeune.

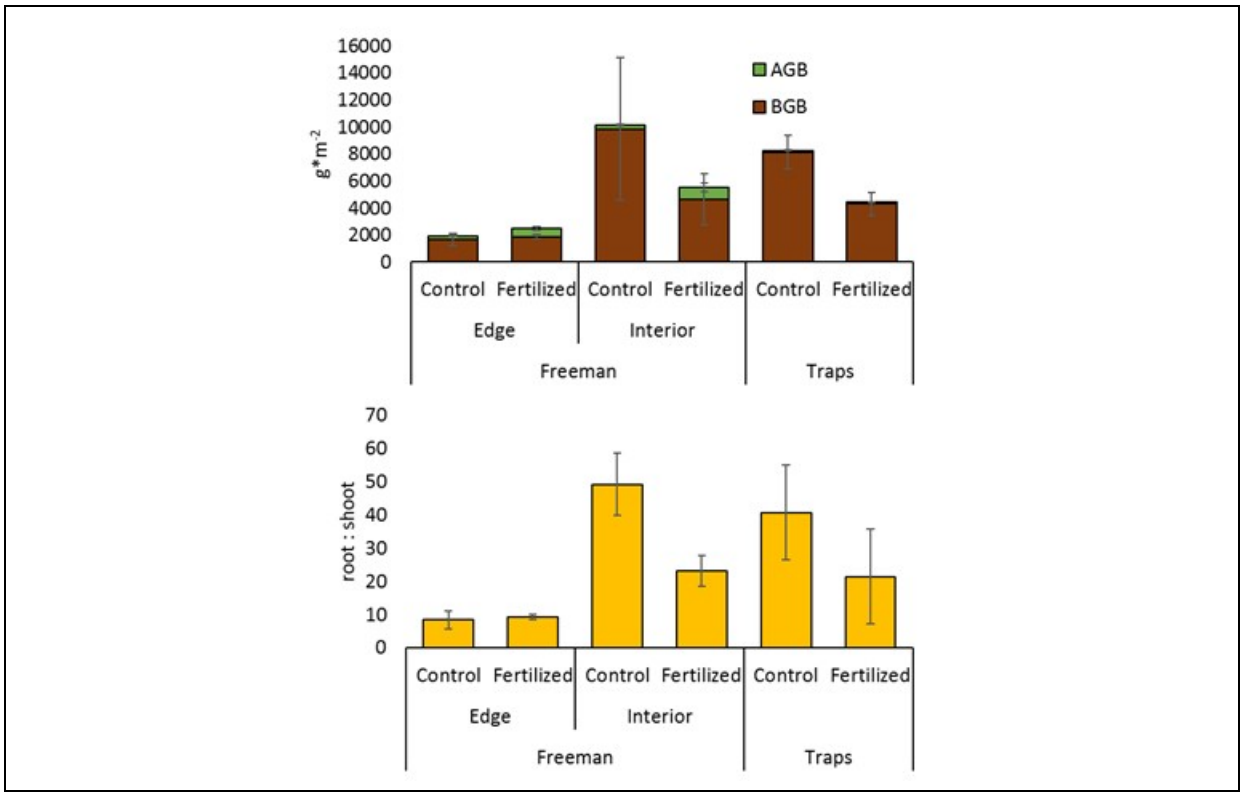

Figure 14-12. Above-ground biomass (AGB) versus below-ground biomass (BGB; top) and root:shoot ratio (bottom) observed in fall 2016 at three marsh sites at Marine Corps Base Camp Lejeune.

Metabolism

All metabolic parameters, respiration, GPP, and NCM varied by season, location, and treatment. Annual respiration (**Figure 14-13**) was significantly greater on the edge than at the interior of Freeman Creek ($p=3e^{-4}$) and Traps Bay Creek ($p=1e^{-4}$), but was not significantly different between Freeman Creek and Traps Bay Creek. Fertilized plots had significantly greater rates of respiration than control plots ($p=2e^{-16}$), but there was a significant interaction between treatment and location ($p=0.033$), indicating that fertilization had a greater effect on respiration at the Freeman Creek edge and a diminished effect at Traps Bay Creek. Annual GPP (**Figure 14-13**) was significantly greater at the Freeman Creek edge ($p<0.001$) and at Traps Bay Creek ($p=0.011$) than at the Freeman Creek interior. Greater GPP was found in fertilized plots than control plots ($p=3.3e^{-12}$). A significant interaction between treatment and location ($p=0.011$) indicated that fertilization stimulated GPP more in the Freeman Creek interior than at the Freeman Creek edge or Traps Bay Creek.

NCM (metabolism per square meter), which includes both plant metabolism and microbial metabolism in the sediment, varied by season and by location. For non-fertilized plots at all marsh sites, the NCM tended to be net heterotrophic in fall and winter, but was net autotrophic in the spring and varied in the summer depending on location (**Figure 14-14**). The NCM was significantly more heterotrophic in the fall than in the spring ($p<1e^{-7}$), winter ($p=6e^{-4}$), and summer ($p=1e^{-7}$), with winter significantly more heterotrophic than spring ($p=2e^{-4}$) and summer

(p=0.02). On an annual basis, Traps Bay Creek was net autotrophic, but Freeman Creek was net heterotrophic in both the edge and the interior (**Figure 14-15**). This finding is consistent with the observation that Traps Bay Creek had greater GPP, but similar respiration compared with the Freeman Creek interior. Analysis with a linear mixed-effect model revealed that Freeman Creek and Traps Bay Creek had significantly different net metabolic rates ($p=4e^{-4}$). In addition, fertilized plots were significantly more heterotrophic than control plots at Freeman Creek ($p=4e^{-8}$). Location and treatment had a significant interaction (p=0.01), indicating that fertilization had a stronger effect on NCM at Freeman Creek edge and a diminished effect on Traps Bay Creek.

Thus, on an annual basis, marshes within the same coastal system may differ in trophic status depending on location. These differences are likely driven by pore water chemistry, which varies in response to physical factors such as flushing rates, tidal amplitude, elevation in the tidal framework, and pore water residence time. Results at Freeman Creek demonstrate that not all marshes accumulate carbon only through autochthonous primary production. Net heterotrophic marshes such as Freeman Creek must rely on external sources to accumulate carbon and maintain elevation relative to sea level. Increasing nitrogen pollution in coastal waters may speed the loss of salt marsh carbon as CO_2 into the atmosphere by stimulating respiration more than GPP. The varying concentrations of pore water H_2S, NH_4, and DOC in these different locations may drive observed differences in metabolism.

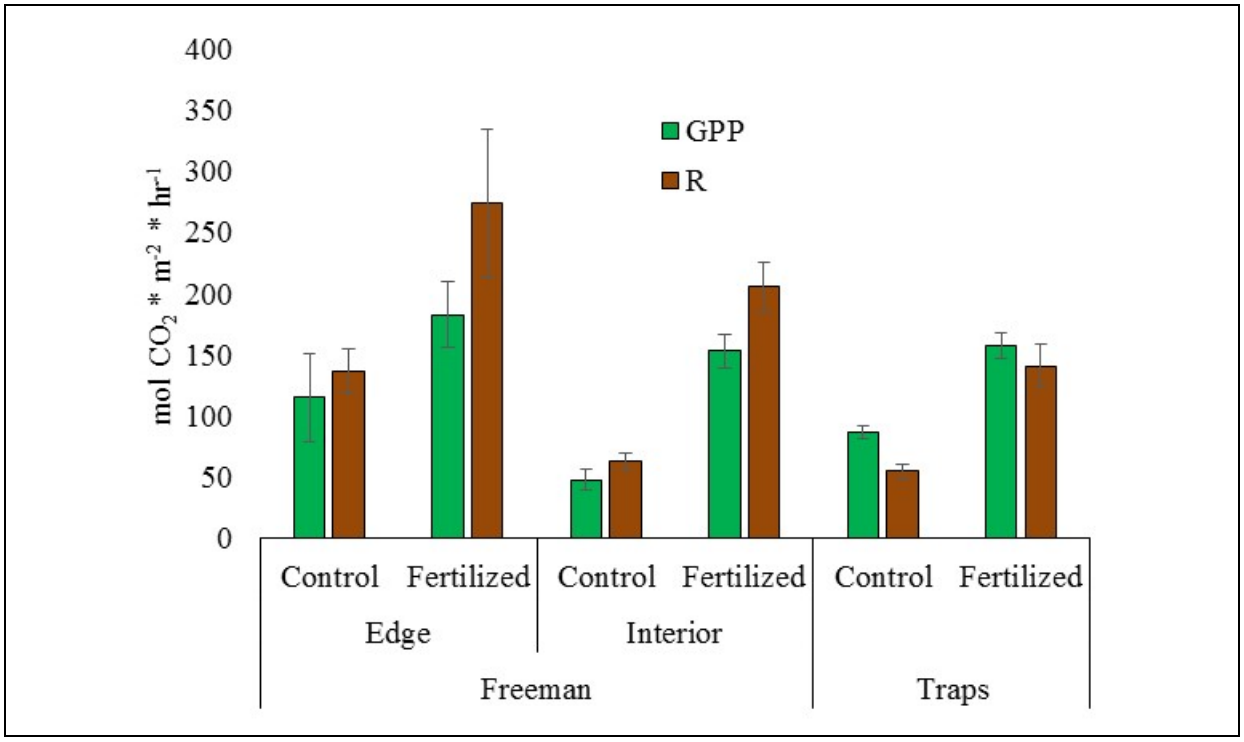

Figure 14-13. Annual GPP and respiration (R) rates for the three marsh sites at Marine Corps Base Camp Lejeune.

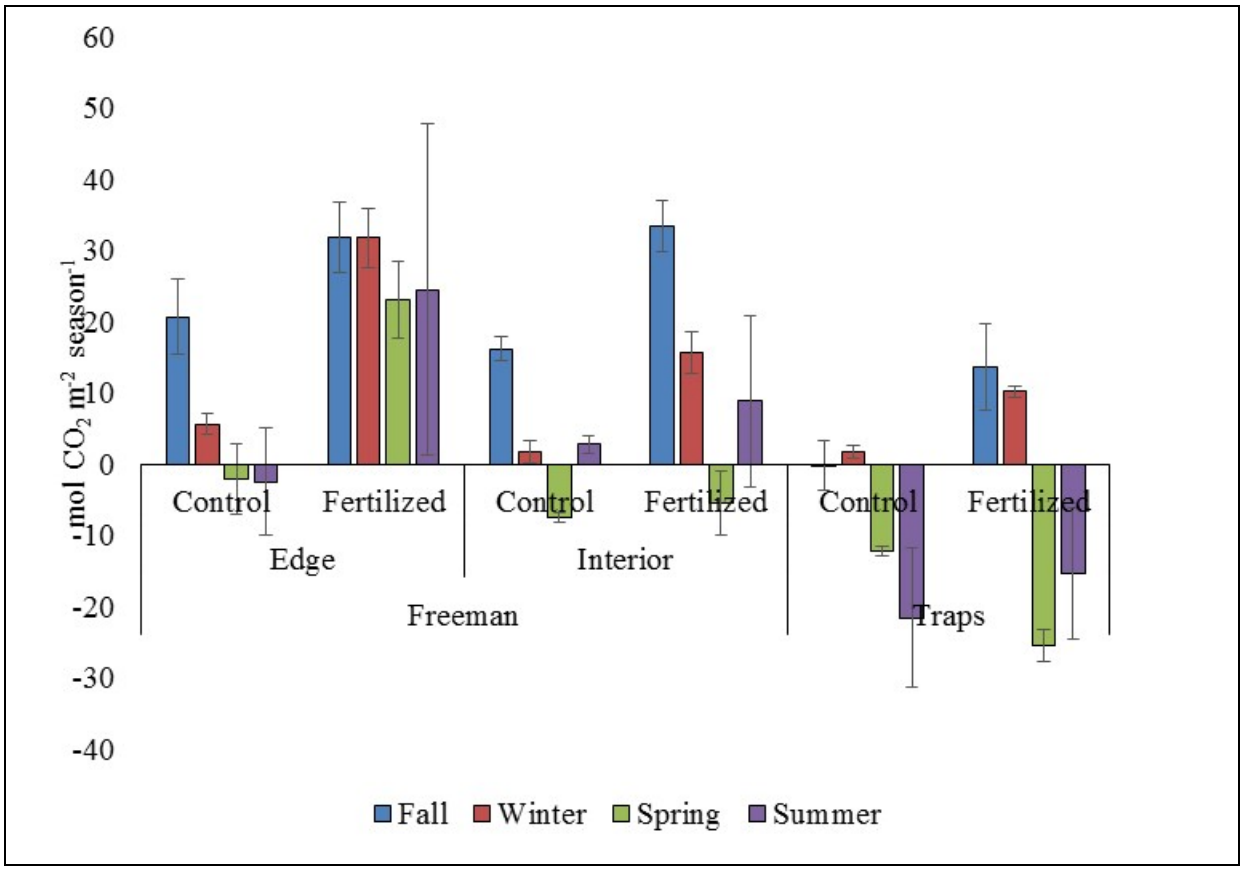

Figure 14-14. Seasonal net community metabolism. Positive values represent net heterotrophy and CO_2 emissions. Negative values represent net autotrophy and CO_2 uptake for the three marsh sites at Marine Corps Base Camp Lejeune.

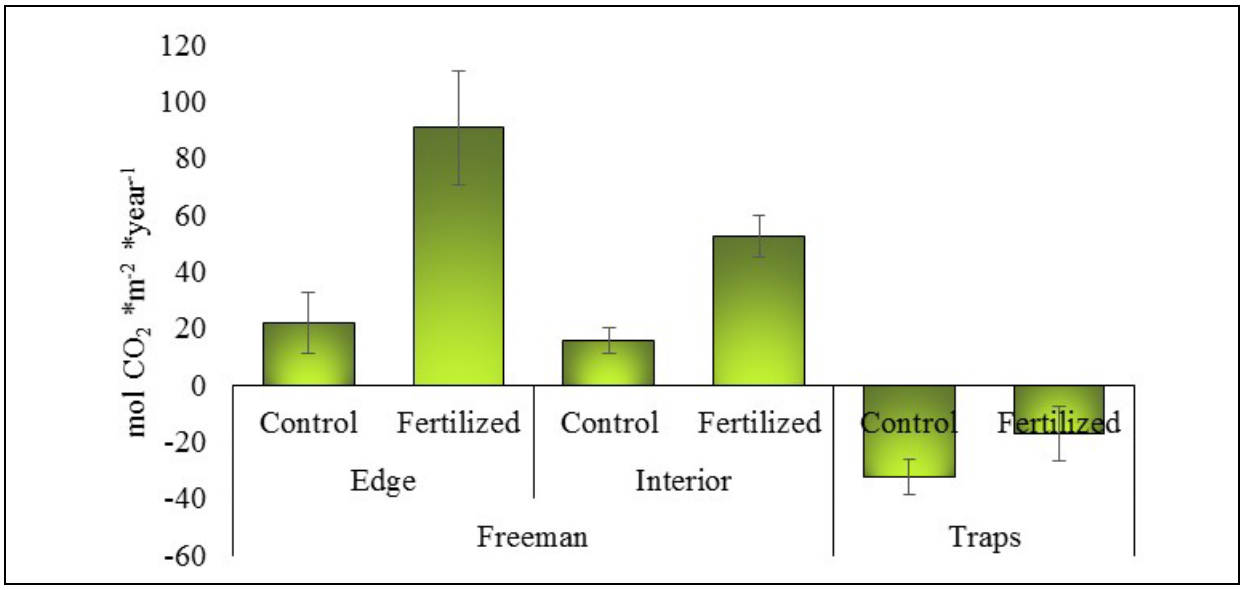

Figure 14-15. Net community metabolism extrapolated to annual scale. Positive values represent net heterotrophy and CO_2 emissions. Negative values represent net autotrophy and CO_2 uptake at three marsh sites at Marine Corps Base Camp Lejeune.

NCM Measured with Static Chambers vs. an Eddy Covariance Tower

The pattern of hourly NCM extrapolated from seasonal static chamber measurements at Freeman Creek control plots appeared to match closely with those made by the Freeman Creek eddy covariance tower (**Figure 14-16**). However, nighttime respiration from the chamber tended to be higher than tower measurements, and the tower captured several brief spikes not predicted by chamber extrapolations. Because fluxes measured by the tower were lower during periods of tidal inundation, we performed preliminary calculations to correct for the effects of inundation on chamber measurements. We determined that by reducing the uptake of CO_2 by GPP during daytime inundation and reducing CO_2 effluxes due to R to zero during nighttime inundation, the chamber and eddy covariance fluxes were in excellent agreement. However, because these corrections are preliminary, they were made only for the Freeman Creek marsh where the eddy covariance tower was located, and because the variations in inundation period over space and time are currently not well understood, the data reported below do not include these corrections.

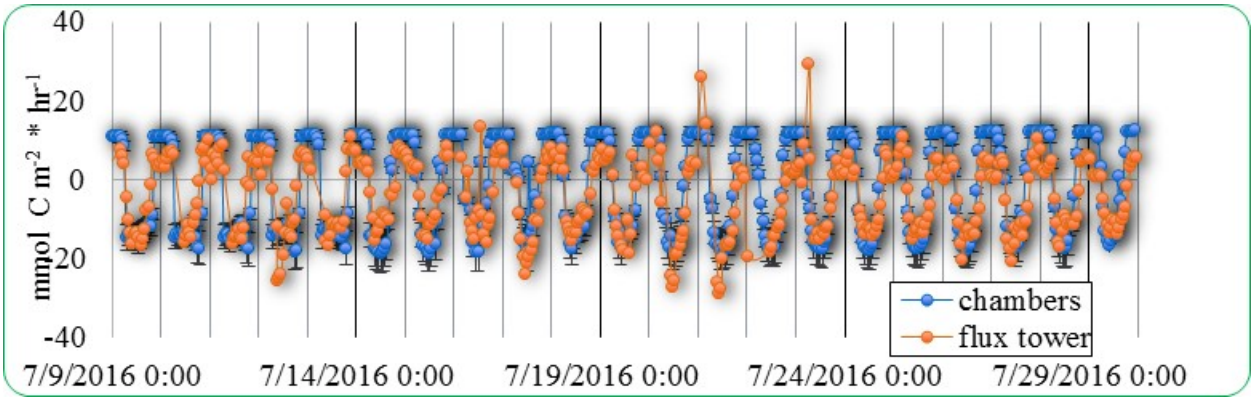

Figure 14-16. Comparison of net CO_2 exchange at Freeman Creek measured with a static chamber system and with an eddy covariance tower from July 9 through 30, 2016.

Net Ecosystem Metabolism

"NEM" is defined here as the net metabolism for the total area of *S. alterniflora* marsh at Freeman Creek. A spatial analysis conducted for Freeman Creek yielded a total *S. alterniflora* marsh (combined tall-form and short-form) area of 0.47 km^2 (**Figure 14-17**) with a marsh edge area (within 5 m of a tidal creek) composing 0.14 km^2 (or 29.3%) of the total *S. alterniflora* marsh area. Thus, edge marsh is an important component of total marsh area for Freeman Creek and other systems with complex networks of branching tidal creeks. The Freeman Creek NEM was extrapolated to the edge and interior marsh areas separately, and compared with the NEM extrapolated by using only interior CO_2 flux values to represent the entire marsh area (**Table 14-3**). Because the NCM of the edge was greater than the interior under fertilized conditions, the fertilized marsh NEM was underestimated by 21.4% when differences in edge and interior fluxes were ignored. Thus, for marshes with high nitrogen availability and a significant percentage of edge area, the difference in NCM between the edge and the interior are important to consider when spatially extrapolating CO_2 fluxes to entire marsh systems.

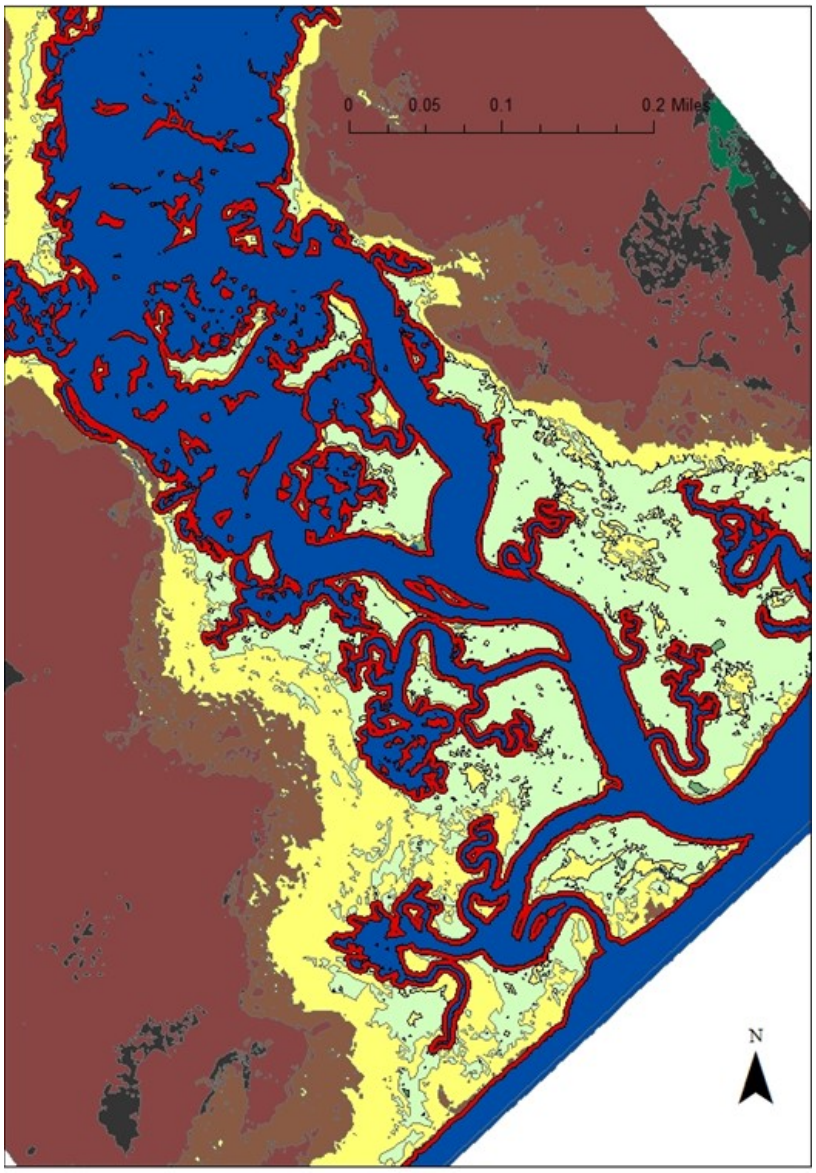

Figure 14-17. Spatial analysis of Freeman Creek performed with ArcGIS showing tall-form *S. alterniflora* marsh (yellow), short-form *S. alterniflora* marsh (green), and *S. alterniflora* marsh within 5 m of creek bank (red).

The Freeman Creek vegetation layer was originally produced by Research Project CW4, see Chapter 13, Section 3.

Table 14-3. Freeman Creek NEM (10^5 kg C/year) Estimates Compared with and without Considering Edge Differences for Both Control and Fertilized Scenarios

Treatment	Without Edge	With Edge	% Difference
Control	0.89	0.99	11.4%
Fertilized	2.98	3.61	21.4%
% difference	234.1%	263.8%	

Greenhouse Gas Emissions

N_2O fluxes were below detection limit. CH_4 was detectable in every location during every season (**Figure 14-18**), but emissions were three orders of magnitude lower than CO_2. CH_4 emissions were significantly higher at Traps Bay Creek than Freeman Creek edge (p=0.007), but were statistically the same as in Freeman Creek interior. Emissions were significantly higher during summer than winter ($p=9e^{-5}$). Fertilization caused an increase in CH_4 emissions (p=0.02), which has also been observed in other studies and may be the result of greater above-ground biomass, which may increase the efficiency of plant-mediated gas transport (Tong et al., 2012).

CH_4 emission appears to be negligible to marsh carbon emissions because it is several orders of magnitude lower than CO_2 emissions. However, because CH_4 has 45 times the 100-year sustained flux radiative forcing of CO_2 (Neubauer and Megonigal, 2015), CH_4 emissions are still a significant component of salt marsh GHG emissions; in some plots, they nearly offset the climate benefits of CO_2 uptake.

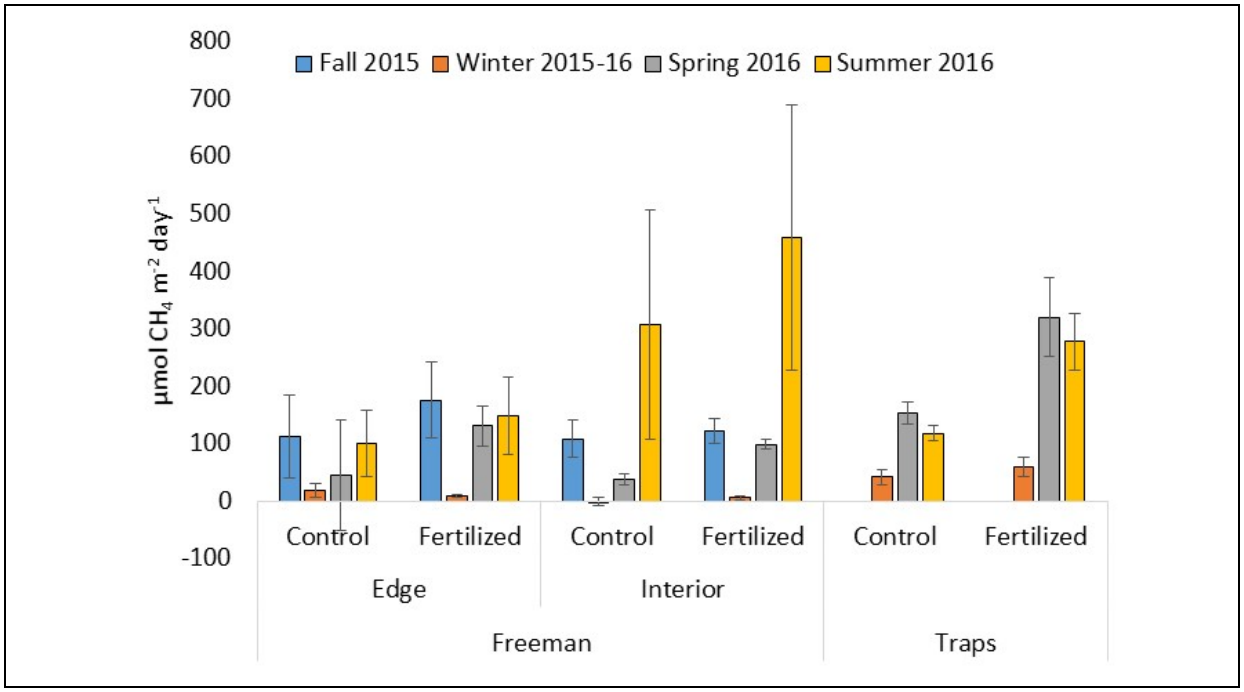

Figure 14-18. Daily CH_4 fluxes at three marsh sites at Marine Corps Base Camp Lejeune.

Note: There are no values for Traps Bay Creek in fall 2015.

Total Carbon Accumulation at Freeman Creek Marsh

Although we have established that NCM may represent either a gain or loss term depending upon the location of the marsh, NCM alone does not determine whether a salt marsh is gaining or losing carbon. Net heterotrophic marshes may continue to accumulate carbon if sediment carbon input exceeds CO_2 emissions and lateral carbon export (**Figure 14-19**).

Lateral Carbon Export

Tidal DIC export was lower during spring 2016 (28.36 mmol m^{-2} tidal $cycle^{-1}$) than summer 2016 (88.97 mmol m^{-2} tidal $cycle^{-1}$); however, tidal DOC export was greater during spring 2016 (69.66 mmol m^{-2} tidal $cycle^{-1}$) than summer 2016 (22.58 mmol m^{-2} tidal $cycle^{-1}$). Annual DIC export (**Table 14-4**) was similar in magnitude to DOC export, and annual groundwater carbon export was less than tidal export. However, carbon export was at a similar magnitude to the observed gains of carbon due to NCM plus sediment OM import rates. It was recently suggested that eddy covariance towers underestimate marsh NCM by missing the DIC export component during inundation (Wang et al., 2017). Inundation can potentially reduce CO_2 uptake due to light limitation of GPP (Kathilankal et al., 2008). Inorganic carbon produced by R may accumulate in overlying water as DIC with a decrease in CO_2 efflux into the atmosphere. At Freeman Creek, marsh inundation had a marked effect on CO_2 exchanges with the atmosphere, as previously shown by a comparison between CO_2 exchanges based upon the covariance tower and chamber measurements (**Figure 14-16**).

Table 14-4. Annual Tidal, Groundwater, and Total Carbon Export for DIC, DOC, and Total Dissolved Carbon (mol m^{-2} $year^{-1}$) at Freeman Creek

Export	DIC	DOC	Total Dissolved Carbon
Tidal export	42.83	33.67	76.49
Groundwater export	3.05	0.18	3.23
Total export	45.88	33.85	79.72

Sediment Carbon Input

Marker Horizons at Freeman Creek interior and Traps Bay Creek indicated an average accretion rate of 3.65 and 1.83 cm per year, respectively (see Research Project CW-4, Chapter 13, Sections1 and 2 of this final report for full details). Sediment carbon input was greater in fertilized plots in both locations, 8.03 cm per year at Freeman Creek interior and 2.56 at Traps Bay Creek. Sediment carbon input (**Table 14-5**), which was calculated from accretion rates, bulk density (0.28 g m^{-2} at Freeman Creek and 0.18 at Traps Bay Creek), %OM (15.7 at Freeman Creek and 27.4 at Traps Bay Creek), and 45% carbon composition in surface OM (based on data from Research Project CW-4), was of the same order of magnitude as the observed CO_2 exchange.

Net Carbon Accumulation

Salt marsh carbon accumulation is primarily governed by the balance between NCM, lateral carbon export and sediment carbon input (**Figure 14-19**). Calculations of lateral carbon export and net marsh carbon accumulation require that we take into account the effects of inundation on NCM. Inundation will reduce GPP because of light limitation and will change the distribution of products of R between CO_2 and DIC. The importance of lateral export and its regulation by inundation is being actively studied by several research groups, including ours. **Figure 14-19** shows the balance between NCM and sediment OM input disregarding losses due to lateral export. The Freeman Creek edge was the only location with net loss of carbon, the result of net

heterotrophy and low sediment deposition. However, in the interior, enough sediment carbon was deposited to offset the loss as CO_2 and result in net carbon accumulation. Although CO_2 emission increased with fertilization, sediment carbon deposition also increased, acting as a negative feedback on marsh carbon gains and losses. At Traps Bay Creek, sediment carbon input added significantly to the total carbon accumulation.

Table 14-5. Sediment Carbon Input Rates (mol C m^{-2} yr^{-1})

Marsh Site	Control	Fertilized	Source of Data
Freeman Creek edge	3.2	3.2	Research Project CW-4 predictive model (Ellen Herbert) (See Chapter 13 of this report)
Freeman Creek interior	62.1	126.4	Marker Horizons
Traps Bay Creek	34.5	42.4	Marker Horizons

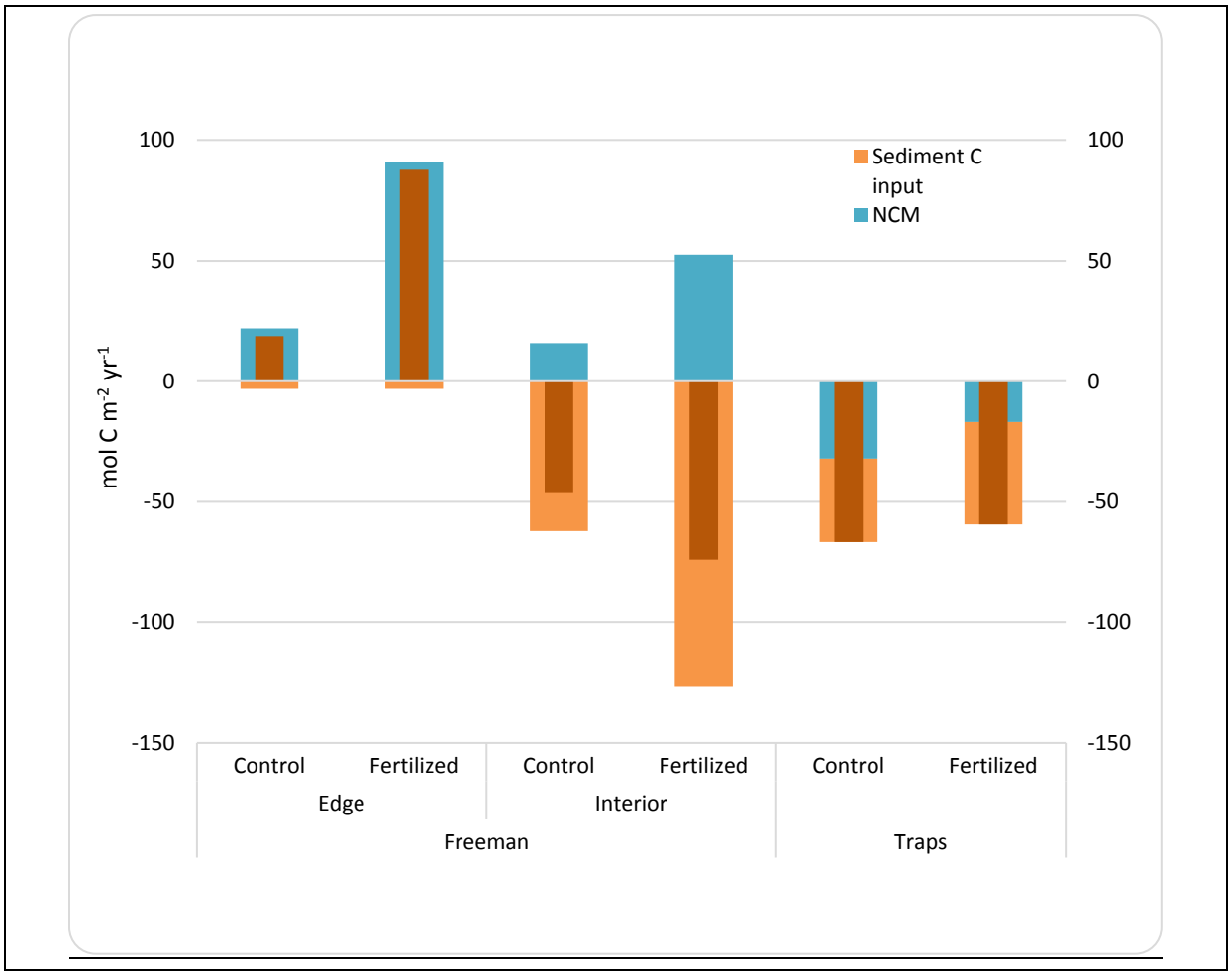

Figure 14-19. Comparison of carbon (C) fluxes and total short-term C accumulation for each treatment.

Note: Negative values represent accumulation, and positive values represent loss.

Total carbon accumulation per square meter was quantified by a mass balance of NCM and sediment OM input, ignoring losses due to lateral carbon export and the effects of inundation on NCM (**Figure 14-19**). Although Freeman Creek interior lost carbon to the atmosphere because of net heterotrophy, the magnitude of sediment carbon input resulted in an overall net gain of carbon; under fertilized conditions, the net carbon gain increased relative to control conditions. Along the edge, where sediment deposition is low because of high elevation and decreased inundation time, we predicted a net loss of carbon, which will become much more severe under fertilized conditions due to the strong impact of fertilization on edge NCM. Although Traps Bay Creek receives somewhat less sediment input, total carbon accumulation is greater than at Freeman Creek interior because it is a net autotrophic marsh. Total carbon accumulation at Traps Bay Creek was similar under both natural and fertilized conditions because of comparable levels of sediment carbon input and a relatively small impact of fertilization on NCM. It remains unclear whether the primary source of substrate used for respiration is derived from allochthonous sediment carbon input or from autochthonous GPP.

Carbon Mass Balance in Freeman Creek Marsh

To scale per square meter measurements of carbon gains and losses to the entire Freeman Creek *S. alterniflora* marsh area, we adjusted GPP, R, and NCM to match results of our static chamber measurements with those of the eddy covariance tower for the same period, July 2016, and calculated lateral carbon export during inundation periods. Once scaled to total marsh area, Freeman Creek was calculated to lose a total of 115,000 kg carbon per year (**Figure 14-20**). If the entire Freeman Creek marsh was fertilized with excess nitrogen, the marsh would be expected to shift to a net gain of 49,000 kg carbon per year (**Figure 14-21**). Ignoring the differences on the edge in the mass balance budget would cause an overestimation of sediment carbon input and underestimation of CO_2 emission. Therefore, the difference in metabolism and sediment input between edge and interior is crucial to quantify to accurately determine salt marsh carbon accumulation. The increase in carbon accumulation efficiency with fertilization at Freeman Creek interior was due mainly to the increased sediment accretion rate (Davis et al., 2017). Therefore, fertilization may be considered as a management strategy in the interior marsh to increase elevation at the cost of reduced carbon accumulation. Although the below-ground biomass was observed to decrease, this impact may be offset by the increase in sediment input (Graham and Mendelssohn, 2014). However, it is important to avoid increasing nitrogen availability on the edge marsh, where negative effects appear to outweigh positive effects.

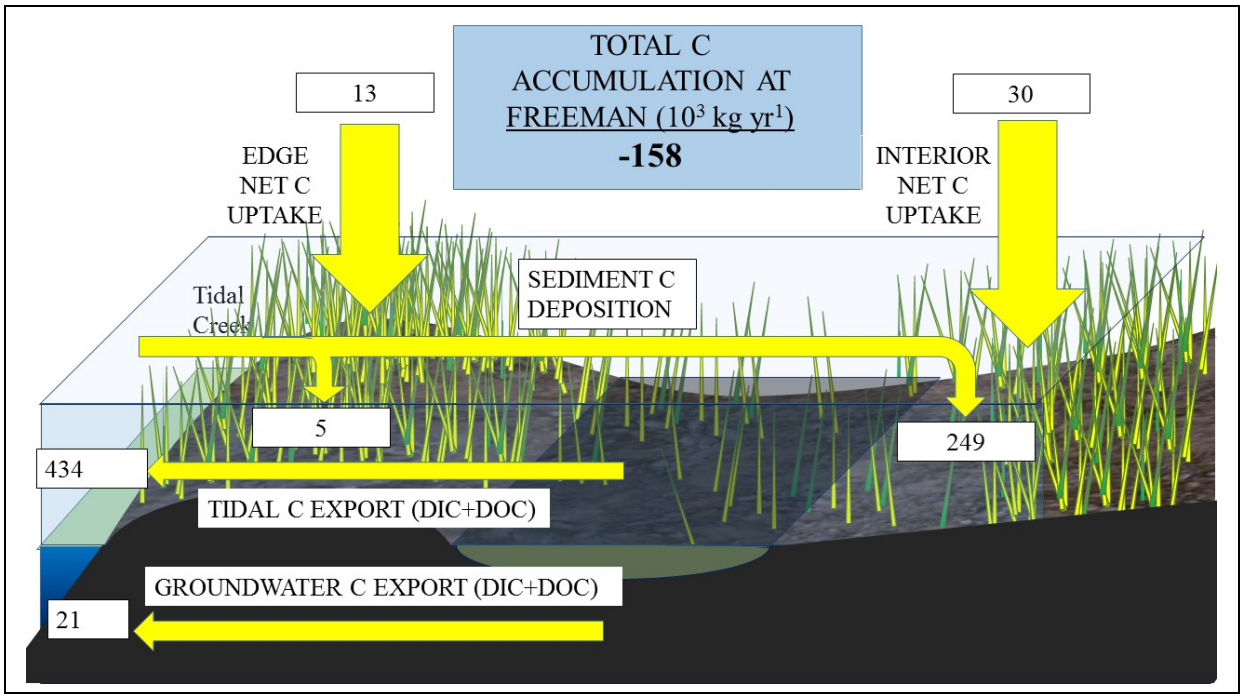

Figure 14-20. Mass balance carbon (C) budget in Freeman Creek marsh to estimate net carbon accumulation.

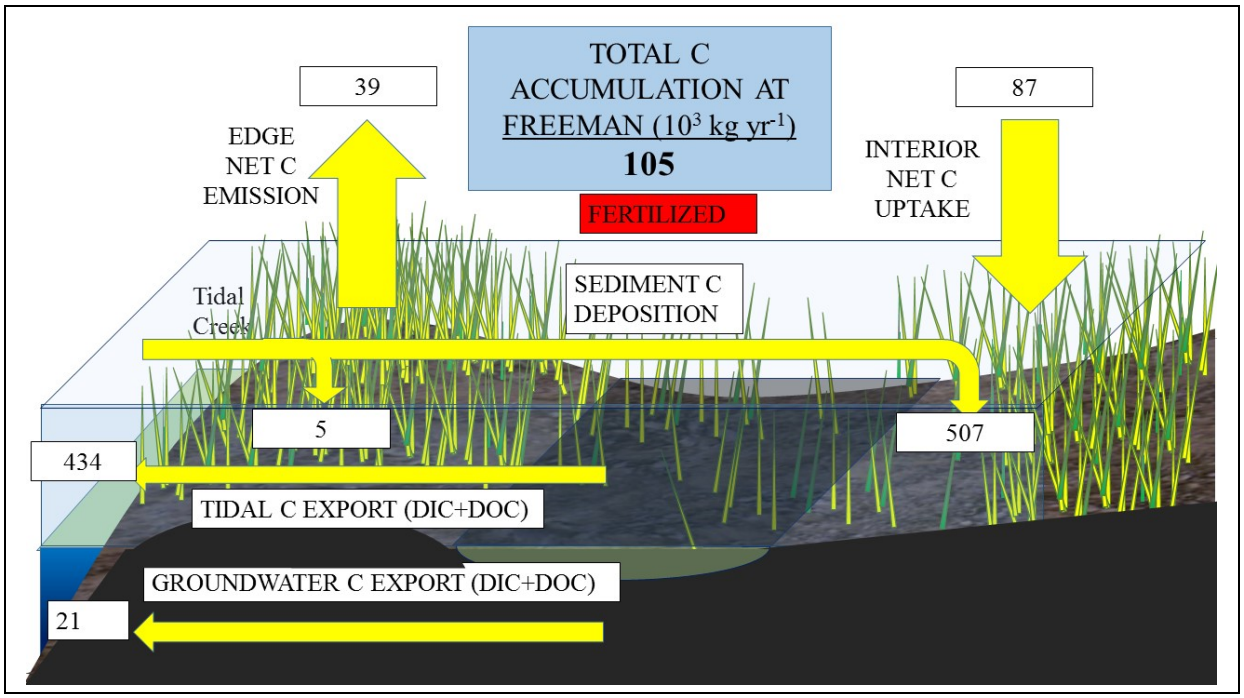

Figure 14-21. Mass balance carbon (C) budget in Freeman Creek marsh with fertilization.

Conclusions and Implications for Future Research and Implementation

Key Scientific Findings

Salt marshes are generally thought to be net autotrophic, accumulating CO_2 through rates of GPP that are higher than respiration. However, here we showed that marshes in specific locations may be net heterotrophic with higher rates of respiration than GPP and net loss of CO_2. Much of the observed loss of CO_2 is likely due to microbial respiration of the dissolved organic matter delivered by sediments. Physical characteristics of a marsh location such as elevation in the tidal framework, tidal amplitude, distance from creek bank, pore water flushing, and pore water residence time influence pore water chemistry, which in turn drives differences in plant primary production and sediment carbon and nitrogen processing. For example, H_2S accumulation in interior marsh sites is greater than in well-flushed marsh edge sites. The high H_2S may reduce plant uptake of nitrogen necessary for primary production and result in the observed accumulation of NH_4^+ in interior marsh pore water.

Carbon exchanges in coastal marshes may occur via influxes or effluxes of CO_2 to the atmosphere, via lateral exchanges of DIC and DOC between the marsh surface and sub-surface and the adjacent creek, and by inputs or exports of sediment carbon. Lateral export in tidal water and sediment carbon inputs were larger in magnitude than CO_2 exchanges between marsh and atmosphere in these marshes; CH_4 emissions were negligible. In both Freeman Creek and Traps Bay Creek, sediment carbon input was the largest net source and lateral export was the largest net loss of carbon to and from the marsh. Even though Freeman Creek as a whole was net autotrophic based upon its CO_2 exchanges with the atmosphere, lateral carbon export resulted in net loss of carbon. However, fertilization reversed the loss of carbon from Freeman Creek, primarily due to increased sediment OM input. Because of low sediment OM input and low below-ground biomass, Freeman Creek edge is likely to be more unstable than Freeman Creek interior and more susceptible to erosion as has been observed in some New England marshes (Deegan et al., 2012). It is, therefore, imperative that salt marshes, especially those that are net heterotrophic, maintain their supply of sediment to continue to accumulate carbon and sustain their elevation relative to sea level rise. Future research may include determining whether the source of the accreted sediment carbon is from terrestrial uplands, eroded material from other marshes, or from the coastal ocean. The magnitude and variability of lateral carbon export from salt marshes and, thus, the contribution of marsh derived DIC to estuaries and the coastal ocean are of major concern and require additional research.

Previous studies at the NRE have suggested that fertilization can potentially increase sustainability of *S. alterniflora* marshes (Davis et al., 2017). Fertilization increases above-ground biomass, which in turn increases sediment trapping, enabling the marsh to keep pace with sea level rise. At both Freeman Creek and Traps Bay Creek, fertilization caused an increase in above-ground biomass and resulted in increased sediment carbon inputs; however, at the same time, fertilization increased net losses of CO_2 and CH_4 at Freeman Creek edge marsh through metabolism and decreased below-ground biomass in Freeman Creek and Traps Bay Creek interior marshes. Fertilization had a greater impact on marsh locations with short pore water residence times and low H_2S concentrations. Specific marsh locations are more vulnerable to nitrogen pollution than others, depending upon the physical characteristics of the marsh. Based on the calculated carbon mass balance for Freeman Creek, if the entire marsh was fertilized, then

it would slightly increase the net carbon accumulation in that marsh; however, the losses of carbon on the edges of the marsh would be greatly increased. The strong response of edge marsh fertilization has a great effect on the overall mass balance because edge comprises nearly 30% of the entire *S. alterniflora* marsh area. Further research is needed to determine the source and lability of the carbon that is deposited on the marsh surface and its time scale of retention. Results of this study support the use of thin-layer sediment addition to the marsh surface as a method to enhance sustainability.

Research Questions

1. **In *Spartina alterniflora*–dominated salt marsh at similar elevations, how does tide range affect GPP?**
   Longer inundation time corresponded to a decrease in GPP. However, the direct effects of tidal range on GPP in a typical NRE marsh were difficult to determine from our chosen sites because the site with low tidal range (Traps Bay Creek) possessed atypical salt marsh hydrology and longer inundation times than the site with higher tidal range (Freeman Creek) and shorter inundation time. Longer inundation time is expected to increase lateral export of carbon as DIC rather than as CO_2 into the atmosphere; however, we were unable to test this hypothesis because there was only an eddy covariance tower in Freeman Creek marsh and not in Traps Bay marsh.

2. **How will the production to respiration ratio vary with sediment accretion rate and elevation?**
   Production to respiration and sediment accretion were found to be inversely correlated in the NRE. Freeman Creek had a greater sediment accretion rate than Traps Bay Creek (3.1 versus 1.8 cm/yr), but a lower production to respiration. Within both sites, fertilization increased sediment accretion rates, but decreased production to respiration. No pattern was detected with elevation. Freeman Creek marsh, a net heterotrophic site, must import sufficient sediment organic carbon to remain sustainable and accumulate carbon.

3. **On an annual time scale, will NRE salt marshes demonstrate a net uptake of CO_2?**
   Freeman Creek marsh, the site that represents most of the salt marsh area in the marshes adjacent to the ICW, was slightly net autotrophic, demonstrating net uptake of CO_2; however, there was net loss of CO_2 at sites close to the creek edge, especially when fertilized.

4. **Is methane an important fate of fixed carbon in the salt marshes of the NRE?**
   Methane fluxes were several orders of magnitude lower than CO_2 fluxes at all sites, and so were a minor fate of fixed carbon in the salt marshes of the NRE.

5. **What are the contributions of DIC, pCO_2, and DOC to diffusive and advective losses of carbon from salt marshes to the overlying water and adjacent tidal creeks?**
   Lateral exports of carbon as DIC and DOC were determined only for Freeman Creek marsh because the water level data for Traps Bay marsh were uncertain. Lateral export was a major factor determining net carbon accumulation for Freeman Creek marsh. The contribution of DIC and DOC from marshes to the NRE was negligible relative to other sources of carbon because of the marsh limited aerial extent (120 ha marsh to 7872 ha estuary).

6. **On an annual time scale, will NRE salt marshes demonstrate a net uptake of dissolved inorganic nitrogen (DIN) and phosphorus from overlying water?**
   Patterns of DIN uptake and release in the dark were highly variable by location and season, but generally displayed a larger net release of phosphorus and ammonium and a smaller uptake of nitrate, resulting in an overall net release of phosphorus and DIN on an annual time scale.

Findings with Implications for Future Base Management

The observations of net loss of carbon at Freeman Creek marsh, slight accumulation of carbon in response to fertilization, and the need for sediment carbon input to sustain the marsh especially at edge locations, highlights the need for managers to control eutrophication in the NRE and to seek methods to implement sediment carbon inputs. Fertilization should be avoided on the creek bank habitats, where negative impacts outweigh positive effects.

Literature Cited

Bradley, P.M., and J.T. Morris. 1990. Influence of oxygen and sulfide concentration on nitrogen uptake kinetics in *Spartina alterniflora*. *Ecology 71*(1):282–287.

Burgin, A.J., and S.K. Hamilton. 2007. Have we overemphasized the role of denitrification in aquatic ecosystems? A review of nitrate removal pathways. *Frontiers in Ecology and the Environment 5*(2):89–96.

Cline, J.D. 1969. Spectrophotometric determination of hydrogen sulfide in natural waters. *Limnology and Oceanography 14*(3):454–458.

Darby, F.A., and R.E. Turner. 2008. Effects of eutrophication on salt marsh root and rhizome biomass accumulation. *Marine Ecology Progress Series* 363:63–70.

Davis, J., C. Currin, and J.T. Morris. 2017. Impacts of fertilization and tidal inundation on elevation change in microtidal, low relief salt marshes. *Estuaries and Coasts 40*(6):1677–1687.

Deegan, L.A., D.S. Johnson, R.S. Warren, B.J. Peterson, J.W. Fleeger, S. Fagherazzi, and W.M. Wollheim. 2012. Coastal eutrophication as a driver of salt marsh loss. *Nature 490*:388–392.

Duarte, C.M., J.J. Middelburg, and N. Caraco. 2005. Major role of marine vegetation on the oceanic carbon cycle. *Biogeosciences 2*:1–8.

Ensign, S., C. Currin, M. Piehler, and C. Tobias. 2017. A method for using shoreline morphology to predict suspended sediment concentration in tidal creeks. *Geomorphology 276*:280–288.

Fredrichs, C.T., and J.E. Perry. 2001. Tidal salt marsh morphodynamics: A synthesis. *Journal of Coastal Research 27*:7–37.

Graham, S.A., and I.A. Mendelssohn. 2014. Coastal wetland stability maintained through counterbalancing accretionary responses to chronic nutrient enrichment. *Ecology 95*(12):3271–3283.

Howarth, R.W., and A. Giblin. 1983. Sulfate reduction in the salt marshes at Sapelo Island, Georgia. *Limnology and Oceanography 28*:70–82.

Howes, B.L., J.W.H. Dacey, and G.M. King. 1984. Carbon flow through oxygen and sulfate reduction pathways in salt marsh sediments. *Limnology and Oceanography 29*(5):1037–1051.

Jassby, A.D., and T. Platt. 1976. Mathematical formulation of the relationship between photosynthesis and light for phytoplankton. *Limnology and Oceanography 21*(4):540–547.

Joye, S.B., and J.T. Holibaugh. 1995. Influence of sulfide inhibition of nitrification on nitrogen regeneration in sediments. *Science 270*:623–625.

Kathilankal, J.C., T.J. Mozdzer, J.D. Fuentes, P. D'Odorico, K.J. McGlathery, and J.C. Zieman. 2008. Tidal influences on carbon assimilation by a salt marsh. *Environmental Research Letters 3*:044010.

Kirwan, M.L., S. Temmerman, E.E. Skeehan, G.R. Guntenspergen, and S. Fagherazzi. 2016. Overestimation of marsh vulnerability to sea level rise. *Nature Climate Change 6*:253–260.

Koop-Jakobsen, K., and A.E. Giblin. 2010. The effect of increased nitrate loading on nitrate reduction via denitrification and DNRA in salt marsh sediments. *Limnology and Oceanography 55*(2):789–802.

Lettrich, M. 2011. *Nitrogen Advection and Denitrification Loss in Southeastern North Carolina Salt Marshes*. Unpublished master's thesis, University of North Carolina at Wilmington, Wilmington, NC.

Liao, N. 2001. Determination of Ammonia by Flow Injection Analysis. QuikChem Method 10-107-06-1-J. Lachat Instruments, Loveland, CO.

Miller, W.D., S.C. Neubauer, and I.C. Anderson. 2001. Effects of sea level induced disturbances on high salt marsh metabolism. *Estuaries 24*(3):357–367.

Morris J.T. and P.M. Bradley. 1999. Effects of nutrient loading on the carbon balance of coastal wetland sediments. *Limnology and Oceanography 44*(3):699–702.

Morris, J.T., G.P. Shaffer, and J.A. Nyman. 2013. Brinson review: Perspectives on the influence of nutrients on the sustainability of coastal wetlands. *Wetlands 33*:975–988.

Morris J.T., P.V. Sundareshwar, C.T. Nietch, Bjorn Kjerfve, and D.R. Cahoon. 2002. Responses of coastal wetlands to rising sea level. *Ecology 83*(10):2869–2877.

Nelson, J.L., and E.S. Zavaleta. 2012. Salt marsh as a coastal filter for the oceans: Changes in function with experimental increases in nitrogen loading and sea-level rise. *PLoS One 7*(8):e38558.

Neubauer, S.C., and J.P. Megonigal. 2015. Moving beyond global warming potentials to quantify the climatic role of ecosystems. *Ecosystems 18*:1000–1013.

Neubauer, S.C., and I.C. Anderson. 2003. Transport of dissolved inorganic carbon from a tidal freshwater marsh to the York River Estuary. *Limnology and Oceanography 48*(1):299–307.

Neubauer, S.C., K. Givler, S. Valentine, and J.P. Megonigal. 2005. Seasonal patterns and plant-mediated controls of subsurface wetland biogeochemistry. *Ecology 86*(12):3334–3344.

Neubauer, S.C., W.D. Miller, and I.C. Anderson. 2000. Carbon cycling in a tidal freshwater marsh ecosystem: A gas flux study. *Marine Ecology Progress Series 199*:13–30.

Poffenbarger, H.J., B.A. Needelman, and J.P. Megonigal. 2011. Salinity influence on methane emissions from tidal marshes. *Wetlands 31*(5):831–842.

R Core Team. 2014. *R: A Language and Environment for Statistical Computing*. R Foundation for Statistical Computing, Vienna, Australia.

Scavia, D., and S.B. Bricker. 2006. Coastal eutrophication assessment in the United States. *Biogeochemistry 79*:187–208.

Silsbe, G.M., and S.M. Malkin. 2015. *Phytotools: Phytoplankton Production Tools*. Technical Report. February. Available at https://www.researchgate.net/publication/272294040_Phytotools_Phytoplankton_Production_Tools

Tobias, C., and S.C. Neubauer. 2009. Salt marsh biogeochemistry—An overview. Pp. 445–492 in *Coastal Wetlands: An Integrated Ecosystem Approach*. Edited by Perillo, G.M.E., E. Wolanski, D.R. Cahoon, and M.M. Brinson. Elsevier.

Tong, C., W.Q. Wang, J.F. Huang, V. Gauci, L.H. Zhang, and C.S. Zeng. 2012. Invasive alien plants increase CH_4 emissions from a subtropical tidal estuarine wetland. *Biogeochemistry 1–3*:677–693.

Valiela, I. 2015. The Great Sippewissett salt marsh plots—Some history, highlights, and contrails from a long-term study. *Estuaries and Coasts 38*(4):1099–1120.

Wang, S.R., D. Di Lorio, W. Cai, and C.S. Hopkinson. 2017. Inorganic carbon and oxygen dynamics in a marsh-dominated estuary. *Limnology and Oceanography*. doi: 10.1002/lno.10614

Wang, Z.A., K.D. Kroeger, N.K. Ganju, M.E. Gonneea, and S.N. Chu. 2016. Intertidal salt marshes as an important source of inorganic carbon to the coastal ocean. *Limnology and Oceanography 61*(5):1916–1931.

Wiegert, R.G. and B.J. Freeman. 1990. *Tidal Salt Marshes of the Southeast Atlantic Coast: A Community Profile.* Biological Report 85(7.29). Fish and Wildlife Service, U.S. Department of the Interior. Available at https://www.nwrc.usgs.gov/techrpt/85-7-29.pdf

Zervas, C. 2004. *Carolina Bathymetry/Topography Sea Level Rise Project: Determination of Sea Level Trends*. NOAA Technical No. NOS CO-OPS 041. p. 31. Available at https://tidesandcurrents.noaa.gov/publications/techrpt41.pdf

Zhang Y., L. Wang, X. Xie, L. Huang, and Y. Wu. 2013. Effects of invasion of *Spartina alterniflora* and exogenous N deposition on N_2O emissions in a coastal salt marsh. *Ecological Engineering 58*:77–83.

Appendix 14-A
Influence of Salt Marshes on Nitrogen, Phosphorus, and Carbon in Tidal Creek Channels

Influence of Salt Marshes on Nitrogen, Phosphorus, and Carbon in Tidal Creek Channels

Conducted by Dr. Scott Ensign

Objectives

A goal of Research Project CW-5 was to measure the influence of salt marshes on nitrogen, phosphorus, and carbon in tidal creek channels. Salt marsh sediment microbial communities and vegetation may affect nitrogen, phosphorus, and carbon in creek water overlying the marsh during high tide. These concentration changes would subsequently alter the flux of nitrogen, phosphorus, and carbon in the tidal creek channel during low tide. The objective of this research was to measure the rate of concentration change in nitrogen, phosphorus, and carbon in a volume of water isolated on the marsh during high tide. This rate of concentration change can be extrapolated across a salt marsh surface to estimate the mass export of nitrogen, phosphorus, and carbon back to the tidal creek channel at low tide.

Materials and Methods

Plexiglass chambers were created to isolate a volume of water on the marsh, that could be sampled repeatedly over a period of several hours while the marsh was flooded. The square chambers were 0.45-m wide by 1.5-m tall. A 0.025-m hole was drilled on each side 0.1 m from the bottom edge. The chambers were pushed into the marsh surface at low tide until the holes were at the sediment surface to allow water to enter during flood tide. Once the chambers had filled with approximately 10 cm of water during flood tide, stoppers were placed in the holes. To counteract the pressure head gradient that developed as the water elevation continued to rise outside the chamber, we added 1-gallon Ziploc bags of water to the chamber. The Ziploc bags displaced water inside the chamber and raised the water level inside the chamber to match the water level outside the chamber. This method prevented intrusion of water from outside the chamber during the incubation.

Water samples were withdrawn from the chamber every hour for 3 hours, beginning after the chambers were stoppered. Acid-washed syringes and plastic tubing were used to pull water from the chamber to minimize disturbance of the sediment surface. Water was filtered onsite through 0.2-µm polysulfone filters for dissolved organic carbon (DOC), nitrate (NO_3^-), ammonium (NH_4^+), and phosphate (PO_4^{3-}) analysis; stored on ice during transport to the laboratory; and then frozen until analysis. Samples for dissolved inorganic carbon (DIC) were stored in Hungate tubes containing 0.1 mL of HgCl.

Sampling was conducted during daylight, and therefore benthic microalgae and ultraviolet photolytic processes may contribute to changes in nitrogen, phosphorus, and carbon concentrations. Because the rates of concentration change may differ between day and night, we employed light and dark chambers to capture this variability. Two types of chambers were made

and deployed: dark chambers were made of black acrylic with black acrylic tops, and light chambers were made with ultraviolet-transparent acrylic. Dark chambers were shaded by using beach umbrellas to prevent heating and subsequent effects on biogeochemical processes inside the chamber.

During each field deployment, three sets of chambers (three light and three dark per set) were deployed from boardwalks. Chambers were positioned in relatively low elevations on the marsh to ensure that they filled with water quickly as the tide rose and allowed sufficient time for sampling. Additionally, samples were collected from the creek channel, coinciding with each chamber sampling. Water temperature was measured inside the chambers during each sampling.

The rates of concentration change were calculated for each constituent (i.e., DIC, DOC, NO_3^-, NH_4^+, and PO_4^{3-}) during each deployment. Concentrations in each chamber were normalized by subtracting the initial concentration measured by the first sample after the holes in the chambers were stoppered. This normalization allowed the application of a linear regression between concentration (dependent variable) and elapsed time of incubation (independent variable), with a sample size of 24 for each constituent on each sampling date. Data from the dark and light chambers were combined in each regression to provide an integrated, diurnal rate of concentration change.

Results and Discussion

Sampling was conducted at Freeman Creek on 16 April 2016 and 26 August 2016, and at Traps Bay Creek on 18 November 2015 and 2 November 2016. Isolation of water inside the chambers from water outside was achieved in Traps Bay Creek, where Ziploc bags were added to maintain the water level inside at the same elevation as outside the chamber. However, chambers in Freeman Creek did not show development of a water level difference inside versus outside. We assume that the chamber walls were not deep enough to cut off fiddler crab burrows that allowed pore water connectivity between the inside and outside of the chamber. Only two sets of chambers (four total chambers instead of six deployed on all other dates) were measured in Traps Bay Creek on 18 November 2015 because flood tide elevation did not flood the chambers adequately at all locations. The average temperature of water inside the light chambers was, on average, 0.4°C higher than the dark chambers.

Table 14A-1. Water Temperature Inside Chambers During Marsh Incubations

Creek	Date	Mean Temperature of Light Chambers (°C)	Mean Temperature of Dark Chambers (°C)
Freeman	16 April 2016	16.6	16.0
Freeman	26 August 2016	31.1	30.5
Traps Bay	18 November 2015	19.0	19.2
Traps Bay	2 November 2016	17.6	17.5

DIC increased by 0.104 mmol L^{-1} hr^{-1} at Traps Bay Creek in November 2015 (**Table 14A-2 and Figure 14A-1**). In contrast, DIC decreased by 0.013 mmol L^{-1} hr^{-1} in Freeman Creek in August 2016. No significant change in DOC occurred over the course of the incubations. NO_3^- decreased by 0.02 and 0.091 µmol L^{-1} hr^{-1} in Freeman Creek on 26 August 2016 and in Traps Bay Creek on

18 November 2016, respectively. NH_4^+ decreased by 0.416 µmol L^{-1} hr^{-1} in Freeman Creek 26 August 2016. Finally, PO_4^{3-} decreased by 0.045 and 0.020 µmol L^{-1} hr^{-1} in Freeman Creek on 26 August 2016 and in Traps Bay Creek on 2 November 2016, respectively.

Table 14A-2. Results of Linear Regression of Concentration Change as a Function of Incubation Time for Marsh Chamber Incubations During Flood Tide

Creek	Date	Constituent	Units	p	Slope	Intercept
Freeman	16 April 2016	DIC	mM hr^{-1}	0.164	—	—
Freeman	26 August 2016	DIC	mM hr^{-1}	0.005	−0.013[a]	0.002
Traps Bay	18 November 2015	DIC	mM hr^{-1}	0.026	0.104[a]	−0.015
Traps Bay	2 November 2016	DIC	mM hr^{-1}	0.398	—	—
Freeman	16 April 2016	DOC	µM hr^{-1}	0.905	—	—
Freeman	26 August2016	DOC	µM hr^{-1}	0.205	—	—
Traps Bay	18 November 2015	DOC	µM hr^{-1}	0.841	—	—
Traps Bay	2 November 2016	DOC	µM hr^{-1}	0.9615	—	—
Freeman	16 April 2016	NO_3^-	µM hr^{-1}	0.258	—	—
Freeman	26 August 2016	NO_3^-	µM hr^{-1}	0.004	−0.020[a]	0.005
Traps Bay	18 November 2015	NO_3^-	µM hr^{-1}	0.081	−0.091[a]	−0.033
Traps Bay	2 November 2016	NO_3^-	µM hr^{-1}	0.411	—	—
Freeman	16 April 2016	NH_4^+	µM hr^{-1}	0.162	—	—
Freeman	26 August 2016	NH_4^+	µM hr^{-1}	0.009	−0.416[a]	0.263
Traps Bay	18 November 2015	NH_4^+	µM hr^{-1}	0.169	—	—
Traps Bay	2 November 2016	NH_4^+	µM hr^{-1}	0.165	—	—
Freeman	16 April 2016	PO_4^{3-}	µM hr^{-1}	0.386	—	—
Freeman	26 August 2016	PO_4^{3-}	µM hr^{-1}	<0.001	−0.045[a]	−0.006
Traps Bay	18 N 2015	PO_4^{3-}	µM hr^{-1}	0.353	—	—
Traps Bay	2 November 2016	PO_4^{3-}	µM hr^{-1}	0.013	−0.020[a]	−0.002

[a] Significantly different from zero at a=0.05.

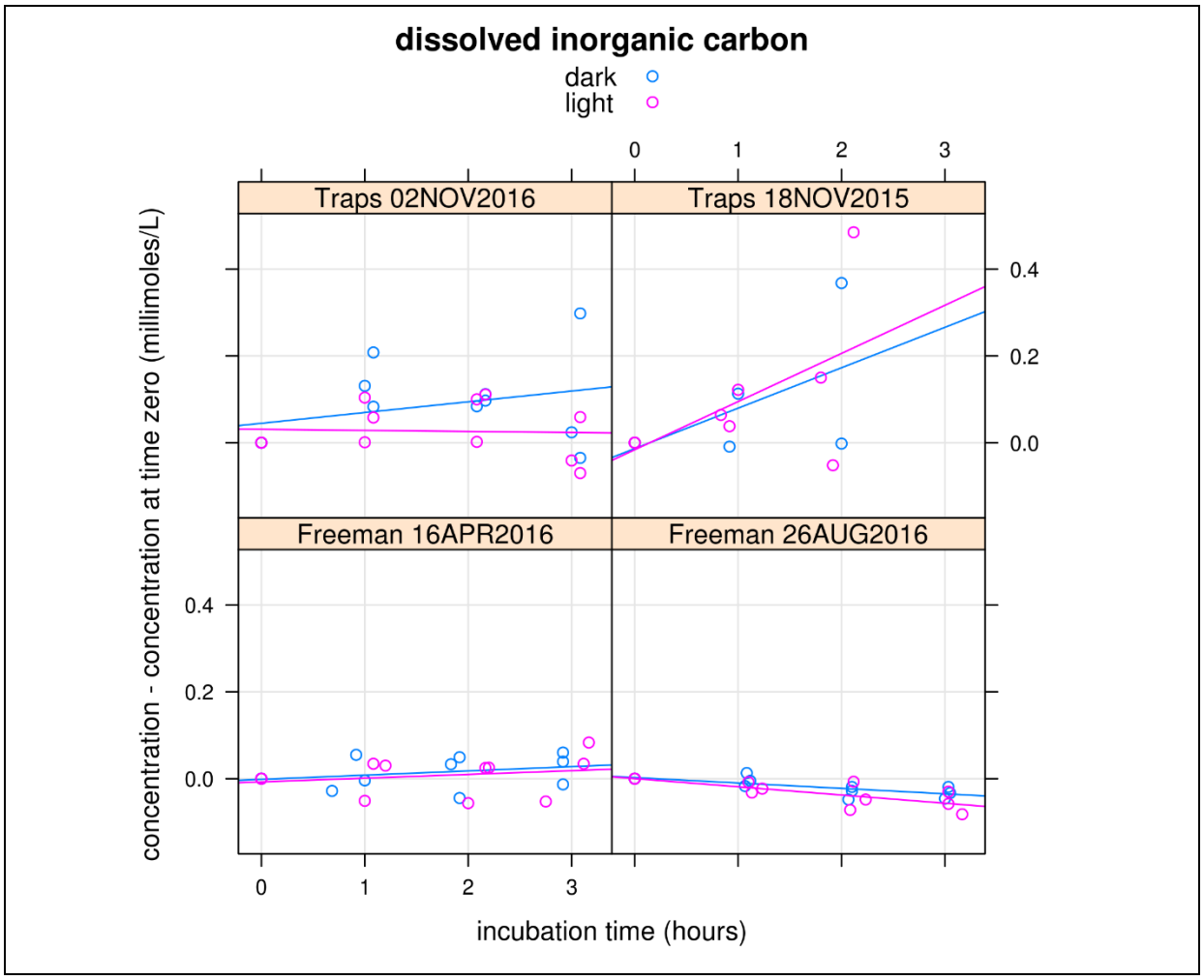

Figure 14A-1. Dissolved inorganic carbon (DIC) concentration changes over time in incubation chambers.

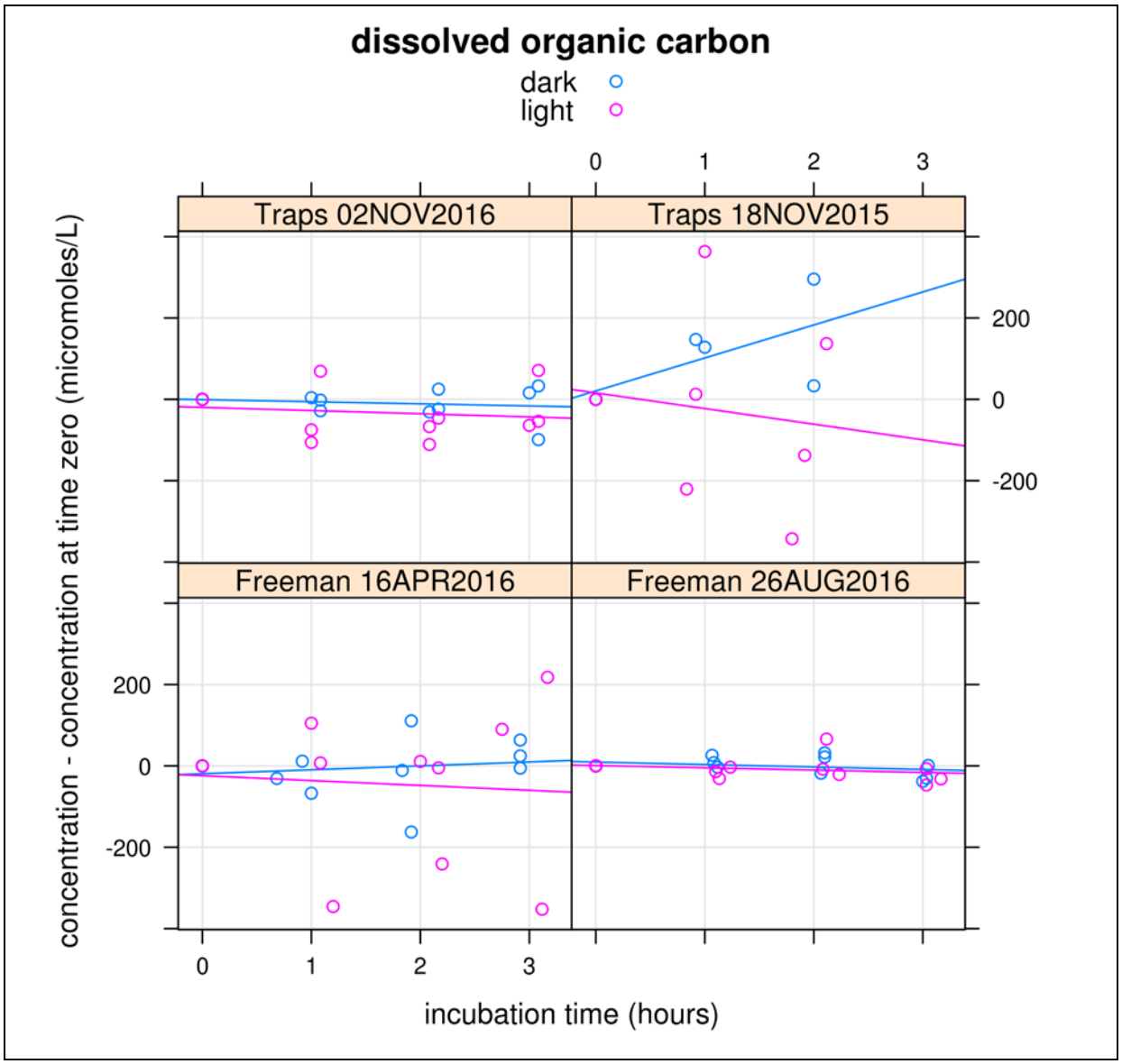

Figure 14A-2. Dissolved organic carbon (DOC) concentration changes over time in incubation chambers.

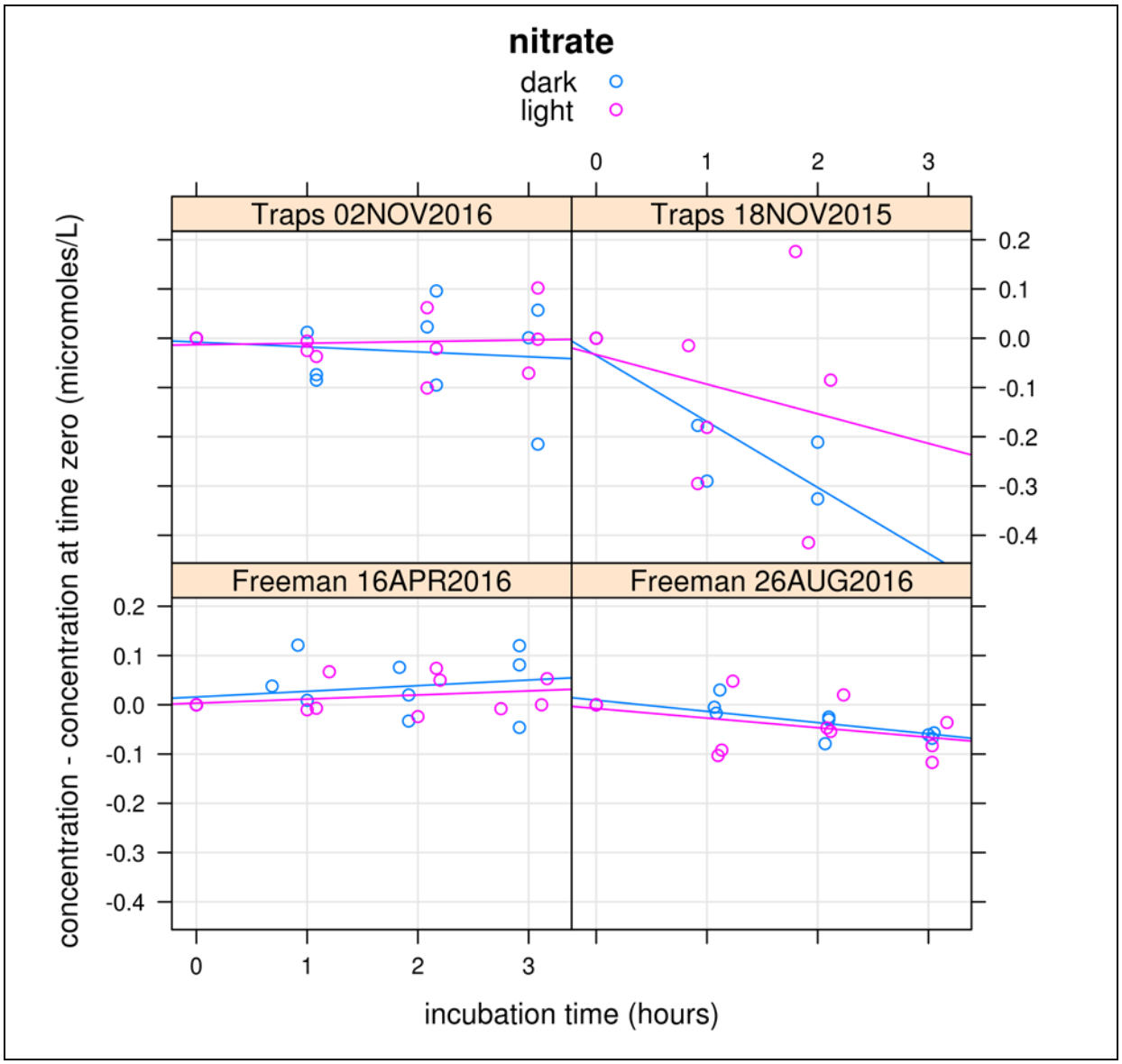

Figure 14A-3. Nitrate (NO_3^-) concentration changes over time in incubation chambers.

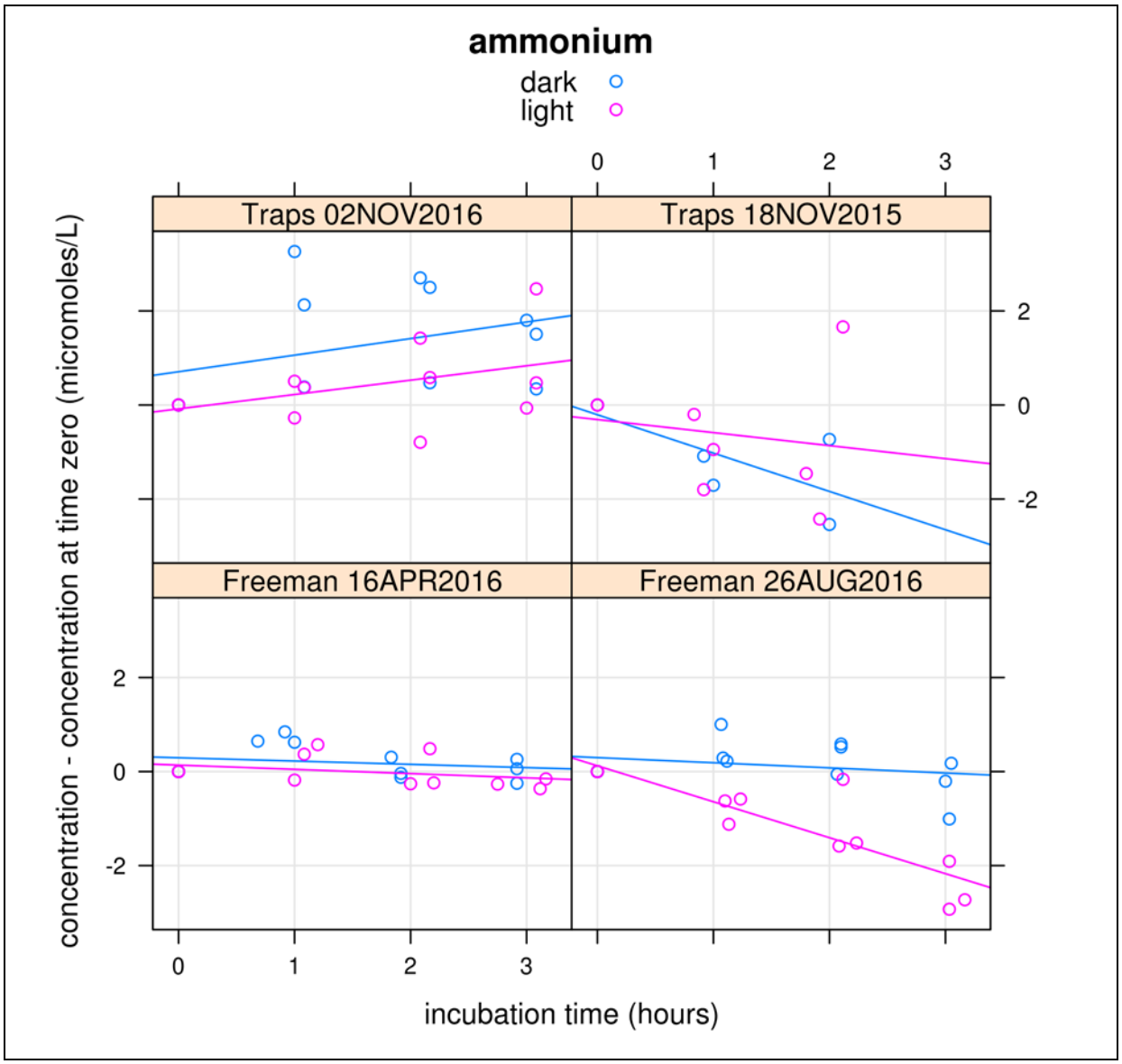

Figure 14A-4. Ammonium (NH_4^+) concentration changes over time in incubation chambers.

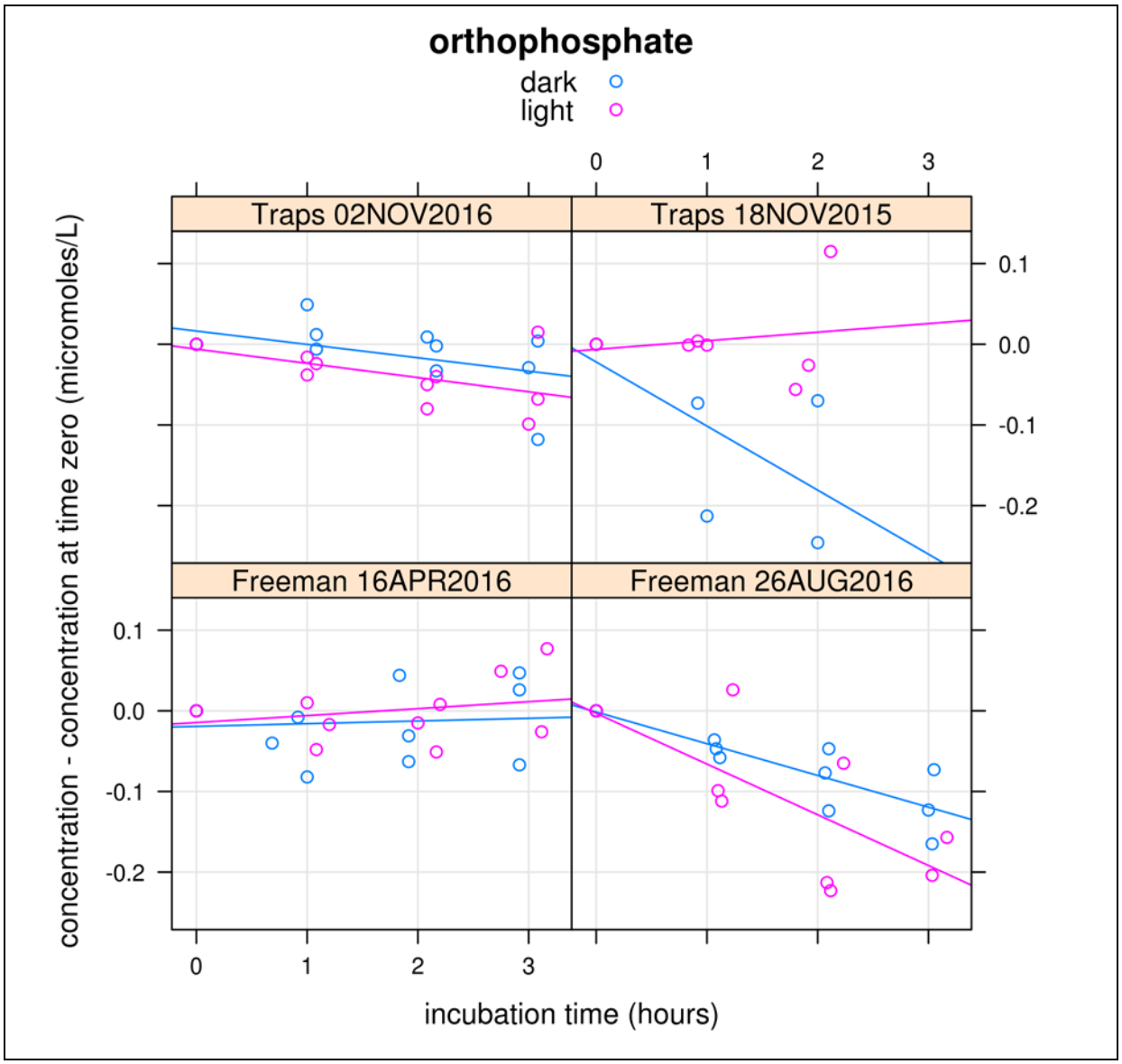

Figure 14A-5. Phosphate (PO_4^{3-}) concentration changes over time in incubation chambers.

Appendix 14-B
List of Scientific/Technical Publications

Papers

None

Thesis

Ken Czapla, doctoral dissertation, in progress (anticipated completion in 2018)

Presentations

Anderson, I., J. Crosswell, K. Czapla, and B. Van Dam. 2017. *Carbon Transformations and Source-Sink Dynamics Along a River, Marsh, Estuary, Ocean Continuum*. To be presented at the American Geophysical Union, New Orleans LA. December. (Invited speaker).

Anderson, I., C. Currin, C. Tobias, K. Czapla, N. McTigue, and S. Ensign. 2017. *Lateral Export of Carbon from Salt Marshes to Adjacent Aquatic Systems*. To be presented at the Conference of the Coastal Estuarine Research Federation, Providence, RI. November.

Czapla, K., I. Anderson, J. Stanhope, M. Fogarty, C. Currin, N. McTigue, and E. Herbert. 2017. *Spatial Patterns of Net Community Production in Response to Fertilization in a Polyhaline Marsh*. To be presented at the Conference of the Coastal Estuarine Research Federation, Providence, RI. November.

Anderson, I., K. Czapla, and E. Herbert. 2017. *Salt Marsh Metabolism and Carbon Accumulation*. Presented at Ocean Carbon and Biogeochemistry, Woods Hole, MA. June. (Invited speaker).

Czapla, K., I. Anderson, E. Herbert, and M. Fogarty. 2017. *Salt Marsh Metabolism and Carbon Accumulation: Effects of Location and Fertilization*. Poster presented at Ocean Carbon and Biogeochemistry, Woods Hole, MA. June.

Anderson, I., M. Brush, J. Stanhope, J. Crosswell, H. Paerl, M. Piehler, B. McKee, and B. Van Dam. 2017. *Carbon Budget of a Shallow, Lagoon Estuary: Transformations and Source-Sink Dynamics*. Presented at the University of South Alabama, Dauphin Island Sea Laboratory, AL. April. (Invited plenary speaker).

Anderson, I., J. Crosswell, and B. Van Dam. 2017. *Carbon Transformations and Source—Sink Dynamics Along a River, Estuary, Ocean Continuum*. Presented at the Annual Meeting of the North America Carbon Program, Bethesda, MD. February. (Invited speaker)

Czapla, K., I. Anderson, and J. Stanhope. 2016. *Effective Edges: Salt Marsh Creek Banks as Hotspots for N Removal*. Presented to the Atlantic Estuarine Research Society, Virginia Beach, VA. March.

Anderson, I., J. Stanhope, B. Van Dam, N. Hall, J. Croswell, H. Paerl, and M. Brush. 2015. *Bio-physical Controls of CO_2 Fluxes Along a River–Estuary Continuum*. Presented at the Conference of the Coastal and Estuarine Research Federation, Portland, OR. November.

Stanhope, J., I. Anderson, J. Croswell, B. Van Dam, H. Paerl, and H. Walker. 2015. *A Shallow Photic Estuary in North Carolina: A Source or Sink of Carbon Dioxide?* Presented at the Conference of the Coastal and Estuarine Research Federation, Portland, OR. November.

Van Dam, B., J. Stanhope, I. Anderson, and H. Paerl. 2015. *Estuarine CO_2 Flux: A Comparison of Two North Carolina Estuaries*. Presented at the Conference of the Coastal and Estuarine Research Federation, Portland, OR. November.

Paerl, H.W., I.C. Anderson, W.S. Gardner, M.J. McCarthy, N.S. Hall, B.L. Peierls, and K.L. Rossignol. 2015. *Controlling Eutrophication Along the Freshwater–Marine Continuum: Why the Need for Dual Nutrient Input Constraints?* Presented at the Conference of the Coastal and Estuarine Research Federation, Portland, OR. November.

Stanhope, J.W., I.C. Anderson, M.J. Brush, C.A. Currin, and M.F. Piehler. 2013. *Benthic Microbial Responses to Interacting Physical-Biological Drivers in a Shallow Estuary*. Presented at the Conference of the Coastal and Estuarine Research Federation, San Diego, CA.

Anderson, I.C.. 2014. *Interacting Drivers Regulating the Fate of Nitrogen in Shallow Photic Marine Systems*. Presented at the Joint Aquatic Sciences Meeting, Santa Fe, NM. May.

Anderson, I.C. 2012. *Responses of the Benthic Filter to Physical Drivers*. Presented at the University of Parma, Parma, Italy. October. (Invited)

Anderson, I.C. 2012. *The Role of the Benthic Filter in Shallow Estuaries*. Presented at the East China Normal University, Shanghai, China. June 2012. (Invited)

Anderson, I.C. 2012. *Tracking the Fate of Carbon and Nitrogen in a Shallow Photic Coastal Lagoon*. Presented at East China Normal University, Shanghai, China. June. (Invited)

Appendix 14-C
List of Students

- Ken Czapla, Ph.D., Virginia Institute of Marine Sciences, in progress

Chapter 15

Predicting Sustainability of Coastal Military Training Environments: Developing and Evaluating a Simplified, Numerical Morphology Model

SERDP Project Number: RC-2245

Coastal Barrier Module

Research Project CB-4

Lead Researcher:

Dr. Jesse McNinch,
U.S. Army Corps of Engineers,
Engineer Research and Development Center, Coastal & Hydraulics Laboratory
Jesse.McNinch@usace.army.mil

Supporting Researchers:

Dr. Richard Luettich, UNC-IMS
Dr. Brad Johnson, USACE
Dr. Janelle Fleming, Seahorse Coastal Consulting
Dr. Jason Fleming, Seahorse Coastal Consulting

November 2017

Final

This report was prepared under contract to the U.S. Department of Defense (DoD) Strategic Environmental Research and Development Program (SERDP). The publication of this report does not indicate endorsement by DoD, nor should the contents be construed as reflecting the official policy or position of DoD. References herein to any specific commercial product, process, or service by trade name, trademark, manufacturer, or otherwise, do not necessarily constitute or imply its endorsement, recommendation, or favoring by DoD.

Table of Contents

Acronyms 15-v
Abstract 15-1
Objectives of the Research Project 15-2
Background 15-2
Model Formulation 15-4
Methods 15-5
Beach Morphology Model CSHORE-C15 15-5
Beach Topography and Nearshore Bathymetry 15-6
Waves 15-7
Water Level: Tides, Storm Surge, and Sea Level Rise 15-9
Sea Level: Future Projections 15-11
Climate: Winds 15-12
Results and Discussion 15-15
Hindcast Results: 1989–2009 15-15
Forecast Results: 2017–2065 15-17
Conclusions and Implications for Future Research and Implementation 15-24
Key Scientific Findings 15-24
Research Questions 15-24
Findings with Implications for Future Base Management 15-25
Literature Cited 15-25
Appendix 15-A: List of Scientific/Technical Publications 15-A-1

List of Figures

Figure 15-1. Location map of Onslow Beach, North Carolina showing the varying topography and uses along the barrier island. 15-3
Figure 15-2. Examples of high-resolution LiDAR topography collected at Onslow Beach during DCERP1 for initiation of CSHORE-C15 morphology model. 15-7
Figure 15-3. Climate signals embedded within winds and WIS wave results from Onslow Beach. 15-8
Figure 15-4. Relationship of observed local winds and significant wave height at Onslow Beach. 15-9
Figure 15-5. Relationship of observed local winds and water level (without astronomical tide) at Onslow Beach. 15-11
Figure 15-6. Sea level rise curves developed for Onslow Beach region 2010–2065; x-axis label refers to calendar year (Hall et al., 2016). 15-12

Figure 15-7. Mean and standard deviation of 13 MACA down-scaled wind model deltas from the Onslow Beach region. 15-14

Figure 15-8. Mean and standard deviation of 13 MACA down-scaled wind model deltas from the Onslow Beach region comparing the two 20-year periods, 1989–2009 (hindcast) and 2045–2065 (forecast). 15-14

Figure 15-9. Running 20-year means of 13 MACA down-scaled wind forecasts for Onslow Beach from 1989–2065 in units of wind power $(m/s)^3$ in top panel. Percent difference from 20-year mean between 1989 and 2065 (bottom panel). 15-15

Figure 15-10. CSHORE-C15 hindcast results, 1989–2009, showing a 20.7-m cumulative root mean square error (RMSE) of shoreline prediction versus observed. 15-17

Figure 15-11. Modeled shoreline change rates (in m/yr) in three regions of Onslow Beach from 2017–2065 under different sea level rise rates. 15-18

Figure 15-12. CSHORE-C15 predictions of shoreline and beach position in 2040 across the Onslow Beach recreational and training areas under highest and lowest sea level rise scenarios. 15-20

Figure 15-13. CSHORE-C15 predictions of shoreline and beach position in 2065 across the Onslow Beach recreational and training areas under highest and lowest sea level rise scenarios. 15-20

Figure 15-14. CSHORE-C15 predictions of shoreline and beach position in 2065 across the Onslow Beach central training area under highest and lowest sea level rise scenarios. 15-21

Figure 15-15. CSHORE-C15 predictions of shoreline and beach position in 2065 across the Onslow Beach northern training area under highest and lowest sea level rise scenarios. 15-21

Figure 15-16. Modeled mean, annual shoreline change rate (in m/yr) 2015–2065 at Onslow Beach under different sea level rise rates. 15-22

Figure 15-17. Predictions of shoreline and beach position in 2100 by using extrapolated long-term shoreline change rates (CSHORE-C15 simulations 2017–2065) across the Onslow Beach recreational and training area under highest and lowest sea level rise scenarios. 15-23

Figure 15-18. Predictions of shoreline and beach position in 2100 using extrapolated long-term shoreline change rates (CSHORE-C15 simulations 2017–2065) across the Onslow Beach southern training area under highest and lowest sea level rise scenarios. 15-23

List of Tables

Table 15-1. Sea Level Rise Equation Coefficients Developed for Onslow Beach (Hall et al., 2016) 15-12

Table 15-2. MACA downscaled, wind forecast models used in study 15-13

Acronyms

2-D	two dimensional
3-D	three dimensional
ADCIRC	Advanced Circulation (Model)
CB	Coastal Barrier (Module)
CDIP	Coastal Data Information Program (Waverider)
cm	centimeter
DCERP	Defense Coastal/Estuarine Research Program
DCERP1	first cycle of DCERP
DCERP2	second cycle of DCERP
DoD	U.S. Department of Defense
ENSO	El Niño-Southern Oscillation
ft	feet, foot
GEOMBEST	Geomorphic Model of Barrier, Estuarine, and Shoreface Translations
ICW	Intracoastal Waterway
km	kilometer
km^2	square kilometer
LiDAR	light detection and ranging
m	meter
m^3/s	cubic meters per second
MACA	Multivariate Adaptive Constructed Analogs
MCBCL	Marine Corps Base Camp Lejeune
m/yr	meters per year
NAO	North Atlantic Oscillation
RC	Resource Conservation and Climate Change (a SERDP program area)
RCP	representative concentration pathway
RMSE	root mean squared error
SERDP	Strategic Environmental Research and Development Program
UNC-IMS	University of North Carolina at Chapel Hill's Institute of Marine Sciences
USACE	U.S. Army Corps of Engineers
WIS	Wave Information Studies

Abstract

Sustaining beach training environments is a necessary element for expeditionary exercises at Marine Corps Base Camp Lejeune (MCBCL). Although training on Onslow Beach has not yet been interrupted by beach erosion, pre-existing infrastructure has been destroyed (e.g., Riseley Pier, parking lots), and the dramatic changes following recent storms pose a concern to long-term sustainability of this critical asset. Strategies to sustain dynamic environments, such as beaches, that are exposed to a range of natural pressures (e.g., storms, sea level rise) and military uses (e.g., vehicular and amphibious-vessel traffic) are dependent upon assessing the effects of military uses and forecasting changes due to climate forces. Changes to the beach, as measured by shoreline position, beach width, and overwash fans, were evaluated in historical imagery (1932–2009) and maps. DCERP1 findings indicated that storms (defined here by decadal hurricane frequency), not military training use, had the largest influence on beach position and overwash. In lieu of simply extrapolating past shoreline change rates to predict future shoreline position, a simplified numerical morphology model, CSHORE-C15, was developed so that beach changes could be forecast under different scenarios of sea level rise and storms. CSHORE-C15 computes a complete hydrodynamic and sediment transport solution within the breaking wave region and is computationally efficient enough for use in a stochastic framework for long simulated time periods. Model skill was evaluated by using observed forcing conditions and shoreline positions from 1989–2009, and revealed a 20.7 m error in the final shoreline position after 20 years of hourly, cumulative solutions.

Forecast simulations were carried out by using guidance from SERDP regarding five sea level rise rates developed for the Onslow Beach region. Scenarios to encapsulate likely changes in regional storminess were developed through evaluation of 13 down-scaled climate models. The total envelope of forecast wind magnitude indicates minimal changes through 2065, with a maximum delta increase of 8% and a decrease of 10% relative to the ensemble mean. Variations in wave and water level boundary conditions for the model were developed by using simple measurement-based empirical relations. CSHORE-C15 simulations using these possible extremes in wind magnitude revealed negligible differences in shoreline position. However, modeled shoreline position demonstrated a sensitivity to sea level rise scenarios. CSHORE-C15 forecasts of shoreline position, using the highest and lowest sea level rise rates, all indicate substantial loss of infrastructure south of the Onslow Beach Bridge within 20 years, and a complete loss (defined by the primary dune located west of Ocean Drive) within 50 years. Island width, defined by the distance from the primary dune to the Intracoastal Waterway, will be less than 100 m in the northern portion of the training area within 50 years. Conversely, model forecasts using the same range of sea level rise rates and climate forces indicate shoreline position and its associated beach and dune will remain stable and likely grow seaward along the entire reach of Onslow Beach north of the bridge.

Keywords: Beach, CSHORE-C15, erosion, morphology, Onslow Beach, sea level rise, shoreline

Objectives of the Research Project

The overarching objective of Research Project CB-4 was to predict beach morphology and shoreline position, hourly, under varying climate change scenarios from 2015 to 2065. Specifically, a simplified numerical morphology model (CSHORE-C15), along with regional observations and models of relevant hydrodynamics, were used to forecast the response of the Onslow Beach shoreline to variations in storm frequency and relative sea level rise at Marine Corps Base Camp Lejeune (MCBCL). This objective and designed research plan were motivated, in part, to provide actionable management information for sustaining the training function of Onslow Beach into the future.

The goals that were required to meet this objective included the following: (1) the development of CSHORE-C15 and creation of model boundary conditions by using DCERP1 data, (2) the development and assessment of localized waves and water levels (e.g., tides, storm surge) required to force CSHORE-C15, and (3) skill assessment by using beach morphology data observed over the past 26 years (1989–2015) and CSHORE-C15 morphology results. In addition, the required goals included the following: (4) development of forecast scenarios, namely, winds, waves, and water level under varying climate conditions; and (5) CSHORE-C15 simulations under varying climate forcing conditions from 2015–2065.

The hypotheses that were tested included: (1) beach changes, specifically shoreline position, will be spatially consistent along the length of Onslow Beach under each simulated climate forcing scenario, (2) beach morphology changes will be attenuated relative to increases or decreases in winds, and (3) the highest rates of sea level rise generate the highest shoreline change along Onslow Beach.

Background

Onslow Beach is a transgressive barrier island located on the eastern coast of the United States along the chain of barrier islands extending from Cape Lookout to Cape Fear in North Carolina (**Figure 15-1**). Bordered by Brown's Inlet to the northeast and the New River Inlet to the southwest, the island is approximately 12 km in length and covers an area of approximately 5 km^2. The northeastern half of the island is characterized by well-developed dune ridges and a stable to accretionary shoreline with few overwash fans. In contrast, the southwestern half of the island is characterized by poorly-developed segmented dunes, experiences chronic, long-term erosion (>3 m/yr near New River Inlet; Morton et al., 2005) and is the site of extensive active and historical overwash. Onslow Beach is a mixed energy/wave-dominated barrier island (Hayes, 1979). The mean tidal range is approximately 1 m, mean significant wave height 0.91 m, and dominant wave period 7.4 seconds (National Data Buoy Center, 2009). The dominant wave direction is from the SE during the spring and summer and from the NE during the winter. The impact of winter storm waves approaching from the northeast, however, is dampened due to partial sheltering provided by Cape Lookout.

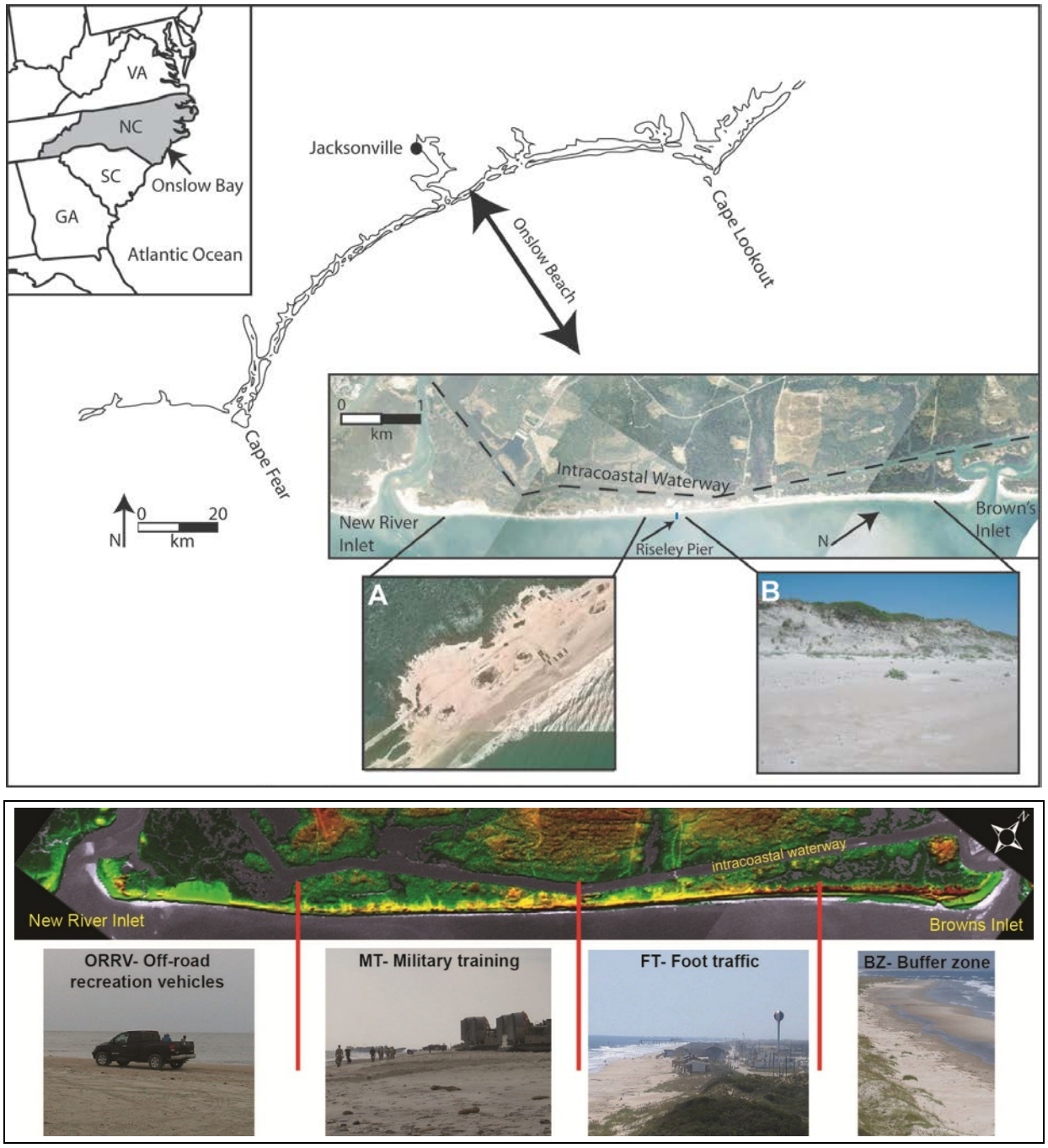

Figure 15-1. Location map of Onslow Beach, North Carolina showing the varying topography and uses along the barrier island.

Offshore sediment availability in Onslow Bay is severely limited. The elongate shoals at Cape Fear and Cape Lookout limit exchange from adjacent embayments (McNinch and Wells, 1999), and with no significant local fluvial inputs, the accumulation of recent nearshore sediment which is well-developed elsewhere on the southeastern US Atlantic shelf is essentially absent here (Cleary and Pilkey, 1968). More than 200 box dredge samples collected on the continental shelf of Onslow Bay reveal a patchwork of primarily relict or residual sediments (Cleary and Pilkey, 1968). Recent acoustic mapping by Wadman et al. (2008) reveals the only significant nearshore

sand is a narrow wedge approximately 4-m thick just offshore of Brown's Inlet that tapers both offshore and towards the southwest. Sidescan and sub-bottom data indicate that the rest of the nearshore (water depths up to 11 m) is characterized by either a thin (<20 cm) veneer of sand overlying indurated hard bottom; or relict sediments (Wadman et al., 2008). An 1872 U.S. Coast and Geodetic Survey topographic sheet shows that Onslow Beach was historically connected to the mainland by a marshy habitat containing narrow, sinuous channels. In 1932, the landward boundary of the barrier island was drastically altered with the construction of the Atlantic Intracoastal Waterway (ICW) (Cleary and Riggs, 1999), which separated the island from the mainland with a 60-m wide linear channel. The modern ICW averages 130 meters in width and is maintained to a depth of approximately 3.7 m (12 ft mean low water) by the U.S. Army Corps of Engineers (http://www.saw.usace.army.mil/nav/aiww.htm).

A chronic challenge to managing coastal facilities and their associated environments is obtaining accurate and up-to-date predictions of where the shoreline, beach, and dunes will be located in the coming decades. Most engineering projects strive for 30- to 50-year time spans, but knowledge of how these coastal environments will change and how they can best be used from a military training perspective is very limited over decadal time scales. The difficulty in predicting future shoreline position partly stems from the fact that simply extrapolating past shoreline change is problematic when considering that many of the environmental conditions forcing shoreline behavior (e.g., sea level rise, storms) are likely to vary in the coming decades with climate change. The difficulty is further complicated because numerical models that have been developed to predict coastal morphology change are expensive to execute and do not easily scale-up from seconds to hours (e.g., storm wave events) to longer, annual-decadal time periods. Simply put, how a beach may respond to a particular storm event in most locations is not what one may expect over the coming decade, nor can long-term shoreline change data be scaled down to predict what one may expect from the next storm event. During Research Project CB-4, the team developed and evaluated a simplified numerical coastal morphology model (CSHORE-C15) that retains detailed sediment transport calculations. In addition, CSHORE-C15 can respond to changes in forcing conditions on an hourly basis, yet can be simulated over longer, management-relevant time periods.

Model Formulation

Currently, there are three general categories of shoreline change models: box models, equilibrium models, and deterministic physical models. Geology box models operate over large time and spatial scales and essentially undertake an accounting exercise that tracks the volume of sand encompassed within the island as it migrates under different scenarios of relative sea level change (e.g., the Geomorphic Model of Barrier, Estuarine, and Shoreface Translations [GEOMBEST]). Although the geology box models can incorporate varying stratigraphy and the influence of shifts in relative sea level rise, they are not designed to provide predictions of shoreline position on a storm-by-storm basis.

Equilibrium models, used by researchers such as Yates et al. (2009) and Plant et al. (1999), can demonstrate skill for morphology change predictions, but the method is completely dependent upon an extensive set of training data, which are exceptionally uncommon. Furthermore, the level of uncertainty in the predictions is large for any previously unobserved conditions, such as transgression into different geology, or climate and sea level variations.

Deterministic physical models for nearshore change (e.g., MIKE21, Delft3D, XBeach) are based on the solution of a two-dimensional (2-D) or three-dimensional (3-D) horizontal hydrodynamic balance and sediment transport equations. These more resolved and computationally intensive methods have reached some level of maturity in the prediction of waves and currents (Dietrich et al., 2010). However, without a focus on the importance of breaking waves and without a representation of the swash zone, the predictions of nearshore sediment transport and morphology have not approached a similar level of accuracy. Indeed, the practical ability to predict coastal morphology over storms and the intervening quiescent periods remains a challenge to the coastal community, and is ultimately necessary to correctly predict shoreline change over seasonal–decadal time periods to be relevant for U.S. Department of Defense (DoD) installation management. CSHORE-C15 is a deterministic model (details described in later section) that has been simplified to enable execution over longer time periods.

Sea level rise and associated shoreline transgression are important to coastal DoD installations such as MCBCL at time scales spanning storm events (hour–days) to decades because the geology underlying the migrating beach and nearshore dictates the: (1) morphology and bathymetry of the surf zone, and sometimes (2) the volume of sand that may be recycled and contributed to the modern sediment budget. For example, regions of the barrier island that migrate into rock behave differently from regions that migrate into largely muddy sediments. Interestingly, it is not just a simple matter of one region being more erosion resistant than others or one region providing more sand than another. The characteristics of the geology exposed in the surf zone influence the bathymetry which, in turn, influences the wave energy and sediment transport at very small spatial scales (0–1,000 m; McNinch, 2004; McNinch et al., 2012). Recognizing this complex feedback between underlying geology and hydrodynamic processes at short time scales (hours–days) and its implications to shoreline management over longer periods (seasons–decades), represents a significant advancement in the coastal processes community (developed, in part, from DCERP1 findings). Additionally, barrier islands have a limited retreat and can have overtopping, and the application of the idealized methods for evolution of a mainland coast are not applicable. The dynamic response of the beach to these varying influences (e.g. waves, sea level, geology, sediment supply) highlight the likely error of simply projecting a new shoreline position based solely on raising water level to a matching topographic elevation (i.e., bathtub flooding approach) or extrapolating shoreline change by using past shoreline behavior. Much of the literature over the past couple of decades (e.g., Browder and McNinch, 2006; Houser et al., 2008; McNinch, 2004; Riggs et al., 1999; Schupp et al., 2006) correctly argued that geology played an important role in shoreline processes, but it was a very simplistic understanding based largely on spatial association and did not transition to physics-based equations that could be used in forecast models.

Methods

Beach Morphology Model CSHORE-C15

The CSHORE-C15 is a generalization of the one-dimensional cross-shore hydrodynamic and morphological evolution model CSHORE to include gentle variation in the longshore direction.

The CSHORE beach morphology model, developed by the U.S. Army Corps of Engineers (USACE) for the past several years, has reached some level of maturity and provided practical

and accurate code to predict beach profile evolution over the nearshore region in a computationally efficient manner. The interested reader is referred to Johnson et al. (2012) for a complete description of the one-dimensional model. The majority of the CSHORE development effort was in the new and physically defensible sediment transport algorithms for a nearshore breaking wave environment. The model accounts for wave and current interaction, bedload and suspended loads, and wave-related sediment transport within the surf and swash zones. The CSHORE model, however, only predicts morphological evolution on the basis of cross-shore transport, and is appropriate for application in cases of strict longshore uniformity.

While Onslow Beach is characterized by a continuous and relatively smooth coast, variations in shoreline orientation along the island can drive gradients in the longshore transport and result in persistent shoreline change. To properly include the impact of the longshore gradients, the generalized CSHORE-C15 model was developed. In the new formulation, sediment transport gradients in both the cross-shore and alongshore are computed and result in morphological change. The sand transport in the cross-shore direction is rapidly varying, and the resultant bed changes are computed frequently in accordance with the numerical stability criteria. Alongshore transport gradients, in contrast, have a smaller but cumulative impact. The newly-developed model computes bottom position changes through the domain with a global sediment conservation statement enacted daily. Within this framework, divergence of longshore transport between transects manifests as shoreline change. The CSHORE-C15 model, however, does not account for pronounced longshore variation in sediment transport potential. A groin field, for instance, would limit the sediment transport in a manner that would violate the CSHORE-C15 model assumptions. For gradually varying coast, the model is as accurate as a fully 3-D morphology model that is difficult to run over longer climate-relevant time periods, and the model is applicable for the gently varying coast at Onslow Beach.

Beach Topography and Nearshore Bathymetry

Initial bathymetry and beach topography conditions for the initiation of CSHORE-C15 were garnered from the extensive bathymetry and topography data already collected along Onslow Beach during DCERP1 (RTI International, 2013), as well as from historical shorelines (Foxgrover, 2009). High-resolution light detection and ranging (LiDAR) topography of the upper beach, primary dune face, and dune crest was critical initial conditions for modeling morphology change, including the effects of wave runup, overwash, and nearshore sediment transport (**Figure 15-2**).

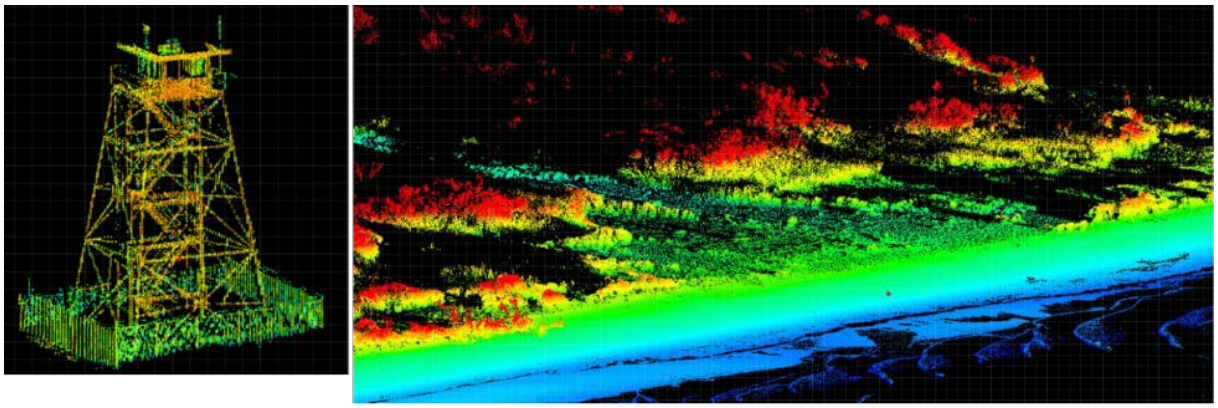

North observation tower

Onslow Beach topography showing dunes in warm colors across the beach to waves in the surf zone.

Figure 15-2. Examples of high-resolution LiDAR topography collected at Onslow Beach during DCERP1 for initiation of CSHORE-C15 morphology model.

Waves

Other funded research projects near MCBCL since 2011 were leveraged to deploy a continuous, real-time wave buoy (Coastal Data Information Program [CDIP#190] Waverider) in shallow water to provide recent observations of waves on the inner shelf near Onslow Beach. These wave data were consistent with the virtual Wave Information Studies (WIS) station located in the nearshore of Onslow Beach. Wave data from the past 30 years were obtained from a WIS modeled nearshore station node located just seaward of Onslow Beach. The WIS is a USACE–sponsored project that generates consistent, hourly, long-term (30+ years) wave climatologies along all U.S. coastlines, including the Great Lakes and U.S. island territories. The WIS program originated in the Great Lakes in the mid-1970s and migrated to the Atlantic and Pacific Oceans and the Gulf of Mexico. Unlike a forecast, a wave hindcast predicts past wave conditions by using a computer model and observed wind fields. By using value-added wind fields, which combine ground and satellite wind observations, hindcast wave information is generally of higher accuracy than forecast wave conditions and compares well with observed wave conditions. The WIS database provides hindcast wave information for a densely spaced series of "virtual wave gauges" in water depths between 15 m and 20 m and for a less-dense series in deeper water (100 m or more). Hindcast data available from each site include hourly wind speed, wind direction, and bulk wave parameters (significant wave height, period, and direction). For more information about WIS, see the Field Research Facility's Web site at http://wis.usace.army.mil/WIS_Documentation.shtml.

The hourly time series of wave data from 1989–2009, located in 9-m depth just seaward of Onslow Beach, was used to force CSHORE-C15 during the hindcast simulations. The observed wind fields used by WIS encompassed past meteorological climate signals embedded in the winds such as the North Atlantic Oscillation (NAO) and El Nino Southern Oscillation (ENSO) and are mirrored in the wave climate near Onslow Beach (**Figure 15-3**). To preserve these well-documented climate signals in the forecast simulations, the same hourly time series of wave data from 1989–2009 was used to forecast through 2065. The magnitude of this wrapped-forward wave time series was manipulated to reflect varying climate changes in nearshore winds (see the

section title Climate: Winds) in CSHORE-C15 forecast simulations. Simulations using varying storm frequencies (expressed as varying numbers of storm occurrences during ENSO and NAO periodicities), however, were outside the scope of this effort and not investigated.

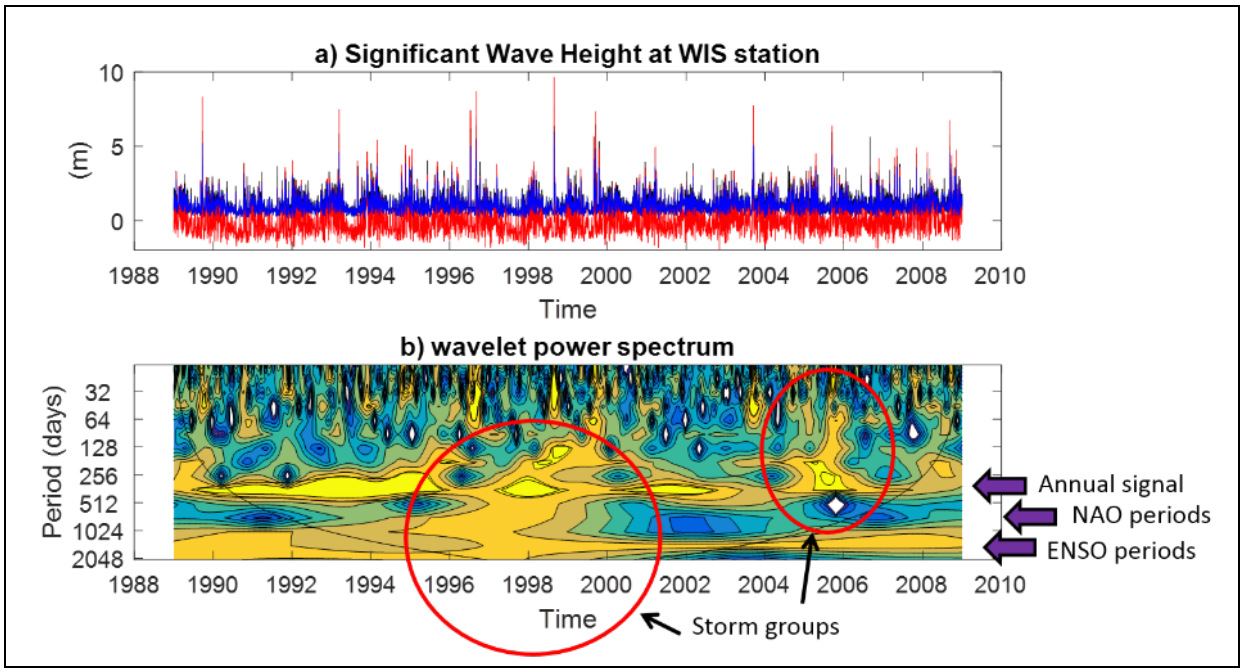

Figure 15-3. Climate signals embedded within winds and WIS wave results from Onslow Beach.

The top panel shows raw, hourly significant wave height and the blue line has the mean removed for wavelet analysis shown in the bottom panel.

Wave fields develop due to wind, but evolve over days and over a spatial range of 0 km to thousands of kilometers. The sea surface conditions at a point are a combination of locally generated waves and energy that advects from remote waters. The waves at the Onslow Beach WIS Station 63279, then, are related to the local wind field, but not exclusively. Nevertheless, directly relating forecasts of varying local wind magnitudes to modify the wave field provides a tractable method for forecasting waves, under the limitations of our project scope, and is consistent with the level of confidence in the climate predictions. **Figure 15-4** shows the WIS wind speed and wave height for the 20 years of MCBCL data, 1989–2009. Considering the importance of incident wave energy in morphology modeling, the provided data include only cases in which the mean wave direction was within ±45 degrees of an Onslow Beach cross-shore transect. It is clear from the data that wind magnitude and wave height were correlated, although the degree of scatter was considerable (**Figure 15-4**). An empirical fit to the results is provided in **Figure 15-2** and is expressed as calculated by using Equation 15-1:

$$H_s = 14\left\{1 - e^{-0.02u}\right\} \qquad \text{(Eq. 15-1)}$$

With a simple expression for the wind and wave relationship, the enhanced wave time series $\hat{H}_s$ was readily developed as an expansion of the hindcast record as calculated by using Equation 15-2:

$$\hat{H}_s = H_s + \frac{\partial H_s}{\partial u}\Delta u = H_s + .28e^{-0.02u}\Delta u \qquad \text{(Eq. 15-2)}$$

The expression in Equation 15-2 was used to compute the enhanced wave field and reverted to the hindcast record for a case without altered winds. Note that this rudimentary analysis only resulted in changes to the magnitude of the waves and does not account for increases in the storm frequency or possible alterations in direction.

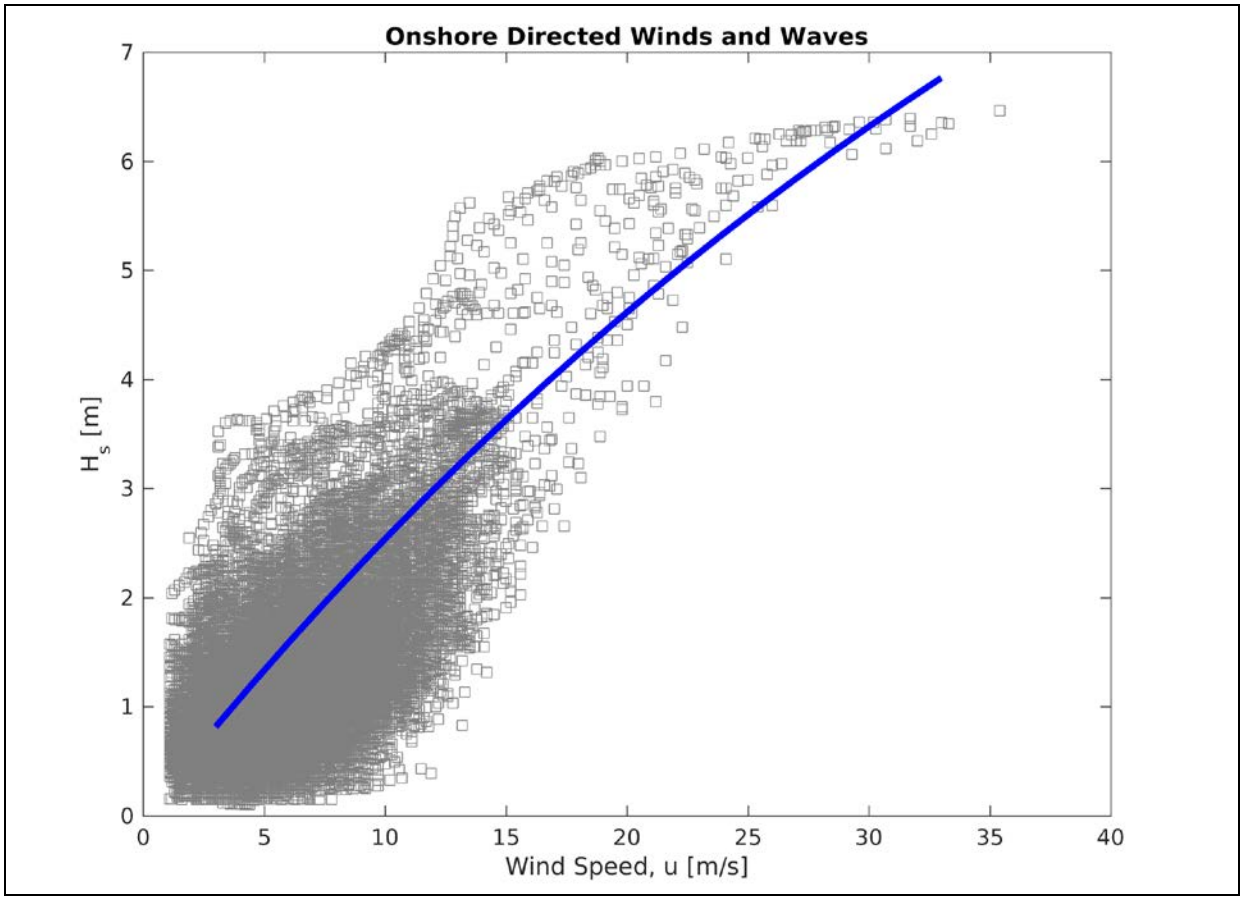

Figure 15-4. Relationship of observed local winds and significant wave height at Onslow Beach.

Water Level: Tides, Storm Surge, and Sea Level Rise

A time-varying sea level is a required boundary condition for implementation of CSHORE-C15. Water level (η) in the Onslow Beach region was forced, in general, by four factors and can be expressed as a linear superposition as shown in Equation 15-3:

$$\eta = \eta sea\ level + \eta tide + \eta storm + \eta wave \qquad \text{(Eq. 15-3)}$$

where ηsea is water level and is the slowly varying sea level, ηtide is the combined harmonic tidal variation, ηstorm is the atmospherically driven short-term departure of the water levels from the tidally driven variation, and ηwave is the additional setup due to the wave radiation stress.

Regionally observed water-level data (National Oceanic and Atmospheric Administration Beaufort and Wrightsville, NC stations) transformed to Onslow Beach and verified by results from the Advanced Circulation (ADCIRC) model (Luettich et al., 1992) were used to simulate tides, currents, and water surface elevations for hindcast modeling. During DCERP1, the ADCIRC model was applied to North Carolina coastal waters with focus on the Onslow Beach area (Reynolds-Fleming et al., 2012). Results were evaluated from previous ADCIRC model simulations, taking advantage of their existing bathymetric grid and previously validated results, and to ensure observations from regional stations were transformed correctly to Onslow Beach. This hourly reconstruction of water level for the past 20 years was used to force CSHORE-C15 in hindcast simulations.

In a consistent strategy employed for forecasting waves, a time series of water level containing the tide, storm, and wave components was created by wrapping the historic, 1989–2009, signal forward to 2065. Regional climate signals were embedded within this time series, and the wind-driven components (ηstorm + ηwave) were manipulated for varying scenarios of wind forecasts by the empirical relationship observed at Onslow Beach in the past (**Figure 15-5**; see Equation 15-4):

$$\eta = 0.014u2 \times g - 0.073 \qquad \text{(Eq. 15-4)}$$

Where ux is the onshore-directed wind component. Consistent with Equation 15-2, the enhanced wave time series is expressed as an extension of the base case:

$$\hat{\eta} = \eta + \partial\eta\ \partial ux \Delta ux = \eta + 0.028\ gux \Delta u \qquad \text{(Eq. 15-5)}$$

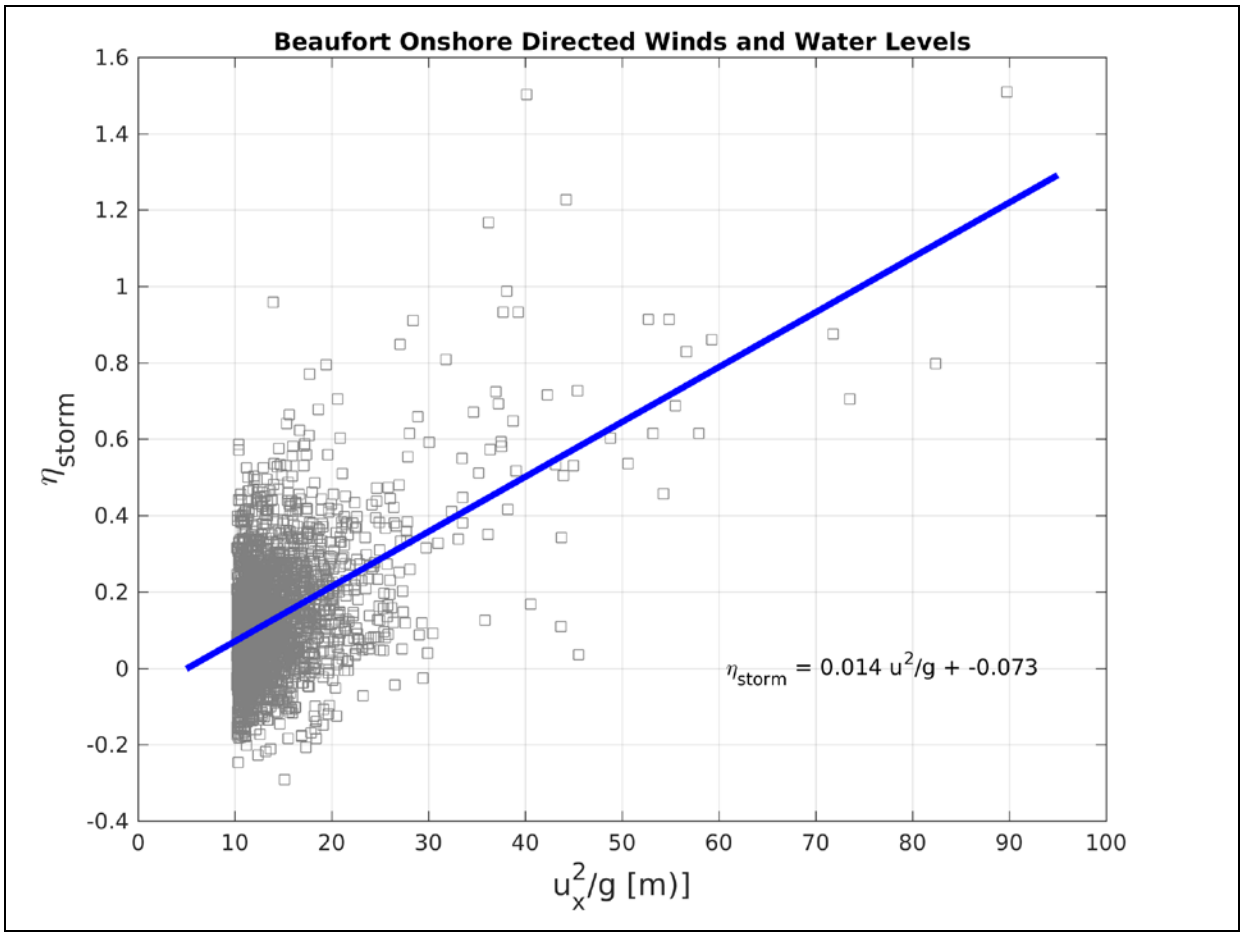

Figure 15-5. Relationship of observed local winds and water level (without astronomical tide) at Onslow Beach.

Sea Level: Future Projections

An extensive review of regional data and literature pertaining to the local changes in sea level was conducted by Hall et al. (2016). Taken with the expected global change, the projections are cast as quadratic dependent on the departure of time (*t*) from 1992 (see Equation 15-6):

$$SLR = a \times (t - 1992) + b \times (t - 1992)^2 \qquad \text{(Eq. 15-6)}$$

Where a and b are empirical coefficients. Considering the uncertainties associated with local and global changes, the sea level rise estimates were provided with a range of coefficients as presented in **Table 15-1**. These sea level rise curves, plotted through 2065 in **Figure 15-6**, were used in this investigation without modification for all simulated scenarios.

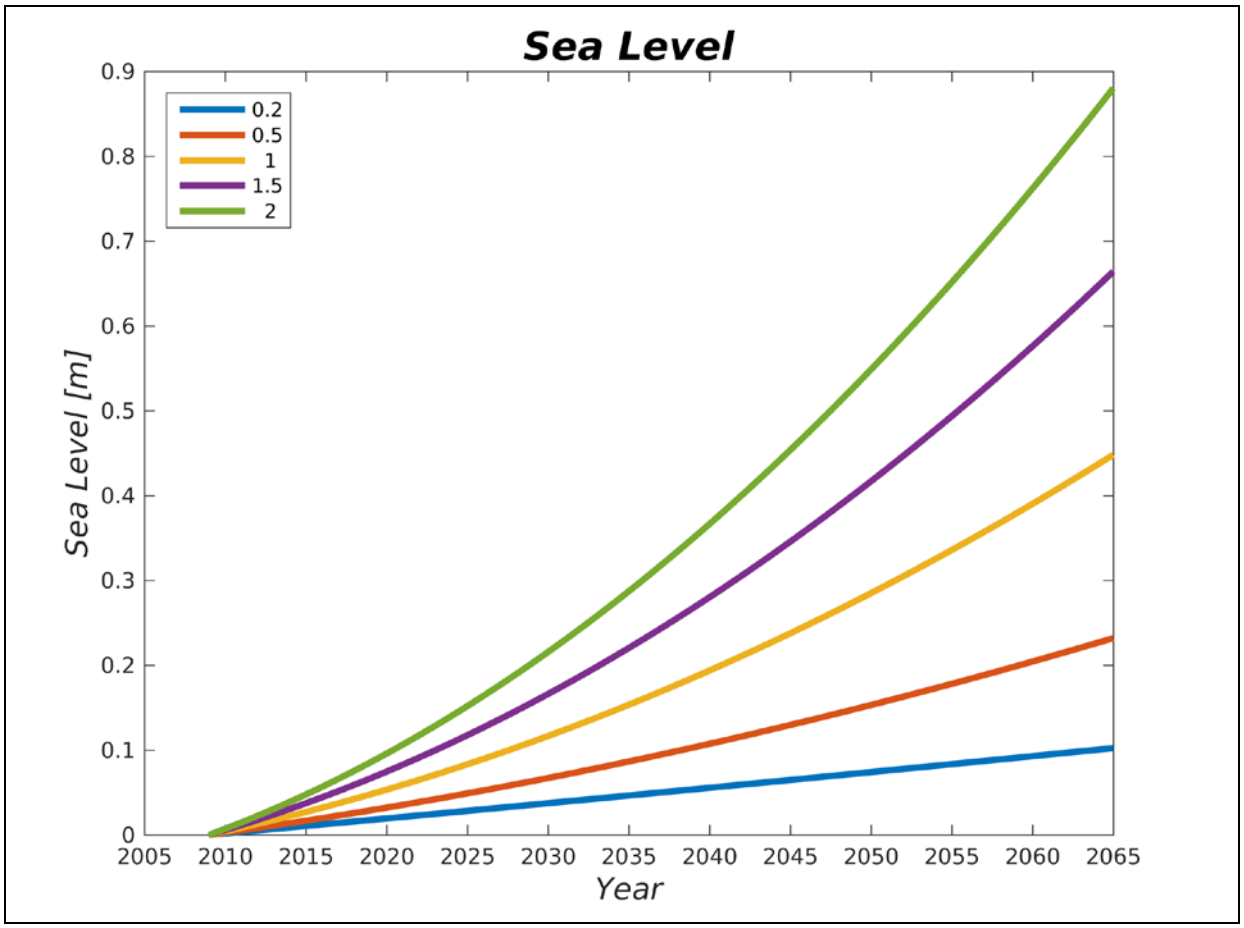

Figure 15-6. Sea level rise curves developed for Onslow Beach region 2010–2065; x-axis label refers to calendar year (Hall et al., 2016).

Table 15-1. Sea Level Rise Equation Coefficients Developed for Onslow Beach (Hall et al., 2016)

Category	Scenario (m)	*a* (m/yr)	*b* (m/yr^2)
Lowest	0.2	1.7×10^{-3}	1.406036×10^{-6}
Low	0.5	1.7×10^{-3}	2.7126200×10^{-5}
Moderate	1.0	1.7×10^{-3}	6.9993141×10^{-5}
High	1.5	1.7×10^{-3}	1.12860082×10^{-4}
Highest	2.0	1.7×10^{-3}	1.55727023×10^{-4}

Climate: Winds

Potential fluctuations in wind magnitude from present to 2065, and the resulting response in the morphology of Onslow Beach, were examined by using the Multivariate Adaptive Constructed Analogs (MACA) data set (Abatzoglou and Brown, 2012) provided by DCERP2 Research Project CC-1. MACA was designed to provide guidance about future climate conditions at spatial scales that are useful for localized management, specifically approximately 6-km resolution at daily time steps (for details regarding downscaling and model comparisons, see

http://climate.ncsu.edu/hadinon/pinemap/MACA_FAQs.php). The MACA wind forecasts used in this study spanned a climate model baseline period of 1950–2005 and a future period of 2006–2099 under a representative concentration pathway (RCP 8.5) of future emissions based on current or higher levels of relevant factors such as economic activity, energy sources, and population growth.

Thirteen down-scaled global climate models were investigated for CSHORE-C15 simulations at Onslow Beach. **Table 15-2** lists model names and their corresponding number abbreviations used in the subsequent figure. An average wind magnitude from each model was determined from 1989–2099, as well as a running 20-year mean by using a forward and backward, zero-phase filter. The difference between the 20-year means and the overall average, or model delta, was computed for each model. Statistics of model deltas, namely mean and standard deviation, for the down-scaled global models revealed close agreement between all 13 models in the Onslow Beach region (**Figure 15-7**). For the purposes of modeling morphology with CSHORE-C15, we compared all 13 model deltas (mean and standard deviation) between the hindcast period, 1989–2009, and a 20-year period from 2045–2065 (**Figure 15-8**). This comparison revealed larger model delta averages in the 2045–2065 period, but no clear trend of wind magnitude increase or decrease (four models had higher delta means, and nine had lower delta means). Similarly, the standard deviations of model deltas between the two 20-year periods, 1989–2009 and 2045–2065, were mixed with no clear trend.

Table 15-2. MACA downscaled, wind forecast models used in study

Model Name	Model Abbreviation
bcc-csm1	1
BNU-ESM	2
CanESM2	3
CNRM-CM5	4
CSIRO-Mk3-6	5
GFDL-ESM2G	6
GFDL-ESM2M	7
inmcm4	8
MIROC5	9
MIROC-ESM-CHEM	10
MIROC-ESM	11
MRI-CGM3	12
NorESM1	13

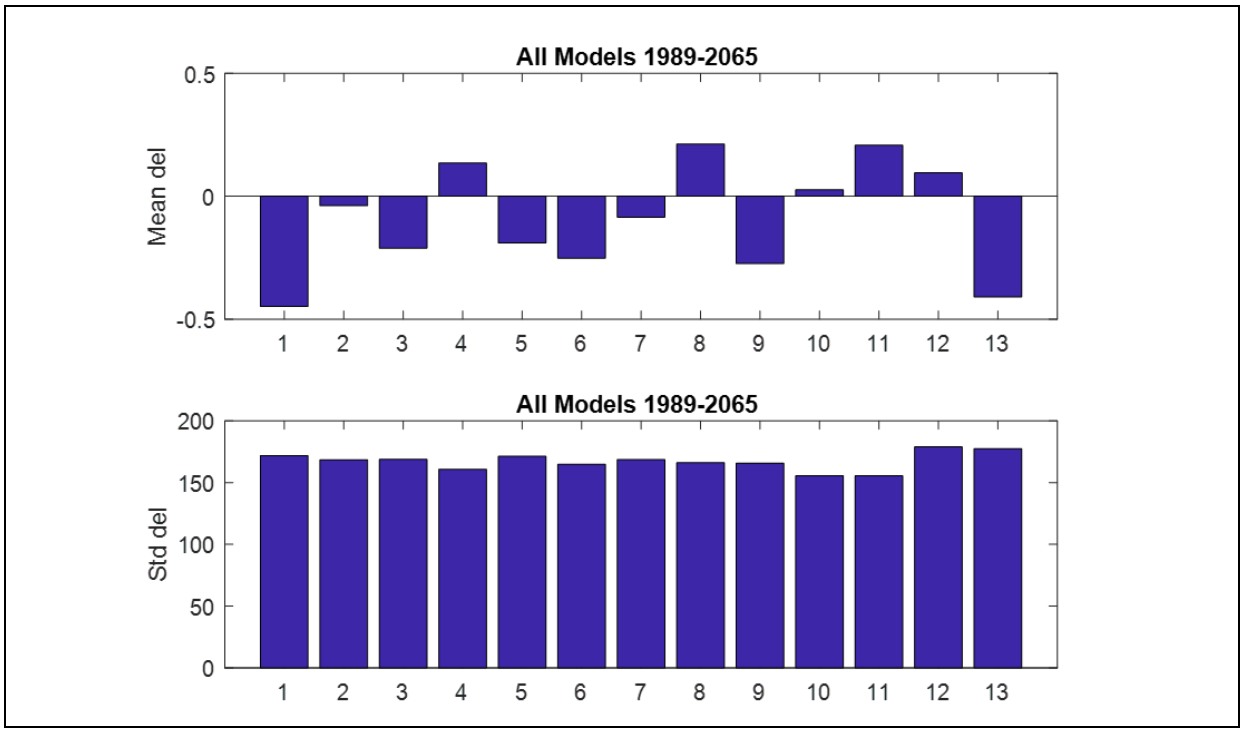

Figure 15-7. Mean and standard deviation of 13 MACA down-scaled wind model deltas from the Onslow Beach region.

Note: Models number are defined in **Table 15-2**.

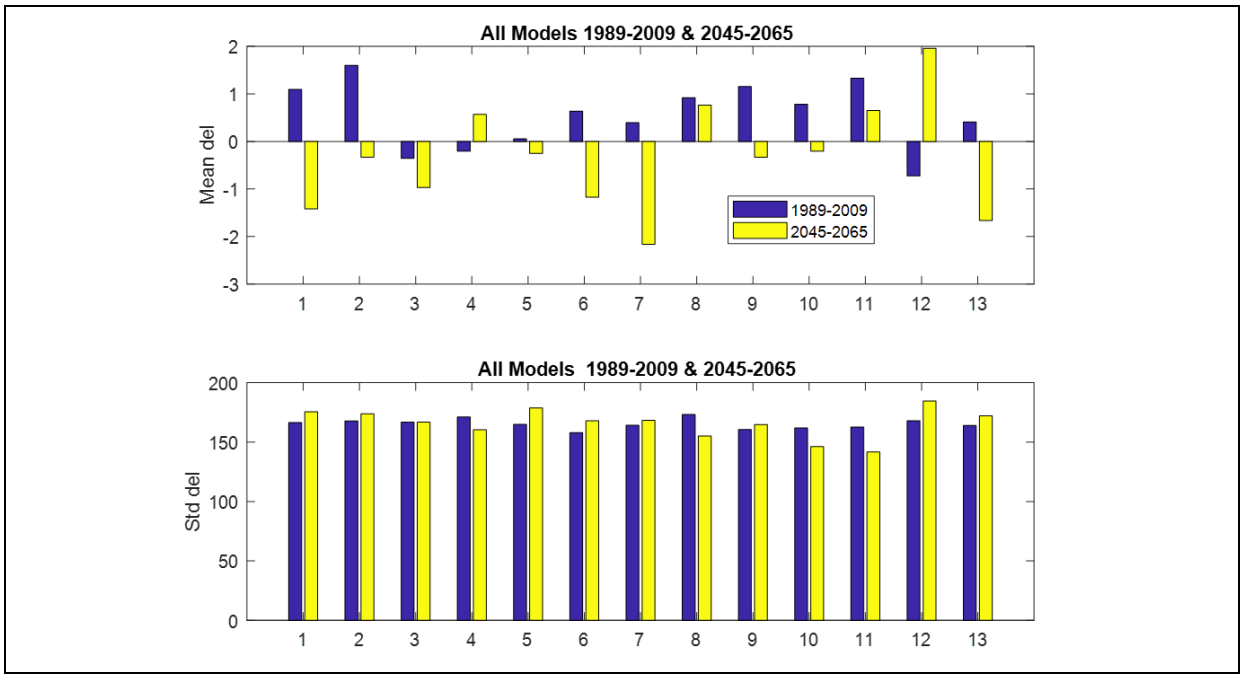

Figure 15-8. Mean and standard deviation of 13 MACA down-scaled wind model deltas from the Onslow Beach region comparing the two 20-year periods, 1989–2009 (hindcast) and 2045–2065 (forecast).

Note: Models number are defined in **Table 15-2**.

To develop climate change scenarios that may reflect a maximum of potential differences in modeled winds between our historical data (1989) and 2065, we measured the percent difference between the running 20-year mean of all models in 1989 and 2065 (**Figure 15-9**). The CSHORE-C15 simulations were run by using the most extreme increase and decrease wind model forecasts to capture a likely window of possibilities and resulting shoreline responses. Interestingly, the highest percentage increase in 20-year model deltas, of all 13 models, between 1989 and 2065 was 7.8%, and the highest percentage decrease was 10.2%. The empirical relationships established from Onslow Beach relating winds to waves and water level were applied to the forcing time series used by CSHORE-C15 to test the response of the beach to this range of forecast winds.

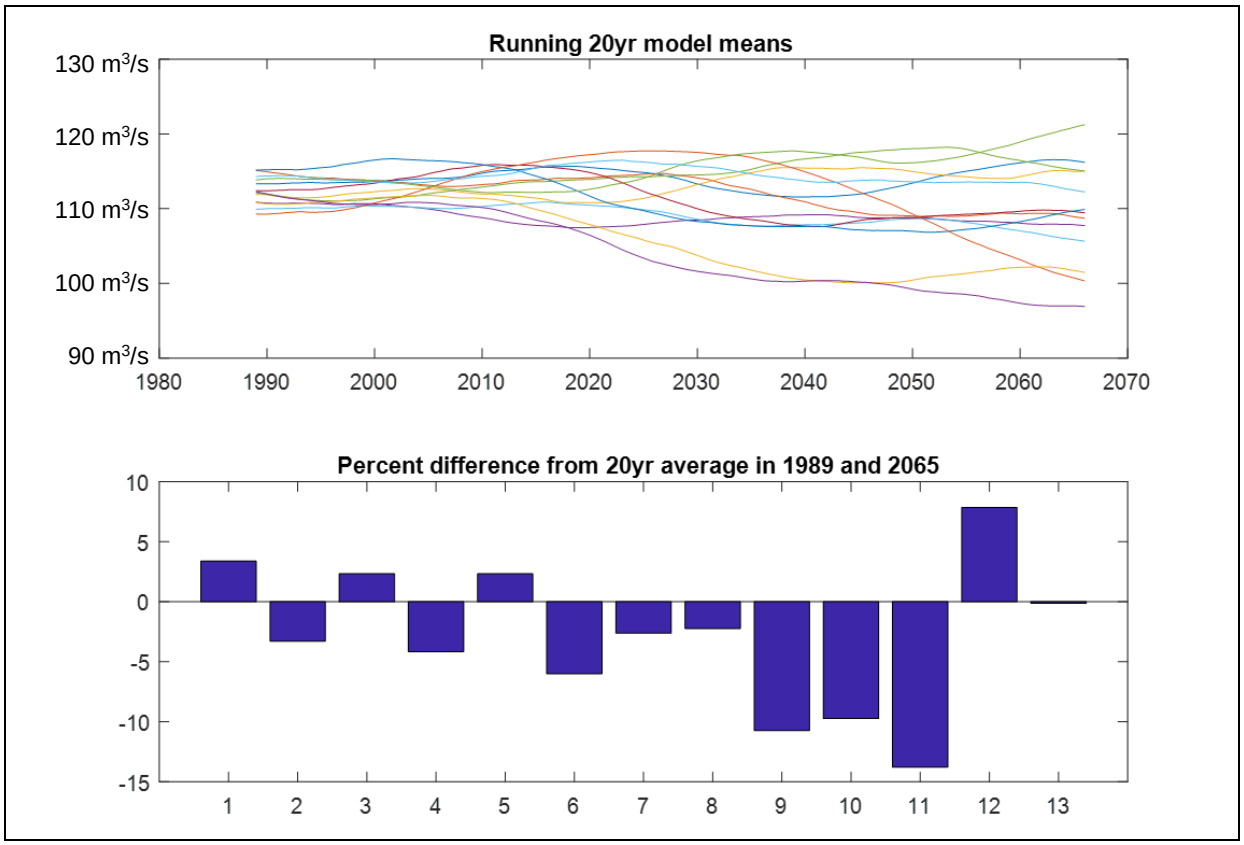

Figure 15-9. Running 20-year means of 13 MACA down-scaled wind forecasts for Onslow Beach from 1989–2065 in units of wind power (in m^3/s) in top panel. Percent difference from 20-year mean between 1989 and 2065 (bottom panel).

Results and Discussion

Hindcast Results: 1989–2009

To prepare to test our proposed hypotheses and provide a prediction of shoreline position at Onslow Beach from 2015 through 2065, under varying climate scenarios, we first assessed the skill of CSHORE-C15 through hindcast simulations of the previous 20 years (1989–2009). The CSHORE-C15 validation simulation was initiated by using beach topography and nearshore bathymetry collected at Onslow Beach during DCERP1. Modeled shoreline positions and the

associated nearshore bathymetry and beach topography were driven by hourly nearshore conditions of waves and water level. The regional observations of waves and water level, verified by the DCERP1 ADCIRC model simulations, and WIS, from the past 20 years, were used by CSHORE-C15 to compute hourly sediment transport rates and cross-shore morphology change and, ultimately, predict the shoreline position. Because the modeled shoreline simulations were run without adjustments to the observed historic shoreline, the modeled results represent a gauge of model accuracy in decadal shoreline change predictions. The 1989 shoreline was used to initiate the simulation, and results thereafter were determined purely on the forcing oceanographic conditions and CSHORE-C15 theoretical underpinnings.

For the purposes of model simulations and ease in evaluating results, a local rectilinear coordinate system was created for Onslow Beach such that the shoreline was rotated along a truer north–south axis, termed alongshore, and a cross-shore axis that was more aligned with a local seaward-landward axis. **Figure 15-10** illustrates Onslow Beach modeled and observed shorelines starting in 1989 and ending in 2009. The root mean square error (RMSE), comparing all modeled shoreline positions along Onslow Beach with observed, was 20.7 m. CSHORE-C15 hindcast results do not suggest a persistent bias as modeled predictions, compared with historic shoreline positions, erred in both under-predicting and over-predicting shoreline change. The Onslow Beach shoreline has been rotating, over the long term (at least since 1932–2009), with the northern one-third of the island shoreline accreting seaward and the southern one-third of the island shoreline rapidly shifting landward (RTI International, 2013; see DCERP1 Final Research Report Chapter 10 for more details). This complexity in shoreline behavior over such a small spatial scale is particularly challenging for morphology modeling. Nevertheless, CSHORE-C15 captured the overall trends of shoreline change at Onslow Beach and demonstrated skill (RMSE= 20.7 m) after 20 years of hourly determinations that were well within typical seasonal or storm-driven shoreline change for the region (Brodie and McNinch, 2011; Rodriguez et al, 2009).

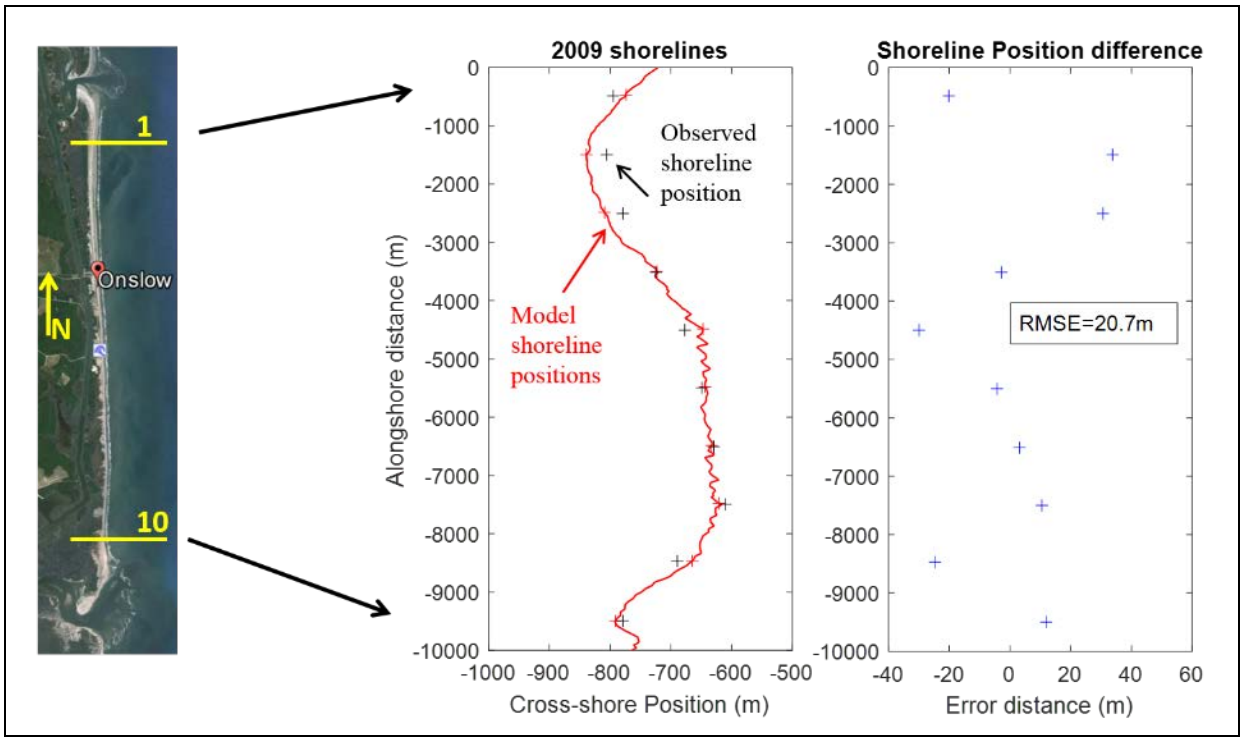

Figure 15-10. CSHORE-C15 hindcast results, 1989–2009, showing a 20.7-m cumulative root mean square error (RMSE) of shoreline prediction versus observed.

Forecast Results: 2017–2065

Predictions of Onslow Beach morphology, from the dunes seaward to depths of 10 m, were determined by employing CSHORE-C15, which used multiple climate scenarios of sea level rise and changes in wind magnitude (storm intensity). For the sake of clarity and to capture the entire range of possible outcomes, we focused on the extreme scenarios, namely, CSHORE-C15 results using the highest and lowest sea level rise rates and the highest and lowest wind forecasts. All CSHORE-C15 results, highlighted in subsequent figures by shoreline position, fell within this window of possible outcomes.

Evaluation of the shoreline position under the 10% decrease and 7.8% increase in daily wind magnitude, representing the range of MACA forecast winds through 2065, revealed no significant differences at Onslow Beach. Those small differences in wind magnitude translated to even smaller variations to waves and water level in the Onslow Beach region. Thus, predictions of shoreline position were within several meters of one another (well within CSHORE-C15 precision). Future evaluations should explore how changes in storm frequency, not just wind magnitude, may affect Onslow Beach.

CSHORE-C15 modeled shoreline change rates, an annual mean, and a running 10-year mean, are shown in **Figure 15-11** at three representative regions: the northern pedestrian recreational area, military training area, and the southern vehicular recreational area, under a lowest, moderate, and highest sea level rise rate. The military training area will likely undergo the most rapid shoreline change over the next decade, slowing to a more moderate rate of between 1 to 2 m/yr transgression from 2030–2060. Interestingly, the moderate sea level rise rate causes a greater

shoreline change rate than the highest sea level rise after 2055. Similarly, the highest sea level rise causes the highest shoreline change rate in the southern region until approximately 2040, but then shifts to the smallest change rate as compared with the low and moderate sea level rise scenarios. We suspect this results from greater morphology changes around the existing washover fans over the next 20 years under the highest sea level scenario. The northern one-third of Onslow Beach, as reflected by the area near the North Range Tower, shows a sustained accretion (seaward growth) and/or stability through 2065.

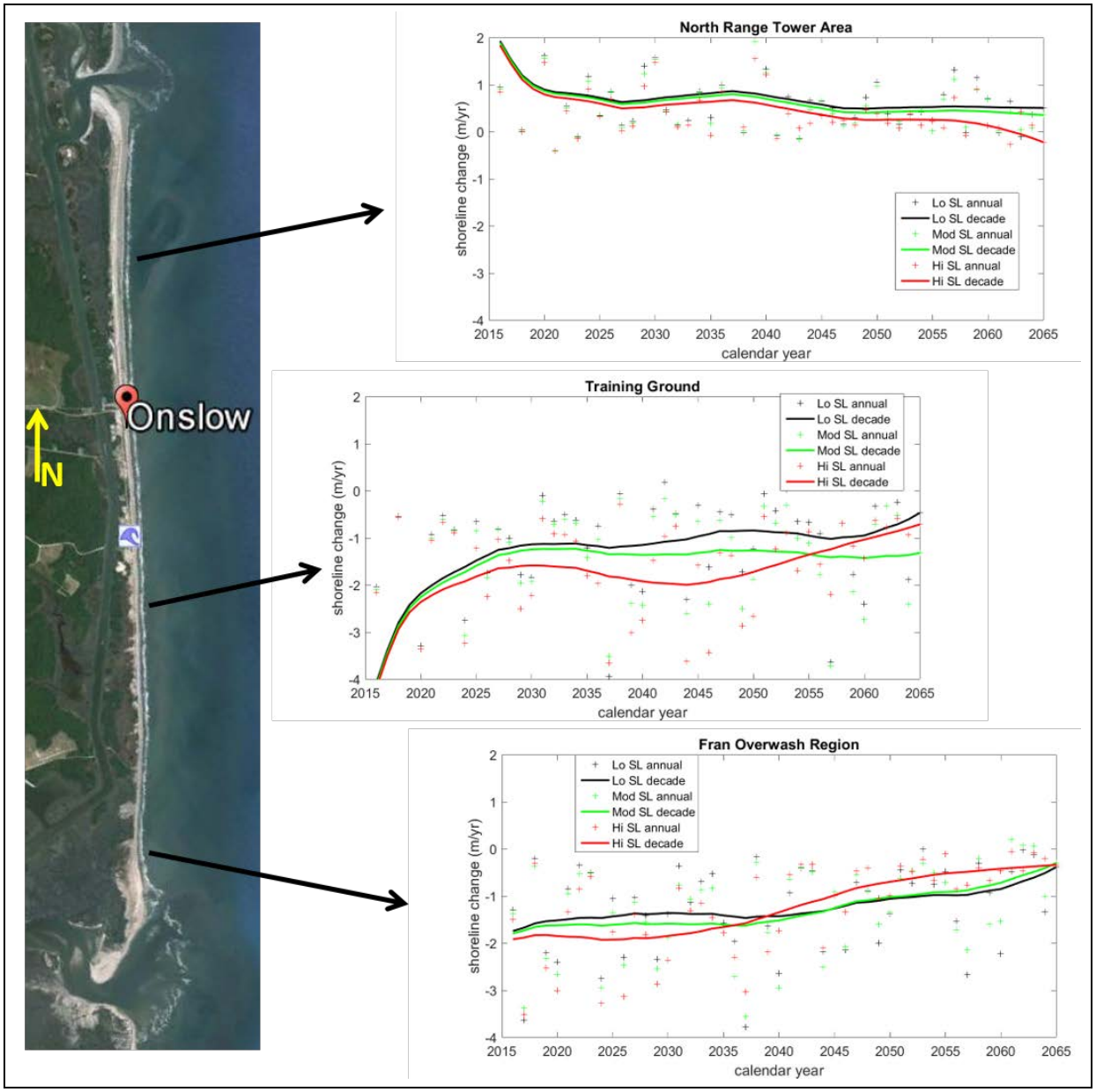

Figure 15-11. Modeled shoreline change rates (in m/yr) in three regions of Onslow Beach from 2017–2065 under different sea level rise rates.

A more short-term, actionable prediction for the recreational and military training areas of Onslow Beach to 2040 is shown in **Figure 15-12**. The predicted shoreline position under both

the highest (red lines) and lowest (yellow lines) sea level rise scenarios will likely threaten the current location of Ocean Drive south of the Onslow Beach bridge by 2040 (**Figure 15-12**) when considering the computed beach width. Predictions of shoreline position and beach width to 2065 are shown on **Figures 15-13, 15-14, and 15-15**. **Figure 15-13** focuses on the recreational and military training grounds just south of the bridge and shows the beach to extend west of Ocean Drive and cutting into much of the existing infrastructure under both the highest and lowest sea level rise rate. Similarly, the shorelines under either sea level extremes across the central training region are west of the existing sand access road, and the beach extends across the present dune field (**Figure 15-14**). The area of Onslow Beach that is most narrow, as defined by the current ocean shoreline and the ICW, is shown in **Figure 15-15.** Shoreline and beach positions under both the highest and lowest sea level rise scenarios indicated a continued narrowing of Onslow Beach through 2065 such that the beach will extend within 100 m of the ICW shoreline.

The bar plot in **Figure 15-16** shows the mean annual shoreline change rate along Onslow Beach from CSHORE-C15 model predictions 2017–2065 by using several potential sea level rise rates. These values are relatively similar to shoreline behavior at Onslow Beach from 1932–2009 (Foxgrover, 2009) in that the northern one-third of the island was accreting or stable and the lower two-thirds of the island was transgressing toward the mainland. The CSHORE-C15 model predictions did, however, indicate greater erosion in the northern training areas and into the recreational area just south of the Onslow Beach Bridge, as well as greatest sensitivity to which sea level rise scenario was used. Simply put, the shoreline position transgressed farther under higher sea level rise rates in this central region, whereas the shoreline in the southern one-third of the island (near existing, extensive washover fans) continued to erode and transgress westward at similar rates regardless of which sea level rise curve was applied. These mean long-term annual shoreline change rates (2017–2065) were extrapolated from 2065–2100 to provide a crude estimate to possible shoreline positions through the end of this century. Similar to all extrapolations, they reflect the forcing conditions under which the values were determined and limit the generality of the results. Nevertheless, given that these long-term change rates were relatively consistent under a range of climate change scenarios and similar observations over the past 70 years, extrapolating beyond 2065 is as reasonable as simulating morphology change by using CSHORE-C15 with forecasts of forcing conditions that are well beyond current model skill. Extrapolation of the shoreline and beach to 2100 suggests inundation of all current infrastructure south of the Onslow Beach Bridge (**Figure 15-17**), as well as loss of all current egress points in the military training area (**Figure 15-18**).

Figure 15-12. CSHORE-C15 predictions of shoreline and beach position in 2040 across the Onslow Beach recreational and training areas under highest and lowest sea level rise scenarios.

Figure 15-13. CSHORE-C15 predictions of shoreline and beach position in 2065 across the Onslow Beach recreational and training areas under highest and lowest sea level rise scenarios.

Figure 15-14. CSHORE-C15 predictions of shoreline and beach position in 2065 across the Onslow Beach central training area under highest and lowest sea level rise scenarios.

Figure 15-15. CSHORE-C15 predictions of shoreline and beach position in 2065 across the Onslow Beach northern training area under highest and lowest sea level rise scenarios.

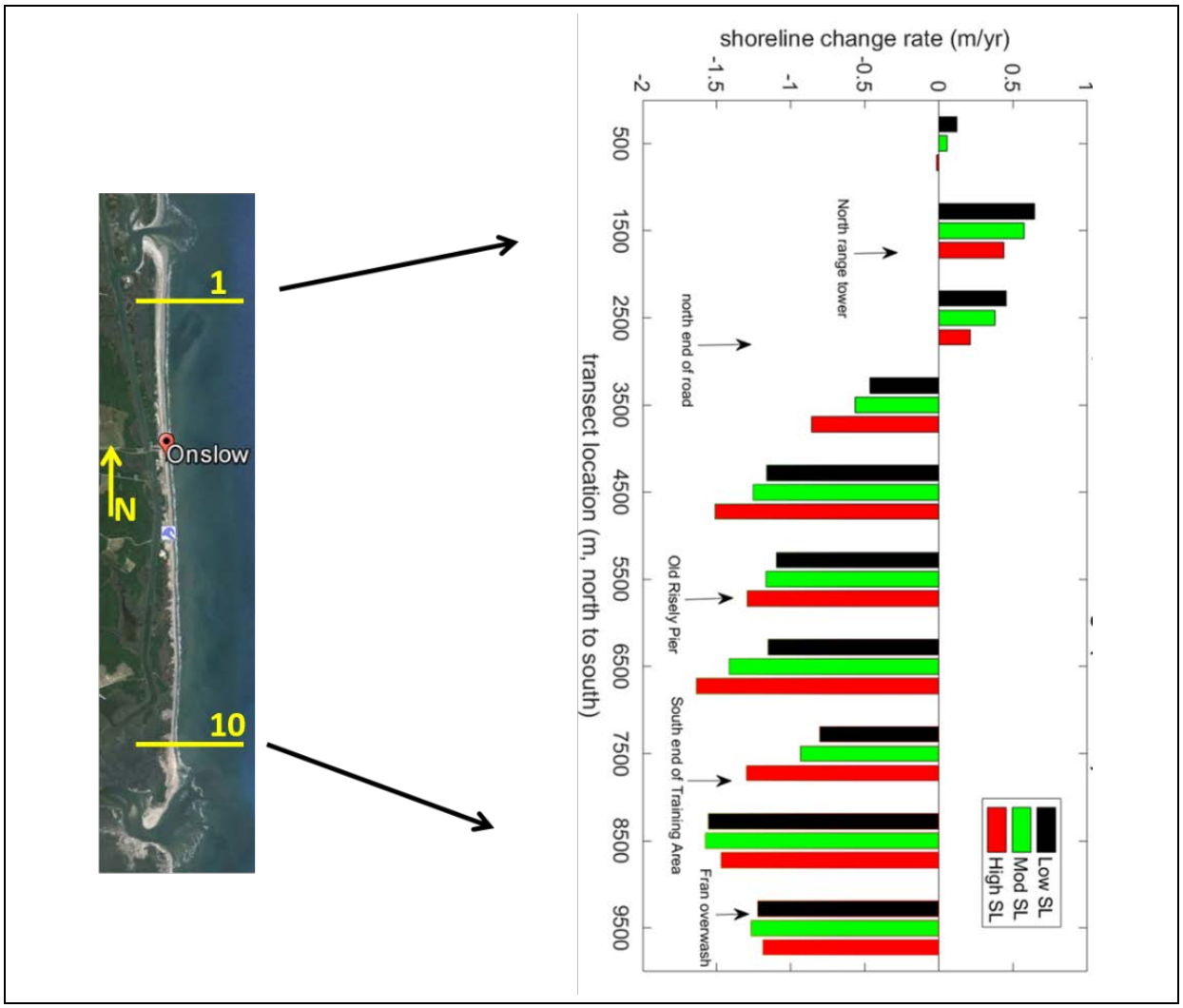

Figure 15-16. Modeled mean, annual shoreline change rate (in m/yr) 2015–2065 at Onslow Beach under different sea level rise rates.

Each of the 10 solutions of annual shoreline change correspond to the 10 cross-shore transects modeled down the length of Onslow Beach (illustrated in map view on left panel).

Figure 15-17. Predictions of shoreline and beach position in 2100 by using extrapolated long-term shoreline change rates (CSHORE-C15 simulations 2017–2065) across the Onslow Beach recreational and training area under highest and lowest sea level rise scenarios.

Figure 15-18. Predictions of shoreline and beach position in 2100 using extrapolated long-term shoreline change rates (CSHORE-C15 simulations 2017–2065) across the Onslow Beach southern training area under highest and lowest sea level rise scenarios.

Conclusions and Implications for Future Research and Implementation

Key Scientific Findings

Military training activities on Onslow Beach have not caused measurable changes to shoreline position or beach topography or to the frequency or scale of overwash processes. Decadal storm frequency, instead, appears to have been closely linked to overwash from the 1940s to the early 2000s. A beach and nearshore morphology model, CSHORE-C15, was developed for Onslow Beach to predict future beach changes under varying climate change scenarios and to ultimately forecast the sustainability of the beach for expeditionary training at MCBCL. Climate model forecasts of winds through 2065 suggest little change in wind magnitude near Onslow Beach over the next five decades, and the resulting beach changes to these potentially small variations in wind are minimal. Beach and shoreline position changes to sea level rise, in contrast, are substantial at Onslow Beach, even under the most conservative sea level rise rate (0.2 m by 2100). Future investigations should explore what level of increase in wind magnitude is needed to generate significant changes to the beach (i.e., is there a trigger threshold) and whether variations in storm occurrences within known climate periodicities (e.g., ENSO, NAO) would cause significant morphology changes at Onslow Beach. Model predictions of shoreline change from this study are also being used in Research Project CB-5 to estimate the amount of carbon exported to the coastal ocean at Onslow Beach from the southern portion of the beach.

Research Questions

Our overarching research question explored how Onslow Beach responds to varying scenarios of climate change; specifically, to sea level rise and stronger storms.

1. Will shoreline position be spatially consistent down the length of Onslow Beach under each simulated climate forcing scenario?

Findings revealed that the morphological response is distinctly different in three regions of Onslow Beach: (1) north of the Onslow Beach Bridge remained stable and accretive, (2) south of the Onslow Beach Bridge to the southern end of the training area will likely experience the highest rates of erosion in the coming decades, and (3) south of the training area to the New River Inlet will remain erosive, but likely stabilize to slower rates of recession after the next decade

2. Will beach morphology changes at Onslow Beach be attenuated relative to small increases and decreases in wind magnitude?

Model results show that beach morphology at Onslow Beach is not sensitive to small variations in wind magnitude.

3. Will the highest rates of sea level rise generate the highest shoreline change along Onslow Beach?

Results indicate that the highest shoreline change does occur with the highest sea level rise scenario except for the southern one-third of Onslow Beach. Model simulations indicate that beach morphology across both the military training area and the southern one-third of Onslow

Beach will be extensively modified in the near future under high sea level rise rates, leading to a redistribution of sediment and shoreline shape and ultimately to smaller shoreline position change rates across the southern one third in later decades. In contrast, the moderate and lower sea level rise scenarios do not force as extensive of morphology change across the region in the earlier years leading to a steadier erosional response through 2065.

Findings with Implications for Future Base Management

The current military training area and the recreational area south of the Onslow Beach Bridge will likely be threatened by 2040 and severely affected within 50 years, even under the lowest of sea level rise (0.2 m by 2100) curve. Higher sea level rise rates (2.0 m by 2100) will exacerbate these effects, such that loss of most existing infrastructure on both sides of Ocean Drive will occur. Conversely, the beach and associated environments will remain stable and build seaward along the entire reach of Onslow Beach north of the Onslow Beach Bridge.

Literature Cited

Abatzoglou, J.T., and T.J. Brown. 2012. A comparison of statistical downscaling method suited for wildfire applications. *International Journal of Climatology 32*:720–780.

Brodie, K.L., and J.E. McNinch. 2011. Beach change during a nor'easter: Relationships to wave steepness and inner surf zone dissipation. Pp. 1360–1374 in *The Proceedings of the Coastal Sediments 2011 1*. Edited by J.D. Rosati, P. Wang, and T.M. Roberts.

Browder, A., and J.E. McNinch. 2006. Linking framework geology of the nearshore: Correlation of paleo-channels with shore-oblique sandbars and gravel outcrops. *Marine Geology 231*:141–162.

Cleary, W.J., and O.H. Pilkey. 1968. *Sedimentation in Onslow Bay. Guidebook for Field Excursions: Durham, North Carolina, Geological Society of America, Southeastern Section, Southeastern Geology. Special Publication 1*:17.

Cleary, W.J., and S.R. Riggs. 1999. Beach erosion and hurricane protection plan for Onslow Beach. Camp Lejeune: Comprehensive Geologic Characteristics Report: Camp Lejeune, North Carolina. U.S. Marine Corps. 137 pages.

Dietrich, J.C., S. Bunya, J.J. Westerink, B.A. Ebersole, J.M. Smith, J.H. Atkinson, R.E. Jensen, D.T. Resio, R.A. Luettich Jr., C.N. Dawson, V.J. Cardone, A.T. Cox, M.D. Powell, H.J. Westerink, H.J. Roberts. 2010. A high-resolution coupled riverine flow, tide, wind, wind wave, and storm surge model for southern Louisiana and Mississippi, Part II: Synoptic description and analysis of Hurricanes Katrina and Rita. *Monthly Weather Review 138*:378–404.

Foxgrover, A.C. 2009. Quantifying the overwash component of barrier island morphodynamics: Onslow Beach, NC. Master's thesis, The College of William and Mary, Williamsburg, VA.

Hall, J.A., S. Gill, J. Obeysekera, J., W. Sweet, K. Knuuti, and J. Marburger. 2016. *Regional Sea Level Scenarios for Coastal Risk Management: Managing the Uncertainty of Future Sea Level Change and Extreme Water Levels for the Department of Defense Coastal Sites Worldwide*. U.S. Department of Defense, Strategic Environmental Research and Development Program (SERDP). 224 pages. Available at https://www.serdp-estcp.org/Program-Areas/Resource-Conservation-and-Resiliency/Infrastructure-Resiliency/Regional-Sea-Level-Scenarios-for-Coastal-Risk-Management

Hayes, M.O. 1979. Barrier island morphology as a function of tidal and wave regime. Pp. 1–28 *Barrier Islands: From the Gulf of St. Lawrence to the Gulf of Mexico.* Edited by Leatherman, S.P. Academic Press: New York.

Houser, C., C. Hapke, and S. Hamilton. 2008. Controls on coastal dune morphology, shoreline erosion, and barrier island response to extreme storm. *Geomorphology 100*:223–240.

Luettich, R.A., Jr., J.J. Westerink, and N.W. Scheffner. 1992. *ADCIRC: An Advanced Three-Dimensional Circulation Model for Shelves Coasts and Estuaries, Report 1: Theory and Methodology of ADCIRC-2DDI and ADCIRC-3DL*. Dredging Research Program Technical Report DRP-92-6. U.S. Army Engineers Waterways Experiment Station, Vicksburg, MS. 137 pages.

McNinch, J.E. 2004. Geologic control in the nearshore: Shore-oblique sandbars and shoreline erosional hotspots, Mid-Atlantic Bight, USA. *Marine Geology 211*(1–2):121–141.

McNinch, J.E., and J.T. Wells. 1999. Sedimentary processes and depositional history of a cape-associated shoal, Cape Lookout, North Carolina. *Marine Geology 158*(1–4):233–252.

McNinch, J.E., K.L. Brodie, H.M. Wadman, K.K. Hathaway, R.K. Slocum, R.P. Mulligan, J.L. Hanson, and W.A. Birkemeier. 2012. Observations of wave run-up, shoreline hot-spot erosion, and sound-side seiching during Hurricane Irene at the Field Research Facility. Shore & Beach *80*(2).

Morton, R.A., T. Miller, and L. Moore. 2005. Historical shoreline changes along the U.S. Gulf of Mexico: A summary of recent shoreline comparisons and analyses. *Journal of Coastal Research 21*(4):704–709.

National Data Buoy Center. 2009. Station 41159—Onslow Bay Outer, NC. Available at http://www.ndbc.noaa.gov/station_page.php?station=41159

Plant, N.G., R.A. Holman, and M.H. Freilich. 1999. A simple model for interannual sandbar behavior. *Journal of Geophysical Research 104*(C7):15755–15776.

Reynolds-Fleming, J.V., R.A. Luettich, and J.G. Fleming. 2012. Comparative hydrodynamics during events along a barrier island: Explanation for overwash. *Estuaries and Coasts*. doi: 10.1007/s12237-012-9578-8

Riggs, S.R., S.W. Snyder, D. Ames, and P. Stille. 1999. Chronostratigraphy of upper cenozoic phosphorites on the north carolina continental margin and oceanographic implications for phosphogenesis. Pp. 369–385 in *Marine Authigenesis: From Global to Microbial: Journal of Sedimentary Research Special Publication Number 66*. Edited by C.R. Glenn, C.R., and J. Lucas.

RTI International. 2013. *DCERP1 Final Research Report*. Strategic Environmental Research and Development Program (SERDP) Research Project RC-1413. RTI International, Research Triangle Park, NC.

Schupp, C.A., J.E. McNinch, and J.H. List. 2006. Shore-oblique bars, gravel outcrops and correlation to shoreline hotspots. *Marine Geology 233*:63–79.

Yates, M.L., R.T. Guza, and W.C. O'Reilly. 2009. Equilibrium shoreline response: Observations and modeling. *Journal of Geophysical Research 114*:C09014. 16 pages.

Wadman, H.M., J.E. McNinch, A.C. Foxgrover, and A.B. Rodriguez. 2008. Spatial variation of shoreline change along an important Marine Corps amphibious training ground, Onslow Beach, NC; Part 1: Nearshore geology and morphology. Abstract for the Fall 2008 Geological Society of America Meeting, Houston, TX.

Appendix 15-A
List of Scientific/Technical Publications

Papers

Johnson, B.D., N. Kobayashi, and M. Gravens. 2012. *Cross-Shore Numerical Model CSHORE for Waves, Currents, Sediment Transport and Beach Profile Evolution ERDC/CHL TR-12-22*. Available at http://acwc.sdp.sirsi.net/client/en_US/default/search/detailnonmodal/ent:$002f$002fSD_ASSET$002f0$002f1011469/ada/?qf=AUTHOR%09Author%09Kobayashi%2C+Nobuhisa%09Kobayashi%2C+Nobuhisa&qu=Wamsley%2C+Ty+V

Thesis

None.

Presentations

None

Chapter 16

Linking Barrier Island Transgression Induced by Storms and Sea Level Rise to the Carbon Cycle, Changes in Ecosystem Function, and Management Decisions

SERDP Project Number: RC-2245

Coastal Barrier Module

Research Project CB-5

Lead Researcher:

Dr. Antonio Rodriguez
University of North Carolina at Chapel Hill's Institute of Marine Sciences (UNC-IMS)
abrodrig@email.unc.edu

Supporting Researchers:

Dr. Stephen Fegley, srfegley@email.unc.edu
Ethan Theuerkauf, ejtheu@email.unc.edu
Beth VanDusen, beth.vandusen@gmail.com

November 2017

Final

This report was prepared under contract to the U.S. Department of Defense (DoD) Strategic Environmental Research and Development Program (SERDP). The publication of this report does not indicate endorsement by DoD, nor should the contents be construed as reflecting the official policy or position of DoD. References herein to any specific commercial product, process, or service by trade name, trademark, manufacturer, or otherwise, do not necessarily constitute or imply its endorsement, recommendation, or favoring by DoD.

Table of Contents

Acronyms 16-vi
Abstract 16-1
Objectives of the Research Project 16-2
Background 16-2
Barrier Island Transgression 16-2
Carbon Storage and Export in Transgressive Barrier Islands over Centennial to Millennial Time Scales 16-4
Carbon Storage and Export in Transgressive Barrier Islands over Yearly to Centennial Time Scales 16-6
Materials and Methods 16-7
Carbon Budget Model 16-7
Washover Fan Evolution 16-13
Shorebird Nesting Activity 16-13
Sea Turtle Nesting Activity 16-14
Results and Discussion 16-14
Carbon Budget Model 16-14
Changes in Carbon 16-17
Carbon Budgets at Different Phases of Island Transgression 16-19
Washover Fan Evolution 16-21
Sea Turtle Nesting Activity 16-29
Conclusions and Implications for Future Research and Implementation 16-34
Research Questions 16-35
Findings with Implications for Future Base Management 16-36
Literature Cited 16-36
Appendix 16-A: Supporting Data 16-A-1
Appendix 16-B: List of Scientific/Technical Publications 16-B-1
Appendix 16-C: List of Students 16-C-1
Appendix 16-D: Other Supporting Information 16-D-1

List of Figures

Figure 16-1. The southern two-thirds of Onslow Beach is a typical transgressive barrier and ideal location for deriving a carbon budget, while examining the process of island rollover as it pertains to marsh accretion, marsh burial, island morphology, beach erosion, and ecosystem function..... 16-3

Figure 16-2. Conceptual model of transgressive barrier island evolution. As the barrier island moves landward towards the previous highstand shoreline, the backbarrier lagoon (A) transforms into a wide saltmarsh (B), which decreases in width as island migration progresses..... 16-5

Figure 16-3. (A) Map showing sample locations. Red dots indicate cores sampled for percent organic carbon. (B) Elevation profiles across Sites F1 and F2 showing that the morphology is similar to the transgressive barrier island settings shown in Figure 16-2. 16-9

Figure 16-4. Illustration of the parameterization of the transgressive barrier island carbon-budget model (not to scale)..... 16-12

Figure 16-5. Time series of physical processes and data collection at the study site from May 2012 to November 2014. 16-14

Figure 16-6. Stratigraphic cross section of (A) Site F1 and (B) Site F2 used to parameterize the barrier carbon-budget model. 16-16

Figure 16-7. Time series of photographs showing the impact of overwash on marsh width. Onslow Beach Site F1 (A) experienced marsh loss during Hurricanes Fran and Bonnie; Site F2 (B) experienced marsh loss during Hurricanes Irene and Sandy. 16-18

Figure 16-8. Carbon reservoirs from 1872 to 2014 for Sites F1 (A, B) and F2 (C, D). 16-20

Figure 16-9. Time series showing changes in washover volume, area, and the average vegetation percent cover at Site F2 (top) and the duration of overwash each month (bottom). 16-22

Figure 16-10. Time series showing changes in washover volume, area, and the average vegetation percent cover at Site F2.1 (top) and the duration of overwash each month (bottom). 16-23

Figure 16-11. Percent cover of sand in each vegetation plot sampled at Sites F1 (top panel), F2 (middle panel), and F2.1 (bottom panel) over a 6-year interval. 16-27

Figure 16-12. The alongshore frequency of turtle nesting events parsed into contiguous regions of shoreface geologic activity. 16-30

Figure 16-13. The elevation above MSL (in m, top panel) and linear distance to MHW (in m, bottom panel) of turtle nesting events in each of the 3 years. 16-33

Figure 16-14. Regression tree showing the mean number of unhatched eggs found under the combinations of date when the nest was laid, nest elevation, nest distance from MHW, and number of times the nest was inundated. 16-34

List of Tables

Table 16-1. Oceanfront and Backbarrier Shoreline Erosion Rates Used in the Carbon Budget Model..... 16-11

Table 16-2. Carbon Data and Age Dates Used in the Carbon Budget Model..... 16-12

Table 16-3. Number of Nests Containing Eggs for Each Species of Ground-Nesting Shorebird in Each Year Discovered on Each Washover Fan. 16-28

Acronyms

AD	Anno Domini
ANOVA	analysis of variance
cal BP	calendar years before present
CB	Coastal Barrier (Module)
cm	centimeter
cm^2	centimeter squared
CO_2	carbon dioxide
DCERP	Defense Coastal/Estuarine Research Project
DCERP1	first cycle of DCERP
DCERP2	Second cycle of DCERP
DoD	U.S. Department of Defense
EMD	Environmental Management Division
ESR	emergence success rate
$g\ C\ m^{-2}$	grams of carbon per square meter
$g\ C\ yr^{-1}\ m^{-1}$	grams of carbon per year per meter
$g\ m^{-1}$	grams per meter
$g\ m^{-2}$	grams per square meter
ICW	Intracoastal Waterway
ka	kilo-annum
km	kilometer
m	meter
$m\ km^{-1}$	meter per kilometer
$m\ yr^{-1}$	meter per year
m^2	meters squared
MCBCL	Marine Corps Base Camp Lejeune
MHW	mean highwater
MSL	mean sea level
NAVD 88	North Atlantic Vertical Datum of 1988
RC	Resource Conservation and Climate Change (a SERDP program area)
RTK-GPS	real-time kinematic global positioning system
SERDP	Strategic Environmental Research and Development Program
UNC-IMS	University of North Carolina at Chapel Hill's Institute of Marine Sciences

Abstract

Backbarrier saltmarshes are considered to be carbon sinks; however, barrier island transgression and the associated processes of erosion and overwash are typically not included in coastal carbon budgets. Here, we present a carbon-budget model for Onslow Beach that includes a dynamic carbon-storage term, driven by backbarrier-marsh width, and a carbon-export term, driven by ocean and backbarrier shoreline erosion. The model was parameterized from remote sensing data showing the rates of shoreline erosion, cores that sampled the carbon-rich sediment preserved at depth in the island, and radiocarbon dates from the base of the carbon-rich sediment from which carbon burial rates were determined. Overwash processes are important for barrier island transgression, and we present monitoring data that show changes in aerial extent, shorebird use, and vegetation of three washovers. Water-level loggers and cameras deployed on two washovers recorded overwash over a 2-year period, during which vegetation, shorebird, and topographic data were periodically collected. Results show that shoreline erosion and burial of backbarrier marsh from washover deposition and dredge-spoil disposal temporarily transitioned each site into a net exporter (source) of carbon. Overwash is a more continuous process than previously thought, and one of our sites continues to overwash 6 years after initial formation of the washover deposit. Carbon reservoirs of the study sites decreased for over a decade because carbon storage in the backbarrier marsh could not keep pace with ocean-shoreline erosion. With progressive narrowing of the backbarrier marsh, Onslow Beach will begin to function more persistently as a carbon source until the reservoir is depleted at the point where the coastal barrier welds with the mainland. With accelerated sea level rise and an increase in storminess expected in the future, erosion of carbonaceous sediment at the ocean shoreline will more frequently shift the carbon budget of Onslow Beach toward being a net source of carbon to adjacent environments and the atmosphere. Onslow Beach will also experience more overwash and washover deposition in the future, making the southwestern portion of the island difficult to access because of inundation during high tides and unsuitable for nesting shorebirds and sea turtles.

Keywords: Barrier island, transgression, carbon, sea level rise, sea turtle, shorebird, overwash, washover, dune, beach, erosion, saltmarsh, peat

Objectives of the Research Project

The technical objectives for Research Project CB-5 included developing a carbon-budget model for Onslow Beach and examining the role of overwash and washover deposition in island transgression (island rollover toward the mainland). The technical objectives for Research Project CB-5 included measuring the following: (1) the rate of island transgression, (2) organic carbon from initial accumulation in the backbarrier marsh to final erosion of peat in the shoreface, and (3) the duration and efficacy of carbon burial as the barrier rolls over the backbarrier marsh during transgression. The technical objectives for Research Project CB-5 also included measuring the following: (4) the flux of carbon into the ocean as peat erodes in the shoreface, (5) the contribution of barrier sand to backbarrier marsh accretion as the island moves landward, and (6) the changes in habitat quality for flora, nesting sea turtles, and shorebirds, as well as the loss of military training area resulting from island rollover. To improve understanding of barrier island transgression by including information about the cycling of materials and the changes in island morphology and associated ecosystem services (e.g., the presence of an amphibious training ground and carbon sequestration) resulting from island rollover, we addressed the following research questions:

1. How does the age, volume, and carbon content of the peat change with increasing distance from the saltmarsh to the ocean?

2. What are the relationships between the rate of island transgression and the volume of peat preserved within the barrier and the flux of carbon to the ocean from the erosion of peat in the foreshore?

3. What are the differences in abundance of nesting shorebirds at young washover fans with no vegetation and older vegetated washover fans?

4. What are the relationships between sea turtle nest survivorship to hatching and backbeach width, elevation, and beach slope?

5. Questions 1 and 2 were addressed by developing a carbon-budget model. Questions 3 and 4 were addressed by monitoring the vegetation density and shorebird utilization of two washover fans and by collecting beach-morphology data around turtle nests.

Background

Barrier Island Transgression

In response to sea level rise, increased storminess, and reduced sediment supply, barrier islands migrate landward (transgress) by aeolian processes and storm overwash (Leatherman and Williams, 1977), flood tidal delta formation (Leatherman, 1979; Riggs and Ames, 2007) and erosional shoreface retreat (Bruun, 1962; Dubois, 1995, Miselis and McNinch, 2006; Niedoroda et al., 1985; Pilkey et al., 1993; Rodriguez et al., 2001; Swift, 1976). This general conceptual model has been thoroughly tested from examining modern barriers (e.g., Moslow and Heron, 1978; Timmons et al., 2010; Wilkinson and Byrne, 1977) and barrier remnants preserved on the inner continental shelf (e.g., Belknap and Kraft, 1985; Rodriguez et al., 2004). However, it is

unclear how the process of barrier rollover contributes to the coastal carbon budget and impacts the distribution and function of saltmarsh habitats. It is also unclear how the process will be modified by climate change and associated changes in the rate of sea level rise and storminess. In the absence of more detailed, quantitative data on these processes, management preparations, responses, and practices to preserve military training assets and environmentally sensitive habitats can only be informed by anecdotal information.

Transgressive barrier islands, such as the southwestern two-thirds of Marine Corps Base Camp Lejeune's (MCBCL's) Onslow Beach **(Figure 16-1**), sequester carbon principally through accretion of backbarrier marshes and peat burying this carbon below meters of sand by overwash and aeolian processes (**Figure 16-2**). These barriers also export carbon to adjacent environments when the buried peat deposit is eroded at the ocean and backbarrier shorelines. The deposition of washover fans (i.e., the landform created during overwash) provides substrates for saltmarshes and dune flora (Johnston, 1998), is the mechanism of carbon burial, and creates important habitat for some nesting shorebirds (including the federally listed piping plover [*Charadrius melodus*]; Maslo et al., 2011). However, deposition of washover fans also adversely impacts MCBCL's infrastructure, including egresses, access roads, buildings, back-beach staging areas, and the Intracoastal Waterway (ICW). In addition, the process of overwash produces a beach that presents a different landscape to nesting sea turtles with the potential of altering their choice of nesting location and influencing nesting success in ways that lead to necessary changes in MCBCL's wildlife management practices involving decisions about nest relocation practices (Mazaris et al., 2006; Pfaller et al., 2008; Rizkalla and Savage, 2011; Spanier, 2010).

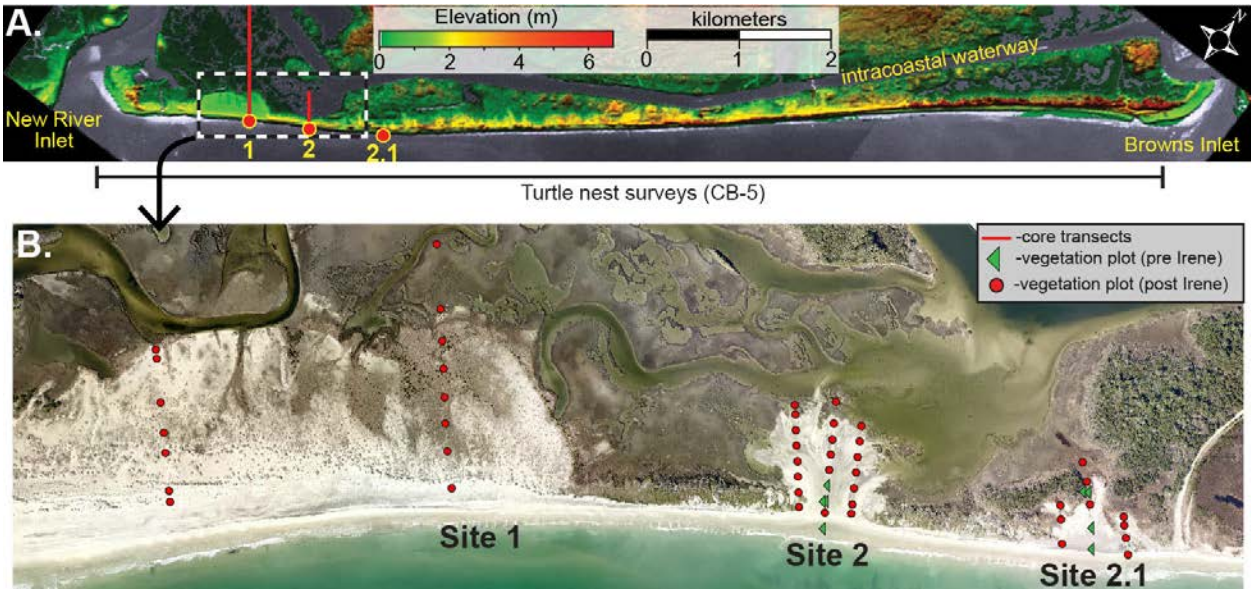

Figure 16-1. The southern two-thirds of Onslow Beach is a typical transgressive barrier and ideal location for deriving a carbon budget, while examining the process of island rollover as it pertains to marsh accretion, marsh burial, island morphology, beach erosion, and ecosystem function.

The aerial photograph was taken June 6, 2012.

This research project builds on the monitoring and research efforts of DCERP1. During DCERP1, we learned that MCBCL military training activities at their present level have little impact on the historical washover fans (associated with Hurricane Fran in August 1996) and ancient washover fans (greater than 200 years old) that were mapped, as well as the associated fronting beach and intertidal areas. Research conducted by Rodriguez et al. (2012) shows significant variability in erosion rates and depths along Onslow Beach at decadal and yearly time scales, which MCBCL manages by employing spatially defined restoration strategies (e.g., grass planting, turtle nest relocation, sand-fence construction). Management of the amphibious training and recreational resources is becoming more challenging in the future because scientists have shown that the rate of sea level rise is increasing (Church and White, 2006; Jevrejeva et al., 2008; Rahmstorf, 2007). Another challenge is that tropical and extratropical storm intensity (Elsner et al., 2008; Emanuel, 2005; Knuston et al., 1988) and frequency (Goldenberg et al., 2001; Webster et al., 2005) in the North Atlantic Ocean are also increasing (Carter and Draper, 1988), which will lead to increases in degradation of protective coastal dunes, more frequent overwash across Onslow Beach and other analogous U.S. Department of Defense coastal installations, and more rapid erosion of peat deposits on the beach.

Carbon Storage and Export in Transgressive Barrier Islands over Centennial to Millennial Time Scales

Carbon storage in transgressive barrier islands is directly related to the width of backbarrier saltmarsh, whereas carbon export occurs in response to erosion associated with the landward movement of the island. Sea level rise principally forces barrier islands to migrate landward across continental shelves and during migration the width of backbarrier marsh changes due to erosion and storm overwash. This width change can be positive if overwash creates new marsh width through washover or flood-tidal delta deposition, or negative if erosion and overwash (burial of marsh) reduces marsh width.

Coastal-plain gradients are low along the U.S. Atlantic and Gulf coasts (typically less than 0.5 m km^{-1}; Mattheus and Rodriguez, 2011); however, along the coastal-plain edge, shorelines that formed during sea level highstands (periods when sea levels are at their highest) are preserved as a series of scarps (paleoshoreline scarps; Stephenson, 1912). The Suffolk Scarp is the most seaward scarp that parallels the modern shoreline along the U.S. mid-Atlantic coast (Winker and Howard, 1977). Barrier islands migrated landward from the outer continental shelf during the last deglaciation (lowstand of −135 m below mean sea level (MSL) at 20 ka; Yokoyama et al., 2000), towards the steep paleoshoreline scarp at the edge of the coastal plain. The mainland-estuarine shoreline behind barrier islands also moved landward with sea level rise and the rate of transgression and extent of intertidal habitat along that shoreline was strongly controlled by the topography of the land being inundated (Rodriguez et al., 2005 and 2008; Simms and Rodriguez, 2014).

Johnson (1919) described changes in barrier island environments that take place during landward migration, including changes in backbarrier saltmarsh width (**Figure 16-2**). During island migration, carbon-rich marsh sediment is eroded at the backbarrier marsh shoreline (Eulie et al., 2016; Leonardi and Fagherazzi, 2014) and on the shoreface (Fisher, 1961; Johnson, 1919; Kraft, 1971). Once the migrating barrier island approaches the steep gradient of the paleoshoreline scarp, backbarrier lagoon expansion is prevented from keeping pace with landward barrier

movement. Eventually, the lagoon will decrease in size, fill with sediment, and transform into an extensive marsh confined to the area between the barrier and the coastal plain (**Figure 16-2B**). As the island continues to migrate landward, the backbarrier saltmarsh will narrow, and the barrier will ultimately weld with the paleoshoreline scarp. Modern transgressive barrier islands exist within the settings presented in **Figure 16-2**, and adjacent barrier islands or segments of the same barrier can be located different distances from the previous highstand shoreline. Along a single coastal margin, differences among modern barrier island settings can be attributed to spatial variations in the topography of the land being inundated, sediment supply, and/or relative sea level.

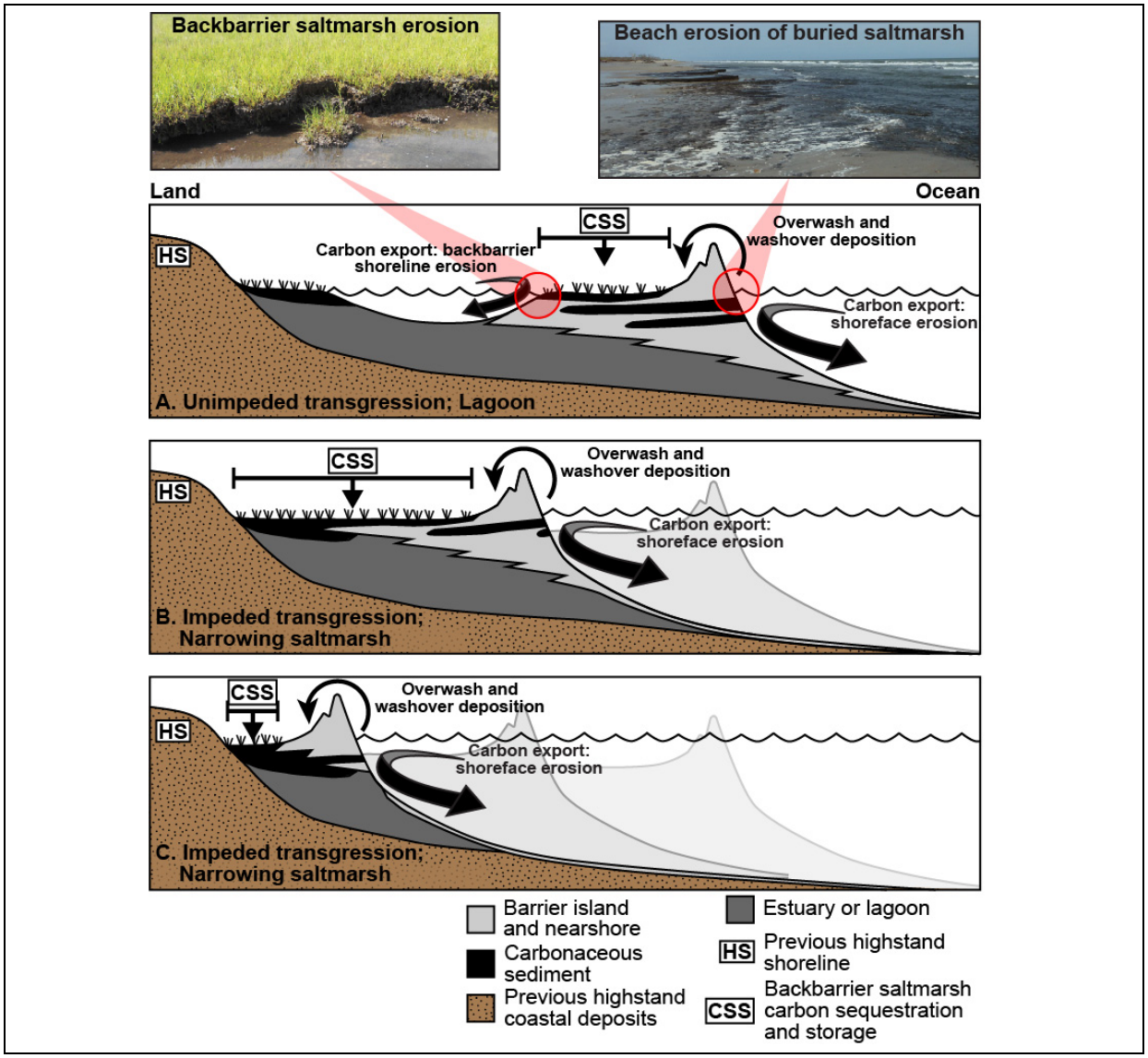

Figure 16-2. Conceptual model of transgressive barrier island evolution. As the barrier island moves landward towards the previous highstand shoreline, the backbarrier lagoon (A) transforms into a wide saltmarsh (B), which decreases in width as island migration progresses.

Barrier-island transgression is associated with overwash, washover deposition, and erosion of carbonaceous saltmarsh sediment at the shoreface and estuarine shoreline.

Carbon Storage and Export in Transgressive Barrier Islands over Yearly to Centennial Time Scales

The carbon budget of transgressive barrier islands such as Onslow Beach is largely modulated by storminess and relative sea level rise over yearly to centennial time scales. Substrate for backbarrier marsh colonization is primarily created during storms through overwash and island breaching, which result in the deposition of washover fans and terraces, as well as flood-tidal deltas (Godfrey and Godfrey, 1976). Washover deposits form from overwash during storms when the water level exceeds the maximum elevation of the barrier and waves and currents transport eroded beach, dune, and shoreface sand across the island, where it is deposited in backbarrier open water and/or fringing marsh environments (Donnelly et al., 2006; Lorenzo-Trueba and Ashton, 2014). Washover deposition builds island width and helps to sustain transgressive barrier islands through time by balancing erosion at the ocean and backbarrier shoreline (Leatherman and Williams, 1983; Timmons et al., 2010).

Marsh colonization likely occurs rapidly on washover deposits once the substrate reaches an intertidal elevation and conditions are optimal for marsh growth (Gunnell et al., 2013). Once saltmarsh is established, the carbon reservoir of the barrier island increases rapidly as the marsh accretes vertically to keep pace with sea level rise through autochthonous (i.e., internal) and allochthonous (i.e., external) sediment deposition (Nyman et al., 2006; Redfield and Rubin, 1962). Autochthonous deposition occurs in response to the marsh grass life cycle. Allochthonous deposition takes place as the marsh grass decreases flow velocity during inundation, promoting deposition of the suspended sediment load, which contains inorganic and organic material from terrestrial and other aquatic sources (Ember et al., 1987). Marshes sequester carbon by removing carbon dioxide (CO_2) from the atmosphere through photosynthesis and storing organic carbon in both above-ground and below-ground biomass. This sequestered carbon also accumulates in marsh sediments, and the fraction of carbon that remains in the soil over longer time scales (decades to millennia) after microbial degradation is considered to be buried. We define “carbon storage” as the along-shore averaged carbon reservoir of the marsh, partitioned across the lifetime of the marsh (i.e., a rate derived from the marsh surface to its base). The process of marsh-soil formation results in an increase in the total amount of carbon contained within the entire marsh reservoir through time.

Transgressive barrier islands may represent an important carbon sink because the carbon reservoir will increase through time if backbarrier marshes keep pace with sea level rise and maintain their extent; however, if export exceeds storage, the barrier may function as a net source of carbon. Carbon export from backbarrier-marsh shoreline and ocean shoreline erosion, therefore, must also be included in the transgressive island carbon budget. Backbarrier marshes erode in response to waves and currents that are amplified by human disturbances (e.g., boat wakes and installation of hard structures), strong winds, and storm events (Elliott et al., 2015; Mattheus et al., 2010; Mariotti and Carr, 2014; Riggs and Ames, 2007; Timmons et al., 2010).

The erosion of organic-rich marsh deposits, from both the shoreface and the backbarrier shoreline, will export carbon from the barrier island system to the coastal ocean and estuary. Some portion of that carbon will be converted back into CO_2, whereas other more refractory portions will likely become redeposited in adjacent environments (Cai et al., 2003; Canuel et al., 2012). Regional and global carbon budgets should account for carbon exported from

transgressive barrier islands because some of this carbon will be an input term for adjacent marine and coastal environments. The ultimate fate of the eroded carbon is difficult to discern; therefore, we are simply treating it as being lost from the barrier island and are neither tracing subsequent pathways nor modifications of the organic material.

The net carbon budget (g C yr^{-1} m^{-1}) of a transgressive barrier island over any time scale is the difference between the amount of carbon stored across the marsh platform and the amount of carbon exported from shoreface erosion and backbarrier shoreline erosion (**Figure 16-2**). The trajectory (positive or negative g C yr^{-1} m^{-1}) of the carbon budget will dictate whether the carbon reservoir increases or decreases through time. For example, if carbon storage exceeds export, then the barrier island will function as a carbon sink, and the reservoir will increase through time. Changes in storminess, sea level rise, and coastal development influence the rates of erosion and the distribution of saltmarsh, which will alter carbon export and storage rates and ultimately the carbon budget and reservoir of a barrier island.

Materials and Methods

Carbon Budget Model

The conceptual framework for barrier island rollover and associated implications to the carbon budget of a transgressive barrier island were examined by developing a numerical along-shore averaged carbon-budget model and parameterizing that model with data collected at two sites along survey transects on Onslow Beach. Our methods were chosen to elucidate those main processes responsible for transitioning transgressive barrier islands from being carbon sinks to sources and to evaluate the timescale over which that transition can occur.

Study Sites

Carbon budgets were developed at Site F1, a setting where a wide backbarrier saltmarsh that is narrowing due to beach erosion is confined between the barrier island and an increase in coastal slope, thus impeding upland marsh transgression and Site F2, a setting similar to Site F1, but with a narrow backbarrier saltmarsh. The two sites are located along the southwestern portion of the island (**Figure 16-1**). Over the past century, both sites have been characterized by low barrier elevations (less than 2 m) and a history of ocean overwash during storms. Four hurricanes altered the morphology of these two sites within the past 21 years. In September 1996, Hurricane Fran formed a large washover terrace at Site F1, which subsequently increased in landward width during Hurricane Bonnie in August 1998. Hurricane Irene, which made landfall near Cape Lookout, NC, in August 2011 created a washover terrace at Site F2. This terrace was subsequently modified into a washover fan during Hurricane Sandy in October 2012 and during frequent nor'easters in the winter months (late 2012 through early 2013; VanDusen et al., 2016). Hurricane Irene also formed a washover deposit at Site F2.1. That site was not included in the carbon budget, but we did monitor post-storm changes in morphology, vegetation, and shorebird use.

Data Collection

To estimate the net carbon budget at both sites, carbon storage and export were calculated. The rate of carbon storage (g C yr^{-1} m^{-1}) was estimated from measuring saltmarsh sedimentation rates, sediment composition, and marsh width changes. The rate of carbon export (g C yr^{-1} m^{-1}), was estimated from measuring saltmarsh sediment thickness and composition and the rates of backbarrier and shoreface erosion. Carbon budgets were computed along shore-perpendicular transects (**Figure 16-3**), and the model was subsequently parameterized with information from vibracores and a time series of aerial photographs.

Vibracores. To sample the entire thickness of the marsh, vibracores were collected along shore-normal transects at Sites F1 and F2 from the ocean shoreline landward to the ICW (**Figure 16-3**). Elevation and positional data (vertical position relative to the North Atlantic Vertical Datum of 1988 [NAVD 88]) were gathered with a Trimble real-time kinematic global positioning system (RTK-GPS) at each core location, as well as along a profile at each coring transect. Cores were split on the long axis, photographed, described, and sampled to define sedimentary facies, determine the carbon inventory, and age date marsh-plant material. Carbonaceous units were subsampled in continuous 5-cm increments from half of the split cores for organic carbon analysis. Samples were dried and homogenized by using a grinder and a mortar and pestle. A Costech ECS4010 Elemental Analyzer was used to measure percent organic carbon on subsamples of the carbonaceous sediment, and values were reported with a ±0.17% analytical error. The percent organic carbon was converted into grams of carbon per square meter based on the mass of the sample and the area of the core (45.6 cm^2). To determine when saltmarsh first colonized the site, above-ground biomass (e.g., grass blades, stems, seeds) was sampled from the base of the marsh units and sent to Beta Analytic for carbon-14 dating. This technique assumes that the material dated was preserved in situ (Redfield and Rubin, 1962). Radiocarbon dates were calibrated with the IntCal13 radiocarbon calibration curve by using Calib 7.1 (Reimer et al., 2013; Stuiver and Reimer, 1993).

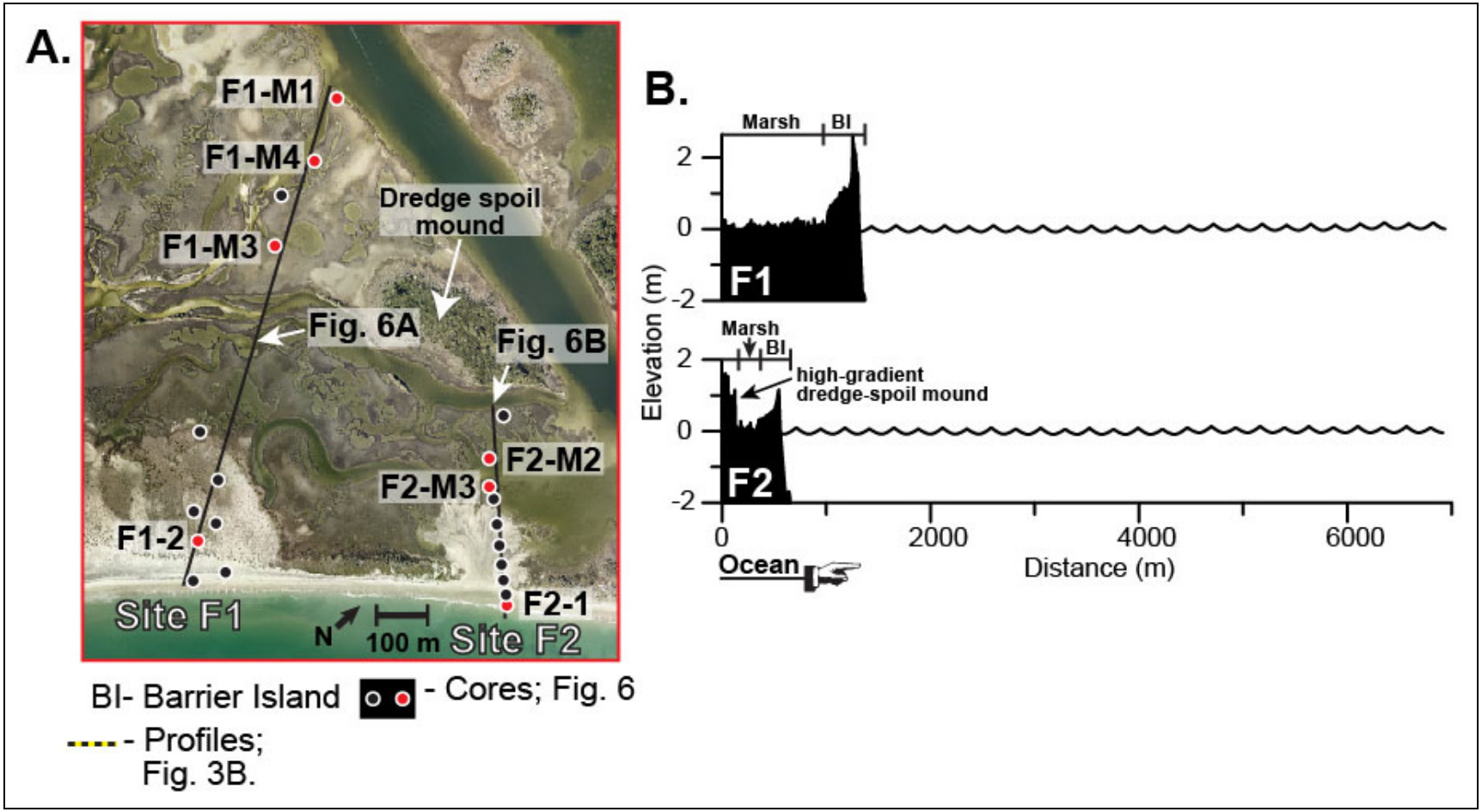

Figure 16-3. (A) Map showing sample locations. Red dots indicate cores sampled for percent organic carbon. (B) Elevation profiles across Sites F1 and F2 showing that the morphology is similar to the transgressive barrier island settings shown in Figure 16-2.

Changes in Shoreline Position and Marsh Width. Backbarrier and oceanfront shoreline erosion rates were measured by using aerial photographs from the U.S. Department of Agriculture, digitized shorelines downloaded from the North Carolina Division of Coastal Management, and terrestrial laser scanning data. Erosion rates were calculated by using the ArcGIS extension Digital Shoreline Analysis System (Thieler et al., 2009), which calculates the distance each shoreline is from a baseline along defined transects. The rates of shoreline erosion were calculated for each period by using the end-point method.

Ocean shoreline retreat rates over decadal to centennial time scales were developed by using shoreline shapefiles from the North Carolina Division of Coastal Management. The shoreline shapefiles were digitized from a combination of T-sheets and aerial photographs and have resolutions ranging from 1.5m to 10.8 m. The dates of the ocean shorelines used were 1872, 1934, 1997, and 2004. Ocean shoreline retreat rates over annual time scales for the last decade were measured during biannual surveys from 2007 to 2014 by using a terrestrial laser scanner (Theuerkauf and Rodriguez, 2014). These data capture shoreline changes associated with extensive washover deposition during Hurricanes Fran, Bonnie, Irene, and Sandy. The shoreline position was extracted from Digital Elevation Models constructed by using topographic data from the laser scans. The shoreline is defined by the mean high water line, which is approximated as the 0.36 m NAVD 88 contour (Weber et al., 2005).

A constant rate of backbarrier-shoreline retreat, calculated over multiple decades, was used to parameterize the model at both sites. After construction of the ICW in the 1930s, backbarrier-marsh shoreline retreat rates were measured at Sites F1 and F2 by using aerial photographs from 1983 and 2014. Aerial photographs and historical maps were also used to measure changes in marsh width from dredging of the ICW and burial by washover deposits during storms. The initial marsh width (from the backbarrier-marsh shoreline towards the dune) was measured from AD 1872, the earliest available map. Aerial photographs from 1938, 1998, 2002, 2011, and 2013 were used for marsh width measurements. Decreases in marsh width from ICW dredging and washover deposition were modeled as being instantaneous in the year that the loss occurred. Visual inspection of the aerial photographs did not reveal fragmentation of backbarrier marsh through time resulting from sea level rise and expansion of the tidal-creek network. Marsh can only be lost in our carbon-budget model by burial, shoreline erosion, and/or dredging.

Carbon Budget and Reservoir

The first known position of the ocean shoreline at AD 1872 was used as the starting point for the model, which was run forward in time to 2014. Carbon storage was parameterized through a combination of data from the coring surveys and aerial photographs (**Figure 16-4 and Table 16-1**). The rate of carbon storage (Sr; g C yr^{-1} m^{-1}) is the product of the rate of carbon accumulation (Ar; g m^{-2} yr^{-1}) in the backbarrier marsh and the width of the marsh (m; **Figure 16-3**). The Ar was estimated from cores collected in the backbarrier marsh along each transect and calculated by dividing the backbarrier marsh carbon inventory (Ib; g m^{-2}) by the age of initial marsh colonization (yr), determined from the radiocarbon date collected at the base of the marsh. We defined Ib at Site F1 as an average of the carbon sampled in three cores (± standard deviation), and Ib at Site F2 as the median of the carbon sampled in two cores from each site (± range/2; **Figures 16-4 and 16-5; Table 16-2**). The rate of shoreface carbon export (Er_s; g C yr^{-1} m^{-1}) is the product of the shoreface carbon inventory (Is; g m^{-2}), measured by using

one core on the shoreface at each site (**Figure 16-4**) and the shoreface erosion rate (ds/dt; m yr^{-1}; **Figure 16-4**). The rate of backbarrier carbon export (Er_b; g C yr^{-1} m^{-1}) is the product of the backbarrier marsh carbon inventory (Ib; g m^{-2}), and the rate of backbarrier marsh shoreline erosion (ds/dt; m yr^{-1}; **Figure 16-4**). The marsh carbon inventory for carbon export at the backbarrier-marsh shoreline was computed by using the same cores as those used to compute carbon storage.

Table 16-1. Oceanfront and Backbarrier Shoreline Erosion Rates Used in the Carbon Budget Model

Ocean Shoreline Erosion Rates	(m/yr)
Site F1	
Onslow Beach F1 1872–1934	−1.3
Onslow Beach F1 1934–1995	−1.1
Onslow Beach F1 1996 (Hurricane Fran)	−7.3
Onslow Beach F1 1997–2004	0.2
Onslow Beach F1 2004–2007	−3.6
Onslow Beach F1 2007–2014	2.9
Site F2	
Onslow Beach F2 1872–1934	0.1
Onslow Beach F2 1934–1995	−1.1
Onslow Beach F2 1996 (Hurricane Fran)	−5.2
Onslow Beach F2 1997–2004	−5.3
Onslow Beach F2 2004–2007	−3.1
Onslow Beach F2 2007–2010	−0.8
Onslow Beach F2 2011	−10.1
Onslow Beach F2 2012	−7.5
Onslow Beach F2 2013–2014	−0.8
Backbarrier Shoreline Erosion Rates	
Onslow Beach F1 1983–2014	−0.9
Onslow Beach F2 1983–2014	0.0

Table 16-2. Carbon Data and Age Dates Used in the Carbon Budget Model

Site	Core Name	Inventory (g C m^{-2})	Age (Years Before 2014)	Accumulation Rate (g C m^{-2} yr^{-1})
F1 Backbarrier Marsh Carbon	F1-M1	10,423.1 ±17.7	288.0	36.2
	F1-M3	67,68.8 ±11.5	465.0	14.6
	F1-M4	12,274.6 ±20.9	719.0	17.1
	Average	*9,822.2 ±16.7*	*490.7*	*22.6 ±11.8*
F1 Shoreface	F1-7	*13,394.0 ±22.8*	—	—
F2 Backbarrier Marsh Carbon	F2-M2	9,913.8 ±16.9	228.0	43.5
	F2-M3	10,107.3 ±17.2	243.0	41.6
	Average	*10,010.5 ±17.0*	*235.5*	*42.5 ±0.95*
F2 Shoreface	F2-1	10,388.2 ±17.7	—	—

The carbon reservoir (R; g m^{-1}) at each site for the first year of the model was calculated as (Ib [g m^{-2}] × the initial backbarrier marsh width [m]) + (Is [g m^{-2}] × the initial beach width [m]). For each subsequent year, the calculated net carbon budget was either added to or subtracted from the reservoir. At Site F1, the initial backbarrier marsh width was 1,400 m, and the beach width was 100 m. At Site 2, the initial backbarrier marsh width was 455 m, and the beach width was 100 m. The carbon reservoir was computed every year from AD 1872 to 2014 at each site.

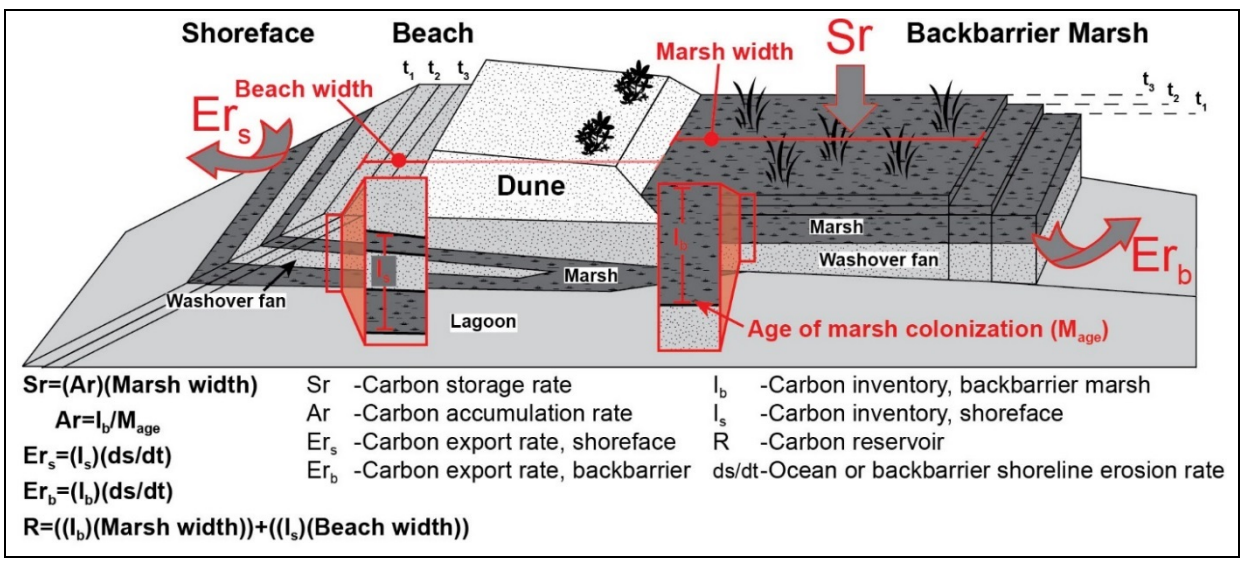

Figure 16-4. Illustration of the parameterization of the transgressive barrier island carbon-budget model (not to scale).

The net carbon budget (g yr^{-1} m^{-1}) is the difference between the carbon storage rate (Sr) and the rate of carbon export from shoreface erosion and backbarrier shoreline erosion (Er_s + Er_b).

Washover Fan Evolution

Morphologic Change and Overwash Record

Morphologic changes were measured by using a Riegl three-dimensional LMSZ210ii terrestrial laser scanner to collect millions of X, Y, and Z points from SF2 and F2.1 (more details are presented in *DCERP2 Research Plan* [RTI, 2013]). Those point data were processed and Digital Elevation Models were created, from which measures of change were extracted. We collected 19 point data sets at Site F2 from May 2011 to October 2015 and 12 point data sets at Site F2.1 from January 2012 to October 2014 (**Figure 16-5**). We used water-level loggers deployed in shallow wells to derive overwash records at Onslow Beach. Details about this method appear in VanDusen et al. (2016). The record is only applicable for the area around the well and contains information about the occurrence of inundation overwash, which is associated with a height value. Height values are relative to the ground surface near the well. Inundation overwash occurs when storm-surge elevation, measured independently from wave run-up, is greater than dune-crest elevation, resulting in water consistently flowing over the barrier.

Ecological Succession

We used data collected seasonally from long-term fixed plots to quantify changes to the flora assemblages that occurred in the washover fans (Site F1 [fan from 1996 Hurricane Fran], Site F2 [fan from 2011 Hurricane Irene and subsequent storms], and Site F2.1 [fan from 2012 Hurricane Sandy]) and contiguous saltmarshes. To quantify ecological succession in the younger washover fans at Sites F2 and F2.1 and to compare the structure of the floral series documented in those washover fans to the floral communities on the older washover fan (Site F1), we established a total of 43 permanent, 5-m × 20-m vegetation plots parsed among several across-island transects (one new transect at Site F1, two new transects at Site F2, and three new transects at Site F2.1 to add to the 12 existing plots at Site F1 [eight plots] and Site F2 [four plots]). We used a modified form of the Carolina Vegetation Survey protocol (Peet et al., 1988) to sample these plots (and resampled the existing ones) semi-annually starting in February 2013 to determine which species were present in each plot and their respective percent cover within each 100 m^2 plot (**Figures 16-1 and 16-5**).

Shorebird Nesting Activity

During nesting season (late April through mid-June), we documented ground-nesting shorebird use of three washover fans in 2013, 2014, and 2016. At bi-weekly intervals during nesting season, we censused ground-nesting bird nests, identified the species making the nest, and followed the fate of each nest until it was abandoned, predated, or any eggs hatched. Because of their smaller size, we were able to survey the entire area of each younger washover fan (Site F2 [formed in 2011] and Site F2.1 [formed in 2012]) for bird nesting activity each time we were in the field. At the older Site F1 washover fan (formed in 1996), we surveyed bird nesting activity along three, approximately 80-m wide transects that extended across the island from the exposed beach to the saltmarsh. The easternmost transect crossed dense dune-field vegetation, while the two western transects, which were contiguous, covered areas more sparsely vegetated. The total areas covered at Sites F2 and F2.1 are comparable to the surveyed area at Site F1: Site F1

western transects = 37,000 m^2; Site F1 eastern transect = 11,000 m^2; Site F2 fan =35,000 m^2; and Site F2.1 fan =10,000 m^2.

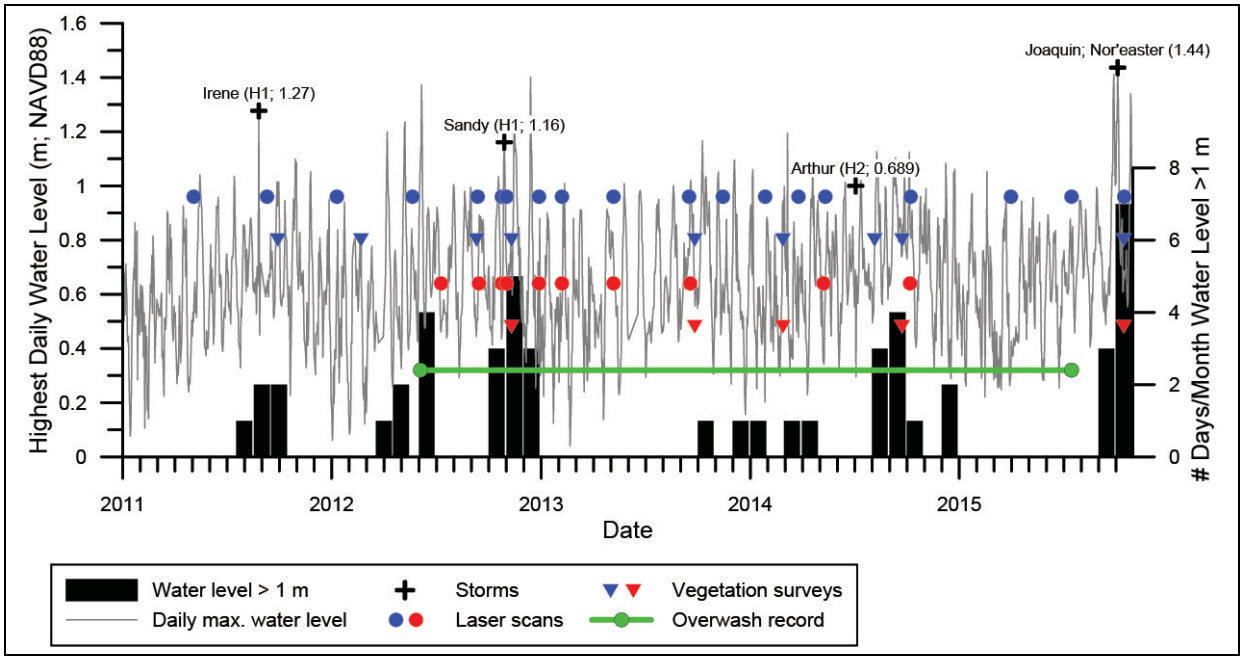

Figure 16-5. Time series of physical processes and data collection at the study site from May 2012 to November 2014.

Water levels at the National Oceanic and Atmospheric Administration Station 8658163, located 53 km southwest of the study site on an ocean-side pier is shown by the gray line and black bars. Data collected at Sites F2 and F2.1 are shown in blue and red, respectively.

Sea Turtle Nesting Activity

Throughout sea turtle nesting season (May through August), personnel in MCBCL's Environmental Management Division (EMD) conduct daily surveys to make initial discovery and global positioning system (GPS) location recordings of all sea turtle false crawls and nests. In each of 3 years, we visited the location of a majority of false crawl and turtle nesting events that occurred, within the succeeding week. A Trimble RTK-GPS was used to collect data regarding the sea turtle nest elevations (coordinates) and nearby landscape morphology to enable us to relate nest location and site-specific hatching success to elevation and dune-beach morphology (for details, see *DCERP2 Research Plan* [RTI, 2013]).

Results and Discussion

Carbon Budget Model

Sedimentology and Stratigraphy

Cores collected at Sites F1 and F2 sampled a classic transgressive barrier sequence, including a basal Pre-Holocene unit overlain successively by lagoonal, saltmarsh, washover, beach and dune deposits (**Figure 16-6**). The Pre-Holocene unit ranged in character from stiff clay to fine-grained sand and is indicative of subaerial exposure during a period of lower sea level. The lagoonal unit

was a muddy sand with silty laminae that contains less than 1% organic carbon. Washover deposits at Sites F1 and F2 were sampled in our cores immediately seaward of the modern backbarrier marsh (**Figure 16-6**). At Site F1, these deposits formed during Hurricanes Fran (1996) and Bonnie (1998); at Site F2, the deposits formed during Hurricanes Irene (2011) and Sandy (2012). The seaward cores at Sites F1 and F2 sampled modern beach and dune sand perched above the lagoonal unit and organic-rich saltmarsh sediment.

The backbarrier marsh extends seaward underneath the washover and dune deposits and was sampled at both sites as a carbonaceous (1% to 11% of carbon) muddy sand to sandy silt unit with abundant plant material (**Figure 16-6**). Cores collected in the modern marsh at Site F1 sampled saltmarsh with organic carbon ranging from 1% to 11%. A radiocarbon date from the base of the backbarrier marsh unit at Site F1 indicates that the marsh colonized the site between 225 ± 57 calendar years before present (cal BP) and 681 ± 28 cal BP. The carbon accumulation rates calculated from the backbarrier marsh cores increase towards the ICW shoreline at Site F1 (**Table 16-2 and Figure 16-6**). The marsh unit sampled in the beach cores at Site F1 was thinner than the backbarrier marsh and intercalated with sand beds interpreted as washover deposits. Vegetation from the base of the marsh unit sampled below the beach sand was radiocarbon dated as 300 ±33 cal BP and organic carbon ranged from 4% to 11%.

The modern backbarrier saltmarsh sediment at Site F2 ranged in organic carbon from approximately 1% to 13% and ranged in age from 80 ±68 cal BP to 300 ±19 cal BP (**Figure 16-6**). Similar to the other sites, backbarrier marsh carbon accumulation rates increased towards the ICW; however, given that dredge-spoil mounds are situated between the marsh and the ICW, the percent difference between the two cores was only 4.4%, less than at Site F1. Approximately 60 cm of older marsh material was sampled below sand in cores collected on the beach at Site F2 (**Figure 16-6**). A radiocarbon date at the base of this seaward marsh unit yielded an age of 504 ±32 cal BP and organic carbon ranges from 1% to 6%.

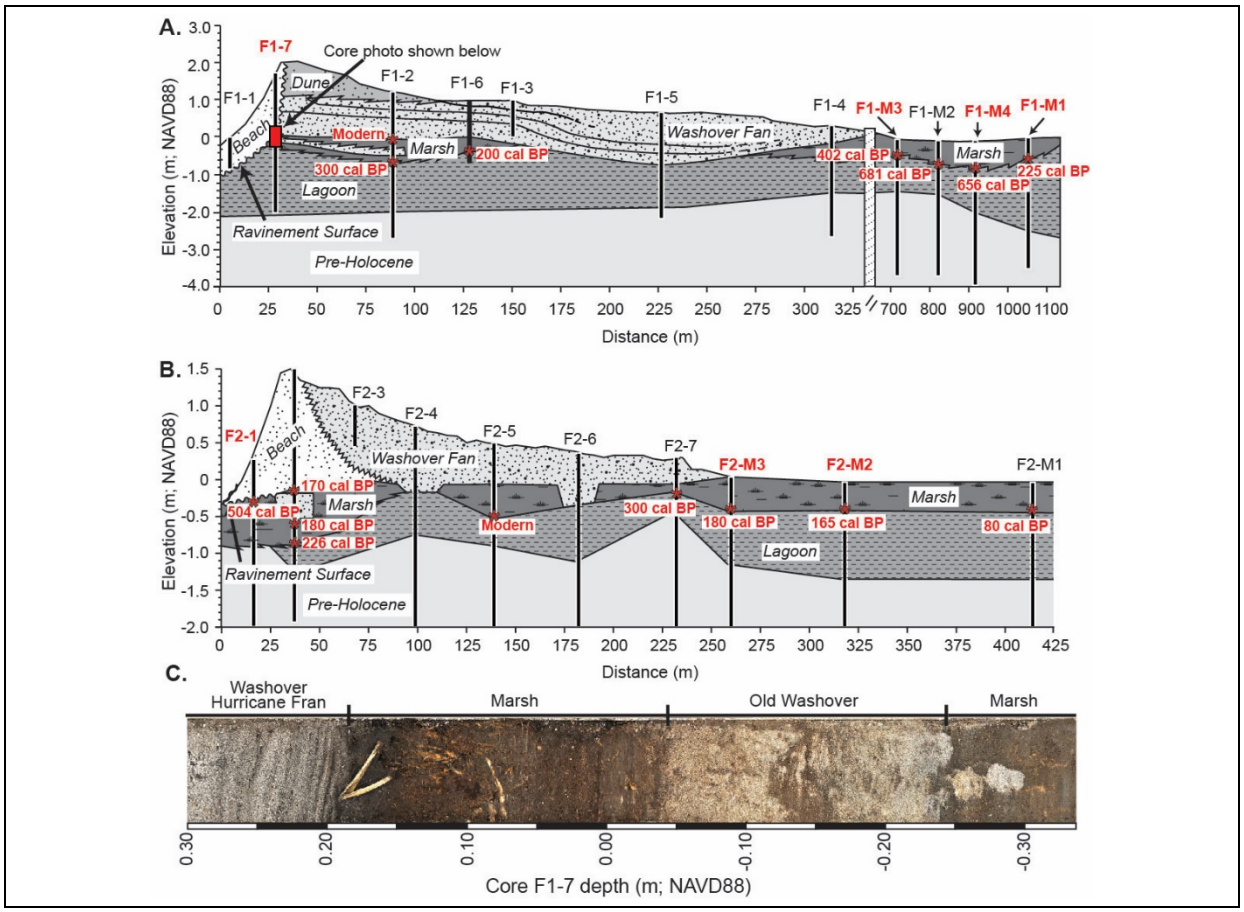

Figure 16-6. Stratigraphic cross section of (A) Site F1 and (B) Site F2 used to parameterize the barrier carbon-budget model.

Carbon analyses of saltmarsh sediment conducted on those cores are labeled in red. Transects and core locations are shown on Figure 16-3.

Changes in Erosion Rates and Marsh Width

From 1872 to 2014, the ocean shoreline moved landward approximately 255 m at Site F1 and approximately 200 m at Site F2 (**Table 16-1**). The ocean shoreline at Site F1 oscillated between accretion and erosion after 1996. Since 2007, the shoreline has been moving seaward. This accretion is likely related to a post-storm recovery after Hurricane Fran. At Site F2, the rate of shoreline change increased across the twentieth century (**Table 16-1**). After 2010, higher shoreline retreat rates were observed at Site F2, likely due to storm events in 2011 and 2012 (**Table 16-1**).

The marsh shorelines at Site F1 are eroding approximately 0.26 m/yr^{-1}, calculated as an end-point rate based on two aerial photographs taken more than 30 years apart. Although this method for measuring backbarrier erosion cannot resolve variability due to storms, Leonardi et al. (2016) argue that large storms are not as important for eroding marsh shorelines as average wave conditions are. The marsh shoreline is not eroding at Site F2 because when the ICW was constructed, dredged material was placed on top of the marsh, adjacent to the ICW, and formed an approximately 1.5-m high sand mound that has since been colonized by maritime forest, and

it buffers the marsh shoreline from erosion. This high-elevation mound presents a landscape that resembles a backbarrier marsh lapping against the previous highstand shoreline.

Marsh width has decreased at variable rates since construction of the ICW. Marsh narrowing due to backbarrier erosion is likely a relatively continuous process (Leonardi et al., 2016); however, washover deposition during storms and human disturbances that bury marsh can result in large and abrupt marsh loss. In 1932, there was a rapid reduction in backbarrier marsh width behind Onslow Beach when the ICW was excavated and dredged material was disposed of into the marsh. Sites F1 and F2 lost approximately 460 m and 130 m of marsh width, respectively, from burial and loss of marsh during construction of the ICW. Overwash from Hurricanes Fran (1996) and Bonnie (1998) abruptly buried 180 m and 110 m of marsh at Site F1, respectively (**Figure 16-7**). In 2011, approximately 30 m of marsh was buried at Site F2 during Hurricane Irene (**Figure 16-7**). During the following year, approximately 150 m of marsh was buried at Site F2 during Hurricane Sandy and subsequent nor'easters (**Figure 16-7;** VanDusen et al., 2016).

Changes in Carbon

The core data, combined with shoreline erosion and marsh width change data, were used to determine the along-shore averaged carbon storage and export rates. At Site F1, the marsh carbon accumulation rate is 22.6 ±11.8 g C m^{-2} yr^{-1}, which is based on cores F1-M1, F1-M3, and F1-M4 (**Table 16-2**). The marsh carbon accumulation rate at Site F2 is 42.5 ± 0.95 g C m^{-2} yr^{-1}, which is based on cores F2-M2 and F2-M3 (**Table 16-2**). Sudden decreases in marsh width from dredging of the ICW and burial by washover deposits caused the decreases in carbon storage at Onslow Beach (**Figure 16-7**). After dredging of the ICW at Site F1, carbon storage progressively decreased through time in response to marsh-shoreline erosion; which was not observed at Site F2, given that the landward edge of the marsh is in contact with the dredge-spoil mound and is stationary (**Figure 16-7**). At both sites, variability in oceanfront erosion rates is the main driver of variations in carbon export. The shoreface carbon inventories at Sites F1 and F2 are assumed to be constant through time and were measured as 13,394 ±22.8 g C m^{-2} (core F1-2) and 10,388 ±17.7 g C m^{-2} (core F2-1), respectively. Carbon export rates are highest during storms that cause high erosion rates (**Figure 16-7**). For example, high export rates in 1996 at Sites F1 and F2 are associated with Hurricane Fran, and high export rates at Site F2 in 2011 were associated with Hurricane Irene. During storm-recovery phases, such as at Site F1 after Hurricane Fran, or other instances when the beach is not eroding, no carbon was being exported on the ocean side (**Figure 16-7**).

The carbon budget has varied considerably over the past century, but both sites remained carbon sinks until the 1990s (**Figure 16-7**). The net carbon budget decreased more rapidly at Site F2 than Site F1 around 1932 because of higher oceanfront shoreline erosion rates and a proportionally larger loss of carbon storage capacity from excavation and burial of marsh during ICW construction. Throughout this earlier part of the record, however, the carbon reservoir progressively increased at both sites. Both sites became carbon sources in 1996 during Hurricane Fran, which resulted in the loss of some of the carbon reservoir. At Site F1, the transition to a carbon source during Hurricane Fran resulted from high shoreface erosion rates and washover deposition that reduced backbarrier marsh carbon storage. At Site F2, the transition was only the result of high shoreface erosion rates. There was no washover deposition at Site F2 during

Hurricane Fran. Site F1 transitioned back and forth between a carbon sink and source after the storm because the beach fluctuated between accreting and eroding. A similar pattern was observed at Site F2; however, that site only temporarily transitioned back to a carbon sink after Hurricane Fran because erosion persisted (**Figure 16-7**). The carbon reservoir at Site F2 has generally been declining since 1996.

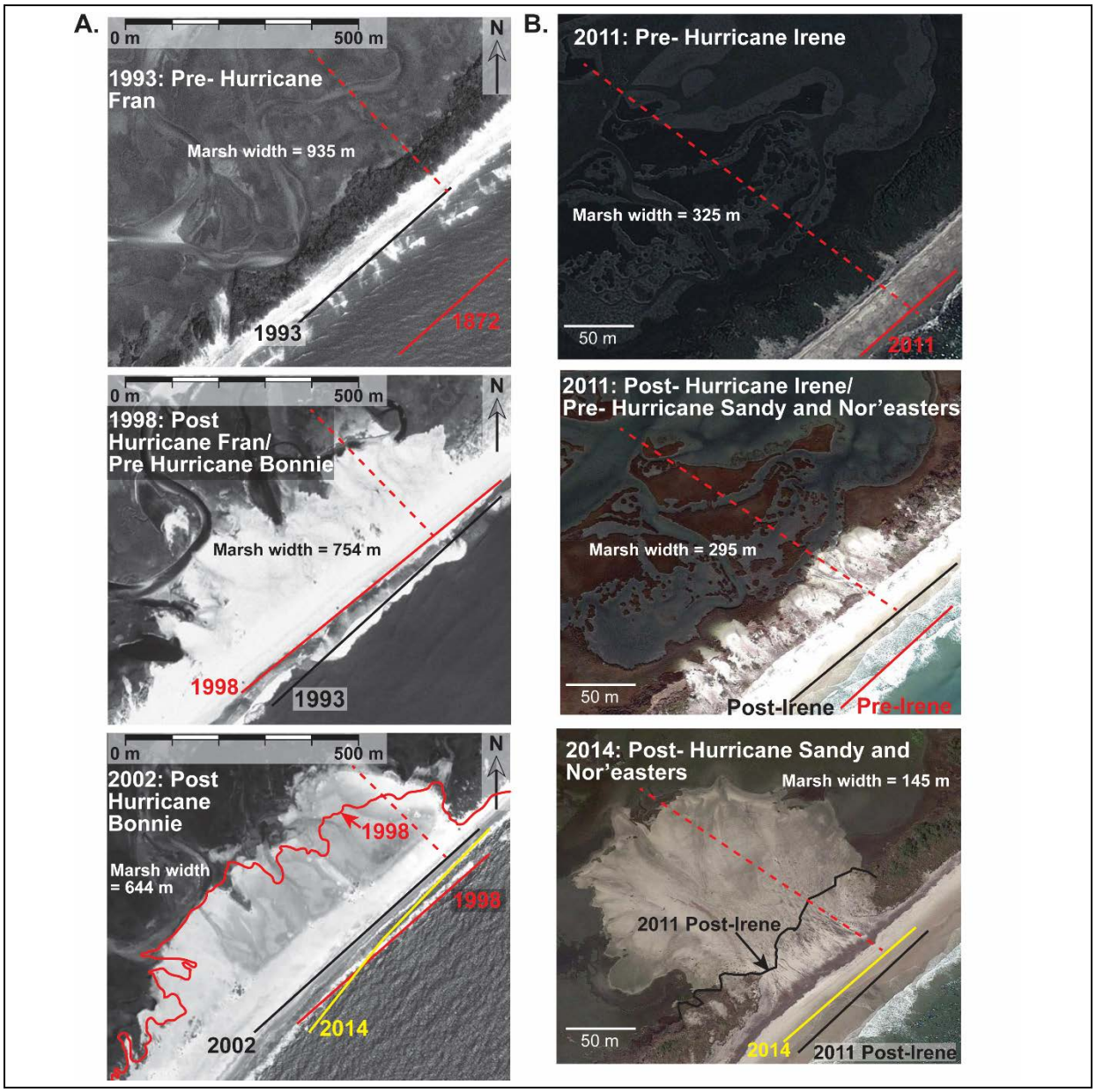

Figure 16-7. Time series of photographs showing the impact of overwash on marsh width. Onslow Beach Site F1 (A) experienced marsh loss during Hurricanes Fran and Bonnie; Site F2 (B) experienced marsh loss during Hurricanes Irene and Sandy.

Transects used for the carbon-budget model are denoted in each photograph with a dashed red line. Shorelines used in the erosion rate calculations are denoted with solid red, black, and yellow lines. Marsh width is annotated on each photograph. The landward extent of the Hurricane Fran washover deposit is denoted by a solid red line on the 2002 photograph, and the landward extent of the Hurricane Irene washover deposit is annotated by a solid black line on the 2014 photograph.

Hurricanes Irene and Sandy resulted in a decrease in the carbon reservoir at Site F2 due to high erosion rates and burial of backbarrier marsh by washover deposition. Presently, Site F2 remains a carbon source because of diminished backbarrier marsh width and sustained carbon export from shoreface erosion.

Carbon Budgets at Different Phases of Island Transgression

Placing results into context with the transgressive barrier island evolution conceptual model (**Figure 16-2**) indicates that as a barrier migrates closer to the mainland, carbon export from shoreline erosion and overwash exceeds carbon storage more frequently and by greater amounts (**Figure 16-8**). Unimpeded transgressive barriers are separated from the mainland by an open-water lagoon. Approximately 54% of the 1,390 km of transgressive barrier island shoreline along the U.S. East Coast is in this setting. The wide backbarrier lagoon allows for the formation of large flood-tidal deltas that are eventually colonized by saltmarsh after the tidal inlet closes. Similar to Site F2, expansive marsh stores a large amount of carbon annually. As barrier island transgression continues, the backbarrier lagoon narrows, shallows, and will be converted to a saltmarsh platform with tidal creeks. Once the backbarrier lagoon is filled in, carbon storage in the transgressive barrier island is likely high because of the increased backbarrier marsh width that occurs when the mainland and backbarrier fringing marshes merge. Even though islands with no backbarrier lagoon account for 46% of the transgressive barrier shoreline length along the U.S. East Coast, they account for approximately 71% of the backbarrier marsh area. Storms do not form inlets and subsequent extensive flood-tidal deltas along impeded transgressive barriers because no lagoon exists to maintain tidal flow, thus new marsh formation can only occur in association with storm overwash and washover deposition. Site F1, with its wide backbarrier marsh, represents this setting, and carbon storage outpaced carbon export there during non-storm periods (**Figure 16-8**). During Hurricane Fran, the site temporarily transitioned to a carbon source due to increased carbon export from shoreface erosion and a decrease in carbon storage from washover burial (**Figure 16-8**).

Island transgression is impeded when the narrowing backbarrier marsh laps against the higher gradient of the previous highstand shoreline. At this setting, the barrier is near the mainland, the backbarrier marsh is narrow, the island is functioning as a sustained source of carbon to adjacent depositional environments and the atmosphere, and the carbon reservoir is continuously decreasing. Site F2, with its narrow backbarrier marsh, relatively small carbon reservoir and steep-gradient dredge-spoil mound, and analogous to the previous highstand shoreline scarp, represents this setting. Erosion and overwash during the late twentieth century and early twenty-first century caused Site F2 to function primarily as a carbon source, which reduced the carbon reservoir. The large washover deposit that formed in response to Hurricanes Irene and Sandy could eventually be recolonized by saltmarsh, which would increase backbarrier marsh carbon storage and transition the site back to a carbon sink. Given that the washover fan is currently above tidal elevation, sea level would need to reach the elevation of the fan before intertidal saltmarsh formation will occur. With continual sea level rise and transgression, the island will merge with the mainland, but could transition back into a barrier island as the coastal plain is inundated landward forming a new lagoon or extensive backbarrier marsh.

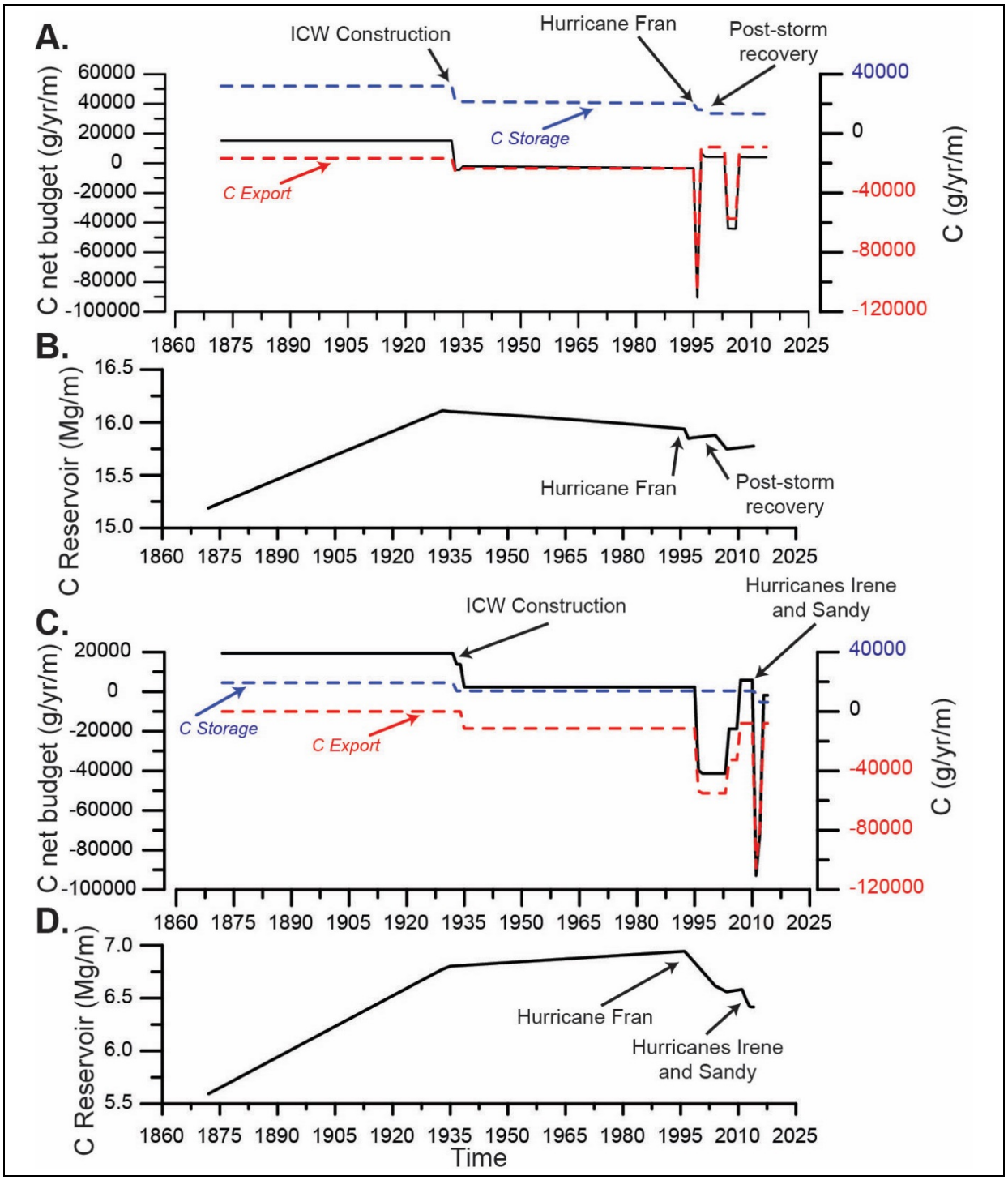

Figure 16-8. Carbon reservoirs from 1872 to 2014 for Sites F1 (A, B) and F2 (C, D).

In A and C, carbon storage is depicted as a dashed blue line and carbon export as a dashed red line. The net carbon budget (storage + export) is represented with a solid black line. Note the difference in limits for carbon export and storage on the secondary *y*-axis in panels A and C. The timing of the ICW dredging and storm impacts are annotated on each graph.

On undeveloped transgressive barrier islands, storms drive the transition from a carbon sink to a source because they induce carbon export through shoreface erosion and reduce carbon storage through washover deposition onto backbarrier marsh. The resilience of the barrier island carbon reservoir to storms decreases from unimpeded to impeded island transgression. For impeded transgressive barriers, such as Onslow Beach, an increase in storminess will hasten the islands transition to a sustained carbon source because of the associated increase in erosion and overwash and lack of backbarrier accommodation to support additional marsh formation (for more information, see Chapter 15 of this report).

Rates of carbon storage can increase or decrease with changes in the rate of sea level rise, even if the backbarrier marsh width remains constant, because of changes in marsh productivity (Kirwan and Mudd, 2012). Higher rates of sea level rise increase carbon storage by increasing accommodation space for marsh accretion (Morris et al., 2002 and 2012), but if the rate is too high, then marsh will collapse (DeLaune et al., 1986; Reed, 1990). Accelerating sea level rise also increases the rate of barrier island rollover (FitzGerald et al., 2008; Lorenzo-Trueba and Ashton, 2014). More rapid barrier rollover will accelerate the loss of the backbarrier lagoon, shift the island toward the mainland, and decrease the resilience of the carbon reservoir as the backbarrier saltmarsh habitat is squeezed between the previous highstand shoreline scarp and the migrating barrier island. The rate of carbon export at the ocean shoreline will increase, and carbon storage in the backbarrier will decrease in response to rapid barrier rollover and associated increase in marsh-burial from washover deposition at impeded transgressive barrier islands. This will likely offset some of the increased carbon storage induced by sea level rise and associated increased productivity (Kirwan and Mudd, 2012).

Washover Fan Evolution

Morphologic Change and Overwash Record

The washover deposits at Sites F2 and F2.1 experienced multiple overwash events after they formed in 2011 during Hurricane Irene. At Site F2, each year from June 2012 to 2015, we documented 64, 16, and 6 overwash events, respectively (**Figure 16-9**). Over the same time period at Site F2.1, we documented 29, 2, and 10 overwash events, respectively (**Figure 16-10**). Site F2.1 is higher in elevation than Site F2, which makes it more resistant to overwash and explains the smaller number of overwash events. During the 7 months after Hurricane Sandy, the washover fan at Site F2 increased in area from 3,300 ±170 m^2 to 29,000 ±1,500 m^2 and in volume from 2,200 ±130 m^3 to 66,700 ±1,100 m^3 (see **Appendix 16-A**). During the same time period, the washover at Site F2.1 maintained its area and only increased in volume about 400 m^3. After that 10-fold increase in size of the Site F2 washover fan over a 7-month period, its morphology stabilized and vegetation began to recolonize (**Figure 16-9**). At Site F2, more sand was transported across the island by overwash processes after storms than during storms. The higher density of vegetation at Site F2.1 and higher elevation made the morphology of this washover less dynamic than Site F2. Almost 4 years after the Site F2 washover formed it continued to experience overwash, notably, overwash produced by the Joaquin/Nor'easter in October of 2015 (at the end of our study) dramatically reduced the floral cover that had been developing and increased washover volume by 43% and area by 22% (see **Appendix 16-A**).

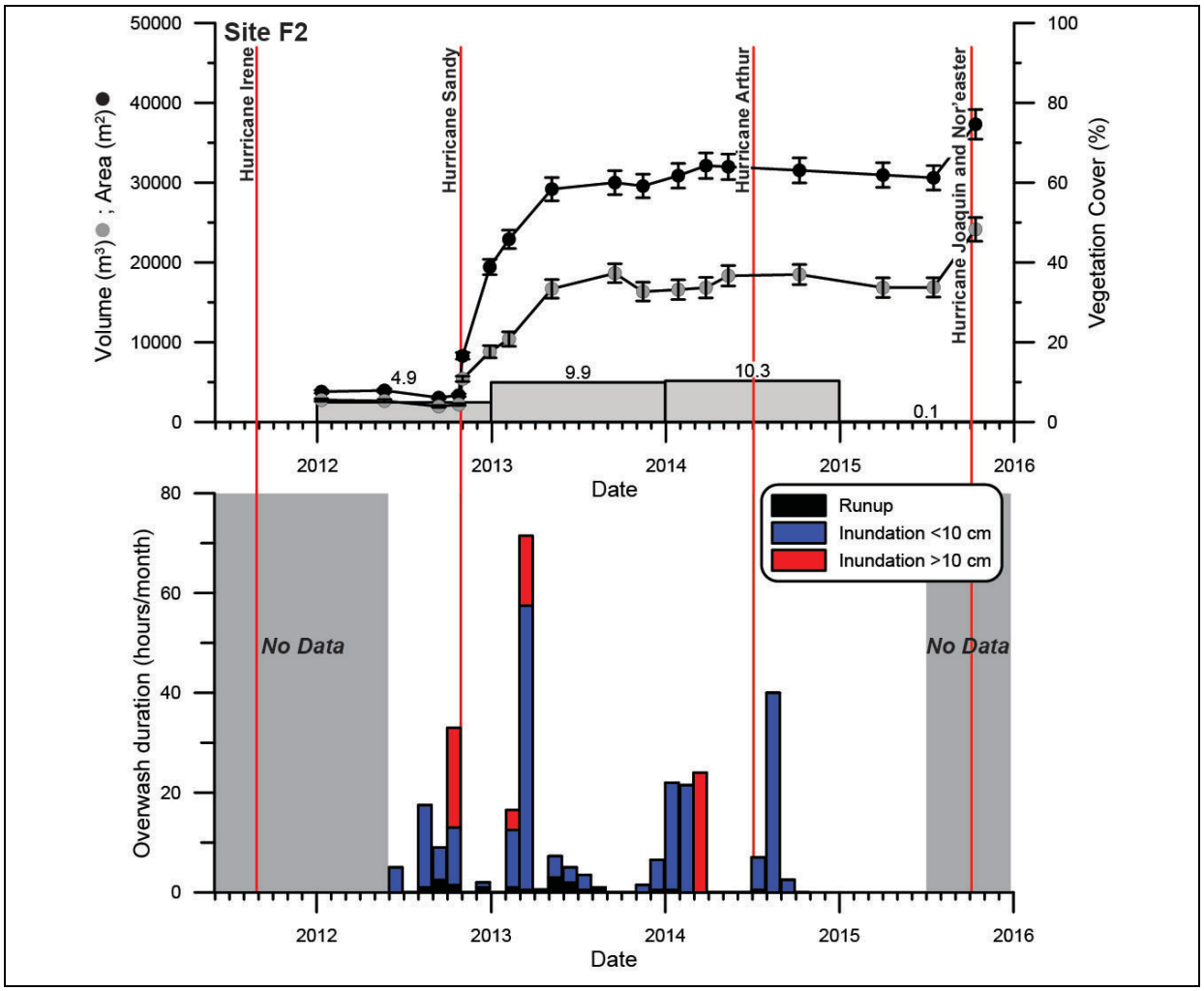

Figure 16-9. Time series showing changes in washover volume, area, and the average vegetation percent cover at Site F2 (top) and the duration of overwash each month (bottom).

The changes in washover volume from one observation to the next are accurate and precise, but the absolute volumes are not. This is because we do not know how the thickness of the washover deposit varies spatially. We assumed that the base of the washover was consistently at an elevation of 0.0 m NAVD 88 when measuring volume.

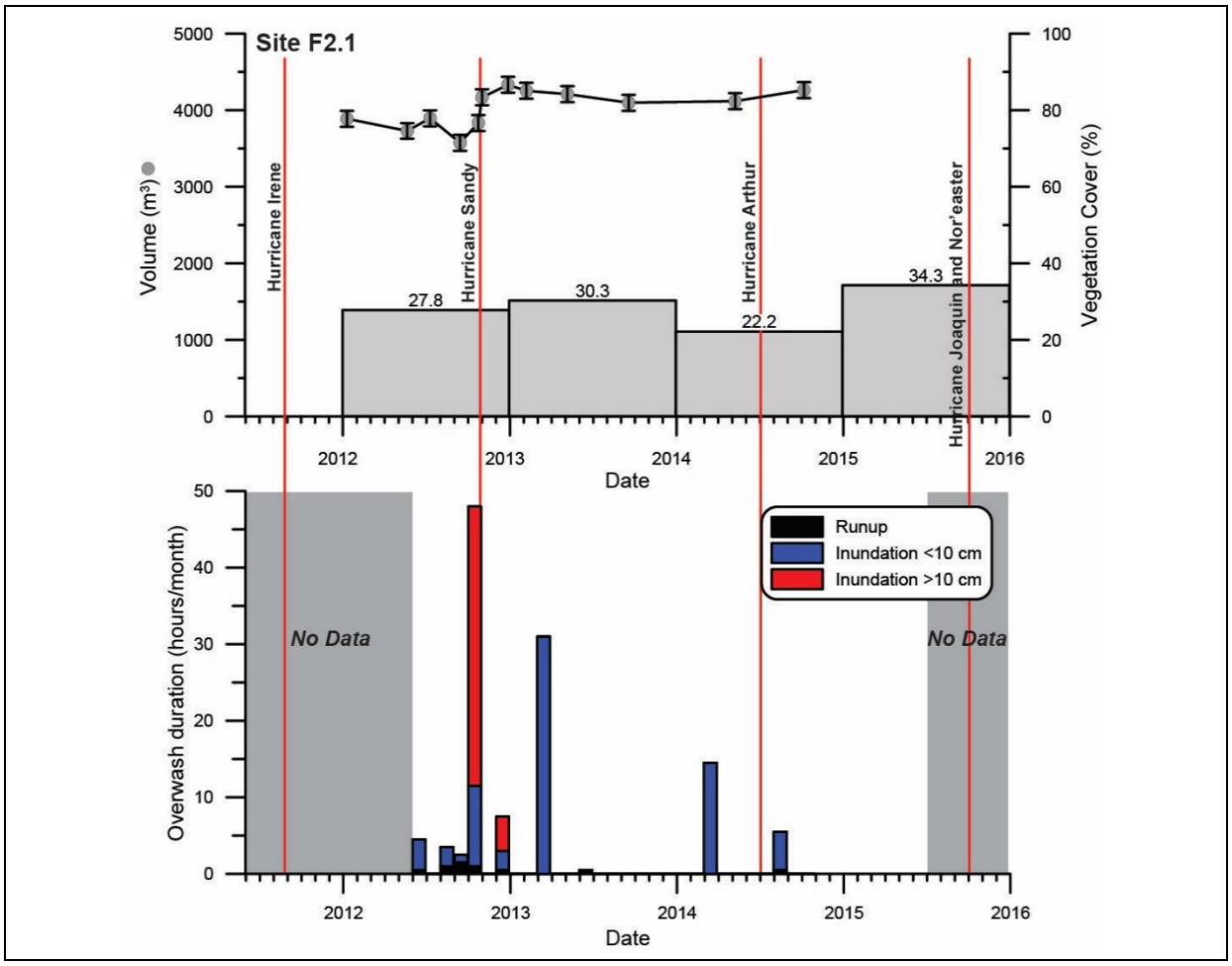

Figure 16-10. Time series showing changes in washover volume, area, and the average vegetation percent cover at Site F2.1 (top) and the duration of overwash each month (bottom).

The changes in washover volume from one observation to the next are accurate and precise, but the absolute volumes are not. This is because we do not know how the thickness of the washover deposit varies spatially. We assumed that the base of the washover was consistently at an elevation of 0.0 m NAVD 88 when measuring volume.

Ecological Succession

The most important effects of vegetation in washover fan evolution and shorebird nesting depends upon the areal extent and density of the individual plants. As plant percent cover increases so does the accumulation and stability of the sediment. Most shorebirds prefer sparse vegetation cover for nesting, between 5% and 10% (Ray, 2010). Consequently, we present here the percentage of each vegetation plot that was unvegetated during each sampling (i.e., how much of the surface was unvegetated sand (**Figure 16-11**).

At Site F1, we never observed any overwash or evidence of overwash during the 6 years we sampled. With the exception of Plot V02 on the southern transect, the percentage of the surface that was sand decreased or stayed approximately the same (**Figure 16-11**). The loss of vegetation in Plot V02 appeared to be related to a blowout (dune deflation and subsequent dispersal of the sediment by wind resulting in a loss of vegetation in dune fields; McLachlan and Brown, 2006).

At Site F2, the frequent overwash events resulted in the virtual absence of vegetation and the areal dominance of sand in all plots after Hurricanes Irene and Sandy, especially in the middle transect (**Figure 16-11**). Disturbance from flooding or sand movement (both erosion and accretion) determine barrier island plant survival (Miller, 2015). Some vegetative growth on some of the lateral transects (north and south) can be seen prior to the nor'easter combined with Hurricane Joaquin. These areas were protected from most flooding and wind events. Although it is not readily apparent in **Figure 16-12**, at the last sampling in the summer of 2016, much of the washover fan had vegetative cover ranging from 2% to 7% (instead of the 0% observed during preceding years). Based on visual field observations, Site F2.1 was densely vegetated before Hurricane Irene. This storm produced a tongue-shaped fan that extended across the island and ended at the backbarrier saltmarsh (Plots V05 and V06 of the middle transect, **Figure 16-11**). Over the years, substantial vegetative regrowth occurred throughout this entire fan until 2015. Sand movement associated with the nor'easter combined with Hurricane Joaquin covered vegetation in the plots closest to the beach (e.g., V01 in the north transect), which subsequently led to sand transport into inshore plots that reduced vegetative cover.

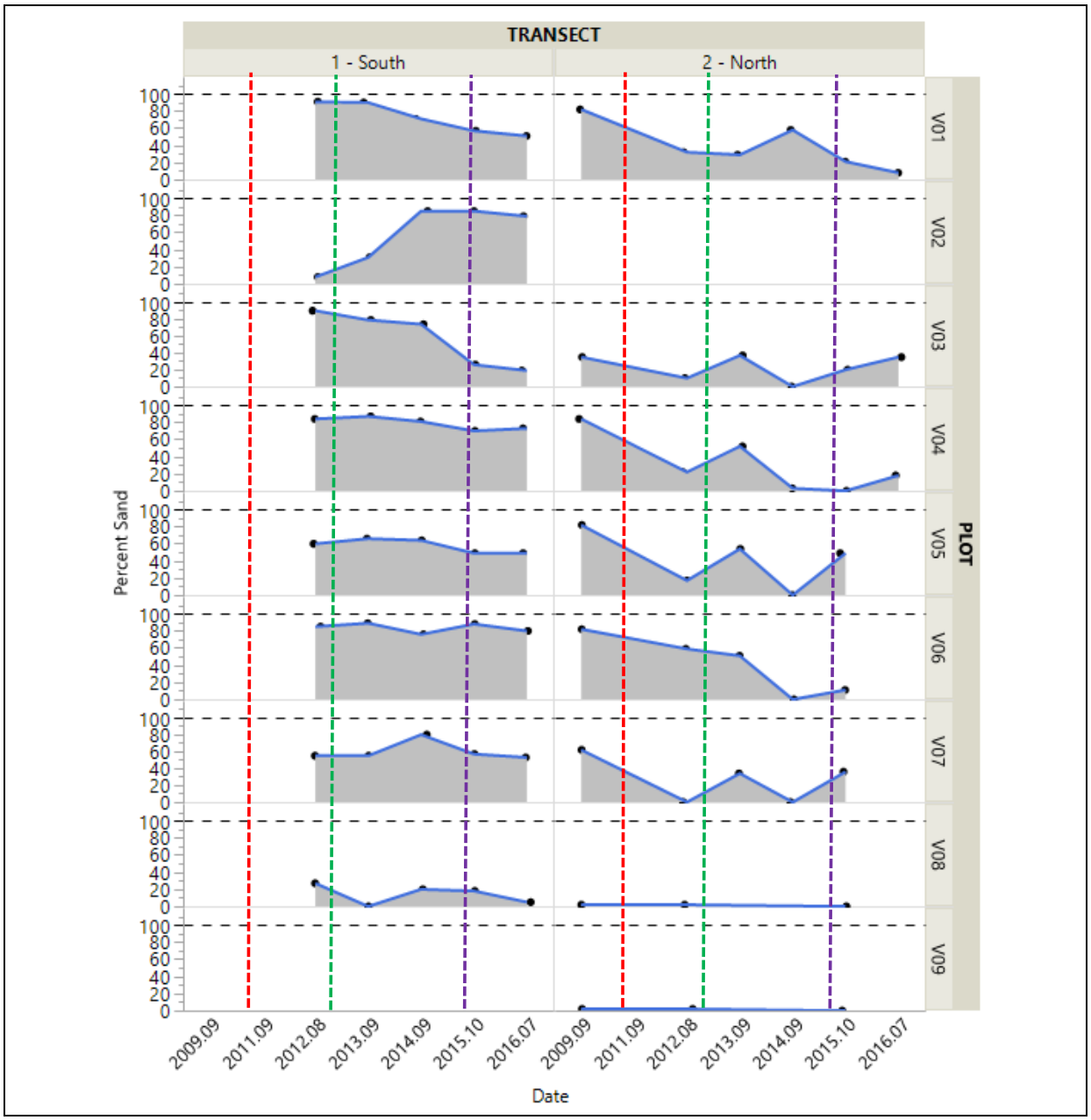

Figure 16-11. Percent cover of sand in each vegetation plot sampled at Sites F1 (top panel), F2 (middle panel), and F2.1 (bottom panel) over a 6-year interval (continued below).

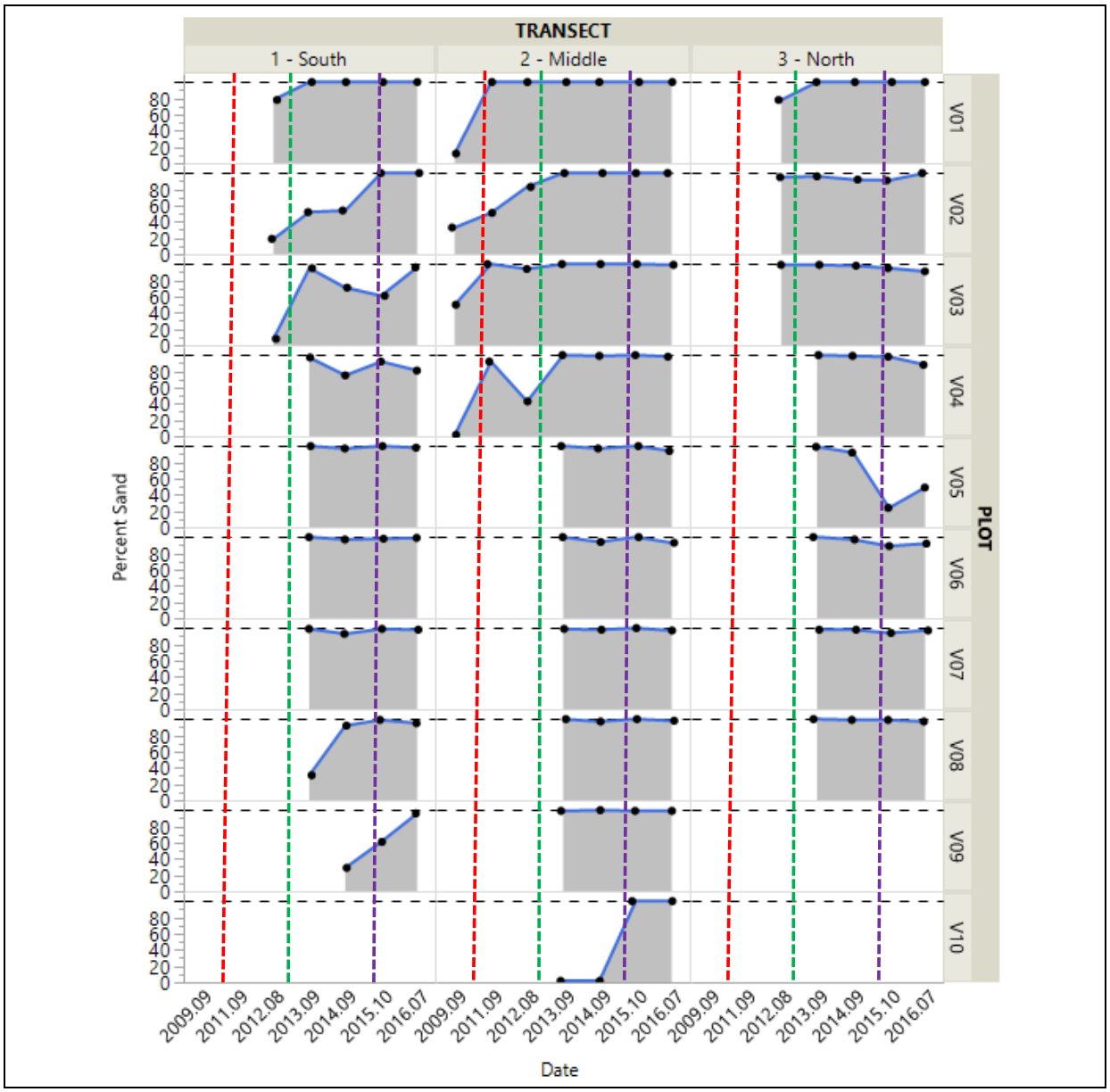

Figure 16-11. Percent cover of sand in each vegetation plot sampled at Sites F1 (top panel), F2 (middle panel), and F2.1 (bottom panel) over a 6-year interval (continued below).

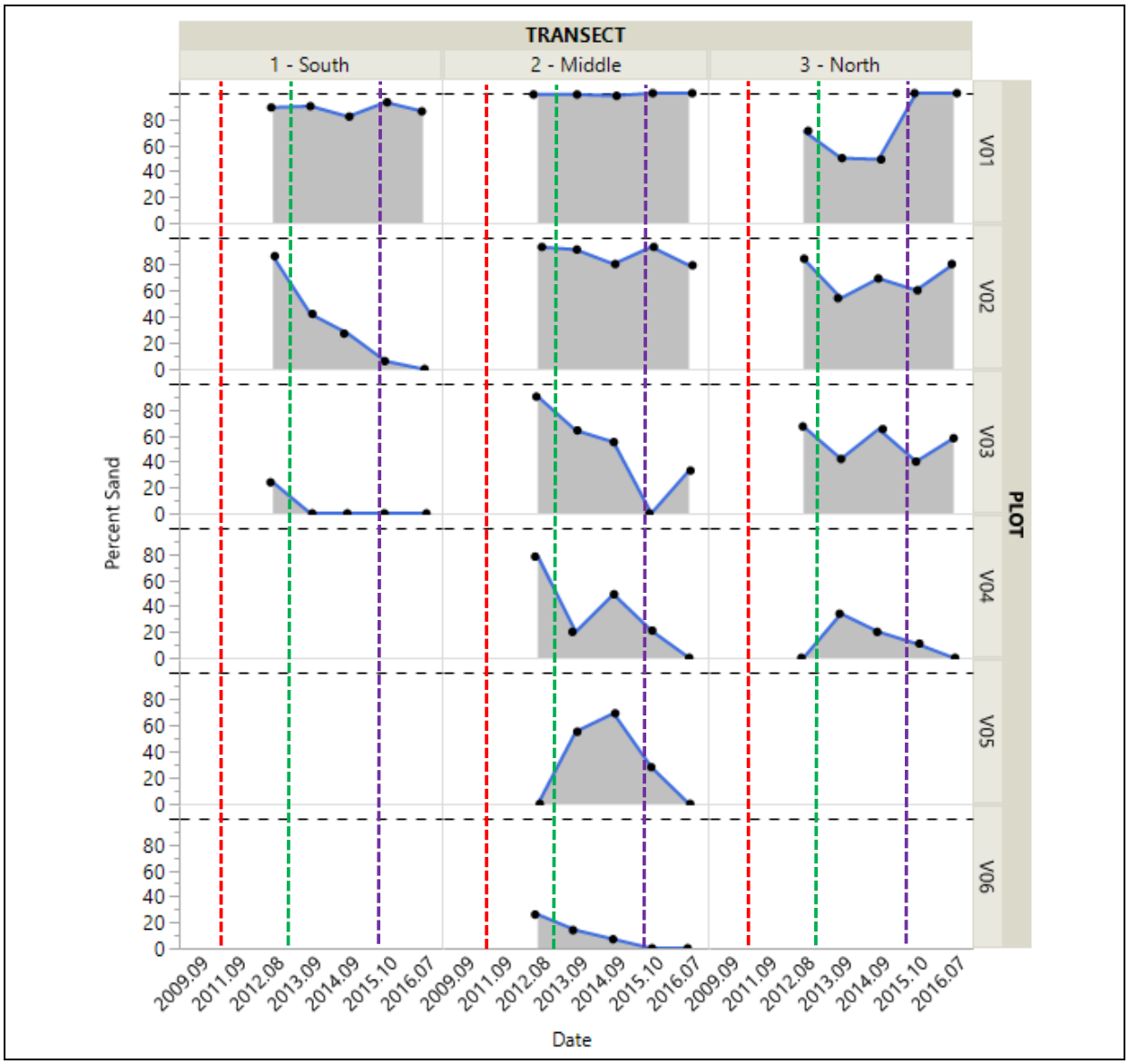

Figure 16-11. Percent cover of sand in each vegetation plot sampled at Sites F1 (top panel), F2 (middle panel), and F2.1 (bottom panel) over a 6-year interval.

The vertical dashed lines show the approximate occurrence of Hurricane Irene (red), Hurricane Sandy (green), and the nor'easter associated with Hurricane Joaquin (purple). On each transect, the lowest number plot (e.g., V01) is always closest to the beach and is located on the primary dune (at initiation). Subsequent plots increase in distance at 30- to 40-m intervals from the beach, and the last plot is on the backbarrier. No dots or shading indicate that either a plot was not established in that location or that it was not sampled on that date. The horizontal dashed lines indicate 100% exposed sand (i.e., no vegetation). **Figure 16-1** shows the location of these transects on Onslow Beach.

As expected, based on other studies examining the roles of island morphologies and physical energy characteristics on barrier island dynamics (Stallins and Parker, 2003), changes in floral cover followed different trajectories at each of the three sites. Site F1 (**Figure 16-11**) showed only marginal changes associated with the presence and absence of annual species. Overall, this site was dominated by vegetation rather than exposed sand (notice the large gaps in most plots between the dashed line indicated 100% sand cover and the actual cover measured). Site F2 was the antithesis to this pattern because it was characterized by little to no vegetation in the seaward

and central portions until the last 2 years of the study. Some increases in floral cover by vegetated growth occurred along the margins. It was only in 2015, after a decrease in the frequency of overwash, that seedlings began to survive over much of the fan. The large overwash event associated with the combination of a nor'easter and Hurricane Joaquin devastated vegetation in a narrow corridor across the flat, leaving most of the vegetation intact. Subsequently, a sparse, but widespread, vegetation cover was present in 2016 throughout much of the fan (except in the most seaward plots that still experienced substantial aeolian sand transport). Site F2 was dominated by overwash and aeolian transport throughout most of the study; vegetation only began to influence the fan in 2016. Site F2.1 showed rapid vegetative regrowth along its margins and in a backbarrier portion. Only the most seaward plots were affected after the initial overwash produced by Hurricane Irene. Consequently, Site F2.1 was largely vegetation dominated, except in the most shoreward portion where occasional overwash, erosion, and aeolian transport occurred throughout the study.

Shorebird Nesting Activity

Each of the three fans demonstrated different patterns of shorebird nesting (**Table 16-3**). We found several nests, by four different species, at Site F1 in 2013, but surprisingly little nesting during subsequent years. In 2014 and 2016, we observed as many Wilson's plover (*Charadrius wilsonia*) pairs and as many scrapes (areas hollowed out by birds in preparation for nest construction) at this site as in 2013, but nesting was much more infrequent.

Table 16-3. Number of Nests Containing Eggs for Each Species of Ground-Nesting Shorebird in Each Year Discovered on Each Washover Fan.

No Data Were Collected in 2015.

Washover Fan	Year	Wilson's Plover	Willet	Killdeer	Oyster-Catcher	Least Tern	Total
Site F1	2013	4	3	2	1	0	10
	2014	1	0	1	2	0	4
	2016	1	0	0	0	1	2
Site F2	2013	0	0	0	1	1	2
	2014	0	0	0	0	0	0
	2016	3	1	0	1	8	13
Site F2.1	2013	1	0	0	0	0	1
	2014	1	0	0	0	0	1
	2016	0	0	0	0	0	0

Note: Wilson's plover = *Charadrius wilsonia*; willet = *Tringa semipalmata*; killdeer = *Charadrius vociferus*; oystercatcher = *Haematopus palliatus*; least tern = *Sternula antillarum*.

At Site F2, nesting was rare or absent until 2016, when 13 nests produced by four different species were documented. The majority of the nests were produced by least terns, but the number of Wilson's plover nests was the second highest observed at any location in the entire study. In 2013 and 2014, we rarely observed Wilson's plover pairs on the fan, but in 2016 at least six pairs were observed on several occasions. The fewest nests and least amount of bird activity was

observed at Site F2.1. The two nests observed there were near the middle transect, nearest the beach.

Nest success varied by site and year. At Site F1 in 2013, two plover nests, one killdeer () nest, and the oystercatcher nests produced hatchlings. The other nests were predated or eroded away. All observed nests failed due to predation in 2014. In 2016, the fate of many nests could not be determined with certainty. Two weeks after discovery (too short an interval for hatching) the locations were found, but the eggs were not present. No predator tracks or broken shell pieces were observed in either case. At Site F2, both of the nests in 2013 failed to produce hatchlings. The least tern nest was washed away and the oystercatcher nest was predated (probably by a coyote based on tracks in the sand). In 2016, hatching success was higher with six nests (two plovers and four least terns) producing hatchlings. The remaining nests were either eroded by an overwash event or predated. At Site F2.1, the nest in 2013 was eroded away, but the nest in 2014 produced one hatchling.

We can offer no explanation as to why few nests were found in Site F1 in 2014 and 2016. We found several nests at Site F1 in 2013, and this area was a prime Wilson's plover nesting area during DCERP1 (Ray, 2010). There were no apparent changes to vegetation or fan topography in 2014 and 2016 compared with 2013 and, as previously mentioned, potential breeding pairs were observed in the latter years. Anecdotally, a discussion with MCBCL's EMD wildlife personnel in 2014 revealed that greater numbers of plover nests were found further south on Onslow Beach. The lack of nests at Site F2 in most years was almost certainly a function of the absence of sufficient vegetation to cue nesting behavior. The dramatic increase in nesting activity in 2016 corresponded with the time, when most of Site F2 was covered by sparse vegetation. Site F2.1 was never an ideal shorebird nesting site because even in 2012, dense vegetation surrounded the fan. Ground nesting shorebirds avoid locations with dense vegetation nearby, presumably because it serves as cover for nest predators (DeRose-Wilson et al., 2013). Notably, the only two nests found here were both located the farthest from surrounding vegetation.

Sea Turtle Nesting Activity

The majority of sea turtles that nest on Onslow Beach are loggerheads (*Caretta caretta*). The only beachfront location that these sea turtles avoid is near the inlets (**Figure 16-12**). Both false crawls and nests are significantly fewer ($P<0.0011$ and <0.0002, respectively) near the inlets, and no significant differences exist in the number (or linear density) of these events among other sections of the island. This implies that, except for inlet areas, turtles show no preference for approaching the beachface of Onslow Beach. In addition, there is no significant difference ($P=0.123$) between the number of false crawls and nests along most of the island. This suggests that abandoning a nesting attempt or producing a nest depends on proximate cues (e.g., beach slope, dune height, distance from the water, vegetation) at the specific location where the turtle explores. There is no evidence that the turtles perceive characteristics associated with longer term beachface dynamics.

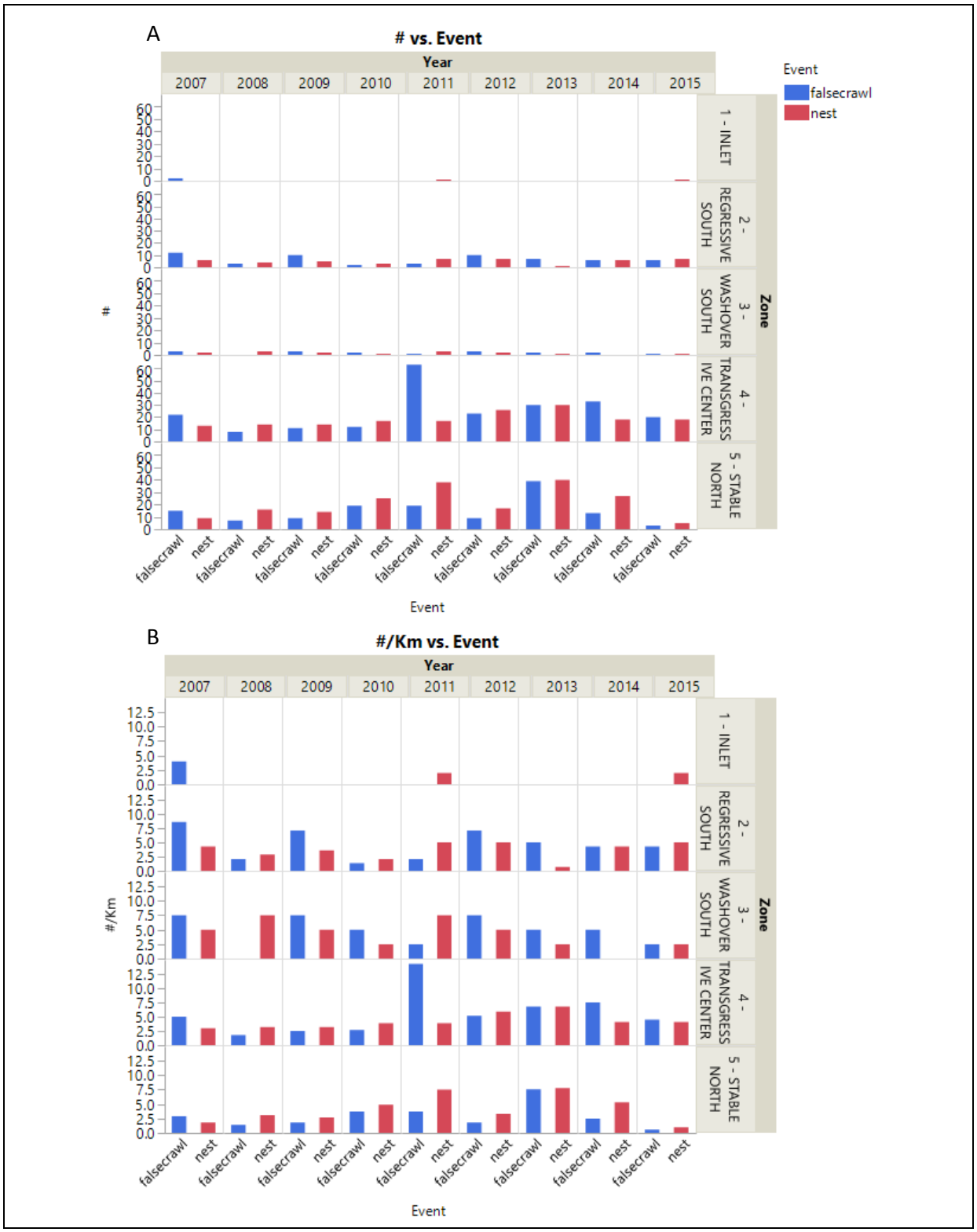

Figure 16-12. The alongshore frequency of turtle nesting events parsed into contiguous regions of shoreface geologic activity.

The absolute number of events in each year are presented in the top panel. Because the regions differ in alongshore length, the density of nesting events is presented in the bottom panel.

Among the specific cues that may be used by both sea turtles and MCBCL EMD personnel for selecting nest placement sites, which are unlikely to be inundated, are absolute elevation above MSL and the distance from mean highwater (MHW; **Figure 16-13**). A two-way analysis of variance (ANOVA) reveals that false crawls occur at lower elevation ($P<0.0001$) in every year (interaction of elevation × year $P = 0.304$), suggesting that the sea turtles abandon a crawl generally before reaching the back beach. There are no significant differences among elevation heights of nests, regardless of whether they are in an original or relocated location. A two-way ANOVA of distances of nesting events from MHW indicated different patterns. Both factors (year and type of nest event) were significant ($P<0.0001$ and $P<0.0001$, respectively) as is the interaction of the factors ($P<0.0065$). Analysis of the means associated with the type of nest event showed that nests relocated by EMD personnel were farthest from MHW followed by nests that were not relocated. The shortest distances to MHW were associated with nests that were relocated and false crawls. This finding is not surprising, given that most of the nests that were relocated were those in the military training zone, a section of the island that typically has a narrow backbeach. The pattern of the year × type interactions among nest events were similar across years with only marginal variation; most nests relocated by EMD personnel and most false crawls were closest to the MHW in every year (the interaction occurred because in 2 years, the distance from MHW to all nest events were not significantly different). No significant relationships were found between type of nest activity and beach slope.

We explored whether nest hatching success was affected by the elevation of the nest or its distance from MHW. The most widely used measure of nest hatching success is the emergence success rate (ESR; Caderas, 2016), which is the percentage of hatchlings that leave a nest. This measure is estimated by conducting an inventory of the hatched nest and counting the number of unhatched eggs, hatched eggs, hatchlings dead in the nest, and hatchlings alive in the nest. An examination of nest inventory records revealed that the component that dictates variation in this measure the most is the number of unhatched eggs. We used regression tree analysis to examine how the number of unhatched eggs at the time of nest inventory was affected by nest elevation, distance to MHW, date when the nest was laid (nests made later in the season typically do not have sufficient time for the hatchlings to develop to full term), and the number of times a nest was inundated by high water during incubation. The number of times a nest was inundated was not important in our study. This may seem surprising, given that nest inundation was found to be a leading cause of turtle nest failures (McElroy et al., 2015; Pike et al., 2015), but of the 120 nests measured in our study over the 3 years, only 14 of them were inundated; out of those 14, only five were inundated more than twice. Too few nests were inundated to affect our results. More than 40% of the variation in the number of unhatched eggs was explained by the remaining three factors, with date when the nest was laid accounting for almost half of the explained variation (45.5%; **Figure 16-14**).

An interesting interaction was revealed in the analysis. Nests lower in elevation (less than 1.9 m) had fewer unhatched eggs if they were closer to MHW (less than 22 m) than farther away. Nests higher in elevation (greater than 1.9 m) had fewer unhatched eggs if they were farther from MHW (greater than 21.8 m). This unusual result arises from the large number of relocated nests (38.3% of all nests) in the study. Almost all relocated nests were moved to a location on the northern end of the island that is high and far from MHW. If the relocated nests were removed from the analysis, then the nest elevation and the date when the nest was laid account for almost all variations (higher in elevation and earlier in the season producing fewer unhatched eggs).

Any negative effects of nest location on nest success was mediated by the aggressive and effective practices of the MCBCL EMD personnel who produced an ESR (mean ±1 standard error = 99.4 ±0.1%), which far exceeds most turtle nest management programs along the North Carolina coast. In addition, although nest relocation remains a controversial management practice in North Carolina (Cornwell and Campbell, 2012), the remarkably high ESR values associated with relocated nests on Onslow Beach indicate that MCBCL EMD personnel are adept at the procedure and should not change their current practices.

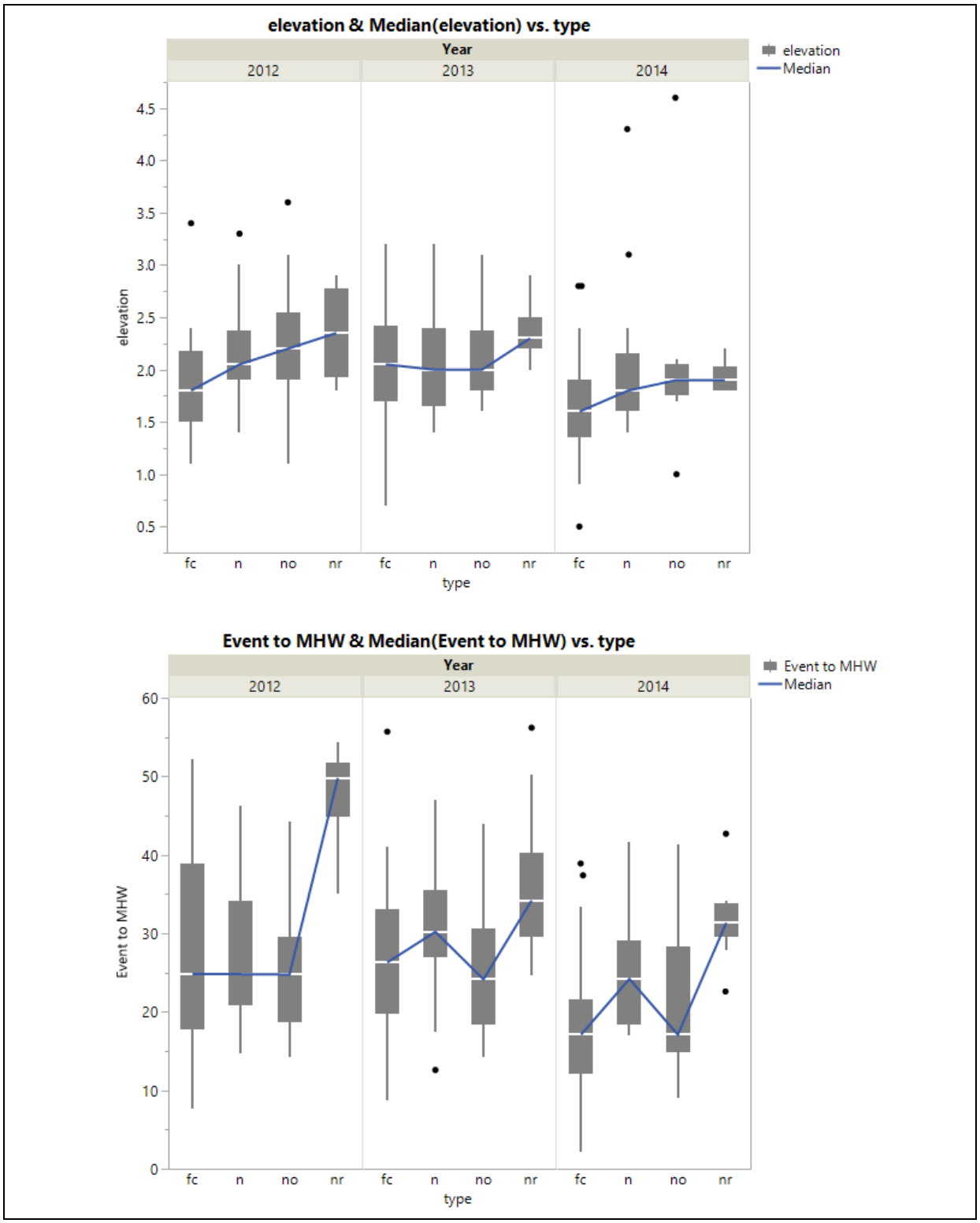

Figure 16-13. The elevation above MSL (in m, top panel) and linear distance to MHW (in m, bottom panel) of turtle nesting events in each of the 3 years.

Box plots show the distribution of individual false crawl (fc), nest (n), nest that is moved by EMD personnel (no), and nest relocation site (nr). The lines indicate the trends associated with the respective medians.

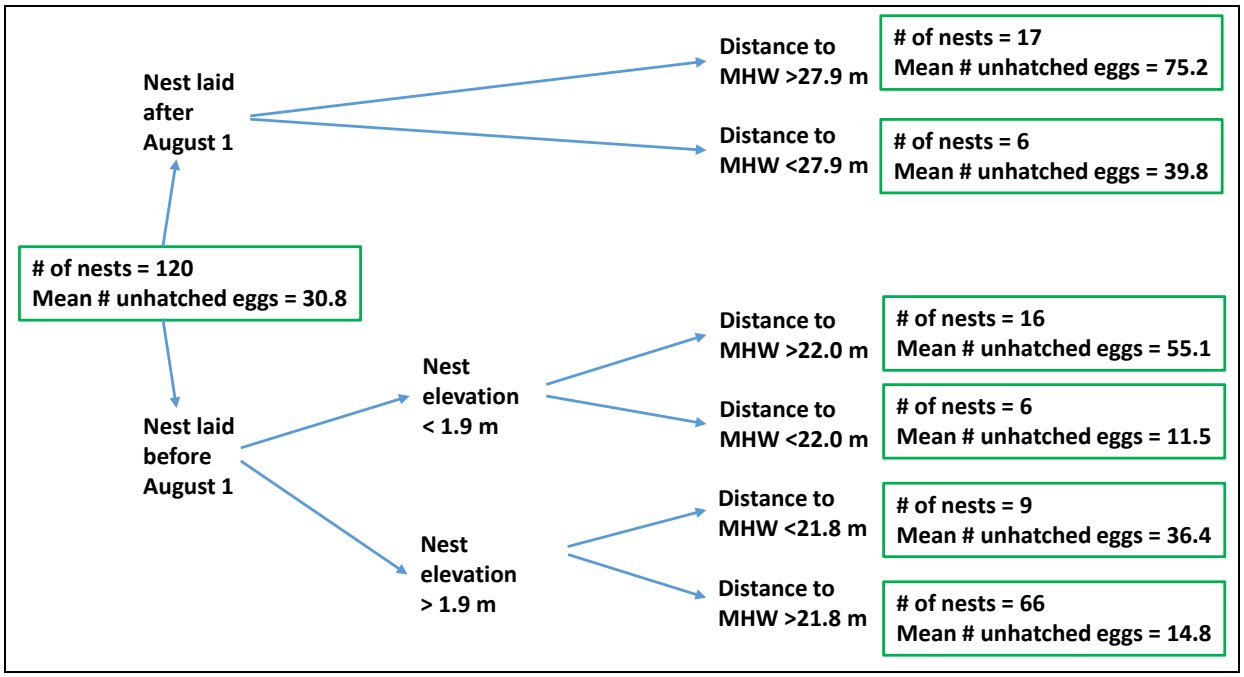

Figure 16-14. Regression tree showing the mean number of unhatched eggs found under the combinations of date when the nest was laid, nest elevation, nest distance from MHW, and number of times the nest was inundated.

Boxes contain the number of nests in each part of the tree and the mean number of unhatched eggs.

Conclusions and Implications for Future Research and Implementation

The processes associated with barrier island transgression have not previously been considered in the context of coastal carbon budgets, and our results showed that a barrier island carbon budget is sensitive to changes in shoreline erosion rate and to marsh width. Barrier island transgression can increase the carbon reservoir within a barrier by creating new marsh substrate through flood-tidal delta formation and washover-fan deposition, but will also export carbon through shoreface and backbarrier erosion. Backbarrier shoreline erosion, burial of marsh by overwash transport and deposition, and dredge-spoil disposal are all processes that reduce marsh width and consequently decrease the carbon storage capacity of a barrier island. Global wetland inventories consider only backbarrier marsh area in assessments of carbon storage and thus are ignoring the processes associated with barrier island response to storms, sea level rise, and anthropogenic disturbance.

The integrity of the barrier island carbon reservoir is mainly a function of the setting of the barrier island. Transgressive barrier islands with a wide backbarrier marsh primarily function as carbon sinks, but will transition to sources temporarily during storms when ocean shoreline erosion rates increase and overwash deposition onto backbarrier marshes occurs. As a barrier island continues to migrate landward, the backbarrier marsh narrows beyond a critical width where the island primarily functions as a carbon source and the reservoir is decreasing. During this phase of barrier island transgression, carbon export rates will likely continuously exceed storage rates across the narrow backbarrier marsh. This decreasing (negative) trajectory of the carbon reservoir endures until the reservoir is depleted when the barrier merges with the

mainland (the previous highstand shoreline). Our modeling results and field observations on Onslow Beach advocate for the consideration of barrier island transgressive processes in regional and global coastal carbon budgets. Proper assessment of present and future transgressive barrier island carbon budgets must consider erosion and overwash, as well as the island's backbarrier setting.

Our data highlight that overwash during fair weather conditions is an important process of transporting sand across a barrier island. The current paradigm is that washover deposition takes place during overwash associated with a single large storm event, such as a hurricane, and subsequent recovery of the dune line after the storm occurs rapidly (within a year) as vegetation recolonizes the area, trapping wind-blown sand. After a storm, washover development is thought to be strongly driven by biogeomorphic feedbacks such as ecological plant succession and aerial sediment accumulation. Our data set represents the only long-term ecological study of washover fans and shows that this conceptual model is incomplete and needs modification. Although washover evolution at Site F2.1 follows the accepted paradigm, we discovered that washover development at narrow portions of an island where backbarrier elevation is low, such as Site F2, is modified by overwash processes frequently for years after the initial storm event.

Research Questions

1. **How does the age, volume, and carbon content of the peat change with increasing distance from the saltmarsh to the ocean?**

There is little difference between the age, volume, and carbon content of the peat sampled near the ocean versus the peat sampled in the saltmarsh. This is mainly due to the rapid transgression and young age of Onslow Beach.

2. **What are the relationships between the rate of island transgression and the volume of peat preserved within the barrier and the flux of carbon to the ocean from the erosion of peat in the foreshore?**

The rate of island transgression ended up being very similar for both sites examined. However, during storms and erosive events, the flux of carbon to the ocean from the erosion of peat in the foreshore was greater than the rate of carbon storage in the backbarrier marsh.

3. **What are the differences in abundance of nesting shorebirds at young washover fans with no vegetation and older vegetated washover fans?**

The age of a washover fan does not determine abundances of nesting shorebirds. In our study, both the oldest and the youngest fans demonstrated, in different years, the greatest nesting activity. What does influence shorebird nesting activity are proximate cues such as frequency of overwash and aeolian transport and the density and distribution of vegetation on the fans.

4. **What are the relationships between sea turtle nest survivorship to hatching and backbeach width, elevation, and beach slope?**

Nest survivorship to sea turtle hatching is high on Onslow Beach as long as the nest locations are not inundated. Our results show that both sea turtles and MCBCL personnel, place nests in

locations that are high in elevation (relative to mean sea level) and farther from MHW. Beach slope did not appear to play a role in nest siting or nest success. No recommendations for changing current EMD turtle nest management need be made.

Findings with Implications for Future Base Management

The southwestern end of Onslow Beach will become increasingly unsuitable for amphibious training exercises, nesting shorebirds, and sea turtles in the future. This is because overwash at this portion of the island will continue to become more frequent as sea level rises. We recorded 86 overwash events over approximately a 2-year period during DCERP2. We did not have instrumentation deployed to sense overwash during DCERP1, but MCBCL personnel who drove the beach every day only mentioned two overwash events during that 5-year study (2008–2012). The northeastern end of the island is currently used for recreational activities, and based on our findings that show the northeastern beach is more stable than the southwestern beach, MCBCL is considering extending its training activities to the northeastern portion of the island, where a wider and higher elevation beach allows more vehicles to maneuver. This northeastern portion of the barrier island is also prime sea turtle habitat. As human activities on Onslow Beach move to the northeast, areas for turtle nest relocation should be delineated and protected from human disturbance.

Literature Cited

Belknap, D.F., and J.C. Kraft. 1985. Influence of antecedent geology on stratigraphic preservation potential and evolution of Delaware's barrier systems. *Marine Geology 63*:235–262.

Bruun, P. 1962. Sea-level rise as a cause of shore erosion. In *Proceedings of the American Society of Civil Engineers, Journal of the Waterway Harbors Division 88*:117–130.

Caderas, J. 2016. *Beach Nourishment: Effects on the Hatching and Emergence Success Rates of Leatherback* (Dermochelys coriacea)*, Loggerhead* (Caretta caretta)*, and Green* (Chelonia mydas) *Sea Turtles.* Master's thesis, Nova Southeastern University, Fort Lauderdale, FL.

Cai, W.-J., Z.A. Wang, and Y. Wang, Y. 2003. The role of marsh-dominated heterotrophic continental margins in transport of CO_2 between the atmosphere, the land–sea interface and the ocean. *Geophysical Research Letters 30*(16).

Canuel, E.A., S.S. Cammer, H.A. McIntosh, and C.R. Pondell. 2012. Climate change impacts on the organic carbon cycle at the land-ocean interface. *Annual Review of Earth and Planetary Sciences 40*(1):685–711.

Carter, D.J.T., and L. Draper. 1988. Has the northeast Atlantic become rougher? *Nature 332*:494.

Church, J.A., and N.J. White. 2006. A 20th century acceleration in global sea-level rise. *Geophysical Research Letters 33*(1).

Cornwell, M.L., and L.M. Campbell. 2012. Co-producing conservation and knowledge: citizen-based sea turtle monitoring in North Carolina, USA. *Social Studies of Science 42*:101–120.

DeLaune, R.D., C.J. Smith, and W.H. Patrick. 1986. Sedimentation patterns in a Gulf Coast backbarrier marsh: Response to increasing submergence. *Earth Surface Processes and Landforms 11*(5):485–490.

DeRose-Wilson, A., J.D. Fraser, S.M. Karpanty, and D.H. Catlin. 2013. Nest-site selection and demography of Wilson's plovers on a North Carolina barrier island. *Journal of Field Ornithology 84*:329–344.

Donnelly, C., N. Kraus, and M. Larson. 2006. State of knowledge on measurement and modeling of coastal overwash. *Journal of Coastal Research 224*:965–991.

Dubois, R.N. 1995. The transgressive barrier model—An alternative to 2-dimensional volume balanced models. *Journal of Coastal Research 11*(4):1272–1286.

Elliott, E.A., B.A. McKee, and A.B. Rodriguez. 2015. The utility of estuarine settling basins for constructing multi-decadal, high-resolution records of sedimentation. *Estuarine, Coastal Shelf Science 164*:105–114.

Elsner, J.B., T.H. Jagger, and K.-B. Liu. 2008. Comparison of hurricane return levels using historical and geological records. *Journal of Applied Meteorology & Climatology 47*(2):368–374.

Emanuel, K. 2005. Increasing destructiveness of tropical cyclones over the past 30 years. *Nature 436*(7051):686–688.

Ember, L.M., D.F. Williams, and J.T. Morris. 1987. Processes that influence carbon isotope variations in salt marsh sediments. *Marine Ecology Progress Series 36*:33–42.

Eulie, D.O., J. Walsh, D.R. Corbett, and P.R. Mulligan. 2016. Temporal and spatial dynamics of estuarine shoreline change in the Albemarle-Pamlico estuarine system, North Carolina, USA. *Estuaries and Coasts* 1–17.

Fisher, A.G. 1961. Stratigraphic record of transgressing seas in light of sedimentation on Atlantic coast of New Jersey. *American Association of Petroleum Geologists Bulletin, 45*(10):1656–1667.

FitzGerald, D.M., M.S. Fenster, B.A. Argow, and I.V. Buynevich. 2008. Coastal impacts due to sea-level rise. *Annual Review of Earth and Planetary Sciences, 36*:601–647.

Godfrey, P.J., and M.M. Godfrey. 1976. Barrier island ecology of Cape Lookout National Seashore and vicinity, North Carolina. *National Park Service Scientific Monograph Series 9*. Edited by Service, N.P.

Goldenberg, S.B., C.W. Landsea, A.M. Mestas-Nunez, and W.M. Gray. 2001. The recent increase in Atlantic hurricane activity: Causes and implications. *Science 293*(5529):474–479.

Gunnell, J.R., A.B. Rodriguez, and B.A. McKee. 2013. How a marsh is built from the bottom up. *Geology 41*:859–862.

Jevrejeva, S., J.C. Moore, A. Grinsted, and P.L. Woodworth. 2008. Recent global sea level acceleration started over 200 years ago? *Geophysical Research Letters 35*.

Johnson, D.W. 1919. *Shore Processes and Shoreline Development*. John Wiley & Sons, Inc.: Boston, MA.

Johnston, M.K. 1998. *The Inherited Geologic Framework of the New River Submarine Headland Complex, North Carolina, and Its Influence on Modern Sedimentation*. MS thesis, University of North Carolina at Wilmington, Wilmington, NC. 83 pages.

Kirwan, M.L., and S.M. Mudd. 2012. Response of salt-marsh carbon accumulation to climate change. *Nature 489*(7417):550–553.

Knuston, T.R., R.E. Tuleya, and Y. Kurihara. 1988. Simulated increase of hurricane intensities in a CO_2–warmed climate. *Science 279*:1018–1020.

Kraft, J.C. 1971. Sedimentary facies patterns and geologic history of a Holocene marine transgression. *Geological Society of America Bulletin 82*:2131–2158.

Leatherman, S.P. 1979. Migration of Assateague Island, Maryland, by inlet and over-wash processes. *Geology 7*(2):104–107.

Leatherman, S.P., and A.T. Williams. 1983. Vertical sedimentation units in a barrier island washover fan. *Earth Surface Processes and Landforms 8*:141–150.

Leatherman, S.P., and A.T. Williams. 1977. Lateral textural grading in overwash sediments. *Earth Surface Processes 2*(4):333–341.

Leonardi, N., N.K. Ganju, and S. Fagherazzi. 2016. A linear relationship between wave power and erosion determines salt-marsh resilence to violent storms and hurricanes. *Proceedings of the National Academy of Sciences 113*(1):64-68.

Leonardi, N., and S. Fagherazzi. 2014. How waves shape salt marshes. *Geology 42*(10):887–890.

Lorenzo-Trueba, J., and A.D. Ashton. 2014. Rollover, drowning, and discontinuous retreat: Distinct modes of barrier response to sea-level rise arising from a simple morphodynamic model. *Journal of Geophysical Research: Earth Surface 119*(4):779–801.

Mariotti, G., and J. Carr. 2014. Dual role of salt marsh retreat: Long-term loss and short-term resilience. *Water Resources Research 50*(4):2963–2974.

Maslo, B., S.N. Handel, and T. Pover. 2011. Restoring beaches for Atlantic coast piping plovers (*Charadrius melodus*): A classification and regression tree analysis of nest-site selection. *Restoration Ecology 19*:194–203.

Mattheus, C.R., and A.B. Rodriguez. 2011. Controls on late quaternary incised-valley dimension along passive margins evaluated using empirical data. *Sedimentology 58*(5):1113–1137.

Mattheus, C.R., A.B. Rodriguez, B.A. McKee, and C.A. Currin. 2010 Impacts of land-use change and hard structures on evolution of fringing marsh shorelines. *Estuaries, Coastal and Shelf Science 88* (3): 365-376.

Mazaris, A.D., Y.G. Matsinos, and D. Margaritoulis. 2006. Nest site selection of loggerhead sea turtles: The case of the island of Zakynthos, W Greece. *Journal of Experimental Marine Biology and Ecology 336*:157–162.

McElroy, M.L., M.G. Dodd, and S.B. Castleberry. 2015. Effects of common loggerhead sea turtle nest management methods on hatching and emergence success at Sapelo Island, Georgia, USA. *Chelonian Conservation and Biology 14*:49–55.

McLachlan, A. and A.C. Brown. 2006. *The Ecology of Sandy Shores*. Second edition. Elsevier Press: Amsterdam, The Netherlands.

Miller, T.E. 2015. Effects of disturbance on vegetation by sand accretion and erosion across coastal dune habitats on a barrier island. *AoB PLANTS 7*:plv003.

Miselis, J.L., and J.E. McNinch. 2006. Calculating shoreline erosion potential using nearshore stratigraphy and sediment volume: Outer Banks, North Carolina. *Journal of Geophysical Research: Earth Surface 111*(F2).

Morris, J.T., J. Edwards, S. Crooks, and E. Reyes. 2012. Assessment of carbon sequestration potential in coastal wetlands. Pp. 517–531 in *Recarbonization of the Biosphere*. Edited by Lal, R., K. Lorenz, R.F. Hüttl, B.U. Schneider, and J. von Braun. Springer: Dordrecht, The Netherlands.

Morris, J.T., P.V. Sundareshwar, C.T. Nietch, B. Kjerfve, and D.R. Cahoon. 2002. Responses of coastal wetlands to rising sea level. *Ecology 83*:2869–2877.

Moslow, T.F., and D.S. Heron. 1978. Relict inlets: preservation and occurrence in the Holocene stratigraphy of southern Core Banks, North Carolina. *Journal of Sedimentary Petrology 48*:1275–1286.

Niedoroda, A.W., D.J.P. Swift, A.G. Figueiredo Jr., and G.L. Freeland. 1985. Barrier island evolution, middle Atlantic shelf, USA. Part II: Evidence from the shelf floor. *Marine Geology 63*(1–4):363–396.

Nyman, J.A., R.J. Walters, R.D. Delaune, and W.H. Patrick. 2006. Marsh vertical accretion via vegetative growth. *Estuarine, Coastal and Shelf Science 69*(3–4):370–380.

Peet, R.K., T.R. Wentworth, and P.S. White. 1998. A flexible, multipurpose method for recording vegetation composition and structure. *Castanea 63*:262–274.

Pfaller, J.B., C.J. Limpus, and K.A. Bjorndal. 2008. Nest-site selection in individual loggerhead turtles and consequences for doomed-egg relocation. *Conservation Biology 23*:72–80.

Pike, D.A., E.A. Roznik, and I. Bell. 2015. Nest inundations from sea-level rise threatens sea turtle population viability. *Royal Society Open Science 2*:150127.

Pilkey, O.H., R.S. Young, S.R. Riggs, A.W.S. Smith, H.Y. Wu, and W.D. Pilkey. 1993. The concept of shoreface profile of equilibrium—A critical review. *Journal of Coastal Research 9*(1):255–278.

Rahmstorf, S. 2007. A semi-empirical approach to projecting future sea-level rise. *Science 315*:368–370.

Ray, K.L. 2010. *Factors Affecting Wilson's Plover (*Charadrius wilsonia*) Demography and Habitat Use at Onslow Beach, Marine Corps Base Camp Lejeune, North Carolina.* M.S. thesis, Virginia Polytechnic and State University, Blacksburg, VA.

Redfield, A.C., and M. Rubin. 1962. The age of salt marsh peat and its relation to recent changes in sea level at Barnstable, Massachusetts. *Proceedings of the National Academy of Sciences 48*(10):1728–1735.

Reed, D.J. 1990. The impact of sea-level rise on coastal salt marshes. *Progress in Physical Geography 14*:24–40.

Reimer, P.J., E. Bard, A. Bayliss, J.W. Beck, P.G. Blackwell, C. Bronk Ramsey, C.E. Buck, H. Cheng, R.L. Edwards, M. Friedrich, P.M. Grootes, T.P. Guilderson, H. Haflidason, I. Hajdas, C. Hatté, T.J. Heaton, D.L. Hoffmann, A.G. Hogg, K.A. Hughen, K.F. Kaiser, B. Kromer, S.W. Manning, M. Niu, R.W. Reimer, D.A. Richards, E.M. Scott, J.R. Southon, R.A. Staff, C.S.M. Turney, and J. van der Plicht. 2013. IntCal13 and Marine13 Radiocarbon Age Calibration Curves 0–50,000 Years cal BP. *Radiocarbon 55*(4):1869–1887.

Riggs, S.R., and D.V. Ames. 2007. Effect of storms on barrier island dynamics, Core Banks, Cape Lookout National Seashore, North Carolina, 1960–2001. Scientific Investigations Report 2006–5309. Available at https://pubs.usgs.gov/sir/2006/5309/pdf/sir2006-5309.pdf

Rizkalla, C.E., and A. Savage. 2011. Impact of seawalls on loggerhead sea turtle (*Caretta caretta*) nesting and hatching success. *Journal of Coastal Research 27*:166–173.

Rodriguez, A.B., P.L. Rodriguez, and S.R. Fegley. 2012. One-year along-beach variation in the maximum depth of erosion resulting from irregular shoreline morphology. *Marine Geology*, 291–294:12–23.

Rodriguez, A.B., D.L. Greene, J.B. Anderson, and A.R. Simms. 2008. Response of Mobile Bay and eastern Mississippi Sound, Alabama, to changes in sediment accommodation and accumulation. Pp. 13–29 in *Response of Upper Gulf Coast Estuaries to Holocene Climate Change and Sea-Level Rise*. Special Paper, 443. Edited by Anderson, J.B., and A.B. Rodriguez. Geological Society of America, Boulder, CO.

Rodriguez, A.B., J.B. Anderson, and A.R. Simms. 2005. Terrace inundation as an autocyclic mechanism for parasequence formation: Galveston estuary, Texas, USA. *Journal of Sedimentary Research 75*:608–620.

Rodriguez, A.B., J.B. Anderson, F.P. Siringan, and M. Taviani. 2004. Holocene evolution of the east Texas coast and inner continental shelf: along-strike variability in coastal retreat rates. *Journal of Sedimentary Research 74*:406–422.

Rodriguez, A.B., M.L. Fassell, and J.B. Anderson. 2001. Variations in shoreface progradation and ravinement along the Texas coast, Gulf of Mexico. *Sedimentology 48*:837–853.

RTI International. 2013. *DCERP2 Research Plan.* RTI International, Research Triangle Park, NC. Prepared for Strategic Environmental Research and Development Program (SERDP), Arlington, VA.

Simms, A.R., and A.B. Rodriguez. 2014. Where do coastlines stabilize following rapid retreat? *Geophysical Research Letters 41*(5):1698–1703.

Spanier, M.J. 2010. Beach erosion and nest site selection by the leatherback sea turtle Dermochelys coriacea (Testudines: Dermochelyidae) and implications for management practices at Playa Gandoca, Costa Rica. *International Journal of Tropical Biology 58*:1237–1246.

Stallins, J.A., and A.J. Parker. 2003. The influence of complex systems interactions on barrier island dune vegetation pattern and process. *Annals of the Association of American Geographers 93*:13–29.

Stephenson, L. 1912. The coastal plain of North Carolina: The Cretaceous, Lafayette, and Quaternary formations. *North Carolina Geological Survey Bulletin 3*:73–171.

Stuiver, M., and P.J. Reimer. 1993. Extended 14C database and revised CALIB radiocarbon calibration program. *Radiocarbon 35*:215–230.

Swift, D.J.P. 1976. Coastal sedimentation. Pp. 255–310 in *Marine Sediment Transport and Environmental Management*. Edited by Stanley, D.J., and D.J.P. Swift. John Wiley and Sons: New York.

Theuerkauf, E.J., and A.B. Rodriguez. 2014. Evaluating proxies for estimating subaerial beach volume change across increasing time scales and various morphologies. *Earth Surface Processes and Landforms 39*(5):593–604.

Thieler, E.R., E.A. Himmelstoss, J.L. Zichichi, and A. Ergul. 2009. *Digital Shoreline Analysis System (DSAS) Version 4.0—An ArcGIS Extension for Calculating Shoreline Change*. Open-File Report 2008-1278. U.S. Geological Survey Publication. Available at https://pubs.er.usgs.gov/publication/ofr20081278

Timmons, E.A., A.B. Rodriguez, C.R. Mattheus, and R. DeWitt. 2010. Transition of a regressive to a transgressive barrier island as a function of back-barrier erosion, climate change, and low sediment supply, Bogue Banks, North Carolina, USA. *Marine Geology 278*:100–114.

VanDusen, B.M., E.J. Theuerkauf, S.R. Fegley, and A.B. Rodriguez. 2016. Monitoring overwash using water-level loggers resolves frequent inundation and run-up events. *Geomorphology 254*:32–40.

Weber, K.M., J.H. List, and K.L.M. Morgan. 2005. *An Operational Mean High Water Datum for Determination of Shoreline Position from Topographic Lidar Data*. Open-File Report 2005–1027. U.S. Geological Survey Publication. Available at https://pubs.er.usgs.gov/publication/ofr20051027

Webster, P.J., G.J. Holland, J.A. Curry, and H.R. Chang. 2005. Changes in tropical cyclone number, duration, and intensity in a warming environment. *Science 309*(5742):1844–1846.

Wilkinson, B.H., and J.R. Byrne. 1977. Lavaca Bay—Transgressive deltaic sedimentation in central Texas estuary. *American Association of Petroleum Geologists Bulletin 61*:527–545.

Winker, C.D., and J.D. Howard. 1977. Correlation of tectonically deformed shorelines on the southern Atlantic coastal plain. *Geology 5*:123–127.

Yokoyama, Y., K. Lambeck, P. De Deckker, P. Johnston, and L.K. Fifield. 2000. Timing of the last glacial maximum from observed sea-level minima. *Nature 406*(6797):713–716.

Appendix 16-A
Supporting Data

We mapped the morphology of the washover at Site F2 16 times using a terrestrial laser scanner. The images in **Figure 16A-1** highlight the morphologic changes that we captured. The washover deposit increased in size the most during the 6 months after Hurricane Sandy (October 2012), which passed far offshore of Onslow Beach. Tropical storm Joaquin passed offshore during a nor'easter event in October 2015 and also changed the morphology of the washover. The large impact from Hurricanes Sandy and Joaquin to the morphology of the washover was mainly because of the high vulnerability of the island to overwash, initially a result of Hurricane Irene (August 2011), which lowered the dune elevation. This underscores the importance of storm recurrence interval as a mechanism for driving coastal change.

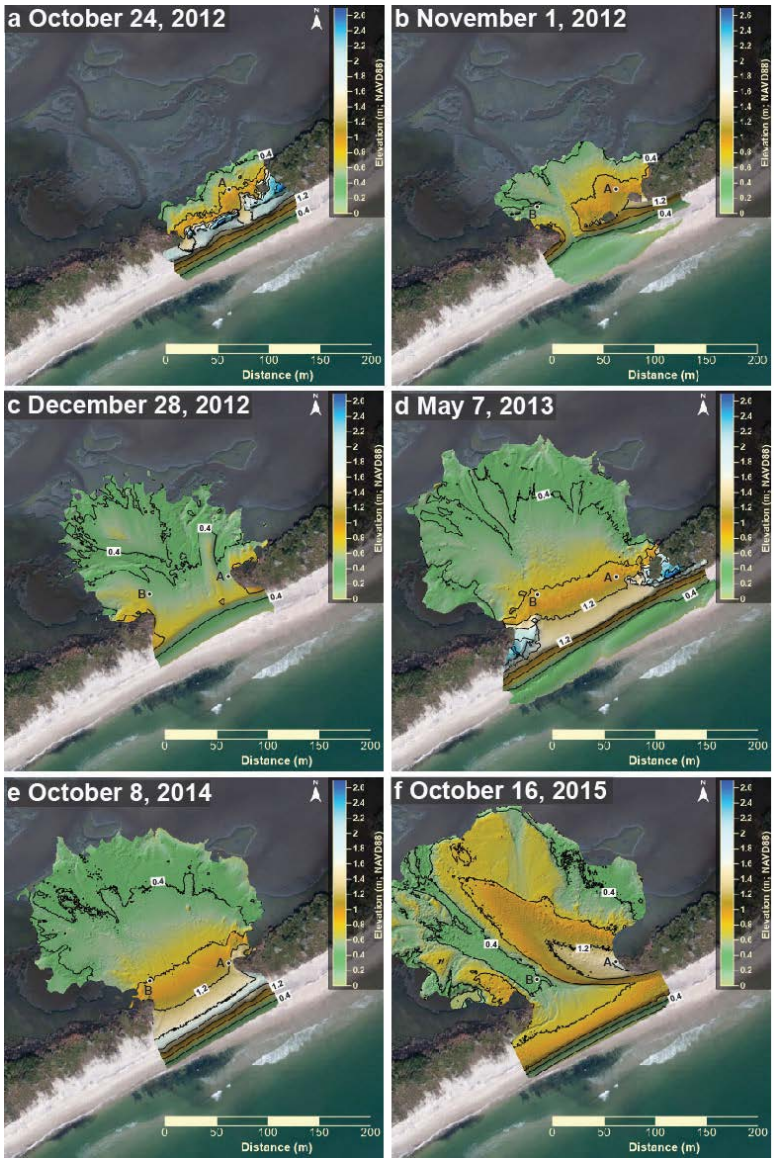

Figure 16A-1. Supporting Data

Appendix 16-B
List of Scientific/Technical Publications

Papers

Rodriguez, A.B., W. Yu, and E.J. Theuerkauf. Accepted. Abrupt increase in washover deposition along a transgressive barrier island during the late 19th century acceleration in sea-level rise. In *The Response of Barrier Islands and Barrier Spits to Climate Change*. Edited by Moore, L., and B. Murray. Springer Geography.

Theuerkauf, E.J., and A.B. Rodriguez. 2017. Placing barrier-island transgression in a blue-carbon context. *Earth's Future 5*(7):789–810. doi: 10.1002/2017EF000568

VanDusen, B.M., E.J. Theuerkauf, S.R. Fegley, and A.B. Rodriguez. 2016, Monitoring overwash using water-level loggers resolves frequent inundation and runup events. *Geomorphology 254*:32–40.

Theuerkauf, E.J., J.D. Stephens, J.T. Ridge, F.J. Fodrie, and A.B. Rodriguez. 2015. Carbon export from fringing saltmarsh shoreline erosion overwhelms carbon storage across a critical width threshold. *Estuarine, Coastal and Shelf Science 164*:367–378. doi: 10.1016/j.ecss.2015.08.001

Theuerkauf, E.J., A.B. Rodriguez, S.R. Fegley, and R. Leuttich. 2014. Sea-level anomalies as drivers of beach erosion. *Geophysical Research Letters 41*:5139–5147. doi: 10.1002/2014GL060544

Theuerkauf, E.J., and A.B. Rodriguez. 2014, Evaluating proxies for estimating subaerial beach volume change across increasing time scales and various morphologies. *Earth Surface Processes and Landforms 39*:593–604. doi: 10.1002/esp.3467

Thesis

Theuerkauf, E. 2016. *Field and Modeling Investigations into the Drivers and Implications of Beach and Saltmarsh Shoreline Erosion: Examining the Impacts of Geomorphic Change on Coastal Carbon Budgets and the Role of Sea-Level Anomalies in Facilitating Beach Erosion*. PhD, University of North Carolina at Chapel Hill, Chapel Hill, NC.

Theuerkauf, E. 2012. *Evaluating Proxies of Subaerial Beach Volume Change Across Various Time Scales and Morphologies at Onslow Beach, North Carolina, USA*. M.S., University of North Carolina at Chapel Hill, Chapel Hill, NC.

Yu, W. 2012. *Impacts of Storms and Sea-Level Rise on Coastal Evolution Between Two Capes: Onslow Bay, North Carolina*. M.S., University of North Carolina at Chapel Hill, Chapel Hill, NC.

Presentations

Atencio, A.N., A.B. Rodriguez, and B.A. McKee. 2017. *Temperature Effects on the Carbon Content of Marsh Core Subsamples Through Time*. Presented at the Geological Society of America Southeastern Section's 66th Annual Meeting, Richmond, VA. Abstracts with programs.

Rodriguez, A.B., E. Theuerkauf, J. Ridge, and W. Yu. 2017. *Stratigraphic Record of Washover Deposition Shows Rapid Response of Barrier Islands to Sea-Level Rise*. Presented at the American Association of Petroleum Geologists' Annual Convention and Exhibition, Houston, TX.

McTigue, N., J. Davis, C.R. Tobias, B.A. McKee, A.B. Rodriguez, and C. Currin. 2016. *Measuring Organic Carbon Sequestration, Burial, and Preservation in Salt Marsh Sediments over the Past Two Millennia*. Presented at the American Geophysical Union's Fall Meeting, San Francisco, CA.

Rodriguez, A.B., and E.J. Theuerkauf. 2016. *Depositional Record of Washover Reveals Rapid Response of a Transgressive Barrier to Accelerated Sea-Level Rise*. Presented at the Geological Society of America Southeastern Section's 65th Annual Meeting, Columbia, SC. 48(3). Abstracts with programs.

Theuerkauf, E.J., A.B. Rodriguez, B. VanDusen, and S.R. Fegley. 2016. *Variability in Overwash Frequency and Magnitude of Washover Terraces at Yearly Time Scales and Implications for the Evolution of Transgressive Barrier Islands*. Presented at the Geological Society of America Southeastern Section's 65th Annual Meeting, Columbia, SC. 48(3). Abstracts with programs.

Theuerkauf, E.J., A.B. Rodriguez, J.T. Ridge, and C. White-Nockleby. 2015. *Impacts of Geomorphic Change on the Carbon Budgets of Estuarine Fringing Marshes and Transgressive Barrier Islands: Insights from a Simple Box Modelling Approach*. Presented at the Geological Society of America's Annual Meeting, Baltimore, MD. 47(7). Abstracts with programs.

Rodriguez, A.B., E.J. Theuerkauf, B. VanDusen, S.R. Fegley, J.T. Ridge, and C.D. Deaton. 2015. *Variations in Barrier Island Resistance to Overwash at Monthly to Decadal Time Scales*. Presented at the Geological Society of America's Annual Meeting, Baltimore, MD. 47(7). Abstracts with programs.

Theuerkauf, E.J., J.D. Stephens, C. White-Nockleby, J.T. Ridge, F.J. Fodrie, and A.B. Rodriguez. 2015. *Including Saltmarsh Erosion and Barrier-Island Transgression in Blue Carbon Budgets*. Presented at the Atlantic Estuarine Research Society's Spring Meeting, Wanchese, NC.

Theuerkauf, E.J., A.B. Rodriguez, S.R. Fegley, and R.A. Luettich. 2014. *Sea-Level Anomalies Facilitate Beach Erosion and Increase Barrier Island Vulnerability to Storms and Sea-Level Rise*. Presented at the American Geophysical Union's Fall Meeting, San Francisco, CA.

Appendix 16-C
List of Students

- Ethan Theuerkauf, Ph.D., University of North Carolina at Chapel Hill (UNC-CH), 2016.
- Ethan Theuerkauf, M.S., UNC-CH, 2012.
- Winnie Yu, M.S., UNC-CH, 2012.

Appendix 16-D
Other Supporting Information

Dr. Ethan Theuerkauf received the University of North Carolina at Chapel Hill's Impact Award in 2015. This award recognizes graduate students and recent graduate alumni whose research directly contributes to the educational, economic, physical, social or cultural well-being of North Carolina citizens in the near future.

Chapter 17

Effects of Different Understory/Midstory Restoration Management Options on Terrestrial Ecosystem Plant and Bird Communities

SERDP Project Number: RC-2245

Terrestrial Module

Research Project T-1

Lead Researcher:

Norman L. Christensen
Duke University
Durham, NC
normc@duke.edu

Supporting Researchers:

Stephen Mitchell
Duke University
Durham, NC
stephen.mitchell@duke.edu

November 2017

Final

This report was prepared under contract to the U.S. Department of Defense (DoD) Strategic Environmental Research and Development Program (SERDP). The publication of this report does not indicate endorsement by DoD, nor should the contents be construed as reflecting the official policy or position of DoD. References herein to any specific commercial product, process, or service by trade name, trademark, manufacturer, or otherwise, do not necessarily constitute or imply its endorsement, recommendation, or favoring by DoD.

Table of Contents

List of Acronyms 17-v
Abstract 17-1
Objectives of the Research Project 17-3
Background 17-3
Materials and Methods 17-6
    Experimental Blocks 17-6
    Vegetation, Arthropod, and Bird Sampling 17-7
    Statistical Analyses 17-8
Results and Discussion 17-8
    Pre- and Post-Treatment Variations in Vegetation and Bird Communities 17-8
Conclusions and Implications for Future Research and Implementation 17-14
    Research Questions 17-14
    Other Key Scientific Findings 17-16
    Findings with Implications for Future Base Management 17-16
Literature Cited 17-16
Appendix 17-A: Supporting Data 17-A-1
Appendix 17-B: List of Scientific/Technical Publications 17-B-1
Appendix 17-C: List of Students 17-C-1

List of Figures

Figure 17-1. Conceptual model for the DCERP Research Project T-1 Module. 17-4

Figure 17-2. (Left) A typical loblolly pine site before understory/midstory thinning occurred. (Middle) The HydroAx is being used to mulch woody stems less than 20 cm in diameter at dbh. (Right) A typical site after understory/midstory thinning occurred. 17-7

Figure 17-3. The location of experimental blocks and treatment plots for Research Project T-1 at MCBCL. 17-7

Figure 17-4. Post-treatment density of understory woody stems in 2010 or 2011 (blue) and 2016 (orange). 17-10

Figure 17-5. Post-treatment understory plant diversity (number of taxa per 0.1 ha) in 2010 or 2011 (blue) and 2016 (orange). 17-11

Figure 17-6. Post-treatment bird diversity (number of species per plot) in 2010 or 2011 (blue) and 2016 (orange). 17-11

Figure 17-7. A comparison of understory plant species richness and bird species richness for all plots and sample years. 17-12

Figure 17-8. NMS ordination of plant species composition in 24 experimental plots. 17-13

Figure 17-9. NMS ordination of bird species composition in 24 experimental plots. 17-14

List of Tables

Table 17-1. Summary of Pre-treatment and Post-treatment Data of Stems Between 1 cm and 20 cm in diameter at dbh for Experimental Plots. 17-9

List of Acronyms

µg/g	micrograms per gram
Al	aluminum
ANOVA	analysis of variance
BD	bulk density
°C	degrees Celsius
C	unthinned control
Ca	calcium
CEC	cation exchange capacity
cm	centimeter
D	dormant season
dbh	diameter at breast height (1.5 m)
DCERP	Defense Coastal/Estuarine Research Program
DCERP1	first cycle of DCERP
DCERP2	second cycle of DCERP
DF	degrees of freedom
DoD	U.S. Department of Defense
F	F ratio
g	gram
G	growing season
g/cm^3	gram per cubic centimeter
ha	hectare
K	potassium
m	meter
m^2	square meter
m^2/ha	square meter per hectare
MCBCL	Marine Corps Base Camp Lejeune
mEq	milliequivalent
Mg	magnesium
N/A	missing data
NMS	non-metric multi-dimensional scaling
PCA	principal components analysis
PO_4–P	orthophosphate
R^2	R squared
RC	Resource Conservation and Climate Change (a SERDP program area)
RCW	red-cockaded woodpecker
SERDP	Strategic Environmental Research and Development Program
SOM%	percent soil organic matter
T	Terrestrial (Module)

Abstract

Changing patterns of land use, agriculture, and forest management have greatly altered forest ecosystems across much of the mid-Atlantic lower Coastal Plain. In particular, vast areas that were once dominated by open longleaf pine (*Pinus palustris*) savanna now support closed canopy stands of loblolly pine (*Pinus taeda*) with a dense understory and midstory of broadleaved shrubs and trees. The absence of fire on these landscapes has exacerbated this trend. This situation is typical for large areas of Marine Corps Base Camp Lejeune (MCBCL). In recent years, longleaf pine restoration at MCBCL has focused on the use of understory and midstory thinning to produce savanna-like conditions and allow restoration of historical fire regimes by using prescribed burning. There were three objectives of this study. The first objective was to determine the effects of different understory/midstory thinning treatments (hereafter referred to as thinning) and prescribed burning in 50- to 60-year-old loblolly pine stands on plant and avifaunal communities. The second objective was to determine the interrelationships among the vegetation and avifaunal communities across sites representing a wide range of soil conditions and red-cockaded woodpecker (RCW) habitat qualities. The last objective was to assess the implications of these results for forest management and restoration at MCBCL. These three objectives were pursued by using a randomized block design field experiment consisting of eight blocks with three treatments in each block. Individual blocks were located on MCBCL to represent a range of soil site conditions. Treatments included an unthinned control (C), dormant season (D) thinning, and growing season (G) thinning. All experimental plots (including controls) were prescribed burned 6 to 18 months after thinning. The first post-treatment prescribed burns were completed during 2010 and 2011. The second post-treatment prescribed burn was attempted in 2014 and 2015; however, weather and air quality conditions did not meet prescribed burn standards in either year. Vegetation and bird species were sampled in 2016 and compared to results from 2010 and 2011.

The density of the understory plants (defined as stems 1- to 20-cm dbh) was decreased in all treatments following thinning treatment application and prescribed burning. However, understory stem density was considerably higher in the C treatment than either the D or G thinning treatment. Understory stem density was significantly lower in the G treatment than the D treatment in 2010 or 2011. In the absence of prescribed burning, understory stem density increased significantly in all plots, and the treatment differences disappeared. Understory plant species richness was significantly higher in D and G treatment compared with the C treatment in 2010 or 2011. However, plant species richness was lower in all plots in 2016 compared with 2010 or 2011, and differences among treatments disappeared. Bird species richness was consistently lower in 2016 compared with 2010 or 2011, with no differences among treatments at either sample time. Non-metric multi-dimensional scaling (NMS) ordinations of 2010–2011 plant and bird data revealed clear differences in the species composition of plant and bird communities related to site moisture characteristics of experimental blocks. NMS ordinations of 2016 plant and bird data indicate significant changes in species composition away from restoration goals. These changes are likely related to the absence of prescribed burning in the interval between 2010–2011 and 2016. Probably the most important conclusion of this study is that mechanical restoration treatments such as understory thinning must be accompanied by regular prescribed burning to be effective.

Keywords: Bird species composition and richness, forest restoration, understory or midstory thinning, loblolly pine, longleaf pine, ordination, plant species composition and richness, high pocosin, prescribed burning, red-cockaded woodpecker, soils.

Objectives of the Research Project

This research project focuses on critical knowledge gaps related to efforts to restore longleaf pine ecosystems on sites across Marine Corps Base Camp Lejeune (MCBCL) that have been modified by past land-use and forest management activities. Specifically, we examined the effects of alternative understory restoration strategies (dormant and growing season thinning of understory and midstory trees and shrubs) on understory plant and avian communities. Research Project T-1 activities were focused on the following three primary objectives:

1. To determine the effects of different understory/midstory thinning treatments (henceforth referred to as thinning treatments) and prescribed burning aimed at restoring longleaf pine (*Pinus palustris*) forest habitat in 50- to 60-year-old loblolly pine (*Pinus taeda*) stands on plant and avifaunal communities.
2. To determine the interrelationships among the vegetation and avifaunal communities across sites representing a wide range of soil conditions and red-cockaded woodpecker (RCW) habitat qualities.
3. To assess the implications of these results for forest management and restoration at MCBCL.

Objectives 1 and 2 were pursued in close collaboration with Dr. Jeff Walters and his colleagues working on Research Project T-4 (see Chapter 19 of the *DCERP2 Final Report* [RTI, 2017]). This experimental work was begun during DCERP1 and continued in DCERP2 to allow sufficient time to assess vegetation and bird community responses to treatments. This work was also continued into DCERP2to provide adequate time between the first prescribed burns 1 year following thinning treatments (in 2010 or 2011) and a subsequent burn 3 or 4 years later (planned for 2014 and 2015). Our DCERP1 work allowed us to assess the effects of experimental treatments after only a single growing season. DCERP2 allowed us to evaluate treatment effects after nearly 6 years on these same treatment sites. However, because weather and/or air quality conditions did not meet prescribed burn standards, subsequent burn was not possible. This significant departure from our research plan had important consequences and implications for management.

Background

The terrestrial vegetation of North Carolina's lower Coastal Plain is known for its diversity across a wide range of spatial scales. MCBCL lands capture much of that variation (**Figure 17-1**). At the landscape scale, geomorphic variations such as relict dune and estuarine deposits and subtle changes (±1 m) in elevation of the soil surface relative to the shallow water table produce remarkable variations in ecosystem structure, composition, and processes. Within a few kilometers of the coast, vegetation composition is heavily influenced by salt aerosol and maritime climatic gradients. In pre-settlement times, inland vegetation varied along a continuum from shrub bog (pocosin) wetlands on deep peat soils to pine-dominated flatwoods with an understory of shrubs on poorly drained mineral soils and longleaf pine savannas on well-drained sands (Christensen, 2000). There is nearly complete turnover of plant species composition from one end of this gradient to the other. Some of these ecosystems display remarkable species richness and high levels of species endemism at very local scales. For example, longleaf pine

savannas may support more than 60 vascular plant species per square meter and more than 120 species per hectare (Walker and Peet, 1983).

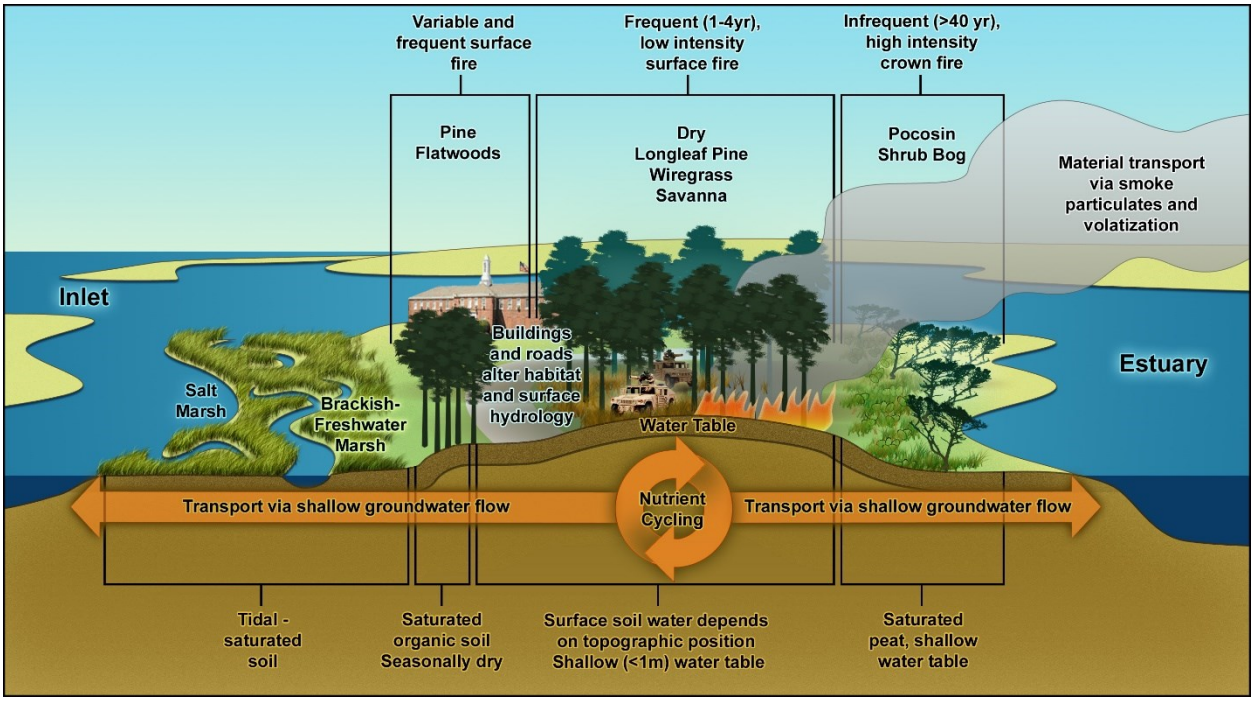

Figure 17-1. Conceptual model for the DCERP Research Project T-1 Module.

Ecosystem composition and structure were also heavily influenced by variations in pre-settlement fire regimes along this gradient. Pocosins typically experience intense, crown-killing fires at return intervals of more than 40 years, whereas longleaf pine savannas are maintained by light surface fires at intervals of between 1 and 5 years (Bailey et al., 2007; Christensen, 1981, 1992, and 2000). The relative amount and distribution of pocosin, flatwood, and savanna ecosystems on pre-settlement landscapes was heavily influenced by the frequency and behavior of fire. Repeated, low severity fires can maintain savannas on very moist soils with relatively high amounts of organic matter. Indeed, it is just these situations that support the highest plant species richness at small (m^2) spatial scales. It is also these sites that support many unique endemic species, including several insectivorous plant species. On all but very well-drained sites, the absence of fire for periods longer than 5 or 6 years results in the invasion of shrubs and a variety of understory trees. This invasion also changes the amounts and distribution of fuels such that subsequent fires are likely to be severe enough to kill, and even consume, canopy trees.

Today, post-settlement land use and disturbance influence the mosaic of terrestrial ecosystems on lower Coastal Plain landscapes such as on MCBCL. Except for the wettest and driest sites, forests on much of this landscape were cleared for agriculture during the eighteenth and nineteenth centuries (Crowley, 1996). Longleaf pine savannas that were not cut were heavily managed for naval stores (Early, 2004). Much of this farmland was abandoned in the years after the Civil War and Reconstruction up to World War II; post-abandonment succession generally produced an even-aged overstory of loblolly pine with an understory dominated by shrubs and understory trees on all but the driest sites (Christensen, 2000; Mitchell et al., 2015). Fire was not only excluded from these forests, but the successional changes promoted understory vegetation

and fuels that are comparatively difficult to burn (Nowacki and Abrams, 2008). From 1940 through 1960, large tracts of such land were acquired by timber companies that managed them to maintain loblolly pine dominance.

Across the southeastern United States, this history of land use led to the transformation of more than 95% of the land once dominated by longleaf pine savanna to loblolly pine dominated flatwoods. Even where longleaf pine remained, fire suppression often led to the invasion of woody understory plants and the loss of endemic plant and animal species. In many places, longleaf pine ecosystems are represented by relatively small and often isolated stands.

Altered fire regimes and habitat loss and fragmentation have contributed to the significant number of plant and animal species found in communities dominated by longleaf pine that are currently listed as threatened or endangered under the Endangered Species Act. The RCW is probably most notable among these listed species. These listings, along with general concerns about the loss of longleaf pine habitat, have been the impetus for restoration of loblolly pine flatwoods to longleaf pine savannas. Indeed, maintenance and restoration of longleaf pine habitat and associated populations of RCWs have been prominent objectives of forest management over much of the MCBCL landscape.

In some areas of MCBCL, restoration has taken the form of clear-cutting, followed by planting of longleaf pine and the eventual re-establishment of an appropriate prescribed fire regime. Restoration of mature longleaf pine habitat by using this approach will, of course, require many decades. As an alternative strategy to accelerate habitat restoration, MCBCL staff have implemented mechanical thinning treatments to remove understory and midstory hardwoods (generally stems less than 20 cm in dbh). This strategy mimics natural open savanna–like stand structures and understory composition with fuels that are more typical of longleaf pine ecosystems. Such management is currently being applied to hundreds of MCBCL acres each year. Variations on this management theme include different seasons (growing and dormant) of mechanical control of the woody understory. Restoration of low- severity, high- frequency fire regimes is a key objective. Therefore, all thinned areas receive a late winter or early spring prescribed burn in the following year.

Dr. Joan Walker of the U.S. Department of Agriculture's Forest Service has performed SERDP–sponsored research (SI-1474) to examine patterns of establishment and growth of longleaf pine seedlings in response to thinning treatments. The effects of similar understory thinning on avifaunal communities have been examined in longleaf pine forests of the sand hills of northwestern Florida (Provencher et al., 2002 and 2003). The specific effects of these treatments on other understory components (e.g., vegetation, forest floor, and fuels), insects, and avifauna have not been studied in loblolly dominated ecosystems such as on MCBCL. Loblolly-dominated flatwoods occur on a range of soil site situations, but the variation in the response to such thinning treatments (i.e., restoration success) across this range has not been studied.

The effects of restoration treatments on understory vegetation are especially relevant because the composition of this community is a major determinant of RCW habitat quality (USFWS, 2003). The needs of RCWs are well known, but virtually nothing is known about the relationships between the diversity and composition of the plant communities and the diversity and composition of avian communities (USFWS, 2003).

Data gathered during DCERP1 provided information about the effects of different seasons of understory thinning (followed by prescribed burning) 1 year after treatment. As expected, thinning significantly reduced the density of understory woody stems, and this effect was greatest in plots treated during the growing season. There was a significant increase in the richness of understory plant species with thinning, but no difference was observed between plots thinned in the dormant season when compared with the growing season. Bird species richness was unaffected by thinning treatments. These results are found in the *DCERP1 Final Research Report* (RTI International, 2013).

Our DCERP1 research revealed very significant correlations between soil site conditions (soil organic matter and pH in particular), plant species composition and bird species composition. A year after treatment, thinning (regardless of season) appeared to have little, if any, effect on these relationships.

Materials and Methods

Experimental Blocks

In 2008, stands that were slated for forest restoration (i.e., understory/midstory thinning treatment) were identified by MCBCL staff. These stands or restoration treatment units were dominated in the canopy by 50- to 60-year-old loblolly pine, with a dense midstory of woody trees and shrubs. Based on general appearance, soil series, and dominant species, the stands were designated as mesic (well-drained soils, dominated by loblolly pine [Goldsboro series] and some longleaf pine [Baymeade series]), wet-mesic (moister soils, dominated by loblolly pine only [Lynchburg series]), or high pocosin (wet, organic soils, dominated by loblolly and with some pond pine [Torhunta series]).

Restoration treatment units were selected to be sufficiently large (greater than 5 ha) to accommodate experimental treatment blocks and simultaneous studies of bird communities. Each experimental treatment block included three 1-ha treatment plots, as follows: (1) no woody understory and midstory removal control (C), (2) dormant season mechanical understory and midstory removal (D), and (3) growing season mechanical understory/midstory removal (G). A 25-m treated buffer surrounded each 1-ha treatment plot. Understory/midstory removal was conducted by using a Hydro-Ax® mulching device, which typically cuts and mulches all trees less than 20 cm in diameter at dbh, leaving behind the shredded biomass (**Figure 17-2**). Dormant season (D) treatments were installed during January and February 2009, and growing season (G) treatments were installed in June and July 2009. Restoration treatment units were selected to establish three blocks in each of the mesic, wet-mesic, and high pocosin designations for a total of nine blocks. However, one of the wet-mesic blocks was lost to a wildfire in 2009, leaving eight blocks (**Figure 17-3**). All treatments were to receive non-growing season prescribed burns at 3-year intervals. The first post-treatment prescribed burns were completed during 2010 and 2011. Our expectation was that a second post-treatment prescribed burn would be completed in each treatment block in 2014. However, only the HA block was burned in 2014. As of 2017, additional prescribed burning was not possible on any additional plots. This was largely because the weather and/or air quality conditions did not meet prescribed standards for burning. The impacts of these changes in prescribed burning applications on vegetation and avian sampling are discussed in the remainder of this subsection.

Figure 17-2. (Left) A typical loblolly pine site before understory/midstory thinning occurred. (Middle) The Hydro-Ax is being used to mulch woody stems less than 20 cm in diameter at dbh. (Right) A typical site after understory/midstory thinning occurred.

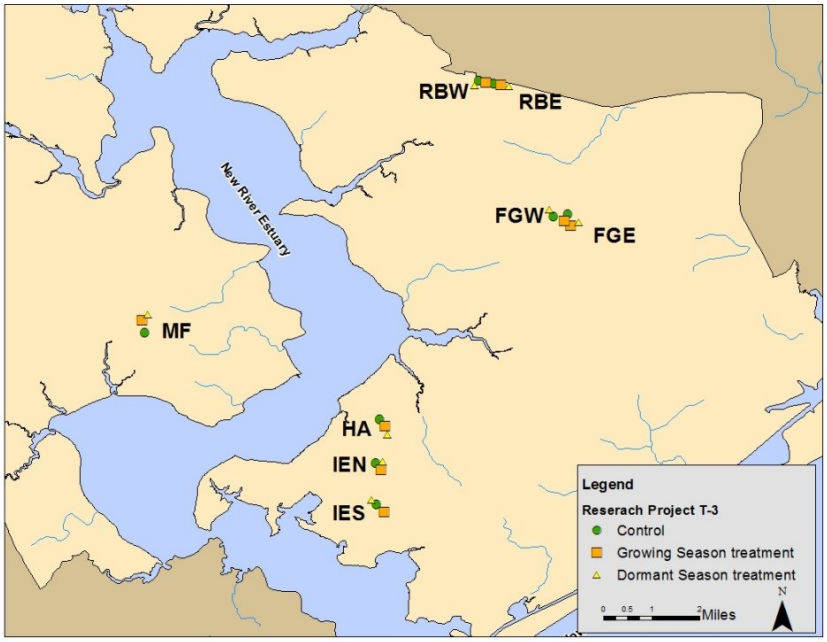

Figure 17-3. The location of experimental blocks and treatment plots for Research Project T-1 at MCBCL.

Vegetation, Arthropod, and Bird Sampling

During December 2008 and January 2009, before thinning treatment applications, woody stems between 1 and 20 cm in diameter at dbh (henceforth referred to as understory stems) were censused by species and diameter class in each of the three 1-ha experimental plots in each of the eight blocks. The size range of between 1 and 20 cm in diameter at dbh was selected because these are the stems typically removed during the thinning treatment. Within an 8-m radius of each of the five randomly located points in each plot, the dbh and species identity were recorded for each stem greater than or equal to 5 cm in diameter at dbh. All stems less than 5 cm were recorded by species and dbh along a 1 m × 8 m transect traversing each point.

After thinning treatment and prescribed burning, a 20 m × 50 m (0.1-ha) plot was located and permanently marked in the center of each treatment plot, and each plot was censused for

vegetation species abundance and diversity, cover of herbs, and biomass of woody plants by using the Carolina Vegetation Survey methodology (Peet et al., 1998). Censuses were performed during the growing season after the post-thinning prescribed burning. Thus, some plots were censused during the 2010 growing season and some in 2011. We had planned to re-census the vegetation in these plots after prescribed burning in 2014 or 2015; however, by April 2016 only one experimental block was burned. Notwithstanding the fact that the planned prescribed burns were not completed, we resampled the vegetation in all plots in June and August 2016.

Bird composition and abundance were assessed from point count samples at the center of each treatment plot at several times throughout the breeding season the same year as the vegetation census in that plot. These assessments were conducted in collaboration with staff from Research Project T-4. The details of avian sampling methods are described in the final report for DCERP 1 Research Project T-2 (Walters, 2013). As with the herbs, birds were sampled in each experimental plot 1 year after the post-treatment prescribed burn (either in 2010 or 2011) and again in 2016.

Statistical Analyses

Data were analyzed by using standard statistical tools for product–moment correlation and analysis of variance (ANOVA) provided in the data analysis and graphics system R (Venables and Smith, 2011). Non-metric multi-dimensional scaling (NMS) ordination (Kruskal and Wish, 1978) was used to analyze trends in species composition in experimental plots. Each NMS axis represents a component of variation in the multivariate data set that is similar to a principal components analysis (PCA). However, NMS ordination is much better suited for use with non-normal species composition data than PCA. Plots with similar scores for a particular NMS axis are more similar to one another with respect to the trends in species composition represented by that axis than stands with less similar scores. Our NMS analyses used the Sørenson dissimilarity metric for 1,000 iterations to derive two-dimensional ordination axes, which represent the main axes of compositional variation. We ran PC-ORD software with random starting configurations for 100 runs with real data with a maximum of 1,000 iterations per run and a stability criterion of 0.00001. Indicator species analysis (Dufrêne and Legendre, 1997), and correlation and regression tree analyses (McCune and Grace, 2002) were used to identify those species and site measures that are most highly correlated to variations in species composition represented in the NMS ordination (McCune and Grace, 2002).

Results and Discussion

Pre- and Post-Treatment Variations in Vegetation and Bird Communities

Pre-treatment density of understory woody stems averaged 24,440/ha and varied from 5,500 to 57,000/ha across all treatment blocks (**Table 17-1**). There was considerable within-block variation in pretreatment stem density, and there was no apparent relationship between pre-treatment stem density and block moisture condition. Thinning and prescribed fire reduced the density of understory woody stems by more than 90% in most plots. This finding was true even for control plots because they had been prescribed burned in either 2010 or 2011 along with the thinned plots. One year after treatment, there were no significant differences in understory woody stem density among blocks (F ratio [F]=0.98, degrees of freedom [DF]=7, P>0.48).

However, there were significant differences among treatments (F=47.56, DF=2, P<0.00001). Specifically, stem density was uniformly highest in control plots, lower in dormant season thinning plots, and lowest in growing season thinned plots (**Figure 17-4**). However, after 5 or 6 years without regular prescribed burning, there were no differences among controls and thinning treatments. These results indicate that, in the short term, growing season thinning may be more effective than dormant season thinning in reducing understory hardwood density. However, if thinning treatments are not followed by regular prescribed fire, then the benefits from thinning are quickly lost.

Table 17-1. Summary of Pre-treatment and Post-treatment Data of Stems Between 1 cm and 20 cm in diameter at dbh for Experimental Plots.

Blocks are Ordered Top to Bottom as High Pocosin (FGE, FGW, and IES), Wet-Mesic (IEN, HA, and MF), and Mesic (RBE and RBW).

Treatment Block	Age (Year) in 2010	1 Year Pre-treatment	Post-treatment (2010 or 2011)	Post-treatment (2016)
FGE-C	50	Not applicable	2,660	2,880
FGE-D	50	11,020	920	2,690
FGE-G	50	21,440	150	1,910
FGW-C	50	Not applicable	2,170	2430
FGW-D	50	11,520	790	2,690
FGW-G	50	22,370	160	2,160
IES-C	60	47,260	380	250
IES-D	60	7,390	770	2,160
IES-G	60	11,880	620	7,410
IEN-C	50	57,120	2,070	2,875
IEN-D	50	11,520	1,000	2,440
IEN-G	50	16,670	220	2,980
HA-C	53	28,360	1,430	1,220
HA-D	53	17,100	90	1,490
HA-G	53	9,340	380	1,370
MF-C	63	34,980	2,770	2,140
MF-D	65	7,3320	350	2,790
MF-G	65	11,760	570	3,310
RBE-C	60	13,330	2,710	2,550
RBE-D	64	6,830	1,080	1,970
RBE-G	64	10,800	200	2,320
RBW-C	56	11,880	1,280	2,550
RBW-D	56	6,650	1,020	2,920
RBW-G	56	9,710	190	2,320

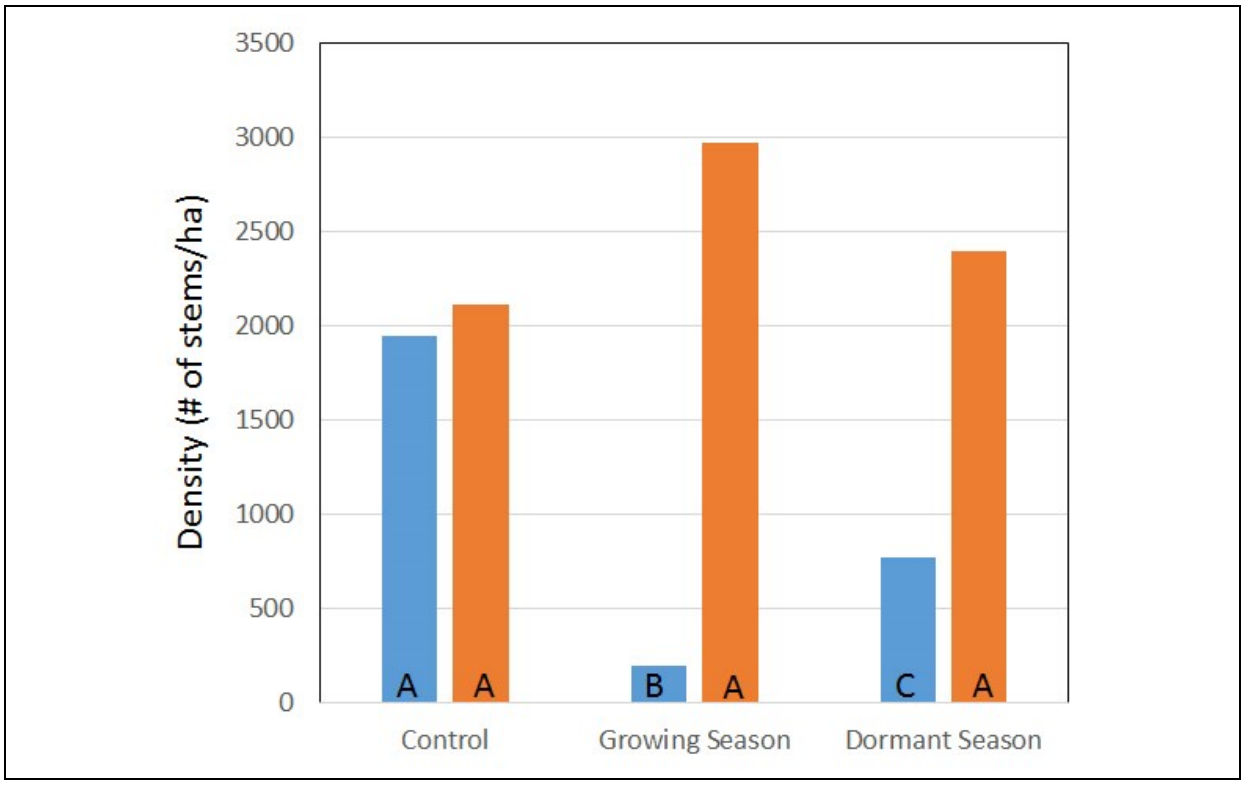

Figure 17-4. Post-treatment density of understory woody stems in 2010 or 2011 (blue) and 2016 (orange).

Significant differences (P<0.05, Duncan's Multiple Range Test) by the letter in each bar. Bars sharing the same letter are statistically homogeneous.

Average species richness (number of taxa per 0.1 ha) of understory plants for each treatment is presented in **Figure 17-5**. Total plant species richness (number of species per 0.1 ha) ranged from as low as 7 in FGW-C (a pocosin plot) to as high as 52 in RBW-G (a wet-mesic plot). Richness was highest in thinned plots immediately after treatment, although the season when thinning occurred did not have a significant effect. There were no significant differences among treatments in 2016; species richness in the thinned plots had returned to levels similar to the unthinned controls.

This increase in plant species richness in thinned treatment plots during the growing season after treatment applications and prescribed burning is very likely a consequence of increased light to the understory, owing to diminished canopy cover, reduced amounts of litter, and diminished competition from understory shrubs. Differences between the growing season and dormant season thinning treatments were not evident after 1 year.

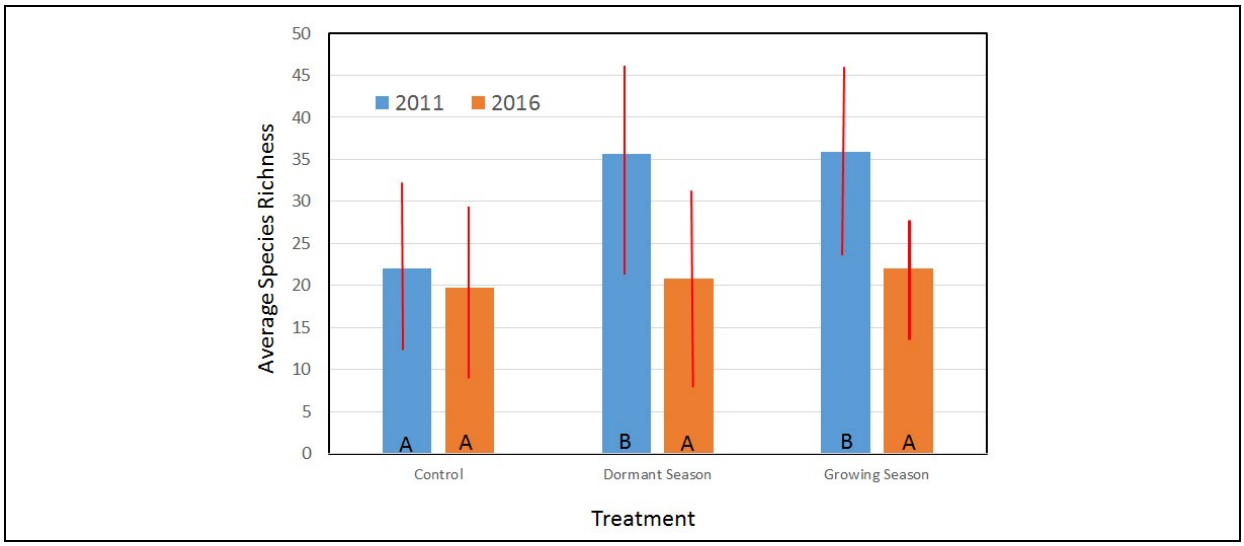

Figure 17-5. Post-treatment understory plant diversity (number of taxa per 0.1 ha) in 2010 or 2011 (blue) and 2016 (orange).

Significant differences (P<0.05, Duncan's Multiple Range Test) are indicated by the letter in each bar. Bars sharing the same letter are statistically homogeneous. Vertical red lines indicate a ±1 standard deviation.

There were no significant differences among treatments in avian species diversity at either sampling date (**Figure 17-6**). However, bird species richness was significantly lower across all treatments and blocks in 2016 compared with 2010–2011. This finding is very likely a direct consequence of changes in plant species composition and vegetation structure such as the increased density of woody stems in the understory caused by the absence of prescribed burns.

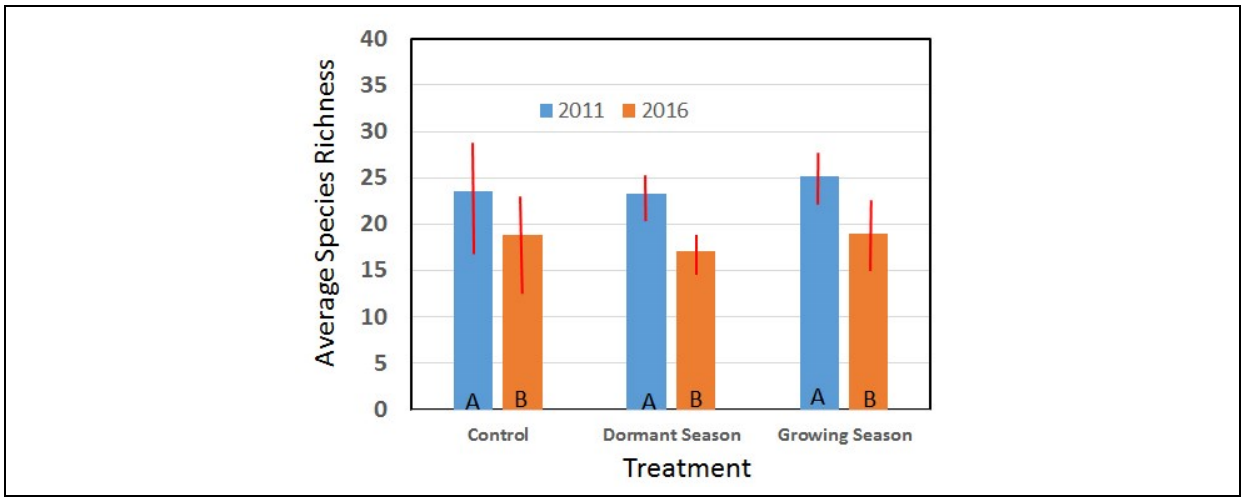

Figure 17-6. Post-treatment bird diversity (number of species per plot) in 2010 or 2011 (blue) and 2016 (orange).

Significant differences (P<0.05, Duncan's Multiple Range Test) by the letter in each bar. Bars sharing the same letter are statistically homogeneous. Vertical red lines indicate a ±1 standard deviation.

There was a strong correlation between the plant species richness and bird species richness among plots and treatments and across years (r=0.495, P<0.001, **Figure 17-7**). This correlation

was strongest among the plots sampled in 2010 or 2011 (r=0.53, P<0.01) than in 2016 (r=0.18, P<0.10).

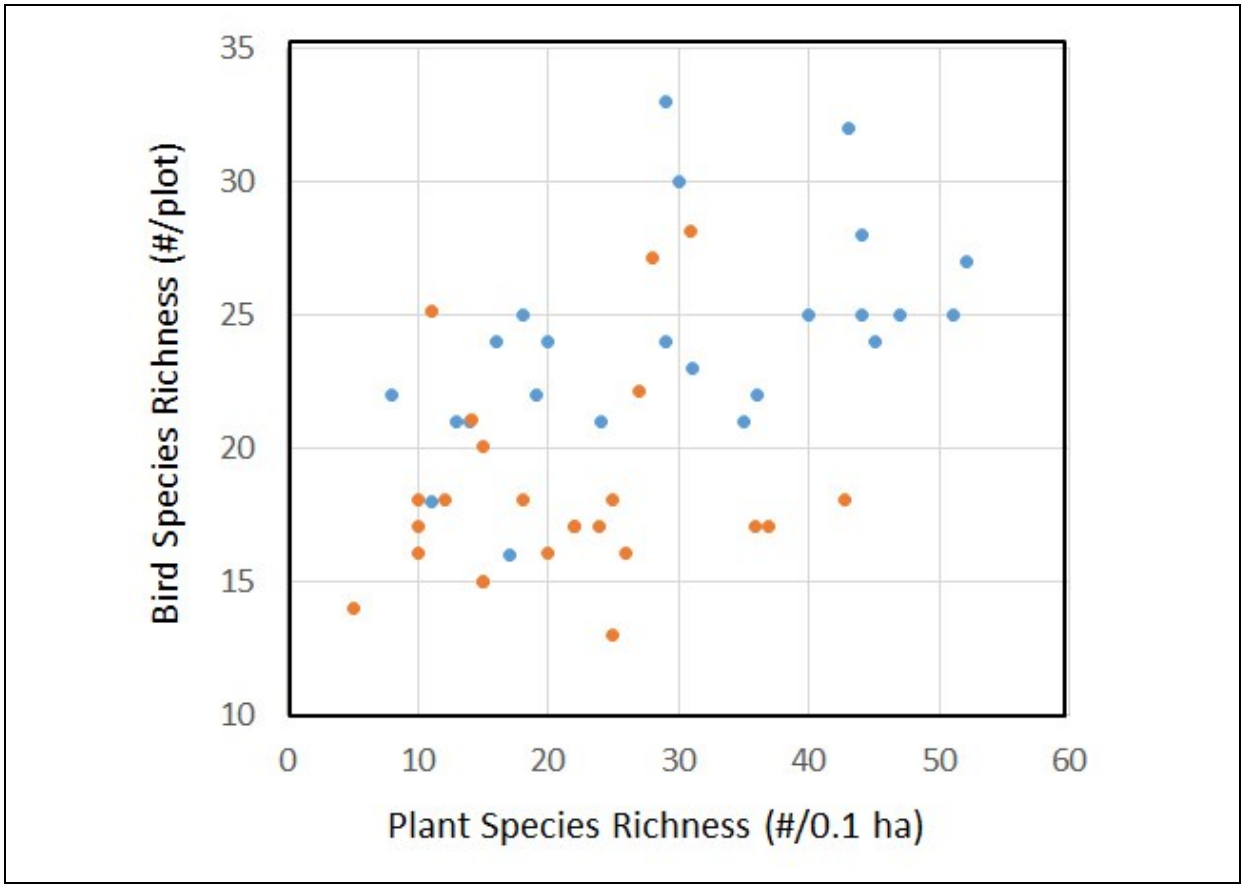

Figure 17-7. A comparison of understory plant species richness and bird species richness for all plots and sample years.

Blue circles represent 2010 or 2011 samples; orange dots denote 2016 samples.

Compositional variation in the community of plants among treatment plots based on NMS ordination is presented in **Figure 17-8**. Treatment blocks are arrayed in this ordination as a continuum from high pocosin, with low Axis 1 and Axis 2 scores, to wet mesic, with intermediate Axes 1 and 2 scores, and mesic plots, with high Axis 1 and Axis 2 scores. This gradient also correlates with plant species richness, which increases from high pocosin stands to mesic stands (R^2=0.65, P<0.0001, multiple regression species richness versus Axis 1 and Axis 2). Based on NMS scores, understory composition of thinned stands is generally more similar to that of high diversity longleaf pine savannas than their respective controls. However, there no obvious difference was observed between plots thinned in the dormant versus the growing season. These trends are absent among 2016 NMS scores. Indeed, high pocosin and wet mesic plot 2016 NMS scores are uniformly less similar to the longleaf pine restoration target compared with 2010 or 2011. It is very likely that this shift in understory plant species composition away from restoration goals is a direct consequence of the absence of prescribed fire and the rapid ingrowth of woody stems.

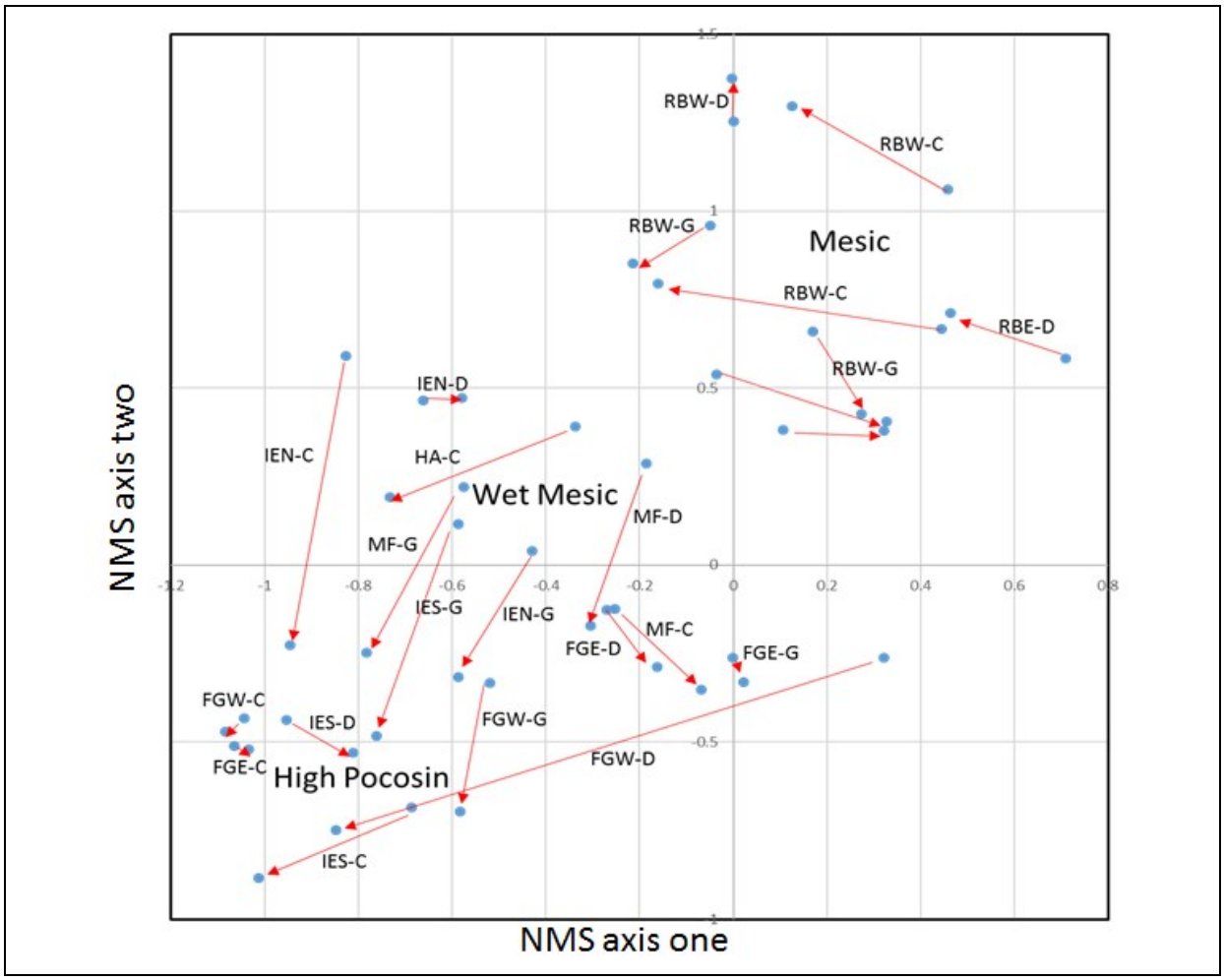

Figure 17-8. NMS ordination of plant species composition in 24 experimental plots.

The point at the base of each arrow represents the 2010–2011 sample. The point at the tip of each arrow is that same plot sampled in 2016.

Compositional variation in the community of birds among treatment plots based on NMS ordination is displayed in **Figure 17-9**. Although the **Figure 17-9** is oriented differently, the general arrangement of plots relative to one another is remarkably similar, particularly among the 2010 or 2011 samples. The high pocosin blocks have low NMS Axis 2 scores, and the mesic plots have high NMS Axis 2 scores. There is a very clear separation of the 2010 and 2011 samples from the 2016 samples along Axis 1, indicating a very consistent change in the composition of the bird communities in these plots over this time interval. This change is because of notable increases in the prevalence of eastern bluebirds (*Sialia sialis*), gray catbirds (*Dumetella calolinensis*), Connecticut warblers (*Oporornis agilis*), Acadian flycatchers (*Empidonax virescens*), and brown thrashers (*Toxostoma rufum*) in 2016, and diminished importance of Bachman's sparrows (*Aimophila aestivalis*), blue-gray gnatcatchers (*Polioptila caerulea*), eastern kingbirds (*Tyrannus tyrannus),* and white-eyed vireo (*Vireo griseus*). It is impossible to assign a single cause to these changes. The changes are almost certainly due in part to normal year-to-year variations in population sizes that occur in many bird species. The differences are also likely because of changes in the vegetation structure (e.g., increased density

of understory woody stems) and plant species composition of these plots that has occurred in the absence of prescribed fire.

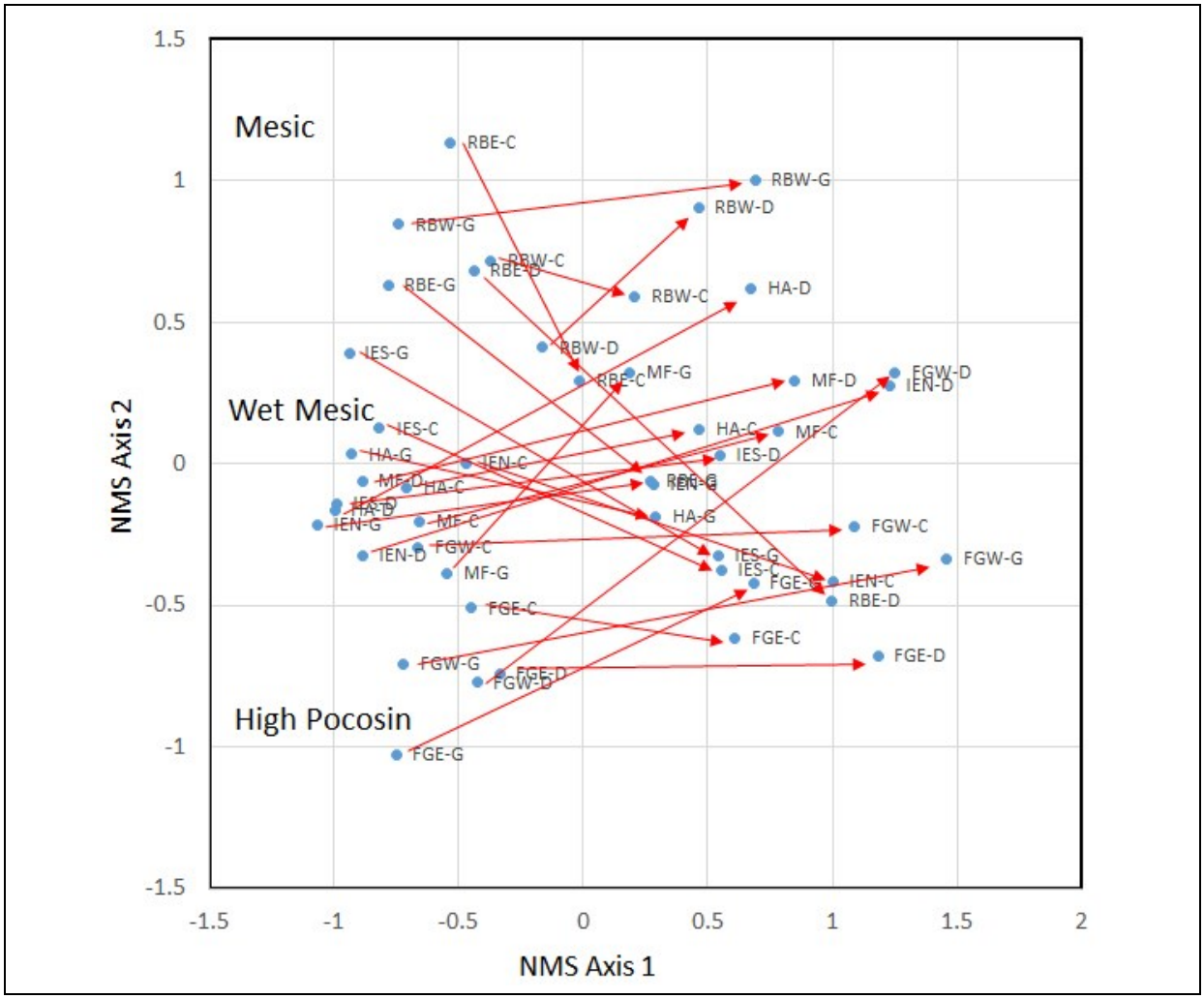

Figure 17-9. NMS ordination of bird species composition in 24 experimental plots.

The point at the base of each arrow represents the 2010 or 2011 sample. The point at the tip of each arrow is that same plot sampled in 2016.

Conclusions and Implications for Future Research and Implementation

Research Questions

1. **What are the effects of dormant season understory thinning or growing season understory thinning, followed by prescribed burning, on the density of small woody stems in the understory?**

Prescribed burning alone and thinning followed by prescribed burning significantly reduced the density of small stems (less than 5 cm and between 5 cm and 20 cm) 1 year after thinning treatments. This effect was greatest in growing season treatments, less in dormant season treatments and lowest in controls (prescribe burn only). After 5 years in the absence of additional

prescribed burn, differences in understory stem density among treatments disappear entirely, which has several important ecosystem consequences. Woody sprouts compete with understory herbs for light and other resources, and they change the physical structure of the understory in ways that influence feeding and nesting habitat for birds. Woody sprouts also result in a general increase in the quantity of understory fuel and potentially increase the severity of future fires.

2. What are the effects of dormant season understory thinning or growing season understory thinning, followed by prescribed burning, on the diversity of understory herbs?

In the first year after treatment, the diversity of understory herbs significantly increased in thinned treatments compared to controls. There was no difference between dormant and growing season thinning. Without subsequent prescribed burns, the effects of thinning on plant species diversity disappeared. By 2016, there were no differences among the unthinned control and thinned plots.

3. What are the effects of dormant season understory thinning or growing season understory thinning, followed by prescribed burning, on the diversity of birds?

Thinning treatments did not have any impacts on the richness of bird species compared with the unthinned controls 1 year after treatment. However, in the absence of prescribed burning, bird species richness declined across all treatments.

4. What are the effects of dormant season understory thinning or growing season understory thinning, followed by prescribed burning, on the composition of understory plant species?

The composition of understory herbaceous vegetation was highly correlated with the conditions (organic matter and pH) among plots. In the year following thinning treatment, there was a detectable shift in understory plant species composition toward that characteristic of longleaf pine savannas (the restoration goal) in the thinned treatments. There was no apparent effect due to thinning season. Absent additional prescribed burning, treatment plot herb composition moved away from this restoration goal.

5. What are the effects of dormant season understory thinning or growing season understory thinning, followed by prescribed burning, on the species composition of bird communities?

Bird species composition was highly correlated with the composition of understory plants. However, thinning treatments did not have any effects on bird species composition compared with controls. Bird species composition changed significantly between 2010–2011 and 2016 in all plots regardless of thinning treatment. This finding is likely a consequence of normal year-to-year variation in population sizes of individual species and of directional changes in wood stem density and understory plant species composition that resulted from the absence of fire.

Other Key Scientific Findings

Our results signify a very strong relationship between soil characteristics, plant community composition, and avian community composition. However, the exact mechanisms underlying these relationships remain poorly understood, but they provide strong assurance that management strategies focused on particular ecosystem components, such as the restoration of plant community composition, are likely to have favorable effects on other ecosystem components.

Findings with Implications for Future Base Management

Although short-term results indicated significant benefits of both dormant and growing season thinning for restoration plant diversity and composition of 50- to 60-year-old loblolly-dominated forests to conditions similar to those of longleaf pine savannas, those benefits were lost without subsequent prescribed burning. Without prescribed burning, differences in the density of understory woody stems between thinned treatments and unthinned controls quickly disappeared. This ingrowth resulted in an increase in understory fuels and may increase the severity of future fires. Finally, the lack of prescribed burning was likely a contributing factor to significant changes in bird species diversity and composition over the duration of this study. Probably the most important conclusion of this study is that the mechanical restoration treatments (e.g., understory thinning) must be accompanied by a regular prescribed burning to be effective.

Literature Cited

Andrews, P.L., and L.S. Bradshaw. 1997. *FIRES: Fire Information Retrieval and Evaluation System—A Program for Fire Danger Rating Analysis*. General Technical Report INT-GTR-367. U.S. Department of Agriculture, Forest Service, Intermountain Research Station.

Bailey, A.D., R. Mickler, and C. Frost. 2007. Pre-settlement fire regime and vegetation mapping in southeastern Coastal Plain forest ecosystems. Pp. 275–286 in *Conference Proceedings of The Fire Environment—Innovations, Management, and Policy*, Destin, FL. Proceedings RMRS-P-46CD. March 26–30. Edited by Butler, B.W., and W. Cook. U.S. Department of Agriculture, Forest Service, Rocky Mountain Research Station, Fort Collins, CO.

Christensen, N.L. 2000. Vegetation of the Coastal Plain of the southeastern United States. Pp. 397–448 in Vegetation of North America. 2nd edition. Edited by Barbour, M., and W.D. Billings. Cambridge University Press.

Christensen, N.L. 1992. Variable fire regimes on complex landscapes: Ecological consequences, policy implications, and management strategies. Pp. ix–xiii in *Fire in the Environment*. U.S. Department of Agriculture's Forest Service General Technical Report SE-69. Edited by Waldrop, T.

Christensen, N.L. 1981. Fire regimes in southeastern ecosystems. Pp. 112–136 in *Fire Regimes and Ecosystem Properties*. U.S. Department of Agriculture's Forest Service General

Technical Report WO-26. 594 pages. Edited by Mooney, H.A., T.M. Bonnicksen, N.L. Christensen, J.E. Lotan, and W.A. Reiners.

Crowley, A.E. 1996. *This Land, This South: An Environmental History*. University of Kentucky Press: Lexington, KY.

Dufrêne, M., and P. Legendre. 1997. Species assemblages and indicator species: The need for a flexible assymetrical approach. *Ecological Mongographs 67*:345–366.

Early, L.S. 2004. *Looking for Longleaf*. University of North Carolina Press: Chapel Hill, NC.

Kruskal, J.B., and M. Wish. 1978. *Multidimensional Scaling*. Sage Publications: Beverly Hills, CA.

McCune, B., and J.B. Grace. 2002. *Analysis of Ecological Communities*. MjM Software Design: Gleneden Beach.

Mitchell, S., K. Palmquist, S. Cohen, and N.L. Christensen. 2015. Patterns of vegetation composition and diversity in pine-dominated ecosystems of the Outer Coastal Plain of North Carolina: Implications for ecosystem restoration. *Forest Ecology and Management 356*:64–73.

Nowacki, G.J., and M.D. Abrams. 2008. The demise of fire and the "mesophication" of forests in the eastern United States. *Bioscience 58*:124–138.

Peet, R.K., T.R. Wentworth, and P.S. White. 1998. A flexible, multipurpose method for recording vegetation composition and structure. *Castanea 63*:262–274.

Provencher L., A.R. Litt, and D.R. Gordon. 2003. Predictors of species richness in northwest Florida longleaf pine sandhills. *Conservation Bioliology 17*:1660–1671.

Provencher, L., N.M. Gobris, L.A. Brennan, D.R. Gordon, and J.L. Hardesty. 2002. Breeding bird response to midstory hardwood reduction in Florida sandhill longleaf pine forests. *Journal of Wildlife Manage*ment *66*:641–661.

RTI International. 2017. *Final DCERP2 Report*. Prepared for the Strategic Environmental Research and Development Program (SERDP), Arlington, VA. RTI International, Research Triangle Park, NC.

RTI International. 2013. *DCERP1 Final Research Report*. Strategic Environmental Research and Development Program (SERDP) Research Project RC-1413. RTI International, Research Triangle Park, NC.

USFWS (U.S. Fish and Wildlife Service). 2003. *Red-Cockaded Woodpecker (Picoides borealis) Recovery Plan*. Second Revision. U.S. Fish and Wildlife Service, Atlanta, GA.

Venables, W.N. and D.M. Smith. 2011. *An Introduction to R: Version 2.13.2*. Available at http://cran.r-project.org/doc/manuals/R-intro.pdf

Walker, J., and R.K. Peet. 1983. Composition and species diversity of pine-wire grass savannas of the Green Swamp, North Carolina. *Vegetatio 55*:163–179.

Walters, J.R. 2013. Effects of Habitat management for red-cockaded woodpeckers on bird communities. Chapter 14 in SERDP project RC1413 final report.

Appendix 17-A
Supporting Data

Table 17A-1. List of Plant Species Encountered in Eight Treatment Blocks (Note: Species Codes refer to Acronyms Used in the Field Notes and During Various Computer Analyses)

	Species Name	Species Code
1.	*Andropogon ternarius, A. elliottii, Schizachyrium scoparium, A. virginicus*	ANDCOM
2.	*Acer rubrum*	ACERUB
3.	*Agalinis fasciculata*	AGAFAS
4.	*Agalinis setacea*	AGASET
5.	*Aletris farinosa*	ALEFAR
6.	*Amelanchier canadensis*	AMECAN
7.	*Amorpha herbacea*	AMOHER
8.	*Andropogon capillipes*	ANDCAP
9.	*Andropogon glaucopsis*	ANDGLA
10.	*Andropogon glomeratus var. glomeratus*	ANDGLO
11.	*Andropogon glomeratus var. hirsutior*	ANDGLOH
12.	*Andropogon mohrii*	ANDMOH
13.	*Antennaria plantaginifolia*	ANTPLA
14.	*Aristida stricta*	ARISTR
15.	*Aristida virgata*	ARIVIR
16.	*Aronia arbutifolia*	AROARB
17.	*Aronia melanocarpa*	AROMEL
18.	*Arundinaria tecta*	ARUTEC
19.	*Asclepias*	ASCSPP
20.	*Asclepias amplexicaulis*	ASCAMP
21.	*Asclepias humistrata*	ASCHUM
22.	*Asclepias pedicellata*	ASCPED
23.	*Asteraceae*	ASTSPP
24.	*Baccharis halimifolia*	BACHAL
25.	*Bacopa*	BACOPA
26.	*Baptisia tinctoria*	BAPTIN
27.	*Bigelowia nudata var. nudata*	BIGNUD
28.	*Callicarpa americana*	CALAME
29.	*Carex*	CARSPP
30.	*Carex reniformis*	CARREN
31.	*Carex striata var. brevis*	CARSTR
32.	*Carphephorus paniculatus*	CARSPP
33.	*Carphephorus paniculatus + odor*	CARTOM
34.	*Carphephorus tomentosus*	CAROPP

	Species Name	Species Code
35.	*Carya glabra*	CARGLA
36.	*Carya pallida*	CARPAL
37.	*Centella erecta*	CENERE
38.	*Cercis canadensis*	CERCAN
39.	*Chamaecrista [nictitans + fasciculata]*	CHANPF
40.	*Chamaecyparis thyoides*	CHATHY
41.	*Chasmanthium*	CHAMAN
42.	*Chasmanthium laxum*	CHALAX
43.	*Chrysopsis gossypina*	CHRGOS
44.	*Chrysopsis mariana*	CHRMAR
45.	*Cirsium*	CIRSIU
46.	*Cirsium horridulum*	CIRHOR
47.	*Cirsium lecontei*	CIRLEC
48.	*Cirsium repandum*	CIRREP
49.	*Cirsium virginianum*	CIRVIR
50.	*Cirsium vulgare*	CIRVUL
51.	*Cleistes [bifaria + divaricata]*	CLEBPD
52.	*Clethra alnifolia*	CLEALN
53.	*Cnidoscolus stimulosus*	CNISTI
54.	*Comptonia*	COMPTON
55.	*Coreopsis falcata*	CORFAL
56.	*Coreopsis linifolia*	CORLIN
57.	*Coreopsis Unknown*	CORUK
58.	*Coreopsis verticillata*	CORVER
59.	*Crataegus aprica*	CRAAPR
60.	*Crocanthemum carolinianum*	CROCAR
61.	*Crotalaria purshii*	CROPUR
62.	*Ctenium aromaticum*	CTEARO
63.	*Cuscuta*	CUSCUT
64.	*Cyperus retrorsus*	CYPRET
65.	*Cyrilla racemiflora*	CYRRAC
66.	*Desmodium*	DESSPP
67.	*Desmodium ciliare*	DESCIL
68.	*Desmodium glabellum*	DESGLA
69.	*Desmodium lineatum*	DESLIN
70.	*Desmodium marilandicum*	DESMAR
71.	*Desmodium obtusum*	DESOBT
72.	*Desmodium paniculatum*	DESPAN
73.	*Desmodium perplexum*	DESPER

	Species Name	Species Code
74.	*Desmodium tenuifolium*	DESTEN
75.	*Dichanthelium*	DICSPP
76.	*Dichanthelium [longiligulatum + ensifolium]*	DICLPE
77.	*Dichanthelium strigosum*	DICSLS
78.	*Dichanthelium aciculare*	DICACI
79.	*Dichanthelium angustifolium*	DICANG
80.	*Dichanthelium arenicoloides*	DICARE
81.	*Dichanthelium chamaelonche ssp. chamaelonche*	DICCHA
82.	*Dichanthelium commutatum*	DICCOM
83.	*Dichanthelium commutatum var. ashei*	DICCOM
84.	*Dichanthelium consanguineum*	DICCON
85.	*Dichanthelium dichotomum*	DICDIC
86.	*Dichanthelium dichotomum var. dichotomum*	DICDID
87.	*Dichanthelium ensifolium*	DICENS
88.	*Dichanthelium mattamuskeetense*	DICMAT
89.	*Dichanthelium ovale*	DICOVA
90.	*Dichanthelium ovale var. addisonii*	DICOVA
91.	*Dichanthelium ovale var. ovale*	DICOPO
92.	*Dichanthelium portoricense*	DICPOR
93.	*Dichanthelium portoricense ssp. Patulum*	DICPSP
94.	*Dichanthelium portoricense ssp. Portoricense*	DICPSO
95.	*Dichanthelium portoricense X*	DICPSX
96.	*Dichanthelium scoparium*	DICSCO
97.	*Dichanthelium species 2*	DICSP2
98.	*Dichanthelium sphaerocarpon*	DICSPH
99.	*Dichanthelium strigosum*	DICSTR
100.	*Dichanthelium strigosum var. glabrescens*	DICSPG
101.	*Dichanthelium strigosum var. leucoblepharis*	DICSPL
102.	*Dichanthelium strigosum var. strigosum*	DICSPS
103.	*Dichanthelium tenue*	DICTEN
104.	*Dichanthelium villosissimum var. villosissimum*	DICVIL
105.	*Diodia virginiana*	DIOVIR
106.	*Dionaea*	DIONAE
107.	*Dionaea muscipula*	DIOMUS
108.	*Dioscorea*	DIOSCO
109.	*Diospyros virginiana*	DIOVIR
110.	*Drosera [brevifolia + capillaris]*	DROBPC
111.	*Drosera brevifolia*	DROBRE
112.	*Elephantopus nudatus*	ELEPHA

	Species Name	Species Code
113.	*Eragrostis refracta*	ERAREF
114.	*Eragrostis spectabilis*	ERASPE
115.	*Erigeron strigosus var. strigosus*	ERISTR
116.	*Erigeron vernus*	ERIVER
117.	*Eubotrys racemosa*	EUBRAC
118.	*Eupatorium*	EUPSPP
119.	*Eupatorium [mohrii + recurvans]*	EUPMPR
120.	*Eupatorium album*	EUPALB
121.	*Eupatorium capillifolium*	EUPCAP
122.	*Eupatorium hyssopifolium*	EUPHYS
123.	*Eupatorium leucolepis*	EUPLEU
124.	*Eupatorium linearifolium*	EUPLIN
125.	*Eupatorium mohrii*	EUPMOH
126.	*Eupatorium pilosum*	EUPPIL
127.	*Eupatorium rotundifolium*	EUPROT
128.	*Euphorbia curtisii*	EUPCUR
129.	*Euphorbia ipecacuanhae*	EUPIPE
130.	*Eurybia compacta*	EURCOM
131.	*Eurybia paludosa*	EURPAL
132.	*Euthamia caroliniana*	EUTCAR
133.	*Fimbristylis annua*	FIMANN
134.	*Galactia [regularis + volubilis var. volubilis]*	GALRVV
135.	*Galactia erecta*	GALERE
136.	*Galactia regularis*	GALREG
137.	*Galactia volubilis var. volubilis*	GALVPV
138.	*Gaylussacia dumosa*	GAYDUM
139.	*Gaylussacia frondosa*	GAYFR
140.	*Gaylussacia tomentosa*	GAYTOM
141.	*Gelsemium sempervirens*	GELSEM
142.	*Gentiana autumnalis*	GENAUT
143.	*Gleditsia triacanthos*	GLETRI
144.	*Gnaphalium*	GNAPHA
145.	*Gordonia lasianthus*	GORLAS
146.	*Gymnopogon brevifolius*	GYMBRE
147.	*Helianthus angustifolius*	HELANG
148.	*Helianthus atrorubens*	HELATR
149.	*Helianthus heterophyllus*	HELHET
150.	*Hexastylis*	HEXAST
151.	*Hieracium gronovii*	HIEGRO

	Species Name	Species Code
152.	*Hieracium marianum*	HIEMAR
153.	*Hydrocotyle bonariensis*	HYDBON
154.	*Hypericum cistifolium*	HYPCIS
155.	*Hypericum crux-andreae*	HYPCRU
156.	*Hypericum hypericoides*	HYPHYP
157.	*Hypericum setosum*	HYPSET
158.	*Hypericum tenuifolium*	HYPTEN
159.	*Hypoxis hirsuta*	HYPHIR
160.	*Hypoxis juncea*	HYPJUN
161.	*Ilex coriacea*	ILECOR
162.	*Ilex glabra*	ILEGLA
163.	*Ilex opaca var. opaca*	ILEOPA
164.	*Ilex vomitoria*	ILEVOM
165.	*Ionactis linariifolia*	IONLIN
166.	*Ipomoea*	IPOMOE
167.	*Iris verna var. verna*	IRIVER
168.	*Juncus*	JUNSPP
169.	*Juncus acuminatus*	JUNACU
170.	*Juncus biflorus*	JUNBIF
171.	*Juncus canadensis*	JUNCAN
172.	*Juncus dichotomus*	JUNDIC
173.	*Juncus scirpoides*	JUNSCI
174.	*Kalmia carolina*	KALCAR
175.	*Lachnocaulon anceps*	LACANC
176.	*Lactuca canadensis*	LACCAN
177.	*Lechea [pulchella var. ramosissima + torreyi var. congesta]*	LECPRT
178.	*Lechea minor*	LECMIN
179.	*Lechea pulchella var. ramosissima*	LECPPR
180.	*Lechea tenuifolia*	LECTEN
181.	*Lespedeza angustifolia*	LESANG
182.	*Lespedeza capitata*	LESCAP
183.	*Lespedeza hirta*	LESHIR
184.	*Lespedeza hirta var. curtissii*	LESHPC
185.	*Lespedeza hirta var. hirta*	LESHPH
186.	*Lespedeza virginica*	LESVIR
187.	*Leucothoe axillaris*	LECAXI
188.	*Liatris [pilosa + virgata]*	LIAPPV
189.	*Liatris spicata*	LIASPI
190.	*Liatris spicata var. resinosa*	LIASPI

	Species Name	Species Code
191.	*Linum floridanum*	LINFLO
192.	*Liquidambar styraciflua*	LIQSTY
193.	*Liriodendron tulipifera*	LIRTUL
194.	*Lobelia nuttallii*	LOBNUT
195.	*Ludwigia virgata*	LUDVIR
196.	*Lycopodiella alopecuroides*	LYCALO
197.	*Lycopodium*	LYCOPO
198.	*Lyonia ligustrina*	LYOLIG
199.	*Lyonia ligustrina var. foliosiflora*	LYOLIG
200.	*Lyonia lucida*	LYOLUC
201.	*Lyonia mariana*	LYOMAR
202.	*Lysimachia loomisii*	LYSLOO
203.	*Magnolia virginiana*	MAGVIR
204.	*Marshallia graminifolia*	MARGRA
205.	*Mikania scandens*	MIKSCA
206.	*Mitchella repens*	MITREP
207.	*Morella caroliniensis*	MORCAR
208.	*Morella cerifera*	MORCER
209.	*Morella pumila*	MORPUM
210.	*Muhlenbergia expansa*	MUHEXP
211.	*Nyssa sylvatica*	NYSSYL
212.	*Orbexilum pedunculatum var. psoralioides*	ORBPED
213.	*Osmunda cinnamomea var. cinnamomea*	OSMCIN
214.	*Osmunda regalis*	OSMREG
215.	*Osmunda regalis var. spectabilis*	OSMRPS
216.	*Oxypolis denticulata*	OXYDEN
217.	*Panicum amarum*	PANAMA
218.	*Panicum anceps*	PANANC
219.	*Panicum anceps var. rhizomatum*	PANAPR
220.	*Panicum virgatum*	PANVIR
221.	*Parthenium*	PARSPP
222.	*Parthenocissus quinquefolia*	PARQUI
223.	*Paspalum praecox var. praecox*	PASPRA
224.	*Paspalum setaceum var. stramineum*	PASSET
225.	*Persea palustris*	PERPAL
226.	*Picea*	PICSPP
227.	*Pinus palustris*	PINPAL
228.	*Pinus serotina*	PINSER
229.	*Pinus taeda*	PINTAE

	Species Name	Species Code
230.	*Pityopsis graminifolia*	PITGRA
231.	*Platanthera*	PLATAN
232.	*Platanthera ciliaris*	PLACIL
233.	*Pleea tenuifolia*	PLETEN
234.	*Pluchea baccharis*	PLUBAC
235.	*Polygala [brevifolia + hookeri + cruciata]*	POLBHC
236.	*Polygala brevifolia*	POLBRE
237.	*Polygala cruciata*	POLCRU
238.	*Polygala incarnata*	POLINC
239.	*Polygala lutea*	POLLUT
240.	*Potentilla*	POTSPP
241.	*Prenanthes*	PRESPP
242.	*Prunus serotina*	PRUSER
243.	*Pteridium aquilinum var. pseudocaudatum*	PTEAQU
244.	*Pterocaulon pycnostachyum*	PTEPYC
245.	*Pycnanthemum flexuosum*	PYCFLE
246.	*Pyxidanthera barbulata*	PYXBAR
247.	*Quercus*	QUESPP
248.	*Quercus falcata*	QUEFAL
249.	*Quercus geminata*	QUEGEM
250.	*Quercus hemisphaerica*	QUEHEM
251.	*Quercus incana*	QUEINC
252.	*Quercus incana X marilandica*	QUEIXM
253.	*Quercus laevis*	QUELAE
254.	*Quercus laevis X marilandica*	QUELXM
255.	*Quercus margaretta*	QUEMAR
256.	*Quercus marilandica*	QUEMVM
257.	*Quercus marilandica var. marilandica*	QUEMPM
258.	*Quercus michauxii*	QUEMIC
259.	*Quercus nigra*	QUENIG
260.	*Quercus stellata*	QUESTE
261.	*Quercus virginiana*	QUEVIR
262.	*Quercus xashei*	QUEXASH
263.	*Quercus xcaduca*	QUEXCA
264.	*Quercus xincomita*	QUEXIN
265.	*Rhexia [nashii + mariana var. mariana]*	RHENMM
266.	*Rhexia alifanus*	RHEALI
267.	*Rhexia lutea*	RHELUT
268.	*Rhexia mariana*	RHEMAR

	Species Name	Species Code
269.	*Rhexia nashii*	RHENAS
270.	*Rhexia petiolata*	RHEPET
271.	*Rhizophora*	RHIZOP
272.	*Rhododendron atlanticum*	RHOATL
273.	*Rhus copallinum*	RHUCOP
274.	*Rhynchosia tomentosa*	RHYTOM
275.	*Rhynchospora*	RHYSPP
276.	*Rhynchospora baldwinii*	RHYBAL
277.	*Rhynchospora divergens*	RHYDIV
278.	*Rhynchospora fascicularis var. distans*	RHYFVD
279.	*Rhynchospora fascicularis var. fascicularis*	RHYFVF
280.	*Rhynchospora grayi*	RHYGRA
281.	*Rhynchospora harveyi*	RHYHAR
282.	*Rhynchospora plumosa*	RHYPLU
283.	*Robinia nana*	ROBSPP
284.	*Rubus*	RUBSPP
285.	*Sabatia difformis*	SABDIF
286.	*Saccharum*	SACCHA
287.	*Salix caroliniana*	SALCAR
288.	*Sarracenia flava*	SARFLA
289.	*Sarracenia rubra x flava*	SARRXF
290.	*Sassafras albidum*	SASALB
291.	*Schizachyrium scoparium*	SCHSCO
292.	*Scleria [ciliata var. ciliata + elliottii]*	SCLCCE
293.	*Scleria [ciliata var. glabra + pauciflora var. pauciflora]*	SCLCGP
294.	*Scleria [nitida + triglomerata]*	SCLNPT
295.	*Scleria ciliata*	SCLCIL
296.	*Scleria ciliata var. ciliata*	SCLCVC
297.	*Scleria ciliata var. glabra*	SCLCVG
298.	*Scleria nitida*	SCLNIT
299.	*Scleria oligantha*	SCLOLI
300.	*Scleria pauciflora var. pauciflora*	SCLPVP
301.	*Scleria triglomerata*	SCLTRI
302.	*Sericocarpus asteroides*	SERAST
303.	*Sericocarpus linifolius*	SERLIN
304.	*Sericocarpus tortifolius*	SERTOR
305.	*Seymeria cassioides*	SEYCAS
306.	*Silphium compositum*	SILCOM
307.	*Sisyrinchium capillare*	SISCAP

	Species Name	Species Code
308.	*Smilax bona-nox*	SMIBON
309.	*Smilax glauca*	SMIGLA
310.	*Smilax laurifolia*	SMILAU
311.	*Smilax rotundifolia*	SMIROT
312.	*Solidago arguta*	SOLARU
313.	*Solidago odora*	SOLODO
314.	*Solidago odora var. odora*	SOLOVO
315.	*Solidago pulchra*	SOLPUL
316.	*Solidago stricta*	SOLSTR
317.	*Sophronanthe pilosa*	SOPPIL
318.	*Sorbus americana*	SORAME
319.	*Spiranthes*	SPISPP
320.	*Spiranthes eatonii*	SPIEAT
321.	*Spiranthes lacera var. gracilis*	SPILVG
322.	*Spiranthes praecox*	SPIPRA
323.	*Sporobolus pinetorum*	SPOPIN
324.	*Stylosanthes biflora*	STYBIF
325.	*Symphyotrichum concolor*	SYMCON
326.	*Symphyotrichum concolor var. concolor*	SYMCVC
327.	*Symphyotrichum dumosum var. dumosum*	SYMDVD
328.	*Symphyotrichum tenuifolium*	SYMTEN
329.	*Symphyotrichum walteri*	SYMWAL
330.	*Symplocos tinctoria*	SYMTIN
331.	*Tephrosia florida*	TEPFLO
332.	*Tephrosia hispidula*	TEPHIS
333.	*Toxicodendron pubescens*	TOXPUB
334.	*Toxicodendron radicans*	TOXRAD
335.	*Toxicodendron radicans var. radicans*	TOXRVR
336.	*Tragia urens*	TRAURE
337.	*Uvularia puberula*	UVUPUB
338.	*Vaccinium arboreum*	VACARB
339.	*Vaccinium corymbosum*	VACCOR
340.	*Vaccinium crassifolium*	VACCRA
341.	*Vaccinium formosum*	VACFOR
342.	*Vaccinium fuscatum*	VACFUS
343.	*Vaccinium stamineum*	VASTA
344.	*Vaccinium tenellum*	VACTEN
345.	*Viola primulifolia*	VIOPRI
346.	*Viola septemloba*	VIOSEP

	Species Name	Species Code
347.	*Vitis rotundifolia*	VITROT
348.	*Vitis rotundifolia var. rotundifolia*	VITRVR
349.	*Woodwardia areolata*	WOOARE
350.	*Woodwardia virginica*	WOOVIR
351.	*Xyris ambigua*	XYRAMB
352.	*Xyris caroliniana*	XYRCAR
353.	*Zigadenus glaberrimus*	ZIGGLA
354.	*Zenobia pulverulenta*	ZENPUL

Table 17A-2. List of Bird Species Encountered in Eight Treatment Blocks (Note: Species Codes refer to Acronyms Used in the Field Notes and During Various Computer Analyses)

Species Code	Common Name
ACFL	Acadian flycatcher
AMCR	American crow
AMGO	American goldfinch
AMRO	American robin
BACS	Bachman's sparrow
BAEA	Bald eagle
BARS	Barn swallow
BAWW	Black and white warbler
BDOW	Barred owl
BGGN	Blue-gray gnatcatcher
BHCO	Brown-headed cowbird
BHNU	Brown-headed nuthatch
BLGR	Blue grosbeak
BLJA	Blue jay
BRTH	Brown thrasher
BTGR	Boat-tailed grackle
BWHA	Broad-winged hawk
CACH	Carolina chickadee
CAGO	Canada goose
CARW	Carolina wren
CHSP	Chipping sparrow
COGR	Common grackle
CONI	Common nighthawk
COYE	Common yellowthroat
DOWO	Downy woodpecker
EABL	Eastern bluebird
EAKI	Eastern kingbird
EAME	Eastern meadowlark
EATO	Eastern towhee
EAWP	Eastern wood-pewee
ECDO	Eurasian collared-dove
FICR	Fish crow
FISP	Field sparrow
GBHE	Great blue heron
GCFL	Great crested flycatcher
GHOW	Great horned owl
GRCA	Gray catbird

Species Code	Common Name
HAWO	Hairy woodpecker
HOFI	House finch
HOWA	Hooded warbler
HOWR	House wren
INBU	Indigo bunting
KEWA	Kentucky warbler
KILL	Killdeer
LAGU	Laughing gull
MIKI	Mississippi kite
MODO	Mourning dove
NOBO	Northern bobwhite
NOCA	Northern cardinal
NOFL	Northern flicker
NOMO	Northern Mockingbird
NOPA	Northern parula
NRWS	Northern rough-winged swallow
OROR	Connecticut warbler
OSPR	Osprey
OVEN	ovenbird
PIWA	Pink-headed warbler
PIWO	Pileated woodpecker
PRAW	Prairie warbler
PROW	Prothonotary warbler
RBWO	Red-bellied woodpecker
* Not on list	Ruby-crowned kinglet
RCWO	Red-cockaded woodpecker
REVI	Red-eyed vireo
RHWO	Red-headed woodpecker
RSHA	Red-shouldered hawk
RTHA	Red-tailed hawk
RTHU	Ruby-throated hummingbird
RWBL	Red-winged blackbird
SCTA	Scarlet tanager
SOSP	Song sparrow
SUTA	Summer tanager
SWWA	Swainson's warbler
TUTI	Tufted titmouse
TUVU	Turkey vulture
WBNU	White-breasted nuthatch

Species Code	Common Name
WEVI	White-eyed vireo
WEWA	Worm-eating warbler
WITU	Wild turkey
WOTH	Wood Thrush
WPWI	Eastern Whip-poor-will
WTSP	White trailed sparrow
YBCH	Yellow-breasted chat
YBCU	Yellow-billed cuckoo
YTVI	Yellow-throated vireo
YTWA	Yellow-throated warbler

Table 17A-3. For 85 Marine Corps Base Camp Lejeune (MCBCL) pine-dominated monitoring plots, averaged values for species richness (number per 0.1 ha), stems less than 15 cm (number per ha), basal area (m^2/ha), cation exchange capacity (CEC; mEq/100 g soil), bulk density (BD, in g/cm^3), pH, percent soil organic matter (SOM%), and orthophosphate (PO_4−P), calcium (Ca), magnesium (Mg), potassium (K), and aluminum (Al) in each of the experimental treatment plots.

Extractable element concentrations are expressed in µg/g. "N/A" indicates missing data.

Plot Name	Species Richness	Stems <15 cm	Basal Area	CEC	BD	pH	SOM %	P	Ca	Mg	K	Al
1. 6x-01-0053	48	50	10.69	3.78	1.33	4.15	2.15	2.25	140.00	31.00	18.50	110.50
2. 6x-01-0054	46	20	30.34	5.01	1.16	4.28	3.28	1.00	221.75	32.50	24.75	119.75
3. 6x-01-0058	75	160	42.28	2.91	1.40	4.00	1.01	1.00	98.25	18.00	9.00	292.50
4. 6x-02-0054	45	120	56.81	5.22	1.16	4.40	3.97	2.25	228.00	42.25	36.00	186.00
5. 6x-02-0058	68	90	51.94	5.11	1.16	4.18	3.75	3.25	183.50	33.50	54.75	306.50
6. 6x-02-0059	91	50	28.03	3.66	1.24	4.18	2.90	1.50	126.00	23.00	20.75	391.25
7. 6x-03-0051	34	190	72.82	4.85	1.18	4.13	3.67	1.25	183.75	30.75	22.00	101.00
8. 6x-03-0053	118	160	33.05	2.68	1.26	4.18	2.43	1.50	100.50	16.00	20.00	798.00
9. 6x-04-0053	49	130	19.56	4.27	1.30	3.95	3.09	1.00	109.50	40.00	25.75	117.75
10. 6x-04-0054	32	130	11.59	4.23	1.14	4.80	4.46	2.50	254.50	34.00	26.75	89.25
11. 6x-04-0056	57	20	10.59	5.84	1.26	3.80	3.50	1.25	162.50	43.25	22.00	145.50
12. 6x-04-0057	49	130	45.43	2.89	1.36	4.10	1.90	1.00	101.25	20.75	14.75	52.50
13. 6x-04-0058	61	280	42.12	2.33	1.34	4.20	1.75	1.00	88.75	15.00	11.75	578.75
14. 6x-04-0059	68	110	27.10	6.06	1.26	4.30	3.16	2.75	286.75	31.00	31.75	172.75
15. 6x-05-0054	55	250	30.15	3.85	1.39	4.00	2.84	1.00	105.25	35.00	20.75	122.00
16. 6x-05-0055	72	140	26.24	2.55	1.40	4.38	1.45	1.25	121.75	19.50	16.00	401.50
17. 6x-05-0058	32	30	37.99	3.21	1.36	4.08	1.73	4.00	128.50	16.25	13.75	80.50
18. 6x-05-0059	84	190	41.45	3.01	1.14	3.88	4.01	2.75	77.25	21.00	20.25	713.00
19. 6x-05-0060	56	260	41.58	3.20	1.25	4.08	2.36	5.25	111.50	21.50	18.25	233.25

Plot Name	Species Richness	Stems <15 cm	Basal Area	CEC	BD	pH	SOM %	P	Ca	Mg	K	Al
20. 6x-08-0001	91	110	110.88	8.30	0.95	3.85	10.64	2.50	267.50	50.00	37.75	277.75
21. 6x-08-0002	92	50	18.95	9.50	0.96	3.83	10.28	1.50	276.25	65.75	36.50	424.75
22. 6x-08-0003	57	30	20.81	5.40	1.21	4.20	3.52	1.25	218.50	28.25	26.00	149.25
23. 6x-08-0004	60	70	6.38	11.12	1.04	3.73	10.51	1.25	302.50	83.50	56.25	149.75
24. 6x-08-0005	46	160	77.93	5.86	1.11	4.10	3.54	4.25	230.75	45.50	23.50	135.50
25. CR1	37	760	8.11	3.29	1.23	4.68	2.24	6.00	170.00	39.75	13.50	87.00
26. CT1	23	90	9.95	2.07	1.21	4.85	2.10	5.25	116.50	23.75	14.00	76.00
27. CR2	20	250	13.99	N/A	N/A	N/A	N/A	N/A	N/A	N/A	N/A	N/A
28. CT4	38	490	11.19	3.06	1.04	4.60	4.49	4.25	160.25	28.00	12.50	102.25
29. DC2	28	0	12.52	4.17	0.90	4.33	18.35	4.00	159.25	35.75	20.00	89.00
30. FGE-C	10	2,880	26.28	9.57	0.22	3.78	67.83	3.25	216.75	96.00	46.50	231.25
31. FGW-C	7	2,430	25.60	9.88	0.39	3.78	51.44	3.00	251.00	84.75	46.75	208.50
32. FGE-G	18	2,060	19.69	6.89	0.54	3.98	34.27	3.00	243.25	52.75	24.00	198.50
33. FGW-G	17	2,060	19.69	7.36	0.41	4.00	37.39	3.75	235.75	60.25	31.25	400.75
34. FGE-D	18	2,060	19.69	7.19	0.53	3.78	41.19	6.25	196.75	47.50	46.50	574.50
35. FGW-D	30	2,060	19.69	9.47	0.81	4.08	11.91	4.25	351.25	63.25	37.00	118.25
36. GT1	48	280	12.72	3.83	1.09	4.73	2.75	9.00	233.50	36.25	22.50	131.75
37. GT2	38	50	20.28	3.04	1.12	4.63	2.21	7.50	149.75	31.25	21.00	126.25
38. GT4	39	590	8.38	4.46	1.01	4.80	3.74	6.50	272.75	36.75	19.25	167.00
39. GT5	53	110	13.69	7.13	0.98	4.45	7.19	4.25	347.75	59.75	20.50	220.00
40. GT6	30	40	10.96	4.56	1.02	4.50	8.17	4.25	180.50	44.00	28.00	230.25
41. HAC	24	1,580	18.11	6.21	0.69	4.10	13.83	5.50	186.25	56.00	34.50	527.00
42. HAG	35	360	8.48	6.57	0.93	4.45	6.07	4.25	301.25	39.00	25.75	658.50
43. HAD	41	360	8.48	8.60	0.76	4.18	13.37	6.75	390.75	54.75	30.00	640.50
44. IEN-C	14	5,470	7.66	6.68	0.55	3.88	30.33	10.25	172.50	48.25	41.00	868.25
45. IES-C	12	100	19.78	7.93	0.30	3.73	68.12	3.75	93.75	103.00	77.25	167.75
46. IEN-G	21	0	17.66	11.29	0.45	3.85	43.43	6.50	336.75	80.75	48.50	496.00
47. IES-G	13	350	13.59	10.74	0.50	3.93	33.82	5.00	346.75	69.75	43.25	418.75
48. IEN-D	23	1,880	10.23	7.42	0.59	3.85	33.67	6.25	170.50	71.75	41.00	786.00
49. IES-D	15	590	18.51	7.65	0.44	3.85	53.26	6.00	193.25	72.00	29.50	379.25
50. MFC	24	4,940	21.36	5.71	0.74	3.93	14.38	12.25	172.25	42.00	31.75	866.50
51. MFG	21	240	16.50	5.54	0.39	3.90	30.22	10.25	170.00	40.50	30.25	841.75
52. MFD	32	60	23.64	6.98	0.58	3.95	25.49	9.00	193.75	59.25	43.00	626.75
53. NE2	43	230	10.93	4.52	1.07	4.23	3.29	4.75	177.75	33.25	20.25	159.25
54. NE4	41	160	11.74	3.57	0.93	4.25	5.52	4.50	129.75	35.25	20.50	351.25
55. PN17	25	340	3.17	3.42	1.22	4.43	1.41	2.50	170.25	24.50	8.25	70.75
56. PN17	14	800	1.82	4.11	1.34	4.68	1.03	2.50	265.75	22.25	11.00	62.25
57. PN18	32	1,080	4.35	3.86	1.37	4.55	0.91	5.00	226.75	21.75	11.25	60.25
58. PN23	28	870	0.07	8.16	0.98	4.85	4.96	148.50	741.00	48.25	24.00	473.25

Plot Name	Species Richness	Stems <15 cm	Basal Area	CEC	BD	pH	SOM %	P	Ca	Mg	K	Al
59. PN33	30	4,330	39.71	5.75	0.98	4.18	8.98	8.50	229.00	42.00	17.75	504.25
60. PN34	29	270	4.33	4.37	0.97	4.43	5.95	6.75	186.75	40.00	27.75	498.50
61. PN39	30	1,540	8.96	4.20	1.00	4.68	5.10	5.75	215.75	49.00	29.25	352.25
62. PN47	37	630	0.42	4.29	1.13	4.65	2.86	5.25	207.00	57.75	72.25	501.25
63. PN51	33	1,290	8.34	N/A	N/A	N/A	N/A	N/A	N/A	N/A	N/A	N/A
64. PN60	30	100	10.59	4.67	1.00	4.10	5.15	6.00	153.75	41.00	24.00	391.00
65. PN62	39	4,020	7.18	7.59	0.91	4.30	7.91	6.00	309.00	50.25	25.25	579.75
66. PN65	38	280	12.70	10.64	0.82	4.08	9.56	8.75	450.50	57.50	16.75	322.00
67. PN66	19	1,390	1.19	5.17	0.92	4.28	5.26	9.25	231.50	39.25	23.00	220.00
68. PN69	36	290	15.32	3.26	1.11	4.40	4.36	4.50	130.50	33.50	18.25	206.50
69. RBE-C	15	3,660	23.89	8.09	0.80	4.45	16.05	7.00	401.00	56.75	37.75	692.00
70. RBW-C	13	3,340	26.08	4.97	1.01	4.43	5.69	7.50	229.25	47.00	36.00	852.00
71. RBE-G	33	110	13.31	9.64	0.85	4.03	7.95	10.50	369.50	64.50	33.00	545.00
72. RBW-G	32	30	19.07	8.03	0.90	4.23	6.52	7.25	359.00	56.75	30.50	393.75
73. RBE-D	29	910	18.37	4.54	1.05	4.60	5.18	6.50	242.00	40.25	28.50	382.75
74. RBW-D	40	2,920	22.05	10.04	0.66	4.23	17.92	8.25	458.75	83.50	66.50	361.50
75. SC1	29	1,010	9.20	4.82	1.08	4.15	5.96	5.50	171.75	43.00	17.00	232.25
76. SC2	24	1,120	12.86	3.95	1.21	4.30	2.51	3.75	160.75	31.50	16.75	131.00
77. VL2	40	0	13.54	5.26	0.85	4.05	8.05	3.50	176.50	44.25	20.25	254.75
78. VL3	44	50	12.85	4.77	0.90	3.98	9.39	4.75	120.00	53.00	17.00	256.50
79. VL4	43	880	12.64	1.63	0.96	4.10	5.34	3.38	9.13	30.25	12.00	462.75
80. VL5	33	3,530	12.89	3.92	0.86	4.08	6.91	5.50	122.50	36.00	27.25	339.25
81. VL6	30	50	8.77	5.38	0.94	4.05	4.91	6.25	174.75	47.25	27.00	137.25
82. POC11	9	N/A	N/A	3.78	0.71	4.95	21.69	3.50	138.00	98.00	23.75	127.75
83. POC12	10	N/A	N/A	4.38	0.44	4.55	41.41	3.50	167.25	74.25	23.25	174.50
84. POC9	14	N/A	N/A	6.70	0.78	4.58	8.01	9.25	410.50	56.00	30.75	604.25
85. POC10	28	N/A		3.79	0.92	4.70	5.12	3.50	175.75	48.50	17.75	170.00

Appendix 17-B
List of Scientific/Technical Publications

Published Papers

Smart, L., J.J. Swenson, N.L. Christensen, and J.O. Sexton. 2012. Three-dimensional characterization of pine forest type and red-cockaded woodpecker habitat by small-footprint, discrete-return lidar. *Forest Ecology and Management 281*:100–110.

K. Baumann, Mitchell S.R., N.L. Christensen, J.J. Schauer, D.R. Blake, J.M. Fort, and E.S. Edgerton. 2013. Effects of mechanical thinning on fuel consumption and smoke emissions from prescribed burning in coastal North Carolina in Wade, D. D. and Fox, R., Proceedings of Fourth Fire Behavior and Fuels Conference: at the crossroads: looking toward the future in a changing environment. Raleigh, NC; St. Petersburg, Russia. International Association of Wildland Fire, Missoula, MN. p. 84-121.

Christensen, N.L. 2014. An historical perspective on forest succession and its relevance to ecosystem restoration and conservation practice in North America. *Forest Ecology and Management 330*:312–322.

Mitchell, S., K. Palmquist, S. Cohen, and N.L. Christensen, Jr. 2015. Patterns of vegetation composition and diversity in pine-dominated ecosystems of the Outer Coastal Plain of North Carolina: Implications for ecosystem restoration. *Forest Ecology and Management 356*:64–73.

Mitchell, S.R. 2015. Carbon dynamics of mixed- and high-severity wildfires: Pyrogenic CO2 emissions, post-fire carbon balance, and succession. In: The Ecological Importance of Mixed-Severity Fires: Nature's Phoenix. Elsevier.

Palmquist, K.A., R.K. Peet, and S.R. Mitchell. 2015. Scale-dependent responses of longleaf pine vegetation to fire frequency and environmental context across two decades. *Journal of Ecology* 103:998-1008.

Papers in Preparation

Mitchell S.R., N.L. Christensen, J.W. Walters, S.A. Cohen, V. Garcia, K. Rose, and K. Palmquist. In preparation. Herbaceous layer plant composition as a determinant of breeding bird communities in Atlantic Coastal Plain pine forests. For *Ecological Applications*.

Mitchell, S.R. and N.L. Christensen. In preparation. Dormant and growing season understory thinning to restore herbaceous plant communities typical of longleaf pine ecosystems. For *Forest Ecology and Management*.

Presentations

Mitchell, S.R., and N.L. Christensen. 2011. Vegetative diversity and composition correlates with avifaunal diversity and composition in pine forests of the Atlantic coastal plain. Presented at the Ecological Society of America conference in Austin, Texas

Mitchell, S.R., and N.L. Christensen. 2012. Soil properties drive differences in taxonomic groups among pine forests of the Atlantic coastal plain. Presented at the Ecological Society of America conference in Portland, Oregon

Appendix 17-C
List of Students

- Lindsey Smart – Master of Environmental Management, Nicholas School of the Environment, Duke University, Durham, NC. Graduated May 2009. *Three-dimensional characterization of pine forest type and red-cockaded woodpecker habitat by small-footprint, discrete return radar*. Master's thesis.
- Rachel Roberts – Master of Environmental Management, Nicholas School of the Environment. Graduated May 2011.
- Courtney Colwell – Master of Environmental Management, Nicholas School of the Environment. Graduated May 2013.
- Kyle Palmquist, Ph.D. Department of Biology, University of North Carolina at Chapel Hill, Chapel Hill, NC. Graduated May 2013. *Species turnover and compositional shifts of the longleaf pine ecosystem after 18 years.* Doctoral Thesis.

Chapter 18

Forest Management, Species Habitat, and Implications for Carbon Flux and Storage

SERDP Project Number: RC-2245

Terrestrial Module

Research Project T-3

Lead Researcher:

Dr. Stephen R. Mitchell, Duke University
E-mail: srm12@duke.edu

Supporting Researcher:

Dr. Norman L. Christensen, Duke University
E-mail: normc@duke.edu

January 2018

Final

This report was prepared under contract to the U.S. Department of Defense (DoD) Strategic Environmental Research and Development Program (SERDP). The publication of this report does not indicate endorsement by DoD, nor should the contents be construed as reflecting the official policy or position of DoD. References herein to any specific commercial product, process, or service by trade name, trademark, manufacturer, or otherwise, do not necessarily constitute or imply its endorsement, recommendation, or favoring by DoD.

Table of Contents

Acronyms 18-v
Abstract 18-1
Objectives of the Research Project 18-3
Background 18-3
Materials and Methods 18-5
The LANDIS-II Model Overview 18-5
LANDIS-II Model Calibration 18-6
Synthetic Landscape Simulations 18-8
Forest Management Scenarios 18-9
Climate Scenarios 18-11
Statistical Comparisons 18-13
Decision Support Tools and Technology Transfer 18-13
Results and Discussion 18-14
Forest Management and Carbon Storage 18-14
Future Climate Effects 18-16
Decision Support Tools and Technology Transfer 18-18
Conclusions and Implications for Future Research and Implementation 18-20
Research Questions 18-20
Findings with Implications for Future Base Management 18-21
Literature Cited 18-22
Appendix 18-A: Supporting Data 18-A-1
Appendix 18-B: List of Scientific/Technical Publications 18-B-1

List of Figures

Figure 18-1. Relationships of LiDAR, MCBCL Geodatabase, and field data used for estimating forest growth rates for use to calibrate the LANDIS-II model. 18-7
Figure 18-2. The range of carbon storage values for loblolly pine and longleaf pine, based on silvicultural yield tables (i.e., not derived from model simulations). 18-8
Figure 18-3. Time series comparison of total ecosystem carbon (C) storage + harvested C stored in timber products from forested landscapes of loblolly versus longleaf pine in our synthetic landscape simulations. 18-14
Figure 18-4. Carbon stored (in g C m^{-2}) across MCBCL's landscape in each management scenario with an MFRI of 3 years. 18-16

Figure 18-5. Changes in above-ground carbon storage for each climate scenario, including the baseline (control) for the No Management (MFRI = 3 years) scenario. 18-17

Figure 18-6. Map of carbon storage (g C m^{-2}) at MCBCL assuming No Management (and no prescribed fire) under the ECHAM5 climate scenario (left) and the MIROC-ESM-CHEM scenario (right). 18-19

List of Tables

Table 18-1. Management Treatments Simulated by Using the LANDIS-II Model and Their Projected impacts 18-9

Table 18-2. Global Climate Models Used for Climate Change Projections 18-12

Table 18-3. Global Climate Models Used for Climate Projections for 2090–2100. 18-13

Table 18-4. Average Carbon Stored (g C m^{-2} ± SD) in the Year 2100 Across MCBCL's Landscape in Each Management and MFRI Scenario for Current Climate Conditions. 18-15

Table 18-5. Total Carbon Stored in the Year 2100 Across the MCBCL Landscape in Each Management and MFRI Scenario for Each of Four Climate Models. Units are in g C m^{-2}. 18-18

Acronyms

°C	degree Celsius
°F	degree Fahrenheit
C	carbon
CC	Climate Change (Module)
cm	centimeter
dbh	diameter at breast height
DCERP	Defense Coastal/Estuarine Research Program
DCERP1	first cycle of DCERP
DCERP2	second cycle of DCERP
DIMS	Data and Information Management System
DoD	U.S. Department of Defense
ECONet	North Carolina Environment and Climate Observing Network
g C m-2	grams of carbon per square meter
GIS	geographic information systems
ha	hectare
iMAP	interactive mapping application
kg C m-2	kilograms of carbon per square meter
LiDAR	light detecting and ranging
m	meter
MACA	Multivariate Adaptive Constructed Analogs
MCBCL	Marine Corps Base Camp Lejeune
METDATA	University of Idaho's Gridded Surface Meteorological Data
MFRI	mean fire return interval
Mg C ha-1	megagrams of carbon per hectare
mm	millimeter
MRPP	Multi-Response Permutation Procedure
NLDAS-2	North American Land Data Assimilation System version 2
NOAA	National Oceanic and Atmospheric Administration
ppt	parts per thousand
PRISM	Parameter-elevation Regressions on Independent Slopes Model
RC	Resource Conservation and Climate Change (a SERDP program area)
RCW	red-cockaded woodpecker
RMSE	root mean squared error
SD	standard deviation
SERAP	Southeast Regional Assessment Project
SERDP	Strategic Environmental Research and Development Program
T	Terrestrial (module)
TSP	Translating Science into Practice

Abstract

Support of the military training mission is the primary goal for management of the pine-dominated forests of Marine Corps Base Camp Lejeune (MCBCL). However, restoring and maintaining biodiversity and endangered species habitat (most notably the red-cockaded woodpecker (RCW, *Picoides borealis*) and timber production are also important goals. In the future, carbon storage might be added to these goals as a strategy to mitigate emissions of greenhouse gases and their impacts on climate.

The primary objective of this research project was to provide MCBCL managers with the information and tools needed to monitor and manage carbon stores while supporting military training goals and restoring and maintaining key elements (e.g., biodiversity, endangered species habitat) of longleaf pine (*Pinus palustris*) and loblolly pine (*Pinus taeda*) ecosystems in the context of potential changes in climate. To accomplish this goal, we used field data from DCERP1 and from MCBCL's Environmental Management Division to calibrate a forest landscape simulation model, LANDIS-II.

We used the LANDIS-II model to compare carbon storage capacity over time in synthetic stands dominated by either loblolly pine or by longleaf pine under simulated harvest frequencies of 25, 40, 60, 80, 100, and 120 years. Carbon storage is highest in the control (no harvest) and is progressively lower when harvesting frequency is increased in synthetic stands. The differences between control and harvested stands were greater for longleaf than for loblolly pine. Longleaf stands store more carbon for all harvest rotations greater than 40 years. These differences are largely a consequence of higher longevity among longleaf as compared with loblolly pine trees. These results from synthetic stands help us understand what occurs in real-world forest stands such as those at MCBCL. The differences in landscape level carbon storage resulting from different longevities of longleaf versus loblolly pine explained many of our findings in the spatially explicit simulations.

We also used the LANDIS-II model to simulate management scenario across the MCBCL landscape out to the year 2100. The six different management scenarios are as follows: control (No Management), application of prescribed fire only (Prescribed Fire Only), 25-year rotation commercial harvest (Commercial Harvest Cycle I), 60-year rotation commercial harvest (Commercial Harvest Cycle II), midstory thinning of loblolly pine with longleaf pine planted in the understory (Longleaf Savanna Restoration I), and clearcutting loblolly pine followed by longleaf pine restoration (Longleaf Savanna Restoration II). We ran each management scenario by using mean fire return intervals (MFRIs) of both 3 years and 6 years and based each scenario on the continuation of current climate conditions (1980–2011) until 2100. Simulations show that management practices that promoted longleaf pine restoration resulted in higher carbon storage compared with all other management scenarios. However, clearcutting loblolly pine and replanting with longleaf (Longleaf Savanna Restoration II) resulted in less stored carbon than understory and midstory thinning of loblolly and replanting with longleaf (Longleaf Savanna Restoration I). Regardless of harvest protocols, application of prescribed fire every 6 years resulted in higher carbon storage than application of prescribed fires every 3 years, although the marginal benefit of the longer MFRI on carbon storage (less than 5% for most management

scenarios) is probably not sufficient to compensate for likely negative impacts on biodiversity and military training uses of the forest land.

To examine the potential impacts of future climate on carbon storage at MCBCL, we used climate projections derived from general circulation models, representing a range of plausible climate futures. Each of these climate scenarios produced lower overall carbon storage by the year 2100 compared with the historic climate data as a baseline scenario; however, the magnitude of the difference varied widely among the various climate models. The lowest levels of carbon storage result from the model that predicts average monthly and annual temperatures to be much higher (9°C) than those forecast by other models. Combined with a significant reduction in mean summer precipitation, this model produced conditions quite different than those that characterized the range of climatic conditions where loblolly and longleaf pine grow today. Climate change of this sort would require very significant changes in forest management practices, goals, and protocols. Given the wide divergence in model climate forecasts and their effects on the change in future carbon storage, these results provide a measure of the range of possible outcomes, but not meaningful predictions.

Keywords: Carbon cycle, carbon sequestration, fire ecology, climate change, forest management, forest restoration

Objectives of the Research Project

The primary objective of Research Project T-3 was to provide Marine Corps Base Camp Lejeune (MCBCL) managers with the information and tools needed to monitor and manage carbon stores, while supporting military training goals and restoring and maintaining key elements (e.g., biodiversity, endangered species habitat) of longleaf pine (*Pinus palustris*) and loblolly pine (*Pinus taeda*) ecosystems in the context of potential changes in climate at MCBCL. Specific objectives of Research Project T-3 included the following:

1. Adapt and calibrate the LANDIS-II model for carbon storage and changes in the pine-dominated ecosystems of the MCBCL landscape by using monitoring and research data gathered during DCERP1.

2. Run the LANDIS-II model for the MCBCL landscape based on forest management scenarios representative of current and future practices. These practices included no management (Control), prescribed fire application only, 25-year harvest rotation for pulpwood production (Commercial Harvest Cycle I), 60-year harvest rotation for saw timber production (Commercial Cycle II), midstory removal of loblolly pine followed by planting of longleaf pine (Longleaf Savanna Restoration I), and a complete removal of loblolly pine (via clearcutting) followed by planting of longleaf pine (Longleaf Savanna Restoration II).

3. Assess the effects of variation in prescribed fire return intervals (3 year versus 6 year) regarding forest carbon storage for each of the management scenarios.

4. Assess the effects of future climate at MCBCL regarding each management scenario and prescribed fire interval.

5. Develop decision-support tools based on simulation results to allow managers to assess potential tradeoffs among training, harvest, conservation, and carbon management goals.

6. Transfer knowledge gained during this study to managers at MCBCL and other military installations on similar landscapes.

Background

The majority (72%, 112,320 acres) of MCBCL's landscape is occupied by pine-dominated forests and wetlands that have been described by Mitchell et al. (2015). These forested lands are centrally important to MCBCL's training mission, and its timber is a source of revenue for the Base. These forest lands also provide habitat for a diverse array of plant and animal species (most notably populations of the federally endangered red-cockaded woodpecker [RCW, *Picoides borealis*]) and store large amounts of carbon. These lands could potentially be managed to maximize carbon storage to mitigate greenhouse gas emissions. The U.S. Department of Defense (DoD) supports contemporary notions of sustainable forest management and aims to balance military mission support with the maintenance of native biodiversity and sustainable yields of forest products. However, no specific mandate currently exists regarding managing MCBCL pine forests for carbon storage.

Changing patterns of land use, agriculture, and forest management over the past century have already altered MCBCL's forest ecosystems. In particular, large areas that were once dominated by open longleaf pine savanna now support closed canopy stands of loblolly pine (Mitchell et al., 2015). Fire suppression in these pine stands has resulted in the accumulation of a dense midstory of hardwood vegetation and a thick layer of soil organic matter (Varner et al., 2005). The accumulation and thick layer impede regeneration of longleaf pine in two ways. First, the accumulation of a hardwood midstory severely limits the recruitment of longleaf pine seedlings, which regenerate best in an open, park-like savanna (Brockway et al., 1998). Second, the surface soil organic layer prevents regeneration of longleaf pine seedlings and many endemic herbaceous species (Cohen et al., 2004). Successful longleaf ecosystem restoration depends upon removal of midstory hardwoods and reduction in accumulated soil surface organic (Brockway et al., 2009). Compared with open longleaf pine forests, closed-canopied loblolly pine stands have diminished value, both for military training and for biodiversity conservation.

For more than two decades, MCBCL managers have pursued strategies to restore loblolly stands to more open longleaf savanna conditions that would increase suitability for training and biodiversity conservation. In some areas, these strategies have involved complete removal (clearcutting) of loblolly pine followed by planting of longleaf pine. In other MCBCL locations, longleaf pine restoration has used understory and midstory thinning to produce savanna-like conditions. In both situations, prescribed fire has been used to simulate historical fire regimes and maintain savanna-like conditions. The goal has been to apply such fires at 3-year intervals, although weather conditions, air quality constraints, and limited human resources have made achievement of this goal difficult in recent years.

The impacts of restoration treatments on carbon stores and carbon flux to and from longleaf and loblolly ecosystems are not well understood. Understory hardwood thinning and repeated low-severity burns must reduce carbon storage in restored compared to unrestored loblolly pine stands in the short term. This reduction might be offset in the long term by increased productivity of remaining trees and reduced frequency and severity of wildfire. Climate influences the frequency and severity of disturbances, as well as the trajectory of post-disturbance changes. Thus, persistent changes in temperature, precipitation, and evapotranspiration may significantly affect both long-term carbon storage and dynamics. Studies in other pine-dominated ecosystems suggest understory thinning aimed at fuel reduction significantly decreases carbon storage in the long term because wildfires consume a relatively small fraction (less than 30%) of carbon stored in stems wood, branches, coarse woody debris (Campbell et al., 2012; Mitchell et al., 2009). Thus, the effects of variations in restoration management, including variations in thinning protocols and in return intervals, on carbon flux and storage must be understood to provide maximum flexibility in meeting habitat restoration and carbon sequestration goals within the constraints of costs and personnel resources.

Martin et al. (2015), working at Fort Bragg, NC, have recently shown that longleaf pine forests can provide habitat for RCWs, while continuing to store large amounts of carbon. However, high-quality (i.e., frequently burned) RCW habitat may store slightly less carbon than low-quality (i.e., infrequently burned, with a hardwood midstory) habitat (although frequently burned longleaf pine savanna may store more carbon than infrequently burned loblolly pine stands). Similar trade-offs may exist for MCBCL forests, but, until now, the effects of different restoration strategies on long-term carbon storage have not been examined. Longleaf pine trees

generally live longer than loblolly pines and, therefore, have the potential for higher long-term carbon storage (Kush et al., 2004). Recent work has confirmed the higher carbon storage capacities of longleaf pine (Samuelson et al., 2014 and 2017). However, loblolly pine has considerably higher growth rates early in succession compared with longleaf pine and might, depending on the time frame, result in increased carbon storage compared with longleaf pine. Thus, the relative effects of different forest management strategies on carbon storage remain uncertain.

Climate change has the potential to alter patterns of forest carbon storage in the future. What remains uncertain is whether future climate will be amenable to increased forest growth rates and carbon sequestration, or whether future climate will result in increased growth stress and consequently result in a reduction in carbon sequestration. Climate models broadly agree that temperatures throughout the Atlantic Coastal Plain will rise in the twenty-first century (Liu et al., 2013), but projections regarding the magnitudes (and seasonality) of precipitation are uncertain, with some models predicting an increase in precipitation, and others predicting a decrease in precipitation. It is also worth noting that the seasonality of precipitation can impact potential growth rates. An increase in annual precipitation can be essentially nullified in the event of a loss of precipitation during the growing season (approximately April through October), which could lead to growing season drought stress. Changing precipitation regimes can also have significant impacts on the prescribed fire regimes during the dormant season (when the application of prescribed fire is safest), as well as during the growing season when fires are more difficult to contain (Clark et al., 2014). An increase in precipitation during the dormant season can decrease the “window” in which forest managers can set prescribed fires under optimal (and safe conditions).

Aggregated estimates of climate change projections suggest that the ecosystems of the Atlantic Coastal Plain will undergo a gradual shift toward those of the Gulf Coast and Florida, in which climatic conditions become more amenable to slash pine (*Pinus elliotii*) and less suitable to loblolly pine, while remaining relatively ideal for longleaf pine (IPCC, 2014). However, there is a considerable range in estimates of precipitation within different climate models.

Materials and Methods

The LANDIS-II Model Overview

To determine what forest management practices best maximize forest carbon storage capacity across MCBCL’s mixed longleaf and loblolly forests, we used the LANDIS-II model (Scheller and Mladenoff, 2004, Scheller et al., 2007). LANDIS-II simulates ecosystem processes, while accounting for the composition and growth of tree species. The model simulates establishment, growth, and death of cohorts of trees at a user-designated model resolution (30-m resolution for our project). LANDIS-II stratifies the heterogeneous landscape into land types based on climate, soil, and terrain attributes. Within the simulation, the size of an individual cell typically represents the resolution of the Geographic information systems (GIS) data dictate the mapping of spatial attributes across the simulated landscape. Mapping units include layers developed from spatially explicit surveys of forest inventory data within different compartments of forest across MCBCL, each with different stand characteristics (i.e., species, stand age, management history). Thus, LANDIS-II simulates change at the scale of individual stands, while simulating changes

across landscapes composed of stands of different tree species in different stages of succession following application of different forest management practices. Because the model is spatially explicit regarding the relationship of cells to one another, cells interact with each other through the propagation of disturbances, such as fire, and the successional processes that such disturbances produce. LANDIS-II also provides spatial data about stand development and carbon storage that can be used to develop forest management plans.

We used the LANDIS-II Century Extension to examine how ecosystem processes respond to patterns of climatic variability (historical and projected) (Scheller et al., 2011). This extension simulates above- and below-ground biogeochemical processes in response to climate and forest management. The Century extension (Parton et al., 1987 and 1993) links above-ground processes of stand dynamics to below-ground processes of soil carbon and nitrogen dynamics. Climate data needed to drive LANDIS-II consisted of average minimum monthly temperature, average monthly maximum temperature, standard deviation of monthly temperatures, average annual precipitation, and standard deviation of annual precipitation. Within the Century Extension, each species-age cohort has an associated leaf biomass, above-ground wood biomass, coarse root biomass, and fine root biomass (Scheller et al., 2011). The size of each cohort component is a function of net primary productivity, carbon allocation, and mortality. Annual fractions of leaf mortality are modeled as the inverse of their longevity and occur during a user-designated month. Monthly fractions of above-ground wood mortality are user determined and included all forms of wood mortality, including thinning and loss of branches. In addition, age-related mortality substantially reduces above-ground biomass after a cohort reaches 80% of maximum longevity (Scheller and Mladenoff, 2004).

LANDIS-II Model Calibration

MCBCL Vegetation Data

DCERP1 vegetation monitoring data from 0.1-ha permanent plots in 89 pine-dominated (longleaf pine and loblolly pine) stands on MCBCL provided important inputs for the LANDIS-II model. Some of these inputs (i.e., field measurements of forest carbon storage) include species composition, tree density, size class distribution, and seedling abundance (**Figure 18-1**). The sampling methods used to generate these data are described by Mitchell et al. (2015). Loblolly pine forests at MCBCL are largely fire suppressed; on average, have higher soil organic matter than longleaf pine stands; and often contain a dense hardwood midstory of sweet gum (*Liquidambar styraciflua*) and red maple (*Acer rubrum*). Historically, lands now occupied by MCBCL were used primarily for timber production and, to a lesser extent, agriculture. No agricultural usage has occurred since MCBCL was designated as a military installation in 1941 (MCBCL, 2006).

Soil Data

We collected a uniform sample of the top 10 cm of mineral soil (soil beneath layers of litter and duff) by using a 5-cm diameter piston corer at four points within each 0.1-ha permanent vegetation plot. Brookside Laboratories (New Knoxville, OH) analyzed each soil sample. Staff at Brookside Laboratories determined the percent soil organic matter by weight loss after ignition at 360°C (**Figure 18-1**). We used these data and the Natural Resources Conservation Service's

soil survey data to map community types across the Base and as necessary inputs for model simulations of carbon and nitrogen turnover.

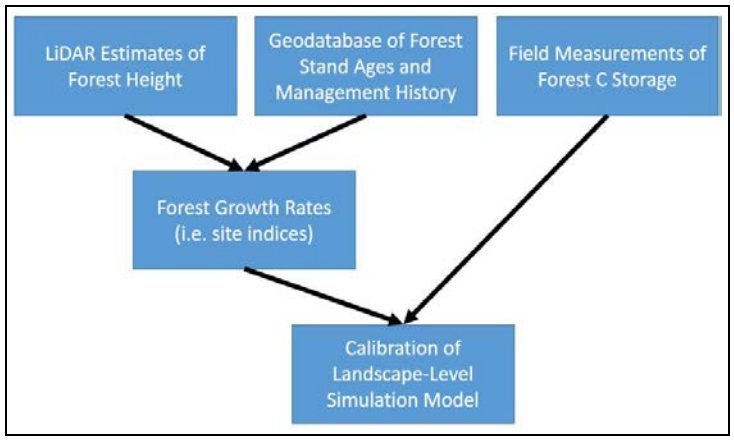

Figure 18-1. Relationships of LiDAR, MCBCL Geodatabase, and field data used for estimating forest growth rates for use to calibrate the LANDIS-II model.

Note: C = carbon.

LiDAR Data

LiDAR (light detection and ranging) data used in the LANDIS-II model were collected in 2010 by MCBCL. We used these LiDAR data to estimate the forest canopy heights in each of the MCBCL management compartments (see Chapter 21 of this *DCERP2 Final Report*). Stand ages and disturbance histories, as well as the identity and relative abundance of the dominant tree species, were also available from MCBCL's Environmental Management Division for each of these compartments. We used the 95th percentile of height as an estimate of average forest canopy height across each compartment, which we used to assign an aggregated estimate of forest height for each forest compartment. We then used this estimate of forest height with age data in a Geodatabase to estimate the site index, a measure of forest growth rates (**Figure 18-1**).

Decomposition

We also used the LANDIS-II model to simulate root decomposition rates, which we derived from work conducted during SERDP Research Project RC-2115. Estimates of loblolly pine root decomposition rates are readily available in the literature (Cybulski et al., 2000; King, 1997; Sanchez, 2001), but there are few studies about the dynamics of tap root decomposition in longleaf pine. Therefore, we used estimates of root decomposition for longleaf pine forests provided by Research Project RC-2115 to aid our model calibration (Anderson et al., 2014; Samuelson et al., 2017), which is calculated as shown in Equation 1:

$$\text{Tap Root Biomass} = \exp\left(-6.69404+0.00461\times\text{AgeAtHarvest}-0.027508\times\text{YearsSinceMortality}+2.01612\times\ln(\text{StumpDiameter (cm)})+1.17653\times\ln(\text{Tmin})\right) \quad \text{(Eq. 1)}$$

where T_{min} is the USDA plant hardiness zone minimum temperature, which, for MCBCL, is 10°F. We used this equation to extrapolate an average annual longleaf pine tap root decomposition rate (0.03) to use in the LANDIS-II model.

Additionally, we measured combustible materials (e.g., needles, leaves, fine and coarse woody debris) on the ground, which are the primary fuel carriers of prescribed fires. These results were obtained from the experimental treatment plots from DCERP1 Research Project T-1. We measured the combustible materials on each plot before and after prescribed fires to obtain estimates of fuel consumption in the 18 loblolly pine plots.

Stochastic and Deterministic Model Attributes

Year-to-year variations in climate are deterministic in LANDIS-II and do not vary among model runs. Variability among LANDIS-II model runs is primarily a consequence of stochastic disturbances (fire and hurricanes) and associated legacy effects on post-fire succession. Changes in light and nutrient availability associated with post-disturbance succession are examples of such legacy effects. We conducted a series of test simulations in which we varied a fuel accumulation parameter (k) in relation to the fire size (in hectares) to derive the parameters that most closely emulated fire regimes practiced at MCBCL under our management scenarios. These regimes included simulations of prescribed burning of the managed stands at MCBCL at a frequency of 3 years and 6 years within management compartments of different sizes. This approach resulted in simulated fires that burned largely within a prescribed severity, but with some variation in fire severity across the simulated landscape. Thus, disturbance and succession are the primary causes of variation in the LANDIS-II model and account for the differences observed between simulations run under the same climatic driving data. Following a disturbance, cohort establishment also depends upon species-specific light availability and its interaction with the level of light that is within the cell. Although levels of light and post-fire successional dynamics are largely similar within cells within a managed fire regime area, there is nevertheless some variation in light availability that can result in variation in post-fire species composition and succession. In summary, variation in the LANDIS-II model is propagated through disturbances and through the emergent properties of the simulated landscape over time.

Synthetic Landscape Simulations

To provide a more focused analysis of the trade-offs involved in managing for loblolly versus longleaf pine, we used the LANDIS-II model to simulate long-term patterns of carbon storage in each of these species on a hypothetical homogeneous landscape. We ran simulations, assuming identical site indices (i.e., potential growth rates) for longleaf and loblolly pine stands such that potential growth rates were similar to those found throughout MCBCL and throughout landscapes of the Atlantic coastal plain. Simulations were on a gridded landscape (100-meter resolution with 100 cells, 100-ha total area) that approximated the growth and carbon storage characteristics observed from our field data and LiDAR measurements. The initial conditions for our landscape assumed a rotation harvest of 50 years, whereby an equal number of cells were aged 1 to 50 years. Longleaf pine has a higher long-term carbon storage capacity (**Figure 18-2**), in part due to its

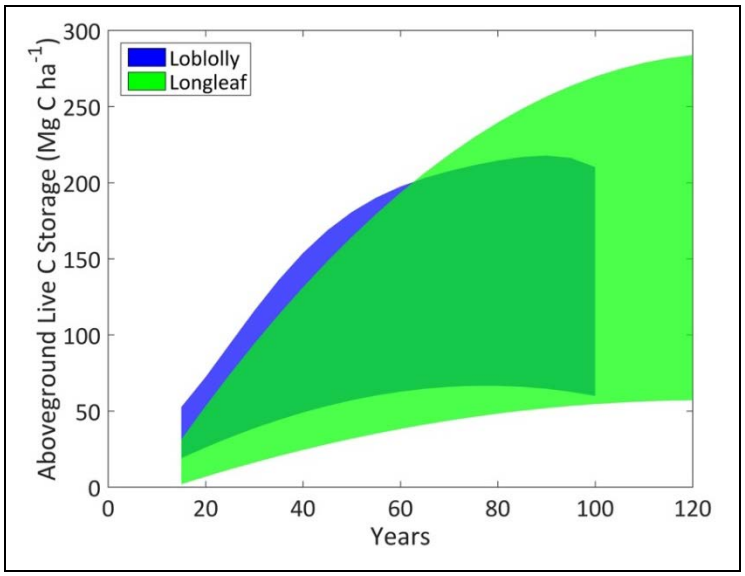

Figure 18-2. The range of carbon storage values for loblolly pine and longleaf pine, based on silvicultural yield tables (i.e., not derived from model simulations).

longevity (200-year life span). In contrast, loblolly pine has higher growth rates in earlier stages of succession, but has an earlier onset of mortality, usually at approximately 100 years of age (Loehle, 1988). Thus, long-term carbon mitigation efforts at MCBCL—and throughout the Atlantic Coastal Plain—are challenged by a trade-off among management goals in which loblolly pine stands will store more carbon early (from age 20 to 60 years). Then, carbon storage plateaus, and these trees will not store additional carbon in the long term (60 to 100 years) compared with longleaf pine, which continues increasing its carbon storage capacity from age 20 through 120 years.

The storage of carbon in forest products after harvest complicates the assessment of how to best manage southeastern pine forests for climate change mitigation. We also examined the effects of the harvest and storage of biomass carbon in long-term forest products (i.e., timber). We simulated forest harvests for stands at frequencies of 25, 40, 60, 80, 100, and 120 years. Our assumptions were that 60% of all harvested biomass was stored in slowly decomposing timber products and decomposed at a rate of 1% per year, and that 40% of the remaining woody materials was lost during harvesting and manufacturing (Harmon and Marks, 2002; Mitchell et al., 2012).

Forest Management Scenarios

We ran the LANDIS-II model with six different management scenarios (**Table 18-1)**. We ran prescribed fires at two different MFRIs: every 3 years and every 6 years. We used these two MFRIs because conducting prescribed burns at MCBCL may occur at a lower frequency in the future because of changes in climate conditions (i.e., changes in the hydrologic cycle that may be characterized by increased drought or increased rainfall events) than have recently occurred. Historically, prescribed fires were set in longleaf pine savannas approximately every 3 years; however, recent dormant season weather conditions have not been conducive to burning and/or smoke dispersal at MCBCL. Thus, we believe it may be important to incorporate these recent conditions as a possibility. Finally, to account for the uncertainty in the LANDIS-II modeling framework and the variability that results from the emergent properties of our simulated landscape, we replicated each combination of management scenario (n=6) and fire regime (n=2) simulation three times. Incorporating replicate simulations also allowed us to calculate a standard deviation (SD) for the mean of each combination and to assess statistical differences among these combinations (see the section titled **Statistical Comparisons** in this chapter).

Table 18-1. Management Treatments Simulated by Using the LANDIS-II Model and Their Projected impacts

Management Treatment	Projected Impacts to Carbon Stores
No Management (Control)	Carbon accumulates in both live and dead pools. There is an increased wildfire risk.
Prescribed Fire Only: No thinning or cutting	Carbon accumulates in both live and dead pools, but it is regulated by prescribed fire.
Commercial Harvest Cycle I: Loblolly pine clear-cut at 25 years for pulpwood	There is an overall reduction in carbon stores, particularly in loblolly pine stands.

(continued)

Table 18-1. Management Treatments Simulated by Using the LANDIS-II Model and Their Projected impacts (continued)

Management Treatment	Projected Impacts to Carbon Stores
Commercial Harvest Cycle II: Loblolly pine clear-cut at 60 years for timber production	This treatment maintains carbon stores.
Longleaf Savanna Restoration I: Loblolly pine understory/midstory thinned, followed by longleaf pine plantings	There is a small, short-term decrease in carbon stores, followed by a long-term increase in carbon stores.
Longleaf Savanna Restoration II: Loblolly pine clear-cut, followed by longleaf pine restoration	There is a short-term decrease in carbon stores, followed by a long-term increase in stores because of the higher carbon storage capacity of longleaf pine.

The following discussion provides additional details about each of the management practices selected.

No Management: No management of any stands, which is not a likely management scenario. Rather, this scenario provided a baseline for comparison with the other model management simulations.

Prescribed Fire Only: No management of any stands other than the application of prescribed fire at specified intervals. Although the incorporation of prescribed fire means that this scenario is not as unlikely as the one previously mentioned, the MCBCL's Environmental Management Division does fund much of its operations from timber-harvesting revenues. We included two scenarios of prescribed fire frequency, MFRI= 3 years and 6 years.

Commercial Harvest Cycle I: In this scenario, loblolly pine stands, including those with dense shrubby undergrowth, were allowed to grow without any understory thinning treatments. Loblolly sites were clear-cut when pines reached approximately 25 years for pulpwood, and the residual understory was burned. A 25-year rotation is not representative of the management practices used at MCBCL, but it is a common practice for pulpwood production throughout the Southeastern United States. We included two scenarios of prescribed fire frequency, in which MFRI=3 years and 6 years.

Commercial Harvest Cycle II. This scenario simulated widely adopted approaches to managing loblolly pine stands for long-term timber yields. Such an approach involved repeated partial stand harvests to reduce competition for sunlight and to increase growth rates of select trees. Stands were thinned at age 20, 35, and 45 years, before being clear-cut at age 60 years. We included two scenarios of prescribed fire frequency, in which MFRI=3 years and 6 years.

Longleaf Savanna Restoration I: In this scenario, shrubs and understory trees (up to 8 inches dbh) were thinned and masticated with debris left onsite. The site was then prescribe burned 1 year after thinning and every 3 years or 6 years thereafter. Longleaf pine seedlings are planted in the understory (though establishment of seedlings may be difficult). After mature loblolly pines reached 70–80 years, stands were selectively cut to encourage new longleaf recruitment and to maintain an uneven-aged population of live trees and snags (potential RCW habitat). Longleaf pine stands were cut (individual or group selection) at 120 years.

Longleaf Savanna Restoration II: In this scenario, loblolly pine stands were clear-cut and replaced with longleaf pine seedlings (though establishment of seedlings may be difficult). Once the longleaf seedlings reached 5 to 10 years of age, stands were prescribe burned every 3 years or 6 years thereafter. Longleaf pine stands were cut at (individual or group selection) 120 years. We included two scenarios of prescribed fire frequency, in which MFRI=3 years and 6 years.

Climate Scenarios

Historical Climate Data

We used historical climate data to formulate the baseline (control) conditions for the LANDIS-II simulations. The DCERP2 Research Project CC-1 Team provided these data as described in Chapter 3 of this *DCERP2 Final Report*. The researchers also evaluated three gridded historical climate data sets: (1) Parameter-elevation Regressions on Independent Slopes Model (PRISM; Daly et al., 2008), (2) North American Land Data Assimilation System version 2 (NLDAS-2; Xia et al., 2012a and 2012b), and (3) the University of Idaho's Gridded Surface Meteorological Data (METDATA; Abatzoglou, 2011).

The DCERP2 Research Project CC-1 Team compared the three historical climate data sets with an independent weather station observational data set called the North Carolina Environment and Climate Observing Network (ECONet), which consists of research-quality measurements of common variables (e.g., temperature, precipitation, winds, relative humidity).

The average root mean squared error (RMSE) for all ECONet stations was compared with each historical climate data set for three daily variables of interest: maximum temperature, minimum temperature, and precipitation. PRISM had the lowest error for minimum and maximum temperature and precipitation. However, the DCERP2 Research Project CC-1 Team selected METDATA for the historical climate baseline because it encompassed the climate variables that were needed by LANDIS-II and the other DCERP2 models. The DCERP2 Research Project CC-1 Team generated daily data were generated for maximum temperature, minimum temperature, and precipitation. Climate data were continuous from 1960 through 2010.

Future Climate Projections

The DCERP2 Research Project CC-1 Team identified the range of possible climate futures to be used by the DCERP2 Team, reducing the 76 possible climate models down to an ensemble of 24 climate models by using a hierarchal clustering technique. However, given time constraints to run LANDIS-II, it was impossible to run all 24 climate models for all the management scenarios. The Research Project CC-1 Team further reduced the number of climate models in the ensemble down to four models that retained a similar range of uncertainty in the climate variables as the ensemble of the 24 models. The four models selected included the ECHAM5, ECHO-G, GFDL-CM2.1 and MIROC-ESM-CHEM models (**Table 18-2**).

From each climate model, we used daily climate data for maximum temperature, minimum temperature, and precipitation from Research Project CC-1 for the period of climate future projections (2011–2099). We only ran each climate model once for each forest management scenario. The climate models assume a "Canopy" photosynthesis model, which calculates

photosynthetic rates as a function of light interception and its attenuation through the canopy and the response of leaf layers to available light within different layers of the canopy.

Three of the models (i.e., ECHAM5, ECHO-G, and GFDL-CM2.1) represented hydrology by using a "bucket" model, in which a single soil layer is conceptualized as a bucket receiving and retaining all incident water until its storage capacity is filled. The MIROC-ESM-CHEM model assumed multiple soil layers in its representation or hydrology. Bucket models are particularly efficient with describing land surface processes and are coupled with large-scale atmospheric models, but may experience problems because of their simple representation of vegetation and estimation of potential evapotranspiration fluxes. It is worth noting that the MIROC-ESM-CHEM, which used multiple layers of soil, had substantially different projections of temperature and rainfall than the other three models, which used a simpler approach and were in greater agreement with each other regarding temperature and precipitation forecasts than with the MIROC-ESM-CHEM model.

Table 18-2. Global Climate Models Used for Climate Change Projections

Projection	Model	Model Origin	Atmospheric Resolution	Ocean Resolution	Hydrology	Physiology
ECHAM5	MACA	Max Plank Institute for Meteorology, Hamburg, Germany	1.9°×1.9°	1.5°×1.5°	Bucket	Canopy
ECHO-G	SERAP	Meteorological Institute of the University of Bonn, Bonn, Germany	3.9°×3.9°	0.5° to 2.8°×2.8°	Bucket	Canopy
GFDL-CM2.1	SERAP	NOAA + the U.S. Department of Commerce	2.0°×2.5°	0.3° to 1°×1°	Bucket	Canopy
MIROC-ESM-CHEM	SERAP	Meteorological Research Institute, Tsukuba, Japan	2.8°×2.8°	0.5° to 2.0°–2.5°	Layers	Canopy

Note: MACA = Multivariate Adaptive Constructed Analogs; NOAA = National Oceanic and Atmospheric Administration; SERAP = Southeast Regional Assessment Project.

Projected values of selected climate variables in the year 2100 are indicated in **Table 18-3** for the control and each of the four climate scenarios. All four climate scenarios predicted higher future temperatures. Differences in summer temperatures were minimal for three of the climate models, with only a 2°C difference from the control. However, projections for the MIROC-ESM-CHEM model were 9°C higher than baseline conditions. Differences were more pronounced between mean annual temperatures, with a 4°C, 5°C, 3°C, and 9°C change for the ECHAM5, ECHO-G, GFDL-CM2.1, and MIROC-ESM-CHEM models, respectively. These differences in temperature over the course of 1 year will result in increased evapotranspiration, which can exacerbate the reductions in annual rainfall seen in all, but one (i.e., GFDL-CM2.1) of the climate models.

Interestingly, the ECHO-G model was the only model with lower annual rainfall in 2090–2100 than baseline conditions, yet this model had higher rainfall than the other climate three models and baseline condition during the summer months. This is because the ECHO-G model had substantially lower precipitation during other months, particularly the winter months. For example, for December 2090–2100, the ECHO-G model's estimates of precipitation were half

(52%) of the estimates from the GFDL-CM2.1 model. It is also worth noting that the MIROC-ESM-CHEM model was the only model that predicted lower precipitation than the baseline condition. This may be a consequence of its far higher temperatures, which may be causing atmospheric water demand to increase to a point at which local hydrological cycles are altered.

Table 18-3. Global Climate Models Used for Climate Projections for 2090–2100.

Model	Summer Precipitation (mean mm, June through August)	Summer Temperature (mean °C, June through August)	Annual Precipitation (mean mm)	Annual Temperature (mean °C)
Baseline conditions (Control)	160	26	1,119	6
ECHAM5	185	28	1,372	10
ECHO-G	240	28	982	11
GFDL-CM2.1	186	28	1,434	9
MIROC-ESM-CHEM	128	35	1,217	15

Statistical Comparisons

We used a Multi-Response Permutation Procedure (MRPP) to test for significant differences in carbon storage among the six management practices and two MFRI treatments and climate scenarios (Mielke and Berry, 2007). MRPP is a non-parametric procedure for testing the hypothesis of no difference between two or more groups of entities. As such, we used the MRPP to examine the magnitude of the differences in carbon storage among the different management and climate projection scenarios. MRPP calculates the chance-corrected within-group agreement (A), a descriptor of within-group homogeneity compared to the random expectation. When all items are identical within groups, then the observed delta (δ, weighted mean within-group distance) is equal to zero, while A=1. However, for ecological data, values for A are commonly below 0.1, even when the observed δ differs significantly from the expected, whereas an A greater than 0.3 is rather high (McCune et al., 2002). Although we expected statistically significant differences between different management scenarios, we were unsure of what to expect regarding different scenarios of climate (i.e., climate scenarios as compared with the historical baseline climate conditions that served as a control) within the same groups of management scenarios. Of particular interest to our study were differences between longleaf pine stands and loblolly pine stands with midstory removal treatments.

Decision Support Tools and Technology Transfer

LANDIS-II generates maps in the ERDAS .img format. We used ArcMap software to convert the .img files to .tiff files, which were subsequently given a geospatial signature that would allow for spatially explicit mapping (i.e., geotiff files) of the carbon storage across MCBCL. The DCERP2 Data Management Team in Research Project TSP-1 used these data to generate maps at 5-year intervals (i.e., the frequency at which the LANDIS-II Century Succession extension was run). Additionally, our georeferenced maps of carbon storage were supplemented by non-georeferenced estimates of Base-wide carbon storage presented as a graph in the interactive mapping application (iMAP). Together, our georeferenced map files and our estimate of Base-

wide carbon storage were incorporated into the DCERP Data and Information Management System (DIMS) iMAP tool to allow land managers at MCBCL to visualize the impacts of different scenarios of forest management practices. Visualizations of the management practices forecast by using the four climate model projects are discussed in the following Results and Discussion section of this chapter.

Results and Discussion

Forest Management and Carbon Storage

Synthetic Landscape Simulation Results

Simulations of carbon sequestration and long-term carbon storage capacities of homogeneous landscapes revealed significant differences between stands dominated by loblolly pine versus longleaf pine. The amount of carbon stored in the unharvested longleaf pine control group was considerably higher (25%) than for the unharvested (control) group for loblolly pine after 50 years (**Figure 18-3**). Carbon storage in young (less than 50 years old) longleaf stands was generally lower than loblolly pine stands, owing in part to the delayed onset of stem growth in longleaf pine.

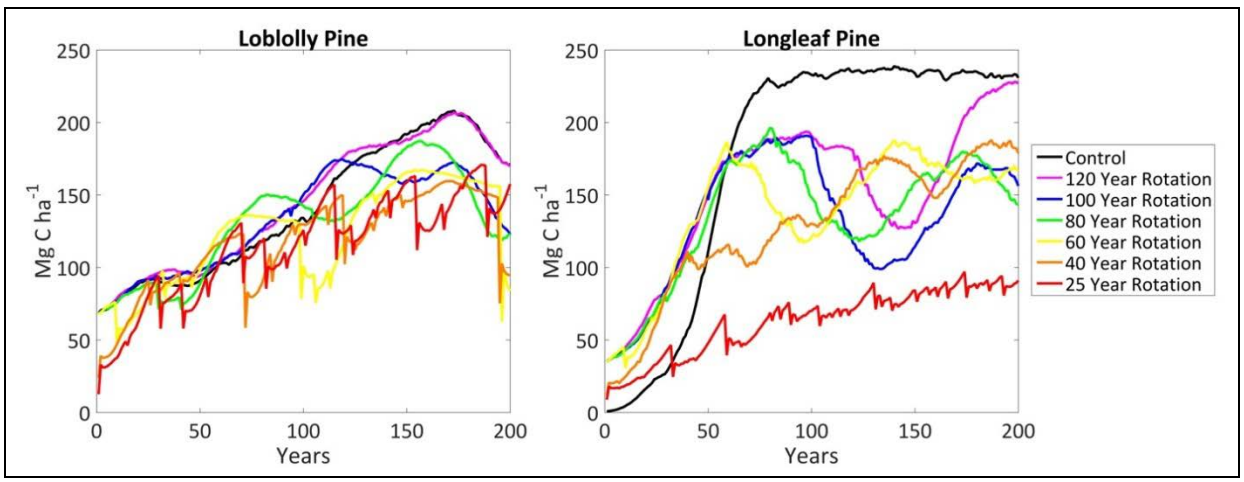

Figure 18-3. Time series comparison of total ecosystem carbon (C) storage + harvested C stored in timber products from forested landscapes of loblolly versus longleaf pine in our synthetic landscape simulations.

In loblolly pine, whether in forest ecosystems or in slowly decomposing timber products, carbon storage was highest in the unharvested control group and was progressively lower with successively shorter harvest regimes. This finding was also true for longleaf pine stands, but the differences between the unharvested (control) group and the harvest treatments were much greater than in loblolly pine. Carbon storage increases in stands that are harvested frequently because of the inclusion of forest products in our estimates of stand carbon storage. However, the harvest of and subsequent storage of carbon in timber products did not compensate for the amount of carbon that could be stored if either of these forest types were to remain unharvested. Thus, efforts to maximize long-term carbon storage in Atlantic coastal plain ecosystems would benefit from the restoration of longleaf pine where site conditions will support that species.

However, the restoration of longleaf pine can be very difficult at sites where fire has been absent, and research regarding the best methods for longleaf restoration are ongoing (Mitchell et al., 2015 and in revision; Palmquist et al., 2015).

MCBCL Landscape Simulation Results

Based on MRPP analyses, the LANDIS-II model results displayed a high degree of statistical significance among the various combinations of forest management, fire frequency, and climate scenarios (A=0.24, p<0.0001, **Table 18-4**). Assuming no change in future climate conditions, there were significant differences in carbon storage among management scenarios. Both Longleaf Savanna Restoration I and II had significantly higher carbon storage than the No Management scenario and the Prescribed Fire Only scenario (A=0.31–0.42, p<0.05). With an MFRI of 3 years, by 2100, these treatments stored 11,986 g C m^2 during the Longleaf Savanna Restoration I scenario and 10,274 g C m^2 during the Longleaf Savanna Restoration II scenario. With an MFRI of 6 years, by 2100, these treatments stored 13,339 g C m^2 during the Longleaf Savanna Restoration I scenario and 11,598 g C m^2 during the Longleaf Savanna Restoration II scenario. There were no significant differences between the Commercial Harvest Cycle I and II scenarios (A=−0.99–0.079, p>0.2). This finding may be because timber harvesting for both scenarios began before simulation year 2099 and because of the small sample size available for each combination of forest management and MFRI. There was no significant difference in the No Management and the Prescribed Fire Only scenarios (A=−0.25, p>0.8). These results suggest that, under historical climatic conditions, carbon storage at MCBCL and throughout the southeastern US can be increased through active management, even if such management involves the partial thinning of longleaf pine stands at 70 years of age.

Table 18-4. Average Carbon Stored (g C m^{-2} ± SD) in the Year 2100 Across MCBCL's Landscape in Each Management and MFRI Scenario for Current Climate Conditions.

Each estimate and SD is based on three independent model runs. Superscript letters denote statistically homogeneous (p>0.05) subsets based on MRPP analysis.

Treatments	Prescribed Fire Frequency (MFRI=3 years)	Prescribed Fire Frequency (MFRI=6 years)
No Management	8,378±106[a]	
Prescribed Fire Only	8,377±108[a]	11,018±242[b]
Commercial Harvest Cycle I	2,663±30[c]	3,627±42[c]
Commercial Harvest Cycle II	9,127±170[c]	9,473±509[c]
Longleaf Savanna Restoration I	11,986±279[b]	13,339±116[b]
Longleaf Savanna Restoration II	10,274±334[b]	11,598±239[b]

In every forest management scenario, the MCBCL landscape burned on an MFRI of 6 years stored slightly more carbon than when burned on an MFRI of 3 years (**Figures 18-4 and 18-5**). This preliminary result suggests that longleaf pine stands can be managed on an MFRI of 6 years to maximize carbon storage. However, longer MFRIs (i.e., 5 to 7 years) produce significant changes in plant and avifaunal composition, and they may diminish RCW habitat quality (see Chapter 9 of this *DCERP2 Final Report*). Furthermore, longer MFRI's lead to increased fuel

accumulation with a higher risk of wildfires, which can further constrain management options for prescribed burning.

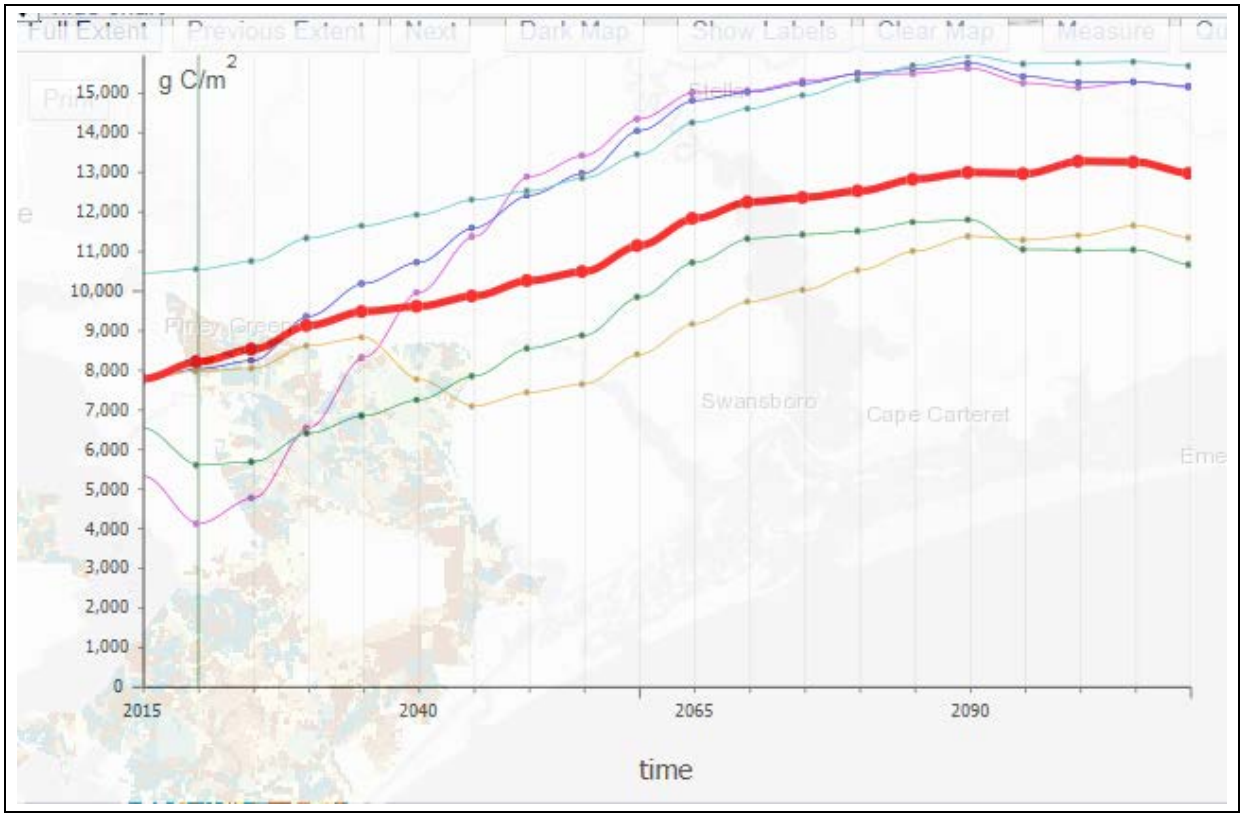

Figure 18-4. Carbon stored (in g C m^{-2}) across MCBCL's landscape in each management scenario with an MFRI of 3 years.

Note: This figure is a screen capture from the DCERP DIMS.

Future Climate Effects

Our estimates of carbon storage under future climate scenarios yielded divergent results, with some simulations showing results similar to the baseline (control) climate simulations; other simulations showed drastically lower carbon storage (**Figure 18-5**). All four climate scenarios project significantly higher temperatures, but the MIROC-ESM-CHEM model predicts substantially lower summer rainfall than the other three models. This difference likely explains the much lower carbon storage levels produced by this climate scenario. However, extreme climatic events, such as particularly high temperatures and extended periods of drought (which are not detectable when looking at long-term averages) may also contribute to large-scale forest dieback. Additionally, extreme flooding, such as that predicted by the GFDL-CM2.1 model for the year 2089, could also result in significant forest dieback. Given the wide divergence in model climate forecasts and their effects on the change in future carbon storage, these results provide a measure of the range of possible carbon storage outcomes.

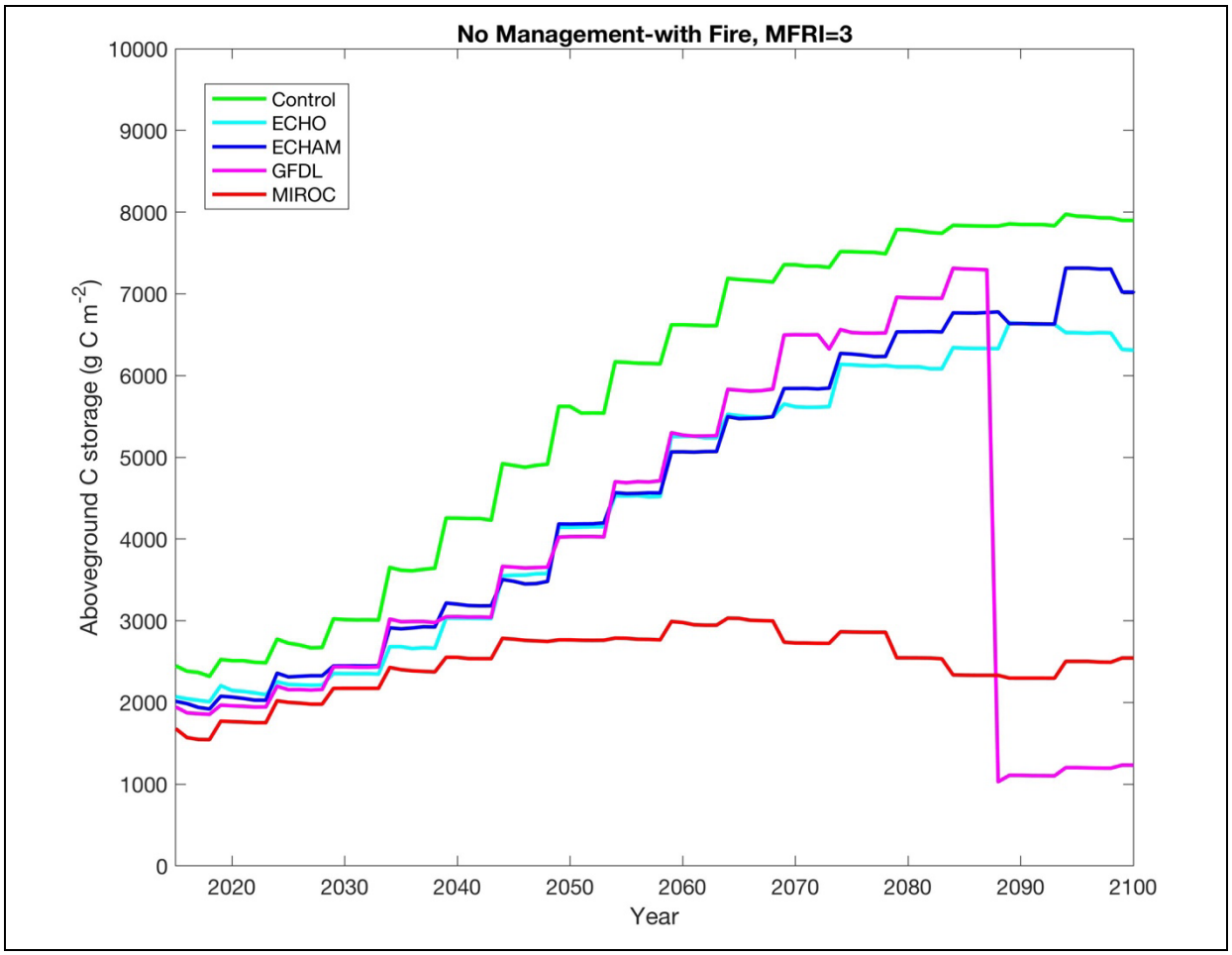

Figure 18-5. Changes in above-ground carbon storage for each climate scenario, including the baseline (control) for the No Management (MFRI = 3 years) scenario.

There is considerable divergence among climate models regarding carbon storage in each of the management and MFRI treatments (**Table 18-5**). Our MRPP analysis found statistically significant effects of our future climate scenarios on long-term carbon storage (2090–2100). Among simulations with similar forest management and MFRIs, differences in carbon storage between the baseline climate scenario and projected future climate scenarios were statistically significant, with the baseline climate simulations storing more carbon in the Commercial Harvest Cycle I group (A=0.42, p<0.05), Commercial Harvest Cycle II group (A=0.42, p<0.05), Longleaf Savanna Restoration I group (A=0.23, p<0.05), Longleaf Savanna Restoration II group (A=0.11, p<0.05), and the Prescribed Fire only group (A=0.42, p<0.05).

Table 18-5. Total Carbon Stored in the Year 2100 Across the MCBCL Landscape in Each Management and MFRI Scenario for Each of Four Climate Models. Units are in g C m^{-2}.

Treatments	MFRI	Current Climate	ECHO-G	ECHAM5	GFDL-CM2.1	MIROC-ESM-CHEM
No Management	Not applicable	8,378±106	9,446	10,343	11416	3,265
Prescribed Fire Only	3	8,377±108	7,429	8,216	9038	3,265
	6	11,018±242	10,346	11,191	11,381	4,358
Commercial Harvest Cycle I	3	2,663±30	1,778	1,891	2,080	1,111
	6	3,627±42	2,169	2,732	3,224	1,423
Commercial Harvest Cycle II	3	9,127±170	8,113	8,993	8,094	3,276
	6	9,473±509	11,026	11,797	12,977	4,562
Longleaf Savanna Restoration I	3	11,986±279	6,702	8,910	9,801	2,302
	6	13,339±116	10,832	12,568	13,825	4,463
Longleaf Savanna Restoration II	3	10,274±334	7,640	9,125	10,038	3,254
	6	11,598±239	11,238	11,828	13,011	4,030

Decision Support Tools and Technology Transfer

Maps of carbon storage were generated every 5 years between 2020 and 100 and displayed in iMAP and available in the DCERP Document Database. MCBCL managers can use these results to examine how different forest management practices and future climate conditions can impact long-term carbon storage. For example, if a forest manager wanted to determine how replacing loblolly pine with longleaf pine may impact carbon storage in both near and long terms, they could look at how the Longleaf Savanna Restoration I and II scenarios differ in their projections of carbon storage in 2020 compared with 2100. Forest managers could also examine how these management scenarios can differ because of different future climate scenarios.

Such differences can be extreme, as shown in **Figure 18-6** (ECHAM5 climate model scenario compared with the MIROC-ESM-CHEM climate model scenario). In this example, the ECHAM5 scenario shows that the MCBCL landscape reaches levels of carbon storage that are close to the maximal levels of carbon storage that can be found at MCBCL today, whereby differences in carbon storage are largely reflective of differences on site quality/soil fertility. Total carbon storage in this scenario is 10,344 g C m^{-2}. Comparable amounts of modeled carbon are stored for the ECHO-G (9,446 g C m^{-2}) and the GFDL-CM2 (11,416 g C m^{-2}) models. However, in the MIROC-ESM-CHEM scenario (shown on the right in **Figure 18-8**) shows very different results because this scenario has the lowest mean summer precipitation (128 mm) and the highest mean summer temperatures (35°C). Together, the effects of the interactions between rising temperatures and decreasing precipitation greatly reduces projected carbon storage capacity. Thus, the differences in site quality and soil fertility that characterize the modern-day differences in how the landscape can store carbon are no longer apparent because of the pervasive impacts of rising temperatures and decreasing precipitation. Here, the MCBCL-wide carbon storage for the MIROC-ESM-CHEM scenario produces the lowest of the four climate scenarios (3,256 g C m^{-2}).

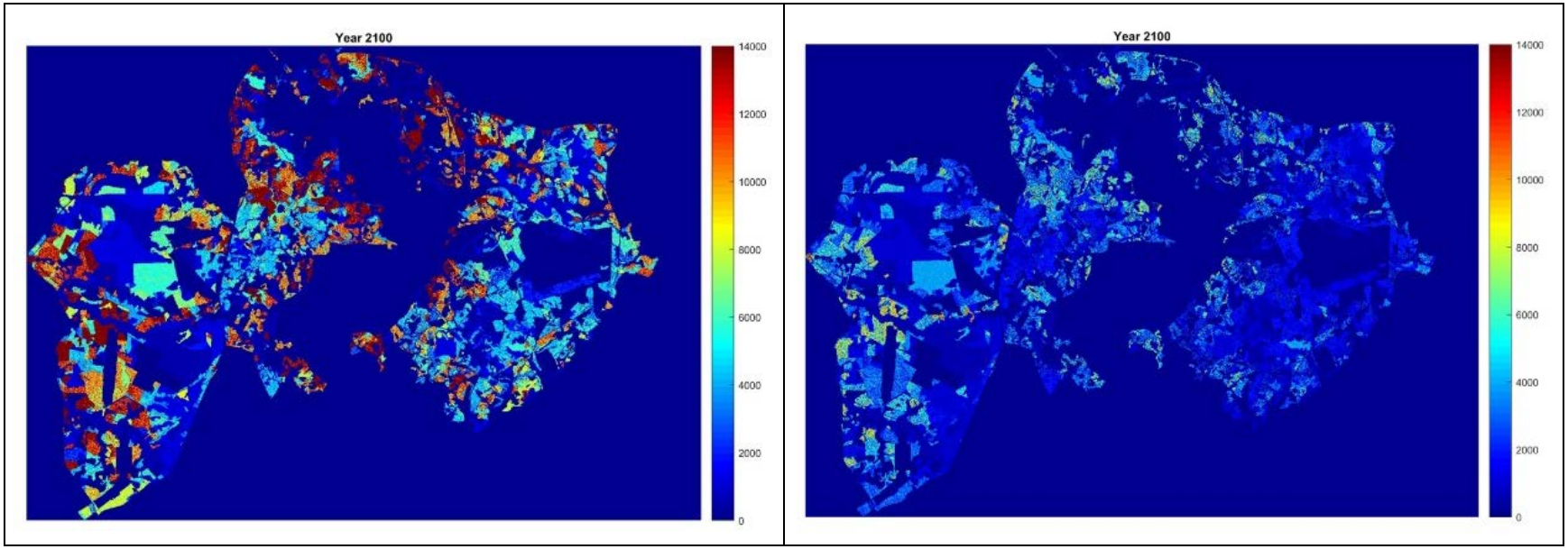

Figure 18-6. Map of carbon storage (g C m^{-2}) at MCBCL assuming No Management (and no prescribed fire) under the ECHAM5 climate scenario (left) and the MIROC-ESM-CHEM scenario (right).

Conclusions and Implications for Future Research and Implementation

Research Questions

1. At the level of individual stands, how do different forest management scenarios influence carbon stores in the near term (less than 10 years), intermediate term (10 to 70 years), and long term (greater than 70 years)?

Carbon storage in stands dominated by either loblolly pine or longleaf pine vary substantially among different forest management scenarios depending on the time frame. At the level of individual stands of both loblolly pine and longleaf pine, carbon storage is highest in the absence of harvest and is progressively lower with successively shorter harvest regimes. The differences between unharvested and harvested stands were, however, greater for longleaf pine than for loblolly pine. Average carbon storage was higher in loblolly pine than in longleaf pine stands for the shortest harvest rotations (less than 25 years). Longleaf pine stands store more carbon for all harvest rotations greater than 40 years. This finding was true even when carbon storage in wood products was included in the carbon storage calculation. These differences are largely a consequence of higher longevity among longleaf pine compared to loblolly pine trees.

2. At the level of the MCBCL landscape, how do variations in the application of different management scenarios influence carbon stores in the near term (less than 10 years), intermediate term (10 to 70 years), and long term (greater than 70 years)?

Carbon storage will be highest across landscapes managed for longleaf pine restoration over the long term. At the level of the MCBCL landscape, clear-cutting loblolly pine and replanting with longleaf pine (Longleaf Savanna Restoration II) results in less stored carbon than understory and midstory thinning of loblolly pine and replanting with longleaf pine (Longleaf Savanna Restoration I). However, both treatments result in more stored carbon across the landscape than commercial timber harvest treatments.

Regardless of forest management practices applied, longer prescribed fire return intervals (6 years versus 3 years) result in 10% or higher carbon storage. Prescribed fire return intervals of 3 years are generally considered to be ideal for maximizing biodiversity, creating ideal RCW habitat conditions, and maintaining training land to support the military's mission. Average fire return intervals have increased over the past several years, owing to weather conditions that have not been conducive to burning and/or smoke dispersal. Future climate may further constrain options for prescribed burning. Longer MFRIs (i.e., 5 to 7 years) produce significant changes in plant and avifaunal composition, and they may diminish RCW habitat quality (see Chapter 17 of this *DCERP2 Final Report*). Furthermore, longer MFRIs lead to increased fuel accumulation that can further increase risk of wildfires and thus constrain options for prescribed burning. The marginal benefit of longer MFRI on carbon storage is probably not sufficient to compensate for likely negative impacts on biodiversity and RCW habitat, as well as increased risk of more severe wildfires.

3. How will likely scenarios of climate change affect stand and landscape level changes in carbon storage associated with variations in forest management scenarios?

There is significant variation in predicted future conditions among different climate models, but all models result in lower carbon storage on the MCBCL landscape in 2100 compared with historical climate baseline conditions. Each of the four climate model scenarios tested in this research project produced lower overall carbon storage by the year 2100 compared with the historical climate baseline; however, the magnitude of this difference varied widely among models. In the ECHO-G and ECHAM5 scenarios, conditions remain suitable for both loblolly pine and longleaf pine ecosystems under all our management scenarios through 2100. Conditions were also suitable for these ecosystems at MCBCL in the GFDL-CM2.1 scenario until 2085–2090. In this scenario, major rain events (84 cm of rain in 2 months) occur during summer 2089 that result in a precipitous reduction in above-ground carbon storage across the landscape (cf. **Figure 18-6**). The MIROC-ESM-CHEM model simulations resulted in the lowest amount of carbon storage on the MCBCL landscape compared with the other climate models. This model produced average monthly and annual temperatures that were far higher than those forecast by other models. Combined with a significant reduction in summer precipitation, this model produced conditions quite different than those that characterized the range of climatic conditions where loblolly pine and longleaf pine grow today. Future climate change of this magnitude would require very significant changes in forest management goals and protocols. Given the wide divergence in model climate forecasts and their effects on the change in future carbon storage capacity, these results provide a measure of the range of possible outcomes, but not meaningful predictions.

Findings with Implications for Future Base Management

Forests at MCBCL have the potential to store far more carbon than they currently do, particularly if they are harvested less frequently. The early rapid growth of loblolly pine results in greater carbon storage than longleaf pine under typical pulpwood management schedules (e.g., 25-year harvest regimes). Under less intensive harvest regimes, longleaf pine stands store more carbon than loblolly pine stands.

Long-term carbon storage was highest in forest management scenarios that promoted the restoration of longleaf pine across the landscape. However, these two scenarios (i.e., Longleaf Savanna Restoration I and II) had very different initial post-treatment carbon stores. Clearcutting all loblolly pine stands (as in Longleaf Savanna Restoration II) resulted in the lowest post-treatment carbon storage across the MCBCL. Carbon storage subsequently remained low for several decades following treatment. By contrast, midstory thinning of loblolly pine stands, followed by planting longleaf pine (as in Longleaf Savanna Restoration I), resulted in only a modest immediate decline in carbon storage, which was quickly reversed by the growth of overstory loblolly pine trees that are retained and the growth of planted understory longleaf pine seedlings.

Literature Cited

Abatzoglou, J.T. 2011. Development of gridded surface meteorological data for ecological applications and modeling. *International Journal of Climatology 33*(1):121–131.

Anderson, P., K. Johnsen, C.A. Gonzalez-Benecke, and L. Samuelson. 2014. *Predicting Taproot Decomposition of Longleaf Pine Across the Southeastern U.S.* Presented at the 99th Annual Convention of the Ecological Society of America, Sacramento, CA. Available at https://www.researchgate.net/publication/267289059_Predicting_taproot_decomposition_of_longleaf_pine_across_the_southeastern_US

Brockway, D.G., K.W. Outcalt, and R.N. Wilkins. 1998. Restoring longleaf pine wiregrass ecosystems: Plant cover, diversity and biomass following low-rate hexazinone application on Florida sandhills. *Forest Ecology and Management 103*(2–3):159–175.

Brockway, D.G., K.W. Outcalt, B.L. Estes, and R.B. Rummer. 2009. Vegetation response to midstorey mulching and prescribed burning for wildfire hazard reduction and longleaf pine (*Pinus palustris Mill.*) ecosystem restoration. *Forestry 82*(3):299–314.

Campbell, J.L., M.E. Harmon, and S.R. Mitchell. 2012. Can fuel-reduction treatments really increase forest carbon storage in the western U.S. by reducing future fire emissions? *Frontiers in Ecology and the Environment 10*(2):83–90.

Clark, K.L., N. Skowronski, H. Renninger, and R. Scheller. 2014. Climate change and fire management in the mid-Atlantic region. *Forest Ecology and Management 327:*306–315.

Cohen, S., R. Braham, and F. Sanchez. 2004. Seed bank viability in disturbed longleaf pine sites. *Restoration Ecology 12*(4):503–515.

Cybulski, W.J., W.T. Peterjohn, and J.H. Sullivan. 2000. The influence of elevated ultraviolet-radiation (UV-B) on tissue quality and decomposition of loblolly pine (*Pinus taeda L.*) needles. *Environmental and Experimental Botany 44*(3):231–241.

Daly, C., M. Halbleib, J.I. Smith, W.P. Gibson, M.K. Doggett, G.H. Taylor, J. Curtis, and P.P. Pasteris. 2008. Physiographically sensitive mapping of climatological temperature and precipitation across the conterminous United States. *International Journal of Climatology 28*:2031–2064. doi: 10.1002/joc.1688

Harmon, M.E., and B. Marks. 2002. Effects of silvicultural practices on carbon stores in Douglas-fir-western hemlock forests in the Pacific Northwest, USA: Results from a simulation model. *Canadian Journal of Forest Research 32*:863–877.

IPCC (Intergovernmental Panel on Climate Change). 2014. *Climate Change 2014–Impacts, Adaptation and Vulnerability: Regional Aspects*. Cambridge University Press.

King, J.S., H.L. Allen, P. Dougherty, and B.R. Strain. 1997. Decomposition of roots in loblolly pine: Effects of nutrient and water availability and root size class on mass loss and nutrient dynamics. *Plant and Soil 195*(1):171–184.

Kush, J.S., R.S. Meldahl, C.K. McMahon, and W.D. Boyer. 2004. Longleaf pine: A sustainable approach for increasing terrestrial carbon in the Southern United States. *Environmental Management 33*:S139–S147.

Liu, Y., S.L. Goodrick, and J.A. Stanturf. 2013. Future U.S. wildfire potential trends projected using a dynamically downscaled climate change scenario. *Forest Ecology and Management 294*:120–135.

Loehle, C. 1988. Tree life history strategies: The role of defenses. *Canadian Journal of Forest Research 18*:209–222.

Martin, K.L., M.D. Hurteau, B.A. Hungate, G.W. Koch, and M.P. North. 2015. Carbon tradeoffs of restoration and provision of endangered species habitat in a fire-maintained forest. *Ecosystems 18*:76–88.

MCBCL (Marine Corps Base Camp Lejeune). 2006. Integrated Natural Resource Management Plan (INRMP). US Marine Corps, Camp Lejeune, NC.

McCune, B., J.B. Grace, and D.L. Urban. 2002. *Analysis of Ecological Communities.* Volume 28. Gleneden Beach, OR: MjM software design.

Mielke, P.W., and K.J. Berry. 2007. *Permutation methods: A distance function approach*. Springer-Verlag: New York.

Mitchell, S.R., M.E. Harmon, and K.E. O'Connell. 2012. Carbon debt and carbon sequestration parity in forest bioenergy production. *GCB Bioenergy 4*:818–827.

Mitchell, S.R., M.E. Harmon, and K.E. O'connell. 2009. Forest fuel reduction alters fire severity and long-term carbon storage in three Pacific Northwest ecosystems. *Ecological Applications 19*(3):643–655.

Mitchell, S., K. Palmquist, S. Cohen, and N.L. Christensen. 2015. Patterns of vegetation composition and diversity in pine-dominated ecosystems of the Outer Coastal Plain of North Carolina: Implications for ecosystem restoration. *Forest Ecology and Management 356*:64–73.

Mitchell, S.R., J.R. Walters, N. Christensen, K. Palmquist, K. Rose, and V. Garcia. In preparation. Herbaceous layer plant composition as a determinant of breeding bird communities in pine forests of the Atlantic Coastal Plain.

Palmquist, K.A., R.K. Peet, and S.R. Mitchell. 2015. Scale-dependent responses of longleaf pine vegetation to fire frequency and environmental context across two decades. *Journal of Ecology 103*(4):998–1008.

Parton, W.J., J.M.O. Scurlock, D.S. Ojima, T.G. Gilmanov, R.J. Scholes, D.S. Schimel, T. Kirchner, J-C. Menaut, T. Seastedt, E. Garcia Moya, A. Kamnalrut, and J.I. Kinyamario. 1993. Observations and modeling of biomass and soil organic matter dynamics for the grassland biome worldwide. *Global Biogeochemical Cycles 7*(4):785–809.

Parton, W.J., D.S. Schimel, C.V. Cole, and D.S. Ojima. 1987. Analysis of factors controlling soil organic matter levels in Great Plains grasslands. *Soil Science Society of America Journal 51*(5):1173–1179.

Samuelson, L.J., T.A. Stokes, J.R. Butnor, K.H. Johnsen, C.A. Gonzalez-Benecke, T.A. Martin, W.P. Cropper, P.H. Anderson, M.R. Ramirez, and J.C. Lewis. 2017. Ecosystem carbon density and allocation across a chronosequence of longleaf pine forests. *Ecological Applications 27*:244–259.

Samuelson, L.J., T.A. Stokes, J.R. Butnor, K.H. Johnsen, C.A. Gonzalez-Benecke, P. Anderson, J. Jackson, L. Ferrari, T.A. Martin, and W.P. Cropper, Jr. 2014. Ecosystem carbon stocks in *Pinus palustris* forests. *Canadian Journal of Forest Research 44*:476–486.

Sanchez, F.G. 2001. Loblolly pine needle decomposition and nutrient dynamics as affected by irrigation, fertilization, and substrate quality. *Forest Ecology and Management 152*(1–3):85–96.

Scheller, R.M., D. Hua, P.V. Bolstad, R.A. Birdsey, and D.J. Mladenoff. 2011. The effects of forest harvest intensity in combination with wind disturbance on carbon dynamics in Lake States Mesic Forests. *Ecological Modelling 222*(1):144–153.

Scheller, R.M., J.B. Domingo, B.R. Sturtevant, J.S. Williams, A. Rudy, E.J. Gustafson, and D.J. Mladenoff. 2007. Design, development, and application of LANDIS-II, a spatial landscape simulation model with flexible temporal and spatial resolution. *Ecological Modelling 201*:409–419.

Scheller, R.M., and D.J. Mladenoff. 2004. A forest growth and biomass module for a landscape simulation model, LANDIS: Design, validation, and application. *Ecological Modelling 180*:211–229.

Varner, J.M., D.R. Gordon, E. Putz, and J.K. Hiers. 2005. Restoring fire to long-unburned *Pinus palustris* ecosystems: Novel fire effects and consequences for long-unburned ecosystems. *Restoration Ecology 13*:536–544.

Xia, Y., K. Mitchell, M. Ek, J. Sheffield, B. Cosgrove, E. Wood, L. Luo, C. Alonge, H. Wei, J. Meng, B. Livneh, D. Lettenmaier, V. Koren, Q. Duan, K. Mo, Y. Fan, and D. Mocko. 2012a. Continental-scale water and energy flux analysis and validation for the North American Land Data Assimilation System project phase 2 (NLDAS-2): 1. Intercomparison and application of model products. *Journal of Geophysical Research, Atmospheres* 117(D3).

Xia, Y., K. Mitchell, M. Ek, B. Cosgrove, J. Sheffield, L. Luo, C. Alonge, H. Wei, J. Meng, B. Livneh, Q. Duan, and D. Lohmann. 2012b. Continental-scale water and energy flux analysis and validation for the North American Land Data Assimilation System project phase 2 (NLDAS-2): 2. Validation of model-simulated streamflow. *Journal of Geophysical Research, Atmospheres* 117(D3).

Appendix 18-A
Supporting Data

The tables in this appendix show modeled estimates of carbon storage for both historical climate data and projections of future climate data based on four climate models recommended by the researchers from DCERP2 Research Project CC-1. We examined the mean of the four climate models despite the fact that they were very different. It is important to note that our examination of mean carbon storage values for different climate change scenarios should not be construed as an examination of four replicate scenarios of climate change. Instead, these should be considered as four distinct scenarios of projections of climate change.

Table 18A-1. Total Carbon Storage (g C m^{-2}) for Prescribed Burn Only, 3-Year Mean Fire Return Interval (MFRI) Management Scenario for Each of the Four Climate Projections

Year	ECHO-G	ECHAM5	GFDL-CM2.1	MIROC-ESM-CHEM
2015	3,518	3,547	3,384	2,951
2035	4,578.	4,452	4,507	3,198
2065	7,860	8,152	8,459	3,656
2100	9,712	10,227	11,503	3,136

Table 18A-2. Modeled Estimates of Carbon Storage (g C m^{-2}) and Associated Uncertainty Estimates for the *No Management* Scenario by Using Baseline Climate Data (1960–2015) and Mean Values of the Four Climate Scenarios

Year	Current Climate Conditions		Projected Climate Change Conditions	
	Mean	(±2SD)	Mean	(±2SD)
2015	3,040	76	3,040	76
2035	5,599	166	6,159	98
2065	8,235	206	9,767	106
2100	8,378	218	10,411	180

Table 18A-3. Modeled Estimates of Carbon Storage (g C m^{-2}) and Associated Uncertainty Estimates for Prescribed Fire Only; Results Are Shown for Two Mean Fire Return Intervals (3 Years and 6 Years)

MFRI	Year	Current Climate Conditions		Projected Climate Change Conditions	
		Mean	(±2SD)	Mean	(±2SD)
3	2015	3,040	76	3,040	76
	2035	5,599	166	5,598	134
	2065	8,235	205	8,194	317
	2100	8,377	217	8,252	132
6	2015	3,040	76	3,040	76
	2035	3,716	224	6,707	152
	2065	10,449	404	10,578	201
	2100	11,018	483	11,048	176

Table 18A-4. Modeled Estimates of Carbon Storage (g C m^{-2}) and Associated Uncertainty Estimates for Managing Forests Under a *Commercial Harvest Cycle I (pulpwood)* Regime by Using Historical Climate Data (1960–2015) and Projections of Future Climate. Results Are Shown for Two Mean Fire Return Intervals (3 Years and 6 Years)

MFRI	Year	Current Climate Conditions		Projected Climate Change Conditions	
		Mean	(±2SD)	Mean	(±2SD)
3	2015	3,040	76	3,040	76
	2035	1,595	16	1,571	34
	2065	2,231	57	2,256	41
	2100	2,653	156	2,655	99
6	2015	3,040	76	3,040	76
	2035	1,818	32	1,832	11
	2065	2,874	55	2,836	40
	2100	3,627	84	3,630	32

Table 18A-5. Modeled Estimates of Carbon Storage (g C m^{-2}) and Associated Uncertainty Estimates for Managing Forests Under a *Commercial Harvest Cycle II* (Timber) Regime by Using Historical Climate Data (1960–2015) and Projections of Future Climate; Results Are Shown for Two Mean Fire Return Intervals (3 Years and 6 Years)

MFRI	Year	Current Climate Conditions		Projected Climate Change Conditions	
		Mean	(±2SD)	Mean	(±2SD)
3	2015	3,040	76	3,040	76
	2035	6,023	209	6,050	151
	2065	2,534	219	2,581	193
	2100	2,755	116	2,816	71
6	2015	3,040	76	3,040	76
	2035	2,519	54	2,935	760
	2065	2,860	28	2,864	65
	2100	3,659	31	3,627	110

Table 18A-6. Modeled Estimates of Carbon Storage (g C m^{-2}) and Associated Uncertainty Estimates for Managing Forests Under *Longleaf Savanna Restoration I* (Understory/Midstory Thinning, Followed by Longleaf Planting) Regime by Using Historical Climate Data (1960–2015) and Projections of Future Climate. Results Are Shown for Two Mean Fire Return Intervals (3 Years and 6 Years)

MFRI	Year	Current Climate Conditions		Projected Climate Change Conditions	
		Mean	(±2SD)	Mean	(±2SD)
3	2015	3,040	76	3,040	76
	2035	7,437	25	7,353	55
	2065	10,053	1775	11,285	1654
	2100	11,986	558	12,378	458
6	2015	3,040	76	3,040	76
	2035	4,692	130	4,643	135
	2065	10,513	65	10,340	179
	2100	13,339	228	13,489	88

Table 18A-7. Modeled Estimates of Carbon Storage (g C m^{-2}) and Associated Uncertainty Estimates for Managing Forests Under *Longleaf Savanna Restoration II* (Clearcutting, Followed by Planting Longleaf) Regime by Using Historical Climate Data (1960–2015) and Projections of Future Climate. Results Are Shown for Two Mean Fire Return Intervals (3 Years and 6 Years)

MFRI	Year	Current Climate Conditions		Projected Climate Change Conditions	
		Mean	(±2SD)	Mean	(±2SD)
3	2015	3,040	76	3,687	55
	2035	6,091	34	6,006	62
	2065	8,617	400	9,673	300
	2100	10,274	668	10,609	50
6	2015	3,040	76	3,040	76
	2035	3,398	90	3,457	106
	2065	8,392	216	8,486	264
	2100	11,598	478	11,634	138

Appendix 18-B
List of Scientific/Technical Publications

Publications

None

Presentations

Mitchell, S.R., N. Christensen, S. Cohen, P. Cunningham, & B. Donnelley. 2015. *Contrasting Patterns of Carbon Flux and Storage in Pine Forest Ecosystems of the Atlantic Coastal Plain: Implications for Ecosystem Restoration and Climate Change Mitigation*. Poster presented at the American Geophysical Union Conference, San Francisco, CA.

Chapter 19

Impacts of Climate Change on Management of Red-Cockaded Woodpeckers at MCBCL

SERDP Project Number: RC-2245

Terrestrial Module

Research Project Number T-4

Lead Researchers:

Dr. Jeffrey R. Walters
Virginia Tech
jrwalt@vt.edu

Dr. Sara Zeigler[1]
Virginia Tech
szeigler@usgs.gov

Supporting Researchers:

Dr. Victoria Garcia, vgarcia@vt.edu

November 2017

Final

[1] Current affiliation: U.S. Geological Survey, Woods Hole Coastal and Marine Science Center; Woods Hole, MA

This report was prepared under contract to the U.S. Department of Defense (DoD) Strategic Environmental Research and Development Program (SERDP). The publication of this report does not indicate endorsement by DoD, nor should the contents be construed as reflecting the official policy or position of DoD. References herein to any specific commercial product, process, or service by trade name, trademark, manufacturer, or otherwise, do not necessarily constitute or imply its endorsement, recommendation, or favoring by DoD.

Table of Contents

Acronyms 19-vii
Abstract 19-1
Objectives of the Research Project 19-2
Background 19-2
Red-Cockaded Woodpeckers and the U.S. Department of Defense 19-2
Impacts of Climate Change on RCWs 19-3
Modeling RCW Population Dynamics and Previous SERDP Research 19-4
Relationships of Background to Objectives 19-5
Materials and Methods 19-5
Forest Dynamic Models—Baseline Models 19-5
Landscape and Management Scenarios 19-10
RCW DSS 19-11
Effects of Climate on RCW Demography 19-12
Results and Discussion 19-15
MCBCL Forest Dynamic Models 19-15
Effects of Climate on RCW Demography 19-15
Conclusions and Implications for Future Research and Implementation 19-20
Effects of Climate on RCW Demography 19-20
Effects of Climate and Management on RCW Habitat 19-22
Research Questions 19-23
Other Key Scientific Findings 19-23
Findings with Implications for Future Base Management 19-23
Literature Cited 19-53
Appendix 19-A: List of Scientific/Technical Publications 19-A-1
Appendix 19-B: List of Students 19-B-1
Appendix 19-C: LANDFIRE Model Settings 19-C-1
Appendix 19-D: ST-Sim User's Guide 19-D-1
Appendix 19-E: ST-Sim Quick Reference Guide 19-E-1

List of Figures

Figure 19-1. Longleaf pine sub-ecosystems modeled within state and transitions models, based on biophysical settings outlined by the LANDFIRE program (Zahn, 2015). 19-35

Figure 19-2. Landscape states, successional pathways, and fire effects for the Central Atlantic Coastal Plain Wet Longleaf Pine sub-ecosystem found within the boundaries of Marine Corps Base Camp Lejeune. 19-36

Figure 19-3. Landscape states, successional pathways, and fire effects for the Atlantic Coastal Plain Upland Longleaf Pine and Other sub-ecosystems found within the boundaries of Marine Corps Base Camp Lejeune, as well as the Atlantic Coastal Plain Fall-Line Sandhill Longleaf Pine Woodland and Other sub-ecosystems found within the boundaries of Fort Bragg..... 19-37

Figure 19-4. Landscape states, successional pathways, and fire effects for the Florida Longleaf Pine Sandhill and Other sub-ecosystems found within the boundaries of Eglin Air Force Base..... 19-38

Figure 19-5. Wind/weather/stress (WWS; e.g., hurricane) and insect/disease (ID) effects for the Atlantic Coastal Plain Upland Longleaf Pine and the Central Atlantic Coastal Plain Wet Longleaf Pine sub-ecosystems found within the boundaries of Marine Corps Base Camp Lejeune, as well as the Atlantic Coastal Plain Fall-Line Sandhill Longleaf Pine Woodland sub-ecosystem found within the boundaries of Fort Bragg. 19-39

Figure 19-6. Wind/weather/stress (WWS [e.g., hurricane]) effects for the Florida Longleaf Pine Sandhill sub-ecosystem found within the boundaries of Eglin Air Force Base..... 19-40

Figure 19-7. The effects of management techniques for the Atlantic Coastal Plain Upland Longleaf Pine, Central Atlantic Coastal Plain Wet Longleaf Pine, and Other sub-ecosystems found within the boundaries of Marine Corps Base Camp Lejeune (MCBCL), as well as the Atlantic Coastal Plain Fall-Line Sandhill Longleaf Pine Woodland and Other sub-ecosystems found within the boundaries of Fort Bragg. 19-41

Figure 19-8. The effects of management techniques for the Florida Longleaf Pine Sandhill and Other sub-ecosystems found within the boundaries of Eglin Air Force Base. 19-42

Figure 19-9. Conceptualization of the linked ST-Sim Landscape Model and the red-cockaded woodpecker (RCW) population model in the RCW Decision Support System (RCW DSS). 19-43

Figure 19-10. Predicted land cover at Marine Corps Base Camp Lejeune (MCBCL) following a 50-year simulation that assumed all management approaches and other natural events (e.g., wildfires, hurricanes) would continue occurring at rates commensurate with present day. 19-44

Figure 19-11. Results of scenarios modeled in the ST-Sim landscape model (for a detailed description of scenario assumptions, see the section of this chapter titled Landscape and Management Scenarios). 19-45

Figure 19-12. Predicted land cover at Marine Corps Base Camp Lejeune (MCBCL) after a simulation of 50 years that assumed longleaf pine stands of low suitability for red-cockaded woodpecker (RCW) nesting would be

prioritized for all habitat management (e.g., prescribed burns, mechanical midstory removal, herbicide application). 19-46

Figure 19-13. Predicted land cover at Marine Corps Base Camp Lejeune (MCBCL) after a simulation of 50 years that assumed the end of all longleaf pine habitat management (e.g., prescribed burns, mechanical midstory removal, herbicide application)..... 19-47

Figure 19-14. Changes in egg-laying dates over time at two study sites in North Carolina: (A) Marine Corps Base Camp Lejeune (MCBCL) and (B) the Sandhills..... 19-48

Figure 19-15. (A) The age at first reproduction and (B) lifespan increased slightly at Marine Corps Base Camp Lejeune (MCBCL). (C) The survival to the first year wavered over time, but the effect was very small..... 19-48

Figure 19-16. Variance in lay dates increased quadratically over time in the Sandhills, NC. 19-49

Figure 19-17. (A) Clutch size and (B) partial brood loss both increased in the Sandhills, NC. 19-49

Figure 19-18. (A) Survival to age 1 increased quadratically over time in Sandhills, NC. (B) Nestling weight and age decreased over time, and (C) the number of fledglings per nest increased slightly. 19-50

Figure 19-19. (A) Age at first reproduction increased in the Sandhills, but (B) lifespan did not change during the same period. 19-51

Figure 19-20. Past temperature trends indicated a mixed pattern in the Southeastern United States compared with the remainder of the United States. 19-51

Figure 19-21. Changes in annual means over time regarding the (A) number of young fledged per group, (B) group size, and (C) breeding male's age in MCBCL, NC. 19-52

Figure 19-22. Changes in annual means over time regarding the (A) number of young fledged per group, (B) group size, and (C) breeding male's age in Sandhills, NC. 19-52

List of Tables

Table 19-1. Characteristics of States Used to Describe Longleaf Pine and Other Sub-ecosystems on Marine Corps Base Camp Lejeune (MCBCL), Fort Bragg, and Eglin Air Force Base in Both the ST-Sim Landscape Model and in the Red-Cockaded Woodpecker (RCW) Population Model as Part of the RCW Decision-Support System (RCW DSS) 19-24

Table 19-2. Management Targets Included in the Baseline Models for Longleaf Pine and Other Sub-ecosystems on Marine Corps Base Camp Lejeune (MCBCL), Fort Bragg, and Eglin Air Force Base (AFB) in the ST-Sim Landscape Model 19-28

Table 19-3. Management and Climate Scenarios Considered for Marine Corps Base Camp Lejeune (MCBCL) 19-28

Table 19-4. The Proportion of the Landscapes at Marine Corps Base Camp Lejeune (MCBCL), Fort Bragg, and Eglin Air Force Base Covered by Each Landscape State Class According to LANDFIRE Data Products for the Year 2014 19-29

Table 19-5. Landscape Composition (in Acres), as Predicted by the ST-Sim Landscape Model, in Response to Altered Climate and Management Regimes at Marine Corps Base Camp Lejeune 19-33

Table 19-6. Summary of How Red-Cockaded Woodpecker Traits Are Changing over Time at Two Sites in North Carolina (See Tables A1 and A2 for Entire Results) 19-34

Table 19-7. Summary of Effects of Local Climate Variables on Red-Cockaded Woodpecker Life History Traits 19-34

Acronyms

°C	degree Celsius
AFB	Air Force Base
AICc	Akaike's Information Criterion corrected for small sample sizes
DCERP	Defense Coastal/Estuarine Research Program
DCERP2	second cycle of DCERP
DoD	U.S. Department of Defense
HA	herbicide application
ID	insect/disease
km	kilometer
m	meter
MCBCL	Marine Corps Base Camp Lejeune
MR	mechanical midstory removal
N/A	not applicable
PB	prescribed burn
PRISM	Parameter-elevation Regressions on Independent Slopes Model
R	replacement fire
R^2	R squared
RC	Resource Conservation and Climate Change (a SERDP program area)
RCW	red-cockaded woodpecker
RCW DSS	Red-Cockaded Woodpecker Decision-Support System
S	surface fire
SERDP	Strategic Environmental Research and Development Program
T	Terrestrial (Module)
WG	wiregrass planting
WWS	wind/weather/stress

Abstract

The overarching goal of Research Project T-4 was to provide Marine Corps Base Camp Lejeune (MCBCL) managers with information they will require to continue to integrate recovery of the endangered red-cockaded woodpecker (RCW; *Picoides borealis*) with military training and other management goals as climate changes. Specific objectives involved evaluating possible impacts of climate change on RCW demography and population dynamics and constructing a modeling tool that will allow managers at MCBCL and Fort Bragg (both in North Carolina) to conduct additional assessments of how management activities might affect RCWs on current and future landscapes. We used long-term data (1980–2013) to examine changes in demographic traits over time, as well as the relationships of these traits to climate, at MCBCL and Fort Bragg. We found that many traits are changing and that these and other traits consistently varied with local temperature and rainfall. At both sites, warmer temperatures had positive effects on several traits, leading to increased production of fledglings. At MCBCL, increased rainfall had some negative effects. As climate continues to change, one may expect increased productivity at Fort Bragg and increased variation in productivity at MCBCL. These results show how climate is affecting this endangered species in the northern end of its range. Changing climate appears to be having negative effects on RCW productivity in the southern portions of the range in Florida.

We developed forest dynamics models specific to longleaf pine (*Pinus palustris*) sub-ecosystems as described by the LANDFIRE Program. In our specific models, we evaluated the landscape in 0.2-acre map cells, and models included states that were characteristic of the land-cover and vegetation types found throughout the relevant military installations in the southeast and that were relevant to RCW habitat needs. As such, each state was associated with a specific RCW habitat suitability value. Landscape cells move from one state to another through probabilistic or deterministic transitions involving natural processes (e.g., succession, aging, natural wildfires) and management (e.g., prescribed burns, herbicide treatments, mechanical midstory removal). As a proof of concept, we simulated several landscape scenarios for MCBCL that explored altered management and climate regimes and compared them to a “baseline” scenario reflecting current conditions. Two scenarios resulted in increases in area with open midstories and dense understories, which are both characteristic of optimal RCW habitats. These scenarios included an increase in the current prescribed fire regime and a management regime in which pine stands currently in poor condition for RCWs were prioritized for habitat management. The remaining scenarios considered resulted in reductions in optimal RCW habitat. A reduction in the frequency of wildfires and the cessation of all habitat management activities resulted in the largest decreases in optimal RCW habitat. Other changes to environmental conditions, including an increased frequency of hurricanes and wildfires, and a management regime in which currently suitable pine stands were prioritized for management also resulted in decreased RCW habitat compared with current conditions. These results suggest that the most efficient management of the landscape for RCW habitat would prioritize prescribed burning, particularly of pine stands currently in poor condition for RCWs. Furthermore, climate change—if it alters wildfire frequencies in either direction or increases the frequency of hurricanes—could negatively affect RCW habitat in the future.

Keywords: Climate change, demography, forest dynamics, LANDFIRE, model, red-cockaded woodpecker, *Picoides borealis*.

Objectives of the Research Project

The overarching goal of Research Project T-4 was to provide Marine Corps Base Camp Lejeune (MCBCL) managers with information they will require to continue to integrate recovery of the endangered red-cockaded woodpecker (RCW, *Picoides borealis*) with military training and carbon sequestration goals as climate changes. This information drives the management of the terrestrial ecosystem. Specific objectives were to: (1) evaluate the possible impacts of climate change on the demography of RCWs; (2) use simulation modeling to assess how the dynamics of the RCW population on MCBCL may be altered by the effects of climate change on RCW demography and forest structure; (3) provide MCBCL with a modeling tool that will allow Base managers to make additional assessments of how management activities might impact the RCW population on current and future landscapes; and (4) provide a refined version of this same tool to an additional North Carolina installation, Fort Bragg. The questions guiding the research included the following:

1. Based on current linkages between weather and RCW productivity, how are projected changes in weather due to climate change predicted to alter RCW productivity on MCBCL and Fort Bragg?
2. Based on simulation modeling, how are projected changes in RCW demography and longleaf pine (*Pinus palustris*) habitat due to climate change predicted to alter RCW population growth on MCBCL?

Background

Red-Cockaded Woodpeckers and the U.S. Department of Defense

The RCW is an endangered species endemic to pine savannas of the southeastern United States. The species became endangered due to loss of habitat, particularly preferred longleaf pine savannas, and alteration of remaining habitat due to fire suppression (U.S. FWS, 2003; Walters, 1991). The species appeared to be on the verge of extinction in the 1980s (Costa and Escano, 1989). Because of the RCWs' endangered status and large area requirements (Conner et al., 2001), their needs have driven habitat management on most military installations in the southeastern United States for the past 30+ years. Recovering the species to a point at which it no longer restricts military training activities is a high priority within the U.S. Department of Defense (DoD).

RCW population dynamics are unusual and derive from two linked peculiarities of its biology: (1) its habit of constructing cavities in living pines and (2) its cooperative breeding system (Conner et al., 2001; Walters and Garcia, 2016). Cavities take many years to construct, but they can be used for years to decades once completed (Harding and Walters, 2002); thus, existing cavities are a highly valuable resource. Birds compete for breeding positions on territories that already contain a set of such cavities, rather than establishing new territories in unoccupied habitat (Walters et al., 1992). The best management strategy for RCWs, therefore, is one that focuses on territory quality, with a specific aim at preventing existing territory abandonment while creating additional new territories. This strategy is preferred over those that focus on demography and that are designed to increase reproduction or reduce mortality (Walters, 1991).

A territory-focused management strategy that combines restoration of longleaf pine ecosystems with new, species-specific management techniques was developed (Walters, 1991), and has proven to be highly effective, especially on DoD lands (Costa, 2004; Walters and Garcia, 2016).

The RCW is highly dependent on DoD lands for its recovery. Fourteen installations support RCW populations, and 10 are among the 39 designated recovery populations. All or a portion of six Primary Core Populations (of 12 such populations region-wide), which are the populations most critical to recovery, are located on military installations (Camp Mackall, Eglin Air Force Base [AFB], Fort Benning, Fort Bragg, Fort Polk, Fort Stewart, and MCBCL) (U.S. FWS, 2003). These include four of the six largest RCW populations. Since publication of the Recovery Plan (U.S. FWS, 2003), these four populations have exceeded the prescribed population size for recovery (i.e., greater than 350 active territories) and have therefore been declared recovered by the U.S. Fish and Wildlife Service.

Similar to other DoD installations in the southeastern United States, the primary conservation objectives of MCBCL natural resource managers for the installation's terrestrial environment are to restore the longleaf pine ecosystem and to recover the RCW within that system while supporting the military training mission. The RCW population on MCBCL has not yet been recovered, but the installation has been a leader in efforts to recover the species. The RCW population on MCBCL has been completely and intensively monitored since 1986, and MCBCL was the first location where the new management strategy was employed, beginning in 1991 (Walters, 2004). Based on the habitat available, the recovery goal for the MCBCL population was set at 173 active territories (U.S. FWS, 2003). When management was initiated in 1991, there were only 35 active RCW territories on MCBCL; only 27 of those territories contained family groups capable of reproduction. By 2017, the population had increased to 128 active territories, 115 of which contained family groups. Clearly the new RCW management strategy met with great and (literally) unprecedented success on MCBCL.

Impacts of Climate Change on RCWs

The DoD has had great success in meeting its RCW recovery objectives, while continuing to support its training mission, but climate change presents a challenge to continued success. When faced with changing habitat selection pressures that can result from a changing climate, only four outcomes are possible for populations: (1) moving to new habitat where the selection pressure is similar to the old habitat; (2) remaining in place, but altering some traits in response to the selection pressure via phenotypic plasticity; (3) adapting to the new selection pressure through changes in genotype frequencies (i.e., microevolution); or (4) local extinction (Gienapp et al., 2008; Holt, 1990). Latitudinal and altitudinal range shifts in response to climate change are widely documented, including in birds (Parmesan and Yohe, 2003; Walther et al., 2002). As a habitat specialist tied to the longleaf pine ecosystem, a range shift is not an option available to RCWs. Similar to other long-lived species with slow life histories, longleaf pine will shift its range at a much slower rate than the rate at which climate is changing (Lenoir et al., 2008), an impact that is augmented by the extremely limited dispersal range of this large-coned species and the RCW's requirement for old growth forest. Hence, RCWs must respond to climate change *in situ* through phenotypic plasticity or microevolution to avoid the outcome of local extinction.

Knowing the extent to which RCWs can adapt to changing climate via means other than range shifts, and knowing the limits to those adaptations, will be critical to determining the proper management and conservation of this and other species that are unlikely to alter their distribution in response to climate change. Advancement of the timing of breeding (lay date) is a widely documented response of avian species to climate change, including RCWs (Schiegg, 2002). How other life history traits of the species are being affected by climate change is unknown. Also, for those traits that are changing, understanding the mechanism (phenotypic plasticity or microevolution) by which the birds are altering life history patterns will provide insight into the extent to which populations are subject to changing natural selection regimes and environmental conditions (Charmantier et al., 2008; Husby et al., 2010), as well as understanding the level of adaptability and possible limits to the changes that the RCW can undergo.

Modeling RCW Population Dynamics and Previous SERDP Research

Determining how alterations in RCW demography are driven by climate change, and how they will impact the future viability of RCWs, requires projecting those impacts to the population level in population dynamics models. Standard models used for population viability analysis, such as matrix models, have limited applicability to RCWs because they do not incorporate the extreme spatial constraints on dispersal that characterize this species (Heppell et al., 1994; Maguire et al., 1995; Walters et al., 2002a; Zeigler and Walters, 2014). Many males and some females, instead of dispering in their first year, remain on their natal territory as non-breeding helpers (Lennartz et al., 1987; Ligon, 1970; Walters et al., 1988). Helpers eventually become breeders by inheriting a breeding position on their natal territory or dispersing to fill a breeding vacancy, but they only compete for breeding vacancies in the neighborhood of their home territory (Daniels and Walters, 2000; Kesler et al., 2010). Helpers represent a pool of replacement breeders and thus can act as a buffer between breeder mortality and population productivity. Thus, the critical breeding population remains stable while the larger population fluctuates, reducing the population-level impacts of environmental stochasticity (Grimm et al., 2005; Letcher et al., 1998). However, this buffering effect occurs only if helpers are within dispersal range of the territories on which breeders perish. As a result, the spatial distribution of territories has impacts on population dynamics comparable to those of population size (Walters et al., 2002a). There are also spatial constraints on dispersal of individuals that disperse in their first year, as most disperse through forays that limit their movement to approximately 6 km (Kesler et al., 2010). A small proportion of these juveniles become jumpers that engage in long-distance dispersal of almost unlimited range, during which these individuals lack the sensitivity to habitat that characterizes helpers and foraying juveniles (Kesler et al., 2010).

Because spatially explicit, individual-based models track the performance and fate of individual organisms (Judson, 1994) and their locations (Dunning et al., 1995), the models can incorporate constraints on movement such as those that occur in RCWs. We constructed such a model for RCWs (Letcher et al., 1998) and demonstrated its utility in accurately projecting the dynamics of RCW populations (Schiegg et al., 2005; Walters et al., 2002a; Zeigler and Walters, 2014). Initially, the use of this model was limited to our research group. During a previous SERDP research project (RC-1472), we developed the Red-Cockaded Woodpecker Decision-Support System (RCW DSS) Tool, which is a user-friendly version of the model for general use on DoD installations with RCW populations. The RCW DSS Tool has been widely used across the southeastern United States, including by MCBCL staff. The DSS Tool has two options for

interaction of RCWs with the landscape, a land-cover option and an RCW matrix option. In the land-cover option, the quality of habitat associated with each RCW group is a simple function of land-cover type and the age of pine stands. In the RCW matrix option, habitat quality is determined by scores produced by the tool that the U.S. Fish and Wildlife Service uses to evaluate RCW foraging habitat (i.e., the RCW matrix).

To develop the RCW DSS further, we added the capability for the model to evaulate potential changes in habitat availability through the use of a state-and-transition model. The state-and-transition model, developed in the generic platform ST-Sim (Daniel and Frid, 2011), allows the user to simulate likely future landscapes that reflect changes to, for example, the climate or local habitat management regime. These simulated landscapes can be used within the RCW DSS to further investigate how landscape change effects the viability of RCW populations. This work began as part of another SERDP research project (RC-1696), in which we developed a forest dynamics model option for the RCW DSS appropriate for longleaf pine sandhills habitat on Eglin AFB (in Florida). Here, we develop a second version of the forest dynamics model option that is appropriate for the pine habitats on MCBCL and a third version that is appropriate for longleaf pine habitat on a third installation, Fort Bragg (in North Carolina).

Relationships of Background to Objectives

The fate of the RCW depends upon its ability to adapt to changing conditions at the locations where it currently exists, perhaps within a restricted range; longleaf pine forest has been predicted to decline under different climate change scenarios (Hansen et al., 2001; Iverson and Prasad, 2001; but see Iverson et al., 2008). One of our objectives was to document the relationships between weather and RCW demography over the past 25 to 30 years, thus as a first step toward projecting the capability of RCWs to persist as the climate and RCW habitat continues to change.

Furthermore, many species with large geographical distributions display variability in habitat selection and use (Collins, 1983; Liles et al., 2015; Noon and McKelvey, 1996), including RCWs (McKellar et al., 2014). Variability in habitat use can make “one-size-fits-all” management plans or models used to support those management plans ineffective. Therefore, our objectives in this and a previous research project (RC-1969) included the development of a suite of site-based habitat models for RCWs, with type-localities for Eglin AFB in Florida and MCBCL and Fort Bragg, both in North Carolina (**Figure 19-1**). These models are linked to our spatially explicit, individual-based model of RCW population dynamics through the RCW DSS.

Materials and Methods

Forest Dynamic Models—Baseline Models

We developed a forest dynamics model for longleaf pine ecosystems throughout the southeastern United States in representative areas within the RCW geographical distribution. These forest dynamics models are specific to longleaf pine sub-ecosystems (or biophysical settings), as described by the LANDFIRE Program (a joint program by the U.S. Department of Agriculture’s Forest Service and the U.S. Department of the Interior; https://www.LANDFIRE.gov/index.php) (Rollins, 2009; Zahn, 2015). Sub-ecosystems modeled in this study include (1) Central Atlantic

Coastal Plain Wet Longleaf Pine (MCBCL), (2) Atlantic Coastal Plain Upland Longleaf Pine (MCBCL and Fort Bragg), (3) Atlantic Coastal Plain Fall-line Sandhills Longleaf Pine Woodland (MCBCL and Fort Bragg), and (4) Florida Longleaf Pine Sandhill (Eglin AFB; **Figure 19-1**). One additional "sub-ecosystem" was modeled for each study area to include forests and land-cover states not reflective of the previously mentioned longleaf pine states. This sub-ecosystem was labeled as "Other," and included states for Bare Land, Other, Water, Hardwood Forest, Mixed Pine/Hardwood Forest, and Other Pine. Models of these sub-ecosystems were designed as state-and-transition models intended for simulation in the program ST-Sim (Daniel and Frid, 2011). A more detailed description of these sub-ecosystems and their representative distributions, vegetation types, and disturbances (based on the LANDFIRE descriptions of biophysical settings) are in **Appendix 19-C**.

Using LANDFIRE products as the foundation of our modeling efforts promoted consistency across sites. LANDFIRE models are based on published literature, local data sets, and expert opinion, and these models undergo a rigorous review process prior to publication. We further refined models for use at finer scales within military installations, added transitions for relevant management activities, and modified states as necessary to make models relevant to RCW management. Original LANDFIRE states and transitions are described in **Appendix 19-C**, and revised foundational successional models for RCW management are shown in **Figures 19-2 through 19-4**.

States

In any ST-Sim model, map units (e.g., map cell, forest stand) in the total study area must fall within a discrete land-cover class known as a "state." In our specific ST-SIM models of longleaf pine ecosystems, we evaluated the landscape in 0.22-acre map cells and included states that were both characteristic of the land-cover and vegetation types found throughout the relevant military installations and relevant to RCW habitat needs. As such, each state was associated with a specific RCW habitat suitability value (ranging from 1 to 5; **Table 19-1**). We included major land-cover classes for Other Pine (e.g., loblolly pine [*Pinus taeda*]), Developed, Hardwood, Water, Bare Land, Mixed (Pine/Hardwood), and Longleaf Pine.

Pine classes further consisted of a series of states that describe stand age as well as midstory and ground-cover characteristics. Generally, preferred habitat for RCWs consists of mature, open longleaf pine savannas with large/old trees, sparse midstory, and lush herbaceous groundcover (Hardesty et al., 1997; James et al., 2001; U.S. FWS, 2003; Walters et al., 2002b). Studies have shown that RCW stand-use declines as the density of small pines (Porter and Labisky, 1986; Walters et al., 2000; Walters et al., 2002b) and the density (Hooper and Harlow, 1986; Jones and Hunt, 1996) and height (Walters et al., 2000; Walters et al., 2002b) of hardwood trees in the midstory increase. In addition, larger, more productive RCW groups are found in areas with a high percentage cover of grasses and forbs in the understory (James et al., 1997). Therefore, the Longleaf Pine states used within the ST-Sim models were characterized by age (0–14 years; 15–74 years; and greater than 75 years), midstory characteristics (Open; Closed); and herbaceous understory characteristics (Sparse; Dense; **Table 19-1**). Similarly, states within the Other Pine classes were described as having an Open or Closed midstory and a Dense or Sparse herbaceous ground cover. Suitability values for Longleaf Pine and Other Pine states reflect the RCWs' preferences for (1) large, old trees over small, young trees for foraging (Bradshaw, 1995;

DeLotelle et al., 1987; Engstrom and Sanders, 1997; Hardesty et al., 1997; Hooper and Lennartz, 1981; Jones and Hunt, 1996; Porter and Labisky, 1986; Walters et al., 2000 and 2002b; Zwicker and Walters, 1999); (2) low midstory height and density (Bradshaw, 1995; Doster and James, 1998; Hardesty et al., 1997; Hooper and Harlow, 1986; Walters et al., 2000 and 2002b); and (3) a high groundcover density of native grasses and herbs (Hardesty et al., 1997; James et al., 1997 and 2001).

Landscape cells categorized as Hardwood and Mixed contain forest stands where most trees are hardwood species or a mixture of pine and hardwood species, respectively. Landscape cells identified by the Other state have been clear-cut, paved, or heavily altered for or by human use, and the Bare Land state describes areas with exposed soil (e.g., shoreline and cleared bombing ranges). Finally, the Water state includes areas covered by waterbodies.

These land-cover types are prevalent throughout the RCW distribution and within the military installations considered. Except for the Longleaf Pine and Other Pine states, we did not consider additional attributes for age or forest structure in other states, because, in some instances, forest structure is irrelevant (i.e., Other, Water, Bare Land) or because, in other instances, RCWs use these land-cover types infrequently irrespective of the forest structure (Hardwood, Mixed) (Bradshaw, 1995; Hardesty et al., 1997; Hooper and Lennartz, 1981; Porter and Labisky, 1986; Repasky, 1984). Although each of these non-pine states is associated with unsuitable land cover (suitability=1), it was important to include these unsuitable states because RCW habitat could be converted to these other states through long-term successional processes or through immediate human modification to the landscape, which could have important consequences for RCW populations.

Transitions

In any ST-SIM model, landscape cells within the model move from one state to another through probabilistic or deterministic transitions. In our modified LANDFIRE models of longleaf pine ecosystems, those transitions occur for each 0.22-acre landscape cell through (1) natural processes (e.g., succession, aging, natural wildfires) and (2) management (e.g., prescribed burns, herbicide treatments, mechanical midstory removal).

Longleaf pine ecosystems transform from savanna-like woodlands to closed canopy forests with higher overstory density and lower understory species richness and abundance when fire is suppressed (Brockway and Lewis, 1997; Gilliam and Platt, 1999; Glitzenstein et al., 2003; Provencher et al., 2001c; Rodgers and Provencher, 1999; Ware et al., 1993). Without fire, longleaf ecosystems ultimately develop into forests of mixed pine and xeric/mesic hardwoods (Myers, 1985; Veno, 1976) that are unsuitable for RCWs (Bradshaw, 1995; Hardesty et al., 1997; Hooper and Lennartz, 1981; Porter and Labisky, 1986; Repasky, 1984). However, variations in soil type, moisture, and fertility can change how specific longleaf pine ecosystems (e.g., spodosol versus ultisol flatwoods) respond to similar fire frequencies based on differences in ecosystem productivity (Glitzenstein et al., 2003; Mitchell et al., 1999). For this reason, we developed separate models for each longleaf pine sub-ecosystem for each focal military installation (**Figures 19-2 through 19-4**).

Although the probability and effects of specific transitions differed slightly among sub-ecosystem models, all models considered the same natural and management transitions (except for wiregrass planting). All land-cover cells proceeded from one state to another on a defined successional pathway as forest stands aged, and cells proceeded along an alternative pathway in the absence of fire or management applications. The speed of succession in each ecosystem modeled was defined by the original LANDFIRE models and considered soil type, moisture, and fertility (**Figures 19-2 through 19-4; Appendix 19-C**).

Three forms of natural disturbance could interrupt these successional pathways, as specified by the original LANDFIRE models: wildfires (**Figures 19-2 through 19-4**), hurricanes (**Figures 19-5 and 19-6**), and insect/disease outbreaks (**Figure 19-5**). Wildfires could occur on the landscape at different intensities and include surface (low intensity), mixed (moderate intensity), and replacement (high intensity) fires. A given landscape cell's probability of experiencing each of these fire types, hurricanes, or insect/disease outbreaks was dependent on that cell's state and was provided in the original LANDFIRE models (**Appendix 19-C**). In general, surface fires maintained the cell's current state, mixed fires reverted the cell to a more open state, and replacement fires, hurricanes, and insect/disease outbreaks reverted the cell to the Early Development (Early:ALL) state (**Figures 19-2 through 19-4**). For all forms of natural disturbance, the ST-SIM model uses probabilities to calculate the approximate area affected by each transition each year for each state.

We also added disturbances for intentional management activities to the original LANDFIRE models. Management transitions included prescribed burns, mechanical midstory removal, herbicide application, and wiregrass planting. Studies examining restoration techniques in longleaf pine ecosystems have shown that prescribed burns decreased oaks in smaller size classes by 20% compared to controls (Provencher et al., 2001b), increased understory densities (Provencher et al., 2001a and 2001b) and created plant, arthropod, herpetofauna, and bird communities that were more similar to frequently those in burned reference plots (Provencher et al., 2001c, 2002a, 2002b, and 2002c). We assumed that prescribed burns would behave in a manner similar to surface or mixed wildfires, reverting a given cell's original state to a more open condition (**Figures 19-7 and 19-8**).

Similarly, a large-scale study of restoration techniques at Eglin AFB also showed that the use of herbicides and the mechanical chainsaw felling and girdling of hardwood species in the midstory (or "mechanical midstory removal") were extremely effective in reducing the hardwood midstory. Oaks in the smallest size classes decreased by 60% after herbicide treatments and by 90% after mechanical removal treatments when compared with control plots (Provencher et al., 2001a and 2001b). Irrespective of the method used, this reduction in hardwood tree density followed by a spring burn ultimately resulted in a higher presence of RCWs and other bird species associated with longleaf pine ecosystems compared with control plots (Provencher et al., 2002b and 2002c). However, although herbicide and mechanical removal improved midstory suitability, these management techniques alone did not improve the condition of the herbaceous understory when compared with control and fire plots (Provencher et al., 2001a). Therefore, we modeled the effects of herbicide and mechanical midstory removal such that the landscape cell's original state was maintained (for already open states), or the state reverted to one with an open midstory, but a sparse understory (**Figures 19-7 and 19-8**).

Finally, we considered a management transition for wiregrass planting at MCBCL because this technique is practiced at the Base over limited spatial scales. We assumed that wiregrass planting would only occur in states that have an open midstory, but a sparse ground cover (**Figure 19-7**).

A target area was set for each management activity in each longleaf pine sub-ecosystem. Target areas were provided by staff at MCBCL (G. Haught, unpublished data) and Eglin AFB (K. Hiers, unpublished data) and reflected the area affected by actual management activities on each Base (**Table 19-2**). Because target areas were unknown for Fort Bragg, we left these values at "0 acres" in the baseline model. However, a user could manipulate target area values for any management transition, sub-ecosystem type, or military installation to explore the effects of different management regimes. We also assigned a probability that each state would experience a prescribed burn, mechanical midstory removal, or herbicide application per data provided by staff at MCBCL (G. Haught, unpublished data; **Figure 19-7**) and Eglin AFB (K. Hiers, unpublished data; **Figure 19-8**). Because probabilities were unknown for Fort Bragg, we used MCBCL probabilities. Unlike the probabilities used for natural disturbances, those associated with management activities instead provided a relative ranking by which cells in each state experience each management activity. For example, cells characterized as Mid-development with an Open midstory and Dense groundcover have a greater probability of being burned (0.3) compared with those characterized as Late development with an Open midstory and Dense groundcover (0.003) in the Atlantic Coastal Plain Upland Longleaf Pine sub-ecosystem on MCBCL (**Figure 19-7**). With this parameterization, the ST-SIM model will always simulate a prescribed burn in enough cells to meet the annual management target; however, cells belonging to states with the highest probability of being burned will experience the transition first, followed by those within the state with the next highest probability, and so on until the management target has been met.

Input Data

Initializing the ST-SIM models requires GeoTiff files that reflect the following: (1) sub-ecosystem types, (2) land-cover states at time 0 (t_0), and (3) stand ages for each study area. In other words, each 30-m × 30-m raster cell (0.22 acre) within the boundaries of every study area contained a value for sub-ecosystem type, ST-SIM land cover state, and stand age. We created these GeoTiff files in ArcGIS version 10.2 from LANDFIRE products (available at https://www.landfire.gov/vegetation.php). At the time this research was conducted, the most recently available LANDFIRE products reflected 2014 land-cover conditions, and we used these data sets.

Boundaries for each sub-ecosystem were derived from the LANDFIRE "Biophysical Settings" raster layer. We then combined this Existing Vegetation Type layer with LANDFIRE'S "Existing Vegetation Type" and "Succession Classes" raster layers to determine the exact ST-SIM land-cover state. Finally, we approximated stand age based on the land-cover state. See the user manual in **Appendix 19-D** for additional information on this procedure.

For each study area, the raster layers for sub-ecosystem (referred to alternately as "Vegetation Type" or "Biophysical Setting" in ST-SIM), state class, and age were projected to North American Datum 1983 with Universal Transverse Mercator Zone 18N, clipped to the boundaries of the study area, and exported as a GeoTiff for use in ST-SIM. GeoTiff files used as input layers

are available for each study area and are stored in the ArcGIS file geodatabase accompanying this *DCERP2 Final Report*.

Landscape and Management Scenarios

As an example of the utility of these landscape models, we modeled several scenarios related to changes (or lack of changes) to current management or other environmental conditions at MCBCL. Scenarios (with additional details provided in **Table 19-3**) included the following:

1. *Baseline*—We assumed that current landscape management and fire regimes would continue for the entire 50-year simulation.
2. *No Management*—We assumed the cessation of all current landscape management efforts, including prescribed fire, midstory removal, herbicide application, and wiregrass planting.
3. *Altered Fire Regime*—We modeled two scenarios related to an altered fire regime. In the first scenario, we assumed a reduction of the acreage currently burned through prescribed fire by half (Half Prescribed Scenario). In the second scenario, we assumed a doubling of the acreage currently burned through prescribed fires (2xPrescribed Scenario). In the 2xPrescribed Scenario, we also assumed that the increase in resources devoted to prescribed burning would come at a cost to other management techniques. Thus, no mechanical midstory removal, herbicide application, or wiregrass planting occurred under this scenario.
4. *Longleaf Management*—We assumed that all landscape management efforts would be focused on the highest quality longleaf sites (Mid- and Late Development states with Open midstories and Dense understories) at the expense of restoring lower quality sites.
5. *Restoration Management*—This scenario offered a contrasting alternative to the Longleaf Management Scenario. In this scenario, we assumed that landscape management efforts would be focused on lower quality sites (Early Development and Mid- and Late Development states with Closed midstories and sparse understories) at the expense of maintaining already high-quality sites.
6. *Climate Regimes*—In this final set of scenarios, we assumed that specific transitions would occur at lower or higher probabilities because of climate change. We explored scenarios in which (1) the probability of hurricanes doubles (2xHurricane Scenario), (2) the probability of hurricanes quadruples (4xHurricane Scenario), (3) the probability of natural wildfires occurring is cut in half (Half Wildfire Scenario), and (4) the probability of wildfires occurring doubles (2xWildfire Scenario).

We modeled both spatially explicit and non-spatially explicit simulations for each scenario. For the spatially explicit simulations, the input GeoTiff layers explicitly dictated initial landscape conditions, and we simulated all models for one iteration of 50 time steps. The output for these simulations was a GeoTiff layer representing land-cover state classes at time step 50. These map outputs could later be used within the RCW DSS tool. For the non-spatially explicit models, the model was initialized by using the proportion of the total landscape area covered by each land-cover state class (per the GeoTiff layers; **Table 19-4**). These models were run for 10 iterations of

50 time steps, and the output consisted of the proportions of the landscape (averaged over 10 iterations) covered by each state class at the end of 50 time steps (years) for that scenario.

Although we did not run scenarios for Eglin AFB or Fort Bragg, we also include landscape state class proportions (**Table 19-4**) and GeoTiff files (see ArcGIS File Geodatabase accompanying this report) for use in initializing scenarios for these military installations.

RCW DSS

The RCW DSS was developed as two independent, but connected models (**Figure 19-9**) under the "metamodel approach." This approach is conceptualized as the linking of often discipline-specific models representing components of a larger system to reveal emergent properties of multi-dimensional interactions (Lacy et al., 2013). In the RCW DSS, the two connected models are the RCW population model and a landscape model. The ST-SIM landscape model represents a new, dynamic landscape option, added to the two, previously-existing static landscape options, for the latter. The ST-Sim model is simulated for a user-specified number of time steps. Resulting predictive land-cover state maps created through the simulation can be exported in temporal increments of the user's choosing (e.g., we created a map for year 50 for each scenario previously listed). These predictive maps can then be uploaded into the RCW population model as input files, thereby allowing users to evaluate RCW population dynamics as habitat suitability changes through time.

The second component of the RCW DSS—the RCW population model (Walters et al., 2011)—runs as an add-on in ArcGIS version 10 (ESRI, Redlands, CA). Although the RCW DSS can be applied to populations anywhere in the RCW distribution range, the model was specifically created to inform critical management decisions for RCW populations on military installations in the southeastern United States (Walters et al., 2011). The model is stochastic and is unique in its incorporation of social behaviors that drive population dynamics (Zeigler and Walters, 2014). In general, simulations developed in the RCW population model are constructed as scenarios in ArcGIS with spatial layers for RCW cavity tree clusters (i.e., territories) and for the underlying landscape. Representations of the underlying landscape can be forecasted through the ST-SIM model in the RCW DSS application. The map of cavity tree clusters shows all occupied and unoccupied territory centers at the start of a simulation. The RCW population model also allows for the creation of new territories through budding (i.e., a process in which a single group splits into two when enough suitable habitat is available) or through the addition of sets of human-created artificial cavities, known as recruitment clusters.

In the RCW population model, the landscape is depicted in seven categories that delineate how that parcel could be used within the model: (1) Pine: suitable for both breeding and foraging; (2–4) Open, Water, or Other (all considered gaps): suitable only for the movement of some RCW classes; and (5–7) Hardwood, low-suitability Pine, or Mixed pine–hardwood stands: suitable only for the movement of RCWs. In the RCW DSS, we derive predictive land-cover maps from the ST-SIM landscape model and reclassify those land cover states to the seven categories recognized by the RCW population model.

During any simulation within the RCW population model, individual RCWs are categorized based on a defined set of life history stage classes, which subsequently determine movement,

mortality, and fecundity rates. At birth, males are added as fledglings that (1) die within their first year; (2) remain in their natal territories as helpers, breeders, or solitary males; or (3) disperse from their natal territories during their first year. Individuals that disperse either fill a breeding vacancy or become a solitary male or floater. Female fledglings exercise Option 1 or Option 3. Dispersal range and land-cover types over which individuals will travel are dependent on the sex and stage of the individual. The user chooses stage-specific transition, mortality, and fecundity rates by selecting one of two demographic sub-models within the RCW population model. The Sandhills sub-model is based on observations of RCW populations in the Sandhills from 1980 to 1994 (Letcher et al., 1998; Walters et al., 1988), and this sub-model is appropriate for modeling interior populations at installations like Fort Bragg. The Coastal sub-model is based on observations on MCBCL in coastal North Carolina from 1986 to 2001 (Walters, 2004), and this sub-model is most appropriate for coastal populations on installations such as MCBCL and Eglin AFB. Demographic and environmental stochasticity are automatically incorporated into the RCW population model through these sub-model-specific survival and fecundity rates (Letcher et al., 1998; Walters et al., 2002). The final outputs produced by the RCW DSS illustrate a likely future RCW population size and composition, as well as territory availability and locations.

Effects of Climate on RCW Demography

We used existing long-term demographic data collected at a coastal site (MCBCL; 1986–2013) and an inland site (Sandhills; 1980–2013) in North Carolina. At both sites, the birds inhabit a mixture of mature pine savanna and more degraded pine stands, including longleaf and loblolly pine. Information about population monitoring and data collection is found in Walters et al. (1988). These data contained the following for each individual in each year: group/territory affiliation, age (in years), status (i.e., breeder, helper, floater, fledgling), and kin relationship (if a helper) to breeders. They also contained the following data for each nesting attempt in each group and each year: number of eggs, identity and number of nestlings, identity and number of fledglings, group size (number of breeding adults plus helpers), nest fate, and age (in days) and weight of each nestling at the time when it was banded. If the age of an individual was unknown because it was banded as an adult, then we substituted the mean adult age for each sex so that data points would not be excluded due to missing values in this covariate. We substituted mean ages for missing ages for 402 out of 2,581 males and 450 out of 3,111 females.

From the data set, we derived the following variables for each occupied territory and individual in each year: the date when the first egg was laid (first attempts only), the variance in laying date (first attempts only), clutch size (first attempts only), nest survival (first attempts only), the difference between clutch size and number of fledglings for successful nests (partial brood loss, first attempts only), the number of fledglings (annual fecundity, excluding rare double broods), fledgling survival to the first year (successful attempts), within-brood variance in nestling weight (hatching asynchrony, all attempts), nestling size (weight/age, all attempts), age at first reproduction, and lifespan. We also included the following random effects as appropriate to the individual analysis: study site, area within the study site (location), territory, and individual identity.

Association Between Habitat Quality and Group Size

RCW habitat has improved at the two sites during the past 30 years due to greatly improved management practices (Conner et al., 2001). Habitat management actions, such as providing artificial cavities, maintaining mature trees, and especially applying prescribed fire and thinning to control midstory vegetation, have been key in increasing and maintaining RCW populations at both MCBCL and Fort Bragg during the period over which we analyzed climate effects. Therefore, changes in traits over this time could be partly or wholly due to improved habitat quality through management rather than changes in climate. Unfortunately, we did not have annual measures of habitat quality at each territory. To separate the effects of habitat improvements from the effects of climate change, we sought to control for changing habitat quality by including a covariate known to be associated with habitat quality, group size (Conner et al., 2001; Heppell et al., 1994; McKellar et al., 2014). Also, male and female age are known to be associated with some of the traits we examined, such as lay date and clutch size, in many species (Clutton-Brock, 1988; Hochachka, 1990; Smith, 1993), so we also included parental age in the analyses to account for age-related effects.

To determine the extent to which group size was an adequate control for changing habitat quality, we examined whether group size predicted a widely used measure of RCW habitat quality, foraging habitat quality scores (R-scores), which are derived from the RCW Matrix Application (for more information, see http://www.fws.gov/rcwrecovery/matrix.html). We only had R-scores for the Sandhills study area in 2009. Thus, we were unable to test the relationship between habitat quality and group size for MCBCL and had to assume that results from the Sandhills analysis also apply to MCBCL due to similar management practices at both sites. We were interested in determining whether group size predicted habitat quality, so we used group size as the explanatory variable and R-score as the response variable. We constructed a global model containing group size and male age in 2009, quadratic and cubic terms for both variables, and an interaction between the two variables. We used Akaike's Information Criterion corrected for small sample sizes (AICc) (Anderson, 2008; Burnham and Anderson, 2002) to compare models nested within the global model, including an intercept-only model, to determine whether group size predicted R-score.

Are Traits Changing Over Time?

To examine how RCW traits have changed over time at each site, we examined the relationship between year and each trait, with the trait as the response variable. We included the identity of the male and female breeders, the territory, and, only in the Sandhills (the larger site), the location as random factors. We tested and included both random intercepts and random slopes to account for pseudoreplication when the random slope and/or intercept explained greater than zero of the variance and did not cause the models to be overfitted (i.e., the random slopes and intercepts had a correlation coefficient close to 1; Schielzeth and Forstmeier, 2009). We included male and female age, as well as higher order polynomials of age, to control for the effects of age on the response variable. We included group size as a covariate to account for territory quality as well as helper effects. For analyses involving hatching asynchrony and nestling weight/age, we only included birds that were weighed before they were 13 days old because the slope of the weight/age ratio continues to rise until 13 days of age, whereupon it begins to asymptote (Garcia, 2014). Additionally, nestlings were banded at older ages only in the early, but not later, years of

the study, and we did not want to bias the results by including these birds in the analyses. Thus, we excluded 439 out of a possible 13,897 records. The analyses that included nestling weight/age were only conducted for the Sandhills because age data for MCBCL were only available for 2 years.

We used data from 1980–2013 to determine whether individuals survived to the first year, but only included individuals that hatched in 2011 or earlier. If a bird that fledged in 2011 had not been seen again by 2013, we considered it to have died. We included birds that hatched before 2007 for the analysis of age at first reproduction because 99% of males and females that attained a breeding position had done so by age 7. We considered birds that hatched in 2006 or earlier that had not attained a breeding position by 2013 to be non-breeders. To examine lifespan, we included birds that hatched before 2001 because only 0.007% (13 out of 1,891) of birds hatched before 2001 were still alive in 2013. In all analyses, we included an autoregressive term (AR1 or AR2) when there was evidence of autocorrelation, and we tested whether the term eliminated the autocorrelation by using a Durbin-Watson test. The data were analyzed in Program R (v.3.1.1; R Development Core Team, 2014) with standard analytical tools, such as linear models, Generalized Linear Models, Generalized Linear Mixed Models, and AICc (Anderson, 2008; Burnham and Anderson, 2002). We constructed a global model by using polynomials for year, number of helpers, female age, and male age. For year and age, we included the highest order polynomial (up to third order) that allowed the model to converge. We then calculated AICc values for models nested within the global model, and we model-averaged across all models to account for uncertainty by using package MuMin in R (Bartoń, 2011). We report the R^2 for the global model, the full model-averaged coefficients for each polynomial of year, and the relative importance of each polynomial of year. Relative importance is the sum of the Akaike weights for that term over all the models in which the term appears. When we discuss effect sizes in terms of percent change, they are based on the exponentiated log odds ratio of the model averaged coefficient from a post-hoc candidate model set in which year is only a linear term (no polynomial) to allow direct interpretation.

Does Local Climate Directly Affect Traits and Are These Traits Changing Over Time?

We then examined whether climate variables at each site were associated with selected traits by using climate data supplied by the State Climate Office of North Carolina, North Carolina State University, Raleigh, NC, obtained from Parameter-elevation Regressions on Independent Slopes Model (PRISM) climate data sets (see http://www.prism.oregonstate.edu). PRISM data are based on observations from a wide range of monitoring networks. The data we used were based on 4-km grid point data for the daily data and 800-m grid point data for the monthly data. The data supplied were monthly mean temperature, total monthly precipitation, daily minimum temperature, daily maximum temperature, daily mean temperature, and daily total precipitation for each study site. We derived annual climate variables such as mean daily minimum temperature for February from these data. We used linear regression or generalized linear regression and AICc to test which of 72–158 climate variables for each site were associated with each trait. We included a 1-year time lag for climate variables for the analysis involving local recruitment, for which weather from the previous year (the recruits' hatch year) may be expected to affect the probability of recruitment. We did not include time lags for other traits because, although time lagged climate variables have been found to be important in other studies, they are difficult to interpret (Jenouvrier, 2013; Thompson and Ollason, 2001). The number of days

above a specific temperature was a count of the number of days that month when the daily maximum was higher than the stated temperature, whereas the number of days below a specific temperature was a count of the number of days that month when the daily minimum was below the stated temperature. For behaviors that occur earlier in the breeding season, such as lay date and clutch size, we examined climate variables from January to April. For the other traits, we examined climate variables for January to June. We present results only for up to five climate variables with a delta AICc less than 2.

We then examined whether some of the climate variables most strongly associated with RCW life history traits changed over time. We used linear regression to test linear, quadratic, and cubic relationships between the climate variable and year.

Results and Discussion

MCBCL Forest Dynamic Models

The scenarios modeled as part of this study for MCBCL suggested that alterations to current management strategies and climate change could impact habitat available for RCWs. All of the scenarios except Longleaf Management resulted in large increases in optimal pine habitat (with open midstories and dense understories) compared to initial conditions. The model predicted that 62,185 acres of optimal pine habitat would be available for RCW nesting and foraging after 50 years under the current management regime ("baseline" scenario; **Figure 19-10**). Only the following two scenarios resulted in an increase in optimal RCW habitat over the baseline estimate (**Table 19-5 and Figure 19-11**): (1) an increase in the area treated by prescribed burns (2xPrescribed; 63,529 acres optimal habitat) and (2) the prioritization of currently unsuitable pine for habitat management over currently suitable stands (Restoration Management; 65,268 acres optimal habitat; **Figure 19-12**). The remaining scenarios resulted in reduced areas of optimal pine habitat (**Table 19-5 and Figure 19-11**). The scenario in which the frequency of wildfires was reduced by half (Half Wildfires) had the largest impact, decreasing optimal RCW habitat to a total of 43,661 acres (**Table 19-5 and Figure 19-11**). The cessation of all habitat management (No Management) reduced optimal pine habitat to 58,003 acres (**Table 19-5 and Figures 19-11 and 19-13**). Increases in the frequencies of hurricanes (2xHurricanes and 4xHurricanes) and a doubling in the frequency of wildfires (2xWildfire) reduced optimal habitat to 56,334 and 61,615 acres, respectively (**Table 19-5 and Figure 19-11**). Finally, changes to the current management regime that reduced the frequency of prescribed burning (Half Prescribed) or that prioritized already suitable pine stands for habitat management (Longleaf Management) also resulted in reduced levels of optimal RCW habitat compared to current conditions to 60,461 and 61,135 acres, respectively (**Table 19-5 and Figure 19-11**).

Effects of Climate on RCW Demography

Association Between Habitat Quality and Group Size

RCW group size predicted R-score ($F_{1,76}$=8.1, p=0.006). The model containing the single linear term group size had the lowest AICc when compared with other models. The second-ranked model contained group size and group size squared, and had a delta AICc of 1.8, indicating support for this model as well. The evidence ratio between the top (group size only) model and the model containing only the intercept was 17.56. The R^2 for the top model, which contained

group size, was 0.10, and the correlation coefficient between group size and R-score was 0.31. Thus, group size is associated with R-score and explains some of the variation in habitat quality as defined by R-score.

One might conclude that because group size is not more strongly associated with R-score that group size is not a very effective surrogate for habitat quality. Indeed, the effectiveness of RCW Matrix R-scores as a measure of habitat quality has been questioned, and a recent study showed that R-scores are not consistently correlated with RCW fitness as measured by productivity and group size across the range of the species (McKellar et al., 2014). However, RCW Matrix R-scores were developed based on Sandhills data, and although McKellar et al. (2014) found that R-score did not predict group size universally, it did predict group size in the Sandhills. In addition, we found that group size was correlated with R-score when only using group size data in the year in which the data for the R-scores were collected. Furthermore, in a regression tree analysis, McKellar et al. (2014) found that habitat features that are associated with productivity, namely herbaceous groundcover and large pines, are positively related to group size. Therefore, we conclude that at least for our analysis of data from North Carolina, group size is an effective control for habitat quality, an assertion that is further supported by previous research (Conner et al., 2001; Heppell et al., 1994). Thus, we attributed the changes in traits over time we report below to changes in climate rather than changes in habitat quality. The associations that we found between climate variables and these traits support this assertion.

Are Traits Changing Over Time?

Some traits changed in ways predicted by climate change (**Table 19-6 and Figures 19-14 through 19-19**). Lay days advanced by a total of 5.4 days over the 27-year study period at MCBCL (**Figure 19-14A**) and 2.6 days over the 32-year study period in the Sandhills. However, the effect was not linear in the Sandhills, indicating that lay dates declined during the first one-third of the study, leveled out, and then declined again during the last one-third of the study (**Figure 19-14B**).

Other traits that changed over time at MCBCL were age at first reproduction and lifespan, which both increased slightly (**Figure 19-15**). The term “Year” was also relatively important (sum of Akaike weights=0.66) in explaining survival to the first year at MCBCL, but the effect was small (**Figure 19-15**). Other traits at MCBCL did not appear to have changed discernibly over time because the term “Year” was of little relative importance in the model-averaged results for the remaining response variables.

Variance in laying date increased in the Sandhills over most of the period of the study, then decreased slightly at the end of the study period (**Figure 19-16**). Clutch size increased linearly over time, although the effect was small (0.2% average increase per year; **Figure 19-17**). Partial brood loss also increased linearly, and although the effect was small (0.5% per year), the relative importance of the linear variable “Year” was 0.99 (**Figure 19-17**). Survival to the first year increased quadratically, with an initial increase followed by a decrease at the end of the study (**Figure 19-18A**). Nestling size decreased during the study in the Sandhills (**Figure 19-18B**). The effect was cubic, and each polynomial of “Year” had a relative importance of 1.00. The linear term “Year” had a relative importance of 0.68 in terms of number of fledglings produced in the Sandhills, but the effect was small (0.1% per year; **Figure 19-18C**).

Age at first reproduction increased linearly in the Sandhills (**Figure 19-19**). Unlike at MCBCL, however, there was no corresponding increase in lifespan (**Figure 19-19**). Nest survival and hatching asynchrony do not appear to have changed over time in the Sandhills (**Table 19-6**).

Our results indicate that RCWs are experiencing changes in life history traits, but that these changes differ in important ways between populations. Most notably, multiple traits in the Sandhills have changed, whereas only lay date, age at first reproduction, and lifespan have changed at MCBCL. Whether this finding is the result of a shorter study period, more variability in the climate variables that matter at MCBCL, or some other factor, is unknown. In the Sandhills, in addition to earlier laying, the annual variance in lay dates has increased, albeit quadratically with a slight decrease at the end (**Figure 19-16**). This finding is contrary to the decreased variance in lay dates that has been predicted to accompany advancing lay dates in migratory species (Winkler et al., 2002). However, RCWs are non-migratory, and migratory and resident species might respond differently in this respect because resident species are not constrained by arrival time or the need to depart the breeding grounds at the end of the breeding season.

In the Sandhills population, birds are experiencing a series of linked changes to life history traits. Earlier laying is associated with larger clutches (Klomp, 1970; Winkler and Walters, 1983), and indeed RCW clutch sizes in the Sandhills have increased slightly (**Table 19-6**). Slight increases in clutch size is one of the effects predicted to occur with climate change (Winkler et al., 2002). Larger clutches are associated with smaller nestlings (Lack, 1947), and correspondingly nestling size decreased over the study period in the Sandhills. Declining body size is one of the widespread predicted responses to climate change (Gardner et al., 2011), but, in this case, the effect may also be linked to increased clutch size. Partial brood loss (in the first nesting attempt) increased throughout the study period. This suggests that birds may be stimulated to lay earlier (perhaps cues indicating food availability are earlier), but have less ability to predict food during the nestling period (perhaps the food peak no longer matches the nestling period well), leading to more partial brood loss. Nevertheless, the number of fledglings produced each year increased, suggesting that larger clutch sizes led to greater productivity overall despite greater partial brood loss during the first nesting attempt. Survival from fledging to age 1 increased quadratically (**Figure 19-18**), indicating that the increased number of fledglings were more successfully recruited into the population during the middle of the study period, which is coincident with a period of relative “cooling” from 1998–2008 or 2001–2010 (Easterling and Wehner, 2009).

The age at first reproduction increased at both study sites, and lifespan increased at MCBCL. These results indicate that RCWs are reproducing later and (in the coastal site at least) are living longer, which suggests a broader life history strategy associated with fewer offspring that survive better. However, we found no clear evidence of such direct trade-offs. Thus, the changes in age at first reproduction and lifespan might be due to the population dynamics associated with improved habitat and increases in the number of available cavities rather than shifting life history strategies. Overall, RCWs in North Carolina appear to be adjusting life history traits such that their populations are not experiencing adverse effects due to climate change thus far.

Our results are similar to those of Schiegg et al. (2002) because both studies found that RCWs laid eggs earlier over time at both sites. However, our study found a cubic rather than linear trend in laying date in the Sandhills (**Figure 19-14B**). This is due to the longer duration of our study.

The data in Schiegg et al. (2002) covered until 1998, which coincided with the beginning of the 10-year period of relative cooling (1998–2008) and a global warming hiatus that may be responsible for the cubic trend in our data (Chen and Tung, 2014; Easterling and Wehner, 2009; Tollefson, 2014).

Does Local Climate Directly Affect Traits and Are These Variables Changing Over Time?

Climate variables directly affected many life history traits in RCWs (**Table 19-7**). In general, warmer spring temperatures had positive effects: warmer spring temperatures were associated with larger clutch sizes and earlier laying dates at both sites, reduced partial brood loss at MCBCL, and increased fledgling production in the Sandhills. Precipitation affected several traits at MCBCL, with greater precipitation having negative effects in terms of increased partial brood loss and decreased fledgling production. Increased winter precipitation had a positive effect on nest survival, but the effect was small (**Table 19-7**). In the Sandhills, the climate variables that affected traits were almost exclusively related to temperature. More days with temperatures below 5°C in May (i.e., cooler minimum and nighttime temperatures) were associated with increased partial brood loss. Higher daily maximum temperatures in April were associated with decreased survival from fledging to age one, so the effects of warmer temperatures were not uniformly positive. At both sites, warmer winter temperatures were associated with decreased hatching asynchrony (**Table 19-7**).

More specifically, at MCBCL, cooler temperatures in March (more days below 5°C) were associated with later mean lay dates, and warmer daily temperatures (mean daily mean and mean daily minimum) in March were linked with earlier mean lay dates (**Table 19-7**). Greater precipitation in January was associated with increased variance in lay date, whereas warmer temperatures in February were linked with decreased variance in lay date. Warmer temperatures in March may be associated with increased clutch size, but the intercept-only model was highest ranked in this analysis. Greater variance in precipitation and increased daily precipitation in January, as well as warmer February nighttime temperatures were associated with increased nest survival. More precipitation in May and cooler temperatures in April were associated with greater partial brood loss (i.e., less May precipitation and warmer April temperatures result in decreased partial brood loss). Increased May precipitation was also associated with decreased fledgling production. Hotter temperatures in May and decreased precipitation in March were associated with decreased survival from fledging to age one. Warmer days in January were associated with decreased hatching asynchrony.

In the Sandhills, warmer March and April temperatures were associated with earlier lay dates (**Table 19-7**). Hotter June temperatures were associated with decreased variance in lay dates. Fewer cold days (the number of days below 5°C) and higher minimum daily temperatures in April were associated with increased clutch sizes, and colder weather in May (the number of days below 5°C) was linked with decreased clutch sizes. Hotter June temperatures (the number of days above 35°C) and decreased February precipitation were associated with higher nest survival. Warmer days (or nights) in May were associated with decreased partial brood loss, and warmer days (or nights) in April were linked with greater fledgling production. As at MCBCL, higher daily maximum temperatures were associated with decreased survival to age 1. Fewer very cold days (or nights) were associated with decreased hatching asynchrony.

Despite clear evidence of changes in temperature and precipitation from long-term climate data sets at the two study sites, we obtained mixed results when we examined changes in climate variables that affected RCW traits over the study period. At MCBCL, the highest ranked model for variance contained a linear "Year" effect, indicating a decreasing trend in daily total precipitation in winter (in January specifically) during the study period. In the Sandhills, models containing the linear term "Year" were competitive with the intercept-only models, suggesting a possible increasing trend in mean daily maximum temperatures in April, but the intercept-only models were nevertheless more highly ranked.

Warmer springs were associated with earlier laying at both sites, and thus global warming can account for changes in lay dates over time. Variance in lay date was associated with winter temperatures and variance in winter precipitation at MCBCL, but with June heat in the Sandhills. These results suggest that variance in lay dates is limited by winter conditions (i.e., the beginning of the breeding season) in MCBCL, but summer heat (i.e., the end of the breeding season) in the Sandhills, where hot June temperatures, may cut off further breeding. High temperatures and exposure can both have negative effects on nest survival and the viability of eggs under some conditions (Beissinger et al., 2005; Conrey et al., 2016; Cook et al., 2005; Rolland et al., 2011; Stoleson and Beissinger, 1999), and cavities retain high temperatures longer than open-cup nests (Godard et al., 2007). Therefore, higher than normal summer heat may cut off further breeding by a variety of mechanisms, including making the eggs susceptible to infection, increasing exposure due to incubation being unnecessary in the heat, or by causing birds heat stress.

Precipitation was most important at the coastal site (MCBCL), where increased precipitation caused greater nest survival (in spring), but also greater partial brood loss and decreased fledgling production (in late spring). Other studies have found that precipitation increased partial brood loss and decreased fledgling production (Fisher et al., 2015; Halupka et al., 2008; Proffitt et al., 2010).

Early laying appears to be a response to early warming, but precipitation then complicates matters because early laying may result in more potential exposure to cool wet periods that may cause egg or nestling loss, particularly at a wetter coastal site such as MCBCL. Therefore, increased precipitation and variance in precipitation could make productivity more difficult to predict at each site.

Long-term climate data collected at these two study sites indicate that (winter) precipitation is decreasing and that temperature is increasing in the Sandhills. These findings suggest that climate change could benefit RCWs in North Carolina, at the northern end of the species range, for at least some traits, but this conclusion may be premature. The amount of climate change has been modest thus far, and the southeastern United States is part of an area that did not experience the same scale of warming from 1900–2012 as most of the remainder of the United States and the globe. This area, dubbed the "warming hole," has been the subject of much research (**Figure 19-20**; Carter et al., 2014; Rogers, 2013; Walsh et al., 2014). Although the warming pattern has been more stable since the 1970s, with an average increase of 1.1°C per year, the high local variability in this area has resulted in mixed patterns locally (Walsh et al., 2014).

Although we found a trend toward decreasing winter precipitation at MCBCL, according to the National Climate Assessment, the long-term record indicates that precipitation has increased in

the MCBCL area, but decreased or remained stable in the Sandhills area (Peterson et al., 2014; Walsh et al., 2014). The lack of clear patterns due to the "warming hole," the variable nature of precipitation in this region, and the cooling period from 1998–2008 (Easterling and Wehner, 2009) may explain why life history trait and climate variable changes were not clearly directional over the study period. These mixed trends may also explain why some of the changes in traits during the study were small. If traits are changing along with climate, and the climate variables do not show clear linear change during the study period, but do show change in the longer term data, the traits could also show larger effects if a longer record were available. Thus, birds may indeed be responding to directional climate change that was not captured directly or within the length of our study, but which is nevertheless associated with the climate variables we examined. In either case, the evidence suggests that some traits are changing and that local climate directly affected RCW traits during the study (**Tables 19-6 and 19-7**).

Despite flat or even cooling trends in parts of the Southeast, temperatures are now expected to increase (with high confidence) over the next century, even given annual and decadal variation (Carter et al., 2014; Walsh et al., 2014). Precipitation is more difficult to predict, but is also expected to increase near MCBCL (Walsh et al., 2014). Thus, we can expect increased temperatures in the Sandhills and increased precipitation in MCBCL to continue to affect life history traits. Thus far, RCWs at these two sites appear to be benefitting, or at least not suffering adverse effects, from climate change. Changes in traits are modest thus far and mostly positive from a management perspective, probably due to direct impacts from climate, as well as from improving habitat quality. Because these sites are at the northern end of the range, we would expect that if RCWs were responding positively to climate change anywhere, they would be doing so here. Thus, these populations could be used as a benchmark for how more southerly populations are faring under changing environmental conditions. For example, at our study site at Eglin AFB in Florida, in the southern portion of the range, fledgling production has decreased over the past 20 years ("Year"=−0.0140 ±0.0082, P=0.0875, n=432) despite improvements in habitat management and increasing group size, indicative of improved habitat quality, at that study site. The negative effects of climate change may counter the positive effects of improving habitat at the southern end of the species' range. Although increased temperatures had positive effects on some traits in our study populations, there may be a point at which increasing temperatures begin to have negative effects even in northern populations.

Conclusions and Implications for Future Research and Implementation

Effects of Climate on RCW Demography

RCW traits have changed over time (**Table 19-6**), and climate variables are associated with changing traits (**Table 19-7**). In many cases, a single climate variable explained approximately one-fifth to one-third of the variation in the trait. The effects of climate on traits were independent of "Year" or any other time variable, suggesting that even if the changing traits were associated with improving habitat quality, there was also a direct association with climate that was not ordered in time. RCWs appeared to be able to shift some traits phenotypically in response to climate. These changes could reflect microevolution in response to changing climate or, more likely, phenotypic plasticity in response to non-directional annual variation in weather. The directional nature of the traits that have changed suggested a response to a directional environmental change, but we found mixed evidence that the local climate variables we

examined were shifting in a straightforward directional manner over the relatively short duration of the study. However, there was clear evidence from longer-term data and other sources that local climate is changing, albeit in less intuitive and more complex ways than simple warming (Boyles and Raman, 2003; Easterling, 2002; Konrad and Fuhrmann, 2013).

Many of the traits that we examined likely were affected by changes in habitat quality or population structure. To account for these possibilities, we included group size in the analyses as a surrogate for habitat quality, and male and female age (as well as group size) to account for changes in population structure. As previously discussed we believe that these variables were effective in controlling for effects of habitat quality and population structure, and thus that the changes in traits we report are due to climate. This is not to say that changes in habitat quality and population structure have not affected the traits we examined, however. At both study sites, productivity has increased over time, group sizes have gotten larger, and the ages of breeding males have gotten older (**Figures 19-21 and 19-22**). Clearly, the magnitude of these changes is well beyond what can be accounted for by the effects of climate we documented, and we believe improved habitat quality is responsible for these trends. It is possible that habitat change is being driven by changes in climate, that is, that climate is affecting traits indirectly through effects on habitat as well as directly through effects of weather. Although we were unable to assess this possibility, we believe that most of the improvement in habitat was due to management. There has been great effort at both MCBCL and the Sandhills to restore habitat through prescribed burning, construction of artificial cavities and other proven management techniques (Rudolph et al., 2004; Walters, 1991), and both study populations have increased dramatically. Thus, due to several factors, conditions for RCWs in these two North Carolina populations have improved greatly over the past 30 years.

As climate change progresses, knowing how populations and species may respond will be important to managing these populations. For species like the RCW that cannot shift range, knowing how particular climate variables may affect life history traits at many different stages (Zeigler, 2013) may allow one to predict likely responses to local conditions and to shift management accordingly. However, to our knowledge, no study has examined how life history traits in an endangered species that cannot alter its range because it persists on habitat islands are changing due to climate change. Few studies have examined multiple traits within a species, and to our knowledge, none have done so this extensively.

A logical next step would be to develop multiple trait and multiple climate variable models to predict how future climate scenarios may affect RCW populations. Additionally, determining the mechanisms by which climate affects RCW traits could be useful in managing these populations in the future. These findings could then be used to project responses of RCWs across the range, both current and, based on climate projections, in the future. Although preliminary, being based on only three populations, our results suggest that impacts of climate change over the next few decades could vary greatly geographically, with positive effects at the northern end of the range but negative effects at the southern end of the range, at least in the eastern portion of the species' range. Studies of more western populations along the Gulf Coast and inland are needed to enable a full assessment of the range-wide impacts of climate change on RCWs, and thus the future of RCWs on DoD lands.

Effects of Climate and Management on RCW Habitat

According to the proof-of-concept scenarios that we simulated for the landscape at MCBCL, climate change and alterations to the current habitat management regime on the Base could have direct and indirect implications for the RCW population. In terms of management, our results suggest that most changes will lead to reductions in optimal RCW habitat over current, baseline management strategies. However, a doubling of the acreage burned each year—even if that increase comes at the expense of other management techniques such as herbicide and midstory removal—could increase RCW habitat by more than 1,000 acres after 50 years. This result was supported by studies at Eglin AFB, where prescribed burning was found to have a substantial positive impact on RCW habitat by decreasing midstory density, increasing herbaceous understory coverage, and promoting arthropod communities (Provencher et al., 2001a, 2001b, 2001c, 2002a, 2002b, and 2002c). Although mechanical midstory removal and herbicide application also promoted RCW habitat, these management techniques alone did not improve the condition of the herbaceous understory compared to control and fire plots (Provencher et al., 2001a), underscoring the importance of fire as a management tool in RCW habitats.

We also found that the way in which longleaf pine stands are prioritized can influence RCW habitat availability. When management efforts are focused on pine stands that are already of high quality (i.e., maintaining already high-quality habitat), the acreage of optimal RCW habitat declined compared with current, baseline strategies. However, the prioritization of currently low-quality pine stands (e.g., with dense midstories and sparse understories) for management results in an increase in optimal RCW habitat by more than 3,000 acres after 50 years. All other changes to the management strategy that we considered, including a cessation of all management and a reduction in the area burned each year, resulted in lower acreage of optimal RCW habitat.

The ST-Sim landscape model and scenarios modeled therein also suggests that climate change could alter RCW habitat availability. Changes to the wildfire regime, which could be influenced by precipitation regimes, reduced optimal RCW habitat by approximately 570 acres to 18,500 acres at the end of the 50-year simulation. Habitat was reduced both when wildfire frequency decreased by half and when frequency doubled, suggesting that either wetter or drier years over current conditions could negatively impact RCW habitat if precipitation levels influence wildfire prevalence. Furthermore, an increase in the frequency of coastal storms, as is projected along the U.S. Atlantic Coast in coming decades (Pachauri et al., 2014), would reduce optimal RCW habitat by approximately 2,000 to 6,000 acres after 50 years, assuming that hurricanes would convert mature stands to early successional habitat as we have modeled their impacts.

These scenarios modeled as part of this report support the use of the ST-Sim landscape model to evaluate the effects of landscape change on habitat availability for RCWs. Next steps include a thorough vetting of the model and “baseline” parameters used by natural resource staff at MCBCL, Fort Bragg, and Eglin AFB. From there, staff can evaluate scenarios related to current needs and scheduled changes to landscape management on relevant Bases as part of an adaptive management strategy.

Research Questions

1. Based on current linkages between weather and RCW productivity, how are projected changes in weather due to climate change predicted to alter RCW productivity on MCBCL and Fort Bragg?

Our results suggest that changing climate will have positive or neutral effects on RCW productivity over the short term, due to the capability of the species to respond to a range of conditions through phenotypic plasticity, coupled with the nature of changing climate at the northern end of the species' range. However, possible negative impacts of changing climate at the southern end of the range suggest that there are limits to the capacity of the species' phenotypic plasticity. Thus, RCWs could experience adverse effects of climate change in North Carolina over the long term, depending on the magnitude of future changes in climate.

2. Based on simulation modeling, how are projected changes in RCW demography and longleaf pine habitat due to climate change predicted to alter RCW population growth on MCBCL?

The spatially explicit, individual-based RCW population model that we intended to use to address this question operates as an ArcGIS extension. Due to the changes that ESRI made to its base code, the model no longer functions reliably. This issue precluded us from investigating this question.

Other Key Scientific Findings

We demonstrated correlations between weather and several life history traits of RCWs such as clutch size and survival from fledging to age one. The mechanisms responsible for these correlations should be investigated to project effects of future climate change on the species.

Findings with Implications for Future Base Management

To date, the impacts of climate change on RCWs at MCBCL and Fort Bragg at the northern end of the species' range have been positive to neutral, resulting in increasing productivity, but possibly reduced survival of juveniles. However, we have evidence of negative effects of climate change on productivity of RCWs on Eglin AFB in Florida at the southern end of the range. If the climate at MCBCL changes sufficiently in the future, then the RCW population may eventually experience negative impacts similar to those occurring at the southern end of the range. These findings are directly applicable to all other DoD installations in the southeastern United States. It is likely that current and future impacts of climate change on other installations are a function of their geographic location. Furthermore, climate change—should it alter wildfire frequencies in either direction or increase the frequency of hurricanes—could negatively affect RCW habitat in the future at MCBCL. Beyond climate change, our results suggest that the most efficient management of the landscape for RCW habitat at MCBCL would prioritize prescribed burning, particularly of currently low-suitability pine stands.

Table 19-1. Characteristics of States Used to Describe Longleaf Pine and Other Sub-ecosystems on Marine Corps Base Camp Lejeune (MCBCL), Fort Bragg, and Eglin Air Force Base in Both the ST-Sim Landscape Model and in the Red-Cockaded Woodpecker (RCW) Population Model as Part of the RCW Decision-Support System (RCW DSS)

Structural characteristics and definitions were derived from the LANDFIRE program (Zahn, 2015). In addition to land-cover type, state classes were also classified by suitability for RCW nesting and foraging (from no suitability=1 to high suitability=5) and stand age in the RCW population model (or RCW DSS).

Site	Sub-ecosystem	Stage	Age (Years)	Time Since Fire (Years)	Ground Cover (% Cover)	Midstory	Pine Canopy Cover	RCW Habitat Suitability	RCW DSS Type	RCW DSS Age
MCBCL	Central Atlantic Coastal Plain Wet Longleaf	Early Development	<15	Not applicable (N/A)	≥40 (Dominated by grasses, small-statured shrubs, and forbs)	N/A	0–50%	1	Open	0
		Mid-Development (Open midstory, Dense understory)	15–75	<10	≥40 (Dominated by grasses, especially wiregrass)	"Minimal" hardwood component	21–50%	5	Pine	60
		Mid-Development (Open midstory, Sparse understory)	15–75	≥10	<40	"Minimal" hardwood component	21–50%	3	Pine	60
		Mid-Development (Closed midstory, Sparse understory)	15–75	≥10	<40	"Substantial" component of hardwood and other pine species	51–80% (Hardwood and encroaching pine cover >50%)	3	Pine	60
		Late Development (Open midstory, Dense understory)	>75	<10	≥40 (Dominated by grasses, especially wiregrass)	"Minimal" hardwood component	11–60%	5	Pine	75
		Late Development (Open midstory, Sparse understory)	>75	≥10	<40	"Minimal" hardwood component	11–60%	3	Pine	75

(continued)

Table 19-1. Characteristics of States Used to Describe Longleaf Pine and Other Sub-ecosystems on Marine Corps Base Camp Lejeune (MCBCL), Fort Bragg, and Eglin Air Force Base in Both the ST-Sim Landscape Model and in the Red-Cockaded Woodpecker (RCW) Population Model as Part of the RCW Decision-Support System (RCW DSS) (continued)

Site	Sub-ecosystem	Stage	Age (Years)	Time Since Fire (Years)	Ground Cover (% Cover)	Midstory	Pine Canopy Cover	RCW Habitat Suitability	RCW DSS Type	RCW DSS Age
		Late Development (Closed midstory, Sparse understory)	>75	≥ 10	<40	"Substantial" component of hardwood and other pine species	61–100%	2	Pine Dispersal Only	75
MCBCL and Fort Bragg	Atlantic Coastal Plain Upland Longleaf Pine and Atlantic Coastal Plain Fall-Line Sandhill Longleaf Pine	Early Development	<15	N/A	≥40 (Dominated by grasses, small-statured shrubs, and forbs)	N/A	0–50%	1	Open	0
		Mid-Development (Open midstory, Dense understory)	15–75	<15	≥40 (Dominated by grasses, especially wiregrass)	"Minimal" hardwood component	21–70%	5	Pine	60
		Mid-Development (Open midstory, Sparse understory)	15–75	≥15	<40	"Minimal" hardwood component	21–70%	3	Pine	60
		Mid-Development (Closed midstory, Sparse understory)	15–75	≥15	<40	"Substantial" component of hardwood and other pine species	71–90% (Hardwood and encroaching pine cover >50%)	3	Pine	60
		Late Development (Open midstory, Dense understory)	>75	<20	≥40 (Dominated by grasses, especially wiregrass)	"Minimal" hardwood component	21–70%	5	Pine	75

(continued)

Table 19-1. Characteristics of States Used to Describe Longleaf Pine and Other Sub-ecosystems on Marine Corps Base Camp Lejeune (MCBCL), Fort Bragg, and Eglin Air Force Base in Both the ST-Sim Landscape Model and in the Red-Cockaded Woodpecker (RCW) Population Model as Part of the RCW Decision-Support System (RCW DSS) (continued)

Site	Sub-ecosystem	Stage	Age (Years)	Time Since Fire (Years)	Ground Cover (% Cover)	Midstory	Pine Canopy Cover	RCW Habitat Suitability	RCW DSS Type	RCW DSS Age
		Late Development (Open midstory, Sparse understory)	>75	≥20	<40	"Minimal" hardwood component	21–70%	3	Pine	75
		Late Development (Closed midstory, Sparse understory)	>75	≥20	<40	"Substantial" component of hardwood and other pine species	71–90%	2	Pine Dispersal Only	75
Eglin AFB	Florida Longleaf Pine Sandhill	Early Development	<15	N/A	≥40 (Dominated by grasses, small-statured shrubs, and forbs)	N/A	0–50%	1	Open	0
		Mid-Development (Open midstory, Dense understory)	15–75	<15	≥ 40 (Dominated by grasses, especially wiregrass)	"Minimal" hardwood component	21–70%	5	Pine	60
		Mid-Development (Open midstory, Sparse understory)	15–75	≥15	<40	"Minimal" hardwood component	21–70%	3	Pine	60
		Mid-Development (Closed midstory, Sparse understory)	15–75	≥15	<40	"Substantial" component of hardwood and other pine species	71–100%	3	Pine	60

(continued)

Table 19-1. Characteristics of States Used to Describe Longleaf Pine and Other Sub-ecosystems on Marine Corps Base Camp Lejeune (MCBCL), Fort Bragg, and Eglin Air Force Base in Both the ST-Sim Landscape Model and in the Red-Cockaded Woodpecker (RCW) Population Model as Part of the RCW Decision-Support System (RCW DSS) (continued)

Site	Sub-ecosystem	Stage	Age (Years)	Time Since Fire (Years)	Ground Cover (% Cover)	Midstory	Pine Canopy Cover	RCW Habitat Suitability	RCW DSS Type	RCW DSS Age
		Late Development (Open midstory, Dense understory)	>75	<15	≥40 (Dominated by grasses, especially wiregrass)	"Minimal" hardwood component	21–70%	5	Pine	75
		Late Development (Open midstory, Sparse understory)	>75	≥15	<40	"Minimal" hardwood component	21–70%	3	Pine	75
		Late Development (Closed midstory, Sparse understory)	>75	≥15	<40	"Substantial" component of hardwood and other pine species	71–100%	2	Pine Dispersal Only	75
All sites and sub-ecosystems		Bare	N/A	N/A	N/A	N/A	0%	1	Bare	0
		Mixed	N/A	N/A	<40	N/A	N/A	1	Mixed	0
		Hardwood	N/A	N/A	<40	N/A	N/A	1	Hard	0
		Other Pine (Open midstory, Dense understory)	N/A	<10–20	≥40	"Minimal" hardwood component	21–70%	4	Pine	60
		Other Pine (Closed midstory, Sparse understory)	N/A	≥10–20	<40	"Substantial" component of hardwood and other pine species	71–100%	2	Pine Dispersal Only	60
		Other	N/A	N/A	N/A	N/A	0%	1	Other	0
		Water	N/A	N/A	N/A	N/A	0%	1	Water	0

Table 19-2. Management Targets Included in the Baseline Models for Longleaf Pine and Other Sub-ecosystems on Marine Corps Base Camp Lejeune (MCBCL), Fort Bragg, and Eglin Air Force Base (AFB) in the ST-Sim Landscape Model

"Non-Fire Management" could include mechanical midstory removal, herbicide application, or wiregrass planting (MCBCL only).

Site	Sub-Ecosystem	Management Technique	Management Target (Acres)
MCBCL	Central Atlantic Coastal Plain Wet Longleaf	Non-fire management	1,300
		Prescribed burn	9,200
	Atlantic Coastal Plain Upland Longleaf Pine	Non-fire management	650
		Prescribed burn	4,600
Fort Bragg[a]	Atlantic Coastal Plain Fall-Line Sandhill Longleaf Pine	Non-fire management	0
		Prescribed burn	0
Eglin AFB	Florida Longleaf Pine Sandhill	Non-fire management	8,000
		Prescribed burn	104,000

[a] Management targets were unknown for Fort Bragg and were input as "0" in the baseline model. Users can alter this value to simulate the effects of management on the military installation.

Table 19-3. Management and Climate Scenarios Considered for Marine Corps Base Camp Lejeune (MCBCL)

Scenario Name	Transitions Affected	Change in Parameter from Baseline
Baseline	Not applicable (N/A)	N/A
No management	Prescribed fire, mechanical midstory removal, herbicide application, and wiregrass planting	Probability of these transitions occurring changed to 0; area of transition targets changed to 0
Altered fire regime—half prescribed	Prescribed fire	Halved the baseline target area for prescribed burns compared with baseline Upland Longleaf=2,300 acres; Wet Longleaf=4,600 acres Left non-fire management targets the same
Altered fire regime—2x prescribed	Prescribed fire mechanical midstory removal, herbicide application, and wiregrass planting	Doubled the baseline target area for prescribed burns compared to baseline Upland Longleaf=9,200 acres; Wet Longleaf=18,400 acres Made transition targets for non-fire management equal to 0
Longleaf management	Prescribed fire, mechanical midstory removal, and herbicide application	Added 0.1 to the probability of management transitions for the Mid- and Late Development states with Open midstories and Dense ground cover Reduced the probability of prescribed burns for all states with Open midstories and Sparse ground covers (to 0.05), which ensured that higher quality longleaf sites were preferentially treated with management applications compared to lower quality sites

(continued)

Table 19-3. Management and Climate Scenarios Considered for Marine Corps Base Camp Lejeune (MCBCL) (continued)

Scenario Name	Transitions Affected	Change in Parameter from Baseline
Restoration management	Prescribed fire, mechanical midstory removal, and herbicide application	Added 0.1 to the probability of management transitions the Mid- and Late Development states with Closed midstories and Sparse ground cover, which ensured that lower quality longleaf sites were preferentially treated with management applications compared to higher quality sites Halved the transition targets for prescribed burns and non-fire management Assumed that more resources would need to go into restoring the least suitable landcover types, reducing the total area that can be treated
Climate regime— 2x hurricane	Hurricanes	Doubled the baseline probability of the wind/weather/stress transition for all states Upland Longleaf=0.002–0.01; Wet Longleaf=0.01–0.0166
Climate regime— 4x hurricane	Hurricanes	Multiplied the baseline the probability of the wind/weather/stress transition by 4 for all states Upland Longleaf=0.004–0.02; Wet Longleaf=0.02–0.0332
Climate regime— half wildfire	Wildfires	Halved the baseline probability for surface, mixed, and replacement fire transitions for all states Upland Longleaf=0.002–0.125; Wet Longleaf=0.005–0.155
Climate regime— 2x wildfire	Wildfires	Doubled the baseline probability for surface, mixed, and replacement fire transitions for all states Upland Longleaf=0.01–0.50; Wet Longleaf=0.008–0.62

Table 19-4. The Proportion of the Landscapes at Marine Corps Base Camp Lejeune (MCBCL), Fort Bragg, and Eglin Air Force Base Covered by Each Landscape State Class According to LANDFIRE Data Products for the Year 2014

These proportions were used to initialize the non-spatially explicit scenario simulations for MCBCL.

Vegetation Type (Stratum)	State Class	Area of Landscape (Acres)	Proportion of Landscape
Marine Corps Base Camp Lejeune			
Atlantic Coastal Plain Upland Longleaf Pine Woodland/Atlantic Coastal Plain Fall-Line Sandhills Longleaf Pine Woodland	Bare:ALL	402.31	0
	Early1:ALL	6,772.58	0.00
	Hard:CLS-SPAR	4.67	0.05
	Late1:CLS-SPAR	0.89	0.00
	Late1:OPN-DEN	818.19	0.00
	Mid1:CLS-SPAR	6,631.14	0.01
	Mid1:OPN-DEN	0.67	0.05
	Mixed:CLS-SPAR	5,375.28	0.00
	Other_Pine:CLS-SPAR	1,547.87	0.04
	Other_Pine:OPN-DEN	10,651.36	0.01
	Other:ALL	402.31	0.07

(continued)

Table 19-4. The Proportion of the Landscapes at Marine Corps Base Camp Lejeune (MCBCL), Fort Bragg, and Eglin Air Force Base Covered by Each Landscape State Class According to LANDFIRE Data Products for the Year 2014 (continued)

Vegetation Type (Stratum)	State Class	Area of Landscape (Acres)	Proportion of Landscape
Central Atlantic Coastal Plain Wet Longleaf Pine Savanna and Flatwoods	Bare:ALL	0	0
	Early1:ALL	2,253.97	0.02
	Hard:CLS-SPAR	3,352.82	0.02
	Late1:CLS-SPAR	204.16	0.00
	Late1:OPN-DEN	5.56	0.00
	Mid1:CLS-SPAR	7,669.94	0.05
	Mid1:OPN-DEN	11,265.39	0.08
	Mixed:CLS-SPAR	39.36	0.00
	Other_Pine:CLS-SPAR	7,972.18	0.06
	Other_Pine:OPN-DEN	4,606.23	0.03
	Other:ALL	5,657.27	0.04
Other	Bare:ALL	2,687.64	0.02
	Early1:ALL	0	0
	Hard:CLS-SPAR	11,257.39	0.08
	Late1:CLS-SPAR	0	0
	Late1:OPN-DEN	0	0
	Mid1:CLS-SPAR	0	0
	Mid1:OPN-DEN	0	0
	Mixed:CLS-SPAR	113.87	0.00
	Other_Pine:CLS-SPAR	19,014.06	0.13
	Other_Pine:OPN-DEN	11,334.56	0.08
	Other:ALL	2,186.58	0.02
Fort Bragg			
Atlantic Coastal Plain Upland Longleaf Pine Woodland/Atlantic Coastal Plain Fall-Line Sandhills Longleaf Pine Woodland	Bare:ALL	426.58	0.00
	Early1:ALL	29.04	0.00
	Hard:CLS-SPAR	1,039.94	0.01
	Late1:CLS-SPAR	16.72	0.00
	Late1:OPN-DEN	9.90	0.00
	Mid1:CLS-SPAR	17,071.56	0.11
	Mid1:OPN-DEN	70,672.80	0.47
	Mixed:CLS-SPAR	0	0
	Other_Pine:CLS-SPAR	3,333.88	0.02
	Other_Pine:OPN-DEN	316.36	0.00
	Other:ALL	21,470.02	0.14

(continued)

Table 19-4. The Proportion of the Landscapes at Marine Corps Base Camp Lejeune (MCBCL), Fort Bragg, and Eglin Air Force Base Covered by Each Landscape State Class According to LANDFIRE Data Products for the Year 2014 (continued)

Vegetation Type (Stratum)	State Class	Area of Landscape (Acres)	Proportion of Landscape
Central Atlantic Coastal Plain Wet Longleaf Pine Savanna and Flatwoods	Bare:ALL	18.70	0.00
	Early1:ALL	21.78	0.00
	Hard:CLS-SPAR	12.32	0.00
	Late1:CLS-SPAR	84.70	0.00
	Late1:OPN-DEN	0.66	0.00
	Mid1:CLS-SPAR	1,897.72	0.01
	Mid1:OPN-DEN	1,325.72	0.01
	Mixed:CLS-SPAR	0	0
	Other_Pine:CLS-SPAR	274.12	0.00
	Other_Pine:OPN-DEN	45.54	0.00
	Other:ALL	159.94	0.00
Other	Bare:ALL	10,251.78	0.07
	Early1:ALL	23.32	0.00
	Hard:CLS-SPAR	3,249.40	0.02
	Late1:CLS-SPAR	37.40	0.00
	Late1:OPN-DEN	163.68	0.00
	Mid1:CLS-SPAR	4,898.08	0.03
	Mid1:OPN-DEN	1,014.20	0.01
	Mixed:CLS-SPAR	0	0
	Other_Pine:CLS-SPAR	5,380.98	0.04
	Other_Pine:OPN-DEN	5991.92	0.04
	Other:ALL	1,231.56	0.01
Eglin Air Force Base			
Atlantic Coastal Plain Fall-Line Sandhills Longleaf Pine	Bare:ALL	29,399.92	0.06
	Early1:ALL	95.92	0.00
	Hard:CLS-SPAR	117.26	0.00
	Late1:CLS-SPAR	15,999.28	0.04
	Late1:OPN-DEN	163,958.96	0.36
	Mid1:CLS-SPAR	0.22	0.00
	Mid1:OPN-DEN	30,869.08	0.07
	Mixed:CLS-SPAR	5,876.64	0.01
	Other_Pine:CLS-SPAR	25,966.82	0.06
	Other_Pine:OPN-DEN	7,166.06	0.02
	Other:ALL	50,401.34	0.11

(continued)

Table 19-4. The Proportion of the Landscapes at Marine Corps Base Camp Lejeune (MCBCL), Fort Bragg, and Eglin Air Force Base Covered by Each Landscape State Class According to LANDFIRE Data Products for the Year 2014 (continued)

Vegetation Type (Stratum)	State Class	Area of Landscape (Acres)	Proportion of Landscape
Other	Bare:ALL	10,478.38	0.02
	Early1:ALL	231	0.00
	Hard:CLS-SPAR	6,613.2	0.01
	Late1:CLS-SPAR	656.04	0.00
	Late1:OPN-DEN	582.56	0.00
	Mid1:CLS-SPAR	58.3	0.00
	Mid1:OPN-DEN	1,007.6	0.00
	Mixed:CLS-SPAR	25,695.78	0.06
	Other_Pine:CLS-SPAR	30,462.52	0.07
	Other_Pine:OPN-DEN	35,282.06	0.08
	Other:ALL	12,663.2	0.03

Table 19-5. Landscape Composition (in Acres), as Predicted by the ST-Sim Landscape Model, in Response to Altered Climate and Management Regimes at Marine Corps Base Camp Lejeune

Landscape changes were modeled over 50 years in the landscape model according to scenarios outlined in the section of this chapter titled Landscape and Management Scenarios.

Landcover Type	Initial	Scenarios									
		Baseline	No Manage	Half Burn	2x Burn	Longleaf Manage	Restore Manage	2x Hurricanes	4x Hurricanes	Half Wildfire	2x Wildfire
Pine: Open-Dense	19,441	62,185	58,003	60,461	63,529	19,441	62,185	59,819	56,334	48,517	61,615
Early Successional	2,628	11,800	11,910	12,430	12,082	2,628	11,800	14,058	17,638	5,962	17,356
Pine: Closed-Sparse	40,616	5,150	9,168	6,282	3,494	40,616	5,150	5,266	5,094	24,619	153
Pine: Open-Sparse	0	1	0	1	0	0	1	1	1	2	0
Non-pine Forest	21,305	21,542	21,533	21,516	21,535	21,305	21,542	21,538	21,556	21,540	21,503
Other	41,785	42,205	42,269	42,194	42,242	41,785	42,205	42,201	42,259	42,244	42,254

Table 19-6. Summary of How Red-Cockaded Woodpecker Traits Are Changing over Time at Two Sites in North Carolina (See Tables A1 and A2 for Entire Results)

Up arrows indicate a positive relationship; down arrows indicate a negative relationship. Striped arrows represent MCBCL, and gray arrows represent Sandhills.

Response Variable (n)	Change over Time	
	MCBCL	Sandhills
Lay date	⇩	⇩
Variance in laying dates	0	⇧
Clutch size	0	⇧
Nest survival	0	0
Partial brood loss	0	⇧
Number of fledglings	0	⇧
Survival to age one	⇧	⇧ ⇩
Hatching asynchrony	0	0
Nestling size	Not applicable	⇩
Age at first reproduction	⇩	⇧
Lifespan	⇧	0

Table 19-7. Summary of Effects of Local Climate Variables on Red-Cockaded Woodpecker Life History Traits

Each arrow represents a climate variable, and only the top 3 highest ranked variables from **Tables A5 and A6** are represented. Up arrows indicate a positive relationship; down arrows indicate a negative relationship. Striped arrows represent MCBCL, and gray arrows represent Sandhills.

Trait	Warmer Winter Temperatures	Warmer Spring Temperatures	Hotter Summers, More Variance in Temperature	More Winter Rain, More Variance in Winter Rain	More Late Spring Rain
Mean lay date		⇩⇩⇩ ⇩⇩	⇩		
Variance in lay date	⇩			⇩ ⇧⇧	
Clutch size		⇧⇧	⇧⇧		
Nest survival	⇧			⇧⇧	⇩
Partial brood loss		⇩	⇧	⇧	⇧⇧
Number fledged			⇧		⇩
Survival to year 1		⇩⇩⇩	⇩		
Hatching asynchrony	⇩	⇩			

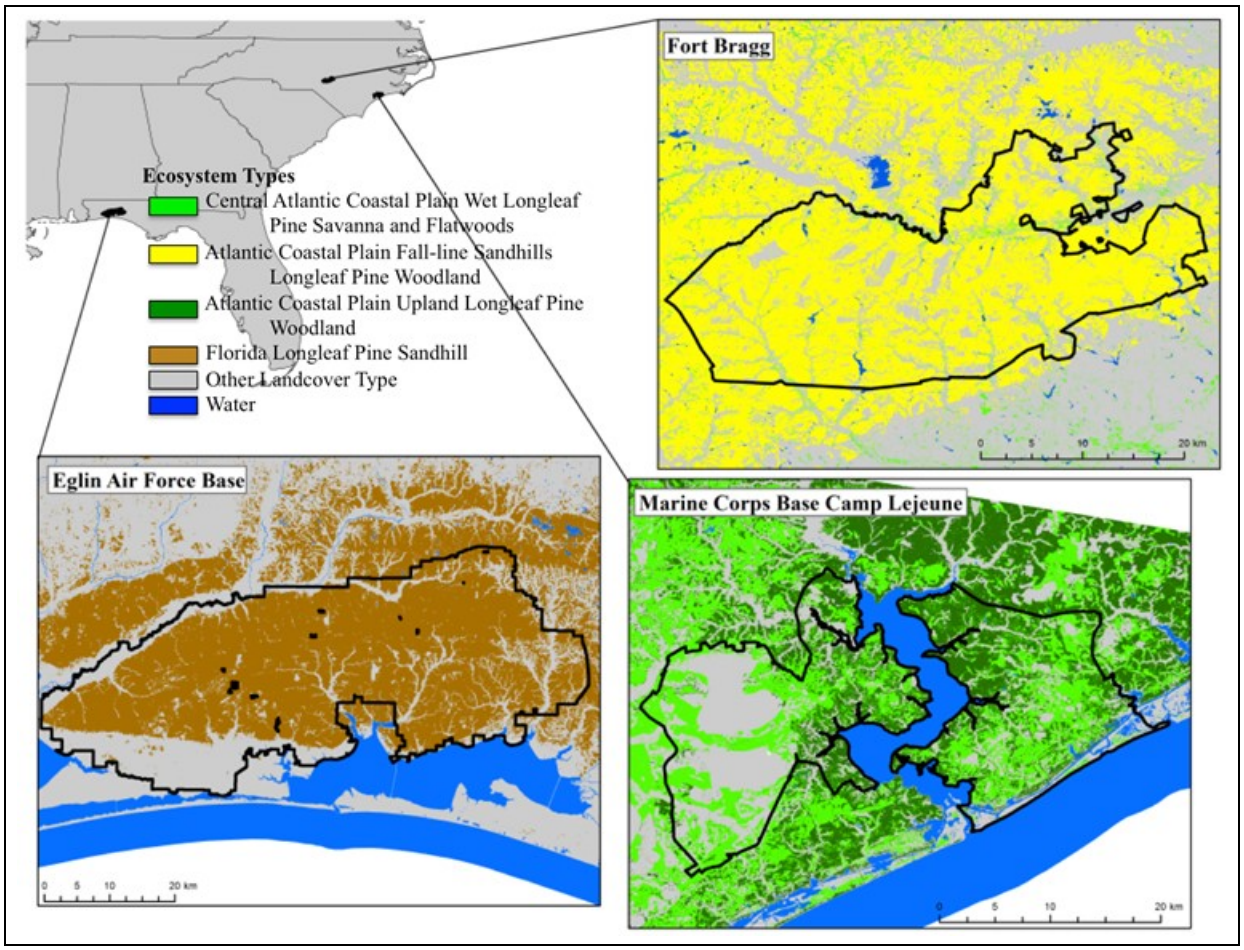

Figure 19-1. Longleaf pine sub-ecosystems modeled within state and transitions models, based on biophysical settings outlined by the LANDFIRE program (Zahn, 2015).

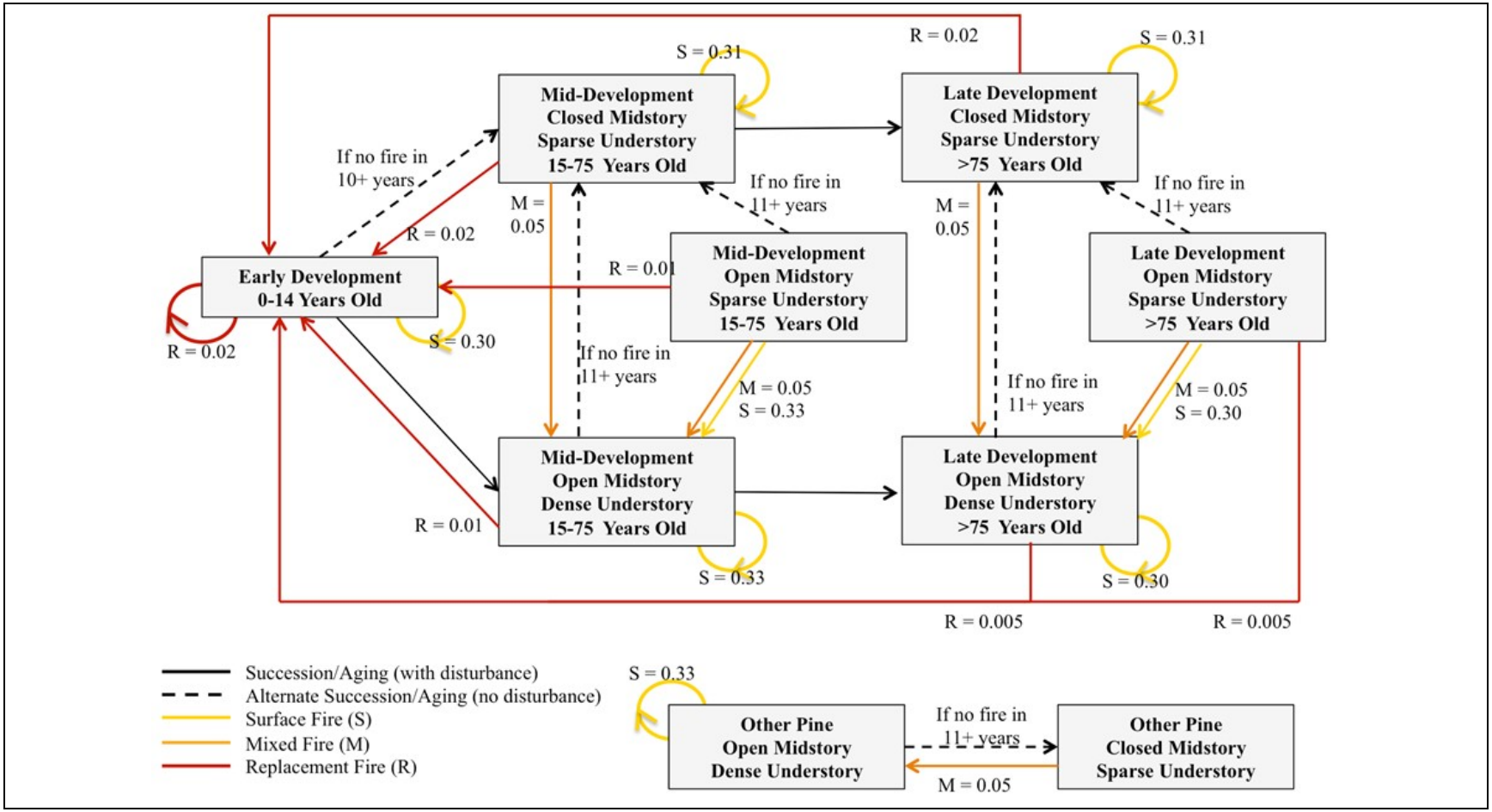

Figure 19-2. Landscape states, successional pathways, and fire effects for the Central Atlantic Coastal Plain Wet Longleaf Pine sub-ecosystem found within the boundaries of Marine Corps Base Camp Lejeune.

The fire types considered included (from lowest severity to highest severity): Surface (S), Mixed (M), and Replacement (R). The values next to fire type indicate the annual probability that the transition will occur for a given landscape cell of that state. Fire and management (or lack thereof) dictated the successional pathway followed. The sub-ecosystem also included states for Hardwood, Mixed Hardwood/Pine, Bare Land, Water, and Other (not shown).

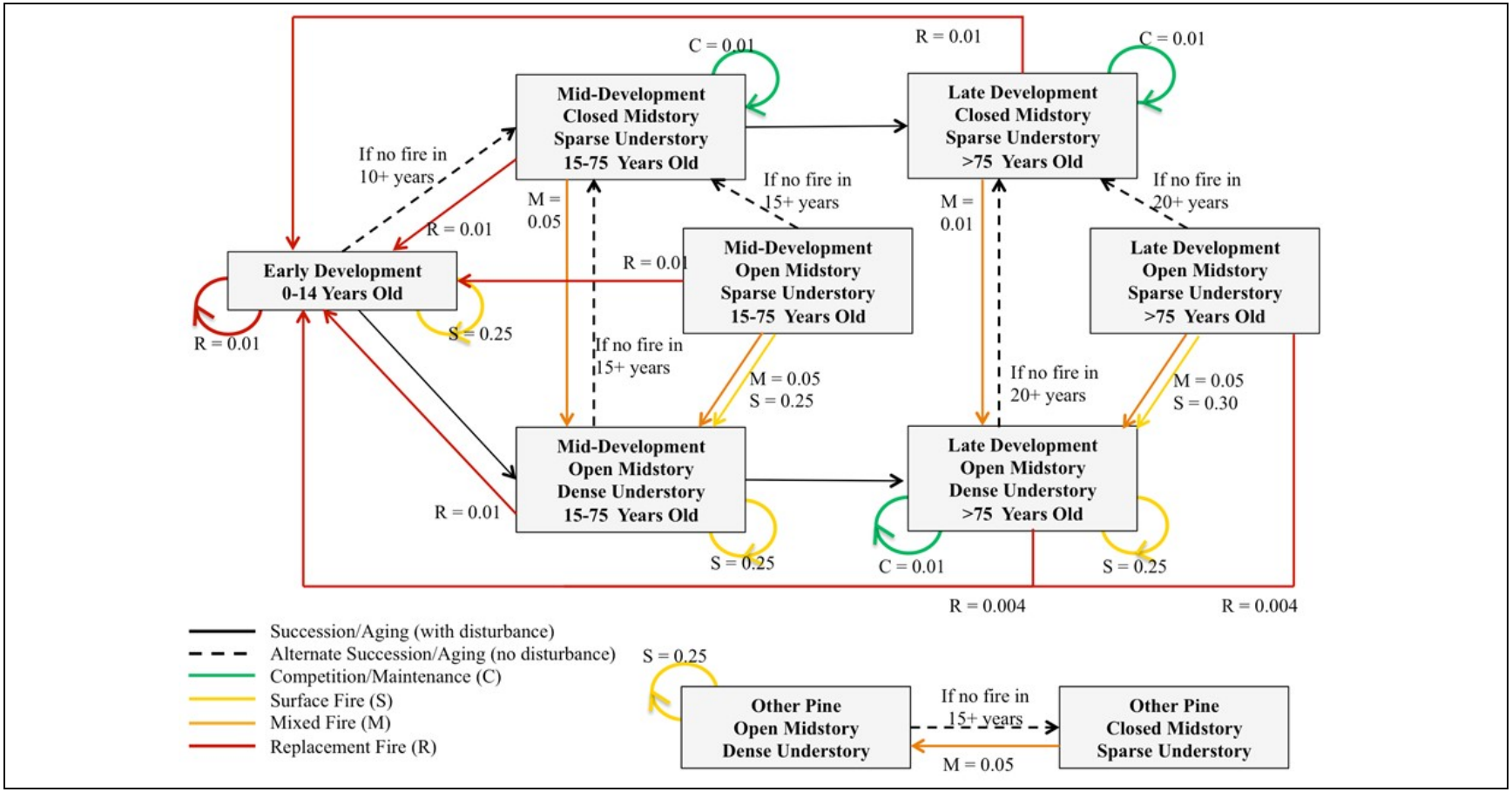

Figure 19-3. Landscape states, successional pathways, and fire effects for the Atlantic Coastal Plain Upland Longleaf Pine and Other sub-ecosystems found within the boundaries of Marine Corps Base Camp Lejeune, as well as the Atlantic Coastal Plain Fall-Line Sandhill Longleaf Pine Woodland and Other sub-ecosystems found within the boundaries of Fort Bragg.

The fire types considered included (from lowest severity to highest severity): Surface (S), Mixed (M), and Replacement (R). The values next to the fire type indicate the annual probability that the transition will occur for a given landscape cell of that state. Fire and management (or lack thereof) dictated the successional pathway followed. These sub-ecosystems also included states for Hardwood, Mixed Hardwood/Pine, Bare Land, Water, and Other (not shown). The Other sub-ecosystems on both military installations did not consider longleaf pine states (e.g., Mid-Development, Late Development).

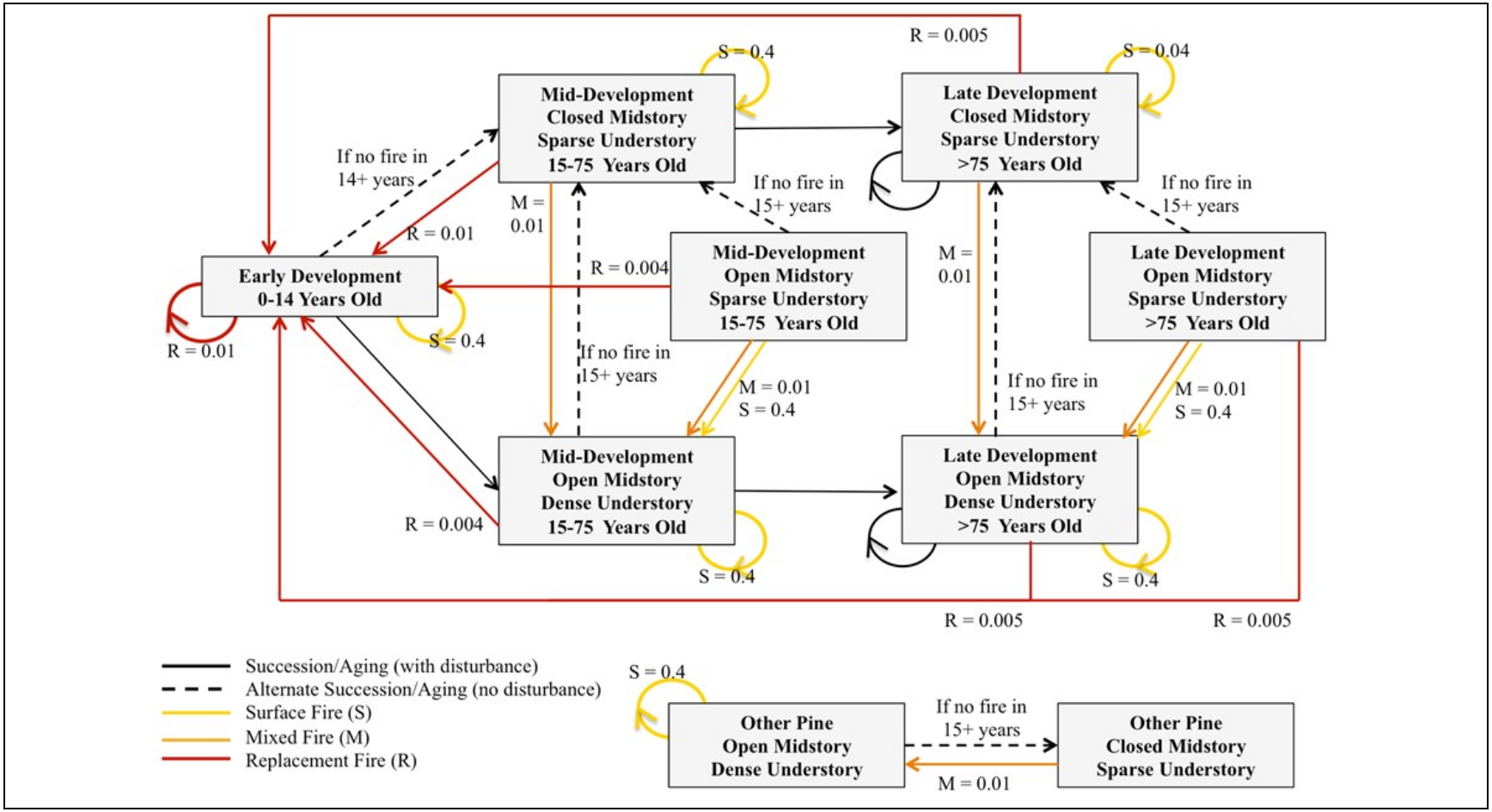

Figure 19-4. Landscape states, successional pathways, and fire effects for the Florida Longleaf Pine Sandhill and Other sub-ecosystems found within the boundaries of Eglin Air Force Base.

The fire types considered included (from lowest severity to highest severity): Surface (S), Mixed (M), and Replacement (R). The values next to the fire type indicate the annual probability that the transition will occur for a given landscape cell of that state. Fire and management (or lack thereof) dictated the successional pathway followed. These sub-ecosystems also included states for Hardwood, Mixed Hardwood/Pine, Bare Land, Water, and Other (not shown). The Other sub-ecosystem did not consider longleaf pine states (e.g., Mid-Development, Late Development).

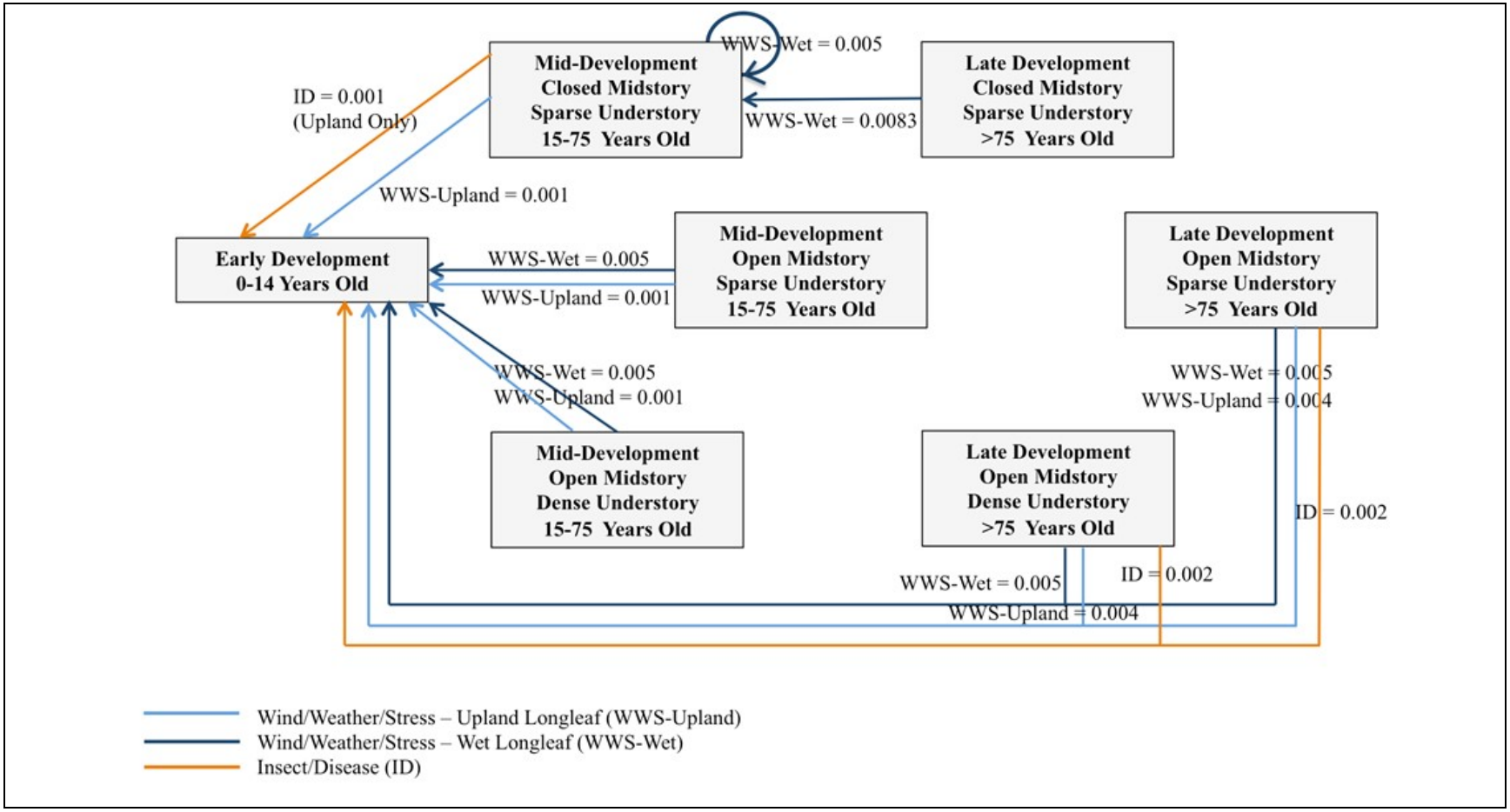

Figure 19-5. Wind/weather/stress (WWS; e.g., hurricane) and insect/disease (ID) effects for the Atlantic Coastal Plain Upland Longleaf Pine and the Central Atlantic Coastal Plain Wet Longleaf Pine sub-ecosystems found within the boundaries of Marine Corps Base Camp Lejeune, as well as the Atlantic Coastal Plain Fall-Line Sandhill Longleaf Pine Woodland sub-ecosystem found within the boundaries of Fort Bragg.

Fort Bragg's transitions follow those shown for the MCBCL Atlantic Coastal Plain Upland Longleaf Pine sub-ecosystem (WWS-Upland and ID transitions).

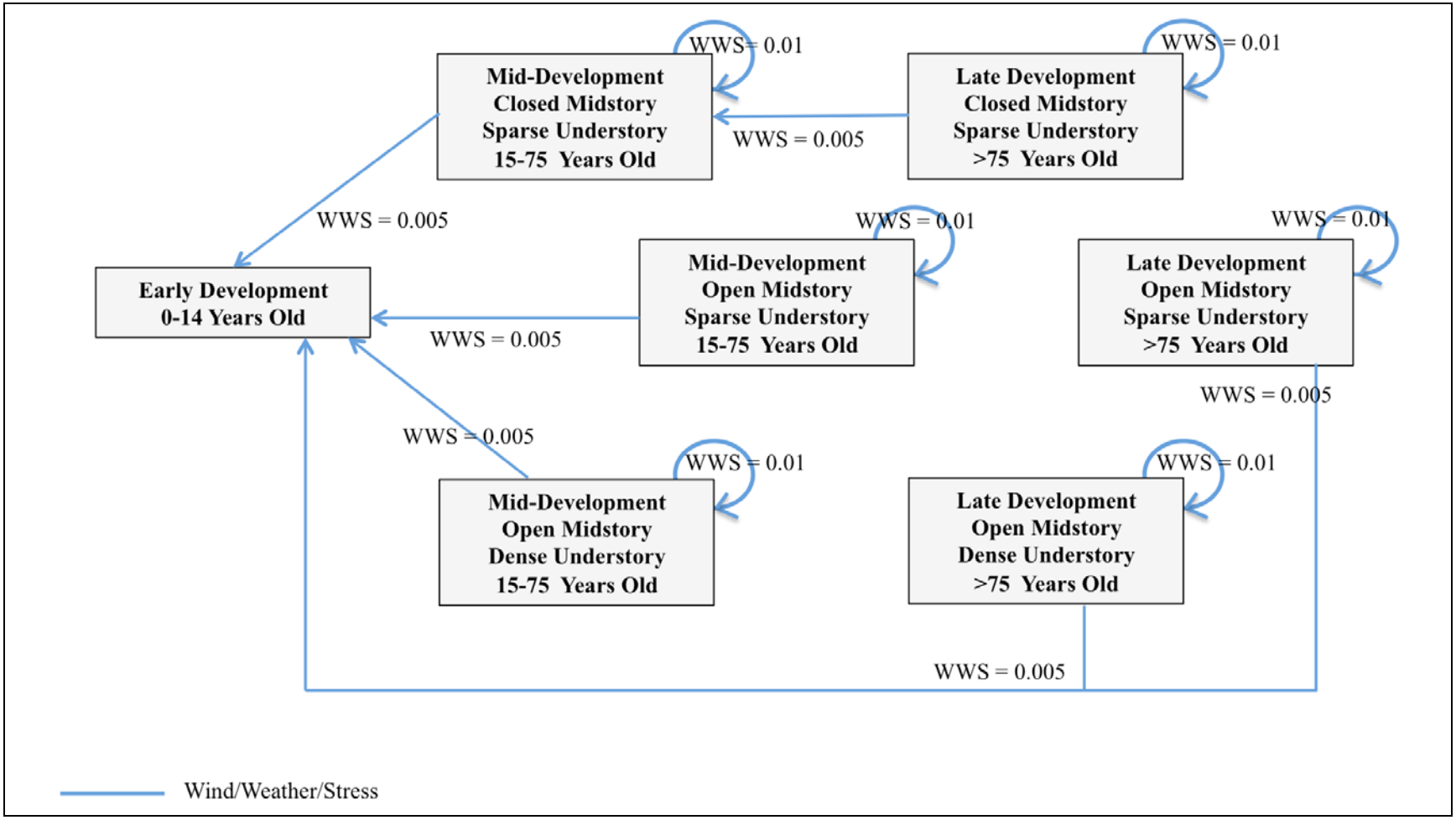

Figure 19-6. Wind/weather/stress (WWS [e.g., hurricane]) effects for the Florida Longleaf Pine Sandhill sub-ecosystem found within the boundaries of Eglin Air Force Base.

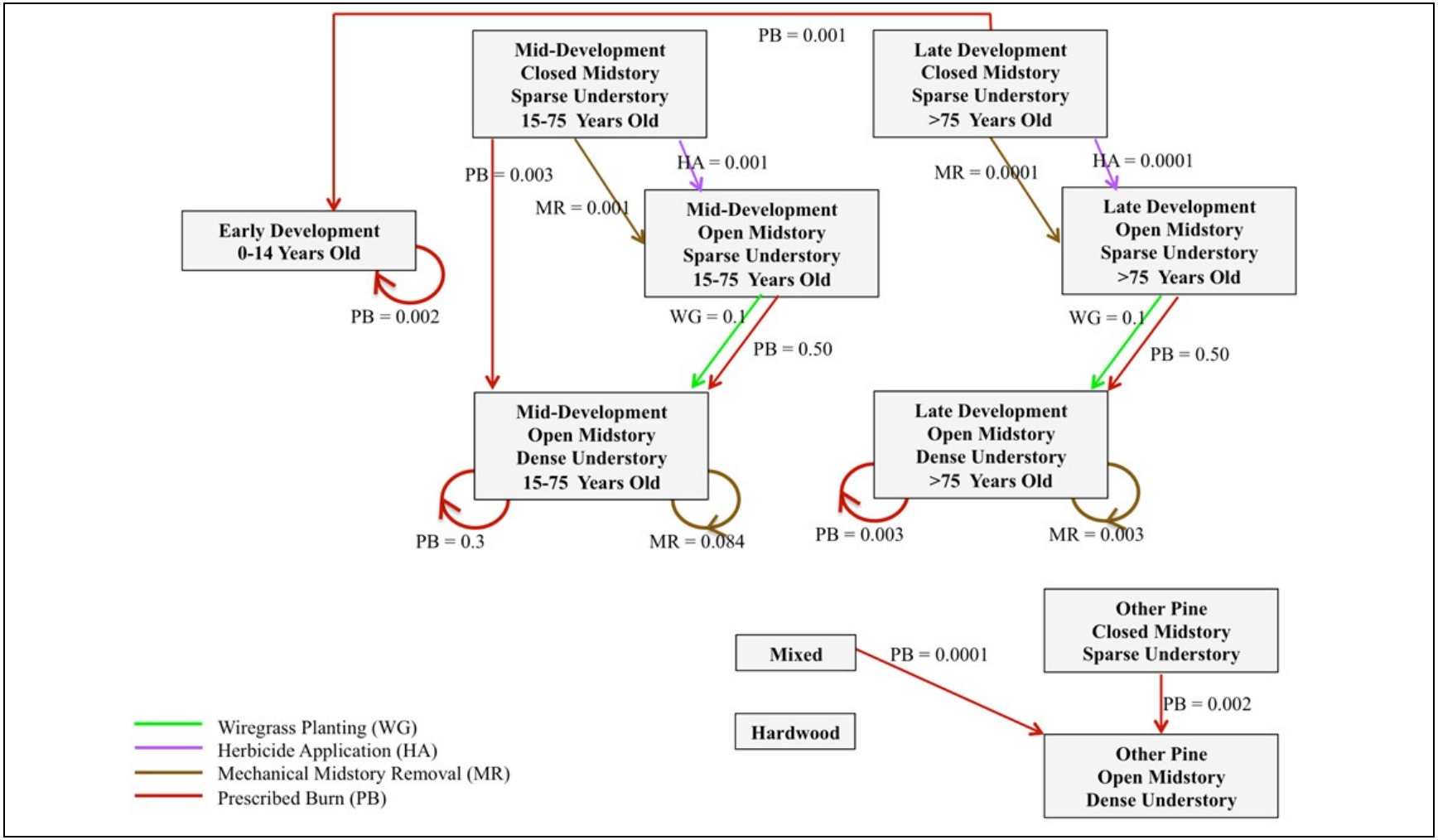

Figure 19-7. The effects of management techniques for the Atlantic Coastal Plain Upland Longleaf Pine, Central Atlantic Coastal Plain Wet Longleaf Pine, and Other sub-ecosystems found within the boundaries of Marine Corps Base Camp Lejeune (MCBCL), as well as the Atlantic Coastal Plain Fall-Line Sandhill Longleaf Pine Woodland and Other sub-ecosystems found within the boundaries of Fort Bragg.

Techniques could include prescribed burn (PB), herbicide application (HA), mechanical midstory removal (MR), and wiregrass planting (WG).

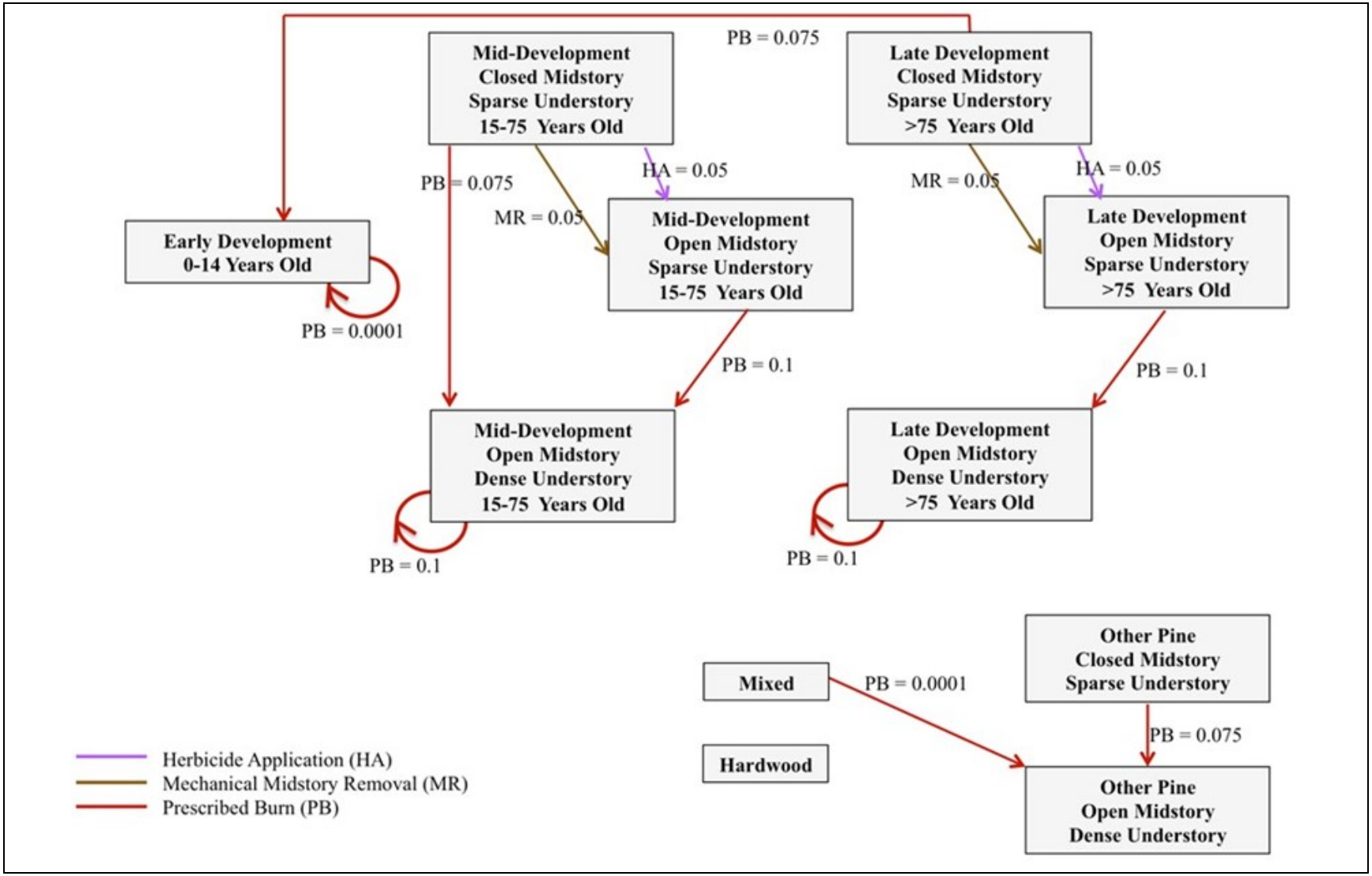

Figure 19-8. The effects of management techniques for the Florida Longleaf Pine Sandhill and Other sub-ecosystems found within the boundaries of Eglin Air Force Base.

Techniques could include prescribed burn (PB), herbicide application (HA), and mechanical midstory removal (MR).

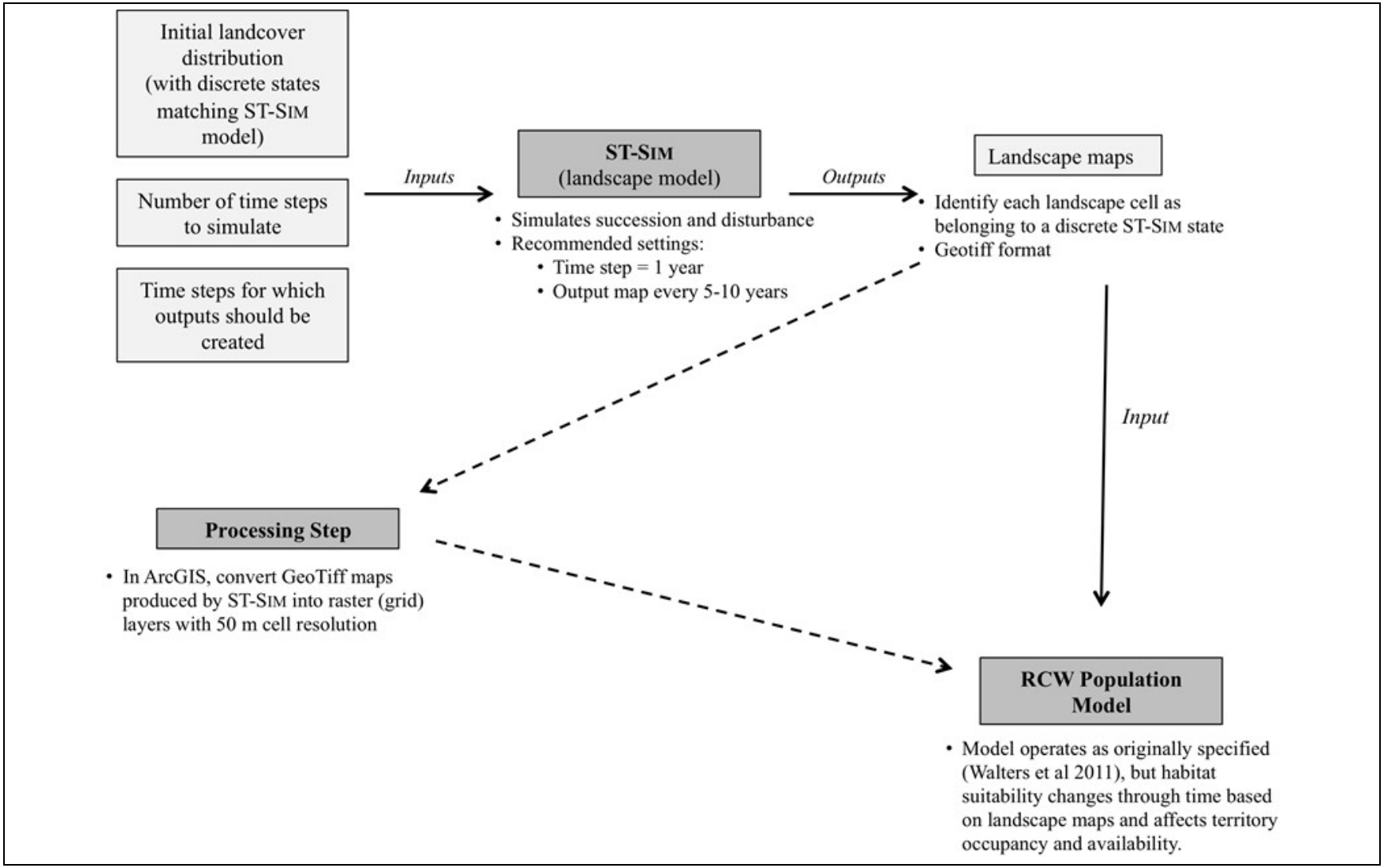

Figure 19-9. Conceptualization of the linked ST-Sim Landscape Model and the red-cockaded woodpecker (RCW) population model in the RCW Decision Support System (RCW DSS).

The RCW DSS is intended for use as an applied tool for RCW conservation and management.

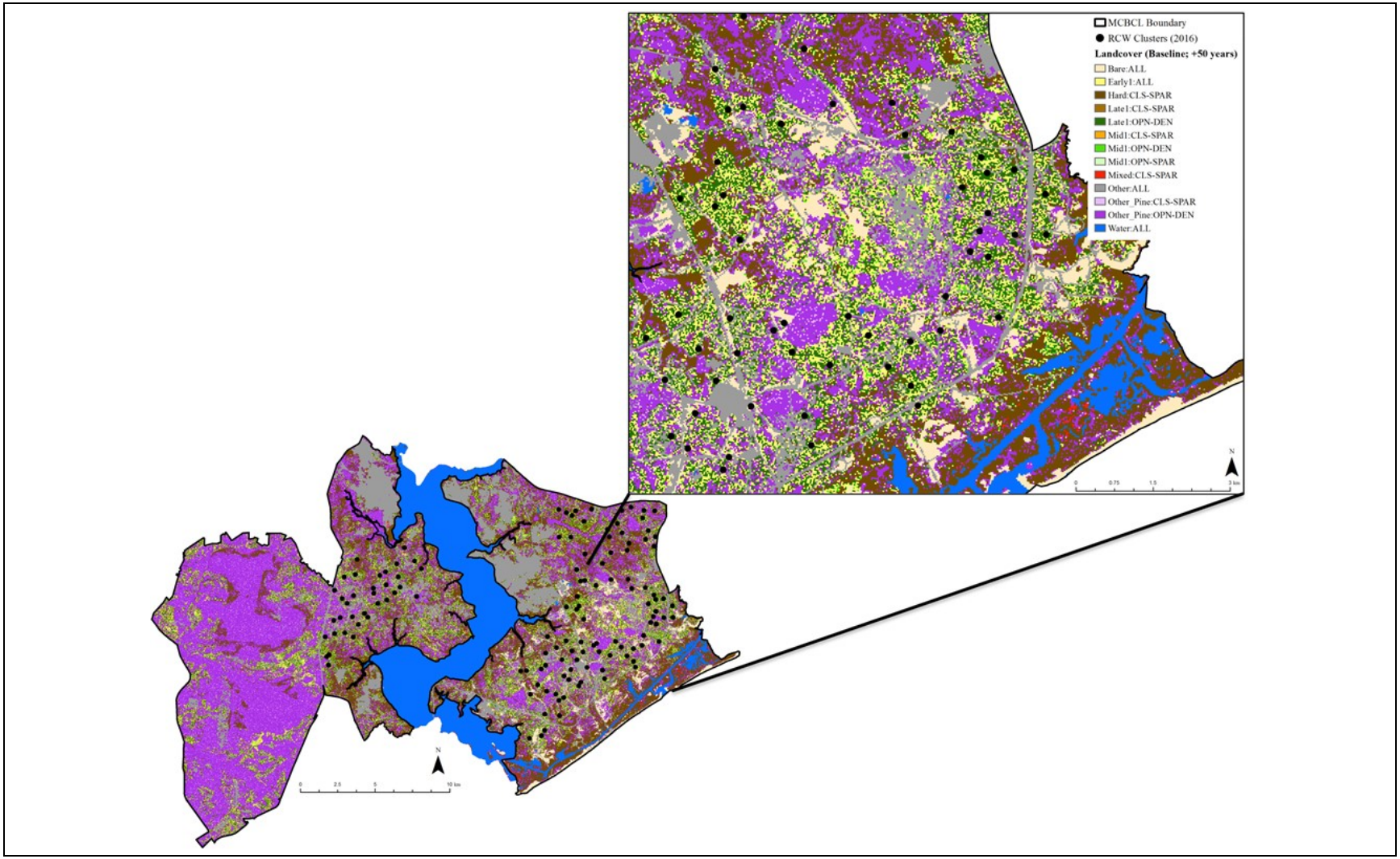

Figure 19-10. Predicted land cover at Marine Corps Base Camp Lejeune (MCBCL) following a 50-year simulation that assumed all management approaches and other natural events (e.g., wildfires, hurricanes) would continue occurring at rates commensurate with present day.

For reference, we included red-cockaded woodpecker (RCW) territory centers, or "clusters," that were present in 2016.

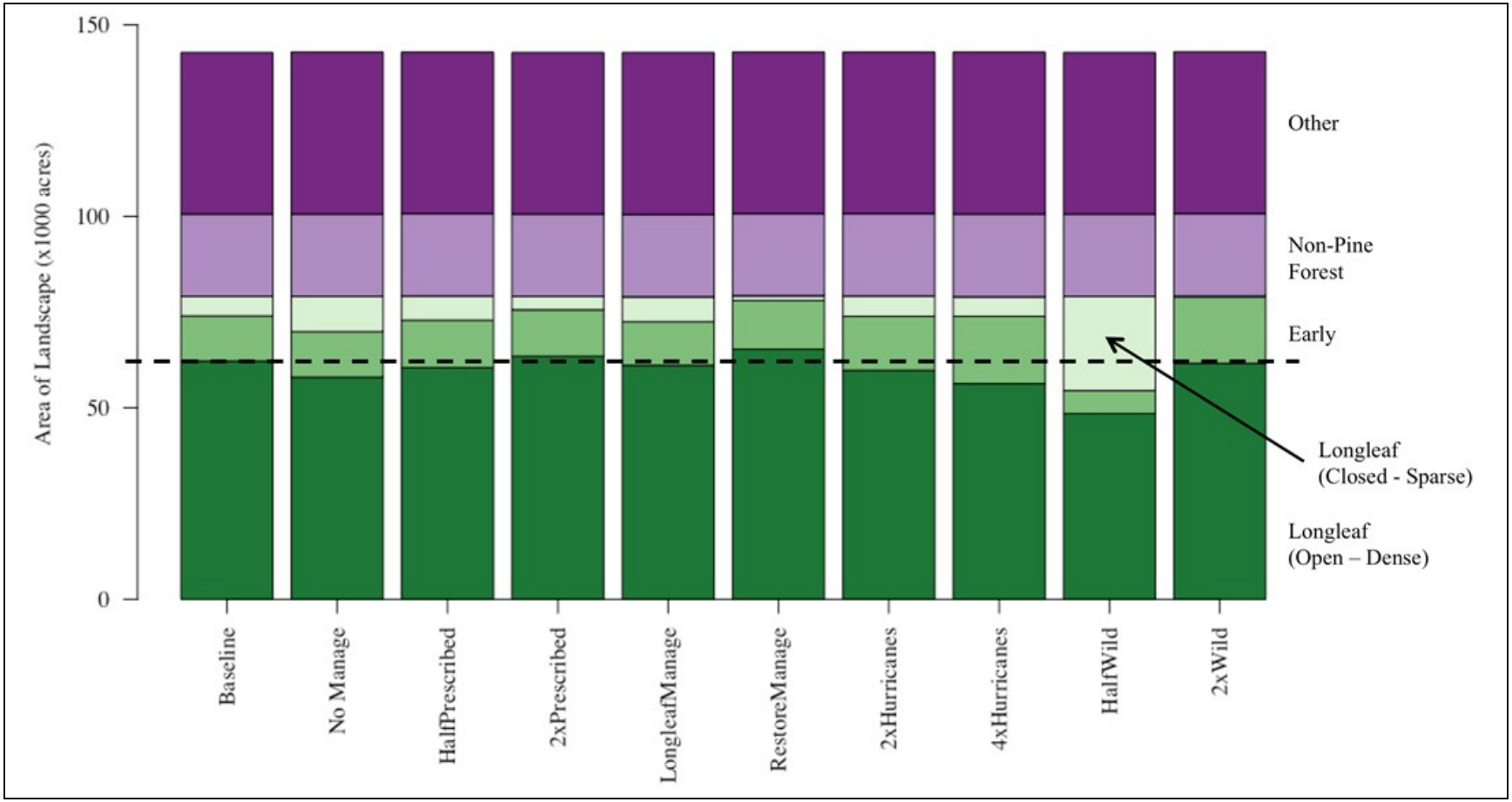

Figure 19-11. Results of scenarios modeled in the ST-Sim landscape model (for a detailed description of scenario assumptions, see the section of this chapter titled Landscape and Management Scenarios).

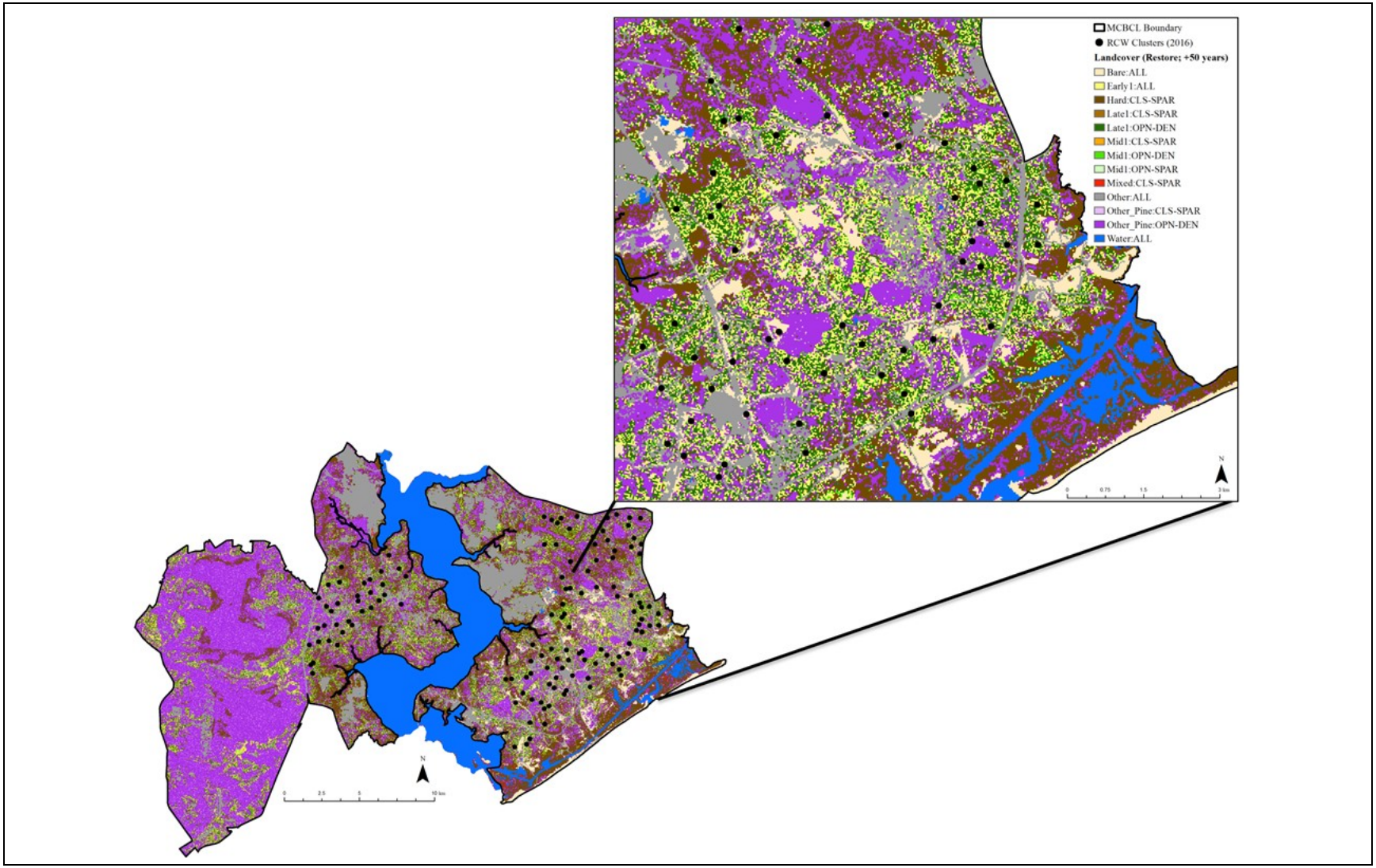

Figure 19-12. Predicted land cover at Marine Corps Base Camp Lejeune (MCBCL) after a simulation of 50 years that assumed longleaf pine stands of low suitability for red-cockaded woodpecker (RCW) nesting would be prioritized for all habitat management (e.g., prescribed burns, mechanical midstory removal, herbicide application).

For reference, we included RCW territory centers, or "clusters," that were present in 2016.

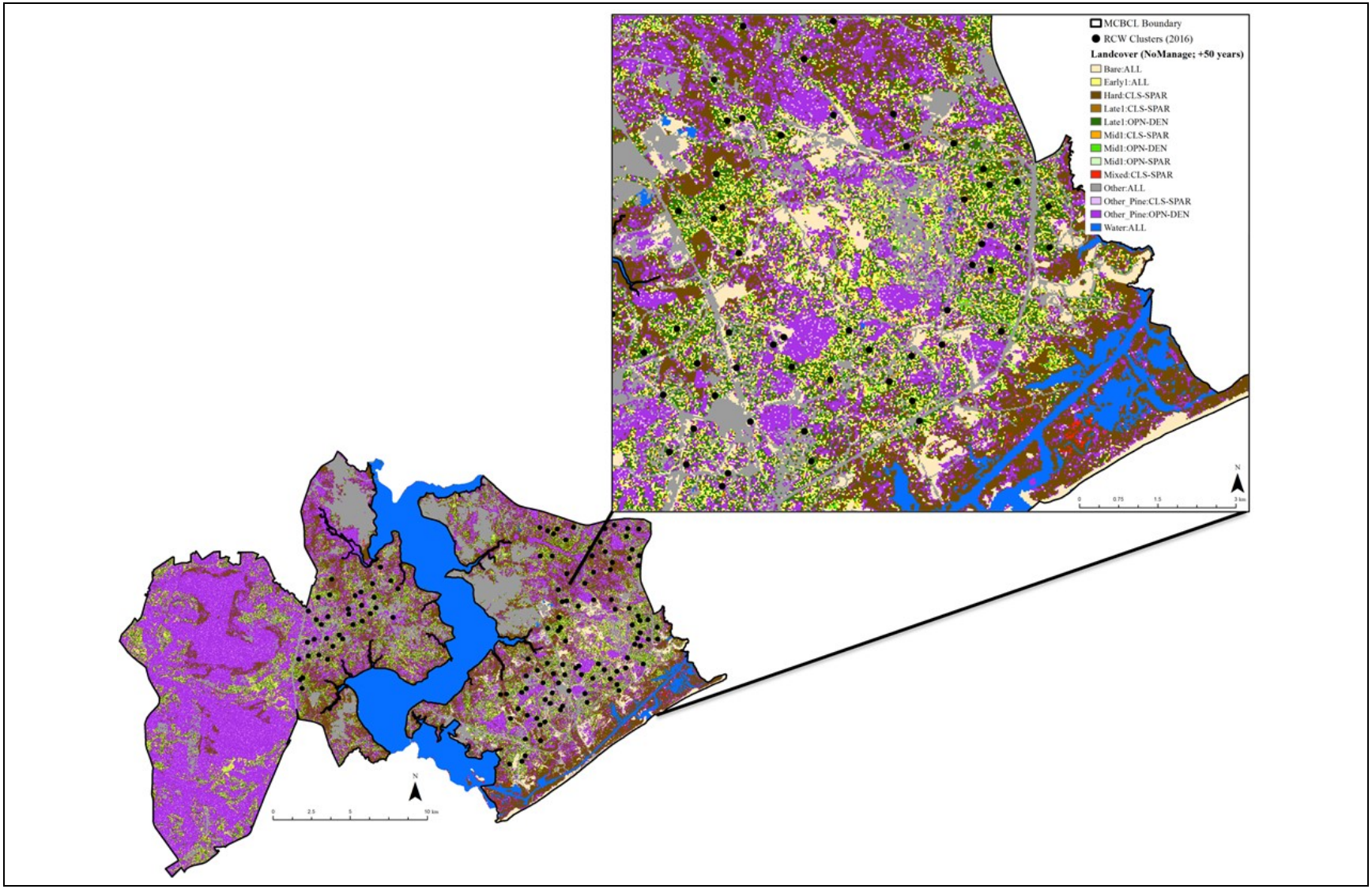

Figure 19-13. Predicted land cover at Marine Corps Base Camp Lejeune (MCBCL) after a simulation of 50 years that assumed the end of all longleaf pine habitat management (e.g., prescribed burns, mechanical midstory removal, herbicide application).

For reference, we included red-cockaded woodpecker (RCW) territory centers, or "clusters," that were present in 2016.

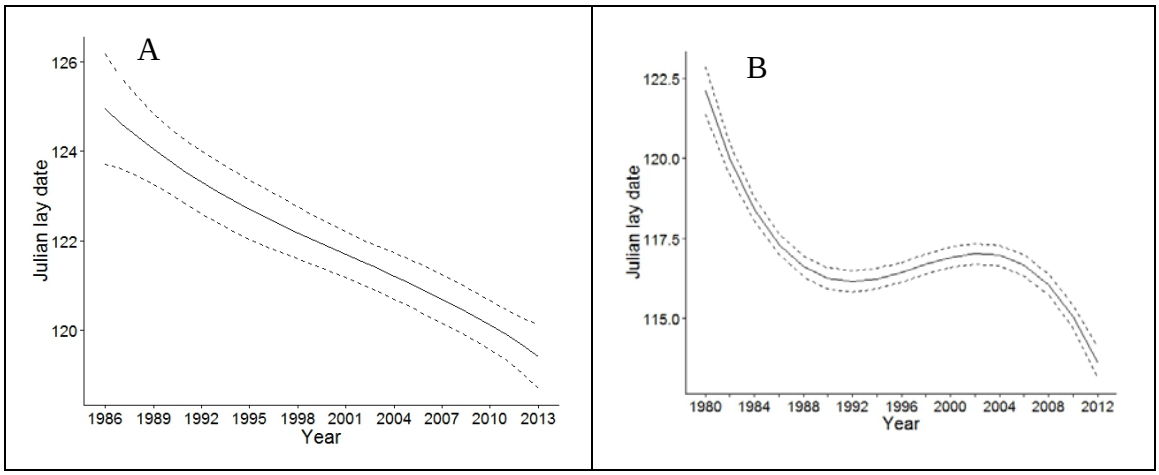

Figure 19-14. Changes in egg-laying dates over time at two study sites in North Carolina: (A) Marine Corps Base Camp Lejeune (MCBCL) and (B) the Sandhills.

Lines are model-averaged predictions and unconditional standard errors.

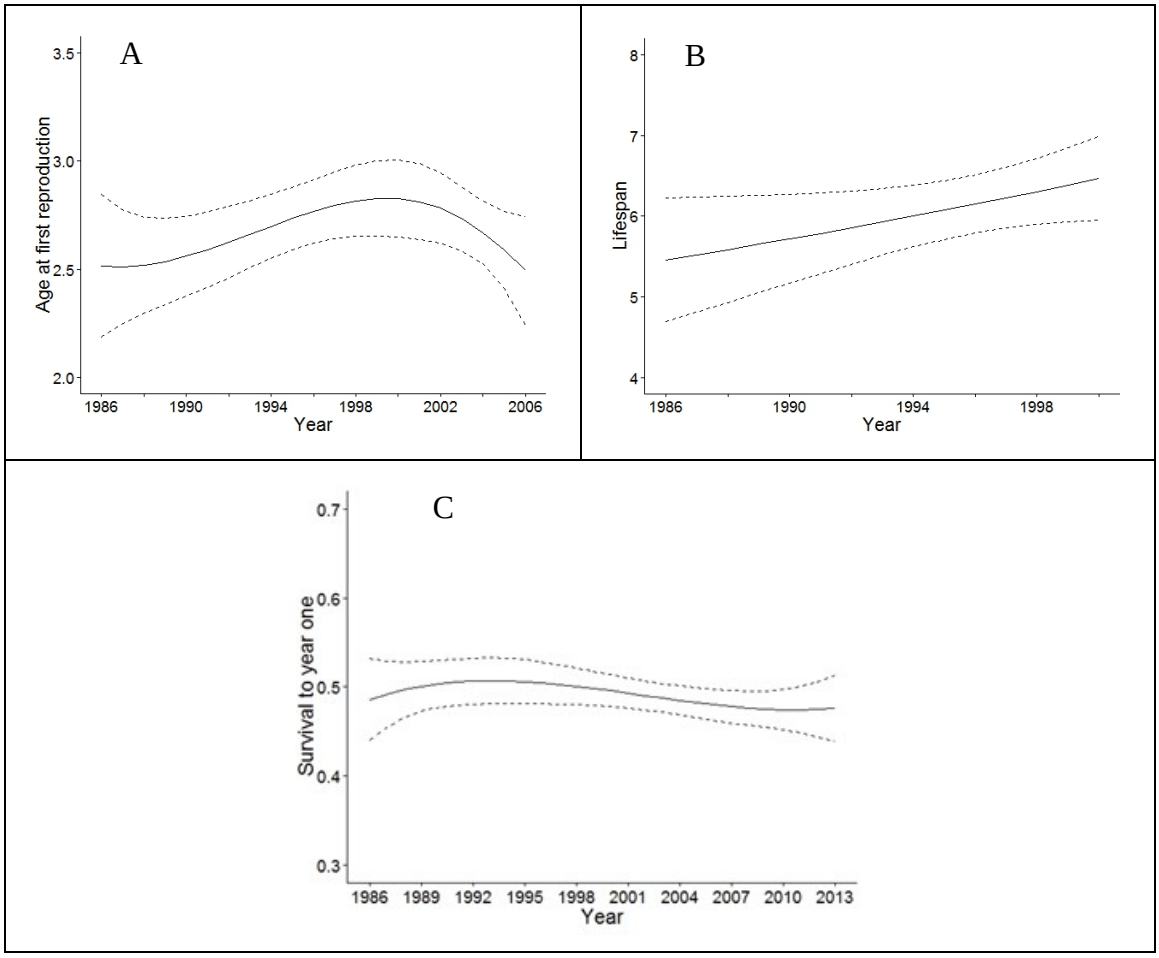

Figure 19-15. (A) The age at first reproduction and (B) lifespan increased slightly at Marine Corps Base Camp Lejeune (MCBCL). (C) The survival to the first year wavered over time, but the effect was very small.

Lines are model-averaged predictions and unconditional standard errors.

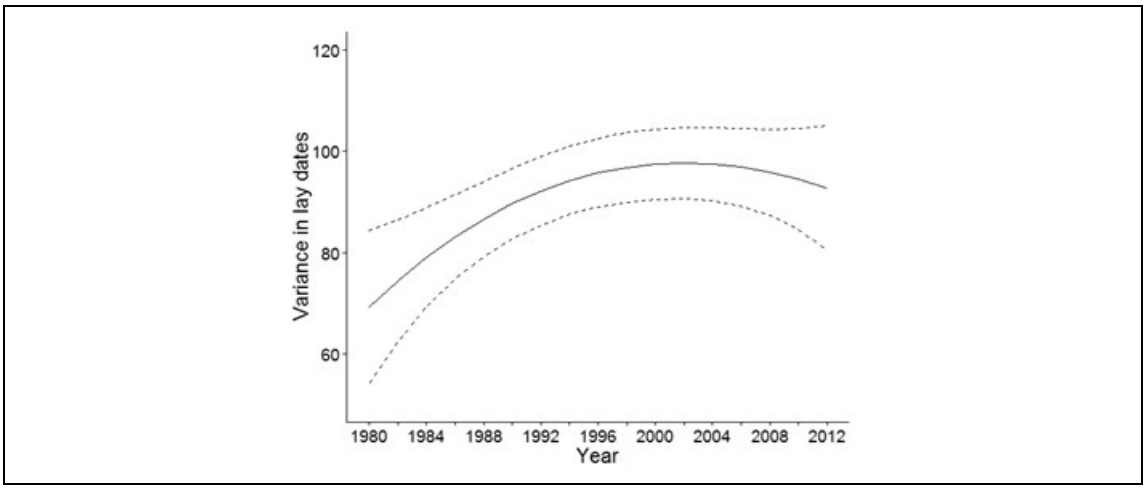

Figure 19-16. Variance in lay dates increased quadratically over time in the Sandhills, NC.

Lines are model-averaged predictions and unconditional standard errors.

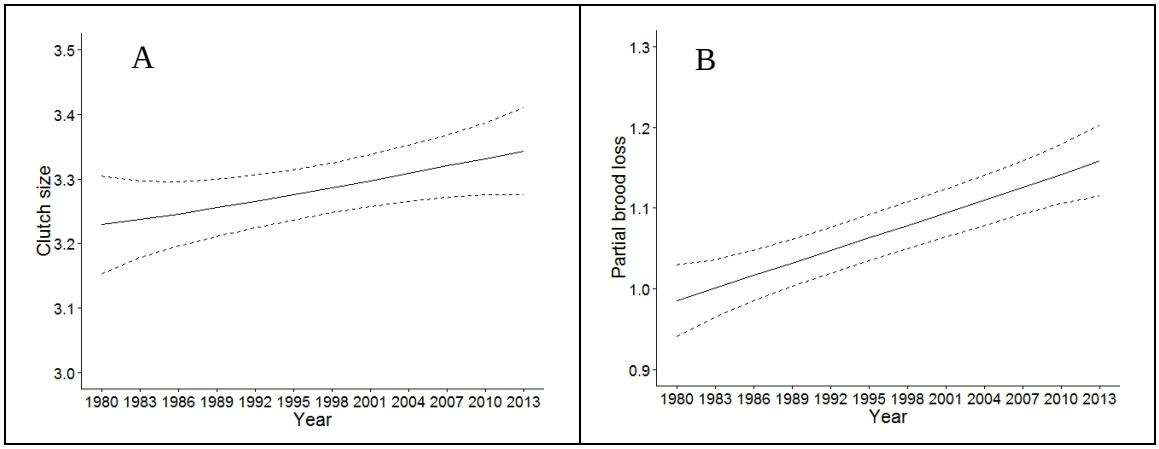

Figure 19-17. (A) Clutch size and (B) partial brood loss both increased in the Sandhills, NC.

Lines are model-averaged predictions and unconditional standard errors.

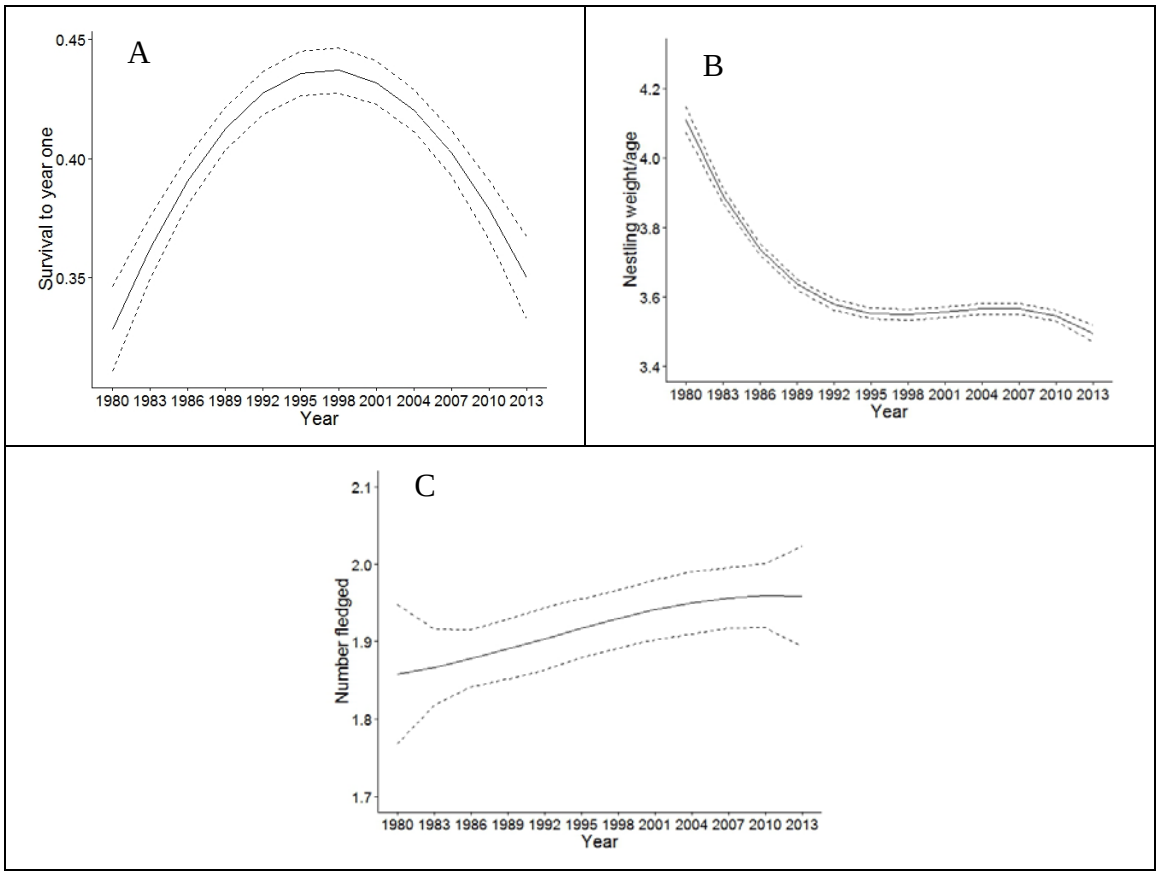

Figure 19-18. (A) Survival to age 1 increased quadratically over time in Sandhills, NC. (B) Nestling weight and age decreased over time, and (C) the number of fledglings per nest increased slightly.

Lines are model-averaged predictions and unconditional standard errors.

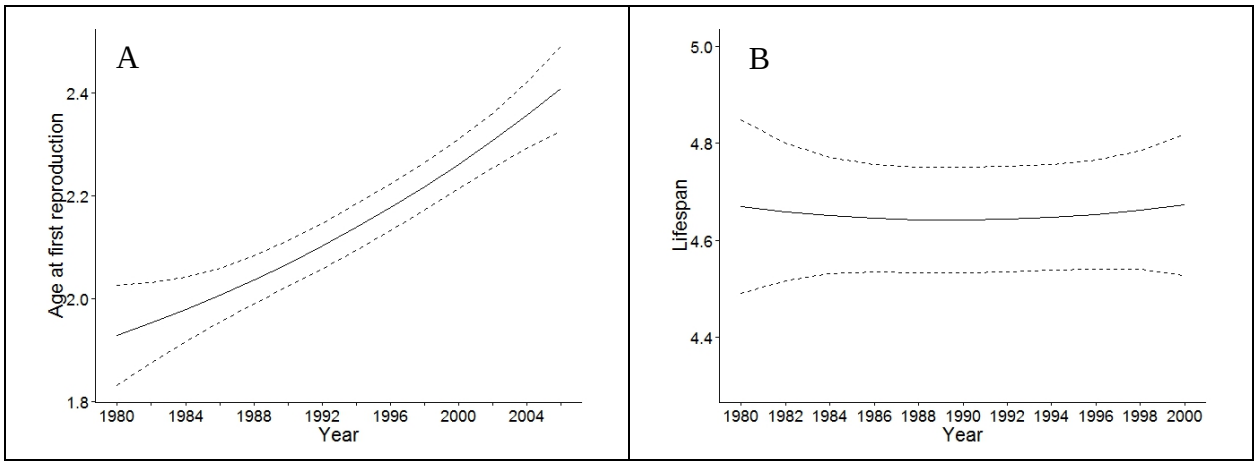

Figure 19-19. (A) Age at first reproduction increased in the Sandhills, but (B) lifespan did not change during the same period.

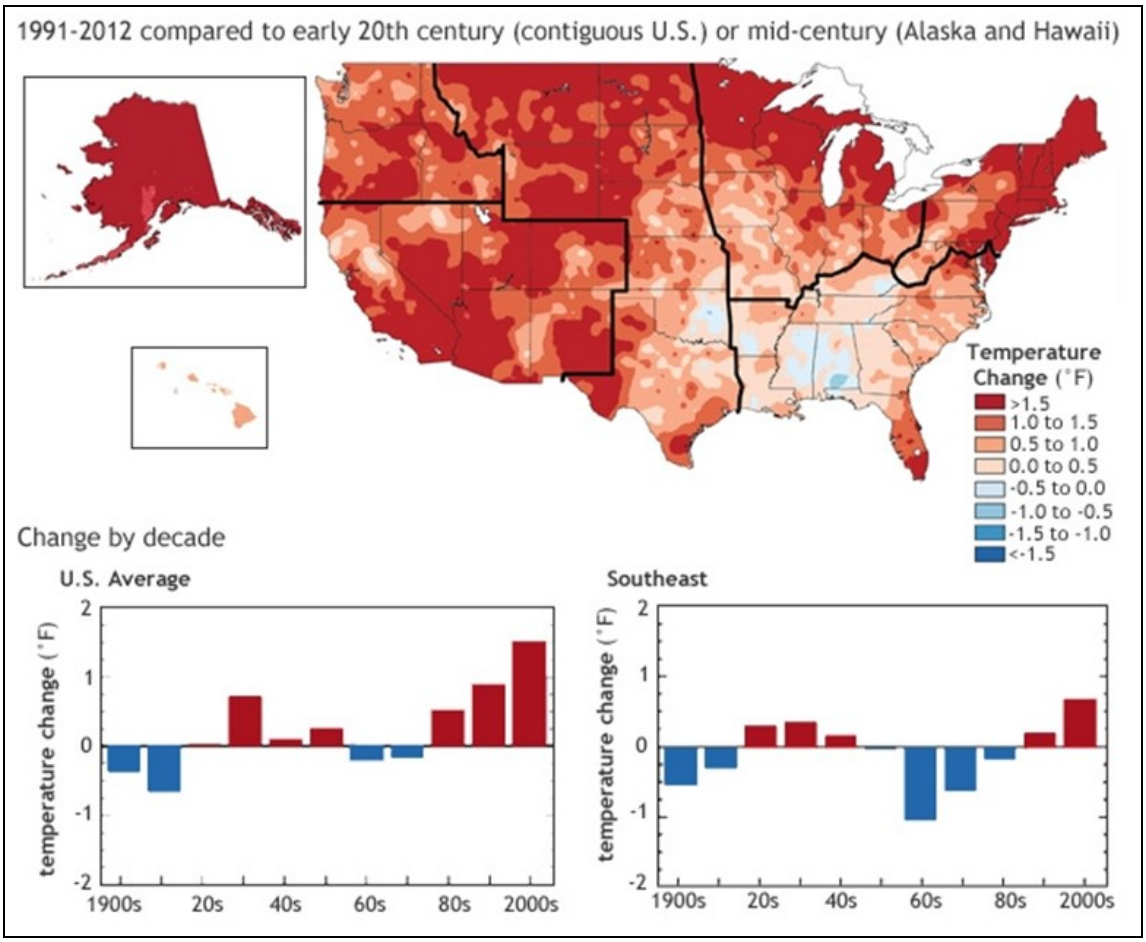

Figure 19-20. Past temperature trends indicated a mixed pattern in the Southeastern United States compared with the remainder of the United States.

Map from Chapter 2 of the 2014 National Climate Assessment, adapted for the Web and reprinted from https://www.climate.gov/news-features/climate-qa/does-global-warming-mean-it%E2%80%99s-warming-everywhere. Original graphic provided by National Oceanic and Atmospheric Administration's National Climatic Data Center and the Cooperative Institute for Climate and Satellites–North Carolina.

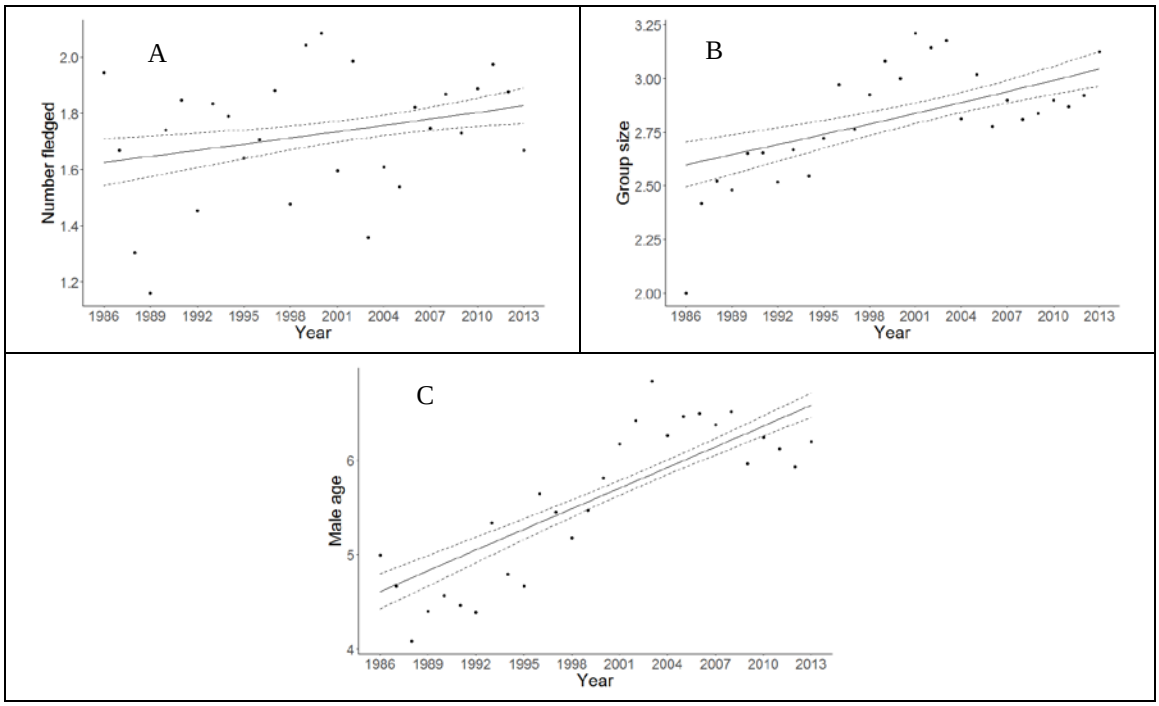

Figure 19-21. Changes in annual means over time regarding the (A) number of young fledged per group, (B) group size, and (C) breeding male's age in MCBCL, NC.

All three variables have increased throughout the study period.

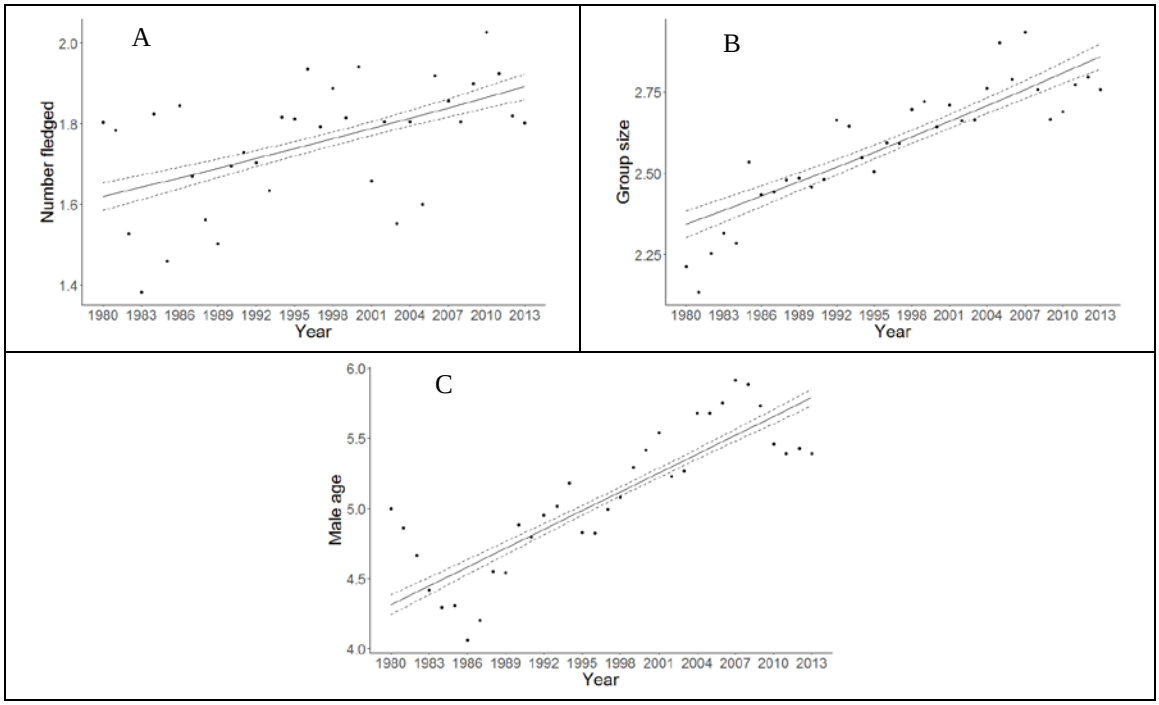

Figure 19-22. Changes in annual means over time regarding the (A) number of young fledged per group, (B) group size, and (C) breeding male's age in Sandhills, NC.

All three variables have increased throughout the study period.

Literature Cited

Anderson, D. 2008. *Model-Based Inference in the Life Sciences: A Primer on Evidence*. Springer, New York, NY.

Bartoń, K. 2011. *MuMIn: Multi-Model Inference. R Package Version 1.0.0*. Available at http://CRAN.R-project.org/package=MuMIn. R Foundation for Statistical Computing, Vienna, Austria.

Beissinger, S., M. Cook, and W. Arendt. 2005. The shelf life of bird eggs: Testing egg viability using a tropical climate gradient. *Ecology 86*:2164–2175.

Boyles, R., and S. Raman. 2003. Analysis of climate trends in North Carolina (1949–1998). *Environment International 29*:263–275.

Bradshaw, D. 1995. Habitat use by a relict population of red-cockaded woodpeckers in southeastern Virginia. *Red-Cockaded Woodpecker: Recovery, Ecology and Management*. Edited by Kulhavy, D., R. Hooper, and R. Costa. Center for Applied Studies in Forestry, Stephen F. Austin State University, Nacogdoches, TX.

Brockway, D., and C. Lewis. 1997. Long-term effects of dormant-season prescribed fire on plant community diversity, structure, and productivity in a longleaf pine wiregrass ecosystem. *Forest Ecology and Management 96*:167–183.

Burnham, K., and D. Anderson. 2002. *Model Selection and Multi-model Inference: A Practical Information–Theoretic Approach*. 2nd Edition. Springer-Verlag, New York, NY.

Carter, L., J. Jones, L. Berry, V. Burkett, J. Murley, J. Obeysekera, P. Schramm, and D. Wear. 2014. Southeast and the Caribbean. Pp. 396–417, Chapter 17 in *Climate Change Impacts in the United States: The Third National Climate Assessment*. U.S. Global Change Research Program. Edited by J.M. Melillo, T.C. Richmond, and G.W. Yohe. Available at http://www.globalchange.gov/sites/globalchange/files/Ch_0a_FrontMatter_ThirdNCA_GovtReviewDraft_Nov_22_2013_clean.pdf

Charmantier, A., R. McCleery, L. Cole, C. Perrins, L. Kruuk, and B. Sheldon. 2008. Adaptive phenotypic plasticity in response to climate change in a wild bird population. *Science 320*:800–803.

Chen, X., and K. Tung. 2014. Varying planetary heat sink led to global-warming slowdown and acceleration. *Science 345*:897–903.

Clutton-Brock, T. (Ed.). 1988. *Reproductive Success: Studies of Individual Variation in Contrasting Breeding Systems*. University of Chicago Press: Chicago, IL.

Collins, S. 1983. Geographic variation in habitat structure of the black-throated green warbler (*Dendroica virens*). *Auk 100*:382–389.

Conner, R., D. Rudolph, and J. Walters. 2001. *The Red-Cockaded Woodpecker: Surviving in a Fire-Maintained Ecosystem*. University of Texas Press: Austin, TX.

Conrey, R., S. Skagen, A. Yackel Adams, and A. Panjabi. 2016. Extremes of heat, drought and precipitation depress reproductive performance in shortgrass prairie passerines. *Ibis 158*:614–629.

Cook, M. I., S. R. Beissinger, G. A. Toranzos, R. A. Rodriguez, and W. J. Arendt. 2005. Microbial infection affects egg viability and incubation behavior in a tropical passerine. *Behavioral Ecology 16*:30-36.

Costa, R. 2004. State of the red-cockaded woodpecker world: Highlights of the previous decade (1992–2002). *Red-Cockaded Woodpecker: Road to Recovery*. Edited by Costa, R., and S.J. Daniels. Hancock House Publishing: Blaine, WA.

Costa, R., and R. Escano. 1989. *Red-Cockaded Woodpecker: Status and Management in the Southern Region in 1986*. Technical publication R8-TP-US. Edited by the U.S. Department of Agriculture, Forest Service, Southern Region.

Daniel, C., and L. Frid. 2011. Predicting landscape vegetation dynamics using state-and-transition simulation models. Pp. 5–22 in P*roceedings of the First Landscape State-and-Transition Simulation Modeling Conference*, U.S. Department of Agriculture and U.S. Forest Service, Pacific Northwest Research Station, Portland, OR. June 14–16. Edited by Kerns, B., A. Shlisky, and C. Daniel.

Daniels, S.J., and J.R. Walters. 2000. Between-year breeding dispersal in red-cockaded woodpeckers: Multiple causes and estimated cost. *Ecology 81*:2473–2484.

DeLotelle, R., R. Epting, and J. Newman. 1987. Habitat use and territory characteristics of red-cockaded woodpeckers in central Florida. *Wilson Bulletin 99*:202–217.

Doster, R.H., and D.A. James. 1998. Home range size and foraging habitat of red-cockaded woodpeckers in the Ouachita Mountains of Arkansas. *Wilson Bulletin 110*:110–117.

Dunning, J.B., Jr., D.J. Stewart, B.J. Danielson, B.R. Noon, T.L. Root, R.H. Lamberson, and E. Stevens. 1995. Spatially explicit population models: current forms and future uses. *Ecological Applications 5*:3–11.

Easterling, D. 2002. Recent changes in frost days and the frost-free season in the United States. *Bulletin of the American Meteorological Society 83*:1327–1332.

Easterling, D., and M. Wehner. 2009. Is the climate warming or cooling? *Geophysical Research Letters 36*:1–3.

Engstrom, R., and F. Sanders. 1997. Red-cockaded woodpecker foraging ecology in an old-growth longleaf pine forest. *Wilson Bulletin 109*:203–217.

Fisher, R., T. Wellicome, E. Bayne, R. Poulin, L. Todd, and A. Ford. 2015. Extreme precipitation reduces reproductive output of an endangered raptor. *Journal of Applied Ecology 52*:1500–1508.

Garcia, V. 2014. *Lifetime fitness and changing life history traits in red-cockaded woodpeckers*. Department of Biological Sciences, Virginia Tech, Blacksburg, VA.

Gardner, J., A. Peters, M. Kearney, L. Joseph, and R. Heinsohn. 2011. Declining body size: A third universal response to warming? *Trends in Ecology and Evolution 26*:285–291.

Gienapp, P., C. Teplitsky, J. Alho, J. Mills, and J. Merila. 2008. Climate change and evolution: Disentangling environmental and genetic responses. *Molecular Ecology 17*:167–178.

Gilliam, F., and W. Platt. 1999. Effects of long-term fire exclusion on tree species composition and stand structure in an old-growth *Pinus palustris* (longleaf pine) forest. *Plant Ecology 140*:15–26.

Glitzenstein, J., D. Streng, and D. Wade. 2003. Fire frequency effects on longleaf pine (*Pinus palustris*) vegetation in South Carolina and northeast Florida, USA. *Natural Areas Journal 23*:22–37.

Godard, R., C. Morgan Wilson, J. Frick, P. Siegel, and B. Bowers. 2007. The effects of exposure and microbes on hatchability of eggs in open-cup and cavity nests. *Journal of Avian Biology 38*:709–716.

Grimm, V., E. Revilla, J. Groeneveld, S. Kramer-Schadt, M. Schwager, J. Tews, M. Wichmann, and F. Jeltsch. 2005. Importance of buffer mechanisms for population viability analysis. *Conservation Biology 19*:578–580.

Halupka, L., A. Dyrcz, and M. Borowiec. 2008. Climate change affects breeding of reed warblers *Acrocephalus scirpaceus*. *Journal of Avian Biology 39*:95–100.

Hansen, A., R. Neilson, V. Dale, C. Flather, L. Iverson, D. Currie, S. Shafer, R. Cook, and P. Bartlein. 2001. Global change in forests: Responses of species, communities, and biomes: Interactions between climate change and land use are projected to cause large shifts in biodiversity. *Bioscience 51*:765–779.

Hardesty, J., K. Gault, and H. Percival. 1997. *Ecological Correlates of Red-Cockaded Woodpecker (Picoides borealis) Foraging Preference, Habitat Use, and Home Range Size in Northwest Florida (Eglin Air Force Base)*. Final report research work order 99. Florida Cooperative Fish and Wildlife Unit, University of Florida, Gainesville, FL.

Harding, S., and J. Walters. 2002. Processes regulating the population dynamics of red-cockaded woodpecker cavities. *Journal of Wildlife Management 66*:1083–1095.

Heppell, S.S., J.R. Walters, and L.B. Crowder. 1994. Evaluating management alternatives for red-cockaded woodpeckers: A modeling approach. *Journal of Wildlife Management 58*:479–487.

Hochachka, W. 1990. Seasonal decline in reproductive performance of song sparrows. *Ecology 71*:1279–1288.

Holt, R. 1990. The microevolutionary consequences of climate change. *Trends in Ecology and Evolution 5*:311–315.

Hooper, R., and R. Harlow. 1986. *Forest Stand Selection by Foraging Red-Cockaded Woodpeckers*. Southeastern Forest Experimental Station Research Paper: SE-259. U.S. Department of Agriculture Forest Service.

Hooper, R., and M. Lennartz. 1981. Foraging behavior of the red-cockaded woodpecker in South Carolina. *Auk 98*:321–334.

Husby, A., D. Nussey, M. Visser, A. Wilson, B. Sheldon, and L. Kruuk. 2010. Contrasting patterns of phenotypic plasticity in reproductive traits in two great tit (*Parus major*) populations. *Evolution 64*:2221–2237.

Iverson, L., and A. Prasad. 2001. Potential changes in tree species richness and forest community types following climate change. *Ecosystems 4*:186–199.

Iverson, L., A. Prasad, and S. Matthews. 2008. Modeling potential climate change impacts on the trees of the northeastern United States. *Mitigation and Adaptation Strategies for Global Change 13*:487–516.

James, F., C. Hess, B. Kicklighter, and R. Thum. 2001. Ecosystem management and the niche gestalt of the red-cockaded woodpecker in longleaf pine forests. *Ecological Applications 11*:854–870.

James, F., C. Hess, and D. Kufrin. 1997. Species-centered environmental analysis: Indirect effects of fire history on red-cockaded woodpeckers. *Ecological Applications 7*:118–129.

Jenouvrier, S. 2013. Impacts of climate change on avian populations. *Global Change Biology 19*:2036–2057.

Jones, C., and H. Hunt. 1996. Foraging habitat of the red-cockaded woodpecker on the D'Arbonne National Wildlife Refuge, Louisiana. *Journal of Field Ornithology 67*:511–518.

Judson, O. 1994. The rise of the individual-based model in ecology. *Trends in Ecology and Evolution 9*:9–14.

Kesler, D., J. Walters, and J. Kappes. 2010. Social influences on dispersal and the fat-tailed dispersal distribution in red-cockaded woodpeckers. *Behavioral Ecology 21*:1337–1343.

Klomp, H. 1970. The determination of clutch size in birds: A review. *Ardea 58*:1–121.

Konrad, II, C., and C. Fuhrmann. 2013. Climate of the southeast USA: Past, present, and future. Pp. 8–42 in *Climate of the Southeast United States*. Edited by Ingram, K., K. Dow, L. Carter, and J. Anderson. Island Press: Washington, DC.

Lack, D. 1947. The significance of clutch-size. *Ibis 89*:302–352.

Lacy, R., P. Miller, P. Nyhus, J. Pollak, B. Raboy, and S. Zeigler. 2013. Metamodels for transdisciplinary analysis of wildlife population dynamics. *PLoS ONE 8*:e84211.

Lennartz, M., R. Hooper, and R. Harlow. 1987. Sociality and cooperative breeding of red-cockaded woodpeckers, *Picoides borealis*. *Behavioral Ecology and Socibiology 20*:77–88.

Lenoir, J., J. Gegout, P. Marquet, P. de Ruffray, and H. Brisse. 2008. A significant upward shift in plant species optimum elevation during the 20th century. *Science 320*:1768–1771.

Letcher, B.H., J.A. Priddy, J.R. Walters, and L.B. Crowder. 1998. An individual-based, spatially-explicit simulation model of the population dynamics of the endangered red-cockaded woodpecker, *Picoides borealis*. *Biological Conservation 86*:1–14.

Ligon, J.D. 1970. Behavior and breeding biology of the red-cockaded woodpecker. *Auk 87*:255–278.

Liles, M., M. Peterson, J. Seminoff, E. Altamirano, A. Nenriquez, A. Gaos, V. Gadea, J. Urteaga, P. Torres, B. Wallace, and T. Peterson. 2015. One-size does not fit all: Importance of adjusting conservation practices for endangered hawksbill sea turtles to address local nesting habitat needs in the eastern Pacific Ocean. *Biological Conservation 184*:405–413.

Maguire, L.A., G.F. Wilhere, and Q. Dong. 1995. Population viability analysis for red-cockaded woodpeckers in the Georgia Piedmont. *Journal of Wildlife Management 59*:533–542.

McKellar, A., D. Kesler, R. Mitchell, D. Delaney, and J. Walters. 2014. Geographic variation in fitness and foraging habitat quality in an endangered bird. *Biological Conservation 175*:52–64.

Mitchell, L.R., L.D. Carlile, and C.R. Chandler. 1999. Effects of southern flying squirrels on nest success of red-cockaded woodpeckers. *Journal of Wildlife Management 63*:538–545.

Myers, R. 1985. Fire and the dynamic relationship between Florida sandhill and sand pine scrub vegetation. *Bulletin of the Torrey Botanical Club 112*:241–252.

Noon, B., and K. McKelvey. 1996. Management of the spotted owl: A case study in conservation biology. *Annual Review of Ecology and Systematics 27*:135–162.

Pachauri, R., M. Allen, V. Barros, J. Broome, W. Cramer, R. Christ, J. Church, L. Clarke, Q. Dahe, P. Dasgupta, and N. Dudash (Eds.). 2014. *Climate Change 2014: Synthesis Report*. Contribution of Working Groups I, II, and III to the Fifth Assessment Report of the Intergovernmental Panel on Climate Change. Intergovernmental Panel on Climate Change (IPCC), Geneva, Switzerland.

Parmesan, C., and G. Yohe. 2003. A globally coherent fingerprint of climate change impacts across natural systems. *Nature 421*:37–42.

Peterson, T., T. Karl, J. Kossin, K. Kunkel, J. Lawrimore, J. McMahon, R. Vose, and X. Yin. 2014. Changes in weather and climate extremes: State of knowledge relevant to air and water quality in the United States. *Journal of the Air and Waste Management Association 64*:184–197.

Porter, M., and R. Labisky. 1986. Home range and foraging habitat of red-cockaded woodpeckers in northern Florida. *Journal of Wildlife Management 50*:239–247.

Proffitt, K., T. McEneaney, P. White, and R. Garrott. 2010. Productivity and fledging success of trumpeter swans in Yellowstone National Park, 1987–2007. *Waterbirds 33*:341–348.

Provencher, L., K. Galley, A. Litt, D. Gordon, L. Brennan, G. Tanner, and J. Hardesty. 2002a. Fire, herbicide, and chainsaw-felling effects on arthropods in fire-suppressed longleaf pine sandhills at Eglin Air Force Base, FL. In *Proceedings: The Role of Fire for Nongame Wildlife Management and Community Restoration: Traditional Uses and New Directions*. U.S. Department of Agriculture and the U.S. Forest Service, Newton Square, PA.

Provencher, L., N. Gobris, and L. Brennan. 2002b. Effects of hardwood reduction on winter birds in northwest Florida longleaf pine sandhill forests. *Auk 119*:71–87.

Provencher, L., N. Gobris, L. Brennan, D. Gordon, and J. Hardesty. 2002c. Breeding bird response to midstory hardwood reduction in Florida sandhill longleaf pine forests. *Journal of Wildlife Management 66*:641–661.

Provencher, L., B. Herring, D. Gordon, H. Rodgers, K. Galley, G. Tanner, J. Hardesty, and L. Brennan. 2001a. Effects of hardwood reduction techniques on longleaf pine sandhill vegetation in northwest Florida. *Restoration Ecology 9*:13–27.

Provencher, L., B. Herring, D. Gordon, H. Rodgers, G. Tanner, J. Hardesty, L. Brennan, and A. Litt. 2001b. Longleaf pine and oak responses to hardwood reduction techniques in fire-suppressed sandhills in northwest Florida. *Forest Ecology and Management 148*:63–77.

Provencher, L., A. Litt, D. Gordon, H. Rodgers, B. Herring, K. Galley, J. McAdoo, S. McAdoo, N. Gobris, and J. Hardesty. 2001c. Restoring fire and hurricanes in longleaf pine sandhills. *Ecological Restoration 19*:92–98.

R Development Core Team. 2014. *R: A Language and Environment for Statistical Computing*. R Foundation for Statistical Computing, Vienna, Austria.

Repasky, P. 1984. *Home Range and Habitat Utilization of the Red-Cockaded Woodpecker*. M.S. thesis, North Carolina State University, Raleigh, NC.

Rodgers, H., and L. Provencher. 1999. Analysis of longleaf pine sandhill vegetation in northwest Florida. *Castanea 64*:138–162.

Rogers, J. 2013. The 20th century cooling trend over the southeastern United States. *Climate Dynamics 40*:341–352.

Rolland, V., J. Hostetler, T. Hines, H. Percival, and M. Oli. 2011. Factors influencing reproductive performance of northern bobwhite in South Florida. *European Journal of Wildlife Research 57*:717–727.

Rollins, M. 2009. LANDFIRE: A nationally consistent vegetation, wildland fire, and fuel assessment. *International Journal of Wildland Fire 18*:235–249.

Rudolph, D., R. Conner, and J. Walters. 2004. Red-cockaded woodpecker recovery: An integrated strategy. Pp. 70–76 in *Red-Cockaded Woodpecker: Road to Recovery*. Edited by Costa, R., and S. Daniels. Hancock House Publishers: Blaine, WA.

Schiegg, K., J.R. Walters, and J.A. Priddy. 2005. Testing a spatially explicit, individual-based model of red-cockaded woodpecker population dynamics. *Ecological Applications 15*:1495–1503.

Schiegg, K., J.R. Walters, and J.A. Priddy. 2002. The consequences of disrupted dispersal in fragmented red-cockaded woodpecker (*Picoides borealis)* populations. *Journal of Animal Ecology 71*:710–721.

Schielzeth, H., and W. Forstmeier. 2009. Conclusions beyond support: Overconfident estimates in mixed models. *Behavioral Ecology 20*:416–420.

Smith, H. 1993. Parental age and reproduction in the marsh tit *Paras palustris*. *Ibis 135*:196–201.

Stoleson, S., and S. Beissinger. 1999. Egg viability as a constraint on hatching synchrony at high ambient temperatures. *Journal of Animal Ecology 68*:951–962.

Thompson, P., and J. Ollason. 2001. Lagged effects of ocean climate change on fulmar population dynamics. *Nature 413*:417–420.

Tollefson, J. 2014. The case of the missing heat. *Nature 505*:276–278.

U.S. FWS (Fish and Wildlife Service). 2003. *Recovery Plan for the Red-Cockaded Woodpecker (Picoides borealis)*. U.S. Fish and Wildlife Service, Atlanta, GA.

Veno, P. 1976. Successional relationships of five Florida plant communities. *Ecology 57*:498–508.

Walsh, J., D. Wuebbles, K. Hayhoe, J. Kossin, K. Kunkel, G. Stephens, P. Thorne, R. Vose, M. Wehner, J. Willis, D. Anderson, S. Doney, R. Feely, P. Hennon, V. Kharin, T. Knutson, F. Landerer, T. Lenton, J. Kennedy, and R. Somerville. 2014. Our changing climate. Pp. 19–67, Chapter 2 in *Climate Change Impacts in the United States: The Third National Climate Assessment*. U.S. Global Change Research Program. Edited by J.M. Melillo, T.C. Richmond, and G.W. Yohe. Available at http://www.globalchange.gov/sites/globalchange/files/Ch_0a_FrontMatter_ThirdNCA_GovtReviewDraft_Nov_22_2013_clean.pdf

Walters, J. 2004. Unusual dynamics in a rapidly increasing population of red-cockaded woodpeckers at Camp Lejeune, North Carolina. Pp. 256–267 in *Red-Cockaded Woodpecker: Road to Recovery*. Edited by Costa, R., and S.J. Daniels. Hancock House Publishing: Blaine, WA.

Walters, J. 1991. Application of ecological principles to the management of endangered species: The case of the red-cockaded woodpecker. *Annual Review of Ecology and Systematics 22*:505–523.

Walters, J., and V. Garcia. 2016. Red-cockaded woodpeckers: Alternative pathways to breeding success. Pp. 58–78 in *Cooperative Breeding in Vertebrates: Studies in Ecology, Evolution, and Behavior*. Edited by Koenig, W., and J. Dickinson. Cambridge University Press: Cambridge, United Kingdom.

Walters, J., P. Baldassaro, K. Convery, L. Crowder, D. Kessler, R. McGregor, J. Priddy, and S. Tweddale. 2011. *A Decision Support System for Identifying and Ranking Critical Habitat Parcels on and in the Vicinity of Department of Defense Installations*. Final Report to the U.S. Department of Defense. SERDP RC-1472.

Walters, J., L. Crowder, and J. Priddy. 2002a. Population viability analysis for red-cockaded woodpeckers using an individual-based model. *Ecological Applications 12*:249–260.

Walters, J., S. Daniels, J. Carter, and P. Doerr. 2002b. Defining quality of red-cockaded woodpecker foraging habitat based on habitat use and fitness. *Journal of Wildlife Management 66*:1064–1082.

Walters, J., S. Daniels, J. Carter III, P. Doerr, K. Brust, and J. Mitchell. 2000. *Foraging Habitat Resources, Preferences, and Fitness of Red-Cockaded Woodpeckers in the North Carolina Sandhills*. Fort Bragg Project Final Report. Virginia Tech, Blacksburg, VA, and North Carolina State University, Raleigh, NC.

Walters, J., C. Copeyon, and J. Carter. 1992. Test of the ecological basis of cooperative breeding in red-cockaded woodpeckers. *Auk 109*:90–97.

Walters, J., P. Doerr, and J. Carter. 1988. The cooperative breeding system of the red-cockaded woodpecker. *Ethology 78*:275–305.

Walther, G.-R., E. Post, P. Convey, A. Menzel, C. Parmesan, T. Beebee, J-M. Fromentin, O. Hoegh-Guldberg, and F. Bairlein. 2002. Ecological responses to recent climate change. *Nature 416*:389–395.

Ware, S., C. Frost, and P. Doerr. 1993. Southern mixed hardwood forest: The former longleaf pine forest. *Biodiversity of the Southeastern United States: Lowland Terrestrial Ecosystems*. Edited by Martin, W., S. Boyce, and A. Echternacht. Wiley: New York.

Winkler, D., and J. Walters. 1983. The determination of clutch size in precocial birds. *Current Ornithology 1*:33–68.

Winkler, D., P. Dunn, and C. McCulloch. 2002. Predicting the effects of climate change on avian life-history traits. In *Proceedings of the National Academy of Sciences 99*:13595–13599.

Zahn, S. 2015. *LANDFIRE: U.S. Geological Survey Fact Sheet 2015–3047*. Available at http://dx.doi.org/10.3133/fs20153047

Zeigler, S. 2013. Predicting responses to climate change requires all life-history stages. *Journal of Animal Ecology 82*:3–5.

Zeigler, S., and J. Walters. 2014. Population models for social species: Lessons learned from models of red-cockaded woodpeckers (*Picoides borealis*). *Ecological Applications 24*:2144–2154.

Zwicker, S., and J. Walters. 1999. Selection of pines for foraging by red-cockaded woodpeckers. *Journal of Wildlife Management 63*:843–852.

Appendix 19-A
List of Scientific/Technical Publications

Papers

Garcia, V., and J.R. Walters. In review. Association between climate and changing life history traits in red-cockaded woodpeckers. *Ecology and Evolution*.

Zeigler, S.L., and J.R. Walters. 2014. Population models for social species: Lessons learned from models of red-cockaded woodpeckers (*Picoides borealis*). *Ecological Applications 24*:2144–2154.

Thesis

Garcia, V. 2014. *Lifetime Fitness and Changing Life History Traits in Red-Cockaded Woodpeckers*. Ph.D. dissertation, Virginia Tech, Blacksburg, VA.

Presentations

Garcia, V., and J.R. Walters. 2011. *Changes in Demographic Traits of Red-Cockaded Woodpeckers in Response to Climate Change*. Poster presented at Virginia Tech's Department of Biological Sciences Research Day, Blacksburg, VA.

Garcia, V., and J.R. Walters. 2012. *What Factors Contribute Most to Lifetime Fitness in Red-Cockaded Woodpeckers?* Invited presentation at the North American Ornithological Conference, Vancouver, BC.

Garcia, V., and J.R. Walters. 2013. *Long-Term Changes in Red-cockaded Woodpecker Life History Traits*. Presented at a joint meeting of American Ornithologists' Union and the Cooper Ornithological Society, Chicago, IL.

Garcia, V., and J.R. Walters. 2014. *Association Between Climate and Changing Life History Traits in Red-Cockaded Woodpeckers*. Poster presented at a joint meeting of American Ornithologists' Union, the Cooper Ornithological Society, and the Canadian Society of Ornithologists, Estes Park, CO; and Longleaf Alliance Conference, Mobile, AL.

Garcia, V., and J.R. Walters. 2015. *Lifetime Fitness and Changing Life History Traits in Red-Cockaded Woodpeckers*. Seminar presented to the Biological Sciences Department, Old Dominion University, Norfolk, VA.

Garcia, V., J.R. Walters, and K.R. Rose. 2010. *Effects of Restoring Vegetation Communities for the Benefit of Endangered Red-Cockaded Woodpeckers on the Rest of the Avian Community*. Poster presented at a joint meeting of the Cooper Ornithological Society, the American Ornithologists' Union, and the Society of Canadian Ornithologists, San Diego, CA; and at Virginia Tech's Department of Biological Sciences Research Day, Blacksburg, VA.

Rose, K.R., J.R. Walters, L.A. Blanc, and V. Garcia. 2012. *Impacts of Managing Pine Habitat for Red-Cockaded Woodpeckers on the Avian Community Aboard Marine Corps Base Camp Lejeune, North Carolina*. Poster presented at the Wildlife Society 19th Annual Conference, Portland, OR.

Walters, J.R., V. Garcia, K.R. Rose, and L.A. Blanc. 2010. *How Managing Forests to Benefit Red-Cockaded Woodpeckers Impacts the Rest of the Avian Community*. Presented at the Department of Defense's Strategic Environmental Research and Development Program, Washington DC. November 30–December 2.

Appendix 19-B
List of Students

- Vicki Garcia, Ph.D., Virginia Tech, Blacksburg, VA, 2014.

Appendix 19-C
LANDFIRE Model Settings

Descriptions of LANDFIRE biophysical settings and models that form the basis for landscape models developed in this study (for additional details, see https://www.landfire.gov/NationalProductDescriptions24.php).

LANDFIRE Biophysical Setting Model

***Biophysical Setting* 5813460** **Atlantic Coastal Plain Fall-Line Sandhills Longleaf Pine Woodland**

☐ *This BPS is lumped with:*
☐ *This BPS is split into multiple models:*

General Information

Contributors (also see the Comments field **Date** 7/27/2006

Modeler 1 Philip E. Hyatt phyatt@fs.fed.us
Modeler 2
Modeler 3

Reviewer Chris Szell cszell@tnc.org
Reviewer Ken Outcalt koutcalt@fs.fed.us
Reviewer Mike Schafale michael.schafale@ncmail.net

Vegetation Type

Forest and Woodland

Dominant Species*

PIPA2	QUMA6
QULA2	QUST
QUIN	ARBE7
QUMA3	ARST5

General Model Sources

☑ Literature
☐ Local Data
☑ Expert Estimate

Map Zone

58

Model Zone

☐ Alaska
☐ California
☐ Great Basin
☐ Great Lakes
☐ Northeast
☐ Northern Plains
☐ N-Cent.Rockies
☐ Pacific Northwest
☐ South Central
☑ Southeast
☐ S. Appalachians
☐ Southwest

Geographic Range

This system occurs in the Fall-line Sandhills region of central NC extending into central GA -- see Ecoregion 65c of EPA 2004 (NatureServe 2006).

Biophysical Site Description

This system predominates its range, covering most of the natural landscape of the region (NatureServe 2006). It occurs on upland sites ranging from gently rolling, broad ridgetops to steeper side slopes, as well as locally in mesic swales and terraces. Most soils are well- to excessively drained. Non-wetland conditions and frequent fire unify this system within the Fall-line Sandhills region. Soil texture appears to be the most important driver of differences among associations within the system, with biogeography also important (NatureServe 2006).

Vegetation Description

The vegetation is naturally dominated by longleaf pine (*Pinus palustris*). Most associations have an understory of scrub oaks (*Quercus laevis*, *Q. marilandica*, *Q. incana* and *Q. margarettiae*), expect maybe the more mesic examples. Low shrubs, most ericaceous, may be abundant. Grasses dominate the well-developed herb layer. Wiregrass (*Aristida stricta* in the north, *A. beyrichiana* in the south) dominates in most of the range, but other grasses dominate where it is absent. For example, in central SC, both species of *Aristida* are absent and various other grass species dominate. Forbs, including many legumes, are also present (NatureServe 2006). Associations on deep, coarse sands

may have low species richness but have a distinct set of xerophytic herbs and dwarf-shrubs (NatureServe 2006).

Disturbance Description

Frequent, low-intensity fire provides the dominant natural ecological force. Component communities naturally burned every few years, many averaging as often as every three years. Fires are naturally low to moderate in intensity. They burn above-ground parts of herbs and shrubs, but have little effect on the fire-tolerant trees. Vegetation recovers very quickly from fires, with live herbaceous biomass often restored in just a few weeks. Many plants have their flowering triggered by burning. Fire is important in creating the structure of the vegetation. In the absence of fire, less fire-tolerant species increase and others invade the system. The scrub oaks and shrubs, kept to low density and mostly reduced to shrub size, become tall and dense and can suppress tree regeneration. Herb layer density and diversity decline. However, even in the absence of fire, given the poor soil conditions of most sites, it would take a number of years for a hardwood mid-story to develop and even then some longleaf regeneration continues to occur.

Canopies are believed to naturally be many-aged, consisting of a fine mosaic of small even-aged groves driven by gap-phase regeneration. Longleaf pine is shade-intolerant and slow to reach reproductive age, but is very long-lived. Most plants in these systems appear to be conservative, living a long time and only rarely sexually reproducing or colonizing new sites (NatureServe 2006).

Adjacency or Identification Concerns

This system is distinguished from Atlantic Coastal Plain Upland Longleaf Pine Woodland (CES203.281 or BpS 1347) based on differences in landscape patterns, prevailing associations and some floristic differences. Dissected topography with much higher relief, predominance of interbedded sands and clays, and the interspersion with seepage wetlands all charactize the Fall-line Sandhills, in contrast to the low relief, pure sands or loams, and mosaics containing other wetland types in the rest of the Coastal Plain. Some matrix associations in the Fall-line Sandhills, such as *Pinus palustris*/ *Quercus marilandica*/ *Gaylussacia dumosa*/ *Aristata stricta* Woodland (CEGL003595) are nearly absent in the rest of the Coastal Plain. The abundance of legumes in most Sandhills region associations and their scarcity in most Outer Coastal Plain associations is striking, and probably relates to the differences in prevailing soil textures. The abundance of legumes distinguishes this system from Atlantic Coastal Plain Upland Longleaf Pine Woodland (CES203.281 or BpS 1347).

The system does not have a biogeographic break in southern SC, as the Outer Coastal Plain systems do. It includes areas with both forms of *Aristata stricta sensu lato* (*A. stricta*, *sensu stricto* and *A. beyrichiana*). Gopher tortoises (*Gopherus polyphemus*), absent here, help break this system from the Outer Coastal Plain systems where they serve as a keystone species. The ecological role of saturated wetland conditions in the Atlantic Coastal Plain Northern Wet Longleaf Pine Savanna and Flatwoods (CES203.265 or BpS 1449) distinguishes that system from Fall-line Sandhills.

Adjacent ecological systems include: Atlantic Coastal Plain Sandhill Seep (CES203.253); Atlantic Coastal Plain Small Blackwater River Floodplain Forest (CES203.249 see BpS 1473); Atlantic Coastal

Plain Streamhead Seepage Swamp, Pocosin, and Baygall (CES203.252 or BpS 1468) (NatureServe 2006).

Native Uncharacteristic Conditions

Much of this area of longleaf pine has been fire suppressed, managed and farmed to the point that little intact habitat exists.

Scale Description

The landscape is adequate in size to contain the natural variation in vegetation and disturbance regimes. Topographically, areas could be very large and extend continuously over a large expanse of the landscape, or occur as small patches.

This system is naturally a matrix system, covering most of the landscape in its range. Most occurrences now are artificially bounded remnants or naturally small islands. Extensive occurrences usually have embedded wetland systems, especially Atlantic Coastal Plain Streamhead Seepage Swamp, Pocosin, and Baygall (CES203.252 or BpS 1468) (NatureServe 2006).

Natural patches once would have been contiguous over hundreds of square miles, covering most of the landscape in the region and broken only by river systems. Most occurrences are now artificially bounded remnants of small to fairly large size. A few landscape matrix areas of thousands of acres remain (NatureServe 2006).

Issues/Problems

Notes taken from the Rapid Assessment Model R9LLSH -- this model includes areas with *Aristida stricta sensu lato* and bluestems dominating the understory. This fall line sandhill ecosystem may have two distinct xeric communities in the landscape. Longleaf pine-scrub oak sandhills and longleaf pine-turkey oak sandhills can make up this BpS within its geographic range. Also, no insect and disease disturbances were noted during the succession pathway of this BpS. It was suggested that some level of disturbance from a bark beetle infestation be added to this pathway. Most likely classes B and D would be where the problem would occur.

In creating this BpS the bark beetle infestation concern was taken into consideration and is reflected in the VDDT model.

Comments

This model description was developed from NatureServe (2006) ecological description for CES203.254 and the Rapid Assessment model (R9LLSH). The VDDT model was designed using the Rapid Assessment model (R9LLSH).

This model was reviewed at Durham, NC model review held 23 Jan. 2007.

Vegetation Classes

Indicator Species* and Structure Data (for upper layer lifeform)

Class A 13%

Canopy Position

Early Development 1 All Structure PIPA2 Upper
ARBE7 Lower
ARST5 Lower
SCSCS3 LoWERw-

	Min	*Max*
Cover	0 %	100 %
Height	Herb 0m	Herb >1.1m
Tree Size Class	None	

☑ **Upper Layer Lifeform**
☐
☐ Herbaceous
Shrub ☐ Upper layer lifeform differs from dominant lifeform. Tree **Fuel Model** 2

Description

Canopy gaps, most single tree to a quarter acre size characterize class A. Pine regeneration grows here up to 15yrs old, or site lacks pine regeneration because no mast year has occurred since the gap opened. The native grassy ground cover is dominated by various grasses, with *A. stricta sensu lato* infrequently present in this region. Tree cover ranges from 0-50%.

Indicator Species* and Structure Data (for upper layer lifeform)

Class B 5%

Canopy Position

Mid Development 1 Closed PIPA2 Upper
QULA2 Mid-Upper
RHCO Low-Mid

	Min	*Max*
Cover	71 %	90 %
Height	Tree 5.1m	Tree 25m
Tree Size Class	Medium 9-21" BH	

Upper Layer Lifeform
☐
☐
☑ Herbaceous
Shrub SAAL5 Low-Mid ☐ Upper layer lifeform differs from dominant lifeform. Tree **Fuel Model** 6

Description

Class B is characterized by patches, most ¼ acre or less, of canopy pines 15-75yrs old, and a substantial component of hardwoods or other pine species encroaching in the absence of fire. Hardwood and encroaching pine cover is >50%. The pine canopy cover ranges from 25-75%.

Indicator Species* and

Class C 40%

Canopy Position **Structure Data (for upper layer lifeform)**

Mid Development 1 Open

PIPA2 Upper
ARBE7 Lower
ARST5 Lower
SCSCS3 Lower

	Min	*Max*
Cover	21 %	70 %
Height	Tree 5.1m	Tree 25m
Tree Size Class	Large 21-33"D H	

Upper Layer Lifeform
☐
☐ Herbaceous
☑
Shrub Tree **Fuel Model** 2

☐ Upper layer lifeform differs from dominant lifeform.

Description

Class C includes patches, most ¼ acre or less, with canopy pines 15-75yrs old, and a minimal hardwood component due to frequent fire. The ground cover is dominated by grasses. The pine canopy cover ranges from 25-75%.

Class D 40%

Late Development 1 Open

Upper Layer Lifeform

- ☐
- ☐
- ☑ Herbaceous
- Shrub
- Tree

Fuel Model 2

Indicator Species* and Canopy Position

PIPA2	Upper
ARBE7	Lower
ARST5	Lower
SCSCS3	Lower

Structure Data (for upper layer lifeform)

	Min	*Max*
Cover	21 %	70 %
Height	Tree 25.1m	Tree >50.1m
Tree Size Class	Very Large >33"DBH	

☐ Upper layer lifeform differs from dominant lifeform.

Description

Class D includes patches, most ¼ acre or less, with canopy pines 75yrs+ old, and a minimal component of hardwoods. The ground cover is dominated by grasses. The pine canopy cover ranges from 25-75%.

Class E 2%

Late Development 1 Closed

Upper Layer Lifeform

- ☐ Herbaceous
- ☐
- ☑ Shrub Tree

Fuel Model 9

Indicator Species* and Canopy Position

PIPA2	Upper
QULA2	Mid-Upper
QUIN	Mid-Upper
QUST	Mid-Upper

☐ Upper layer lifeform differs from dominant lifeform.

Structure Data (for upper layer lifeform)

	Min	*Max*
Cover	71 %	90 %
Height	Tree 25.1m	Tree >50.1m
Tree Size Class	Very Large >33"DBH	

Description

Class E is characterized by patches with canopy pines 75yrs+ old, and a substantial component of hardwoods or pines other than longleaf in either the overstory or understory. The ground cover is shrubby or sparse. Hardwood and encroaching pine cover is >50%.

Disturbances

Fire Regime Group:** I

Historical Fire Size (acres)

Avg 1000

Min 1

Max 100000

Fire Intervals	Avg FI	Min FI	Max FI	Probability	Percent of All Fires
	132			0.00758	3
Mixed	370			0.00270	1
Surface	4			0.25	96
All Fires	4			0.26028	

Fire Intervals (FI):
Fire interval is expressed in years for each fire severity class and for all types of fire combined (All Fires). Average FI is central tendency modeled. Minimum and maximum show the relative range of fire intervals, if known. Probability is the inver of fire interval in years and is used in reference condition modeling. Percent of all fires is the percent of all fires in that severity class.

Replacement

☑ **Sources of Fire Regime Data**

☐ Literature

☑ Local Data

Expert Estimate

☑ **Additional** ☐ **Disturbances** ☐ **Modeled**

☑ Insects/DiseaseNative GrazingOther (optional 1)

☑ Wind/Weather/StressCompetitionOther (optional 2)

References

Brown, J.K. and J. Kapler-Smith, eds. 2000. Wildland fire in ecosystems: effects of fire on flora. Gen. Tech. Rep. RMRS-GTR-42. vol 2. Ogden, UT: USDA Forest Service, Rocky Mountain Research Station. 257 pp.

Christensen, N.L. 1981. Fire regimes in southeastern ecosystems. Pages 112-136 in: Mooney, H.A., Bonnickson, T.M., Christensen, N.L., Lotan, J.E. and Reiners, W.A., eds. Fire regimes and ecosystem properties. USDA Forest Service General Technical Report WO-26. .

EPA [Environmental Protection Agency]. 2004. Level III and IV Ecoregions of EPA Region 4. U.S. Environmental Protection Agency, National Health and Environmental Effects Research Laboratory, Western Ecology Division, Corvallis, OR. Scale 1:2,000,000.

Frost, Cecil. 1993. Four Centuries of Changing Landscape Patterns in the Longleaf Pine Ecosystem. In Hermann, Sharon M., ed. The Longleaf Pine Ecosystem: ecology, restoration and management. Proceedings of the Tall Timbers Fire Ecology Conference, No. 18. Tallahassee, FL: Tall Timbers Research Station.

Gan, Jianbang. 2004. Risk and damage of southern pine beetle outbreaks under global climate change. Forest Ecology and Management. 61-71.

Landers, J. Larry. 1991. Disturbance influences on pine traits in the southeastern United States. Pages 61-
98 in: High intensity fire in wildlands: management challenges and options. Proceedings, 17th Tall Timbers fire ecology conference, 1989 May 18-21, Tallahassee, FL. Tallahassee, FL: Tall Timbers Research Station.

NatureServe. 2006. International Ecological Classification Standard: Terrestrial Ecological Classifications.

NatureServe Central Databases. Arlington, VA, U.S.A. Data current as of 18 July 2006.

Palick, Brian J. and Neil Pederson. 1996. Overstory mortality and canopy disturbances in longleaf pine ecosystems. Can. J. For. Res. 26: 2035-2047.

Price, T., Doggett, C., Pye, J. and Smith, B. 1998. A History of Southern Pine Beetle Outbreaks in the Southeastern United States. Atlanta, GA: Georgia Forestry Commission.

Schmidt, K.M., J.P. Menakis, C.C. Hardy, W.J. Hann and D.L. Bunnell. 2002. Development of coarse-scale spatial data for wildland fire and fuel management. Gen. Tech. Rep. RMRS-GTR-87. Fort Collins, CO: USDA Forest Service, Rocky Mountain Research Station. 41 pp. + CD.

Wade, D.D., Brock, B.L., Brose, P.H., Grace, James B., Hoch, Greg A. and Patterson, William A. III, 2000. Fire in eastern ecosystems. Pages 53-96 in: Brown, J.K. and J. Kapler- Smith, eds. Wildland fire in ecosystems: effects of fire on flora. Gen. Tech. Rep. RMRS-GTR-42. Ogden, UT: USDA Forest Service, Rocky Mountain Research Station.

USDA Forest Service, Rocky Mountain Research Station, Fire Sciences Laboratory (2002, December). Fire Effects Information System, [Online]. Available: http://www.fs.fed.us/database/feis/.

LANDFIRE Biophysical Setting Model

Biophysical Setting 5813470 Atlantic Coastal Plain Upland Longleaf Pine Woodland

☐ *This BPS is lumped with:*
☐ *This BPS is split into multiple models:*

General Information

Contributors (also see the Comments field **Date** 7/27/2006

Modeler 1 Philip E. Hyatt phyatt@fs.fed.us **Reviewer** Chris Szell cszell@tnc.org

Modeler 2 **Reviewer** Mike Schafale michael.schafale@ncmail.net

Modeler 3 **Reviewer**

Vegetation Type

Forest and Woodland

Map Zone

58

Model Zone

☐ Alaska ☐ N-Cent.Rockies
☐ California ☐ Pacific Northwest
☐ Great Basin ☐ South Central
☐ Great Lakes ☑ Southeast
☐ Northeast ☐ S. Appalachians
☐ Northern Plains ☐ Southwest

Dominant Species*

PIPA2	QUMA3
QULA2	ARST5
QUIN	SCSC
QUMA6	SONU2

General Model Sources

☑ Literature
☐ Local Data
☑ Expert Estimate

Geographic Range

The ecological system that corresponds to this BpS is noted by NatureServe (2006) to be found in the
Atlantic Coastal Plain (exclusive of the Fall-line Sandhills) from southern VA to northeastern FL (see CES203.281).

Biophysical Site Description

Once perhaps the most extensive system in the Outer Coastal Plain within its range. Examples and associations share the common feature of upland (non-wetland) moisture regimes and natural exposure to frequent fire (NatureServe 2006).

Occurs on upland sites of the Middle to Outer Atlantic Coastal Plain, on landforms that include loamy to sandy flats, relict beach system deposits, eolian sand deposits, Carolina bay rims and occasional low rolling hills. Soils range from mesic to xeric and from sandy to loamy or occasionally clayey. Most natural remnants are on coarse sands, but most examples probably once occurred on loamy soils. Soils are largely acidic and infertile, and the coarsest sands are excessively drained and sterile.

The unifying feature of this system is non-wetland sites that naturally supported frequent fire. As such, it once covered much of the landscape of the Coastal Plain. Variations in soil texture

and drainage appear to be a primary driver of differences between associations within the system, with biogeography also important (NatureServe 2006).

Vegetation Description

Vegetation is a set of associations that are most naturally woodlands or savannas dominated by *Pinus palustris* and having a well-developed grassy herb layer. A few associations have sparse herb layers due to excessively drained soils, and a few are dominated by scrub oaks. Other pine species may sometimes be present. Scrub oaks (*Quercus laevis*, *Quercus incana*, *Quercus margarettiae*, *Quercus hemisphaerica* and others) form an understory in most associations, all but the mesic ones. Low shrubs, most ericaceous, are often an important component. In most of the range, *Aristida stricta* is the dominant herb. In the southern and northern parts of the range, it is absent, and various other grass species dominate. Forbs, especially composites, are usually also an important herb component, and lichens are abundant in some associations. Many associations have moderate species richness, with most of the species in the herb layer. Some mesic associations have very high species richness, among the highest values ever measured at the 1/10-hectare scale. Associations on deep, coarse sands may have low species richness but have a distinct set of xerophytic herbs and dwarf-shrubs.

Disturbance Description

Frequent, low-intensity fire is the predominant natural force in this system. Component communities naturally burned every few years, many averaging as often as every three years. Fires are naturally low to moderate in intensity. They burn above-ground parts of herbs and shrubs but have little effect on the fire tolerant trees. Vegetation recovers very quickly from fire, with live herbaceous biomass often restored in just a few weeks. Many plants have their flowering triggered by burning. In the absence of fire, less fire tolerant species increase and others invade the system. The scrub oaks and shrubs, kept to low density and mostly reduced to shrub size by fire, become tall and dense and can suppress tree regeneration. Herb layer density and diversity decline. Only on the most excessively drained coarse sands does the vegetation not undergo substantial structural alteration and reduction in species richness after just a few years without burning (NatureServe 2006).

Canopies are believed to naturally be many-aged, consisting of a fine mosaic of small even-aged groves driven by gap-phase regeneration. Longleaf pine is shade-intolerant and slow to reach reproductive age but is very long-lived. Most plants in these systems appear to be conservative, living a long time and only rarely sexually reproducing or colonizing new sites (NatureServe 2006).

Adjacency or Identification Concerns

This system is distinguished from Atlantic Coastal Plain Northern Wet Longleaf Pine Savanna and Flatwoods (CES203.265 or BpS 1449) because of the ecological role of saturated wetland conditions in the latter. The two systems have much in common, including frequent fire and the same primary dominant tree and herb species. They often occur in the same landscapes. However, floristic differences are well marked, and no associations are shared. This system is distinguished from the Atlantic Coastal Plain Fallline Sandhills Longleaf Pine Woodland

(CES203.254 or BpS 1346) based on the differences in landscape patterns and prevailing associations in the two regions. Dissected topography with much higher relief, predominance of interbedded sands and clays, and interspersion with seepage wetlands all characterize the Fall-line Sandhills, in contrast to the low relief, pure sands or loams, and mosaics containing other wetland types in the rest of the Coastal Plain. Some matrix associations in the Fall-line Sandhills, such as *Pinus palustris* / *Quercus marilandica* / *Gaylussacia dumosa* / *Aristida stricta* Woodland (CEGL003595) are nearly absent in the rest of the Coastal Plain, and there are systematic floristic differences. If this were to be split into a northern and southern component, the distinction would be justified based on differences in climate, flora, and some differences in ecological dynamics. Gopher tortoises (*Gopherus polyphemus*) are an important keystone species in the southern portion of the range. The dominant grass also changes at this approximate point, with *Aristida beyrichiana* dominating herb layers to the south (NatureServe 2006).

Similar Ecological Systems: Atlantic Coastal Plain Fall-line Sandhills Longleaf Pine Woodland

(CES203.254 or BpS 1346); Atlantic Coastal Plain Northern Wet Longleaf Pine Savanna and Flatwoods (CES203.265 or BpS 1449).

Adjacent Ecological Systems: Atlantic Coastal Plain Northern Wet Longleaf Pine Savanna and Flatwoods (CES203.265 or BpS 1449) or Atlantic Coastal Plain Peatland Pocosin and Canebrake (CES203.267 or BpS 1452) are the most commonly associated systems, often forming mosaics. Atlantic Coastal Plain Southern Depression Pondshore (CES203.262) and small floodplain systems may be embedded in matrices of this system. Other adjacent systems include the Atlantic Coastal Plain Clay-Based Carolina Bay Wetland (CES203.245 or BpS 1459).

Native Uncharacteristic Conditions

Most natural remnants are on coarse sands, but most examples probably once occurred on loamy soils (NatureServe 2006).

Scale Description

This system is naturally a matrix system, probably once the most extensive system in its range. Most occurrences now are artificially bounded remnants or naturally small islands. Occurrences often form mosaics with Atlantic Coastal Plain Northern Wet Longleaf Pine Savanna and Flatwoods (CES203.265 or BpS 1449) or Atlantic Coastal Plain Peatland Pocosin (CES203.267 or BpS 1452) and may have smallpatch systems embedded in them. A few landscape matrix areas of several thousand acres remain (NatureServe 2006).

Issues/Problems

Comments

This model description was created using the corresponding NatureServe (2006) ecological description for CES203.281. The VDDT model was based on the Rapid Assessment model (R9LLSH -- Longleaf Sandhills) as were the class percentages given below.

Vegetation Classes

Indicator Species* and Structure Data (for upper layer lifeform)

Class A 13%

Canopy Position

Early Development 1 All Structure PIPA2 Upper
ANVI2 Lower
SCSCS3 Lower
ARST5 Lower

	Min	*Max*
Cover	0 %	100 %
Height	Herb 0m	Herb >1.1m
Tree Size Class	None	

☑ **Upper Layer Lifeform**
☐
☐ Herbaceous
Shrub ☐ Upper layer lifeform differs from dominant lifeform. Tree **Fuel Model** 2

Description

Canopy gaps, most single tree to a quarter acre size characterize class A. Pine regeneration grows here up to 15yrs old, or site lacks pine regeneration because no mast year has occurred since the gap opened. The native grassy ground cover is dominated by various grasses, with A. stricta the dominant herb. Tree cover ranges from 0-50%.

Indicator Species* and Structure Data (for upper layer lifeform)

Class B 5%

Canopy Position

Mid Development 1 Closed PIPA2 Upper
QULA2 Mid-Upper
RHCO Low-Mid

	Min	*Max*
Cover	71 %	90 %
Height	Tree 5.1m	Tree 25m
Tree Size Class	Medium 9-21" BH	

Upper Layer Lifeform
☐
☐
☑ Herbaceous
Shrub SAAL5 Low-Mid ☐ Upper layer lifeform differs from dominant lifeform. Tree **Fuel Model** 6

Description

Class B is characterized by patches, most ¼ acre or less, of canopy pines 15-75yrs old, and a substantial component of hardwoods or other pine species encroaching in the absence of fire. Hardwood and encroaching pine cover is >50%. The pine canopy cover ranges from 25-75%.

Class C 40%

Indicator Species* and Canopy Position

PIPA2 Upper
ARST5 Lower
SCSCS3 Lower

Structure Data (for upper layer lifeform)

	Min	*Max* Mid Develo
Cover	21 %	70 %
Height	Tree 5.1m	Tree 25m
Tree Size Class	Large 21-33"D H	

pment 1 Open

Upper Layer Lifeform
☐
☐ Herbaceous
☑ ☐ Upper layer lifeform differs from dominant lifeform.
Shrub Tree **Fuel Model** 2

Description

Class C includes patches, most ¼ acre or less, with canopy pines 15-75yrs old, and a minimal hardwood component due to frequent fire. The ground cover is dominated by grasses. The pine canopy cover ranges from 25-75%.

Class D 40%

Late Development 1 Open

Indicator Species* and Canopy Position

PIPA2	Upper	
ARST5	Lower	
SCSCS3	Lower	

Structure Data (for upper layer lifeform)

	Min	Max
Cover	21 %	70 %
Height	Tree 25.1m	Tree 50m
Tree Size Class	Very Large >33 'DBH	

☐ Upper layer lifeform differs from dominant lifeform.

☐
☐ **Upper Layer Lifeform**
☑ Herbaceous
Shrub
Tree

Fuel Model 2

Description

Class D includes patches, most ¼ acre or less, with canopy pines 75yrs+ old, and a minimal component of hardwoods. The ground cover is dominated by grasses. The pine canopy cover ranges from 25-75%.

Class E 2%

Late Development 1 Closed

Indicator Species* and Canopy Position

PIPA2	Upper
QUFA	Mid-Upper
QUNI	Mid-Upper
QULA3	Mid-Upper

Structure Data (for upper layer lifeform)

	Min	Max
Cover	71 %	90 %
Height	Tree 25.1m	Tree 50m
Tree Size Class	Very Large >33 'DBH	

☐ Upper layer lifeform differs from dominant lifeform.

☐ **Upper Layer Lifeform**
☐
☑ Herbaceous
Shrub
Tree

Fuel Model 9

Description

Class E is characterized by patches with canopy pines 75yrs+ old, and a substantial component of hardwoods or pines other than longleaf in either the overstory or understory. The ground cover is shrubby or sparse. Hardwood and encroaching pine cover is >50%.

Disturbances

Fire Regime Group:** I

Historical Fire Size (acres)

Avg

Min

Max

Fire Intervals	Avg FI	Min FI	Max FI	Probability	Percent of All Fires
	132			0.00758	3
Mixed	370			0.00270	1
Surface	4			0.25	96
All Fires	4			0.26028	

Replacement

Fire Intervals (FI):

Fire interval is expressed in years for each fire severity class and for all types of fire combined (All Fires). Average FI is central tendency modeled. Minimum and maximum show the relative range of fire intervals, if known. Probability is the inver of fire interval in years and is used in reference condition modeling. Percent of all fires is the percent of all fires in that severity class.

☑ **Sources of Fire Regime Data**

☐ Literature

☑ Local Data

Expert Estimate

☑ **Additional** ☐ **Disturbances** ☐ **Modeled**

☑ Insects/DiseaseNative GrazingOther (optional 1)

Wind/Weather/StressCompetitionOther (optional 2)

References

Brown, J.K. and J. Kapler-Smith, eds. 2000. Wildland fire in ecosystems: effects of fire on flora. Gen. Tech. Rep. RMRS-GTR-42. vol 2. Ogden, UT: USDA Forest Service, Rocky Mountain Research Station. 257 pp.

Christensen, N.L. 1981. Fire regimes in southeastern ecosystems. In Mooney, H.A., Bonnickson, T.M., Christensen, N.L., Lotan, J.E. and Reiners, W.A., eds. Fire regimes and ecosystem properties. USDA Forest Service General Technical Report WO-26. pp. 112-136.

Frost, Cecil. 1993. Four Centuries of Changing Landscape Patterns in the Longleaf Pine Ecosystem. In Hermann, Sharon M., ed. The Longleaf Pine Ecosystem: ecology, restoration and management. Proceedings of the Tall Timbers Fire Ecology Conference, No. 18. Tallahassee, FL: Tall Timbers Research Station.

Gan, Jianbang. 2004. Risk and damage of southern pine beetle outbreaks under global climate change. Forest Ecology and Management. 61-71.

Landers, J. Larry. 1991. Disturbance influences on pine traits in the southeastern United States. Pages 61-98 in: High intensity fire in wildlands: management challenges and options. Proceedings, 17th Tall Timbers fire ecology conference, 1989 May 18-21, Tallahassee, FL. Tallahassee, FL: Tall Timbers Research Station.

NatureServe. 2006. International Ecological Classification Standard: Terrestrial Ecological Classifications. NatureServe Central Databases. Arlington, VA, U.S.A. Data current as of 18 July 2006.

Palick, Brian J. and Neil Pederson. 1996. Overstory mortality and canopy disturbances in longleaf pine ecosystems. Can. J. For. Res. 26: 2035-2047.

Price, T., Doggett, C., Pye, J. and Smith, B. 1998. A History of Southern Pine Beetle Outbreaks in the Southeastern United States. Atlanta, GA: Georgia Forestry Commission.

Schmidt, K.M., J.P. Menakis, C.C. Hardy, W.J. Hann and D.L. Bunnell. 2002. Development of coarse-scale spatial data for wildland fire and fuel management. Gen. Tech. Rep. RMRS-GTR-87. Fort Collins, CO: USDA Forest Service, Rocky Mountain Research Station. 41 pp. + CD.

Wade, D.D., Brock, B.L., Brose, P.H., Grace, James B., Hoch, Greg A. and Patterson, William A. III, 2000. Fire in eastern ecosystems. Pages 53-96 in: Brown, J.K. and J. Kapler- Smith, eds. Wildland fire in ecosystems: effects of fire on flora. Gen. Tech. Rep. RMRS-GTR-42. Ogden, UT: USDA Forest Service, Rocky Mountain Research Station.

USDA Forest Service, Rocky Mountain Research Station, Fire Sciences Laboratory (2002, December). Fire Effects Information System, [Online]. Available: http://www.fs.fed.us/database/feis/.

LANDFIRE Biophysical Setting Model

***Biophysical Setting* 5814490** **Central Atlantic Coastal Plain Wet Longleaf Pine Savanna and Flatwoods**

☐ *This BPS is lumped with:*
☐ *This BPS is split into multiple models:*

General Information

Contributors (also see the Comments field **Date** 8/29/2006

Modeler 1 Brent Wilson brentrw@earthlink.net **Reviewer** Chris Szell cszell@tnc.org

Modeler 2 John Mangus john.mangus@usmc.mil **Reviewer**

Modeler 3 **Reviewer**

Vegetation Type

Wetlands/Riparian

Map Zone

58

Model Zone

☐ Alaska ☐ N-Cent.Rockies
☐ California ☐ Pacific Northwest
☐ Great Basin ☐ South Central
☐ Great Lakes ☑ Southeast
☐ Northeast ☐ S. Appalachians
☐ Northern Plains ☐ Southwest

Dominant Species*

PIPA2 QUERC
PISE
ARIST
ARUND2

General Model Sources

☐ Literature
☐ Local Data
☑ Expert Estimate

Geographic Range

This system ranges from southern VA to southern SC (NatureServe 2006)

Biophysical Site Description

This BpS occurs in seasonally wet woodlands on nearly level, moderately well to somewhat poorly drained sandy soils of an acid character. Examples of occupied soil series include Foreston, Rains and Altavista. This BpS is typically dissected by wet hardwood or coniferous communities.

NatureServe (2006) note this was once one of the most extensive systems in the coastward part of its range. This system occurs on wet mineral soil sites (see modeler's description above), primarily in the Middle and Outer Coastal Plain but occasionally in the Fall-line Sandhills. Landforms include low areas in relict beach ridge systems and eolian sand deposits, and poorly drained clayey, loamy, or sandy flats. They occasionally occur on river terraces above current flood levels. Soils range from clayey to sandy, with no accumulated organic surface layer. Soils are seasonally saturated, due to high water table or poor soil drainage. The unifying feature of this system is wet mineral soils associated with a high frequency of fire.

Vegetation Description

Northern Wet Longleaf Pine Savanna is characterized by an open, savanna-like to nearly closed canopy of longleaf pine (*Pinus palustris*), with a component of pond pine (*Pinus serotina*) or

slash pine (*Pinus elliottii*). Hardwoods are present in any abundance only in examples altered by fire suppression (NatureServe 2006).The understory consists of predominantly wiregrasss (*Aristida* spp), blueberries (*Vaccinium* spp) and various perennial herbs. Switchcane (*Arundinaria* spp) and evergreen shrubs are present on the wettest sites. The ground cover is a dense combination of herbs and low shrubs. A variety of ericaceous shrubs and hollies is common, with density determined by fire history. Grasses naturally dominate the ground cover. *Aristida stricta* often dominates within its range, but *Ctenium aromaticum*, *Sporobolus pinetorum*, *Sporobolus teretifolius*, or other grasses may dominate. A great diversity of other herbs is often present, including composites, sedges, insectivorous plants and variety of showy forbs (NatureServe 2006).

Canopy trees are patchy in distribution, with regeneration in canopy gaps generally less than an acre in size. Mid-successional clumps occur in similar sized patches as regeneration. The oldest trees occur as isolated individuals. The reference classes are aggregates of numerous patches well dispersed over the landscape. Canopy gaps are created by fire mortality, lightning and wind-throw at the scale of individual to several trees.

Communities in this system are often very high in species richness, with some of the highest values measured anywhere at the 1/10-hectare, 1/100-hectare, and 1-square-meter levels. However, some associations are naturally low to moderate in species richness.

Disturbance Description

Frequent, low -intensity fires are the dominant natural ecological force, often occurring every 1-3yrs but ranging up to five year intervals, with seasonally wet areas excluded. Fires are usually low to moderate in intensity overall, generally resulting in topkill of the lower and middle layers, but periodically will kill young regeneration patches and occasionally individual older trees. Although fire can occur in any season, in pre-European settlement times lightning fires were most prevalent in the April-May period, although Native Americans were common in these areas and represented a significant ignition source. In this landscape, frequency is more important than seasonality, as long as the season of burn is varied periodically. This community is subjected to hurricanes which may cause thinning of stands, localized blowdown or uprooting of stands, or perhaps rarely blowdowns on larger areas.

Frequent fire is crucial in determining its structure and even its identity. They burn above-ground parts of herbs and shrubs but have little effect on the fire-tolerant trees. Vegetation recovers very quickly from fire, with live herbaceous biomass often restored in just a few weeks. Many plants have their flowering triggered by burning. In the absence of fire, the shrubs increase and hardwoods may invade the system. Herb layer density and diversity decline after just a couple of years without fire. In time, unburned examples will become nearly indistinguishable from the drier associations of Atlantic Coastal Plain Peatland Pocosin (CES203.267) (NatureServe 2006).

Canopies are believed to naturally be many-aged, consisting of a fine mosaic of small even-aged groves driven by gap-phase regeneration. Longleaf pine is shade-intolerant and slow to reach reproductive age but is very long-lived (NatureServe 2006).

Adjacency or Identification Concerns

Northern Wet Longleaf Pine Savanna occurs within the landscape on Carolina Bay rims to large flats adjacent to pocosin types.

This system is distinguished from Atlantic Coastal Plain Southern Wet Pine Savanna and Flatwoods (CES203.536) because of substantial biogeographic differences. The break is placed at the northern range limit of *Aristida beyrichiana*, which is a keystone species in the communities where it occurs. This corresponds roughly with the geographic break in the upland longleaf pine systems (NatureServe 2006).

This system is distinguished from Atlantic Coastal Plain Upland Longleaf Pine Woodland (CES203.281) because of its more upland character. However, the two systems have much in common, including frequent fire and the same primary dominant tree and many herbaceous species. They can also occur in the same landscapes. However, floristic differences are well marked, and no associations are shared. This system occurs primarily in the Outer Coastal Plain, but small patches may occur in atypical landforms in the Fallline Sandhills. Sandhills examples are not treated as a separate system, as the upland longleaf pine systems are, because they are confined to sites that more resemble the Outer Coastal Plain. They are distinguished in the Sandhills from Atlantic Coastal Plain Sandhill Seep (CES203.253) by landform and apparent hydrology that is driven by seasonal high water table rather than seepage. Similar Ecological Systems also include Atlantic Coastal Plain Fall-line Sandhills Longleaf Pine Woodland (CES203.254) (NatureServe 2006).

Adjacent Ecological Systems noted by NatureServe (2006) include: Atlantic Coastal Plain Upland Longleaf Pine Woodland (CES203.281) and Atlantic Coastal Plain Peatland Pocosin (CES203.267) are the most frequently associated systems. Atlantic Coastal Plain Southern Depression Pondshore (CES203.262) patches may be embedded, and Atlantic Coastal Plain Small Blackwater River Floodplain Forest (CES203.249), Atlantic Coastal Plain Small Brownwater River Floodplain Forest (CES203.250), and Atlantic Coastal Plain Mesic Hardwood and Mixed Forest (CES203.242) may adjoin. Atlantic Coastal Plain Clay-Based Carolina Bay Wetland (CES203.245) is also an adjacent system.

Native Uncharacteristic Conditions

Scale Description

This system naturally occurs as large to small patches, sometimes part of extensive matrix mosaics with other systems. It was naturally one of the most abundant systems on the lower terraces of the Outer Coastal Plain. Many remaining examples are naturally bounded islands (NatureServe 2006).

Low intensity fires may have ranged in size from very small to thousands of acres. Replacement fires may have been localized to less than an acre, or as large as hundreds of acres. Hurricane and wind damage may have ranged from single trees, to entire timber stands scattered in the landscape. Flooding disturbance probably was limited to a few acres associated with storm events. Patch size of this type may range from 10ac to thousands of acres, forming the matrix within which other types are imbedded.

Issues/Problems

Uncharacteristic vegetation types include even-aged canopy stands in which age structure has been influenced by plantation establishment and mechanical treatments. Site conversion to other species, primarily loblolly pine has reduced acreage in longleaf communities. Suitability for development for agriculture, commercial and residential development has eliminated forest land acreage. Site preparation methods have altered microsite hydrology and impacted movement in the landscape. Fire suppression activities have negatively impacted natural regeneration of longleaf pine.

Comments

Some information excerpted from Rapid Assessment for Longleaf Pine Mesic Uplands.

After reviewing the VDDT model developed by Wilson/Mangus, Szell noted that the correction of several violations of the usage of alternate succession changed model outputs. Therefore, the fire frequency values reflect the output from K. Outcalt model BpS 1450 which Szell adapted for BpS 1449.

Vegetation Classes

Indicator Species* and Structure Data (for upper layer lifeform)

Class A 15%

Canopy Position

Early Development 1 All Structure PIPA2 Upper
PISE Upper
ARIST Lower

	Min	Max
Cover	0 %	50 %
Height	Tree 0m	Tree 5m
Tree Size Class	Sapling >4.5ft; <5"DBH	

☐ **Upper Layer Lifeform**
☐
☑ Herbaceous
ARUND2 Lower
Shrub
☐ Upper layer lifeform differs from dominant lifeform.
Tree **Fuel Model** 2

Description

Class age 0-14yrs: Class A is a post replacement stage with canopy gaps, mostly single tree to quarter acre in size, of pine regeneration up to 15yrs old. The native ground cover is dominated by wiregrass and other grasses, small statured shrubs, and forbs. Subject to ice damage in the northern part of model zone.

Class B 5%

Mid Development 1 Closed

Indicator Species* and Canopy Position

PIPA2 Upper
PISE Upper
QUERC Mid-Upper

Structure Data (for upper layer lifeform)

	Min	*Max*
Cover	51 %	80 %
Height	Tree 10.1m	Tree 25m
Tree Size Class	Medium 9-21" BH	

Upper Layer Lifeform

- ☐ Herbaceous
- ☐ Shrub
- ☑ Tree

ARUND2 Lower

☐ Upper layer lifeform differs from dominant lifeform.

Fuel Model 7

Description

Class age 15-74yrs: Class B is characterized as a mid-seral closed stage with patches, mostly quarter acre or less in size, of canopy pines 15-75yrs old and a substantial component of hardwoods (e.g., oaks, titi and bays) or other pine species encroaching in the absence of fire. The hardwood and encroaching pine cover is >50%. The canopy pine cover ranges from 50-75%. Older age classes potentially impacted by hurricanes.

Class C 48%

Mid Development 1 Open

Indicator Species* and Canopy Position

PIPA2 Upper
PISE Upper
ARIST Lower

Structure Data (for upper layer lifeform)

	Min	*Max*
Cover	21 %	50 %
Height	Tree 10.1m	Tree 25m
Tree Size Class	Medium 9-21" BH	

Upper Layer Lifeform

- ☐ ARUND2 Lower
- ☐ Herbaceous
- ☑ Shrub
- Tree

☐ Upper layer lifeform differs from dominant lifeform.

Fuel Model 2

Description

Class age 15-74yrs: Class C is characterized by a mid-seral open condition with patches, most ¼ acre or less in size, of canopy pines 15-75yrs old and a minimal hardwood component due to frequent fire. The ground cover is grass-dominated, generally by wiregrass. The canopy pine cover ranges from 25-70%. Older age classes potentially impacted by hurricanes.

Class D 29%

Late Development 1 Open

Indicator Species* and Canopy Position

PIPA2	Upper
PISE	Upper
ARIST	Lower
ARUND2	Lower

Structure Data (for upper layer lifeform)

	Min	*Max*
Cover	11 %	60 %
Height	Tree 25.1m	Tree 50m
Tree Size Class	Large 21-33"D H	

☐ ☐ **Upper Layer Lifeform**

☑ Herbaceous

Shrub

Tree

Fuel Model 2

☑ Upper layer lifeform differs from dominant lifeform.

Description

Class age 75yrs+: Class D is classified as a late-seral open stage with patches, most ¼ acre or less in size, of canopy pines 75yrs+ old and a minimal component of hardwoods. The ground cover is grass-dominated, generally by wiregrass. The canopy pine cover ranges from 11-60%. Large crowned older trees susceptible to windthrow from hurricanes.

Class E 3%

Late Development 1 Closed

Indicator Species* and Canopy Position

QUERC	Upper
PIPA2	Upper
PISE	Upper

Structure Data (for upper layer lifeform)

	Min	*Max*
Cover	61 %	100 %
Height	Tree 25.1m	Tree 50m
Tree Size Class	Large 21-33"D H	

☐ **Upper Layer Lifeform**

☐

☑ Herbaceous

Shrub

Tree

Fuel Model 8

☐ Upper layer lifeform differs from dominant lifeform.

Description

Class age 75yrs+: Class E is characterized by a late-seral closed stage with patches of canopy pines 75yrs+ old, and a substantial component of hardwoods or pines other than longleaf in either the overstory or understory. The ground cover is shrubby or sparse. The hardwood and encroaching pine cover is >50%. Subject to some hurricane windthrow damage.

Disturbances

Fire Regime Group:** I

Historical Fire Size (acres)

Avg 1000

Min 1

Max 100000

Fire Intervals	*Avg FI*	*Min FI*	*Max FI*	*Probability*	*Percent of All Fires*
	90	50		0.01111	3
Mixed	256			0.00391	1
Surface	3.19	3	4	0.31348	95
All Fires	3			0.3285	

Replacement 200

Fire Intervals (FI):
Fire interval is expressed in years for each fire severity class and for all types of fire combined (All Fires). Average FI is central tendency modeled. Minimum and maximum show the relative range of fire intervals, if known. Probability is the inver of fire interval in years and is used in reference condition modeling. Percent of all fires is the percent of all fires in that severity class.

☐ **Sources of Fire Regime Data**

☐

☑ Literature

Local Data

Expert Estimate

☑ **Additional** ☐ **Disturbances** ☐ **Modeled**

☑

Insects/DiseaseNative GrazingOther (optional 1)

Wind/Weather/StressCompetitionOther (optional 2)

References

Brown, J.K. and J. Kapler-Smith, eds. 2000. Wildland fire in ecosystems: effects of fire on flora. Gen. Tech. Rep. RMRS-GTR-42. vol 2. Ogden, UT: USDA Forest Service, Rocky Mountain Research Station. 257 pp.

NatureServe. 2006. International Ecological Classification Standard: Terrestrial Ecological Classifications. NatureServe Central Databases. Arlington, VA, U.S.A. Data current as of 18 July 2006.

Schmidt, K.M., J.P. Menakis, C.C. Hardy, W.J. Hann and D.L. Bunnell. 2002. Development of coarse-scale spatial data for wildland fire and fuel management. Gen. Tech. Rep. RMRS-GTR-87. Fort Collins, CO: USDA Forest Service, Rocky Mountain Research Station. 41 pp. + CD.

USDA Forest Service, Rocky Mountain Research Station, Fire Sciences Laboratory (2002, December). Fire Effects Information System, [Online]. Available: http://www.fs.fed.us/database/feis/.

LANDFIRE Biophysical Setting Model

Biophysical Setting 9913560 Florida Longleaf Pine Sandhill

☐ *This BPS is lumped with:*
☐ *This BPS is split into multiple models:*

General Information

Contributors (also see the Comments field **Date** 7/19/2006

Modeler 1 Dennis Hardin hardind@doacs.state.fl. **Reviewer** Chris Szell cszell@tnc.org us

Modeler 2 **Reviewer** Keith Fisher kfisher@tnc.org

Modeler 3 **Reviewer** Amanda Stevensamanda.stevens@eglin.af.mil

Vegetation Type

Forest and Woodland

Dominant Species*

PIPA2
QULA2
QUIN
ARBE7

General Model Sources

☐ Literature
☑ Local Data
☑ Expert Estimate

Map Zone

99

Model Zone

☐ Alaska
☐ California
☐ Great Basin
☐ Great Lakes
☐ Northeast
☐ Northern Plains
☐ N-Cent.Rockies
☐ Pacific Northwest
☐ South Central
☑ Southeast
☐ S. Appalachians
☐ Southwest

Geographic Range

This type occurs from northeastern FL at the St. Mary's River to central FL to a line between about Sarasota County and Indian River County, and westward into the panhandle along a band between the inner and outer coastal plain.

NatureServe 2006 lists the range as found in the Outer Coastal Plain and adjacent Inner Coastal Plain of FL, including the central Florida Peninsula (Ocala National Forest, Brooksville Ridge, southern end of the Lake Wales Ridge) (Abrahamson et al. 1984) and the panhandle (e.g., Eglin Air Force Base).

Biophysical Site Description

Longleaf pine sandhills occur as dry woodlands/savannas on excessively drained or other xeric soils. Soils are deep coarse sands. It occurs on upland, gently rolling, broad ridge tops.

Soils are typically Entisols (Psamments), with very limited profile development. Some soil series associated with this system include the Astatula series (Kalisz 1982), as well as the Lake, Tavares and Orsino series (Abrahamson et al. 1984). In some cases the soils may be unusually dark in color at the surface, which has been attributed, in part, to the presence of charcoal. Soils are strongly acidic (pH 4.75.0). At least some of these sites have silt or clay in the subsoil contributing to significantly higher extractable bases at the surface when compared to nearby

scrub sites (Kalisz 1982). Excluded are areas with a "shallow sand cap" (K. Outcault pers. comm.). On Eglin Air Force Base, habitat for this system includes areas covered by the Citronelle Formation. Psamments are the dominant soil suborder in the areas of Florida where this system is found (NRCS n.d.) (paragraph taken from NatureServe 2006).

Vegetation Description

The canopy is strongly dominated by longleaf pine (*Pinus palustris*). Xerophytic scrub oaks, predominately turkey oak (*Quercus laevis*), bluejack oak (*Quercus incana*), sand live oak (*Quercus geminata*) or sand post oak (*Quercus margaretta*), are present as sparsely scattered midstory individuals or clumps and shrub-size fire-sprouts under the reference condition. The oaks become denser with fire exclusion. Other less xerophytic oaks are absent or extremely rare.

A rich herbaceous layer is present. Characteristic species in this stratum are *Aristida beyrichiana*, over most of the range, and *Licania michauxii* (NatureServe 2006).
Also with bluestems (*Schizachyrium* spp. or *Andropogon* spp.) and dropseed (*Sporobolus* spp.) in places. The herb layer is moderately dense, with a variety of other xerophytic herbs present. In addition, a number of species found primarily in central Florida may also be present, among the most frequent of which is *Chapmannia floridana*. Other geographically limited species may include *Sabal etonia*, *Polygonella ciliata* and *Arnoglossum floridanum* (NatureServe 2006).

Low shrubs are sparse in the reference condition, but can become dense with fire exclusion.

Canopy trees are patchy to dense in distribution, with regeneration in canopy gaps of ¼ acre to a few acres in size, occasional mid-successional clumps in similar sized patches and the oldest trees occurring as isolated individuals or as large patches. Canopy gaps are created by fire mortality, lightning and wind throw at the scale of individual trees or several trees. Because of the irregular seed production of longleaf pine, canopy gaps may lack regeneration for several years.

Disturbance Description

Frequent surface fires, every 1-4yrs generally burn across large expanses. Fires are usually low in intensity overall, but will occasionally kill young regeneration patches and rarely kill individual older trees. Hurricanes and accompanying tornadic winds may result in blowdowns that occur as thinnings, patches, or, rarely, large patches.

Fire is absolutely essential to maintain this system, without which it may be almost completely replaced by scrub vegetation (in the Florida Peninsula) (NatureServe 2006).

Adjacency or Identification Concerns

This type is distinguished from other longleaf pine-dominated groups by the presence of xerophytic oaks and the absence of other oaks, and by the absence of mesophytic or wetland herbs.

Adjacent to Central Florida Wet Prairie and Herbaceous Seep (CES203.491) and Central Florida Pine Flatwoods (CES203.382). It can be surrounded by Florida Peninsula Inland Scrub (CES203.057) (NatureServe 2006).

Longleaf pine sandhills are abundant in the Sandhills Region of North and South Carolina, and scattered on relict beach ridge systems of the outer coastal plain and on sand dune systems associated with rivers. Rare extreme sandhills (sand barrens) are so excessively drained that all strata are low in density, leaving much bare sand even in the absence of fire. Fuels are too discontinuous to support regular fire. This model does not cover these extreme communities.

Uncharacteristic vegetation types include even-aged canopy stands in which age structure has been homogenized by logging or clearing. Examples include where loblolly or slash pine have replaced some or all of the longleaf pine, where midstory oaks and/or low shrubs have become dense due to inadequate burning, and where the grass-dominated ground cover has been lost due to soil disturbance or past canopy closure.

Native Uncharacteristic Conditions

On Eglin and some surrounding areas some sandhills have been invaded by the native sandpine (from surrounding old planted plantations and natural areas) due to fire suppression. This creates a monoculture of sandpine overstory with little to no understory (usually consisting of lichen and bareground) and little midstory.

Scale Description

The landscape is adequate in size to contain the natural variation in vegetation and disturbance regimes. Topographically, areas could be very large and extend continuously over a large expanse of the landscape, or occur as small patches.

This system represents larger patches of *Pinus palustris* Sandhills (in FL), ranging from 60-4000ha in size (NatureServe 2006).

Issues/Problems

Longleaf pine-scrub oak sandhills and longleaf pine-turkey oak sandhills can make up this BpS within its geographic range. Also, no insect and disease disturbances were noted during the succession pathway of this BpS. It was suggested that some level of disturbance from a bark beetle infestation be added to this pathway. Most likely classes B and D would be where the problem would occur. This addition has not been done.

Comments

NOTE: 1/23/09: As a result of final QC for LANDFIRE National by Jennifer Long the user-defined min and max fire return intervals for mixed severity fire were deleted because they were not consistent with the modeled fire return interval for this fire severity type.

The information from the RA model R9LLSH by C. Bailey and K. Hiers was used as a starting point for this BpS LANDFIRE VDDT Model and then adapted by D. Hardin.

This model was reviewed during a model review workshop held 09/19/2006 Tallahassee, FL.

Vegetation Classes

Indicator Species* and Structure Data (for upper layer lifeform)

Class A 13%

Canopy Position

Early Development 1 All Structure PIPA2 All
ARBE7 All

☐ **Upper Layer Lifeform** Herbaceous
☐
☑ Shrub ☐ Upper layer lifeform differs from dominant lifeform.
Tree **Fuel Model** 2

	Min	*Max*
Cover	0 %	50 %
Height	Tree 0m	Tree 5m
Tree Size Class	Sapling >4.5ft; <5"DBH	

Description

Class A is characterized by canopy gaps, perhaps 1/4 to two acres in size, with pine regeneration up to 15yrs old, or lacking pine regeneration because no mast year has occurred since the gap opened. The native grassy ground cover is dominated by Aristida stricta. Tree cover ranges from 0-50%.

Indicator Species* and Structure Data (for upper layer lifeform)

Class B 2%

Canopy Position

Mid Development 1 Closed PIPA2 Upper
QULA2 Middle
QUGE2 Middle

☐ **Upper Layer Lifeform**
Herbaceous
☐
☑ Shrub ARBE7 Lower ☐ Upper layer lifeform differs from dominant lifeform. Tree **Fuel Model** 6

	Min	*Max*
Cover	71 %	100 %
Height	Tree 0m	Tree 25m
Tree Size Class	Pole 5-9" DBH	

Description

Class B includes patches, perhaps 1/4 to 2 acres in size, with canopy pines 15-75yrs old. A substantial component of mid-story hardwoods or shrubs is encroaching in the absence of fire. The hardwood/shrub cover is >50%. Canopy pine cover ranges between 25-75%. This class would also establish in fire shadows created by geologic or hydrologic changes.

Class C 37%

Mid Development 1 Open

Indicator Species* and Canopy Position

PIPA2	Upper
QULA2	Middle
QUGE2	Middle
ARBE7	Lower

Structure Data (for upper layer lifeform)

	Min	*Max*
Cover	21 %	70 %
Height	Tree 0m	Tree 25m
Tree Size Class	Medium 9-21" BH	

☐ Upper layer lifeform differs from dominant lifeform.

Upper Layer Lifeform

☐ Herbaceous
☐ Shrub
☑ Tree

Fuel Model 6

Description

Class C includes patches, perhaps 1/4 to two acres in size, with canopy pines 15-75yrs old. There is a minimal hardwood component and only sparse shrubs due to frequent fire. Aristida stricta dominates the ground cover. Canopy pine cover ranges between 25-75%.

Class D 44%

Late Development 1 Open

Indicator Species* and Canopy Position

PIPA2	Upper
QULA2	Middle
QUGE2	Middle
ARBE7	Lower

Structure Data (for upper layer lifeform)

	Min	*Max*
Cover	21 %	70 %
Height	Tree 0m	Tree 25m
Tree Size Class	Large 21-33"D H	

☐ Upper layer lifeform differs from dominant lifeform.

Upper Layer Lifeform

☐ Herbaceous
☐ Shrub
☑ Tree

Fuel Model 2

Description

Class D is characterized by patches, perhaps 1/4 to two or more acres in size, with canopy pines 75yrs+ old up to hundreds of years old. There is a minimal hardwood component and only sparse shrubs due to frequent fire. Aristida stricta dominates the ground cover. Canopy pine cover ranges between 25-75%.

Class E 4%

Late Development 1 Closed

Indicator Species* and Canopy Position

PIPA2	Upper
QUGE2	Middle
QULA2	Middle
ARBE7	Lower

Structure Data (for upper layer lifeform)

	Min	*Max*
Cover	71 %	100 %
Height	Tree 0m	Tree 50m
Tree Size Class	Large 21-33"D H	

☐ Upper layer lifeform differs from dominant lifeform.

Upper Layer Lifeform

☐ Herbaceous
☐ Shrub
☑ Tree

Fuel Model 9

Description

Class E includes patches with a few remnant canopy pines 75yrs+ old, with a substantial component of hardwoods and/or shrubs in either the overstory or understory. The ground cover is shrubby or sparse. The hardwood/shrub cover is >50%. This class would also establish in fire shadows created by geologic or hydrologic changes.

Disturbances

Fire Regime Group:** I

Historical Fire Size (acres)

Avg 10000

Min 1

Max 100000

Fire Intervals	*Avg FI*	*Min FI*	*Max FI*	*Probability*	*Percent of All Fires*
	190			0.00526	1
Mixed	10000			0.0001	0
Surface	2.5	1	10	0.4	99
All Fires	2			0.40536	
Replacement		150			250

Fire Intervals (FI):
Fire interval is expressed in years for each fire severity class and for all types of fire combined (All Fires). Average FI is central tendency modeled. Minimum and maximum show the relative range of fire intervals, if known. Probability is the inver of fire interval in years and is used in reference condition modeling. Percent of all fires is the percent of all fires in that severity class.

☐ **Sources of Fire Regime Data**

☑ Literature

☑ Local Data

☐ Expert Estimate

☐ **Additional** ☐ **Disturbances** ☐ **Modeled**

☑ Insects/DiseaseNative GrazingOther (optional 1)

Wind/Weather/StressCompetitionOther (optional 2)

References

Abrahamson, W.G., A.F. Johnson, J.N. Layne and P.A. Peroni. 1984. Vegetation of the Archbold Biological Station, Florida: An example of the southern Lake Wales Ridge. Florida Scientist 47: 209-250.

Boyer, W.D. 1993. Long-term development of regeneration under pine seed tree and shelter wood stands. Southern Journal of Applied Forestry 17: 10-15.

Brewer, J.S. and Platt, W.J. 1994a. Effects of fire season and herbivory on reproductive success in a clonal forb, Pityopsis graminifolia. Journal of Ecology 82: 665-675.

Brewer, J.S. and Platt, W.J. 1994b. Effects of fire season and soil fertility on clonal growth in the pyrophilic forb, Pityopsis graminifolia (Asteraceae). American Journal of Botany 81: 805-814.

Brown, James K., Smith, Jane Kapler, eds. 2000. Wildland fire in ecosystems: effects of fire on flora. Gen. Tech. Rep. RMRS-GTR-42-vol. 2. Ogden, UT: USDA Forest Service, Rocky Mountain Research Station. 257 pp.

Christensen, N.L. 1981. Fire regimes in southeastern ecosystems. In Mooney, H.A., Bonnickson, T.M., Christensen, N.L., Lotan, J.E. and Reiners, W.A., eds. Fire regimes and ecosystem properties. USDA Forest Service General Technical Report WO-26. pp. 112-136.

Croker, T.C., and Boyer, W.D. 1984 . Regenerating longleaf pine naturally. USDA Forest Service Research Paper SE-105.

Frost, Cecil C. 1993. Four centuries of changing landscape patterns in the longleaf pine ecosystem. In Hermann, S.M., ed. The longleaf pine ecosystem: ecology, restoration and management. Proc. Tall Timbers Fire Ecol. Conf. No. 18: 17-43.

Frost, Cecil C. 1997. Presettlement vegetation and fire history of the Savannah River Site and vicinity, South Carolina. Savannah River Forest Station (map and text). U.S. Department of Energy. 186 pp. [with 2 GIS maps].

Glitzenstein, J.S., Harcombe, PA, and Streng, D.R. 1986. Disturbance, succession, and maintenance of species diversity in an east Texas forest. Ecological Monographs 56: 243258.

Hainds, M.J., Mitchell, R.J., Palik, B.J. and Boring, L.R. 1999. Abundance and distribution of native legumes (Leguminosae) in frequently burned longleaf pine (Pinaceae)—wiregrass (Poaceae) ecosystems. American Journal of Botany 86: 1606-1614.

Hermann, S.M., Van Hook, T., Flowers, R.W., Brennan, L.A., Glizenstein, J.S., Streng, D.R., Walker, J.L. and Myers, R.L. 1998. Fire and biodiversity: studies of vegetation and arthropods. North American Wildland and Natural Resource Conference 63: 384-401.

Hiers, J.K., Wyatt, R. and Mitchell, R.J. 2000. The effects of fire regime on legume reproduction in longleaf pine savannas: is a season selective? Oecologia 125: 521-530.

Jacqmain, E.I., Jones R.H. and Mitchell, R.M. 1999. Influences of frequent cool-season burning across a soil moisture gradient on oak community structure in longleaf pine ecosystems. American Midland Naturalist 141: 85-100.

Jose, S., Jokela, E.J. and D.L. Miller, eds. 2006. The Longleaf Pine Ecosystem Ecology, Silviculture, and Restoration. Springer, New York. 438 pp.

Kalisz, PJ. 1982. The longleaf pine islands of the Ocala National Forest: A soil study. Ph.D. dissertation, University of Florida, Gainesville. 126 pp.

Kirkman, L.K., Drew, M.B. and Edwards, D. 1998. Effects of experimental fire regimes on the population dynamics of Schwalbea americana L. Plant Ecology 137: 115-137.

NatureServe. 2007. International Ecological Classification Standard: Terrestrial Ecological Classifications. NatureServe Central Databases. Arlington, VA. Data current as of 10 February 2007.

NatureServe. 2006. International Ecological Classification Standard: Terrestrial Ecological Classifications.

NatureServe Central Databases. Arlington, VA, U.S.A. Data current as of 18 July 2006.

NRCS [Natural Resources Conservation Service]. No date. Entosols map. USDA Natural Resources Conservation Service. [http://soils.usda.gov/technical/classification/orders/entisols_map.html]. (accessed 27 June 2006).

Outcalt, Ken. Personal communication. Research Plant Ecologist, USDA Forest Service, Southern Research Station, Asheville, NC. E-mail: koutcalt@fs.fed.us . Phone: (706) 559-4309.

Palik, B.J. and Engstrom, R.T. 1999. Species composition. In M.L. Hunter, Jr., ed. Maintaining biodiversity in forest ecosystems. Cambridge University Press: 65-94.

Palik, B.J., Mitchell, R.J., Houseal, G. and Pederson, N. 1997. Effects of canopy structure on resource availability and seedling responses in a longleaf pine ecosystem. Canadian Journal of Forest Research 27: 1458-1464.

Palik, B.J. and Pederson, N. 1996. Natural disturbance and overstory mortality in longleaf pine ecosystems. Canadian Journal of Forest Research 26: 2035-2047.

Peet, R.K. and Allard, D.J. 1993. Longleaf pine vegetation of the Southern Atlantic and Eastern Gulf Coast regions: a preliminary classification. In Proceedings of the 18th Tall Timbers Fire Ecology Conference. Tallahassee, FL: Tall Timbers Research Station.

Platt, W.J., Evans, G.W. and Davis, M.M. 1988. Effects of fire season on flowering of forbs and shrubs in longleaf pine forests. Oecologia 76: 353-363.

Platt, W.J., Evans, G.W. and Rathbun, S.L. 1988. The population dynamics of a long-lived conifer (Pinus palustris). American Naturalist 131: 491-525.

Platt, W.J. and Rathbun, S.L. 1993. Population dynamics of an old-growth population of longleaf pine (Pinus palustris). In Proceedings of the 18th Tall Timbers Fire Ecology Conference. Tallahassee, FL: Tall Timbers Research Station.

Schmidt, Kirsten M., Menakis, James P., Hardy, Colin C., Hann, Wendel J. and Bunnell, David L. 2002. Development of coarse-scale spatial data for wildland fire and fuel management. Gen. Tech. Rep. RMRSGTR-87. Fort Collins, CO: USDA Forest Service, Rocky Mountain Research Station. 41 pp. + CD.

Streng, D.R., Glitzenstein, J.S. and Platt, W.J. 1993. Evaluating effects of season of burn in longleaf pine forests: a critical literature review and some results from an ongoing long-term study. Proceedings of the Tall Timbers Fire Ecology Conference 18: 227-259.

Robbins, L.E. and Myers, R.L. 1992. Seasonal effects of prescribed burning in Florida. Miscellaneous Publications of the Tall Timbers Research Station 8: 1-97.

USDA Forest Service, Rocky Mountain Research Station, Fire Sciences Laboratory (2002, December). Fire Effects Information System, [Online]. Available: http://www.fs.fed.us/database/feis/.

Walker, J. and Peet, R.K. 1983. Composition and species diversity of pine-wiregrass savannas of the Green Swamp, North Carolina. Vegetation 55: 163-179.

Walters, J. R. 1991. Application of ecological principals to the management of endangered species: the case of the red-cockaded woodpecker. Annual Review of Ecology and Systematics 22: 505-523.

Ware, S., Frost, C. and Doerr, P.D. 1993. Southern mixed hardwood forest: The former longleaf pine forest. In Martin, W.H., Boyce, S.G. and Echternacht, A.C., eds. Biodiversity of the southeastern United States. New York, NY: John Wiley and Sons, Inc: 447-493.

Appendix 19-D
ST-Sim User's Guide

User's Guide for the Longleaf Pine State-and-Transition Model

Developed for Red-Cockaded Woodpecker modeling applications

Author: Sara Zeigler
Parameterization: Sara Zeigler and Jeffrey Walters (Virginia Tech)
Model: Parameterization and screenshots specific to ST-SIM (ApexRMS) version 3.0.44
Date: August 2017

Table of Contents

1. Introduction 3
2. Downloading ST-SIM 4
3. Quick Run 4
4. Parameterizing the Model 5
4.1 Landscape States 6
4.2 Transitions 11
4.3 Organization of States and Transitions 16
4.3.1 Deterministic Transitions (Succession and Aging) 16
4.3.2 Alternative Succession in the Absence of Disturbance 22
4.3.3 Fire 28
4.3.4 Herbicide Treatment 36
4.3.5 Mechanical Removal 38
4.3.6 Wiregrass Planting 38
4.3.7 Other "Natural" Transitions 40
4.4 Simulation Controls and Initial Conditions 44
4.4.1 Run controls 44
4.4.2 Initial landscape conditions 44
4.4.3 Output options 48
5. Running an ST-SIM Model 49
6. ST-SIM Results and Outputs 51
7. Advanced Model Parameterization – Spatial Multipliers 52
8. Landscape Input Values and Maps in ArcGIS 56
8.1 Vegetation Type map 56
8.2 State Class map 57
8.3 Age map 57

1. Introduction

We developed a model of successional-disturbance dynamics in a longleaf pine (*Pinus palustris*) ecosystem in order to simulate red-cockaded woodpecker (RCW; *Picoides borealis*) population-level responses to landcover change. Outputs from the landscape model, which include both spatially explicit and non-spatially explicit descriptions of the landcover types that comprise a given area, can be used as inputs into an RCW-specific population model (Walters et al. 2011; Figure 1). Our landscape model was constructed within the existing program ST-SIM (Daniel & Frid 2011), which is a state-and-transition model that simulates future landcover conditions by considering interactions between successional processes, unplanned disturbances, and planned changes to the landscape. In this manual, we focus on the parameterization of the ST-SIM landscape model that is specific to Marine Corps Base Camp Lejeune (MCBCL). However, this model has also been modified for use at Fort Bragg and Eglin Air Force Base. Models for all locations were based on forest dynamics models developed by the LANDFIRE Program (joint program by the U.S. Department of Agriculture Forest Service and the Department of the Interior; https://www.LANDFIRE.gov/index.php)(Rollins 2009; Zahn 2015).

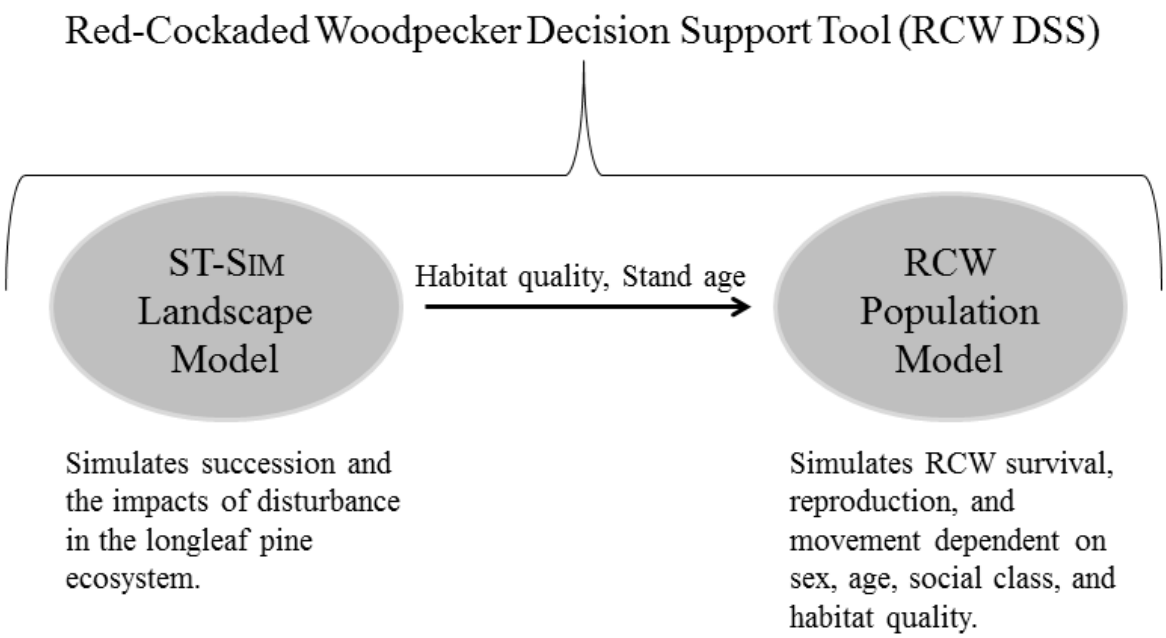

Figure 1. Conceptualization of the linked ST-SIM landscape – red-cockaded woodpecker population model, an applied tool for red-cockaded woodpecker (RCW) conservation.

2. Downloading ST-SIM

ST-SIM is a free state-and-transition modeling platform available from ApexRMS at http://www.apexrms.com. Download the zip file for the most recent version of the software (current version at time this guide was written: 3.0.44). Unzip the file's contents to the location of your choice, and run the setup application to install the software.

3. Quick Run

As the user, you can choose to construct a state and transition model from scratch from the steps outlined in *Section 4. Parameterizing the Model* in this user's manual. This section also details how to adjust certain parameters to test potential landcover changes and management approaches in longleaf pine ecosystems.

However, to immediately run the ST-SIM model, you can open the ST-SIM library that accompanies this user manual. Unzip the file "Longleaf_RCW", and extract the files and folders within this zip file onto your desktop. Then, open the ST-SIM program (which may appear on your computer as "SyncroSim"). Click on "File" along the top menu bar in the main ST-SIM window, and select "Open Library".

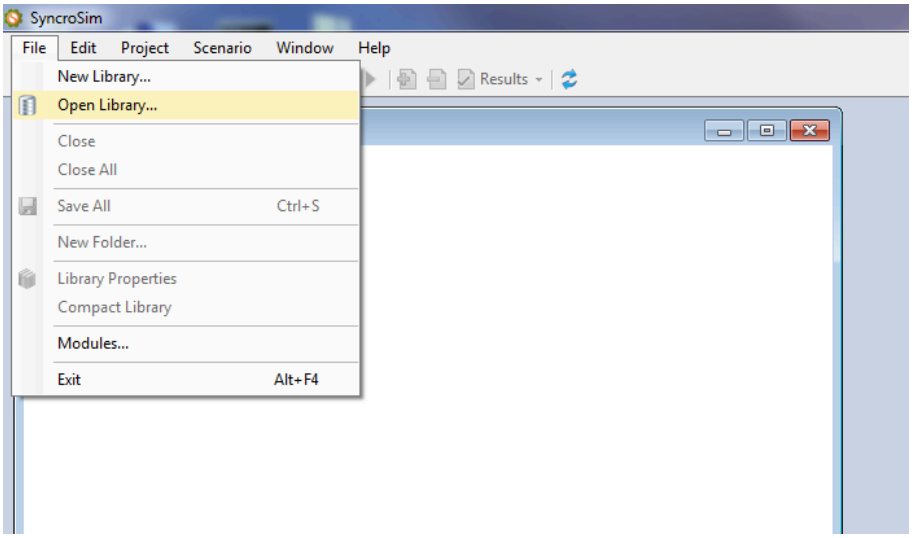

In the "Open Library" window that appears, navigate to the unzipped folder that accompanied this manual, and select the ST-SIM file "Longleaf_RCW.ssim". This library contains modified versions of LANDFIRE forest dynamics models for MCBCL, Fort Bragg, and Eglin Air Force Base. Site-specific models appear as separate projects in this library.

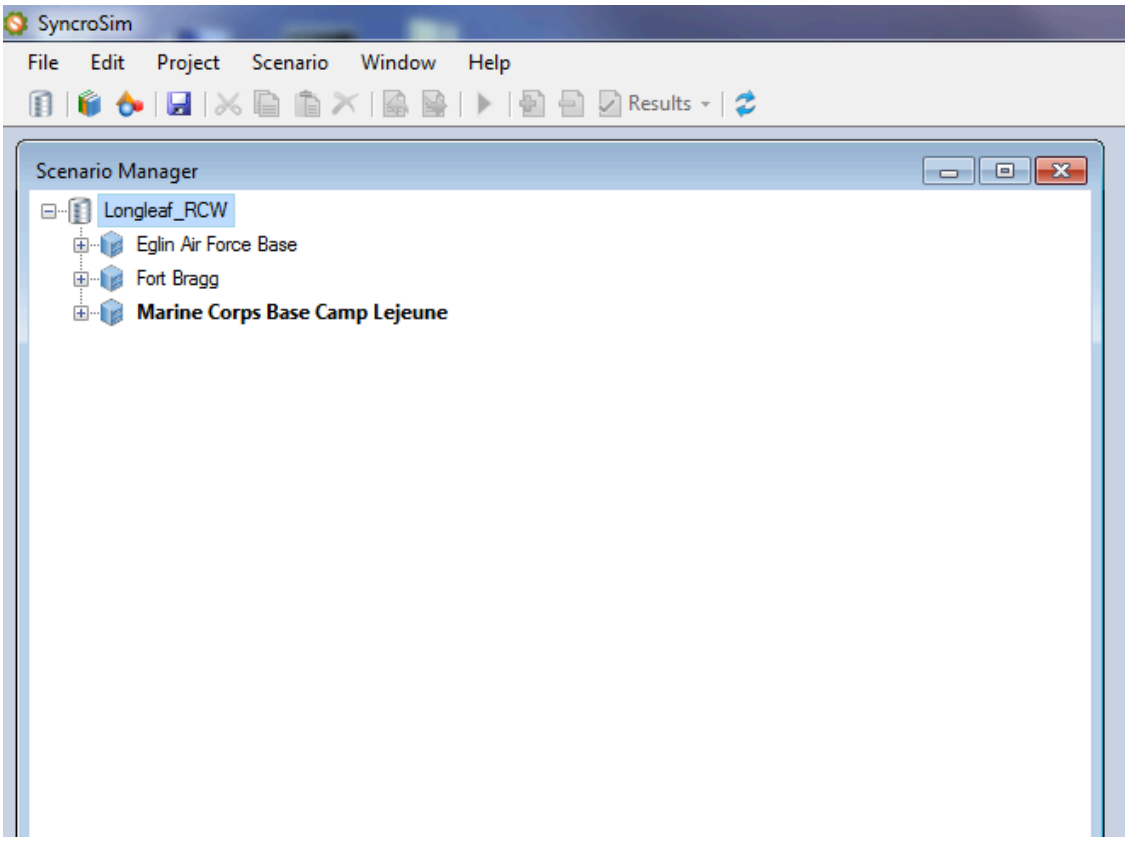

You can then set the initial conditions (*Section 4.5 Simulation Controls and Initial Conditions*), run the model (*Section 5. Running the ST-SIM Model*), and evaluate the results (*Section 6. ST-SIM Results and Outputs*).

4. Parameterizing the Model

In this section, we describe how the user can build an ST-SIM landscape model from scratch. Throughout this section, we specifically describe the steps taken to construct the baseline model of longleaf pine ecosystem dynamics for MCBCL. After downloading and opening ST-SIM, go to "File" and "New Library" to create a new project library. You will be prompted to name and save this library at the location of your choice (currently saved as "Longleaf_RCW"). Next, right-click on the library's name, and select "New" and "Project". You will again be prompted to name and save this project at the location of your choice (currently saved as "Marine Corps Base Camp Lejeune"). From there, you will be able to specifically parameterize the ST-SIM model to simulate the dynamics of the longleaf pine ecosystem.

Data and published literature used to select parameters for our model are described in more detail in the report that accompanies this user's manual. In addition, these models were derived from LANDFIRE products. For more information, see https://www.LANDFIRE.gov/index.php (Rollins 2009; Zahn 2015).

4.1 Landscape States

The basic units of any ST-SIM model are the landscape strata, states, and transitions that govern changes between specific landscape classes. This information is added through the "Project Definitions" window that is accessed by right-clicking on the project name in the "Libraries" window and selecting "Project Definitions".

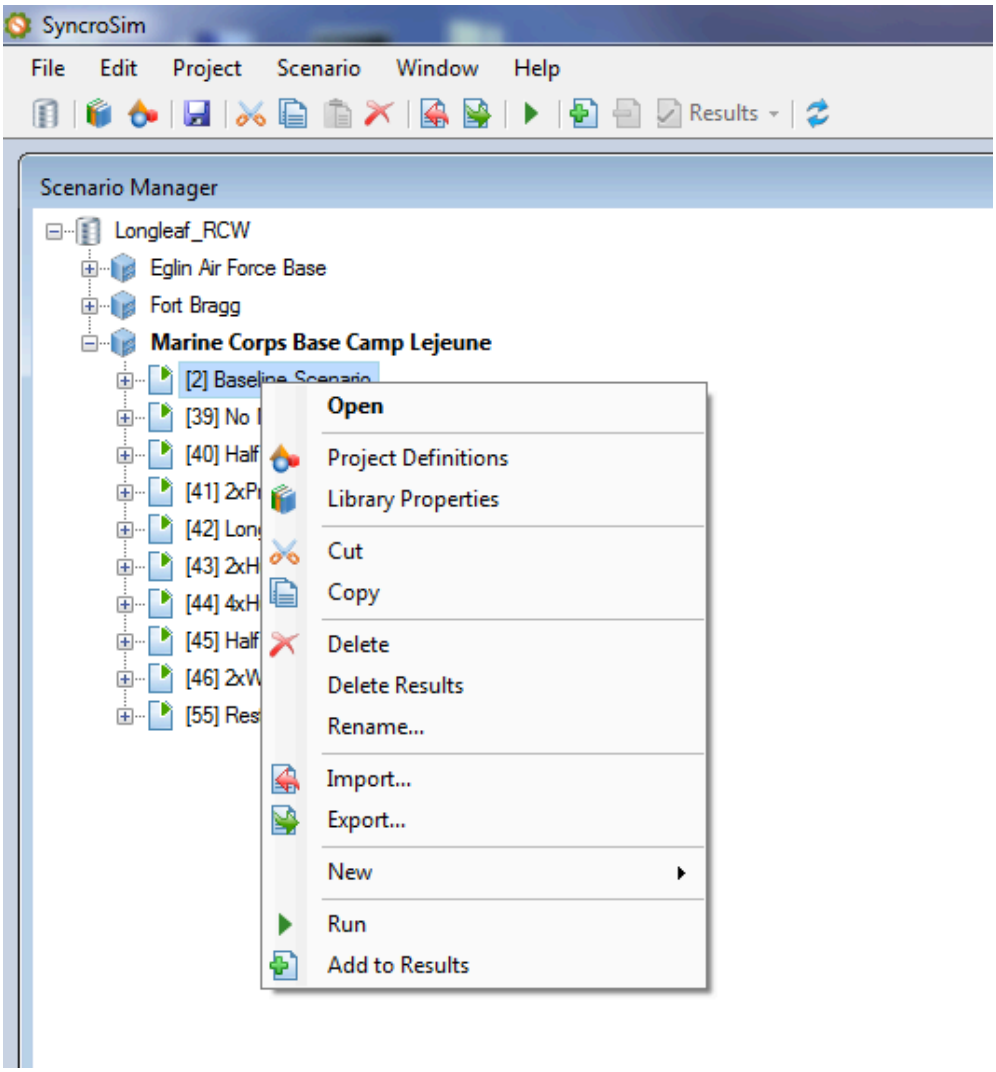

In the first tab ("Strata"), the types of strata represented in the model can be added. These are the major underlying classifications of the landscape, such as ecoregions or soil types, that govern the type of vegetation that can grow in specific areas. According to the LANDFIRE program, the area within the boundaries of MCBCL is primarily composed of the biophysical settings (or "vegetation types" or "settings") for "Atlantic Coastal Plain Upland Longleaf Pine Woodland (biophysical setting 5813470)" and "Central Atlantic Coastal Plain Wet Longleaf Pine Savanna and Flatwoods (biophysical setting 5814490)". These biophysical settings, which differ in soil moisture, successional speed, etc., serve as separate Vegetation Types within the MCBCL

model. We also added a third Vegetation Type for “Other” for all landcover types not found in these longleaf pine biophysical settings. Therefore, add “Upland Longleaf (ID:1)”, “Wet Longleaf (ID:2)”, and “Other (ID:3)” under Strata – Vegetation Type (Table 1). ID values given in this window and in all others represent the identification value associated with this vegetation type on maps used in spatially explicit simulations. (To add a column for “ID”, right-click on the cell in the top-left corner of the table and selecting this additional column). In general, the states, time scales of succession, and effects of disturbances can be unique to each of these Vegetation Types.

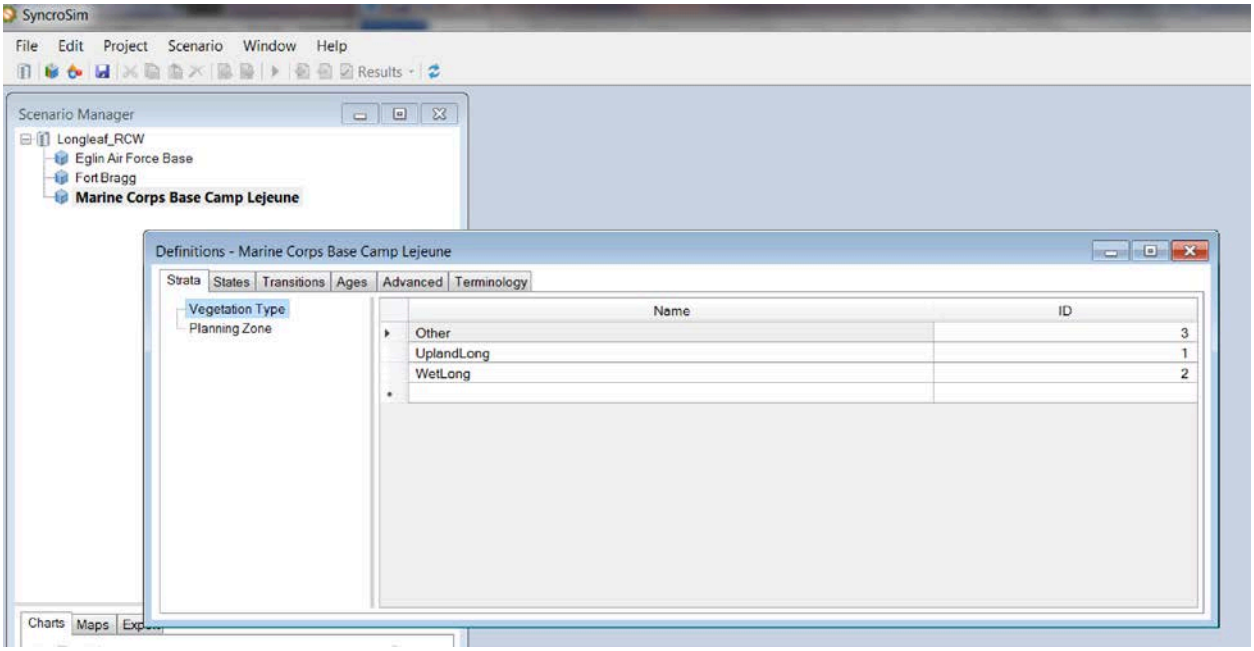

Table 1. Strata, Cover Types, Structural Stages, and State Classes that define the landscape at Marine Corps Base Camp Lejeune in the ST-SIM landscape model (derived from the LANDFIRE project; https://www.landfire.gov/).

Project Definitions - States	ST-Sim Name (ID)	Description[1]
Strata – Vegetation Type		
Upland Longleaf Pine	UplandLong (1)	Atlantic Coastal Plain Upland Longleaf Pine Woodland (biophysical setting 5813470)
Wet Longleaf Pine	WetLong (2)	Central Atlantic Coastal Plain Wet Longleaf Pine Savanna and Flatwoods (biophysical setting 5814490)
Other	Other (3)	Landcover not contained in the above biophysical settings
States - Cover Type		
Early Development 1	Early1	Longleaf pine ≤ 15 years old
Mid-Development 1	Mid1	Longleaf pine 15- 75 years old
Late Development 1	Late1	Longleaf pine > 75 years old
Bare Land	Bare	Areas of bare land (e.g., bombing ranges)
Hardwood	Hard	Stands containing hardwood species
Mixed	Mixed	Stands containing a mix of hardwood and pine species
Other	Other	Other "human-modified" landcover (e.g., development)
Water	Water	Bodies of water
Other Pine	Other_Pine	Stands containing species of pine not considered in the Upland and Wet Longleaf strata (e.g., loblolly, slash pine)
States – Structural Stage		
All	ALL	Midstory and understory conditions are irrelevant.
Open - Dense	OPN-DEN	Contains a minimal hardwood component due to frequent fire. The ground cover is dense (> 40%) and dominated by grasses. The pine canopy cover ranges from 25-75%.
Open - Sparse	OPN-SPAR	Contains a minimal hardwood component but a sparse (<40%) cover of understory grasses. Condition results from mechanical midstory removal or herbicide application in the absence of fire.
Closed - Sparse	CLS-SPAR	Contains a substantial component of hardwoods or other pine species encroaching in the absence of fire. Hardwood and encroaching pine cover is >50%. The pine canopy cover ranges from 25-75%. Understory cover is sparse (< 40%).
State Class		
Early Development 1:ALL	Early1:ALL (2)	Canopy gaps, most single tree to a quarter acre size, characterize this class. Pine regeneration grows here up to 15 years old, or the site lacks pine regeneration because no mast year has occurred since the gap opened. The native grassy ground

		cover is dominated by various grasses, with *A. stricta* the dominant herb. Tree cover ranges from 0-50%.
Mid-Development1:Closed-Sparse	Mid1:CLS-SPAR (7)	Characterized by patches, most a quarter acre or less, of canopy longleaf pine 15-75 years old and a substantial component of hardwoods or other pine species encroaching in the absence of fire. Understory grasses and other herbaceous plants cover < 40% of the area. Hardwood and encroaching pine cover is >50%. The pine canopy cover ranges from 25-75%.
Mid-Development1:Open-Sparse	Mid1:OPN-SPAR (9)	Characterized by patches, most a quarter acre or less, with canopy longleaf pine 15-75 years old and a minimal hardwood component due to mechanical mid-story removal or herbicide application. Ground cover, usually dominated by grasses, is sparse (<40%) in the absence of fire.
Mid-Development1:Open-Dense	Mid1:OPN-DEN (8)	Characterized by patches, most a quarter acre or less, with canopy longleaf pine 15-75 years old and a minimal hardwood component due to frequent fire. The ground cover is dense (>40%) and dominated by grasses. The pine canopy cover ranges from 25-75%.
Late Development1:Closed-Sparse	Late1:CLS-SPAR (4)	Characterized by patches with canopy pines 75years+ old and a substantial component of hardwoods or pines other than longleaf in either the overstory or understory. The ground cover is shrubby or sparse (<40% cover). Hardwood and encroaching pine cover is >50%.
Late Development1:Open-Sparse	Late 1:OPN-SPAR (6)	Characterized by patches, most a quarter acre or less, with canopy pines 75years+ old and a minimal component of hardwoods due to mechanical mid-story removal or herbicide application. Ground cover, usually dominated by grasses, is sparse (<40% cover) in the absence of fire.
Late Development1:Open-Dense	Late 1:OPN-DEN (5)	Characterized by patches, most a quarter acre or less, with canopy longleaf pine 75years+ old and a minimal component of hardwoods. The ground cover is dense (>40% cover) and dominated by grasses. The pine canopy cover ranges from 25-75%.
Bare Land:ALL	Bare:ALL (1)	Bare land with no pine or hardwood component.
Hardwood:Closed-Sparse	Hard:CLS-SPAR (3)	Stands of hardwood species with a substantial mid-story hardwood component and sparse cover (<40%) of understory plants.
Mixed:Closed-Sparse	Mixed:CLS-SPAR (10)	Stands of hardwood and pine species with a substantial mid-story hardwood component and sparse cover (<40%) of understory plants.
Other:ALL	Other:ALL (11)	Other landcover types (e.g., development) with no pine or hardwood component.
Water:ALL	Water:ALL (14)	Water bodies with no pine or hardwood component.
Other Pine: Closed-Sparse	Other Pine:CLS-SPAR (12)	Characterized by patches of non-longleaf pine species > 15 years old and a substantial component of hardwoods or other pine species encroaching in the absence of fire. The ground cover is shrubby or sparse (<40% cover).
Other Pine:Open-Dense	Other Pine:OPN-DEN (13)	Characterized by patches of non-longleaf pine species > 15 years old and a minimal hardwood component due to frequent fire. The ground cover is dense (>40%) and dominated by grasses.

Next, specify the landscape state classes, which are the basic units of any ST-SIM model and are discrete classes representing specific landcover types, successional states, or other landscape characteristics (e.g., tree density, species composition, etc.). State classes are a defined combination of "Cover Type" and "Structural Stage". In developing this ST-SIM model, it was necessary to create states that were relevant both to the longleaf pine ecosystem and to RCW biology/ecology while also being compatible within the RCW population model. We also adhered closely to existing LANDFIRE models. Here, you would add Cover Type, Structural Stage, and State Class as shown in Table 1. (To add columns for "ID" and "Description", right-click on the cell in the top-left corner of the table and selecting these additional columns).

In general, the states represented here reflect two major successional pathways: (1) a pathway where fire is frequent, the mid-story is open, and the understory is dense and dominated by herbaceous plants as well as (2) a pathway where fire is absent, the mid-story is closed and dominated by hardwood species, and the understory is sparse or shrubby.

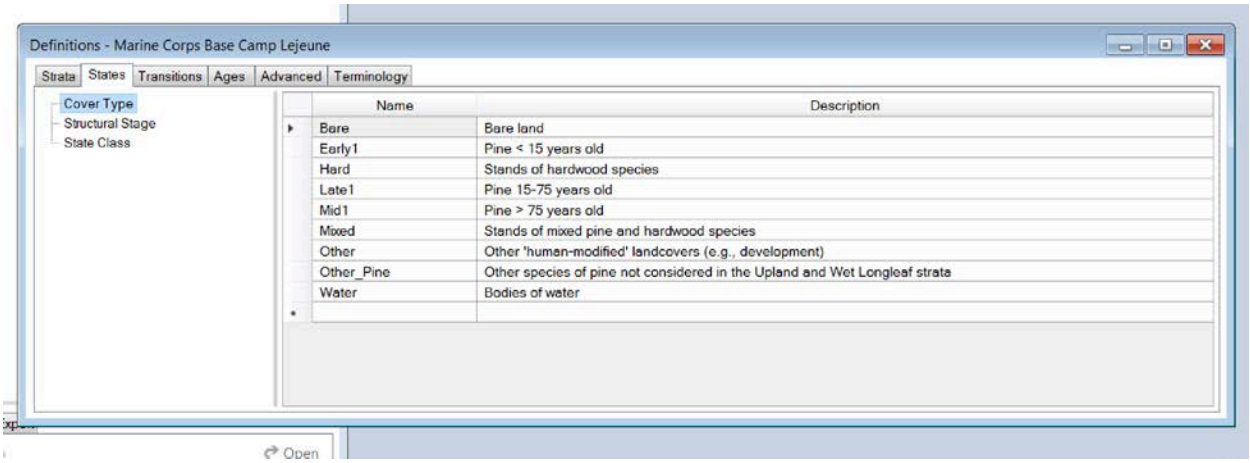

Name	Description
Bare	Bare land
Early1	Pine < 15 years old
Hard	Stands of hardwood species
Late1	Pine 15-75 years old
Mid1	Pine > 75 years old
Mixed	Stands of mixed pine and hardwood species
Other	Other 'human-modified' landcovers (e.g., development)
Other_Pine	Other species of pine not considered in the Upland and Wet Longleaf strata
Water	Bodies of water

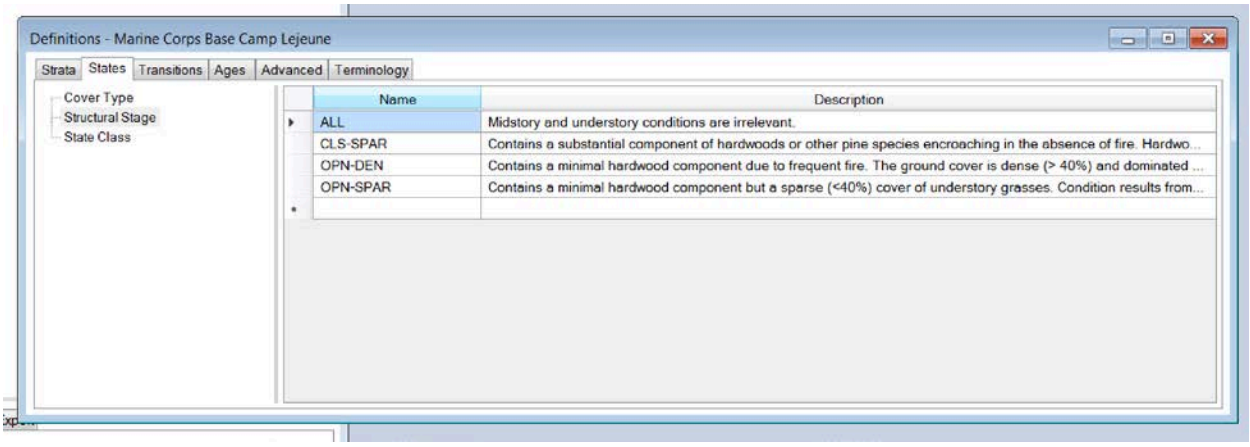

Name	Description
ALL	Midstory and understory conditions are irrelevant.
CLS-SPAR	Contains a substantial component of hardwoods or other pine species encroaching in the absence of fire. Hardwo...
OPN-DEN	Contains a minimal hardwood component due to frequent fire. The ground cover is dense (> 40%) and dominated ...
OPN-SPAR	Contains a minimal hardwood component but a sparse (<40%) cover of understory grasses. Condition results from...

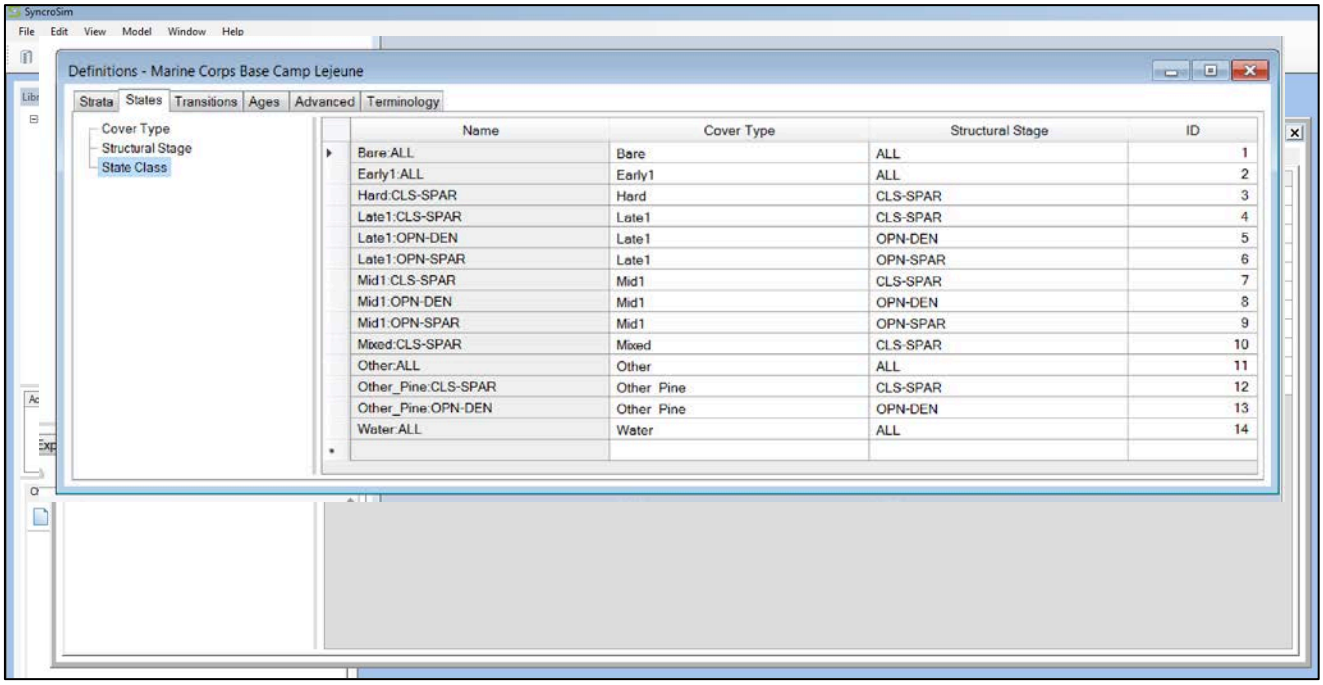

Name	Cover Type	Structural Stage	ID
Bare:ALL	Bare	ALL	1
Early1:ALL	Early1	ALL	2
Hard:CLS-SPAR	Hard	CLS-SPAR	3
Late1:CLS-SPAR	Late1	CLS-SPAR	4
Late1:OPN-DEN	Late1	OPN-DEN	5
Late1:OPN-SPAR	Late1	OPN-SPAR	6
Mid1:CLS-SPAR	Mid1	CLS-SPAR	7
Mid1:OPN-DEN	Mid1	OPN-DEN	8
Mid1:OPN-SPAR	Mid1	OPN-SPAR	9
Mixed:CLS-SPAR	Mixed	CLS-SPAR	10
Other:ALL	Other	ALL	11
Other_Pine:CLS-SPAR	Other_Pine	CLS-SPAR	12
Other_Pine:OPN-DEN	Other_Pine	OPN-DEN	13
Water:ALL	Water	ALL	14

4.2 Transitions

In ST-SIM, discrete landscape cells within the model move from one state class to another through probabilistic or deterministic transitions. In our model, those transitions occur through (*i*) natural processes (e.g., succession, natural wildfires), (*ii*) management (e.g., prescribed burns, herbicide treatments, mechanical midstory removal), or (*iii*) other human modification (e.g., development).

The specific parameters for each transition will be added elsewhere, but, for now, the identification and description of each type of transition can be added through the “Project Definitions” window that is accessed by right-clicking on the project name in the “Libraries” window and selecting “Project Definitions”. Click on the “Transitions” tab.

First, add each broad type of transition group shown in Table 2 by clicking on “Transition Group” to the left of the “Project Definitions” window (add a column for “Description” by right-clicking on the cell in the top-left corner of the table and selecting this additional column). Transition types are organized into these groups for later model parameterization.

Table 2. Transition groups and types that define the landscape at Marine Corps Base Camp Lejeune in the ST-SIM landscape model (derived from the LANDFIRE project; https://www.landfire.gov/).

Project Definitions - Transitions	ST-Sim Name (ID)	Description[1]
Transition Group		
All Fire	AllFire	All disturbances related to wildfire and management-related burns.
Alternative Succession	AlternativeSuccession	All transitions related to successional pathways that occur in the absence of fire.
Competition/Maintenance	Competition/Maintenance	All transitions that occur that maintain a landscape cell in its current state class.
Development	Develop	All transitions related to the development of a landscape cell (to the "Other" state class).
Insect/Disease	Insect/Disease	All disturbances related to insect infestations or disease outbreaks.
Mixed Fire	MixedFire	All fires of mixed severity.
Non-fire Disturbances	NonFireDisturbances	All natural disturbances not related to fire.
Non-fire Management	NonFireManagement	All transitions related to the management of the landscape
Non-replacement Fire	NonReplacementFire	All types of wildfires except for replacement fire
Prescribed Burn	PrescribedBurn	All fires related to an intentional management-related burn.
Replacement Fire	ReplacementFire	All fires of stand replacement-level severity.
Surface Fire	SurfaceFire	All fires of surface-level (mild) severity.
Wind/Weather/Stress	Wind/Weather/Stress	All natural disturbances related to weather.
Transition Type		
Alternative Succession	AltSuccession (1)	An alternative successional pathway that occurs in the absence of fire.
Competition/Maintenance	Competition/Maint (2)	Transition that maintains a landscape cell in its current state.
Development	Development (3)	Transition from any state class to the "Other" state class through human modification or development.
Grass Planting	GrassPlant (4)	Management-related planting of wiregrass to improve the density and quality of the understory.
Herbicide Application	HerbApp (5)	Application of herbicide to reduce the mid-story hardwood and non-longleaf pine component.
Insect/Disease	Insect/Disease (6)	An insect or disease infestation that causes the death of the stand and movement to the Early Development state.
Mechanical Midstory Removal	MidRemove (7)	Mechanical mid-story removal to reduce the mid-story hardwood and non-longleaf pine component.
Mixed Fire	MixedFire (8)	Wildfire or other non-management related fire with a top-kill 25-75%.
Prescribed Burn	PrescribedBurn (9)	Management-related use of fire to maintain an open mid-story and dense herbaceous ground cover.

Replacement Fire	ReplacementFire (10)	Wildfire or other non-management related fire with a top-kill >75%.
Surface Fire	SurfaceFire (11)	Wildfire or other non-management related fire with a top-kill < 25%.
Wind/Weather/Stress	Wind/Weather/Stress (12)	Natural weather-related disturbance (e.g., hurricanes).
Transition Types by Group		
All Fire		Contains transition(s): MixedFire, PrescribedBurn, ReplacementFire, SurfaceFire
Alternative Succession		Contains transition(s): AltSuccession
Competition/Maintenance		Contains transition(s): Competition/Maint
Development		Contains transition(s): Develop
Insect/Disease		Contains transition(s): Insect/Disease
Mixed Fire		Contains transition(s): MixedFire
Non-fire Disturbances		Contains transition(s): Competition/Maint, Insect/Disease, Wind/Weather/Stress
Non-fire Management		Contains transition(s): GrassPlant, HerbApp, MidRemove
Non-replacement Fire		Contains transition(s): MixedFire, SurfaceFire
PrescribedBurn		Contains transition(s): PrescribedBurn
Replacement Fire		Contains transition(s): ReplacementFire
SurfaceFire		Contains transition(s): SurfaceFire
Wind/Weather/Stress		Contains transition(s): Wind/Weather/Stress

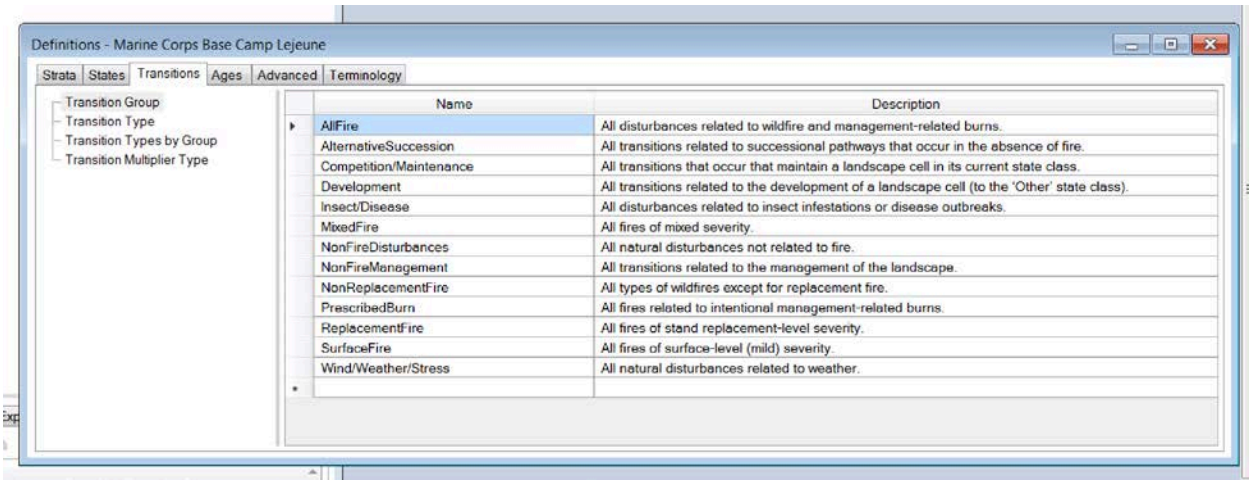

Name	Description
AllFire	All disturbances related to wildfire and management-related burns.
AlternativeSuccession	All transitions related to successional pathways that occur in the absence of fire.
Competition/Maintenance	All transitions that occur that maintain a landscape cell in its current state class.
Development	All transitions related to the development of a landscape cell (to the 'Other' state class).
Insect/Disease	All disturbances related to insect infestations or disease outbreaks.
MixedFire	All fires of mixed severity.
NonFireDisturbances	All natural disturbances not related to fire.
NonFireManagement	All transitions related to the management of the landscape.
NonReplacementFire	All types of wildfires except for replacement fire.
PrescribedBurn	All fires related to intentional management-related burns.
ReplacementFire	All fires of stand replacement-level severity.
SurfaceFire	All fires of surface-level (mild) severity.
Wind/Weather/Stress	All natural disturbances related to weather.

Then, indicate the identity of specific transitions by clicking "Transition Type" to the left of the "Project Definitions" window (add columns for "ID" and "Description" by right-clicking on the cell in the top-left corner of the table and selecting these additional columns). Transition types are organized into these groups for later model parameterization. Transition types should be added according to Table 2.

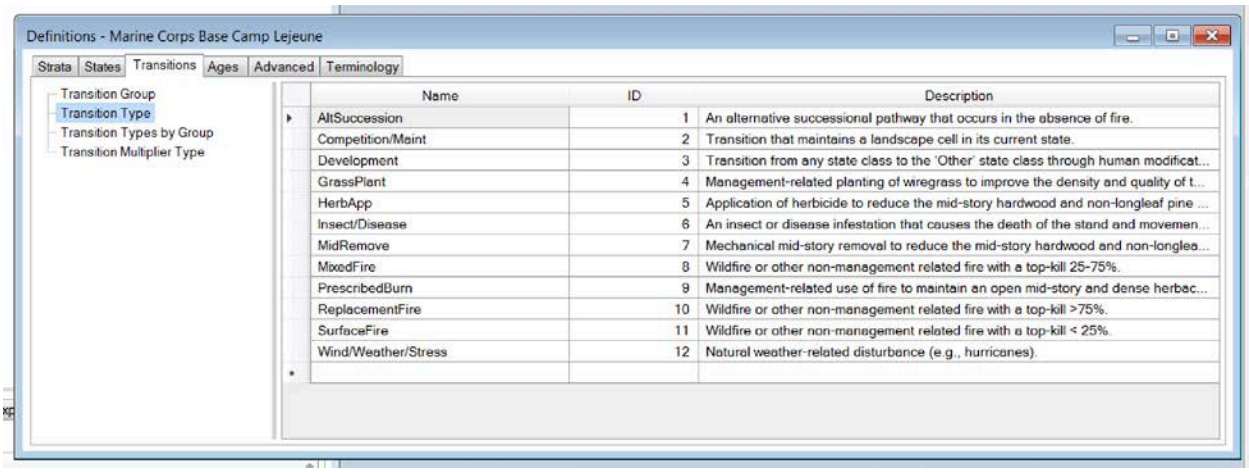

Name	ID	Description
AltSuccession	1	An alternative successional pathway that occurs in the absence of fire.
Competition/Maint	2	Transition that maintains a landscape cell in its current state.
Development	3	Transition from any state class to the 'Other' state class through human modificat...
GrassPlant	4	Management-related planting of wiregrass to improve the density and quality of t...
HerbApp	5	Application of herbicide to reduce the mid-story hardwood and non-longleaf pine ...
Insect/Disease	6	An insect or disease infestation that causes the death of the stand and movemen...
MidRemove	7	Mechanical mid-story removal to reduce the mid-story hardwood and non-longlea...
MixedFire	8	Wildfire or other non-management related fire with a top-kill 25-75%.
PrescribedBurn	9	Management-related use of fire to maintain an open mid-story and dense herbac...
ReplacementFire	10	Wildfire or other non-management related fire with a top-kill >75%.
SurfaceFire	11	Wildfire or other non-management related fire with a top-kill < 25%.
Wind/Weather/Stress	12	Natural weather-related disturbance (e.g., hurricanes).

Finally, organize the transition types into groups by clicking on "Transition Type by Group" in the "Project Definitions" window. Under "Transition Type", select the specific transition, and, under "Transition Group", select the group to which it belongs according to Table 2.

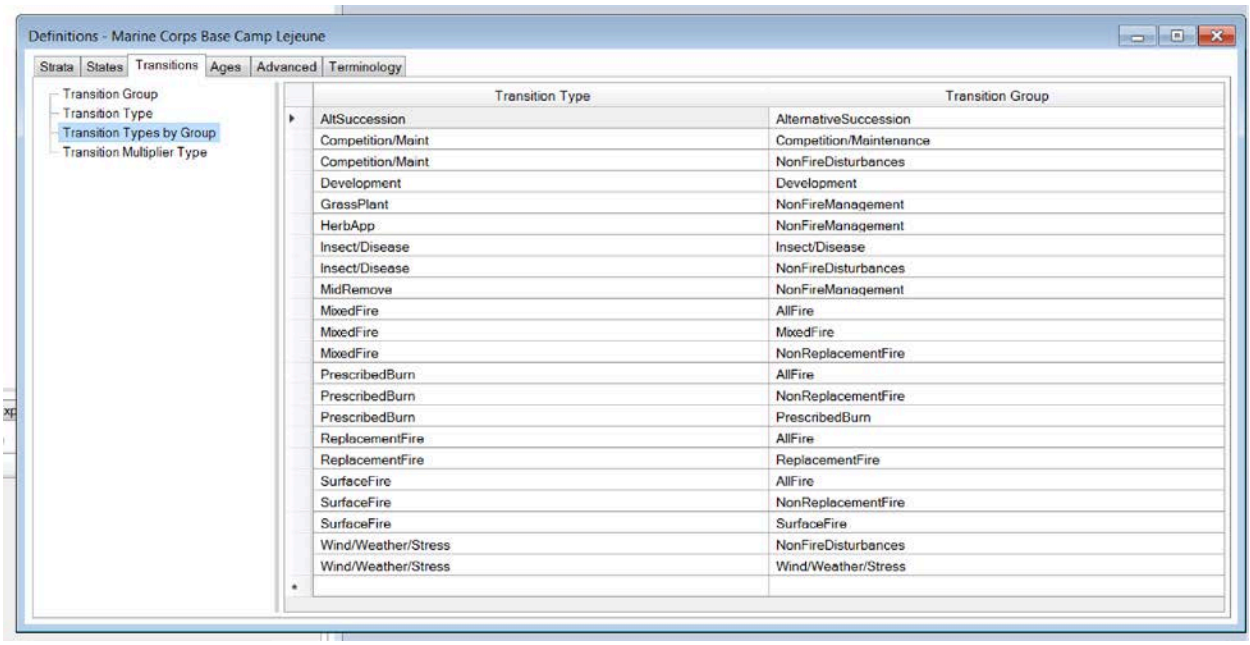

Transition Type	Transition Group
AltSuccession	AlternativeSuccession
Competition/Maint	Competition/Maintenance
Competition/Maint	NonFireDisturbances
Development	Development
GrassPlant	NonFireManagement
HerbApp	NonFireManagement
Insect/Disease	Insect/Disease
Insect/Disease	NonFireDisturbances
MidRemove	NonFireManagement
MixedFire	AllFire
MixedFire	MixedFire
MixedFire	NonReplacementFire
PrescribedBurn	AllFire
PrescribedBurn	NonReplacementFire
PrescribedBurn	PrescribedBurn
ReplacementFire	AllFire
ReplacementFire	ReplacementFire
SurfaceFire	AllFire
SurfaceFire	NonReplacementFire
SurfaceFire	SurfaceFire
Wind/Weather/Stress	NonFireDisturbances
Wind/Weather/Stress	Wind/Weather/Stress

The last project definition to define is related to the tracking and reporting of stand ages in the model. Because the age of the stand is important for the quality of nesting and foraging habitat for RCWs, we want to report stand ages with our results. Click on the “Ages” tab in the “Project Definitions” window. Click on “Age Types” and indicate that the model should age types every time step up to a maximum report age of 9,999 years. Then click on “Age Groups” and indicate groups for maximum ages of “15”, “60”, “75”, and “9999” with identical IDs. The model will thus group state classes according to age classes of $\leq$ 15 years, 15-60 years, 60-75 years, and > 75 years. Then save the project and close the “Project Definitions” window.

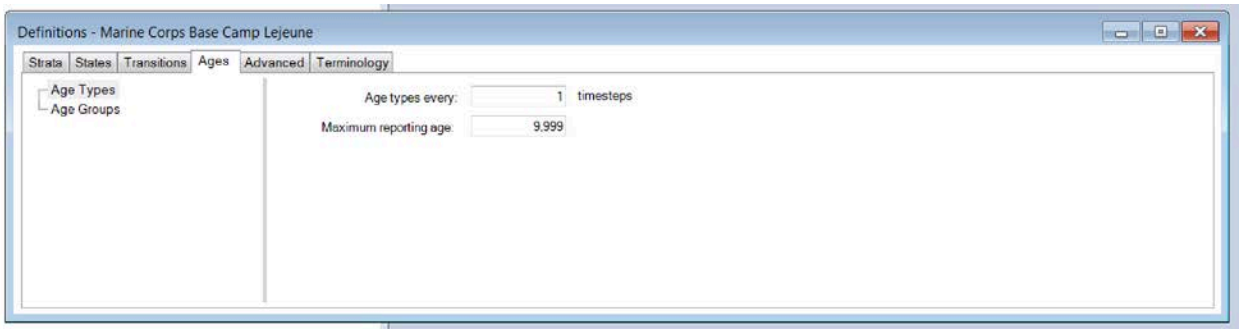

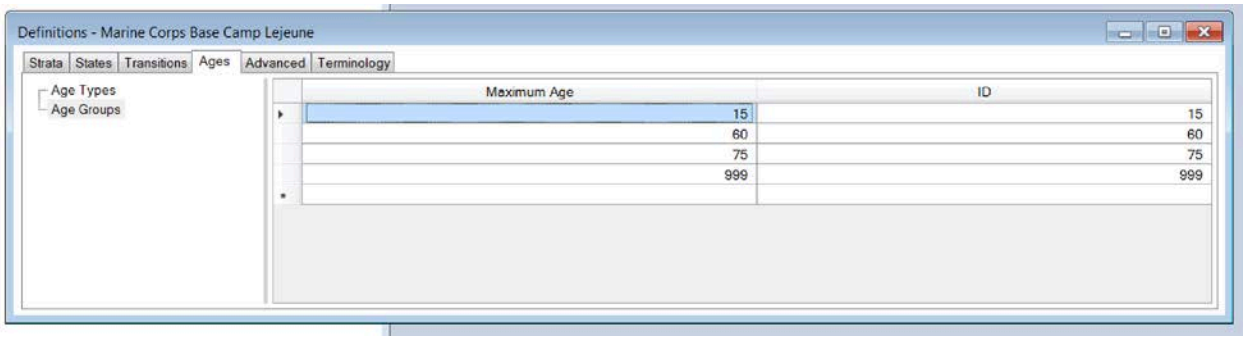

4.3 Organization of States and Transitions

Landscape cells within the ST-SIM model move from one state class to another through probabilistic or deterministic transitions. For probabilistic transitions, the user indicates the probability that a specific transition will occur for a given state class. This probability typically reflects the percentage of the landscape that will be impacted by a given transition each time step and is dependent on the availability of the state classes in which that transition is eligible to occur. In contrast, deterministic transitions always occur after some user-specified period of time or event has occurred.

Management transitions, such as Prescribed Burn, Herbicide Application, Mechanical Removal, and Grass Planting, have both probabilistic and deterministic elements in their parameterizations. These transitions are probabilistic in that they will occur only in certain state classes (where the user has given that class a probability > 0). However, we also model management actions as targets (described in *Sections 4.3.3 Fire, 4.3.4 Herbicide Treatment,* and *4.3.5 Mechanical Removal*). This allows the user to specify the area over which each management action will be applied on the landscape.

In the remainder of this section, we will describe the transitions that were simulated in the Baseline Scenario in more detail as well as how those transitions link the landscape states. This scenario is based on current landscape conditions (2014 LANDFIRE products) and management regimes at MCBCL.

4.3.1 Deterministic Transitions (Succession and Aging)

To visually organize state classes and connect those classes through the transitions described in the previous section, begin by creating a new scenario within the main project by right-clicking on the project name (“Marine Corps Base Camp Lejeune”) in the “Libraries” window and selecting “New” and “Scenario”.

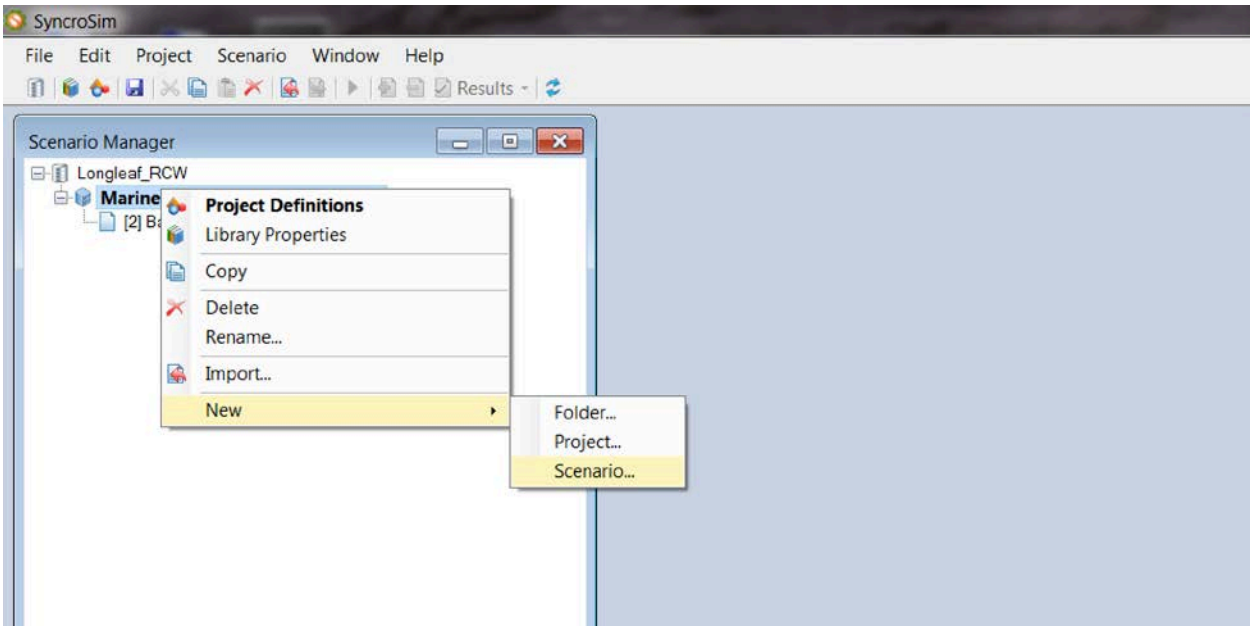

The “New Scenario” window will appear, where the user can name the scenario, indicate the author, and add any pertinent information pertaining to the scenario. In this first scenario, we will be modeling baseline conditions and management targets, so we named this scenario “Baseline”.

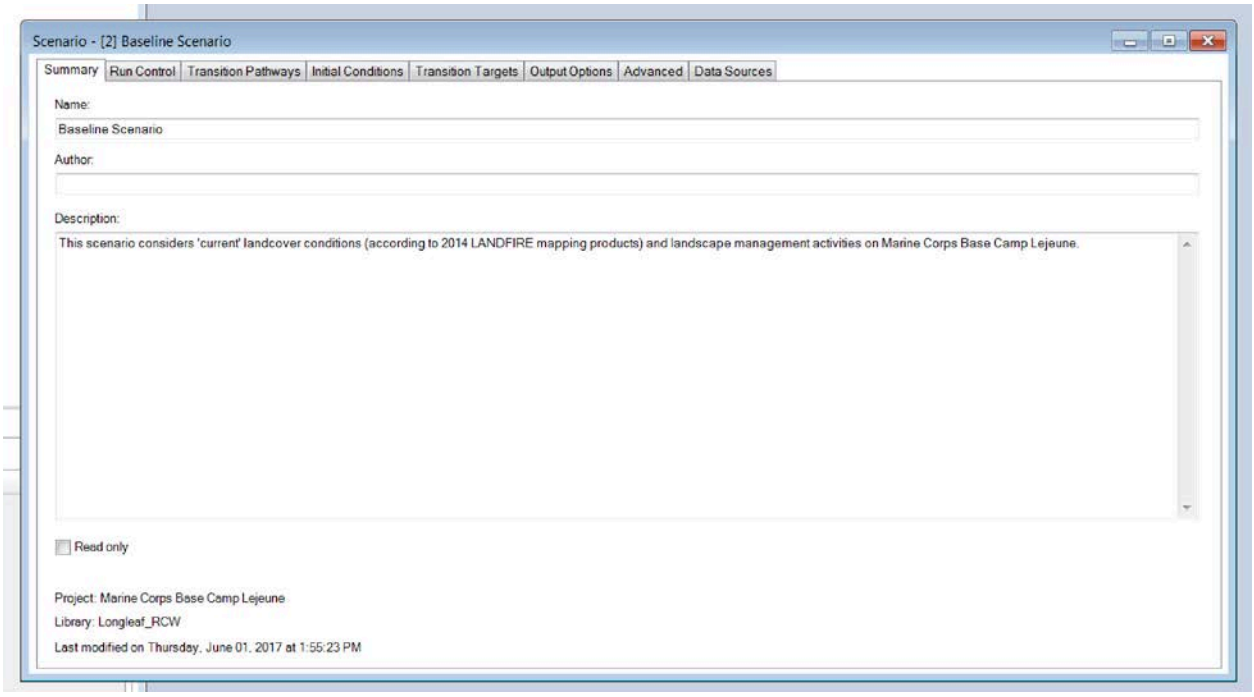

Then, double-click the scenario name in the “Libraries” window to open the scenario’s input window. Click on the “Transitions Pathways” tab, and select the “UplandLong” stratum worksheet at the bottom of the window. Right-click anywhere in this window, and select “Add State Class…”. The “Add State Class” window will appear where the Cover Type and appropriate Structural Stage can be selected.

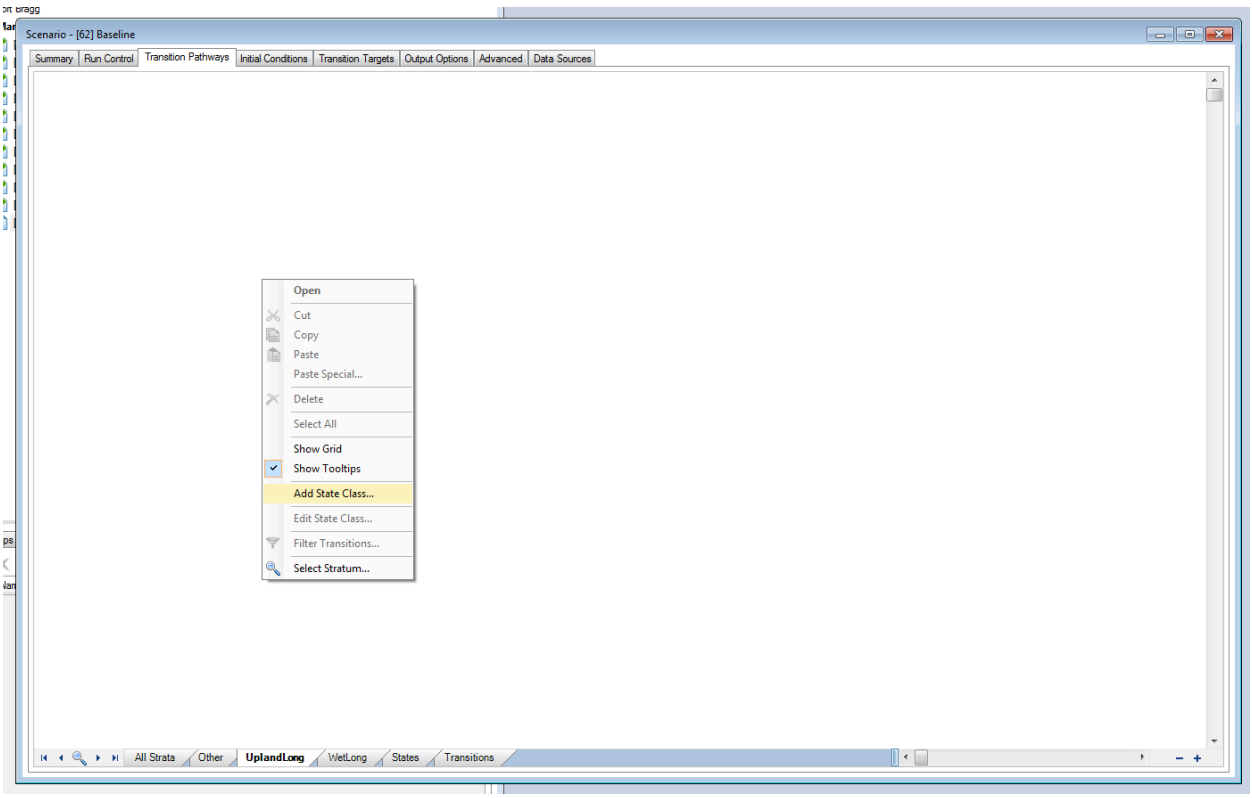

Select a Cover Type with its appropriate Structural Stage (e.g., Bare: ALL). A small gray box will appear representing the state class. This box can be moved and organized based on the user’s preference by clicking on the box and dragging it to a more suitable location.

The top line of each box represents the Cover Type, the middle line represents the Structural Stage, and the bottom line represents the Age Class that landscape cells of that Cover and Structural Type must fall within (Figure 2).

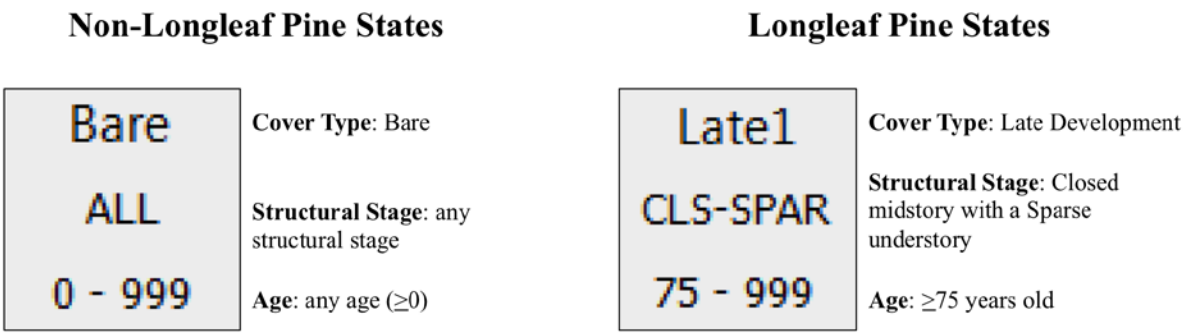

Figure 2. Information contained in the landscape state boxes in ST-SIM.

You will repeat the process for adding states until all states described in *Section 4.1 Landscape States* have been added to this screen.

We will now add deterministic transitions to link relevant state classes. These transitions tend to be related to aging. Go to the States tab at the bottom of the Transition Pathways tab. In the first row, select "UplandLong" under Vegetation Type, "Bare:ALL" under From Class, "Bare:ALL" under To Class, "0" under Age Min, "999" under Age Max, and "A4" under Location. This signifies that, in the absence of a probabilistic transition, a landscape cell classified as Bare:ALL will remain in that state class permanently. The Location simply specifies the position of that state class in the Transition Pathways window.

In the second row, select "UplandLong" under Vegetation Type, "Mid1:CLS-SPAR" under From Class, "Late1:CLS-SPAR" under To Class, "15" under Age Min, "74" under Age Max, and "B1" under Location. This indicates that, in the absence of a probabilistic transition, a landscape cell in the Mid-Development/Closed-Sparse state class will remain in that age class as long as the stand's age is between 15 and 74 years old. After the stand reaches 75 years old, the state class will then transition to the Late-Development/Closed-Sparse state class. Generally, the longleaf pine states will remain on the same successional pathway (Closed-Sparse vs. Open-Sparse vs. Open-Dense) in the absence of a probabilistic transition.

Repeat this process for every deterministic transition shown in the screenshot in Figure 3.

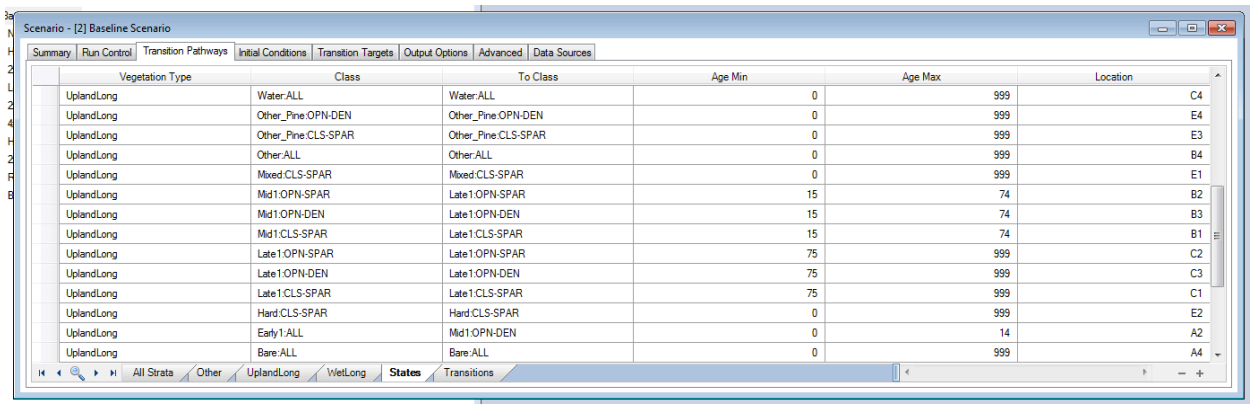

Scenario - [2] Baseline Scenario

Summary | Run Control | Transition Pathways | Initial Conditions | Transition Targets | Output Options | Advanced | Data Sources

Vegetation Type	Class	To Class	Age Min	Age Max	Location
UplandLong	Water:ALL	Water:ALL	0	999	C4
UplandLong	Other_Pine:OPN-DEN	Other_Pine:OPN-DEN	0	999	E4
UplandLong	Other_Pine:CLS-SPAR	Other_Pine:CLS-SPAR	0	999	E3
UplandLong	Other:ALL	Other:ALL	0	999	B4
UplandLong	Mixed:CLS-SPAR	Mixed:CLS-SPAR	0	999	E1
UplandLong	Mid1:OPN-SPAR	Late1:OPN-SPAR	15	74	B2
UplandLong	Mid1:OPN-DEN	Late1:OPN-DEN	15	74	B3
UplandLong	Mid1:CLS-SPAR	Late1:CLS-SPAR	15	74	B1
UplandLong	Late1:OPN-SPAR	Late1:OPN-SPAR	75	999	C2
UplandLong	Late1:OPN-DEN	Late1:OPN-DEN	75	999	C3
UplandLong	Late1:CLS-SPAR	Late1:CLS-SPAR	75	999	C1
UplandLong	Hard:CLS-SPAR	Hard:CLS-SPAR	0	999	E2
UplandLong	Early1:ALL	Mid1:OPN-DEN	0	14	A2
UplandLong	Bare:ALL	Bare:ALL	0	999	A4

All Strata | Other | UplandLong | WetLong | States | Transitions

Figure 3. Deterministic transitions between state classes present in the model for the Upland Longleaf Pine (UplandLong) Vegetation Type at Marine Corps Base Camp Lejeune.

Click on the “UplandLong” tab at the bottom of the “Transition Pathways” tab. You should now see all state classes present in the Upland Longleaf Pine Vegetation Type linked through green arrows depicting deterministic transitions

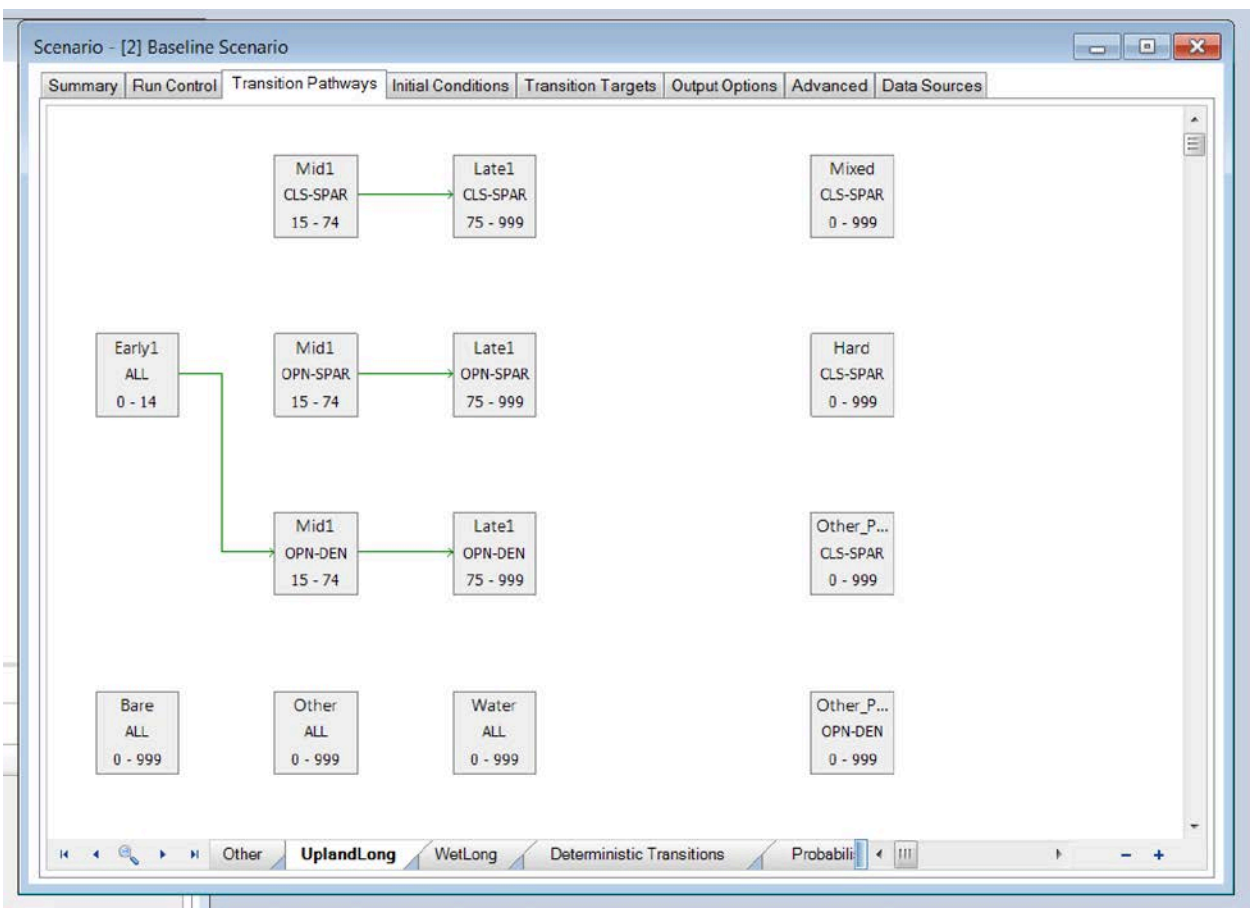

Repeat this process for both the Wet Longleaf Pine (WetLong) and Other Vegetation Types according to Figures 4 and 5.

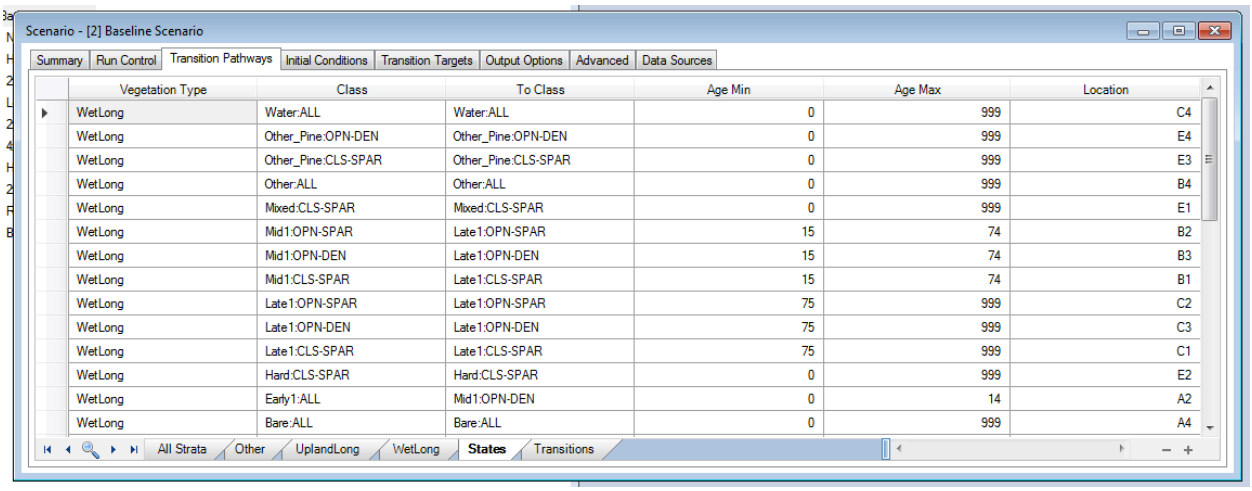

Scenario - [2] Baseline Scenario

Summary | Run Control | Transition Pathways | Initial Conditions | Transition Targets | Output Options | Advanced | Data Sources

Vegetation Type	Class	To Class	Age Min	Age Max	Location
WetLong	Water:ALL	Water:ALL	0	999	C4
WetLong	Other_Pine:OPN-DEN	Other_Pine:OPN-DEN	0	999	E4
WetLong	Other_Pine:CLS-SPAR	Other_Pine:CLS-SPAR	0	999	E3
WetLong	Other:ALL	Other:ALL	0	999	B4
WetLong	Mixed:CLS-SPAR	Mixed:CLS-SPAR	0	999	E1
WetLong	Mid1:OPN-SPAR	Late1:OPN-SPAR	15	74	B2
WetLong	Mid1:OPN-DEN	Late1:OPN-DEN	15	74	B3
WetLong	Mid1:CLS-SPAR	Late1:CLS-SPAR	15	74	B1
WetLong	Late1:OPN-SPAR	Late1:OPN-SPAR	75	999	C2
WetLong	Late1:OPN-DEN	Late1:OPN-DEN	75	999	C3
WetLong	Late1:CLS-SPAR	Late1:CLS-SPAR	75	999	C1
WetLong	Hard:CLS-SPAR	Hard:CLS-SPAR	0	999	E2
WetLong	Early1:ALL	Mid1:OPN-DEN	0	14	A2
WetLong	Bare:ALL	Bare:ALL	0	999	A4

All Strata | Other | UplandLong | WetLong | States | Transitions

Figure 4. Deterministic transitions between state classes present in the model for the Wet Longleaf Pine (WetLong) Vegetation Type at Marine Corps Base Camp Lejeune.

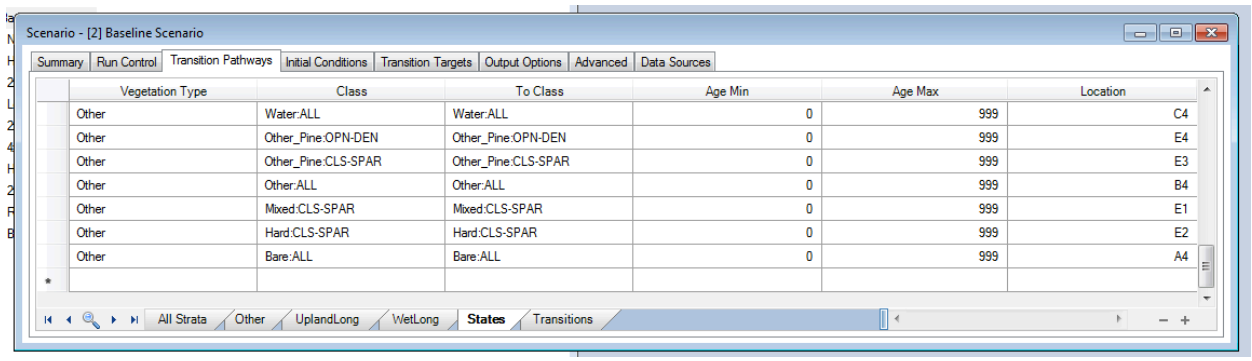

Scenario - [2] Baseline Scenario

Summary | Run Control | Transition Pathways | Initial Conditions | Transition Targets | Output Options | Advanced | Data Sources

Vegetation Type	Class	To Class	Age Min	Age Max	Location
Other	Water:ALL	Water:ALL	0	999	C4
Other	Other_Pine:OPN-DEN	Other_Pine:OPN-DEN	0	999	E4
Other	Other_Pine:CLS-SPAR	Other_Pine:CLS-SPAR	0	999	E3
Other	Other:ALL	Other:ALL	0	999	B4
Other	Mixed:CLS-SPAR	Mixed:CLS-SPAR	0	999	E1
Other	Hard:CLS-SPAR	Hard:CLS-SPAR	0	999	E2
Other	Bare:ALL	Bare:ALL	0	999	A4

All Strata | Other | UplandLong | WetLong | States | Transitions

Figure 5. Deterministic transitions between state classes present in the model for the Other (Other) Vegetation Type at Marine Corps Base Camp Lejeune.

4.3.2 Alternative Succession in the Absence of Disturbance

Our model (and the original LANDFIRE models) includes two main successional pathways: (1) where frequent disturbance maintains an open midstory condition and a dense understory as well as (2) where infrequent disturbance creates closed midstory and sparse understory conditions. Aging, disturbance, and succession will cause a landscape cell's state class to move among these pathways (Figures 6-7).

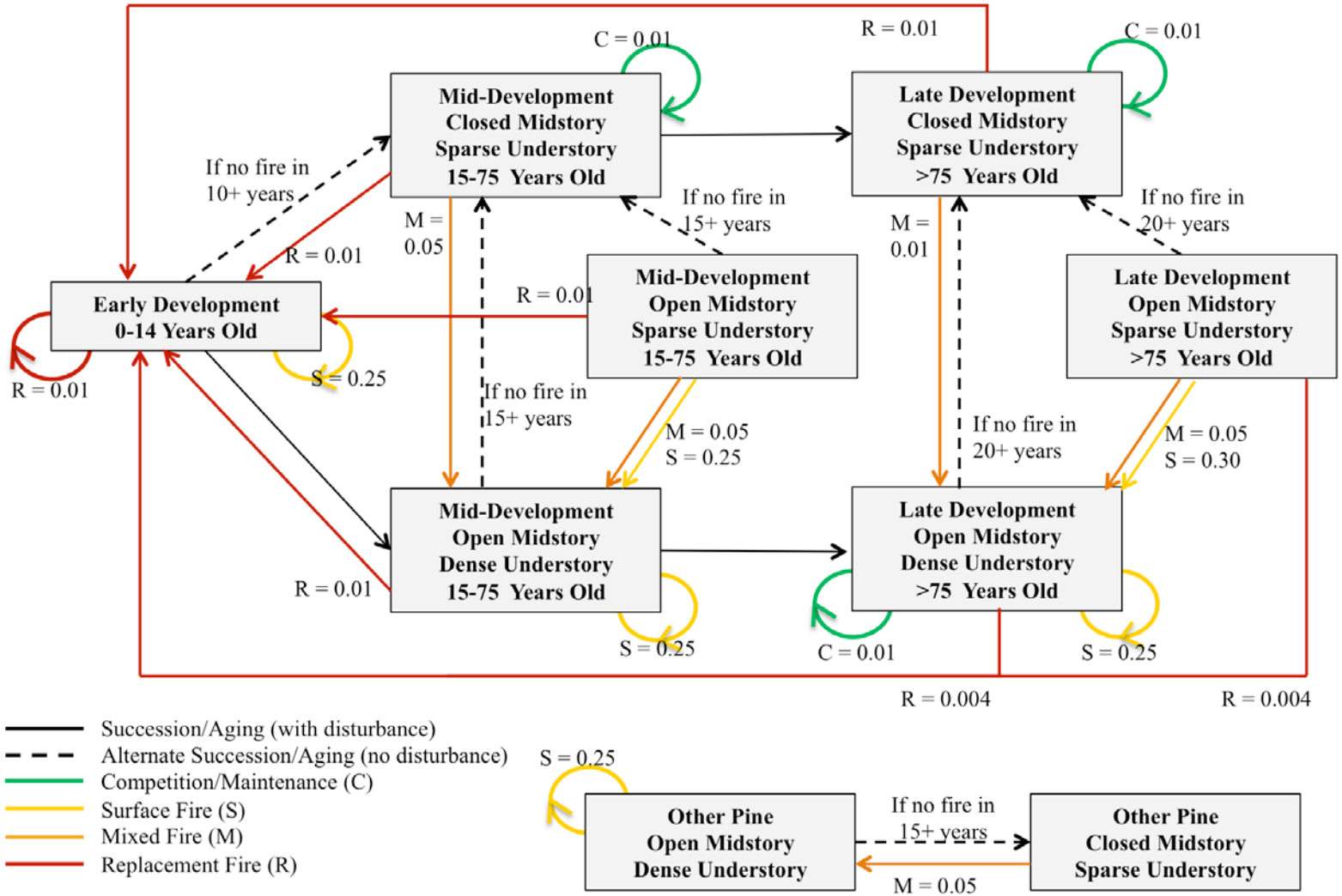

Figure 6. State classes and transitions (with probabilities) related to succession, aging, and wildfires for longleaf pine and other pine state classes in the *Atlantic Coastal Plain Upland Longleaf Pine* (DryLong) and *Other* biophysical setting (or vegetation type) at Marine Corps Base Camp Lejeune. Additional possible state classes not shown include: Bare Land, Other, Hardwood, Mixed, and Water. The *Other* biophyscial setting does not include transitions for longleaf pine states (e.g., Mid-Development1:OPN-DEN; etc.).

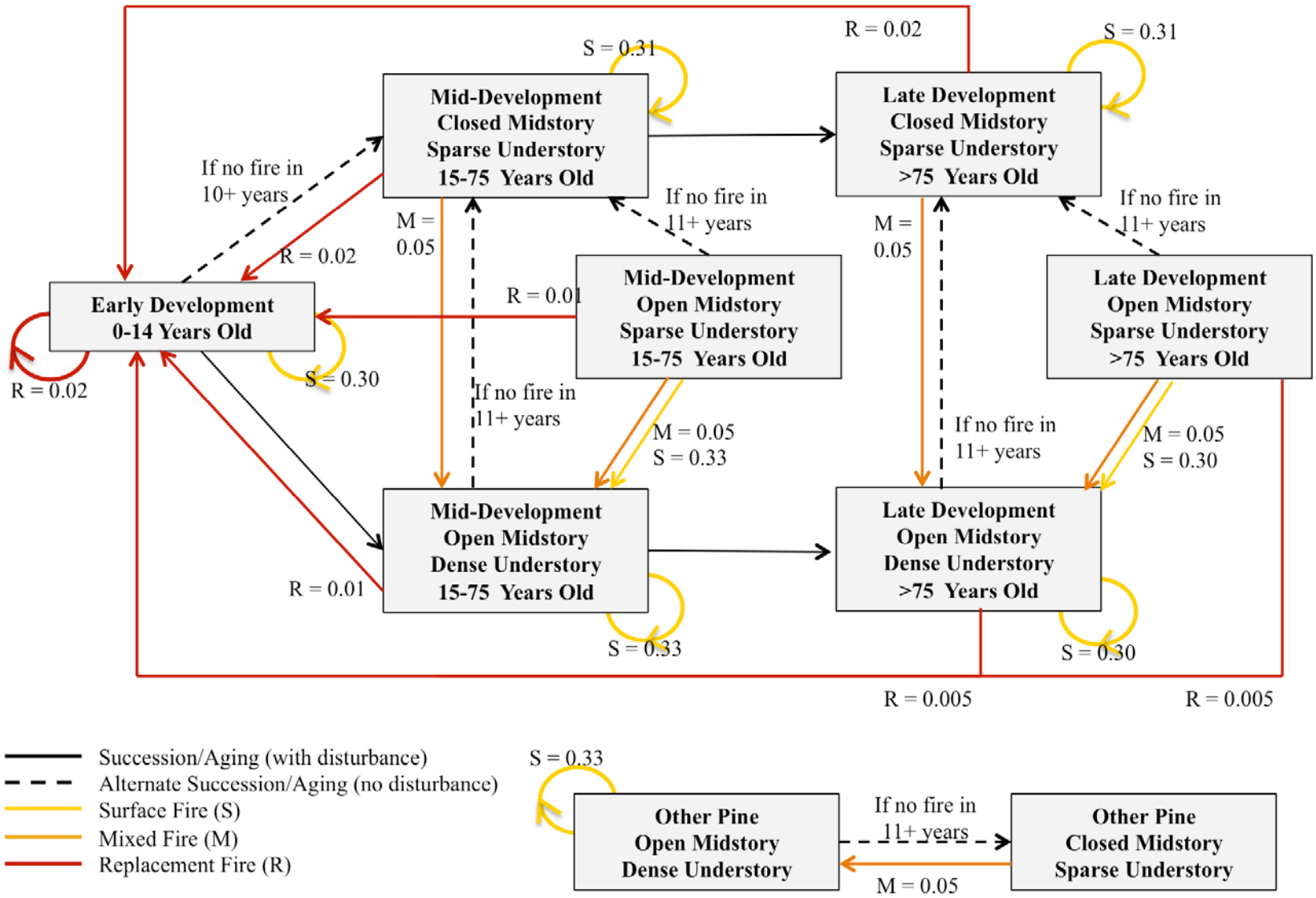

Figure 7. State classes and transitions (with probabilities) related to succession, aging, and wildfires for longleaf pine and other pine state classes in the *Central Atlantic Coastal Plain Wet Longleaf Pine* (WetLong) biophysical setting (or vegetation type) at Marine Corps Base Camp Lejeune. Additional possible state classes not shown include: Bare Land, Other, Hardwood, Mixed, and Water.

We assume that succession only occurs in the absence of management and disturbances. To create this condition in ST-SIM, go to the “Advanced” tab in the “Baseline Scenario”, click the “+” icon next to “Time-Since-Transition” in the list on the left side of this screen, and select “Time-Since-Transition Group”. Then, create separate rows for each of the following Transition Types: “AltSuccession”, “Competition/Maint”, “Insect/Disease”, “MixedFire”, “ReplacementFire”, “SurfaceFire”, and “Wind/Weather/Stress”. In each of these rows, add “AllFire” as the Transition Group.

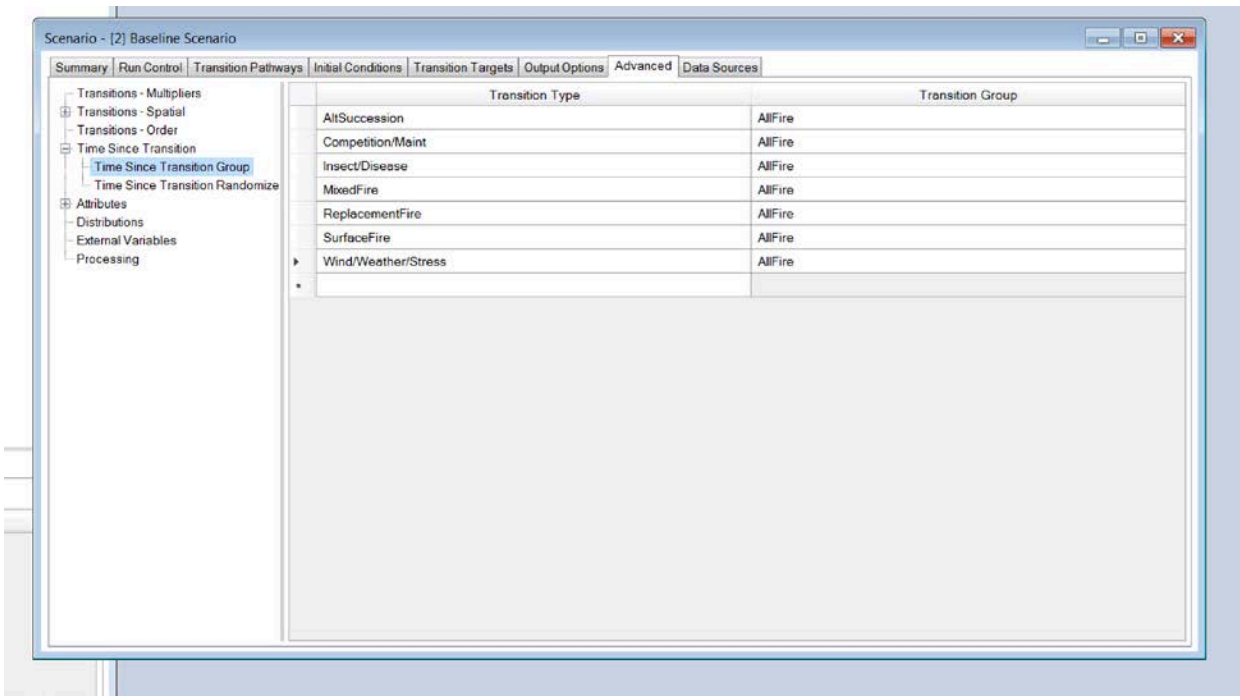

Changes related to succession in the presence of fire (i.e., pathway 1) have already been added to the model. Changes related to succession in the absence of fire or other disturbances (i.e., pathway 2) are added to the model as Alternative Succession. Go back to the Transitions Pathways tab in the Baseline Scenario window, and select the Transitions tab at the bottom of the window. Here, you will add an entry for each transition depicted by the dashed black lines in Figures 6-7.

For example (highlighted in Figure 8), to depict the transition from Mid-Development1: Open-Dense to Mid-Development1: Closed-Sparse in the *Atlantic Coastal Plain Upland Longleaf Pine* biophysical setting, you would select “UplandLong” as the From Vegetation Type and To Vegetation Type; “Mid1:OPN-DEN” as the From Class; “Mid1:CLS-SPAR” as the To Class; and “AltSuccession” as the Transition Type. Type “1.00” for both the Probability and Proportion; “15” for Age Min; “74” for Age Max; “0” for Age Shift; “Yes” for Age Reset; “15” for TST Min; “9999” for TST Max; and “-9999” for TST Shift. This indicates that all longleaf pine stands between the ages of 15 and 74 in the Mid-Development1: Open-Dense state class (within the Upland Longleaf Pine biophysical setting) will transition to the Mid-Development1:

Closed-Sparse class with certainty if a fire (or other relevant disturbance) does not occur in 15 or more years. If this transition occurs, the age of the stand will remain as is (and will not revert to 0).

Repeat this process for all 17 transitions related to Alternate Succession (dashed lines in Figures 6-7) as shown in Figure 8. State classes for Bare Land, Other, Hardwood, Mixed, and Water do not experience succession in this model, and the Alternative Succession transition will not be added as probabilistic transitions for these states.

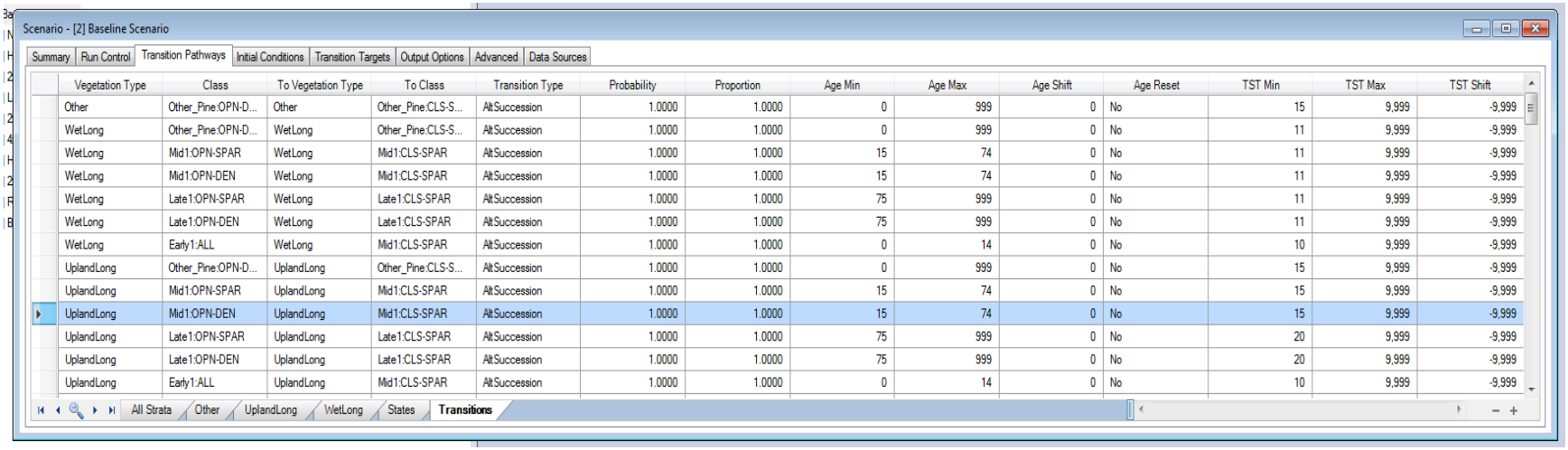

Scenario - [2] Baseline Scenario

Summary | Run Control | Transition Pathways | Initial Conditions | Transition Targets | Output Options | Advanced | Data Sources

Vegetation Type	Class	To Vegetation Type	To Class	Transition Type	Probability	Proportion	Age Min	Age Max	Age Shift	Age Reset	TST Min	TST Max	TST Shift
Other	Other_Pine:OPN-D...	Other	Other_Pine:CLS-S...	AltSuccession	1.0000	1.0000	0	999	0	No	15	9,999	-9,999
WetLong	Other_Pine:OPN-D...	WetLong	Other_Pine:CLS-S...	AltSuccession	1.0000	1.0000	0	999	0	No	11	9,999	-9,999
WetLong	Mid1:OPN-SPAR	WetLong	Mid1:CLS-SPAR	AltSuccession	1.0000	1.0000	15	74	0	No	11	9,999	-9,999
WetLong	Mid1:OPN-DEN	WetLong	Mid1:CLS-SPAR	AltSuccession	1.0000	1.0000	15	74	0	No	11	9,999	-9,999
WetLong	Late1:OPN-SPAR	WetLong	Late1:CLS-SPAR	AltSuccession	1.0000	1.0000	75	999	0	No	11	9,999	-9,999
WetLong	Late1:OPN-DEN	WetLong	Late1:CLS-SPAR	AltSuccession	1.0000	1.0000	75	999	0	No	11	9,999	-9,999
WetLong	Early1:ALL	WetLong	Mid1:CLS-SPAR	AltSuccession	1.0000	1.0000	0	14	0	No	10	9,999	-9,999
UplandLong	Other_Pine:OPN-D...	UplandLong	Other_Pine:CLS-S...	AltSuccession	1.0000	1.0000	0	999	0	No	15	9,999	-9,999
UplandLong	Mid1:OPN-SPAR	UplandLong	Mid1:CLS-SPAR	AltSuccession	1.0000	1.0000	15	74	0	No	15	9,999	-9,999
UplandLong	Mid1:OPN-DEN	UplandLong	Mid1:CLS-SPAR	AltSuccession	1.0000	1.0000	15	74	0	No	15	9,999	-9,999
UplandLong	Late1:OPN-SPAR	UplandLong	Late1:CLS-SPAR	AltSuccession	1.0000	1.0000	75	999	0	No	20	9,999	-9,999
UplandLong	Late1:OPN-DEN	UplandLong	Late1:CLS-SPAR	AltSuccession	1.0000	1.0000	75	999	0	No	20	9,999	-9,999
UplandLong	Early1:ALL	UplandLong	Mid1:CLS-SPAR	AltSuccession	1.0000	1.0000	0	14	0	No	10	9,999	-9,999

All Strata | Other | UplandLong | WetLong | States | Transitions

Figure 8. Probabilistic transitions between state classes related to alternative successional pathways (i.e., successional that occurs in the absence of fire and other disturbances) in *Atlantic Coastal Plain Upland Longleaf Pine* (UplandLong), *Central Atlantic Coastal Plain Wet Longleaf Pine* (WetLong), and *Other* biophyscial settings present in the model for Marine Corps Base Camp Lejeune.

4.3.3 Fire

The longleaf pine ecosystem is highly adapted to and dependent on fire. In the ST-SIM model (and in the original LANDFIRE model), we assumed that landscape experienced fires as wildfires (i.e., occurring through lightning strikes, vandalism, or other means; Figures 6-7) and as prescribed burns intentionally initiated as part of a management protocol (Figure 9).

In the model, wildfires can occur at high (replacement), medium (mixed), or low (surface) intensities depending on the preceding period of fire suppression as reflected in the current state of the stand (Figures 6-7). Low intensity surface fires typically maintain the landscape cell in its current state. In contrast, high intensity replacement fires tend to revert landscape cells back to an open, early successional state (Figure 6-7).

Wildfires are added to the model as probabilistic transitions. To add this transition, open the Transitions tab at the bottom of the Transition Pathways screen. You will then add a row for each transition related to wildfires for each state class, biophysical setting, and wildfire type. For example (highlighted in Figure 9), to depict the transition that would occur if a surface fire burned a landscape cell in the state Late Development1: Open-Dense in the *Central Atlantic Coastal Plain Wet Longleaf Pine* biophysical setting, you would select “WetLong” as the From Vegetation Type and To Vegetation Type; “Late1:OPN-DEN” as the From Class; “Late1:OPN-DEN” as the To Class; and “SurfaceFire” as the Transition Type. Type “0.3” for Probability; “1.0” for Proportion; “75” for Age Min; “999” for Age Max; “0” for Age Shift; “No” for Age Reset; “0” for TST Min; “9999” for TST Max; and “-9999” for TST Shift. This indicates that all longleaf pine stands > 75 years old in the Late Development1: Open-Dense state class (within the Wet Longleaf Pine biophysical setting) have a 30% chance of experiencing a surface fire in any given year of a model simulation. If a surface fire does occur, the landscape cell will remain in its current state, and the stand age will remain as is (and will not revert to 0). For this transition and landscape state, it does not matter if another disturbance has impacted the landscape cell (hence, the range from 0 to 9999 for TST Min and TST Max).

Repeat this process for all 15 Surface Fire transitions (yellow lines in Figures 6-7) as shown in Figure 10. Mixed fires (orange lines in Figures 6-7) and replacement fires (red lines in Figures 6-7) are added in a similar manner according to Figure 11 and Figure 12, respectively. Note the differences in values for transition probabilities by landscape states. This indicates that some landscape states are more likely than others to experience each wildfire type, and landscape cells in states with higher probabilities will be more likely to experience each type of wildfire compared to cells in states with lower probabilities. These probabilities were derived for the original LANDFIRE models through expert opinion. State classes for Bare Land, Other, Hardwood, Mixed, and Water do not experience surface fires in this model.

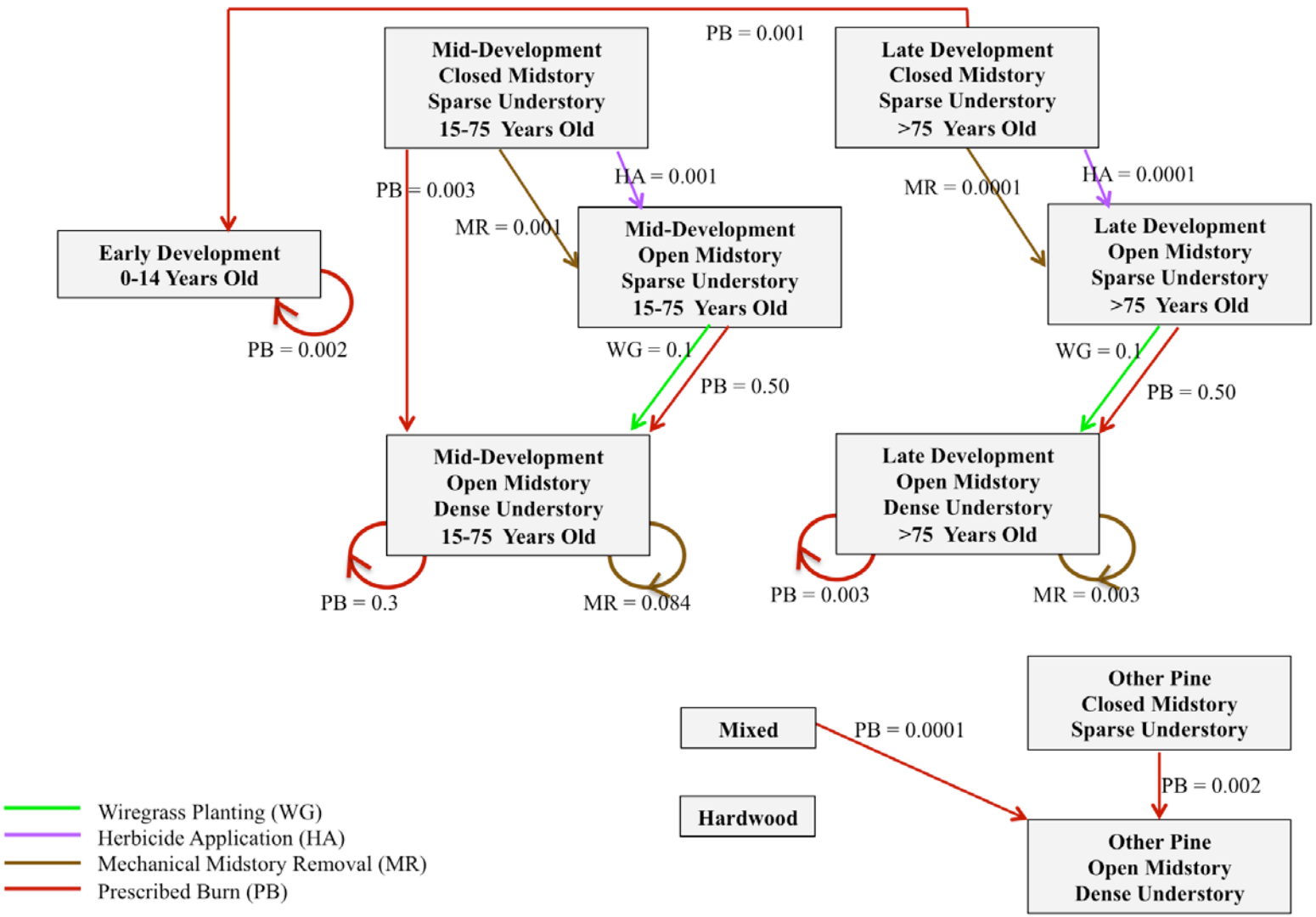

Figure 9. Transitions between state classes related to management techniques typically employed at Marine Corps Base Camp Lejeune. Management transitions included in the ST-SIM model include prescribed burns, herbicide application, mechanical midstory removal and wiregrass planting. These transitions occurred in an identical fashion for landscape cells in the *Atlantic Coastal Plain Upland Longleaf Pine* (UplandLong), *Central Atlantic Coastal Plain Wet Longleaf Pine* (WetLong), and *Other* biophyscial settings.

Scenario - [2] Baseline Scenario

Summary | Run Control | Transition Pathways | Initial Conditions | Transition Targets | Output Options | Advanced | Data Sources

Vegetation Type	Class	To Vegetation Type	To Class	Transition Type	Probability	Proportion	Age Min	Age Max	Age Shift	Age Reset	TST Min	TST Max	TST Shift
Other	Other_Pine:OPN-D...	Other	Other_Pine:OPN-D...	SurfaceFire	0.2500	1.0000	0	999	0	No	0	9,999	-9,999
WetLong	Other_Pine:OPN-D...	WetLong	Other_Pine:OPN-D...	SurfaceFire	0.3300	1.0000	0	999	0	No	0	9,999	-9,999
WetLong	Mid1:OPN-SPAR	WetLong	Mid1:OPN-DEN	SurfaceFire	0.3300	1.0000	15	74	0	No	0	9,999	-9,999
WetLong	Mid1:OPN-DEN	WetLong	Mid1:OPN-DEN	SurfaceFire	0.3300	1.0000	15	74	0	No	0	9,999	-9,999
WetLong	Mid1:CLS-SPAR	WetLong	Mid1:CLS-SPAR	SurfaceFire	0.3100	1.0000	15	74	0	No	0	9,999	-9,999
WetLong	Late1:OPN-SPAR	WetLong	Late1:OPN-DEN	SurfaceFire	0.3000	1.0000	75	999	0	No	0	9,999	-9,999
WetLong	Late1:OPN-DEN	WetLong	Late1:OPN-DEN	SurfaceFire	0.3000	1.0000	75	999	0	No	0	9,999	-9,999
WetLong	Late1:CLS-SPAR	WetLong	Late1:CLS-SPAR	SurfaceFire	0.3100	1.0000	75	999	0	No	0	9,999	-9,999
WetLong	Early1:ALL	WetLong	Early1:ALL	SurfaceFire	0.3000	1.0000	0	14	-999	Yes	0	9,999	-9,999
UplandLong	Other_Pine:OPN-D...	UplandLong	Other_Pine:OPN-D...	SurfaceFire	0.2500	1.0000	0	999	0	No	0	9,999	-9,999
UplandLong	Mid1:OPN-SPAR	UplandLong	Mid1:OPN-DEN	SurfaceFire	0.2500	1.0000	15	74	0	No	0	9,999	-9,999
UplandLong	Mid1:OPN-DEN	UplandLong	Mid1:OPN-DEN	SurfaceFire	0.2500	1.0000	15	74	0	No	0	9,999	-9,999
UplandLong	Late1:OPN-SPAR	UplandLong	Late1:OPN-DEN	SurfaceFire	0.2500	1.0000	75	999	0	No	0	9,999	-9,999
UplandLong	Late1:OPN-DEN	UplandLong	Late1:OPN-DEN	SurfaceFire	0.2500	1.0000	75	999	0	No	0	9,999	-9,999
UplandLong	Early1:ALL	UplandLong	Early1:ALL	SurfaceFire	0.2500	1.0000	0	14	-999	Yes	0	9,999	-9,999

All Strata | Other | UplandLong | WetLong | States | Transitions

Figure 10. Probabilistic transitions between state classes related to the surface fire transition in *Atlantic Coastal Plain Upland Longleaf Pine* (UplandLong), *Central Atlantic Coastal Plain Wet Longleaf Pine* (WetLong), and *Other* biophyscial settings present in the model for Marine Corps Base Camp Lejeune.

Scenario - [2] Baseline Scenario

Summary | Run Control | Transition Pathways | Initial Conditions | Transition Targets | Output Options | Advanced | Data Sources

Vegetation Type	Class	To Vegetation Type	To Class	Transition Type	Probability	Proportion	Age Min	Age Max	Age Shift	Age Reset	TST Min	TST Max	TST Shift
Other	Other_Pine:CLS-S...	Other	Other_Pine:OPN-D...	MixedFire	0.0500	1.0000	0	999	0	No	0	9,999	-9,999
WetLong	Other_Pine:CLS-S...	WetLong	Other_Pine:OPN-D...	MixedFire	0.0500	1.0000	0	999	0	No	0	9,999	-9,999
WetLong	Mid1:OPN-SPAR	WetLong	Mid1:OPN-DEN	MixedFire	0.0500	1.0000	15	74	0	No	0	9,999	-9,999
WetLong	Mid1:CLS-SPAR	WetLong	Mid1:OPN-DEN	MixedFire	0.0500	1.0000	15	74	0	No	0	9,999	-9,999
WetLong	Late1:OPN-SPAR	WetLong	Late1:OPN-DEN	MixedFire	0.0500	1.0000	75	999	0	No	0	9,999	-9,999
WetLong	Late1:CLS-SPAR	WetLong	Late1:OPN-DEN	MixedFire	0.0500	1.0000	75	999	0	No	0	9,999	-9,999
UplandLong	Other_Pine:CLS-S...	UplandLong	Other_Pine:OPN-D...	MixedFire	0.0500	1.0000	0	999	0	No	0	9,999	-9,999
UplandLong	Mid1:OPN-SPAR	UplandLong	Mid1:OPN-DEN	MixedFire	0.0500	1.0000	15	74	0	No	0	9,999	-9,999
UplandLong	Mid1:CLS-SPAR	UplandLong	Mid1:OPN-DEN	MixedFire	0.0500	1.0000	15	74	0	No	0	9,999	-9,999
UplandLong	Late1:OPN-SPAR	UplandLong	Late1:OPN-DEN	MixedFire	0.0100	1.0000	75	999	0	No	0	9,999	-9,999
UplandLong	Late1:CLS-SPAR	UplandLong	Late1:OPN-DEN	MixedFire	0.0100	1.0000	75	999	0	No	0	9,999	-9,999

All Strata | Other | UplandLong | WetLong | States | Transitions

Figure 11. Probabilistic transitions between state classes related to the mixed fire transition in *Atlantic Coastal Plain Upland Longleaf Pine* (UplandLong), *Central Atlantic Coastal Plain Wet Longleaf Pine* (WetLong), and *Other* biophyscial settings present in the model for Marine Corps Base Camp Lejeune.

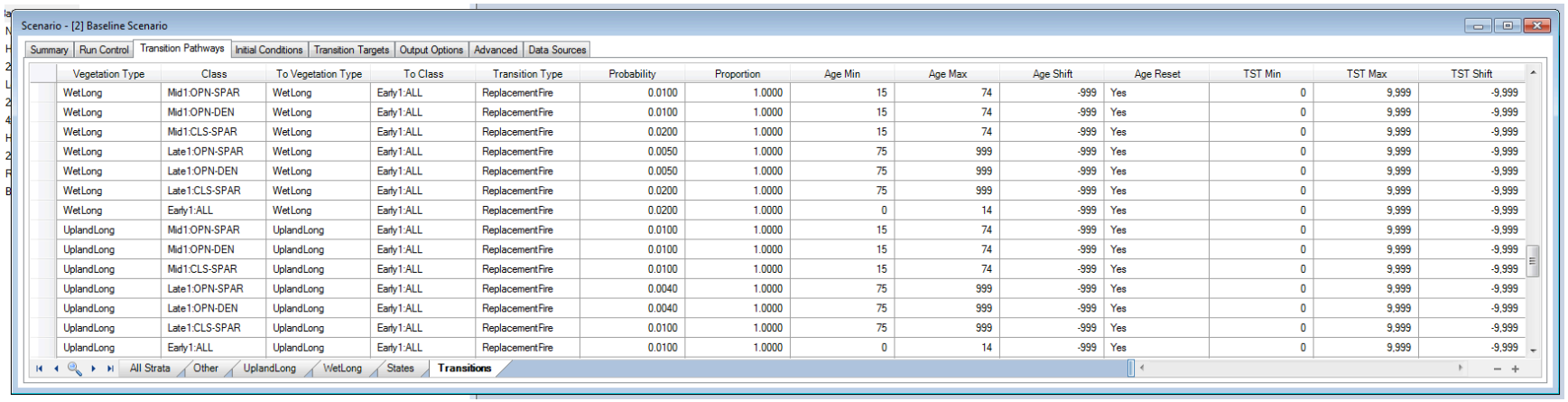

Scenario - [2] Baseline Scenario

Summary | Run Control | Transition Pathways | Initial Conditions | Transition Targets | Output Options | Advanced | Data Sources

Vegetation Type	Class	To Vegetation Type	To Class	Transition Type	Probability	Proportion	Age Min	Age Max	Age Shift	Age Reset	TST Min	TST Max	TST Shift
WetLong	Mid1:OPN-SPAR	WetLong	Early1:ALL	ReplacementFire	0.0100	1.0000	15	74	-999	Yes	0	9,999	-9,999
WetLong	Mid1:OPN-DEN	WetLong	Early1:ALL	ReplacementFire	0.0100	1.0000	15	74	-999	Yes	0	9,999	-9,999
WetLong	Mid1:CLS-SPAR	WetLong	Early1:ALL	ReplacementFire	0.0200	1.0000	15	74	-999	Yes	0	9,999	-9,999
WetLong	Late1:OPN-SPAR	WetLong	Early1:ALL	ReplacementFire	0.0050	1.0000	75	999	-999	Yes	0	9,999	-9,999
WetLong	Late1:OPN-DEN	WetLong	Early1:ALL	ReplacementFire	0.0050	1.0000	75	999	-999	Yes	0	9,999	-9,999
WetLong	Late1:CLS-SPAR	WetLong	Early1:ALL	ReplacementFire	0.0200	1.0000	75	999	-999	Yes	0	9,999	-9,999
WetLong	Early1:ALL	WetLong	Early1:ALL	ReplacementFire	0.0200	1.0000	0	14	-999	Yes	0	9,999	-9,999
UplandLong	Mid1:OPN-SPAR	UplandLong	Early1:ALL	ReplacementFire	0.0100	1.0000	15	74	-999	Yes	0	9,999	-9,999
UplandLong	Mid1:OPN-DEN	UplandLong	Early1:ALL	ReplacementFire	0.0100	1.0000	15	74	-999	Yes	0	9,999	-9,999
UplandLong	Mid1:CLS-SPAR	UplandLong	Early1:ALL	ReplacementFire	0.0100	1.0000	15	74	-999	Yes	0	9,999	-9,999
UplandLong	Late1:OPN-SPAR	UplandLong	Early1:ALL	ReplacementFire	0.0040	1.0000	75	999	-999	Yes	0	9,999	-9,999
UplandLong	Late1:OPN-DEN	UplandLong	Early1:ALL	ReplacementFire	0.0040	1.0000	75	999	-999	Yes	0	9,999	-9,999
UplandLong	Late1:CLS-SPAR	UplandLong	Early1:ALL	ReplacementFire	0.0100	1.0000	75	999	-999	Yes	0	9,999	-9,999
UplandLong	Early1:ALL	UplandLong	Early1:ALL	ReplacementFire	0.0100	1.0000	0	14	-999	Yes	0	9,999	-9,999

All Strata | Other | UplandLong | WetLong | States | Transitions

Figure 12. Probabilistic transitions between state classes related to the replacement fire transition in *Atlantic Coastal Plain Upland Longleaf Pine* (UplandLong), *Central Atlantic Coastal Plain Wet Longleaf Pine* (WetLong), and *Other* biophyscial settings present in the model for Marine Corps Base Camp Lejeune.

The transition for prescribed burns was similarly parameterized in the ST-SIM model (Figure 9). For example (highlighted in Figure 13), to depict the transition that would occur if prescribed burn impacted a landscape cell in the state Mid-Development1: Open-Sparse in the *Atlantic Coastal Plain Upland Longleaf Pine* biophysical setting, you would select "UplandLong" as the From Vegetation Type and To Vegetation Type; "Mid1:OPN-SPAR" as the From Class; "Mid1:OPN-DEN" as the To Class; and "PrescribedBurn" as the Transition Type. Type "0.5" for the Probability; "1.0" for Proportion; "15" for Age Min; "74" for Age Max; "0" for Age Shift; "No" for Age Reset; "0" for TST Min; "9999" for TST Max; and "-9999" for TST Shift. This indicates that all longleaf pine stands between 15 and 74 years old in the Mid-Development1: Open-Sparse state class (within the Upland Longleaf Pine biophysical setting) have a 50% chance of experiencing a surface fire in any given year of a model simulation. If a burn does occur, the landscape cell will transform to one in which the understory is dense, and the stand age will remain as is (and will not revert to 0). For this transition and landscape state, it does not matter if another disturbance has impacted the landscape cell (hence, the range from 0 to 9999 for TST Min and TST Max). This particular example describes the use of prescribed burns on landscape cells that typically follow herbicide or mechanical removal treatments (Provencher et al. 2001a; Provencher et al. 2002).

Repeat this process for all 23 Prescribed Burn transitions (red lines in Figure 9) as shown in Figure 13. In addition to the longleaf pine states, state classes for Hardwood and Mixed were also eligible for treatment with prescribed burns; however, state classes for Bare Land, Other, and Water can not experience prescribed burns in this model. Again, note the differences in values for transition probabilities by landscape states. This indicates that some landscape states are more likely than others to be treated with prescribed burns, and landscape cells in states with higher probabilities will be more likely to be treated than cells in states with lower probabilities. These probabilities were derived from data on management activities on MCBCL (G. Haught, unpublished data).

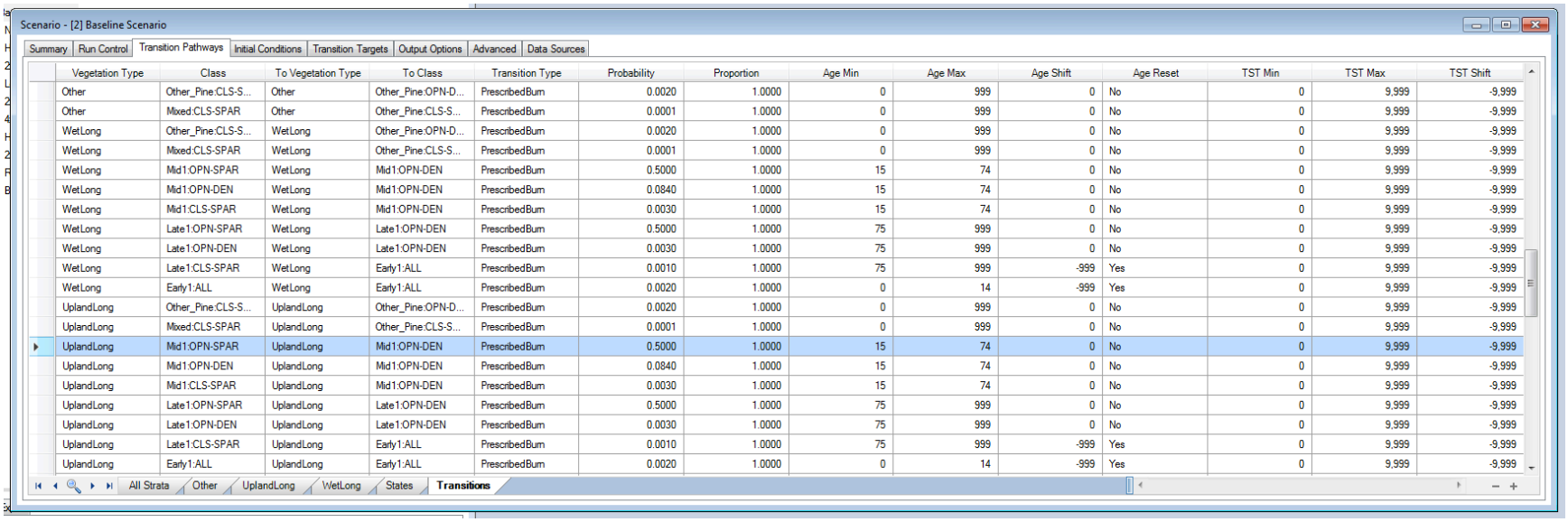

Scenario - [2] Baseline Scenario

Summary | Run Control | Transition Pathways | Initial Conditions | Transition Targets | Output Options | Advanced | Data Sources

Vegetation Type	Class	To Vegetation Type	To Class	Transition Type	Probability	Proportion	Age Min	Age Max	Age Shift	Age Reset	TST Min	TST Max	TST Shift
Other	Other_Pine:CLS-S...	Other	Other_Pine:OPN-D...	PrescribedBurn	0.0020	1.0000	0	999	0	No	0	9,999	-9,999
Other	Mixed:CLS-SPAR	Other	Other_Pine:CLS-S...	PrescribedBurn	0.0001	1.0000	0	999	0	No	0	9,999	-9,999
WetLong	Other_Pine:CLS-S...	WetLong	Other_Pine:OPN-D...	PrescribedBurn	0.0020	1.0000	0	999	0	No	0	9,999	-9,999
WetLong	Mixed:CLS-SPAR	WetLong	Other_Pine:CLS-S...	PrescribedBurn	0.0001	1.0000	0	999	0	No	0	9,999	-9,999
WetLong	Mid1:OPN-SPAR	WetLong	Mid1:OPN-DEN	PrescribedBurn	0.5000	1.0000	15	74	0	No	0	9,999	-9,999
WetLong	Mid1:OPN-DEN	WetLong	Mid1:OPN-DEN	PrescribedBurn	0.0840	1.0000	15	74	0	No	0	9,999	-9,999
WetLong	Mid1:CLS-SPAR	WetLong	Mid1:OPN-DEN	PrescribedBurn	0.0030	1.0000	15	74	0	No	0	9,999	-9,999
WetLong	Late1:OPN-SPAR	WetLong	Late1:OPN-DEN	PrescribedBurn	0.5000	1.0000	75	999	0	No	0	9,999	-9,999
WetLong	Late1:OPN-DEN	WetLong	Late1:OPN-DEN	PrescribedBurn	0.0030	1.0000	75	999	0	No	0	9,999	-9,999
WetLong	Late1:CLS-SPAR	WetLong	Early1:ALL	PrescribedBurn	0.0010	1.0000	75	999	-999	Yes	0	9,999	-9,999
WetLong	Early1:ALL	WetLong	Early1:ALL	PrescribedBurn	0.0020	1.0000	0	14	-999	Yes	0	9,999	-9,999
UplandLong	Other_Pine:CLS-S...	UplandLong	Other_Pine:OPN-D...	PrescribedBurn	0.0020	1.0000	0	999	0	No	0	9,999	-9,999
UplandLong	Mixed:CLS-SPAR	UplandLong	Other_Pine:CLS-S...	PrescribedBurn	0.0001	1.0000	0	999	0	No	0	9,999	-9,999
UplandLong	Mid1:OPN-SPAR	UplandLong	Mid1:OPN-DEN	PrescribedBurn	0.5000	1.0000	15	74	0	No	0	9,999	-9,999
UplandLong	Mid1:OPN-DEN	UplandLong	Mid1:OPN-DEN	PrescribedBurn	0.0840	1.0000	15	74	0	No	0	9,999	-9,999
UplandLong	Mid1:CLS-SPAR	UplandLong	Mid1:OPN-DEN	PrescribedBurn	0.0030	1.0000	15	74	0	No	0	9,999	-9,999
UplandLong	Late1:OPN-SPAR	UplandLong	Late1:OPN-DEN	PrescribedBurn	0.5000	1.0000	75	999	0	No	0	9,999	-9,999
UplandLong	Late1:OPN-DEN	UplandLong	Late1:OPN-DEN	PrescribedBurn	0.0030	1.0000	75	999	0	No	0	9,999	-9,999
UplandLong	Late1:CLS-SPAR	UplandLong	Early1:ALL	PrescribedBurn	0.0010	1.0000	75	999	-999	Yes	0	9,999	-9,999
UplandLong	Early1:ALL	UplandLong	Early1:ALL	PrescribedBurn	0.0020	1.0000	0	14	-999	Yes	0	9,999	-9,999

All Strata | Other | UplandLong | WetLong | States | Transitions

Figure 13. Probabilistic transitions between state classes related to the Prescribed Burn transition in *Atlantic Coastal Plain Upland Longleaf Pine* (UplandLong), *Central Atlantic Coastal Plain Wet Longleaf Pine* (WetLong), and *Other* biophyscial settings present in the model for Marine Corps Base Camp Lejeune.

Although probabilities dictate which state classes are more likely to experience management applications than others, we can set targets to control the total area of the landscape that actually experiences management each year. This is in contrast to more natural transitions (like wildfires), where the values given for each transition probability ultimately determine how much of the landscape is affected by that transition. To set management targets, go to the Transition Targets tab of the Baseline Scenario window. As an example (highlighted in Figure 14), select "UplandLong" as the Vegetation Type and "Prescribed Burn" as the Transition Group. Input "4,700" under Target Area (acres). (Note: if a column for Vegetation Type is not visible, right-click on the small square in the top left corner of the Transition Targets table and select "Vegetation Type"). This parameterization indicates that, within the *Atlantic Coastal Plain Upland Longleaf Pine*, a total of 4,600 acres will be affected by the Prescribed Burn transition each simulation year. Only landcover cells that are characterized by an eligible state class (probability for Prescribed Burn > 0) can be affected by this transition, and landcover cells in state classes with higher probabilities will be treated by Prescribed Burns preferentially. In other words, landcover cells characterized by state classes with the highest probabilities (e.g., Mid-Development1: Open-Sparse) will be treated with Prescribed Burns first, followed by landcover cells with the next highest probabilities, and so on until the Prescribed Burn transition target has been met. Add Prescribed Burn targets for both biophysical settings according to Figure 14. These targets were derived from recent management protocols on MCBCL (G. Haught, unpublished data). We calculated the average total area treated with prescribed burns on the installation (total = ~ 13,800 acres). We then assumed, because the *Central Atlantic Coastal Plain Wet Longleaf Pine* biophysical setting covers roughly twice as much area than the *Atlantic Coastal Plain Upland Longleaf Pine*, that 9,200 acres of prescribed burns occur within the UplandLong biophysical setting and 4,600 acres of burns occur in the WetLong biophyscial setting.

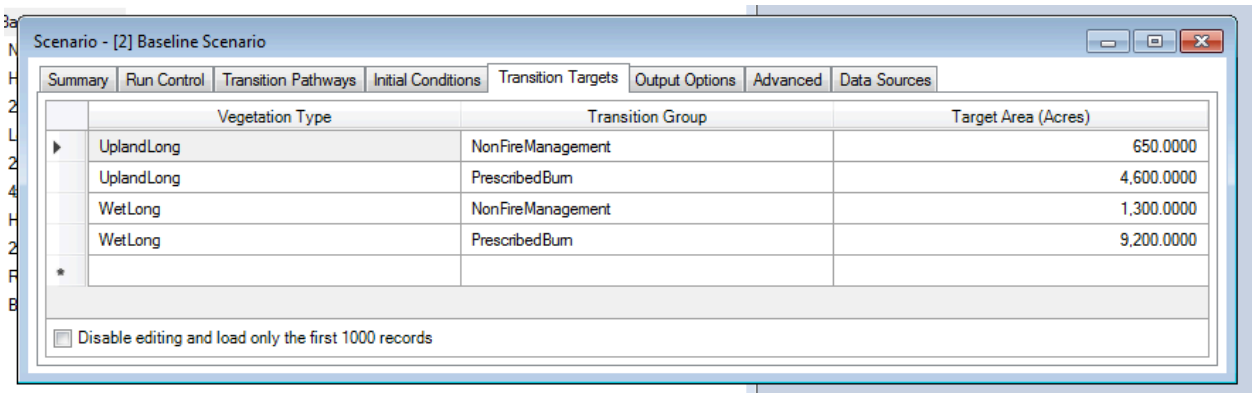

Figure 14. Transition targets for Prescribed Burns and all other non-fire management transitions (Mechanical Midstory Removal, Herbicide, Wiregrass Planting) in the *Atlantic Coastal Plain Upland Longleaf Pine* (UplandLong) and *Central Atlantic Coastal Plain Wet Longleaf Pine* (WetLong) biophyscial settings present in the model for Marine Corps Base Camp Lejeune.

If transition targets were not specified, each eligible landscape cell would have an independent, user-specified probability (probability given in Figure 9, Figure 13) of experiencing a Prescribed Burn each time step. In addition, if one cell is affected by the Prescribed Burn transition, the probability of any other cell experiencing the Prescribed Burn transition would not change. As a result, there could be some simulation years where a prescribed burn does not occur in any cell and other years where a prescribed burn occurs in every eligible cell (although this would be unlikely, particularly in large landscapes). However, by setting a transition target, the user forces the model to simulate this transition in a user-specified number of landscape cells (here, the number of cells comprising 13,800 acres) each simulation year. The transition can still only occur in cells that are within the eligible landscape states, and the transition will preferentially occur in states with the highest probability of experiencing that transition (so it remains critical that the probabilistic Prescribed Burn transition is added for the longleaf pine states as described earlier in this section). If specific states are preferentially burned, then this can be added to the simulation by increasing the prescribed burn for those states relative to others.

In should be noted, however, that there is no guarantee that this transition target will be met each simulation year. For example, in the scenario developed in this manual, there may be years where there are fewer than 13,800 acres of longleaf pine on the landscape (although this is unlikely given our parameterization). If this happens, then the transition target cannot be met because there will not be enough landscape cells in the eligible landscape states.

The user can also specify that targets be used only for certain simulation years and/or that a target occurs within an area range (instead of a single target value). This can be done by right-clicking on the cell in the top-left corner of the Transition Targets table; selecting “Time Step”, “Target Area Min”, and “Target Area Max”; and inputting the appropriate values in the table.

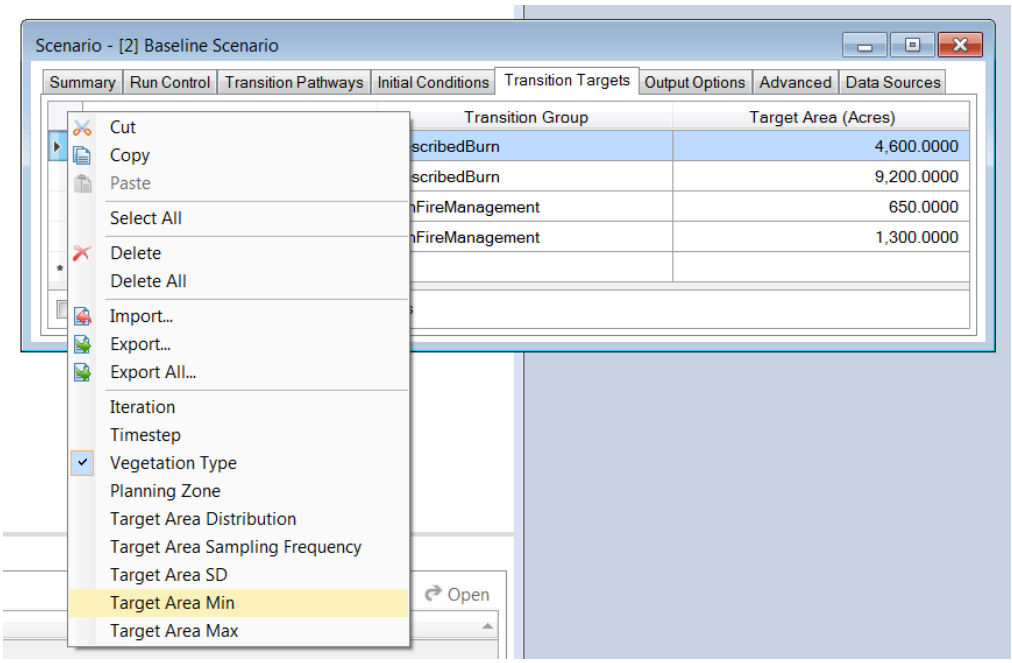

4.3.4 Herbicide Treatment

In addition to fire, a large-scale study of restoration techniques at Eglin Air Force Base also showed that the use of herbicides, specifically the ULW®-form of hexazinone, was extremely effective in reducing the hardwood midstory (Provencher et al. 2001a; Provencher et al. 2001b). Given the effectiveness of the use of herbicide in restoring longleaf pine communities and its use on MCBCL, we included herbicide as a potential management option in the ST-SIM landscape model. In this model, herbicide application primarily affects the density of the midstory (Figure 9).

The transition for Herbicide Application is parameterized in the same way as Prescribed Burns in the ST-SIM model. For example (highlighted in Figure 15), to depict the transition that would occur if herbicide was applied to a landscape cell in the state Late Development1: Closed-Sparse in the *Central Atlantic Coastal Plain Wet Longleaf Pine* biophysical setting, you would select "WetLong" as the From Vegetation Type and To Vegetation Type; "Late1:CLS-SPAR" as the From Class; "Late1:OPN-SPAR" as the To Class; and "HerbApp" as the Transition Type. Type "0.0001" for the Probability; "1.0" for Proportion; "75" for Age Min; "999" for Age Max; "0" for Age Shift; "No" for Age Reset; "0" for TST Min; "9999" for TST Max; and "-9999" for TST Shift. This indicates that all longleaf pine stands 75 year or older in the Late Development1: Closed-Sparse state class (within the Wet Longleaf Pine biophysical setting) have a 0.01% chance of being treated with herbicide in any given year of a model simulation. If herbicide is applied, the landscape cell will transform to one in which the midstory is closed to one in which is open, and the stand age will remain as is (and will not revert to 0). For this transition and landscape state, it does not matter if another disturbance has impacted the landscape cell (hence, the range from 0 to 9999 for TST Min and TST Max).

Repeat this process for all four Herbicide transitions (purple lines in Figure 9) as shown in Figure 15. Probabilities associated with the Herbicide transition were derived from data on management activities on MCBCL (G. Haught, unpublished data). These probabilities again designated which state classes are preferentially treated with herbicide (i.e., those with the highest probabilities) each year on the installation.

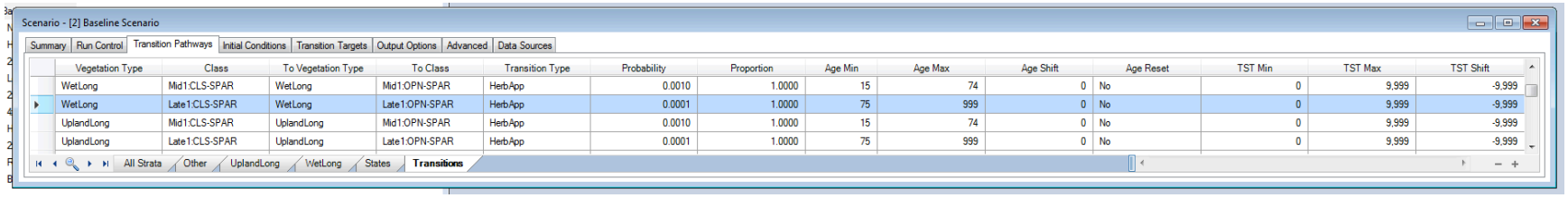

Scenario - [2] Baseline Scenario

Summary | Run Control | Transition Pathways | Initial Conditions | Transition Targets | Output Options | Advanced | Data Sources

Vegetation Type	Class	To Vegetation Type	To Class	Transition Type	Probability	Proportion	Age Min	Age Max	Age Shift	Age Reset	TST Min	TST Max	TST Shift
WetLong	Mid1:CLS-SPAR	WetLong	Mid1:OPN-SPAR	HerbApp	0.0010	1.0000	15	74	0	No	0	9,999	-9,999
WetLong	Late1:CLS-SPAR	WetLong	Late1:OPN-SPAR	HerbApp	0.0001	1.0000	75	999	0	No	0	9,999	-9,999
UplandLong	Mid1:CLS-SPAR	UplandLong	Mid1:OPN-SPAR	HerbApp	0.0010	1.0000	15	74	0	No	0	9,999	-9,999
UplandLong	Late1:CLS-SPAR	UplandLong	Late1:OPN-SPAR	HerbApp	0.0001	1.0000	75	999	0	No	0	9,999	-9,999

All Strata | Other | UplandLong | WetLong | States | Transitions

Figure 15. Probabilistic transitions between state classes related to the Herbicide Application transition in *Atlantic Coastal Plain Upland Longleaf Pine* (UplandLong) and *Central Atlantic Coastal Plain Wet Longleaf Pine* (WetLong) biophyscial settings present in the model for Marine Corps Base Camp Lejeune.

Transition targets for Herbicide Application are also added in the same manner as those associated with the Prescribed Burn transition. We combined all non-fire management techniques (i.e., herbicide application, mechanical midstory removal, and wiregrass planting) into a single "Non-Fire Management" transition group. Based on management activity data on MCBCL (G. Haught, unpublished data), these three non-fire management techniques are applied to an average of 1,950 acres per year. We again assumed that 66% of this acreage would be associated with the more pervasive *Central Atlantic Coastal Plain Wet Longleaf Pine* (1,300 acres) and 33% would be associated with *Atlantic Coastal Plain Upland Longleaf Pine* (650 acres). Add these management targets as shown in Figure 14.

4.3.5 Mechanical Removal

Mechanical chainsaw felling and girdling of hardwood species in the midstory is also a commonly used restoration technique in the longleaf pine ecosystem on MCBCL, and we included this technique as a possible management option in the ST-SIM landscape model (brown lines in Figure 9). Like the herbicide application, mechanical midstory removal primarily impacts the midstory for eligible landscape states.

Add transitions for Mechanical Midstory Removal ("MidRemove") in the same manner as transitions were added for Herbicide Application (see *Section 4.3.4 Herbicide Treatment*) according to Figure 16. Management targets related to Mechanical Midstory Removal were already added to the model as part of the "NonFireManagement" group shown in Figure 14.

4.3.6 Wiregrass Planting

Finally, the manual planting of wiregrass in the understory of longleaf pine stands is occasionally used on a limited basis on MCBCL, and we included this technique as a possible management option in the ST-SIM landscape model (green lines in Figure 9). This management transition primarily impacts the understory for eligible landscape states.

Add transitions for Wiregrass Planting ("GrassPlant") in the same manner as transitions were added for Herbicide Application (see *Section 4.3.4 Herbicide Treatment*) according to Figure 17. Management targets related to Wiregrass Planting were already added to the model as part of the "NonFireManagement" group shown in Figure 14.

Scenario - [2] Baseline Scenario

Summary | Run Control | Transition Pathways | Initial Conditions | Transition Targets | Output Options | Advanced | Data Sources

Vegetation Type	Class	To Vegetation Type	To Class	Transition Type	Probability	Proportion	Age Min	Age Max	Age Shift	Age Reset	TST Min	TST Max	TST Shift
WetLong	Mid1:OPN-DEN	WetLong	Mid1:OPN-DEN	MidRemove	0.3000	1.0000	15	74	0	No	0	9,999	-9,999
WetLong	Mid1:CLS-SPAR	WetLong	Mid1:OPN-SPAR	MidRemove	0.0010	1.0000	15	74	0	No	0	9,999	-9,999
WetLong	Late1:OPN-DEN	WetLong	Late1:OPN-DEN	MidRemove	0.0030	1.0000	75	999	0	No	0	9,999	-9,999
WetLong	Late1:CLS-SPAR	WetLong	Late1:OPN-SPAR	MidRemove	0.0001	1.0000	75	999	0	No	0	9,999	-9,999
UplandLong	Mid1:OPN-DEN	UplandLong	Mid1:OPN-DEN	MidRemove	0.3000	1.0000	15	74	0	No	0	9,999	-9,999
UplandLong	Mid1:CLS-SPAR	UplandLong	Mid1:OPN-SPAR	MidRemove	0.0010	1.0000	15	74	0	No	0	9,999	-9,999
UplandLong	Late1:OPN-DEN	UplandLong	Late1:OPN-DEN	MidRemove	0.0030	1.0000	75	999	0	No	0	9,999	-9,999
UplandLong	Late1:CLS-SPAR	UplandLong	Late1:OPN-SPAR	MidRemove	0.0001	1.0000	75	999	0	No	0	9,999	-9,999

All Strata | Other | UplandLong | WetLong | States | **Transitions**

Figure 16. Probabilistic transitions between state classes related to the Mechanical Midstory Removal transition in *Atlantic Coastal Plain Upland Longleaf Pine* (UplandLong) and *Central Atlantic Coastal Plain Wet Longleaf Pine* (WetLong) biophyscial settings present in the model for Marine Corps Base Camp Lejeune.

Scenario - [2] Baseline Scenario

Summary | Run Control | Transition Pathways | Initial Conditions | Transition Targets | Output Options | Advanced | Data Sources

Vegetation Type	Class	To Vegetation Type	To Class	Transition Type	Probability	Proportion	Age Min	Age Max	Age Shift	Age Reset	TST Min	TST Max	TST Shift
WetLong	Mid1:OPN-SPAR	WetLong	Mid1:OPN-DEN	GrassPlant	0.1000	1.0000	15	74	0	No	0	9,999	-9,999
WetLong	Late1:OPN-SPAR	WetLong	Late1:OPN-SPAR	GrassPlant	0.1000	1.0000	75	999	0	No	0	9,999	-9,999
UplandLong	Mid1:OPN-SPAR	UplandLong	Mid1:OPN-DEN	GrassPlant	0.1000	1.0000	15	74	0	No	0	9,999	-9,999
UplandLong	Late1:OPN-SPAR	UplandLong	Late1:OPN-SPAR	GrassPlant	0.1000	1.0000	75	999	0	No	0	9,999	-9,999

All Strata | Other | UplandLong | WetLong | States | **Transitions**

Figure 17. Probabilistic transitions between state classes related to the Wiregrass Planting transition in *Atlantic Coastal Plain Upland Longleaf Pine* (UplandLong) and *Central Atlantic Coastal Plain Wet Longleaf Pine* (WetLong) biophyscial settings present in the model for Marine Corps Base Camp Lejeune.

4.3.7 Other "Natural" Transitions

Several additional non-management transitions were included in the original LANDFIRE model for the biophysical settings represented on MCBCL. These include hurricanes ("Wind/Weather/Stress"), "Insects/Disease", and "Competition/Maintenance". Like the three wildfire transitions, the probability associated with a given landscape state and each of these transitions determines the likelihood of that transition occurring in a given simulation year. For instance, landscape cells characterized by states with higher probabilities for the "Insects/Disease" transition will be more likely to experience that transition in a given year. Probabilities and transition pathways for these transitions can be seen in Figure 18 (Wind/Weather/Stress, Insect/Disease) and Figure 6 (Competition/Maintenance).

Add these transitions as you would for any of the other fire or management transitions (e.g., see *Section 4.3.4 Herbicide Treatment*) according to Figures 19-21.

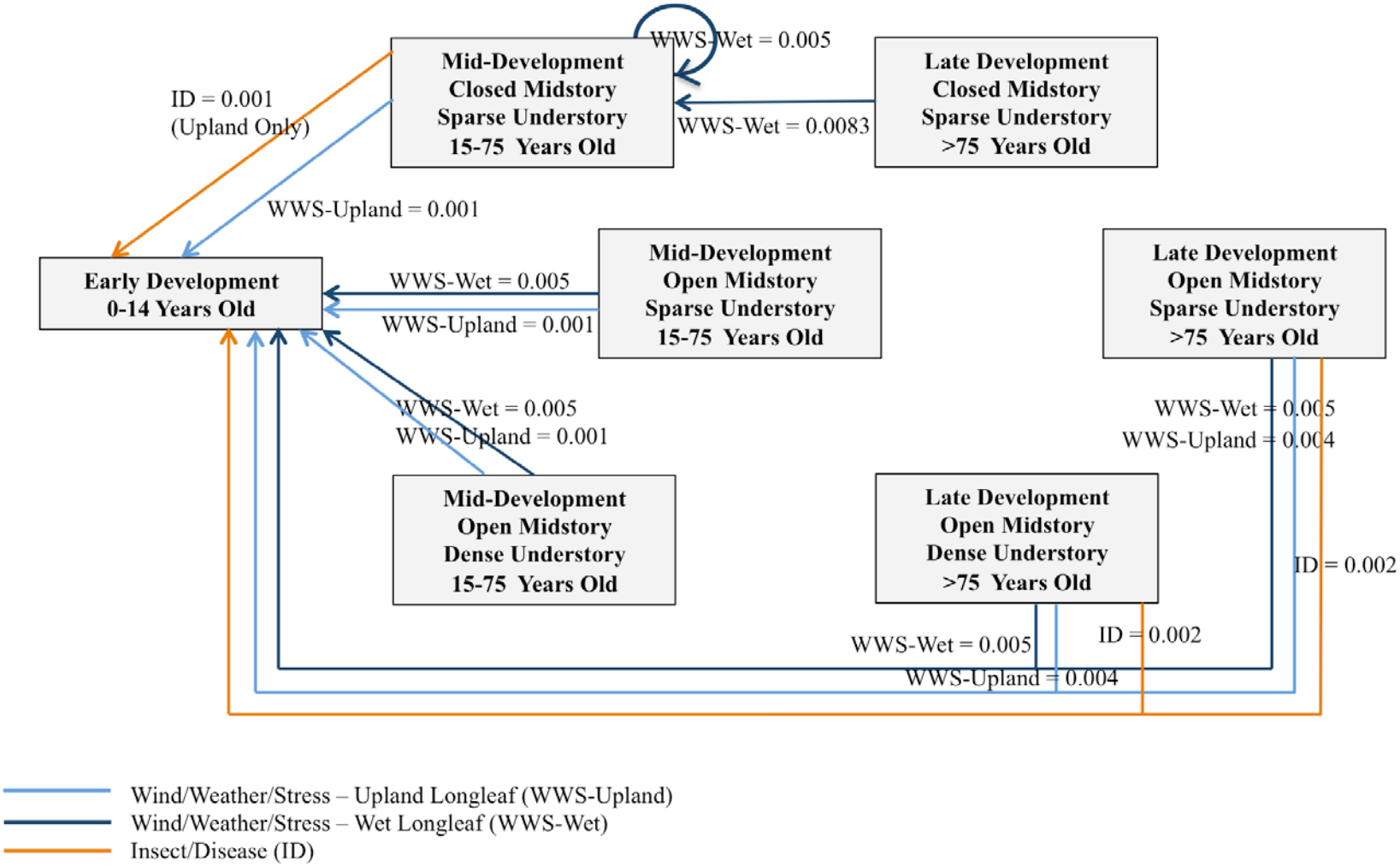

Figure 18. Transitions between state classes related to Wind/Weather/Stress (e.g., hurricanes), Insects/Disease, and Competition/Maintence on Marine Corps Base Camp Lejeune.

Scenario - [2] Baseline Scenario

Summary | Run Control | Transition Pathways | Initial Conditions | Transition Targets | Output Options | Advanced | Data Sources

Vegetation Type	Class	To Vegetation Type	To Class	Transition Type	Probability	Proportion	Age Min	Age Max	Age Shift	Age Reset	TST Min	TST Max	TST Shift
WetLong	Mid1:OPN-SPAR	WetLong	Early1:ALL	Wind/Weather/...	0.0050	1.0000	15	74	-999	Yes	0	9,999	-9,999
WetLong	Mid1:OPN-DEN	WetLong	Early1:ALL	Wind/Weather/...	0.0050	1.0000	15	74	-999	Yes	0	9,999	-9,999
WetLong	Mid1:CLS-SPAR	WetLong	Mid1:CLS-SPAR	Wind/Weather/...	0.0050	1.0000	15	74	0	No	0	9,999	-9,999
WetLong	Late1:OPN-SPAR	WetLong	Early1:ALL	Wind/Weather/...	0.0050	1.0000	75	999	-999	Yes	0	9,999	-9,999
WetLong	Late1:OPN-DEN	WetLong	Early1:ALL	Wind/Weather/...	0.0050	1.0000	75	999	-999	Yes	0	9,999	-9,999
WetLong	Late1:CLS-SPAR	WetLong	Mid1:CLS-SPAR	Wind/Weather/...	0.0083	1.0000	75	999	0	No	0	9,999	-9,999
UplandLong	Mid1:OPN-SPAR	UplandLong	Early1:ALL	Wind/Weather/...	0.0010	1.0000	15	74	-999	Yes	0	9,999	-9,999
UplandLong	Mid1:OPN-DEN	UplandLong	Early1:ALL	Wind/Weather/...	0.0010	1.0000	15	74	-999	Yes	0	9,999	-9,999
UplandLong	Mid1:CLS-SPAR	UplandLong	Early1:ALL	Wind/Weather/...	0.0010	1.0000	15	74	-999	Yes	0	9,999	-9,999
UplandLong	Late1:OPN-SPAR	UplandLong	Early1:ALL	Wind/Weather/...	0.0040	1.0000	75	999	-999	Yes	0	9,999	-9,999
UplandLong	Late1:OPN-DEN	UplandLong	Early1:ALL	Wind/Weather/...	0.0040	1.0000	75	999	-999	Yes	0	9,999	-9,999

All Strata | Other | UplandLong | WetLong | States | Transitions

Figure 19. Probabilistic transitions between state classes related to the Wind/Weather/Stress transition in *Atlantic Coastal Plain Upland Longleaf Pine* (UplandLong) and *Central Atlantic Coastal Plain Wet Longleaf Pine* (WetLong) biophyscial settings present in the model for Marine Corps Base Camp Lejeune.

Scenario - [2] Baseline Scenario

Summary | Run Control | Transition Pathways | Initial Conditions | Transition Targets | Output Options | Advanced | Data Sources

Vegetation Type	Class	To Vegetation Type	To Class	Transition Type	Probability	Proportion	Age Min	Age Max	Age Shift	Age Reset	TST Min	TST Max	TST Shift
WetLong	Late1:OPN-SPAR	WetLong	Early1:ALL	Insect/Disease	0.0020	1.0000	75	999	-999	Yes	0	9,999	-9,999
WetLong	Late1:OPN-DEN	WetLong	Early1:ALL	Insect/Disease	0.0020	1.0000	75	999	-999	Yes	0	9,999	-9,999
UplandLong	Mid1:CLS-SPAR	UplandLong	Early1:ALL	Insect/Disease	0.0010	1.0000	15	74	-999	Yes	0	9,999	-9,999
UplandLong	Late1:OPN-SPAR	UplandLong	Early1:ALL	Insect/Disease	0.0020	1.0000	75	999	-999	Yes	0	9,999	-9,999
UplandLong	Late1:OPN-DEN	UplandLong	Early1:ALL	Insect/Disease	0.0020	1.0000	75	999	-999	Yes	0	9,999	-9,999

All Strata | Other | UplandLong | WetLong | States | Transitions

Figure 20. Probabilistic transitions between state classes related to the Insect/Disease transition in *Atlantic Coastal Plain Upland Longleaf Pine* (UplandLong) and *Central Atlantic Coastal Plain Wet Longleaf Pine* (WetLong) biophyscial settings present in the model for Marine Corps Base Camp Lejeune.

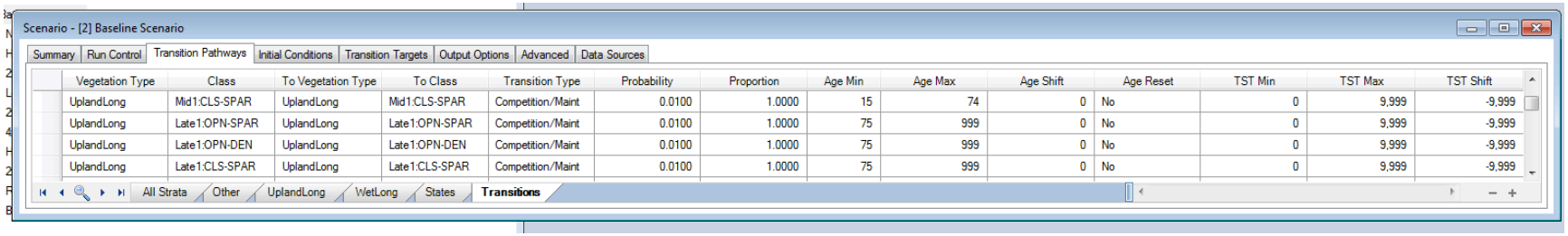

Scenario - [2] Baseline Scenario

Summary | Run Control | Transition Pathways | Initial Conditions | Transition Targets | Output Options | Advanced | Data Sources

Vegetation Type	Class	To Vegetation Type	To Class	Transition Type	Probability	Proportion	Age Min	Age Max	Age Shift	Age Reset	TST Min	TST Max	TST Shift
UplandLong	Mid1:CLS-SPAR	UplandLong	Mid1:CLS-SPAR	Competition/Maint	0.0100	1.0000	15	74	0	No	0	9,999	-9,999
UplandLong	Late1:OPN-SPAR	UplandLong	Late1:OPN-SPAR	Competition/Maint	0.0100	1.0000	75	999	0	No	0	9,999	-9,999
UplandLong	Late1:OPN-DEN	UplandLong	Late1:OPN-DEN	Competition/Maint	0.0100	1.0000	75	999	0	No	0	9,999	-9,999
UplandLong	Late1:CLS-SPAR	UplandLong	Late1:CLS-SPAR	Competition/Maint	0.0100	1.0000	75	999	0	No	0	9,999	-9,999

All Strata | Other | UplandLong | WetLong | States | Transitions

Figure 21. Probabilistic transitions between state classes related to the Competition/Maintenance transition in *Atlantic Coastal Plain Upland Longleaf Pine* (UplandLong) and *Central Atlantic Coastal Plain Wet Longleaf Pine* (WetLong) biophyscial settings present in the model for Marine Corps Base Camp Lejeune.

4.4 Simulation Controls and Initial Conditions

4.4.1 Run controls

Before running an ST-SIM model, parameters for the simulation characteristics and initial conditions must be selected. Click on the tab "Run Control" in the "Baseline Scenario" window. There, input the number of times steps, the number of iterations, and whether the model should be run spatially or not. The length of the time step and the number of time steps will vary depending on the scenario. As an example, we will simulate the model for 50 years assuming that one time step equals a single year. In addition, because this is a stochastic simulation of landscape dynamics, each iteration could result in a different distribution of landscape states. If you want to create an averaged distribution of landscape states, run the model for multiple iterations by adding a number > 1 next to "Iterations" in this window. For example, if you select "10" here, ST-SIM will simulate the model from year 0 to year 50, repeating this process 10 times. Finally, the model can be run spatially by adding a check next to "Run model spatially" in this window. In this case, the model will use maps of the study area to determine the areas of the landscape states and their distributions (described in next section), and it will output predictive maps as the simulation progresses. If this box is not checked, the user must indicate the percentage of the total landscape that is comprised of each landscape state (described in next section). Accordingly, the model will not be spatially explicit, and maps will not be output at the end of the simulation. Instead, ST-SIM will indicate a predictive percentage of the total landscape that is comprised of each landscape state at the end of the simulation.

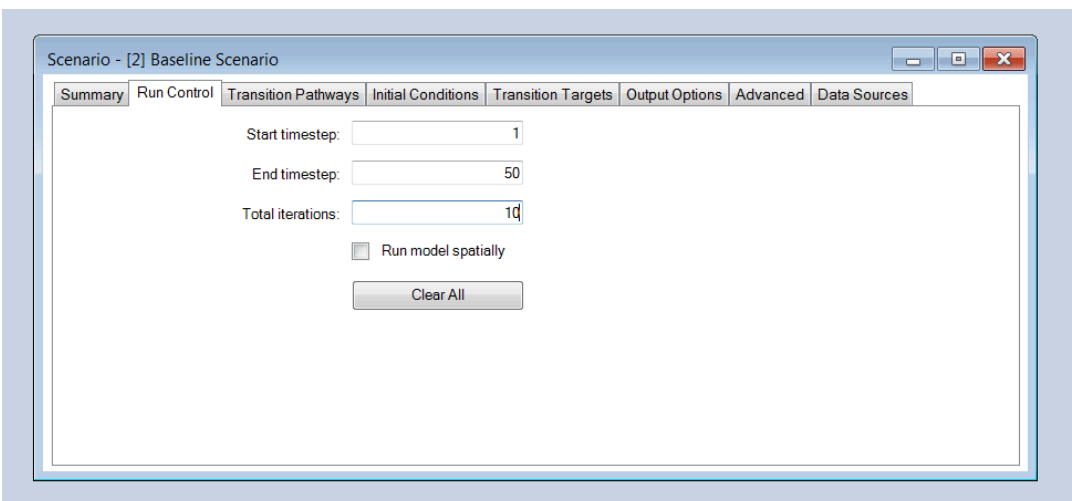

4.4.2 Initial landscape conditions

The proportional areas for each landscape state can be added by selecting the tab "Initial Conditions" in the "Baseline Scenario" window. Here, either a spatially explicit or a non-

spatially explicit description of what the landscape looks like at the start (t = 0) of the simulation must be supplied.

If the simulation will be run non-spatially (the box in the previous screen was left unchecked), click on “Non-Spatial” to the left of this window. In this new window, indicate the total size of the landscape (in acres) and the number of simulation cells associated with the landscape in the corresponding input boxes. In the map we created for the distribution of all landscape states (Section *8.2 State Class map*) based on LANDFIRE products, the landscape covered a total area of 142,882.4616 acres and was composed of 642,473 cells. ST-Sim will automatically calculate the cell size in acres based on this information, which calculates to 0.2224 acres.

Then, in the table associated with this window, you will add a row for each landscape state and each vegetation type. For example (see highlighted row in Figure 22), add a row for the area of the landscape covered by the Late Development1: Open-Dense state within the *Atlantic Coastal Plain Upland Longleaf Pine* biophysical setting. Based on the map we created for this landscape based on LANDFIRE products, we found that only a small portion of the landscape is characterized by this state and biophysical setting (0.89 acres or 0.0006% of the total landscape). To input this information, select “UplandLong” under “Vegetation Type” and “Late1:OPN-DEN” under state class. Because the late development state class contains stands 75 years or older, input “75” under “Age Min” and “9999” under “Age Max”. Finally, input “0.0006” under “Total Amount”. Note that the “Total Amount” column specifies the percentage of the landscape covered by that landscape state and biophysical setting. You would add a row for each state class and biophysical setting initially represented on the MCBCL landscape, as shown in Figure 22.

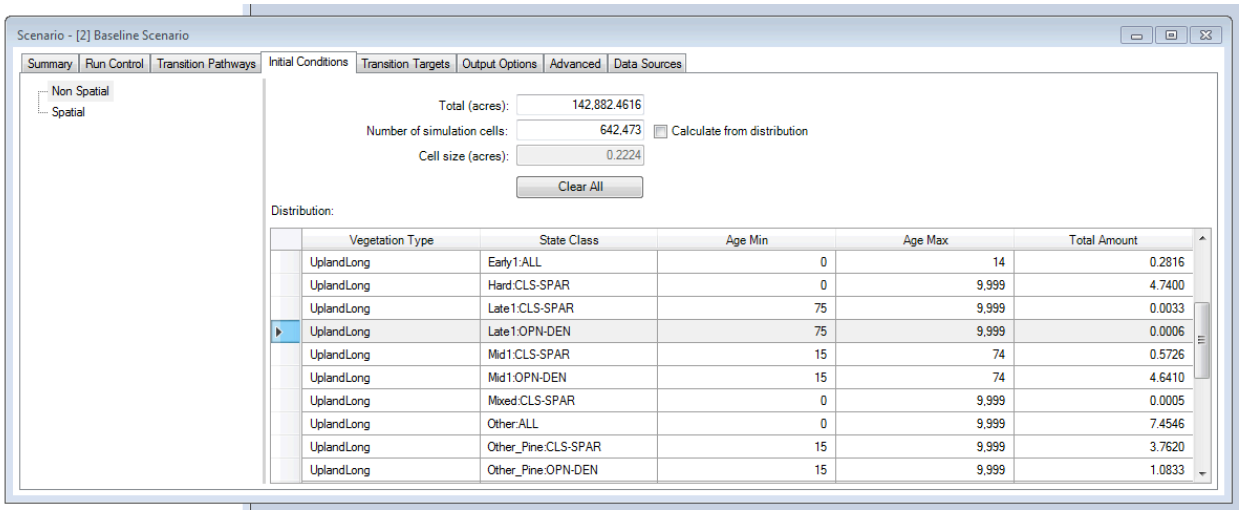

Vegetation Type	State Class	Age Min	Age Max	Total Amount
UplandLong	Early1:ALL	0	14	0.2816
UplandLong	Hard:CLS-SPAR	0	9,999	4.7400
UplandLong	Late1:CLS-SPAR	75	9,999	0.0033
UplandLong	Late1:OPN-DEN	75	9,999	0.0006
UplandLong	Mid1:CLS-SPAR	15	74	0.5726
UplandLong	Mid1:OPN-DEN	15	74	4.6410
UplandLong	Mixed:CLS-SPAR	0	9,999	0.0005
UplandLong	Other:ALL	0	9,999	7.4546
UplandLong	Other_Pine:CLS-SPAR	15	9,999	3.7620
UplandLong	Other_Pine:OPN-DEN	15	9,999	1.0833

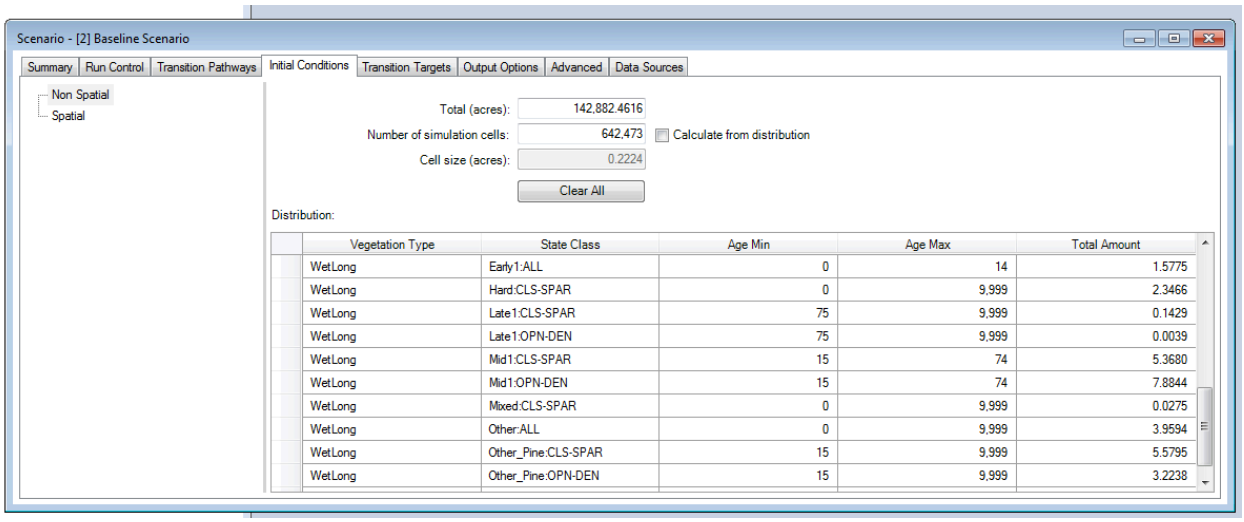

Vegetation Type	State Class	Age Min	Age Max	Total Amount
WetLong	Early1:ALL	0	14	1.5775
WetLong	Hard:CLS-SPAR	0	9,999	2.3466
WetLong	Late1:CLS-SPAR	75	9,999	0.1429
WetLong	Late1:OPN-DEN	75	9,999	0.0039
WetLong	Mid1:CLS-SPAR	15	74	5.3680
WetLong	Mid1:OPN-DEN	15	74	7.8844
WetLong	Mixed:CLS-SPAR	0	9,999	0.0275
WetLong	Other:ALL	0	9,999	3.9594
WetLong	Other_Pine:CLS-SPAR	15	9,999	5.5795
WetLong	Other_Pine:OPN-DEN	15	9,999	3.2238

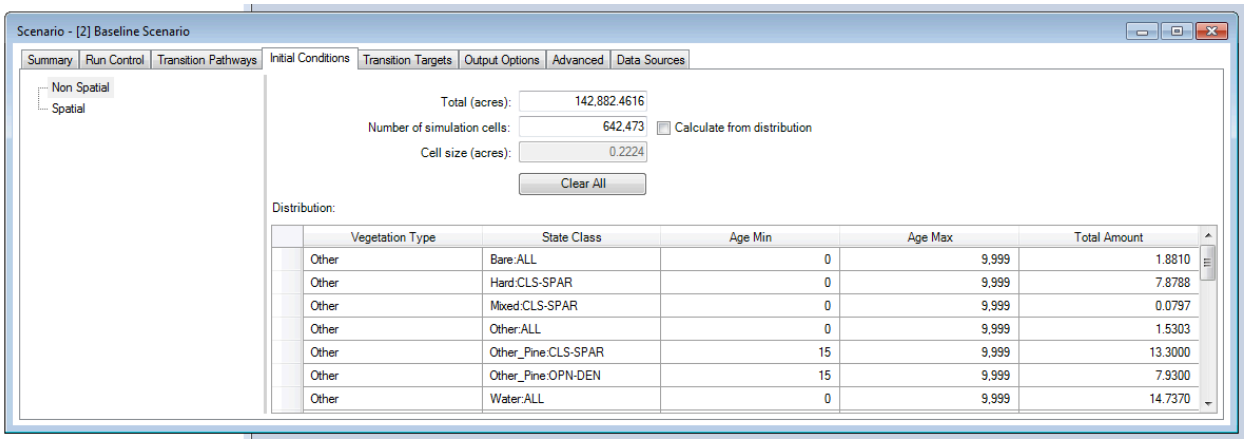

Vegetation Type	State Class	Age Min	Age Max	Total Amount
Other	Bare:ALL	0	9,999	1.8810
Other	Hard:CLS-SPAR	0	9,999	7.8788
Other	Mixed:CLS-SPAR	0	9,999	0.0797
Other	Other:ALL	0	9,999	1.5303
Other	Other_Pine:CLS-SPAR	15	9,999	13.3000
Other	Other_Pine:OPN-DEN	15	9,999	7.9300
Other	Water:ALL	0	9,999	14.7370

Figure 22. Percentage of landscape covered by each landscape state in the *Atlantic Coastal Plain Upland Longleaf Pine* (UplandLong), *Central Atlantic Coastal Plain Wet Longleaf Pine* (WetLong), and *Other* biophyscial settings present in the model for Marine Corps Base Camp Lejeune. Percentages are based on data derived by the LANDFIRE project in 2014.

If you choose to run a spatially explicit simulation (the box in the previous screen was checked), click on “Spatial” to the left of this window. Here, a series of Geo.TIFF maps must be uploaded, which together show the underlying biophysical setting (“Vegetation Type”), the distributions of each landscape state (“State Class”), and the ages of each landscape cell (“Age”). For each file type in this window, click “Browse”, navigate to the appropriate file, and click “Open” to upload the correct Geo.TIFF map. For this Baseline Scenario, we do not consider a “Planning Zone”. See *Section 8. Landscape Input Values and Maps in ArcGIS* for guidance in creating these input maps. All maps uploaded in this step must have the same extents (i.e., number of rows and columns) and cell sizes. If this is not the case, an error message will appear, and the simulation will not run.

The ST-SIM program will then automatically calculate appropriate values for the numbers of rows and columns, the cell size, the number of cells, and the total landscape area based on the attributes associated with the uploaded map files.

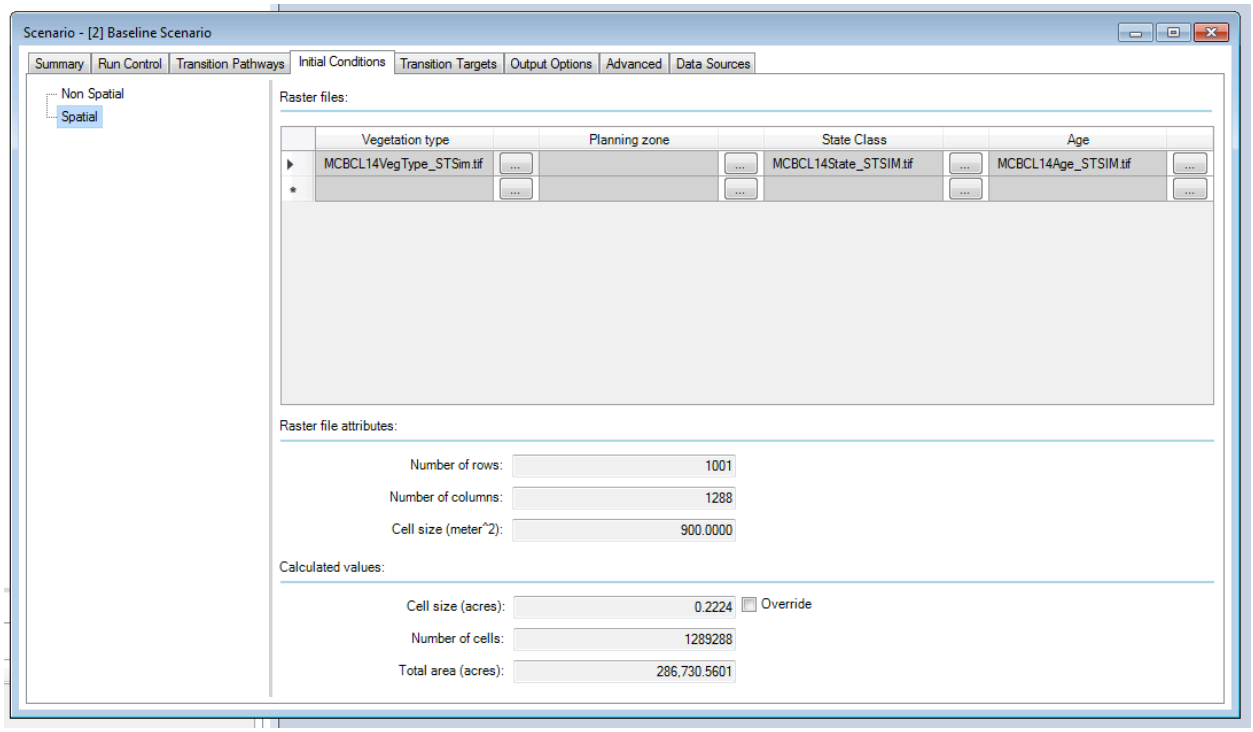

4.4.3 Output options

To set the final simulation controls in ST-SIM, click on the tab "Output Options" in the "Baseline Scenario" window. On this screen you can indicate what types of outputs you would like the model to generate throughout a simulation and at what point(s) in the simulation you would like those outputs created. For example, if you select "State classes every 1 time step(s)" for both the Summary and Spatial Outputs, the model will track the area and location of every state class for every iteration (depending on the number of iterations given in the "Run Control" tab) and time step of the simulation. If you select "State classes every 50 time steps", however, the model will only save that information for the 50th time step (for every iteration). Check the box for "Include zero values" so that the output files will contain rows for all landscape states, even those not represented in the simulated outputs.

In non-spatial simulations, the summary outputs are the only available output options (see selection possibilities in the "Summary output" box on the "Output Options" screen; Table 3). However, in a spatially explicit simulation (i.e., Geo.TIFF maps have been uploaded to parameterize the model's initial conditions), the user can choose to select spatially explicit outputs (see selection possibilities in the "Spatial output" box on the "Output Options" screen; Table 3). These outputs include maps of the landscape showing the locations of state classes and transition events for the specified times steps and iterations. See Table 3 for a description of each major available output. Click on the box next to one or more output names; each checked output will be produced during the course of the ST-SIM simulation. The simulation running time will be a function of the number of outputs you select, whether or not you produce output maps, the number of iterations you run, and how often you want outputs produced.

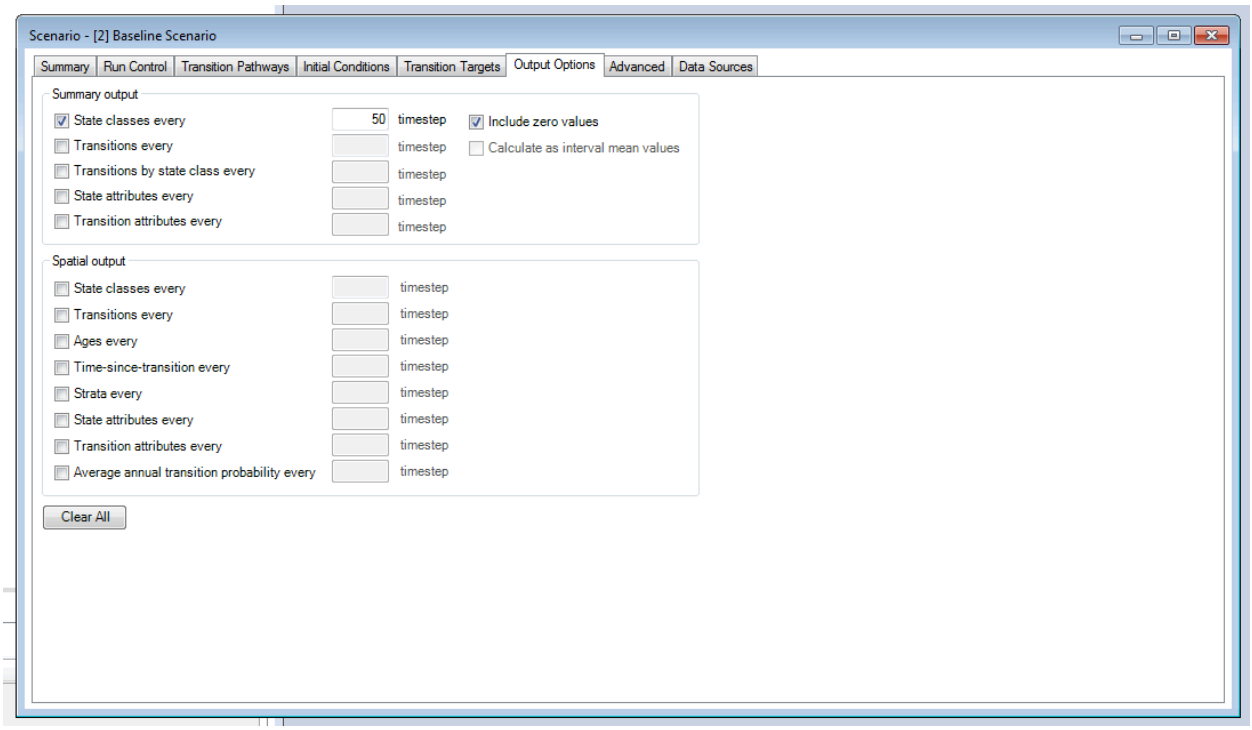

Table 3. Major outputs from an ST-SIM model. Spatial outputs can only be produced for spatially explicit simulations where Geo.TIFF files have been uploaded to parameterize the model's initial conditions.

Output Name	Description
Summary Outputs	*Format: Exported as Microsoft Excel files*
State classes	Area of the landscape in each state class (for iterations and time steps chosen)
Transitions	Area of the landscape affected by each transition type (for iterations and time steps chosen)
Transitions by state class	Area of each state class affected by each transition type (for iterations and time steps chosen)
Spatial Outputs	*Format: Exported as Geo.TIFF files*
State classes	Map of landscape showing state classes, produced for each iteration and time step indicated
Transitions	Map of landscape showing the locations of specific transition types; produced for each iteration and time step indicated. An individual map is produced for each transition type.
Ages	Map of landscape showing the "age" of each landscape cell; applicable primarily for forest stands

5. Running an ST-SIM Model

After all states, transitions, input values (or maps), and other parameters have been added to the ST-SIM model, you are ready to simulate your landscape model. Highlight the scenario name in the "Libraries" window (for example, "Baseline Scenario"), and click on the "Run" button along the menu bar at the top of the "SyncroSim" screen.

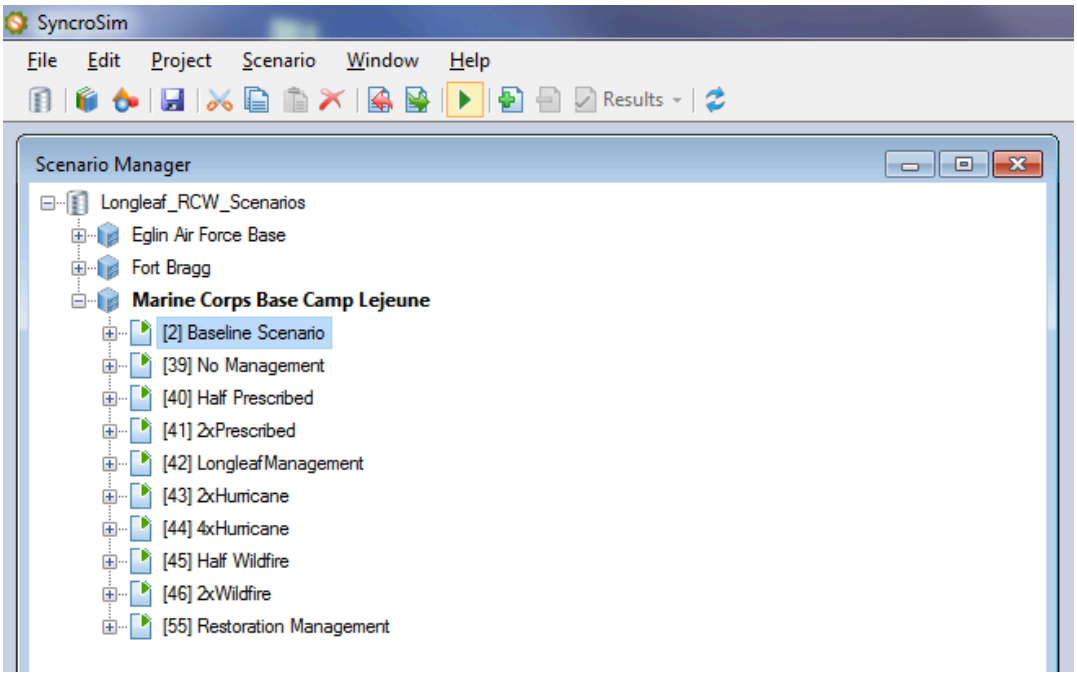

After you hit the run button, a task window should appear indicating that the model is running, and a simulation bar at the bottom of the screen indicates the current iteration and time step that the model is on. The simulation can be stopped at any time by clicking the “Stop” symbol in the task window.

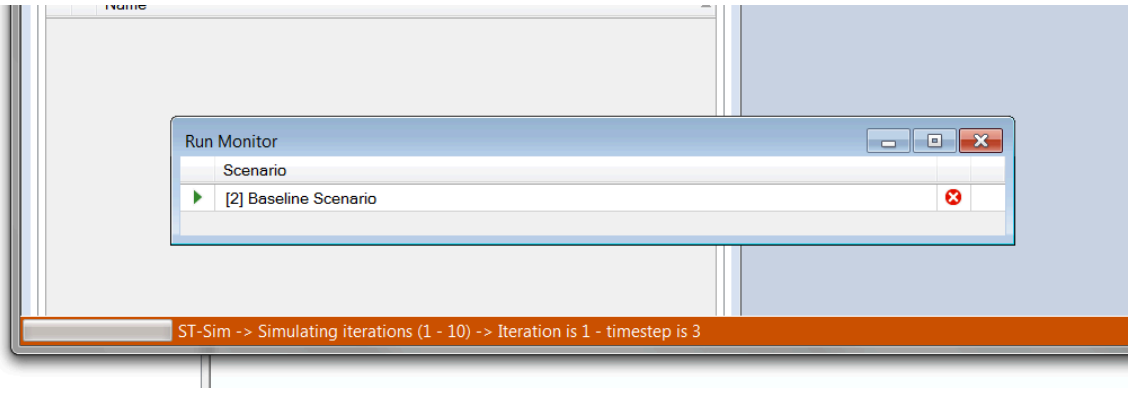

When the simulation has completed, a checkmark should appear in the “Run Monitor” window next to the scenario name, and a results folder will appear under the scenario name in the “Libraries” window.

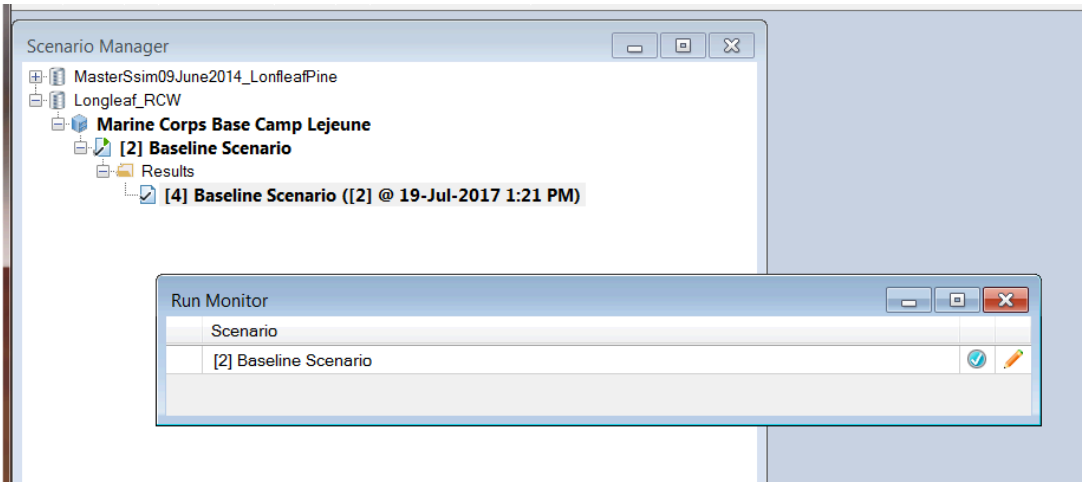

6. ST-SIM Results and Outputs

After the simulation has completed, the user can either view results within the ST-SIM program, export tables for viewing in other programs (like Microsoft Excel), or open Geo.TIFF maps in a GIS platform (e.g., ArcGIS).

Right-click on the appropriate results listed under the scenario name (here, “Baseline Scenario”) in the “Libraries” window. This will make those particular results the “active” results if more than one results folder is available.

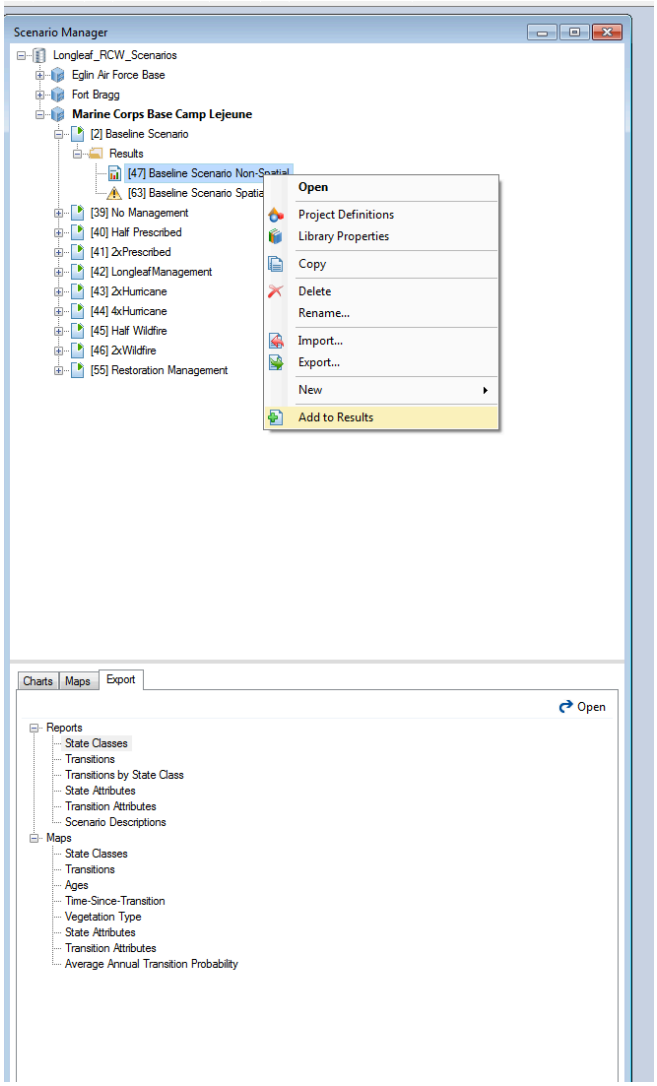

To generate a report, click on the “Export” tab at the bottom of the “Libraries” window, double click on the type of report you would like to create (e.g., “State Classes”), and save the new report. This will create a Microsoft Excel file showing, for example, the area of each state class

for every iteration (depending on the number of iterations you chose in the “Run Control” tab) and every time step you selected in the “Output Options” tab.

If the model was parameterized as spatially explicit, maps showing the locations of landscape states and specific transitions can also be produced. Click on the “Export” tab at the bottom of the “Libraries” window, double click on the type of map you would like to create (e.g., “State Classes”), and browse to or create a folder where maps will be saved. The ST-SIM model will then produce maps of the specified category (e.g., state classes, transitions) for every iteration (depending on the number of iterations you chose in the “Run Control” tab) and every time step you selected in the “Output Options” tab. The names of each map produced contain information about the scenario, model iteration, model time step, and map type (Figure 23). These maps can then be opened in a mapping platform like ArcGIS.

Figure 23. An example of an identification name associated with result maps produced through the ST-SIM model.

7. Advanced Model Parameterization – Spatial Multipliers

In addition to the baseline parameters discussed in the preceding sections, the user can also choose to add a number of more advanced parameters or processes to the ST-SIM landscape model. In this section, we describe how transitions can be constrained within specific locations in the study region or to specific time steps throughout a simulation.

For some transitions, the user may wish to constrain those events to specific areas. For example, a user may wish to determine the impact of a development project in a particular area of the base on the entire RCW population. Similarly, a user may wish to better understand how focusing limited management resources into one area might impact the availability of habitat for RCWs. Adding a spatial constraint to a transition event in the ST-SIM landscape model is done through the use of spatial multipliers under the “Advanced” tab in the scenario window.

As an example, lets assume that you want to predict RCW habitat availability over 20 years, given that a potential development project will convert all landscape cells within a 3,547 acre

plot in the eastern half of the base to the Developed state class in year 10 (Figure 24). In order to parameterize this scenario, a transition group containing the Development transition must be created in the project definitions for this scenario. This group has already been created for the baseline model (described in *Section 4.2 Transitions*).

Next, a probabilistic value for the Development transition must be added to every landscape state in the same manner that, for example, the fire transition was added to the Longleaf Pine landscape states. For probability, you can use any value, as long as all landscape states have the same value (unless you want to parameterize the model such that some landscape states have a higher probability of being developed than others, in which case you would give landscape states that will be preferentially converted a higher probability). For simplicity, we recommend using a probability of 1.

Add this transition by clicking on the "Transitions" tab at the bottom of the "Transition Pathways" tab. Here you will add a new row for each landscape state in each vegetation type for the development transition. For example (highlighted in Figure 24), add a development transition for hardwood stands in the *Atlantic Coastal Plain Upland Longleaf Pine* (UplandLong) vegetation type by selecting "UplandLong" under "Vegetation Type" and "Hard:CLS-SPAR" under "Class". Under "To Vegetation Type", select "Other", and select "Other:ALL" under "To Class". Select "Development" under "Transition Type" with a Probability and Proportion of "1", and "Age Min" and "Age Max" of 0 and 999, and an "Age Shift" of "-9999". Indicate "Yes" under "Age Reset" as well as "0" and "9999" under "TST Min" and "TST Max". Finally, add "-9999" under "TST Shift". In this example, these inputs specify that a landscape cell containing a hardwood stand will move to the Other state class (and the vegetation type will become Other as well) due to the Development transition with certainty, no matter how long it has been since a disturbance last occurred. When this happens, the age of the stand (or landscape cell) will reset to 0. This transition should be added to all landscape states (except Water) in each of the three vegetation types with identical parameters (with the exception of the "From Class" field).

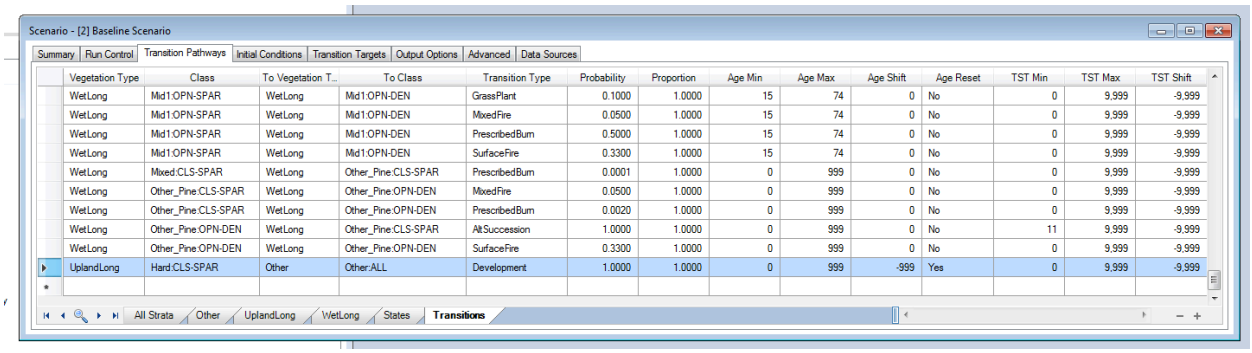

Vegetation Type	Class	To Vegetation T...	To Class	Transition Type	Probability	Proportion	Age Min	Age Max	Age Shift	Age Reset	TST Min	TST Max	TST Shift
WetLong	Mid1:OPN-SPAR	WetLong	Mid1:OPN-DEN	GrassPlant	0.1000	1.0000	15	74	0	No	0	9,999	-9,999
WetLong	Mid1:OPN-SPAR	WetLong	Mid1:OPN-DEN	MixedFire	0.0500	1.0000	15	74	0	No	0	9,999	-9,999
WetLong	Mid1:OPN-SPAR	WetLong	Mid1:OPN-DEN	PrescribedBurn	0.5000	1.0000	15	74	0	No	0	9,999	-9,999
WetLong	Mid1:OPN-SPAR	WetLong	Mid1:OPN-DEN	SurfaceFire	0.3300	1.0000	15	74	0	No	0	9,999	-9,999
WetLong	Mixed:CLS-SPAR	WetLong	Other_Pine:CLS-SPAR	PrescribedBurn	0.0001	1.0000	0	999	0	No	0	9,999	-9,999
WetLong	Other_Pine:CLS-SPAR	WetLong	Other_Pine:OPN-DEN	MixedFire	0.0500	1.0000	0	999	0	No	0	9,999	-9,999
WetLong	Other_Pine:CLS-SPAR	WetLong	Other_Pine:OPN-DEN	PrescribedBurn	0.0020	1.0000	0	999	0	No	0	9,999	-9,999
WetLong	Other_Pine:OPN-DEN	WetLong	Other_Pine:CLS-SPAR	AltSuccession	1.0000	1.0000	0	999	0	No	11	9,999	-9,999
WetLong	Other_Pine:OPN-DEN	WetLong	Other_Pine:OPN-DEN	SurfaceFire	0.3300	1.0000	0	999	0	No	0	9,999	-9,999
UplandLong	Hard:CLS-SPAR	Other	Other:ALL	Development	1.0000	1.0000	0	999	-999	Yes	0	9,999	-9,999

Figure 24. Probabilistic transitions between state classes related to the Development transition in *Atlantic Coastal Plain Upland Longleaf Pine* (UplandLong), *Central Atlantic Coastal Plain Wet Longleaf Pine* (WetLong), and *Other* biophyscial settings present in the model for Marine Corps Base Camp Lejeune.

Given this parameterization alone, all landscape cells would be converted to the Developed state during a simulation. Therefore, we also need to set transition targets and use a spatial multiplier file to further govern this transition. Spatial multipliers are generally used to tell the model when and where to apply a given transition.

In the scenario window, click on the “Advanced” tab, and expand the menu for “Transitions-Spatial” on the menu along the left-hand side of the screen. Then select “Transition Spatial Multipliers”. Next, choose “Development” in the dropdown for “Transition Group”. In the final parameterization step for this option, you then need to upload a Geo.TIFF map that will act as a spatial multiplier. In ArcGIS, create a raster file where all cells that should be developed during the simulation have a value of “1” and all cells that should not be developed a value of “0”. This raster must be in the same projection and have the same size and extent as the Geo.TIFF files used to initialize the model. Export this raster file as a Geo.TIFF. See Figure 25 for an example of what this spatial multiplier landscape map should look like.

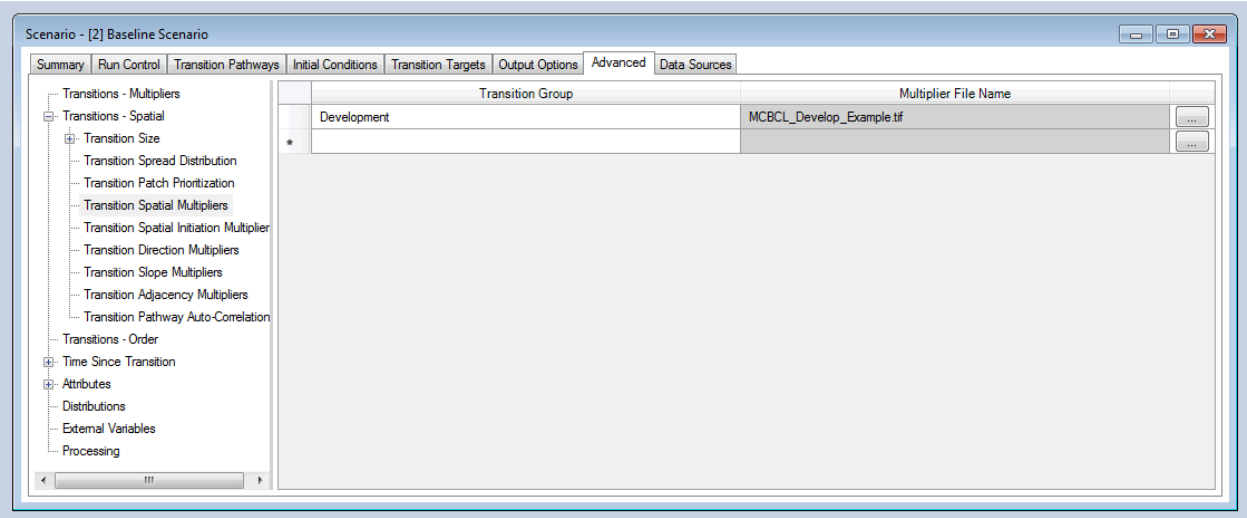

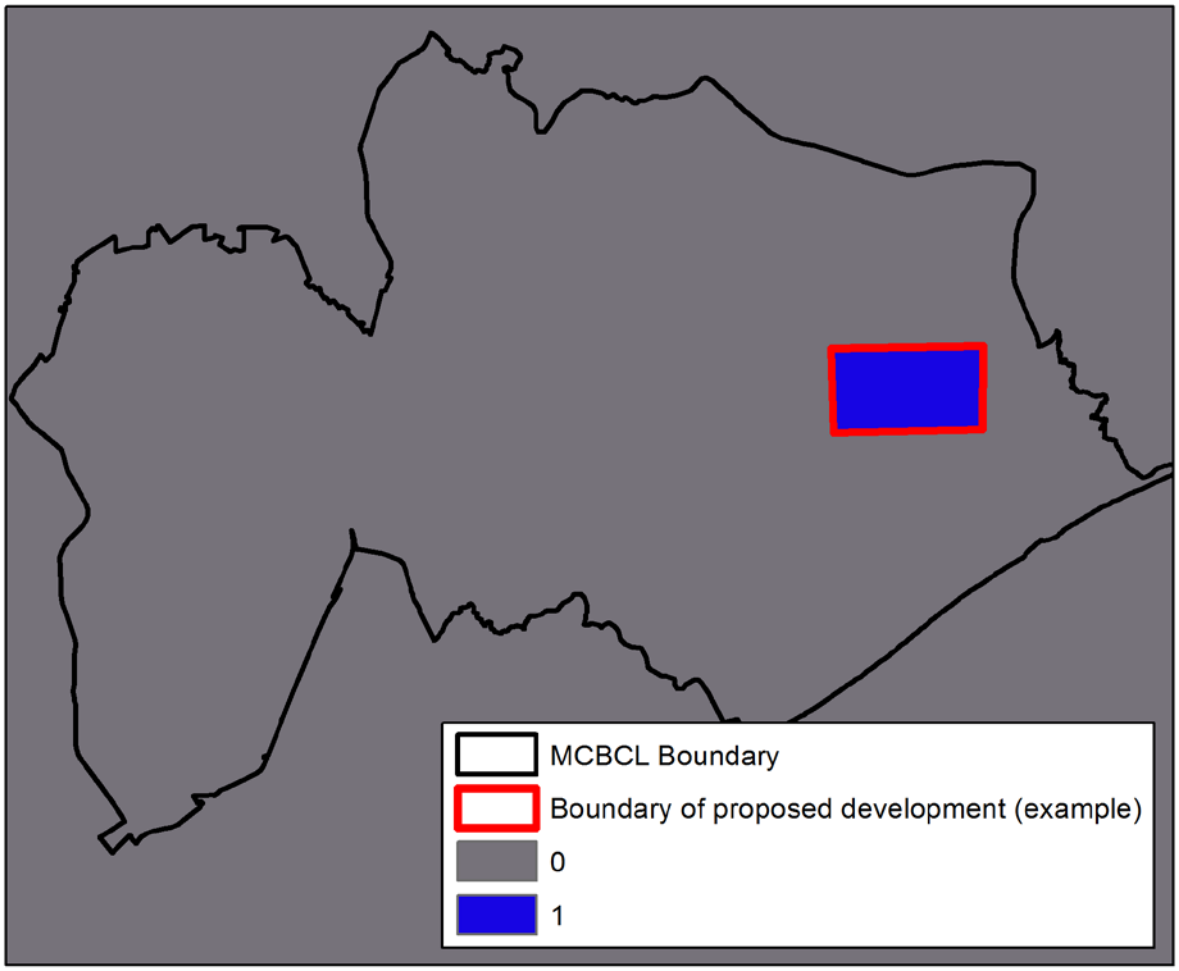

Figure 25. An example of spatial multiplier files (file type: Geo.TIFF) used to spatially constrain the development transition within a specific area on Marine Corps Base Camp Lejeune (MCBCL).

Under this parameterization, the ST-SIM model will evaluate each landscape cell such that the cell's state-specific probabilities for all transitions in the transition group selected in the Spatial Multipliers table (in this example, Development) are multiplied by the cell's corresponding spatial multiplier value given in the Spatial Multiplier Geo.TIFF. In the example shown in Figure 25, the probability for experiencing the Development transition for all cells outside of the blue development footprint (1) will be multiplied by 0, resulting in a 0 probability that those cells will be development. However, the probability for experiencing the Development transition for all cells inside the blue development footprint (1) will be multiplied by 1, and those cells will transition to the Other:ALL state.

This procedure can also be used to simulate a variety of other scenarios. For instance, instead of using only values of 0 and 1 to turn transitions on and off, you can give landscape cells in the spatial multiplier Geo.TIFF file values between 0 and 1 to increase the probabilities that certain landscape cells will experience specified transitions over others. Using this parameterization, transitions would still occur outside of the specified area, just at a lower probability.

8. Landscape Input Values and Maps in ArcGIS

To run a meaningful simulation of the ST-SIM model, an understanding of the landscape's composition is critical when initializing the model. If you plan to run a non-spatial version of the model, you will need to know the percentage of the total landscape in each landscape state used in the model. In this scenario, the landscape's composition is important, but the spatial distribution of those states will not be considered. On the other hand, a spatially explicit simulation of the model will require that you upload maps of the study area that show both the composition and distribution of the landscape states.

We created maps in ArcGIS version 10 (ESRI) to convey this information for MCBCL. These maps were necessary for calculating the landscape composition for the non-spatial simulation and for providing the necessary parameters for the spatially explicit simulation. The State Class map was used to determine the landscape composition (non-spatial simulation) while the Vegetation Type, State Class, and Age maps were used to parameterize the spatially explicit simulation.

All maps required to initialize an ST-SIM landscape model for MCBCL have been created using LANDFIRE products, representing base characteristics for the year 2014. These files, in both Geo.TIFF and raster formats, accompany this guide.

8.1 Vegetation Type map

To run a spatially explicit model in ST-SIM, a vegetation type map must be uploaded under the "Initial Conditions" tab. This map delineates zones that limit what type of vegetation (and which landscape states) can occur in those areas. For example, these zones could be based on underlying soil or ecoregion types. In this model for MCBCL, we considered separate zones for the *Atlantic Coastal Plain Upland Longleaf Pine* (UplandLong), *Central Atlantic Coastal Plain*

Wet Longleaf Pine (WetLong), and *Other* biophyscial settings. To create this file, we downloaded the Biophysical Settings layer for our area of interest for the year 2014 (https://www.landfire.gov/vegetation.php). In ArcGIS, we exported the .tiff file to a raster and reclassified the layer such that 'Atlantic Coastal Plains Fall-Line Sandhills Longleaf Pine Woodland' and 'Atlantic Coastal Plain Upland Longleaf Pine Woodland' were give a value of '1'; 'Central Atlantic Coastal Plain Wet Longleaf Pine Savanna and Flatwoods' were given a value of '2'; and all other settings were given a value of 3. These represent the Vegetation Types used in the model for (1) Upland Longleaf, (2) Wet Longleaf, and (3) Other. We clipped this map within the confines of the MCBCL footprint and reprojected the map to have a projection of NAD83 UTM Zone 18N. Finally, we exported the map as a tiff file for use in ST-SIM. See Figure 26 for an example of what the vegetation type map should look like.

8.2 State Class map

To create the state class map, we combined information on the biophysical setting, vegetation cover, and successional state for all landscape cells within the boundaries of MCBCL. We downloaded LANDFIRE layers for Biophysical Setting, Existing Vegetation Type, and Succession Classes for the year 2014 for our area of interest (https://www.landfire.gov/vegetation.php). In ArcGIS, we converted each of these layers to a raster, clipped rasters within the boundaries of MCBCL, and reprojected layers to NAD83 UTM Zone 18N.

We reclassified the Existing Vegetation Type layer to depict landcover types represented in our ST-SIM model. This reclassification is shown in Table 4. We then combined this reclassified layer with the reclassified Biophyscial Settings layer (*Section 8.1 Vegetation Type map*) and the Succession Classes raster using the "Combine" tool in ArcGIS. Each landscape cell in the resulting raster had a value for biophysical setting, vegetation type, and succession type. We specified state classes as shown in Table 5. We exported the combined raster such that cells were given the value associated with their state class (see 'ID' in Table 1). Finally, we exported the map as a .tiff file for use in ST-SIM. See Figure 27 for an example of what the vegetation type map should look like.

The attribute table associated with this layer can then be used to specify the composition of landscape states within the study for non-spatially explicit simulations, while the .tiff version of the map can be used to specify the composition and spatial distribution of states in spatially explicit simulations.

8.3 Age map

Finally, a spatially explicit ST-SIM simulation requires a map of stand ages for all relevant states. We created an age layer for the year 2014 using the state class layer (described in *Section 8.2 State Class map*). We made assumptions about the age of the stand based on the state class as shown in Table 5. We exported the State Class raster such that cells were given the value associated with their ages (Table 5). We then exported the map as a .tiff file for use in ST-SIM. See Figure 28 for an example of what the vegetation type map should look like.

Table 4. Reclassification of vegetation types contained in the Existing Vegetation Types LANDFIRE product (https://www.landfire.gov/vegetation.php) to landcover classes contained in the ST-SIM landscape model of longleaf pine ecosystem dynamics at Marine Corps Base Camp Lejeune, Fort Bragg, and Eglin Air Force Base. The ST-SIM landscape model was designed to simulate habitat dynamics for red-cockaded woodpeckers in the southeastern United States. Vegetation types correspond to states listed in Table 1.

LANDFIRE Class Name	LANDFIRE Life Form	LANDFIRE Subclass	Vegetation Type (Reclassified Type)	Reclassified Value
Atlantic Coastal Plain Clay-Based Carolina Bay Wetland	Tree	Hardwood	Hard:CLS-SPAR	200
Atlantic Coastal Plain Fall-line Sandhills Longleaf Pine Woodland	Tree	Conifer	Longleaf (Succession TBD)	600
Atlantic Coastal Plain Peatland Pocosin and Canebrake Shrubland	Shrub	Shrubland	Other Pine (Succession TBD)	400
Atlantic Coastal Plain Peatland Pocosin and Canebrake Woodland	Tree	Shrubland	Other Pine (Succession TBD)	400
Atlantic Coastal Plain Streamhead Seepage Swamp-Pocosin-Baygall	Tree	Riparian	Other Pine (Succession TBD)	400
Atlantic Coastal Plain Upland Longleaf Pine Woodland	Tree	Conifer	Longleaf (Succession TBD)	600
Barren	Barren	Barren	Bare:ALL	100
Central Atlantic Coastal Plain Maritime Forest	Tree	Hardwood	Hard:CLS-SPAR	200
Central Atlantic Coastal Plain Wet Longleaf Pine Savanna and Flatwoods	Tree	Conifer	Longleaf (Succession TBD)	600
Central Atlantic Coastal Plain Wet Longleaf Pine Savanna and Shrubland	Shrub	Conifer	Longleaf (Succession TBD)	600
Developed-High Intensity	Developed	Developed-High	Other:ALL	500
Developed-Low Intensity	Developed	Developed-Low	Other:ALL	500
Developed-Medium Intensity	Developed	Developed-Med	Other:ALL	500
Developed-Roads	Developed	Developed-Roads	Other:ALL	500
East Gulf Coastal Plain Interior Upland Longleaf Pine Woodland	Tree	Conifer	Other Pine (succession TBD)	400
East Gulf Coastal Plain Maritime Forest	Tree	Hardwood	Hard:CLS-SPAR	200
East Gulf Coastal Plain Near-Coast Pine Flatwoods	Tree	Conifer	Other Pine (succession TBD)	400
East Gulf Coastal Plain Savanna and Wet Prairie	Herb	Riparian	Water:ALL	700
East Gulf Coastal Plain Wet Prairie Grassland	Herb	Riparian	Bare:ALL	100
East Gulf Coastal Plain Wet Prairie Shrubland	Shrub	Riparian	Bare:ALL	100
Eastern Cool Temperate Close Grown Crop	Agriculture	Agricultural	Other:ALL	500
Eastern Cool Temperate Developed Ruderal Deciduous Forest	Tree	Developed	Other:ALL	500
Eastern Cool Temperate Developed Ruderal Evergreen Forest	Tree	Developed	Other:ALL	500
Eastern Cool Temperate Developed Ruderal Grassland	Herb	Developed	Other:ALL	500
Eastern Cool Temperate Developed Ruderal Shrubland	Shrub	Developed	Other:ALL	500
Eastern Cool Temperate Fallow/Idle Cropland	Herb	Agricultural	Other:ALL	500
Eastern Cool Temperate Pasture and Hayland	Herb	Agricultural	Other:ALL	500
Eastern Cool Temperate Row Crop	Agriculture	Agricultural	Other:ALL	500
Eastern Cool Temperate Row Crop - Close Grown Crop	Agriculture	Agricultural	Other:ALL	500
Eastern Cool Temperate Undeveloped Ruderal Grassland	Herb	Developed	Other:ALL	500
Eastern Cool Temperate Urban Deciduous Forest	Tree	Developed	Other:ALL	500

Eastern Cool Temperate Urban Evergreen Forest	Tree	Developed	Other:ALL	500
Eastern Cool Temperate Urban Herbaceous	Herb	Developed	Other:ALL	500
Eastern Cool Temperate Urban Mixed Forest	Tree	Developed	Other:ALL	500
Eastern Cool Temperate Urban Shrubland	Shrub	Developed	Other:ALL	500
Eastern Warm Temperate Aquaculture	Agriculture	Agricultural	Other:ALL	500
Eastern Warm Temperate Close Grown Crop	Agriculture	Agricultural	Other:ALL	500
Eastern Warm Temperate Developed Ruderal Deciduous Forest	Tree	Developed	Other:ALL	500
Eastern Warm Temperate Developed Ruderal Evergreen Forest	Tree	Developed	Other:ALL	500
Eastern Warm Temperate Developed Ruderal Grassland	Herb	Developed	Other:ALL	500
Eastern Warm Temperate Developed Ruderal Mixed Forest	Tree	Developed	Other:ALL	500
Eastern Warm Temperate Developed Ruderal Shrubland	Shrub	Developed	Other:ALL	500
Eastern Warm Temperate Fallow/Idle Cropland	Herb	Agricultural	Other:ALL	500
Eastern Warm Temperate Orchard	Tree	Agricultural	Other:ALL	500
Eastern Warm Temperate Pasture and Hayland	Herb	Agricultural	Other:ALL	500
Eastern Warm Temperate Row Crop	Agriculture	Agricultural	Other:ALL	500
Eastern Warm Temperate Row Crop - Close Grown Crop	Agriculture	Agricultural	Other:ALL	500
Eastern Warm Temperate Undeveloped Ruderal Grassland	Herb	Developed	Other:ALL	500
Eastern Warm Temperate Urban Urban Deciduous Forest	Tree	Developed	Other:ALL	500
Eastern Warm Temperate Urban Urban Evergreen Forest	Tree	Developed	Other:ALL	500
Eastern Warm Temperate Urban Urban Herbaceous	Herb	Developed	Other:ALL	500
Eastern Warm Temperate Urban Urban Mixed Forest	Tree	Developed	Other:ALL	500
Eastern Warm Temperate Urban Urban Shrubland	Shrub	Developed	Other:ALL	500
Eastern Warm Temperate Wheat	Agriculture	Agricultural	Other:ALL	500
Florida Longleaf Pine Sandhill	Tree	Conifer	Longleaf (succession TBD)	600
Floridian Highlands Freshwater Marsh Herbaceous	Herb	Riparian	Water:ALL	700
Floridian Highlands Freshwater Marsh Shrubland	Shrub	Riparian	Bare:ALL	100
Gulf and Atlantic Coastal Plain Floodplain Forest	Tree	Riparian	Other Pine (Succession TBD)	400
Gulf and Atlantic Coastal Plain Floodplain Herbaceous	Herb	Riparian	Bare:ALL	100
Gulf and Atlantic Coastal Plain Floodplain Shrubland	Shrub	Riparian	Other Pine (Succession TBD)	400
Gulf and Atlantic Coastal Plain Small Stream Riparian Herbaceous	Herb	Riparian	Bare:ALL	100
Gulf and Atlantic Coastal Plain Small Stream Riparian Shrubland	Shrub	Riparian	Other Pine (Succession TBD)	400
Gulf and Atlantic Coastal Plain Small Stream Riparian Woodland	Tree	Riparian	Other Pine (Succession TBD)	400
Gulf and Atlantic Coastal Plain Sparsely Vegetated Systems	Sparse	Sparse Vegetated	Bare:ALL	100
Gulf and Atlantic Coastal Plain Swamp Systems	Tree	Riparian	Hard:CLS-SPAR	200
Gulf and Atlantic Coastal Plain Tidal Marsh Herbaceous	Herb	Riparian	Bare:ALL	100
Gulf and Atlantic Coastal Plain Tidal Marsh Shrubland	Shrub	Riparian	Bare:ALL	100
Introduced Upland Vegetation-Perennial Grassland and Forbland	Herb	Exotic Herb	Bare:ALL	100
Introduced Upland Vegetation-Treed	Tree	Exotic Tree-Shrub	Hard:CLS-SPAR	200
Introduced Wetland Vegetation-Herbaceous	Herb	Exotic Herb	Bare:ALL	100
Introduced Wetland Vegetation-Tree	Tree	Riparian	Mixed:CLS-SPAR	300

Managed Tree Plantation-Southeast Conifer and Hardwood Plantation	Tree	Conifer	Other Pine (Succession TBD)	400
Open Water	Water	Open Water	Water:ALL	700
Quarries-Strip Mines-Gravel Pits	Barren	Quarries, etc.	Other:ALL	500
Recently Burned-Herb and Grass Cover	Herb	Grassland	Bare:ALL	100
Recently Logged-Herb and Grass Cover	Herb	Grassland	Bare:ALL	100
Ruderal Upland-Treed	Tree	Conifer/Hard	Mixed:CLS-SPAR	300
Southern Atlantic Coastal Plain Dry and Dry-Mesic Oak Forest	Tree	Hardwood	Hard:CLS-SPAR	200
Southern Atlantic Coastal Plain Maritime Forest	Tree	Hardwood	Other Pine (Succession TBD)	400
Southern Atlantic Coastal Plain Mesic Hardwood Forest	Tree	Hardwood	Hard:CLS-SPAR	200
Southern Atlantic Coastal Plain Nonriverine Swamp and Wet Hardwood	Tree	Riparian	Hard:CLS-SPAR	200
Southern Coastal Plain Dry Upland Hardwood Forest	Tree	Hardwood	Hard:CLS-SPAR	200
Southern Coastal Plain Mesic Slope Forest	Tree	Hardwood	Mixed:CLS-SPAR	300
Southern Coastal Plain Nonriverine Cypress Dome Herbaceous	Herb	Hardwood	Hard:CLS-SPAR	200
Southern Coastal Plain Nonriverine Cypress Dome Woodland	Tree	Hardwood	Hard:CLS-SPAR	200
Southern Coastal Plain Seepage Swamp and Baygall Shrubland	Shrub	Riparian	Mixed:CLS-SPAR	300
Southern Coastal Plain Seepage Swamp and Baygall Woodland	Tree	Riparian	Mixed:CLS-SPAR	300

Table 5. Determination of ST-SIM state classes based on LANDFIRE data products depicting Existing Vegetation Types (reclassified according to Table 4) and Succession Classes (https://www.landfire.gov/vegetation.php). These state classes correspond with those listed in Table 1 and are intended to model longleaf pine ecosystem dynamics at Marine Corps Base Camp Lejeune, Fort Bragg, and Eglin Air Force Base. Stand ages were assumed based on succession and state class. The ST-SIM landscape model was designed to simulate habitat dynamics for red-cockaded woodpeckers in the southeastern United States.

Vegetation Type	Succession Class	State Class	State Class Code	Stand Age
Bare Land	Class C - Mid-Development 1, Open	Bare:ALL	1	0
Bare Land	Class D - Late-Development 1, Open	Bare:ALL	1	0
Bare Land	Class A - Early-Development 1	Bare:ALL	1	0
Bare Land	Barren	Bare:ALL	1	0
Bare Land	Uncharacteristic Exotic Veg	Bare:ALL	1	0
Bare Land	Uncharacteristic Native Veg (assumed Closed)	Bare:ALL	1	0
Bare Land	Class B - Mid-Development 1, Closed	Bare:ALL	1	0
Hardwood Stand	Uncharacteristic Native Veg (assumed Closed)	Hard:CLS-SPAR	3	50
Hardwood Stand	Class C - Mid-Development 1, Open	Hard:CLS-SPAR	3	50
Hardwood Stand	Class B - Mid-Development 1, Closed	Hard:CLS-SPAR	3	50
Hardwood Stand	Class D - Late-Development 1, Open	Hard:CLS-SPAR	3	50
Hardwood Stand	Class A - Early-Development 1	Hard:CLS-SPAR	3	50
Hardwood Stand	Class E - Late-Development 1, Closed	Hard:CLS-SPAR	3	50
Hardwood Stand	Uncharacteristic Exotic Veg (assumed closed)	Hard:CLS-SPAR	3	50
Longleaf Pine	Class E - Late-Development 1, Closed	Late1:CLS-SPAR	4	75
Longleaf Pine	Class D - Late-Development 1, Open	Late1:OPN-DEN	5	75
Longleaf Pine	Class C - Mid-Development 1, Open	Mid1:OPN-DEN	8	60
Longleaf Pine	Class B - Mid-Development 1, Closed	Mid1:CLS-SPAR	7	60
Longleaf Pine	Class A - Early-Development 1	Early1:ALL	2	7
Longleaf Pine	Uncharacteristic Native Veg (assumed Closed)	Late1:CLS-SPAR	4	75
Mixed Hardwood/Pine Stand	Class C - Mid-Development 1, Open	Mixed:CLS-SPAR	10	50
Mixed Hardwood/Pine Stand	Class B - Mid-Development 1, Closed	Mixed:CLS-SPAR	10	50
Mixed Hardwood/Pine Stand	Class A - Early-Development 1	Mixed:CLS-SPAR	10	50
Mixed Hardwood/Pine Stand	Class D - Late-Development 1, Open	Mixed:CLS-SPAR	10	50
Mixed Hardwood/Pine Stand	Uncharacteristic Native Veg (assumed Closed)	Mixed:CLS-SPAR	10	50
Mixed Hardwood/Pine Stand	Class E - Late-Development 1, Closed	Mixed:CLS-SPAR	10	50
Other (non-longleaf) Pine Stand	Class B - Mid-Development 1, Closed	Other_Pine:CLS-SPAR	12	60
Other (non-longleaf) Pine Stand	Class C - Mid-Development 1, Open	Other_Pine:OPN-DEN	13	60
Other (non-longleaf) Pine Stand	Class E - Late-Development 1, Closed	Other_Pine:CLS-SPAR	12	60

Other (non-longleaf) Pine Stand	Class A - Early-Development 1	Other_Pine:OPN-DEN	13	60
Other (non-longleaf) Pine Stand	Uncharacteristic Native Veg (assumed Closed)	Other_Pine:CLS-SPAR	12	60
Other (non-longleaf) Pine Stand	Class D - Late-Development 1, Open	Other_Pine:OPN-DEN	13	60
Other Landcover	Urban	Other:ALL	11	0
Other Landcover	Agriculture	Other:ALL	11	0
Water	Water	Water:ALL	14	0
Water	Class A - Early-Development 1	Water:ALL	14	0
Water	Class D - Late-Development 1, Open	Water:ALL	14	0
Water	Class E - Late-Development 1, Closed	Water:ALL	14	0

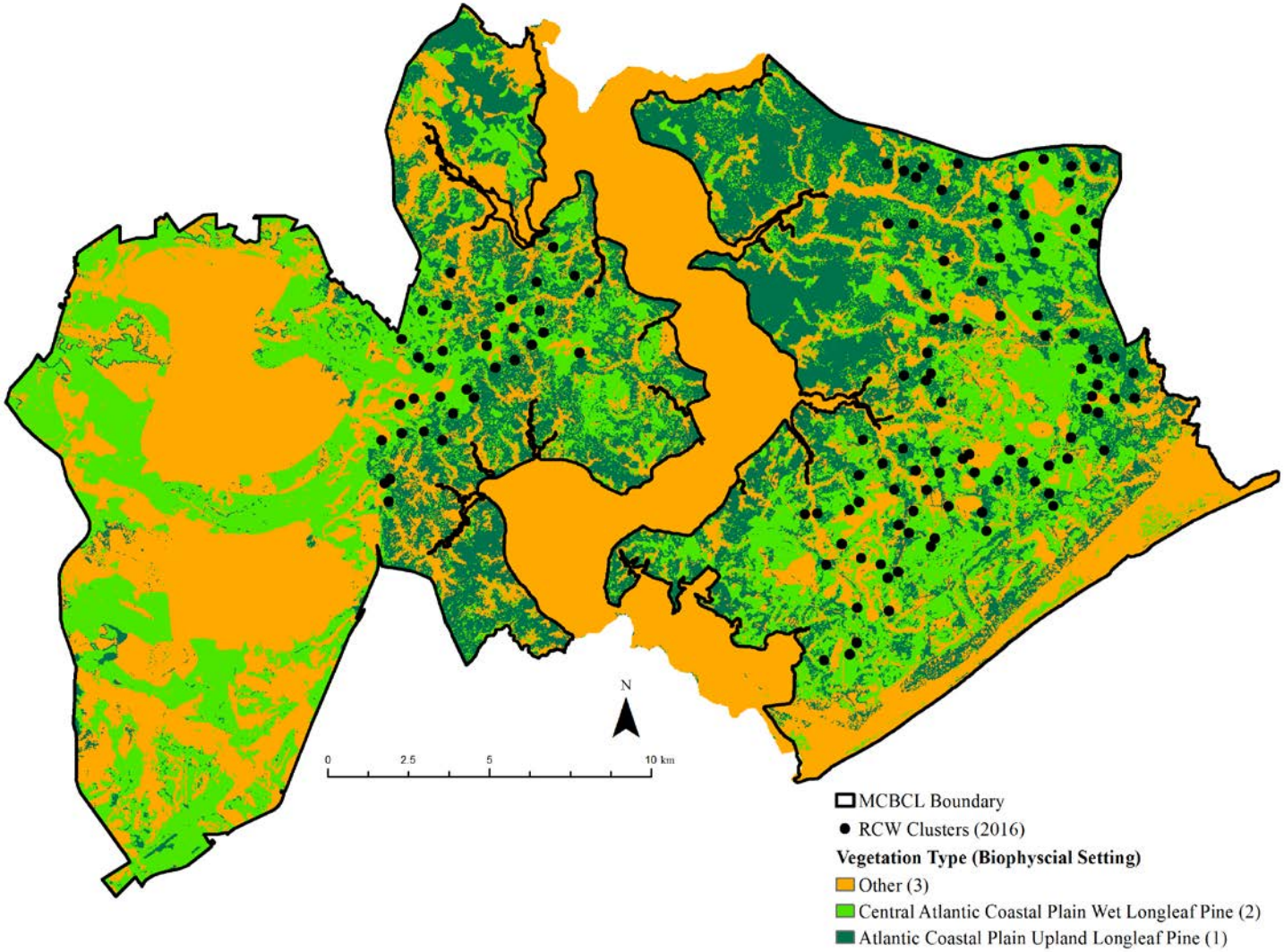

Figure 26. Vegetation types (or biophysical settings) represented on Marine Corps Base Camp Lejeune and included in the ST-SIM landscape model. Information derived from LANDFIRE products.

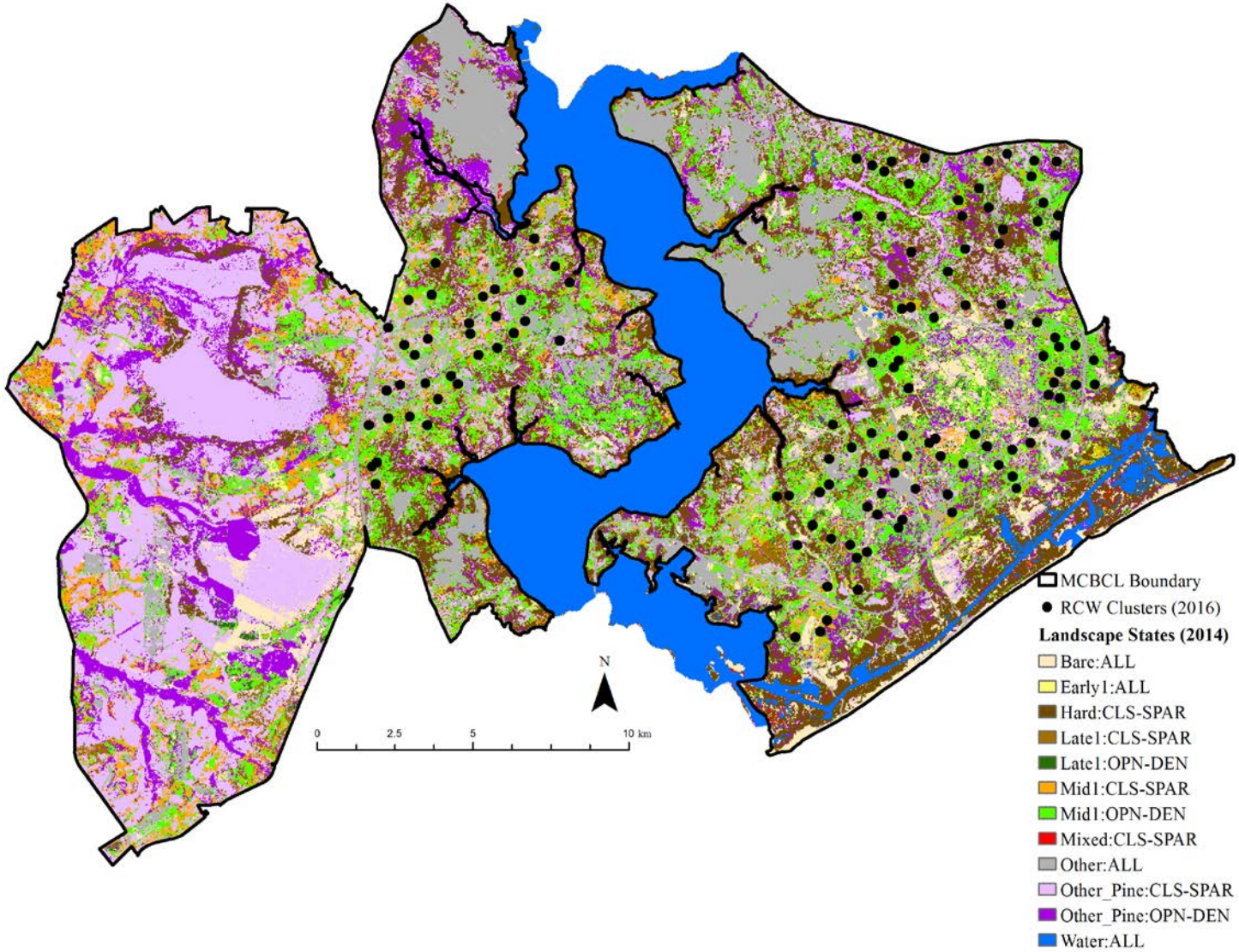

Figure 27. State classes represented on Marine Corps Base Camp Lejeune and included in the ST-SIM landscape model. Information derived from LANDFIRE products.

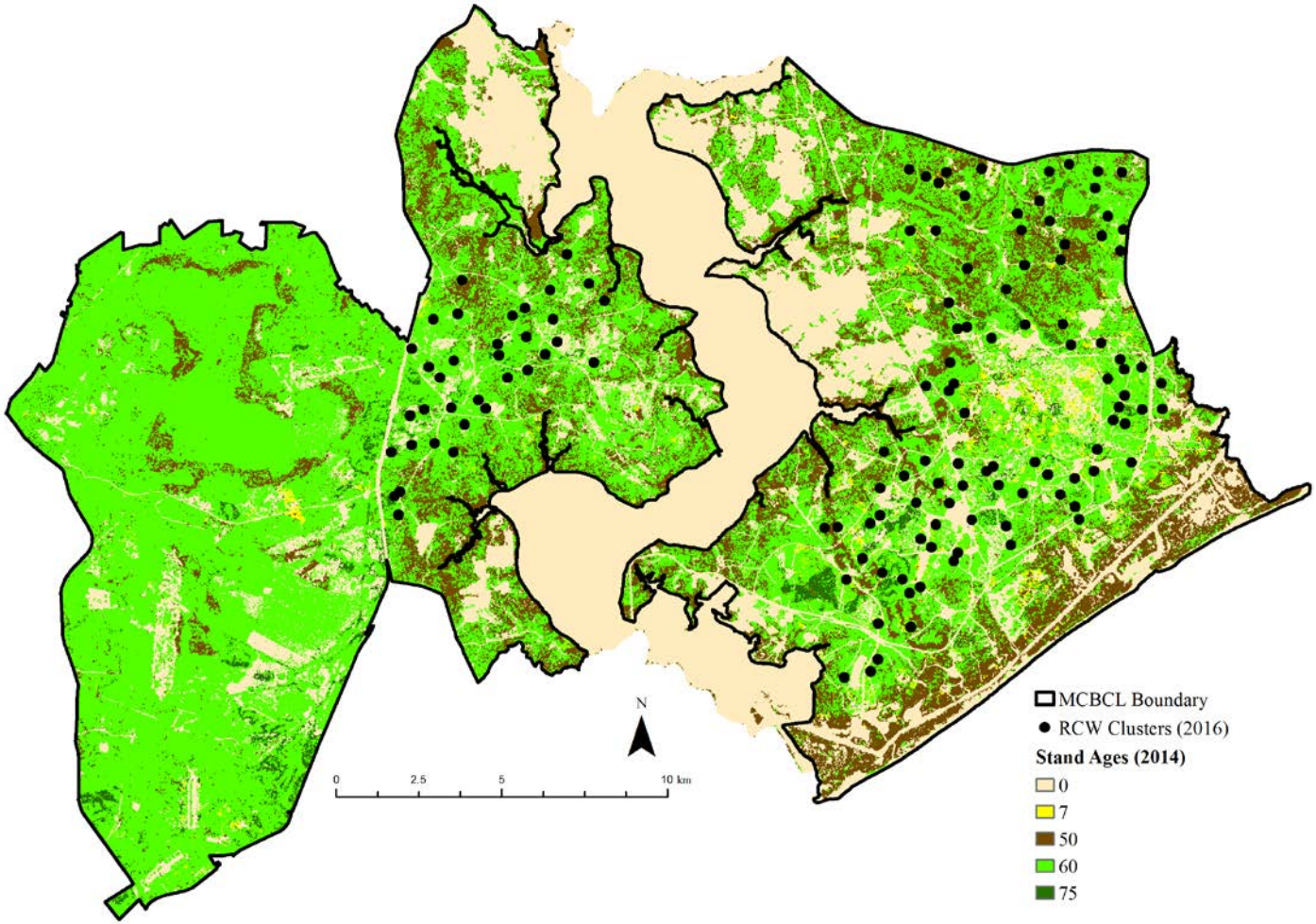

Figure 28. Stand ages represented on Marine Corps Base Camp Lejeune and included in the ST-SIM landscape model. Ages assumed based on state classes (and according to LANDFIRE data products).

References

Daniel, C., and L. Frid. 2011. Predicting landscape vegetation dynamics using state-and-transition simulation models. Pages 5-22 in B. Kerns, A. Shlisky, and C. Daniel, editors. Proceedings of the First Landscape State-and-Transition Simulation Modeling Conference, June 14-16 2011. U.S. Department of Agriculture and U.S. Forest Service, Pacific Northwest Research Station, Portland, OR.

Provencher, L., K. Galley, A. Litt, D. Gordon, L. Brennan, G. Tanner, and J. Hardesty. 2002. Fire, herbicide, and chainsaw-felling effects on arthropods in fire-suppressed longleaf pine sandhills at Eglin Air Force Base, FL. Proceedings: The Role of Fire for Nongame Wildlife Management and Community Restoration: Traditional Uses and New Directions. US Department of Agriculture and the US Forest Service, Newton Square, PA.

Provencher, L., B. Herring, D. Gordon, H. Rodgers, K. Galley, G. Tanner, J. Hardesty, and L. Brennan. 2001a. Effects of hardwood reduction techniques on longleaf pine sandhill vegetation in northwest Florida. Restoration Ecology **9**:13-27.

Provencher, L., B. Herring, D. Gordon, H. Rodgers, G. Tanner, J. Hardesty, L. Brennan, and A. Litt. 2001b. Longleaf pine and oak responses to hardwood reduction techniques in fire-suppressed sandhills in northwest Florida. Forest Ecology and Management **148**:63-77.

Rollins, M. 2009. LANDFIRE: a nationally consistent vegetation, wildland fire, and fuel assessment. International Journal of Wildland Fire **18**:235-249.

Walters, J., P. Baldassaro, K. Convery, L. Crowder, D. Kessler, R. McGregor, J. Priddy, and S. Tweddale. 2011. A Decision Support System for Identifying and Ranking Critical Habitat Parcels On and In the Vicinity of Department of Defense Installations. Final Report to the Department of Defense (SERDP RC-1472).

Zahn, S. 2015. LANDFIRE: U.S. Geological Survey Fact Sheet 2015-3047. Available at http://dx.doi.org/10.3133/fs20153047. Page 2 in U. S. G. Survey, editor, Sioux Falls, SD.

Appendix 19-E
ST-Sim Quick Reference Guide

Quick Reference Guide for the Longleaf Pine State-and-Transition Model
Developed for Red-Cockaded Woodpecker modeling applications

Sara Zeigler and Jeffrey Walters, Virginia Tech
September 2017

Additional resources:
This document is intended to act as a quick reference guide for users wishing to make small changes to baseline longleaf pine ecosystem models in the platform ST-SIM. Additional information can be found in the user's manual specific to this application as well as references available for the modeling platform more generally:

Forum of user questions: http://www.apexrms.com/forumqa/
Video tutorials: http://syncrosim.com/index.php?title=Getting_Started

****Important:** We recommend copying the Baseline scenario before making any changes. Right-click on the scenario name (e.g., Baseline scenario) in the Scenario Manager screen and click 'Copy'. Then, right-click on the project name (e.g., Marine Corps Base Camp Lejeune) and paste the copied scenario. Rename the new, copied scenario by right-clicking on the scenario and selecting Rename.

1. Run controls

The number of time steps and iterations can be set by double-clicking on a scenario name and then clicking on the Run Control tab. Uncheck the box for 'Run model spatially' if you want to run a non-spatially explicit model. See section *4.4 Simulation Controls and Initial Conditions* in the user's manual for additional information.

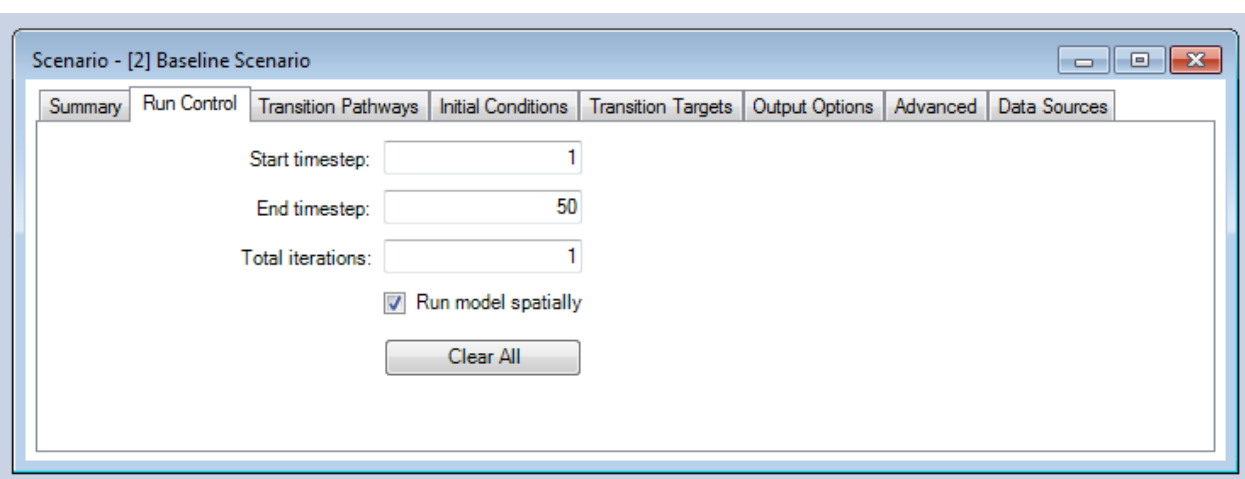

2. Changing initial landscape conditions

See section *8 Landscape Input Values and Maps in ArcGIS* for instructions on how initial landscape conditions can be determined or how initial landscape maps can be created in ArcGIS. New initial landscape maps can be added by double-clicking on the scenario in the Scenario Manager window, clicking the Initial Conditions tab, and then clicking Spatial on the left-hand side of this window. Delete existing maps by right-clicking on the cell on the left-hand side of the first row in the Raster Files table and selecting 'Delete All'. You can then click on the '…' button to navigate to new .tiff files depicting the Vegetation Type, State Class, and Age maps representative of your landscape. Information on the number of rows, cell size, etc. will populate automatically.

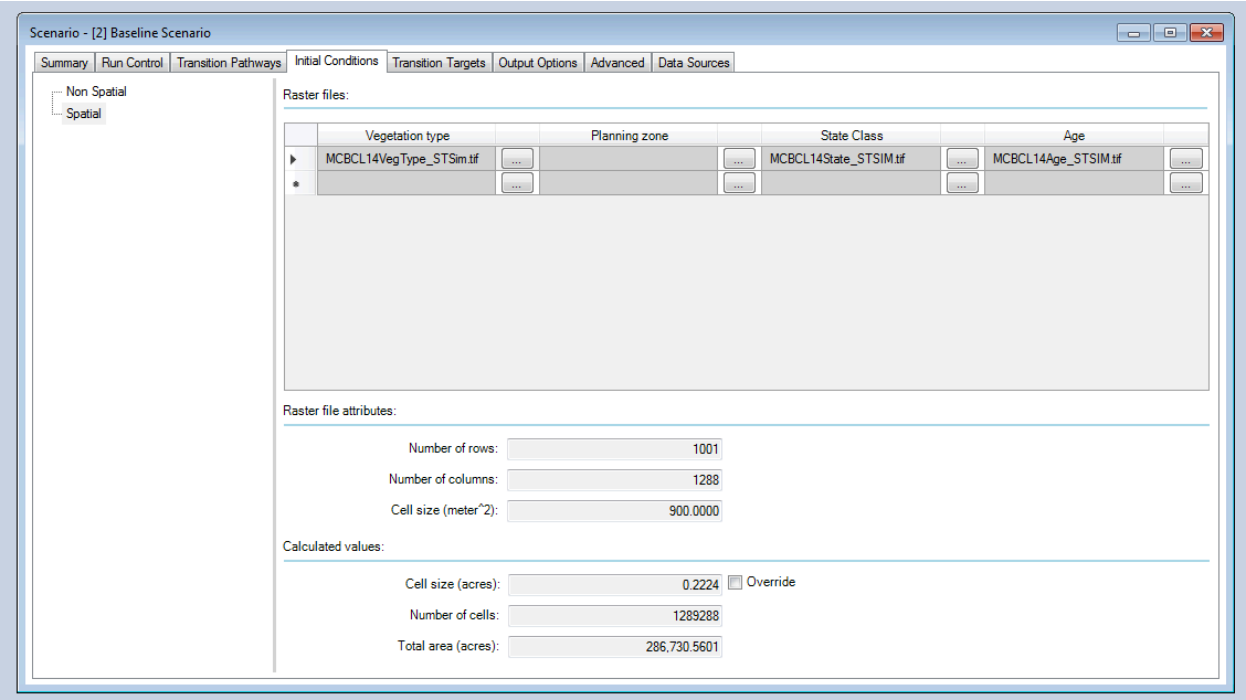

If the box for 'Run model spatially' is left unchecked under Run Controls, you click on 'Non Spatial' on the left-hand side of the Initial Conditions window. Here, you indicate the total percentage of the landscape covered by cells of a specific state class under the column for Total Amount. See section *4.4.2 Initial Landscape Conditions* in the user's manual for additional information.

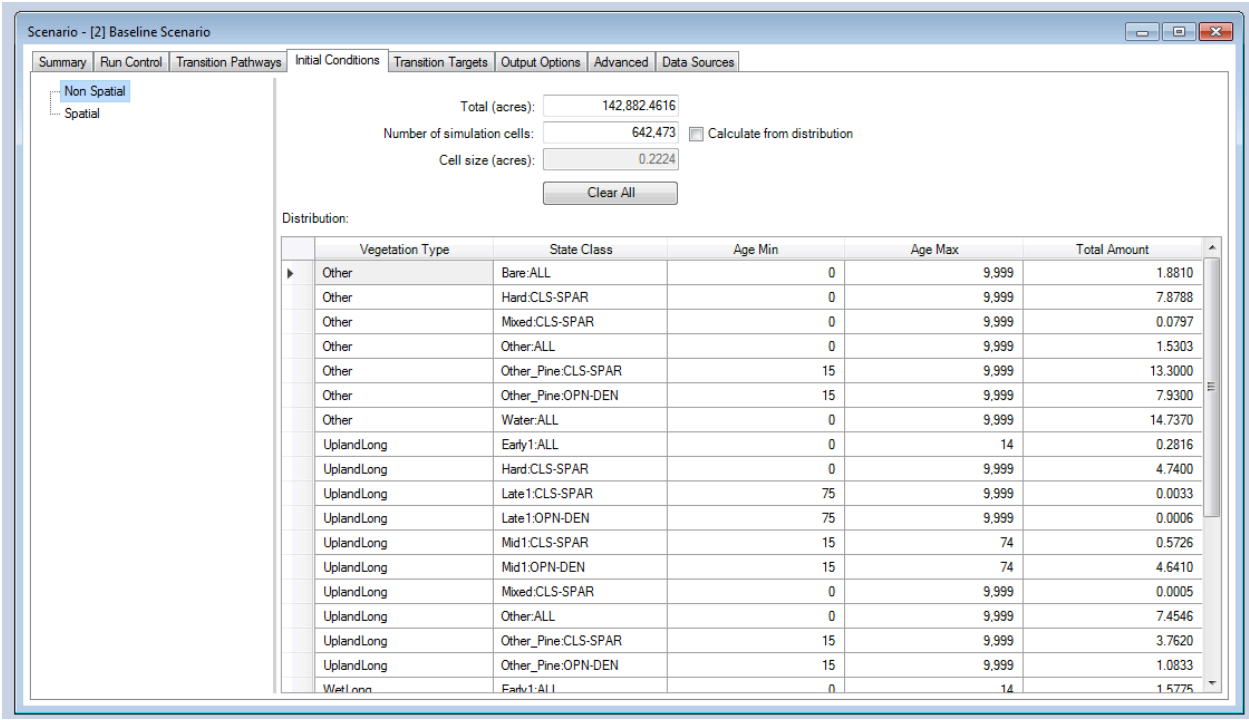

Vegetation Type	State Class	Age Min	Age Max	Total Amount
Other	Bare:ALL	0	9,999	1.8810
Other	Hard:CLS-SPAR	0	9,999	7.8788
Other	Mixed:CLS-SPAR	0	9,999	0.0797
Other	Other:ALL	0	9,999	1.5303
Other	Other_Pine:CLS-SPAR	15	9,999	13.3000
Other	Other_Pine:OPN-DEN	15	9,999	7.9300
Other	Water:ALL	0	9,999	14.7370
UplandLong	Early1:ALL	0	14	0.2816
UplandLong	Hard:CLS-SPAR	0	9,999	4.7400
UplandLong	Late1:CLS-SPAR	75	9,999	0.0033
UplandLong	Late1:OPN-DEN	75	9,999	0.0006
UplandLong	Mid1:CLS-SPAR	15	74	0.5726
UplandLong	Mid1:OPN-DEN	15	74	4.6410
UplandLong	Mixed:CLS-SPAR	0	9,999	0.0005
UplandLong	Other:ALL	0	9,999	7.4546
UplandLong	Other_Pine:CLS-SPAR	15	9,999	3.7620
UplandLong	Other_Pine:OPN-DEN	15	9,999	1.0833
WetLong	Early1:ALL	0	14	1.5775

3. Changing management targets

In ST-SIM, a user can set annual area targets for specific transitions. For example, you may want to model a scenario where 1,000 acres are intentionally burned each year. To set or change these targets, double click on a scenario name in ST-SIM and click on the Transitions Targets tab. Here, you can change the area targets (in acres) for existing transitions (here, Prescribed Burns and Non-Fire Management) by clicking in the appropriate cell under the Target Area column and typing the desired target. New transition targets can be added by selecting the appropriate Vegetation Type, Transition Group, and Target Area in a new row in this table. See section *4.3 Organization of States and Transitions* in the user's manual for additional information.

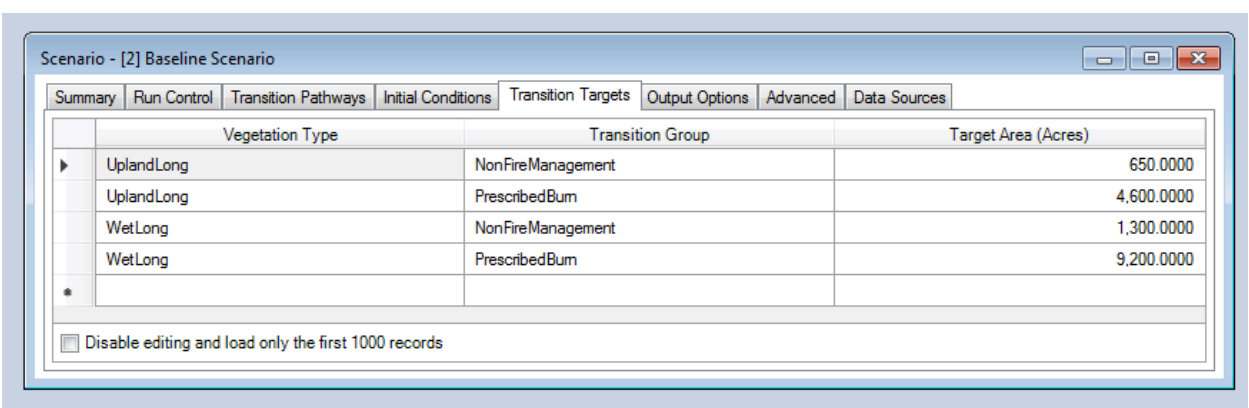

Vegetation Type	Transition Group	Target Area (Acres)
UplandLong	NonFireManagement	650.0000
UplandLong	PrescribedBurn	4,600.0000
WetLong	NonFireManagement	1,300.0000
WetLong	PrescribedBurn	9,200.0000

4. Changing the priority of management targets

Even if transition targets are set for specific transitions, probabilities associated with each state class dictate which states are treated with that management technique first. For example, states for Late1:Open-Sparse and Mid1:Open-Sparse have the highest probabilities (0.50) for experiencing a prescribed burn, followed by the Mid1:Open-Dense state (probability = 0.084). In a given simulation year, landscape cells characterized by the Late1/Mid1: Open-Sparse states will experience the Prescribed Burn transition until all such cells have been burned or until the Prescribed Burn target has been met. If all Late1/Mid1: Open-Sparse cells are burned in a given year before the target is met, then cells characterized by the Mid1:Open-Dense state will be burned until the target is met and so on.

The user can prioritize specific states for management transitions over others. Double click on a scenario name in ST-SIM and click on the Transitions Pathways tab. At the bottom of this screen, click on the Transitions tab. A state's transition probability can be changed here by typing a new value associated with any state and transition under the Probability column. States with higher probability values will preferentially experience a transition over those with lower values. In this parameterization, probabilities control the order in which states experience a transition; however, the Transition Target controls exactly how many cells in the landscape actually experience the transition. For more information, see section *4.3 Organization of States and Transitions* in the user's manual.

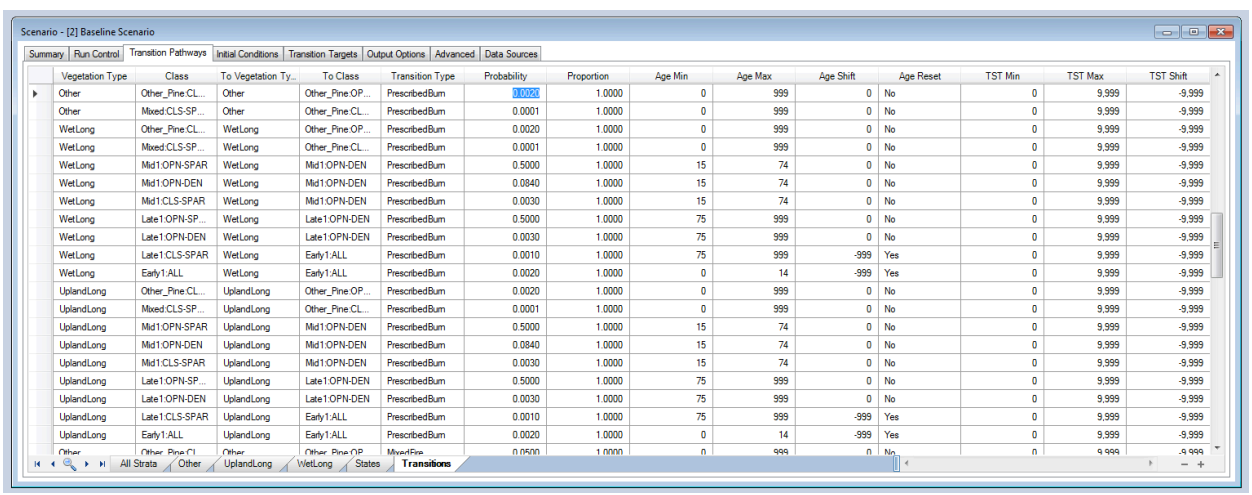

Vegetation Type	Class	To Vegetation Ty...	To Class	Transition Type	Probability	Proportion	Age Min	Age Max	Age Shift	Age Reset	TST Min	TST Max	TST Shift
Other	Other_Pine:CL...	Other	Other_Pine:OP...	PrescribedBurn	0.0020	1.0000	0	999	0	No	0	9,999	-9,999
Other	Mixed:CLS-SP...	Other	Other_Pine:CL...	PrescribedBurn	0.0001	1.0000	0	999	0	No	0	9,999	-9,999
WetLong	Other_Pine:CL...	WetLong	Other_Pine:OP...	PrescribedBurn	0.0020	1.0000	0	999	0	No	0	9,999	-9,999
WetLong	Mixed:CLS-SP...	WetLong	Other_Pine:CL...	PrescribedBurn	0.0001	1.0000	0	999	0	No	0	9,999	-9,999
WetLong	Mid1:OPN-SPAR	WetLong	Mid1:OPN-DEN	PrescribedBurn	0.5000	1.0000	15	74	0	No	0	9,999	-9,999
WetLong	Mid1:OPN-DEN	WetLong	Mid1:OPN-DEN	PrescribedBurn	0.0840	1.0000	15	74	0	No	0	9,999	-9,999
WetLong	Mid1:CLS-SPAR	WetLong	Mid1:OPN-DEN	PrescribedBurn	0.0030	1.0000	15	74	0	No	0	9,999	-9,999
WetLong	Late1:OPN-SP...	WetLong	Late1:OPN-DEN	PrescribedBurn	0.5000	1.0000	75	999	0	No	0	9,999	-9,999
WetLong	Late1:OPN-DEN	WetLong	Late1:OPN-DEN	PrescribedBurn	0.0030	1.0000	75	999	0	No	0	9,999	-9,999
WetLong	Late1:CLS-SPAR	WetLong	Early1:ALL	PrescribedBurn	0.0010	1.0000	75	999	-999	Yes	0	9,999	-9,999
WetLong	Early1:ALL	WetLong	Early1:ALL	PrescribedBurn	0.0020	1.0000	0	14	-999	Yes	0	9,999	-9,999
UplandLong	Other_Pine:CL...	UplandLong	Other_Pine:OP...	PrescribedBurn	0.0020	1.0000	0	999	0	No	0	9,999	-9,999
UplandLong	Mixed:CLS-SP...	UplandLong	Other_Pine:CL...	PrescribedBurn	0.0001	1.0000	0	999	0	No	0	9,999	-9,999
UplandLong	Mid1:OPN-SPAR	UplandLong	Mid1:OPN-DEN	PrescribedBurn	0.5000	1.0000	15	74	0	No	0	9,999	-9,999
UplandLong	Mid1:OPN-DEN	UplandLong	Mid1:OPN-DEN	PrescribedBurn	0.0840	1.0000	15	74	0	No	0	9,999	-9,999
UplandLong	Mid1:CLS-SPAR	UplandLong	Mid1:OPN-DEN	PrescribedBurn	0.0030	1.0000	15	74	0	No	0	9,999	-9,999
UplandLong	Late1:OPN-SP...	UplandLong	Late1:OPN-DEN	PrescribedBurn	0.5000	1.0000	75	999	0	No	0	9,999	-9,999
UplandLong	Late1:OPN-DEN	UplandLong	Late1:OPN-DEN	PrescribedBurn	0.0030	1.0000	75	999	0	No	0	9,999	-9,999
UplandLong	Late1:CLS-SPAR	UplandLong	Early1:ALL	PrescribedBurn	0.0010	1.0000	75	999	-999	Yes	0	9,999	-9,999
UplandLong	Early1:ALL	UplandLong	Early1:ALL	PrescribedBurn	0.0020	1.0000	0	14	-999	Yes	0	9,999	-9,999
Other	Other_Pine:CL...	Other	Other_Pine:OP...	MixedFire	0.0500	1.0000	0	999	0	No	0	9,999	-9,999

5. Changing the probability of natural transitions

The probabilities of natural transitions occurring can be changed in the same way. For example, the user may want to model the effects of more frequent hurricanes. This can be accomplished by double-clicking on a scenario name in ST-SIM and then clicking on the Transitions Pathways tab. At the bottom of this screen, click on the Transitions tab. The state's transition probability can be changed here by typing a new value associated with any state and transition under the Probability column. Unlike management transitions that have a Transition Target, there is no cap on how

many landscape cells experience a given transition – the transition probability value alone dictates the likelihood that a landscape cell in a given state will experience the transition. For more information, see section *4.3.7 Other 'Natural' Transitions* in the user's manual.

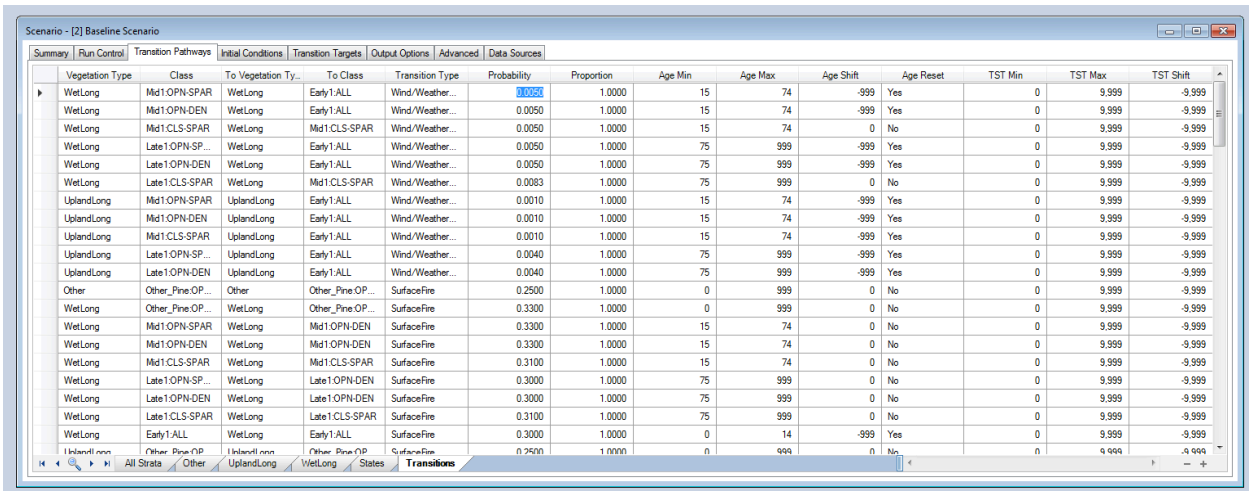

Scenario - [2] Baseline Scenario

Summary | Run Control | Transition Pathways | Initial Conditions | Transition Targets | Output Options | Advanced | Data Sources

Vegetation Type	Class	To Vegetation Ty...	To Class	Transition Type	Probability	Proportion	Age Min	Age Max	Age Shift	Age Reset	TST Min	TST Max	TST Shift
WetLong	Mid1:OPN-SPAR	WetLong	Early1:ALL	Wind/Weather...	0.0050	1.0000	15	74	-999	Yes	0	9,999	-9,999
WetLong	Mid1:OPN-DEN	WetLong	Early1:ALL	Wind/Weather...	0.0050	1.0000	15	74	-999	Yes	0	9,999	-9,999
WetLong	Mid1:CLS-SPAR	WetLong	Mid1:CLS-SPAR	Wind/Weather...	0.0050	1.0000	15	74	0	No	0	9,999	-9,999
WetLong	Late1:OPN-SP...	WetLong	Early1:ALL	Wind/Weather...	0.0050	1.0000	75	999	-999	Yes	0	9,999	-9,999
WetLong	Late1:OPN-DEN	WetLong	Early1:ALL	Wind/Weather...	0.0050	1.0000	75	999	-999	Yes	0	9,999	-9,999
WetLong	Late1:CLS-SPAR	WetLong	Mid1:CLS-SPAR	Wind/Weather...	0.0083	1.0000	75	999	0	No	0	9,999	-9,999
UplandLong	Mid1:OPN-SPAR	UplandLong	Early1:ALL	Wind/Weather...	0.0010	1.0000	15	74	-999	Yes	0	9,999	-9,999
UplandLong	Mid1:OPN-DEN	UplandLong	Early1:ALL	Wind/Weather...	0.0010	1.0000	15	74	-999	Yes	0	9,999	-9,999
UplandLong	Mid1:CLS-SPAR	UplandLong	Early1:ALL	Wind/Weather...	0.0010	1.0000	15	74	-999	Yes	0	9,999	-9,999
UplandLong	Late1:OPN-SP...	UplandLong	Early1:ALL	Wind/Weather...	0.0040	1.0000	75	999	-999	Yes	0	9,999	-9,999
UplandLong	Late1:OPN-DEN	UplandLong	Early1:ALL	Wind/Weather...	0.0040	1.0000	75	999	-999	Yes	0	9,999	-9,999
Other	Other_Pine:OP...	Other	Other_Pine:OP...	SurfaceFire	0.2500	1.0000	0	999	0	No	0	9,999	-9,999
WetLong	Other_Pine:OP...	WetLong	Other_Pine:OP...	SurfaceFire	0.3300	1.0000	0	999	0	No	0	9,999	-9,999
WetLong	Mid1:OPN-SPAR	WetLong	Mid1:OPN-DEN	SurfaceFire	0.3300	1.0000	15	74	0	No	0	9,999	-9,999
WetLong	Mid1:OPN-DEN	WetLong	Mid1:OPN-DEN	SurfaceFire	0.3300	1.0000	15	74	0	No	0	9,999	-9,999
WetLong	Mid1:CLS-SPAR	WetLong	Mid1:CLS-SPAR	SurfaceFire	0.3100	1.0000	15	74	0	No	0	9,999	-9,999
WetLong	Late1:OPN-SP...	WetLong	Late1:OPN-DEN	SurfaceFire	0.3000	1.0000	75	999	0	No	0	9,999	-9,999
WetLong	Late1:OPN-DEN	WetLong	Late1:OPN-DEN	SurfaceFire	0.3000	1.0000	75	999	0	No	0	9,999	-9,999
WetLong	Late1:CLS-SPAR	WetLong	Late1:CLS-SPAR	SurfaceFire	0.3100	1.0000	75	999	0	No	0	9,999	-9,999
WetLong	Early1:ALL	WetLong	Early1:ALL	SurfaceFire	0.3000	1.0000	0	14	-999	Yes	0	9,999	-9,999
UplandLong	Other_Pine:OP...	UplandLong	Other_Pine:OP...	SurfaceFire	0.2500	1.0000	0	999	0	No	0	9,999	-9,999

All Strata | Other | UplandLong | WetLong | States | Transitions

6. Changing the rate of succession

A user may wish to model a scenario where succession occurs faster (or slower) compared to current conditions as, for example, growing conditions are altered through climate change. To model this, double-click on a scenario name in ST-SIM and then click on the Transitions Pathways tab. At the bottom of this screen, click on the Transitions tab. For all rows where the Transition Type is 'AltSuccession' (or Alternative Succession), type a new value under 'TST Min'. Currently, in the MCBCL Baseline scenario, 10 to 20 years must go by without a fire or other management transition occurring before a landscape state with an open midstory and a dense understory is converted to a state with a closed midstory and sparse understory. Increasing the TST Min (or minimum time since a transition has occurred) will model a scenario in which succession occurs more slowly – i.e., more years can go by without a fire before a state transitions to a more closed state. Decreasing the TST Min will model a scenario in which succession occurs more quickly – i.e., fewer years can go by without a fire before a state transitions to a more closed state. For more information, see section *4.3.1 Deterministic Transitions (Succession and Aging)* and section *4.3.2 Alternative Succession in the Absence of Disturbance* in the user's manual.

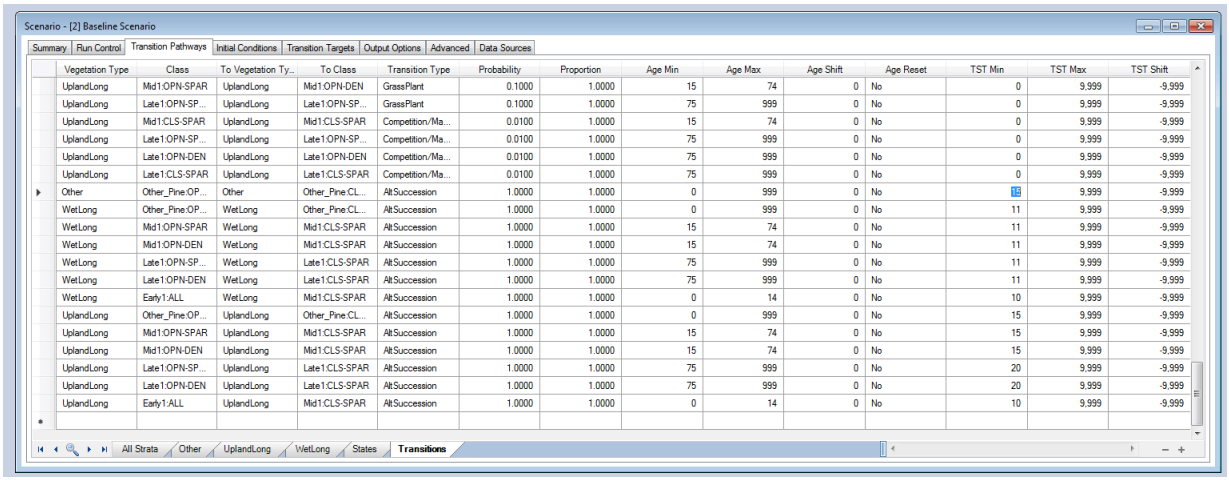

Scenario - [2] Baseline Scenario

Summary | Run Control | Transition Pathways | Initial Conditions | Transition Targets | Output Options | Advanced | Data Sources

Vegetation Type	Class	To Vegetation Ty...	To Class	Transition Type	Probability	Proportion	Age Min	Age Max	Age Shift	Age Reset	TST Min	TST Max	TST Shift
UplandLong	Mid1:OPN-SPAR	UplandLong	Mid1:OPN-DEN	GrassPlant	0.1000	1.0000	15	74	0	No	0	9,999	-9,999
UplandLong	Late1:OPN-SP...	UplandLong	Late1:OPN-SP...	GrassPlant	0.1000	1.0000	75	999	0	No	0	9,999	-9,999
UplandLong	Mid1:CLS-SPAR	UplandLong	Mid1:CLS-SPAR	Competition/Ma...	0.0100	1.0000	15	74	0	No	0	9,999	-9,999
UplandLong	Late1:OPN-SP...	UplandLong	Late1:OPN-SP...	Competition/Ma...	0.0100	1.0000	75	999	0	No	0	9,999	-9,999
UplandLong	Late1:OPN-DEN	UplandLong	Late1:OPN-DEN	Competition/Ma...	0.0100	1.0000	75	999	0	No	0	9,999	-9,999
UplandLong	Late1:CLS-SPAR	UplandLong	Late1:CLS-SPAR	Competition/Ma...	0.0100	1.0000	75	999	0	No	0	9,999	-9,999
Other	Other_Pine:OP...	Other	Other_Pine:CL...	AltSuccession	1.0000	1.0000	0	999	0	No	11	9,999	-9,999
WetLong	Other_Pine:OP...	WetLong	Other_Pine:CL...	AltSuccession	1.0000	1.0000	0	999	0	No	11	9,999	-9,999
WetLong	Mid1:OPN-SPAR	WetLong	Mid1:CLS-SPAR	AltSuccession	1.0000	1.0000	15	74	0	No	11	9,999	-9,999
WetLong	Mid1:OPN-DEN	WetLong	Mid1:CLS-SPAR	AltSuccession	1.0000	1.0000	15	74	0	No	11	9,999	-9,999
WetLong	Late1:OPN-SP...	WetLong	Late1:CLS-SPAR	AltSuccession	1.0000	1.0000	75	999	0	No	11	9,999	-9,999
WetLong	Late1:OPN-DEN	WetLong	Late1:CLS-SPAR	AltSuccession	1.0000	1.0000	75	999	0	No	11	9,999	-9,999
WetLong	Early1:ALL	WetLong	Mid1:CLS-SPAR	AltSuccession	1.0000	1.0000	0	14	0	No	10	9,999	-9,999
UplandLong	Other_Pine:OP...	UplandLong	Other_Pine:CL...	AltSuccession	1.0000	1.0000	0	999	0	No	15	9,999	-9,999
UplandLong	Mid1:OPN-SPAR	UplandLong	Mid1:CLS-SPAR	AltSuccession	1.0000	1.0000	15	74	0	No	15	9,999	-9,999
UplandLong	Mid1:OPN-DEN	UplandLong	Mid1:CLS-SPAR	AltSuccession	1.0000	1.0000	15	74	0	No	15	9,999	-9,999
UplandLong	Late1:OPN-SP...	UplandLong	Late1:CLS-SPAR	AltSuccession	1.0000	1.0000	75	999	0	No	20	9,999	-9,999
UplandLong	Late1:OPN-DEN	UplandLong	Late1:CLS-SPAR	AltSuccession	1.0000	1.0000	75	999	0	No	20	9,999	-9,999
UplandLong	Early1:ALL	UplandLong	Mid1:CLS-SPAR	AltSuccession	1.0000	1.0000	0	14	0	No	10	9,999	-9,999

All Strata | Other | UplandLong | WetLong | States | Transitions

7. Focus transitions on a given area – example, modeling development

Transitions can be constrained to a spatially specific area. For example, the user may wish to model the effects of focusing all longleaf pine management to a specific 10,000 acre plot. Alternatively, the user may wish to explore the impacts of infrastructure development in a particular area of the base. In the Transitions tab, add a new row for the Development transition for every Vegetation Type and State Class, with the Probability equal to '1' and the To Class: equal to 'Other:ALL'. (See section *4.3 Organization of States and Transitions* in the user's manual for information on how to create a new transition). Then, under the Advanced tab, click Transitions-Spatial and Transition Spatial Multipliers. Select Development under Transition Group. Under Multiplier File Name, navigate to a .tiff file previously created to define the boundaries of the development project of interest. Landscape cells in this .tiff file should have a value of 1 where development will occur and a value of 0 where development will not occur. The model will multiply the probability for the Development transition shown in the Transitions tab (in this case 1.0) by the surface depicted by the multiplier .tiff file to create a new probability value for that transition. See section *7 Advanced Model Parameterization – Spatial Multipliers* in the user's manual for more information.

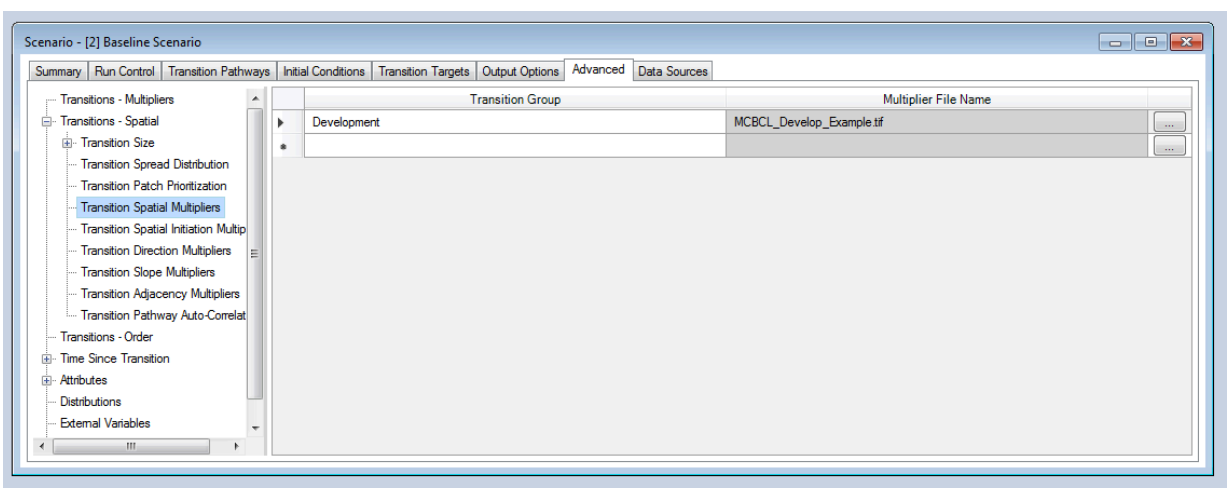

Chapter 20

Using LiDAR to Measure Forests at Marine Corps Base Camp Lejeune

SERDP Project Number: RC-2245

Research Project TSP-1

Lead Researchers:

Peter Harrell
Duke University
Durham, NC
Peter.Harrell@duke.edu

Supporting Researchers:

Pat Halpin
Pat.Halpin@duke.edu

November 2017

Final

This report was prepared under contract to the U.S. Department of Defense (DoD) Strategic Environmental Research and Development Program (SERDP). The publication of this report does not indicate endorsement by DoD, nor should the contents be construed as reflecting the official policy or position of DoD. References herein to any specific commercial product, process, or service by trade name, trademark, manufacturer, or otherwise, do not necessarily constitute or imply its endorsement, recommendation, or favoring by DoD.

Table of Contents

Acronyms 20-v
Abstract 20-1
Objectives of the Research Project 20-3
Background 20-3
Materials and Methods 20-5
LiDAR Data 20-5
Forest Stand Data 20-8
Model Development 20-10
Results and Discussion 20-11
LiDAR Forest Height and Density Measurements 20-11
Forest Stand Data and Basal Area Models 20-16
Conclusions and Implications for Future Research and Implementation 20-22
Research Questions 20-22
Findings with Implications for Future Base Management 20-23
Literature Cited 20-23

List of Figures

Figure 20-1. LiDAR processing units for MCBCL. 20-7
Figure 20-2. Forest stands, colored by age, that were used during the analysis. 20-9
Figure 20-3. Paradise Point forest stands, colored by age, that were used during the analysis. 20-10
Figure 20-4. 2014 LiDAR–derived forest height measurements for MCBCL. 20-12
Figure 20-5. 2014 LiDAR–derived forest height measurements for Training Area K. 20-13
Figure 20-6. The 2014 LiDAR forest height (left) is displayed for Forest Stand 252010000. The 2013 aerial photograph (right) of this forest stand identifies scattered trees. 20-13
Figure 20-7. LiDAR–derived forest density for MCBCL. 20-15
Figure 20-8. LiDAR–derived forest density measurements for Training Area K. 20-15
Figure 20-9. Forest Stand 301984020 shows different densities, which is evidence of row planting. 20-16

List of Tables

Table 20-1. Basal Area Model Scenarios 20-11

Table 20-2. Correlations Between Measured Total Basal Area and the 10 Predictive LiDAR–Derived Variables 20-17

Table 20-3. Model Runs with Summary Stand Statistics and Akaike Information Criterion (AIC) Multiple Regression Model Results 20-18

Table 20-4. Akaike Information Criterion (AIC) Variables, Coefficients, SE, and P-Values for Model Scenarios 1 Through 9, Modeling Basal Area by Forest Stand Type 20-19

Table 20-5. Number of Times When Each Predictor Variable Was Used Among the Nine Models 20-22

Acronyms

AGB	above-ground biomass
AIC	Akaike Information Criterion
ASPRS	American Society of Photogrammetry and Remote Sensing
cm	centimeter
DCERP	Defense Coastal/Estuarine Research Program
DCERP1	first cycle of DCERP
DCERP2	second cycle of DCERP
DEM	Digital Elevation Model
DoD	U.S. Department of Defense
FEMA	Federal Emergency Management Agency
ft	foot, feet
ft^2	square foot, square feet
ft2/acre	square feet per acre
GSRA	Greater Sandy Run Area
ha	hectare
LAS	LASer file format
LiDAR	light detection and ranging
m	meter
m^2	square meter
MCBCL	Marine Corps Base Camp Lejeune
NCFMP	North Carolina Floodplain Mapping Program
r^2	coefficient of determination
RC	Resource Conservation and Climate Change (a SERDP program area)
RMSEz	root mean square error vertical
SD	standard deviation
SE	standard error
SERDP	Strategic Environmental Research and Development Program
TSP	Translating Science into Practice (Module)

Abstract

A primary concern with DCERP2 is sustainability of Marine Corps Base Camp Lejeune (MCBCL), given global climate change scenarios that predict sea level rise and changes in vegetation and carbon storage. For MCBCL to remain a viable training facility, it must be able to manage for these changing conditions, which requires an understanding of the processes involved and being able to monitor the changes as they occur. We focused on the forest stands at MCBCL and proposed a method to directly measure tree height and density by using light detection and ranging (LiDAR) data. We then utilized the LiDAR–derived tree height and density to predict tree basal area, using forest stand data from MCBCL to calibrate the model. The resulting tree height, density, and basal area information provides a baseline to monitor the effects of future change from direct human impacts or climate change and a method to monitor that change as it occurs. An important goal of this project was to determine whether existing LiDAR and MCBCL forest stand data are sufficient for achieving the forest monitoring objectives.

LiDAR data for MCBCL lands were collected between January and March 2014 for the North Carolina Floodplain Mapping Program. The data have an average point density of 2 points per square meter. The vertical accuracy requirements meet or exceed the standard from the American Society of Photogrammetry and Remote Sensing. The LiDAR data were processed to eliminate errors in the point cloud and forest height, and density data sets were produced. Forest stand data from MCBCL were used as ground truth to develop basal area models. The forest height ranged from −3.4 m to 39.6 m. Forest density is the ratio of above-ground returns to all returns and ranges from 0 (low density) to 1 (high density). Basal area was modeled by using 10 LiDAR–derived forest height and density variables (e.g., minimum, maximum, mean, standard deviation [SD], sum for height and density), calibrated with the MCBCL basal area field measurements. Nine model scenarios examined the impacts of forest species composition, age and basal area (high versus low) on the effectiveness of the model. The coefficient of determination (r^2) varied between 32% and 44% for all models. Other studies found better relationships for modeling basal area. These studies all used ground truth data specifically collected for the study. The height variables in the model, particularly mean, maximum, and SD, were the most significant in all models except for hardwood, in which maximum and sum density were most significant.

The MCBCL forest stand data were the limiting factor in the basal area models. These forest stand data lacked height information so the LiDAR–derived height could not be absolutely calibrated. The methods used by MCBCL personnel to determine basal area per stand are a standard cruise procedure. A forest cruise is a coarse measurement that focuses on merchantable timber and does not account for all stems. This method results in a scale mismatch between the stand data and the LiDAR, which measures all stems at a relatively fine scale. Above-ground biomass (AGB) would also be a better measure than basal area because it is more directly related to the LiDAR data. For long-term monitoring that can detect changes in forest height, density, and AGB, new ground-truth data would need to be collected in a subset of stands by using a plot-based measurement method. Not all stands would need this level of sampling; a subset across species, age, and size would provide calibration, thereby greatly improving the basal area models.

Keywords: LiDAR, forest height, forest density, forest monitoring, landscape change, basal area

Objectives of the Research Project

A primary concern with DCERP2 is sustainability of Marine Corps Base Camp Lejeune (MCBCL), given global climate change scenarios that predict sea level rise and changes in vegetation and carbon storage. For MCBCL to remain a viable training facility, it must be able to manage for these changing conditions, which requires an understanding of the processes involved and being able to monitor the changes as they occur. We focused on the forest stands at MCBCL and proposed a method to directly measure tree height and density by using light detection and ranging (LiDAR) data. We then utilized the LiDAR–derived tree height and density to predict tree basal area, using forest stand data from MCBCL to calibrate the model. The resulting tree height, density, and basal area information provides a baseline to monitor the effects of future change from direct human impacts or climate change and a method to monitor that change as it occurs.

Many studies have shown the ability of LiDAR to measure or estimate the biophysical properties of forests; however, these studies collected new LiDAR and forest measurement data specifically for this purpose. We used existing LiDAR and MCBCL–collected forest stand data to determine whether these data are sufficient to measure forest height, density, and model basal area. The LiDAR data were originally collected to produce more accurate Digital Elevation Models (DEMs), not to measure above-ground vegetation structure. The forest stand data were collected by using forestry cruise methods at MCBCL as part of the forest management procedures and were not collected specifically to calibrate LiDAR data. If these data, particularly the forest data, can be effectively used, then MCBCL and other U.S. Department of Defense (DoD) installation locations nation-wide may be able to effectively monitor forest change without collecting new data. If not, then new measurement methods may be necessary for the forest stands at MCBCL to monitor changes in forest stand structure, basal area and above-ground biomass (AGB) and carbon storage.

Background

During a DCERP1 monitoring activity, we developed a methodology to identify where the vegetation change happened and what type of change occurred in the past by using greenness gain and loss measured from a time series of Landsat Thematic Mapper satellite images. This methodology linked management choices in the past to the effects on the landscape of MCBCL. The next logical step was to quantify the current forest condition in terms of forest biophysical parameters such as height, density, and basal area to provide a baseline to monitor the impacts of future change from direct human impacts or climate change. Field measurements are the most accurate, but are extremely time consuming and expensive to collect, particularly because field measurements must be repeated to identify changes in the forest structure over time. Remote sensing can cover large areas at a low cost, but these data require field measurements to calibrate the remote-sensing models.

Various remote-sensing platforms have been used to measure forest structure and biophysical properties such as height, carbon storage, and AGB. Remote sensing has been used for many years to monitor carbon storage and change (Ahern et al., 1991; Cohen et al., 1996; Running et al., 1999). However, optical sensors such as Landsat are limited to mostly the canopy, especially as the forest canopy closes in older, higher biomass forests and so it is less sensitive to forest

structure and AGB (Carlson and Ripley, 1997; Lefsky 2002a and 2002b; Turner et al., 1999; Steininger, 2000; Waring et al., 1995). Radar can penetrate the canopy and measure AGB effectively, but saturates at relatively low biomass levels (Dobson et al., 1995; Hall et al., 2011; Harrell et al., 1997; Shugart et al., 2010).

LiDAR technology is a good option because this system directly measures the vertical structure of a forest, making LiDAR well suited for measuring tree height and density and for modeling basal area and AGB (Hall et al., 2005; Lefsky et al., 2002a and 2002b; Patenaude et al., 2004; Smart et al., 2012; Zolkos et al., 2013). Because the LiDAR sensor is designed to provide a three-dimensional measure, it may overcome the signal saturation problem at high densities found with other sensors (Dobson, 2000; Hall et al., 2005; Lefsky et al., 2001). No evidence has been found that LiDAR experiences signal saturation (Lefsky et al., 2002b). The primary measurement taken with LiDAR data is the distance from the source (aircraft or satellite) to the target. This distance is determined by measuring the time it takes for an emitted pulse to reflect off the target and return to the sensor. This time delay is then multiplied by the speed of light and divided by two (down and back), thereby deriving a distance.

A single pulse from a small footprint direct return LiDAR can reflect multiple times, depending on the surface. Each reflection results in a separate point in the data. Bare ground would have only a single return, and one pulse would result in one point. A complex surface such as a forest would have multiple returns from a single pulse. Current discrete return LiDAR systems record between one and five returns per pulse. Pulse density is then the number of pulses emitted per unit time by the laser. The point density received could be up to five times higher than the emitted pulse density, and one pulse sent out could result in five separate point measurements on the surface. In a forest, the first return would be from at or near the top of the trees. The last return would be from the ground surface. The difference between these two returns equals the forest height. The average number of returns points per pulse can provide an estimate of forest density—an area with many returns per pulse has more or denser vegetation than a location with fewer returns per pulse.

The studies previously mentioned found that LiDAR effectively measured forest biophysical parameters. These studies collected the LiDAR and forest data specifically for their respective analysis. Our goal was to use existing LiDAR data and forest stand measurements collected at MCBCL to determine whether LiDAR and forest measurement data that were not specifically collected for this purpose could produce useful estimates of forest height and density, and whether these parameters can then be used to produce estimates of basal area. This method could be used to monitor changes in the MCBCL forest structure over time. The LiDAR data and the forest data collection methods are not optimized for this application, so this presents several challenges.

Existing LiDAR data were available from the State of North Carolina. These data were collected to produce accurate bare earth elevation data. LiDAR data, which were collected primarily to provide better DEMs, use the last return only, the remaining point cloud of returns from vegetation are interference. To minimize vegetation interference, these LiDAR data are collected during the leaf-off condition in winter. LiDAR optimized for measuring forest stand structure is collected during leaf-on condition in summer. An additional concern was whether the pulse

density of the existing LiDAR was sufficient. In general, pulse density must be higher to effectively describe forest structure than if the goal is only ground surface elevation.

Existing forest stand data were provided by MCBCL's Environmental Management Division. Forest stands are relatively homogenous units in terms of age and species and are measured by using forest cruising methods. These methods differ from a plot sampling method, with multiple plots per stand, which is better suited for measuring forest structure during LiDAR studies. The cruise data do not provide height, diameter, or AGB information. The cruise data do have basal area, but that information is not directly related to LiDAR returns like AGB. The cruise method is also a coarser sampling methodology, spatially, than the procedures designed for use with LiDAR. This coarser resolution results in a spatial mismatch, which can be problematic (Woodcock and Strahler, 1987). If existing LiDAR and forest data can be used effectively, then the data could be used to monitor forest change over time at MCBCL and anywhere these data are available. If not, then MCBCL may need to implement new LiDAR and/or forest measurement methods to monitor forest AGB and carbon storage change because of future climate change.

Materials and Methods

The general approach is to develop measurements of forest height and density from LiDAR data for MCBCL as a management tool and to use these data to predict basal area by using multiple regression as a first step towards a carbon monitoring methodology.

LiDAR Data

Four discrete return LiDAR data sets exist for MCBCL: February 2001, February 2007, March 2013, and January through March 2014. The primary purpose for these collections was to produce DEMs. The data were collected during winter to reduce the effects of vegetation leaf area on the creation of bare earth models. Data collection in the winter reduces the accuracy of these data sets to measure forest stand parameters, but with sufficient pulse density, they can still produce good results. We examined all four LiDAR data sets, which are further described in the following subsections.

2001 Data

The 2001 data were collected for the North Carolina Floodplain Mapping Program (NCFMP) in association with the Federal Emergency Management Agency (FEMA). The primary purpose of the data was to produce highly accurate DEMs to improve floodplain mapping in North Carolina. Data were collected with a discrete return LiDAR with up to four returns (points) per pulse. The point density was approximately 0.11 points per square meter. Accuracy assessments performed for Onslow County (location of MCBCL) confirmed that the data achieved the required 20 cm root mean square error vertical (RMSEz) accuracy. We acquired the full point cloud in LASer (LAS) file format 1.1. LAS is a standardized public file format for the interchange of three-dimensional point cloud data.

The 2001 NCFMP data were one of the earliest LiDAR products mapping such a large area. As such, there were some inconsistencies in the initial data processing. Two different vendors

collected and processed the data that included MCBCL. The vendor that provided the western portion of MCBCL could not provide the full point cloud, so an analysis could not be completed for this area. In addition, the 0.11 points per square meter point density is low for vegetation analysis; therefore, these data were not used in the analysis.

2007 Data

The LiDAR data collected during February 2007 were contracted by MCBCL. We were never able to acquire the full point cloud, making a forest analysis impossible.

2013 Data

The 2013 LiDAR data were contracted by MCBCL and collected on March 8 and 9, 2013. Point data were in a LAS 1.2 format. The data were acquired with a nominal point spacing of 0.6 m, with an average point density of 3 points per square meter m^2. The vertical accuracy requirements met or exceeded the American Society of Photogrammetry and Remote Sensing's (ASPRS's) required RMSEz of 9.25 cm and the 95% confidence level for vertical accuracy of 18.13 cm. Actual measured vertical error was 8 cm. The point cloud was classified by using ASPRS standard classes. The raster data we produced from the 2013 LiDAR point data used a cell size of 3 m, which is approximately four times the nominal point spacing. Given the point spacing/density, this value means there are enough points representing each cell to provide a good average height and density value for that region (ESRI, ArcGIS Help Menu, *Assessing LiDAR coverage and sample density*).

2014 Data

The 2014 LiDAR data collection covering MCBCL was obtained by the NCFMP (2014), in association with FEMA, to further improve floodplain mapping in North Carolina. The data were collected between January 6 and March 21, 2014. Point data were in a LAS 1.3 format. The data were acquired from the NCFMP with a nominal point spacing of 0.7 m, with an average point density of 2 points per square meter. The vertical accuracy requirements met or exceeded the ASPRS–required RMSEz of 9.25 cm and the 95% confidence level for vertical accuracy of 18.13 cm. Actual measured vertical error was 11.7 cm. The point cloud was classified by using ASPRS's standard classes. Raster data produced from the 2014 LiDAR point data used a cell size of 5 m. This cell size is based on being four times the observed point density, 1.03 m for above-ground and 1.17 m for ground point spacing, rather than the nominal point spacing, to be more conservative.

Data Processing

The 2013 and 2014 LiDAR data were processed for further analyses. To improve processing speed, the LAS data files for MCBCL lands were broken into the following four units: the Greater Sandy Run Area (GSRA), the West Side, the North Side, and the East Side (**Figure 20-1**). The classified point cloud data were used for this analysis, which included classes such as bare earth (ground), vegetation, building, noise, and water (ASPRS's standard classes).

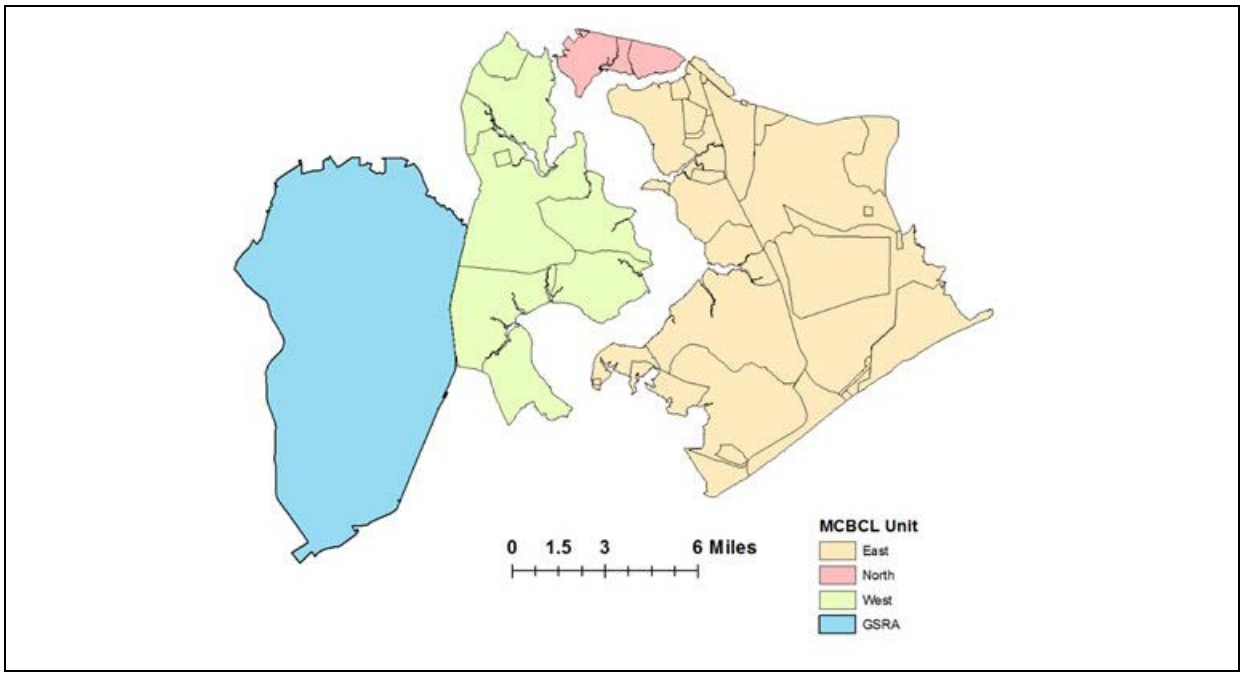

Figure 20-1. LiDAR processing units for MCBCL.

We used ESRI ArcGIS Desktop (2016) to process the LiDAR data. The bare earth (ground) classification was quite accurate for both 2013 and 2014. The bare earth classification was error checked by the vendor to produce the bare earth DEMs at the defined accuracy level. Above-ground points, however, were not checked for class accuracy. For producing a DEM, all that mattered was that the point was not ground. Returns from buildings, birds, and vegetation were all combined into the following two classes: unclassified and vegetation. As such, we used both the vegetation and unclassified classes as inputs and manually checked the point data classifications for errors. To minimize processing time, we limited our efforts to areas at MCBCL defined as forest stands.

We found errors typical with this type of data, with returns from birds and structures labeled as vegetation. These structures and birds were identified manually and re-classified as noise or buildings by following two steps. First, any data with an elevation greater than 90 m were automatically removed from the vegetation class because this is an unrealistic height for trees. Second, the data were then searched tile by tile for any other outliers. Many water, radio, and military observation towers were identified and re-classified to buildings or noise. This process was thorough, but not exhaustive. Undoubtedly, some errors remained in forested compartments, but this affects very few cells in the resulting raster data. If an error occurs in a forest tract, it will not affect the average for the stand.

We used this re-classified data to produce estimates of forest height and density. Forest height was calculated by creating a raster representation of bare earth by using the last return ground class point data and a top-of-forest raster by utilizing the first return above-ground point data. Points were converted to raster by interpolation, going from point data to triangular irregular network then to raster, the standard procedure for data of this type. Appropriate cell sizes were selected, 3 m for 2013 data and 5 m for 2014 data, based on point spacing. The difference between the ground and top-of-the-canopy rasters was calculated to determine the forest height

for each of the four units at MCBCL. The maximum height for a cell was set to 50 m for the 2013 data and 45 m for the 2014 data.

Forest density is measured with LiDAR by the average number of returns per pulse—the more returns, the denser the forest. Rather than a simple average, we used the number of above-ground returns relative to the total returns (ESRI ArcGIS Help Menu, *Estimating forest canopy density and height*). A ratio of all above-ground forest returns divided by the total of all returns (ground and forest) gives a range from near zero (low forest density, bare ground) to 1 (dense forest). By using a ratio, this normalizes the data, helping to standardize it. Forest density was calculated only for the 2014 LiDAR data. The 2013 data produced forest density rasters with stripping, corresponding to the overlap between flight lines. Normalization did not remove this effect, so it was not used.

Forest Stand Data

We used forest stand data collected by MCBCL's Environmental Management Division. Forest stands are relatively homogenous areas defined primarily by species composition, age, and spatial location. Measurements included primary and secondary species, stand birth year, date sampled, site index (base age 50 years) and basal area. "Basal area" is defined as the cross-sectional area of a tree 4.5 ft above ground and describes the degree to which an area is occupied by trees. Basal area is reported as mixed hardwood species and pine (composed of primarily loblolly pine [*Pinus taeda*] and also longleaf pine [*Pinus palustris*] with some slash pine [*Pinus ellioti*] and shortleaf pine (*Pinus echinata*]). The forest stand data were collected by using a standard cruise method with a 10-factor prism to derive the basal area. Stands were re-measured on a regular schedule, with a subset evaluated each year. We added age (2016 – birth year) and total basal area (pine + hardwood) to the data set for analysis.

Unfortunately, the forest stand data did not include directly measured tree height or diameter information; therefore, we had no way to test the accuracy of the LiDAR–derived height. In addition, without height and tree diameter, the AGB could not be calculated, which significantly limited our modeling efforts.

The forest stand data from MCBCL were subset to remove the stands that were defined as non-forested or stands less than 1 ha. Stands missing age or basal area information or with errors were also removed. The remaining stands were buffered inwards by 5 m and 20 m to ensure that all cells were within the stand and to minimize edge effects. This process resulted in 2,447 forest stands (**Figure 20-2**). The closer view of Paradise Point shows the exclusion of developed areas (**Figure 20-3**).

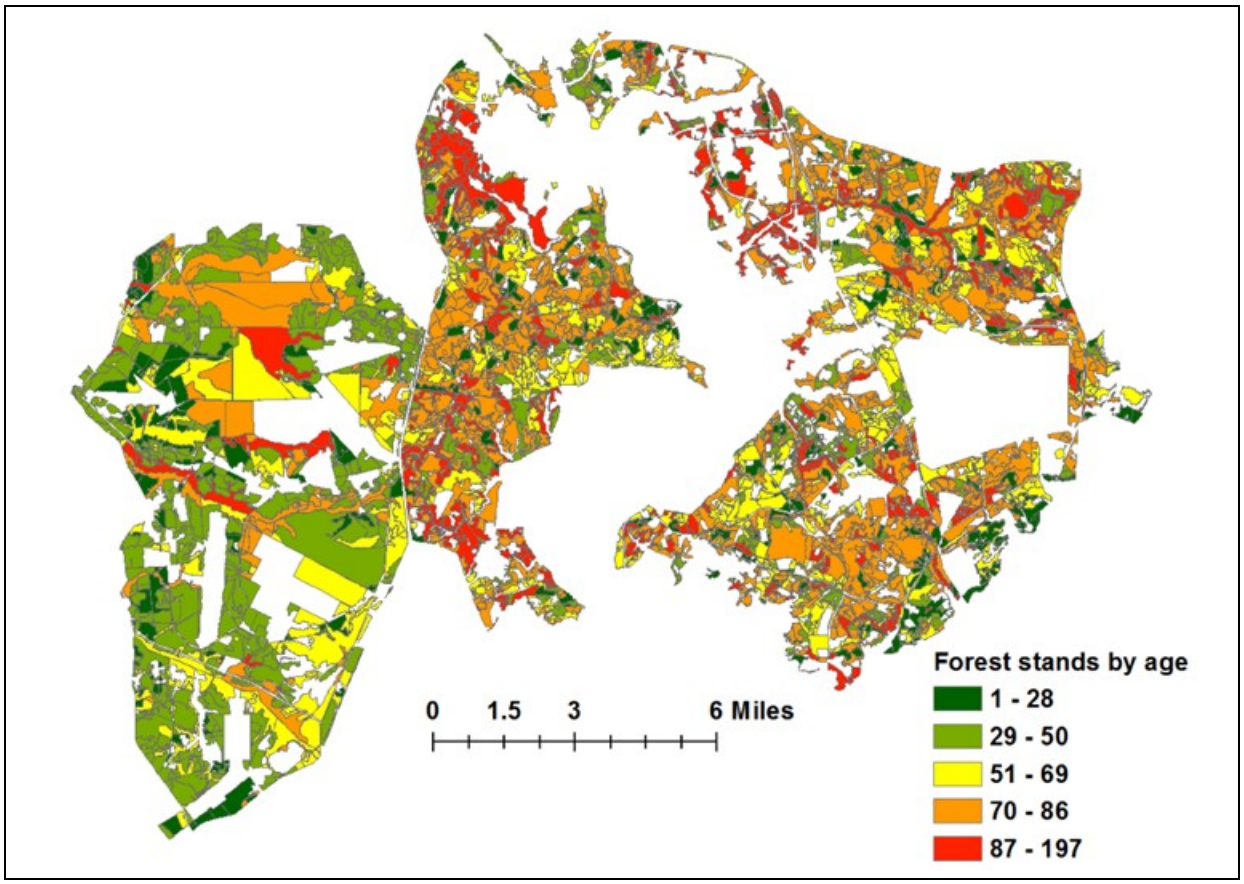

Figure 20-2. Forest stands, colored by age, that were used during the analysis.

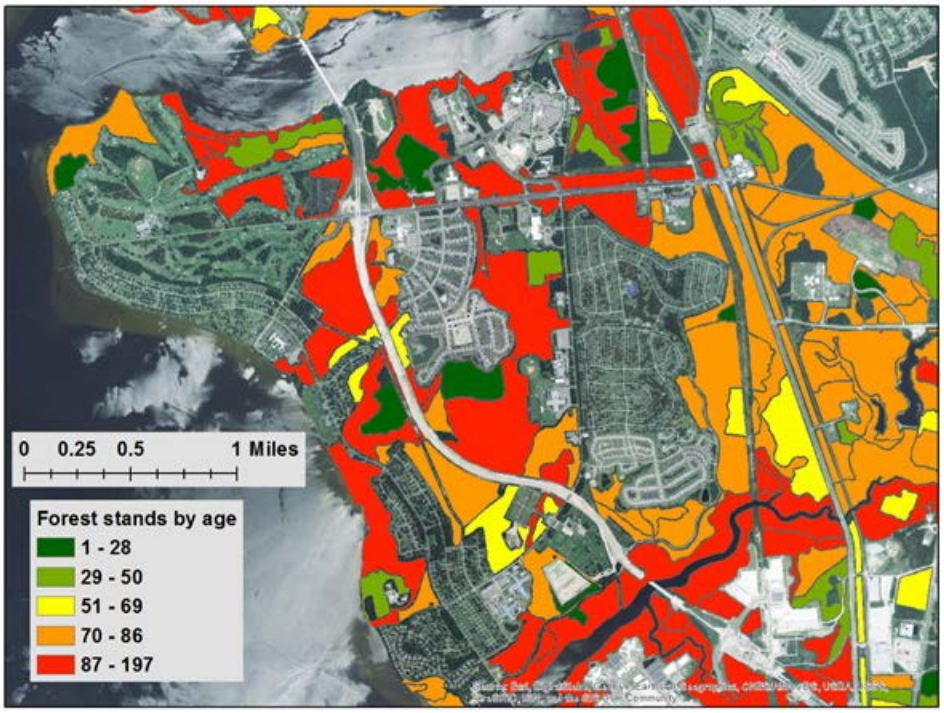

Figure 20-3. Paradise Point forest stands, colored by age, that were used during the analysis.

Model Development

This forest stand polygon data set was used to sample the 2014 LiDAR–derived forest height and density data. The statistical package R was use to run multiple linear regression models with the Akaike Information Criterion (AIC) to predict basal area from stand level variables. AIC is based on information theory and provides a means for model selection that tries to reach the best balance between the goodness-of-fit of a model and the complexity of a model, minimizing the information lost.

The selection of model predictive variables is a primary consideration for studies of this type. We used 10 variables to describe the distribution of LiDAR–derived forest height and density of each stand as the predictor variables for basal area. The 10 variables are minimum height, maximum height, mean height, SD of height and sum of height, minimum density, maximum density, mean density, and the SD of density and sum of density. Sum height and sum density are simply the sum of the height and density values of all cells in a given stand.

Using these 10 variables, we created nine model scenarios (**Table 20-1**). The scenarios were selected by species, basal area, and age to determine whether these factors affected model performance.

Table 20-1. Basal Area Model Scenarios

Model Run and Stand Type	Number of Stands
1. All forest stands	2,447
2. All pine stands	1,058
3. Primarily longleaf pine	319
4. Primarily loblolly pine	515
Pine stands by age	
5. Pine aged ≥50 years	500
6. Pine aged <50 years	558
Pine by basal area	
7. Pine basal area ≥60 ft^2/acre	522
8. Pine basal area <60 ft^2/acre	536
9. Hardwood only	144

We examined the models by using both normal and log transformed data because several studies found stronger results for log-transformed data (Lefsky et al., 1999 and 2002a; Naesset, 2002). However, we found that linear models were a better fit and explained more variance for our data, a pattern that was also described by Hall et al. (2005) for specific models in their results.

Results and Discussion

LiDAR Forest Height and Density Measurements

LiDAR data from 2013 and 2014 produced forest height data. However, 2001 and 2007 LiDAR data were not used in this analysis because of problems with the data as described in the Materials and Methods section of this chapter. LiDAR data from 2014 produced forest density information, but problems with the LiDAR data in 2013 prevented producing forest density results. For consistency, we are reporting results from just the 2014 LiDAR data.

Many studies have shown correlations in a variety of vegetation types between LiDAR returns and biophysical parameters. Tree height and vegetation cover/density were strongly correlated to LiDAR returns in temperate deciduous (Patenaude et al., 2004), temperate evergreen (Hall et al., 2005; Renslow et al., 2000), and boreal forests (Magnussen et al., 1999; Naesset, 1997). Many researchers used LiDAR to model basal area and AGB/carbon storage (Goetz and Dubayah, 2011; Lefsky et al., 2002a and 2002b; Patenaude, 2004; Renslow et al., 2000; Rosette et al., 2012; Zolkos et al., 2013) in a variety of forest types.

There are two concerns with estimates based on LiDAR data. One concern is accurately determining ground returns from above-ground returns, and the second concern is recognizing a return from the very top-of-the-canopy (Lefsky et al., 2002b). Inaccuracies in either or both of these factors result in an underestimation of tree height and the derived estimates of basal area/AGB based on tree height. A high point density helps with both issues, and the 2014 data have a relatively high average point density of 2 points per square meter. We are confident that the resulting DEM represents the ground surface; however, it is likely we underestimated height.

The forest height ranged from −3.4 m to 39.6 m for forest stands at MCBCL (**Figure 20-4**). White areas are exclusion zones that are non-forested areas, stands missing basal area information, or are part of the inward buffer. Orange areas denote low vegetation (small trees, shrubs), and green is used to identify taller vegetation, primarily trees.

Training Area K, which is outlined in red in **Figure 20-4**, is shown in detail in **Figure 20-5**, with forest stand boundaries. Stands that are more uniformly colored contain trees that are more even in height. Stands with multiple colors contain trees that have a wide range in heights. Mature forest stands will often be quite variable in height—large trees with some gaps—and result in the speckled appearance in **Figure 20-5**. Stand 252010000, which is highlighted in red in **Figure 20-5** and shown in detail in **Figure 20-6**, is an extreme example. This stand was a seed tree cut in 1997, leaving mature loblolly pines widely spread apart. This stand was under-planted with longleaf pine in 2009. Seed trees are widely dispersed with lower, mixed vegetation around them. Based on the height data, the seed trees occupy between four and six cells, making the canopy approximately 10 m × 10 m in size and between approximately 20 m and 28 m in height. The surrounding low vegetation is mostly under 1 m with young loblolly trees between 2- and 4-m high scattered in the understory along with shrubs.

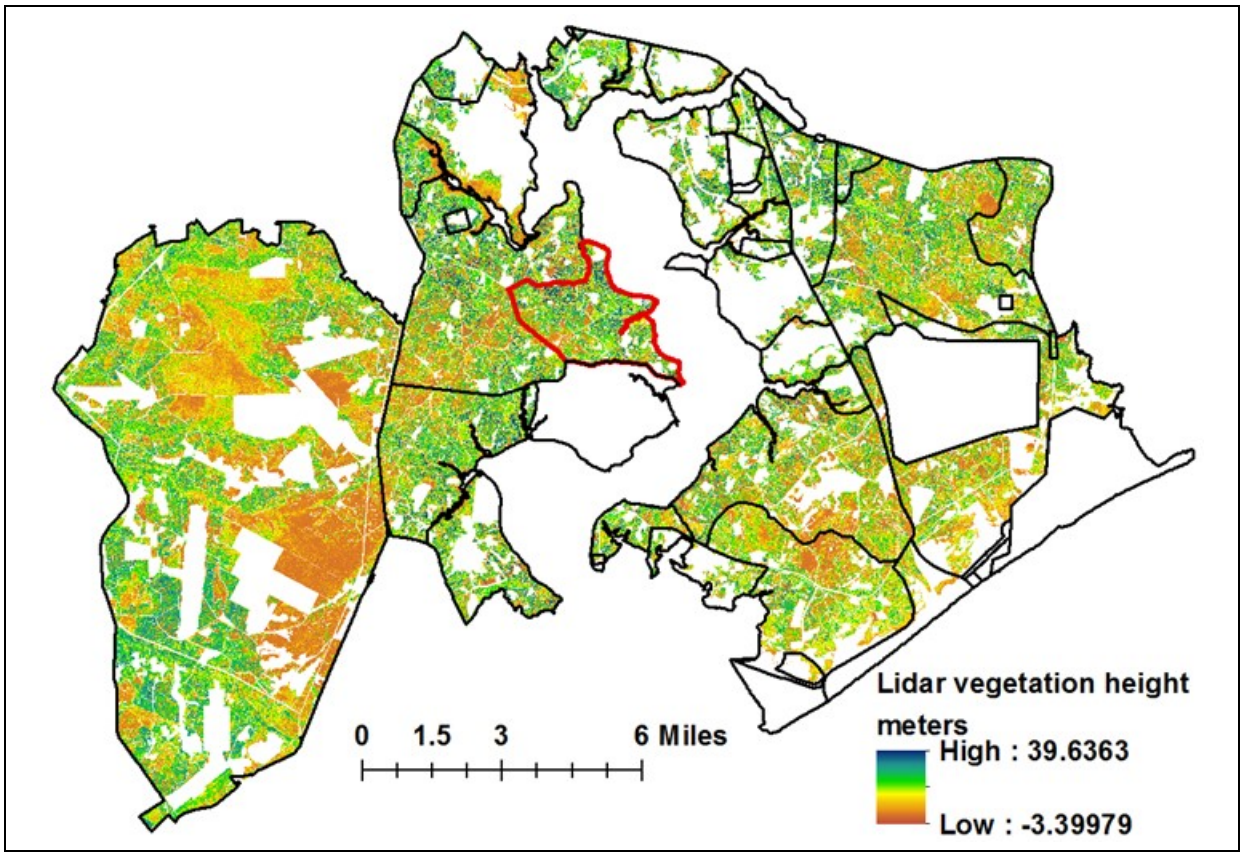

Figure 20-4. 2014 LiDAR–derived forest height measurements for MCBCL.

Note: Training Area K is outlined in red.

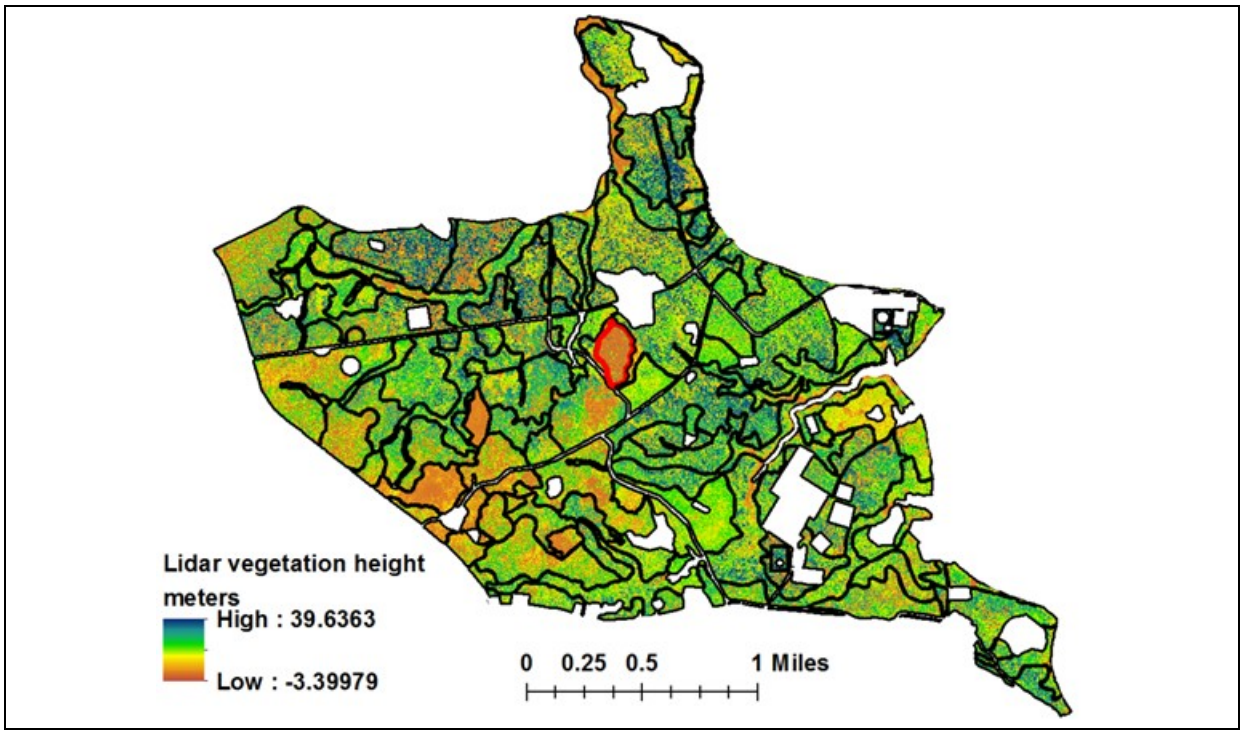

Figure 20-5. 2014 LiDAR–derived forest height measurements for Training Area K.

Note: Stand 252010000 is highlighted in red.

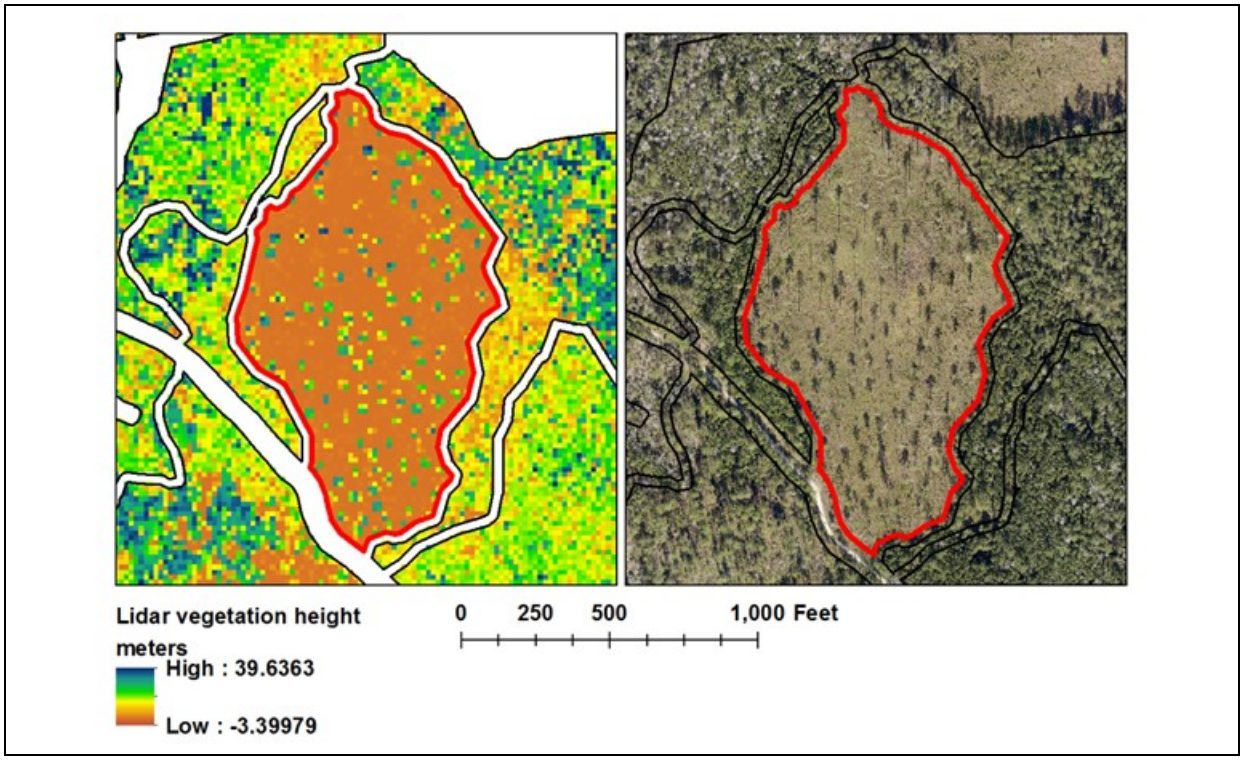

Figure 20-6. The 2014 LiDAR forest height (left) is displayed for Forest Stand 252010000. The 2013 aerial photograph (right) of this forest stand identifies scattered trees.

Negative height values are a measure of error and indicate that the forest height at that location was less than the surface height, which is impossible. We could set these negative values to zero, but this gives us one measure of our error, an error that ranges from 0 to 3.4 m. The distribution of this error gives a mean of 0.1 m, with an SD of 0.2 m, which means the majority of the errors are small, less than 0.5 m. This is a crude measure of error because it likely varies with topography (more in high-slope areas) and vegetation type. The forest stand data do not include tree height, so we cannot conduct a true accuracy assessment. This is a problem with using the forest stand data for this model application.

Another source of error may be the pixel size. Scale has long been recognized as an important factor in measuring biophysical parameters with remote-sensing data because a sensor cannot measure heterogeneity at sub-pixel scales (Woodcock and Strahler, 1987; Zhao et al., 2009). Pixel size was selected to be four times the point density. This size gives a reasonable point sample to determine the height of each cell, but it does have an averaging effect on the height value. This averaging effect results in underestimation of tree height, but it provides a more consistent and reliable estimate. Cell size selection is a trade-off between these two concerns. Unfortunately, the forest stand data do not include height information, so we do not have an independent data set for calibrating pixel size.

In addition to tree height, LiDAR–derived forest density can be a useful monitoring product and may improve the estimates of basal area. Although tree height is an absolute measure, the density is a relative range from 0 (low density) to 1 (high density). **Figure 20-7** shows forest density for MCBCL. **Figure 20-8** shows a closer view of Training Area K (the same area shown in **Figure 20-5** for forest height). Stands that are more uniformly colored are more evenly distributed in terms of density, and stands with multiple colors have a wide range in density. For monitoring forest change, forest density and its distribution statistics in addition to height and its distribution statistics may be a better method to characterize the biophysical parameters of the forest stands than height alone.

Forest stand 301984020 within Training Area K is a good example of the use of forest density because it was a 32-year old loblolly stand in 2014 (**Figure 20-9**). The thinning rows are clearly visible in the aerial photograph on the right (**Figure 20-9**), and low-density areas in the forest are visible on the left. Also visible in **Figure 20-9** are some lower density areas cutting across rows, which may be wet areas or some other factor has caused a reduction of growth in this area, but the forest density measurements clearly identify this pattern.

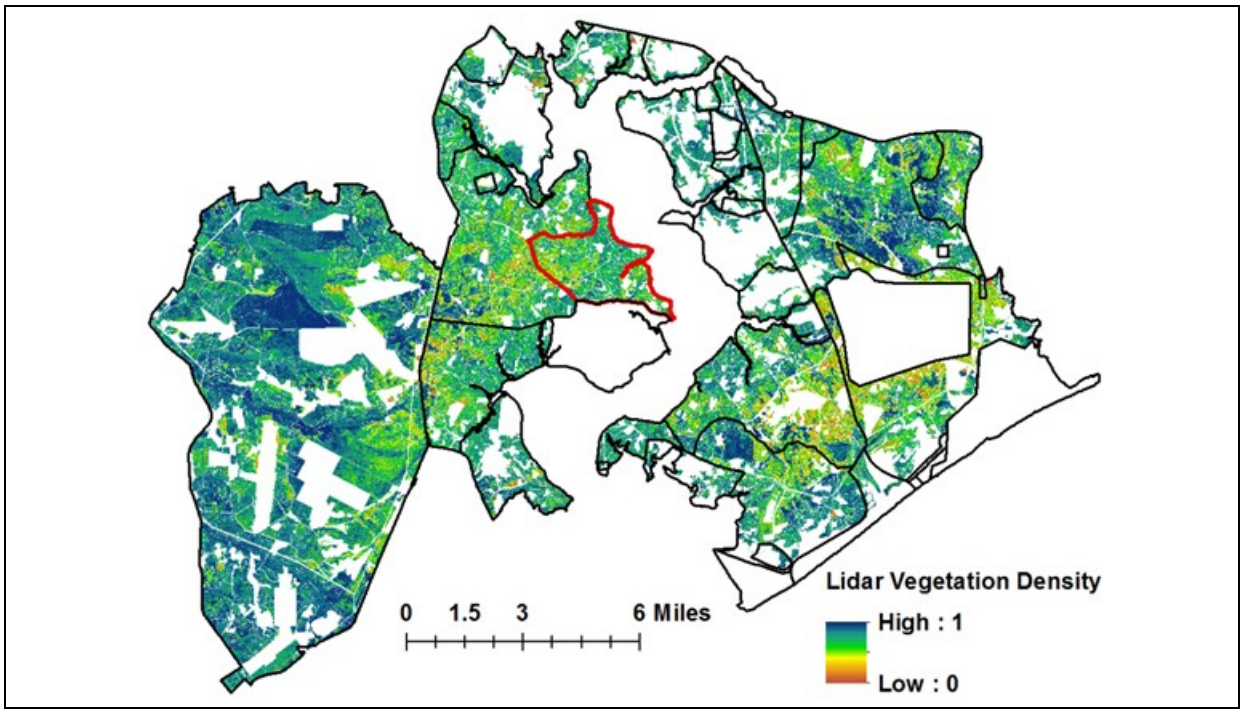

Figure 20-7. LiDAR–derived forest density for MCBCL.

Note: Training Area K is outlined in red.

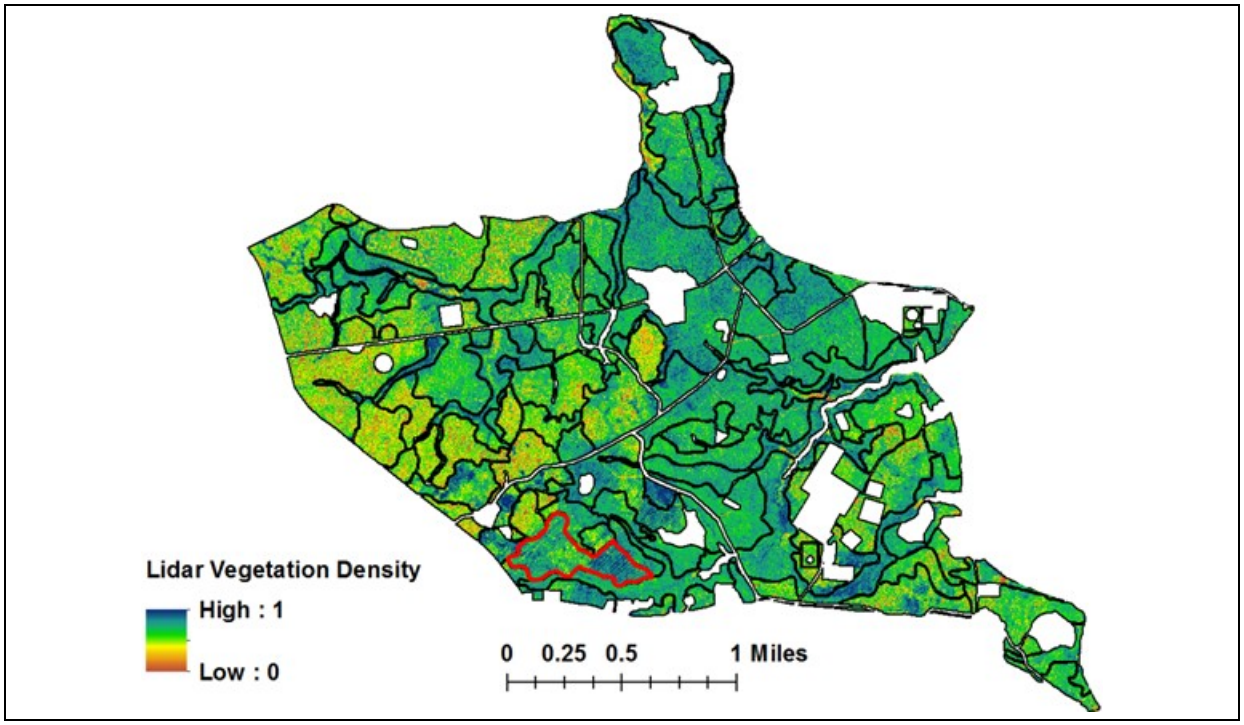

Figure 20-8. LiDAR–derived forest density measurements for Training Area K.

Note: Stand 301984020 is outlined in red.

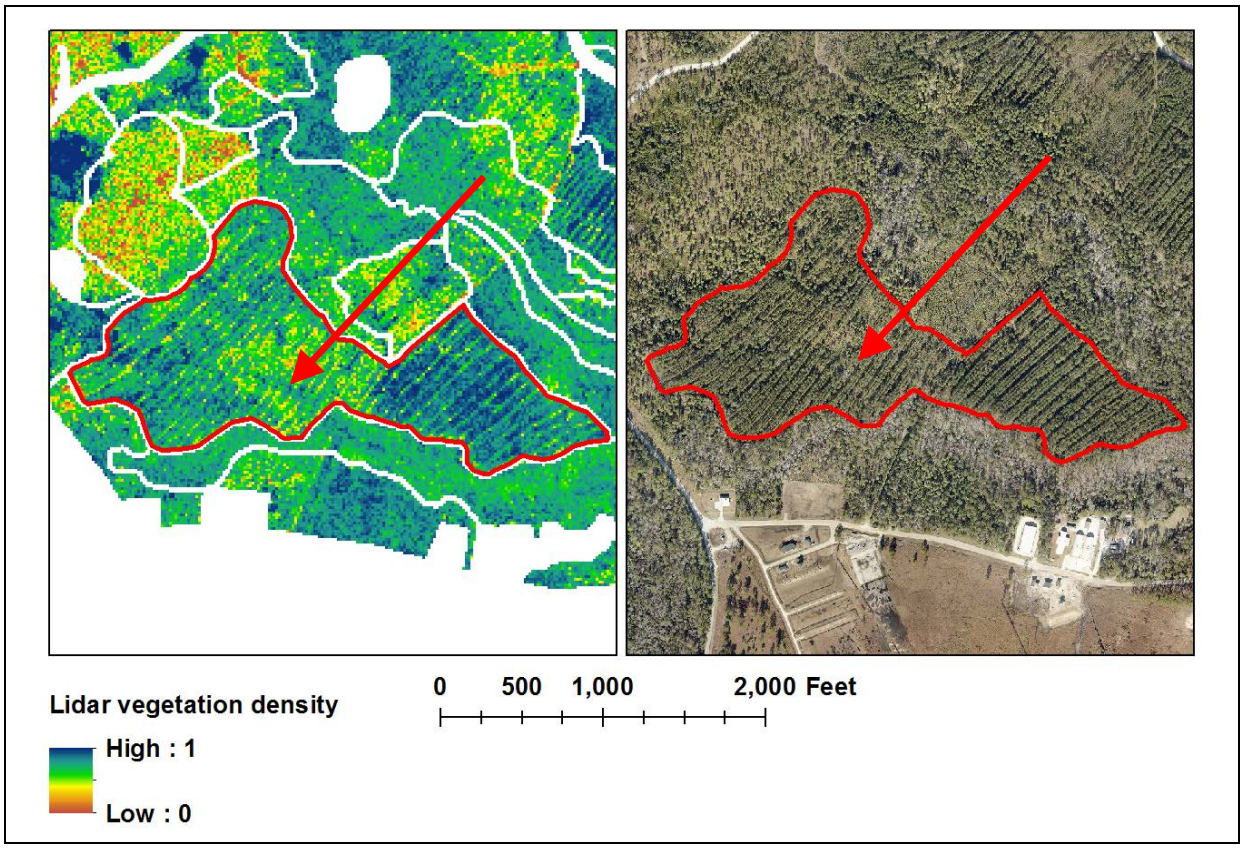

Figure 20-9. Forest Stand 301984020 shows different densities, which is evidence of row planting.

Thinned rows of trees are identified in the 2014 LiDAR forest density (left) and 2013 aerial photograph (right).

Overall, the 2014 LiDAR data calculations of forest height and density are reasonable when compared with aerial photo data. Both calculations would be improved with LiDAR data collected during leaf-on condition in summer. The forest stand data have a significant limitation. These data do not include actual measured tree height data or a measure of forest density other than basal area, so no method is available that can be used to conduct an accuracy assessment and provide an error estimate for LiDAR–derived forest height and density.

Forest Stand Data and Basal Area Models

We used the LiDAR–derived forest height and density to model field measured stand basal area. The 2,447 forest stands with field measurements primarily consist of loblolly pine, longleaf pine, and mixed hardwood. Stand age varied from 1 to 197 years, with an average age of 60 years. The correlations between total basal area and all 10 predictive variables are shown in **Table 20-2**.

Table 20-2. Correlations Between Measured Total Basal Area and the 10 Predictive LiDAR–Derived Variables

Predictive Variables	Total Basal Area
Minimum height	0.14
Maximum height	0.27
Mean height	0.55
SD height	0.33
Sum height	0.16
Minimum density	0.09
Maximum density	0.05
Mean density	0.15
SD density	−0.19
Sum density	0.00

The correlations are not strong, with only mean height above 50%. The remaining correlations are 33% or less. The multiple regressions do somewhat better, but the predictive power is limited primarily because of the nature of the field measurements. The basal area measurements from the MCBCL forest stand data are at a coarser scale than the LiDAR data, resulting in a scale mismatch of the two data sources. The LiDAR data averages 2 sample points per square meter over the entire stand. The cruise methodology to field measure basal area is a much more limited sample and focuses on merchantable timber (trees a specific size or larger), whereas the LiDAR data reflect all vegetation. Scale issues can have a significant impact on the effectiveness of the models (Woodcock and Strahler, 1987; Zhao et al., 2009). Basal area is also less effective for modeling with LiDAR than AGB. AGB is directly related to the LiDAR returns because it is a measure of the total amount of reflective surface in the forest stand, not just a sample of merchantable timber (Hall et al., 2005). As such, models predicting AGB tend to be better than those predicting basal area (Hall et al., 2005; Lefsky et al., 1999). Without height and diameter information about each stand, we cannot calculate AGB.

Our intention was to develop predictive models for basal area by using half the stands for each model scenario (**Table 20-1**) to develop the model, and then to predict the basal area of the other half and produce an accuracy assessment. However, the correlation between total basal area and the individual predictor variables (**Table 20-2**), as well as the initial multiple regression results showed poor predictive ability. Therefore, we focused on an exploratory analysis of describing the relationship by using all stands in each scenario. This information will help define the important predictor variables, even if the variability explained is low.

Table 20-3 shows the results for all nine model scenarios, including stand summary statistics and the variability explained (r^2) of each model. The large number of forest stands, 2,447, allowed us to test a wide range of stand types. The scenarios tested for differences based on tree species, age, and basal area, as we expected model performance to vary relative to these differences. The 2,447 forest stands represent a wide range in basal area, from 2 to 200 ft^2/acre, and age (from very young stands to mature). However, the r^2 values for the model runs are quite consistent, varying from a low of 32% for the model with all pine stands with a basal greater than or equal

to 60 (Model 7) to 44% for pine stands aged less than 50 years (Model 6). There is not much difference based on species, age, or low versus high basal area stands.

Table 20-3. Model Runs with Summary Stand Statistics and Akaike Information Criterion (AIC) Multiple Regression Model Results

Model Run	Stand Type	Stand Measurements			Model Results		
		Mean Basal Area	Minimum Basal Area	Maximum Basal Area	r^2	Standard Error	N
1	All forest stands	68.05	2	200	0.3380	28.55	2447
2	Pine stands	61.11	2	200	0.4040	31.23	1058
3	Longleaf pine	52.71	2	160	0.3427	23.70	319
4	Loblolly pine	72.96	3	197	0.3557	36.38	515
5	Pine aged ≥50 years	53.52	5	160	0.3176	21.94	500
6	Pine aged <50 years	67.91	2	200	0.4396	36.58	558
7	Pine basal area ≥60	93.02	60	200	0.3249	26.36	522
8	Pine basal area <60	30.04	2	58	0.3507	13.09	536
9	Hardwood	54.94	7	158	0.3914	18.98	144

Note: Basal area is in ft^2/acre.

Other studies have found stronger relationships between predictive variables and basal area than were found during our study. Hall et al. (2005) used discrete return LiDAR on low-density ponderosa pine (*Pinus ponderosa*) and found an r^2 of 78.5% for prediction of basal area. Lefsky et al. (1999), using a waveform LiDAR, explained 69% of the variability in their model predicting basal area. Each of these studies collected dedicated field measurements to develop the models.

Table 20-4 presents the variables selected for each model run by the AIC and the coefficients, standard error (SE), and probability for each. The number of predictor variables used in each model varies from 9 of 10 (Model 1, all stands) to 4 of 10 (Model 4, loblolly stands; Model 5, pine stands aged >50 years). For Model 1, only minimum density was removed from the model. The height variables, except for minimum height, are all significant at a *P*-value of <0.0001. Model 4 included maximum height, mean height, and SD height and sum density, and Model 5 used the same height variables, but included maximum density instead of sum density. The height variables in these two models are all significant at a minimum *P*-value of 0.001. Model 6, pine stands aged <50 years, explained the most variability with an r^2 of 44%. This model used the following six variables: maximum height, mean height, SD height, sum height, maximum density, and mean density. All of the height variables are significant at a minimum *P*-value of 0.0005 in Model 6. The P-values for maximum density is 0.07 and for mean density is 0.05.

Table 20-4. Akaike Information Criterion (AIC) Variables, Coefficients, SE, and *P*-Values for Model Scenarios 1 Through 9, Modeling Basal Area by Forest Stand Type

(a) Model Run 1, All Stands

All Stands	Coefficients	SE	*P*-Value
Intercept	−58.9611	22.4343	0.0086
Minimum height	5.2286	2.9362	0.0751
Maximum height	−1.9490	0.1903	<0.0001
Mean height	6.0763	0.2812	<0.0001
SD height	2.8302	0.6561	<0.0001
Sum height	0.0001	0.0000	<0.0001
Maximum density	78.0597	25.3690	0.0021
Mean density	15.0148	7.9379	0.0587
SD density	83.0616	22.2178	0.0002
Sum density	−0.0003	0.0002	0.0723

(b) Model Run 2, Pine Stands

All Pine Stands	Coefficients	SE	*P*-Value
Intercept	−58.3030	27.4756	0.0341
Maximum height	−2.6295	0.3229	<0.0001
Mean height	6.7373	0.3444	<0.0001
SD height	4.3668	0.8711	<0.0001
Sum height	0.0001	0.0000	0.0001
Maximum density	100.5520	28.0743	0.0004
Sum density	−0.0004	0.0002	0.0401

(c) Model Run 3, Longleaf Pine

Longleaf Stands	Coefficients	SE	*P*-Value
Intercept	−53.1646	26.4884	0.0456
Maximum height	−1.9190	0.5187	0.0003
Mean height	4.7629	0.7323	<0.0001
SD height	5.3663	1.5883	0.0008
Minimum density	41.4750	15.3524	0.0073
Maximum density	82.7540	27.6062	0.0029
Sum density	0.0020	0.0010	0.0339

(d) Model Run 4, Loblolly Pine

Loblolly Stands	Coefficients	SE	*P*-Value
Intercept	46.0135	9.5074	<0.0001
Maximum height	−3.3260	0.5061	<0.0001
Mean height	7.6458	0.5119	<0.0001
SD height	4.6664	1.3572	0.0006
Sum density	0.0021	0.0004	<0.0001

Table 20-4. Akaike Information Criterion (AIC) Variables, Coefficients, SE, and *P*-Values for Model Scenarios 1 Through 9, Modeling Basal Area by Forest Stand Type (continued)

(e) Model Run 5, Pine Aged ≥50 Years

Pine, Aged ≥50 Years	Coefficients	SE	*P*-Value
Intercept	−70.0768	24.8799	0.0050
Maximum height	−2.5776	0.3632	<0.0001
Mean height	4.2123	0.5276	<0.0001
SD height	7.2584	1.1825	<0.0001
Maximum density	112.5106	25.5676	<0.0001

(f) Model Run 6, Pine Aged <50 Years

Pine, Aged <50 Years	Coefficients	SE	*P*-Value
Intercept	−68.8343	63.3669	0.2778
Maximum height	−2.7525	0.4827	<0.0001
Mean height	7.7416	0.5367	<0.0001
SD height	5.7167	1.3386	<0.0001
Sum height	0.0001	0.0000	0.0003
Maximum density	124.6880	69.4322	0.0731
Mean density	−33.6810	16.7677	0.0451

(g) Model Run 7, Basal Area ≥60 ft^2/acre

Pine, BA ≥60	Coefficients	SE	*P*-Value
Intercept	85.5092	15.7534	<0.0001
Maximum height	−2.0892	0.4509	<0.0001
Mean height	4.1176	0.5497	<0.0001
Mean density	32.7820	13.8835	0.0186
SD density	−82.3698	44.3469	0.0638
Sum density	0.0017	0.0003	<0.0001

(h) Model Run 8, Basal Area <60 ft^2/acre

Pine, Basal Area <60	Coefficients	SE	*P*-Value
Intercept	8.8147	3.6664	0.0166
Minimum height	8.1523	4.8274	0.0919
Maximum height	−1.1152	0.1577	<0.0001
Mean height	1.4489	0.3049	<0.0001
SD height	4.7501	0.6187	<0.0001
Sum height	0.0000	0.0000	0.1013
SD density	86.9499	17.2556	<0.0001

Table 20-4. Akaike Information Criterion (AIC) Variables, Coefficients, SE, and *P*-Values for Model Scenarios 1 Through 9, Modeling Basal Area by Forest Stand Type (continued)

(i) Model Run 9, Hardwood Stands

Hardwood Stands	Coefficients	SE	*P*-Value
Intercept	869.5256	215.3783	0.0001
Minimum height	19.8131	8.5453	0.0219
Mean height	1.2155	0.8248	0.1429
SD height	3.7948	1.6640	0.0241
Maximum density	−863.4644	214.5155	0.0001
SD density	76.7871	37.3904	0.0419
Sum density	0.0009	0.0002	<0.0001

The height variables are most significant in all models except for the hardwood stands, Table 20-4i, where maximum density and sum density have the highest probability at 0.0001 and <0.0001, respectively. Three of the variables in Model 9 (i.e., minimum height, mean density, and sum density) are kept by the AIC procedure, despite not being significant at the 0.05 level. A few variables in the other models are also not significant at the 0.05 level. By the AIC, keeping these variables improves the model enough to warrant the added complexity of the model.

The model for the hardwood stands is somewhat different than the pine and pine hardwood mix models. The r^2 is similar, at 39%, but the *P*-value of the variables used is quite different. Three height variables are used, but none are significant at better than a probability of 0.05, and three density variables are used. Maximum density and sum density are significant at <0.0001. This finding would suggest that the structural differences between hardwood and pine make the density variables relatively more important to model basal area. This difference may be because the hardwood trees themselves are more variable.

Table 20-5 presents the number of times each variable was used among the nine basal area models. With the AIC procedure of model fitting, one variable may be kept over another, but the importance of both may be similar. Some variables are nearly interchangeable. We looked at which variables are consistently used across all nine models to understand the importance of each. Mean height is used in every model and is significant at *P*-value <0.0001 in all except the hardwood stands model. Mean height is also most highly correlated to basal area in **Table 20-2** at 55%, so mean height's importance as a predictive variable is expected. Maximum height and SD height are used in eight of the nine models, and all at a probability of at least 0.001. The importance of various forms of height measurements is observed in nearly all LiDAR studies predicting basal area and AGB.

Table 20-5. Number of Times When Each Predictor Variable Was Used Among the Nine Models

Predictor Variable	Number of Times Used
Minimum height	3 of 9
Maximum height	8 of 9
Mean height	9 of 9
SD height	8 of 9
Sum height	4 of 9
Minimum density	1 of 9
Maximum density	6 of 9
Mean density	3 of 9
SD density	4 of 9
Sum density	6 of 9

The forest density variables are not as consistently important as the forest height variables, but at least one forest density variable was included in every model. Maximum density and sum density are used in six of the nine models. The remaining forest density variables are used in four or fewer of the models. In several models, the density variables included by the AIC are not significant at the 0.05 level, but they are still included as an improvement to the model. The exception is the hardwood model, in which the density variables have a greater significance than the height variables.

Conclusions and Implications for Future Research and Implementation

Research Questions

1. Can forest height and density be directly measured from LiDAR collected for other purposes?

This study has demonstrated that existing LiDAR data can effectively measure forest height and density at MCBCL. However, the MCBCL forest stand data lack measured tree height. There are several options when processing these data that could potentially affect the accuracy of the height data, such as the pixel size used (too big) and the height data are smoothed and lose maximum height information. If the pixel is too small, then there may not be enough LiDAR points to effectively represent the cell. Without ground truth tree height measurements, we cannot adjust the process to determine the accuracy and to select the best thresholds during processing. Using only the distribution of the LiDAR height data, we have one measure of error of 0 to 3.4 m in height, with a mean of 0.1 m and an SD of 0.2 m.

2. Using the LiDAR−derived forest height and density, can we predict tree basal area and ABG as a method to monitor landscape-level changes?

AGB cannot be modeled. The available stand data do not include AGB, and without measured height and diameter data for each stand, AGB cannot be calculated. Basal area

is available and is determined by using a standard cruise method with a 10-factor prism. Nine different basal area models were created to examine whether the effectiveness of the basal area models varied with species, age, and high versus low basal area of 2,447 homogenous forest stands at MCBCL. The resulting models described between 32% and 44% of the variability. There was not a significant difference between stands composed of different species, ages, and high versus low basal areas. The LiDAR–derived stand height variables, particularly mean height, maximum height, and SD height, were most often used in the AIC multiple regression models. Their relationship is expected, given the importance of various height variables in many published studies. The model using hardwood stands was different because LiDAR forest density variables were more significant than the height variables. This finding may be due to the difference in stand structure between hardwood and pine and perhaps the variability in hardwood stands at MCBCL.

Findings with Implications for Future Base Management

For MCBCL to remain an effective training facility, forest managers must understand how both forest management practices and climate change will affect forest stand structure and carbon storage. This research project has shown that existing LiDAR data can effectively measure stand structure and biophysical parameters. However, the MCBCL forest stand data lacked the height and diameter information necessary for developing the basal area models effectively. The stand data do not include measured height or diameter information about the trees in the stands. Without measured tree height, there was no way to assess the accuracy of the LiDAR–derived height data, improve on the processing of the height data, or calculate AGB for each stand. The basal area estimates are also at a coarser scale than the LiDAR data, the focus being on merchantable timber rather than all trees. This mismatch increases the variability in the LiDAR–derived basal area models.

For MCBCL to measure and monitor forest biophysical parameters during a period of climate change, additional forest measurements will be necessary. To effectively describe a stand for use in modeling, multiple plots per stand are needed to measure tree species, height, diameter, basal area, and AGB. This intensive monitoring is not needed for all stands at MCBCL, but a subset across stands of different species, ages, and basal areas would be needed. A typical sampling procedure that would provide this information is described by Hall et al. (2005). This resulting data could then be used with existing and future LiDAR collections to greatly improve the model results described in this chapter.

Literature Cited

Ahern, F.J., T. Erdle, D.A. Maclean, and I.D. Kneppeck. 1991. A quantitative relationship between forest growth-rates and thematic mapper reflectance measurements. *International Journal of Remote Sensing 12*:387–400.

Carlson, T.N., and D.A. Ripley. 1997. On the relation between NDVI, fractional vegetation cover, and leaf area index. *Remote Sensing of Environment 62*:241–252.

Cohen, W.B., M.E. Harmon, D.O. Wallin, and M. Fiorella. 1996. Two decades of carbon flux from forests of the Pacific Northwest. *Bioscience 46*:836–844.

Dobson, M.C. 2000. Forest information from synthetic aperture radar. *Journal of Forestry 98*:41–43.

Dobson, M.C., F.T. Ulaby, L.E. Pierce, T.L. Sharik, K.M. Bergen, J. Kellndorfer, J.R. Kendra, E. Li, Y.C. Lin, A. Nashashibi, K. Sarabandi, and P. Siqueira. 1995. Estimation of forest biophysical characteristics in Northern Michigan with Sir-C/X-Sar. *IEEE Transactions on Geoscience and Remote Sensing 33*:877–895.

Goetz, S.J., and R.O. Dubayah. 2011. Advances in remote sensing technology and implications for measuring and monitoring forest carbon stocks and change. *Carbon Management 2*:231–244.

Hall, F.G., K. Bergen, J. B. Blair, R. Dubayah, R. Houghton, G. Hurtt, J. Kellndorfer, M. Lefsky, J. Ranson, S. Saatchi, H.H. Shugart, and D. Wickland. 2011. Characterizing 3D vegetation structure from space: Mission requirements. *Remote Sensing of Environment 115*:2753–2775.

Hall, S.A., I.C. Burke, D.O. Box, M.R. Kaufmann, and J.M. Stoker. 2005. Estimating stand structure using discrete-return LiDAR: An example from low density, fire prone ponderosa pine forests. *Forest Ecology and Management 208*:189–209.

Harrell, P.A., E.S. Kasischke, L.L. Bourgeauchavez, E.M. Haney, and N.L. Christensen. 1997. Evaluation of approaches to estimating aboveground biomass in southern pine forests using Sir-C data. *Remote Sensing of Environment 59*:223–233.

Lefsky, M.A., W.B. Cohen, D.J. Harding, G.G. Parker, S.A. Acker, and S.T. Gower. 2002a. LiDAR remote sensing of above-ground biomass in three biomes. *Global Ecology and Biogeography 11*:393–399.

Lefsky, M.A., W.B. Cohen, G.G. Parker, and D.J. Harding. 2002b. LiDAR remote sensing for ecosystem studies. *Bioscience 52*:19–30.

Lefsky, M.A., W.B. Cohen, and T.A. Spies. 2001. An evaluation of alternate remote sensing product for forest inventory, monitoring, and mapping of Douglas fire forest in western Oregon. *Canadian Journal of Forest Research 31*:78–87.

Lefsky, M.A., D. Harding, W.B. Cohen, G. Parker, and H.H. Shugart. 1999. Surface LiDAR remote sensing of basal area and biomass in deciduous forests of Eastern Maryland, USA. *Remote Sensing of Environment 67*:83–98.

Magnussen, S., P. Eggermont, and V.N. LaRiccia. 1999. Recovering tree heights from airborne laser scanner data. *Forest Science 45*:407–422.

Naesset, E. 2002. Predicting forest stand characteristics with airborne scanning laser using a practical two-state procedure and field data. *Remote Sensing of Environment 80*:88–99.

Naesset, E. 1997. Determination of mean tree height of forest stands using airborne laser scanner data. *ISPRS Journal of Photogrammetry and Remote Sensing* 52:49–56.

North Carolina Floodplain Mapping Program. 2014. 2014 LiDAR data. Available at http://www.ncfloodmaps.com

Patenaude, G., R.A. Hill, R. Milne, D.L.A. Gaveau, B.B.J. Briggs, and T.P. Dawson. 2004. Quantifying forest above ground carbon content using LiDAR remote sensing. *Remote Sensing of Environment 93*:368–380.

Renslow, M., P. Greenfield, and T. Guay. 2000. *Evaluation of Multi-Return LIDAR for Forestry Applications*. U.S. Department of Agriculture Forest Service Remote Sensing Applications Center Project Report. RSAC-2060/4810-LSP-000-RPT1. Available at https://www.fs.fed.us/t-d/programs/im/fy00/lidar/report.pdf

Rosette, J., J. Suarez, R. Nelson, S. Los, B. Cook, and P. North. 2012. LiDAR remote sensing for biomass assessment. *Remote Sensing of Biomass—Principles and Applications 24*. 26 pages.

Running, S.W., D.D. Baldocchi, D.P. Turner, S.T. Gower, P.S. Bakwin, and K.A. Hibbard. 1999. A global terrestrial monitoring network integrating tower fluxes, flask sampling, ecosystem modeling and EOS data. *Remote Sensing of Environment 70*:108–127.

Shugart, H.H., S. Saatchi, and F.G. Hall. 2010. Importance of structure and its measurements in quantifying function of forest ecosystems. *Journal of Geophysical Research: Biogeosciences 115*.

Smart, L.S., J.J. Swenson, N.L. Christensen, and J.O. Sexton. 2012. Three-dimensional characterization of pine forest type and red-cockaded woodpecker habitat by small-footprint, discrete-return LiDAR. *Forest Ecology and Management 281*:100–110.

Steininger, M. 2000. Satellite estimation of tropical secondary forest above-ground biomass: Data from Brazil and Bolivia. *International Journal of Remote Sensing 21*:1139–1157.

Turner, D., W. Cohen, R. Kennedy, K. Fassnacht, and J. Briggs. 1999. Relationship between leaf area index and Landsat TM spectral vegetation indices across three temperate zone sites. *Remote Sensing of Environment 70*:52–68.

Waring, R.H., J. Way, E.R. Hunt, L. Morrissey, K.J. Ranson, J.F. Weishample, R. Oren, and S.E. Franklin. 1995. Imaging radar for ecosystem studies. *Bioscience 45*:715–723.

Woodcock, C.E., and A.H. Strahler. 1987. The factor of scale in remote sensing. *Remote Sensing of Environment 21*:311–332.

Zhao, K., S. Popescu, and R. Nelson. 2009. LiDAR remote sensing of forest biomass: A scale-invariant estimation approach using airborne lasers. *Remote Sensing of Environment 113*:182–196.

Zolkos, S.G., S.J. Goetz, and R. Dubayah. 2013. A meta-analysis of terrestrial aboveground biomass estimation using LiDAR remote sensing. *Remote Sensing of Environment 128*:289–298.

Chapter 21

Development of a Spatial Decision-Support Framework: Translating Science into Practice Module

SERDP Project Number: RC-2245

Translating Science into Practice Module

Research Project TSP-1

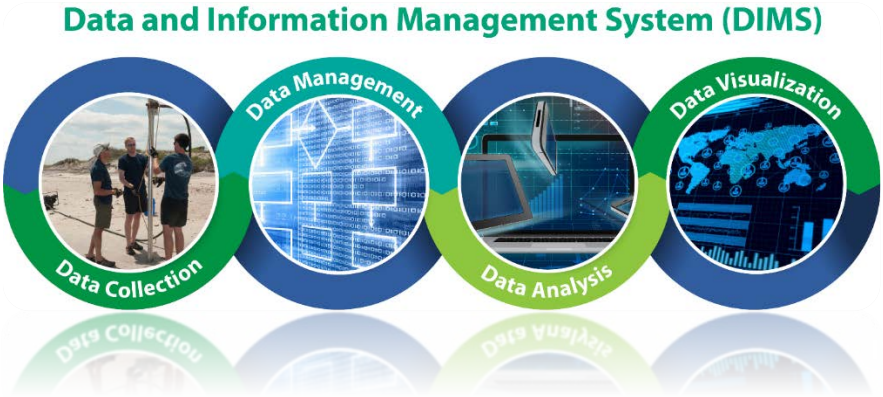

Lead Researchers:

Dr. Patrick N. Halpin and Ms. Danette Boezio
Duke University and RTI International
halpin@duke.edu and dboezio.rti.org

Supporting Researchers:

Jesse Cleary, Duke University
Ben Donnelly, Duke University
Peter Harrell, Duke University
Linda Andrews, RTI International
Anne-Marie Miller, RTI International
Nneka Ubaka-Blackmoore, RTI International
Jennifer Wellard, RTI International

January 2018

Final

This report was prepared under contract to the U.S. Department of Defense (DoD) Strategic Environmental Research and Development Program (SERDP). The publication of this report does not indicate endorsement by DoD, nor should the contents be construed as reflecting the official policy or position of DoD. References herein to any specific commercial product, process, or service by trade name, trademark, manufacturer, or otherwise, do not necessarily constitute or imply its endorsement, recommendation, or favoring by DoD.

Contents

Acronyms 21-v
Abstract 21-1
Objectives of the Research Project 21-2
Background 21-2
Materials and Methods 21-3
Introduction to DIMS 21-3
Components of DIMS 21-4
DCERP Web Sites 21-5
Other Data Portal Products 21-11
Outreach and Engagement of MCBCL and other DoD Installations 21-18
Technical Specifications of DIMS 21-18
Database Design 21-18
Data Life Cycle 21-19
Data Access, Release, and Use Policies 21-22
DIMS Server Environment 21-22
Backup and Recovery System 21-23
Results and Discussion 21-24
Summary of DCERP Data and DIMS User Analytics 21-24
Benefits of DIMS 21-26
Conclusions and Recommendations 21-27
Translating Science into Practice 21-28
Development must be flexible and adapt to the program's and users' needs 21-29
Structural elements of DIMS make it a good data repository for DCERP 21-30
Continuation of DIMS (one component of the DCERP's legacy) 21-31
DIMS provides a centralized location for accessing DCERP data, information, models, tools, and output products, ... 21-31
Appendix 21-A: DCERP Data Policy 21-A-1
Appendix 21-B: Quick Guide: Finding and Exploring DCERP Data, Models, Tools, and Visualization 21-B-1
Appendix 21-C: MCBCL Engagement and Outreach Efforts 21-C-1
Appendix 21-D: Data Dictionaries for Electronic Data Deliverables for DCERP Data Sets 21-D-1
Appendix 21-E: Example of a DCERP Data Fact Sheet 21-E-1
Appendix 21-F: Data Catalogs 21-F-1

List of Figures

Figure 21–1. Components of the Data and Information Management System (DIMS). 21-4
Figure 21–2. The Home page for the DCERP Public Web site. 21-5
Figure 21–3. The DCERP Data Portal. 21-6
Figure 21–4. The MARDIS Home page. 21-7
Figure 21–5. The MARDIS Document Database Search page. 21-8
Figure 21–6. The iMAP Web page. 21-10
Figure 21–7. The Water Quality Explorer..... 21-12
Figure 21–8. Link to data set reports from the Data Portal page. 21-13
Figure 21–9. Link to models and tools from the Data Portal page. 21-13
Figure 21–10. Three story maps in DIMS..... 21-14
Figure 21–11. The Water Quality Dashboard. 21-15
Figure 21–12. The link to the DCERP Data Policy. 21-15
Figure 21–13. The link to the Help and User Guides..... 21-16
Figure 21–14. The DCERP DIMS login. 21-16
Figure 21–15. The link to the iMAP and Data Query from the Data Portal page..... 21-16
Figure 21–16. The Advanced Query Web page in the MARDIS database..... 21-17
Figure 21–17. The Document Database link on the Data Portal page. 21-18
Figure 21–18. Internal MARDIS data-uploading processes and validation checks..... 21-21
Figure 21–19. MARDIS total records and stations. 21-25
Figure 21–20. New versus returning visitors to the DCERP public Web site. 21-25
Figure 21–21. Monthly pages per session. 21-25
Figure 21–22. Monthly average session..... 21-26
Figure 21–23. Document types in the Document Database. 21-26

List of Tables

Table 21-1. Models and Tools Developed and/or Applied During DCERP2 21-10

Acronyms

µg/L	micrograms per liter
AWAC	Acoustic Wave and Current (Profiler)
BMP	Best Management Practice
CAAAC	combined arms amphibious assault course
CB	Coastal Barrier (Module)
CSV	comma-separated value
CW	Coastal Wetlands (Module)
DCERP	Defense Coastal/Estuarine Research Program
DCERP1	first cycle of DCERP
DCERP2	second cycle of DCERP
DIMS	Data and Information Management System
DoD	U.S. Department of Defense
EDD	Electronic Data Deliverable
EMD	Environmental Management Division
ESM	Estuarine Simulation Model
FGDC	Federal Geographic Data Committee
GIS	geographic information systems
ha	hectare
HQMC	Headquarters Marine Corps
ICW	Intracoastal Waterway
ID	identification
iMAP	interactive mapping application
LANDIS-II	Land and Information System (a forest landscape model)
Landsat	Land Remote-Sensing Satellite
LiDAR	Light Detection and Ranging
m	meter
MARDIS	Monitoring and Research Data Information System
MCBCL	Marine Corps Base Camp Lejeune
MCI East	Marine Corps Installation East
NEPA	National Environmental Policy Act
NOAA	National Oceanic and Atmospheric Administration
NRE	New River Estuary
OSC	On-site Coordinator
QA	quality assurance
QC	quality control
RC	Resource Conservation and Climate Change (a SERDP program area)
RCC	Regional Coordinating Committee

RCW	red-cockaded woodpecker
RDBMS	Relational Database Management System
RDMD	Range Development and Management Division
SDSFIE	Spatial Data Standards for Facilities, Infrastructure, and Environment
SDSS	Spatial Decision-Support System
SERDP	Strategic Environmental Research and Development Program
SERPPAS	Southeast Regional Partnership for Planning and Sustainability
SET	surface elevation table
SSL	Secure Sockets Layer
T	Terrestrial (Module)
TAC	Technical Advisory Committee
TSP	Translating Science into Practice (Module)
UNC-IMS	University of North Carolina at Chapel Hill's Institute of Marine Sciences
USACE	U.S. Army of Corps Engineers
USGS	U.S. Geological Survey
VIMS	Virginia Institute of Marine Science

Abstract

The goal of Research Project TSP-1 was to translate science into practice by providing access to DCERP-related research and monitoring data, modeling results, and other decision-support tools to enable staff from Marine Corps Base Camp Lejeune (MCBCL) and other U.S. Department of Defense (DoD) installations to make more informed planning and management decisions about natural resources management. The Data and Information Management System (DIMS), developed by the DCERP Data Management Team, provided the necessary platform needed to accomplish this goal.

DIMS is a comprehensive Web-based repository that documents all DCERP research; offers accessibility to raw monitoring and cross-ecosystem research data, synthesized results, and research models and tools; and provides summaries and visualizations of significant findings. Visualizations were designed to appeal to end users with varying levels of scientific expertise. Visualizations ranged from synthesized summaries developed for installation and coastal managers, such as in the Water Quality Dashboard that summarizes water quality data collected monthly at each of the eight estuarine monitoring stations into annual means, to examination of detailed monthly data collected at multiple monitoring stations over the 10 years of DCERP, such as can be observed in the query-based graphing function.

The development of a public Web site within DIMS and the creation of the Data Portal within the DCERP Web site, where users can register to access the data, allowed DCERP to transition data from MCBCL and the DoD community to other local and regional coastal stakeholders, and other end users including the scientific community.

Keywords: Dashboard, data collection, data management, database, DIMS, Electronic Data Deliverable (EDD), geographic information systems (GIS), geospatial mapping application, interactive mapping application (iMAP), interactive Web mapping, model forecasts and scenarios, modeling tools, data portal, simulation model, Spatial Decision-Support System (SDSS), SQL Server, visualization

Objectives of the Research Project

The goal of Research Project TSP-1 was to ensure that the scientific knowledge and data generated during the entire 10-year DCERP were translated into practical information and tools that were easy to understand and easily accessible so they could be broadly applied in making informed management decisions. Research Project TSP-1 focused on this goal by bringing spatial tools and expanded functionality to the DCERP Data and Information Management System (DIMS). The DCERP Data Portal and the interactive mapping application (iMAP) provided users with project outcomes, helping users to assess each project's findings and their usefulness in making management decisions without requiring specialized analytical tools.

Background

Environmental data collected throughout the duration of the DCERP1 and DCERP2 were critical to research and modeling activities of each project and to the development of decision-support management tools. In support of the data management needs of DCERP and to support accessibility to the complex and voluminous environmental data, members of the DCERP Data Management Team developed DIMS.

Initially, during DCERP1, the primary data management objective was to design and implement the DCERP DIMS to serve as the long-term repository for the program's data and to primarily serve as a data archive, while simultaneously supporting the data management needs of the DCERP Team. Because DCERP2 had specific research and data requirements, the objectives were expanded. DCERP2's objectives were to

- Provide an online portal that Marine Corps Base Camp Lejeune (MCBCL) staff, other U.S. Department of Defense (DoD) installation managers, and public users could employ to access a wide range of data, models, and tools developed by DCERP researchers
- Produce a secure data archive by using standardized data formats that provided the DCERP researchers with the ability to compare data across the different ecosystem modules
- Provide easy-to-understand, actionable information and visualizations to MCBCL managers
- Serve as both a data archive and dynamic exploration tool for MCBCL users for making planning and ecosystem-based management decisions.
- DIMS is a database-driven Internet system that provides a means to access and manage DCERP data collection efforts. DIMS also provides a framework that supports dynamic outreach products and ecosystem-based management tools. DIMS serves as the permanent repository for research and monitoring data and for related information (e.g., documents, reports, photographs, maps) collected during DCERP's 10-year implementation. DIMS includes procedures to manage the data and enable efficient, secure, and accurate input, analysis, integration, display, and sharing of data.

For DCERP2, the third thematic area addressed translating the scientific findings of DCERP's integrated research, monitoring, modeling, and adaptive management activities into actionable

information for installation managers and for federal, state, regional, and local natural resources managers to help them make more informed decisions. Each researcher was responsible for translating the scientific findings into easy-to-understand language. However, it was the role of the Research Project TSP-1 Team to translate the science into useful maps, visualizations, and model scenarios from which MCBCL managers could gain information to make often complex natural resource management decisions.

In support of the programmatic theme for the Translating Science into Practice (TSP), the Research Project TSP-1 Team translated the data for several audiences, including MCBCL and other DoD installation managers, the scientific community, and other coastal managers and stakeholders, including the public. These audiences had different levels of scientific knowledge and understanding of the results; therefore, the significant findings needed to be translated in appropriate ways to each audience. In addition, these audiences had different requirements for the data. For instance, domain experts, both within the DCERP Team, the scientific community, and MCBCL staff require data to be searchable. In addition, coastal managers and regional planners and non-domain experts seeking information about their specific areas of interest require access to general exploration tools. Lastly, public users require access to DCERP's outreach products, including fact sheets, story maps, and the Water Quality Dashboard and other visualizations.

This chapter discusses the implementation of Research Project TSP-1 and the DCERP DIMS, includes the results and conclusions of the project, and provides an overview of DIMS. The overview includes a summary of the DCERP data management functions and addresses common data management aspects such as quality assurance (QA) and quality control (QC), as well as data inventory, processing, validation, submission, storage, and access, release, and use policies.

Materials and Methods

Introduction to DIMS

The Data Management Plan, procedures, functionalities, tools, policies, and guidance evolved as DCERP progressed over the years. Given the size of the DCERP monitoring and research effort, it was vital that the team develop a comprehensive data management system from its inception. Initially, the data management system and policies focused primarily on supporting the scientific work of the DCERP Team. During DCERP1, it was recognized that DCERP would be a data-intensive project; therefore, the program would need to be integrated across the four ecosystem modules, with outreach products varying from reports and fact sheets, to integrated complex visualizations and models. To support these needs, the DCERP Data Management Team developed DIMS to standardize, store, manage, and integrate data from each module so that cross-cutting, inter-module analysis and modeling could be performed. The team's comprehensive DIMS solution provides an integrated analysis of environmental monitoring data from multiple sources that break down the extensive amount of data and information into meaningful, accessible, and manageable solutions that promote better understanding and communication.

As DCERP2 progressed, DIMS became the foundation and framework for housing the findings of the modeling effort and the scientific monitoring and research analyses. These data are

accessible by MCBCL and other DoD installations, the scientific community, and local stakeholders, including the public.

Components of DIMS

The DCERP Data Management Team developed the DIMS data management policies and guidance, as well as the architecture and infrastructure, to effectively and efficiently share and manage data and information products produced by DCERP researchers. DIMS is a flexible framework that is designed to help researchers focus on science. Specifically, DIMS provides the following features and functionalities:

- Data uploading and documentation
- Secure data sharing across the DCERP Team
- Tools to find, organize, and access research project and monitoring products
- Multi-disciplinary integration across the DCERP Team
- Data, information, and metadata accessible through data discovery and visualization tools.

Web-based access and interfaces allow the DCERP researchers, MCBCL staff, and other users, including the public, to access DCERP data from DIMS. DIMS also makes DCERP information available via the DCERP public Web site, provides a secure password-protected Web site for team-only collaboration (i.e., the DCERP Team Web site), and supports the data management needs of DCERP, including data archiving, searching, and retrieval. As part of the approach to meet the many requirements and needs of DCERP, the team developed several distinct systems for DIMS (**Figure 21-1**) that are further described in the following section.

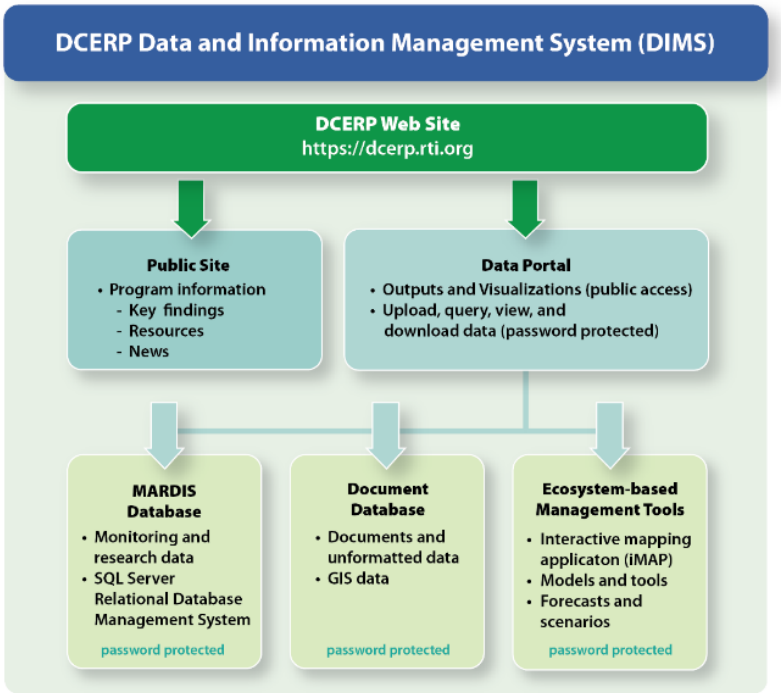

Figure 21–1. Components of the Data and Information Management System (DIMS).

Note: GIS = geographic information systems; MARDIS = Monitoring and Research Data Information System.

DCERP Web Sites

DCERP Team Web Site

The DCERP Team Web site (not shown in **Figure 21-1**) was a password-protected site only available to the DCERP Team. At this site, team members could share administrative planning documents, reports of activities, and other information of interest to facilitate communication and provide a forum for discussing the results and their implications for management. The team maintained this site for the duration of DCERP1 and DCERP2, but because of the internal audience it served, it was not retained beyond the DCERP end date.

DCERP Public Web Site

The DCERP public Web site is a subsection of the DCERP Web site (see https://dcerp.rti.org) and is the long-term face of the program. The public Web site provides comprehensive information about the entire program, including the background, objectives, and approaches of the program and research activities; the benefits to military installations; and descriptions of the research and monitoring efforts. This site also contains contact information for the DCERP management team and DCERP lead investigators and provides links to their respective affiliated organizations. The DCERP Team posted technical reports, presentations, and other outreach materials to this site throughout the duration of the program. **Figure 21-2** is the Home page for the DCERP Public Web site.

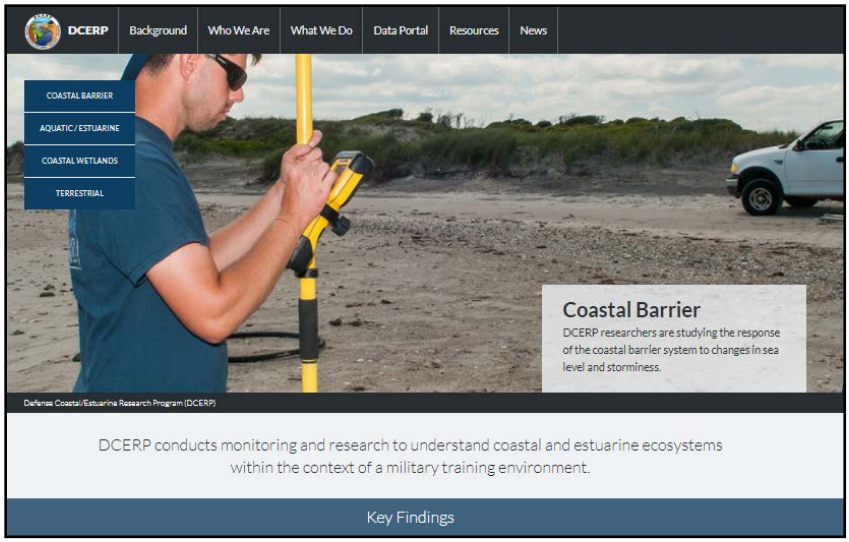

Figure 21–2. The Home page for the DCERP Public Web site.

DCERP Data Portal

The DCERP Data Portal (**Figure 21-3**) is a subsection of the DCERP Web site (see https://dcerp.rti.org/#/data-portal) and is the front-end interface to the data and tool components of DIMS. These components include the Monitoring and Research Data Information System (MARDIS) database, the Document Database, and Ecosystem-based Management Tools such as

iMAP. In addition, the Data Portal provides access to various output products and tools (e.g., story maps) and model pages that contain information and outputs from the models, the Water Quality Dashboard, topic-driven queries, and other ecosystem-based management tools. The components presented in **Figure 21-1** are further described in the following subsections of this chapter, followed by detailed descriptions of the other components that comprise the Data Portal.

Figure 21–3. The DCERP Data Portal.

MARDIS Database

The MARDIS database is a Microsoft SQL Server Relational Database Management System (RDBMS) that provides scalability, security, robustness, user management functionality, data consistency, and the ability to conduct complex queries. The MARDIS database serves as the long-term repository for DCERP tabular and environmental research and monitoring data that have defined content and structure. Although MARDIS was originally designed to be a simple data archive, it has evolved greatly throughout DCERP to now being essential to the overall DCERP DIMS framework. MARDIS offers controlled access to all components, data, and functions and feeds data to the tools that provide visualizations of the data. The MARDIS Home page is presented as **Figure 21-4**.

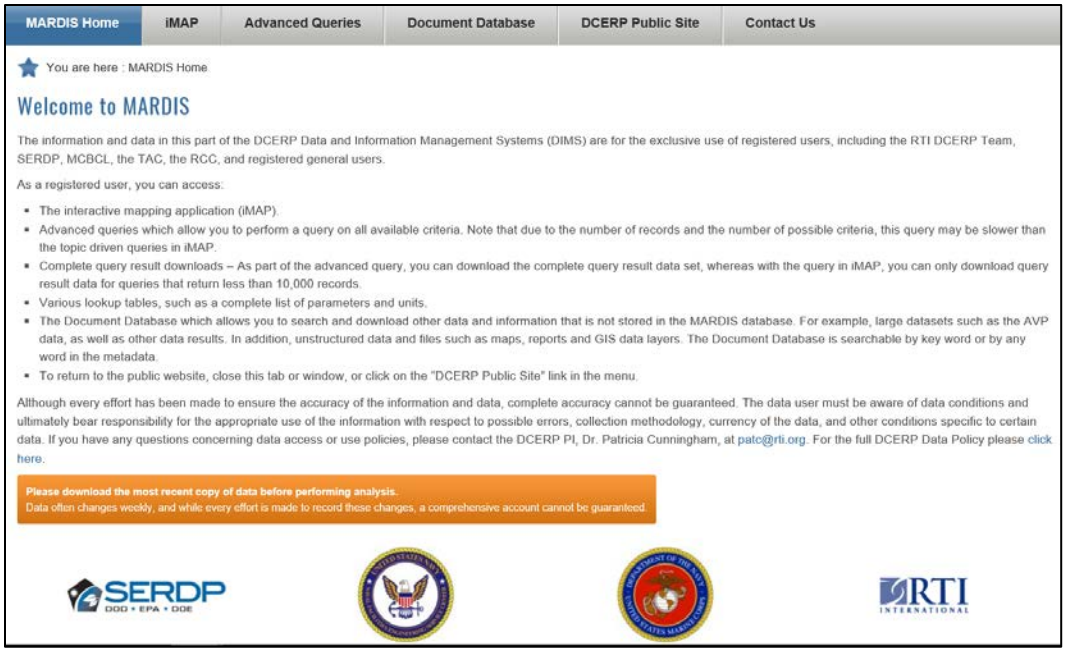

Figure 21–4. The MARDIS Home page.

Document Database

The Document Database is used to store and manage unstructured or derivative DCERP data such as maps, photographs, data files, reports, and other files and documents that cannot be stored as structured data in MARDIS. The Document Database serves as a searchable repository for all of the DCERP Team's finished products such as technical reports for MCBCL and final reports for SERDP directly related to DCERP monitoring, research, and modeling activities. Metadata associated with each document are searchable to facilitate document retrieval, help users understand the content of the documents, and locate files that contain data of value to their research. The Document Database Search page is presented as **Figure 21-5**.

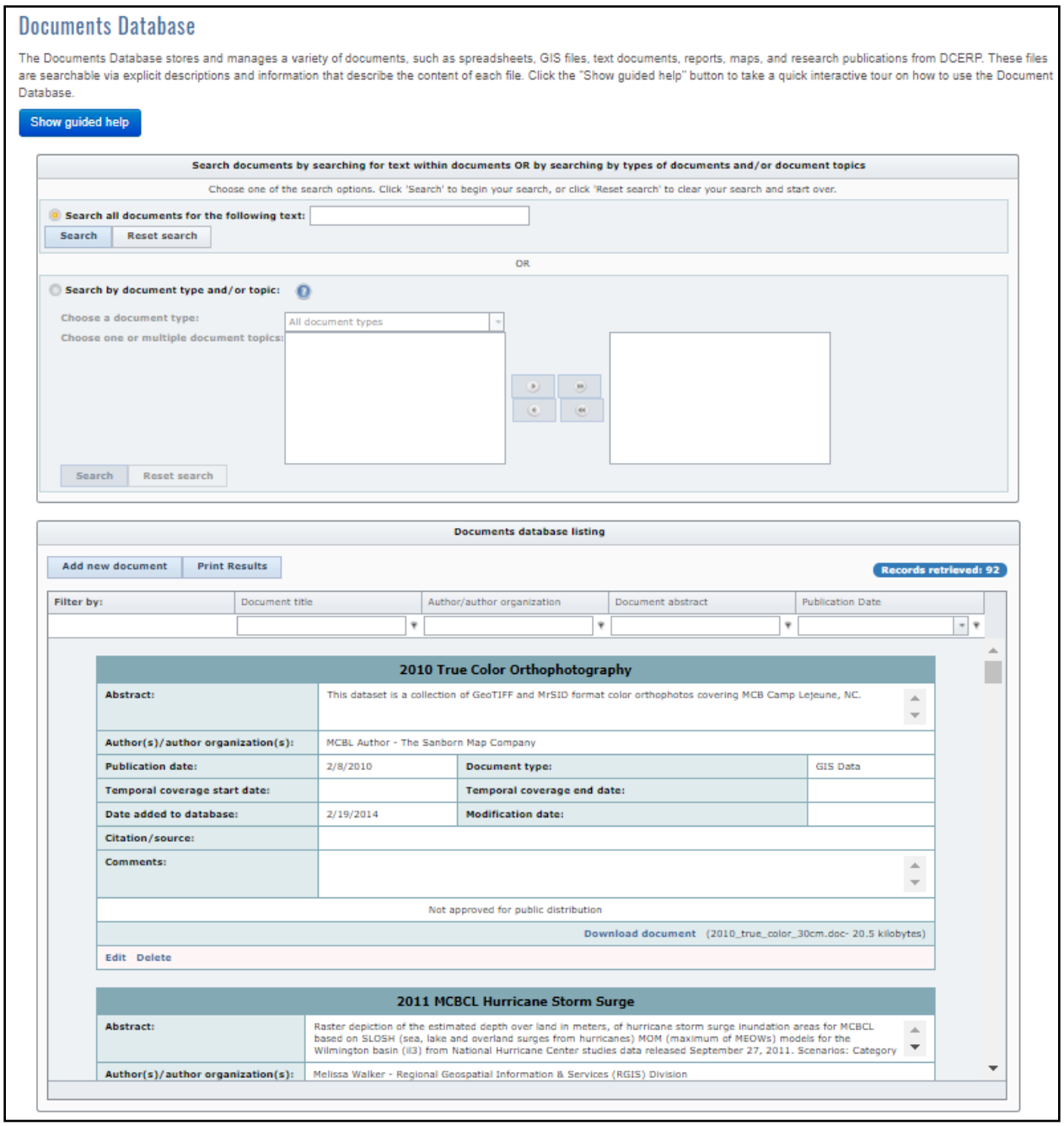

Figure 21–5. The MARDIS Document Database Search page.

Ecosystem-Based Management Tools

During DCERP1, the team developed and provided a simple interactive station map interface as part of the MARDIS Web site. The purpose of the interface was to allow users to query monitoring stations by station name, data set name, geographical location, type of sampling station (i.e., land, ocean, estuarine, stream/river, or wetland), or parameter group.

During DCERP2, these early capabilities and components were greatly expanded in functionality under Research Project TSP-1. Creating a Web framework for presenting data products allowed

for discovery and basic analysis of the data produced by DCERP researchers in the other ecosystem modules without requiring specialized geographic software such as ArcGIS, which was a requirement of SERDP.

During DCERP2, the DCERP Team added three primary components of the Ecosystem-based Management Tools part of DIMS to the framework: iMAP, Models and Tools, and Forecasts and Scenarios. These three components are described further in the following sections.

Interactive Mapping Application

iMAP allows users to visualize DCERP geospatial data and provides spatial and topic-driven search capabilities for data from MARDIS and other sources. The primary objective of iMAP is to allow end users to assess relationships and help them discover data to support management decisions.

The main requirements for creating the online iMAP were to

- Create Web browser–based tools to accommodate different operating systems and minimize the need for specific computer hardware and software
- Use Web visualization technologies developed by ESRI, which is the preferred MCBCL vendor for geographic information systems (GIS), to allow back-end integration and long-term support
- Use authentication rules so users would have different levels of access to data (e.g., publicly available sea level rise models versus restricted access to MCBCL training area designations).

Early in the development of iMAP, it became apparent that to meet the goals of turning science into actionable information, the framework needed to become a decision-support system for all DCERP module research and monitoring data. During DCERP2, the Research Project TSP-1 Team developed the iMAP and MARDIS enhancements side-by-side. The first release of iMAP incorporated the monitoring locations from the Aquatic/Estuarine, Coastal Barrier, Coastal Wetlands, and Terrestrial Modules. The final iMAP system is tightly integrated and represents not only monitoring and modeled data, but also other spatial information (**Figure 21-6**).

The Research Project TSP-1 Team iteratively vetted the iMAP system and MARDIS database with MCBCL staff to ensure that the required data sets were included. MCBCL provided data layers to the team to add the military context to DCERP data, such as training and firing ranges. DCERP researchers contributed other data, such as analysis of shoreline change, to iMAP and MARDIS. DCERP Team members met with Base staff to obtain their crucial feedback, which was used to refine data sets to customize the iMAP and better meet the installation's management needs.

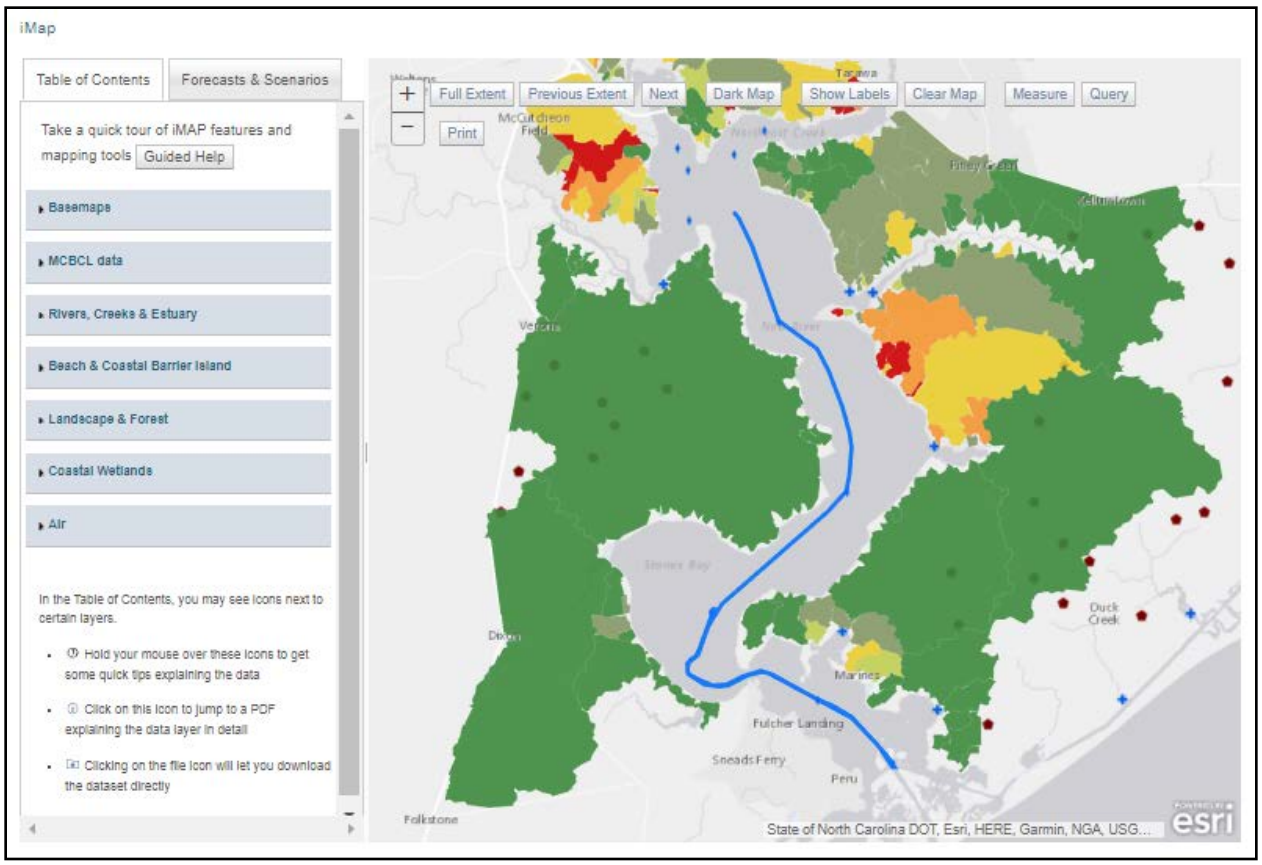

Figure 21–6. The iMAP Web page.

Models and Tools

The Model and Tools component provides integrated decision-support models and tools developed by DCERP researchers. These models and tools, or scenario outputs from those models that take too long for users to run directly, are accessible through the framework. **Table 21-1** summarizes the models and tools that were developed or applied during DCERP2 and identifies the purpose of each model for installation managers.

Table 21–1. Models and Tools Developed and/or Applied During DCERP2

Model Name and Research Project	Purpose of the Model for Installation Managers
Estuarine Simulation Model (Research Project TSP-2)	To identify water quality impairment from nutrients and sediment, as well as carbon dynamics in the New River Estuary under current and future land-use and climate scenarios
Geospatial Marsh Model (Research Project CW-4)	To estimate the sustainability of marshes under different sea level rise scenarios specified by SERDP (Hall et al., 2016) through 2100
Beach Morphology Model (Research Project CB-4)	To predict shoreline location and elevation of Onslow Beach under different sea level rise scenarios specified by SERDP and storminess scenarios (i.e., future wind speed) through 2100

(continued)

Table 21-1. Models and Tools Developed and/or Applied During DCERP2 (continued)

Model Name and Research Project	Purpose of the Model for Installation Managers
Forest Carbon Management Tool (Research Project T-3)	To estimate the carbon storage capacity of forested areas based upon different forestry management practices and climate scenarios through 2100 by using a LANDIS-II (Land and Information System) model
Red-Cockaded Woodpecker (RCW) Decision-Support System (Research Project T-4)	To predict the demographics of RCW populations in MCBCL based on habitat changes from future climate and forest management practices derived from the Forest Carbon Management Tool

The integration of MARDIS with iMAP facilitated the development of decision-support systems, visualizations, model output results, and custom tools that allow users to interact with, query, and visualize the spatial and non-spatial data in DIMS. This integration enabled installation managers to make informed decisions to support their long-term goals of military training and preparedness while sustaining the natural resource assets of MCBCL for the future.

Forecasts and Scenarios

The Forecasts and Scenarios component allows users who do not need customized scenario results to review a library of previously generated management and climate change scenario outputs prepared by the model and tool developers. This library contains vetted scenarios for the following models:

- Geospatial Marsh Model
- Beach Morphology Model
- Forest Carbon Management Tool.

Other Data Portal Products

The DCERP Data Portal also incorporates custom tools, such as story maps, to help turn the complex scientific DCERP data into actionable information and to more effectively communicate DCERP results and findings to various end users. Other tools summarize MARDIS data, such as the Water Quality Explorer shown in **Figure 21-7**.

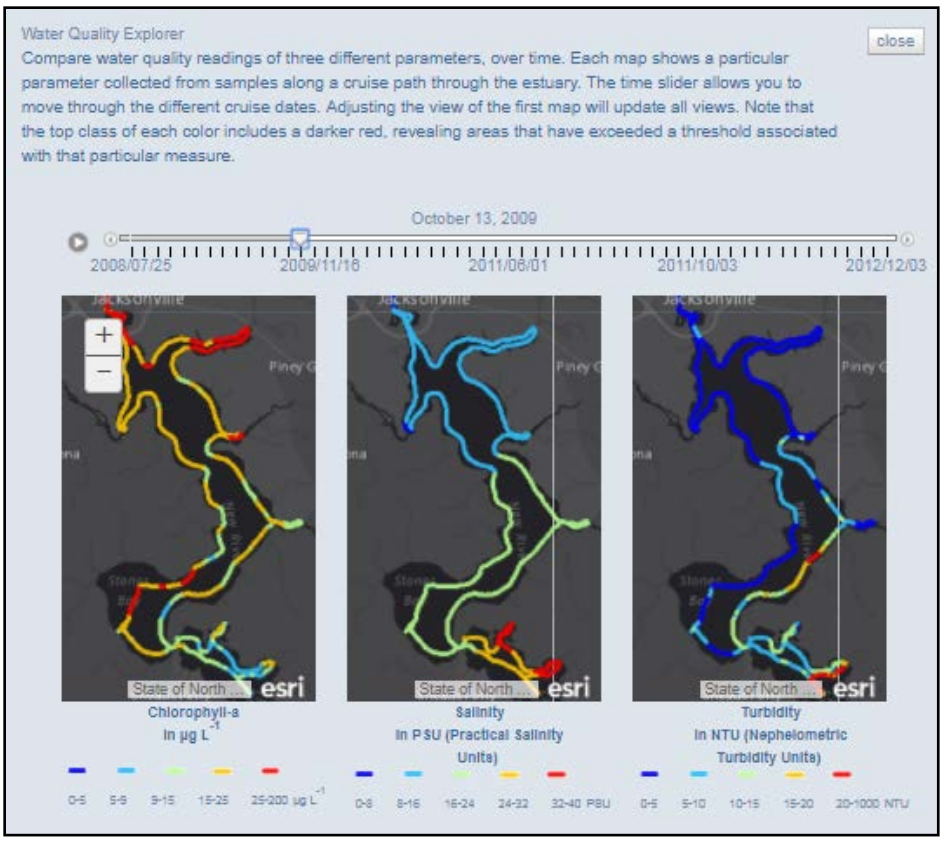

Figure 21–7. The Water Quality Explorer.

There is a wide variety of data and information available through the Data Portal. Some data are openly available to users; other data require user registration for a login identification (ID) and password to obtain access to the data. Note: Anyone can register for access to the Data Portal and obtain a user login by providing basic information such as the user's name, organization or affiliation, e-mail address, and intended use of the data and products. The DCERP Data Portal and the products to which it provides access are described below in the following subsections in the same order as presented on the Data Portal page (**Figures 21-3 and 21-8**).

What Data Does DCERP Have? *(Openly Accessible)*

This link on the Data Portal page (**Figure 21-8**) provides access to a variety of data set reports that describe the data available within DIMS. These Web pages include a current data report, a GIS data report, and an "other" data report. A current data report represents data that are currently available in MARDIS via the advanced query and iMAP. A GIS data report represents spatial data available from iMAP and the Document Database. An "other" data report represents data and results that are not available in MARDIS, but are available as spreadsheets and CSV (comma-separated value) files in the Document Database. Although these reports are openly accessible, access to the data itself is not (for more information, see the section titled Requires Basic User Registration).

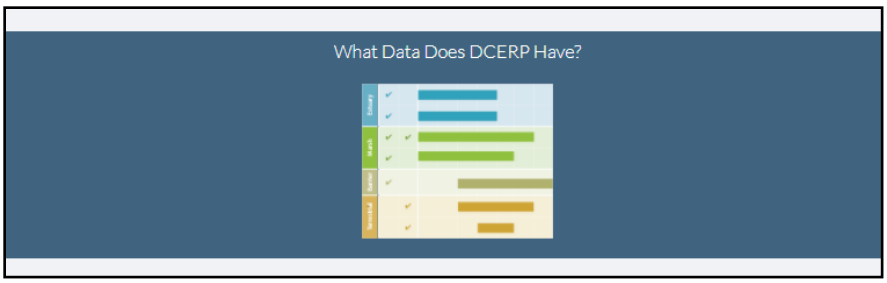

Figure 21–8. Link to data set reports from the Data Portal page.

Models and Tools (Openly Accessible)

This link on the Data Portal page (**Figure 21-9**) provides access to many ecosystem models, tools, and output products developed for DCERP, including links to externally hosted products such as the Estuarine Simulation Model, which is maintained at the Virginia Institute of Marine Science. Descriptions are provided for each model and tool, with links to more information and in many cases links to model outputs in iMAP, story maps, or other methods.

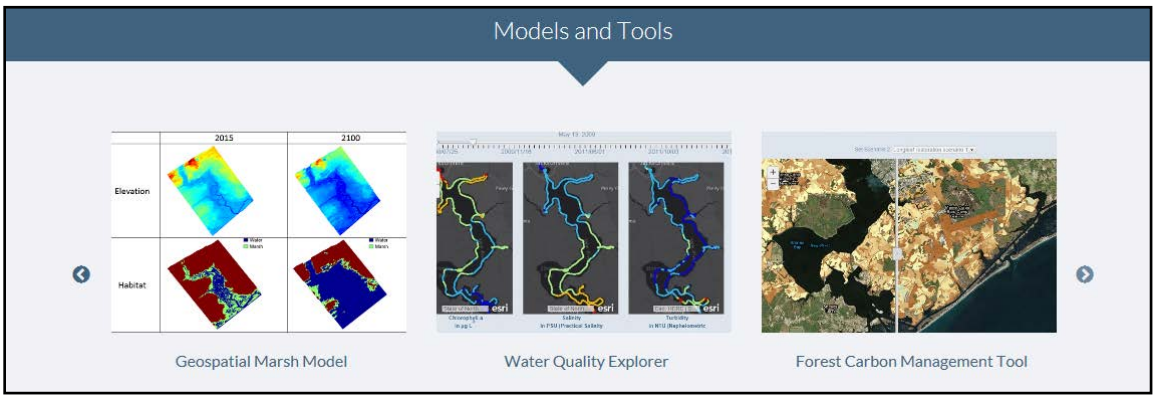

Figure 21–9. Link to models and tools from the Data Portal page.

Story Maps (Openly Accessible)

Story maps are short, highly visual presentations of key findings or concepts. Story maps use photographs, tables, and other graphical elements to help communicate information to users, who can click through the presentation at their own speed. Story maps translate DCERP scientific findings and results into easy-to-understand information by summarizing the findings and results and telling a story. Story maps are intended for non-technical audiences, but they are also used to summarize issues and key findings for managers and decision makers. The following two story maps are available for viewing in DIMS (**Figure 21-10**):

- Coastal Barrier Morphology story map titled *Onslow Beach: A Barrier Island of Shifting Sands and Migrating Shorelines*
- New River Estuary (NRE) story map titled *The New River Estuary: Human and Climatic Factors Affecting Water Quality Now and in the Future*

Also available for viewing is the Geospatial Marsh Model (**Figure 21-10**), which provides visual outputs of what occurs at three different marshes on MCBCL under five scenarios of rising sea level.

Figure 21–10. Three story maps in DIMS.

Water Quality Dashboard (Openly Accessible)

The Water Quality Dashboard (**Figure 21-11**) provides a graphical and numerical summary of 8 years of mean monthly water quality conditions from MARDIS. Some of the water quality conditions include concentrations of chlorophyll *a*, total suspended solids, bottom-water dissolved oxygen, total nitrogen, and total phosphorus that were monitored from 2008 to 2015 at eight monitoring stations in the NRE. Users can select one station or more from the station map and obtain a visualization of annual mean parameters over the 8 years when data were collected. In addition, users can obtain information about monthly values of each of the water quality parameters monitored from 2008 through 2016.

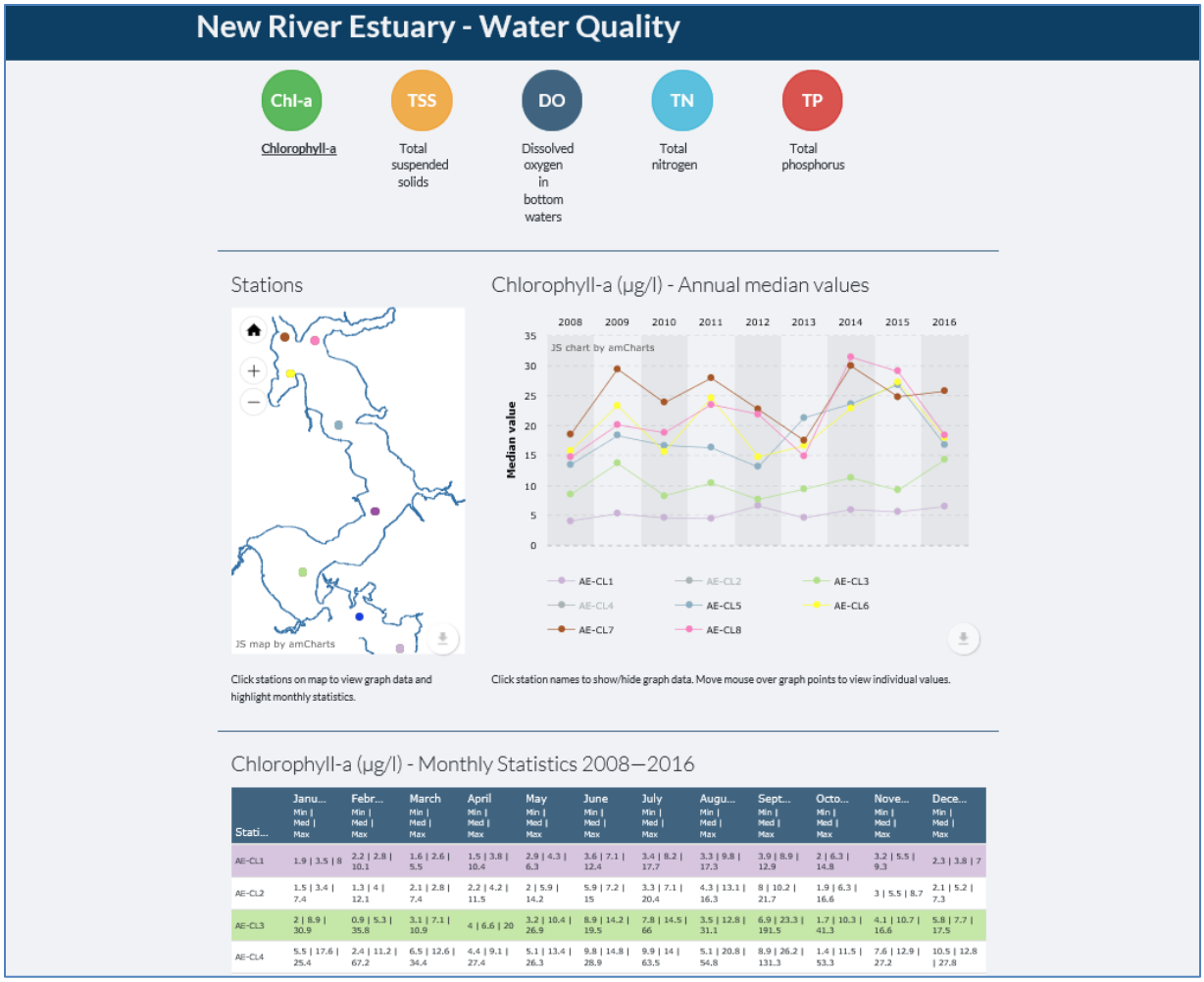

Figure 21–11. The Water Quality Dashboard.

DCERP Data Policy (Openly Accessible)

The link for the DCERP Data Policy (**Figure 21-12**) provides access to this document. The DCERP Data Policy, which is provided in **Appendix 21-A** of this chapter, specifies the general roles, responsibilities, and the rights of the various data users regarding the use of DCERP data and describes the data access, release, and use agreements of all parties.

Figure 21–12. The link to the DCERP Data Policy.

Help and User Guides (Openly Accessible)

This link for the Help and User Guides (**Figure 21-13**) provides access to the Resources page where the Help documents are available. Some of these documents include the *DCERP Quick Guide*, the *EDD (Electronic Data Deliverable) Reference Guide*, and the *MARDIS Quick Tips for the Advanced Query*. **Appendix 21-B** of this chapter is example user's guide titled *Quick Guide: Finding and Exploring DCERP Data, Models, Tools, and Visualizations*.

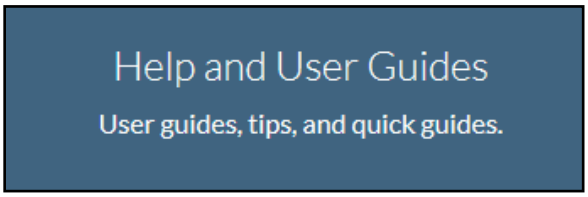

Figure 21–13. The link to the Help and User Guides.

Login (Requires Basic User Registration for a Login ID and Password)

A login to access DCERP data and products, as well as advanced components of the DCERP DIMS, is required (**Figure 21-14**).

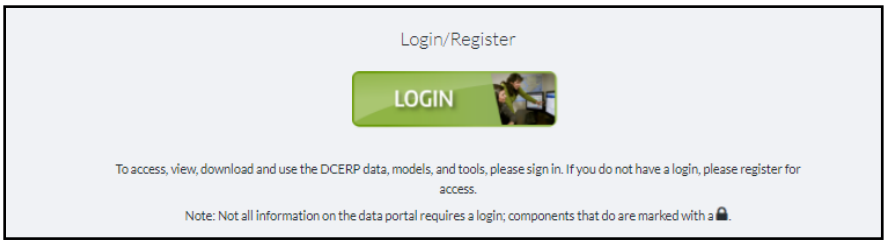

Figure 21–14. The DCERP DIMS login.

iMAP and Data Query (Requires Basic User Registration for a Login ID and Password)

Users can view DCERP stations and model scenarios on an interactive map, can use the Map/Topic Queries link to query DCERP data, and can view and download query results in tabular form or generated in graphs. A link from the Data Portal page is shown in **Figure 21-15**.

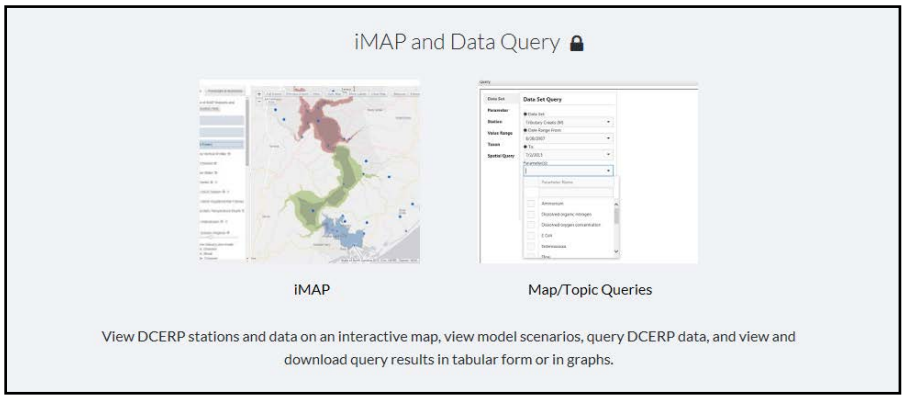

Figure 21–15. The link to the iMAP and Data Query from the Data Portal page.

Advanced Query and Download Data (Requires Basic User Registration for a Login ID and Password)

The Advanced Query link in the MARDIS database (**Figure 21-16**) allows users to query every combination of criteria, find stations, access large data downloads, and view look-up tables such as a full list of all parameters.

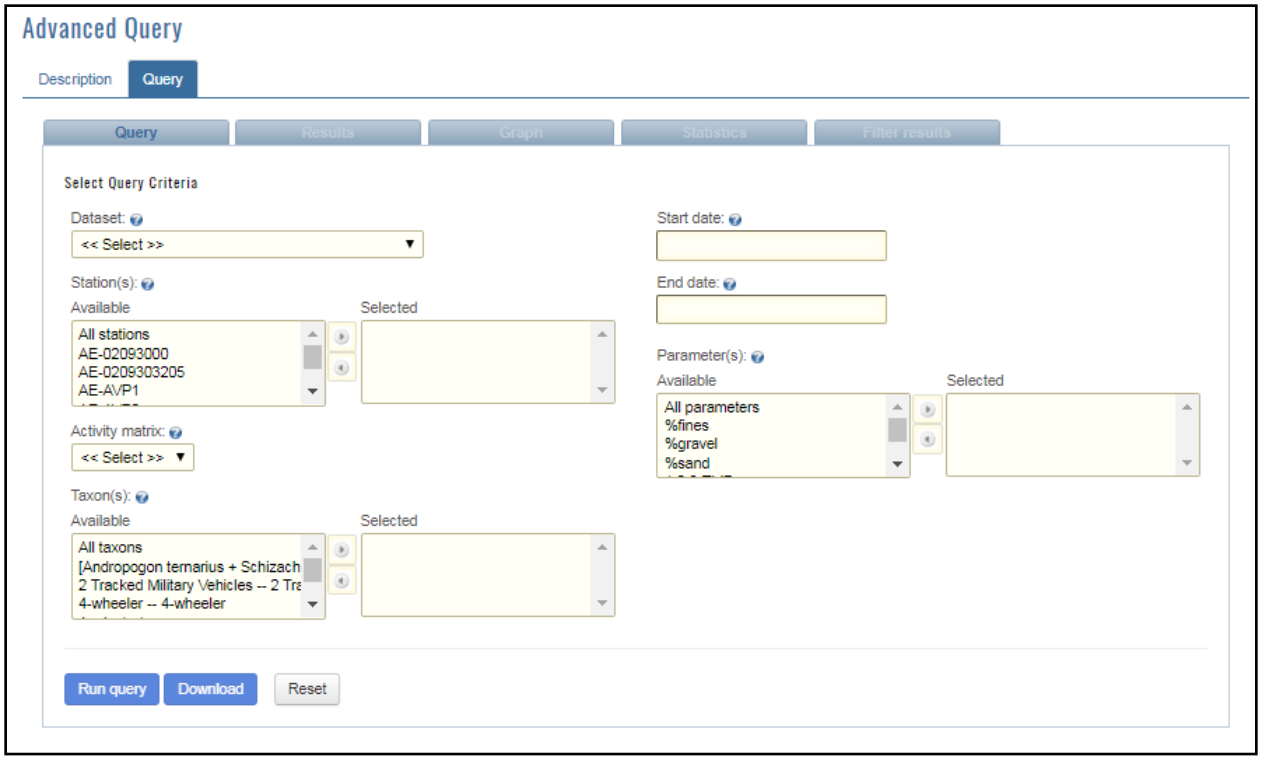

Figure 21–16. The Advanced Query Web page in the MARDIS database.

Document Database (Requires Basic User Registration for a Login ID and Password)

The Document Database link on the Data Portal page (**Figure 21-17**) allows users to access the database, which stores and manages a wide variety of documents such as spreadsheets, GIS files, text documents (including reports), maps, and research publications.

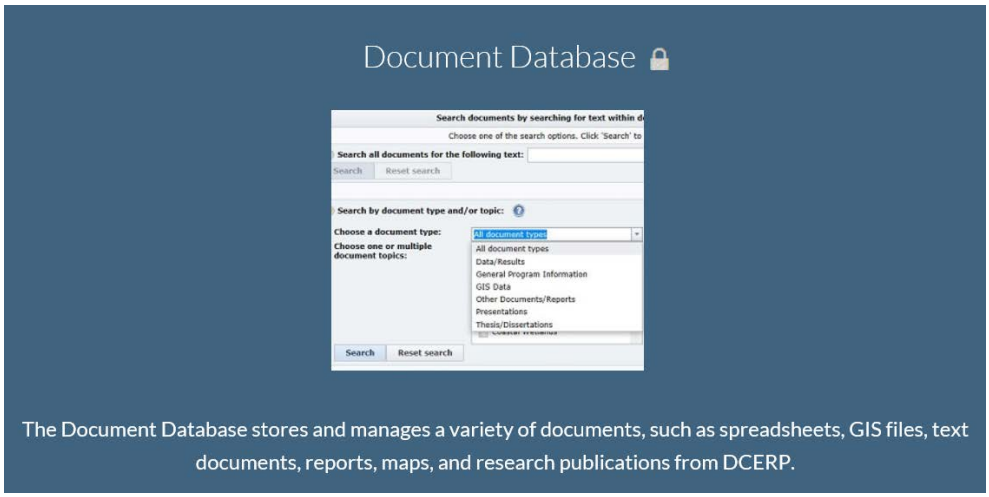

Figure 21–17. The Document Database link on the Data Portal page.

Outreach and Engagement of MCBCL and other DoD Installations

The Research Project TSP-1 Team and DCERP2 researchers sought assistance from installation staff with evaluating DIMS products (i.e., reviewing and providing feedback about iMAP, data layers, and model scenarios) and providing feedback about how these products could be improved to better address MCBCL management's needs.

To improve communication with target DoD installations, the DCERP2 Team invited managers from MCBCL and three other installations to the annual DCERP2 Technical Advisory Committee (TAC) meetings at MCBCL. The three installations were and Marine Corps Air Station (MCAS) Cherry Point and Fort Bragg (both in North Carolina) and Eglin Air Force Base (in Florida). The purpose of this outreach effort was to obtain additional perspectives about tool development needs and ways to translate research results into clear actionable statements for installation managers. In addition, Research Project TSP-1 researchers and DCERP2 Team members participated in on-site presentations to installation staff to demonstrate how to properly use the various tools and products, and then obtained their feedback regarding recommended improvements. **Appendix 21-C** of this chapter lists MCBCL engagement and outreach efforts.

Technical Specifications of DIMS

Database Design

The database design selected for MARDIS was based on recognized ecological and environmental data standards and was adapted to provide support for DCERP monitoring and research data. This comprehensive design supported structured results from each ecosystem module by using the typical relationships between sample locations, parameters, and result values, including all attributes needed to support any analysis or modeling activities using the data.

Access to the DCERP data is managed via a comprehensive security and access model built into the MARDIS database. User accounts, with roles that define access privileges, have been

implemented to prevent unauthorized access or the accidental or intentional compromising of data quality.

Data Life Cycle

This subsection discusses the data life cycle, specifically DCERP data and metadata standards; data submission by the DCERP Team; QA, QC, and validation efforts; and data transition associated with MARDIS.

Data and Metadata Standards

Adopting database design standards for DCERP was of paramount importance to facilitate the data exchange within the DCERP Team and between data collection operations and the MARDIS database. Standard data and metadata fields aid in identifying, discovering, assessing, and managing the data and in ensuring the known quality of the data. Standard data and metadata fields also allow for cross-cutting and inter-module analysis and modeling.

The DCERP geospatial data structure for spatial vector data maintains compatibility, to the extent possible, with the Spatial Data Standards for Facilities, Infrastructure, and Environment (SDSFIE) format (http://www.sdsfie.org), which was developed by the U.S. Armed Forces and the U.S. Army Corps of Engineers. Military installations across the United States use this standard to obtain their geospatial data. Because MCBCL personnel currently uses the SDSFIE standard for the Base's geospatial data, translation between MCBCL vector data and DCERP vector data were relatively straightforward.

The Federal Geographic Data Committee's (FGDC's) Content Standard for Digital Geospatial Metadata defines dozens of metadata elements to promote the coordinated development, use, sharing, and dissemination of geographic data. This coordinated effort is important because it helps to ensure that potential users of those data sets can reasonably determine the fitness of a data set for the purpose(s) for which they intend to use it. The DCERP GIS data metadata standard was based on—and is compatible with—the FGDC's metadata standards.

Data Submission

Data submitted to the MARDIS database must comply with the database standards and contain metadata that conform to the policies developed for DIMS and the MARDIS database. One method used to assist users in complying with these standards and policies is to use EDD templates. An EDD is an electronic, formatted file for sharing and manipulating data that is used to standardize and import data into MARDIS. A standardized EDD format is required to maintain compatibility across ecosystem modules and to reduce complexity of the data-loading process. There are three types of core EDDs: results, biological, and stations. Each core EDD handles many different data sets; the EDDs used for DCERP data sets are presented in **Appendix 21-D** of this chapter.

DCERP researchers were responsible for processing raw monitoring data results (e.g., laboratory and field results) into the EDD templates for uploading into MARDIS. To assist the DCERP Team with data sets that were too labor intensive to manually transform, including the large, consistent, and continuous automated data sets (e.g., the tidal gauge and Dataflow cruise data

sets), the Data Management Team developed custom transformation tools. These tools automated the process of converting the raw data into the EDD templates.

Additional data processing methods were required for mapping and visualization of data. Outputs from DCERP ecosystem modules were submitted in a wide variety of formats, from simple text tables of longitude–latitude coordinates (for the coastal barrier modeling) to multi-dimensional rasters (for historic and future climate forecasts). Research Project TSP-1 Team developed processing methods on a case-by-case basis, with considerable collaboration from DCERP researchers and MCBCL staff. In addition to the technical requirements, specific subjective decisions had to be made about what to visualize and the best way to visualize the data.

QA, QC, and Data Validation

DCERP researchers were responsible for conducting QA and QC procedures on the data that they collected.

The MARDIS data-loading processes included appropriate built-in data constraints to help ensure data integrity, whereby data were rejected if specific standard referential data were not provided. The processes also provided basic validation checks to ensure that, when possible, data values that were invalid or out of range were detected before uploading and that the data being uploaded were valid and sensible before being entered into MARDIS. As a result, data quality was maintained through the automated processes by reducing the possibility of human-introduced data entry and processing errors.

Figure 21-18 demonstrates the MARDIS upload process, including internal processing, which automatically performs the various validation checks during the data-uploading process.

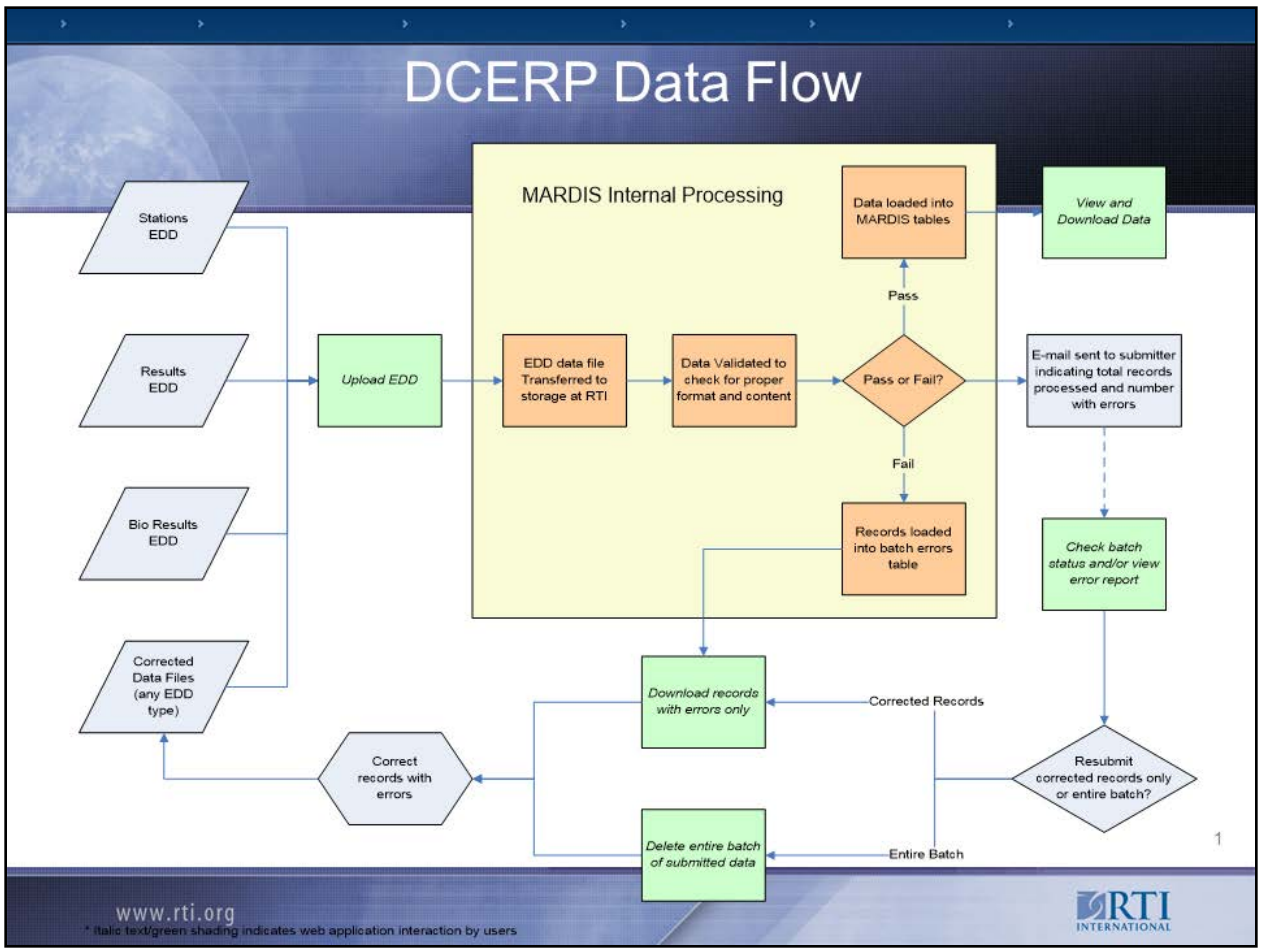

Figure 21–18. Internal MARDIS data-uploading processes and validation checks.

Data Transition

All data collected and developed under DCERP have been archived in DIMS. The Transition Plan transitioned data in a variety of formats to end users, depending upon the various end-user requirements. Military installations may want a SQL and geospatial export of the data, but SERDP and other users may want Microsoft Access or Excel versions of the data. Documents and files stored in the Document Database will be burned to DVDs and distributed, as appropriate, to SERDP staff and various users. RTI and the DCERP Team will also load some data into long-term, Web-accessible databases that are appropriate for DCERP data.

In addition, SERDP staff explored a long-term option to transfer DIMS to a third party to support DIMS for a period of 2 to 3 years beyond the DCERP contract period. This option would allow the third party to support MARDIS, the Document Database, iMAP, and the various visualizations and outputs. By employing this option, DIMS would still be accessible to MCBCL, other DoD installations, and other registered users. It is important to note that the software that was used to develop DIMS is at the end of its life cycle; therefore, the software and technologies will require upgrades to ensure that DIMS continues to function properly in the future.

Data Access, Release, and Use Policies

The DCERP Data Policy (**Appendix 21-A** of this chapter) was developed and implemented by the Data Management Team to define data access and use policies and guidelines. DCERP data are made available to authorized users via access to the DCERP Data Portal. Varying levels of data access have been implemented in DIMS via user groups and roles to prevent unauthorized access to sensitive MCBCL installation information or compromising data quality.

DIMS Server Environment

During the 10 years of DCERP, RTI's Information Technology Services (ITS) Department housed and managed the computer hardware to support DIMS, including MARDIS, the Document Database, the DCERP Team Web site, and the public Web site. ITS Department staff provided professional services and a secure environment for computer technology applications at RTI.

The DIMS hardware environment consisted of the following items:

- A standard set of development, staging, and production database servers to handle the development, testing, and final production duties required in a complex database environment
- A standard set of development, staging, and production Web application servers to handle the development, testing, and final production of Web interfaces and other applications that allow users to interact with the MARDIS databases through the Internet
- A Web server that supports the DCERP Team Web site
- An external storage device that serves as a file server and stores large imagery files for long-term archival purposes
- The following leased software applications:
    - Microsoft Windows Operating System
    - BackupAgent
    - Patch Management
    - McAfee security software
    - Microsoft SQL 2008 (standard license).

In addition, three Secure Sockets Layer (SSL) certificates (https) were purchased; these certificates are renewed yearly to handle encrypted communications between the data servers and client Web browsers. One ArcGIS software program was purchased; this program was renewed annually.

Backup and Recovery System

DIMS includes user management functions (e.g., account management, managing user roles, access) and standard data management functions (e.g., rollback, backup, archiving, disaster recovery [multi-storage locations], other operational and system administration tasks).

RTI's ITS Department staff implemented a back-up and recovery system for the production servers by using the following standard methods, as defined and operated by the Department:

- A full backup was performed weekly between the close of business on the last workday of the week and Sunday evening.
- Differential backups were performed once nightly Monday through Thursday (excluding holidays).
- Full backups of Microsoft SQL Server databases included both the data and transaction log devices. Full backups were performed once nightly, Monday through Thursday (excluding holidays), and once between the close of business on the last workday of the week and Sunday evening.
- On the last workday of the week, a courier picked up the previous week's full back-up tapes and the current week's last differential set of tapes. These tapes were stored at an approved off-site location, which used a concrete and steel-reinforced media vault to store these tapes. The media vault met the American National Standards Institute's guidelines for safe, climate-controlled storage of tapes. The vault was certified at a 4-hour fire rating with highly sensitive ionization fire detectors, and it was monitored 24 hours per day by an independent security firm.
- In the event of a disaster, these back-up tapes were used for recovery. All other back-up tapes were stored in the computing facility of RTI's ITS Department. Both locations were secured; only authorized personnel had access to these locations.
- Differential backups were retained for 28 days. At the end of the 28 days, a differential tape was reused for a current differential backup.
- Full backups were retained for 90 days. At the end of the 90 days, a full tape was reused for a current full backup.

Results and Discussion

Summary of DCERP Data and DIMS User Analytics

The types and volumes of data that were created during DCERP were extensive and consisted of multimedia data collected across more than 943 discrete sampling locations in a variety of formats and structures. A summary of the types and amounts of data and information in DIMS is presented in the text box to the right. DIMS Data Management staff used Google Analytics to track the use of DIMS during different phases in the development of DIMS. The different phases that were tracked include after the first release of DIMS to MCBCL staff, after its release to the Regional Coordinating Committee and TAC members, and after the City of Jacksonville (in NC) stakeholders meeting in May 2017. A summary of the Google Analytic analyses is provided in the following subsections.

DCERP Data by the Numbers

47 data sets in MARDIS

1,332 stations in MARDIS

Over **18.5 million** total records in MARDIS

Over **60** data layers in iMAP

More than **100** documents in the Document Database

More than **200** registered users

Public Web site 2015 through 2017:

- **88,183** page views
- Users viewed at least **6 pages per session**
- Users spent at least **4.5 minutes** on the site

In 2017, the numbers increased to:

- More than **13 pages per session**
- **8 minutes** per user on the site

Monitoring and Research Data in MARDIS

By the end of DCERP2, there were 44 data sets; 1,354 distinctly named stations (at 943 discrete locations); and a total of 17,796,801 records in the MARDIS database. **Figure 21-19** shows the growth of stations and records over the course of DCERP.

iMAP Data Layers

The iMAP visualizes more than 60 data layers (for a detailed list, see the iMAP data catalog in **Appendix 21F [Table 21F-2]** for detailed list). iMAP includes station locations, model forecast and scenario spatial outputs, spatially analyzed and processed data, and summarized spatial data.

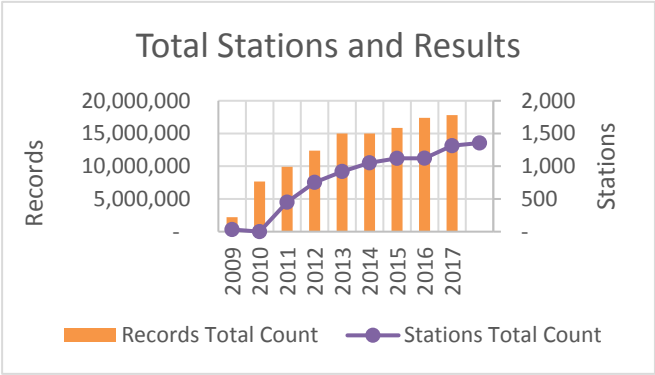

Figure 21–19. MARDIS total records and stations.

Registered Users

Parts of DIMS require user registration for access. Currently, there are more than 200 DIMS registered users, including more than 60 users from DoD.

Pubic Web Site

As shown in **Figure 21-20**, from 2015 through 2017, on average, more than 35% of users were new visitors to the site, and the total number of DCERP public Web site pages (different pages within the site) viewed by all users was more than 68,000. Users spent on average at least 4.5 minutes on the site and viewed at least six pages per session. In 2017, usage of the DCERP public Web site increased significantly, and these metrics increased to users spending an average of 8 minutes on the site and viewing more than 13 pages per session (**Figures 21-21 and 20-22)**. The DCERP Team believes this increase can be attributed to several factors. First, the team significantly redesigned the Web site and made the data and tools accessible to the general public (with basic registration). Second, the team participated in additional outreach efforts (i.e., at the TAC meetings, MCBCL meetings, local stakeholder's meeting in May 2017, and DCERP Symposium in October 2017).

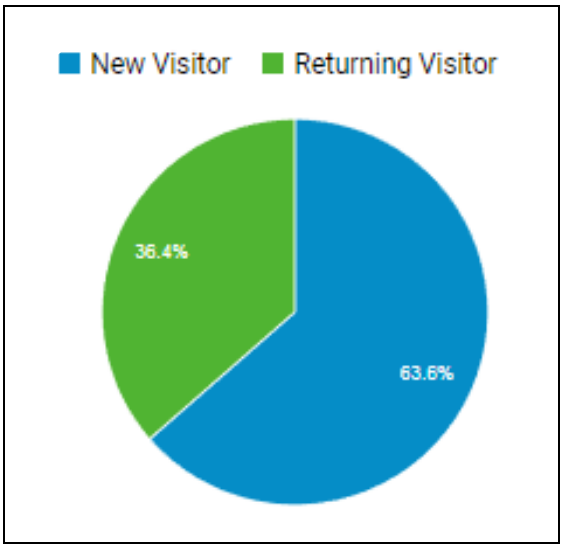

Figure 21–20. New versus returning visitors to the DCERP public Web site.

Figure 21–21. Monthly pages per session.

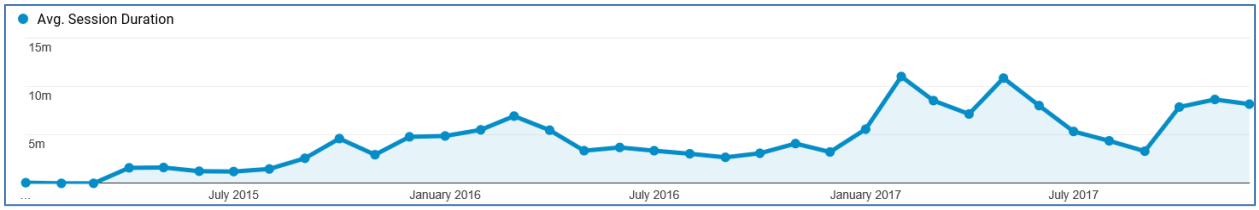

Figure 21–22. Monthly average session.

Documents and Files in the Document Database

The Document Database holds more than 100 documents and files of various types, from reports and program information, to data and results and GIS files. **Figure 21-23** shows the distribution by document type.

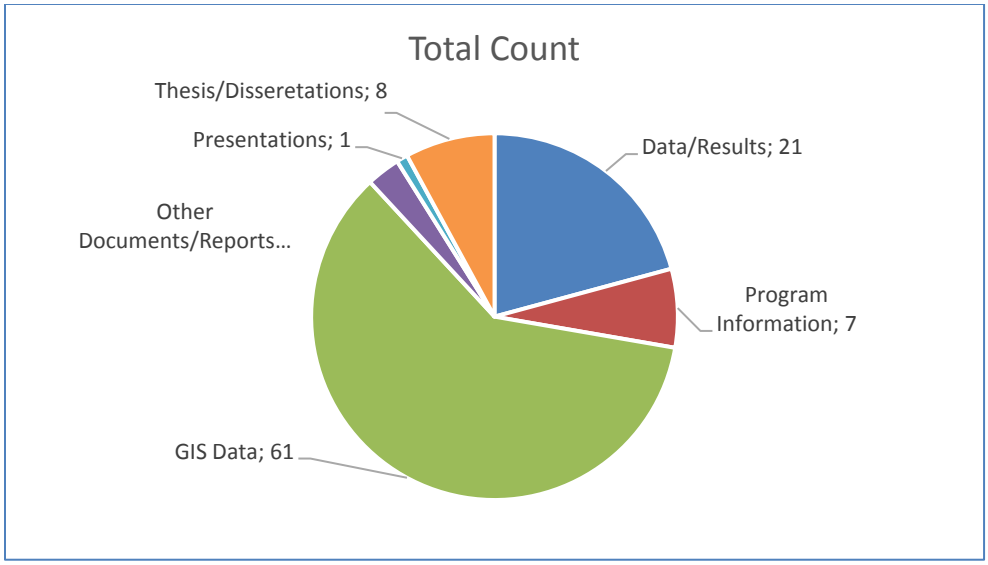

Figure 21–23. Document types in the Document Database.

Benefits of DIMS

DIMS offers many benefits to DCERP researchers, MCBCL, and other users. For instance, DIMS

- Allows for multi-disciplinary data integration and analysis
- Facilitates the sharing and reuse of data
- Keeps data in a safe, secure, and central location
- Provides integrity and validation of research results
- Makes it easier for users to find, understand, and access data
- Provides various levels of data synthesis from raw data to pre-generated model runs.

Integrating DIMS with additional functionalities under Research Project TSP-1 resulted in the implementation of a common framework that provides a centralized location for improved access

to DCERP data, models, and tools. In addition, the integration resulted in a common Internet mapping framework and tools for viewing data synthesized over space and time. Lastly, the effort helped to integrate specific models directly with DIMS and the DCERP data and to provide model outcomes in formats directly accessible by MCBCL and other DoD installation staff. Development of online tools, which make the GIS data, models, and research and monitoring results of the DCERP modules accessible via the Web, can all be accessed via the DCERP Data Portal.

Conclusions and Recommendations

The goal of the Research Project TSP-1 was to translate the data and results generated by DCERP researchers into clear and easy-to-understand language and products and to convey results by transitioning relevant scientific findings into actionable information. DIMS was developed as a comprehensive data management system that supports integrated data collection, management, analysis, and visualization of cross-ecosystem data. DIMS, and the comprehensive suite of tools, help translate the extensive amount of DCERP data into accessible, searchable, and usable information. The consistent format and standardized structure provided by DIMS allows for the comprehensive data integration from virtually any type of source and fosters efficient integrated analysis and synthesis. Developing DIMS as a Web-based system provided a centrally located data-driven Web application that requires no special software from users and allows easy assembling and downloading of data needed for models and research analysis. The suite of tools help users access, share, and view the data and break down the extensive amount of data into a meaningful, accessible, and manageable solution for decision makers and other users.

The primary focus early in DCERP2 involved refining the online tools to engage the DCERP Team. Specifically, mapping tools were structured to emphasize output from the four ecosystem modules. This activity has allowed researchers supporting Research Project TSP-1 to vet early progress with the MCBCL audience that is most capable of refining the data display. This research-centric approach helped guide the goals of including as many data layers as possible in iMAP and setting up workflows for processing future model outputs. Subsequent feedback from MCBCL staff further improved this structure.

The Research Project TSP-1 Team identified several major recommendations that may be valuable to other SERDP projects when developing a data and information management system as large in scope as the one that encompassed 10 years of the DCERP research and monitoring efforts. These recommendations are provided in the remainder of this chapter to address the following four major areas:

- Translating science into practice
- Development must be flexible and adapt to the program’s and users’ needs
- Structural elements of DIMS make it a good data repository for DCERP
- Continuation of DIMS (one component of the DCERP’s legacy).

Translating Science into Practice

Data and information must be made useable and understandable to users.

Environmental research, monitoring, and forecast modeling results do not easily provide actionable information in a format directly useable by Base managers and planners. The data that help answer scientific questions are not inherently valuable outside of the domain of scientific research without being translated to meet decision-making needs of installation managers.

As the Research Project TSP-1 Team met with researchers supporting other DCERP ecosystem modules, MCBCL staff, and regional stakeholders, the practical uses of DCERP data continually evolved. Early on, it became apparent that integrating MARDIS and iMAP user interfaces would involve continuing updates and obtaining MCBCL feedback to continue to improve the usefulness of the product to the installation.

It is important to understand what data are important to stakeholders.

Involvement and interactions with DoD installation staff and stakeholders allowed the DCERP Data Management Team to understand what data were important to MCBCL staff and the context within which they understood data. MCBCL staff found the research data more comprehensible when they could juxtapose the information with familiar data sets. MCBCL forestry data were tightly integrated with the LANDIS-II (Land and Information System) modeling process, and because of this, MCBCL forest managers could provide early feedback about the usefulness of the visualizations. As the DCERP Team added more MCBCL data (i.e., military training area boundaries, footprints of future infrastructure construction, locations of storm water retention ponds), Base staff found that the entire decision-support system was more useful. When the users have their own data in a data system, they are more likely to use the information to generate quick maps, figures, and screen shots, and they become more interested in all data in the system.

Summarizing the data is as important as visualizing and synthesizing the data.

The DCERP Team created many tools for multidimensional exploration—comparing temporal and spatial extents and visualizing results of different ecological process model scenarios. Feedback sessions with MCBCL staff emphasized that, although these tools were useful, it was also important to summarize the research findings and modeling results. These summaries could be visual images, such as a graphic that illustrates the total carbon stored across MCBCL's forest lands that are associated with a current management practice or future climate scenarios.

Making the research results relevant to non-experts is a major challenge.

The full value of data and analysis from DCERP research is revealed when it directly informs decisions made by installation planners. Practical application of DCERP information involves bridging the gap between expert reporting, in which researchers have comprehensive knowledge of a domain, and installation planners, who may interface with the data only infrequently. Making research results relevant to non-experts required synthesizing and, in some cases, simplifying the results. Summarizing data and giving the results context was vital to incorporating research results into installation operations.

Communicating complex information by using story maps is an effective tool for delivering data to non-experts.

Story maps are effective methods for translating the science of DCERP into effective communication tools for DoD installation managers; local, regional, state, and federal natural resources managers; and other interested stakeholders, including the public. One key benefit of using story maps is that once a few templates are created, additional story maps can be developed at minimal cost. Therefore, staff will have more time to write the content of the story map to ensure that these effectively convey the complex science into understandable concepts and results. Another benefit is that MCBCL staff have been using story maps for their own work, so they were supportive of using them in DIMS.

Development must be flexible and adapt to the program's and users' needs

Changes in scope over the course of DCERP were necessary to improve DIMS.

With the broad goal of turning science into practice, the final data management system that was developed by the DCERP Team was ultimately created in ways that could not have been planned at the outset of the program. The original goal of the Spatial Decision-Support System (SDSS) of Research Project TSP-1 was to link Light Detection and Ranging (LiDAR) data, LANDIS-II modeling results, and RCW habitat analysis into a single, loosely linked system for exploring terrestrial management scenarios. Although outputs from these three projects were integrated into the LANDIS-II and RCW models, the final iMAP framework does not try to run the models live through the interface. iMAP and other tools (e.g. Geospatial Marsh Model) present the outputs as discreet data products. This approach was guided by the feedback from the MCBCL staff because the end users wanted summarized data that could be compared with existing data, not on-the-fly modeling capability.

By the end of Year 1 of DCERP2, researchers and TAC members requested that many more capabilities be developed from Research Project TSP-1 and DIMS than originally proposed. The scope moved beyond the terrestrial ecosystem models and MARDIS monitoring stations to include representative data from all research projects, as well as other non-DCERP data models (e.g., the National Oceanic and Atmospheric Administration's [NOAA's] sea level rise outputs).

As the Research Project TSP-1 Team met with MCBCL staff, more data were cataloged and added to iMAP, steering the application towards a general-purpose GIS, less specifically tied to DCERP modeling. In addition, data results and model outputs were visualized and presented in customized tools, thereby providing a thorough interface for the researchers to more easily interpret the data.

Each presentation to the TAC and round of feedback from MCBCL staff led to refinements that suggested new changes in subsequent sessions. The data system delivered at the end of the decade of DCERP research is both a reflection of scientific findings and the day-to-day interests of the MCBCL management staff.

Data displays must be customized to fit the outputs.

The iMAP user interface included representative data sets from all research projects and ecosystem modules. The DCERP Team maintained this requirement from the outset because we wanted iMAP to serve as a hub for data discovery and an overview of DCERP research, as well as an analytical tool. However, the outputs of some modules did not always display well in the application. Monitored storm effects, such as overwash fans, provided information that was of interest to the Base, but the geographic features were not at a scale that was useful in visualizing them in the mapping tool. Data such as these were better developed as story map presentations for viewing outside of iMAP. Story map settings also provided more flexibility for developing the context and for using illustrative figures and photographs to explain the significance of the data findings. Other data, such as the Geospatial Marsh Model, were better displayed as image and table outputs from the model.

Structural elements of DIMS make it a good data repository for DCERP

Data must be put into a standardized format.

Standardized data enforce consistency across the various data sets and enables analysis. DIMS standardizes, stores, manages, and integrates data from each ecosystem module so that cross-cutting, inter-module analysis, and modeling can be performed. Research Project TSP-1's comprehensive DIMS solution provides an integrated analysis of environmental monitoring data from multiple sources that improves our ability to communicate the information to users so they can easily understand it.

Development of an integrated, standardized, data management system from the start has many benefits.

Developing an integrated data management system, such as DIMS, helps keep data in a safe, secure, and central location; eliminates version-control issues; provides data integrity and validation; and fosters efficient integrated analysis and synthesis.

Providing accurate and detailed metadata is important so users fully understand the limitations and uncertainty of the data or findings.

Providing accurate and detailed metadata is important so that the users of the data can understand the limitations and uncertainty of the data or findings. Through the iMAP framework, the DCERP Team developed many techniques to provide in situ documentation of data sets, such as pop-up informational windows and links to the original data. The MCBCL staff also requested the DCERP Team to develop succinct text summaries. This work led to an effort by the Research Project TSP-1 Team to develop fact sheets with DCERP Team researchers. Links to fact sheets and metadata are accessed in iMAP's data layer table of contents, through the DCERP Data Portal, and in the Document Database. An example fact sheet is included in Appendix 21-E of this chapter.

Providing preliminary model outputs can help streamline technical development.

Preliminary data provided by some researchers greatly aided in the refinement of the related user interface in DIMS. The example output data helped to reveal technical challenges, drove interface improvements, provided re-usable code, and allowed the Research Project TSP-1 Team to develop the best visualization methods for the data, while simultaneously allowing the researchers to continue working on their models, scenarios, and/or data outputs.

Development of more DIMS functionalities during DCERP1 would have facilitated earlier distribution of final products in DCERP2.

Initially during DCERP1, the objective of DIMS was to serve as the long-term repository for DCERP data and to primarily serve as a data archive. During DCERP1, it was proposed that more functionalities (e.g., iMAP, visualizations, more query tools) be added early in the program to help obtain early buy-in from the Base and other users. During DCERP2, the objective included implementing more functionalities and tools; however, the development of DIMS was constrained during DCERP1, which slowed implementation of several applications during DCERP2 until near the end of the program. Had DIMS been more robustly developed during DCERP1, then the products may have been completed earlier during DCERP2. An iterative process of providing tools and products beginning in DCERP1 would also have led to earlier buy-in from the MCBCL staff, recommendations for additional tools that were of use to the Base and other users, and the ability to make results and products available sooner to users.

Continuation of DIMS (one component of the DCERP's legacy)

DIMS provides a dynamic vehicle for archiving and disseminating DCERP research and monitoring data and findings to users.

DIMS provides a centralized location for accessing DCERP data, information, models, tools, and output products, and the system provides accessibility to all the various users. DIMS is a database-driven Internet system that provides a means to access and manage the DCERP data collections and provides useful and scientifically sound data and information in a framework that will support ecosystem-based management analysis, tools, and decisions. The various tools that assist users in accessing, sharing, and viewing the data enable users to look at the vast amounts of DCERP data in more meaningful and manageable ways, thus turning the data into usable information. Users can more easily view the available data, and these tools will allow them to screen variables that are important to them. Users can then download more specific subsets of the data for use in further analysis or for running various models and decision-support tools.

DIMS allows for the widest continuing distribution of data, models, tools, and other products to interested users. Open access to all registered users will make DCERP information available for comparison with other coastal research and monitoring data and will allow the use of tools and models to analyze data. In addition, open access to all registered users will provide examples of translating complex information into easy-to-understand and actionable information for a wide variety of audiences. The DCERP data represent results from one of the longest running and most intensively monitored ecological programs sponsored by the federal government in recent years.

The DCERP DIMS provided MCBCL with an extensive source of baseline data.

The extensive amount of baseline data provided by DCERP can ultimately support MCBCL's long-term ecosystem-based data management needs. The 10 years of monitoring data, for example, can provide data for comparison with future monitoring results and the ability to assess significant changes in ecosystem function and trends in the data over time.

Appendix 21-A
DCERP Data Policy

Defense Coastal/Estuarine Research Program (DCERP)

SERDP RC-2245

DCERP Data Policy Version 2.0

November 13, 2009 (Version 1)
February 2016 (Version 2)

Prepared by:

RTI International*
3040 Cornwallis Road
P.O. Box 12194
Research Triangle Park, NC 27709-2194

* RTI International is a registered trademark and a trade name of Research Triangle Institute.

Table of Contents

Definitions....iii

1.0 Introduction....1
- 1.1 Background....1
- 1.2 Purpose....1

2.0 Data Management Responsibilities....2
- 2.1 Responsibilities of the DCERP Data Management Team....2
- 2.2 Responsibilities of the DCERP Researchers....2
- 2.3 Responsibilities of Data Users....2

3.0 Data Types, Data Users, and Data Access Privileges....3
- 3.1 Data and MetadataTypes....3
  - 3.1.1 Data Types....3
  - 3.1.2 Metadata Types....3
- 3.2 Data Users....4
- 3.3 Data and DIMS User-Access Privileges....4

4.0 DCERP Data Use Guidelines....6
- 4.1 Data Use Agreement....6
- 4.2 Disclaimer and Acknowledgments (DCERP Research Team Only)....6
  - 4.2.1 U.S. Department of Defense Disclaimer....6
  - 4.2.2 SERDP Acknowledgment....6

5.0 References....6

List of Tables

Table 1. Data and DIMS User-Access Privileges for DCERP Research and Monitoring Data....5

Appendix

A. Data Use Agreement

Definitions

Data Requestor or Data User—For the purposes of this document, the terms "data requestor" or "data user" are often used interchangeably, depending on context.

DCERP (Defense Coastal/Estuarine Research Program)—This program is a Strategic Environmental Research and Development Program (SERDP)–funded study sited at Marine Corps Base Camp Lejeune (MCBCL). The first cycle of DCERP is referred to as DCERP1 and was conducted from July 2006–January 2013. DCERP2, the second cycle of DCERP, is being conducted from February 2013–October 2017. This document is inclusive of both cycles of the DCERP.

DIMS (Data and Information Management System)—The DCERP DIMS is a comprehensive system that supports and provides a repository for DCERP's collection and storage of environmental data. DIMS supports DCERP's geospatial data management, statistical analysis, model integration, and document sharing. The DCERP DIMS consists of the following systems: the Monitoring and Research Data Information System (MARDIS), the DCERP public Web site, the Document Database, and the Spatial Decision-Support System (SDSS), which consists of the interactive mapping applications (iMAP) and ecosystem-based management tools.

Ecosystem Module Team—DCERP uses four ecosystem modules to facilitate its research and monitoring activities at MCBCL. The following four ecosystem modules were included in both DCERP1 and DCERP2: Aquatic/Estuarine, Coastal Wetlands, Coastal Barrier, and Terrestrial Modules.

iMAP (Interactive Mapping Applications)—The iMAP is the component of the SDSS for visualizing DCERP geospatial data and providing spatial search capabilities for data from MARDIS and other sources.

MARDIS (Monitoring and Research Data Information System)—MARDIS is the long-term repository for all DCERP monitoring and research data.

MCBCL (Marine Corps Base Camp Lejeune)—Located in Jacksonville, NC, MCBCL is the largest U.S. Marine Corps installation on the East Coast and serves as the main host site for DCERP.

Monitoring Data—This term refers to data collected under activities specified in the *DCERP Baseline Monitoring Plan* (RTI International, 2007a), the *DCERP2 Monitoring Plan* (RTI International, 2013a), or added by approved supplemental funding requests as new monitoring activities.

RCC (Regional Coordinating Committee)—The RCC is a group of local, state, and regional stakeholders whose organizations conduct research similar to that conducted under DCERP. These stakeholders provide input about their organization's findings and how their results may be used by DCERP researchers, as well as valuable input to the RTI International DCERP Team regarding the application of results to real-world natural resource management issues.

Research Data—This term refers to data collected under research project activities specified in the *DCERP Research Plan* (RTI International, 2007b), the *DCERP2 Research Plan* (RTI International, 2013b), or added by approved supplemental funding requests as new research projects.

RTI DCERP Team or Researchers—The RTI DCERP Team includes the DCERP Principal Investigator, other environmental scientists from RTI, and researchers from seven universities, three federal agencies, and five small businesses.

SERDP (Strategic Environmental Research and Development Program)—This program is the U.S. Department of Defense's environmental science and technology program, implemented in partnership with the U.S. Department of Energy and the U.S. Environmental Protection Agency. SERDP invests in basic and applied research and provides funding and oversight for numerous research projects including DCERP.

SDSS (Spatial Decision-Support System)—The SDSS is the information system that brings together research and monitoring data from MARDIS, geographic information system (GIS) maps, various management and climate scenarios, and models and tools in interactive, and mostly spatial, interfaces.

TAC (Technical Advisory Committee)—The DCERP TAC consists of scientific experts from a variety of disciplines from academia, federal agencies, and the private sector who are selected by SERDP to review the science conducted in DCERP and make recommendations to assist the team in attaining the research objectives of the program. The TAC provides third-party review of the program and recommends course corrections when needed.

1.0 Introduction

The DCERP Team created the DCERP Data Policy version 1.0 in 2009 and updated it in 2016 as version 2.0. This section of the policy provides the background for the data management strategy for the Defense Coastal/Estuarine Research Program (DCERP) and discusses the purpose of the Data Policy for this program.

1.1 Background

The data management strategy for DCERP is designed to address the needs of the program, individual DCERP researchers, Marine Corps Base Camp Lejeune (MCBCL), the larger scientific community, and other stakeholders. Central to this strategy is the timely submission and sharing of data and metadata collected during the monitoring and the research programs. DCERP researchers have a strong commitment to data integrity and to meeting the data management requirements established by the Strategic Environmental Research and Development Program (SERDP) for storing and sharing this data with MCBCL and other U.S. Department of Defense (DoD) installations, the scientific community, and other local, state, and regional stakeholders.

To facilitate data management, the DCERP Data and Information Management System (DIMS) was implemented by the Data Management Team in DCERP1. The first objective of DIMS is to support the data collection and research efforts of DCERP that better enable DCERP researchers to communicate, collaborate, and contribute to DCERP objectives. The second objective of DIMS is to make DCERP data readily available and usable by MCBCL staff to support ecosystem-based data management. DIMS includes the Monitoring and Research Data Information System (MARDIS), Spatial Decision-Support System (SDSS), and the Document Database. MARDIS is a centralized database that stores and presents data collection activities from each ecosystem module in a consistent format and standardized structure. The SDSS is the information system that brings together data from MARDIS, geographic information system (GIS) maps, various management and climate scenarios, and models and tools in interactive and mostly spatial interfaces. The Document Database is a repository for unstructured data, maps, reports, and documents.

1.2 Purpose

The purpose of the DCERP Data Policy is to encourage openness and sharing of DCERP data for the mutual benefit of SERDP, DCERP, MCBCL, other DoD installations, the scientific community, and other stakeholders. The Data Policy applies to current and future access to research and monitoring data collected or information produced by using SERDP funds that are contained in the DCERP DIMS, including the MARDIS, the interactive mapping applications (iMAP), and the Document Database. The goals of the Data Policy presented in this document are to allow access to DCERP data consistent with the following:

- Protecting the security interests of MCBCL
- Protecting the intellectual rights of DCERP researchers to have first rights to publish the results of their work
- Maintaining an open and cooperative relationship between DCERP researchers and MCBCL staff
- Enhancing the use of publicly funded data to meet multiple scientific, DoD installation, and other end-user purposes.

This DCERP Data Policy also specifies the general roles and responsibilities of the DCERP Data Management Team, the DCERP researchers, and the various data users regarding the use of DCERP data;

describes the data access and release processes; and discusses the acceptance of the Data Use Agreement by all parties.

2.0 Data Management Responsibilities

This section of the Data Policy describes the data management responsibilities of the various parties: the DCERP Data Management Team, the DCERP researchers, and other data users.

2.1 Responsibilities of the DCERP Data Management Team

The Data Management Team is responsible for providing and maintaining the DCERP DIMS. The team also develops and implements policies, guidelines, standards, and procedures for DCERP data management activities, thus ensuring the integrity, security, accessibility, and usefulness of data and information maintained in DIMS. In addition, the Data Management Team ensures that data are maintained in a secure environment and are suitably controlled to ensure that only authorized users can access the data. The team defines data standards that allow for integration and standardization across the various types of DCERP data and information and provides basic validation checks of data to ensure compliance with MARDIS standards and data integrity. The Data Management Team also provides Web-based user interfaces that will allow authorized users to view and download data and information. Finally, the team serves as the liaison with the DCERP researchers, the DCERP On-Site Coordinator, MCBCL, SERDP, and other users to encourage and evaluate feedback, ensure that user community needs are being met, and ensure that all levels of data and metadata are available in the appropriate time frame.

2.2 Responsibilities of the DCERP Researchers

DCERP researchers are responsible for the timely submission of all data and metadata generated during monitoring activities and research projects to DIMS. DCERP researchers also have primary responsibility for the quality and correctness of data submitted to DIMS and should interact with the Data Management Team to ensure that

- Data comply with DIMS standards and contain metadata that conform to the policies developed for the DCERP DIMS
- Data are uploaded into DIMS by using the approved format and appropriate templates
- Data subject to revision are promptly updated in MARDIS and revisions are thoroughly documented
- Each data set or product in DIMS has metadata or a fact sheet (described in Section 3.1.2 of this Data Policy)
- Questions and concerns related to submitted data or metadata are promptly resolved.

2.3 Responsibilities of Data Users

SERDP recognizes the legitimate rights of data originators and collaborating DCERP researchers regarding the first use of the data they collect. In addition, SERDP encourages data sharing with the scientific community at large and with other local, state, and regional stakeholders. All data users must abide by the terms and policies outlined in this DCERP Data Policy, must follow the data access and release processes outlined in Section 3.0 of this document, and agree to the Data Use Agreement in **Appendix A** of this Data Policy. These terms and processes include, but are not limited to, working in cooperation with the DCERP researchers, properly citing the DCERP data used, agreeing to the terms of acceptable use, and understanding and agreeing that DCERP data are provided for use solely by the approved data requestor. Any redistribution of the DCERP data or metadata to other unauthorized parties is prohibited.

Access to DCERP data is subject to registration to enable the Data Management Team to track usage, evaluate the data's impacts in the scientific community, and confirm the data user's agreement to the terms of acceptable use. Once registered, approved data users will be allowed access to DCERP data.

The following information will be required for registration to access DIMS and is also required when transferring any data to a data requestor via methods other than DIMS:

- Name of the data requestor
- Affiliation of the data requestor
- E-mail address of the data requestor
- Complete contact information (i.e., street address, city, state, zip code, and telephone number)
- Acceptance of the Data Use Agreement, as applicable.

3.0 Data Types, Data Users, and Data Access Privileges

To ensure data integrity, DCERP data should be acquired directly from DIMS and not from other third-party sources that may alter the data or may not include the latest updates and revisions to the data. This section of the DCERP Data Policy describes the types of DCERP data available and accessibility, defines the various users, and discusses the user access privileges.

3.1 Data and Metadata Types

3.1.1 Data Types

DCERP data include monitoring and research data. These two different types of data will be available for access to data users within the following time frames:

- **Monitoring data**—DCERP monitoring data, which are identified in the *DCERP Baseline Monitoring Plan* (RTI International, 2007a), and the *DCERP2 Monitoring Plan* (RTI International, 2013a) are available in MARDIS within 6 months after collection.
- **Research data**—DCERP research data, which are identified in the *DCERP Research Plan* (RTI International, 2007b), and the *DCERP2 Research Plan* (RTI International, 2013b), are available in MARDIS within 2 years of the data collection date or by June 2017 to allow time for the DCERP researchers to perform analyses, conduct quality assurance and quality control on the data, and publish the final results.

A third type of data available in DIMS is MCBCL–generated data. These data were provided by MCBCL and are only available to the DCERP Team, SERDP, and DoD users.

3.1.2 Metadata Types

Metadata are needed so that data and products are accurately understood and used in an appropriate manner. Different formats and methods were used to develop this information, but clarity and completeness were the objectives for all metadata. There are three main types of metadata associated with data archived in the DCERP DIMS: metadata required with each MARDIS record (research and monitoring data), geospatial metadata, and data fact sheets. These three types of metadata are discussed further as follows:

- **Research and monitoring data in MARDIS**—Metadata provide supporting information about monitoring and research data that include, but are not limited to, a description of the location where the data were collected, the field and laboratory methods used to collect and analyze the data, and the spatial extent and temporal frequency of the data collected. In MARDIS, metadata fields have been combined with the actual sampling data fields; therefore, DCERP metadata are

not a separate element, table, or document, but instead they are an integral component of each data record.

- G**eospatial metadata (including modeling results)**—Geospatial data generated by DCERP are available in the Document Database and iMAP. When possible, the geospatial metadata uses the format established by the Federal Geographic Data Committee Content Standard for Digital Geospatial Metadata (FGDC-STD-001-1998) and is available in the Document Database.
- **Data fact sheets**—These documents provide general descriptions of the data set, describe the methods used to collect or produce the data, and explain how the data were or can be used and where to find additional information about the data set. The fact sheets are available for the data sets and products displayed in iMAP. Fact sheets are also available on the DCERP public Web site.

3.2 Data Users

This section of the DCERP Data Policy identifies the specific types of data users and the level of access to DCERP research and monitoring data for each type of data user. The primary data users are defined as follows:

- RTI International DCERP Team and DCERP researchers (to be identified by RTI)
- SERDP Management Team (to be identified by the SERDP/Environmental Security Technology Certification Program [ESTCP] Executive Director)
- MCBCL personnel (to be identified by MCBCL)
- Other DoD installation personnel (to be identified by the SERDP/ESTCP Program Manager for Resource Conservation and Climate Change)
- Non-DCERP SERDP/ESTCP researchers (to be identified by the SERDP/ESTCP Program Manager for Resource Conservation and Climate Change)
- Technical Advisory Committee (TAC) and Regional Coordinating Committee ([RCC], both to be identified by the SERDP Resource Conservation and Climate Change Program Manager)
- Registered users (including local, state, and federal personnel, as well as private sector, university, and public individuals)
- Unregistered users (no password or registration required; however, user access is limited to the DCERP public Web site only).

3.3 Data and DIMS User-Access Privileges

There are three types of access privileges to DIMS: upload, view, and download. Currently, only the DCERP Team, including the Data Management Team, has the ability to upload or edit data directly to DIMS. **Table 1** describes the different data users and the access privileges for each user group based on the type of data (monitoring or research data).

Table 1. Data and DIMS User-Access Privileges for DCERP Research and Monitoring Data[a]

Data Users	MARDIS and iMAP Access	Document Database Access	DCERP1 Monitoring and Research Data	DCERP2 Monitoring Data	DCERP2 Research Data[b]
DCERP Research Team	Yes	Yes	View and download[c] data privileges	View and download[c] data privileges	View and download[c] data privileges
SERDP Management Team	Yes	Yes	View and download[c] data privileges	View and download[c] data privileges	View and download[c] data privileges
MCBCL personnel	Yes	Yes	View and download[c] data privileges	View and download[c] data privileges	View and download[c] data privileges
Other DoD installation personnel	Yes	Yes	View and download[c] data privileges	View and download[c] data privileges	View and download[c] data privileges
Non-DCERP SERDP/ESTCP researchers	Yes	No	View and download[c] data privileges	View and download[c] data privileges	View data privileges
TAC and RCC members	Yes	No	View and download[c] data privileges	View and download[c] data privileges	View data privileges
Registered users	Yes	No	View and download[c] data privileges	View and download[c] data privileges	No
Public access (unregistered users)[d]	No	No	No	No	No

[a] MCBCL and SERDP have the right to limit the release of sensitive DoD installation data as appropriate.

[b] Access to DCERP2 research data is limited until October 2017 for some users. After that time, DCERP1 and 2 data will be available to all registered users for viewing and downloading.

[c] Prior to downloading data, the user must agree to the Data Use Agreement (see Appendix A of this DCERP Data Policy).

[d] Unregistered users only have access to the DCERP public Web site. Unregistered users, however, can register to obtain data privileges.

4.0 DCERP Data Use Guidelines

Monitoring and research data acquired from DIMS will be accompanied by the Data Use Agreement, which describes the general roles, obligations, and rights enjoyed by each data user regarding the use of the released data sets. The Data Use Agreement is available in Appendix A of this DCERP Data Policy. This section of the DCERP Data Policy also describes the required DoD disclaimer and acknowledgments associated with the use of the DCERP data in presentations, publications, and reports for the DCERP Research Team.

4.1 Data Use Agreement

The Data Use Agreement pertains to the DCERP Team, SERDP, MCBCL, other DoD installation personnel, non-DCERP SERDP/ESTCP researchers, members of the DCERP TAC and RCC members, and registered users.

The use of DCERP data has the potential to greatly increase communication, collaboration, and synthesis within and among various disciplines, and thus is fostered, supported, and encouraged by SERDP. By accepting DCERP data, the data user agrees to abide by the terms of the Data Use Agreement. The DCERP Principal Investigator (PI) has the right to immediately terminate this agreement by written notice if the data user fails to comply with any of the terms outlined in this agreement. The data user may be held responsible for any misuse that is caused or encouraged by his or her failure to abide by the terms of this agreement. In accordance with the Data Use Agreement (for additional details, see Appendix A of this DCERP Data Policy).

4.2 Disclaimer and Acknowledgments (DCERP Research Team Only)

4.2.1 U.S. Department of Defense Disclaimer

All publications or reports prepared as part of DCERP must conspicuously display the following disclaimer on the cover page or in the front matter of the report:

> "Views, opinions, and/or findings contained in this report are those of the author(s) and should not be construed as an official U.S. Department of Defense position or decision unless so designated by other official documentation."

4.2.2 SERDP Acknowledgment

The following acknowledgment statement must also be included in any report prepared as part of DCERP:

> "This research was conducted under the Defense Coastal/Estuarine Research Program (DCERP), funded by the Strategic Environmental Research and Development Program (SERDP)."

In addition to the SERDP acknowledgment previously mentioned, DCERP Team members should also recognize and acknowledge the services provided by MCBCL as the host installation or specific MCBCL staff who provided assistance, as appropriate, in the conduct of their research.

5.0 References

Federal Geographic Data Committee. FGDC-STD-001-1998. Content standard for digital geospatial metadata (revised June 1998). Federal Geographic Data Committee. Washington, D.C. Available at https://www.fgdc.gov/standards/projects/FGDC-standards-projects/metadata/base-metadata/v2_0698.pdf

RTI International. 2007a. *DCERP Baseline Monitoring Plan*. Prepared for SERDP, Arlington, VA. Available at https://dcerp.rti.org/DCERPPublicSite/PublicDocuments

RTI International. 2007b. *DCERP Research Plan*. Prepared for SERDP, Arlington, VA. Available at https://dcerp.rti.org/DCERPPublicSite/PublicDocuments

RTI International. 2013a. *DCERP2 Monitoring Plan*. Prepared for SERDP, Arlington, VA. Available at https://dcerp.rti.org/DCERPPublicSite/PublicDocuments

RTI International. 2013b. *DCERP2 Research Plan*. Prepared for SERDP, Arlington, VA. Available at https://dcerp.rti.org/DCERPPublicSite/PublicDocuments

Appendix A

Data Use Agreement

(To accompany all data transfers)

Defense Coastal/Estuarine Research Program Data Use Agreement

Version 2.0: February 2016

By accepting Defense Coastal/Estuarine Research Program (DCERP) data, the data user agrees to abide by the terms of the Data Use Agreement. The DCERP Principal Investigator (PI) has the right to immediately terminate this agreement by written notice if the data user fails to comply with any of the terms outlined in this agreement. The data user may be held responsible for any misuse that is caused or encouraged by his or her failure to abide by the terms of this agreement. If you have any questions concerning data access or use policies, please contact the DCERP PI, Dr. Patricia Cunningham, via e-mail at patc@rti.org or the DCERP Data Manager, Ms. Danette Boezio, via e-mail at dboezio@rti.org. Permission to use DCERP data is granted to the data user subject to the following terms and conditions:

- ***Acceptable use*.** Use of the DCERP data is restricted to academic, research, educational, government, or other not-for-profit professional purposes. Distribution and/or release of this information and/or data for other purposes are strictly prohibited.
- ***Data liability*.** Although substantial efforts are made to ensure the accuracy of data and documentation contained in the Data and Information Management System (DIMS), complete accuracy of data and metadata cannot be guaranteed; all data and metadata are made available "as is." The data user agrees not to hold the RTI International DCERP Team or the individual DCERP researcher liable or responsible for any loss, damage, claim, cost, or expense as a result of DCERP data contents or their use or interpretation. The data user must be aware of data conditions and ultimately bears responsibility for the appropriate use of the information.
- ***Redistribution*.** DCERP data are provided for use only by the data requestor or user. Redistribution of the data or metadata to other unauthorized parties is strictly prohibited.
- ***Citation*.** The data user must properly cite the DCERP data in any publications, presentations, posters, or other materials and/or in the metadata of any derived data products that were produced using the DCERP data. A citation should appear in the following general format: *DCERP researcher's name, year of data collection, title of data set: DCERP Data and Information Management System (database), and date accessed.* An example of a citation is presented as follows:

  Baumann, K. 2009. EPA Criteria Pollutants (Ozone, Sulfur Dioxide, Particulate Matter): DCERP Data and Information Management System (database). Accessed April 6, 2009.
- ***Collaboration*.** DCERP data have been released in the spirit of open scientific collaboration; therefore, data users should consider consultation, collaboration, and/or co-authorship with the DCERP researcher who collected the data.
- ***Notification*.** The data user will notify the DCERP PI (Dr. Cunningham) and the DCERP On-Site Coordinator (Dr. Susan Cohen via e-mail at susan.cohen@usmil.gov) when any derivative work or publication, based on or derived from the DCERP data, is being prepared for distribution in posters, presentations, or publications.

Appendix 21-B
Quick Guide: Finding and Exploring DCERP Data, Models, Tools, and Visualization

Quick Guide:

Finding and Exploring DCERP Data, Models, Tools, and Visualizations

The purpose of this document is to give users a high-level introduction to the data available in DCERP and where to find it. This is not meant as a comprehensive guide. Please see the other DCERP and MARDIS help documents for complete details and instructions.

Data Portal

The Data Portal page is the portal to all the DCERP data, models, tools, and visualizations.

Many components are openly accessible, but access to the data and certain components require basic registration (name, organization, and purpose) and a login.

- Components that require login are marked with a 🔒.
- Select the "Login" button or 🔒 on the Data Portal page to Register or login using the username and password generated during registration.
- Scroll down the Data Portal page to further explore each product.

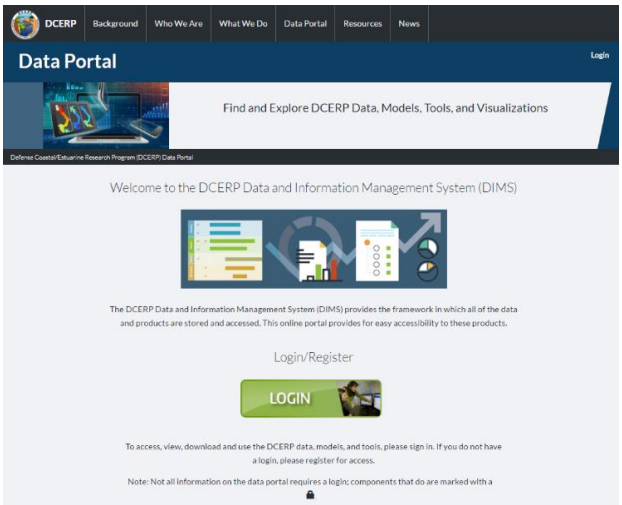

Components of the Data Portal

What Data Does DCERP Have

This link provides access to a variety of dataset reports that describe the data available within DIMS, including in MARDIS, GIS data, and other data and results available in spreadsheets and CSV files.

Models and Tools

- Step through using the arrows or carousel. Select a model icon for information on that model or tool, or to link directly to the layer in iMAP.
- Models Overview provides a summary of the models developed during DCERP1 and DCERP2.

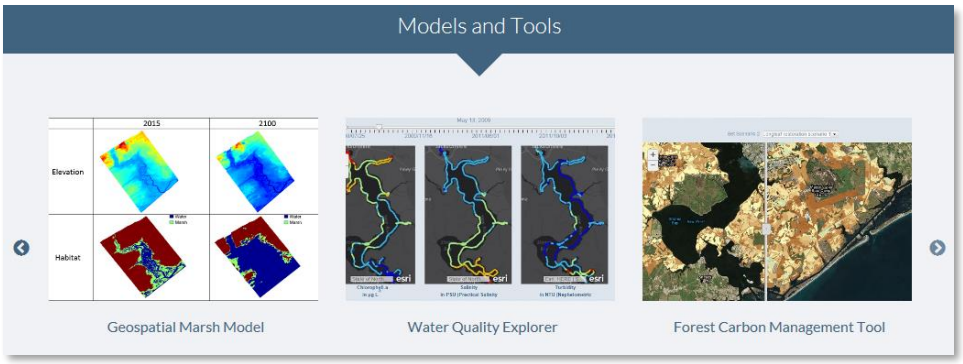

iMAP and Data Query

- View DCERP stations and their data, and model scenarios on an interactive map. Use the Map/Topic Queries to query DCERP data and download results in tabular form or in graphs. See *iMAP and iMAP Query Tips* section below.

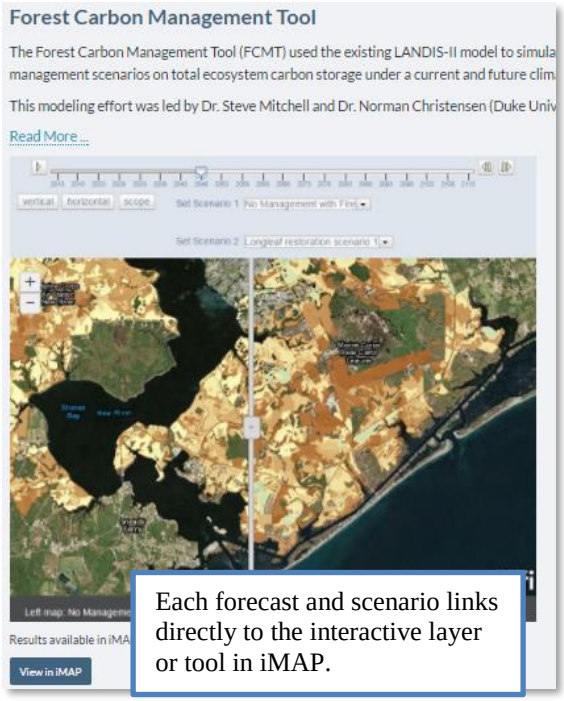

Each forecast and scenario links directly to the interactive layer or tool in iMAP.

Story Maps

Story maps guide you through an interactive visual narrative of research data and information. The three current story maps are:

- Coastal Barrier Morphology: *Onslow Beach: A barrier island of shifting sands and migrating shorelines*

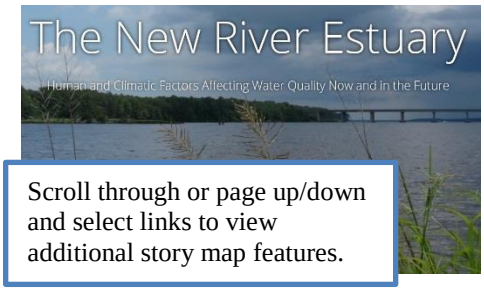

Scroll through or page up/down and select links to view additional story map features.

- The New River Estuary: *Human and climatic factors affecting water quality now and in the future*
- Geospatial Marsh Model story map.

Water Quality Dashboard

- Provides an at-a-glance summary of water quality conditions at 8 monitoring station in the New River Estuary, from Jacksonville, NC to the New River Inlet.
- Dynamic map, graph, and table update to display parameter data and highlight selected stations.

Advanced Query and Download Data

- Query every possible combination of criteria, find stations, and view lookup tables.
- The Description tab provides advanced query instructions and access to the *MARDIS Quick Tips for the Advanced Query* help document.
- View large data downloads exceeding 10,000 records. Results are graphed and linked to iMAP.

Document Database

The Document Database stores and manages documents such as spreadsheets, GIS and Raster data, text documents, reports, maps, and research publications from DCERP. *A Guided Help* is available on the Document Database.

Help and User Guides

Provides links to additional guides, tips, and quick guides.

Login Required

MARDIS Menu

Once logged in, the MARDIS menu navigates through login-required DCERP data pages.

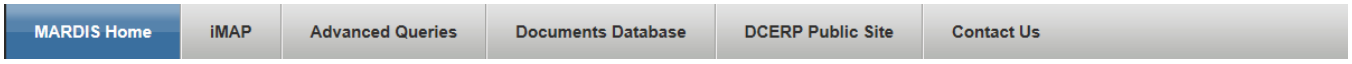

iMAP and iMAP Query Tips

Login to MARDIS for access to the Interactive Mapping Application (iMAP) and Query tools.

iMAP contains geographic data and analytical tools developed by DCERP. iMAP can be used to visualize data and overlay diverse datasets to explore the environment at Marine Corps Base Camp Lejeune (MCBCL).

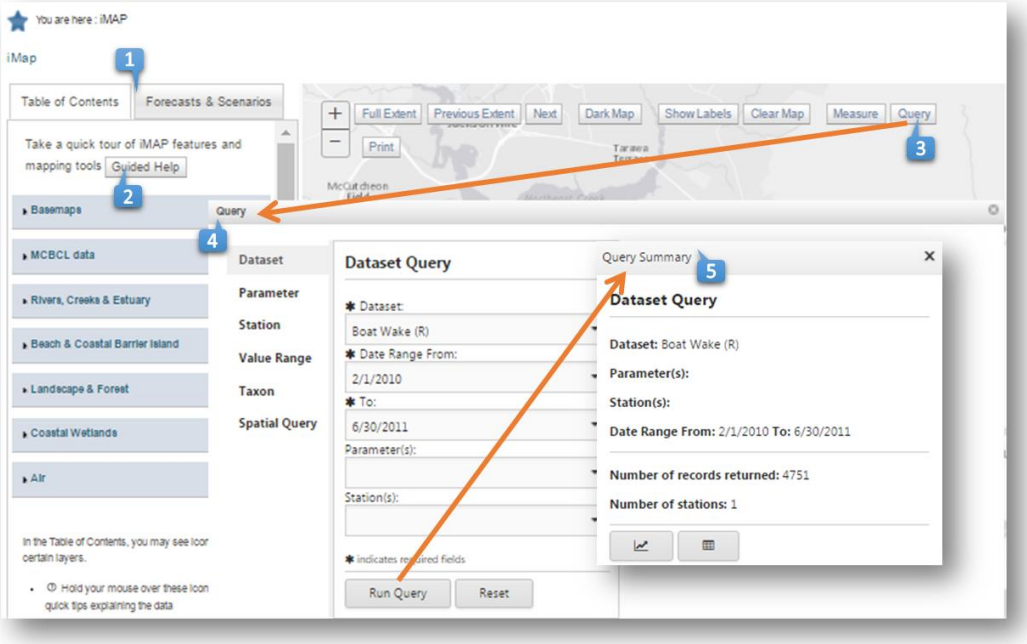

1. **Table of Contents** tab displays iMAP data layers organized by ecosystem. Select a layer to view it on the map. Click on a station icon to view station information. Select **Forecast & Scenarios** for interactive explorer and comparison tools.
2. iMAP **Guided Help** walks you through using iMAP and its features.
3. **Query** button on the map triggers the Query wizard pop-up.

4. The Query wizard has 6 query topics: Dataset; Parameter; Station; Value Range; Taxon; and Spatial Query.
5. **Query Summary** wizard displays results of the query in graph or tabular form.

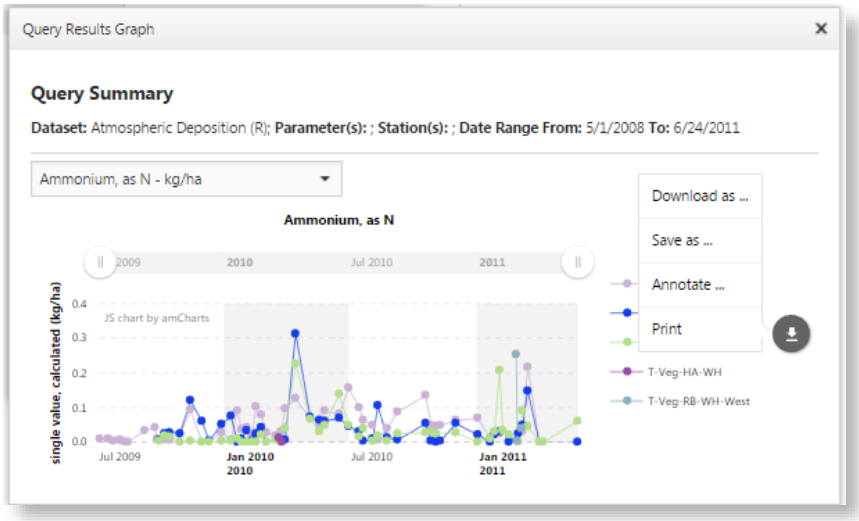

- You cannot view or download data from a query search if there are more than 10,000 records.
- Date ranges default to dates within which data is available for the selected criteria.
- Close the Query Summary to view the highlighted station on the map.
- Select the Table of Contents icons in each panel to view layer details or download datasets. Hover over tooltips to display pop-up information.

Forecasts & Scenarios

The **Forecasts & Scenarios** tab contains dynamic data and a library of modeled management and climate change scenarios for the various ecosystems studied by DCERP. Compare model scenarios on the map or in interactive explorer tools with side-by-side displays.

Data Downloads

Data can be downloaded in a number of formats from several features in DIMS:

1. **Perform an iMAP query** on station data to download results from the Query Results Graph or Query Results Table pop-up. The iMAP Query will return no more than 10,000 results.
2. Perform an Advanced Query for download options for returned query results and returned filter results. The Advanced Query can return the first 10,000 results, or can download all matching query results including complete datasets.
3. My Downloads page displays a list of the download files available to you, generated using the large download option on the "Advanced Query" page.
   To download a file, click the "Download" link on the applicable row in the table.
4. Search Stations Query to query and download complete Station data by name, station type, and parameter group in Excel or tab delimited format.
5. Search the Document Database to download document files.

Appendix 21-C
MCBCL Engagement and Outreach Efforts

Summary of Marine Corps Base Camp Lejeune's Participation in DCERP2 Activities

2012

November: DCERP2 Planning Meeting. The DCERP2 Research Team met with Marine Corps Base Camp Lejeune (MCBCL) staff from the Environmental Management Division (EMD), Marine Corps Installation East (MCI East) Natural Resources, Operations and Training, and National Environmental Policy Act (NEPA). The purpose of the meeting was to discuss the objectives for DCERP2 compared with DCERP1, present the new organization for the team and thematic areas, and obtain feedback from MCBCL staff about proposed research and monitoring activities for DCERP2. The DCERP Team used this feedback to finalize these activities before DCERP2 commenced in February 2013.

2013

April: Joint Meetings of the Regional Coordinating Committee (RCC) and the Technical Advisory Committee (TAC). Over 2 days, MCBCL staff attended presentations and participated in ecosystem-specific break-out sessions to share information about their management needs. MCBCL staff attended a special working luncheon to learn about the DCERP Data and Information Management System (DIMS) and the planned models and tools, and then the staff completed a survey to determine their needs. Specifically, members of the Research Project TSP-1 Team demonstrated the Data Portal application to MCBCL and other installation staff to obtain the first round of feedback for refining the management and planning tools. Early feedback suggested that it was important for the Data Portal to provide simple functionality and data summarization to present a generalized sense of portal capabilities and data holdings, with links to the full data and advanced tools.

April: Living Shoreline Planning Meeting. Members of the DCERP2 Team met with MCBCL staff to design the Implementation Plan for three Living Shorelines sites, which were a collaborative effort between Mr. John DeLuca of MCBCL's EMD and Dr. Carolyn Currin of the National Oceanic and Atmospheric Administration's (NOAA's) Beaufort Laboratory.

2014

- **March: RCC Meeting.** MCBCL staff attended this 1-day meeting with other stakeholders for an overview of findings from Year 1 of DCERP2 and to plan for the upcoming year. Stakeholders, including MCBCL, shared information that was relevant to the DCERP.
- **March: TAC Meeting.** MCBCL staff attended this 2-day meeting that focused on presenting detailed information from each research project and monitoring activity. Staff participated in break-out sessions that focused on the impacts of climate change and other management needs. MCBCL staff also hosted a site tour, which included tours of the New River Estuary and forest management areas.
- **April: Southeast Regional Partnership for Planning and Sustainability (SERPPAS).** SERPPAS and Dr. Currin, a member of the DCERP Coastal Wetlands Module Team,

discussed overlapping areas of interest and possible coordinated efforts regarding the installation of Living Shorelines at MCBCL.

- **April: U.S. Department of Defense (DoD) Climate Action Task Force.** MCBCL's EMD staff requested input from Dr. Ryan Boyles (of the Southeast Climate Science Center), a member of the DCERP Climate Change Module Team, to identify data sets in completing a Headquarters Marine Corps (HQMC) survey regarding quantifying and qualifying past impacts and future "predictable" impacts and vulnerabilities because of climate change. Orders came out of the Office of the Secretary of Defense, from DoD's Climate Change Action Task Force.
- **June: Living Shorelines Implementation.** Dr. Currin (of NOAA) collaborated with staff from MCBCL's EMD and the N.C. Coastal Federation to install 1,100 *Spartina alterniflora* plants and 500 *Spartina patens* plants at three different locations along eroding edges of the Intracoastal Waterway and the New River Estuary.
- **June: Estuarine Simulation Model (ESM) Demonstration**. Drs. Mark Brush and Sam Lake (both from the Virginia Institute of Marine Science [VIMS] and Research Project TSP-2) met with natural resources managers from MCBCL and Marine Corps Air Station Cherry Point. The purpose of the meeting was to present the ESMs developed for the New and Neuse Rivers, obtain user feedback, and discuss application of the tool to answer real-world water quality questions.
- **July: DCERP DIMS Update**. Ms. Danette Boezio (of RTI International) met with Ms. Debbie Moffit and Mr. Scott Miller (both of MCBCL) to discuss DCERP data and to incorporate and share the data with MCBCL's data systems. DCERP data will most likely be classified as third-party data. The MCBCL geographic information systems (GIS) will retain the data before the information is posted, so metadata can be reviewed and updated.
- **September: DCERP Terrestrial Module Update.** Dr. Susan Cohen, the DCERP On-site Coordinator (OSC), briefed MCBCL's new EMD forestry staff about DCERP's research activities.
- **October: Marsh Adaptation Implementation Project.** Dr. Currin (of NOAA) met with staff from MCBCL's Range Development and Management Department (RDMD) and EMD to review the thin-layer dredge spoil disposal project proposed for the coastal marshes.

2015

- **April: RCC Meeting.** MCBCL staff and other stakeholders participated in this 1-day meeting at the MCBCL Officers' Club. This meeting included an open session for individual tutorials about the use of DIMS.
- **April: TAC Meeting**. MCBCL staff attend this 2-day meeting to hear progress about research and monitoring activities, with a focus on new project starts and synthesis of results at the thematic level. MCBCL and other DoD installation representatives provided input about their management needs. MCBCL hosted members of the TAC and DCERP Team and provided a briefing and tour of the Marine Corps Special Operations Command and demonstration of working dog training.

- **June: ESM at Eglin Air Force Base.** Drs. Brush and Lake (both of VIMS; Research Project TSP-2) visited Eglin Air Force Base in Florida to meet with Base personnel and local environmental groups. The purpose of the meeting was to present the DCERP planned modeling of Choctawhatchee Bay, the DCERP online modeling capabilities, and solicit feedback about key management issues and potential uses for the online model from Eglin staff and local non-governmental organizations.
- **July: Forest Carbon Management Tool.** Dr. Steve Mitchell (of Duke University) met with MCBCL foresters to discuss the LANDIS-II (Land and Information System) model, review the input variables (and whether they are representative of MCBCL forests), and discuss the potential model outputs and scenarios. In addition, Dr. Mitchell reviewed management scenarios proposed in the Research Plan and discussed how the results would be transferred to MCBCL.
- **December: Ecosystem Module Meetings.** Members of the DCERP Team from Research Project TSP-1 (Mr. Ben Donnelly of Duke University), RTI (Ms. Kimberly Matthews), and the Aquatic/Estuarine (Dr. Michael Piehler of the University of North Carolina at Chapel Hill's Institute of Marine Sciences [UNC-IMS]), Coastal Wetlands (Dr. Currin of NOAA), and Terrestrial (Dr. Mitchell of Duke University) Modules met with Base staff at MCBCL. Separate meetings were held for each ecosystem. During these meetings, MCBCL staff provided extensive feedback about what types of data they wanted in the interactive mapping application (iMAP) and the functionalities in which they were most interested. MCBCL staff completed electronic surveys to evaluate the effectiveness of each training session and obtain additional feedback about the functionality of DIMS. After the meetings, Dr. Cohen (the DCERP OSC) conducted individual meetings with MCBCL staff to obtain additional feedback about DIMS, including the inclusion of additional MCBCL data layers in iMAP that would be helpful to MCBCL staff.

2016

- **February: Coastal Barrier Module Meeting**. Members of the DCERP Team from Research Project TSP-1 (Ms. Boezio of RTI), RTI (Ms. Matthews), and the Coastal Barrier Module (Drs. Steve Fegley and Tony Rodriguez, both of UNC-IMS) met with MCBCL staff. MCBCL staff provided extensive feedback about what types of data they wanted visualized in iMAP and the functionalities in which they were most interested with regards to management of Onslow Island and its resources.
- **April: RDMD**. Dr. Cohen (the DCERP OSC) participated in a meeting organized by Mr. Chip Olmstead, the Deputy Director of the G3/5, RDMD at MCBCL. The RDMD would like to develop a combined arms amphibious assault course (CAAAC) at MCBCL. The potential CAAAC would allow amphibious assault vehicles to storm the beach, cross the Intracoastal Waterway along one of three routes, and travel to combat town. Dr. Cohen provided an overview and demonstrated DIMS and its usefulness to contribute to the decision-making process regarding site selection on short to medium (20- to 30-year) time scales.

- **April: RCC Meeting.** MCBCL staff and other stakeholders participated in this 1-day meeting at the MCBCL Officers' Club. This meeting included an open session for individual tutorials about the use of DIMS.

- **April: TAC Meeting.** MCBCL staff attended this 2-day meeting to hear about progress regarding research and monitoring activities, with a focus on synthesis of results and discussion of the schedule for remaining activities. MCBCL and other DoD installation representatives provided input about their management needs.

- **August: Onslow Beach: Support to Amphibious Landing Operations.** DCERP Team member, Dr. Rodriguez (of UNC-IMS), briefed U.S. Navy staff from Norfolk, VA; Marines from MCBCL, staff from MCBCL's Range Control (i.e., Col. Davis, LtCol. Kruse, LtCol. Warner, and Mr. Olmstead) and staff from other MCBCL groups who participate in these large (multi-country) training exercises. The meeting objectives were to

- Determine the range and training area requirements to support current and future combined arms amphibious assault training at MCBCL. Specifically, this objective involved determining the baseline beach requirements needed to support Marine Expeditionary Brigade–sized amphibious exercises and training and identifying guiding doctrine and publications. This objective also involved identifying key elements of the amphibious landing process that can be enhanced and/or developed through physical improvements, regulatory easements, or new or expanded range capabilities.
- Synchronize Bold Alligator plans with range regulations, limitations, and safety requirements. To address this objective, the following questions were discussed: What is actually going to be exercised? What is going to be simulated? What is going to be constructed? What safety regulations and features will be in play? Dr. Rodriguez delivered a presentation about the morphologic changes of Onslow Beach and showed the audience changes to the beach in terms of shoreline position, width, and elevation. Dr. Rodriguez also discussed the changes that he has personally observed since 2007.
- **October:** Dr. Cohen provided an update about DCERP research, with an emphasis on DIMS.
- **November: Sustainability of Onslow Beach Training Area.** Dr. Rodriguez met with Mr. Olmstead, MCBCL's RDMD, about the high rate of shoreline erosion in the training area and potential problems that could occur to military training as a result.

2017

- **February: DIMS Review Workshops.** Ms. Matthews and Research TSP-1 Team member (Ms. Boezio, both of RTI) conducted three 2-hour workshops at MCBCL. Base staff reviewed DIMS, with a focus on the response to previous comments from MCBCL.
- **May: DIMS Update.** Ms. Matthews and Research TSP-1 Team member (Ms. Boezio, both of RTI) facilitated a meeting with MCBCL staff to present recent updates to DIMS and obtain feedback about how to incorporate model results in DIMS.

- **May: Stakeholders' Meeting.** MCBCL staff and local stakeholders attended this 1-day conference in Jacksonville, NC. The meeting focused on management-relevant results from DCERP2.
- **August: Out brief: MCBCL Water Quality Management.** Dr. Piehler (of UNC-IMS) presented findings from research and monitoring investigations regarding MCBCL's storm water management and water quality impacts to the environment. Feedback from MCBCL staff will be incorporated into the Final Report.
- **August: Out brief: Change in the Upland Pine Forests of MCBCL: Ten Years of Study and Its Relevance to Forest Management.** Dr. Norman Christensen (of Duke University) presented recommendations to forest management practices at MCBCL.
- **September: Out brief: ESM.** Dr. Brush (VIMS) presented management-relevant findings from the ESM and provided training about how to properly use the online ESM. Dr. Brush will conduct briefings for Marine Corps Air Station Cherry Point and MCBCL.
- **September: Out brief: Red-Cockaded Woodpecker (RCW) Decision-Support System.** Drs. Sara Zeigler and Jeffrey Walters (both of Virginia Tech) presented management relevant findings from the RCW landscape model via a Webinar to MCBCL and Fort Bragg personnel.
- **September: NOAA Regional Congressional Roundtable: Science and Service in Support of North Carolina's Coastal Communities**. Dr. Cohen (DCERP OSC) presented DCERP findings highlighting NOAA's Science Maintains Military Readiness.
- **November: Out brief: ESM.** Dr. Brush (of VIMS) presented management-relevant findings from the ESM to federal staff and local stakeholders at Eglin Air Force Base in Florida.
- **December: Out brief: Coastal Barrier Morphology Model.** Dr. Jesse McNinch (of the Army Corps of Engineers) presented findings from the model regarding barrier island sustainability over the next 50 years.

Appendix 21-D
Data Dictionaries for Electronic Data Deliverables for DCERP Data Sets

Table 21D-1. Data Dictionary for Stations Electronic Deliverable.

Field Name	Required	Length	Field Type	Description
Activity group	no	40	Text	activity group name
Dataset_Name	no	20	Text	name of the dataset to be displayed in MARDIS
Station_Name	yes	40	Text	station name used by project (displayed in iMAP)
Station_Long_Name	yes	100	Text	longer more descriptive station name (displayed in iMAP)
Station_Type_Name	yes	40	Text	station type - from existing list
Latitude_Measure	yes		Numeric	latitude (decimal degrees)
Longitude_Measure	yes		Numeric	longitude (decimal degrees)
Collection_Method_ Name	yes	50	Text	collection method - from existing list
Reference_Datum_ Name	yes	40	Text	reference datum - from existing list
Agency	no	100	Text	agency responsible for station
Contact_Name	yes	100	Text	station contact name (first and last name)
Contact_Information	yes	200	Text	station contact information (e-mail address)
URL_Information	no	300	Text	URL for data stored external from MARDIS
Data_External	no	3	Text	yes/no - If yes, then data is not stored in MARDIS
Station_Comments	no	200	Text	Comments or additional station information

Table 21D-2. Data Dictionary for Results Electronic Deliverable.

Field Name	Required	Length	Field Type	Description
Station_Name	yes	40	Text	station name used in MARDIS - must be loaded in MARDIS prior to Results EDD upload
Sample_Name	no	40	Text	sample name created by user
Activity_Matrix_Name	yes	40	Text	activity matrix - from existing list
Activity_Type_Name	yes	40	Text	activity type - from existing list
Start_Date	yes		datetime	start date/time
End_Date	no		datetime	end date/time
Exceptional_Event	no	50	Text	indicates exceptional event sample - from existing list
Sampling_Equipment	yes	50	Text	sample collection equipment - from existing list
Sample_Collection_Method_Name	yes	40	Text	sample collection method - from existing list
Depth	no		Numeric	depth value for applicable samples
Depth_Min	no		Numeric	minimum depth value for applicable values
Depth_Max	no		Numeric	maximum depth value for applicable samples
Depth_Unit	no	60	Text	units of depth for applicable sample - from existing list
Depth_Type_Code	no	5	Text	type of depth (i.e. S - surface or B - bottom)
Parameter_Name	yes	60	Text	parameter being sampled - parameter must be loaded in MARDIS prior to Results EDD upload
Result_Value	yes	40	Text	measured result value
Measurement_Unit_Name	yes	60	Text	units of measurement - from existing list
Qualifier_Code	no	4	Text	result qualifier codes to further qualify or explain result (or lack of result) - from existing list
Statistic_Type_Name	no	40	Text	statistic type - from existing list
Standard_Deviation	no		Numeric	standard deviation - only applies to applicable statistic types
Analytical_Method_Name	no	70	Text	analytical method - from existing list
Detection_Quantitation_Limit	no		Numeric	detection limit value

(continued)

Table 21D-2. Data Dictionary for Results Electronic Deliverable (continued).

Field Name	Required	Length	Field Type	Description
Detection_Quantitation_Limit_Type_Name	no	40	Text	detection limit type - from existing list
Result_Comment	no	300	Text	result comment
Latitude_Measure	no		Numeric	latitude (decimal degrees)
Longitude_Measure	no		Numeric	longitude (decimal degrees)
Collection_Method_Name	no	50	Text	location collection method - from existing list
Reference_Datum_Name	no	40	Text	reference datum - from existing list

Table 21D-3. Data Dictionary for Biological Results Electronic Deliverable.

Field Name	Required	Length	Field Type	Description
Station_Name	yes	40	Text	station name used in MARDIS - must be loaded in MARDIS prior to Results EDD upload
Sample_Name	no	40	Text	sample name created by user
Activity_Matrix_Name	yes	40	Text	activity matrix - from existing list
Activity_Type_Name	yes	40	Text	activity type - from existing list
Start_Date	yes		datetime	start date/time
End_Date	no		datetime	end date/time
Exceptional_Event	no	50	Text	indicates exceptional event sample - from existing list
Sampling_Equipment	yes	50	Text	sample collection equipment - from existing MARDIS list (
Sample_Collection_Method_Name	yes	40	Text	sample collection method - from existing list
Depth	no		Numeric	depth value for applicable samples
Depth_Min	no		Numeric	minimum depth value for applicable values
Depth_Max	no		Numeric	maximum depth value for applicable samples
Depth_Unit	no	60	Text	units of depth for applicable sample - from existing list
Depth_Type_Code	no	5	Text	type of depth (e.g. S - surface or B - bottom)

(continued)

Table 21D-3. Data Dictionary for Biological Results Electronic Deliverable (continued).

Field Name	Required	Length	Field Type	Description
Subject_Taxon	yes	120	Text	taxonomic name of the subject - from existing list
Biological_Descriptor	no	40	Text	biological type description (e.g life stage, habitat)- from existing list
Biological_Description	no	60	Text	biological description (e.g. egg, hatchling, foraging) - from existing list
Individual_Identifier	no	20	Text	unique identifier for an individual being monitored
Parameter_Name	yes	60	Text	parameter being sampled - parameter must be loaded in MARDIS prior to Results EDD upload
Result_Value	yes	40	Text	measured result value
Measurement_Unit_Name	yes	60	Text	units of measurement - from existing list
Qualifier_Code	no	4	Text	result qualifier codes to further qualify or explain result (or lack of result) - from existing list
Statistic_Type_Name	no	40	Text	statistic type - from existing list
Standard_Deviation	no		Numeric	standard deviation - only applies to applicable statistic types
Analytical_Method_Name	no	70	Text	analytical method - from existing MARDIS list
Detection_Quantitation_Limit	no		Numeric	detection limit value
Detection_Quantitation_Limit_Type_Name	no	40	Text	detection limit type - from existing list
Result_Comment	no	300	Text	result comment
Latitude_Measure	no		Numeric	latitude (decimal degrees)
Longitude_Measure	no		Numeric	longitude (decimal degrees)
Collection_Method_Name	no	50	Text	location collection method - from existing list
Reference_Datum_Name	no	40	Text	reference datum - from existing list

Appendix 21-E
Example of a DCERP Data Fact Sheet

DCERP DATA FACTSHEET

Tributary Creeks – Estimated Monthly Yield

Data Set Name:	Estimated Monthly Yield
Outputs:	Tributary Creeks—stream flow, nutrient and sediment concentrations
Temporal Resolution:	1 year
Data Years	2008-2016

Description of data set

This data set was developed to identify the amounts of sediments and nutrients (nitrate, ammonia, dissolved organic nitrogen, and phosphate) that flow into the New River Estuary (NRE) and assess how land use on Marine Corps Base Camp Lejeune (MCBCL) affects estuarine water quality. In DCERP1 (2007–2011), 10 watersheds that drain into headwater creeks were monitored for in-stream water quality. In DCERP2 (2011–2015), five of the stations were monitored, with each representing a gradient in the amount of land development from 3% to 63%.

Land cover and watershed area in hectares (ha) of study sites.

Percent impervious is indicated in parentheses (source: Homer et al., 2007).

Site	Forested Land (ha)	Impervious Surface (ha)	Developed Land (ha)	Total Area (ha)
Air Station	14.76	20.96 (26.55%)	39.42	78.93
Tarawa	24.48	32.28 (23.2%)	63.9	139.14
Courthouse Bay	3.06	4.85 (15.5 %)	19.62	31.32
Cogdel	280.53	115.25 (13.8%)	209.16	835.83
Traps	5.76	2.11 (4.13%)	6.39	51.03
Southwest Creek	35.55	2.33 (3%)	6.66	77.49
Gillets	70.74	12.94 (2.86%)	35.28	452.97
Freeman	151.56	9.32 (1.6%)	21.69	588.24
French	80.28	8.56 (1.1%)	27.72	807.3
Camp Johnson	16.47	0.06 (0.27%)	0	22.32

Methods

A graphical separation technique was utilized to delineate between the baseflow component and total stream flow during storm events (Ward and Robinson, 2000). Groundwater contribution during storms was determined by extending antecedent conditions by interpolating from baseflow before the rain event to the point of greatest inflection on the falling limb of the hydrograph. A mass balance equation was used to determine the resultant storm flow contribution to nutrient (nitrate, ammonia, dissolved organic nitrogen, and phosphate) and TSS yield.

Collection of water samples at sites when automatic water samplers were deployed was at a fine temporal resolution throughout storms, which enabled development of a continuous record of nutrient and TSS concentrations by interpolating between measured samples. When automatic water samplers were not present, extrapolating measured data to half hour intervals was accomplished by applying quality control

(QC; flow versus concentration) generated polynomials to calculate concentration based on water flow. QC relationships were created using all available data within the study period, but applied only to those times and sites when automatic water samplers were not present.

New River Estuary tributary creek watershed yield was calculated by using loading rates from the gauged area in each zone of the estuary and then extrapolated based on total tributary creek watershed area in each zone.

Assessment of Data Variability

There were general patterns in annual loading, with higher loads of all constituents in years with higher precipitation. Seasonal patterns in discharge and loading were generally higher water volumes and loading in winter and lower water volumes and loads in summer. Exceptions to this annual pattern included large events in summer months that elevated loads.

Limitations of the Data

The loads are calculated for tributary creeks that drain to the New River Estuary and were determined for the portion of the watersheds that are located with Marine Corps Base Camp Lejeune.

Uncertainty in the Estimates

To assess the uncertainty of extrapolation of the loading from the tributary creeks, we chose the creek with the central value for yield (median) to make a central estimate, then used the 2nd ranked and 4th ranked yields to calculate a minimum and maximum yield, respectively.

Data Owner

Name	Mike Piehler
Affiliation	University of North Carolina at Chapel Hill's Institute of Marine Sciences
E-mail	piehler@unc.edu

Selected Publications

Stumpf, C.H., R.T. Noble, M.F. Piehler, and S. Thompson. 2010. Loading of fecal indicator bacteria in tidal creek headwaters: Hydrographic, meteorological, and terrestrial runoff relationships. *Water Research* 44(16):4704–4715.

Von Korff, BH, MF Piehler, and SH Ensign. 2014 Comparison of denitrification between river channels and their adjoining tidal freshwater wetlands. *Wetlands, 34*: 1047-1060.

Stumpf, C.H. 2011. *New Approaches and Technologies for Quantifying Fecal Contamination in Tidal Creek and Coastal Receiving Waters.* Doctoral Dissertation, University of North Carolina at Chapel Hill, Chapel Hill, NC.

Von Korff, B. 2011. *Spatial Variability of Denitrification in Tidal Freshwater Rivers*. Master of Science in Marine Sciences, University of North Carolina at Chapel Hill, Chapel Hill, NC.

Schwartz, R. 2010. *Land Use Affects the Timing and Magnitude of Material Delivery to Headwater Streams in Coastal North Carolina*. Master of Science in the Curriculum for the Environment and Ecology, University of North Carolina at Chapel Hill, Chapel Hill, NC.

Appendix 21-F
Data Catalogs

Table 21F-1. MARDIS Data Catalog

Dataset	Description	Total Stations	Parameters	Start Date	End Date	Number of Records
ATMOSPHERIC DEPOSITION (R)	Rainfall collectors (MDN) and throughfall collectors	5	pH; Sulfate; Total nitrogen; Precipitation, throughfall; Chloride; Nitrite-nitrogen; Nitrate-nitrogen; Phosphate, as P; Sodium; Ammonium, as N; Potassium; Magnesium; Calcium; Precipitation, volume collected	07-06-2009	05-27-2011	5,603
AWAC (M)	Nearshore (Oceanographic) - Hydrodynamic Acoustic Wave and Current (AWAC) data	2	Pressure; Wave height, significant; Wave height, 1/3; Wave height, 1/10; Wave height, maximum; Wave period, dominant; Wave period, peak; Wave period, mean zerocrossing; Wave direction, peak; Wave direction, spread; Wave direction, dominant; Unidirectivity index; Surface current speed; Surface water direction	03-18-2008	08-03-2010	277,816
BOAT WAKE (R)	Wave height resulting from boat wakes in the ICW	1	Wave height	02-01-2010	06-30-2011	4,762
CARBON BURIAL – DEEP CORES	Carbon burial in marsh and estuary sites	10	Carbon to nitrogen molar ratio; Total nitrogen; Bulk density; Total organic carbon; 13C, isotopic ratio; 15N, isotopic ratio; Total Pb-210; Excess Pb-210; Sediment accumulation rate; Mass accumulation rate; Carbon accumulation rate	09-13-2013	01-08-2016	2,236
EMISSION FACTORS (R)	Emission factors (EF) calculated assuming that the fuel-carbon content by mass is 42.6 % and all fuel-C species produced and emitted during PB were captured	10	Ammonium; Barometric pressure; Particulate matter (PM2.5); Temperature, air; Relative humidity; Sulfur Dioxide; Sulfate; Nitrate; Chloride; Potassium; Magnesium; Calcium; Aluminum; Copper; Zinc; Manganese; Iron; Sulfur; Carbon monoxide; Carbon monoxide, hi-res; Carbon dioxide; Carbon dioxide, hi-res; Particulate matter (PM2.5), hi-res; 1,2,3-TMBenzene; 1,2,4-Benzenetricarboxylic acid; 1,2,4-TMBenzene; 1,3-	03-19-2010	03-03-2011	3,900

Dataset	Description	Total Stations	Parameters	Start Date	End Date	Number of Records
			Butadiene; 1-Butene; 1-Methylchrysene; 1-Pentene; Butyl nitrate; 2-Ethyltoluene; 2-Hydroxy-4-isopropyl Adipic acid; 2-Methylpentane; 3-Ethlytoluene; 3-Methylpentane; 4-Ethyltoluene; 7-Oxodehydroabietic acid; Abietic acid; Acephenanthrylene; Acetate; Acetic; Adipic acid; a-Pinene; Azelaic acid; Benz(a)anthracene; Benzene; Benzo(a)pyrene; Benzo(b)fluoranthene; Benzo(e)pyrene; Benzo(GHI)fluoranthene; Benzo(GHI)perylene; Benzo(j)fluoranthene; Benzo(k)fluoranthene; b-Pinene; b-Sitosterol; Tetrachloroethylene; Trichloroethylene; Calcium, ionic; Campesterol; Cadmium; Dichloromethane; Bromomethane; Chloromethane; Methyl iodide; Methane; Chloroform; Cholesterol; Chrysene; cis-2-Butene; Coronene; Carbonyl sulfide; Chromium; Cyclopenta(cd)pyrene; Decanoic acid; Dehydroabietic acid; Dibenz(ah)anthracene; Dimethyl sulfide; Docosane; Docosanoic acid; Dodecanoic acid; Dotriacontane; Carbon, elemental; Eicosane; Eicosanoic acid; Ethane; Ethene; Ethylbenzene; Ethyne (Acetylene); Ethyl nitrate; Fluoride; Fluoranthene; Formate; Formic acid; Glutaric acid; Hydrochloric acid; Heneicosane; Heneicosanoic acid; Hentriacontane; Heptacosane; Heptatriacontane; Hexacosane; Hexacosanoic acid; Hexatriacontane; Nitric acid; Nitrous acid; i-Butane; i-Butene; Indeno(1,2,3-cd)pyrene; i-Pentane; Isopropyl nitrate; Isophthalic acid; Isopimaric acid; Isoprene; Isopropylbenzene; Potassium, ionic; Levoglucosan; Lithium; Linoleic acid; Linolenic acid; Methyl Nitrate; Magnesium, ionic; mp-Xylene; Sodium, ionic; n-Butane; Ammonia; n-Heptane; n-Hexane; Nickel; n-Octane; Nonacosane; Nonacosanoic acid; Nonadecanoic acid; n-Pentane; N-Propyl nitrate; Organic carbon; Octacosane; Octacosanoic acid; Octanoic acid; Octatriacontane; Oleic acid; Oxalate; Oxalic acid;			

Dataset	Description	Total Stations	Parameters	Start Date	End Date	Number of Records
			o-Xylene; Palmitic (Hexadecanoic) acid; Palmitoleic acid; Pentacosane; Pentatriacontane; Perylene; Phthalic acid; Picene; Pimaric acid; Pimelic acid; Propane; Propene; Propylbenzene; Pyrene; Rubidium; Retene; Sandaracopimaric acid; Antimony; Sebacic acid; Silicon; volume of air, Quartz filter; volume of air, Teflon filter; Strontium; Stearic (Octadecanoic) acid; Stigmastanol; Stigmasterol; Suberic acid; Succinic acid; Terephthalic acid; Tetracosane; Tetracosanoic acid; Tetradecanoic acid; Tetratriacontane; Titanium; Toluene; trans-2-Butene; Triacontane; Triacontanoic acid; Tricosane; Tricosanoic acid; Tritriacontane; Barium; 1,3,5-TMBenzene; Arsenic; Chlorine			
EPA CRITERIA (M)	EPA Criteria Pollutants -(Ozone, Sulfur Dioxide, Particulate Matter)	8	Particulate matter (PM2.5); Particulate matter (PM10); Ozone; Sulfur Dioxide	07-01-2008	09-30-2011	369,693
HISTORIC MET DATA - LAND STATIONS (M)	Historic Meteorology - land stations, on and off Base	3	Particulate matter (PM2.5); Particulate matter (PM10); Wind speed; Wind direction; Temperature, air	03-04-2005	09-30-2011	328,479
INVERTEBRATES/FISH/GHOST CRABS (M)	Benthic invertebrates, surf fish, and ghost crab monitoring	80	Count; Length	10-08-2007	09-13-2011	20,361
MARSH BIOMASS - FERTILIZED PLOTS (R)	Marsh Biomass - Fertilized plots	3	Dry Biomass (Live); Dry Biomass (Dead); Dry Biomass (Total Below Ground); Dry Weight (Dead) - Control 1; Dry Weight (Dead) - Control 2; Dry Weight (Dead) - Control 3; Dry Weight (Dead) - Fertilized 1; Dry Weight (Dead) - Fertilized 2; Dry Weight (Dead) - Fertilized 3; Dry Weight (Dead) - Nitrogen 1; Dry Weight (Dead) - Nitrogen 2; Dry Weight (Dead) - Nitrogen 3; Dry Weight (Dead) - Phosphorus 1; Dry Weight (Dead) -	03-29-2008	03-28-2010	854

Dataset	Description	Total Stations	Parameters	Start Date	End Date	Number of Records
			Phosphorus 2; Dry Weight (Dead) - Phosphorus 3; Dry Weight (Live) - Control 1; Dry Weight (Live) - Control 2; Dry Weight (Live) - Control 3; Dry Weight (Live) - Fertilized 1; Dry Weight (Live) - Fertilized 2; Dry Weight (Live) - Fertilized 3; Dry Weight (Live) - Nitrogen 1; Dry Weight (Live) - Nitrogen 2; Dry Weight (Live) - Nitrogen 3; Dry Weight (Live) - Phosphorus 1; Dry Weight (Live) - Phosphorus 2; Dry Weight (Live) - Phosphorus 3			
MARSH CARBON FLUX (R)	Continuous measurements of the net CO2 exchanges between the Freeman Creek marsh and the atmosphere, and between the upper New River Estuary (NRE) at the Officer's Club dock and the atmosphere were collected.	1	Barometric pressure; Wind speed; Wind direction; Temperature, air; Relative humidity; Solar irradiation, local; Water depth; Carbon dioxide flux, air-marsh, positive upward	10-20-2015	10-04-2016	373,785
MARSH GROUNDWATER & NUTRIENTS (M)	Shallow groundwater and nutrients in the New River Estuary marshes	60	Ammonium; Temperature, water; Specific conductance; Salinity; Dissolved organic carbon; Dissolved organic nitrogen; Nitrate/Nitrite; Orthophosphate; Total dissolved nitrogen; Water level, relative to NAVD88; Ferrous; Hydrogen sulfide; Sulfate	02-01-2008	11-06-2009	1,435,425
MARSH SEDIMENT CORES	Sediment carbon stock values from Marsh Sediment core	42	Sediment carbon stock	12-04-2013	05-16-2016	42

Dataset	Description	Total Stations	Parameters	Start Date	End Date	Number of Records
MARSH SEDIMENT ORGANIC MATTER/PARTICLE SIZE (M)	Marsh Sediment organic matter content percentage and sediment particle size	12	Gravel; Organic matter; Silt; Sand	02-19-2008	05-01-2011	52
MARSH VEGETATION (M)	Marsh composition and abundance	175	Count; Stem height; Percent cover; Length; Dry Biomass (Live); Dry Biomass (Dead)	09-08-2008	07-28-2016	7,557
MET DATA - LAND STATIONS (M)	Meteorology - land stations, on and off Base	13	Barometric pressure; Ceiling; Wind speed; Wind direction; Temperature, air; Photosynthetically active radiation; Relative humidity; Solar irradiation, local; Precipitation; Visibility; Moisture, fuel; Temperature, fuel	07-01-2008	09-30-2011	2,323,611
NEW RIVER - TIDAL FRESHWATER	Stationary samplers	2	Temperature, water; Specific conductance; Salinity; Dissolved oxygen concentration; Dissolved oxygen saturation; Water level, relative to instrument	05-10-2016	10-05-2016	20,404
NEW RIVER (USGS STATION) (M)	Streamflow and nutrient concentrations at New River at Gum Branch. Streamflow, tide, velocity, nutrient concentrations, salinity, dissolved oxygen, pH, and water temperature at New River at Jacksonville.	2	Chlorophyll a; Ammonium; Temperature, water; Salinity; Turbidity; Dissolved inorganic carbon; Dissolved oxygen concentration; Dissolved organic carbon; Dissolved oxygen saturation; Nitrate/Nitrite; Orthophosphate; Particulate nitrogen; Particulate organic carbon; Particulate phosphorus; Total dissolved nitrogen; Total dissolved phosphorus; Suspended sediment concentration; Conductivity; Total nitrogen; Total phosphorus; Ammonium, as N	04-07-2008	10-09-2016	1,938
NEW RIVER (USGS SUPPLEMENTAL TRANSECT) (M)	Nutrients and chlorophyll a at supplemental locations between the primary USGS stations	4	Chlorophyll a; Ammonium; Nitrate/Nitrite; Orthophosphate; Particulate nitrogen; Particulate organic carbon; Particulate phosphorus; Total dissolved nitrogen; Total dissolved phosphorus	03-29-2011	12-14-2011	108

Dataset	Description	Total Stations	Parameters	Start Date	End Date	Number of Records
NRE - ADCP (M)	New River Estuary - Acoustic Doppler Current Profiler	1	Water level, relative to instrument; Current speed, east-west; Current speed, north-south; Current speed, vertical; Current speed, magnitude; Current direction	02-20-2008	05-25-2008	2,569,581
NRE - DATAFLOW - MAINSTREAM (M)	Mainstream New River Estuary - Dataflow	103	Temperature, water; pH; Salinity; Turbidity; Barometric pressure; Dissolved oxygen concentration; Dissolved oxygen saturation; Chlorophyll in vivo; Carbon dioxide, partial pressure	02-11-2009	07-16-2015	1,252,766
NRE - DATAFLOW - SHALLOW (R)	Shallow water New River Estuary – Dataflow	44	Chlorophyll a; Temperature, water; pH; Specific conductance; Salinity; Turbidity; Colored dissolved organic matter; Chlorophyll b; Dissolved oxygen concentration; Dissolved oxygen saturation; Diffuse light attenuation coefficient; Chlorophyll in vivo; Nitrate/Nitrite; Organic matter; Total nitrogen; Bulk density; Total organic carbon; Chlorophyll c; Phaeophytin; Nitrate/Nitrite, extractable; Ammonium, extractable; Colored dissolved organic matter 440nm; Carbon dioxide, partial pressure	07-23-2007	07-17-2015	1,654,706
NRE- BENTHIC AND WATER COLUMN (R)	Benthic Functional Responses in the New River Estuary	19	Chlorophyll a; Ammonium; Temperature, water; pH; Specific conductance; Salinity; Turbidity; Colored dissolved organic matter; Dissolved inorganic carbon; Dissolved oxygen concentration; Dissolved organic carbon; Dissolved organic nitrogen; Dissolved oxygen saturation; Diffuse light attenuation coefficient; Photosynthetically active radiation; Chlorophyll in vivo; Nitrate/Nitrite; Orthophosphate; Particulate nitrogen; Particulate organic carbon; Total dissolved nitrogen; Total suspended solids; Nitrate; Nitrite; Phaeophytin; Respiration, DIC; Net community production, DIC; Gross primary production, DIC; Gross nitrogen mineralization; Nitrate/nitrite flux; Ammonium flux; Phosphate flux; Dissolved organic nitrogen flux; Colored dissolved organic matter 440nm; Carbon dioxide, partial pressure, delta	07-23-2007	07-16-2015	233,183

Dataset	Description	Total Stations	Parameters	Start Date	End Date	Number of Records
NRE- CTD (M)	New River Estuary - Conductivity, Temperature, Depth Sensor	2	Temperature, water; Specific conductance; Pressure	02-20-2008	08-11-2008	226,077
NRE- WATER COLUMN (M)	Mainstem New River Estuary water quality, nutrient chemistry, and phytoplankton biomass and productivity	10	Chlorophyll a; Ammonium; Dissolved silica; Temperature, water; pH; Salinity; Turbidity; Barometric pressure; Colored dissolved organic matter; Dissolved inorganic carbon; Dissolved oxygen concentration; Dissolved organic carbon; Dissolved organic nitrogen; Dissolved oxygen saturation; Diffuse light attenuation coefficient; Photosynthetically active radiation; Chlorophyll in vivo; Depth, Secchi disk depth; Nitrate/Nitrite; Orthophosphate; Particulate nitrogen; Particulate organic carbon; Particulate phosphorus; Primary productivity; Total dissolved nitrogen; Total dissolved phosphorus; Total suspended solids	10-11-2007	12-05-2016	79,738
NRE-YSI-SHALLOWS	Bimonthly sampling and sampling after episodic events at stations: AE-SW-1, AE-SW-3, AE-SW-9	3	Chlorophyll a; Temperature, water; pH; Specific conductance; Salinity; Turbidity; Dissolved oxygen concentration; Dissolved oxygen saturation; Chlorophyll in vivo; Water depth, total	07-15-2013	07-16-2015	69,614
OVERWASH SENSORS	Water-level loggers deployed in shallow wells derived the overwash records at Onslow Beach	4	Water level, relative to ground surface near well	06-04-2012	06-06-2015	218

Dataset	Description	Total Stations	Parameters	Start Date	End Date	Number of Records
PHYTOPLANKTON PHOTOPIGMENTS (R)	Phytoplankton Photopigments	10	ß-Carotene; 19'-Hexanoyloxyfucoxanthin; 9' cis-Neoxanthin; Alloxanthin; Antheraxanthin; Chlorophyll c1 and c2; Chlorophyll b; Chlorophyllide a; Diadinoxanthin; Diatoxanthin; Fucoxanthin; 19'-Butanoyloxyfucoxanthin; Chlorophyll a HPLC; Gyroxanthin; Lutein; Monadoxanthin; Myxoxanthophyll; Peridinin; Violaxanthin; Zeaxanthin	10-11-2007	10-04-2012	20,480
RAINFALL (R)	Rainfall from manual rain gauges and tipping bucket gauges	33	Precipitation	05-01-2008	06-24-2011	357,451
RCW - AVIAN POINT COUNT (R)	RCW - Avian point count data	148	Radial distance; Cluster size	04-10-2009	06-22-2010	33,102
RCW - CAVITY NEST (R)	RCW - Cavity Nest data	30	Nest count	04-10-2009	04-10-2011	950
RCW - SNAGS (R)	RCW - Snag data	30	Density	07-10-2009	07-25-2009	75
RCW - TREE CONTENTS (R)	RCW - Tree Contents	21	Tree cavity contents	04-16-2009	04-10-2010	1,251
RCW - VEGETATION (R)	RCW - Veg plot data	148	RCW habitat quality score	04-10-2009	04-10-2011	246
SEDIMENT ELEVATION TABLE (M)	Sediment elevation table	16	Sediment Elevation, relative to NAVD88	02-19-2008	11-18-2016	571
SHOREBIRDS - PRODUCTIVITY (R)	Shorebird nest productivity, nest success	65	Hatched; Nest found; Nest lost; Egg count	04-23-2008	06-23-2009	182
SHOREBIRDS - SURVEY (R)	Shorebird survey	65	Count	01-09-2008	08-03-2009	8,996

Dataset	Description	Total Stations	Parameters	Start Date	End Date	Number of Records
SHOREBIRDS - WASHOVER FANS	Bird nesting activity was assessed biweekly by walking along established transects on each of the three washover fans on the southern Onslow Beach.	6	Egg count	04-16-2013	06-14-2016	32
SHOREFACE BATHYMETRY - SEDIMENT CORE (M)	Sediment core data from Onslow Beach	13	%sand; %fines; %gravel; D50 (sand size); Sediment Description	09-23-2007	09-23-2007	703
SURFICAL BEACH SEDIMENT (M)	Sediment texture and composition	100	Calcium Carbonate; Gravel; Particle size	10-08-2007	09-08-2010	1,287
SUSPENDED SEDIMENTS	SSC and Turbidity measurements from Marsh Tidal Creeks	36	Temperature, water; Specific conductance; Salinity; Turbidity; Suspended sediment concentration; Water depth; Current speed, magnitude; Suspended sediment concentration, inorganic	06-28-2013	08-10-2015	7,010
TERRESTRIAL INSECTS (R)	Terrestrial insect composition and abundance	27	Count	06-15-2010	06-15-2010	3,785
TERRESTRIAL SOILS (R)	Soils research dataset	78	pH; Organic matter; Bulk density; Sodium; Potassium; Magnesium; Calcium; Aluminum; Boron; Copper; Estimated Nitrogen Release; Total Exchange Capacity; Zinc; Manganese; Calcium, percent base saturation; Iron; Hydrogen, percent base saturation; Potassium, percent base saturation; Magnesium, percent base saturation; Sodium, percent base saturation; Other bases, percent base saturation; Sulfur; Phosphorus; Tree cavity contents	05-04-2009	06-15-2010	7,122

Dataset	Description	Total Stations	Parameters	Start Date	End Date	Number of Records
TERRESTRIAL VEGETATION (M)	Terrestrial Vegetation	124	Percent cover; Basal Area; Stem diameter; Stem count; Fuel particles; Fuel weight	05-18-2009	06-01-2016	8,618
TRIBUTARY CREEKS - ISOTOPES (R)	Stable isotope analysis	8	13C, isotopic ratio; 18O, isotopic ratio; 15N, isotopic ratio	06-14-2010	05-07-2012	2,208
TRIBUTARY CREEKS (M)	Tributary Creeks - stream flow, nutrient and sediment concentrations	10	Ammonium; Temperature, water; Specific conductance; Dissolved oxygen concentration; Dissolved organic nitrogen; E Coli; Enterococcus; Flow; Precipitation; Nitrate/Nitrite; Orthophosphate; Total dissolved nitrogen; Total suspended solids; Total coliforms	08-28-2007	07-02-2015	2,434,309
WATER LEVEL/TIDE GAUGE (M)	New River Estuary water level/tide gauge data	2	Temperature, water; Salinity; Water level, relative to NAVD88; Water level, preliminary, relative to NAVD88	02-21-2008	12-24-2016	4,347,096
WET DEPOSITION (R)	MDN collectors	4	pH; Precipitation; Sulfate; Total nitrogen; Total organic carbon; Chloride; Nitrite-nitrogen; Nitrate-nitrogen; Phosphate, as P; Sodium; Ammonium, as N; Potassium; Magnesium; Calcium	06-23-2009	06-05-2011	7,852

Table 21F-2. iMAP Data Catalog

Data Set Title	Data Provider	Description
MCBCL BOUNDARY	Marine Corps Base Camp Lejeune (MCBCL) data	This data set is the installation boundary.
CANTONMENT	MCBCL data	This data set shows the areas of development that support the U.S. Marines and Sailors living aboard MCBCL. Development consists of operational, maintenance, and supply facilities in addition to troop billeting, family housing, academic and applied instruction, dependent schools, and commercial, community, medical, recreation, and other supporting facilities. Cantonment areas are separated from range training areas.
TRAINING AREAS	MCBCL data	Polygons represent areas where military training is conducted. Data are subtyped between the individual training areas and the large training blocks.
RANGES	MCBCL data	This data set displays a designated land or water area set aside, managed, and used to conduct research on, develop, test, and evaluate military munitions and explosives, other ordnance, or weapon systems, or to train military personnel in their use and handling. This data set does not include airspace.
SPLASH POINTS	MCBCL data	Points represent amphibious splash points where amphibious vehicles embark and disembark on shore from open water.
TANK TRAILS	MCBCL data	Arcs depict tank trail center lines.
FUTURE PROJECTS	MCBCL data	This data set displays the location where a proposed use of land and/or water has been made, but a project has yet to be created. Planned construction footprints can be labeled with the “Label Features” button on the map. A user can click on a footprint to bring up more information.
STORM WATER BEST MANAGEMENT PRACTICES (BMPS)	MCBCL data	This data set displays an accumulation of storm water that is impounded by a dam or weir. Owing to different regulatory and management practices, storm water ponds have been separated out from other types of impoundments, including bioretention basins, wet ponds, holding ponds, and sand filter basins. Storm water BMPs can be labeled with the “Label Features” button on the map.
AUTONOMOUS VERTICAL PROFILER	Rivers, creeks, and estuary	This data set shows the data that have been collected continuously by the autonomous vertical profilers (AVPs), which are anchored floating platforms, measure water column conditions every 30 minutes at two sites in the New River Estuary (NRE). This data set provides detailed information about the impacts of events (e.g., severe rain event, high winds from storm events) on surface to near-bottom water quality conditions.

Data Set Title	Data Provider	Description
NRE MAIN CHANNEL	Rivers, creeks, and estuary	Water quality data are collected monthly from sampling locations along the length of the NRE. The data set includes physical, chemical, and phytoplankton parameters for surface and near-bottom water samples. Data are used to assess the spatial and temporal variabilities in water quality, productivity, trophic state, and habitat conditions along the estuarine salinity gradient from the estuary's head to the New River Inlet.
NRE SHALLOW WATER	Rivers, creeks, and estuary	The Dataflow system continuously measured water quality parameters as the boat traveled around the perimeter of the NRE. At six stations along the Dataflow route, additional samples were taken for dissolved inorganic and organic nutrients and for organic carbon. These data were used to calculate nutrient and carbon concentrations and transformations throughout the NRE.
TRIBUTARY CREEKS	Rivers, creeks, and estuary	Routine monitoring of nutrient and sediment concentrations and stream flow were collected on MCBCL creeks that drain into the NRE or the Intracoastal Waterway (ICW). Stations were located above tidal influence and were used to calculate nutrient and sediment loadings to the NRE, representing different land cover types.
NEW RIVER U.S. GEOLOGICAL SURVEY (USGS) STATION	Rivers, creeks, and estuary	Stream flow, river stage, and water quality conditions were monitored at the USGS stream gaging stations at Gum Branch and at Jacksonville on the New River to understand conditions in the upper and lower reaches of the New River watershed and to quantify nutrient loading to the NRE from watershed sources.
NEW RIVER USGS SUPPLEMENTAL TRANSECT	Rivers, creeks, and estuary	Supplemental measurements of river discharge and nutrient concentrations were collected between the Gum Branch and Jacksonville USGS stream gaging stations in 2011 to better define the head of tide and the study processes affecting nitrogen concentrations in this area of the New River.
NRE CONDUCTIVITY–TEMPERATURE–DEPTH	Rivers, creeks, and estuary	High-resolution data regarding the salinity and temperature of the NRE were collected along with current and flow data to understand the tidal influence on circulation within the NRE.
DATAFLOW MAINSTREAM	Rivers, creeks, and estuary	The Dataflow system continuously measured water quality parameters as the boat traveled along the mainstem of the NRE from the estuary's head near Jacksonville to the New River Inlet. The purpose of the data set is to expand the spatial resolution of monthly fixed station monitoring data.
DATAFLOW SHALLOWS	Rivers, creeks, and estuary	The Dataflow system continuously measured water quality parameters as the boat traveled along the shallow shoals of the NRE from the estuary's head near Jacksonville to the New River Inlet. The purpose of the data set is to expand the spatial resolution of monthly fixed station monitoring data on the shoals.
WATER QUALITY EXPLORER	Rivers, creeks, and estuary	Water quality parameters from measurements made during estuary Dataflow cruises are summarized.

Data Set Title	Data Provider	Description
ESTIMATED MONTHLY NITRATE YIELD	Rivers, creeks, and estuary	The MCBCL tributary creek watershed nitrate yield was calculated in each zone of the NRE, and then was extrapolated based on total tributary creek watershed area in each zone. The data years were 2008 through 2016.
ESTIMATED MONTHLY TOTAL SUSPENDED SOLIDS	Rivers, creeks, and estuary	The sediment yield for the MCBCL tributary creek watershed was calculated in each zone of the estuary, and then was extrapolated based on total tributary creek watershed area in each zone. The data years were 2008 through 2016.
NRE BATHYMETRY	Rivers, creeks, and estuary	Interferometric swath bathymetry was used to produce this high-resolution (5-m) bathymetric map of the NRE in 2009 by the DCERP Team.
NRE REGIONS	Rivers, creeks, and estuary	For DCERP, the NRE was divided into three regions (i.e., upper, middle, and lower) to aid in reporting results and running predictive models. The estuary was further divided by water depth into shoal (less than 0.5-m average water depth) and channel (greater than 0.5-m average water depth).
ACOUSTIC WAVE AND CURRENT (AWAC) PROFILER	Beach and coastal barrier island	Wave and current data were collected continuously (every 15 minutes) by a Nortek AWAC instrument located near Riseley Pier offshore of Onslow Beach that provided simultaneous sampling of wave burst and current profile data. These data were used to verify the hydrodynamic models of the Onslow Bay region developed based on wave and wind data from several off-shore buoys.
BARRIER VEGETATION	Beach and coastal barrier island	Coastal barrier stations were sampled as part of the Terrestrial Module's vegetation monitoring program during DCERP1.
INVERTEBRATES, FISH, GHOST CRABS	Beach and coastal barrier island	Biological samples were collected along transects from the dune to the sub-tidal zone at focus sites across Onslow Beach and Bear Island. The purpose of this sampling effort was to determine whether military training activities on the beach affected the abundance of organisms that play important roles in supporting the bird and coastal fish populations in the region.
SHOREBIRD COUNTS	Beach and coastal barrier island	Shorebird surveys were conducted along established transects on the Onslow Beach at least once every 7 to 10 days in 2008 and 2009. Surveyors walked along the beach and boated or kayaked through the marsh to conduct surveys from 6:30 through 10:30 a.m. Surveys focused on 15 focal shorebird and tern species. Stations in this set were defined by the geographic coordinates of the species observed at the time of identification.
SHOREBIRD NESTS	Beach and coastal barrier island	From March through July in 2008 and 2009, researchers surveyed Onslow Beach for shorebird and tern nests. Nest locations were monitored with motion-triggered cameras to track nest outcomes: successful nest (at least one egg hatched), nest abandoned (eggs did not hatch 5 days after the predicted hatch date or adults were not observed defending a nest containing eggs for more than 72 hours), or nest lost (due to predation or other factors).

Data Set Title	Data Provider	Description
SHOREFACE SEDIMENT CORES	Beach and coastal barrier island	Detailed sediment analyses were performed on marine sediment vibracores, and results were used to characterize the bottom geology and nearshore sediment offshore along Onslow Beach. These cores were used to develop the history of the island overwash and washover fan deposition over the past 3,000 years and to measure the maximum annual depth of erosion on the beach.
SURFICIAL BEACH SEDIMENT	Beach and coastal barrier island	Sediment samples were collected along transects from the dune to the sub-tidal zone at focus sites across Onslow Beach and Bear Island. Sediment texture and composition, which can vary with the intensity of hydrodynamic processes, were measured to characterize habitat quality.
SHORELINE AND VEGETATION HISTORY	Beach and coastal barrier island	The locations of the shoreline (i.e., water line) and vegetation lines were digitized from aerial photographs. The vegetation line is an estimate of the landward extent of active overwash.
ONSLOW BAY BATHYMETRY: 2007	Beach and coastal barrier island	Bathymetry data are from the shallow region of Onslow Bay, adjacent to Onslow Beach, NC. Data were collected in 2007 by the DCERP Team.
AERIAL IMAGERY: 1938	Beach and coastal barrier island	Historic aerial photographs of the study area (from April 24, 1938) were provided by the Wilmington (NC) District of the U.S. Army Corps of Engineers (USACE).
AERIAL IMAGERY: 1989	Beach and coastal barrier island	Historic aerial photographs of the study area (from November 25, 1989) were provided by the Wilmington (NC) District of USACE.
SEA TURTLE NESTING (MCBCL)	Beach and coastal barrier island	Sea turtle nesting data were provided by MCBCL's Environmental Management Division. Surveys were conducted every morning during the nesting season (from May 1 through October 1) along Onslow Beach. Nests laid in locations on shore were low enough to be at risk of erosion or flooding, and any nests found in the active military training zone were moved to more protected locations on Onslow Beach.
AVIAN CAVITY NEST	Landscape and forest	This data set provides the count of nests for cavity-nesting birds on 30 9-ha plots at MCBCL. Plots were selected in upland stands dominated by longleaf pine (*Pinus palustris*) at least 60 years of age and that reflected the range of red-cockaded woodpecker (RCW) cavity tree densities available.
AVIAN CAVITY NEST SUCCESS	Landscape and forest	The contents of tree cavities included diameter at breast height of the cavity tree, tree type (hardwood, live pine, and dead pine; species for pines only), bird species, nest contents, whether cavity entrances were normal or enlarged, species of excavator if known (2009 to 2010), decay class of dead cavity trees (i.e., snags), cavity height and orientation, and location.
RCW AVIAN POINT COUNTS	Landscape and forest	A survey of breeding birds was conducted in 2009 and 2010 at 146 points spanning the range of RCW foraging habitat quality on MCBCL, as measured by the RCW foraging habitat matrix tool developed by the U.S. Fish and Wildlife Service.

Data Set Title	Data Provider	Description
AVIAN SNAG DENSITY	Landscape and forest	Data were collected regarding the availability of nesting substrates (e.g., pines, hardwood) to determine the strength of interactions between cavity-nesting bird communities on MCBCL. Data reported were snag density or number of snags per hectare.
TERRESTRIAL INSECTS	Landscape and forest	Terrestrial insect and spider community composition and abundance were determined at experimental forestry management plots.
TERRESTRIAL SOILS	Landscape and forest	Physical and chemical soil properties were determined from each experimental forestry plot.
TERRESTRIAL VEGETATION	Landscape and forest	Terrestrial forest communities were sampled for species composition and abundances of the floral species. Fuel load estimations were assessed by using standard U.S. Forest Service protocols.
TOTAL CARBON STORAGE FROM LANDIS-II (FOREST LANDSCAPE MODEL)	Landscape and forest	This data set presents the total live biomass carbon scenarios. Values are from a preliminary 2013 baseline, showing the total live carbon that is expected under different forest management practices.
SOIL TYPE	Landscape and forest	This data set identifies the soil type from the Onslow County Soil Survey.
FOREST STANDS (MCBCL)	Landscape and forest	This data set displays MCBCL forestry data from 2015. “Compartment” and “Stand” numbers can be displayed with the “Label Features” button on the map
BASAL AREA AND SITE INDEX (MCBCL)	Landscape and forest	This data set provides MCBCL forestry data from 2015.
VEGETATION LOSS AND GAIN	Landscape and forest	The change in green vegetation was determined from Land Remote-Sensing Satellite (Landsat) system images between 1984 and 2010 to examine the change in vegetation patterns and human development at MCBCL. Greenness gain is largely timber harvest areas that have regrown. Greenness loss is a good indicator of human impact and development. Permanent change indicates a change to impervious surface. Reduced vegetation is indicative of understory/mid-story thinning. Intense loss is indicative of clear-cutting or removal of all vegetation.
VEGETATION HEIGHT	Landscape and forest	The height of vegetation was determined from the 2013 MCBCL Light Detection and Ranging (LiDAR) data.
RED-COCKADED WOODPECKER HABITAT	Landscape and forest	RCW Habitat Quality Scores were determined by DCERP Researcher, Dr. Jeffrey Walters. RCW habitat quality scores ranged from 0 to 5 and are classified as non-habitat (0), unsuitable (1), potentially suitable (2 or 3), or suitable (4 or 5). Pine basal area were determined from MCBCL’s forest stand data.

Data Set Title	Data Provider	Description
FIRE AND BURN	Landscape and forest	This data set identifies the type of wildland fire: wildfire or prescribed fire. Wildfire is any unplanned or unwanted fire. Prescribed fire is ignited by management actions to meet specific objectives. Data were from 1995 through 2015.
MARSH BIOMASS FERTILIZED PLOTS	Coastal wetlands	Three experimental marsh plots were treated with the addition of nutrients (nitrogen and/or phosphorus) to measure the response of marsh vegetation (change in above-ground and below-ground biomass over time).
MARSH SEDIMENTS	Coastal wetlands	Marsh sediment data were collected at marsh sites before the installation of surface elevation tables (SETs) to analyze the relationship between elevation and site characteristics.
MARSH SHALLOW GROUNDWATER NUTRIENTS	Coastal wetlands	Shallow groundwater and nutrients were measured at marsh sites to determine the flow of nutrients from upland areas to the marshes and from the marshes to adjacent surface waters (ultimately to the NRE or the ICW).
MARSH SURFACE ELEVATION TABLES	Coastal wetlands	SETs were used to precisely measure small-scale (millimeter) changes in marsh elevation. These data were used to test models predicting marsh response to sea level rise and to measure the effects of fertilizer additions on marsh surface elevation change.
MARSH VEGETATION	Coastal wetlands	Marsh plant composition and density were quantified and peak annual above-ground biomass were estimated in permanent plots at each marsh site. The data were used to determine the relationships between environmental parameters and marsh distribution and production, to document changes in plant community composition, and to document marsh die-off and recovery.
WATER LEVEL TIDE GAUGE	Coastal wetlands	Water level data were collected every 6 minutes at two locations in the NRE to calculate tidal datums and to determine how tidal range, temperature, and salinity vary temporally and spatially.
VEGETATION ALONG SHORE	Coastal wetlands	Shoreline marsh vegetation species or general vegetation community were determined during field surveys in 2009.
SHORELINE TYPE	Coastal wetlands	Shoreline types (swamp forest, marsh, sediment bank, or modified) along the NRE and ICW were determined based on observations made in 2009 from a small boat. The shoreline type classification scheme was developed in consultation with MCBCL and the N.C. Division of Coastal Management staff.
SHORELINE MODIFICATIONS	Coastal wetlands	Further description of the type of modification for shoreline types was classified as “modified” or “miscellaneous.” Modifications were determined during field surveys in 2009 and were based on the classification scheme developed in consultation with MCBCL and the N.C. Division of Coastal Management staff.

Data Set Title	Data Provider	Description
SHORELINE HISTORY	Coastal wetlands	The NRE and ICW shoreline locations were digitized by using aerial photography from 1938 (ICW only), 1956, 1989, and 2004.
SHORELINE CHANGE 1956–2004	Coastal wetlands	Aerial photography from 1956, 1989, and 2004 was used to digitize the NRE shoreline edge. The wet–dry line was delineated on sediment shorelines, and the vegetation boundary was used on vegetated shorelines. The point-based method (Cowart et al., 2010) was used to measure the shoreline change rate at 50-m intervals.
MARSH AREA	Coastal wetlands	A combination of aerial imagery and field observations was used to determine extent of marsh area at MCBCL.
RAINFALL GAUGES	Air	Rainfall measurements from manual rain gauges and automatic tipping bucket gauges were collected across MCBCL from 2008 to 2010 to determine spatial variability in rainfall across MCBCL.
WEATHER STATIONS—LONG TERM	Air	A long-term record of weather data was recorded at the Marine Corps Air Station New River. Limited data from 2008 through 2011 are available in the Monitoring and Research Data Information System (MARDIS). Comprehensive data are available through MesoWest (see http://mesowest.utah.edu).
WEATHER STATIONS—SHORT TERM	Air	Temporary weather stations were established during DCERP to supplement the long-term record at the Marine Corps Air Station New River to characterize weather conditions at MCBCL.
ATMOSPHERIC WET DEPOSITION CHEMISTRY	Air	Data about the chemical composition of precipitation (i.e., wet deposition) across MCBCL were used to determine sources of nutrients to the NRE.
THROUGHFALL WET DEPOSITION CHEMISTRY	Air	Data about the chemical composition of precipitation (i.e., wet deposition) to the forest floor under forest communities at MCBCL are included in this data set.
NOAA NATIONAL SEA LEVEL RISE MODEL	National Oceanic and Atmospheric Administration (NOAA) National Sea Level Rise Model	This data set illustrates the scale of potential flooding.
TOTAL LIVE BIOMASS CARBON SCENARIOS		This data set shows total live carbon expected under different forest management practices. Values are from a preliminary 2015 baseline.
CLIMATE FORECASTS FOR EASTERN NORTH CAROLINA	Climate	Downscale forecasts of Eastern North Carolina climate parameters (i.e., temperature and precipitation) are included in this data set.